FEB - FRESENIUS ENVIRONMENTAL BULLETIN
Founded jointly by F. Korte and F. Coulston
Production by PSP - Vimy Str. 1e, 85354 Freising, Germany in
cooperation with PRT-Parlar Research & Technology
Vimy Str 1e, 85354 Freising

Printed in Germany-ISSN 1018-4619

Fresenius Environmental Bulletin is abstracted/indexed in:
Biology & Environmental Sciences, BIOSIS, CAB International, Cambridge Scientific abstracts, Chemical Abstracts, Current Awareness, Current Contents/Agriculture, CSA Civil Engineering Abstracts, CSA Mechanical & Transportation Engineering, IBIDS database, Information Ventures, NISC, Research Alert, Science Citation Index (SCI), Scisearch, Selected Water Resources Abstracts

CONTENTS

ORIGINAL PAPERS

PROBABILITY TO BUY AGRICULTURAL PRODUCTS FROM DIFFERENT SALES POINTS DURING COVID-19: AN EXEMPLARY SCENARIO ANALYSIS 4719
Rahmiye Figen Ceylan, Ilkay Kutlar, Mehmet Guven, Cagri Bayraktar

RESPONSES TO DROUGHT STRESS IN GERMINATING SEEDS OF *AGRIOPHYLLUM SQUARROSUM* (L.) AND *SETARIA VIRIDIS* (L.) 4730
Juanli Chen, Xueyong Zhao, Yaqiu Zhang, Yongqing Luo, Zhaoquan He, Rui Zhang, Hailun Yu, Runxia Zhang

CURRENT STATUS OF *TERMINALIA ARJUNA* AND *ALBIZIA LEBBECK* IN AGROFORESTRY SYSTEMS OF SOUTHERN PUNJAB, PAKISTAN 4742
Muhammad Farooq Azhar, Muhammad Arslan Pervez, Ihsan Qadir, Muhammad Zubair, Muhammad Farooq, Jahanzaib, Ghulam Yasin

AN EXAMPLE OF THE EFFECT OF DIET QUALITY ON THE IMMUNE SYSTEM OF AN INFECTED INSECT: *URESIPHITA GILVATA* (FABRICIUS, 1794) 4749
Oguzhan Yanar, Elif Fatma Topkara, Gizem Aykol, Fatma Gonul Solmaz, Sevcan Mercan, Ardahan Eski

STUDY ON CALORIFIC VALUE OF SEMI-COKE AND DESULFURIZATION EFFECT DURING PYROLYSIS OF BITUMINOUS COAL 4756
Chen Jihao, Li Yue, Chen Xinjuan, Zhang Lei, Yang Dongfeng

EFFECTS OF GENOTYPIC VARIATION AND SOME NEW PROTOCOLS ON GYNOGENESIS EFFICIENCY OF CUCUMBER 4763
Hasan Pinar, Seher Toprak, Fatih Hanci, Duran Simsek

THE INFLUENCE OF PERLITE AND IRRIGATION MANAGEMENT ON THE PROPERTIES OF POTATOES IN GYPSIFEROUS SOIL 4771
Wael Fahmi Abdulrahman Al- Shamary, Bassam A A H Alkhateb, Emad Telfah Abdel Ghani, Tawfiq M Al-Antary, Abdel-Monnem S Kahlel

ENERGY ANALYSIS OF WASTEWATER TREATMENT PLANT IN PAPER AND PAPERBOARD MILL 4779
Mehmet Recai Durgut, Busra Yarar

EFFECTS OF CADMIUM AND CHICKEN MANURE ON DRY WEIGHT AND SOME HEAVY METAL AMOUNTS FOR HEALTHY LETTUCE (*LACTUCA SATIVA* L.) CONSUMPTION 4787
Hakan Celik, Sita Sanele Kunene

EVALUATION AND ANALYSIS OF COORDINATED DEVELOPMENT OF ECOLOGICAL ENVIRONMENT AND ECONOMY 4798
Wanchun Zhu, Song Liu

ON-FARM IRRIGATION MANAGEMENT FOR SHALLOW WATER TABLE SOILS AT NORTH NILE DELTA EGYPT BASED ON TILLAGE PRACTICES AND ECONOMICS 4804
Abdelaziz Okasha, Alaa El-Bably, Amira Eid

RESEARCH ON THE COOPERATIVE COUPLING DEVELOPMENT OF RURAL TOURISM AND URBANIZATION CONSTRUCTION FROM THE PERSPECTIVE OF ECOLOGICAL CIVILIZATION 4823
Huijuan Ye, Li Mao

RESEARCH ON CYCLIC REDESIGN OF PRODUCT BASED ON INDOOR ECOLOGICAL ENVIRONMENT PROTECTION 4830
Yujie Shu, Sheng Kang, Jianping Jiang

RESEARCH ON THE ROLE OF AGRICULTURAL INFORMATIZATION CONSTRUCTION IN AGRICULTURAL DEVELOPMENT: BASED ON BIG DATA PLATFORM 4836
Tongzhou Yang, Shanlang Lin, Shijun Chen

MORPHOLOGICAL AND BIOCHEMICAL COMPARISON OF Bt CORN SEEDLINGS WITH NON TRANSGENIC COUNTERPARTS 4842
Oksal Macar, Kultigin Cavusoglu, Tugce Kalefetoglu Macar, Emine Yalcin

RESEARCH ON CONDENSATION HEAT RECOVERY PERFORMANCE OF R410A MULTIFUNCTIONAL HEAT PUMP SYSTEM 4850
Qing Luo, Jinping Li, Yuping Deng

COORDINATED DESIGN OF TOURISM AND ECOLOGICAL HABITAT ENVIRONMENT IN URBAN DEVELOPMENT 4855
Yuefang Guo

RESEARCH ON CORRELATION BETWEEN ECOTOURISM SERVICE QUALITY AND ENVIRONMENTAL POLLUTION 4861
Hanfei Lv, Wei Zhou

IN VITRO ANTIOXIDANT, ANTIMICROBIAL, ANTICANCER ACTIVITIES ASSESSMENT OF *THYMUS PECTINATUS*, SCREENING OF ENZYME INHIBITORY 4868
Merve Ergul, Gulsen Guclu, Mehmet Atas, Metin Durmus Cetin, Nuraniye Eruygur, Esra Ucar, Huseyin Askin Akpulat

EFFECT OF NaCl ON THE PHOTOSYNTHESIS PARAMETERS IN *SALIX MATSUDANA* KOIDZ 4875
Yi Jiang, Jiahui Han, Wenxiu Xue, Jinhua Zou

STUDY ON RISK ASSESSMENT OF URBAN GAS PIPELINE LEAKAGE BASED ON ECOLOGICAL PLANNING 4888
Jixin Zhang, Haoyuan Dai, Jian Kang, Maomao Li, Ruishen Wang, Qiuju You

CORRELATION BETWEEN WEATHER AND COVID-19 PANDEMIC IN JORDAN 4893
Eman Abdelhafez, Mohammad Hamdan

ANALYSIS OF CLIMATIC VARIATION AND DETECTION OF LAND USE CHANGES USING GEO-SPATIAL TECHNIQUES IN BAHAWALPUR DISTRICT, PAKISTAN 4901
Tanveer Ahmed, Rab Nawaz, Alia Ahmed

STUDY ON ENVIRONMENTAL PERFORMANCE EVALUATION OF GREEN BUILDING BASED ON BIM TECHNOLOGY 4911
Sen Xu

EFFECT OF POTASSIUM IODIDE IN WHEAT (*TRITICUM AESTIVUM* L.) 4921
Ozcan Caglar

MOLECULAR CHARACTERIZATION AND YIELD LEVELS OF LOCAL BEAN (*PHASEOLUS VULGARIS* L.) GENOTYPES GROWING IN EASTERN MEDITERRANEAN REGION 4928
Okkes Akin Boylu, Umit Girgel, Alihan Cokkizgin

EFFECT OF PHOSPHORIC ACID SPRAY ON RICE GROWTH AND YIELD UNDER SALINE SODIC SOILS 4935
Mahmoud Abdlehamed Elhity, Abdel Hamed Mohammed Omer, Bassiouni Abdelrazik Zayed, Abdelaziz Ali Assra, Montaser M Hassan, Yaser M Hafez, Khaled A Abdelaal

BIOLOGICAL MECHANISM OF THE REMOVAL OF *MICROCYSTIS* USING LOW INTENSITY ULTRASONIC IRRADIATION 4943
Bo Wang, Lingxi Luo, Ximing Zeng, Hui Zeng

SYSTEM REALIZATION PATH OF VISUAL SORTING ROBOT SYSTEM UNDER BIG DATA ECOLOGICAL ENVIRONMENT 4953
Zhe Yan, Hongda Liu, Qixian Cao

MORPHOMETRIC ANALYSIS TO INFER HYDROLOGICAL BEHAVIOUR OF CORUH RIVER BASIN (NORTHERN TURKEY) USING GIS TECHNIQUE 4962
Umit Yildirim

STUDIES ON NUTRITIONAL PHYSICOCHEMICAL AND FUNCTIONAL COMPOSITION OF FOUR SELECTED PLANTS OF NAMAL VALLEY (MIANWALI) PUNJAB PAKISTAN 4975
Muhammad Rizwan, Kafeel Ahmad, Zafar Iqbal Khan, Iftikhar Ahmed, Sonaina Nazar, Humayun Bashir

DIETARY VITAMIN E AMELIORATES ZINC-TISSUE CONCENTRATION IN ZINC-DEFICIENT PREGNANT RATS 4984
Amamra Sabrina, Khaldi Fadila, Sayah Sarra, Amamra Fatima

RESEARCH ON ECO-EFFICIENCY COMPENSATION MEASUREMENT OF ECOLOGICAL FUNCTION ZONE IN HUAIHE RIVER BASIN BASED ON CARBON EMISSION REDUCTION 4994
Shuhang Zhao, Yu Du, Gang He, Tiantian Wang

PERFORMANCE EVALUATION OF CMIP5 MODELS FOR PRECIPITATION AND TEMPERATURE OVER HAIHE RIVER BASIN, CHINA 5002
Hao Yang, Xiaofeng Chen, Ying Feng, Wei Jiao, Tiezhu Yan

EVALUATION OF COTTON GENOTYPES FOR DROUGHT TOLERANCE AND THEIR CORRELATION STUDY AT SEEDLING STAGE 5015
Nasreen Fatima Veesar, Wajid Ali Jatoi, Qurban Ali Channa, Shahnaz Memon, Naila Gandahi, Ghulam Aisha, Tarique Ali Jatoi, Wazir Ali Maitlo, Altaf Hussain Solangi, Lubna Rajput

APPLICATION OF MULTI SENSOR KALMAN FILTER IN ULTRASONIC WATER METER 5026
Fuqiang Zuo, Yu Liu

STUDY ON LOW POWER CONSUMPTION OF KALMAN FILTER 5033
Fuqiang Zuo, Yu Liu

STUDY ON THE INHIBITION EFFECT OF DIFFERENT ORGANIC FERTILIZERS ON KONJAK SOUTHERN BLIGHT 5040
Changming Liu, Juan Lin

STUDY ON THE CONTROL OF SOIL-BORNE DISEASES OF KONJAK BY WALNUT SHELL WOOD VINEGAR 5047
Changming Liu, Feng Xian, Juan Lin

DETERMINATION OF LOST FISHING GEAR IN THE INDLAND WATER OF TURKEY: SAMPLE OF KEBAN DAM LAKE (ELAZIG) 5054
Murside Dartay

RESEARCH ON THE COUNTERMEASURES OF PROMOTING THE INTEGRATED DEVELOPMENT OF RURAL THREE INDUSTRIES IN THE CONSTRUCTION OF BEAUTIFUL COUNTRYSIDE 5059
Tianbin Mao, Qian Li

DIAGNOSIS OF THE DURATION OF HEAVY RAINSTORMS UNDER SUBTROPICAL ENVIRONMENTAL CONDITIONS IN LOW-LATITUDE PLATEAU AREAS 5067
Jing Zhou, Yan Sun, Haiying Wu, Yang Shen

RESEARCH ON THE COUPLING AND COORDINATED DEVELOPMENT OF REGIONAL ECOLOGICAL ENVIRONMENT AND FINANCIAL SUPPORT IN THE PROCESS OF URBANIZATION 5075
Xueqing Kang, Yuanxin Zhang

RESEARCH ON CARBON RISK MANAGEMENT OF HIGH-POLLUTING PORT ENTERPRISES: BASED ON IOT TECHNOLOGY AND ECOLOGICAL PERSPECTIVE 5084
Qi Zhao, Bing Yang

MOLECULAR EPIDEMIOLOGY AND CHARACTERIZATION OF HEPATITIS DELTA VIRUS FROM PESHAWAR DIVISION KPK-PAKISTAN 5093
Izhar ul Haq, Muhammad Mumtaz Khan, Adnan Khurshid, Anees Muhammad, Mohammad Ejaz, Waqas Hussain Shah, Sajid Ali, Sadia Alam

TOXICITY OF FIVE PLANT EXTRACTS AGAINST CALLOSOBRUCHUS MACULATUS FAB. (COLEOPTERA BRUCHIDAE) A MAJOR INSECT PEST OF STORED PULSES 5098
Rasheed Akbar, Imtiaz Ali Khan

AN EXPERIMENTAL AND NUMERICAL STUDY OF TURBIDITY CURRENTS ENTERING A STRATIFIED RESERVOIR 5108
Rui Wang, Xi Mao, Lu Gao, Lijian Qi, Xiuyuan Lu, Yong Wang, Jidong Li, Chunhang Xie, Hao Yuan, Zhongluan Yan, Leilei Qin

IN SILICO SCREENING OF SHORT CHAIN FATTY ACIDS FROM ALGAE TARGETING ACE2 RECEPTOR FOR SARS-CoV-2: MOLECULAR DOCKING AND MOLECULAR DYNAMICS SIMULATION 5119
Selin Sayin

DETERMINATION OF GENETIC VARIABILITY OF POTATO VIRUS Y IN SAUDI ARABIA 5131
Adel A Rezk, Sherif M El-Ganainy, Khalid A Alhudaib, Mohamed Z Alyami, Muhammad N Sattar

ANALYSIS AND APPLICATION OF EXPONENTIAL STRENGTH CRITERION IN WELLBORE STABILITY INVESTIGATION DURING OIL AND GAS DEVELOPMENT 5140
Zhe Liu, Liang Zhu, Yishan Lou, Qing He, Chengfu Han

AGROINJECTION TECHNIQUE FOR TRANSIENT GENE EXPRESSION AS RAPID AND HIGHLY EFFICIENT METHOD FOR POTATO AGROBACTERIUM-BASED TRANSFORMATION BY CRY1CA GENE 5149
Mohei El-Din Solliman, Heba Allah A Mohasseb, Abdullatif A Al-Khateeb, Suliman A Al-Khateeb, Wael F Shehata, Mohammed I Aldaej

TECTONIC EVOLUTION OF THE NORTHWESTERN MARGIN IN THE JUNGGAR BASIN AND CALCULATION OF ITS STRUCTURAL SHORTENING 5161
Baocheng Wu, Zongyu Lu, Jiangang Shi, Chao Xiong, Wei Zhang

RESEARCH ON SEISMIC RESISTANCE OF SIMPLE SUPPORTED BEAM BRIDGES IN MOUNTAINOUS AREAS BASED ON THE NEW SEISMIC RESISTANCE CODE 5169
Miao Zhang, Chunxia Xie

ANALYSIS OF ULTIMATE BEARING CAPACITY FACTOR OF BURIED STRIP FOUNDATION ADJACENT TO SLOPE BASED ON TERZAGHI THEORY OF FOUNDATION ULTIMATE BEARING CAPACITY 5176
Yang Jiang, Wenhu Gu, Jiarui Chen

A SURVEY RESEARCH ON ENVIRONMENTALLY FRIENDLY CONSUMPTION BEHAVIOR 5187
Sule Turhan, SefaCakir, SelinTugba Varoglu

A STUDY ABOUT RECYCLING INTO THE NATURE AND THE REHABILITATION OF OPEN MINES THROUGH "MURGUL" SAMPLE CASE 5194
Hilal Surat, Mustafa Aybar

A DYNAMIC MODEL FOR CALCULATING THE THERMAL PARAMETERS OF HORIZONTAL WELLS WITH STEAM HUFF AND PUFF 5211
Qingchun Gao, Zhiming Wang, Quanshu Zeng

RESEARCH ON THE CONSTRUCTION STRATEGY OF GREEN CIVILIZATION MORAL EDUCATION IN COLLEGES AND UNIVERSITIES FROM THE PERSPECTIVE OF ECOLOGICAL CIVILIZATION 5220
Jia Liu

OPTIMIZATION OF ENERGY-SAVING AND ENVIRONMENTALLY FRIENDLY B & B BUILDING UNDER THE CONCEPT OF GREEN COUNTRYSIDE-TAKING SOUTHWEST ZHEJIANG AREA FOR EXAMPLE 5230
Yuchun Zheng

COMPARATION AMONG SORPTIVE CHARACTERISTICS OF CADMIUM BY SOLID WASTES-DERIVED BIOCHAR FROM AQUEOUS SOLUTION 5238
Hao Yang, Chengchun Sun, Can Zhang, Wei Jiao, Dan Zheng

EXPERIMENTAL STUDY ON THE THERMAL MANAGEMENT AND ACTIVE CONTROL OF DIESEL ENGINE EXHAUST PRODUCTS BASED ON ENERGY SAVING AND ENVIRONMENTAL PROTECTION REQUIREMENTS 5244
Ke Sun, Da Li, Hao Liu, Haiyang Zhao, Guodong Zhang, Shuzhan Bai

EVALUATION OF CARBONIFEROUS-PERMIAN HYDROCARBON SOURCE ROCKS IN HUANGHUA SAG, BOHAI BAY BASIN, CHINA 5254
Yun Zhao, Tao Li

ANALYSIS OF CHINA'S ENVIRONMENTAL KUZNETS CURVE FROM THE PERSPECTIVE OF PM2.5 INDEX 5262
Yan Yue, Yirong Ying

THE STRUCTURE OF SPERMATHECA IN THE SUBGENUS C*ASSIDA* (*CASSIDA*) LINNAEUS, 1758 (COLEOPTERA: CHRYSOMELIDAE: CASSIDINAE) AND ITS TAXONOMIC SIGNIFICANCE 5270
Huseyin Ozdikmen, Neslihan Bal

STUDY ON LIGHT REFLECTION MATERIAL CHARACTERISTICS OF DELINTED COTTONSEED AND ITS RELATIONSHIP WITH GERMINATION 5292
Hongzhou Zhang, Qiaohua Wang

COMPARISONS OF AGRICULTURAL USING BETWEEN SEWAGE SLUDGE AND LIVESTOCK MANURE FOR NUTRIENT LOADING, ECOLOGICAL RISK AND POTENTIAL IN TAIYUAN METROPOLITAN AREA 5302
Baoling Duan, Qiang Feng, Yushan Bu

SORPTIVE REMOVAL OF CADMIUM BY SULFURIC ACID/ULTRASONIC-MODIFIED STRAW BIOCHAR FROM SIMULATED EUTROPHIC WATER 5312
Chunxue Yu, Weikang Gao, Bai Yu, Wei Jiao

MONITORING THE VEGETATION PHENOLOGICAL CHARACTERISTICS IN MEADOW STEPPE USING SOLAR-INDUCED CHLOROPHYLL FLUORESCENCE 5320
Tong Dong, Hongqi Wu, Pingan Jiang, Junhui Cheng, Nurmemet Erkin, Haibin Gu, Yongkang Li

A NOVEL MASS METEOROLOGICAL DATA STORAGE SYSTEM BASED ON HADOOP ECOSYSTEM 5332
Quanpeng Ji

COMPARATIVE EFFICIENCY OF NEW HERBICIDES FOR WEED CONTROL ON QUALITY YIELD AND ITS COMPONENT IN MAIZE (*ZEA MAYS*) 5340
Abd El-Wahed A El-Sayed, Azza E Khaffagy, Fatma E M Shaheen, Yaser Hafez, Khaled Abdelaal, Fahmy A S Hassan, Dalia A Elhag

A NOVEL MEASUREMENT METHOD OF KEY NODES IN ECOSYSTEM PUBLIC OPINION COMMUNICATION NETWORK 5350
Huaibin Qin

THE EVALUATION OF INDIGENOUS GRAPEVINE PRODUCTION KNOWLEDGE BY SOIL CARBON IN A SEMI-ARID REGION SOUTHEASTERN TURKEY 5356
Gokhan Buyuk, Ceren A Bayram, Erhan Akca

RESEARCH ON CALCULATION METHOD OF STEAM ABSORPTION IN STEAM INJECTION THERMAL RECOVERY TECHNOLOGY 5362
Rui Deng, Ming Li, Song Linghu, Ruixiang Yang, Jingping Xie

DETERMINATION OF DESIGN PARAMETERS OF DAIRY CATTLE FOOT BATH WITH OZONATED WATER SYSTEM 5370
Erkan Gonulol, Goksel Tirpanci Sivri, Mehmet Recai Durgut, Ahmet Refik Onal

MICRO-PORE STRUCTURE CHARACTERISTICS OF THE CHANG 6 MEMBER SANDSTONE RESERVOIR IN HUANGJIANG OILFIELD ORDOS BASIN CHINA 5377
Jianmin Yang, Fu Leng, Haisheng Yu, Yuping Zhao

SENSITIVITY ANALYSIS OF STEAM INJECTION PARAMETERS OF STEAM INJECTION THERMAL RECOVERY TECHNOLOGY 5385
Rui Deng, Ming Li, Song Linghu, Ruixiang Yang

INVESTIGATION OF THE ANTIMICROBIAL AGENT POTENTIAL OF 1,5-DIKETONE DERIVATIVES 5395
Gursel Korkmaz, Ugur Tutar, Hayreddin Gezegen

ANTIOXIDANT ANTIMICROBIAL OXIDANT AND ELEMENTS CONTENTS OF *XYLARIA POLYMORPHA* AND *X. HYPOXYLON* (XYLARIACEAE) 5400
Beste Gizem Ozbey Saridogan, Cemil Islek, Hayri Baba, Ilgaz Akata, Mustafa Sevindik

COAL SEAM PERMEABILITY ENHANCEMENT TECHNOLOGY AND HIGH-VOLTAGE ELECTRICAL PULSE NEW TECHNOLOGY RESEARCH PROGRESS AND TREND 5405
Bin Li, Sheng Xue

EVALUATION OF YIELD AND QUALITY CHARACTERISTICS OF BREAD WHEAT GENOTYPES GROWN IN THE TYPIC HAPLOXERERT SUBGROUP SOILS 5415
Duygu Boyraz Erdem, Ferruh Feza Yilmaz

THE EFFECT OF DIFFERENT SALINITY LEVELS ON BIOMASS PRODUCTIVITY OF DIATOM SPECIES AND ACCUMULATION OF FUCOXANTHIN 5421
Leyla Uslu, Oya Isik, Mahamad Ahmat Hamid, Burcu Ak Cimen

LOW-ALTITUDE UAV REMOTE SENSING TECHNOLOGY AND ITS APPLICATION IN SURVEYING AND MAPPING OF A BAUXITE MINE 5429
Jiuling Tian

RESEARCH ON THE INTERNATIONAL DEVELOPMENT OF CHINESE THIRD-PARTY PAYMENT PLATFORMS BASED ON THE TWO-SIDE MARKET THEORY-A PERSPECETIVE OF GREEN DEVELOPMENT 5437
Cheng Cheng, Xiaobin Li, Jiapeng Wang

FOLIAR-APPLIED HYDROGEN PEROXIDE AND PROLINE MODULATES GROWTH, YIELD AND BIOCHEMICAL ATTRIBUTES OF WHEAT (*TRITICUM AESTIVUM L.*) UNDER VARIED N AND P LEVELS 5445
Naila Asghar, Nudrat Aisha Akram, Amina Ameer, Huma Shahid, Shameem Kausar, Ansa Asghar, Tayyaba Idrees, Sahar Mumtaz, Hafiz M Asfahan, Muhammad Sultan, Istakhar Jahangir

THE EFFECT OF HEAT STRESS ON THE COMPOSITION AND MICROBIOLOGICAL QUALITY OF BULK TANK MILK IN DAIRY CATTLE 5466
Ayse Deniz Cardak

POPULATION FLUCTUATIONS OF THE PISTACHIO TWIG BORER, *KERMANIA PISTACIELLA* AMSEL AND ITS PARASITOIDS 5476
Cevdet Kaplan, Mustafa Cemal Ciftci

WATER STRESS EFFECT ON CONFECTIONERY HYBRID SUNFLOWER (*HELIANTHUS ANNUUS* L.) CULTIVARS IN DIFFERENT GROWTH PERIODS 5486
Ismail Naneli, Ferzat Turan

COMPARABLE ANALYSIS ATMOSPHERIC DEFICITS AND WATER REGIME DURING DIFFERENT SEASON ON ALLUVIAL FLOOD FOREST HABITAT AT EAST SREM 5498
Milena A Andelic

RESEARCH ON THE DEVELOPMENT OF CULTURAL CREATION PRODUCTS OF ENVIRONMENTAL CERAMICS UNDER THE BACKGROUND OF DIGITAL CREATIVE INDUSTRY 5510
Xiaobo Lian, Sangyoung Lee

STUDY ON PROPERTIES OF CHEMICALLY MODIFIED DIAMOND LIKE CARBON FILMS 5516
Jin-mei Wu

EVALUATION ON CONSUMER ATTITUDES TOWARDS TO THE PURCHASE OF ECO-LABELED PRODUCTS 5521
Mirela Panainte-Lehadus, Valentin Nedeff, Narcis Barsan, Emilian Mosnegutu, Antonina Temea, Claudia Tomozei, Oana Irimia, Dana Chitimus

NOTICE

RESEARCH ON COORDINATED DEVELOPMENT OF REGIONAL ECOLOGICAL ENVIRONMENT AND ECONOMY 5529
Qiyue Chen, Shijun Chen, Tao Fan

COVID-19 MANAGEMENT: TRADITIONAL CHINESE MEDICINE VS. WESTERN MEDICINAL ANTIVIRAL DRUGS, A REVIEW AND META-ANALYSIS 5537
Muhammad Adnan Shereen, Nadia Bashir, Mubarak Ali Khan, Abeer Kazmi, Suliman Khan, Luo Zhen, Jianguo Wu

STUDY ON LOW-CARBON ECONOMY BASED ON ECOLOGICAL PERSPECTIVE 5550
Shuling Wang

ANALYSIS OF LOGISTICS EFFICIENCY BASED ON GREEN SUPPLY CHAIN 5557
Li Zhang

© by PSP Volume 30– No. 05/2021 pages 4719-4729 Fresenius Environmental Bulletin

PROBABILITY TO BUY AGRICULTURAL PRODUCTS FROM DIFFERENT SALES POINTS DURING COVID-19: AN EXEMPLARY SCENARIO ANALYSIS

Rahmiye Figen Ceylan*, Ilkay Kutlar, Mehmet Guven, Cagri Bayraktar

Akdeniz University, Faculty of Agriculture, Department of Agricultural Economics, 07059, Antalya, Turkey

ABSTRACT

The world has been facing a challenge. We have remembered that our way of living might change due to outer effects in a very short time period. COVID-19 pandemic that entered into our agenda in the first quarter of 2020 had led to many changes in our daily routines. Survival of lives includes not only being alive but also maintenance of daily needs. The most important need of livelihoods is daily nutrition of course. Yet, both our demand and way of meeting this demand have been facing with challenges as well. When accompanied with rising product prices and amount of products purchased, the operation of the sector was motivated with online sales opportunities. Departing from this view, it was intended to compare changing marketing tool preferences of individuals for fresh agricultural products. In this regard probabilities of 499 individuals surveyed online to maintain their agricultural purchases on district bazaars, on supermarkets or malls and via online order and delivery was compared under different scenarios for Turkey. The findings indicated that with rising spendable income and share of income on fresh product expenditures, probability to use online tools had raised during the pandemic process. Besides, there observed clues that tendency for online shopping was higher under lower or no loss of income during the pandemic. Under these conditions, the tendency to make agricultural and fresh product purchases and tools and media of marketing seem to be more challenging for educated and relatively young population in the future.

KEYWORDS:
COVID-19, agricultural products, sales point, consumer preference, logit, scenario analysis

INTRODUCTION

Change is one of the main subjects of livelihoods and we face with change every day. People can predict forthcoming events frequently and adapt themselves to changes. But some occasions are unpredictable and it is both hard to adapt and it requires changing many attitudes in life. By the end of 2019, the world had faced with the novel Coronavirus (COVID-19). By the time the virus disease appeared, the apparent global effects were not even considered. Within the passing months, a lot of lives were lost, health management systems were devastated, and many industries were stopped at least partly due to lock-down measures and services sectors were shut down almost in everywhere. Besides, face-to-face education from primary to tertiary level seems to be delayed in many countries, and adapting the education system still requires too much time.

In addition to these overwhelming challenges, economic processes were disrupted both on the producer and consumer levels. However, livelihoods have to meet their nutrition demand and agricultural and food products supply systems have to be maintained. In this regard, the observed changing preferences and attitudes of consumers seem to affect the future of agro-food markets as well. Departing from this point of view, this research intended to measure changing sales point preferences of consumers in their agricultural purchases with a random sample surveyed online in Turkey. With the survey and analysis, it was aimed to understand in which way the individuals maintained their fresh product purchases during the COVID-19 pandemic process that they have passed through until the time the survey was completed. The factors affecting the way that the randomly surveyed 499 individuals have made purchases on district markets or bazaars, on supermarkets or malls and online via internet orders, were analysed within a binomial logistic regression modelling. The aim was to estimate probabilities to make agricultural expenditures from different sales points and to build scenarios for comparing these agricultural shopping methods. Therefore, the paper follows with the provision of general background information on consumption on pandemic times, and the comparative analysis results were provided and discussed.

BACKGROUND INFORMATION

Since the announcement of the COVID-19 pandemic, the change in individuals' consumption attitudes had become visible directly. There appeared new needs like masks or disinfectants and the suppliers of these products have been experiencing a rather significant rising market share. In addition, lock-down implementations lead to over purchases of both durable and non-durable products in supermarkets. Especially, sanitation products or durable consumer goods like flour and dried legumes were sold out worldwide [1].

The changing consumption attitudes of households have been measured within the process and some projections for future were set forward. In addition to home office working in many sectors and maintenance of collaborative activities through social media and recently developed software, rising home orders and home delivery for consumables had become visible and the change seems to be sustainable even after the pandemic [2]. This change seemed to bring new regulations for consumption in the close future departing from the USA example [3].

The changing online and offline consumption volume was estimated for 214 cities of China [4]. It was understood from monitoring and evaluation of credit card operations that daily offline consumptions for goods and services fell by 32 % within the 12-weeks period. The fall in spending for services was much higher as 64 % for entertainment and 59 % for travel. Yet, face to face transactions for goods had declined significantly as well. The overall declination signed a reduction in the GDP of China by 1,2 % in comparison with 2019. The difference estimate findings also indicated a shift to online spending for consumer goods.

The effect of the pandemic was measured for Japanese households utilising credit card operation records focusing on sustainability of online consumption after the pandemic [5]. It was understood that most of the audience that had rising tendency for online shopping were composed of people having experience prior to the pandemic. Yet, there appeared new online shoppers and rising share was more for younger households. However, the findings did not infer a significant rise which will sustain after the pandemic. This inference was attributed to already high online consumption tendency of Japanese households.

Credit card transactions were observed for French consumers to compare online and offline consumption activities from the end of January to mid of April 2020 [6]. It was found out that despite the declining offline consumption for many sectors, the rising online consumption activities involving home delivery seem to compensate loss for consumption. Considering our main interest, purchases from grocery stores, markets and food stores had declined at beginning. The declination remained for offline purchases and it was compensated with online transactions afterwards. Therefore, consumers tended to shift online consumption in France within the considered time period. It was inferred that the online shopping tendency will be sustainable for many sectors involving agricultural purchases. Another inference was related with purchases of fresh products in the USA. 900 grocery shoppers were surveyed online and on-time change in consumer preferences was detected [7]. As much the COVID-19 process continues consumers' willingness to buy grocery products from the shop declines. This brought development of online order and home delivery systems for grocery stores into the agenda.

This situational change confirmed by the recent literature was valid globally and Turkey was no different. This was related not only with health considerations but also with trust in economics and maintenance of economic activities (Baltaci and Akaydin, 2020). Besides, households had directed their spendable income mostly on necessities within the process [8,9]. Mainly middle and upper classes have been shopping online for technological devices, textiles, or some sort of durable products before the pandemic as well. Yet, the changing attitudes were also visible on agro-food purchases, even for fruits and vegetables. Within the process, many households started to avoid from shopping in fresh markets or district bazaars for their FFV requirements [10]. Therefore, with lock-down implementations, neighbourhood markets that belong in supermarket chains had started to receive online orders and make home delivery as well.

However, demand and supply for agricultural products, especially those that are non-durable should be evaluated in order to estimate the future of the market. These products have low supply and demand elasticity and there expected no significant change in demand of households or services sectors. Meanwhile, countries had realised the importance of fresh product supply systems and the sustainability of farming practices [8]. Checking out the fresh fruits and vegetables supply system in Turkey, farmers used to bring their products either to wholesale markets or preferred direct sales, through personal communication or street vending. One of the main customer groups of wholesale markets and dealers has always been the services sector (hotels, restaurants and cafes) in Turkey. It is definite that the demand from organised retailers (outdoor catering services, touristic enterprises, public institutes, and educational institutes) had declined within the pandemic process. In the meanwhile, neighbourhood markets or exporters had become more important customers of the wholesale marketing system [11].

Yet, home orders and delivery had become a visible developing services branch throughout the

world [12] and the trend has been the same for Turkey as well. In the process, the credit card operations could be monitored and used as clues for improving online services. With regards to these transactions, the statistics published by the Interbank Card Centre provided us with some insights. The statistics indicated that 24 % of credit card operations took place online in Turkey in April 2020. Besides, it was found out that around 5 million credit cards were used for online transactions for the first time between March and April 2020 [13]. Therefore, households that were not very fond of online purchases, had started to involve in these sorts of activities and many people started to buy even their necessities online [14]. The challenge cannot be related just with durable products with respect to shrinking services sector and rising tendencies to cook and stay at home. Therefore, many households had started to buy fresh products online as well [15,16]. Accordingly, online purchases have become a developing tendency and modern commercial tools have been acknowledged even by those that call themselves as traditional customers [1].

Checking out a recent research conducted in Turkey with 200 households online, the elementary changes were observed [17]. Accordingly, 64,5 % of participants declared that their preferences towards online shopping had changed. While 52,5 % indicated that they started to make online shopping occasionally within the process, 46 % declared that they buy products online between one and three times per week. Besides, 61,5 % of the target group declared that they had started to buy agro-food products online as well. Another online survey conducted with 1.000 Turkish households by a private research company indicated that the households demand for pickles, sauces, packed food and flour and bread yeast had risen almost by 100 % within March and April 2020 [18]. These findings confirmed the need for food security of the individuals. In addition, demand for electronic devices to make yeast, bread or cake had risen significantly in March 2020, as measured by the number of searches recorded by Google [19].

Within the process rising tendency for online shopping of households on fresh agricultural products had been a significant observation. Accordingly, not the individual demand but the tools utilised to fulfil this demand seems to be changing [20]. Departing from this view, measuring the changing marketing tool or sales point preferences seems to be an important subject for the close future. Whether the observed rising tendency for online shopping will be sustainable or not should be clarified in order to organise supply systems of especially small size producers and suppliers. Accordingly, this paper aimed to measure the factors that were effective in preference of sales outlets to project potential changes for the future.

MATERIALS AND METHODS

The research data is based on an online survey conducted in the first two weeks of August 2020 via random distribution of the survey. The consumption data was collected from 499 Turkish consumers widespread in the country. The aim was to estimate the probability of individuals to maintain their agricultural purchasing activities in three different settings within the COVID-19 pandemic process. Agricultural purchases encompassed fresh and packed FFVs and animal products for the concerned analyses. The analysis aimed to search and compare the following probabilities.

- Probability to maintain agricultural purchases in district markets – bazaars during the pandemic
- Probability to maintain agricultural purchases in supermarkets or malls during the pandemic
- Probability to maintain agricultural purchases via online delivery systems during the pandemic

The probability to do so and factors affecting this probability were estimated departing from detected probabilities taking two variables, 0 and 1. Therefore, while the detected probability refers to taking an action (1) or not taking (0), estimated probability refers to a number ranging between 0 and 1 indicating the chance of occurrence by percentages. For the concerned analyses binomial logistic regression was used to estimate the non-normally distributed dependent variable including information on detected probability (0 and 1) which was developed by McFadden [21]. Logistic regression is used to estimate these sorts of models having a dependent variable with dichotomous nature and that invalidate classical OLS estimation assumptions [22,23].

In the estimated logistic regression equation, Y is the dependent variable taking 0 and 1 with regards to individuals' purchasing preferences. In addition, x represents quantitative and D represents qualitative independent variables that affect the detected probability via their parameter estimates.

The dependent variables of three equations were retrieved from five scaled preference data. The preferences were 1: none, 2: rarely, 3: occasionally, 4: frequently, and 5: very frequently. Therefore these three dependent variables were demonstrated in the Table 1 and incorporated independent variables were demonstrated in the consecutive Table 2.

$$log[Pr(Y = 1|x)] = \ln\left[\frac{Pr(Y = 1|x)}{1 - Pr(Y = 1|x)}\right] = \sum \beta_i x_i + \sum \alpha_i D_i + u_i$$

TABLE1
Estimated Dependent Variables

Y_b	1 if the individual has bought agricultural products from district markets/bazaars frequently or very frequently; 0 otherwise
Y_m	1 if the individual has bought agricultural products from supermarkets frequently or very frequently; 0 otherwise
Y_o	1 if the individual has bought agricultural products online frequently or very frequently; 0 otherwise

TABLE 2
List of Estimators

A_i	**Age of the participant**	Quantitative - Continuous
G_i	**Gender of the participant**	Binary - 1, if the participant is female
HHI_i	**Household Income**	Binary – 1 if the income is higher than 4.500 TL ($ 613,14)*
HHS_i	**Household Size**	Quantitative – numerical
VE_i	**Expenditure on FFVs and Food**	Quantitative – Continuous, TL
AE_i	**Expenditure on Animal Products**	Quantitative – Continuous, TL
TO_i	**Online Shopping Tendency**	Binary – 1 if the participant has a willingness to make purchases online hereafter
DI_i	**Downsizing in Household Income**	Quantitative – Continuous, TL

*: 4.500 TLs were considered as a moderate level of income for the analyses. Official exchange rate as of 31.08.2020 announced by the Central Bank of Turkey was $ 1 = 7,3393 TL. This rate is used hereafter.

RESULTS

Descriptive Layout. Firstly, it is important to note that many demographic characteristics of the correspondents were collected via the online survey implemented in August 2020. Around 60 % of the correspondents were female. Most of the survey participants were settled in the Mediterranean province of Antalya with 44 %. Although the sample was random, geographical dispersion was limited due to the time restriction of the survey. As the group was analysed with respect to education level, it was understood that the average education level was significantly high. College or bachelor's graduates referred to 54 % of the audience and this group was followed by post-graduates with 30 %. This finding can partly be explained by the methodology used, online survey. Yet, due to low variation in inhabitancy and education information of the group, these were not considered as factors explaining the probability to make agricultural shopping in targeted centres. The average age of the group was 39, but many age groups were represented in the sample. When the household size was overviewed, it was understood that 45 % of individuals were living in households with 4 or more members. Yet, 59 % of the audience indicated that they do not have children and they mostly live with their families or companions as friends.

Lately, data related to employment information of the audience were checked. It was understood that 300 people (60 % of the group) were employed on full-time basis while 12 % were either student or non-employed and 8,82 % were retired. 5 % of the audience were working part-time and the remaining 14 % were out of labour force. This inference continues with the distribution of calculated household income demonstrated in Figure 1.

Accordingly, 43 % of participants seemed to have a household income between minimum wage (2.318 TLs = $ 315,83) and $ 885,64. Yet, 52 % of participants declared that they have a monthly household income more than $ 885,64, which could be referred as more than moderate income. The detected more than average household income level can again be attributed to online survey implementation procedure.

The change in the employment status of the participants and their family members during the pandemic process were surveyed as well. It was understood that 15 % of individuals have a family member (either herself or another member) who has lost his or her job at least partly. Yet, 54 % of those who lost their jobs were still unemployed at the time of the survey, while 39 % declared that they lost their jobs temporarily (between 1 and 3 months). Among those having lost their jobs, 80 % (70 participants) declared receipt of no compensation wage. While 8 % of the audience indicated receipt of compensation wage between 3 months at most, 12 % declared they have been receiving this supportive payment by the time of the survey. In addition to changing employment situation, the

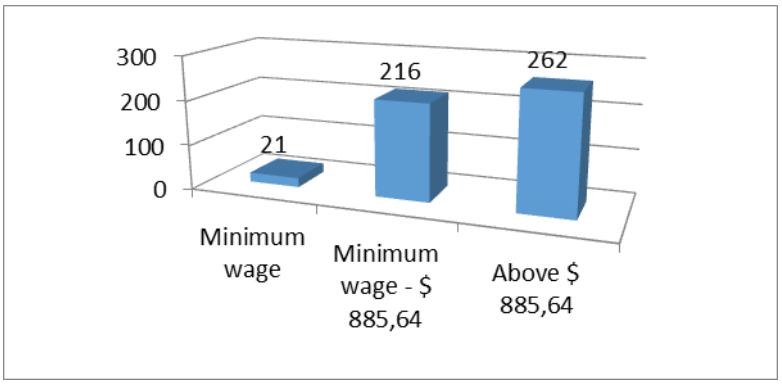

FIGURE 1
Income Scales of Surveyed Participants

changing household income was considered as well. It was understood that 70,67 % of participants have lost more than $ 136,25 of their household income. This group was followed with loss between $ 68,26 and $ 136,25 by 9,33 % and lower than $ 68,13 with 8 %. This signed possible changing consumption attitudes and preferences. After this brief explanation of the sample, the comparative probability estimation in terms of different sales points were made and evaluated.

Probability to make agricultural purchases in district bazaars. Initially, it is noteworthy to indicate that 57 of 499 individuals maintained going to bazaars within the COVID-19 process. This refers to 11 % of the individuals and provides us with the inference that many households avoided to go open markets. Accordingly, the probability was estimated against selected indicators and the magnitudes of these effects were measured. Table 3demonstrates the estimation findings.

Referring to estimation outputs, it can be indicated that single significances of parameter estimates are low, which is not a serious consideration for binary estimation procedures. The Mc Fadden R^2 produced for this dataset was low. However, significance of parameter estimates has been measured by Likelihood Ratio test [24] which provided a 90 % joint significance data. Yet, two distinguished statistics indicated that the results can be interpreted. Hosmer Lemeshow statistic indicated the goodness of fit of parameter estimates with a probability value higher than 0,05 [25,26]. Andrews statistic confirmed the interpretability of results with again probability greater than 0,05 [27,28]. Departing from this evaluation, the estimated probabilities were calculated for different variations of explanatory variables via antilog transformation and scenario evaluation was made with respect to average agricultural expenditure per month [29].

Checking the scenarios set forward, the indicative findings are rather significant. The alternative probability of maintaining agricultural purchases on district markets during COVID-19 process was calculated for female individuals having a monthly income more than $ 613,14. The differentiation was made with respect to age, potential tendency to make online shopping after the process, and the value of monthly expenditures on FFVs. Accordingly, the possibility to shop on bazaars for a 30 years old female having tendency to shop on online ranges from 21 % to 14 % due to average FFVs expenditures. The same scale reduces to from 9 % to 5 % for individuals not having intention to make online shopping. When the female is 40 years old, the scale changed from 22 % to 16 % for ones having online shopping tendency and from 9 % to 6 % for those that do not have online shopping willingness. These findings led us to draw the consecutive indications.

- Younger females have a lower tendency to shop on bazaars, even though the scales are not quite different statistically.

TABLE 3
Probability to Shop on District Markets/Bazaars during the COVID-19 pandemic

Parameter	Estimate	Z-statistic (probability)
Constant	-1,39	-2,80 (0,00)***
TO_i – Online Shopping Tendency	-0,26	-0,86 (0,38)
G_i – Gender	-0,38	-1,29 (0,19)
VE_i – Expenditure on FFVs and Food	-0,0002	-1,82 (0,06)*
HHI_i – Household Income	-0,49	-1,47 (0,13)
A_i - Age	0,01	0,83 (0,40)
Mc Fadden R^2 = 0,03	**MDV= 0,11**	**H-L (prob)= 4,53 (0,81)**
LR (prob)= 10,98 (0,05)*		**Andrews (prob)= 5,09 (0,89)**

TABLE 4
Estimated Probability to Shop on District Markets/Bazaars during the COVID-19 pandemic

	VE=$ 68,13	VE=$ 136,25	VE= $204,38	VE= $ 272,51
Female, Age 30 Tendency for Online Shopping + $ 613,14 monthly income	0,21	0,18	0,16	0,14
Female, Age 30 No tendency for Online Shopping + $ 613,14 monthly income	0,09	0,07	0,06	0,05
Female, Age 40 Tendency for Online Shopping + $ 613,14 monthly income	0,22	0,19	0,18	0,16
Female, Age 40 No tendency for Online Shopping + $ 613,14 monthly income	0,09	0,08	0,07	0,06

- The possibility to make agricultural purchases on bazaars reduces significantly with respect to the amount devoted for FFVs purchases from their budgets. Reduction in the possibility for 30 years old females that allocate $ 68,13 or $ 272,51 of her income was 33 % and 44 % with respect to having the tendency for online shopping afterwards. The differentiation for 40 years old females was 27 % and 33 % respectively. This finding indicated that the reduction in the estimated probability is higher for younger females.
- The detected difference in favour of having tendency for online shopping even after the pandemic process needs further assessment as it is not in conformity with the expectations.

Probability to make agricultural purchases in supermarkets/malls. The number of individuals that maintained shopping for fresh agricultural products on supermarkets or market sections of shopping malls was 198. This meant 40 % of the overall sample. Therefore, the probability of an individual to shop on these stores was estimated against properly selected indicators and the findings were indicated in the Table 5.

Considering the statistical findings and referring to the methodological approach indicated in the analysis for bazaars, the probability to shop on markets were estimated on age, household income and household size and expenditure on FFVs and animal products. Using these estimates, different scenarios were produced for households that have one companion in the house and have more than $ 613,14 of monthly income. The differentiation was made with respect to monthly expenditures on FFVs and animal products and for two different age scales. The findings were demonstrated in the Table 6.

In the first instance, the expenditure of an individual who spends $ 68,13 on animal products per month and lives with one other person was compared for his/her age, taking 30 and 40 years as base, and for FFVs expenditure per month. For 30 years old individuals the probability ranged from 39 % to 43 % due to expenditure on FFVs, while the scale ranged from 34 % to 38 % for 40 years old. However, when the same comparison was made for those who spend $ 136,25 on animal products per month the possibility ranged from 35 to 40 % and

TABLE 5
Probability to Shop on Supermarkets/malls during the COVID-19 pandemic

Parameter	Estimate	Z-statistic (probability)
Constant	-0,50	-1,05 (0,29)
HHI_i – Household Income	0,35	1,49 (0,14)
VE_i – Expenditure on FFVs and Food	0,00011	1,09 (0,27)
AE_i – Expenditure on Animal Products	0,00028	-1,50 (0,13)
A_i - Age	-0,02	-2,51 (0,01)
HHS_i – Household Size	0,22	2,16 (0,03)
Mc Fadden R^2 = 0,02	**MDV= 0,39**	**H-L (prob)= 14,08 (0,08)**
LR (prob)= 16,40 (0,00)* **		**Andrews (prob)= 15,87 (0,11)**

TABLE 6
Estimated Probability to Shop on Super-markets/malls during the COVID-19 pandemic

	VE=$ 68,13	VE=$ 136,25	VE= $204,38	VE= $ 272,51
Age 30 + $ 613,14 monthly income Household size – 2 (fixed) Expenditure on Animal Products – $ 68,13	0,39	0,40	0,42	0,43
Age 40 + $ 613,14 monthly income Household size – 2 (fixed) Expenditure on Animal Products – $ 68,13	0,34	0,35	0,36	0,38
Age 30 + $ 613,14 monthly income Household size – 2 (fixed) Expenditure on Animal Products – $ 136,25	0,35	0,37	0,38	0,40
Age 40 + $ 613,14 monthly income Household size – 2 (fixed) Expenditure on Animal Products – $ 136,25	0,30	0,32	0,33	0,34

30 % to 34 % with respect to age and expenditure on FFVs. The inferences retrieved from the findings were discussed respecting the features of the purchaser.

- For individuals that spend more on animal products, the probability declined for both age groups and FFVs expenditure scales. This can be read as less dependence on vegetable or packed food consumption of individuals that prefer more protein content in their daily nutrition.
- Despite the declining probability to make agricultural purchases on bazaars with respect to rising share of expenditures on FFVs, the tendency to go to supermarkets or malls rises hereby. The declination for those that spend $ 68,13 for animal products rose by 11 % and by 14 % for those that spend $ 136,25 for both age groups. The rise is higher for people that spend more on animal products. This might seem controversial. However, the comparison was made within the group and overall declination in the possibility for all scales respecting expenditure on FFVs is valid. This finding just means a higher rise for people having higher expenditure on animal products.
- The aggregate difference can be set forward as 13 % declination in the estimated probability from ones that spend $ 68,13 both for FFVs and animal products to individuals that spend $ 272,51 on FFVs and $ 136,25 on animal products. Accordingly, this confirmed the declined tendency of individuals that depend more on protein-based consumption.

Probability to make online agricultural purchases. It was first important to note that 98 individuals referring to 20 % of the sample indicated that they used online tools for fresh product purchases. Considering the number of individuals that have willingness to maintain online purchases after the pandemic process was 209, it is possible to note that most of the targeted audience were satisfied with

TABLE 7
Probability to Shop Online during the COVID-19 pandemic

Parameter	Estimate	Z-statistic (probability)
Constant	-0,87	-1,42 (0,15)
G_i – Gender	0,29	1,18 (0,23)
HHI_i – Household Income	1,38	3,96 (0,00)***
VE_i – Expenditure on FFVs and Food	0,00034	0,33 (0,73)
DI_i – Downsizing in Household Income	-0,20	-1,29 (0,19)
A_i - Age	-0,04	-3,28 (0,00)***
HHS_i – Household Size	-0,10	-0,81 (0,41)
Mc Fadden R^2 = 0,06	**MDV= 0,19**	**H-L (prob)= 5,87 (0,66)**
LR (prob)= 29,01(0,00)* **		**Andrews (prob)= 5,63 (0,85)**

online tools and orders for this probability analysis. 73 out of 98 individuals confirmed the maintenance of online agricultural purchases hereafter. This can be read that 75 % of online purchasers considered the online tools as sustainable, while the remaining individuals had to do online shopping due to lock-down measures. Finally, the estimated probability to make online purchases for agricultural consumption was calculated with the same methodology. Yet, the tendency to maintain online purchases was not considered as an explanatory due to its high correlation with the probability.

Depending on the results, the estimated probability to make agricultural purchases online was explained by gender, age, expenditure on FFVs, household size and household income and reduction in monthly income during the COVID-19 process. The analyses lead us to set forward six scenarios to estimate the probability with respect to age and reduction in monthly income. Females having more than $ 613,13 household income and living with a companion was compared due to age, 30 or 40, and from lower than $ 68,13 and to more than $ 136,25 income loss. The final calculations were made with respect to the value of FFVs expenditures. The estimated probabilities and explanations were indicated in the Table 8.

The probability of an individual being more than 30 years old was higher when her share of FFVs expenditure was higher and it reduced by the rising lost income during the pandemic. The scale ranged between 36 % and 48 % for income loss lower than $ 68,13, between 31 %, 43 % for income loss between 68,13 and $ 136,25 and between 27 % and 38 % for loss more than $ 136,25. For females older than 40 years, the same scales started from a lower level. While the highest probability for females that lose less than $ 68,13 of her income was 42 % for the highest share of FFVs expenditures, the individual having lost more than $ 136,25 seemed to have a probability to shop online by 32 %. Accordingly, there are significant inferences withdrawn.

TABLE 8
Estimated Probability to Shop Online during the COVID-19 pandemic

	VE=$ 68,13	**VE=$ 136,25**	**VE= $204,38**	**VE= $ 272,51**
Female, Age 30 + $ 613,14 monthly income Household size – 2 (fixed) Downsizing in household income – $ 68,13	0,36	0,40	0,44	0,48
Female, Age 30 + $ 613,14 monthly income Household size – 2 (fixed) Downsizing in household income – $ 136,25	0,31	0,35	0,39	0,43
Female, Age 30 + $ 613,14 monthly income Household size – 2 (fixed) Downsizing in household income – + $ 136,25	0,27	0,31	0,34	0,38
Female, Age 40 + $ 613,14 monthly income Household size – 2 (fixed) Downsizing in household income – $ 68,13	0,30	0,34	0,38	0,42
Female, Age 40 + $ 613,14 monthly income Household size – 2 (fixed) Downsizing in household income – $ 136,25	0,24	0,27	0,31	0,34
Female, Age 40 + $ 613,14 monthly income Household size – 2 (fixed) Downsizing in household income – + $ 136,25	0,22	0,25	0,28	0,32

- While the amount devoted for FFVs expenditures and the probability to shop online changes in the same line, the change with respect to rising income loss is vice versa.
- The rise for 30 years old individuals that have lost less than $ 68,13 of their income, having agricultural expenditures between $ 68,13 and $ 136,25 is 33 % on average. Despite starting from a lower estimated level, the same change for females that were 40 years old was 40 %.
- The rise for 30 years old that have lost more than $ 136,25, was 42 % and it was 46 % for those older than 40.
- Younger females with higher household income and lower declination in income during the pandemic process seemed to have higher tendency to buy fresh agricultural products online.

Evaluation and Conclusion. We have been living in an era that many things in our lives have been changing. The COVID-19 pandemic has many unfortunate effects on people and the operation of the global world. Yet, nobody is sure whether the health dimension can be controlled soon or whether the challenges we have been facing can be reverted. In addition to global and macro changes, our daily lives were affected as well. We are much less social and our intention to reach outdoor leisure activities has declined desperately. In line with these challenges, our consumption preferences and attitudes have been changing. Considering these micro-challenges, it was intended to determine how individuals had maintained their purchases and consumption of agricultural products within the pandemic process. The sales point preference of consumers and factors affecting this preference appeared as a concept to be assessed. Accordingly, with utilisation of survey data withdrawn from 499 individuals in Turkey in August 2020, the probabilities of individuals shopping on district markets, super-markets and with utilisation of online delivery services were estimated and compared within different scenarios for their agro-food purchases.

The findings were considerably interesting. It can be definitely inferred that young and educated part of the society has been shifting to online purchases of anything possible including agricultural products. There is not a significant difference for shopping on district bazaars with respect to age for females, if they do have a tendency or experience for online shopping. However, with the rising share of income devoted for vegetative products, the tendency to shop on bazaars seemed to decline within the sample. The dependence of individuals for shopping in super-markets or malls seemed to be higher. People seemed to shop in supermarkets more irrespective of their gender, if they are younger and if they spend less on animal products. When the probability of online fresh product purchases was considered, younger females that have lost less income compared to others and that devote more of their income to vegetable expenditures seemed to maintain their fresh product purchases via online tools more. As an important share of the audience (more than 70 %) indicated that they have lost more than $ 136,25 of their income, the possible shift leads us to consider future challenges.

These findings showed us that more individuals might shift to make online shopping for any sort of product. Up until now, online shopping was a preferable alternative for purchases of durable products as technical devices, textiles, furniture or sanitary products. These sort of purchasing attitudes have been mostly related with the need to save time. Yet, the pandemic had brought online delivery systems as alternative channels for nutrition demand as well. Online sales outlets might constitute an important supplier for both durable and non-durable agro-food product purchases in the close future. A sign for this challenge is developing delivery systems of retail chains. Online agro-food shopping might be more widespread as more retail chains have been adapting to online order and home-delivery. In addition to individuals that want to save time during their purchases, individuals having health and sanitation considerations will prefer online shopping more. This attitude change related with the COVID-19 pandemic process seems to be continuous. In other words, shopping tendencies and sales point preferences of individuals mostly with more than moderate income will maintain their shopping activities even after the pandemic ends. This can be understood from the rising tendency of younger population with relatively higher income and lower income loss to shop online.

Yet, within this comparative evaluation, it is not possible to infer that the whole society will decline face to face shopping. Many households have the intention to make agro-food purchases in physical outlets, and many people will continue to buy fresh agricultural products from bazaars or district markets. However, it is also apparent that the tendency to shift online purchasing has been rising and will become more widespread. Accordingly, both producers and primary and secondary level suppliers need to get prepared for this tendency of the society composed of educated individuals with higher income.

Departing from this brief field study, it can be inferred that the future of agro-food markets will be much more challenging and the whole system from production to final sales should get prepared. In this regard, producers and wholesalers of fresh products need to adapt to online marketing systems and improve their technological infrastructure and technology use.

REFERENCES

[1] Baker, S.R., Farrokhnia, R.A., Meyer, S., Pagel, M., ve Yannelis, C. (2020) How does household spending respond to an epidemic? Consumption during the 2020 COVID-19 Pandemic. NBER WP: 26949. National Bureau of Economic Research.

[2] Cohen, M.J. (2020). Does the COVID-19 outbreak mark the onset of a sustainable consumption transition? Sustainability: Science, Practice and Policy. 16(1), 1-3.

[3] Sheth, J. (2020). Impact of Covid-19 on consumer behavior: Will the old habits return or die? Journal of Business Research. 117, 280-283.

[4] Chen, H., Qian, W., and Wen, Q. (2020). The Impact of the COVID-19 Pandemic on consumption: Learning from high frequency transaction data. SSRN Electronic Journal. https://ssrn.com/abstract=3568574 . pp: 51 (Accessed: 25.08.2020)

[5] Watanabe, T. and Omori, Y. (2020). Online consumption during the COVID-19 crisis: Evidence from Japan. JSPS Grant-in-Aid for Scientific Research (S), Central Bank Communication Design, Working Paper Series. No.023 (June 2020), https://www.centralbank.e.u-tokyo.ac.jp/wp-content/uploads/2020/06/cb-wp023.pdf (Accessed: 30.08.2020)

[6] Bounie, D., Camara, Y. and Galbraith, J.W. (2020). Consumers' mobility, expenditure and online-offline substitution response to COVID-19: Evidence from French transaction data. SSRN Electronic Journal. https://ssrn.com/abstract=3588373. pp: 54. (Accessed: 15.07.2020).

[7] Grashuis, J., Skevas, T. and Segovia, M. (2020). Grocery Shopping Preferences during the COVID-19 Pandemic. Sustainability. 2020(12), 5369.

[8] Dogan, Y. and Dogan, S. (2020) Coronavirus-Pandemic and its effect on crops production in Turkey. Artuklu Kaime International Journal of Economics and Administrative Researches. 3(1), 41-55.

[9] Duygun, A. (2020) Evaluation of consumers' lifestyles during the COVID-19 pandemic. International Academic Journal, Econder. 4(1), 232-247.

[10] Duran, M.S. and Acar, M. (2020) What a virus could do to the world: Macroeconomic effects of covid-19 pandemic. International Journal of Social and Economic Sciences. 10(1), 54-67.

[11] Erdal, H. and Kablan, M.S. (2019) Evaluation of consumer perception on E-commerce marketing of agricultural products on the internet: Example of Samsun province. 4th International Symposium on Innovative Approaches in Engineering and Natural Sciences. 4(6), 85-89.

[12] Stephens, E.C., Martin, G. and VanVijk, M., Timsina, J., Snow, V. (2020). Impacts of COVID-19 on agricultural and food systems world wide and on progress to the sustainable development goals. Agricultural Systems. 183, 1-2.

[13] Baltaci, A. Akaydin, H. (2020) Effect of COVID-19 Pandemia period on consumers' buying behavior of food products: A literature review. Journal of Health Science Yuksek Ihtisas University. 1, 57-64.

[14] Arslan, İ., Karagul, S. (2020) A global threat (COVID-19 Pandemic) and the journey to change. Uskudar University Journal of Social Sciences. 10 (May2020), 1-36.

[15] Yildiz, A. (2020) Investigation of consumer behavior in crisis Periods. International Journal of Social Sciences Academy. 2(3), 377-390.

[16] Ongan, D., Bozdag, A.N., Ayer, Ç. (2020) Food supply and (in) security during COVID-19 outbreak. Izmir Kâtip Çelebi University Journal of Health Sciences Faculty. 5(2), 215-220.

[17] Danışmaz, A. (2020) The Effect of Covid-19 Epidemic to consumers' online shopping behavior. Social Sciences Research Journal. 9(2), 83-90.

[18] IPSOS (2020) IPSOS household survey report. https://www.ipsos.com/tr-tr/hane-ici-hizli-tuketim-urunleri-satin-aliminda-icecek-urunleri-dikkat-cekti. (Accessed date: 20.05.2020)

[19] Guven, H. (2020) Changes in e-Commerce in the Covid-19 Pandemic crisis process. Eurasian Journal of Researches in Social and Economics (EJRSE). 7(5), 251-268.

[20] Gunduz, O. (2020) Self-Sufficiency in agriculture and food sector during the Covid-19 outbreak. Turkish Academy Political Social Strategic Research Foundation (TASAV) Health, Agriculture and Food. 65-71.

[21] McFadden, D. (1973) Conditional Logit Analysis of Qualitative Choice Be. In: Zarembka, P., Ed., Frontiers in Econometrics (1974), Academic Press, NewYork. 105-142.

[22] Efron, B. (1988) Logistic Regression, survival analysis, and the Kaplan-Meier curve. Journal of the American Statistical Association. 83(402), 414-425.

[23] Cox, D.R. and Snell, E.J. (1989) Analysis of Binary Data. Chalpman Hall/ CRC, 2nd ed. pp: 240.

[24] Gujarati, D.N. (2003) Basic Econometrics. NewYork: McGraw Hill Book Co. pp: 545-546, 555.

[25] Hosmer, W. and Lemeshow, S. (1989) Applied Logistic Regression. Wiley Series in Probability and Statistics, New York. pp: 375.

[26] Canary, J.D. (2013) Grouped Goodness-of-Fit Tests for Binary Regression Models, Unpublished PhD thesis, University of Tasmania. pp: 162.
[27] Andrews, D.W.K. (1988a) Chi-square diagnostic tests for econometric models: Introduction and applications. Journal of Econometrics. 37(1), 135-156.
[28] Andrews, D.W.K. (1988b) Chi-Square diagnostic tests for econometric models: Theory. Econometrica. 56, 1419–1453.
[29] Semple, H.M. and Brierley, J.S. (2000) A Logit analysis of problems affecting domestic food production in Guyana. Social and Economic Studies (Sir Arthur Lewis Institute of Social and Economic Studies, University of the WestIndies). 49(1), 211-224.

Received: **25.09.2020**
Accepted: **31.01.2021**

CORRESPONDING AUTHOR

Rahmiye Figen Ceylan
Akdeniz University,
Faculty of Agriculture,
Department of Agricultural Economics,
Antalya – Turkey

e-mail: ceylan.figen@gmail.com

© by PSP Volume 30– No. 05/2021 pages 4730-4741 Fresenius Environmental Bulletin

RESPONSES TO DROUGHT STRESS IN GERMINATING SEEDS OF *AGRIOPHYLLUM SQUARROSUM* (L.) AND *SETARIA VIRIDIS* (L.)

Juanli Chen[1,2,3,4,*], Xueyong Zhao[2,4], Yaqiu Zhang[5], Yongqing Luo[2,4], Zhaoquan He[2,3,4], Rui Zhang[2,3,4], Hailun Yu[2,3,4], Runxia Zhang[2,3,4]

[1]Ecological Security and Protection Key Laboratory of Sichuan Province, Mianyang Normal University, Mianyang, China
[2]Northwest Institute of Eco-environment and Resources, CAS, Lanzhou, China
[3]University of Chinese Academy of Sciences, Beijing, China
[4]Naiman Desertification Research Station, Northwest institute of Eco-environment and Resources, CAS, Tongliao, Inner Mongolia Autonomous Region, China
[5]Horticultural Technology Department, Hanzhong Agricultural Technology Extension Center, Hanzhong, China

ABSTRACT

To understand how germinating psammophyte seeds adapt to drought stress in China's Horqin Sandy Land, we examined how the seedling growth and physiological properties of *Agriophyllum squarrosum* (L.) and *Setaria viridis* (L.) respond to drought. Results showed that *Agriophyllum squarrosum* had stronger drought stress resistance compared with *Setaria viridis*. The seed germination rate, plumule length, single-seed fresh weight, and seed water content of both species decreased under drought. At a water potential of -0.30 MPa, seed germination of *A. squarrosum* was 15.7% and that of *S. viridis* was only 2.7%. Mild and moderate drought increased radicle length and superoxide dismutase (SOD) activity of *A. squarrosum* and *S. viridis*, the soluble proteins and soluble sugars contents of *A. squarrosum* and catalase (CAT) activity of *S. viridis*, but severe drought decreased these values. The radicle length of *A. squarrosum* was highest at -0.09 MPa (at 45.8% greater than in the control), and was significantly larger than in other treatments. With prolonged drought stress, the SOD and CAT activities and the soluble sugars and proteins contents of *A. squarrosum* were higher than those of *S. viridis.* However, the free proline content of *A. squarrosum* was lower than that of *S. viridis* when the water potential was higher than -0.30 MPa. Our results demonstrate different physiological adaptability to drought for the two species, and will support more effective vegetation restoration in the Horqin Sandy Land.

KEYWORDS:
Horqin Sandy Land, water potential, drought stress, germination, physiological response

INTRODUCTION

About one-third of the world's land is arid or semi-arid, versus nearly half of the land in China [1]. Economic development and population expansion make the shortage of water resources in these areas increasingly serious [2], and exacerbate drought sufficiently that it seriously affects plant growth and development, yield and gene expression [3-6]. China Horqin Sandy Land is in a semi-arid region, water loss and soil erosion have exacerbated and the vegetation cover has been reduced by long-term human interference with the region's natural ecosystems and by drought [7].

Drought and plant adaptability are closely related to plant succession, and knowing how plants respond to drought improves our understanding of plant ecophysiology [8,9]. Seed germination is the first stage of plant life, and therefore is crucial in determining the success of plant establishment. Water is the main factor that affects seed germination in arid and semi-arid regions [10]. Many studies have found that seed germination and seedling emergency were linked with the intensity of drought. For example, the seeds of *Periploca sepium* could endure moderate osmotic stress (-0.6 MPa), but seed fresh weight and seed water content decreased with increasing osmotic stress [11]. The radicle and plumule lengths of cotton decreased by osmotic stress, and seed germination was significantly negatively correlated with the intensity of drought stress [12].

The physiological responses to drought stress are responses to disruption of the balance of the active oxygen metabolism system, leading to the accumulation of reactive oxygen species (ROS). The accumulation of ROS activated the antioxidant protection system, which includes the generation of enzymes such as superoxide dismutase (SOD) and catalase (CAT) [13,14]. For example, leaf antioxidase activity of *Artemisia halodendron* increased with increasing soil drought intensity, but decreased with irrigation in an artificial soil under repeated cycles of

drought and rewatering [15]. Under natural conditions, leaf antioxidase activities of *Lycium ruthenicum* increased with drought stress [16]. Other studies have found that plant cells often reduced their osmotic potential (i.e., make it more negative) in response to drought by increasing the solute concentrations (soluble proteins, soluble sugars, free proline) These solutes may reduce the water stress that increases ROS levels and maintain the integrity of membranes, while also functioning as nitrogen and carbon sources [17,18].

Agriophyllum squarrosum and *Setaria viridis* are pan-temperate plant species. *A. squarrosum*, which often colonizes mobile dunes, is one of the most common pioneer species, and its successful establishment provides a solid foundation for subsequent plant invasion and vegetation establishment [19]. *S. viridis*, as it can survive on sites subject to moderate drought, making it suitable for promoting the establishment of plant communities and improving soil conditions [20]. There have been many studies of plant responses to light, temperature and other environmental factors during seed germination, but few studies of the physiological responses of germination of these psammophyte species under drought stresses. Given their importance in the restoration of vegetation communities in degraded sandy land, it's important to understand how these species respond to drought stress. In particular, we need to learn more about their germination characteristics and physiological responses and whether solute concentrations respond to drought similarly to what has been observed in other species. This will provide theoretical guidance for vegetation restoration in China's semi-arid regions and support the development of a more scientific basis for more rational utilization of plant resources in the country's arid and semi-arid regions. Understanding the adaptations of these species to the sandy environment of these areas will also guide their use in biological stabilization of mobile sands.

We hypothesized that our study species would exhibit responses to drought stress similar to those that have been reported in other species, but with differences in the relative importance of the responses. Thus, the objectives of the present study were to (1) describe the seed germination characteristics of *A. squarrosum* and *S. viridis* under a gradient of drought stress, (2) seek their physiological responses to drought during seed germination, and reveal the relationship between their physiological adaptations and seed germination strategy.

MATERIALS AND METHODS

Experiment design. Our experiments were carried out in June 2018 at the Naiman Desertification Research Station, Chinese Academy of Sciences, which is located in the southeastern part of the Horqin Sandy Land, in the eastern part of China's Inner Mongolia Autonomous region. This region has a continental semi-arid monsoon climate. The land's physiognomy is characterized by a mosaic of mobile dunes, semi-fixed dunes, fixed dunes, interdunes, lowlands, steppe and desert steppe grassland [21,22].

In October 2017, we collected mature seeds of *A. squarrosum* and *S. viridis* from semi-mobile dunes near the study area (42°58′N, 120°43′E) and stored them in a dry chamber at room temperature (15 to 25 °C). The mean seed weights of *A. squarrosum* and *S. viridis* were 2.25 ± 0.15 g (mean ± SD) and 1.02 ± 0.02 g (N = 1000). Seed water contents of *A. squarrosum* and *S. viridis* were 6.49 ± 0.77% w/w and 5.82 ± 0.61% w/w before the experiments.

We selected seeds with good kernel plumpness and uniform shape, then placed them evenly in a 12-cm-diameter Petri dish containing a double-layer filter paper. Each dish had 100 seeds and the paper was moistened with 5 mL of water with a different osmotic content in each treatment. Seed germination was carried out in an incubator at 25 °C, and germination was defined as visible protrusion of the radical.

Osmotic stress was created using polyethylene glycol (PEG-6000) at different concentrations to simulate six levels of drought stress. We used PEG-6000 concentration of 0, 2.5, 5, 7.5, 10.0 and 15.0% w/v. We used the equation of Michel and Kaufmann (1973) to calculate the water potential of these solutions at 25 °C. These were 0 MPa, -0.02 MPa, -0.05 MPa, -0.09 MPa, -0.15 MPa, and -0.30 MPa, respectively. The water potential of 0 MPa was used as the control.

We used 30 Petri dishes for each drought treatment. Seeds were continuously cultured for 7 days until no additional seeds germinated, and we recorded the number of germinated seeds daily. On days 3, 5, 7, we randomly selected 10 seedlings from each dish to measure the radicle and plumule length. We used 20 dishes to measure the activity of antioxidant enzymes and the content of osmoregulatory substances. The other remaining 10 dishes were used to measure seed weight and water content. These seeds were removed from the treatment solutions and weighed immediately to determine their fresh weight, and then placed in an oven to be dried at 105 °C for 20 min followed by 60 °C for 72 h.

Analytical methods and statistical analysis. We removed and cleaned surface treatment solutions from the seed before measuring biochemical and physiological indicators. Each sample was ground using a mortar and pestle until no large fragments were visible. We extracted the random 0.1 g fresh samples with chilled extraction

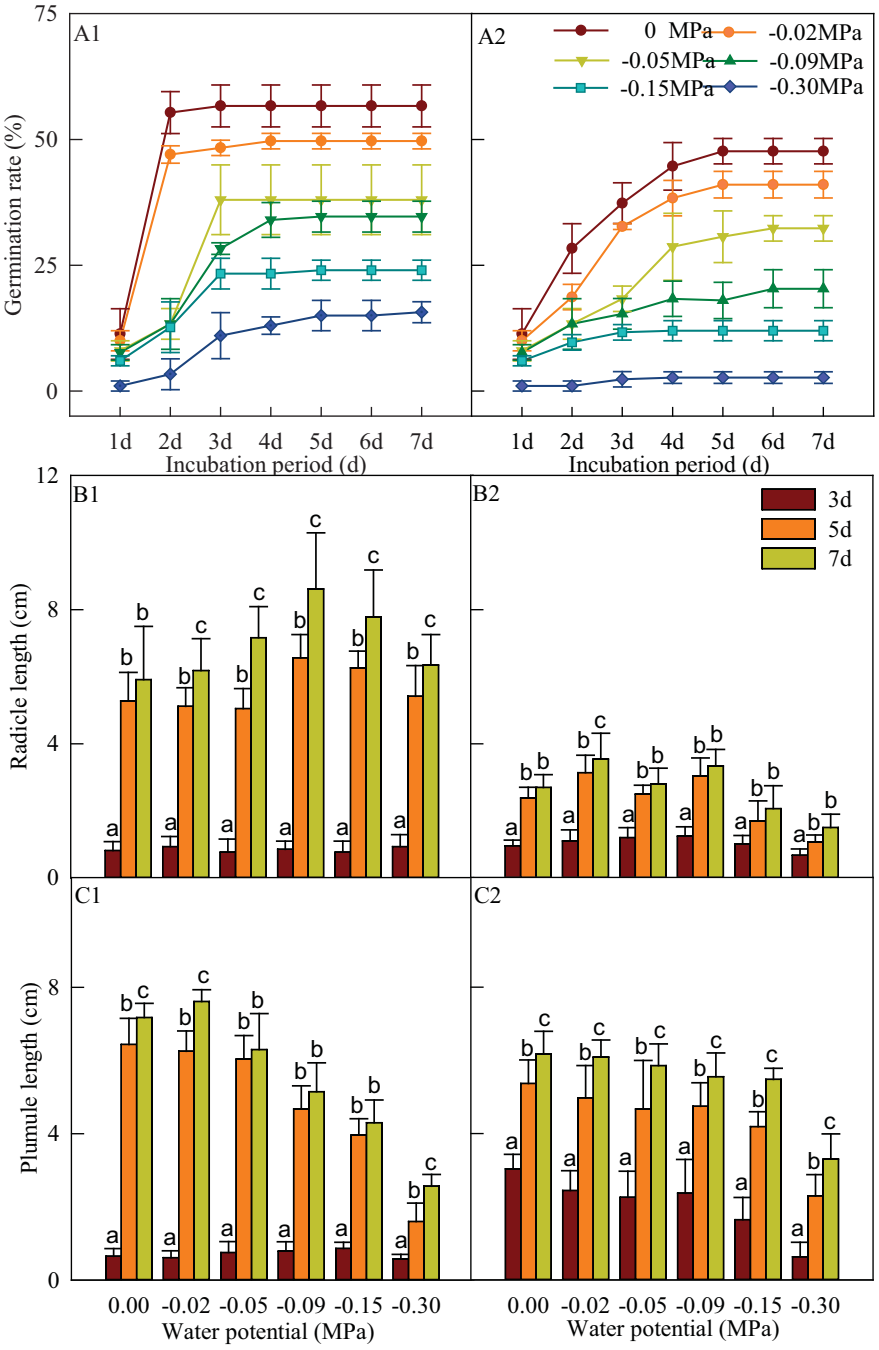

FIGURE 1

Effects of water potential on germination rate and seedling growth characteristics.

A1: Germination rate of *A. squarrosum*; A2: Germination rate of *S. viridis*; B1: Radical length of *A. squarrosum*; B2: Radical length of *S. viridis*; C1: Plumule length of *A. squarrosum*; C2: Plumule length of *S. viridis.*
Values are mean ± SD.

buffer (50 mM phosphate, 1% (w/v) polyvinylpyrrolidone) and centrifuged the extract at 15,000 *g* for 20 minutes. The supernatants were stored at 4 ºC until they could be analyzed. SOD activity was determined spectrophotometrically with nitroblue tetrazolium (NBT) and one unit of SOD was defined as the amount of enzyme required to produce a 50% inhibition of NBT. CAT activity was measured using iodine–starch method and one unit of CAT was defined as the quantity of enzyme required to reduce 10^{-6} mol H_2O_2 per minute [21,23,24]. The malondialdehyde (MDA) content, which represents the extent of membrane lipid peroxidation, was measured using the thiobarbituric acid method [25]. The Soluble proteins content was measured spectrophotometrically using Coomassie blue dye combination method [26]. The free prolines concentration was measured spectrophotometrically with ninhydrin method [27]. The soluble sugars content was determined spectropho-

tometrically with anthrone-sulfuric [21]. The contents of MDA and soluble osmolytes and the activity of SOD were determined using a spectrophotometer (Shimadzu Corporation, Japan).

Statistical analysis of the data was conducted using version 20.0 of SPSS for Windows. We used one-way analysis of variance (ANOVA) to identify significant differences among the treatments. When the ANOVA result was significant, we used least significant difference (LSD) tests to identify significant differences between pairs of treatments. We defined significant differences as $P < 0.05$.

RESULTS

Changes in germination rate and seedling growth characteristics. With increasing drought stress, the seed germination rate decreased for *A. squarrosum* (Figure 1A1) and *S. viridis* (Figure 1A2). In the control for *A. squarrosum*, at a water potential of 0 MPa, the final germination rate of was 56.7 %. By day 3, most of the seed that was capable of germination had germinated. As the water potential decreased below -0.15 MPa, the number of germinating seeds decreased to less than half of the value in the control and the seed germination rate decreased further, to 15.7%, when drought stress increased to -0.30 MPa. For *S. viridis* in the control, the final germination rate was 47.7%. Germination continued to increase until day 6. When the water potential decreased to -0.15 MPa, the germination rate decreased to 12%, and it was only 2.7% when drought stress increased to -0.30 MPa.

In order to understand seedling growth characteristics of *A. squarrosum* (Figure 1B1) and *S. viridis* ((Figure 1B2) and their responses to drought stress, we measured the length of the radicle. Before day 3, radicle length of *A. squarrosum* increased slowly. The radicle length on day 3 was < 1 cm under all levels of stress and did not differ significantly between treatments. The growth rate from day 3 to day 7 was much higher than the growth before day 3. As drought stress increased to -0.09 MPa, the radicle length first increased and then decreased until day 7. Its length reached 5.9 cm in the control. Radicle length increased gradually when drought stress increased to -0.09 MPa and decreased when drought stress increased from -0.09 MPa to -0.30 MPa. At -0.09 MPa, the length was 8.6 cm, 45.8% higher than that in the control and significantly greater than the length in other treatments. When drought stress was weaker than -0.09 MPa, the radicle length of *S. viridis* in each treatment was greater than that in the control on days 5 and days 7. The length was 3.5 cm and 3.3 cm at the water potential of -0.02 MPa and -0.09 MPa, respectively, and were 29.6% and 22.2% higher than in the control When drought stress increased beyond -0.09 MPa, the radicle length decreased gradually.

Plumule lengths also differed in their responses and values between species. For *A. squarrosum* (Figure 1C1) on day 3, the difference (max - min) of plumule lengths among the treatments was 0.8 cm, versus 6.0 cm on day 5 and 7.1 cm on day 7. At a drought stress increased beyond -0.02 MPa, the plumule length decreased with increasing drought stress. The plumule length was greatest (7.6 cm) at -0.02 MPa, but did not differ significantly from the control. When drought stress was greater than -0.05 MPa, the plumule length was lower and differed significantly from the control. For *S. viridis* (Figure 1C2) on day 3, the difference in plumule length among the treatments was 2.9 cm. Furthermore, the difference increased 5.2 cm on day 5 and 5.7 cm on day 7. As drought stress increased, the plumule length of *S. viridis* decreased. When drought stress was weaker than -0.05 MPa, there was no significant difference from the control. When drought stress was greater than -0.05 MPa, the plumule length was significantly lower than in the control. There was no significant difference between treatments as drought stress increased from -0.05 MPa to -0.15 MPa.

Changes in seed fresh weight and water content. Before germination, the single-seed weight and seed water content of *A. squarrosum* were higher than those of *S. viridis*. In the control, the single-seed fresh weight and seed water content of both species showed three phases (Figure 2), with sharp initial growth (until day 3), followed by a moderate change (day 3 to 5), and finally a rapid increase (day 5 to 7). The single-seed fresh weight and seed water content of both species decreased with increasing drought stress. When drought stress was -0.05 MPa on day 7, the seed water content of *A. squarrosum* was 229%, but that of *S. viridis* was only 135%. As drought stress increased, the content of both species decreased rapidly, followed by a small change at the highest levels of drought stress. As the drought duration increased, water absorption of *A. squarrosum* was greater than that of *S. viridis.*

Changes in malondialdehyde and antioxidant enzymes. The malondialdehyde (MDA) content of both species was low at all water potentials (Figure 3A1 and Figure 3A2), with values below 0.5 mmol g^{-1} DW, and the MDA content of *A. squarrosum* was lower than that of *S. viridis* at all levels of drought stress. For *A. squarrosum*, the MDA content gradually increased with increasing drought stress. The content was greater than that in the control at all levels except -0.09 MPa on day 3 and increased gradually until day 5. However, there were no significant difference among the treatments. By day 7, the MDA content increased by 27.2%、41.7%、42.6% and 40.1%, respectively, compared with the control as the water potential decreased from -0.02 MPa to -0.15 MPa, but did not differ significantly among the treatments. The MDA content was 63.7%

greater than in the control at -0.30 MPa, and there were significant differences on day 7. For *S. viridis*, in addition to the water potential of -0.30 MPa, the MDA content also increased over time and with increasing drought stress. On day 7, the MDA contents were significantly higher at -0.02 MPa，-0.09 MPa and -0.15 MPa than that in the control.

Superoxide dismutase (SOD) activity of *A. squarrosum* was higher than that of *S. viridis* (Figure 3B1; Figure 3B2). SOD activities of *A. squarrosum* was increased from 0 MPa to -0.09 MPa and then decreased (as stress increased from -0.09 MPa to -0.30 MPa) during the 7 days. When the water potential decreased from 0 MPa to -0.09 MPa, SOD activity of *A. squarrosum* increased and became significantly different from that in the control. When the water potential was -0.15 MPa and -0.30 MPa, SOD activity first increased (day 3 to 5) and then decreased (day 5 to 7). As drought stress increased, SOD activity was greater than that in the control but did not differ significantly among the treatments on day 3. On day 7, SOD activity reached its maximum (76.378 U g^{-1} DW) at a water potential of -0.09 MPa, and was significantly higher than in other treatments. For *S. viridis*, SOD activity increased significantly with time and as water potential decreased from 0 MPa to -0.30 MPa. On day 7, SOD activity was highest at a water potential of -0.09 MPa, and was significantly higher than in the control (by 54.6%).

Catalase (CAT) activity of *A. squarrosum* was higher than that of *S. viridis* (Figure 3C1; Figure 3C2). For *A. squarrosum*, CAT activity in the control was higher than in other treatments. CAT activity first decreased (day 3 to 5) and then increased (day 5 to 7) except for opposite trends at a water potential of -0.30 MPa. As drought stress increased, CAT activity showed an inconsistent trend of changes. On day 7, when the water potential was -0.02 MPa, CAT activity was lower than the control (by 2.6%) but the two values did not differ significantly. As drought stress increased from -0.02 MPa to -0.30 MPa, CAT activities in all treatments became significantly lower than in the control. For *S. viridis*, CAT activity increased over time when the water potential decreased from 0 MPa to -0.09 MPa. CAT activity first increased (day 3 to 5) and then decreased (day 5 to 7) as the water potential decreased from -0.15 MPa to -0.30 MPa. On day 7, CAT activity first increased and then decreased, reaching its highest value (79.9 U g^{-1} DW) at water potential of -0.09 MPa.

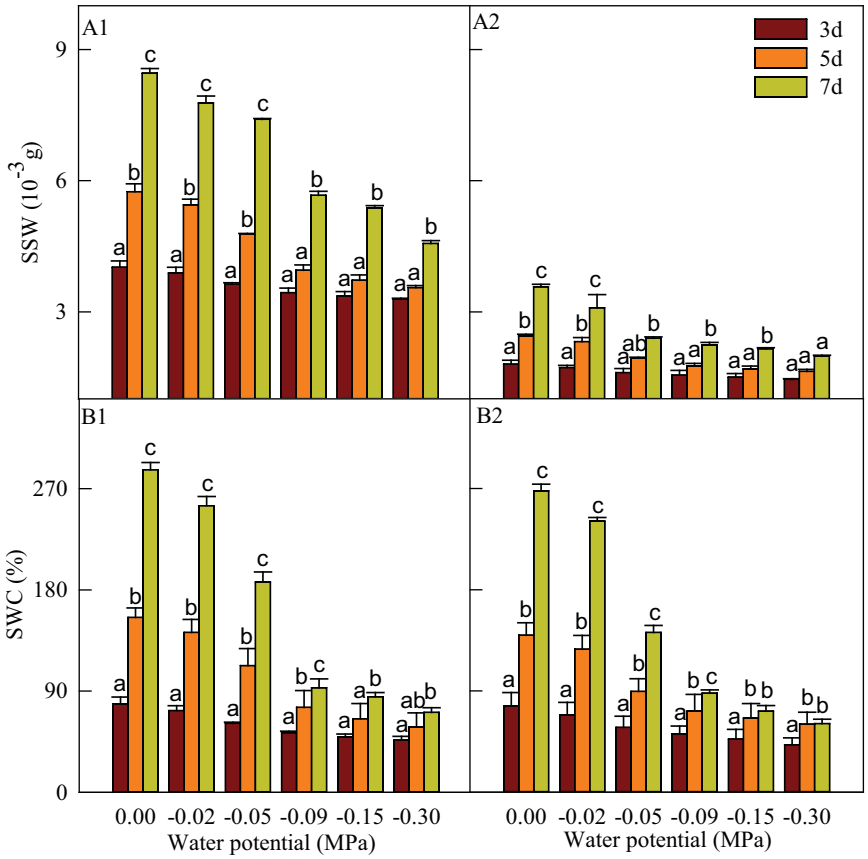

FIGURE 2

Effects of water potential on single-seed weight (SSW) and seed water content (SWC).

A1: SSW of *A. squarrosum*; A2: SSW of *S. viridis*; B1: SWC of *A. squarrosum*; B2: SWC of *S. viridis*. Values were assigned as mean ± SD.

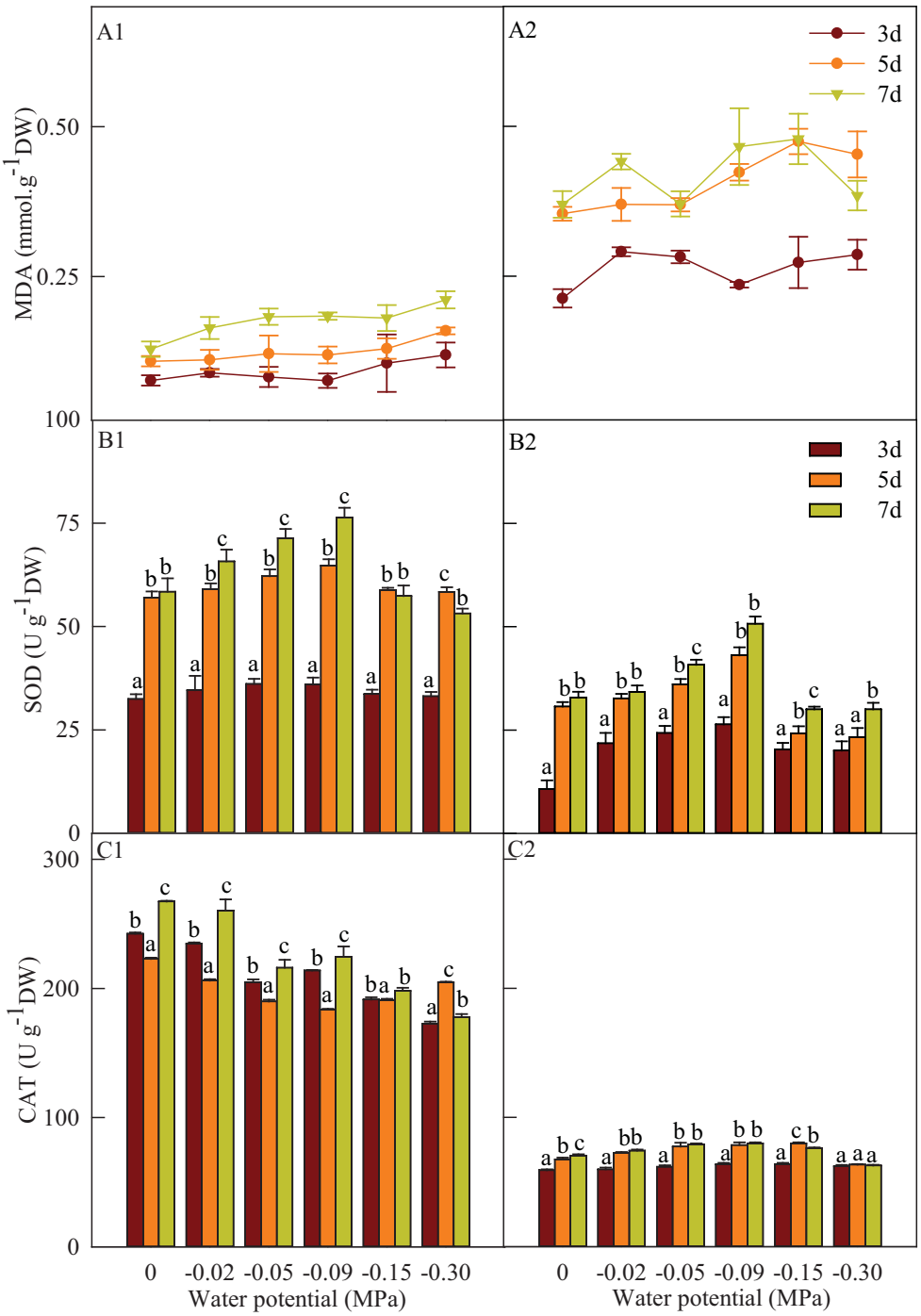

FIGURE 3

Effects of water potential on the content of malondialdehyde (MDA) and two antioxidant enzymes.

A1: MDA of *A. squarrosum*; A2: MDA of *S. viridis*; B1: SOD of *A. squarrosum*; B2: SOD of *S. viridis*; C1: CAT of *A. squarrosum*; C2: CAT of *S. viridis*. Values were assigned as mean ± SD. Bars for a species labeled with different letters are significantly different at $P < 0.05$ in different time of the same treatment.

Changes in osmoregulatory substance. The soluble proteins content of *A. squarrosum* was higher than that of *S. viridis* (Figure 4A1 and Figure 4A2). The soluble proteins content of *A. squarrosum* ranged from 69.943 mg·g^{-1} DW to 84.380 mg·g^{-1} DW, versus from 23.947 mg·g^{-1} DW to 34.769 mg·g^{-1} DW for *S. viridis*. From day 0 to day 7, when water potential decreased from 0 MPa to -0.09 MPa, the soluble proteins content of *A. squarrosum* increased gradually and higher than in the control; as the water potential decreased from -0.15 MPa to -0.30 MPa the content first decreased (day 3 to 5), and then increased (day 5 to 7). On day 5, the soluble proteins content of *A. squarrosum* was significantly higher than that in the control when drought stress was greater than -0.09 MPa. On day 7, the soluble proteins contents of *A. squarrosum* and *S. viridis* first increased and then decreased with increasing

drought stress. The content was highest for *A. squarrosum* at -0.09 MPa (84.38 mg·g^{-1}DW) and this value was significantly greater than in other treatments. For *S. viridis*, the soluble proteins content increased as drought stress increased, except at -0.05 MPa and -0.09 MPa. On day 7, the content of *S. viridis* increased gradually and higher than that in the control as drought stress increased from 0 MPa to -0.09 MPa, but the content was lower than in control as drought stress increased beyond -0.09 MPa.

Figure 4B1 and Figure 4B2 shows the changes in the soluble sugars content in response to increasing drought stress. The soluble sugars of *A. squarrosum* was higher than that of *S. viridis.* For both species, the soluble sugars content first decreased (day 3 to 5) and then increased (day 5 to 7), except for -0.30 MPa of *S.viridis.* On day 7, the soluble sugars contents of both species increased gradually and were higher than in the control when drought stress increased from 0 MPa to -0.09 MPa. On day 7, when water potential was -0.09 MPa, the soluble sugars

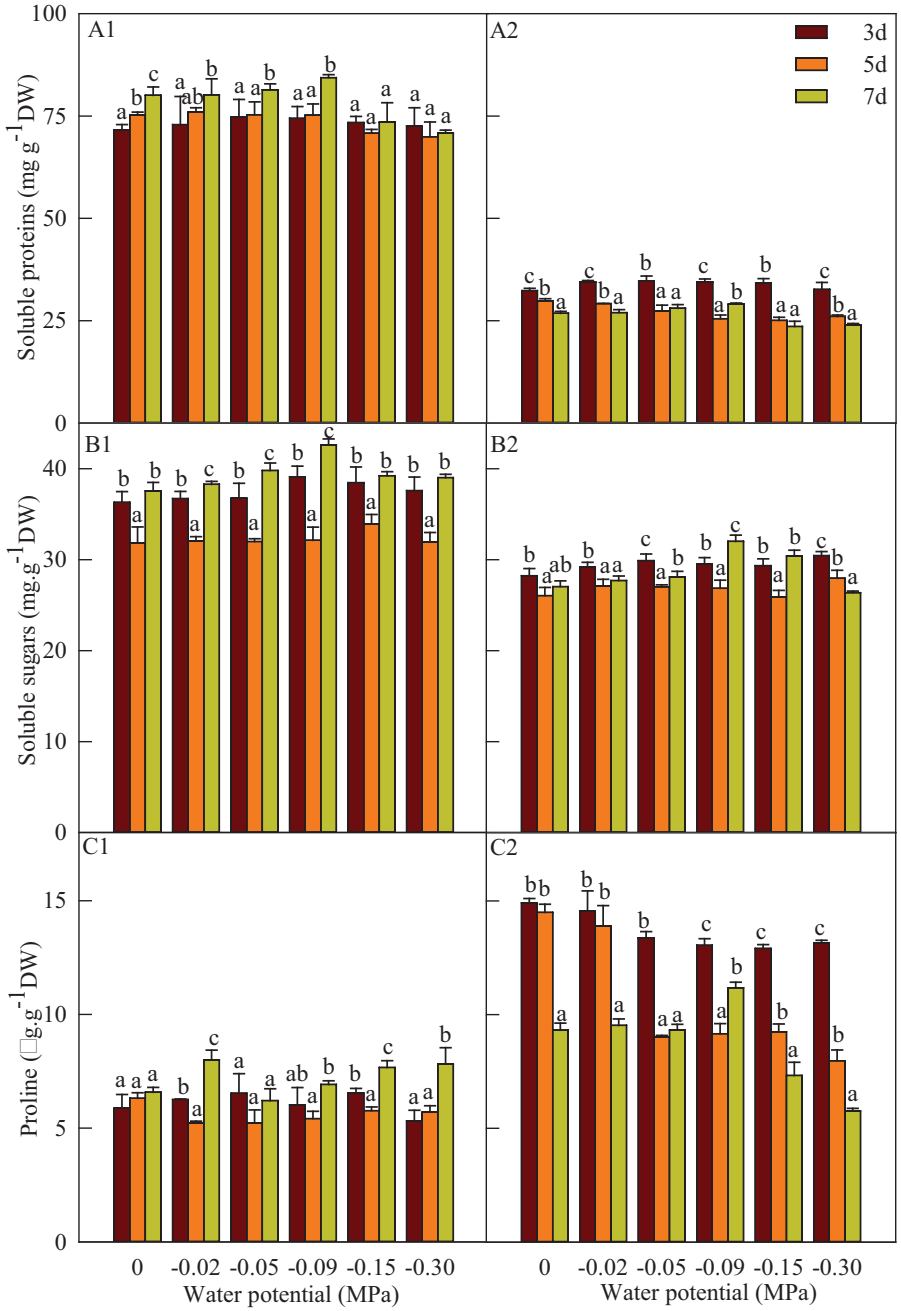

FIGURE 4

Effects of water potential on osmoregulatory substances.

A1: Soluble proteins of *A. squarrosum*; A2: Soluble proteins of *S. viridis*; B1: Soluble sugars of *A. squarrosum*; B2: Soluble sugars of *S. viridis*; C1: Free proline of *A. squarrosum*; C2: Free proline of *S. viridis.*

content of *A. squarrosum* reached 42.606 mg g^{-1} DW and was significantly higher than in other treatments; the content of *S. viridis* reached its maximum (32.018 mg·g^{-1}DW), which was 54.6% higher than in the control.

The free proline content of *A. squarrosum* ranged from 5.230 μg g^{-1} DW to 8.002 μg g^{-1} DW, versus from 5.766 μg g^{-1} DW to 14.918 μg g^{-1} DW for *S. viridis* (Figure 4C1; Figure 4C2). The free proline content of *A. squarrosum* first decreased (day 3 to 5) and then increased (day 5 to 7) as drought stress increased from -0.02 MPa to -0.150 MPa. On day 7, the free proline content in the control was lower than in other treatments, except at water potential of -0.05 MPa; as drought stress increased from -0.05 MPa to -0.30 MPa, free proline content increased gradually, but was lower than that of -0.02 MPa. For *S. viridis*, the free proline content decreased with increasing duration of drought stress, except at water potential of -0.05 MPa and -0.09 MP. On day 7, at drought stress weaker than -0.09 MPa, the content was higher than in the control but did not differ significantly; the free proline content was highest at -0.09 MPa, and significantly greater than in other treatments, but significantly lower than in the control when drought stress was greater than -0.09 MPa.

Correlation analysis. We also performed a correlation analysis to identify significant relationships between seedling growth and physiological characteristics for the two species (Table 1). For *A. squarrosum*, germination was significantly positively correlated with CAT. The radicle length was significantly positively correlated with MDA and SOD, and the plumule length was significantly positively correlated with SOD and soluble proteins. The single-seed weight and seed water content were significantly positively correlated with SOD, CAT and soluble proteins. SOD was significantly positively correlated with MDA and soluble proteins, and CAT was significantly positively correlated with soluble proteins. For *S. viridis*, germination, single-seed weight and seed water content were not significantly correlated with any of the other parameters. The radicle and plumule lengths were significantly positively correlated with MDA, SOD and CAT, but significantly negatively correlated with soluble proteins. MDA was significantly positively correlated with SOD and CAT, but significantly negatively correlated with soluble proteins and free proline. SOD was significantly positively correlated with CAT, and CAT was significantly negatively correlated with the soluble proteins content. The soluble proteins content was significantly positively correlated with free proline.

TABLE 1
Correlations between seedling growth parameters and physiological indices for *A. squarrosum and S. viridis*.

Species	Item	Germination	Radicle	Plumule	SSW	SWC	MDA	SOD	CAT	Proteins	Sugars
A. squarrosum	MDA	-0.363	0.803**	0.429	0.444	0.443					
	SOD	0.111	0.948**	0.839**	0.628**	0.628**	0.692*				
	CAT	0.776*	0.034	0.350	0.657**	0.658**	-0.115	0.114			
	Proteins	0.437	0.452	0.661*	0.753**	0.753**	0.291	0.599*	0.509*		
	Sugars	-0.175	0.023	-0.138	0.229	0.228	0.363	-0.053	0.207	0.437	
	Proline	-0.005	0.315	0.167	0.420	0.419	0.560*	0.165	0.311	0.250	0.634*
S. viridis	MDA	-0.119	0.595*	0.611*	0.350	0.349					
	SOD	0.183	0.851**	0.714*	0.443	0.443	0.604*				
	CAT	0.158	0.797*	0.765*	0.373	0.374	0.743*	0.783*			
	Proteins	0.090	-0.504*	-0.609*	-0.397	-0.397	-0.853**	-0.459	-0.626*		
	Sugars	-0.330	-0.221	-0.313	-0.297	-0.297	-0.182	0.009	-0.153	0.465	
	Proline	0.370	-0.283	-0.366	-0.236	-0.237	-0.720*	-0.408	-0.474	0.865**	0.259

DISCUSSION

Studies have shown that drought affects the growth of most plants in arid and semi-arid regions, and although most plants have a certain ability to resist drought, their drought tolerance varies widely [11,28]. Seed germination6 and seedling growth are the prerequisite for species to become established at site, and we focused on those processes in the present study, as they are highly important for individual development, population formation and community composition [29]. These eco-physiological responses differ among species. For example, the germination of *Anthephora pubescens* seed was severely inhibited at a water potential of -0.15 MPa [30]. The germination of canola decreased significantly at a water potential of -0.10 MPa and germination did not occur when the water potential reached -0.6 MPa [31]. The seeds germination of *Periploca sepium* could germinate under drought stress as serve as -0.6 MPa. [11]. We also found that seed germination of *A. squarrosum* and *S. viridis* decreased significantly with increasing drought stress, and that the impact was greater for *S. viridis*. When the water potential reached -0.30 MPa, seed germination of *A. squarrosum* was 15.7%, but the rate for *S. viridis* was even lower, at only 2.7%. Thus, the drought tolerance of *A. squarrosum* seeds was greater than that of *S. viridis* seeds.

The growth of radicle and plumule is the first stage of the morphogenesis of new plant after seed germination, and therefore plays an important role in the subsequent growth and reproduction of the plant [32]. As the duration of drought stress increased, the radicle length of *A. squarrosum* first increased and then decreased. The radicle length of *A. squarrosum* was longest when the water potential reached -0.09 MPa, For *S. viridis*, the radicle length was greater than in the control at a drought stress weaker than -0.09 MPa and decreased gradually, and became lower than in the control when drought stress increased beyond -0.09 MPa. We therefore found that mild to moderate drought improved the radicle length of both species, but the radicle length decreased after the stress reached a certain threshed (i.e., -0.09 MPa). These results were consistent with those of previous studies about the relationship between drought stress and early seeding growth, suggesting that radicle elongation could be a survival strategy for plants that helped them obtain moisture from deeper soil layers, thereby mitigating the effects of drought [33,34]. Except at a water potential of -0.02 MPa, the plumule length of both species decreased gradually with increasing drought stress, as this stress inhibited plumule elongation. Under drought stress, plants can adjust the balance between their aboveground and underground organs to prioritize the use of limited nutrients by the organ that is most crucial for survival, such as the roots in water-limited arid environment [35]. Although our experiments were carried out in Petri dishes, our results agree with this description.

The seed is a dormant or resting embryo before germination, and water absorption is the beginning of growth for most seeds. In general, this process can generally be divided into three stages, with rapid initial water absorption, followed by a slower increase, and finally a rapid increase [36,37]. The water absorption process of both species agreed with this description. However, water absorption decreased as drought stress increased, leading to decreased single-seed fresh weight and seed water content in both species. As the duration of drought stress increased, water uptake was increasingly severe inhibited and with little change. Our results were similar to those for *P. sepium* [11]. When the duration of stress increased, the water uptake capacity of *S. viridis* became weaker than that of *A. squarrosum.* This may explain why the drought tolerance of *A. squarrosum* seeds was greater than that of *S. viridis*.

Under drought and other stresses, the balance between the generation of reactive oxygen species (i.e., free radicals) in cells and elimination of these toxins is disrupted. As a result, large amounts of free radicals can accumulate, leading to peroxidation of membrane lipid. This is accompanied by accumulation of MDA and damage to cell membrane, thereby inhibiting plant growth, and possibly even causing death [38,39]. We found that MDA content of both species was higher under drought than in the control, but the content was lower in *A. squarrosum*, indicating that drought damaged both plants, but more so in *S. viridis*. However, the MDA content remained less than 0.5 $mmol \cdot g^{-1}DW$ and did not change significantly, probably because the content of protective enzymes and osmoregulatory substances increased after drought, thereby protecting the cell membrane [40]. Under adverse conditions, membrane-protective enzyme systems are stimulated in plants, particularly for antioxidant enzymes such as SOD and CAT, which reduce the damage to membrane [41]. SOD may be the first defense when plants are subjected to peroxidation of membrane lipid by ROS, and higher SOD activity could decrease the rate or intensity of peroxidation, thereby reducing damage to the plant [42,43]. CAT is also active, and catalyzes the decomposition of H_2O_2 in cells to prevent peroxidation, thereby protecting the plant and maintaining a dynamic balance between oxidation and reduction [44,45]. The changes of the antioxidant enzyme activities differed between our two species under prolonged drought stress. SOD activity in *A. squarrosum* and *S. viridis* and CAT activity in *S. viridis* were first showed increase when drought stress was weaker than -0.09 MPa, and then decreased.as drought stress increased. Our correlation analysis indicated that SOD in *A. squarrosum* and *S. viridis* and CAT in *S. viridis* were significant positive correlated with radicle length, plumule length and MDA.

As an additional method of mitigating stress, plants make their cytoplasmic osmotic potential more negative to retain water, and prevent leakage of cytoplasm through increasing the content of cytosol under adversity conditions, thereby maintaining cell turgor and permitting growth [46]. The stress tolerance of plants is therefore closely related to the changes in the content of osmoregulatory substances under stress. Changes in soluble proteins and sugars contents in *A. squarrosum* showed similar trends under prolonged drought stress, with both contents first increasing and then decreasing. The osmoregulatory substance in *S. viridis* were increased when drought stress was weaker than -0.09 MPa. Our correlation analysis showed that the soluble proteins content was significantly positively correlated with the catalase content, and the free prolines content was significantly positively correlated with malondialdehyde in *A. squarrosum* but significantly negatively correlated in *S. viridis*.

Mild and moderate drought increased SOD activity in *A. squarrosum* and *S. viridis* and CAT activity in *S. viridis*, but severe drought decreased activities of both enzymes. When drought stress was weaker than -0.09 MPa, only the SOD activity and the soluble proteins content in *A. squarrosum* increased. As the duration of the stress increased, the content of the soluble sugars and the free proline in *A. squarrosum* increased under severe drought stress, but both the enzymes activities and soluble proteins content decreased to levels below those in the control. With prolonged drought stress, the antioxidant enzymes and the osmoregulatory substances increased in both species to varying degrees, but the contents of antioxidant enzymes, soluble proteins, and soluble sugars were higher in *A. squarrosum* than in *S. viridis*. Therefore, *A. squarrosum* had stronger drought resistance than *S. viridis,* probably because the activity of its protective enzymes and the content of osmoregulatory substances increased greatly after the imposition drought stress, and these responses effectively alleviated damage to cell membrane.

CONCLUSIONS

Our results confirmed our research hypotheses: although the response mechanisms that underlie drought adaptation were similar in the two species, and agreed with previous reports in the literature for other species, the magnitudes and trends of the response differed. The germination rate, plumule length, seed fresh weight and seed water content of both species decreased under osmotic stress of polyethylene glycol, and *A. squarrosum* showed stronger drought resistant than *S. viridis.* When drought stress increased to -0.30 MPa, the seed germination of *A. squarrosum* decreased to 15.7%, but the rate for *S. viridis* was even lower, at only 2.7%. The radicle length of *A. squarrosum* was highest at a water potential of -0.09 MPa, reaching a value 45.8% higher than in the control, and this length was significantly greater than in other treatments. Under drought stress, the MDA contents of *A. squarrosum* and *S. viridis* were higher than in the control, but the contents in all treatments were less than 0.5 $mmol \cdot g^{-1}$DW and did not change significantly. SOD activity of the two species and CAT activity of *S. viridis* first increased while drought stress was weaker than -0.09 MPa, and then decreased as drought stress increased. *A. squarrosum* had stronger drought resistance, probably because its greater contents of SOD, CAT, soluble sugars and soluble proteins strengthen its ability to mitigate the negative effects of drought stress.

ACKNOWLEDGEMENTS

This study was financially supported by the National Basic Resources Investigation Program of China (2017FY100200), the National Natural Science Foundation of China (31770762; 41371053). We thank all members of the Naiman Desertification Research Station, Chinese Academy of Sciences, for their help in field and laboratory work. We also thank the anonymous reviewers for their valuable comments on the manuscript.

REFERENCES

[1] Chen, J.L., Zhao, X.Y.,Zhang, Y.Q., Li, Y.Q., Luo, Y.Y., Ning, Z.Y., Wang, R.X., Wang, P.Y., Cong, A.Q. (2019) Effects of drought and rehydration on the chlorophyll fluorescence parameters and physiological responses of *Artemisia halodendron*. Water. 11(4), 793.

[2] He, Z.Q., Zhang, T.H., Liu, X.P., Shang, X. (2018) Water-yield relationship responses of maize to ridge-furrow planting systems coupled with multiple irrigation levels in China's Horqin Sandy Land. Agronomy. 8(10), 221.

[3] Bray, E.A. (1993) Molecular responses to water deficit. Plant Physiology. 103(4), 1035-1040.

[4] Cellier, F., Conéjéro, G., Breitler, J.C., Casse, F. (1998) Molecular and physiological responses to water deficit in drought-tolerant and drought-sensitive lines of sunflower: accumulation of dehydrin transcripts correlates with tolerance. Plant Physiology. 116(1), 319-328.

[5] Shinozaki, K., Yamaguchishinozaki, K. (1997) Gene expression and signal transduction in water-stress response. Plant Physiology. 115(2), 327-334.

[6] Shinozaki, K., Yamaguchi-Shinozaki, K., Mizoguchi, T., Urao, T., Katagiri, T., Nakashima, K., Abe, H., Ichimura, K., Liu, Q., Nanjyo, T. (1998) Molecular responses to water stress in *Arabidopsis thaliana*. Journal of Plant Research. 111(1102), 345-351.

[7] Liu, X.P., He, Y.H., Zhao, X.Y., Zhang, T.H., Zhang, L.M., Ma, Y.H., Yao, S.X., Wang, S.K., Wei, S.L. (2015) Characteristics of deep drainage and soil water in the mobile sandy lands of Inner Mongolia, northern China. Journal of Arid Land. 7(2), 238-250.

[8] Kent, M., Owen, N.W., Dale, P., Newnham, R.M., Giles, T.M. (2001) Studies of vegetation burial: a focus for biogeography and biogeomorphology? Progress in Physical Geography. 25(4), 455-482.

[9] Qu, H., Zhao, H.L., Zhou, R.L., Wang, J., Li, J., Orr, B.J. (2012) Effects of sand burial stress on maize (*Zea mays* L.) growth and physiological responses. Australian Journal of Crop Science. 6(5), 869-876.

[10] Liu, X.P., He, Y.H., Zhao, X.Y., Zhang, T.H., Li, Y.L., Yun, J.Y., Wei, S.L., Yue, X.F. (2016) The response of soil water and deep percolation under *Caragana microphylla* to rainfall in the Horqin Sand Land, northern China. Catena. 139, 82-91.

[11] An, Y.Y., Liang, Z.S. (2013) Drought tolerance of *Periploca sepium* during seed germination: antioxidant defense and compatible solutes accumulation. Acta Physiologiae Plantarum. 35(3), 959-967.

[12] Li, D.X., Li, C.D., Sun, H.C., Liu, L.T., Zhang, Y.J. (2012) Photosynthetic and chlorophyll fluorescence regulation of upland cotton (*Gossiypium hirsutum* L.) under drought conditions. Plant Omics. 5(5), 432-437.

[13] Apel, K., Hirt, H. (2004) Reactive oxygen species: metabolism, oxidative stress, and signal transduction. Annual Review of Plant Biology. 55(1), 373-399.

[14] Blokhina, O., Virolainen, E., Fagerstedt, K.V. (2003) Antioxidants, oxidative damage and oxygen deprivationstress: a review. Ann. Bot. 91(2), 179-194.

[15] Luo, Y.Y., Zhao, X.Y., Zhou, R.L., Zuo, X.A., Zhang, J.H., Li, Y.Q. (2011) Physiological acclimation of two psammophytes to repeated soil drought and rewatering. Acta Physiologiae Plantarum. 33(1), 79-91.

[16] Guo, Y.Y., Yu, H.Y., Yang, M.M., Kong, D.S., Zhang, Y.J. (2018) Effect of drought stress on lipid peroxidation, osmotic adjustment and antioxidant enzyme activity of leaves and roots of *Lycium ruthenicum* Murr. seedling. Russian Journal of Plant Physiology. 65(2), 244-250.

[17] Ashraf, M., Foolad, M.R. (2007) Roles of glycine betaine and proline in improving plant abiotic stress resistance. Environmental and Experimental Botany. 59(2), 206-216.

[18] Rai, V.K. (2002) Role of amino acids in plant responses to stresses. Biologia Plantarum. 45(4), 481-487.

[19] Tobe, K., Zhang, L.P., Omasa, K. (2005) Seed germination and seedling emergence of three annuals growing on desert sand dunes in China. Annals of Botany. 95(4), 649-659.

[20] Mao, W., Li, Y.L., Zhao, X.Y., Zhang, T.H., Liu, X.P. (2016) Variations of leaf economic spectrum of eight dominant plant species in two successional stages under contrasting nutrient supply. Polish Journal of Ecology. 64(1), 14-24.

[21] Li, J., Qu, H., Zhao, H.L., Zhou, R.L., Yun, J.Y., Pan, C.C. (2015) Growth and physiological responses of *Agriophyllum squarrosum* to sand burial stress. Journal of Arid Land. 7(1), 94-100.

[22] Zhao, H.L., Li, J., Liu, R.T., Zhou, R.L., Qu, H., Pan, C.C. (2014) Effects of desertification on temporal and spatial distribution of soil macroarthropods in Horqin sandy grassland, Inner Mongolia. Geoderma. 223, 62-67.

[23] Drazkiewicz, M., Skórzyńska-Polit, E., Krupa, Z. (2004) Copper-induced oxidative stress and antioxidant defence in *Arabidopsis thaliana*. Biometals. 17(4), 379-387.

[24] Sundar, D., Perianayaguy, B., Reddy, A.R. (2004) Localization of antioxidant enzymes in the cellular compartments of sorghum leaves. Plant Growth Regulation. 44(2), 157-163.

[25] Heath, R.L., Packer, L. (1968) Photoperoxidation in isolated chloroplasts: I. Kinetics and stoichiometry of fatty acid peroxidation. Archives of Biochemistry and Biophysics. 125(1), 189-198.

[26] Bradford, M.M. (1976) A rapid and sensitive method for the quantitation of microgram quantities of protein using the principle of protein dye binding. Analytical Biochemistry. 72(12), 248–254.

[27] Yemm, E.W., Cocking, E.C. (1955) The determination of amino-acids with ninhydrin. Analyst. 80, 209-214.

[28] Talbi, S., Romero-Puertas, M.C., Hernández, A., Terrón, L., Ferchichi, A., Sandalio, L.M. (2015) Drought tolerance in a Saharian plant *Oudneya africana*: Role of antioxidant defences. Environmental and Experimental Botany. 111, 114-126.

[29] Gutterman, Y. (1993) Seed germination in desert plants. Springer Verlag, Berlin.

[30] Den Berg, L., Zeng, Y. (2006) Response of South African indigenous grass species to drought stress induced by polyethylene glycol (PEG) 6000. South African Journal of Botany. 72(2), 284-286.

[31] Heshmat, O., Saeed, H.A., Fardin, K. (2011) The improvememt of seed germination traits in canola (*Brassica napus* L.) as affected by saline and drought stress. International Journal of Agricultural Technology. 7(3), 611-622.
[32] Abbas, M.K., Ali, A.S. (2012) Abstract: Effect of the extract of Schanginia aegyptiaca on seed germination and seedling growth of roselle (*Hibiscus sabdariffa* L.). Asian Journal of Agricultural Research. 6(2), 83-90.
[33] Rohamare, Y., Dhumal, K.N., Nikam, T.D. (2014) Response of Ajowan to water stress induced by polyethylene glycol (PEG) 6000 during seed germination and seedling growth. Journal of Environmental Biology. 35(5), 789-793.
[34] Shukla, N., Verma, Y., Shukla, P.K., Misra, P. (2016) Effect of polyethylene glycol (PEG) 6000 on seed priming in drought tolerant and sensitive barley (*Hordeum vulgare* L.) seeds. International Journal of Plant Sciences. 11(1), 75-78.
[35] Sack, L., Grubb, P.J., Marañón, T. (2003) The functional morphology of juvenile plants tolerant of strong summer drought in shaded forest understories in southern Spain. Plant Ecology. 168(1), 139-163.
[36] Bradford, K.J. (1990) A water relations analysis of seed germination rates. Plant Physiology. 94(2), 840-849.
[37] Koller, D., Hadas, A. (1982) Water relations in the germination of seeds. Encyclopedia of Plant Physiology New. 12, 401-431.
[38] Izanloo, A., Condon, A.G., Langridge, P., Tester, M., Schnurbusch, T. (2008) Different mechanisms of adaptation to cyclic water stress in two South Australian bread wheat cultivars. Journal of Experimental Botany. 59(12), 3327-3346.
[39] Pagter, M., Bragato, C.H. (2005) Tolerance and physiological responses of *Phragmites australis* to water deficit. Aquatic Botany. 81(4), 285-299.
[40] Zhao, H.L., Li , J., Zhou, R.L., Yun, J.Y., Qu, H., Pan, C.C. (2015) Effects of strong wind-drift blowing on the growth and physiological properties of *Pinus sylvestris* var. mongolica seedlings. Chinese Journal of Ecology. 34(4), 901-906.(in Chinese)
[41] Jouili, H., El, F.E. (2003) Changes in antioxidant and lignifying enzyme activities in sunflower roots (*Helianthus annuus* L.) stressed with copper excess. Comptes Rendus Biologies. 326(7), 639-644.
[42] Monk, L.S., Fagerstedt, K.V., Crawford, R.M.M. (2010) Oxygen toxicity and superoxide dismutase as an antioxidant in physiological stress. Physiologia Plantarum. 76(3), 456-459.
[43] Mittler, R. (2002) Oxidative stress, antioxidants and stress tolerance. Trends in Plant Science. 7(9), 405-410.
[44] Jiménez, A., Hernández, J.A., Río, L.A.D., Sevilla, F. (1997) Evidence for the presence of the ascorbate-glutathione cycle in mitochondria and peroxisomes of pea leaves. Plant Physiology. 114(1), 275-284.
[45] Navari-Izzo, F., Quartacci, M.F., Sgherri, C.M. (1996) Superoxide generation in relation to dehydration and rehydration. Biochemical Society Transactions. 24(2), 447-451.
[46] Qayyum, A., Razzaq, A., Ahmad, M.Z., Jenks, M.A. (2011) Water stress causes differential effects on germination indices, total soluble sugar and proline content in wheat (*Triticum aestivum* L.) genotypes. African Journal of Biotechnology. 10(64), 14038-14045.

Received: **06.08.2019**
Accepted: **03.02.2021**

CORRESPONDING AUTHOR

Juanli Chen
Ecological Security and Protection Key Laboratory of Sichuan Province,
Mianyang Normal University,
Mianyang – China

e-mail: juanlic@163.com

© by PSP Volume 30– No. 05/2021 pages 4742-4748 Fresenius Environmental Bulletin

CURRENT STATUS OF *TERMINALIA ARJUNA* AND *ALBIZIA LEBBECK* IN AGROFORESTRY SYSTEMS OF SOUTHERN PUNJAB, PAKISTAN

Muhammad Farooq Azhar[1], Muhammad Arslan Pervez[1], Ihsan Qadir[1], Muhammad Zubair[1], Muhammad Farooq[1], Jahanzaib[1], Ghulam Yasin[1,2,*]

[1]Department of Forestry and Range Management, Bahauddin Zakariya University, Multan, Punjab, Pakistan
[2]Department of Forestry, Range and Wildlife Management, The Islamia University, Bahawalpur, Punjab, Pakistan

ABSTRACT

Pakistan comprises of lowest forest resources and its southern region is facing the worst deforest conditions. Farm forests are providing 90% fuelwood and 76% timber wood of the country's demand but the forest cover area is declining day by day. Therefore, it is the need of time to promote agroforestry on private lands to meet the requirements of the community for tangible and intangible purposes. The objective of this study was to identify the uses and benefits of less familiar tree species such as *Terminalia arjuna* and *Albizia lebbeck* by visiting timber merchants, farmers, nursery owners and traditional healers locally known as Hakims. Data were collected from 11 different localities of the Multan division of Southern Punjab. The results indicated that both species were preferred by the grower for specific uses: *A. lebbeck* is preferably grown on agricultural lands due to more market value, fuelwood and fodder demand, but *T. arjuna* was found to be important for hakims and was reported as more important medicinal plant than *A. lebbeck*. An important source of information in the study area about tree cultivation was the neighbor farmers (42.2%) and major problems were lack of technical assistance (28.7%) and less availability of seedlings (22%). To overcome the pressure of wood production by some specific tree species, the government should focus on the planting of *T. arjuna* and other fast-growing trees. Moreover, the Government should also give incentives, financial subsidies, and market assistance to the farmers to promote the cultivation of less familiar fast-growing trees in conventional farming systems.

KEYWORDS:
Agroforestry, *Albizia lebbeck*, Fuelwood, Medicinal tree, Tangible, *Terminalia arjuna*

INTRODUCTION

Trees are custodians of terrestrial vegetation and provide various services and products. The cultivation of other crops was started in forests by clearing trees. Later on, a combination of both was started to practice for getting multiple benefits and named this type of cultivation as Agroforestry. It is a sustainable land-use system where overall production and options for products increases. Besides, it ensures soil protection and employment source for the local community. Agroforestry is a little focused at govt. level in Pakistan but as farm forestry, it has been practiced in irrigated areas on private farms. About 0.2 billion trees are present on cultivated lands of Punjab mostly on irrigated areas (95%). *Dalbergia sissoo* (Shisham) has about 42% share, *Acacia modesta* (Phulai) 20%, Va*chellia nilotica* (Kikar) 11% and *Melia azedarach* (Bakain) has 7% share [1]. Southern Punjab is warmer and dry; therefore, mostly indigenous tree species like *Zizyphus muaritiana*, *Albizzia labbeck* are grown. Some tree species of moist areas are also being cultivated due to their good performance and fast growth. *T. arjuna* is one of them and can be seen on roads and public places.

Terminalia arjuna is commonly known as 'Arjuna'. It is native to India and has importance in Ayurveda medicine system [2]. *Terminalia* belongs to the *Combretaceae* family and it is a useful forest tree species with numerous medicinal and fodder values. It is also a good shady tree and planted as an ornamental tree in parks and avenues [3]. It has the potential to grow in a variety of soils, preferably fertile loamy and humid soils [4] and consider an exotic tree. *Albizia lebbeck* is a deciduous woody tree having a normal height of 12–21m of Mimosaceae family and locally known as siris or sharin. It is native to Pakistan and can be cultivated in a variety of soil types and mostly preferred to cultivate on farms, along rivers and roadsides, irrigated forests. It has a pleasing look and can be cultured in gardens as an aesthetic plant [5]. Its noteworthy repute is due to its medicinal value, feed and nutritious food.

Tree planting is associated with multiple benefits still its adoption on farmlands has hesitations due

to different socio-economic issues. The challenges in adopting agroforestry are various but social and economic variables are still addressed while explaining problems related to agroforestry adoption [6-7]. The smallholding is also a mentioned fact in agroforestry adaptation [8]. Preferences, biophysical and market with future uncertainty and risk are other factors of tree cultivation by farmers. Tree planting at the farm level also been studied by focusing on socio-psychological factors, like perceptions and attitudes [9]. Long-awaited economic return from trees in addition to crops and market response may also be a hindrance. The indigenous trees sometimes have less market value doubled with slow growth becomes a challenge for farmers to cultivate trees on farms. Exotic trees with fast growth could be a more acceptable option in this context but the non-availability of these species at nursery level and local marketing trends during marketing could hinder this option. A study of all stakeholders from nursery to end-user gives a clearer picture of problems associated with the adaptation of agroforestry systems. Together, all stakeholders' attitude decides the status of a species in a local agroforestry system.

The current study was designed to assess the farmers' attitude towards planting the exotic and indigenous tree species on farmlands. Actual hindrances of adopting exotic species like *T. arjuna* from nursery to end-user levels were also studied to frame their attitude at all levels. The selected tree species are ranked as fast-growing. A detailed study was carried out from seedling (germplasm) availability in nurseries to cultivation on farms and at the end the personnel from the market (including timber merchants and traditional medicinal healers/ herb sellers). Status and problems at each stakeholder level were also assessed which could be helpful in agroforestry expansion.

MATERIALS AND METHODS

Study Area. The current study was conducted in agricultural areas of the Multan division of Southern Punjab in 2017. The altitudinal height of the selected area is 160m to 500m. The soil is alluvial with 150-250 mm mean annual rainfall. Temperature is high and reached at 50°C in summer with winter frost at some places. Agriculture is the mainland use system with a total of 36% cultivated area. Canal and tube well water is the major source of irrigation. A major proportion of about 2.7 million ha area is wildland and practiced as grazing land. About 0.15 m ha is under the control of South Punjab Forest Company (SPFC) for tree cultivation. The area has semi-arid climatic conditions and experiences comparatively less rainfall than central Punjab [10-11].

Questionnaire preparation and data collection. A well-equipped questionnaire was drafted by consulting relevant literature and pre-tested [12]. The data was collected from all personnel present in the chain from farmers to market like nursery growers, timber merchants, furniture makers and traditional healers (Hakims) about the selected trees. Information regarding different parameters such as germplasm availability in nurseries, cultivation, and choice of farmers, usage and marketing at traditional healers' shops (Hakims) and timber markets were collected along with all possible constraints. Primary data was taken by adopting a systematic random sampling method. A total of 375 persons were interviewed from 11 different rural and urban localities of Multan division such as union councils and towns (Table 1). Focus groups and key informants were identified and interviewed at an individual level to provide detail information regarding the availability of selected trees at nursery level, their cultivation, marketing and role in medicines.

Data Analysis. After the completion of the survey, the collected data was divided into logical groups coded and analyzed using SPSS statistical software version 16.0.

RESULTS

The information regarding the age of all respondent categories: farmers, nursery growers, timber merchants, and traditional hakims is presented in Fig.1. Most of the farmers (40.15 %), traditional hakims (42.30 %) and timber merchants (37.14 %) were over 45 years of age while maximum nursery growers (40 %) fell in the age category of 35-45. Education is an important aspect of life and has positive impacts on the developmental processes and decision-making abilities of individuals. The highest literacy level was computed for traditional hakims (91.02%) while the lowest literacy level (80.30 %) was computed for farmers. Most of the people from all categories had secondary school education irrespective of the resources available except farmers as depicted in Table 2. Maximum farmers (29.54 % and 25.75 %) had primary (≤ 5th grade) and middle-level education (8th grade) respectively while only 11.36 % of farmers had intermediate level education when compared with other respondent's classes.

Table 3 reveals the information about farmer purpose, source of information and constraints in the cultivation of selected species. It was found that about half of the farmers (50.8%) were planting these tree species for obtaining fuelwood while 23.5 % farmers were cultivating for fodder during drought periods, windbreaker (9.9 %), soil fertility (9.09 %) and agricultural implements (6.8%). The major source of information for the majority of the farmers was neighbor farmers as most people in villages were illiterate or primary level education. About one-third of the respondent (26.51%) revealed

television as their information source and only 6.81% of respondents in the study area told that they got information from the forest department. Lack of technical assistance was reported by farmers (28.7 %) as the major problem in cultivating trees, followed by less availability of seedlings (22 %) and water shortage (18.2 %).

Most of the nurseries in the study area were dealing mostly with ornamental and fruit plants as compared to trees because of their more demand. Around 60 nursery owners acknowledged the tree seedlings demand and purchase by buyers according to their needs. Data was obtained from nursery growers about the demand and their recommendation and constraints of both plant seedlings. About one third (25 %) nursery growers recommend *T. arjuna* seedlings to buyers for promoting this species in the agricultural land use system of the country. However, 35 % of nursery growers reported that buyers mostly prefer to purchase *A. lebbeck* seedlings as compared to *T. arjuna*. A remarkable difference regarding the sale of seedlings was noticed and about 20 % of nursery growers were selling *A. lebbeck* seedlings whereas only 13.3% were selling *T. arjuna* seedlings (Table 4). The major problem faced by nursery growers in establishing and marketing of these tree species was lack of technical assistance: 33.3 % nursery growers reported lack of technical assistance about *T. arjuna* while 30 % about *A. lebbeck* followed by consumer interest (21.7 %) for both species.

TABLE 1
Detail of localities where survey and interviews were conducted regarding current status of *Terminalia arjuna* and *Albizia lebbeck* in agroforestry systems

Localities	Traditional Healers (Hakims)	Farmers	Nursery	TM, FM, Wood Carpenters	Total
UC-68	5	15	2	8	30 (8)
UC-70	8	10	4	6	28 (7.46)
UC-72	3	7	3	11	24 (6.4)
UC-74	9	14	1	9	33 (8.8)
UC-75	4	8	5	6	23 (6.13)
UC-76	7	10	3	11	31 (8.26)
UC-77	2	9	2	4	17 (4.53)
Khanewal	11	15	9	10	45 (12)
Multan	9	20	15	17	61 (16.26)
Mian Chanu	12	12	6	18	46 (12.26)
Kacha Khu	8	12	10	7	37 (9.86)
Total	78 (20.8)	132 (35.2)	60 (16)	105 (28)	375

Note: TM (Timber merchants), FM (Furniture manufactures), UC (Sub administrative unit of a District); Values in parenthesis are the percentages

TABLE 2
Respondents distribution according to their educational status and literacy level the in study area

Respondents categories	Illiterate	<5th grade	5-8th grade	8-10th grade	>10th grade	Literacy level (%)
Farmers	26 (19.7)	39 (29.5)	34 (25.8)	18 (13.6)	15 (11.4)	80.30
Nursery Growers	8 (13.3)	9 (15)	13 (21.7)	19 (31.7)	11 (18.3)	86.66
Traditional Healers	7 (8.9)	11 (14.1)	13 (16.6)	28 (35.9)	19 (24.4)	91.02
Timber Merchants	11 (10.5)	15 (14.3)	28 (26.8)	33 (31.4)	18 (17.1)	89.52

N=375, Values in parenthesis are the percentages

TABLE 3
Purpose of cultivation, source of information and constraints about cultivation of *T. arjuna* and *A.* by farmers in the study area

Purpose of tree cultivation		Information Source		Constraints in Cultivating trees	
Fuelwood	67 (50.8)	Radio/FM	19 (14.4)	Lack of Capital	22 (16.7)
Fodder	31 (23.5)	Television	35 (26.51)	Small land holding	19 (14.4)
Wind Breaker	13 (9.9)	Printed Material	13 (9.84)	Water shortage	24 (18.2)
Soil Fertility	12 (9.09)	Forest Department	9 (6.81)	Lack of technical assistance	38 (28.7)
Agricultural implements	9 (6.8)	Neighbor farmers	56 (42.4)	Less availability of seedlings	29 (22)

N=132, Values in parenthesis are the percentages

TABLE 4
Preference and constraints of nursery growers for establishing and marketing nurseries of *T. arjuna* and *A. lebbeck*

Preference of Nursery growers	*T. arjuna*	*A. lebbeck*	Constraints	*T. arjuna*	*A. lebbeck*
Recommend seedling to buyers	15 (25)	12 (20)	Lack of education	8 (13.3)	6 (10)
Buyers choice of purchasing seedling	12 (20)	21 (35)	Lack of technical skills	9 (15)	14 (23.3)
Preparation of Nursery	10 (16.7)	6 (10)	Lack of technical assistance	20 (33.3)	18 (30)
Purchase of seedling from Forest Department	15 (25)	9 (15)	Lack of marketing facilities	10 (16.7)	9 (15)
Sale of seedling	8 (13.3)	12 (20)	Lack of consumer interest	13 (21.7)	13 (21.7)

N=60, Values in parenthesis are the percentages

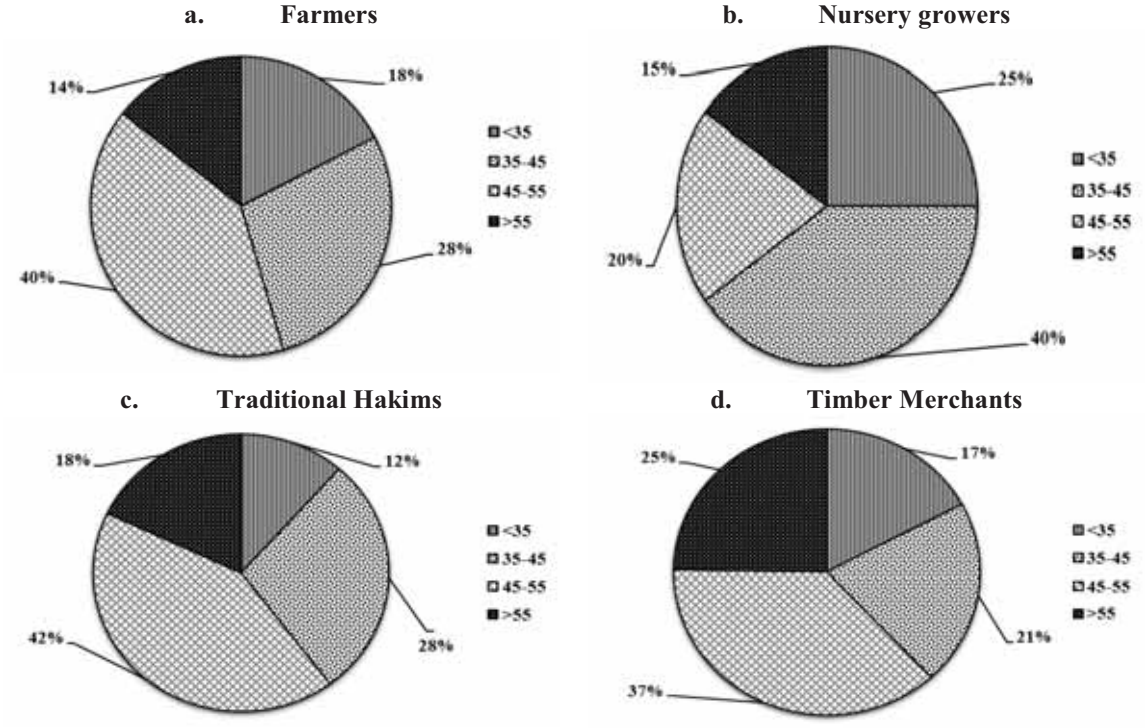

FIGURE 1 (a, b, c & d)
Respondents distribution according to their age in study area.

The data regarding medicinal uses of *T. arjuna* and *A. lebbeck* is presented in Fig. 2. A total of 78 traditional healers from the study area were surveyed. All Hakims were familiar and used *T. arjuna* and *A. lebbeck* extracts in their medicines singly and combined with other trees extracts. More than half of the respondents (60 %) reported the use of *T. arjuna* in treating heart diseases followed by skin treatment (18 %) whereas, 41 % respondents mentioned to use *A. lebbeck* in stomach related problems followed by dysentery (27 %) and skin treatment (14 %).

The data regarding the availability and utilization of *T. arjuna* and *A. lebbeck* is presented in Table 5. The results about the purchase of wood by timber merchants to further retail sale of *A. lebbeck* were maximum (90%) from farmers. About 49.5 % of respondents mentioned the higher demand of buyers regarding *A. lebbeck* wood as compared to *T.* arjuna. The latter species was not sold as wood by respondents, neither recommended to buyers and nor even demanded by buyers.

DISCUSSION

Socio-economic is an important factor in determining the behavior of people towards innovations and technologies. The productive, economic, human, social and protective services of agroforestry were assigned higher values due to their socioeco

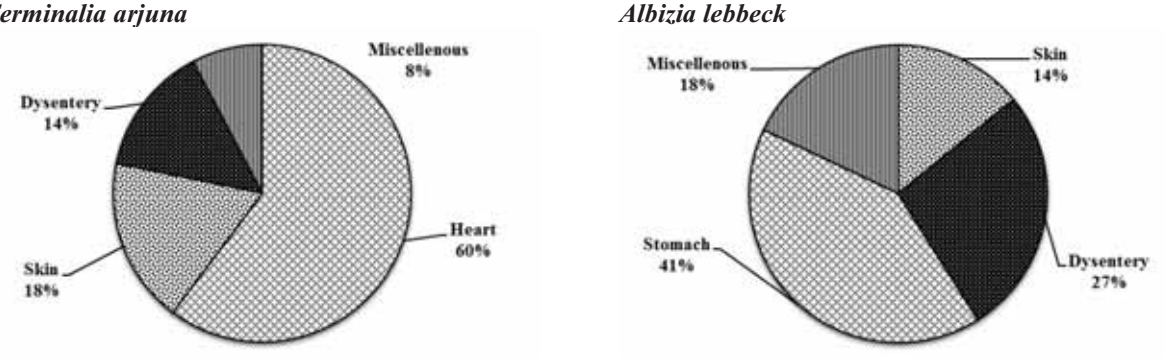

FIGURE 2
Utilization of *T. arjuna* and *A.lebbeck* by traditional hakims in treating diseases.

TABLE 5
Availability and utilization of *A.lebbeck* and *T. arjuna* in Timber market as compared to others tree species

	Timber merchants Preferences (%)				
	Purchase for sale		Sale of Timber	Recommendation to buyers	Buyers demand
	Farmer	Forest department			
A.lebbeck	90 %	10%	30%	20.5%	49.5%
T. arjuna	0	0	0	0	0

nomic and life-supporting impact on the rural societies, which is consistent with the previous workers [13-14]. The character like age and education make people more aware of the ongoing issues and challenges [15]. The majority of the respondents were middle-aged in the present study. Middle-aged farmers are the main earners as they are generally and economically active, innovative and hardworking in villages [16]. Our findings are similar to [17], reported 41% of respondents with over 40 years of age in district Chiniot of Pakistan. The low education in the study area reflects the unstable socioeconomic conditions, the involvement of young people in livelihood earnings and dispiritedness towards higher education [18]. More or less similar results have been reported by [19] who described the majority of farmers in the southern region of Pakistan were less educated. Tree planting along crops was emerged greatly till 2000 all over Pakistan and then decreased gradually due to marketing concerning issues and government policies etc. [1]. Moreover, other studies have advised farmers to grow trees on problematic soils and recommended tree species like *Albizia*, *Populus*, and *Eucalyptus* [20]. In developing countries like Pakistan, most people plant trees for obtaining fuelwood [12, 17]. It is quite obvious from our findings as more than half of the farmers cultivate *T. arjuna* and *A. lebbeck* for getting fuelwood. [21] also reported trees role in increasing soil fertility and providing other marketable products like food, timber, etc.

A. lebbeck was not cultivated in the study area for medicinal purposes but has been reported by various researchers as a medicinal tree. The above findings have similarities to [22] and [23] who described the use of leaves to be good for night blindness, syphilis and ulcer [22], respiratory disorders, cold and cough [23]. The pod extract is believed to possess antiprotozoal, hypoglycemic, antidiabetic, and anticancer properties [24]. The wood of *T. arjuna* is not much known in the market as compared to other contemporary local species like *D. sissoo*, P. deltoides, *A. lebbeck*, etc. This may be another reason for its less demand as wood, though the wood has almost similar qualities as the wood of *D. sissoo* [1]. The findings of this study regarding its use as medicine are similar to those reported by [25-26] as it has been widely reported as cardiotonic in heart failure and skin and dysentery related diseases. The bark of tree helps to decrease cardiovascular disease risk by lowering the blood pressure, improving the endothelial function, reducing blood cholesterol levels, having anti-inflammatory activity and improving the antioxidant defense of the cardiovascular system [27-28].

CONCLUSION

There is a relationship between tree cultivation and marketing. Farmers preferably cultivate only those trees which are easily available in nurseries and have more market value. Therefore, fruit trees are more cultivated as compared to purely timber-producing tree species. It provides a supplementary income source in the long run whereas cash crops are seasonal, low cast and main income sources of farmers. Similarly, only those plant nurseries are available which are demanded by farmers or cultivators. Farmers identified factors associated with decision making for the selection of tree species on their land. They are influenced by neighboring farmers more

than any other source. It supports the selection of local tree species rather than the newly introduced tree species. New exotic species also need special considerations for their introduction in local wood-based industries. *A. lebbeck* is an indigenous tree species and has already established a timber market, therefore, it has not any issue regarding seedling availability and marketing. *T. arjuna* is not well known by the farmers and mostly considered as an ornamental tree, therefore it has less acceptability in farmers and timber markets. It has importance in traditional medicines and its medicinally used parts are available from pansar stores who purchased it from the middle man without knowing or considering its production at the local level. The publicity of multipurpose trees should be promoted at the farmer level. The government can evolve the Agroforestry institutes to focus on the farmer's problems involved in agroforestry practices.

REFERENCES

[1] Qureshi, M. A. A. (2005) Basics of Forestry and Allied Sciences. 2nd Ed. A. One Publishers Lahore, Pakistan. 145-149.

[2] Seelinger, G., Merfort, I. and Schempp, C. M. (2008) Anti-oxidant, anti-inflammatory and anti-allergic activities of luteolin. Planta Medica. 74, 1667-1677.

[3] Orwa, C. (2009) Agroforest tree Database: a tree reference and selection guide, version 4.0. http://www.worldagroforestry. org/sites/treedbs/treedatabases.asp.(13-6-2009)

[4] Dwivedi, S. (2007) *Terminalia arjuna* Wight & Arn. a useful drug for cardiovascular disorders. Journal of Ethnopharmacology. 114, 114-129.

[5] Burkil, H. M. (2000) The Useful Plants of West Tropical Africa. Royal Botanic Gardens, Kew. London. 11–13.

[6] Kiptot, E., Hebinck, P., Franzel, S. and Richards, P. (2007) Adopters, testers or pseudo-adopters? Dynamics of the use of improved tree fallows by farmers in western Kenya. Agricultural Systems. 94, 509-519.

[7] Meijer, S.S., Catacutan, D., Ajayi, O. C., Sileshi, G. W. and Nieuwenhuis, M. (2015) The role of knowledge, attitudes and perceptions in the uptake of agricultural and agroforestry innovations among smallholder farmers in sub-Saharan Africa. International Journal of Agricultural Sustainability. 13, 40-54.

[8] Pattanayak, S. K., Mercer, D. E., Sills, E. and Yang, J. C. (2003) Taking stock of agroforestry adoption studies. Agroforestry Systems. 57, 173-186.

[9] Sileshi, G. W., Kuntashula, E., Matakala, P. and Nkunika, P. O. (2008) Farmers' perceptions of tree mortality, pests and pest management practices in agroforestry in Malawi, Mozambique and Zambia. Agroforestry Systems. 72, 87-101.

[10] Baig, M. B., Shabbir, A., Nowshad, K. and Muhammad, K. (2008) Germ plasm Conservation of Multipurpose Trees and their Role in Agroforestry for Sustainable Agricultural Production in Pakistan. International Journal of Agriculture & Biology. 10, 340-348.

[11] FAO. (1987) Pakistan's experience in rangeland rehabilitation and improvement. Food and Agriculture Organization of the United Nations. Rome, Italy. pp. 70.

[12] Farooq, T. H., Nawaz, M. F., Khan, M. W., Gilani, M. M., Buajan, S., Iftikhar, J., Tunon, N. and Wu, P. (2017) Potentials of agroforestry and constraints faced by the farmers in its adoption in District Nankana Sahib, Pakistan. International Journal of Development and Sustainability. 6, 586-593.

[13] Kareemulla, K., Rizvi, R. H., Yadav, R. S. and Dhyani, S. K. (2009) Agroforestry for rural development – cooperatives as viable institutions. Agricultural Situation in India. 61-67.

[14] Bijalwan, A., Sharma, C.M. and Kediyal, V.K. (2011) Socioeconomic status and livelihood support through traditional agroforestry systems in hill and mountain agroecosystem of Garhwal Himalaya, India. The Indian Forester. 138, 1423-1430.

[15] Talebi, K. and Tajeddin, M. (2011) The adoption of new and innovative knowledge by small and medium enterprises for Iran. Opportunities and constraints for growth. African Journal of Business Management. 5, 39-49.

[16] Islam, M. A., Masoodi, T. H., Gangoo, S. A., Sofi, P. A., Bhat, G. M., Wani, A. A. and Malik, A. R. (2015) Perceptions, attitudes and preferences in agroforestry among rural societies of Kashmir, India. Journal of Applied and Natural Science. 7, 976-983.

[17] Nawaz, M. F., Gul, S., Farooq, T. H., Siddiqui, M. T., Asif, M., Ahmad, I. and Niazi, N. K. (2016) Assessing the actual status and farmer's attitude towards agroforestry in Chiniot, Pakistan. International Journal of Forestry and Wildlife Sciences. 3, 393-397.

[18] Pal, G. (2011) Socio-economic characteristics of lac growers in Kanker district of Chhattisgarh. The Indian Forester. 137, 1294-1297.

[19] Luqman, M., Saqib, R., Karim, M., Nawab, K., Rehman, A. and Yaseen, M. (2018) Socio-economic impacts of agroforestry on livelihoods of rural households in Southern Region of the Punjab, Pakistan. Sarhad Journal of Agriculture. 34, 880-887.

[20] Owino, F. (2005) Improving multipurpose tree and shrub species for agroforestry systems. Agroforestry Systems. 19, 131-137.
[21] Ajake, A. O. (2012) The role of forest trees in indigenous farming systems as catalyst for forest resources management in the rural villages of Cross River State, Nigeria. Global Journal of Human Social Sciences, Geography and Environmental Geosciences. 12, 13-24.
[22] Pathak, N., Gohil, P., Patel, N. B., Kasture, S., Jivani, N. and Bhalodia, Y. (2009) Curative effect of *Albizia lebbeck* methanolic extract against adjuvant arthritis with special reference to bone erosion. International Journal of Pharmaceutical Sciences and Drug Research. 1, 183-187.
[23] Saha, A. and Ahmed, M. (2009) The analgesic and anti-inflammatory activities of the extract of *Albizia lebbeck* in animal model. Pakistan Journal of Pharmaceutical Sciences. 22, 74-77.
[24] Faisal, M., Singh, P. P. and Irchhaiya, R. (2012) Review on *Albizia lebbeck* a potent herbal drug. International Research Journal of Pharmacy. 3, 63-68.
[25] Prusti, A. B. and Behera, K. K. (2007) Ethnobotanical exploration of Malkangiri district of Orissa, India. Ethnobotanical Leaflets. p. 14.
[26] Kumar, G. P., Navya, K., Ramya, E. M., Venkataramana, M., Anand, T., and Anilakumar, K. R. (2013) DNA damage protecting and free radical scavenging properties of Terminalia arjuna bark in PC-12 cells and plasmid DNA. Free radicals and antioxidants. 3, 35-39.
[27] Kumar, S., Ma, J., Pankaj, P., Km, S. and Kg, S. (2017) *Terminalia arjuna* (Roxb.) reverses the molecular signature of fibrosis induced by Isoproterenol in rat heart. American Journal of Phytomedicine and Clinical Therapeutics. 5, 3-22.
[28] Ambika, S. P. P. and Chauhan, S. M. S. (2014) Activity-guided isolation of antioxidants from the leaves of *Terminalia arjuna.* Natural Product Research. 28, 760-763.

Received: **14.10.2019**
Accepted: **31.01.2021**

CORRESPONDING AUTHOR

Ghulam Yasin
Department of Forestry and Range Management,
Bahauddin Zakariya University,
Multan Punjab – Pakistan

e-mail: yasin_2486@yahoo.com

© by PSP Volume 30– No. 05/2021 pages 4749-4755 Fresenius Environmental Bulletin

AN EXAMPLE OF THE EFFECT OF DIET QUALITY ON THE IMMUNE SYSTEM OF AN INFECTED INSECT: *URESIPHITA GILVATA* (FABRICIUS, 1794)

Oguzhan Yanar[1,*], Gizem Aykol[1], Elif Fatma Topkara[1], Fatma Gonul Solmaz[1], Sevcan Mercan[2], Ardahan Eski[3]

[1]Department of Biology, Science and Art Faculty, Ondokuz Mayis University, 55139, Samsun, Turkey
[2]Vocational School of Health Services, Ondokuz Mayıs University, 55139, Samsun, Turkey
[3]Program of Biomedical Equipment Technology, Vocational School, Bilecik Seyh Edebali University, 11230, Bilecik, Turkey

ABSTRACT

The aim of this study was to determine the changes in cellular and humoral immunity of *Uresiphita gilvata* larvae fed with diets containing different amounts of protein and carbohydrate and infected with *Bacillus thuringiensis* subsp. *kurstaki*. In this context, it has been determined how diet contents and infection affect superoxide dismutase (SOD), manganese superoxide dismutase (MnSOD), catalase (CAT), glutathione peroxidase (GSH-Px), phenoloxidase (PO) enzyme activities and total hemocyte counts of larvae. For this purpose, four different diets were prepared by changing the amounts of protein and carbohydrate. Except for the control groups, other groups were infected with bacteria. In control and infected groups, superoxide dismutase and manganese superoxide dismutase enzymes showed the highest activity in the groups with the highest amount of protein. The catalase enzyme showed inhibition in all infected groups compared to control groups. As the amount of protein in the control groups increased, the phenoloxidase enzyme was found to be activated. It was found that the number of hemocytes decreased with infection (except H). Larvae exposed to infection and diet imbalance try to protect themselves with both cellular and humoral defense to combat these negativities.

KEYWORDS:
Bacillus thuringiensis, Protein, Carbohydrate, Enzyme, Infection

INTRODUCTION

Nutrition is very crucial for all animals, including herbivorous insects [1, 2]. All herbivorous insects, including caterpillars, require the same nutrients [3]. These include amino acids (mostly derived from the protein in the nutrients), carbohydrates (sugars and starch), lipids (fatty acids, phospholipids, and sterols), vitamins, and minerals. Lipids, vitamins, and minerals are classified as micronutrients. These micronutrients are found at low levels in plants, and often herbivorous insects need only small amounts of these nutrients. A large amount of macronutrients, such as protein and carbohydrate is needed in nutrition [4].

It is unquestionable that both pathogens and insecticides significantly affect insect populations. Generally, pathogens invade insects in two ways. They can enter the intestines through consumption, or they can enter the hemolymph by penetrating wounds on the body surface or integument or the intestine tissue [5].

Insect immunity consists of three parts: Cuticle, which provides physical and chemical obstacles to the external world of microbes, cellular immunity, and humoral immunity [6]. Pathogens that enter the body through a cuticle lead to infection through the enzymatic digestion of the cuticle or wounds that occur in the cuticle. In addition to being vital components of the defense system, hemocytes have many functions, including synthesis and transport of nutrients and hormones, the formation of connective tissue, and wound healing [7]. Humoral immunity involves the production of antimicrobial peptides, reactive oxygen and nitrogen intermediates, as well as enzymatic complex cascades that regulate hemolymph clotting and melanization [8, 9].

There is an antioxidant defense system in organisms that is responsible for destroying or counteracting endogenous or exogenous reactive chemicals. Superoxide dismutase (SOD), catalase (CAT), glutathione peroxidase (GPx), glutathione S-transferase (GST), glutathione reductase (GR), ascorbate peroxidase, thioredoxin peroxidase, disulfide reductase, and methionine sulfoxide reductase are antioxidant enzymes found in insects [10]. The antioxidant mechanism becomes active in response to stress in insect tissues and allows insects to survive in chemically unsuitable environmental conditions [11].

Superoxide dismutase is the enzyme that converts superoxide radicals (O_2^-) to hydrogen peroxide (H_2O_2) and molecular oxygen (O_2) [12]. It is known that manganese superoxide dismutase (MnSOD) is an essential antioxidant enzyme found in the mitochondrial matrix of aerobic organisms

[13]. MnSOD is crucial for aerobic cells and is biologically significant. Catalase converts hydrogen peroxide (H_2O_2) to water and oxygen. Glutathione peroxidase is the enzyme responsible for the reduction of hydroperoxides.

The *Bacillus thuringiensis* used in the research is a Gram-positive soil bacterium with entomopathogenic properties that produce insecticidal proteins (so-called Cry proteins or δ-endotoxins) during sports formation [14, 15]. *Uresiphita gilvata* Fabricius 1974 is widespread in Europe and North Africa. Having commercial plants of the genus Trifolium in Turkey also cause serious economic losses.

This research aimed to investigate the effects of macronutrients (protein and carbohydrate) found in artificial diet contents of *U. gilvata* larvae infected by *B. thuringiensis* subsp. *kurstaki* on the cellular and humoral immunity of larvae.

MATERIALS AND METHODS

Collecting larvae. *Uresiphita gilvata* larvae were collected from the plants of the *Sophora alopecuroides* (Fabaceae) in the Kızılırmak Delta in the Bafra district of Samsun Province in September 2017.

Artificial diet contents. In this research, *U. gilvata* larvae fed in artificial diets prepared by using different concentrations of protein and carbohydrates. The control diet (CD) was used as an artificial diet developed by Yamamoto [16]. The amount of protein (casein) and carbohydrate (sucrose) was changed, and four different diets were prepared (Table 1).

Feeding experiment. In this experiment, larvae fed with diets for a particular period. Following this step, except for the control groups, various other assays were performed after the other larvae infected with *B. thuringiensis* subsp. *kurstaki*. This experiment was carried out in 2 stages, and each was put the determined number of *U. gilvata* larvae. To determine the total hemocyte count, 50 larvae were placed in the first stage, and 100 larvae were placed in plastic containers for each group to determine the enzyme activity. The larvae were subjected to overfeed with artificial diets. After five days of feeding, the hemolymph of control larvae was taken. 1 ml of bacteria was applied for infected groups, and three days more larvae were allowed to be fed in related diets. Then, the hemolymphs were taken, and the enzymes activities and hemocyte counts were analyzed.

TABLE 1
Diet groups and diet contents

Diet groups	Diet contents
A	P:C 30:30 (CD) (Control)
B	P:C 30:30 (Infected)
C	P:C 50:10 (Control)
D	P:C 50:10 (Infected)
E	P:C 10:50 (Control)
F	P:C 10:50 (Infected)
G	P:C 15:15 (Control)
H	P:C 15:15 (Infected)

P:C Protein: Carbohydrate

Giemsa dyeing of preparations to be used in hemocyte counting. After the insect hemolymph to be used in the hemocyte count were placed in the Eppendorf tubes, full preservative preparations were obtained by dyeing with Giemsa in order not to deteriorate the hemocyte structures. After the hemolymph was removed from the larvae in each group and placed in Eppendorf tubes, 10 µl of hemolymph was spread for each slide. After drying the hemolymph spreading the slide, the Giemsa dyeing steps were applied.

TABLE 2
Mean hemocyte counts of *Uresiphita gilvata* larvae

Diet contents	Diet groups	Groups	Mean±standard error (n/10µl)	t	*P*
P:C 30:30	A	Control	2072±3.8	-316.2	<0.001
	B	Infected	1188±4.1		
P:C 50:10	C	Control	1921±2.7	-594.3	<0.001
	D	Infected	1495±5.3		
P:C 10:50	E	Control	1634±6.1	-436.3	<0.001
	F	Infected	1085±1.9		
P:C 15:15	G	Control	1742±3.5	-231.3	<0.001
	H	Infected	1930±3.0		

Enzyme analysis. Protein determination was made according to Lowry et al. method [17]. Catalase activity was determined by Lück method [18], the superoxide dismutase activity was determined by the spectrophotometric method of McCord and Fridovich [19] and Flohé and Ötting method [20]. Benov and Fridovich's method [21] was used for manganese superoxide dismutase activity. Glutathione peroxidase enzyme activity was determined by Lawrence and Burk method [22]. The phenoloxidase activity was determined by the method of Ashida and Söderhall [23].

Statistical analysis. To determine the relationship between hemocyte count and enzyme activation depending on the diet content, two independent samples t-test were used. SPSS 21 version was used for these tests.

RESULTS AND DISCUSSION

Among the control groups, the least hemocyte count is in the E diet group with the lowest amount of protein (P:C 10:50). It was found that the highest count of hemocytes was in the A diet group (P:C 30:30). It is an adequate and balanced diet in terms of nutrients, proteins, and carbohydrates. Protein and carbohydrate equilibrium is crucial for this species, as in all living things. Among the control groups and the infected groups, the lowest hemocyte counts are in the diet groups with the minimum amounts of protein (E and F diets; P:C 10:50). It shows how important protein is in cellular defense (Table 2).

In the comparison of the number of hemocytes involved in cellular defense, the effect of infection, as well as the diet content, is crucial. It is evident that the hemocyte count of larvae fed in the groups infected with bacteria (except H) is less than that of the control groups. In a study with *Trichoplusia ni* [24], the hemocyte count of larvae infected with *B. thuringiensis* was found to be less than that of the control larvae. In comparison to the control group, it has been found that there is a decrease in hemocyte count of *Plodia interpunctella* larvae infected with *B. thuringiensis* [25]. These studies coincide with the results of our research.

It was found when the amount of protein in the diet increased in the infected groups, the hemocyte count increased. A remarkable result was found in the diet group H (P:C 15:15), whose protein and carbohydrate amounts were reduced by half. While hemocyte counts of bacterial infection and other groups were decreased compared to control groups, an increase was observed in the count of hemocytes of the larvae fed into this diet. While the hemocyte counts decreased compared to the control groups due to bacterial infection, an increase in the hemocyte counts of the larvae fed to this diet was recorded. All animals need a balanced diet [26]. In addition to both protein and carbohydrate in inadequate nutrition, as well as infection with the larvae have to fight against the infection may have increased the hemocyte counts.

An increase in phenoloxidase enzyme activity was noted as the amount of protein added to the diet increased (except for G) in the control groups. Phenoloxidase is an important enzyme used against many pathogens [27]. In insects, prophenoloxidases (PPO) are converted to phenoloxidases (PO), and activated to induce melanization after pathogen infection [28]. Melanin production is often triggered by cellular responses [29, 30]. The melanization pathway is activated by hemocytes that release serine proteases and induce PO cascade [31, 32] (Table 3).

It has been noted that phenoloxidase enzyme activity changes with a bacterial infection. It was found that this enzyme was activated by an infection in all groups (except D). The highest activation (412%) is in the diet group (H) which reduced the

TABLE 3
Phenoloxidase activities of *Uresiphita gilvata* larvae

Diet contents	Diet groups	Groups	Mean±standard error (Iu/ml)	t	*P*
P:C 30:30	A	Control	2.2	9.8	<0.001
	B	Infected	2.6		
P:C 50:10	C	Control	3.3	-739.2	<0.001
	D	Infected	1.6		
P:C 10:50	E	Control	1.4	62.8	<0.001
	F	Infected	1.5		
P:C 15:15	G	Control	1.1	2061.6	>0.05
	H	Infected	5.8		

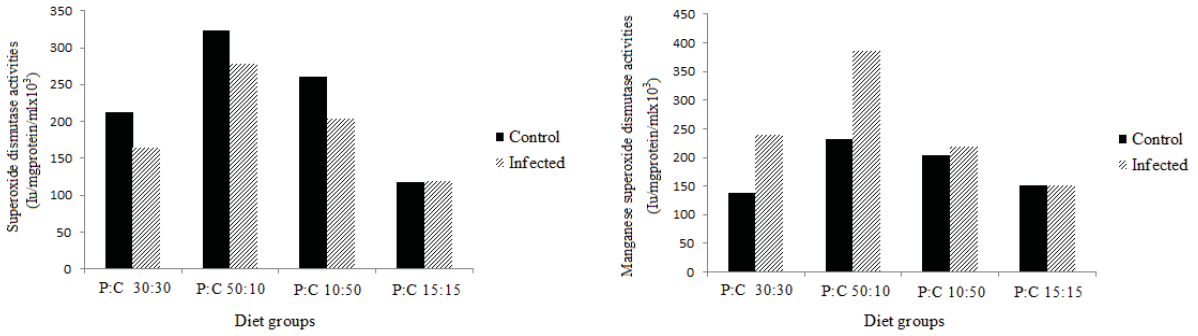

FIGURE 1
Comparison of superoxide dismutase and manganese superoxide dismutase enzyme activities according to diet groups of *Uresiphita gilvata* larvae

amount of protein and carbohydrate by half. The phenoloxidase enzyme activity in this group, where the count of hemocytes increased only, was maximal. The increase in infection, insufficient nutrient content (P:C 15:15), and the increase in the count of hemocytes involved in humoral defense led to high activation of the phenoloxidase enzyme compared to the control group (G).

The lowest phenoloxidase activity among the infected groups is in the group (F) with the least amount of protein. In this group, the minimum hemocyte count as a result of the infection caused the phenoloxidase enzyme activity to be minimal. This suggests that both phenoloxidase activities depend on the number of hemocytes and also the role of protein and infection in enzyme activity.

The highest levels of superoxide dismutase enzyme activity in both control and infected groups were found in diet groups (C and D) with the highest protein content (C=324±2.2, p<0.001; D=279±1.5, p<0.001). In our study, inhibition occurred in all groups (except H) by the bacterial infection. Various insecticides are known to suppress the activity of key enzymes such as superoxide dismutase [33, 34]. The decrease in enzyme activity by infection may mean that bacteria suppress oxidative stress (Figure 1).

Manganese superoxide dismutase is an antioxidant enzyme found in the mitochondrial matrix of aerobic organisms [13]. This enzyme is essential for aerobic cells and is biologically crucial [35]. The highest manganese superoxide dismutase enzyme activity in both control and infected groups is in diet groups with the highest amount of protein (C and D) (C=232±3.0, p<0.001; D=387±3.0, p<0.001). The highest levels of superoxide dismutase enzyme activities are also in these groups. It suggests that the amount of protein directly affects both cytoplasmic and mitochondrial radical scavenging mechanisms.

Manganese superoxide dismutase plays a role in the innate immune response of the animal in the presence of bacteria [36, 37]. In a research with *Hyphantria cunea*, it was found that manganese superoxide dismutase expression in *Pseudomonas aeruginosa* and *Candida albicans* infected larvae was two times lower than in controls [38]. In our study, activation in all groups (except H) with bacterial infection occurred. As the amount of carbohydrate added to the diet increased in the infected groups (except H), the enzyme activity decreased. In the diet group (F), which has the highest carbohydrate content, the activation is minimal (7.8%) (F=220±3.1; p<0.001). This shows that the infection and carbohydrate cause inhibition of the activation of the manganese superoxide dismutase enzyme.

The amount of protein and carbohydrate in the diet has been associated with the ability to overcome stresses such as the immune responses of herbivore insects [39]. As the amount of protein added to the diet increased in the control groups, an increase in catalase enzyme activity was recorded. Among these groups, the highest catalase enzyme activity (C= 9955±3.9; p<0.001) was found in the diet group C with the maximum protein content (P:C 50:10). In this group, both superoxide dismutase and manganese superoxide dismutase activities are maximal. The high activity of these enzymes led to the high activity of the catalase enzyme (Figure 2).

Dubovskiy et al. [40] found that catalase enzyme activity in the midgut of *G. mellonella* larvae infected with *B. thuringiensis* decreased compared to the control groups. In a study on catalase activities in the midgut of *Lymantria dispar* larvae fed in different plants, a decrease in enzyme activity was found [41]. In our research, it was shown that all groups showed inhibition in catalase enzyme due to bacterial infection. It suggests that free radicals in the environment may be held by *B. thuringiensis*.

Diet content can have a wide variety of effects on immune responses [42, 43]. A reduction in the activity of glutathione peroxidase enzyme was noted as the amount of carbohydrate added to the diet decreased in the control groups (except for G). It shows that carbohydrate is crucial in the removal of hydrogen peroxide.

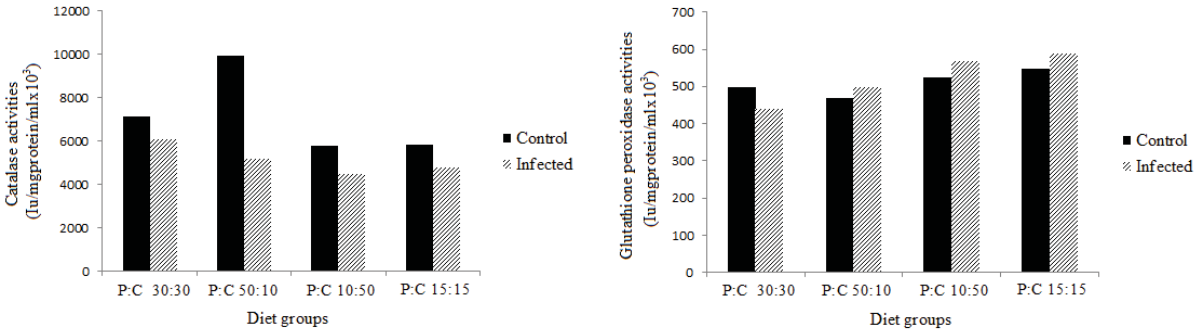

FIGURE 2
Comparison of catalase and glutathione peroxidase enzyme activities according to diet groups of *Uresiphita gilvata* larvae

Glutathione peroxidase removes a low concentration of hydrogen peroxide. Catalase removes the high hydrogen peroxide concentration [44]. Among the control groups, the catalase activity was maximal in the C diet group in which superoxide dismutase and manganese superoxide dismutase enzymes showed maximum activity. However, glutathione peroxidase enzyme activity showed minimum activity in this group (C=468±3.7; $p<0.001$). It shows that catalase and glutathione peroxidase enzymes work in a coordinated manner.

CONCLUSION

In our study, we examined the effects of protein and carbohydrate from the most basic macronutrients for nutrition on *U. gilvata* larvae. We also investigated how cellular and humoral defense systems are affected by these two variables when the larvae are infected with *B. thuringiensis*. Differences were observed in the cellular and humoral defenses of the larvae fed in diets with different contents under normal conditions (except infection) depending on the diet content. When an infection is included, larvae activate defense systems against infection. Sometimes this activity of enzymes is inhibited by infection.

ACKNOWLEDGEMENTS

This study was supported by the Ondokuz Mayıs University Research Foundation.

REFEFENCES

[1] Behmer, S.T. (2009) Insect herbivore nutrient regulation. Annu. Rev. Entomol. 54, 165-187.
[2] Simpson, S.J. and Raubenheimer, D. (2012) The Nature of Nutrition: A Unifying Framework from Animal Adaptation to Human Obesity. Princeton University Press, New Jersey. 256 pp.
[3] Chapman, R.F., Simpson, S.J. and Douglas, A.E. (2013) The Insects. Cambridge University Press, England. 959p.
[4] Bernays, E.A. (1994) Host-Plant Selection by Phytophagous Insects. Chapman and Hall, London. 312p.
[5] Wu, K., Yang, B., Huang, W., Dobens, L., Song, H. and Ling, E. (2016) Gut immunity in Lepidopteran insects. Dev. Comp. Immunol. 64, 65-74.
[6] James, R.R. and Xu, J. (2012) Mechanisms by which pesticides affect insect immunity. J. Invertebr. Pathol. 109, 175-182.
[7] Pandey, J.P. and Tiwari, R.K. (2012) An overview of insect hemocyte science and its future application in applied and biomedical fields. Am. J. Biochem. Mol. Biol. 2, 82-105.
[8] Gillespie, J.P., Kanost, M.R. and Trenczek, T. (1997) Biological mediators of insect immunity. Annu. Rev. Entomol. 42, 611-643.
[9] Marmaras, V.J. and Lampropoulou, M. (2009) Regulators and signalling in insect haemocyte immunity. Cell. Signal. 21, 186-195.
[10] Missirlis, F., Rahlfs, S., Dimopoulos, N., Bauer, H., Becker, K., Hilliker, A. and Phillips, J.P. (2003) A putative glutathione peroxidase of *Drosophila* encodes thioredoxin peroxidase that provides resistance against oxidative stress but fails to complement a lack of catalase activity. J. Biol. Chem. 384, 463-472.
[11] Hyršl, P., Buyukguzel, E. and Buyukguzel, K. (2007) The effects of boric acid-induced oxidative stress on antioxidant enzymes and survivorship in Galleria mellonella. Arch. Insect Biochem. Physiol. 66, 23-31.
[12] Özelçi-Kavas, G. (1994) Physiopathological approach to reactive oxygen metabolites. J. Ankara Univ. Fac. Med. 47, 579-592. (in Turkish)
[13] Cadenas, E. and Davies, K.J. (2000) Mitochondrial free radical generation, oxidative stress, and aging. Free Radic. Biol. Med. 29, 222-230.

[14] Avisar, D., Eilenberg, H., Keller, M., Reznik, N., Segal, M., Sneh, B. and Zilberstein, A. (2009) The *Bacillus thuringiensis* delta-endotoxin Cry1C as a potential bio insecticide inplants. Plant Sci. 176, 315-324.

[15] Vachon, V., Laprade, R. and Schwartz, J.L. (2012) Current models of the mode of action of *Bacillus thuringiensis* insecticidal crystal proteins: A critical review. J. Invertebr. Pathol. 111, 1-12.

[16] Yamamoto, R.T. (1969) Mass rearing of tobacco hornworm. II. Larval rearing and pupation. J. Econ. Entomol. 62, 1427-1431.

[17] Lowry, O.H., Rsebrough, N.T., Farr, A.L. and Randall, R.J. (1951) Protein measurement with the folin phenol reagent. J. Biol. Chem. 193, 265-275.

[18] Lück, H. (1963) Catalase. In: Bergmeyer, H. U. (ed.) Methods of Enzymatic Analysis. Weinheim and Academic Press, New York. 885-888.

[19] McCord, J.M., Fridovich, I. (1969) Superoxide dismutase: An enzymic function for erythrocuprein (hemocuprein). J. Biol. Chem. 244, 6049-6055.

[20] Flohé, L. and Ötting, F. (1984) Superoxide dismutase assays. Methods Enzymol. 105, 93-104.

[21] Benov, L. and Fridovich, I. (1998) Growth in iron-enriched medium partially compensates *E. coli* for the lack of Mn and Fe SOD. J. Biol. Chem. 273, 10313-10316.

[22] Lawrence, R.A. and Burk, R.F. (1976) Glutathione peroxidase activity in selenium deficient rat liver. Biochem. Biophys. Res. Commun. 71, 952-958.

[23] Ashida, M. and Söderhall, K. (1984) The prophenoloxidase activating system in crayfish. Comp. Biochem. Physiol. B Biochem. Mol. Biol. 77, 21-26.

[24] Ericsson, J.D., Janmaat, A.F., Lowenberger, C. and Myers, J.H. (2009) Is decreased generalized immunity a cost of *Bt* resistance in cabbage loopers *Trichoplusia ni*? J. Invertebr. Pathol. 100, 61-67.

[25] Orozco-Flores, A.A., Valadez-Lira, J.A., Oppert, B., Gomez-Flores, R., Tamez-Guerra, R., Rodríguez-Padilla, C. and Tamez-Guerra, P. (2017) Regulation by gut bacteria of immune response, *Bacillus thuringiensis* susceptibility and hemolin expression in *Plodia interpunctella*. J. Insect Physiol. 98, 275-283.

[26] Clissold, F.J. and Simpson, S.J. (2015) Temperature, food quality and life history traits of herbivorous insects. Curr. Opin. Insect Sci. 11, 63-70.

[27] Cerenius, L. and Söderhäll, K. (2004) The prophenoloxidase-activating system in invertebrates. Immunol. Rev. 198, 116-126.

[28] Lu, A., Zhang, Q., Zhang, J., Yang, B., Wu, K., Xie, W., Luan, Y.X. and Ling, E. (2014) Insect prophenoloxidase: The view beyond immunity. Front. Physiol. 5, 1-15.

[29] Jiang, H.B., Wang, Y. and Kanost, M. R. (1998) Pro-phenol oxidase activating proteinase from an insect, *Manduca sexta*, a bacteria-inducible protein similar to *Drosophila easter*. Proc. Natl. Acad. Sci. U.S.A. 95, 12220-12225.

[30] Goldsworthy, G., Mullen, L., Opoku-Ware, K. and Chandrakant, S. (2003) Interactions between the endocrine and immune systems in locusts. Physiol. Entomol. 28, 54-61.

[31] Kurihara, Y., Shimazu, T. and Wago, H. (1992) Classification of hemocytes in the common cutworm, *Spodoptera litura* (Lepidoptera: Noctuidae) II. Possible roles of granular plasmatocytes and oenocytoids in the cellular defense reactions. Appl. Entomol. Zool. 27, 237-242.

[32] Gajewski, K.M., Sorrentino, R.P., Lee, J.H., Zhang, Q., Russell, M. and Schulz, R.A. (2007) Identification of a crystal cell-specific enhancer of the black cells prophenoloxidase gene in *Drosophila*. Genesis. 45, 200-207.

[33] Adamski, Z., Ziemnicki, K., Fila, K., Žikić, R. and Štajn, A. (2003) Effects of long-term exposure to fenitrothion on *Spodoptera exigua* and *Tenebrio molitor* larval development and antioxidant enzyme activity. Biol. Lett. 40, 43-52.

[34] Buyukguzel, E. (2009) Evidence of oxidative and antioxidative responses by *Galleria mellonella* larvae to malathion. J. Econ. Entomol. 102, 152-159.

[35] Candas, D., Li, J.J. (2014) MnSOD in oxidative stress response-potential regulation via mitochondrial protein influx. Antioxid. Redox Signal. 20, 1599-1617.

[36] Cheng, W., Tung, Y.H., Liu, C.H. and Chen, J.C. (2006) Molecular cloning and characterization of copper/zinc superoxide dismutase (Cu, Zn-SOD) from the giant freshwater prawn *Macrobrachium rosenbergii*. Fish Shellfish Immun. 21, 102-112.

[37] Bao, Y., Li, L. and Zhang, G. (2008) The manganese superoxide dismutase gene in bay scallop *Argopecten irradians*: Cloning, 3D modelling and mRNA expression. Fish Shellfish Immun. 25, 425-432.

[38] Kim, Y.I., Kim, H.J., Kwon, Y.M., Kang, Y.J., Lee, I.H., Jin, B.R., Han, Y.S., Cheon, H.M., Ha, N.G. and Seo, S.J. (2010) Modulation of MnSOD protein in response to different experimental stimulation in *Hyphantria cunea*. Comp. Biochem. Physiol. B Biochem. Mol. Biol. 157, 343-350.

[39] Deans, C.A., Sword, G.A. and Behmer, S.T. (2016) Nutrition as a neglected factor in insect herbivore susceptibility to Bt toxins. Curr. Opin. Insect Sci. 15, 97-103.
[40] Dubovskiy, I.M., Martemyanov, V.V., Vorontsova, Y.L., Rantala, M.J., Gryzanova, E.V. and Glupov, V.V. (2008) Effect of bacterial infection on antioxidant activity and lipid peroxidation in the midgut of *Galleria mellonella* L. larvae (Lepidoptera, Pyralidae). Comp. Biochem. Physiol. C: Toxicol. Pharmacol. 148, 1-5.
[41] Peric-Mataruga, V., Blagojevic, D., Spasic, M.B., Ivanovic, J. and Jankovic-Hladni, M. (1996) Effect of the host plant on the antioxidative defence in the midgut of *Lymantria dispar* L. caterpillars of population origins. J. Insect Physiol. 43, 101-106.
[42] Koella, J.C. and Sorense, F.L. (2002) Effect of adult nutrition on the melanization immune response of the malaria vector *Anopheles stephensi*. Med. Vet. Entomol. 16, 316-320.
[43] Brunner, F.S., Schmid-Hempel, P. and Barribeau, S.M. (2014) Protein-poor diet reduces host-specific immune gene expression in *Bombus terrestris*. Proc. R. Soc. Lond. B. 281, 20140128.
[44] Özcan, O., Erdal, H., Çakırca, G. and Yönden, Z. (2015) Oxidative stress and its impacts on intracellular lipids, proteins and DNA. J. Clin. Exp. Invest. 6, 331-336.

Received: **05.11.2019**
Accepted: **20.01.2021**

CORRESPONDING AUTHOR

Oguzhan Yanar
Department of Biology,
Science and Art Faculty,
Ondokuz Mayis University,
55139 Samsun – Turkey

e-mail: oyanar46@gmail.com

© by PSP Volume 30– No. 05/2021 pages 4756-4762 Fresenius Environmental Bulletin

STUDY ON CALORIFIC VALUE OF SEMI-COKE AND DESULFURIZATION EFFECT DURING PYROLYSIS OF BITUMINOUS COAL

Chen Jihao[1,2,*], Li Yue[1,2], Chen Xinjuan[1,2], Zhang Lei[3], Yang Dongfeng[1,2]

[1] Shaanxi Coal Geological Laboratory Co. Ltd., Xi'an, 710054, China
[2]Key Laboratory of Coal Resources Exploration and Comprehensive Utilization, Ministry of Natural Resources, Xi'an, 710021, China
[3] Xi'an University of Technology, Xi'an 710048, China

ABSTRACT

Taking bituminous coal with medium sulfur content as experimental coal sample, the effect of desulfurization, calorific value and volatile matter were studied. Pyrolysis of coal samples was conducted in a high temperature furnace with different pyrolysis time, different temperature and different mass. The effects of pyrolysis conditions on desulfurization efficiency, semicoke volatilization and calorific value were investigated. The results showed that:(1) Pyrolysis had the effect of desulfurization, which was affected by pyrolysis temperature, pyrolysis time and pyrolysis quality; (2) The desulfurization efficiency of coal pyrolysis reached 29.91% in 16 min, the desulfurization efficiency was good, and the calorific value of semicoke was 22.99kJ/g; (3) In the temperature range of 450℃ to 650℃, the desulfurization efficiency had little change, at this time, semicoke had the effect of sulfur fixation; (4) The maximum specific surface area of semicoke was 102.78m^2/g at 650℃ and the reduction of C-S and S-O functional groups in the FTIR spectrum of semicoke result in desulfurization during pyrolysis.

KEYWORDS:
Semi-coke, desulfurization, calorific value, pyrolysis

INTRODUCTION

China was rich in coal resources, which provided an important energy guarantee for the development and progress of the country and society. However, the quality of coal resources was uneven, the content of low rank coal was more, and the utilization rate of direct combustion as fuel was low, resulting in waste of resources. Through pyrolysis coal, high value products were extracted from coal, and the potential value of coal was developed. The preparation of coal into tar, pyrolysis gas and semi-coke by pyrolysis was achieved[1]. Due to the abundant sulfur in coal, semi-coke, pyrolysis gas and tar were produced during pyrolysis, and many harmful sulfur-containing substances such as SO_2, H_2S and thiols were released[2]. Therefore, it was of great significance to study the desulfurization effect in the process of coal pyrolysis and realize the clean utilization of coal resources.

In the process of coal pyrolysis, combustible materials were released or oxidized, gasified, decomposed and polymerized on the surface or inside of coal particles. According to the sulphur content of coal, there were three types: low sulfur coal (St.d<1%), medium sulphur coal (1% ≤St.d≤3%) and high sulfur coal (St.d >3%)[3]. There were two main types of sulfur in coal: inorganic sulfur and organic sulfur. Inorganic sulfur in coal mainly included pyrite sulfur, sulfate sulfur, elemental sulfur and so on. Organic sulfur in coal mainly existed in macromolecule of coal in the form of mercaptan, thiophene and so on, and according to the structure, it can be divided into heterocyclic group, aromatic group and aliphatic group sulfur, including mercaptan, thioether, thiophene and so on[4-5]. Some of iron sulfide sulfur can be pyrolyzed to form sulfide and element S, then S can react with H and CO to form H_2S and COS, or can be directly polymerized to Sn; H_2S, COS and CS_2 can be obtained by the direct reaction of H_2, CO and C with iron sulfide and other sulfides at different temperatures[6]. Sulfate sulfur can be directly decomposed or oxidized by CO to SO_2. Organic sulfur was relatively complex, so there were many ways to transform: it usually decomposed to form free radical S, and then the free radical s was transformed into various sulfides.The three kinds of sulfur can also be transformed into each other. The active component in pyrite or organic sulfur can react with the active part of inorganic matrix to form new sulfate or organic substance and stay in semi-coke, while the sulfur in semi-coke can continue to react with organic matrix or inorganic substance to form stable organic thiophene[7]. Studies had shown that[8], most of the sulfur in lignite was mercaptan and

TABLE 1
Industrial analysis and element analysis of coal sample(%)

industrial analysis				Q(KJ/g)	element analysis/%				
M_{ad}	A_{ad}	V_{ad}	FC_{ad}		C	H	O	N	S_t
1.39	18.82	29.75	50.04	25.52	62.22	3.720	12.28	0.89	1.12

aliphatic thioether, while it was mainly dibenzothiophene in bituminous coal. Therefore, it was of great significance to study the desulfurization of coal pyrolysis process and realize for clean utilization of coal.

The middle sulfur bituminous coal was selected as the experimental coal sample to carry out pyrolysis under different conditions. By measuring the volatile, calorific value and total sulfur content of pyrolysis semi-coke, the influence of pyrolysis conditions on desulfurization efficiency, semi-coke volatile and calorific value was studied, which was conducive to the clean and efficient utilization of coal and provided technical support for the establishment of coal pyrolysis desulfurization.

EXPERIMENTS

Experimental materials. Preparation of experimental coal sample. The raw coal produced in Cuimu coal mine of China was taken as the experimental coal sample, and the medium sulfur coal was selected for the experiment.The raw coal was crushed to less than 3cm by crusher, dried in a drying oven at 75℃ for 40min, and the experimental coal sample was prepared by using the powder of the powder mill. Industrial analysis and element analysis of coal samples were shown in Table 1.

Preparation of pyrolysis semi-coke. Preparation of semicokes with different pyrolysis time: 3g coal sample was placed in a volatilizing dish, which was covered and pyrolyzed in an oxygen isolated muffle furnace at 850℃. The pyrolysis time was 3min, 5min, 7min, 11min and 16min respectively. The semi-cokes with different pyrolysis time were prepared.

Preparation of semi-cokes at different pyrolysis temperatures: 3g coal sample was placed in a volatilizing dish, which was covered and pyrolyzed in an oxygen isolated muffle furnace for 5min The pyrolysis temperatures were 450℃, 550℃, 650℃, 750℃ and 850℃ respectively. The semi-cokes with different pyrolysis temperatures were prepared.

Preparation of semi-cokes with different pyrolysis quality:1g, 2g, 3g and 5g coal samples were respectively placed in a volatilizing dish, which was covered and pyrolyzed in an oxygen isolated muffle furnace at 850 ℃ for 5min. Semi-cokes with different pyrolysis quality were prepared.

Test sample and equipment. The muffle furnace used in the experiment was a box type muffle furnace(5E-MF6000), which was produced by Changsha Kaiyuan Co., Ltd. and used for industrial analysis of experimental samples.

The model of the sulfur determinator used in the experiment was SDS-IVa, which was produced by Hunan Sande Technology Co., Ltd. The sulfur determinator was mainly used to determine the total sulfur in coal samples and semi-coke samples.

The model of the rapid calorimeter used in the experiment was 5E-KC5410, which was produced by Changsha Kaiyuan Co., Ltd. The calorific value of coal sample and pyrolysis semi-coke was measured.

Calculation formula of coal desulfurization efficiency:

$$\omega = \frac{m_{coal\ sample} \times S_{coal\ sample} - m_{semi\text{-}coke} \times S_{semi\text{-}coke}}{m_{coal\ sample} \times S_{coal\ sample}} \times 100\%$$

ω—desulfurization efficiency/%,$m_{coal\ sample}$—coal sample quality/g, $m_{semi\text{-}coke}$—semicoke quality/g, $S_{coal\ sample}$—coal sample total sulfur/%, $S_{semi\text{-}coke}$—semicoke total sulfur/%.

Characterization of semi-coke. Specific surface area (BET): The JW-BK122W type surface and pore size analyzer was used to measure the specific surface area of semi-coke and coal sample.

The Vario EL III element analyzer (Elementar company in Germany) was used for elemental detection of coal samples and semi-coke.

FT-IR characterization: the FT-IR spectrometer was manufactured by Bruker company, and the model was VERTEX70. The infrared spectrometer can scan in the range of 4000~400cm-1 and 28 times, and the resolution was in the range of $4cm^{-1}$.

RESULTS AND DISCUSSIONS

Analysis of coal samples with different pyrolysis time. Figure 1 showed the change rule of mass loss and desulfurization efficiency with pyrolysis time in the pyrolysis process of 3g coal sample at 850℃. It can be seen from the figure

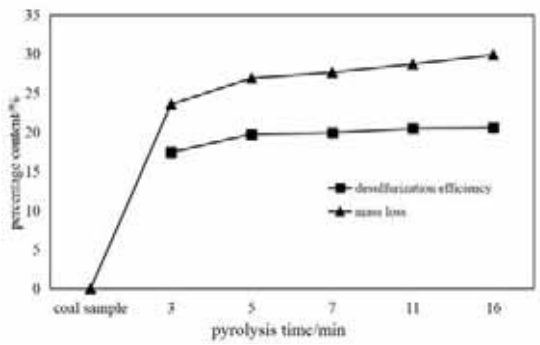

FIGURE 1
Variation of mass loss and desulfurization efficiency of coal samples with pyrolysis time

that the mass loss and desulfurization efficiency of coal sample increase with the increase of pyrolysis time. The pyrolysis of coal samples at high temperature produces water, pyrolysis gas and tar, which made the quality of coal samples less. The longer pyrolysis time was, the more pyrolysis reaction was, the more pyrolysis gas and tar were produced, and the more mass loss of coal samples was. When the pyrolysis time was 3 minutes, the mass loss of coal sample was 23.56%. When the pyrolysis time was 16 minutes, the mass loss of coal sample was 29.91%. There were many sulfur compounds in coal. Sulfur was divided into organic sulfur and inorganic sulfur. Organic sulfur was mainly composed of some sulfur functional groups, such as mercaptan, thioether and thiophene; inorganic sulfur was mainly the sulfur element contained in mineral composition, such as FeS_2, sulfate, etc. The sulfur will change chemically with the pyrolysis process and precipitate with the pyrolysis gas and tar, so as to remove the sulfur from coal. With the increase of pyrolysis time, the amount of precipitation will increase, so that the desulfurization efficiency will increase. When the pyrolysis time was 3 minutes, the desulfurization efficiency was 17.42%. When the pyrolysis time was 11 minutes and 16 minutes, the desulfurization efficiency was 20.45% and 20.52%, respectively; there was little difference between the desulfurization efficiency and the desulfurization efficiency tended to be stable.

Figure 2 showed the variation of volatilization and calorific value of semi-coke with pyrolysis time at 850℃. It can be seen that both volatilization and calorific value of semi-coke decrease with the increase of pyrolysis time. Water, pyrolysis gas and tar gas were separated from

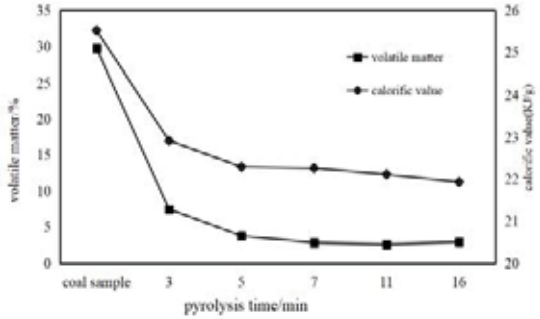

FIGURE 2
Variation of volatile matter and calorific value of pyrolysis semi-coke with pyrolysis time

coal samples during pyrolysis, and with the increase of pyrolysis time, the amount of pyrolysis gas in coal sample also increased, so the volatile content of pyrolysis semi-coke decreased with the increase of pyrolysis time. The main components of the pyrolysis gas were methane, hydrogen, carbon dioxide, carbon monoxide and various hydrocarbon gases. The main components of the tar were hydrocarbons, aromatic hydrocarbons, etc., which contain a lot of heat. As a result of the large amount of heat removed by the precipitation of pyrolysis gas and tar, the calorific value of pyrolysis semicoke was less. Therefore, with the increase of pyrolysis time, the calorific value of semi-coke decreased. The volatile content of raw coal was 29.75%, and that of semi-coke was reduced to 2.93% after 16 min pyrolysis. The calorific value of raw coal was 25.52KJ/g. When the pyrolysis time was 11min and 16min, the calorific value was 22.91KJ/g and 22.99KJ/g, respectively. The calorific value of 11min and 16min had little difference. It was found in Figure 2 that when the pyrolysis time continued to increase from 11min, the calorific value tended to be stable.

Analysis of coal samples with different pyrolysis temperature. Figure 3 showed the change rule of mass loss and desulfurization efficiency with pyrolysis time when 3g coal sample was pyrolysis for 5min. With the increase of pyrolysis temperature, the mass loss and desulfurization efficiency of coal sample increased. In the process of coal pyrolysis, with the increase of temperature, water and gas were first separated out, then the decomposition reaction was carried out to generate pyrolysis gas and tar, and finally the polycondensation reaction was carried out to

generate semi-coke and hydrogen. As the whole process of pyrolysis will be accompanied by the precipitation of substances, so with the increase of pyrolysis temperature, the mass loss of coal sample was increasing. The conversion of inorganic sulfur to organic sulfur also occurred in the pyrolysis process, and the desulfurization efficiency changed greatly from 450℃ to 650℃, so the conversion of inorganic sulfur to organic sulfur occurred in this temperature range. When the temperature increased to 650℃, the desulfurization efficiency increased from 17.46% at 650℃ to 19.73% at 850℃.

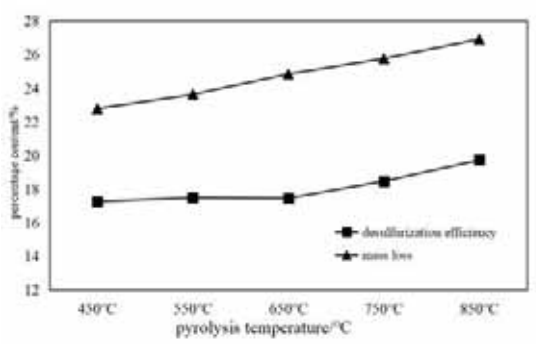

FIGURE 3
Variation of loss and desulfurization efficiency of coal sample with pyrolysis temperature

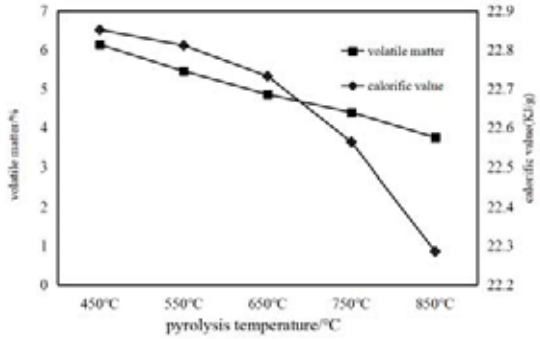

FIGURE 4
Variation of volatile and calorific value of pyrolysis semicoke with pyrolysis temperature

Figure 4 showed the change rule of mass loss and desulfurization efficiency with pyrolysis time when 3g coal sample was pyrolysis for 5min. With the increase of pyrolysis temperature, the volatilization and calorific value of semi-coke decreased. The calorific value of semicoke was 22.85KJ/g at 450℃ and 22.29KJ/g at 650℃. The pyrolysis temperature was between 300℃ ~ 600℃, which resulted in the depolymerization and decomposition reaction, and the gas and tar were separated out. Except for the pyrolysis water, carbon monoxide and carbon dioxide, the gas composition was mainly gaseous hydrocarbon with high calorific value. The pyrolysis temperature was above 600 ℃, the main reaction was condensation, the amount of tar was very little, the main volatile was gas. After 700 ℃, the gas was mainly composed of hydrogen, which took away a lot of calorific value. Therefore, with the increase of pyrolysis temperature, the volatiles and calorific value of semi-coke decreased.

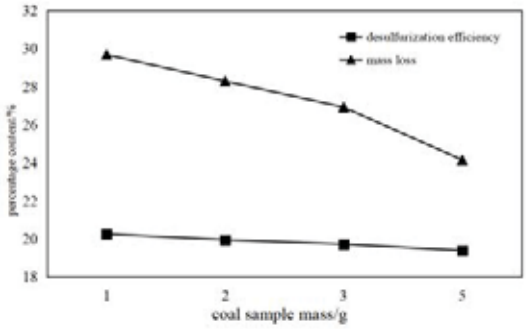

FIGURE 5
Variation of loss and desulfurization efficiency of coal samples with pyrolysis quality

Analysis of coal sample with different pyrolysis quality. As shown in Figure 5, different quality coal sample were pyrolyzed at 850℃ for 5min. The mass loss of coal and the calorific value of semi-coke change with the pyrolysis quality. With the increase of pyrolysis coal quality, the loss of coal quality and desulfurization efficiency were reduced. The more the quality of the coal sample, the less the pyrolysis was, the less the pyrolysis gas and tar gas were produced, the less the mass loss was, and the higher the calorific value of the pyrolysis semi-coke was. Therefore, with the increase of pyrolysis quality, the loss of coal sample was less, and the heat of semi-coke was greater.

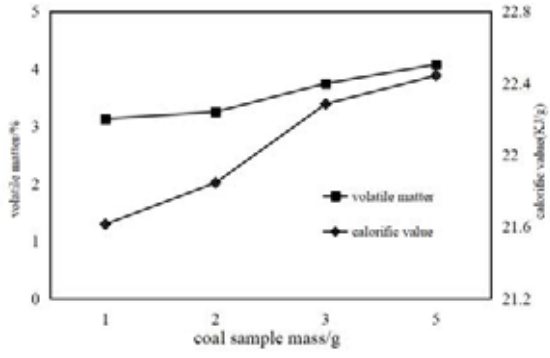

FIGURE 6
Variation of volatile and calorific value of pyrolysis semi-coke with pyrolysis quality

Figure 6 showed the change of volatile and total sulfur of pyrolysis semi-coke with pyrolysis quality. The more pyrolysis quality, the higher volatile and calorific value of semicoke. When

the quality of the coal sample was more, the organic matter in the coal can't be pyrolyzed in time. In the residual coal sample, the volatile matter in the coal increased. At the same time, the gas and tar with high heat released less, and the heat of the remaining semi-coke was higher. Therefore, the calorific value of semi-coke increased with the pyrolysis quality.

CHARACTERIZATION

Specific surface area of semi-coke and coal sample. Table 2 was the characterization of specific surface area and pore volume of semi-coke at different pyrolysis temperatures. It can be seen from the table that the surface area of raw coal was relatively small, only 9.45m^2/g. With the increase of pyrolysis temperature, the specific surface area of coal increased first and then decreased. When the pyrolysis temperature was 650℃, the specific surface area of pyrolysis semi-coke was the largest, 102.78m^2/g. The reason why the specific surface area of coal pyrolysis increased first and then decreases was that: in the initial stage of pyrolysis coal, the specific surface area of coal began to increase with the increase of temperature, the depolymerization reaction was intense and the polycondensation reaction occurred at the same time, the specific surface area was still increased; when the pyrolysis reached a certain temperature, the severity of the depolymerization reaction and the polycondensation reaction was normal, and the specific surface area reached the maximum; when the temperature continued to rise, the depolymerization reaction weakened, and the polycondensation reaction was violent, which reduced the specific surface area [9-10].

TABLE 2
Specific surface area (m^2/g) and pore structure at different pyrolysis temperatures

Semi-cok	Specific sur-	Pore vol-	Average pore
coal sample	9.45	0.0127	3.8781
450℃	47.12	0.0389	3.6329
550℃	68.45	0.0552	3.4539
650℃	102.78	0.0813	3.1817
750℃	45.32	0.0425	3.9442
850℃	35.54	0.0401	4.6169

Fourier infrared analysis. It can be seen from Figure 7 that the functional groups of coal sample had changed greatly before and after pyrolysis. The stretching vibration of C-O (1330-1110cm^{-1}), C-S (800-700cm^{-1}), S-O (700-900cm^{-1}, 1300-1350cm^{-1}) and other single bonds of alcohols, phenols, ethers and esters decreased gradually, indicating that the removal of organic thioethers, mercaptans, sulfones and disulfides occurred in the pyrolysis process. The

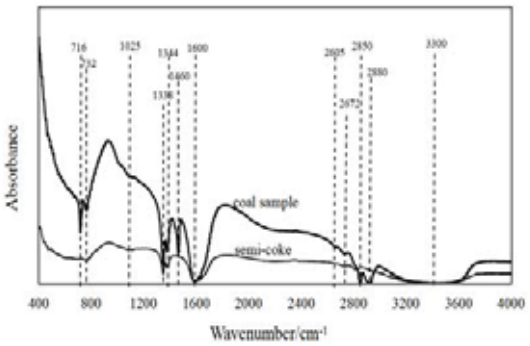

FIGURE 7
Fourier infrared spectrum of raw coal and semi-coke

stretching vibration of [SiO-], [=C=O] and [-O-] functional groups appeared at 1150cm-1. In the range of 1460cm^{-1}-1380cm^{-1}, deformation vibration of [CH_2-] and [CH_3-] on the alkyl chain was strong, and the strength in the same semi-coke was significantly reduced [11-12]. At 1600cm-1, the expansion vibration of [-C=C-] aromatics was strong, and the pre vibration strength of [-C=C-] aromatics in pyrolysis semi-coke was obviously reduced. At 2850cm^{-1} and 2880cm^{-1}, there were aliphatic [CH_2-] symmetric stretching vibration and [CH_2-] asymmetric stretching vibration, and the aliphatic [CH_2-] vibration before reaction was stronger. About 3400cm^{-1} was the absorption peak formed by the [-OH] vibration of alcohol, phenol, carboxyl, etc., but the [-OH] vibration peak before the reaction was stronger, and the [-OH] strength after the reaction was weaker, mainly due to the consumption of [-OH] in the reaction process [13-14]. Therefore, in the process of pyrolysis coal, more functional groups and sulfur-containing functional groups were consumed,pyrolysis gas and tar was generated , more heat and sulfur elements was taken away.

CONCLUSION

(1) In the process of coal pyrolysis, pyrolysis components were separated, which made the volatile matter and calorific value of semi-coke reduced. Pyrolysis had the effect of desulfurization, and the effect of desulfurization was affected by pyrolysis temperature, pyrolysis time and pyrolysis quality.

(2) In the pyrolysis process of 3g coal sample at 850℃, the desulfurization efficiency reached 29.91% in 16 minutes, the desulfurization effect was good, and the calorific value of semi-coke was 22.99KJ/g. In the pyrolysis process of 3g coal sample for 5 minutes, the desulfurization efficiency increased with the increase of temperature, but in the temperature range of 450℃-650℃, the desulfurization efficiency changed little, and semi-coke had the effect of sulfur fixation. The main reason for the desulfurization effect of coal sample quality was the insufficient pyrolysis.

(3) Through pyrolysis at different temperatures, the change of specific surface area of semi-coke was studied. It was found that the specific surface area increased first and then decreased with the increase of temperature. The maximum specific surface area at 650℃ was 102.78m^2/g. After pyrolysis, the infrared analysis of raw coal and semi-coke showed that the functional groups of C-S and S-O in the semi-coke were reduced, so the desulfurization was carried out.

ACKNOWLEDGEMENTS

Financial support of this research was provided by Key Laboratory of Coal Resources Exploration and Comprehensive Utilization, Ministry of Land and Resources (Program No.KF2020-10) in P.R. China.Project 51704230 supported by National Natural Science Foundation of China. Key Research and Development Program of Shaanxi (2019ZDLSF05-05-01). Natural Science Basic Research Program of Shaanxi (2019JL-01)

REFERENCES

[1] Ren, L., Yang, F.L., Jia, Y.J., Di, Z.C., Chen, F.Q., Meng, A.G. (2019) Effect of Conditions of Low-rank Coal Pyrolysis on Gas Phase Product Distribution and Semi-coke Structure.Coal Conversion. 42(6), 17-27.

[2] Zhao, H., Li, L., and Liu Z.H. (2017) Experimental Study on Sulphur Escape from Coal at Different Temperatures under Nitrogen Atmosphere.Coal Technology. 36(2), 318-320.

[3] Cai, C.C., Yang, M.H., Pan, L.L., Zhang, M.X., Ge, T. (2018) Study of types and content of sulfur in coal samples of different densities using X-ray photoelectron spectroscopy (XPS).Coal Preparation Technology. (5), 56-59.

[4] Yang, F.L., Ren, L., Jia, Y.J., Wu, H.B., Di, Z.C., Chen, F.Q. (2019) Research progress on volatiles and sulfur removal during low temperature pyrolysis of coal. Clean Coal Technology. 25(1):47-56.

[5] Liu, S.W., Zou, C., Zhao, J.X., Li, X.M., She, Y., Wu, H., Ma, C. (2018) Speciation of Sulfur and Regularity of Pyrolysis Gas Evolution in Different Coking Coals.Coal Conversion. 41(2), 24-30.

[6] Liu, Z.H., Tu, W., and Han, Z.W. (2018) Experimental Study on Migration Patterns of Sulfur in Coal under Argon Atmosphere. Coal Technology. 37(2), 310-312.

[7] Frigge, L., Elserafi, G., Strohle, J., Epple, B. (2016) Sulfur and Chlorine Gas Species Formation during Coal Pyrolysis in Nitrogen and Carbon Dioxide Atmosphere . Energy & Fuel. 30(9), 7713-7720.

[8] Torres-Ordoñez, R.J., Calkins, W.H., Klein,, M.T. (1990) Distribution of Organic-Sulfur-Containing Structures in High Organic Sulfur Coals . Acs. Symposium Series. 197(10), 288-295.

[9] Yin, Z.Y., Xu, H., Tang, D.Z., Chen, Y.P., Zhao, T.T. (2019) Study on pore structure change during different coal grade pyrolysis.Coal Science and Technology. 47(9), 74-79.

[10] Tang, J., Wang, Q.H., Zhang, R., Shi, Z.L., Cen, K.F. (2015) Effect of Specific Surface Area and Ash Content on the Mechanisms of Bituminous Coal Char Gasification. Proceedings of the CSEE. 35(20), 5244-5250.

[11] Liang, H.Z., Wang, C.G., Zeng, F.G., Li, M.F., Xiang, Jian-hua. (2014) Effect of demineralization on lignite structure from Yinmin coalfield by FT-IR investigation.Journal of Fuel Chemistry and Technology. 42(2), 129-137.

[12] Zhang, L., Shu, H., Jia, Y., Zhang, L., Xu, D. (2020) Study on Solid Waste Pyrolysis Coke Catalyst for Catalytic Cracking of Coal Tar. International Journal of Hydrogen Energy. 45, 19280-19290.

[13] Zhang, L., Jia, Y., Shu, H., Zhang, L., Wen, X., Luo, M., Wang, Y.S., Xu, D. (2020) Application of Surfactant-modified Cordierite-based Catalysts in Denitration Process. Fuel. 268, 117242.

[14] Zhang, L., Shu, H., Zhang, L., Jia, Y. (2020) Gas modified pyrolysis coke for in-situ catalytic cracking of coal tar. ACS Omega. 5, 14911–14923.

Received: **22.03.2020**
Accepted: **17.11.2020**

CORRESPONDING AUTHOR

Chen Jihao
Shaanxi Coal Geological Laboratory Co. Ltd.
Xi'an 710054 – China

e-mail: 15929995059@163.com

© by PSP Volume 30– No. 05/2021 pages 4763-4770 Fresenius Environmental Bulletin

EFFECTS OF GENOTYPIC VARIATION AND SOME NEW PROTOCOLS ON GYNOGENESIS EFFICIENCY OF CUCUMBER

Hasan Pinar[1,*], Seher Toprak[1], Fatih Hanci[1], Duran Simsek[2]

[1]Erciyes University, Faculty of Agriculture, Department of Horticulture, Kayseri, Turkey
[2]Areo Seed Co., Antalya, Turkey

ABSTRACT

In this study, gynogenesis capacity of different Cucumber germplasm, including some commercial varieties, was evaluated and optimized. Unfertilized female flowers of 23 hybrid cucumber genotypes were used as explant source after the two or three weeks of emergence. For each genotype, 30 Petri dishes were prepared with five explants per dish. The study was planned in three stages. In the first stage, the ovarian culture efficiency was tried to be determined by using three ovarian culture protocols which were used in previous studies and obtained successful results. The highest result of embryo unit for per Petri and callus unit for per Petri were obtained from protocol-1 (MS + 1 mg L-1 TDZ + 1 mg L-1 IBA) according to the average of all genotypes at this stage (1.57 units / Petri). In the second stage of the study, the best protocol selected from the first stage, and two new protocols (P-4 and P-5) created with modifications were tested. At the end of this stage, the best protocol selected from the first stage (P-1) and the P-4 (MS + NAA 1.5 mg L-1 + BAP 1.8 mg L-1 + 2,4D 0.7 mg L-1 + Kinetin 1.0 mg L-1) yielded the highest embryo results. In the last stage of the study, two new protocols were tried, but none of them were as good as the previously tried protocols. The results showed that the interaction between genotype x media components was found to be statistically significant at all stages.

KEYWORDS:
Cucumber breeding, embryogenesis, haploidy

INTRODUCTION

According to the most recent data of the United Nations Food and Agriculture Organization, worldwide cucumber (*Cucumis sativus* L.) production was approximately 83,649,161 tons in 2017. Turkey produces 1,827,782 tons of cucumber annually, which is 2.19% of world cucumber production, and it ranks as the 4th largest producer. The cucumber is grown on more than 37,600 ha in Turkey and its productivity is 4.85 t da^{-1}, which is high in comparison with the productivity of 3.69 t/ha worldwide [1].

Recently, conventional breeding methods have been replaced by biotechnological methods in the production of commercial hybrids. One of these new methods is the double haploid (DH) technique. DH plants, which are completely homozygous, can only be obtained in one generation [2]. Haploids are plants (sporophytes) that include a gametic chromosome number (n). These plants can occur spontaneously in nature or as a result of various induction techniques in the laboratory condition. Spontaneous haploid plants have been known since 1922 when Blakeslee first explained this phenomenon in *Datura stramonium* [3]. This was after followed by similar reports in other plants such as wheat (*Triticum aestivum*), tobacco (*Nicotiana tabacum*) [4]. However, the spontaneous emergence of haploid plants is a rare event, and therefore its practical value is very limited. The potential for use of haploid plants for plant breeding programs was increased in 1964 by obtaining haploid embryos from in vitro culture of Datura anthers [5], [6]. This was followed by similar developments in tobacco [7]. Numerous attempts have been made to obtain haploid plants by various methods and protocols have been published for more than 250 plant species [8].

DH technique, which shortens the plant breeding process, is widely used in vegetable breeding. The major advantage of DHs is the rapid production of fully homozygous lines even in cross-pollination species. Production of inbred lines by traditional methods 10-12 years in cross-pollinated plants; self-fertilized plants can last 6-7 years. However, even in Dioic species such as spinach which it is impossible to selfing, inbred lines can be produced in 1-2 years with the DH method. DH plants show normal meiosis and do not lose the desired properties in the next generations [9]. Also, since the lines obtained by DH technique are absolute homozygous, it is very easy to detect and

TABLE 1
Gynogenesis media protocols used in the study

	Stage I			Stage II		Stage III	
Media	**Protocol I** [21]	**Protocol II** [18]	**Protocol III** [22]	**Protocol IV**	**Protocol V**	**Protocol VI**	**Protocol VII**
MS	4.3 g	4.4 g	4.3 g	4.3 g	4.3 g	4.3 gr	4.3 gr
Sucrose	30 g	30 g	30 g	30 g	30 g	30 gr	30 gr
TDZ	1 mg l^{-1}	-	-	-	0.04 mg l^{-1}	1 mg l^{-1}	-
IBA	1 mg l^{-1}	-	-	-	-	-	-
NAA	-	2 mg	0.05 mg\l	1.5 mg l^{-1}	-	-	0.5 mg l^{-}
BAP	-	3 mg l^{-1}	0.2 mg l^{-1}	1.8 mg l^{-1}	-	1 mg l^{-1}	1 mg l^{-1}
AA	-	20 mg l^{-1}	-	-	-	-	-
2,4 D	-	-	-	0.7 mg l^{-1}	-	-	0.7 mg l^{-}
Kinetin	-	-	-	1 mg l^{-1}	-	-	1 mg l^{-1}
Glutamin	-	-	-	-	-	800 mg l^{-1}	-
$AgNO_3$	-	-	-	-	-	-	10 mg l^{-1}
Prolin	-	100 mg l^{-1}	-	-	-	-	-
pH	5.7	5.7	5.7	5.8	5.7	5.8	5.8
Agar	4 gr	4 gr	4 gr	6 gr	8 gr	6 gr	6 gr

TABLE 2
Results of Stage I

Genotypes	**Number of Embryos**			**Number of Callus**		
	Protocol 1	**Protocol 2**	**Protocol 3**	**Protocol 1**	**Protocol 2**	**Protocol 3**
K1	1.33 g	1.03 cd	1.50 c	2.67 b	0,00 e	0.53 l
K2	1.89 de	0.20 k	1.50 c	1.53 hi	0.17 bcd	1.23 f
K3	1.17 gh	0.23 jk	0.73 e	1.20 jkl	0.12 bcd	0.27 m
K4	1.37 g	0.50 hi	1.50 c	2.24 cd	0,00 e	1.07 h
K5	1.87 def	0.43 ij	1.07 d	1.40 ij	0.19 abcd	1.63 d
K6	1.76 def	1.10 c	0.70 ef	1.73 fgh	0,00 e	1.20 fg
K7	2.70 a	1.70 a	0.67 efg	2.33 c	0.23 ab	1.07 h
K8	1.67 f	1.13 bc	1.48 c	1.30 jk	0.20 abc	1.17 g
K9	1,00 hij	1.10 c	1.40 c	1.77 fg	0.10 cde	1.20 fg
K10	2.27 c	0.83 def	1.40 c	2.03 e	0,00 e	2.00 c
K11	1.81 def	0.63 fghi	0.53 efg	1.13 kl	0,00 e	0.63 k
K12	1.92 d	1.31 b	0.47 g	1.80 f	0.30 a	0.80 j
K13	1.80 def	0.44 i	1.17 d	1.10 kl	0.00 e	1.20 fg
K14	1.8 def	0.97 cde	1.17 d	2.10 de	0.11 cde	2.07 b
K15	0.93 ij	0.93 cde	1.00 d	0.87 mn	0.00 e	0.83 j
K16	1.07hi	0.19 k	0.62 efg	3.47 a	0.00 e	1.07 h
K17	2.48 b	0.57 ghi	2.13 a	1.57 ghi	0.12 bcd	1.40 e
K18	1.07 hi	0.16 k	0.50 fg	0.57 o	0.00 e	0.67 k
K19	2.28 bc	0.77 efg	0.97 d	1.81 f	0.00 e	0.93 i
Erciyes	0.63 k	0.67 fgh	0.67 efg	1.77 fg	0.00 e	1.07 h
Lemas	0.83 jk	0.53 hi	0.67 efg	1,00 lm	0.00 e	0.97 i
Silyon	1.70 ef	0.83 def	1.73 b	1.27 jk	0.13 bcd	3.03 a
ZYMV	0.87 ij	0.19 k	0.47 g	0.77 no	0.08 de	1.20 fg
Mean	*1.57 A*	*0.72 C*	*1.04 B*	*1.63 A'*	*0.08 C'*	*1.18 B'*
F Ratios	*61.88**	*30.65**	*37.96**	*81.72**	*5.43**	*613.41**
LSD	*0.20*	*0.21*	*0.22*	*0.21*	*0.11*	*0.07*

*: Means within a column that have a different small letter are significantly different from each other and means within a row that have different capital letter are significantly different from each other ($p < 0.05$).

isolate recessive mutations. By using DH plants, the dominance effect in the plant breeding process is eliminated and the additive gene effect is doubled. Another advantage of double haplodization is that it can be purified in a short time for the mixed varieties or populations grown [10]. In a cucumber breeding program, the establishment of homozygous parental lines using the traditional self-pollination method takes from six to eight years [11]. However, it is

possible to reduce this period to one or two years using DH technique.

There are three commonly used techniques in Cucurbits: (a) haploid parthenogenesis (using irradiated pollen during pollination for induction), in vitro gynogenesis (during in vitro culture of ovules and ovaries) and in vitro androgenesis (during in vitro culture of microspores and anthers) [12]. Ovary culture technique is widely used in the *Cucurbitaceae* family. However, as a result of many gynogenesis studies performed in different species (cucumber, pumpkin, sweet potato, onion, etc.), genotype factor was found to be important for the success of the protocols [13]; [14], [15]; [16]. Also, different combination of media has been tested for in vitro gynogenesis induction in cucumber. Moqbeli *et al.* [17] used ovarian culture in six hybrid cucumber cultivars and reported the most successful results in MS medium containing 0.04 mg L^{-1} TDZ. Among the varieties, the highest number of embryogenesis was observed in "summer star" cultivar. Gemes *et al.* [11] reported that pre-application of cucumber at 32°C had a positive effect on haploid embryo development in ovule culture. Similarly, Diao *et al.* [18] reported that embryo formation is affected by high temperature. Metwally *et al.* [19] reported Murashige and Skoog (MS) medium [27] supplemented with 1-5 mg dm^{-3} 2,4D and 30 g dm^{-3} for successful embryogenesis. Xie *et al.* [20], 2,4-Dichlorophenoxyacetic acid (2,4D), naphthalene-1-acetic acid and benzyladenine (BA) added N6 basal medium used for the same purpose.

The main objectives of this study were:1) to evaluate the effect of genotypes on callus and embryo induction in ovary culture, 2) to develop an effective ovarian culture protocol that could be used in different Cucumber genotypes.

MATERIALS AND METHODS

The study was conducted between 2017-2019 at Erciyes University (Kayseri, Turkey) greenhouses and laboratories. Totally twenty-three different cucumber genotypes were used as explant source. The seeds of the genotypes were planted in 3:1 peat-perlite medium and transferred to the greenhouse when two true leaf stages reached. The plants were grown as single stems with routine practical applications. Two or three weeks after the emergence of the first female flowers, and one or three days before the anthesis, the female flowers were taken and quickly transported to the laboratory in cold storage boxes. Modified method of Gemes *et al.* [11] and Diao *et al.* [18] was used for disinfection of explants. Female buds were incubated for 15 minutes in a 20% commercial hypo-solution with a few drops of Tween-20, then washed three times with sterile distilled water for five minutes each. The ovaries were then cut into 1 mm pieces and placed in Petri dishes. For each genotype, 30 Petri dishes were prepared with five explants per dish.

The studies to obtain callus and embryo from female flower explants were planned in three stages. The first stage of the study was conducted in the spring season of 2017. In this stage, three protocols were tested: Protocol-I (P-I) ([21]), Protocol-II (P-II) ([18]) and Protocol-III (P-III) ([22]). During the second stage of study, two new Protocols (P-IV and P-V) were tested in addition to the best protocol of the first stage. The second stage of the study was conducted in the autumn season of 2017. According to the results obtained in the first and second stage, the two new protocol (P-VI) and P-VII) were created in the third stage in the spring season of 2018 (Table 1).

MS medium ([17]) was used as a basal medium in all experiments. In the process of establishing new protocols, different concentrations of 2,4-Dichlorophenoxyacetic acid (0, 1, 3, 5 mg L^{-1}) as auxin ([19], [23] and Thidiazuron (0, 0.01 , 0.02, 0.04 mg L^{-1}) (as cytokinin [11]) were added to the basal medium. All the media contained 30 g L^{-1} sucrose and 6 gr/l agar as a solidifying agent. The medium was adjusted to pH 5.7 or 5.8 with 1 N HCl and 1 N KOH.

In the first protocol, the Petri dishes were kept in the darkness for 14 days at 25°C conditions [21]. It was then incubated for 11 days at 25°C ±2 and 16/8 hour photoperiod (light intensity 35 µmol m^{-2} s^{-1}; 3200 lux approximately). At the end of the 25th day, embryo and callus formation were observed from the explants, and they are subcultured to MS + 20 mg ascorbic acid, 100 mg proline, 3 mg BA, 2 mg NAA medium at same climatic condition. In the second protocol, Petri dishes were kept at 35°C for 3 days in darkness [18]. Followed, incubated at 25°C±2 temperature and 16/8 hour photoperiod (light intensity 35 µmol m^{-2} s^{-1}; 3200 lux approximately). When the embryos output was observed in the explants, these were transferred to the subculture under same conditions (MS basal media + 0.3 mg L^{-1} BAP). In the third protocol, the Petri dishes were incubated at 25°C ± 2 and 16/8 hour photoperiod (light intensity 35 µmol m^{-2} s^{-1}; 3200 lux approximately). It was subcultured on day 30. MS + 0.6 mg L^{-1} BAP was used as subculture medium. Temperature and light conditions have not changed [22]. Ambient conditions for other protocols were set at 24±1 ºC, and 16/8 hr light / dark photoperiod. In the experiments, the amount of callus and embryo obtained from each petri dish was recorded separately. Analysis of variance ANOVA was employed to compare the means of genotypes, protocols and their interactions. The significance of differences between results was determined by LSD multiple comparison techniques. Statistical analysis was conducted using the PAST3 software [28].

TABLE 3
Results of Stage II

Genotypes	Number of Embryos			Number of Callus		
	Protocol I	**Protocol IV**	**Protocol V**	**Protocol I**	**Protocol IV**	**Protocol V**
K1	1.43 jkl	1.83 fgh	1.83 def	0.57 abc	2.40 abc	0.67 b-e
K2	2.13 bcd	1.48 ij	1.73 f	0.70 a	1.67 ijk	0.73 bcd
K3	1.83 efg	1.50 ij	1.73 f	0.53 a-d	1.23 m	0.83 b
K4	1.71 ghi	1.81 gh	1.23 hij	0.37 c-h	2.53 ab	0.70 b-e
K5	1.50 ijk	2.03 ef	0.90 k	0.50 a-e	1.60 jk	0.40 gh
K6	1.73 fgh	1.83 fgh	1.43 gh	0.67 ab	2.00 fgh	0.77 bc
K7	2.03 cde	2.07 de	1.90 c-f	0.43 c-g	2.60 a	1.20 a
K8	1.83 efg	1.87 e-h	1.37 gh	0.23 gh	1.87 ghi	0.60 c-g
K9	2.27 ab	1.67 hi	1.97 cde	0.33 d-h	2.23 cde	0.83 b
K10	2.40 a	2.27 cd	2.07 bc	0.40 c-h	2.07 efg	0.63 b-f
K11	2.10 bcd	2.33 bc	1.90 c-f	0.33 d-h	1.60 jk	0.53 d-h
K12	2.20 abc	2.47 bc	2.07 bc	0.43 c-g	2.17 def	0.77 bc
K13	1.97 de	2,00 efg	1.37 gh	0.27 fgh	1.81 hij	0.77 bc
K14	2.37 a	1.87 e-h	2.23 b	0.47 b-f	2.33 bcd	0.67 b-e
K15	2.13 bcd	1.40 j	2.57 a	0.40 c-h	1.27 m	0.83 b
K16	1.50 ijk	0.80 m	1.07 jk	0.30 e-h	2.20 c-f	0.77 bc
K17	1.53 h-k	2.77 a	1.13 ij	0.27 fgh	2.23 cde	0.57 c-h
K18	1.50 ijk	1.33 jk	1.33 ghi	0.20 h	0.9 n	0.37 h
K19	1.93 def	2.50 b	1.47 g	0.23 gh	2.2 c-f	0.73 bcd
Erciyes	0.77 m	1.10 l	1.77 ef	0.57 abc	1.67 ijk	0.77 bc
Lemas	1.33 kl	1.10 l	2.00 cd	0.40 c-h	1.13 m	0.43 fgh
Silyon	1.27 l	1.87 e-h	1.27 g-j	0.37 c-h	1.5 kl	0.59 c-g
ZYMV	1.63 g-j	1.17 kl	1.43 gh	0.33 d-h	1.3 lm	0.50 e-h
Mean	*1.79 A*	*1.79 A*	*1.64 B*	*0.40 C'*	*1.85 A'*	*0,68 B'*
F Ratios	*27.62**	*41.35**	*29.25**	*3.23**	*37.43**	*5.35**
LSD	*0.22*	*0.22*	*0.22*	*0.22*	*0.22*	*0.22*

*: Means within a column that have a different small letter are significantly different from each other and means within a row that have different capital letter are significantly different from each other ($p < 0.05$).

RESULTS AND DISCUSSION

According to the variance analysis results, the difference between the responses of different genotypes to different protocols was found to be statistically significant for both embryo and callus induction. These results are similar to those of Diao *et al.* [18] and Shalaby [16] indicating that gynogenesis protocols should be optimized for each different genotype.

The number of callus and embryos observed in all protocols throughout the study are shown in Table 2. In first stage of the study, the highest result of embryo unit for per Petri and callus unit for per Petri were obtained from P-I according to the average of all genotypes, 1.57 units / Petri dishes and 1.63 units / Petri dishes respectively. Similarly, when all the results of the first stage are evaluated for each genotype separately, the maximum number of embryos (2.70 per petri dish) was observed in P-I from the K7 genotype. However, the highest callus rate was observed in the same protocol but in K16 genotype (3.47 per petri dish). The lowest number of embryos observed was obtained from the P-II according to the average of all genotypes (0.72 per petri dish). The most striking result obtained at this stage is that the "K7" genotype, which gives the highest number of embryos in the first protocol, reaches the highest value (1.70 units / Petri dishes) in P-II. Another interesting result was that the genotype "Erciyes" having the lowest embryo value in P-I (0.63 units / Petri dishes) gave almost the same result in the second protocol (0.67 units / Petri dishes). However, the K2 genotype, which produces 1.89 embryos per petri dish in the first protocol, was able to give only 0.20 embryos for each Petri in the second protocol. Similar decreases were observed in K16 and K18 genotypes. In the first stage of our study, TDZ was used only in the first protocol. In parallel with the other literature data Moqbeli *et al.* [17], Li *et al.* [24], Özsan and Onus [25] the highest embryo formation was obtained from this protocol according to the average of all genotypes. However, IBA was used in addition to TDZ in this protocol. The second protocol includes NAA, AA, proline, and BAP as an alternative to TDZ and IBA. However, this protocol has the lowest embryo rates. In the P-III, low amounts of NAA and BAP were used and relatively high embryo results were obtained compared to the second protocol.

TABLE 4
Results of Stage III

Genotypes	Number of Embryos		Number of Callus	
	Protocol V1	**Protocol VII**	**Protocol V1**	**Protocol VII**
K1	0.73 gh	0.11	0.17 defg	1.67 cde
K2	1.43 a	0.17	0.20 cdefg	1.40 fgh
K3	0.43 j	0.27	0.27 abcdef	2.04 ab
K4	1.07 cde	0.13	0.13 efg	1.60 def
K5	0.50 ij	0.23	0.33 abcd	1.50 ef
K6	0.87 efg	0.09	0.13 efg	1.83 bc
K7	1.33 ab	0.07	0.40 ab	1.07 i
K8	0.87 efg	0.12	0.30 abcde	1.53 def
K9	0.50 ij	0.20	0.23 bcdef	1.13 i
K10	0.98 def	0.20	0.43 a	1.47 ef
K11	0.77 fgh	0.33	0.17 defg	0.73 jk
K12	1.17 bcd	0.20	0.37 abc	2.17 a
K13	0.97 def	0.47	0.12 efg	0.60 k
K14	1.48 a	0.13	0.09 fg	1.23 ghi
K15	0.60 hij	0.13	0.17 defg	1.87 bc
K16	0.70 ghi	0.13	0.03 g	0.83 j
K17	0.90 efg	0.11	0.17 defg	2.23 a
K18	1.17 bcd	0.17	0.11 efg	1.59 def
K19	1.50 a	0.20	0.27 abcdef	1.07 i
Erciyes	1.00 cde	0.30	0.12 efg	1.43 fg
Multistar	1.37 ab	0.23	0.09 fg	1.17 i
Zymv (HA)	1.20 bc	0.20	0.11 efg	1.20 hi
Zymv (x)	0.87 efg	0.17	0.13 efg	1.73 cd
Mean	*0.97 A*	*0.19 B'*	*0.20 B*	*1.44 A'*
F Ratios	*16.95**	*1.44^{ns}*	*2.37**	*32.44**
LSD	*0.22*	*0.21*	*0.20*	*0.22*

*: Means within a column that have a different small letter are significantly different from each other and means within a row that have different capital letter are significantly different from each other, ns: not significant ($p < 0.05$).

During the second stage of the study, in addition to the best protocol selected from the first stage (P-I), two new protocols were tested. P-IV was obtained with the addition of NAA, BAP, 2,4D, and Kinetin, an alternative to TDZ and IBA. In the other protocol (P-V), TDZ was used in very low amounts (0.04 mg L^{-1}). Based on the average of all genotypes, the highest result of the embryo unit per petri dish was obtained from P-IV and P-I (1.79 units / Petri dishes). When the results at this stage were evaluated separately for each genotype, the maximum number of embryos (2.77 per petri dish) from the K17 genotype was observed in P-IV. The lowest number of embryos in the second stage of the study was obtained from P-V according to the average of all genotypes (1.64 per petri dish). Considering that the lowest embryo unit observed in the first stage of the study was 0.72 units / Petri dishes compared to the average of all genotypes, it was understood that the modifications made during the second stage were appropriate.

Although the "lowest embryo numbers" were different between the first and second stage, no significant increase was observed in the "highest embryo" numbers. Therefore, protocols were modified, and the third stage was started in the spring season of 2018. At this stage, two different protocols were prepared and the experiment was re-established. In the third stage of the study, glutamine (800 mg L^{-1}) and BAP (1 mg L^{-1}) were added, and IBA was removed to the prescription of P-I. In addition, the search for alternatives to TDZ and IBA continued and the first protocol of the second stage was modified using $AgNO_3$. However, the highest results in the first and second stages could not be reached. In the P-VI, maximum embryo numbers were recorded as 1.48 and 1.50 units / Petri dishes in K14 and K19 genotypes, respectively. Specifically, in the P-VII, the number of embryos per petri dish did not exceed 0.5 units / Petri dishes in any genotype.

The embryos obtained from all three stages were separated from the ovule with the help of sterile scalpel and transferred to five different media pre-

pared to form shoots. The percentages of transformation from embryos to plants were determined after 28 days (Table 4). The obtained plantlets were taken to standard rooting medium. Three days later, root formations were observed. The obtained plantlets were removed from the medium and transferred to growth chambers, where they were planted in pots containing peat: perlite (3:1).

As in many other plant species, it is important to obtain homozygous pure lines as soon as possible in cucumber breeding programs. Although some studies have been tried with cucumber anther culture, it has been reported that successful results can be obtained with ovule/ovarium culture applications as in other members of *Cucurbitaceous* family. However, the success of ovule/ovarium culture depends on many factors such as culture media or genotype [26].

Moqbeli *et al.* [17] cultured six un-fertilized female flowers belonging to six different cucumber hybrids in MS basal media modified with various hormones. The explants were pre-shocked at 35±1 ° C for 0, 2, 3 or 4 days. The first visual embryo-like structures were observed after three weeks in culture. The highest embryogenesis rate was obtained from the "summer star" variety in medium modified with 0.04 mg L^{-1} TDZ.

In the study of Li *et al.* [24], different concentrations of TDZ and $AgNO_3$ were added to CBM media to increase the effectiveness of cucumber ovule culture. According to the results, it was reported that the media containing 0.03 - 0.07 mg dm^{-3} TDZ constitutes the highest number of embryos. Furthermore, the highest plant regeneration rate was reported to be obtained from CBM medium supplemented with 0.05 mg dm^{-3} α-naphthalenetic acid, 0.2 mg dm^{-3} 6-benzyladenine and 5-10 mg dm^{-3} $AgNO_3$. According to flow cytometry findings, 80% of regenerated plants were identified as haploid.

Golabadi *et al.* [22] investigated the effect of various factors on the success of cucumber ovule culture, and planned three different trials for this purpose. In the first trial, the following four factors were investigated: pre-temperature shock, genotypes, hormonal combinations, and $AgNO_3$. According to the findings, the highest embryogenesis rate was obtained in pre-temperature shock and NAA + 2,4-D + KIN + BAP applications. After the second experiment, it was reported that the interaction of genotype and hormone combinations had a statistically significant effect on embryo production. As a result of the third experiment, the highest embryogenesis (24.93%) was determined in the genotype of NBDC6*6/32441 which is local Iranian variety. According to all findings, temperature shock, hormone combinations, and genotype have been reported to be effective in embryo formation.

Similarly, Özsan and Onus [25] collected the unfertilized female flowers of different cucumber genotypes one day before the anthesis to determine the effects of different media on gynogenesis and cultured in eight different cucumber basal media (CBM). All explants were maintained in dark conditions at 35 ° C for three days and then transferred to 25°C in dark conditions for two days. According to the findings, the highest embryo formation and plant growth ratio were obtained in the 0.03 mg L^{-1} TDZ + CBM media and genotype "0703". These results are consistent with our findings. In our study, as the results of ANOVA showed, the interaction between genotype x media components was found to be statistically significant at all stages. Accordingly, as with many other plant species, it would not be appropriate to propose a single recipe for all genotypes of a species. However, our findings have proved that the success of ovarian culture in cucumber can be increased by some hormonal modifications to be made in the media. According to the average of all genotypes, the mean comparison for hormonal composition showed that TDZ + IBA (1.0 + 1.0 mg L^{-1}) or combination of NAA + BAP + 2.4D + Kinetin (1.5 + 1.8 + 0.7 + 1.0 mg L^{-1}) embryogenesis

CONCLUSIONS

The study revealed the findings of genotype and media component factors. On average, the rate of gynogenesis was low in all treatments. But this was an expected result for Cucumber. Significant differences for embryo induction were found among all treatments. However, these differences were more associated with the difference in supplemental plant growth regulator. A future study utilizing additional genotypes and hormones could be conducted to verify the effects.

ACKNOWLEDGEMENTS

This work was supported by Research Fund of the Erciyes University. Project Number: FSI-2017-7182.

REFERENCES

[1] FAO,(2018). http://www.fao.org/faostat/en/#data/QC

[2] Eduardo, I., Arus, P., Monforte, A.J. (2005). Development of a Genomic Library of Near Isogenic Lines (NILS) in Melon (*Cucumis melo* L.) from the Exotic Accession PI161375. Theorical and Applied Genetic. 112, 139–148.

[3] Blakeslee, A.F., Belling, J., Farnham, M.E., Begner, A.D. (1922) A Haploid Mutant in the Jimson Weed, "*Datura stramonium*". Science. 55, 646.
[4] Forster, B.P. Heberle-Bors, E., Kasha, K.J., Touraev, A. (2007). The resurgence of haploids in higher plants. Trends Plant Science. 12, 368–375.
[5] Guha, S. and Maheshwari, S.C. (1964). In Vitro Production of Embryos from Anthers of Datura. Nature. 204, 497.
[6] Guha, S. and Maheshwari, S.C. (1967). Development of embryoids from pollen grains of Datura in vitro. Phytomorphology. 17, 97-9.
[7] Nitsch, J. P., & Nitsch, C. (1969). Haploid plants from pollen grains. Science, 163(3862), 85-87.
[8] Maluszynski M, Kasha KJ, Forster BP, Szarejko I (2003). Doubled haploid production in crop plants: A manual. Kluwer Academic Publishers, Dordrecht, The Netherlands.
[9] Reinert J Bajaj PS (1977). Applied and Fundamental Aspects of Plant Cell, Tissue, and Organ Culture, Springer Verlag Berlin, Heidelberg, New York.
[10] Comlekcioglu, N., Buyukalaca, S., and Abak, K. (2001). Effect of silver nitrate on haploid embryo induction by anther culture in pepper (*Capsicum annuum*) In: K. Abak, Buyukalaca S, Dasgan Y. (Eds.). Proceeding of the XI EUCARPIA Meeting on Genetics and Breeding of Capsicum and Eggplant, Eucarpia. 133–135.
[11] Gémes-Juhász, A., Balogh, P., Ferenczy, A. and Kristóf, Z. (2002). Effect of optimal stage of female gametophyte and heat treatment on in vitro gynogenesis induction in cucumber (*Cucumis sativus* L.). Plant Cell Reports. 21, 105–111.
[12] Gałązka, J. and Niemirowicz-Szczytt, K. (2013). Review of research on haploid production in cucumber and other cucurbits. Folia Horticulturae. 25, 67–78.
[13] Dumas de Vaulx, R., Chambonnet, D. (1986). Obtention of embryos and plants from in vitro culture of unfertilized ovules of *Cucurbita pepo* L. In: Horn W, Jensen CJ, Odenbach, W, Schieder O (Eds.), Genetic Manipulation in Plant breeding. Proceedings of the International Symposium organised by EUCARPIA, Walter de Gruyter & Co., Berlin. 295–297.
[14] Kobayashi, S., Ohgawara, T., Saito, W., Nakamura, Y., Omura, M. (1997). Production of triploid somatic hybrids in Citrus. Journal of the Japanese Society for Horticultural Science. 66, 453-458.
[15] Alan, A.R., Brants, A., Cobb, E., Goldschmied, A., Mutschler, M.A., Earle, E.D. (2004). Fecund gynogenic lines from onion (*Allium cepa* L.) breeding materials. Plant Science. 167(5), 1055-1066.
[16] Shalaby, T.A. (2007). Factors affecting haploid induction through in vitro gynogenesis in summer squash (*Cucurbita pepo* L.). Scientia Horticulturae. 115(115):1-6
[17] Moqbeli, E., Peyvast, G., Hamidoghli, Y., Olfati, J.A. (2013). *In vitro* cucumber haploid line generation in several new cultivars. Asia Pacific Journal of Molecular Biology. 21, 18–25
[18] Diao, W., Jia, Y., Hui, S., Zhang, X., Lou, Q., Chen, J.F. (2009). Efficient embryo induction in cucumber ovary culture and homozygous identification of the regenerants using SSR markers. Scientia Horticulturae. 119, 246–251.
[19] Metwally, I.O.E., Abd El-All, A.M. and Leilah, A.A. (1998). Effect of preceding summer crops and nitrogen fertilizer levels on growth, yield and yield components of wheat. Proc 8th Conf. Agron. Suez., Canal Univ. Ismailia. 28-29.
[20] Xie B, Wang XF, Fan ZC (2006). Improved conditions of in vitro culture of unpollinated ovules and production of embryonary sac plants in summer squash (*Cucurbita pepo* L.) Scientia Agricultura Sinica 39(1):132-138.
[21] Tantasawat, P.A., Sorntip, A., Pornbungkerd, P. (2015). Effects of Exogenous Application of Plant Growth Regulators on Growth, Yield, and *In Vitro* Gynogenesis in Cucumber. Hortscience. 50(3), 374–382.
[22] Golabadi, M., Ghanbari, S., Keighobadi, K., Ercisli, S. (2017). Embryo and callus induction by different factors in ovary culture of cucumber. Journal of Applied Botany and Food Quality. 90, 68–75.
[23] Rekha, K., Jayashree, R., Sushamakumari, S., Sankariammal, L., Thulaseedharan, A. (2007). Endosperm culture in Hevea brasiliensis. In: Keshavachandran R, Nazeem PA, Girija D, John PS and Peter KV (Eds) Recent Trends in Horticultural Biotechnology, New India Publishers. 111-116.
[24] Li, J.W., Si, S.W., Chang, J.Y., Li, J.X., Liu, J.Q. (2013). Thidiazuron and silver nitrate enhanced gynogenesis of unfertilized ovule cultures of *Cucumis sativus*. Biologia Plantarum. 57, 164-168.
[25] Ozsan, T., Onus, N. (2017). In vitro Pepper (*Capsicum annuum* L.) Anther Culture: Can be Affected Via Vitamins B?, Biotechnology Journal International. 20(1), 1-13.
[26] Ashok Kumar, H.G., Murthy, H.N., Paek, K.Y. (2003). Embryogenesis and plant regeneration from anther cultures of *Cucumis sativus* L. Sci Hortic. 98, 213–222.
[27] Murashige, T., Skoog, F. (1962). A revised medium for rapid growth and bioassays with tobacco cultures. Physiology Plants. 15, 473–497.

[28] Hammer, Ø., Harper, D. A., & Ryan, P. D. (2001). PAST: Paleontological statistics software package for education and data analysis. Palaeontologia electronica, 4(1), 9.

Received: **10.04.2020**
Accepted: **16.09.2020**

CORRESPONDING AUTHOR

Hasan Pinar
Erciyes University,
Faculty of Agriculture,
Department of Horticulture,
Kayseri – Turkey

e-mail: hpinarka@yahoo.com

© by PSP Volume 30– No. 05/2021 pages 4771-4778 Fresenius Environmental Bulletin

THE INFLUENCE OF PERLITE AND IRRIGATION MANAGEMENT ON THE PROPERTIES OF POTATOES IN GYPSIFEROUS SOIL

Wael Fahmi Abdulrahman Al- Shamary[1], Bassam A A H Alkhateb[2], Emad Telfah Abdel Ghani[3], Tawfiq M Al-Antary[4,*], Abdel-Monnem S Kahlel[5]

[1]College of Agriculture, Al-Hawija, University of Kirkuk, 9487, Kirkuk, Iraq
[2]College of Agriculture, University of Anbar, 31001, Anbar, Iraq
[3]Upper Euphrates Basin Development Center, Planning & Databases Dept., University of Anbar, 31001, Anbar, Iraq
[4]Plant Protection Department, School of Agriculture, the University of Jordan, 11942 Amman, Jordan
[5]Technical Agricultural College Northern Technical University, Mosul, Iraq

ABSTRACT

A field experiment is carried out in Anbar province for the spring of 2018 in a gypsiferous soil with a sandy clay loam to study the effect of perlite (PL), quantity and intervals of irrigation (IQ & IT) on the consumption and efficiency of water use (WC & WUE) and total yield (TY) of potatoes. PL is added at 0, 4 and 8% of soil volume (SV). IQ is added at 100 and 50% of net depth of irrigation (NDI) are applied. Two ITs every 3 and 6 days are applied. The treatments are distributed according split-split plots system within the design of completely randomized blocks (RCBD) with three replications. The irrigation is scheduled based on the American evaporation basin Class A. PL of 8% of SV led to the WUE of 22.78 kg.m-3 at 50% NDI and IT every 3 days, while it is less WUE when compared to control treatment, reaching 7.15 kg.m-3 at 100% IQ every 6 days IT. The addition of PL of 8% SV achieved the highest TY of 29 tons.ha-1 at the level of 100% IQ and every 3 days IT compared to control treatment, where it gave the lowest TY of 11.2 tons.ha-1 at IQ of 50% NDI with IT every 6 days. The stabilization of the perlite addition factor with 50% NDI and IT of 3 days have led to save (987.875 m3. ha-1) of irrigation water.

KEYWORDS:
Perlite, Irrigation intervals, Yield, Growth, Potato plant

INTRODUCTION

The gypsiferous lands consist 20% of the total area of Iraq; which have formidable physical and fertility problems, such as low agricultural production capacity [1] .Water is the most important determinant of agricultural production in gypsiferous soils. The increasing water demands due to the high population density makes people use many approaches to mitigate the aquatic scarcity, including the reduction of hydraulic inputs during the season by scheduling irrigation [2]. The lack of water available to plants leads to a reduction in production and quality of yield with increasing the disease infestation [3], therefore, water use management and rationalization of irrigation is essential. Iraq suffers from water scarcity due to the shortage of annual hydraulic flow incomes of the Tigris and Euphrates rivers[4]. In all of the world, several procedures followed to reduce crop water consumption by creative scientific methods, such as deficit irrigation, which adds less water than actual requirements [5]. The decreased yield of crops is related to the quantity of available water for irrigation [6] In addition, water stress and reduced irrigation cause insignificant drop in yield [7]. In modern agriculture, precise application and management of irrigation and water requirements of crops is critical successful cropping program. The soil and plant properties, as well as climatic factors controlled the process of hydrous transfer in rhizosphere [8]. Thus, many organic and inorganic compounds if applied to soil can significantly change and improve soil water holding capacity and water use efficiency by cropping systems [9] , for example perlite granules that are produced under high (1500 0C) temperature, can reach a 4-20 times of their original size and generally a 430% increase in their volume that can better hold water and support plant roots particularly under deficit irrigation conditions, also perlite is the optimal germination medium sterilized and free from weeds, pathogens and other shrubs [10].

Potatoes are widely grown in the world because they are highly nutritious and energy-rich, and despite the increase in the area under cultivation, Their production in Iraq still fails to meet their local needs [11], where the area of potato cultivation in Iraq is 40,000 hectares [12]. It worth noting that the potato crop endures the deficit irrigation without a decrease in the quality or quantity of yield during the period preceding the tubers composition [13].Badr et al. [14] showed that drip-irrigated potatoes at 40, 60, 80 and 100 % of evaporated water have led to a significant rise in growth indicators and tubers with increasing

irrigation levels. Water stress-sensitive crops such as potatoes need a structured program to manage the irrigation cycle [15]. The main objective of the study is to investigate the influence of perlite addition, the amount of irrigation and the intervals on the consumption and use efficiency of water for the potato crop.

MATERIALS AND METHODS

This study is done as field experiment in Al-Anbar Province/Heet City (180 km to the west of Baghdad) that lies on 42.842597o E longitude, 33.637479o N latitude, at 34 m elevation above sea level during the period from February till May 2018, in a gypsiferous soil. The soil physical and chemical properties are presented in (table 1). The soil saturation capacity, permanent wilting point and volumetric moisture are determined in laboratory [82].

Study Treatments: The experiment included three factors:

1. Perlite treatment in three levels (PL): 0, 4 and 8% of soil volume mixed with soil particles for 30 cm width [17].
2. Irrigation water quantity (IQ): 50% and 100% of the net irrigation depth (NDI) counted from the US evaporation pan class A.
3. Irrigation intervals (IT): Two irrigation intervals of 3 and 6 days.

Experimental Design: Distribution of treatments are done according to the Split – Split Plot Pattern within Randomized Complete Block Design (RCBD) with three replicates. ITs treatment placed in the main plots. Every main plot divided into two sub-plots that irrigated randomly. Every sub-plot partitioned to three lines; in which, PL application distributed randomly. Treatment number reached 2 x 2 x 3 = 12.

Farm Preparation And Cultivation: The farm tilled, leveled and separated into three blocks. Each block divided into plots as defined in the experimental design and the split plots also divided into lines with a length of 10 m and a width of 0,75 m. Diammonium phosphate (DAP) and potassium sulphate fertilizers applied as 300 kg P_2O_5 and K_2O per hectare in respective; the addition of half potassium was before cultivation and the other half after 45 days of cultivation with urea fertilizer, which used as 300 kg per hectare[18] . The cultivation of (Riviera) potato cultivar tubers at a depth of 8 cm and a space of 0.4 m between plants after soaking in a fungicide called (Aggressive) with a concentration of 250 ml/100L of water for 10 minutes. The tubers were then added to the gibberellic solution as a single disk per 200 L of water to stimulate the growth of the tubers.

Scheduling Of Irrigation: All treatments irrigated as 40 mm deep for germination. Irrigation then scheduled to compensate vaporized water from the American evaporation class A pool every 4 and 6 days using 50 % and 100 % NDI. The NDI computed after that by the following equations:

1. Calculation of evaporation reverse transpiration by the equation mentioned by Al-Hadithi and Al-Kubaisi [23].

$$ET_0 = K_p \times E_{pan} \quad \text{.....(1)}$$

TABLE 1
Some of the physical and chemical characteristics of farm soil

Soil properties		Units	Value
Hydrogen potential pH		---	8.0
Electrical Conductivity (I : I)		$dS.m^{-1}$	2.5
Available Nutrients	Nitrogen	$mg.kg^{-1}$	60
	Phosphorus		30
	Potassium		220
Organic Matter			9.6
$CaSO_4$		$g.kg^{-1}$	180
$CaSO_3$			80
Soil Separates	Sand	$g.kg^{-1}$	528
	Silt		232
	Clay		240
Soil Texture			Sandy Clay Loam
Volumetric Moisture at Saturation		%	44.88
Volumetric Moisture at Field Capacity			29.74
Volumetric Moisture at Wilting Point			940
Bulk Density		$Mgm.m^{-1}$	1.27

Where:

ET0: evapotranspiration potential (mm.day-1).

Epan: evapotranspiration measured in the pan (mm.day-1).

Kp: evaporation pan's specific coefficient, that differs according to pan's type, vegetative cover surrounding the pan, and soil surface nature, as mentioned by Allen et al [37]. The value 0.8 was depended here depending on meteorological conditions of study area according to the method mentioned by ÇETIN et al [24] .

Calculating the actual evapotranspiration that equals the practical water consumption of potato crop irrigated superficially and by spraying; according to the following equation:

$$ET_a = K_c \times ET_0 \ldots\ldots\ldots \quad (2)$$

Where:

ETa: actual evapotranspiration (mm.day-1).

Kc = Crop coefficient

Values 0.75,1.15,1.00 and0.80 that are listed by Shiri-e-Janagrad et al [21] were desired to represent crop coefficient values for the durations (03/7 – 03/27), (27/03 – 04/16), (04/16 – 05/11) and (05/11 –05/20) successively.

Water balance equation was based on the calculation of water consumption:

$$\mathrm{ETa} = (\mathrm{P} + \mathrm{Ir}) - (\mathrm{D} + \mathrm{R} + \mathrm{In} + \Delta\mathrm{s}) \quad (3)$$

Where:

Eta is water consumption (ml), P is water quantity, D is deep percolation, R is superficial flow, In is water blocked by plant, ΔS is soil moisture difference; and if we suppose that both superficial flows, water blocked by plant and deep percolation are zero, then; the equation becomes as follows:

$$\mathrm{ETa} = (\mathrm{P} + \mathrm{Ir}) - \Delta\mathrm{s} \quad (4)$$

Water quantity that should be applied for saline leaching according to the equation of[22] which is special for the drip irrigation system was estimated as below:

$$LR = \frac{\mathrm{Ecw}}{(2\mathrm{Max\ Ece})} \times 100 \ \ldots\ldots\ldots \quad .(5)$$

Where L.R represents leaching requirements (%), Ecw is the electrical conductivity (dS. m-1) and Max ECe is the maximum electrical conductivity (dS. m-1) of the cultivated soil when the crop yield is zero, it's a tabulated value that differs with the crop; it equals 10 for potato crop[19] .

Drip irrigation systems have been used for droppers that discharge 4 liters. hour-1 and the irrigation water was applied according to the dual application system to split the quantity of water introduced into two bursts that are separated with 6 hours[20]. The irrigation time was calculated according to the equation mentioned in (AL – Hadithi, 2002).

$$\mathrm{q} \times \mathrm{t} = \mathrm{a} \times \mathrm{d} \ldots\ldots \quad (6)$$

Where:

q: discharge is given for the lateral lines (m3.hr-1), t: irrigation time (hour), a: the cultivated area (m2) and d: applied water depth (m).

Total yield (TY) for each treatment (average treatment area for three replicates in m2) separately and related to hectare using the equation mentioned by AL – Zobaie [26] as in the following:

$$TY = \frac{Experimentunityield\ (kg)}{Experimentunityield\ (m^2)} \times 10000 \quad (7)$$

Water use efficiency (WUE) or water productivity (WP) was estimated by Hillel[27] by dividing the total crop (kg.ha-1) to the added water volume (m3.ha-1) as mentioned by Doorenbos [25] .

$$WUE\ (\mathrm{kg.m^{-3}}) = \frac{TotalYied\ (kg.ha^{-1})}{Addedwaterquantity\ (m^3.ha^{-1})} \ldots \quad (8)$$

Data have been analyzed according to the followed experimental design and averages were tested according to the least significant difference (L.S.D.) test with probability level 0.05 [28] using GenStat Program.

RESULTS

Water Consumptive (Wc): Table 2 displays the LR-free WC values of the potato crop for germination and the other four phases of development for 3-and 6-day IT and 50 % and 100 % NDIs. During the growing season, the WC hit 235.595, 235.995, 471.19 and 471.99 mm respectively for the above listed IT and NDI. Escalation in water consumption for 100 % deep irrigation treatment attributed to increase of plant transpiration and soil evaporation which is consistent with several workers [29,5]. The highest ETa recorded in complete irrigation compared to zero irrigation treatment. It has been shown that cultivation and fertilization can significantly affect plant water uptake [30,31].

At the vegetative growth stage, WC values increased to 64.63 and 54.13 ml for 50 and 100 % NDIs. In addition, the progressive growth of the plant continued to increase to 148.66 and 130.26 ml water consumption at the nodulation stage, reaching 133.2 and 124.2 ml during the nodule swelling stage. In order to meet the nodulation requirements and also because of the rise in temperature during the growing season as a result of climate change, the cause of this continuous increase can be attributed to the extreme irrigation and nutritional needs of plants with decreased leaf area. At the end of the season, the WC values dwindled to 105 and 103.1 mm during the maturation phase. The diminished plant need for water could be due to end of developmental stage and senescence, as most areas of the plant have dried.

Total Yield (Ty) (Ton. Ha^{-1}): Figure 1 shows how research treatments impact TY quantity. The addition of PLs shows high variations in TY. Where the highest value for other additional NDIs can be seen at 8% PL compared to 0 and 4% PL. The lowest TY values for levels 0 and 4 % PLs are 11.2 and 16 ton.ha^{-1} compared with 19.5 ton.ha^{-1} for 8 % PL.

TABLE 2
Water Consumption of Potato Crop mm.season-1

Growth Stage	Stage Duration (day)	Water Consumption (WC) (mm) Irrigation Interval (IT) (day) 3 Irrigation Level 100 %	3 Irrigation Level 50%	6 Irrigation Level 100 %	6 Irrigation Level 50%	NDI ($m^3.ha^{-3}$)
Germination	27	40	20	40	20	167.44
Vegetative Growth	20	54.13	27.065	64.63	32.315	226.588 270.541
Nodulation	20	148.66	74.33	130.26	65.13	622.290 545.268
Tuber Swelling for Two Rains (16 and 20) mm	25	124.2	62.1	133.2	66.6	519.901 557.575
Maturity	10	105	52.5	103.1	51.55	439.53 431.576
Grand Total		471.99	235.995	471.19	235.595	1975.75 1972.4

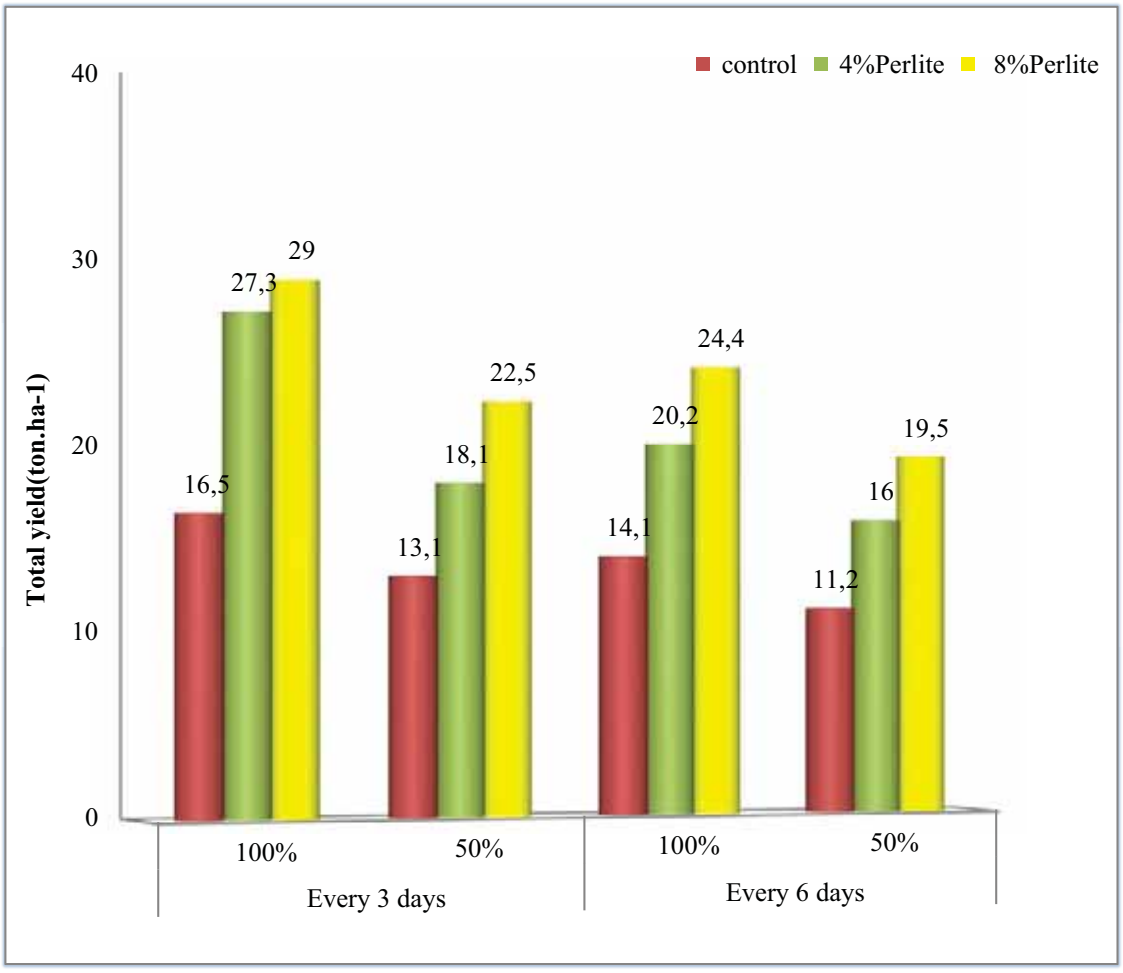

L.S.D 0.05	A	B	C	A*B	A*C	B*C	A*B*C
	2.966	2.532	1.949	2.800	2.727	2.980	3.924

FIGURE 1
Perlite application and irrigation interval effect on total yield (ton.ha-1)

This result is because of perlite properties of covering soil particles with hydration shells which encourage the penetration of the roots to increase the ability of plants to retain free water. The penetration of roots in the soil will create more spaces for water movement which reduces its bulk density. This reduction will positively reflect vegetative growth characteristics; improve the yield and its components. The PLs can enhance soil structure and boost aggregate stability to increase water permeability. The perlite plays positive role in enhancing both physical and chemical properties of the soil. Furthermore, PL has a large surface area that would improve the retention of water in the soil. The increase in yield could also be attributed to the slight evaporation of water in soil body, The increasing of excessive water content in soil as well as the availability of stored water in the soil caused by perlite application will, therefore, cause more vegetative growth and for all of this, the yield will increase [32].

The results of Figure 1 shows significant differences in the TY values caused by the difference in the irrigation intervals for any PL added. At 3 days IT, they reached the highest values of 16.5, 27.3 and 29 ton.ha^{-1}. Whereas they were 14.1, 20.2 and 24.4 ton.ha^{-1} for PLs 0, 4 and 8% respectively for 6 days IT. This drop in TY values could be attributed to the extensive irrigation intervals as well as the reduced content of water in [33] .

Figure 1 reveals that 100 % of deep NDIs are significantly higher than 50 % NDIs. Since 100 NDI for 3 and 6 ITs improved the TY value significantly relative to 50 % NDI for 6 days IT. The values reached 14.1, 20.2 and 24.4ton.ha^{-1} for NDI of 100% if irrigated every 6 days; compared to 11.2, 16.0 and 19.5 ton.ha^{-1} for 50% deep NDI with 6 days of IT with PLs of 0, 4 and 8% in successive. The reduction of TY values for 50% NDI, 6 days IT treatments in comparison with 100% NDI for 3 and 6 days ITs could be attributed to the effect of water stress on tubers crop which agreed with El-Latif et al. [34] . They found that water stress is the main reason of yield reduction that could be 50% or more.

Water Use Efficiency (Kg.M^{-3}) (Wue): Figure 2 demonstrates the impact of research treatments on WUE values that ranged from PLs to achieve a peak value of 8 % PL relative to 0 and 4 % for any NDIs applied but they have reached the lowest values of 13.82 and 8.35 kg.m^{-3} for 0 and 4% PLs compared with 14.86 kg.m^{-3} for 8% PL. This results maybe because of the increased yield and its components due to perlite addition, which reduce evaporation losses along with increased excess water in soil after the addition of perlite. The increased water storage raises the vegetative growth of branches that increase tubers' yield and its components .

Figure 2 shows significant variations between WUE values by various ITs for every application of PLs, where they reach their top values for IT of 3 days and 50% IQ and recorded 13.26 ,18.32 and 22.78 kg.m-3 in comparison with IT of 6 days, 50% IQ where they were 11.36, 16.22 and 19.77 kg.m-3 for PLs of 0, 4 and 8% successively. WUE declined with high levels of irrigation where the maximum WUE existed in treatment with the lowest IQ [35].

Results cited in Fig. 2 stated that irrigation at 50 % IQ increased the WUE values significantly compared to 100 % IQ during 6 days IT, where it reached 11.36, 16.22 and 19.77 kg.m-3 for 50% IQ by 6days IT compared with 7.15, 10.24 and 12.37 kg.m-3 for 100% IQ at 6 days IT for PLs 0, 4 and 8% successively. The increasing WUE values could be attributed to the few IQs added to the farm. The reduced WUE resulting from increased supply of IQ water due to the lack of aeration of roots caused by increased soil moisture In addition to the increased loss of nutrients by percolated water and the reduction of their concentration and therefore the reduction in productivity in relation to the overall IQ water, The listing of 50 % added IQ influences WUE and water reserves that irrigated additional areas to expand farmland [36].

CONCLUSIONS

This study shows the evident improvements in soil characteristics due to perlite addition, which increased soil's water holding capacity, saved more water volumes and reduced water requirements of plant to increase irrigation intervals; Irrigation at 50 % of NDI together with 3-day IT saved (987,875 m3. ha-1) irrigation water with stabilization of perlite factor, and this led to the possibility of cultivation in gypsiferous soils and partial reclamation and correction of their physical properties.

ACKNOWLEDGEMENTS

This research was funded by the University of Anbar Grant Vote no. 9442500. The authors would like to thank all, who provided the insight and expertise that greatly assisted in the research. The authors also appreciate the efforts of academic and support staffs of the Department of Soil and Water Resources - College of Agriculture, in providing all the required assistance and materials in conducting this research .In addition, the authors would like to thank the University of Jordan for help in publishing this research.

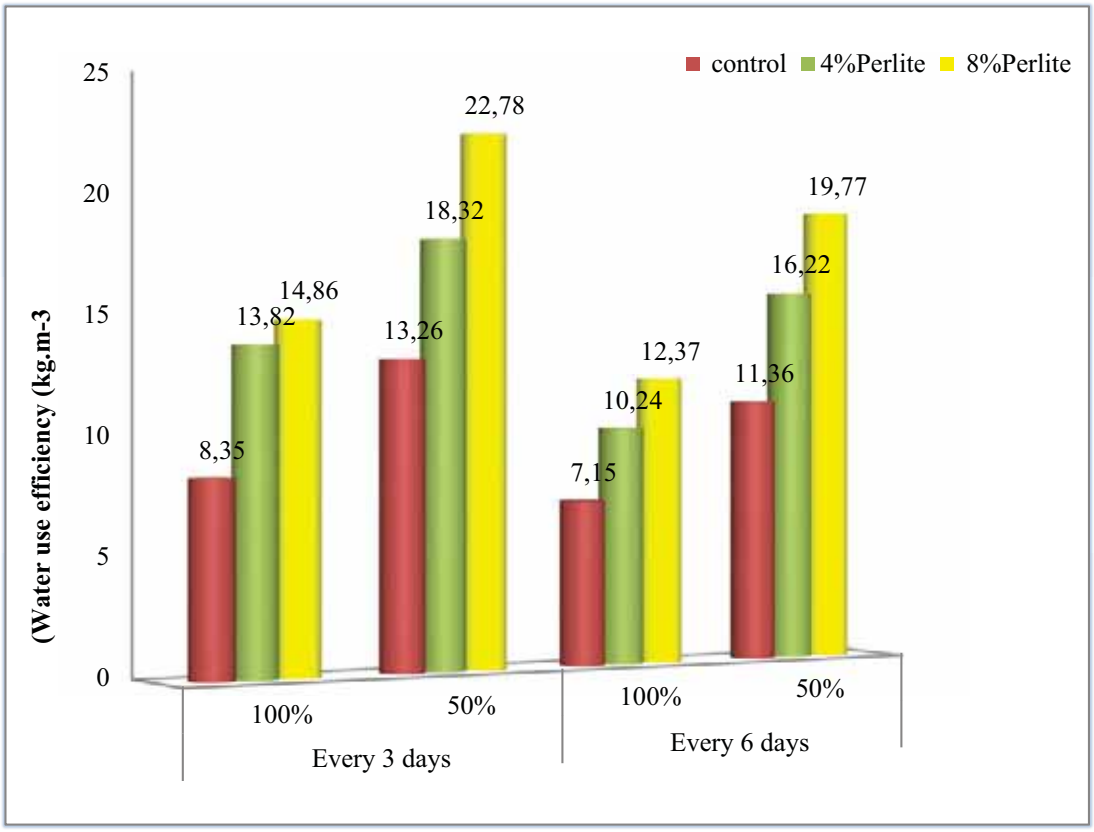

L.S.D	A	B	C	A*B	A*C	B*C	A*B*C
0.05	2.275	1.915	1.518	2.130	2.111	2.287	3.028

FIGURE2
Effect of perlite addition and irrigation brake level on water use efficiency(kg.m-3)

REFERENCES

[1] Saliem, K.A. (2001) The Effect of Irrigation Water Quality and Application on The Properties Gypsiferous Soils for AL-Dour Area. College of Agriculture University of Baghdad.Iraq.

[2] Oweis, T., Zhang, H.and Pala, M. (2000) Water use efficiency of rainfed and irrigated bread wheat in a Mediterranean Environment. Agronomy Journal. 92(2), 231–238.

[3] Pereira, A.B.and Shock, C.C. (2006) Development of irrigation best management practices for potato from a research perspective in the United States. Sakia. Org e-Publish. 1(1), 1–20

[4] Al-Shahrabali, Q. (2009) Surface water resources in Iraq current and future senarios. Iraq Soil Salinity and Water Management. 7, 15-17.

[5] Ati, A.S. (2009) Effect of irrigation deficit and addition of corn cobs on consumptive use and yield of wheat Triticum aestivum L. J. Agric. Sci. Mansoura Univ. 34 (6), 7103–7113.

[6] Geerts, S.and Raes, D. (2009) Deficit irrigation as an on-farm strategy to maximize crop water productivity in dry areas. Agricultural Water Management. 96(9), 1275–1284.

[7] Al-Najim, H.J.M. (2013) The Impact of Irrigation water Salinity Water Magnatization and Soil Available Moisture Depletion Percent on Some Soil Physical and Potato and Growth. College of Agriculture- University of Al-Anbar Iraq.

[8] Shankar, V., Prasad, K.S.H., Ojha, C.S.P.and Govindaraju, R.S. (2013) Optimizing Water Use in Irrigation-A Review. Journal of the Indian Institute of Science. 93(2), 209–226.

[9] Evans, M.R. (2004) Ground bovine bone as a perlite alternative in horticultural substrates. HortTechnology. 14(2), 171–175.

[10] Hanna, H.Y. (2006) A stir and disinfect technique to recycle perlite for cost-effective greenhouse tomato production. J. Veg. Sci. 12(1), 51-63.

[11] AL-Thalage, A.A. and AL-Najjar, E.Y. (2012) An Analytical study of the reality of the production of potato crop in some Arab countries for the period 1981-2010 (Iraq Model) : A Comparative study. Al- Rafidain Journal. 40(4), 77-91.

[12] FAOSTAT (2013) The Statistics Division of the Food and Agriculture Organization of the United Nations. Rome, Italy .

[13] Shock, C.C., Zalewski, J.C., Stieber, T.D.and Burnett, D.S. (1992) Impact of early-season water deficits on Russet Burbank plant development, tuber yield and quality. American Potato Journal. 69(12), 793–803.
[14] Badr, M.A., El-Tohamy, W.A.and Zaghloul, A.M. (2012) Yield and water use efficiency of potato grown under different irrigation and nitrogen levels in an arid region. Agricultural Water Management. 110, 9–15.
[15] Ayas, S. (2013). The effects of different regimes on potato (Solanum tuberosum L. Hermes) yield and quality characteristics under unheated greenhouse conditions. Bulgarian Journal of Agricultural Science. 19(1), 87–95.
[16] Page, A.L., Miller, R.H. and Keeney, D.R. (1982) Methods of soil analysis. Part 2. Chemical and microbiological properties. Agronomy, No. 9. Soil Science Society of America, Madison, WI. 1159.
[17] Hamdi, G.J. (2017) Effect of perlite in reducing water stress for three genotypes of tomato. M. Sc. Thesis. College of Agriculture. University of Diyala. Iraq.
[18] AL–Fadhiy, J.T.M. (2006) Foliar Application on Growth, Yield and Components of Potato Plants Tubers (Solanum Tuberosum L.). College of Agriculture University of Baghdad.
[19] Ayer, R.S. and Westcot, D.W. (1985) Water quality for agriculture, irrigation and drainage. FAW Irrigation and Drainge Paper No, 29,Rev 1.
[20] AL-Khateeb, B.A.,Yousif, B.M. and Abed Al Rhman, W.F. (2016) Measurement of water consumptive use, growth, and yield of potato(Solanum tuberosum L) under drip irrigation system. AL-Anbar Journal of Agricultural Sciences. 14(2),36-52.
[21] Shiri-e-Janagrad, M., Tobeh, A., Abbasi, A., Jamaati-e-Somarin, S. and Hokmalipour, S. (2009) Vegetative growth of potato (Solanum tuberosum L.) cultivars, under the effects of different levels of nitrogen fertilizer. Research Journal of Biological Sciences. 4(7), 807–814.
[22] Haman, D.Z. and Yeager, T.H. (2000) Foliar Deposits and Stains from Irrigation Water. Citeseer. Fact Sheet ENH 150, a series of Environmental Horticulture Department, Florida Cooperative Extension Service, Institute of Food and Agricultural Sciences, University of Florida.
[23] Al-Hadithi,I. And Al-Kubaisi,A.(2010). Modern Irrigation Technlogies and Other Issues in Water Issue. (First Edit). Baghdad , Iraq.
[24] Çetin, Ö., Yildirim, O., Uygan, D. and Boyaci, H. (2002) Irrigation scheduling of drip-irrigated tomatoes using Class A pan evaporation. Turkish Journal of Agriculture and Forestry. 26(4), 171–178.
[25] Doorenbos, J. (1975) Guidelines for predicting crop water requirements. Food and Agriculture Organization. Rome, Irrig. Drainage. 24.
[26] AL-Zobaie, A.A.A. (2016) The Effect of Planting date and Spraying of nutrient Organic (Siapton 10 L.) growth and Yield five varieties of Potatoes Solanum Tuberosum L. University of Al-Anbar. MS Thesis. College of Agriculture Iraq.
[27] Hillel, D. (2008) Years of drip irrigation reviewing the past, prospects for the future. Crops Soils. 41, 38–42.
[28] Al-Sahaf, F.H. (1989) Practical Plant Nutrition. Ministry of Higher Education and Scientific Research. Dar Al-Hikma Printing Press. Iraq.
[29] AL–Hadithi, S.A.S. (2002) Deficit irrigation scheduling of Zea mayz L. Ph.D. Dissertation College of Agriculture University of Baghdad.Iraq.
[30] Souri, M.K. and Hatamian, M. (2019) Aminochelates in plant nutrition: a review. Journal of Plant Nutrition. 42(1), 67–78.
[31] Souri, M.K., Neumann, G. and Römheld, V. (2009) Nitrogen forms and water consumption in tomato plants. Horticulture Environment and Biotechnology. 50(5), 377–383.
[32] Salas-Pérez, L., Garcia-Hernández, J.L., Márquez-Hernández, C., Fortis-Hernández, M., Estrada-Arellano, J.R., Esparza-Rivera, J.R. and Preciado-Rangel, P. (2017) Yield and nutraceutical quality of tomato fruits in organic substrates. Ecosistemas y Recursos Agropecuarios. 4(10), 169–175.
[33] Farooq, M., Wahid, A., Kobayashi, N., Fujita, D. and Basra, S.M.A. (2009) Plant drought stress: effects, mechanisms and management. In Sustainable Agriculture. Springer. 153–188.
[34] El-Latif, K.M.A., Osman, E.A.M., Abdullah, R. and El Kader, N.A. (2011) Response of potato plants to potassium fertilizer rates and soil moisture deficit. Adv. Appl. Sci. Res. 2(2), 388–397.
[35] Fouda, T., Elmetwalli, A.and Eltaher, A. (2012) Response of potato to nitrogen and water deficit under sprinkler irrigation. Scientific Papers Series-Management, Economic Engineering in Agriculture and Rural Development. 12(1), 77–81.
[36] Feddes, R.A., Kowailk, P.J. and Zaradny, H. (1978) Simulation of field water use and crop yield, PUDOC, Wangeningen. 189.
[37] Allen, R.G., Pereira, L.S., Raes, D. and Smith, M. (1998) Crop evapotranspiration-Guidelines for computing crop water requirements-FAO Irrigation and drainage. FAO, Rome. 300(9), 56. D05109.

Received: **16.01.2021**
Accepted: **10.02.2021**

CORRESPONDING AUTHOR

Tawfiq M Al Antary
Plant Protection Dept.,Faculty Of Agriculture ,
The University Of Jordan,
Amman – Jordan

e-mail: tawfiqalantary@yahoo.com

© by PSP Volume 30– No. 05/2021 pages 4779-4786 Fresenius Environmental Bulletin

ENERGY ANALYSIS OF WASTEWATER TREATMENT PLANT IN PAPER AND PAPERBOARD MILL

Mehmet Recai Durgut*, Busra Yarar

Department of Biosystem Engineering, Faculty of Agriculture, Tekirdag Namik Kemal University Tekirdag, Turkey

ABSTRACT

Water is one of the most important raw materials used in the production of paper and cardboard. For this reason, the production of paper and cardboard is always a process in which high amounts of water should be used. Water contaminates during this operations. For this reason, water used in paper and cardboard production should be treated. This study; It was carried out in a treatment plant located in a factory that produces cardboard in various weights. The treatment plant operates 24 hours with an installed capacity of 4020 m³/day. The aim is; to compare and interpret energy consumption by using the data of this facility. The wastewater treatment plant consists of physical and biological treatment units and the active sludge system has the capacity to handle 4000 kg BOD/day, 4020 m³/day hydraulic load. In this study, energy consumed during the treatment process; electrical, manual, mechanical and chemical energy as kWh/m³. The initial data were collected through field monitoring and supported by interviews with facility operators and recorded data (entering-exiting wastewater values, laboratory analyzes, consumables and chemical consumptions) for the research period. The field monitoring was carried out for 6 months in the 2017- 2018 period. As a result energy; Electrical, mechanical, manual and chemical energy are calculated separately. Total energy expenditure was found to be 1.9587 kWh/m³. It has been concluded that electrical energy has a share of 80.6% and chemical energy 18.05%.

KEYWORDS:
Wastewater treatment, electrical energy, manual energy, chemical energy, mechanical energy, paper and cardboard

INTRODUCTION

Energy efficiency is on the agenda in many areas due to the rapidly depleting energy resources. There is a significant amount of energy use in wastewater treatment plants, both in treatment processes and in units where wastewater is collected and transported. Today, increasing energy prices and tighter discharge standards brought by new legal regulations increase the operating costs of wastewater treatment plants worldwide. Energy optimization becomes even more important from an economic and environmental perspective, with increased energy costs and sustainability efforts. In this context, it is important to monitor energy consumption and treatment capacities on the basis of units from the entrance to the exit of the facility for the optimization of the operating cost in waste water treatment plants [1].

Wastewater treatment plants not only use fossil fuel resources that are decreasing day by day, but also create carbon footprints and emit greenhouse gases (carbon dioxide, methane and nitrous oxide) into the atmosphere during the treatment processes. It is known that ~ 0.1-0.4% of the total energy spent worldwide is used in these facilities, which consume a significant amount of energy [15]. While this rate is 1% in Sweden, it is 3% in the USA and UK. In Israel, a country with insufficient water resources, it is 10% due to the high rate of advanced treatment of wastewater for beneficial use [10].

Each wastewater treatment method causes various environmental impacts due to energy consumption, use of chemical consumables, emissions to the atmosphere, water and soil from related processes [6].

In water and wastewater treatment, collection and treatment units are units with very high energy needs. First of all, the wastewater collection systems designed and operated by considering the environment and human health ensure the transmission of wastewater from the pollutant source to the treatment unit. The wastewater reaching the treatment plant is delivered to the receiving environment by reaching the targeted discharge standards within the facility. The treatment process also consists of processes with high energy requirements such as pumping, mixing, ventilation and sludge disposal. Organic load in wastewater is eliminated by introducing the oxygen required for aerobic biomass into the system [1].

When the treatment processes of wastewater are examined, a high amount of energy is required in processes such as transport, treatment, discharge of wastewater and disposal of the formed sludge. The energy required for pumping and ventilation (in biological treatment) among these processes is the most important part of the energy used in the facility. In a study conducted by Lingsten et al. [9], the amount of

energy required for the pumping at the treatment plants in Sweden was determined as ~ 20 kWh / person-year [9]. In another study conducted in the USA, the energy required for the treatment and transportation of water and wastewater was determined as approximately 3% of the energy used on a country basis (~ 21x106 kWh/year) [5].

The paper industry is one of the leading industries creating serious environmental problems in terms of both the water used in production and the amount of waste water generated. In the paper industry, which holds an important place in our country economically, the pollution load caused by the water used per unit production and the amount of waste water released is quite high compared to other industry branches [4].

The paper industry is among the industries that produce the most waste water, and the characteristics of the waste water produced vary depending on the type and quality of the paper produced. In general, since paper industry wastewater is wastewater with high organic pollution and high suspended solids concentrations, it is preferable to treat it using biological treatment processes. However, their purification in biological treatment does not always give good results due to the difficult degradable substances they contain. In this case, chemical treatment, chemical oxidation, anaerobic treatment etc. alternatives are also being evaluated. One of the most important issues while determining the appropriate treatment alternative is investment and operating cost [3, 8].

Energy management in wastewater treatment plants means "ensuring the use of energy in an appropriate value and continuously in order to achieve the desired wastewater treatment discharge standards with minimum cost and to ensure sustainable development". This very comprehensive definition covers many processes from the design of the waste water treatment plant to the operation of the waste water treatment plant at an appropriate value. Energy management can be achieved through the examination and optimization of many processes. A high amount of energy is consumed in wastewater treatment plants [13].

Alternative equipment applications stand out in the studies for energy conservation. These equipment that are effective in facility consumption; inlet pumping pump, ventilation equipment and equipment used for the operation of sludge, etc. examples can be given [7].

In wastewater treatment plants, electrical, manual, mechanical, chemical, etc. energy types are used. Most of the studies on this subject have focused on electricity consumption only for benchmarking. Electrical energy is only half of the total energy consumption. It has an important share in labor energy; this means that small-scale treatment plants provide significant employment opportunities in new industrialized countries and fossil fuel-based energy is replaced by renewable energy. The duplication of similar studies and the production of data in this area will provide guidelines to decide on the scale of the wastewater treatment process, taking into account the energy and climate change mitigation strategies [2, 12].

High energy consumption, energy recovery, energy efficiency practices in equipment and processes, and the importance of energy cost management have led to the implementation of energy optimization efforts in wastewater treatment plants. The energy consumption of a wastewater treatment plant varies depending on different parameters such as the population in the city, industrial wastewater, population growth, discharge criteria. Efforts to reduce energy use are also important as they reduce energy costs at the facilities. For this reason, in order to be able to comment and make suggestions about the energy consumption of the facilities, the current situation and the operations of the facilities must first be examined in this respect. The daily routines of the wastewater treatment plant subject to this study and the activities performed were revealed with real data and energy; electrical, mechanical, workforce and chemically determined.

MATERIALS AND METHODS

Although the installed capacity of the facility under study is 4020 m³/day, the flow rate is around 2000 m³/day. The vast majority (99%) of the water coming to the facility is industrial wastewater; 1% is domestic waste water arising from the daily needs of the factory staff.

The data required for the realization of this study are the values used and realized during the operation of the facility between September 2017 and February 2018. During the determination of these values, observations were made at the facility between 08:00 and 18:00 on weekdays and between 13:00 and 16:00 on weekends, and the values were monitored. The wastewater treatment scheme is shown in Figure 1.

Determination of electrical energy input. In order to reach the information of the equipment belonging to the facility, the flow chart of the facility was first examined and an equipment list was created. Then, the usage procedures of the equipment were examined and the values were confirmed by comparing the label values of the equipment in the field.

The electrical energy input is determined by the formula given in Equation 1. Considering the electrical load of the pump / motor (kW), the time in hours the engine is running (h) and the total amount of waste water treated.

$$E_p = \frac{P \times T}{Q} \quad (1)$$

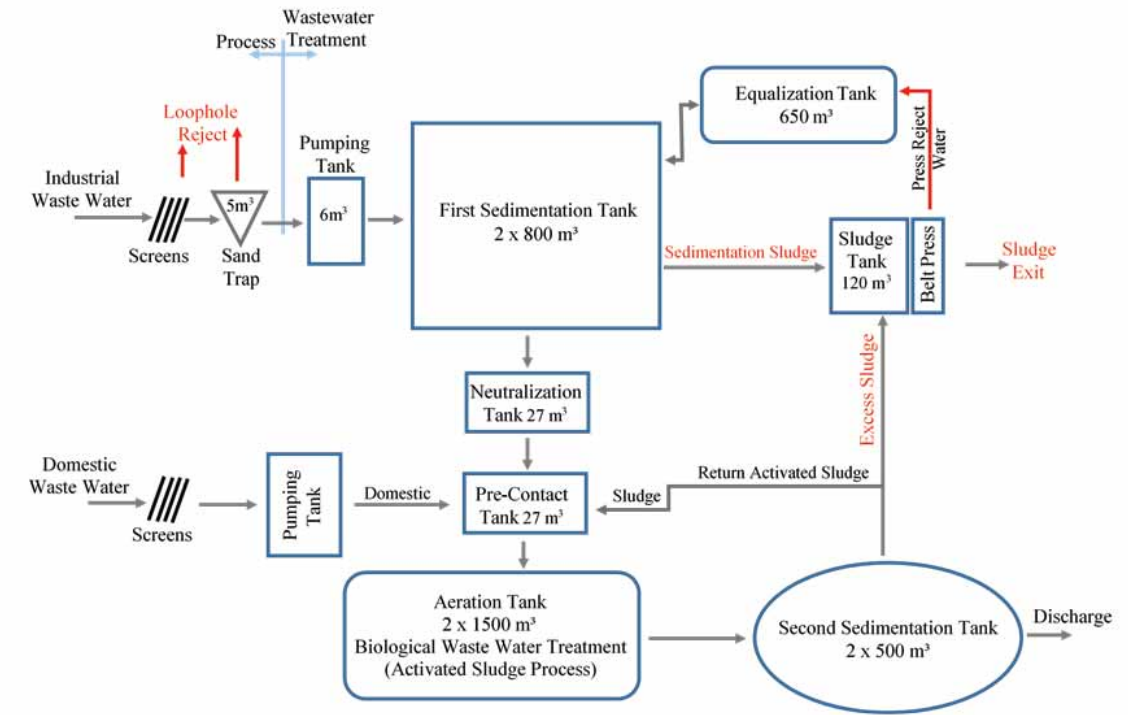

FIGURE 1
Process flow diagram of the WWTP

where, Ep is the electrical energy kWh/m^3, Q the total flow of wastewater in m^3/day, P the rated power of the electrical motor in kilo Watt (kW), and T is the operation hours in a day (h/day) [12].

The power of the equipment used in the facility and the working hours during the day were determined for each equipment. While making the determinations, the motor efficiency was accepted as 80% [12].

Determination of mechanical energy. The diesel generator did not work as there were no power cuts during the six months period when the measurements were made. However, since the loader is used during the transportation of the sludge generated in the facility, there is a constant consumption of diesel fuel. Determination of diesel fuel quantities was achieved by measuring the fuel used by the plant authorities.

Mechanical or fuel energy; It represents diesel fuel spent on operating the generator used in power outages and diesel fuel consumed during the use of the loader. Mechanical energy was determined using in Equation 2.

$$E_f = \frac{10\ D}{Q} \qquad (2)$$

Where, 10 is the energy density value of diesel in kWh/L and represents the amount of energy stored within 1 L of diesel and D is the amount of diesel consumed in L/day [2].

Determination of manual energy. For the purpose of carrying out this study, observations were made between 08:00 and 18:00 on weekdays and between 13:00 and 16:00 on weekends, and observations were made by the employees.

Later, it was added to this study by getting information about the reasons for the activities, the times they took and their difficulty, by meeting with the facility officials.

Consumption of workforce energy is a function of the sexes of the operators and the activities they perform. Based on these issues, workforce energy was determined with equality in Equation 3.

$$E_m = \frac{\sum_{i=0}^{i=n}\sum_{j=0}^{j=m} E_{ij}N_{ij}T_{ij}}{Q} \qquad (3)$$

Where, Em is manual energy in kWh/m^3, n the number of nature of activities (light, active, and heavy), m the number of gender (male, female), E the human power equivalent (kW), N the number of persons engaged in an activity and T is the total time devoted in the activity (h/day) [2].

Determination of chemical energy. In order to determine chemical energy; Chemical reactions in the biological units of the treatment plant and consumable chemicals used for pH balancing are considered.

Daily consumption is recorded by the operators on business shift forms. Therefore; the data on their chemical consumption were obtained from these records.

Based on these issues, its chemical energy has been determined with equality in Equation 4. Thus, chemical energy (Ec) in kWh/m^3 is determined.

$$E_c = \frac{n[\sum \Delta H_p - \sum \Delta H_r]}{Q} \times 0{,}000278 \quad (4)$$

Where, n is the number of moles (mol/day), 0.000278 is the conversion factor from KJ to kWh, ΔHp the enthalpy (heat) of formation of products (kJ/mol), and ΔHr is enthalpy (heat) of formation of reactants (kJ/mol) [12].

RESULTS AND DISCUSSION

Daily flow rates to be used in calculations; It is created by taking the 6-month averages of the meter values that are read separately every day. The final average of the incoming wastewater flow was determined as 1934.36 m³/day. The reasons for the incoming wastewater flow rate to be higher than the wastewater flow rate are; evaporation and purification sludge occurring in the units and the amount of moisture away from the facility.

The electricity consumption determined separately for each equipment was collected and the electrical energy consumed during the purification of 1 m water for the whole facility was found to be 1.5789 kWh/m3 found. Percentage shares of the electricity consumption values of the wastewater treatment plant are given in Figure 2.

It is seen that the highest electricity consumption in the facility is in aerators. Aerators account for 76% of 1.5789 kWh/m³ of electricity consumption per 1 m3 of water. The facility has 12 aerators that make up 76% of this. When the energy consumption of aerators is examined, it is determined that 96% of aerators are in aeration pools.

Typically in a conventional wastewater treatment plant, the aeration of the mixed liquid, which makes the main contribution to energy consumption, varies between 55-70% [13]. In a wastewater treatment plant, ventilation systems reported that they may contain 54% or more of the total energy use. The study in 2010 showed that 50-60% of the energy consumed by the treatment plants is related to the ventilation process [11]. Considering these values, it is seen that there is an above-average electricity consumption in the ventilation processes of the facility under examination.

A power outage is an emergency for the waste water treatment plant. If emergency situations are not intervened; it means that the aerators providing the oxygen required for the biological system do not work and therefore the active sludge population in the system is destroyed. Therefore; there is a diesel generator in the waste water treatment plant to be used during possible power outages. In addition, the loader that works to send the sludge from the belt press to disposal is also diesel fueled. Diesel consumption per day was found to be 2.44 L on average. Considering these activities, mechanical energy has been determined as 0.0126 kWh/m³.

The wastewater treatment plant where the study is carried out does not have any automation system. For this reason, many processes such as analyzing the pollution values, starting and stopping the equipment, operating the system and cleaning the unit are carried out with work force energy (with the body strength of the employees). The activities in which the workforce energy is spent, the type of activities, the number of people participating in the activities and the time spent during the activities are shown in Table 1.

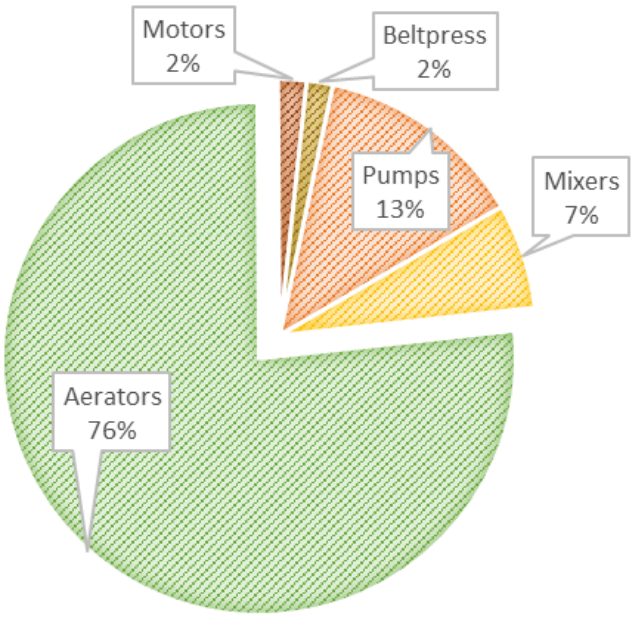

FIGURE 2
Distribution of electrical energy consumption

TABLE 1
Manual labour input in WWTP

Treatment unit	Nature of activity	Gender	Number of people	Average labour time input (h/day)	Treatment unit	Nature of activity	Gender	Number of people	Average labour time input (h/day)
Pumping tank float control	Light	Male	1	0.5	Reading flow meter values	Light	Male	1	0.5
Sludge tank level control	Light	Male	1	1	Cleaning the grills in the entrance structures	Heavy	Male	2	1
Preparation of polymer solution	Heavy	Male	2	1	Sedimentation tank cleaning	Heavy	Male	2	2
Shift book and writing reports	Light	Male	1	0.5	Domestic pumping tank cleaning	Heavy	Male	2	1
Pumps controls	Heavy	Male	2	1	Process pumping tank cleaning	Heavy	Male	2	0.5
Aerators controls	Heavy	Male	2	1	Neutralization tank cleaning	Heavy	Male	2	0.5
Mixer controls	Heavy	Male	2	1	Cleaning the front contact tank	Heavy	Male	2	1
Device verifications	Light	Male	1	1	Cleaning the aeration tank	Heavy	Male	2	4
Sampling procedures	Moderate	Male	1	3	Cleaning the final settling tank	Heavy	Male	2	3
Cleaning and control of laboratory devices	Light	Male	1	0.5	Beltpress Cleaning	Heavy	Male	1	1
Wastewater analysis in the laboratory	Moderate	Male	2	10	Sludge tank cleaning	Heavy	Male	2	3
Chemical storage control	Light	Male	1	0.5	Filtration pool cleaning	Heavy	Male	2	1

TABLE 2
Human power equivalent (E) in kW (WHO 1985)

Input	Male	Female	Activities in the treatment plant
Light	0.13	0.10	Switch on/off the raw water pump, maintain the log-book, check motor temperature
Moderate	0.14	0.11	Open/close the sludge drain valve, operation of valves for backwashing
Heavy	0.54	0.44	Prepare the chemical solution for dosing, fill the chemical solution in the dosing tank, collect the dried sludge in gunny bags

The manpower equivalent table published by WHO in 1985 is given in Table 2. Based on the manpower equivalents, the workforce energy was determined using the data in Table 2 [2, 12].

The manual energies determined separately for each activity were collected and the manual energy spent for the overall plant was found to be 0.0139 kWh/m³.

Organic compounds in wastewater entering the facility in 1 day contain approximately 100 kg/day of C atoms. In order to carry out the reaction, 50 kg of urea fertilizer (CH_4N_2O) is added per day and 10 kg of DAP fertilizer ($(NH_4)\ 2HPO_4$) is added. In cases where the pH of the wastewater is higher than 9; In order to balance pH, aluminum sulfate ($Al_2(SO_4)_3$) is added to the water.

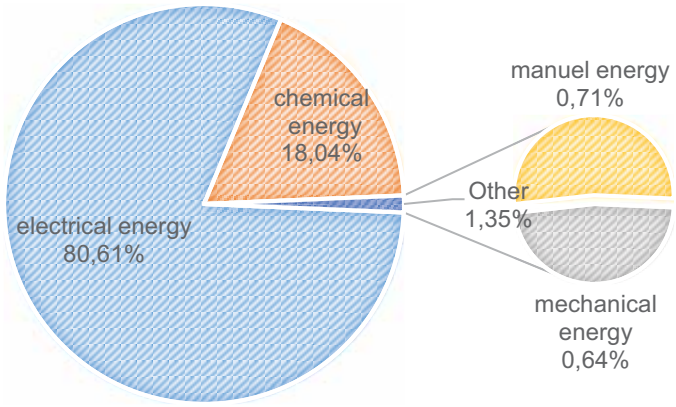

FIGURE 3
Percentage distribution of energy consumption

Total chemical energy consumed in the facility was found to be 0.3533 kWh/m³, including the chemical energy spent during the biological system's treatment and the chemical energy spent during the pH balancing process.

CONCLUSIONS

As a result, the total energy spent; it was found as 1.9587 kWh/m³ and Percentage distribution of energy consumption was shown in Figure 3. Energy consumption, respectively; electrical energy 1.5789 kWh/m³, mechanical energy 0.0126 kWh/m³, manual energy 0.0139 kWh/m³, chemical energy 0.3533 kWh/m³ determined as.

Considering the world average of energy consumption of wastewater treatment plants; values are seen to vary between 0.079 and 1.122 kWh/m³. This is because all wastewater treatment plants have the same level of treatment, waste quality standards, process technology, employee experience, etc. is not having. The worldwide widespread technology is the activated sludge system and when it is not specified by the authors, it is understood to be the process adopted [14]. The energy consumption value we detected in our study is above the world average. Also; It is known from the literature and administrative experience that 25-40% of operating costs in a traditional wastewater treatment plant are caused by energy consumption. This value varies in the range of approximately 0.3-2.1 kWh/m³ of treated wastewater [13]. The wastewater treatment plant subject to this project is close to the upper limit in terms of consumption.

Sing et al. [12], in a study in his energy; It was made by classifying as electrical, mechanical, workmanship and chemical, and the total energy consumption of the wastewater treatment plant was found to be 1.046 kWh/m³. Compared to this study, the energy consumption in our facility was found 1.87 times higher than our energy consumption.

Belloir et al. [2], energy consumption was found to be 3.3 kWh/m³. According to this study, it was concluded that we consume 1.68 times less energy. These differences are thought to arise from process differences in treatment plants.

The distribution of energy consumption in the wastewater treatment plant by department is given in Figure 4. It has been determined that the electricity consumption of the aerators in the aeration tanks is the most energy consumed in the aeration tanks with a 77% share in the energy consumption since the consumption of the aerator has a 96% share in the energy consumption. In belt press, which belongs to the sludge dewatering process, it is concluded that it has a 10% share in energy consumption due to the consumption of electricity, mechanical and workforce energy types.

There are two methods of treatment applied in the waste water treatment plant subject to the study. The first one is physical treatment and the second one is biological treatment. The average consumption determined as a result of the data obtained for six months in the Physical Treatment units of the facility is 0.37145 kWh/m³. Units that cause energy consumption in the physical treatment process; The pumps in the domestic and process pumping tanks and the workforce expended in the tanks, balancing tank pumps, the moving spherical bridges and pumps in the sedimentation tanks and the workforce expended in the tanks, and the sludge dewatered belt press. In biological treatment units; ventilation pools, settling pools, neutralization tank constitute the main consumption of the facility. It causes an average of 1.5468 kWh/m³ energy consumption in the biological treatment process.

As a result of the evaluation of the energy consumption, the suggestions given below are expected to provide optimization in terms of energy efficiency.

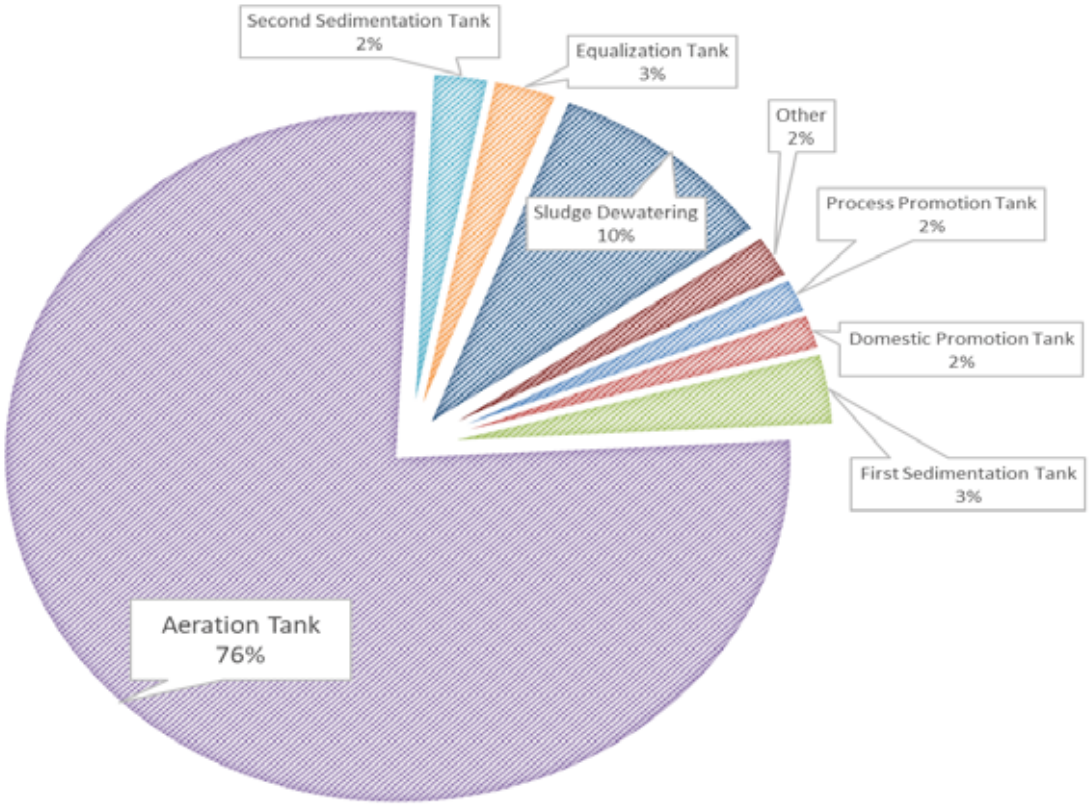

FIGURE 4
Distribution of energy consumption on a process basis

It has been 19 years since the installation of the facility and it was observed that no investment was made in the facility during this period. Therefore; it is recommended to renew the 15 kW aerators supplied during the installation phase of the facility with new technology and low energy consumption aerators.

During the 6-month field monitoring period, it has been observed that the staff working in the treatment plant are experienced employees working in the facility for many years. Experienced employee factor is useful in many respects; it is also a fact that it makes negative effects on the unnecessary use of energy in the facilities operated by making use of intuition and experience instead of laboratory results and technical data.

As a requirement of the cardboard process, the organic materials that will create nutrients for the biological treatment system in the wastewater coming to the facility are low and therefore cause nutrient deficiency for the activated sludge bacteria in the biological treatment process. Therefore, the facility has extra chemical consumption for nutrient purposes and this increases the chemical energy consumption. A review of the auxiliary chemicals used in the production process and the use of chemicals with organic content will increase the amount of nutrients in wastewater. In addition; it may be suggested that domestic wastewater, which can create nutrients for wastewater, be accepted into the biological treatment system.

There is no automation system in the wastewater treatment plant, which is the subject of the research, and therefore body power is at the forefront. It is predicted that labor force energy will decrease as a result of increasing automation systems.

For the realization of all these suggestions; it is thought that it would be beneficial to get support from the engineering companies operating in the field of waste water treatment plants in the effective and efficient energy use.

ACKNOWLEDGEMENTS

This study; It was produced from a MSc. Thesis by Busra YARAR at the Institute of Natural and Applied Sciences, Tekirdag Namik Kemal University, 2019.

REFERENCES

[1] Aynur, Z. (2014) Energy efficiency in wastewater treatment plants. Master Thesis, Istanbul Technical University, Institute of Science, Istanbul.

[2] Belloir, C., Stanford, C. and Soares, A. (2015) Energy Benchmarking in Wastewater Treatment Plants: the İmportance of Site Operation and Layout. Environmental Technology. 36, 260-269.
[3] Bierbaum, S., Escabasse, J.Y., Well, A., Kompare, B., Drev, D. and Klemencic, A.K. (2012) Reducing Fresh Water Consumption In Paper Industry By Recycling Aop-Treated Effluents Fresen. Environ. Bull. 21(8a), 2178–2184.
[4] Dogan, E., Aydıner, C., Mert, B., Narcı, A., Kılıncoglu, O., Durna, E. and Akbacak, U. (2017) Determination of nanofiltration membranes for reuse of paper mill industry wastewater. Pamukkale University Journal of Engineering Sciences. 23(3), 279.
[5] Horne, A.J., Jasper, J.T., Nguyen, M.T., Jones, Z.L., Ismail, N.S., Sedlak, D.L., Sharp, J.O., Luthy, R.G. and Nelson, K.L. (2013) Unit Process Wetlands for Removal of Trace Organic Contaminants and Pathogens from Municipal Wastewater Effluents. Environmental Engineering Science, Reinventing Urban Water Infrastructure. 30, 8.
[6] Georgiopoulou, M., Abeliotis, K., Kornaros, M. and Lyberatos, G. (2008) Selection of The Best Available Technology For Industrial Wastewater Treatment Based on Environmental Evaluation Of Alternative Treatment Technologies: The Case Of Milk Industry. Fresen. Environ. Bull. 17(1), 1-12.
[7] Kılınc, O. (2017) Evaluation of Waste Water Treatment in Terms of Energy Efficiency. Master Thesis, Selcuk University, Institute of Science, Konya.
[8] Koken, E., Buyukkamaci, N. (2010) Effect of sludge management systems on overall pulp and paper industry wastewater treatment plant cost. ITU Journal Series E: Water Pollution Control. 20, 66-76.
[9] Lingsten, A., Lundkvist, M., Hellström, D. and Balmer, P. (2011) VA-verkens energianvändning 2008 (Swedish Water and Wastewater Utilities Use of Energy in 2008). Svenskt Vatten Utveckling, Stockholm, Sweden (In Swedish), Rapport Nr 2011-04.
[10] Olsson, G. (2012) Water and Energy Threats and Opportunities. IWA Publishing, London. 465
[11] Saghafi, S., Mehrdadi, N., Hendy, G.N.B. and Rad, H. (2015) Energy Efficiency in Wastewater Treatment Plant Emphasizing On Cod Removal: A Case Study Of Amol Industrial Zone, Iran, Canadian Journal of Pure and Applied Sciences. June. 9(2), 3441-3448.
[12] Singh, P., Carliell-Marquet, C., Kansal, A. (2012) Energy Pattern Analysis of a Wastewater Treatment Plant. Appl. Water Sci. 2, 221-226.
[13] Turkmenler, H. (2017) Energy Efficiency in Wastewater Treatment Plants. Journal of Polytechnic. 20(2), 495-502.
[14] Wakeel, M., Chen, B., Hayat, T., Alsaedi, A. and Ahmad, B. (2016) Energy Consumption for Water use Cycles in Different Countries: A review, Applied Energy. 178, 868–885.
[15] WEF (1997) Energy Conservation in Wastewater Treatment Facilities Manual of Practice, Water Environment Federation, Alexandria, USA. 1–142

Received: **23.04.2020**
Accepted: **15.02.2021**

CORRESPONDING AUTHOR

Mehmet Recai Durgut
Department of Biosystem Engineering,
Faculty of Agriculture,
Tekirdag Namik Kemal University,
Tekirdag – Turkey

e-mail: rdurgut@nku.edu.tr

© by PSP Volume 30– No. 05/2021 pages 4787-4797 Fresenius Environmental Bulletin

EFFECTS OF CADMIUM AND CHICKEN MANURE ON DRY WEIGHT AND SOME HEAVY METAL AMOUNTS FOR HEALTHY LETTUCE (*LACTUCA SATIVA* L.) CONSUMPTION

Hakan Celik[1,*], Sita Sanele Kunene[2]

[1]Department of Soil Science and Plant Nutrition, Faculty of Agriculture, Bursa Uludag University, Bursa, Turkey
[2]Department of Soil Science and Plant Nutrition, Institute of Natural and Applied Science, Bursa Uludag University, Bursa, Turkey

ABSTRACT

Although the plants might be grown without showing any toxicity symptoms in the soils having cadmium (Cd) concentrations within the permissible ranges, it may give harm to human health depending to its' metal concentrations and also to the consuming amounts. Regarding to analyse such problem, a greenhouse experiment was conducted to evaluate the effects of cadmium and chicken manure on the dry weight amounts of lettuce (*Lactuca sativa* L.) leaves and roots and on some heavy metal concentrations, under Cd containing soil conditions. Increasing doses of Cd (0, 10, and 20 mg kg^{-1} Cd) and increasing doses of chicken manure (0, 500, 1000, and 2000 kg da^{-1}) were applied to soil. Although the applied Cd concentrations were within the maximum limits mentioned in various countries, increased the Cd concentrations both in the roots (68.50 mg kg^{-1}) and in the leaves (39.52 mg kg^{-1}) and found over the limits of WHO. It was observed that not only Cd but also Pb, Cr, Zn, Fe, Mn and Cu were accumulated in lettuce roots rather than leaves without giving any chlorotic toxicity symptoms. However, decreased the dry weight amounts of lettuce both in leaves and in roots and also the amounts of other elements. The least leaf (6.43 g pot^{-1}) and root (2.54 g pot^{-1}) dry weight yield was obtained from the highest dose of cadmium (Cd2). Adding chicken manure to the soil under Cd improved the dry weight of the plants, and lessen the amounts of Cr, Pb, and the other micro nutrients but not found proficient to decrease Cd amounts. Because of health-related risks, there is a need to control and rearrangement for the limits of Cd in soils and in plants consumed by humans.

KEYWORDS:
Accumulation, cadmium, dry yield, health, heavy metals, toxicity

INTRODUCTION

Heavy metals are known as the natural components of the rocks. However, in parallel with the increase in the human population, the development of today's technology, and in addition to the industrial activities; anthropogenic activities such as excessive usage of fertilizers and pesticides, and irrigation with wastewater significantly increased the concentrations and the natural distribution pattern of the heavy metals [1, 2, 3].

Some heavy metal trace elements are known as necessary for the plants growth, development and physiological life functions such as copper (Cu), zinc (Zn), iron (Fe), manganese (Mn), molybdenum (Mo), nickel (Ni), and cobalt (Co). However, it has been reported that excessive doses of these elements and the trace amounts of many heavy metals other than this group, including arsenic (As), mercury (Hg), cadmium (Cd) and lead (Pb) may be toxic to plants [2, 4, 5, 6, 7].

High concentrations of these heavy metals in plants cause deterioration of many physiological events such as photosynthesis, water intake, germination, transpiration, stoma movements, protein synthesis, membrane stability, enzyme activity and hormonal balance [8, 9]. Due to the accumulation of heavy metals in plants and the bodies of humans and animals which fed with these plants over time, may cause serious damage to the human body and can negatively affect their lives [2, 10, 11, 12, 13].

Of the related heavy metals, Cd concentrations of uncontaminated soils were reported below 0.5 mg kg^{-1} and may reach up to 3.0 mg kg^{-1} depending to the parent material [14]. Especially as a result of intensive and continuous use of phosphorus fertilizers Cd has the potential to accumulate in soils and the maximum allowable concentration in agricultural soils in various countries were indicated between 1-20 mg kg^{-1} [12]. Depending on the accumulated concentrations of cadmium in the soil, cause also accumulation in plants and can negatively

TABLE 1
Some Properties of the soil

Properties	Amounts	Properties	Amounts
Texture	Clay	Lime, $CaCO_3$, %	4.68
Sand, %	44.76	Organic matter, %	2.21
Silt, %	14.00	Total nitrogen (N), %	0.092
Clay, %	41.24	Available phosphorus (P), mg kg^{-1}	14.51
pH (1:2.5 soil:water)	7.91	Iron (Fe) mg kg^{-1}	12.49
EC, µS cm^{-1}	530	Cupper (Cu) mg kg^{-1}	1.56
Sodium (Na)) mg kg^{-1}	175.6	Zinc (Zn) mg kg^{-1}	0.95
Potassium (K)) mg kg^{-1}	375.5	Manganese (Mn) mg kg^{-1}	31.64
Calcium (Ca)) mg kg^{-1}	10048	Cadmium (Cd) mg kg^{-1}	0.02
Magnesium (Mg) mg kg^{-1}	390.2	Lead (Pb) mg kg^{-1}	1.82
Boron (B) mg kg^{-1}	0.65	Chromium (Cr) mg kg^{-1}	0.02

affect human health through the food chain [11, 14, 15, 16]. The mean concentrations of Cd has been reported between 0.013-0.22 mg kg^{-1} in grains, 0.07-0.28 mg kg^{-1} in grasses, and 0.08-0.28 mg kg^{-1} in legumes [14]. Plants may be grown in normal appearance in the soils contaminated with Cd, however its element contents may not be safe for human consumption. It was also pointed out according to the WHO report that the daily consumption of Cd was limited as 1 µg Cd per kg^{-1} of the body weight and is equivalent to a daily intake of 70 µg kg^{-1} [17]. Lettuce, as well as being a popular vegetable because of its widespread consumption, in recent years it has also become important plant that can affect human health and nutrition due to its hyper accumulator properties [8].

The uptake of these harmful heavy metals by plants may be lessen with some materials applied to soil. Some agricultural practices such as phosphorites, zeolites, montmorillonites, humic organic matter, and some wastes have also been tried to prevent mobilization of trace metals [9, 12]. In various studies, it has been reported that some organic materials applied to the soil reduce the mobility and uptake of heavy metals in the soil [8]. Organic amendments such as animal manure, crop residues and biosolids has been used to immobilize the heavy metals [5, 9, 18]. Chicken manure with its high nutrient content which is used as an organic fertilizer source increasing the efficiency, aeration and water holding capacity of the soil may also be useful to prevent the mobility or accumulation of heavy metals in plants.

This research was carried out to determine the effects of cadmium and chicken manure applied to the soil on growth of lettuce and some heavy metals amounts and also to state the concentrations in soil and also in plants were harmful or not for human nutrition.

MATERIALS AND METHODS

A greenhouse experiment was conducted in randomized plots designed with three replicates. The soil sample used in the experiment was collected from 0–20 cm deep in a field located at the Agricultural Research and Application Centre of Bursa Uludag University (39°35′, 40°40′ and 28°10′, 30°00′) in Turkey. The soil used in the experiment had a clay texture and 7.91 pH. Additionally, it had low lime content and Electrical Conductivity (EC). The soil also had adequate concentrations of organic matter and nutrient elements and not excessive heavy metals (Table 1).

Air-dried soil was passed through a 4 mm sieve, and 3.5 kg of soil placed into each polyethylene covered plastic pots which were 20 cm in diameter and 18 cm deep. Three different rates of cadmium (0, 10 and 20 mg kg^{-1} Cd) that are mentioned in the maximum limits of various countries were applied to the soil as cadmium sulphate ($3CdSO_4.8H_2O$) (Extra pure, Merck, Germany). According to the nutrient treatments, the N, P, and K concentrations of the related pots were arranged at a constant value of 50 mg kg^{-1} N, with ammonium nitrate (NH_4NO_3) (Extra pure, Merck, Germany), 40 mg kg^{-1} P and 50 mg kg^{-1} K with monopotassium phosphate (KH_2PO_4) (Emprove, Merck, Germany) before planting.

Five lettuce (*Lactuca sativa* L.) seed cultivars 'Lettuce Batavia Maritima' were planted in each pot, and three plants were left in each pot after germination. The water content of the pots was adjusted to 70% of the field capacity during the experiment. After 45 days, the lettuce were cut over the soil level and then the leaves and roots were immediately transferred to the laboratory. In order to avoid possible contamination from dust, the samples were washed in tap water and twice with deionized water. The samples were dried in a hot air oven (Nuve KD 400, Turkey) at 70°C for 72 h, weighed and then ground using a laboratory mill

TABLE 2
Some properties of the chicken manure used in the trial

Properties	Amounts	Properties	Amounts
pH (1:2.5 w/v)	9.82	Iron (Fe) g kg^{-1}	8.84
EC. µS cm^{-1}	11.72	Cupper (Cu) mg kg^{-1}	61.41
Organic matter %	42.45	Zinc (Zn) mg kg^{-1}	376.97
Nitrogen (N) g kg^{-1}	13.89	Manganese (Mn) mg kg^{-1}	642.75
Phosphorus (P) g kg^{-1}	16.13	Boron (B) mg kg^{-1}	44.48
Sodium (Na) g kg^{-1}	4.55	Cadmium (Cd) mg kg^{-1}	0.22
Potassium (K) g kg^{-1}	23.35	Lead (Pb) mg kg^{-1}	0.21
Calcium (Ca) g kg^{-1}	60.73	Chromium (Cr) mg kg^{-1}	54.00
Magnesium (Mg) g kg^{-1}	7.49		

TABLE 3
Effects of increasing doses of cadmium and chicken manure on dry weight of leaf and root of lettuce (g pot^{-1})

Plant Parts	Cadmium Doses (mg kg^{-1})	Chicken Manure (kg da^{-1})													
		CM0			CM1			CM2			CM3			Mean	
Leaves	Cd0	10.68	a	A	9.68	a	A	10.11	a	A	10.02	a	A	10.12	a
	Cd1	7.43	b	A	7.69	b	A	7.65	b	A	6.76	b	A	7.38	b
	Cd2	4.30	c	C	5.58	c	BC	8.52	ab	A	7.33	b	AB	6.43	b
	Mean	**7.47**			**7.65**			**8.76**			**8.03**				
A $_{LSD}$		öd			B $_{LSD<0.01}$			1.294			AxB $_{LSD< 0.05}$			1.911	
Roots	Cd0	4.63			3.53			4.86			4.36			4.35	a
	Cd1	2.44			6.63			6.13			3.17			4.59	a
	Cd2	0.93			3.06			3.34			2.81			2.54	b
	Mean	**2.67**	**B**		**4.41**	**A**		**4.78**	**A**		**3.45**	**AB**			
A $_{LSD< 0.05}$		1.372			B $_{LSD<0.01}$			1.609			AxB $_{LSD}$			öd	

The differences between values by different letters are significant. Capital letters for each row and small letters for each column.

(Foss CT 193 cyclotec, Denmark) passing through 0.5 mm sieve. For the evaluation of the nutrient uptake in leaves and roots, the ground samples were digested using a mixture of 3 mL of nitric acid (HNO_3) (65 %, Emplura, Merck) and 3 mL of hydrogen peroxide (H_2O_2) (35 %, Emprove, Merck, Germany) in a microwave oven (Berghof MWS 2, Germany) [19]. Heavy metals (Cd, Pb and Cr), and the nutrients (Fe, Zn, Mn, and Cu) amounts were determined by inductively coupled plasma-optical emission spectrometry (ICP-OES) (Perkin Elmer Optima 2100DV, USA) [20]. Data from all of the experiments were subjected to statistical analysis and the mean values were compared using the least significant difference (LSD) multiple range test with the computer program MINITAB 17.1.0.0 (Minitab Inc., State College, Pennsylvania, USA).

RESULTS AND DISCUSSION

Effects of Cd on Dry Weight Amounts. Increasing doses of cadmium applied to the soil significantly decreased the leaf and root dry weight yield of lettuce ($p<0.01$). While the highest dry weight amounts of leaves (10.12 g pot^{-1}) were determined in control, the least leaf (6.43 g pot^{-1}) and root (2.54 g pot^{-1}) dry weight yield was obtained from the highest dose of cadmium (Cd2) (Table 3). Stolt et al. [21] on bread and durum wheat, Milone et al. [22] also on wheat reported that root development was prevented with high concentrations of cadmium significantly. Canal and Bozkurt [23] also stated decreases on plant height, plant weight, and number of lettuce leaf, under toxic Cd conditions. Bitiktaş [24] stated that the decrease in the development of plants was caused by the fact that the roots were damaged by heavy metals and that they could not get enough nutrients. Some previous researches shown nutrient imbalances of Mg, Ca, and Fe which affects the photosynthesis, chlorophyll content, membrane stability and enzymes as reason on inhibited growth of the plants under increased Cd [25]. Some studies have been reported the synergistic or antagonistic effects on the uptake of the nutrients [26]. Yang et al. [27] reported the decreased growth rate, dry matter yield and the accumulation of the nutrients in cabbage, ryegrass, maize and white clover.

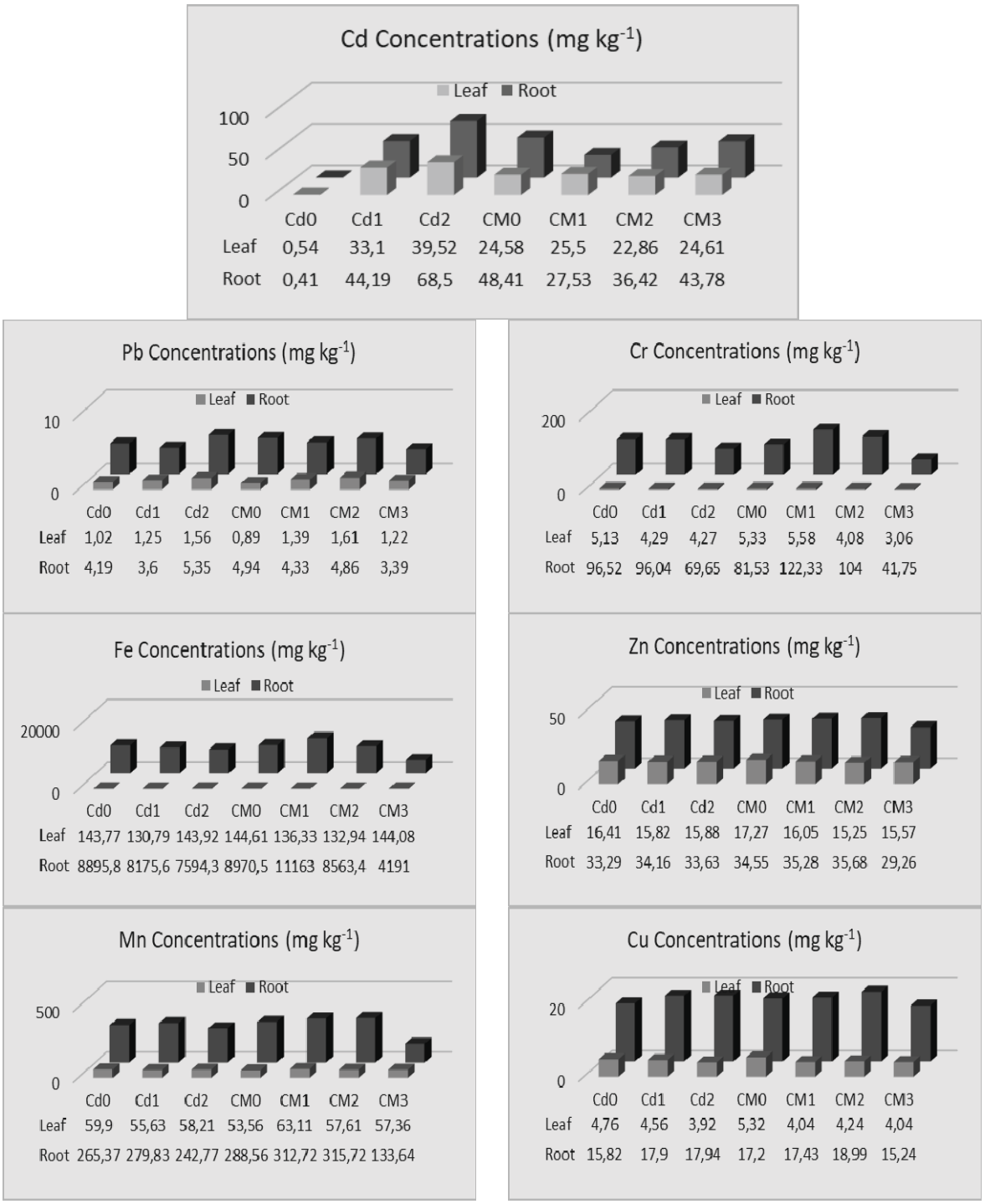

FIGURE 1
Effects of increasing doses of cadmium (Cd) and chicken manure (CM) on some heavy metal contents of leaf and root of lettuce

Effects of Cd on Cadmium Amounts. The cadmium doses applied increased the cadmium concentrations and the up taken amounts in the leaves and roots of lettuce, and the increase was found statistically significant ($p<0.01$). The average Cd concentration of plants in the applications without cadmium (Cd0) was determined as 0.54 mg kg^{-1} in leaves and 0.41 mg kg^{-1} in roots (Figure 1). The concentrations increased with cadmium applications and found as 33.1 mg kg^{-1} and 39.52 mg kg^{-1} in leaves. It was observed that cadmium accumulated in the roots, concentration in the roots were increased more than leaves and were found as 44.19 mg kg^{-1} and 68.50 mg kg^{-1} (Figure 1). The least up taken amount of cadmium in leaf (5.43 µg pot^{-1}) and in root (0.40 µg pot^{-1}), were also obtained from the control dose (Cd0) where cadmium was not applied (Table 4). Since the accumulation of cadmium in the roots adversely affects root development, the up taken amount of cadmium was detect-

ed more in the leaves rather than in the roots. The highest up taken cadmium amount in leaf (243.41 µg pot^{-1}) was obtained from the first dose of cadmium (Cd1). The amount decreased at the highest dose of Cd in relation to the decrease in dry weight and found as 241.46 µg pot^{-1} in leaves. The highest up taken cadmium amount in roots (68.50 µg pot^{-1}) was determined at the second dose (Cd2). Li et al. [28] and Bakhshayesh et al. [29] also reported elevated plant Cd concentrations parallel with increased Cd doses in their study. Lehoczky et al. [30] reported that cadmium accumulation differs according to plant varieties, and lettuce and spinach which are in the group of vegetables that leaves are edible may accumulate the cadmium element the most. In another study, it was reported that the lettuce plant had the ability to accumulate high amounts of Cd and that the toxic effects of Cd can be observed in people who regularly consume plants which contain Cd more than 3 mg kg^{-1} in their tissues [31]. Various researches indicated the sufficiency level of Cd in mature leaf tissues as 0.05-0.2 mg kg^{-1} and excessive or toxic range as 5-30 mg kg^{-1} and tolerable limit for agronomic crops as 0.05-0.5 mg kg^{-1} [12]. In our research, the lettuce plants which was grown under normal soil conditions had Cd concentrations in the safe limits. However, the plants grown on the soils on which Cd applied in the range of maximum limits have taken the Cd over this dedicated limits both in the roots and in the leaves. And also the amounts were found harmful for regular consumption according to the daily intake limits of WHO (70 µg kg^{-1}) mentioned by Smolders [17].

TABLE 4
Effects of increasing doses of cadmium and chicken manure on Cd, Cr and Pb uptake of leaf and root of lettuce

	Plant Parts	Cadmium Doses (mg kg^{-1})	Chicken Manure (kg da^{-1}) CM0			CM1			CM2			CM3			Mean	
Cd (µg pot^{-1})	Leaves	Cd0	5.31	b	A	5.50	b	A	5.06	b	A	5.84	c	A	5.43	b
		Cd1	194.69	a	B	269.51	a	A	280.19	a	A	229.26	b	AB	243.41	a
		Cd2	189.28	a	C	228.13	a	BC	264.23	a	AB	284.17	a	A	241.46	a
		Mean	**129.76**	**B**		**167.71**	**AB**		**183.16**	**A**		**173.09**	**A**			
		A $_{LSD<0.01}$	40.163			B $_{LSD<0.01}$	34.782			AxB $_{LSD<0.05}$	51.366					
	Roots	Cd0	0.50	c	A	0.33	c	A	0.33	b	A	0.42	b	A	0.40	c
		Cd1	36.17	b	B	26.50	b	B	45.33	a	AB	68.75	a	A	44.19	b
		Cd2	92.50	a	A	55.75	a	B	63.58	a	B	62.17	a	B	68.50	a
		Mean	**43.06**			**27.53**			**36.42**			**43.78**				
		A $_{LSD}$	ns			B $_{LSD<0.01}$	16.546			AxB $_{LSD<0.05}$	24.434					
Cr (µg pot^{-1})	Leaves	Cd0	82.30	a	A	38.98	a	B	44.39	a	B	41.78	a	B	51.86	a
		Cd1	34.17	b	AB	49.00	a	A	29.92	a	AB	16.66	a	B	32.44	b
		Cd2	18.24	b	A	36.72	a	A	33.78	a	A	18.86	a	A	26.90	b
		Mean	**44.90**	**A**		**41.57**	**A**		**36.03**	**AB**		**25.76**	**B**			
		A $_{LSD<0.01}$	11.360			B $_{LSD<0.01}$	13.323			AxB $_{LSD<0.01}$	26.647					
	Roots	Cd0	496.51	a	A	286.45	b	A	721.98	a	A	247.32	a	A	438.06	ab
		Cd1	164.12	a	B	1226.23	a	A	866.77	a	A	40.29	a	B	574.35	a
		Cd2	70.28	a	A	308.74	b	A	151.62	b	A	172.18	a	A	175.70	b
		Mean	**243.64**	**B**		**607.14**	**A**		**580.12**	**A**		**153.26**	**B**			
		A $_{LSD<0.05}$	322.590			B $_{LSD<0.05}$	279.371			AxB $_{LSD<0.05}$	558.742					
Pb (µg pot^{-1})	Leaves	Cd0	4.69			9.35			9.35			17.28			10.17	
		Cd1	8.59			10.70			12.70			4.98			9.24	
		Cd2	4.81			9.53			21.15			8.82			11.08	
		Mean	**6.03**			**9.86**			**14.40**			**10.36**				
		A $_{LSD}$	ns			B $_{LSD}$	ns			AxB $_{LSD}$	ns					
	Roots	Cd0	18.00			22.29			13.09			17.38			17.69	
		Cd1	13.04			10.95			19.34			10.83			13.54	
		Cd2	4.96			13.97			25.93			8.13			13.25	
		Mean	**12.00**			**15.74**			**19.45**			**12.11**				
		A $_{LSD}$	ns			B $_{LSD}$	ns			AxB $_{LSD}$	ns					

The differences between values by different letters are significant. Capital letters for each row and small letters for each column.

Effects of Cd on Some Other Heavy Metal Amounts. The effect of increasing cadmium doses applied to the soil, on the up taken amounts of Cr with leaves ($p<0.01$) and roots ($p<0.05$) of lettuce was found statistically significant (Table 4). Along with the increased cadmium doses, the up taken amount of Cr by the leaves and roots of the plant was decreased. The up taken amounts in the roots were found higher than leaves. While the highest chromium uptake in the leaves (51.86 μg pot^{-1}) was obtained from the control dose (Cd0) where cadmium was not applied, and in the roots (574.35 μg pot^{-1}) it was determined at the first dose of Cd (Cd1). The lowest Cr amount in the leaves (26.90 μg pot^{-1}) and in the roots (175.70 μg pot^{-1}) was obtained from the highest dose of cadmium (Cd2). Although the chromium concentrations were not found statistically significant, the highest Cr concentrations in the leaves (5.13 mg kg^{-1}) and in the roots (96.52 mg kg^{-1}) was found at the control dose (Cd0) and tended to decrease with increasing cadmium doses (Figure 1). This results shows, also the competition of Cr with Cd.

The effect of increasing cadmium doses applied to the soil, on the up taken amounts of Pb of leaves and roots of the lettuce was not statistically significant, however the effect, was found significant on the concentrations of the roots ($p<0.01$). Highest concentrations of Pb were found at the highest doses of Cd both in the leaves (1.56 mg kg^{-1}) and in the roots (5.35 mg kg^{-1}) because of the inhibited development as a consequence of applied Cd. The highest up taken Pb was obtained in the root (17.69 μg pot^{-1}) from the control dose (Cd0), along with the increased cadmium doses, the up taken amount of Pb by the roots decreased, and the lowest up taken Pb amount in roots (13.25 μg pot^{-1}) was obtained from the highest cadmium dose (Cd2) (Table 4). Even though the inhibited development was more severe in the roots, the up taken amount of Pb was found more in the roots rather than in the leaves because of the highest accumulated amount of Pb in the roots. Benavides et al. [32] reported that, cadmium is in competition with the elements K, Ca, Mg, Fe, Mn, Cu, Zn, and Ni. In addition to the findings, negative effect of cadmium to Pb uptake were found in our study.

The effect of increasing cadmium doses applied to the soil, on the up taken amounts of Fe on leaves and roots of the lettuce was found statistically significant ($p<0.01$) (Table 5). However the concentrations were not found significant. Along with the increased cadmium doses, the up taken amount of iron by the leaves and roots of the plant was decreased. While the highest iron uptake in the leaf (1455.64 μg pot^{-1}) was obtained from the control dose (Cd0) where cadmium was not applied, in the root (43051.5 μg pot^{-1}) it was determined from the first dose of Cd (Cd1). However, the lowest iron up take in the leaves (924.07 μg pot^{-1}) and in the roots (19756.1 μg pot^{-1}) was obtained from the highest dose of cadmium (Cd2) (Table 5). Although the accumulation of cadmium in the roots affected the root development more than leaves, over accumulation of iron in the roots caused the up taken amount of iron to be found higher in the roots compared to the leaves. If the plant has Cd in the nutrient medium, a significant decrease on Fe transport and a lack of Fe in the shoots and also a mutual relationship between Cd and Fe was reported. Just as Cd complicates the Fe uptake of the plant, Fe also affects the uptake of the Cd by the plant and its transport from the roots to the shoots [33].

The effect of increasing cadmium doses applied to the soil, on the up taken amounts of Zn of leaves and roots of the lettuce was found statistically significant ($p<0.01$). Although the effect, was not significant on the concentrations, the amount of Zn was found high in the roots rather than leaves (Figure 1). However the up taken amounts were found a little high in the leaves because of the inhibited root development. Along with the increased cadmium doses, the up taken amount of Zn by the plant's leaves and roots decreased. The highest up taken Zn was obtained in the leaf (166.14 μg pot^{-1}) from the control dose (Cd0) where cadmium was not applied, and in the root (159.25 μg pot^{-1}) it was determined at the first dose of Cd. However, the lowest up taken Zn amount, in leaves (101.29 μg pot^{-1}) and in roots (82.94 μg pot^{-1}) was obtained from the highest cadmium dose (Cd2). Wu and Zhang [26] reported a substantial reduction in Zn concentrations of roots and shoots with increasing Cd concentration in the medium. As mentioned in the previous research results a significant influence of Cd addition have been occurred on the uptake of Zn in roots and leaves of lettuce.

The effect of increasing cadmium doses applied to the soil, on the up taken amounts of Mn was found statistically significant on leaves ($p<0.01$) and roots ($p<0.05$) of the lettuce plant. Manganese concentrations in the roots were found higher than leaves but not found significant. Along with the increased cadmium doses, the up taken amount of Mn by the plant's leaves and roots decreased. The highest up taken Mn was obtained in the leaf (602.78 μg pot^{-1}) from the control dose (Cd0) where cadmium was not applied, and in the root (1459.33 μg pot^{-1}) it was determined at the first dose of Cd. The lowest up taken Mn amount, in leaves (377.97 μg pot^{-1}) and in roots (610.41 μg pot^{-1}) was obtained from the highest cadmium dose (Cd2). This results shows, also the competition of Mn with cadmium clearly.

It was observed that Cu also accumulated in the roots, and Cu concentration was found higher in the roots than leaves but not found statistically significant (Figure 1). However the effect of increasing Cd was found statistically significant on the up taken amounts of Cd ($p< 0.01$). The highest

TABLE 5
Effects of increasing doses of cadmium and chicken manure on Fe, Zn, Mn and Cu uptake of leaf and root of lettuce

	Plant Parts	Cadmium Doses (mg kg^{-1})	Chicken Manure (kg da^{-1}) CM0			CM1			CM2			CM3			Mean	
Fe (µg pot^{-1})	Leaves	Cd0	1607.94			1172.58			1427.32			1614.71			1455.64	a
		Cd1	1099.69			889.40			922.78			993.63			976.37	b
		Cd2	638.98			956.53			1162.94			937.83			924.07	b
		Mean	**1115.54**			**1006.17**			**1171.01**			**1182.06**				
		A $_{LSD}$		ns		B $_{LSD<0.01}$			447.36			AxB $_{LSD}$			ns	
	Roots	Cd0	56586.4	a	A	24269.6	a	A	59479.0	a	A	20528.8	a	A	40215.9	ab
		Cd1	18656.5	ab	BC	95350.9	b	A	52600.2	ab	B	5598.2	a	C	43051.5	a
		Cd2	6781.5	b	A	37739.6	b	A	16085.1	b	A	18418.0	a	A	19756.1	b
		Mean	**27341.5**	**BC**		**52453.4**	**A**		**42721.4**	**AB**		**14848.3**	**C**			
		A $_{LSD<0.01}$	23906.994			B $_{LSD<0.01}$			20704.064			AxB $_{LSD<0.01}$			41408.128	
Zn (µg pot^{-1})	Leaves	Cd0	197.19			162.64			147.05			157.69			166.14	a
		Cd1	129.17			110.28			123.64			107.19			117.57	b
		Cd2	72.22			93.72			126.94			112.26			101.29	b
		Mean	**132.86**			**122.21**			**132.55**			**125.71**				
		A $_{LSD}$		ns		B $_{LSD<0.01}$			30.729			AxB $_{LSD}$			ns	
	Roots	Cd0	170.39	a	AB	105.37	b	B	194.58	a	A	116.29	a	AB	146.66	a
		Cd1	79.83	b	B	240.55	a	A	225.48	a	A	91.12	a	B	159.25	a
		Cd2	32.34	b	A	114.49	b	A	92.21	b	A	92.72	a	A	82.94	b
		Mean	**94.18**	**B**		**153.47**	**AB**		**170.76**	**A**		**100.04**	**B**			
		A $_{LSD<0.01}$	68.247			B $_{LSD<0.01}$			59.104			AxB $_{LSD<0.05}$			87.283	
Mn (µg pot^{-1})	Leaves	Cd0	630.77	a	A	604.59	a	A	601.18	a	A	574.57	a	A	602.78	a
		Cd1	378.30	b	A	478.92	b	A	405.46	b	A	386.89	b	A	412.39	b
		Cd2	217.73	c	C	358.94	b	B	514.36	ab	A	420.85	b	AB	377.97	b
		Mean	**408.93**			**480.82**			**507.01**			**460.77**				
		A $_{LSD}$		ns		B $_{LSD<0.01}$			84.987			AxB $_{LSD<0.05}$			125.507	
	Roots	Cd0	1761.53	a	A	704.79	b	A	1712.78	ab	A	635.93	a	A	1203.76	ab
		Cd1	611.74	ab	B	2549.10	a	A	2436.84	a	A	239.63	a	B	1459.33	a
		Cd2	217.19	b	A	1095.60	b	A	588.95	b	A	539.92	a	A	610.41	b
		Mean	**863.49**	**AB**		**1449.83**	**A**		**1579.52**	**A**		**471.82**	**B**			
		A $_{LSD<0.01}$	939.944			B $_{LSD<0.05}$			601.060			AxB $_{LSD<0.05}$			1202.119	
Cu (µg pot^{-1})	Leaves	Cd0	62.25	a	A	46.21	a	AB	39.17	a	B	41.14	a	B	47.19	a
		Cd1	48.79	a	A	26.38	b	B	28.63	a	B	30.85	a	AB	33.66	b
		Cd2	14.62	b	B	20.75	b	B	41.94	a	A	25.27	a	AB	25.65	b
		Mean	**41.89**			**31.11**			**36.58**			**32.42**				
		A $_{LSD}$		ns		B $_{LSD<0.01}$			12.76			AxB $_{LSD<0.05}$			18.779	
	Roots	Cd0	80.88	a	A	51.39	b	A	89.21	ab	A	56.32	a	A	69.45	ab
		Cd1	35.96	ab	B	124.97	a	A	127.52	a	A	48.52	a	B	84.24	a
		Cd2	17.23	b	A	56.70	b	A	49.55	b	A	49.98	a	A	43.36	b
		Mean	**44.69**	**B**		**77.69**	**AB**		**88.76**	**A**		**51.61**	**B**			
		A $_{LSD<0.01}$	36.226			B $_{LSD<0.01}$			31.372			AxB $_{LSD<0.05}$			46.330	

The differences between values by different letters are significant. Capital letters for each row and small letters for each column.

up taken amount of Cu in leaf (47.19 µg pot^{-1}) were obtained from the control dose (Cd0) where cadmium was not applied and in root (84.24 µg pot^{-1}) it was determined at the first dose of Cd (Table 5). The lowest up taken Cu amount was obtained from the second dose of cadmium (Cd2), both in leaf (25.65 µg pot^{-1}) and in root (43.36 µg pot^{-1}). Wu and Zhang [26] determined a reduction on Cu concentration in barley with the addition of Cd to the growing media. Competition of cadmium with the elements K, Ca, Mg, Fe, Mn, Cu, Zn, and Ni were also reported in past researches [27, 32]. Contami-

nation degree of the soil, the plant species, plant parts, and rhizosphere are important factors on nutrient uptake. However, not only Cd but also the nutrient elements concentrations, their interactions with each other for precipitation, absorption ability from the roots and bindings with organic compounds within the medium are quite important. These were also found compatible with the previous results.

Effects of Chicken Manure on Dry Weight Amounts. Increasing doses of chicken manure applied to the soil have statistically significant effect ($p<0.05$) on the dry weight yield of lettuce roots. Although its effect on leaf dry weights was not found significant, chicken manure first elevated the dry weight and then tend to decrease. The highest leaf (8.76 g pot^{-1}) and root (4.78 g pot^{-1}) dry weight yield was obtained from the second application dose of chicken manure (CM2) and decreased at the last dose (Table 3). The least leaf (7.47 g pot^{-1}) and root (2.67 g pot^{-1}) dry weight amounts were determined at the control pots. According to the interactions of cadmium and the chicken manure; the highest leaf dry weight yield (10.68 g pot^{-1}) was obtained from lettuce in pots (Cd0xCM0), where no cadmium and chicken manure applied dose. In contrast, the least leaf dry weight yield (4.30 g pot^{-1}) was obtained from lettuce plants in pots (Cd2xCM0), where no chicken manure applied and the highest level of cadmium. It has been reported that humic compounds may be an important alternative in terms of increasing nutrient availability and regulating the toxicity problems in some areas [34]. With its high nutrient content chicken manure is used as an organic fertilizer source increasing the efficiency, aeration and water holding capacity of the soil may also be useful to prevent the mobility or accumulation of heavy metals in plants. Chicken manure was indicated as a good soil amendment and fertilizer, and perform increases nutrient element concentrations in soils and in leaves [18, 35]. It has been also stated that humic substances in chicken manure exhibit behaviours similar to growth hormones in plants, increase the intake of plant nutrients, promote plant growth and have a positive effect on increasing the amount of dry matter [36, 37]. The findings obtained from our experiment were found to be compatible with previous studies. Many researchers have found that humic acids are effective on plant growth and development, and when applied in small quantities, it positively affects development; however, they stated that when applied in large quantities, they had ineffective or negative effects on development [38].

Effects of Chicken Manure on Cd Amounts. The effect of increasing doses of chicken manure applied to the soil on the up taken amount of cadmium of the leaves was found statistically significant ($p<0.05$), but not in the roots. In parallel with the increasing chicken manure applications, concentrations and the up taken amount of cadmium by the plant has increased (Figure 1 and Table 4). The highest cadmium up take in the leaf (183.16 µg pot^{-1}) was obtained from the second application dose of chicken manure (CM2) and in the root (43.78 µg pot^{-1}) it was determined at the highest dose (CM3)(Table 4). According to the interactions of cadmium and the chicken manure; the highest leaf Cd uptake (284.17 µg pot^{-1}) was obtained from lettuce in pots (Cd2xCM3) where the highest doses of Cd and chicken manure. In contrast, the least leaf Cd uptake (5.06 µg pot^{-1}) was obtained from lettuce plants in pots (Cd0xCM2), where no Cd applied and the second level of chicken manure. While the highest root Cd uptake (92.50 µg pot^{-1}) was occurred in (Cd2xCM0), the least amounts (0.33-0.42 µg pot^{-1}) were determined at no Cd added but chicken manure applied pots (Cd0xCM1-3). Pierzynski et al. [39] has been reported that the ability of soils to absorb these trace elements depends on their ability to form pH-dependent surface loads of organic matter, clay minerals and hydrated metal oxides. In various studies, it has been reported that some organic materials applied to the soil reduce the mobility and uptake of heavy metals in the soil if Cd bound to chelate complex to prevent its entrance in to roots [14]. Organic amendments including humic substances, increase the surface charge and can form complexes with metal cations, and organic bond fractions and therefore increase intake or, conversely, compete with roots and reduce the uptake [9, 40].

Effects of Chicken Manure on Some Heavy Metal Amounts. The effect of increasing doses of chicken manure applied to the soil, on the Cr uptake of the leaves ($p<0.01$) and the roots ($p<0.05$) of the lettuce was found statistically significant. Although the highest Cr uptake in leaves was found (44.90 µg pot^{-1}) at control pots (CM0) and 607.14 µg pot^{-1} in the roots tended to decrease with the increasing chicken manure and found least at the highest dose (CM3) both in leaves (25.76 µg pot^{-1}) and in the roots (153.26 µg pot^{-1}) (Table 4).

The effect of increasing doses of chicken manure applied to the soil, on the up taken amount of Pb of the leaves and the roots of the lettuce was not found statistically significant. However the up taken amount of Fe, Zn, Mn, and Cu were found significant in roots ($p<0.01$). The highest up taken amounts and also the concentration was found at the roots and decreased with the highest chicken manure applications (Table 4 and Figure 1).

In parallel with the increasing chicken manure applications, the amount of up taken Fe, Zn, Mn, and Cu by the plant has increased, but tend to decrease with the highest dose of chicken manure. The highest up taken amounts of Fe were obtained

from the first application dose of chicken manure (CM1) in the roots as (52453.4 µg pot^{-1}), and Zn, Mn, an Cu was found at the second dose of chicken manure as (170.76 µg pot^{-1}), (1579.52 µg pot^{-1}), and (88.76 µg pot^{-1}) respectively (Table 5). It has been reported that the stimulating effect of humic substances on plant growth is associated with increasing the intake of macro nutrients. Formation of organo-metal compounds in the soil may increase heavy metal availability in plants. Arroyo et al. [41] pointed increased concentrations of Cu in plants grown on the poultry manure amended soils. On the other hand, interaction between metal and solid phase of humic substances may cause degradation on heavy metal availability. In addition to macro and micro plant nutrients, poultry manure can also contain many heavy metals depending on the production and management process. It has been stated that the amount of As, Cd, Cu and Mn of the soils increased compared to the control with chicken manure applications [42].

CONCLUSION

Increasing doses of Cd decreased the dry weight amounts of lettuce both in leaves and in roots and also decreased the amounts of other heavy metals. Not only Cd but also Pb, Cr, Zn, Fe, Mn and Cu were accumulated in roots rather than leaves. However, no visual chlorotic or necrotic deformation and toxicity symptoms was appeared. Adding chicken manure to the soil under toxic conditions of Cd improved the dry weight of the plants, and lessen the amounts of heavy metals but not proficient to decrease them to permissible limits. Cd were accumulated in the roots rather than leaves, however high amounts of Cd in the soil gave rise to the amounts be found also high in the leaves. The tolerance of the plants to elevated concentrations of trace metals in soils may result a health risk to humans and also to animals. Although the applied Cd concentrations were within the maximum limits mentioned various countries, increased the amounts in the leaves and found over the limits of WHO, so consumption of lettuce plant which were grown on such conditions without showing any symptoms may be dangerous for human health. Because of health-related risks, limits of these elements in soils and in plants consumed by humans have to be carefully controlled and the thresholds must be re arranged.

ACKNOWLEDGEMENTS

The manuscript was prepared from the thesis data of MSc.

REFERENCES

[1] Intawongse, M., Dean, J.R.. (2006). Uptake of heavy metals by vegetable plants grown on contaminated soil and their bioavailability in the human gastrointestinal tract. Food Additives and Contaminants. 23(1), 36-48.

[2] Ali, A.S.M., Ahmed, H.A.M., Emara, H.A.E.A., Janjua, M.N., Alhafez, N. (2019). Estimation and Bio-Availability of Toxic Metals between Soils and Plants. Polish Journal of Environmental Studies. 28(1), 15-24.

[3] Dorak, S., Çelik, H. (2020). Seasonal Variation of Some Trace Element and Heavy Metal Concentrations in a Turkish Stream. Polish Journal of Environmental Studies. 29(1), 589-600.

[4] Hashem, H.A., Hassanein, R.A., El-Deep, M.H., Shouman, A.I. (2013). Irrigation with Industrial Waste Water Activates Antioxidant System and Osmoprotectant Accumulation in Lettuce, Turnip And Tomato Plants. Ecotoxicology and Environmental Safety. 95, 144–152.

[5] Adesoye, A.M., Adekola, F.A., Olukomaiya, K.O., Olukomaiya, O.O., Iwuchukwu, P.O. (2014). Evaluation of physical properties and heavy metal composition of manure of some domestic animals. International Journal of Innovation and Scientific Research. 9(2), 293-296.

[6] Zhang, X., Gao B., Xia, H. (2014). Effect of Cadmium on Growth, Photosynthesis, Mineral Nutrition and Metal Accumulation of Bana Grass and Vetiver Grass. Ecotoxicology and Environmental Safety. 106, 102–108.

[7] Mathur, S., Kalaji, H.M., Jajoo, A. (2016). Investigation of deleterious effects of chromium phytotoxicity and photosynthesis in wheat plant. Photosynthetica. 54, 1-9.

[8] Canal, S.B, Bozkurt, M.A., Kipcak, S. (2018). The effects of organic amendments on cadmium uptake of spinach (Spinacia oleracea L.) and plant growth under cadmium toxicity. Fresen. Environ. Bull. 27(5), 3174-3179.

[9] Hina, K., Kanwal, S.S., Arshad, M., Gul, I. (2019). Effect of cadmium (Cd) stress on spinach (Spinacea oleracea) and its retention kinetics in soil in response to organic amendments. Pakistan Journal of Agricultural Sciences. 56(1).

[10] Khan, S., Cao, Q., Zheng, Y.M., Huang, Y.Z., Zhu, Y.G. (2007). Health Risks of Heavy Metals in Contaminated Soils and Food Crops Irrigated with Wastewater in Beijing, China. Environmental Pollution. 152, 686-692.

[11] Monteiro MS, Santos, C., Soares, A., Mann, R. (2009). Assessment of biomarkers of cadmium stres in lettuce. Exotoxicology and Environmental Safety. 72, 811-818.
[12] Kabata-Pendias, A. (2010). Trace Elements in Soils and Plants. Boca Raton: CRC Press. 548 pp.
[13] Morgan, R. (2012). Soil, Heavy Metals, and Human Health, In: Soils And Human Health, Edited By: Brevik E. C. And Burgess L. C., Boca Raton F.L., USA, CRC Press. 74-97.
[14] Nazar, R., Iqbal, N., Masood, A., Khan, M.I.R., Syeed, S., Khan, N.A. (2012). Cadmium toxicity in plants and role of mineral nutrients in its alleviation. American Journal of Plant Sciences 3(10), 1476-1489.
[15] Gul, I., Manzoor, M. Silvestre, J., Rizwan, M., Hina, K., Kallerhoff, J., Arshad, M. (2018). EDTA−Assisted phytoextraction of lead and cadmium by pelargonium cultivars grown on spiked soil.Int. J. Phytorem. 21(2), 101-110.
[16] Manzoor, M., Gul, I., Silvestre, J., Kallerhoff J., Arshad, M. (2018). Screening of indigenous ornamental species from different plant families for Pb accumulation potential exposed to metal gradient in spiked soils. Soil Sediment. Contam. 27, 439–453.
[17] Smolders, E. (2001). Cadmium uptake by plants. International Journal of Occupational Medicine and Environmental Health. 14(2), 177-183.
[18] Dikinya, O., Mufwanzala, N. (2010). Chicken manure-enhanced soil fertility and productivity: effects of application rates. J. Soil Sci. Environ. Manage. 1, 46-54.
[19] Çelik, H., Turan, M.A., Aşık, B.B., Katkat, A.V. (2017). Evaluation of analytical methods for boron determination in maize shoots. Communications in Soil Science and Plant Analysis, 48(21):2573-2581.
[20] Hansen, T.H., de Bang, T.C., Laursen, K.H., Pedas, P., Husted, S., Schjorring, J.K. (2013). Multi element plant tissue analysis using ICP spectrometry, In: Plant Mineral Nutrients. Methods in Molecular Biology (Methods and Protocols). Maathuis, F.J. (ed). Humana Press, Totowa, NJ. 953, 121-141.
[21] Stolt, J.P., Sneller, F.E.C., Bryngelsson, T., Lundborg, T., Schat, H. (2003). Phytochelatin and Cadmium Accumulation in Wheat. Environmental and Experimental Botany. 49, 21-28.
[22] Milone, M.T., Sgherri, C., Clijsters, H., Navari-Izzo, F. (2003). Antioxidative Responses of Wheat Treated with Realistic Concentration of Cadmium. Environmental and Experimental Botany, 50, 265–276.
[23] Canal, S.B., Bozkurt, M.A. (2018). The Influence of Iron Fertilizer and Sewage Sludge on Plant Growth and Anti-oxidative Enzyme Activity Against Cadmium Toxicity in Lettuce (Lactuca sativa L. var. longifolia). Yuzuncu Yıl University Journal of Agricultural Sciences. 28(1), 19-26. (in Turkish).
[24] Bitiktaş A. (2007). The Effect of Zinc and Cadmium Toxicity on Lettuce Plant Growth and Activity of Some Enzymes. Yuzuncu Yıl University, Institute of Natural and Applied Sciences, Van, Turkey. (in Turkish).
[25] Azevedo, H., Glória Pinto, C.G., Santos, C. (2005). Cadmium effects in sunflower: membrane permeability and changes in catalase and peroxidase activity in leaves and calluses. Journal of Plant Nutrition. 28(12), pp.2233-2241.
[26] Wu, F., Zhang, G., (2002). Alleviation of cadmium-toxicity by application of zinc and ascorbic acid in barley. Journal of Plant Nutrition. 25(12), 2745-2761.
[27] Yang, M.G.; Lin, X.Y., Yang, X.E. (1998). Impact of Cd on Growth and Nutrient Accumulation of Different Plant Species. Chinese J. Appl. Ecol. 9, 89–94.
[28] Li S., Wang, F., Ru, M., Ni, W. (2014). Cadmium Tolerance and Accumulation of Elsholtzia Argyi Oriıgining from a Zinc/Lead Mining Site – a Hydroponics Experiment. International Journal of Phytoremediation. 16, 1257–1267.
[29] Bakhshayesh, B.E., Delkash, M., Scholz, M. (2014). Response of Vegetables to Cadmium Enriched Soil. Water. 1246-1256.
[30] Lehoczky, E., Szabo, L., Horvath, Sz. (1998). Cadmium uptake by lettuce in different soils. Commun. Soil Sci. Plant Anal., 29(11-4): 1903-1912.
[31] Pais, I., Jones, J.B. Jr. (2000). The Handbook of Trace Elements. Published by St. Lucie Pres, Boca Raton, Florida. 240 p.
[32] Benavides, M.P., Gallego, M.S., Tomaro, L.M. (2005). Cadmium Toxicity in Plants. Braz. J. Plant Physiol. 17 (1), 21-34.
[33] Siedlecka, A., Krupa, Z. (1999). Cd/Fe interaction in higher plants. Its consequence for the photosynthetic apparatus. Photosynthetica. 36(3), 321-331.
[34] Karaman, M.R., Turan, M., Tutar, A., Dizman, M. (2012). Relationship Between Humic Substances and Micronutrients Availability in Plant Production. Sakarya University Faculty of Arts and Science, The journal of Arts and Science. 14(1), 165-175. (in Turkish).

[35] Agbede, T.M., Ojeniyi, S.O., Adeyemo, A.J. (2008). Effect of poultry manure on soil physical and chemical properties, growth and grain yield of sorghum in southwest, Nigeria. American-Eurasian Journal of Sustainable Agriculture. 2(1), 72-77.
[36] Çelik, H., Katkat, A.V., Asik, B.B., Turan, M.A., (2010). Effects of humus on growth and nutrient uptake of maize under saline and calcareous soil conditions. Žemdirbystė (Agriculture). 97(4), 15-22.
[37] Aşık, B. B., Çelik H., Turan M. A., Katkat, A. V. (2012). Effects of Foliar Applications of Humic Acid on Plant Growth and Mineral Nutrients Uptake of Plant under Saline and Calcareous Conditions. Sakarya University Faculty of Arts and Science, The journal of Arts and Science.14(1), 541-548. (in Turkish).
[38] Padem, H., Öcal, A. (1999). Effect of humic acid applications on yield and some characteristics of processing tomato. Acta Horticulturae. 487, 159-164.
[39] Pierzynski, G.M., Vance, G.F., Sims, J.T. (2005). Soils and environmental quality. CRC press. 584 p.
[40] Khan, M.A., Khan, S., Khan, A., Alam, M. (2017). Soil contamination with cadmium, consequences and remediation using organic amendments. Sci Total Environ. 601–602:1591–1605.
[41] Arroyo, M.D.M.D., Hornedo, R.M.D.I., Peralta, F.A., Almestre, C.R., Sánchez, J.V.M. (2014). Heavy metals concentration in soil, plant, earthworm and leachate from poultry manure applied to agricultural land. Revista Internacional de Contaminación Ambiental. 30(1), 43-50.
[42] Gupta, G., Charles, S. (1999). Trace elements in soils fertilized with poultry litter. Poultry Science. 78(12), 1695-1698.

Received: **27.04.2020**
Accepted: **07.02.2021**

CORRESPONDING AUTHOR

Hakan Celik
Department of Soil Science and Plant Nutrition,
Faculty of Agriculture,
Bursa Uludag University,
Bursa – Turkey

e-mail: hcelik@uludag.edu.tr

© by PSP Volume 30– No. 05/2021 pages 4798-4803 Fresenius Environmental Bulletin

EVALUATION AND ANALYSIS OF COORDINATED DEVELOPMENT OF ECOLOGICAL ENVIRONMENT AND ECONOMY

Wanchun Zhu[1,*], Song Liu[2]

[1]Higher Vocational and Techical shool, Guizhou Minzu University, Guiyang 550025, Guizhou, China
[2]Business School of Guizhou Minzu University, Guiyang, 550025, Guizhou, China

ABSTRACT

Coordinated development of ecological environment and economy has become a hot spot of sustainable development research. This study analyzed the coordination between ecological environment and economic development in Guangdong Province so that guidance and suggestions can be provided. Based on the comprehensive evaluation index of ecological environment and economy in Guangdong Province in recent years, coordination degree model of ecological environment and economic development was established, and trend and coordination degree relationships of ecological environment and economy were analyzed. Coordination degree of economy and ecological environment in Guangdong Province has been getting higher and higher, showing that environmental protection is attached more importance with rapid economic development. Ecological environment and economy are mutually dependent and mutually stimulating. The higher the coordination degree between them, the better the sustainable development can be achieved.

KEYWORDS:
Ecological environment, Economic development, Sustainable, Coordinated development

INTRODUCTION

Since reform and opening, China has devoted to developing all kinds of industries, so that the national economy has soared rapidly and the life of the Chinese people has transferred from poverty to food and clothing, and then to the overall well-off [1]. However, when economy developed quickly, the neglect of ecological environment protection restricted economy to further develop. Ecological environment and economic development are mutually dependent and mutually stimulating [2]. A good ecological environment can greatly promote economic development, and the constant development of economy will also guide people to put more emphasis on the ecological environment protection [3]. It is an urgent problem that how to deal with the relationships between ecological environment and economic development. And realizing the coordinated development of ecological environment and economy is the key to implement the strategic core of sustainable development. Therefore, on the basis of the idea of sustainable development, this study took Guangdong Province as an example and analyzed the coordination degree of ecological environment and economic development in recent 15 years to reveal the dynamic evolution track of ecological environment and economic development in Guangdong Province, which is not only essential for the ecological environment protection and economic development of Guangdong Province in the future , but also it provided reference for other regions in terms of ecological protection and economic development.

MATERIALS AND METHODS

Overview of Research Area. Located in the southernmost part of mainland China with an area of 179800 square kilometers, Guangdong Province accounts for about 1.87% of the national land area. It neighbors Fujian in the East, Guangxi in the west, Jiangxi and Hunan in the north, South China Sea in the south, and Hong Kong and Macau Special Administrative Regions on both sides of the Pearl River estuary. By the end of 2018, the permanent population of Guangdong Province was 113.46 million, which grew by 1.77 million compared with the end of 2017. Guangdong Province is one of the regions which embraces the richest water, heat and light resources in China. It is equipped with abundant animal and plants resources. Guangdong situates in the East Asian monsoon region, therefore, south subtropical and tropical monsoon climate types locates in most areas and mid-subtropical monsoon climate locates in a few areas. Guangdong Province is rich in water resources, in which an annual precipitation can be up to 319.4 billion cubic meters with abundant rainfall and numerous rivers. The main water systems are the east river, west river, north river and delta water systems of the Pearl River and the Hanjiang River system.

TABLE 1
Indicator system for coordinated development of ecological environment and economy

Serial number	System layer	Indicator layer	unit	index
1	ecosystem	Forest cover rate	%	positive
2		Urban green area	%	positive
3		Total afforestation area	Thousand hectares	positive
4		Nature reserve area	Thousand hectares	positive
5		Per capita arable land area	Square meter	positive
6		Sewage treatment rate	%	positive
7		Industrial wastewater discharge	10,000 tons	negative
8		Acid rain frequency	%	negative
9	economic development	GDP	100 million yuan	positive
10		GDP per capita	yuan	positive
11		GDP growth rate	%	positive
12		Total imports and exports	100 million yuan	positive
13		Per capita disposable income of urban residents	yuan	positive
14		Per capita disposable income of rural residents	yuan	positive
15		Proportion of primary industry to GDP	%	positive
16		Proportion of tertiary industry to GDP	%	positive

Guangdong Province was the pioneer of carrying out the reform and opening up in China, promoting prosperity of economy. Since 1989, annual GDP in Guangdong Province has ranked first in the country and its total economic aggregate volume has reached 1 / 8 of the national total, becoming the largest economic province and one of the regions with the most developed domestic economy, the most dynamic market and the most attractive investment. In 2018, Guangdong's GDP reached 9727.777 billion yuan, an increase of 6.8% compared with 2017. The per capita GDP reached 86412 yuan, converted into US $13058 at the annual average exchange rate. Among the three major industries, firstly, the added value of the primary industry reached 383.144 billion yuan, an increase of 4.2% year on year; secondly, the added value of the secondary industry reached 4069.515 billion yuan, an increase of 5.9% year on year; and thirdly, the added value of the tertiary industry reached 5275.118 billion yuan, an increase of 7.8% year on year. In the tertiary industry, the accommodation and catering industry grew by 2.7%, the financial industry grew by 6.3%, the wholesale and retail industry grew by 4.5%, the private economy grew by 7.3%, the real estate industry grew by 3.3%, the productive service industry grew by 7.9%, and the modern service industry grew by 8.6%. However, the remarkable achievements of Guangdong Province were with diverse environmental problems. In terms of water resources, random discharge of sewage and ignorance of sewage treatment resulted in a certain contamination in water quality. In terms of atmospheric environment, the emissions of exhaust gas and smoke and dust have been apt to be increased in recent years; In contrast, the degree of air pollution in the Pearl River Delta was more serious than that in the eastern, western and northern Guangdong which were relatively backward in economic development. The atmospheric environment was directly affected by the economic development, especially the industrial development; In terms of land resources, the heavy use of pesticides and fertilizers in rural areas and the discharge of heavy metals in urban industries aggravated the burden of land resources, indicating that the treatment of land environmental pollution has been of great urgency. In addition, the irrational development and utilization of cultivated land and natural disasters resulted in serious soil erosion, causing the decline of the per capita cultivated land area year by year.

Establishment of Evaluation Index System. Index Selection. The establishment of evaluation index system is the foundation and key of the evaluation of the coordinated development of ecological environment and economy [4]. Aiming at ensuring the index to become scientific, systematic, concise, reasonable and operable, the coastal advantages and development history of Guangdong Province was integrated. The pattern of coordinated development of ecological environment and economic development was chosen as basis and eight indexes were selected respectively from ecological environment and economic development to conduct research on the coordinated development of ecological environment and economy in Guangdong Province [5, 6]. Details are shown in Table 1.

Research Method and Model. Data Standardization. Because of different index units and variation degree, in order to narrow the magnitude differences among different indexes to make the selected indexes comparable and maximize the elimination of the impact of dimensions on the analysis results, the range transformation method was used to

standardize the data, which can be specifically divided into positive indexes and negative indexes [7, 8].

$A_i^{'} = \frac{A_i - A_{min}}{A_{max} - A_{min}}$ Positive index (1)

$A_i^{'} = \frac{A_{max} - A_i}{A_{max} - A_{min}}$ Negative index (2)

$A_i^{'}$ in formula (1) (2) is standardized index value, A_i is original standard index value. A_{min} and A_{max} are the minimum standard index value and the maximum standard index value which came from the same series before treatment.

Determination of Weight. This study adopted entropy method of objective weighting method according to the variation of each index to determine objective weight. This method laid a foundation of the amount of information provided by each index. Compared with the subjective weight method, it can reduce the interference caused by human in index evaluation [9].

Construction of Coordination Degree Model. Coordination degree is an important index to describe the interaction degree of system or elements [10]. In order to better define the degree of coordinated development of ecological environment and economic development in Guangdong Province, the research adopted the coordination degree model and coordinated degree of development, which is of great significance to judge the strength of the system or the interaction between elements and the corresponding time interval of the interaction. The calculation formula is as follows:

$f(x) = \sum_{i=1}^{9} a_i \times X_i^{'}$ (3)

$\mathrm{g}(y) = \sum_{j=1}^{7} b_j \times Y_j^{'}$ (4)

a_i and $b_j$are the index weights of the i-th ecological environment and the j-th economic development respectively, and $X_i^{'}$and$Y_j^{'}$are the values of ecological environment and economic development index respectively after data standardization.

Calculating the comprehensive evaluation function of ecological environment and economic development can obtain the deviation coefficient C of ecological environment and economic development. The size of the deviation coefficient can reflect the degree of relationship between them [10, 11]. The calculation formula is as follows:

$\mathrm{C} = \sqrt{f(x) \times \mathrm{g}(y) \div [(f(x) + \mathrm{g}(y) \div 2)]^2}$ (5)

The coordination degree can reflect the comprehensive evaluation value between ecological environment and economic development, expressed by T, but coordination development degree is indispensable to reflect the coordination level of ecological environment and economic development more truly and more comprehensively, expressed by D. The coordination degree between ecological environment and economic development can be really reflected by the degree of coordinated development. The smaller the degree is, the more harmonious the ecological environment and economic development are, and vice versa [11-13]. The calculation formula is as follows:

$\mathrm{T} = \alpha f(x) + \beta \mathrm{g}(y)$ (6)

$\mathrm{D} = \sqrt{\mathrm{C} \times \mathrm{T}}$ (7)

In formula (6) (7), T represents the development degree between ecological environment and economic development; $f(x)$and $\mathrm{g}(y)$are the comprehensive evaluation functions of ecological environment and economic development respectively; α, β are undetermined coefficients. This study regarded both ecological environment and economic development as equally important and chose them as the starting point, so α and β are valued as 0.5; D represents the coordination degree of ecological environment and economic development [14, 15].

RESULTS AND DISCUSSION

Result Measurement of Ecological Environment and Economic Development. This study collected the relevant index data of Guangdong Province from 2005 to 2019. First of all, Data was standardized and then the weight value of each evaluation index was determined by entropy method. The comprehensive evaluation index of ecological environment and economic development were gained after analysis. Result can be seen in Table 2.

In accordance with the calculation results of the above formula, the dispersion coefficient C, the coordination degree T and the coordination development degree D of Guangdong Province from 2005 to 2019 were respectively obtained through the coordination degree, the coordination development degree model and the discrimination standard. The coordination degree and the coordination development degree level were divided according to Table 3, which can better reflect the coordination condition and coordination type of the ecological environment and economic development of Guangdong Province [16, 17]. The results are shown in Table 4.

TABLE 2
Comprehensive evaluation index of ecological environment and economy

years	2005	2006	2007	2008	2009	2010	2011	2012	2013	2014	2015	2016	2017	2018	2019
Ecological development status	0.230	0.220	0.256	0.376	0.378	0.412	0.535	0.590	0.688	0.762	0.834	0.897	0.924	0.983	1.034
The level of economic development	0.176	0.189	0.247	0.378	0.276	0.401	0.567	0.631	0.691	0.831	0.972	1.034	1.139	1.250	1.414

TABLE 3
Division of coordinated development

Coordinated Development Division	Coordinated Development Type
0.00~0.10	Severe disorders
0.11~0.3	Moderate disorder
0.31~0.4	Mild disorders
0.41~0.5	Barely Coordinating
0.51~0.6	Primary coordinated development
0.61~0.7	Intermediate Coordinated Development
0.71~0.9	Well coordinated development
>0.9	High-quality coordinated development

TABLE 4
Evaluation results of coordinated development of ecological environment and economy in Guangdong Province

years	Coefficient of dispersion	Coordination	Coordinated development	Coordination type
2005	0.083	0.442	0.204	Moderate disorder
2006	0.091	0.478	0.259	Moderate disorder
2007	0.103	0.499	0.313	Mild disorders
2008	0.114	0.534	0.367	Mild disorders
2009	0.12	0.561	0.4	Mild disorders
2010	0.141	0.582	0.457	Barely Coordinating
2011	0.169	0.611	0.511	Primary coordinated development
2012	0.193	0.632	0.576	Primary coordinated development
2013	0.234	0.663	0.634	Intermediate Coordinated Development
2014	0.279	0.701	0.699	Intermediate Coordinated Development
2015	0.324	0.73	0.785	Well coordinated development
2016	0.398	0.778	0.846	Well coordinated development
2017	0.478	0.815	0.893	Well coordinated development
2018	0.59	0.849	0.967	High-quality coordinated development
2019	0.671	0.919	1.026	High-quality coordinated development

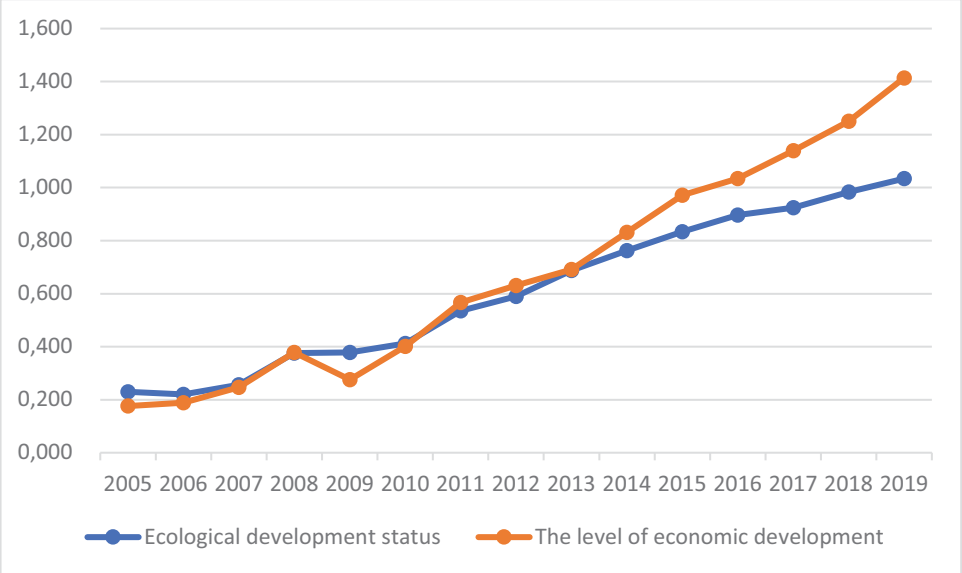

FIGURE 1
Comprehensive Evaluation Index of Ecological Environment and Economy

Analysis of Coordinated Development of Ecological Environment and Economy. On the basis of the comparative analysis of the coordination between the ecological environment and economic development in Table 3 and Table 4, the coordination between the ecological environment and economic development in Guangdong Province tended to escalate from 2005 to 2019. From 2005 to 2006,

the coordination was of serious imbalance, uncovering that Guangdong Province has paid a heavy price of ecological environment destruction while economic development. In 2007-2009, the condition has been improved, transferring into moderate maladjustment, and in 2010, it changed into mild maladjustment. Since 2012, the coordination between the ecological environment and economic development has changed from imbalance to coordination, and from 2011 to 2012, it reached the level of barely coordination. From 2013 to 2019, the level of primary coordination has gone to the level of high-quality coordinated development, indicating that since 2013, Guangdong Province has paid more attention to the protection and governance of the ecological environment while developing its economy, and the coordination between the ecological environment and economic development has been constantly enhanced.

According to Table 4, the evolution track of coordinated development between ecological environment and economy in Guangdong Province from 2005 to 2019 is drawn.

In Figure 1, the broken line of square node represents ecological development status, and the broken line of circular node represents the level of economy development. From the figure, it is obvious that from 2005 to 2019, ecological development status has always been on the rise, while the level of economy development has always been on the rise except for 2008. Before 2013, except 2008, the growth rate of ecological development and economy development was generally remained balanced, showing that the ecological environment was also constantly improving while the economic development of Guangdong Province was constantly developing. After 2013, the growth rate of the level of economy development is higher than that of ecological environment. In the past seven years, ecological development status has increased from 0.688 to 1.034, and the level of economy development has increased from 0.691 to 1.414, which shows that the economy of Guangdong Province was developing at a faster speed while protecting ecological environment.

Above all, in recent 15 years, ecological development status in Guangdong Province has been on the rise, but the level of economy development dropped significantly in 2008, because of the global financial storm happened in 2008. The economic development of various industries in Guangdong Province was restricted on a different level. In 2009, in order to deal with the global financial crisis, all countries have conducted policies so that the global economic situation has been alleviated, the level of economy development in Guangdong Province has gradually increased, and the coordination degree of both of them has been constantly improved.

Measure and Suggestion for Coordinated Development of Ecological Environment and Economy. Not only is Guangdong Province the largest economic province in China, but also it is one of the regions equipped with the most developed economy, the most dynamic market and the most attractive investment [18]. Economy development is accompanied with increasing pressure on the ecological environment [19]. Provided that Guangdong Province intends to ensure that the ecological environment and economic development can maintain in a high degree of coordination for a long time, strategies of sustainable development must be carried out to the harmonize delicate relationships between them. Therefore, the suggestions are as follows:

(1) Construction of legal system should be strengthened, laws and regulations on the coordinated development of ecological environment and economy should be improved, and the legal system based on the coordinated development of ecological environment and economy should be strictly implement.

(2) Waste recycling are supposed to be strongly supported, the use of renewable resources should be encouraged, and illegal heavy polluting enterprises should be urged to strictly punish by law enforcement departments.

(3) Usage proportion of coal in the overall energy should be diminished, the change of energy structure and the use of relatively clean energy, renewable energy are supposed to be encouraged.

(4) Investment in environmental protection ought to be strengthened, urban green coverage should be increased, and the pace of urban landscape construction should be sped up.

CONCLUSIONS

Based on the comprehensive evaluation index of ecological environment and economy in Guangdong Province in recent years, coordination degree model of ecological environment and economic development was established, and trend and coordination degree relationships of ecological environment and economy were analyzed. Coordination degree of economy and ecological environment in Guangdong Province has been getting higher and higher, showing that environmental protection is attached more importance with rapid economic development. Ecological environment and economy are mutually dependent and mutually stimulating. The higher the coordination degree between them, the better the sustainable development can be achieved.

REFERENCES

[1] Sun, Q., Zhang, X.H., Zhang, H.W., Niu, H.P. (2018) Coordinated development of a coupled social economy and resource environment system: A case study in Henan Province, China. Environment Development and Sustainability. 20, 1385 – 1404.

[2] Cheng, X., Chen, L.D., Sun, R.H., Kong, P.R. (2018) Land use changes and socio-economic development strongly deteriorate river ecosystem health in one of the largest basins in China. Science of the Total Environment. 616, 376-385.

[3] Wu, D., Ning, S. (2018) Dynamic assessment of urban economy - environment - energy system using system dynamics model: A case study in Beijing. Environ. Res. 164, 70-84.

[4] Cheng, C.C. (2015) The Overall Framework and Strategy of the Yangtze River Economic Zone 's Coordinated Equilibrium Development. Journal of Nantong University. 1, 1-8.

[5] Sun, X. (2017) Multi-indicator Evaluation and Analysis of Coordinated Industrial Development of Urban Agglomerations. Urban and Environmental Studies. 05(2).

[6] Gultekin, U. (2019) Renewable electricity generation for sustainable development and environmental management in Turkey. Fresen. Environ. Bull. 28, 8171-8174.

[7] Zeng, G., Wang, F.L. (2016) Research on the Evaluation of the Coordinated Development Capability of the Cities Along the Yangtze River Economic Belt. Frontiers. 2, 58-64.

[8] Ran, Y.C., Xie, J.X., Li, X.L. (2016) Socio-economic Development and Its Effects on the Ecological Environment of the Yellow River Source Zone. Landscape and Ecosystem Diversity, Dynamics and Management in the Yellow River Source Zone. 1, 331-351.

[9] Li, A.H., Su, J., Jia, C.L. (2017) The Coordinated Development and Consistent Model Between Economic Growth and Carbon Emissions. Chinese Journal of Management Science. 25(4), 1-6.

[10] Han, F., Li, E.L. (2015) The Evaluation of Coordinated Development between Urban and Rural Areas in Central Plains Economic Zone. Economic Survey. 120(7), 4638-4653.

[11] Vasseur, L., Horning, D., Thornbush, M., Cohen-Shacham, E., Andrade, A., Barrow, E., Edwards, S.R., Wit, P., Jones, M. (2017) Complex problems and unchallenged solutions: Bringing ecosystem governance to the forefront of the UN sustainable development goals. Ambio. 46(7), 731-742.

[12] Zhou, J.K. (2016) On the Overall Strategic Significance of Coordinated Development of Beijing, Tianjin and Hebei. Frontiers. 4, 40-50.

[13] Zheng, D.F., Zang, Z., Zhao, L.S., Sun, C.Z. (2014) Analyzing the spatial-temporal correlation of the economic growth and resource-environment with the model of coordinated development degree. Journal of Glaciology and Geocryology. 36(3), 740-750.

[14] Du, X.H., Zhang, T. (2015) The Simulation to Coupling Development Between Water Resource and Environment and Socio-economic System: Dongting Lake Ecological Economic Zone as an Example. Scientia Geographica Sinica. 35(9), 1109-1115.

[15] Zhou, B., Zhao, K., Zhong, L.S., Chen, T., Yu, H. (2015) Coordinated development evaluation of the ecosystem health and the tourism economy Zhoushan Islands. Acta Ecologica Sinica. 35(10), 3437-3446.

[16] Moore, S.E., Logerwell, E., Eisner, L., Farley Jr., E.V., Harwood, L.A., Kuletz, K., Lovvorn, J., Murphy, J.R., Quakenbush, L.T. (2014) Marine Fishes, Birds and Mammals as Sentinels of Ecosystem Variability and Reorganization in the Pacific Arctic Region. Springer Netherlands.

[17] Seidl, A. (2014) Cultural ecosystem services and economic development: World Heritage and early efforts at tourism in Albania. Ecosystem Services. 10, 164-171.

[18] Tang, X., McLellan, B.C., Snowden, S., Zhang, B., Hook, M. (2015) Dilemmas for China: Energy, economy and environment. Sustainability. 7, 5508-5520.

[19] Ma, J.Y. (2015) Hunan Normal University. Dongjiang Lake Reservoir Area Evaluation of Water Environmental Carrying Capacity and the Research of the Coordinated Development. Economic Geography. 35(11), 184-189.

Received: **28.05.2020**
Accepted: **04.09.2020**

CORRESPONDING AUTHOR

Wanchun Zhu
Higher Vocational and Technical School
Guizhou Minzu University
Guiyang 550025, Guizhou – China

e-mail: zhuwanchun88@tom.com

© by PSP Volume 30– No. 05/2021 pages 4804-4822 Fresenius Environmental Bulletin

ON-FARM IRRIGATION MANAGEMENT FOR SHALLOW WATER TABLE SOILS AT NORTH NILE DELTA EGYPT BASED ON TILLAGE PRACTICES AND ECONOMICS

Abdelaziz Okasha[1,*], Alaa El-Bably[2], Amira Eid[2]

[1]Agric. Eng. Dept., Faculty of Agric, Kafrelsheikh University, Egypt
[2]Soils, Water and Environment Res. Inst., Agric. Res. Center, Giza, Egypt

ABSTRACT

Proper management of water irrigation by labouration reduces irrigation water saving, increases crop yields, reduces irrigation costs and maximizes water productivity. The integrative effects of irrigation control on farm, through controlled irrigation run length and stream size, under different tillage depths on the crop yield and its water relation are not well documented in the shallow water table soils. Over a two-year field analysis, therefore, the impact of irrigation run length and stream size on wheat yield and water productivity under different tillage depths and the contribution from the water table to the requirement of wheat water was assessed. A split-split plot design with three replicates was used. Two tillage depths occupied the main plots, at 10-20 cm (T1) and 20-30cm (T2) depth. The stream size treatments; 2 (S1) , 3 (S2) and 4(S3) $LS^{-1}m^{-1}$ were arranged in the sub plots, where the sub-sub plots were devoted to irrigation run length treatments ; 100% of run length without cut-off (C1), cut-off at 90% (C2) and at 80% (C3) of strip length. Results showed that, the combination of (T2), (S3) and (C2) had the highest during the two growing seasons and the average values of water productivity were ($2.29 kg.m^{-3}$),water application efficiency was 73.42%, water saving was 42.84%, wheat grain and straw yield were 10.297 and 10.708$ton.ha^{-1}$, and the highest contribution of ground water (CGW) was 21.4% compared with control treatment (T1S1C1) that had no CGW. Also, results revealed that the T2S3C2 treatment achieved the highest net return (NR) that was 1173.99$US $ha^{-1}$and benefit cost ration (BCR) was 0.9 compared with the control treatment T1S1C1 that was 522.77$US.$ha^{-1}$ and 0.36, respectively. Therefore, cut off irrigation at 90% of strip length with stream size $4LS^{-1}m^{-1}$ under tillage depth 20-30cm resulted in a promising strategy to maximize wheat yield and to improve the water productivity under the conditions of shallow water table areas.

KEYWORDS:
On-Farm Irrigation Management, Water Productivity, Tillage Practices, Economic Efficiency, Wheat (Triticum aestivum L.), Water Table

INTRODUCTION

The most important cereal crop in Egypt is wheat (Triticum aestivum L.) and the grain, in turn, is the largest cereals. The value of agriculture is nearly 10 percent and of all agriculture imports about 20 percent. [1]. As wheat production in Egypt is some 10,0 million tons, produced from 1,5 million hectares, covering approximately 40 % of the population, Egypt is the world's largest importer of wheat [2]. Egypt has two major issues, with an increasing population and a lack of water. Irrigated agriculture in Egypt is the dominant form of agriculture and the restriction of water supplies due to the substantial population growth makes it imperative to find ways to conserve the irrigation water and improve crop productivity. The water shortage facing Egypt is growing continually and the threshold of less than 500 m^3Y^{-1} $capita^{-1}$ is expected to be reached. Hens increasing production of wheat and saving water are the key techniques to address these challenges. [3].

Improvements in irrigation practices by means of an irrigation cuts or high stream sizes are required in areas that include shallow ground water table (SGWT), such as the North Nile Delta soil of Egypt, to avoid excessive irrigation and to save water. A shallow water table's contribution to crop water usage can have positive effects on yield and decrease annual change [4]. One option is to high irrigation water by using low ground water to control crops when irrigation is scheduled. [5]. Many studies illustrate the significance of the shallow water table in arid and semiarid regions as a possible crop water source. For arid and semiarid irrigated districts, the SGWT will contribute between 20 to 40% of water consumption. However, several variables, including water table depth and the seasonally applied water depend on the contribution of the SGWT to netting crops water needs. [6]. In the case of water table depth (WTD), the ratio of a seasonally average

ground water contribution to the winter wheat production has reached up to 75% equal to 1.0 m, not irrigated, and in the case of WTD equal to 3.0 m, three applications for irrigation [7]. The effect of shallow soil water levels on the use of crop water in large drainage lysimeters has been investigated. If a table of ground water was held at a depth of 0.5 m, the whole system uses what ground water sources [8]. More than 65% of the possible evapotranspiration of winter wheat with precipitation as a depth of the water table amounted to over 40-150 cm, along with seasonal contributions from ground-water. Because the depth of the water table was not less than 110cm from the field, the contribution from the water table almost satisfies the whole water requirement for winter wheat, with the total plumage in winter. It could satisfy the complete water demand at a depth of 110cm or more [9]. The ground-water table has contributed 29% of the consumption of wheat-water in the period from maturation to harvest yields, and wheat-biomass increases water productivity as irrigation water is reduced and ground-water levels decrease, so a shallow water table can decrease the irrigation water needs and can provide an important source for farm water [10]. Wheat could obtain 32 percent of its water requirement on a loam ground with a water table at less than 1.0 m. [11].

Cut-off wheat irrigation is an effective technique for improving water management in the area north of the Nile Delta with a 90% stream-length ratio of water saving, compared to irrigation without cut-off, of water irrigation. Furthermore, the highest values of efficiency in water use (1.73kg.m^{-3}) and productivity of water (1.61 kg.m^{-3}) were obtained from a 90 percent strip length of irrigation cut off [12]. The loss of runoff increased and the loss of deep percolation decreased with the increase in the stream. The appropriate water flow and running length can achieve a uniform application of water and reduce depth, run-off and erosion. The best flux size is the one that films water to the end of the border according to the cut-off ratio requirement [13]. In comparison with the conventional method, deep percolation and ruin are less in the cut-back procedure. Therefore, in heavy textured soils the cut-back process was more efficient than in light textured soils [14]. Cut-off berseem (Clover), crop irrigation at 90% strike length in the North Nile Delta of Egypt, yields 95% that is irrigated, 95% strip length, 7.9% irrigation water and maximum efficiency of water use 16.58 kg m^{-3}. Agronomic practices for high crop yields must be optimized. Soil tillage plays an important role in crop yields by activating the physical properties of soil and by ensuring a proper laundering system will increase the water available for crops by promoting root growth soils Agronomic practices [15]. The results of the statistical analyses show that winter wheat was considerably affected by soil tillage and nitrogen fertilization processes. Subsequent to the therapy, the water was improved and the soil water stored, thereby improving wheat yield. The yields of wheat grain increased as root conditions were improved and soil water supplemented. [16]. Deep labour, such as chisel or plow plowing, performed better than shallow laying, as deep lawns improved soil moisture content, bulk density and resistance to penetrate under irrigated wheat in silty clay loam soil. These deep labouring practices in semiarid environments are therefore recommended for silty clay loam soil for better crop growth. No tillage could, however, improve the soil water content and physical quality in drought conditions as compared with conventional tillage, which results in significant increases in the yield of wheat and water consumption. [17]. Further evidence indicated that no tillage could not affect crop yields significantly. [18]. Two tillage systems; traditional tillage (CT), reduced tillage (RT), with the incorporation on the grain yield and nitrogen production (NUE) of wheat of the prior crop and without incorporation of the straw of the previous crop. They found that CT yields and NUE were the most consistent and that RT can be used to produce the CT-like spring wheat yields [19].

The conventional method of irrigation caused a great deal of water to be wasted and thus a low degree of output is achieved. Egypt is now suffering from extreme water shortages, while the Nile is the main source of fresh water, and Egypt's agriculture sector is also considered to be one of the largest water consumers, which is why we had to solve irrigation problems. [20]. At the back of the Egyptian wheat irrigation system, especially in clay soils, the weeding front is permitted. Water can be retained for a long time in the upper part of the irrigated stream, contributing to a greater loss of percolation. In order to produce a horizontal movement advantage, the irrigation front should be stopped outside the cultivated borders (cut off irrigation technique). Following a cut off irrigation event, the waterside will proceed to irrigate more cropland and water percolates before it stops. This is known to save water efficiently. Therefore, the objective of this study is to: (1) assess the effect of cut-off irrigation and the stream size under different soil tillage on saving irrigation water, (2) maximizing water productivity and (3) the contribution of the table of groundwater to wheat water in Egypt's North Nile Delta area under shallow water conditions.

MATERIALS AND METHODS

The study area. A field experiment was carried out at the Experimental Farm of Sakha Agricultural Research Station, Agricultural Research Center (ARC) during the two growing seasons 2017/18 and 2018/19. The site is located at 31° 07' N Latitude, 30°05' E Longitude with an elevation of about 6 meters above mean sea level. The site represents the

conditions and circumstances of North Nile Delta region. The prevailing climate of the area is semiarid. It is characterized by a cool winter with a mean air temperature of around 13°C. Summer is hot with no rain, and mean air temperature of about 26 °C with mean relative humidity of 72% during the day time. The amount of annual rainfall is low and fall mostly in winter, reaching about 130 mm year-1. The meteorological data of the experimental site as shown in Table 1 were measured in an agro-meteorological station about 100 m in distance from the experimental field. Soil of the experimental site was clayey in texture (58.3% clay, 23.2% silt and 18.5% sand), with an average bulk density of 1.25 Mg m^{-3} for 0-60 cm depth and is alkaline in reaction with pH value (1:2.5 soil and water) of 8.03. Field capacity, wilting point and available water values were 41.54, 20.50 and 21.04% respectively. The soil topography is flat with shallow water table level in such area is ranged from 70-110 cm using observation well. Average soil electric conductivity in saturated paste extract (EC) and organic matter content, in 0-60 cm depth, were about 1.94 dSm^{-1} and 2.48%, respectively. The average EC of irrigation water was 0.48 $dSm^{-1}$and the soil profile is fairly uniform without distinct change in texture.

Treatments and experimental design. The experimental design was a split split-plot design with three replicates. Two tillage depths occupied the main plots, at 10-20 cm (T1) and 20-30 cm (T2). The stream size treatments; 2 (S1), 3 (S2) and 4(S3) $LS^{-1}m^{-1}$were arranged in the sub plots, where the sub-sub plots were devoted to irrigation run length treatments ; 100% of strip length without cut-off (C1) (control), cut-off at 90% (C2) and at 80% (C3) of strip length. Length of each cultivated strip was 25 m and width 4 m, irrigation was stopped when water front reached 25.0 (control) treatment, 22.5 and 20.0 m for C1, C2 and C3, respectively. Figure (1) showed the layout of the experimental plots for one replicate only. To avoid lateral movement of water, Plots isolated by ditches of 1.5 m in width. The leveling was 0.1% ground surface slop.

Agronomic practices. Wheat (Triticum aestivum L.). Variety Misr-1 cultivar was planted at the rate of 140 kg seeds $hectare^{-1}$ on 10th and 15th November and harvested 5th and 10th May in the first and second seasons, respectively. All agricultural practices were performed as recommended by the Egyptian Ministry of Agricultural and Land Reclamation for the crop and the area except the three factors of study i.e., tillage practices, stream size and cut- off irrigation. At harvest, three square meters were randomly selected from each sub-sub plot to estimate the grain and straw yield.

TABLE 1
Mean values of some Meteorological of the experimental area during the two-growing seasons of wheat 2017/18 and 2018/19.

Season	Month	Temperature, c°			Relative humidity, %			Wind velocity, km/d at 2m height	Pan evaporation (mm/day)	Rainfall, mm/month	Sun Shine hours
		Max.	Min.	Mean	Max.	Min.	Mean				
Season 2017/2018	Nov.	23.7	9.9	16.8	84.70	58.60	71.65	53.50	2.06	9.3	8.0
	Dec.	21.3	8.4	14.9	88.20	64.80	76.50	42.90	1.47	5.60	6.6
	Jun.	18.9	3.6	11.3	89.40	64.40	76.90	44.90	2.63	36.40	7.0
	Feb.	21.6	4.6	13.1	87.60	63.40	75.50	34.70	2.78	16.60	7.7
	Marc.	25.4	6.6	16.0	82.30	48.30	65.30	46.40	4.22	---	8.6
	Apr.	27.8	10	18.9	80.90	43.90	62.40	74.00	5.32	---	9.6
Season 2018/2019	Nov.	25.0	7.4	16.2	86.60	54.60	70.60	24.20	1.60	---	8.2
	Dec.	19.5	3.9	11.7	88.70	62.40	75.55	24.50	0.83	21.70	6.8
	Jun.	18.9	2.3	10.6	82.30	53.30	67.80	33.10	1.14	14.90	7.0
	Feb.	19.	4.3	12.0	86.90	58.20	72.55	28.60	1.78	17.60	7.9
	Marc	21.7	7.6	14.7	87.80	56.60	72.20	45.70	2.86	17.30	8.5
	Apr.	25.1	11.3	18.2	80.80	48.90	64.85	44.80	3.65	7.60	9.4

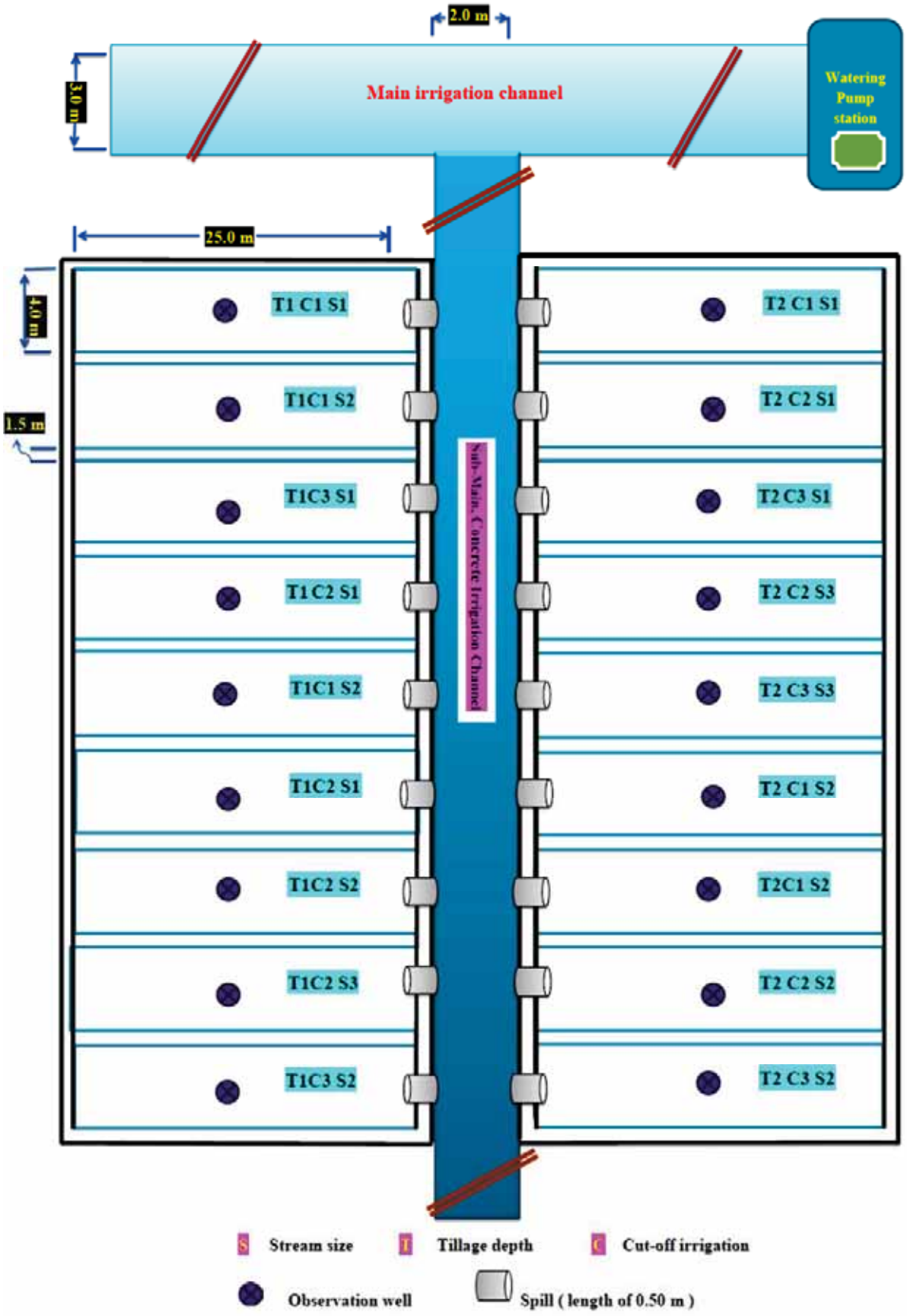

FIGURE 1
Schematic diagram showing the distribution of treatments as related to the layout of the experiment for one replication.

Irrigation water management. Irrigation water was conveyed to the experimental plots and measured by spills, inserted beneath the strip bank, according to **[21]** using the following formulas:

$$\mathbf{Q = CA\sqrt{2gh}} \ldots\ldots\ldots\ldots (1)$$

Where: Q: Discharge of irrigation water (cm^3s^{-1}),

C: Coefficient of discharge =0.62 (determined experimentally),

A: Inner cross section area of the irrigation spiel (cm^2)

g: Gravity acceleration (981cm/s^2)and

h: Average effective head (13cm).

The length of each cultivated strip was 25m, therefore, irrigation water was stopped when the water front reached 25, 22.5, 20m of the strip length for treatments C_1, C_2 and C_3 respectively. Five station were arranged every 5 m along the strip to measure the flow advance pattern. According to the equation (1) the spile tube with two inches inner diameter gives discharge of $2LS^{-1}m^{-1}$, therefore one and two spilles were used for stream size treatment S_1 and S_3, respectively. For the stream size treatment of (S_2) spile tube with 2.5 inches inner diameter was used to give the discharge of $3LS^{-1}m^{-1}$

The effective rainfall (ER). It was estimated according to [22] as:

$$\mathrm{ER} = \text{Incident rainfall} \times 0.7 \ldots\ldots\ldots\ldots (2)$$

Crop evapotranspiration (ETc). It was calculated according to [23], using the equation**:**

$$ET_C = ET_\circ \times K_C \ldots\ldots\ldots\ldots\ldots\ldots\ldots\ldots (3)$$

Where:

$ET_\circ$: Reference crop evapotranspiration, and

Kc: Crop coefficient**.**

The reference crop evapotranspiration ($ET_\circ$). It was calculated from the FAO- Penman Monteith method [23] using CROPWAT model v.8.0 [24] based on the agro-metrological data collected for the studied area.

The crop coefficient (Kc). Values were quoted from FAO [23] and Kc values were 0.4, 0.8, 1.2, 0.7 for growth wheat stages initial (20 day), development (60 day), mid-season (70 day) and late season (30 day), respectively.

Advance time (Ta). Wooden stakes were installed along each strip at 5 m interval where advance time was recorded.

Soil moisture depletion (SMD). Soil moisture depletion (SMD) was calculated using the following equation [21].

$$SMD = \sum_{i=1}^{i=n} \left(\frac{\theta_2 - \theta_1}{100} \times \rho_{bi} \times D_i\right) \ldots\ldots (4)$$

Where:

SMD: Soil moisture depletion,

i : Number of soil layers (1-4),

Di : Soil layer thickness (15 cm),

ρ_{bi} : Bulk density (kg m^{-3}) of the layer,

θ_1 : Soil moisture percentage before the next irrigation, and

θ_2 : Soil moisture percentage, 48 hours after irrigation.

Fluctuation of the water table depth (WTD). To determine the diagram of the fluctuation of the groundwater table (GWT) under wheat crop during the growing season, eighteen observation wells were installed along different treatments. The observation well was a 5 cm in diameter and 200 cm long, perforated plastic tube. WTD readings were recorded before each irrigation, 2 days after irrigation or rainfall and at an interval of 7 days between irrigations with the help of a metallic sounder fixed in a sealed top to measure the depth of the water table.

Contribution of ground water (GW). It has been estimated using equation of the water balance as follows [9] and [25]:

$$\mathrm{GW, \%} = \left((\mathrm{ET_C} - \mathrm{SMD})/\mathrm{ET_C}\right) \times 100 \ldots\ldots (5)$$

Where:

The GWT % is the percentage of the contribution of ground water table to the crop evapotranspiration (ETc) and SMD is the soil moisture depletion.

Soil moisture monitoring. Time Domain Reflect meter (TDR) probe was used to measure soil moisture, Figure (2) before each irrigation, 2 days after irrigation or rainfall, at intervals of 7 days between irrigation and harvesting, drilling the soil profile from 0 to 60 cm in 15 cm.

FIGURE 2
Time Domain Reflect meter (TDR).

Water application efficiency (Ea). It was calculated for the 60 cm soil depth according to [21] and [26] as follow:

$$Ea = \frac{Ws}{Wf} \times 100 \ldots\ldots\ldots\ldots (6)$$

Where:

Ea: Water application efficiency, in percent,

Ws: Amount of water stored in the crop root zone, and

Wf : Amount of water delivered to field.

Distribution uniformity (Du). Distribution uniformity is expressed as a decimal as suggested by [27].

$$Du = \frac{\bar{X}_{LQ}}{\bar{X}} \times 100 \ldots\ldots\ldots\ldots (7)$$

Where:

$\bar{X}_{LQ}$: Low-quarter average -depth/volume amount caught/infiltrated, and

$\bar{X}$: Average amount depth/volume caught/infiltrated.

Water distribution efficiency (Ed). It was calculated according to [28] as follows**:**

$$Ed = \left(1 - \frac{\bar{Y}}{\bar{d}}\right) \ldots\ldots\ldots\ldots (8)$$

Where:

$\bar{Y}$: Average numerical deviation from $\bar{d}$, and

$\bar{d}$: Average depth of soil water stored along the run during the irrigation.

Irrigation water productivity (IWP). IWP is defined as the crop yield per cubic meter of irrigation water supplied [29].

$$IWP = \frac{\text{Crop yield}}{\text{Applied irrigation water}} \ldots\ldots\ldots\ldots (9)$$

Economic efficiency (EE). According to [30] as:

$$EE = \frac{\text{Net return } (return - cost)}{\text{Applied irrigation water}} \ldots\ldots\ldots\ldots (10)$$

Economic evaluation (profitability). Profitability was calculated according to the equations outlined by [31] as:

1- Gross revenue = (grain yield × price) + (straw yield × price),

2-Net return (NR) =total return – total cost, and

3- Benefit cost ratio BCR = NR /total cost.

Gross revenue has been calculated by multiplying total yield in kg ha^{-1} and wheat market price per kilogram, the farm-gate price for wheat grain in this study was 0.222 $US kg-1 and 0.04$US for kilogram straw (Exchange rate 1 EGP=0.06 $US in 2018)

Statistical analysis. Data were statistically analyzed as split-split- plot design by model of CoStat Version 6.45 as statistical program. Treatment means were compared at a probability level of 0.05 according to the (Duncan, 1955) test, in order to estimate significant treatment differences.

RESULTS

Advance time: Figures (3 to 10) show strip length versus advance time with other treatments. The highest values of advance time (64.68 and 31.30 min.) for the first and second irrigation were recorded under (C1S1T1) treatment during the 1st and 2nd seasons, respectively. On the other hand, the lowest values of advance time (35.33) and 17.16 min) for 1st and 2nd irrigation were detected under treatment (C3S3T2) during both seasons, respectively.

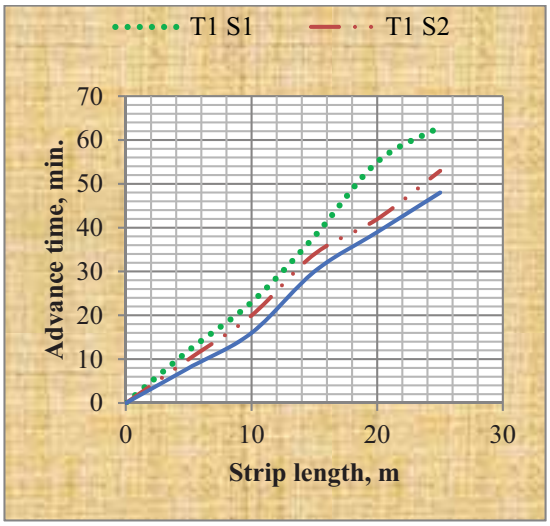

FIGURE 3
Advance time vs. strip length as affected by stream size (S) and 10-20cm depth of tillage (T1) for first irrigation during 1st season.

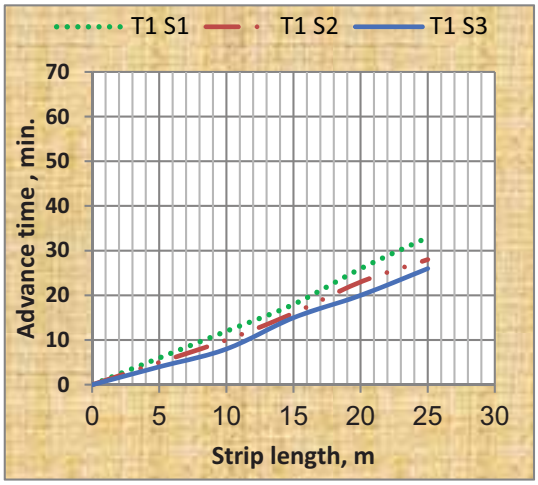

FIGURE 4
Advance time vs. strip length as affected by stream size (S) and 10-20cm depth of tillage(T1) for second irrigation during 1st season.

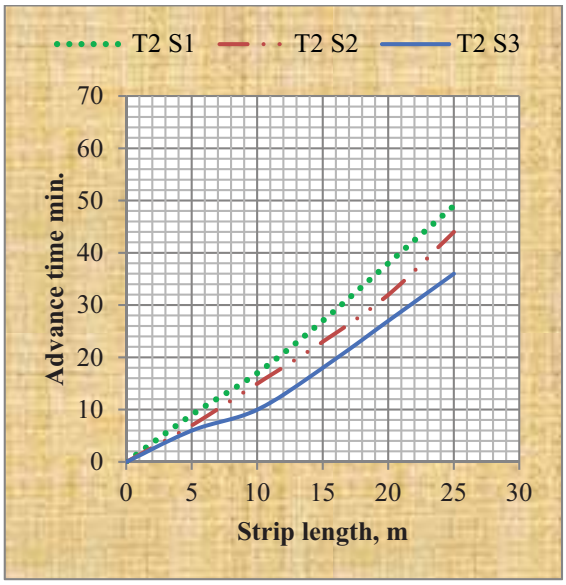

FIGURE 5
Advance time vs. strip length as affected by stream size (S) and 20-30cm depth of tillage (T2) for first irrigation during 1st season

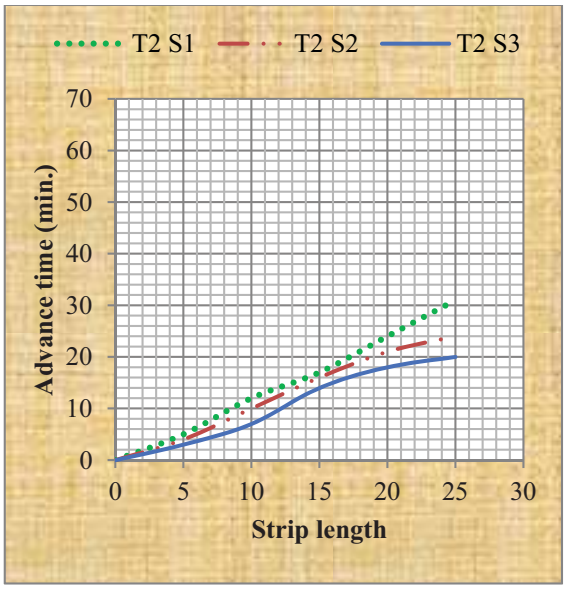

FIGURE 6
Advance time vs. strip length as affected by stream size (S) and 20-30cm depth of tillage(T2) for second irrigation during 1st season.

It was noticed that advance time was increased with increasing cut-off irrigation treatments under stream size rates during both seasons of cultivation. Also, data in Table (5&6) reveal that, the advance time under stream size treatments, were in the following order: S1> S2> S3. On the other hand, the total amount of advance time under cut-off irrigation treatments were in the following order C1> C2 > C3. The advance time of the stream size $4LS^{-1}m^{-1}$ (S3) treatment was the lowest, and the amount for the $2LS^{-1}m^{-1}$ treatment was the highest. From the data also, it is revealed that the stream size of $4LS^{-1}m^{-1}$ is more appropriate than the normal $2LS^{-1}m^{-1}$one. It is clearly revealed that discharge and depth of tillage played great role in the variation of the advance time. In fact, the advance time also varied from site to site. Regardless of differences in discharge and cut-off irrigation, on average the advance time range from 49-36 min and 26-19 min between sites at first and second irrigation under 10-20 cm tillage depth while it was 64-48 and 28-20min, respectively. This was attributed to differences in surface roughness, slope and field leveling or depressions. In the first irrigation, due to the confounding effect of high surface roughness, the effect of cut-off irrigation was not clearly observed.

Total applied water (Wa). Under conditions of the present study the total applied water (Wa) in season for wheat crop consists of three components which were irrigation water (IW), effective rainfall (ER) and contribution of ground water (GW) from water table depth (WTD).

Effective rainfall (ER). Wheat as a spring crop, received 47.5mm of the effective rainfall amounted and 51.1mm in the 1st season during the period from November to February and in the 2nd season during the period from December to March, respectively, as shown in the previous Table 1. It was calculated according to equation (2). The overall average of rainfall in the area of study is about 60 mm. The amount of rains is considered less and unreliable for irrigation, but it works to separate the irrigation periods and thus saves the amount of irrigation water.

Water table depth (WTD). The area of study is characterized by a shallow water table which can meet partially the crop water needs depending on its depth. Seasonal average of maximum and minimum values of water table depth, under each treatment, during the two growing seasons is given in Table 2. Seasonal average of minimum values of WTD varied from 34 to 63 cm and from 37 to 66 cm in the 1st and 2nd seasons respectively. The corresponding values of the maximum values varied from 90 to 115 cm. the seasonal average during the two seasons were 76 79.7 cm for the 1st and 2nd respectively. Therefore, it may be considered that the study area is a shallow water table region. It worth to mention that WTD reached its lowest value immediately before irrigation, whereas the maximum values reached at 2 days after irrigation. Following irrigation, the WTD decrease gradually in between irrigations. An example for the daily fluctuation WTD under the irrigation cut-off treatments (C) is illustrated in Figure (11). The fluctuation of WTD defines the cut-off irrigation, stream size and the tillage depth treatments. The absolute values of both minimum and maximum depth of water table increased with increasing the stream size and with tillage depth, i.e S3> S2 > S1 and T2> T1. While it decreases with increasing irrigation cut-

off, i.e, C1< C2<C3. As shown in table 2, the treatment combinations C1 S1 T1 recorded the highest WTD, whereas the treatment C3 S3 T2 had the lowest WTD. The management of irrigation cut-off at 80% from border length with a water discharge rate of 4L $S^{-1}m^{-1}$ (S3) under tillage depth 20-30 cm (T2) in north Nile Delta have the advantage proper aeration in effective root zone, minimizing the water logging hazard in the area and save a reasonable amount of irrigation water.

Irrigation water (IW). IW decreased significantly with decreasing the irrigation cut-off (C) and with increasing the stream size (S) and the tillage depth (T) at ($p<0.05$). The highest amount of IW was 4892 m^3 ha^{-1} over two seasons for the control treatment (C1). Meanwhile, the lowest one was 685 m^3 ha^{-1} for treatment of C3, distributed on five irrigations event as shown in Table 3. In comparison with the control treatment (C1), average IW saving was 5.4% (267m^3ha^{-1}) and 24.6% (1206 m^3ha^{-1}) for the cut-off treatments C2 and C3, respectively. The lowest IW amount of C3 than C2 or C1 treatments could be explained on the basis that the wetting front following stop irrigation in C3 treatment (80% cut-off) never reached the end of the strip, while under C2 (90% cut-off) wetting front following stop irrigation almost reached the end of the strip, which resulted in less water than under C2, as well as, under the control treatment C1 (without cut-off). The results, also, showed that the stream size treatment S3 ($4LS^{-1}m^{-1}$) had the lowest IW amount (4174 m^3ha^{-1}) and was less than S1 and S2 by 28.1 and 12.0%, respectively. This is due to the action of high discharge water rapidly trapping air in the cracks and thus tells the largest area in a short time and the opposite of little disposition these is room to penetrate the water from the cracks and then to deep percolation. Therefore, it is a practical means for on farm effective water management since it reduces the amount of the irrigation water. These results are in a great harmony with these obtained by [12] and [32] who reported that the lowest values of applied water for wheat crop were detected under irrigation discharge 4.0 $LS^{-1}m^{-1}$ and cut-off irrigation at 85% of border length during wheat growing season. Regarding the tillage depth, the amount of IW, over the two seasons, under T2 treatment was 4628 m^3ha^{-1} lower than that of T1 which was 4824 m^3ha^{-1}. i.e, deep tillage (T2) saves water by about 4.1%. This may be due to the physical soil properties improvement. Deep tillage improves the soil bulk density, water storage capacity and soil penetration resistance [33]. Pertaining the combination of cut-off irrigation with the stream size and tillage practices, the treatment of C2 S3 T2 had the lowest IW values to be 3868 m^3 ha^{-1} and the highest one was 5671 m^3ha^{-1} for the control treatment (C1 S1 T1) table (5) and Figure 4, i.e, values of water saving amounted 2238m^3 ha^{-1} which formed 38.9 % and 2056 m^3ha^{-1} which formed 36.7% were recorded with the treatment of C3 S3T2 during the 1st and 2nd seasons, respectively.

TABLE 2
Maximum, minimum and mean values of the depth of water table during the two growing seasons of wheat 2017/18 and 2018/19.

Observation well no	Treatments	1st season			2nd season		
		Max.	Mini.	Mean	Max.	Mini	Mean
1	$C_1S_1T_1$	34	90	62	37	94	66
2	$C_2S_1T_1$	38	92	65	41	96	69
3	$C_3S_1T_1$	39	95	67	42	99	71
4	$C_1S_2T_1$	43	96	70	47	100	73
5	$C_2S_2T_1$	48	100	74	51	104	78
6	$C_3S_2T_1$	44	99	72	47	103	75
7	$C_1S_3T_1$	45	105	75	48	109	79
8	$C_2S_3T_1$	50	108	79	54	112	83
9	$C_3S_3T_1$	47	105	76	50	109	80
10	$C_1S_1T_2$	44	100	72	47	104	76
11	$C_2S_1T_2$	49	106	78	52	110	81
12	$C_3S_1T_2$	47	110	79	50	116	82
13	$C_1S_2T_2$	49	110	80	53	114	83
14	$C_2S_2T_2$	52	110	81	55	114	85
15	$C_3S_2T_2$	54	110	82	57	114	86
16	$C_1S_3T_2$	48	112	80	51	116	84
17	$C_2S_3T_2$	60	115	88	64	119	91
18	$C_3S_3T_2$	63	115	89	66	119	93
Average		47	104	76	51	108	80

T= Tillage depth S=Stream size C=Cut-off irrigation

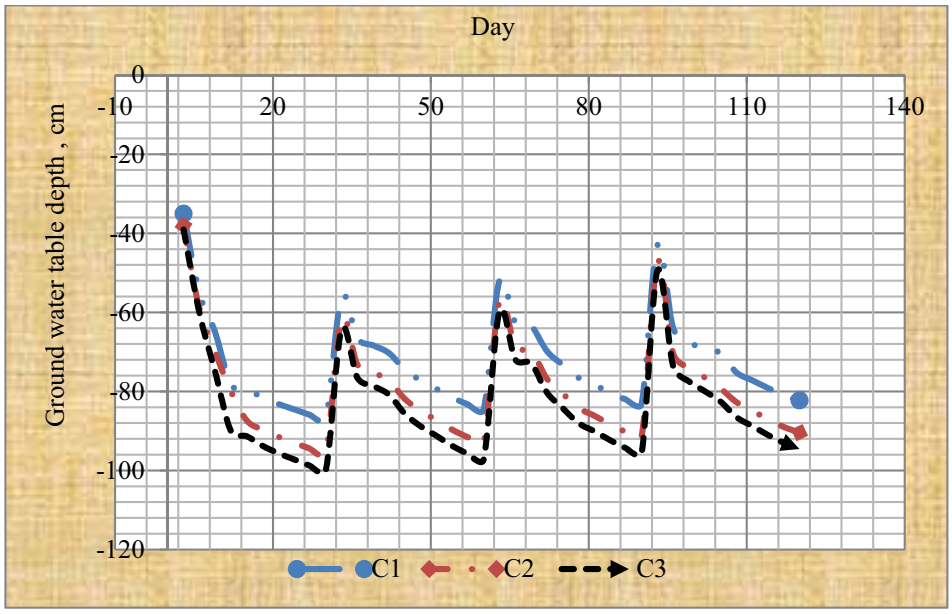

FIGURE 11
Fluctuation of ground water table depth after irrigation days as affected by cut-off irrigation (C).

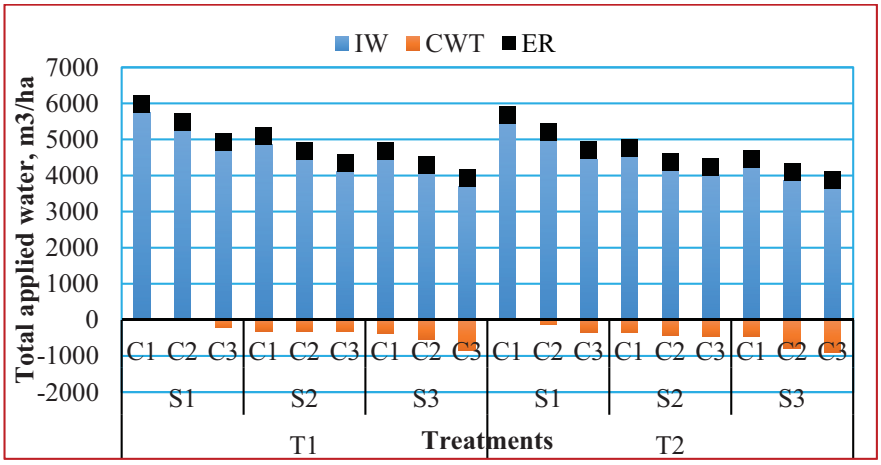

FIGURE 12
The relationship between total applied water from irrigation water (IW), effective rainfall (ER) and contribution of ground water (GW) and treatments during the first season.

T= Tillage depth S=Stream size C=Cut-off irrigation

Contribution of ground water (GW). Values of GW to crop evapotranspiration (ETc) during the two seasons are given in Table 3, Table 4 and (Figure 12 to 13). Data revealed that GW values increased significantly at ($p<0.05$) with decreasing cut-off irrigation (C3 >C2 > C1 and with increasing stream size (S3 >S2> S1) and with tillage depth (T2 > T1). Also, data revealed that by increasing irrigation applied water (Table 3), less GW values was obtained. For the maximum applied water treatment (C1 S1 T1) the control treatment there was no contribution from the water table. The highest values of GW were 902 m^3ha^{-1} (22.57%) and 755 m^3ha^{-1} (20.22%) during the 1st and 2nd season respectively, with an overall average of 829 m^3ha^{-1} (20.4%) for treatment C3 S3 T2). Under the condition of the present study, the GW percentage of the ETc varied from 1.62 to 21.4%. as an average of the two seasons except the control treatment which had no GW. The most probable explanation for these finding is due to the fact that as the mount of applied water increased, the contribution of the water table is decreased. So, irrigating wheat plant with 4L S^{-1} m^{-1} discharge with cut-off irrigation at 80% of the strip length under tillage depth 20-30 cm received the lowest irrigation water and therefore achieved the highest values of GW percent. these results are in agreement with these obtained by [4], [9] [32], [33] and [34]. In general, GW decreased with the increase of WTD or irrigation quantity [5]. When WTD is very shallow, irrigation may be eliminated to maximize GW and avoid water logging problem. It is obvious from the above results that the ground water contribution is important and should be operated as a system for effective water

management. This will save water, energy and labor. The water table contribution should be recognized as a source of ETc when water table is very shallow and the irrigation system should be managed to maximize the water use efficiency WUE and yield of wheat by controlling the cut-off irrigation and the stream size.

Water application efficiency (Ea, %). Water application efficiency reflects the capacity of roots to utilize the moisture stored in the soil between irrigation intervals, data in Table 5 and Figure (14 to 15) and revealed that the highest values of water application efficiency (Ea) were 74.78and 72.05% resulted from C2S3T2 treatment during the1st and 2nd seasons, respectively, while, the lowest values of water application efficiency were 43.55 and 42.32% resulted from C1S1T1 treatment during both seasons, respectively. Also, it was noticed that mean values of water application efficiency were increased with increasing deep tillage, stream size and cut-off irrigation during both seasons. These results are somewhat agreed with those obtained by [13], [33], [37] and [38].

Distribution uniformity (Du). Water distribution uniformity is defined as the average of low 25% of measurements; divided by the average volume of all measurements. Water distribution uniformity gives an indication of the magnitude of the distribution problem. As shown in Table 5 and Figure. (16 to 17). Du were 94.72 and 93.6% resulted from C2S3T2 treatment during the1st and 2nd seasons, respectively, while, the lowest values of Du were 56.55 and 54.99% resulted from C1S1T1 treatment during both seasons, respectively. Also, it was noticed that mean values of Du were increased with increasing deep tillage, stream size and cut-off irrigation during both seasons. and take the same trend curves of water application efficiency. These results are somewhat agreed with those obtained by [13], [33], [37] and [38].

Water distribution efficiency (Ed, %). Presented data in Table 5 and Figure. (18 to19) show that the highest values of water distributed efficiency (90.25 and 93.86%) were recorded with cut-off irrigation at 100% of border length (C1) and stream size 4 $Ls^{-1}m^{-1}$ under 20-30cm tillage depth (T2) during the1st and 2nd seasons, respectively. While, the lowest values of water distribution efficiency (63.34 and 67.95%) were resulted from cut-off irrigation at 80% of border length and irrigation discharge 2.0L $s^{-1}m^{-1}$ under 10-20 cm tillage depth (T1) during both seasons, respectively. It is obvious from the obtained data that the values of water distribution efficiency increased with increasing stream size and decreased with increasing cut-off irrigation treatments during both seasons. These results are in the same agreement with those obtained by [33], [37] and [38].

TABLE 3
Irrigation water (IW), contribution of ground water (GW), rainfall (RF) and total applied water (Wa).

Treatments			Season 2017/2018				Season 2018/2019			
			IW m^3ha^{-1}	GW m^3ha^{-1}	RF m^3ha^{-1}	Wa m^3ha^{-1}	IW m^3ha^{-1}	GW m^3ha^{-1}	RF m^3ha^{-1}	Wa m^3ha^{-1}
		C_1	5741	0	475	6076	5601	0	511	6252
	S_1	C_2	5252	0	475	5628	5153	0	511	5763
		C_3	4701	219.91	475	5281	4586	0	511	5212
		C_1	4862	312.26	475	5563	4776	189.92	511	5563
T_1	S_2	C_2	4449	321.78	475	5191	4394	379.85	511	5340
		C_3	4100	331.3	475	4906	4152	559.78	511	5223
		C_1	4439	373.66	475	5288	4388	479.81	511	5379
	S_3	C_2	4062	543.59	475	5056	4037	564.63	511	5138
		C_3	3687	855.37	475	5017	3693	754.77	511	4959
		C_1	5446	0	475	5840	5365	0	511	5957
	S_1	C_2	4983	129.95	475	5541	4936	0	511	5494
		C_3	4460	349.86	475	5285	4393	149.94	511	5054
		C_1	4534	361.76	475	5327	4490	181.83	511	5227
T_2	S_2	C_2	4148	427.45	475	5032	4130	326.89	511	4986
		C_3	4000	474.57	475	4950	3911	531.69	511	4954
		C_1	4223	450.77	475	5128	4202	481.33	511	5215
	S_3	C_2	3864	784.45	475	5123	3866	641.55	511	5019
		C_3	3635	902.5	475	5013	3682	788.26	511	4981

T= Tillage depth S=Stream size C=Cut-off irrigation

Grain yield (GY). Grain yield (GY) was influenced significantly at p(<0.05) by the irrigation management treatments (irrigation cut-off and stream size) and had the same trend in both seasons as shown in Table 6. The highest GY, over two seasons, (8600.50 kg ha^{-1}) was obtained from the cut-off irrigation at 90% of strip length(C2). The lowest values of Gy (6681.0 and 7321.0 kg ha^{-1}) were detected under C1 and C3 respectively. The increase due to C2 relative to C1 and C3 treatments were 14.8% and 22.3%, respectively. This finding might be attributed to that, under treatment C2 (90% cut-off), wetting front following stop irrigation almost reached the end of strip. Meanwhile, under treatment C3 (80% cut-off), the wetting front following stop irrigation never reached the end of strip induced less water than the actual needs of the growing plants. On the other hand, irrigation tell the end of strip (treatment C1), resulted in excess water more than the actual need of the growing plants. Both excess/or less water leads to reduction in grain yield. These results are in a good agreement with these obtained, in the same area of this study, by [12] they reported that yield of wheat and its components was the highest under treatment 90% cut-off in comparison with 80% cut-off and 100% without cut-off. Concerning the effect of stream size, S3 treatment ($4LS^{-1}m^{-1}$) gave the highest GY (7736.70 kg ha^{-1}), over both seasons and was 6.0 and 2.2% higher than in S1 and S2 treatments, respectively. This could be attributed to that higher stream size (S3) moves water to the end of the strip better than lower ones (S1 and S2), resulting in uniform water application which reflected in higher grain yield.

Regarding the effect of tillage practices, values of GY was greatest with T2 treatment (7750.95 kg ha^{-1} as an average of two seasons, and was 5.9% higher than in T1 treatment. These results are in the same trend of [35] they should that deep tillage practices performed better than shallow tillage by facilitating soil physical properties in silty clay loam soil under irrigated wheat crop.

TABLE 4
Contribution of ground water (GW) to wheat evapotranspiration (ETc) under different treatments during the two growing seasons.

Treatments		Season 2017/2018				Season 2018/2019			
		GW m^3ha^{-1}		GW %		GW m^3ha^{-1}		GW %	
		T_1	T_2	T_1	T_2	T_1	T_2	T_1	T_2
	C_1	0.00	0.00	0.00	0.00	0.00	0.00	0.00	0.00
S_1	C_2	0.00	129.95	0.00	3.25	0.00	0.00	0.00	0.00
	C_3	219.91	349.86	5.50	8.75	0.00	149.94	0.00	3.85
	C_1	312.26	361.76	7.81	9.05	189.92	181.83	4.87	4.66
S_2	C_2	321.78	427.45	8.05	10.69	379.85	326.89	9.74	8.39
	C_3	331.30	474.57	8.29	11.87	559.78	531.69	14.36	13.64
	C_1	373.66	450.77	9.35	11.27	479.81	481.33	12.31	12.35
S_3	C_2	543.59	784.45	13.60	19.62	564.63	641.55	14.48	16.46
	C_3	855.37	902.50	21.39	22.57	754.77	788.26	19.36	20.22
Means of C	C_1	248.9 c				218.4 c			
	C_2	367.5 b				318.8 b			
	C_3	503.8 a				447.3 a			
Means of S	S_1	121.8 c				39.7 c			
	S_2	371.2 b				324. 2 b			
	S_3	627.3 a				620.7 a			
Means of T	T_1	312.4 b				334.9 a			
	T_2	434.5 a				321.5 b			
T*S*C		**				**			

T= Tillage depth S=Stream size C=Cut-off irrigation
Numbers within a column with the different letter are significantly by LSD and ** mean highly significant

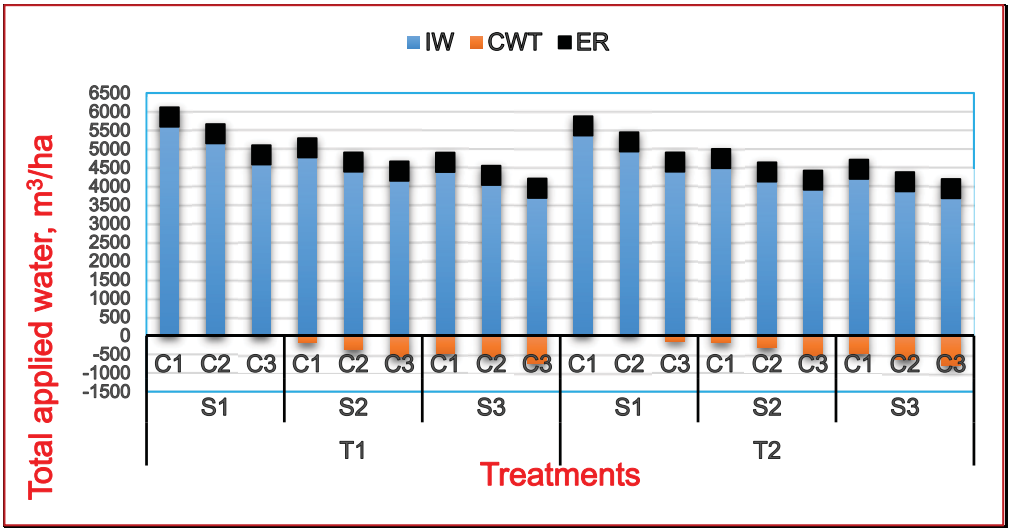

FIGURE 13
The relationship between total applied water from irrigation water (IW), effective rainfall (ER) and contribution of ground water (GW) and treatments during the second season.
T= Tillage depth S=Stream size C=Cut-off irrigation

TABLE 5
Water application efficiency (Ea%), distribution uniformity (Du%) and water distribution efficiency (Ed, %) as affected by cut-off irrigation. Stream size and depth of tillage during the 1st and 2nd seasons.

Treatments		Season 2017/2018						Season 2018/2019					
		Ea, %		Du %		Ed %		Ea, %		Du %		Ed %	
		T_1	T_2	T_1	T_2	T_1	T_2	T_1	T_2	T_1	T_2	T_1	T_2
	C_1	43.5	45.5	56.55	59.15	75.90	58.24	42.3	45	54.99	58.5	78.94	82.14
S_1	C_2	52.9	55.6	68.77	72.28	70.89	70.05	52.4	55	68.12	71.5	73.73	72.85
	C_3	47.3	49.7	61.49	64.61	63.34	65.15	46.8	49.2	60.84	63.96	67.95	69.43
	C_1	51.1	53.6	66.43	69.68	79.43	80.76	50.6	53.1	65.78	69.03	82.61	83.99
S_2	C_2	60.2	63.1	78.26	82.03	73.40	75.65	59.6	62.5	77.48	81.25	76.34	78.68
	C_3	55.9	58.5	72.67	76.05	68.09	70.76	55.3	57.9	71.89	75.27	70.81	73.59
	C_1	55.9	58.7	72.67	76.31	88.40	90.25	55.3	58.1	71.89	75.53	91.94	93.86
S_3	C_2	71.0	74.4	92.3	94.72	83.07	87.02	70.3	72.0	91.39	93.6	86.39	90.50
	C_3	67.1	70.1	87.23	91.13	70.51	75.98	66.4	69.4	86.32	90.22	73.33	79.02

T= Tillage depth S=Stream size C=Cut-off irrigation

The interaction between irrigation management (cut-off and stream size) and tillage practices treatments was significant ($p<0.05$). The highest GY was 8665. and 9051 kg ha^{-1} in the 1st and 2nd season, respectively, under the treatment C2 S3 T2. While the lowest one was 6386 and 6959 kg ha^{-1} under the treatment C1 S1 T1, respectively.

Straw yield (SY). Straw yield (SY) was significantly influenced by the different irrigation management treatments and tillage practices. All treatments were significantly differing from each other as shown in Table 6. Treatment C2 (90% cut-off) yielded the highest SY (12785.0 kg ha^{-1}) and was higher by 17.5 and 12.2% than in C1 and C3, over both seasons, respectively. SY under the stream size treatments had the same trend in both seasons as that of GY, and increased with increasing the stream size, the highest SY was 11763.8 kg ha^{-1} for the treatment of S3 followed by S2 to be 11559.0 kg ha^{-1} and S1 to be 11228.5 kg ha^{-1} over the two seasons. The results pertaining to tillage practices showed that T2 treatment had the highest SY to be 11785.85 kg ha^{-1}, over two seasons, and was higher by 4.7% than T1 treatment (10-20 cm depth). The interaction effect between the irrigation management and tillage practices was significant ($p<0.05$) and reveled that treatment of C2 S3 T2 had the highest SY to be 12147 kg

ha^{-1} over the two seasons. The lowest value of SY was 9314 kg ha^{-1} was obtained from C1 S1 T1 treatment. The reason of higher grain and straw yield and might be due to the optimum supply of soil moisture which created by the proper irrigation cut-off at 90% of strip length (C2) and the high stream size 4 $LS^{-1}m^{-1}$ (S3) as well as, the appropriate tillage practices 20-30 cm depth (T2) for wheat crop cultivation under the condition of the study area. Similar results were found by [12].

It is evident from the results that grain and straw yield in the 2nd season was higher than that of the 1st season.

Irrigation water productivity (WP). Water productivity is used to measure the relationship between the amount of crop produced and amount of water involved in crop production and is expressed as crop production per unit volume of water. Different water productivity indices results from different water input options. It was defined as a ratio between crop yield achieved and the consumptive water use, total water use or the irrigation water with drawl when that assessment aims at evaluating the performance of given irrigation systems [39]. In the present study the water productivity was calculated as a ratio between crop yields achieved from the irrigation water input [40]. A higher crop water productivity (WP) resulted in either the same production from less water resources, or a higher production from the same water resources, depending on irrigation water management, tillage practices and soil fertility.

TABLE 6
Wheat grain and straw yield (kg ha^{-1}) as influenced by irrigation cut-off (C), stream size (S) and tillage depth (T) during the two growing seasons.

Treatment.		Grain yield				Straw yield			
		1st Season		2nd Season		1st Season		2nd Season	
		T_1	T_2	T_1	T_2	T_1	T_2	T_1	T_2
S_1	C_1	6674	7110	9463	10004	6960	7418	9849	10400
	C_2	7963 a	8513	11059	11740	8313	8891	11478	12173
	C_3	6101	6503	8754	9252	6358	6781	9224	9922
S_2	C_1	6970	7419	9830	10386	7271	7743	10224	10791
	C_2	8281	8655	11454	11916	8648	9040	11880	12352
	C_3	6348	6771	9060	9584	6618	7062	9636	10170
S_3	C_1	7168	7656 b	10075	10679	7478	7991	10473	11090
	C_2	8411	8665	11614	11929	8784	9051	12044	12366
	C_3	6555	6973	9316	9834	6835	7274	9897	10425
C_1		7166.0 b		7476.0 b		11024.8 b		11423.1 b	
C_2		8414.0 a		8787.0 a		12570.5 a		13000.9 a	
C_3		6541.0 c		6821.o c		10252.0 c		10831.1 c	
S_1		7144.0 c		7453.5 c		10997.3 c		11459.7 c	
S_2		7407.6 b		7730.3 b		11323.7 b		11794.3 b	
S_3		7571.2 a		7902.2 a		11526.4 a		12001.2 a	
T_1		7163.4 b		7474.0 b		11021.4 b		11474.7 b	
T_2		7585.1 a		7916.8 a		11543.4 a		12028.7 a	
T*C*S		**		**		**		**	

T= Tillage depth S=Stream size C=Cut-off irrigation
Numbers within a column with the different letter are significantly by LSD and ** mean highly significant

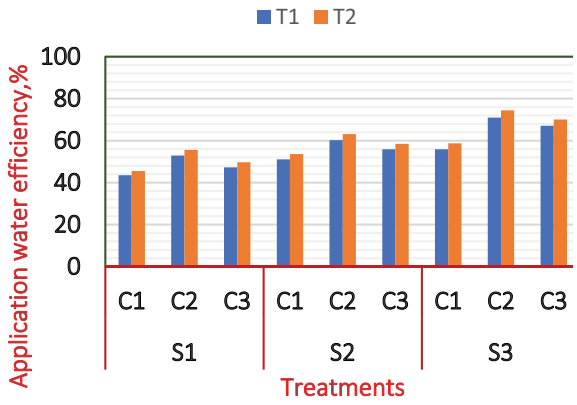

FIGURE 14
Effect of cut-off irrigation(C), stream size (S) and depth of tillage (T) on water application efficiency (Ea, %) for 1st season.

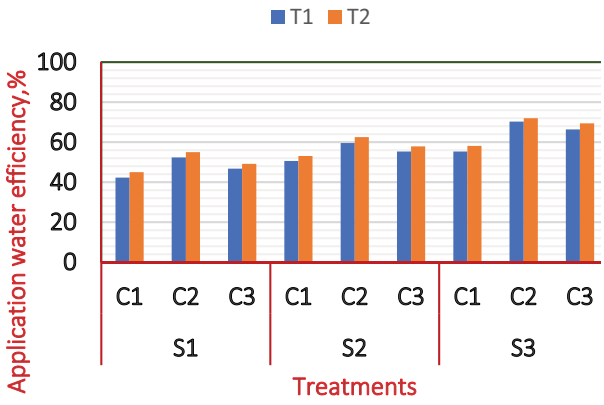

FIGURE 15
Effect of cut-off irrigation(C), stream size (S) and depth of tillage (T) on water application efficiency (Ea, %) for 2nd season.

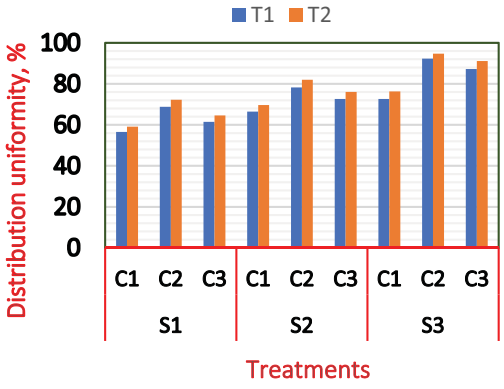

FIGURE 16
Effect of cut-off irrigation(C), stream size (S) and depth of tillage (T) on distribution uniformity (Du) for 1st season

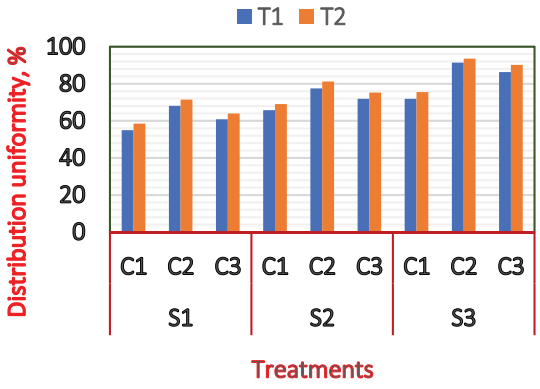

FIGURE 17
Effect of cut-off irrigation(C), stream size (S) and depth of tillage (T) on distribution uniformity (Du) for 2nd season.

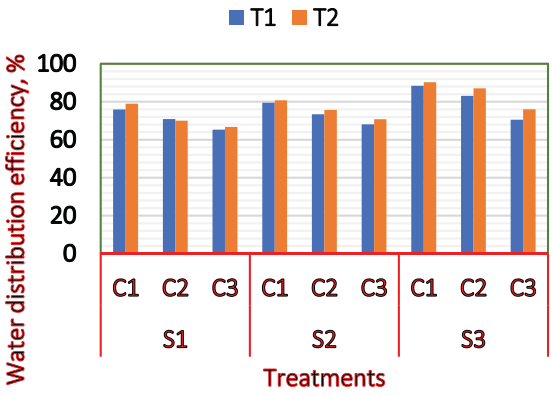

FIGURE 18
Effect of cut-off irrigation(C), stream size (S) and depth of tillage (T) on water distribution uniformity (Ed%) for 1st season.

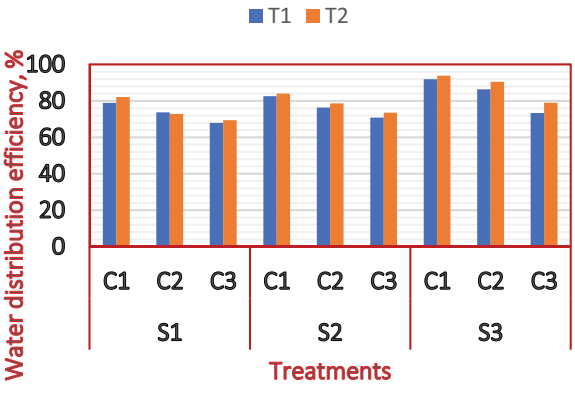

FIGURE 19
Effect of cut-off irrigation(C), stream size (S) and depth of tillage (T) on water distribution uniformity (Ed%) for 2nd season.

As shown in Table 7, WP increased significantly at (P< 0.05%) with increasing the cut-off irrigation. The cut-off irrigation at 90% of the strip length (C2), the highest values were 1.88 and 1.77 kg m^{-3} during the 1st and 2nd seasons, respectively. The lowest one was 1.46 and 1.29 kg m^{-3} were recorded for the treatment of C1 (the control) for the same two seasons. Regarding the stream size effect, results revealed that WP increased significantly with increasing the stream size in the following order S3 >S2 > S1, i.e., the stream size 4 $LS^{-1}m^{-1}$ (S3) had the highest values (1.88 and 1.73 kg m^{-3}) for the 1st and 2nd seasons respectively. The lowest values were 1.37 and 1.34 kg m^{-3} were obtained from treatment of S1 (the control) for the same two seasons respectively. Also, WP affected significantly at P< 0.05% by the tillage practices. The tillage depth 20-30 cm (T2) treatment had higher values to be 1.73 and 1.63 kg m^{-3} than the tillage depth 10-20 cm (T1) treatment which were 1.56 and 1.43 $kg.m^{-3}$, for the 1st and 2nd seasons respectively. These results are similar to these obtained by [12], 33] and [41]. [The interaction between irrigation water management (cut-off and stream size) and tillage depth treatments was highly significant (P> 0.05%). The obtained results revealed that the highest values of WP (2.24 and 2.34 kg m^{-3}) were recorded for T2 S3 C2 treatment during the 1st and 2nd seasons respectively, while the lowest one (1.13 and 1.24 kg m^{-3}) were detected under T1 S1 C1 for the same two seasons. This means that WP under the treatment T2 S3 C2 is higher than the control treatment T1 S1 C1 by about 48% as an overall average of two seasons. The obtained values of wheat WP in the present study exceed in all cases those reported by FAO (0.8-1.0 kg m^{-3}) earlier given by [42]. According to [43] the range of WP for irrigated wheat is very large (0.6-1.7 kg m^{-3}). They ascribed the variability of WP to climate, water management and soil (nutrient) management, among others. The high values of WP obtained by C2 and S3 and T2 treatments could be attributed to the less delivered amount of irrigation water which induced from the application of C2 ,S3 and T2 treatment relative to the other treatments (Table 5), and to the better performance of the deep tillage (T2) than the shallow depth (T1) by facilitating the soil physical properties which reflected in higher grain yield. The most outstanding conclusion is that WP can be increased significantly if irrigation water is reduced. On other words, producing more food from less water can be achieved by increasing the WP. So, cut-off irrigation at 90% of strip length with stream size 4L $S^{-1}m^{-1}$ under tillage depth 20-30 cm can be a promising strategy to maximize wheat yield and to improve the water productivity. When water supplies are limiting, the farmers goal should to maximize net income per unit water rather than per land unite.

Economic efficiency (EE): Economic efficiency (EE) takes into account values of output, opportunity costs of inputs, and externalities and is achieved when scarce resources (as well as in Egypt) are allocated and used such that net value or net returns (returns minus costs) is maximized [30]. Regarding the effect of cut-off irrigation on EE was highly significant with C2 as compared with the other two treatments. Both C1 and C3 treatments were similar in the two seasons these trends occurred under all stream size treatments as shown in Table 7. The highest values 0.239and 0.272 \$US m^{-3} during the 1st and 2nd seasons respectively. The lowest one 0.139 and 0.169 \$US m^{-3} were recorded under treatment C1 (the control) for the same two seasons. Regarding the stream size effect, results revealed that EE increased significantly with increasing the stream size in the following order S3 >S2 > S1, i.e the stream size $4LS^{-1}m^{-1}$ (S3) had the highest values (0.199 and 0.244 \$US m^{-3}) for the 1st and 2nd seasons respectively. The lowest values (0.142 and 0.156 \$US m^{-3}) were obtained from treatment S1 (the control) for the same two seasons respectively. Also, EE affected significantly at P< 0.05% by the tillage practices. The tillage depth 20-30 cm (T2) treatment had higher values (0.187 and 0.216\$US m^{-3}) than the tillage depth 10-20 cm (T1) treatment (0.153 and 0.186 \$US m^{-3}), for the 1st and 2nd seasons, respectively.

Net return (NR). Regarding the effect of the tillage practices, stream size and cut off irrigation during the two growing seasons, the highest NR (1118.93 and 1223.06 \$US ha^{-1}) occurred with T2S3C2 and the lowest (428.34 and 617.20 \$US ha^{-1}) occurred with T1S1C3 during the 1st and 2nd seasons, respectively. Concerning the effect of stream size NR was greatest with S3 followed by S2 then S1. This occurred under each of the three-cut-off irrigation (C1, C2and C3) and two depths of tillage (T1 and T2) as shown in Table 8.

Concerning the effect of cut-off irrigation, NR was greatest with C2 followed by C1 then C3. This occurred under each of the three-stream size (S1, S2 and S3) and two depths of tillage (T1 and T2). The mean values for NR as an average of the two growing seasons due to C1, C2 and C3 were 802.41, 1152.99 and 631.05. \$US ha^{-1} respectively. The percent of increase in NR given by C2 was 30.4 % as compared with C1and 45.2 % as compared C3.Thus the cut-off irrigation treatments of C2 was superior to the C1 and C3 treatments

Benefit cost ratio BCR. Regarding the effect of water regimes and depth of tillage as shown in Table 8. The highest BCR (0.86 and 0.94) occurred with T2S3C 90% and the lowest (0.33 and 0.39) occurred with T1S1C3 during the 1st and 2nd seasons respectively. The mean BCR (over the two seasons) due to C1, C2 and C3 were 0.61, 0.89 and 0.48, re-

spectively (Table 6). The increases due to C2 in relation to the C1 and C3 regimes were 31.4% and 46.0%. Concerning the effect of stream size, BCR was greatest with S3 followed by S2 then S1. This occurred during the two growing seasons The mean values for BCR in the two growing seasons due to S1, S2 and S3 were 0.61, 0.67 and 0.71 respectively. The percent of increase in BCR given by S3 was 15.55 % as compared with S1and 5.7 % as compared S2 .Thus the discharge treatments of S2 and S3 were superior to the S1treatment.

CONCLUSIONS

In irrigation areas, particularly in which rainfall is unreliable for irrigation, the integrated irrigation management with suitable tillage practices is necessary to find ways for saving water and maximizing crops yield and water productivity. In addition, when the ground water table is shallow it can be used as a partial source for the needs of plant water, this leads to decrease the amount of water used for irrigation. The irrigation management through 90% cut-off irrigation of strip length with a stream size 4 $LS^{-1}m^{-1}$ under tillage depth of 20-30 cm (treatment of T2 S3 C2), could be applied for increase wheat yield and water productivity as well. Treatment of T2 S3 C2 had the highest values of wheat grain yield to be 10.297 ton ha^{-1}, straw yield to be 10.708 ton ha^{-1}, water application efficiency to be 73.43%, water productivity to be 2.29 $kg.m^{-3}$ and the BCR to be 0.90 compared to the control treatment (T1 S1 C1) which produced 6.67 ton ha^{-1}, 8.40 ton ha^{-1}, 42.9%, 1.2 and 0.36, respectively. Treatment of T2 S3 C2 also, saved the irrigation water amount by 42.84%. It is a particle mean for on farm effective water management since it reduces the amount of irrigation water. The shallow ground water table contributed to the needs of wheat to water by about 21.4% under the condition of the study area.

TABLE 7
Irrigation water (IW), water productivity (WP kg m^{-3}) and economic water productivity (EE$US m^{-3}) under different treatments during the two-growing season

Treatments		Season 2017/2018						Season 2018/2019					
		IW m^3 ha^{-1}		WP (kg m^{-3})		EE $US m^{-3}		IW m^3 ha^{-1}		WP (kg m^{-3})		EE $US m^{-3}	
s	Cut-off	T_1	T_2	T_1	T_2	T_1	T_2	T_1	T_2	T_1	T_2	T_1	T_2
S_1	C_1	5741	5446	1.13	1.27	0.10	0.13	5601	5365	1.24	1.38	0.12	0.15
	C_2	5252	4983	1.47	1.67	0.18	0.22	5153	4936	1.61	1.80	0.20	0.24
	C_3	4701	4460	1.25	1.42	0.09	0.12	4586	4393	1.39	1.54	0.11	0.14
S_2	C_1	4862	4534	1.39	1.60	0.14	0.17	4776	4490	1.52	1.72	0.16	0.19
	C_2	4449	4148	1.82	2.06	0.23	0.27	4394	4130	1.97	2.19	0.26	0.30
	C_3	4100	4000	1.55	1.65	0.12	0.15	4152	3911	1.59	1.81	0.14	0.18
S_3	C_1	4439	4223	1.61	1.79	0.16	0.20	4388	4202	1.70	1.90	0.18	0.22
	C_2	4062	3864	2.04	2.24	0.26	0.29	4037	3866	2.18	2.34	0.29	0.32
	C_3	3687	3635	1.76	1.87	0.15	0.18	3693	3682	1.85	1.98	0.17	0.20
Means of C	C_1	4618 a		1.46 c		2.31 b		5166 a		1.29 c		2.82 b	
	C_2	4784 b		1.88 a		3.89 a		4466 b		1.77 a		4.53 a	
	C_3	4335 c		1.58 b		2.31 b		3036 c		1.52 b		2.61 b	
Means of S	S_1	5385 a		1.37 c		2.37 c		5318 a		1.34 c		2.66 c	
	S_2	4929 b		1.68 b		2.38 b		4422 b		1.51 b		3.42 b	
	S_3	4423 c		1.88 a		3.32 a		3925 c		1.73 a		4.06 a	
Means of T	T_1	5082 a		1.56 b		2.55 b		4566 a		1.43 b		3.10 b	
	T_2	4743 b		1.73 c		3.12 a		4513 b		1.63 a		3.6 a	
T*S*C		**		**		**		**		**		**	

Numbers within a column with the different letter are significantly by LSD and ** mean highly significant

TABLE 8
Net return NR ($US) and benefit coast ratio BCR as affected by cut-off irrigation, stream size and depth of tillage during the two growing seasons

Treatments		Season 2017/2018				Season 2018/2019			
		NR ($US)		BCR		NR ($US)		BCR	
		T_1	T_2	T_1	T_2	T_1	T_2	T_1	T_2
S_1	C_1	585.66	694.68	0.45	0.53	665.52	779.82	0.51	0.60
	C2	939.66	1079.94	0.73	0.83	1035.24	1182.36	0.80	0.91
	C_3	428.34	527.94	0.33	0.40	504.96	617.22	0.39	0.47
S_2	C_1	667.02	779.52	0.52	0.60	750.48	868.62	0.58	0.67
	C2	1027.08	1118.94	0.79	0.86	1126.74	1223.04	0.87	0.94
	C_3	496.20	601.56	0.38	0.46	579.90	690.42	0.45	0.53
S_3	C_1	721.38	844.56	0.56	0.65	807.06	936.42	0.62	0.72
	C2	1062.72	1121.7	0.82	0.86	1163.88	1226.10	0.90	0.94
	C_3	553.02	657.06	0.43	0.50	639.18	748.32	0.49	0.57
C_1		763.98 b		0.58 b		840.84 b		0.64 b	
C2		1106.88 a		0.85 a		1199.10 a		0.92 a	
C_3		592.56 c		0.45 c		669.54 c		0.51 c	
S_1		757.92 c		0.58 c		840.60 c		0.64 c	
S_2		830.28 b		0.63 b		910.92 b		0.70 b	
S_3		875.22 a		0.67 a		957.90 a		0.74 a	
T_1		768.60 b		0.59 b		845.82 b		0.65 b	
T_2		879.66 a		0.67 a		960.48 a		0.73 a	
T*C*S		**		**		**		**	

Numbers within a column with the different letter are significantly by LSD and ** mean highly significant
The price of a kilo of grain wheat=0.226 $US and kilo straw =0.04 $US (1 Dollar=16 L.E (2018)

ACKNOWLEDGEMENTS

The authors wish to express sincere thanks to Prof. Dr. Said Mohamed Khalifa (May ALLAH have mercy on him), Agric. Engineering Dept., Faculty of Agriculture, Kafrelsheikh University, for his sincere supervision, encouragement, helpful advices in field irrigation engineering during our research.

REFERENCES

[1] McGill, J., Prikhodko, D., Sterk, B. and Talks, P. (2015). Egypt: Wheat sector review. FAO Investment Centre. Country Highlights (FAO) Eng. 21, 11.

[2] Cafpmas C.A.F.P.M.A.S. (2014). Central Agency for Public Mobilization and Statistics CAPMAS. Available: http://www.capmas.gov.eg/. Accessed date: 10/12/2014

[3] El-Marsafawy, S., Swelam, A. and Ghanem, A. (2018). Evolution of crop water productivity in the Nile Delta over three decades (1985–2015). Water. 10(9), 1168.

[4] Mensegue, H.R.V., Degioanni, A.J. and Cisneros, J.M. (2015). Estimating shallow water table contribution to soybean water use in Argentina. European Scientific Journal. 11(14), 1857–7881.

[5] Ayars, J.E., Christen, E.W., Soppe, R.W. and Meyer, W.S. (2006). The resource potential of in-situ shallow ground water use in irrigated agriculture: a review. Irrigation Science. 24(3), 147-160.

[6] Liu, E.K., Mei, X.R., Yan, C.R., Gong, D.Z. and Zhang, Y.Q. (2016). Effects of water stress on photosynthetic characteristics, dry matter translocation and WUE in two winter wheat genotypes. Agricultural Water Management. 167, 75-85.

[7] Luo, Y. and Sophocleous, M. (2010). Seasonal groundwater contribution to crop-water use assessed with lysimeter observations and model simulations. Journal of Hydrology. 389(3-4), 325-335.

[8] Kahlown, M.A. and Azam, M. (2002). Individual and combined effect of waterlogging and salinity on crop yields in the Indus basin. Irrigation and Drainage: The journal of the International Commission on Irrigation and Drainage. 51(4), 329-338.

[9] Liu, T. and Luo, Y. (2011). Effects of shallow water tables on the water use and yield of winter wheat ('Triticum aestivum'l.) Under rain-fed condition. Australian Journal of Crop Science. 5(13), 1692-1697.
[10] Zhong-feng, H.U.O., Qian, Z.H.A.O. and Ying-hua, Z.H.A.N.G. (2011). Experimental Study on effects of magnetization on surface tension of water. Procedia Engineering. 26, 501-505.
[11] Kahlown, M.A. and Ashraf, M. (2005). Effect of shallow groundwater table on crop water requirements and crop yields. Agricultural Water Management. 76(1), 24-35.
[12] Kassab, M.M. and Ibrahim, M.A.M. (2007). Cut off Wheat (triticum Sp.) Irrigation as an Effective Technique for Improving Water Management. Alexandria Science Exchange. 28(4), 158.
[13] Soares, A.A., Oliveira, R.A., Ramos, M.M., Rasch, A. and D'Ávila, J.H.T. (2000). Cutting-back furrow irrigation design-a new methodology. Engenharia Agrícola. 20(2), 119-129.
[14] Mostafazadeh, B., Farzamnia, M., Mostafazadeh, B. and Farzamnia, M. (2000). The study of hydraulic performance of furrow irrigation under different methods of discharge management. Journal of Science and Technology of Agriculture and Natural Resources. 4(3), 1-11.
[15] Kassab, M.M., Darwesh, R.K. and Ibrahim, M.A.M. (2012). Response of Egyptian Clover to Cutoff Irrigation Technique on Clay Soils at North Nile Delta. Alexandria Science Exchange. 33(3), 196-205.
[16] Jug, D., Đurđević, B., Birkás, M., Brozović, B., Lipiec, J., Vukadinović, V. and Jug, I. (2019). Effect of conservation tillage on crop productivity and nitrogen use efficiency. Soil and Tillage Research. 194, 104327.
[17] Amin, M., Khan, M. J., Jan, M.T., Ur Rehman, M., Tariq, J.A., Hanif, M. and Shah, Z. (2014). Effect of different tillage practices on soil physical properties under wheat in semi-arid environment. Soil Environ. 33(1), 33-37.
[18] Jin, H., Qingjie, W., Hongwen, L., Lijin, L. and Huanwen, G. (2009). Effect of alternative tillage and residue cover on yield and water use efficiency in annual double cropping system in North China Plain. Soil and Tillage Research. 104(1), 198-205.
[19] Brennan, J., Hackett, R., McCabe, T., Grant, J., Fortune, R. A. and Forristal, P. D. (2014). The effect of tillage system and residue management on grain yield and nitrogen use efficiency in winter wheat in a cool Atlantic climate. European Journal of Agronomy.54, 61-69.
[20] Khalifa, E.S., Okasha, A. and Shawat, S. (2019). Development of surface irrigation using surge irrigation technique. Fresen. Environ. Bull. 28(4A), 3121-3130.
[21] Majumdar, D.K. (2002). Irrigation Water Management: Principles and Practice. 2nd ed. Prentice Hall of India, New Delhi. 110001, 487. 261-283.
[22] Chavan, M.L, Khodke U.M. and Changade, N.M. (2010) Estimation of crop water requirement for irrigation planning in a semi-arid region. International Journal of Agricultural Engineering. 2(2), 236-242.
[23] Allen, R.G., Pereira, L.S., Raes, D. and Smith, M. (1998). Crop evapotranspiration-Guidelines for computing crop water requirements-FAO Irrigation and drainage paper 56. FAO Rome. 300(9), D05109.
[24] Smith, M. (1992). CROPWAT-a computer program for irrigation planning and management. FAO Irrigation and Drainage Paper. 46, 126.
[25] Ibrahim, I.M., Gaheen, S.A. and Ismail, S.M. (1995). Role of irrigation management on water parameters and yield of Sugar Beet in Shallow water Table soils of Nlie delta. Water Resources Management in Arid counturies, Muscat Sultanate of Oman. 98-106.
[26] Michael, A.M. (2008). Irrigation Theory and Practice. Vikas Publishing House Pvt.Ltd. New Delhi. pp.455-516.
[27] James, L.G. (1988). Principles of farm irrigation systems design. John Wiley and Sons Limited. 92.
[28] Ismail, S. M. (2014). Surface irrigation system-Planning and design of irrigation system. Bostan EL-Mearfa, Egypt (in Arabic). 86.
[29] Singh, R., Kundu, D.K. and Tripathi, V.K. (2006). Contribution of Upward Flux From Shallow Ground Water Table to Crop Water Use in Major Soil Groups of Orissa Jour. Agric. Physics. 6(1), 1-6
[30] Wichelns, D. (1999). Economic efficiency and irrigation water policy with an example from Egypt. International Journal of Water Resources Development. 15(4), 543-560.
[31] Li, J., Eneji, A.E., Duan, L., Inanaga, S. and Li, Z. (2005). Saving irrigation water for winter wheat with phosphorus application in the North China Plain. Journal of Plant Nutrition. 28(11), 2001-2010.
[32] El-Hadidi, E., Ibrahim, M., Abdel-hafez, S. and Eid, M. (2015). Effect of deficit irrigation and raised bed on wheat yield, water productivity and water saving in north Nile Delta, Egypt. Journal of Soil Sciences and Agricultural Engineering. 6(7), 845-862.
[33] EL-Hadidi, E., Saied, M., Ghaly, F. and Khalifa, R. (2016). Assessing the effect of water discharge rates and cut-off irrigation on wheat production and some water relations at North Nile Delta Region. Journal of Soil Sciences and Agricultural Engineering. 7(6), 397-407.

[34] Karimov, A.K., Šimůnek, J., Hanjra, M.A., Avliyakulov, M. and Forkutsa, I. (2014). Effects of the shallow water table on water use of winter wheat and ecosystem health: Implications for unlocking the potential of groundwater in the Fergana Valley (Central Asia). Agricultural Water Management. 131, 57-69
[35] Amin, M., Khan, M.J., Jan, M.T., Rehman, M., Tariq, J.A., Hanif, M. and Shah, Z. (2014). Effect of different tillage practices on soil physical properties under wheat in semi-arid environment. Soil Environ. 33(1), 33-37.
[36] Khan, M.J., Khattak, M.K. and Wahab, S. (2006). Influenced of Various tillage practices on selected Physical properties of sandy loam soil under Rainfred area. Sarhad Journal of Agriculture. 22(1), 71-80.
[37] Mosalm, W.M. (2009). Evaluation of surface irrigation under different rates of water discharge and nitrogen fertilization levels (Doctoral dissertation, Ph. D. Thesis, Fac. Agric. Mansoura Univ. Egypt), 45-115.
[38] Amer, A.M. (2011). Evaluation of surface irrigation as a function of water infiltration in cultivated soils in the Nile Delta. Irrigation and Drainage Systems. 25(4), 367-383.
[39] Cao, X., Wang, Y., Wu, P. and Zhao, X. (2015). Water productivity evaluation for grain crops in irrigated regions of China. Ecological Indicators. 55, 107-117.
[40] Pereira, L.S., Oweis, T. and Zairi, A. (2002). Irrigation management under water scarcity. Agricultural Water Management.57(3), 175-206.
[41] Moursi, E.A., Aziz, M.A. and ELMansoury, M.A. (2014). Effect of length of irrigation run and nitrogen rates on productivity of some wheat cultivars, some water relations and nitrogen content in heavy clay soils. J. Agric. Kafr. EL-Sheikh Univ. 40 (3), 630-658.
[42] Doorenbos, J. and Kassam, A.H. (1979). Yield response to water. Irrigation and drainage. FAO. Rome, Italy. (33),164-170.
[43] Zwart, S.J. and Bastiaanssen, W.G. (2004). Review of measured crop water productivity values for irrigated wheat, rice, cotton and maize. Agricultural Water Management. 69(2), 115-133.

Received: **15.06.2020**
Accepted: **20.01.2021**

CORRESPONDING AUTHOR

Abdelaziz Okasha
Agricultural Engineering Department,
Faculty of Agriculture,
Kafrelsheikh University,
Kafrelsheikh 33516 – Egypt

e-mail: abdelaziz.okasha@agr.kfs.edu.eg

© by PSP Volume 30– No. 05/2021 pages 4823-4829 Fresenius Environmental Bulletin

RESEARCH ON THE COOPERATIVE COUPLING DEVELOPMENT OF RURAL TOURISM AND URBANIZATION CONSTRUCTION FROM THE PERSPECTIVE OF ECOLOGICAL CIVILIZATION

Huijuan Ye*, Li Mao

Jiangsu Agri-Animal Husbandry Vocational College, Taizhou, Jiangsu Province 225300, China

ABSTRACT

Based on the tourism resources of Langshan Town, this paper explores the current situation of cooperative coupling development between rural tourism and urbanization construction in Langshan Town from the perspective of ecological civilization construction. By constructing the cooperative coupling model of rural tourism and new urbanization construction, the degree of cooperative coupling between rural tourism industry and urbanization construction in Langshan Town from 2014 to 2019 is analyzed. The research results show that the overall development level of rural tourism industry in Langshan Town is gradually rising from 2014 to 2019, and the overall level of urbanization construction in 6 years is on the rise. At the same time, the level of cooperative coupling between rural tourism and urbanization construction is generally improving. The improvement of coordination between the two systems is not only conducive to the coordinated development of economy, but also advocates the concept of ecological civilization construction, promotes the development of urbanization industry chain and provides economic support for the urbanization construction.

KEYWORDS:
Ecological civilization, Rural tourism, Urbanization construction, Cooperative coupling

INTRODUCTION

The 18th National Congress of the Communist Party of China advocates "vigorously promoting the construction of ecological civilization" and puts forward the development concept of new urbanization. The Party leadership points out that to accelerate the urbanization construction and improve the urbanization quality, it is necessary to integrate the concept of ecological civilization with the process of urbanization, and take a sustainable green, low-carbon, intelligent new urbanization path [1-2]. In order to coordinate the healthy development of urbanization, the State Council has adopted the National New Urbanization Plan (2014-2020) to encourage the accelerated development of urbanization. Compared with traditional industries, tourism is an emerging industry with unique advantages of environmental protection, low resource consumption, large employment capacity, low pollution and good comprehensive effect. In the process of urbanization development, tourism will gradually replace the former tertiary industry and become the key force leading the urbanization development. In the past, tourism products mainly focused on single sightseeing products. With the rapid development of the Internet era, high-tech technologies such as artificial intelligence and 5G communication have penetrated into all fields of life, including tourism. Modern tourism is no longer a single sightseeing, but is constantly upgrading into a supporting service industry with diversified sectors, such as clothing, food, housing, travel, tourism, shopping, entertainment, etc., and a diversified service system that is often dominated by leisure and vacation [3-4]. Moreover, the urban population is more and more inclined to take vacations at tourist destinations in rural areas during holidays, which greatly promotes the development of other tertiary industries. In cities and towns rich in tourism resources, tourism is often the leading industry to promote urbanization development. The coordinated development of the two is of great significance to promote regional economic development and accelerate urbanization construction. This paper studies the development of rural tourism in Langshan Town, Shaoyang City, Hunan Province and the cooperative coupling degree of urbanization construction, providing theoretical basis for the cooperative development of rural tourism industry and new urbanization in Langshan Town.

Analysis on the Cooperative Coupling Development Foundation of Rural Tourism and Urbanization Construction in Langshan Town. Analysis on the Current Situation of Tourism Industry in Langshan Town. Langshan Town is a small town located in Nanjun, Xinning County, Hunan Province. It is located at the junction of Hunan

and Guangxi, with Zhangjiajie in the north and Guilin in the south. It has unique features and pleasant landscape. Langshan has the title of national scenic spot, with a total area of 270 square kilometers and a total population of 30,000. Langshan Town has gained rich tourism resources due to its unique geographical features. In 2003, Langshan was listed as the national eco-tourism demonstration base, and successfully completed the application for the "China Danxia" project in 2010. All along, Langshan Town has been working hard towards the goal of 5A-level scenic spot. At present, the tourism industry in Langshan Town and the tertiary industry driven by it have become the economic pillar industries of local residents. With the continuous development of tourism, the per capita GDP of residents has continuously increased, and has even exceeded the national per capita GDP level in recent years (see Table 1).

Rural tourism is mainly composed of tourists, tourism resources, tourism industry and tourism products. The following conclusions can be drawn from the questionnaire survey of tourism in Langshan Town: (1) From the source of tourists, most of them are from local province, accounting for about 80%, while few from outside the province accounting for less than 20%. From the age of tourists, most of them are students, tourists aged 20-30 account for 45% while tourists aged 30-45 account for 34%, and tourists over 50 are relatively few, accounting for about 17%. (2) From the perspective of tourism motivation, tourists choose Langshan as their tourism destination mainly because of its close distance, beautiful environment and drop-by route. Among them, 35% of tourists, mainly from the province and aged over 40 years old, choose Langshan because of close distance, while 20% of tourists choose Langshan because of its unique style and beautiful environment, and about 10% of tourists choose Langshan in case of business trip or drop-by route [5-7].

Analysis on the Cooperative Coupling Interaction between Rural Tourism and Urbanization Construction in Langshan Town. The cooperative coupling of rural tourism and urbanization construction in Langshan Town is mainly reflected in the development foundation and opportunities. Good policies are not only conducive to attracting investment from tourism, but also strengthen the development of other tertiary industries closely combined with tourism, accelerate the industrial integration, and provide economic support for the development of urbanization [8]. The coupling on the basis of development is mainly reflected in the continuous growth of the national economic foundation, which brings essential basic resources such as transportation and talents to the development of rural tourism and urbanization construction. In addition, the growth of residents' income also promotes the continuous increase of people's spending on tourism [9]. The relationship between the development of rural tourism industry and the new urbanization construction in Langshan Town is as follows: first, the development of new urbanization and the continuous growth of economy have provided the development of rural tourism industry with the support of transportation, materials, talents and technologies, including the government's support, implementation of tax and fee reduction policies, further improvement of residents' land system, introduction of technologies, etc. On the other hand, Langshan Town's urbanization has injected new vitality, technology and talents into the development of tourism industry, which are the core strength to speed up economic construction [10-12]. Urbanization has also provided support for the development of rural tourism in Langshan Town. Furthermore, the development of rural tourism industry has not only driven the construction of urban culture and spiritual civilization, but also significantly promoted the construction and development of new urbanization and accelerated the urban-rural integration. As shown in Figure 1, it is the cooperative coupling interaction mechanism between rural tourism and urbanization construction in Langshan Town [13-14].

MATERIALS AND METHODS

Cooperative Coupling Model Design of Rural Tourism and New Urbanization Construction in Langshan Town. The development of rural tourism and the level of new urbanization construction in Langshan Town complement each other. In view of the fact that the two subsystems are similar to the coupling coordination system, they have the same analysis process. In the process of system development from disorder to order, the coupling degree is the main measure of the co-evolution effect. In this paper, the physical concept of coupling degree is used to define and measure the degree of correlation between the key factors in two sub-systems of rural tourism and urbanization construction in Langshan Town as the degree of cooperative coupling [15].

Comprehensive Development Level Evaluation Model. In this paper, the comprehensive development level of rural tourism and urbanization construction in Langshan Town is analyzed, and the linear weighting method is used. The formula is as follows: $u_i = \sum_{j=1}^{p} \lambda_{ij} u_{ij}, \sum_{j=1}^{p} \lambda_{ij} = 1$. In the formula, u_{ij} represents the characteristic index value, u_i represents the comprehensive development level value of the system, and λ_{ij} represents the weight, which is obtained through entropy weight method in physics [16]. In order to eliminate the difference in the order of magnitude of evaluation indexes, the original data are processed by the following formula to

TABLE 1
Comparison between GDP Per Capita of Langshan Town and National GDP Per Capita

Years	GDP per capita in Langshan Town (yuan)	Per capita GDP growth rate of Langshan Town (%)	China's GDP per capita (yuan)	China's per capita GDP growth rate (%)
2016	37889.9	18.77	35642.8	14.55
2017	41245.9	10.22	39997.2	9.81
2018	49986.3	12.56	45365.8	8.99
2019	57168.3	14.37	49562.1	9.25

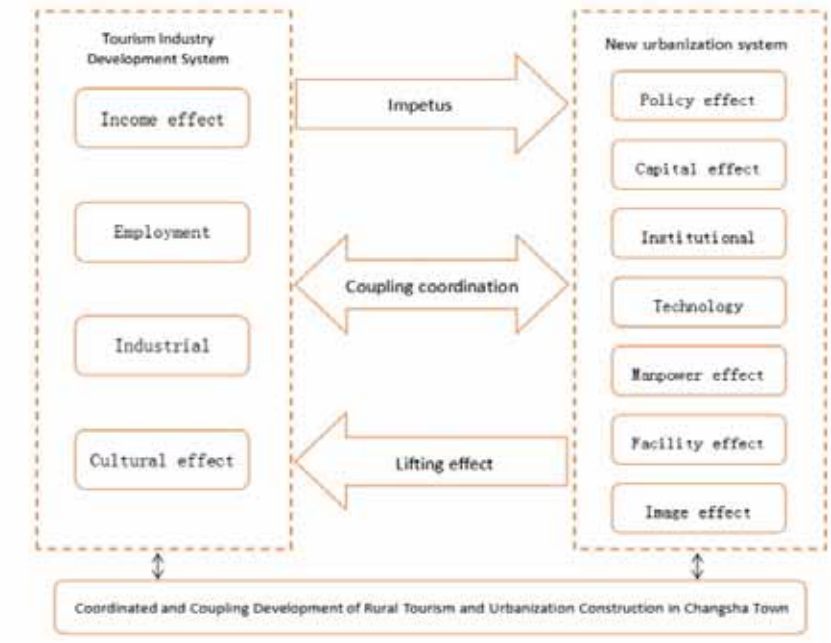

FIGURE 1
Cooperative Coupling Development Mechanism of Rural Tourism and Urbanization Construction in Langshan Town

obtain the u_{ij}, and the calculation formula is: $u_{ij} = \frac{x_{ij} - \min(x_j)}{\max(x_j) - \min(x_j)} \times 0.99 + 0.01$.

Cooperative Coupling Evaluation Model. The coupling evaluation model of rural tourism and urbanization construction in Langshan Town is established, and the calculation formula is as follows: $C = \frac{2\sqrt{u_1 \times u_2}}{u_1 + u_2}$. In the formula, C represents the coupling degree of the system, u_1 represents the comprehensive development level of rural tourism in Langshan Town, and u_2 represents the comprehensive development level of urbanization construction. In the evaluation process, the formula can only express the interaction strength of the two systems, so the conclusion may deviate from the actual situation. Therefore, in the actual evaluation process, the cooperative coupling degree model is introduced, as follows: $D = \sqrt{C \times T}$, $T = \alpha_{u_1} + \beta_{u_1}$. D represents the cooperative coupling degree of the two research systems, T is the comprehensive evaluation index, α and β are the specific weight. There are many factors that promote the urbanization construction of Langshan Town. In addition to tourism, other industries, such as hotel accommodation, transportation, agricultural products, are providing the basis for the urbanization construction. Through consultation with relevant professionals, the specific weight scores of α and β are set as 0.35 and 0.65 respectively.

First of all, according to the cooperative coupling development level (see Table 2), the general context of rural tourism and urbanization construction in Langshan Town is analyzed. The developable space is defined, and the lagging development system in the two systems is identified [17].

Construction of Two System Indexes. Rural tourism and urbanization construction in Langshan Town are complex multi-factor systems, not simple linear systems, so it is often necessary to use multiple indicators for comprehensive evaluation, draw

on the existing evaluation system, and construct the cooperative coupling measurement index system, as shown in Table 3. The table includes indicators that represent the development of rural tourism, such as total tourism revenue, number of tourists, etc. In addition, indicators such as GDP per capita and the proportion of non-agricultural population are cited to reflect the current situation of urbanization construction [18].

TABLE 2
Classification Criteria for Cooperative Coupling Level of Rural Tourism and Urbanization Construction

Cooperative coupling	Collaboration level	Cooperative coupling	Collaboration level
0.000-0.090	Extreme disorder	0.500-0.590	Barely coordinated
0.100-0.190	Severe disorder	0.600-0.690	Primary coordination
0.200-0.290	Moderate disorder	0.700-0.790	Moderate coordination
0.300-0.390	Mild disorder	0.800-0.890	Good collaboration
0.400-0.490	Imminent imbalance	0.900-1.000	High-quality collaboration

TABLE 3
Cooperative Coupling Measurement Index System of Rural Tourism and Urbanization Construction in Langshan Town

Coupling system	Indicator type	Evaluation index	Weights	Unit
Rural Tourism Development System	/	Tourism revenue	0.527	Ten thousand yuan
/	/	Total number of tourists	0.361	Ten thousand
/	/	Total accommodation and food consumption	0.457	Ten thousand yuan
Urbanization system	Population urbanization	Proportion of non-agricultural population	0.147	%
/	Economic urbanization	GDP per capita	0.315	yuan
/	/	Coefficient of income difference between urban and rural residents	0.077	%
/	Social urbanization	Basic pension insurance coverage	0.099	%
/	Environmental urbanization	Deep forest coverage	0.081	%
/	/	Urban sewage treatment rate	0.233	%

TABLE 4
Evaluation of Cooperative Coupling Development between Rural Tourism and Urbanization Construction in Langshan Town

Year	Comprehensive development level of rural tourism (u_1)	Comprehensive development level of urbanization (u2)	Cooperative coupling (D)	Evaluation
2014	0.010	0.245	0.251	Imminent imbalance
2015	0.511	0.523	0.505	Barely coordinated
2016	0.374	0.453	0.472	Imminent imbalance
2017	0.792	0.740	0.871	Good collaboration
2018	0.899	0.907	0.943	High-quality collaboration
2019	0.967	0.758	0.898	Good collaboration

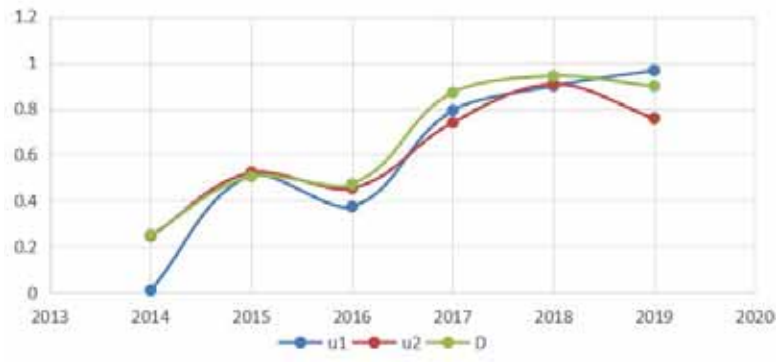

FIGURE 2
Cooperative Coupling Development of Rural Tourism and Urbanization Construction in Langshan Town

RESULTS AND DISCUSSION

Research and Analysis on the Cooperative Coupling Development of Rural Tourism and Urbanization Construction in Langshan Town. Data Processing and Research Analysis Results. This paper makes statistics on the data of Langshan Town's tourism industry development in the six years from 2014 to 2019, uses relevant formulas to deal with the original data related to indicators with dimensionless processing, and calculates the processed data using the model. See Table 4 for the analysis results. According to the data in Table 4, the trend is plotted to obtain Figure 2.

Description and Analysis of Results. Based on the analysis of the data in Table 4 and the trend in Figure 2, it can be seen that the overall development level of the rural tourism industry in Langshan Town is gradually rising from 2014 to 2019. From 2015 to 2016, although the overall development level is slightly declining, it is soon rise again and continuously rising until 2019. From 2014 to 2019, the overall level of urbanization construction showed a trend of rising first then falling, and rising then falling. Although the development level declined from 2018 to 2019, the overall development level in 2019 still reached 0.758, maintaining a high level. Therefore, the overall level of urbanization construction in the six years is a rising trend. As can be seen from Figure 2, the degree of cooperative coupling between rural tourism and urbanization construction (D) is also steadily increasing year by year. The development trend is similar to the level of rural tourism development. The level of cooperative coupling has gradually improved from the initial imbalance state to a good coordination state, and even reached a high-quality coordination state by 2018, which shows that the synergistic effect and interaction between rural tourism and urbanization construction in Langshan Town are gradually increasing. With the convening of the 18th National Congress of the Communist Party of China, the concept of ecological civilization construction has gradually become popular among the people. In order to coordinate the healthy development of urbanization and promote the innovation of relevant systems and policies, the government has also issued numerous policies to support the development of local tourism industry, which has continuously greatly promoted the development speed of urban economy. At the same time, it has improved the cooperative coupling degree between rural tourism and new urbanization construction, from the initial imbalance state to the later harmonious, unified and sustainable high-quality coordinated development state [19-20].

Through the research and analysis of the cooperative coupling degree between rural tourism development and urbanization construction in Langshan Town from 2014 to 2019, it can be seen that firstly, the cooperative coupling level between rural tourism and urbanization construction in Langshan Town is generally improving, and the improvement of the coordination level of the two systems is not only conducive to the coordinated development of economy, but also advocates the concept of ecological civilization construction, promotes the development of rural tourism and the rise of other tertiary industries driven by tourism, which in turn provide economic support for the urbanization construction; Secondly, the promotion of rural tourism development to urbanization construction needs to be enhanced. Although Langshan Town has unique features and rich tourism resources, the current driving force of urbanization construction in this town is limited. The development of rural tourism industry should be further standardized and needs the support of relevant policies. However, we can also see that the rural tourism industry and its coordination with urbanization construction in Langshan Town is continuously improving. Therefore, it is believed that under the government's active guiding policies, the degree of cooperative coupling between rural tourism and urbanization construction will continue to develop towards the goal of high quality and coordination, thus promoting the construction of tourism culture and the development process of new urbanization in Langshan Town.

CONCLUSIONS

This paper explores the current situation of cooperative coupling development between rural tourism and urbanization construction in Langshan Town from the perspective of ecological civilization construction. By constructing the cooperative coupling model of rural tourism and new urbanization construction, the degree of cooperative coupling between rural tourism industry and urbanization construction in Langshan Town from 2014 to 2019 is analyzed. The research results show that the overall development level of rural tourism industry in Langshan Town is gradually rising from 2014 to 2019, and the overall level of urbanization construction in 6 years is on the rise. At the same time, the level of cooperative coupling between rural tourism and urbanization construction is generally improving. The improvement of coordination between the two systems is not only conducive to the coordinated development of economy, but also advocates the concept of ecological civilization construction, promotes the development of urbanization industry chain and provides economic support for the urbanization construction.

ACKNOWLEDGEMENTS

The study was supported by "Research on School-level Topics of Jiangsu Agri-animal Husbandry Vocational College (Grant No. NSFR 201901)".

REFERENCES

[1] Zhang, H.G. (2018) Analysis on development of green economy in Tibet from the perspective of ecological civilization. Journal of Landscape Research. 10(5), 72-75.
[2] Luan, Y.L., Hu, S.E. (2018) Construction of a community of human destiny from the perspective of ecological civilization. Journal of Central University for Nationalities (Natural Science Edition). 27(1), 11-14.
[3] Wang, X. (2016) Strategy of sustainable development of rural tourism in China from the perspective of ecological civilization. Journal of Central South University of Forestry and Technology: Social Science Edition. 10(3), 20-23.
[4] Yan, D. (2019) Analysis of environmental governance from the perspective of ecological civilization construction. Northern Environment. 31(6), 194-195.
[5] Zhang, L. (2018) Research on enterprise environmental accounting information disclosure from the perspective of environmental protection—taking Sinopec as an example. IOP Conference. 452(3).
[6] Gao, J., Yang, W., Tian, M. (2016) Countermeasures for sustainable development of urbanization in China based on the perspective of ecological civilization. China Development. 16(1), 7-11.
[7] Huang, Z., Huang, R. (2018) Rural culture research in the context of urbanization and tourism development: academic contention and research direction. Geographical Research. 37(2), 233-249.
[8] Caihong, Z. (2016) Research on application of edible landscape in rural tourism: A case of dendrobium landscape in Pu'er City. Campus English (Teaching and Research Edition). 9, 250-252.
[9] Baohua, W.U. (2016) Research on the influential factors of rural human resources development of Tianjin in the context of new-type urbanization. Chinese Journal of Urban and Environmental Studies. 3(4), 1550029.
[10] Lu, X., Li, C. (2016) Research on the interaction between tourism development and urbanization in rural tourism destinations. Journal of Dalian University of Technology: Social Science Edition. 37(4), 85-90.
[11] Wang, Y., Lu, Z., Zhao, H., Ma, Y. (2020) The impact of urbanization development on the meteorological and environmental elements in the central cities of Liaoning Province. IOP Conference Series Earth and Environmental Science. 446, 032107.
[12] Huang, H., Shen, W.N., Yuan, S. (2019) Research on coupling degree of green development and urbanization in Beijing-Tianjin-Hebei Region. Journal of Hunan University of Finance and Economics. 35(3), 87-93.
[13] Zhang, C.H. (2016) Research on application of edible landscape in rural tourism: A case of dendrobium landscape in Pu'er City. English on Campus. 9, 250-252.
[14] Wang, D., Li, Q. (2019) Research on coupling relationship between new-type urbanization and family farm development. Qiushi Academic Journal. 46(4), 64-71.
[15] Dhiab, L.B., Dkhili, H. (2019) Impact of income, trade, urbanization, and financial development on CO_2 emissions in the GCC countries. International Journal of Advanced and Applied Sciences. 6(7), 36-42.
[16] Sun, Y., Xia, X. (2015) Research on Rural Tourism Development in Liaoning Province from the Perspective of New Urbanization. Journal of Central South University of Forestry and Technology: Social Science Edition. 9(3), 69-72.
[17] Yu, B. (2019) Research on the relationship between rural tourism and new rural construction in the context of new urbanization—Taking Henan Province as an example. Journal of Xuchang University. 38(1), 127-131.
[18] Chi, N., Xue, B., Ren, C. (2017) How to retain the nostalgia in rural tourism. Asian Agricultural Research. 04, 103-104.
[19] Li, T. (2016) Theoretical exploration and practice of the coupled development of ecological agriculture and ecotourism in China from the perspective of ecological civilization. Heihe Journal. 4, 7-9.
[20] Chen, L, Peng, D., Jia, B., Xiang, S., Cao, S. (2013) Research on Rural Tourism Development from the Perspective of Ecological Civilization--Taking Fuling District of Chongqing as an Example. Green Technology. 9, 257-260.

Received: **04.06.2020**
Accepted: **17.10.2020**

CORRESPONDING AUTHOR

Huijuan Ye
Jiangsu Agri-Animal Husbandry
Vocational College,
Taizhou, Jiangsu Province 225300 – China

e-mail: liuqiaobin8889@sina.com

© by PSP Volume 30– No. 05/2021 pages 4830-4835 Fresenius Environmental Bulletin

RESEARCH ON CYCLIC REDESIGN OF PRODUCT BASED ON INDOOR ECOLOGICAL ENVIRONMENT PROTECTION

Yujie Shu, Sheng Kang*, Jianping Jiang

School of Art and Design, Shaoyang University, Shaoyang, Hunan 422000, China

ABSTRACT

With the growing prosperity of Internet, resource shortage, environmental pollution are becoming increasingly severe. Green development have become national strategy, and the limitation and urgency constantly prompt designers to attach more importance to environment protection. Meanwhile, designers begin to pay attention to cyclic reuse of resource and take the responsibility for society and environment. This study focused on the significance of cyclic redesign on environmental protection, resource conservation and sustainable development based on indoor ecological environment protection, studied and summarized four design methods of cyclic redesign, advocated to innovatively realize recycling by redesign waste product and old material, so as to achieve the purpose of alleviating resource shortage, reducing waste generation and protecting environment.

KEYWORDS:
Environmental pollution, Ecological resource, Cyclic redesign, Ecological environment protection

INTRODUCTION

Cyclic redesign is a design mode to reduce the impact of products on indoor environment based on the idea of environmental protection. It is not only conducive to cyclic utilization, but also it is an important part of green design [1-2]. Green design under the concept of ecological environment protection is based on the theory of ecological environment protection and applied the original ecological concept to the whole process of design. Ecological design puts emphasis on the management process of considering environmental factors in an all-round way, minimizing the impact of the designed products on the environment in the whole life cycle. The concept of "redesign" coincides with the ecological design. Both of them consider the environment as a whole, balances the use value of products and the energy consumption of reproducing as well as the relationships between human and environment, economic development and resource conservation [3-5]. In traditional product design, the environmental cost of product almost originates from design. In contrast, the cyclic redesign of product requires higher demand in reducing waste, saving resources and reducing energy consumption. "Redesign" also popularly known as "reuse" - is to give full play to the innovative application of existing products, to use one thing for many purposes, or to recycle, to innovate, or to reuse the product or the packaging of the product that have been used by simple processing and decoration. Reuse, a part of the concept of redesign, gives priority to using old materials or old products as new materials for design so as to reduce waste and energy consumption. Meanwhile, it seizes the creative opportunity from new process and redesigned products and optimizes the environmental protection performance of products [6].

MATERIALS AND METHODS

The Significance of Cyclic Redesign on Ecological Environment Protection. Alleviation of Environmental Pollution from Discarded Products. The advocacy of cyclic redesign and the reuse of discarded products exerts a positive effect on alleviating the environmental problems caused by discarded products and old materials. Product design is one of the important means to bring about business opportunities in the market competition. During the process of interior product design, many enterprises accelerate the frequency of product upgrading while chasing popularity, so that the products which are designed and manufactured can be replaced by more fashionable and powerful products in a short time. Therefore, design has become an essential medium to promote the unrestrained consumption of many consumers [7-8], which will greatly shorten the life of products, resulting in some products with use value or recycling value being abandoned prematurely. This "various design styles" make people concern about the environmental deterioration caused by a mass of abandoned and obsolete products and discarded materials while enjoying prosperity of the consumer market. Severe ecological environment situation hides behind the booming consumption market. Designers can reuse the concept of "design" again to digest or transform existing products and their wastes. For example,

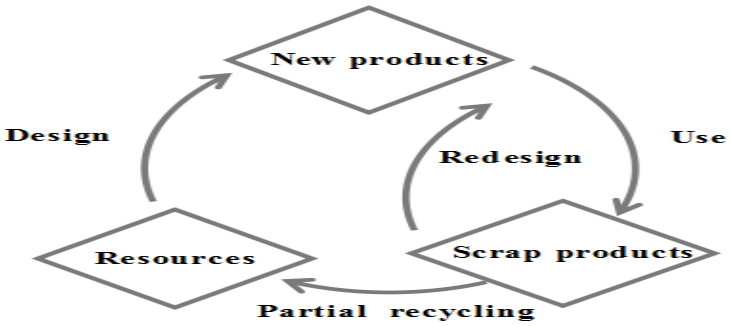

FIGURE 1
Material Circulation Diagram of Product Recycle

mineral water bottles can be remade as a wide variety of "small flowerpots", which is not only beautiful and convenient to decorate indoor environment, but also it increases the cyclic reuse of resources, reduces waste and protects the natural environment.

Settlement of Resource Shortage in Product Design and Manufacturing. The advocacy of cyclic redesign is beneficial to settle resource shortage emerged in the process of product design and manufacturing. In product manufacturing, it is inevitable to use processing technology with serious pollution and consume plenty of raw materials, but it is also accompanied by a large amount of energy consumption while using products. In addition, abandoned products need a long degradation time and it will exert a negative effect on environment. In order to alleviate the resource shortage crisis and make great full use of precious limited resources on the earth, designers must high value the whole life cycle of products from design to discard, so that the design,usage and discard of products can have many opportunities for re-innovation, redesign, reproducing and recycling to reduce the influence on the environment. Advocating the concept of cyclic redesign of products can focus on energy conservation at all stages of the product life cycle and fundamentally cope with resource shortage, which is also conducive to the sustainable development of the ecosystem as well [9-11].

RESULTS AND DISCUSSION

Research on the Design Method of Cyclic Redesign. The purpose of cyclic redesign of indoor ecological environment protection is to develop the second and third life cycle of products (or packaging materials, components) or to extend the life cycle of products. After the products are scrapped, the wastes can be cyclic redesigned as much as possible, so that the products can be developed in another function or form continuously, or the waste can be transformed into the raw materials for another product cycle production, extending or starting a new life cycle. Cyclic redesign and reuse of products can digest and transform existing products and their wastes well [12-14]. The cyclic redesign makes the discarded products and abandoned materials involve in the circulation system of "resources- products-renewable resources" (Figure 1), which can greatly reduce the waste of resources and promote the sustainable development of resources and ecological environment.

Extension of Life Cycle by Innovative Usage of Cyclic Resign. The application of innovative design idea to products should take full consideration of the potential innovative use value and extend products' service life . When a product is scrapped, its using way and diversity of functions are supposed to be developed as much as possible, forming a circular process of "resource-product-use-one time scrapped-(multiple) innovative use- recycle waste ", so as to extend service life of product. For example, the growth speed of children determines that children's furniture will not serve a very long time. Therefore, it results in a large amount of waste of resources because the furniture is not old enough to be discarded [15]. At the same time, new children's furniture tends to contain formaldehyde and other pollutants. It is easy to pollute the indoor environment if seats and trolleys are replaced at a fast speed, which will seriously affect children's health. Product redesign based on the concept of indoor environmental protection will redesign and reconstruct these "outdated" furniture, innovating its use way and endowing children's furniture with "growable capacity", so that the purpose of extending life cycle and realizing cyclic reuse can be achieved [16]. As shown in Figure 2, the designers innovated the baby cradle with a short service life, transforming the cradle which was of no use significance into a chair cradle. With the growth of children, cradle was not long enough and it would be further developed into the back of the seat to serve children again. A baby cradle with a short service life is transformed from a predictable waste into a long-

FIGURE 2
Continuous Use of Children Seat with Different Growth Stages

FIGURE 3
Recycling of Abandoned Mineral Water Bottles

lived furniture brimmed with interest and "growth" by innovative transformation from designers.

Cyclic Redesign of Product Materials. Products are composed of only one material or more materials. After the products are knocked out or scrapped, the properties and uses of most of the materials have not been changed substantially. For example, obsolete chairs is still wood, discarded plastic bag is still plastic, discarded aluminum products is still metal. In these waste products, if the materials are easy to regenerate, such as metal, wood, paper, are directly discarded with materials which are with high cost of regeneration, such as glass and ceramics, it will not only lead to a huge waste of social resources, but also it will result in incalculable pollution to the environment. The material cyclic redesign of waste products is an innovative design of resource reorganization and reproduction by recycling the materials still valued [17]. Art design, innovation and transformation will help to relocate the function of these waste materials, endow them with new forms, bring about secondary lives to these discarded products and old materials, and stimulate the environmental awareness of consumers. In daily life, the used mineral water bottles will be discarded at will, which will result in great pressure on the ecological environment. In fact, the abandoned mineral water bottles can be made into various indoor decorations by simple reprocessing. As shown in Figure 3, it is a handicraft made from redesigning abandoned mineral water bottles. From left to right, it is followed by handicraft of mineral water bottles, flower pots of mineral water bottles, humidifiers of mineral water bottles. These indoor decorations and appliances not only ornament life, but also they are more eco-friendly and good for the cyclic reuse of waste materials.

Cyclic Redesign of Product Function. Electrical and electronic products with booming development and shorter renewal cycle are all composed of multiple components. The elimination of these products do not indicate that all components are required to be abandoned. Many of them are still intact and can be used. The purpose of cyclic redesign of product function is to recycle the intact components in the scrapped products, and reuse them in the reproducing of new products, or adopt the law of product modeling design to redesign and transform them, create a new combination mode, and form a new product and life cycle on the basis of the original function of components. For example, designers recycled and redesigned the intact CPU fans after the computer was scrapped and then they assembled multiple CPU fans together to create a creative "computer fan". In addition, a bicycle's seat is usually intact even though the cycle is scrapped. In order to avoid the waste of resources, designers made a bench by using the discarded seats, so that

FIGURE 4
Birdcage and Desk Made by Abandoned Microwave Oven

FIGURE 5
Wine Box Lamp Made by Abandoned Red Wine Packing Box

the bicycle seat can remain the original "sitting" function[18-19]. As shown in Figure 4, the desk and birdcage are made by the abandoned microwave oven which still can accommodate. After appropriate transformation, the microwave oven still can used for accommodation and storage, which not only reduces the generation of waste, but also creates a new service life of the product. It can also be designed into another indoor appliance, which is beneficial to the cyclic reapplication of indoor products and reducing the waste of resources.

Cyclic Redesign of Product Emotion. Consumers not only eager to buy durable goods, but also keep a watchful eye on more fashionable and beautiful goods. Generally speaking, buying new products shows weeding out the old one. However, not all the people are obsessed with the new one and dislike the old one and not all the people are rich enough to upgrade the existing products. Some consumers will rely on old products or even resonate with them. Therefore, old items can not be replaced by ordinary new products. This guides some designers start focusing on the cyclic redesign in the product emotion, providing a new idea for the closer relationships between the creators and the products [20-21]. For example, designers recreate the abandoned products with keen emotions, so that they can continue to serve with a more elegant life cycle and extend the emotion. As shown in Figure 5, it is very regrettable to to discard the abandoned high-grade red wine packing box and the beautiful and elegant wine box directly. Designers created a "wine box lamp" by simply redesigning and reproducing the wine box. It's not only beautiful, artistic and it can enrich new vitality to the indoor decoration. Besides, the paper lampshade is more environmental-friendly than the plastic lampshade.

CONCLUSIONS

Huge impetuses are contained in design, pushing the continuous progress of society and environmental improvement. Cyclic redesign based on the concept of indoor ecological and environmental protection embodies an environmental and green life style and concept, with its creative idea originating from daily life. There is no so-called waste, but the misplaced resources, from daily necessities to lamps, to electronic products, to furniture. Redesigning waste of products

and old materials can not only extend the service life of products, endow the products with second life cycles, but also improve indoor living environment and create a more healthy living condition. Product redesign gives full play to the values of abandoned products and components, extends the service life of products, reduces waste of resources, and protects ecosystem and natural environment.

ACKNOWLEDGEMENTS

This paper is supported by 2019 Hunan Provincial Department of Education Scientific Research Project: Application of Regional Traditional Patterns in Home Design in Southwest Hunan (19C1681).

REFERENCES

[1] Zheng, B.J. (2012) Green Packaging Materials and Modern Packaging Design. Applied Mechanics and Materials. 271-272, 77-80.
[2] Zhang, L., Chu, X.N., Xue, D.Y. (2019) Identification of the to-be-improved product features based on online reviews for product redesign. International Journal of Production Research. 57(8), 2464-2479.
[3] Yung, W.K.C., Chan, H.K., Wong, D.W.C., So, J.H.T., Choi, A.C.K., Yue, T.M. (2012) Eco-redesign of a personal electronic product subject to the energy-using product directive. International Journal of Production Research. 50(5), 1411-1423.
[4] Yung, W.K.C., Chan, H.K., So, J.H.T., Wong, D.W.C., Choi, A.C.K., Yue, T.M. (2011) A life-cycle assessment for eco-redesign of a consumer electronic product. Journal of Engineering Design. 22(2), 69-85.
[5] He, D.W., Yuan, D.H., Song, Z.J., Xu, Y.P., Liu, Z.M. (2019) Eco-friendly synthesis of high silica zeolite Y with choline as green and innocent structure-directing agent. Chinese Journal of Catalysis. 40(1), 52-59.
[6] Xu, H.R., Zhang, W.C., Li, M., Qin, F.W. (2019) Generating Quantitative Product Profile Using Char-Word CNNs. Applied Mathe-matics: A Journal of Chinese Universities. 34(3), 356-378.
[7] Vanvliet, B. (2015) Marketing green products through package design. Packaging World. 22(9), 188-194.
[8] Zhou, F.F., Liao, J.J., Teng, J. (2014) Green Ecological Design Research of Tourism Product Packaging. Applied Mechanics and Materials. 670-671, 960-963.
[9] Helbert, V.S., Gaillet, L., Chaussadent, T., Gaudefroy, V., Creus, J. (2020) Rhamnolipids as an eco-friendly corrosion inhibitor of rebars in simulated concrete pore solution: evaluation of conditioning and addition methods. Corrosion Engineering Science and Technology. 55(2), 91-102.
[10] Wang, R., Gu, X.S. (2010) Redesign of Products Based on Ecological Ethics. Packaging Engineering. 31 (18), 22-24.
[11] Mäkimattila, M., Melkas, H., Uotila, T. Redesign of Home Care Service Delivery: A Systemic Approach to IT Innovations. International Journal of Information Systems and Social Change (IJISSC). 8(2), 1-24.
[12] Paparoidamis, N.G.,Tran, T.T.H., Leonidou, L.C., Zeriti, A. (2019) Being Innovative While Being Green: An Experimental Inquiry into How Consumers Respond to Eco-Innovative Product Designs. Journal of Product Innovation Management. 36(6), 824-847.
[13] Zheng, Z.F., Su, K. (2014) The Development of Green Design and Research on Product Design for Recycling. Applied Mechanics and Materials. 3629(1372), 702-706.
[14] Lemke, F., Luzio, J.P.P. (2014) Exploring Green Consumers' Mind-Set toward Green Product Design and Life Cycle Assessment. Journal of Industrial Ecology. 18(5), 619-630.
[15] Gultekin, U. (2019) Renewable electricity generation for sustainable development and environmental management in Turkey. Fresen Environ Bull. 28, 8171-8174.
[16] Howard, B., Acha, S., Shah, N., Polak, J. (2019) Implicit Sensing of Building Occupancy Count with Information and Communication Technology Data Sets. Building and Environment. 157, 297-308.
[17] Batabyal, A.A., Beladi, H. (2019) The optimal provision of information and communication technologies in smart cities. Technological Forecasting and Social Change. 14, 216-220.
[18] Ringen, G., Schulte, K.Ø.(2017) Continuous vs Step Change Production Process Improvement as Enablers for Product Redesign and New Market Opportunities. APMS 2017: Advances in Production Management Systems. The Path to Intelligent, Collaborative and Sustainable Manufacturing, 57-64.
[19] Hilmi, B., Najman, N.S.M., Azhar, D.D., Noor, S.N.F.M., Hamid, Z.A.A. (2019) Eco-friendly denture adhesives (EFDAs) filled with different types of natural starches: mechanical and biological performance evaluation. Journal of Adhesion Science and Technology. 34(1), 76-90.
[20] Romli, A., Prickett, P., Setchi, R., Shoe, S. (2014) A Conceptual Model for Sustainable Product Design. Key Engineering Materials. 572, 3-6.

[21] Gama-Lara, S.A., Natividad, R., Vilchis-Nestor, A.R., Lopez-Castanares, R., Garcia-Orozco, I., Gonzalez-Pedroza, M.G., Morales-Luckie, R.A. (2019) Ultra-Small Platinum Nanoparticles with High Catalytic Selectivity Synthesized by an Eco-friendly Method Supported on Natural Hydroxyapatite. Catalysis Letters. 149(12), 3447-3453.

Received: **05.06.2020**
Accepted: **16.11.2020**

CORRESPONDING AUTHOR

Sheng Kang
School of Art and Design, Shaoyang University, Shaoyang Hunan 422000 – China

e-mail: nihaobeijing999@aliyun.com

© by PSP Volume 30– No. 05/2021 pages 4836-4841 Fresenius Environmental Bulletin

RESEARCH ON THE ROLE OF AGRICULTURAL INFORMATIZATION CONSTRUCTION IN AGRICULTURAL DEVELOPMENT: BASED ON BIG DATA PLATFORM

Tongzhou Yang[1], Shanlang Lin[2], Shijun Chen[3,*]

[1]School of Intelligence and Computing, Tianjin University, Shanghai 300350, China
[2]School of Economic and Management, Tongji University, Shanghai 200092, China
[3]Institute of New Rural Development, Tongji University, Shanghai 200241, China

ABSTRACT

Agricultural informatization construction is a series of measures taken to serve agriculture and improve the utilization value of agricultural information resources, which has achieved fruitful results in decades of development. However, with the rapid growth of agricultural informatization data, the amount of data is increasing, the data structure is becoming more and more complex, and the data analysis and application is becoming more and more difficult. The use of big data platform can solve the problems of diversity, redundancy and complexity of agricultural data, making data search, comparison, clustering and analysis simple and effective. This paper summarizes the application of big data in agricultural informatization construction, and points out its application prospect in agricultural development in combination with the characteristics of big data, providing reference for agricultural information resource management.

KEYWORDS:
Big data, Agricultural informatization, Agricultural development, Information technology

INTRODUCTION

Agricultural informatization construction is an important part of the construction of socialist new countryside in China, and it is an important way and measure to improve agricultural productivity and solve the "three agricultural problems". Agricultural informatization resource management refers to the collection of a series of data such as planning, measurement, coordination, control, and service obtained in the process of agricultural resources, agricultural production, agricultural product operation, service and supervision through various means such as policy, technology and economy. Due to the diverse sources of agricultural informatization resources, the complex data format, and the relatively scattered distribution, at present, most agricultural resource management still uses traditional distributed databases to store and manage agricultural data.

Big data is a new generation of information technology collection, also an application-driven technology service field. However, the existing software tools cannot effectively extract, store, search, share, analyze and process massive and complex data collection. With the rapid development of communication technology, various sensors are increasingly popular, and network infrastructure is developing at a high speed. More and more fields, such as e-commerce, finance, advertising, biology, medical treatment, logistics and so on, begin to consciously collect and accumulate a large number of data, and dig out the value that had never been before [1]. The amount of data generated in the past two years is 90% of the total amount of historical data, among which the total amount of data generated by China in 2019 is more than 0.8ZB (equivalent to 800 million TB), twice the amount of data generated in 2017, equivalent to the total amount of global data in 2010 [2]. Big data has penetrated into various industries, setting off another wave of information technology, bringing a new direction for industry development and technological progress. With the rapid growth of agricultural informatization resource data, the amount of data is increasing, the data structure is more and more complex, and the data analysis and application is more and more difficult. In the era of big data, agricultural workers introduce big data technology into agriculture, which makes data search, comparison, clustering and analysis simple and effective.

MATERIALS AND METHODS

Application of Big Data in Agricultural Informatization Construction. Application Basis of Big Data in Agricultural Informatization Resource Management. Agricultural informatization is mainly characterized by its dependence on information, high input and public welfare, long-term and arduousness, diversity, dynamics and high efficiency

[3]. After years of development, agricultural informatization resources have accumulated a large amount of distributed management data, and due to the diversity of types of agricultural informatization resources, there are a large number of unstructured data. With the development of agricultural science and technology, and the application of new information means such as cloud computing and Internet of Things, unstructured data is growing rapidly, and agricultural informatization resources have developed into real big data. As shown in Figure 1, agricultural big data is condensed by means of value mining, raw reveal, knowledge discovery, etc. the data is analyzed by means of real-time analysis technology, artificial intelligence technology, statistical analysis technology, online analysis technology, etc., then the data is processed by means of structured transformation technology, data warehouse technology, data preprocessing technology, etc. finally the data is stored to form an agricultural cloud computing platform [4].

Facing the Breadth of Agricultural Informatization Resources, Giving Full Play to the Functions of Big Data Distribution and Integration. Based on the existing data, build the deployment and application of distributed data, with regional and departmental data as the core, with the help of Distributed File System (DFS) to optimize efficiency and distributed data management engine, break through the distributed non-relational data processing and management technology, integrate the heterogeneous data of agricultural informatization resources, build the big data index model, and break the application limitation of unilateral and scattered agricultural resources, realize the movement, replication and backup of agricultural resources between departments and regions, optimize the storage and calculation efficiency, integrate basic data such as environment, land and hydrology, and cover the data of planting, forestry, animal husbandry, aquaculture and agricultural product processing industry. Starting from the specialization and breadth of data, use big data association and mining technology to build the data application in the non-professional field and the inherent association with agricultural informatization resources [5].

Facing the Depth of Agricultural Industry Chain, Giving Full Play to the Functions of Big Data Mining and Analysis. Through big data, all links of the agricultural industry are connected, vertical application of big data is carried out according to the industry needs, special group mining is carried out on production, processing, logistics, marketing and backtracking with big data, object-oriented data fusion and connection are broken through, NoSQL application and semantic-based big data analysis and mining are carried out only from the data itself, agricultural resources are mined and managed in sequence mode, decision support is carried out on statistical data, spatial data and temporal data, and application and management are carried out in loose coupling mode [6-7]. At present, in order to facilitate management, the majority of agricultural management have divided the agricultural industry chain, but it has lost the intrinsic connection of agricultural resources, such as agricultural production, storage, circulation and management, and allocation of agricultural machinery by different departments. With the help of big data, the data is coupled in the form of DFS through big data engine without copying and moving data of all departments. In specific application, the target data is extracted and analyzed through filtering and mapping to obtain the best data set. Big data can process and model a large amount of data, thus studying, analyzing and judging agricultural resources, establishing an information system to make decisions more scientific [8].

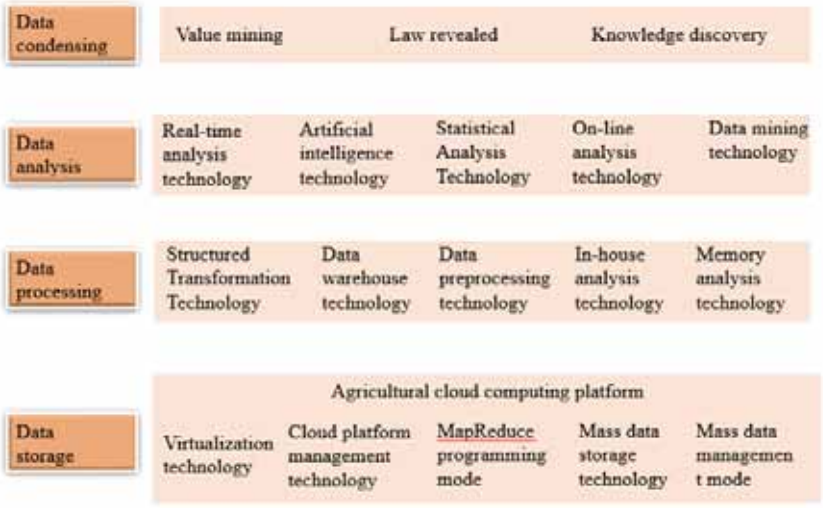

FIGURE 1
Agricultural Big Data Processing Platform

Facing the Agriculture and External Industry Data, Constructing the "Big Data-Driven Agriculture" Mode. The collection and application of agricultural resource data not only involves agriculture, but also includes other industries such as society, economy and service. Considering agriculture purely from itself will inevitably lead to deviation in agricultural production. Driven by big data, take agricultural informatization resources as the core, link other industry data with it in sequence and parallel mode, use the bottom technology of big data to simulate and stratify the association, make various targeted solutions for agricultural informatization resources, manage on the basis of data analysis, achieve scientific management of agriculture, thus carrying out more effective supervision and support, and formulating more reasonable policies and measures [9]. Through the integration of internal and external data of agricultural informatization resources, agricultural and external industry data, to establish data models, apply and implement in terms of various agriculture, to achieve data exchange and sharing benefiting agriculture, farmers and rural areas, and to form the network support for big data, are the ultimate goals of big data application in agriculture.

RESULTS

Role of Agricultural Informatization Construction in Agricultural Development under Big Data Platform. Production Link Can Realize Intelligent, Refined and Standardized Production. The world agricultural development shows that agriculture is in the process of transformation from 1.0 small-scale production, 2.0 mechanized production, 3.0 precise production to 4.0 intelligent production [10]. The agricultural development in China is also transforming from extensive management and over-reliance on resources to intelligence, refinement and standardization. As shown in Figure 2, in the process of agricultural production, agricultural informatization construction is mainly used for data platform services, UAV plant protection, refined farming and automatic driving of agricultural machinery [11].

Under the big data platform, a number of new information technologies such as the Internet of things and artificial intelligence emerge as the times require, which will bring great changes to agricultural production, realize mechanization of production means, automation of production process, precision of production mode. People and machinery can realize communication with each other, so agricultural producers can control agricultural production machinery and master agricultural production information without leaving their homes, making agriculture develop in the direction of refinement and standardization so as to obtain maximum benefits, which is the agricultural development trend in the future [12]. As shown in Figure 3, with the help pf Internet of things, artificial intelligence and other emerging information technologies, the proportion of China's automatic production in recent years has increased from 9% in 2014 to 27% in 2019, and the agricultural output value has increased significantly. From 0.2 million in 2014 to 2.22 million in 2019, it can be seen that the informatization construction has a huge role in promoting the agricultural economy [13].

Operation Link Can Achieve Networked and Effective Docking with the Consumption Market. Traditional agricultural sales and operation are blind and disorderly, mainly because of difficulties in obtaining market information, restrictions on agricultural operation, circulation channels and circulation methods, and difficulties in opening up the market and expanding the sales scope and channels of agricultural products. Traditional agriculture mainly supplies the surrounding areas, which easily leads to the situation of excess capacity and unsalable products. In recent years, news of unsalable agricultural products is common in various news media. The new generation of Internet technology can realize network sales and operation. For example, the emergence of electronic commerce has changed the way of agricultural product sales and circulation. In the future, e-commerce will break through the bottleneck of information asymmetry in the past and realize rapid and effective docking with the agricultural product consumption market. Big data on agricultural product consumption market formed by e-commerce can also further promote the establishment of a market mechanism to guide production by consumption, enhance the connection between farmers and consumers, and improve the pertinence and scientificity of agricultural operation. Figure 4 takes Taobao, Jingdong and Pingduoduo, the largest domestic sales platforms, as examples. In 2019, the online sales ratio of agricultural products on the three platforms reached 28%, 21% and 17%, with sales of 1.53 billion, 1.02 billion and 950 million respectively, a year-on-year increase of22%, 23% and 30% compared with 2018 [14].

Management Link Can Realize Datamation, Scientific Decision-Making and Efficient Management. In the context of big data, technologies such as cloud computing and big data are widely used in industrial management, providing technical support for the realization of scientific management, including agriculture. With the gradual improvement of the collection, development and utilization of agricultural information data in the future, a comprehensive agricultural information cloud service platform that integrates all agricultural management data such as agricultural policy information, production information, technical information, meteorological information and market information will be estab-

lished [15-17]. This platform can monitor crop production process and growth environment in an all-round way, balance market demand and planting scale, guide production and operation based on market demand, resolve the contradiction between decentralized small-scale production and unified large market, realize retrospective management of agricultural product quality and safety, and realize scientific decision-making and efficient management [18]. Data from a sampling survey conducted by relevant research institutions (Table 1) show that the use of cloud service platform by farmers has a significant impact on agricultural production. Among them, the farmers in southwest and south China who use cloud service platform have more than 95% higher income than the farmers who do not use cloud service platform. In the rest areas, compared with those without cloud service platform, the agricultural income of farmers using cloud service platform almost increases by more than 50% [19].

Service Link Can Realize Online and Comprehensive Exchange and Sharing of Information Resource. Emerging Internet technologies have integrated various information terminals such as computer terminals, mobile phone terminals, radio terminals and television terminals. People have more convenient and diversified ways to obtain information, and more and more farmers are closely connected to the Internet through television, computer, mobile phone and radio. Relying on the existing Internet terminal platform, agricultural producers can share technical information and market information related to production, conveniently obtain service information such as agricultural policies, laws and financing, and also realize instant interaction and communication with other agricultural producers and agricultural experts. It changes the scattered and relatively backward state, solve the problems existing in agriculture, and improve the service level of agricultural information [20]. It can be said that the big data platform has brought new opportunities and new directions for the development of agricultural informatization, as well as a new way of thinking and development path for agricultural informatization and agricultural modernization.

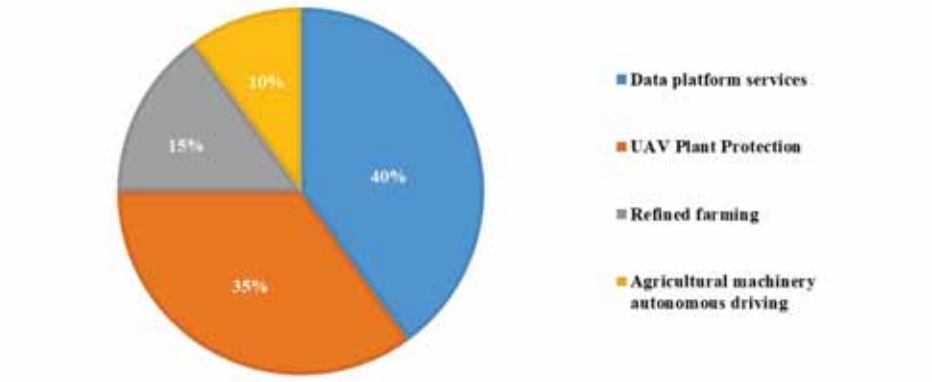

FIGURE 2
Application Scenario of Agricultural Informatization Production Link

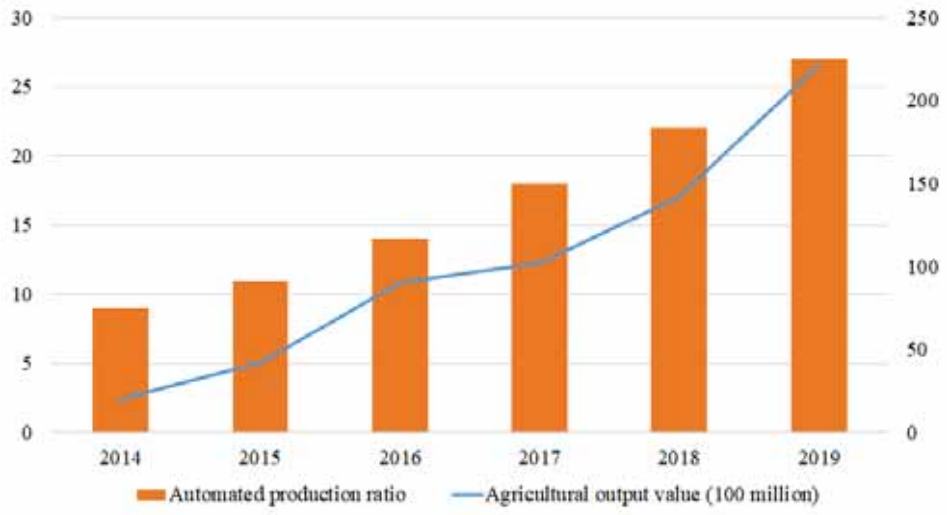

FIGURE 3
China's Agricultural Output Value and Automatic Production Proportion

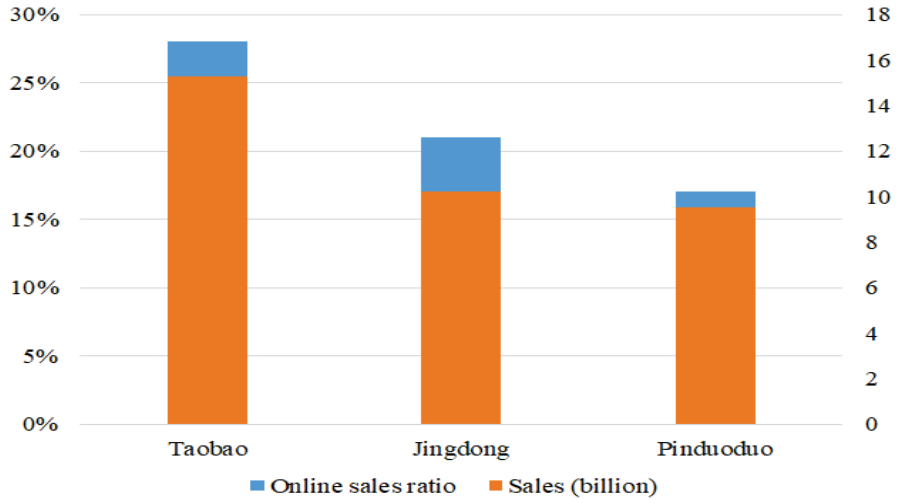

FIGURE 4
Proportion and Sales of Agricultural Products on E-Commerce Platforms

TABLE 1
Impact of Using Cloud Service Platform on Agricultural Production

Areas	Revenue (using cloud service platform)	Revenue (without using cloud service platform)	Income increase (%)
Huadong Region	156.3	100.2	56.0
South China	435.7	221.4	96.8
Central China	356.9	198.4	79.9
North China	358.5	241.2	48.6
North-west region	169.4	112.8	50.2
Southwest Region	184.6	92.3	100.0
North-east area	274.4	159.8	71.7

CONCLUSION

Under the market economy, the agriculture production mode and decentralized management make the participants in market competition more dependent on information than ever before. Through big data, not only can agricultural production be regulated and controlled by establishing of a comprehensive data platform, but also the dynamic changes in the process of agricultural planting and circulation can be recorded and analyzed. By the data analysis, corresponding management and regulation measures can be formulated to promote the efficient and orderly development of agriculture. Therefore, it is essential for the "modern tool", big data, to fully play its role in China's agricultural production. No matter from the overall deployment of the country or the actual needs, the agricultural big data platform should be in the forefront of the construction of big data in various industries. The national and local agricultural authorities should take the lead and jointly organize scientific research institutions, large-scale agricultural enterprises and farmers, improve the mechanism for sharing, collecting, analyzing and using agricultural big data, establish a unified platform for agricultural big data nationwide, assist scientific decision-making in all links of the industrial chain, and realize sustainable industrial development and industrial structure optimization.

REFERENCES

[1] Wang, X. (2016) Agricultural Informatization and Big Data. [J]. Big Data Research. 2(1), 2016002.
[2] Han, X., Wang, L., Wang, H., Wang, S. (2015) Efficiency Evaluation of Agricultural Informatization Based on CCR and Super-Efficiency DEA Model. In: Li D., Chen Y. (eds) Computer and Computing Technologies in Agriculture VIII. CCTA 2014. IFIP Advances in Information and Communication Technology, Springer, Cham. 452.
[3] Bai, Y. (2017) Construction of Agricultural Information Service Platform Based on Mobile Internet. [J]. Agricultural Engineering. 5, 54-56
[4] Wei, M., Chen, X.H. (2015) Resource Construction of Agricultural Information and "Last Kilometer" Problem Correlation Study. [J]. Heilongjiang Agricultural Sciences. 1, 150-155.

[5] Zhao, R., Kou, Y., Du, R., Gu, L., Yang, H. (2015) Research on Construction of Cloud Service Platform of Sci-tech Information for Agricultural Research System. In: Li D., Chen Y. (eds) Computer and Computing Technologies in Agriculture VIII. CCTA 2014. IFIP Advances in Information and Communication Technology, Springer, Cham. 452.
[6] Xu, L., He, Z., Wang, Z., Zhang, Y. (2015) Development Model of Agricultural Product Information Platform Based on RFID Technology. [C]. In: Proceedings of the 2015 International Conference on Network and Information Systems for Computers (ICNISC). 404-407.
[7] Chen, X., Zhong, S., Wei, C. (2016) Potential Evaluation Method on Plow Layer Soil-Stripping of Cultivated Land Occupied by Non-Agricultural Construction. [J]. Transactions of the Chinese Society of Agricultural Engineering. 32, 289-296.
[8] Wu, L., Huo, Z.-G., Zhang, L., Yu, C., Yang, J., Zhang, G. (2015) Level Indicators Construction and Temporal-Spatial Distribution Features of Agricultural Flood in the Southwest of China. [J]. 26(8), 2473-2481.
[9] Wang, H.Z., Lin, G. W., Wang, J.Q., Gao, W.L., Chen, Y.F., Duan, Q.L. (2014) Management of Big Data in the Internet of Things in Agriculture Based on Cloud Computing. Applied Mechanics and Materials. 548–549, 1438–1444.
[10] Bendre, M., Thool, R.C., Thool, V.R. (2015) Big data in Precision Agriculture: Weather Forecasting for Future Farming. 2015 1st International Conference on Next Generation Computing Technologies (NGCT). 744-750.
[11] Kamilaris, A., Kartakoullis, A., Prenafeta-Boldú, Francesc, X. (2017) A Review on the Practice of Big Data Analysis in Agriculture. [J]. Computers and Electronics in Agriculture. 143, 23-37.
[12] Yadav, R., Rathod, J., Nair, V. (2015) Big Data Meets Small Sensors in Precision Agriculture. International Journal of Computer Applications. 975, 8887.
[13] Stubb, M. (2016) Big Data in US Agriculture. Washington, DC: Congressional Research Service.
[14] Sekhar, C.C. (2017) Productivity Improvement in Agriculture Sector Using Big Data Tools. 2017 International Conference on Big Data Analytics and Computational Intelligence (ICBDAC). 169-172.
[15] Mi, C.Q. (2016) Agriculture Big Data Technology and Its Application in Agriculture Disaster Mapping. [J]. Agricultural Engineering. 6(6), 15-17.
[16] Bendre, M.R., Thool, R.C., Thool, V.R. (2016) Big Data in Precision Agriculture through ICT: Rainfall Prediction Using Neural Network Approach. In: Satapathy S., Bhatt Y., Joshi A., Mishra, D. (eds) Proceedings of the International Congress on Information and Communication Technology. Advances in Intelligent Systems and Computing, Springer, Singapore. 438.
[17] Basso, B., Dobrowolski, J., McKay, C. (2017) From the Dust Bowl to Drones to Big Data: The Next Revolution in Agriculture. [J]. Georgetown Journal of International Affairs. 18(3), 158-165.
[18] Sabarina, K., Priya, N. (2015) Lowering Data Dimensionality in Big Data for the Benefit of Precision Agriculture. [J]. Procedia Computer Science. 48, 548-554.
[19] Rao, N H. (2017) Big Data and Climate Smart Agriculture - Review of Current Status and Implications for Agricultural Research and Innovation in India. SSRN Electronic Journal.
[20] Cougot, D. (2015) Smart Agriculture in the 21st Century: A Discussion on Innovation, Biotechnology, and Big Data. [C]. No 205015, Agricultural Outlook Forum 2015, United States Department of Agriculture, Agricultural Outlook Forum.

Received: **05.06.2020**
Accepted: **14.09.2020**

CORRESPONDING AUTHOR

Shijun Chen
Institute of New Rural Development
Tongji University
Shanghai 200241 – China

e-mail: chenshijun877@protonmail.com

© by PSP Volume 30– No. 05/2021 pages 4842-4849 Fresenius Environmental Bulletin

MORPHOLOGICAL AND BIOCHEMICAL COMPARISON OF Bt CORN SEEDLINGS WITH NON TRANSGENIC COUNTERPARTS

Oksal Macar[1,*], Kultigin Cavusoglu[2], Tugce Kalefetoglu Macar[1], Emine Yalcin[2]

[1]Giresun University, Sebinkarahisar School of Applied Sciences, Department of Food Technology, Giresun, Turkey
[2]Giresun University, Faculty of Science and Arts, Department of Biology, Giresun, Turkey

ABSTRACT

Bt-corn, which is one of the most cultivated transgenic corn lines in the world, can synthesize the Cry1 Ab insecticidal protein produced by *Bacillus thuringiens* subsp. kurstaki bacteria. In this study, possible effects of genetic modifications in genetically modified Bt corn on germination and early seedling the periods were determined. Micronucleus formation, chromosomal aberrations, germination success and morphological characteristics were examined during the germination phase. Stomatal density, pigment content, malondialdehyde and proline contents of leaves and seedling morphology were examined in the early seedling period. According to the results of this study, Bt corn had a shorter seedling length but larger leaf area. In addition, anthocyanin content and proline levels and anterior and posterior stomatal densities were higher in Bt corn. Consequently, genetic modification did not lead to noticeable changes which may affect the yield. However, the increased levels of anthocyanin and proline in Bt corn indicated an oxidative stress that the plant was able to overcome.

KEYWORDS:
Antioxidant, Corn, GMO, Seedling, Transgenic, *Zea mays* L.

INTRODUCTION

Since the rapid development in the industrial zones and the increasing world population cause both the decrease in agricultural areas and environmental pollution, significant losses in the quantity and quality of agricultural products have become inevitable. Transgenic plants have become a technological revolution in agriculture that effectively increases production efficiency. While genetically modified organisms (GMOs) containing one or more new genes from foreign organisms promised undeniable benefits for developing countries, they have also caused controversy from the moment they first emerged [1, 2].

Corn (*Zea mays* L.), one of the major crops, is as source of food, forage, and raw material for industrial products [3]. Corn is most produced crop around the world with 1,123.84 million tons in 2019 [4]. Due to its versatility and high yield makes genetically modified (GM) corn is one of the most grown transgenic plants [5]. GM corn constituted 32% of the global corn production in 2017 [6]. Corn is an ideal candidate for genetic engineering for insect resistance, as its production is severely restricted by insect attack [7]. Bt corn can synthesize the Cry1 Ab insecticidal protein produced by *Bacillus thuringiens* subsp. kurstaki bacteria thanks to the changes made in its genetics. The insects die within 1-2 days after the endotoxins produced by transferred genes become active in the alkaline environment of the insect gut [8]. These endotoxins are harmful for certain lepidopteran pests of corn [9]. Bt corn can show some agronomic and physiological differences compared to no- transgenic near isolines [10]. Since there is still too much uncertainty about the application methods and side effects of transgenic technology, an ongoing concern remains for plant physiology, human health and the environment due to GM crops.

The goal of this work is to demonstrate the potential effects of genetic modifications in genetically modified Bt corn on germination and early seedling the periods by the terms of micronucleus formation and morphological characteristics during germination, germination success, and stomata number, morphology of seedling, pigment content, malondialdehyde and proline contents.

MATERIALS AND METHODS

Materials. Transgenic Bt corn and non - genetically modified corn seeds were obtained commercially.

Seed surface sterilization. Seed surface sterilization was performed by treating the shell of the seeds with 12% sodium hypochlorite (NaOCl) solution for 10 minutes and washing with distilled water for 24 hours.

Germination period analyses. Seeds were placed in 10 pieces of petri dishes with Whatman no

1. paper under aseptic conditions. The papers in the petri dishes were soaked with distilled water and distilled water was added to the petri dishes to compensate for the moisture lost daily. Seed development was followed for 7 days in the dark and at 25 ºC [11].

The germination percentages of genetically modified and non-genetically modified seeds were calculated with the following equation (Equation 1).

Equation 1. Germination (%) = (Germinated seeds / total seeds) x 100 [11].

Root elongation was determined by measuring the length of the radicle with the help of a ruler. Weight gain of seeds, defined as the difference in weights measured before and after germination, were measured with precision scales.

Same preparation procedure and slides used for micronucleus test and mitotic ındex. Corn seeds were germinated in petri dishes with distilled water for 72 hours at 25 ºC. Root tips of germinated corn seeds were cut and fixed in Clarke fixator (3: 1 glacial acetic acid and distilled water) for 2 hours. Fixed root tips were washed with 96% ethanol for 15 minutes and stored in 70% ethanol at 4 ºC until microscopic preparations. After that, the root tips were hydrolyzed in 1 N HCl at 60 ºC for 13 minutes and were stained with feulgen stain for 35 minutes. Stained root tips were squashed in 45% CH3COOH solution to prepare slides. Cells were examined under a binocular microscope (Japan, Nikon) at 1000X magnification [12]. To determine MN frequencies, 500 cells were examined in ten slides (total 5,000) to calculate the frequency of MN. MI was accepted as the total number of cells in mitosis per 5,000 cells observed [13].

Seedling period analyses. Seedlings were grown in a controlled laboratory environment. Equally sized seeds were surface sterilized then sown in pots containing one kilogram of soil. The pots were kept at 25 oC temperature and 12-hours light period. Seedlings were watered daily. Harvest was made at the end of the third week.

The lengths of the seedlings were found by measuring the height of the seedlings with a ruler. Fresh seedling weight was found by weighing the aerial parts of the plant in a precision scale. Dry seedling weight was determined by weighing the seedlings in a precision scale after drying at 80 °C for 48 hours. Leaf area was obtained by examining the images obtained from the fourth leaves in "Digimizer" software [14]. To determine the relative water content (RWC), 3 parts (1 cm2) from fourth leaves of the seedlings were immediately weighed to obtain their fresh weight (W). Then, the samples were hydrated in distilled water for 24 hours and reweighed to obtain a turgid weight (TW). Finally, leaves were dried at 80 °C for 48 hours and weighed to get a dry weight (DW). RWC of the leaf is calculated according to equation 2.

Equation 2. RWC (%) = [(W-DW) / (TW-DW)] x 100.

Transparent nail polish was applied to on both the front (adaxial) and back (abaxial) of the fourth leaf of each seedling to evaluate the number of the stoma per mm2. When the nail polish dried, a transparent adhesive tape was attached to the polish and then peeled off. Stoma molds were obtained by sticking this tape to the slides later on. Stomata were counted in four areas of 1mm2 on both the upper and lower parts of the leaves of five seedlings. Stoma molds were obtained by sticking this tape to the slides later on. Stomata were counted in four areas (1 mm2) on both the top and bottom of the leaves of the five seedlings (total 20 areas for each seed) [15].

The total amount of chlorophyll and carotenoids in the leaves of three-week-old corn seedlings were determined according to Lichtenthaler [16]. In order to determine the total chlorophyll (a + b) and carotenoid content, 3 ml of 100% acetone was added onto the small pieces (1g) taken from the 4th leaves. The samples were kept in a refrigerator (+4 ºC) in the dark for 1 week to allow the pigments to pass from the leaf tissue to the solution. At the end of this period, the absorbances of the samples were read in a spectrophotometer (Shimadzu Mini-1240 UV-Vis) at wavelengths of 470, 644.8 and 661.6 nm.

Anthocyanin content was determined according to Mancinelli et al. [17]. To determine the amount of anthocyanin in leaf tissues, 1 gr of leaf sample was homogenized with 2 ml of mixture containing 79% methanol (pure), 20% distilled water and 1% HCl. The samples were kept in the dark in the refrigerator (4 ºC) for 1 week. At the end of this period, the absorbances of the samples were read in the spectrophotometer (Shimadzu Mini-1240 UV-Vis) at 530 and 657 nm wavelengths.

The amount of malondialdehyde (MDA) in the leaves investigated using the method of Ohkawa et al. [18]. The weighed 0.1 g fresh leaf sample was cut into small pieces and homogenized with 1.5 ml of 5% trichloroacetic acid (TCA). This mixture was centrifuged at 12,000 rpm at 25 °C and for 15 minutes and the supernatant was used to determine the amount of malondialdehyde. Equal volume of supernatant and 20% TCA solution containing 0.5% thioborbutyric acid (TBA) were mixed and kept in a water bath at 95 °C for 30 minutes. The reactions were stopped by placing the reaction tubes in the ice bath. The tubes were centrifuged at 1,000 rpm for 5 minutes and their absorbance at 532 and 600 nm wavelengths were measured in a spectrophotometer (Shimadzu Mini-1240 UV-Vis).

The extracts were prepared according to the method of Weimberg [19] to determine the amount of proline in the leaves. Leaf samples taken from the seedlings were weighed 20 mg. 10 ml of distilled water was added to the sample and the material was kept at 95 °C for 10 minutes in a hot water bath, followed by cooling and filtration. Proline amounts of

samples were analyzed according to the acid-ninhydrin method and the absorbances of the samples were read at 520 nm in a spectrophotometer (Shimadzu Mini-1240 UV-Vis).

RESULTS AND DISCUSSION

Since germination is the first and most important stage of the plant, the growth and yield of the crops depends on this period [20]. Any disorder arising from genetic manipulation can be observed during germination. At the end of the 7th day of germination process, it was determined that the germination percentage of Bt corn seeds was 2% lower than the germination percentage of the non Bt corn seeds (Table 1). Although the root elongation levels of the two genotypes were not statistically significant, a remarkable difference between the weight gains of Bt corn and non-Bt corn (% 16,6) was determined ($p < 0.05$). The greater weight gain of Bt corn at the germination stage might indicate an unintended genetic change, but this change did not affect root elongation and more importantly, the percentage of germination. Our results in accordance with Graeber et al. [21] who reported that Bt and non – Bt corn similar yield performance under non insect infestation conditions.

Possible chromosomal damage that may affect the survival rate of cells caused by genetic intervention on Bt corn was investigated using MN, CAs and MI (Table 2). While the CAs test shows clastogenicity, the MI test can be used to determine both clastogenicity and mitotic damage [22]. MI is a reliable marker of cell division frequency and a well-known indicator of genotoxicity [23]. In our study, nuclei and chromosomes were clearly observed on slides prepared from both Bt corn and non-Bt corn groups, but micronucleus was not detected. Results of MN, CAs and MI were consistent with each other.

Various physiological and morphological parameters in the early seedling stage were investigated to understand the possible changes caused by genetic modifications on Bt corn and non - Bt corn seedlings (Table 3). Bt corn seedlings were determined to be significantly shorter (%16.11) than non - Bt corn seedlings ($p < 0.05$). On the other hand, mean leaf area of Bt corn was significantly larger (% 12,35) than non - Bt corn. Additionally, no statistically significant difference was found between fresh and dry weights as well as relative water contents of Bt corn and non - Bt corn. Both front and back stomatal densities of Bt corn were significantly higher than non - Bt corn. Genetic transformation process could cause undesirable effects, which are unrelated to the nature of the particular transgene [24]. In addition, Poerschmann et al. [25] reported higher lignin levels and composition in the stem of Bt corn compared to the isogenic line. Manetti et al. [26] also noted some unexpected changes in the nitrogen pathway in Bt corn varieties. Similar to our results, Xiaogang et al. [27] stated that stomatal structure and density in cotton unintentionally were affected by genetic modifications. Furthermore, Balsamo et al. [28] mentioned unstable physiological variations between Bt corn (MON 810) and non - GMO corn. It is difficult to determine whether the observed physiological and morphological differences will affect yield without testing all possible field conditions.

Chlorophyll content is one of the main factors affecting the photosynthetic capacity of plants [29]. Stress factors are usually resulted in a decrease in chlorophyll content in leaves [30]. On the other hand, carotenoids play a role in combating oxidative stress by eliminating singlet oxygen [31]. Chlorophyll and carotenoid levels in the leaves of Bt corn and non - Bt corn seedlings were not significantly different (Figures 2 and 3). The results of chlorophyll content were consistent with fresh and dry weights of seedlings and indicated unaffected photosynthetic capacity in Bt corn. Similarly, genetic modification did not cause a remarkable change in carotenoid levels of the Bt corn seedling.

TABLE 1
Germination percentage, root elongation and weight gain of non Bt corn and Bt corn.

	Non - Bt corn	Bt corn
Germination percentage (%)	93	91
Root elongation (cm)	6.88±0.224	6.87±0.222
Weight gain (g)	0.307±0.015	0.368±0.011

TABLE 2
Genetic damage parameters of non Bt corn and Bt corn.

	Non - Bt corn	Bt corn
Micronucleus	0.00±0.00	0.00±0.00
Chromosomal aberrations	0.00±0.00	0.00±0.00
Mitotic index (%)	7.58±0.16	7.46±0.22

TABLE 3
Physiological and morphological parameters of non Bt corn and Bt corn seedlings.

	Non - Bt corn	Bt corn
Seedling length (cm)	42.20±1.16	35.40±0.75
Leaf size (cm^2)	44.50±1.81	50.00±2.85
Seeding fresh weight (gr)	3.10±0.16	2.97±0.25
Seedling dry weight (gr)	0.33±0.03	0.32±.03
Relative water content (%)	86.33±1.36	87.44±0.98
Front stoma density (count/mm^2)	38.40±1.20	43.20±2.13
Back stoma density (count/mm^2)	71.30±4.10	81.60±3.15

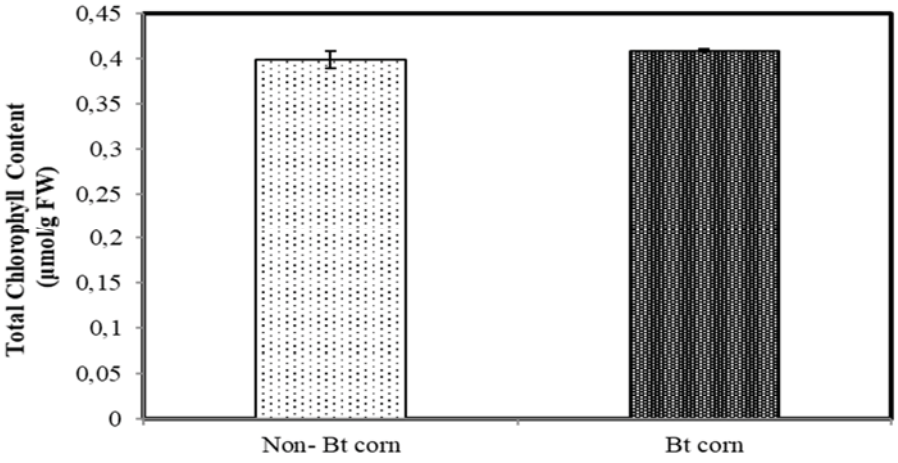

FIGURE 1
Chlorophyll contents of non Bt corn and Bt corn seedlings.

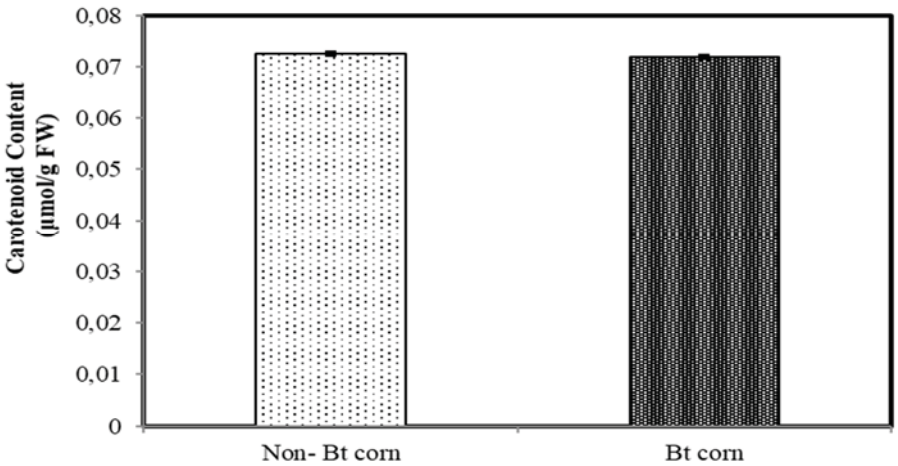

FIGURE 2
Carotenoid contents of non Bt corn and Bt corn seedlings.

Unlike chlorophyll and carotenoid levels, anthocyanin amounts in Bt corn seedlings were significantly higher than those in the leaves of the non - Bt corn seedlings (Figure 3) ($p < 0.05$). Anthocyanins are among the secondary metabolites that occur naturally in plant tissues [32]. Both environmental and anthropogenic stress factors are usually resulted in an accumulation of anthocyanins in various plant species. Indeed, it is well documented that anthocyanins play multifunctional roles in stressful conditions such as UV-irradiation, high light, chilling, pathogens, wounding and osmotic stress [33]. Reactive oxygen species are so sensitive to anthocyanins that in case of oxidative stress generated from ROS, maintenance of photosynthetic capacity is only possible with an increase in anthocyanin content [34]. From this point of view, anthocyanin accumulation in Bt corn was a clear sign of oxidative stress.

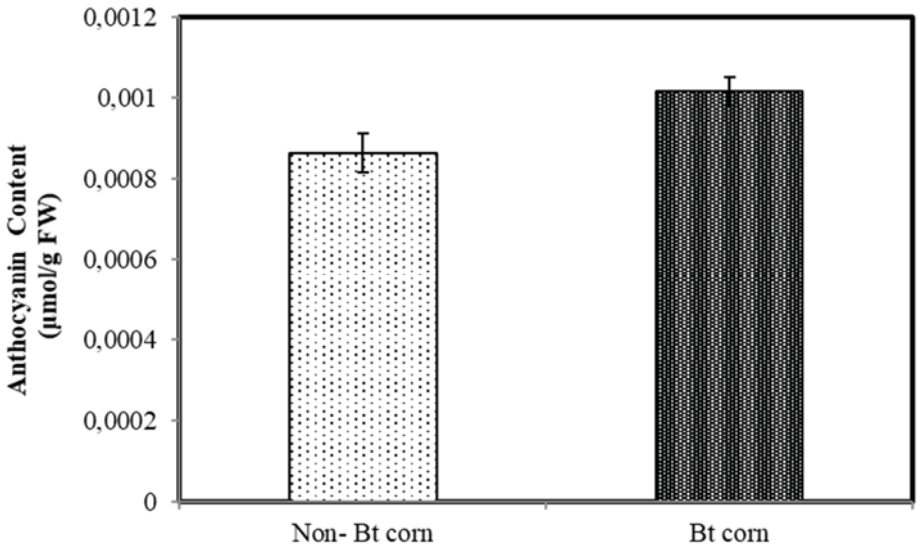

FIGURE 3
Anthocyanin content of non Bt corn and Bt corn seedlings.

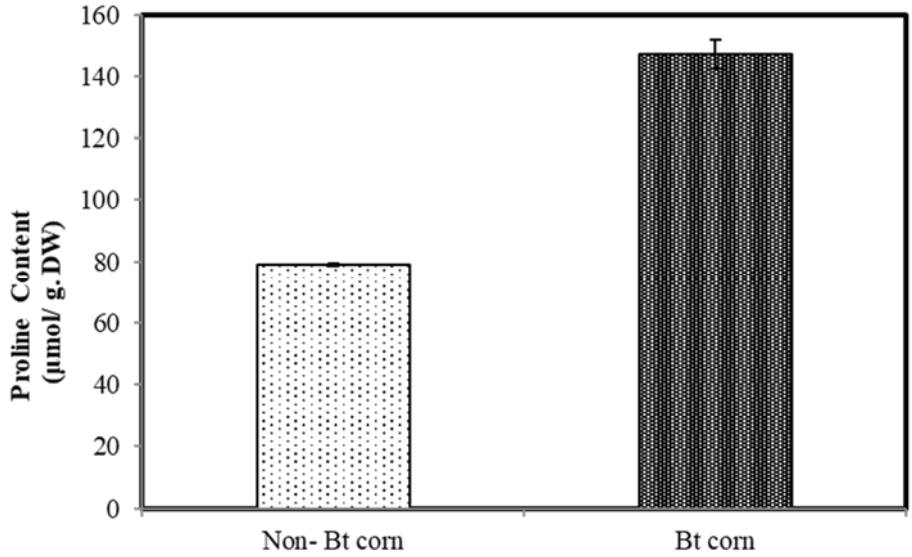

FIGURE 4
Proline content of non Bt corn and Bt corn seedlings.

As an osmoprotectant, proline is extremely important for the plant to combat stress through reduce oxidative stress [35]. The proline content of Bt corn seedlings was about 1.9 times that of non - Bt corn seedlings (Figure 5). The difference was statistically significant ($p < 0.05$). These results were consistent with the previously mentioned increased proline level in Bt corn grain [36]. Parallel to the anthocyanin results, increased proline levels in Bt corn were signs of oxidative stress induced by genetic modification. Molinari et al. [37] stated that under stress conditions, the role of proline in the oxidative defense system is more important than its role in osmotic regulation in transgenic sugar.

An increase in MDA level is a parameter for evaluating oxidative stress damage to lipid membranes [38]. MDA amounts were determined in order to investigate oxidative damage to leaf cell membranes (Figure 4). According to the results of this study, there was no statistically significant difference between MDA amounts of non - Bt corn and Bt corn. Similar to our results, Kalefetoglu Macar et al. [36] reported increased MDA level in grains of Bt corn. Although elevated anthocyanin and proline levels of Bt corn indicated an induced defense mechanism, gene manipulation-related oxidative stress did not initiate a lipid peroxidation in cell membranes. It can be inferred that due to increased proline and anthocyanin synthesis in corn, membrane integrity is preserved against oxidative stress.

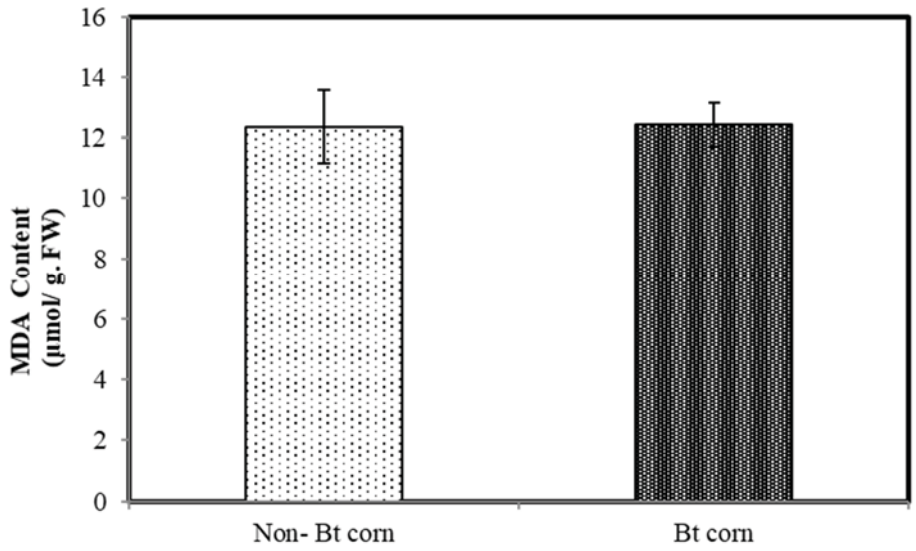

FIGURE 5
MDA content of non Bt corn and Bt corn seedlings.

CONCLUSIONS

In this study, possible unwanted effects of genetic manipulation on Bt corn in germination and early seedling periods were investigated with multifaceted approach. Various physiological, chemical and morphological alterations in Bt corn were observed. It is unclear to what extent these alterations will affect plant yield gene insertion resulted in. In addition, signs of oxidative stress were observed in Bt corn, but oxidative stress could be overcome by defense systems of plant. Thus, further investigations are needed to obtain a comprehensive understanding of possible effects of transgene technology on corn plant.

ACKNOWLEDGEMENTS

This research was supported financially by the Giresun University Scientific Research Unit (Project No. FEN-BAP-C-220413-26).

REFERENCES

[1] Magaña-Gómez, J.A., Calderón de la Barca, A.M. (2009) Risk assessment of genetically modified crops for nutrition and health. Nutrition Reviews. 67, 1-16.

[2] Téllez, P., Ayra, C., Morán-Bertot, I., Rodríguez-Cabrera, L., Sosa, A.E., Oliva, O., Ponce, M., Riverón, A., Hernández, D., Rodríguez-de la Noval, C. (2016) New knowledge on insect-resistance management for transgenic Bt corn. Biotecnología Aplicada. 33, 1511-1513.

[3] Ostrý, V., Malíř, F., Pfohl-Leszkowicz, A. (2015) Comparative data concerning aflatoxin contents in Bt maize and non-Bt isogenic maize in relation to human and animal health–a review. Acta Veterinaria Brno. 84, 47-53.

[4] USDA. (2021) World Agricultural Supply and Demand Estimates. https://www.usda.gov/oce/commodity/wasde/wasde0221.pdf. (Accessed on March 01, 2021)

[5] Rótolo, G.C., Francis, C., Craviotto, R.M., Viglia, S., Pereyra, A., Ulgiati, S. (2015) Time to re-think the GMO revolution in agriculture. Ecological Informatics. 26, 35-49.

[6] ISAAA. (2017). Global Status of Commercialized Biotech/GM Crops: 2017. ISAAA Brief No. 53. ISAAA: Ithaca, NY.

[7] Asmaa, A.H., Lary, S., Edwards, M.G., Qusti, S., Cockburn, A., Poulsen, M., Gatehouse, A.M. (2019) A proteomic-based approach to study underlying molecular responses of the small intestine of Wistar rats to genetically modified corn (MON810). Transgenic Research. 28, 479-498.

[8] OECD (2007) Consensus document on safety information on transgenic plants expressing Bacillus thuringiensis derived insect control protein", Organisation for Economic Co-operation and Development. 7, 1-107

[9] du Pisanie, A., du Preez, L., van den Berg, J., Pieters, R. (2019) The rate of release of Cry1Ab protein from Bt maize leaves into water. Water SA. 45, 710-715.

[10] Ma, B.L., Subedi, K.D. (2005) Development, yield, grain moisture and nitrogen uptake of Bt corn hybrids and their conventional near-isolines. Field Crops Research. 93, 199-211.

[11] Çavuşoğlu, K., Yalçın, E., Şengül, B., Şengül Ü. (2009) Protective role of lycopene on refinery wastewater-induced cytotoxicity in maize root tip cells. Fresen. Environ. Bull. 18, 1779-1787.
[12] Fenech, M., Chang, W.P., Kirsch-Volders, M., Holland, N., Bonassi, S., Zeiger, E. (2003) Human micronucleus project, HUMN project: detailed description of the scoring criteria for the cytokinesis-block micronucleus assay using isolated human lymphocyte cultures. Mutation Research. 534, 65-75.
[13] Inceer, H., Ayaz, S., Beyazoglu, O. (2003) Cytogenetic effects of copper chloride on the root tip cells of *Helianthus annuus* L. Turkish Journal of Biology. 27, 43-46.
[14] Digimizer. (2016) Free image analysis software. http://www.digimizer.com/download.php.
[15] Gülen, H., Köksal, N., Atilla, E. (2004) Stoma density and stoma size of some cherry and apple cultivars grafted on different rootstocks. Bahçe. 33, 1-5.
[16] Lichtenthaler, H.K. (1987) Chlorophylls and carotenoids: pigments of photosynthetic biomembranes. Methods in Enzymology. 148, 350-382.
[17] Mancinelli, A.L., Yang, C.P.H., Lindquist, P., Anderson, O.R., Rabino, I. (1975) Photocontrol of anthocyanin synthesis III. The action of streptomycin on the synthesis of chlorophyll and anthocyanin. Plant Physiology. 55, 251-257.
[18] Ohkawa, H., Ohishi, N., Yagi, Y. (1979) Assay of lipid peroxides in animal tissue by thiobarbituric acid reaction. Analytical Biochemistry. 95, 351-358.
[19] Weimberg, R. (1987) Solute adjustments in leaves of two species of wheat at two different stages of growth in response to salinity. Physiologia Plantarum. 70, 381-388.
[20] Khayatnezhad, M., Gholamin, R., Jamaatie-Somarin, S.H., Zabihi-Mahmoodabad, R. (2010) Effects of peg stress on corn cultivars (*Zea mays* L.) at germination stage. World Applied Sciences Journal. 11, 504-506.
[21] Graeber, J.V., Nafziger, E.D., Mies, D.W. (1999) Evaluation of transgenic, Bt-containing corn hybrids. Journal of Production Agriculture. 12, 659-663.
[22] Dimitrov, B., Gadeva, P., Benova, D., Bineva, M. (2006) Comparative genotoxicity of the herbicides Roundup, Stomp and Reglone in plant and mammalian test systems. Mutagenesis. 21, 375-382.
[23] Antonsie-Wiez, D. (1990) Analysis of the cell in the root meristem of *Allium cepa* under the influence of Ledakrin. Folia Histochemica et Cytobiologica. 28, 79-95.
[24] Blechl, A.E., Vensel, W.H. (2013) Variant high-molecular-weight glutenin subunits arising from biolistic transformation of wheat. Journal of Cereal Science. 57, 496-503.
[25] Poerschmann, J., Gathmann, A., Augustin, J., Langer, U., Gorecki, T. (2005) Molecular composition of leaves and stems of genetically modified Bt and near-isogenic non- Bt maize characterization of lignin patterns. Journal of Environmental Quality. 34, 1508-1518.
[26] Manetti, C., Bianchetti, C., Casciani, L., Castro, C., Enrica Di Cocco, M., Miccheli, A., Motto, M., Conti, F. (2006) A metabonomic study of transgenic maize (*Zea mays*) seeds revealed variations in osmolytes and branched amino acids. Journal of Experimental Botany. 57, 2613-2625.
[27] Xiaogang, L., Changfeng, D., Wang, X., Liu, B. (2015) Comparison of the physiological characteristics of transgenic insect-resistant cotton and conventional lines. Scientific Reports. 5, 8739.
[28] Balsamo, G.M., Cangahuala-Inocente, G.C., Bertoldo, J.B., Terenzi, H., Arisi, A.C. (2011) Proteomic analysis of four Brazilian MON810 maize varieties and their four non-genetically-modified isogenic varieties. Journal of Agricultural and Food Chemistry. 59, 11553-11559.
[29] Bowes, G. (1991) Growth at elevated CO_2 photosynthetic responses mediated through Rubisco. Plant, Cell & Environment. 14, 795-806.
[30] Ibrahim, M., Ahmad, N., Shinwari, Z.K., Bano, A., Ullah, F. (2013) Allelopathic assessment of genetically modified and non modified maize (Zea mays L.) on physiology of wheat (Triticum aestivum L.). Pakistan Journal of Botany. 45(1), 235-240.
[31] Knox, J.P., Dodge, A.O. (1985) Singlet oxygen and plants. Photochemistry. 24, 889-896.
[32] Trojak, M., Skowron, E. (2017) Role of anthocyanins in high-light stress response. World Scientific News. 81, 150-168.
[33] Neill, S.O. (2002) The functional role of anthocyanins in leaves, The University of Auckland, Auckland. 1-179.
[34] Xu, Z., Mahmood, K., Rothstein, S.J. (2017) ROS induces anthocyanin production via late biosynthetic genes and anthocyanin deficiency confers the hypersensitivity to ROS-generating stresses in Arabidopsis. Plant and Cell Physiology. 58, 1364-1377.
[35] Matysik, J., Alia, A., Bhalu, B., Mohanty, P. (2002) Molecularmechanisms of quenching of reactive oxygen species byproline under stress in plants. Current Science. 82, 525-532.
[36] Kalefetoglu Macar, T., Yalcin, E., Macar, O., Cavusoglu, K. (2021) A comparative assessment of the unintended effects of genetic modification on Bt corn. Fresen. Environ. Bull. 30, 1344-1352.

[37] Molinari, H.B.C., Marur, C.J., Daros, E., De Campos, M.K.F., De Carvalho, J.F.R.P., Filho, J.C.B., Pereira, L.F.P., Vieira, L.G.E. (2007) Evaluation of the stress-inducible production of proline in transgenic sugarcane (Saccharum spp.): osmotic adjustment, chlorophyll fluorescence and oxidative stress. Physiologia Plantarum. 130, 218-229.

[38] Arbona, V., Hossain, Z., López-Climent, M.F., Pérez-Clemente, R.M., Gómez-Cadenas, A. (2008) Antioxidant enzymatic activity is linked to waterlogging stress tolerance in citrus. Physiologia Plantarum. 132, 452-466.

Received: **12.01.2021**
Accepted: **21.02.2021**

CORRESPONDING AUTHOR

Oksal Macar
Sebinkarahisar School of Applied Sciences,
Department of Food Technology,
Giresun University,
Giresun – Turkey

e-mail: oksal.macar@giresun.edu.tr

© by PSP Volume 30– No. 05/2021 pages 4850-4854 Fresenius Environmental Bulletin

RESEARCH ON CONDENSATION HEAT RECOVERY PERFORMANCE OF R410A MULTIFUNCTIONAL HEAT PUMP SYSTEM

Qing Luo[1,2], Jinping Li[1,2,*], Yuping Deng[3]

[1]West Energy and Environmental Research Center, Lanzhou University of Technology, Lanzhou 730050, Gansu, China
[2]School of Energy and Power Engineering, Lanzhou University of Technology, Lanzhou 730050, Gansu, China
[3]Qingdao Hisense Hitachi Air Conditioning System Co., Ltd., Qingdao 266510, Shandong, China

ABSTRACT

R410A multifunctional heat pump system is generally considered to have stronger heat recovery performance than R134A system. In this paper, two reagents are tested and compared. The experimental results show that the new system can reliably operate in the low-temperature heating range of -15°C and above. The compressor exhaust temperature can be controlled between 56.3-83.0°C. Unit heating capacity is increased by 17% compared to R134a system, and the overall energy efficiency above 0°C is improved by 21%. The new system solves the problems of high exhaust temperature and severe attenuation of heating performance under low temperature conditions of the R134a system.

KEYWORDS:
Air conditioning, Heat pump energy efficiency, Refrigerant, R410A

INTRODUCTION

At present, most automotive air conditioners generally use the high-temperature refrigerant R134a. However, when the ambient temperature of the R134a refrigerant is lower than 10°C, the compressor exhaust temperature can reach 120°C, and the heating capacity of the system will be seriously attenuated or even abnormal work, heating still needs to be equipped with auxiliary heating equipment [1]. Some scholars have proposed a heat pump system using CO_2 as the refrigerant [2]. Its system performance is better than that of R134a refrigerant. Especially at low temperatures, CO_2 has good thermal performance, and CO_2 is a natural refrigerant [3-5]. It is more environmentally friendly than R134a. However, the pressure of the heat pump system using CO_2 as the refrigerant is too high, and the reliability and safety of the system are poor. R410A has good thermal conductivity and flow characteristics, has lower permeability than R134a, which is less prone to leakage, and has a wide operating temperature range. R134a is not required for system dryness. And its higher operating pressure and higher gas density make it easier to adapt to smaller flow compressors and thinner pipes than R134a, and the manufacturing cost will be reduced. Aiming at the problems of the current application of R134a automotive air conditioner at low temperature, the compressor exhaust temperature is high and the heating performance is seriously attenuated, the author has developed a set of R410A supplemental air enthalpy heat pump type automotive air conditioning unit for a certain model. The heating performance of the new system was tested and the performance was compared with the original R134a system. The application of R410A in heat pump car air conditioners was analyzed to provide a reference for the subsequent development of car air conditioners.

MATERIALS AND METHODS

Heat-pump air-conditioning system for enthalpy-enhancing heat pump of pure electric vehicle. Considering the energy-saving requirements for battery energy consumption of pure electric vehicles, combined with the structure of automobile air conditioners and the operating temperature range of the developed model batteries, an air-enriched heat pump type pure electric vehicle air-conditioning system using R410A was developed. The minimum operating temperature of the battery system on the development model is -15°C, so the air-conditioning system only needs to operate to a heating temperature of -15°C. The system consists of a rotor compressor with an air supply port, a four-way valve, a gas-liquid separator, an external condenser, an internal evaporator, a throttle valve, parts of an air supply valve, and PTC electric auxiliary heat in the vehicle, as shown in Figure 1. In the cooling mode, the refrigerant is discharged through the compressor, flows through the four-way valve, the external heat exchanger, the throttle valve 1, the supplemental tank, the throttle valve 2, the internal heat exchanger,

and then enters the air through the four-way valve. The liquid separator returns to the compressor. In heating mode, the compressor air valve is opened, and the high-temperature and high-pressure gaseous refrigerant enters the car's heat exchanger through the four-way valve to condense and release heat. The throttle valve 2 performs a throttling and pressure reduction to become a gas-liquid two-phase refrigerant. Flashing occurs in the supplemental gas tank, and the medium-pressure saturated vapor in the upper part of the supplemental gas tank enters the compressor through the supplementary gas valve. Due to the continuous flashing of the vapor, the liquid refrigerant in the lower part of the supplemental gas tank is too cold. After the agent is throttled again by the throttle valve 1, it enters the external heat exchanger of the vehicle, flows back to the compressor through the main circuit, and the heating cycle is completed.

Test conditions and test plans. There are two methods for performance test of automobile air conditioner: balanced room calorimeter method and air enthalpy difference method. The balance room calorimeter method has the advantages of high accuracy, but the disadvantages are higher test requirements and higher test costs. This test uses the enthalpy difference method. The formulation of the test plan mainly refers to the following national standards or industry standards regarding the performance test standards for automotive air conditioning benches, including: GB / T 21361—2008 "Automotive Air Conditioners", QC / T 657- -2000 “Test method of automobile air-conditioning refrigeration device “, JB / T 6914-93" Test method of automobile air-conditioner performance " and QC / T656-2000 “Performance requirements of automobile air-conditioning refrigeration device”. Enterprises will also learn from some foreign standards in actual tests, such as GMW 3037-2001 (A / C system maximum performance validation for passenger vehicles) which is commonly used in the United States. The test unit was tested on the automotive air-conditioning enthalpy difference test bench. The unit was installed on a bench. The car heat exchanger and supporting assembly (HVAC) were placed on the indoor side of the laboratory. The outdoor heat exchanger included the main body of the bench such as the compressor Place on the outdoor side.

The instruments used in the experiments met the relevant national standards QC / T72.2 ~ 93 [6]. The test plan is shown in Table 1. The on-board wind speed of the external heat exchanger is 4.5 m/s.

RESULTS AND DISCUSSION

The application of R134a ordinary heat pump system and newly developed application R410A supplemental gas enthalpy heat pump system compressor exhaust temperature changes with ambient temperature as shown in Figure 1. It can be seen from Figure 1 that as the ambient temperature decreases, the exhaust temperature of the compressor of the R134a refrigerant system increases from 100°C to approximately 130°C. This is mainly because as the ambient temperature outside the car decreases, the evaporation pressure of the heat exchanger outside the car also decreases, resulting in a decrease in the suction pressure of the unit, an increase in the unit compression ratio, and an increase in the exhaust temperature, which is close to 130°C The temperature has exceeded the exhaust limit of the unit operation. Here is just to test the limit of the exhaust temperature of the unit. In actual operation, when the unit runs to an ambient temperature of about 4°C, the exhaust temperature has exceeded 120°C, and the system should stop operation. To ensure safety, heat extraction at lower ambient temperature can only be compensated by auxiliary electric heating. Obviously, this system will cause extra consumption of electric vehicle battery energy, and is not suitable for electric vehicle air-conditioning systems without engine waste heat utilization. Because the new system uses R410A and the supplementary air structure, the air conditioning system can control the temperature within a reasonable range throughout the heating zone, so that the new system can operate reliably throughout the heating zone. It can be seen that as

TABLE 1
Test scheme

	Car inlet air Dry bulb temperature / °C Wet bulb temperature / °C		Car outside entrance air Dry bulb temperature / °C
R410A system	20	15	- 15/ - 12/ - 7/ - 5/0/2/4/6/ 7/8/10/12/15
R134a system	20	15	0/2/4/6/7/8/10/12/15

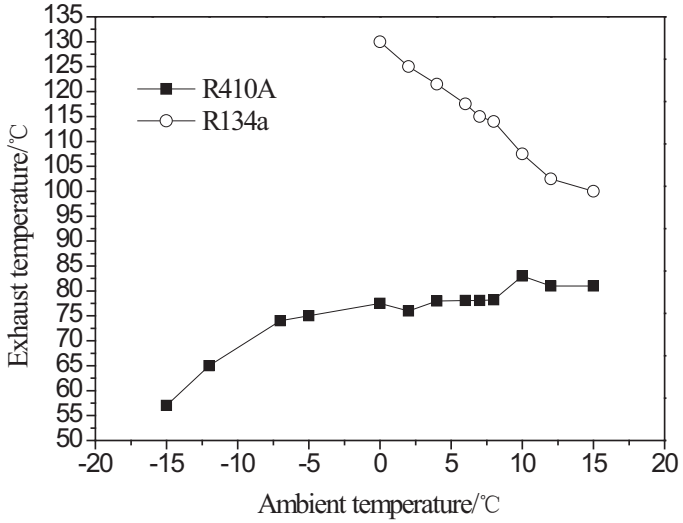

FIGURE 1
Changes in exhaust temperature of two systems with ambient temperature

the ambient temperature decreases, the exhaust temperature of the R410A system gradually decreases. When the ambient temperature is 10°C, the maximum exhaust temperature of the unit is 83°C, and when the ambient temperature is －15°C, the unit It can still maintain an exhaust temperature of 55°C.

The heating performance of the two systems is shown in Figure 2. It can be seen from Figure 2 that as the ambient temperature decreases, the heating capacity and COP of the two systems generally decrease. R134a system at ambient temperature from 15. When the temperature changes from 0 to 0°C, the heating capacity of the unit is reduced from 3674 W to 1885 W, and the COP is reduced from 2.7 to 1.7. The main reasons are lower ambient temperature, lower system suction pressure, and larger refrigerant specific volume, resulting in a decrease in the mass flow rate of the circulating working fluid of the unit, and a reduction in the heating capacity and COP of air conditioners. For the R410A system, due to the supply air and enthalpy, when the ambient temperature is －15°C, the unit still has 2822 W heating capacity, and the COP is 1.6 at 15°C, the unit heating capacity is 4156 W, and COP is 2.9. The heating capacity of the R410A system is 17% higher than that of the R134a system, and the overall energy efficiency above 0°C is increased by 21%.

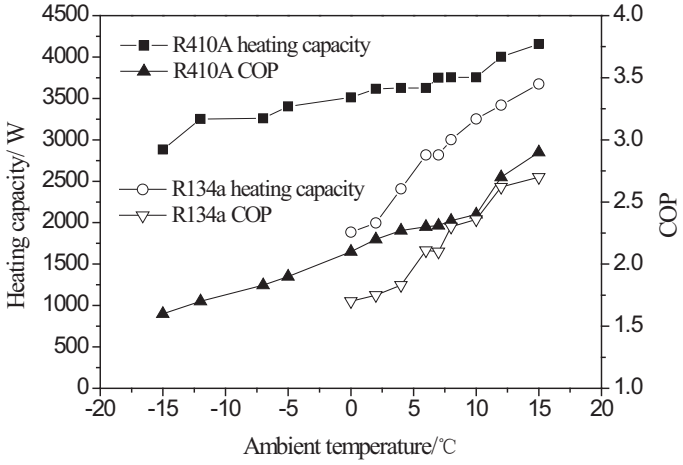

FIGURE 2
Variation of heating performance parameters of two systems with ambient temperature

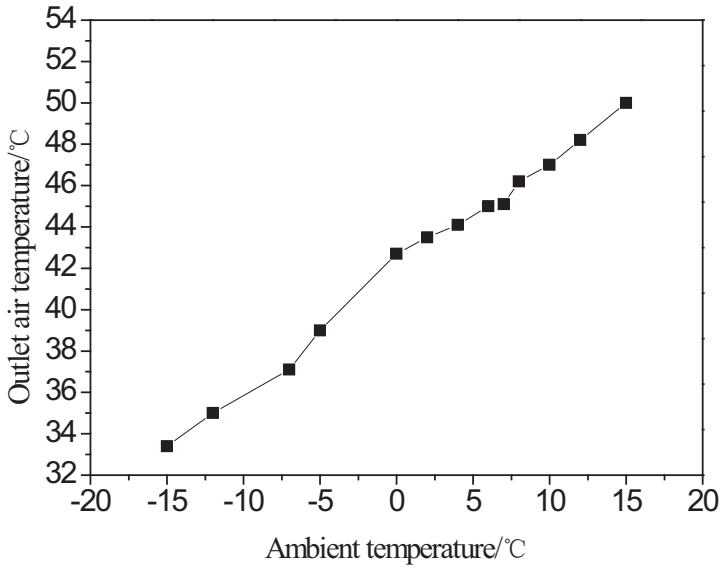

FIGURE 3
Changes in the temperature of the outlet air in the R410A refrigerant system with ambient temperature

The temperature test of the new system in the heating zone car is shown in Figure 3. In order to test the heat output of the heat pump separately, the PTC electric heating was shielded during the test. According to the comfort of "head cool feet", the test thermocouple was placed in the air outlet of the car in the blower mode. It can be seen from Figure 3 that as the ambient temperature decreases, the air temperature inside the car shows a trend of overall decrease. The main reason is that the heating capacity of the air conditioner is gradually decreasing at this time, causing the air temperature inside the car to decrease. When the unit is at －15℃, the temperature of the air in the car is 33.4℃, at 7℃, the temperature of the air is 37.1℃, and at 5℃, the temperature of the air is 39.0℃. It is indicated that －5°C and above ambient temperature can be used to meet the heating requirements of the car without the need to turn on electric auxiliary heat. When the temperature is below 5°C, appropriate electric auxiliary heat can be used for temperature compensation. Because of the nature of R410A, the heating range of the system is wider than that of R134a. R134a cannot be used well in environments below 0°C. Excessive exhaust temperature causes the system to rely on electricity when the ambient temperature is lower than 0°C. Heating for heating. At this point, the R410A system can effectively save battery power consumption. In addition, because R410A has a higher pressure than R134a during operation, it will have lower flow loss and better heat transfer performance. At the same time, due to higher gas density, the system can use more finesse under the same heating requirements. The pipes and smaller valves get the same mass flow working medium as R134a, which directly reduces manufacturing costs.

CONCLUSIONS

The newly designed pure electric vehicle air-conditioning unit based on the characteristics of R410A refrigerant and the supplemental enthalpy heat pump technology is more suitable for low-temperature heating environments than the original R134a refrigerant ordinary heat pump automobile air-conditioning unit. The experiments show that: (1) The R410A supplemental gas enthalpy heat pump system has a wider heating operation range than the R134a system. The ambient temperature is 156.3°C when the ambient temperature is 15°C, and the maximum exhaust temperature is 83.0°C when the temperature is 10°C. The reasonable exhaust temperature can be controlled in the heating zone. When the ambient temperature is －5°C, the temperature of the air in the car is 39.0°C without the use of electric auxiliary heat, which has already met the heating requirements in the car. The lower temperature only needs to take a certain power of electric auxiliary heat compensation, the new system has a significant effect on reducing battery power consumption. (2) The heating capacity of the new system is 17% higher than that of the R134a system, and the overall energy efficiency above 0°C is increased by 21%. The new system solves the problems of severe degradation of heating performance and excessively high exhaust temperature of the R134a refrigerant ordinary heat pump air-conditioning unit under low-temperature conditions, and provides a technical reference for the development and application of R410A refrigerant system products for automotive air conditioning in the future. (3) For electric vehicles that do not use engine waste heat and have strict requirements for battery energy saving, the use of

R410A, which is more suitable for low temperature, as a refrigerant, can fully reflect the advantages of heat pump heating, which has a great effect on saving battery energy of electric vehicles It helps, but because R410A and R134a both have high global warming potential GWP, it is still necessary to develop more environmentally friendly refrigerants in the future.

REFERENCES

[1] Hosoz, M., Direk, M. (2006) Performance evaluation of an integrated automotive air conditioning and heat pump system. Energy Conversion and Management. 47, 545-559.

[2] Kim, S.C., Kim, M.S., Hwang, I.C., Lim, T.W. (2007) Performance evaluation of a CO_2 heat pump system for fuel cell vehicles considering the heat exchanger arrangements. International Journal of Refrigeration. 30, 1195-1206.

[3] Yang, J.L., Ma, Y.T., Feng, G., Li, M.X. (2009) Optimization and Experimental Study on Transcritical CO_2 Heat Pump System. Fluid Machinery. 37, 53-58.

[4] Ma, Y.T., Wang, W. (2010) Substitution and Postponable Technology of Refrigerants. Journal of Refrigeration. 31, 11-17.

[5] Yu, J.T., Tian, D.L., Xiao, G.Y.. (2012) Research on Auto Air-Conditioning System Performance Test and Evaluation Method. Automobile Technology. 10, 47-51.

[6] Zhou, G.H., Li, H.J., Li, X.G., Su, Z.Y., Xu, Y.T., Zhou, T. (2016) Experimental study on heat pump air conditioning system for pure electric vehicle at ultra low temperature. Refrigeration and Air-Conditioning. 16, 73-77.

Received: **14.06.2020**
Accepted: **24.09.2020**

CORRESPONDING AUTHOR

Jinping Li
West Energy and Environmental Research Center,
Lanzhou University of Technology,
Lanzhou 730050 Gansu – China

e-mail: mingtian88ww@163.com

© by PSP Volume 30– No. 05/2021 pages 4855-4860 Fresenius Environmental Bulletin

COORDINATED DESIGN OF TOURISM AND ECOLOGICAL HABITAT ENVIRONMENT IN URBAN DEVELOPMENT

Yuefang Guo*

School of Business, Xinyang Normal University, Xinyang 464000, Henan, China

ABSTRACT

According to the principle of coordination, the coordinated development of tourism and ecological environment will produce greater overall coordination effect. Taking Wuhan city as an example, a model for measuring the coordination degree of the complex system is established based on the related data of tourism and ecological environment development in Wuhan. The quantitative analysis method of complex correlation coefficient weighting is used to make an empirical analysis on the coordinated development degree of the tourism and ecological environment complex system in Wuhan. It is concluded that the tourism industry and the ecological environment system in Wuhan are on the rise, but the coordination degree of the complex system has not reached the ideal state of coordinated development. The overall coordination effect of tourism and ecological environment has a positive and mutual promotion trend, which is of great significance to the development of the city.

KEYWORDS:
Tourism industry, Ecological environment, Coordinated development, Coordination model

INTRODUCTION

As a newly emerging strategic pillar industry, tourism plays a crucial role in promoting economic development [1]. The discussion on its sustainable development has gradually become the focus of research at home and abroad. In 2014, the State Council issued a number of opinions on promoting the reform and development of tourism industry and stressed that we should accelerate the transformation of the development mode, promote the tourism development to the intensive change, pay more attention to the protection of the ecological environment, and realize the sustainable development [2-4]. It is very important for the sustainable development of tourism to see the coordinated development of tourism and ecological environment. On the other hand, tourism is a highly mobile industry. There is a general spatial correlation between adjacent areas. Exploring the current situation of the coordinated development of tourism and ecological environment is of great significance for the sustainable development of tourism and ecological environment in China [5].

Wuhan is a famous tourist city in China. It is rich in tourism resources and receives tens of millions of tourists every year [6-10]. At the same time, Wuhan is a green city with beautiful ecology and pleasant environment. It is close to Weihe River, the Loess Plateau and the Qinling Mountains, and has beautiful natural landscape. It has been awarded the National Health City, the National Garden City, the excellent tourism city of China and the happiest city in China. This paper takes Wuhan as an example to study the coordination between the tourism industry and the ecological environment [11-15].

Based on the linkage development index system proposed by Wang Zhenzhen and Chen Gongyu, this paper selects 5 indicators, including the total number of tourists, the total income of tourism, the total number of passengers, the number of tourism employees and the total number of travel agencies, to simulate the development level of the tourism industry. The author also selects 5 indicators of green coverage rate, the days of ambient air quality two or above, urban cleaning rate, no public interest rate of domestic waste and green area of per capita park to simulate the development level of ecological environment system. According to this, the evaluation index system of coordination degree is set up as Table 1.

MATERIALS AND METHODS

Coordination degree model of tourism and ecological environment system. Subsystem order degree model. The coordinated development of tourism and ecological environment is considered as a complex system $S=\{S_1,S_2\}$, S_1 represents the tourism subsystem, and S_2 represents the ecological environment subsystem S_{ji}, $j \in [1,2]$. Suppose the tourism or ecological environment subsystem, in which j is the subscript of the subsystem, and i is the subscript of the order parameter of the subsys

TABLE 1
Evaluation index system for coordination degree of tourism and ecological environment in Wuhan

System layer	Subsystem layer	Symbol	Index layer
Coordinated development of tourism industry and ecological environment S	Tourism S_1	X_{11}	Total number of visitors (ten thousand people)
		X_{12}	Total tourism income (Billion)
		X_{13}	Total passenger volume (ten thousand people)
		X_{14}	The number of employees in the tourism industry (peo-
		X_{15}	Total number of travel agencies
	Ecological environment S_2	X_{21}	Green coverage rate (%)
		X_{22}	The days of ambient air quality two or above (days)
		X_{23}	Cleaning rate of urban cleaning (%)
		X_{24}	No public interest rate of domestic waste (%)
		X_{25}	Park green area per capita (square meter)

$$SS_j(P_j) = \sum_{i=1}^{n} \lambda_i SS_j(P_{ji}), \lambda_i \geq 0 \text{且} \sum_{i=1}^{n} \lambda_i = 1 \quad (2)$$

$$CI = \xi\left\{\left(f(SS_1,\ t) \times f(SS_2,\ t)/\left[\left(f(SS_1,\ t) + f(SS_2,\ t)\right)^2\right]\right\}^{\frac{1}{2}} \quad (4)$$

tem. It is assumed that the order parameter variable in the coordinated evolution process is P_j= *(*X_{j1}, X_{j2},... X_{ji}*)*, of which $i = 1,2,\cdots\cdots,n$, $m_{ji} \leq P_{ji} \leq M_{ji}$. The order parameter component $P_{j1}, P_{j2,\ldots\ldots,} P_{ji}$ is assumed to be a positive index. The definition formula (1) is the order degree of the order parametric component P_{ji} of the subsystem S_j.

$$SS_j(P_{ji}) = \begin{cases} \dfrac{X_{ji} - m_{ji}}{M_{ji} - m_{ji}}, i \in [1,k] \\ \dfrac{M_{ji} - X_{ji}}{M_{ji} - m_{ji}}, i \in [k+1,n] \end{cases} \quad (1)$$

In formula (1): M_{ji} and M_{ji} are the upper and lower limits of the P_{ji} of the subsystem order parameter variables, respectively. According to the coordination theory $SS_j(P_{ji}) \in [-1,1]$, the more the value of $SS_j(P_{ji})$ is closer to 1, the greater the contribution of the order parameter component to the development level of the subsystem S_1 or S_2. The value of $SS_j(P_{ji})$ is closer to 0, which indicates that the contribution of the order parameter component to the development level of the subsystem S_1 or S_2 is smaller. In general, the contribution of the order parameter component P_{ji} in each subsystem to its corresponding subsystem S_1 or S_2 can be described by the integration of the $SS_j(P_{ji})$. The results of $SS_j(P_{ji})$ can be affected by the size of each component and the difference in the combination mode. The integration of $SS_j(P_{ji})$ is carried out by the linear weighting method, shown in formula (2):

In form (2): λ_i represents the weight of each index in the development of the subsystem S_j, that is, the weight of each order parameter. It is known by the formula (2) that $SS_j(P_j) \in [0,1]$. The value of $SS_j(P_j)$ is closer to 1, indicating that the greater the contribution of P_j to the subsystem S_1 or S_2, the smaller the vice versa.

System development coordination model. Composite system coordination degree reflects positive matching relationship between the two subsystems and the degree of coordinated development of tourism and ecological environment in a period of time. It is assumed that the comprehensive development level function of the tourism subsystem S_1 in the t period is $f(SS_1,\ t)$, and the comprehensive development level function of the ecological environment subsystem S_2 in the t period is $f(SS_2,\ t)$. The comprehensive development level function of the composite system is calculated in formula (3):

$$F = \eta f(SS_1,\ t) + \sigma f(SS_2,\ t) \quad (3)$$

In Formula 3, $f(SS_j, t) = \sum_{i=1}^{n} \lambda_i P_i$, η and σ are the undetermined coefficients. Considering the equal contribution of tourism and ecological environment to regional coordinated development, we will take $\eta = \sigma = 0.5$.

On this basis, the coordination degree of the tourism industry and the ecological environment system is calculated. In this paper, the coupling degree function is used to define the coordination degree of tourism and ecological environment system. (4):

In formula 4, CI is the degree of system coordination, $CI \in [0,1]$, and the CI value is closer to 1, which indicates that tourism industry is more coordinated with the development of ecological environment system. On the contrary, it is more uncoordinated; ξ is the adjustment coefficient ($\xi \geq 2$), this paper takes $\xi = 2$.

But the coordination degree of CI can only reflect the degree of coordinated development of the two systems of tourism and ecological environment, and cannot reflect the actual development level of

coordination degree of composite system and subsystem. In order to avoid the exceptional situation of "the comprehensive development level of tourism and ecological environment is low, but the coordination degree of the two industries are high". We need to further integrate the coordination degree *CI* with the comprehensive development level function of the tourism industry and the ecological environment subsystem, and establish the coordination degree measurement model of the composite system, that is, the formula (5):

$$R = \sqrt{CI \times F} \tag{5}$$

In formula (5): R represents the coordination degree of the composite system, $R_{(t)} \in (0,1)$. When $R_{(t)}$ approaches 1, shows that the complex system of tourism and environment is going to the coordinated development under the ideal condition. The two industries or systems have developed orderly, showing a state of mutualism and mutual improvement. When the function $R_{(t)}$ approaches 0, it indicates that the coordination degree of the composite system is relatively small, and the tourism industry (or ecosystem) system even hinders the development of the ecosystem (or Tourism) system. The two industries may have competing relations.

Coordination grade division. In order to evaluate the coordinated development degree of the tourism industry and the ecological environment complex system more intuitively, the classification of the co scheduling is divided, and the results are shown in Table 2.

RESULTS AND DISCUSSION

Data sources and processing. According to the evaluation index system of coordination degree, the 2005-2014 year tourism and ecological environment related data in Wuhan were collected and collate (Table 3). The data are derived from the Shaanxi statistical yearbook and the Chinese statistical yearbook. Because the data units of each index are inconsistent, it may lead to a great difference between the observed value and the real value. Therefore, in order to avoid the effect of the different dimension differences on the real coordination results, the standardized transformation method is applied to deal with the index data in Table 3.

Index weight calculation. Index weight is the important degree of reflecting index in the system of compound system evaluation. The weight assignment can directly affect the accuracy and scientificity of the evaluation results. At present, the methods of determining the weight of the index are: the analytic hierarchy process (AHP), the correlation matrix weighting method, the variation coefficient method and the entropy method. This paper selects the correlation matrix weighting method to determine the weight of each evaluation index in the subsystem.

The concrete steps are as follows:

$$r_{ij} = \frac{\sum (x_i - \bar{x_i})(x_i - \bar{x_j})}{\sqrt{\sum (x_i - \bar{x_i})^2 (x_i - \bar{x_j})^2}} \tag{6}$$

According to the formula (6), the correlation coefficient matrix D and the complex correlation coefficient K_i can be obtained for the m index.

$$D = \begin{bmatrix} 1 & r_{21} & \cdots & r_{m1} \\ r_{12} & 1 & \cdots & r_{m2} \\ \cdots & \cdots & \cdots & \cdots \\ r_{1m} & r_{2m} & \cdots & 1 \end{bmatrix} \tag{7}$$

$$k_i = \sqrt{r_i^T D_{-i}^{-1} r_i} \quad (i=1,2, \ldots, m) \tag{8}$$

In formula (8), D_{-i} represents the correlation coefficient matrix for removing the index X_i. The larger the complex correlation coefficient K_i is, the greater the possibility that the x_i will be influenced by the remaining *m-1* indicators. The smaller the contribution to the comprehensive development level, the smaller the corresponding weight.

The correlation coefficient of K_i and the countdown after normalization can get the weight λ_i of each evaluation index, shown in the formula (9).

$$\lambda_i = \frac{1/K_i}{\sum_{i=1}^{m} 1/K_i} \tag{9}$$

According to the formula (6) - (9), we can calculate the index weight of each subsystem's parameters in the subsystem with SPSS19.0 measurement and statistics software and DPS data processing system, and the calculation results are shown in Table 4. Determination of order and coordination degree. The initial data is introduced into the formula (1), and the order degree of S_1 and S_2 ordinal parameter P_{ji} is calculated. The results are taken into the formula (2). Combined with the weight coefficient λ_i of each index, we get the order degree of the S_1 system of Wuhan tourism system and the eco system S_2 from 2005 to 2014. According to the formula (3) - (5), the coordination degree R of the tourism and ecological environment complex sys tem of Wuhan city was obtained for 2005-2014 years, as shown in Table 5.

TABLE 2
Coordination degree classification and its standard

Coordination grade	0.3—0.45	0.45—0.55	0.55—0.65	0.65—0.75	0.75—0.85	0.85—0.95	0.95—1.0
Coordination degree	Imbalance	On the verge of maladjustment	Grudging coordination	Primary coordination	Intermediate coordination	Good coordination	Better coordination

TABLE 3
Order parameter index of tourism and ecological environment subsystem

Year	Tourism S_1					Ecological environmentS_2				
	X_{11}	X_{12}	X_{13}	X_{14}	X_{15}	X_{21}	X_{22}	X_{23}	X_{24}	X_{25}
2005	280.3	165.6	18927	139	2763	41.55	200	68.31	90.11	2.46
2006	437.0	204.0	19366	158	3677	41.25	190	69.32	90.31	2.91
2007	619.3	254.4	21007	179	4564	43.95	220	72.39	90.93	3.2
2008	968.9	274.6	27630	209	5620	40.32	241	69.51	91.32	3.6
2009	1317.2	301.3	29368	234	6125	41.63	230	70.31	91.45	4.2
2010	5201	362.8	31118	260	8161	40.37	200	72.92	93.21	5.78
2011	6553	478.9	34333	333	10970	41.41	196	72.92	95.7	6.85
2012	7863	594.5	36154	378	12776	41.42	210	89.09	94.47	6.67
2013	8289	761.77	38289	420	13736	42.2	212	91.5	99.86	7.54
2014	8379.6	799.4	40289	466	14396	42.8	193	93.6	99.85	7.76

TABLE 4
Weight index weight of the sub system of tourism and ecological environment

The index weight of S_1 in the tourism industry system					The weight of each index of the ecological environment system S_2				
X_{11}	X_{12}	X_{13}	X_{14}	X_{15}	X_{21}	X_{22}	X_{23}	X_{24}	X_{25}
0.2160	0.2093	0.1457	0.2203	0.2088	0.2031	0.1111	0.3068	0.1915	0.1875

TABLE 5
Coordination of tourism and ecological environment system in Wuhan

Year	$SS_1(P_1)$	$SS_2(P_1)$	The coordination degree of the composite system RR	Coordination grade
2005	0.50011362	0.59	—	
2006	0.510286869	0.625475704	0.519865884	On the verge of maladjustment
2007	0.581668341	0.605032788	0.6525908416	Primary coordination
2008	0.485875248	0.623923796	0.4112530905	Imbalance
2009	0.576248318	0.654906733	0.3727571386	Imbalance
2010	0.62826876	0.683463491	0.6385815	Grudging coordination
2011	0.687958417	0.6700881	0.7155317	Primary coordination
2012	0.737328269	0.695088686	0.7075138717	Primary coordination
2013	0.827173959	0.675636706	0.7212571517	Primary coordination
2014	0.944326905	0.68998417	0.8587500408	Intermediate maladjustment

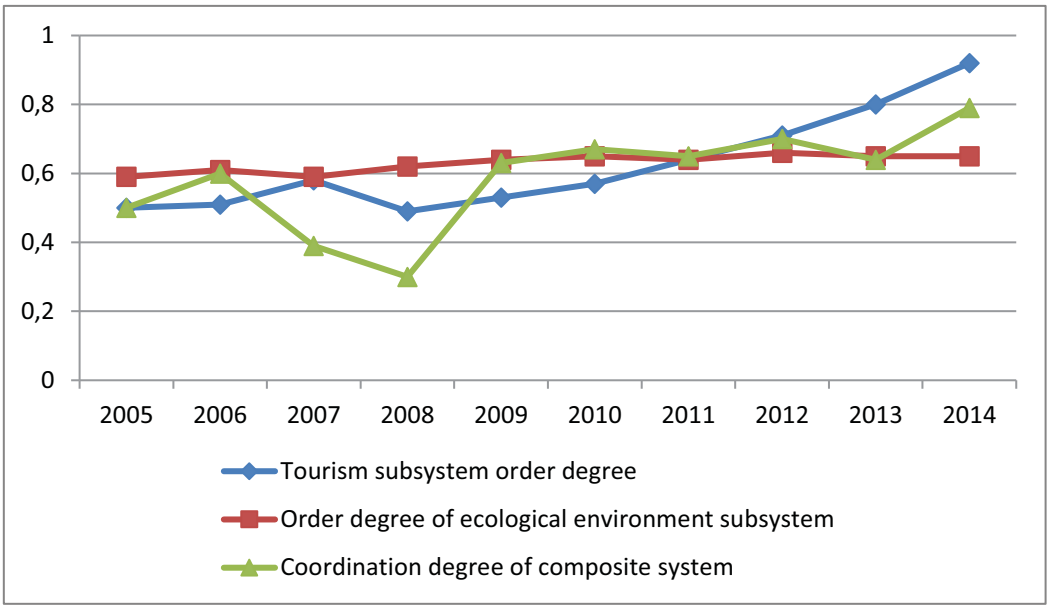

FIGURE 1
The trend map of the coordinated development of the tourism industry and the ecological environment complex system

In order to facilitate the analysis of the order characteristics of the subsystem and the trend characteristics of the coordinated development of the composite system, we draw the coordinated development and change trend map of the tourism industry and the eco environment system based on the data in Table 5, as shown in Figure 1.

From 2005 to 2014, the level of tourism economic development and the level of ecological environment in Wuhan are fluctuating. In the past ten years, the tourism industry in Wuhan has achieved an annual average growth of 7.79%. The total tourism revenue has increased from 15.44 billion to 81.144 billion, and the total number of tourist in Wuhan has increased from 21.4903 million to 101.3 million. But the impact of the international financial crisis in 2008 led to a low tourism industry in 2008. However, after the settlement of the crisis, Wuhan's tourism economy has developed rapidly to its previous level or even explosive growth. This shows that Wuhan's tourism economy has great elasticity and great potential for development.

The ecological environmental system of Wuhan has achieved an average annual growth of 2.03% from 2005 to 2014. Wuhan actively promotes transformation projects of river networks and lakes, and implements "big green project" to improve the level of road greening. The above measures make the comprehensive evaluation function of the ecological environment in Wuhan maintain a steady state of growth. The improvement of the environmental situation in Wuhan has given the tourism industry a broader space. But in 2013, the proportion of heavy air quality in Wuhan and the number of days that better than grade two account for the proportion of the whole year is reduced, which resulted in the small order of the ecological environment system in Wuhan in 2013. The problems of the ecological environment in Wuhan should arouse the attention of the relevant departments of environmental protection.

In the past ten years, the complex coordination degree of the tourism economic ecological environment system in Wuhan has been on the rise. The degree of coordination has changed from being on the verge of maladjustment to intermediate maladjustment. It shows that the coordination and interaction between Wuhan's tourism economic system and eco environment system is close and positive. The coordination type of tourism economy ecosystem environment in Wuhan changed from tourism economy lag type (2004 to 2011) to lagged ecosystem (2002 to 2014). The tourism economy of Wuhan has developed rapidly, and the development level of the tourism economy exceeds the level of the ecological environment.

CONCLUSIONS

The development of tourism has brought great pressure to the ecological environment as well as the development of the economy. Developing ecotourism industry and actively promoting transformation and upgrading of tourism industry and promoting sustainable development of tourism is of great significance for economic development and social progress. In urban development, the economic income

obtained by the tourism industry should be put into the environment protection and construction, and the ecological environment level should be gradually improved.

REFERENCES

[1] Sun, T., Shen, Q.Q. (2020) Coupling and coordination analysis between tourism development and ecological environment in Jiangsu province. Fresen. Environ. Bull. 29(5), 3671-3678.

[2] Yao, H.Q., Liu, B. (2020) Study on the problems of rural tourism eco-environment and its countermeasures. Fresen. Environ. Bull. 29(3), 1489-1492.

[3] He, J. (2019) Progress in ecotourism research: 20 years retrospective analysis. Fresen. Environ. Bull. 28(8), 5712-5718.

[4] Zhou, R. (2019) Study on the environmental capacity of ecotourism based on theory of sustainable development. Fresen. Environ. Bull. 28(5), 4293-4296.

[5] Wang, Q.Y., Li, M., Yang, Y.L. (2019) Study on the issues of rural tourism eco-environment and governance strategy. Fresen. Environ. Bull. 28(12A), 10083-10088.

[6] Yao, T.T. (2017) Study on the Coordinated Development of Tourism Economy and Ecological Environment in Resource-based City of Taiyuan. Sci-tech Innovation and Productivity. 4, 4-7.

[7] Guo, X.D., Li, Y.F. (2014) Research on the Relationship of Coordinated Development between Urban Tourism Economy and Ecological Environment: Taking Beijing as an Example. Research on Development. 2, 78-81.

[8] Zhou, L, Wang, C. (2016) Research on Coupling Coordination Degree of Tourism Industry—New Urbanization—Ecological Environment in China. Journal of Southwest Jiaotong University. 17(6), 122-129.

[9] Nie, X.Y., Shi, P.J., Wang, X.M. (2014) Data Processing in Ecological Development and Environment Improvement by Analysis of the Relationship between Tourism Development and Urban Development. Advanced Materials Research. 978, 169-173.

[10] Shi, H.C., Liu, L., Wang, B.L., Liu, W. (2012) Study on coordinated development of tourism economy and urban ecological environment in Lanzhou City. Journal of Northwest Normal University. 48(4), 108-114.

[11] Liu, J. (2016) Research on the Coordination of Urban Development and Ecological Environment in Aksu City. Science Technology & Industry. 16(12), 35-37.

[12] Weng, G.M., Lu, C. (2010) A Study on the Coordinated Development Evaluation of Tourism Economy and Urban Environment-Take Qinhuangdao City as Example. Ecological Economy. 3, 28-31.

[13] Li, S.J., Li, M.X. (2016) Research on Coupling Relation between Tourism Economy and Ecological Environment System of China's Costal Cities. Commercial Research. 466, 185-192.

[14] Guo, X.Y., Ming, Q.Z., Mu, X.Q., Wu, J.L. (2017) Study on Spatial and Temporal Evolution of Urban Tourism and Ecological Civilization——Taking Henan Province as an Example. Resource Development & Market. 33(6), 732-738.

[15] Nie, X.Y., Shi, P.J., Jiao, B.B., Wang, X.M., Chen, X. (2015) Analysis of the Coordination and Trend of Tourism and Urban Development in Dunhuang City. Areal Research & Development. 4, 89-94.

Received: **14.06.2020**
Accepted: **16.10.2020**

CORRESPONDING AUTHOR

Yuefang Guo
School of Business,
Xinyang Normal University,
Xinyang 464000 Henan – China

e-mail: maigood889@sina.com

© by PSP Volume 30– No. 05/2021 pages 4861-4867 Fresenius Environmental Bulletin

RESEARCH ON CORRELATION BETWEEN ECOTOURISM SERVICE QUALITY AND ENVIRONMENTAL POLLUTION

Hanfei Lv*, Wei Zhou

Hotel Industry Development Center, Tianjin Vocational Institute, Tianjin 300350, China

ABSTRACT

After rapid development, eco-tourism has become a new growth point of my country's tourism industry, and has received extensive attention from academia. The correlation between tourism service quality and environmental pollution, as a result of specialized division of labor, can provide a good perspective for the study of ecotourism development. In this paper, a literature review of relevant studies is conducted, summarizing relevant research results, and a large number of reviews on the correlation between ecotourism service quality and environmental pollution. This article combines the literature reading and its own observation and thinking to give a definition and interpretation of the concept of the relationship between ecotourism service quality and environmental pollution, analyzes the characteristics of the relationship between ecotourism service quality and environmental pollution, and gives ecotourism The concept of the core value of the correlation between service quality and environmental pollution is mainly used to clarify the development direction of the correlation between ecotourism service quality and environmental pollution. The research conclusions of this paper are as follows: by selecting the question of assessing the relevance of ecotourism service quality and environmental pollution from the perspective of tourist satisfaction, using SPSS to conduct mean, T sample test analysis and IPA analysis on the data, the problems in ecotourism are given Relevant opinions and suggestions on tourism service quality and environmental pollution control.

KEYWORDS:
Ecotourism, Service quality, Environmental pollution, Correlation

INTRODUCTION

Ecotourism originated from the urban people's lifestyle to escape industrial pollution and block rhythm. Ecotourism came into being and has developed to a certain extent. With the rapid development of railways and other means of transportation, the expansion and popularization of ecotourism has gradually become a popular social activity in some developed countries. my country's eco-tourism emerged after the reform and development, and the main form of the early period was the unique sightseeing agriculture [1]. In 1998, China's urban and rural tourism kicked off the development of domestic ecotourism. In 2006, driven by the theme of the National Tourism Administration's China Ecotourism Year, the development of the ecotourism market entered a period of vigorous development, which also caused serious ecological and environmental pollution problems. Since the late 1990s, the village has undergone four stages of spontaneous development, quantitative expansion, standardized development and quality improvement. The eco-tourism industry has germinated to key cultivation. After more than 20 years of active exploration, a unique development path has been established and formed eco-tourism model [2-4]. In 2009, in order to promote the upgrading of ecotourism, the Tourism Bureau combined with the development practices of ecotourism and environmental pollution control, summed up and launched a new ecotourism industry. The new format is a brand-new concept proposed for the creation of second-generation ecotourism. It is of great significance to improve the quality of ecotourism and environmental protection. On the whole, there are still some serious environmental pollution problems in the development of eco-tourism for more than 20 years, and the environmental satisfaction of eco-tourism is low [5].

The study of ecotourism in Europe was earlier and began in the 1950s. The rise of ecotourism is seen as a grassroots phenomenon, and its main purpose is to provide support for agricultural economic development. The European Union and the World Economic Cooperation and Development Organization define ecotourism as a tourism activity that occurs in rural areas. Yusof et al. [6] believe that the tourism environmental pollution that occurs in rural areas is not entirely eco-tourism. The scale, culture and social structure of eco-tourism should have traditional characteristics of rural areas. At the same time, the environmental pollution of eco-tourism in different countries and regions will rely

on different Geographical characteristics show different forms. In addition to this definition, Kaffashi et al. [7] made a comprehensive description of the concept of eco-tourism: eco-tourism is a multi-faceted tourism activity, not just a tourism activity that occurs in rural areas. The true form of eco-tourism environmental pollution should occur in rural areas, and tourism activities are linked to traditional rural culture. Dekhili and Achabou [8] believe that the pollution of buildings and residents' accommodation environment has the characteristics of small-scale villages, local pollution is related to tourism activities, and tourism activities are subject to local control. Enggraini et al. [9] believe that due to different regions relying on different natural, economic, historical and geographical environments, eco-tourism environmental pollution has different types. Ndirima [10] believe that because the concept of ecotourism has not yet reached an international consensus, the above terms are often used interchangeably abroad. Although scholars have different definitions of the concept of ecotourism, they generally agree with the characteristic of rural nature, which is an important symbol for defining ecotourism. Bălteanu et al. [11] believe that the problem between sustainable development and environmental protection is the core of ecotourism development. If the development efforts are within the range of the ecological environment, the development of ecotourism can meet the needs of economic development in rural areas, so that local residents gain profit. Bhattacharya et al. [12] believe that for eco-tourism to achieve sustainable development, financial and technical support must be guaranteed, and scientific management must be conducted to strengthen cooperation between regions. Machado and Conto [13] believes that ecotourism community participation is the core issue of ecotourism. Ecotourism sites need to benefit from tourism development, but also can not ignore the feelings of local residents and mobilize Residents are actively involved in the development of ecotourism.

MATERIALS AND METHODS

Connotation Analysis of Correlation between Ecotourism Service Quality and Environmental Pollution. Concept definition. Regarding the definition of the concept of the relationship between ecotourism service quality and environmental pollution, some domestic scholars have also given their own views. The correlation between the quality of ecotourism services and environmental pollution is the degree of horizontal and vertical functional destruction of the eco-environment in order to meet the needs of tourists to relax and relax. However, more scholars give the concepts of tourism service quality and environmental pollution, and there are fewer literatures concerning the concepts of tourism and environmental pollution. This paper defines the correlation between the quality of ecotourism services and environmental pollution as the chain of environmental pollution formed by various departments supporting ecotourism activities through a certain economic relationship. It appears as a network structure composed of horizontal collaboration and vertical supply and demand. In this concept, there is a horizontal cooperative relationship between the eco-tourism service quality and some departments of environmental pollution. Every industry that is related to the quality of ecotourism services and environmental pollution can provide tourism products for direct tourists, but to provide tourists with complete environmental protection tourism products, it is necessary for industries that are related to tourism service quality and environmental protection to cooperate with each other. Such as poor collaboration or poor performance in one of these industries will cause consumers to weaken the service quality of the entire eco-tourism.

Construction of Ecotourism Tourist Service Quality Measurement System. This paper selects the quality of eco-tourism catering services, quality of eco-tourism accommodation services, eco-tourism atmospheric environment, and eco-tourism natural environment as project indicator layers. Each indicator layer contains several factor layers, which is shown in Table 1.

RESULTS AND DISCUSSION

Case Analysis of the Correlation between Ecotourism Service Quality and Environmental Pollution. Questionnaire design and data collection. The questionnaire is divided into two parts. The first part is the demographic characteristics and travel characteristics of tourists. This part includes two aspects: tourist demographic characteristics and tourist service quality and environmental pollution characteristics. The second part is the survey of tourism service quality and environmental pollution. This survey uses Likert's five-point scale as the evaluation standard for index measurement, and divides the measurement of all factors into 5 levels. The survey targets are two aspects of service quality and environmental pollution.

The data sources used in this article have two parts: the first part is a field survey of various eco-tourism destinations in December 2017, and the second part is the distribution of online questionnaires. A total of 280 questionnaires were

TABLE 1
Ecotourism Tourist Service Quality Measurement System

Target layer	Indicator layer	Factor layer
Eco-tourism	Quality of Ecotourism Catering Service	Country features
		Environmental sanitation
		Catering price
		Catering Services
		Catering taste
	Ecotourism Accommodation Service Quality	Country features
		Environmental sanitation
		Accommodation price
		Accommodation Service
	Ecotourism atmospheric environment	Rural characteristic air quality
		Air pollution cost
		Air pollution level
		Types of air pollution
	Ecotourism natural environment	Impact of rural environmental characteristics
		Environmental protection
		Environmental governance level
		Environmental protection infrastructure

TABLE 2
Demographic characteristics of ecotourism tourists

Item	Eigenvalues	Proportion
Gender	Male	47.4
	Female	52.6
Age	Below 18	4.1
	19-25	28.1
	26-35	34.3
	36-50	24.0
	Over 51	9.5

distributed, and 252 valid questionnaires were recovered.

Data reliability analysis. Reliability refers to the credibility of the questionnaire in the sense of measurement, also called reliability. Questionnaires with good reliability will show good stability and consistency. Reliability analysis is an analysis method to obtain the reliability of the questionnaire through surveying methods, and to evaluate whether the questionnaire has good reliability and stability by reliability. Generally speaking, the same question tends to be consistent in the questionnaires of different test subjects, which means that there is no large sample-to-sample error in this questionnaire, the reliability of the questionnaire is higher, and the reliability of the questionnaire is low. Reliability generally uses the α coefficient as its measurement index. The α coefficient is generally between 0 and 1. The higher the reliability, the closer the α coefficient is to 1, indicating that the questionnaire is more stable. Cronbach pointed out that under normal circumstances, the α coefficient is above 0.70, indicating that the questionnaire has good reliability and can be used for further analysis. If the α coefficient is less than 0.35, the reliability is low, and the questionnaire is not stable enough to be used. In between, the questionnaire reliability is acceptable. In this study, SPSS data analysis software was used to perform reliability analysis on the questionnaires used to check their consistency to ensure the quality and credibility of the questionnaires. After testing, the overall reliability of the questionnaire adopted in this survey is α=0.958, the reliability of service quality α=0.956, and the reliability of environmental pollution α=0.963, all of which meet Cronbach's standard (greater than 0.70), showing that the questionnaire is good The reliability can be analyzed in the next step.

Sample descriptive analysis. In this survey, males accounted for 47.4% of the total sample, and females accounted for 52.6%. The gender ratio was relatively balanced. In terms of age structure, the proportion of tourists in the 26-35 age group is the highest.

In the way of eco-tourism, most people choose to drive to their destination by car, and 71.1% choose to travel with relatives and friends. Regarding the acquisition channels of ecotourism information, relatives and friends accounted for 51.3%, that is to say, the information transmission method of ecotourism is very traditional, and marketing activities need to be strengthened. The occupancy rate of ecotourism is only 31.7%, indicating that ecotourism has fewer attractions and there is a short-chain problem between the quality of tourism services and environmental pollution, resulting in short stays for tourists. For the overall satisfaction of ecotourism, the ratio of very satisfied and satisfied is 60.5%, and the satisfaction and satisfaction rates of

TABLE 3
Eco-tourism evaluation factor service quality ranking

Indicator layer	Factor layer	Very dissatisfied	Dissatisfied	General	Satisfied	Very satisfied	Mean	Sort
Quality of Ecotourism Catering Service	Country features	5	8	126	90	13	3.40	2
	Environmental sanitation	6	20	152	58	6	3.16	16
	Catering price	12	46	95	76	13	3.13	18
	Catering Services	4	47	91	64	6	3.20	14
	Catering taste	0	25	116	96	5	3.34	3
Ecotourism Accommodation Service Quality	Country features	0	13	127	83	19	3.45	1
	Environmental sanitation	7	45	97	74	19	3.22	10
	Accommodation price	4	39	103	90	6	3.22	10
	Accommodation Service	6	20	120	88	8	3.29	5
Ecotourism atmospheric environment	Rural characteristic air quality	7	25	126	71	13	3.24	7
	Air pollution cost	5	65	108	58	6	2.98	20
	Air pollution level	5	52	121	57	7	3.03	19
	Types of air pollution	3	29	148	50	12	3.15	17
Ecotourism natural environment	Impact of rural environmental characteristics	6	33	112	78	13	3.24	7
	Environmental protection	4	34	117	75	12	3.23	10
	Environmental governance level	6	63	128	32	13	3.24	7
	Environmental protection infrastructure	6	26	109	82	19	3.34	4

accommodation quality, accommodation price, and tourist services are all above 90%. This shows that the overall service quality of ecotourism has much room for improvement. As the overall service quality is not high, the environmental protection level of eco-tourism destinations is also not high. The average and standard deviation of the service quality of the evaluation indicators are calculated, and sorted according to the average size. It can be seen from the observation that among the three-level indicators, tourists are more satisfied with the impact of the rural environmental characteristics of tourism accommodation, the rural characteristics and tastes of tourism and catering; and the quality of service ranked second in the tourist environment pollution situation.

Calculate the average and standard deviation of the environmental pollution of the evaluation indicators, and sort them according to the average size. It can be seen from the observation that among the three-level indicators, tourists consider that the environmental protection of tourism scenic spots, the level of environmental governance and the environmental protection of tourism accommodation are the most important; while the environmental pollution ranks secondarily is the parking capacity of tourist traffic and the Prices and types of tourist goods. The paired sample T test is a statistical method to test whether there is a significant difference between the two paired sample population means. A paired sample can be two sets of sampled data referred to by the same variable, or it can be regarded as two different sides of a problem. When performing the paired sample T test, you need to find the difference between each pair of samples, and then compare the relationship between the mean and the overall mean of 0. Weak samples have no difference, and the mean should be near 0, otherwise it means that the samples are different. In this study, the paired sample T test was used to analyze the differences in environmental pollution and service quality in the questionnaire. If the difference is not significant, it means that the environmental pollution and service quality of this indicator are different in the completion of the test. On the contrary, it is significant, that is, there is a certain distinction between the subjects' evaluation of environmental pollution and service quality. In terms of the mean value, service quality is less than environmental pollution, and the mean difference is negative, indicating that tourists have high expectations for each indicator, but the actual evaluation is slightly dissatisfied, and there is a certain difference between the two.

IPA Analysis of Ecotourism Environmental Pollution and Service Quality. The IPA analysis of eco-tourism environmental pollution and service quality is a tool for studying the environmental development strategy of the tourism market.

Because of its ease of operation and diagnostics, it has been popularized in recent years. The theory takes service quality and environmental pollution as attribute models. It establishes the horizontal and vertical coordinate system and places the measurement factors in four quadrants to reflect the actual problems, and then gives specific suggestions for management. In this paper, the IPA analysis method is used to study the relative difference between environmental pollution and service quality of each measurement factor of ecotourism tourist service quality. In this paper, service quality is taken as the horizontal axis, and environmental pollution is taken as the vertical axis. The total average of 3.23 and 3.86 is used as the boundary between the horizontal and vertical axes to divide the four quadrants of the coordinate system. By analyzing the position of the measurement factor in the quadrant, the current status of ecotourism and the areas for improvement are analyzed. The first quadrant is Good Work (high environmental pollution, high service quality). The factors of the quadrant service quality and environmental pollution assessment meet or exceed the ecological quality standards. They play a pillar role in the organization and should continue to maintain and protect these indicators. Advantage, continue to maintain and develop competitiveness. The second quadrant is Low Priority (high environmental pollution, low service quality), and the service quality does not meet the eco-tourism quality standards. The factors belonging to this quadrant are the key areas that need to be improved. The indicators distributed in this area include the environmental protection of tourism and catering, the environmental protection of tourism accommodation, the environmental protection of tourist attractions and recreational activities. It is necessary to analyze the reasons and propose corresponding solutions. The third quadrant is Concentrate Here (low environmental pollution, low service quality), and neither environmental pollution nor service quality meet the ecotourism quality standards. The fourth quadrant is Possible Overskill (low environmental pollution, high service quality). The service quality exceeds the eco-tourism quality standard, but the environmental pollution has not reached. Therefore, organizations should allocate more resources to deal with the first quadrant indicators. This shows that the rural characteristics and services of tourism accommodation, the environmental management level of tourism scenic spots and environmental protection infrastructure are doing very well, so there is no need to spend more time and energy to improve the status quo.

Countermeasures and Suggestions for Coordinated Development of Ecotourism Service Quality and Environmental Protection. Eco-tourism departments strengthen collaboration. Pay attention to horizontal collaboration, that is, attach importance to the industrial matching between departments. First, the government should formulate a tourism industry development plan based on the actual situation of the eco-tourism destination, do a good job in forecasting market demand prospects, and construct and adjust the quantity structure and hierarchy of each department; second, each eco-tourism department should actively participate in cooperation The division of labor and cooperation in the correlation between the quality of ecotourism services and environmental pollution, the emphasis on the balance of links, and the establishment of a scientific interest distribution mechanism to ensure that the overall benefits of ecotourism service quality and environmental pollution are greater than the interests of all participants. The vertical extension of tourism ecotourism service quality and environmental protection refers to the extension of ecotourism to the survey and planning of tourist attractions and scenic spots, the planning and development of tourism products and services, and the sales and after-sales services of tourism products and services. Follow-up optimization and other links.

Strengthen industrial collaboration between ecotourism destinations. The concept of industrial clusters first refers to a series of geographically close and interconnected enterprises that exist in a common or complementary manner through mutual resources or cooperative division of labor. For ecotourism, the cultivation of industrial clusters between ecotourism destinations can actively leverage the advantages of ecotourism and drive the development of the ecotourism industry. The excellent operation of the industrial cluster area can connect related enterprises in the area as a whole, orderly division of labor and cooperation, sharing production resources, environmental protection infrastructure equipment, business information and mutual supervision and promotion in the area. Eco-tourism areas form industrial clusters, sharing eco-tourism resources, tourist sources, and tourism environmental protection infrastructure, etc., which will virtually enhance core competitiveness and form an eco-tourism brand effect.

Eco-tourism industry departments improve management. Today, in many eco-tourism destinations in my country, environmental protection is a relatively lacking aspect in product development. This is because sanitation protection awareness is lacking for operators and tourists, and there is a lack of efficient and feasible sanitation management measures and means. Therefore, when considering the construction and protection of eco-tourism destinations, the protection of tourist destination environments urgently needs to be resolved. This requires developers of tourist areas to start from both inside and outside. Internally, it is

necessary to strengthen investment in environmental protection facilities, strengthen the construction of tourist destinations themselves, regulate the behavior of service providers, and increase supervision and management measures. Externally, the government, media, and educational institutions are used to take feasible and effective environmental governance measures, increase investment in remediation, and promote good tourist habits to the public.

CONCLUSIONS

The concepts of ecotourism service quality and environmental pollution are different from the general manufacturing tourism service quality and environmental protection. This article defines it as a chain relationship formed by various departments supporting ecotourism activities through a certain economic relationship. Some departments show a horizontal collaboration relationship, and some departments show a vertical supply and demand relationship. My research believes that the correlation between the quality of ecotourism services and environmental pollution has three characteristics. First, the quality of ecotourism services and environmental protection are horizontally related to each industry. Each industry faces consumers at the same time, and secondly, the quality of ecotourism services and environmental protection. Individual links can directly provide ecological services for tourists. Finally, the quality of ecotourism services and environmental protection are different from the general quality of tourism services, and their chain cores are diversified. Therefore, the core value of ecotourism service quality and environmental protection is the experience of rural culture.

REFERENCES

[1] Dong, H.M. (2010) Study on sustainable development of ecotourism in the Northern Piedmont in the Qinling Mountains. Journal of Sustainable Development. 3(1), 104-108.

[2] Li, Y.H., Xiang, B. (2014) Research Progress in the Ecotourism Environmental Carrying Capacity. Advanced Materials Research. 869-870, 781-785.

[3] Ma, J.Z., Cheng, K. (2008) Impacts of ecotourism on wildlife in nature reserves: Monitoring and management. Acta Ecologica Sinica. 43, 539-568.

[4] Chen, J., Ge, J.F., Liang, Y.Q. (2010) Discussion on ecotourism development model in Taihang Mountain Area of Hebei Province. Journal of Arid Land Resources & Environment. 24(2), 122-125.

[5] Yi, X.L., Fu, Q.M. (2016) Vulnerability of Ecotourism Resource Development of Wujiang Gallery and Its Protection Measures. Journal of Anhui Agricultural Sciences. 34, 167-169.

[6] Yusof, N., Rahman, S., Iranmanesh, M. (2015) Effects of resort service quality, location quality and environmental practices on the loyalty of guests within the Malaysian ecotourism industry. Pertanika Journal of Social Science & Humanities. 23(4), 1015-1030.

[7] Kaffashi, S., Radam, A., Shamsudin, M.N., Yacob, M.R., Nordin, N.H. (2015) Ecological conservation, ecotourism, and sustainable management: the case of Penang National Park. Forests. 6(7), 2345-2370.

[8] Dekhili, S., Achabou, M.A. (2015) The perception of ecotourism. Semantic profusion and tourists' expectations. Rimhe Revue Interdisciplinaire Management Homme & Entreprise. 19(5), 3-20.

[9] Enggraini, R., Yulianda, F., Krisanti, M. (2013) Ecological Condition and Ecotourism Potency at Timbulun Waterfall area, Sungai Nanam Village, Solok District, West Sumatera. MT - Fisheries.

[10] Ndirima, Z.K. (2002) Ecotourism and its effects on the livelihoods of the host community and natural resource management: a case study of Amboseli, Kenya. University of Nairobi, Nairobi.

[11] Bălteanu, A.D., Dincă, A.I., Surugiu, C., Dumitraşcu, M., Micu, D., Felciuc, M. (2008) Ecotourism and Environmental Change in the Romanian Carpathians. Global Environmental Research. 12 (2008), 161-172.

[12] Bhattacharya, A.K., Saksena, V., Banerjee, S. (2006) Environmental auditing in ecotourism: a study on visitors' management in Van Vihar National Park, Bhopal, M.P. (India). Indian Forester. 132(2), 1-3.

[13] Machado, Á.L.D.M., Conto, S.M.D. (2013) Environmental practices to minimize environmental impacts of ecotourism: information managers of travel agencies of Rio Grande do Sul. Cultur Revista De Cultura E Turismo. 2013, 31-46.

Received: **16.06.2020**
Accepted: **17.10.2020**

CORRESPONDING AUTHOR

Hanfei Lv
Tianjin Vocational Institute,
Hotel Industry Development Center,
Tianjin 300350 – China

e-mail: lizha888@outlook.com

© by PSP Volume 30– No. 05/2021 pages 4868-4874 Fresenius Environmental Bulletin

IN VITRO ANTIOXIDANT, ANTIMICROBIAL, ANTICANCER ACTIVITIES ASSESSMENT OF *THYMUS PECTINATUS*, SCREENING OF ENZYME INHIBITORY

Merve Ergul[1], Gulsen Guclu[2,*], Mehmet Atas[3], Metin Durmus Cetin[4], Nuraniye Eruygur[5], Esra Ucar[6], Huseyin Askin Akpulat[7]

[1]Department of Pharmacology, Faculty of Pharmacy, Sivas Cumhuriyet University, Sivas, Turkey
[2]Department of Health Care Services, Health Services Vocational School, Sivas Cumhuriyet University, Sivas, Turkey
[3]Department of Pharmaceutical Microbiology, Faculty of Pharmacy, Sivas Cumhuriyet University, Sivas, Turkey
[4]Department of Field Crops, Batı Akdeniz Agriculture Research Institute, Antalya, Turkey
[5]Department of Pharmacognosy, Faculty of Pharmacy, University of Selcuk, Konya, Turkey
[6]Department of Crop and Animal Production, Sivas Vocational School, Sivas Cumhuriyet University, Sivas, Turkey
[7]Department of Biology, Faculty of Sience, Sivas Cumhuriyet University, Sivas, Turkey

ABSTRACT

According to the data obtained in this study, *Thymus pectinatus* has antioxidant and enzyme inhibitory activities while has not showed antimicrobial activities. The results of the current study provide valuable information, showing that the major component of the water extract of *T. pectinatus* is "1,3-Propanediol, 2-methyl-, dipropanoate" (59.34 %). This is the first investigation of the antioxidant and enzyme inhibitory activity of *T. pectinatus*. The results showed that the water extract had high antioxidant, anti-amylase, and anticancer effects, and a higher total phenolic content. Therefore, further phytochemical and bioactivity-guided isolation of *T. pectinatus* water extract could be carried out to identify the active compounds.

KEYWORDS:
Thymus pectinatus, Antimicrobial, Antioxidant, Enzyme inhibitory, Anticancer

INTRODUCTION

Thymus is a perennial plant of the Lamiaceae family [1]. This genus, known as "thyme" in English and "kekik" in Turkish, has 38 species and 64 taxa, 24 of which are endemic in Turkey [2,3]. The leaves of *Thymus* are used as alternative medicine in bronchitis, arthritis, rheumatism, and for the removal of intestinal gas [4]. It has been reported to have antimicrobial and antioxidant activities [4-6].

In recent years, the essential oil or extracts of medicinal and aromatic plants have been the focus of increasing interest in therapy and phytotherapy fields because of the abundant secondary metabolite content [4,7-9]. The use of these components is increased in particular in the treatment of or protection against diseases such as cancer, Alzheimer's disease, diabetes mellitus, cardiovascular disease, and to delay the aging process. The components can show different physiological activity on living [10-12]. The effects may be due to only one compound or the synergistic effect of several compounds. Phenols; it is a chemical component in essential oils that has antioxidant effects and provides the body with protection from reactive oxygen types and damage caused by oxidative stress caused by free radicals [13,14].

Alzheimer's disease and Diabetes mellitus (DM) are major diseases in the general population. Butyrylcholinesterase (BChE) and Acetylcholinesterase (AChE) are effective target enzymes in the treatment of Alzeihmer's disease. In DM treatment, α-amylase and α-glucosidase play an important role in hydrolyzing carbohydrates that lead to an increase in the blood glucose level. Therefore, people have to use such enzyme inhibitors to control and regulate levels of enzymes which are related to Alzheimer's disease and diabetes [15]. Drugs used for such diseases are available, but there are no specific solutions, and they have many side-effects. This has motivated researchers to search for new plants and their active substances for the treatment of such diseases.

Cancer is a disease that has a fatal outcome worldwide and develops due to multiple variable causes. The frequency of different types of cancer in men and women can vary. While breast cancer occurs in 1 out of every 10 women, this rate is much lower in men and the treatment touches are generally not at pleasant levels. Traditional treatments used in the clinic have several serious side effects and can cause damage to non-cancerous tissues [16]. Hereby, the usage of the essential oil or extracts of medicinal and aromatic plants has crucially increased in recent years [17].

The *Thymus* plant is readily available as it is widely consumed by the public. Although the plant is known to be useful, there have been no published studies of the effects of the water extract of the essential oil of *T. pectinatus* on antioxidants and inhib-

itory enzyme activity. In this study, it is aimed to determine the different biological properties of *Thymus pectinatus*, which is an endemic species, such as antioxidant, antimicrobial activity, activity of enzyme and cytotoxicity.

MATERIALS AND METHODS

Plant materials and preparation of extracts. *Thymus pectinatus* plant materials, an endemic region in terms of wild plants in Turkey, which were collected from Sivas. (B6 Sivas: Sivas-Karayün 25 km, roadside, 25 June 2015, Akpulat 4589). Antimicrobial activity and cytotoxicity experiments were conducted at the Faculty of Pharmacy laboratories while *in vitro* antioxidant and enzyme inhibition activity tests were carried out at the Advanced Technology Research and Application Center (CÜTAM), Sivas Cumhuriyet University, Sivas, in 2019.

The Chemical Composition. The plants were dried and ground with a blender (Blue house). 10 g of dried plant sample was taken and soaked in 50 mL of water for 24 hours with intermittent agitation. After the extract was filtered, it was dried in a furnace at 40 ° C. The extracts obtained were analyzed by GC-MS method known as Gas Chromatography-Mass Spectrometry.

***In vitro* Antioxidant Activity.** The antioxidant activity of the water extract of *Thymus pectinatus* aerial parts was tested using different methods. The DPPH radical scavenging activity of the extract was evaluated according to the Blois method (1958) with slight modification. ABTS radical scavenging activity was evaluated by the method of Re et al. (1999) with minor modifications [18]. Total phenolic content was determined using the Folin-Ciocalteu spectrophotometric method and expressed as milligrams of gallic acid equivalents per gram of the dry weight of the extract [19]. The flavonoid content was determined with the aluminum chloride colorimetric method of Molan and Mahd (2014) [20]. The content of total flavonoids was expressed as milligrams of catechine equivalent per gram of the dry weight of the extract.

***In vitro* enzyme inhibition assay.** The AChE/BChE inhibition assay was carried out according to the Ellman method as described by our previous study [21,33]. The α-glucosidase inhibition method was reported by Kumar et al. (2012) [22]. The α-amylase inhibition activity of the extract was investigated by the method reported by Kumar et al. (2013) [23]. In both of the α-glucosidase and α-amylase inhibition method, acarbose was used as a positive control. In the same time, tyrosinase inhibitory activity was determined using the 96-well plate spectrophotometric method as described by Jeong et al. (2009) with slight modifications [24].

In vitro cytotoxicity assay. The cytotoxicity of the *Thymus pectinatus* water extract was tested against MDA-MB-231 (human breast adenocarcinoma) and L-929 (mouse fibroblast) cell lines. Both cell lines were cultured in DMEM containing 10% FBS, 1% L-glutamine, 100 IU/mL penicillin, and 10 mg/mL streptomycin in 25cm^2 polystyrene flasks and sustained in a humidified atmosphere with 5% CO_2 at 37°C. Cells were passaged when they had reached 85-90% confluence.

Antiproliferative activity of the extract was evaluated on the MDA-MB-231 and L-929 cell lines by the XTT cell proliferation method. Initially, the cells were seeded at a density of 5x10^3 cells per well in 96-well culture plates in 100 µl of culture medium and were allowed to attach overnight before treatment. Then these cells were treated with various concentrations (0,0625, 0,125, 0,25, 0,5, 1 mg/ml) of extract for 24 h. Following treatments, the medium was removed and wells were washed twice with 200 µl phosphate-buffered saline (PBS). At the end of these periods, for determination of living cells, 100 µl DMEM without phenol red and 50 µl XTT labeling mixture were added to each well, and then the plates were incubated for another 4 h. The absorbance of XTT-formazan was measured using a microplate (ELISA) reader at 450 nm against the control (the same cells without any treatment). All experiments were carried out as three different independent experiments and cell viability was expressed as % of control (100% viability).

Antimicrobial Activity. Microdilution broth method. The broth microdilution method was applied to 96-well microtiter plates, and the minimum inhibitory concentration (MIC) of *T. pectinatus* was determined [25]. The bacterial and yeast test strains used in this study were *Escherichia coli* (ATCC 25922), *Staphylococcus aureus* (ATCC 29213), *Pseudomonas aeruginosa* (ATCC 27853), *Bacillus cereus* (ATCC 27853), *Candida albicans* (ATCC10231) and *Candida tropicalis* (DSM11953). Mueller-Hinton broth (Accumix®AM1072) was utilizated as a culture media for bacteria and Sabouraud Dextrose Broth (Himedia ME033) was used for Candida spp. [26,27].

The extract was dissolved in DMSO (50 mg/mL). 90 µl of media were added to the first row of the microtiter plates and 50 µl of the remaining wells. The 11th wells were used as the reproductive controls and 100 µL broth was added. 10 µL extract was added in the first line of the microtiter plate and serial two-fold dilutions were prepared. The extract concentration in the wells was between 2.5 and 0.004 mg/mL. The bacteria and fungi suspensions (50µL) were added to prepared samples. The final inoculum size was 5×10^5 CFU/mL in the bacteria wells and

0.5-2.5×10^3 CFU/mL in the Candida sp. wells (CLSI, 2002, CLSI, 2012). The MIC concentration of the extract was determined as the lowest concentration that prevents visible growth of bacteria and yeast after incubation at 37°C overnight.

RESULTS AND DISCUSSION

The Chemical Composition. In the water extract of *Thymus pectinatus*, eight components were obtained by GS-MS method. 1,3-propanediol, 2-methyl-, dipropanoate (59.34 %) was determined as the major component (Table 1). The following main components are; hexadecanoic acid, methyl ester (CAS) (7.87 %), propanoic acid, pentyl ester (7.00 %), 2-methoxy-4-vinyl phenol (4.20 %), thietane (2.66 %), benzene, 1-(1,1-dimethyl ethoxy)-4-methyl (2.44 %), 2-oxazolidinethione, 4,4-dimethyl (1.81 %), 2-hexenal, (E)- (CAS) (1.10 %). Vardar-Ünlü et al. (2003) reported that the essential oil of *Thymus pectinatus* was analyzed with GC-MS and thymol, γ-terpinene, p-cymene, carvacrol, and borneol were identified as major components [28].

Antioxidant activity. DPPH and ABTS radical scavenging activity. *In vitro* antioxidant activities were determined by comparing the total phenolic and flavonoid contents of *Thymus pectinatus* water extract with DPPH and ABTS radical scavenging activity with standard antioxidant components, BHT and BHA. The lower the IC_{50} value, the higher the radical scavenging activity of the extract. The water extract showed DPPH radical scavenging activity with the IC_{50} value of 120.52 ± 0.36 µg/mL and ABTS radical scavenging activity with the IC_{50} value of 59.39 ± 1.69 µg/mL, although these values were lower than the reference BHT and BHA (8.68 ± 0.16 and 6.93 ± 0.65 µg/mL, respectively) (Table 2). Other investigators have confirmed that *T. pectinatus* has powerful antioxidant activity [4;28]. As a result of DPPH analysis, it was determined that methanol extract (IC50 = 76.24 ± 1.84 µg / mL) had better activity than water extract (168.64 ± 0.91 µg / mL)

Total phenol and flavonoid content. As shown in Table 2, the total phenolic content values for the water extract of *T. pectinatus* was 57.47 ± 4.07 mg gallic acid equivalents (GAE)/g dried extract, while total flavonoid content value was 4.06 ± 0.87 mg catechin equivalents (CE)/g dry weight of the extract. Phenolic compounds have antioxidant properties and protect living organisms from oxidative damage [29-31].

Enzyme Inhibiton Activity. Anti-cholinesterase Activity. Both AChE and BChE play important role in controlling against Alzheimer's disease and related dementia. When the inhibitory activity of AChE and BChE of the water extract of *T. pectinatus* was examined, the AChE inhibitory activity was 50.92 ± 4.85 %, and no BChE inhibition activity was observed (Table 3). But the AChE inhibitory activity was lower than that of the reference drug Galanthamine (93.87 ± 0.56).

TABLE 1
The chemical composition of the water extract of *Thymus pectinatus*

No	RT	Components	Relative percentage (%)Water Extract
1	4.740	Thietane	2.66
2	5.925	Propanoic acid, pentyl ester	7.00
3	6.102	1,3-Propanediol, 2-methyl-, dipropanoate	59.34
4	6.755	2-Oxazolidinethione, 4,4-dimethyl	1.81
5	18.714	2-Hexenal, (E)- (CAS)	1.10
6	22.633	2-Methoxy-4-vinylphenol	4.20
7	32.601	Benzene, 1-(1,1-dimethylethoxy)-4-methyl	2.44
8	37.739	Hexadecanoic acid, methyl ester (CAS)	7.87
Total			**86.42**

TABLE 2
***In vitro* antioxidant activities of the water extract of *T. pectinatus* (IC_{50} value in µg/mL)**

Extracts	DPPH Radical Scavenging Activity	ABTS Radical Scavenging Activity	Total Phenolic Content	Total Flavonoid Content
Water	120.52 ± 0.36	59.39 ± 1.69	57.47 ± 4.07	4.06 ± 0.87
Reference Drugs				
BHT	8.68 ± 0.16	-		
BHA	-	6.93 0.65		

TABLE 3
In vitro* enzyme inhibitory activities of the water extract of *Thymus pectinatus

Extracts	*Anticholinesterase Activity*		*Antidiabetic Activity*		*Skin Whitening*
	AChE	*BChE*	*a-Glucosidase*	*a-Amylase*	*Tyrosinase*
Water	50.92± 4.85	-	49.41±1.94	17.34±1.50	78.55±0.30
Reference Drugs					
Galanthamine Hydrobromide	93.87± 0.56	89.89± 0.01			
Acarbose			57.56±0.52	58.40±0.63	
Kojic Acid					56.42 ±1.59

α-Glucosidase and α-Amylase Inhibition Activity. α-Glucosidase and α-Amylase are catalyzing the hydrolysis of polysaccharides and disaccharides to monosaccharides in digestive organs, therefore, they can be a therapeutical approach to treat diabetes mellitus by reducing postprandial hyperglycemia [21]. The inhibitory activity of the water extract of *T. pectinatus* was evaluated against α-glucosidase and α-amylase enzyme (Table 3) in comparison with the positive control drug acarbose. According to the data, the water extract demonstrated vigorous inhibitory activity both against α-glucosidase (49.41 ± 1.94%) and α-amylase (17.34 ± 1.50%) compared to the reference drug acarbose (57.56 ± 0.52% and 58.40 ± 0.63%, respectively) at the same concentration.

Tyrosinase Inhibitory Activity. The tyrosinase inhibitory activities of water extracts of *T. pectinatus* are presented in Table 3 as a percentage. The study results revealed that water extract showed higher tyrosinase inhibitory activity (78.55 ± 0.30%) than the kojic acid, which was used as the positive control and showed an inhibition level of 56.42 ± 1.59% at the same concentration (i.e., 2 mg/mL).

Cell viability. *In vitro* cytotoxicity of the water extract of *T. pectinatus* was appreciated on MDA-MB-231 and L-929 cell lines by XTT assay and results are shown in Figure 1. According to experimental results, in the presence of water extract at all concentrations reduced significantly MDA-MB-231 cell proliferation ($p<0.05$) in a dose-dependent manner when compared with the control group. The IC_{50} of the water extract of *T. pectinatus* in MDA-MB-231 cell lines was calculated as 0.206 mg/mL. Conversely, the water extract did not show evident cytotoxicity on the L929 cell line at the IC_{50} concentrations. In general, the results suggest that *T. pectinatus* extracts may have strong anti-proliferative activity against MDA-MB-231 cell lines and may be a potential anticancer agent. However, in order to evaluate this possibility correctly, the anticancer properties of *T. pectinatus* need to be further investigated.

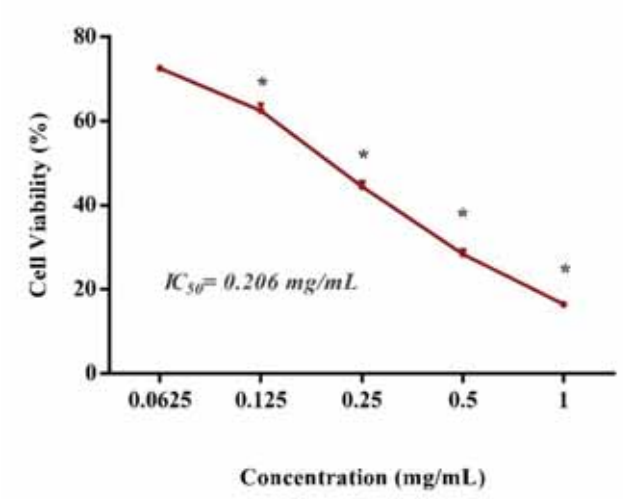

FIGURE 1
Effects of water extract from *T. pectinatus* on viability of MDA-MB-231 cell line, after treatment with different concentrations (range: 0,065-1 mg/mL) for 24 h.

TABLE 4
The antimicrobial activity values of *Thymus pectinatus* water extract

Microorganisms and MIC values (mg/mL)

	E. coli	*S. aureus*	*P. aeruginosa*	*B. cereus*	*C. albicans*	*C. tropicalis*
	ATCC 25922	ATCC 29213	ATCC 27853	ATCC 11778	ATCC 10231	DSM 11953
Thymus	2,5	2,5	>2,5	>2,5	>2,5	2,5

Antimicrobial Activity. The antimicrobial activities of *Thymus pectinatus* water extract against *E. coli, S. aureus, P. aeruginosa, B. cereus, C. albicans and C. tropicalis* were detected using the microdilution technique at the concentration range 2,5 to >2.5mg/mL (Table 4).

In the study conducted by Holetz et al in 2002, antimicrobial activity is good if the MIC of the extract was less than 100 µg/ml; It is reported to be moder at between 100 and 500 µg/ml and weak at between 500 and 1000 µg/ml. Values above 1000 µg/ml are considered inactive [32]. According to these criteria, the water extract of *Thymus pectinatus* not showed antimicrobial activities on tested microorganisms.

CONCLUSION

As far as we know, this study is the first study of the antioxidant, antimicrobial and enzyme inhibitory activity of *T. pectinatus* water extract. In the light of the results obtained, it was seen that water extract has high antioxidant, anti-amylase and antiproliferative effects. The water extract also showed a higher amount of total phenolic content. However, it was determined that the water extract of the plant did not have antimicrobial effect. Therefore, further studies are needed for phytochemical and bioactivity-guided isolation of *T. pectinatus* to identify active compounds.

ACKNOWLEDGEMENTS

This study was presented as poster presentation at the Turkey 13. national 1. international field crops congress.

REFERENCES

[1] Könemann, B. (1999) The illustrated AZ of over 10,000 garden plants and how to cultivate them. Hong Kong: Gordon Cheers Publication. 51-3.
[2] Davis, P.H. (1982) Flora of Turkey and the East Aegean Islands. University Press: Edinburgh. 7, 349-382.
[3] Davis, P.H. (1988) Flora of Turkey and the East Aegean Islands. University Press: Edinburgh. Supplementum, 209.
[4] Saygın, A. G., Göze, İ., Alim, A., Ercan, N., Durmuş, N., Vural, N., Alim, B. A. (2018) Essential oil of Thymus pectinatus Fisch&Mey. var. Pectinatus: Chemical formation, antimicrobial, antioxidant, antispasmodic and angiogenic activities. African Journal of Traditional, Complementary and Alternative Medicines. 15(1), 34-41.
[5] Dob, T., Dahmane, D., Benabdelkader, T., & Chelghoum, C. (2006) Composition and Antimicrobial Activity of the Essential Oil of Thymus fontanesii. Pharmaceutical Biology. 44(8), 607-612.
[6] Eruygur, N., Ataş, M., Çevir, Ö., Tekin, M. (2017) Investigating of Phytochemicals, Antioxidant, Antimicrobial and Proliferative Properties of Different Extracts of Thymus spathulifolius Hausskn. and Velen. Endemic Medicinal Plant from Sivas, Turkey. International Journal of Secondary Metabolite. 4(3, Special Issue 1), 155-166.
[7] Sezik, E., Zor, M., Yesilada, E. (1992) Traditional medicine in Turkey II. Folk medicine in Kastamonu. International Journal of Pharmacognosy. 30(3), 233-239.
[8] Sokmen, A., Jones, B. M.,Erturk, M. (1999) The in vitro antibacterial activity of Turkish medicinal plants. Journal of Ethnopharmacology. 67(1), 79-86.
[9] Yeşilada, E., Honda, G., Sezik, E., Tabata, M., Goto, K., Ikeshiro, Y. (1993) Traditional medicine in Turkey IV. Folk medicine in the Mediterranean subdivision. Journal of Ethnopharmacology. 39(1), 31-38.
[10] Do, J. R., Kang, S. N., Lee, S. W., Kim, K. J.,Jo, J. H. (2004) Antimicrobial and antioxidant activities and phenolic contents in the water extract of medicinal plants. Food Science and Biotechnology. 13(5), 640–645.
[11] Albayrak, S., Sağdiç, O., Aksoy, A. (2010) The assays used for assessing antioxidant capacities of herbal products and foods. Erciyes University Journal of Institute of Science and Technology. 26(4), 401-409.

[12] Gaweł-Bęben, K., Bujak, T., Nizioł-Łukaszewska, Z., Antosiewicz, B., Jakubczyk, A., Karaś, M., Rybczyńska, K. (2015) Stevia rebaudiana Bert. leaf extracts as a multifunctional source of natural antioxidants. Molecules. 20(4), 5468-5486.

[13] Ames, B. N. (1983) Dietary carcinogens and anticarcinogens: oxygen radicals and degenerative diseases. Science. 221(4617), 1256-1264.

[14] Do, Q.D., Angkawijaya, A. E., Tran-Nguyen, P. L., Huynh, L. H., Soetaredjo, F. E., Ismadji, S., and Ju, Y. H. (2014) Effect of extraction solvent on total phenol content, total flavonoid content, and antioxidant activity of Limnophila aromatica. Journal of Food and Drug Analysis. 22(3), 296-302.

[15] López, S., Bastida, J., Viladomat, F., Codina, C. (2002) Acetylcholinesterase inhibitory activity of some Amaryllidaceae alkaloids and Narcissus extracts. Life Sciences. 71(21), 2521-2529.

[16] Birjandian, E., Motamed, N.,Yassa, N. (2018) Crude methanol extract of Echinophora platyloba induces apoptosis and cell cycle arrest at S-phase in human breast cancer cells. Iranian Journal of Pharmaceutical Research: IJPR. 17(1), 307.

[17] Grollino, M. G., Raschellà, G., Cordelli, E., Villani, P., Pieraccioli, M., Paximadas, I., Pacchierotti, F. (2017) Cytotoxicity, genotoxicity and gene expression changes elicited by exposure of human hepatic cells to Ginkgo biloba leaf extract. Food and Chemical Toxicology. 109, 486-496.

[18] Re, R., Pellegrini, N., Proteggente, A., Pannala, A., Yang, M., Rice-Evans, C. (1999) Antioxidant activity applying an improved ABTS radical cation decolorization assay. Free Radical Biology and Medicine. 26(9-10), 1231-1237.

[19] Clarke, G., Ting, K. N., Wiart, C., and Fry, J. (2013) Radical Scavenging, Ferric Reducing Activity Potential and Total Phenolics Content Indicates Redundancy in Use of All Three Assays to Screen for Antioxidant Activity of Extracts of Plants from the Malaysian Rainforest. Antioxidants. 4, 2(1), 1-10.

[20] Molan, A.L., and Mahdy, A.S. (2014) Iraqi medicinal plants: Total flavonoid contents, free-radical scavenging and bacterial beta-glucuronidase inhibition activities. IOSR Journal of Dental and Medical Sciences. 13(5), 72-77.

[21] Ergül, M., Ergül, M., Eruygur, N., ATAŞ, M., Ucar, E. (2019) In Vitro Evaluation of the Chemical Composition and Various Biological Activities of Ficus carica Leaf Extracts. Turkish Journal of Pharmaceutical Sciences. 16(4), 401-409.

[22] Kumar, D., Kumar, H., Vedasiromoni, J. R., Pal, B. C. (2012) Bio-assay guided isolation of α-glucosidase inhibitory constituents from Hibiscus mutabilis Leaves. Phytochemical Analysis. 23(5), 421-425.

[23] Kumar, D., Gupta, N., Ghosh, R., Gaonkar, R. H., and Pal, B. C. (2013) α-Glucosidase and α-amylase inhibitory constituent of Carex baccans: Bio-assay guided isolation and quantification by validated RP-HPLC–DAD. Journal of Functional Foods. 5(1), 211-218.

[24] Jeong, S. H., Ryu, Y. B., Curtis-Long, M. J., Ryu, H. W., Baek, Y. S., Kang, J. E., Park, K. H. (2009) Tyrosinase inhibitory polyphenols from roots of Morus lhou. Journal of Agricultural and Food Chemistry. 57(4), 1195-1203.

[25] Eloff, J.N. (1998) A sensitive and quick microplate method to determinate the minimal inhibitory concentration of plant extracts for bacteria. Planta Med. 6, 711–713.

[26] [26] CLSI. (2002) Reference Reference Method for Broth Dilution Antifungal Suscept- ibility Testing of Yeasts, Approved Standard, 2nd ed., NCCLS document M27- A2. CLSI, 940 West Valley Road, Suite 1400, Wayne, Pennsylvania 19087- 1898, USA.

[27] CLSI. (2012) Methods for Dilution Antimicrobial Susceptibility Tests for Bacteria that Grow Aerobically, Approved Standard, 9th ed., CLSI document M07-A9. Clinical and Laboratory Standards Institute, 950 West Valley Road, Suite 2500, Wayne, Pennsylvania 19087, USA.

[28] Vardar-Ünlü, G., Candan, F., Sökmen, A., Daferera, D., Polissiou, M., Sökmen, M.,Tepe, B. (2003) Antimicrobial and antioxidant activity of the essential oil and methanol extracts of Thymus pectinatus Fisch. et Mey. Var. pectinatus (Lamiaceae). Journal of Agricultural and Food Chemistry. 51(1), 63-67.

[29] Duthie, S. J., Collins, A. R., Duthie, G. G., Dobson, V. L. (1997) Quercetin and myricetin protect against hydrogen peroxide-induced DNA damage (strand breaks and oxidised pyrimidines) in human lymphocytes. Mutation Research/Genetic Toxicology and Environmental Mutagenesis. 393(3), 223-231.

[30] Skaper, S. D., Fabris, M., Ferrari, V., Dalle Carbonare, M., Leon, A. (1997) Quercetin protects cutaneous tissue-associated cell types including sensory neurons from oxidative stress induced by glutathione depletion: cooperative effects of ascorbic acid. Free Radical Biology and Medicine. 22(4), 669-678.

[31] Saddiqe, Z., Naeem, I., Maimoona, A. (2010). A review of the antibacterial activity of Hypericum perforatum L. Journal of Ethnopharmacology. 131(3), 511-521.

[32] Holetz, F.B., Pessini, G.L., Sanches, N.R., Cortez, D. A. G., Nakamura, C. V., Dias Filho, B. P. (2002) Screening of some plants used in the Brazilian folk medicine for the treatment of infectious diseases. Memórias do Instituto Oswaldo Cruz. 97(7), 1027-1031.
[33] Ellman, G. L., Courtney, K. D., Andres Jr, V., & Featherstone, R. M. (1961) A new and rapid colorimetric determination of acetylcholinesterase activity. Biochemical Pharmacology. 7(2), 88-95.

Received: **25.06.2020**
Accepted: **03.02.2021**

CORRESPONDING AUTHOR

Gulsen Guclu
Department of Health Care Services,
Health Services Vocational School,
Cumhuriyet University,
Sivas – Turkey

e-mail: gulsenguclu@cumhuriyet.edu.tr

© by PSP Volume 30– No. 05/2021 pages 4875-4887 Fresenius Environmental Bulletin

EFFECT OF NaCl ON THE PHOTOSYNTHESIS PARAMETERS IN *SALIX MATSUDANA* KOIDZ

Yi Jiang, Jiahui Han, Wenxiu Xue, Jinhua Zou*

Tianjin Key Laboratory of Animal and Plant Resistance, College of Life Sciences, Tianjin Normal University, China

ABSTRACT

In order to evaluate the effects of NaCl stress on seedlings of *Salix matsudana* Koidz, the effects of different NaCl concentrations (0, 0.1%, 0.2%, 0.4%) on one-month-old *S. matsudana* seedlings grown in an environment-controlled chamber for 28 days was examined. Responses of *S. matsudana* were monitored in relation to physiological parameters, leaf fall ratio, relative water content (RWC), photosynthetic gas exchange characteristics and chlorophyll fluorescence parameters and chlorophyll concentration. The plants did not show any effect on survival and grew normally without toxic symptoms under 0.1% NaCl, and had different numbers of yellow leaves at the base of the seedlings and new leaves dried under 0.2% and 0.4% NaCl for 28 days. Plant growth, biomass and RWC decreased linearly with an increase in salinity and duration. After the experiment, over a half of the leaves that were treated with 0.4% NaCl had fallen. The chlorophyll contents in the leaves decreased with increasing of NaCl salinity. Leaf photosynthetic gas exchange parameters (net photosynthetic rate, transpiration rate, intercellular CO_2 concentration and stomatal conductance) showed varying correlations and an overall decrease in these parameters under NaCl treatment period compared with the control. The decrease tendency in photochemical efficiency of PSII (F_v'/F_m'), actual photochemical efficiency of PSII (ΦPSII), electronic transfer rate (ETR) and photochemical quenching (qP) were observed, whereas qN had an increasing tendency.

KEYWORDS:
Gas exchange attributes, chlorophyll fluorescence characteristics, chlorophyll concentration, NaCl

INTRODUCTION

At present, nearly 20% of the world's cultivated land and nearly half of all irrigated land are affected by soil salinity and the area is increasing day by day [1]. NaCl is ubiquitous in the environment, increase in salinity is one of the most adverse environmental factors that is predicted to affect plant growth and survival in most arid and semiarid regions worldwide [2, 3], which may cause serious salinization of more than 50% of all arable lands by the year 2050 [4]. A recent review indicated that salt tolerance ability of trees have wide variations among tree species, which can thrive at soil salinities ranging from 200 to 450 mM [5]. Plants have involved several changes in various physiological and biochemical processes in order to survive in soils with high salt concentration [6]. This adverse effect of salt stress appears on whole plant level at almost all growth stages [7].

Salinity influences many aspects of plant physiology including dehydration, ion cytotoxicity, nutritional imbalance, osmosis, oxidation, membrane permeability, and decreased photosynthetic rate [8, 9, 10]. Osmotic stress and ion toxicity are both effects caused by salinity. The salt in the growth solution reduces the capacity of the plant to absorb water and results in osmotic stress, while ion toxicity is caused by an excessive amount of salts entering the transpiration flow and damaging leaf cells [11]. The osmotic effect can lead to various physiological and morphological changes, such as changes in plant water status, cell expansion, cell division, and nutrient balance, decrease activity and denaturation of structural proteins and leakiness of membranes caused by phospholipid bilayer disruption [12, 13]. Furthermore, salt-stressed plants have low leaf area [14] and stomatal conductance [15], decreased biomass [16], photosynthetic gas-exchange rate [17], PSII activity [18], and increased water use efficiency (WUE) [19] and protective enzyme activity [20]. It is important to understand the mechanisms that confer tolerance in saline environments because the ability of plants to grow under salinity is a

feature that determines plant distribution in many areas [11].

Photosynthesis is one of the most important process for the green plants to convert light energy. The light energy is captured and used to convert water, carbon dioxide, and minerals into oxygen and energy-rich organic compounds. Salt stress lead to absorption moisture and nutrients blocked, caused malnutrition, and decreased chlorophyll content, thus inhibited photosynthetic capacity. NaCl inhibits photosynthetic capacity by decreasing CO_2 fixation, stomatal conductance, and transpiration. The negative impact of salinity stress on the photosynthetic apparatus, especially photosystem II (PSII), could be detected before the irreversible morphological damage. Moreover, the accumulation of NaCl in the leaf to toxic concentrations is known to reduce the photosynthesis rate through the destruction of chlorophyll ultra-structure and an inhibition of PSII at both donor and acceptor sides [21]. NaCl stress has a negative effect on the operating effciency of PSII which damages the oxygen-evolving complex and inhibits the quantum yield of PSII electron transport and photochemical efficiency [22]. Injury to PSII can lead to a change in chlorophyll fluorescence. Therefore, chlorophyll fluorescence can be used as a reliable non-invasive method to evaluate changes in the function of PSII and to examine the primary photosynthetic processes under salt stress conditions [23, 24].

S. matsudana (Chinese willow), a member of the Salicaceae family, is widely cultivated in China and has been introduced as an ornamental tree in many areas, including Australia, Europe and North America, etc. As a saline alkali tolerant plant, *S. matsudana* is known to have several characteristics including easy propagation and cultivation, large biomass, fast growing, deep root system, high transpiration rate, tolerance tolerant to drought and salinity, which make them adapt to the saline areas [25].

It is reported that *S. matsudana* is considered to be moderate sensitive to salinity [26]. Thus, it is of utmost importance to exploit its potential against salinity. Herein, we assessed the toxic effects of NaCl by examining photosynthetic parameters (physiological parameters, relative water content (RWC), photosynthetic gas exchange characteristics, chlorophyll fluorescence and chlorophyll content) in leaves of *S. matsudana* in the presence of different concentrations of NaCl.

MATERIALS AND METHODS

Growth conditions and treatment. Healthy and similar-sized woody cuttings of *S. matsudana* approximately 20 cm long were germinated in plastic boxes filled with distilled water for two weeks under glasshouse conditions of 23 ± 5 ℃ and 55 ± 10 % relative humidity. When the seedlings burgeoned, which were transferred and cultivated to 1/2 Hoagland nutrient solution. After an initial growth period, healthy (without leaf chlorotic spots and withered) and uniform (similar height) plants were used in the experiment which were divided into four groups (42 seedlings/group) and irrigated with half-strength Hoagland solution supplemented with 0 (control), 0.1%, 0.2% and 0.4% NaCl. The nutrient solution consisted of 0.75 mM K_2SO_4, 0.65 mM $MgSO_4$, 0.01 mM KCl, 0.25 mM KH_2PO_4, 2 mM $Ca(NO_3)_2$, 100 μM FeEDTA, 10 μM H_3BO_3, 1 μM $MnSO_4$, 0.1 μM $CuSO_4$, 0.05 μM $(NH_4)_6Mo_7O_4$ and 1 μM $ZnSO_4$, adjusted to pH 5.5. The solutions were constantly aerated with an aquarium air pump and replaced every week. All treatments were done in five replicates. Macroscopic observations and all determinations were conducted at the end of each time interval (7 days). The seedlings were used to determine growth characteristics and RWC of leaves, leaf gas exchange and photosynthetic parameter measurements, chlorophyll fluorescence parameter measurements and content of chlorophyll in the present investigation.

Growth measurements. Shoot height, the dry weight (DW) of roots and aerial part, leaf fall ratio and RWC were determined after 7 and 28 days treatment. The growth index determined was the shoot DW/root DW (shoot/root). Leaf fall ratio was collected during the growing season and the cumulative number of these leaves per plant was recorded and calculated as a percentage. RWC was measured for the middle part of a sun-exposed and fully expanded leaf of each stem assayed ($\boldsymbol{n}$ = 5) and was determined according to Barrs's formula [27]: RWC (%) = [(FW − DW)/(TW − DW)] × 100%, where FW is fresh weight, DW is dry weight and TW represents turgid weight (fully hydrated leaf weight determined by keeping them in water for 24 h at 5 ± 1 ℃ in the dark) [28]. The seedlings were carefully divided into leaves, stems, and roots. Dry weight was obtained after drying at 80 ℃ until a constant weight was reached. Shoot height was measured after 7 and 28 days treatment of different concentrations of NaCl.

Measurement of chlorophyll contents. After measuring non-destructive traits (leaf gas exchange and photosynthetic and chlorophyll fluorescence), the same leaves were gathered to measure their photosynthetic pigment concentrations after NaCl treatment for 7 days and 28 days. 0.2 g leaf samples were homogenized in 10 mL of 80 % acetone. Mixture were poured into conical flask and sealed. Conical flasks were stored in the dark at 4 °C for 12 h prior to spectrophotometric measurements. Pigmentation of the sample was centrifuged (4,000 g) for 20 min and the spectral absorbances of supernatant solution were estimated at 663, 646, and 470 nm using a spectrophotometer (UV/Vis Spectrometer, Perkin Elmer Lambda35, Boston, USA).

The chlorophyll and carotenoids contents were calculated as follows according to He et al. [29]:

Chl a (mg g^{-1} FW) = (12.21 × A663 – 2.81 × A646)/FW

Chl b (mg g^{-1} FW) = (20.13 × A646 – 5.03 × A663)/FW

Car (mg g^{-1} FW) = (1000 × A470 – 3.27 × Chl a - 104 × Chl b)/(229 × FW)

Where Aλ = absorbance at λ (nm); FW, leaf fresh weight.

Leaf gas exchange and photosynthetic parameters measurement. Leaf gas exchange and photosynthetic parameters: net photosynthetic rate (Pn), transpiration rate (Tr), stomatal conductance (Gs) and intercellular CO_2 concentration (Ci), were measured in the fifth fully expanded leaf from the top shoot at the end of each time interval (7 days) with five replications per treatment, using portable photosynthesis system (LI-6400, LI-COR, Lincoln, USA) at ambient relative humidity (50 – 60 %), a reference CO_2 of 380 μmol mol^{-1}, a flow rate of 500 μmol s^{-1}, and photosynthetically active radiation (PAR) of 1,000 μmol m^{-2} s^{-1}. The measurements were performed between 10:00 and 12:00 a.m. under the greenhouse conditions described above. Data were given and recorded by the machine.

Chlorophyll fluorescence parameters measurement. Chlorophyll fluorescence parameters quenching analysis was carried out at room temperature with a portable fluorometer (LI-6400, LI-COR, Lincoln, USA). The plants of each treatment were darkened for 12 h prior to measurement. The fifth fully expanded leaf from the top shoot at the end of each time interval (7 days) were selected to measure the chlorophyll fluorescence parameters with five replications per treatment. The minimal Chl fluorescence (F_0) level was measured after applying a far-red pulse for 6 s and the maximal fluorescence (F_m) was registered after applying a 0.8 s saturating flash. Maximal photochemical

TABLE 1
Effects of different NaCl concentrations on growth parameters

	Concentration (mg/ml)	Days	
		7	28
Shoot height (cm)	Control	19.386 ± 0.749 a	25.309 ± 0.957 a
	0.1%	17.167 ± 0.628 a	22.717 ± 1.035 b
	0.2%	15.771 ± 0.532 a	18.954 ± 1.115 c
	0.4%	12.614 ± 0.502 b	14.443 ± 0.660 d
Plant dry weight (g)	Control	18.544 ± 0.111 a	27.918 ± 1.302 a
	0.1%	18.470 ± 0.094 a	25.297 ± 0.900 ab
	0.2%	18.105 ± 0.093 ab	22.696 ± 1.450 bc
	0.4%	17.982 ± 0.204 b	18.807 ± 0.416 c
Leaf fall (%)	Control	3.333 ± 0.003 a	6.333 ± 0.003 a
	0.1%	3.667 ± 0.003 a	10.333 ± 0.003 b
	0.2%	4.000 ± 0.006 a	25.333 ± 0.018 c
	0.4%	4.667 ± 0.003 a	68.333 ± 0.009 d
Shoot/root	Control	2.546 ± 0.354 a	2.322 ± 0.020 a
	0.1%	2.435 ± 0.207 a	2.123 ± 0.017 b
	0.2%	2.349 ± 0.050 a	1.837 ± 0.012 c
	0.4%	2.294 ± 0.057 a	1.648 ± 0.024 d
RWC (%)	Control	0.898 ± 0.011 a	0.845 ± 0.003 a
	0.1%	0.873 ± 0.006 b	0.830 ± 0.001 a
	0.2%	0.860 ± 0.008 b	0.812 ± 0.001 b
	0.4%	0.816 ± 0.003 c	0.780 ± 0.004 c

Different letters indicate significant differences according to t-test ($P < 0.05$).

efficiency of PSII (F_v/F_m) was expressed as: $F_v/F_m = (F_m - F_0)/F_m$. Efficiency of energy harvesting by open reaction centres of photosystem II for light-adapted leaves were calculated as follows: $F_v'/F_m' = (F_m' - F_0')/F_m'$, where, F_0' is minimal fluorescence of a momentarily darkened leaf, and Fm' is maximal fluorescence during a saturating flash light of > 7 mmol m^{-2} s^{-1}. Photochemical quenching (qP) was calculated as indicated by the manufacturer's manual for the LI-6400 leaf chamber fluorometer, $qP = (F_m' - F_s)/(F_m' - F_0')$, where, Fs is the Chl fluorescence yield during actinic illumination. Other fluorescence parameters were measured on light-adapted leaves using the equations of Genty et al. [30] (quantum yield of PSII electron transport, $\Phi PSII = (F_m' - F_s)/F_m'$; apparent electron transport rate, $ETR = (F_m' - F_s)/F_m' \times PPFD \times 0.5 \times 0.84$; non-photochemical quenching, $qN = 1 - (F_m' - F_0')/(F_m - F_0)$). For the calculation of electron transport rate (ETR), photosynthetic photon flux density (PPFD) was the photosynthetic photon flux density of actinic illumination, and 0.5 was assumed as the fraction of the excitation energy distributed to PSII whereas 0.84 was the fractional light absorption of the leaf.

Statistical analysis. All statistical values were calculated using the Statistical Package for Social Sciences (SPSS) program release 17.0 for Windows (SPSS, Chicago, IL, USA) and Sigma Plot 10.0 using means ± standard error (SE). For equality of averages the t-test was applied. Results were considered statistically significant at $p < 0.05$. Pearson's correlation coefficients were used when calculating correlations between different studied parameters.

RESULTS

Effects of NaCl on seedlings. The effects of NaCl on the morphology of the leaves varied with the different concentrations of NaCl. At the first week, *S. matsudana* showed no obvious toxicity symptom in leaves under different concentrations of NaCl treatment. However, after one week, visual leaf symptoms due to NaCl toxicity in *S. matsudana* appeared, at the 0.2% and 0.4% NaCl, drying tips were observed in young leaves, chlorosis and edge drying appeared in the old leaves. Meanwhile, the leaf length and area were obviously shorter than the control and 0.1% NaCl treatment. With the treatment time extended, leaf symptom under excess NaCl became more obvious, some leaves were dried seriously under the 0.4% NaCl treatment (Figure 1).

The growth and development of the plants of *S. matsudana* stressed with different concentrations of NaCl was also obviously affected (Table 1). The effects of NaCl on shoot height of *S. matsudana* varied with the concentration and treatment time (Table 1). There was no toxic effect on shoot growth after 7 days except that under concentration 0.4% NaCl. After 28 days

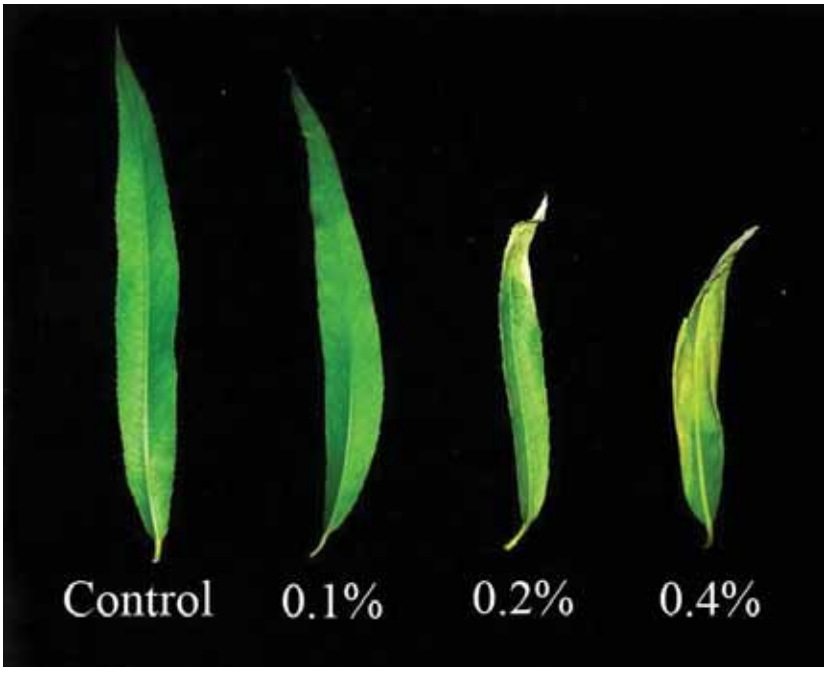

FIGURE 1
Visible symptoms in leaves of *S. matsudana* exposed to NaCl for 28 days.

TABLE 2
Effects of NaCl on photosynthetic gas exchange parameters

Time, days	Treatment (mg/ml)	Photosynthetic gas exchange			
		Pn,μmol m^{-2} s^{-1}	Tr,mmol m^{-2} s^{-1}	Gs,μmol m^{-2} s^{-1}	Ci,μmol mol^{-1}
7	Control	9.95 ± 0.77 a	4.42 ± 0.54 a	0.16 ± 0.02 a	312.58 ± 6.00 a
	0.1%	9.56 ± 0.98 a	3.58 ± 0.26 a	0.12 ± 0.02 a	306.51 ± 6.58 a
	0.2%	6.43 ± 0.95 b	0.81 ± 0.31 b	0.05 ± 0.02 b	244.91 ± 4.34 b
	0.4%	2.92 ± 0.76 c	0.57 ± 0.08 c	0.01 ± 0.00 c	208.14 ± 4.29 c
14	Control	9.92 ± 0.27 a	4.67 ± 0.92 a	0.15 ± 0.01 a	306.61 ± 1.27 a
	0.1%	8.47 ± 1.20 b	2.32 ± 0.52 b	0.08 ± 0.01 b	287.91 ± 1.44 a
	0.2%	6.28 ± 0.66 c	1.31 ± 0.17 c	0.05 ± 0.01 c	236.35 ± 3.78 b
	0.4%	1.92 ± 0.18 d	0.53 ± 0.43 d	0.02 ± 0.00 d	231.23 ± 3.19 b
21	Control	10.39 ± 0.10 a	4.79 ± 0.65 a	0.15 ± 0.01 a	324.21 ± 2.81 a
	0.1%	7.59 ± 0.39 b	1.68 ± 0.18 b	0.06 ± 0.01 b	293.89 ± 5.38 b
	0.2%	3.42 ± 0.57 c	1.39 ± 0.24 b	0.05 ± 0.01 b	246.59 ± 2.31 c
	0.4%	1.52 ± 0.57 d	0.40 ± 0.10 c	0.01 ± 0.01 c	225.30 ± 4.98 c
28	Control	11.05 ± 0.39 a	5.81 ± 0.86 a	0.19 ± 0.02 a	330.50 ± 2.10 a
	0.1%	5.82 ± 0.34 b	2.20 ± 0.02 b	0.07 ± 0.01 b	281.38 ± 5.17 b
	0.2%	2.36 ± 0.52 c	0.49 ± 0.12 c	0.01 ± 0.01 c	223.38 ± 4.08 c
	0.4%	1.36 ± 0.20 d	0.30 ± 0.02 c	0.00 ± 0.00 c	204.48 ± 7.13 c

Values are means ± standard deviation (SD) (n = 5). Different letters indicate significant differences according to t-test ($P < 0.05$).

of treatment, obvious toxic effect appeared in the all treatment and NaCl inhibited the shoot height significantly ($P < 0.05$).

Exposure of *S. matsudana* seedlings to NaCl stress has resulted in gradual reduction in total plant dry mass (Table 1). During early treatment, there was no obvious decrease under 0.1% and 0.2% NaCl treatment. Different NaCl concentration decreased plant DW of *S. matsudana* gradually with the prolonged treatment time. The effect was most pronounced under the highest concentration of NaCl (0.4%). Comparing with the control, 0.4% NaCl reduced the plant DW by 32.63% after 28 days of treatment, which indicates the growth of *S. matsudana* was seriously affected under high concentration of NaCl. Similar response patterns were also observed for the shoot/root ratios for the NaCl-treated seedlings compared to the control.

Leaf fall ratio didn't significantly affected after 7 days of NaCl treatment except for 0.4% NaCl treatment. After long time treatment, the quantity of the damaged leaves defoliated and had a close relation with the NaCl concentration. When treated with 0.4% NaCl, the leaf fall ratio reached 68.33%.

The RWC of leaves decreased to 7.69% in 0.4% NaCl-treated plants when compared to control. Non-treated plants were able to maintain significantly greater RWC than NaCl-treated plants and higher concentrations of NaCl produced a greater decrease in RWC (Table 1).

Effects of NaCl on Chlorophyll and total carotenoid contents. It is clearly shown that NaCl stress decreased the content of chlorophyll a, chlorophyll b, chlorophyll a+b and carotenoids as the concentration of NaCl increased from Figure 2. Small or non significant differences were found in Chl a+b contents under low NaCl concentration in 7 days. The contents of leaf pigments exposed to NaCl for 28 days decreased significantly ($P < 0.05$) when compared with control.

Effects of NaCl on photosynthetic gas exchange parameters. The effects of NaCl on Pn, Tr, Gs and Ci in leaves of *S. matsudana* varied with the different concentrations of NaCl and the duration of treatment (Table 2). When compared to the control, the Pn decreased markedly under NaCl stress. The reduction was the most obvious in the plants treated with 0.4% when compared with other groups during the whole experiment. The Tr in NaCl treated groups were inhibited, and the inhibition was more and more obvious with increasing NaCl concentration and prolonged duration of treatment in comparison with control. At 0.1%, 0.2% and 0.4% NaCl treatments for 28 days, the Tr was reduced by 62.13, 91.57 and 94.84%, respectively when compared to the control. The Gs in control leaves was the highest during 28 days treatment, the Gs in all NaCl treatment groups were inhibited (Table 2). The Gs in 0.4% NaCl treatment was the lowest during the treatment period and decreased with the prolonged

duration of treatment. NaCl could induce the decrease in Ci in leaves of *S. matsu dana* treated with NaCl when compared with control (Table 2). 0.4% NaCl had most toxic effects on Ci in leaves in comparison with control and the other treatment groups.

Effects of NaCl on Chlorophyll Fluorescence parameters. The chlorophyll fluorescence parameters of *S. matsudana* varied with the NaCl concentration and duration of treatment (Table 3). F_v/F_m in *S. matsudana* exposed to 0.4% NaCl was significantly lower ($P < 0.05$) than that in control, and showed a decreasing tendency with the prolonging treatment time. With NaCl concentration increasing, decreasing tendency in ΦPSII, ETR and qP were observed, whereas qN had an increasing tendency.

DISCUSSION

Salinity is one of the major abiotic stresses that seriously affect plant survival through bringing changes in various morphological, biochemical and physiological processes. Although *S. matsudana* is considered as a relatively salt-tolerant plant, presence of excessive salt in long-term exposure may cause adverse effects on plant growth and development [26]. Adaptive responses in morphology and biomass are the primary tolerance indicators which *S. matsudana* can cope with the NaCl contaminated environment [31].

The symptom caused by salt damage was more severe with increased salt concentration in leaves. After 28 days, leaves treated with 0.1% NaCl grew similarly to that in control, and appeared to be healthier than other NaCl treatment. However, visible symptoms, such as wilting,

TABLE 3
Effects of NaCl on chlorophyll fluorescence parameters

Parameter	Concentration (mg/ml)	Days			
		7	14	21	28
Fv/Fm	Control	0.844 ± 0.003 a	0.836 ± 0.002 a	0.832 ± 0.007 a	0.832 ± 0.004 a
	0.1%	0.841 ± 0.002 b	0.835 ± 0.004 a	0.831 ± 0.004 a	0.830 ± 0.004 a
	0.2%	0.840 ± 0.003 b	0.833 ± 0.004 ab	0.829 ± 0.002 a	0.828 ± 0.005 a
	0.4%	0.837 ± 0.002 c	0.831 ± 0.002 b	0.825 ± 0.008 a	0.820 ± 0.004 b
Fv'/Fm'	Control	0.752 ± 0.002 a	0.553 ± 0.003 a	0.526 ± 0.004 a	0.519 ± 0.002 a
	0.1%	0.716 ± 0.001 b	0.517 ± 0.002 b	0.514 ± 0.009 ab	0.507 ± 0.003 b
	0.2%	0.696 ± 0.003 c	0.504 ± 0.006 c	0.508 ± 0.002 b	0.497 ± 0.005 c
	0.4%	0.658 ± 0.003 c	0.501 ± 0.003 c	0.504 ± 0.006 b	0.468 ± 0.004 d
Φ_{PSII}	Control	0.402 ± 0.009 a	0.327 ± 0.02 a	0.374 ± 0.001 a	0.330 ± 0.004 a
	0.1%	0.331 ± 0.006 b	0.279 ± 0.005 b	0.285 ± 0.002 b	0.256 ± 0.014 b
	0.2%	0.304 ± 0.003 b	0.257 ± 0.013 b	0.208 ± 0.002 c	0.153 ± 0.001 c
	0.4%	0.254 ± 0.003 c	0.184 ± 0.002 c	0.184 ± 0.002 c	0.096 ± 0.004 d
ETR	Control	48.383 ± 0.415 a	41.431 ± 0.578 a	37.583 ± 0.725 a	34.166 ± 0.831 a
	0.1%	41.731 ± 0.831 b	37.513 ± 1.370 b	30.280 ± 1.069 b	25.173 ± 0.329 b
	0.2%	37.737 ± 0.405 c	31.714 ± 0.332 c	26.469 ± 0.367 c	21.813 ± 0.361 c
	0.4%	26.338 ± 0.308 d	23.217 ± 0.303 d	21.798 ± 0.619 d	17.524 ± 0.610 d
qN	Control	0.724 ± 0.103 a	0.809 ± 0.019 a	1.034 ± 0.068 a	1.081 ± 0.053 a
	0.1%	0.748 ± 0.080 b	0.851 ± 0.008 a	1.101 ± 0.038 b	1.136 ± 0.087 b
	0.2%	0.791 ± 0.084 c	0.859 ± 0.016 a	1.168 ± 0.034 c	1.172 ± 0.053 c
	0.4%	0.840 ± 0.038 d	0.915 ± 0.003 a	1.215 ± 0.074 d	1.238 ± 0.045 d
qP	Control	0.610 ± 0.033 a	0.541 ± 0.008 a	0.503 ± 0.007 a	0.503 ± 0.007 a
	0.1%	0.589 ± 0.007 a	0.453 ± 0.005 b	0.358 ± 0.027 b	0.348 ± 0.012 b
	0.2%	0.516 ± 0.018 b	0.311 ± 0.029 c	0.213 ± 0.002 c	0.213 ± 0.033 c
	0.4%	0.275 ± 0.014 c	0.189 ± 0.008 d	0.168 ± 0.003 d	0.158 ± 0.008 d

Values are means ± standard deviation (SD) (n = 5). Different letters indicate significant differences according to t-test ($P < 0.05$).

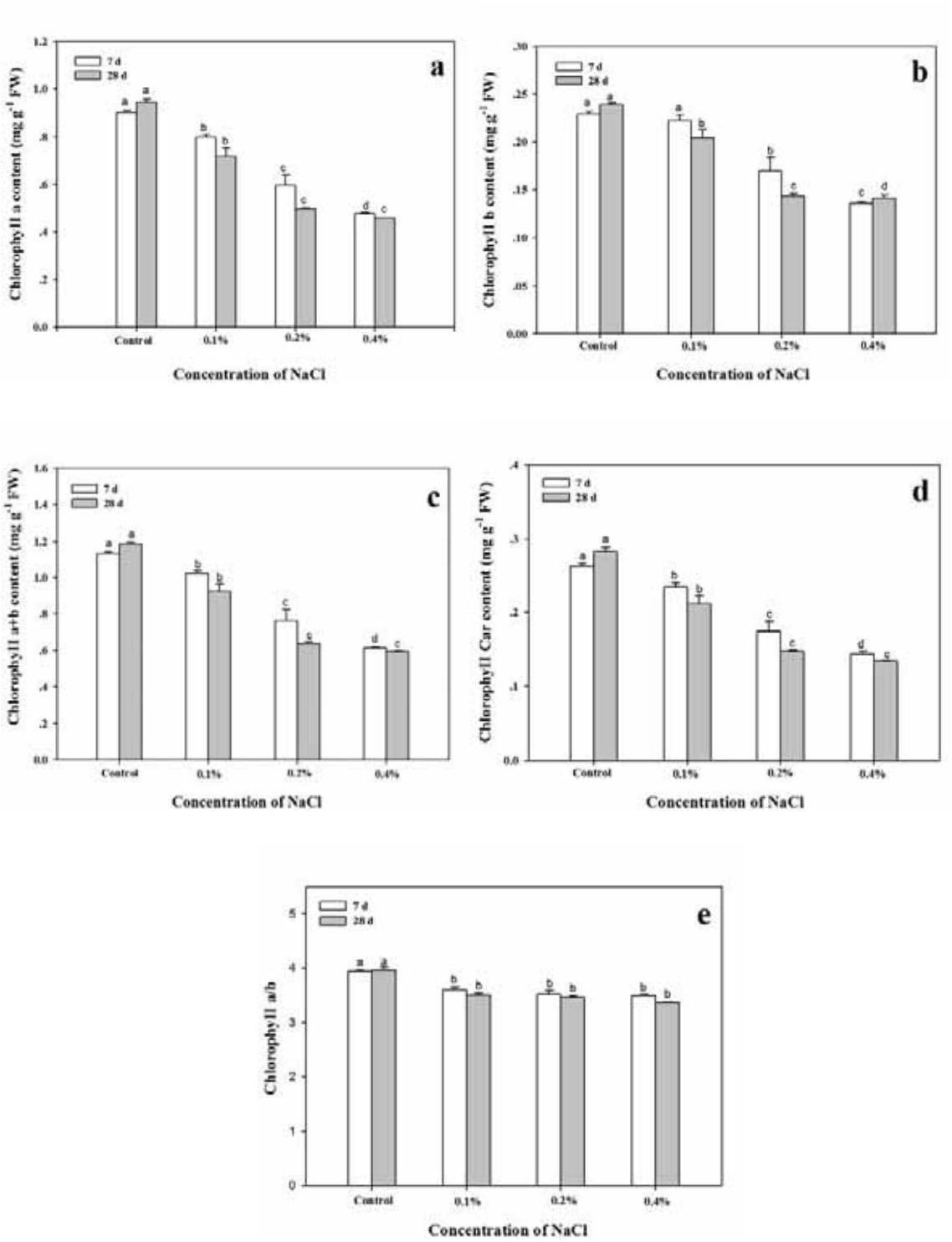

FIGURE 2

Chlorophyll a, b, a+b, carotenoid contents and chlorophyll a/b ratio of *S. matsudana* (a, b, c, d, e) exposed to NaCl stress for 7 and 28 days.

Vertical bars denote SE (n = 5). Different letters indicate significant differences according to t-test ($P < 0.05$).

curling and necrosis of stem tip, were observed in *S. matsudana* seedlings that survive in 0.2% and 0.4% NaCl solution. The stunting observed in salt-tolerant plants has been associated with shorter height, thinner shoot, smaller leaves, and fewer nodes [32]. During long-term exposure to NaCl, plant shoots have been inhibited and show symptoms of injuries such as yellowing or death of older leaves [9].

Growth parameters and RWC content de-

creased under salinity condition in *S. matsudana*. Similar decrease in growth including shoot height and dry weight had been reported in other salinity studies conducted in *M. piperita* [33] and *M. pulegium* [34]. During the experimental period, we found NaCl also had detrimental effects on the plant growth after plant heights were recorded at weekly interval. Shoot height of *S. matsudana* was not inhibited under 0.2% NaCl for short time (7 days), suggesting that seedlings can grow in slightly saline water. However, shoot height decreased with increased NaCl concentration and prolonged treatment time. When the NaCl concentration reached in 0.4%, growth of *S. matsudana* was inhibited seriously ($P < 0.05$). There were many studies indicated suppressive effects on plant growth and biomass production in high salt stress concentrations [35, 36, 37], which were consistent with our results. In this investigation, dry mass of *S. matsudana* were also significantly reduced with the increase of NaCl concentrations. The biomass of *Rosa chinensis* and *Medicago sativa* decreased as the salinity in irrigation water increased [38, 39]. Furthermore, the results of our experiment were similar to that reported significant reductions in shoot/root of walnut cultivars with increasing irrigation water salinity [40].

Either under control or under saline conditions, morphological measurements of biomass were frequently used as evaluating salt tolerance [41]. Salt stress adaptation affected by internal constitutive salt tolerance mechanisms and external environmental factors in plants. The decreased rate of leaf growth was due to the change of osmotic potential which was the one of the primarily factors affected leaf growth. Plant morphology changed by salinity excess the certain threshold, caused stomata less responsive to environmental changes and leaf thickness reduced [42]. After several weeks of salt treatment, cell elongation and cell division reduced unequally lead to more reduction in area than depth, so leaves were smaller and thicker [43]. Netondo et al. [44] suggested that increased salinity lead to decrease of the leaf area, might affect photosynthesis, finally loss the carbon gain thereby a decrease in biomass accumulation. The retarded growth of salt-stressed plants might due to toxic ions accumulated, essential nutrients uptake impaired, or cellular organelles damaged [45]. The decrease of shoot/root ratio is a common response under salt stress [46]. The results of our experiment were similar to the reported significant reductions in shoot/root of walnut cultivars with increasing irrigation water salinity [40]. *S. matsudana* irrigated with excess NaCl probably decreased the capacity to absorb water and nutrients, because a high shoot/root ratio mean that the plant was more likely to suffer from water stress [47].

Leaf drop is one of the mechanisms of salt elimination. When NaCl reached high concentration, defoliation rate obviously rise. This was due to 0.4% NaCl of *S. matsudana* dropped the damaged leaves to eliminate excessive NaCl, and the fewer damaged leaves remained on the plant. The accumulation of NaCl was higher in the older leaves, because they had longer growth period to accumulate salt [44]. The leaves absorbed additional salt to prevent salinity accumulation in plants by shedding, in order to ensure the normal physiological metabolism of plant.

The relative water content is a vital factor for the metabolic and survival of leaves, and maintaining it at an adequate level seems to be salt stress tolerance criteria [48]. Our results were similar with those of previous studies showing that NaCl stress decreased relative leaf water content [24]. The decrease in RWC because of loss of turgor resulted in limited water availability for cell expansion process [49]. Thus, the growth inhibition in *S. matsudana* could be related to the decrease of RWC provoked by the presence of NaCl.

In this study, pigment contents and ratios were reduced significantly by increasing NaCl concentrations. Chlorophyll a, chlorophyll b and carotenoid content decreased significantly in the 0.2% and 0.4% NaCl treatments, and the inhibition strengthened with the duration of stress. In addition, the ratio of chlorophyll a to b was significantly higher under the control than saline treatments. This suggested that NaCl exerted a negative influence on the processes of chlorophyll biosynthesis. The results here were consistent with the findings of Netondo et al.[44] who reported a decline of chlorophyll a, chlorophyll b, carotenoid and chlorophyll a to b ratio in salt-tolerant cultivars of sorghum by increasing NaCl. The decrease in chlorophyll content with increasing NaCl dose had been described in the literature repeatedly [50, 51]. Chlorophyll b was reduced greater than chlorophyll a in salt-sensitive cultivars of rice, that indicated the susceptibility of chlorophyll b to saline stress [52]. Lipid peroxidation and reactive oxygen species (ROS) are thought to be related to direct inhibition of chlorophyll pigment synthesis, which played an essential role in damaging various photosynthetic membranes [53]. The another reason is that the destructed thylakoid membrane lead to reduce the affinity between chlorophylls and proteins of the chloroplast. That would lower the activity of chlorophyll

synthesis enzymes causing a decrease in chlorophyll stability [54].

Photosynthesis is the most fundamental and intricate physiological process that all green plants undergo as it considerably affects the plant growth [55]. It is well known that salinity inhibit photosynthesis in several plant species [56, 57]. In this study, Pn was decreased under salinity stress accompanied with decrease in Gs, Ci, and Tr. One reason might be that salinity caused the reduction of leaf area, destroied the structure of chlorophyll and affected the photosynthetic process [58]. The other reason partially was attributed to the stomatal factor. There were reports indicated that inhibition of photosynthesis was caused by stomatal or non-stomatal factors [59, 60]. Turgor losed and stomatal closed caused by lower leaf water potential, which result in CO_2 assimilation limited and finally the photosynthetic rate reduced. Salinity-induced decrease in Pn might be due to stomatal conductance via a reduction in guard cell turgor and intercellular CO_2 partial pressure had occurred [61]. Furthermore, at high salinity, salts might detroied in the structure of chloroplast and exerted a direct toxic effect on photosynthetic processes [43].

By measuring different chlorophyll fluorescence parameters, it was possible to detect the negative impact of salt stress on photosynthetic performance before the irreversible morphological damage became visible [62]. Chlorophyll fluorescence parameters are sensitive to the ability of plants to tolerate environmental stresses [63]. In this study, *S. matsudana* clearly showed significant variation in all chlorophyll fluorescence parameters. Gitelson et al. [64] pointed out that chlorophyll fluorescence parameters depend on to a great extent pigment contents and the leaf ability to photosynthesis. F_v/F_m could be frequently used as an indicator of photoinhibition or of other kinds of stress [65]. In our experiment, F_v/F_m was variously reduced by the different concentrations of NaCl, which strongly indicate impairment of PSII. Reduction of PSII photochemical efficiency could be attributed partly to the destruction of antennae pigments [14]. qN as a measure of photoprotective thermal dissipation of excess excitation energy (from singlet state chlorophyll a), reflect the capacity of plants to carry out non-radiative dissipation of excess energy [66]. The increase in qN and decrease in qP caused by NaCl suggested that less of absorbed energy by leaves was used in photosynthesis. In addition, the Fv/Fm might decrease as a result of an increase in protective nonradiative energy dissipation (nonphotochemical quenching) associated with a regulated decrease in photochemistry and photosynthesis rates, showed in the decrease of qP values and increase of qN values [65], as borne out by the results of chlorophyll content assays in our study. F_v'/F_m' decreased significantly when exposed to high NaCl. This decrease suggested that high NaCl could lower the quantum yield of PSII. Decrease in actual ΦPSII was closely correlated with the quantum yield of non-cyclic electron transport observed in plants because of decreased carbon metabolism capacity and/or by low utilization of ATP and NADPH in the dark phase of photosynthesis [67].

CONCLUSION

Based on the obtained results, various physiological processes were affected by NaCl on *Salix matsudana* Koidz. As result of NaCl-induced, plant growth, biomass and RWC decreased linearly with an increase in salinity and treatment time. The decline in growth subjected to NaCl was associated with a reduction in photosynthetic capacity. The Pn, Tr, Gs and Ci were reduced in the presence of NaCl. NaCl had a significant effect on the primary photochemistry of PSII. ΦPSII, ETR and qP were decreased, whereas qN increased. In addition, pigment contents were also affected in the treatment of NaCl. Chl a, b and carotenoids content and the chl a/b ratio significantly decreased in the 0.2% and 0.4% NaCl treatments. The information available in this work was an important step towards obtaining a better understanding of the effect of NaCl on the photosynthesis process.

ACKNOWLEDGEMENTS

This project was supported by Natural Science Foundation of China (grant No. 31901184) and Doctor Foundation of Tianjin Normal University (grant No. 52XB1914). The authors wish to express their appreciation to the reviewers for their comments and suggestions.

REFERENCES

[1] Abid, M., Zhang, Y.J. Li, Z., Bai, D.F., Zhong, Y.P. and Fang, J.B. (2020). Effect of salt stress on growth, physiological and biochemical characters of Four kiwifruit genotypes. Sci. Hortic. 271, 109473.

[2] Bidalia, A., Hanief, M. and Rao, K.S. (2017). Tolerance of *Mitragyna parvifolia* (Roxb.) Korth. Seedlings to NaCl salinity. Photosynthetica. 55, 231-239.

[3] Hoire, T., Karahara, I. and Katsuhara, M. (2012). Salinity tolerance mechanisms in glycophytes: An overview with the central focus on rice plants. Rice. 5, 1-18.

[4] Kamanga, R.M., Echigo, K., Yodoya, K., Mekawy, A.M.M. and Ueda, A. (2020). Salinity acclimation ameliorates salt stress in tomato (*Solanum lycopersicum* L.) seedlings by triggering a cascade of physiological processes in the leaves. Sci. Hortic. 270, 109434.

[5] Polle, A. and Chen, S. (2015). On the salty side of life molecular, physiological and anatomical adaptation and acclimation of trees to extreme habitats. Plant Cell Environ. 38, 1794-1816.

[6] Gupta, B. and Huang, B. (2014). Mechanism of salinity tolerance in plants: physiological, biochemical, and molecular characterization. Int. J. Genomics. 2014, 701596.

[7] Nawaz, K., Hussain, K., Majeed, A., Khan, F., Afghan, S. and Ali, K. (2010). Fatality of salt stress to plants: morphological, physiological and biochemical aspects. Afr. J. Biotechnol. 9, 5475-5480.

[8] Zhang, Y.X., Zhang, Y., Yu, J.J., Zhang, H., Wang, L.Y., Wang, S.N., Guo, S.Y., Miao, Y.C., Chen, S.X., Li, Y. and Dai, S.J. (2019). NaCl-responsive ROS scavenging and energy supply in alkaligrass callus revealed from proteomic analysis. BMC Genomics. 20, 990.

[9] Sharifi, P. and Bidabadi, S.S. (2020). Strigolactone could enhances gas-exchange through augmented antioxidant defense system in *Salvia nemorosa* L. plants subjected to saline conditions stress. Ind. Crops Prod. 151, 112460.

[10] Calzone, A., Cotrozzi, L., Pellegrini, E., Guidi, L., Lorenzini, G. and Nali, C. (2020). Differential response strategies of pomegranate cultivars lead to similar tolerance to increasing salt concentrations. Sci. Hortic. 271, 109441.

[11] Morales, S.G., Trejo-Téllez, L.I., Gómez Merino, F.C., Caldana, C., Espinosa-Victoria, D., and Herrera Cabrera, B.E. (2012). Growth, photosynthetic activity, and potassium and sodium concentration in rice plants under salt stress. Acta Sci-Agron. 34, 317-324.

[12] Hamamoto, S., Horie, T., Hauser, F., Deinlein, U., Schroeder, J.I. and Uozumi, N. (2015). HKT transporters mediate salt stress resistance in plants: from structure and function to the field. Curr. Opin. Chem. Biol. 32, 113-120.

[13] Marček, T., Vidaković-Cifrek, Ž., Tkalec, M., Ježić, M. and Ćurković-Perica, M. (2017). Response of dihaploid tobacco roots to salt stress. Acta Bot. Croat. 76, 49-54.

[14] Singh, S.K., Reddy, V.R., Fleisher, D.H. and Timlin, D.J. (2017). Relationship between photosynthetic pigments and chlorophyll fluorescence in soybean under varying phosphorus nutrition at ambient and elevated CO_2. Photosynthetica. 55, 421-433.

[15] Chaves, M.M., Flexas, J. and Pinheiro, C. (2009). Photosynthesis under drought and salt stress: regulation mechanisms from whole plant to cell. Ann. Bot-London. 103, 551-560.

[16] Wu, X., Zhu, Z., Li, X. and Zha, D. (2012). Effects of cytokinin on photosynthetic gas exchange, chlorophyll fluorescence parameters and antioxidative system in seedlings of eggplant (*Solanum melongena* L.) under salinity stress. Acta Physiol. Plant. 34, 2105-2114.

[17] Maimaiti, A., Yunus, Q., Iwanaga, F., Mori, N., Tanaka, K. and Yamanaka, N. (2014). Effects of salinity on growth, photosynthesis, inorganic and organic osmolyte accumulation in *Elaeagnus oxycarpa* seedlings. Acta Physiol. Plant. 36, 881-892.

[18] Kalaji, H.M., Govindjee Bosa, K., Kościelniak, J. and Żuk-Gołaszewska, K. (2011). Effects of salt stress on photosystem II efficiency and CO_2 assimilation in two Syrian barley landraces. Environ. Exp. Bot. 73, 64-72.

[19] Li, J., Zhao, C., Li, J., Yan, Y.Y., Yu, B. and Han, M. (2013). Growth and leaf gas exchange in *Populus euphratica* across soil water and salinity gradients. Photosynthetica. 51, 321-329.

[20] Farhangiabriz, S. and Torabian, S. (2017). Antioxidant enzyme and osmotic adjustment changes in bean seedlings as affected by biochar under salt stress. Ecotox. Environ Safe. 137, 64-70.

[21] Chen, T.H. and Murata, N. (2011). Glycinebetaine protects plants against abiotic stress: mechanisms and biotechnological applications. Plant Cell. Environ. 34, 1-20.

[22] Steponkus, P.L. and Lanphear, F.O. (1967). Refinement of the triphenyl tetrazolium chloride method of determining cold injury. Plant Physiol. 42, 1423-1426.

[23] Hajiboland, R., Aliasgharzadeh, N., Laiegh, S.F. and Poschenrieder, C. (2010). Colonization with arbuscular mycorrhizal fungi improves salinity tolerance of tomato (*Solanum lycopersicum* L.) plants. Plant Soil. 331, 313-327.

[24] Wang, Y., Gu, W., Meng, Y., Xie, T., Li, L., Li, J. and Wei, S. (2017). γ-aminobutyric acid imparts partial protection from salt stress injury to maize seedlings by improving photosynthesis and upregulating osmoprotectants and antioxidants. Sci. Rep-Uk. 7, 43609.

[25] Wu, H.F., Wang, J.Y., Li, B.B., Ouyang, J., Wang, J.R., Shi, Q.Y., Jiang, W.S., Liu, D.H. and Zou, J.H. (2016). *Salix matsudana* koidz tolerance mechanisms to cadmium: uptake and accumulation, subcellular distribution, and chemical forms. Pol. J. Environ. Stud. 25, 1739-1747.

[26] Qiao, G., Zhang, X., Jiang, J., Liu, M., Han, X., Yang, H. and Zhuo, R. (2014). Comparative proteomic analysis of responses to salt stress in chinese willow (*salix matsudana* koidz). Plant Mol. Biol. Rep. 32, 814-827.

[27] Barrs, H.D. (1968). Determination of water deficits in plant tissues. New York: Academic Press.

[28] Kaczmarek, M., Fedorowicz-Strońska, O., Głowacka, K., Waśkiewicz, A. and Sadowski, J. (2017). $CaCl_2$ treatment improves drought stress tolerance in barley (*Hordeum vulgare* L.). Acta Physiol. Plant 39, 41.

[29] He, F., Sheng, M. and Tang, M. (2017). Effects of rhizophagus irregularis on photosynthesis and antioxidative enzymatic system in *Robinia pseudoacacia* L. under drought stress. Front Plant Sci. 8, 183.

[30] Genty, B., Briantais, J.M. and Baker, N.R. (1989). The relationship between the quantum yield of photosynthetic electron transport and quenching of chlorophyll fluorescence. BBA-Gen Subjects. 990, 87-92.

[31] Rossi, L., Zhang, W., Lombardini, L. and Ma, X. (2016). The impact of cerium oxide nanoparticles on the salt stress responses of *Brassica napus* L. Environ. Pollut. 219, 28-36.

[32] Hamayun, M., Khan, S.A., Khan, A.L., Shinwari, Z.K., Hussain, J., Sohn, E.Y., Kang, S.M., Kim, Y.H., Khan, M.A. and Lee, I.J. (2010). Effects of salt on growth attributes and endogenous growth hormones of soybean cultivar Hwangkeumkong. Pak. J. Bot. 42, 3103-3112.

[33] Khorasaninejad, S., Mousavi, A., Soltanloo, H., Hemmati, K. and Khalighi, A. (2010). The effect of salinity stress on growth parameters, essential oil yield and constituent of peppermint (*Mentha piperita* L.). World Appl. Sci. J. 11, 1403-1407.

[34] Farissi, M., Faghire, M., Bargaz, A., Bouizgaren, A., Makoudi, B. and Ghoulam, C. (2014). Growth, nutrients concentrations, and enzymes involved in plants nutrition of alfalfa populations under saline conditions. J. Agr. Sci. Tech. 16, 301-314.

[35] De Sedas, A., Turner, B.L., Winter, K. and Lopez, O.R. (2020). Salinity responses of inland and coastal neotropical trees species. Plant Ecol. 221(8), 695-708.

[36] Zorb, C., Geilfus, C.M., Dietz, K.J. (2019). Salinity and crop yield. Plant Biology. 21, 31-38.

[37] Shelden, M.C., Gilbert, S.E. and Tyerman, S.D. (2020). A laser ablation technique maps differences in elemental composition in roots of two barley cultivars subjected to salinity stress. Plant J. 101, 1462-1473.

[38] Li, X., Wan, S., Kang, Y., Chen, X. and Chu, L. (2016). Chinese rose (*Rosa chinensis*) growth and ion accumulation underirrigation with waters of different salt contents. Agric. Water Manag. 163, 180-189.

[39] Farissi, M., Ghoulam, C. and Bouizgaren, A. (2013). Changes in water deficit saturation and photosynthetic pigments of alfalfa populations under salinity and assessment of proline role in salt tolerance. Agric Sci Res J 3, 29-35.

[40] Akca, Y. and Samsunlu, E. (2012). The effect of salt stress on growth, chlorophyll content, proline, nutrient accumulation, and K/Na ratio in walnut. Pakistan J. Bot. 44, 1513-1520.

[41] El-Hendawy, S.E., Hassan, W.M., Al-Suhaibani, N.A., Refay, Y. and Abdella, K.A. (2017). Comparative performance of multivariable agro-physiological parameters for detecting salt tolerance of wheat cultivars under simulated saline field growing conditions. Front Plant Sci. 8, 435.

[42] Loreto, F. and Bongi, G. (1987). Control of photosynthesis under salt stress in the olive. International Conference on Agrometeorology, Fondazione Cesena Agricoltura, Cesena, Italy.

[43] Munns, R., Tester, M. (2008). Mechanisms of salinity tolerance. Annu. Rev. Plant Biol. 59, 651-681.

[44] Lemanowicz, J. (2019). Activity of selected enzymes as markers of ecotoxicity in technogenic salinization soils. Environ. Sci. Pollut. R. 26, 13014-13024.

[45] Chatzigianni, M., Ntatsi, G., Theodorou, M., Stamatakis, A., Livieratos, L., Rouphael, Y. and Savvas, D. (2019). NaCl effects on tomato seed germination, cell activity and ion allocation. Front Plant. Sci. 10, 1040.

[46] Fernández-García, N., Olmos, E., Bardisi, E., Garma, G.D.L., López-Berenguer, C. and Rubio-Asensio, J.S. (2014). Intrinsic water use efficiency controls the adaptation to high salinity in a semi-arid adapted plant. henna (*Lawsonia inermis* L.). J. Plant Physiol. 171, 64-75.

[47] Tanaka, H., Yamada, S., Masunaga, T., Yamamoto, S., Tsuji, W. and Murillo-Amador, B. (2018). Comparison of nutrient uptake and antioxidative response among four Labiatae herb species under salt stress condition. Soil Sci. Plant. Nutr. 64, 589-597.

[48] Karimi, S., Tavallali, V. and Wirthensohn, M. (2018). Boron amendment improves water relations and performance of Pistacia vera under salt stress. Sci. Hortic-Amsterdam. 241, 252-259.

[49] Katerji, N., Hoorn, J.W., Hamdy, A., Mastrorilli, M. and Mou Karzel E. (1997). Osmotic adjustment of sugar beets in response to soil salinity and its influence on stomatal conductance, growth and yield. Agr. Water Manage. 34, 57-69.

[50] Madhana Kumari, P. and Sekar, K. (2008). Effect of plant growth regulators on chlorophyll and carotenoid content of salinity stressed okra seedlings. Asian J. Hortic. 3, 54-55.

[51] Weisany, W., Sohrabi, Y., Heidari, G.R., Siosemardeh, A. and Ghassemi-Golezani, K. (2011). Physiological responses of soybean (*Glycine max* L.) to zinc application under salinity stress. Aust. J. Crop. Sci. 5, 1441-1447.

[52] Raja Babu, C. and Vijayalakshmi, C. (2008). Impact of salt stress on chlorophyll fraction in rice (*Oryza sativa* L.) leaves. Plant Arch. 8, 969-971.

[53] Sayyad-Amin, P., Jahansooz, M.R., Borzouei, A. and Ajili, F. (2016). Changes in photosynthetic pigments and chlorophyll-a fluorescence attributes of sweet-forage and grain sorghum cultivars under salt stress. J. Biol. Phys. 42, 601-620.

[54] Xing, W., Wang, J., Liu, H., Zou, D. and Zhao, H. (2013). Influence of natural saline-alkalistress on chlorophyll content and chloroplast ultrastructure of two contrasting rice (*Oryza sativa* L. japonica) cultivars. Aust. J. Crop. Sci. 7, 289-292.

[55] Ferdous, J., Mamun, M. and Ali, M.S. (2017). Impact of Environmental and Stress Factors on the Photosynthetic Capabilities of Plants. Univers. J. Agr. Res. 5, 113-118.

[56] Moradi, F. and Ismail, A.M. (2007). Responses of photosynthesis, chlorophyll fluorescence and ROS-Scavenging systems to salt stress during seedling and reproductive stages in rice. Ann. Bot .99, 1161-1173.

[57] Nathawat, N.S., Kuhad. M.S., Patel, A.L., Kumar, R. and Goswami, C.L. (2008). Nitrogen mitigates effect of salinity on plant water relations and photosynthesis in indian mustard (*Brassica juncea*). Acta Agron. Hung. 56, 463-476.

[58] Hakim, M.A., Juraimi, A.S., Hanafi, M.M., Ali, E., Ismail, M.R., Selamat, A. and Karim, R. (2014). Effect of salt stress on morpho-physiology, vegetative growth and yield of rice. J. Environ. Biol. 35, 317.

[59] Farquhar, G.D. and Sharkey, T.D. (1982). Stomatal conductance and photosynthesis. Ann. Rev. Plant. Physiol. 33, 317-345.

[60] López-Serrano, L., Penella, C., San-Bautista, A., López-Galarza, S. and Calatayud, A. (2017). Physiological changes of pepper accessions in response to salinity and water stress. Span. J. Agric. Res. 15, e0804.

[61] Dionisio-Sese, M.L. and Tobita, S. (2000). Effects of salinity on sodium content and photosynthetic responses of rice seedlings differing in salt tolerance. J. Plant. Physiol. 157, 54-58.

[62] Zarco-Tejada, P.J., Pushnik, J.C., Dobrowski, S.Z. and Ustin, S.L. (2003). Steady state chlorophyll a fluorescence detection from canopy derivative reflectance and double-peak red-edge effects. Remote Sens. Environ. 84, 283-294.

[63] Murchie, E.H. and Lawson, T. (2013). Chlorophyll fluorescence analysis: a guide to good practice and understanding some new applications. J. Exp. Bot. 64, 3983-3998.

[64] Gitelson, A.A., Buschmann, C. and Lichtenthaler, H.K. (1999). The chlorophyll fluorescence ratio F735/F700 as an accurate measure of the chlorophyll content in plants. Remote Sens. Environ. 69, 296-302.

[65] Xue, W.X., Jiang, Y., Shang, X.S. and Zou, J. (2020). Effects of different concentrations Cd on mineral accumulation and photosynthesis parameters in *Salix matsudana* Koidz. Fresen. Environ. Bull. 29, 1443-1451.
[66] Murchie, E.H. and Harbinson, J. (2014). Non-photochemical fluorescence quenching across scales: from chloroplasts to plants to communities. Dordrecht: Springer.
[67] Goharrizi, K.J., Amirmahani, F. and Salehi, F. (2019). Assessment of changes in physiological and biochemical traits in four pistachio rootstocks under drought, salinity and drought plus salinity stresses. Physiol. Plantarum. 168, 973-989.

Received: **08.07.2020**
Accepted: **06.02.2021**

CORRESPONDING AUTHOR

Jinhua Zou
Tianjin Key Laboratory of Animal and Plant Resistance,
College of Life Sciences,
Tianjin Normal University,
China

e-mail: zjhmon@126.com

© by PSP Volume 30– No. 05/2021 pages 4888-4892 Fresenius Environmental Bulletin

STUDY ON RISK ASSESSMENT OF URBAN GAS PIPELINE LEAKAGE BASED ON ECOLOGICAL PLANNING

Jixin Zhang[1,*], Haoyuan Dai[1], Jian Kang[1], Maomao Li[1], Ruishen Wang[1], Qiuju You[2]

[1]Department of Safety Engineering, Beijing Institute of Petrochemical technology, Beijing 102617, China
[2]Beijing Research Center of Urban System Engineering, Beijing 100044, China

ABSTRACT

At present, there are few researches on the risk assessment of urban gas pipeline leakage in China. However, with the improvement of urban infrastructure, especially the gradual construction of natural gas pipelines, the risk of urban gas leakage has increased. Therefore, the risk assessment of urban gas transmission and distribution network system is an essential basis for future gas pipeline maintenance and renewal. In view of the existing risks of urban gas pipeline system, this paper puts forward a complete risk assessment method. Based on the method of combining fault tree with event tree to identify the risk of urban gas pipeline system, the model and process of risk assessment of urban gas pipeline system and system-based risk assessment are constructed, and the effectiveness of risk assessment is verified by example evaluation.

KEYWORDS:
Ecological planning, Urban gas pipeline, Risk assessment, Model

INTRODUCTION

With the development of energy, the application of natural gas has become an important foundation of urban construction [1]. The development of urban gas utilization mode can not only optimize the urban energy structure, but also reduce the environmental pollution caused by fossil energy processing [2], which is of great significance to China's sustainable development strategy [3]. At the same time, the construction and configuration of gas pipeline is a vital part of urban public infrastructure [4]. Different from traditional liquid pipeline, gas pipeline transmission system is a repairable, complex and networked comprehensive infrastructure [5]. In recent years, China's urban gas industry has entered a period of high development, with "West-East Gas Transmission Project", "Guangdong Import Project" and "Russian Gas Transmission to the South Project" successively constructed or entered the preliminary work [6]. At present, the main project of "West-East Gas Transmission" has been completed, and gas has been supplied to Beijing and Shanghai. The Zhongwu Line is under intense construction, and other large-scale projects are progressing smoothly [7]. With the successful implementation of these large-scale gas transmission projects, it will inevitably lead to changes in the structure of urban gas pipeline network system in passing and terminal cities. At present, the total length of urban gas pipelines in China has reached tens of thousands of kilometers. The current development of urban gas in China is characterized by natural gas, which develops rapidly and gradually replaces artificial gas. Artificial gas will remain in some cities for a period of time, but the construction of urban gas pipeline network system will be fully carried out [8].

However, the urban gas transmission and distribution network system is not always in a safe state, and it has failures caused by various reasons, which can lead to heavy casualties and property losses. Every year, there are many disasters caused by it. That is to say, there are risks in the urban gas transmission and distribution network system [9]. Li Taijia, academician of Chinese Academy of Engineering, listed "Reliability and Risk Assessment of Gas Pipeline Network" as one of the key topics in the "Main Report for Technological Progress and Development of Urban Gas Industry in 2001-2005". In fact, in China, the risk assessment of urban gas pipeline network is rarely studied [10]. However, the risk control of the whole gas transmission and distribution system in a city, or a subsystem or a component in the system, is the basis of risk decision [11] and the main content of risk management, so it is urgent to study the risk assessment of urban gas transmission and distribution network system [12]. Combined with the definition of risk, this paper puts forward the model and process of risk assessment of urban gas pipeline system, analyzes the favorable conditions of risk assessment, and puts forward the risk assessment model and process based on ecological planning system.

MATERIALS AND METHODS

Assessment System Construction. Risk Assessment Model. Through fault tree analysis and event tree analysis of urban gas distribution pipeline [13], 15 possible consequence events can be obtained by event tree analysis, and the probability of each consequence event can be obtained by comprehensive analysis of fault tree and event tree, then the consequence value of each consequence event can be calculated by further analysis [14]. The risk value of a certain pipeline section can be calculated by the following formula:

$$R = \sum_{I=1}^{15} P_i C_i$$

In which: R is the risk value of a certain pipe section; P_i is the probability of the i-th consequence event ; C_i is the consequence value of the i-th consequence event.

Overview of Urban Geographic Information System. Geographic information system is a system supported by computer hardware and software to collect, store, retrieve, analyze, process and display geographic data information [15]. Geographical data describes the things and phenomena in nature from the following three aspects: ① The position in a certain coordinate system, namely spatial data. ② Attributes that describe the characteristics of things, namely, non-spatial data, such as pipe material, equipment model, etc. The spatial relationship between things is called topological data [16]. ③ The research object of urban geographic information system is the information related to urban spatial geographic distribution. Urban gas pipeline network information system is an integral part of urban geographic information system [17].

Establishment of Urban Gas Pipeline Network Information System. Gas pipeline in geographic information system is usually composed of line entities and point entities. Point entities include elbow, tee of pipeline characteristic points and valves, pressure regulators, compensators, drains of accessory equipment points. Line entities include straight pipe sections and arc pipe sections. The starting point and terminal point of pipe sections are represented by points, which usually include pipeline characteristic points, accessory equipment points, diameter changing points, material changing points, buried age changing points, ownership unit changing points and other important information changing points [18]. The coding of pipeline can be compiled according to the national standard GB/T14395 *Urban Geographical Elements-Urban Roads, Road Intersections, Neighborhoods, Municipal Engineering Pipeline Coding Structure*

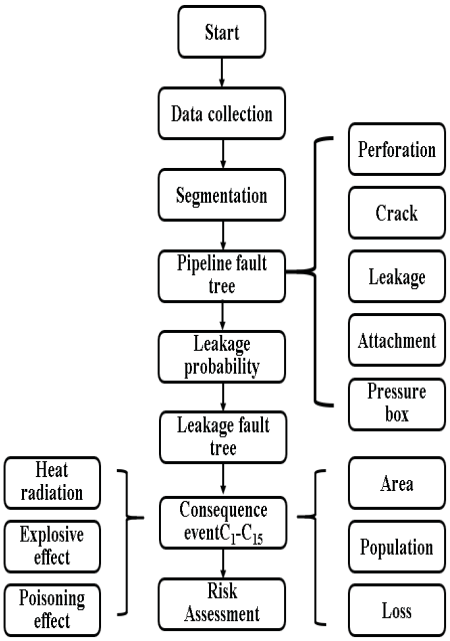

FIGURE 1
Risk assessment model of gas pipeline distribution

Rules, and the coding consists of orientation code, classification code and serial number. The coding of gas pipeline should be hierarchical and unique. Point entities use geographical coordinates (x, y, z) to express the position, while line entities use start nodes and stop nodes to express the position, and arc pipe sections can be represented by multiple groups of start and stop points according to their accuracy requirements. Without accurate position information of the pipeline in service, exploratory measures should be taken to determine its spatial position [19].

In addition to spatial data coding and non-spatial data coding of the gas pipeline network itself, the gas pipeline network information system should also include the topological relationship between the gas pipeline and other adjacent objects and other related non-spatial information. The spatial information of these objects includes ① Soil information adjacent to the pipeline. Soil is usually surface entity or polygon data, and the topological relations between polygon vectors or between polygon vectors, line and point vectors include topological adjacency, topological association and topological inclusion. The attribute data of soil include soil type, soil resistivity, redox potential, water content, salt content, pH value and so on. After the topological relationship between pipeline and soil is established, the soil environment in which pipeline is located can be conveniently inquired. ② Distribution of underground grooves, culverts and wells adjacent to or containing pipelines. The attributes of mainly include groove name, purpose, size, etc.

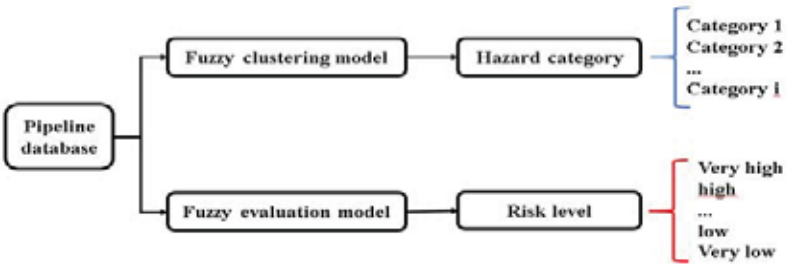

FIGURE 2
Classification and comprehensive evaluation process of gas pipeline

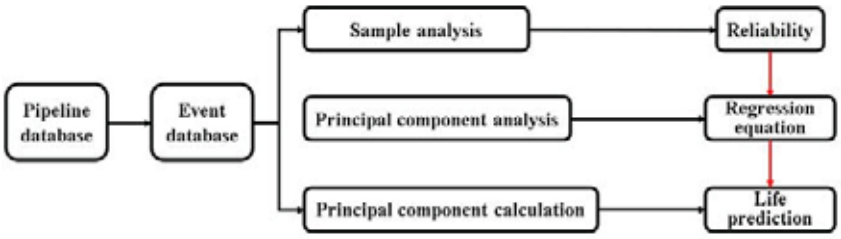

FIGURE 3
Schematic diagram of prediction method of pipeline life and leakage probability

③ Distribution of other underground engineering pipelines adjacent to gas pipelines. The attributes mainly include the purpose and materials of engineering pipelines [20].

Risk Assessment Model of Gas Pipeline Distribution. Based on the foregoing, the risk assessment model of the gas pipeline distribution is summarized as shown in Figure 1.

RESULTS AND DISCUSSION

Risk Assessment of Gas Pipeline Distribution. Classification and Comprehensive Evaluation of Gas Pipeline. Through the method of fuzzy clustering and fuzzy comprehensive evaluation, the situation of dangerous pipelines can be prompted more accurately and timely, and the specific analysis process is shown in Figure 2.

The evaluation model established in this paper needs to collect and record the detailed information of each pipe section. Therefore, the data of all pipe sections can be read through the information base data. By risk assessment, the cluster and comprehensive evaluation results of each pipe section can be obtained, so it is easy to understand which pipe sections of the whole pipe network are similar and the risk status of each pipe section. The end point of middle pipe section is usually point entity, that is, pipeline characteristic point and accessory equipment point. There may be some attribute changes inside the pipe section, for example, the value of some soil parameters is not at the same level, the pipeline laying years are not consistent, and the pipeline anti-corrosion is inconsistent, etc. At this time, this pipe section should be represented as a number of small pipe sections, each of which belongs to this pipe section, but has its own attribute table.

Analysis on Life and Leakage Probability of Gas Pipeline. Figure 3 shows a schematic diagram of prediction method of pipeline life and leakage probability. The data of all leakage accidents of each component, namely pipeline corrosion perforation, pipeline cracking, pipeline leakage, valve leakage, compensator leakage, drainer leakage and pressure adjusting box leakage, can be obtained from the urban gas pipeline network. With life as independent variable and all other parameters as dependent variables, multivariate statistical analysis is carried out on these data by programming according to statistical inference method, and finally the regression equation between component life and other parameters can be obtained. According to the regression equation and the parameters of pipeline system, the life of all components can be predicted, and then the life of pipeline system can also be predicted. On the other hand, according to the leakage data, the life distribution can be obtained, so as to obtain the pipeline unreliability, i.e. leakage probability.

Risk Assessment of Gas Pipeline. Based on the above consequence analysis on risk assessment of gas pipeline, the probability of gas gathering in the confined space and the formation of gas cloud in the open space can be obtained through the simulation of leakage gas diffusion. The probability of each subsequent event in the event tree diagram of each pipe section can be obtained according to the fire probability analysis of leakage source, the analysis of on-site detonating and the analysis of gas composition. Combined with the analysis on gas leakage probability and consequence event, the risk estimation value of each pipe section can be

TABLE 1
Comparison results of pipeline risk assessment methods

Pipeline	Traditional method	Modeling method	Measured
Pipeline1	89	91	93
Pipeline2	69	83	87
Pipeline3	72	68	65
Pipeline4	67	43	47
Pipeline5	79	81	85
Pipeline6	69	65	62
Pipeline7	67	58	59
Pipeline8	88	89	92
Pipeline9	87	88	91
Pipeline10	90	91	89

calculated according to the definition of risk and the above formula.

Examples of Risk Assessment of Urban Gas Pipeline. Based on the commonly used risk assessment form of urban gas pipeline, combined with the failure consequence analysis results, five experts are invited to come to the site to score the multi-section pipeline. According to their opinions, the average score is obtained. With the final evaluation result of the pipeline, the risk level of the corresponding pipeline is evaluated by the constructed risk assessment model, and the leakage possibility can be actually measured by ultrasonic detection means. The differences between the assessment model established in this paper and the traditional assessment methods is compared, and the specific results are shown in Table 1. In order to evaluate the differences among the three methods, the results are analyzed by T-test with SPSS software. The results show that when the confidence interval $P<0.01$, there are obvious differences between the traditional analysis and the measured results, but there is no obvious difference between the values evaluated by the analysis method and the measured values, which indicates that the pipeline risk assessment method established in this paper can better predict the existing state of pipelines and reduce the leakage risk of urban pipelines. However, based on the requirements of green ecological planning, this method needs to collect data and establish information files for all pipelines. Based on the accuracy of data collection, it can directly reflect the risk level of pipelines through the model, thus realizing the risk assessment of pipelines.

CONCLUSIONS

Everything has two sides. On the one hand, urban gas pipeline system brings convenience to urban residents' life and industrial production. On the other hand, due to the flammable, explosive, toxic and easy-to-leak nature of the transmission medium, the urban gas pipeline system often causes safety accidents, leading to casualties and property losses. In view of its existing risks, this paper puts forward a complete risk assessment method. Firstly, the method of combining fault tree with event tree is proposed to identify the risk of urban gas pipeline system. Gas leakage is selected as the top event of the fault tree and the initial event of the event tree, and the failure reasons of the bottom event of the gas distribution pipeline leakage are summarized, the possible consequences caused by gas leakage are deduced, and the reasons for subsequent events in the event tree analysis are summarized by fault tree analysis. Secondly, a fuzzy comprehensive assessment method and the fuzzy clustering analysis are put forward to judge the degree of pipeline corrosion, construction damage, leakage consequence and risk state. Finally, the model and process of risk assessment of urban gas pipeline system and system-based risk assessment are constructed, and the effectiveness of risk assessment is verified by example evaluation.

ACKNOWLEDGEMENTS

This paper is supported by China.National Key R&D Program of China (2018YFC0809700); Science and Technology Project of Beijing Education Commission (KM20181001701 & KM202010017009); Beijing Municipal Natural Science Foundation (9192009); National Natural Science Foundation of China (71901029).

REFERENCES

[1] Cai, B.P., Shao, X., Liu, Y.H., Kong, X.D., Wang, H.F., Xu, H.Q., Ge, W.F. (2020) Remaining Useful Life Estimation of Structure Systems Under the Influence of Multiple Causes, Subsea Pipelines as a Case Study. IEEE Transactions on Industrial Electronics. 67(7), 5737-5747.

[2] Weller, Z.D., Hamburg, S.P., von Fischer, J.C. (2020) A National Estimate of Methane Leakage from Pipeline Mains in Natural Gas Local Distribution Systems. Environmental Science & Technology. 54(14), 8958-8967.

[3] Santiago-Duran, M., Gonzalez-Compean, J.L., Brinkmann, A., Reyes-Anastacio, H.G., Carretero, J., Montella, R., Toscano Pulido, G. (2020) A gearbox model for processing large volumes of data by using pipeline systems encapsulated into virtual containers. Future Generation Computer Systems. 106, 304-319.
[4] Valdivia, P., Barraza, R., Saldivia, D., Gacitua, L., Barrueto, A., Estay, D. (2020) Assessment of a Compressed Air Energy Storage System using gas pipelines as storage devices in Chile. Renewable Energy. 147(1), 1251-1265.
[5] Al-Masri, W.M.F., Abdel-Hafez, M.F., Jaradat, M.A. (2020) Inertial Navigation System of Pipeline Inspection Gauge. IEEE Transactions on Control Systems Technology. 28(2), 609-616.
[6] Li, S.Z., Peng, R.Z., Liu, Z.L. (2020) A surveillance system for urban buried pipeline subject to third-party threats based on fiber optic sensing and convolutional neural network. Structural Health Monitoring-An International Journal. June.
[7] Wang, Y., Hou, X., Zhang, P., Qin, G. (2020) Reliability assessment of multi-state reconfiguration pipeline system with failure interaction based on Cloud inference. Process Safety and Environmental Protection. 137, 116-127.
[8] Wang, T., Guo, Z., Shen, Y., Cui, Z., Goodwin, A. (2020) Accumulation mechanism of biofilm under different water shear forces along the networked pipelines in a drip irrigation system. Scientific Reports. 10(1), 6960.
[9] Vakharia, K., Waqas, M., Shakir, H.J., Chin, F., Hartke, J.N., Shallwani, H., Beecher, J.S., Siddiqui, A.H., Levy, E.I. (2020) Versatile use of catheter systems for deployment of the Pipeline embolization device, a comparison of biaxial and triaxial catheter systems. Journal of Neurointerventional Surgery. 12(6), 585-590.
[10] Merkert, L., Castro, P.M. (2020) Optimal Scheduling of a District Heat System with a Combined Heat and Power Plant Considering Pipeline Dynamics. Industrial & Engineering Chemistry Research. 59(13), 5969-5984.
[11] Tsunoda Meira, W.H, Magatao, L., Neves,-Jr. F., Arruda, L.V.R., Vaqueiro, J.P., Relvas, S., Barbosa-Povoa, A.P. (2020) Scheduling of a single-source multiproduct pipeline system by a matheuristic approach, Combining simulated annealing and MILP. Computers & Chemical Engineering. 136(106784).
[12] Li, W., Huang, Q., Wang, W., Gao, X. (2020) Advances and Future Challenges of Wax Removal in Pipeline Pigging Operations on Crude Oil Transportation Systems. Energy Technology. 8(19014126).
[13] Yang, Y., Li, B., Wu, X., Yang, L. (2020) Application of Adaptive Cubature Kalman Filter to In-Pipe Survey System for 3D Small-Diameter Pipeline Mapping. IEEE Sensors Journal. 20(12), 6331-6337.
[14] Abate, F., Di Caro, D., Di Leo, G., Pietrosanto, A. (2020) A Networked Control System for Gas Pipeline Cathodic Protection. IEEE Transactions on Instrumentation and Measurement. 69(3), 873-882.
[15] Swiercz, M., Mroczkowska, H. (2020) Multiway PCA for Early Leak Detection in a Pipeline System of a Steam Boiler-Selected Case Studies. Sensors. 20(6), 1561.
[16] Ayadi, A., Ghorbel, O., Bensalah, M.S., Abid, M. (2020) Spatio-temporal correlations for damages identification and localization in water pipeline systems based on WSNs. Computer Networks. 171, 107134.
[17] Liu, M., Yang, S.S., Zhang, K.X., Li, J.J., Liu, H.Y., Dai, Y.J. (2018) The study of smart growth of salt lake city and Nottingham city using the entropy method to explore the social, environment and economic changes. Fresen. Environ. Bull. 27, 4631-4636.
[18] Giannoccaro, N.I., Persico, G., Strazzella, S., Lay-Ekuakille, A., Visconti, P. (2020) A System for Optimizing Fertilizer Dosing in Innovative Smart Fertigation Pipelines, Modeling, Construction, Testing and Control. International Journal of Precision Engineering and Manufacturing. 21(8), 1581-1596.
[19] Lukonge, A.B., Cao, X.W. (2020) Leak Detection System for Long-Distance Onshore and Offshore Gas Pipeline Using Acoustic Emission Technology. A Review. Transactions of the Indian Institute of Metals. 73, 1715-1727.
[20] Shang J, An W, Liu Y, Han B, Guo Y. (2020) Oil Pipeline Weld Defect Identification System Based on Convolutional Neural Network. KSII Transactions on Internet and Information Systems. 14(3), 1086-1103.

Received: **30.07.2020**
Accepted: **28.10.2020**

CORRESPONDING AUTHOR

Jixin Zhang
Department of Safety Engineering,
Beijing Institute of Petrochemical Technology,
Beijing 102617, China

e-mail: zjx1163@163.com

© by PSP Volume 30– No. 05/2021 pages 4893-4900 Fresenius Environmental Bulletin

CORRELATION BETWEEN WEATHER AND COVID-19 PANDEMIC IN JORDAN

Eman Abdelhafez[1], Mohammad Hamdan[2,*]

[1]Al-Zaytoonah University of Jordan, Faculty of Engineering and Technology, Department of Alternative Energy Technology, Amman 11733, Jordan
[2]The University of Jordan, School of Engineering, Department of Mechanical Engineering, Amman 11942, Jordan

ABSTRACT

This study aims to correlate weather variables with COVID-19 active cases by using Artificial neural network (ANN) method. Three types of Artificial Neural Network namely; Elman, NARX, and Feedforward networks, were designed and tested using MATLAB software. The COVID-19 active cases in Jordan data was obtained from the Ministry of Health in Jordan, while that of the weather data was obtained from Jordan Metrological Department. Both data were used in the development process of the models to approximate and estimate the actual performance of proposed models. The obtained results from training part were used to validate the ANN results. The performance of the three models was compared was decided based on the three statistics of metrology variables (R, RMSE, and MBE).

Using the average daily temperature and wind speed as the input indicators to the network provided, it was found that Elman model exhibits the best performance and most accurate coefficient of correlation (R) and hence the most accurate correlation between weather variables and COVID-19 active cases in Jordan. while the predictive capability of Feedforward and NARX models were the least.

KEYWORDS:
COVID-19, Coronavirus, weather data, Artificial Neural Network

INTRODUCTION

It is well known that influenza is seasonal and its incidence increases during Winter reasons, it is believed that this due to the existence of physical factors that activate the virus during cold weather conditions. Most recent research work indicated that the transmission route of COVID-19 is bat-human, with unknown intermediate host so far, with the transmission being mainly caused by respiratory droplet suspended in air and human-human contacts [1,2]. Dalziel et al. [3] have found out that climate conditions are considered to be significant predictors of coronavirus illnesses.

Similarly, COVID-19 may be linked to weather conditions as may be concluded from different recent research work. It was reported by Yuan et al. [4] that wind speed, humidity, temperature and wind speed were found to be critical in the transmission of infectious diseases. Also, Bull [5] concluded that pneumonia's mortality rate is highly correlated with weather changes.

Bukhari and Jameel [6] conducted a research work on the influence of temperature and humidity on the transmission intensity of COVID-19 using data from January to February for 100 Chinese cities and for 1005 counties in USA during the period from 15 March to 25 April this year. They found that there exists influence of both temperature and relative humidity on transmission of COVID-19 in both countries.

Tosepu et al. [7] obtained data of COVID-19 from the Ministry of Health in Indonesia and weather data from Metrological department. They conducted analysis on a correlation between weather and covid-19 in Jakarta in Indonesia. They concluded that temperature significantly affects the incidence rate of COVID -19.

Duojiao and Bashir [8] used data obtained from New York city health services and metrological data obtained from National weather service, USA, to investigate the association between COVID-19 and climate indicators in New York City, USA. The weather data used included are average temperature, minimum temperature, maximum temperature, rainfall, average humidity, wind speed and air quality. They conducted the tests using Kendall and Spearman rank correlation. It was found that average temperature, minimum temperature, and air quality were the most weather indicators associated with the COVID-19 pandemic.

Sahin [9] conducted a study on nine cities in Turkey to examine a correlation between examined correlation between weather data and COVID-19, the weather data included temperature, dew point, wind speed and humidity, the effect of each parameter within 1, 3, 7, and 14 days were examined. In addition, the population was taken as an effective parameter in the analysis, which was based on Spearman's correlation coefficients. They concluded

that highest correlations were observed for population, wind speed 14 days ago, and temperature on the day, respectively.

Yueling et al. [10] explored the influence of temperature, humidity and diurnal temperature range on the death number caused by Corona Virus Disease 2019 (COVID-19) during the period from 20 January 2020 to 29 February 2020 in Wuhan, China using generalized additive model. They reviled that a positive association with daily death counts for the diurnal temperature range, while negative one exists for the relative humidity.

Since the announcement made by WHO that COVID-19 is a pandemic, the number of confirmed COVID-19 cases is continuously escalating worldwide [11]. In Jordan the first confirmed of COVID-19 case was confirmed on the second day of March. As of October 14th, 2020, it has increased to 30550 cases. 6466 cases have recovered, 923 cases under treatment, and 257 cases deaths.

The main objective of this study is to correlate weather variables with COVID-19 active cases by using an Artificial neural network (ANN) and to conduct a sensitivity test to find the most effective input parameters on the positive cases of COVID-19 in Jordan.

MATERIALS AND METHODS

Study Area. Jordan lies between longitudes 35^0 40' and 39^0 E and between latitudes 29^0 30' and 34^0 N in the transition region between the zonobiome (with moist cold winters and dry hot summers) and the arid one [12]. The area of Jordan is 89,342 km^2. Currently, the total population of Jordan exceeds ten million.

Data Collection. In this work, the daily data on confirmed COVID -19 cases in Jordan over the period from 15 March to 31 May, 2020, was obtained from the Jordanian Ministry of health, while the weather data including the average daily temperature (^{0}C), relative humidity (%), wind speed (m/s), amount of Rainfall (mm), and average daily solar radiation (W/m^2) was obtained from Jordan Metrological Department.

Data Analysis. Three types of Artificial Neural Network (ANN) were designed and tested using MATLAB software. A total data consists of 78 samples were used as the inputs to the ANN network., In addition, the average daily temperature (T), relative humidity (RH), wind speed (WS), amount of Rainfall (R) and average daily solar radiation (SR) were also used as the inputs to the ANN network. The number of daily new coronavirus positive cases in Jordan is used as the output of the ANN network.

RESULTS AND DISCUSSION

Elman, NARX and Feedforward models were designed and tested using the MATLAB software. These models were used to correlate the weather variables with the covid-19 active cases in Jordan, Levenberg-Marquardt (trainlm) was used as a training algorithm. The performance of the designed models has been conducted using root mean squared error (RMSE), mean bias error (MBE) and the coefficient of correlation (R). More details and description about the proposed three models of ANN were found in [13].

Artificial Neural Network (ANN). Table (1) shows the coefficient of correlation (R) of each model for different numbers of hidden layers. As indicated in the table, the maximum value of R is equal to 0.86789 for Elman model, that corresponds to 45 hidden layers, this was followed by 0.72844 for Feedforward model that corresponds to 15 hidden layer and finally the lowest value of R was 0.64839 for NARX model, which corresponds to 10 hidden layers. Figures (1) and (2) show the comparison of variation of gradient error and validation checks and scatter plots of the models used for the selected models.

TABLE 1
Coefficient of correlation (R) for the proposed models.

Number of Hidden layers	Elman Model	NARX Model	Feedforward Model
10	0.63126	0.64839	0.51455
15	0.70491	0.58698	0.72844
20	0.6912	0.47529	0.6055
25	0.71346	0.50527	0.48039
30	0.47663	0.38188	0.37113
35	0.7356	0.47673	0.56233
40	0.62219	0.62413	0.48554
45	0.86789	0.41989	0.51287
50	0.64635	0.20462	0.156
55	0.68423	0.5029	0.53304

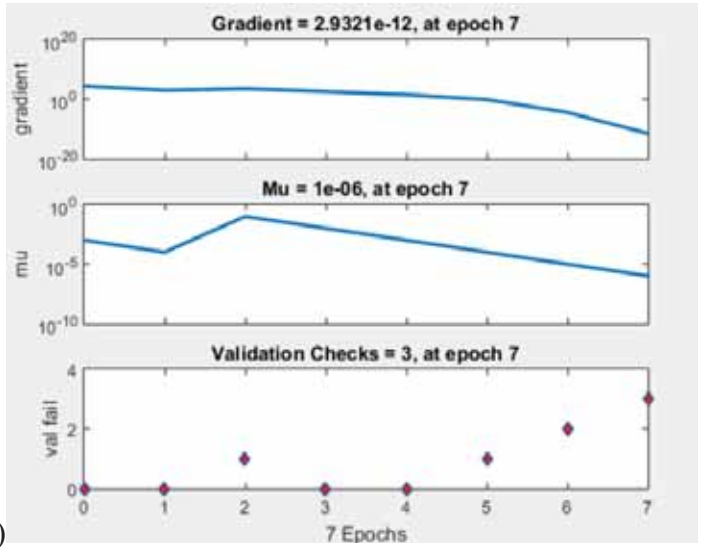

(a)

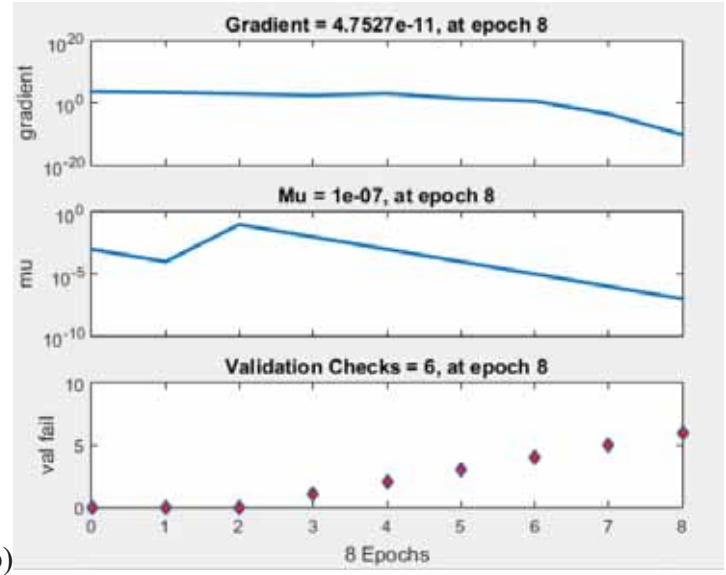

(b)

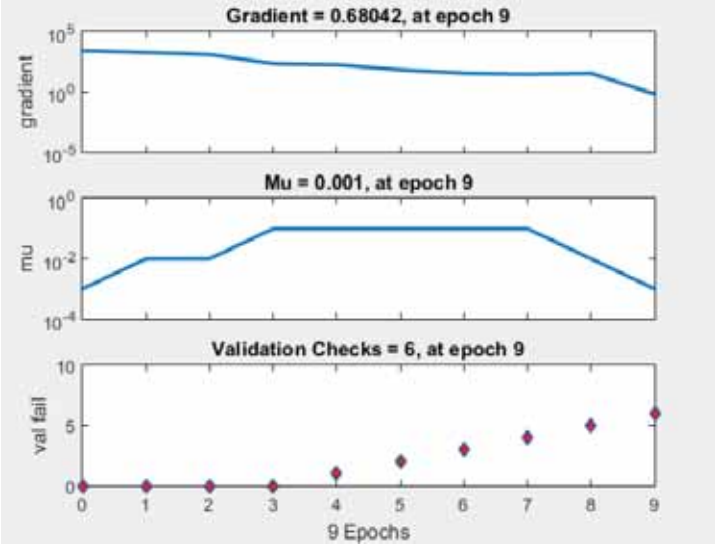

(c)

FIGURE 1
Comparison of variation of gradient error and validation checks for the selected models using (a) Elman, (b) NARX and(c) Feedforward.

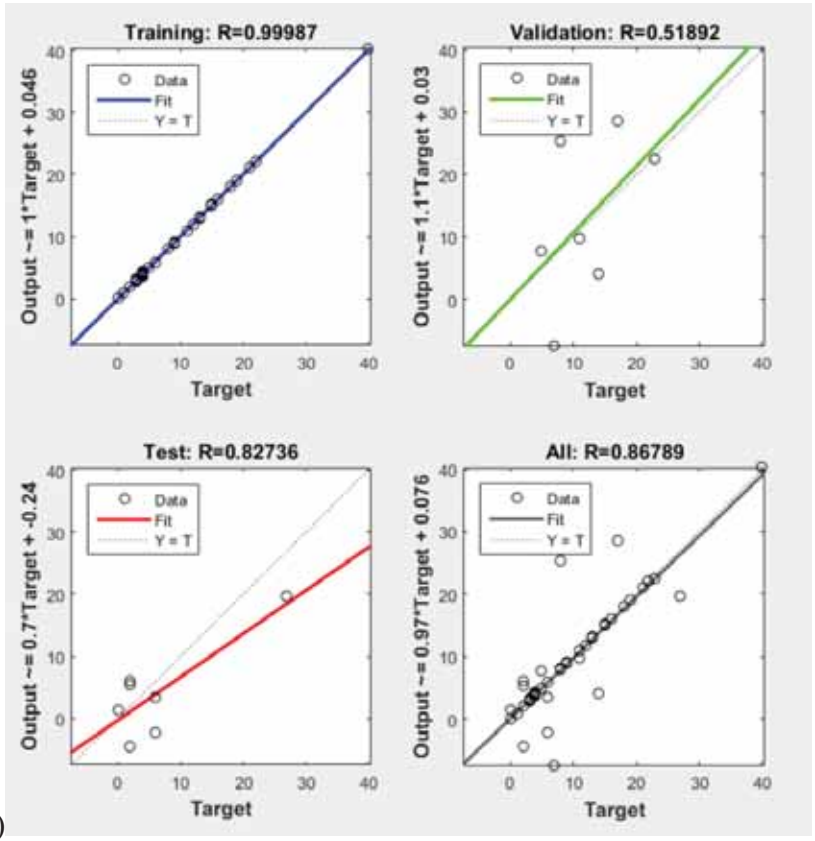
Training: R=0.99987
Validation: R=0.51892
Test: R=0.82736
All: R=0.86789
Data
Fit
Y = T
Target
Output ~= 1*Target + 0.046
Output ~= 1.1*Target + 0.03
Output ~= 0.7*Target + -0.24
Output ~= 0.97*Target + 0.076

(a)

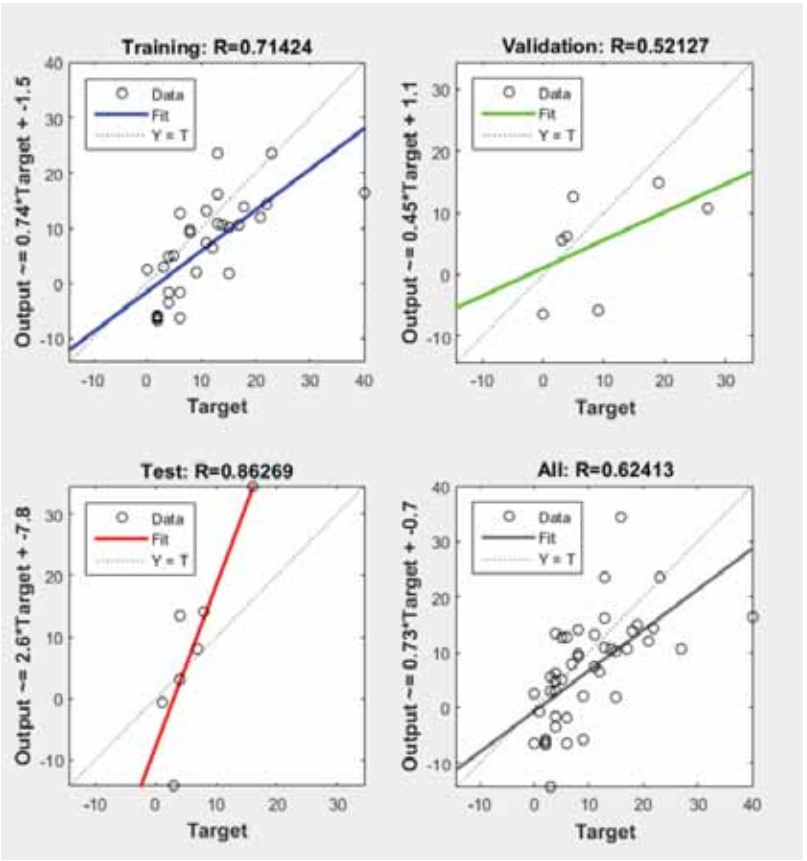
Training: R=0.71424
Validation: R=0.52127
Test: R=0.86269
All: R=0.62413
Data
Fit
Y = T
Target
Output ~= 0.74*Target + -1.5
Output ~= 0.45*Target + 1.1
Output ~= 2.6*Target + -7.8
Output ~= 0.73*Target + -0.7

(b)

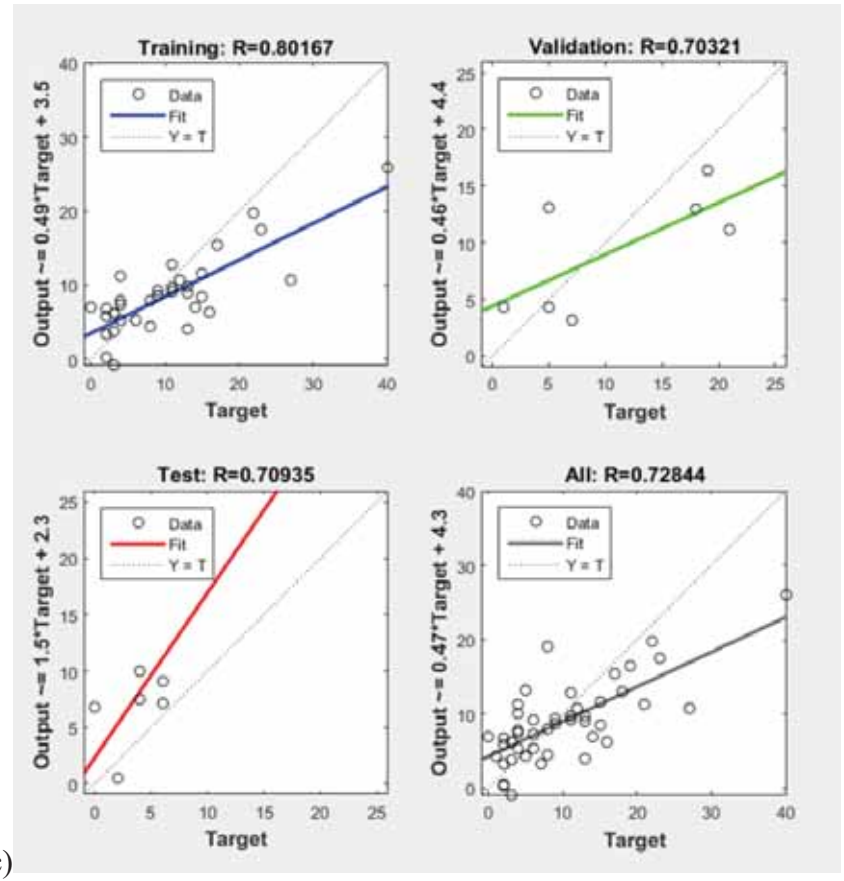

(c)

FIGURE 2
Comparison of scatter plots of the models used for the selected models (a) Elman, (b) NARX and(c) Feedforward.

TABLE 2
Comparison of maximum performance of the used models.

Model	RMSE		MBE		R
	Validation	Training	Validation	Training	
Elman	5.5985	0.1453	4.7523	0.1132	0.86789
NARX	10.3169	7.6585	8.2256	6.0562	0.62413
Feedforward	9.3660	5.5855	7.7227	4.1270	0.72844

The comparative analysis of the different training models using some basic statistics (R, RMSE, and MBE) has been carried out, the obtained result is presented in Table (2). It may be noticed that, Elman model gave the best performance to predict the active cases of CODIV-19. Furthermore, and as shown in the table the predictive capability of Feedforward and NARX models for positive cases of COVID -19 is the least.

Sensitivity test. As mentioned above, Elman model has the best predictive capability to positive cases. The next step was to conduct sensitivity test to find the most effective input parameters on positive cases. Table (3) shows the coefficient of correlation (R) for different types and numbers of inputs to Elman model. From this table, it may be noticed that, the maximum value of R (0.86789), occurred at 45 hidden layers by using five inputs to the model namely; average daily temperature (T), relative humidity (RH), wind speed (WS), amount of rainfall (R) and average daily solar radiation (SR)

For Four inputs and using the four input parameters to the model (average daily temperature, wind speed, amount of Rainfall, and average daily solar radiation), it was found that the maximum value of R (0.96749), which obtained for 10 hidden layers. Furthermore, using three input parameters to the model (average daily temperature, relative humidity and wind speed), the maximum value of R was found to be (0.99664), which was obtained for 30 hidden layers., which was obtained for. When using the input parameters (average daily temperature and wind speed) the maximum value of R was found to be (0.88876), which corresponds to 20 hidden layers and obtained when the average daily temperature was used as input parameter.

TABLE 3
Comparison of maximum performance of the used models.

Number of Hidden layers	T,RH, WS,R ,SR	T	RH	WS	R	SR	T,RH, WS,R	T,RH,WS, SR	T,WS,R, SR	RH,WS ,R,SR
10	0.63126	0.20894	0.26335	0.78558	0.73201	0.77912	0.8463 4	0.87188	0.96749	0.42922
15	0.70491	0.39431	0.40643	0.31509	0.63255	0.36851	0.8661 1	0.3163	0.56703	0.70681
20	0.691 2	0.88876	0.12824	0.62917	0.20464	0.6122	0.5161 4	0.86981	0.68794	0.31632
25	0.713 46	0.57887	0.03839 8	0.04939 5	0.13624	0.64991	0.8951 1	0.82506	0.70721	0.85802
30	0.476 63	0.67252	0.37006	0.462	0.84936	0.74383	0.6101 2	0.71658	0.56113	0.62226
35	0.735 6	0.54938	0.3723	0.16083	0.63158	0.37744	0.7806 6	0.86361	0.51155	0.58826
40	0.622 19	0.73783	0.35963	0.69367	0.64407	0.39504	0.8791 4	0.61512	0.78966	0.75005
45	0.867 89	0.21364	0.26566	0.17036	0.12557	0.28245	0.4322 9	0.51503	0.64989	0.46569
50	0.646 35	0.7064	0.76995	0.71097	0.77784	0.78692	0.8639 3	0.40267	0.60358	0.73671
55	0.684 23	0.41147	0.62605	0.56855	0.59279	0.23198	0.8803 9	0.8034	0.53477	0.50473

Number of Hidden layers	T,RH,WS	T,RH,R	T,RH,SR	T,WS,R	T,WS,SR	RH,WS,R	RH,R,SR	RH,WS,SR	WS,R,SR
10	0.58318	0.99302	0.99031	0.99247	0.98335	0.35098	0.7329	0.54053	0.24696
15	0.96449	0.99282	0.983	0.97827	0.99163	0.31037	0.58288	0.67522	0.61916
20	0.89393	0.89888	0.73501	0.43456	0.92858	0.37405	0.26906	0.81343	0.72883
25	0.83465	0.90251	0.86248	0.80544	0.96894	0.74764	0.57428	0.73049	0.62775
30	0.99664	0.93167	0.99524	0.79984	0.993	0.61364	0.78608	0.88432	0.42244
35	0.49159	0.90039	0.91589	0.91512	0.84973	0.10853	0.56976	0.74274	0.44629
40	0.84306	0.88274	0.81952	0.92245	0.87125	0.82255	0.5752	0.70619	0.65555
45	0.53113	0.9026	0.54781	0.86371	0.67547	0.44728	0.73916	0.70148	0.66848
50	0.91785	0.97616	0.95815	0.94974	0.96365	0.46215	0.48468	0.71804	0.82839
55	0.54418	0.90542	0.83927	0.78365	0.7801	0.39902	0.54005	0.61165	0.6245

Number of Hidden layers	T,RH	T,WS	T,R	T,RS	RH,WS	RH,R	RH,SR	WS,R	WS,SR	R,SR
10	0.9961	0.98991	0.99243	0.98778	0.092637	0.70045	0.644	0.28003	0.66475	0.15103
15	0.95758	0.99106	0.97649	0.96383	0.50752	0.36946	0.35124	0.75692	0.73243	0.53976
20	0.99938	0.99971	0.99383	0.99885	0.90038	0.68474	0.73549	0.6652	0.81657	0.40208
25	0.89521	0.88654	0.9684	0.8244	0.31694	0.80637	0.12477	0.6042	0.23506	0.33761
30	0.98727	0.9891	0.98435	0.9958	0.329	0.843	0.81371	0.2833	0.70959	0.80036
35	0.98608	0.9856	0.97543	0.99149	0.087008	0.51091	0.59141	0.77443	0.76332	0.71755
40	0.98888	0.97041	0.98142	0.9958	0.20252	0.70195	0.53225	0.4377	0.51668	0.60893
45	0.94976	0.98651	0.94908	0.98489	0.19891	0.4193	0.53666	0.2604	0.60012	0.69796
50	0.9976	0.98638	0.97647	0.96152	0.81299	0.88621	0.12905	0.22658	0.59461	0.40015
55	0.85011	0.88017	0.9872	0.98418	0.66331	0.013579	0.71655	0.76087	0.77356	0.50216

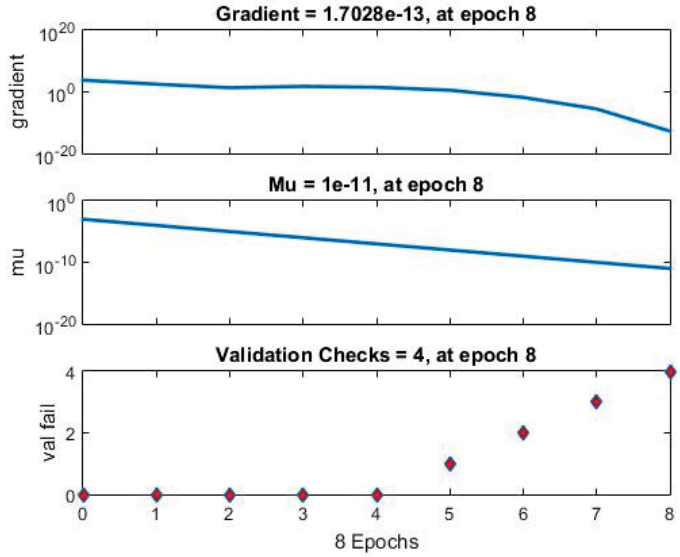

FIGURE 3
Variation of gradient error and validation checks for of the best performance model.

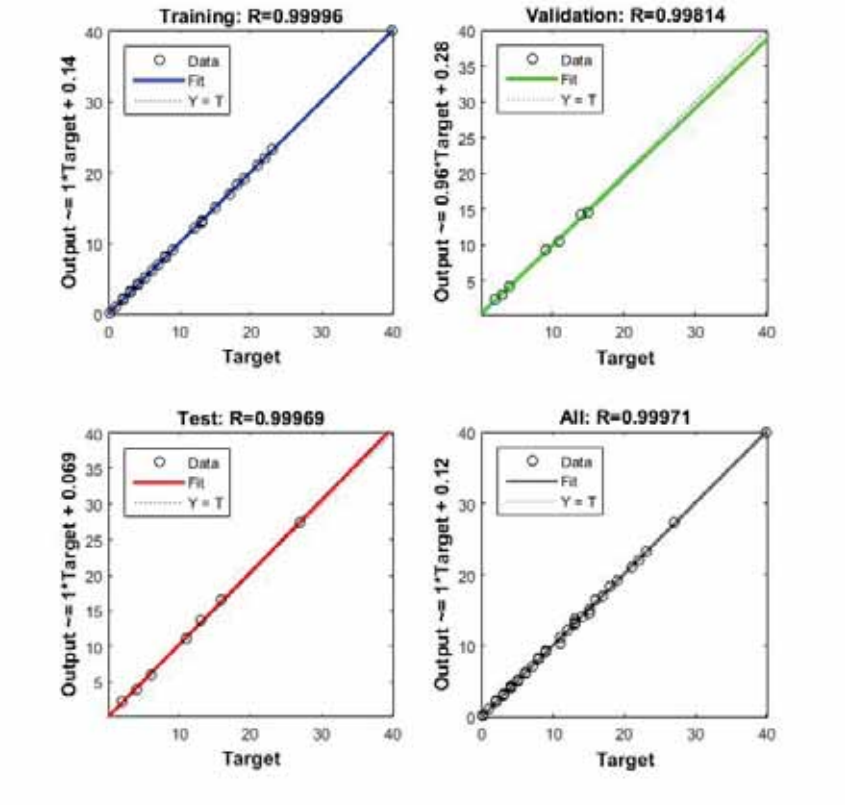

FIGURE 4
Scatter plots for the best performance model.

It is to be noted that, this result is in agreement with that outlined in Ref. [7].

Figure (3) shows the variation of the gradient error, validation checks, and value of μ for each epoch results produced by Elman model when using the average daily temperature (T) and wind speed (WS) as input parameters. It can be noticed from this, that using average daily temperature (T) and wind speed (WS) as inputs to Elman model, its trained converges faster than other models and the training truncated after 8 epochs.

The scatter plots of training, testing, and validation are shown in Figure (4), which shows quite close results of the scatter plot during training, validation, and testing of the COVID-19 active cases in Jordan using average daily temperature (T) and wind speed (WS) as an input for the training model. For

the Elman model when using the average daily temperature (T) and wind speed (WS) as input parameters, it was found that it has the highest values of R in training, validation, and testing, these values are 0.99996, 0.99814, and 0.99969 respectively. Also, the validation RMSE, validation MBE, training RMSE, and training MBE are 0.3524, 0.2880, 0.1466, and 0.1235 respectively.

CONCLUSION

In this study, three types of Artificial Neural Network (ANN), Elman, NARX, and Feedforward networks, were designed and tested using MATLAB software. The daily data of positive COVID-19 cases in Jordan was obtained from the Ministry of Health in Jordan, while the weather data were obtained from Jordan Metrological Department. Both data were used in the development process of the models to approximate and estimate the actual performance of proposed dynamical models in simulation. Statistical results are demonstrated to show the effectiveness of the proposed ANNs.

The comparative analysis of different training models using some basic statistics (R, RMSE and MBE) has been carried out. It was found that Elman model, when using average daily temperature and wind speed as the input to the network has the best predictive capability to positive COVID-19 cases, while Feedforward and NARX models have is the least predictive capability.

REFERENCES

[1] Ge, XY., Li, JL., Yang, XL., Chmura, A., Zhu, G., Epstein, J., Mazet, J., Hu, B., Zhang, W., Peng, C., Zhang, YJ., Luo, MC., Tan, B., Wang, N., Zhu, Y., Crameri, G., Zhang, SY., Wang, LF., Daszak, P., Shi, ZL. (2013). Isolation and characterization of a bat SARS-like coronavirus that uses the ACE2 receptor. Nature. 503503 (7477), 535–538.

[2] Huang, C., Wang, Y., Li, X., Ren, L., Zhao, J., Hu, Y., Zhang, L., Fan, G., Xu, J., Gu, X. (2020). Clinical features of patients infected with 2019 novel coronavirus in Wuhan, China. Lancet. 395 (10223), 497–506.

[3] Dalziel, B.D., Kissler, S., Gog, J.R., Viboud, C., Bjørnstad, O.N., Metcalf, C.J.E. (2018). Urbanization and humidity shape the intensity of influenza epidemics in U.S. cities. Science. 362(6410), 75–79.

[4] Yuan, J., Yun, H., Lan,W.,Wang,W., Sullivan, S.G., Jia, S., Bittles, A.H. (2006). A climatologic investigation of the SARS-CoV outbreak in Beijing, China. Am. J. Infect. Control. 34 (4), 234–236.

[5] Bull, G. (1980). The weather and deaths from pneumonia. Lancet. 315(8183), 1405–1408.

[6] Bukhari, Q., Jameel, Y., 2020. Will Coronavirus Pandemic Diminish by Summer? SSRN Electron. J. https://doi.org/10.2139/ssrn.3556998

[7] Tosepu, R., Gunawan, J., Effendy, D.S., Lestari, H., Bahar, H., Asfian, P. (2020). Correlation between weather and Covid-19 pandemic in Jakarta, Indonesia. Science of the Total Environment. 725. Article ID: 138436.

[8] Duojiao, T., and Bashir, M. (2020). Correlation between climate indicators and COVID-19 pandemic in New York, USA. Science of the Total Environment. 728. Article ID: 138835.

[9] Şahin, M. (2020). Impact of weather on COVID-19 pandemic in Turkey. Science of the Total Environment 728. Article ID: 138810

[10] Yueling, M., Yadong, Z., Jiangtao, L., Xiaotao, H., Bo, W., Shihua, F., Jun, Y., Jingping, N., Ji, Z. and Bin, L. (2020) Effects of temperature variation and humidity on the death of COVID-19 in Wuhan, China. Science of the Total Environment. 724. Article ID: 138226

[11] Cucinotta, D., Vanelli, M. (2020). WHO Declares COVID-19 a Pandemic. Acta Biomedica: Atenei Parmensis. 91(1), 157-160.

[12] Al-Quraín, S. (2008). Taxonomical and Pharmacological Survey of Therapeutic Plants in Jordan. Journal of Natural Products. 1, 10-26.

[13] Al-Naami, B., Abu Mallouh, M., Abdelhafez, E. (2014). Performance Comparison of Adaptive Neural Networks and Adaptive Neuro-Fuzzy Inference System in Brain Cancer Classification. Jordan Journal of Mechanical and Industrial Engineering. 8(5), 305 - 312.

Received: **02.08.2020**
Accepted: **26.01.2021**

CORRESPONDING AUTHOR

Mohammad Hamdan
The University of Jordan,
School of Engineering,
Department of Mechanical Engineering,
Amman 11942 – Jordan

e-mail: mhamdan@ju.edu.jo

© by PSP Volume 30– No. 05/2021 pages 4901-4910 Fresenius Environmental Bulletin

ANALYSIS OF CLIMATIC VARIATION AND DETECTION OF LAND USE CHANGES USING GEO-SPATIAL TECHNIQUES IN BAHAWALPUR DISTRICT, PAKISTAN

Tanveer Ahmed[1], Rab Nawaz[1,2,*], Alia Ahmed[1]

[1]Department of Environmental Management, National College of Business Administration and Economics (NCBA & E), Lahore, Pakistan
[2]Department of Environmental Sciences, The University of Lahore, Lahore, Pakistan

ABSTRACT

Climate change is directly related to our live-lihoods and needs to be studied in order to form mitigation and adaptation policies. Climate change is a global phenomenon and poses diverse implications in form and type for different ecologies. Human activities are greatly disturbing the nature through using the land for different types of anthropogenic activities like cultural, financial matters, environmental aspects, land policy and land development plans. The present study aims to analyze the climatic variation and assess the land use change of district Bahawalpur having total area of 24,830 km^2. Climatic data (minimum temperature, maximum temperature and rainfall) were collected for a period of 30 years (1989-2018). Monthly mean minimum and maximum temperature, annual rainfall, Diurnal Temperature Range (DTR) and their anomalies were calculated using secondary data for the study area. Land use data were collected in the form of Landsat satellite images of last 30 years (1990-2019) with 10 yeas interval from different online sources. Landsat ETM and ETM + satellite imagery were processed in ArcGIS software. Results showed that there is a great variation in maximum temperature anomaly during the entire study period. Minimum temperature anomaly shows positive and negative trend during the entire study period from 1989 to 2019. There is a great variation in DTR anomaly during the study period. 10-years moving average of DTR anomaly remained positive during most of the time. There is variation in annual rainfall anomaly, with both positive and negative values. As in the whole time span of 30 years, built-up land increased from 2.54% (631 Km^2) in 1990 to 4.66% (1,157 Km^2) at the end of 2019. Agricultural land use also increased from 3,439 Km^2 (13.85%) to 5,168 Km^2 (20.81%). Forest land use decreased from the 1,321 Km^2 (5.32%) to 775 Km^2 (3.12%) at end of 2019. Water occupied land with the high fluctuation was 109 Km^2 (0.44%) in 1990 and in 2019 it recorded 148 Km^2 (0.60%). The main land use class desert land also decreased from an area of 19,330 Km^2 (77.85%) to 17,582 Km^2 (70.81%). Correlation of land use change classes in last 30 years showed relationship intensity between different land use changes. Agricultural land and built up land have strong relationship with the value of 0.98. Desert land and agricultural land have strongly negative relationship with the value of -0.94. This study found how rapidly changes occurred in the land use with rate of land use change is a mile stone for the planners, researchers and scholars for the better understanding towards land use change in district Bahawalpur.

KEYWORDS:
Climate change, Land cover change, Agricultural land, Spatio-temporal change, Desertification

INTRODUCTION

Pakistan's economy largely depends on agriculture sector and is at risk due to climatic variability, changes in seasons of the country, droughts and large floods. Climate change may cause energy crisis, food insecurity and water scarcity in the country. Now a days, desertification and land deterioration are also critical global issues. But in Pakistan they are more damaging as three fourth of the total area has already been affected or at the risk to get affected. There are so many factors which are leading to desertification and land deterioration, but population explosion is significant cause [1]. Land cover on the regional and global scale climate has a huge impact. Land-use change accelerates the emission of carbon dioxide into the atmosphere through soil disturbance. Vegetation reduction due to deforestation and burning in agricultural activities result in the release of carbon from the crop again and again [2, 3]. It is also found that land use changes in land surface are caused by non-native animals, plants and diseases that spread and change primary biodiversity [4]. Land use change is the use and change of the earth surface by human. Forecasting land use change and predicting the consequences of the land use change are based on the skills of the researcher [5-6]. Land use change detection and mapping by Remote Sensing Techniques is more accurate and helpful for researcher in predicting the

urban growth pattern by applying different kinds of analysis [7]. Remote sensing and geographic information system approaches are very important techniques and tools to identify the urban land use change. Such techniques are also applied at world level for land use change detection. Land cover term refers to the biological and physical cover on the land surface including plans, mountains, forests and structures, resulted by anthropogenic activities [8-9]. Remote sensing is very necessary tool to observe the land use change because it is more reliable than other earth surface based observation systems. Remote sensing accomplished by different types of cameras, scanners, sensors, which are fixed on the space and air born platforms, gathers information by aerial photography in form of satellite images and LIDAR and RADAR data sets. Remote sensing data vary from time to time and space to space on the basis of the ground reality, different resolution and height of the sensors. In remote sensing, data collected by some sensors and cameras like IKONOS, Quick bird, LIDAR, RADAR, MODIS, LANDSAT and SPOT is used for different type of analysis [10]. This study was conducted to observe the climatic changes and land use changes in Bahawalpur city of Punjab Province of Pakistan. It is important to see the changes that have occurred due to climate change and propose sustainable solutions and recommendations.

MATERIALS AND METHODS

Study Area. The present research has been carried out to detect land use change under climatic variability in semi-arid area of Bahawalpur district using geo-spatial techniques. This study has been conducted in District of Bahawalpur (Figure 1). After 1727, the Kingdom of Bahawalpur was founded by his ruler Amir Sadiq Muhammad Khan with an area of 24,830 square kilometers. Bahawalpur is the 12th largest city in the Punjab province of Pakistan. Bahawalpur lies between the latitude of (29◦ -21 'to 29◦-25') north and (71◦-36 'to 71-46') east. Bahawalpur is the southernmost part of the province. The altitude from sea level is 152 meters [11]. The climate is very hot and dry during summer with cold and dry in winter. The mean maximum temperature of the area is 44 with mean minimum temperature 28 centigrade. Dust storms are often frequent during the summer season. Annual precipitation is 125 to 200 millimeters, which usually occurs in the months of July and August in moon soon season with average rainfall of 10 to 25 cm [2].

Data Collection. The present research comprised of last 30 years. The climatic data (maximum temperature, minimum temperature, rainfall) was collected from Pakistan Meteorological Department (PMD) from 1989 to 2018, located in Shadman Colony, Lahore. Land use data was collected for 30 years (1990 to 2019). Satellite images of Landsat Enhanced Thermal Mapper and ETM+ were downloaded from Global Land Cover Facility, United States Geological Survey's Earth Explorer with equal time intervals. Four satellite images from 1990 to 2019 with the interval of ten years were collected (Table 1).

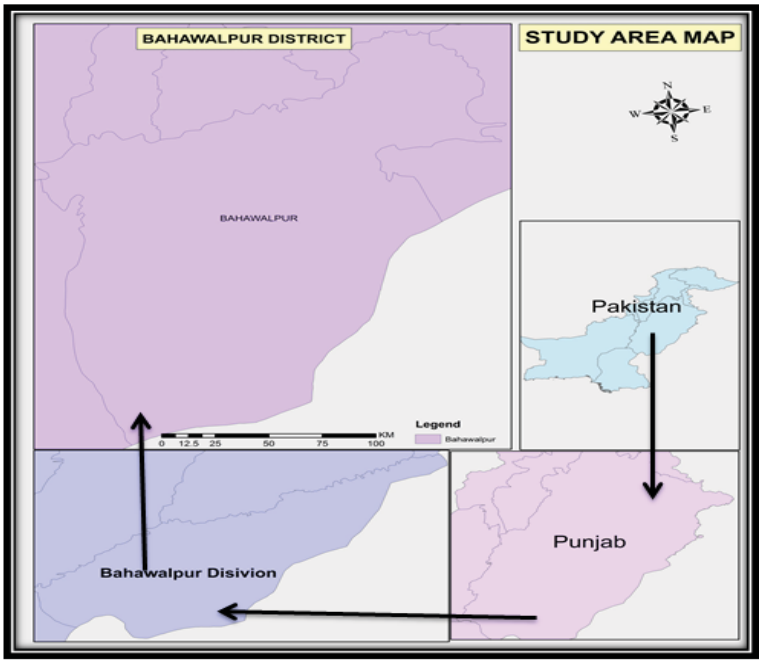

FIGURE 1
Map showing study area of Bahawalpur

TABLE 1
Satellite Images Details

Satellite Sensor	Path Number	Raw Number	Acquisition Date	Resolution
Landsat 5 TM	150	39,40,41	December 03, 1990	30 Meter
Landsat 7 ETM+	150	39,40,41	December 23, 2000	30 Meter
Landsat 7 ETM+	150	39,40,41	December 03, 2010	30 Meter
Landsat 8 OLI	150	39,40,41	October 22, 2019	30 Meter

Image classification. These images were used to detect the land use change in the different time spans and also calculated that how much land use was changed in the study area. For this purpose, different remote sensing techniques e.g., layer stacking, image classification and class differencing calculation were used. Historical imagery was used to analyze the land use pattern of the study area. Spatio-temporal increase and decrease in the specific class of the land use or land cover were measured in ArcMap10.5 software. Satellite images and their acquisition date with path /raw and resolution details are given in table 1 [12]. Name of different classes and their description is given in table 2. Figure 2 represents methodological frame work used in detection of land use change in the study area.

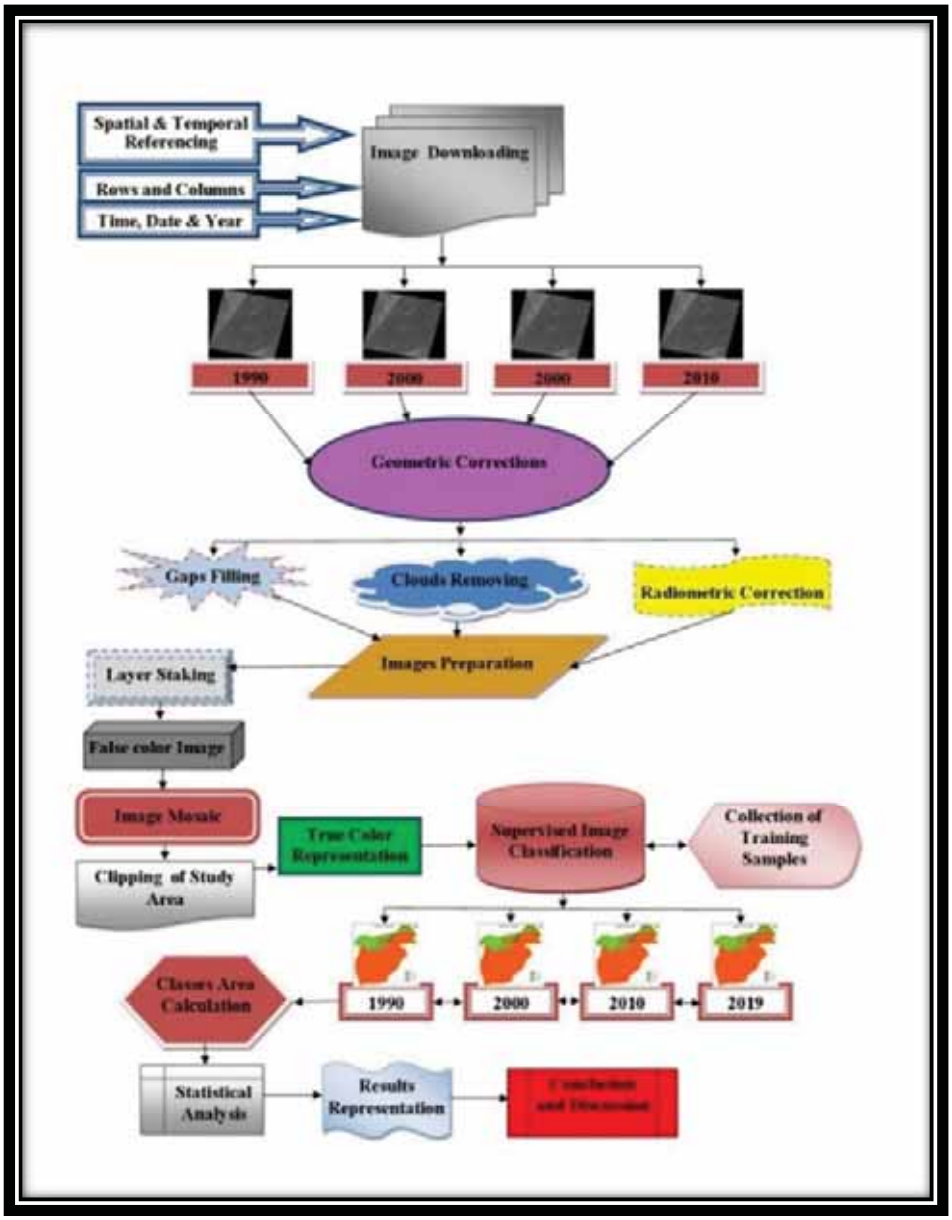

FIGURE 2
Methodological frame work of detection of land use change

TABLE 2
Classes detected in supervised classification

Sr. No.	Name of class	Description
1	Built-up land	Residential, commercial , rods and mixed urban land
2	Desert land	Desert land and barren land of the Cholistan
3	Agricultural land	Crop filed and agricultural forms
4	Forest land	Forest land and tree covered area like roads sides, river sides etc.
5	Water land	River, canals and lakes

Statistical Analysis. Microsoft Excel was used to calculate monthly mean minimum and maximum temperature, annual rainfall and Diurnal Temperature Range (DTR) for the study areas. Anomalies for temperature and precipitation was also calculated using MS excel. Different graphs and charts were also prepared. Following parameters were calculated using data;

- Annual Mean Minimum Temperature Anomaly = Annual Mean Minimum Temperature for a year - Annual Mean Minimum Temperature for 30 years
- Annual Mean Maximum Temperature Anomaly = Annual Mean Maximum Temperature for a year - Annual Mean Maximum Temperature for 30 years
- Minimum Temperature 10-Years Moving Anomaly = Average of Last 10 Years Annual Mean Minimum Temperature Anomaly
- Maximum Temperature 10-Years Moving Anomaly = Average of Last 10 Years Annual Mean Maximum Temperature Anomaly
- Diurnal Temperature Range (DTR) = Mean Maximum Temperature – Mean Minimum Temperature
- Diurnal Temperature Anomaly = Annual Mean DTR for a year - Annual Mean DTR for 30 years
- DTR 10-Years Moving Anomaly
- Annual Total Rainfall Anomaly = Annual Total Rainfall for a year - Annual Total Rainfall for 30 years
- Annual Rainfall 10-Years moving Anomaly = Average of Last 10 Years Annual Rainfall Anomaly

Correlation was calculated to check the relationship between the land use change classes' values from 1990 to 2019 [13]. Following equation was used to find the correlation between different categories of land use;

$$r_{xy} = \frac{\sum_{i=1}^{n}(x_i - \bar{x})(y_i - \bar{y})}{\sqrt{\sum_{i=1}^{n}(x_i - \bar{x})^2 \sum_{i=1}^{n}(y_i - \bar{y})^2}}$$

Where:

- $r_{xy,}$ represents correlation relationship between the variables x and y
- $x_{i,}$ represents x-variable values
- $\bar{x}$, represents mean of x-variable values
- $y_{i,}$ represents values of y-variable
- $\bar{y}$, represents mean of the of y-variable values

RESULTS AND DISCUSSIONS

Variation in Annual Maximum Temperature. Figure 3 shows mean annual maximum temperature for Bahawalpur for a period of 30 years (1989-2018). It also presents 10-years moving average of mean annual maximum temperature. There is a great variation in maximum temperature anomaly during the entire study period. 10-years moving average of maximum temperature anomaly remained positive between 2001 and 2012, reached maximum (0.58) in 2006.

Variation in Annual Minimum Temperature. Figure 4 shows mean annual minimum temperature for Bahawalpur for a period of 30 years (1989-2018). It also presents 10-years moving average of mean annual minimum temperature anomaly. Minimum temperature anomaly shows positive and negative trend during the entire study period from 1989 to 2019. 10-years moving average of minimum temperature anomaly remained negative till 2005. Maximum 10-years moving average of minimum temperature anomaly was found to be around 0.14 ^{o}C in 2007 and 0.16 ^{o}C in 2018.

Diurnal Temperature Range. Diurnal temperature range (DTR) is measured as the dissimilarity between annual maximum temperature and annual minimum temperature. Figure 5 shows diurnal temperature range (DTR) anomaly for Bahawalpur for a period of 30 years (1989-2018). It also presents 10-years moving average of DTR. There is a great variation in DTR anomaly during the study period. 10-years moving average of DTR anomaly remained positive during most of the time. Shifting of season is due to climate change which damages not only crops but also the habitats [14]. This season shifting and severity of weather badly affect maturation cycle of the crops, which in turn lower the crop yield [15].

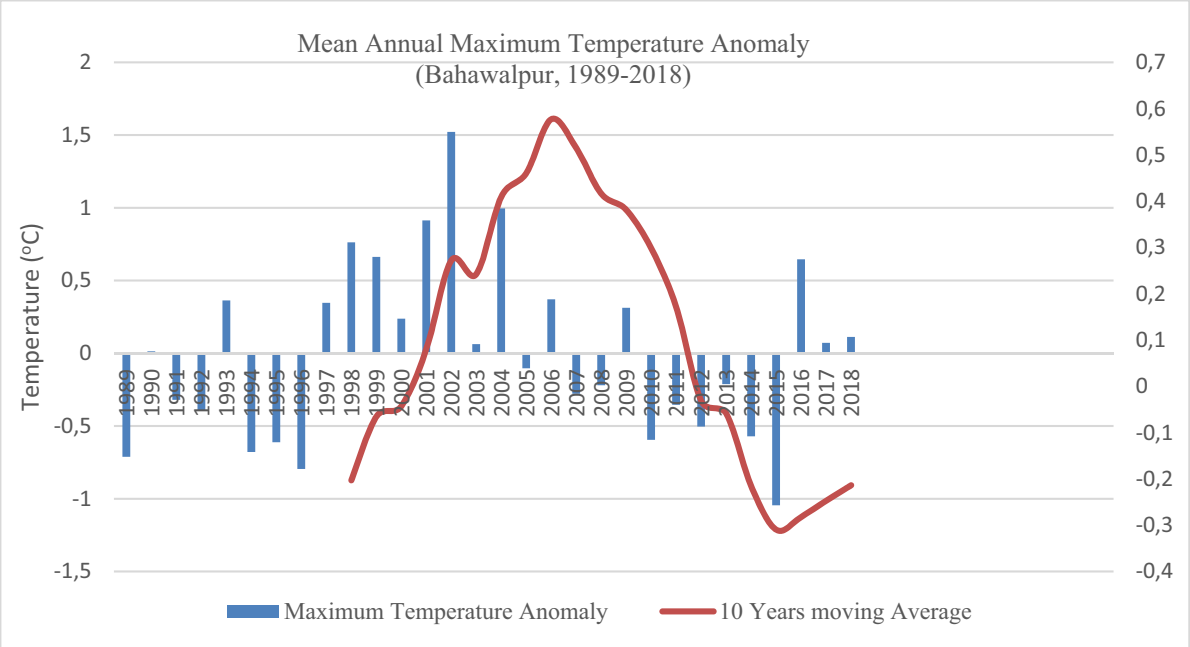

FIGURE 3
Mean annual maximum temperature anomaly with 10-years moving average in Bahawalpur from 1989-2018

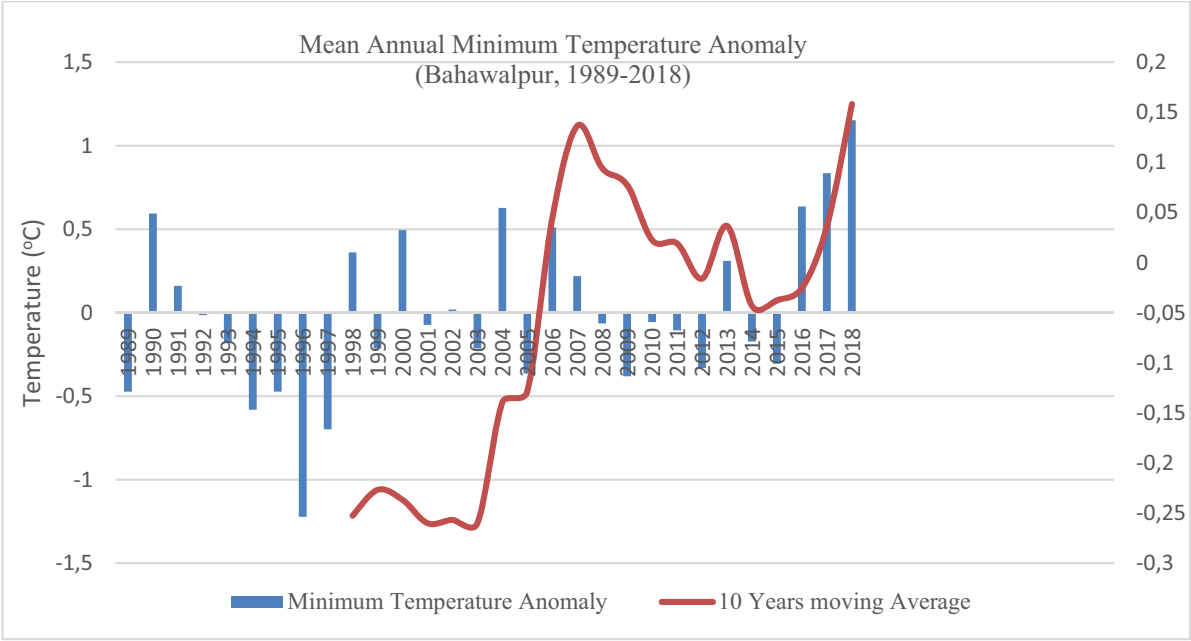

FIGURE 4
Mean annual minimum temperature anomaly with 10-years moving average in Bahawalpur from 1989-2018

Variation in Annual Rainfall. Annual rainfall anomaly for Bahawalpur for a period of 30 years (1989-2018) is presented in the Figure 6. It also shows 10-years moving average of annual rainfall. There is variation in annual rainfall anomaly, with both positive and negative values. 10-years moving average of annual rainfall anomaly remained positive before 2002, became negative between 2002 and 2010 and became positive again from 2012 and onwards.

Land Use Classes from 1990 to 2019. Table 3 shows area of different land use classes during the study duration of 30 years. In 1990, built up land class was comprised of an area of 631 km^2 (2.54%) of total land, desert land was spread on an area of 19,330 Km^2 (77.85%) of land, agricultural land was covering 3,439 km^2 (13.85%), forest land was on an area of 1,321 km^2 (5.32%) of total land and water bodies was spread on an area of 109 km^2 (0.44%). Land use changes assessed in year 2000 like, built-

up land changed as 894 km^2 (3.60%) of total land, desert land changed as 19,131 km^2 covering 77.05%, agricultural land was 4,229 km^2 (17.03%), forest land was detected as 532 km^2 (2.16%) and water land became 39 km^2 (0.16%). In 2010, land use change detected as built-up land was 1018 km^2 (4.10%), desert land changed as 17,877 km^2 (72.00%), agricultural land became 4,929 km^2 (19.85%), forest land covered 962 km^2 (3.87%) of area and water land changed as 44 km^2 (0.18%). After the last decade in 2019, land use change observed as built-up land was detected as 1,157 km^2 (4.44%) of the total area, desert land was detected as an area of 17,582 km^2 (70.81%) of total land, agricultural land became 5,168 km^2 (20.81%), forest land was found with an area of 775 km^2 (3.12%) of total land and water land changed as 148 km^2 with 0.60% of the total land. Area of different land use classes from 1990 to 2019 is shown in Figure 7.

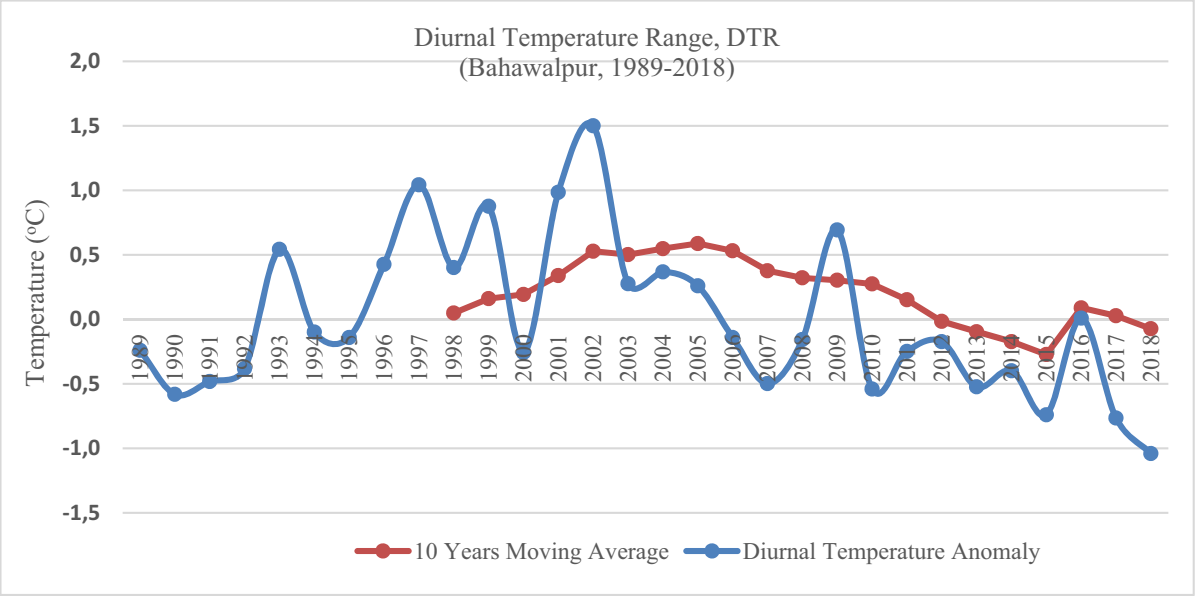

FIGURE 5
Diurnal temperature range anomaly with 10-years moving average in Bahawalpur from 1989-2018

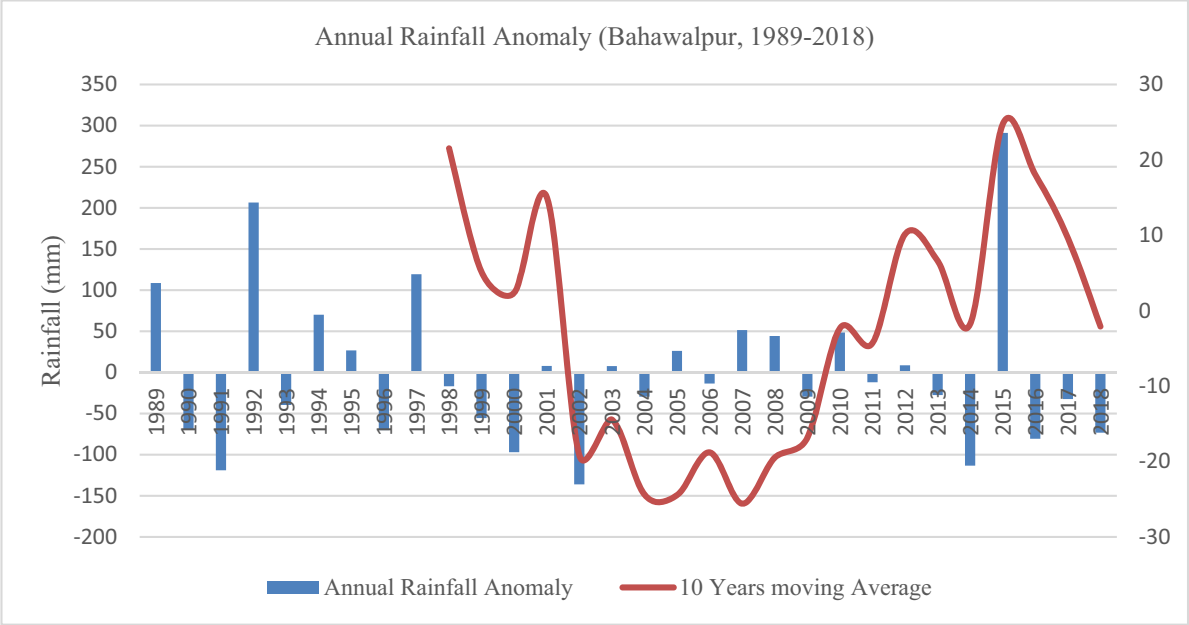

FIGURE 6
Annual rainfall anomaly with 10-years moving average in Bahawalpur from 1989-2018

TABLE 3
Land use change from 1990 to 2019

Land Use	1990		2000		2010		2019	
	Area (Km^2)	%	Area (Km^2)	%	Area (Km^2)	%	Area (Km^2)	%
Built-up land	631	2.54	894	3.60	1,018	4.10	1,157	4.66
Desert land	19,330	77.85	19,131	77.05	17,877	72.00	17,582	70.81
Agricultural	3,439	13.85	4,229	17.03	4,929	19.85	5,168	20.81
Forest land	1,321	5.32	537	2.16	962	3.87	775	3.12
Water land	109	0.44	39	0.16	44	0.18	148	0.60
Total	**24,830**	**100**	**24,830**	**100**	**24,830**	**100**	**24,830**	**100**

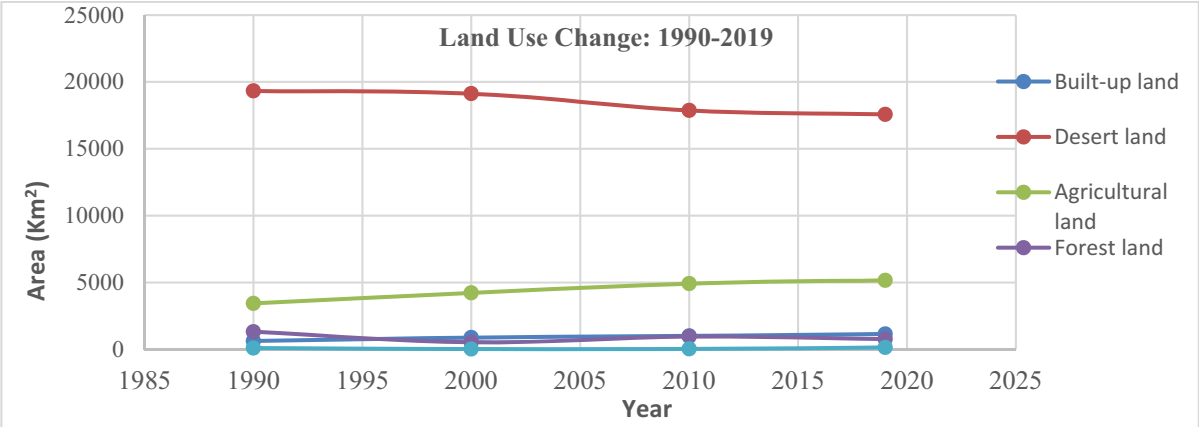

FIGURE 7
Classified Land use change maps of 1990 to 2019

Mapping of Land Use Classes from 1990 to 2019. Figure 8 shows different land use classes on maps of Bahawalpur from 1990 to 2019. Changes in the land use are happening rapidly which may cause changes in compositions of animal diets and population of species due to depletion of rangelands [16]. There is need to formulate and implement adaptation strategies in southern Punjab to minimize impacts of extreme climatic conditions.

Percent Land Use Change. Table 4 shows the percentages increase and decrease of all land use change classes from 1990 to 2000. Results indicated that built-up land increased by 1.06% while desert land decreased by 0.8% in first decades from 1990 to 2000. Agricultural land increased by 3.18% but forest land decreased by 3.16%. There was a decrease of -0.28% in water bodies. Changes in precipitation and rise in temperature are affecting availability of water and causing stresses for crops with adverse effects on yield of crops, farmers' income, and poverty. There is need to reconsider management strategies in agriculture under changing conditions. Crop selections according to climatic changes might cause land use change in developing countries [17].

Table 4 shows the percent land use change in all the classes from 2000 to 2010. Change has been observed as built-up land increased by 0.5 %, desert land decreased by 5.05%, agricultural land increased by 2.82%, forest land increased by 1.71% and water land increased by 0.02% in this period. Agricultural and food production sector is also facing impacts of varying climate. Climatic extremes, such as droughts, may cause food scarcity, further causing an increase in prices of food in recent years. It was found that droughts had been taking place in areas, which are suitable for crop production, turning them into less favorable areas. Climate change can be a biggest threat for the agriculture sector [18]. Table 4 shows the percent change in land use change in classes from 2010 to 2019. In this time span, built-up land increased by 0.56% but desert land decreased by 1.19%. Agricultural land increased by 0.96% and forest land decreased by 0.75% with increased in water land by 0.43%. Different behavioral and structural factors are responsible for land use changes that affect the nature of environment of interest [19]. Climate change is also affecting land use change [20].

Correlation between Land Use Classes from 1990 to 2019. Correlation matrix elaborates the relationship of different kinds of land use changes from 1990 to 2019 (Table 5). Matrix of correlation shows that built up land has strong negative correlation with desert land with a value of r = -0.90 and built-up land has a strong positive rela-

tionship with the agricultural land with a value of r = 0.98. Built-up land has negative relationship with forest land with a value of r = -0.61 and slightly positive with water land under value of r = 0.14. Desert land has strong negative relationship with agriculture land with value of r = -0.94. Matrix showed positive relationship between desert land and forest land with a value r = 0.22. Desert land showed also negative relationship with water land value r = -0.29. Matrix showed the negative value of r = -0.52 between agricultural land and forest land. At the end forest land has near moderate positive value of r = 0.30 with water land.

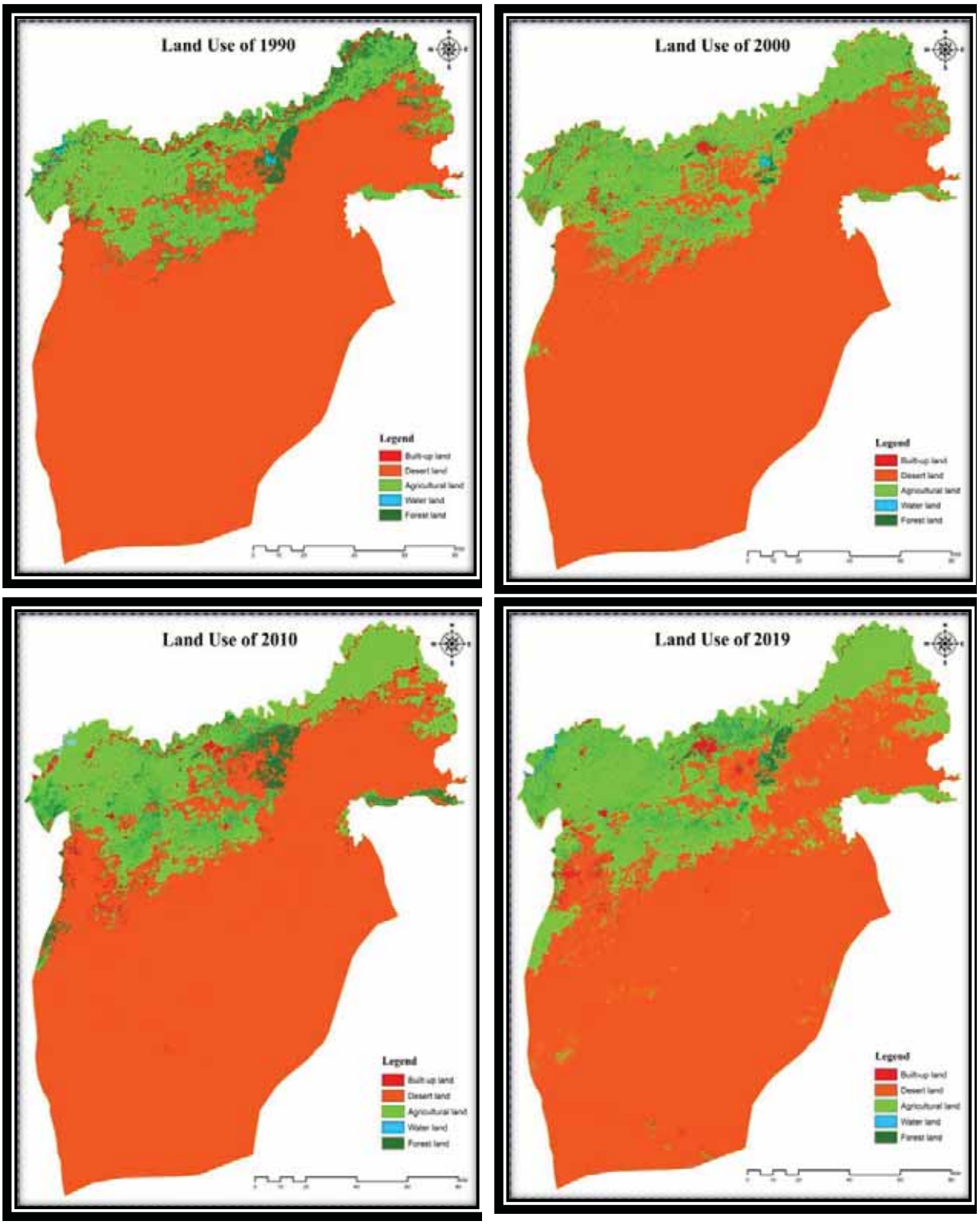

FIGURE 8
Classified Land use change maps from 1990 to 2019

TABLE 4
Percent Land use change from 1990 to 2019

	Area (%) of Land Use Classes			Area (%) of Land Use Classes			Area (%) of Land Use Classes		
Class	1990	2000	Percentage Change	2000	2010	Percentage Change	2010	2019	Percentage Change
Built-up land	2.54	3.60	1.06	3.60	4.10	0.50	4.10	4.66	0.56
Desert land	77.85	77.05	-0.80	77.05	72.00	-5.05	72.00	70.81	-1.19
Agricultural land	13.85	17.03	3.18	17.03	19.85	2.82	19.85	20.81	0.96
Forest land	5.32	2.16	-3.16	2.16	3.87	1.71	3.87	3.12	-0.75
Water land	0.44	0.16	-0.28	0.16	0.18	0.02	0.18	0.60	0.42

TABLE 5
Correlation matrix calculated between classes from 1990 to 2019

	Built-up land	Desert land	Agricultural land	Forest land	Water land
Built-up land	1				
Desert land	-0.90	1			
Agricultural land	0.98	-0.94	1		
Forest land	-0.61	0.22	-0.52	1	
Water land	0.14	-0.29	0.09	0.31	1

CONCLUSION

A great variation in maximum temperature anomaly was observed during the entire study period. Minimum temperature anomaly shows positive and negative trend during the entire study period from 1989 to 2019. A great variation in DTR anomaly was found during the study period. 10-years moving average of DTR anomaly remained positive during most of the time. There is variation in annual rainfall anomaly, with both positive and negative values. On the basis of results of this study obtained by the geo-spatial techniques, it is concluded that land use change occurred with significant pressure and altered the land use areas in last 30 years. In land use changes comparison, agricultural land use increased from 13.85% to 20.81%. Forest land use decreased from 5.32% in 1990 to 3.12% in 2019. Water land was 0.44% in 1990 and increased to 0.60% in 2019. Desert land also decreased from 77.85% in 1990 to 70.81% in 2019. Built-Up land increased from 2.54% in 1990 to 4.66% 2019. Agricultural land and built up land had a very strong positive correlation (r = 0.98). It means that these two types of land uses have strong influence on each other. Forest land has a slightly positive relationship with two other land uses, desert land (r = 0.22) and water land (r = 31). Water management policies should be lunched for the management of the intense fluctuation of water land use. There should be tree plantation by the concerned government departments in this area with the collaboration of local people and non-governmental organizations. Government must implement regulations and policies regarding protection of trees.

ACKNOWLEDGEMENTS

The authors gratefully acknowledge the Department of Environmental Management, National College of Business Administration and Economics (NCBA & E) for the support of this research project. Thanks are extended to Pakistan Meteorological Department (PMD) and United States Geological Survey (USGS) for providing access to the research data. Authors also thank experts for reviewing the manuscript and giving useful suggestions during this study. The authors declare that there is no potential conflict of interest. This research article is a part of dissertation of first author, a student of Ph.D. Program in Environmental Management at NCBA & E Lahore, Pakistan.

REFERENCES

[1] MoCC (2013) The Environment and Climate Change Outlook of Pakistan. Ministry of Climate Change (MoCC). Government of Pakistan (GoP) and United Nations Environment Program (UNEP). 1-25. http://www.mocc.gov.pk/moclc/userfiles1/file/ECCO/exectiv-sumery.pdf (Accessed on 25.06.2019)

[2] Ahmed, T., Shakeel, M., Khalid, S., Ali, A. (2015) Change of Agricultural Land Use in Residential Land and Its Impact on the Socio-Economic Status of the Farmer in Bahawalpur City. Asian Journal of Social Sciences & Humanities: 4, 3.

[3] Foresman, T.W., Pickett, S.T., Zipperer, W. C. (1997) Methods for spatial and temporal land use and land cover assessment for urban ecosystems and application in the greater Baltimore-Chesapeake region. Urban Ecosystems. 1(4), 201-216.

[4] Foley, J.A., DeFries, R., Asner, G. P., Barford, C., Bonan, G., Carpenter, S. R., Gibbs, H. K. (2005) Global consequences of land use. Science. 309(5734), 570-574.

[5] Rindfuss, R. R, Walsh, S. J., Turner, B. L., II, Fox, J., Mishra, V. (2004) Developing a science of land change: Challenges and methodological issues. Proceedings of the National Academy of Sciences of the United States of America. (39), 13976-13981.

[6] Egbenta, R. I. (2009): Analysis of Residential Land Use Change in Enugu Urban. Journal of Environmental Management and Safety. 1(1), 110-123.

[7] Kombe, W.J. (2005): Land use dynamics in peri-urban areas and their implications on the urban growth and form: the case of Dar es Salaam, Tanzania. Habitat International. 29, 113–135.

[8] Ellis, E., and Pontius Jr, R. (2006) Land-use and land-cover change—encyclopedia of earth. Environ. Protect. 2, 142-153.

[9] Thakkar, A. K., Desai, V. R., Patel, A., Potdar, M. B. (2017): Post-classification corrections in improving the classification of Land Use/Land Cover of arid region using RS and GIS: The case of Arjuni watershed, Gujarat, India. The Egyptian Journal of Remote Sensing and Space Science. 20(1), 79-89.

[10] Ellis, E., and Pontius, R. (2013): Land-use and land-cover change. Environmental Information Coalition, National Council for Science and the Environment. 5. Page No. 1-4.

[11] Javed, N.I.A. (2010). Bahawalpur City Profile. Retrieved from www.urbanunit.gov.pk/ (Accessed on 13.08.2019)

[12] Kangabam, R.D., Selvaraj, M., Govindaraju, M. (2019) Assessment of land use land cover changes in Loktak Lake in Indo-Burma Biodiversity Hotspot using geospatial techniques. The Egyptian Journal of Remote Sensing and Space Science. 22(2), 137-143.

[13] Haque, M. I., Basak, R. (2017): Land cover change detection using GIS and remote sensing techniques: A spatio-temporal study on Tanguar Haor, Sunamganj, Bangladesh. The Egyptian Journal of Remote Sensing and Space Science. 20 (4), 251-263.

[14] Bates, B.C., Kundzewicz, Z.W., Wu, S., Palutikof, J.P. (2008): Climate Change and water. IPCC Technical Paper VI, Geneva. [Online]. 1-136. Retrieved from https://www.ipcc.ch/site/assets/uploads/2018/03/climate-change-water-en.pdf (Accessed on 17.2.2019)

[15] Vikas, K.S. (2012): Climate Change and its impact on agriculture: A review. International Journal of Agricultural Environment Biotech. 5(3), 297-302.

[16] PILDAT. (2016): Development in the Livestock and Dairy Development Sector Punjab, Pakistan. Background Paper. Pakistan Institute of legislative Development and Transparency. Page 1-162.

[17] Rounsevell, M.D.A., Evans, S.P., Bullock, P. (1999): Climate change and agricultural soils: impacts and adaptation. Climate Change. 43, 683–709.

[18] Rosenzweig, C., Parry, M.L. (1994) Potential impact of climate change on world food supply. Nature. 367, 133-138.

[19] Verburg, P.H., van Eck, J.R., de Hijs, T.C., Dijst, M.J., Schot, P. (2004) Determination of land use change patterns in the Netherlands. Environment and Planning B - Planning and Design. 31, 125–150.

[20] Dale, V. H. (1997) The relationship between land-use change and climate change. Ecological Applications. 7(3), 753-769.

Received: **03.08.2020**
Accepted: **06.02.2021**

CORRESPONDING AUTHOR

Rab Nawaz
Department of Environmental Sciences,
The University of Lahore,
Lahore – Pakistan 54000

e-mail: rab.nawaz@envs.uol.edu.pk

© by PSP Volume 30– No. 05/2021 pages 4911-4920 Fresenius Environmental Bulletin

STUDY ON ENVIRONMENTAL PERFORMANCE EVALUATION OF GREEN BUILDING BASED ON BIM TECHNOLOGY

Sen Xu*

Management School, Xi'an University of Finance and Economics, Xi'an, Shaanxi 710100, P.R. China

ABSTRACT

The main goal of green building is to address the issue of how energy savings can improve water efficiency, increase application capacity, and ensure that the region's built and natural environments develop together. The indoor and outdoor environmental performance of green building is the research object of this paper, and the feasibility and rationality of the application of BIM technology in the green building environmental performance evaluation system is discussed. Green building indoor and outdoor wind, sound and indoor light environment green indicators are established, BIM technology is used to carry out parametric modeling through data conversion. 3D models within the relevant simulation tools to carry out a variety of performance tests, the use of BIM technology to carry out the assessment of specific aspects and methods are summarized. Based on the proposed evaluation process, the environmental performance of the project, including outdoor wind environment, outdoor acoustic environment, indoor natural ventilation and indoor natural lighting is analyzed and evaluated based on the project case. The results are of great significance to the establishment and improvement of the green building environmental performance evaluation system.

KEYWORDS:
Green building, energy savings, environment, feasibility, BIM technology, performance

INTRODUCTION

The extreme shortage of energy, and the worsening environment have brought great challenges to the sustainable development of the global economy in the 21st century [1-5]. Among many energy consumption fields, the energy consumption of the construction industry accounts for about half [6]. While improving the daily life quality of the general public, how to build a harmonious, stable and long-term development of the construction industry is an important way to ensure that the industry's resource consumption is reduced [7,8]. To comprehensively solve the practical problems encountered in the industry, excessive building energy consumption is a problem that will be encountered in the social and economic development ,and must be dealt with [9]. People also pay more and more attention to the sustainable use of construction resources and environmental protection, and formulate a series of standards and regulations, focusing on the development of green buildings [10,11].

Bossink et al. proposed that construction waste is a large part of garbage, which should be paid enough attention by all walks of life [12]. In 2003, the British Energy Agency first pointed out the low-carbon economy plan [13]. Kumar et al. proposed to use the Fourier transform (FFT) technology in MATLAB to write the simulation code of building roof, and use the simulation code to carry out component simulation [14,15]. In 2008, through the interpretation of the above evaluation system, Germany issued the DGNM evaluation system in combination with its national conditions [16]. For the first time, it comprehensively calculated the building carbon emissions, and summarized the perfect statistical methods. The neural network was used to predict the loss of building thermal parameters after they are known, which has a positive impact on the development of energy conservation in the industry [17]. Liu et al. studied the control forms of the construction industry, estimated the loss of this industry, and evaluated the impact of different regulatory forms on the loss [20]. Cai et al. used BIM to analyze and discuss the design and performance research of buildings in the industry [21]. Wang et al. integrated BIM Technology with regional building development, and used the technology to evaluate and optimize the design of construction industry [22,23].

With the rapid development of green building in the domestic construction industry, most developers do not really understand the concept of green building, but instead, at the cost of high consumption of the project's internal space of constant temperature and humidity, space, supernatural high comfort features advertised as green building, thus eventually forming a high consumption, high waste, high pollution of pseudo-green building [24]. The development and application of green building evaluation system has solved such social problems to a great extent. It is mainly to reasonably determine the quantitative

requirements and evaluation system of building "green", standardize the industrial development efficiently, and publicize the advantages and future trend of this kind of building form. In this paper, the current situation of green building at home and abroad, as well as the problems in the design period and environmental research period are studied. BIM Technology is used to explore the actual impact of green building environment. The application mode of green design is verified by the research results of practical cases.

MATERIALS AND METHODS

Using BIM technology to create a full-fidelity simulation of the building model, the environmental factors corresponding to the green goals of the project decision period are selected for simulation and analysis. This paper uses Autodesk Revit software to create the BIM model, then the model is transferred to Autodesk Ecotect, Swell Vent 2014, Cadna/A software, through the data interface [25]. The basic environmental performance of the case project is analyzed, and through the analysis of the simulation results and the comparison of the two project design objectives, the design phase defects are identified and optimized.

Green building environmental assessment process. (1) Establishment of BIM model. An important prerequisite for carrying out BIM research activities is the use of BIM modeling software to create a dynamic 3D model that includes all of the external shape, size, material type, facility type, etc. Before analysis, structural analysis of the model is required to ensure the accuracy of the model. (2) Definition of boundary conditions. Boundary conditions refer to the software parameters of environmental performance analysis, such as building height, surrounding road information, pedestrian height, indoor house type map and local climatic conditions. In BIM software analysis, boundary conditions need to be calculated and integrated with tools to provide data support for simulation environment performance. (3) Green building environment performance analysis. Simplify the model, complete the transformation through the data transmission interface, and then check the simple model in the software to supplement the building information lost in the transmission process. The object and content of the simulation are clearly defined, and the indoor and outdoor environmental performance simulation is carried out with boundary conditions as simulation parameters. (4) Simulation Results Processing. The final results of indoor and outdoor environmental performance simulations based on BIM green analysis software are expressed in the form of cloud diagrams , and integrated data sheets.The results are intuitive, easy to understand, and easy to compare directly with the corresponding standards and specifications.

Comprehensive evaluation of green building environmental performance. In the comprehensive evaluation of the above environmental performance, it is necessary to score each single performance index, and use the comprehensive weight coefficient to complete the statistics. The evaluation grade of the buildings to be evaluated is divided into: unqualified, qualified, medium, good, excellent, and each evaluation grade gives different rating standards [26]. By looking up the table, the weight B and the score V of the single evaluation element were calculated, and the comprehensive score of the item was obtained by substituting into equation (1):

$$G = \sum_{i=1}^{n} B_j V_j \tag{1}$$

Where, G is the overall score of green building environmental performance assessment. Bj is the weight of the J index factor. Vj is a separate score for the J index factor. In practice, there will still be one point difference without meeting the design level or specification requirements. Therefore, the membership function, which is simple and easy to use, is adopted to fuzzy the clear boundary of the grade and evaluate the green design degree of the building object with its results [27]. The grade of green building environment performance is usually divided by the interval of points, as shown in Table 1. The fuzzy level of grade i control is ai, which belongs to degree function, as shown in equation (2) and (3).

$$\mu_1 = \begin{cases} 1, & a \le a_2 \\ \dfrac{a - b_2}{a_2 - b_2}, & a_2 < a < b_2 \\ 0, & other \end{cases} \tag{2}$$

$$\mu = \begin{cases} 1, & a_i \le a_{i+1} \\ \dfrac{a - b_{i-1}}{a_i - b_{i-1}}, & b_{i-1} < a < a_i \quad i = 2,3...n-1 \\ \dfrac{a - b_{i+1}}{a_{i+1} - b_{i+1}}, & a_{i+1} < a < b_{i+1} \\ 0, & other \end{cases} \tag{3}$$

TABLE 1
Original classification

Grade	*A*	*B*	*C*	.....	*I*
Evaluation interval	(a_1,a_2)	(a_2,a_3)	(a_3,a_4)	.....	(a_i,a_{i+1})
Median value	b_1	b_2	b_3	.....	b_i

RESULTS

Project overview. The project is a residential and supporting business of plot S in the subordinate area of Xi'an city. The project has a large span with a total of 10 pieces of land. The construction contents are mainly residential, commercial, residential centers, schools and game parks of various specifications. Kindergartens, middle schools and commercial equipment are to be built in the north of the site, with a comprehensive area of 42806m2 and a total project area of 126542.38m2. Residences are planned for the south and east, and central Park is planned for the west. About 500 meters to the south of the site is xi 'an North Ring Highway, and about 250 meters to the southeast of the site is a high-speed toll station. The high-speed land has a shelter forest of 50 meters between the residential land, and the project is far from the expressway directly, with little impact of relevant noise. The project is carried out in accordance with the three-star green building assessment in China.

Modeling based on BIM technology. Through the full modeling of the project by BIM software and importing green software, the overall outdoor wind environment and acoustic environment of the project are simulated and analyzed. Firstly, the CAD drawings of the general layout plan are imported into the Autodesk Revit software to locate the project. Then, the volume concept of the Autodesk Revit software isused to simulate the building volume. Finally, the external wall and other parts are defined,get the distribution of the basic residential buildings in the project area.

By setting the sun path to the project location and determining the time period of project analysis in Revit, and turning on the command button of shadow tracking, we can get the rough analysis results of the lighting of each house in each stage of the project. The advantage of this function is most easily reflected in the design phase of the project,This paper uses BIM Technology to establish the general overall model of the project in the Revit software, and carries out the simulation research on all sunshine, wind and sound conditions of the project by using the created complete model, and adjusts it in the design period, to determine the scientific pattern of the building.And adjust it to the reasonable distribution position.

Environmental performance index of green building. The environmental performance index of green building mainly includes building sunshine and radiation analysis, indoor and outdoor wind environment analysis and building indoor and outdoor acoustic environment analysis. (1) Taking the local geographical location and sunshine time and intensity as the analysis environment, BIM parameterized model is used as the simulation ontology. The indoor lighting of buildings in different times is simulated in three-dimensional state. The results of simulation cloud images are calculated and analyzed , and compared with the local standard indexes. The green design goal of buildings is achieved by modifying the design scheme. (2) The velocity field and pressure field of indoor and outdoor wind environment in each region are different. According to the local climate characteristics, the seasonal work research is carried out, and the indoor and outdoor wind conditions are deeply studied by using the BIM tool sville vent, and the feasibility of the design scheme is verified. (3) Through the design speed and traffic flow of the road around the building, the noise level is calculated as the simulation parameters, and the outdoor acoustic environment is analyzed. Then,the outdoor acoustic environment is used as the influence parameter of the indoor environment.Combined with the indoor building structure, the BIM green analysis software Cadna/A is used to simulate. The simulation results are compared with the standard to find out the insufficient design,deepening to achieve green design indicators.

Analysis of outdoor wind environment. In this paper, the whole building 3D model is established by using the Revit software, and then imported into the PHOENICS 2012 software through the parameter mode of gbxml. Finally, the outdoor wind environment of the project is simulated by PHOENICS. The specific working conditions are set as the average wind speed of the dominant wind direction in winter,wind direction is N, wind speed is 2.38m/s. We can get the detailed cloud map of the average wind speed of the dominant wind direction in winter within working condition 1, and the simulation results of the wind speed amplification factor at the average wind speed 1.5m above the ground are shown in Figure 1.

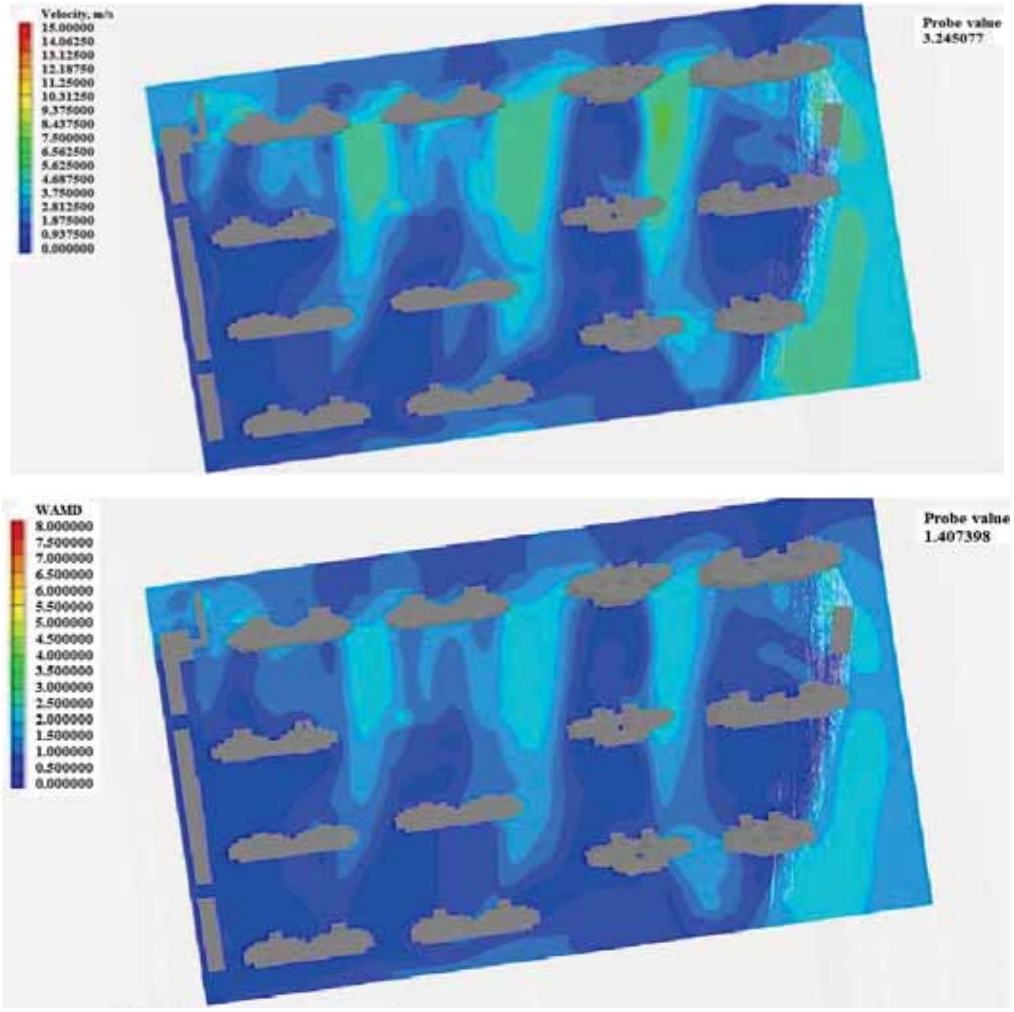

FIGURE 1
Cloud maps of wind speed and wind speed amplification factor at a height of 1.5m from the ground

By the figure above, in the NE wind field,the most outside the wind in the winter average wind speed is 2.38 m/s , the project of outdoor pedestrian height of 1.5 m height maximum wind speed less than 4.88 m/s, amplification coefficient is the highest value is about 1.80, in line with the green building evaluation standard GB/50378-2014 that in the dominant wind speed and wind direction environment in winter, the wind speed in the pedestrian area around the building is lower than 5m/s, in addition, the outdoor wind speed amplification factor is lower than 2. According to Figure 2, in the period of dominant outdoor wind direction in winter, the wind pressure on the windward side of the house is located in the range of -10Pa~4Pa and the wind pressure on the leeward side is -11Pa~2Pa, meeting the requirement that the pressure difference between the front and rear of the building should not be greater than 5Pa in winter. At a height of 1.5m from the ground, the wind pressure on the windward surface of the house is in the range of -1PA~2Pa, and the wind pressure on the leeward surface of the house is in the range of -5PA~0Pa. The outdoor pedestrian area of the project has smooth air flow. By adjusting the simulation parameters to change the working conditions, it is found that in the S wind field of 2.80m/s, the flow field in the pedestrian area around the project is evenly distributed, usually no eddy currents are generated, and the comprehensive ventilation level is relatively high. The maximum wind speed in the pedestrian area around the building is 5.00m/s, among which the maximum amplification factor is 2.10. In addition, there is no vortex or wind area in the pedestrian area.

During the dominant outdoor wind direction in summer, the wind pressure on the windward side of the house is in the range of -2Pa~12Pa and the leeward side is in the range of -6Pa~0Pa. At a height of 1.5m from the ground, the wind pressure on the windward surface of the building is between 0Pa~5Pa, and the wind pressure on the leeward surface is within the range of -3Pa~2Pa. Natural ventilation is easy to occur in pedestrian areas, which facilitates the air transmission around the building. All of the above are in line with the Green Building Evaluation Standard.

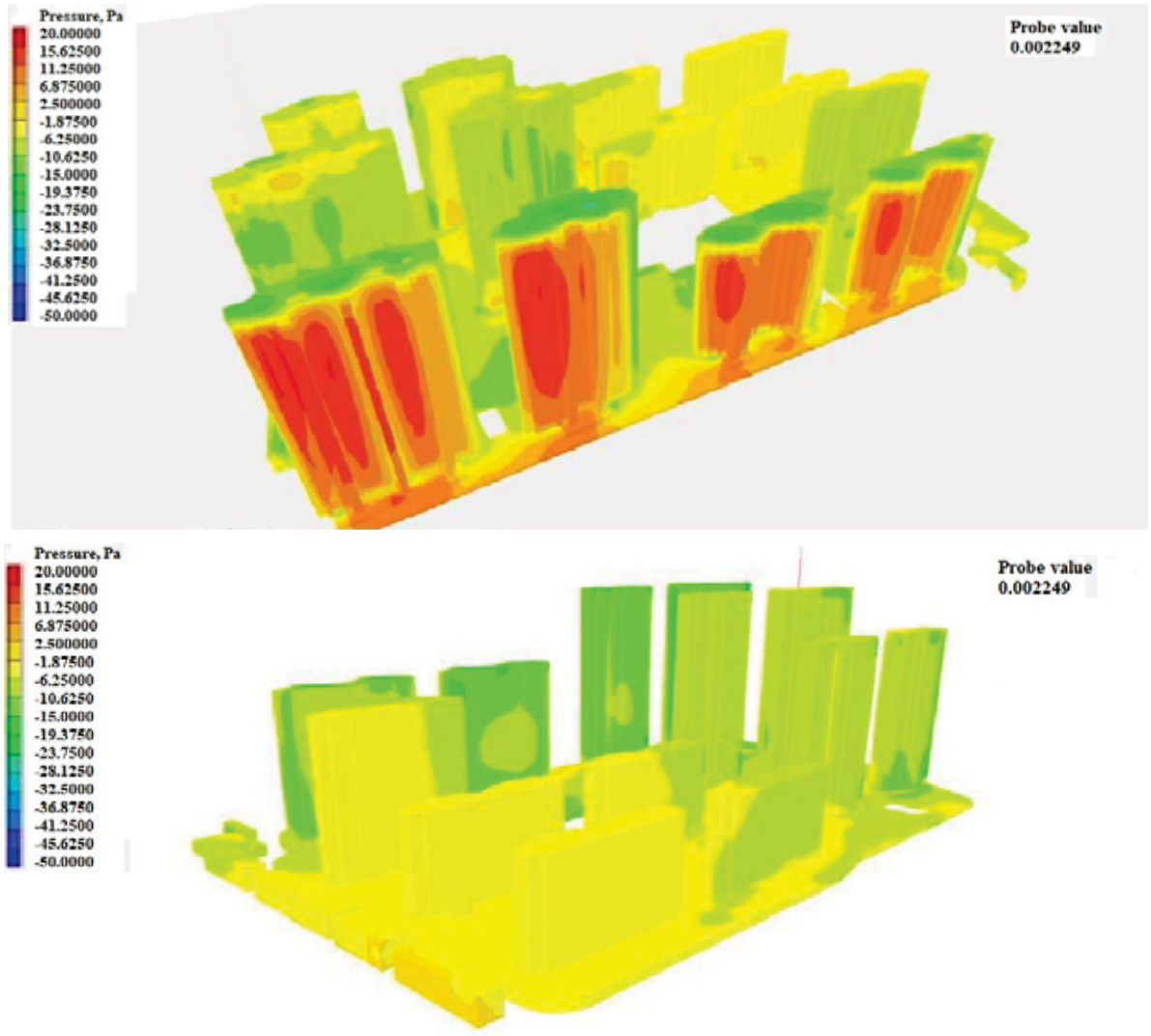

FIGURE 2
Cloud maps of wind pressure on the windward and leeward sides of buildings in winter

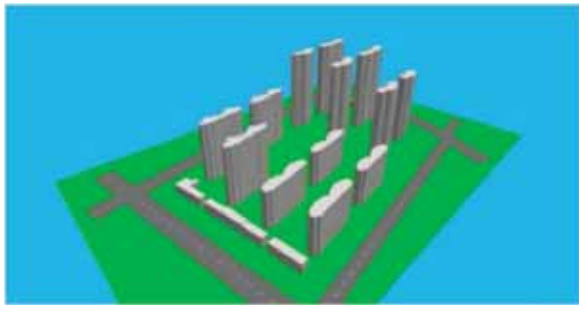

FIGURE 3
3D rendering of the model in Cadna/A software

The model was built and the environmental parameters of the area were added for simulation. Through calculation, it was concluded that in winter (wind direction is NE, wind speed is 2.39m/s) and summer (wind direction is S, wind speed is 2.90m/s), the external wind speed and amplification factor of the project were in line with "the wind speed in the pedestrian area around the building was lower than 5m/s, and the wind speed amplification factor was lower than 2". In summer and transition period (wind direction is E, wind speed is 2.47m/s) when the dominant wind direction, there are no vortices and wind areas in the active area of the project,more than half of the windows can be opened, and the wind pressure difference between the indoor and outdoor surface layer is greater than 0.5Pa.

In this paper, the acoustic environment of this project is divided into two parts: daytime and nighttime, and the most unfavorable point of noise. The overall model of the project established in Revit software is shared with Cadna/A software.Through the decibel analysis of the impact on the project buildings, whether it meets the requirements for residential noise in the standard is determined. Through the simulation of the noise around the whole residential area and the most unfavorable point of the residential area in the daytime, the results are shown in Figure 4.

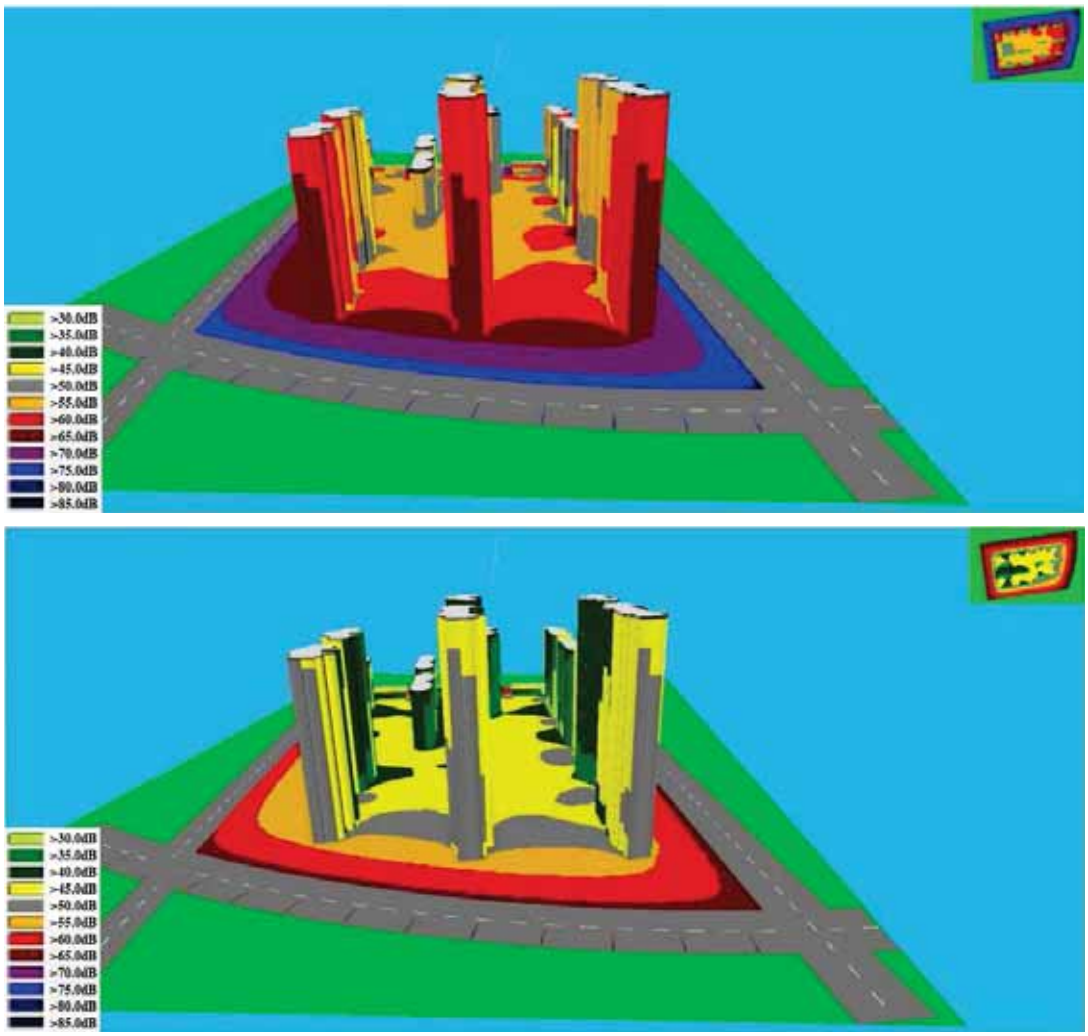

FIGURE 4
Distribution of daytime and nighttime road side noise

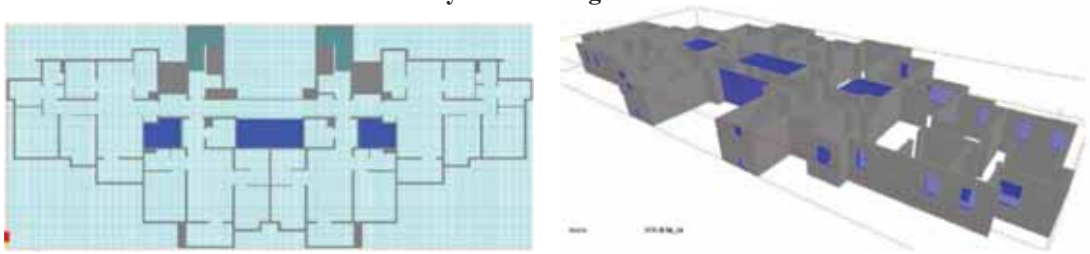

FIGURE 5
Standard floor plan and 3D model diagram of 3# building

It can be seen from the figure that the interior of the project area is basically at 55dB in daytime,and the edge of the residential complex is slightly higher, which is 60dB. The regional noise decibel between the residential area and the road can be divided into two stages, 70dB and 75db.The closer to the road, the higher the noise decibel. In addition, it can be seen that the most unfavorable point of daytime noise in the area is Shantou, with the highest value of 66.5 dB. At night, the eastern residential area is basically at 45dB, while the west residential area is basically at 40dB. The area noise decibels between the residential area and the road are divided into three stages: 55dB, 60dB and 65dB. The closer to the road, the higher the noise decibel. In addition, according to the upper body, we can know that the most unfavorable noise point in the nighttime area is around Shantou,The maximum value is 54.8dB. Therefore, the ambient noise of the road side in the project site conforms to the environmental quality standard for noise.

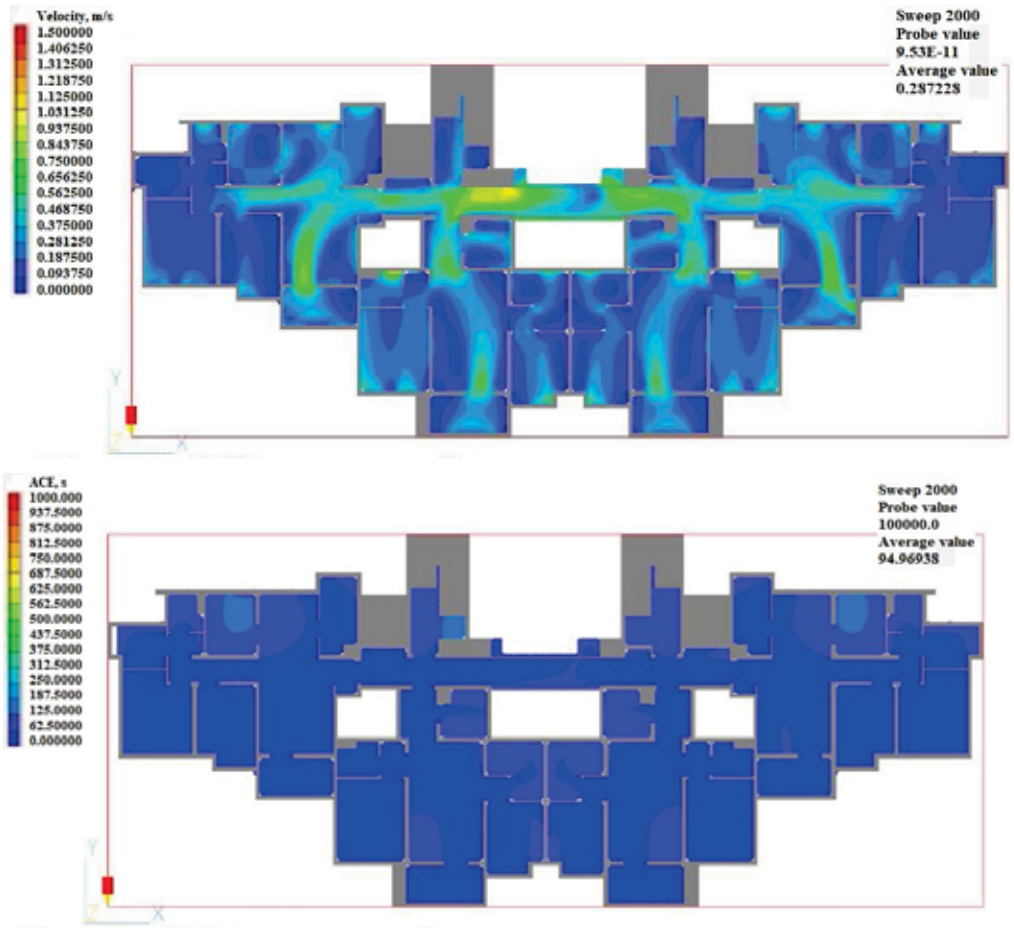

FIGURE 6
Wind speed cloud map of 1.2m height and air age cloud map of standard floor of 3# building

Analysis of indoor natural ventilation. According to the simulation diagram of outdoor wind environment in transition season, the indoor natural ventilation condition of the residential building of the project is simulated and analyzed. In the typical period of transition season, the average natural ventilation frequency of relevant functional rooms in the project exceeds the area ratio of twice per hour. In this simulation, two typical standard floors of the project are selected for relevant simulation, i.e. 3# and 13# buildings.Firstly, the comprehensive design content prepared by the owner was added into the BIM modeling software Revit software to create a complete three dimensional model,which was imported into FLAIR module to carry out a complete simulation study. Figure 5 shows the calculation model of standard floor of 3# building in the module, and 13# building is similar to it.

An in-depth simulation analysis is carried out for the standard floor of 3# building and 13# building. It can be found from the wind speed vector diagram of 1.2m pedestrian height in the standard floor of 3# building， at 1.2m pedestrian height, there is a blank of wind speed vector in two guest toilets in the east and west of the standard floor. The remaining rooms are well ventilated. The average wind speed is within the range of 0.37m/s~0.56m/s.Vectors in the living room and stairway are relatively concentrated here, and the wind speed ranges from 0.65m/s to 0.85m/s, that is, 3# house type conforms to the standard of residential ventilation. Figure 6 shows the simulation results of wind speed and air age at 1.2m pedestrian height for the standard floor type of 3# building.

It can be seen that, at the height of 1.2m pedestrian, the standard 3# floor house type is north-south transparent, the living room and corridor are all the best ventilated parts. The wind speed in the room is 0.65m/s~0.93m/s, and the natural ventilation is poor in the east and west side rooms， because there are walls in the room. The wind speed is generally 0.29m/s. The bedroom is the place where the air residence time is the longest, about 250s. As it is a north-south transparent house, the ventilation ability of the living room is the strongest, and the air residence time is about 20s~60s. At present, the average value of air age of standard layer is 94.97s. The indoor air circulation efficiency is high, and the indoor comprehensive ventilation effect is good. The standard level of building 13# has similar results, which will not be repeated here.

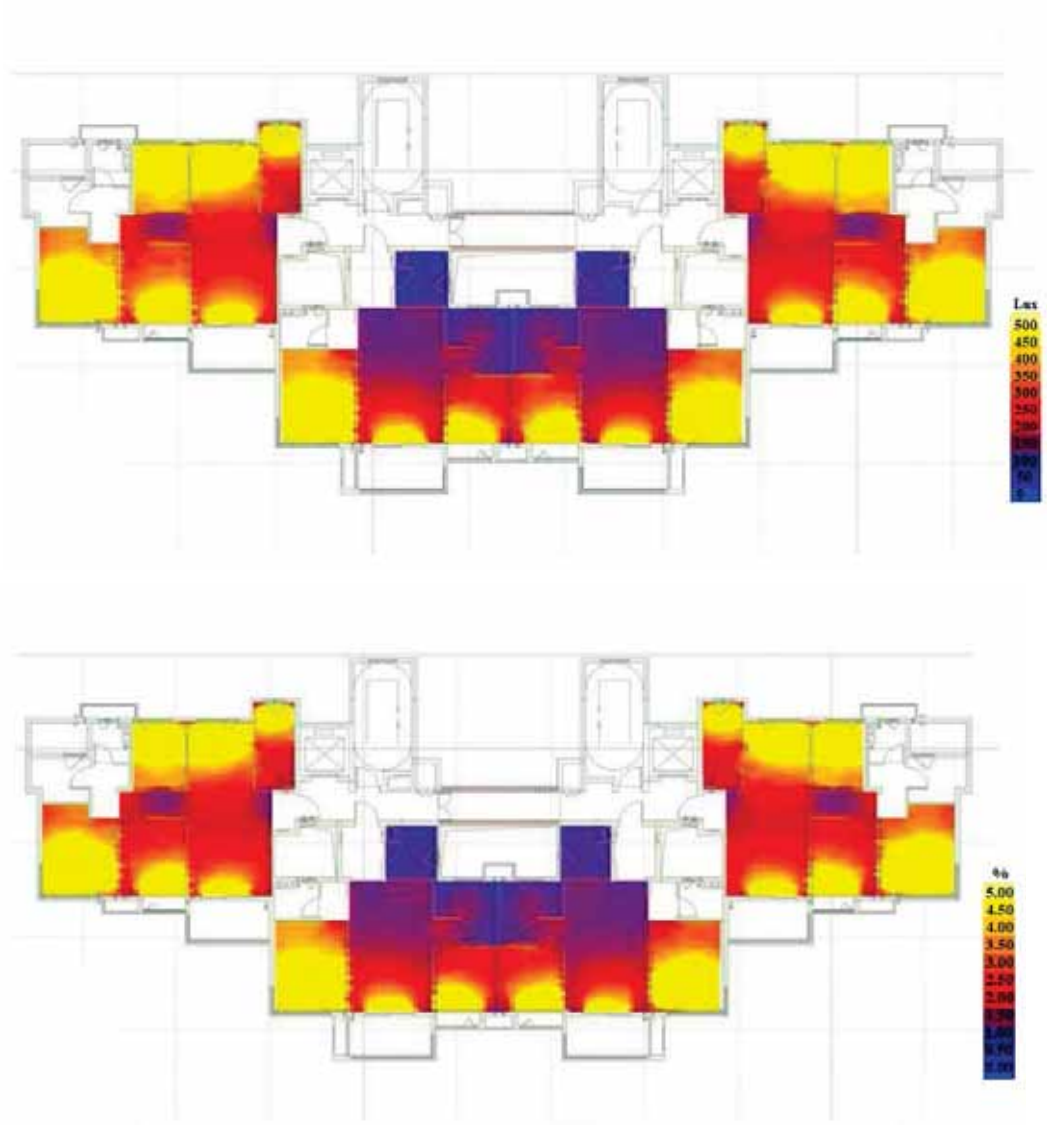

FIGURE 7
Lighting coefficient of standard floor of 3# building and natural lighting illuminance diagram

TABLE 2
Calculation results of daylighting coefficient of standard floors of 3# and 13# buildings

Contour	3#				13#			
	Within		Above		Within		Above	
0~1.1	1088	7.85	13854	100	1025	16.9	6064	100
1.1~2.2	2801	20.22	12766	92.15	1987	32.77	5039	83.1
2.2~3.3	3494	25.22	9965	71.93	1044	17.22	3052	50.33
3.3~4.4	1977	14.27	6471	46.71	587	9.68	2008	33.11

Analysis of indoor natural lighting. Natural light is the light source with the least loss and the most suitable for human beings. Making full use of natural light can save resources and maintain the environment, showing the ecological concept of scientific development in an all-round way. The natural light environment is the environment for the public to live and like for a long time. The visual test results of different light sources show that under the same illumination standard, the recognition level of natural light is higher than that of artificial light, which is convenient for people's daily life,Besides,making full use of natural lighting can save the resources consumed by lighting, and further optimize the office environment, which is of great value to reduce the loss of resources and develop an economical economy.

In this simulation, two standard floors and underground garages of typical house types of this project are selected for relevant simulation. Typical house types are 3# building and 13# building respectively. By studying the sky and indoor and outdoor

reflection components under the sky illumination, daylighting and natural lighting illumination were calculated, and the CIE model of all-cloudy sky was used to design the sky. Figure 7 shows the simulation results of indoor natural lighting coefficient, and natural lighting illumination of standard floor of 3# building. The calculation results of lighting coefficient are shown in Table 1.

It can be seen from the table that the average value of daylighting coefficient in the important functional areas of 3# and 13# buildings is 4.33% and 3.44% respectively, while the natural light illmination is 456.01lx and 354.04lx. It meets the requirements of "building lighting design standard" GB 50033-2013 that "the side lighting coefficient exceeds 2.2%, and the natural lighting illumination exceeds 300 lx". At the same time, according to Table 1, the ratio of area where the daylighting coefficient of important functional rooms in the two buildings is higher than 2.2% is 71.93% and 50% respectively.

CONCLUSIONS

In this paper, the environmental performance evaluation of green building based on BIM Technology is carried out, and the green indexes of indoor and outdoor wind, sound and indoor light environment of green building are established. Combined with the engineering case, the indoor and outdoor environmental performance is evaluated and analyzed. The main conclusions are as follows:

(1) In winter (wind direction NE, wind speed 2.38m/s) and summer (wind direction S, wind speed 2.88m/s), the external wind speed and amplification factor of the project meet the requirements. In summer and transition period (wind direction E, wind speed 2.47m/s) when the dominant wind direction, there is no vortex or wind area in the project's active area, more than half of the windows can be opened, and the wind pressure difference between the indoor and outdoor surface layer is greater than 0.5Pa.

(2) The ambient noise of the road side around the project site is in line with the "environmental quality standard for noise", The 3# standard floor house belongs to the North-South transparent type, and the living room and corridor are the best ventilation parts. The air residence time of the middle room type in the standard floor of 13# building is longer than that of the East-West type, about 600s, and the indoor air circulation speed is fast, indoor overall natural ventilation ability is good.

(3) In the project, the daylighting coefficient and natural light illminance of the important functional areas of 3# and 13# buildings meet the standard, and the ratio of the daylighting coefficient of the two important functional rooms higher than the standard value is 71.93% and 50%, respectively.

ACKNOWLEDGEMENTS

We thank LetPub (www.letpub.com) for its linguistic assistance during the preparation of this manuscript.

REFERENCES

[1] Zhang, L. (2014) Application study of green building based on BIM technology. Applied Mechanics & Materials. 587-589, 2275-2278.
[2] Huang, M., Wang, B. (2015) Evaluating green performance of building products based on gray relational analysis and analytic hierarchy process. Environmental Progress & Sustainable Energy. 33(4), 1389-1395.
[3] Yu, L., Sun, Z., Ding, R., Wang, S., Feng, G. (2015) Research on the post occupancy evaluation of green public building environmental performance combined with carbon emissions accounting. Procedia Engineering. 121, 1454-1460.
[4] Moon, C.H. (2014) Sustainability and floating architecture. International Journal of Sustainable Building Technology & Urban Development. 5(2), 123-127.
[5] Zhang, Y. (2014) Study on corporate environmental performance evaluation based on circular economy. Applied Mechanics and Materials. 675-677, 1815-1818.
[6] Ahmed, A., Korres, N.E., Ploennigs, J., Elhadi, H., Menzel, K. (2011) Mining building performance data for energy-efficient operation. Advanced Engineering Informatics. 25(2), 341-354.
[7] Chang, V.P., Chu, X.Z., Huang, Z.L., Lin, Z.D. (2015) Study of PDRI for the project management of intelligent green building. Journal of Quality. 22(4), 299-320.
[8] Wu, Q., Jia, R., Yu, H. (2014) Study on environmental efficiency of electric power industry based on DEA optimization model. Journal of Information & Computational Science. 11(3), 781-795.
[9] Xie, J.M., Tang, X.W., Shao, Y.F. (2012) Research on stratified cluster evaluation of enterprise green technology innovation based on the rough set. Technology & Investment. 03(2), 68-73.
[10] Passer, A., Sébastien, L., Allacker, K., Lathauwer, D.D., Spirinckx, C., Wittstock, B. (2015) Environmental product declarations entering the building sector: critical reflections based on 5 to 10 years experience in different European countries. The International Journal of Life Cycle Assessment. 20(9), 1199-1212.

[11] Utkucu, D., Hatice, S. (2020) Interoperability and data exchange within BIM platform to evaluate building energy performance and indoor comfort. Automation in Construction. 116(8), 103225.
[12] Ansah, M.K., Chen, X., Yang, H., Lu, L., Lam, P.T.I. (2019) A review and outlook for integrated bim application in green building assessment. Sustainable Cities and Society. 48(7), 101-109.
[13] Samer, M. (2013) Towards the implementation of the green building concept in agricultural buildings: a literature review. Agricultural Engineering International Cigr. Journal. 15(2), 25-46.
[14] Zhen, Z.H., Yang, P., Pei, L.T. (2015) A review for researches and applications of BIM-based operation and maintenance management. Journal of Graphics. 11(5), 66-72.
[15] Gao, X., Pishdad, B.P. (2019) BIM-enabled facilities operation and maintenance: a review. Advanced Engineering Informatics. 39(1), 227-247.
[16] Ramli, A., Akasah, Z.A., Masirin, M.I.M. (2014) Factors contributing to safety and health performance of Malaysian low-cost housing: partial least squares approach. Research Journal of Applied Science Engineering & Technology. 7(21), 4612-4620.
[17] Ukhisia, B.G., Astuti, R., Hidayat, A. (2013) Analysis of the occupational health and safety effects on productivity of employees using partial least squares methods. Psychopharmacology. 143(3), 280-285.
[18] Li, Y., Tang, J., Noakes, C., Hodgson, M.J. (2015) Engineering control of respiratory infection and low-energy design of healthcare facilities. Science & Technology for the Built Environment. 21(1), 25-34.
[19] Lu, Y., Wu, Z., Chang, R., Li, Y. (2017) Building information modeling (BIM) for green buildings: a critical review and future directions. Automation in Construction. 83(11), 134-148.
[20] Chan, A.P.C., Xiao, M.A., Wen, Y.I., Zhou, X., Xiong, F. (2018) Critical review of studies on building information modeling (BIM) in project management. Engineering Management Frontier. 5(3), 394-406.
[21] Jin, R., Zhong, B., Ma, L., Hashemi, A., Ding, L. (2019) Integrating BIM with building performance analysis in project life-cycle. Automation in Construction. 106, 102861.
[22] Maltese, S., Tagliabue, L.C., Cecconi, F.R., Pasini, D., Ciribini, A.L.C. (2017) Sustainability assessment through green BIM for environmental, social and economic efficiency. Procedia Engineering. 180, 520-530.
[23] Cavalliere, C., Dellosso, G.R., Favia, F., Lovicario, M. (2020). BIM-based assessment metrics for the functional flexibility of building designs. Automation in Construction, 107, 1205-1212.
[24] Gerrish, T., Ruikar, K., Cook, M., Johnson, M., Phillip, M., Lowry, C. (2017) BIM application to building energy performance visualisation and management: challenges and potential. Energy and Buildings. 144(6), 218-228.
[25] Ilhan, B., Yaman, H. (2016) Green building assessment tool (GBAT) for integrated BIM-based design decisions. Automation in Construction. 70(10), 26-37.
[26] Cheng, Z., Shahmir, N.R., Lu, T. (2018) BIM-based investigation of total energy consumption in delivering building products. Advanced Engineering Informatics. 38(10), 370-380.
[27] Capozziello, S., Nojiri, S., Odintsov, S.D., Troisi, A. (2006) Cosmological viability of f(r)-gravity as an ideal fluid and its compatibility with a matter dominated phase. Physics Letters B. 639(3), 135-143.

Received: **07.08.2020**
Accepted: **01.02.2021**

CORRESPONDING AUTHOR

Sen Xu
Management School,
Xi'an University of Finance and Economics,
Xi'an Shaanxi 710100 – P.R. China

e-mail: phnwsn@163.com

© by PSP Volume 30– No. 05/2021 pages 4921-4927 Fresenius Environmental Bulletin

EFFECT OF POTASSIUM IODIDE IN WHEAT (*TRITICUM AESTIVUM* L.)

Ozcan Caglar*

Department of Organic Farming Business Management, School of Applied Sciences, Igdir University, 76000, Igdir, Turkey

ABSTRACT

The objective of this study was to determine the effect of irrigation/drought and potassium iodide applications on yield, some yield and quality components in wheat. This study was carried out in the location of Atatürk University Faculty of Agriculture, Erzurum, Turkey in 2004-2005 and 2005-2006 cropping seasons. Four bread wheat genotypes were used (Bezostaja-1, Karasu-90, Doğu-88 and Palandöken-97). Samples for determining minerals were taken at tillering period (Zadoks 20-29), flowering period (Zadoks 60-69), Three treatments (Irrigated, no irrigation and potassium iodide) were used. Seed weight per spike, seed yield, SPAD, test weight and thousand seed weight well responded to water supply, whereas protein and proline contents increased in water stress conditions. Similarly, irrigated treatment allowed increase in yield components that means growth conditions positive. Whereas, there are negative growth conditions in KI and no irrigation treatments. Bezostaja-1 and Karasu-90 were determined as the best genotypes in irrigated and stress conditions. Potassium iodide (KI) is more likely to be used in simulation of effect of water stress conditions on plant growth in irrigated conditions in breeding programs.

KEYWORDS:
Bread wheat genotypes, Water stress, Irrigation, Yield components, Proline, Potassium iodide

INTRODUCTION

Cereals, are the largest group of crops and are the main source of human nutrition in the world. Almost 90% of the daily diet in humans is constituted by plant nutrients, and most of which comprise cereal-derived foods [1,2,3]. With a planting area exceeding 220 million hectares wheat is the most produced grain in the world. This feature makes wheat widespread crop in many regions. Lots of countries take into consideration that wheat as a strategic crop in the world. Being one of the environmental stresses, drought is limiting factor and serious problems in crop production and dry farming areas in the world [4]. Available water for crop development is vital limiting factor in crop production in arid and semi-arid areas [5,6,7]. Water has a vital role in the cellular and plant levels of plant metabolism. Plants grown in arid environment make some physiological and morphological changes to adapt to these conditions. When plants coincide drought environments, their physiological and biochemical changes occur in crop metabolism. Crop structures such as changes in stomata, reducing leaf area, increasing leaf thickness, increasing hairiness and raising the root/shoot ratio could be considered to select drought resistant genotypes in breeding programs [4]. Much research has been carried out on changes in wheat under dry conditions. In particular, the initial development of the plant is sensitive to constipation during the flowering and milk stages, and significant changes in physiological, morphological and biochemical structures have occurred during these periods, and the determination of these changes has been found in previous researches that will provide significant contributions to breeding programs in breeding programs [8,9]. Certain effective techniques can be applied to determine the tolerances of the plant without exposing the plant to the set. One of these techniques is potassium iodide, which when applied during the formation of one third (about 1%) destroys the photosynthetic systems of the plant, causing development retardation. It has been stated that this technique can be used successfully in the selection of tolerant plants in breeding studies by creating a similar situation in the drought caused by the drought [4]. The objective of this study was to determine the effect of irrigation/drought and potassium iodide applications on yield, some yield and quality components in wheat.

MATERIALS AND METHODS

This study was carried out in the location of Atatürk University Faculty of Agriculture, Erzurum, Turkey in 2004-2005 and 2005-2006 cropping seasons. Soil was loamy texture (41.6% sand, 37.4% silt, and 21.0% clay); 0.43% CaCO3, 275.8 mmol kg^{-1} P2O5, 368.4 mmol kg^{-1} K_2O, 6.83 pH, 2.64% organic matter and 3.63 dS m^{-1} electrical conductivity. Average, minimum and maximum temperatures, precipitations in 2004-05 and 2005-06 and long term

years in Erzurum were given in Table 1. Precipitations in 2004-05 and 2005-06 and long term years were 351.9 mm, 284.6 mm and 377.1 mm, respectively.

Maximum, minimum and average temperatures in 2004-05 and 2005-06 and long term years were 23.87, 25.75 and 29.56, -11.75, -11.76 and -12.37; 7.92, 8.98 and 10.05, respectively. Four bread wheat genotypes used were: 1) Palandöken-97, winter-habit, suggested to no irrigation conditions, white seed, 41.5 g 1000-seed weight, 13.5% protein content, 97 cm tall, resistant to lodging, cold, and yellow rust; 2) Doğu-88, winter-habit, suggested to no irrigation conditions, red seed, 39.6 g 1000-seed weight, 12.4 % protein content, 95 cm tall, resistant to lodging, cold, and yellow rust; 3) Karasu-90, winter-habit, suggested to irrigated conditions, red and 42.7 g 1000-seed weight, 12.9 % protein content, 103 cm tall, resistant to lodging, cold, and stripe rust resistant; 4) Bezostaja-1, winter-habit, suggested to irrigated conditions, red seed, 43.3 g 1000-seed weight, 14.2% protein content, 100 cm tall, resistant to lodging, cold, and yellow rust. Fertilizers given were Urea 48 % N, 60 kg N ha^{-1} for no irrigation and KI treatments, 100 kg N ha^{-1} for irrigated treatments, half at sowing stage and half at tillering stage) and triple superphosphate (46% P_2O_5, 60 kg ha^{-1} P_2O_5 for no irrigation and KI treatments, 100 kg ha^{-1} P_2O_5 for irrigated treatments, once at sowing). Seeds were planted at the second weeks of September with 475 seed/m^2 rate. Split-split plot design was as an experimental design with three replications. Plot size was 6 m/1.2 m (7.2 m^2). Applications were; irrigated (at sowing, at stem elongation (Feekes 6.0) and at flowering (Feekes 10.51); no irrigation and KI treatment. 0.6% potassium iodide was applied to simulate drought conditions. KI was sprayed when the grain was one-third developed (Feekes 10.54) under irrigated conditions [4]. Grain yield, SPAD, seed weight per spike, thousand seed weight, test weight, protein content and proline [5,6,7,10] were evaluated. Seed protein content was determined by using Kjedahl method. Proline was extracted from leaf samples of 100 mg fresh weight with 2 ml of 40% methanol. 1 ml extract was mixed with 1 ml of a mixture of glacial acetic acid and orthophosphoric acid (6 M) (3.2 v/v) and 25 ml ninhydrin. After 1 h incubation at 100 ^oC, the tubes were cooled and 5 ml toluene was added. The absorbance of upper phase was spectrophotometrically determined at 528 nm. The proline concentration was determined using a standard curve [5]. ANOVA for data was made using SAS statistic software program. Means were compared by LSD test. Biplot analysis was made by Minitab statistic software program.

RESULTS

Drought is defined a naturally occurring phenomenon that occurs when the amount of precipitation is below the normal level, causing severe hydrological imbalances by adversely affecting land resources and production systems [11]. The main reason for the drought is that the area receives less precipitation for longer than normal. When we combine this with increasing temperature and decreasing humidity, meteorological drought occurs. When irrigation water and soil nutrition in agriculture are not enough, drought can also return to agricultural drought. Simultaneously, the decrease in river flows and underground water forms hydrological drought. The change in global climate pattern lies behind the increase in the frequency and severity of meteorological droughts in our country and it is expected that these changes will make drought a regular part of daily life [2,4]. Variance analysis of irrigation, genotypes and potassium iodide application for characters were given in Table 2.

TABLE 1
Average, minimum and maximum temperatures, precipitations in 2004-05 and 2005-06 and long term years in Erzurum

Climatic Parameters	Years	October	November	December	January	February	March	April	May	June	July	Tot./Av.
Max. Tem. (ºC)	2004-05	20.3	19.5	15.7	13.6	18.5	20.6	26.1	30.2	36.7	37.5	23.87
	2005-06	27.3	22.3	18.5	16.3	17	25.1	26.5	27.8	32.6	39.1	25.25
	Long	32.5	26.8	22.6	19.5	21.1	29.2	32.8	35.1	34.8	41.2	29.56
Min.Tem. (ºC)	2004-05	-7	-15.6	-26.7	-31.7	-17.3	-16.9	-7.5	-3.5	3.9	4.8	-11.75
	2005-06	-6.8	-16.8	-24.7	-33.7	-26.8	-14.8	-4.8	-4.9	6.8	8.9	-11.76
	Long	-7.2	-13.5	-27.2	-28.2	-31.3	-17.3	-5.3	-4.9	4.5	6.7	-12.37
Av.Tem. (ºC)	2004-05	8.7	2.1	1.4	-4.3	-6.2	3.1	14.2	16.3	19.3	24.6	7.92
	2005-06	9.2	4.5	3.6	-5.3	-7.4	3.8	15.3	17.7	23.6	24.8	8.98
	Long	13.4	7.3	4.6	-3.6	-5.6	6.3	11.7	16.4	24.7	25.3	10.05
Tot. Ra. (mm)	2004-05	6.1	6.3	42.1	44.7	47.2	61.4	25.3	66.3	17.3	35.2	351.9
	2005-06	7.9	8.8	55.3	61.7	55.2	45.7	36.3	65.7	35.4	12.6	384.6
	Long	10.2	33.1	45.3	42.3	53.6	44.7	42.3	35.6	46.5	23.5	377.1

*Data of regional meteorology station, Erzurum, **Long years include years of 1970-2006.

TABLE 2
Variance analysis of irrigation, genotypes and potassium iodide application for characters

		F Values						
Source	df	Yield	SPAD	Seed Weight per Spike	Protein Content	Thou. Seed Weight	Test Weight	Proline Content
Year	1	2.36ns	168.99**	30.01*	7.994ns	5.44ns	6.56ns	4.08ns
$Error_1$	2							
Applications	2	544.331**	165.70**	384.61**	49.92**	92.17**	199.76**	2762.97**
Year x Appl.	2	0.896ns	2.28ns	13.62**	0.39ns	0.16ns	0.64ns	4.19ns
$Error_2$	8							
Genotypes	3	3.109*	4.41**	1.39ns	23.89**	2.86ns	2.34ns	16.45**
Year x Genot.	3	2.332ns	4.54**	7.54**	1.61ns	2.11ns	0.54ns	2.37ns
Appl. x Genot.	6	0.507ns	2.73*	1.36ns	0.37ns	0.37ns	1.26ns	5.53**
Year x Ap. x Gen, $Error_3$	6 36	1.083ns	1.074ns	2.09ns	0.49ns	0.68ns	0.78ns	2.14ns
Total	71							
C.V. (%)	71	16.61	14.23	12.36	5.05	11.40	4.39	23.59

*Significant at the 0.05 probability level, **Significant at the 0.01 probability level, ns no significant.

Years, significantly affected SPAD ($p<0.01$) and seed weight per spike ($p<0.05$). Once effect of applications (irrigation and KI) in all characters were significant at 1%, differences in genotypes for yield, SPAD, protein content and proline content were found to be significant at 5%, 1%, 1% ,and 1%, respectively. Year x application in SPAD, year x genotype interactions in SPAD, seed weight per spike, and application x genotype interaction in proline content were determined as significant at 1%. Only %5 significant level was found in application x genotype interaction for SPAD (Table 2).

Yield is one of the most commonly considered feature in lots of studies and determining high yielding genotypes in favorable and unfavorable climatic conditions including well-watered and water stress conditions [1,2,4,7]. The highest seed yield with 5.02 t/ha belonged to irrigated treatment, while lower seed yields were taken from no irrigation (2.63 t/ha) and KI (2.50 t/ha) treatments (Table 3). Seed yield decreased with increasing water stress and this decrease in no irrigation and KI applications occurred as 47.7% and 52.3%, respectively. Besides, the highest seed yield was taken from Bezostaja-1 (3.49 t/ha) and Doğu-88 wash the lowest one (3.22 t/ha). KI treatment gave similar result to no irrigation.

This means that KI could be applied successfully to simulate drought conditions when it is used breeding programs. It was reported that water supply in flowering heading stage that is vital for dry matter accumulation is so vital. Water shortage in that period reduce seed yield [7,12,13,14,15]. KI in the grain was one-third developed creates early senescence and decreases seed yield [14]. SPAD, chlorophyll meter, is fast and dependable method to measure chlorophyll content that assign plant growth [7]. With 51.44, Bezostaja-1 gave the highest SPAD value, while Doğu-88 had the lowest SPAD (48.55). Decreases in no irrigation and KI treatments were 17.8% and 27.5%, in comparison with irrigated treatment. Irrigated treatment had the highest SPAD (58.87) and KI gave the lowest SPAD (42.70). It was pointed out that gain weight per spike is sensitive to environmental conditions specifically water availability in the flowering and seed development stages and significant variabilities were found between irrigated and unirrigated applications [16,17]. No irrigation and KI treatments had 19.4% and 35.4% reductions in seed weight per spike. The highest seed weight per spike belonged to irrigated treatment (1.81 gr), KI had the lowest value (1.17 gr). Similar to seed yield, grain yield per spike significantly decreases with KI application [14]. Once no significant differences occurred among genotypes, the highest value was found in Doğu-88.

Applications had a significant effect ($p<0.01$) on protein content (Table I). No irrigation and KI application caused increase about 5% and 6.6%, respectively. The highest protein contents were found in no irrigation and KI application (12.97% and 13.18%), irrigated one had the lowest value (12.35%). The highest protein content was in Bezostaja-1 (13.46%), but Doğu-88 gave the lowest protein content (12.38%). Water shortage has significant effect in protein content.

TABLE 3
The effect of water and potassium iodide effect on yield and yield components and proline in wheat genotypes

	Applications				
	Yield (t/ha)				
	Palandöken-97	Doğu-88	Karasu-90	Bezostaja-1	Mean
Irrigated	4.92	4.96	5.05	5.14	5.02 A
No irrigation	2.59	2.33	2.85	2.77	2.63 B
KI	2.53	2.37	2.63	2.55	2.5 B
Mean	3.23 AB	3.22 B	3.51 A	3.49 A	3.39
LSD (%):	Application: 0.29, Genotype: 0.23				
	SPAD				
	Palandöken-97	Doğu-88	Karasu-90	Bezostaja-1	Mean
Irrigated	61.83	55.83	58.83	59.00	58.87 A
No irrigation	49.16	47.00	46.00	51.50	48.41 B
KI	41.66	42.83	42.50	43.83	42.70 C
Mean	50.88 AB	48.55 B	49.11 AB	51.44 A	50.00
LSD (%):	Year: 4.53, Application: 286.9, Genotype: 3.02, Year x Genotype: 3.57, Application x Genotype: 4.37				
	Seed Weight per Spike (gr)				
	Palandöken-97	Doğu-88	Karasu-90	Bezostaja-1	Mean
Irrigated	1.87	1.79	1.81	1.76	1.81 A
No irrigation	1.46	1.50	1.48	1.38	1.46 B
KI	1.15	1.19	1.16	1.19	1.17 C
Mean	1.49	1.50	1.48	1.44	1.48
LSD (%):	Year: 0.05, Application: 0.07, Year x Application: 0.10, Year x Genotype: 0.11				
	Protein Content (%)				
	Palandöken-97	Doğu-88	Karasu-90	Bezostaja-1	Mean
Irrigated	12.32	12.03	12.15	12.90	12.35 B
No irrigation	12.98	12.51	12.81	13.60	12.97 A
KI	13.28	12.60	12.96	13.90	13.18 A
Mean	12.86 B	12.38 C	12.64 BC	13.46 A	12.84
LSD (%):	Application: 0.29, Genotype: 0.36				
	Thousand Seed Weight (gr)				
	Palandöken-97	Doğu-88	Karasu-90	Bezostaja-1	Mean
Irrigated	38.50	39.53	38.30	40.91	39.31 A
No irrigation	34.25	33.98	33.48	35.36	34.27 B
KI	31.68	31.13	29.01	31.83	30.91 C
Mean	34.81	34.88	33.60	36.03	34.83
LSD (%):	Application: 2.09				
	Test Weight (kg/hl)				
	Palandöken-97	Doğu-88	Karasu-90	Bezostaja-1	Mean
Irrigated	80.36	79.45	80.71	81.81	80.58 A
No irrigation	77.28	77.81	76.45	77.40	77.23 B
KI	73.71	73.45	72.30	74.35	73.45 C
Mean	77.12	76.90	76.48	77.85	77.09
LSD (%):	Application: 1.20				
	Proline Content (mmol g-1)				
	Palandöken-97	Doğu-88	Karasu-90	Bezostaja-1	Mean
Irrigated	0.30	0.21	0.27	0.19	0.24 C
No irrigation	3.71	3.58	4.57	3.85	3.93 B
KI	5.92	5.99	6.95	6.79	6.41 A
Mean	3.31 C	3.26 C	3.93 A	3.61 B	3.53
LSD (%):	Application: 0.28, Genotype: 0.29, Application x Genotype: 0.51				

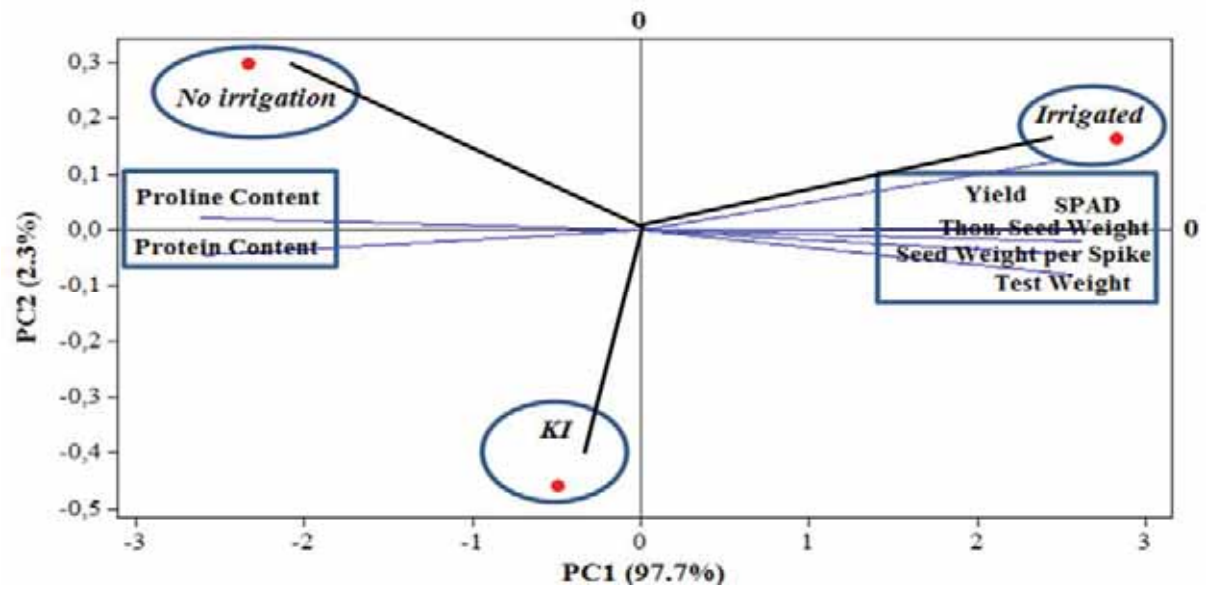

FIGURE 1
Biplot analysis in treatments, yield and yield components in bread wheat genotypes.

Water deficit probably cause reduction in plant water intake, it has a negative impact on the speed of photosynthetic activities and slows down. In this case, the proportion of protein relatively increased in seed of plant [18,19]. Water supply is essential input in plant growth, plant physiological activities and dry matter content, grain filling period and seed development. Water deficit significantly forms yield and yield components including 1000 seed weight [11,20]. Irrigated treatment had the highest 1000 seed weight (39.31 gr) and KI treatment had the lowest value (30.91 gr). Genotype x environment interaction is so complex phenomenon or water deficit environments. Test weight as a quality criterion is essential quality character and selected promising genotypes should have more than 80 kg/hl test weight in breeding programs [21,22,23]. Having significant and positive correlation with grain yield, test weight is highly influenced by water stress and selection for higher test weight helps to increase selection processes [23]. Reductions on test weight in no irrigation and KI application were about 4.2% and 8.9%, respectively. The highest test weight was taken from irrigated treatment (80.58 kg/hl), but KI treatment had 73.45 kg/hl test weight. In water deficit conditions, proline accumulation occur in plants, water stress cause some metabolic disorders such dysfunction of photosynthesis and mitochondria, and impaired protein synthesis [24]. Proline plays important role in the adaptation of plant tissues to water deficit by assisting osmotic regulation, protection of plasma membrane structure [25,26]. KI and no irrigation treatments had 2670.6% and 1637.5% increase in proline content. The highest proline content belonged to KI treatment (6.41 mmol g-1), irrigated treatment had the lowest value (0.24 mmol g-1). The highest proline content was in Karasu-90 (3.93 mmol g-1), but Doğu-88 gave the lowest protein content (3.26 mmol g-1). Biplot analysis in treatments, yield and yield components was given in Figure 1.

Figure 1 shows that yield components and treatments were classified in two and three groups, respectively. While seed weight per spike, SPAD, test weight, seed yield and thousand seed weight grouped in one group; protein and proline contents constituted of same group. Moreover, irrigated, KI and no irrigation treatments formed separate groups.

Seed weight per spike, seed yield, SPAD, test weight and thousand seed weight well responded to water supply, whereas protein and proline contents increased in water stress conditions. Similarly, irrigated treatment allowed increase in yield components that means growth conditions positive. Whereas, there are negative growth conditions in KI and no irrigation treatments. Bezostaja-1 and Karasu-90 were determined as the best genotypes in irrigated and stress conditions. Potassium iodide (KI) is more likely to be used in simulation of effect of water stress conditions on plant growth in irrigated conditions in breeding programs.

ABBREVIATIONS

Potassium iodide, KI; volume to volume, v/v; *soil plant analysis development, SPAD; least significant differences, LSD*.

ACKNOWLEDGEMENT

Author is *grateful* to Atatürk University, Faculty of Agriculture, Field Crop Department for their assistance and financial support.

REFERENCES

[1] Fischer, R.A., Maurer, R. (1978) Drought Resistance in Spring Wheat Cultivars. I. Grain Yield Response. Aust. J. Agric. Res. 29, 897-907.

[2] Blum, A. (1979) Genetic Improvement of Drought Resistance in Crop Plants. A Case for Sorghum. In: Hussell, H. and Staples R.C. (Eds.) Stress Physiology in Crop Plants. Wiley Inter Science, New York, 495-545.

[3] Dencic, S., Kastori, R., Kobiljski, B., Duggan, B. (2000) Evaluation of Grain Yield and Its Components in Wheat Cultivars and Landraces under Near Optimal and Drought Conditions. Euphytica. 113, 1, 43-52.

[4] Blum, A., Shipler, L., Golan, G., Mayer, J. (1989) Yield Stability and Canopy Temperature of Wheat Genotypes under Drought Stress. Field Crops Res. 22, 289-296.

[5] Bates, L., Waldren, R.P., Teatre, J.D. (1973) Rapid Determination of Free Proline for Water Stress Studies. Plant Soil. 39, 205-207.

[6] Ceylan, A. (1994) Field Crop Production, Aegean University Press, Bornova, Izmir, 520.

[7] Paknejad, F., Nasri, M., Tohidi Moghadam, T.H., Zahedi, H., and Alahmadi, M.J. (2007) Effect of Drought Stress on Chlorophyll Fluorescence Parameters, Chlorophyll Content and Grain Yield of Cultivars. Journal of Biological Sci. 7, 6, 841-847.

[8] Lanceras, J.C., Pantuwan, G., Jongdee, B., Toojinda, T. (2004) Quantitative Trait Loci Associated with Drought Tolerance at Reproductive Stage in Rice. Plant Physiology. 135, 384-399.

[9] Farooq, M., Wahid, A., Kobayashi, N., Fujita, D., Basra, S.M.A. (2009) Plant Drought Stress: Effects, Mechanisms and Management. Agron. Sustain. Dev. 29, 185-212

[10] Singh, B., Singh, Y., Ladha, J.K., Bronson, K.F., Balasubramanian, V., Singh, J., Khind, S. (2002) Chlorophyll Meter and Leaf Color Chart-Based Nitrogen Management for Rice and Wheat in Northwestern India. Agron. J. 94, 821-829.

[11] Lopes, M., Reynolds, M., Jalal-Kamali, M., Moussa, M., Feltaous, Y., Tahir, I., Barma, N., Vargas, M., Mannes, Y., Baum, M. (2012) The Yield Correlations of Selectable Physiological Traits in a Population of Advanced Spring Wheat Lines Grown in Warm and Drought Environments. Field Crops Res. 128, 129-136.

[12] Kong, X.X., Ren, S.K., Kou, C.L., Cui, J.M. (1997) Filling Characteristics of Winter Wheat and Effect of Water And Fertilizer on Grain Filling in Sandy Land. Acta Agric. Boreali Sinica. 12, 5964.

[13] Garabet, S., Ryan, J., Wood, M. (1998) Nitrogen and Water Effects on Wheat Yield in a Mediterranean-Type Climate. II. Fertilizer Use Efficiency with Labelled Nitrogen. Field Crops Research. 58, 213-221.

[14] Acevedo, E., Ceccarelli, S. (1989) Role of Physiology in a Breeding Programme for Drought Resistance Conditions. In F.W.G. Baker, ed. Drought resistance in cereals, Wallingford, UK, CAB International, 117-139.

[15] Rong-Hua, L., Baum, P., Grando, S., Ceccarelli, S. (2006) Evaluation of Chlorophyll Content and Fluorescence Parameters as Indicators of Drought Tolerance in Barley. Agriculture Science in China. 5, 10, 751-757.

[16] Knezevic, D., Brankovic G., Surlan-Momirovic, G., Stamenkovic, S., Knezevic, J. (2010) Phenotypic variability of the mass of the primary class of wheat Triticum aestivum L. Arhiv Za Poljoprivredne Nauke. 71(3), 15-20 (in Bosnian).

[17] Knezevic, D., Kondic, D., Markovic, S., Markovic, D., Knezevic, J. (2012) Variability of Trait of Spike in Two Wheat Cultivars (Triticum aestivum L.). Növenytermeles, Suppl. 61, 49-52.

[18] Kattimani, K.N., Naik, V.R., Patil, B.N., Hanchinal, R.R., Kulkarni, V.N. (1996) Effects of Irrigation on Yield, Protein Content and Seedling Vigour in Wheat. Journal of Agricultural University. 21, 295-296.

[19] Panozzo, J.F., Eagles, H.A. (2000) Cultivar and Environmental Effects on Quality Characters in Wheat. II. Protein. Australian Journal of Agricultural Research. 51, 629_636.

[20] Rasmusson, D.C, Chanel, R.Q. (1970) Selection for Grain Yield and Components of Yield in Barley. Crop Sci. 10, 51-54.

[21] Williams, P., El-Haramein, F.J., Nakkoul, H., Rihavi, S. (1988) Crop Quality Evaluation Methods and Guidelines, International Center for Agricultural Research in the Dry Areas (ICARDA), Aleppo, Syria. 145.

[22] Özkaya, H., Özkaya, B. (2005) Analyse Methods I Cereal and Cereal Products, 2nd Press., Food Tech Ass. Pub. No:31, Ankara. 157.

[23] Ali, M.A., Abbas, A., Awan, S.I., Jabran, K., Gardezi, S.D.A. (2011) Correlated Response of Various Morpho-Physiological Characters with Grain Yield in Sorghum Landraces at Different Growth Phases. J. Animal Plant Sci. 21, 4, 671-679.

[24] Bajji, M., Lutts, S., Kinet, J.M. (2000) Physiological Changes After Exposure to and Recovery from Polyethylene Glycol-Induced Water Deficit in Callus Cultures Issued from Durum Wheat (Triticum Durum Desf.) Cultivars Differing in Drought Resistance. J. Plant. Physiol. 156, 75-83.

[25] Hare, P.D., Cress, W.A. (1997) Metabolic Implications of Stress-Induced Proline Accumulation in Plants. Plant Growth Regul. 21, 79-102.
[26] Capell, T., Bassie, L., Christou, P. (2004) Modulation of the Polyamine Biosynthetic Pathway in Transgenic Rice Confers Tolerance to Drought Stress. PNAS. 101(26), 9909– 9914.

Received: **18.08.2020**
Accepted: **10.02.2021**

CORRESPONDING AUTHOR

Ozcan Caglar
Department of Organic Farming Business Management
Igdir University
Igdir 76000 – Turkey

e-mail::ozcan.caglar@igdir.edu.tr

© by PSP Volume 30– No. 05/2021 pages 4928-4934 Fresenius Environmental Bulletin

MOLECULAR CHARACTERIZATION AND YIELD LEVELS OF LOCAL BEAN (*PHASEOLUS VULGARIS* L.) GENOTYPES GROWING IN EASTERN MEDITERRANEAN REGION

Okkes Akin Boylu[1], Umit Girgel[2], Alihan Cokkizgin[3,*]

[1]Kahramanmaras Sutcu Imam University, Field Crops Department, Kahramanmaras, Turkey
[2]Kahramanmaras Sutcu Imam University, Vocational School of Higher Education in Goksun, Kahramanmaras, Turkey
[3]Gaziantep University, Vocational School of Higher Education in Nurdagi, Gaziantep, Turkey

ABSTRACT

This research was carried out in Kahramanmaras Sutcu Imam University, Faculty of Agriculture, Department of Field Crops treatment area in 2014 and 2015 years. As seed material, 15 local bean genotypes (Turtul, Turtul-1, Turtul-2, Turtul-4, Turtul-5, Turtul-6, Turtul-7, Calikiran, Elazıg 1, Cali Bean, Horoz, Black, Kozan 3, Kozan 4, Susehri) of Adana, Hatay, Mersin, Kahramanmaras, Osmaniye, Sivas provinces and varieties "Onceler-98" and "Dermason" were used.

Genetic similarity index values were determined by using 22 primer pairs. The genotypes with the lowest similarity index were Turtul-5 and Calikıran (0.183), Calikiran and Cali (0.204), Elazig-1 and Kozan-3 (0.257), Calikiran and Onceler-98 (0.273), Calikiran and Turtul-2 (0.293), Onceler-98 and Turtul 2 (0.293) and Calikiran and Horoz (0.378).

The genetic similarity index values are examined, the most similar genotype pairs were; Turtul-4 and Kozan-4 (1.000), Dermason and Cali (1.000), Siyah and Turtul-6 (1.000), Susehri and Turtul 1 (1,000), Turtul and Turtul 4 (0.904), Turtul and Kozan-4 (0.904) and Turtul and Turtul-2 (0.904) genotypes.

KEYWORDS:
Ph. vulgaris, Genotype, Molecular markers, SSR, Dry Bean, Yield

INTRODUCTION

Beans (*Phaseolus vulgaris* L .; 2n = 2x = 22) *Papilionoideae* subfamily, *Phaseoleae* class, is a plant included in the *Leguminosae* family. Legumes (*Leguminosae*) family has a wide and rich variety of plants with 650 genus and 18.000 species [1, 2].

The 5 most important species in the genus *Phaseolus* are *P. lanatus* var. *lanatus*, *P. acutifolius*, *P. coccineous* and *P. vulgaris* [3].

Among these species, *P. vulgaris* covers more than 85% of the production areas in the *Phaseolus* species grown in the world. On the other hand, it is known to be the most cultivated species [4, 5]. All of fresh and dry beans are grown commercially in Turkey belong to the species *P. vulgaris* [6].

There are 30.4 million tons of dry beans and 24.8 million tons of green beans in the worldwide. On the other hand, 220 thousand tons of dry beans and 581 thousand tons of green beans are produced in Turkey [7].

In plant breeding, the gene pool needs to be well defined because it is important to avoid repetitions of similar studies and to better evaluate the possibilities. In this case, the morphological indicators being affected by the environmental conditions limit its use [8].

For this reason, in this study, PCR-based ISSR technique, which is one of the increasingly used molecular techniques, has been used in order not to be affected by environmental conditions besides morphological features [9, 10, 11].

In the study, bean genotypes obtained from different locations of Kahramanmaraş province were investigated by molecular methods in which they are related.

MATERIALS AND METHODS

Treatment area. The study was carried out in Republic Of Turkey Ministry Of Agriculture And Forestry East Mediterranean Transitional Zone Agricultural Research Of Institute treatment area (37,5353 latitude, 36,9171 longitude and 560 m altitude) in 2014 and 2015 years.

The treatment was carried out with 4 replications according to the randomized completely block design (RCBD).

Seeds were planted at a depth of 5-6 cm, with 70 cm between row spacing and 10 cm plant spacing. Bean plants were planted 4 rows each plot. The parcel size was calculated as 5.0 m x 2.8 m = 14 m^2.

Seed material. As seed material, 15 local bean genotypes (Turtul, Turtul-1, Turtul-2, Turtul-4, Turtul-5, Turtul-6, Turtul-7, Calikiran, Elazıg 1,

Cali Bean, Horoz, Black bean, Kozan 3, Kozan 4, Susehri) of Adana, Hatay, Mersin, Kahramanmaras, Osmaniye, Sivas provinces and varieties "Onceler-98" and "Dermason" were used.

Plant Growing Practices. In the first year, irrigation was carried out 14 times during the growing period of bean plants, and in the second year, irrigation was done 17 times.

Considering the amount of nutrients in the soil; at the same time with planting, 2.4 kg/da pure Nitrogen fertilizer and 6 kg/da pure P_20_5 fertilizer was applied. Weed control was carried out by hand or pesticides according to the weed development in the field. Chemical pesticides used to control disease and pest.

The physiologically mature bean plots were harvested between September 7-19 in 2014 and between September 9-13 in 2015.

Measurement Parameters. Single Plant Yield. Seeds from 10 plants randomly selected from each plot were weighed separately, and their mean weight (g) values were determined as a single plant yield [12, 13].

Seed Yield. After the harvest, the seed from each plot were weighed and calculated in kg/da and seed yield values were found [12, 14, 15, 16].

Statistical Analysis. The analysis of variance results were evaluated by using the Statistical Analysis System Software (v.9.0) [17]. The experimental design was Randomized Completely Block Design with three replicates and means of treatment were considered significantly different at $p<0.05$. and mean separation was performed according to Duncan's Multiple Range test (DMRT) [18]. On the other hand genetic similarity index was determined in the Spss statistical analysis program v. 24.0.

Plant Material Obtained. Approximately 10 g samples were taken from the young leaves of several plants at different points of the parcel during the period when it was 4-5 leaves from the plants in the field for use in molecular investigations.

SSR Analysis. 22 SSR primer pairs were used in the study (Table 1). The published primer information was used when determining the primers. On the other hand, those related to certain cultivation characteristics in beans were selected [19, 20, 21, 22, 23, 24, 25, 26, 27, 28].

DNA Isolation. 0.5 mg leaf samples taken for DNA isolation were kept in liquid nitrogen and processed in mortar. Then 0.5 ml 10x buffer solution was added to 1.5 ml tubes. Leaf samples were added to these tubes. Then, the tubes were shaken and kept in metal blocks at 65 °C for 15-60 minutes. Then 0.5 ml of chloroform isoamyl alcohol (24:1) was added.

The upper part of the liquid was taken with a pipette in the tubes. The collected liquid was transferred to a new eppendorf tube and 0.5 ml of isopropanol was added. These tubes were then kept at -20 °C for about an hour. These samples were then centrifuged at 12000rpm for 10 minutes. DNA samples accumulated at the bottom of the tubes and the supernatant was poured out. The tubes containing the samples were centrifuged for 2 minutes at 13000 rpm by adding 0.5 ml 70% ethanol.

The tubes were then left to dry and 300 ml of Tris-EDTA was added to them. Thus, DNA isolation was performed. The amount and purity of the isolated DNAs were processed in a 1% (w/v) agarose gel and A260 / A280 and A260 / A230 were determined by measuring in the spectrophotometer (NanoDrop ND-1000) [28].

1% agarose gel was prepared and poured into the tank apparatus. The DNA standard was loaded in the first well on the gel. 8 µl of the isolated genomic DNA samples were taken and 2 µl gel loading buffer (6x) was added. It is mixed and loaded on the gel.

PCR products were run in high resolution 4% (SSR) agarose gel for 4-6 hours at 70 V electric current and staining in 0.5 µg ml^{-1} Ethidium Bromide solution.

RESULTS AND DISCUSSION

Genetic similarity matrix [30] between 17 bean genotypes based on SSR markers was given in Table 2.

The genotypes with the lowest similarity index were Turtul-5 and Calikıran (0.183), Calikiran and Cali (0.204), Elazig-1 and Kozan-3 (0.257), Calikiran and Onceler-98 (0.273), Calikiran and Turtul-2 (0.293), Onceler-98 and Turtul-2 (0.293) and Calikiran and Horoz (0.378). on the other hand genetic similarity index values are examined, the most similar genotype pairs were; Turtul 4 and Kozan-4 (1.000), Dermason and Cali (1.000), Siyah and Turtul-6 (1.000), Susehri and Turtul 1 (1,000), Turtul and Turtul-4 (0.904), Turtul and Kozan-4 (0.904) and Turtul and Turtul-2 (0.904) genotypes (Table 2).

In the dendrogram created using SSR data (Fig.1.), genotypes were collected in 3 main groups (1, 2 and 3). The first two main groups consist of A and B, and two subgroups as C and D. There are only 2 varieties in the third and last group. It was determined that 8 of the genotypes were in the first main group, 7 of them were in the second main group and 2 of them were in the third main group. According to the dendogram, the closest varieties among the genotypes were Elazig-1 and Calikiran,

Susehri and Turtul-1, Dermason and Cali, Turtul-4 and Kozan-4, and Turtul and Turtul-2. This situation showed that some genotypes are very different and some are very close. Similar results gained by [31].

The gel was separated by electrophoresis according to their molecular size. In the polymorphic ones of the displayed DNA bands, DNA bands were scored as band (1) and absent (0) and binary matrix data was created (Table 3).

TABLE 1
Size, melting temperature, function and sequence of SSR primer pairs

Primer	bp	Tm(°C)	Gene relation		Sequence of SSR primer pairs
BM146	281	58	-	**F**	GAGATGAGTCCTTTCCCTACCC
				R	TGCAGACACAATTTATGAAGGC
BM210	166	52	Cyclopropane synthesizer gene resemblance	**F**	ACCACTGCAATCCTCATCTTTG
				R	CCCTCATCCTCCATTCTTATCG
PH7B3	161	49	Pathogen-related protein	**F**	AGTCGCCATAGTTGAAATTTAGGTG
				R	CTTATTAAAACGTGAGCATATGTATCATTC
PH10B11	157	49	Pathogen-related protein	**F**	GAGGGTGTTTCACTATTGTCACTGC
				R	TTCATGGATGGTGGAGGAACAG
DROUGH1	213	55	-	**F**	CAGACATGCAAATTGGAAC
				R	GGAGCACCAAAGATCATAGA
BMd-8	176	47	Giberellin20-oxidase	**F**	TTCATCCTCTCTCCCGAACTT
				R	CTTTTGTGGCTGAGACATGGT
BMd45AIA	129	47	IAA-protein match	**F**	GGTTGGGAAGCCTCATACAG
				R	TAGTCCTTGCTTTCTTTTGC
BMd-48	131	47	Beta-glucan binding protein	**F**	CCCCACCAACTCTTTCTTCC
				R	CAGAATTGACTTGGCGAGAA
SSR-IAC14	221	56	-	**F**	GCTGCATGTTTATCCACCTT
				R	TTGTTACTCACCCCACCATAC
SSR-IAC26	148	56	-	**F**	TTGGATGGCAATAAAATAGCA
				R	TGTTGGACTCAAAGGTGTTCTC
SSR-IAC63	210	59,8	-	**F**	TCGTAGCACTAAGATGGAAGA
				R	GTTTTGTGAACTGTTGAATGTG
SSR-IAC84	154	60	-	**F**	TTGCACTCTTGTTGTTTATGGA
				R	CACAATGACGACAGATGACAGA
SSRIAC116	185	60	-	**F**	AGACATTGTTGATACGGGAGAT
				R	CACCTTGACTTGCCTTTGAC
PV-atcc001	171	49	Beta-phaseolin	**F**	ATGCATGTTCCAACCACCTTCTC
				R	GGAGTGGAACCCTTGCTCTCATC
PV-aaat001	203/158	49/50	-	**F**	TGGAGCCATCTGTCTCTTACCCAC
				R	GAGCACGAGTCACGTTTGCAAC
PV-ag004	201	48	Phytohemagglutinin pseudogene	**F**	TTGATGACGTGGATGCATTGC
				R	AAAGGGCTAGGGAGAGTAAGTTGG
PV-atcc003	176	49	Alpha-phaseolin	**F**	TCTCCATGCATGTTCCAACCAC
				R	GGAGTGGAACCCTTGCTCTCATC
PV-tttc001	161	50	Nitrate reducing	**F**	TTTACGCACCGCAGCACCAC
				R	TGGACTCATAGAGGCGCAGAAAG
PV-gaat001	164	49	the subunit of Ribulose 1,5-bisphosphate carboxylase / oxygenase	**F**	AAGGATGGGTTCCGTGCTTG
				R	CACGGTACACGAAACCATGCTATC
PVat007	192	49	NADP-dependent enzyme	**F**	AGTTAAATTATACGAGGTTAGCCTAAATC
				R	CATTCCCTTCACACATTCACCG
PV-at008	161	49	Ribonuclease-Like Pathogenesis-Related Protein Gene	**F**	AGTCGCCATAGTTGAAATTTAGGTG
				R	CTTATTAAAACGTGAGCATATGTATCATTC
PV-atct001	193	49	Leaf spot disease durability	**F**	CAATTAAAACTCAACCAACCCAAATA
				R	TTTCCCGCCATAGAATATGTGAGA

TABLE 2
Genetic similarity matrix (Nei and Li, 1979) between 17 bean genotypes based on SSR markers

Geno-types	1	2	3	4	5	6	7	8	9	10	11	12	13	14	15	16	17
1	1,000																
2	0,624	1,000															
3	0,516	0,828	1,000														
4	0,467	0,748	0,904	1,000													
5	0,467	0,748	0,904	1,000	1,000												
6	0,418	0,671	0,598	0,677	0,677	1,000											
7	0,370	0,594	0,717	0,794	0,794	0,886	1,000										
8	0,370	0,594	0,717	0,794	0,794	0,886	1,000	1,000									
9	0,257	0,552	0,498	0,581	0,581	0,896	0,794	0,794	1,000								
10	0,418	0,671	0,598	0,677	0,677	1,000	0,886	0,886	0,896	1,000							
11	0,467	0,748	0,904	0,790	0,790	0,677	0,794	0,794	0,581	0,677	1,000						
12	0,418	0,671	0,810	0,896	0,896	0,771	0,886	0,886	0,677	0,771	0,677	1,000					
13	0,418	0,671	0,810	0,896	0,896	0,771	0,886	0,886	0,677	0,771	0,677	1,000	1,000				
14	0,418	0,671	0,810	0,896	0,896	0,542	0,642	0,642	0,458	0,542	0,677	0,771	0,771	1,000			
15	0,516	0,828	0,804	0,904	0,904	0,810	0,717	0,717	0,701	0,810	0,701	0,810	0,810	0,810	1,000		
16	0,488	0,183	0,378	0,488	0,488	0,204	0,325	0,325	0,098	0,204	0,293	0,408	0,408	0,612	0,378	1,000	
17	0,293	0,548	0,378	0,488	0,488	0,612	0,542	0,542	0,683	0,612	0,293	0,612	0,612	0,408	0,567	0,273	1,000

1.Elazig-1, 2.Turtul-5, 3.Turtul, 4.Turtul-4, 5.Kozan-4, 6.Dermason, 7.Siyah, 8.Turtul-6, 9.Kozan-3, 10.Cali, 11.Turtul-2, 12.Susehri, 13.Turtul-1, 14.Turtul-7, 15.Horoz, 16.Calikiran, 17.Onceler-98

When looking at the band patterns created by genotypes, it was determined that 18 of 22 primer pairs formed bands and BMd-8, PVat007, PV-atcc001 and PV-atcc003 primers did not form bands (Table 3).

Single Plant Dry Bean Yield (g). In the study carried out with 17 bean varieties under Kahramanmaras conditions, it was noted that the single plant yield of bean varieties in the statistical study varied between 25.92- 39.55 g and 9 different groups were formed (Table 4).

It was determined that Turtul-2 cultivar had the lowest single plant yield with 25.92 g and Dermason cultivar with the highest single plant yield with 39.55 g. Therefore, it is determined that the averages were statistically different. Single plant yield is a feature determined by genetic characteristics and affected by environmental factors. This is the reason for the difference between genotypes. Our results are similar to the [12, 32].

Dry Bean Seed Yield (kg/da). In terms of seed yield, it was determined that the average varies between 20.76-362.06 kg da^{-1} and 9 different groups were formed. The highest seed yield was 362.06 kg da^{-1} with Dermason cultivar and the lowest seed yield was 20.76 kg da^{-1} with the Kozan-3 genotype (Table 4).

Different seed yield values were obtained from genotypes and this difference may be due to especially genetic structure, geographical conditions, climate characteristics or soil structure. [33] report the impact of the environment on efficiency in their study. Because seed yield is affected by environmental factors as well as genetic structure. Similar results gained by [12, 31, 32].

TABLE 3
DNA marker bands were scored as either present (1) or absent (0) and entered into a binary matrix

		Bean samples																
Primer	Tm value	1	2	3	4	5	6	7	8	9	10	11	12	13	14	15	16	17
DROUGH1	46-47 °C	0	0	0	1	1	1	1	1	1	1	0	1	1	1	1	1	1
SSR-IAC14	47-47 °C	0	0	1	1	1	1	1	1	1	1	1	1	1	1	1	1	0
SSR-IAC63	49-49 °C	0	1	1	1	1	1	1	1	1	1	1	1	1	1	1	0	1
SSR-IAC116	50-50 °C	0	1	1	1	1	1	1	1	1	1	1	1	1	1	1	0	1
SSR-IAC84	50-51 °C	1	1	1	1	1	1	1	1	1	1	1	1	1	1	1	0	0
SSR-IAC26	50-51 °C	0	1	1	1	1	1	1	1	1	1	1	1	1	1	1	0	0
BMd-45AIA	51-47 °C	0	0	1	1	1	0	1	1	0	0	1	1	1	1	0	1	0
BM146	52-52 °C	0	1	1	1	1	1	1	1	1	1	1	1	1	1	1	0	1
BMd-8	52-53 °C	0	0	0	0	0	0	0	0	0	0	0	0	0	0	0	0	0
BMd-48	53-50 °C	1	1	1	1	1	1	1	1	0	1	1	1	1	1	1	1	0
BMD-210	53-54 °C	0	0	0	0	0	1	1	1	1	1	0	1	1	0	0	0	1
PVat007	53-57 °C	0	0	0	0	0	0	0	0	0	0	0	0	0	0	0	0	0
PH7B3	55-55 °C	1	1	1	1	1	1	1	1	1	1	1	1	1	1	1	1	1
PV-at008	55-55 °C	1	1	1	1	1	1	1	1	1	1	1	1	1	1	1	1	1
PH10B11	56-56 °C	1	1	1	1	1	1	1	1	1	1	1	1	1	1	1	1	1
PV-gaat001	56-57 °C	1	1	1	1	1	1	1	1	1	1	1	1	1	1	1	1	1
PV-ag004	57-55 °C	1	1	1	1	1	1	1	1	1	1	1	1	1	1	1	1	1
PV-atcc001	57-58 °C	0	0	0	0	0	0	0	0	0	0	0	0	0	0	0	0	0
PV-aaat001	58-57 °C	0	0	0	0	0	1	1	1	1	1	1	0	0	0	0	0	0
PV-atct001	57-57 °C	0	0	0	0	0	0	0	0	0	0	0	0	0	1	0	1	0
PV-atcc003	57-58 °C	0	0	0	0	0	0	0	0	0	0	0	0	0	0	0	0	0
PV-tttc001	59-57 °C	0	1	1	1	1	1	1	1	1	1	1	1	1	1	1	1	1

TABLE 4
Single Plant Yield and Seed Yield Values for 17 Bean Genotypes in 2014-2015 Years Means

Genotypes	Single Plant Yield*	Seed Yield*
Cali	26.05 G	190.30 F
Calikiran	29.15 D	215.19 E
Dermason	39.55A	362.06 A
Elazig-1	28.60 D	299.50 B
Horoz	28.93 D	140.33 G
Kozan-3	26.83 FG	20.76 H
Kozan-4	26.53 G	21.26 H
Onceler-98	27.98 DEF	307.33 B
Siyah	26.93 FG	22.24 H
Susehri	28.28 DE	306.77 B
Turtul	28.05 DEF	268.19 C
Turtul-1	26.30 G	293.72 B
Turtul-2	25.93 G	157.33 G
Turtul-4	27.20 EFG	236.20 DE
Turtul-5	37.65 B	304.93 B
Turtul-6	31.93 C	303.22 B
Turtul-7	28.30 DE	246.93 CD

*Means are shown that similar letter groups were not significant according to the Duncan Multiple Range Test (DMRP) P<.001

CONCLUSION

The results obtained in our research show that the genetic distances between the genotypes are close, the herbal material used may be due to the collection of a limited or narrow area, or the genetic contraction resulting from self-fertilization.

It can be concluded that there is a high probability of variation in possible hybridization studies with, Turtul-5 with Calikiran, Calikiran with Cali, Elazig-1 with Kozan3, Calikiran with Onceler-98, Calikiran with Turtul-2, Onceler-98 with Turtul-2 and Calikiran with Horoz. On the other hand, it is recommended that breeders further this work with larger populations.

REFERENCES

[1] Gepts, P., Beavis, W.D., Brummer, E.C., Shoemaker, R.C., Stalker, H.T., Weeden, N.F. and Young, N.D. (2005). Legumes as a model plant family. Genomics for food and feed report of the cross-legume advances through genomics conference. Plant Physiology. 137, 1228-1235.

[2] Moreira, D.D.L., Leitão, S.G., Goncalves, J.L.S., Wigg, M.D. and Leitão, G.G. (2005). Antioxidant and antiviral properties of *Pseudopiptadenia contorta* (*Leguminosae*) and of quebracho (*Schinopsis* sp.) extracts. Química Nova. 28(3), 421-425.

[3] Bliss, F.A. (1980). Common bean in hybridization of crop plants (Eds.W.R. Fehr and H.H. Handley), American Society of Agronomy-Crop Singh Science Society of America, Madison, Wisconsin. 273-284.

[4] Singh, S.P. (1999). Integrated genetic improvement. In: Common bean improvement in the twenty-first century. S. P. Singh (ed.). Kluwer Academic Publishers, Dordrecht, The Netherlands. 133-165.

[5] Broughton, W.J., Hernández, G., Blair, M., Beebe, S., Gepts, P. and Vanderleyden, J., (2003). Beans (*Phaseolus* spp.) model food legumes. Plant Soil. 252, 55-128.

[6] Balkaya, A., Yanmaz, R. (2003). Identification of Some Selected French Bean Cultivars by Morphological Properties and Protein Markers, Journal of Agricultural Sciences. 9(2), 182-188.

[7] FAO (2018). Food and Agricultural Organization of United Nations Statistical Database, Dry Bean Production values for World and Turkey,http://www.fao.org/faostat/en/#data/QC (Accessed date: 19.08.2019)

[8] Ekincialp, A. (2012). Determination of genetic relatedness anthracnose diseae (*Colletotrichum lindemuthianum*) (Sacc. and Magnus) Lambs. Scrib.) resistance with phenotypic and molecular methods among bean genotypes in Lake Van basin. Van Yuzuncu Yil University, Institute Of Natural And Applied Sciences, PhD Thesis Van/Turkey. 238 pp.

[9] Tar'an, B., Thomas, E., Michaels and Pauls, K.P. (2002) genetic mapping of agonomic traits in common bean. Crop Science. 42, 544-556.

[10] Coelho, R.C., Faria, M.A., Rocha, J., Reis, A., Oliveira, M .B. P. P., Nunes, E. (2009). Assessing genetic variability in germplasm of *Phaseolus vulgaris* L. collected in Northern Portugal. Scientia Horticulturae. 122, 333-338.

[11] Blair, M. M., Gonzalez, F.L., Kimani and P. M. Butare, L. (2010). Genetic diversity, intergene pool introgression and nutritional quality of common beans (*Phaseolus vulgaris* L.) from Central Africa, Theor. Appl. Genet. 121, 237–248.

[12] Anlarsal, A.E., Yucel, C., Ozveren, D. (2000). The Determination of Seed Yield and Yield Components in Some Bean (*Ph. vulgaris*) Cultivars and Correlations Between These Characters Under the Çukurova Conditions. Turk. J. Agric. For. 24, 19-29.

[13] Girgel, U. (2013). The Determination Of Agronomic And Biological Properties Of Some Culture And Wild Pea Genotypes In Kahramanmaras Conditions. Kahramanmaras Sutcu İmam University Institute for Graduate Studies in Science and Technology,Departmant of Field Crops, PhD Thesis. 123 pp.

[14] Sozen, O., Karadavut, U. (2017a). Determination of the Relationship between Yield and Yield Components of Winter Red Lentil Genotypes under the Conditions of Amik Plain. Turkish Journal of Agricultural and Natural Sciences. 4(4), 468-476.

[15] Bicer, B.T., Albayrak, O., Akinci, C. (2017). Effect of Different Sowing Dates on Yield and Yield Characters in Chickpea. Journal Of Adnan Menderes University Agricultural Faculty. 14(1), 51-57.

[16] Bulyaba, R., Winham D.M., Lenssen, A.W., Moore, K.J., Kelly, J.D., Brick, M.A., Wright, E.M., Ogg J.B. (2020). Genotype by Location Effects on Yield and Seed Nutrient Composition of Common Bean. Agronomy. 10, 347.

[17] SAS (2004) SAS/STAT 9.1. User's guide: Statistics. SAS institute Inc., Carry, NC, USA. 5121 pp.

[18] Duzgunes O, Kesici T, Gurbuz F. (1983). Statistical Methods I. Ankara University, Agricultural Engineering Faculty Press, Ankara, Turkey. 229 pp.

[19] Yu, K., Park, S. J., Poysa, V., Gepts, P. (2000). Integration of simple sequence repeat (SSR) markers into a molecular linkage map of common bean (*Phaseolus vulgaris* L.). The American Genetic Association. 91, 429-434.

[20] Gaitan-Solís, E., Duque, M. C., Edwards, K. J., Tohme, J. (2002). Microsatellite repeats in common bean (*Phaseolus vulgaris*): Isolation, characterization, and cross-species amplification in *Phaseolus* spp. Crop Science. 42, 2128-2136.

[21] Blair, W. M., Pedraza, F., Buendia, H. F., Gaitan, S. E., Beebe, S. E., Gepts, P., Tohme, J. (2003). Development of a genome-wide anchored microsatellite map for common bean Phaseolus vulgaris. Theoretical and Applied Genetics. 107, 1362-1374.

[22] Silva, G. F., Dos Santos, J. B., Ramalho, M. A. P. (2003) Identification of SSR and RAPD markers linked to a resistance allele for angular leaf spot in the common bean (*Phaseolus vulgaris*) line ESAL 550. Genetics and Molecular Biology. 26(4), 459- 463.

[23] Guerra-Sanz, J. M. (2004). New SSR markers of *Phaseolus vulgaris* from sequence databases. Plant Breeding. 123, 87-89.

[24] Sicard, D., Nanni, L., Porfiri, O., Bulfon, D., Papa, R., 2005. Genetic Diversity of *Phaseolus vulgaris* L. and *P. coccineus* L. Landraces in Central Italy. Plant Breeding. 124, 464-472.

[25] Teixeira, F. F., Santos, J. B., Ramalho, M. A. P., Abreu, A. F. B., Guimaraes, C. T., Oliviera, A. C. (2005) QTL Mapping for angular leaf spot in common bean using microsatellite markers. Crop Breeding and Applied Biotechnology. 5(3), 272-278.

[26] Blair, W. M., Giraldo, M. C., Buendia, H. F., Tovar, E., Duque, M. C., Beebe, S.E. (2006). Microsatellite marker diversity in common bean Phaseolus vulgaris L.. Theoretical and Applied Genetics. 113, 100-109.

[27] Benchimol, L. L., De Campos, T., Carbonell, S. A. M., Colombo, C. A., Chioratto, A. F., Formighieri, E. F., Gouvea, L. R. L., De Souza, A. P. (2007). Structure of genetic diversity among common bean (*Phaseolus vulgaris* L.) varieties of Mesoamerican and Andean origins using new developed microsatellite markers. Genetic Resources and Crop Evolution. 54(8), 1747-1762.

[28] Mahuku, G. S., Iglesias, A. M., Jara, C. (2009). Genetics of angular leaf spot resistance in the Andean common bean accession G5686 and identification of markers linked to the resistance genes. Euphytica. 167(3), 381-396

[29] Sambrook, J.F., Russell, D.W. (2001). Molecular Cloning: A Laboratory Manual, 3rd ed., Cold Spring Harbor Laboratory Press. 2100 pp.

[30] Nei, M., Li, W.H., 1979. Mathematical model for studying genetic variation in terms of restriction endonucleases. Proceedings of the National Academy of Sciences of the United States of America. 76, 5269-5273.

[31] Yilmaz, N. (2020). Morphological And Molecular Characterization Of Local Faba Bean (*Vicia faba* L.) Accessions Using Inter-Simple Sequence Repeat (ISSR) Markers. Fresen. Environ. Bull. 29(5), 3756-3763.

[32] Peksen, E., 2005. Comparison Of Some Common Bean (*Phaseolus vulgaris* L.) Genotypes For Seed Yield And Yield Related Characteristics Under Samsun Conditions. J. of Fac. of Agric. OMU. 20(3), 88-95.

[33] Sozen, O., Karadavut, U. (2017b.) The Determination Of Some Genotypic And Phenotypic Parameters For Chemical Composition Of Some Bean Genotypes. Fresen. Environ. Bull. 26(10), 5761-5768.

[34] Yohannes, S., Loha, G., Gessese, M.K. (2020). Performance Evaluation of Common Bean (*Phaseolus vulgaris* L.) Genotypes for Yield and Related Traits at Areka, Southern Ethiopia. Hindawi Advances in Agriculture. 1-8. Article ID:1497530.

Received: **18.08.2020**
Accepted: **07.02.2021**

CORRESPONDING AUTHOR

Alihan Cokkizgin
Gaziantep University,
Vocational School of Higher Education in Nurdagi, Gaziantep – Turkey

e-mail: acokkizgin@gantep.edu.tr

© by PSP Volume 30– No. 05/2021 pages 4935-4942 Fresenius Environmental Bulletin

EFFECT OF PHOSPHORIC ACID SPRAY ON RICE GROWTH AND YIELD UNDER SALINE SODIC SOILS

Mahmoud Abdlehamed Elhity[1], Abdel Hamed Mohammed Omer[1], Bassiouni Abdelrazik Zayed[2], Abdelaziz Ali Assra[3], Montaser M Hassan[4], Yaser M Hafez[5], Khaled A Abdelaal[5,*]

[1]Agronomy Department, Faculty of Agriculture, Kafrelsheikh University, Egypt
[2]Rice Research Department, Field Crops Research Institute, ARC, Egypt
[3]Private Sector, Kafrelshiekh, Egypt
[4]Department of Biology, College of Science, Taif University, P.O.Box 11099, Taif 21944, Saudi Arabia
[5]EPCRS Excellence Center, Plant Pathology and Biotechnology Laboratory, Agricultural Botany Department, Faculty of Agriculture, Kafrelsheikh University, 33516, Egypt

ABSTRACT

The present study was carried out at the farm of El-Sirw Agricultural Research Station Dommitta province during 2018 and 2019 seasons. The main objective of this attempt to finding out the response of Giza 179 rice variety to phosphorous foliar spray at various concentrations and growth stages using phosphoric acid (PA) under saline sodic soil. The experiments were performed in randomized complete block with four replications for each soil. The treatments involved the application of control, 1.5%PA once at mid tillering stage(MT),twice at MT+ panicle initiation stage(PI), thrice at MT+PI+mid booting stage (BT), 2.5% PA once, twice, thrice and 3.5% PA ,once, twice and thrice, basal application of recommended phosphorous in form of calcium superphosphate (P_2O_5) at the rate of 36kg ha^{-1}. The obtained results could be summarized as follows; the tested phosphorous treatments significantly influenced the studied growth characteristics, phosphors uptake kg P, leaf phosphorus content, grain yield and its attributes, in the two seasons of study under both soils. Elevating concentration of PA applied more than one fold up to three folds including mid booting stage showed high efficient effective to improve rice growth, yield attributes and grain yield under saline sodic soil. Calcium superphosphate as a basal application and 3.5% PA as a foliar spray applied three times at mid tillering+ panicle initiation+ mid booting stage were at apar and significantly introduced the highest value of the most studied characteristics under normal and salinity soil during the study seasons. It could be concluded that phosphoric acid applied at the rate of 3.5%PA applied thrice could be equivalent to the recommended dose of calcium superphosphate under saline sodic soil.

KEYWORDS:
Rice, phosphorus spray, saline sodic soil, chlorophyll content

INTRODUCTION

Egypt is classified as semi-arid country with large salt affected soil particularly saline sodic soil sort. The nutrient availability, especially P availability is restricted under saline sodic soils. At the same time, rice crop in Egypt is cultivated at the northern part of Delta, whereas, saline sodic soils are prevailing and improving rice production under such condition obtained by proper management of nutrient involving phosphorous[1]. Salt stress is one of the most harmful factors affect growth and yield in many plants [2-8]. Generally, in Egypt, the phosphorus availability in soil solution is relatively low, because they are mainly fixed on the soil complex as insoluble forms and that hold true under saline sodic soil with high pH value [9]. Furthermore, optimum nutrient management of rice is deemed one of the important factors that control production levels of rice [10-13]. Phosphorus is one of the essential elements required for rice growth and development; it occupied the second order next to nitrogen. It plays a vital roles in the plants such as; early root and seedling growth, promotion of early heading and uniform maturity, seed formation and quality. Also, it acts a physiological role in photosynthesis, energy storage and transfer, respiration and cell division [14]. Zayed et al. [1] stated that applying phosphorous either foliar or basal addition induced apparent improvement in rice growth and yields of rice under salt affected soil. Moreover, farmers used to add the entire amount of phosphorus during soil tillage. As a result, a high percent of the added phosphorus is fixed in an insoluble phase unavailable for plant uptake. Therefore, phosphorus management must focus on the buildup and maintenance of adequate available phosphorus level in the soil to ensure that it does not limit rice growth [15]. Nutrients foliar application could be used to replace soil-applied fertilizer, in which, it overcomes soil fertilization limitations such as; leaching, insoluble fertilizer precipitation,

TABLE 1
Chemical and physical analysis of the experimental site of saline sodic soil in 2018 and 2019 seasons.

Character	2018	2019	Character	2018	2019
pH	8.3	8.2	Soluble anions meq.l-1	-	-
ECe dSm^{-1}	7.3	7.0	CO3--	-	-
SAR %	17	16.1	HCO3-	9.6	8.60
Available N, mg kg^{-1}	29	30	CL-	53.0	50.0
Available P, mg kg^{-1}	10	11	SO4--	10.4	11.4
Available K, mg kg^{-1}	400	380	Available micronutrients ppm	-	-
Soluble cations meq.l^{-1}	-	-	Fe^{++}	5.23	5.95
Ca^{++}	10.0	11.3	Zn^{++}	0.90	1.01
Mg^{++}	9.40	8.0	Mn^{++}	4.60	4.50
K^{+}	0.50	0.70	Soil texture	Clayey	Clayey
Na^{+}	54.0	50.0			

antagonism between certain nutrients, heterogenic soils unsuitable for low rates and fixation/absorption reactions like in the case of phosphorus and potassium [9]. Phosphoric acid, is a rich source for phosphorous and it is also called orthophosphoric acid, (H_3PO_4), the most important oxygen acid of phosphorus as well as it is used to make phosphate salts for fertilizers. Mohamed and Ali [16], showed that application of phosphoric acid reflected the highest values of plant growth, chemical constituent, head yield and its quality compared with calcium super phosphate and rock phosphate. Mosali et al. [17] clarified that foliar application of phosphoric acid was effective in compensating mid-season phosphorus deficiency in winter wheat by low rates of foliar applied and subsequently resulted in higher phosphorus use efficiency. Zayed et al. [18] found that applying phosphoric acid as foliar spray at mid tillering + panicle initiation significantly improved rice growth, yield attributes and rice grain yield under both normal and saline soils. The current research was undertaken to address the benefit role of phosphoric acid as foliar application or phosphorus as a basal application for rice grown under saline sodic soil conditions.

MATERIALS AND METHODS

The present study was carried out at the farm of El-Sirw Agricultural Research Station, Dommitta province during 2018 and 2019 seasons. The attempt was design is finding out the response of Giza 179 rice variety to phosphorous foliar spray at various concentrations and growth stages using phosphoric acid (PA) under saline sodic soils. The experiments were performed in randomized complete block design with four replications. The treatments involved the application of control, 1.5%PA once at mid tillering stage(MT), twice at MT+ panicle initiation stage(PI), thrice at MT+PI+mid booting stage (BT), 2.5% PA once, twice, thrice and 3.5% PA ,once, twice and thrice, basal application of recommended phosphorous in form of calcium superphosphate (% P_2O_5) at the rate of 36kg ha^{-1}. The used phosphoric acid was (orthophosphoric acid H_3PO_4) was 70%, with density of 1.60gcm^3 and concentration of 345gm L^{-1}. The soil chemical physical properties of experimental sites in both soils were analyzed and presented in Table1.

Seedlings aged 30 days were transplanted at spacing of 20X20cm between rows and plants with 4 seedlings hill^{-1} on May25 in each site. The plot size was 2m wide x 5 m length (10 m^2). Phosphorous was applied as indicated in the treatments. Nitrogen in the form of urea at the rate of 165 kg ha^{-1} was applied in three equal doses in the saline soil and two doses in the normal soil. Potassium in the form of potassium sulfate at the rate of 57 kg k_2O ha^{-1}was applied as basal application.

At heading, five hills were randomly taken from each plot, transferred to lab to estimate, leaf area index (LAI),flag leaf area (cm$^{2)}$, flag lea dry weight (g), and chlorophyll content (SPAD) as well as phosphorous leaf content and dry matter production (DM m^{-2}) according to Yoshida et al. [19]. At harvest, panicles of ten hills for each plot were counted to determine the number of panicles hill^{-1}and plant height (cm) was measured. Ten main panicles from each subplot were used to determine panicle length (cm), number of filled and unfilled grains panicle $^{-1}$ and 1000-grain weight. The plants of the six inner rows of each subplot were harvested, dried, threshed, then grain and straw yields were determined at 14 % moisture content and converted into t ha^{-1}. All data collected were subjected to standard statistical analysis of variance following the methods described by Gomez and Gomez [20] using the computer program (COSTAT). The treatment means were compared using Duncan's multiple range test [21]. * and ** symbol used in all Tables indicate the significant at 5% and 1% levels of probability, respectively, while NS means not significant.

RESULTS AND DISCUSSIONS

Data in Table 2 showed that the effect of phosphorous foliar application had significant effect on, leaf area index, flag leaf area and chlorophyll content of Giza 179 rice cultivar in 2018 and 2019 seasons. It is obviously that p addition either as foliar or basal application had positive and significant effect on above-mentioned traits in both seasons. Gradual increasing P foliar concentration with application frequent including late growth stage significantly boosted the mentioned parameters in both seasons. The highest values of above-mentioned traits were obtained with the treatment of calcium super phosphate as basal application without any significant differences among 3.5% liters ha^{-1} of phosphoric acid as a foliar spray application in both seasons. The lowest value of chlorophyll content was recorded by control treatment without any significant differences with those obtained by 1.5% PA sprayed once or twice. The positive role of P application on both chlorophyll content and LAI is mainly contributed to its role in increasing the ATP energy compound in plant tissue reflect on cell division and elongation reflected on large leaf area. Increasing ATP had a beneficial effect of on plant pigments formation resulted in high chlorophyll content. Applying phosphoric at late growth stage ensured well and healthy growth of flag leaf resulted in large flag leaf area. Phosphorous spraying is rapid correct for phosphorus deficiency because of high alkalinity and salinity of soils reflecting on good growth performance. Similar findings were obtained by Zayed [1], Mohamed and Ali [16] and Zayed et al. [18].

Data in Table 3 showed that phosphors treatments as a basal application had significant effect on flag leaf dry weight, P% and dry matter production of Giza 179 rice cultivar in 2018 and 2019 seasons. Gradual increment of phosphoric acid foliar concentration up to 3.5% was significantly induced gradual increment in the above mentioned traits. The highest values of dry matter production of plant and flag leaf and P% were obtained with the treatment of calcium super phosphate as a basal application in 2018 and 2019 seasons without any significant differences between 3.5%PA sprayed thrice at mid tillering + panicle initiation+ mid booting stages in both seasons. The lowest values of above-mentioned traits were recorded with control treatment without significant in both seasons (Table 3). Qadar [22] and Naheed et al. [23] reported that phosphorous application either basal or foliar spray encourage rice growth involving shoot and root systems resulted in high capability for nutrient uptake and foliar spray of P increased its content in leaf and thus avoiding the problem happened under saline sodic soil. Phosphorus has a significant effect to reduce the adverse effects of salinity on growth. As phosphorus increased, it ameliorated the effect of salinity on shoot length and dry weight of different parts of plants. Furthermore, the enhancing effect of phosphoric acid on vegetative growth may be due to the main role in reducing soil pH, which can improve the availability of mineral elements, and make them more soluble and available for absorption by plants, and in turn increased the vegetative growth. The current findings are in agreement with those of Zayed et al. [18], Marschner [24], Ragab et al. [25] and Hafez et al. [26].

TABLE 2
Leaf area index (LAI), flag leaf area (cm^2) and total chlorophyll content (SPAD value) of rice affected by phosphorus treatments under normal and saline soils in 2108 and 2019.

Factor	Leaf area index		Flag leaf area (cm^2)		Total Chlorophyll (SPAD)	
control	4.83g	4.60g	19.7h	20.6g	40.3e	38.9h
1.5% PA once	4.90g	4.63g	20.5gh	21.0g	40.5de	39.0gh
1.5% PA twice	5.10fg	4.83f	20.7g	21.5f	40.6de	39.3gh
1.5% PA thrice	5.36def	5.20e	21.6f	22.2e	40.8cd	39.8ef
2.5 %PA once	5.13efg	4.93f	22.2ef	21.7f	40.7d	39.5fg
2.5 %PA twice	5.56cd	5.30de	22.7de	22.5e	41.1c	40.1de
2.5 % PA thrice	5.80bc	5.56c	23.4d	23.1d	41.7b	40.6c
3.5%%PA once	5.30def	5.40d	23.1de	23.0	41.1c	40.4cd
3.5% PA twice	5.50cde	5.70c	25.6c	24.7c	41.6b	41.1b
3.5 PA thric	6.20ab	6.13ab	29.6ab	27.93ab	42.0a	41.7a
Basal CSP	6.40a	6.23a	30.3a	28.30a	42.1a	41.2b
F test	**	**	**	**	**	**
LSD0.05	0.28	0.15	0.84	0.42	0.29	0.39

PA= phosphoric acid, once at mid tillering(MT), twice,at MT+ panicle initiation(PI). Thrice, MT+PI+ mid booting stage(MB)

TABLE 3
Flag leaf dry weight g , leaf phosphorus content (P%) and dry matter gm^{-1}of rice affected by phosphorus treatments under normal and saline soils in 2108 and2019.

treatment	Flag leaf dry weight		P%		Dry matter g m^{-1}	
	2018	2019	2018	2019	2018	2019
control	0.247h	0.217h	0.188g	0.186g	957.6i	975.3i
1.5% PA once	0.258gh	0.220gh	0.191fg	0.187fg	965.0i	976.0i
1.5% PA twice	0.262g	0.231fg	0.197efg	0.191efg	978.3hi	1060h
1.5% PA thric	0.272fg	0.234f	0.204de	0.197e	1065g	1155f
3 %PA once	0.279ef	0.232fg	0.200ef	0.195ef	994.3h	1113.3g
3 %PA twice	0.287e	0.255e	0.208de	0.208d	1168.3f	1240e
3 % PAthric	0.326d	0.272d	0.219c	0.217c	1240d	1283.3d
3.5%PA once	0.327d	0.273d	0.212cd	0.211cd	1196.6e	1288.3d
3.5 % PA twice	0.354c	0.300c	0.243b	0.254b	1360c	1336.6c
3.5% PA thric	0.386b	0.344b	0.315a	0.309a	1456.6b	1493.3b
Basal CSP	0.426a	0.388a	0.315a	0.303a	1593.3a	1616.6a
F test	**	**	**	**	**	**
LSD0.05	0.011	0.010	0.008	0.006	18.87	21.05

PA= phosphoric acid, once at mid tillering(MT), twice,at MT+ panicle initiation(PI). Thrice, MT+PI+ mid booting stage(MB)

TABLE 4
Plant height (cm), number of panicles hill-^{1} and panicle length (cm)of rice affected by phosphorus treatment under saline sodic soils in 2108and 2019 seasons.

treatment	Plant height (cm)		Panicle number		Panicle length (cm)	
	2018	2019	2018	2019	2018	2019
control	72.6d	76.0f	16.3f	17.1e	18.7e	17.8e
1.5% PA once	73.0d	76.3ef	16.8ef	17.0e	19.05e	18.0e
1.5% PA twice	74.3cd	77.3def	18.1cd	18.1d	19.8d	18.6d
1.5% PA thrice	75.6cd	78.0def	18.5c	18.5d	19.7d	19.00d
2.5% %PA once	74.6cd	77.6def	17.4de	18.4d	20.2c	19.00d
2.5 %PA twice	78.0bc	79.3d	18.8c	19.0cd	20.5b	19.4bc
2.5 % PA thrice	78.3bc	81.3c	18.9c	19.5c	20.7ab	19.7ab
3.5%PAL once	77.3bc	78.3de	18.9c	19.4c	20.8ab	19.4bc
3.5 % PA twice	81.0bc	82.6c	20.7b	21.5b	20.90ab	20.04ab
3.5% PA thrice	84.3a	84.3ab	21.4b	22.4b	21.1a	20.30a
Basal CSP	84.6a	85.3a	23.06a	24.0a	21.12a	20.35a
F test	**	**	**	**	**	**
LSD0.05	3.00	1.46	0.86	0.72	0.30	0.4

PA= phosphoric acid, once at mid tillering(MT), twice,at MT+ panicle initiation(PI). Thrice, MT+PI+ mid booting stage(MB)

Phosphorous application either as basal or spray markedly increased the nutrient content that may be due to their roles in fixing atmospheric nitrogen, reducing soil pH and increasing solubility of phosphorus and potassium in root rizhosphere and consequently increased nutrient uptake and accumulation by plants. Furthermore, addition of phosphorous as foliar spray or basal application might be relieved the phosphorus deficiency happened under saline sodic soil resulted higher concentration of leaf content of phosphorus. The present results are agreed with those reported by Mohamed and Ali [16], Elkelish et al. [27] and Abdelaal et al. [28].

The results presented in Table 4 indicated that plant height, panicle number hill^{-1} and panicle length were significantly influenced and improved by phosphorous treatment involving phosphoric acid foliar application and basal application in 2018 and 2019 seasons. Rising concentration of phosphorus acid with more than two round application including late foliar application significantly increased plant height, panicle number hill^{-1} and panicle length compared with control in both seasons. The highest value of above-mentioned traits were obtained by applied 36 kg P_2O_5 ha^{-1} as a basal application followed by 3.5% PA applied thrice at mid tillering, panicle imitation and mid booting stages in both seasons, Couple treatment of PA foliar with 3.5% concentration three times and basal application of phosphorous were comparable in both seasons with respect to plant height, panicle number and panicle length. Phosphorus deficiency decreased plant height, tiller and panicles number plant^{-1} of rice plant [29,30].

Matsua et al. [31] referred that it is necessary to apply much P fertilizers to beef up rice plants to promote the P absorption for increased effective tillering and consequently increased panicles. Calcium super phosphate application on soil ensured optimum environment for rice growth under salt stresses with high pH as seen in Table1 resulted in higher tillers and bearing tillers. Generally, the phosphorous application enriched rice plants ATP energy compound that might be activated the cell elongation and division lead to more bud formation. The present findings are in an agreement with those reported by Zayed [1] and El-Arqan et al. [32].

Data in Table 5 stated that panicle weight, number of filled and unfilled grains panicle^{-1} and 1000 grain weight were significantly affected by phosphoric acid spray and basal application of calcium super phosphate salinity soils during 2018 and 2019 seasons. It was obviously that foliar spray of phosphoric acid at the concentration of 3.5% applied at mid tillering + panicle initiation + mid booting stages showed high efficiency to improve the grain characteristics; panicle weight, number of filled grains panicle^{-1}, panicle, fertility and 1000-grain weight in both study seasons(Table 5). The latter mentioned treatment possessed the heaviest panicle and 1000 grain and the highest values of filled grain panicle^{-1} as well as the lowest values of unfilled grains number panicle^{-1} without any significant difference was those obtained by basal application of phosphorous treatment in both seasons (Table 5). Low concentration of 1.5%PA sprayed once or twice and control treatments were comparable regarding panicle weight, number of filled grains, number of unfilled grains panicle^{-1} and 1000grain weight in both seasons. From going discussion, addition P as foliage application with more two folds at certain rice growth stages including late growth one is very benefit and effective under saline sodic soil to overcome the problem of poor availability of phosphorous. Interestingly, phosphoric acid application via foliage system at critical growth stage including late ones showed improvement in flag leaf characteristics such measured ones in this study resulted in apparent improvement in current photosynthesis that conflict on grain filling producing heavy panicle and grain and ultimately grain yield. The positive role of phosphorous application in salt stress alleviation might increase panicle exertion and panicle quality. Furthermore, applying phosphorus increased P leaf content, particularly active ones such as flag leaf, first and second leaves ensuring high ATP content with high plant pigments content that resulted in high photosynthesis rate with higher net assimilation at pre and post heading reflected on good grain filling and heavy grains in the terms of heavy panicle.). The phosphorous application involving foliar or basal application might be reduced the Na^+ accumulation and uptake in active leaf might increase its photosynthesis rate that attributed to higher filled grain [13,23]. The current findings are in conformity with those reported by Sahar and Burbey [33], Kalyanasundaram and Surrndirakumar [24], Elayaraja and Angayarkanni [35] and Reddy et al. [36].

TABLE 5
Panicle weight, number of filled and unfilled grains panicle^{-1} and 1000 grain weight (g) of rice affected by phosphorus treatment under saline sodic soils in 2018 and 2019.

Treatment	Panicle weight (g)		No of filled grains panicle^{-1}		No of unfilled grains panicle^{-1}		1000-grain weight (g)	
	2018	2019	2018	2019	2018	2019	2018	2019
control	2.61d	2.71i	88.0h	85.3g	28.0a	34.3a	22.9e	23.1e
1.5% PA once	2.67d	2.77hi	89.1h	88.0g	21.6b	30.6b	23.1de	23.2de
1.5% PA twice	2.76d	2.82gh	90.6h	93.0f	19.3c	24.6c	23.2de	23.4de
1.5% PA thric	2.81d	2.93ef	99.6f	110.3d	15.6e	21.0c	23.5cde	23.7cde
2.5 %PA once	2.78d	2.87fg	94.3g	97.3e	17.6d	18.3e	23.2de	23.4de
2.5 %PA twice	2.88cd	2.98e	104.3e	109.0d	15.3e	14.6g	23.6cd	23.8cd
2.5 % PA thrice	3.06bc	3.10d	118.6d	117.0c	12.6f	13.3g	24.1b	24. 3b
3.5%PA once	2.68d	2.99e	98.6f	107.0d	15.3e	16.6f	23.5cde	23.7cde
3.5 % PA twice	3.26b	3.25c	125.6c	119.0c	11.6f	10.3h	23.8bc	24.1bc
3.5% PA thrice	3.51a	3.62a	136.6ba	134.0a	3.33h	3.33j	25.8a	25.6a
Basal CSP	3.41ab	3.50ab	135.0ab	130.0ab	4.66h	4.00j	25.1ab	25.4ab
F test	**	**	**	**	**	**	**	**
LSD0.05	0.20	0.16	2.46	3.08	1.66	1.43	0.40	0.38

PA= phosphoric acid, once at mid tillering(MT), twice,at MT+ panicle initiation(PI). Thrice, MT+PI+ mid booting stage(MB)

TABLE 6
Yields of rice affected by phosphorus treatment under saline sodic soils in 2108 and 2019.

Factors	Grain yield t ha^{-1}		Biological yield t ha^{-1}		Harvest index	
	2018	2019	2018	2019	2018	2019
control	6.00f	6.13h	15.7g	15.4g	0.38de	0.39cd
1.5% PA once	6.20ef	6.23h	15.8g	15.6fg	0.39d	0.40c
1.5% PA twice	6.23e	6.33g	16.0g	15.8ef	0.39d	0.40c
1.5% PA thrice	6.76cd	6.90e	16.3f	16.5cde	0.41c	0.42b
2.5 %PA once	6.53de	6.60f	16.2f	16.1efg	0.40cd	0.41bc
2.5%PA twice	6.83cd	6.86e	16.87de	16.5cde	0.40cd	0.42b
2.5 % PA thrice	6.96cd	7.16d	17.00d	16.86cd	0.41c	0.42b
3.5%PA once	6.83cd	7.16d	16.6e	16.5cde	0.41c	0.43ab
3.5 % PA twice	7.200c	7.36c	17.5c	16.9c	0.41c	0.43ab
3.5% PA thrice	7.70ab	8.0ab	18.5b	18.3b	0.44a	0.44a
Basal CSP	8.03a	8.20a	19.0a	18.7a	0.42ab	0.44a
F test	**	**	**	**	*	**
LSD0.05	0.33	0.23	0.40	0.330	0.019	0.013

PA= phosphoric acid, once at mid tillering(MT), twice,at MT+ panicle initiation(PI). Thrice, MT+PI+ mid booting stage(MB)

Data in Table 6 indicate that different P treatments had a significant improvement on rice yields and harvest index such condition in 2018 and 2019seasons. Furthermore, harvest index was significantly responded to P spray and basal application in both seasons (Table 6). It is worthy to mention that the treatment of 3.5% PA sprays at mid tillering, panicle initiation and mid booting stages and basal application treatments were comparable in both study seasons. The last finding confirmed that spraying phosphoric acid of 3.5% three times at certain growth stages, mid tillering, panicle initiation and mid booting stage is equivalent to basal application at rate of 36kg P_2O_5 ha^{-1}. Also, spraying phosphoric acid at low concentration of 1.5% during only mid tillering stage or twice at mid tillering and panicle initiation did not bring more yields improvement over control treatment (Table 6). By the way the highest values of yields were obtained by basal application of basal application of phosphorous without significant differences with the treatment of 3.5% PA spray at mid tillering, panicle initiation+ mid booting stages in both seasons (Table 6). Phosphorus fixation in soil involves both adsorption and precipitation reactions, although adsorption is dominant over a short period [38]. Root P uptake during grain filling contributes up to 70% of final grain P content [38]. Kwanho [39] suggest that when exogenous P supply during grain filling is limited, the P demand of developing seeds necessitate premature remobilization of P from vegetative tissues, with consequent reductions in photosynthesis, this study include foliar spray of P at booting stage. Phosphorous application either as basal or spray, markedly increased chlorophyll content in rice, and contribute to high photosynthetic rate. Moreover, P application at late booting stage might increase some biochemical compounds such as RNA and DNA as well as the energetic compound i.e. NADP, FADP and ATP result in cell division and elongation and leading to for heavy and large flag leaf. Both large leaf area and heavy weight of flag leaf with higher chlorophyll consequently the greatest amount of photosynthetic metabolism stream which is directly transformed to spikelet resulted in higher yield components and finally higher yields. Our results are in agreement with those found by Zayed et al. [18], Reddy et al. [36] and Ehsan et al. [40].

CONCLUSION

Under saline sodic soil, appropriate implementation of phosphorus fertilizer application could be brought out by applying phosphoric acid by foliage application three times at mid tillering, panicle initiation and mid booting stage in the concentration of 3.5%. Using phosphoric acid as foliar spray at the concentration of 3.5% at mid tillering, panicle initiation and mid booting stages was equivalent to the recommended dose of calcium superphosphate as a basal application under saline sodic soil. Furthermore, foliar spray of phosphorous late growth stage in the term of booting stage is much needed to fetch high rice grain yield under saline sodic soil.

ACKNOWLEDGEMENTS

The authors of this work deeply appreciate the deanship of scientific research for funding this work by researchers supporting Project number (TURSP-2020/119), Taif University, Saudi Arabia. The authors would like to thank all members of Plant Pathology and Biotechnology Lab. and EPCRS Excellence Centre, Department of Agricultural Botany, Faculty of Agriculture, Kafrelsheikh University, Egypt.

REFERENCES

[1] Zayed, B.A. (2012) The role of phosphorous management in salinity tolerance alleviation in rice crop. Egyptian J. of Agric. Res. 90 (2), 667-685.

[2] Al Kahtani, M. D. F., Attia, K. A., Hafez, Y.M., Khan, N., Eid, A.M., Ali, M.A.M., and Abdelaal, Kh.A.A. (2020) Chlorophyll Fluorescence Parameters and Antioxidant Defense System Can Display Salt Tolerance of Salt Acclimated Sweet Pepper Plants Treated with Chitosan and Plant Growth Promoting Rhizobacteria, Agronomy. 10, 1180.

[3] Hafez, Y., Elkohby, W. Mazrou, Y.S.A., Ghazy, M., Elgamal, A., Abdelaal, Kh.A.A. (2020) Alleviating the detrimental impacts of salt stress on morpho-hpysiological and yield characters of rice plants (*Oryza sativa* L.) using actosol, Nano-Zn and Nano-Si. Fresen. Environ. Bull. 29(8), 6882-6897

[4] Abdelaal, Kh.A.A., Mazrou, Y.S.A. and Hafez, Y.M. (2020) Silicon Foliar Application Mitigates Salt Stress in Sweet Pepper Plants by Enhancing Water Status, Photosynthesis, Antioxidant Enzyme Activity and Fruit Yield. Plants. 9, 733.

[5] Hasan, M. K., El Sabagh, A., Md, S. I., Sikdar, Md., Alam, J., Ratnasekera, D., Barutcular, C., Abdelaal, Kh.A. A. and Islam, M. S. (2017) Comparative adaptable agronomic traits of Blackgram and mungbean for saline lands, Plant Archives. 17(1), 589-593.

[6] Abdelaal, Kh. A.A., EL-Maghraby, L.M., Elansary, H., Hafez, Y.M., Ibrahim, E.I., El-Banna, M., El-Esawi, M. and Elkelish, A. (2020) Treatment of Sweet Pepper with Stress Tolerance-Inducing Compounds Alleviates Salinity Stress Oxidative Damage by Mediating the Physio-Biochemical Activities and Antioxidant Systems. Agronomy. 10, 26.

[7] El-Banna, M. F. and Abdelaal, Kh. A. A. (2018) Response of Strawberry Plants Grown in the Hydroponic System to Pretreatment with H_2O_2 Before Exposure to Salinity Stress J. Plant Production, Mansoura Univ. 9 (12), 989-1001.

[8] Helaly, M.N., Mohammed, Z., El-Shaeery, N. I., Abdelaal, Kh. A.A. and Nofal, I.E. (2017) Cucumber grafting onto pumpkin can represent an interesting tool to minimize salinity stress. Physiological and anatomical studies. Middle East Journal of Agriculture Research. 6 (4), 953-975.

[9] Alshaal, T. and El-Ramady, H. (2017) Foliar Application: from Plant Nutrition to Biofortification. The Environment, Biodiversity & Soil Security. 1, 71- 83.

[10] Singh, B. and Singh, V.K. (2017) Chapter 10 Fertilizer Management in Rice. Springer International Publishing AG 2017 217 Chauhan, B., Jabran, K., Mahajan, G. (eds.), Rice Production Worldwide.

[11] Abd El-Lattef, A.S., Elkhoby, W.M., Abdelaal, Kh. A.A., and Mohamed, A.A.A. (2014) Genetic behavior of morphology, yield, yield components and grain quality in Rice (*Oryza sativa* L.), J Plant Production, Mansoura Univ. 5, 1945-1963.

[12] Elkhoby, W. M., El-khtyar, A.M., Hassan, H. M., Mikhael, B. B. and Abdelaal, Kh.A.A. (2013) Effect of spilt application of nitrogen fertilizer on morpho-physiological attributes and grain yield of broadcast seeded Egyptian hybrid rice (1) J Plant Production, Mansoura Univ. 4, 1259-1280.

[13] Hafez, Y., Elkohby, W., Mazrou, Y.S.A., Ghazy, M., Elgamal, A. and Abdelaal, Kh.A.A. (2020) Alleviating the detrimental impacts of salt stress on morpho-physiological and yield characters of rice plants (*Oryza sativa* L.) using actosol, nano-Zn and nano-Si. Fresen. Environ. Bull. 29, 6882-6897

[14] El-Ghamry, A.M., Mosa, A.A. and El-Naggar, E. M. (2009) Optimum Time for Phosphorus Fertilization on Egyptian Alluvial Soil. Acta Agronomica Hungarica. 57(3), 363–370.

[15] Fairhurst, T,H., Dobermann, A., Quijano-Guerta, C., Balasubramanian, V. (2007) Mineral deficiencies and toxicities. In: Fairhurst TH, Witt C, Buresh RJ, Dobermann A, editors. Rice: a practical guide to nutrient management, 2nd ed. International Rice Research Institute, Los Baños; International Plant Nutrition Institute, Norcross. International Potash Institute, Berne. 46–86

[16] Mohamed M. HM. and Ali, M.M. (2016) Effect of Phosphorus Fertilizer Sources and Foliar Spray with Some Growth Stimulants on Vegetative Growth, Productivity and Quality of Globe Artichoke. International Journal of Plant & Soil Science. 13 (1), 1-15.

[17] Mosali, J., Desta, K. R., Teal, K., Freeman,K.W., Martin, K.L., Lawles, J.W. and Raun, W.R. (2006) Effect of foliar application of phosphorus on winter wheat grain yield, phosphorus uptake, and use efficiency. J. Plant Nutr. 29, 2147-2163.

[18] Zayed, B.A., Okasha, A.M. and Rashwan, E. (2019) Impact of different rates of phosphoric acid foliar spraying on rice growth and yield traits under normal and saline soils conditions. East African Scholars Journal of Agriculture and Life Sciences. 2 (2), 56-66.

[19] Yoshida, S., Forno, D.A., Cock, J.H. and Gomez, K.A. (1971) Laboratory manual for physiological studies of rice .IRRI, Los Banos, Philippines. Pp 61.

[20] Gomez, K .A. and Gomez, A.A. (1984) Statistical procedures for agricultural research. 2nd Ed. John Wiley and Sons, New York, USA.
[21] Duncan, B.D. (1955) Multiple ranges and multiple F-test. Biometrics. 11, 1-42.
[22] Qadar, A. (1998) Alleviation of sodicity stressed rice genotypes by phosphorus fertilization. Plant Soil. 203 (2), 269-277.
[23] Naheed, G., Shahbaz, M. and Akram N. A. (2008) Interactive effect of rooting medium application of phosphorous and NaCl on plant biomass and mineral nutrient of rice (*Oryza sativa* L.). Pak. J. Bot. 40 (4), 1601-1608.
[24] Marschner, H. (1997) Mineral nutrition of higher plants. Second Printing, Academic Press INC. San Diego. 889.
[25] Ragab, A.Y, Geries, L.S.M, Abdelaal, Kh.A.A. and Hanna, S.A. (2019) Growth and productivity of onion plant (*Allium cepa* L.) as affected by transplanting method and NPK fertilization. Fresen. Environ. Bull. 28(11), 7777-7786.
[26] Hafez, Y. M., Attia, K.A., Alamery, S., Ghazy, A., Al-Dosse, A., Ibrahim, E., Rashwan, E., El-Maghraby, L., Awad, A. and Abdelaal, Kh. A.A. (2020) Beneficial Effects of Biochar and Chitosan on Antioxidative Capacity, Osmolytes Accumulation, and Anatomical Characters of Water-Stressed Barley Plants, Agronomy. 10, 630.
[27] Elkelish, A., Qari, S.H., Mazrou, Y.M., Abdelaal, Kh.A.A., Hafez, Y.M., Abu-Elsaoud, A. M., Batiha, G., El-Esawi, M., El Nahhas, N. (2020) Exogenous Ascorbic Acid Induced Chilling Tolerance in Tomato Plants Through Modulating Metabolism, Osmolytes, Antioxidants, and Transcriptional Regulation of Catalase and Heat Shock Proteins. Plants. 9, 431.
[28] Abdelaal, Kh.A.A., Hafez, Y.M., El Sabagh, A. and Saneok H. (2017) Ameliorative effects of Abscisic acid and yeast on morpho-physiological and yield characteristics of maize plant (*Zea mays* L.) under water deficit conditions. Fresen. Environ. Bull. 26(12),7372-7383.
[29] Alam, M.M., Ali, M. H., Amin, A.K.M. and Hasanuzzaman, M. (2009) Yield attributes, yield and harvest index of three irrigated rice varieties under different levels of phosphorous. Advances in Biological Research. 3(3-4), 132-139
[30] Aide, M. and Picker, J. (1996) Potassium and Phosphorus Nutrition in Rice. Information from 1996 Missouri Rice research Update.
[31] Matsua, T., Kumazawa, K., Ishii, R., Ishihara, K. and Hirata, H. (1995) Science of the plant. Volume Two phyliosophy. Food and Agriculture Policy Research Centre, Tokyo. Japan. pp. 1240.
[32] El-Arqan, M. Y., El-Hamdi, Kh. H., Seleem, E. M. and El- Tantawy, I. M. (2002) Nutrient uptake of sugar beet as affected by NPK fertilization and soil salinity levels. Egypt. J. Soil Sci. 42 (4), 783-797.
[33] Sahar, A, and Burbey, N. (2003) Effect of nitrogen, phosphorus and potassium (NPK) compound dosages on the growth and yield of lowland rice. J. Stigma (Indonasia). 11(1), 26-29.
[34] Kalyanasundaram, D. and Surrndirakumar, P.S. (2003) Integrated nutrient management in hybrid rice ADTRH1. Advances in Plant Sciences. 16(1), 171-175.
[35] Elayaraja, D. and Angayarkanni, A. (2007) Effect of foliar spray of nitrogen and phosphorous on yield attributes, yield and harvest index of rice follow black gram. J. of Ecology. 21(3), 231-234.
[36] Reddy, N. M., Keshhavulu, K., Durga, K.K., Ankaiah, R. and Kumar, A. (2009) Effect of nutrients alternate to GA3 on yield and quality in hybrid rice seed production. Research on Crop. 10(3), 718-727.
[37] Choudhury, A.T.M.A., Kennedy, I.R., Ahmed, M.F. and Kecskes, M.L. (2007) Phosphorus Fertilization for Rice and Control of Environmental Pollution Problems Pakistan Journal of Biological Sciences. 10 (13), 2098-2105.
[38] Julia, C., Wissuwa, M., Kretzschmar, T.,, Jeong K. and Rose, T. (2016) Phosphorus uptake, partitioning and redistribution during grain filling in rice. Annals of Botany. 118 (6), 1151–1162
[39] Kwanho J. (2016) Phosphorus remobilization during grain filling in rice. PHD thesis submitted to Southern Cross University. Chapter 5 pp: 95
[40] Ehsan, U., Rehman, A., Arshad, Q. and Shah, S.S. (2009) Yield response of fine rice to NP fertilizer and weed management practices. Pak. J. Bot. 41(3), 1351-1357.

Received: **25.08.2020**
Accepted: **02.02.2021**

CORRESPONDING AUTHOR

Khaled A Abdelaal
EPCRS Excellence Center,
Plant Pathology and Biotechnology Laboratory,
Agricultural Botany Department,
Faculty of Agriculture,
Kafrelsheikh University, 33516 Egypt

e-mail: khaled_elhaies@yahoo.com

© by PSP Volume 30– No. 05/2021 pages 4943-4952 Fresenius Environmental Bulletin

BIOLOGICAL MECHANISM OF THE REMOVAL OF *MICROCYSTIS* USING LOW INTENSITY ULTRASONIC IRRADIATION

Bo Wang[1], Lingxi Luo[2], Ximing Zeng[1], Hui Zeng[1,*]

[1]Peking University, ShenZhen Graduate School, Shenzhen 518055, China
[2]Ier Environmental Protection Engineering Technique Co. Ltd., Shenzhen 518071, China

ABSTRACT

Low intensity ultrasound (80 kHz, 40 W, 10 s) irradiation can significantly improve the sedimentation and cohesion of *Microcystis*, which facilitates sediment removal. Low intensity ultrasonic treatment of *Microcystis* cells resulted in low levels of plasmolysis, although the cell wall, cell membrane, and thylakoid structure remained intact. In addition, cell viability was not significantly affected and extracellular polymers slightly increased. There were no significant increases in cell membrane permeability or extracellular Microcystin-LR, while there were significant increases in phycocyanin and malondialdehyde contents, which were associated with *Microcystis* antioxidant activity. Consequently, low intensity ultrasound irradiation enhances sedimentation and cohesion of *Microcystis*, potentially through low amounts of extravasations or pseudo-cavitation of microcystis cells, which could also be protective mechanisms in *Microcystis*.

KEYWORDS:
Low intensity ultrasound, *Microcystis, Coherence, Settle-ability, Cellular characteristics,* Protein expression

INTRODUCTION

In recent years, the high frequency of blue-green algae blooms caused by eutrophication in lakes and watercourses in China has adversely affected aquatic ecosystem environments, greatly increased the cost of water treatment, in addition to threatening water safety for adjacent residents [1,2].

Ultrasonic irradiation has recently been proposed as an alternative method of controlling algal blooms [3]. Some previous studies have focused on eliminating algal cells from aquatic environments using high intensity and high frequency ultrasonic irradiation [4,5]. Ultrasonic cavitation can physically injure algal cells by exposing their surfaces to high pressure, impulse waves, efflux forces, and shear stress [6,7]. In addition, hydroxyl radicals released by ultrasonic cavitation could also eliminate algae by inactivating algae cells [8,9]. Recently, low intensity ultrasonic irradiation has drawn great attention as a potential method for controlling algae [10,11], considering its superior performance with regard to efficiency and cost, in addition to minimal hazards associated with the potential release of algal toxins following cell disruption. However, few studies have examined the mechanisms by which low intensity ultrasound irradiation eliminates algae [12], particularly the biological mechanisms. Based on the results of previous studies, the present study investigates the biological mechanism of increasing *Microcystis* cohesion and settlement using low intensity ultrasound stress both at the cellular and molecular level, to provide a scientific basis for algae removal technologies using low intensity ultrasound irradiation.

MATERIALS AND METHODS

Sample sources and cultivation. The selected algal species, *Microcystis aeruginosa*, is one of the most common blue-green algae in China's eutrophic waters. The samples (FACHB-905) were purchased from the Institute of Hydrobiology, Chinese Academy of Sciences, and *M. aeruginosa* is classified as a toxigenic algae. Samples for experiments were cultivated at 27±1 °C in axenic BG-11 medium with incandescent light intensity of 36 $\mu E \cdot m^{-2} \cdot s^{-1}$ (12 h dark, 12 h with light) in the illumination incubator (YGZ-400F, Yaoshi Inc.). All the experimental samples were in the exponential growth stage and the cultured algae solutions were diluted to a concentration around 1.0×10^9 cells/L (OD_{680}=0.1). The treatment group were exposed to ultrasonic radiation using an ultrasonic generator (2010 D, Taiheda Inc.) for 10 s(80 kHz , 40 W) ,which compared to unprocessed control group.

Methods. Coherence and settleability influenced by low intensity ultrasonic irradiation. The cell number of treatment group and control group was calculated by using the

haemocytometer (AP-0650010, Marienfeld Inc.) and UV spectrophotometer at 680 nm(UV2450, SHIMADZU Inc.) as two common methodologies used [13,14]. In addition, variations in hydrophobic parameters of the cell surfaces [15] in both groups were measured to investigate the impact on coherence.

Effect of low intensity ultrasonic irradiation on cellular structure and metabolic activity. (1) Impact on cell surface. After centrifuging, both the treatment group and the control group were ① fixed for 2 h in 2.5% glutaraldehyde 2.5%; ② rinsed in phosphate buffer solution (0.1 M，pH 7.0) for 15 min; ③ fixed for 2 hours using osmic acid solution (1%); ④ rinsed again using phosphate buffer solution (0.1 M，pH 7.0) for 15 min; ⑤ dehydrated using ethanol solution (30%~100%); ⑥ which was replaced by tertiary butanol. ⑦ After critical point drying with CO_2 and gold plating by ion sputtering, ⑧ the samples were observed and photographed under a scanning electron microscope (S-570, Hitachi Inc.).

(2) Impact on internal cell structures. After centrifuging, both groups were ① fixed overnight using 2.5% glutaraldehyde(2.5%); ② rinsed using phosphate buffer solution (0.1 M, pH 7.0) for 15 min; ③ fixed for 2 h using osmic acid solution (1%); ④ rinsed again using phosphate buffer solution (0.1 M，pH 7.0) for 15 min; and ⑤ dehydrated using ethanol solution (30%~100%); ⑥ which was replaced by pure acetone; ⑦ The samples were then permeated and embedded using embedding medium; ⑧ sectioned using an ultramicrotome; ⑨ double stained by uranyl acetate and lead citrate; ⑩ and observed and photographed under a transmission electron microscope (H-7650, Hitachi Inc.).

(3) Impact on cell activity. Cell activity in both groups was measured using a hemocytometer and algae cell autofluo-rescence detection [16].

(4) Impact on cytomembrane permeability. Variation in conductivity in both groups was measured using a conductivity meter (HQ14D, Hach Inc) [17].

(5) Impact on the concentration of extra-cellular algae toxins. After filtering with a 45 μm filter, the Microcystin-LR concentrations of the filtrates of both groups were measured using high-performance liquid chromatography (LC-2010HT, Shimadzu Inc.). Chromatographic Column: ODS column (4.6 mm × 150 mm)；temperature of the column : 40°C; detector: UV detector or diode array detector; detection wavelength: 238 nm; flow phase: solvent A was methanol and solvent B was phosphoric acid, which accounted for 55% and 45%, respectively; total flow rate was 0.8 mL/min, with a 30-μL injection volume .

(6) Impact on the stress on cells. The treatment and control groups were ① subjected to multigelation with phosphate buffer Solution (0.05 M) at -20°C and 4°C； ② centrifuged (10,000/rpm ，4°C) for 20 min using a centrifuge(3K15, Sigma Inc.), then the supernatant was extracted. A test kit from Nanjing Jiancheng Biological Engineering Institute was to measure peroxidase (POD), catalase (CAT) and superoxide dismutase (SOD) activity and content of malondialdehyde (MDA) contents.

Protein expression. Protein extraction and measurement. ① 1 mL protein lysate (PL039, Shanghai Sangon) was added to the samples; ② the cell samples were disrupted using a sonicator (JY92-IIN, Ningbo Xinzhi Inc.) and centrifuged (4°C, 12,000 rpm, 30 min); ③ 1 mL precooled acetone (-20°C precipitated overnight); ④ and the supernatant obtained by centrifugation (4°C, 12,000 rpm, 30 min); ⑤ adding 50 μL protein lysate (PL039, Shanghai Sangon Inc); ⑥ measured by non-interfering protein concentration determination kits (SK3071, Shanghai Sangon).

(1) Two-dimensional electrophoresis. Isoelectric focusing electrophoresis analysis was carried out using an isoelectric focusing instrument (IPGhor, GE Healthcare). A solution (9 mol/L urea, 4% CHAPS, 2% IPG buffer solution, 40 mmol/L DTT, 40 mmol/L Tris base protein samples) was added into the 400 μg protein sample to make up a mixture with a total volume of 450 μL. The mixture was placed into the standard strip manifold. 17-cmIPG strips were placed face down covering the mixture. After assimilation under indoor temperature, the mixture was covered with 2 mL mineral oil and hydrated for 14 h and the isoelectric focusing electrophoresis process was carried out (50 μA current, 20°C). After isoelectric focusing, the strip was balanced in equilibrium liquidI(6 mol/L urea, 2% SDS，0.5 mol/L Tris-HCl，pH 8.8 ，30% glycerin，0.25% Bromophenol Blue，5% DTT) and equilibrium liquidII(6 mol/L urea，2% SDS，0.5 mol/L Tris-HCl，pH 8.8，30% glycerin ，0.25% Bromophenol Blue, 5.5% IAA), for 15 min in each case. SDS-PAGE electrophoresis (Amersham Ettan DALT Six, GE Healthcare) was then carried out following by silver staining.

(2) Image scanning analysis. Electrophoresis images were captured using ImageScanner(GE Healthcare) and analyzed by PDQuest 8.0(Bio-rad). Images were processing image through background subtraction, spot detection, and gel matching. The spotted proteins were normalized. Processing abundance analysis of same location spotted point. Calculating the variation in protein content. Protein

point with double variation ratio counted as differential expression point.

(3) MALDI-TOF-MS mass spectrometry and data retrieval. Prepared samples were sent to Sangon Biotech (Shanghai) Co., Ltd for mass spectrometric analyses using a MALDT-TOF-MS mass spectrometer(*Autoflex* speed, Bruker Daltonics Inc.). After removing contaminants from the mass spectra peaks, the data were searched against the data available at http://www.ncbi.nlm.nih.gov.

(4) Statistical analysis. Results were analyzed by student's t-test, which "*" indicates $p < 0.05$, "**" indicates $p < 0.01$ in the figure and table. Each experiment had three replicates.

RESULTS AND DISCUSSION

Coherence and settleability influenced by low intensity ultrasonic irradiation. After processing treatment with low intensity ultrasonic irradiation (80 kHz, 40 W, 10 s), settleability of *Microcystis* increased significantly. Compared to the control group, with 1h sedimentation, algae cells removal rate and OD_{680} removal rate of treatment group increased by 55.83% ($p < 0.01$) and 37.98% ($p < 0.01$) respectively (Table 1). If the natural sedimentation time increases to 3 h or 5 h, the algae removal rate was higher.

Cell surface hydrophobicity indicates strength of cell coherence. The higher the hydrophobicity, the greater the adhesion of cell surface, and in turn greater cell coherency. Hydrophobic values of the treatment groups were significantly higher compared to those of the control group. Therefore, cell coherence was significantly enhanced by low intensity ultrasonic irradiation (Fig. 1)

Influence of low intensity ultrasonic irradiation on cellular structure and metabolic activity. SEM results. *Microcystis* cells in both the control and the treatment group were undamaged following observation under a scanning electron microscope (Fig. 2). Extracellular polymeric substances were relatively higher in the treated group. The extracellular substances were potentially caused by exosmosing of cytoplasmic inclusions due to damage to the cytomembrane after low intensity ultrasonic irradiation. Alternatively, low intensity ultrasonic irradiation could have stimulated *Microcystis* cells to secrete extracellular polymeric substances.

TEM results. Cytoderm, cytomembranes, and thylakoids in both groups were intact. Phycocyanobilins inside Microcystis cells in the treatment group increased compared to in the control group (Fig. 3). Phycocyanobilins increased when Microcystis were exposed to environmental stress [18-20]. In addition, minor plasmolysis was observed in the cells of the treatment group, which could have been due to the rupture of gas vesicles in Microcystis or exosmosing of cytoplasmic inclusions.

TABLE 1
Removal rate of control group and treatment group by natural sedimentation

	C1	O1	C3	O3	C5	O5
Control group	5.24%	4.38%	7.29%	6.20%	8.62%	7.44%
Treatment group	61.07%	42.36%	71.61%	57.02%	83.82%	73.33%
Difference	55.83%**	37.98%**	64.32%**	50.82%**	75.20%**	65.89%**

Note: C1: Algae cells removal rate after 1h sedimentation. O1: Algae OD_{680} removal rate with 1 h sedimentation.

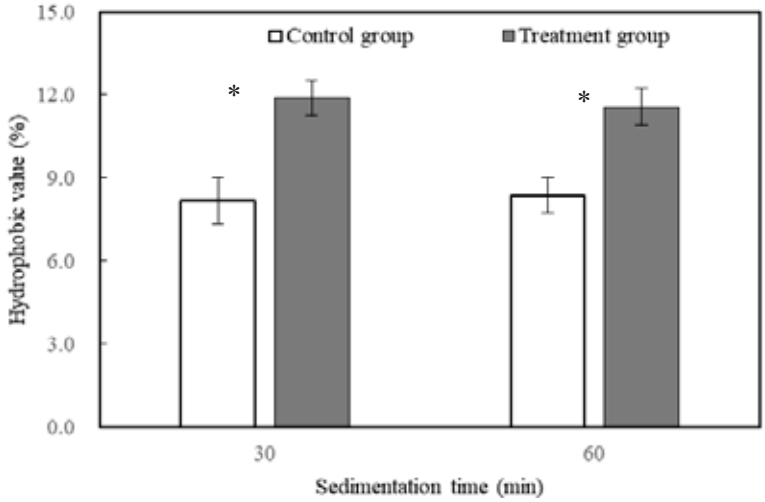

FIGURE 1
Hydrophobic values of control group and treatment group

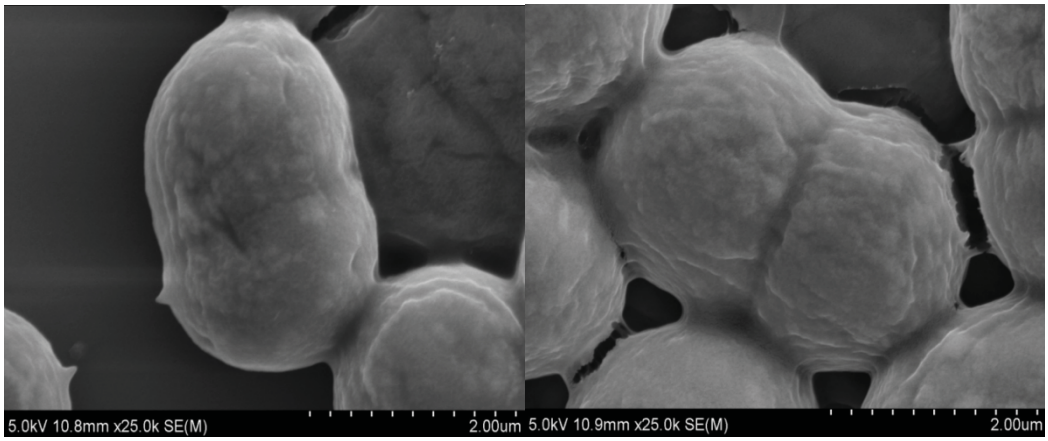

A B

FIGURE 2
Scanning electron microscopy results of control group and treatment group (A:Control group, 25,000×; B: Treatment group, 25,000×).

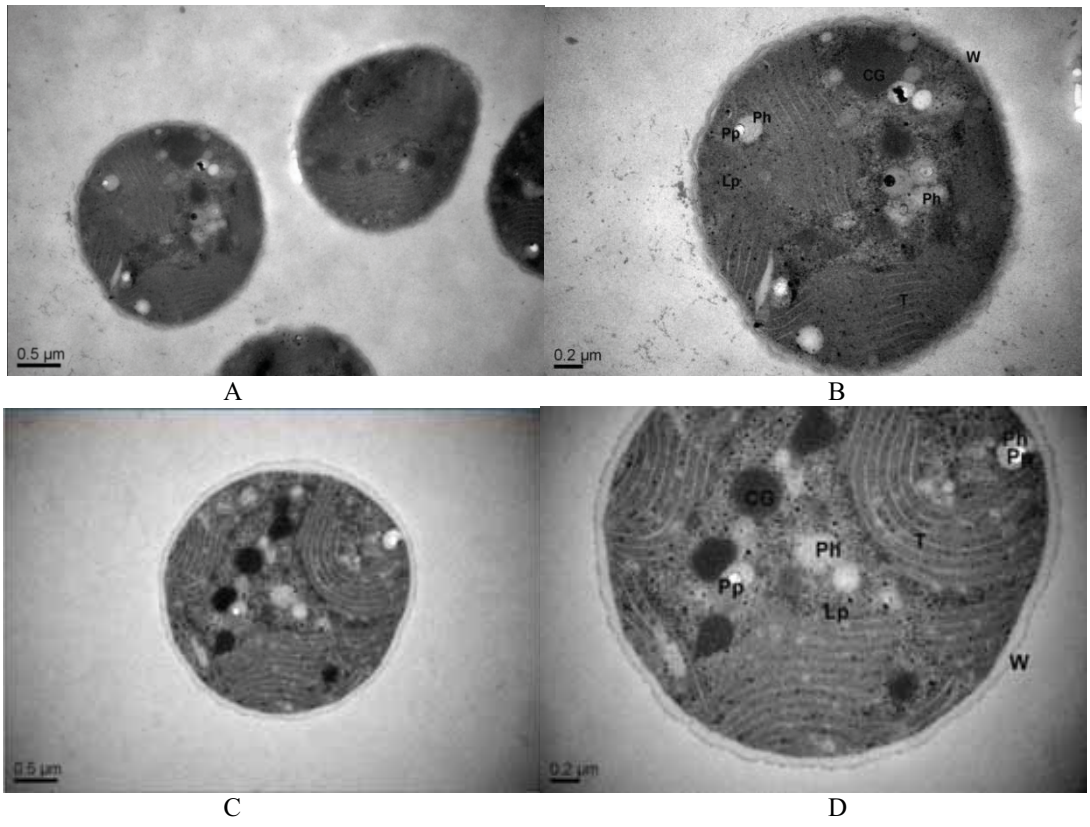

A B

C D

FIGURE 3
TEM results of control group and treatment group.
(Control group, 7,000×; B: control group, 25,000×; C: treatment group, 7,000X; D: treatment group, 25,000×)

Impact on cell activity. Cell activity is an important indicator for evaluating cell integrity [20]. Only *Microcystis* cells with complete cytomembranes present red fluorescence. Low intensity ultrasonic irradiation had no significant influence ($p > 0.05$) on cell activity (Fig. 4).

Impact on cytomembrane permeability. Cytomembrane represents the interface between cell and the external environment. Therefore, its role is to maintain the internal cell microenvironment and normal cell metabolism. When adverse environmental conditions cause damage to the cytomembrane, selective permeability of cytomembrane would be impaired. In addition, the conductivity of extracellular fluid would increase on account of electrolyte leakage. Conductivity in treatment group was marginally than in the control group (Fig. 5). However, the difference was not significantly ($p > 0.05$).

Therefore, the effect of low intensity ultrasonic irradiation on cytomembrane permeability was not significant.

Impact on the concentration of extracellular algal toxins. The concentrations of extracellular Microcystin-LR marginally increased after treatment with low intensity ultrasonic irradiation. However, the change was not significant ($p > 0.05$). (Fig. 6)

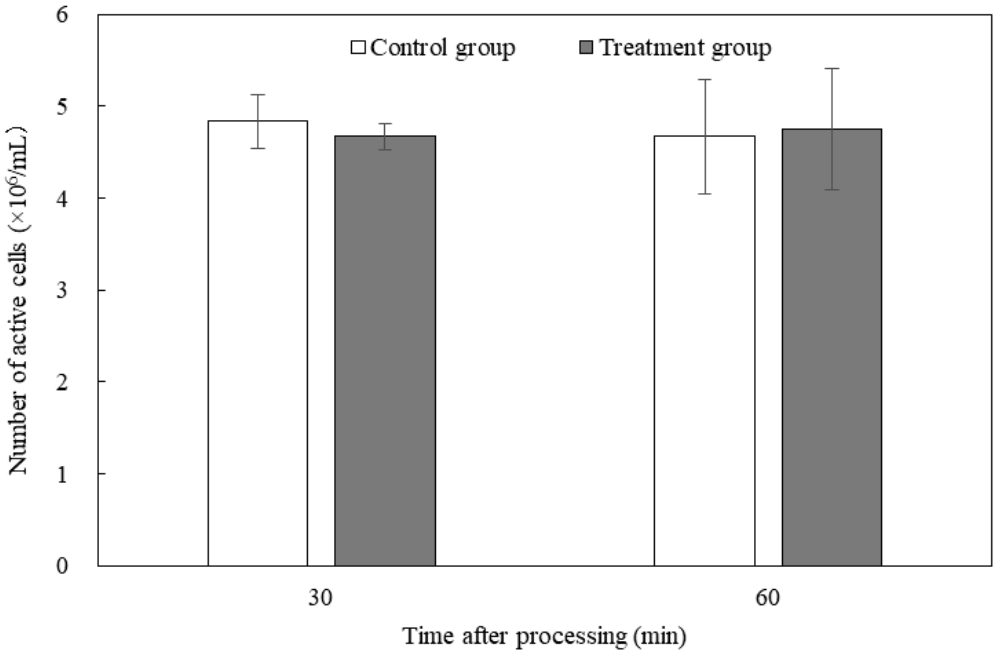

FIGURE 4
The number of active cells of control group and treatment group

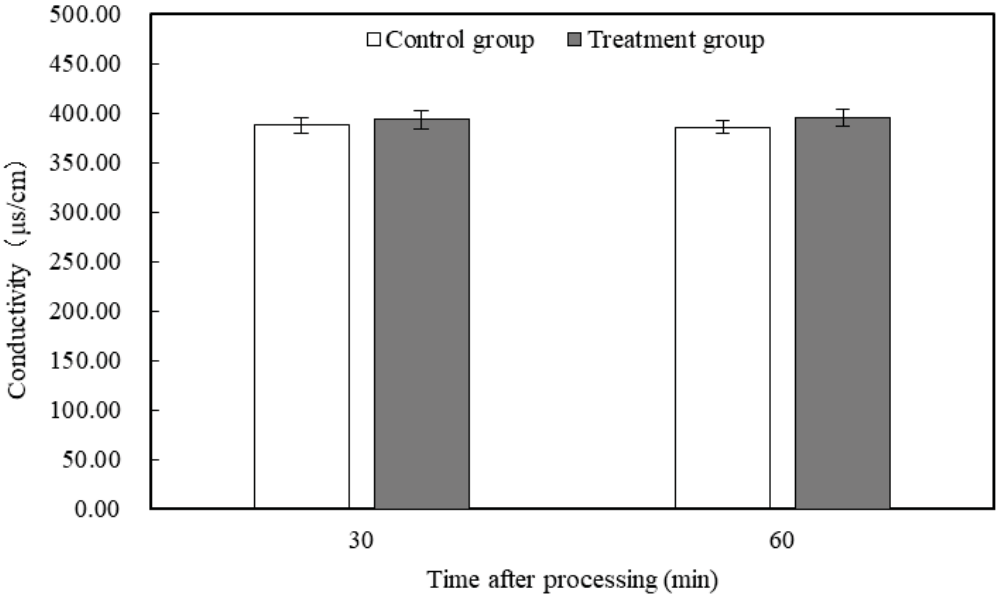

FIGURE 5
Electrical conductivity of control group and treatment group

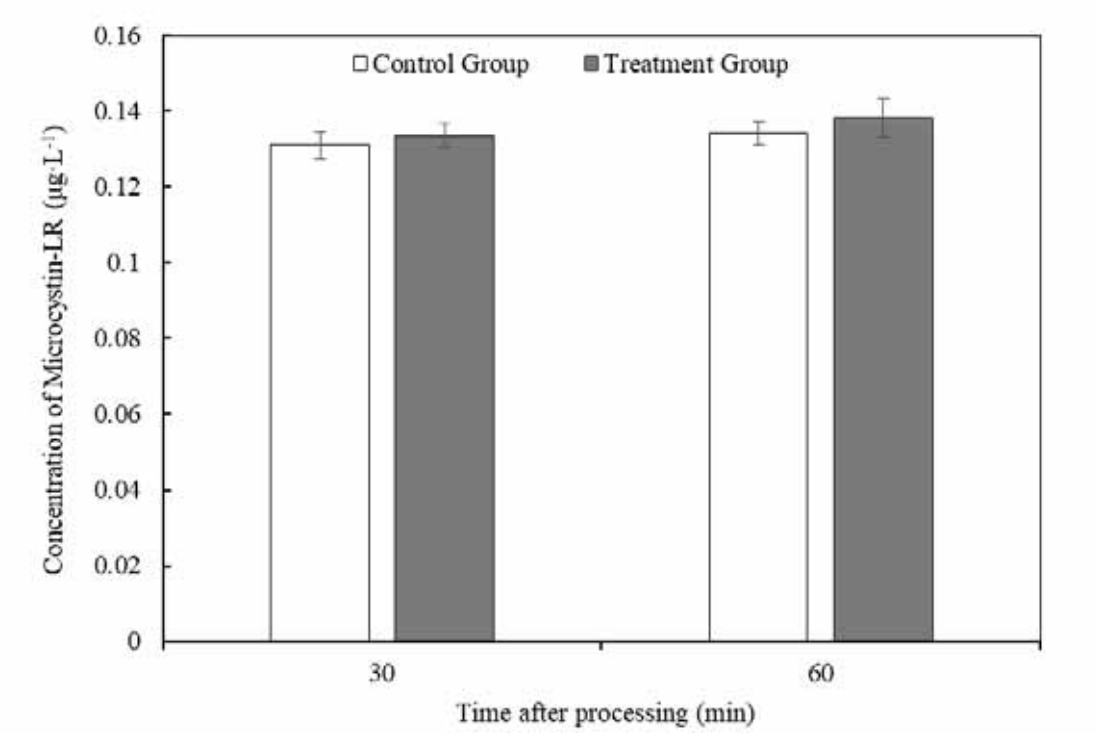

FIGURE 6
Concentrations of extracellular Microcystin-LR in the control and treatment groups

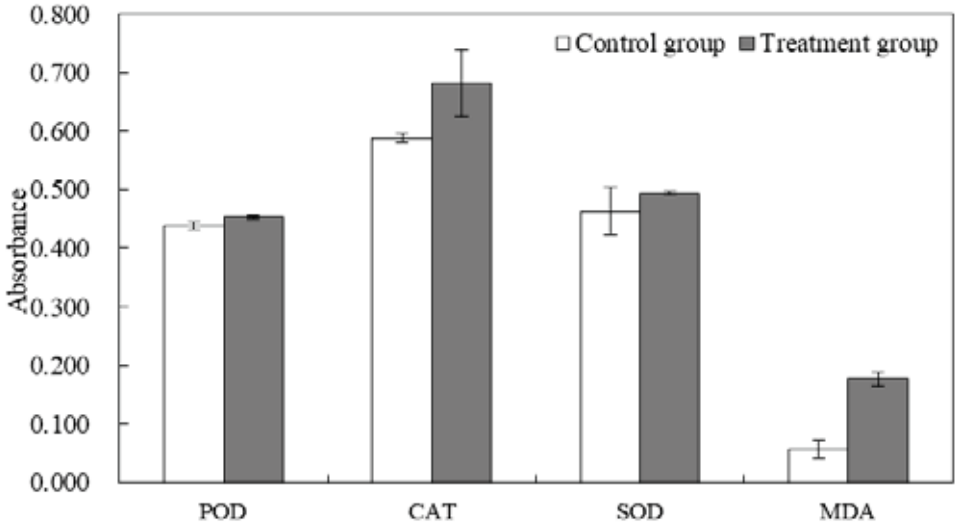

FIGURE 7
Antioxidant enzyme activity and malondialdehyde content in the control and treatment groups

Impact on the stress on cell. Reactive oxygen species contents, including POD, CAT and SOD, in addition to and MDA, could reveal the levels of stress in cells. Particularly, higher contents indicated higher levels of stress in cells. The POD, CAT and SOD levels in treatment group increased by 3.09% ($p > 0.05$), 13.73% ($p > 0.05$), and 6.14% ($p > 0.05$), respectively, compared to in the control group. Notably, MDA contents increased significantly, by 67.92% ($p < 0.01$) (Fig. 7).

Protein expression. Two-dimensional electrophoresis. Separating total proteins from *Microcystis* in both the control and treatment groups using two-dimensional electrophoresis, we obtained clear and satisfactory results of 2-DE gels. Comparison of results from the treatment group and the control group using PDQuest 8.0 revealed that there were 127 significantly differentially expressed proteins, based on their isoelectric points. In addition, 56 were down-expressed and 71 were up-expressed (Fig. 8).

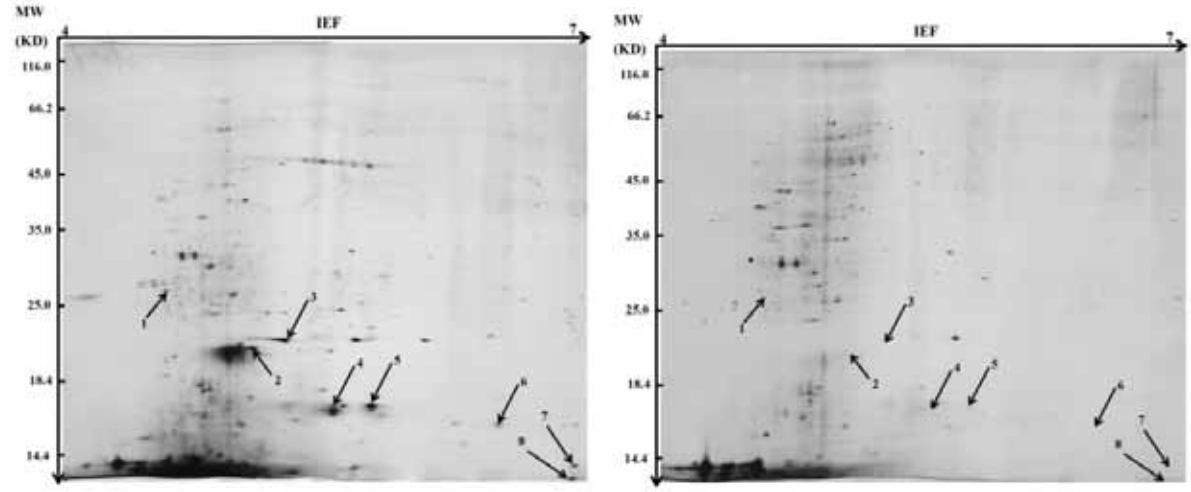

A B

FIGURE 8
2-DE gels for the proteins in *Microcystis* in the control and treatment groups

TABLE 2
2-DE identification of some isoelectric points in *Microcystis* in both the control and the treatment group

Protein spots	Ratio of change of expression	Most similar protein	Serial Number	Similarity degree
1	163.0	unnamed protein product [*Microcystis aeruginosa* PCC 7806]	gi|159027542	10%
2	290.1	cpcB [Microcystis aeruginosa PCC 7806]	gi|159029495	51%
3	3.8	unnamed protein product[*Microcystis aeruginosa* PCC 7806]	gi|159026977	18%
4	52.6	cpcA [*Microcystis aeruginosa* PCC 7806]	gi|159029496	43%
5	16.6	cpcA [*Microcystis aeruginosa* PCC 7806]	gi|159029496	41%
6	644.3	phycocyanin alpha subunit, partial [*Microcystis aeruginosa* PCC 7806]	gi|2673679	26%
7	109.6	psaD [*Microcystis aeruginosa* PCC 7806]	gi|159027390	8%
8	11.0	ribulose 1,5-bisphosphate carboxylase/oxygenase small subunit [*Microcystis aeruginosa* PCC 7806]	gi|112821113	38%

Mass spectrum identification. Twenty-six differentially expressed proteins with abundances greater than 2 and distinct separation effect were chosen for mass spectrometry identification, of which eight were successfully identified (Table 2). The results showed that two points represented unknown proteins and six points represented functional proteins. The most similar proteins were protein represented by points 2, 4, 5, and 6 was the phycocyanin subunit, which exhibited the most apparent increase. Phycocyanins are typically storage units and antioxidants inside living cells. The protein most associated with isoelectric point 7 was a protein subunit of PS I complex in the photosystem, and PS I complex is part of the photosynthetic electron transport chain inside the mesenchyme of the thylakoid membrane. The protein most associated with the isoelectric point 8 was a small protein subunit of 1,5-bisphosphate carboxylase/oxygenase ,which is critical in the Calvin cycle of photosynthesis. Plant enzymes use 1,5-bisphosphate carboxylase as a substrate to fix carbon dioxide and generate hexose phosphate, which break up into two molecules of glycerol-3-phosphate. The abovementioned functional proteins were associated with several physiological processes, such as antioxidant activity, electron transfer, and carbon dioxide fixation. Such physiological processes enhance metabolic balance and self-defense when *Microcystis* are subjected to stress, which in the present case, was low intensity ultrasonic irradiation.

Acceleration of removal of *Microcystis* sediment by low intensity ultrasonic irradiation. In the present study, exposing *Microcystis* to low intensity(40W) ultrasound irradiation for a short time (10s) significantly increased removal result of natural settlement of *Microcystis*. When used in combination with flocculants, the removal efficiency of *Microcystis* was higher [10,12]. Power dissipation in the present study was low compared to previous studies [12,14,21]. In addition, low intensity ultrasound did not cause *Microcystins* to rupture and release algae toxins.. The present study laid the foundation for the establishment of an efficient, economical and safe algae removal technology.

Biological effects of controlling *Microcystis* using low intensity ultrasonic irradiation. Settleability and coherence increased significantly after treatment with low intensity ultrasonic irradiation in the present study, which facilitated the removal of *Microcystis*. Aggregation and subsidence in algae are regulatory mechanisms that are observed in algae subjected changing environmental conditions or stress factors. For example, illumination and ultraviolet light cause aggregation of algae [22-25]. In addition, high temperature can cause subsidence of algae [22,26-27]. The reason for subsidence is may be related to the accumulation of carbohydrates in algae cells [22], and also to the breakage and gas exhaust of gas vesicles [28].

Low intensity ultrasonic irradiation is a gentle strategy for removing algae from eutrophic aquatic environments. After treatment with low intensity ultrasonic irradiation, damage to the cell surfaces or internal cellular structures *Microcystis* was minimal. Among them, cell wall, cell membrane, and thylakoid were intact, and cell activity, cell membrane permeability, and extracellular algal toxin concentration did not change significantly. A small amount of extravasation of the cell contents and the rupture of pseudo-cavitation [11] could be responsible for the increase in cohesiveness and sedimentation of *Microcystis* cells.

In addition, low intensity ultrasonic radiation is a potential stress factor for *Microcystis* cells, because antioxidant enzyme activity and malondialdehyde contents in the treatment group increased at varying degrees, particularly malondialdehyde content, which increased significantly. In addition, the results of transmission electron microscopy and protein expression analyses revealed that phycocyanin increased significantly and it had antioxidant effects on algae cells [18-20]. Consequently, it can be concluded that low intensity ultrasonic irradiation could trigger *Microcystis* self-healing and defensive mechanisms, which may increase the cohesion and settlement of *Microcystis* cells.

CONCLUSION

(1) After treatment with low intensity ultrasonic irradiation (80 kHz, 40 W, 10 s), removal of naturally settling *Microcystis* improved significantly. In addition, the coherence of *Microcystis* cells increased significantly.

(2) After treatment with low intensity ultrasonic irradiation, surface and internal structures of cells displayed minor damage. The cytoderm, cytomembrane, and thylakoid remained intact and there was no significant increase in membrane permeability. In addition, there was no significant change in cell activity. Extracellular polymers and intracellular phycocyanins increased and there was marginal plasmolysis, which could have been due to extravasation of intracellular contents or the rupture of gas vesicles. Intracellular antioxidant enzyme activity and MDA contents increased, with MDA contents increasing significantly.

(3) Analysis of differential expression of proteins revealed that low intensity ultrasonic irradiation significantly increased the expression of antioxidant, electron transfer, and carbon dioxide immobilization proteins in *Microcystis*, particularly phycocyanins.

(4) Low-intensity ultrasound irradiation can increase the cohesion and settlement of *Microcystis* cells, potentially due to low levels of extravasation of intracellular contents and rupture of pseudovacuoles in *Microcystis*. It could also be protective mechanism against low-intensity ultrasound in *Microcystis*.

ACKNOWLEDGEMENT

This work was supported by the National Natural Science Foundation of China (51308006) and Shenzhen's Strategic Emerging Industries Development Foundation of China (JSGG20170413113438810).

REFERENCES

[1] Zhang, J., Zhai, H.-Y., Ji, M. (2016) Removal Of Algal Organic Matter And Control Of Disinfection By-Products By Coagulation. China Water & Wastewater. 32(3), 56-60.

[2] Zhang, C., Zhao, L., Zhang, Y., Zhao, Q.L. (2015) Research Progress Of The Hazard And Control Technology Of Algae Bloom. Environmental Protection Science. 41(3), 107-112.

[3] Shi, H.X., Qu, J.H., Liu, H.J., Mu, Y.L., Xiao, K.T., Wang, L. (2008) Effect Of Ultrasound Irradiation On The Coagulation And Inactivation Of *Microcystis*. Water Supply Research & Technologyaqua. 57(2), 101-108.

[4] Nakano, K., Lee, T.J., Matsumura, M. (2001) In Situ Algal Bloom Control By The Integration Of Ultrasonic Radiation And Jet Circulation To Flushing. Environmental Science & Technology. 35, 4941-4946.

[5] Ma, B.Z., Chen, Y.F., Hao, H.W., Wu, M.S., Wang, B., Lv, H.G., Zhang, G.M. (2005) Influence Of Ultrasonic Field On Microcystins Produced By Bloom-Forming Algae. Colloids & Surfaces (B, Biointerfaces), 41, 197-20l.

[6] Bowen, C.C., Jensen, T.E. (1965) Blue-Green Algae: Fine Structure Of The Gas Vacuoles. Science. 147, 1460-1462.

[7] Liu, X.H. , Wache, P., Wang, X., Chen, H.Q. (2003) Effects Of Fluid Shear Stresses On The Deformation Of Endothelial Cell. Acta Biophysica Sinica. 19, 333-337.

[8] Schafer, F.Q., Qian, S.Y., Buettner, G.R. (2000) Iron And Free Radical Oxidations In Cell Membranes. Cell Mol. Biol. 46, 657-662.

[9] Feril, L.B., Kondo, T., Ogawa, R., Zhao, Q.L. (2003) Dose-Dependent Inhibition Of Ultrasound-Induced Cell Killing And Free Radical Production By Carbon Dioxide. Ultrason. Sonochem. 10, 81-84.

[10] Li, Y. (2011) Study On Effect Of Algal Control By Low-Frequency and Low-Power Ultrasonic Irradiation. Fuxin: Liaoning Technical University.

[11] Zhu, C., Ding, K.Y., Cong, H.B., Ni, J.C., Wang, M.Z., Wang, Q. (2015) Experimental Study On The Safe Removal Of Cyanobacteria With Dynamic Ultrasound Enhanced Coagulation. Acta Scientiae Circumstantiae. 35(8), 2429-2434.

[12] Hu, Y. (2013) Experimental Research Of The Low-Power Ultrasonic Irradiation On The Growth Of Algae. Chongqing: Chongqing University: 23.

[13] Rajaskehar, P., Fan, L., Nguyen, T., Roddick, F.A. (2012) Impact Of Sonication At 20 Khz On *Microcystis Aeruginosa*, *Anabaena Circinalis* And *Chlorella* Sp. Water Research. 46(5), 1473-1481.

[14] Ma, M., Liu, R.P., Liu, H.J., Qu, J.H. (2012) Effect Of Moderate Pre-Oxidation On The Removal Of *Microcystis Aeruginosa* By $Kmno_4$-Fe(Ii) Process: Significance Of The In-Situ Formed Fe(Iii). Water Research. 46 (1), 73-81.

[15] Chen, H., Pan, G., Zhang, M.M. (2004) Effect Of Growth Phase On The Flocculation Of Algal Cells Using Clays. Environmental Science. 25(6), 85-88.

[16] Ho, L., Dreyfus, J., Boyer, J., Lowe, T., Bustamante, H., Duker, P., Meli, T., Newcombe, G. (2012) Fate Of Cyanobacteria and their Metabolites During Water Treatment Sludge Management Processes. Science Of The Total Environment. 424(4), 232-238.

[17] Peng, G.Y., Chen,Y.L., Han, Y.Z., Zhang, T.T. (2016) The Inhibitory Effect Of Lactic Acid On Microcystis Aeruginosa And Its Mechanisms. China Environmental Science. 36(4), 1167-1172.

[18] Yu, H., Huang, J.J., Hu, H.Y. (2009) Effects Of A Novel Allelochemical Ethyl 2-Methyl Acetoacetate (Ema) On The Ultrastructure And Pigment Composition Of Cyanobacterium *Microcystis Aeruginosa*. Bulletin Of Environmental Contamination And Toxicology. 83(4), 502-508.

[19] Churro, C., Fernandes, A.S., Alverca, E., Sam-Bento, F., Paulino, S., Figueira, V.C., Bento, A.J., Prabhakar, S., Lobo, A.M., Martins, L.L. (2010) Effects Of Tryptamine On Growth, Ultrastructure, And Oxidative Stress Of Cyanobacteria And Microalgae Cultures. Hydrobiologia. 649(1), 195-206.

[20] Daly, R.I., Ho, L., Brookes, J.D. (2007) Effect Of Chlorination On Microcycis Aeruginosa Cell Integrity And Subsequent Microcystin Release And Degradation. Environmental Science Technology. 41(12), 4447-4453.

[21] Wan, L., Shao, L.L., Lu, K.H., Zhu, J.Y., Yang, W. (2014) Effects Of Ultrasond Wave On The Ultrastructure And Physiological Characteristics Of Blue-Green Algae (*Microcystis Aeruginosa*). Acta Hydrobiologica Sinica. 38(3), 516-523.

[22] Liang, Z.Y., Lin, X.Z., Ma, M., Zhang, J., Yan, X.B., Liu, T. (2008) A Preliminary Study Of The *Enteromorpha Prolifera* Drift Gathering Causing The Green Tide Phenomenon. Periodical Of Ocean University Of China. 38(4), 601-604.

[23] Dong, J., Li, G.B. (2016) Influencing Factors And Mechanisms On Colony Formation Of *Microcystis*:A Review. Acta Hydrobiologica Sinica. 40(2), 378-387.

[24] Zhou, Y.L. (2007) Effect Of High Temperature And Solar Uv Radiation On Growth And Physiology Of Spirulina And *Arthrospira Platensis*. Shandong: Ocean University Of China. 36-38.

[25] Wang, W.D., Zhang, K., Xu, H.B., Liu, G.Q. (2016) Effect Of Uv Radiation On The Coagulation Of Chlorella And Its Mechanisms. Environmental Science. 37(1), 187-192.

[26] Jin, X.C., Chu, Z.S., Yang, B., Zheng, S.F., Pang, Y., Zeng, Q.R. (2008) Effect Of Temperature On Growth, Photosynthesis And Buoyancy Regulation Of The Cyanobacteria *Microcystis Flosaquae* And *Planktothrix Mougeoti*i. Acta Scientiae Circumstantiae. 28(1), 50-55.

[27] Jia, H. (2010) Research On The Sediment And Float Mechanism Of *Spirulina* Cell. Inner Mongolia: Inner Mongolia Agricultural University: 22.

[28] Hao, H.W., Wu, M.S., Chen, Y.F., Tang, J.W., Wu, Q.Y. (2004) Cavitation Mechanism In Cyanobacterial Growth Inhibition By Ultrasonic Irradiation. Colloids And Surfaces B: Biointerfaces. 33(3-4), 151-156

Received: **09.09.2020**
Accepted: **23.10.2020**

CORRESPONDING AUTHOR

Hui Zeng
Peking University,
ShenZhen Graduate School,
Shenzhen 518055 – China

e-mail: jiankang12ww@163.com

© by PSP Volume 30– No. 05/2021 pages 4953-4961 Fresenius Environmental Bulletin

SYSTEM REALIZATION PATH OF VISUAL SORTING ROBOT SYSTEM UNDER BIG DATA ECOLOGICAL ENVIRONMENT

Zhe Yan*, Hongda Liu, Qixian Cao

School of Automation, Harbin University of Science and Technology, Heilongjiang, Harbin 150080, China

ABSTRACT

Big data ecological environment is the key direction of global science and technology development, which will be conducive to the construction of global science and technology ecosystem. Industrial intelligence has become the development trend of various countries' industries, and the application of machine vision technology to industrial robots has become an important way of industrial intelligence. The main breakthrough point of industrial robot machine vision technology lies in the intelligent classification and positioning of targets. Most of the existing visual industrial robots perform simple workpiece classification based on traditional graphics processing technology. This article introduces the principle and architecture of big data Hadoop technology, designs the motion model and positioning navigation model of the visual sorting robot, proposes the process path to realize the positioning and navigation algorithm of the visual sorting robot, and finally gives the overall implementation and remotely control the operation of the visual sorting robot. At the same time, the hardware design of the visual sorting robot is introduced, the realization path of the image processing of the sorting robot system is discussed, and theoretical research and practical testing are carried out. There are two core problems in the visual robot sorting system, one is image recognition and target tracking based on image processing, and the other is the capture and sorting control strategy based on actual industrial robots. The target to be recognized is goods. This article also expounds the overall scheme of the intelligent sorting process, expounds the functional principle of the system, and verifies the feasibility of the system through specific practices. The experimental results show that the visual sorting system can sort workpieces placed at any position in the working area, with a maximum positioning error of 0.65mm, and the sorting effect is good, meeting the sorting requirements. This study can provide a reliable reference for the construction of global science and technology ecosystem.

KEYWORDS:
Big data environment, ecological, machine vision, sorting robot, system realization path

INTRODUCTION

The sorting robot is a kind of digital management equipment with a wide range of uses and greatly improved technical value. With the increasing popularity of automatic manufacturing in the industrial field, robots are widely used in various industrial production lines to complete various tasks. Figure 1 is a sorting robot performing sorting operations. To use common industrial production methods, various special robots have been developed to perform corresponding tasks, such as electronic welding of parts, processing of industrial devices, and automobile manufacturing and sorting of painted and spliced parts [1-4]. Various professional industrial robots with a clear division of labor and special measures continue to improve social productivity and reduce the workload of employees. Although industrial robots have the characteristics of long-term, continuous and continuous work, the robot sorter can overcome many difficulties. In current practical applications, many robots perform offline landline teaching or programming activities. Although the overall level of industrialization has improved, they still cannot adapt to the smarter industrial production projects that people expect [5-6]. To understand the sorting function, when the workpiece is moving on the conveyor belt, the robot needs to know the type and real-time information of the workpiece to be sorted. Therefore, the robot must be equipped with image sensors to obtain external image information and improve adaptability, meet the sorting requirements of various mechanical parts, and can view and obtain a lot of external information. If this function is used for a robot, the robot can capture the changes in external information and report it to the administrator, thus making the application more extensive.

The American Adept company has developed a software called Adept Sight vision system software, which can add vision functions to the robot, can process smaller parts, and achieve high-quality products [7-8]. The iRVision system developed by the Ameri-

can Fanuc company can realize online or Offline detection, classification and identification. Lex Picker is a high-speed sorting system developed by ABB in Sweden to realize user modular programming, realize machine offline programming, and the shortest sorting cycle can reach 0.3s. The industry 4.0 era is also called the era of big data and the era of intelligence. The simple explanation refers to the realization of the intelligent transformation of the manufacturing industry through the combination of communication technology, virtual network and physical network. The development and design of machine vision technology can raise the robot's external perception ability to a new level [9-12]. Robots with visual perception technology in industrial production can not only greatly improve work efficiency, but also reduce the workload of staff. This paper studies the development of robot visual sorting on a large scale, and introduces the process of collecting, analyzing and displaying environmental information, location information, operating parameters and big data from running robots using experimental testing and optimization techniques.

MATERIALS AND METHODS

Big data analysis methods. Hadoop is an open source software written in the Java programming language, which can process large amounts of data in a parallel/distributed computing environment. HDFS and MapReduce (MR) are two key elements of ApacheHadoop: HDFS is a distributed file system of Hadoop, which can provide data access throughput, and has high availability and fault tolerance. MapReduce is a software framework that supports writing. The program can run on clusters of thousands of computers [13]. It is mainly responsible for all cluster maintenance tasks and scheduling processes, and allows programmers to focus on application logic. When a MapReduce job is sent to the master node, the "file" input is divided into several blocks, which are processed by parallel map making and project reduction. Since HDFS is replicated, tasks are executed on nodes that already have the required data blocks, thereby minimizing unnecessary data transmission [14-15]. The key function that big data Hadoop technology must implement is Map and

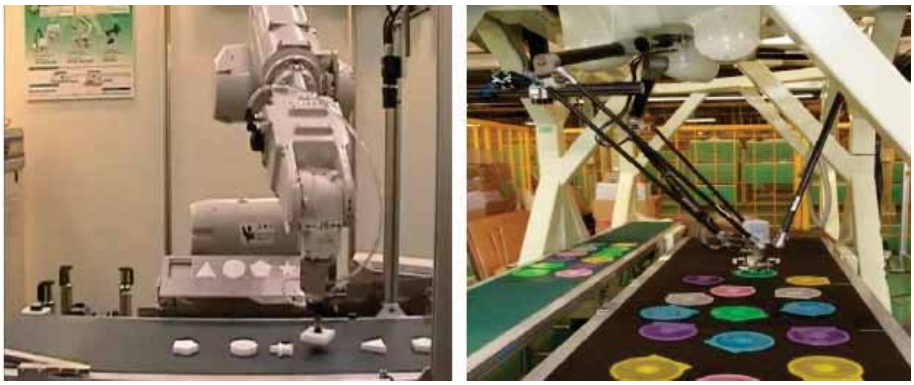

FIGURE 1
Visual sorting robot on the assembly line.

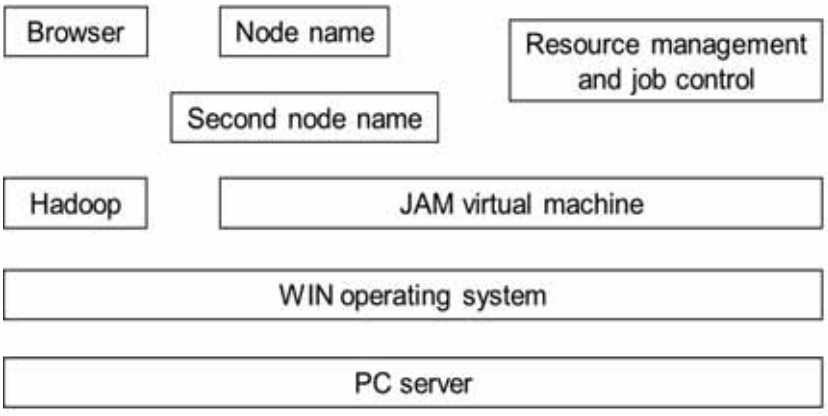

FIGURE 2
Hadoop master node design.

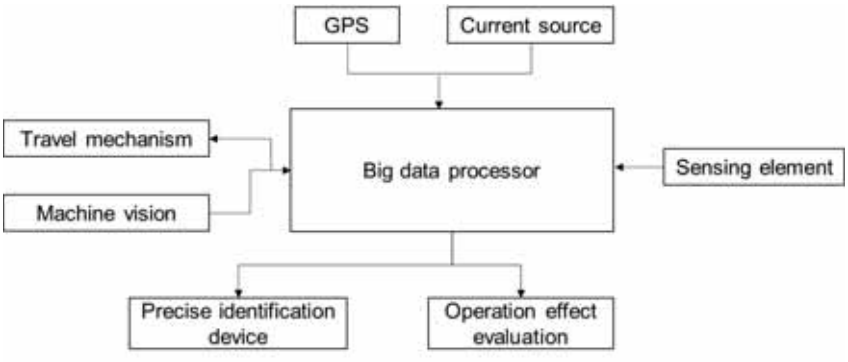

FIGURE 3
The overall design of the visual sorting robot.

Reduce. The MapReduce framework operates on key values, and each mapping item works on separator blocks and creates intermediate data in the form of key value protectors. These keys are then used to sort and split the data, use the same keys during recovery and combine value pairs into the same memory for further processing. The Hadoop master node design is shown in Figure 2.

Design of Big Data Vision Sorting Robot. The scenario of this research is an AS-R vision robot, a four-wheel device, and a smart mobile device with independent power supply and power options. Each part of the robot is divided into four parts according to function: machine vision, GPS location, intelligence and intelligent management. The data generated during the operation includes environmental information, location information, operating parameters and operating effects for analysis and storage [7, 16]. Big data analysis and processing are completed by a small server equipped with robots, and determine the position information of the robot based on GPS position signals, calculate the deviation from the expected route, and identify self-control by controlling hikers. Environmental information is collected through machine vision equipment and various sensors. If big data analysis collects information about objects, it will control the opening of the identification equipment and the position of the robot to achieve precise identification. In addition, sensors can collect various operating factors and operating dimensions of the robot, and provide a basis for evaluating the impact of the operation after analyzing big data. The overall structure of the visual sorting robot is shown in Figure 3.

The vision part of the machine includes the Nikon COOLPIXP60 camera and the TICO UB570 grid handle. The camera has 8 megapixels and is connected to the robot through the shaking process. The angle between the shooting direction and the vertical direction is 60°. The camera captures the image in JPEG format, uses the capture card to convert it into a digital signal, performs visual analysis to draw the outline of the target, and extracts a lot of data from it. The robot's GPS locator is Trigble's AgGPS132 product, which consists of a GPS receiving antenna, a receiver and a radio modem, and an antenna suitable for base stations [17-18].

The wireless transmitter between the robot and the base station is a PacificCrest product of the RFM96W series, which has a high positioning accuracy and can meet the operational requirements of a vision robot. The above-mentioned equipment uses the differential driver of the dispatcher computer to capture the GPS signal, capture it as big data and send it to the server to accurately identify and control the robot. The content of robot intelligence is information about industrial environment, equipment operation and equipment operation status. The acquisition of environmental information includes the DHT11 sensor for measuring temperature and humidity, the WTF-B200 wind speed and direction indicator for moving parts, and the NHZD10 sensor for recording brightness, such as HAL41F Hall element operation positioning device sensing power supply Turn signal to obtain engine speed. The TJP-1 pressure gauge converts pressure into electrical signals to record the workload of related components. Environmental information and information about the operating status of sensors are collected in the form of big data, and then analyzed and processed as the basis for intelligent management decisions [19-21]. The mechanical management of the robot aims to achieve independent walking and accurate identification. The robot adopts four-wheel drive. The drive controller receives information about the position and the direction of travel transmitted by the main control unit from the angle sensor, and then combines it with the recommended wheel drive method, so that it is independently deflected by the fluid valve. The sorting device is controlled by solenoid valves. The main control unit sends a pulse width forming signal through vision and positioning to control the solenoid valve to open and close the appropriate time to accurately identify the parts.

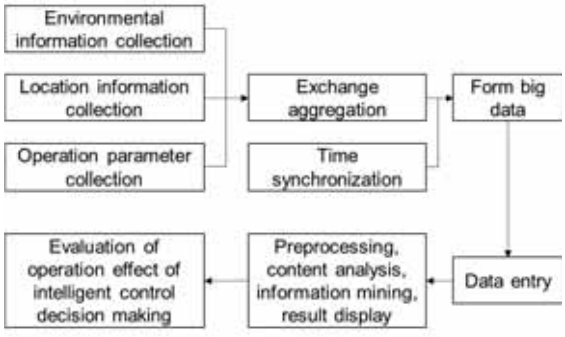

FIGURE 4
Schematic diagram of big data processing.

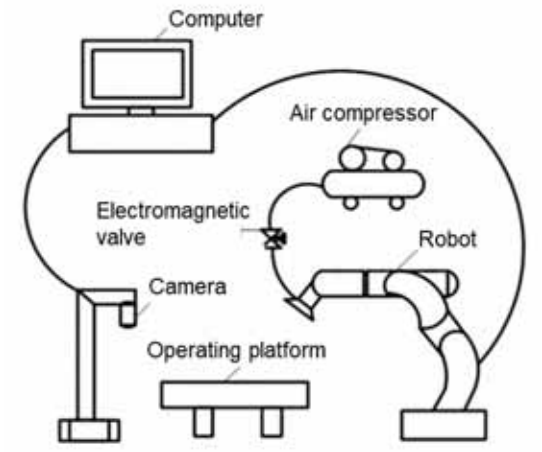

FIGURE 5
Schematic diagram of the working principle of the robot sorting system.

Big data processing process. Big data is a collection of data captured by the vision engine, GPS location and sensors. These contain information about the use of the robot and can be called through various diagnostic procedures. The analysis of a large amount of data involves the recording and reading of PB data, so a large number of calculation models and calculations are required. The big data analysis hardware of the robot is a PCServer server based on x86. Configuration includes Ryzen AMD Ryzen7 dual-core 8-core processor, DDR4 128 GB memory and IntelI350T2 Gigabit network card. Computer speed and memory may meet actual requirements [11, 22]. In this article, Hadoop technology is used as a Java-based framework for distributed big data processing as a big data analysis method. The Hadoop framework consists of a common unit, a distributed file system and other components. We set up cluster files in the distributed file system and create distributed files on the appropriate nodes. This technology can be accurately implemented through calculation models, has high error resistance and flexibility, and has good identification and recognition of large amounts of data. The data recorded by various devices transmitted by the robot reaches the switch through the network and the transmission interface. The switch which is connected to data collection, performs data exchange and aggregation processes, and finally sends them to the large data processor. The above migration process implements the IEEE1588 time synchronization process, which can reduce time delay, thereby improving the accuracy of real-time data. After the processor receives the big data, it records the data according to the specified format, quickly divides the data according to the analysis purpose, and then performs analysis and processing. The process of big data analysis is processing the content analysis of mining information and publishing results to achieve data-centric analysis [23]. Parallel processing is based on the characteristics of different types of big data structures to improve analysis speed. Parallel processing includes comprehensive monitoring and real-time sorting of big data during the data recording process, assigning the data to the corresponding program system according to the model, and then making decisions with the help of professional knowledge bases, laying the foundation for data mining, and finally, comprehensively monitoring the results of the analysis in the storage and management unit to form a database with operating actions and make intelligent management decisions for the robot and evaluate the effect of the operation. The big data processing process is shown in Figure 4.

RESULTS

Components. The hardware sorting system studied is shown in Figure 5, which is composed of a 6-axis robot, an optical unit, a pneumatic module and a computer. The 6-axis manipulator is mounted on an aluminum substrate. The optical unit is composed of a camera and a lens, and is installed outside the robot. The pneumatic module includes a pneumatic aspirator, air compressor, solenoid valve, control circuit and vacuum generator. We write the application program on the computer to combine these modules to form a vision-based robotic sorting system.

6-axis robot: Since the weight of the sorted workpiece is within 400 g and the maximum transport distance is 500 mm, Nachi Corporation chose the light 6-axis high-speed robot MZ04. The robot can process 4kg parts with a 600mm high-precision motor.

Pneumatic module: The pneumatic unit includes an aspirator, an air compressor, a solenoid valve and a vacuum source. The suction hood and vacuum generator are installed at the end of the motor. The vacuum generator converts the compressed air from compressed air to a lower pressure, so that the suction cup attracts the workpiece.

The overall design of the industrial robot sorting system based on image processing is designed in

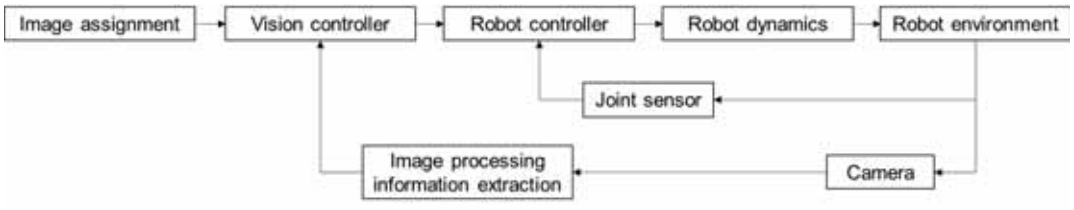

FIGURE 6
Block diagram of image-based visual servo system.

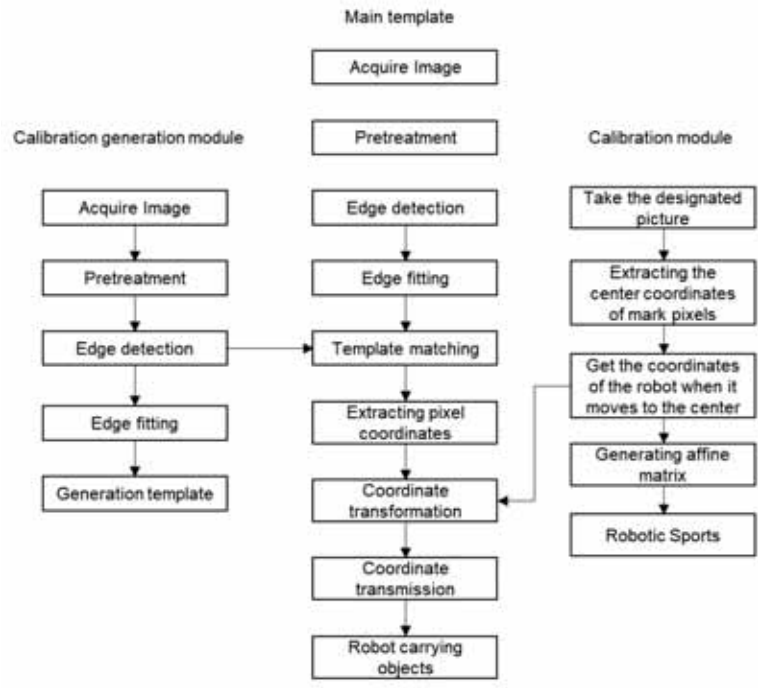

FIGURE 7
Process flow chart of vision-based robotic sorting system.

the system, and the main components of the system are specified, including the sorting and acquisition subsystem, the image system and the analysis of the subsystem based on Guangshu Robot. According to the camera calibration attempts in the HALCON software database, the principles of camera and lens selection for image acquisition are determined. The positioning average first divides the color attributes of the algorithm, and then inverts the curve into a bar graph. Then, it explains the iterative algorithm of subtracting the average offset, explaining the iterative process with image modification, and then specifying the basis and execution of the computer steps. Finally, using the algorithm to complete the component measurement experiment, the real-time coordinates of the target can be obtained. We first find the image processing and extract the action on the target, then use imaging to complete the training of the nervous system, and finally introduce an algorithm to optimize the performance of the nervous system [15, 24-25]. In principle, it explains the principles and specific implementation steps of the analysis algorithm. Finally, the components are determined through experiments, confirming the improved recognition accuracy of neurotransmitter sorting. The sorting method based on industrial robots is as follows:

(1) The D-H parameter method is a general method proposed by Denavit and Hartenberg in 1955. The D-H parameter adds a coordinate system to each robot connection, and then uses 4×4 unit conversion mass to describe the land part between two adjacent connections. The continuous transformation can finally reach the position of the final power source relative to the basic coordinate system, thereby generating robot balance. The visual servo system is shown in Figure 6.

(2) The standard D-H parameter method should be used to establish the kinematic model of the industrial robot, and determine the method and selection criteria of the reverse Chinese solution. At the same time, the relationship between engineering robots and workstations was analyzed in detail, and a sorting strategy based on optimal positions was obtained. Finally, the task of sorting components on the visual platform is completed.

The industrial robot controller uses the Guangzhou CNC (Guangzhou) industrial robot RB-08, the camera uses a USB camera to collect images in real time, and the signal acquisition and control uses

HALCON visual software for real-time processing. According to the sorting activity of the vision robot, it is basically based on the continuous images collected by the camera to identify the type of the target to be sorted, and monitor the position of the target to be sorted, and send the above information to the robot operator to complete the joint management, and further obtain the sorting action.

Sorting system workflow. The process of the whole system is shown in Figure 7. The whole process can be divided into three units, namely the template type unit, the system calibration unit and the main unit. The role of the template model is to process various component types, create class templates and prepare for subsequent template matching [26]. The function of the calibration unit is to establish a business relationship between the visual coordinate system and the mechanical coordinate system. The main function of the host is to establish communication between the computer and the robot and perform automatic sorting operations.

Template extraction and matching in template production is an important part of machine vision and recognition. Features such as the shape and gray value of the target image can be used for template matching. When choosing a matching action, you must first consider directly affecting the accuracy of the game and in different environments. Different lighting conditions for action intensity. The process of creating a template file is divided into the following 3 steps:

(1) Image processing. Due to the long working distance and wide field of view of the system, ordinary light sources are not suitable for workplaces. The linear crop function is used to make the image gray. Customizing large light sources to improve the quality of the collected images is very expensive. We should enlarge the gray area of the image, increase the contrast of the image and improve the quality of the generated image.

(2) Edge extraction. The Canny controller is used to draw the edge of the contour on the workpiece. Canny Operator is a comprehensive bridge analyzer, including filtering, cleaning, inspection and other stages, which can effectively remove static electricity and obtain high-quality edges.

(3) Create a template. Call the Create_shape_model operator in Halcon, enter the edge of the workpiece, set the template angle, zoom ratio and other variables of the template, create the template, and finally call the write_shape_model administrator to save the created template file to the computer.

The calibration units in Eye_in_hand and Eye_to_hand can be divided according to the relative positions of the camera and the operator. Eye_in_hand is a camera mounted on the robotic arm. As the motor arm moves, it has greater flexibility rather than stability. Eye_to_hand fixes the camera at a fixed position outside the robot. It has better stability and broader vision, which can meet the needs of the project.

Using the Eye_to_hand system, the essence of calibration is the relationship between the hardware system node and the camera coordinate system. The traditional calibration method requires the business relationship between the tool hardware and the tool coordinate system, the conversion relationship between the tool coordinate system and the working plane coordinate system, and the business relationship between the working plane coordinate system and the coordinate system. Finally, based on these three relationships, to find the relationship between the camera coordinate system and the robot coordinate system, this method is cumbersome and time-consuming, and can only be completed by many mechanical movements. Therefore, a quick correction method is proposed, which can directly establish the business relationship between the mechanical hardware mechanism and the visual coordinate system in the work area. We place the calibration chart with 3 markers on the work area and take a picture of it with the Acler-1300 g Basler camera. Then, based on the gray value of the image, the unmarked boundary area is extracted, and the pixel coordinate centers of these three points are calculated. Finally, the transformation model is called to obtain the affine transformation matrix. The main part is the backbone of the entire system. The host will sort the templates, call the calibration array to sort the workpiece, and obtain the center part of the workpiece, and finally guide the robot to complete the automatic sorting. As shown in Figure 8, the host computer is composed of a computer program, a communication program for the robot, and a motor program for the robot.

Sorting experiment results. In order to test the performance of the software and hardware of the entire system, a multi-object sorting experiment was designed. Three types of workpieces, several of each type, were placed at any position within the working area. Then the robot communication program and the robot motion program were started on the robot side. Then we start the host computer program on the industrial computer, send a connection request to connect the entire system, and then call the camera's SDK function to open the camera, take pictures of the work area. The pictures obtained through the camera will be transmitted to the industrial computer through the TCP/IP protocol After receiving the image, the host computer program of the industrial computer performs preprocessing, template matching, centroid extraction, coordinate conversion and other operations on the image, and finally sends the centroid coordinates of the workpiece and the coordinates of the corresponding category placement

area of the workpiece to Robot communication program. After the robot communication program receives the coordinate data, it will be stored in the real number register in turn. The robot motion program will call the workpiece centroid coordinate information in the register and the placement area coordinate information of this type of workpiece in an orderly manner to complete the sorting. Figure 9 is the sorting effect diagram of the sorting system.

The area within the rectangular frame in Figure 9a is the placement area of the workpiece to be sorted, and the workpiece to be sorted can be placed at any position in the working area. Figure 9b shows the state of all workpieces after sorting. There are three rectangular areas in the figure, which are rectangular workpiece placement area, triangular workpiece placement area, and circular workpiece placement area. As shown in Figure 9b, each workpiece was successfully sorted to the corresponding area. The position of the geometric center point of the workpiece obtained from the sorting experiment is shown in Table 1.

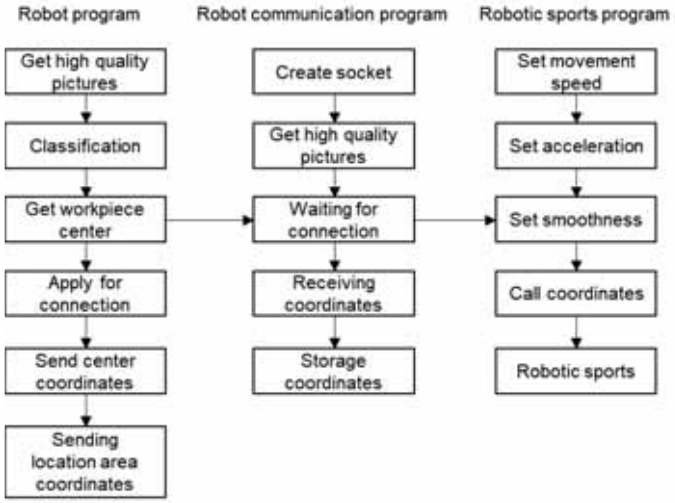

FIGURE 8
Flow chart of the main module.

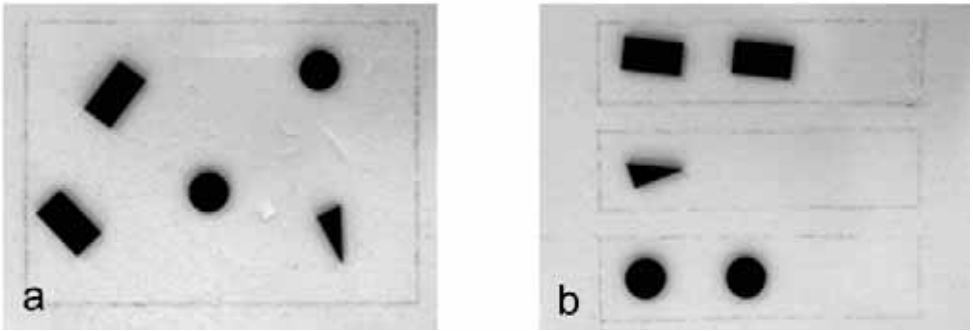

FIGURE 9
Sorting effect diagram (a, before sorting; b, after sorting).

TABLE 1
Workpiece positioning data table

Job type	Actual coordinates (x，y)	Theoretical coordinates (x'，y')	Δx(mm)	Δy(mm)
Rectangle	(215.36,132.41)	(215.06,132.69)	0.30	0.28
Rectangle	(236.20,201.33)	(235.89,201.12)	0.31	0.21
Triangle	(389.06,212.17)	(389.57,211.77)	0.51	0.40
Round	(241.18,192.68)	(241.83,192.26)	0.65	0.42
Round	(305.74,135.87)	(305.53,135.61)	0.21	0.26

The error between the coordinates of the geometric center point of the workpiece obtained by the entire system and the coordinates of the actual geometric center point of the workpiece is between 0.21mm and 0.65mm. The average position error of the robot body measured by the laser tracker is 0.41mm. It can be explained that the positioning error of the robot body is the main error of the whole system. The system error of 0.65mm can meet the requirements of the vision-based robot sorting system. After many experiments and observations, the workpieces in the working area can be sorted successfully.

CONCLUSIONS

(1) We develop a complex visual sorting robot based on the big data ecological environment, collect information about the machine operating environment, collect the position and operation information in the big data, and analyze it to intelligently manage and manage the robot Assess operational impact. With the support of big data, the robot has performed recognition operations on 5 kinds of objects, and the offset distance is small, which can realize self-control. The robot has the ability to accurately recognize objects, and the evaluation result of the operation impact is close to the actual value.

(2) In the robot sorting process, the target moves with the conveyor belt. In order to achieve strong target recognition, it is necessary to combine graphics technology. This paper studies the sorting process and imaging methods. At the same time, the realization path of the visual sorting robot is studied.

(3) The design scheme of the visual robot sorting system is given and the function of each component is explained. The selection of industrial cameras, lenses and light sources in the hardware part of the sorting system is explained, and image processing is also designed. The software and the communication protocol between the control systems are selected.

ACKNOWLEDGEMENTS

This research was not supported by any funds. The authors would like to thank all the techniques who have helped this research.

REFERENCES

[1] Li, X., Wu, P., Wang, R. (2015) Design and manufacture of a small sorting and conveying robot system based on machine visual recognition. Machine Tool & Hydraulics. 58(12), 1718-23.

[2] Liu, Y., Zhong, S., Tian, Z., He, K. (2020) Design of vision servo sorting robot system based on SVM. Journal of Physics Conference Series. 1550, 022032.

[3] Yang, X. (2018) Mobile robot path planning with a non-dominated sorting genetic algorithm. Applied Sciences. 8(11), 2253.

[4] Muhammad, A., Naoshi, K., Tomoo, S. (2011) Use of Machine Vision to Sort Tomato Seedlings for Grafting Robot. Engineering in Agriculture Environment and Food. 4(4), 119-125.

[5] Sun, L., Yuan, G., Zhang, J., Liu, Z., Sun, L. (2013) Automatic button cell sorting manipulator system research based on visual servo control. Advanced Materials Research. 712-715(3), 2285-2289.

[6] Mazlum, Y., Gunduz, M., Gurlek, O., Yazici, M. (2019) Effects of soybean oil supplementation on the growth and survival performance of red claw crayfish Cherax Quadricarinatus in culture condition. Fresen. Environ. Bull. 28(4), 2679-2687.

[7] Raghavan, K., Sastry, P. (1970) Effects of temperature on acetylcholine synthesis and release in perfused human placenta. Indian Journal of Medical Research. 58(12), 1718-1723.

[8] Shaukat, A., Gao, Y., Kuo, J., Bowen, B., Mort, P. (2016) Visual classification of waste material for nuclear decommissioning. Robotics and Autonomous Systems. 75, 365-378.

[9] Uyar, E., Levent, Ç., Aytaç, G. (2003) A computer controlled visual system for object classification. IFAC Proceedings Volumes. 36(7), 101-104.

[10] Chhaniyara, S., Brunskill, C., Yeomans, B., Matthews, M., Saaj, C., Ransom, S., Richter, L. (2012) Terrain trafficability analysis and soil mechanical property identification for planetary rovers: a survey. Journal of Terramechanics. 49(2), 115-128.

[11] Kim, S., Simeral, J., Hochberg, L., Donoghue, J., Black, M. (2008) Neural control of computer cursor velocity by decoding motor cortical spiking activity in humans with tetraplegia. Journal of Neural Engineering. 5(4), 455-476.

[12] Wang, H., Noguchi, N. (2019) Navigation of a robot tractor using the centimeter level augmentation information via quasi-zenith satellite system. Engineering in Agriculture Environment and Food. 12(4), 414-419.

[13] Pechanec, V., Vondrakova, A., Sterbove, L., Cudlin, P. (2020) Environmental data visualization: Stocks of the stored carbon in Czechia. Fresen. Environ. Bull. 29(3), 1630-1636.

[14] Marturi, N., Dembele, S., Piat, N. (2014) Scanning electron microscope image signal-to-noise ratio monitoring for micro-nanomanipulation. Scanning. 36(4), 419-429.

[15] Li, W., Kleeman, L. (2011) Segmentation and modeling of visually symmetric objects by robot actions. International Journal of Robotics Research. 30(9), 1124-1142.
[16] Stein, R., Aoyagi, Y., Weber, D., Shoham, S., Normann, R. (2015) Encoding mechanisms for sensory neurons studied with a multielectrode array in the cat dorsal root ganglion. Revue Canadienne De Physiologie Et Pharmacologie. 82(8-9), 757-768.
[17] Cheng, Y., Wang, S., Yu, D. (2017) Multi-objective optimization design of a bionic parallel oculogyric mechanism. Robot. 39(2), 176-181.
[18] Lin, W., Ross, J., Ziegler, M. (2010) Semiautomatic calibration of robot manipulator for visual inspection task. Journal of Field Robotics. 3(1), 19-39.
[19] Li, M., Jian, C., Zhao, S., Cui, X., Ma, S. (2020) The effect of the measured data on evaluating the structural safety of shield tunnel based on the real-time environment monitoring. Fresen. Environ. Bull. 29(6), 4723-4729.
[20] Wang, J. (2020) Innovating ionic liquids as repairable electronics for liquid robots. Green Energy & Environment. 5(2), 122-123.
[21] Zhang, R., Kan, Z., Yan, X., Hu, W. (2011) Analysis on actuating mechanism for tomato color sorting robot based on high-speed photography. Advanced Materials Research. 308-310, 384-387.
[22] Lin, Y., Min, H., Zhou, H., Pei, F. (2018) A human–robot-environment interactive reasoning mechanism for object sorting robot. IEEE Transactions on Cognitive and Developmental Systems. 10(3), 611-623.
[23] Zhang, T., Pang, M., Yan, Z., Ma, L. (2013) Design of mobile platform based food sorting robot. Information & Communications. 200, 520-523.
[24] Mehdian, M., Rahnejat, H. (1992) An intelligent part sorting robot in unstructured manufacturing environments. Robotica. 10(2), 155.
[25] Zhang, H., Su, T., Wu, S., Zheng, J., Wang, Y. (2017) Sorting route optimization of parallel robot based on improved genetic algorithm. Journal of South China University of Technology. 45(10), 93-99.
[26] Hou, D., Guo, W. (2013) The design for express sorting based on image recognition of barcode. Applied Mechanics & Materials. 303-306, 1013-1016.

Received: **14.09.2020**
Accepted: **19.01.2021**

CORRESPONDING AUTHOR

Zhe Yan
School of Automation,
Harbin University of Science and Technology,
Heilongjiang Harbin 150080 – China

e-mail: huajing9966961@163.com

© by PSP Volume 30– No. 05/2021 pages 4962-4974 Fresenius Environmental Bulletin

MORPHOMETRIC ANALYSIS TO INFER HYDROLOGICAL BEHAVIOUR OF CORUH RIVER BASIN (NORTHERN TURKEY) USING GIS TECHNIQUE

Umit Yildirim*

Bayburt University, Faculty of Arts and Designing, Department of Interior Architecture and Environmental Designing, Bayburt, Turkey

ABSTRACT

Morphometric analysis is a very practical approach for evaluating hydrological processes for watersheds. The combination of morphometric, geological, and geomorphological characteristics of the river basin helps to gain further insights in forecasting hydrological phenomena (such as flooding, soil erosion, and groundwater potential). In this study, the morphometric analysis of the Coruh River Basin was conducted using GIS to establish effective water management. Firstly, the basic morphometric parameters (basin area, basin length, basin perimeter, stream order, stream number, and total stream length) were calculated for both CRB and its subbasins. Then, characteristic morphometric parameters (drainage density, drainage texture, form factor, length of the overland flow, topographic wetness index, and stream power index) were determined. Results showed that the infiltration capacity of the subsurface material was low, and the surface runoff was slow in the subbasins located close to the CRB's outlet. Therefore, these subbasins are more sensitive to flooding, erosion, and landslides compared to others. Soil erosion and thus sediment loss is higher in 1st, 2nd, 3rd, and 5th subbasins, and the groundwater potential is higher in headwater areas of the basin. This study revealed that the GIS-based morphometric analysis is beneficial to implement water management tool at the watershed scale.

KEYWORDS:
Morphometric analysis, water management, watershed hydrology, geographic information system, soil erosion, flooding risk

INTRODUCTION

The water, which is the most basic need of living, is getting more and more importance under changing climate conditions and growing population worldwide. The design of water structures for its direct use (such as dams and lakes) and its indirect effects on the land (such as flood and erosion) need to be controlled by effective management. River basin-based management forms the basis of this effective management, and it plays an essential role in various phases of the hydrological cycle. Climate patterns, topography, geology, and soil property of related catchment are highly affected by the hydrological processes and drainage characteristics (such as drainage pattern and drainage density) of concerned catchment's fluvial system [1-3]. Since surface flow affects weathering, stream erosion, and sediment transportation within watersheds, it causes topological changes and assigns the watershed characteristics. Many researchers have identified a good relation among streamflow, geographic, hydro-chemical and geomorphic features within the watersheds [4-9]. The geomorphic characteristics of a river basin, have long been indicated to be essential indices of hydrological events of surface water [10-13]. Thus, the quantitative analysis of the catchments is the major aspect [4] should be the first step for water management.

Geographic Information System technology has brought a quantitative approach to surface characterization and has created a new mechanism for the explication and running of quantitative data sets for watersheds [9, 14-15]. The present study aimed to deeply investigate the Coruh River Basin (CRB) which is one of the 25 primary river basins in Turkey, through morphometric analysis using GIS technology in the aspect of surface hydrology.

MATERIALS AND METHODS

Basin characteristics. The CRB is a transboundary catchment between Georgia and Turkey. It is located in the NE of Turkey, south of the Black Sea (Figure 1). Approximately 91% of the drainage area of the CRB is in Turkey, while the rest is in Georgia. The primary characteristics of the CRB are summarized in Table 1. The CRB, chiefly extending in the SW–NE direction from the Gümüşhane, Bayburt, and Erzincan provincial borders to the Eastern Blacksea border (Artvin province), covers an area of about 20,257.96 km^2 between latitudes 39°54′16.32″ to 41°31′29″ N and longitudes 39°40′03″ to 42°36′29″ E. The length of the CRB is 399.53 km, which is the catchment with the fastest flowing river in Turkey. The largest share of land use with 46.92%,

33.05%, and 19.76% of the basin is located in Erzurum, Artvin, and Bayburt, respectively, and the rest is in Ardahan, Erzincan, Gümüşhane, Kars, Rize, and Trabzon (Figure 1).

The Coruh River, which is the longest river of the East Black Sea region and has the third-highest runoff coefficients of the 25 main river basin in Turkey, originates in the Mescit Mountains in the Bayburt province. After passing Bayburt, the river enters the Artvin province at the location of the village of Yokuşlu in Yusufeli district. It joins with Oltu water in a place called water convergence. Then, after the combining with Barhal creek close to Yusufeli district, the Coruh River runs in the northwest direction. Ortaköy water next to Artvin, Murgul water, Içkale water, and Kaynarca water in Borçka join into the main river, and it passes through the Muratlı District and flows into the Black Sea from the southwest of Batumi. The part of 22 km of the Coruh River is located in Batumi-Georgia.

The headwaters of the Coruh River in Turkey reach up to ca. 3928 m above mean sea level (amsl) (Figure 2a) with a mean elevation of 1885 m amsl. The CRB comprehends a strongly rough mountainous terrain (Figure 2b). 81.63% of the area lies between 1000-2500 m amsl (Table 1). Especially in the central part of the northern border of the basin (5th subbasin), the heights rise above 3000 m over a short horizontal distance (Figure 2a). According to the slope map (Figure 2b), derived from the 20-m digital elevation model (DEM) of the CRB (Figure 2a), slopes variety from 0.0° to 86.9°, with a mean of 21.2°. Slopes ranging from 0° to 20° cover 45.73% of the basin (Table 1) and commonly located to 4th subbasin (53.63 %), 6th subbasin (79.34 %), and 7th subbasin (57.02 %) (Figure 2b). Areas with a slope of 20 ° to 40 ° are seen in 1st subbasin, 2nd subbasin, 3rd subbasin, and 4th subbasin with a prevalence of 71.44 %, 55.62 %, 70.86 % and 61.61%, respectively.

Since the CRB is located between the Black Sea region and the Eastern Anatolia Region, it covers different climatic conditions of these regions. 99.73% of the CRB is situated within the borders of Artvin, Erzurum, and Bayburt. Therefore, the climate characteristics of these provinces reflect the climate and hydrologic characteristics of the CRB, which has 6.3×109 m^3 annual water potential (Table 1). In Artvin, winters are warmish, summers are hot and very high rainfall, while in Erzurum winters are cold and snowy, summers are hot and dry (Figure 3). Bayburt has a transitional climate between the Eastern Black Sea climate and the Eastern Anatolian climate and in this province, summers are hot and dry, while winters are cold and rainy (Figure 3). For whole CRB, the annual total precipitation and mean temperature are computed as 652.88 mm/year and 8.9 °C respectively by means of the Thiessen polygon method using to spatially interpolate and calculate precipitation and temperature (Table 1 and Figure 2c-d).

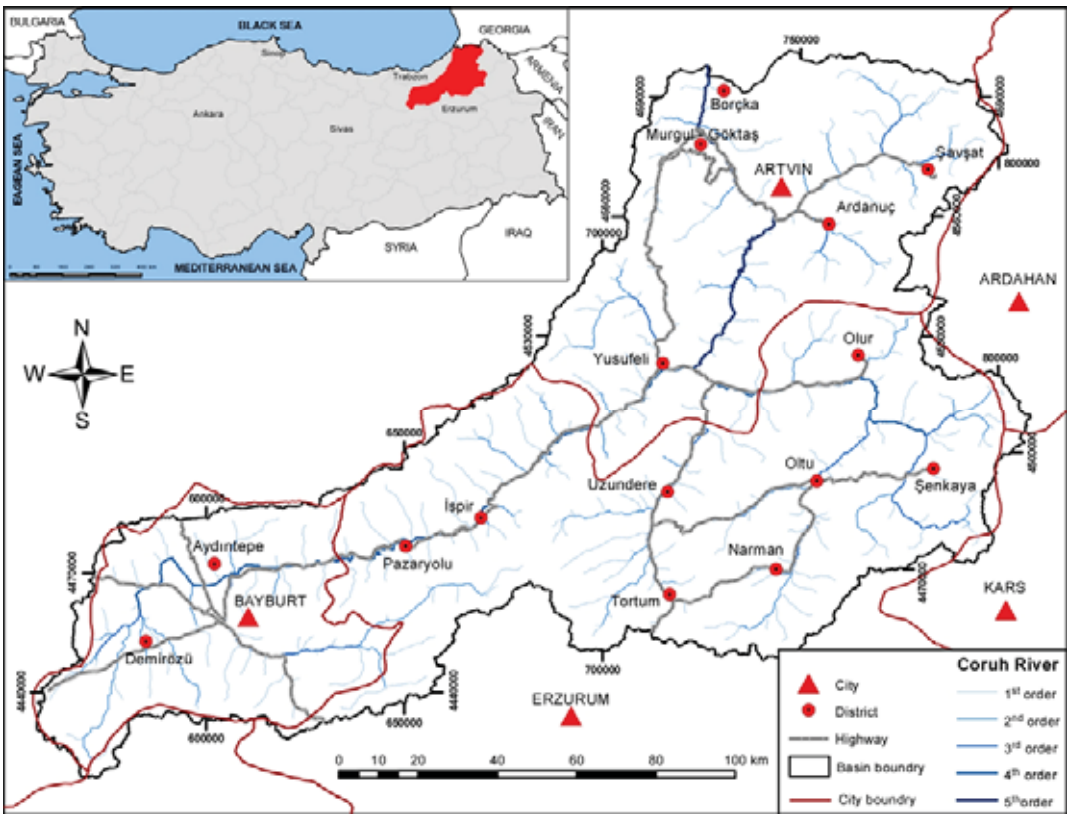

FIGURE 1
The location map of Coruh River Basin.

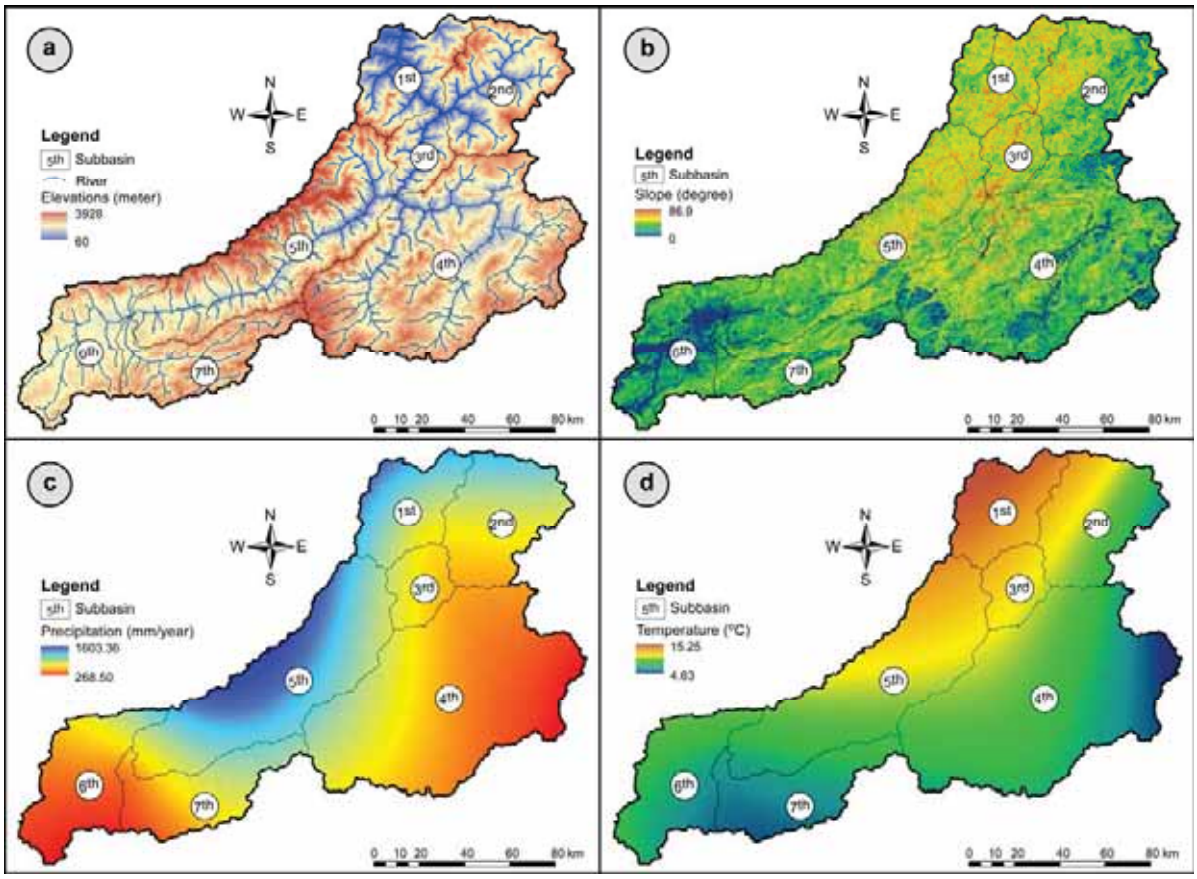

FIGURE 2

Terrestrial changes of elevation (a), slope (b), precipitation (annual mean between the periods 1981-2010) (c) and temperatures (annual mean between the periods 1981-2010) (d) in the CRB basin.

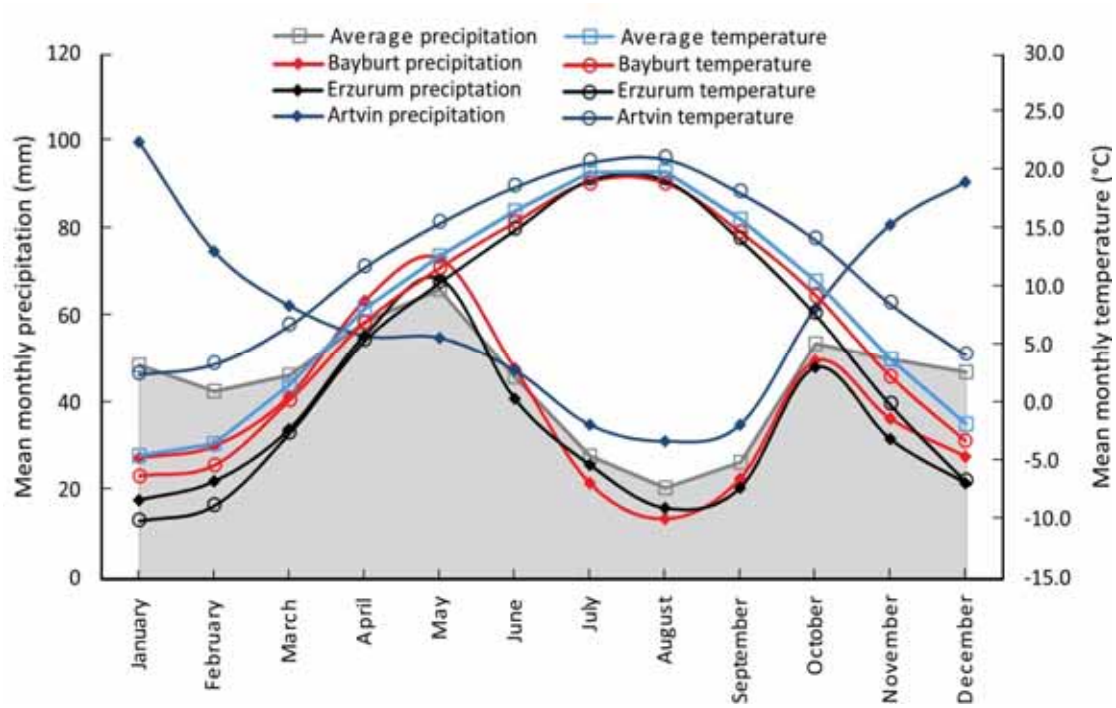

FIGURE 3

The mean monthly temperature and precipitation graphics of Artvin, Erzurum, and Bayburt provinces between the periods 1981 and 2010 [16]. The average precipitation area is shaded with grey to separate from other.

TABLE 1
Basic characteristics of the Coruh River Basin (CRB).

Characteristics	Unit	Value	Characteristics	Unit	Value
Basin area (total)	km^2	20,257.96	*Land use*		
Coruh River Length	km	399.53	Pasture	% area	42.24
Hydrology			Forest	% area	27.70
Discharge (Annual total)	m^3/y	6.3×10^9	Agriculture	% area	9.95
Precipitation (total mean)[a]	mm/y	652.88	Bare Rock	% area	7.12
Temperature (mean)[a]	°C	8.9	Scrub	% area	6.28
Lithology			Arable Land	% area	5.08
Sedimentary rocks	% area	39.55	Settlement	% area	0.93
Carbonate rocks	% area	25.95	Permanent Crop	% area	0.40
Volcanic rock	% area	18.99	Floodplain	% area	0.17
Plutonic rock	% area	8.84	River	% area	0.09
Unconsolidated sediments	% area	3.74	Lake	% area	0.05
Ophiolitic rocks	% area	1.70	*Soil type*		
Metamorphic rocks	% area	1.23	Brown forest	% area	27.49
Elevation range			Brown	% area	17.67
60–500 m	% area	1.19	Basaltic	% area	14.39
500–1000 m	% area	5.04	Maroon	% area	10.24
1000–1500 m	% area	14.57	High-level mountain meadow	% area	7.65
1500–2000 m	% area	35.83	Barerock	% area	7.12
2000–2500 m	% area	31.23	Non-calcic brown forest	% area	4.44
2500–3000 m	% area	10.73	Red yellow podzolic	% area	3.59
3000–3500 m	% area	1.40	Alluvium	% area	2.92
3500–3928 m	% area	0.01	Colluvium	% area	1.65
Slope range			Non-calcic brown	% area	1.58
0°–10°	% area	19.82	Settlement	% area	0.93
10°–20°	% area	25.91	Floodplain	% area	0.17
20°–30°	% area	28.11	River	% area	0.09
30°–40°	% area	21.19	Lake	% area	0.05
40°–50°	% area	4.43	Gray brown podzolic	% area	0.02
> 50°	% area	0.54			

[a]The measured temperature and precipitation data between the period 1981 and 2010 were used.

The geology of the basin is comprised of Cenozoic aged rocks and unconsolidated sediments to Paleozoic aged metamorphic rocks and granitoids which form the basis of the study area. The CRB is located in the eastern Pontides belt. The Eastern Pontites belt is divided into three different geological groups as northern, southern, and axial regions according to their lithological and tectonic characteristics [17-19]. These three zones are separated by NE – SW, and NW – SE directional faults (Figure 4). The Mesozoic-Cenozoic aged volcanic rocks have generally spread in the northern regions whereas Mesozoic and Eocene aged sedimentary rocks and pre-liassic plutonic and metamorphic rocks have spread in the southern zone (Figure 4) [20-22]. The volcanic sequences in the northern region include calderas, massive sulfide deposits, and granitic intrusions [23, 24. Mesozoic Alpine type peridotites and gabbro-diorites spread over most of the axial zone [25, 26. The volcanic rocks of the eastern Pontides lie unconformably on basement rocks and are commonly intruded by granitoids which are intruded during the Late Cretaceous to Late Eocene [27-29]. Jurassic–Cretaceous neritic and pelagic carbonates overlie on this unit. These carbonates are overlain by sedimentary rocks in the south while it's overlain by volcanic rocks in the north (Figure 4) [30, 31]. The volcanic rocks aged upper cretaceous include rhyolites, dacites, andesites, and basalts [24]. The Eocene rocks that are collected of volcanic, volcano-sedimentary, and interbedded turbiditic members unconformably overlie the Upper Cretaceous series [32, 33]. Terrestrial sedimentation continues in limited areas from Middle Eocene to the present [23]. The areal coverages (in %) of different lithologies found in the CRB and its subbasins are presented in Table 1 and Table 2, respectively.

In the CRB, the soils are product of weathering of the underlying volcanic, plutonic, metamorphic, and sedimentary rock formations (Figure 5a). Soil depths are generally in the range of 0-20 cm and have a lithosolic character in mountainous areas where the slope is high. 71% of the basin soils vary at depths of 0-50 cm, and the depth of it exceeds 90 cm in areas where the slope is low [37]. The most dominant soil types are the brown forest (27.49%), brown (17.67%) and basaltic soils (14.39%) (Table 1), which respectively cover downstream (1^{st}, 2^{nd}, 3^{rd},

4th and 5th subbasin), upstream (4th, 5th, 6th, and 7th subbasin) and upstream portions (4th subbasin) of the CRB (Table 2 and Figure 5a). The rest of the soil classes consist of maroon, high-level mountain meadow, bare rock, non-calcic brown forest, red-yellow podzolic, alluvium, colluvium, non-calcic brown, and gray-brown podzolic soils, with a total areal coverage less than about 41% (Table 1).

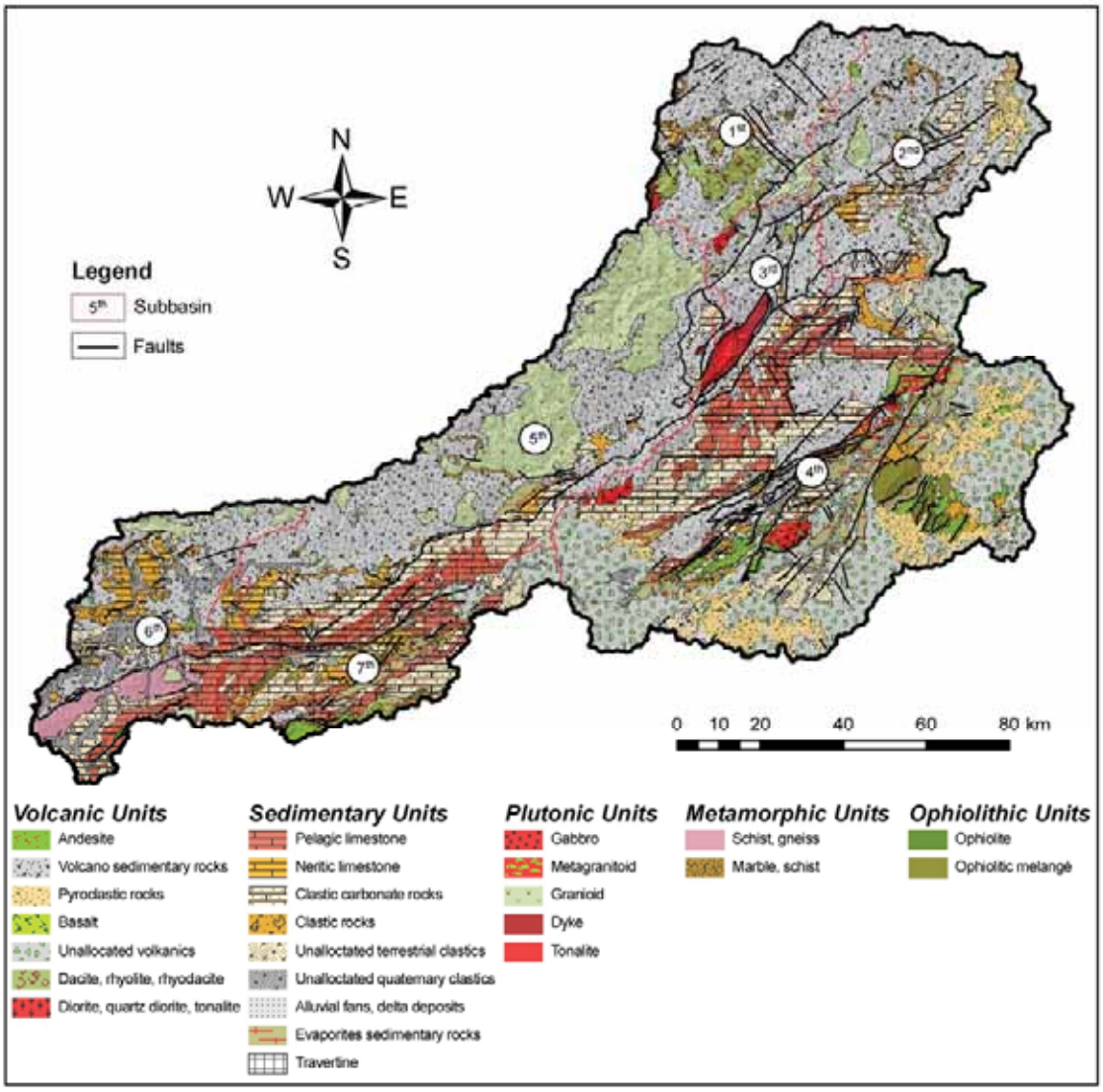

FIGURE 4
Geology map of CRB. The map is modified from [34-36].

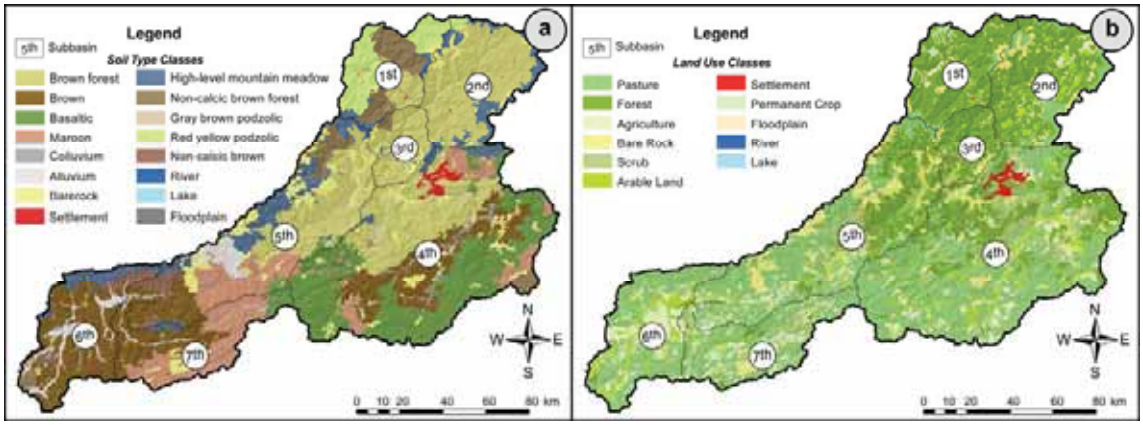

FIGURE 5
Soil [37] (a) and Land use classes (b) maps of CRB.

TABLE 2
Basic characteristics of the subbasins of the Coruh River Basin (CRB).

Characteristics	Unit	Value						
		SB 1	***SB 2***	***SB 3***	***SB 4***	***SB 5***	***SB 6***	***SB 7***
Area	km^2	1,660.88	2,307.78	818.75	7,042.48	4,428.26	2,155.82	1,844.00
Mean Elevation	meter	1,294.00	1,737.60	1,454.71	1,969.88	2,019.02	1,888.29	2,171.22
Mean Slope	degree	34.45	28.77	36.65	24.55	30.26	17.72	23.26
Lithology								
Sedimentary rocks	% area	73.03	68.87	68.35	19.05	51.93	38.20	10.73
Carbonate rocks	% area	5.09	17.14	11.80	27.67	17.48	28.90	72.38
Volcanic rock	% area	18.52	9.34	5.06	43.38	0.71	1.19	8.49
Plutonic rock	% area	2.94	3.39	12.99	2.13	28.75	6.33	–
Unconsolidated sediments	% area	0.42	1.26	0.55	3.99	1.13	14.78	3.78
Ophiolitic rocks	% area	–	–	–	3.49	–	0.57	4.56
Metamorphic rocks	% area	18.52	–	1.26	0.29	–	10.03	0.05
Soil Type								
Brown forest	% area	19.35	74.72	79.12	22.43	28.85	0.78	0.12
Brown	% area	–	–	–	16.27	11.08	60.27	34.97
Basaltic	% area	–	–	–	38.56	2.07	–	5.84
Maroon	% area	–	0.14	–	7.84	15.38	–	45.44
High-level mountain meadow	% area	6.13	15.98	3.84	2.16	13.99	11.20	1.87
Barerock	% area	3.39	7.04	11.60	5.72	13.56	0.46	6.22
Non-calcic brown forest	% area	28.80	–	5.06	1.36	4.97	2.97	–
Red yellow podzolic	% area	41.26	1.74	–	–	0.03	–	–
Alluvium	% area	0.06	0.04	–	0.06	5.49	13.44	2.90
Colluvium	% area	0.07	0.10	–	3.24	0.32	2.44	1.93
Non-calcic brown	% area	–	–	–	–	3.56	7.56	–
Settlement	% area	0.30	0.20	0.10	1.93	0.32	0.74	0.62
Floodplain	% area	0.37	–	–	0.25	0.22	0.07	–
River	% area	0.25	0.02	0.29	0.02	0.16	0.02	0.07
Lake	% area	0.01	0.01	–	0.10	0.01	0.06	–
Gray brown podzolic	% area	–	–	–	0.06	–	–	–
Land Use								
Pasture	% area	6.60	16.43	4.61	53.30	43.78	58.24	58.67
Forest	% area	76.73	60.97	72.96	18.17	22.61	0.65	2.01
Agriculture	% area	5.39	8.03	2.00	6.95	7.21	24.65	20.86
Bare Rock	% area	3.39	7.04	11.60	5.72	13.56	0.46	6.22
Scrub	% area	1.21	0.10	6.01	8.57	9.36	1.27	8.40
Arable Land	% area	0.94	7.17	2.37	4.99	2.76	13.83	3.14
Settlement	% area	0.30	0.20	0.10	1.93	0.32	0.74	0.62
Permanent Crop	% area	4.80	0.02	0.05	–	–	–	–
Floodplain	% area	0.37	–	–	0.25	0.22	0.07	–
River	% area	0.25	0.02	0.29	0.02	0.16	0.02	0.07
Lake	% area	0.01	0.01	–	0.10	0.01	0.06	–

The CRB is represented by many land use types that spread in a different part of the basin (Figure 5b). In the CRB, the most dominant land-use types are the pasture, forest, and agriculture areas, which respectively covers the area of 42.24%, 27.70%, and 9.95% of the whole basin (Table 1 and Figure 5b). The remaining about 20% of the basin is covered by bare rock, scrub, arable land, settlement, permanent crop, floodplain, river, and lake respectively in terms of the covered area (Table 1). Nearly two-thirds of the 1st, 2nd, and 3rd subbasins are forest, while about half of the 4th, 5th, 6th, and 7th subbasins are pasture areas (Table 2). While 24.65% and 20.86% of the 6th and 7th subbasins where the slope is low are used as agricultural areas, the areas covered by agricultural areas in other subbasins vary between 2% and 7.2% (Table 2 and Figure 5b).

TABLE 3
Methodologies perceived for computations of morphometric parameters.

Morphometric Parameter	Basic Parameters Method, Formula and unit	Reference
Basin Area (A)	Area of the basin (km^2)	Arc measurement tools
Basin Perimeter (P)	Perimeter of the basin (km)	[44]
Basin Length (L_b)	Longest distance parallel to the main stream (km)	[44]
Stream Order (U)	Hierarchical rank	[4]
Stream number (N_u)	Number of the stream	[1]
Total Stream Length (L_u)	Total channel length of the stream (km)	[1]
Mean Stream Length (L_{sm})	L_u/N_u (km)	[4]
Characteristic Parameters		
Morphometric Parameters	**Method and Formula**	**References**
Drainage Density (D_d)	L_u/A	[45]
Drainage texture (D_t)	N_u/P	[1]
Form Factor (R_f)	A/L_b^2	[45]
Length of overland flow (L_g)	$1/2D_d$	[1]
Stream Power Index (SPI)	$A_s \times \tan_\beta$ "where A_s is specific catchment area (m^2/m), $_\beta$ is slope gradient (°)"	[46]
Topographic Wetness Index (TWI)	$\ln(a/\tan b)$ "where a is the local upslope area draining through a certain point per unit contour length and $\tan b$ is the local slope in radians"	[47]

Methodology. Geomorphometry is firmly related with hydrology, geology, landscape, soil type, and climate, is a reflection of measuring and mathematical analysis of the physical aspect of landforms such as surface and shape [1, 38- 40]. Many studies on morphometric analysis of river basins concerns the geometry of river basin and stream connection to soil erosion and streamflow on the basin. There are many morphometric parameters to determine the hydrological characterization of river basins [1, 38, 39, 41-43]. The parameters are used in this study, are grouped such as basic parameters and characteristic parameters. The methods and formulas of all parameters which are used in this study have shown in Table 3.

The basis of the morphometric analysis is the digital elevation model (DEM) of the basin. The DEM may create by digitizing the isohips from topographical maps. The present study is based on 1/50,000 scaled topographic map sheets (Turkey E47; c-d, F46; b-c, F47; a-b-c-d, F48; a-b-c-d; F49; a-d, G44; c-d, G45; c-d, G46; a-b-c-d, G47; a-b-c-d, G48; a-b-c-d, G49; a-d, H43; b-c-d, H44; a-b-c-d, H45; a-b-c-d, H46; a-b-c, H47; a-b-c-d, H48; a-b-d, H49; a, I43; a-b) which are published by Turkish Ministry of National Defence, General Command of Mapping. These topographical maps were rectified geographically and the whole study area was delineated in the GIS environment utilizing ArcGIS 9.3 software assigning Universal Transverse Mercator (UTM), World Geodetic System (WGS 1984) and 37N, 38N Zone Projection System. The isohips of the whole study area were digitized on ArcGIS, and the DEM was created using digitized isohips of the basin. Then, the created DEM has been reconditioned by the Fill tool using the Hydrology toolset in ArcGIS for clear of the errors as sinks. Then, flow direction, flow accumulation, stream order (according to Strahler's method), stream to feature, snap pour point, and watershed tools have been used, respectively, to create the layer that is needed to compute basic morphometric parameters values. The snap pour points are selected on joining points of the main Coruh River and outlet of the basin to delineate the boundary of subbasins and whole basin. The CRB was divided into 7 subbasins and the basic morphometric parameters, such as basin area, basin perimeter, basin length, stream order, stream number, and total stream length have been calculated for all subbasins and whole CRB using suitable tools in ArcGIS. Characteristic parameters such as drainage density, drainage texture, form factor, and length of the overland flow were calculated for all subbasin and whole basin using basic parameters. Furthermore, slope, aspect, topographic wetness index (TWI), and stream power index (SPI) which are derived from DEM were also expected through GIS.

RESULTS AND DISCUSSION

The results of the morphometric parameters of CRB and its subbasins are shown in Table 4 and Table 5. Results are discussed under the following subtitle such as Basic Parameters and Characteristic Parameters.

TABLE 4
Results of morphometric analysis.

Basic Parameters							
SB ID	***A***	***P***	***L_b***	***U***	***N_u***	***L_u***	***L_{sm}***
1	1,660.64	257.44	71.56	3	37	221.44	5.98
2	2,307.45	314.92	83.20	4	71	333.54	4.70
3	818.63	167.14	60.11	3	27	135.41	5.02
4	7,041.50	583.98	162.85	4	203	1,106.73	5.45
5	4,427.64	527.02	178.64	4	125	739.64	5.92
6	2,155.52	366.03	104.99	4	63	352.10	5.59
7	1,843.74	389.98	121.91	3	48	297.10	6.19
CRB	20,255.12	1,297.37	399.53	5	581	3,185.96	5.48
Characteristic Parameters							
SB ID	***D_d***	***L_g***	***D_t***	***R_f***	***SPI***	***TWI***	
1	0.13	3.22	0.14	0.32	1.69	4.41	
2	0.14	3.46	0.23	0.33	1.46	4.75	
3	0.17	3.02	0.16	0.23	1.73	4.30	
4	0.16	3.18	0.35	0.27	1.26	5.08	
5	0.17	2.99	0.24	0.14	1.50	4.66	
6	0.16	3.06	0.17	0.20	0.94	5.88	
7	0.16	3.10	0.12	0.12	1.24	5.13	
CRB	0.16	3.14	0.45	0.13	1.35	4.94	

Basic Parameters. The basic parameters are the basic inputs of the characteristic parameters that explain the basin characteristics, although, they do not provide key information in the hydrological evaluation of the basins. The results of the basic parameters of the CRB and its subbasins are shown and discussed below.

Basin area (A) is not sufficient in terms of comparing neighboring basins, but it is one of the most important basic parameters of morphometric analysis. This value represents the area covered by the basin. In this study, while the lowest area belongs to the 3rd subbasin as 818.63 km^2, the highest area belongs to the 4th subbasin as 7,041.50 km^2 (Table 4). The CRB covers a total of 20,255.12 km^2 (Table 4). Basin perimeter (P) value represents the length of the boundary line surrounding the basin [44]. In the present study, the lowest P value belongs to the 3rd subbasin as 167.14 km, whereas the highest P value belongs to the 4th subbasin as 583.98 km (Table 4). The CRB perimeter is 1,297.37 km (Table 4). It has been observed that the perimeters of 6th and 7th subbasins located in the southwestern region of the CRB are relatively higher compared to the area-perimeter relationships of other subbasins. This is due to the headward erosion of various river basins developed in the plateau scarps [14]. Basin Length (Lb) is the length of the line of maximum length that can be drawn parallel to the mainstream that runs along the basi. The basin length of the CRB is 399.53 km (Table 4). While the lowest L_b belongs to the 3rd subbasin (60.11 km) and the highest L_b belongs to the 5th subbasin (178.64 km) (Table 4).

Stream order (U) is one of the most important morphometric parameters in terms of physiographic and structural evaluation of river basins. Stream order refers to the hierarchical link between stream segments. There are several stream order systems such as Horton [1], Shreve [48], Hack [49], and Strahler [4] in the literature. In this study, Strahler's method [4], which is the most widely used in these methods, has been selected. According to Strahler's method, the first branch of the stream is called the first order. The second stream orders are formed by combining the first orders, and the third orders are formed by the meeting of the second orders and so forth. The CRB has fifth-order as a whole (Table 4 and Figure 1). 1st, 3rd, and 7th subbasins are of third-order whereas 2nd, 4th, 5th, and 6th subbasins are of fourth-order (Table 4). It shows that the 2nd, 4th, 5th, and 6th subbasins have a greater potential of discharge than rest. Basin area and basin shape are the highly affecting factors of the distribution of the stream orders in the basin. However, the relief, structural factors, climate variables, geology, and vegetation thickness of the basin affect the flow sequence [9].

Stream number (N_u) is the number of stream segments both in each stream orders and throughout the basin. This parameter mostly influenced by permeability and infiltration of the subsurface soil. The higher Nu value shows the lesser infiltration and permeability. The CRB has 581 stream segment (Table 4). 80.5% of these segments connected to the first order, 15.6% to the second-order, 2.8% to the third-order, 0.8% to the fourth-order, 0.3% to the fifth-order (Table 5). The count of stream segments has been decreased as the stream order increases (Table 5). The N_u of the first orders of the subbasins varies between 75% and 86%. Such a high proportion of first order of these streams specify the current structural weakness in these basins dominantly in the system of lineaments and folding.

TABLE 5
Stream number (N_u), Stream length (L_u), Mean stream length (L_{sm}) of the stream orders, and the bifurcation ratio between the stream orders.

SB ID	1st order			2nd order			3rd order			4th order			5th order		
	N_u	L_u	L_{sm}	N_u	L_u	L_{sm}	N_u	L_u	L_{sm}	N_u	L_u	L_{sm}	N_u	L_u	L_{sm}
1	19	119.2	6.3	5	65.3	13.1	1	37.0	37.0						
2	36	165.2	4.6	8	82.6	10.3	3	49.0	16.3	1	36.8	36.8			
3	14	69.7	5.0	3	38.2	12.7	1	27.5	27.5						
4	100	611.9	6.1	18	239.1	13.3	3	172.4	57.5	1	83.3	83.3			
5	62	437.3	7.1	12	128.5	10.7	2	164.9	82.4	1	9.0	9.0			
6	33	171.6	5.2	8	127.8	16.0	2	10.3	5.2	1	42.4	42.4			
7	24	169.6	7.1	3	72.4	24.1	1	55.1	55.1						
CRB	289	1,750.7	6.1	56	701.1	12.5	10	311.9	31.2	3	321.1	107.0	1	101.2	101.2

Total stream length (L_u), is the total length of all branches of the stream and its orders in a basin. This parameter is a very important parameter in terms of hydrological structures of the underlying rock, landscape, and soil characteristics of the basin due to it represents the runoff features of the stream. The presence of longer streams in less number indicates that the surface is less impermeable, while the presence of shorter streams indicates a more impermeable underlying rock formation [50]. In the present study, as a whole CRB, the total stream length is 3,185.96 km (Table 4). The lowest value of Lu is 135.41 km with a 27 stream segment for 3rd subbasin, while the highest value of total stream length is 1,106.73 km with 203 stream segments for 4th subbasin (Table 4).

Mean stream length (L_{sm}) is the total stream length and stream number ratio in both the basin and in each stream order. The mean stream length value of CRB is 5.48 km (Table 4). The L_{sm} varies between 4.70 km (2nd subbasin) and 6.19 km (7th subbasin) (Table 4). There is a direct proportion between the stream order and mean stream length in the basins that show the basin evolution with uniform weathering-erosion characteristics affecting homogeneous geological material [14]. This proportion has deteriorated between 4th and 5th orders in CRB, between 3rd and 4th orders in 5th subbasin, and between 2nd and 3rd orders in 6th subbasin (Table 5).

Characteristic Parameters. Drainage density (D_d) is one of the most important morphometric parameters, in which erosion and surface runoff status are evaluated, throughout and different parts of a basin [51, 52]. This parameter describes the landscape dissection, the vegetation status, porosity and permeability of the land, and surface runoff potential of the basins [45]. The value of D_d in the present study ranges from 0.13 km^{-1} to 0.17 km^{-1} (Table 4). The lowest value belongs to the 1st subbasin whereas the highest value belongs to the 3rd and 5th subbasins. The CRB has a 0.16 km^{-1} D_d value (Table 4). D_d shows the lower value in the region with the presence of less resistant underlying geology, or those with high infiltration capacities while high D_d shows the subsoil materials may impermeable, infrequent vegetation [52, 53].

Drainage texture (D_t) is the ratio of the length of the basin perimeter to the total stream number of all stream order of the basin [1]. D_t is associated with underlying materials properties (infiltration capacity, permeability, etc.), climate conditions of the region, vegetation type, and relief of the basin [41]. Smith [41] divided the D_t into the five different classes such as very coarse, coarse, medium, fine, and very fine. The D_t is higher in the basins consisting of sparse vegetation or bare underlying lithology, and fine texture is seen, while the basins with massive and resistant rocks have lower D_t representing coarse drainage texture [41]. D_t values range from 0.12 (7th subbasin) to 0.34 (4th subbasin) between the subbasins of CRB (Table 4). The whole CRB has a 0.45 D_t value (Table 4). According to Smith's classification [41], all subbasin and whole basin (CRB) has very coarse drainage texture. These values show the permeability and infiltration capacity of the underlying material is good, and the recharge of the groundwater is considerable. The low values of D_d and D_t illustrate that the surface runoff in the basin is slow and therefore the basin is very sensitive to flooding, erosion, and landslides.

Form factor (R_f) is the most widely used morphometric parameter related to basin shape. The shape of the basin is substantially controlled by the state of erosion in the basin and, is a result of the geological structure of the basin and tectonic evolution. R_f greatly assists in the evaluation of hydrological conditions such as erosional status and flooding risk etc. in basins. R_f is determined by the ratio of the basin area to the square of the basin length [45] and it is generally lower than 0.78 for circular basins [54]. Basins, where the R_f value is lower than 0.22, are represented by elongated shapes [43]. Shorter duration high peak flows are observed in basins with high R_f values, while longer duration and low peak flows are observed in elongated basins with low R_f values [54]. The form factor value of the CRB is 0.13, and the R_f values of its subbasins vary between 0.12 (7th subbasin) and 0.33 (2nd subbasin) representing the elongated shape both the whole CRB and its subbasin (Table 4). The R_f values of the

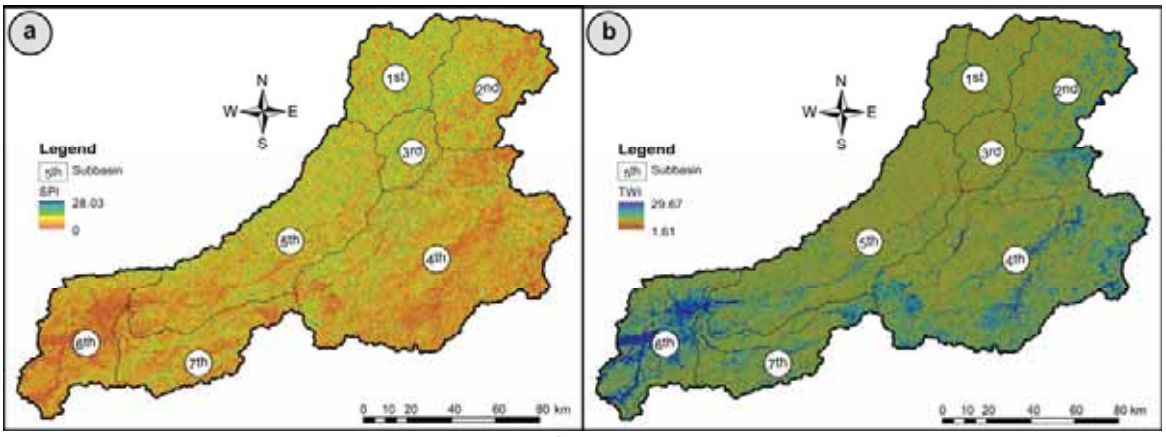

FIGURE 6
Spatial variations of Stream Power Index (SPI) (a) and Topographic Wetness Index (TWI) (b) of Coruh River Basin (CRB).

subbasins that are located close to the basin outlet are greater than 0.22 (Table 4), but the shape of these basins is also near to elongated. The low value of R_f shows that all subbasins and whole CRB are elongated, which means that flood flows can be managed more easily in these basins. When the CRB evaluated within its subbasins, the flash flooding risk is higher in basins (1st, 2nd, and 3rd subbasins) close to the basin outlet compared to the rest of all.

Length of the overland flow (L_g) is a parameter that describes the length of the flow of water over the surface before it reaches a channel flow [1]. Overland flow occurs on the surface in a relatively thin layer and disappears within a few minutes as a result of infiltration through the soil, absorption by plants, and evapotranspiration after precipitation has ended. The flow on the surface is one of the most important independent variables depends on both the physiographic and hydrologic characteristics of the basins [1]. In addition to these basin properties that affect surface runoff, rainfall intensity of the region is also has great importance for overland flow [1]. The L_g of CRB is 3.14 km (Table 4). The values of this parameter vary between 2.99 km (5th subbasin) and 3.46 km (2nd subbasin) for subbasins of CRB (Table 4). The subbasins located around Artvin city, close to the CRB outlet, have higher values of L_g than other subbasins. While the dominant factor causing these differences is rainfall concentration, the geology of the region, soil type, and vegetation may cause differences in values of L_g.

Stream Power Index (SPI), as a measure of the destructive power of flowing water, is one of the important terrain index used in solid mass transport and erosion estimation. SPI shows the erosive power of the flowing water by supposing the proportional to the specific catchment area of discharge and slope [55]. The high values of SPI represent the high slope and flow accumulation exists in the areas of the landscape. In these areas, the flow has high erosive potential. Therefore, this index is a very important parameter to assess in which areas to focus on soil conservation measures to reduce erosion caused by surface runoff. The SPI values range from 0.94 (6th subbasin) and 1.73 (3rd subbasin) within CRB, which has the 1.35 SPI value as a whole (Table 4). The spatial variation of SPI within the CRB has shown in Figure 6a. The density of areas sensitive to soil erosion in the 1st, 2nd, 3rd, and 5th subbasins is higher than other subbasins (Figure 6a). It is observed that the slope (Table 2 and Figure 2b) is higher in these subbasins than others.

Topographic Wetness Index (TWI) is a model developed by Beven and Kirkby [47] as a function of slope and upstream contributing area per unit width perpendicular to the flow direction. The effect of topography on hydrological processes can be determined with this index [56, 57]. TWI can predict areas with a high ability to groundwater accumulation, so it is a very important parameter for determining groundwater potential. The regions with high TWI are the areas richer in groundwater potential where can be evaluated as wetlands. The TWI values of subbasins of CRB vary between 4.30 (3rd subbasin) and 5.88 (6th subbasin) as shown in Table 4. The CRB has the 4.94 TWI as a whole. It is observed that areas with high TWI values are more intense in the 4th, 6th, and 7th subbasins (Figure 6b) and the groundwater potential is high in these areas.

CONCLUSIONS

1st, 3rd, and 7th subbasins are third-order while 2nd, 4th, 5th, and 6th subbasins are fourth-order basins in CRB. The Coruh River Basin is a fifth-order basin as a whole. The D_d, R_f, L_g, SPI, and TWI are the most beneficial morphometric criteria for the CRB in the aspect of evaluating the runoff pattern, sediment yield, and other hydrological parameters. Among these parameters, D_d, R_f, and L_g play an important role in the evaluation of the surface runoff potential. This assessment is also very efficient for estimating flooding risk in the basins. SPI is an extremely useful

parameter for the estimation of gully erosion within subbasins and spatially in a basin. TWI is a very important parameter for predicting groundwater potential zones.

Both D_d and D_t are lower in the first subbasin, indicating that the infiltration capacity of the subsurface material is higher, surface runoff is slow and, therefore, the basin is very sensitive to flooding, erosion, and landslides in this subbasin then others. These values higher in the subbasins on top regions of CRB indicating that the surface runoff is higher in these subbasins. CRB and its subbasins are generally elongated shaped. Among the subbasins of CRB, the 1st and 2nd subbasins are closer to the circular shaped. High R_f and L_g values in these basins reveal that flooding risk in these areas is higher compared to the other subbasins. SPI of 1st, 2nd, 3rd, and 5th subbasin are relatively higher than other subbasins. TWI values are lower in these subbasins. These high values of SPI reveal that higher erosive energy of stream and hence more sediment loss may occur in these subbasins. 4th, 6th, and 7th subbasins, where TWI is high, are valuable in terms of groundwater potential.

The quantitative analysis of morphometric parameters evaluating the various terrain properties such as the nature of underlying rock formation, surface runoff, and infiltration in river basins using GIS, provides considerable benefits in river basin prioritization and management of natural resources for the conservation of soil and water.

REFERENCES

[1] Horton, R.E. (1945). Erosional development of streams and their drainage basins: hydrophysical approach to quantitative morphology. Geological Society of America Bulletin. 56(3), 275–370.

[2] Frissel, C.A., Liss, W.J., Warren, C.E., Hurley, M.D. (1986). A hierarchical framework for stream habitat classification-viewing streams in a watershed context. Environmental Management. 10, 199–214.

[3] Liu, F., Parmenter, R., Brooks, P.D., Conklin, M.H., Bales, R.C. (2008). Seasonal and interannual variation of streamflow pathways and biogeochemical implications in semi-arid, forested catchments in Valles Caldera, New Mexico, Ecohydrology. 1, 239–252.

[4] Strahler, A.N. (1964). Quantative geomorphology of drainage basins and channel networks. In: Handbook of applied hydrology. Chow, V.T. (ed.), McGraw Hill, New York. 439–476.

[5] Zavoianu, I. (1985). Morphometry of drainage basins. Elsevier, Amsterdam. 238 pp.

[6] Robinson, K.W., Lazaro, T.R., Pak, C. (1996). Associations between water-quality trends in New Jersey streams and drainage-basin characteristics, 1975-86. U.S. Geological Survey, Water Resources Investigations Report. 96–4119.

[7] Chen, C.Y., Yu, F.C. (2011). Morphometric analysis of debris flows and their source areas using GIS. Geomorphology. 129, 387–397.

[8] Mahmoud, S.H., Alazba, A.A. (2015). Geomorphological and geophysical information system analysis of major rainwater-harvesting basins in Al-Baha region, Saudi Arabia. Arabian Journal of Geosciences. 8, 9959–9971.

[9] Abboud, I.A., Nofal, R.A. (2017). Morphometric analysis of wadi Khumal basin, western coast of Saudi Arabia, using remote sensing and GIS techniques. Journal of African Earth Sciences. 126, 58–74.

[10] Chorley, R.J. (1969). The drainage basin as the fundamental geomorphic unit. In: Water, earth, and man: a synthesis of hydrology, geomorphology and socio-economic geography. Chorley, R.J. (ed.). Methuen, London. 77–99.

[11] Jenson, S.K. (1991). Applications of hydrologic information automatically extracted from digital elevation models. Hydrological Processes. 5, 31–41.

[12] McDonnell, J., Sivapalan, M., Vaché, K., Dunn, S., Grant, G., Haggerty, R., Weiler, M. (2007). Moving beyond heterogeneity and process complexity: A new vision for watershed hydrology. Water Resources Research. 43(7).

[13] Ross, C.A., Ali, G., Spence, C., Oswald, C., Casson, N. (2019). Comparison of event-specific rainfall-runoff responses and their controls in contrasting geographic areas. Hydrological Processes. 33, 1961–1979.

[14] Thomas, J., Joseph, S., Thrivikramji, K.P., Abe, G., Kannan, N. (2012). Morphometrical analysis of two tropical mountain river basins of contrasting environmental settings, the southern Western Ghats, India. Environmental Earth Sciences. 66, 2353–2366.

[15] Jakada, H., Chen, Z., Luo, M., Zhou, H., Wang, Z., Habib, M. (2019). Watershed characterization and hydrograph recession analysis: A comparative look at a karst vs. non-karst watershed and implications for groundwater resources in Gaolan River Basin, Southern China. Water. 11(4), 743.

[16] Turkish State Meteorological Service (TSMS) (2020). https://www.mgm.gov.tr/veridegerlendirme/il-ve-ilceler-istatistik.aspx. (Accessed date: 13.02.2020)

[17] Bektaş, O., Yilmaz, C., Taslı, K., Akdağ, K., Özgür, S. (1995): Cretaceous rifting of the eastern Pontide carbonate platform (NE Turkey): the formation of carbonates breccias and turbidites as evidences of a drowned platform. Geologia. 57, 233–244.

[18] Eyuboglu, Y., Bektas, O., Seren, A., Maden, N., Jacoby, W.R., Özer, R. (2006). Three axial extensional deformation and formation of Liassic rift basins in the eastern Pontides (NE Turkey). Geologica Carpathica. 57(5), 337–346.
[19] Sipahi, F., Sadıklar, M.B. (2014). Geochemistry of Dacitic Volcanics in the Eastern Pontides (NE Turkey). Geochemistry International. 52, 296–315.
[20] Arslan, M., Tüysüz, N., Korkmaz, S., Kurt, H. (1997). Geochemistry and petrogenesis of the Eastern Pontide volcanic rocks, Northeast Turkey. Chemie der Erde. 57, 157–187.
[21] Şen, C., Arslan, M., Van, A. (1998). Geochemical and petrological characteristics of the Pontide Eocene (?) alkaline province, NE Turkey. Turkish Journal of Earth Sciences. 7, 231–239.
[22] Şen, C. (2007). Jurassic volcanism in the Eastern Pontides: is it rift related or subduction related? Turkish Journal of Earth Sciences. 16, 523–539.
[23] Okay, A.I., Şahintürk, Ö. (1997). Geology of the eastern Pontides. In: Regional and Petroleum Geology of the Black Sea and Surrounding Region, Robinson, A.G. (ed.), American Association of Petroleum Geologists (AAPG) Memoir. 68, 291–311.
[24] Kaygusuz, A., Arslan, M., Siebel, W.S., Şen, C. (2011). Geochemical and Sr–Nd isotopic characteristics of postcollisional calc-alkaline volcanics in the eastern Pontides (NE Turkey). Turkish Journal of Earth Sciences. 20, 137–159.
[25] Kaygusuz, A., Arslan, M., Siebel, W.S., Şen, C., Satir, M. (2008). Petrochemistry and petrology of I-type granitoids in an arc setting: the composite Torul pluton, Eastern Pontides, NE Turkey. International Journal of Earth Sciences. 97, 739–764.
[26] Eyuboglu, Y., Dilek, Y., Bozkurt, E., Bektas, O., Rojay, B., Sen, C. (2010). Structure and geochemistry of an Alaskan type ultramafic–mafic complex in the eastern Pontides, NE Turkey. Gondwana Research. 18, 230–252.
[27] Moore, W.J., McKee, E., Akıncı, O. (1980). Chemistry and chronology of plutonic rocks in the Pontide mountains, northern Turkey. In: Symposium of European Copper Deposits. Jankovic, S., Sillitoe, R.H (eds.), Belgrade Univ. Faculty. Geology Mining. 209–215.
[28] Yılmaz, C. (1997). Dimentological records Cretaceous platformbasin transition Gumushane region (NE Turkey). Géologie Méditerranéenne. Tome. 24(1–2), 125–135.
[29] Kaygusuz, A., Chen, B., Aslan, Z., Wolfgang, S., Şen, C. (2009). U–Pb zircon SHRIMP ages, geochemical and Sr– Nd isotopic compositions of the Early Cretaceous I type Sarıosman pluton, Eastern Pontides, NE Turkey. Turkish Journal of Earth Sciences. 18, 549–581.
[30] Bektaş, O., Van, A., Boynukalin, S. (1987). Jurassic volcanism and its geotectonics in the eastern Pontides (NE Turkey). Geological Bulletin of Turkey. 30, 9–18.
[31] Saydam Eker, C., Korkmaz, S. (2011). Mineralogy and whole rock geochemistry of late Cretaceous sandstones from the eastern Pontides (NE Turkey). Neues Jahrbuch für Mineralogie – Abhandlungen. 188(3), 235–256.
[32] Yılmaz, C., Korkmaz, S. (1999): Basin development in the eastern Pontides, Jurassic to Cretaceous, NE Turkey. Zentralblatt für Geologie und Paläontologie. Teil. I (10–12), 1485–1494.
[33] Saydam Eker, C. (2012). Petrography and geochemistry of Eocene sandstones from eastern Pontides (NE Turkey): implications for source area weathering, provenance and tectonic setting. Geochemistry International. 50, 683–701.
[34] GDMRE (General Directorate of Mineral Research and Exploration) - a (2002). 1:500.000 scale Geological Map of Turkey, Erzurum sheet. Geological Research Department, MTA, Ankara.
[35] GDMRE (General Directorate of Mineral Research and Exploration) - b (2002). 1:500.000 scale Geological Map of Turkey, Trabzon sheet. Geological Research Department, MTA, Ankara.
[36] GDMRE (General Directorate of Mineral Research and Exploration) - c (2002). 1:500.000 scale Geological Map of Turkey, Kars sheet. Geological Research Department, MTA, Ankara.
[37] GDRS (General Directorate of Rural Services) (2001). Soil Characteristics Maps of scale 1/25.000. Ankara.
[38] Strahler, A.N. (1952a). Dynamic basis of geomorphology. Geological Society of America Bulletin. 63(9).
[39] Strahler, A.N. (1952b). Hypsometric (area-altitude) analysis of erosional topography. Geological Society of America Bulletin. 63(11), 1117–42.
[40] Chirala, U., Kinthada, N.R., Gurram, M.K. (2012). Correlation of geomorphometric parameters for the hydrological characterization of Meghadrigedda Watershed, Visakhapatnam, India – A GIS Approach. International Journal of Engineering Science and Technology (IJEST). 4(7).
[41] Smith, K. (1950). Standarts for grading texture of erosional topography. American Journal of Science. 248, 655–668.
[42] Pankaj, A., Kumar, P. (2009). GIS based morphometric analysis of five sub-watersheds of Song River, Dehradun district, Uttarakhand with special reference to landslide incidences, Journal of the Indian Society of Remote Sensing. 37,157–166.

[43] Hajam, R.A., Hamid, A., Bhat, S. (2013). Application of morphometric analysis for geo-hydrological studies using geo-spatial technology –A case study of Vishav drainage basin. Hydrology Current Research. 4(3).
[44] Schumm, S.A. (1956). Evolution of drainage systems and slopes in badlands at Perth Amboy, New Jersey. Geological Society of America Bulletin. 67, 597–646.
[45] Horton, R.E. (1932). Drainage basin characteristics. Transactions of the American Geophysical Union. 13, 350–361.
[46] Moore, I.D., Gesseler, P.E., Nielsen, G.A., Peterson, G.A. (1993). Soil attribute prediction using terrain analysis. Soil Science Society of America Journal. 57, 443–452.
[47] Beven, K.J., Kirkby, M.J. (1979). A physically based, variable contributing area model of basin hydrology. Hydrological Sciences Bulletin. 24(1), 43–70.
[48] Shreve, R.L. (1966). Statistical law of stream numbers. The Journal of Geology, 74(1), 17–37.
[49] Hack, J. (1957). Studies of longitudinal stream profiles in Virginia and Maryland. U.S. Geological Survey Professional Paper. 294–B, 45–97.
[50] Nageswara, R.K. (2020). Analysis of surface runoff potential in ungauged basin using basin parameters and SCS-CN method. Applied Water Science. 10(47).
[51] Bates, N. (1981). Valley shapes. In: Practical foundations of physical geography. Knap, B. (ed.) George Allen & Unwin, London. 25–29.
[52] Eze, E.B., Efiong, J. (2011). Morphometric parameters of the Calabar River Basin: Implication for hydrologic processes. Journal of Geography and Geology. 2 (1), 18–26.
[53] Prasannakumar, V., Vijith, H., Geetha, N. (2011). Terrain evaluation through the assessment of geomorphometric parameters using DEM and GIS: case study of two major sub-watersheds in Attapady, South India. Arabian Journal of Geosciences. 6, 1141–1151.
[54] Ramu Mahalingam, B., Jayashree, P. (2013). Morphometric analysis of Tungabhadra Drainage Basin in Karnataka using geographical information system. Journal of Engineering Computer & Applied Sciences. 2(7).
[55] Moore, I.D., Burch, G.J. (1986). Physical basis of the length-slope factor in the universal soil loss equation. Soil Science Society of America Journal. 50, 1294–1298.
[56] Sørensen, R., Zinko, U., Seibert, J. (2006). On the calculation of the topographic wetness index: evaluation of different methods based on field observations. Hydrology and Earth System Sciences. 10, 101–112.
[57] Lee, S., Kim, J.C., Jung, H.S., Lee, M.J., Lee, S. (2017). Spatial prediction of flood susceptibility using random-forest and boosted-tree models in Seoul metropolitan city, Korea. Geomatics Natural Hazards & Risk. 8(2), 1185–1203.

Received: **17.09.2020**
Accepted: **17.02.2021**

CORRESPONDING AUTHOR

Umit Yildirim
Faculty of Arts and Designing,
Department of Interior Architecture and
Environmental Designing,
Bayburt University,
Bayburt – Turkey

e-mail: umit.yildirim.1907@gmail.com

© by PSP Volume 30– No. 05/2021 pages 4975-4983 Fresenius Environmental Bulletin

STUDIES ON NUTRITIONAL PHYSICOCHEMICAL AND FUNCTIONAL COMPOSITION OF FOUR SELECTED PLANTS OF NAMAL VALLEY (MIANWALI) PUNJAB PAKISTAN

Muhammad Rizwan, Kafeel Ahmad, Zafar Iqbal Khan, Iftikhar Ahmed, Sonaina Nazar*, Humayun Bashir

Department of Botany, University of Sargodha, Sargodha, Pakistan

ABSTRACT

Research study was carried out to assess the geo-environmental interaction of the vegetation of Namal valley. Namal valley is located about 30 km from Mianwali city in the eastern direction.This valley is located in the Salt range. The vegetation of Namal valley is still unobserved and unnoticed. Anthropogenic disturbances like accidental fires by the herds' men and illegal honey hunters, agricultural activities and harvesting of medicinal plants by uprooting have markedly disturbed the natural plant vegetation in this valley. Experimental results of four selected plants (Grewia tanax, Tephrosia purpurea, Pulicaria edmondsonii, Pentatropis spiralis) revealed that Tephrosia purpurea scored maximum frequency and density i.e 61.04% and 29.48% respectively. These plants differed considerably in term of importance value . The importance value of G.tanax, T.purpurea, P.edmondsonii and P. spiralis was 16.30, 64.27, 58.62and 19.10 % respectively. Phytochemicals analysis confirmed the presence of phytochemicals such as tannins, saponin, alkaloids, flavanoids, terpenoids and steroids in all plant samples. All the four plants found rich in flavonoids. Proximate analysis presented that moisture content of G.tanax, T.purpurea, P.edmondsonii and P. spiralis leaves were 26.02, 21.36, 20.95and 43.39% . All four plants showed variation in terms of minerals and amino acids content.

KEYWORDS:
Biodiversity, Namal valley, Salt range, amino acids

INTRODUCTION

Environmental parameters influence the distribution, abundance and life of plants. Local meteorological conditions such as air temperature, pH, rainfall or sunlight may affect the behaviour of vegetation [1]. In order to be aware of terrestrial ecosystems, it is important to study the relationship between environmental factors and plants in these ecosystems. One of the main components of terrestrial ecosystems is vegetation, the absence and presence of which is controlled by environmental variables such as climate, soil and topography. Among different environmental factors, soil is of high importance in plant growth [2].

Plants of same species found in different zones of world have different morphological and anatomical characters which make them successful to adopt in local environmental conditions. Each plant species has its own nutrient composition besides having pharmacologically important phytochemicals. These nutrients are essential for the physiological functions of human body. Such nutrients and biochemical's like carbohydrates, fats and proteins play an significant role in satisfying human requirements for energy and life processes [3,4].

The Salt Range in the Punjab covers an area of 175 km between the foot hills of Himalayan Mountains and Indus plains extending irregularly in arc appearance from the Jhelum River near Tilla Jogian in the east to the Indus River near Kalabagh in the west [5]. Bio diversity is a key feature of Salt Range and it is enriched with natural resources. Different researchers have worked on the flora of salt range specifically on Soon valley but no specific work has been done on the mountains of salt range near Namal valley in district Mianwali and this valley is still unexplored [6].

District Mianwali is positioned in the North West of the Punjab province. It represents the plains of the western part of the Salt Range near the Sakesar hill. It has boundaries with eight districts; district Attock in the North, Chakwal in the North East, Bhakkar district in the South, Khushab in the East, Laki Marwat in the West, Kohat and Karak districts in the North West and Dera Ismail Khan district in the South West .Most of the area is the continuation of Potohar Pleatue and Salt Range [7].

Namal valley is located about 30 km from Mianwali city in the eastern direction. This valley is famous due to Namal lake. The vegetation of Namal valley is still unobserved and unnoticed. Anthropogenic disturbances like accidental fires by the herds'

men and illegal honey hunters, agricultural activities and harvesting of medicinal plants by uprooting have markedly disturbed the natural plant vegetation in this valley. The remaining plant communities are also losing their species richness at an alarming rate due to clear cutting, extensive exploitation of grasslands for raising cattle and worsening environmental conditions. These circumstances also demand that undocumented unique plant communities of this valley must be documented and special strategies formulation for the conservation of this vegetation [8].

The present research aimed to explore of unseen and unobserved vegetation of Namal valley.

MATERIALS AND METHODS

Study area The study was conducted in Namal valley, district Mianwali. This valley is located about 30 km from Mianwali city in the eastern direction ranging at 71 °48°45° E longitude and 32°40°10° N latitude [9] (Figure 1). The Valley is characterized by cold, dry weather at high altitudes and humid, warm in low altitude areas. The summer season is moderate and hot, June and July are the hottest months. The maximum and minimum temperature during June was recorded 49.52 C° and 29.67 C° respectively. The winter season is cold, and temperature rapidly decreases from November onward, December and January are the coldest months. In January maximum and minimum temperature was recorded 11.22C° and -1.00C° respectively. Six ecologically diverse study sites namely Dhok Peera, Dhok Satala, Dhok Lataka, Dhok Garori, Namal village and Rikhi within diameter of 20 km were selected mainly on the basis of differences in their environmental attributes especially variations in elevation, altitude, slope, aspect, topography, soil composition, habitat and vegetation type. The sites selected for detailed study of vegetation and environmental factors were of adequate size, visually uniform and relatively free from recent anthropogenic disturbances.

Data collection Vegetation data of plant species was taken by quadrat method from the sites considering differences in their elevation, ground position and soil type. Within each quadrat, herbaceous plants and their estimated cover values were recorded using visual estimation. Plots measuring 10 × 10 m were used for trees and shrubs and 1 × 1 m quadrates were used for herbs and grasses. Data of 10 to 15 random quadrates was collected in every season. Data of vegetation will be collected in all four seasons. Only data on woody vegetation (trees and shrubs) and grasses was collected in this study.

After data collection of vegetation, four plants species (*Grewia tanax, Tephrosia purpurea, Pulicaria edmondsonii, Pentatropis spiralis*) (Figure 2) were picked for further experiments on the basis of their uniqueness as these species were abundant only in Namal valley and not found abundantly in other parts of Salt range.

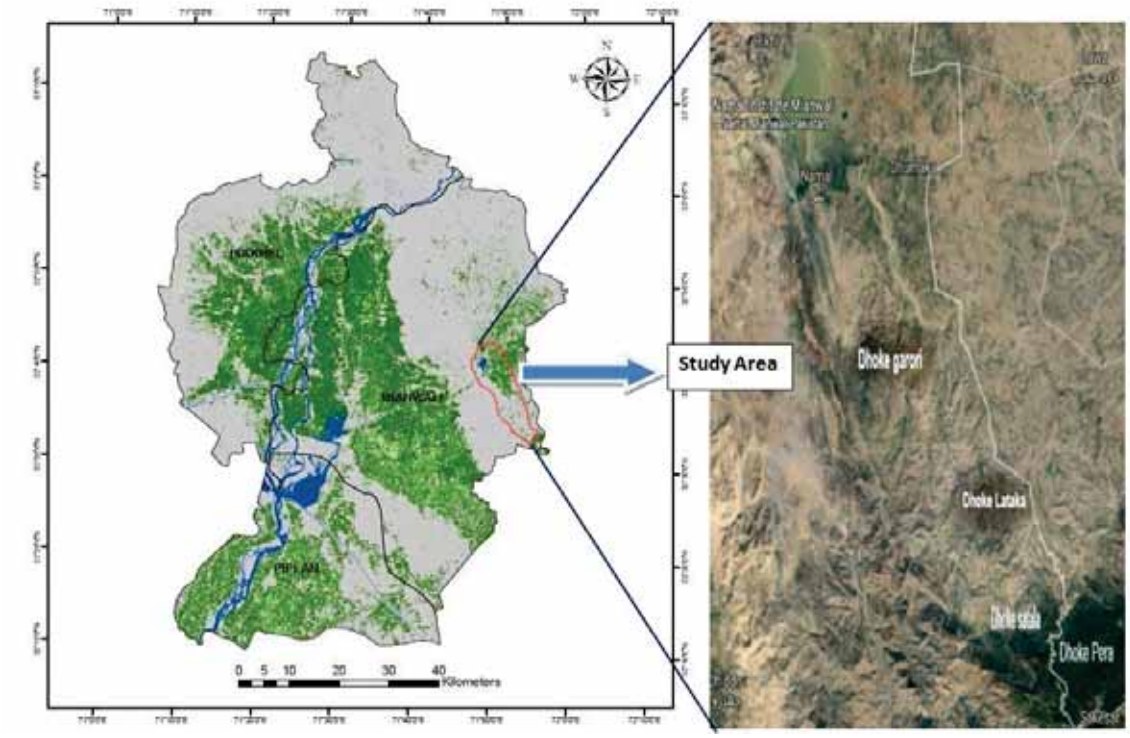

FIGURE 1
Study area


Grewia tanax


Pulicaria edmondsonii


Tephrosia purpurea


Pentatropis spiralis

FIGURE 2
Picked four plants species for the vegetation

Following attributes of four plant species were worked out by using formulas.

1. Species frequency
2. Species density
3. Coverage/ Dominance
4. Relative frequency
5. Relative density
6. Relative coverage/ Dominance
7. Importance value

Number of quadrates in which a species occurred

Frequency % = ---------- x 100

Total number of quadrates taken

Total number of individuals of a species in a quadrate

Density % = ---------- x 100

Total number of individuals of all the species in a quadrate

Area covered by a species in a quadrate

Coverage/dominance% = ----- ----x 100

Total area covered by all the species

Frequency value of a particular species

Relative frequency% = ----------x 100

Total frequency values for all the species

Density of a particular species in a site

Relative density% = ----------x 100

Total density for all the species in that site

Coverage/dominance of a particular species

Coverage/dominance % = ---------- x 100

Total coverage/dominance for all the species within a stand

Importance value = Relative density + relative frequency +relative coverage

Proximate Analysis For proximate analysis fresh and dry plants, samples were grinded into fine powder. The AOAC [10,11] method was used to determine the proximate nutrient composition. Following experiments were performed in Food Science Department, University of Sargodha, Sargodha.

Phytochemical Screening The extract of each powdered parts of plants were used for phytochemical tests and to identify the constituents, Tannins, saponins, reducing sugars, alkaloids, terpenoides, flavonoids, cardiac glycosides and anthraquinones

were estimated following standard methods.[12,13]

Amino Acid Analysis Amino acids composition were determined according to the modified AOAC method [14] and method performed by other researchers[15,16]

Statistical Analysis Statistical analysis was carried out using Microsoft Excel 2007 along with least significant.difference.(LSD) test [17].

RESULTS

Data of plant species were collected from six sites of Namal valley from 2015-2018 representing all the seasons following the method of Henderson and researchers working afterward in this field [18,19,20]. The study area was located at the elevation of 598 m to 1600 m while the slope angle lies between the 30º to 60º. Table 1 gives the site locations, latitude, longitude and topographic characteristics of all six sites of Namal valley. This table also provides the information about habitat, soil texture and vegetation type. Data of plants were collected at different aspects. The soil texture was found different at sites. There was great variety in vegetation on different sites. These types of results were also obtained by different researchers in the past in similar studies [21,22,23]. A total of 191 plant species belonging to 159 genera and 62 families were collected from the Valley. Mostly grasses and herbs dominated the vegetation of most sites followed by the shrubs. The species variation in plants from site to site may be due to the soil type, composition of soil, elevation of selected sites, moisture content of soil, nature of disturbance like grazing pressure, human interference, distance of study site from population area etc. All the factors determine the category of species in which the species fall [24].

The results of proximate analysis (in %) of *Grewia tanax, Tephrosia purpurea, Pulicaria edmondsonii, Pentatropis spiralis* leaves are shown on Table 2. This study has revealed the presence of phytochemicals considered as active medicinal chemical constituents which is found in accordance to the work of Alsir et al [25]. Important medicinal phytochemicals such as tannins, saponin, alkaloids, flavanoids, terpenoids and steroids were present in the samples. The result of the phytochemical analysis shows that the four plants are rich in flavonoids. Both tanax and *Tephrosia purpurea* showed high concentration of flavanoids while P. edmondsonii and P. spiralis showed slightly high concentration of flavanoids. These results are in accordance to the results of Li et al [26]. Tannin concentration was reported very low in all plants except T. purpurea which showed low concentration. Tannin decrease feed intake, growth rate, feed efficiency and protein digestibility. Therefore, foods that have high tannin contents are harmful for health [27,28]. Saponin concentration was reported very low in all four plants. Terpenoid concentraion was higher in T. purpurea and P. spiralis than the other two plants. P. edmondsonii showed the least concentraion of alkaloids while all other plants reported almost same proportion of alkaloids. Concentration ratio of phytochemicals in these four plants is comparatively low than reported by other different scientist in similar studies on these plants[29,30,31,32,33].This comparatively low concentration is probably due to xerophytic condition of area, low precipitation and soil structure. The four species differed significantly in term of frequency however, Tephrosia purpurea was the species which surpassed all of other 3 (Table 3). It scored the highest value of (61.04%) followed by Pulicaria edmondsonii (49.16%). Grewia Tanax and Pentatropis spiralis showed significant differences both from T. purpurea and P. edmondsonii and showed 16.66 and 21.46 % frequency respectively. The data have clearly indicated that species density varied . Lowest value (2.13%) was calculated for G. tanax which was very close to the P. spiralis density (2.85%). Both these plants showed significant variation with T. purpurea (29.48%) and P. edmondsonii (13.19%). Minimal coverage was observed by P. spiralis (4.11%) while T. purpurea expressed maximum coverage (18.31 %). Relative frequencies of all species were different and T. purpurea (38.44%) surpassed all three plants while the relative frequency of G. tanax was least (10.67%).

G.tanax also showed lowest relative density (0.24%) while T. purpurea, P. edmondsonii and P. spiralis showed 2.93,1.41 and 0.31 % respectively. Relative coverage of T. purpurea was found maximum(22.89%) and minimal for P. spiralis (5.14%).

These plants differed considerably in term of importance value . The importance value of *G.tanax, T.purpurea, P.edmondsonii and P. spiralis* was 16.30, 64.27, 58.62and 19.10 % respectively. The spatial variations might be due to the soil type and its composition, elevation of sites, moisture contents of soil, nature of disturbance like grazing pressure, human interference and isolation of study site populated regions [34,35].

This species was successful in maintaining its high diversity that might also be due to strong root system, which may facilitate absorption of moisture as well as nutrients from in different type of soils [36,37].

Table 4 shows the proximate analysis results of selected plants.The moisture content (in %) of *G.tanax, T.purpurea, P.edmondsonii* and P. spiralis leaves were 26.02, 21.36, 20.95 and 43.39% . The ash content of these plants ranged from 2.11 % for *P.edmondsonii* leaves to 4.67% for *G.tanax*. These data were low when compared with the result obtained by Senhaji et al [38].

TABLE 1
Summary of topographic variables and site characteristics of Namal valley

S.No	Location and sites	Coordinates	Elevation (m)	Slope (º)	Aspect	Soil Texture	Habitat description	vegetation type	Plant community
1	Dhok Peera	32.41 N and 71.51 E	716	30-35	Western	sandy clay, loam	Hills with less steep slopes	Dominant grasses & shrubs	*Grewia tanax*
2	Dhok Satala	32.43 N and 71.50 E	680	30-40	Northern	sandy clay, Loam	Hills with moderate slopes	small shrubs with grasses	*Grewia tanax Pentatropis spiralis*
3	Dhok Lataka	32.38 N and 71.53 E	663	35-45	Eastern	sandy stone	Hills with moderate slopes	Dominant sedges & shrubs	*Tephrosia purpurea*
4	Dhok Garori	32.39 N and 71.49 E	632	50-60	Western	Loam	plain surface in the periphery	mixture of grasses, herbs & shrubs	*Pulicaria edmondsonii*
5	Namal village	32.40 N and 71.48 E	602	30-45	Eastern	Loam and clay	within the valley	Dominant grasses & herbs	*Pentatropis spiralis Pulicaria edmondsonii*
6	Rikhi	32.43 N and 71.50 E	598	35-45	Eastern	lime stone with sand stone	more or less flatten peripheral area	mixture of grasses & herbs	*Tephrosia purpurea*

TABLE 2
Qualitative analysis of Phytochemicals present in four selected plants of Namal valley

		Phytochemical results					
s no	Plant	Tannin	Saponin	Alkaloids	Flavanoids	Terpenoids	steroids
1	*Grewia Tanax*	+	+	++	++++	+	++
2	*Tephrosia purpurea*	++	+	++	++++	++	+
3	*Pulicaria edmondsonii*	+	+	+	+++	+	+
4	*Pentatropis spiralis*	+	+	++	+++	++	-

SYMBOLS	EXPLANATION
+	Presence
-	absent
+	very low concentration
++	low concentration
+++	slightly high concentration
++++	high concentration
+++++	very high concentration

TABLE 3
Different attributes of four selected plants of Namal valley

s no	species	frequency(%)	density(%)	coverage/Dominance (%)	Relative frequency(%)	Relative density(%)	Relative coverage/Dominance (%)	Importance value (RF+RD+RC)
1	*Grewia Tanax*	16.66±3.58	2.13±1.06	4.3±1.13	10.67±2.65	0.24±0.16	5.49±1.41	16.40±4.14
2	*Tephrosia purpurea*	61.04±9.90	29.48±8.07	18.31±2.97	38.44±2.80	2.93±0.31	22.89±3.71	64.27±5.97
3	*Pulicaria edmondsonii*	49.16±12.51	13.19±1.52	15.97±3.78	37.24±5.58	1.41±0.41	19.68±4.23	58.62±9.3
4	*Pentatropis spiralis*	21.46±8.55	2.85±1.17	4.11±1.66	13.63±3.05	0.31±0.17	5.14±2.03	19.10±7.43

TABLE 4
Proximate analysis of four selected plants of Namal valley

		Parameters %					
s no	Plant	moisture	ash	crude protein	crude fats	crude fibres	carbohydrate
1	*Grewia Tanax*	26.02±2.31	4.67±0.30	10.74±0.82	1.43±0.04	21.03±0.02	42.14±0.07
2	*Tephrosia purpurea*	21.36±3.16	4.25±0.05	14.03±0.35	10.85±0.23	9.39±1.11	59.51±1.43
3	*Pulicaria edmondsonii*	20.95±1.87	2.11±0.15	11.38±0.31	5.98±1.1	6.01±0.04	49.58±2.21
4	*Pentatropis spiralis*	43.39±2.62	3.87±0.31	8.39±0.05	11.02±0.65	11.02±0.06	32.33±1.06

TABLE 5
Qualitative analysis of amino acids present in selected plants of Namal valley

S No	Name of Amino Acid and Amides	*Grewia Tanax*	*Tephrosia purpurea*	*Pulicaria edmondsonii*	*Pentatropis spiralis*
1	Leucines	+	+	-	+
2	Isoleucine	-	+	+	-
3	Phenylalanine	+	-	-	+
4	Valine	-	-	-	+
5	Tyrosine	+	-	+	-
6	Protine	+	-	+	-
7	Alanine	-	+	+	-
8	Glutamic acid	-	+	+	-
9	Threonine	+	-	+	-
10	Arginine	+	-	-	+
11	Aspartic acid	+	-	+	-
12	Serine	+	-	+	+
13	Glycine	-	-	-	-
14	Asparagines	+	+	-	+
15	Glutamine	+	+	+	-
16	Histidine + Lysine	+	-	+	-
17	Cysteric acids	-	+	-	-

The crude protein of plants ranged from 14.03% for T.purpurea leaves to 8.39% for P. spiralis leaves. The crude fat content of plants varied and was found least in G.tanax (1.43%) and maximum in P. spiralis (11.38). Crude fat content of T.purpurea and P.edmondsonii was 10.85 and 5.98% respectively. However, these values were comparable to that obtained by Murray et al. [39] for and higher than the results obtained by Yadav [40].The values of crude

fibre content of G.tanax, T.purpurea, P.edmondsonii and P. spiralis leaves were 21.03, 9.39, 6.01and 11.02 %. The crude fibre content of studied Grewia species was high when compared with the results of Martos et al. [41].Carbohydrate constitutes a main class of naturally occurring organic compounds that are necessary for the maintenance and nourishment of life in plants and animals and also provide raw materials for many industries [42,43]. The leave is a good source of carbohydrate when consumed because it meets the Recommended Dietary Allowance (RDA) values [44]. The leaves of G.tanax, T.purpurea, P.edmondsonii and P. spiralis contained higher amount of carbohydrates content which were 42.14, 59.51, 49.58 and 32.33% respectively.

The percentage of inorganic matter (ash), moisture crude protein and crude fibers remained low in leaves for plant under investigation. This may be due to the increase of total ion accumulation as a result of increasing soil moisture stress and soil salinity, which agreed with the results obtained by Alli and Smith[45].

Amino acids content Results of the composition of amino acids were shown in Table 5. Amino acids, as constituents of proteins play the most important role in living body[46]. Qualitative results reflected that Eleven amino acids were present in G. tenax .Total seven amino acids were found in T. purpurea. In Pulicaria edmondsonii ten amino acids were found. Six types of amino acids were found in P.spiralis.

CONCLUSIONS

It can be concluded that species diversity in Namal Valley is dependent mainly on rainfalls, nutrient availability and particularly suitable temperature during summer. Similarly sites with better nutritional status and high moisture retaining capacity showed more diversity of plant species. It is need of the time to explore the vegetation of this area and investigate the nutritive value of vegetation of this valley.

REFERENCES

[1] Kohali, M. and Atri, M. (2014) Plant Diversity, Life Form and Phytochoria of Hamedan Alvand Region in Iran.Open Access Library Journal. 1(7), 1-12.

[2] Hussain, J., Ullah. R., Rehman. N., Khan, A.L., Muhammad, Z., Khan, F.U., Hussain, S.T. and Anwar, S. (2010) Endogenous transitional metal and proximate analysis of selected medicinal plants from Pakistan. Journal of Medicinal Plants Research. 4(3), 267-270.

[3] Adnan, M., Hussain, J., Shah, M.T., Shinwari, Z.K., Ullah, F., Bahader, A., Khan, N., Khan, A.L. and Watanabe, T. (2010) Proximate and nutrient composition of medicinal plants of humid and sub-humid regions in North-west Pakistan. Journal of Medicinal Plants Research. 4(4), 339-345.

[4] Zheng, X.L., Xing, F.W. (2009), Ethnobotanical study on medicinal plants around Mt.Yinggeling, Hainan Island, China. Journal of Ethnopharmacology. 124(2), 197-210.

[5] Ahmad, I., Hussain, M., Sajid, M., Ahmad, A. and Hameed, M. (2008) Spatio-Temporal Effects On Association of Plant Species in Soone Valley of Pakistan. Pakistan Journal of Botany. 40(5), 1865-1876.

[6] Ahmad, H. and Waseem, M. (2004) Conservation status of some medicinal plants of Salt Range. Zonas Ardis Research Journal. 22-31

[7] Shah, A. and Rahim, S. (2017), Ethnomedicinal uses of plants for the treatment of malaria in Soon Valley, Khushab, Pakistan. Journal of Ethnopharmacology. 200, 84-106.

[8] Qureshi, R.A., Gilani, S.A. and Ghufran, M.A. (2007). Ethnobotanical studies of plants of Mianwali District Punjab, Pakistan. Pakistan Journal of Botany. 39(7), 2285-2290.

[9] Shah, A., Sarvat, R., Shoaib, S., Ayodele, A., Nadeem, M., Qureshi, T., Ishtiaq, M. and Abbas, A. (2018), An ethnobotanical survey of medicinal plants used for the treatment of snakebite and scorpion sting among the people of Namal valley, Mianwali district, Punjab, Pakistan. Applied Ecology and Environmental Research. 16(1), 111-143.

[10] AOAC (Association of Official Analytical Chemist) (1990) Official Methods of Analysis, Association of Official Analytical Chemists. 15th Edn., AOAC Press, Gaithersburg, USA.

[11] AOAC (1995) Official Methods of Analysis of the AOAC international, 16th ed. Method 970.12. Association of Official Analytical Chemists International. Washington, DC, USA.

[12] Sofowara, A. (1993). Medicinal plants and Traditional medicine in Africa. Spectrum Books. Ltd, Ibadan, Nigeria. 10-15.

[13] Trease, G.E. and Evans, W.C. (1989) Pharmacognosy. 11th Edn., Macmillan Publishers, London, UK. 882.

[14] AOAC. (1990) Official methods of analysis of the AOAC, 15th edn. Methods 932.06, 925.09, 985.29, 923.03. Association of Official Analytical Chemists Arlington, VA, USA.

[15] Arnold, R. (2014) Qualitative Assay Of Amino Acids And Amides In Seeds And Seedlings Of Tephrosia Purpurea In Vindhyan Egion.World Journal of Pharmaceutical Research. 4(1), 1489-1495.

[16] Thonn, A., Bolanle, O., Funmilola, A.S. and Adedayo, A. (2014) Proximate Analysis, Mineral Contents, Amino Acid Composition, Anti-Nutrients and Phytochemical Screening of Brachystegia Eurycoma Harms and Pipper Guineense . American Journal of Food and Nutrition. 2(1), 11-17.

[17] Steel, R.G.D., Torrie, J.H. and Dickey, D.A. (2006) Principles and procedures of statistics. A biometrical approach. 3rd Ed. McGraw Hill Company, New York, USA. 1-5.

[18] Henderson, P.A. (2016). Ecological Methods. Wiley-Blackwell. 200-205.

[19] Sultan, M.W., Saima, S., Dasti, A.A. and Subhan, M. (2007) Ethnobotanical importance of salt range species of district Karak, Pakistan. Pakistan Journal of Plant Sciences. 13(1), 29-31.

[20] Baydoun, S., Chalak, L., Dalleh, H., Arnold, N. (2015), Ethnopharmacological survey of medicinal plants used in traditional medicine by the communities of Mount Hermon, Lebanon. Journal of Ethnopharmacology. 173, 139-156.

[21] Adnan, M., Bibi1, B., Azizullah, A., Andaleeb, R., Mussarat, S., Tariq, A., Naser Khan, A.L. and Begum, S. (2015) Ethnomedicinal Plants Used Against Common Digestive Problems. The African Journal of Traditional, Complementary and Alternative Medicines. 12(5), 99-117.

[22] Khan, M., Hussainm, F. and Musharaf, S. (2013) Conservation status of trees in Tehsil Takht-e-Nasratti, Karak Pakistan. African Journal of Plant Science. 7(6), 201-207.

[23] Siddiqui, M.F., Shaukat, S.S. and Din, M. (2014)Topographic And Edaphic Control Of Arboreal Vegetation and the distribution and growth of Tree Species In Moist Temperate Areas Of Himalayan And Hindukush Regions of Pakistan. Pakistan Journal of Botany. 46(4), 1187-1196.

[24] Ahmad, K., Hussain, M., Ashraf, M., Luqman, M., Ashraf, M.Y. and Khan, Z.I. (2007) Indigenous vegetation of Soone Valley at the risk of extinction. Pakistan Journal of Botany. 39(3), 679-690.

[25] Alsir, E., Aboagarib, A., Yang, R. and Hua, X. (2015) Physicochemical, Nutritional, and Functional Characteristics of Seeds, Peel and Pulp of Grewia tenax (Forssk) Fiori Fruits.Tropical Journal of Pharmaceutical Research. 14 (12), 2247-2254.

[26] Li, H., Wang, Z. and Liu, Y. (2003) Review in the studies on tannins activity of cancer prevention and anticancer. Zhong-Yao-Cai. 26(6), 444-448.

[27] Chung, K.T., Wong, T.Y., Wei, C.I., Hung, Y.W. and Lin, Y. (1998) Tannin and human health. CRC Cr. Rev. Food Sci. 38, 421-464.

[28] Sheikh, M.A. and Kumar, M. (2010) Nutrient status and economic analysis in oak and pine forests in Garhwal Himalaya. Journal of American Science. 6, 117-122.

[29] Elhassan, G.O.M. and Yagi, S.M. (2010) Nutritional Composition of Grewia Species (Grewia tenax (Forsk.) Fiori, G. flavescens Juss and G. Villosa Willd) Fruits G.O. Mohammed Advance Journal of Food Science and Technology. 2(3), 159-162.

[30] Al-Numair, K.S., Ahmed, S.E.B., Al-Assaf, A.H., Alamri, M.S.(2009) Hydrochloric acid extractable minerals and phytate and polyphenols contents of sprouted faba and white bean cultivars. Food Chemistry. 113, 997–1002.

[31] Okwu, D.E. and Ukanwa, N.S. (2007) Nutritive value and phytochemical contents of fluted pumpkin (Telfaria OccidentalisHook f.) vegetable grown with different levels of Turkey droppings. African Crop Science Conference Proceedings. 8, 1759-1964.

[32] Avijit, J., Chakraborthy, G.S. and Seema, G. (2014) []Phytopharmacological Uses Of Tephrosia purpurea - A Review. Pharmacophore. 5 (4), 658-665.

[33] Dastagir, G., Hussain, F., Khattak, F. and Khanzadi, J. (2013) Proximate Analysis of plants of Family Zygophyllaceae and Euphorbiaceae during winter. Sarhad Journal of Agriculture. 3, 29-33.

[34] Alhassan, A.B., Chiroma, A.M. and Kundiri, A.M. (2006) Properties and classification of soils of Kajimaram oasis of Northeast Nigeria. International Journal Of Agriculture & Biology. 8, 256-261.

[35] Iqbal, S. and Bhanger, M. (2006) Effect of Season and Production Location on Antioxidant Activity of Moringa Oleifera Leaves Grown in Pakistan. Journal of Food Composition and Analysis. 19, 544 .

[36] Ahmed, M., Wahab, M., Khan, N., Siddiqui, M.F., Khan, M.U. and Hussain, S.T. (2009) Age and growth rates of some Gymnosperms of Pakistan. A Dendrochronological approach. Pakistan Journal of Botany. 41 (2), 849-860.

[37] Hussain, I., Khan, F. A., Khan, H., Rehman, S.U. and Badrullah. A, (2011) Antimicriobial, phytochemical and fluorescence studies on Tribulus teresstris. Journal of Pharmacy Research. 4(5), 1556-1558.

[38] Senhaji, B., Chebli, B., Mayad, E., Hamdouch A., Heimeur, N., Chahid, A. and Ferji, Z. (2017) Phytochemical screening, quantitative analysis and antioxidant activity of Asteriscus imbricatus and Pulicaria mauritanica organic extracts International Food Research Journal. 24(6), 2482-2489.

[39] Murray, S.S., Schoeninger, M.J. and Bunn, H.T. (2001) Nutritional composition of some wild plant foods and honey used by Hadza foragers of Tanzania. Journal of Food Composition and Analysis. 14, 3-13.
[40] Yadav, A.K., Phalsa, A. (1999) Potential New Small Fruit for Georgia. In, Janick, J. (Ed.), Perspectives on New Crops and New Uses. ASHS Press. 348-352.
[41] Martos, V.M., Navajas, R.Y., Sánchez, M.A., Sánchez, E., López, J., Sendra, E. (2012) Chemical, physico–chemical and functional properties of Grewia tanax. Journal of Food Engineering. 110, 220-224.
[42] Rehman, S., Wazir, S.M., Khan, R.U., Khan, S.U. and Farooq, A. (2013) Ethnobotanically Important Plants of Humzoni, Nwa, KPK, Pakistan. International Journal of Herbal Medicine. 1 (2), 89-101.
[43] Mushtaq, A., Rahmatullah, Q., Muhammad, A., Mir, A.K. and Muhammad, Z. (2009) Traditional herbal remedies used for the treatment of diabetes from district Attock (Pakistan) Pakistan Journal of Botany. 41(6), 2777-2782.
[44] Saeed, M., Khan, H., Khan, M.A., Khan, F., Khan, S.A. and Muhammad, N. (2010) Quantification of Various Metals and Cytotoxic Profile of Aerial Parts of Pollygonatum verticillatum. Pakistan Journal of Botany. 42(6), 3995-4002.
[45] Alli, A. and Smith,Y.R. (2009) Determination of chemical composition of Senna- siamea (Cassia leaves). Pakistan Journal of Nutritions. 8(2), 119-121.
[46] Han, J., Ye, M., Guo, H., Yang, M., Wang, B. R., Guo, D.A. (2007) Analysis of multiple constituents in a Chinese herbal preparation Shuang-Huang-Lian oral liquid by HPLC-DAD-ESI-MSn. Journal of Pharmaceutical and Biomedical Analysis. 44(2), 430-438.
[47] Hussain, J., Ullah, R., Rehman, N., Khan, A.L., Muhammad, Z., Khan, F.U., Shinwari, Z.K., Khan, I.U., Zohaib, M., Din, I.M. and Hussain, A.M. (2011) Nutrient Evaluation And Elemental Analysis of Four Selected Medicinal Plants Of Khyber Pakhtoon Khwa, Pakistan Pakistan Journal of Botany. 43(1), 427-434

Received: **18.09.2020**
Accepted: **16.12.2020**

CORRESPONDING AUTHOR

Sonaina Nazar
Department of Botany,
University of Sargodha,
Sargodha – Pakistan

e-mail: sonaina.nangiana@gmail.com

© by PSP Volume 30– No. 05/2021 pages 4984-4993 Fresenius Environmental Bulletin

DIETARY VITAMIN E AMELIORATES ZINC-TISSUE CONCENTRATION IN ZINC-DEFICIENT PREGNANT RATS

Amamra Sabrina[1],Khaldi Fadila[2,*], Sayah Sarra[2], Amamra Fatima[1]

[1]Laboratory of Aquatic and Terrestrial Ecosystems, Department of Biology, Faculty of Life and Natural Sciences, Mohamed Cherif Messaadia University, Souk Ahras, 41000, Algeria
[2]Laboratory of Sciences and Technology of Water and Environment, Department of Biology, Faculty of Life and Natural Sciences, Mohamed Cherif Messaadia University, Souk Ahras, 41000, Algeria

ABSTRACT

Zinc is an essential nutritional trace element whose activity promotes various vital functions in the body. Further, vitamin E, α-tocopherol, is a potent antioxidant against oxidative stress and changes in tissue mineral content. Thus, the present study was aimed to investigate the beneficial role of vitamin E in improving zinc tissue concentration in rats fed a zinc-deficient diet. Forty pregnant rats were equally divided into four animal groups (n=10), received respectively, adequate zinc-diet (54mg/kg diet; Control G1); zinc-deficient diet (1mg/kg; G2); adequate zinc plus vitamin E supplemented diet (54mg zinc + 500mg vitamin E/kg; G3); and zinc-deficient diet plus and vitamin E (1mg zinc + 500mg vitamin E/kg; G4) over 21 days. Zinc deficiency caused decreased body weight gain, food intake, and concentration of zinc in kidney, liver, and femur tissues excluding the pancreas. Consequently, the insufficiency of dietary zinc levels in pregnant rats decreases zinc tissue concentration in the placenta and fetus.

KEYWORDS:
Zinc Deficiency, Pregnancy, Vitamin E, Reproduction, Rats

INTRODUCTION

Trace elements or trace minerals are essentially found at low concentrations in nature and living organisms (less than 0.01% of the organism weight), although of their importance in various physiological and metabolic processes occurring within living tissues [1-3]. Zinc is one of the most important trace elements contributing to some molecular structures in the body, including enzymes (cofactor for over 300 enzymes) and nearly 2000 transcription factors [4], in addition to many biological functions (eg, protein synthesis, cell division and nucleic acid metabolism [5]). Additionally, zinc promotes fertility, embryo development, fetal maturation, child growth, intellectual development and immunity, healing, and maintenance of the bone matrix [6].

It also acts as an efficient antioxidant in the non-enzymatic cell structures and leads to delay in the antioxidant protein induction, such as metallothioneins [7, 8]. Several previous studies have reported a direct relationship between zinc deficiency, fetal growth restriction, and fetal malformations [9], evidencing thus that the preservation of zinc balance is of critical importance in avoiding the possible consequences of low zinc levels on pre- and post-natal life. Insufficient quantities of zinc during embryogenesis may influence the final phenotype of all organs. Maternal zinc restriction during pregnancy influences fetal growth, while adequate zinc supplementation during pregnancy may result in a reduction of the preterm birth risk [10].

It has been reported also that some pathophysiological conditions resulting in oxidative stress-mediated reactive oxygen species (ROS) generation are able to alter the zinc tissue concentration, as well as obesity can cause zinc deficiency, and subsequently oxidative tissue damages, and cell death and diseases accompanied by alterations in the antioxidant defense systems [11,12].

The latter include enzymatic antioxidants (e.g catalase, superoxide dismutase, and glutathione peroxidase) and non-enzymatic antioxidants evidenced mainly by glutathione; an abundant peptide that can be oxidized by glutathione peroxidase can be effectively deactivated. In addition, some natural exogenous substances like tocopherols (vitamin E), carotenoids, ascorbic acid, flavonoids, and tannins are considered as efficient non-enzymatic able to attenuate the oxidative stress effects [13,14].

Vitamin E is a powerful antioxidant scavenging free radicals (FR), and was first discovered in 1922 as a vital substance for reproduction, and accordingly, it was extensively studied and has become widely used owed to its powerful lipid-soluble antioxidant and anticancer activity. The biological activities of vitamin E, including roles in anti-proliferation, anti-survival, pro-apoptotic, cancer anti-angiogenesis therapy, and anti-inflammation have been well documented. There are various

reports on the benefits of vitamin E on health in general [15].

However, up to now, the biological effect of vitamin E on reproduction is poorly elucidated. This paper was written to provide a review of the known roles of vitamin E as an antioxidant in female reproductive health. Very limited research studies investigating the effect of vitamin E on zinc deficiency mediated oxidative tissue injuries in experimental animals [16,17] have reported that vitamin E supplemented diet is effectively able to reduce the effect of zinc deficiency resulting in oxidative tissue damages via free radicals generation causing oxidation of cell macromolecules (lipids, proteins, and nucleic acids). Therefore, the present study was designed to investigate the beneficial effect of dietary vitamin E on zinc tissue concentration in zinc-deficient pregnant albino rats.

MATERIALS AND METHODS

Animals. Forty adult female albino rats weighing between 180 and 210g were used. The animals were obtained from the Pasteur Institute of Algiers, Algeria. They were housed in polypropylene cages with free access to food and water and maintained during two weeks before the study at room temperature (22 ± 2°C), relative humidity of 40%, and 12/12 hour light/dark cycle. All experimental procedures were approved by the Animal Care Committee and Ethics Committee of our institution (AFRO. No 478, 2009).

Experimental Design. Animals were used at the pregnancy stage and divided equally into 4 groups as the control group and treated groups: Group 1 (G1), rats fed a diet containing adequate zinc level (54mg zinc/kg diet, control group); group 2 (G2), rats fed on a zinc-deficient diet (1mg zinc/kg diet) [18]; group 3 (G3), rats fed vitamin E plus adequate zinc supplemented diet (54mg zinc + 500mg of vitamin E/kg diet) [8]; group 4 (G4), rats fed zinc-deficient diet plus vitamin E (500mg vitamin E/kg and 1mg zinc/kg) [19]. Bodyweight and food intake of control and experimental rats were measured every day during the last ten days of the experimental treatment. Thereafter, animals of all groups were sacrificed by decapitation and subsequently, liver, kidney, pancreas, femur, fetus, and placenta were immediately removed, washed in 9 % sodium chloride solution (NaCl), weighed, and dried at 80°C for 16 hours for determination of zinc tissue concentration.

TABLE 1
Body weight gain (g) and food intake (g diet/ day) in control and experimental groups.

	G1	G2	G3	G4
Body weight gain (g)		**Mean ± SD**		
	16,39± 0,97	11,31± 1,48****	17,1± 0,85 NS	14,96± 1,38*
Food intake (g / d)	21,87± 1,71	18,05± 1,21****	21,32± 1,886 NS	20,36± 1,06*

G1: Control diet rats (54mg zinc/kg diet); G2: Zn- deficient rats (1mg zinc/kg diet); G3: adequate zinc + vitamin E (54mg zinc + 500mg vitamin E/kg diet); G4: zinc deficient diet + vitamin E (1mg zinc + 500mg vitamin E/kg diet) (n= 10 rats/group).

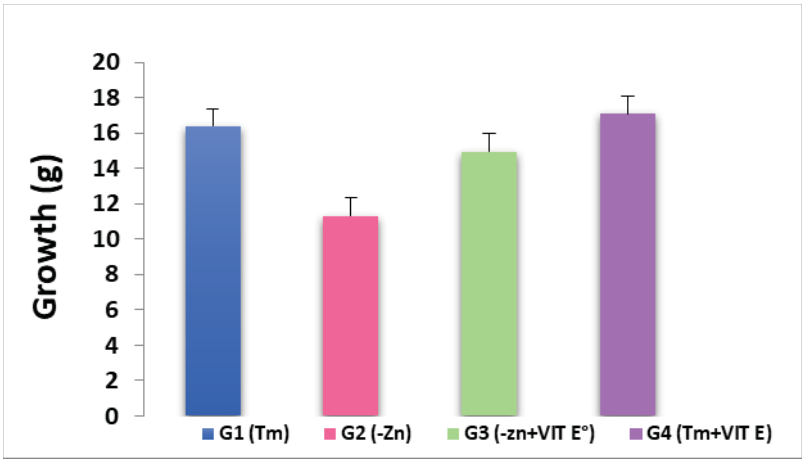

FIGURE 1
Bodyweight gain in pregnant rats

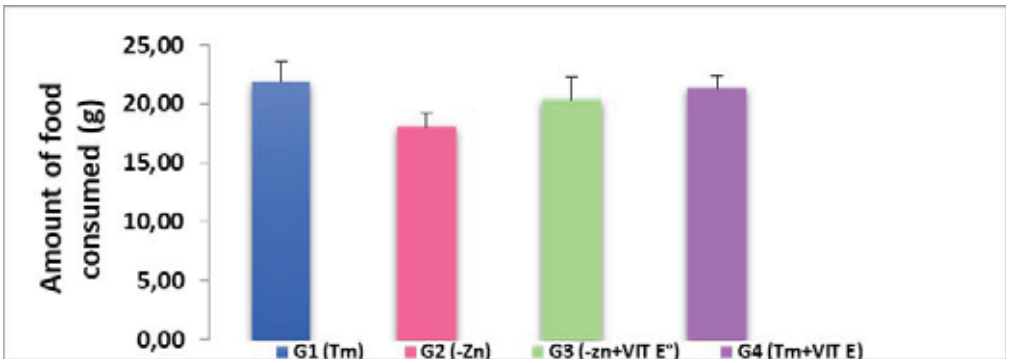

FIGURE 2
Food intake in control and experimental pregnant rats

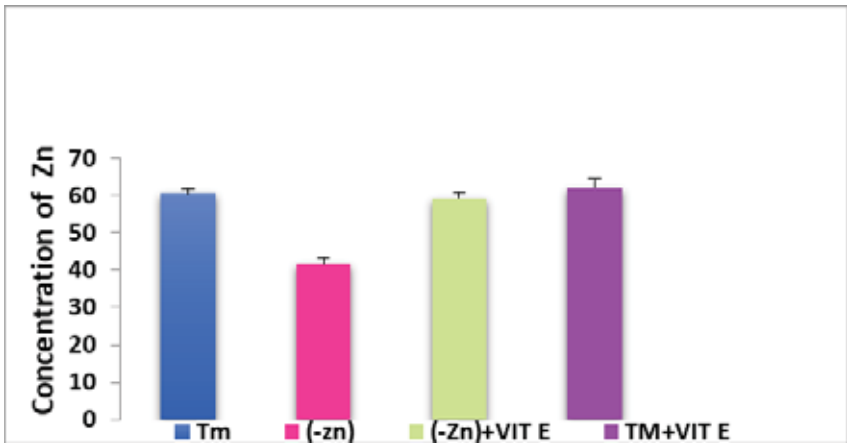

FIGURE 3
Zinc tissue concentration in the liver

TABLE 2
Fresh and dry liver weights (g), water content (%), and tissue zinc concentration (µg / g) in the liver of control and experimental groups.

	Liver			
	G1	**G2**	**G3**	**G4**
	Mean ± SD			
Fresh weight (g)	3,552± 0.46	4,486± 0.34****	3,57± 0.37 NS	3,31± 0.29 NS
Dry weight (g)	1,001± 0,22	1,352± 0,28**	0,98± 0,22 NS	0,99± 0,18 NS
Water content (%)	28,5± 0,69	25,34± 0,69****	29,4± 1,20 NS	28,55± 0,42 NS
Zinc tissue concentration (µg/g)	60,64± 1,36	41,64± 1,59****	62,2± 2,43 NS	59,39± 1,42 NS

G1: Control diet rats (54mg zinc/kg diet); G2: Zn- deficient rats (1mg zinc/kg diet); G3: adequate zinc + vitamin E (54mg zinc + 500mg vitamin E/kg diet); G4: zinc deficient diet + vitamin E (1mg zinc + 500mg vitamin E/kg diet) (n= 10 rats/group).

Determination of Zinc Tissue Concentration. The dried organs were dry-mineralized in a muffle furnace at 458°C for 48 hours. Then, samples were washed, dissolved in 10 ml of 1 M HNO3, and filtered using filter paper (Whatman No. 542). The tissue zinc content in the prepared mineralizes (after dilution with HNO3) in the samples (after dilution wither distilled water) were measured by atomic absorption spectrophotometry (ICP-AES) at Materials Research Unit, Nanomaterials and Ecosystems, Faculty of Sciences of Bizerte, University of Carthage (Tunisia) as described elsewhere [20]. The obtained values of zinc concentration were compared with a standard guideline of zinc nitrate concentration (1 mg/ml) provided in the same conditions.

Statistical analysis. The data were given as Mean ± SD and pairwise comparisons were tested for statistical significance by unpaired Student's t-

test. Statistical tests were performed using Minitab software (Ver, 14, 0) where $p < 0.05$ was considered significant [21].

RESULTS

As shown in Table 1, Figure 1 and 2, body gain and food intake were highly significantly decreased ($P < 0.0001$) in rats fed a zinc-deficient diet (G2) as compared with control-diet (G1), since rats fed zinc deficiency and vitamin E supplemented diet (G4) revealed significant increase ($P < 0.05$) in these parameters as compared with rats fed zinc deficiency diet (G2).

Table 2 and Figure 3 revealed a highly significant decrease ($P < 0.0001$) in zinc liver concentration of rats fed zinc No significant difference was noticed in rats fed a normal diet plus vitamin E (G3) and those fed zinc deficiency diet plus vitamin E (G4).

Zinc tissue concentration showed a highly significant ($P<0,0001$) decrease in rats fed a zinc deficiency diet, a long with a highly significant increase in the group treated with a normal diet and supplemented with the control diet-rats. No significant difference between control group(G1) and G3 was noticed (Table3, Figure4).

TABLE 3
Fresh weight (g), dry weight (g), water content (%), and zinc tissue concentration (µg / g) in the kidney of control and experimental groups

	Kidney			
	G1	G2	G3	G4
	Mean ± SD			
Fresh weight (g)	0,90± 0,05	1,12± 0,11****	0,91± 0,05 NS	0,967± 0,10 NS
Dry weight (g)	0,20± 0,12	0,39± 0,05***	0,22± 0,01 NS	0,20± 0,03 NS
Water content (%)	28,33± 0,99	26,18± 0,25****	30,2± 1,89*	28,4± 2,26 NS
Zinc tissue concentration (µg/g)	164,6± 5,56	84,87± 4,36****	183,8± 3,80****	165,9± 6,45 NS

G1: Control diet rats (54mg zinc/kg diet); G2: Zn- deficient rats (1mg zinc/kg diet); G3: rats fed on diet composed of adequate zinc level + vitamin E (54mg zinc + 500mg vitamin E/kg diet); G4: rats fed on zinc deficiency diet + vitamin E (1mg zinc + 500mg vitamin E/kg diet) (n=10 rats / group).

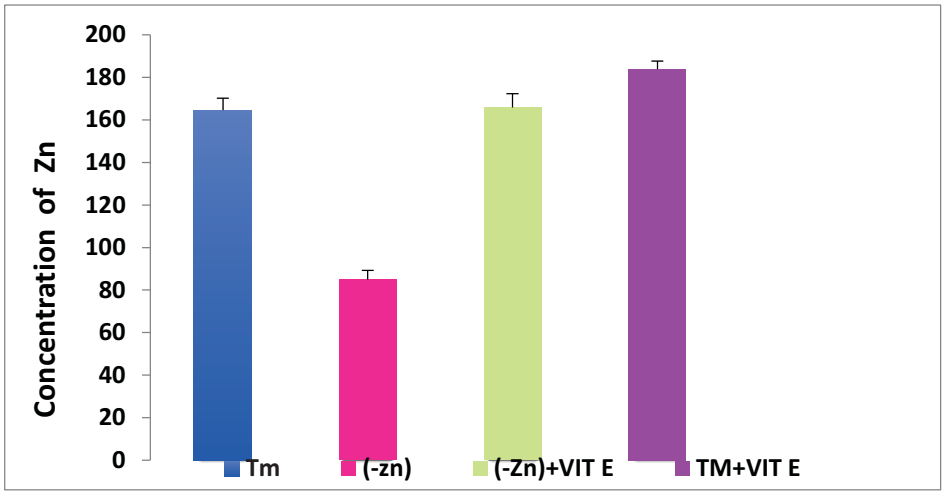

FIGURE 4
Zinc tissue concentration in the kidney

TABLE 4
Fresh weight (g), dry weight (g), water content (%), and zinc tissue concentration (µg / g) in the pancreas of control and experimental groups

	Pancreas			
	G1	G2	G3	G3
	Mean ± SD			
Fresh weight (g)	0,59± 0,03	0,48± 0,075***	0,68± 0,175 NS	0,64± 0,15 NS
Dry weight (g)	0,41± 0,04	0,33± 0,04**	0,48± 0,13 NS	0,45± 0,15 NS
Water content (%)	61,41± 1,44	58,65± 3,327*	69,4± 1,75****	55,92± 3,45***
Zinc tissue concentration (µg/g)	50,62± 2,32	146,3± 3,54****	62,67± 2,32****	52,07± 6,68 NS

G1: Control diet rats (54mg zinc/kg diet); G2: Zn- deficient rats (1mg zinc/kg diet); G3: adequate zinc + vitamin E (54mg zinc + 500mg vitamin E/kg diet); G4: zinc deficient diet + vitamin E (1mg zinc + 500mg vitamin E/kg diet) (n= 10 rats/group).

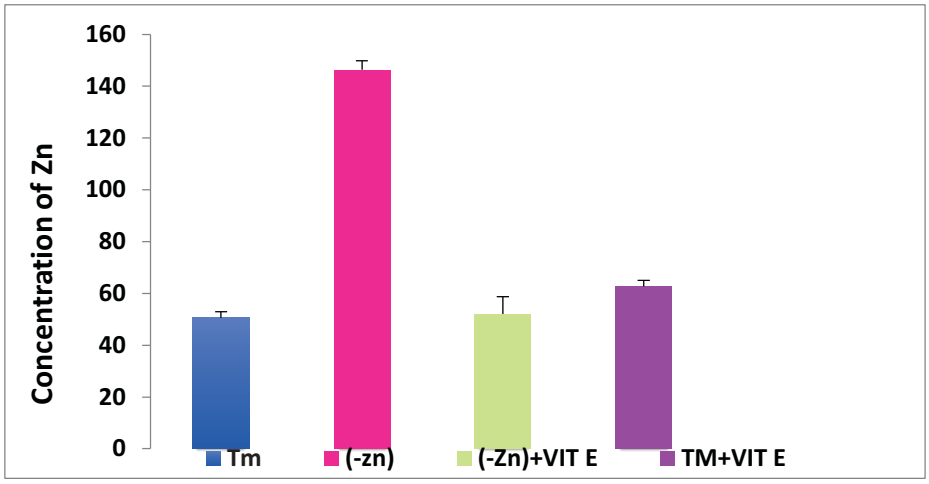

FIGURE 5
Zinc tissue concentration in the pancreas

TABLE 5
Fresh weight (g), dry weight (g), water content (%), and zinc tissue concentration (µg / g) in the femur of control and experimental groups

	Femur			
	G1	G2	G3	G4
	Mean ± SD			
Fresh weight (g)	0,89± 0,07	1,109*± 0,30	1,01± 0,26 NS	0,91± 0,04 NS
Dry weight (g)	0,61± 0,06	0,764± 0,07***	0,63± 0,02 NS	0,60± 0,04 NS
Water content (%)	37,64±0,91	72,77± 4,70****	40,22± 1,98**	40,69± 2,26***
Zinc tissue concentration (µg/g)	157,6±3,67	90,78± 3,62****	156,9± 1,19 NS	170± 8,56***

G1: Control diet rats (54mg zinc/kg diet); G2: Zn- deficient rats (1mg zinc/kg diet); G3: adequate zinc + vitamin E (54mg zinc + 500mg vitamin E/kg diet); G4: zinc deficient diet + vitamin E (1mg zinc + 500mg vitamin E/kg diet) (n= 10 rats/group).

TABLE 6
Fresh weight (g), dry weight (g), water content (%), and zinc tissue concentration (µg / g) in the fetus of control and experimental groups

	Fetus			
	G1	G2	G3	G4
	Mean ± SD			
Fresh weight (g)	3,56±0,45	1,99±0,29****	3,3±0,43 NS	3,85±0,46 NS
Dry weight (g)	1,2±0,04	0,10±0,02****	1,05±0,30 NS	1,58±0,05****
Water Content (%)	20,43±2,29	40,52±1,69****	22±3,14 NS	21,82±1,55 NS
Zinc tissue concentration (µg/g)	138,63±1,70	88,03±4***	140,60±2,03*	42,37±2,88**

G1: Control diet rats (54mg zinc/kg diet); G2: Zn- deficient rats (1mg zinc/kg diet); G3: adequate zinc + vitamin E (54mg zinc + 500mg vitamin E/kg diet); G4: zinc deficient diet + vitamin E (1mg zinc + 500mg vitamin E/kg diet) (n= 10 rats/group).

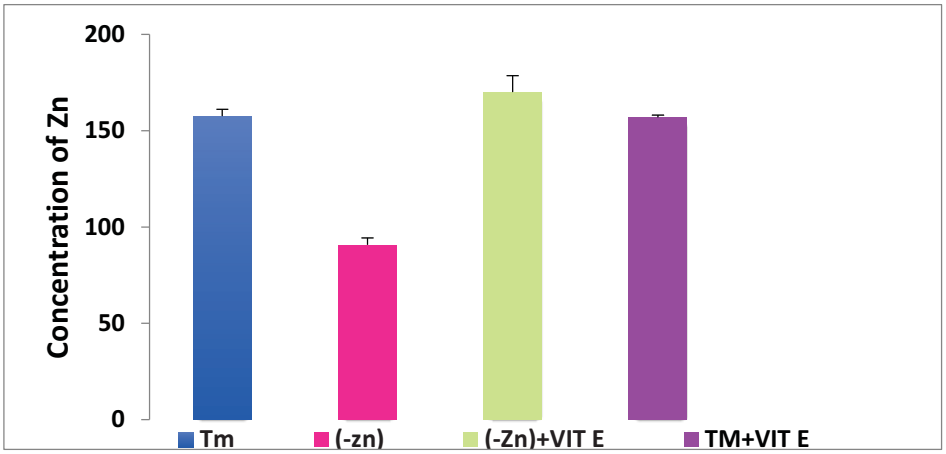

FIGURE 6
Zinc tissue concentration in the femur

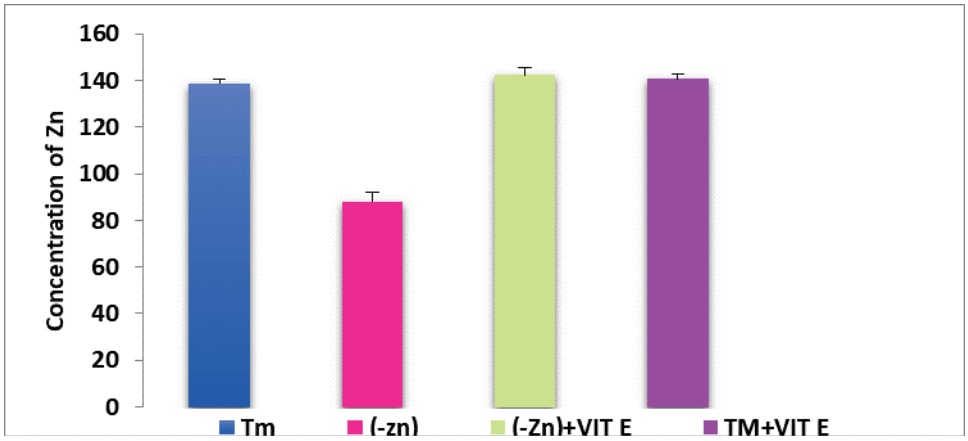

FIGURE 7
Zinc tissue concentration in the fetus

TABLE 7
Fresh weight (g), dry weight (g), water content (%), and zinc tissue concentration (µg / g) in the placenta of control and experimental groups

	Placenta			
	G1	G2	G3	G4
	(Mean ± SD)			
Fresh weight (g)	1,08±0,13	1,12±0,15 NS	1±0,23 NS	0,99±0,29 NS
Dry weight(g)	0,84±0,06	0,77±0,10 NS	0,81±0,02 NS	0,09±0,02****
Water content (%)	70,94±1,14	74,45±5,84 NS	72,39±1,98 NS	70,47±2,19 NS
Zinc tissue concnetration (µg/g)	190,5±5,96	92,65±6,14****	193,9±4,80 NS	187,1±5,52 NS

G1: Control diet rats (54mg zinc/kg diet); G2: Zn- deficient rats (1mg zinc/kg diet); G3: adequate zinc + vitamin E (54mg zinc + 500mg vitamin E/kg diet); G4: zinc deficient diet + vitamin E (1mg zinc + 500mg vitamin E/kg diet) (n= 10 rats/group).

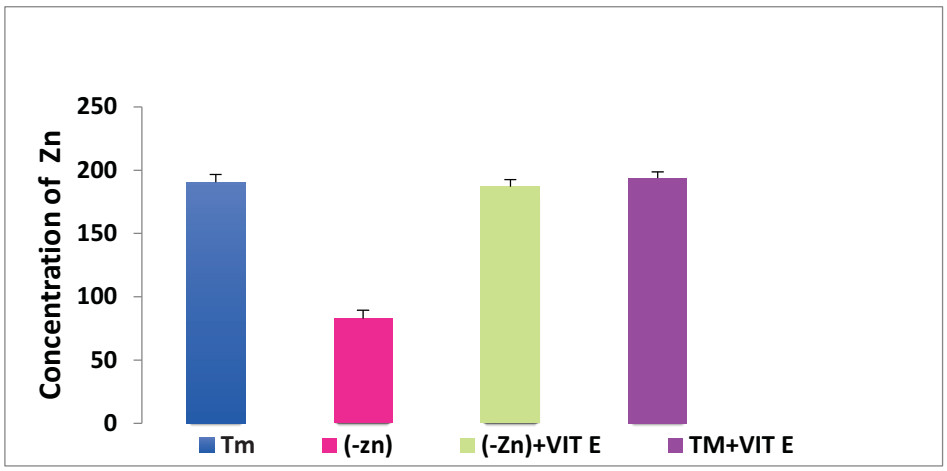

FIGURE 8
Zinc tissue concentration in the placenta

As shown in Table 4 and Figure 5, a highly significant (P<0.0001) decrease in zinc tissue concentration in the pancreas was observed in rats fed zinc deficiency diet, and a highly significant increase in rats receiving adequate zinc diet plus vitamin E as compared with the control diet rats. No significant difference in zinc concentration was noticed in a zinc-deficient diet plus vitamin E.

A highly significant (P <0.0001) decrease in zinc concentration in the femur was noticed in rats fed zinc deficiency diet (G2) as compared with control diet rats (G1), whereas no significant differences were noticed in rats fed adequate zinc level with vitamin E supplemented diet (G3) and those fed zinc deficiency diet plus vitamin E (G4) (Table 5, Figure 6).

Table 6 and Figure 7 reveal a highly significant (P <0.0001) decrease in zinc tissue concentration in the fœtus of rats fed a zinc deficiency diet (G2) as compared with control diet rats. No significant difference was noticed in rats fed an adequate zinc diet plus vitamin E (G3) and those fed zinc deficiency diet plus vitamin E (G4).

The results shown in Table 7 and Figure 8 reveal a highly significant (P<0.0001) decrease in zinc tissue concentration in the placenta of rats fed a zinc deficiency diet (G2) as compared with control-diet rats (G1), since rats fed a combination of adequate zinc and vitamin E (G3) and those fed zinc deficiency diet plus vitamin E did not show any significant differences.

DISCUSSION

Owing to the importance of nutritional zinc in fetal development, growth, and immune function, zinc insufficiency in food during pregnancy may lead to serious teratogenic effects which can be effectively reduced by exogenous antioxidants, including vitamin E [22, 23].

Therefore, the present study was devoted to investigating the beneficial role of vitamin E supplemented diet in attenuating the effect of zinc deficiency on zinc tissue concentration in the main target organs of pregnant female rats. In this study, a marked decrease in body weight gain and food intake was noticed in rats receiving zinc-deficiency diet (G2) as compared with those fed adequate dietary zinc (G1) and, in this regard, the same findings were previously reported [24, 25].

Furthermore, zinc deficiency is able to induce anorexia in humans and animals through the central role of zinc in activating many enzymes involved in the synthesis and breakdown of biologically active peptides commonly known as neuropeptides, contributing to the regulation of food intake [26-28].

Also, the pituitary gland modulating food intake receives metabolic signals and, subsequently transmits them to other target peripheral tissues or organs [29, 30]. Zinc deficient diet in many animal species leads to serious digestive disorders associated with lack of appetite, bodyweight loss, and growth retardation resulting mainly from the deterioration of taste and smell [31, 32].

On the other hand, vitamin E-treated pregnant rats were found to increase food intake and body weight [33]. In the present study, zinc deficiency caused a marked decrease in zinc concentration in the main target organs: liver, kidney, and femur. This finding is in line with that found by [34] and [35] suggesting the strong relationship of the zinc concentration in tissue and the diet.

Unlike other organs, the pancreas showed an increase in zinc tissue concentration proving thus its high sensibility to variation in zinc dietary intake [36]. Herein, the experimental animals exhibit an effective mechanism for retaining zinc from the body through homeostatic reaction according to the increased needs of low zinc dietary intake. This mechanism leads to increased zinc tissue concentration in the pancreas of zinc-deficient diet, although

its concentration is fifty times lower than that in rats fed a normal diet.

It is well-documented, that animals and humans receiving low dietary minerals are often able to retain zinc and other minerals found in some of their tissues, even in the state of severe deficiency [37]. The results revealed also a significant increase in the concentration of zinc in the studied organs of pregnant rats receiving adequate zinc and vitamin E supplemented diet. This is in agreement with the results of [38] who proved the effect of vitamin E in improving zinc tissue concentration in tests in lead intoxicated rats.

Conversely, zinc deficiency showed a significant decrease in zinc tissue concentration in the placenta and fetus of pregnant rats in comparison with those fed a normal zinc diet (G1), and this may be related to the low maternal zinc received by fetus and placenta under dietary zinc deficiency [35]. Other studies have shown that maternal zinc deficiency has long-term effects on the growth, immunity, and metabolic state of offspring [39, 40]. Additionally, previous studies using experimental animals such as rats, mice, pigs, and ewes showed that severe zinc deficiency increases fetal death due to spontaneous abortions or multiple birth defects [41], including organ malformations evidenced by abnormal synthesis of nucleic acids and proteins, decreased cell growth and morphogenesis, abnormal tubulin polymerization, chromosomal defects and excessive lipid peroxidation of cell membranes.

CONCLUSION

Conclusively, vitamin E has effectively improved body weight loss, decreased food intake, and zinc tissue concentration in liver, kidney, femur, placenta, and fetus in zinc-deficient rats. Thus, a zinc-deficient diet proved to be able to disrupt growth rate, dietary intake, and zinc status in vital tissues of pregnant rats, meanwhile vitamin E can act as a powerful antioxidant in attenuating generation of free radicals leading to a decrease of Intracellular zinc concentration.

ACKNOWLEDGEMENTS

No any support or grant were used.

REFERENCES

[1] Mehri, A., Marjan, R.F. (2013) Trace Elements in Human Nutrition: A. Review. Int. J. Medinvest. 2 (3), 115-128.

[2] Beausir, A., Kim, I., Séguy, D., Michaud, L., Lannoy, D. (2011) Micronutrients in parenteral nutrition The Hospital Monitor. 238, 15-28.

[3] Bhattacharya, P., Satya Ranjan., M, Mohsina, H. (2016) Nutritional Aspects of Essential Trace Elements in Oral Health and Disease. An Extensive Review. J. Sci. 2012 pages.

[4] Marreiro, D., Cruz, K.J.C., Morais, J.B.S., Beserra, J.B., Severo, J.S., Oliveira, R.S. (2017) Zinc and Oxidative Stress: Current Mechanisms. Antioxidants. 6(24), 1-9.

[5] Chaffee, B.W., King ,J.C. (2012) Effect of Zinc Supplementation on Pregnancy and Infant Outcomes.A Systematic Review.Paediatr Perinat Epidemiol. 26(01), 118-137.

[6] Girodon, F., Galan, P., Monget, A.L., Boutron-Ruault, M.C., Brunet-Lecompte, P., Preziosi, P., Arnaud, J., Manuguerra, J.C., Herchberg, S. (1999) Impact of trace elements and vitamin supplementation on immunity and infections in institutionalized elderly patients. A randomized controlled trial. Arch. Intern. Med. 159, 748-754.

[7] Sidhu, P., Garg, M.L., Dhawan, D.K .(2004) Protective effects of zinc on oxidative stress enzymes in liver of protein deficient rats. Nutr. Hosp. 19(6) ,341-347.

[8] Miao, X., Wang, Y. (2013) Zinc protects against diabetes-induced pathogenic changes in the aorta: Roles of metallothionein and nuclear factor (erythroid-derived 2)-like 2. Cardiovasc. Diabetol. 12- 54.

[9] Norrozi, M., Borna, S., Parichehr, H., Soghrat, F., Fedyeh, H., Shokoufeh, G .(2012) Evaluation of Zinc Supplementation Effect on Fetal Outcomes in Pregnant Women with Lower-than-Median Serum Zinc Concentration. J. Fam. Repr .Hea. 6(2), 85 – 89.

[10] Terrin, G., Bernicanani, R., Chiara, M., Pietravalle ,A., Aleandri ,V., Conte ,F., De curtis , M. (2015) Zinc in early life: akeyelement in the fetus and preterm neonate. Nutrients. 11, 7(12), 10427-10446 .

[11] Martins, L.M., Oliveira, A.R.S. (2014) Influence of cortisol on zinc metabolism in morbidly obese women. Nutr. Hosp. 29, 57–63.

[12] Sulibuska, J., Bogdanski, P. (2014) Changes in mineral status are associated with improvements in insulin sensitivity in obese patients followingL-arginine supplementation. Eur. J. Nutr. 53, 387–393.

[13] You, H.J., KIM, J.Y., Jeong ,H.G. (2003) 17 beta-estradiol increases inducible nitricoxide synthase expression in macrophages. Biochem. Biophys. Res. Commun. 303(17), 1129-1134.

[14] Naskar, S., Islam, A., Mazumder, U.K., Saha, P., Haldar, P.K., Gupta, M. (2010) *In Vitro* and *In Vivo* Antioxidant Potential of Hydromethanolic Extract of Phoenix dactylifera Fruits. J. Sci. Res. 2(1), 144-157.

[15] Siti Syairah, M.M., Sharaniza, A., Mohd Hamim , R.(2018) Vitamin E as an Antioxidant in Female Reproductive Health. Anti. J. 7(2), 22 .
[16] Kinalski, M., Śledziewski, A., Telejko, B., Zarzycki, W., Kinalska , I. (2000) Lipid peroxidation and scavenging enzyme activity in streptozotocin-induced diabetes. Acta-Diabetologica. 37 (4), 179-183 .
[17] Evans, J.L. (2007) Antioxidants: do they have a role in the treatment of insulin resistance .Ind. J. Med. Res. 125 (3), 355.
[18] Southon, S., Kechrid, Z., Wright, A.J.A., Fairweather-Tait, S. (1988) Effect of reduced dietary zinc intake on carbohydrate and zinc metabolism in the genetically diabetic mouse (C57BL/KsJdb+/db+). Brit. Nutr. 60 (3), 499-507.
[19] Demiralay, R,,Gürsan, N., Erdem, H. (2007) Regulation of nicotine-induced apoptosis of ulmonary artery endothelial cells by treatment of N-acetylcysteine and vitamin E. Hum. Exp. Toxicol. 26 (7), 595-602.
[20] Southon, S., Gee, J., Johnson, I.T. (1984) Hexose transport and mucosal morphology in the small intestine of the zinc-deficient rat. Brit. Nutr. 58, 371-380.
[21] Dagnelie, P.(1999) Theoretical and appliquation. Tome 2 statistics: statistical references to one and two dimensions. Brussels. Univ. of Boeck and Larcier. 659 Pp.
[22] Keen, C.L., Taubeneek, M.W., Daston, G.P., Rogers, J.M., Gershwin, M.F. (1993) Primary and factors underlying abnormal CNS development. Annals of New York Academy of Sciences. 678, 37-47.
[23] Vallee, B.L., Falchuk, K.H. (1993) The biochemical basis of zinc physiology. Physiol Rev. 73, 79-118.
[24] Kechrid, Z., Hamdi, M., Nazıroğlu, M., Flores-Arce, M. (2012) Vitamin D supplementation modulates blood and tissue zinc, liver glutathione and blood biochemical parameters in diabetic rats fed on a zinc-deficient diet. Biol. Trace Elem. Res. 148 (3), 371-377.
[25] Kumari, D., Nair, N., Bedwal, R.S. (2011) Effect of dietary zinc deficiency on testes of Wistar rats: Morphometric and cell quantification studies. Trace Elem. in Med .Bio. 25, 47-53.
[26] Levin, G., Cogan, U., Mokady, S. (1992) Food restriction and membrane fluidity. Mech. Ageing . Dev. 62, 137-141.
[27] Ploysangam, A., Falciglia ,GA., Brehm, B.J. (1997) Effect of marginal zinc deficiency on human growth and development. Trop. Pediatr. 43, 192-197.
[28] Lee, S.L., Kwak, E.H., Kim, Y.H, Choi, J.Y., Kwon, S.T., Beattie, J.H., Kwun ,I.S.(2003) Leptin gene expression and serum leptin levels in zinc deficiency: implications for appetite regulation in rats. Med. Food. 6 (4), 281-289.
[29] Song, H.D., Hu, R.M., Peng, Y., Huang, Q. (2000) Study on the gene expression profiling in the normal human pituitary. Chin. Endocrinol. Metab. 16, 292-296.
[30] Bjursell, M., Egecioglu, E., Gerdin, A. K., Svensson , L.,Oscarsson , J., Morgan, D., Snaith, M., Törnell, J., Bohlooly, Y.M. (2005) Importance of melanin- concentrating hormone receptor for the acute effects of ghrelin. Biochem. Biophys. Res. Commun. 326, 759-765.
[31] Shay, N., Mangian, H. F. (2000) Neurobiology of zinc-influenced eating behavior. Nutr. 130, 1493-1499.
[32] Merrells, K.J., Blewett, H., Jaamieson, J.A., Taylor, C.G., Suh, M. (2009) Relationship between abnormal spermophysiology induced by dietary zinc deficiency and lipid composition in testes of growing rats. Br. Nutr. 102, 226-232.
[33] Badr, G., Bashandy, S., Ebaid, H., Mohany, M., Sayed, D. (2012) Vitamin C supplementation reconstitutes polyfunctional T cells in streptozotocin-induced diabetic rats. Eur. Nutr. 51 , 623-633.
[34] Williams, A.R., Mills, C.E., (1970) The experimental production of zinc deficiency in the rats. Brit. Nutr. 24, 989-1003.
[35] Kechrid, Z., Amamra, S., Bouzerna, N. (2007) The effect of zinc deficiency on zinc status, carbohydrate metabolism and progesterone level in pregnant rats. Turk.Med. Sci. 36, 337-342.
[36] Huber, A.M., Gershoff, S.N. (1970) Effect of dietary zinc and calcium on the retention and distribution of zinc in rats fed semi-purified diets. Nutr.100, 949-954.
[37] Kechrid, Z., Bouzerna, N., Zio M.S. (2001) Effect of low zinc diet on (65)Zn turnover in non-insulin dependent diabetic mice. Diabetes Metab. 27, 580-583.
[38] Ayinde, O.C., Ogunnowo, S., Ogedegbe, R.A. (2012) Influence of vitamin C and vitamin E on testicular zinc content and testicular toxicity in lead exposed albino rats. Pharm. Toxic. 14, 13-17.
[39] Mcardle, H.J., Andersen, H.S., Jones, H., Gambling, L. (2006) Fetal programming: causes and consequences as revealed by studies of dietary manipulation in rats. A review. Placenta. 27 (Suppl A),56-60.
[40] Jou, M.Y., Philipps, A.F., Lonnerdal, B. (2010) maternal zinc deficiency in rats affects growth and glucosemetabolism in the offspring by inducing insulin resistance postnatally. J. Nutr. 140, 1621-1627.

[41] King, J.C. (2000) Determinants of maternal zinc status during pregnancy .Amer. J. Clin. Nutr. 71,1334-1343.

Received: **23.09.2020**
Accepted: **19.01.2021**

CORRESPONDING AUTHOR

Khaldi Fadila
Laboratory of Sciences and Technology of Water and Environment,
Department of Biology, Faculty of Life and Natural Sciences,
Mohamed Cherif Messaadia University,
Souk Ahras 41000 – Algeria

e-mail: f.khaldi@univ-soukahras.dz

© by PSP Volume 30– No. 05/2021 pages 4994-5001 Fresenius Environmental Bulletin

RESEARCH ON ECO-EFFICIENCY COMPENSATION MEASUREMENT OF ECOLOGICAL FUNCTION ZONE IN HUAIHE RIVER BASIN BASED ON CARBON EMISSION REDUCTION

Shuhang Zhao, Yu Du*, Gang He, Tiantian Wang

School 232001, China of Economics and Management, Anhui University of Science and Technology, Huainan, Anhui, China

ABSTRACT

The Huaihe River Basin has a very important position in China's economic and social development. Under the environment where economic development and the environment are coordinated, the upstream ecological function area protects the environment, and the downstream area feeds back the upstream is the general trend. Ecological compensation has become a coordinated and sustainable area. As an important direction of development, a reasonable measurement of ecological compensation efficiency is particularly important. Based on the statistical yearbook data of the Huaihe River Basin and literature surveys, this paper revises the equivalent factors in the ecosystem service value and the service value per unit area. Based on this, the service value per unit area of the Huaihe River Basin is obtained, and the ecological service value of the basin is calculated. According to the carbon emission method, the carbon emission value of the upstream ecological function area is obtained, which proves that vegetation and construction land are the main carbon emission methods. According to the analytic hierarchy process, the efficiency of ecological compensation in different dimensions is measured. The results show that the overall efficiency of ecological compensation in this region is low, and the coordinated development of the region needs to be strengthened in the policy formulation process. The research conclusions of this article can provide some reference for the formulation of related policies.

KEYWORDS:
Carbon emission reduction, ecological compensation, analytic hierarchy process, ecological function zone, Huaihe River Basin

INTRODUCTION

The Huai River Basin is located between the Yangtze River and the Yellow River, with a drainage area of 270,000 square kilometers. The Huai River originates from Henan Province and flows through Henan, Hubei, Anhui, and Jiangsu provinces, with a total length of 1,000 kilometers. The basin is densely populated and rich in resources [1-3]. It is the main grain producing area in China and occupies a very important position in the overall economic and social development of China. It has a population of 183 million and spans 181 counties. The area of arable land accounts for 12% of the country, and the grain output accounts for 1/6 of the country [4-5]. The west, southwest and northeast of the Huaihe River Basin are mountainous and hilly areas, and the hilly area accounts for 1/3 of the basin. On the whole, there are many hills in the west and many plains in the east. In terms of economic development, the development of the west is worse than that of the east and the development is slow [6]. Under the environment where economic development and the environment are coordinated, it is a general trend for the west to protect the environment and the east to feed back the west. Therefore, reasonable ecological compensation has become an important direction for the coordinated and sustainable development of the region.

In Europe, the EU issues ecological compensation funds to farmers through the Agri-environment Scheme every year to protect the ecological environment and biodiversity [7]. In the United States, through the Conservation Reserve Program and Wildlife Habitat Incentives Program, ecological compensation is issued to farmers that meet the requirements. China has carried out projects of returning farmland to forests for many years, which has increased the forest coverage rate year by year [8]. Developing countries such as Costa Rica and Mexico have also launched similar projects [9-10].

Birner et al. [11] put forward a basic analysis standard, they decide the cost effectiveness of ecological compensation from three aspects: the efficiency of output cost, the efficiency of decision cost and the efficiency of implementation cost. Watzold et al. [12] believes that the efficiency of decision-making costs cannot be accurately estimated, but there are correlations among the three. Ferraro et al. [13] proposed that budget efficiency is the best measure, which coincides with the government's

TABLE 1
Service value equivalent factor table

Ecotype	Field	Vegetation	Water system
Food	1.00	0.21	0.5
Climate	0.68	2.20	12.38
Hydrology	0.72	3.55	19.55
Biodiversity	0.81	1.82	2.64
Environmental protection	1.38	1.25	12.54

TABLE 2
Table of service value per unit area (unit: yuan/(mu·year))

Ecotype	Field	Vegetation	Water system
Food	134.98	28.35	67.49
Climate	91.79	296.96	1671.09
Hydrology	97.19	479.19	2638.91
Biodiversity	109.34	245.67	356.35
Environmental protection	186.28	168.73	1692.69
Total	619.57	1218.90	6426.53

requirements. The government values budget efficiency more than cost effectiveness.

Although many countries around the world have carried out hundreds of ecological compensation projects, their measurement methods and results are also different based on the development of different countries. At the same time, due to the limitation of ecological compensation funds, how to formulate ecological compensation plans more efficiently has also become a difficult problem for various ecological compensation projects. For the makers of ecological compensation schemes, the issues need to be considered: ①The policies formulated can achieve the expected ecological compensation goals; ②How to coordinate ecological protection and economic development; ③How to meet the efficiency requirements of ecological compensation policies; ④How to compare different ecological compensation schemes and choose the best compensation scheme.

MATERIALS AND METHODS

Ecosystem service value assessment. The method includes two important contents: the correction of the equivalent factor and the correction of the service value per unit area. Combining the relevant data from the statistical yearbooks of the four provinces in the Huaihe River Basin, it is obtained that the average grain output of Henan Province in the Huaihe River Basin in recent years is 61.35 million tons, accounting for about 9.24% of the total in China. In the table of farmland biological factors in China, the correction coefficient of Henan Province is 1.39. At the same time, based on the existing literature on vegetation and water systems, the equivalent factor data of the Huai River Basin is obtained.

Based on the data in Table 1, the economic value of an ecological service value equivalent to 1/7 of the average grain value is used as the basis, and the average grain price in 2019 (1.24 yuan/500g) is used as the basis, combined with the per capita value given by the National Bureau of Statistics in 2019. The average grain yield per mu is 381kg/mu, and the service value per unit area of the Huai River Basin is obtained, as shown in Table 2

According to the analytic hierarchy process, the measurement of ecological compensation efficiency in the Huaihe River Basin is divided into four dimensions, and each dimension extends four indicators. According to calculations, different indicators and weights of each dimension are obtained. See Table 4 for details.The index data of the upstream area is standardized through SPSS software, combined with the weights of the measurement index system in Table 4, and the results of the ecological compensation efficiency measurement shown in Table 5.

According to the remote sensing satellite data, the area of different ecological types is classified, and the ecological service value data is calculated according to the ecological service value calculation formula [9, 14].

$$V_E = \sum_{n=1}^{m} (A_n \times V_C) \quad (1)$$

$$V_{Ef} = \sum_{n=1}^{m} (A_n \times V_{Cf}) \quad (2)$$

Carbon emission assessment. Both fields and vegetation will have an impact on carbon emissions. According to the research of relevant literature, the net carbon emission coefficient of fields is 0.0422kg/(m2·a), and the net carbon emission coefficient of vegetation is -3.25 kg/(m2·a). We multiply the actual area of fields and vegetation in the Huaihe

River Basin and the emission coefficients to obtain the carbon emissions. Among them, the carbon emission of construction land is calculated according to the following formula [15]:

$$E_i = \delta_f \times E_x \quad (3)$$

Among them, E_i is the carbon emission of construction land, δ_f is the carbon emission conversion coefficient of energy consumption, and E_x is the standard value of energy consumption, taking 0.733t/t.

According to domestic practice for many years, the calculation unit price of carbon emissions is 273.3 yuan/t, and the total economic value of carbon emissions in the Huaihe River Basin can be evaluated based on this. The relevant calculation formula is as follows:

$$E = (A_t \times S_t + A_z \times S_z) \times 2773.3 \times 10^{-3} \quad (4)$$

Among them, A_t is the field area, S_t is the field emission coefficient, A_z is the vegetation area, and S_z is the vegetation emission coefficient.

AHP. The Analytic Hierarchy Process, the AHP method, was created to study the contribution of the industrial sector to the country. The focus is on building an accurate hierarchical model. For the ecological measurement of the Huaihe River Basin, the efficiency measurement is divided into the aspects: economic efficiency, ecological environmental protection efficiency, political efficiency, and social efficiency.

Determine the weight of each indicator according to the analytic hierarchy process, combine the relationship of each indicator, and calculate the weight of each indicator according to the normalized calculation formula. The normalized calculation formula is [16-17]:

$$X'_{ij} = \frac{X_{ij}}{\sqrt{\sum_{i=1}^{m} x_{ij}^2}} \quad (5)$$

Among them, X_{ij} is the data matrix to be normalized, and X'_{ij} is the normalized data, which is between 0 and 1.

First, multiply each row of data:

We take the nth root of M_i and perform normalization processing to obtain the feature vector.

According to the weight calculation method, the weight of each index in the comprehensive efficiency model of water resources ecological compensation in the river basin is calculated

$$M_i: M_i = \prod x'_{ij}, (i, j = 1,2. \ldots, n) \quad (6)$$

We take the nth root of M_i and perform normalization processing to obtain the feature vector.

According to the weight calculation method, the weight of each index in the comprehensive efficiency model of water resources ecological compensation in the river basin is calculated

RESULTS

Measurement of ecological compensation standards in the Huaihe River Basin. According to the calculation formula of the ecological service value, combined with the data in Table 2, the ecological service value of the ecological function area of the Huaihe River Basin can be calculated, which is listed in Table 3. Among them, the field value is calculated based on the area of cultivated land in the basin. The vegetation area is calculated based on the leaf area index LAI of the Huai River Basin and combined with remote sensing satellite data, but some seasonal green plants should be removed from the cultivated land [18-20]. The LAI formula is as follows and perform normalization processing to obtain the feature vector.

According to the weight calculation method, the weight of each index in the comprehensive efficiency model of water resources ecological compensation in the river basin is calculated.

Measurement of ecological compensation standards in the Huaihe River Basin. According to the calculation formula of the ecological service value, combined with the data in Table 2, the ecological service value of the ecological function area of the Huaihe River Basin can be calculated, which is listed in Table 3. Among them, the field value is calculated based on the area of cultivated land in the basin. The vegetation area is calculated based on the leaf area index LAI of the Huai River Basin and combined with remote sensing satellite data, but some seasonal green plants should be removed from the cultivated land. The LAI formula is [21]:

$$LAI = \frac{\sum_{i=1}^{n} LAI_i}{n} \quad (7)$$

TABLE 3
Ecological Service Value Table of the Ecological Function Zone of the Huaihe River Basin (Unit: 100 million yuan/year)

Ecotype	Field	Vegetation	Water system
Food	242.96	34.45	10.22
Climate	165.22	360.81	253.17
Hydrology	174.94	582.22	399.79
Biodiversity	196.81	298.49	53.99
Environmental protection	335.30	205.01	256.44
Total	1115.24	1480.96	973.62

Among them, LAI_i is the LAI value of the i-th scene, and n is the number of LAI in the researched time series

From the data in Table 3, it can be seen that the ecological service value of the ecological function zone in the Huaihe River Basin is 356.983 billion yuan, of which the ecological service value of vegetation is the highest at 148.096 billion yuan, which makes the greatest contribution to the ecological service of the Huaihe River Basin ecological function zone. This is because vegetation can better purify the air, retain moisture, prevent soil erosion, regulate the climate, and protect biodiversity. Rivers and lakes and other water systems are also of higher value for ecological services, because they can provide abundant water sources and aquatic products, and can also regulate climate [22]. Therefore, in terms of ecological compensation, investment in vegetation can be increased, and the value of ecological services in the Huai River Basin can be more effectively improved.

According to the carbon emission method, the ecological compensation value of the ecological function zone in the upper reaches of the Huaihe River Basin can be calculated. Among them, the field carbon source effect is 5.064 million tons, the carbon emission value is 1.384 billion yuan. The vegetation carbon sink effect is 263 million tons, and the carbon emission value is -71.947 billion yuan. The carbon source effect of construction land is 177 million tons, and the carbon emission value is 48.421 billion yuan. The total carbon emission value of the ecological function zone in the upper reaches of the Huaihe River Basin is -22.142 billion yuan. Therefore, from the calculation results, it can be seen that the fields and construction land are the main carbon emission methods of the ecological function zone in the upper reaches of the Huaihe River Basin, and they play a vital role in the carbon emission of the Huaihe River Basin. The vegetation can better reduce carbon emissions and provide support for protecting the ecological environment.

Ecological compensation measurement of the ecological function zone in the upper reaches of the Huaihe River Basin. Based on the statistical yearbooks of the provinces and counties and cities of the Huai River Basin, combined with data from the Huai River Basin resource bank, and data obtained from the research team's fixed-site field surveys and interviews in the Huai River Basin over the years, the ecological compensation efficiency was measured.

The Huaihe River Basin as a whole shows the phenomenon that the upstream development is slower than the downstream [23-24]. From the perspective of industrial structure, the proportion of employees in the primary industry is the highest in the upstream region and the lowest in the downstream region, reflecting the unevenness of the level of economic development from the side. In order for the downstream area to have good water resources, the upstream area must carry out ecological protection, and it is particularly important to carry out reasonable ecological compensation in the downstream area.

From the data in Figure 1, it can be seen that the proportion of people engaged in the primary industry in the upstream ecological function zone is relatively high, and the proportion of people engaged in the tertiary industry is low. According to the data in Figure 2, the average annual net income of rural residents is much lower than that of urban residents, and there is a large income gap between urban and rural residents. In order to ensure the ecological sustainability of the faster downstream areas, the upstream areas will inevitably need to reduce the development of energy-intensive industries, which will

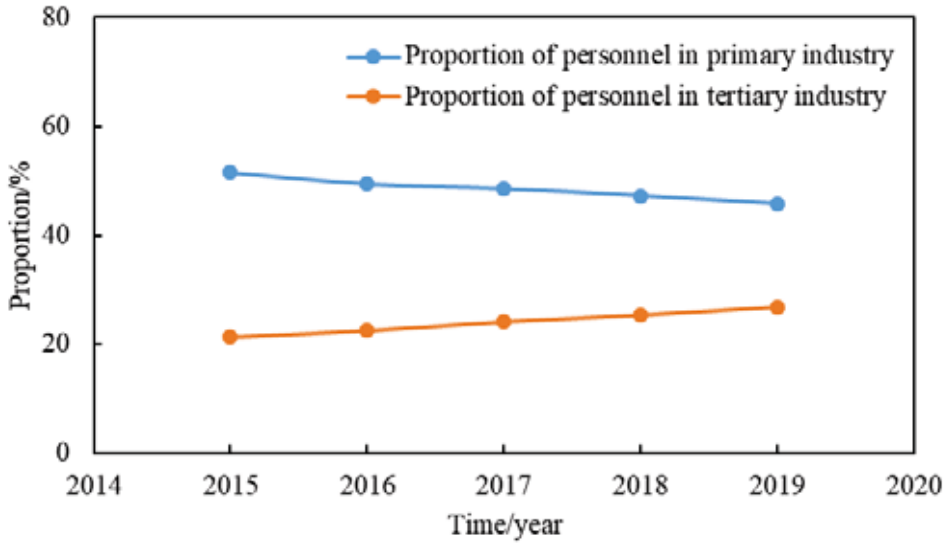

FIGURE 1
The proportion of employees in the primary and tertiary industries in the upper reaches of the Huaihe River Basin from 2015 to 2019.

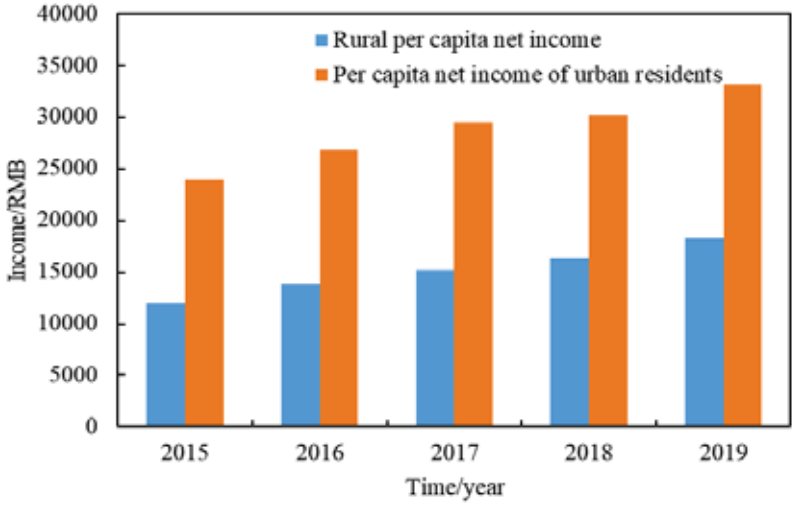

FIGURE 2
2018-2019 Per capita disposable income in the upper reaches of the Huaihe River Basin

lead to the imbalance of urban and rural development, which can be better compensated by reasonable ecological compensation measures It can be seen from Table 5 and Figure 3 that the efficiency of ecological compensation in the upper reaches of the Huaihe River Basin has shown an upward trend, indicating that in terms of ecological compensation, the upper reaches of the area pay more attention to it and have achieved certain results. According to the results of the comprehensive efficiency calculation, the ecological compensation efficiency is low, and the overall efficiency of the area still has a lot of room for improvement. Among the four dimensions, the efficiency of eco-environmental protection is the highest [25]. This is because the upstream area is located in the upper reaches of the Huai River Basin. The safety of downstream water sources must be guaranteed, which has a profound impact on the ecological environment of the downstream area. Economic efficiency is second, but the overall situation is also low, reflecting the region's "environmental priority" strategy. In order to ensure water safety in downstream areas, upstream areas have made great economic sacrifices. The low economic efficiency and ecological efficiency are also reflected in social efficiency [26]. The social efficiency measurement includes per capita net income, employment population growth rate, per capita disposable income rate growth rate, and per capita water resource share. The low social efficiency is directly reflected in people's lack of significant improvement in living standards. For the development of the downstream, the upstream has sacrificed a lot of its own development opportunities. Therefore, the "backfeeding" of the downstream area to the upstream area is particularly important [27]. The existence of the ecological efficiency compensation mechanism provides the possibility to solve this imbalance. Among the four dimensions, political efficiency is relatively low, which has a greater relationship with the level of economic development. In areas with high levels of economic development, people's participation in political life is significantly higher. Judging from the

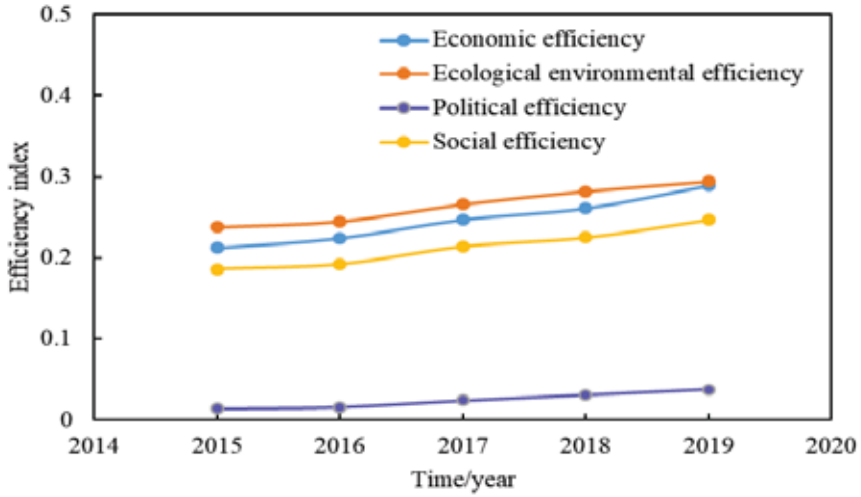

FIGURE 3
Trends of ecological compensation efficiency in the upper reaches of the Huaihe River Basin from 2015 to

TABLE 4
List of comprehensive efficiency measurement of ecological compensation

Dimension	Index
Economic efficiency (0.242)	GDP growth rate/% (0.024) Growth rate of added value of agricultural production/% (0.082) Growth rate of the tertiary industry/% (0.066) Resource consumption per unit GDP/yuan (0.015) Special compensation income/yuan (0.055)
Ecological environmental protection efficiency (0.211)	Industrial waste emission reduction rate/% (0.03) Returning farmland to forest area/mu (0.051) Percentage of environmental protection expenditure/% (0.071) Forest coverage rate/% (0.044) Soil erosion area/mu (0.015)
Political efficiency (0.0624)	Reduction rate of the number of ecological compensation policy formulation meetings/% (0.0281) Ecological compensation policy document reduction rate/% (0.0124) People's satisfaction/% (0.0219)
Social efficiency (0.385)	Per capita net income/yuan (0.104) Employment population growth rate/% (0.0832) Per capita disposable income growth rate/% (0.118) Per capita share of water resources/% (0.0798)

TABLE 5
Ecological compensation measurement results in the upper reaches of the Huaihe River Basin

Year	2015	2016	2017	2018	2019
Economic efficiency	0.212	0.224	0.247	0.261	0.289
Ecological environmental protection efficiency	0.238	0.245	0.266	0.282	0.294
Political efficiency	0.014	0.016	0.024	0.031	0.038
Social efficiency	0.186	0.192	0.214	0.225	0.247
Overall efficiency	0.1625	0.16925	0.18775	0.19975	0.217

law of political efficiency development in the past five years, the growth rate of political efficiency is the highest, which shows that with the popularization of the concept of rule of law in recent years and the improvement of people's lives, people's ideological level has gradually improved. According to the calculation results, the overall efficiency of the region is low, and the coordinated development of the region needs to be strengthened in the policy formulation process. At the same time, we must try our best to improve people's living standards, accelerate economic development, and appropriately increase the value of ecological compensation Kalacska, M., Sanchez-Azofeifa, G., Rivard, B., Calvo- Alvarado, J., Quesada, C. (2008) Baseline assessment for environ-mental services payments from satellite imagery: A case study from Costa Rica and Mexico. Journal of Environmental Management. 88(2), 348- 359

CONCLUSIONS

(1) The ecological service contribution of vegetation in the ecological function zone of the Huaihe River Basin is the largest, which is 148.096 billion yuan. It is necessary to increase the ecological compensation for vegetation.

(2) The ecological compensation value calculated by the carbon emission method shows that construction and is the main source of carbon emissions, with a carbon emission value of 48.421 billion yuan, and vegetation as a carbon sink can better reduce carbon emissions, with a reduction value of 71.947 billion yuan.

(3) The ecological compensation measurement of the ecological function area in the upper reaches of the Huaihe River shows that the efficiency of ecological environmental protection and economic efficiency are the focus of the efficiency of ecological compensation in this area. However, the overall efficiency of the region is relatively low, and it is necessary to focus on strengthening regional coordinated development in the policy formulation process.

ACKNOWLEDGEMENTS

This work was financially supported by the Social Science Innovation Development Research in Anhui Province of 2019 (Project Number: 2019CX110) and the Humanities and Social Sciences Research in Anhui Province of 2019 (Project Number: SK2019A0099).

REFERENCES

[1] Villarroya, A., Persson, J., Puig, J. (2014) Ecological compensation: From general guidance and expertise to specific proposals for road developments. Environmental Impact Assessment Review. 45, 54-62.

[2] Sierra, R., Russman, E. (2006) On the efficiency of environmen-tal service payments: a forest conservation assessment in the Osa Peninsula, Costa Rica. Ecological Economics. 59(1), 131-141.

[3] Kalacska, M., Sanchez-Azofeifa, G., Rivard, B., Calvo- Alvarado, J., Quesada, C. (2008) Baseline assessment for environ-mental services payments from satellite imagery: A case study from Costa Rica and Mexico. Journal of Environmental Management. 88(2), 348- 359.

[4] Pechanec, V., Vondrakova, A., Sterbove, L., Cudlin, P. (2020) Environmental data visualization: Stocks of the stored carbon in Czechia. Fresen. Environ. Bull. 29(3), 1630-1636.

[5] Li, W., Zhang, S., Lu, C. (2019) The semi-centennial timescale dynamic assessment on carbon emission trajectory determinants for Hebei Province within the new normal pattern shock. Science of the Total Environment. 689, 494-504.

[6] Yuan, K., Zhang, M., Gan, C., Chen, Y., Zhu, Q., Yang, H. (2020) Provincial Eco-Compensation of Carbon Based on the Target of Carbon Emission Reduction. Resources and Environment in the Yangtze Basin. 1, 21-29.

[7] Liu, C., Zhang, F., Zhang, H. (2020) Comparative analysis of off-site precast concrete and cast-in-place concrete in low-carbon built environment. Fresen. Environ. Bull. 29(3), 1804-1812.

[8] Li, Q. (2015) Basin water resources ecological compensation system and efficiency measurement. Wuhan: Huazhong Agricultural University (Dissertation).

[9] Sun, J. (2015) Study on the optimization of the measurement methods for the ecological compensation of the basin. Hefei: Anhui Agricultural University (Dissertation).

[10] Gao, H., Zhang, X., Liu, M., Gao, J., Wei, W. (2020) Research on Ecological Compensation Standard and Level for Key Ecological Functional Areas of the Huaihe River Source. Journal of Xinyang Normal University (Natural Science Edition). 33(2), 244-249.

[11] Birner, R., Wittmer, H. (2004) On the efficient boundaries of the State- The contribution of transaction costs economics to the analysis of decentralization and devolution in Natural Resource Management. Environment and Planning C: Government and Policy. 22(5), 667-685.

[12] Watzold, F., Schwerdtner, K. (2005) Why be wasteful when pre-serving a valuable resource A review article on the cost- effectiveness of European biodiversity conservation policy. Biological Conservation. 123, 327-338.

[13] Ferraro, P. (2008) Asymmetric information and contract design for payments for environmental services. Ecological Economics. 65, 810-821.

[14] Huan, Y., Wang, Y., Liu, S., Hou, F. (2015) Value Measure and Ecological Compensation Research of Main Carbon Sink Factors Affected by Coal Mining. Forestry Economics. 37(4), 88-93.

[15] Chen, W., Yu, X., Xiong, X. (2018) Study on the measurement of ecological compensation efficiency of government led River Basin - A case study of major coastal cities in the Yangtze River Economic Belt. Jianghuai Tribune. 289(03), 43.

[16] Xie, G., Xiao, Y., Zhen, L., Lu, C. (2005) Study on ecosystem services value of food production in China. Chinese Journal of Eco-agriculture. 13(3), 10-13.

[17] Sakin, E., Yanardag, I. (2019) Effect of application of sheep manure and its biochar on carbon emissions in salt affected calcareous soil in Sanliurfa Region SE Turkey. Fresen. Environ. Bull. 28(4), 2553-2560.

[18] Li, J., Guo, Q. (2012) Estimation and temporal and spatial distribution of net primary productivity of terrestrial vegetation in Henan Province. The 27th Annual Meeting of China Meteorological Society. 1-9.

[19] Villarroya, A., Puig, J. (2010) Ecological compensation and environmental impact assessment in Spain. Environmental Impact Assessment Review. 30(6), 357-362.

[20] Brown, M., Clarkson, B., Barton, B., Joshi, C. (2013) Ecological compensation: an evaluation of regulatory compliance in New Zealand. Impact Assessment and Project Appraisal. 31(1), 34-44.

[21] Nentwig, W., Frank, T., Lethmayer, C. (1998) Sown weed strips: Artificial ecological compensation areas as an important tool in conservation biological control. In Conservation Biological Control. 133-153.

[22] Simmonds, J., Sonter, L., Watson, J., Bennun, L., Costa, H., Dutson, G., Kiesecker, J. (2020) Moving from biodiversity offsets to a target-based approach for ecological compensation. Conservation Letters. 13(2), Article ID: 12695.

[23] Ma, J. (2019) Study on innovation path of China's carbon emission trading market construction. Fresen. Environ. Bull. 28(10), 7382-7387.

[24] Yu, A., Lin, X., Zhang, Y., Jiang, X., Peng, L. (2019) Analysis of driving factors and allocation of carbon emission allowance in China. Science of The Total Environment. 673, 74-82.

[25] Koh, N., Hahn, T., Ituarte-Lima, C. (2017) Safeguards for enhancing ecological compensation in Sweden. Land Use Policy. 64, 186-199.
[26] Meineri, E., Deville, A., Grémillet, D., Gauthier-Clerc, M., Béchet, A. (2015) Combining correlative and mechanistic habitat suitability models to improve ecological compensation. Biological Reviews. 90(1), 314-329.
[27] Burgio, G., Ferrari, R., Pozzati, M., Boriani, L. (2004) The role of ecological compensation areas on predator populations: an analysis on biodiversity and phenology of Coccinellidae (Coleoptera) on non-crop plants within hedgerows in Northern Italy. Bulletin of Insectology. 57, 1-10.

Received: **28.09.2020**
Accepted: **16.11.2020**

CORRESPONDING AUTHOR

Yu Du
School of Economics and Management
Anhui University of Science and Technology
232001 Huainan Anhui – China

e-mail: tomato8521@sina.com

© by PSP Volume 30– No. 05/2021 pages 5002-5014 Fresenius Environmental Bulletin

PERFORMANCE EVALUATION OF CMIP5 MODELS FOR PRECIPITATION AND TEMPERATURE OVER HAIHE RIVER BASIN, CHINA

Hao Yang[1], Xiaofeng Chen[2], Ying Feng[3], Wei Jiao[4], Tiezhu Yan[5,*]

[1]Beijing Academy of Social Sciences, Beijing 100101, China
[2]State Grid Economic and Technological Research Institute Co., Ltd., Beijing 102209, China
[3]State Key Laboratory of Water Environment Simulation, School of Environment, Beijing Normal University, 19 Xinjiekouwai Street, Beijing 100875, China
[4]Shandong Provincial Key Laboratory of Water and Soil Conservation and Environmental Protection, College of Resources and Environment, Linyi University, Linyi 276000, China
[5]Institute of Agricultural Resources and Regional Planning, Chinese Academy of Agricultural Sciences, Beijing 100081, China

ABSTRACT

The quantitative evaluation of GCMs' performance is vital to reduce the uncertainty of regional climate change impact research. A cascade progressive-like analysis approach is applied to evaluate the five phase of the Coupled Model Intercomparison Project (CMIP5) models' ability by comparing the models' outputs with ground observations (i.e., precipitation and temperature) over the Haihe River Basin from 1960 to 2004. The results show that for the chosen seventeen GCMs after preliminary screening, all models can reproduce the intra-annual characteristics of temperature and precipitation well, and show much better agreement with temperature than precipitation. However, the majority of the models tend to underestimate the annual mean temperature, with a mean underestimation of 0.34-2.82℃. For precipitation, all models overestimate the annual mean precipitation, with a mean overestimation of 11%-97%. The step of performance evaluation for large-scale atmospheric variables and preliminary screening of models carried out before performance evaluation for ground climate variables can reduce uncertainties from the subjective selection of model and model error between large-scale atmospheric variables (i.e., relative humidity at 500hPa and 850hPa) and ground precipitation. Overall, the five models, namely, HadGEM2-ES, CESM1-BGC, MPI-ESM-LR, CNRM-CM5 and ACCESS1.3, are recommended as optimal choice for regional impact studies over the HRB.

KEYWORDS:
CMIP5 models, Haihe River Basin, temperature and precipitation, performance evaluation, large-scale atmospheric variable

INTRODUCTION

In term of the impact of climate change on earth system, the hydrological cycle is of particular concern due to its severe consequences for societies and ecosystems [1-4]. For climate change impact research, General Circulation Models (GCMs) are the primary instrument available for simulation and projection of climate change, and have been applied extensively to the research on the response of natural system to future climate change [5-6]. However, the reliability of GCMs is subject to three distinct sources of uncertainties, stemming from internal variability, scenario uncertainty and model uncertainty [7-8]. Although complexity and resolution of GCMs have been gradually increasing and CMIP5 models have been proved to improve the simulation of precipitation and temperature in different regions [9-12], the uncertainty of their projections still remains large [13-14]. It is crucial, therefore, to evaluate the performance of GCMs, both individually and collectively, in the application for the regional impact studies which is sufficiently credible for policy and decision-making on adaptation to and mitigation of climate change [15-16].

It is widely accepted that the agreement of the results from models with present observations is the only feasible way to build confidence for the application of the model [17-18]. In general, the performance of individual model depends on the climate variables concerned, geographical region, evaluation approach and evaluation metrics. At present, in addition to the common climate variables concerned (i.e., precipitation and temperature), some large-scale atmospheric variables are also considered [19-22]. For models to predict future climate conditions reliably, not only must they accurately simulate the mean state of the current climate system, they should also skillfully simulate changes of the climate system, such as annual cycle, interannual variability, trend and so on [23]. Hence, this paper aims at providing a comprehensive performance evaluation of CMIP5

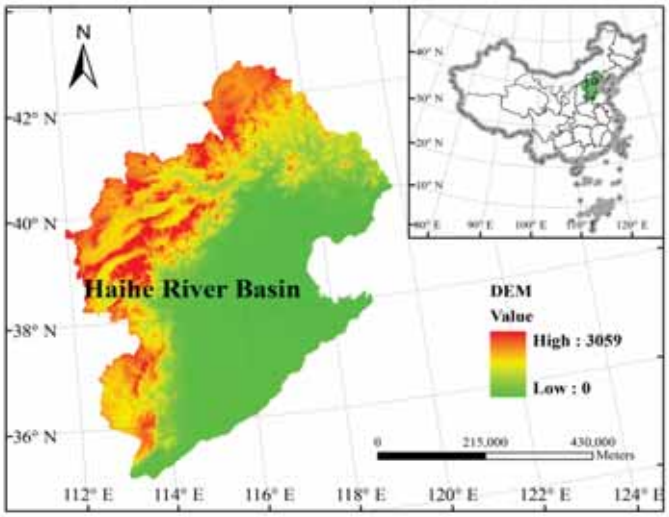

FIGURE 1
Location of the Haihe River Basin

models by comparing models' outputs and corresponding observations at monthly time-scale for the period 1961-2004 in the HRB, China.

MATERIALS AND METHODS

Study area. The Haihe River Basin (HRB), stretching between 112-120°E and 35-43° N, covers an area of approximately 31.8×10^4 km^2, which accounts for 3.3% of the total area of China. The elevation of the basin varies between 100-3,059m above mean sea level. The basin comprises the mountains and plateaus in the north and west occupying nearly 60% of the total area, and the North China Plain in the east and south occupying the remaining 40% (Figure 1). All rivers in the basin flow westward and drain into the Bohai Sea. The basin is located in the transition zone from arid to humid climate in China. The predominant climate is the Asian Monsoon climate characterized by cold and dry winters and hot and rainy summers. The multi-year average rainfall in the basin, 75% of which mainly occurs during the period from July to September, ranges from 350 to 750 mm, and shows the trend that gradually decreases from southeast to northwest; the average annual temperature varies between -4.9 and 15℃ [24-25].

Data sources. The simulations and observations were at monthly time-scale and the study period was from 1961 to 2004. The observation data used in this study includes the following threefold: 1) The observed gridded dataset of surface air temperature and precipitation (0.5°×0.5° grid) was derived from the China Meteorological Administration (available at http://cdc.cma.gov.cn/home.do). The method of spatial interpolation used in data processing was the Thin Plate Smoothing Spline, and the quality of the dataset was verified by cross-validation and error analysis. Compared to other gridded dataset, such as the dataset of the Climatic Research Unit at University of East Anglia, UK, the advantage of this dataset is that it is more appropriate to application in China because all existing meteorological stations were used to generate the gridded dataset. 2) The monthly large-scale atmospheric variables, derived from the National Center for Environmental Prediction/National Center for Atmospheric Research (NCEP/NCAR) Reanalysis Project, was used as a reference to carry out the evaluation of historical simulation of CMIP5 models. 3) The chosen GCM outputs with respect to the variables of interest are derived from the PCMDI (available at http://pcmdi9.llnl.gov/esgf-web-fe/). Detailed information on these models can be found in The Coupled Model Intercomparison Project (CMIP). In CMIP5, the historical run was mainly performed from 1850 to 2005, and the CMIP5 includes 42 models.

Due to the relatively small area for the HRB (only 5 grids with a spatial resolution of 2.5°×2.5°), and avoiding the error introduced by the interpolation method, the performance of CMIP5 models was evaluated by comparing the simulation of areal precipitation and temperature along with relative humidity at 500hPa, 850hPa (hereafter, hur500 and hur850, respectively) by the CMIP5 models and the observations in the HRB.

Methodology. A method adopted for evaluating GCMs' performance in this study is a cascade progressive-like analysis approach, and includes preliminary screening of models, performance evaluation of large-scale atmospheric variables and ground observational variables (i.e., precipitation and surface mean temperature), and

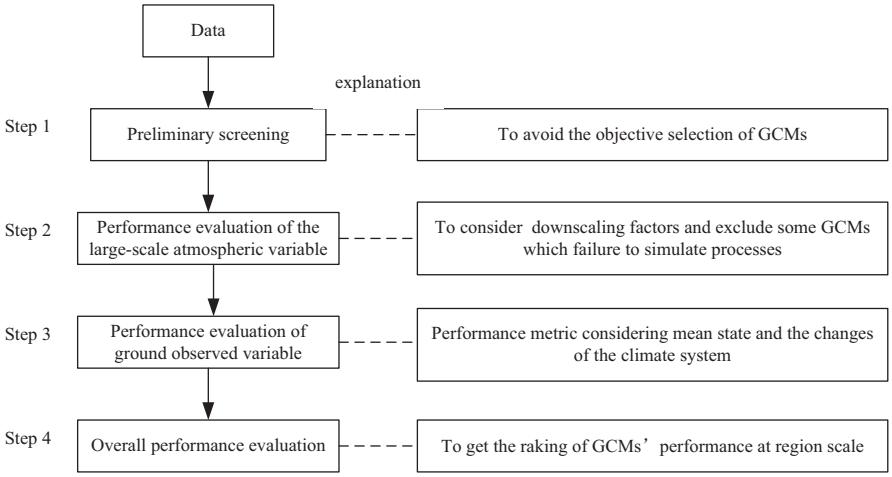

FIGURE 2

Flowchart of the method used for evaluating the performance of GCMs

overall performance evaluation. The detained description of each step is illustrated under next subsection and the flowchart of the method is showed in Figure 2.

Preliminary screening of GCMs. The GCMs, which perform well at the large scale, provide a guarantee for the following performance evaluation of GCMs at regional and local scales [26]. Therefore, GCMs' simulation ability at the large scale should be assured before the application of GCMs in regional and local scales. The main purpose of preliminary screening of GCMs, on the basis of the exiting research results on the simulation ability of GCMs at the large scale, is to ensure that the subsequent regional and local performance evaluation of climate models possesses higher reliability by avoiding subjective selection of a subset of GCMs. Moreover, it can effectively lessen the workload for regional and local performance evaluation for all GCMs in the regional scale.

Performance evaluation of large-scale atmospheric variables and ground observed variables. Generally, the common climate variables in impact studies of climate change, which is the representation of climate change, are surface air temperature and precipitation and are always used to assess the simulation performance of GCMs. Some large-scale atmospheric variables (e.g., mean sea level pressure) are also adopted. It is an acknowledged fact that the simulation ability of GCMs for precipitation is worse than that for temperature [21, 27]. Given that the precipitation possesses larger impact on the earth system, selection of GCM which have better simulation ability for precipitation is helpful to reduce uncertainty of the impact studies(for example, impact studies on regional hydrological cycle). Although the GCMs are capable of realistically simulating the major physical processes of climate system, the model error for the large-scale atmospheric variable exits, further influencing ground climate variables. Therefore, hur500 and hur850 are chosen as large-scale atmospheric variables to assess simulation performance of GCMs, for which are the main source of water vapour for precipitation in the HRB, and are also the common predictors (i.e., large-scale atmospheric variables) for statistical downscaling of precipitation [28]. Different from the previous studies [19, 21, 29], the evaluation of performance of GCMs for the large-scale atmospheric variables in this study is conducted as an independent step before performance evaluation for the ground observational climatic variable in this study, rather than just with gourd climatic variables as a whole for performance evaluation of GCMs.

Overall performance evaluation. In this study, the overall performance of GCMs, identified after the preliminary screening of GCMs and performance evaluation for large-scale atmospheric variables, are evaluated on the basis of the multi-criteria score-based method [21]. The specific evaluation process is depicted as follows: Firstly, a rank score (RS) value ranging from 0 to 9 is computed for each individual evaluation metrics based on the equation (1):

$$RS_i = \frac{x_i - x_{min}}{x_{max} - x_{min}} \times 9 \qquad (1)$$

where x_i is the relative error or statistic values between the modeled and observed evaluation metrics for the i th GCM, xmax and xmin represent the maximum and minimum value of relative error or statistic value. Secondly, the total RS value of the individual variable of interest for the specific GCM is product of each individual evaluation metrics' RS and their weight, and the weight for each evaluation metrics is determined according to the previous

TABLE 1

Evaluation metrics and its mathematical methods and weights.

Evaluation metrics	Mathematical Method	Weights
Mean	Mean	1.0
Standard deviation	Standard deviation	1.0
Temporal variation	NRMSE	1.0
Monthly distribution	Correlation coefficient	1.0
Annual trend and its magnitude	Mann-Kendall test	0.5
	Sen's slope estimator	0.5
Probability density functions	S_{score}	1

study [21] and is showed in Table 1. Finally, the overall performance of GCMs, considering multi-performance indices, is assessed by means of the sum of the RS of each performance indices (i.e., climatic variable and large-scale atmospheric variable).

The choice of performance indices and evaluation metrics. It is a fundamental step to choose the performance indices and evaluation metrics for evaluating GCMs' credibility in impact modeling of climate change. As shown in the previous subsection, the precipitation, temperature, hur850 and hur500 are chosen as performance indices to assess the GCMs' performance. Meanwhile, the six evaluation metrics, which can present the mean state of the current climate change and changes of the climate system, are chosen to provide a more comprehensive assessment of the GCMs and to avoid a biased assessment due to individual performance metrics. The chosen evaluation metrics in this study is listed in Table 1. The specific equation of these six metrics could be found in the previous studies [21, 30-34].

RESULTS

Preliminary screening of GCMs. Based on Gleckler' research result [17], some GCMs with relatively poor simulation performance could be excluded in the light of the research purpose. In this study, the future regional or local precipitation and surface temperature, which are derived from GCMs' output by mean of downscaling technology, will be applied to regional impact study of climate change on watershed hydrological cycle. In additional, most of the above mentioned thirteen climate variables are always used as the candidate predictor adopted by statistical downscaling technology for resolving the scale mismatch between the results supplied by the GCMs and that required by relevant models. Therefore, the model, which has the ability of better presentation of two thirds of climate variables, is chosen to be the candidate model for subsequent evaluation over the HRB. Eventually, seventeen CMIP5 models were chosen for further performance evaluation in the HRB.

Performance evaluation of large-scale atmospheric variables. The performance of CMIP5 models for hur500 and hru850 is shown in Figure 3. It shows the multi-annual mean hur500 and hur850 in the HRB are 40.87 and 52.62%, while the variation of GCMs is from 39.34 to 51.74% (hur500) and 42.34 to 64.06% (hur850) with median and mean values of 46.5 and 45.16%, and of 51.32 and 52.08%, respectively. Meanwhile, most of GCMs overestimated annual mean hur500 and hur850. The highest bias of estimate for annual mean hur500 is showed with CMCC-CMS (GCM 10), and for hur850 with CESM1-WACCM (GCM 8).

Overall, all GCMs can reproduce the annual cycle of the hur500 and hur850, but the annual cycle of monthly hur850 is simulated more accurately than that of hur500 (Figure 4). For hur850, the correlation coefficient clustered primarily in the range of 0.77-0.94, with a minimum correlation coefficient of 0.07 for BCC-CSM1.1 (GCM 3), which performs poorly. For hur500, the correlation coefficient clustered primarily in the range of 0.67 and 0.88, with a minimum correlation coefficient of -0.30 for CESM1-CAM5 (GCM 7). It is obvious that most GCMs for hur500 overestimated in ascending stage and underestimated in descending stage, conversely, slightly underestimate in the overall stage for hur850.

Figure 5 depicts that empirical cumulative probability distributions for the observed and GCM monthly mean hur500 and hur850 in the study area. Overall, for hur500 and hur850, 17 GCMs did not simulate the probability distribution. For hur500, eight out of 17 GCMs simulated probability distribution close to the observation, and the others do not capture the probability distribution; for hur850, GCMs' ability of simulation of probability distribution is lightly better than that for hur500.

According to the mathematical formula of the score-based method, it is found that the lower the ranking score of GCMs is, the better the simulation performance of GCMs is. The ranking score for hur500, hur850 and the combination of the above two variables in the simulation performance of GCMs is given in Figure 6. Both ACCESS1.0 and HadGEM2-CC (GCM 1 and 13) have the highest

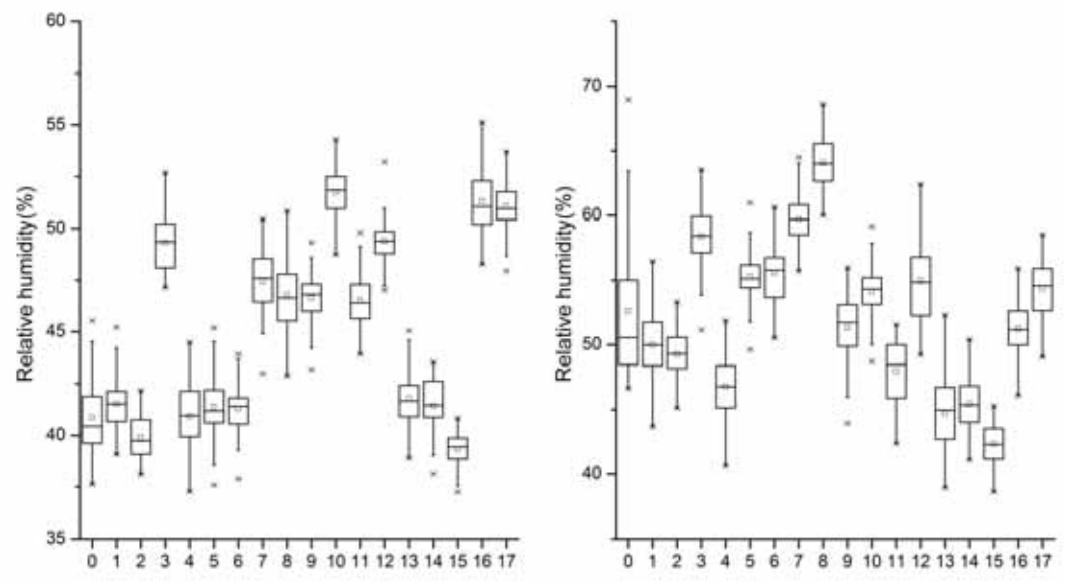

FIGURE 3
Box plots of annual mean relative humidity at 500hPa (left) and 850hPa (right) of observed and simulated by GCMs. The abscissa depicts observations (0) and the number of GCMs (1~17).

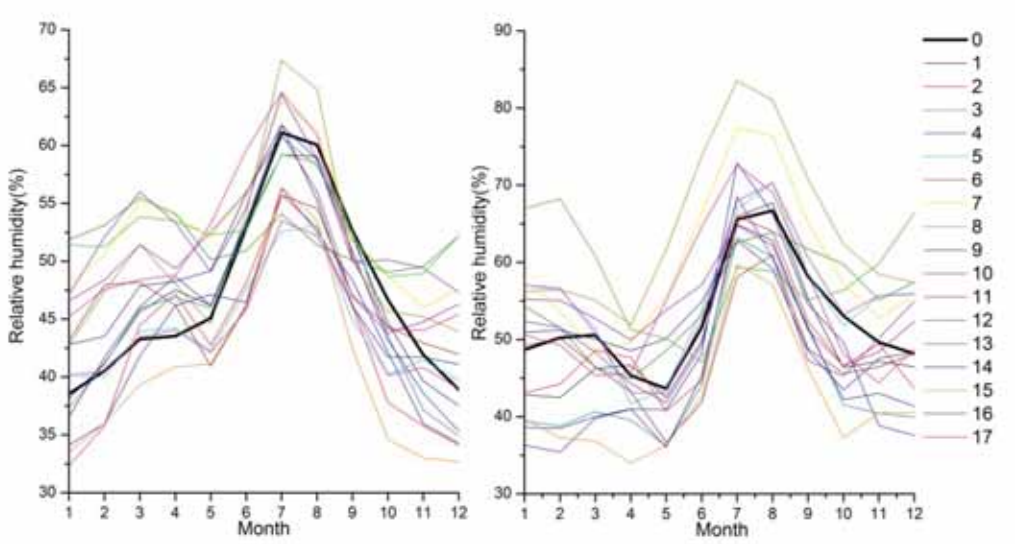

FIGURE 4
Annual cycle of observation (thick black line) and GCMs' simulation (thin colored line) of monthly mean relative humidity at 500hPa (left) and 850hPa (right).

ability to simulate historical characteristics for the change of hur500 atmospheric variable. However, the MPI-ESM-LR and MIROC5 (GCM 16 and 17) have the highest ability for simulation of hur850. From the results of overall evaluation for both large-scale atmospheric variables, ACCESS1.0 (GCM1) performs the best.

The BCC-CSM1.1, CESM1-CAM5, CESM1-WACCM, CMCC-CMS, GFDL-ESM2M, MIROC4h (GCM3, 7, 8, 10, 12 and 15) is the last six one in the list of ranking scores of GCMs (Figure 6). They performed more poorly in the simulation of hur500 and hur850 than the other GCMs, for higher than average ranking scores of the combination of the above two atmospheric variables. These six GCMs were, therefore, excluded in the subsequent consideration of the simulation ability of GCMs for precipitation and surface temperature. Specifically, GFDL-ESM2M and MIROC4h (GCMs 12 and 15) performed poorly in simulations of hur500 and hur850; however, they performed relatively well in simulation of precipitation. This implied that there was a simulation distortion for GCMs in some regions so that the performance of some GCMs which performed well in the simulation of precipitation, performed poorly in simulations of the process of water vapour circulation at these regions, this verifying that the performance evaluation of large-scale atmospheric variables as the intermediate process is essential. Moreover, it should be pointed out that

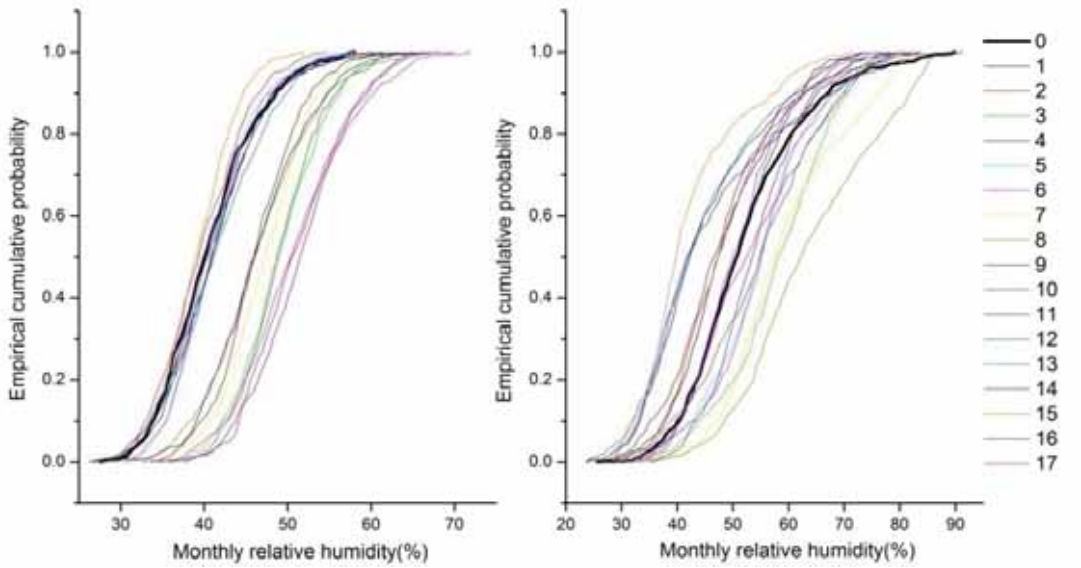

FIGURE 5
Empirical cumulative probabilities of observed (thick black line) and simulated by GCMs (thin colored line) monthly relative humidity at 500hPa (left) and 850hPa (right)

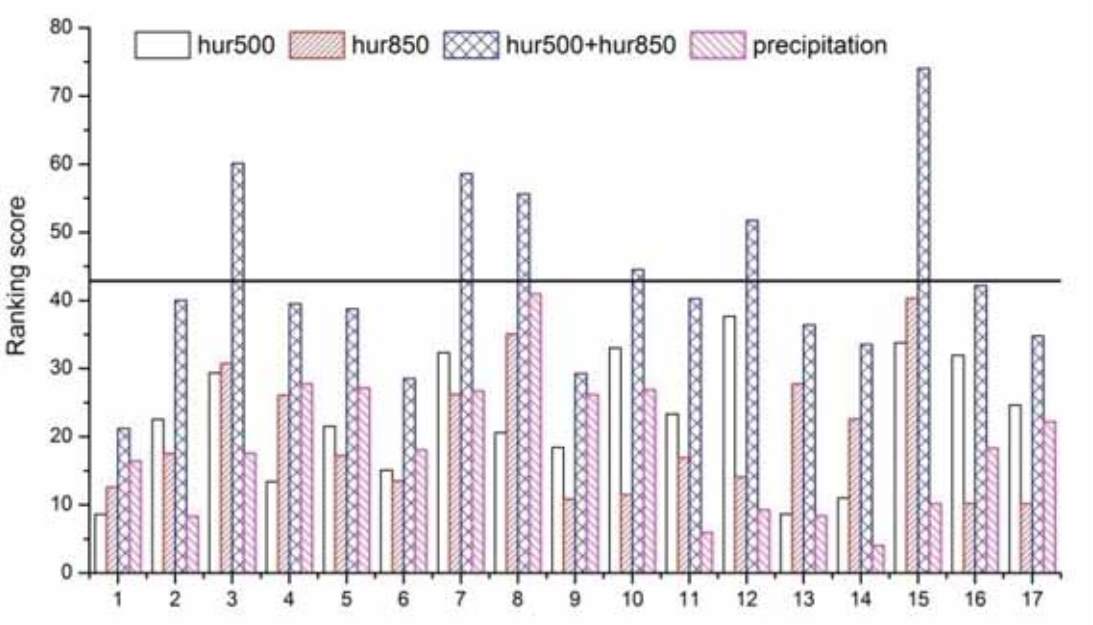

FIGURE 6
Ranking score for relative humidity at 500hPa and 850hPa, the combination of the above two variables and precipitation. The horizontal thin line shows the mean ranking score for the combination. The abscissa depicts the number of GCMs.

Figure 6 also showed that the ranking score of the combination of hur500 and hur850 versus that of the precipitation was not inconsistent for some GCMs. Therefore, the performance evaluation of large-scale atmospheric variables as intermediate processes is also necessary to reduce uncertainty of GCMs' application and the exclusion of the six GCM whose ranking score were at the bottom of the list in this study is essential and sensible for the reduction of uncertainty.

Performance evaluation of ground observed variables. The performance of precipitation. The multi-annual mean precipitation in the HRB is 527.62mm, while the variation of GCMs is from 544.79 to 1038.42mm with median and mean values of 678.56 and 709.11mm, respectively. Figure 7 depicts that the box plot of the annual mean precipitation simulated by 17 GCMs and observed for the period of 1961-2004. It shows that all the GCMs overestimated annual mean precipitation, and that CESM1-WACCM (GCM 8) has the highest bias of estimate for annual mean precipitation. The standard deviation of annual precipitation for the GCM simulations vary from 73.96 to 162.58mm compared to the observed value of 90.48mm.The

NRMSE values of annual precipitation range from 0.67 to 1.27.

The GCMs' ability to simulate an actual annual cycle of precipitation is an important measure for the performance assessment. Figure 8 compares the simulated monthly distribution of mean precipitation to observation for the period 1961-2004. It shows that the monthly distribution of mean precipitation simulated by GCMs has a higher variation and that nearly all GCMs overestimated the monthly precipitation within the year, except in July and August for some GCMs. All GCMs can also capture the annual cycle of precipitation, with a minimum correlation coefficient of 0.86 for CMSS-CMS (GCM 10), and all GCMs simulated the annual pattern of precipitation, i.e., the precipitation is not distributed evenly and maximum precipitation occurs mainly from June to September. For annual cycle of precipitation, the CESM1-WACCM (GCM 8) has the relative highest error.

Observed annual precipitation has a statistically insignificant decreasing trend for 1961-2004 with a Kendall Z statistics of -1.41. Different GCMs present different change trend of precipitation, with Z statistics ranging from -1.69 to 1.63. Nine out of 17 GCMs have the same trend as that of observed annual precipitation. The trend magnitude of observed annual precipitation is -1.66mm/a, while that of GCMs range from -2.12 to 2.11mm/a. The median and mean values of trend magnitude simulated by GCMs are -0.24 and -0.07mm/a, respectively.

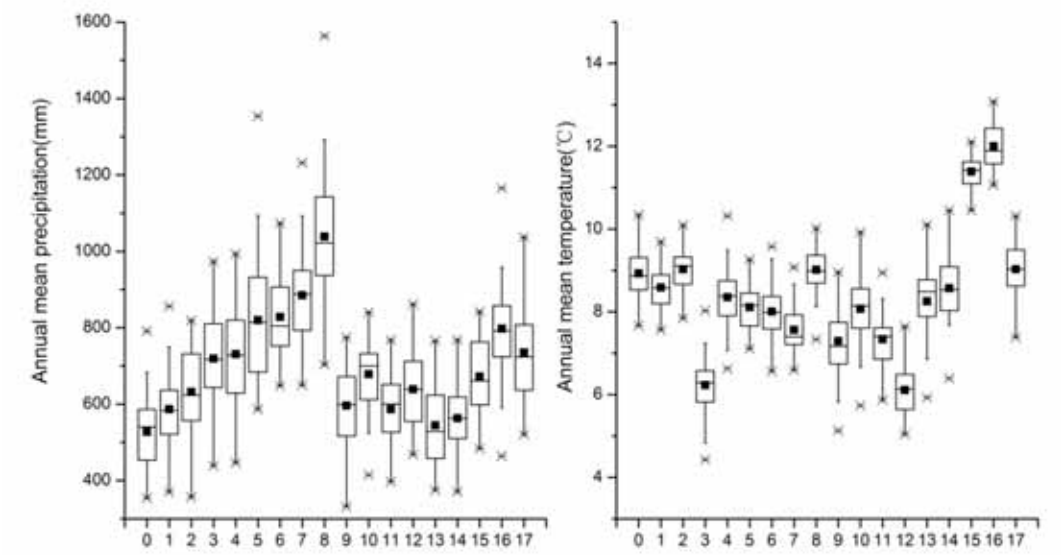

FIGURE 7
Box plots of annual mean precipitation (left) and temperature (right) as observed and simulated by GCMs during 1961-2004

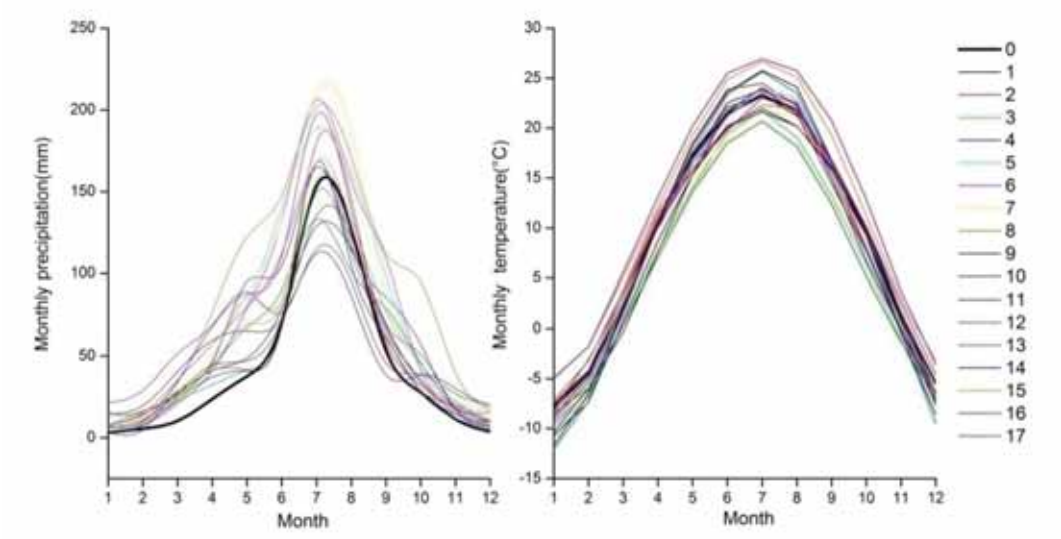

FIGURE 8
Annual cycle of observed (thick black line) and GCMs (thin colored line) monthly precipitation (left) and temperature (right)

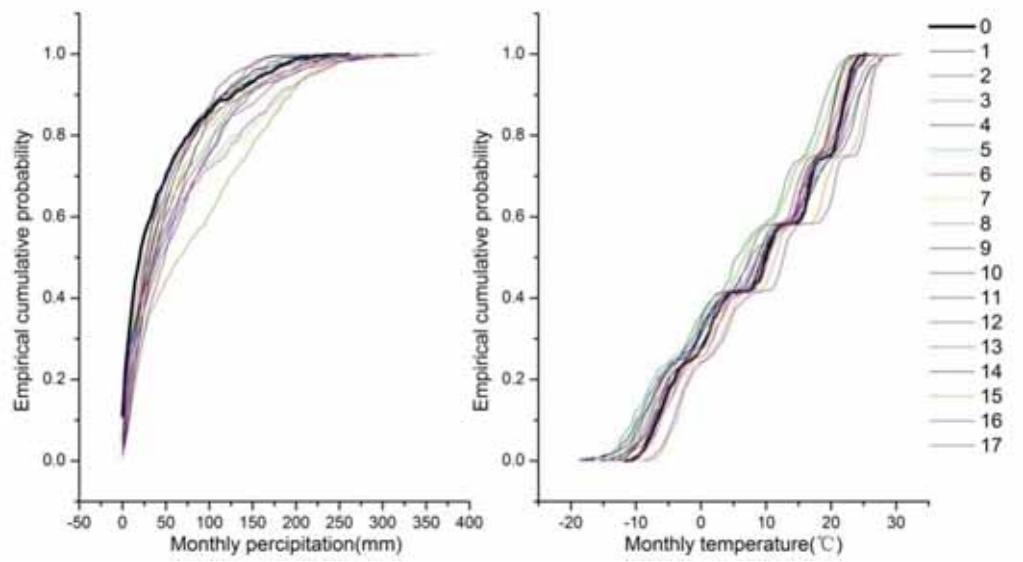

FIGURE 9
Empirical cumulative probabilities of observed value (thick black line) and simulated by GCMs (thin colored line) monthly precipitation (left) and temperature (right)

Figure 9 depicts the empirical cumulative probability distributions for the observed and GCM monthly mean precipitation over the HRB. Overall, for the probability distribution of the occurrence of precipitation simulated by 17 GCMs, there are obvious difference between more than 50mm and lower than 150mm, with CESM1-WACCM (GCM8) performing relatively poorly. The Sscore of 17 GCMs is mainly from 0.75 to 0.80.

According to the total ranking score in Figure 10, the derived results with respect to the simulation ability of 17 GCMs for precipitation in the HRB demonstrated that the HadGEM2-ES (GCMs 14) is the best relative performer, and the CESM1-WACCM (GCMs 8) performs the worst.

The performance of temperature. The multi-annual mean surface temperature in the HRB is 8.93℃, while the variation of GCMs is from 6.11 to 12℃ with median and mean values of 8.25 and 8.4℃, respectively. According to Figure 7, the results show that most models, 12 out of 17 GCMs, tend to underestimate the annual mean surface temperature over the basin relative to observations. Conversely, the others overestimate it. It is noted that the MIROC4h model and MIROC5 model (GCMs 15 and 16) show the maximum bias of estimate for annual mean surface temperature compared to the observation. The standard deviations of annual surface temperature for the GCMs' simulations vary from 0.4 to 0.89 compared to the observed value of 0.6. Moreover, the NRMSE value of annual surface temperature ranges from 0.18 to 0.33.

Although all GCMs can reproduce the annual cycle of the surface temperature, with a minimum correlation coefficient of 0.99 showing that the GCMs simulated well the change characteristics of mean surface temperature within a year (i.e. a single peak in summer), the simulation value of annual cycle of surface temperature fluctuated above and below the observation in the range of ±2℃ and most models underestimated monthly mean surface temperature in winter (Figure 8). Generally, the models showed much better agreement with the observed surface mean temperature than precipitation.

For the annual surface temperature, all GCMs show an upward trend for the period 1961-2004, as do observation. The 17 GCMs' Z-statistics varies from 0.92 to 5.25 with median and mean values of 2.44 and 2.81, respectively, while that of observation is 4.08. The 15 GCMs underestimated the surface temperature trend and the other two GCMs overestimated the current climate. The magnitude of the observed annual surface temperature trend is 0.03℃/a, most GCMs underestimate change magnitude of temperature, with a range between 0.01 and 0.03℃/a. The observed annual surface temperature trend was statistically significant at the 95% probability level, while 15 out of 17 GMCs also showed a statistically significant trend.

Overall, 17 GCMs simulated the probability distribution close to observation (Figure 9). Nevertheless, the variation of Sscore primarily focused in the range of 0.5-0.7. The MIROC4h model and MIROC5 model (GCMs 15 and 16) appeared to be the relatively weak with low Sscore values.

In summary, according to the total ranking score in Figure 10, the derived results with respect to the simulation ability of the 17 GCMs for surface temperature in the HRB demonstrated that the MPI-ESM-LR (GCMs 17) is the best relative performer, and the MIROC4h (GCMs 15) performs the worst.

After performance evaluation of CMIP5 models for the intermediate process (i.e., lager-scale atmospheric variables), the remaining eleven CMIP5

models are assessed to validate the simulation of ground observed variables, including surface temperature and precipitation. From the performance of the CMIP5 models in the simulation of precipitation and temperature, we concluded that HadGEM2-ES (GCMs 14) is the best for precipitation simulation, while MPI-ESM-LR (GCM 17) is the best for temperature simulation. It also shows that for all GCMs the result of precipitation simulation is inferior to that of temperature.

Overall performance evaluation. After preliminary screening, performance evaluation of intermediate process and ground observation variables, the overall performance evaluation of GCMs for surface temperature and precipitation was conducted by means of summing the ranking scores of surface temperature and precipitation.

Figure 11 presents the rank of overall performance evaluation of the CMIP5 models for surface temperature and precipitation in the HRB. Due to the limited number of GCMs adopted for the research on climate change, the five top ranked GCMs, which have the higher capability of simulating the current climate condition, are recommended as optimal choice for studies on climate change in the HRB. They were HadGEM2-ES, CESM1-BGC, MPI-ESM-LR, CNRM-CM5 and ACCESS1.3 (GCM 14, 6, 17, 11 and 1), respectively.

DISCUSSION

The choice of GCMs is a major contributor to uncertainty in the modeling chain of climate change impact research [35-36], so the effective reduction of uncertainty caused by the selection of GCMs is vital to ensure confidence for end user in the use of models in regional application. Thus, the five phase of the Coupled Model Intercomparison Project (CMIP5) models' ability for ground observations (i.e., precipitation and temperature) are evaluated over the Haihe River Basin (HRB) for the period 1960-2004 from the perspective of simulation of the mean state and variability of climate system.

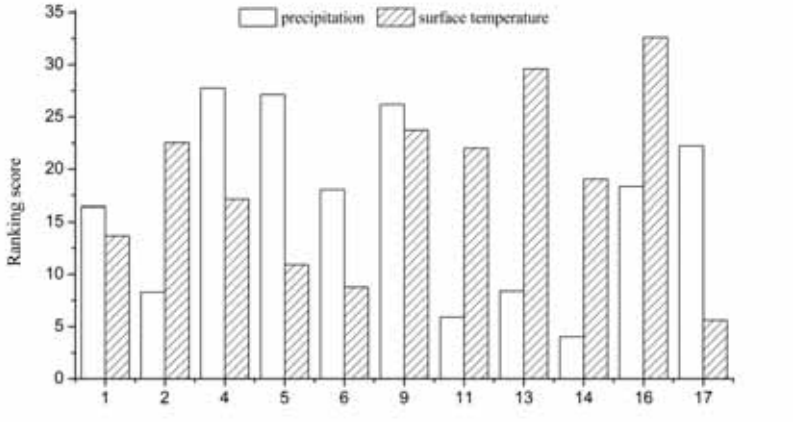

FIGURE 10
Overall ranking score of performance evaluation of GCMs. The abscissa depicts the number of GCMs.

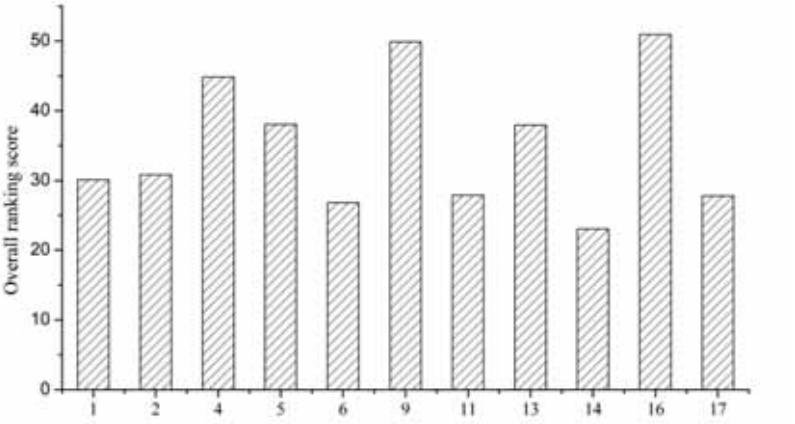

FIGURE 11
Overall ranking score of performance evaluation of GCMs. The abscissa depicts the number of GCMs.

This study shows that all chosen models can reproduce the intra-annual characteristics of surface air temperature and precipitation and the result of precipitation simulation is inferior to that of temperature. In addition, the majority of the GCMs tend to underestimate the annual mean temperature. Although all models show increasing trend as same as the observation, the majority of model show cold bias and underestimate the magnitude of warming trend. The result is consistent with the previous research in China [37]. For precipitation, all models overestimate the annual mean precipitation over the HRB. The precipitation over the HRB is mainly influence by the East Asian summer monsoon. Because the Ease Asian summer monsoon has weakened since the end of 1970s [38], the precipitation shows a decreasing trend during the period 1961-2004. For CMIP5 models, nine models show the same decreasing trend and the great difference for change magnitude of precipitation trend exit. Meanwhile, probability distribution of the occurrence of precipitation are different between more than 50mm and lower than 150mm.

The method used in this study including preliminary screening and performance evaluation for large-scale atmospheric variable can reduce uncertainty of the following aspects to identify model credibility with more confidence: 1) uncertainty caused by the subjective selection of GCM; 2) uncertainty due to model bias between atmospheric processes presented by large-scale atmospheric variable and ground observational variables. The atmospheric water vapor content and transportation have the important role for regional precipitation occurrence and precipitation amount. The water vapor content and transportation, in turn, is determined by the combined contributions from thermodynamic (specific humidity) and dynamic (wind) factors [39]. Thus, hur850 and hur500 are also evaluated to performance of models in this study because the precipitation is paid more attention in subsequent impact studies of climate change on hydrological cycle over the HRB. The obvious model bias between water vapor content presented by hur850 and hur500 and regional precipitation exist. The models which have big model bias should be excluded to reduce uncertainty for subsequent application in impact studies. It should be noted that some other large-scale atmospheric variables can be chosen to evaluate GCMs' credibility, such as sea pressure level, geopotential height and wind speed [21-22, 29, 40]. Meanwhile, the mean state of climate system research has largely ignored effects of atmospheric circulation on climate variability [41]. Hence, evaluation metrics presenting mean state and variability of climate system should be used to more systematically assess the performance of GCMs.

Although it is advisable to remove the models that seriously fail to meet observational constraints on large scales [42], in the preliminary screening of GCMs in this study, due to the lack of the literature relevant to the performance evaluation of all CMIP5 in China or Asia, the simulation ability of every CMIP5 model at global scale is also an option to exclude some CMIP5 models that perform relative poorly. The above result may reasonably be used to preliminarily evaluate model performance in regional application within the scope of Pacific Northwest USA. Therefore, it is essential to conduct the performance evaluation of GCMs at continental scale for regional climate change impact research.

This study also demonstrated again that different GCMs present different simulation ability and none of GCMs can perform well for all used performance indices and evaluation metrics. In addition, the amount of performance indices and evaluation metrics, the choice of evaluation method, and the weight of evaluation metrics can affect the result of the evaluation of GCMs [21-22, 43]. The interpolation method used to obtain the areal average precipitation and temperature, and the time scale of climate variables used in performance evaluation, can also affect final evaluation result. Thus, it should also been pointed out that the ranking of GCMs in the HRB does not represent a hierarchical order. For example, GFDL-ESM2M model perform wore in the simulation of annual temperature in HRB, however, it perform well in Northern Eurasia [44]. The result from this study can be helpful for selection of CMIP5 models applied in impact studies of climate change over the HRB. For example, future temperature projections could be obtained directly from better performing GCMs' outputs. Meanwhile, the method adopted in this study can provide an effective reference for other research regions.

CONCLUSIONS

The results show that for the chosen seventeen GCMs after preliminary screening, all models can reproduce the intra-annual characteristics of temperature and precipitation well, and show much better agreement with temperature than precipitation. However, the majority of the models tend to underestimate the annual mean temperature, with a mean underestimation of 0.34-2.82°C. For precipitation, all models overestimate the annual mean precipitation, with a mean overestimation of 11%-97%. The step of performance evaluation for large-scale atmospheric variables and preliminary screening of models carried out before performance evaluation for ground climate variables can reduce uncertainties from the subjective selection of model and model error between large-scale atmospheric variables (i.e., relative humidity at 500hPa and 850hPa) and ground precipitation. Overall, the five models, namely, HadGEM2-ES, CESM1-BGC, MPI-ESM-LR, CNRM-CM5 and ACCESS1.3, are recommended as optimal choice for regional impact studies over the HRB. This method used in this study can easily be

extended to different study regions and the results can provide informative support for climate change impact research over the HRB.

ACKNOWLEDGEMENTS

The study was supported by the National Social Science Fund of China (No.41562017) and Beijing Social Science Foundation Youth Project, China (No. 2019 CN016). We acknowledge the World Climate Research Programme's Working Group on Coupled Modelling, which is responsible for CMIP, and we thank the climate modeling groups (listed in Table 1 of this paper) for producing and making available their model output. For CMIP the U.S. Department of Energy's Program for Climate Model Diagnosis and Intercomparison provides coordinating support and led development of software infrastructure in partnership with the Global Organization for Earth System Science Portals.

REFERENCES

[1] Beniston, M. (2002) Climatic change: possible impacts on human health. Swiss Medical Weekly. 132(25-26), 332-337.
[2] Kundzewicz, Z.W. and Somlyody, L. (1997) Climatic Change Impact on Water Resources in a Systems Perspective. Water Resources Management. 11(6), 407-435.
[3] Walther, G.R., Post, E., Menzel, A., Parmesan, C., Beebee, T., Fromentin, J.M., Hoegh-Guldberg, O. and Bairlein, F. (2002) Ecological responses to recent climate change. Nature. 416(6879), 389-395.
[4] Whitehead, P.G., Wilby, R.L. Battarbee, R.W., Kernan, M. and Wade, A.J. (2009) A review of the potential impacts of climate change on surface water quality. Hydrological Sciences Journal-Journal Des Sciences Hydrologiques. 54(1), 101-123.
[5] Yan, T.Z., Bai, J.W., Arsenio, T., Liu, J. and Shen Z.Y. (2019) Future climate change impacts on streamflow and nitrogen exports based on CMIP5 projection in the Miyun Reservoir Basin, China. Ecohydrology & Hydrobiology. 19(2), 266-278.
[6] Jha, M.K., Gassman, P.W. and Panagopoulos, Y. (2015) Regional changes in nitrate loadings in the Upper Mississippi River Basin under predicted mid-century climate. Regional Environmental Change. 15(3), 449-460.
[7] Hawkins, E. and Sutton, R. (2009) The potential to narrow uncertainty in regional climate predictions. Bulletin of the American Meteorological Society. 90(8), 1095-1108.
[8] Knutti, R. (2008) Should we believe model predictions of future climate change? Philosophical Transactions of the Royal Society a-Mathematical Physical and Engineering Sciences. 366(1885), 4647-4664.
[9] Chen, L. and Frauenfeld, O.W. (2014) Surface Air Temperature Changes over the Twentieth and Twenty-First Centuries in China Simulated by 20 CMIP5 Models. Journal of Climate. 27(11), 3920-3937.
[10] Joetzjer, E., Douville, H., Delire, C. and Ciais, P. (2013) Present-day and future Amazonian precipitation in global climate models: CMIP5 versus CMIP3. Climate Dynamics 41(11-12), 2921-2936.
[11] Sperber, K.R., Annamalai, H., Kang, I.S., Kitoh, A., Moise, A., Turner, A., Wang, B. and Zhou, T. (2013) The Asian summer monsoon: an intercomparison of CMIP5 vs. CMIP3 simulations of the late 20th century. Climate Dynamics. 41(9-10), 2711-2744.
[12] Wei, K., Xu, T., Du, Z.C., Gong, H.N. and Xie, B.H. (2014) How well do the current state-of-the-art CMIP5 models characterise the climatology of the East Asian winter monsoon? Climate Dynamics. 43(5-6), 1241-1255.
[13] Hua, W., Chen, H. and Sun, S. (2014) Uncertainty in land surface temperature simulation over China by CMIP3/CMIP5 models. Theoretical and Applied Climatology. 117(3-4), 463-474.
[14] Huang, D.Q., Zhu, J., Zhang, Y.C. and Huang, A.N. (2013) Uncertainties on the simulated summer precipitation over Eastern China from the CMIP5 models. Journal of Geophysical Research-Atmospheres. 118(16), 9035-9047.
[15] Collins, M., Chandler, R.E., Cox, P.M., Huthnance, J.M., Rougier, J. and Stephenson, D.B. (2012) Quantifying future climate change. Nature Climate Change. 2(6), 403-409.
[16] Knutti, R., Furrer, R., Tebaldl, C., Cermak, J. and Meehl, G.A. (2010) Challenges in Combining Projections from Multiple Climate Models. Journal of Climate. 23(10), 2739-2758.
[17] Gleckler, P.J., Taylor, K.E. and Doutriaux, C. (2008) Performance metrics for climate models. Journal of Geophysical Research-Atmospheres. 113(D6). 1-20.
[18] Reichler, T. and Kim, J. (2008) How well do coupled models simulate today's climate? Bulletin of the American Meteorological Society. 89(3), 303-312.
[19] Errasti, I., Ezcurra, A., Saenz, J. and Ibarra, G. (2011) Validation of IPCC AR4 models over the Iberian Peninsula. Theoretical and Applied Climatology. 103(1-2), 61-79.

[20] Sheffield, J., Barrett, A., Colle, B. and Fernando, D.N. (2013) North American Climate in CMIP5 Experiments. Part I: Evaluation of Historical Simulations of Continental and Regional Climatology. Journal of Climate. 26(23), 9209-9245.

[21] Fu, G.B, Liu, Z.F., Charles, S.P., Xu, Z.X. and Yao, Z.J. (2013) A score-based method for assessing the performance of GCMs: A case study of southeastern Australia. Journal of Geophysical Research-Atmospheres. 118(10), 4154-4167.

[22] Schaller, N., Mahlstein, I., Cermak. R. and Knutti, R. (2011) Analyzing precipitation projections: A comparison of different approaches to climate model evaluation. Journal of Geophysical Research-Atmospheres. 116,1-14.

[23] Stoner, A.M.K., Hayhoe, K. and Wuebbles, D.J. (2009) Assessing General Circulation Model Simulations of Atmospheric Teleconnection Patterns. Journal of Climate. 22(16), 4348-4372.

[24] Wang, W., Shao, Q., Peng, S., Xing, W., Sun, F. and Luo, Y. (2013) Quantitative assessment of the impact of climate variability and human activities on runoff changes: a case study in four catchments of the Haihe River basin, China. Hydrological Processes. 27(8), 1158-1174.

[25] Yang, Y. and Tian, F. (2009) Abrupt change of runoff and its major driving factors in Haihe River Catchment, China. Journal of Hydrology. 374(3-4), 373-383.

[26] Overland, J.E., Wang, M.Y., Bond, N.A., Walsh, J.E., Kattsov, V.M. and Chapman, W.L. (2011) Considerations in the Selection of Global Climate Models for Regional Climate Projections: The Arctic as a Case Study. Journal of Climate. 24(6), 1583-1597.

[27] Su, F., Duan, X., Chen, D., Hao, Z. and Cuo, L. (2013) Evaluation of the Global Climate Models in the CMIP5 over the Tibetan Plateau. Journal of Climate. 26(10), 3187-3208.

[28] Chu, J.T., Xia, J., Xu, C.Y. and Singh, V.P. (2010) Statistical downscaling of daily mean temperature, pan evaporation and precipitation for climate change scenarios in Haihe River, China. Theoretical and Applied Climatology. 99(1-2), 149-161.

[29] Watterson, I.G., Hirst, A.C. and Rotstayn, L.D. (2013) A skill score based evaluation of simulated Australian climate. Australian Meteorological and Oceanographic Journal. 63(1), 181-190.

[30] Yan, T., Shen, Z. and Bai, J. (2017) Spatial and Temporal Changes in Temperature, Precipitation, and Streamflow in the Miyun Reservoir Basin of China. Water. 9(2), 1-15.

[31] Perkins, S.E., Pitman, A.J., Holbrook, N.J. and Mcaneney, J. (2007) Evaluation of the AR4 climate models' simulated daily maximum temperature, minimum temperature, and precipitation over Australia using probability density functions. Journal of Climate. 20(17), 4356-4376.

[32] Suryavanshi, S., Pandey, A., Chaube, U.C. and Joshi, N. (2014) Long-term historic changes in climatic variables of Betwa Basin, India. Theoretical and Applied Climatology. 117(3-4), 403-418.

[33] Hirsch, R.M., Slack, J.R.and Smith, R.A. (1982) Techniques of trend analysis for monthly water-quality data. Water Resources Research. (18), 107-121.

[34] Sen, P.K. (1968) Estimates of the regression coefficient based on Kendall's tau. Journal of the American Statistical Association. 63, 1379-1389.

[35] Chen, H., Xu, C.-Y. and Guo, S. (2012) Comparison and evaluation of multiple GCMs, statistical downscaling and hydrological models in the study of climate change impacts on runoff. Journal of Hydrology. 434, 36-45.

[36] Chen, J., Brissette, F.P. and Poulin, A. (2011) Overall uncertainty study of the hydrological impacts of climate change for a Canadian watershed. Water Resources Research. 47, 1-16

[37] Chen, L. and Frauenfeld, O.W. (2014) A comprehensive evaluation of precipitation simulations over China based on CMIP5 multimodel ensemble projections. Journal of Geophysical Research-Atmospheres 119(10), 5767-5786.

[38] Yu, R.C., Wang, B. and Zhou, T.J. (2004) Tropospheric cooling and summer monsoon weakening trend over East Asia. Geophysical Research Letters. 31(22), 1-4.

[39] Li, L. and Li, W. (2015) Thermodynamic and dynamic contributions to future changes in regional precipitation variance: focus on the Southeastern United States. Climate Dynamics. 45(1-2), 67-82.

[40] Li, Y., Leung, L.R., Xiao, Z., Wei, M. and Li, Q. (2013) Interdecadal Connection between Arctic Temperature and Summer Precipitation over the Yangtze River Valley in the CMIP5 Historical Simulations. Journal of Climate. 26(19), 7464-7488.

[41] Perez, J., Menendez, M., Mendez, F.J. and Losada, I.J. (2014) Evaluating the performance of CMIP3 and CMIP5 global climate models over the north-east Atlantic region. Climate Dynamics. 43(9-10), 2663-2680.

[42] Thibeault, J.M. and Seth, A. (2014) A Framework for Evaluating Model Credibility for Warm-Season Precipitation in Northeastern North America: A Case Study of CMIP5 Simulations and Projections. Journal of Climate. 27(2), 493-510.

[43] Rupp, D.E., Abatzoglou, J.T., Hegewisch, K.C. and Mote, P.W. (2013) Evaluation of CMIP5 20th century climate simulations for the Pacific Northwest USA. Journal of Geophysical Research-Atmospheres 118(19), 10884-10906.
[44] Miao, C., Duan, Q.Y., Sun, Q.H., Huang, Y., Kong, D.X., Yang, T.T., Ye, A., Di, Z.H and Gong, W. (2014) Assessment of CMIP5 climate models and projected temperature changes over Northern Eurasia. Environmental Research Letters. 9(5), 1-12.

Received: **20.10.2020**
Accepted: **13.01.2021**

CORRESPONDING AUTHOR

Tiezhu Yan
Institute of Agricultural Resources and Regional Planning,
Chinese Academy of Agricultural Sciences,
Beijing 100081 – China

e-mail: yanxiaoshi1984@126.com

© by PSP Volume 30– No. 05/2021 pages 5015-5025 Fresenius Environmental Bulletin

EVALUATION OF COTTON GENOTYPES FOR DROUGHT TOLERANCE AND THEIR CORRELATION STUDY AT SEEDLING STAGE

Nasreen Fatima Veesar[1], Wajid Ali Jatoi[1,*], Qurban Ali Channa[1], Shahnaz Memon[2], Naila Gandahi[1], Ghulam Aisha[1], Tarique Ali Jatoi[3], Wazir Ali Maitlo[4], Altaf Hussain Solangi[1], Lubna Rajput[5]

[1]Department of Plant Breeding and Genetics, Sindh Agriculture University Tandojam, Pakistan
[2]Cotton Research Institute Tandojam Pakistan
[3]Department of Soil Science, Sindh Agriculture University Tandojam, Pakistan
[4]Department of Molecular Biology and Genetics, Shaheed Benazir Bhutto University, Benazirabad, Pakistan
[5]Agriculture Research Center Tandojam Pakistan

ABSTRACT

Drought stress is considered as the most limiting factor that reduces crop productivity all over the world. Among the abiotic stresses, drought adversely affects the plant growth and development, consequently the yield. The current research experiment was conducted in RCBD factorial arrangement with two irrigation treatments (non-stress and water stress at seedling stage) in four replications at experimental field, Department of Plant Breeding and Genetics, Sindh Agriculture University, Tandojam during 2010. Twelve most popular upland cotton cultivars viz. CRIS-134, CRIS-342, Sadori, Chandi, Sindh-1, NIAB-78, CIM-496,CIM-499, CIM-506, CIM-534, BH-160 and Bt cotton (Australian origin) with diverse characters and origin were selected for the study at seedling stage for physiological as well growth parameters under water stress conditions. The growth and physiological traits were comprised of shoot length (cm), root length (cm), number of lateral roots (NLR) , leaf area (cm^2) (LA) , leaf relative water content (RWC), excised leaf water loss (ELWL%) , stomatal density(ST) and stomatal conductance (SC) was calculated. The significance of treatments x genotypes interactions revealed that cotton cultivars performed variably over irrigation regimes. Water stress significantly affected shoot length, root length, number of lateral roots, leaf area, relative water content, excised leaf water loss, stomatal conductance, and stomatal density. Further correlation coefficient revealed that traits were positively and significantly associated except that stomatal conductance was negatively associated with shoot length, root length, and no of lateral roots.

KEYWORDS:
Cotton, screening, seedling stage, correlations

INTRODUCTION

The cotton varieties cultivated in Pakistan encounter various biotic and abiotic stresses. Among the abiotic stresses, water stress poses a severe concern which restricts the cotton productivity in Pakistan and in numerous other parts of the globe [1]. By now, it is well recognized that drought tolerance is a multifaceted phenomenon that adversely affects cotton plant at seedling stage. The developmental stages for cotton plant may be separated into five main growth phases; 1) germination and emergence, 2) seedling establishment, 3) leaf area and canopy development, 4) flowering and boll development and 5) boll maturation. Water stress at beginning developmental phase can deteriorate plant stand due to non-survival of seedlings.

Longer duration of drought at seedling stage may become catastrophic for cotton plant, while water stress at peak flowering stage is very critical for seed cotton yield. Water requirement is comparatively higher for cotton plant to retain flowers and young bolls; nonetheless this moisture demand is relatively high at early seedling stages [2]. Combination of both root architecture and physiological characters associated with water stress tolerance may end-up in evolving improved moisture stress tolerant cotton genotypes [3]. Another facet of water stress tolerance is the capability of plants to condense down the water evapotranspiration with increased stomatal closure and smaller but thicker leaves [4]. Generally, plant breeders use elite plant varieties as parents to develop breeding material through hybridization and selection programmes, which decreases the genetic distance of popular varieties, yet utilizing public germplasm in breeding programmes can enhance genetic base of breeding material. Hence, it becomes indispensable to discover potential alleles for moisture deficit environment which are present in adapted genetic stock or transmit unique genes from exotic germplasm to widen genetic base for water stress tolerance. Characterization of moisture stress resistant genotypes is

a big issue to identify and develop the phenotypic characters which contribute towards stress tolerance and establish their comparative significance. There has been a lack of knowledge regarding physiological traits associated with water stress tolerance that can be used as indicators for drought tolerance. Several physiological attributes were considered as prospective indicators for water stress tolerance, for instance reticence of photosynthesis and low stomatal conductance [5]. Due to genetic variability there may be two types of reactions of cultivars for drought increase in root length and decrease in root length. Root length of crop plants imposed to low soil moisture content of water content sometimes have shown significant increases in root length against those plants which are irrigated adequate water without water stress [6,7]. And compete for receiving moisture from deeper levels of soil than plants grown under non-stress water conditions [8,9,10,11]. Shoot length is also considerably sensitive to water stress, thus cause severe decline in shoot length [12,7]. The Root/shoot length ratio is regarded as stress adaptive system in response to water shortage conditions; hence it is considered an important indicator for drought stress tolerance.

Some physiological attributes like relative water content (RWC) which measures the amount of water retained by the plant in the leaf tissue, thus high RWC in water stress conditions would be preferable to sustain water stress. Higher RWC in leaf tissue has been considered as reliable selection criteria to evolve crop varieties for water shortage environments [13,14].

Various morphological, physiological and yield characters are being used to measure drought tolerance when they are correlated with each other. Cotton subjected to water deficient since cotton originates from areas that are often exposed to water-deficit stress [15,16]. Therefore, selection for drought tolerance is a major interest of plant breeders in cotton. A number of different morphological (leaf, stem and root growth parameters) and physiological traits (more than 30 traits) have been suggested as important selection criteria relative to drought tolerance in cotton [17]. However, none of the above physiological traits has so far been consistently correlated positively with drought tolerance [17]. The difficulty in identification of a physiological parameter as a reliable indicator of yield in drought conditions has suggested that yield performance over a range of environments should be used as the main indicator for drought tolerance [18]. Several morphological traits belonging to seedling traits have been reported showing importance in relation to water stress tolerance in cotton [2]. Such traits include taproot mass, density of lateral roots, seedling vigor, rapidity in root development and root/shoot ratio [19]. For drought tolerance, longer taproot was supported by [20]. Two schools of thought exist among the researchers regarding root length under water stress conditions. Some scientists reported that root length of plants subjected to water stress registered significant increase in root length against those plants irrigated with optimum level of water [6,7]. On the contrary, some scientists found that root length under drought conditions has decreased seriously [20,21]. It is often recommended that the identification and selection of morpho-physiological traits can be successful endeavor to breed varieties which produce higher yields, hence may be highly successful approach to be used in combination with appropriate plant breeding techniques. Quite a number of phenotypic traits have been recognized which could be applied to enhance the yield of parental genotypes under moisture deficit situations or may be adopted as indirect criteria for selection, particularly for improving yield under water stress environment. Therefore thus study was planned to investigate the influence of water stress upon physiological parameters and their interrelationship at seedling stage.

MATERIALS AND METHODS

The research was carried out in the experimental area of the Department of Plant Breeding and Genetics at Sindh Agriculture University Tandojam, Pakistan during the years 2010.Twelve most popular upland cotton cultivars viz. CRIS-134, CRIS-342, Sadori, Chandi, Sindh-1, NIAB-78, CIM-496, CIM-499, CIM-506, CIM-534, BH-160 and Bt cotton (Australian origin) with diverse characters and origin were studied. The experiment was carried-out in factorial design with two irrigation treatments, non stress and water stress with four replications. The water regimes were considered as the main factor while varieties as sub-factor. All agricultural inputs and practices like spraying, fertilization, weeding, irrigation and cotton production technology were adopted as recommended for the cotton crop. The data were collected from ten tagged plants in each replication. The seedlings were t part; the plant material was screened at seedling stage against water stress with some developmental and physiological traits.

Field screening for drought tolerance at seedling stage. Two irrigation regimes i.e. non-stress in which normal irrigations were applied, first after 25 days of sowing and second at 44 days after sowing whereas in water stress treatment, the stress was imposed from sowing till 44 days of the crop growth and development. For developmental and physiological traits, the observations were recorded for shoot length (cm), root length (cm), number of lateral roots, leaf area (cm^2), leaf relative water content with formula RWC = [(Fresh weight–Dry weight) / (Turgid weight–Dry weight)] x 100, excised leaf water loss (ELWL%) was calculated by following

[22] with formula E LWL = (Fresh weight –wilted weight) / Dry weight x 100, stomatal conductance ($mmolm^{-2}s^{-1}$) was determined in $mmolm^{-2}s^{-1}$ by Prometer-AP4 and stomatal density (mm^2) by impression method according to technique developed [23]. The soil type of the experimental area was loam and sandy loam in texture. For the cotton experiment area, water content at field capacity varied from 20.3 to 27.6 %, and wilting point varied from 7.2 to 9.7 % on dry weight basis. The dry soil bulk densities ranged from 1.42 to 1.50 g cm-3 throughout the 1.2 m deep profile.

RESULTS AND DISCUSSION

Analysis of variance and mean performance of cotton genotypes under water stress conditions at seedling stage The results revealed that moisture deficit inflicted considerable influence on all the developmental and physiological characters at seedling stage (Table 1). Inconsistent responses of genotypes to water stress were observed because mean squares due to treatment × genotypes interactions were significant for all the studied characters. Analogous to these results, [24] observed significant influence of water stress on root and shoot length of 80 accessions of cotton examined. The significance of accessions × treatment interactions revealed differential response of accessions to the two moisture environments. Significant differences for stomatal conductance, water content in leaves and water loss from excised leaves due to drought stress were also noted by [25]. The mean performance of cotton genotypes for various developmental and physiological traits under water stress are discussed here under.

Shoot length (cm). Compared with non-stressed control, drought stress reduced the shoot lengths of cotton genotypes ranging from -4.85 (Sadori) to -15.00cm (Chandi). The maximum drought-induced reduction in shoot length, therefore was noted in Chandi (-15.00cm), though this genotype recorded the maximum shoot length under optimum irrigation conditions (Table 2). Cultivars, Chandi, Bt-cotton and BH-160 with maximum declines in shoot length as -15.00, -13.50 and -10.75cm respectively were found rather more susceptible to drought stress conditions. In water stress, the shoot lengths of Sadori (45.15 cm) followed by CRIS-134 (45.10 cm) were relatively longer. These genotypes also showed greater tolerance to drought stress due to the fact that the shoot lengths of Sadori and CRIS-134 genotypes were reduced to only -4.85 and -5.65cm respectively under drought stress conditions. Similar to our findings, [26] found that shoot length of cotton seedlings were decreased due to exposure of drought stress [27] suggested that shoot growth modifications may influence the root growth and development, thus may interfere with the cotton susceptibility to water stress. Response of cotton genotypes to water stress involves osmotic adjustment, elasticity to photochemical apparatus and stomatal conductance; hence the nature of shoot and root growth and development determine responses of genotypes to water stress [27,28] stated that water deficiency at initial vegetative stage has substantially reduced the shoot and root dry-matter in cotton plant.

Root length (cm). It is by now well understood that, all the root parameters are essential for water stress tolerance. A number of researchers have observed the prospective function of roots under moisture-deficit conditions [29]. The cotton genotypes evaluated under water stress responded differentially to drought stress. However, water stress reduced the root length of varieties CIM-499, CRIS-342, NIAB-78, Chandi, BH-160 and Bt-cotton by -4.75, -4.63, -2.75, -2.50, -1.00, and -0.75 cm, respectively, yet cultivars CRIS-342 and CIM-499 were found more susceptible to drought stress because these cultivars recorded higher reductions in root length attributable to moisture stress. Contrary to above findings, the root length of varieties like CIM-534, CRIS-134, CIM-506, Sindh-1, CIM-496 and Sadori were increased rather declined by 4.75, 4.50, 3.75, 3.38, 3.25 and 3.00 respectively under water stress indicating their drought tolerance (Table 2). In consonance with our findings, [30,26] observed that moderate water stress at seedling stage caused increase in root length while moisture stress at reproductive stage or longer period have condensed the root development. In another study, [31] pointed-out that genetically modified cottons were more tolerant to water stress because of good rooting system against wild type cotton. Profuse and deeper root systems are often desirable characteristics for drought adaptation. Deep root system also imparts drought resistance in many crop plants. In cotton, diploid species have high degree of drought tolerance by virtue of their deep root system [32,33]. Generally deep rooted plants exhibit greater drought tolerance than shallow rooted genotypes. Therefore, first irrigation is usually delayed in cotton up to 40 days, so that roots may become longer in natural conditions for search of deep soil moisture.

Number of lateral roots. The important characteristic of roots in drought-tolerant plants is the presence of young lateral roots which are also called as focal sites of water uptake [34]. Water stress induced significant variations in lateral roots of cotton seedlings (Figure 1), yet the genotypes also responded variably under water stress conditions. Exposure of water stress reduced the number of lateral roots in cultivars NIAB-78, CIM-499, Bt-cotton, Chandi, CRIS-342 and BH-160 and by -

3.00, -3.00, -3.00, -2.75 -1.75, and -1.25 roots respectively (Table 3). Inversely, the number of lateral roots of varieties like Sindh-1, CRIS-134, Sadori, CIM-534, CIM-499 and CIM-506 were increased by 5.50, 5.00, 4.50, 4.00, 3.75, and 3.50 respectively revealing their water stress tolerance. Under drought stress as well as control conditions, CRIS-134, Sadori and Sindh-1 recorded more number of lateral roots than rest of the genotypes (Table 3). Analogous to present results [35], found two drought tolerant cotton genotypes while [33] observed six cotton genotypes which produced higher number of lateral roots indicating their drought tolerance while [36] observed that severe water stress reduced the root proliferation.

Leaf area (cm^2). Leaf area is one of the main determinants of crop yield as it regulates plant water balance through its influence on transpiration [37]. Results regarding leaf area of cotton genotypes showed significant variations under the influence of drought stress, yet some varieties showed higher reductions in leaf area than the others due to water stress (Table 3). Drought stress generally reduced the leaf area of all the twelve cotton genotypes evaluated with the range of -6.00 to -28.75cm^2. Under water stress, the maximum reductions in leaf area however was recorded in BH-160 (-28.75cm^2) closely followed by CIM-499 (-25.00 cm^2) and Bt-cotton (-21.00 cm^2) revealing their vulnerability to water stress. While other groups of cultivars like CIM-496, CIM-534, and Sindh-1 showed tolerance to drought stress due to reason that leaf area of these genotypes was less affected by stress and reduction was noted as -6.50, 6.50, and -6.00cm^2 respectively [38] in his study observed that water stress resulted in reductions of all plant organs including total plant weight. However, he stated that declines in the leaf area below the optimum leaf area index will decrease crop growth rate and total photosynthesis per plant which ultimately will decrease the yield. Under well water condition, leaf area index increases along with growth rate, but it decreases in water deficit condition due to leaf area adjustment process. [39] conducted a pot experiment in green house on two cotton varieties and observed 24% and 29% decrease in leaf area of two genotypes respectively in drought-stressed plants [40] noted the consequence of drought stress on leaf area at various reproductive stages of cotton and concluded that drought stress decreased leaf area in all the stages of the crop except maturity.

Relative water content (RWC %). High RWC% under drought stress conditions may be preferable to maintain water balance, thus higher RWC% may be adopted as good criteria to breed plants for water stress tolerance [14]. Moisture stress tolerance can be achieved through the capability of plants to minimize evaporation via stomatal shutting and also modifications in leaf phenotype [4]. In present study, drought stress caused considerable declines in RWC% of the genotypes under screening and the reduction ranged from -26.50 to -48.50% (Table 4). The maximum reductions in RWC% due to drought stress was recorded in varieties CIM-499 (-48.50%) closely followed by NIAB-78 (-47.50%) and Bt-cotton (-45.50%). On an average, decline of -36.25% was recorded due to water stress. However, other cultivars such as CIM-506, CRIS-134 and CIM-534 showed tolerance to drought stress by showing less declines in RWC% and these genotypes recorded reductions of -26.750, -26.50 and -28.25% due to water stress. Moisture stress caused substantial decline in yield, growth and leaves water content as reported by [25]. However some varieties recorded higher growth and yield and also sustained higher leaf water content and more photosynthesis. Leaf relative water content was observed as 69% and 45% in transgenic and wild-type plants, respectively at 10-day drought stress. Similarly, transgenic plants showed better performance due to stress responsive genes for photosynthesis, stomatal conductance, transpiration, and osmotic potential as compared to wild type [41].

Excised leaf water loss (ELWL%). The cultivars possessing ability of low rate excised leaf water loss how drought resistance. Therefore, ELWL% was recommended as best measure for tolerance to water stresses [14]. Variable response of cotton genotypes was observed for ELWL% under water stress at seedling stage. Drought stress increased the excised leaf water loss of all the cotton genotypes in the range of -14.50 to -27.50%. The maximum reduction in ELWL% nevertheless was recorded in varieties Bt-cotton followed by NIAB-78 and BH-160 (Table 4). Some genotypes like CIM-496, CRIS-134 and CIM-534 showed lower ELWL% under drought stress, the relative ELWL% of these genotypes was with -13.00, -14.50 and -17.50%, hence demonstrated their stress tolerance. Analogous to our findings, [25] also observed negative effects of water stress on excised leaf water loss in water shortage conditions.

Stomatal conductance (mmol $m^{-2}s^{-1}$). Stomatal conductance of cotton genotypes was significantly altered under the influence of drought stress. Likewise, the cotton genotypes responded differentially to drought stress conditions. Under drought stress, cotton genotypes decreased the stomatal conductance varying from -55.50 to -101.50mmol $m^{-2}s^{-1}$. In drought stress, the maximum drop in stomatal conductance was recorded in Sadori (-101.50mmol $m^{-2}s^{-1}$) distantly followed by CIM-506 (-90.50mmol $m^{-2}s^{-1}$), hence indicating their less vulnerability in water stress conditions (Table 5).

Nonetheless, Chandi, NIAB-78 and CIM-499 genotypes recorded less declines in stomatal conductance under drought stress showing their higher susceptibility to water stress. Drought stress significantly affected stomatal conductance which declined by 41.52% across the 182 genotypes from 39.53 mmol m^{-2} s^{-1} in the control to 23.12 mmol m^{-2} s^{-1} under drought stress [42].Since water use efficiency is higher in genotypes which are characterized by stomatal conductance, often resulting from a lower water status, but such genotypes disadvantageously extract more water from the soil [43,44], whilst maintaining higher stomatal conductance, can produce higher yields. Conversely, under conditions of limited soil moisture, low water use efficiency (WUE) resulting from excessive evapotranspiration will not allow sustained accumulation of dry matter and its partitioning to reproductive organs [45,46,25] found that the water stress lowered the stomatal conductance, thus some varieties were less affected by water stress and maintained their stomatal conductance.

Stomatal density (mm^2). Decline of moisture via leaves is an important occurrence in cotton plants in water stress conditions [47]. Cotton genotypes under present study exhibited significant variations in stomatal density of under the influence of drought stress. Likewise, the cotton genotypes responded changeably to drought stress (Figure 2), some being less affected than the others (Figure 3). On an average, the stomata numbers declined by -16.85mm^2. Against non-stressed control, drought stress decreased the stomatal density of cotton genotypes in the range of -10.00 to -23.00mm^2. Among the genotypes, the maximum drought-induced reductions in stomatal density were recorded in CIM-506 followed by CIM-534, Sadori and CRIS-134 as

TABLE 1
Mean squares from analysis of variance for physiological traits of cotton genotypes grown under non-stress and water stress conditions

Traits	Replication (D.F.=3)	Genotypes (G) (D.F.=11)	Treatment (T) (D.F.=1)	G x T (D.F.=11)	Error (D.F.= 69)
Shoot length	2.16	125.21**	1647.56**	21.55**	2.74
Root length	2.59	185.32**	6.51**	26.16**	1.00
No. lateral roots	1.26	61.58**	22.04**	26.54**	0.79
Leaf area	1.50	1317.62**	4620.38**	121.01**	1.13
Relative water content	2.30	399.50**	31537.50**	135.40**	0.90
Excised leaf water loss	14.43	217.69**	9263.01**	37.15**	9.06
Stomatal conductance	26.00	29650.00**	143685.00**	459.00**	22.00
Stomatal density	0.09	35.40**	6919.01**	24.76**	0.36

** = Significant at 1% of probability level.

TABLE 2
Mean performance for shoot length and root length of cotton genotypes grown under non-stress and water stress conditions

Genotypes	Shoot length (cm)		R.D*	Root length (cm)		R.D*
	Non-stress	Water stress		Non-stress	Water stress	
CRIS-134	50.75	45.10	-5.65	23.50	28.00	4.50
CRIS-342	42.25	35.33	-6.93	18.63	14.00	-4.63
Sadori	50.00	45.15	-4.85	21.75	24.75	3.00
Chandi	51.50	36.50	-15.00	16.75	14.25	-2.50
Sindh-1	49.50	43.50	-6.00	20.63	24.00	3.38
NIAB-78	46.25	36.75	-9.50	15.00	12.25	-2.75
CIM-496	51.00	45.00	-6.00	19.50	22.75	3.25
CIM-499	41.00	32.50	-8.50	17.25	12.50	-4.75
CIM-506	47.50	41.50	-6.00	21.75	25.50	3.75
CIM-534	48.25	41.50	-6.75	21.25	26.00	4.75
BH-160	45.75	35.00	-10.75	14.00	13.00	-1.00
Bt (Aust)	45.50	32.00	-13.50	13.25	12.50	-0.75
Mean	47.44	39.15	-8.29	18.60	19.13	0.25
LSD(5%) Genotypes (G)	1.65			0.99		
Treatment (T)	0.67			0.40		
G x T	2.33			1.41		

*RD = Relative difference between non-stress and water stress treatments.

TABLE 3
Mean performance for number of lateral roots and leaf area of cotton genotypes grown under non-stress and water stress conditions

Genotypes	No. of lateral Roots		R.D*	Leaf area (cm^{-2})		R.D*
	Non-stress	Water stress		Non-stress	Water stress	
CRIS-134	15.50	20.50	5.00	116.00	107.25	-8.75
CRIS-342	14.00	12.25	-1.75	103.00	92.00	-11.00
Sadori	16.00	20.50	4.50	107.00	98.00	-9.00
Chandi	13.00	10.25	-2.75	109.00	90.25	-18.75
Sindh-1	15.00	20.50	5.50	106.75	100.75	-6.00
NIAB-78	14.00	11.00	-3.00	107.50	92.25	-15.25
CIM-496	15.00	18.75	3.75	130.75	124.25	-6.50
CIM-499	15.50	12.50	-3.00	125.75	100.75	-25.00
CIM-506	15.50	19.00	3.50	121.25	111.25	-10.00
CIM-534	14.75	18.75	4.00	117.25	110.75	-6.50
BH-160	13.75	12.50	-1.25	119.50	90.75	-28.75
Bt (Aust)	12.00	9.00	-3.00	86.00	65.00	-21.00
Mean	14.50	15.46		112.48	98.60	-13.88
LSD(5%) Genotypes (G)	0.88		0.96	1.06		
Treatment (T)	0.36			0.43		
G x T	1.25			1.49		

*RD = Relative difference between non-stress and water stress treatments.

TABLE 4
Mean performance for relative water content and excised leaf water loss of cotton genotypes grown under non-stress and water stress conditions

Genotypes	RWC (%)		R.D*	Excised leaf water loss (%)		R.D*
	Non-stress	Water stress		Non-stress	Water stress	
CRIS-134	91.50	65.00	-26.50	81.50	67.00	-14.50
CRIS-342	87.25	52.50	-34.75	85.25	66.00	-19.25
Sadori	92.00	61.25	-30.75	87.75	70.00	-17.75
Chandi	90.50	49.00	-41.50	79.50	60.00	-19.50
Sindh-1	89.50	58.25	-31.25	85.00	67.25	-17.75
NIAB-78	88.00	40.50	-47.50	78.00	51.75	-26.25
CIM-496	98.00	66.00	-32.00	84.50	71.50	-13.00
CIM-499	90.50	42.00	-48.50	79.00	58.50	-20.50
CIM-506	87.50	60.75	-26.75	76.75	58.00	-18.75
CIM-534	84.75	56.50	-28.25	80.75	63.25	-17.50
BH-160	82.75	41.00	-41.75	86.50	63.00	-23.50
Bt (Aust)	80.50	35.00	-45.50	76.50	49.00	-27.50
Mean	88.56	52.31	-36.25	81.75	62.10	-19.65
LSD(5%) Genotypes (G)	0.95			3.02		
Treatment (T)	0.38			1.22		
G x T	1.34			4.24		

*RD = Relative difference between non-stress and water stress treatments.

compared to other cultivars screened (Table 5 and Figure 3). These cultivars performed better due to the fact that maximum reduction in stomata helped them to sustain water stress and retain more water with less evapo-transpiration from leaves, [48] noted that stomatal density increased as water stress increased, while the maximum stomatal aperture reduced only in the severe stressed plants, [49] observed a reduction of 14.24% in stomatal density in low moisture. The time of the maximum stomatal aperture was delayed in the mild and severe stressed plants. When severe stress occurred, the stomata were kept open until the transpiration decreased to nearly zero, suggesting that the stomata might not be the main factor in adjusting transpiration in cotton. Different plant traits are reported to enhance water stress tolerance which include chunky leaves, thicker palisade cells, stout epidermis, more hairs on plan parts, thicker parenchyma cells, smaller stomata, more palisade cells against to spongy cells [50,51,52] stated that stomata hole very important functions of plant like maintaining cellular function and producing energy. Stomata conductance may also be important gauge for measuring drought tolerance in cotton because of

TABLE 5
Mean performance for stomatal conductance and stomatal density of cotton genotypes grown under non-stress and water stress conditions

Genotypes	Stomatal conductance ($mmols^{-2}s^{-1}$)		R.D*	Stomatal density (mm^2)		R.D*
	Non-stress	Water stress		Non-stress	Water stress	
CRIS-134	210.00	132.75	77.25	40.00	30.00	10.00
CRIS-342	316.25	245.00	71.25	46.25	26.50	19.75
Sadori	242.25	140.75	101.50	41.00	28.00	13.00
Chandi	340.00	283.75	56.25	46.00	24.75	21.25
Sindh-1	230.50	146.50	84.00	40.00	26.75	13.25
NIAB-78	343.00	286.00	57.00	45.00	28.00	17.00
CIM-496	218.75	145.50	73.25	40.00	24.25	15.75
CIM-499	380.00	289.50	90.50	42.00	24.25	17.75
CIM-506	216.00	130.00	86.00	46.00	30.25	15.75
CIM-534	242.50	150.50	92.00	40.75	25.00	15.75
BH-160	284.50	200.50	84.00	48.00	28.00	20.00
Bt (Aust)	247.25	191.75	55.50	49.00	26.00	23.00
Mean	272.58	195.21	77.38	43.67	26.81	16.85
LSD(5%) Genotypes (G)	4.66			0.60		
Treatment (T)	1.90			0.24		
G x T	6.60			0.84		

*RD = Relative difference between non-stress and water stress treatments.

TABLE 6
Correlation co-efficient between developmental and physiological trait of cotton genotypes under water stress condition

Traits	SL	RL	NLR	LA	RWC	ELWL	SC
RL	0.486**						
NLR	0.400**	0.872**					
LA	0.631**	0.476**	0.487**				
RWC	0.849**	0.273**	0.189	0.682**			
ELWL	0.774**	0.196	0.160	0.606**	0.914**		
SC	-0.020	-0.640**	-0.597**	0.062	0.336**	0.314**	
SD	0.639**	-0.098	-0.148	0.382**	0.855**	0.790**	0.537**

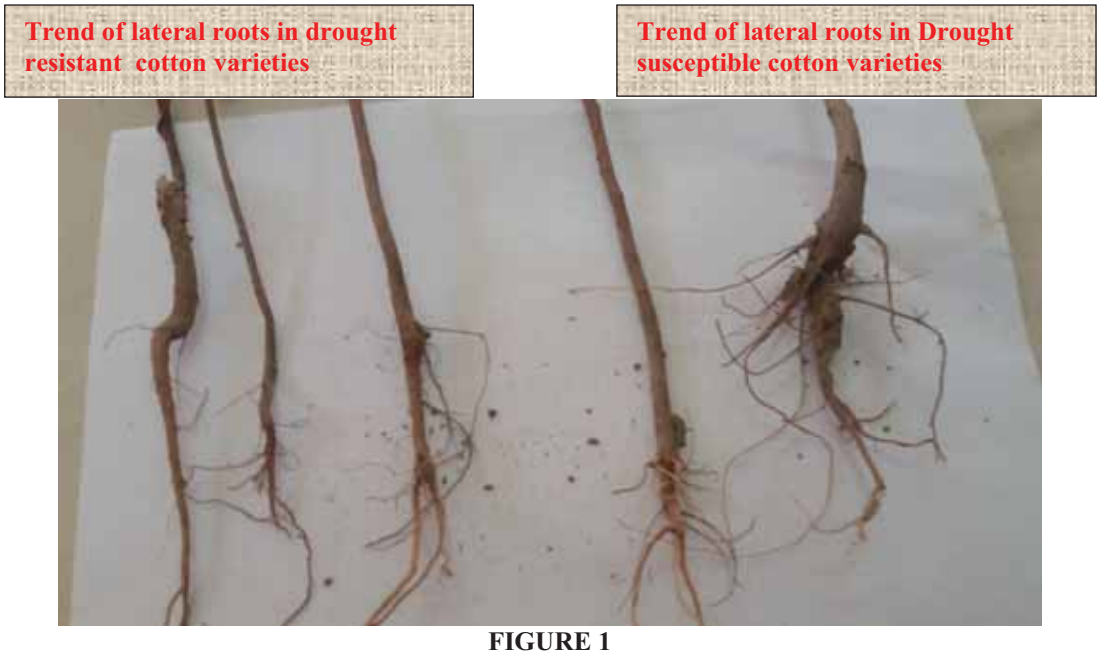

FIGURE 1
Trend of lateral root architecture in drought resistant and drought susceptible cotton varieties

Stomata of drought susceptible varieties

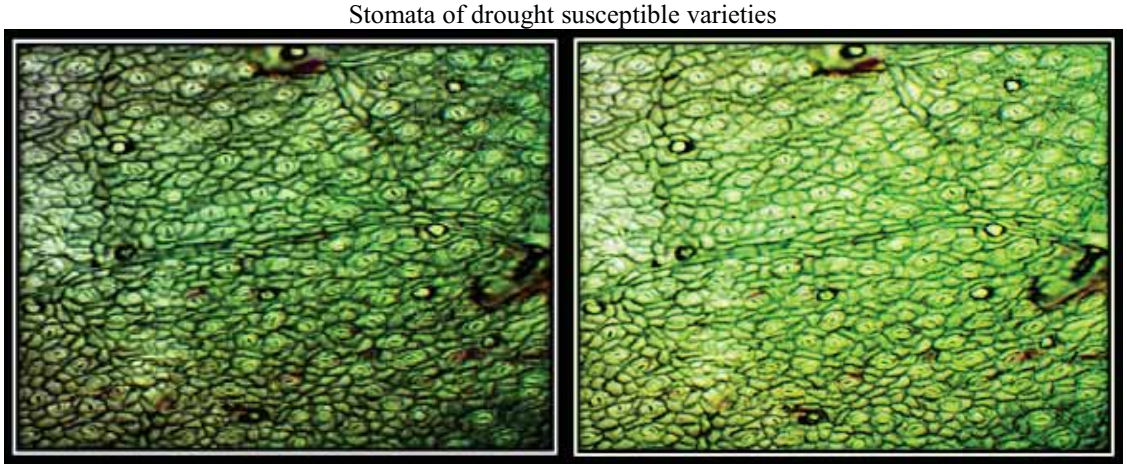

FIGURE 2
Presentation of cotton stomata of drought susceptible varieties

Stomata of drought tolerant varieties

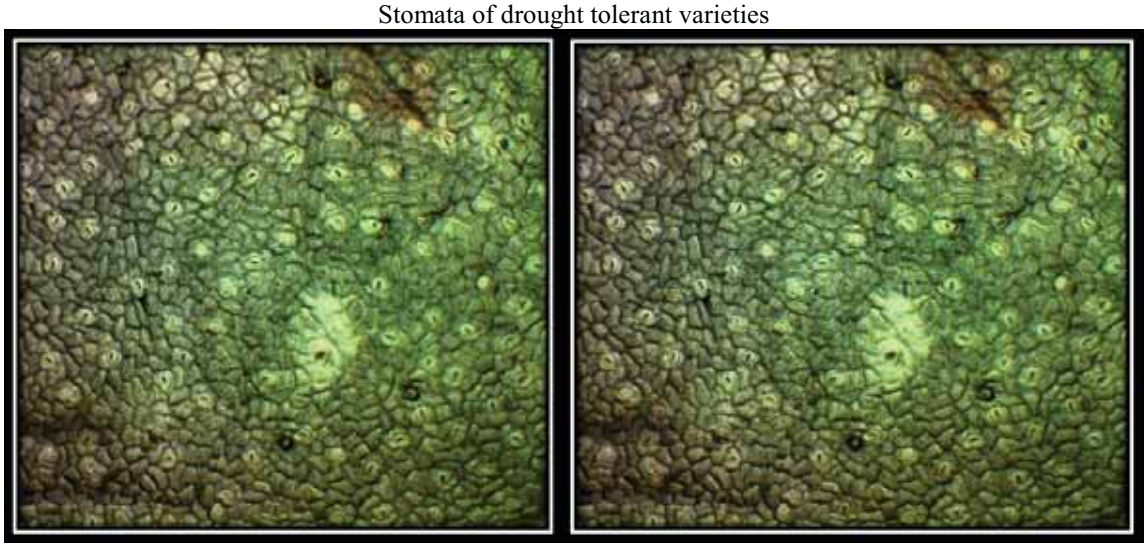

FIGURE 3
Presentation of cotton stomata of drought tolerant varieties

negative association of drought tolerance with stomata conductance.

Correlations (r) between development and physiological traits. There was a significant positive association of shoot length with root length, number of lateral roots, leaf area, relative water content and stomatal density (Table 6). These results indicated that when shoot length increases, it correspondingly increases the plant roots, smaller lateral roots, leaf area, RWC and stomatal count per unit area. Root length showed significant positive associations with number of lateral roots, leaf area and relative water content, while significantly negative association of root length was observed with stomatal conductance and number of lateral roots. The negative correlations of root length with stomatal conductance and lateral roots revealed that as the length of roots increase, it causes more evapotranspiration. Leaf area showed significant and positive relationship with water content in leaves. The relationship of stomatal density with leaf area, water content in leaves, water loss from excised leaves, and stomatal conductance was also significant and positive. The relationships of leaf area with characters related to evapo-transpiration are well documented. It has been stated that RWC was considered as impotent parameter for determining water status in plant leaves. The preference of RWC to be important illustration of plant water status due to genetic variation also hold true because of close alliance between relative water content and yield in water stress Available reports revealed that drought tolerant species reduce the water loss by reducing the leaf area and also restricting stomatal opening.

Data availability statement. The data mentioned in the manuscript are available at any time for the guidance of researchers and scientists.

REFERENCES

[1] Saranga, Y., Menz, M., Jiang, C., Robert, D. Yakir, J., and Andrew, H. (2001). Genomic dissection of genotype x environment interactions conferring adaptation of cotton to arid conditions. Genome Res. 11, 1988-1995.

[2] Riaz, M., Farooq, J., Sakhawat, G., Mahmood, A., Sadiqand, M., and Yaseen, M. (2013). Genotypic variability for root/shoot parameters under water stress in some advanced lines of cotton (*Gossypiumhirsutum* L.). Genet. Mol. Res. 12(1), 552-561.

[3] Basal, H., Smith, C.W., Thaxton, P.M., and Hemphill, J.K. (2005). Seedling drought tolerance in upland cotton. Crop. Sci. 45, 766-771.

[4] Franca, M., Thi, A., Pimental, C., Rossiello, R., Fodil, Y. and Laffary, D. (2000). Differences growth and water relations among *Phaseolus vulgaris* cultivars in response to induced drought stress. Environ. Exp. Bot. 43, 227-237.

[5] Athar, H.R. and Ashraf, M. (2005). Photosynthesis under drought stress. In: Hand Book of photosynthesis (2ed). M. Pessarakli. CRC Press, New York, USA. Pp. 795-810.

[6] Chaitante, D., Iorio, D., Maiuro, L. and Scippa, S. (2000). Effect of water stress on root meristems in woody and herbaceous plants during the first stage of development. Function and Physiology. 245-258.

[7] Abdalla, M.M. and El-Khoshiban, N.H. (2007). The influence of water stress on growth, relative water content, photosynthetic pigments, some metabolic and hormonal contents of two *Triticum aestivum* cultivars. J. Appl. Sci. Res. 3(12), 2062-2074.

[8] Kamara, A., Menkir, A., Babu-Apraku, B. and Ibikunle, O. (2003). The influence of drought stress on growth, yield and yield components of stressed maize genotypes. J. Agric. Sci. 141, 43-50.

[9] Rizza, F., Badeck, F., Cattivelli, L. and Lidestri, O. (2004). Use of a water stress index to identify barley genotypes adapted to rainfed and irrigated conditions. Crop Sci. 44, 2127-2137.

[10] Moinuddin, R., Fisher, A., Sayre, K. and Reynolds, M. (2005) Osmotic adjustment in wheat in relation to grain yield under water deficit environments. Agron. J. 97, 1062-1071.

[11] Hufstetler, V., Boerma, R., Carter, T. and Earl, H. (2007). Genotypic variation for three physiological traits affecting drought tolerance in soybean. Crop Sci. 47, 25-35.

[12] Schuzendubel, A., Rudolf, N.P.C. and Polle, A. (2002). Cadmium and H 2 O 2 -induced oxidative stress in populous x canescens roots. Plant Physiol. Biochem. (40), 577-584.

[13] Malik, T., Wright, D., and Virk, D. (1999). Inheritance of net photosynthesis and transpiration efficiency in spring wheat, *Triticum aestivum* L., under drought. Plant Breed. 118, 93-95.

[14] Rahman, S., Shaheen, M., Rahman, M. and Malik, T. (2000). Evaluation of excised leaf water loss and relative water content as screening techniques for breeding drought resistant wheat. Pak. J. Biol. Sci. 3, 663-665.

[15] Pettigrew, W. and Meredith, W. (1994) Leaf gas exchange parameters vary among cotton genotypes. Crop Sci. 34, 700-705.

[16] Lacape, M., Wery, J. and Annerosa, D. (1998) Relationship between plant and soil water status in five field-growing cotton (*Gossypiumhirsutum*L.) cultivars. Field Crops Res. 57, 29-48.

[17] Loka, D., Oosterhuis, D., and Ritchie, G. (2011) Stress Physiology in Cotton: Water-deficit stress in cotton. The Cotton Foundation, Cordova, Tennessee (USA). 37-72.

[18] Voltas, J., Lopez-Corcoles, H. and Borras, G. (2005). Use of biplot analysis and factorial regression for the investigation of superior genotypes in multi environment trials. Eur. Journal Agronomy. 22, 309–324.

[19] Cook, C. (1985). Identifying root traits among MAR and non-MAR cotton, *Gossypium hirsutum* L. cultivars that relate to performance under limited moisture conditions. Master Thesis. Texas A&M University, USA.

[20] Pace, P., Cralle, T., El-Halawany, S., Cothren, J. and Senseman, S. (1999). Drought-induced changes in shoots and root growth of young cotton plants. The J. Cotton Sci. 3, 183-187.

[21] Adil, J., Shahid, M., Aftab, B., Rashid, B., Sarwar, M., Mohamed, B., Hassan, S. and Husnain, T. (2014) Water stress mediated changes in morphology and physiology of *Gossypiumarboreum* (Var. FDH-786). J. Plant Sci. 2, 179-186.

[22] Clark, J.H. and McCaig, T.M. (1982) Evaluation of techniques for screening for drought resistance in wheat. Crop Sci. 22, 1036-1040.

[23] Radoglou, K. and Jarvis, P. (1990) Effects of CO_2 enrichment on four poplar clones. II. Leaf surface properties. Annals of Botany. 65, 627–632.

[24] Iqbal, K., Azhar, F., Khan, I. and Ullah, E. (2010). Assessment of cotton (*Gossypiumhirsutum* L.) germplasm under water stress condition. Int. J. Agric. Biol. 12, 251-255.

[25] Soomro, M., Markhand, G. and Soomro, B. (2011). Screening Pakistani cotton for drought tolerance. Pak. J. Bot. 44 (1), 383-388.

[26] Shah, A., Khan, T., Sadaqat, H. and Chatha, A. (2011). Alterations in leaf pigments in cotton (*Gossypium hirsutum* L.)genotypes subjected to drought stress conditions. Int. J. Agric. Biol. 13, 902-908.

[27] Brito, G., Sofiatti, D., Lima, M., Carvalho, L. and Filho, J. (2011) Physiological traits for drought phenotyping in cotton. Acta Scientiarum Agronomy. 33 (1), 117-125.

[28] Cardenal, L., Mora-Oberlaender, J. and Chaparro-Giraldo, A. (2013) Study Of Gene Flow From Gm Cotton (Gossypium Hirsutum) Varieties In "El Espinal" (Tolima, Colombia). Acta Biol. Colomb. 18 (3), 489-498.

[29] Comas, L., Becker, S., Cruz, V., Byrne, P. and Dierig, D. (2013) Root traits contributing to plant productivity under drought. Front Plant Sci. 4, 442.

[30] Luo, H., Zhang, Y., and Zhang, W. (2016) Effects of water stress and re-watering on photosynthesis, root activity, and yield of cotton with drip irrigation under mulch. Photosynthetica. 54, 65–73.

[31] Liu, G., Li, X., Jin, S., Liu, X., Zhu, L., Nie, Y., and Zhang, X. (2014). Overexpression of rice NAC gene *SNAC1*improves drought and salt tolerance by enhancing root development and reducing transpiration rate in transgenic cotton. PLoS ONE. 9. Article ID: e86895. http://journals.plos.org/plosone/article?id=10.1371/journal.pone.0086895

[32] Bhatt J and Andal R. 1979. Variation in foliar anatomy of cotton. Proc. Ind. Acad. Sci. 8, 451-453.

[33] Mvula, J, James, M., Bokosi, V. and Banda, M. (2018) Screening cotton (*Gossypium hirsutum* L.) genotypes for drought tolerance under screen house conditions in Malawi. J. Plant Breed. and Crop. Sci. 10(2), 48-57.

[34] Peterson, C., Murrmann, M. and Steudle, E. (1993) Location of the major barriers to water and ion movement in young roots of *Zea mays* L. Planta. 190, 127–13.

[35] Basal, H., Smith, C., Thaxtonand, P., and Hemphill, J. (2004). Seedling drought tolerance in upland cotton. American Society Agronomy. 45, 766-771.

[36] Imran, M., Kamaran, S., Khan, T., Muneer, M., Rashid, M., Munir, M., and Azhar, F. (2016). Genetic analysis of fiber quality parameter under water stress in upland cotton (*Gossypium hirsutum* L.) J. Agri. and Envi. Sci. 5, 134-139.

[37] Levitt, J. (1980. Responces of plants to environment. 2nd ed. Academic press, New York.

[38] Singh, S., and Singh, D. (2004). Genetic analysis of morph-physiological parameters in cotton (*Gossypium hirsutum* L.). Indian J. Genet. PlantBreed. 61, 57–60.

[39] Parida, A., Dagaonka, V., Phalak, M. and Aurangabadkar, L.P. (2007). Differential responses of the enzymes involved in proline biosynthesis and degradation in drought tolerant and sensitive cotton genotypes during drought stress and recovery. Acta Physiol. Plant. 30, 619-627.

[40] Norren, S., Athar, U. and Ashraf, M. (2013). Interactive effects of watering regimes and exog enously applied osmoprotectants on earliness indices and leaf area index in cotton (Gossypium hirsutum L.) crop. Pakistan Journal of Botany. 45(6), 1873-1881.

[41] Sarwar, M., Saleem, M., and Ullah, N. (2017. Exogenously applied growth regulators protect the cotton crop from heat-induced injury by modulating plant defense mechanism. Sci. Rep. 8 (17), 1-15.

[42] Aboughadareh, A., Ahmadi, A., Mehrabi, J., Etminan, A., Moghaddam, M., Kadambot, H., and Siddique, M. (2017). Physiological responses to drought stress in wild relatives of wheat: implications for wheat improvement. Acta Physiol. Plant. 39, 106-114.

[43] Blum, A. (2009) Effective use of water (EUW) and not water-use efficiency (WUE) is the target of crop yield improvement under drought stress. Field Crops Res. 112, 119-123.

[44] Blum, A. (2011) Plant Breeding for Water-Limited Environments. New York, N.Y., Springer.

[45] Clarke, J. and McCaig, T. (1982) Evaluation of techniques for screening for drought resistance in wheat. Crop Sci. 22, 1036-1040.

[46] Barnabas, B., Jager, K., and Feher, A. (2008) The effect of drought and heat stress on reproductive processes in cereals. Plant Cell Environ. 31, 11-38.

[47] Sinclair, T., Zwieniecki, M. and Holbrook, N. (2008) Low leaf hydraulic conductance associated with drought tolerance in soybean. Physiol. Plant. 132, 446-451.

[48] Fang, Y. and Xiong, L. (2015). General mechanisms of drought response and their application in drought resistance improvement in plants. Cell. Mol. Life Sci. 72, 673-689.

[49] Wang, C., Isoda, A., Li, M., and Wang, D. (2007) Growth and eco-physiological performance of cotton under water stress conditions. Agricultural Sciences in China. 6, 949-955.

[50] Jatoi, W.A., Baloch, M.J., Khan, N., Munir, M., Khakwani, A.A., Vessar, N.F., Panhwar, S.A., and Gul, S. (2014) Heterosis for yield and physiological traits in wheat under water stress conditions. The J. Animal and Plant Sci. 24(1), 252-261.

[51] Hetherington, A. and Woodward, F. (2003). The role of stomata in sensing and driving environmental change. Nature. 424, 901-908.

[52] Iqbal, M., Khan, M., Naeem, M., Aziz, U., Afzal, J. and Latif, M. (2013). Inducing drought tolerance in upland cotton (*Gossypium hirsutum* L.), accomplishments and future prospects. World Appl. Sci. J. 21(7), 1062-1069.
[53] Wang, J., Griffiths, R., Ying, J., McCourt, P. and Huang, Y. (2009) Development of drought-tolerant (*Brassica napus* L.) through genetic modulation of ABA mediated stomata responses. Crop Sci. 49, 1539-1554.

Received: **25.10.2020**
Accepted: **07.11.2020**

CORRESPONDING AUTHOR

Wajid Ali Jatoi
Department of Plant Breeding and Genetics,
Sindh Agriculture University
Tandojam – Pakistan

e-mail: jatoiwajid@yahoo.com

© by PSP Volume 30– No. 05/2021 pages 5026-5032 Fresenius Environmental Bulletin

APPLICATION OF MULTI SENSOR KALMAN FILTER IN ULTRASONIC WATER METER

Fuqiang Zuo[1,2,3], Yu Liu[1,2,3,*]

[1]Research and Development Center of Healthcare Electronics, Institute of Microelectronics of Chinese Academy of Sciences,Beijing 100029, China
[2]University of Chinese Academy of Sciences, Beijing 100049, China
[3]Beijing Key Laboratory of RFIC Technology for Next Generation Communications, Institute of Microelectronics of Chinese Academy of Sciences, Beijing 100029, China

ABSTRACT

In this paper, Kalman filter algorithm was applied to the current ultrasonic flow measurement technology, and the application of Kalman filter algorithm in ultrasonic water meter was improved by multi parameter modification. The establishment of multi parameter model made the improved Kalman filter algorithm more suitable for flow measurement. By selecting the control factors, temperature and ion concentration were determined as the medium control parameters. Temperature T and concentration variable C were added to the model as control parameters. The research results show that the temperature and concentration exhibit a negative correlation with the measurement accuracy, and a Kalman filter algorithm based on multi-sensor is constructed. The measurement error range is reduced from 3-5% to about 1%. The measurement process not only ensures the accuracy and stability of flow measurement, but also reduces the computational complexity and considers the low power consumption.

KEYWORDS:
Multi parameter, Kalman filter, Ultrasonic water meter

INTRODUCTION

Ultrasonic is a kind of mechanical vibration wave with frequency higher than 20kHz, which is equipped with good directivity and elasticity, strong penetration ability, relatively concentrated energy and other characteristics [1]. It is widely used in industrial and military fields, such as velocity detecting, ranging, positioning, etc. Ultrasonic will be affected by different media and environmental noise [2] or cause refraction and reflection when it encounters various obstacles [3] during its spread. The application of ultrasonic properties in detecting technique has become the key of research in the 21st century [4]. At present, the basic principle of velocity detecting of the opposite-type ultrasonic is the same as that of the reflective, which estimates the subject position by receiving the ultrasonic emitted from different fixed positions [5]. The difference is that the opposite-type ultrasonic velocity detecting method needs to determine how to allocate the ultrasonic probe when building the system [6]. At present, the system structure of ultrasonic velocity detecting is simplified, which can complete the velocity detecting by two ultrasonic modules. However, high precision and high resolution are still a potential obstacle limited the further development, for the main reason that the decrease of measurement accuracy caused by the existence of transit time error [7].

There are many theories and methods to eliminate the transit time error. For example, after receiving the echo signal, AGC amplification is applied in the signal to avoid triggering error, and different threshold values are selected in accordance with the actual measurement distance [8]. The double comparator shaping circuit is used to estimate the arrival time of the echo signal; a circuit where the threshold voltage can be decreased with time increase is designed to conduct multiple measurements to get the average value, in order to effectively eliminate the error caused by single measurement [9]. Either the ill conditioned mathematical method is used to fit the relationship between the measured value and the real value, or the BP neural network is used for nonlinear correction of the measurement results [10]. The method of parameter compensation is mainly used in the elimination of sound velocity error for the reason that the sound velocity V of ultrasonic depends on the temperature, pressure, density and other characteristics of the transmission media [11]. Therefore, in this research, control parameters such as temperature, pressure and ion concentration were investigated respectively to detect accuracy and stability, and finally, a Kalman filter algorithm based on multi-sensor was constructed.

MATERIALS AND METHODS

Principle of Ultrasonic Measurement. The principle of ultrasonic measurement is a flow measurement principle based on the ultrasonic transit time difference method, specifically showing

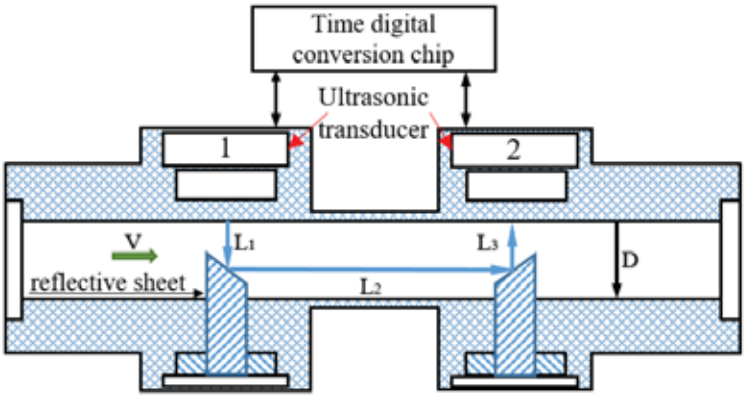

FIGURE 1
Schematic Diagram of Ultrasonic Flow Measurement Principle

$$t_{downstream} = \frac{L_1 + L_3}{C} + \frac{L_2}{C + v} \quad (1)$$

$$t_{countercurrent} = \frac{L_1 + L_3}{C} + \frac{L_2}{C - v} \quad (2)$$

$$\Delta t = t_{countercurrent} - t_{downstream} = \frac{L_2}{C - v} - \frac{L_2}{C + v} = \frac{2vL_2}{C^2 - v^2} \approx \frac{2vL_2}{C^2} \quad (3)$$

$$v \approx \frac{\Delta tC^2}{2L_2} \quad (4)$$

that there is a certain time difference between the time when the downstream transducer emits the ultrasonic wave and the counter current transducer receives the ultrasonic wave and the time when the counter current transducer emits the ultrasonic wave the downstream transducer receives the ultrasonic wave [12]. There is a functional relationship between time difference and the current flow velocity, therefore, fluid velocity can be obtained by measuring the time difference [13]. The schematic diagram is shown in Figure 1.

The process of ultrasonic flow measurement principle are (please see the equations above):

Where, $t_{countercurrent}$ represents the transit time of counter current ultrasonic wave; $t_{downstream}$represents the transit time of downstream ultrasonic wave; L_1 represents the distance between ultrasonic transducers; D represents the pipe diameter; C represents the transit speed of ultrasonic wave in water; Δt represents the transit time difference of ultrasonic wave between downstream and counter current; υ represents the fluid velocity in the pipe.

Empirical Model. Kalman filter algorithm is an algorithm for estimating model parameters without the ability of modeling [14], so an existing empirical model is required. Ultrasonic is provided with three important characteristics as follows:

1) Similarity: the waveform of echo signals at different positions are similar;

2) Correlation: for the same device and the same object, with the change of distance, the ultrasonic echo signal only changes in strength while the waveform changes little, that is to say, the echo signals are closely related;

3) Narrowband: the frequency of ultrasonic signal is mainly distributed in the narrow frequency domain centered in the resonant frequency of transducer.

Therefore, the parameterization of prediction noise Q in Kalman filter algorithm is related to temperature T, pressure P and time t, forming a parametric model[15]; Measured values of pressure and temperature sensors are introduced into the Kalman filter algorithm to further improve accuracy and stability of flow measurement; There is a certain relationship between the transit speed of ultrasound in water and the state of medium, directly linked with temperature and pressure [15]. Based on this, equation $Q=f(T, P, t)$ is established, and the corresponding function relationship or empirical formula is found. The measured velocity, temperature and pressure are comprehensively filtered by Kalman filter algorithm; Time-drift caused by time t is properly taken into consideration to make some modification; It is necessary to extend Kalman filter algorithm because it integrates multiple sensors and there is a certain functional relationship between sensor values.

A measuring tube with a diameter of 20 mm was selected, and the flow rate of ultrasonic test was set as a fixed value q to compare with the data measured by later experiments. In this experiment, the actual flow rate was set as $q1$=10 L·h^{-1}, $q2$=16 L·h^{-1},

and *q3*=4000 L·h^{-1} respectively, and the corresponding flow velocity was set as *v1*=8.84mm/s, *v2*=14.15mm/s, *v3*=3.537m/s; the accuracy and stability of measurement were improved by introduction of temperature and pressure, especially at low flow rate.

Composition of Model Parameters. In the conventional Kalman filter framework, when the actual fluid model of the target matches the theoretical model of the frame, the residual information meets the following requirements:

$$\mathrm{E}[\gamma_k \gamma_i^T] = \begin{cases} H_k P_{k|k-1} H_k^T + R_k, j = k \\ 0, \ j \neq k \end{cases} \quad (5)$$

Where, H_k is the system state transition matrix; $P_{k|k-1}$ is the state prediction error variance matrix; R_k is the state process variance matrix. When the model is mismatched, the predicted $X_{k|k-1}$ will appear error, and the residual sequence will no longer meet the above equation. At this time, prediction error variance can be calculate:

$$P_{k|k-1} = \emptyset_{k|k-1} P_{k-1|k-1} \emptyset_{k|k-1}^T + Q_k \quad (6)$$

Since the target state transition matrix $\Phi_{k|k-1}$ and process noise variance matrix Q_k are related to model parameters, parameters of fluid model can be established to adjust the in real time by considering the actual statistical characteristics of residual sequence and $P_{k|k-1}$. It can be expressed as:

$$V_k = \mathrm{E}[\gamma_k \gamma_\emptyset^T] \quad (7)$$

$$V_k = \frac{\sigma V_{k-1} + \gamma_k \gamma_k^T}{1+\emptyset}, V_0 = 0 \quad (8)$$

$$\begin{cases} N_k = V_k - R_k \\ M_k = H_k(\emptyset_{k|k-1} P_{k-1|k-1} \emptyset_{k|k-1}^T + Q_k) H_k^T \end{cases} \quad (9)$$

$$\lambda_k \begin{cases} \frac{trance(N_k)}{trance(M_k)}, \frac{trance(N_k)}{trance(M_k)} > 1 \\ 1, \frac{trance(N_k)}{trance(M_k)} \leq 1 \end{cases} \quad (10)$$

After fully consideration, the extended Kalman filter algorithm mainly contains five updated equations:

① Predicted value:

$$\hat{x}_k^- \cong f(\hat{x}_{k-1}, u_{k-1}, 0); \quad (11)$$

② Covariance matrix update:

$$P_k^- = A_{k-1} P_{k-1} {A_{k-1}}^T + Q_{k-1}, \ Q_{k-1} = f_w'(\hat{x}_{k-1}, 0) q f_w'(\hat{x}_{k-1}, 0)^T; \quad (12)$$

③ Kalman gain:

$$K = P_k^- H_k^T (H_k P_k^- H_k^T + R_k)^{-1}, \ R_k = h_v'(\hat{x}_k^-, 0) r h_v'(\hat{x}_k^-, 0)^T; \quad (13)$$

④ Correction value:

$$\hat{x}_k = \hat{x}_k^- + K(Z_k - h(\hat{x}_k^-, 0)); \quad (14)$$

⑤ Covariance matrix update:

$$P_k = (I - K_k H_k) P_k^-. \quad (15)$$

Parameter Verification of Multi Sensor. The system model of ultrasonic flow measurement is established based on extended Kalman filter algorithm, consisting of ten components [16, 17]:

① The state variable $X = (T, \upsilon)^T$, medium temperature (℃), pressure (MPa) and flow rate (m/s) of the model are defined;

② The control variable, usually the motor control of valve opening is input. It can be direct current or duty cycle of PWM wave. There is no control variable in this system;

③ Observed variable $Z = (c, \Delta t)^T$, velocity of ultrasound in medium (m/s) and transit time difference (ns) are defined. The number of observed variable is less than state variable;

④ System description: the flow rate and temperature are large inertial variables, so the prediction is the same as that of the previous moment, and the smaller the sampling interval is, the more accurate the system; the system is out of external control; the observed value of the system is also consistent with the filter value;

⑤ State equation:

$$\hat{x}_k^- = f(\hat{x}_{k-1}, u_{k-1}, w_{k-1}) = A\hat{x}_{k-1} + Bu_{k-1} + n(Q), \quad (16)$$

⑥ Observation equation:

$$Z_k = H(\hat{x}_k, v) = H(\hat{x}_k, 0) + HRH^T = H(\hat{x}_k, 0) + V, \quad (17)$$

⑦ The observation value corresponds to the state equation, that is, time difference:

$$h_2: \Delta t = \frac{L}{c-v} - \frac{L}{c+v} = 2L\frac{v}{c^2} = 2Lvc^{-2} \quad (18)$$

Numerical verification: the correlation between the estimated value of parameters calculated in Kalman filter algorithm and the measured value is established, and the significant difference between the estimated value and the measured value of different parameter pairs is investigated respectively. If there is no significant difference between the estimated value and the measured value within the parameter range, it can be proposed that the model parameters are applicable for Kalman filter algorithm to measure ultrasonic water meter flow.

RESULTS AND DISCUSSION

Analysis of Temperature Effect. In order to optimize the extended Kalman filter algorithm, the influence of external temperature on the accuracy was investigated. The ultrasonic data was obtained through the measurement system. The experiment was carried out by testing the fixed flow rate through ultrasonic. Since the stability and accuracy of the algorithm were affected by low flow velocity [18], the actual flow velocity was set as Q=10 L·h^{-1} in this experiment. Because of the fast recursive speed of extended Kalman filter algorithm, a total of 80 measurements were launched to ensure enough measured data for operation. Aiming at starting the extended Kalman filter algorithm, an initial state value of *d1* was input, that was, the value of $X_{0|0}$, which can be arbitrarily determined, so $X_{0|0}$= 1 was set. After inputting the initial value, the filter and detector started to collaboratively work. The data was analyzed after 80 operations. In order to highlight the effect of modal optimization, four groups of measurements were conducted. Each group of measurements corresponds to 4 different testing temperatures, and the results are shown in Figure 2.

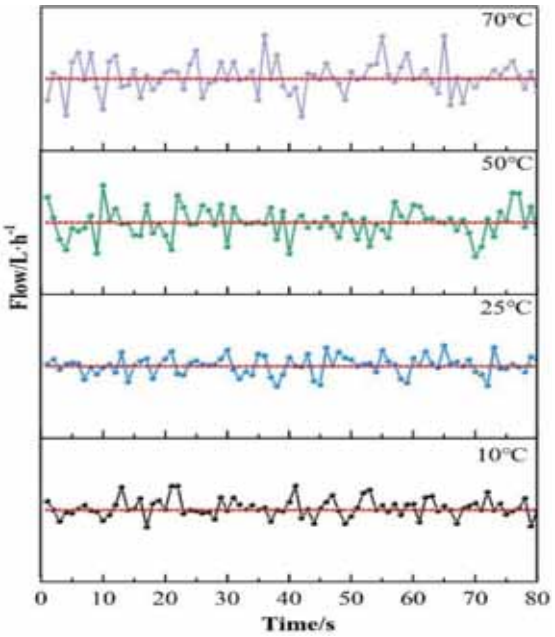

FIGURE 2
Influence of Different Temperature on Test Results

In Figure 2, the red line represents the standard flow rate value set by the testing system; the lines of other colors respectively the test values corrected by the extended Kalman filter algorithm at 10°C, 25°C, 50°C and 70°C respectively. It can be figured out that the influence of environmental noise and the hardware property of the system contribute to some certain errors in the accuracy of ultrasonic velocity measurement. The error range of measurement value is still controlled at about 2% when the temperature is 25 °C at room temperature and 10 °C at low temperature. Obviously, this is acceptable for the overall flow rate. However, with the increase of temperature, the error range gradually increases from 1% to 1-2% at 50 °C and 3-5% at 90 °C. Apparently, it greatly limits ultrasonic velocity measurement. Therefore, through the adjustment of model parameters, the parameters are reasonably modified according to the negative correlation observed by the model state variable $X=(T,\upsilon)^T$ [19]. The water flow velocity at 90 °C is measured by the modified model, and the results are shown in Figure 3.

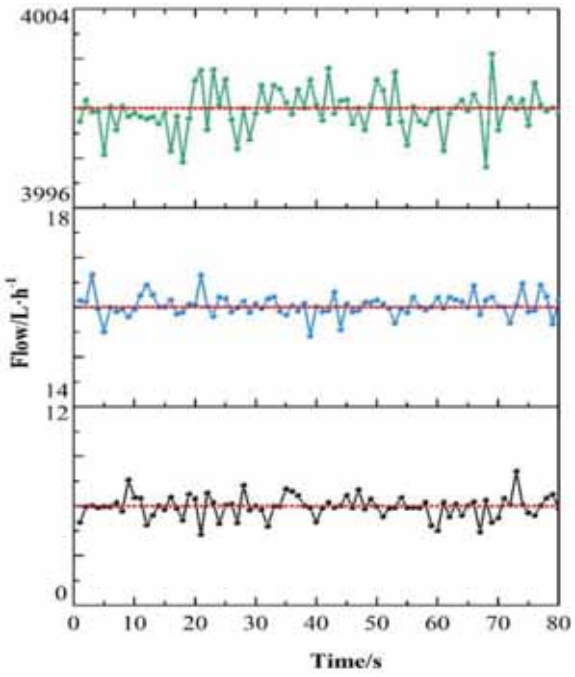

FIGURE 3
Testing Results of Extended Kalman Filter Algorithm at Different Flow Rates at 90 °C

It is obvious that the accuracy of the testing results is improved after the modification. The error range is only about 2% at the flow rate of 10 L/h and 16 L/h, and less than 5% at the flow rate of 4000 L/h, which indicates that the accuracy of Kalman filter in water flow measurement at different temperatures can be improved by adjusting the temperature. In addition, it is worth noting that the testing values do not fluctuate violently and basically float up and down along the actual value in the 80 times testing. The extension of time do not result in fluctuation, therefore, it also demonstrates that the extended Kalman filter algorithm system has good testing stability.

Analysis of Pressure Effect. Aimed to optimize the extended Kalman filter algorithm, the influence of external water pressure on the accuracy was investigated. The ultrasonic data was obtained through the measurement system. In the experiment, ultrasonic was used to test the fixed flow rate. Since low flow velocity easily gave rise to problems on the

stability and accuracy of the algorithm, the actual flow velocity was set as Q=10 L·h^{-1} in this experiment. Because of the fast recursive speed of extended Kalman filter algorithm, a total of 80 measurements were organized to ensure enough measured data for operation. An initial state value of *d1* needed to be input before starting the extended Kalman filter algorithm, that is, the value of $X_{0|0}$, which can be arbitrarily determined, so $X_{0|0}$= 1 was set. After inputting the initial value, the filter and detector started to work cooperatively. The data was analyzed after 80 operations. In order to stress on the effect of modal optimization, four groups of measurements were conducted. Each group of measurements corresponds to 4 different testing pressures, and the results are shown in Figure 4.

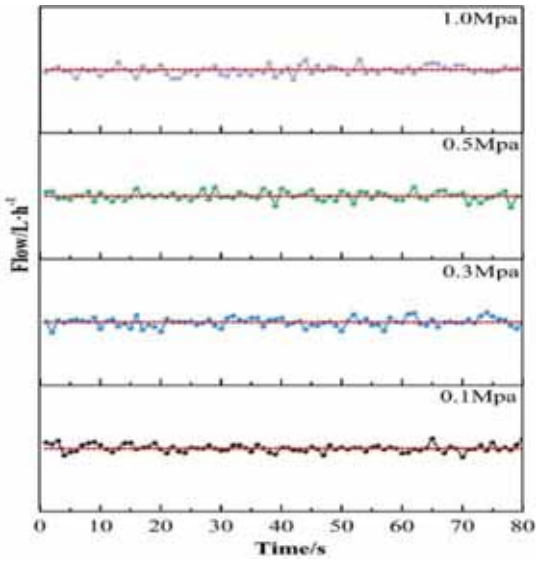

FIGURE 4
Influence of Different Pressures on Testing Results

In Figure 4, the red line represents the standard flow rate value set by the testing system; the lines with other colors represent the testing values modified by the extended Kalman filter algorithm at 0.1 MPa, 0.3 MPa, 0.5 MPa, 1.0 MPa respectively. It can be seen that influencing by environmental noise and the hardware property of the system, a certain error exists in the accuracy of ultrasonic velocity measurement. However, the overall error range is very small, and the error range does not increase significantly with the increase of pressure, which reveals that the water pressure do not produce direct interference on the transmission of ultrasonic, so the detection of pressure in external parameters is not a necessary control factor [20].

Analysis of Ion Concentration in Water Effect. Water is the benign solvent of most solutions, so the dissolved ions in water often change the flow parameters. Therefore, the water flow with different ion concentration was measured to expand the application range of this method.The ultrasonic data was obtained through the measurement system. The experimental process was to test the fixed flow rate through ultrasonic. Since problems on the stability and accuracy of the algorithm could be triggered by low flow velocity, the actual flow velocity was set as Q=16 L·h^{-1} in this experiment. Because of the fast recursive speed of extended Kalman filter algorithm, a total of 80 measurements were conducted to make sure that there was enough measured data for operation. In order to make the extended Kalman filter algorithm work, an initial state value of *d1* was input, that is, the value of $X_{0|0}$, which was given arbitrarily, so $X_{0|0}$= 1 was set. After inputting the initial value, the filter and detector started to collaboratively work. The data was analyzed after 80 operations. In order to stress on the effect of modal optimization, four groups of measurements were conducted. Each group of measurements corresponds to 4 different chloride concentrations, and the results are shown in Figure 5.

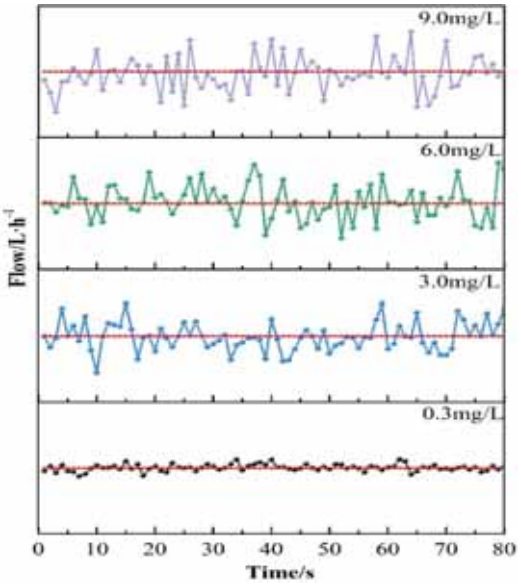

FIGURE 5
Influence of Different Chloride Concentration on Testing Results

It can be clearly seen from Figure 5 that with the increase of ion concentration, the accuracy of the testing results directly decreases, and the error range increases from 1% to 3-5%. Apparently, it is unacceptable for the overall testing [21]. Therefore, the addition of ion concentration as a parameter in the model state variable $X=(T,\upsilon)^T$ also has a negative correlation with the results. The water with different chloride concentration was measured by the modified model, and the results are shown in Figure 6. It can be found out that the accuracy of the testing results is improved after the correction. whatever ion concentration it is, the measurement error maintains at about 1%.

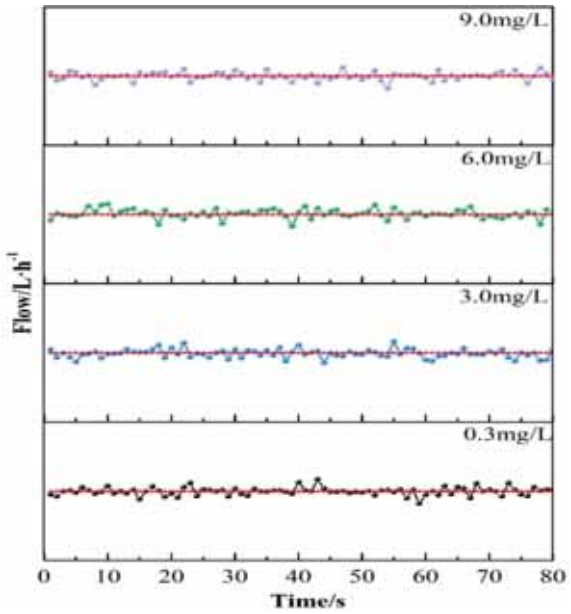

FIGURE 6
Influence of Different Chloride Concentration on Testing Results from Modified Model

CONCLUSIONS

In this paper, Kalman filter algorithm was applied to the current ultrasonic flow measurement technique, and the improvement of the application of Kalman filter algorithm in ultrasonic water meter by multi-sensor correction was proposed. Establishing multi parameter model help the improved Kalman filter algorithm more suitable for flow measurement, ensuring and the accuracy and stability of flow measurement. Through the screening of media parameters, the final parameters affecting the ultrasonic transmission were temperature and ion concentration. The appropriate ultrasonic measurement technique was obtained by modified model, controlling the measurement error of water flow velocity at high temperature and high ion concentration from 3-5% to about 1%, which proved that the multi parameter Kalman filter algorithm can better adapt the application of ultrasonic water meter in different conditions.

ACKNOWLEDGEMENTS

1. National Science and Technology Major Project of China (under Grants 2018ZX01031201-001), National Key R&D Program (under Grants 2018YFC2001100)

2. National Natural Science Foundation of China (under Grants 61574165)

REFERENCES

[1] Yuan, H., Dai, H.F., Wei, X.Z., Ming P.W. (2019) A Novel Model-Based Internal State Observer of a Fuel Cell System for Electric Vehicles Using Improved Kalman Filter Approach. Applied Energy. 268, 115009.

[2] Park, S., Kim, K., Shin, C., Min, J.H., Na, E.H., Park L J. (2020) Variable Update Strategy to Improve Water Quality Forecast Accuracy in Multivariate Data Assimilation Using the Ensemble Kalman Filter. Water Research. 176, 115711.

[3] Thenaisie, G., Park, C.H., Lee, S.G. (2020) A Real-Time Entropy Estimation Algorithm for Lithium Batteries Based on a Combination of Kalman Filter and Nonlinear Observer. Ieee Transactions on Industrial Electronics. 67(9), 8034-8043.

[4] Cao, R.W., Jiang, N., Lu, M.H. (2015) Sensorless Control of Linear Flux-Switching Permanent Magnet Motor Based on Extended Kalman Filter. Ieee Transactions on Industrial Electronics. 67(7), 5971-5979.

[5] Pogorelyuk, L., Rowley, C.W., Kasdin, N.J. (2020) An Efficient Approximation of The Kalman Filter for Multiple Systems Coupled Via Low-Dimensional Stochastic Input. Automatica. 117, 108972.

[6] Zhang, C., Yan, Q., Kuczynska-Kippen, N., Gao, X.P. (2015) An Ensemble Kalman Filter Approach to Assess the Effects of Hydrological Variability, Water Diversion, and Meteorological Forcing on the Total Phosphorus Concentration in a Shallow Reservoir. Science of the Total Envi-ronment. 724, 138215.

[7] Song, R., Chen, X.Y., Fang, Y.C., Huang, H.Q. (2020) Integrated Navigation of Gps/Ins Based on Fusion of Recursive Maximum Likelihood Imm and Square-Root Cubature Kalman Filter. Isa Transactions. 105, 387-395.

[8] Narayanan, H., Behle, L., Luna, M.F., Sokolov, M., Guillen-Gosalbez, G., Morbidelli, M., Butte, A. (2020) Hybrid-Ekf: Hybrid Model Coupled with Extended Kalman Filter for Real-Time Monitoring and Control of Mammalian Cell Culture. Biotechnology and Bioengineering. 117(9), 2703-2714.

[9] Ebrahimi, F., Abedi, M. (2016) Design of a Robust Central Difference Kalman Filter in the Presence of Uncertainties and Unknown Measurement Errors. Signal Processing. 172, 107533.

[10] Hage, D.A., Conde, M.H., Loffeld, O. (2020) Sparse Signal Recovery Via Kalman-Filter-Based L(1) Minimization. Signal Processing. 171, 107487.

[11] Phogat, K.S., Chang, D.E. (2020) Discrete-Time Invariant Extended Kalman Filter on Matrix Lie Groups. International Journal of Robust and Nonlinear Control. 30(12), 4449-4462.
[12] Ravi, A., Narasimhan, S., Kaisare, N.S. (2020) Sampled Output Augmentation Method for Handling Measurement Delays in Multirate Kalman Filter. Chemical Engineering Science. 224, 115763.
[13] Van Leeuwen, P.J. (2020) A Consistent Interpretation of the Stochastic Version of the Ensemble Kalman Filter. Quarterly Journal of the Royal Meteorological Society. 146 (731), 2815-2825.
[14] Yang, Y, Li, B., Wu, X.J., Yang, L.J. (2018) Application of Adaptive Cubature Kalman Filter to In-Pipe Survey System for 3d Small-Diameter Pipeline Mapping. Ieee Sensors Journal. 20(12), 6331-6337.
[15] Chu, C.B., Yang, S.D. (2020) Keyframe-Based Rgb-D Visual-Inertial Odometry and Camera Extrinsic Calibration Using Extended Kalman Filter. Ieee Sensors Journal. 20(11), 6130-6138.
[16] Wang, J., Zhang, T., Jin, B.N., Zhu, Y.Y., Tong, J.W. (2020) Student's T-Based Robust Kalman Filter for a Sins/Usbl Integration Navigation Strategy. Ieee Sensors Journal. 20(10), 5540-5553.
[17] Arasaratnam, I., Haykin, S. (2009) Cubature Kalman Filters. IEEE Transactions on Automatic Control. 54(6), 1254-1269.
[18] Man, J., Zheng, Q., Wu, L.S., Zeng, L.Z. (2020) Adaptive Multi-Fidelity Probabilistic Collocation-Based Kalman Filter for Subsurface Flow Data Assimilation: Numerical Modeling and Real-World Experiment. Stochastic Environmental Research and Risk Assessment. Stochastic Environmental Research and Risk Assessment. 34(8), 1135-1146.
[19] Amirat, Y., Oubrahim, Z., Ahmed, H., Benbouzid, M., Wang, T.Z. (2020) Phasor Estimation for Grid Power Monitoring: Least Square Vs. Linear Kalman Filter. Energies, 13(10), 2456.
[20] Bajo, M. (2019) Improving Storm Surge Forecast in Venice with a Unidimensional Kalman Filter. Estuarine Coastal and Shelf Science. 239, 106773.
[21] Emami, A., Sarvi, M., Bagloee, S.A. (2020) Short-Term Traffic Flow Prediction Based on Faded Memory Kalman Filter Fusing Data from Connected Vehicles and Bluetooth Sensors. Simulation Modelling Practice and Theory. 102, 102025.

Received: **26.10.2020**
Accepted: **28.10.2020**

CORRESPONDING AUTHOR

Yu Liu
Research and Development Center of Healthcare Electronics, Institute of Microelectronics of Chinese Academy of Sciences,
Beijing 100029, China

e-mail: makiafeng8888@outlook.com

© by PSP Volume 30– No. 05/2021 pages 5033-5039 Fresenius Environmental Bulletin

STUDY ON LOW POWER CONSUMPTION OF KALMAN FILTER

Fuqiang Zuo[1,2,3], Yu Liu[1,2,3,*]

[1]Research and Development Center of Healthcare Electronics, Institute of Microelectronics of Chinese Academy of Sciences, Beijing 100029, China
[2]University of Chinese Academy of Sciences, Beijing 100049, China
[3]Beijing Key Laboratory of RFIC Technology for Next Generation Communications, Institute of Microelectronics of Chinese Academy of Sciences, Beijing 100029, China

ABSTRACT

In the 21st century, high-precision and high-resolution velocity measurement has been realized, and ultrasonic flow measurement technology has been greatly improved. However, the flow measurement algorithms of mature products are relatively confidential at home and abroad. Research shows that the Kalman filter algorithm has application potential in the monitoring and measurement of ultrasonic flow. Therefore, this paper applies the Kalman filter algorithm to the current ultrasonic flow measurement technology and proposes an improved Kalman filter algorithm that adapts to the change of flow characteristics. The Kalman filter algorithm is successfully applied to the ultrasonic velocity measurement system by introducing an adaptive factor into the algorithm. When the flow rate is 1000 $mL \cdot min^{-1}$, the measurement error range is reduced from ±50 $mL \cdot min^{-1}$ to ±5 $mL \cdot min^{-1}$. At the same time, correction parameters *a* and *b* are introduced respectively, finally the accurate measurement of the flow rate by the ultrasonic testing system at low flow rate and high flow rate is realized, and the error ranges are reduced to ±0.1 $mL \cdot min^{-1}$ and ±2 $mL \cdot min^{-1}$ respectively, which ensures the accuracy and stability of flow measurement, reduces the calculation complexity and takes into account the low power consumption performance.

KEYWORDS:
Kalman filter, Ultrasonic water meter, Low power consumption, Energy

INTRODUCTION

In the late 20th century and the early 21st century, with the continuous in-depth study of the fluid distribution law, especially with the development of electronic technology, chip technology, microprocessor technology (MCU, MPU), digital signal processing technology (DSP, FPGA, CPLD) and other related technologies, the resolution and accuracy of time measurement are increasingly high [1]. Moreover, in the 21st century, there is a special chip TDC for time-to-digital conversion, which can achieve high-precision and high-resolution time measurement [2]. The ultrasonic flow measurement technology has been significantly improved, with its measurement accuracy and stability greatly improved, and it has been gradually promoted and applied in many fields [3], such as petroleum, national defense, chemical industry, smelting, water supply, drainage and other fields of scientific research, production, life [4,5]. Overseas research, invention and manufacturing of ultrasonic flow measurement products are relatively early, and related technologies, patents, papers are rich, so there are a lot of mature and commercial ultrasonic flow measurement products abroad [6]. For example, the United States, Germany, Japan and other countries are in the international leading position, with rich research and manufacturing experience, currently dominating the development trend of ultrasonic flow measurement [7]. The research and manufacturing of ultrasonic flow measurement in China is immature. However, due to the strong domestic market demand and the increasing number of engineering students year by year, the corresponding scientific researchers and engineers in China also show a blowout trend [8]. With the deepening of domestic and foreign exchanges, the domestic ultrasonic flow measurement products have also made great progress. Some enterprises not only have put their products into market in large quantities, but also own relatively mature and stable technologies, and many of them have entered the international market [9].

The flow measurement algorithms of mature products are relatively confidential at home and abroad, and only a few literatures have studied the monitoring and measurement of ultrasonic flow [10]. Leopoldo Angrisani et al. [11] proposed to use the Kalman filter algorithm for flow measurement of ultrasonic time difference method, and to process the data. Zhen-Jing Yao et al. [12] proposed to use multiple SR-UKF filtering algorithm to improve the accuracy of ultrasonic time difference distance measurement system, which can be used for

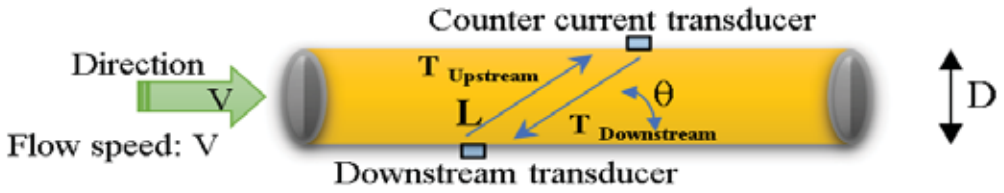

FIGURE 1
Schematic diagram of ultrasonic flow measurement

$$T_{Upstream} = \frac{L}{c - V\cos\theta}$$

$$T_{downstream} = \frac{L}{c + V\cos\theta}$$

$$\Delta T = T_{Upstream} - T_{downstream} = \frac{\frac{D}{\sin\theta}}{c - V\cos\theta} - \frac{\frac{D}{\sin\theta}}{c + V\cos\theta}$$

$$= \frac{2DV\cos\theta}{\sin\theta\,(c^2 - V^2\cos^2\theta)} \approx \frac{2DV\cos\theta}{c^2\sin\theta} = \frac{2DV}{c^2\tan\theta}$$

$$v \approx \frac{\Delta T c^2\tan\theta}{2D} = \frac{c^2\tan\theta}{2D}(T_{Upstream} - T_{downstream}) \quad (1)$$

reference in ultrasonic flow measurement. Leopoldo Angrisani et al. [13] proposed to use Kalman filter algorithm and UKF for the estimation of ultrasonic time difference method and its performance evaluation. Obviously, the Kalman filter algorithm has application potential in the monitoring and measurement of ultrasonic flow [14]. However, there is little research on the application of Kalman filter algorithm in ultrasonic water meter at present. In this paper, the Kalman filter algorithm is applied to the current ultrasonic flow measurement technology, and an improved Kalman filter algorithm adapted to the change of flow characteristics is proposed. By establishing a multi-parameter model, the improved Kalman filter algorithm is more suitable for flow measurement, and ensures the accuracy and stability of flow measurement, while reducing the computation complexity and taking into account the low power consumption performance.

MATERIALS AND METHODS

Principles of Ultrasonic Measurement. The principle of ultrasonic measurement is a flow measurement principle based on the ultrasonic propagation time difference method, which is embodied in a certain time difference between the time when the ultrasonic wave is transmitted by the downstream transducer and received by the counter-current transducer and the time when the ultrasonic wave is transmitted by the countercurrent transducer and received by the downstream transducer. The time difference has a functional relationship with the current flow rate, so the flow rate of fluid can be obtained by measuring the time difference [15]. The principle diagram is shown in Figure 1.

The principle process of ultrasonic flow measurement (see the equation above).

In the formula, $T_{upstream}$ represents the countercurrent ultrasonic propagation time; $T_{downstream}$ represents the downstream ultrasonic propagation time; L represents the distance between ultrasonic transducers; D represents the pipe diameter; c represents the propagation speed of ultrasonic in water; θ represents the included angle between the central line of the downstream and countercurrent transducer and the pipe axis, which can be 0 °; ΔT represents the propagation time difference of downstream and countercurrent ultrasonic; V represents the flow velocity in the pipe.

Empirical Model. Kalman filter algorithm is an algorithm for estimating model parameters, which does not have the ability of modeling, so an existing empirical model is needed [16]. As ultrasound has the following three important characteristics:

1) Similarity: Echo signal waveforms at different positions are similar;

2) Correlation: For the same device and the same object, with the change of distance, the ultrasonic echo signal changes only in strength, but little in waveforms, that is to say, the echo signals are closely related;

3) Narrowness: The frequency of ultrasonic signal is mainly distributed in a narrow frequency domain centered on the resonant frequency of the transducer.

Therefore, the following empirical model can be adopted for ultrasonic single echo:

$$A(t) = A_0\left(\frac{t-\tau}{T}\right)^{\alpha} e^{\frac{-t+\tau}{T}} \quad (2)$$

$$r(t) = A(t)\sin(2\pi f_c t + \theta) \quad (3)$$

In the formula, *A(t)* is the envelope of the echo signal, A_0 is the amplitude. *T* and α, determined by the ultrasonic sensor and some environmental factors, control the shape of the echo envelope, τ is the required transit time, *r(t)* is the entire echo signal, f_c and θ are the frequency and initial phase of the ultrasonic wave respectively.

Composition and Adjustment Process of Model Parameters. In the traditional Kalman filter framework, when the actual fluid model of the target matches the theoretical model of the framework, the residual information satisfies [17]:

$$E[\gamma_k \gamma_i^T] = \begin{cases} H_k P_{k|k-1} H_k^T + R_k, j = k \\ 0, \ j \neq k \end{cases} \quad (4)$$

Among them, H_k is the system state transition matrix; $P_{k|k-1}$ is the state prediction error variance matrix; R_k is the state process variance matrix. When the model is mismatched, according to the state value $X_{k|k-1}$ predicted by the model, there is drift deviation, and the residual sequence no longer meets the above equation characteristics. At this time, the state prediction error variance can be calculated as:

$$P_{k|k-1} = \emptyset_{k|k-1} P_{k-1|k-1} \emptyset_{k|k-1}^T + Q_k \quad (5)$$

Since the state transition matrix $\phi_{k|k-1}$ and the process noise variance matrix Q_k of the target are related to the model parameters, the relationship between the actual statistical characteristics of the residual sequence and $P_{k|k-1}$ can be established to adjust the fluid model parameters in real time [18]. The specific construction process can be expressed as follows:

$$V_k = E[\gamma_k \gamma_\emptyset^T] \quad (6)$$

$$V_k = \frac{\sigma V_{k-1} + \gamma_k \gamma_k^T}{1+\emptyset}, V_0 = 0 \quad (7)$$

$$\begin{cases} N_k = V_k - R_k \\ M_k = H_k(\emptyset_{k|k-1} P_{k-1|k-1} \emptyset_{k|k-1}^T + Q_k) H_k^T \end{cases} \quad (8)$$

$$\lambda_k \begin{cases} \frac{trance(N_k)}{trance(M_k)}, \frac{trance(N_k)}{trance(M_k)} > 1 \\ 1, \frac{trance(N_k)}{trance(M_k)} \leq 1 \end{cases} \quad (9)$$

Among them, V_k is statistical characteristic, $0 \leq \sigma \leq 1$ is forgetting factor, λ_k is regulating factor, and parameter adjustment can be expressed as follows:

$$\alpha_k = \lambda_k \alpha \quad (10)$$

λ_k is the coefficient regulating factor under the condition of state mutation. Generally, in the case of weak state change, the smaller empirical value is usually taken. When the state changes greatly, the time-varying adjustment method is adopted, and the proportion coefficient *c* is introduced:

$$\lambda_k = c \times \lambda \quad (11)$$

Model Parameter Verification. Model simulation:

1) The ultrasonic with a center frequency of 4MHz is sampled at a sampling frequency of 15MHz.

2) The envelope of the sampled digital signal is extracted by Hilbert transform. The so-called Hilbert transform is to make the signal as fast Fourier transform (FFT) first, set the negative frequency component of the result to zero, and then make an inverse Fourier transform (IFFT). It should be noted that Hilbert transform can only extract the envelope, not suppress the noise.

3) The extracted envelope and a certain number of data points before and after it are used as observation signals in Kalman filter algorithm, then the estimated value of parameters can be obtained.

Numerical verification:

In this paper, the correlation between the estimated value of parameters calculated in Kalman filter algorithm and the measured value is established, and the significant differences between the estimated value and the measured value for different parameters are investigated respectively. When there is no significant difference, it can be considered that the model parameters are suitable for the measurement of ultrasonic water meter flow by Kalman filter algorithm.

RESULTS AND DISCUSSION

Analysis of Simulation Results. In order to study the performance of the optimized extended Kalman filter algorithm for transit time estimation, the simulation test system for ultrasonic measurement of fixed flow velocity is set as the research object; the experimental process is the process of the fixed velocity measurement by ultrasonic wave. A measuring pipe with a diameter of 20mm is selected, and the flow velocity of ultrasonic measurement is set as a fixed value Q to compare with the data measured in later experiments. In this experiment, the actual flow velocity are respectively set as Q_1 = 10 L/h, Q_2 = 16 L/h, and Q_3 = 4000 L/h. Because of the fast recursive speed of the extended Kalman filter algorithm, the Q is measured 80 times by simulation software to

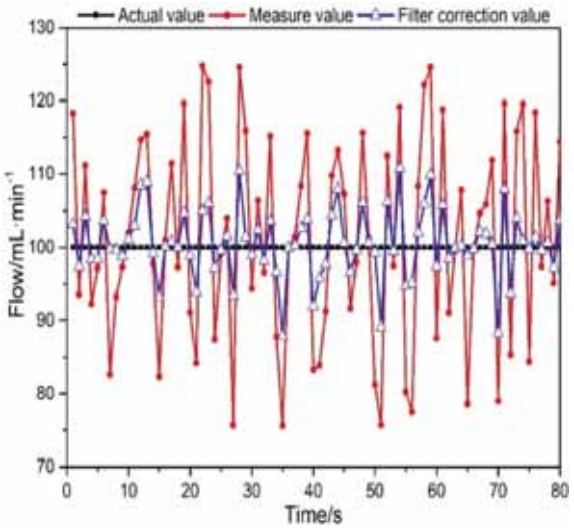

(a) Measurementsimulation of 100mL·min^{-1} flow velocity

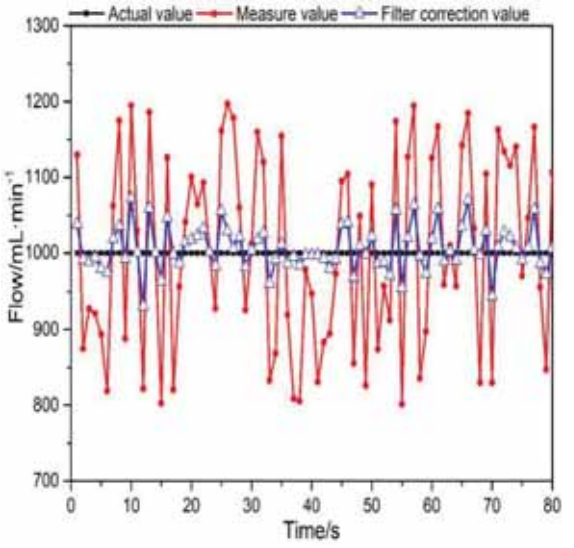

(b) Measurement simulation of 1000mL·min^{-1} flow velocity

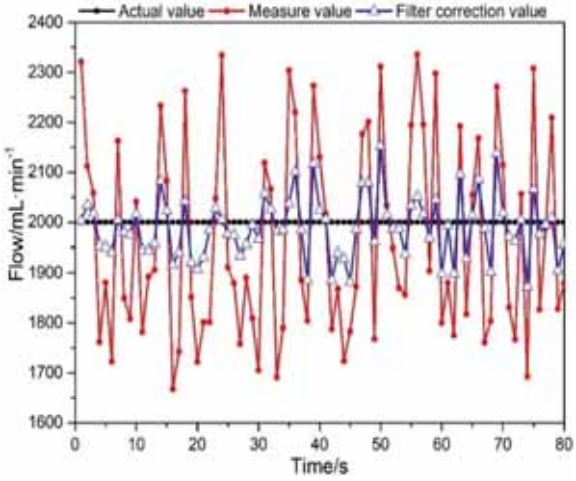

(c) Measurement simulation of 2000mL·min^{-1} flow velocity

FIGURE 2
Simulation of flow velocity measurement by extended Kalman filter

obtain enough measured data for calculation, so as to necessary to input an initial state value of d1, that is, the value of $X_{0|0}$, which can be arbitrarily given. achieve the experimental purpose. In order to make the extended Kalman filter algorithm work, it is Set $X_{0|0}$ = 3.8 mL·min^{-1}. After the initial value is input, the extended Kalman filter and T1 start to work together, and perform data analysis after 80 operations [19]. To highlight the effect of modal optimization, two groups of measurements are carried out. In the first group, the received ultrasonic signal is directly processed by extended Kalman filter without modal optimization, and the measurement data is shown in Figure 2.

In Figure 2, the red line represents the measure value of velocity by the test system; the blue line represents the value modified by the extended Kalman filter algorithm; and the black line is the actual value. It can be seen that due to the influence of environmental noise and the hardware characteristics of the system itself, the accuracy of ultrasonic velocity measurement has a considerable error. The error range is different under different flow rates. When the flow rate is 100mL·min^{-1}, the error range is about ±25mL·min^{-1}. When the flow rate is increased to 1000mL·min^{-1}, the error range is about ±200mL·min^{-1}, further increasing the flow rate to 2000mL·min^{-1}, the error range extends to about ±350mL·min^{-1}. Obviously, there is a great limitation for the ultrasonic velocity measurement. However, after the processing of the extended Kalman filter algorithm, the ranging error is greatly reduced, and the corrected value is closer to the actual value than the system measured value. In the 80 times of measurement, the circle line representing the modified distance value by the extended Kalman filter algorithm is closer to the line of actual value. Under the three conditions of Q= 100mL·min^{-1}, Q = 1000mL·min^{-1}, Q= 2000mL·min^{-1}, the error range of each condition is reduced to ±10mL·min^{-1}, ±50mL·min^{-1}, ±100mL·min^{-1} after Kalman filtering. Obviously, the measurement accuracy is improved by Kalman filter, but the error still exists and cannot be ignored, so the accuracy of the test system needs to be further improved. The extended Kalman filter algorithm after modal optimization is used to process the ultrasonic signal in the second group of measurement, and the measurement data is shown in Figure 3. It can be seen from the figure that after the modal optimization, the accuracy of the measured value is significantly improved, and the correction value represented by the blue line is gradually close to the actual value. In the three cases of Q = 100mL·min^{-1}, Q = 1000mL·min^{-1}, Q = 2000mL·min^{-1}, after the Kalman filtering with modal optimization, the error range under each condition is reduced to ±5mL·min^{-1}, ±5mL·min^{-1}, ±50mL·min^{-1}

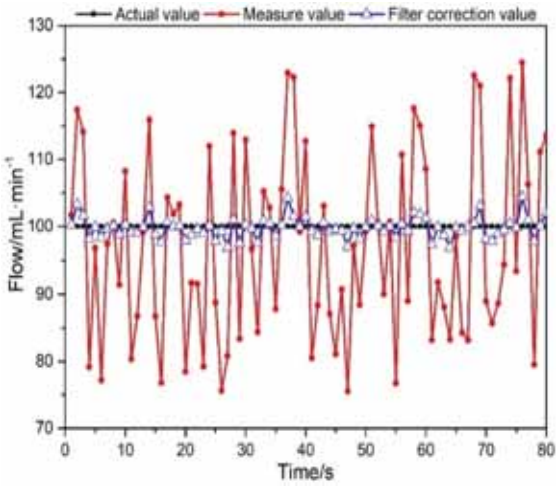

(a) Measurement simulation of 100mL·min^{-1} flow velocity

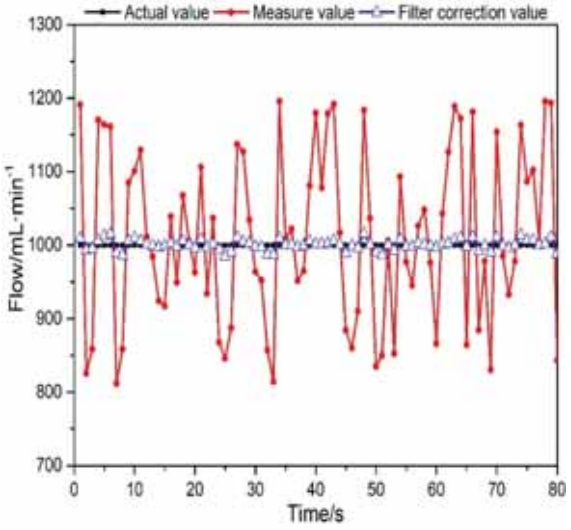

(b) Measurement simulation of 1000mL·min^{-1} flow velocity

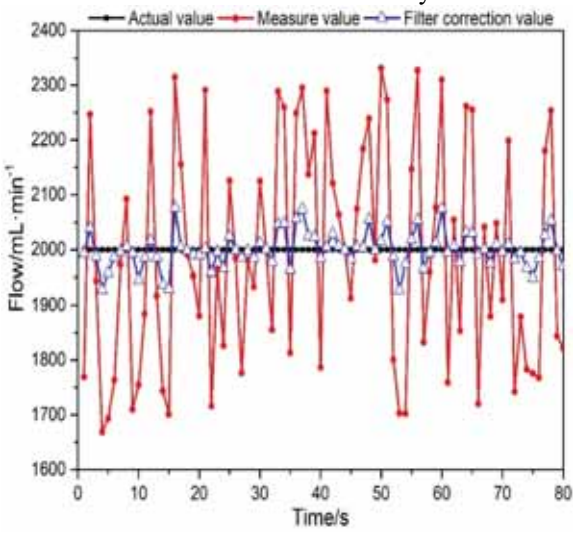

(c) Measurement simulation of 2000mL·min^{-1} flow velocity

FIGURE 3
Simulation of flow velocity measurement by extended Kalman filter with modal optimization

respectively. Obviously, when Q = 1000mL·min^{-1}, the measurement has a high degree of accuracy, and the fluctuation is more difficult to be directly optimized through filtering processing. Therefore, which may be due to the difference between the parameters in the pipeline at low flow and high flow, parameter adjustment is carried out for the test system with low flow and high flow.

Parameter Correction. Low Velocity Correction. As the flow rate increases from 100mL·min^{-1} to 1000mL·min^{-1}, the measurement accuracy increases gradually. Therefore, the parameter correction should ensure the system measurement error caused by the difference of flow rate. The correction parameter α and the sudden change regulating factor of flow rate λ is introduced to establish the correlation $\lambda_k = \lambda / \alpha$ [20]. The corrected measurement data is shown in Figure 4. It can be seen from the figure that with the increase of test times, the measurement error of flow rate gradually reduces from ±3 mL·min^{-1} to about ±0.1 mL·min^{-1}, which indicates that the accuracy of the test system under low flow is effectively improved by modifying parameters. The results show that the improved Kalman filter with modal optimization can be applied to the ultrasonic testing system with low velocity.

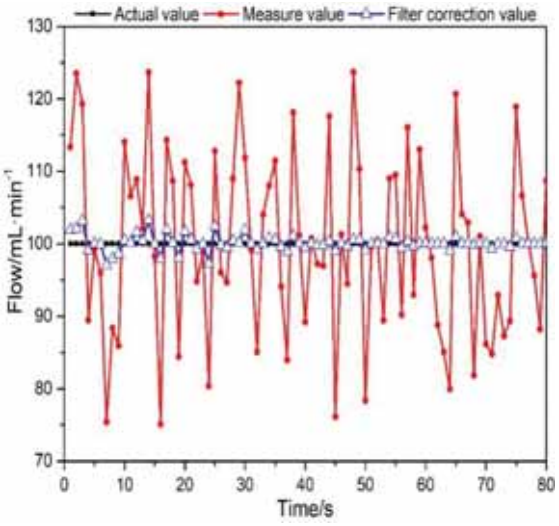

FIGURE 4
Simulation of low flow velocity measurement by extended Kalman filter with parameter adjustment and optimization

High Velocity Correction. As the flow rate increases from 1000mL·min^{-1} to 2000mL·min^{-1}, the measurement accuracy decreases gradually. Therefore, the parameter correction needs to ensure the system measurement error caused by the difference of flow rate. The correction parameter *b* and the sudden change regulating factor of flow rate λ is introduced to establish the correlation

$\lambda_k = b\lambda$ [21].

The corrected measurement data is shown in Figure 5. It can be seen from the figure that with the increase of test times, the measurement error of flow rate gradually decreases from ±10mL·min^{-1} to ±2 mL·min^{-1}, which shows that the accuracy of the test system in high flow situation is effectively improved by modifying parameters, and the error shows a gradual convergence process after the increase of test times, indicating that the flow rate can be accurately measured under the premise of sufficient test times.

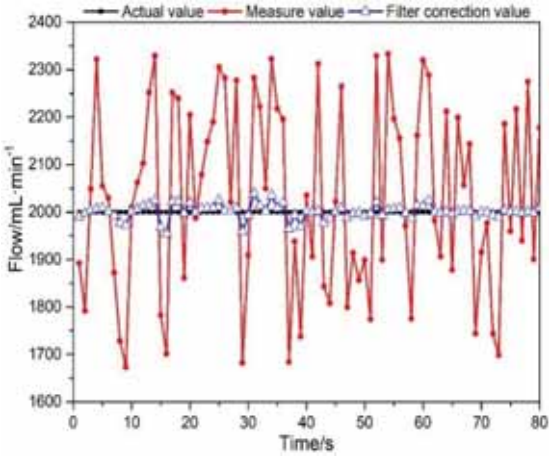

FIGURE 5
Simulation of high flow velocity measurement by extended Kalman filter with parameter adjustment and optimization

CONCLUSIONS

In this paper, the Kalman filter algorithm is applied to the current ultrasonic flow measurement technology, and an improved Kalman filter algorithm adapted to the change of flow characteristics is proposed. By establishing a multi-parameter model, the improved Kalman filter algorithm is more suitable for flow measurement, and ensures the accuracy and stability of flow measurement, while reducing the computation complexity and taking into account the low power consumption performance. The Kalman filter algorithm is successfully applied to the ultrasonic velocity measurement system by introducing an adaptive factor into the algorithm. When the flow rate is 1000 mL·min^{-1}, the measurement error range is reduced from ±50 mL·min^{-1} to ±5 mL mL·min^{-1}, which significantly improves the accuracy of the measurement system. In addition, due to the difference between the low flow rate and the high flow rate, correction parameters *a* and *b* are introduced respectively, finally the accurate measurement of the flow rate at low flow rate and high flow rate by the ultrasonic testing system is realized, and the error ranges are reduced to ±0.1 mL·min^{-1} and ±2 mL·min^{-1} respectively.

ACKNOWLEDGEMENTS

This research was supported by the National Science and Technology Major Project of China (under Grants 2018ZX01031201-001), National Key R&D Program (under Grants 2018YFC2001100), National Natural Science Foundation of China (under Grants 61574165).

REFERENCES

[1] Kostoglou, K., Lunglmayr, M. (2020) Root tracking using time-varying autoregressive moving average models and sigma-point Kalman filters. Eurasip Journal on Advances in Signal Processing. 1, 6.

[2] Luong, Q.H.,Tran, D.T., Trung, N.L., Huynh, H.T., Do, M.N. (2019) Simulation study of two-dimensional viscoelastic imaging of soft tissues using the extended Kalman filter for tumor detection. Simulation-transactions of the Society for Modeling and Simulation International. 96(5), 0037549719873381.

[3] Park, C., Ryu, S.J., Jeong, B.H., Lee, S.P., Hong, C.K., Kim, Y.B., Lee, B. (2019) Real-Time Noninvasive Intracranial State Estimation Using Unscented Kalman Filter. IEEE Transactions on Neural Systems and Rehabilitation Engineering. 27(9), 1931-1938.

[4] Hamelmann, P., Vullings, R., Mischi, M., Kolen, A.F., Schmitt, L., Bergmans, J.W.M. (2019) An Extended Kalman Filter for Fetal Heart Location Estimation During Doppler-Based Heart Rate Monitoring. IEEE Transactions on Instrumentation and Measurement. 68(9), 3221-3231.

[5] Kostoglou, K., Robertson, A.D., Macintosh, B.J., Mitsis, G.D. (2019) A Novel Framework for Estimating Time-Varying Multivariate Autoregressive Models and Application to Cardiovascular Responses to Acute Exercise. IEEE Transactions on Biomedical Engineering. 66(11), 3257-3266.

[6] Kostoglou, K., Schondorf, R., Mitsis, G.D. (2019) Modeling of multiple-input, time-varying systems with recursively estimated basis expansions. Signal processing. 155, 287-300.

[7] Lapouge, G., Troccaz, J., Poignet, P. (2018) Multi-rate unscented Kalman filtering for pose and curvature estimation in 3D ultrasound-guided needle steering. Control Engineering Practice. 80, 116-124.

[8] Ma, F.Q., Liu, F.J., Zhang, X.T., Wang, P., Bai, H.Y., Guo, H. (2018) An ultrasonic positioning algorithm based on maximum correntropy criterion extended Kalman filter weighted centroid. Signal image and video processing. 12(6), 1207-1215.

[9] Zhao, S., Li, G.R., Zhang, W., Gu, J.J. (2018) Automatical Intima-Media Border Segmentation on Ultrasound Image Sequences Using a Kalman Filter Snake. IEEE Access. 6, 40804-40810.
[10] Bordoy, J., Traub-Ens, A., Sadr, A., Wendeberg, J., Hoeflinger, F., Schindelhauer, C., Reindl, L. (2016) Bank of Kalman Filters in Closed-Loop for Robust Localization Using Unsynchronized Beacons. IEEE Sensors Journal. 16(19), 7142-7149.
[11] Angrisani, L., Baccigalupi, A., Lo Moriello, R.S. (2006) Ultrasonic time-of-flight estimation through unscented Kalman filter. IEEE Transactions on Instrumentation and Measurement. 55(4), 1077-1084.
[12] Yao, Z.J., Meng, Q.H., Zeng, M. (2010) Improvement in the accuracy of estimating the time-of-flight in an ultrasonic ranging system using multiple square-root unscented Kalman filters. Review of Scientific Instruments. 81(10), 104901.
[13] Angrisani, L., Baccigalupi, A., Lo Moriello, R.S. (2006) A measurement method based on Kalman filtering for ultrasonic time-of-flight estimation. IEEE Transactions on Instrumentation and Measurement. 55(2), 442-448.
[14] Lai, T.Y., Chen, H.I., Shih, C.C., Kuo, L.C., Hsu, H.Y., Huang, C.C. (2016) Application of a novel Kalman filter based block matching method to ultrasound images for hand tendon displacement estimation. Medical Physics. 43(1), 148-158.
[15] Boashash, B., Khan, N.A., Ben-Jabeur, T. (2015) Time-frequency features for pattern recognition using high-resolution TFDs: A tutorial review. Digital Signal Processing. 40, 1-30.
[16] Amin, H.U., Malik, A.S., Ahmad, R.F., Badruddin, N., Kamel, N., Hussain, M., Chooi, W. (2015) Feature extraction and classification for EEG signals using wavelet transform and machine learning techniques. Australasian Physical & Engineering Sciences in Medicine. 38(1), 139-149.
[17] Nazem, F., Ahmadian, A., Seraj, N.D., Giti, M. (2014) Two-stage point-based registration method between ultrasound and CT imaging of the liver based on ICP and unscented Kalman filter: a phantom study. International Journal of Computer assisted Radiology and Surgery. 9(1), 39-48.
[18] Myers, M.R., Jorge, A.B., Yuhas, D.E., Walker, D.G. (2013) Using Ultrasound and the Extended Kalman Filter for Characterizing Aerothermodynamic Environments. AIAA Journal. 51(10), 2410-2419.
[19] De Senneville, B.D., Roujol, S., Hey, S., Moonen, C., Ries, M. (2013) Extended Kalman Filtering for Continuous Volumetric MR-Temperature Imaging. IEEE Transactions on Medical Imaging. 32(4), 711-718.
[20] Snare, S.R., Mjolstad, O.C., Orderud, F., Dalen, H., Torp, H. (2012) Automated septum thickness measurement-A Kalman filter approach. Computer Methods and Programs in Biomedicine, 108(2), 477-486.
[21] Myers, M.R., Jorge, A.B., Mutton, M.J., Walker, D.G. (2012) A comparison of extended Kalman filter, particle filter, and least squares localization methods for a high heat flux concentrated source. International Journal of Heat and Mass Transfer. 55(9-10), 2219-2228.

Received: **26.10.2020**
Accepted: **13.02.2021**

CORRESPONDING AUTHOR

Yu Liu
Research and Development Center of Healthcare Electronics, Institute of Microelectronics of Chinese Academy of Sciences,
Beijing 100029, China

e-mail: makiafeng8888@outlook.com

© by PSP Volume 30– No. 05/2021 pages 5040-5046 Fresenius Environmental Bulletin

STUDY ON THE INHIBITION EFFECT OF DIFFERENT ORGANIC FERTILIZERS ON KONJAK SOUTHERN BLIGHT

Changming Liu[1,*], Juan Lin[2]

[1]Shangluo University, Shangluo, Shaanxi 726000, China
[2]Rural Energy Station of Shangluo, Shangluo, Shaanxi 726000, China

ABSTRACT

Southern blight is a common disease on crops, and also a major disease affecting the cultivation and production of konjak. Studies have shown that its sclerotium has no dormancy period, and has the characteristics of strong tolerance to extreme environment, long incubation period and easy transmission. Therefore, removing the pathogen with pesticides is the main method for planting konjak. In order to reduce the incidence of southern blight during the cultivation of konjak, organic fertilizers were used for the inhibition of the pathogen, and three kinds of organic fertilizers, including livestock manure, biogas residue and wood vinegar, were selected to analyze the growth inhibition of the pathogen by single factor and response surface methodology. The test accuracy was systematically analyzed from three aspects: fertilizer concentration, fertilizer amount and fertilizer frequency. The results show that when the fertilizer concentration is 20g/L, the fertilizer frequency is 2 and the fertilizer amount is 3g, the growth of southern blight pathogen can be well inhibited.

KEYWORDS:
Organic fertilizer, Konjak, Southern blight, Antibacterial growth

INTRODUCTION

Southern blight is a common disease on crops [1], and also a major disease affecting the production of konjak. It often occurs simultaneously with soft rot, which aggravates the damage. The host range of southern blight pathogen is extremely wide, and infects more than 200 kinds of plants [2]. It mainly damages tomato, eggplant, pepper, tobacco and potato of Solanaceae; cowpea, soybean, kidney bean and peanut of Leguminosae; pumpkin, watermelon and muskmelon of Cucurbitaceae, and rarely cause death of Gramineae [3]. In recent years, it has been reported that the southern blight of hawthorn, water chestnut, clover, konjak, vanilla, bean, tea seedling, apple, mulberry, alfalfa, pomegranate, Dichondra repens, legume and other crops have occurred in different areas to varying degrees [4]. In terms of pathogenic mechanism, many studies have shown that the pathogen can produce some enzymes that can decompose the cell wall of host, such as ß-1,4-mannosidase and mannanase, which can damage the cell wall of host and cause disease [5]. In addition, the pathogen hardly produces xylanase and cellulase, but can produce hemicellulase, acetate esterase, α-arabinase and α-galactosidase, which also makes it easier for the pathogen to cause damage to the tissue structure of host [6]. The pathogen can be dormant for a winter, mainly with sclerotium in the soil, occasionally with hyphae, rhizomorph and other forms [7]. Maranzano [8] has found that the sclerotium has no dormancy period, and has strong adaptability to extreme environment, and can be latent in disease residue, weeds and soil for up to 6 months. When the external ecological environment is suitable for its growth, the sclerotium germinates and produces hyphae, which is transmitted by rain water, irrigation water and fertilizer with bacteria, and directly invades konjak. After the hyphae invades, it destroys konjak cells by secreting cell wall degradation enzymes, thus leading to southern blight [9, 10].

Studies have shown that one of the main reasons for the disease of konjak is the bacteria on the surface of the seed taro and the residual bacteria in the soil, so both the seed taro and the soil need to be disinfected [11]. At present, soil disinfection is mainly carried out by sprinkling quicklime powder or spraying 72% pesticide streptomycin, and 72% pesticide streptomycin and 75% copper hydroxide wettable powder are mainly used for the surface disinfection of seed taro, which can achieve better results [12]. However, there many limitations of the application of pesticides in the development of green ecology, so the development of organic fertilizers with the efficacy of preventing pathogens is a vital research direction to prevent the konjak disease [13]. Studies have shown that common organic fertilizers, including biogas residue, livestock manure and organic compost, have an inhibitory effect on some bacteria [14, 15]. However, the research on the effect of organic fertilizers on the konjak southern blight is rare. Therefore, on the basis of summarizing the common organic fertilizers at present, the organic fertilizers with antibacterial growth effect were

screened, and the effects of biogas residue, wood vinegar and livestock manure on the konjak southern blight were compared. By single factor test and response surface test, the effects of fertilizer concentration, fertilizer amount and fertilizer frequency on the sclerotium growth of southern blight were systematically analyzed. Finally, the kinds of organic fertilizers and their application conditions were selected to inhibit the incidence of konjak disease.

MATERIALS AND METHODS

Experimental Conditions and Methods. Inhibition Experiment of Southern Blight. Acquisition of Plant Pathogen. Spray super-clean worktable with 70% alcohol, 2.0% phenol soap, 5.0% carbolic acid, etc., then irradiate with ultraviolet lamp for 20-30 min, wipe the table with 70% alcohol, soak knives, scissors, tweezers and needles in 70% alcohol, and sterilize petri dishes, gauze, culture medium and sterile water in high-pressure steam sterilizers at 121℃ for 30 min. Place the required items on the workbench in sequence, wash hands with soap and wipe hands with 70% alcohol.

Fresh diseased leaves with typical symptoms were selected as separation materials, and the diseased leaves or branches were washed down by tap water for 30min, and then cut from the healthy tissue parts where the diseased spots were turned around by 1-2 mm (in case of branches, the cortex with diseased spots was peeled off). Take 10 mL beaker, disinfect it with alcohol, put the separation material, pour in 50% sodium hypochlorite solution, pour out the disinfectant after 1min, rinse it with sterile water for 2-3 times, and take appropriate amount of the last sterile water to coat the culture plate for sterility test control. Use sterile scissors to cut the separation materials into squares with the size of 2-3 mm between diseased and healthy tissues, clamp the cut materials with tweezers, put them on the beef extract-peptone culture medium plate, and press them gently. Each dish has 4-5 pieces, which are evenly discharged. Mark the separation code, date and name on the petri dish with a marker, and turn the petri dish upside down and place it in an incubator at 25-28℃. After 3-4 days, select typical colonies without mixed bacteria from the separation materials, pick them with inoculation needles at the edge of the colonies, re-inoculate them on another plate, and culture in a 28℃ incubator [16].

Growth Inhibition Experiment of Plant Pathogen. Pick the edge of the target pathogen colony with a inoculation needle, and inoculate it onto another plate to obtain a plate with colonies. The organic fertilizer was soaked in a certain amount of water, and the representative organic fertilizer leaching solution was obtained by leaching method. The leaching solution was diluted by different times, and the rated leaching solution was dripped on the colony plate. Observe the colony growth status after 24 hours, and further confirm the colony growth status after 3-4 days. By staining with aniline blue-emulsifiable phenol and observing under microscope, the mycelia of pathogenic bacteria were observed [17].

Response Surface Analysis Method. Single Factor Test Design. The single factor test was completed according to the above method, and the specific parameters are shown in Table 1.

Box-Beheken Test. According to the results of single factor test, three factors which have significant effects on colony growth inhibition were selected as response variables, namely, fertilizer concentration (A), fertilizer amount (B) and fertilizer frequency (C). The levels of variables were expressed as - 1, 0 and 1. The data offset was taken as the response value. The response surface test of three factors and three levels was designed by using Box-Beheken central combination software. The Box-Beheken test design with optimized test location is shown in Table 2.

TABLE 1
Single factor tests for test locations selection

Num.	Concen-	Amount/g	Fre-
1	5	1	1
2	10	2	2
3	15	3	3
4	20	4	4
5	25	5	5
6	30	6	6
7	35	7	7

TABLE 2
Factors and levels of Box-Beheken test

Level	Concen-trate/g/L	Amount/g	Fre-quency
-1	**10**	**3**	**4**
0	**15**	**4**	**5**
1	**20**	**5**	**6**

RESULTS AND DISCUSSION

Single Factor Test Analysis on the Antibacterial Effect of Organic Fertilizer. The inhibition of three kinds of organic fertilizer extracts on the growth of southern blight pathogen was investigated respectively, and the statistical results of livestock manure, biogas residue and wood vinegar extracts on the growth of flora are shown in Figure 1-3. As can be seen from Figure 1, with the increase of the concentration of livestock manure leaching solution, the number of flora shows a stable trend at first and then decreases, which indicates that the leaching solution of livestock manure can effectively inhibit the growth of southern blight pathogen, and the amount

of leaching solution also shows the same reaction trend. In addition, by analyzing the fertilizer frequency, it can be found that livestock manure can inhibit the growth of flora only after about 6 releases. This may be due to the existence of some trace heavy metals in livestock manure, which affects the growth environment of flora and inhibits its growth [18]. Figure 2 shows the effect of biogas residue leaching solution on the growth of flora. It can be seen that low concentration biogas residue can obviously inhibit the growth of flora, and at the same time, its amount is lower than that of livestock manure at low concentration. Only 2g leaching solution can successfully inhibit the growth of flora, and its frequency can be controlled within 3 times, which indicates that the existence of specific components in biogas residue can effectively inhibit the southern blight pathogen [19]. However, it can be seen from Figure 3 that the leaching solution of wood vinegar shows different reaction results, and no matter the concentration, amount and frequency have no direct effect on the growth of flora, indicating that wood vinegar has no inhibitory effect on the growth of southern blight pathogen.

Response Surface Analysis on the Growth Inhibition of Southern Blight Pathogen by Biogas Residue. According to the results of single factor test, three factors which have significant effects on the growth of flora, namely, the fertilizer concentration (A), the fertilizer amount (B) and the fertilizer frequency (C), were selected as response variables, and the number of colonies after growth was taken as response value (Y). Design-Expert 8.0.6 software was used to design a response surface test with three factors and three levels, and the design and results are shown in Table 3. The variance analysis of the test data was carried out with the software Design-Expert 8.0.6, and the results are shown in Table 4. The regression model equation between each factor and the response value is :
(Eq.1)

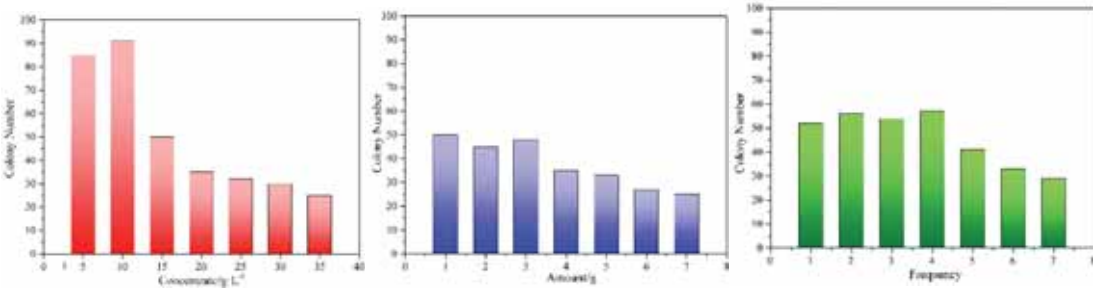

FIGURE 1
Effect of livestock manure on the growth of southern blight pathogen

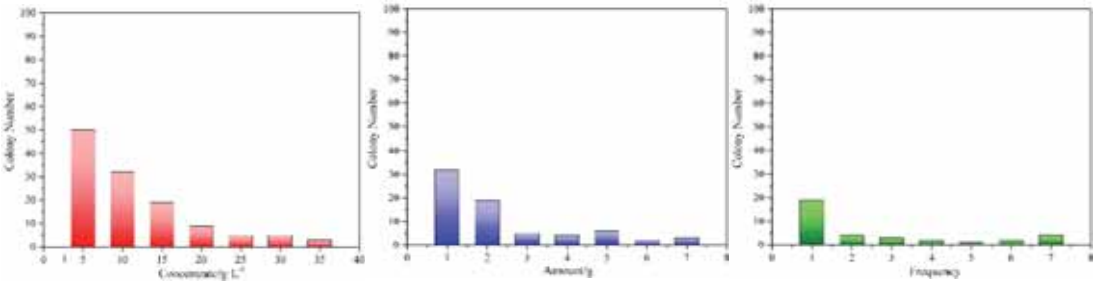

FIGURE 2
Effect of biogas residue on the growth of southern blight pathogen

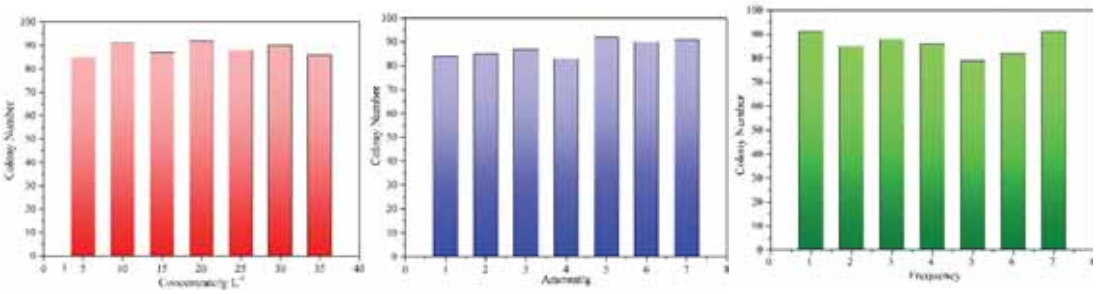

FIGURE 3
Effect of wood vinegar on the growth of southern blight pathogen

$$R=96.1-3.175A+1.575B-0.075C-0.025AB-0.475AC+3.325BC-3.1625A^2-0.9625B^2-5.3625C^2 \quad \text{(Eq. 1)}$$

The P value of the model is 0.0225, which indicates that the regression model established by this method is significant. The decision coefficient of the regression model is 0.8225, which shows that the model can be used to predict the effect of different test positions on test accuracy. In the model, the quadratic term B^2 has a significant effect on the response value ($P<0.01$), while the other terms have no significant effect on the response value, indicating that there may be interaction between different factors, not a single linear relationship. The effect of each factor on the response value can be evaluated by the F value in variance analysis. The larger the F value, the more significant the effect on the response value. Therefore, the order of the effect of selected factors on the test accuracy is: fertilizer concentration (A) > fertilizer frequency (C) > fertilizer amount (B).

The multiple regression analysis was carried out on the test results by using Design-Expert 8.0.6 software, and three response surfaces of the interactive effect of fertilizer concentration (A), fertilizer amount (B) and fertilizer frequency (C) on the number of colonies were obtained, as shown in Figure 4.

Contour is the horizontal projection of response surface, which reflects whether there is interaction between various factors. Ellipse contour indicates that the interaction between two factors is significant, while circular contour indicates that the interaction between two factors is not significant [20]. The response surface results in Figure 3b show that the slope in the B-axis direction is flatter than that in the A-axis, indicating that the effect of fertilizer concentration on colony growth is greater than that of fertilizer amount. The response surface in Figure 3d shows that the slope of C-axis is flatter than that of A-axis, which also shows that the fertilizer concentration has greater effect on colony growth than the fertilizer frequency. By further comparing the two factors BC, it can be seen from Figure 3f that compared with the fertilizer amount, the fertilizer frequency has a greater effect on colony growth.

TABLE 3
Response surface test design and results

Num.	C./g/L	Amount/g	Frequency	Colony	Num.	C./g/L	Amount/g	Frequency	Colony
1	0	0	0	7	10	0	0	0	7
2	1	1	0	7	11	0	0	0	1
3	-1	0	1	9	12	0	1	-1	3
4	0	-1	-1	9	13	1	0	1	6
5	1	0	-1	6	14	0	0	0	7
6	-1	-1	0	6	15	1	-1	0	7
7	0	0	0	7	16	-1	0	-1	6
8	0	1	1	6	17	-1	1	0	3
9	0	-1	1	3					

TABLE 4
Analysis of variance table

Source	Sum of Squares	df	Mean Square	F Value	p-value Prob > F
Model	7.5788	9	6.17542	3.605182	0.0225
A-A	8.645	1	8.645	8.036945	0.0252
B-B	9.845	1	9.845	0.004485	0.2024
C-C	0.045	1	0.045	1.977719	0.9485
AB	0.0025	1	0.0025	0.000249	0.9878
AC	0.9025	1	0.9025	0.089942	0.7730
BC	4.2225	1	4.2225	4.40714	0.0739
A^2	2.11118	1	2.11118	4.19673	0.0797
B^2	3.900658	1	3.900658	0.388733	0.0052
C^2	1.0796	1	1.0796	12.06659	0.0104
Residual	7.24	7	10.03429		
Lack of Fit	3.34	3	10.78	1.137731	0.1347
Pure Error	37.9	4	9.475		
Cor Total	5.8188	16			

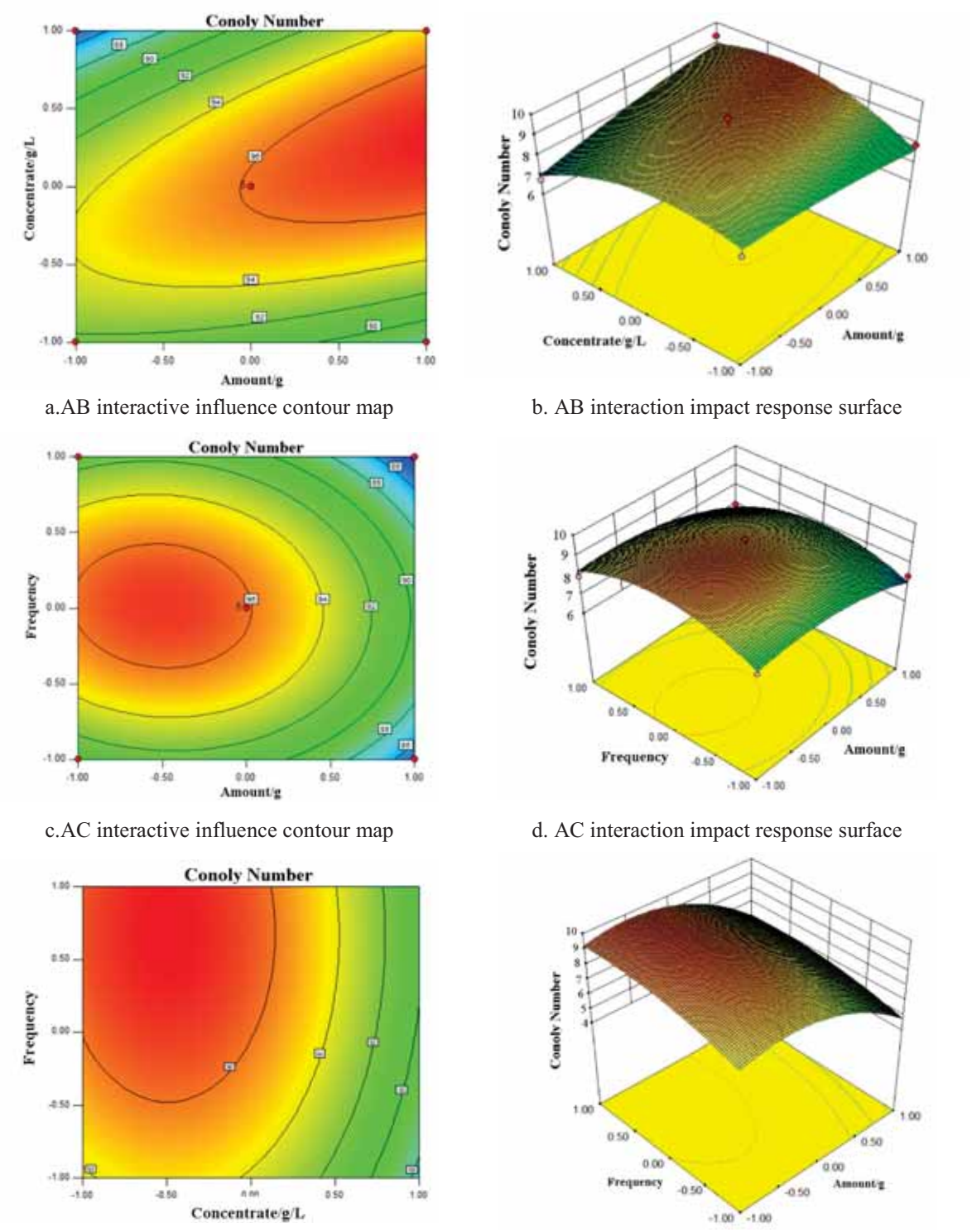

a.AB interactive influence contour map

b. AB interaction impact response surface

c.AC interactive influence contour map

d. AC interaction impact response surface

e. BC interactive influence contour map

f. BC interaction impact response surface

FIGURE 4

Contour and response surface of two-factor interaction on the growth of southern blight pathogen

This result is consistent with the result of variance analysis. In addition, it is worth noting that in Figure 2(a,c,e), ellipse projection is shown in the interactive contour map, which indicates that there is obvious interaction between factors, among which AB and BC show more obvious interaction, and although there is interaction between AC, the interaction between each other is weaker. According to the analysis, the growth process of southern blight pathogen is affected by three factors: fertilizer concentration (A), fertilizer amount (B) and fertilizer frequency (C), following the order of fertilizer concentration (A) > fertilizer frequency (C) > fertilizer amount (B),

which is consistent with the analysis results. When the fertilizer concentration is 20g/L, the fertilizer frequency is 2, and the fertilizer amount is 3g, the growth of southern blight pathogen can be well inhibited, and the number of colonies can be controlled within 3.

CONCLUSION

In order to control the growth of southern blight pathogen by organic fertilizer and reduce the disease incidence during the cultivation of konjak, three kinds of organic fertilizers, including livestock manure, biogas residue and wood vinegar, were selected to analyze the growth inhibition of the pathogen by single factor analysis and response surface methodology. From the single factor results, it can be seen that wood vinegar has no direct inhibitory effect on the growth of southern blight pathogen, while livestock manure and biogas residue have obvious inhibitory effect on the growth of southern blight pathogen, and biogas residue can achieve good inhibitory effect at low concentration, low amount and low frequency. The interaction between the selected factors was analyzed by response surface methodology. The results show that there is an obvious interaction between the fertilizer concentration and the fertilizer amount. The fertilizer amount and the fertilizer frequency also has obvious interaction, but the interaction between the fertilizer concentration and the fertilizer frequency is weak. The comprehensive analysis show that when the fertilizer concentration is 20 g/L, the fertilizer frequency is 2, and the fertilizer amount is 3g, the growth of southern blight pathogen can be well inhibited, and the number of colonies can be controlled within 3.

ACKNOWLEDGEMENT

Major Research and Development Program of Shaanxi Province, China (No. 2020NY-054); Science and Technology Innovation Team of Shangluo University (No. 18SCX004).

REFERENCES

[1] Fransen, N.L., Hsiao, C., Van Der Poel, M., Engelenburg, H.J., Verdaasdonk, K., Vincenten, M.C.J., Remmerswaal, E.B.M., Kuhlmann, T., Mason, M.R.J., Hamann, J., Smolders, J., Huitinga, I. (2020) Tissue-Resident Memory T Cells Invade The Brain Parenchyma In Multiple Sclerosis White Matter Lesions. Brain. 143(6), 1714-1730.

[2] Geraldes, R., Jurynczyk, M., Dos Passos, G.E., Prichler, A., Chung, K., Hagens, M., Palace, J. (2020) Distinct Influence Of Different Vascular Risk Factors On White Matter Brain Lesions In Multiple Sclerosis. Journal Of Neurology Neurosurgery And Psychiatry. 91(4), 388-391.

[3] Van Wageningen, T.A., Vlaar, E., Kooij, G., Jongenelen, C.A.M., Geurts, J.J.G., van Dam, A.M. (2019) Regulation Of Microglial Tmem119 And P2ry12 Immunoreactivity In Multiple Sclerosis White And Grey Matter Lesions Is Dependent On Their Inflammatory Environment. Acta Neuropathologica Communications. 7(1), 206.

[4] Elkjaer, M.L., Frisch, T., Reynolds, R., Kacprowski, T., Burton, M., Kruse, T.A., Thomassen, M., Baumbach, J., Illes, Z. (2019) Molecular Signature Of Different Lesion Types In The Brain White Matter Of Patients With Progressive Multiple Sclerosis. Acta Neuropathologica Communications. 7(1), 205.

[5] Pons, A.L., Higginbottom, A., Cooper-Knock, J., Alrafiah, A., Alofi, E., Kirby, J., Shaw, P.J., Wood, J.D., Highley, J.R. (2020) Oligodendrocyte Pathology Exceeds Axonal Pathology In White Matter In Human Amyotrophic Lateral Sclerosis. Journal Of Pathology. 251(3), 262-271.

[6] Teuber-Hanselmann, S., Meinl, E., Junker, A. (2020) Micrornas In Gray And White Matter Multiple Sclerosis Lesions: Impact On Pathophysiology. Journal Of Pathology. 250(5), 496-509.

[7] Lu, L., Xie, A.S., Serkova, N., Malykhina, A. (2020) Comparative Evaluation Of White Matter Demyelination By Magnetic Resonance Imaging And Neurogenic Voiding Dysfunction In A Viral Murine Model Of Multiple Sclerosis. Journal of Urology. 203(4), E700-E701.

[8] Maranzano, J., Dadar, M., Zhernovaia, M., Arnold, D.L., Collins, D.L., Narayanan, S. (2020) Automated Separation Of Diffusely Abnormal White Matter From Focal White Matter Lesions On Mri In Multiple Sclerosis. Neuroimage. 213, 116690.

[9] Planche, V, Su, J.H., Mournet, S., Saranathan, M., Dousset, V., Han, M., Rutt, B.K., Tourdias, T. (2020) White-Matter-Nulled Mprage At 7t Reveals Thalamic Lesions And Atrophy Of Specific Thalamic Nuclei In Multiple Sclerosis. Multiple Sclerosis Journal. 26(8), 987-992.

[10] Brier, M.R., Snyder, A.Z., Tanenbaum, A., Wu, G., Cross, A., Benzinger, T.L., Naismith, R. (2020) Multiple Sclerosis Disability Correlates With Abnormalities In Normal Appearing White And Gray Matter Measured In Routine Clinical Images. Multiple Sclerosis Journal. 261(1), 91-92.

[11] Mackay, K.B., Shenoy, V.B., Demesa, J., Rolland, A. (2020) Oral Administration Of Ehp-101 Promotes Remyelination In White Matter In The Cuprizone/Rapamycin Mouse Model Of Multiple Sclerosis. Multiple Sclerosis Journal. 261 (1), 146-147.

[12] De Jong, J.M., Wang, P., Oomkens, M., Baron, W. (2020) Remodeling Of The Interstitial Extracellular Matrix In White Matter Multiple Sclerosis Lesions: Implications For Remyelination (Failure). Journal Of Neuroscience Research. 98(7), 1370-1397.

[13] Radetz, A., Koirala, N., Kraemer, J., Johnen, A., Fleischer, V., Gonzalez-Escamilla, G., Cerina, M., Muthuraman, M., Meuth, S.G., Groppa, S. (2020) Gray Matter Integrity Predicts White Matter Network Reorganization In Multiple Sclerosis. Human Brain Mapping. 41(4), 917-927.

[14] Filip, P., Svatkova, A., Carpenter, A.F., Eberly, L.E., Nestrasil, I., Nissi, M.J., Michaeli, S., Mangia, S. (2020) Rotating Frame Mri Relaxations As Markers Of Diffuse White Matter Abnormalities In Multiple Sclerosis. Neuroimage-Clinical. 26, 102234.

[15] Steinbach, R., Batyrbekova, M., Gaur, N., Voss, A.,Stubendorff, B., Mayer, T.E., Gaser, C., Witte, O.W., Prell, T., Grosskreutz, J. (2020) Applying The D50 Disease Progression Model To Gray And White Matter Pathology In Amyotrophic Lateral Sclerosis. Neuroimage-Clinical. 25, 102094.

[16] Sinnecker, T., Ruberte, E., Schaedelin, S., Canova, V., Amann, M., Naegelin, Y., Penner, I.K., Mueller, J., Kuhle, J., Decard, B., Derfuss, T., Kappos, L., Granziera, C., Wuerfel, J., Magon, S.,Yaldizli, O. (2020) New And Enlarging White Matter Lesions Adjacent To The Ventricle System And Thalamic Atrophy Are Independently Associated With Lateral Ventricular Enlargement In Multiple Sclerosis. Journal Of Neurology. 267(1), 192-202.

[17] Rachmadi, M.F., Valdes-Hernandez, M.D.C., Li, H.W., Guerrero, R., Meijboom, R., Wiseman, S., Waldman, A., Zhang, J.G., Rueckert, D., Wardlaw, J., Komura, T. (2020) Limited One-Time Sampling Irregularity Map (Lots-Im) For Automatic Unsupervised Assessment Of White Matter Hyperintensities And Multiple Sclerosis Lesions In Structural Brain Magnetic Resonance Images. Computerized Medical Imaging And Graphics. 79, 101685.

[18] Gabel, M.C., Broad, R.J., Young, A.L., Abrahams, S., Bastin, M.E., Goldstein, L.H., Turner, M.R., Cercignani, M., Leigh, P.N. (2020) Reply To: Early White Matter Changes On Diffusion Tensor Imaging In Amyotrophic Lateral Sclerosis. Annals Of Clinical And Translational Neurology. 7(7), 1266-1267.

[19] Finsterer, J., Scorza, F.A., Scorza, C.A. (2020) Early White Matter Changes On Diffusion Tensor Imaging In Amyotrophic Lateral Sclerosis. Annals Of Clinical And Translational Neurology. 7(7), 1265-1266.

[20] Gabel, M.C., Broad, R.J., Young, A.L., Abrahams, S., Bastin, M.E., Menke, R.A.L., Al-Chalabi, A., Goldstein, L.H., Tsermentseli, S., Alexander, D.C., Turner, M.R., Leigh, P.N., Cercignani, M. (2020) Evolution Of White Matter Damage In Amyotrophic Lateral Sclerosis. Annals Of Clinical And Translational Neurology. 7(5), 722-732.

Received: **27.10.2020**
Accepted: **01.12.2020**

CORRESPONDING AUTHOR

Changming Liu
Shangluo University,
Shangluo Shaanxi 726000 – China

e-mail: lidingyun2016@163.com

© by PSP Volume 30– No. 05/2021 pages 5047-5053 Fresenius Environmental Bulletin

STUDY ON THE CONTROL OF SOIL-BORNE DISEASES OF KONJAK BY WALNUT SHELL WOOD VINEGAR

Changming Liu[1,*], Feng Xian[2], Juan Lin[3]

[1]Shangluo University, Shangluo, Shaanxi 726000, China
[2]Inner Mongulia Academy of Agriculture & Animal Husbandry Science, Huhehaote 010031, China
[3]Rural Energy Station of Shangluo, Shangluo, Shaanxi 726000, China

ABSTRACT

Konjak is not only a kind of food, but also a kind of medicinal material and an economic crop, which is widely distributed in Yunnan, Guizhou, Sichuan, southwestern Shanxi and western Hubei. However, two soil-borne diseases of konjak, soft rot and southern blight, restrict the development of konjak planting industry. In recent years, there are many researches on the control of konjak soft rot and southern blight, including the application of biological bacteria or biological fertilizer, soil disinfection, crop rotation and so on. Studies have shown that wood vinegar can inhibit and kill bacteria, regulate plant growth, promote plant photosynthesis, promote nutrient absorption and improve the quality of trees and fruits. In this paper, the white konjak was used as the test material to carry out field experiments, and the control effects of walnut shell wood vinegar at different temperatures and different dilutions on soil-borne diseases of konjak were explored in order to obtain the best treatment conditions. The results showed that when the walnut shell wood vinegar was diluted 600 times in K_2 (180~300°C), the highest seeding rate of konjak reached 99.17%; the disease resistance was the best, and the diseased plant rate was only 3.36%; the average yield was the largest, reaching 148 g/clump.

KEYWORDS:
Walnut shell wood vinegar, Konjak, Soil-borne disease, Prevention

INTRODUCTION

Konjak, which is both food and medicinal material, is mainly distributed in Southeast Asia and Africa; China, Japan, Myanmar, Vietnam, Indonesia and other countries [1]. The production areas in China are mainly distributed in Yunnan, Guizhou, Sichuan, southern Shanxi and Western Hubei, with the most abundant resources in mountainous areas around Sichuan Basin. The production areas in Sichuan are mainly distributed in Dabashan Mountain Area in the east of Sichuan, and Jinsha River Valley in the southwest is the most important production area of white Konjak in China [2,3]. There are many disease types of Konjak, mainly including southern blight, soft rot, leaf blight and ring spot disease, among which soft rot and southern blight are the two major soil-borne diseases. Soft rot, also known as ball rot and stem fall disease, can cause Konjak to rot from the base root and lodging in pieces, resulting in bulb rot, thus reducing production. Southern blight, also known as black limp disease and root limp disease, mainly affects the base of petiole, resulting in the damage of petiole or corm. When the petiole base is infected with southern blight, dark brown spots will appear and expand continuously. Finally, the petiole will grow white silk-like hyphae and show light red color. The pathogen grows well in high temperature, humid air and long sunshine. The soil-borne diseases of konjak has seriously affected the large-scale konjak planting industry, reduced its profit, and seriously affected the economic income of growers [4-7]. Therefore, in recent years, many researchers have focused on the control of soil-borne diseases of konjak, and constantly explored effective methods for it, generally including deep ploughing, application of biological fertilizer or biological agents, application of sterilization agents for soil sterilization, crop rotation, etc. [8-10]. However, the current control effect needs to be further strengthened.

With the rapid development of biotechnology, the use of biotechnology to control soil-borne diseases of konjak has become a new solution to agricultural problems [11, 12]. Wood vinegar is a kind of clear reddish brown liquid obtained by dry distillation of plant material residues and other products after condensation and standing, while separating precipitated wood tar. It has wide sources, low cost and no pollution, and has been mainly used as soil improver, plant growth regulator, food preservative, beverage additive, feed additive, environment-friendly snow melting agent, bactericide, anti-inflammatory agent, etc. It is widely used in agriculture and forestry production, environmental protection, food processing, animal husbandry production, medical and health fields [13-16]. Walnut shell wood vinegar is a kind of clear acid mixture obtained from walnut shell after dry condensation and standing, while separating wood tar. Studies have shown that

walnut shell wood vinegar contains more than 40 kinds of organic substances, including phenols, acids, ketones and heterocyclic compounds, among which phenols with strong antibacterial activity are much higher than other substances. Therefore, walnut shell wood vinegar has good antibacterial properties and can be used as bactericides in agricultural production [17]. Its chemical composition is complex, and the components of wood vinegar extracted from different temperatures are not the same. Therefore, the control effects of walnut shell wood vinegar on soil-borne diseases of konjak at different temperatures are different. In this paper, four temperature stages and dilution times of walnut shell wood vinegar were used as independent variables, and the seedling rate (%), diseased plant rate (%) and average yield (%) of konjak were taken as dependent variables. The factors influencing the control effect of walnut shell wood vinegar on soil-borne diseases were explored, and the differences of various combination factors were analyzed, finally the best condition was obtained, which provided certain reference for controlling soil-borne diseases by using wood vinegar.

MATERIALS AND METHODS

Test Materials and Equipment. Materials: walnut shell wood vinegar was provided by CAU Guangdong Biopharmaceutical Co., Ltd., the raw material was walnut shell, the extraction temperature was 90-500℃; the variety of konjak: white konjak from Jinyang County; the test equipment: electronic analytical balance (Shimazu, Japan).

Test Methods. In this study, the field experiment [18] was used to study the control effects of walnut shell wood vinegar collected at different temperatures and different dilutions on konjak soil-borne diseases. The temperatures were 90℃~180℃, 180℃~300℃, 300℃~500℃ and the whole temperature stage was 90℃~500℃. The dilution times were 200, 400, 600 and 800 respectively, totally 17 treatments in the test, as shown in Table 1. The method of random block was adopted to divide the experimental plot, and each block is 1m apart. 120 konjak seeds were planted and labeled in each plot, and 2040 konjak seeds were shared for experiment in total. Konjak, white konjak from Jinyang County, was planted on April 1, 2019. The number of seedlings and the number of plants with soil-borne diseases were recorded every 10 days after planting, and the yield was measured on October 30. 3-5 days before planting, the walnut shell wood vinegar was irrigated with water, and at the same time, the same amount of walnut shell vinegar at different temperatures and dilution times was applied. The groups with the same method and the same amount of clear water in the same period was compared, and the unified routine management was adopted for other management measures after planting.

Data Analysis and Processing. Origin 2016 was used to plot the data, and also for One-Sample t-Test [19].

TABLE 1
Processing parameters of konjak with walnut shell wood vinegar

Processing	Temperature Section	Dilution Factor
1	CK	CK
2	K_0(90℃~500℃)	200
3	K_1(90℃~180℃)	200
4	K_2(180℃~300℃)	200
5	K_3(300℃~500℃)	200
6	K_0(90℃~500℃)	400
7	K_1(90℃~180℃)	400
8	K_2(180℃~300℃)	400
9	K_3(300℃~500℃)	400
10	K_0(90℃~500℃)	600
11	K_1(90℃~180℃)	600
12	K_2(180℃~300℃)	600
13	K_3(300℃~500℃)	600
14	K_0(90℃~500℃)	800
15	K_1(90℃~180℃)	800
16	K_2(180℃~300℃)	800
17	K_3(300℃~500℃)	800

RESULTS AND DISCUSSION

Effect of Walnut Shell Wood Vinegar on the Seeding Rate of Konjak. Figure 1 shows the effect of walnut shell wood vinegar diluted with different times at different temperatures on the seeding number and seedling rate of konjak. It can be seen from Figure 1 that walnut shell wood vinegar with different dilution times and different temperatures have different effects on the seeding rate of konjak. The seeding rate of konjak treated with walnut shell wood vinegar diluted different times but at the same temperature is different, and the seeding rate of konjak treated with walnut shell wood vinegar diluted the same times but at different temperatures is also different, which indicates that both collection temperature and dilution times have effects on the control of soil-borne diseases of konjak. The specific data are shown in Table 2. It can be seen that when the dilution times of walnut shell wood vinegar is 200 times at different temperatures, compared with the blank control group, the seedling rate decreases, which may be due to the high concentration of walnut shell wood vinegar and the high organic acid composition, resulting in the destruction of bacterial colonies in the soil conducive to the seeding of konjak, thus affecting the seedling rate [20]. When the dilution times of walnut vinegar are 400, 600 and 800 times, the seeding number and seeding rate are higher than those of the blank control group. When the temperature is K_2, i.e. 180 ~ 300 ℃ and the dilution times is 600 times, the seedling rate of konjak is the best, with 119 seedlings and 99.17% seeding rate. Using origin 2016 to analyze the significant difference of the data, the P values at dilution times of 200, 400, 600 and 800 times are 0.053, 0.018, 0.015 and 0.191 respectively. Therefore, when the dilution times are 200 and 800 times, the P value is greater than 0.05, which is not a significant difference factor. When the dilution times are 400 and 600 times, the P value is less than 0.05, which is a significant difference factor, showing that when the dilution times are 400 and 600 times, the wood vinegar at different temperatures has a significant effect on promoting the seeding of konjak; but when the dilution times are 200 and 800 times, the effects of wood vinegar at different temperatures on the seeding of konjak is not obvious.

Effect of Walnut Shell Wood Vinegar on the Disease Resistance of Konjak. The disease resistance of konjak can be characterized by the diseased plant rate [21]. Figure 2 shows the effect of walnut shell wood vinegar diluted with different times at different temperatures on the diseased plant number and diseased plant rate of konjak. It can be seen that walnut shell wood vinegar at different temperatures and dilution times has different effects on the disease resistance of konjak. The diseased plant rate of konjak with the same temperature and different dilution times is different; and the diseased plant rates of konjak treated with walnut shell vinegar at different temperatures with the same dilution times are also different, which indicates that the collected temperature

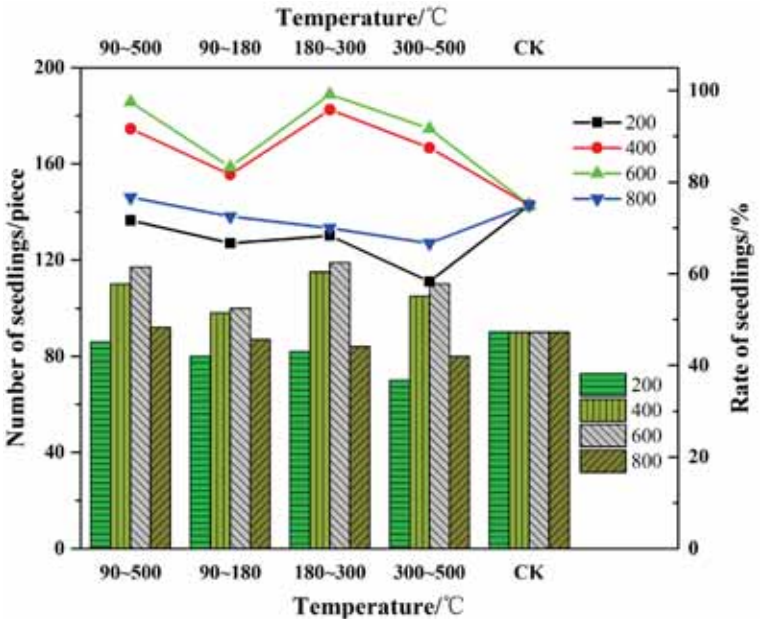

FIGURE 1
Effect of walnut shell wood vinegar diluted by different times at different temperatures on the seeding number and seeding rate of konjak

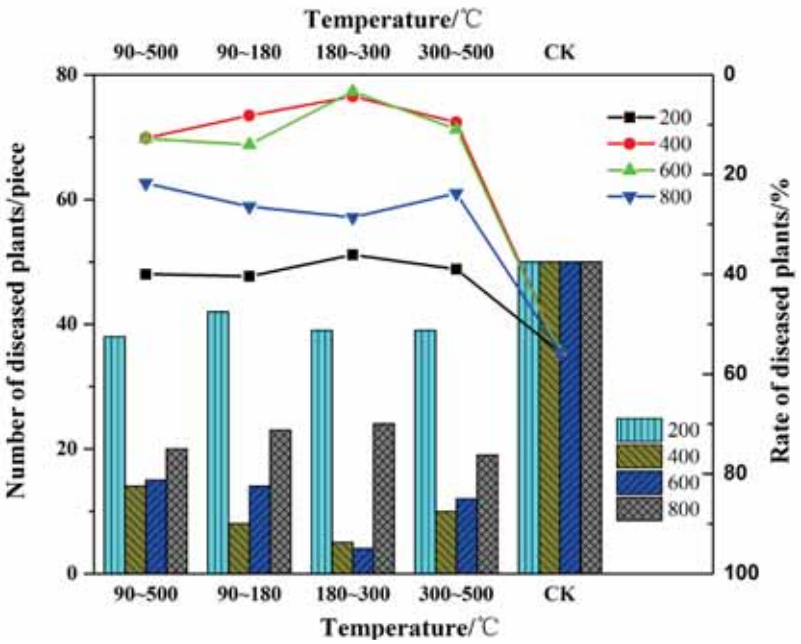

FIGURE 2
Effect of walnut shell wood vinegar diluted by different times at different temperatures on the disease resistance of konjak

and dilution times have effects on the disease resistance of walnut shell vinegar to konjak. Specific data are shown in Table 2. When the dilution times of walnut shell wood vinegar are 200, 400, 600 and 800 times, compared with the blank control group, the diseased plant rate decreases. When the dilution times of walnut shell wood vinegar are 400 and 600, the trend of the number and rate of diseased plants are the same, but the effect difference is not obvious. When the dilution times is 600 times and the temperature is K_2, the disease resistance is the best, and the number of diseased plants is only 4, with diseased plant rates of 3.36%, indicating that the disease resistance of konjak can be increased by wood walnut shell vinegar at all temperatures under different dilution times. Origin 2016 was used to analyze the significant difference of the data. The P values of 200, 400, 600 and 800 times of dilution are all less than 0.05. Therefore, all dilution times are significant difference factors, indicating that under these dilution times, wood vinegar at each stage of temperature has a significant role in promoting the disease resistance of konjak.

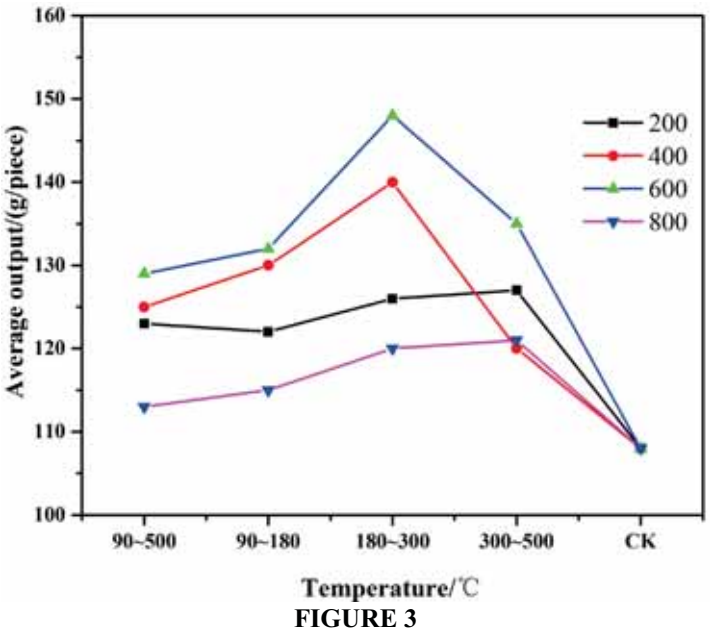

FIGURE 3
Effect of walnut shell wood vinegar diluted by different times at different temperatures on the average yield of konjak

TABLE 2
Effect of walnut husk wood vinegar diluted in different temperature sections on the seedling rate, disease resistance and yield of konjac

Processing	Conditions		Seedling Situation			Resistance to disease		Output		
	Temperature/°C	Dilution factor	Planting base/piece	Number of seedlings/piece	Rate of seedlings/%	Number of diseased plants	Rate of diseased plants/%	Total output/g	Number of harvests/piece	Average output/g//piece
1	CK	CK	120	90	75.00	50	55.56	4320	40	108
2	90~500	200	120	100	83.33	38	38.00	6000	48	123
3	90~180	200	120	104	86.67	42	40.38	5244	38	122
4	180~300	200	120	108	90.00	39	36.11	6450	43	126
5	300~500	200	120	104	86.67	39	37.50	3720	31	127
6	90~500	400	120	116	96.67	14	12.07	12384	96	125
7	90~180	400	120	114	95.00	8	7.02	11520	90	130
8	180~300	400	120	119	99.17	5	4.20	16280	110	140
9	300~500	400	120	115	95.83	10	8.70	12825	95	120
10	90~500	600	120	117	97.50	15	12.82	12546	102	129
11	90~180	600	120	113	94.17	14	12.39	10492	86	132
12	180~300	600	120	119	99.17	4	3.36	14490	115	148
13	300~500	600	120	116	96.67	12	10.34	12446	98	135
14	90~500	800	120	92	76.67	20	21.74	8136	72	113
15	90~180	800	120	87	72.50	23	26.44	7680	64	115
16	180~300	800	120	84	70.00	24	28.57	6900	60	120
17	300~500	800	120	80	66.67	19	23.75	7381	61	121

Effect of Walnut Shell Wood Vinegar on the Average Yield of Konjak. The average yield of konjak is also directly reflecting the control effect [22]. Figure 3 shows the effect of walnut shell wood vinegar diluted with different times at different temperatures on the average yield of konjak. It can be seen from Figure 3 that walnut shell wood vinegar with different dilution times and different temperatures has different effects on the average yield of konjak. The average yield of konjak treated with walnut shell wood vinegar at the same temperature but different dilution times is different, and the average yield of konjak treated with walnut shell vinegar at different temperatures with the same dilution times is also different, which indicates that both collection temperature and dilution times have effects on the average yield of konjak. The specific data are shown in Table 2. When the dilution times of walnut shell wood vinegar is 200, 400, 600 and 800 times, the average yield increases compared with the blank control group, indicating that the application of walnut shell wood vinegar can promote the yield increase. When the dilution times of walnut shell wood vinegar is 400 and 600 times, the average yield increases significantly. When the temperatures are K_0, K_1, K_2, the effect of promoting yield is 600 > 400 > 200 > 800; when the temperature is K_3, the effect of promoting yield is 600 > 200 > 800 > 400. When the dilution times is 600 times and the temperature is K2, the average yield is 148g/clump, which shows that walnut shell wood vinegar at all temperatures under different dilution times can improve the average yield of konjak. Origin 2016 was used to analyze the significant difference of the data. The P values of 200, 400, 600 and 800 times are all less than 0.05, so all dilution times are significant difference factors, indicating that under these dilution times, wood vinegar at each stage of temperature has a significant effect on the average yield of konjak.

CONCLUSION

In this test, the effects of walnut shell wood vinegar diluted by different times at different temperatures on controlling soil-borne diseases of konjak were studied. The results showed that different temperatures and different dilution times have obvious effects on the control effect, and different combination factors have great differences on the control effect. When the walnut shell wood vinegar diluted 600 times at temperature of K_2(180~300°C), the highest seeding rate of konjak can reach 99.17%. The disease resistance is the best, and the diseased plant rate is only 3.36%; the average yield is the largest, reaching 148g/clump. This test provides a certain reference for the control of crop diseases with wood vinegar.

ACKNOWLEDGEMENT

Major Research and Development Program of Shaanxi Province, China (No. 2020NY-054); Science and Technology Innovation Team of Shangluo University (No. 18SCX004).

REFERENCES

[1] Zhang, S.L., Purwadaria, H.K., Borompichaichartkul, C., Tripetch, P. (2020) Konjac Industry in Major Producing Countries// Konjac Glucomannan. 223-254.

[2] Lu, Q.Z. (2019) Potential and Countermeasures of Developing Konjac Industry Under Hainan Rubber Plantation. Modern Agricultural Science and Technology. 21, 102-103.

[3] Zhang, Y., Li, L.P., Yang, F.M. (2019) Green Development Countermeasure of Konjac Industry in Chuxiong Prefectre. Journal of Anhui Agricultural Sciences. 47(7), 232-234.

[4] He, F., Zhang, Z.L., Cui, M., Liu, L.P., Xue, Q.H. (2018) Soft rot disease alters soil characteristics and root-associated, culturable microbial community of Amorphophallus konjac. Journal of General Plant Pathology. 84(1), 44-57.

[5] Li, M.F., Chen, T.Y., Xiang, L.Y., X., Wang, H.Y., Li, G., Shi, Y.L., Zhu, W. (2019) Bacillus megaterium Strain ZX001: Isolation and Identification and Its Relationship with Konjac Soft Rot Disease. Chinese Agricultural Science Bulletin. 35(21), 103-109.

[6] Gong, M.F., Lin, T.X., Huang, J., Zeng, B. (2018) Screening of endophytic bacteria isolated from two kinds of antarctic plant antagonistic konjac soft rot disease[C]// 2017 International Conference On Biotechnology And Bioengineering (Icbb-2017). 235-237.

[7] Tsror, L., Lebiush, S., Meshulam, M., Aharon, M., Matan, E., Tregerman, M., Gamliel, A. (2015) Biofumigation for the control of soilborne diseases. Acta Horticulturae. 747, 389-394.

[8] Malandrakis, A.A., Kavroulakis, N., Chrysikopoulos, C.V. (2019) Use of copper, silver and zinc nanoparticles against foliar and soilborne plant pathogens . Science of the Total Environment. 670, 292-299.

[9] Pan, D.J., Tang, W.W., Zeng, D.Q. (2019) Effects of Soil-applied Herbicides on Soil-borne Plant Diseases. Molecular Plant Breeding. 17(11), 3799-3806.

[10] Pugalendhi, L., Tamilselvi, N.A., Thangamani, C. (2019) Vegetable grafting – A Boon for soilborne pest and disease management- A Review. Madras Agricultural Journal. 106 (10-12), 561-570.

[11] Lu, X.C., Jiang, J.C., Sun, K., Sun, Y.J. (2017) Review on Preparation and Application of Wood Vinegar. Chemistry and Industry of Forest Products. 37(3), 21-30.

[12] Yang, F., Han, R.Y., Li, R.R., Wang, L.Y., Guo, Y.X. (2018) Effect of Wood Vinegar on Seed Germination and Seedling Growth of Red Bean. Anhui Agricultural Science Bulletin. 24(8), 9-10.

[13] Diógenes, G.V., Magalhães Teixeira, E.N., Pimenta, A.S., de Souza, J.G., Moreira, J.A., Marinho, A.L., Veras, A., Chemane, I.A. (2019) Wood vinegar from eucalyptus as an additive in broiler quail feed. Archives of Environmental Health An International Journal. 9(3), 164-181.

[14] Han, R.Y., Yang, F., Li, R.R., Liu, S.X., Zhang, Q.F., Wang, L.Y., Guo, Y.X. (2018) Inhibitory Effects of Wood Vinegar and its Combined with Pesticides on 13 Plant Pathogenic Fungi. Farm Products Processing, 6, 47-50.

[15] Liu, L., Guo, X.P., Wang, S.Q., Li, L., Zeng, Y., Liu, G.H. (2018) Effects of wood vinegar on properties and mechanism of heavy metal competitive adsorption on secondary fermentation based composts. Ecotoxicology & Environmental Safety. 150, 270-279.

[16] Zhang, L.Y., Wang, L.C., Liu, X., Li, Y.G. (2018) Research Progress on Comprehensive Utilization of Wood Vinegar. Henan Science and Technology. 633, 129-132.

[17] Chen, L.B., Wang, J.G. (2017) Chemical Constitution Analysis of Wood Vinegar from Walnut Shell by Gas Chromatography-Mass Spectrometry. Shandong Chemical Industry. 46(17), 74-76.

[18] Banerjee, A.V. (2017) An Introduction to the "Handbook of Field Experiments". Handbook of Economic Field Experiments. 1, 1-24.

[19] Hess, A.S., Hess, J.R. (2017) One- and two-sample t tests. Transfusion. 57(10), 2319-2320.

[20] Wang, J.G. (2017) Chemical Constitution Analysis of Wood Vinegar from Rice Husk by Gas Chromatography-Mass Spectrometry. Journal of Anhui Agricultural Sciences. 45(31), 15-17.

[21] Pruteanu, M., Lobato, J.I.H., Stach, T., Hengge, R. (2020) Common plant flavonoids prevent the assembly of amyloid curli fibres and can interfere with bacterial biofilm formation. Environmental Microbiology. 22(12), 5280-5299.

[22] Yang, L.H. (2019) Effects of Different Planting Densities on Yield and Disease of Hybrid Konjac. Journal of Yangtze University (Natural Science Edition). 16(7), 62-64.

Received: **27.10.2020**
Accepted: **01.12.2020**

CORRESPONDING AUTHOR

Changming Liu
Shangluo University,
Shangluo Shaanxi 726000 – China

e-mail: lidingyun2016@163.com

© by PSP Volume 30– No. 05/2021 pages 5054-5058 Fresenius Environmental Bulletin

DETERMINATION OF LOST FISHING GEAR IN THE INDLAND WATER OF TURKEY: SAMPLE OF KEBAN DAM LAKE (ELAZIG)

Murside Dartay*

Firat University, Fisheries Faculty, Department of Fisheries Technology, 23119, Elazig, Turkey

ABSTRACT

This study was detected the gross quantity of lost fishing gear in the indland waters of Turkey. We also consider ghost catches resulting from lost gear in other types of fisheries, and the extent to which the value of ghost catches has been quantified. By doing so, the study ultimately aims to contribute to reducing pollution by suggesting more efficient and practical management solutions for these problems. In fact ,of all the thrown fishing nets found in the indland waters areas, 95 % are tramel-nets, gill-nets and traps. This study has indicated that gillnets, trammel nets and traps could be a considerable threat to indland water species once control of the nets has been lost. Using regression analysis it is that 4.4 km trammel nets, 7.2 km gill-nets and 500 set traps are lost gears annually. In conclusion; traditional fishing gears with eco-friendly designs must and establishment of incentive programmes for the fishermen in the indland waters.

KEYWORDS:
Ghost fishing, lost gear, gillnets, trammel nets, traps, indland waters, Turkey

INTRODUCTION

Ghost fishing refers to derelict fishing gear, either lost or abandoned, which continues to function in the water; continuing to induce mortality of aquatic organisms without human control or refers to the potential catch of lost fishing gear, that is catching fish and adding to fishing mortality but in a cryptic way [1-3].

Modern gears are mostly made of non-biodegradable synthetic fibres and can persist in the environment for long periods. They can therefore theoretically continue to catch fish for long periods of time. Graphic and emotive images of dead fish, crustaceans, seabirds and marine mammals in nets and pots which have been lost, have heightened public and political concern over ghost fishing as an issue [4] .

Research on ghost fishing became active in the late 1980s. Ghost fishing has been confirmed for traps, gillnets, trammel-nets and small seine nets. Some lost traps are functional for a long period of time, even in shallow waters.

Fish traps can also be lost as a result of bad weather, chaffing and cutting of set ropes or floats, traps being snagged on the waterbed, faulty gear, vandalism, human error, or traps being inadvertently towed away by other boat traffic Lost fish traps also have the potential to continue to fish. Consequences for gillnets after loss depend on seabed conditions. The ghost fishing function of gillnets remaining on flat seabeds declines rapidly with decreasing heights and increasing visibility.

Ghost fishing occurs when passive gears such as gillnets, trammel nets, wreck nets, pots and traps, are lost or discarded and continue to catch commercially important species of fish and crustaceans as well as non-commercial species of fish and crustaceans, birds, marine mammals and turtles [3-5]. Derelict fishing gear is not necessarily ghost-fishing gear. Ghost fishing was defined as the ability of fishing gear to continue fishing after all control of that gear is lost by the fisherman [1].

Prevention of gear loss is the most fundamental solution against ghost fishing. The reasons for fishing gear loss are: entanglement of gear or its accessory parts which prevents hauling; misplacement during operations; and dropped fishing gear either accidentally or intentionally [6]. The vertical profile and invisibility of gillnets are the primary characteristics that determine their effectiveness. Depth and sea bottom type and the lost gear's exposure to environmental incidents such as storms, surge and fouling are therefore key determinants of the effective catching efficiency of individual ghost gillnets [7–8].

This study was performed to estimate the gross number of lost fishing nets in the indland water of Turkey. By doing so, the study ultimately aims to contribute to reducing pollution by suggesting more efficient and practical management solutions for these problems. In fact, of all the thrown fishing nets found in the indland waters areas, 95 % are tramel-nets, gill-nets and crabs. In this context, this paper attempts to determine the number of lost nets in the

three fishing gears and explores some feasible management solutions for the problems based on the estimate and advice from the experts on the issue.

MATERIALS AND METHODS

This study was occured between 2013 and 2014 fishing seasons in the Keban Dam lake/Turkey (Figure 1). Keban Dam Lake, the second largest dam lake in terms of surface area. Its area is 645 km^2. Monthly samples were taken between 2013 and 2014 years in order to detect lost gears at Keban Dam Lake locality of Turkey.

In this study; the surveys were designed: Face-to-face field surveys (interviews) were applied to fishermen in the Keban Dam Lake/Turkey. The survey use done dependent variable and independent variables and included different indicators to measure the variables. The dependent variable,the number of used nets,was measured by investigating the number of the traps and nets lost.

The respondents were asked to answer the questions regarding the number of fishing boats, fishery months per year, number of fishing days per, , the number of nets used per fishing, ,the number of lost nets, the causes of lossing of nets of fishermen.

The analyses of the data were conducted in using regression analysis, this study constructed a regressione quation to detect the number of lost fishing nets.

RESULTS AND DISCUSSION

In this study were conducted at at the end of the fishing season in the indlan water. All of the surveys were conducted from March 2 th to 28 th, 2014.

As shown in Table 1, a total of 285 fisherman are available. Through face-to-face interviews, 139 (trap,23; gill-net, 72; trammel nets,44) from 120 fishing days unions in the Keban dam lake were collected. The length of lost gear were detected 7.2 km of gillnets,4.4 km trammel nets, 500 unıon traps. This research utilized independent variables including operating months per year, days of fishing per month, number of fishing gears used year.

As shown in Table 2, gill-net fishery, trammel fishery and trap fishery involved use of montly different number of boats. These frequency distributions imply the used fishing boats and amount of lost gear being performed. Crayfish fishing is carried out between July and December. A total of lost traps detected for 500 union. Maximum amount of lost gillnets detected in june. Minumum amount of lost gillnets in August. Maximum amount of lost tramelnets detected in june. Minumum amount of lost tramel nets in August and September (Figures 2,3,4). This study has indicated that gillnets, trammel nets and traps could be a considerable threat to indland water species once control of the nets has been lost.

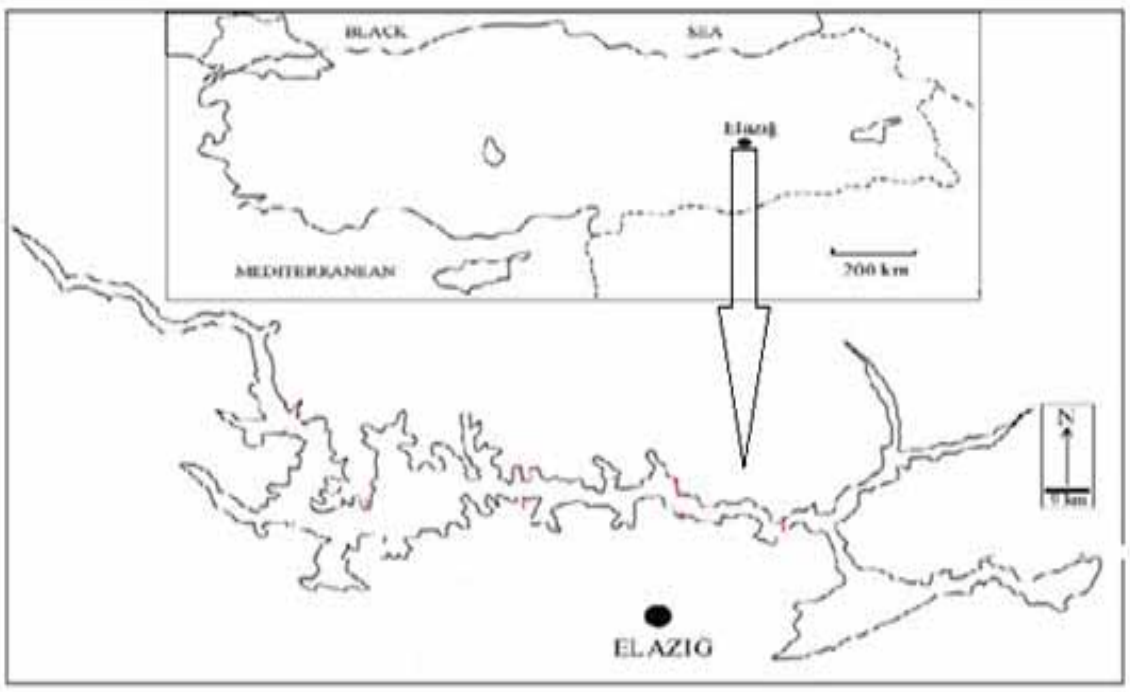

FIGURE 1
Research area (Keban Dam Lake/Elazıg/Turkey)

TABLE 1
Number of fisherman surveyed in the Keban Dam Lake

Source of data	Number of gillnets fisherman (unıon)	Number of trammel nets fisherman	Number of traps fisherman	Total
Number of fisherman	285	186	42	285
Number of lost gear fisherman	72	44	23	139
Length of lost gear (m/unıon)	7200	4400	500	-

*1 union 100 meter

TABLE 2
Distribution of lost gear according to monthly in the research area (2013-2014)

Years	Months	Number of Boats	Amount of determined lost gear		
			Gillnets (m)	Trammel nets(m)	Traps (unıon)
2013	July	118	-	-	-
2013	August	96	100	250	50
2013	September	129	400	250	150
2013	October	135	600	350	50
2013	November	139	850	300	200
2013	December	139	1500	500	Forbidden month
2014	January	118	1800	1200	F. month
2014	February	118	1100	800	F. month
2014	March	118	850	750	F. month
Sum	-	-	7200	4400	500

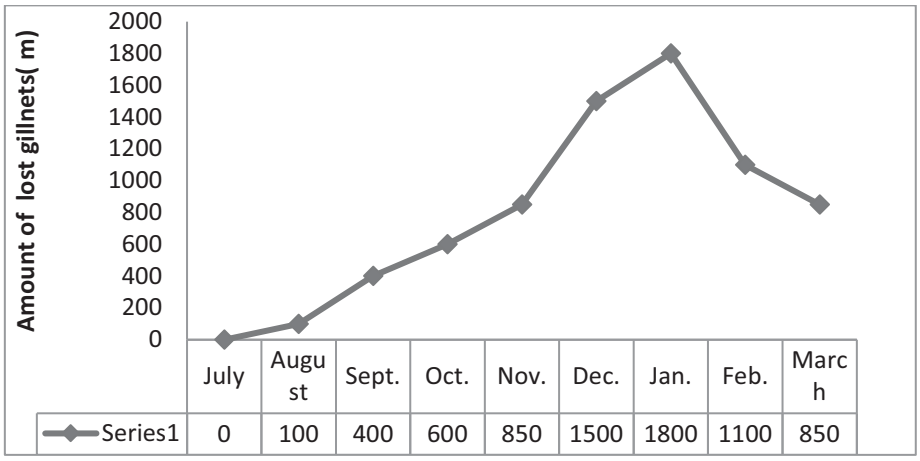

FIGURE 2
Amount of lost gillnets.

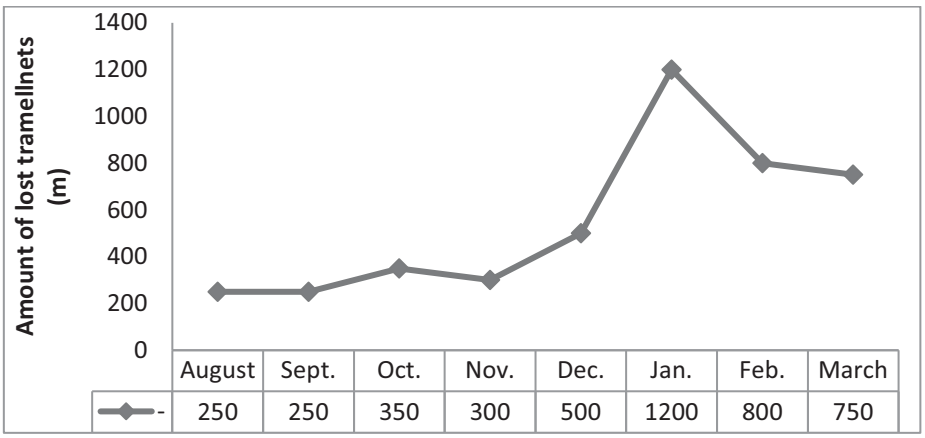

FIGURE 3
Amount of lost trammel nets.

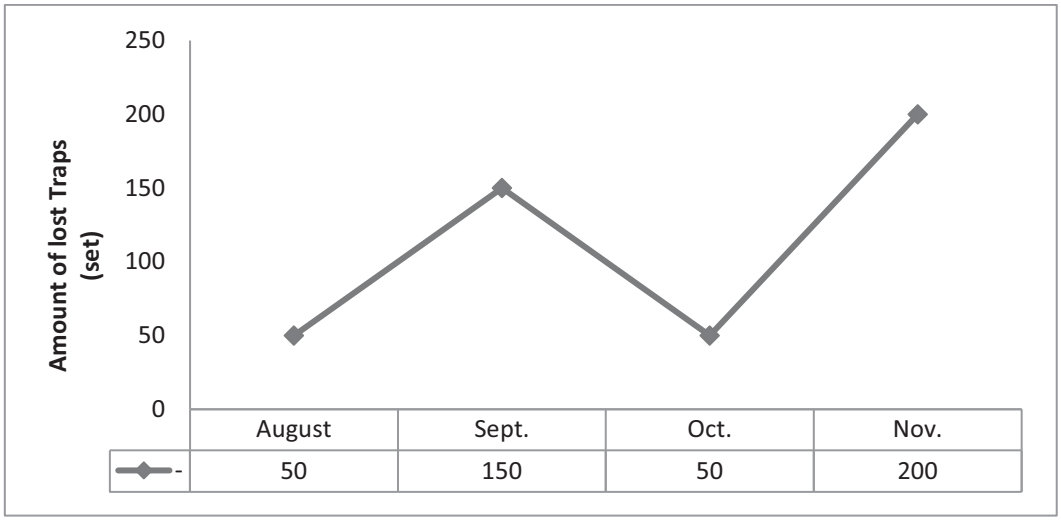

FIGURE 4
Amount of lost traps

TABLE 3
The main reasons for their loss nets of fishermen

Reasons	Weather Conditions	Rupture of buoys	Installation of nets on the boats	Installation of nets on the ground	Total
Number of Fishermen	84	17	13	25	139

Fishermen were asked why they lost their nets. The answers given by the fishermen are given in Table 3.

As shown in Table 3, Number of fishermen who lost nets due to weather conditions, rupture of buoys, ınstallation of nets on the boats, installation of nets on the ground were detected 84, 17, 13, 25 recpectively.

Studies on ghost fishing are limited. A survey of 123 fishermen (about 28% of the fishermen in Izmir Bay) found that about 78.5 km of set nets have been lost in 2002 in Izmir Bay The lost set nets were mainly (97%) multifilament, with mesh sizes varying between 24 and 240 mm. The main reason for their loss was gear conflict [9]. In this study were detected 4.4 km trammel nets, 7.2 km gill-nets and 500 set traps are lost gears annually.

Kaiser *et al* [7], it is that lost gear at 90 meter length of gillnet and trammel nets in the UK, Erzini *et al.* [10], 100 meter gillnet in the Portugal , Nakashima and Matsuoka [11], 72 meter gillnet in the Japan, Sancho et al., [12]. 50 meter gillnet in the Spain, Santos et al. [13], 53 meter gillnet in the p Portugal, Humborstad et al. [14], 27.5 meter gillnets in the Norway, Nakashima and Matsuoka [15],16 meter in the Japan have been reported.

In conclusion; ghost fishing has a number of negative impacts that may be environmental, social or economic in nature. This research were detected the lost gillnets, trammel nets and trap fisheries. While the environmental impacts of lost gear may be considerable, these impacts It harms underwater creatures and cause water pollution. Lost gears as environmental generates some negative impacts in the water. Lost gears as environmental generates some negative impacts in the water. ghost nets act as reefs actively catching fish and generate Potential habitat damage. Therefore traditional fishing gears with eco-friendly designs must and establishment of incentive programmes for the fishermen.

REFERENCES

[1] Smolowitz, R.J. (1978) Trap design and ghost fishing: Discussion. Mar. Fish. Rev. 40, 59–67.
[2] Matsushita, Y., Honda, N., Fujita, K., Watanabe, T. (2004) Time series changes in gillnets abandoned at shallow water. Bull. Fish. Res. Agen. 10, 15–17.
[3] Newman , S., Craig, L., Skepper, G., Mitsopoulos, E. A., Corey, B., Wakefield, H. E. S. (2011) Assessment of the Potential Impacts of Trap Usage and Ghost Fishing on the Northern Demersal Scalefish Fishery. Reviews in Fisheries Science . 19 (2), 74-84.
[4] Brown, J., Macfadyen, G. (2007) Ghost fishing in European waters: Impacts and management responses. Marine Policy. 31, 488–504.
[5] Kim, S.G, Lee, W., Moon, Y. (2014) The estimation of derelict fishing gear in the coastal waters of South Korea:Trapandgill-net fisheries Marine Policy. 46, 119–122.

[6] Matsuoka, T., Osako, T., Miyagi, M. (1997) Underwater observation and assessment on ghost fishing by lost fish-traps. In: ZhouY, Zhou H, Yao C, Lu Y, Hu F, Chui H, Din F., Fourth Asian Fish. Forum. Asian Fisheries Society, Beijing. 179–183.
[7] Kaiser, M.J., Bullimore, B., Newman, P., Lock, K., Gilbert, S. (1996) Catches in 'ghost fishing' set nets. Mar. Ecol. Prog. Ser. 145, 11–16.
[8] Bullimore, B.A., Newman, P.B., Kaiser, M.J., Gilbert, S.E., Lock, K.M. (2001) A study of catches in a fleet of 'ghost-fishing' pots. Fishery Bulletin. 99, 247–53.
[9] Ayaz, A., Unal, V., Ozekinci, U. (2004) An investigation on the determination of amount of lost set net which cause to ghost fishing in Izmir Bay. J. Fish. Aquat. Sci. 21, 35–38.
[10] Erzini, K., Monteiro, C.C., Ribeiro, J., Santos, M.N., Gaspar, M., Monteiro, P., Borges, T.C. (1997) An experimental study of gill net and trammel net 'ghost fishing' off the Algarve (southern Portugal). Mar. Ecol. Prog. Ser. 158, 257–265.
[11] Nakashima, T., Matsuoka, T. (2004) Ghost-fishing ability decreasing over time for lost bottom-gillnet and estimation of total number of mortality. Nippon Suisan Gakk. 70, 728–737.
[12] Sancho, G., Puente, E., Bilbao, A., Gomez, E., Arregi, L. (2003) Catch rates of monkfish (Lophius spp.) by lost tangle nets in the Cantabrian Sea (northern Spain). Fish. Res. 64, 129–139.
[13] Santos, M.N., Saldanha, H.J., Gaspar, M.B., Monteiro, C.C. (2003) Hake (Merluccius merluccius L., 1758) ghost fishing by gill nets off the Algarve (southern Portugal). Fish. Res. 64, 119–128.
[14] Humborstad, O.,Løkkeborg, S., Hareide, NR., Furevik, D.M.(2003) Catches of Greenland halibut (*Reinhardtius hippoglossoides*) in deep-water ghost fishing gillnets on the Norwegian continental slope. Fish. Res. 64, 163–170.
[15] Nakashima, T., Matsuoka, T. (2004) Ghost fishing ability decreasing over time for lost bottom-gillnet and estimation of total number of mortality. Nippon Suisan Gakkaishi. 70, 728–737.

Received: **30.10.2020**
Accepted: **20.01.2021**

CORRESPONDING AUTHOR

Murside Dartay
Firat University,
Fisheries Faculty,
Fisheries, Technology Department,
23119, Elazig – Turkey

e-mail:mdartay@firat.edu.tr

© by PSP Volume 30– No. 05/2021 pages 5059-5066 Fresenius Environmental Bulletin

RESEARCH ON THE COUNTERMEASURES OF PROMOTING THE INTEGRATED DEVELOPMENT OF RURAL THREE INDUSTRIES IN THE CONSTRUCTION OF BEAUTIFUL COUNTRYSIDE

Tianbin Mao[1,*], Qian Li[2]

[1]Department of Architecture, Faculty of Architecture and Civil Engineering, Chengdu University, Chengdu 610106, China
[2]Department of Environmental Art, Faculty of Art and Design, Chengdu University, Chengdu 610106, China

ABSTRACT

The integrated development of rural three industries enriches the structure of rural industrial chain and increases farmers' income, which is an important measure to accelerate the development of rural economy. The construction of beautiful countryside, as an essential means to solve the problem of rural contradictions at this stage, plays a key role in narrowing the gap between urban and rural areas and provides a solid foundation for the integrated development of rural three industries. By analyzing the two major rural reform policies of the construction of beautiful countryside and the integrated development of rural three industries, this study puts forward the current positive situation of the construction of beautiful countryside and the problems faced by the integrated development of rural three industries, analyzes the coupling relationship between the two, and finally puts forward the corresponding countermeasures to promote the integrated development of rural three industries in the construction of beautiful countryside, which has certain guiding significance for accelerating the rural modernization construction, balancing urban and rural development, narrowing the gap between urban and rural development and realizing the rural sustainable development.

KEYWORDS:
Beautiful countryside, Integration, Countermeasure, Sustainable development

INTRODUCTION

With the rapid development of urbanization and urban-rural integration in China, a large number of surplus labor in rural areas are gradually transferred to cities, resulting in problems such as hollowization of rural productivity and deterioration of agricultural ecological environment. In 2013, the No. 1 Document of the Party Central Committee took the construction of beautiful countryside as an significant part of the rural work for the first time. According to the actual situation of the development of rural areas, it put forward the beautiful countryside strategy to strengthen the rural environmental protection, ecological construction and comprehensive control [1]. Document No.1 of 2015 clearly proposed to promote the development of "integration of three industries" in rural areas, and determines that "integration of three industries" is a major direction for China's agricultural development at present. The integrated development of rural three industries will change the mode of rural economic development and realize the construction of beautiful countryside by rectifying the development of rural areas without destroying the ecological and natural environment. For the development of "integration of three industries" in rural areas, beautiful countryside can create a good development environment, guide the sustainable development of the three industries and create economic benefits, while the integrated development of rural three industries will promote the coordinated development of economy, society and ecology in rural areas, ensure the protection of rural culture and ecology, and form a real beautiful countryside with "livable ecology, efficient production, beautiful life and harmonious humanity" [2-3].

MATERIALS AND METHODS

Study on Related Concepts and Development Status. Study on Related Concepts. Construction of Beautiful Countryside. In the process of exploring the construction of new socialist countryside, through continuous theoretical practice, China has determined the new direction of rural planning and upgrading and the construction goal of new countryside, gradually derived the concept of "beautiful countryside" [4]. The construction of beautiful countryside is the most powerful guarantee to effectively change the mode of production and operation in rural areas and narrow the gap between rural and urban areas by solving the three agricultural issues relating to "agriculture, rural areas and rural people" in combination with China's basic national

conditions. "Beautiful countryside" aims at livable ecological environment, beautiful rural life, efficient production mode, and harmonious coexistence between human and nature, to show the beauty of vision, practicality, artistic conception and connotation of beautiful countryside. Its conceptual connotation map is shown in Figure 1. The concept of "beautiful countryside" was first put forward in Anji, Zhejiang Province in 2008. In order to promote the development of urban-rural integration and accelerate the construction of new countryside, Anji, Zhejiang Province, has carried out specific actions for the construction of beautiful countryside. Starting from the conceptual planning, it has carried out the research on development strategy and rural features, then carried out the specialized design and village planning of beautiful countryside, and through integration and upgrading, finally completed the construction of "county town scenic area". These processes have formulated a complete set of evaluation criteria, the specific planning process is shown in Figure 2. After the promotion of "beautiful countryside" mode in Anji, Zhejiang Province, the construction of beautiful countryside has gradually become popular all over the country. Tourism modes such as "rural cultural town" and "ecological countryside" based on the mode of beautiful countryside have also become popular throughout the country. The beauty of "beautiful countryside" is not only reflected in the beauty of natural rural scenery, but also in the beauty of rural history and culture, as well as the beauty of villagers' hard work and wealth [5-6].

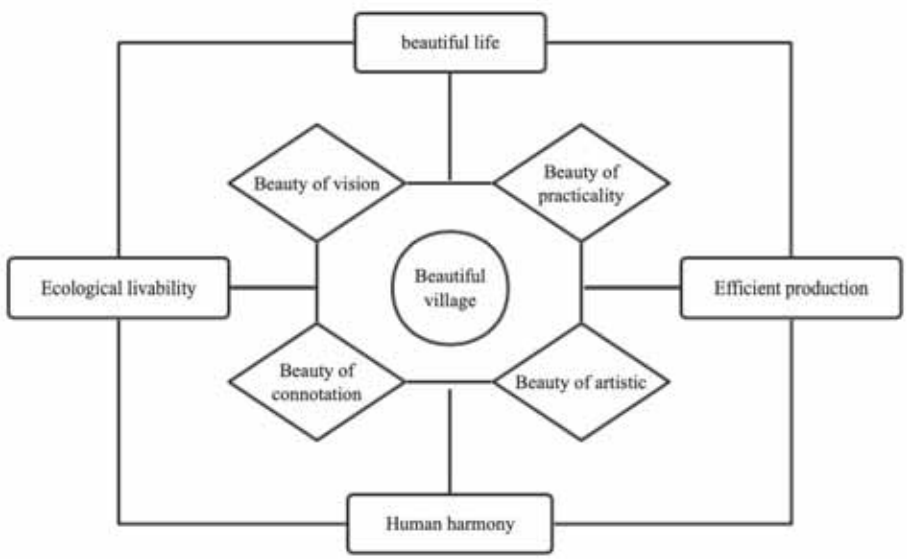

FIGURE 1
Connotation of "Beautiful Countryside"

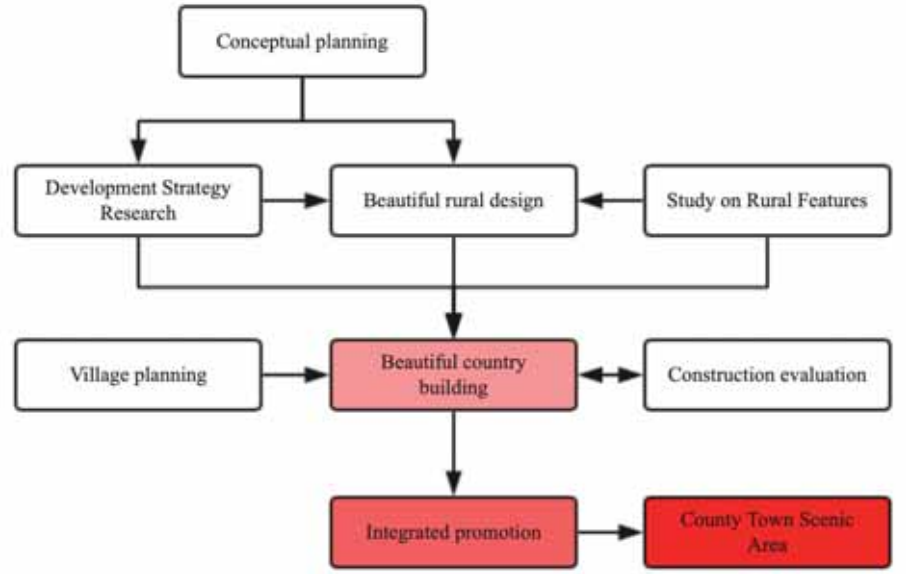

FIGURE 2
"Beautiful Countryside" Planning in Anji, Zhejiang Province

Integrated Development of Rural Three Industries Promoting the integrated development of rural three industries is clearly put forward in the No. 1 Document of the Party Central Committee in 2018 [7]. The proposal of this strategy is based on the existing rural problems: strong restriction of agricultural resources, complex circulation links of agricultural products and fewer rural industrial chain, etc. The fundamental reason lies in the low efficiency of rural industrial chain. Only by promoting the integrated development of rural three industries, extending the rural industrial chain and expanding the scope of rural industries can the current rural problems in our country be solved. The specific series of processes are shown in Figure 3. Through the reorganization and optimization of the three rural industries, the integration of rural three industries will cross each other, thus widening the scope of the rural industries, extending the structure of the rural industrial chain, increasing the functions of the rural industries, upgrading the level of the rural industries, and comprehensively optimizing the overall structure of the rural industries. Promoting the integrated development of rural three industries will be beneficial to break the imbalance between urban and rural development, increase the number of jobs in rural areas sharply and improve the income of farmers. Furthermore, it can also realize the innovation of rural production mode, while traditional agriculture will get a certain transformation after technical development, which is also an important means to promote the development of modern agriculture [8]. Although the development of modern agriculture and the integration of rural three industries have some overlap in the implementation plan, the strategic objectives of the two are the same, both of which are to promote the development of modernization and improve people's happiness.

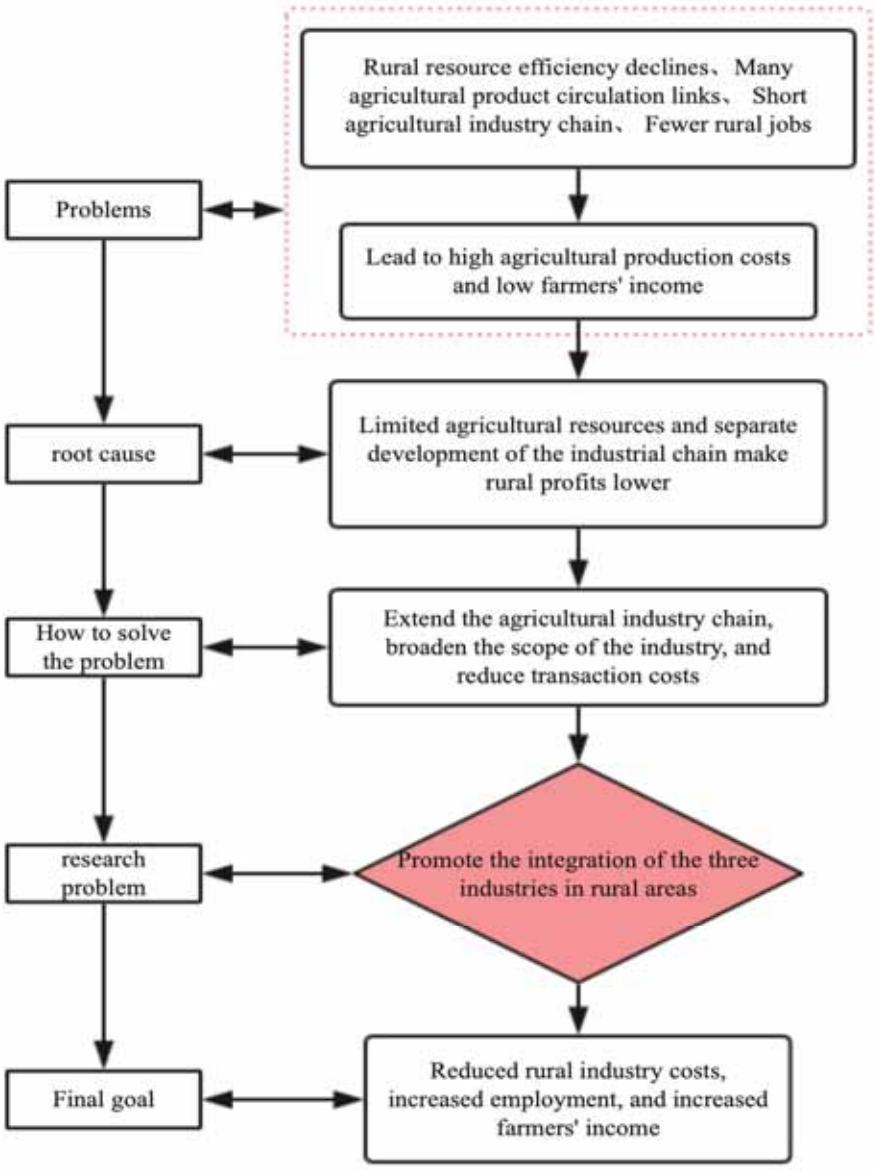

FIGURE 3
Proposal of "Integration of Three Industries in Rural Areas"

Development Status The construction of beautiful countryside and the integrated development of rural three industries are both strategic directions for the development of rural modernization, and complement each other. The ultimate goal of the integrated development of rural three industries is the construction of beautiful countryside, which must start with the problems existing in the integration of rural three industries. Therefore, clarifying the relationship between the two is of great significance to the construction of modern rural areas [9-10].

Current Situation of Construction of Beautiful Countryside As an essential strategic objective for building beautiful China, the construction of beautiful countryside is an important means to reduce the gap between urban and rural areas and promote the development of urban and rural areas, and is a key indicator for China to enter a well-off society in an all-round way [11]. In recent years, with the promulgation and implementation of various national policies and the drive and support of government, all localities have achieved fruitful results in the construction of beautiful countryside.

First, the ecological environment in the countryside has been greatly improved. China's rural areas are extensive, and there have been many environmental problems such as ecological pollution, random discharge of domestic sewage, soil erosion caused by cultivated land and pesticide pollution. On the road of building beautiful countryside, sustainable development is one of the strategic objectives to be implemented. In order to realize this strategic objective, we must improve the ecological environment in the countryside [12]. Under the implementation and promotion of the policies, rural greening has been continuously strengthened, the domestic sewage and garbage has been recycled, thus realizing the sustainable development of energy resources, promoting modern agricultural technology and reducing the pressure on cultivated land.

Second, the rural culture has been inherited and preserved. On the road of building beautiful countryside, cultural resources in rural areas have been fully explored, and ancestral temples, cultural stations and other buildings have been established to preserve and inherit traditional rural culture. The inheritance of intangible cultural heritage not only carries forward the traditional characteristic culture in rural areas, but also enriches the business and cultural life of the local countryside [13].

Third, the rural infrastructure is improving day by day. In order to build beautiful countryside, since the 17th National Congress of the Communist Party of China, the government has invested huge sums of money to improve the infrastructure in rural areas, built more than 1.56 million kilometers of new roads, and the hardening rate of rural roads has exceeded 99.2% [14]. At the same time, the network infrastructure has basically achieved full coverage. In the past, rural areas could only obtain external information through television, while in modern rural areas, network facilities will be the most basic living requirement. In terms of entertainment facilities, through introduction and promotion, the long-term development has been achieved in rural areas, and rural life has become more and more colorful.

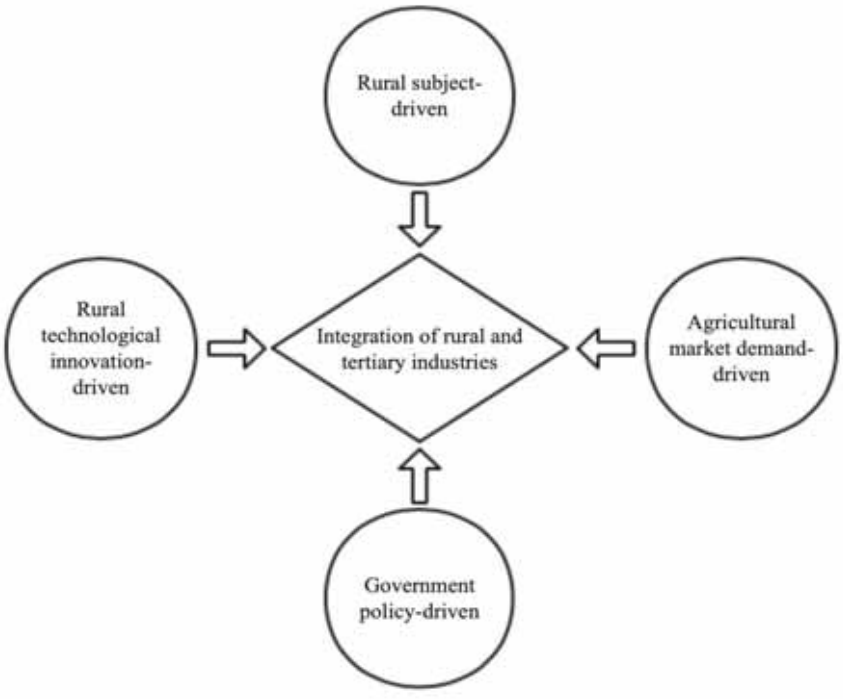

FIGURE 4
Driving Factors for the Integrated Development of Rural Three Industries

Fourth, the rural modernization construction is obvious. In the process of promoting the construction of beautiful countryside, the transformation of traditional agriculture has achieved remarkable results. With the support of policies, advanced modern agricultural technologies have been introduced, which not only reduces manpower, but also greatly increases the output of agricultural products and diversifies sales channels, thus greatly increasing the income of farmers. In addition, the vigorous development of modern ecological countryside and rural tourism has significantly increased rural revenue and employment, showing the quite effective construction of beautiful countryside [15-16].

On the whole, the construction of beautiful countryside has provided a good foundation for promoting the integrated development of rural three industries.

Problems Faced by the Integrated Development of Rural Three Industries The integrated development of rural three industries is driven by rural main interests, agricultural technology innovation, agricultural product market demand and government policies (as shown in Figure 4), which are indispensable. Although the construction of beautiful countryside has provided a good foundation for promoting the integrated development of rural three industries, there are still some problems in the integration of rural three industries from its current development situation and its own driving factors.

First, the construction of rural infrastructure cannot keep pace with the process of promoting the integrated development of rural three industries. The rural infrastructure is an important condition for promoting the integrated development of rural three industries, while it has always been in a relatively backward stage, which is bound to affect the process of integrated development of rural three industries [17]. Although the roads in rural areas extend in all directions, the traffic conditions are backward, the quality is difficult to guarantee, the area is too small or with potholes everywhere, and there are also various problems in later maintenance. In addition, water conservancy facilities are relatively lagging behind, which makes it more difficult to realize the large-scale of agricultural production and promote the integrated development of rural three industries.

Second, there is a lack of connection between the rural industrial chain and supply chain. The so-called integrated development of rural three industries has its first essence to realize the integration of the three major industries in rural areas, to extend the rural industrial chain, to broaden the scope of rural industries, to abandon the traditional single industrial chain and supply chain, to closely linked the three major industries by modern technology and to realize the maximization of the industrial structure in rural areas. To quickly achieve the integrated development of the three major industries in rural areas, we must first improve and expand the industrial chain and supply chain in rural areas and realize their joint effect [18].

Third, production factors in rural areas are blocked. In the process of promoting the integrated development of rural three industries, the circulation of rural production factors has been blocked, resulting in a big gap with the economic development of cities, especially in terms of talents, modern technology and capital flow. With the continuous development of the modernization process, the countryside needs to introduce more talents, technology and funds, to scientifically plan and manage the development of rural agriculture, and to accelerate the integrated development of rural three industries.

Therefore, there are still some problems in the integrated development of rural three industries, which will become obstacles to the construction of beautiful countryside. Only with the support of government policies can the rural areas receive more attention and use the strength of the whole society to promote the integrated development of rural three industries.

RESULTS

Research on the Countermeasures of the Integrated Development of Rural Three Industries in the Construction of Beautiful Countryside. With the rapid development of our country's economy, the government's investment in rural areas is also increasing, which has changed the rural industrial structure, accelerated the construction of modern and beautiful countryside, and laid a solid foundation for the realization of sustainable development.

Connection between the Construction of Beautiful Countryside and the Integrated Development of Rural Three Industries. As an important means to promote agricultural development, the integration of rural three industries has realized the integrated development of rural characteristics and various industries. By extending the rural industrial chain, broadening the scope of rural industries, and realizing new breakthroughs in rural industries, it has provided sufficient impetus for the modernization transformation of traditional agriculture and the sustainable development of agriculture, not only realizing the substantial increase in farmers' income, but also maximizing the protection of ecological environment [19].

In the process of building beautiful countryside, the integrated development of rural three industries plays a significant role in promoting the coordinated development of the rural economy. The integrated development of rural three industries pays more attention to the effective combination of the major industries and the rural areas, and builds a construction

mode in which the industries drive the rural economic development and the rural areas promote the industrial development, which lays a solid foundation for the construction of beautiful countryside and brings the greatest economic benefits to the rural areas. In addition, the integrated development of rural three industries has provided sufficient impetus for narrowing the gap between urban and rural areas and building urban-rural integration. On the premise of the common development of rural three industries, the rural resources in all aspects should be effectively integrated and utilized to promote the construction of modern rural management entities and realize the common transformation and development of the rural industrial structure. The integrated development of rural three industries can also promote the modernization of rural agriculture and provide a good foundation for the construction of beautiful countryside [20]. Moreover, the integrated development of rural three industries has better realized the inheritance and development of rural culture. In the process of promotion, the cultural characteristics and details of the rural areas in the region are fully explored, the economic development and the protection of cultural resources are integrated to form a new cultural industry chain and realize the inheritance and development of culture.

Countermeasures of Promoting the Integrated Development of Rural Three Industries in the Construction of Beautiful Countryside Improve Rural Infrastructure. The perfect rural infrastructure plays a decisive role in achieving the integrated development of rural three industries. Nowadays, in the process of continuously strengthening the modernization construction in China, the rural modernization construction has become particularly important. The government should invest more manpower and material resources, comprehensively guarantee rural roads, water conservancy, bridges, electricity and other infrastructure, and promote the rural modernization construction. Otherwise, through the support and encouragement of policies, the amount of foreign capital investment in rural construction is guaranteed to provide a solid foundation for promoting the integrated development of rural three industries [21].

Deepen the Interest Relationship between Subjects. The ultimate goal of promoting the integration of rural three industries is to reduce the cost of rural industry, improve the economic efficiency, increase the income of farmers and the number of jobs. Starting from the purpose, the government should strengthen the support and supervision of rural areas, formulate corresponding policies to strengthen the regulation of agricultural products sales in rural areas, improve the rural credit system, build more rural industry participants, enrich the industrial chain structure of rural areas, deepen the interest relationship of the participants in the industrial chain, and realize the regional rural interest community. In addition, the government should encourage more farmers to participate in the industrial chain of the integrated development of rural three industries, expand the industrial scope, increase the industrial structure, and achieve the smooth progress of the integration of rural three industries.

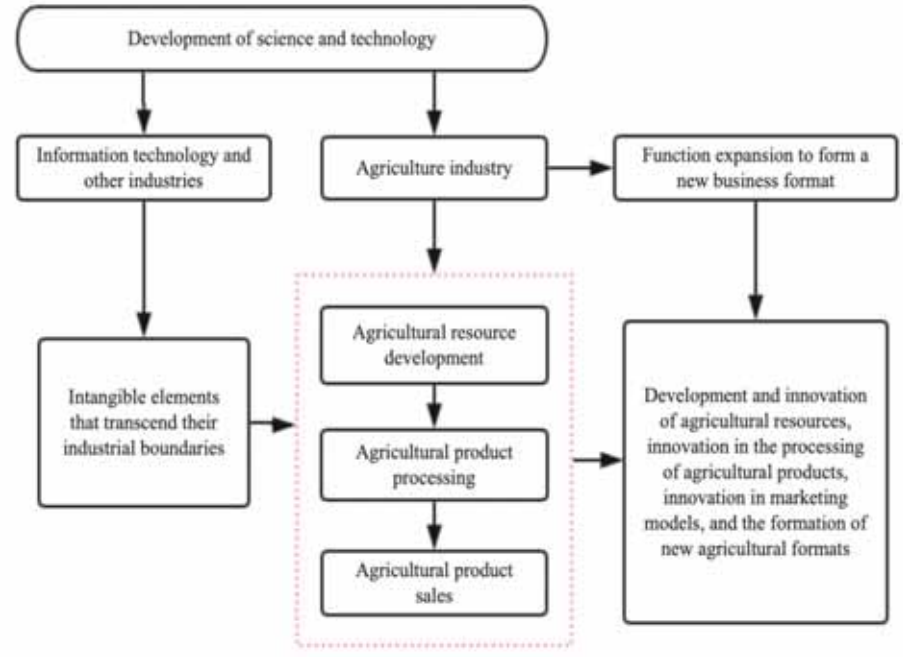

FIGURE 5
Infiltration and Integration of Scientific and Technological Development into Agriculture

Encourage Scientific and Technological Innovation and Achieve the Strategic Goal of Sustainable Development Science and technology are the primary productive forces, and the development of modern agriculture cannot be separated from the development and innovation of science and technology. For one thing, the development of science and technology can promote the internal development of various industries. In terms of agriculture, it is reflected in the development of agricultural resources, the processing and sales of agricultural products. For another, other industries can penetrate into the development of agriculture through the development of science and technology, fully tap the economic benefits of agriculture and expand new rural businesses, as shown in Figure 5. Additionally, the introduction of advanced agricultural production technologies and modern agricultural management programs can speed up the reform of traditional agriculture and the development of modern agriculture in the process of the integrated development of rural three industries. While ensuring the quality of agricultural products, it is necessary to greatly increase the output of agricultural products, reduce the production cost of agricultural products, and ensure the growth of farmers' income. Furthermore, ensure the development of ecological agriculture, reduce rural pollution, protect rural ecological resources, apply modern science and technology to strengthen the recycling of rural waste materials, so as to lay the foundation for the sustainable development of rural areas. Finally, introduce technical personnel, strengthen the cultivation of talents' ability in agricultural science and technology innovation, thereby providing sufficient power for the integrated development of rural three industries.

CONCLUSIONS

At present, there is still a big gap between urban and rural development in our country. In order to realize the overall development of urban and rural areas, the construction of beautiful countryside and the integrated development of rural three industries are indispensable. In the context of the construction of beautiful countryside, the integrated development of rural three industries is progressing smoothly, the rural economy has developed rapidly, and the rural income has generally increased, greatly increasing the happiness of farmers' life, protecting the rural ecological environment, providing an important guarantee for the sustainable development of the rural areas, which is a step towards the full realization of a well-off society.

ACKNOWLEDGEMENTS

The study was supported by "Chengdu Key Research Base Of Philosophy And Social Sciences – The Funded Project of the Construction and Development of Beautiful Village Research Center in 2019 (Grant No.CCRC 06)".

REFERENCES

[1] Cao, L.M. (2018) Beautiful Rural Construction Under Background of Urban-Rural Integration. Agricultural Engineering. 8(1), 132-133.
[2] Manning, D.B., Bemmann, A. (2015) Linking the Producers and Consumers of Woodfuel to Contribute to the Sustainable Development of Rural Areas: An Introduction to AgroForNet. John Wiley & Sons Hoboken. 1-4.
[3] Emelyanova, L.L., Kropinova, E.G., Voloshenko, K.J. (2015) The integrated approach to sustainable development of rural areas: the case for the agricultural sector in the Kaliningrad region of the Russian Federation. Int. J. Agricultural Resources Governance and Ecology. 11(2), 158-177.
[4] Gyawali, N.P. (2017) Microhydro-Based Mini grid for Sustainable Development of Rural Communities: A Case Study of Nepal. Springer, Singapore. 151-174.
[5] Zhang, C.J. (2015) Sustainable Development of Agriculture from the Perspective of Rural Urbanization. Asian Agricultural Research. 7(3), 8-10.
[6] Sun, T., Shen, Q.Q. (2020) Coupling and coordination analysis between tourism development and ecological environment in Jiangsu province. Fresen. Environ. Bull. 29(5), 3671-3678.
[7] Ma, L.B., Tian, Y.Y., Xie, Z.L., Guo, X.D., Gu, Y. (2018) Evaluation of quality and spatial reconstruction of oasis rural settlements based on micro-scale. Transactions of the Chinese Society of Agricultural Engineering. 34(5), 227-234.
[8] Qin, Y.D., Sun, Y.P. (2020) Study on the construction of sports training venues. Fresen. Environ. Bull. 29(4), 2469-2474.
[9] Chowdhury, T.A. (2015) Development of a Multidimensional Sustainable Livelihoods Model for Rural Bangladesh. The Journal of Developing Areas. 49(5), 153-168.
[10] Li, Z.X., Molnar, J.J., Sun, S.Q. (2016) An Analysis of Policy Optimization concerning Sustainable Agricultural Development in China Based on 2014 US Farm Bill. Asian Agricultural Research. 8(3), 8-11.
[11] Chirozva, C. (2015) Community agency and entrepreneurship in ecotourism planning and development in the Great Limpopo Transfron-tier Conservation Area. Journal of Ecotourism. 14, 1-19.

[12] Zhang, X.H., Qin, Y., Yang, P. (2017) Hollow Village Problems in Rural Areas Under the Perspective of the Balanced Development. Journal of Yunnan Agricultural University. 11(4), 22-26.
[13] Zainoddin, A.I., Amran, A., Shaharudin, M.R. (2017) Factor That Impacts the Capability Development and Sustainable Income of the Rural Development Programme in Malaysia. Advanced Science Letters. 23(11), 10621-10624.
[14] Qin, Z.C. (2016) Integrated Development of Urban and Rural Areas: National Strategy Oriented to the Future. Frontiers. 4, 6-17.
[15] Kumar, H.D., Kumar, N.T., Suresh, K.R., Mitavachan, H., Shankar, G. (2015) Advanced Solar-Irrigation Scheduling for Sustainable Rural Development: A Case of India. Springer Proceedings in Energy Springer, Cham. 123-131.
[16] Castro, A.D., Fronza, C.F. (2015) Sustainable development in agriculture: a socio-ecological approach. International Journal of Engineering Research and Applications. 5(11), 12-15.
[17] Qin, B.T. (2015) Sustainable Agricultural Development in Rural China: The Way of Addressing Agricultural Pollution. Springer, Berlin, Heidelberg. 13-22.
[18] Soliman, I. (2015) Diagnosis and Challenges of Sustainable Agricultural Development in Egypt. Sustainable Agricultural Development. 19-64.
[19] Loch, C., Rebollar, P.B.M., Rosenfeldt, Y.A.Z., Walkoski, M. (2015) Landscape multifuncionality evaluation as a subsidy to public policies for sustainable rural development. Ciencia Rural. 45(1), 171-177.
[20] Pan, D.H., Zhang, Y., Lei, G.Y. (2015) Construction and Sustainable Development Countermeasures of Agricultural Science and Technology Park in Counties of Heilongjiang. Heilongjiang Agricultural Sciences. 7, 171-174.
[21] Liu, J. (2015) Sustainable Development of Agriculture from Perspective of Agricultural Mechanization. Agricultural Engineering. 5(4), 43-44.

Received: **01.11.2020**
Accepted: **19.01.2021**

CORRESPONDING AUTHOR

Tianbin Mao
Department of Architecture,
Faculty of Architecture and Civil Engineering,
Chengdu University,
Chengdu 610106 – China

e-mail: saksalaskjkj88@aliyun.com

© by PSP Volume 30– No. 05/2021 pages 5067-5074 Fresenius Environmental Bulletin

DIAGNOSIS OF THE DURATION OF HEAVY RAINSTORMS UNDER SUBTROPICAL ENVIRONMENTAL CONDITIONS IN LOW-LATITUDE PLATEAU AREAS

Jing Zhou[1,2], Yan Sun[2,*], Haiying Wu[3], Yang Shen[3]

[1]School of Atmospheric Science, Nanjing University of Information Science & Technology, Nanjing 210044, China
[2]Jiangsu Institute of Meteorological Science, Nanjing 210009, China
[3]Jiangsu Meteorological Observatory, Nanjing 210008, China

ABSTRACT

The research on the characteristics of low-latitude plateau rainstorm is the current hot spot of meteorological research. Therefore, in this paper, we take China's Yunnan Province as the research object, and systematically carry out the diagnosis study of the duration of heavy rainstorms in low-latitude plateau areas. Yunnan belongs to the subtropical plateau area, with sufficient rainfall and distinct dry and wet seasons. The vertical change of temperature with the topography is particularly significant. Through the analysis of the geographical and climatic characteristics, combined with the research on the background of the influence of atmospheric circulation on the heavy rain in Yunnan, the duration of heavy rains in Yunnan in multiple time periods in 2019 is analyzed. Under the interaction of the East Asian cold trough and the south branch trough, and under the influence of the subtropical high in the western Pacific and the south branch trough continues to move southward, a water vapor channel is formed from the Bay of Bengal to southwestern Yunnan. The mesoscale low pressure is affected by the strong cold air, which promotes the development of convection, and strengthens the tropical mesoscale cyclones and causes the instability of convection. Combined with the complex topography of Yunnan, it has resulted in long-term continuous heavy rain in Yunnan. Finally, through the test of the rainfall from 0:00 on July 28 to 12:00 on July 31, the results show that the rainfall during this period is mainly concentrated from 0:00 on July 29 to 12:00 on July 30. The amount of precipitation changes from high to low, and the rainfall in some areas has exceeded 13mm, which lasts for a long time.

KEYWORDS:
Low latitudes environment, plateau areas, heavy rain, weather, duration, diagnosis

INTRODUCTION

Different from other degrees of precipitation, rainstorm weather is usually accompanied by serious natural disasters, which is the key content of meteorology research. For example, there are many kinds of meteorological disasters in Jiangsu province, mainly including rainstorm, strong convection, thunder and lightning, etc. Jiangsu is low-lying and flat, which is not conducive to catharsis [1-2]. Especially in early summer, there will be heavy rains and floods, which will harm the growth of crops and seriously affect people's economy and life. The existing research on rainstorm weather is mainly concentrated in South China and the vicinity of the Huai River Basin. Meteorological studies and climate studies for such topographic features include the formation of the boundary layer convergence system, the mechanism of cold air triggering rainstorms in warm areas, and the effect of the boundary layer convergence system on the Meso-scale Convective System (MCS). These research results help us understand the mechanism of mesoscale rainstorm [3]. Although the research on the mechanism of heavy rain near the Huai River Basin is sufficient, there are few studies on the low-latitude plateau (Yun-Gui Plateau) area, especially the Yunnan area. In recent years, many weather stations have been established in Yunnan, but the research results on heavy rains are not sufficient [4].

As a representative region of the low-latitude plateau, Yunnan is one of the regions with the best ecological environment in the middle and low-latitude regions of the northern hemisphere. The whole area of Yunnan has complex topography, special geographical location, diverse climate changes, and distinct dry and wet climates. The terrain of Yunnan is complex and there is a lot of precipitation in summer. The rainfall starts from mid to late May and lasts until the end of October [5-7]. During the rainy season, precipitation is concentrated and heavy rains occur frequently. However, rainstorms and precipitation are mainly concentrated in local areas with obvious geographical features. Rainstorms are coming

quickly and precipitation is swift and violent, leading to major natural disasters such as landslides and mudslides in the mountains, which pose a great threat to the lives and property safety of the local people in Yunnan.

Regarding the problem of long duration of torrential rains in low-latitude plateaus such as Yunnan, in this paper, we have carried out a systematic diagnosis of the duration of heavy rains in low-latitude plateaus. In addition, the reasons for the formation of torrential rains in this area are analyzed to provide a reliable basis for future environmental disaster management.

RESEARCH AREA AND METHODS

Research area. Yunnan Province is located in southwestern China with a total area of 390,000 square kilometers, and lies between 21°8' and 29°15' north latitude. This area is a low-latitude region, with Guangxi and Guizhou in the east, Myanmar to the west, Vietnam, Laos and other countries in the south, and the Tibet Plateau to the northwest. The terrain of Yunnan is high in the west and low in the east. It gradually decreases from north to south in a stepped form. The average elevation of the province is above 1 500 m, which is a low-latitude mountainous plateau area. The wide valley in the southern section of the Yunling Mountains is the boundary of the entire Yunnan Province [8]. The Yunnan-Guizhou Plateau is composed of the Yunnan-Guizhou Plateau in the east and the western Guizhou Plateau, with an average elevation of about 2 000 m. The valleys and mountains in the western region are separated from each other, forming the famous Hengduan Mountains, with an average elevation of about 4 000 m. The southern and southwestern border areas are river valley landforms, which are flat and open, with an average elevation of less than 1 000 m [9]. The specific topography is shown in Figure 1.

The southern Yunnan is severely affected by the monsoon due to it is close to Myanmar and Vietnam. Its northwest side connects to the Qinghai-Tibet Plateau, so it is simultaneously affected by two tropical ocean climates, the Bay of Bengal and the South China Sea. The East Asian summer monsoon and the southwest Indian monsoon affect the climate of Yunnan in summer together with the high-latitude weather system. Yunnan is the dry season from April to November of the second year each year [10-11]. During this time, the western dry heating group controls the climate in Yunnan. Meanwhile, the climate is warm and sunny with a small amount of precipitation, and the precipitation in the dry season is less than 10% of the whole year. From May to October each year is the rainy season in Yunnan, and the warm and humid ocean air currents dominate the climate and precipitation in the region. At this time, precipitation is frequent and often extreme rainstorms, which account for 90% of the total annual precipitation. Therefore, this area is a typical low-latitude plateau. The temperature difference in the four seasons is small and the climate is distinct between dry and wet seasons. At the same time, it has the characteristics of vertical variation due to the influence of mountain environment [12].

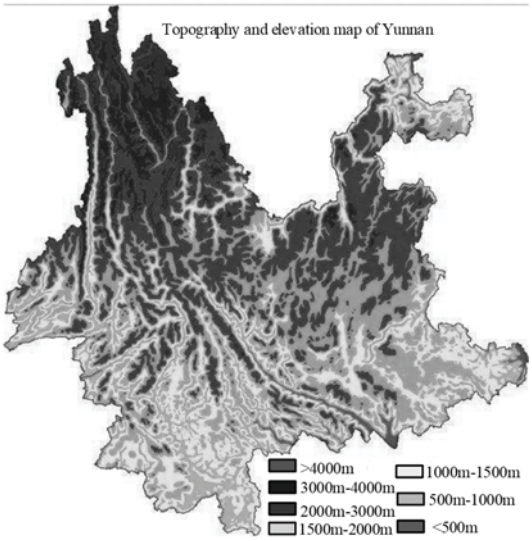

FIGURE 1
Overall topography and altitude of Yunnan.

Background of the influence of atmospheric circulation. Figure 2 records the average change of the heavy precipitation process under different atmospheric pressures from 8 pm on May 28, 2019 to 8 pm on June 1, 2019. It can be seen from Figure 2(a) that the mid-high latitudes in Asia and Europe under the 550 hPa condition mainly show the characteristics of two grooves and two ridges. Judging from latitude and longitude, the Sea of Okhotsk and Caspian Sea areas are trough areas, while the Aleutian Islands and Lake Baikal areas are ridge areas. Near 30° north latitude, there is a shear from east to west between the mid-latitude high ridge area and the subtropical high. At the same time, this shear, together with the East Asian groove line, extends westward to a position of 90°E. The southwestern region of China is influenced by the cold air in the middle and high latitudes that is guided by this form [13]. In the mid-to-low latitude area, near the north is a subtropical high pressure area. The 597 gpm line is between 18° and 25° north latitude and belongs to the northern part of the South my country Sea and the central part of Taiwan. The west ridge point extends to about 108° east longitude, and forms a thick and deep trough (south branch trough) at the junction of India and Myanmar.

The Yunnan area is affected by the interaction between the southern branch trough and the subtropical high and is affected by the warm humid air from the Bay of Bengal. Figure 2(b) clearly shows that the low-level 900 hPa process averages, the East Asian cold trough exists in the Yangtze River basin, and the warm zone is on the west side of the Bay of Bengal. A cold center appears in the western section of the Sichuan Basin and the southeast of the Qinghai-Tibet Plateau. A low-pressure circulation is formed in the areas of India, Myanmar and the Bay of Bengal, which makes the cold and warm air flow converge in Yunnan [14-15]. Figure 2(c) shows the process flow field at 900 hPa. A strong cross-equatorial air flow is formed in the region of 35°-55° east longitude, and the air flow forms a reentry at 11° north latitude. The airflow has reached the east side of the Bay of Bengal and turned into a southwesterly airflow extending to southwestern my country. It formed a low-altitude southwest rapid in the southwest of Yunnan Province, and also causes the instability of torrential rain.

RESULTS

Analysis of ground shear line and mesoscale diagnosis. From the night of July 28 to the early morning of July 31, 2019, Yunnan ushered in extremely heavy rain. Figure 3 shows the results of surface weather analysis from the beginning to the end of the rainstorm. At 16:00 on the evening of the 19th, under the large-scale cold high pressure in eastern Yunnan, the southwestern shear line in central Yunnan moved from northwest to southeast. However, a strong air current appeared in the southwest of Yunnan. It moves the tangent northward, but the tangent is blocked by the cold high pressure [16-17]. By 20:30 on the 19th, the shear line reached central Yunnan. The newly born mesoscale low pressure is continuously developed and strengthened by the invasion of cold air. At this time, the center of pressure is located in the southwestern region of central Yunnan (southwest of Chuxiong). Thunderstorms appeared in the southern part of the shear line, and showers appeared around the shear line and in the north [10, 18]. At 22:30, the position of the shear line and the mesoscale low pressure no longer changed. Cold air continues to invade. The interaction of mesoscale low pressure and cold air forms two airflows, the southwest airflow and the easterly airflow. These two air currents bring warm and humid air to Yunnan Province. In northern Yunnan, the shear line converged with this warm and humid air current, and caused the extremely heavy rain in central Yunnan that has rarely

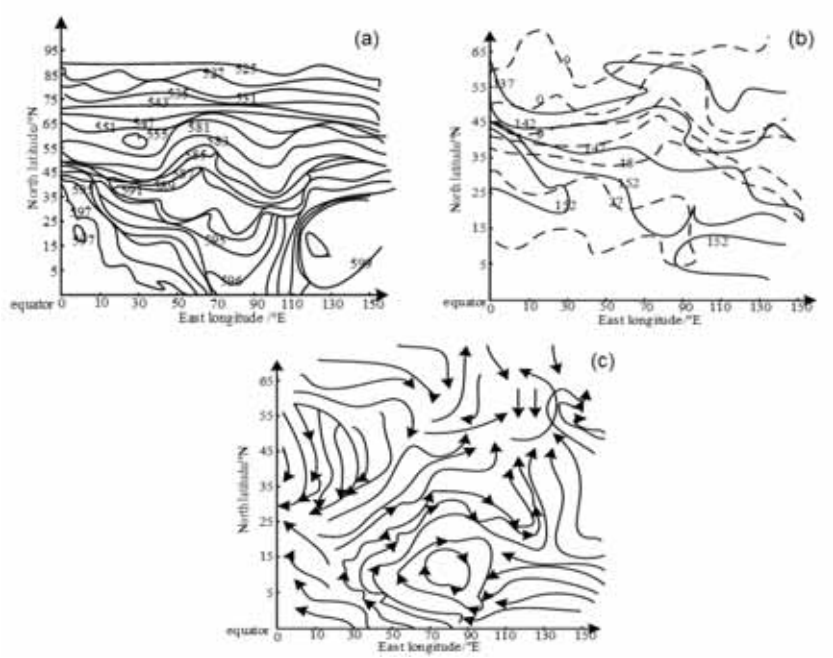

FIGURE 2

Average situation of heavy rainfall process under different atmospheric pressure.

Notes: (a) 550 hPa process average (interval of each line is 40 gpm), (b) 900 hPa process average (where the dotted line represents the temperature field, the interval between each line is 9°C; the solid line represents the height field, and the interval between each line is 50 GPM), (c) Average flow field of 900 hPa process.

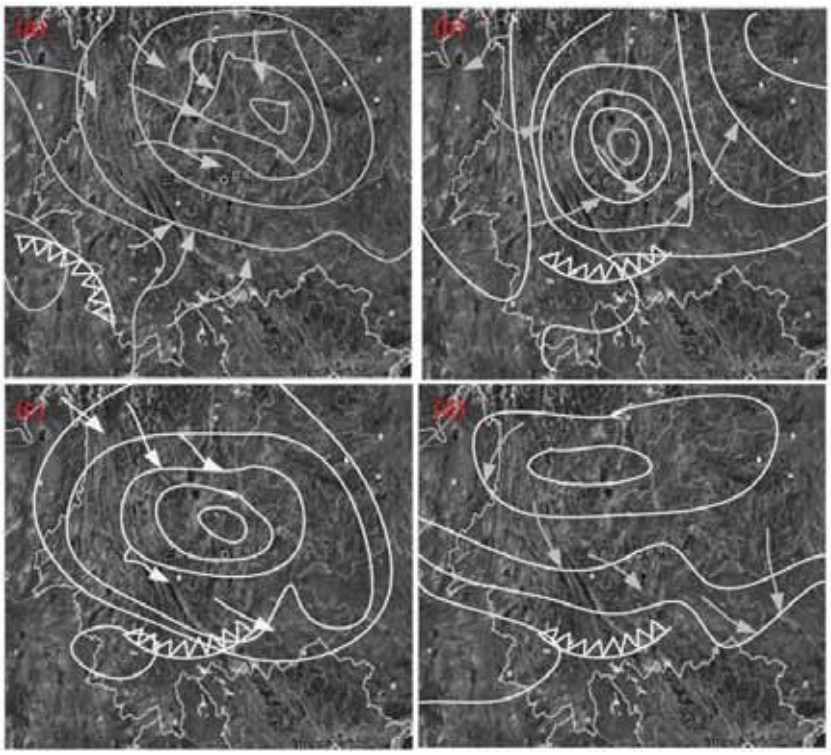

FIGURE 3

Analysis of surface mesoscale low pressure shear line of heavy rain duration.

Notes: (a) Early stage of Rainstorm at 16:00 on the 19th, (b) The rainstorm continued at 20:30 on the 19th, (c) The rainstorm intensified at 22:30 on the 19th, (d) The rainstorm weakened at 03:00 on the 20th.

been seen in recent years. After more than 4 hours of heavy rainfall, the wind speed in the area south of the mesoscale shear line increased. The large-scale cold high pressure moves to the southeast, while the mesoscale low pressure moves to the northwest and gradually weakens. The precipitation process continued until about 4 am on the 20th. During the last 12 hours of torrential rain and precipitation, most parts of Yunnan Province experienced torrential rains to extreme torrential rains [19]. During the continuous rainstorm, it is always located in the south of the shear line and in the meso-scale low pressure area. The precipitation in the area south of the shear line is only 0.45 mm, which indicates that the heavy rain is mainly concentrated in the center of the mesoscale and the location north of the shear line.

Diagnosis of factors affecting continuous precipitation. (1) The influence of cold air and south branch trough. From July 28, 2019 to July 31, 2019, heavy rains and extremely heavy rains continued to occur in many areas of Yunnan Province. The 550 hPa altitude field is shown in Figure 4. It can be seen from Figure 4(a) that there is a low trough in the Bay of Bengal, but it is not a complete south branch trough. Affected by the low trough, the southwest warm and humid air currents formed in Yunnan Province are weak, and the cold air is mainly formed in the northern part of the Yellow River. In the north of Yunnan, a vortex is formed in the Qinghai-Tibet Plateau. The weak cold air spreads southward from this low vortex, forming weak precipitation in the southwest of Yunnan [11, 20]. It can be seen from Figure 4(b) that the low vortex on the Qinghai-Tibet Plateau continues to move eastward and gradually strengthens. The cold air moved eastward into Yunnan Province under the influence of the South Branch Channel [21]. The subtropical high moves westward. The northwestern part of the Qinghai-Tibet Plateau has been intensified by the influence of the South Asian High, leading to gradual precipitation in central and western Yunnan. As shown in Figure 4(c), affected by the western Pacific subtropical high, the southern branch trough continues to move south. A water vapor channel has been formed from the Bay of Bengal to southwestern Yunnan. The cold air continued to move south and merged with the water vapor channel in central and western Yunnan, forming heavy rainfall. Figure 4(d) shows that the subtropical high and the Qinghai-Tibet Plateau high confront each other. The southern branch trough can only maintain a small amount of movement, and the water vapor transport in the southwest of Yunnan is strong and stable, which has caused many areas to continue to maintain heavy rainfall. The cold air continued to move eastward, and the subtropical high still moved westward and showed an upward trend. Although the low vortex from the Qinghai-Tibet

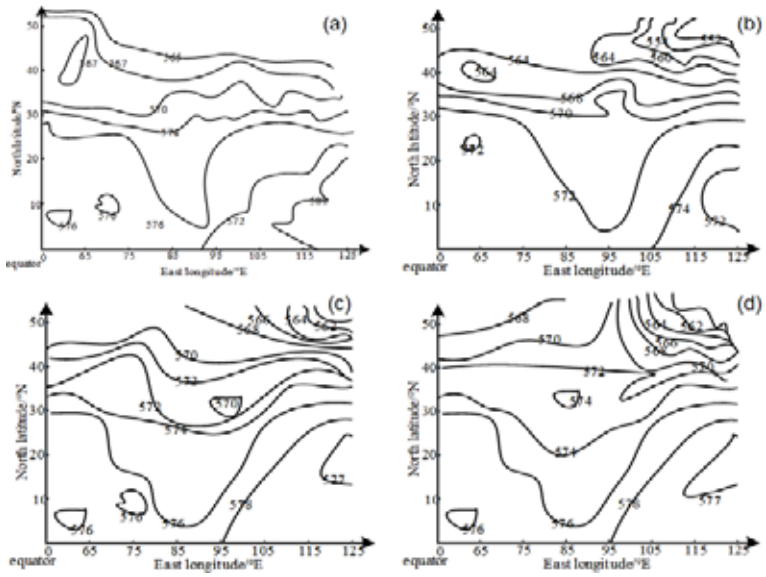

FIGURE 4
550 hPa geopotential height field.

Notes: (a) Before 0:00 rain on July 28, 2019; (b) Precipitation starts at 8:00 p.m. on July 28, 2019; (c) On July 29, 2019, the heavy rainfall appears at 0:00 p.m; (d) Continuous heavy rain on July 30, 2019.

Plateau weakened, it kept moving eastward. The south branch trough shrinks to the north and gradually weakens, and the trough lines are distributed from northeast to southwest. This situation led to the westward shift of water vapor transport and concentrated heavy precipitation in southern Yunnan [15, 22]. After 8:00 p.m. on July 31, due to the interruption of water vapor supply, the south branch trough dissipated and the rainstorm ended.

From the above analysis, it can be seen that during the duration of heavy rainfall, the appearance of the southern branch trough caused a large amount of warm and humid airflow to trigger auxiliary coalescence in Yunnan. The cold air on the Qinghai-Tibet Plateau played a role in fueling the flames of the cold and warm air in Yunnan, forming mesoscale convective weather. Many unstable factors and the emergence of complex energies have caused heavy rain on the low-latitude plateau.

(2) The impact of low jet stream. From the above analysis, it can be seen that water vapor transportation is the main cause of heavy rains in Yunnan. The main channel for water vapor transport is the low-level jet stream. The results of the study of heavy precipitation in South China indicate that the low-level jet is an important image factor of the precipitation process [23]. The low-level jet stream in Yunnan is mainly closely related to the summer monsoon. Yunnan belongs to the low-latitude plateau and generally has a high altitude, so it is necessary to study the water vapor transport under the 800 hPa atmospheric pressure. Let's take the heavy precipitation process from July 28, 2019 to July 31, 2019 as an example. At that time, the low vortex on the Qinghai-Tibet Plateau moved eastward and met the southern branch trough. The subtropical high continues to strengthen while traveling westward. The warm and humid air flow in the water vapor channel extending from the Bay of Bengal to Yunnan has increased. In turn, a strong low-altitude jet stream is formed. This low-altitude jet zone is also accompanied by a strong wind speed center with a smaller scale. The strong wind speed center moved to the territory of Yunnan and continued to increase, resulting in the formation of strong precipitation centers in some parts of Yunnan several times. Studies have shown that large-scale environments can lead to the appearance of low-level jets, but the specific causes need to be further studied.

Under 800 hPa atmospheric pressure, no jet stream formed between the Bay of Bengal and Yunnan before the rain at 0:00 on July 28, 2019. Only two wind speed centers with obvious characteristics appear in Yunnan, but the values are relatively small. As time passed, the south branch trough formed and gradually stabilized, and the jet stream also formed and gradually strengthened. It moved to the northeast with strong wind speed along the jet stream, and superimposed with the wind speed core area in Yunnan, causing the wind speed core to be continuously strengthened. After the heavy rainfall began, a 13 m/s jet center appeared at 0:00 on July 9, 2019, and heavy rains and extremely heavy rain appeared on both sides of the jet center. After that, the cold air moved eastward, and the subtropical high moved westward and rose northward. The south branch trough shifted from

TABLE 1
Statistical results of precipitation (mm).

Time	Chuxiong	Mouding	Eshan	Xinping
0 o'clock on July 28	0.54	0.68	3.12	0.28
12:00 on July 28	0.83	0.97	4.28	6.59
0 o'clock on July 29	6.72	8.95	6.57	8.42
12:00 on July 29	8.43	10.37	6.43	9.05
0 o'clock on July 30	10.49	10.58	12.15	14.34
12:00 on July 30	11.35	13.34	11.36	12.69
0 o'clock on July 31	0.64	0.57	2.61	5.33
12:00 on July 31	0.52	0.49	1.73	0.16

the northeast to the southwest. This led to the movement of the jet stream from northeast to southwest, which caused the jet stream in Yunnan to shift to the south. In the middle and late period of heavy rain, the intensity of the jet center had increased to 17 m/s, and heavy rainfall appeared in the northwest of the jet center. The southwesterly airflow then changed to the westerly airflow. The wind speed in the rainy area was still high, but the water vapor supply was insufficient. The intensity and range of the center of the jet stream gradually reduced and moved eastward, and the heavy rain and precipitation ended [19-20]. The vertical superimposition and enhancement of jet pulsation led to unstable convective development and caused heavy rain in Yunnan [22].

Diagnosis of low-level mesoscale cyclones. In order to study the meso-scale cyclone system of heavy precipitation from July 28, 2019 to July 31, 2019, we used the nine-point smoothing filter method to obtain the meso-scale field in Yunnan. There was no mesoscale system when precipitation did not occur on July 28, 2019, and a mesoscale depression appeared in the northern part of the rainstorm area after the heavy rain on July 29. After heavy rainfall lasted for more than two hours, the meso-scale low pressure increased, and the mesoscale low pressure in central Yunnan showed a sharp rise in convergence, which led to the rare and extremely heavy rain in this area. On July 31, 2019, the cold air gradually weakened, and the mesoscale low pressure moved to the northwest, weakened and disappeared.

Analysis and diagnosis of precipitation. In order to further diagnose the characteristics of the continuous rainstorm, four test points were selected during the precipitation process from July 28, 2019 to July 31, 2019 to analyze and diagnose the precipitation of each test point. The four test points are Mouding, Xinping, Chuxiong and Eshan, and the statistical results are shown in Table 1.

In Table 1, the Chuxiong and Mouding monitoring points are associated with the first precipitation center. Precipitation is mainly concentrated from 0:00 on July 29th to 12:00 on July 30th, and precipitation ranges from high to low. Both monitoring points changed to light rain at 0:00 on July 31st until the heavy rain stopped. During the rainstorm stage, the precipitation exceeded 10 mm. At 12:00 on July 30, the highest precipitation in Mouding area exceeded 13 mm. Xinping and Eshan belong to the second precipitation center. The precipitation in Eshan has reached 3 mm since 0:00 on July 28. The rainfall in Xinping area has gradually increased since 12:00 on July 28, and the continuity of precipitation is not strong. Two different mesoscale systems caused two heavy precipitation centers respectively. From the point of view of the time period of the torrential rain and the central area of the heavy rainfall, the precipitation range is wide, the duration is long, and the mesoscale characteristics are obvious.

CONCLUSIONS

Yunnan is a low-latitude plateau with complex terrain. The whole province is like spring in all seasons, warm in winter and cool in summer, with sufficient precipitation and distinct wet and dry conditions. Affected by air currents such as the Qinghai-Tibet Plateau, the southern branch trough, and subtropical high pressure, extreme weather phenomena such as heavy rains are prone to occur during the rainy season. We tested the rainstorm conditions in various areas of Yunnan from 0:00 on July 28 to 12:00 on July 31. The results showed that the highest precipitation reached 13mm from July 29 to July 30. During the rainstorm period, the precipitation is more than 10mm, the rainfall time is longer and the range is wide. The following results are obtained through analysis:

(1) The continuous strengthening of the subtropical high and the continuous development of the southern branch trough provide a large-scale atmospheric circulation background for the occurrence of extremely heavy rains in Yunnan.

(2) The tropical depression in southern Yunnan converges with two warm and humid air currents in the Beibu Gulf and the Bay of Bengal to guide the

low-level jet stream, which provides sufficient water vapor transportation for precipitation in Yunnan.

(3) Affected by the cold air and subtropical high pressure brought by the Qinghai-Tibet Plateau and high latitudes, the tropical mesoscale low pressure will rise in convergence, and cold air will trigger precipitation.

(4) Studies have shown that the East Asian cold trough and the south branch trough interact, and the westerly belt system plays an important role in causing heavy rainfall.

(5) Affected by the low-level mesoscale convergence line, the northern cold air and the southern branch trough, combined with the influence of the topographical characteristics of Yunnan, the area is prone to strong precipitation.

ACKNOWLEDGEMENTS

This work was financially supported by the National Natural Science Foundation of China (No. 41575070) and the Natural Science Foundation of Jiangsu Province (BK20201506).

REFERENCES

[1] Lei, L., Lei, X. (2018) Influence of typhoon in the east china sea on the southwest vortex rainstorm in Sichuan Province. Journal of Tropical Meteorology. 034(003), 314-323.

[2] Sun, Y., Wang, Y., Shen, X., Zhou, Y., Deng, G. (2018) Diagnostic Analysis on a Heavy Rainfall Associated with the Northeast Cold Vortex and Atmospheric River. Plateau Meteorology. 037(004), 970-980.

[3] Liu, X., Wang, Y., Hu, Z., Zhou, Y. (2019) Diagnostic Analysis and Radar Echo Features of a Hailstorm Severe Convective Weather Process over the Tibetan Plateau. Climatic and Environmental Research. 24(5), 611-625.

[4] Zhu, L., Zhang, T., Li, H., Yin, L. (2018) Analysis on Meso-scale Features and Forming Reasons of a Short Time Intensive Precipitation Case in Yunnan Province. Journal of Chengdu University of Information Technology. 33(03), 112-120.

[5] Longyang, Q. (2019) Assessing the effects of climate change on water quality of plateau deep-water lake - A study case of Hongfeng lake. Science of the Total Environment. 647, 1518-1530.

[6] Sun, J., Wei, J., Fu, S., Zhang, Y., Wang, H. (2018) The Multi-scale Physical Model for Persistent Heavy Rainfall Events in the Yangtze? Huaihe River Valley. Chinese Journal of Atmospheric Sciences. 042(004), 741-754.

[7] Xu, J., Bi, B., Shen, Y., Chen, T., Gong, Y., Li, J. (2018) Mesoscale characteristics and mechanism analysis of the unexpected local torrential rain in Guangzhou on 7 May 2017. Acta Meteorologica Sinica. 076(004), 511-524.

[8] Qin, Y., Zhou, S., Zhang, R., Yang, S., Yan, Z. (2017) Seasonal Variations of Occurrence Frequencies of Two Types of Tropopause over the Tibetan Plateau and Their Differences from Those in the Same Latitudes. Climatic and Environmental Research. 022(004), 508-518.

[9] Long, Y., Wu, F., Que, Z., Deng, D., Zhang, K. (2018) Analysis of a Local Heavy Rainstorm Process in Northern Jiangxi. Meteorological Science and Technology. 46(06), 149-158.

[10] Yang, Z., Yin, X., Hu, Y., Zhou, Q. (2018) Correlation between Atmospheric Instability Parameters and Lightning Activities over Low-Latitude Plateau. Meteorological Science and Technology. 46(05), 1020-1025.

[11] Huang, X., Fang, N., Zhu, T., Wang, L., Shi, Z., Hua, L. (2018) Hydrological response of a large-scale mountainous watershed to rainstorm spatial patterns and reforestation in subtropical China. Science of The Total Environment. 645, 1083-1093.

[12] Gao, H., Li, G. (2020) Mesoscale Synoptic Meteorology Analysis and Numerical Experiment of Local Sudden Rainstorm Affected by Topography in Southeast Part of Guizhou Province. Plateau Meteorology. 39(02), 301-310.

[13] Liu, G., Lai, Z., Zhong, X., Huang, R., Zhai, L. (2017) Analysis of multi-scale characteristics of a july 2015 persistently long heavy rainfall in Guangxi. Journal of Tropical Meteorology. 033(003), 357-367.

[14] Yuan, K., Lu, Y., Li, M., Yao, W., Liu, H. (2018) Diagnosis and Analysis of Storm Process in Middle and Lower Reaches of Yangtze River by One-dimensional Moist Vorticity and One-dimensional Moist Divergence. Journal of China Hydrology. 38(04), 64-69.

[15] Zhao, Y., Wang, Y. (2017) A Numerical Investigation of the Formation Mechanism for the Extremely Heavy-Rain Event in Southern Fujian Induced by Westward-Moving Typhoon Soulik in 2013. Climatic and Environmental Research. 22(003), 365-380.

[16] Wang, H., Wang, C., Gao, F., Gao, Y., Wang, W., Hu, S., Wu, X. (2017) Comparative Analysis on Mesoscale Characteristics of Two Local Short-Time Severe Rainstorm Processes in Chengde. Meteorological Monthly. 516(12), 1507-1516.

[17] Teruyuki, K. (2018) Representative Height of the Low-Level Water Vapor Field for Examining the Initiation of Moist Convection Leading to Heavy Rainfall in East Asia[J]. Journal of the Meteorological Society of Japan. 96(2), 69-83
[18] Prenner, D., Kaitna, R., Mostbauer, K., Hrachowitz M. (2018) The Value of Using Multiple Hydrometeorological Variables to Predict Temporal Debris Flow Susceptibility in an Alpine Environment. Water Resources Research. 54(9), 6822-6843.
[19] Do Nascimento, C., Mary, W., Da Silva, L. (2018) Hydrological performance of modular-tray green roof systems for increasing the resilience of mega-cities to climate change. Journal of Hydrology. (573), 1057-1066.
[20] Elkamhawy, E., Wang, H., Zhou, B., Yang, Z. (2018) Failure mechanism of a slope with a thin soft band triggered by intensive rainfall. Environmental Earth Sciences. 77(9), 340.
[21] Yasumitsu, M., Takemasa, M., Masaru, K., Hiromu, S., Kae, S. (2019) Impact of Dense and Frequent Surface Observations on 1-Minute-Update Severe Rainstorm Prediction: A Simulation Study. Journal of the Meteorological Society of Japan. 97(1), 253-273.
[22] Shrestha, S., Laza, M., Mende, C., Bhosale, S., Dingkuhn, M. (2020) The blaster: A methodology to induce rice lodging at plot scale to study lodging resistance. Field Crops Research. 245, 107663.
[23] Prenner, D., Kaitna, R., Mostbauer, K., Hrachowitz, M. (2018) The Value of Using Multiple Hydrometeorological Variables to Predict Temporal Debris Flow Susceptibility in an Alpine Environment. Water Resources Research. 54(9), 6822-6843.

Received: **03.11.2020**
Accepted: **24.11.2020**

CORRESPONDING AUTHOR

Yan Sun
Jiangsu Institute of Meteorological Science,
Nanjing 210008 – China

e-mail: jsshqxtsy@sina.com

© by PSP Volume 30– No. 05/2021 pages 5075-5083 Fresenius Environmental Bulletin

RESEARCH ON THE COUPLING AND COORDINATED DEVELOPMENT OF REGIONAL ECOLOGICAL ENVIRONMENT AND FINANCIAL SUPPORT IN THE PROCESS OF URBANIZATION

Xueqing Kang[1], Yuanxin Zhang[2,*]

[1]School of Economics, Sichuan University, Chengdu 610065, China
[2]Chengdu Institution of New Economic Development, Chengdu 610000, China

ABSTRACT

Financial support is the basic support for the development of the ecological environment, and urbanization is the only way to ensure rapid economic development and modernization. In this paper, we conducted a systematic study on the coordinated development of regional ecological environment and financial support under the process of urbanization, and constructed a corresponding quantitative evaluation index system. According to the relevant data of the standardization evaluation index, the entropy method is used to calculate the evaluation index weight, and then we construct a coupling and coordination evaluation model. In addition, based on the results of the internal coordination of the system, the coupling between subsystems, and the overall coordination, the degree of coupling and coordination between the regional ecological environment and financial support under the urbanization process is judged. Finally, taking a province in China as the research area, a coupled and coordinated empirical study was conducted based on the relevant data of the area from 2005 to 2019. The results show that the overall coordination degree of the study area shows a gradual improvement trend, which can be roughly divided into four main stages: a rapid rise period, a slow rise period, a small fall period and a stable period. During 2005-2008, the number of sub-regions with financial support synchronized with the ecological environment increased from 3 to 7. From this analysis, it is known that the main factor leading to the low degree of early coupling and coordination of the research area is that financial support lags behind the development of the ecological environment.

KEYWORDS:
Urbanization process, ecological environment, financial support, coupling and coordination, evaluation index, weight

INTRODUCTION

Financial support is the basic support for the development of the ecological environment, and urbanization is the only way to ensure rapid economic development and modernization [1]. China's urbanization related plans clearly pointed out that the purpose is adaptability, economy, greenness, and beauty, adheres to resource conservation and environmental friendliness, and aims to improve economic output [2-3]. The ecological environment is the core and foundation for realizing regional sustainable development. Finance, as a financial innovation that supports the green transformation and development of the national economy, can rationally allocate and guide limited resources to the direction of environmental protection [4]. Therefore, through scientific methods to reduce resource costs and reduce environmental pollution, the coordinated development of economy and environment can be achieved. In the context of the close relationship between the urbanization process and economic growth, how to deal with the contradiction between the deterioration of the regional ecological environment and the rapid development of the financial economy under the urbanization process is one of the main problems that my country urgently needs to solve at present [5]. In this context, it is very important to study the coordinated development of regional ecological environment and financial support under the process of urbanization. The financial ecological environment is actually a bionic concept in the financial field. There are also precedents for scholars to introduce ecological theory into other disciplines [6]. Some scholars have conducted a lot of research on the coordinated development of economy and environment, the relationship between population and resource development, the conflict and resolution of economic and social benefits of enterprises, and ecological benefits.

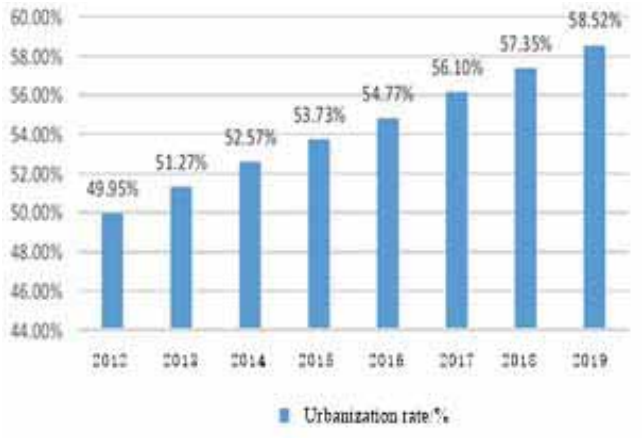

FIGURE 1
China's urbanization rate from 2012 to 2019.

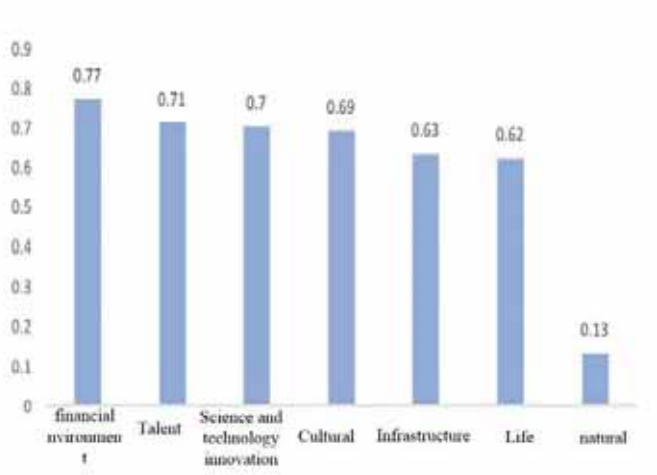

FIGURE 2
The correlation between each factor and urbanization process.

As a result, emerging sciences such as ecological economics and environmental economics and a large number of economic and social sustainable development theories have emerged. Ecological environment and finance are an organic whole that interacts and restricts each other. A good regional ecological environment is the basic condition for sustainable economic development [7].

RESEARCH METHODS

Index system construction. China's urbanization path is a complex process with multiple factors and multiple links, which is affected by economic, political, cultural and other aspects. Moreover, China's urbanization road started late and the development speed is relatively slow. Figure 1 shows the statistics of China's urbanization process in recent years.

Based on the status quo of China's social development and the data in Figure 1 and Figure 2, it is known that with the continuous improvement of social living standards, the development of financial standards is closely related to the process of urbanization. Economy and ecology are complementary and interactive. While economic development, the protection of the ecological environment cannot be ignored. The construction of an evaluation index system that can fully reflect the correlation between the regional ecological environment and financial support under the process of urbanization is the key to studying the coordinated development of them [8]. A few scholars have conducted theoretical research on the coupling of finance and ecological environment. They construct the conditions for economic growth of the ecological environment based on the close internal relationship between finance and the ecological environment. Generally, as the economy grows, environmental quality will deteriorate first and then be improved. Based on this, the correlation between the regional ecological

TABLE 1
Evaluation indicator system.

System partition	First level indicator	Secondary indicators	Calculation method	unit	Indicator direction
Ecological environment under the process of urbanization	Population urbanization	Population urbanization rate	Urban population/total population	(%)	Positive
		Urban population density	City population/city area	(people/km^2)	Positive
		Natural population growth rate	Raw statistics	(%)	Positive
	Ecological urbanization	Harmless treatment rate of domestic garbage	Raw statistics	(%)	Positive
		Park green area per capita	Park green area / urban population	(m^2/person)	Positive
		Green coverage rate of built-up area	Raw statistics	(%)	Positive
		Sewage treatment rate	Raw statistics	(%)	Positive
	Social urbanization	Urban unemployment rate	Urban registered unemployment rate	(%)	Negative
		Every 10,000 people own buses	Raw statistics	(Vehicles)	Positive
		City medical level	Number of health technicians per 1,000 people in urban areas	(people)	Positive
		Road area per capita	Area of urban roads/total urban population	(m^2/person)	Positive
		Urban education technology investment level	Education, technology expenditure/general public budget expenditure	(%)	Positive
		Urban construction process	Urban construction land area	(km^2)	Positive
Financial support in the process of urbanization	Financial scale	Urban maintenance and construction funds expenditure	Raw statistics	(Ten thousand yuan)	Positive
		Commercial bank loan growth	Increment of the loan in the current period / beginning balance	(%)	Positive
		Financial practitioners	Raw statistics	(people)	Positive
		Financial correlation rate	Total deposits and loans of financial institutions/GDP	(%)	Positive
		Per capita deposit level	Savings balance of urban and rural residents / permanent population	(Yuan / person)	Positive
	Financial structure	Proportion of medium and long-term loans	Medium and long-term loan balance/loan balance	(%)	Positive
		Insurance depth	Premium income/GDP	(%)	Positive
	Financial efficiency	Insurance density	Premium income / permanent population	(Yuan / person)	Positive
		Efficiency of financial intermediary	Resident savings/loan balance	(%)	Positive
		Deposit ratio	Loan balance/deposit balance	(%)	Positive

environment and financial support under the urbanization process needs to consider the ecological environmental factors under the urbanization process, which include society, economy, population, environment, etc. [9]. In this paper, based on the criteria of data availability, comprehensiveness, and science and rationality, we select 13 detailed indicators from the three aspects of population, ecology, and cities to construct the ecological environment indicator subsystem under the urbanization process [10]. In addition, 10 detailed indicators are selected from three aspects: scale, structure and efficiency to construct

the financial support indicator subsystem in the process of urbanization. The financial support index subsystem (shown in Table 1) is used to study the level of coupling and coordination between them. The data involved in Table 1 comes from the statistical yearbooks of the province in the past 15 years in the study area, the statistical yearbooks of cities in China, and the statistical reports on national economic and social development over the years [11-12].

Data source and processing. The main task of the data processing process is to standardize the indicators and determine the weight of each indicator. The commonly used weight calculation methods include analytic hierarchy process, entropy method and principal component analysis. Entropy method is an objective weighting method, which can avoid the weighting bias caused by subjective judgments such as analytic hierarchy process [13]. We use the entropy method to assign weights to the indicators in the indicator system in Table 1. The weight coefficients of different indicators are determined based on the level of difference between different indicators [14] to objectively describe the importance of different indicators in the load indicator system.

In order to reduce the influence caused by the directional difference and category difference between the indicators, the normalization method should be selected to implement standardization processing for different indicators before determining the index entropy value [15]. The specific process is as follows:

First, the normalization of the positive indicators is as follows:

$$Z_{ij} = \left[\frac{x_{ij} - x_{ij,\min}}{x_{ij,\max} - x_{ij,\min}} \right] \times 100\% \quad (1)$$

The normalization processing for negative indicators is as follows:

$$Z_{ij} = \left[\frac{x_{ij,\max} - x_{ij}}{x_{ij,\max} - x_{ij,\min}} \right] \times 100\% \quad (2)$$

Among them, Z_{ij} and x_{ij} respectively represent the standardized value of the index and the initial value of the index, and $x_{ij,max}$ and $x_{ij,min}$ respectively represent the upper limit and lower limit of the index.

After normalizing X_{ij}, the proportion F_{ij} of X_{ij} is determined:

$$F_{ij} = \frac{X_{ij}}{\sum_{i=1}^{n} X_{ij}} \left(j = 1,2,\cdots,m \right) \quad (3)$$

Equation (3) is used to determine the entropy value S_j of the j-th index:

$$S_j = k \sum_{i=1}^{n} F_{ij} \ln\left(F_{ij} \right) \quad (4)$$

Among them, k=-1/ln(n) represents the adjustment coefficient. Normally, $S_j \geq 0$.

Equation (5) is used to determine the utility value E_j of the jth index:

$$E_j = 1 - S_j \quad (5)$$

Equation (6) is used to determine the weight W_j of the j-th index:

$$W_j = \frac{E_j}{\sum_{i=1}^{m} X_{ij} E_j} \quad (6)$$

Coupling coordination evaluation model. (1) Calculation of internal coordination of the system. Let $x_j = \left(x_{1j}, x_{2j}, \cdots, x_{mn} \right)^T$ represent the ordinal parameter of the subsystem index, where $n \geq 0$, $x_{\min} \leq x_{ij} \leq x_{\max}$, $i = 1,2,\cdots,m$, $j = 1,2,\cdots,n$.

Let L_{ij} represent the degree of order of the order parameter x_j, under the condition that L_{ij} is equal to $\frac{x_{ij} - x_{\min}}{x_{\max} - x_{\min}}$ and $\frac{x_{\max} - x_{ij}}{x_{\max} - x_{\min}}$, they have positive and negative effects respectively [16]. x_{max} represents the upper limit value of the sequence parameter at the critical point of the stable state of the system, and x_{min} represents the lower limit value.

The weighted *TOPSIS* method [17] and the L_{ij} calculation results are selected to determine the internal coordination degree of the subsystem Y_i:

$$Y_i = \sum_{i=1}^{m} L_{ij} w_j \left(Y_i = a_i, b_i \right) \quad (7)$$

Among them, a_i and b_i respectively represent ecological environment subsystem and financial support subsystem. $0 \leq Y_i \leq 1$, the closer the Y_i value is to 1, the greater the internal coordination rate of the subsystem, and the closer the Y_i value is to 0, the smaller the internal coordination rate of the subsystem.

(2) Calculation of coupling degree between subsystems. The calculation formula of the coupling degree O_i between subsystems is as follows:

$$O_i = \left(\frac{a_i \times b_i}{\left[\frac{a_i + b_i}{2} \right]^2} \right)^{\frac{1}{2}} \quad (8)$$

The coupling degree between subsystems O_i ranges from 0 to 1. The closer the O_i value is to 1, the higher the coupling degree between subsystems [18]. The closer the O_i value is to 0, the lower the coupling degree between subsystems.

(3) Overall coordination calculation. The linear weighting method is selected to determine the overall coordination degree Ti between the regional ecological environment and financial support in the process of urbanization, and the formula is as follows [19]:

$$T_i = \lambda\left(\alpha a_i + \beta b_i\right) + \gamma O_i \quad (9)$$

Among them, λ represents the degree of coordination within the system, and γ represents the importance of the coupling degree between subsystems. Normally, the λ value and the γ value are consistent, and both are 0.5. α represents the importance of the ecological environment subsystem, β represents the importance of the financial support subsystem, and defines the importance of the two subsystems to be the same, and both are 0.5. The overall coordination degree T_i ranges from 0 to 1. The closer the T_i value is to 1, the higher the overall coordination of the system; the closer the T_i value is to 0, the lower the overall coordination of the system.

(4) Coupling coordination model. The results of the coupled and coordinated development model of regional ecological environment and financial support under the process of urbanization are as follows [20]:

$$D_i = \sqrt{O_i \times T_i} \quad (10)$$

According to the research conclusions of related scholars [21], Table 2 shows the level and evaluation criteria of the coupling and coordinated development of the regional ecological environment and financial support under the process of urbanization.

TABLE 2
Standards and grades of coupling coordination degree.

Coupling	Low coupling		
Coordination	0.00—0.10	0.11—0.20	0.21—0.30
Coordination level	Extreme imbalance	Severe Disorder	Moderate disorder
Coupling	Antagonistic stage		
Coordination	0.31—0.40	0.41—0.50	
Coordination level	Mild disorder	On the verge of disorder	
Coupling	Run-in stage		
Coordination	0.51—0.60	0.61—0.70	0.71—0.80
Coordination level	Basic coordination	Primary coordination	Intermediate coordination
Coupling	Highly coupled		
Coordination	0.81—0.90	0.91—1.00	
Coordination level	Well coordinated	Quality coordination	

TABLE 3
Calculation results of the weight of each indicator.

Ecological environment subsystem in the process of urbanization		Financial support subsystem in the process of urbanization	
Secondary indicators	Weights	Secondary indicators	Weights
1	0.065 9	1	0.112 3
2	0.072 6	2	0.089 4
3	0.081 4	3	0.087 5
4	0.065 8	4	0.086 2
5	0.071 4	5	0.118 3
6	0.063 3	6	0.096 5
7	0.052 5	7	0.095 2
8	0.102 4	8	0.103 3
9	0.086 1	9	0.089 7
10	0.082 0	10	0.121 6
11	0.079 6		
12	0.090 3		
13	0.086 7		

RESULTS

The coupling and coordination of finance and the ecological environment not only emphasizes the quantitative growth of economic development, but also emphasizes the improvement of the quality of economic development while the quantity of economic development increases. Coupling degree model, coupling coordination degree model and other methods are used to conduct qualitative research on the relationship between China's financial and ecological environment coupling and coordination development.

Coordinated and coupled development degree. The weight is determined according to the entropy method, and then the relative weight of each index is calculated separately. After implementing standardization of the indicators in the evaluation indicator system in this method, the entropy method is used to determine the weight of each indicator. The results are shown in Table 3.

From 2005 to 2019, the research results of the internal coordination degree, coupling degree, overall coordination degree and coupling coordination degree between the ecological environment and financial support in the study area are shown in Table 4 and Table 5.

Through the analysis of Table 4 and Table 5, the overall coordination degree of the ecological environment and financial support in the study area from 2005 to 2019 showed a gradual increase trend. It can be roughly divided into four main stages: rapid rise period, slow rise period, small fall period and stable period.

TABLE 4

The degree of internal coordination and coupling between the ecological environment and financial support in the study area.

Years	Internal coordination		System coupling
	Ecosystem	financial support	
2005	0.41	0.02	0.05
2006	0.39	0.04	0.27
2007	0.44	0.09	0.52
2008	0.32	0.16	0.84
2009	0.43	0.25	0.91
2010	0.44	0.31	0.91
2011	0.52	0.48	0.98
2012	0.63	0.53	0.97
2013	0.59	0.67	0.98
2014	0.48	0.81	0.92
2015	0.48	0.98	0.82
2016	0.63	0.85	0.95
2017	0.64	0.78	0.96
2018	0.59	0.73	0.97
2019	0.64	0.69	0.99

TABLE 5

Overall coordination degree and coupling coordination degree between ecological environment and financial support.

Years	Overall coordination	Coupling degree	Coupling and coordinated development stage
2005	0.16	0.10	Extreme imbalance
2006	0.25	0.27	Moderate disorder
2007	0.37	0.44	On the verge of disorder
2008	0.55	0.69	Primary coordination
2009	0.63	0.75	Intermediate coordination
2010	0.66	0.78	Intermediate coordination
2011	0.74	0.86	Well coordinated
2012	0.77	0.88	Well coordinated
2013	0.79	0.89	Well coordinated
2014	0.75	0.84	Well coordinated
2015	0.71	0.78	Intermediate coordination
2016	0.80	0.88	Well coordinated
2017	0.79	0.88	Well coordinated
2018	0.78	0.88	Well coordinated
2019	0.80	0.90	Well coordinated

(1) Rapid rise period. The rapid rise of the coupling and coordination between the ecological environment and financial support of the research object is mainly in the period from 2005 to 2008. At this stage, the degree of coupling and coordination has increased by 170%, 63%, and 57% respectively compared with the previous year. The development level of coupling coordination developed from an extreme imbalance in 2005 to a moderate imbalance in 2006, to a near imbalance in 2007, and finally to primary coordination in 2008. The degree of coupling and tuning has increased rapidly.

(2) Slow rise period. The period of rapid rise in the coupling and coordination between the ecological environment and financial support of the research object is mainly from 2009 to 2013. It can be seen that the degree of coupling and coordination in this stage has increased by 9%, 4%, 10%, 2% and 1% each year compared with the previous year. The level of development of coupling coordination has gone from intermediate coordination in 2009 and 2010 to good coordination in 2011, 2012 and 2013, and the degree of coupling tuning has increased slowly.

(3) Slight fall period. The small fall period of the coupling and coordination between the ecological environment and financial support of the research object is mainly from 2014 to 2016. In this stage, the degree of coupling coordination increased by -6%, -7% and 13% each year compared with the previous year. The level of development of coupling coordination ranges from good coordination in 2014, to intermediate coordination in 2015, to good coordination in 2016. The coupling tuning degree appears to drop slightly.

(4) Stable period. The small decline period of the coupling and coordination between the ecological environment and financial support of the research object is mainly from 2017 to 2019. In this stage, the degree of coupling and coordination increased by 0%, 0% and 2.5% respectively compared with the previous year. The level of coupling and coordination development is well coordinated.

Restrictive factors for the coordinated development of regional ecological environment and financial support in the process of urbanization. In order to analyze the main constraints of the coordinated development of the ecological environment and financial support in the study area under the urbanization process, the development state of the ecological environment and financial support in different sub-regions in the four time nodes of the study area in 2005, 2006, 2007 and 2008 is analyzed. The result is shown in Figure 3. The black cylinder indicates that financial support lags behind the development of the ecological environment, the gray cylinder indicates that financial support is synchronized with the development of the ecological environment, and the white cylinder indicates that financial support is ahead of the development of the ecological environment.

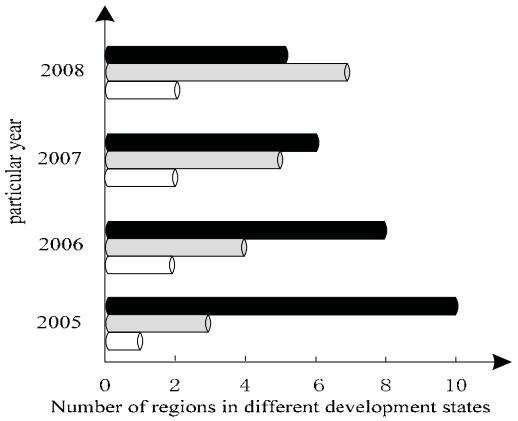

FIGURE 3
The development status of the ecological environment and financial support at different time nodes.

Analysis of Figure 3 shows that in 2005, the number of sub-regions where financial support lags behind the development of the ecological environment in the study area was the largest, reaching 10. There are only 3 sub-regions where financial support is synchronized with the ecological environment. The number of sub-regions where financial support is ahead of the ecological environment is the least, only one. Compared with 2005, the number of sub-regions where financial support is synchronized with the ecological environment in 2006 increased to 4, and it has been increasing year by year. By 2008, the number of sub-regions where financial support was synchronized with the ecological environment reached 7. The degree of coordination between the ecological environment of the study area and financial support has reached an intermediate level. It is found that in the study area, the main factor leading to a low degree of coordination between the ecological environment and financial support is that financial support lags behind the development of the ecological environment. The main reason for this phenomenon is that the urbanization process of the research area is relatively early and the financial support is relatively backward, so the coupled and coordinated development of the research area is at a low level. The lack of financial support in the study area is mainly reflected in indicators such as urban maintenance and construction fund expenditure, loan-to-deposit ratio and financial intermediary efficiency. The shortage of funds for urban maintenance

and construction has resulted in the inability to implement the resources required for infrastructure construction in the process of regional development. The loan-to-deposit ratio reflects the efficiency of fund utilization in the research area. Its low value indicates that the ability to transfer funds and investment in the study area is poor, and restricts the urbanization process of the study area. The low efficiency of financial intermediary means that the valuable financial resources in the research area cannot be used scientifically, which severely restricts the coordinated development of the ecological environment and financial support in the process of urbanization.

CONCLUSIONS

In this paper, we conducted a systematic study on the coordinated development of regional ecological environment and financial support under the process of urbanization, and constructed a corresponding quantitative evaluation index system. The overall coordination degree of the study area shows a gradual improvement trend, which can be roughly divided into four main stages: a rapid rise period, a slow rise period, a small fall period and a stable period. During 2005-2008, the number of sub-regions with financial support synchronized with the ecological environment increased from 3 to 7. From this analysis, it is known that the main factor leading to the low degree of early coupling and coordination of the research area is that financial support lags behind the development of the ecological environment.

In view of the analysis results of the coupling coordination degree between the regional ecological environment and financial support under the urbanization process of the study area, we propose the following suggestions: (1) Expand financial scale and encourage financial development; (2) Optimize the financial structure and implement financial reforms; (3) Promote financial development and improve financial efficiency.

ACKNOWLEDGEMENTS

This work was not supported by any funds. We want to thank all the techniques who have helped this research and all authors of the references.

REFERENCES

[1] Liu, S., Zhu, J., Xu, J., Wu, X., Zhao, S., Hou, X. (2018) Impact of urbanization on regional ecological footprint and its coupling relationship. Acta Zoologica Sinica. 38(24), 227-239.

[2] Wang, Y., Wang, P. (2019) spatiotemporal pattern and aggregation characteristics of county urbanization from the perspective of new urbanization: A case study of Zhejiang Province Geography of Arid Regions. 42(2), 423-432.

[3] Paziliam, M., Sima, Y., Jie, Y., Zheng, L. (2017) Evaluation of spatial and temporal differences in coordinated development of urbanization and ecological environment in Xinjiang. Environmental Pollution and Prevention. 39(9), 1043-1047.

[4] Mario, B., Vincenzo, A. (2018) Towards a more 'Sustainable' Human Development Index: Integrating the environment and freedom. Ecological indicators: Integrating, Monitoring, Assessment and Management. 91(8), 220-231.

[5] Duan, X., Dai, S., Liao, K. (2020) Research on the coordinated development of regional scientific and technological innovation, economic development and ecological environment -- An Empirical Analysis Based on Provincial Panel Data. Science and Technology Management Research. 40(1), 89-100.

[6] Bavarian, N., Sumstine, S., Cruz, S. (2018) Confirming the Prevalence, Characteristics, and Utility of Ecological Theory in Explaining Prescription Stimulant Misuse. Journal of Drug Issues. 48(1), 118-133.

[7] Mamipour, S., Yahoo, M., Jalalvandi, S. (2019) An empirical analysis of the relationship between the environment, economy, and society: Results of a PCA-VAR model for Iran. Ecological Indicators. 102(7), 760-769.

[8] Kang, J., Tang, A., Yu, L. (2018) Analysis of coordinated development of financial ecological environment and technological innovation based on physical coupling coordination model. Editorial Department of Natural Science Journal of Xiangtan University. 145(2), 112-116.

[9] Pang, Q., Li, M., Li, H. (2019) Spatial coupling and coordinated development of financial agglomeration, regional innovation and ecological efficiency in the Yangtze River economic belt. Industrial Technology Economy. 38(2), 68-76.

[10] Emelyanova, N., Naprasnikova, E., Sorokovoi, A. (2018) The Ecological State of a Large City of Eastern Siberia in the Process of Urbanization. Geography and Natural Resources. 39(4), 324-331.

[11]Zhou, X., Yang, L. (2018) research on coordinated development of regional economy and ecological environment based on innovation driven. Economic Issues Exploration. (7), 174-183.
[12]Shen, T., Lei, L. (2018) Analysis on the difference of coupling coordination degree between financial ecological environment and economic growth in ASEAN countries. Reform and Strategy. 34(8), 63-71.
[13]Deng C. (2018) Analysis of coordinated development of tourism industry urbanization ecological environment coupling in Shanxi Province. Regional Research and Development. 37 (6), 85-89.
[14]Cai, B., Zhao, W., Li, Y., Li, Z. (2019) Spatial pattern and influencing factors of coupling coordination degree of regional innovation and regional economy in China. Science and Technology Management Research. 39(9), 96-105.
[15]Peng, C., Wu, Y. (2017) Evaluation and difference analysis of the coupling and coordinated development of China's ecological economic science and technology system. Science and Technology Management Research. 4(4), 250-250.
[16]Guo, Q., Ding, C. (2017) Research on the regional pattern of coordinated development of China's "three modernizations" and its influencing factors -- An Empirical Study Based on Provincial Panel Data. Journal of Hebei University of Economic and Trade. 38(1), 101-109.
[17]Huo, Y., Zhu, L. (2018) Research on the coupling and coordinated development of science and technology finance, scientific and technological innovation and regional economy: a case study of nine provinces along the Silk Road Economic Belt. Wuhan Finance. 9, 57-56.
[18]Li, H., Yuan, Y., Wang, N. (2019) Evaluation of coupling and coordinated development of regional green finance and ecological environment. Statistics and Decision Making. 35(8), 161-164.
[19]Gupta, K., Chatur, P. (2020) Gradient self-weighting linear collaborative discriminant regression classification for human cognitive states classification. Machine Vision and Applications. 31(3), 1-16.
[20]Zimmerer, K., Lambin, E., Vanek, S. (2018) Smallholder telecoupling and potential sustainability. Ecology & Society. 23(1), 30.
[21]Zhou Y., Shi S. (2019) Study on coupling coordination evaluation of urbanization and ecological environment in Ethnic Area - Taking 10 counties (cities) in Fujian Province as examples. Forestry Economy. 325(8), 96-102.

Received: **07.11.2020**
Accepted: **20.01.2021**

CORRESPONDING AUTHOR

Yuanxin Zhang
Chengdu Institution of New Economic Development, Chengdu 610000 – China

e-mail: zyxrd2020@163.com

© by PSP Volume 30– No. 05/2021 pages 5084-5092 Fresenius Environmental Bulletin

RESEARCH ON CARBON RISK MANAGEMENT OF HIGH-POLLUTING PORT ENTERPRISES: BASED ON IOT TECHNOLOGY AND ECOLOGICAL PERSPECTIVE

Qi Zhao, Bing Yang*

Department of Business Administration, Chaohu University, Chaohu 238000, China

ABSTRACT

With the continuous improvement of socialist informatization, the development speed of current logistics enterprises has gradually increased. However, due to the impact of informatization, the logistics situation has gradually become severe, and the current port logistics pressure has gradually increased. In order to comprehensively improve logistics enterprises' Marketing quality, and comprehensively improve the carbon risk management quality of high-polluting port companies. This article combines current relevant research content to conduct an effective analysis of the current actual situation of port logistics carbon emissions, in order to better determine the new type of high-polluting port company carbon Risk management plan, comprehensively sort out the shortcomings in the current management system plan, and formulate relevant intensive technical management equipment in a targeted manner, so as to better promote the quality of logistics management, give play to the advantages of logistics management, and promote the overall development of logistics capabilities Upgrade and realize continuous reform of carbon risk management for high-polluting port enterprises.

KEYWORDS:
Internet of Things, Ports, Informatization, Carbon risk

INTRODUCTION

According to estimates from the International Environmental Organization's Global Carbon Plan, China's CO_2 emissions per capita in 2013 ranked first in the world [1-4]. Extensive economic growth produces huge carbon emissions, which not only pollutes the environment, but also raises the operating costs of China's economy and society, and restricts the potential for endogenous economic growth. According to the requirements of the National Climate Change Regulations, China's carbon emission intensity in 2020 should be reduced by 40%-45% compared to 2005 (Figure 1). Therefore, various localities have introduced policies to set total carbon emission indicators and allocate basic emissions based on historical emission models or benchmark models [5-9].

The port industry is a basic industry and strategic industry of the national economy and society. The characteristics of the industry determine the need to consume a lot of energy. Therefore, it is urgent to promote low-carbon [10-13]. Corporate carbon risk refers to the uncertainty of the impact of carbon factors on corporate goals. Today, with increasing attention to environmental protection, carbon risks are becoming more prominent, but Chinese companies are far from paying enough attention to carbon risks. The vast majority of companies have not yet incorporated carbon risk management into the risk management framework [14]. Therefore, research on the potential of corporate carbon risk management mechanisms must do.

In the process of management, as managers, they should fully understand the status quo of environmental pollution caused by carbon emissions, so as to formulate targeted measures and management methods based on the status quo of management, fully realize the carbon risk management of high-polluting port enterprises, and promote effective application of networking [15-18]. In the current process, the main source of pollution is the polluted gas produced by various transportation equipment. In order to better reduce the environmental pollution caused by various transportation equipment, we have formulated targeted air pollution protection measures and unlimited sensors. Network equipment, etc., implement real-time monitoring and placement of current logistics and transportation management, thereby comprehensively improving the quality of air protection, realizing the effective implementation of the carbon risk management business of high-polluting port enterprises, and promoting the overall deve lopment of environmental protection.

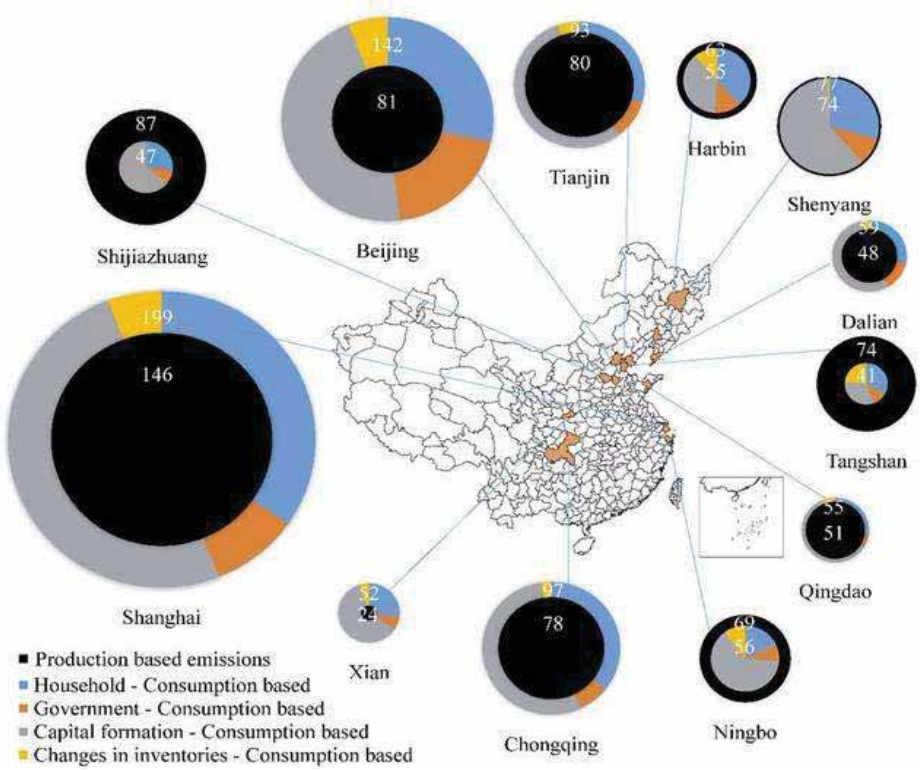

FIGURE 1
Production- and consumption-based CO_2 emissions at the city level

MATERIALS AND METHODS

Cargo automatic stacking algorithm. In order to better promote the orderly development of port logistics work, first, as managers, they should make full use of information network transmission equipment to actively transmit the current transportation content and container carrying situation to the information system through data transmission. Not only can it effectively supervise the current physical transportation management line sharing, but also can fully collect and organize various basic data. Then exchange the control information of the yard with the network to realize the automatic stacking of containers. The algorithm of automatic container stacking mainly has the following six steps: First, through the effective division of a variety of container storage parts, comprehensively sort out the current container carrying and distribution conditions, and decompose all the container conditions. Use these data to establish the correct digital model size and so on. The second is to sort out the actual situation of the cu rrent containers to better clarify the delivery time, transportation information, and transportation items of each container, so as to ensure that different containers can be fully optimized and managed in a standardized location. Effectively reduce the generation of security risks. The third is to re -standardize all logistics content according to current logistics management practices, effectively reduce the occurrence of safety risks, and fully realize informatization and intensive management. Four is. Re-integrate repeated time and logistics information to ensure that there will be no omissions and failures. Fifth, according to the type of cargo information (such as refrigeration or stacking failure), the remaining effective stacking point is based on the number of containers stacked at the stacking point, the distance between the stacking point and the berth of the container, and the stacking point. The shipping time of the above container and the quality of the current container a re weighted. Sixth, after weighting, sort all the effective stacking points according to the weight value to get a list of available stacking points from good to bad. Through the information collection of the Internet of Things technology such as frequency radio identification, the data model supporting the algorithm is automatically established.

Car automatic scheduling algorithm. First of all, according to the actual situation of the current logistics, use the video supervision and management system of the positioning system to effectively analyze the actual situation of the current transportation logistics, clarify the specific time of each delivery work and the actual situation of the operation, so as to guide the management personnel Effectively conduct targeted management. At the same time, make full use of the information network to sort out and

TABLE 1
Carbon risk rating standards

Classification	Grade standard
Low risk	X≤1
Medium risk	1＜X≤1.0747
High risk	X＞1.0747

Note: X is the calculation result of carbon emission data.

interact with all the delivery site conditions, and finally effectively ensure that various scheduling tasks can be carried out in accordance with the established location and time, ensure the actual situation of each logistics and transportation equipment, and fully ensure that the management personnel are in limited.

RESULTS AND DISCUSSION

System function requirements. At present, the management of port logistics in our country has gradually been evidenced, but the carbon emission quality of logistics is still high, not only that its scope is relatively wide, management objectives, etc., there are no targeted measures and management methods for intensive management , This requires managers to fully analyze the actual status of port logistics, formulate targeted measures and methods, effectively promote the effective implementation of information management, establish an effective management and control platform, and promote the intensive management of port carbon emissions. Automatic collection, identification and transmission of carbon emission information.

(1) Logistics equipment and personnel real-time dispatch management function. At this stage, it can be found in the logistics and transportation management process that due to the large number of value-added transportation vehicles currently moving in various ports, equipment management personnel should make full use of various information equipment and information management methods to comprehensively deepen their understanding of vehicle information. Effective management and mastery, so as to better analyze the dispatching situation of transportation equipment and transportation personnel in different transportation environments, formulate relevant measures and methods in a targeted manner, comprehensively promote the effective implementation of information management, and master through the implementation of personnel Analyze, carry out the orderly transfer of personnel and the timely arrangement of equipment at an appropriate time and price adjustment, so as to promote the effective implementation of port carbon emission management.

(2) Statistical analysis function of carbon emission data, ability to accumulate carbon. Only through a special information system can we make a clear analysis of the actual situation of current carbon emissions, so as to carry out timely warning and problem sorting through the relevant information management system, so as to comprehensively analyze the detailed light trucks of carbon emissions and formulate relevant decision reports The content lays a solid theoretical and data foundation for the orderly development of energy conservation and emission reduction in the later period. Specifically, carbon emission data is the basis of carbon risk management, but the data needs to be scientifically and accurately analyzed to determine whether there is a carbon risk and the carbon risk level. The level standards are shown in Table 1. The analysis of carbon emission data not only requires the system to have statistical analysis functions, but also can realize the classification and judgment of the data content, so as to ensure that the various positions of the management department can quickly obtain the data information related to their own work. Based on the collected data, the calculation can be carried out based on the formula $E_T=G_0\cdot(1+\lambda)t\cdot X_0\cdot(1-\mu)$. The result can be compared with the grade rating standard to confirm the risk level, so as to provide reliable in accordance with (Figure 2).

(3) Integration function with the management system of relevant departments of the enterprise. In order to promote the effective implementation of carbon risk management for high-polluting port companies, based on the information management of carbon emissions, as a management department, an effective communication mechanism between multiple departments and multiple agencies should be established in accordance with the current actual logistics situation. Therefore, through the establishment and improvement of the carbon risk management system of high-polluting port enterprises, the main responsibility of environmental supervision and management can be clarified, and the occurrence of environmental pollution problems can be reduced. The realization of this function will integrate the management resources of various departments of the enterprise and realize the comprehensive utilization of resources, so as to ensure that each department in the enterprise has a clear understanding of its own role and function in carbon risk management, thereby reducing carbon risk management. Inaction, and ensure that each management resource can give full play to its value and benefits. For example, when the management work is carried out on the basis of detailed summary data, there will be a detailed summary of the carbon emissions in different regions and different time periods in high-polluting ports. According to the information content, the

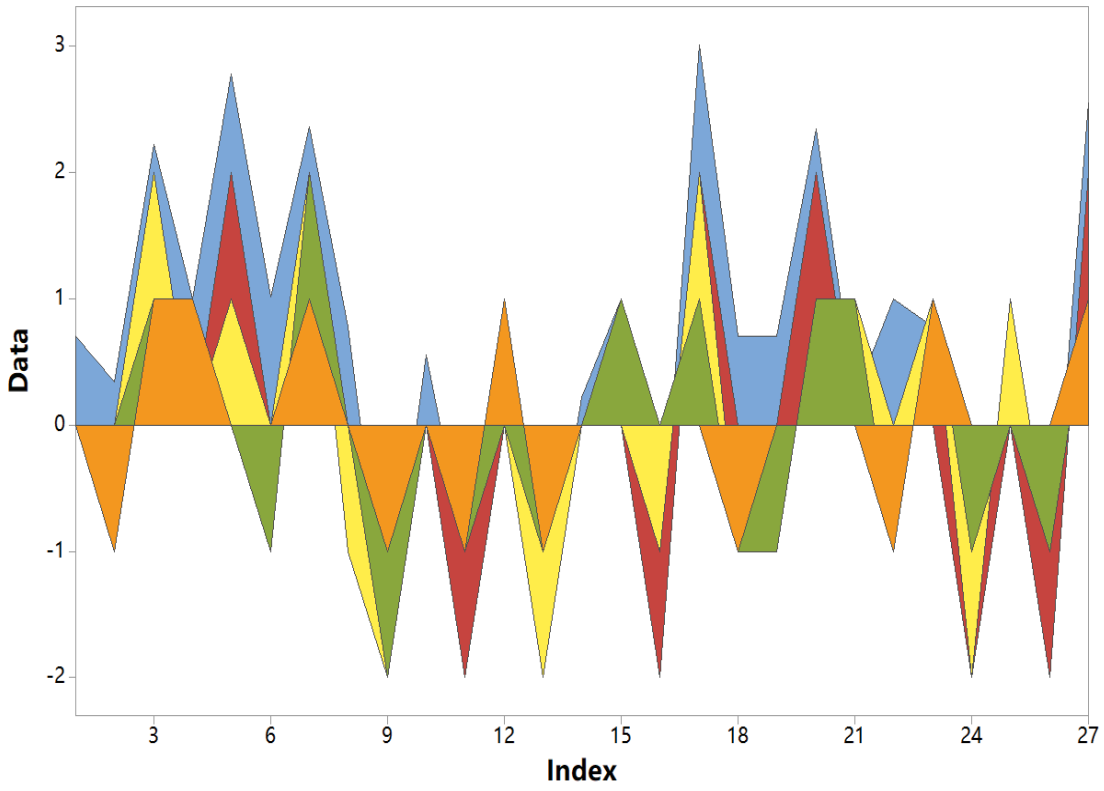
Data
Index
3
2
1
0
-1
-2
3
6
9
12
15
18
21
24
27

(a)

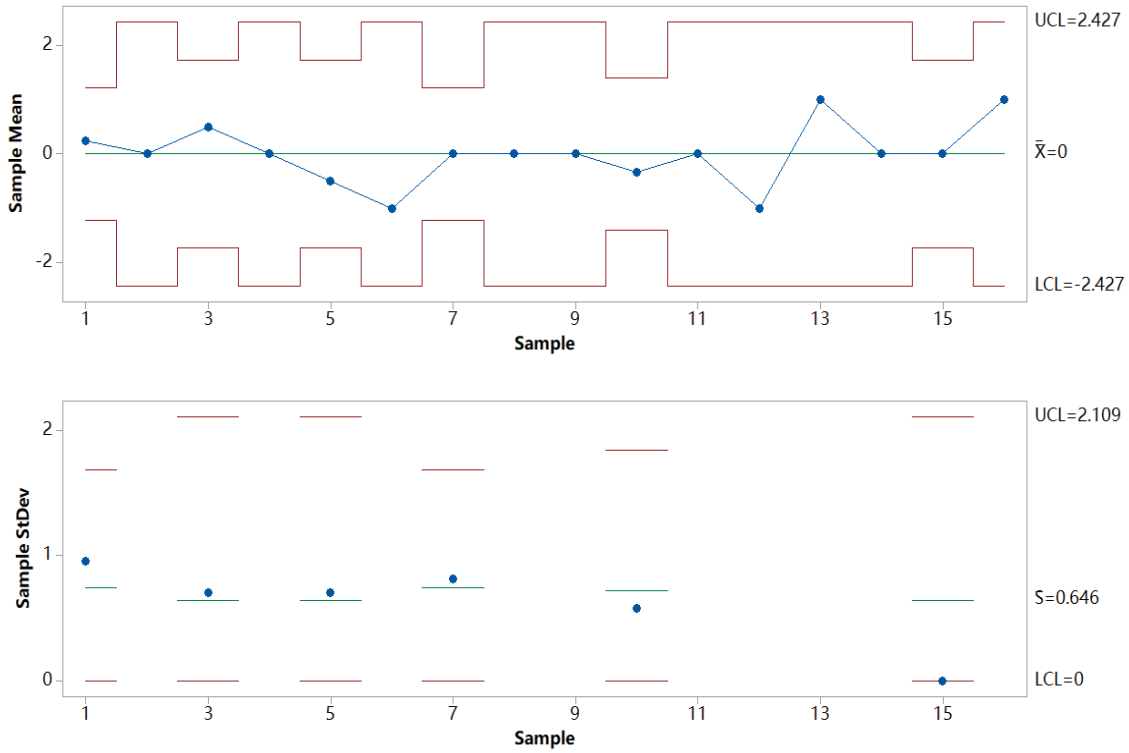
Sample Mean
Sample
UCL=2.427
X̄=0
LCL=-2.427
Sample StDev
Sample
UCL=2.109
S=0.646
LCL=0

(b)

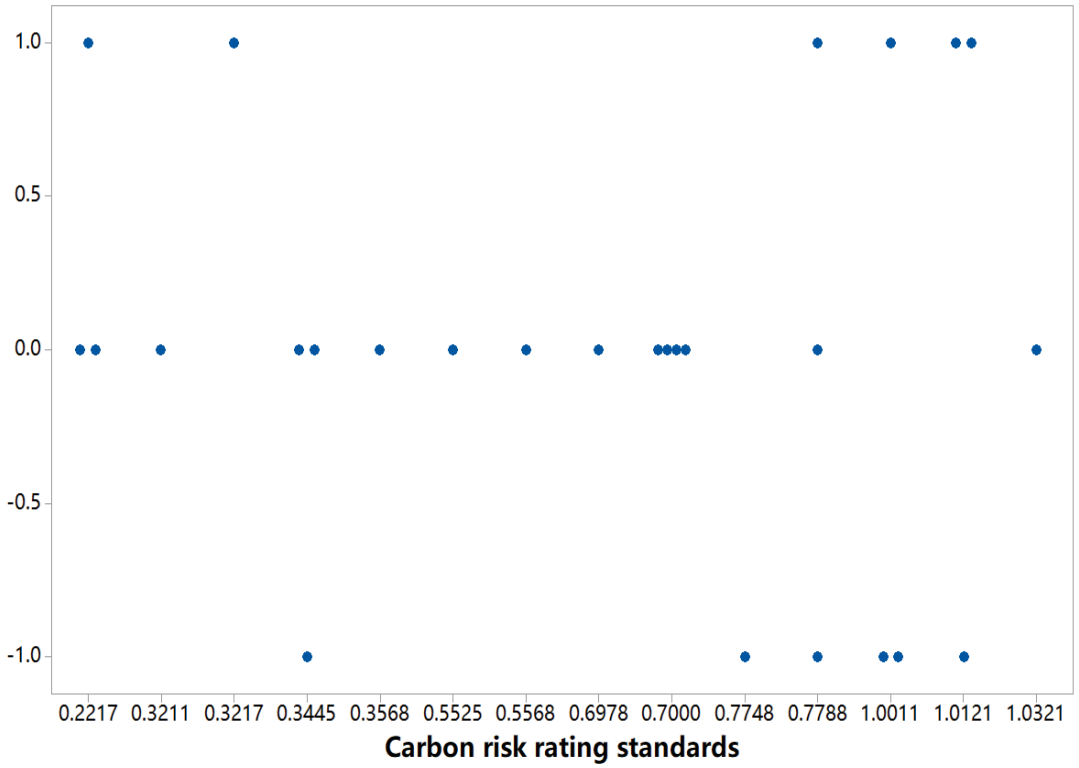

(c)

FIGURE 2
Result statistics and analysis

main subjects that cause carbon risks can be identified and targeted measures can be taken. Optimize the allocation of management resources, which leads to effective control of carbon risk management and prevention in the bud. This is the top priority for maximizing the benefits of highly polluting ports.

Basic principles of the system. The effective implementation of carbon risk management work for high-polluting port companies not only requires a large amount of data for effective support, but also requires intensive management of the current actual brain-bearing management equipment, which mainly integrates various logistics and transportation information effectively, and RFID readers and wireless sensor nodes are combined to form an intelligent node, which collects and effectively organizes data by combining a variety of logistics and transportation information content and the actual situation of logistics operations, and at the same time, effective data collection in each key operation loading area Supervise, realize intelligent overall management, different intelligent power-saving internally built delayed data transmission induction device, through series operation, thus establish a complete supervision system. When all vehicles with data in the database enter the data sensing area, the intelligent management equipment will directly transmit the current vehicle information, owner's name, transportation content, etc. to the information computer IQ in a timely manner, thereby effectively To realize the comprehensive supervision and management of the supervision system, once the carbon emissions are found to exceed the established indicators, they will promptly perform the operation in the supervision system platform and require the management personnel to enter the site in time to conduct on-site operations to reduce carbon emissions produce.

System structure. The production of the carbon risk management and supervision system for high-polluting port companies is mainly realized through a variety of network nodes and data transmission monitoring devices. The effective installation of intelligent nodes is mainly for the current transportation process of vehicles and various transportation equipment. Effective supervision and management of carbon emissions. In order to better explore the actual carbon emission indicators in the current detection area, effective supervision and management can be carried out through intelligent nodes, and all data will be fed back to the monitoring center to ensure that the carbon emission indicators are qualified. The main purpose of King Joint Point is to better realize the timely monitoring and management of various transportation equipment

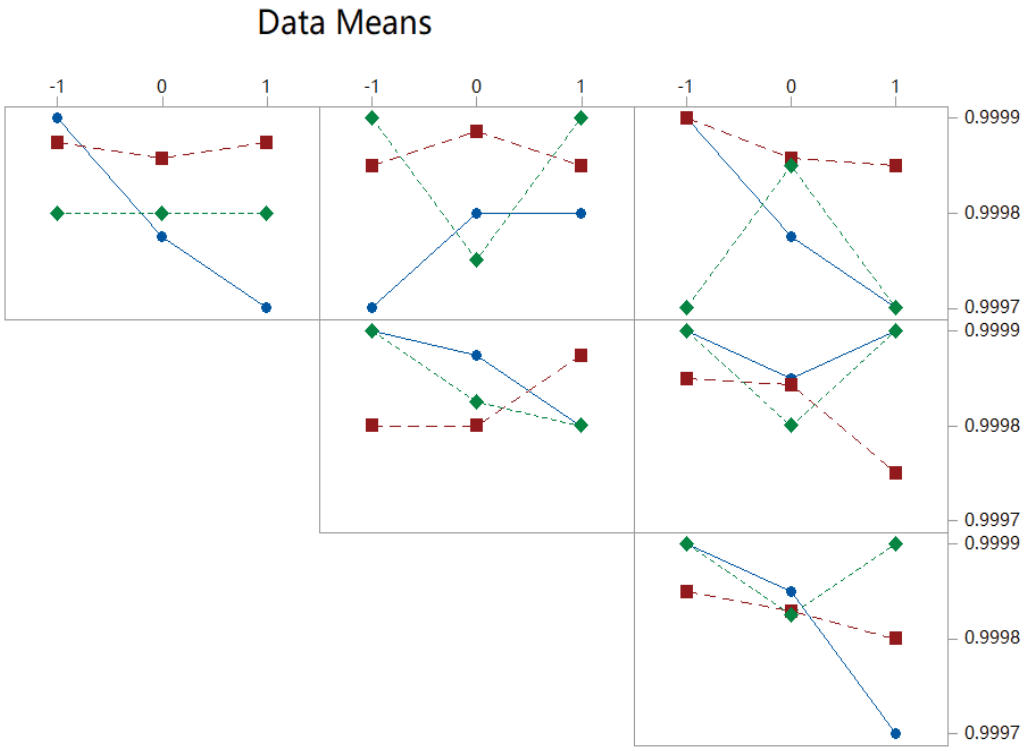
Data Means
-1
0
1
0.9999
0.9998
0.9997

(a)

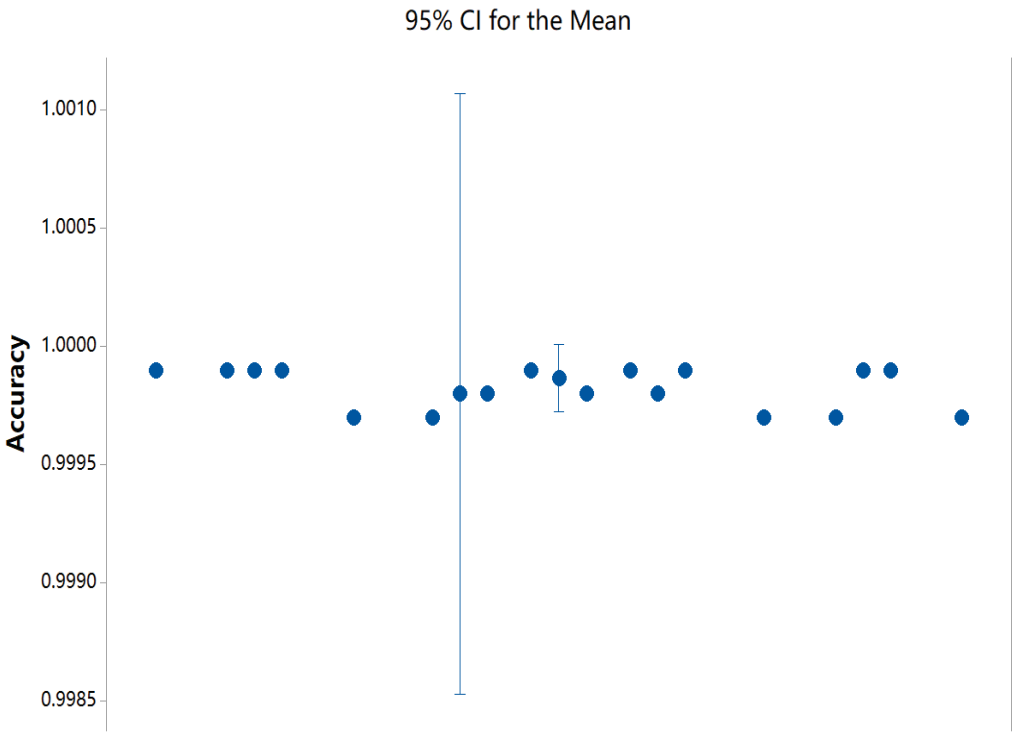
95% CI for the Mean
Accuracy
1.0010
1.0005
1.0000
0.9995
0.9990
0.9985

(b)

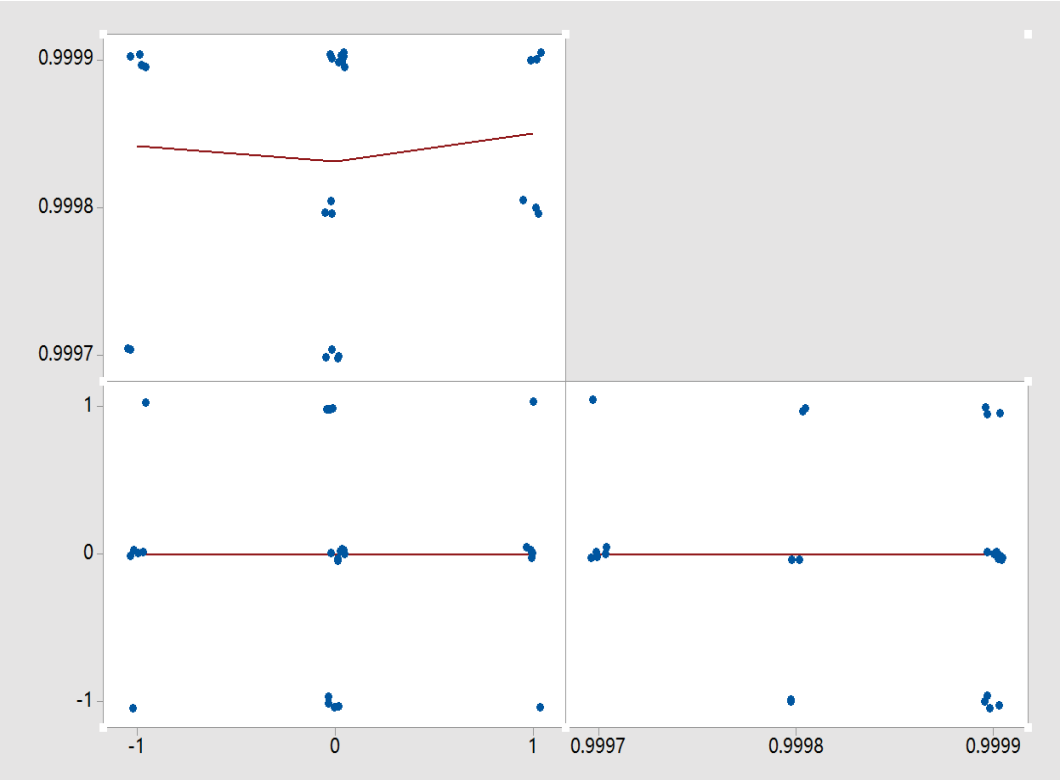

(c)

FIGURE 3
Plot for Accuracy

through the effective maintenance of data. On the one hand, it promotes the overall improvement of the quality of monitoring and management, and on the other hand, it also promotes the overall management of transportation equipment to effectively ensure The requirement that unqualified vehicles not be released. Through the establishment of a variety of network information modules, all current actual transportation conditions can be timely connected to the financial control center, and the timeliness and effectiveness of supervision and management can be improved. The effective realization of network transmission is mainly through the circulation of the network to ensure that there is sufficient network data between each key node for effective support, so as to ensure that the network data is not interrupted. The monitoring center is mainly the core department to realize the carbon risk management of high-polluting port enterprises. It has not only established a complete data management center, but also effectively arranged special supervision and management equipment, which effectively promoted the overall improvement of data management quality. Good promotion of the full implementation of informatization. The monitoring center is responsible for the issuance and execution of monitoring management instructions, and the analysis and processing of monitoring data. The effective establishment of the remote control system will more realize the comprehensive connection between multiple departments, further promote the effective communication between various information, better promote the coordination between multiple departments, and realize the informationization of high-pollution port enterprises. Comprehensive improvement of carbon risk management capabilities (Figure 3).

System hardware design. In order to further realize the effective design and management of the hardware of the carbon risk management system for high-polluting port enterprises, firstly, the smart node should be fully optimized. During the installation of the smart node, a variety of transmission sensory devices, signal control devices and system equipment should be required. Unified management of identification devices. In the management process, the data collection management and the effective management of the gas transmission management should be well coordinated, so as to realize the effective conversion between the two in the process of following. The overall optimization of the gas sensing device is actually to concentrate a variety of hardware devices on one transmission medium, and better use carbon emission gas detection as the main content of the current intelligent node, so as to better play the role of hardware equipment processing In order to do a good job in the overall optimization of

network management nodes, it is mainly to reorganize and optimize the basic equipment of the various network management nodes currently used to ensure that various data can be timely and effectively fed back to the current informatization during the transmission process. Among the equipment, a variety of management basic equipment is fully coordinated. Targeted data transmission management equipment is installed in a relatively close environment, and remote network transmission devices are mainly used for supervisory transmission in remote transmissions, thereby comprehensively improving the quality of remote control management.

CONCLUSION

In order to comprehensively improve the management quality of carbon risk management of high-pollution port enterprises, managers should fully understand the positive impact of information management in the establishment of the current carbon risk management system for high-pollution port enterprises. In view of the current environmental protection management situation, Carefully sort out the various problems that exist in the carbon risk management process of high-pollution port companies at this stage, and further give full play to the role of the current remote information sensing device in China, on the one hand, improve the quality of carbon risk management and protection of current high-pollution port companies. On the other hand, it is better to promote the establishment of the Internet of Information and Things. To ensure that under the wired technology, the advantages of informatization supervision and management can be better utilized, the overall improvement of the quality of informatization management is promoted, and the effective establishment of a carbon risk management system for high-polluting port enterprises is realized.

ACKNOWLEDGEMENT

This paper is supported by Anhui Province Social Science Innovation Development Research Project in 2019 (Item Number: 2019CX085) and Key projects of Humanities and Social Sciences Research in Anhui Colleges and Universities in 2016 (Item Number: SK2016A0636).

REFERENCES

[1] Ma, W.J., Gao, B., Guo, Y.D., Liu, Y.Y., Chen, J.Y., Zhang, C.Y., Wang, Z. (2018) Chemical Compositions and Health Risk Assessments of Toxic Metals in the Groundwater Surrounding A Uranium Tailings Ponds. Fresen. Environ. Bull. 27, 8938-8945.

[2] Akkan, T., Yazicioglu, O., Yazici, R., Yilmaz, M. (2018) An Examination of Ecological and Statistical Risk Assessment of Toxic Metals in Sediments at Siddikli Dam Lake: A Case Study in Kirsehir, Turkey. Fresen. Environ. Bull. 27, 8104-8111

[3] Ma, J.Z., Cheng, K. (2008) Impacts of ecotourism on wildlife in nature reserves: Monitoring and Management. Acta Ecologica Sinica. 43, 539-568.

[4] Chen, J., Ge, J.F., Liang, Y.Q. (2010) Discussion on ecotourism development model in Taihang Mountain Area of Hebei Province. Journal of Arid Land Resources & Environment. 24(2), 122-125.

[5] Yi, X.L., Fu, Q.M. (2016) Vulnerability of Ecotourism Resource Development of Wujiang Gallery and Its Protection Measures. Journal of Anhui Agricultural Sciences. 34, 167-169.

[6] Yusof, N., Rahman, S., Iranmanesh, M. (2015) Effects of resort service quality, location quality and environmental practices on the loyalty of guests within the Malaysian ecotourism industry. Pertanika Journal of Social Science & Humanities. 23(4), 1015-1030.

[7] Kaffashi, S., Radam, A., Shamsudin, M.N., Yacob, M.R., Nordin, N.H. (2015) Ecological conservation, ecotourism, and sustainable management: the case of Penang National Park. Forests. 6(7), 2345-2370.

[8] Li, Y.H., Xiang, B. (2014) Research Progress in the Ecotourism Environmental Carrying Capacity. Advanced Materials Research. 869-870. 781-785.

[9] Dong, H.M. (2010) Study on sustainable development of ecotourism in the Northern Piedmont in the Qinling Mountains. Journal of Sustainable Development. 3(1), 104-108.

[10] Bhattacharya, A.K., Saksena, V., Banerjee, S. (2006) Environmental auditing in ecotourism: a study on visitors' management in Van Vihar National Park, Bhopal, M.P. (India). Indian Forester. 132(2), 1-3.

[11] Tahervand, S., Jalali, M. (2017) Sorption and Desorption of Potentially Toxic Metals (Cd, Cu, Ni and Zn) by Soil Amended with Bentonite, Calcite and Zeolite as a Function of pH. J. Geochem. Explor. 181, 148-159.

[12] Yu, H.Y., Liu, C.P., Zhu, J.S., Li, F.B., Deng, D.M.,Wang, Q., Liu, C.S. (2016) Cadmium Availability In Rice Paddy Fields From A Mining Area: The Effects of Soil Properties Highlighting Iron Fractions and Ph Value. Environ. Pollut. 209, 38-45.
[13] Gray, C.W., Dunham, S.J., Dennis, P.G., Zhao, F.J., Zhao, F.J., Mcgrath, S.P. (2006) Field Evaluation of in Situ Remediation of a Heavy Metal Contaminated Soil Using Lime And Red-Mud. Environ. Pollut. 142, 530-539.
[14] Garau, G., Castaldi, P., Santona, L., Deiana, P., Melis, P. (2007) Influence of Red Mud, Zeolite And Lime on Heavy Metal Immobilization, Culturable Heterotrophic Microbial Populations and Enzyme Activities in a Contaminated Soil. Geoderma. 142, 47-57.
[15] Chen, Y.H., Xie, T.H., Liang, Q.F., Liu, M.J., Zhao, M.L., Wang, M.K., Wang, G. (2016) Effectiveness of Lime and Peat Applications on Cadmium Availability in a Paddy Soil Under Various Moisture Regimes. Environ. Sci. Pollut. Res. 23, 7757-7766.
[16] Han, X.Q., Xiao, X.Y., Guo, Z.H., Xie, Y.H., Zhu, H.W., Peng, C., Liang, Y.Q. (2018) Release of Cadmium in Contaminated Paddy Soil Amended with NPK Fertilizer and Lime Under Water Management. Ecotoxicol. Environ. Saf. 159, 38-45.
[17] Cao, X.Y., Hu, P.J., Tan, C.Y., Wu, L.H., Peng, B., Christie, P., Luo, Y.M. (2018) Effects of a Natural Sepiolite Bearing Material and Lime on the Immobilization and Persistence of Cadmium in a Contaminated Acid Agricultural Soil. Environ. Sci. Pollut. Res. 25, 22075-22084.
[18] He, Y.B., Huang, D.Y., Zhu, Q.H., Wang, S., Liu, S.L., He, H.B., Zhu, H.H., Xu, C. (2017) A Three-Season Field Study on the in-Situ Remediation of Cd-Contaminated Paddy Soil Using Lime, Two Industrial By-Products, and a Low-Cd-Accumulation Rice Cultivar. Ecotoxicol. Environ. Saf. 136, 135-141.

Received: **14.11.2020**
Accepted: **10.01.2021**

CORRESPONDING AUTHOR

Bing Yang
Department of Business Administration,
Chaohu University,
Chaohu 23000 – China

e-mail: yangbing888991@163.com

© by PSP Volume 30– No. 05/2021 pages 5093-5097 Fresenius Environmental Bulletin

MOLECULAR EPIDEMIOLOGY AND CHARACTERIZATION OF HEPATITIS DELTA VIRUS FROM PESHAWAR DIVISION KPK-PAKISTAN

Izhar ul Haq[1], Muhammad Mumtaz Khan[1], Adnan Khurshid[2], Anees Muhammad[3], Mohammad Ejaz[1], Waqas Hussain Shah[4], Sajid Ali[5], Sadia Alam[1,*]

[1]Department of Microbiology, University of Haripur, Pakistan
[2]Virologist, WHO Regional Reference Laboratory, National Institute of Health, Islamabad, Pakistan
[3]Department of Medical Lab Technology, University of Haripur, Pakistan
[4]Department of Biotechnology, COMSATS University Islamabad, Abbottabad Campus, Pakistan
[5]Department of Biotechnology, Abdul Wali Khan University Mardan, Pakistan

ABSTRACT

Hepatitis Delta virus (HDV) causes superinfection along with harsh complication as compared to only HBV infection and is the only member of genus delta virus. HDV is considered as a satellite virus of HBV based on the biological principles of HBV and therefore it is unable to cause disease without HBV. The co infection of both HDV and HBV cause more serious liver disorders compared to mono infection of HBV. Chronic infection with HBV and HDV can lead to chronic hepatitis with acute fulminant hepatitis and progression of cirrhosis. The aim of the study was to determine the prevalence of hepatitis D virus in positive samples of hepatitis B virus in Peshawar division of KPK, Pakistan. Two hundred positive samples of hepatitis B virus were collected from different areas of KPK. Furthermore, RT-PCR positive samples (n=80) were screened by ELISA (Enzyme Linked Immunosorbent Assay) for the presence of HDV. Nested PCR was used to confirm the positive HDV samples. Among 200 samples only 80 were confirmed for HDV. Nested PCR shows that only (n=2) 14.3% samples were positive for HDV. Over all data of our study, shows that the prevalence of HDV infection is usually higher in males than female and investigate that the prevalence of hepatitis D virus infection remains high in Peshawar division as compared to other divisions of KPK, Pakistan. The study showed the prevalence and molecular epidemiology of HDV co infection in Hepatitis B infected individuals. The hepatitis D virus may present as a co-infection in an individual recently affected with hepatitis B virus in chronic HBV carriers.

KEYWORDS:
Hepatitis D virus, Hepatitis B virus, RT- PCR, ELISA

INTRODUCTION

Hepatitis Delta virus is a unique, single-stranded RNA virus that is depend on hepatitis B surface antigen for virion propagation and assembly and show similar transmission route like HBV that is via sexual or parenteral route. The genome size of HDV is approximately 17 kb nucleotides having a single circular rod shape RNA structure with 70% similar base pairs [1]. The open reading frame of HDV encodes for delta antigens, LHDAg inhibit the HDV-RNA synthesis and is required for HDV particle formation while sHDAg is essential for HDV genome synthesis.

Hepatitis D virus cause chronic hepatitis D and is the only member of genus delta virus. HDV is considered as a satellite virus of HBV based on the biological principles of HBV and therefore it is unable to cause disease without HBV [2-3]. The co infection of both HDV and HBV cause more serious liver disorders compared to mono infection of HBV. It is estimated that among 240 million chromic HBV carriers, approximately 15-20 million were infected with HDV [4]. Among the infected patients of HBV and HDV, less than 5% of these patients develop chronic HDV infection. Chronic HBV carriers that are super fused with HDV tend to have severe hepatitis at the acute stage; 80% of these patients develop chronic HDV infection. Chronic infection with HBV and HDV can lead to chronic hepatitis with acute fulminant hepatitis and progression of cirrhosis.

In 1980s, the prevalence rate of HDV infection was ranging between 15 – 20 million worldwide [5]. HDV is generally more prevalent in developing countries of Central Asia, the Amazon basin, Mediterranean; Sub Saharan Africa and the Middle East [6]. The rate of chronic HDV infection has been decreased due to proper vaccination against HBV infection, improvement in living condition, sanitation and sexual restrains. The prevalence is variable geographically with the rate of > 20 % in the Amazon basin at South America. In Africa the prevalence of HDV in Gabon is 15.6% to 70.6%, in Cameroon 17.6%, while in sub-Saharan Africa its prevalence was estimated from 1.3% to 50% [7]. In Iran, Pakistan, Turkey, Central Asia and Mongolia prevalence

is also very high [8-9].

Like HBV, HDV is also contagious and can transmit through body fluids such as semen, blood or vaginal fluid. It can rarely transmit vertically from mother to fetus [10]. However, sexual contact is an important form of transmission of HDV in endemic areas.

As the molecular epidemiology and seroprevalence need to be assessed to improve the control measure of coinfection of HBV and HDV. Here in this study we accessed the prevalence and molecular epidemiology of co infection of HBV-HDV in Peshawar province division of Pakistan.

MATERIALS AND METHODS

A total of 200 samples were collected randomly from different hospitals and laboratories of Peshawar division from the patient having age 7-60 (mean 33.3+ 9.33 years) that are HBsAg positive and immediately sent to Microbiology Laboratory of Department of Microbiology, University of Haripur for further diagnosis. Informed consent was taken from the patient while collecting the sample for diagnosis.

Serology All the samples were retested and confirmed for the presence of HBsAg using Rapid Kit method. The negative samples were eliminated from the study. The screening of anti-HDV antibodies were carried out by using ELISA (DIA.PRO, Diagnostic Bioprobes Srl Italy). All the tests were performed according to manufacturer protocols.

HBV-DNA and HDV-RNA detection The serum samples of 150 µl HBV-DNA was extracted through viral HBV-DNA isolation kit (Macherey-NagelGmbH & Co. KG, Germany) according to protocol. The quantitative detection of HBV was carried out by real-time PCR. In this, the quantification and amplification of extracted DNA were amplified with the commercially available HBV DNA quantitative real-time PCR amplification kit (Sansure Biotech Inc® HBV DNA Quantitative Fluorescence Diagnostic kit, China).

HDV RNA was extracted from 140 µl samples using the QIAmp Viral mini RNA extraction kit. The extracted RNA was reverse transcribed into cDNA with reverse transcriptase enzyme (Thermo Scientific) and 1 µl of 10 pmol outer antisense primer. The thermal cycling was carried out in nested PCR for 5 min at 70°C. The preparation of PCR mixture for making cDNA, for a single reaction contained 500 mM KCl, 200 mM Tris HCl (pH 8.4), 10 mM dNTPs, 0.1M DDT, and 200 U of reverse transcriptase of MMLV. The denaturation of cDNA in thermocycler completes in 60 min at 42 0C, followed by inactivation of RT enzyme at 70 0C for 10 minutes.

Qualitative detection of HDV RNA The determination of RNA HDV was performed by means of nested PCR. The qualitative detection of RNA HDV was performed in two rounds. The first round PCR was performed in a PCR reaction mixture of 20 µl having 500 mM KCl, 200 mM Tris HCl (pH 8.4) 2.5mM dNTPs, 25mM MgCl2 and 10 pmol of each outer sense nucleotides 694-717 (5'-CATGGTCCCAGCCTCCTCGCTGGC-3') and anti- outer sense nucleotides 872-895 (5'-CCGCGAGGAGGTGGAGATGCCATG-3') [11] and 1 U of Taq DNA polymerase enzyme. PCR amplification is for 35 cycles. Initial denaturation at 95 0C for 3 minute, Annealing at 64 0C for 1 minute , Extension at 720C for 1 minutes followed by final extension at 72 0C for 10 minutes. The second round nested PCR was also performed in a PCR reaction tube of 20 µl having 500 mM KCl, 200 mM Tris HCl (pH 8.4) 2.5mM dNTPs, 25mM MgCl2 and 10 Pmol of each inner sense nucleotides 728-747 (5'-CATGGTCCCAGCCTCCTCGCTGGC-3') and anti- inner sense primer 845-864 (5'-CCGCGAGGAGGTGGAGATGCCATG-3') [11]. 5µl of PCR product was analyzed on 2% agarose gel electrophoresis. DNA ladder of 100 bps was used as marker to find out the specific size of amplified product. The positive sample for HDV shows band at 137 bps. Both negative and positive controls were included in each run to prevent false negative or false positive uncertainty.

Statistical analysis The data were analyzed through SPSS version 16.0 (IBM Corporation, Armonk, NY, USA). Categorical data was analyzed by Fisher's exact test

RESULTS

Demographic features A total of 200 HBsAg positive samples were collected from Peshawar division that includes the 86 positive sample from district Peshawar (43%), 59 from Nowshera (29.5%) and 55 from Charsadda (27.5%) (Figure 1). Among these positive sample 123 samples were from male and 67 were from female. The mean age of all the patients was 33.03±11.4 years with no significant differences between the age of male (32.80±10.6 years) and female (31.95±10.3 years).

Prevalence of anti-HDV Antibodies Among these positive samples n=80 (40%) shows the positive results of HBV for RT-PCR. These PCR confirmed sample when tested for the presence of anti-HDV antibodies by using ELISA shows about 14 (17.5%) positive and 66 (82.5%) negative samples. The highest prevalence of antibodies were found in Peshawar district of Peshawar division KPK as shown in Table 1.

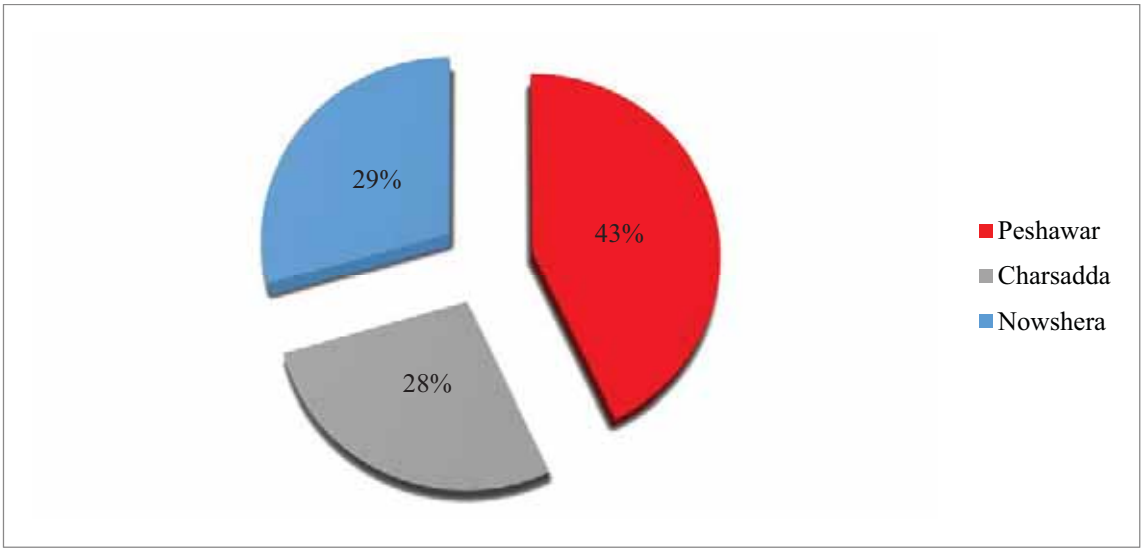

FIGURE 1
Percentage of patient of different regions of Peshawar division enrolled in the study

TABLE 1
District wise prevalence of HDV co-infection

Location	ELISA HDV		Total
	Negative	Positive	
Charsadda	19	1	20
Nowshera	14	6	20
Peshawar	33	7	40
Total	**66**	**14**	**80**

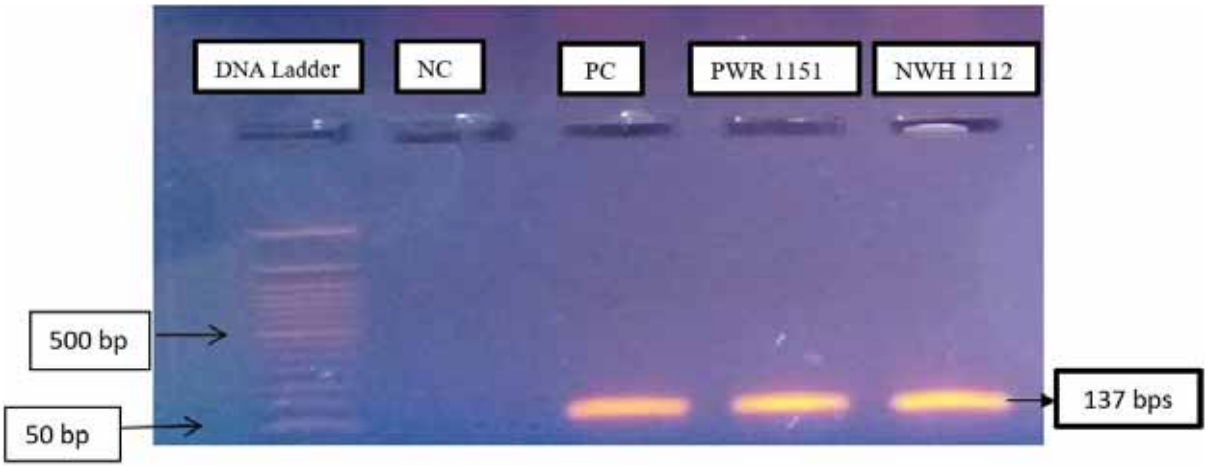

FIGURE 2
Gel electrophoresis of nested PCR

TABLE 2
Frequency of PCR HDV

PCR HDV				
	Frequency	Percent	Valid Percent	Cumulative
Positive	2	14.3	14.3	14.3
Negative	12	85.7	85.7	100.0
Total	**14**	**100.0**	**100.0**	

The anti- HD Ab positive samples were further amplified through nested PCR to amplify the HDV DNA (Figure 2). The overall prevalence of positive samples of HBV by Real-time PCR was found 40% (80/200).

Prevalence of HBV-HDV co infection Among these 80 positive sample 14 were found to have anti-HDV antibodies and n=2 (14.3%) samples shows co-infection when analyzed by nested PCR as shown in Figure 2 and Table 2.

DISCUSSION

The delta hepatitis virus remains a severe worldwide health issue that influences 15-20 million individuals around the world. The hepatitis D virus may present as a co-infection in an individual recently affected with hepatitis B virus in chronic HBV carriers. Many studies have reported a tendency to reduce the formation of hepatitis D virus in patients with hepatitis B throughout the world. Pakistan is amongst the endemic countries where HDV prevalence found to be increased [12]. Although HDV is extremely common in Eastern Europe, Middle East, Africa, and Amazon basin. The incidence is low in United States and northern Europe. The prevalence of HDV is decreasing in the developed world, probably due to vaccination against hepatitis B and the improvement of public health standards, blood product screening and HIV treatment [13].

The frequency of hepatitis D virus infection associated with HBs Ag positive cases has been reported in various provinces of Pakistan including Sindh (16.6%) in 2005 [14] in Punjab 30% in 2010 [15] and in KPK 4% in 2011 [11]. The current study showed that the rate of HDV linked with HBsAg positive patients in Peshawar has increased to 14.3 % that is co-related with the study performed by Mumtaz in 2005 that show the 16.6 % positive cases in Sindh [14].

The results of previous epidemiological studies conducted in Pakistan that the prevalence of hepatitis delta infections was higher in men than in women that are in correlation with our study that also report the high prevalence in male than female [14].

In current study, viral DNA was detected in 40% of the total positive patients that are at higher risk of developing chronic disease. Moreover, due to an active state of their infection, these individuals pose a risk for further dissemination of HBV infection. The finding of the current study proposed the rate of HDV co-infection with HBV is 14.3% that are high compared to the previous study that shows only 2% of the coinfection cases in Karachi city of Pakistan.

In Karachi, it has been reported that only 2% were positive for HDV. These two cases were found in the HBs Ag positive patients. It is recommended that there is a lack of facility of improper diagnosis of co-infection of HDV and HBV [16].

The current study shows improved results as compared to reported study conducted previously in Pakistan (14.3%) that shows decline in prevalence of co-infection of HBV and HDV compared to 44% out of 408 reported cases of Zuberi study [17] and 16.6% prevalence reported by to [14]. This presumes Pakistan has a general decline prevalence rate of HBV contamination because of expanding mindfulness and utilization of HBV vaccination with a divergent increase in HDV co-infection. Awareness of common people played significant role in decreasing the prevalence of HBV.

CONCLUSIONS

Current study contributes significant information with respect to the molecular epidemiology and characterization of HDV circulating in Peshawar division; demonstrate a molecular prevalence of 2 (14.3%) in our study. The data also provide the prevalence and associated risk factors with the onset of dual infection of HBV with Hepatitis D virus (HDV). A significance understanding and research data on HDV with HBV infections prevalence must be needed in order to overcome the associated risk factors of the disease. In this study, we concluded that the prevalence of hepatitis Delta virus is present in the geographical region. Proper implantation of HBV vaccination must be done in the general population to minimize the burden of dual HDV infection in the coming future. The Ministry of Health should consider the risk factors to control the spread of the double infection of Hepatitis B and D.

REFERENCES

[1] Elena, S.F., Dopazo, J., Flores, R., Diener, T.O. and Moya, A. (1991) Phylogeny of viroids, viroidlike satellite RNAs, and the viroidlike domain of hepatitis delta virus RNA. Proceedings of the National Academy of Sciences. 88(13), 5631-5634.

[2] Lai, M.M. (2005) RNA replication without RNA-dependent RNA polymerase: surprises from hepatitis delta virus. Journal of Virology. 79(13), 7951-7958.

[3] Chang, J., Nie, X., Gudima, S. and Taylor, J. (2006) Action of inhibitors on accumulation of processed hepatitis delta virus RNAs. Journal of Virology. 80(7), 3205-3214.

[4] Wedemeyer, H. and Manns, M.P. (2010) Epidemiology, pathogenesis and management of hepatitis D: update and challenges ahead." Nature Reviews Gastroenterology & Hepatology. 7(1), 31.

[5] Rizzetto, M., Ponzetto, A. and Forzani, I. (1990) Hepatitis delta virus as a global health problem. Vaccine. 8, S10-S14.
[6] Noureddin, M. and Gish, R. (2014) Hepatitis delta: epidemiology, diagnosis and management 36 years after discovery. Current Gastroenterology Reports. 16(1), 365.
[7] Opaleye, O.O., Japhet, O.M., Adewumi, O.M., Omoruyi, E.C., Akanbi, O.A., Oluremi, A.S., Wang, B., Van Tong, H., Velavan, T.P. and Bock, C.T. (2016) Molecular epidemiology of hepatitis D virus circulating in Southwestern Nigeria. Virology Journal. 13(1), 61.
[8] Chen, X., Oidovsambuu, O., Liu, P., Grosely, R., Elazar, M., Winn, V.D., Fram, B., Boa, Z., Dai, H., Dashtseren, B. and Yagaanbuyant, D. (2017) A novel quantitative microarray antibody capture assay identifies an extremely high hepatitis delta virus prevalence among hepatitis B virus–infected mongolians. Hepatology. 66(6), 1739-1749.
[9] Shaikh, H., Mobin, A., Manzoor, I. and Ebrahim, M.A. (2018) Hepatitis Delta. The Professional Medical Journal. 25(01), 73-77.
[10] François-Souquière, S., Makuwa, M., Bisvigou, U. and Kazanji, M. (2016) Epidemiological and molecular features of hepatitis B and hepatitis delta virus transmission in a remote rural community in central Africa. Infection, Genetics and Evolution. 39, 12-21.
[11] Khan, A.U., Waqar, M., Akram, M., Zaib, M., Wasim, M., Ahmad, S., Niaz, Z., Ali, S., Ali, H., Idrees, M. and Bajwa, M.A. (2011) True prevalence of twin HDV-HBV infection in Pakistan: a molecular approach. Virology Journal. 8(1), 420.
[12] Abbas, Z. (2012) Hepatitis D in Pakistan. J. Coll. Physicians Surg. Pak. 22(9), 547-548.
[13] Brancaccio, G., Giuberti, T., Verucchi, G., Levantesi, M., Sacchini, D., Fattovich, G., Madonia, S.T., Fasano, M., Gavrila, C., Nardi, A. and Gaeta, G.B. (2014) Epidemiological evolution of Chronic Hepatitis Delta in Italy. An analysis of the Master-B cohort. Digestive and Liver Disease. 46, e12-e13.
[14] Mumtaz, K., Hamid, S.S., Adil, S., Afaq, A., Islam, M., Abid, S., Shah, H.A. and Jafri, W. (2005) Epidemiology and clinical pattern of hepatitis delta virus infection in Pakistan. Journal of Gastroenterology and Hepatology. 20(10), 1503-1507.
[15] Rizzetto, M. (2015) Hepatitis D virus: introduction and epidemiology. Cold Spring Harbor Perspectives in Medicine. 5(7), a021576.
[16] Aftab, M., Amin, I., Idrees, M., Ali, A., Rafique, S. and Naz, S. (2018) Molecular epidemiology of hepatitis delta and hepatitis B viruses circulating in two major provinces (East and North-West) of Pakistan. Infection, Genetics and Evolution. 64, 65-69.
[17] Zuberi, S. (1998) An overview of HBV/HCV in Pakistan. Pakistan Journal of Medical Research. 37(Suppl), 12.

Received: **14.11.2020**
Accepted: **10.01.2021**

CORRESPONDING AUTHOR

Sadia Alam
Department of Microbiology,
The University of Haripur,
Pakistan

e-mail: sadia.alam2004@gmail.com

© by PSP Volume 30– No. 05/2021 pages 5098-5107 Fresenius Environmental Bulletin

TOXICITY OF FIVE PLANT EXTRACTS AGAINST CALLOSOBRUCHUS MACULATUS FAB. (COLEOPTERA BRUCHIDAE) A MAJOR INSECT PEST OF STORED PULSES

Rasheed Akbar[1,2,*], Imtiaz Ali Khan[1]

[1]Department of Entomology, The University of Agriculture Peshawar, Pakistan
[2]Department of Entomology, The University of Haripur, Pakistan

ABSTRACT

Bruchid Beetle, Callosbruchus maculatus Fab. (Coleoptera: Bruchidae) causes huge losses to pulses. In the present experiment aqueous and powder extracts of five plant species, i.e. Azadirichta indica L., Thuja orientalis L., Nicotiana tabacum L., Nicotiana rustica L., Melia azedarach L. at six different concentrations of 0.50%, 1%, 1.5%, 2%, 2.5% and 3%, were tested for their toxicity against C. maculatus under controlled laboratory conditions of 27±5°C temp., 60%±5% R.H. and 12:12h (L:D) photoperiod. The research were replicated four times using Completely Randomized Design. C. maculatus mortalities were significantly higher in aqueous form with all N. tabacum concentrations and in powder form with A. indica significantly lower mortalities were recorded of T. orientalis after 24h, 48h, 72h, and 7d and 14d. Overall means mortalities of C. maculatus were also significantly higher with N. tabacum in aqueous form with all concentrations and A. indica in powder form, where it was significantly lower with T. orientalis in aqueous and T. orientalis in powder form after 24h, 48h, 72h, and 7d and 14d. All the Phyto-chemicals were present in N. tabacum and in N. rustica while in A. indica least number of it were present. Phyto-sterol was present in highest while carbohydrates in moderate concentration. Saponins were present only in N. rustica and N. tabacum aqueous extracts. N. tabacum, A. indica and M. azedarach proves the most effective bio pesticides may be used as alternative to synthetic insecticides for the control of C. maculatus in stored pulses.

KEYWORDS:
C. maculatus, Plant extracts, Toxicity, Insect Mortalities, Phyto-chemicals

INTRODUCTION

In developing countries 10-40% damages is caused in stored grains and pulses due to the attack of *Callosobruchus* species during storage [1]. Caswell [2] reported 50% losses of cowpeas in storage of 3 or 4 months due to infestation caused by *C. maculatus*.Store grain losses from 10-40% caused by insects, microbes and other pests have been estimated globally, while 10-20% in Pakistan [3, 4]. Currently, in Pakistan and other developing countries, chlorinated hydrocarbon, organophosphorus, pyrethroids and fumigants are continuously used for the suppressions of store grain insect pests, which may endanger human and animal health as well as agroecosystem [5]. On the other hand, repeated application of these synthetic chemicals not only disturb biological control systems, which are mainly maintained by natural enemies, but also results into outbreaks of minor insect pests [6]. More than 10,000 arthropods have been reported to trigger serious damage to store grains products worldwide [7]. *A. indica* possess insecticidal activities an indigenous plant widely available in India and Burma. Different parts of this plant have been reported to have antiseptic, wound-healing, skin disease-curing and antiulcer activity [8]. The water soluble part of alcoholic extract of *A. indica* leaves possesses significant antiserotonin, antiinflammatory, antifertility and hepatoprotective activity [8]. Aqueous neem kernel extract has been used for warding off insect attack on crops. Oil from nuts and leaves is a stimulant insecticide and antiseptic. It inhibits feeding in a variety of insects and also inhibits ecdysis at much lower concentrations [9].

T. orientalis L., locally known as "Morpankhi", is extensively cultivated as an ornamental tree in cool and moist places for its attractive dense foliage and bush like habit of growthEssential oils derived from many aromatic plants are well known to possess cytotoxic, antioxidant, antifungal, insecticidal and antimicrobial activities [10].

The Chinaberry tree, *Melia azedarach* L. (Sapindales: Meliaceae), is a deciduous tree often grown for its medicinal uses and for shade or ornament on roadsides. The non-conventional insecticidal effects of extracts or compounds isolated from *M. azedarach* trees include: partial reduction or complete inhibition of fecundity and egg hatchability, reduction of life span of adults, oviposition deterrence, antifeedant effects, and insect growth regulatory effects at molting [11]. *M. azedarach* has been shown to possess many insecticidal effects against different pest species [12,13, 14].

N. tabacum and N. rustica contains nicotine which cause uncontrolled nerve firing and masking acetylcholine in insects [15]. Plant derived bioactive substances are considered a very good and cheap source of medicines that play a significant role for human health improvement as well as used against different types of microbial diseases [15]. Aqueous extract of many allelopathic plants are known to exhibit antifungal properties [16].

Due to injudicious, frequent and high dose use of some insecticides against stored product insect pests, many-fold resistances have been reported against these synthetic chemicals. Because the synthetic insecticides have harmful effects on environment, many safe alternative strategies for the management of insect pests have been tried since decades [17]. The use of plant extracts is one of the safe alternative for controlling stored insect pests. The use of plant extract not only safe for the environment but also safe for the associated natural enemies. Keeping in view the importance of botanical pesticides as one of the major safe alternative to the synthetic insecticides against stored product insect pests, the present study was conducted with the aims to study the toxicity effects five plant extracts against C. *maculatus.*

MATERIALS AND METHODS

For the present study, experiments on toxicity of five botanical extracts (liquid and powder form) against *C. maculatus* were carried out in Completely Randomized Design under control laboratory conditions of 27 ± 5°C temperature, 60% ± 5% RH and 12:12h (L:D) photoperiod during the year of 2018-19.

Insects Collection: *C. maculatus* were collected from different mung bean grains godowns in District Swabi, Khyber Pakhtunkhwa, Pakistan. The collected specimens were shifted in plastic bottles measuring 10 x 12 cm to Entomological Laboratory for identification. The beetles were identified with the help of available literature [18].

Establishment of stock culture: To establish a stock culture of *C. maculatus*, Mung bean was used as host. *C. maculatus* were reared in the Entomological Laboratory on whole Mung bean in plastic jars (10 x 12 cm) covered with Muslin cloth according to the method of [19].

Plant materials: leaves and fruits of the different host plants were collected from various locations of district Swabi and district Haripur, Khyber Pakhtunkhwa Pakistan (Table 1).

Phytochemical screening of selected plant aqueous extracts: The standard solution of 200 ml extracts was prepared by mixture of selected plant extract and distilled water. The extracts were subjected for phytochemical for the following standard methods.

Extraction procedure. Maceration: For maceration (for fluid extract), whole or coarsely powdered plant-drug was kept in contact with the solvent in a stopper container for a defined period with frequent agitation until soluble matter is dissolved [20].

Tests for alkaloids: Wegner s tests: Extracts of the test plants were dissolved individually in dilute hydrochloric acid 1.5% and filtered with Whatman No. 1 filter paper by the treatment filtrates with few drops of iodine in 2 to 3 drops of potassium iodide. The presence of brown reddish precipitates that pointed out the presence of Alkaloids in the samples [21].

Tests for phenols: Ferric Chloride Test: for the screening of phenol plant aqueous extracts was treated with 3-4 drops of ferric chloride solution. The appearance of bluish black color indicated the presence of phenols.

Tests for Phyto-sterols: Salkowski's Test: The test plants aqueous extracts were treated with chloroform and filtered with Whatman no. 1 filter paper. Few drops of concentrated Sulphuric acid were added and then vertexed it and allowed to stand for some time. The golden yellow color indicated the presence of Phyto-sterol [22].

Tests for diterpenes: Copper acetate Test: To observe the presence of diterpenes, the plant aqueous extracts were treated with 3-4 drops of copper acetate solution. Formation of emerald green color indicated the presence of diterpenes.

Tests for Saponins: Foam Test: For dilution about 2 ml of plant aqueous extracts were taken in test tube, in distilled water and vertexed it for 5 minutes. Foam produced and persisted for ten minutes indicated the presence of Saponins [21].

Tests for Flavonoids: Alkaline Reagent Test: For the presence of flavonoids, the plant aqueous extracts were treated with 2-3 drops of lead acetate solutions. The formation of intense yellow color, which becomes colorless on addition of dilute acid, indicated the presence of Flavonoids [21].

Contact Toxicity of Plants aqueous extracts. To investigate the contact action of test plants extracts on newly emerged beetles, Petri dishes (16 cm diam.) were sprayed thoroughly from all sides with the help of a mist sprayer till the runoff and then air dried for 30 minutes. Ten pairs of *C. maculatus* adult beetles of same age were caged by using Camel hair brush. Number of dead adult beetles were then

counted after treatment and converted to percent mortality for each concentration after 24h, 48h,72h, and 7, 14 and 21 days according to method of [23] with some modification, as per formula given below:

Corrected % Mortality = % mortality in treatment - % mortality in control x100

100- % mortality in control

Toxicity of plants powders against *C. maculatus:-* The toxicity studies of selected plant powders were studied according to the methodology of [19]. The experiment was carried out according to CR Design with four replicates. Each plant powder was tested at six concentrations, i.e. 0.5, 1, 1.5, 2, 2.5 and 3% w/w. There were six treatments including a control. Each treatment containing 20g of sterilized pulses treated with different concentrations of plants powders. The treated pulses were kept in Petri dishes and vigorously shaken before the release of beetles for the complete mixing of plant powders. Ten pairs of freshly emerged adult beetles were released in the tested arena. The beetles were starved for an hour before releasing in the arena. The data were recorded on the mortality of the test insect after 24, 48, 72, 168 and 336 hours after treatment. The dead beetles were removed from the Petri dishes on daily basis.

Statistical Analysis. The recorded data were subjected to Analysis of Variance (ANOVA) with two factors CRD (complete randomized design) and means were separated by using the Least Significant Difference (LSD) test at 5% level of probability. Statistical analyses were carried out using STATISTIX8.1 [24].

RESULTS

The results of experiment on the presence or absence of various Phyto-chemicals in aqueous extracts of different plants showed that in *N. tabacum* and in *N. rustica* all the Phyto-chemicals were present while in *A. indica* least number of five phytochemicals were present. The results also revealed that all the tested plants exhibited high concentration of Phyto-sterol and moderate concentration of carbohydrates, while Saponins were present only in *N. rustica* and *N. tabacum* aqueous extracts. The present findings are similar to that of [25].

1. C. maculatus mortalities 24 h after treatment with six aqueous concentrations of five plant species. After 24 hours exposures period with six different concentrations of five plant species crude extract gave significantly (P=0.0000, F=25.01) different C. maculatus mortalities (Figure 1). C maculatus mortalities significantly increased with increase in plant concentration. C. maculatus mortalities were significantly higher (13±1.25%, 18±1.75%, 23±2.25%, 30±3%, 35±3.5% and 40±4%) with all N. tabacum concentrations and significantly lower (5±0.5%, 10±1%, 13±1.25%, 18±1.75%, 20±2% and 23±2.25%) mortalities were recorded of T. orientalis. Overall means mortalities of C. maculatus were significantly higher of 26% with N. tabacum and lower of 15% with T. orientalis.

2. C. maculatus mortalities 48 h after treatment with six aqueous concentrations of five plant species. The results in Figure 2 reveal significantly (F=23.52, P=0.00) higher (20±0.00%, 25±0.50%, 33±0.25%, 38±0.48%, 40±0.71% and 45±0.29%) C. maculatus mortalities with all the N. tabacum concentrations and significantly lower (10±0.00%, 13±0.63%, 20±0.41%, 23±0.48%, 25±0.29% and 30±0.00%) mortalities with all the concentrations of T. orientalis. Overall mean mortalities of C. maculatus were significantly higher of 33% with N. tabacum and lower of 20% with T. orientalis.

3. C. maculatus mortalities 72 h after treatment with six aqueous concentrations of five plant species. Seventy-two hours after treatment, C. maculatus mortalities were significantly (F=29.84, P=0.00) higher (29±0.25%, 32±0.65%, 47±0.41%, 55±0.25%, 61±0.48% and 71±0.25%) with all the N. tabacum concentrations and significantly lower (24±0.25%, 32±0.29%, 39±0.25%, 42±0.29%, 47±0.41% and 50±0.25%) mortalities with all concentrations of T. orientalis. Overall mean C. maculatus mortalities were significantly higher (49%) with N. tabacum and lower (39%) with T. orientalis.

4. C. maculatus mortalities 7 days after treatment with six aqueous concentrations of five plant species. Six aqueous concentrations of five plant species caused significantly different C. maculatus mortalities seven days after treatment (Figure 4) where mortalities increased with increase in concentrations. C. maculatus mortalities were significantly (F=79.23, P=0.00)higher (46±0.25%, 51±0.25%, 60±0.29%, 77±0.00%, 86±0.25% and 94±0.29%) with all the concentrations of N. tabacum and significantly lower (29±0.25%, 37±0.29%, 43±0.41%, 54±0.41%, 66±0.41% and 77±0.41%) with all the concentrations of T. orientalis. Overall mean C. maculatus mortality was significantly higher of 69% with N. tabacum and significantly lower of 51% with C. maculatus.

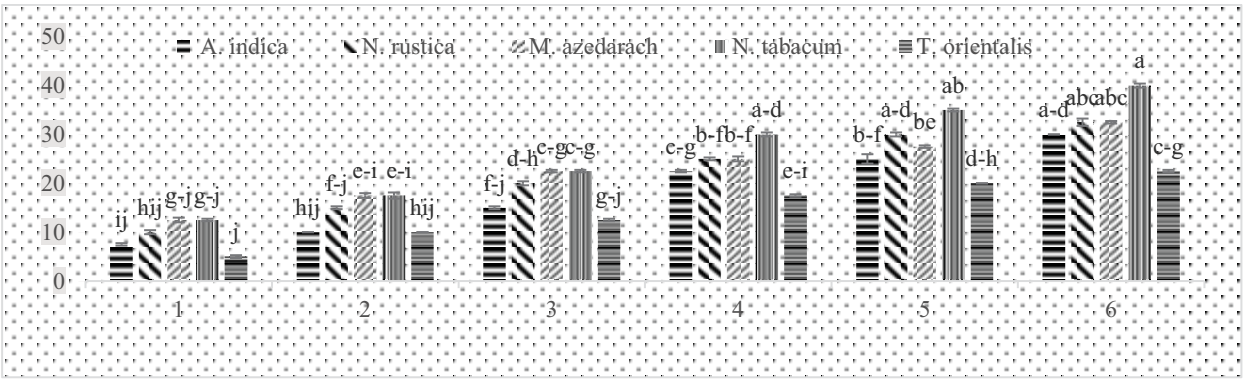

FIGURE 1

Mean C. maculatus mortality (%) after 24 h exposure period to six concentrations of crude- extracts of five plant species under laboratory conditions during 2018-2019.

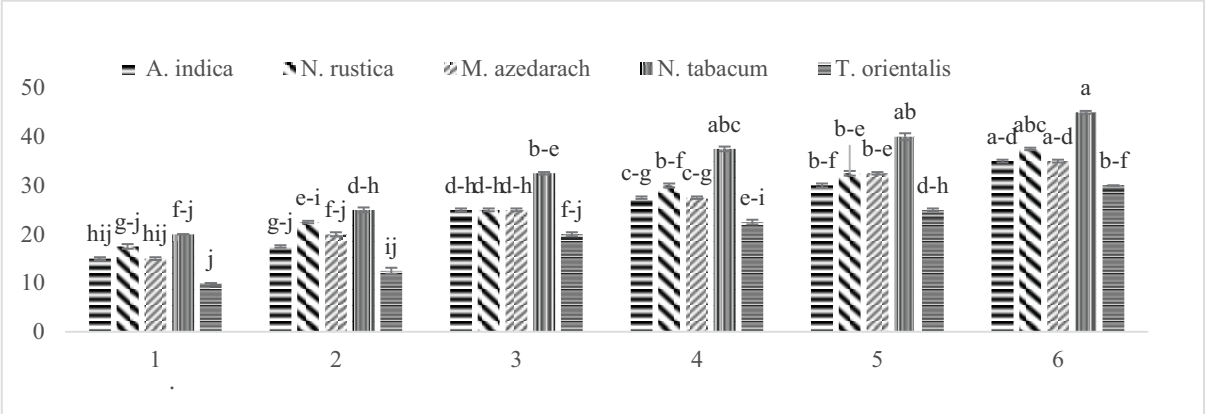

FIGURE 2

Mean C. maculatus mortality (%) after 48 h exposure period to six concentrations of crude- extracts of five plant species under laboratory conditions during 2018-2019

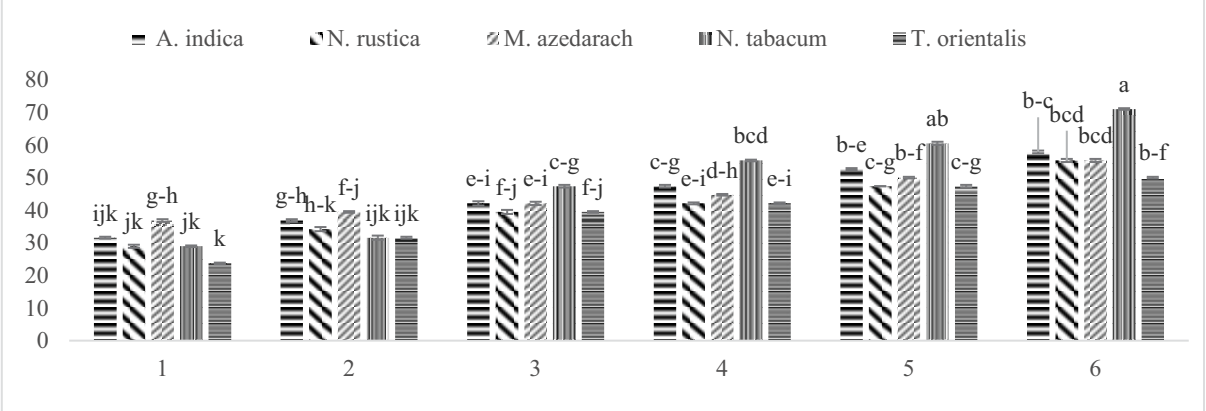

FIGURE 3

Mean C. maculatus mortality (%) after 72 h exposure period to six concentrations of crude- extracts of five plant species under laboratory conditions during 2018-2019

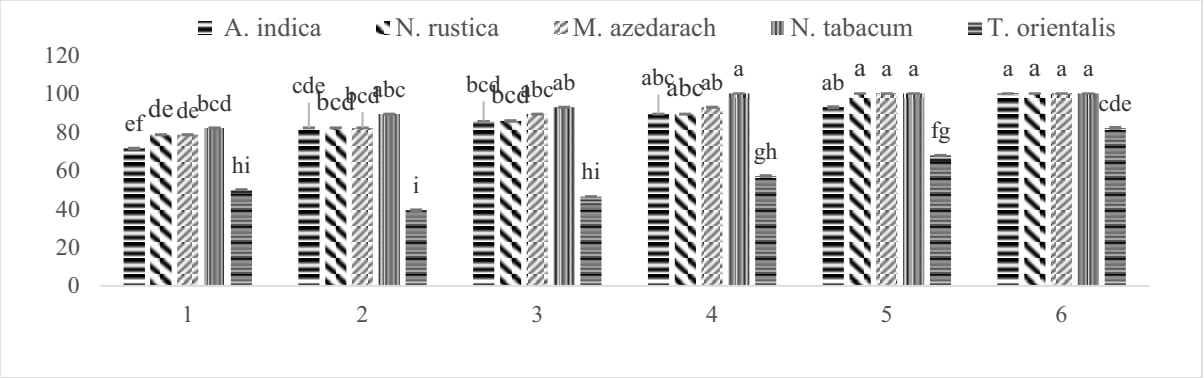

FIGURE 4
Mean C. maculatus mortality (%) after 7 days exposure period to six concentrations of crude- extracts of five plant species under laboratory conditions during 2018-2019

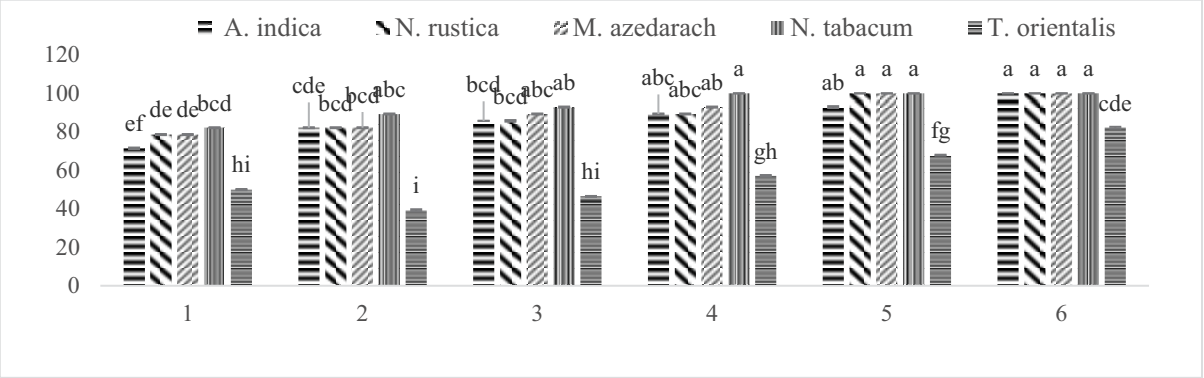

FIGURE 5
Mean C. maculatus mortality (%) after 7 days exposure period to six concentrations of crude- extracts of five plant species under laboratory conditions during 2018-2019

5. C. maculatus mortalities 14 days after treatment with six aqueous concentrations of five plant species. Fourteen days after treatment, C. maculatus mortalities were differently affected by the different concentrations of five plants species as shown in (Figure 5). C. maculatus mortalities were significantly (F=29.92, P=0.00) higher (82±0.25%, 89±0.25%, 93±0.29%, 100±0.00%, 100±0.00% and 100±0.00%) with all concentrations of N. tabacum and significantly lower (32 ±0.29 %, 39±0.48 %, 46±0.25%, 57±0.41%, 68±0.25% and 75 ±0.48%) with T. orientalis. Overall mean C. maculatus mortalities were significantly higher (94%) with N. tabacum and lower (52%) with T. orientalis.

6. C. maculatus mortalities 24h after treatment with six powder concentrations of five plant species. The results in Figure 6 reveal that six powder concentrations of the five plant species yielded significantly different C. maculatus mortalities 24 hours after treatment. C. maculatus mortalities were significantly (F=22.97 P=0.00) higher (8±0.25%, 8±0.25%, 15±0.29%, 18±0.25%, 23±0.25% and 23±0.25%) with all A. indica concentrations and significantly lower (3±0.25%, 3±0.25%, 5±0.29%, 8±0.25%, 10±0.00% and 13±0.25%) with T. orientalis. Overall mean C. maculatus mortalities were significantly higher of 15% with A. indica and lower of 07% with T. orientalis.

7. C. maculatus mortalities 48h after treatment with six powder concentrations of five plant species. Forty-eight hours after treatment, C. maculatus mortalities were significantly (F=18.84, P=0.00.) higher (13±0.48%, 18±0.25%, 20±0.41%, 23±0.25%, 23±0.25% and 28±0.25%) with all the A. indica concentrations and significantly lower (8±0.25%, 10±0.41%, 13±0.25%, 15±0.29%, 18±0.48% and 18±0.48%) with all the concentrations of T. orientalis. (Figure 7). Overall mean C. maculatus mortalities were significantly higher of 20% with A. indica and lower of 13% with T. orientalis.

8. C. maculatus mortalities 72h after treatment with six powder concentrations of five plant species. (In Figure 8) C. maculatus mortalities 72 hours after treatment were significantly (F=38.41, P=0.00) higher (18±0.25%, 24±0.25%, 29±0.25%, 34±0.25%, 39±0.25% and 42±0.29%) with all the A. indica concentrations and significantly lower (13±0.25%, 18±0.25%, 21±0.29%, 29±0.25%, 32±0.29% and 32±0.29%) mortalities with all concentrations of M. azedarach. Overall mean C. maculatus mortalities were higher (30%) with A. indica and lower (18%) with M. azedarach.

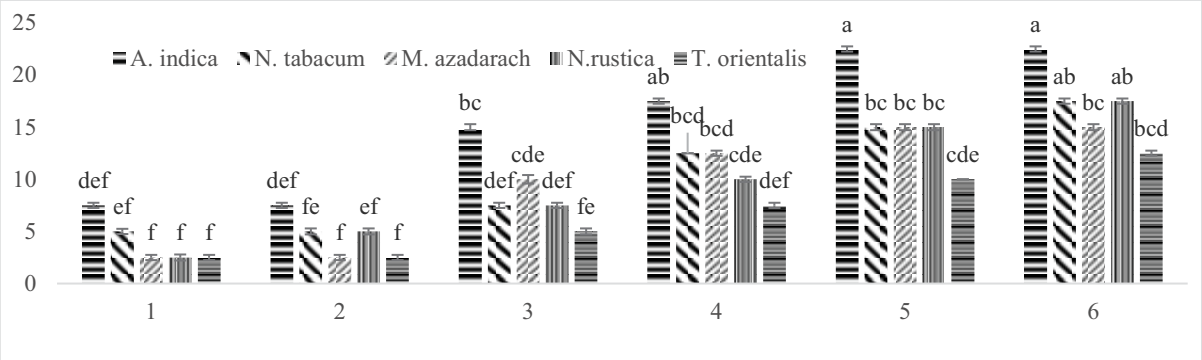

FIGURE 6
Mean percent mortality of C. maculatus after 24 h exposure period treated with six powder concentrations of five plant species during 2018-2019

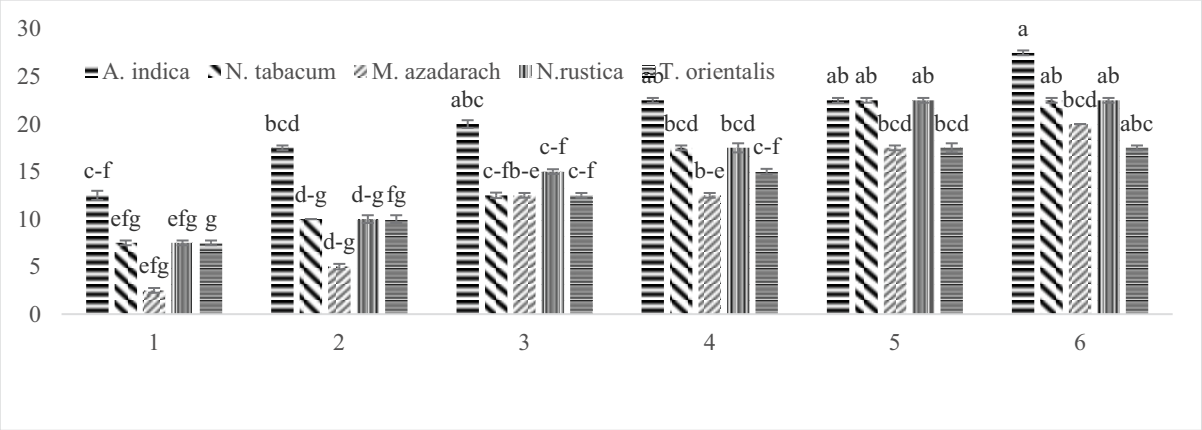

FIGURE 7
Mean percent mortality of C. maculatus after 48 h exposure period treated with six powder concentrations of five plant species during 2018-2019.

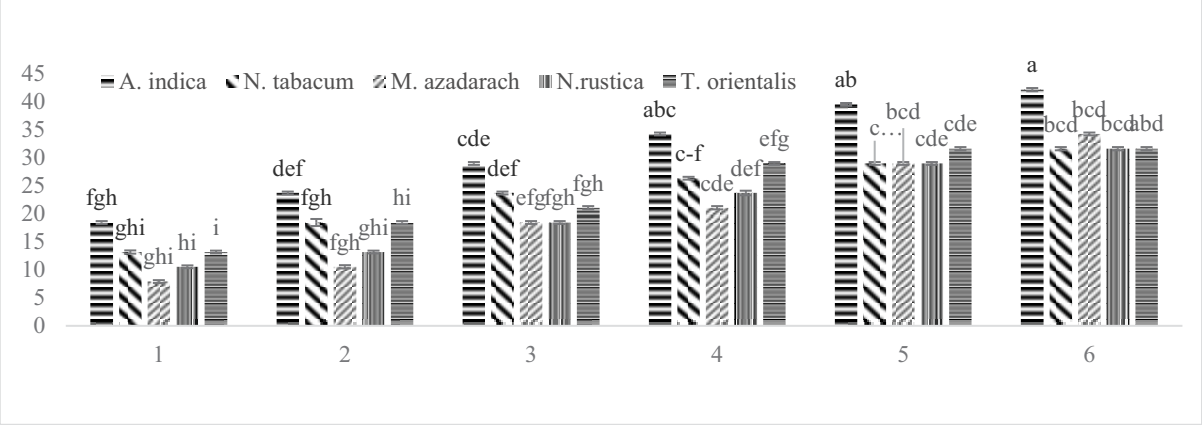

FIGURE 8
Mean percent mortality of C. maculatus after 72 h exposure period treated with six powder concentrations of five plant species during 2018-2019.

9. C. maculatus mortalities 7 days after treatment with six powder concentrations of five plant species. Seven days after treatment, C. maculatus mortalities were significantly (F= 245.52, P=0.00) higher (38±0.25%, 43±0.25%, 51±0.29%, 68±0.00%, 78±0.00% and 89±0.00%) with all the concentrations of A. indica and significantly lower (19±0.29%, 27±0.25%, 38±0.25%, 43±0.25%, 51±0.29% and 62±0.29%) with all the concentrations of T. orientalis (Figure 9). Overall C. maculatus mean mortalities were significantly higher (60%) with T. orientalis and significantly lower (40%) with C. maculatus.

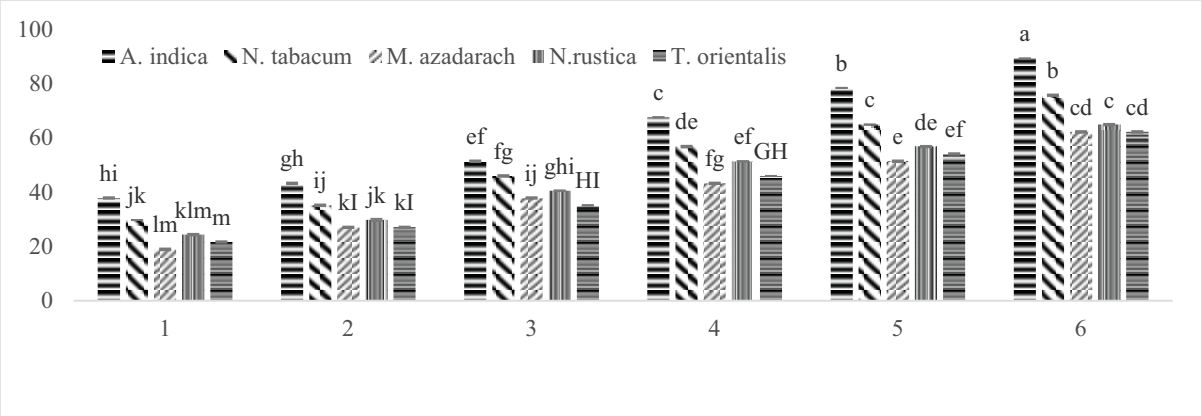

FIGURE 9
Mean percent mortality of C. maculatus after 7 days exposure period treated with six powder concentrations of five plant species during 2018-2019

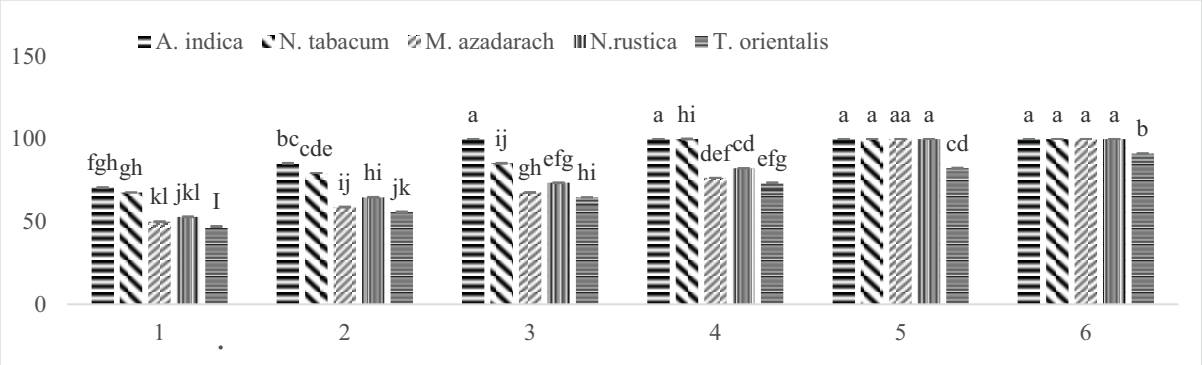

FIGURE 10
Mean percent mortality of C. maculatus after 14 days exposure period treated with six powder concentrations of five plant species during 2018-2019

TABLE 1
List of plant species and plant parts to be used in the experiment with *C. maculatus* during 2018-19.

Sr. No.	Common Name	Botanical Name	Family	Part used
1	Neem	*Azadirachta indica*	Meliaceae	Fruit
2	Bakion	*Melia azedarach*	Meliaceae	Fruit
3	White Patta	*Nicotiana rustica*	Solanaceae	Leave
4	Virginia tobacco	*Nicotiana tabacum*	Solanaceae	Leave
5	Chinese arborvitae	*Thuja orientalis*	Cupressaceae	Fruit

10. C. maculatus mortalities 14 days after treatment with six powder concentrations of five plant species. The results in Figure 10 reveal that C. maculatus mortalities were significantly (F=266.59, P=0.00) higher (71±0.29%, 85±0.25%, 100±0.00%, 100±0.00%, 100±0.00% and 100±0.00%) with A. indica and significantly lower (47±0.29%, 56±0.25%, 65±0.00%, 74±0.25%, 82±0.29% and 91±0.25%) with T. orientalis. Overall mean mortalities of C. maculatus were significantly higher (93%) with A. indica and significantly lower (69%) with T. orientalis.

DISCUSSION

The present results revealed that all the five plant species yielded mortalities in *C. maculatus*, where mortalities increased with increase in plant extract concentrations. Our results are similar to the findings of [26]. *N. tabacum* in aqueous form yielded significantly higher *C. maculatus* mortalities at all concentrations. *N. tabacum* leaves aqueous extracts contained all the phytochemicals, i.e. alkaloids, flavonoids, saponins, phenols, di-terpenes and phytosterol. Alkaloids contain nicotine which is biologically active compound of tobacco leaves, which acts on insect central nervous system causing paralysis

[25]. The results of our study are in agreement to those of [27] who stated that tobacco leaves are useful in the control of aphids. *N. tabacum* was reported to possess contact, stomach and respiratory poisoning properties attributed to the active constituent nicotine [28]. Leaf powder of *N. tabacum* and *N. rustica* was found effective in killing adult insect pests [29]. Seventy-one percent *S. zeamais* mortality was caused with tobacco plant powder on maize grains. It was also reported that 2.0 g of *N. tabacum* applied in 50 g of maize grains resulted 100.00% mortality of *S. zeamais* [30].

In the present results 2.5 % and 3% aqueous extract of *A. indica* and *M. azedarach* yielded significantly higher *C. maculatus* mortalities. The present results are comparable to those of [20] who reported that azadirichtin based insecticides caused maximum mortality to stored insect pests when exposed to both contact and oral methods. *A. indica* contain growth regulators, e.g. azadirichtin and solanin, saponins, alkaloids, flavonoids, tannins and cyanogenic glucosides, which preventing molting in insects. The presence of azadirichtin also enhance the development of an anti-peristaltic sensation in the insect gut which ultimately prevent feeding [31]. Neem leaf and seed extracts also showed toxicity against stored grain pests [32]. Our results are agreement with the findings of [33], who also isolated various compounds from the roots, seeds and leaves of neem extracts, known for their biological activities against insect pests.

In the present findings *M. azedarach* gave significantly higher *C. maculatus* mortalities both in contact and powder form. *M. azedarach* contain numerous secondary metabolites i.e. triterpenoids, the melicarpins, which are not identical to azadirichtin, and these triterpenoids' may have growth regulating functions in insect pests [34] toxicity to mammals [11], and as stomach poison for chewing insects [35]. In our results flavonoids, Saponins, Phyto-sterol, proteins and carbohydrate were obtained from aqueous extracts of *M. azedarach*. Similar compounds have also been reported by [1] from meliaceae plants which can be utilized as insecticides, anti-feedent and growth inhibitor. In our experiments aqueous extracts, both in contact and powder form, of *T. orientalis* gave lowest *C. maculatus* mortalities. The toxic effects of *P. orientalis* oil could be attributed to α-pinene and other components. As major constituents of *P. orientalis* are monoterpenoids, they are typically volatile and rather lipophilic compounds that can penetrate into insects rapidly and interfere with their physiological functions [35]. Due to their high volatility they have fumigant activity that might be of importance for controlling stored-product insects [36].

CONCLUSIONS

It was found in the present results that aqueous extracts of N. tabacum, A. indica and M. azedarach and powder extract of A. indica and N. tabacum yielded significantly higher C. maculatus mortalities at all concentrations. It can be concluded that N. tabacum, A. indica and M. azedarach may be used as safe alternative to synthetic insecticides for the control of C. maculatus. Therefore, the use of plant extracts of these five botanicals, both in aqueous and powder form, will not only efficiently suppress C. maculatus populations, but will also reduce health hazards to human and other non-target living things, environmental pollution, ecological imbalance and toxic residues in market produce.

ACKNOWLEDGEMENTS

My special thanks to my supervisory committee. The University of Haripur and those other researchers who help me a lot for their guidance, precious suggestion which enable me to complete my thesis and publication.

REFERENCES

[1] Shaaya, E., Kostjukovski, M., Eilberg, J. E. and Sukprakarn, C. (1997) Plant oils as fumigants and contact insecticides for the control of stored-product insects. Journal of Stored Products Research. 33(1), 7-15.

[2] Caswell, G. H. and Akibu, S. (1981) The use of Pirimiphos – methyl to control bruchids attacking selected varieties of stored cowpea. Samara Journal of Agriculture Research. 16(1), 85-87.

[3] Khan, I., Afsheen, S., Din, N., Khattak, S., Khalil, S. K. and Lou, Y. H. Y. (2010) Appraisal of different wheat genotypes against angoumois grain moth, *Sitotroga ceralella* (Oliv). Pakistan Journal of Zoology. 42(3), 161-168.

[4] Rashid, A., Sazzad, B., Begum, R. A. and Shahjahan, R. (2012) Mortality effect of BT extracts and esterase variability in three stored grain insects: *Callosobruchus chinensis*, *Sitophilus granarius* and *Tribolium castaneum*. International Journal of Agriculture Food Science. 2(4), 158-163.

[5] Ahmed, A., Ahmad, T., Arian, M. A. and Ahmed, M. (2008) Management of Bagged Wheat godowns to control the stored grain insect pests. Pakistan Entomologist. 30(1), 31-36.

[6] Collins, P. J., Daglish, G.J., Pavic, H., Lambkin, T. M. and Kapittke, R. (2002) Combating storing resistance to phosphine in stored grain pests in Australia. – In: Wright E. J., Highley E., Stored grain in Australia 2000. Preceding of the Australian Postharvest Technical Conference, Adelaide. 1-4 August.

[7] Rajendran, S. and Sriranjini, V. (2008) Plant products as fumigants for stored-product insect control. Journal of Stored Products Research. 44(2), 126-135.

[8] Chattopadhyay, R. R. and Bandyopadhyay, M. (2005) Effect of *Azadirachta indica* leaf extract on serum lipid profile changes in normal and streptozotocin induced diabetic rats. African Journal of Biomedical Research. 8(2), 101-104.

[9] Isman, M. B., Koul, O., Luczynski, A., and Kaminski, J. (1990). Insecticidal and antifeedant bioactivities of neem oils and their relationship to azadirachtin content. Journal of Agricultural and Food Chemistry. 38(6), 1406-1411.

[10] Shah, W. A. and Qadir, M. (2013) Chemical composition, Antioxidant and Antibacterial activity of Thuja orientalis essential oil. World Journal of Pharmacological. Sciences. 2(2), 56-60.

[11] Ascher, K.S. (1993) Nonconventional insecticidal effects of pesticides available from the neem tree, *Azadirachta indica*. Archives of Insect Biochemistry and Physiology. 22(3-4), 433-449.

[12] AL-akhras H. A. (2010) Effect of *Melia azedarach* on Black Aphid Aphis fabae, M.S. Thesis. Beirut, Lebanon: Lebanese University. 51-52

[13] Hammad, E. M. A. F. and McAuslane, H. H. J. (2010) Effect of *Melia azedarach* L. extract on *Liriomyza sativae* (Diptera: Agromyzidae) and its biocontrol agent *Diglyphus isaea* (Hymenoptera: Eulophidae). Journal of Food Agriculture and Environment. 8(3), 1247-1252.

[14] Jazzar, C. and Hammad, E. A. F. (2003) The efficacy of enhanced aqueous extracts of *Melia azedarach* leaves and fruits integrated with the *Camptotylus reuteri* releases against the sweetpotato whitefly nymphs. Bulletin of Insectology. 56(4), 269-276.

[15] Kumar, V. P., Chauhan, N. S., Padh, H., and Rajani, M. (2006) Search for antibacterial and antifungal agents from selected Indian medicinal plants. Journal of Ethnopharmacology. 107(2), 182-188.

[16] Chou, C. H. (1995) Allelopathy and sustainable Agriculture.In: Allelpathy Organisms, Process and Applications. ACS Symposium Series. 582, 211-233.

[17] Margaritopoulos, J. T., Skouras, P. J., Nikolaidou, P., Manolikaki, J., Maritsa, K., Tsamandani, K. and Tsitsipis, J. A. (2007) Insecticide resistance status of *Myzus persicae* (Hemiptera: Aphididae) populations from peach and tobacco in mainland Greece. Pest Management Science: Formerly Pesticide Science. 63(8), 821-829.

[18] Fatima, S. M., Usman, A., Sohail, K., Afzal, M., Shah, B., Adnan, M. and Shah, S. R. A. (2016) Rearing and identification of *Callosbruchus maculatus* (Bruchidae: Coleoptera) in Chickpea. Journal of Entomology and Zoological Studies. 4(1), 264-266.

[19] Zafar, U., Mamoon-Ur–Rashid, M. and Shah, M. (2018) Entomotoxicity of plant powders against Pulse beetle (*Callosobruchus chinensis*) on stored mung bean (*Vigna radiata*). 6(1), 1637-1641.

[20] Eleazu, C.O., Eleazu, K.C., Awa, E. and Chukwuma, S. C. (2012) Comparative study of the phytochemical composition of the leaves of five Nigerian medicinal plants. Journal of Biotechnology and Pharmaceutical Research. 3(2), 42-46.

[21] Ncube, N. S., Afolayan, A. J. and Okoh, A. I. (2008). Assessment techniques of antimicrobial properties of natural compounds of plant origin: current methods and future trends. African Journal of Biotechnology. 7(12), 1797-1806.

[22] Kamal, T., Ahmad, M., Raji, A. A., Muayad, S. R. and Muhammad, N.O. (2012) Preliminary phytochemical screening test of *Garcinia griffithii* Plant. Innova Ciencia. 4(4), 68-74.

[23] Paudyal, S., Opit, G. P. and Arthur, F. H. (2016) Contact Toxicity of Deltamethrin against *Tribolium castaneum* (Coleoptera: Tenebrionidae), *Sitophilus oryzae* (Coleoptera: Curculionidae), and *Rhyzopertha dominica* (Coleoptera: Bostrichidae) Adults. Journal of Economic. Entomology. 109(4), 1936–1942.

[24] Steel, R.G.D. and Torrie, J. H. (1980) Principals and procedures of statistics: A biological approach. 2nd Ed. McGraw Hill Book Co. N.Y. 481 p.

[25] Yash, S., Deepak, S. and Jayaraman, K. S. (2017) Recent trends in antimicrobial peptide prediction using machine learning techniques. Biomedical Informatics Publishing Group. 13(12), 415–416.

[26] Parveen, F., Khan, A. and Zaib, S. (2013) Repellency of red flour beetle, *Tribolium castaneum* caused by leave extract fractions of hill toon, Cedrela serrata. International Journal of Entomological Research. 1(1), 01-10.

[27] Stoll, G. (1988). Natural Crop protection in the Tropics. Agrecol. Margraf Publishers. 188 pp.

[28] Asawalam, E. F., Emosairue, S. O., Ekeleme, F. and Wokocha, R. C. (2007) Insecticidal Effects of Powdered Parts of Eight Nigerian Plant species against Maize weevil, *Sitophilus zeamais* Motschulsky (Coleoptera: Curculionidae). Electronic Journal of Environmental, Agricultural and Food Chemistry. 6(11), 2526–2533.
[29] Danjumma, B. J., Majeed, Q., Manga, S. B., Yahaya, A., Dike, M. C. and Bamaiyi, L. (2009) Effect of Some Plant Powders in the Control of *Sitophilus zeamais* Motsch (Coleoptera: Curculionidae) Infestation on Maize Grains. American-Eurasian Journal of Scientific Research. 4(4), 313–316.
[30] Kestenholzetal, C., Stevenson, P., Belmain, S. R. (2007) Comparative study of field and laboratory evaluations of the ethnobotanical *Cassia sophera* L. (Leguminosae) for bioactivity against the storage pests *Callosobruchus maculatus* (F.) (Coleoptera: Bruchidae) and *Sitophilus oryzae* (L.) (Coleoptera: Curculionidae). Journal of Stored Product Research. 43(1), 79-86.
[31] Sharif, M., Shamshad, A. and Iram, N. (2007) Efficacy of neem (*Azadirachta Indica* A. Juss) leaf extract for the control of *Tribolium castaneum (*Herbst*)*. Biologia. 53(2), 75–81.
[32] Biswas, K., Chattopadhyay, I., Banerjee, R. K. and Bandyopadhyay, U. (2002) Biological activities and medicinal properties of neem (*Azadirachta indica*). Current Science-Bangalore. 82(11), 1336-1345.
[33] Kraus, W. (2002). Azadirachtin and other triterpenoids. See. Ref. 81, 39–111
[34] Chiu, S. F. (1989). Recent advances in research on botanical insecticides in China. 69-77.
[35] Lee, Y. H., Park, E.K. and Lee, S. E. (2002) Adverse effect of essential oil fumigation on *Proisotomaminuta* (Collembola: Entomobryoidae). Journal of Asia. Pacific Entomology. 5(1), 131-133.
[36] Ahn, Y.J., Lee, S.B., Lee, H.S., Kim, G.H. (1998) Insecticidal and acaricidal activity of carvacrol and β-thujaplicine derived from Thujopsis dolabrata var. hondai sawdust. Journal of Chemical Ecology. 24(1), 81-90.

Received: **18.11.2020**
Accepted: **07.02.2021**

CORRESPONDING AUTHOR

Rasheed Akbar
Department of Entomology,
The University of Agriculture Peshawar,
Pakistan

e-mail: rasheedaup@gmail.com,
rasheed.akbar@uoh,edu.pk

© by PSP Volume 30– No. 05/2021 pages 5108-5118 Fresenius Environmental Bulletin

AN EXPERIMENTAL AND NUMERICAL STUDY OF TURBIDITY CURRENTS ENTERING A STRATIFIED RESERVOIR

Rui Wang[1,2], Xi Mao[2,*], Lu Gao[2], Lijian Qi[2], Xiuyuan Lu[2], Yong Wang[2], Jidong Li[2], Chunhang Xie[3], Hao Yuan[3], Zhongluan Yan[4], Leilei Qin[4]

[1]POWERCHINA Chengdu Engineering Corporation Limited, Chengdu, China (Co-first institute)
[2]College of Water Conservancy and Hydropower Engineering, Sichuan Agricultural University, Ya'an, China (Co-first institute)
[3]Southwest Research Institute for Water Transport Engineering, Chongqing Jiaotong University, Chongqing, China
[4]China Three Gorges Corporation, Beijing, China

ABSTRACT

Turbidity currents are helpful for regulating reservoir sedimentation. However, the movement of turbidity currents is affected by the water temperature in a stratified reservoir. It is necessary to analyze the motion of turbidity currents in stratified reservoirs. Flume experiments and a mathematical model were used to study the motion of turbidity currents in a stratified reservoir in this study. The phenomenon that turbidity currents traveled in different water layers was successfully demonstrated in flume experiments. Based on the RNG k-ε turbulence model, we proposed a mathematical model that coupled the heat conduction and sediment transport equations. This model was verified by experimental data. This study confirmed that the interflow or overflow was different than the underflow in the reservoir when low sediment concentration turbidity currents entered the stratified water. The mathematical model established in this study was used to simulate the above phenomenon and was validated by experimental data. This study provides a calculation method for analyzing the turbidity currents entering a stratified reservoir.

KEYWORDS:
Turbidity currents, stratified reservoir, interflow, RNG k-ε turbulence model, flume experiment

INTRODUCTION

Temperature stratification occurs in reservoirs during specific seasons. The differences in the water density in the vertical direction caused by temperature stratification affect the movement of turbidity currents. Therefore, interflow or overflow forms in stratified reservoirs. This phenomenon has been recorded in several reservoirs, such as Mead Lake in the United States [1] and the Xin Anjiang reservoir in China [2].

The influence of a stratified reservoir on the turbidity current is mainly determined by the density differences between the inflow and water in the reservoir. The higher the density of the inflow is, the smaller the influence is. According to the recorded temperature data of stratified reservoirs shown in Table 1, the density difference caused by the temperature difference between the surface and bottom of the stratified reservoirs was 0.320–1.695 kg/m^3 [3]. The influence of temperature stratification can be ignored in reservoirs with a higher sediment concentration inflow. In the southwestern region of China, the average sediment concentration is about 1 kg/m^3, which is within the density difference range mentioned above [1]. With such a low sediment concentration, turbidity currents are more susceptible to reservoir stratification. Thus, the temperature and sediment concentration should be analyzed together in these reservoirs.

Numerical simulations have been applied to study turbidity currents to obtain full insight into the varied physical processes of turbidity currents. Some one-dimensional numerical models have been used in cases with simple boundary conditions and no thermal stratification. Two-dimensional models using the RNG k-ε turbulence model are generally applied to simulate narrow or shallow reservoirs, depth-averaged models are often used to examine the underflow [4], and laterally averaged two-dimensional models are generally used to investigate the flow in stratified reservoirs. A model capable of simulating the flow and thermal characteristics of a reservoir system was used to help identify feasible reservoir operations and the volume of cold water released [5]. The CE-QUAL-W2 hydrodynamics and transport model [6,7] was used to simulate the contaminated density current in the

TABLE 1
The water temperature of the reservoir surface and bottom

Reservoir	Dam height (m)	Surface temperature (℃)	Bottom temperature (℃)	Temperature difference (℃)	Density difference (kg/m^3)
DanJingkou	97	18.44	12.1	6.34	0.974
XinAnjiang	105	21.10	10.4	10.7	1.695
FengMan	90.5	11.80	6.2	5.6	0.410
FouZiling	75	18.21	13.08	5.13	0.811
GuanTing	45	13.70	11.0	2.7	0.320
XinFengjing	105	21.4	12.0	9.4	1.595
Bould	221	19.5	12.8	6.7	1.098
Norris	81	18.2	7.9	10.3	1.298
Shivaxi	94	19.2	6.5	12.7	1.560

stratified Shasta Reservoir to assist in contamination control and remediation after a toxic chemical spill and water quality management. The model of the turbidity in the Schoharie reservoir was studied and validated by simulating the appearance timing and magnitudes of pollutants[8]. Before this, they conducted a simulation of the seasonal hydrothermal density stratification regime of the Schoharie Reservoir to examine the behavior of density currents based on the specific conductance as a conservative tracer. A laterally averaged two-dimensional model was applied and validated by field data from the Ertan reservoir to predict the density current induced by a temperature difference[9]. Other mathematical models and three-dimensional models, such as multiphase models, large eddy simulations (LES), and direct numerical simulation (DNS), are often used to investigate the motion of a denser underflow propagating on a slope into a homogeneous environment[10, 11]. However, most research has focused on one factor or the other, without coupling the temperature and sediment characteristics. Moreover, there are some differences between the sediment and pollutants due to the special characteristics of the sediment[12, 13].

In this study, a two-dimensional mathematical model that accounted for the sediment and temperature was proposed to simulate the turbidity current in a stratified reservoir. A flume system was designed to study the movement of the turbidity current under different water temperature stratification conditions.

MATHEMATICAL MODEL

To simultaneously account for the temperature and sediment, the model must account for both the thermal conductance and sediment transport in water. In this study, a two-dimensional mathematical model for the turbidity current in stratified water was constructed that included the continuity, momentum, transport, and heat conduction equations. In addition, the buoyancy term in the momentum equation should be modified by considering the effects of the temperature and sediment.

Transport Equation for Sediment. The sediment settling velocity should be used to modify the transport term in the transport equation as Formula 1:

$$\frac{\partial(\rho\varphi)}{\partial t}+\frac{\partial[\rho\varphi(u_i-\omega)]}{\partial x_i}=\frac{\partial}{\partial x_i}(\frac{\nu_t}{\sigma_t}\frac{\partial\rho\varphi}{\partial x_i}) \quad (1)$$

where x_i is the space coordinate, t is the time coordinate, u_i (m/s) is velocity in each direction, ρ (kg/m^3) is the density, v_t (kg/m·s) is the kinematic viscosity caused by the turbulence, φ (kg/m^3) is the sediment concentration, and ω (m/s) is the sediment settling velocity.

The sediment settling velocity at low sediment concentrations is as Formula 2 [14]:

$$\frac{\omega_0}{\omega}=1+k_s\frac{D}{s} \quad (2)$$

where ω_0 is the sediment settling velocity in still water (m/s), s is the spacing between two sediment particles (m), D (m) is the particle size of the sediment, and k_s is an empirical coefficient.

D/s can be expressed as Formula 3:

$$D/s=1.24\varphi^{1/3} \quad (3)$$

The sediment settling velocity in still water is denoted by ω_0 (m/s) and expressed as Formula 4:

$$\rho_t=999.939900+4.216485(10^{-2})t_e-7.097451(10^{-2})t_e^{\,2}+3.509571(10^{-5})t_e^{\,3}-9.9037785(10^{-8})t_e^{\,4} \quad (9)$$

$$\omega_0^2 = \frac{4}{3} \cdot \frac{1}{C_D} \cdot \frac{\rho_S - \rho}{\rho} \cdot gD \quad (4)$$

where ρ_s (kg/m^3) is the density of the sediment, $C_D = 24/(\omega_0 D/\nu)$ is the damping coefficient, and g (m/s^2) is the acceleration of gravity.

Heat Conduction Equation. The heat conduction equation was used to model the heat conduction in water as Formula 5:

$$\frac{\partial}{\partial t}(\rho E) + \frac{\partial[u_i(\rho E + P)]}{\partial x_i} = \frac{\partial}{\partial x_j}(k_f \frac{\partial T}{\partial x_j}) \quad (5)$$

where T (K) is the water temperature, k_f (W/m·K) is the heat conduction coefficient determined by the turbulence, $E=h-P/\rho+u^2/2$ is the energy, and h (J) is the enthalpy.

For an incompressible fluid, h is expressed as Formula 6:

$$h = \sum_j Y_j h_j + P/\rho \quad (6)$$

where $h_j = \int_{T_{ref}}^{T} c_{p,j} dT$ is the reference enthalpy and T_{ref} is the reference temperature.

When the turbidity current enters a stratified environment, the temperature and sediment transport equation must be simulated using the coupled momentum and continuity equations. We present the momentum equations that include the temperature and sediment concentration to modify the buoyancy term. According to Boussinesq approximation, the density difference in the inertial terms is negligible and only must be considered in the gravity term. The momentum equations are as Formula 7:

$$\frac{\partial u_i}{\partial t} + u_j \frac{\partial u_i}{\partial x_j} = -\frac{1}{\rho}\frac{\partial P}{\partial x_i} + \nu_t \frac{\partial^2 u_i}{\partial x_j^2} + \frac{\Delta \rho g}{\rho} \quad (7)$$

where x_i is the space coordinate, t is the time coordinate, u_i (m/s) is velocity in each direction, P (Pa) is the pressure, ρ (kg/m^3) is the density, and ν_t (kg/m·s) is the kinematic viscosity caused by the turbulence. The difference between the density and reference density is denoted as $\Delta\rho$ (kg/m^3), and g (m/s^2) is the acceleration of gravity.

The density is determined by the temperature and sediment concentration as Formula 8:

$$\rho = \rho_t + (1 - \frac{\rho_t}{\rho_m})\ \varphi \quad (8)$$

where ρ_t (kg/m^3) is the density of water determined by the temperature, and ρ_m is the density of the sediment.

Changes in the water density due to pressure can be ignored under normal conditions. The values for the water density (ρ_t) (Victor et al., 2003) are calculated as Formula 9:

where t_e (°C) is the water temperature.

The renormalization group (RNG) k-ε turbulence model was adopted to close the model, and the equations for turbulent kinetic energy k and turbulent dissipation rate ε were as Formula 10 ~Formula 12:

$$\frac{\partial(\rho k)}{\partial t} + \frac{\partial(\rho k u_i)}{\partial x_i} = \frac{\partial}{\partial x_j}[\alpha_k \nu_t \frac{\partial k}{\partial x_j}] + G_k + G_b - \rho\varepsilon \quad (10)$$

$$\frac{\partial(\rho\varepsilon)}{\partial t} + \frac{\partial(\rho\varepsilon u_i)}{\partial x_i} = \frac{\partial}{\partial x_j}[\alpha_\varepsilon \nu_t \frac{\partial \varepsilon}{\partial x_j}] + \frac{C_{1\varepsilon}^* \varepsilon}{k} G_k - C_{2\varepsilon}\rho\frac{\varepsilon^2}{k} \quad (11)$$

$$\nu_t = \rho C_\mu \frac{k^2}{\varepsilon} \quad (12)$$

where G_k is the generation term of the kinetic energy caused by the mean velocity gradient, G_b is the generation term caused by the buoyancy, and the empirical constant parameters have the following values: $C_{1\varepsilon} = 1.42$, $C_{2\varepsilon} = 1.68$, $\eta_0 = 4.37$, $\beta = 0.012$, $C\mu = 0.09$, and $\alpha_k = \alpha_\varepsilon = 1.39$.

EXPERIMENTS OF TURBIDITY CURRENTS IN THERMALLY STRATIFIED WATER

Experimental Setup. Turbidity currents in thermally stratified water were produced in a glass flume (Figure 1). This laboratory flume was designed based on the requirements of the turbidity current simulation and mathematical model validation.

Before each experiment, heating devices were used to form vertical temperature stratification in the flume. At the beginning of the experiment, the turbid water was pumped into the inlet region with a specified temperature and sediment concentration. A turbidity current formed in the slope region. When the turbidity current entered the stratified environment of the flat region, its motion, which was affected by the stratified environment, was observed. Two vertical temperature monitoring sections were set at 95 and 215 cm from the inlet of the flume, and ten temperature auto-logging probes with an average vertical spacing of 5.5 cm were placed at different depths for each monitoring section to record the temperature. The precision of the temperature probes was ±0.2°C.

Experimental Conditions. The parameters of the turbidity current experiments are listed in Table 2 with the discharge, sediment concentrations, temperature stratification structure, inflow Reynolds

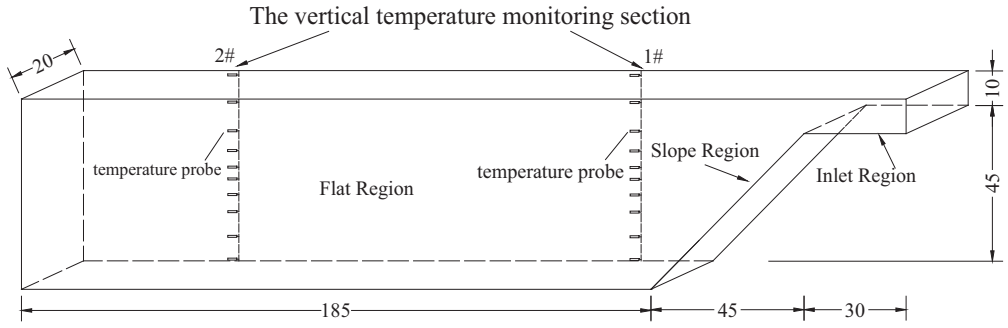

(Unit：cm)

FIGURE 1
Flume design

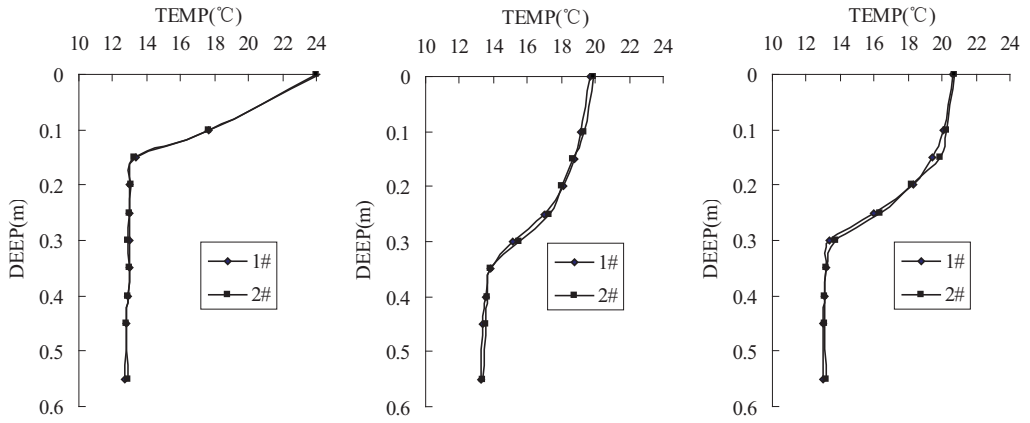

(a) No. 3Y211 (b)No. 3Y221 (c)No. 3Y241

FIGURE 2
Contrast of temperature at the same depth for two monitoring sections

TABLE 2
Experiments conditions

No.	Characteristics of turbid inflow					Characteristics of thermal stratification in the flume			
	Q m^3/h	T ℃	C* kg/m^3	*Fr′*	*Re*	T ℃	Δρ kg/m^3	Depth of thermocline cm	∇T of thermocline ℃/cm
3Y121	0.500	21.9	1.819	0.62	701	11.5~21.8	1.72	30	0.48
3Y221	0.864	20.4	0.864	0.40	1112	13.3~20.7	1.28	25	0.42
3Y241	0.892	21.1	0.892	0.34	582	13.0~20.6	1.30	25	0.49
3Y211	0.752	21.3	0.752	0.45	992	12.7~24.2	2.17	40	0.86
3Y261	0.591	30.0	0.591	0.25	1321	12.1~20.3	1.35	25	0.39
3Y142	1.029	11.9	1.029	0.21	819	12.1~12.1	0	\	\

C*: The sediment concentration

number *Re*, and inflow densimetric Froude number *Fr′*, which reflected the formation conditions of a turbidity current. Silt with a dry density of 1667 kg/m^3 and median grain size of 10.0 μm was used in all the experiments.

The Reynolds number (*Re*) and densimetric Froude number (*Fr′*) were defined as as Formula 13 and Formula 14:

$$Re = \frac{\bar{v}h}{\upsilon} \tag{13}$$

$$Fr' = \frac{\bar{v}}{\sqrt{\frac{\rho' - \rho}{\rho'} gh\cos\beta}} \tag{14}$$

where $\bar{v}$ is the average velocity, h is the water

depth at the inlet, υ is the kinematic viscosity, ρ' is the density of the turbid water, ρ_0 is the density of the water, and β is the slope angle.

The initial vertical temperature distributions at the two monitoring sections are shown in Figure 2 (No. 3Y211, 3Y221, and 3Y241). When the maximum temperature difference between the two monitoring sections was less than 0.4°C at the same depth, the horizontal temperature was considered to be identical. Thus, temperature stratification in the flume was achieved using our experimental setup.

Motion Patterns. Three motion patterns for the turbidity current were observed in the experiments (Figure 3). The results suggest that the movement patterns of the turbidity current in thermally stratified water was determined by the density parameter. The turbidity current traveled along the bottom if the density of the inflow was greater than the ambient water (No. 3Y142), but it flowed over the top of the flume forming overflow when the density of the inflow was smaller than that of the ambient water (No. 3Y261). The inflow propagated as an interflow if the density of the inflow was between the densities of the top and bottom ambient water (No. Y121, Y221, 3Y241, and 3Y211).

When the turbidity current becomes overflow or interflow, the lower interface between the water and turbidity current may be the main location where sediment settling occurs. Thus, a clear interface between the water and turbidity current was observed in addition to the sediment settling in the flume experiments. This phenomenon can be explained by the Bernoulli effect [14], which states that an increase in the speed of the fluid occurs simultaneously with a decrease in the pressure. Hence, the pressure in the lower velocity zone was greater than that in the higher velocity zone, and it caused an uplift force acting on the higher velocity zone. As the turbidity current moved faster than the surrounding water, the Bernoulli effect produced an uplift force to restrain the dispersion and settling of sediment particles at the edge of the lower interface to maintain a clear lower interface.

RESULTS

Model Validation. The experimental and numerical results are shown in Figure 4 (No. 3Y241). Due to the influence of the temperature stratification, the turbidity currents flowed in the middle level of the flume. The turbidity currents had pointed heads and thick bodies, similar to a wedge, due to the friction between the upper and lower water phases. The experiments and simulations showed the same results for the turbidity current shape. Comparisons of the thickness of the turbidity currents (Figure 5) showed an average difference of 17%. The velocities of the front turbidity currents were affected by the inflow. The arrival time of each cross-section is shown in Figure 6. The average error between the calculation and experiment was only 6%.

The vertical structure of the water temperature when the fronts of the turbidity currents were 160 cm from the entrance is shown in Figure 7. The average error of the temperature between the calculation and experiment in section 1 was only 4.7%, and it was only 2.2% in section 2.

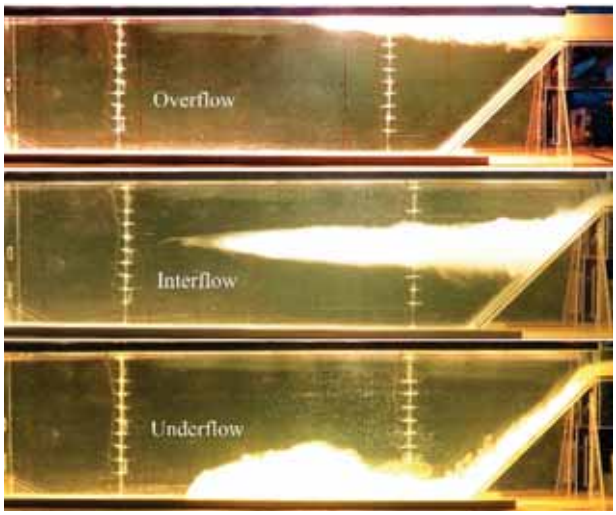

FIGURE 3
Different patterns for the turbidity currents

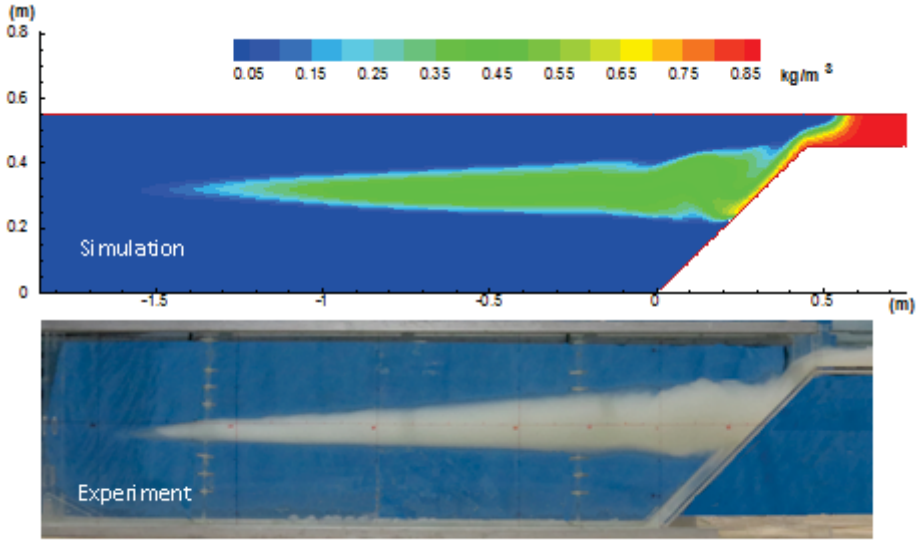

FIGURE 4
The turbidity current shape (No.3Y241)

The experimental and numerical results of the underflow are shown in Figure 8 (No. 3Y142). The thickness of the front was greater than that of the tail in the underflow, which was entirely different between interflow and overflow. The thickness of the turbidity currents (Figure 9) showed an average difference of 9%. Figure 10 shows the time required for the front of the turbidity current to reach each section in the numerical calculations and experiments. The results showed that the average error between the calculated and experimental values was only 8.5%.

Particle image velocimetry (PIV) was used to measure the flow field in the flume (No. 3Y121). The average error between the calculation and experiment was ±9% (Figure 11). The numerical simulation was consistent with our experimental observations, indicating that the numerical simulations could accurately simulate the vortex above the turbidity front.

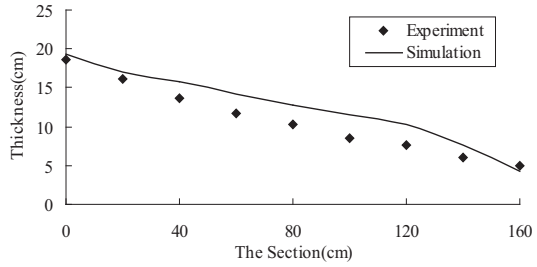

FIGURE 5
The thickness of the turbidity current

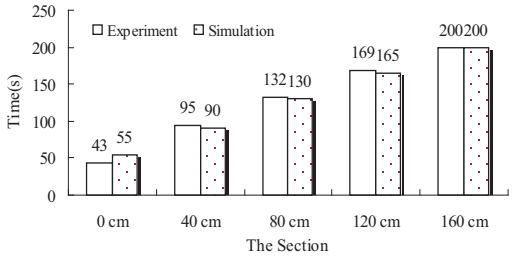

FIGURE 6
The arrival time of the head for each section

Motion of Interflow with Different *Fr′*. The motion characteristics of the interflow, such as the velocity and thickness, are often closely related to the inflow conditions. The validated mathematical model was used to analyze the relationship between the inflow conditions and motion characteristics of the interflow.

Three simulation conditions with different inflow conditions were chosen for the same stratified environment. The boundary conditions for each case are listed in Table 3 and were characterized by the inflow *Fr′*, which is a dimensionless parameter.

Motion Characteristics of Interflow. Figure 12 shows the arrival time at each section of the front of the turbidity current. The results indicated that velocity was positively correlated with the *Fr′* number of the inflow. The thickness of the turbidity current at each section of the flume is shown in Figure 13. The thickness of the back must be larger than the thickness of the front to keep current moving forward. The thickness of the turbidity current at each section was positively correlated to the Fr' number.

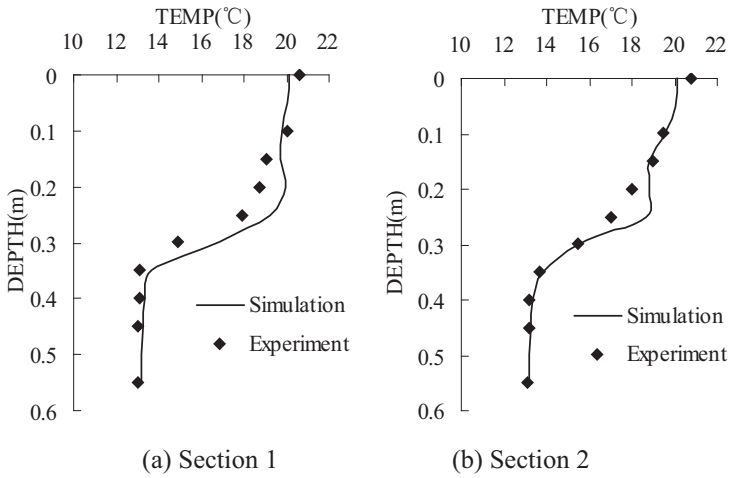

(a) Section 1 (b) Section 2

FIGURE 7
Comparison of temperature in the simulations and experiments

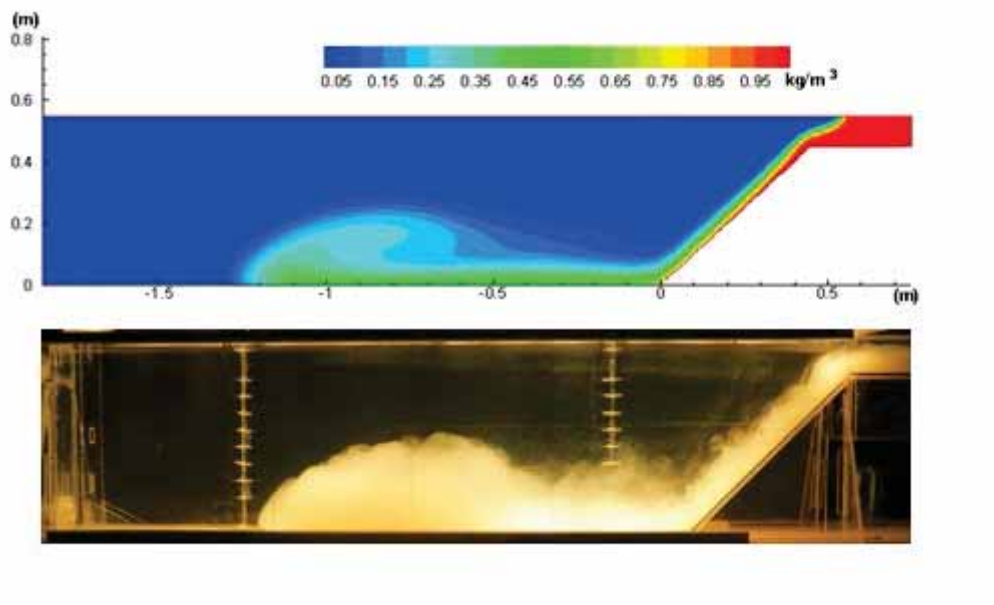

FIGURE 8
Turbidity current shape (No.3Y142)

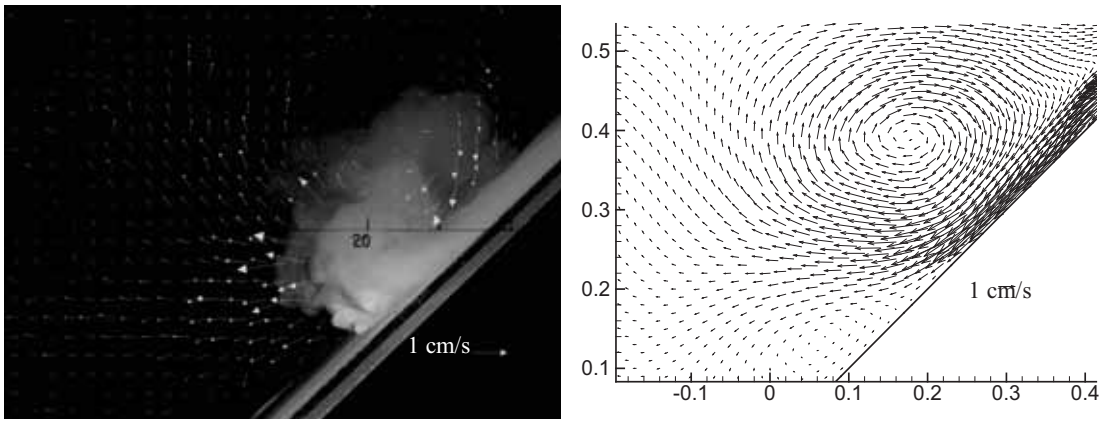

FIGURE 11
Comparison of the PIV measurements and flow field simulations

TABLE 3
Boundary conditions for each case

Case	Q(m^3/h)	*v*(m/s)	*C*(kg/m^3)	T(°C)	*Fr′*
1	0.72	0.01	0.8	21.1	0.41
2	1.44	0.02	0.8	21.1	0.82
3	2.16	0.03	0.8	21.1	1.24

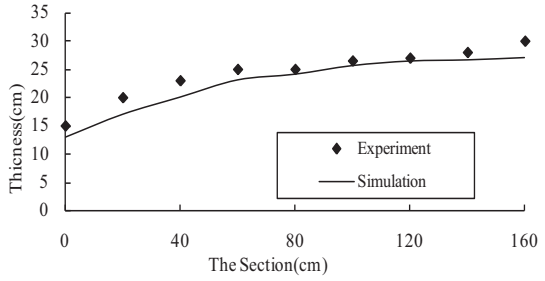

FIGURE 9
The thickness of the turbidity current

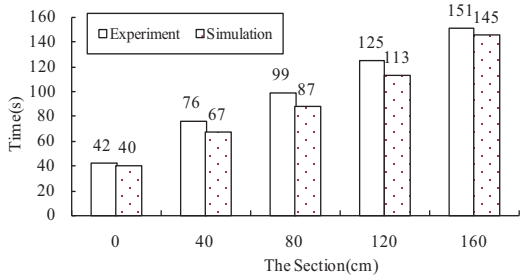

FIGURE 10
The arrival time of the head

Vertical Distribution of Sediment Concentration, Velocity, and Temperature. The vertical distribution of the sediment concentration, velocity, and temperature for five sections of the flume is shown in Figure 14. Figure 14(a) shows the distribution of the sediment concentration. The back of the turbidity current was thicker than the head, and the turbidity current maintained a wedge shape in the flume.

Figure 14(b) shows the distribution structure of the velocity. The velocity of the turbidity current area was larger than the surrounding velocity. Figure 14(c) shows the distribution of the temperature. As the high-temperature water carrying the sediment entered the stratified flume, it replaced the low-temperature water in the middle level, causing the temperature in the middle level to approach that of the top level of the flume. The bottom-level density current exhibited another temperature structure, where the temperatures at the bottom and surface were higher than that in the middle.

The density of the fluid changed due to the temperature and sediment concentration. Accordingly, the density is an important factor for multi-factor coupling analysis. The interflow always moved along a similar density layer. The forms of the turbidity currents in the flume could be estimated by comparing the density of the turbid water inflow to that of the water in the flume.

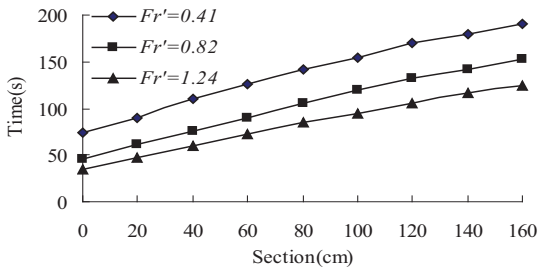

FIGURE 12
Arrival time at each section of the head for each condition

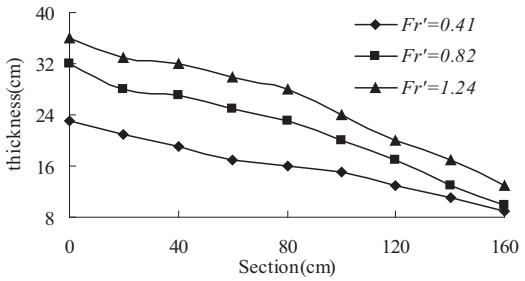

FIGURE 13
Thickness of the turbidity current at each section of the flume for each condition

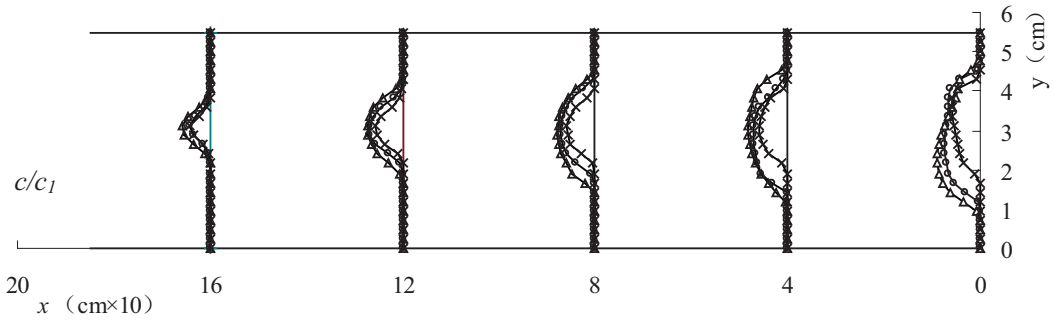

(a) The vertical distribution of the sediment concentration.
(c_1 is the sediment concentration of the inflow)
(×Condition 1; ○Condition 2; △Condition 3)

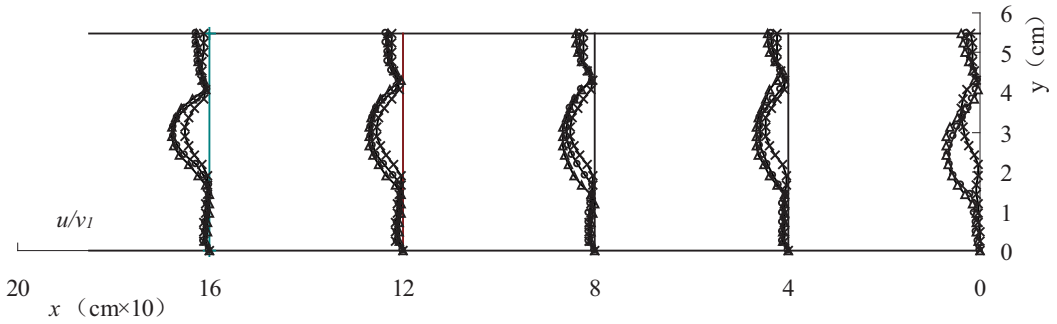

(b) The vertical distribution of the velocity.
(v_1 is the largest velocity of the three conditions, with a value of 0.03 m/s)
(×Condition 1; ○Condition 2; △Condition 3)

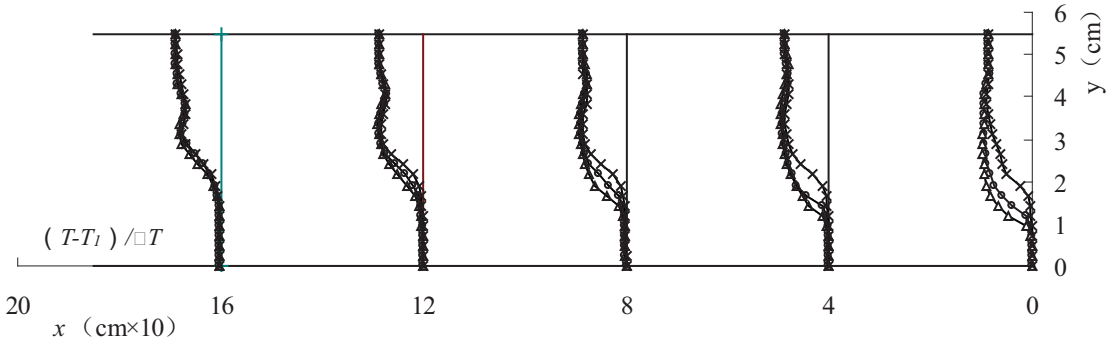

(c) The vertical distribution of the temperature.
(T_1 is the temperature of the inflow and$\triangle T$ is the difference between the highest and lowest temperatures)
(×Condition 1; ○Condition 2; △Condition 3)

FIGURE 14
Vertical distribution of sediment concentration, velocity, and temperature

CONCLUSION

The formation of a turbidity current is beneficial for the regulation of water and sediment in reservoirs. It is necessary to consider the interaction between the temperature stratification and density flow in the analysis of the density flow in low sediment concentration rivers. In this study, laboratory flume tests showed different forms of the turbidity current under the condition of water temperature stratification. Based on the characteristics of the sediment particles, a mathematical model was established to analyze the turbidity current with stratification of the ambient temperature and include the temperature and sediment in the simulation simultaneously. The interaction between the temperature field and sediment content was reflected by the influence of the convection field, which affected the buoyancy term

and turbulent diffusion term in the momentum equation. The simulation results showed that the calculated results were in good agreement with the measured results, which indicated that the correction of the buoyancy term using the sediment content and temperature was correct. The model could be used to analyze and predict the turbidity current under the influence of water temperature stratification. The conclusions of this study were as follows:

(1) The motion of the turbidity current in a stratified water body could be determined by analyzing the density value of the inflow water body (determined by the sediment content and temperature). If the middle layer of the reservoir is formed, it always moved forward in a layer with a similar density.

(2) When a middle or surface turbidity current occurred, the sedimentation of sediment particles was inhibited by the influence of the Bernoulli effect, which caused the muddy water heavy flow effectively to maintain its "wedge" shape in the advancing process.

(3) There was a positive correlation between the forward velocity and the Fr' of the uniform inflow along the thickness of the flow, that is, the larger the Fr' was at the entrance, the greater the forward velocity and the thickness along the flow were.

(4) The high-temperature incoming water carried sediment into the middle or bottom layer of the stratified water body, which destroyed the original stratification structure of the water temperature and rapidly increased the middle or bottom water temperature, accelerating the transition from a stratified to a mixed reservoir.

ACKNOWLEDGEMENTS

This work was supported by Sichuan Agricultural University (grant number: 065H0600, 1921993122, 2021993131).

REFERENCES

[1] Fan, J.H. (2011) Density currents and sedimentation engineering experiments and design. China Water & Power Press, Beijing, China. 14-27.

[2] Huang, S.Y., Mao, G.X. (1997) The reason for Xin'an River reservoir discharged muddy water-continuous. Water Resources Protection. 3, 40-43.

[3] Deng, Y. (2003) Study on the water temperature prediction model for the huge and deep reservoir, Sichuan University, Chengdu.

[4] Imran, J., Parker, G., Katopodes, N. (1998) A numerical model of channel inception on submarine fans. Geophysical Research. 103 (C1), 1219–1238.

[5] Alexander, J., Mulder T. (2002) Experimental quasi-steady density currents. Marine Geology. 186, 195–210.

[6] Chung, S. W., Hipsey, M. R., Imberger, J. (2009) Modelling the propagation of turbid density inflows into a stratified lake. Environment Model. 24(12), 1467–1482.

[7] Gu, R.C., Chung, S.W. (1998) Reservoir flow sensitivity to inflow and ambient parameters. Water Resources Planning and Management. 124(3), 119-127.

[8] Gelda, R.K., Effler, S. W. (2007) Modeling Turbidity in a Water Supply Reservoir: Advancements and Issues. Journal of Environmental Engineering. 133(2), 139-148.

[9] Deng, Y., Li, J., Luo, L., Zhao, W.Q. (2003) Temperature prediction model for reservoirs. Journal of Hydraulic Engineering. 7, 7-11.

[10] Birman, V. K., Meiburg, E., Ungarish, M. (2007) On gravity currents in stratified ambient. Physics of Fluids. 19(8), 086602.

[11] Dai, A. (2013) Experiments on gravity currents propagating on different bottom slopes. Journal of Fluid Mechanics. 731, 117–141.

[12] He, W., Lian, J., Du, H., Ma, C. (2018) Source tracking and temperature prediction of discharged water in a deep reservoir based on a 3-d hydro-thermal-tracer model. Journal of Hydro-environment Research. 20, 9-21.

[13] Niemeyer, R.J., Cheng, Y., Mao, Y., Yearsley, J.R., Nijssen, B. (2018) A thermally-stratified reservoir module for large-scale distributed stream temperature models with application in the Tennessee river basin. Water Resources Research. 54(10), 8103-8119.

[14] Chien, N.,Wan, Z.H. (2003) Mechanics of sediment transport. Science Press, Beijing, China. 45-73.

Received: **19.11.2020**
Accepted: **07.02.2021**

CORRESPONDING AUTHOR

Xi Mao
College of Water Conservancy and Hydropower Engineering,
Sichuan Agricultural University,
Ya'an – China

e-mail: maowhiteknight@163.com

© by PSP Volume 30– No. 05/2021 pages 5119-5130 Fresenius Environmental Bulletin

IN SILICO SCREENING OF SHORT CHAIN FATTY ACIDS FROM ALGAE TARGETING ACE2 RECEPTOR FOR SARS-CoV-2: MOLECULAR DOCKING AND MOLECULAR DYNAMICS SIMULATION

Selin Sayin*

Department of Marine Technologies, Faculty of Marine Sciences and Technology, Iskenderun Technical University, 31200 Iskenderun, Hatay, Turkey

ABSTRACT

Algae contain numerious bioactive compounds. Some of these compounds and their secondary metabolites show antioxidant, antiviral, anti-inflammatory and antifibrotic activities *in vitro* and *in vivo*. It is important for ethnopharmacology that algae can be used for the treatment of diseases. In this study, it was aimed to determine whether the SCFS formed as a result of the degradation of marine algae by microbiota can be effective in preventing the binding of SARS-CoV-2 virus between cellular ACE2 receptor via Spike protein by in silico methods. Molecular docking analyses of thirty-eight Short Chain Fatty Acids (SCFAs) from Algae were applied against ACE2 enzyme to define the mechanism of interaction at the molecular level. Furthermore, molecular dynamics simulation was exerted to probe the stability of angiotensin-converting enzyme 2 (ACE2) with the best selective compound 8. These studies have demonstrated that compound 8 showed selective inhibitory activity for ACE2. Based on this information, it may be possible to treat COVID-19 disease by developing more effective and selective ACE2 inhibitors. Combining the computational results, it is suggested that the reported complex may be a promising structure and maybe deserved more research as an antiviral drug.

KEYWORDS:
ACE2 inhibitors, Algae, molecular dynamics simulation, molecular docking, SCFAs, SARS-CoV-2

INTRODUCTION

The recent outbreak of novel coronavirus disease (COVID-19), occurring from a severe acute respiratory syndrome (SARS) like coronavirus started in Wuhan, China, is spreading rapidly in humans, which is now considered as a global pandemic [1]. Coronaviruses (CoVs) are enveloped viruses containing a single positive-stranded RNA, and causing a wide array of respiratory, gastrointestinal, and neurological diseases in human hosts [2].

The coronavirus surface protein spike (S) mediates entry into target cells by binding to a cellular receptor and subsequently fusing the viral envelope with a host cell membrane [3]. The receptor-binding activity of the S proteins is located within the S1 subunit while the S subunit harbors the functional elements required for membrane fusion [4]. The SARS-CoV S protein (SARS-S) utilizes ACE2 as a receptor for host cell entry [5,6], ACE2, a metallopeptidase, is expressed on major viral target cells, type II pneumocytes and enterocytes [7] and its catalytic domain binds to SARS-S with high affinity [8,9]. Binding of SARS-S to ACE2 triggers subtle conformational rearrangements in SARS-S, which are believed to increase the sensitivity of the S protein to proteolytic digest at the border between the S1 and S2 subunits [8-10].

Previous research efforts to develop antiviral agents against members of Coronaviridae family demonstrated that the ACE2 entry receptor, the RNA-dependent RNA polymerase (RdRp) and the main protease (Mpro) proteins may represent suitable drug targets [11]. Although initially promising, inhibitors targeting ACE2 (hence aiming to block critical coronavirus-host interactions) did not advance clinically due to significant side effects [12]. Likewise, RdRp inhibitors appeared to be not very specific and demonstrated overall lower potency, which also translated into common side effects in patients [13]. Nevertheless, rapid drug repurposing efforts have identified Remdesivir, a RdRp inhibitor, as a promising antiviral drug against COVID-19 [14].

Marine algae have been evaluated as an attractive source of potential drug compounds in several biochemical and pharmacological investigations [15-18]. Algae are a very simple chlorophyll-containing organism composed of one or group of cells together in colonies which are basically not much related to each other making it polyphyletic in nature [19-22]. Natural products from algae have been widely explored, since long time, for human use as food and as medical treatments. Many chemicals and

products from algae have economic importance and are broadly used as it is a good source of fibre, minerals, antioxidants, vitamins, pigments, steroids, lectins, halogenated compounds, polysaccharides, proteins, polyunsaturated fatty acids and other lipids; thus, they are even consumed in many countries [23-26]. Algae are a rich and varied source of pharmacologically active natural products and nutraceuticals. Currently these products are very valuable in the market. Many products are now being commercialized such as carotenoids, phycobilins, fatty acids, polysaccharides, vitamins, and biologically active molecules for use in human and animal health [27-34]. Large ranges of products are being derived from algae which include; antimicrobials, antivirals, therapeutic proteins, drugs, antifungals and many more [35-40].

Volatile Fatty Acids (VFA) is applied to short-chain fatty acids (SCFAs), usually consisted of two to six carbon atoms, such as acetic, butyric, or propionic acid [41]. SCFAs are compounds of algae such as *Acutodesmus obliquus, Auxenochlorella protothecoides*, *Chlamydomonas reinhardtii*, and *Chlorella sorokiniana* which have been evaluated for some medicinal applications [42]. In this article, the binding of thirty-eight SCFAs from algae with ACE2 protein that SARS-CoV-2 using entry receptor in human cells was carried out by computational methods.

MATERIALS AND METHODS

Molecular Docking. Molecular docking studies were carried out with the help of Discovery Studio 2019 (BIOVIA, 2019) sub-protocol, CDOCKER [43] with CHARMm-based grid-enabled docking method that uses soft core potentials and MD-generated random ligand conformations, and poses refinement in the active site using a simulated annealing process. The X-ray crystal structure of angiotensin-converting enzyme 2 (ACE2) (PDB access code: 2AJF) was downloaded from the Protein Database (http://www.pdb.org) [44]. The water and undesired molecules were then removed and hydrogen atoms were added to the target protein, ACE2. The essential oils were extracted from Algae as the ligands (Table S1 in Supplementary File) were drawn and optimized based on DFT / B3LYP / 6-31G * using Gaussian 09 [45]. Finally, the interactions of the relevant molecules with the target were carried out by CDOCKER through molecular docking. As a result of docking calculations, the data were sorted and analyzed according to the calculated docking score, binding energy and root mean square deviation (RMSD) values. In addition to these parameters mentioned above, it should not be overlooked that the types of interaction between the ligand(s) and the target are the most crucial features for determining the best exposure to ACE2 receptor against the treatment of SARS-CoV-2.

Molecular Dynamics Simulation. Molecular Dynamics (MD) simulations were applied for the complex with the best coupling pose to investigate the relative stability of the ligand (compound **8**) within the active region of ACE2 and to sample a series of compliance samples as a function of time. All MD simulations and additional configurations were realized with NAMD program [46]. The MD simulation consisted of a copy of the SARS-COV-2 related protein (ACE2), a copy of the inserted ligand (compound **8**), and 12056 water molecules, 50 $Na^{+,}$ and 32 Cl^{-} ions. In this way, the system was neutralized. The energy minimizations of the complex (1000; 2000 numsteps) were carried out by Steepest Descent and Adopted Basis Newton-Raphson (NR) methods, respectively by using the CHARMM force field [47-48]. Following equilibration for 1000 ps =1 ns in NVT and NPT ensemble were applied for the complex. During the production run, the time steps were set to 2 fs, respectively. When MD simulations were completed, the stability of the generated complexes was analyzed based on analyzing RMSD and root mean square fluctuation (RMSF) values.

RESULTS

Molecular Docking. Molecular docking was applied between thirty-eight SCFAs from algae and ACE2 model structure to investigate docking interactions of the complexes. The docking results were analyzed based on binding energy, CDOCKER scores, and RMSD. They were summarized in Figure 1, It was suggested that compound **8** has the lowest binding energy (-65.460 kcal/mol), CDOCKER energy (-64.385 kcal/mol) and RMSD (0.00791 Å) values in all compounds. Besides, their docked conformations and interactions which are occurred the possible ten conformations of each complex with ACE2 as the target, were analyzed. The best one, compound **8** was chosen and displayed in Figure 2.

The compound **8** was formed eighteen hydrogen bonds including five conventional hydrogen bonds with Thr445, Tyr510, Arg518, and H77 residues and also thirteen carbon-hydrogen bonds with Lys441, Pro346, Glu375, Glu402, His374, Thr371, Glu406 and Asn508 residues in the active site of ACE2. The detailed information about the docked complex was given at Table S2 in supporting information part

TABLE S1
Chemical structures of thirty-eight SCFAs from algae with ACE2

Name	SMILES	Molecular For-	Molecular
1	CSC	C2 H6 S	62.136
2	B.CSC	C2 H9 B S	75.97
3	CC(=O)O	C2 H4 O2	60.054
4	CCCCCCCCCCCCCCCCC	C17 H36	240.475
5	CCCCCCCCCCCCCCCCCCC	C19 H40	268.529
6	CCO	C2 H6 O	46.07
7	C1COCCOCCOCCOCCOCCOCCO1	C14 H28 O7	308.378
8	COC=C.OCCOCCOCCOCCOCCOCCOCCOCCOCCOCCOCCO	C23 H48 O12	516.637
9	C1CCCCC1	C6 H12	84.162
10	CCc1ccccc1	C8 H10	106.168
11	Cc1ccccc1C	C8 H10	106.168
12	Cc1ccc(C)cc1	C8 H10	106.168
13	C[C@H](CC(=C)C)c1ccccc1	C12 H16	160.26
14	CCCCOCCO	C6 H14 O2	118.178
15	CC(=O)C	C3 H6 O	58.081
16	ClCCl	C H2 Cl2	84.933
17	CCCC(C)C	C6 H14	86.178
18	CC(C)C(C)C	C6 H14	86.178
19	CCC(C)CC	C6 H14	86.178
20	CCCCCC	C6 H14	86.178
21	CC1CCCC1	C6 H12	84.162
22	C[C@@H](OC=O)C(C)(C)C	C7 H14 O2	130.189
23	CC(C)CC=O	C5 H10 O	86.135
24	CCCCCC=O	C6 H12 O	100.162
25	CCCCCCCCCCCCCCC	C15 H32	212.421
26	O=C[C@H]1CO1	C3 H4 O2	72.065
27	CCCCCCCCC=O	C9 H18 O	142.243
28	C\C=C\CCCCCCCCCCCCC=O	C16 H30 O	238.416
29	CCCCCCCCCCCCCCCCCOC(=O)OC(=C)C	C20 H38 O3	326.524
30	CCCCCCCCCCCCCCCCCCCCCCCCCCCCCCCCCC	C31 H64	436.853
31	CCCCCCCCCCCCCCCCCCCCCCCCC	C24 H50	338.664
32	CC(=CCCC(=O)C)C	C8 H14 O	126.2
33	CCCCCCCCCC(=O)Oc1ccc(O)c(C)c1	C17 H26 O3	278.395
34	Cc1cccc(OC(=O)CCCCCBr)c1C	C14 H19 Br O2	299.21
35	Cc1ccc2C(=C)CCCC(C)(C)c2c1	C15 H20	200.325
36	CC1(C)C=CC=C2C(C)(C)[C@H]3C[C@@]12C=C3	C15 H20	200.325
37	C[C@@]12CCc3ccccc3C1=CC[C@@H]2O	C14 H16 O	200.282
38	C[C@@H]1C(=C)CC[C@]1(C)c2ccc(C)cc2	C15 H20	200.325

As a result of this process, it is revealed that the interactions, binding affinity, and orientation of the compound **8** are highly important to define and evaluate the interaction mechanism of the ligand-target complex. Furthermore, the stability of compound **8** during the 10000 ps molecular dynamics (MD) simulation was performed to better understand both of the effects of compound **8** upon ACE2 protein.

Molecular Dynamics Simulation. The ACE2-compound **8** complex was subjected for carrying out MD simulation to evaluate the stability of the ACE2's backbone stability and also the stability of compound **8** inside the binding site of ACE2. It was analyzed the time-dependent behavior of MD trajectories for ACE2-compound **8** complex including root

mean square deviation (RMSD) for all backbone atoms and root mean square fluc tuations of the residues (RMSF). The RMSD of the backbone is an indicator to appreciate the stability of the target during the simulation. Figure 3 provides the RMSD for the compound **8**-bound profile. From the data in Figure 3, it is apparent that RMSD for the complex has 600 conformations during 1ns. In the initial stages, while the RMSD values increased, it was fixed and optimized at approximately 100th conformation at the following time intervals which proposed that the compound **8**-ACE2 complex is stable.

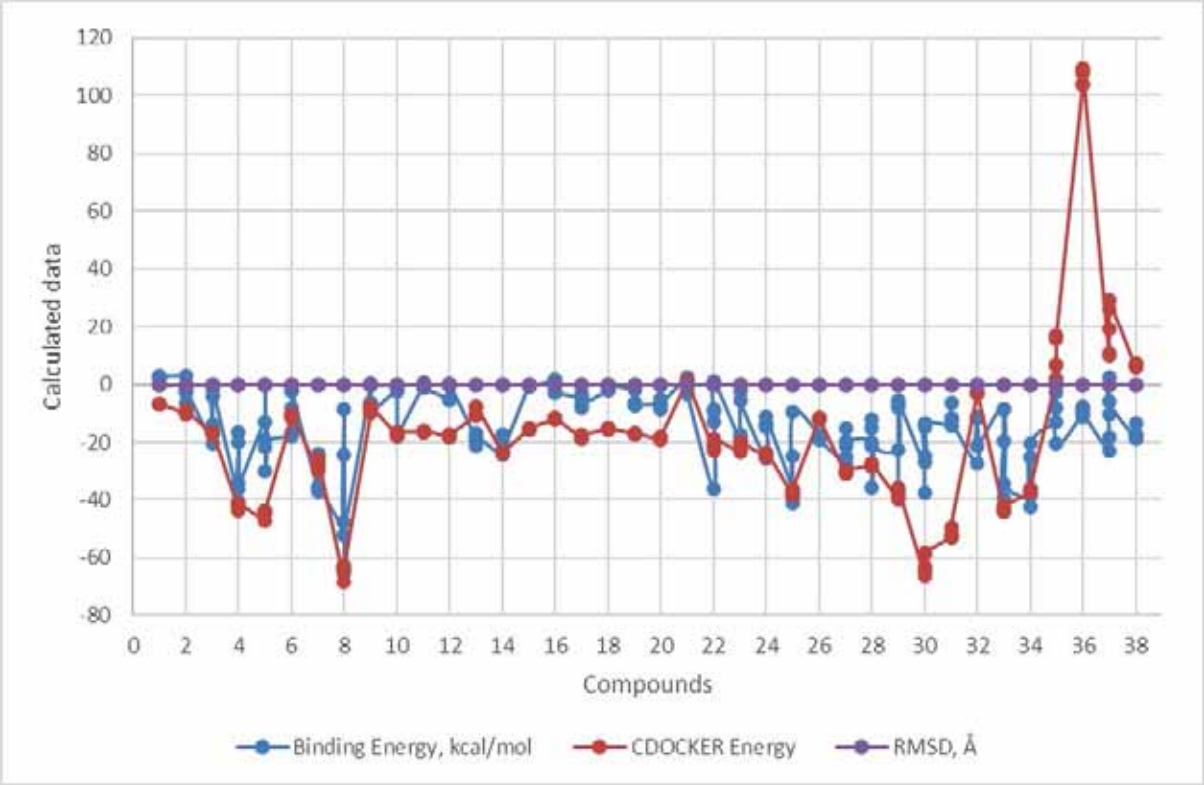

FIGURE 1
The data of calculated binding energy, DOCKER, and RMSD of studied compounds against ACE2.

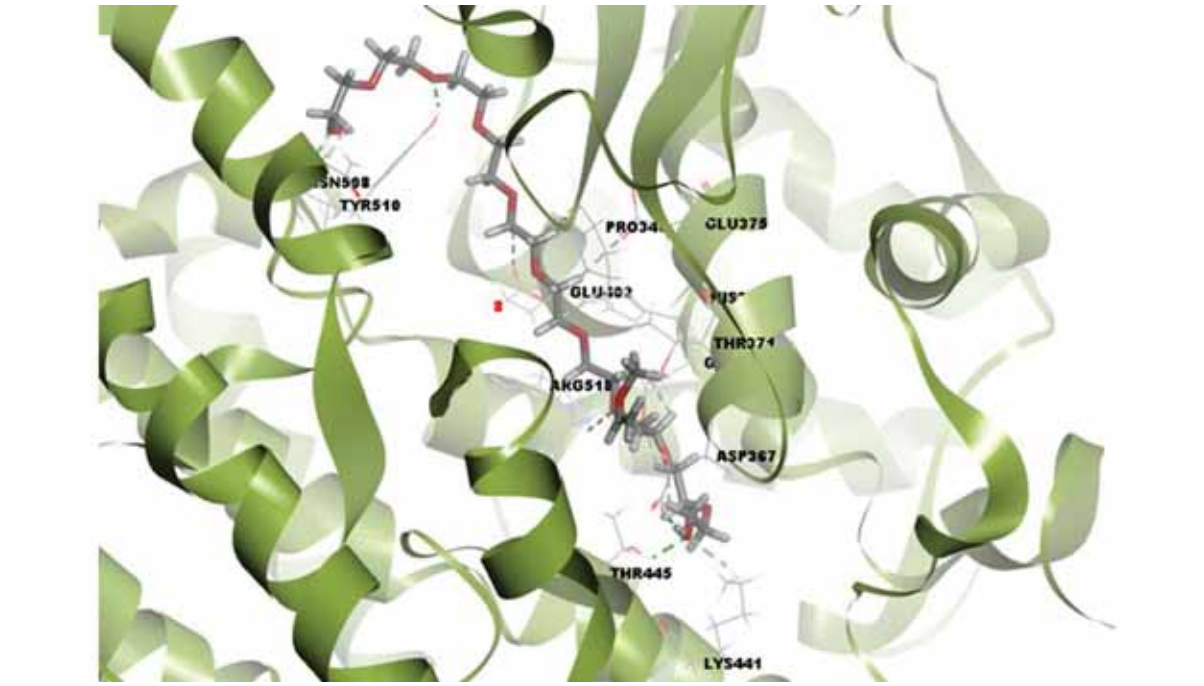

FIGURE 2
Three-dimensional interaction between compound 8 (stick, grey color) and ACE2, shown in the solid ribbon model (green)

TABLE S2
Interactions types and distances of the best compound 8 with ACE2

Interactions	Distance Å	Bonding	Bonding Types	Binding site of Enzyme	Bind-ind site of lig-and
A:THR445:HG1 - 8:O11	2.140	Hydrogen Bond	Conventional Hydrogen Bond	A:THR445:HG1	8:O11
A:TYR510:HN - 8:O10	2.157	Hydrogen Bond	Conventional Hydrogen Bond	A:TYR510:HN	8:O10
A:TYR510:HH - 8:O6	2.334	Hydrogen Bond	Conventional Hydrogen Bond	A:TYR510:HH	8:O6
A:ARG518:HH12 - 8:O5	2.867	Hydrogen Bond	Conventional Hydrogen Bond	A:ARG518:HH12	8:O5
8:H77 - A:ASP367:OD2	2.091	Hydrogen Bond	Conventional Hydrogen Bond	A:ASP367:OD2	8:H77
A:LYS441:HE1 - 8:O11	2.441	Hydrogen Bond	Carbon Hydrogen Bond	A:LYS441:HE1	8:O11
8:H36 - A:PRO346:O	2.424	Hydrogen Bond	Carbon Hydrogen Bond	A:PRO346:O	8:H36
8:H37 - A:PRO346:O	2.673	Hydrogen Bond	Carbon Hydrogen Bond	A:PRO346:O	8:H37
8:H38 - A:GLU375:OE1	2.722	Hydrogen Bond	Carbon Hydrogen Bond	A:GLU375:OE1	8:H38
8:H41 - A:GLU402:OE2	2.665	Hydrogen Bond	Carbon Hydrogen Bond	A:GLU402:OE2	8:H41
8:H42 - A:HIS374:NE2	2.605	Hydrogen Bond	Carbon Hydrogen Bond	A:HIS374:NE2	8:H42
8:H50 - A:THR371:OG1	2.585	Hydrogen Bond	Carbon Hydrogen Bond	A:THR371:OG1	8:H50
8:H51 - A:GLU406:OE2	2.967	Hydrogen Bond	Carbon Hydrogen Bond	A:GLU406:OE2	8:H51
8:H58 - A:GLU406:OE2	2.981	Hydrogen Bond	Carbon Hydrogen Bond	A:GLU406:OE2	8:H58
8:H59 - A:GLU406:OE1	2.910	Hydrogen Bond	Carbon Hydrogen Bond	A:GLU406:OE1	8:H59
8:H62 - A:GLU406:OE1	3.010	Hydrogen Bond	Carbon Hydrogen Bond	A:GLU406:OE1	8:H62
8:H73 - A:ASN508:O	2.702	Hydrogen Bond	Carbon Hydrogen Bond	A:ASN508:O	8:H73

When we consider the interaction in more detail later, in the non-bonding interaction analysis between ACE2 and compound 8, hydrogen bond, hydrophobic interaction, and metal interactions were evaluated by comparing with pre-simulation molecular docking interactions (Figure 4). As a result of comparisons, it reveals that stronger interactions occur by shortening the bonds made by compound **8** with residues Thr371, His 374, Glu402, Glu406, and Tyr510 in the active region of ACE2. The detailed information about the related complex was given at Table S3 in supporting information part.

Another significant parameter of the simulation is root mean square fluctuations of the residues (RMSF) to examine the protein flexibility with compound **8**. The RMSF for ACE2-compound **8** was calculated to define the effect of compound **8** upon the flexibility of ACE2. The compound **8**-ACE2 complex depicted markedly fluctuations Glu87, Gln139, Asn154, Gln325, Phe428, Asn601, and Asp615 residues of ACE2 (Figure 5). These results show that the ACE2- compound **8** complex is stable. Taken together, RMSD and RMSF results suggest that compound **8** has a stable interaction with ACE2.

DISCUSSION

Mammalian gastrointestinal tracts are colonized by a large number of beneficial and pathogenic bacteria. Beneficial gut bacteria such as *Bifidobacterium* spp. and *Lactobacillus* spp. promote human health by providing nutritional metabolites, such as short-chain fatty acids (SCFAs), through fermentation of digestion-resistant carbohydrates in the foods. These carbohydrates, serve as a nutrient source (prebiotics) for probiotic bacteria [49]. The SCFAs are metabolites of the gut microbiota, can

promote health through the regulation of gut hormone release, cholesterol synthesis/metabolism, enhanced satiety as well as exerting anticancer and anti-inflammatory effects [50]. It is estimated that 90% of SCFAs are absorbed from the intestinal lumen by colonocytes or delivered to the liver via the hepatic portal vein while a small portion of them enter systemic circulation with the capacity to influence cells within peripheral tissues [51]. Recent studies have shown that the bioactivities of algal sulfated polysaccharides in the host are related to their metabolites produced by gut microorganisms, which convert carbohydrates into useful metabolites, including SCFAs and that the gut microbiota plays a key role in regulating host metabolism, nutrition, and immunity [52]. The beneficial effects of SCFAs on host health include protection from obesity, chronic respiratory disease or asthma, cancer, and inflammatory bowel disease, modulation of immunity, glucose homeostasis, lipid metabolism, and appetite regulation [53].

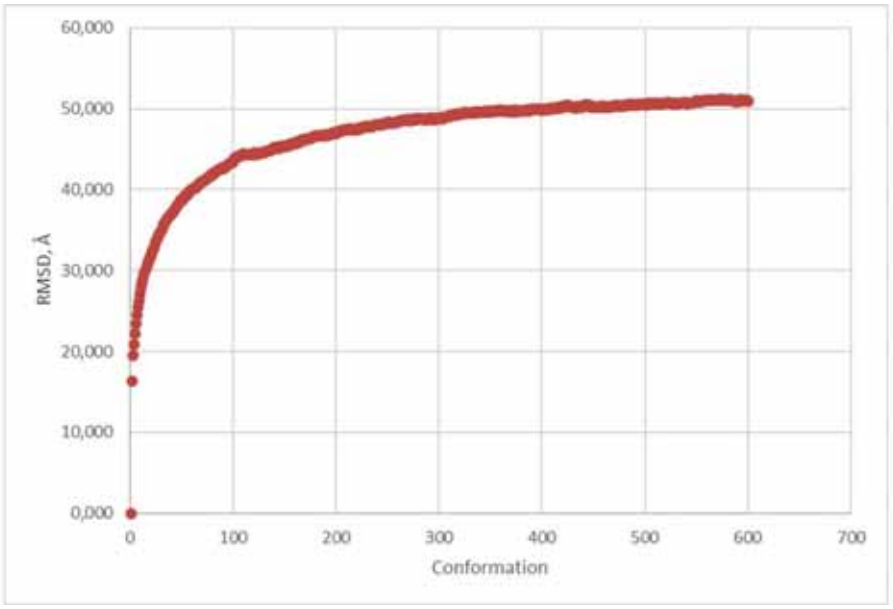

FIGURE 3
RMSD values of ACE2-compound 8 complex during 1ns MD simulation

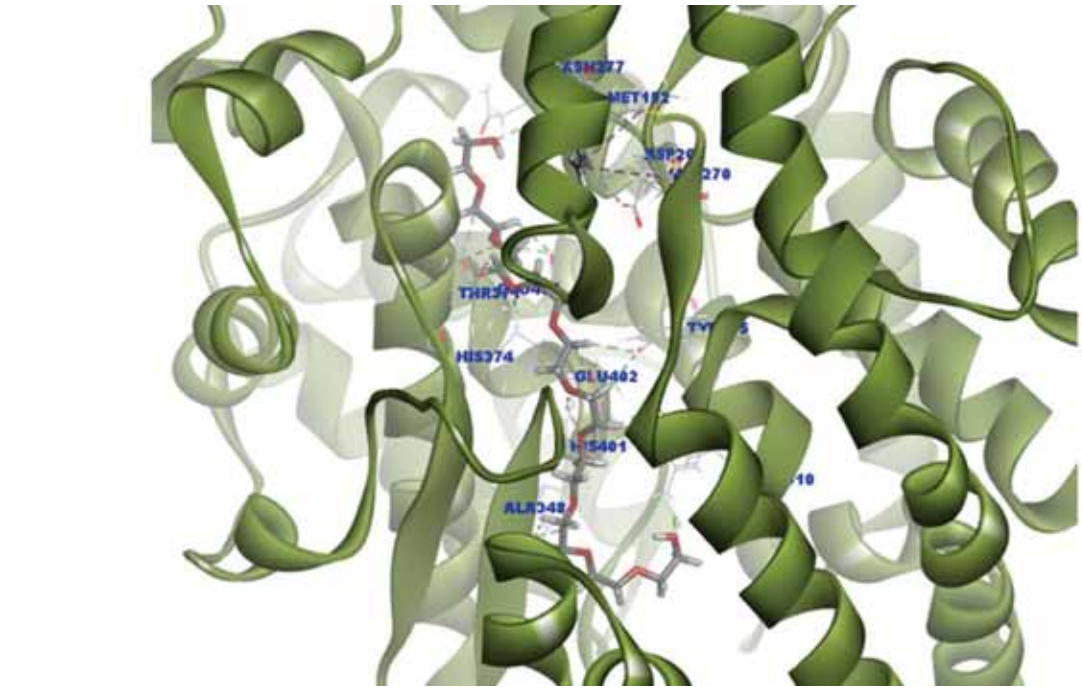

FIGURE 4
Three-dimensional interaction between compound 8 (stick, grey color) and ACE2, shown in the solid ribbon model (green), after the simulation

TABLE S3
Interactions types and distances of the best compound 8 with ACE2, after the simulation. The stable residues of ACE2 and distances with the compound 8 are indicated in red color after MD simulation

Interactions	Distance Å	Bonding	Bonding Types	Binding site of Enzyme	Binding site of ligand
A:ASN277:HD22 - :8:O12	2.860	Hydrogen Bond	Conventional Hydrogen Bond	A:ASN277:HD22	:8:O12
A:HIS374:HD1 - :8:O5	2.082	Hydrogen Bond	Conventional Hydrogen Bond	A:HIS374:HD1	:8:O5
A:ARG514:HH22 - :8:O10	1.700	Hydrogen Bond	Conventional Hydrogen Bond	A:ARG514:HH22	:8:O10
A:GLN442:HA - :8:O11	2.579	Hydrogen Bond	Carbon Hydrogen Bond	A:GLN442:HA	:8:O11
:8:H36 - A:TYR515:OH	2.411	Hydrogen Bond	Carbon Hydrogen Bond	A:TYR515:OH	:8:H36
:8:H41 - A:GLU402:OE2	2.665	Hydrogen Bond	Carbon Hydrogen Bond	A:GLU402:OE2	:8:H41
:8:H41 - A:TYR510:OH	2.280	Hydrogen Bond	Carbon Hydrogen Bond	A:TYR510:OH	:8:H41
:8:H42 - A:GLU402:OE1	2.432	Hydrogen Bond	Carbon Hydrogen Bond	A:GLU402:OE1	:8:H42
:8:H43 - A:TYR515:OH	2.682	Hydrogen Bond	Carbon Hydrogen Bond	A:TYR515:OH	:8:H43
:8:H44 - A:HIS401:O	3.061	Hydrogen Bond	Carbon Hydrogen Bond	A:HIS401:O	:8:H44
:8:H51 - A:THR371:OG1	2.586	Hydrogen Bond	Carbon Hydrogen Bond	A:THR371:OG1	:8:H51
:8:H52 - A:ALA348:O	2.928	Hydrogen Bond	Carbon Hydrogen Bond	A:ALA348:O	:8:H52
:8:H53 - A:ALA348:O	2.635	Hydrogen Bond	Carbon Hydrogen Bond	A:ALA348:O	:8:H53
:8:H55 - A:THR371:OG1	2.585	Hydrogen Bond	Carbon Hydrogen Bond	A:THR371:OG1	:8:H55
:8:H62 - A:GLU406:OE1	2.874	Hydrogen Bond	Carbon Hydrogen Bond	A:GLU406:OE1	:8:H62
:8:H63 - A:GLU406:OE1	2.651	Hydrogen Bond	Carbon Hydrogen Bond	A:GLU406:OE1	:8:H63
:8:H63 - A:GLU406:O	2.468	Hydrogen Bond	Carbon Hydrogen Bond	A:GLU406:O	:8:H63
:8:H67 - A:GLU406:O	2.573	Hydrogen Bond	Carbon Hydrogen Bond	A:GLU406:O	:8:H67
:8:H81 - A:ASP269:OD2	2.788	Hydrogen Bond	Carbon Hydrogen Bond	A:ASP269:OD2	:8:H81
A:ZN803:ZN - :8:O1	2.130	Other	Metal-Acceptor	A:ZN803:ZN	:8:O1
A:ZN803:ZN - :8:O2	2.057	Other	Metal-Acceptor	A:ZN803:ZN	:8:O2
:8:C35 - A:MET152	4.885	Hydrophobic	Alkyl	A:MET152	:8:C35
:8:C35 - A:MET270	5.346	Hydrophobic	Alkyl	A:MET270	:8:C35

SCFAs play important roles as signaling molecules in certain cell signaling pathways in human cells. Therefore, they are also important in disease pathogenesis and treatment. For example, butyrate has antitumorigenic and anti-inflammatory activities through its HDAC inhibitor and HAT activator activities which are important for epigenetic regulation of gene expression in cells. It is showed that SCFAs can regulate cytokine expression in T cells and SCFA-mediated HDAC inhibition in activated T cells results in increased FoxP3 induction through acetylation at FoxP3 locus and generation of regulatory T cells (Tregs). To date, several SCFAs membraneous receptors including free fatty acid receptors type 2 and 3 (FFA2 and FFA3), G protein-coupled receptor 109A (GPR109A) have identified in human. SCFAs and their receptors regulate inflammatory processes through MAPK signaling pathways including ERK, JNK, and p38MAPK and also NF-κB activation pathways. SCFAs increase

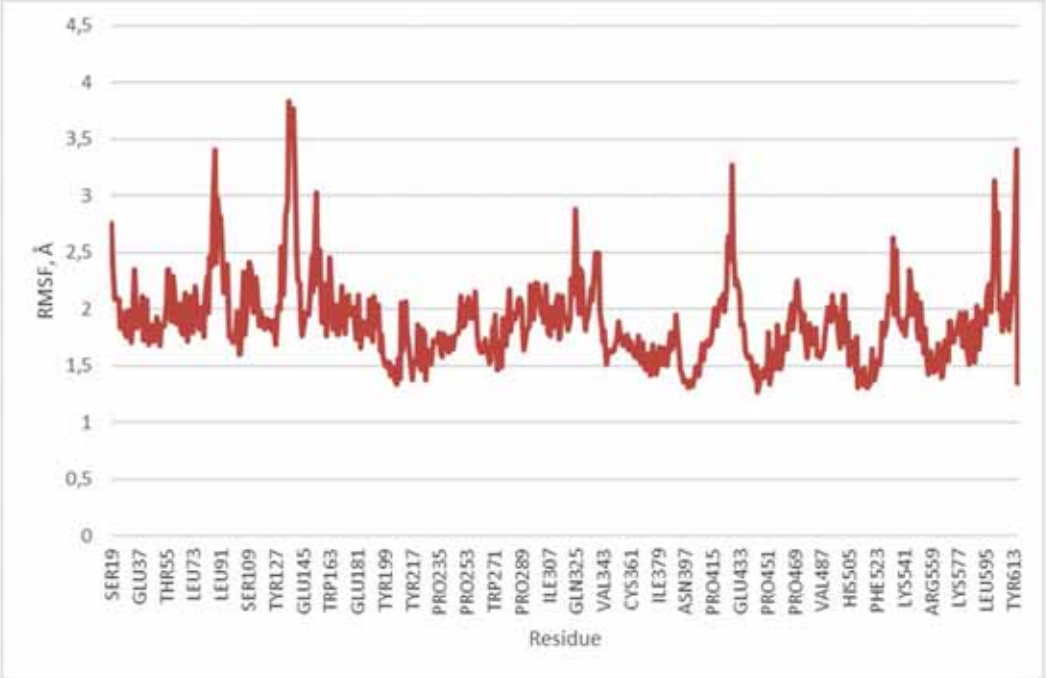

FIGURE 5
RMSF of ACE2 residues backbone with compound 8 during 10 ns MD simulation

Tregs in lung tissue and hematopoiesis of dendritic cells in the bone marrow, and regulate the gut immune system through their receptors [54]. Especially FFA2 receptor is mainly expressed on immune cells, including neutrophils, eosinophils, dendritic cells, and monocytes. Activation of FFA2 receptor results in a down regulated expression of pro-inflammatory cytokines IL-6 and IL-1β through inhibition of NF-κB signaling pathway in immune cells [55]. SCFAs reduce the LPS- and cytokine-stimulated production of pro-inflammatory mediators while increasing the release of the anti-inflammatory cytokines [56]. Also, activation of FFA2 and FFA3 receptors on neutrophils and macrophages by SCFAs reduce IL-8 production in the airways during inflammation [57]. In addition to impacts on pro-inflammatory cytokine expression SCFAs also play important roles in chemotaxis, accelerated pathogen clearance through ROS activation, and epithelial membrane integrity [58]. During influenza infection, SCFAs increase the proliferation of monocyte and dendritic cell progenitors resulting in increased Ly6C− monocytes in the bone marrow and in the lungs. These Ly6C− monocytes can differentiate into alternatively activated macrophages (AAMs) that express lower levels of neutrophil chemoattractant CXCL1. Due to the reduced neutrophil infiltration, influenza-mediated lung immunopathology is found to be decreased [59]. Administration of SCFAs results in recovery from *Kp*-induced lung injury by modulating neutrophils and macrophages activity through binding to their receptor GPR43 in mice [60]. In an animal study, it was shown that; avian influenza induced gut dysbiosis confers susceptibility to respiratory bacterial infection due to reduced production of SCFAs in the gut exogenous and administration of SCFAs and synthetic FFAR2 agonist protects against post-influenza secondary bacterial infection [61]. Oral administration of SCFAs protects against influenza virus infection through leading to the accumulation of AAMs in the lung of influenza-infected mice. These AAMs produce less CXCL1 reducing the neutrophil infiltration into the airway and tissue damage [62]. Influenza virus infections and three major beta coronavirus (CoV) pandemic infections of Middle East Respiratory Syndrome (MERS), Severe Acute Respiratory Syndrome (SARS-CoV-1), and COVID-19; include the dysregulation of acute inflammatory responses involving macrophages, neutrophils, dendritic cells (DCs), toll-like receptors (TLRs), cytokines, chemokines, and CD4+ and CD8+ T-cells, and lung tissue damage and bacterial superinfections [63]. Possible effects of microbiota producing SCFAs in modulating the viral respiratory infections including SARS-CoV-2 through regulating the immune system and endothelial barriers in tissues were discussed recently [64]. Despite the recent findings related to SCFAs and viral lung infections and the effects of SCFAs on systemic immune regulation, there is no report on their possible effects on the COVID-19 pandemic. Therefore, we evaluated that may SCFAs, which could be produced by gut microbiota from indigestible polysaccharides of plants and some algae species, have a protective effect on COVID-19 infection through *in silico* analysis by modeling ACE2 receptor of the SARS-CoV-2 Spike protein.

CONCLUSION

In this study, we analyzed the interaction mechanism of thirty-eight SCFAs from algae against ACE2 at the molecular level with the help of docking and MD simulation. Because, it is quite costly to crystallize the molecular level of all ligands interaction with ACE2 in the experimental study. These studies resulted that compound **8** for ACE2 show good binding affinity in all studied SCFAs. Furthermore, it was observed that the hydrogen bonding interaction between compound **8** and the amino acid **Thr371, His 374, Glu402, Glu406,** and **Tyr510** of ACE2 remained stable during the simulation time (Figure 3).

This study will aid to visualize the molecular mechanism and potential effects of any essential oils from Algae's underlying potential of ACE2 inhibitor to treat the SARS-CoV-2.

Disclosure statement. The corresponding author states that there is no conflict of interest.

Funding. This research did not receive any specific grant from funding agencies in the public, commercial, or not-for-profit sectors.

REFERENCES

[1] Lu, H., Stratton, C.W., and Tang, Y. (2020). Outbreak of pneumonia of unknown etiology in Wuhan, China: The mystery and the miracle. J. Med. Virol. 92, 401-4022.

[2] Zumla, A., Chan, J.F.W., Azhar, E.I., Hui, D.S.C., and Yuen, K-Y. (2016). Coronaviruses-Drug Discovery and Therapeutic Pptions. Nat. Rev. Drug Discov. 15, 327-347.

[3] Gallagher, T.M., and Buchmeier, M.J. (2001). Coronavirus spike proteins in viral entry and pathogenesis. Virology. 279, 371-374.

[4] Hofmann, H., and Pöhlmann, S. (2004). Cellular entry of the SARS coronavirus. Trends Microbiol. 12, 466-472.

[5] Li, W., Moore, M.J., Vasilieva, N., Sui, J., Wong, S.K., Berne, M.A., Somasundaran, M., Sullivan, J.L., Luzuriaga, K., Greenough, T.C., Choe, H., and Farzan, M. (2003). Angiotensin-converting enzyme 2 is a functional receptor for the SARS coronavirus. Nature. 426, 450–454.

[6] Wang, P., Chen, J., Zheng, A., Nie, Y., Shi, X., Wang, W., Wang, G., Luo, M., Liu, H., Tan, L., Song, X., Wang, Z., Yin, X., Qu, X., Wang, X., Qing, T., Ding, M., and Deng, H. (2004). Expression Cloning of Functional Receptor used by SARS Coronavirus. Biochem BiopHYS Res. Commun. 315, 439-44.

[7] Wong, S.K., Li, W., Moore, M.J., Choe, H., and Farzan, M.A. (2003). 193 Amino Acid Fragment of the SARS Coronavirus S Protein Efficiently Binds Angiotensin-converting Enzyme 2. J. Biol. Chem. 27, 3197-201.

[8] Hamming, I., Timens, W., Bulthuis, M., Lely, A., Navis, G., and van Goor, H. (2004). Tissue distribution of ACE2 protein, the functional receptor for SARS coronavirus. A first step in understanding SARS pathogenesis. The J. Pathol. 203, 631–637.

[9] To, K.F., Tong, J.H., Chan, P.K., Au, F.W., Chim, S.S., Chan, K.C., Cheung, J.L., Liu, E.Y., Tse, G.M., Lo, A.W., Lo, Y.M., and Ng, H.K. (2004). Tissue and Cellular Tropism of the Coronavirus Associated with Severe Acute Respiratory Syndrome: Anin-situ Hybridization Study of Fatal Cases. J. Pathol. 202, 157-63.

[10] Li, F., Berardi, M., Li, W., Farzan, M., Dormitzer, P.R., and Harrison, S.C. (2006). Conformational States of the Severe Acute Respiratory Syndrome Coronavirus Spike Protein Ectodomain. J. Virol. 80, 6794-800.

[11] Li, G., and De Clercq, E. (2020). Therapeutic Options for the 2019 Novel Coronavirus (2019-nCoV). Nat. Rev. Drug Discov. 19, 149-50.

[12] Han, D.P., Penn-Nicholson, A., and Cho, M.W. (2006). Identification of critical determinants on ACE2 for SARS-CoV entry and development of a potent entry inhibitor. Virology. 350, 15-25.

[13] Cameron, C.E., and Castro, C. (2001). The mechanism of action of ribavirin: lethal mutagenesis of RNA virus genomes mediated by the viral RNA-dependent RNA polymerase. Curr. Opin. Infect. Dis. 14, 757-64.

[14] Wang, M., Cao, R., Zhang, L., Yang, X., Liu, J., Xu, M., Shi, Z., Hu, Z., Zhong, W., and Xiao, G. (2020). Remdesivir and chloroquine effectively inhibit the recently emerged novel coronavirus (2019-nCoV) in vitro. Cell. Res. 30, 269-71.

[15] Kerr, R.G., and Kerr, S.S. (1999). Marine natural products as therapeutic agents. Exp. Opin. Ther. Patents. 9, 1207-22.

[16] Luescher-Mattli, M. (2003). Algae, a possible source for new drugs in the treatment of HIV and other viral diseases. Curr. Med. Chem. Anti-Infect. Agents. 2, 219-25.

[17] Simmons, T.L., Andrianasolo, E., McPhail, K., Flatt, P., and Gerwick, W.H. (2005). Marine Natural Products as Anticancer Drugs. Mol. Cancer Ther. 4, 333-42.

[18] Lahaye, M., and Robic, A. (2007). Structure and functional properties of ulvan, a polysaccharide from green seaweeds. Biomacromolecules. 8, 1765-74.

[19] Torresa, F.A.E., Passalacquaa, T.G., Velásqueza, A.M.A., de Souzab, R., Colepicolod, P., and Graminhaa, M.A.S. (2014). New drugs with antiprotozoal activity from marine algae: a review. Rev. Bras. Farmacogn. 24, 3.

[20] Kharkwal, H., Joshi, D.D., Bahuguna, P.P., and Kharkwal, A. (2012). Algae as Future Drugs. Asian J. Pharm. Clin. Res. 5, 1-5.
[21] Christaki, E., Bonos, E., Giannenas, I., and Florou-Paneri, P. (2017). Phycobiliproteins: A New Perspective in Natural Pigments Derived from Microalgae. J. Oceanogr. Mar. Res. 4.
[22] Montasser, M.S., Am, Y., Hegazi, M., Dashti, N., El-Sharkawey, A.E., and Beall, G.W. (2016). A Novel Eco-friendly Method of Using Red Algae (Laurencia papillosa) to Synthesize Gold Nanoprisms. J. Nanomed. Nanotechnol. 7.
[23] Mehta, P., Shepard, J., Rouse, K., Sullivan, T., McCarthy, D., Yurko-Mauro, K., Rooney, M., Schallon, D., and Secic, M. (2016). Growth and Tolerability of Healthy Term Infants Fed a New Formula Supplemented with DHA from Schizochytrium sp Microalgae. J. Vasc. Med. Surg. 4.
[24] Kurup, G.M., and Jose, M.G. (2016). In Vitro Antioxidant Properties of Edible Marine Algae Sargassum swartzii, Ulva fasciata and Chaetomorpha antennina of Kerala Coast. J Pharma Reports. 1.
[25] Oramary, S.O.M., Koramarky, D.M.I., Salih, S.A., and Mustafa, A.A. (2016). Feeding Common Carp Fish (Cyprinus carpio) on Natural Foods (Algae, Phytoplankton, Zooplankton and Others) on Tigris River in Mosul Dam / Duhok, Kurdistan Region of Iraq. J. Aquac. Res. Development. 7.
[26] Perez, L. (2014). Biofuels from Microalgae, A Promising Alternative. Pharm. Anal. Chem. 2.
[27] Steudel, B. (2014). Microalgae in Ecology: Ecosystem Functioning Experiments. J. Oceanogr. Mar. Res. 2, 122.
[28] Sanmukh, S.G., Bruno, B., Ramakrishnan, U., Khairnar, K., Sandhya, S., and Paunikar, W.N. (2014). Bioactive Compounds Derived from Microalgae Showing Antimicrobial Activities. J. Aquac. Res. Dev. 5.
[29] Nandi, R., Kakali, M., and Saha, B. (2015). Surfactant Assistant Enhancement of Bioremediation Rate for Hexavalent Chromium by Water Algae. Biochem. Physiol. 4.
[30] El-Sharony, T.F., El-Gioushy, S.F., and Amin, O.A. (2015). Effect of Foliar Application with Algae and Plant Extracts on Growth, Yield and Fruit Quality of Fruitful Mango Trees Cv. Fagri Kalan. J. Horticulture. 2.
[31] Ramirez-Merida, L.G., and Zepka, L.Q. (2015). Microalgae as Nanofactory for Production of Antimicrobial Molecules. J. Nanomed. Nanotechnol. 6.
[32] Abdolsamad, S., Younes, G., and Yaghoobi, M.M. (2015). The effect of Silver nanoparticles [AgNPs] on chlorophyll A and B-carotene content [as two natural antioxidants] in the microalgae Chlorella vulgaris. J. Ecol. Environ. Sci. 3, 41-55.
[33] Stoyneva-Gärtner, M.P., and Uzunov, B.A. (2015). An Ethnobiological Glance on Globalization Impact on the Traditional Use of Algae and Fungi as Food in Bulgaria. J. Nutr. Food Sci. 5, 413.
[34] Suantika, G., Lumbantoruan, G., Muhammad, H., Azizah, F.F.G., and Aditiawati, P. (2015). Performance of Zero Water Discharge (ZWD) System with Nitrifying Bacteria and Microalgae Chaetoceros calcitrans Components in Super Intensive White Shrimp (Litopenaeus vannamei) Culture. J. Aquac. Res. Dev. 6, 1-6.
[35] Tomar, V., and Parab, N. (2012). Raman Spectroscopy of Algae: A Review. J. Nanomed. Nanotech. 3, 131.
[36] Ariyanti, D., Handanyani, N.A., and Hadiyanto, N. (2012). Feasibility of Using Microalgae for Biocement Production through Biocementation. J. Bioprocess. Biotech. 2, 111-115.
[37] Budiyono, and Kusworo, T.D. (2012). Microalgae for Stabilizing Biogas Production from Cassava Starch Wastewater. Internat. J. of Waste Resources. 2, 17-21.
[38] El-Sheekh, M.M., Ghareib, M.M., and Abou-El-Souod, G.W. (2011). Biodegradation of Phenolic and Polycyclic Aromatic Compounds by Some Algae and Cyanobacteria. J. Bioremediat. Biodegradat. 3, 133.
[39] Sulaymon, A.H., Mohammed, A.A., and Al-Musawi, T.J. (2013). Column Biosorption of Lead, Cadmium, Copper, and Arsenic ions onto Algae. J. Bioprocess. Biotech. 3, 128.
[40] Silva, M., Vieira, L.M.M., Almeida, A.P., Silva, A.M.S., Seca, A.M.L., Barreto, M.C., Neto, A.I., Pedro, M., Pinto, E., and Kijjoa, A. (2013). Chemical Study and Biological Activity Evaluation of Two Azorean Macroalgae: Ulva rigida and Gelidium microdon. Oceanogr. 1.
[41] Lee, W.S., Chua, A.S.M., Yeoh, H.K., and Ngoh, G.C. (2010). A review of the production and applications of waste-derived volatile fatty acids. Chem. Eng. J. 235, 83-99.
[42] Lacroux J, Trably E, Bernet N., Steyer JP, and van Lis R. (2020). Mixotrophic growth of microalgae on volatile fatty acids is determined by their undissociated form. Algal. Res. 47, 101870.
[43] Wu, G., Robertson, D.H., Brooks, C.L., and Vieth, M. (2003). Detailed Analysis of Grid-based Molecular Docking: A case Study of CDOCKER- A CHARMm-based MD Docking Algorithm. J. Comput. Chem. 24, 1549-1562.
[44] Fass, D., Bogden, C.E., and Berger, J.M. (1999). Quaternary changes in topoisomerase II may direct orthogonal movement of two DNA strands. Nature Struc. Bio. 6, 322-326.

[45] Frisch, M. J.; Trucks, G. W.; Schlegel, H. B.; Scuseria, G. E.; Robb, M. A.; Cheeseman, J. R.; Scalmani, G.; Barone, V.; Mennucci, B.; Petersson, G. A.; Nakatsuji, H.; Caricato, M.; Li, X.; Hratchian, H. P.; Izmaylov, A. F.; Bloino, J.; Zheng, G.; Sonnenberg, J. L.; Hada, M.; Ehara, M.; Toyota, K.; Fukuda, R.; Hasegawa, J.; Ishida, M.; Nakajima, T.; Honda, Y.; Kitao, O.; Nakai, H.; Vreven, T.; Montgomery, J. A., Jr.; Peralta, J. E.; Ogliaro, F.; Bearpark, M.; Heyd, J. J.; Brothers, E.; Kudin, K. N.; Staroverov, V. N.; Kobayashi, R.; Normand, J.; Raghavachari, K.; Rendell, A.; Burant, J. C.; Iyengar, S. S.; Tomasi, J.; Cossi, M.; Rega, N.; Millam, J. M.; Klene, M.; Knox, J. E.; Cross, J. B.; Bakken, V.; Adamo, C.; Jaramillo, J.; Gomperts, R.; Stratmann, R. E.; Yazyev, O.; Austin, A. J.; Cammi, R.; Pomelli, C.; Ochterski, J. W.; Martin, R. L.; Morokuma, K.; Zakrzewski, V. G.; Voth, G. A.; Salvador, P.; Dannenberg, J. J.; Dapprich, S.; Daniels, A. D.; Farkas, Ö.; Foresman, J. B.; Ortiz, J. V.; Cioslowski, J.; Fox, D. J. (2009) Gaussian, Inc., Wallingford CT.. Gaussian 09, Revision E.01.

[46] Phillips, J.C., Braun, R., Wang, W., Gumbart, J., Tajkhorshid, E., Villa, E., Chipot, C., Skeel, R.D., Kale´, L., and Schulten, K. (2005). Scalable molecular dynamics with NAMD. J. Comput. Chem. 26, 1781-1802.

[47] Brooks, B.R., Bruccoleri, R.E., Olafson, B.D., States, D.J., Swaminathan, S., and Karplus, M. (1983). CHARMM: A program for macromolecular energy, minimization, and dynamics calculations. J. Comput. Chem. 4, 187–217.

[48] Lee, J., Cheng, X., Jo, S., MacKerell, A.D., Klauda, J.B., and Im, W. (2016). CHARMM-GUI Input Generator for NAMD, Gromacs, Amber, Openmm, and CHARMM/OpenMM Simulations using the CHARMM36 Additive Force Field. Biophys. J. 110, 641a.

[49] Liu, J., Kandasamy, S., Zhang, J., Kirby, C.W., Karakach, T., Hafting, J., Critchley, A.T., Evans, F., and Prithiviraj, B. (2015). Prebiotic Effects of Diet Supplemented With the Cultivated Red Seaweed Chondrus Crispus or With Fructo-Oligo-Saccharide on Host Immunity, Colonic Microbiota and Gut Microbial Metabolites. BMC Complement Altern Med. 15, 279.

[50] Strain, C.R., Collins, K.C., Naughton, V., McSorley, E.M., Stanton, C., Smyth, T.J., SoleVila, A., Rea, M.C., Ross, P.R., Cherry, P., and Allsopp, P.J. (2020). Effects of a Polysaccharide-Rich Extract Derived from Irish-sourced Laminaria digitata on the Composition and Metabolic Activity of the Human Gut Microbiota Using an in vitro Colonic Model. Eur. J. Nutr. 59, 309-325.

[51] McLoughlin, R.F., Berthon, B.S., Jensen, M.E., Baines, K.J., and Wood, L.G. (2017). Short-chain Fatty Acids, Prebiotics, Synbiotics, and Systemic Inflammation: A Systematic Review and Meta-Analysis. Am. J. Clin. Nutr. 106, 930-945.

[52] Chen, L., Xu, W., Chen, D., Chen, G., Liu, J., Zeng, X., Shao, R., and Zhu, H. (2018). Digestibility of sulfated polysaccharide from the brown seaweed Ascophyllum nodosum and its effect on the human gut microbiota in vitro. Int. J. Biol. Macromol. 112, 1055-1061.

[53] Charoensiddhi, S., Abraham, R.E., Su, P., and Zhang, W. (2020). Seaweed and seaweed-derived metabolites as prebiotics. Adv. Food Nutr. Res. 91, 97-156.

[54] Koh, A., De Vadder, F., Kovatcheva-Datchary, P., and Bäckhed, F. (2016). From Dietary Fiber to Host Physiology: Short-Chain Fatty Acids as Key Bacterial Metabolites. Cell. 165, 1332-1345.

[55] Li, M., van Esch, B.C.A.M., Wagenaar, G.T.M., Garssen, J., Folkerts, G., and Henricks, P.A.J. (2018). Pro- and anti-inflammatory effects of short chain fatty acids on immune and endothelial cells. Eur. J. Pharmacol. 831, 52-9.

[56] Zeng, H., Umar, S., Rust, B., Lazarova, D., and Bordonaro, M. (2019). Secondary Bile Acids and Short Chain Fatty Acids in the Colon: A Focus on Colonic Microbiome, Cell Proliferation, Inflammation, and Cancer. Int. J. Mol. Sci. 20, 1214.

[57] Halnes, I., Baines, K.J., Berthon, B.S., MacDonald L.K., Gibson, P.G., and Wood, L.G. (2017). Soluble Fibre Meal Challenge Reduces Airway Inflammation and Expression of GPR43 and GPR41 in Asthma. Nutrients. 9, 57.

[58] Tan, J., McKenzie, C., Potamitis, M., Thorburn, A.N., Mackay, C.R., and Macia, L. (2014). The Role of Short-chain Fatty Acids in Health and Disease. Adv. Immunol. 121, 91-119.

[59] Dang, A.T., and Marsland, B.J. (2019). Microbes, metabolites, and the gut-lung axis. Mucosal. Immunol. 12(4), 843-50.

[60] Galvão, I., Tavares, L.P., Corrêa, R.O., Fachi, J.L., Rocha, V.M., Rungue, M., Garcia, C.C., Cassali, G., Ferreira, C.M., Martins, F.S., Oliveira, S.C., Mackay, C.R., Teixeira, M.M., Vinolo, M.A.R., and Vieira, A.T. (2018). The Metabolic Sensor GPR43 Receptor Plays a Role in the Control of Klebsiella pneumoniae Infection in the Lung. Front Immunol. 9, 142.

[61] Sencio, V., Barthelemy, A., Tavares, L.P., Machado, M.G., Soulard, D., Cuinat, C., Queiroz-Junior, C.M., Noordine, M.L., Salomé-Desnoulez, S., Deryuter, L., Foligné, B., Wahl, C., Frisch, B., Vieira, A.T., Paget, C., Milligan, G., Ulven, T., Wolowczuk, I., Faveeuw, C., Le Goffic, R., Thomas, M., Ferreira, S., Teixeira, M.M., and Trottein, F. (2020). Gut Dysbiosis during Influenza Contributes to Pulmonary Pneumococcal Superinfection through Altered Short-Chain Fatty Acid Production. Cell. Rep. 30, 2934-2947.

[62] Trompette, A., Gollwitzer, E.S., Pattaroni, C., LopezMejia, I.C., Riva, E., Pernot, J., Uba,N., Fajas, L., Nicod, L.P., and Marsland, B.J. (2018). Dietary Fiber Confers Protection Against Flu by Shaping Ly6c- Patrolling Monocyte Hematopoiesis and CD8 + T cell Metabolism. Immunity. 48, 992-1005.

[63] Iddir, M., Brito, A., Dingeo, G., Fernandez Del Campo, S.S., Samouda, H., La Frano, M.R., and Bohn, T. (2020). Strengthening the Immune System and Reducing Inflammation and Oxidative Stress through Diet and Nutrition: Considerations during the COVID-19 Crisis. Nutrients. 12, E1562.

[64] Shinde, T., Hansbro, P.M., Sohal, S.S., Dingle, P., Eri, R., and Stanley, R. (2020). Microbiota Modulating Nutritional Approaches to Countering the Effects of Viral Respiratory Infections Including SARS-CoV-2 through Promoting Metabolic and Immune Fitness with Probiotics and Plant Bioactives. Microorganisms. 8, 921.

Received: **29.11.2020**
Accepted: **03.02.2021**

CORRESPONDING AUTHOR

Selin Sayin
Department of Marine Technologies,
Faculty of Marine Sciences and Technology,
Iskenderun Technical University,
31200 Iskenderun Hatay – Turkey

e-mail: selin.sayin@iste.edu.tr

© by PSP Volume 30– No. 05/2021 pages 5131-5139 Fresenius Environmental Bulletin

DETERMINATION OF GENETIC VARIABILITY OF POTATO VIRUS Y IN SAUDI ARABIA

Adel A Rezk[1,5,*], Sherif M El-Ganainy[2,3,5], Khalid A Alhudaib[2,3], Mohamed Z Alyami[2], Muhammad N Sattar[4]

[1]Department of Agricultural Biotechnology, College of Agriculture & Food Sciences. P.O. Box 420, Al-Ahsa 31982, King Faisal University, Saudi Arabia
[2]Department of Arid Land Agriculture, College of Agriculture & Food Sciences, P.O. Box 420, Al-Ahsa 31982, King Faisal University, Saudi Arabia
[3]Plant Pests and Diseases Unit, College of Agriculture & Food Sciences, P.O. Box 420, Al-Ahsa 31982, King Faisal University, Saudi Arabia
[4]Central Laboratories, P.O. Box 400, Al-Ahsa 31982, King Faisal University, Saudi Arabia
[5]Plant Pathology Research Institute, Agricultural Research Center, 12619, Giza, Egypt

ABSTRACT

Among various biotic stresses, potato virus Y (PVY) is one of the most economically important pathogen deteriorating the quality and yield of cultivate potato (*Solanum tubersosum* L.). Precise identification and characterization of PVY in potato tubers is a crucial step for international trade and selection of seed potato for healthy plant material. Nevertheless, PVY genome has high degree of genetic variability and thus detection and classification of isolates is a challenging task. During this study, the genetic variability of PVY was investigated in five different regions of Saudi Arabia. In total, 184 plant leaf samples were collected from Haradh, Qassim, Al-Ahsa, Hail and Wadi Al-Dawasir regions and subjected to PVY specific ELISA assays. The PVY infection rate was ranging from 36.36% in Hail region to 94.47% in the Qassim region, respectively. The strain specific ELISA assay showed that 10.32% of samples were tested positive for PVY^{N} strain while, average rate of PVY infection was 55.98% in all collected samples, respectively. Total RNA was isolated from 25 ELISA positive samples and subjected to RT-PCR using degenerate primers for PVY. The amplicons were sequenced and the partial coat protein (CP) sequence of 23 samples were 99.2-100% identical to the recombinant PVY strains SYRII, SYRIII and 261-4, respectively. While, two isolates showed highest nucleotide (nt) sequence identity at 99.7% to PVY^{N-Wi} recombinant strain. The full-length genome of one isolate was completely sequenced using next generation sequencing, which showed 99.4-99.5% nt sequence identity with PVY^{SYRIII} reported from Syria (AB461454) and Saudi Arabia (KP793715), respectively. The results further support the findings that SYRIII strain has been broadly spreading in the Middle East and thus, potato producers in these regions must be well aware of this spreading epidemic in the potato fields.

KEYWORDS:
Molecular Characterization, Potato virus Y, Recombination, Saudi Arabia, *Solanum tuberosum*, SYRIII

INTRODUCTION

Potato virus Y (PVY, genus *Potyvirus*, family *Potyviridae*) is a major constraint to global production of solanaceous crops [1]. It has a ca. 9.7 kb positive-sense and single stranded RNA (ssRNA) genome flexibly encapsulated in a filamentous protein coat [2]. During infection, the genomic RNA of PVY is translated into a large set of polyprotein, which is then further cleaved into ca. 10 individual proteins through autocatalysis. PVY is a complex of different strains, which have a broad range of host plants encompassing ~495 species of 72 genera in 31 plant families [3]. The differential hypersensitive responses (HR) of PVY isolates against Ny, Nc, Nz and putative N_d hypersensitive genes in potato cultivar or veinal necrotic symptoms in tobacco distinguish them into five biological, non-recombinant strain groups (PVY^{O}, PVY^{C}, PVY^{Z}, PVY^{D}, PVY^{N} and PVY^{E}), respectively [4, 5]. Among them, PVY^{O}, PVY^{C}, PVY^{Z} and PVY^{D} elicit HR in the presence of Ny, Nc, Nz and Nd genes, respectively. Whereas, PVY^{N} (sometimes referred as European N or PVY^{Eu-N}) and PVY^{E} do not elecit any HR in potato (not tested yet with Nd gene) but induce vein necrosis, mosaic and vein clearing symptoms in tobacco, respectively [6, 7]. Recombination is vital between different PVY lineages and approximately 16 PVY recombinants have been identified, mostly originating from non-recombinant PVY^{O} and PVY^{Eu-N} strains [8]. Among them, nine recombinants (PVY^{E}, PVY^{N-Wi}, $PVY^{N:O}$, PVY-NE11, PVY^{NTNa}, PVY^{NTNb} and PVY-SYR-I, -II, and –III) are relatively commonly reported from multiple geographical localities whereas, seven recombinant types (PVY-SCRI-N, PVY-FrN, PVY^{N-Wi}-156var, PVY^{N-Wi}-261-4, PVY-Nicola, PVY-nnp and PVY-T13) are rarely reported

[4]. The completely sequenced genomes of PVY isolates were found non-recombinants (42%) and recombinants (58%) constituting five major phylogroups C, N, O, R1 and R2, respectively [9]. All of the non-recombinants fall within C, N and O phylogroups whereas, recombinants were grouped within R1 and R2 phylogroups, respectively. Moreover, Gibbs et al. [9] also reported two common recombination patterns in the recombinant isolates in R1 and R2 phylogroups. The origin of 5'-terminal region of both phylogroups is commonly shared with PVY^N and PVY^O parents. However, the 3'-terminal region of R1 isolates has been originated from PVY^O wherease, R2 isolates received their 3'-terminal region from PVY^N parents, respectively.

The likely history of PVY origin is in the South America, which is considered as the first potato domestication region [10]. During the current decade, the recombinant strains of PVY have been widely spreading in the potato cultivating areas where these strains cause mild foliage symptoms associated with severely impaired tuber phenotypes in the sensitive potato cultivars [11]. These recombinants produce two major tuber syndromes, potato tuber necrotic ringspot disease (PTNRD) and canoe-shaped cracks [11]. The occurrence of dominant classical and/or recombinant PVY strains differ in different potato producing regions differ in different countries [12, 13]. The stringent quarantine measures undoubtedly assist to control cross-border spreads of specific PVY strains however, the strain-specific resistance of the common potato cultivars may shape the geographical distribution of a particular strain [14].

Potato (*Solanum tuberosum* L.) occupies an imperative rank as food crop after rice and wheat with a global annual production ca. 327 million tons on an area 18.6 million ha [15]. It has been grown in Saudi Arabia to be consumed as fresh as well as processed food. The annual potato cultivation in Saudi Arabia encompasses 18755 ha with 476418 tons annual production (https://www.potatopro.com/saudi-arabia/potato-statistics). Potato has been widely cultivated as primary crop in Riyadh, Eastern province and Tabuk in Saudi Arabia. In Saudi Arabia, potato is cultivated biannually during spring (seed tubers imported from Europe) and fall growing seasons (from local seed tubers), respectively. The aim of the study was to investigate the genetic variability of PVY strains prevailing in the potato cultivation regions in Saudi Arabia.

MATERIALS AND METHODS

Potato leaf samples from 184 samples showing virus-like symptoms leaf yellowing, mosaic and crinkling were collected from five different locations (Harad, Al-Qaseem, Hail, Al-Ahsa and Wadi Al-dawaser) in the Kingdom of Saudi Arabia (Figure 1, Table 1) during the spring and fall, 2019. Each sample was divided into three consecutive portions; long-term storage (at -80°C), ELISA testing (stored at 4°C) and RNA extraction or other downstream applications (stored at -20°C).

DAS-ELISA assay. Initially, all samples were tested for serological reactivity using double-antibody sandwich (DAS) ELISA detection kits antibodies (BIOREBA, Reinach, Switzerland) specific for PVY detection. Subsequently, the ELISA positive samples were further tested for the presence of specific PVY strains using monoclonal antibodies specific for PVY^{NTN} strain. Absorbance values were measured within 30 min at 405 nm using a microplate dual filter read (Awareness Technology, Inc. USA). The samples with DAS-ELISA values at least twice those of the healthy control were considered positive.

RNA Extraction, RT-PCR. Total RNA was extracted from 100 mg of potato leaf samples using RNeasy plant mini kit (QIAGEN, Germany), according to the manufacturer's instructions. One Step RT-PCR was carried out using and "iScript One Step qRT-PCR Kit " (Biomatik, Canada)for the collected potato samples. The RNA extracts were used as templates for RT-PCR amplification reactions on 24 ELISA positive samples using primers CP2 5'-CCAGTCAAACCCGAACAAAGG-3' and CP1 5'-GGCATAGCGTGCTAAACCCA-3' [16] to amplify ~570 bp partial coat protein (CP). RT-PCR mixture prepared for each reaction by combining 12.5 µL of iGreen Mastermix (Biomatik, Candada), 5 µL of total RNA, 10 µM of each sense primer;, 0.5 µL of qRT-PCR Enzyme Mix (50X) and the reaction was completed to 25 µL with Milli Q water. Reverse transcription reaction started with incubation at 42°C for 30 min, followed by denaturation at 95°C for 10 min. PCR amplification was performed by 35 threshold cycles in (ESCO Swift Maxi Thermal Cycler, USA) starting with denaturation at 95°C for 1 minute, primer annealing at 58°C for 1 minute, and extension at 72°C for 1 minute. At the end final extension was performed at 72°C for 7 minutes. Five microliters aliquots of PCR products were analyzed on 1.5% agarose gels in 0.5X TBE buffer and the size of amplified products was determined with 100 bp DNA ladder.

Sequencing and sequence analysis. The amplified products from 25 samples were further purified with Gene JET PCR Purification Kit (ThermoFisher Scientific, USA) and completely sequenced using Sanger sequencing platform at Macrogen (Korea). Two samples (PVYH and PVYW) were further selected for cDNA synthesis using COSMO cDNA synthesis Kit (Willowfort, UK) to carry out whole genome sequencing with Illumina

HiSeq platform X, 150bp PE at Macrogen, Korea. Data output was 5 Gb per sample.

Full genome sequences of PVY isolates representing most prevalent strains were retrieved from NCBI GenBank database for nucleotide (nt) sequence alignment and calculation of pairwise nt identity using species demarcation tool (SDT) [17] (Figure 2). Phylogenetic dendrogram for full-length genome of PVY was constructed using MegaX software with maximum composite likelihood algorithm and the predicted General Time Reversible Model available in MegaX [18].

TABLE 1
Double Antibody Sandwich –Enzyme-linked immunosorbent assay (DAS-ELISA) results using polyclonal antibodies and PVY^N monoclonal antibodies.

Location	Number of samples	Number of infection*	Infection%	PVY^{N**}	PVY^N%
Harad	24	10	41.67	1	10
Al-Qaseem	17	16	94.67	8	50
Al-Ahsa	29	26	86.66	8	30.77
Hail	22	8	36.36	2	25
Wady Al-Dawaser	92	43	46.74	0	0
Total	184	103	55.98	19	10.33

*Polyclonal antibodies (pAbs) (Cat-No: 110577)
** Monoclonal antibodies PVY^N (MAbs) (Cat-No:112777)

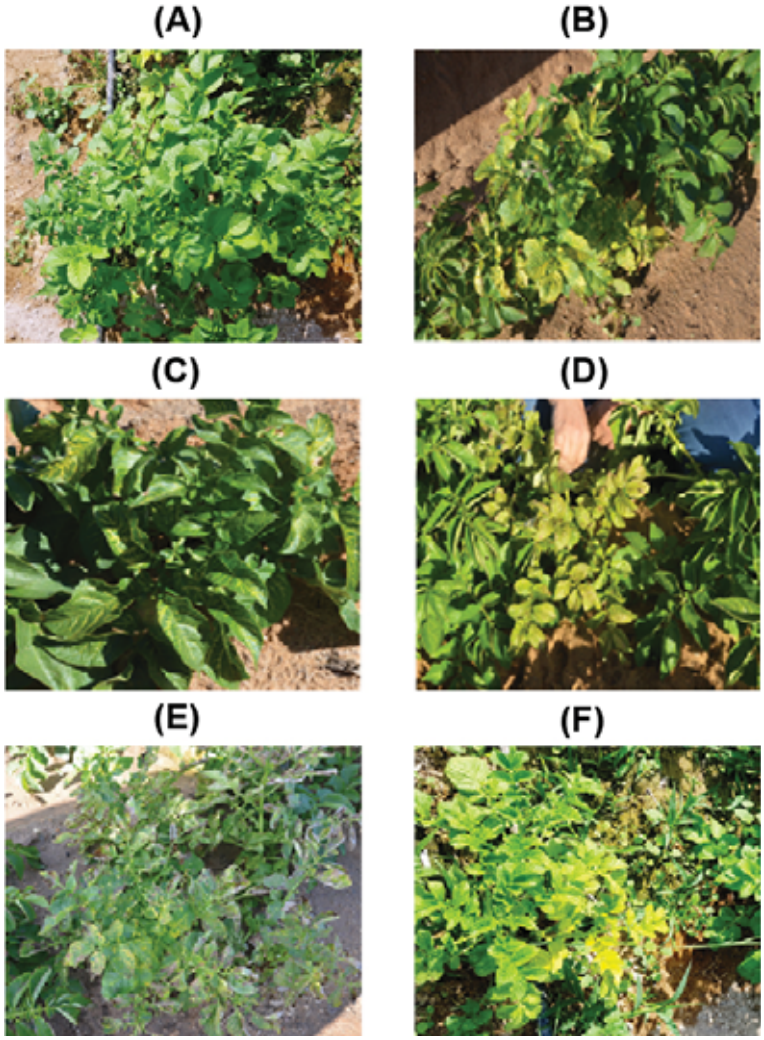

FIGURE 1
Potato plant showing typical symptoms of PVY infection collection from (A) Harad, (B) Al-Qaseem, (C) Al-Ahsa, (D) Hail and (E) Wady Al-dawaser regions of Saudi Arabia, compared to the (F) Healthy plant, respectively.

Recombination analysis. Recombination analysis was carried out with two independent methods genetic algorithm for recombination detection (GARD) and recombination detection program (RDP5), respectively (Figure 3). At least seven different algorithms were employed in RDP4 to endorse any recombination event in the PVY genome. Only those recombination events were contemplated, which were supported with at least four algorithms with minimum acceptable cut-off P-values $1x10^{-5}$.

RESULTS

Serological and RT-PCR assay. In order to identify the occurrence of local virus isolates in the potato crop in Saudi Arabia, potato fields were surveyed in the major potato cultivation regions during spring and fall growing seasons. In total, 184 plant leaf samples were serologically tested and 55.98 % were tested positive through ELISA testing kit (Table 1). Moreover, PVY infection was found in 42, 95, 87, 36 and 46% of leaf samples collected from Harad, Al-Qaseem, Al-Ahsa, Hail and Wady Al-dawasar regions. Of the number of samples tested positive with polyclonal PVY antibodies, 103 leaf samples were further investigated using strain-specific monoclonal antibodies for PVY^N strain. It was found that 10, 50, 31 and 25% of sample from Harad, Al-Qaseem, Al-Ahsa and Hail were tested positive for PVY^N strain (Table 1). However, no sample was tested positive from Wady Al-dawasar with PVY^N monoclonal antibodies. Furthermore, 25 ELISA positive samples were randomly selected for RNA extractions to study the genetic diversity and the presence of any possible PVY recombinant isolates in the local PVY infection.

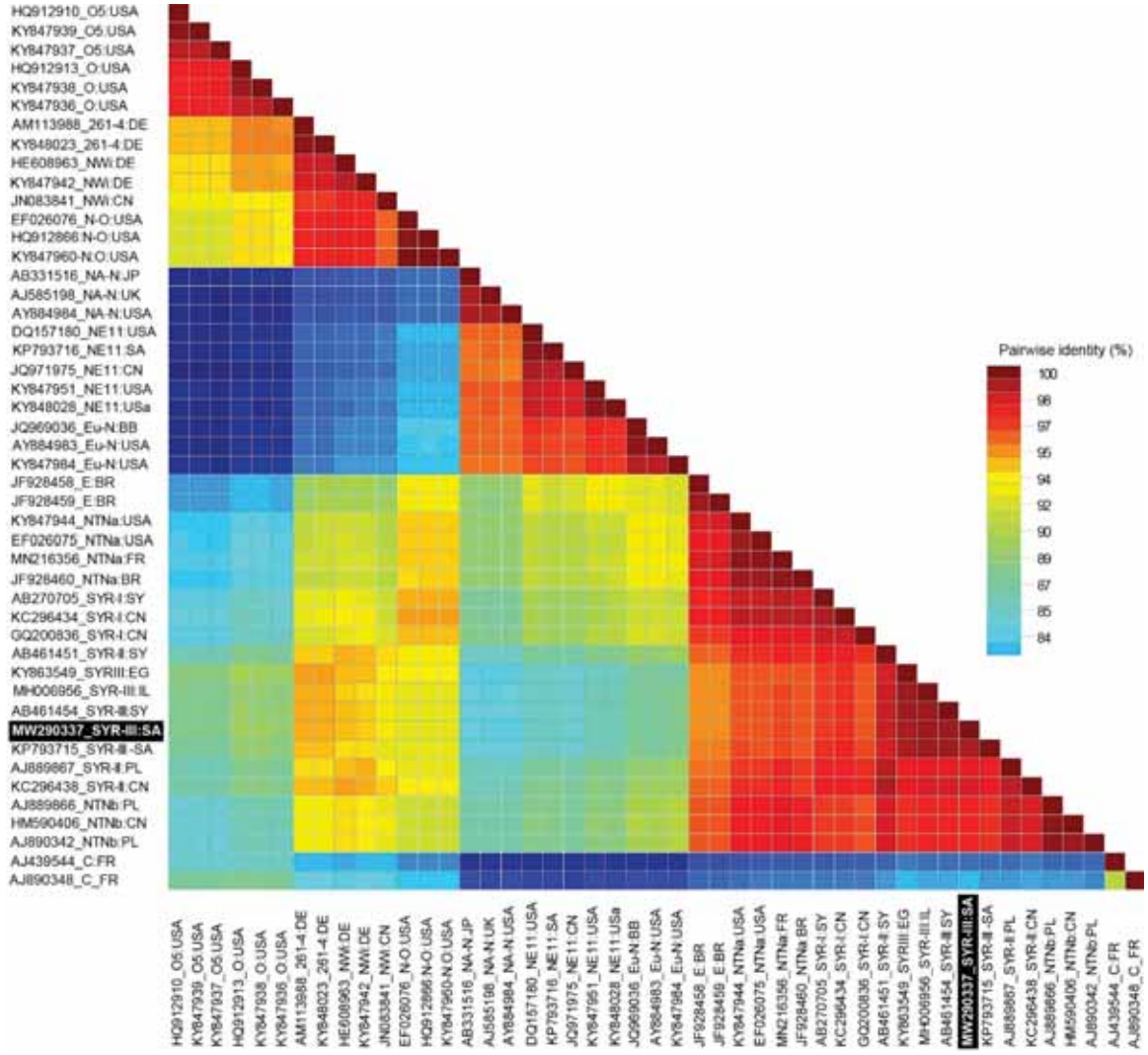

FIGURE 2

Nucleotide sequence comparison of full-length PVY genome to the related PVY strains retrieved from NCBI GenBank database. The PVY isolate identified in this study has been represented with the respective accession number MW290337 and in white text on a black background.

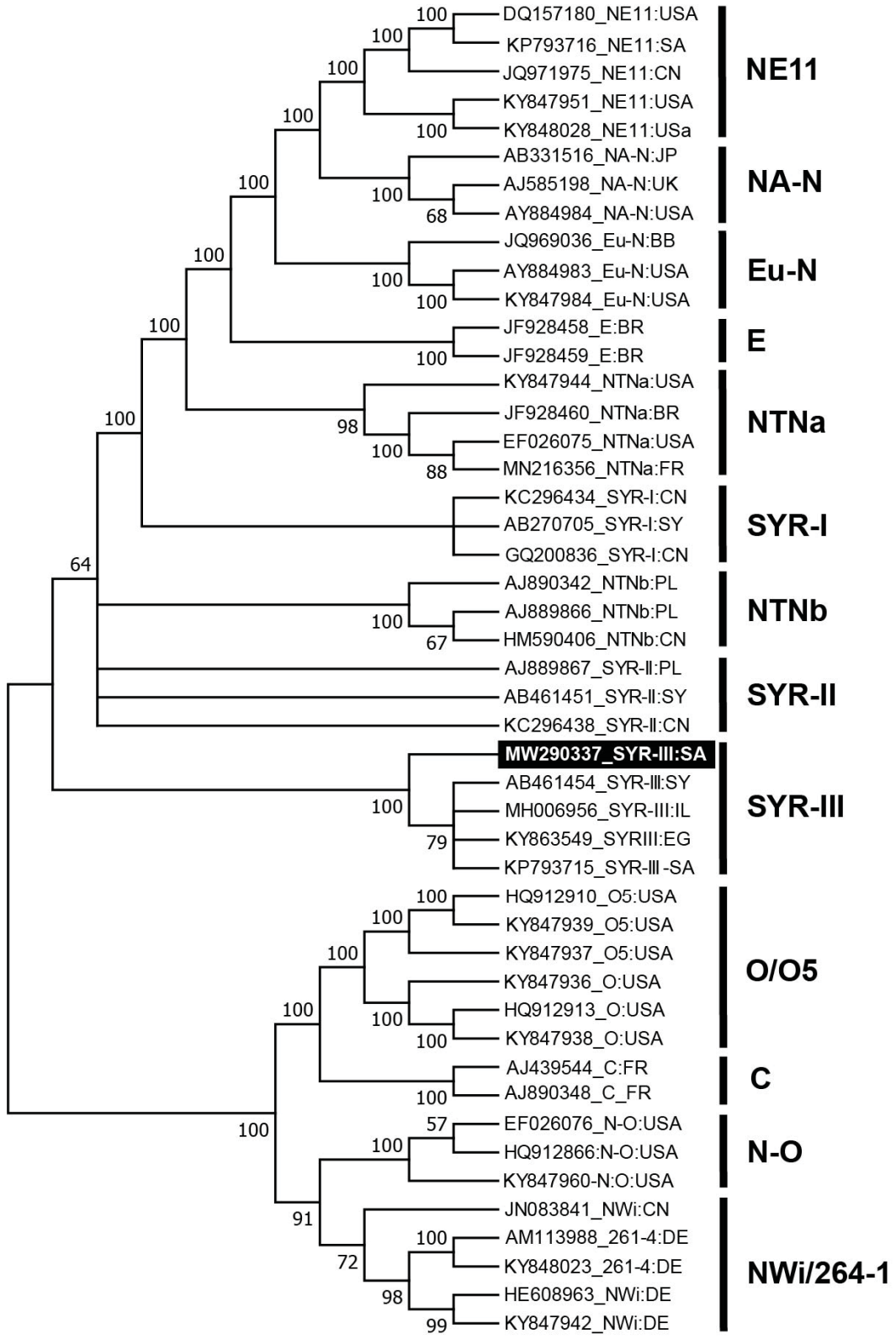

FIGURE 3

Phylogenetic dendrogram based upon full-length genome of PVY to infer evolutionary relationships with other related PVY strains retrieved from NCBI GenBank database.

The isolates shown here are representing the most prevalent PVY strains with their respective accession numbers and country of origin, respectively. The phylogenetic dendrogram was constructed in MegaX software using maximum likelihood algorithm and predicted General Time Reversible Model. The length of each branch is representing the evolutionary relatedness of the isolates whereas, the numbers are representing the % bootstrap values to support each branch. The abbreviations are as: Brazil (BR), China (CN), Egypt (EG), France (FR), Germany (DE), Israel (IL), Japan (JP), Poland (PL), Saudi Arabia (SA), Syria (SY), Unite Kingdom (UK) and United States of America (USA).

TABLE 2
Recombination analysis of PVY full-length genome using RDP5

Recombination event	Recombination breakpoint (nt position)	Major parent	Minor parent	Average P Values using different RDP methods
PVY-H Full-length				
R1	693-2416	O (KY847938)	EuN (AY884983)	RDP 5.967x10^{-129} GENECONV 9.603 x10^{-172} BootScan 3.155 x10^{-125} MaxChi 4.793 x10^{-42} Chimaera 3.399 x10^{-43} SiScan 3.974 x10^{-43} 3Seq 9.762 x10^{-97}
R2	5831-8436	N-Wi (HE608963)	EuN (KY847984)	RDP 1.323 x 10^{-122} GENECONV 6.024 x 10^{-128} BootScan 1.294 x 10^{-109} MaxChi 2.555 x 10^{-45} Chimaera 4.873 x 10^{-48} SiScan 9.009 x 10^{-50} 3Seq 2.526 x 10^{-213}

Strain identification using RT-PCR assays. The cDNA from the selected 25 samples were used as template in RT-PCR reactions using CP specific primers for molecular characterization of the PVY strains. The partial sequencing of CP region showed that the nucleotide (nt) sequence identity of the PVY isolates from 23 samples was 99.2-100% identical to recombinant PVY strains SYRII, SYRIII and a rarely occurring strain 261-4, respectively. While, two isolates showed highest nt sequence identity at 99.7% to PVY^{N-Wi} recombinant strain.

Whole genome sequencing and sequence analysis. Two samples PVYH from Al-Ahsa and PVYW from Wady Al-dawaser region were selected for whole genome sequencing however, at the end the whole genome sequencing of only one sample was completed due to unavoidable experimental errors. The complete genome of PVYH isolate from Al-Ahsa was 9,680 nt and submitted to NCBI GenBank with accession number MW290337. It showed highest nt sequence identity at 99.4-99.5% with PVY^{SYRIII} reported from Syria (AB461454) and Saudi Arabia (KP793715), respectively (Figure 2). The phylogenetic dendrogram grouped the PVY isolate into a well-supported clade (100% bootstrap value) with other SYRIII isolates reported from Egypt, Israel, Saudi Arabia and Syria (Figure 3). The genomic organization of the identified PVY isolate represented typical PVY^{SYRIII} encompassing a complete polyprotein, which was further sub-grouped into nine (09) intact individual proteins (Figure 4).

Recombination analysis. The recombination events were projected through GARD and RDP5, respectively. The GARD analysis detected one recombination event at the nt coordinates 5844–9719 (data not shown). Whereas, the RDP5 detected two recombination events encompassing nt coordinates 693-2416 and 5831-8436, respectively (Figure 4, Table 2). Six algorithms in RDP supported the first recombination event with their respective P-values as RDP 5.967x10^{-129}, GENECONV 9.603 x10^{-172}, BootScan 3.155 x10^{-125}, MaxChi 4.793 x10^{-42}, Chimaera 3.399 x10^{-43}, SiScan 3.974 x10^{-43}, and 3Seq 9.762 x10^{-97}, respectively (Table 2). The respective major and minor parents for the first recombination event were PVY^{O} (KY847938) and PVY^{EuN} (AY884983) (Table 2). Seven algorithms in RDP5 with their respective P-values as RDP 1.323 x 10^{-122}, GENECONV 6.024 x 10^{-128}, BootScan 1.294 x 10^{-109}, MaxChi 2.555 x 10^{-45}, Chimaera 4.873 x 10^{-48}, SiScan 9.009 x 10^{-50}, 3Seq 2.526 x 10^{-213} supported the second recombination event. The major and minor parents were inferred as PVY^{N-Wi} (HE608963) and PVY^{EuN} (KY847984), respectively.

DISCUSSION

Potato production in Saudi Arabia have witnessed a tremendous increase during last couple of decades from ca. 90,000 tons in 1990 [19] to ~476, 418 tons in 2016. In Saudi Arabia, potato has been cultivated during two growing seasons, fall and spring, respectively. The seed tuber for fall growing season crop is mostly locally produced while, for spring crop most of the seed tubers is imported from Europe. The dramatic increase in potato production together with continuous import of potato seed tuber may necessarily increase the virus infection in the local potato crops. Many research studies reported PVY as the main viral infection in potato fields in

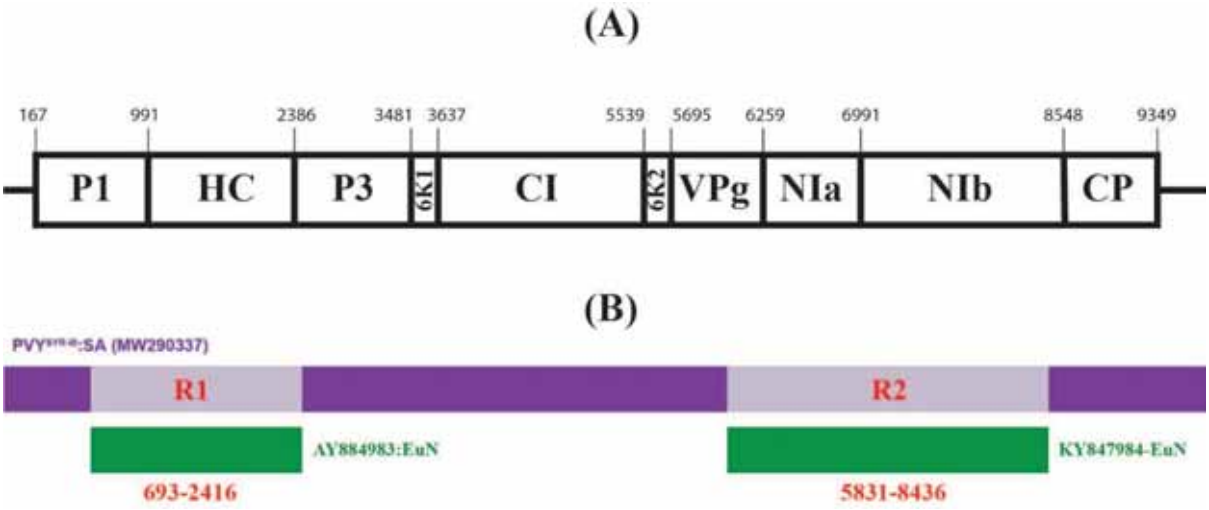

FIGURE 4

Recombination analysis of full-length genome of PVY using recombination detection program (RDP5).
(A) Graphical representation of full-length genome of PVY with typical nine (9) open reading frames (ORF) encoding proteins abbreviated as: 6K1 protein, 6K2 protein, cylindrical inclusion (CI) helicase, coat protein (CP), Helper component protein (HC-Pro), nuclear inclusion protein (NIa), NIb replicase, P3 protein, and virus protein genome-linked (VPg), respectively. (B) Graphical representation of two recombination events in full-length PVY isolate (MW290337) supported by at least four different algorithms in RDP5 with minimum acceptable P-value $1x10^{-5}$. The lilac color rectangles are showing the two recombination events R1 and R2 while two rectangles in green color at the bottom are showing the predicted minor parents for each recombination event, respectively.

Saudi Arabia [19-21] however, the latest strain identification and full-genome characterization of PVY was reported in 2016 [22]. The current study tentatively identified four recombinant PVY strains (SYRII, SYRIII, 264-1 and N-Wi) in the major potato production regions in Saudi Arabia. Besides, the complete genome of PVY^{SYRIII} was determined and completely investigated for its evolutionary background. The recombination analysis GARD and RDP5 conferred the PVY isolate in our current study as a recombinant SRYIII isolate with at least two recombination events. The SYRIII strain is a dominant strain in Egypt, Israel, Jordan, and Syria [13, 23-25]. Furthermore, our results corroborate with Chikh-Ali et al. [22] that this strain has been becoming a dominant strain in the potato cultivating regions in Saudi Arabia. These studies pointed towards an alarming situation for the continuous spread of SYRIII strain in the Middle-Eastern countries. There is no potato trade existed between Syria, Egypt and Israel and thus these countries are not the probable source of SYRIII spread in Saudi Arabia. However, keeping in view the fact that these countries (including Saudi Arabia) import most of the seed tubers from European markets and thus it imply a much wider distribution of SYRIII strain in Saudi Arabia. This hypothesis is further supported by the identification of PVY^{NE-11} strain from Saudi Arabia [22], which is also a recombinant strain originated in United States [26]. It appears that SYRIII strain has been localized in the Middle-East however, broader investigations are highly needed to further explore this hypothesis.

CONCLUSIONS

The data represented in our study further supported the previous findings of Chikh-Ali et al. [22] that SYRIII has been spreading in the Middle East and has broader distribution in almost all potato producing fields. The potato producers in these regions must be well aware of this spreading epidemic in their potato fields. Furthermore, our study implies that potato seed certification must be more vigilant about the potato suppliers from Europe to limit the spread of novel PVY recombinants in Saudi Arabia.

ACKNOWLEDGEMENTS

Authors would like to acknowledge King Faisal University and Deputyship for Research & Innovation, Ministry of Education in Saudi Arabia for funding this research work through the project number IFT20057

REFERENCES

[1] Karasev, A. V. and Gray, S. M. (2013) Continuous and emerging challenges of Potato virus Y in potato. Annu. Rev. Phytopathol. 51, 571-586

[2] Wylie, S. J., Adams, M., Chalam, C., Kreuze, J., López-Moya, J. J., Ohshima, K., Praveen, S., Rabenstein, F., Stenger, D. and Wang, A. (2017) ICTV virus taxonomy profile: Potyviridae. J. Gen. Virol. 98, 352

[3] Gibbs, A. J., Hajizadeh, M., Ohshima, K. and Jones, R. A. (2020) The potyviruses: an evolutionary synthesis is emerging. Viruses. 12, 132
[4] Green, K. J., Brown, C. J., Gray, S. M. and Karasev, A. V. (2017) Phylogenetic study of recombinant strains of Potato virus Y. Virology. 507, 40-52
[5] Fuentes, S., Gibbs, A., Adams, I., Wilson, C. R., Botermans, M., Fox, A., Kreuze, J., Boonham, N., Kehoe, M. and Jones, R. (2020) Potato virus A isolates from three continents: their biological properties, phylogenetics and prehistory. Phytopathology. 111(1), 217-226.
[6] Chikh-Ali, M., Vander Pol, D., Nikolaeva, O. V., Melzer, M. J. and Karasev, A. V. (2016) Biological and molecular characterization of a tomato isolate of potato virus Y (PVY) of the PVYC lineage. Arch. Virol. 161, 3561-3566
[7] Kehoe, M. A. and Jones, R. A. C. (2016) Improving Potato virus Y strain nomenclature: lessons from comparing isolates obtained over a 73-year period. Plant Pathol. 65, 322-333
[8] Green, K. J., Brown, C. J. and Karasev, A. V. (2018) Genetic diversity of potato virus Y (PVY): sequence analyses reveal ten novel PVY recombinant structures. Arch. Virol. 163, 23-32
[9] Gibbs, A. J., Ohshima, K., Yasaka, R., Mohammadi, M., Gibbs, M. J. and Jones, R. A. (2017) The phylogenetics of the global population of potato virus Y and its necrogenic recombinants. Virus Evol. 3 (1), vex002
[10] Fuentes, S., Jones, R. A. C., Matsuoka, H., Ohshima, K., Kreuze, J. and Gibbs, A. J. (2019) Potato virus Y; the Andean connection. Virus Evol. 5 (2), vez037
[11] Benedict, C. A., McMoran, D. W., Inglis, D. A. and Karasev, A. V. (2015) Tuber Symptoms Associated with Recombinant Strains of Potato virus Y in Specialty Potatoes Under Western Washington Growing Conditions. Am. J. Potato Res. 92, 593-602
[12] Green, K., Quintero-Ferrer, A., Chikh-Ali, M., Jones, R. A. C. and Karasev, A. V. (2020) Genetic diversity of nine new non-recombinant potato virus Y isolates from three biological strain groups: historical and geographical insights. Plant Dis.
[13] Elwan, E. A., Abdel Aleem, E. E., Fattouh, F. A., Green, K. J., Tran, L. T. and Karasev, A. V. (2017) Occurrence of diverse recombinant strains of Potato virus Y circulating in potato fields in Egypt. Plant Dis. 101, 1463-1469
[14] MacKenzie, T. D. B., Lavoie, J., Nie, X. Z. and Singh, M. (2018) Differential spread of potato virus Y (PVY) strains O, N:O and NTN in the field: implications for the rise of recombinant PVY strains in New Brunswick, Canada. Am. J. Potato Res. 95, 301-310
[15] Jha, G. (2016) A review on drip irrigation using saline irrigation water in potato (Solanum tuberosum L.). J. Agroecol. Nat. Res. Manag. 3, 43-46
[16] Rigotti, S. and Gugerli, P. (2007) Rapid identification of potato virus Y strains by one-step triplex RT-PCR. J. Virol. Methods. 140, 90-94
[17] Muhire, B. M., Varsani, A. and Martin, D. P. (2014) SDT: A virus classification tool based on pairwise sequence alignment and identity calculation. PloS one. 9 (9), e108277
[18] Kumar, S., Stecher, G., Li, M., Knyaz, C. and Tamura, K. (2018) MEGA X: molecular evolutionary genetics analysis across computing platforms. Mol Biol Evol. 35, 1547-1549
[19] AlShahwan, I. M., Abdalla, O. A. and AlSaleh, M. A. (1997) Viruses in the northern potato-producing regions of Saudi Arabia. Plant Pathol. 46, 91-94
[20] Al-Saikhan, M., Alhudaib, K. and Soliman, A. (2014) Detection of three potato viruses isolated from Saudi Arabia. Int. J. Virol. 10, 224-234
[21] Sabir, J. S. (2012) Identification of six potato virus Y isolates from Saudi Arabia. Afr. J. Biotechnol. 11, 9709-9715
[22] Chikh-Ali, M., Alruwaili, H., Vander Pol, D. and Karasev, A. V. (2016) Molecular characterization of recombinant strains of Potato virus Y from Saudi Arabia. Plant Dis. 100, 292-297
[23] Avrahami-Moyal, L., Tam, Y., Sela, N., Prakash, S., Harel, Y. M., Bornstein, M., Shulchani, R., Dar, Z. and Gaba, V. (2019) Characterization of potato virus Y populations in potato in Israel. Arch Virol. 164, 1691-1695
[24] Anfoka, G., Ahmad, F. H., Altaleb, M., Al Shhab, M., Abubaker, S., Levy, D., Rosner, A. and Czosnek, H. (2014) First report of recombinant Potato virus Y strains infecting potato in Jordan. Plant Dis. 98, 1017-1017
[25] Chikh Ali, M., Maoka, T., Natsuaki, T. and Natsuaki, K. (2010) PVYNTN-NW, a novel recombinant strain of Potato virus Y predominating in potato fields in Syria. Plant Pathol. 59, 31-41
[26] Lorenzen, J., Nolte, P., Martin, D., Pasche, J. S. and Gudmestad, N. C. (2008) NE-11 represents a new strain variant class of Potato virus Y. Arch. Virol. 153, 517-525

Received: **30.11.2020**
Accepted: **19.01.2021**

CORRESPONDING AUTHOR

Adel A Rezk
Department of Agricultural Biotechnology,
King Faisal University,
P.O. Box 420,
Al-Ahsa 31982 – Saudi Arabia

e-mail: arazk@kfu.edu.sa
adelrezk@hotmail.com

© by PSP Volume 30– No. 05/2021 pages 5140-5148 Fresenius Environmental Bulletin

ANALYSIS AND APPLICATION OF EXPONENTIAL STRENGTH CRITERION IN WELLBORE STABILITY INVESTIGATION DURING OIL AND GAS DEVELOPMENT

Zhe Liu[1], Liang Zhu[1,*], Yishan Lou[1], Qing He[2], Chengfu Han[3]

[1]School of Petroleum Engineering, Yangtze University, Wuhan, Hubei, 431000, China
[2]Engineering Technology Research Institute of Sinopec East China Oil and Gas Company, Nanjing, Jiangsu, 210031, China
[3]Changqing drilling company of CNPC Chuanqing Drilling Engineering Co., Ltd, Xi'an, Shaanxi, 710018, China

ABSTRACT

In engineering practice, a linear poroelasticity stress model in combination with a rock strength criterion is commonly used to determine the minimum and pressure required for ensuring wellbore stability. Therefore, a main aspect of wellbore stability analysis is the selection of an appropriate rock strength criterion. The Mohr–Coulomb criterion is the most widely used strength criterion in rock engineering problems. However, the nonlinear strength characteristics of rocks under high in-situ stress can no longer be accurately described and characterized by traditional strength criteria. Bottom-hole rock strength assessment of deep hole is important for optimization of drilling method, drilling parameters and design of bit-tool. In this paper, the distribution characteristics of rock true triaxial strength test data in the main stress space are studied. Then the exponential strength is used to predict the collapse pressure of wellbore based on the linear elastic wellbore stress model. The research results prove that, the present form of Mohr-Coulomb criterion suffers from two major limitations. Firstly, it represents the strength of rock as a linear function of confining pressure. Secondly, the effect of intermediate principal stress is not considered by this criterion. As a result, the collapse pressure predicted by Mohr-Coulomb criterion is conservative. The effect of intermediate principal stress on rock strength is restricted by σ3. Besides, in normal faulting stress regime, horizontal wellbore is most prone to collapse. In reverse faulting regime, the wellbore collapse pressure is smaller when drilling along the direction of horizontal maximum In-situ stress. In strike-slip stress regime, the risk of wellbore instability is highest in vertical wells, while the horizontal borehole is more stable. The quantitative study of drilling fluid density to ensure that the stability of wellbore provides basis and suggestions for well structure, optimization of hole trajectory and reasonable determination of drilling fluid density.

KEYWORDS:
Exponential strength criterion, borehole stability, collapse pressure, true triaxial rock strength, well stress distribution

INTRODUCTION

Wellbore instability is a common problem in the process of oil drilling and has been troubling the oil industry [1]. The wellbore instability accident has caused huge economic losses to oil industry all over the world [2]. With the more precise requirements for the control of critical wellbore pressure, it is more urgent to solve the problem of wellbore instability[3]. Scholars at home and abroad have done a lot of research on wellbore stability in oil and gas exploitation.

The selection of reasonable strength criterion is very important in wellbore stability analysis[4]. The rock strength criterion is the function of stress state and rock strength, which is used to judge whether the rock is destructive or not under certain stress state[5-6]. Due to the lack of accurate interpretation of rock strength characteristics, there are hundreds of strength criteria, because the Mohr-coulomb criterion does not consider the influence of intermediate principal stress to strength, the predicted results of minimum mud pressure for preventing failure of wellbore tend to be safe[7]. The Mohr–Coulomb criterion is the most widely used strength criterion in rock engineering problems. the present form of Mohr- Coulomb criterion suffers from two major limitations. Firstly, it represents the strength of rock as a linear function of confining pressure. Secondly, the effect of intermediate principal stress is not considered all studied the minimum mud pressure for inclined wells with different strength criteria, which proving that Mohr-Coulomb criterion overestimated the collapse pressure of wellbore, while Drucker-Prager criterion overestimated the influence of intermediate principal stress[8]. Islam et al. [9] found that when the In-situ stress difference is small, the collapse pressure predicted by Mohr- Coulomb criterion has little difference from that predicted by Mogi-Coulomb criterion. Compared with the intermediate

principal stress, the in-situ stress and borehole trajectory have a more significant impact on the borehole collapse[10]. However, under the condition of a strong anisotropy in situ stress, the influence of intermediate principal stress on the wellbore collapse pressure cannot be ignored[11-12]. According to Yu et al. [13] et al., the research and design results in many cases depend on the selected strength criteria, it can even be said that the selection of strength criteria is more important than calculation. In addition, under the action of pressure difference, drilling fluid will invade into reservoir fractures, weaken the rock strength, and lead to shear failure of wellbore. Therefore, the failure characteristics of rock should be correctly understood in the analysis of borehole stability [14-16]. The effects of minimum principal stress and intermediate principal stress should be determined theoretically in order to select the appropriate true triaxial strength criterion for rock failure. The nonlinear strength characteristics of rocks under high in-situ stress can no longer be accurately described and characterized by traditional strength criteria. Exponential strength criterion reveals the failure characteristics and triaxial strength characteristics of rocks under high confining pressure, which describes the influence of intermediate principal stress on rock strength [17-19]. According to Exponential strength criterion, the intermediate principal stress improves the strength of rock specimen, but when intermediate principal stress is high enough to cause failure in the σ2-σ3 direction, the strength will decrease with the increasing intermediate principal stress. It is found that the exponential strength criterion completely conforms to the basic characteristics of rock strength on the meridian plane [20-21]. Moreover, it gives much lower misfits than other criteria, which can correctly describe the strength characteristics of soft or hard rocks with different properties, and the physical significance of its parameters is clear [22-23].

The application of exponential strength criterion in shear failure analysis of borehole is still rarely reported. In this paper, the mechanical characteristics of exponential strength criterion in shear stress space and main stress space are studied. Combined with the linear elastic stress model, the wellbore collapse pressure under arbitrary well trajectory is calculated, which compared with the predicted results of Mohr- Coulomb criterion, in order to understand clearly the influence degree of intermediate principal stress and strength criteria in wellbore stability analysis. The borehole collapse pressure under three in-situ stress regimes is also analyzed and discussed. The research results provide more comprehensive guidance for drilling engineering design and wellbore trajectory optimization.

BASIC THEORY AND METHODS

Analytical model of stress distribution around wellbore. The primary In-situ stress is generally expressed by three mutually perpendicular principal stresses σ_H (maximum horizontal stress), σ_h (minimum horizontal stress), σ_v (vertical stress), for convenience, the general coordinate system (x', y', z') can be simply selected to be in the directions of three principal stresses, with x', y', z' respectively in the direction of σ_H, σ_h, σ_v. In inclined wells, when the borehole direction deviates from the main stress direction, i.e. the borehole axis is not parallel to any of the three in-situ stresses, so the coordinate transformation is required. The rectangular coordinate system (x, y, z) and column coordinate system (r, θ, z) of well are established(see Figure 1), the axis Oz corresponds to the borehole axis, Ox and Oy are located in a plane perpendicular to the borehole axis. The stresses $\sigma_{xx}, \sigma_{yy}, \sigma_{zz}, \tau_{yz}, \tau_{yz}, \tau_{xz}$ can be determined from σ_H, σ_h, σ_v by Equation 1 [4, 24-25]:

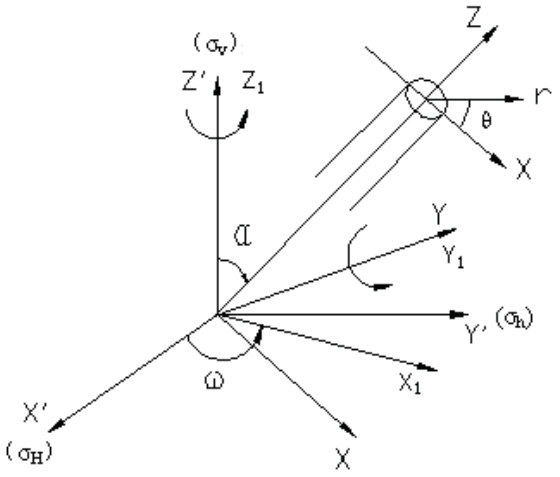

FIGURE 1
Coordination transformation for stress around borehole.

Where σ_H is maximum horizontal stress, MPa; σ_h is minimum horizontal stress, MPa; σ_v is vertical stress, MPa; α and ω represent, respectively, the projected orientation of the wellbore with respect to the x axis and the deviation of the wellbore from vertical, deg (see Figure 1).

The drilling fluid column pressure of wellbore and pore pressure is taken into account, and the stress in the borehole rectangular coordinate system is expressed as the stress in the borehole column coordinate system, and the elastic solution of the stresses at wellbore wall for a deviated well can be obtained by Equation 2 [26-27]:

$$\begin{aligned}
\sigma_{xx} &= \sigma_H \cdot \cos^2\alpha \cdot \cos^2\omega + \sigma_h \cdot \cos^2\alpha \cdot \sin^2\omega + \sigma_v \cdot \sin^2\alpha \\
\sigma_{yy} &= \sigma_H \cdot \sin^2\omega + \sigma_h \cdot \cos^2\omega \\
\sigma_{zz} &= \sigma_H \cdot \sin^2\alpha \cdot \cos^2\omega + \sigma_h \cdot \sin^2\alpha \cdot \sin^2\omega + \sigma_v \cdot \cos^2\alpha \\
\tau_{xy} &= -\sigma_H \cdot \cos\alpha \cdot \cos\omega \cdot \sin\omega + \sigma_h \cdot \cos\alpha \cdot \cos\omega \cdot \sin\omega \\
\tau_{yz} &= -\sigma_H \cdot \sin\alpha \cdot \cos\omega \cdot \sin\omega + \sigma_h \cdot \sin\alpha \cdot \cos\omega \cdot \sin\omega \\
\tau_{xz} &= \sigma_H \cdot \cos\alpha \cdot \sin\alpha \cdot \cos^2\omega + \sigma_h \cdot \cos\alpha \cdot \sin\alpha \cdot \sin^2\omega - \sigma_v \cdot \cos\alpha \cdot \sin\alpha
\end{aligned} \tag{1}$$

$$\begin{cases}
\sigma_r = \dfrac{R^2}{r^2}P_w + \dfrac{\sigma_{xx}+\sigma_{yy}}{2}\left(1-\dfrac{R^2}{r^2}\right) + \dfrac{\sigma_{xx}-\sigma_{yy}}{2}\left(1+\dfrac{3R^4}{r^4}-\dfrac{4R^2}{r^2}\right)cos2\theta + \tau_{xy}\left(1+\dfrac{3R^4}{r^4}-\dfrac{4R^2}{r^2}\right)sin2\theta\text{-}\lambda P_{\mathrm{p}} \\
\sigma_\theta = -\dfrac{R^2}{r^2}P_w + \dfrac{\sigma_{xx}+\sigma_{yy}}{2}\left(1+\dfrac{R^2}{r^2}\right) - \dfrac{\sigma_{xx}-\sigma_{yy}}{2}\left(1+\dfrac{3R^4}{r^4}\right)cos2\theta - \tau_{xy}\left(1+\dfrac{3R^4}{r^4}\right)sin2\theta\text{-}\lambda P_{\mathrm{p}} \\
\sigma_z = -\dfrac{R^2}{r^2}P_w + \sigma_{zz} - \nu\left[2\left(\sigma_{xx}-\sigma_{yy}\right)\dfrac{R^2}{r^2}cos2\theta + 4\tau_{xy}\dfrac{R^2}{r^2}sin2\theta\right]\text{-}\lambda P_{\mathrm{p}} \\
\tau_{r\theta} = \dfrac{\sigma_{yy}-\sigma_{xx}}{2}\left(1-\dfrac{3R^4}{r^4}+\dfrac{2R^2}{r^2}\right)sin2\theta + \tau_{xy}\left(1-\dfrac{3R^4}{r^4}+\dfrac{2R^2}{r^2}\right)cos2\theta \\
\tau_{\theta z} = \tau_{yz}\left(1+\dfrac{R^2}{r^2}\right)cos\theta - \tau_{xz}\left(1+\dfrac{R^2}{r^2}\right)sin\theta \\
\tau_{rz} = \tau_{xz}\left(1-\dfrac{R^2}{r^2}\right)cos\theta + \tau_{yz}\left(1-\dfrac{R^2}{r^2}\right)sin\theta
\end{cases} \tag{2}$$

Where R is the borehole radius, mm; r is the distance from the point around the well to the borehole axis, mm; Pw is the wellbore mud pressure, MPa; λ is Biot's constant, which is commonly used in soil mechanics to consider the effect of pore fluid pressure on the effective stresses acting on rock matrix; θ is the counterclockwise angle from the x axis, °.

Rock strength criteria. (1) Mohr-Coulomb criterion. According to the Mohr Coulomb criterion, shear failure occurs when the shear stress on a plane inside the rock mass exceeds the intermineral cohesion of the rock mass and the friction force on the fracture surface, which is one of the failure criteria commonly used in wellbore stability analysis, namely [22]:

$$\tau_{\max} = c\cos\phi + \sin\phi\sigma_{m,2} \tag{3}$$

$$\tau_{\max} = \frac{1}{2}\left(\sigma_1 - \sigma_3\right), \sigma_{m,2} = \frac{1}{2}\left(\sigma_1 + \sigma_3\right) \tag{4}$$

Where, τ_{max} is the maximum shear stress, MPa; $\sigma_{m,2}$ is the normal stress, MPa; and c and ϕ, respectively, the cohesive and internal friction angle of the rock; σ_1 is the maximum principal stress, MPa, σ_3 is the minimum principal stress, MPa.

(2) Expontial strength criterion. During the true triaxial test, the minimum principal stress and the intermediate principal stress are first applied to the rock specimens, then the maximum principal stress is applied to rock gradually until rock specimens are broken. Therefore, the strength criterion of minimum principal stress and intermediate principal stress can better reflect the failure mechanism of rocks under true triaxial stress tests. Based on the influence characteristics of confining pressure and intermediate principal stress on the strength, You et al. [16] built two exponential formulas to jointly represent true triaxial strength criterion of rocks, and they are defined as:

$$\begin{cases}
\sigma_1 = \sigma_{\mathrm{S}} + H\left(\sigma_2 - \sigma_3, \sigma_3\right) \\
\sigma_{\mathrm{S}} = \sigma_3 + Q_\infty - \left(Q_\infty - Q_0\right)e^{\left[-\frac{(K_0-1)}{Q_\infty - Q_0}\right]} \\
H\left(\sigma_2 - \sigma_3, \sigma_3\right) = Q_{\mathrm{D}}\dfrac{\gamma\left(\sigma_2 - \sigma_3\right)}{\sigma_{\mathrm{S}} - \sigma_3}e^{\left[1-\frac{\gamma(\sigma_2-\sigma_3)}{\sigma_{\mathrm{S}}-\sigma_3}\right]}
\end{cases} \tag{5}$$

Where σ_S is the conventional triaxial strength, which is only related to confining pressure ($\sigma_2 = \sigma_3$), MPa; Q0 is the uniaxial compressive strength, MPa; Q_∞ is limitation of stress deviator or the twice of shear stress limitation. And K0 is the ratio of strength increasing with confining pressure at a confining pressure of 0, QD is the maximum influence value of the intermediate principal stress on the strength, γ is the positional parameter that reaches the maximum strength. You et al. found that γ had no significant effect on the fitting deviation, and it was assumed to be constant 1.7. The criterion is consisting of two parts, three criterion parameters are required to describe the conventional triaxial compression

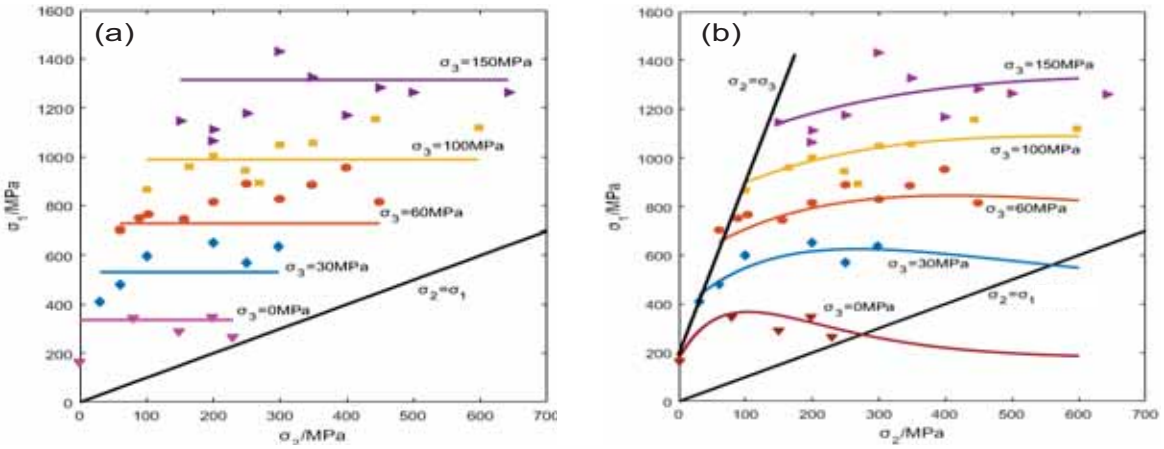

FIGURE 2
Plot of rock failure criteria in principle stress space.
Notes: (a) Mohr-Coulomb criterion, (b) Exponential strength criterion.

strength, which can fit the test results in a larger range and with higher accuracy. There are two parameters to describe the action of the intermediate principal stress, one of which has little influence on the fitting accuracy and can be assumed to be constant 1.7. It is suggested to determine the strength criterion parameters according to the influence coefficients of intermediate principal stress and minimum principal stress on the strength when the stress tends to infinity at $\sigma_2 = \sigma_3$, and the fitting error thus obtained does not increase significantly.

(3) Rock strength criterion analysis. In order to see clearly the distribution characteristics of exponential strength criterion in the main stress (σ_2, σ_1) space and the fitting effect of true triaxial strength data of rocks, this criterion is displayed in (σ_2, σ_1) space, the influence of the second principal stress on rock strength is studied, and the applicability of exponential strength criterion in wellbore stability analysis is analyzed by comparing it with Mohr-Coulomb strength criterion which is often used. As it is difficult to carry out mechanical tests of true triaxial test of rocks, the author used Mohr-Coulomb criterion and exponential strength criterion to fit the KTB amphibolite true triaxial test data in reference [7]. The fitting results of those two criteria mentioned above and true triaxial test data of rock strength in the main stress space are shown in Figure 2(a)~(b).

It can be seen from Figure 2 that Mohr-Coulomb criterion neglects the impact of intermediate principal stress (i.e., σ_2) on rock strength, and compared with the actual triaxial strength test data of rock, the predicted strength of this criterion is relatively weak, which is conservative and always overestimates minimum mud pressure required for wellbore stability. According to the exponential strength criterion, the intermediate principal stress may improve the strength of rock specimen, but its influence will be restricted by σ 3. Also when σ 2 is high enough to cause failure in the σ 2- σ 3 direction, the strength will decrease with the increasing σ 2. The exponential function with three parameters satisfies the basic characteristics of rock strength on the meridian plane [22]. The results show that the proposed exponential true triaxial strength criteria are of good accuracy in predicting rock strength, and can well reflect different types of rock ranged from soft to hard.

In the process of drilling, if the bottom hole column pressure is too high, under the action of pressure difference, the drilling fluid is more likely to invade into the fracture of the surrounding rock, leading to the increase of drilling fluid density, which will aggravate the collapse of the wellbore. In order to accurately predict the minimum drilling fluid density to maintain wellbore stability and achieve the purpose of fine control of bottom-hole drilling fluid column pressure, the exponential strength criterion, which can better describe the true triaxial failure mechanism of rock, should be applied to the wellbore stability analysis, and the accurate prediction for the characteristics of wellbore shear failure can improve the accuracy of the prediction for original in-situ stress[23]. Exponential strength criterion parameters have definite mechanical meaning, which is of great application value in the field of petroleum engineering.

RESULTS

Analytical models for predicting collapse pressure. When the inclination and azimuth are constant, the stress state of the wellbore is only a function of θ. It is not difficult to see that the changing of σθ and σz are the same with the change of θ. Therefore, the maximum and minimum values can be obtained at the same position.

$$d\sigma_\theta / d\theta = 0 \quad (6)$$

By solving the above equation, equ.7 is gotten:

$$\theta_1 = \frac{1}{2}\arctan\left(\frac{2\tau_{xy}}{\sigma_x^o - \sigma_y^o}\right), \quad \theta_1 = \frac{\pi}{2} + \frac{1}{2}\arctan\left(\frac{2\tau_{xy}}{\sigma_x^o - \sigma_y^o}\right) \tag{7}$$

The circumferential stress of the wellbore wall reaches its maximum or minimum value at θ_1 or θ_2. After determining the extreme stress point of the shaft wall, combining the extreme stress value with the corresponding strength criterion, the stability of the shaft wall can be judged. Since the failure criteria adopted in the wellbore stability analysis are mostly expressed in terms of principal stress, Therefore, it is necessary to convert the stress around the well into the expression of the main stress. Combined with the effective stress theory, the main stress at the shaft wall can be expressed as follows:

$$\begin{cases} \sigma_i = \sigma_r \\ \sigma_j = \dfrac{\sigma_\theta + \sigma_z}{2} + \dfrac{\sqrt{(\sigma_\theta - \sigma_z)^2 + 4\tau_{\theta z}}}{2} \\ \sigma_k = \dfrac{\sigma_\theta + \sigma_z}{2} - \dfrac{\sqrt{(\sigma_\theta - \sigma_z)^2 + 4\tau_{\theta z}}}{2} \end{cases} \tag{8}$$

According to Chen et al., wellbore instability can be divided into four modes. When the pressure of the liquid column at the bottom of the well is the minimum principal stress, the wall may be destroyed by wide breakout. As a result, σ_i is the minimum principal stress at wellbore wall, the maximum principal stress and intermediate principal stress can be obtained by comparing the value of σ_j and σ_k. The three main stresses at wellbore wall were substituted into Mohr-Coulomb and exponential strength criterion respectively, and the calculation formula of collapse pressure to maintain the stability of wellbore was obtained as shown in equations (9)~(10) [11, 25]:

$$F_{\mathrm{MC}}(P_{\mathrm{w}}) = c\cos\phi + \sin\phi\sigma_{m,2} - \tau_{\max} \tag{9}$$

$$F_{\mathrm{ESC}}(P_{\mathrm{W}}) = \sigma_1 - \sigma_{\mathrm{S}} - H(\sigma_2 - \sigma_3, \sigma_3) \tag{10}$$

For inclined or horizontal wells, it is difficult to obtain the solution formula of the wellbore collapse pressure directly. When the equation F≤0, the wellbore will collapse. Based on this condition, the author calculated the pressure of minimum mud pressure required for wellbore stability under different inclination and azimuth by numerical method.

Collapse pressure prediction model analysis.

(1) Results comparison. Reservoir parameters in this area are as follows: formation depth H=2050m, vertical stress σ_v=51.57MPa, maximum horizontal stress σ_H =42.8MPa, minimum horizontal stress σ_h=36.2MPa, pore pressure Pp=15.57MPa, the effective stress coefficient of λ =0.75 and Poisson's ratio v=0.33.

Figure 3(a) shows the change cloud diagram of the wellbore collapse pressure calculated by MOHR-COULOMB criterion under any wellbore trajectory, Figure 3(b) shows the change cloud diagram of the wellbore collapse pressure calculated by Exponential strength criterion under any wellbore trajectory. The horizontal axis is borehole azimuth, and the vertical axis is borehole inclination. The color ranges from dark blue to deep red, indicating the collapse pressure from low to high. It can be clearly seen from the figure that the wellbore collapse pressure is distributed in different wellbore trajectory. The wellbore collapse pressure obtained by using Mohr-Coulomb criterion is relatively large, with a variation range of 110MPa~138MPa. When the borehole drilling direction is within the range of inclination Angle of 35°~45° and azimuth Angle of 80°~90°, the borehole instability accident is the least likely to occur. When the borehole drilling direction is in the range of inclination angle 78°~90° and azimuth angle 0°~28°, the pressure of borehole collapse is relatively high and collapse is easy to occur. The predicted results of Exponential strength criterion vary from 90MPa to 121MPa. When the borehole drilling direction is within the range of inclination angle of 40° to 45° and azimuth Angle of 85° to 90°, the value of wellbore collapse pressure is small, which is the best drilling trajectory. When the inclination angle of the well is 78°~90° and the azimuth angle is 0°~28°, the shear failure accident of the wellbore wall is easy to occur.

Those two criteria have little difference in the prediction results of high-occurrence drilling trajectory of collapse accident, but the prediction results of optimal wellbore trajectory are obviously different. The safety range of well trajectory predicted by Mohr- Coulomb criterion is larger than that predicted by exponential strength criterion. The influence of intermediate principal stress on wellbore instability is considered in the wellbore stability predicting by exponential strength criterion, which the description of true triaxial failure mechanism of rock is more reasonable. It is suggested that exponential strength criterion is preferred in the wellbore shear instability analysis.

(2) Influence of original in situ stress regimes. In-situ stress plays an important role in wellbore stability analysis. The in-situ stress regimes [25] are normal faulting (NF) stress regime, reverse faulting (RF) stress regime and strike slip (SS) stress regime. When σ1 is vertical, normal fault occurs, when σ3 is

vertical, reverse fault occurs, and σ2 is vertical strike slip fault occurs, which is illustrated in Figure 4(a) - (c).

In order to analyze and compare the general law of wellbore stability in the above three in-situ stress fields, simulations of minimum mud pressure required for wellbore stability are conducted for a formation at a depth of 2050m with rock maximum principal stress σ1=51.57MPa, intermediate principal stress σ2=42.8MPa, minimum principal stress σ3=36.2MPa, the formation pore pressure is assumed to be 15.57MPa, Poisson's ratio of 0.33, and Biot's constant is assumed to be 0.75 which is a typical value. Based on the above data, the exponential strength criterion was used to study the variation of wellbore collapse pressure in different in-situ stress regimes. The calculation results of different borehole inclination angles (α) and borehole azimuth angles (ω) are shown in Figures 5 - 7.

In normal fault stress regime (Figure 5), the collapse pressures of horizontal wells with different azimuth angles remain at a high level, which indicate that the borehole of horizontal wells is most vulnerable to collapse under NF stress regime. When the borehole azimuth is relatively small, the wellbore collapse pressure increases with the increase of borehole inclination angle. When the borehole was drilled in the direction of minimum horizontal stress (ω=90°), the wellbore collapse pressure showed a trend of decreasing firstly and then increasing with the increase of well inclination angle. However, in this particular example, deviated boreholes with an inclination of 45° and azimuth of 90° required the lowest collapse pressure. This means that wellbore wall collapse problem can be minimized if the well would be deviated 45° from the vertical and parallel to the direction of the minimum in situ stress (i.e., ω=90°).

In reverse fault stress regime, (Figure 6), When the azimuth angle is high, the wellbore collapse pressure is also high, and the change of well inclination angle has no significant effect on the collapse pressure. Compared with other borehole azimuth, if the well would be parallel to the direction of the minimum in situ stress, the wellbore collapse is lower, which decreases firstly and then increases with the increase of borehole inclination angle [28]. The optimum well path associated with the minimum mud pressure required for wellbore stability is for deviated borehole (α=45°) drilled parallel to the maximum in situ stress (i.e., ω=0°).

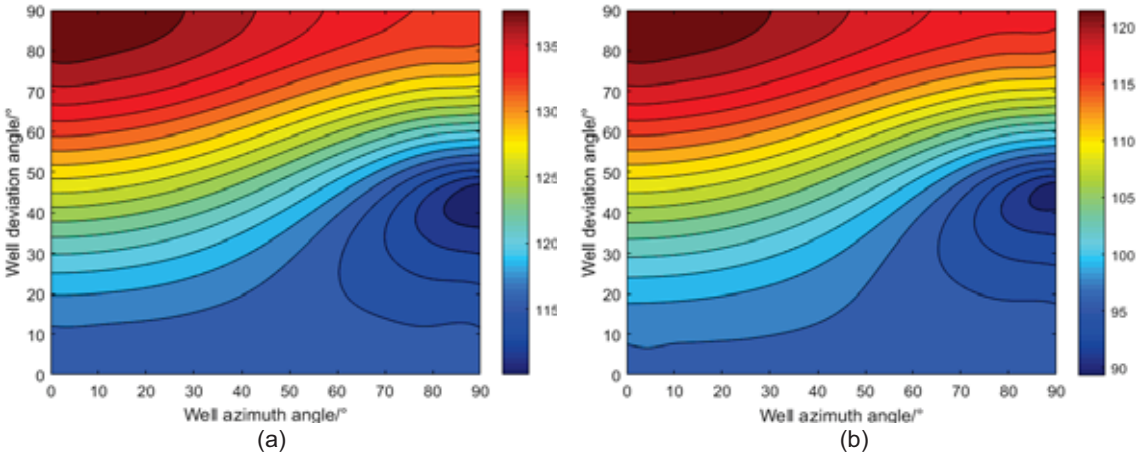

FIGURE 3

Prediction of collapse pressure with full scale well trajectory under three strength criteria.

Notes: (a) Mohr-Coulomb criterion, (b) Exponential strength criterion.

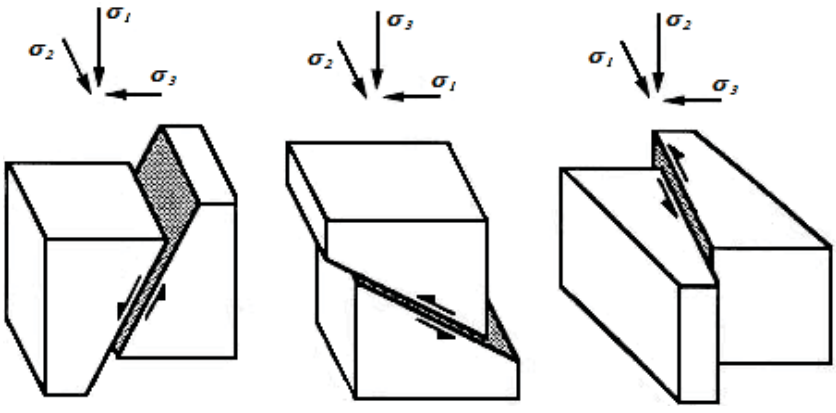

FIGURE 4

In situ stress regimes: (a) Normal fault, (b) reverse fault, (c) strike-slip.

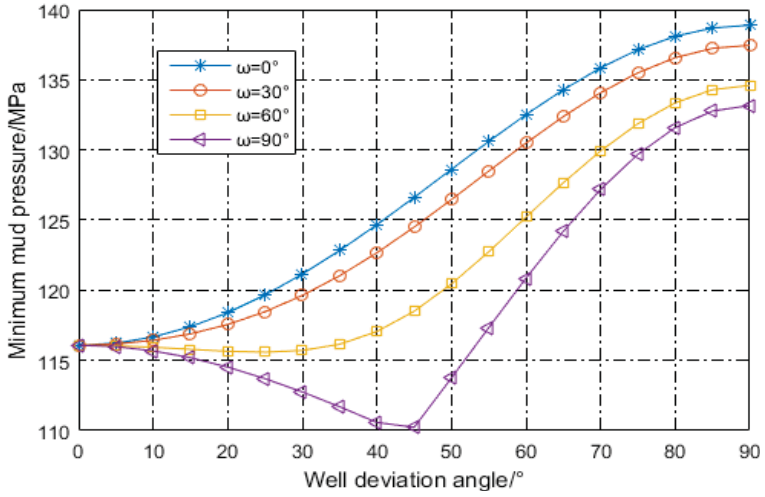

FIGURE 5
Borehole collapse pressure as a function of trajectory in NF stress regime.

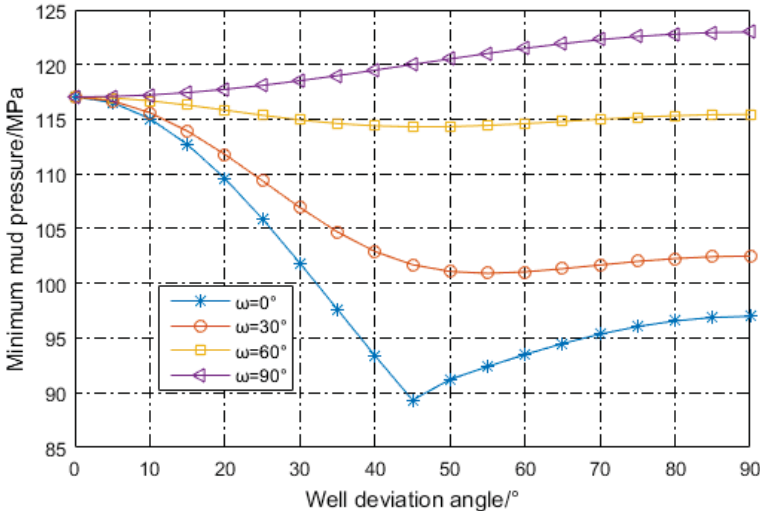

FIGURE 6
Borehole collapse pressure as a function of trajectory in RF stress regime.

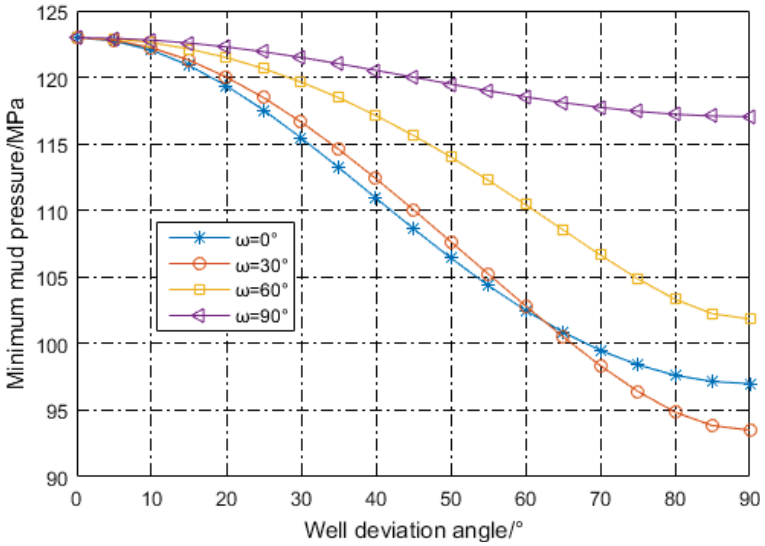

FIGURE 7
Borehole collapse pressure as a function of trajectory in SS stress regime.

In strike-slip fault stress regime with anisotropic horizontal stress, the variation trend of wellbore collapse pressure is shown in Figure 7. It can be found that, under different borehole orientations, the wellbore collapse pressure decreases with the increase of well inclination angle, and the risk of wellbore instability is the highest in vertical wells. In general, the horizontal borehole is more stable, i.e. the minimum mud pressure required for wellbore stability is lower. If the well would be parallel to the minimum in situ stress (i.e., ω=90°), the changing range of wellbore collapse pressure with the well deviation is small, while if the well with an orientation of 30° from the direction of the maximum horizontal in situ stress, the wellbore collapse pressure with the changing of well deviation varies a lot. The collapse pressure is considerably minimized when the borehole is horizontal with an orientation of 30° from the direction of the maximum horizontal in situ stress.

CONCLUSIONS

Based on the linear elastic model for stress distribution around wellbore and the exponential strength criterion considering the intermediate principal stress, the mechanism of wellbore wall collapse is studied, and the following conclusions are drawn:

(1) Mohr-Coulomb criterion neglects the impact of intermediate principal stress (i.e., σ_2) on rock strength, and compared with the actual triaxial strength test data of rock, the predicted strength of this criterion is relatively weak, which is conservative and always overestimates minimum mud pressure required for wellbore stability. According to the exponential strength criterion, the intermediate principal stress may improve the strength of rock specimen, but its influence will be restricted by σ 3. Also when σ 2 is high enough to cause failure in the σ 2- σ 3 direction, the strength will decrease with the increasing σ 2.

(2) The wellbore collapse pressure obtained by using Mohr-Coulomb criterion is relatively large, with a variation range of 110MPa~138MPa, and the predicted results of Exponential strength criterion vary from 90MPa to 121MPa. Those two criteria have little difference in the prediction results of high-occurrence drilling trajectory of collapse accident, but the prediction results of optimal wellbore trajectory are obviously different. It is suggested that exponential strength criterion is preferred in the wellbore shear instability analysis.

(3) In normal fault stress regime, wellbore wall collapse problem can be minimized if the well would be deviated 45° from the vertical and parallel to the direction of the minimum in situ stress (i.e., ω=90°). The optimum well path associated with the minimum mud pressure required for wellbore stability is for deviated borehole (α=45°) drilled parallel to the maximum in situ stress (i.e., ω=0°). In strike-slip fault stress regime with anisotropic horizontal stress, the collapse pressure is considerably minimized when the borehole is horizontal with an orientation of 30° from the direction of the maximum horizontal in situ stress.

(4) Wellbore stability is a very complicated problem. This paper only studies wellbore stability from the mechanical mechanism. The solution of this problem should also consider the influence of rock weak surface structure, seepage stress, temperature and other factors on wellbore stress distribution.

ACKNOWLEDGEMENTS

This study was supported by the National Science and Technology Major Projects of the 13th Five Year Plan (No.2016zx05061) and the Natural Science Foundation of Hubei Province (No.2018cfb770).

REFERENCES

[1] Manshad, A., Jalalifar, H., Aslannejad, M. (2014) Analysis of vertical, horizontal and deviated wellbores stability by analytical and numerical methods. Journal of Petroleum Exploration and Production Technology. 4(4), 359-369.

[2] Zare-Reisabadi, M., Kaffash, A., Shadizadeh, S. (2012) Determination of optimal well trajectory during drilling and production based on borehole stability. International Journal of Rock Mechanics and Mining Sciences. 56, 77-87.

[3] Moos, D., Peska, P., Finkbeiner, T., Zoback, M. (2003) Comprehensive wellbore stability analysis utilizing quantitative risk assessment. Journal of Petroleum Science & Engineering. 38(3), 97-109.

[4] Maleki, S., Gholami, R., Rasouli, V., Moradzadeh, A., Riabi, R., Sadaghzadeh, F. (2014) Comparison of different failure criteria in prediction of safe mud weigh window in drilling practice. Earth-Science Reviews. 136, 36-58.

[5] Al-Shaaibi, S., Al-Ajmi, A., Al-Wahaibi, Y. (2013) Three-dimensional modeling for predicting sand production. Journal of Petroleum Science and Engineering. 109, 348-363.

[6] Ma, T., Yang, Z., Chen, P., Guo, Z. (2017) Collapse Risk for Deviated Borehole in Shale Formations Based on True-triaxial Strength Criterion Journal of Southwest Petroleum University (Science & Technology Edition). 39(1), 161-168.

[7] Zhang, L., Cao, P., Radha, K. (2010) Evaluation of rock strength criteria for wellbore stability analysis. International Journal of Rock Mechanics and Mining Sciences. 47(8), 1304-1316.

[8] Al-Ajmi, A., Zimmerman, R. (2005) Relation between the Mogi and the Coulomb failure criteria. International Journal of Rock Mechanics and Mining Sciences. 42(3), 431-439.
[9] Islam, M. (2013) An experimental investigation of shale mechanical properties through drained and undrained test mechanisms. Rock Mechanics & Rock Engineering. 46(6), 1391-1413.
[10] Chen, J., Hubbard, S., Peterson, J., Williams, K., Fienen, M. and Jardine, P. (2006) Development of a joint hydrogeophysical inversion approach and application to a contaminated fractured aquifer. Water Resources Research. 42(6), 277-279.
[11] Gholilou, A., Far, P., Vialle, S., Madadi, M. (2017) Determination of safe mud window considering time-dependent variations of temperature and pore pressure: analytical and numerical approaches. Journal of Rock Mechanics & Geotechnical Engineering. 9(5), 900-911.
[12] Maleki, S., Gholami, R., Rasouli, V., Moradzadeh, A., Ghavami Riabi, R., Sadaghzadeh, F. (2014) Comparison of different failure criteria in prediction of safe mud weigh window in drilling practice. Earth-Science Reviews. 136(3), 36-58.
[13] Yu, M., Yoshimine, M., Qiang, H., Zan, Y., Xiao, Y., Li, L., Sheng, Z. (2004) Advances and prospects for strength theory. Advances and Prospects for Strength Theory. 21(6), 1-20.
[14] You, M. (2008) Characteristics of exponential strength criterion of rock in principal stress space. Chinese Journal of Rock Mechanics and Engineering. 28(08), 1541-1551.
[15] You, M. (2009) True-triaxial strength criteria for rock. International Journal of Rock Mechanics and Mining Sciences. 46(1), 115-127.
[16] You, M. (2010) Mechanical characteristics of the exponential strength criterion under conventional triaxial stresses. International Journal of Rock Mechanics & Mining Sciences. 47(2), 195-204.
[17] Hadjicontis, V., Mavromatou, C. (2013) Transient electric signals prior to rock failure under uniaxial compression. Geophysical Research Letters. 21(16), 1687-1690.
[18] Singh, M., Raj, A., Singh, B. (2011) Modified mohr–coulomb criterion for non-linear triaxial and polyaxial strength of intact rocks. International Journal of Rock Mechanics & Mining Sciences. 48(4), 546-555.
[19] Gholami, R., Moradzadeh, A., Rasouli, V., Hanachi, J. (2014) Practical application of failure criteria in determining safe mud weight windows in drilling operations. Journal of Rock Mechanics & Geotechnical Engineering. 6(1), 13-25.
[20] Jiang, H. (2015) Failure criteria for cohesive-frictional materials based on Mohr-Coulomb failure function. International Journal for Numerical & Analytical Methods in Geomechanics. 39(13), 1471-1482.
[21] Kou, S., Efron, B. (2002) Smoothers and the cp, generalized maximum likelihood, and extended exponential criteria: a geometric approach. Publications of the American Statistical Association. 97(459), 766-782.
[22] Khoroshun, L., Shikula, E. (2009) Deformation and long-term damage of layered materials with stress-rupture microstrength described by an exponential power function. International Applied Mechanics. 45(8), 873-881.
[23] Nazarenko, L. (2010) Damageability of a material reinforced with unidirectional orthotropic fibers for an exponential function of long-term microstrength. Journal of Mathematical Sciences. 168(5), 653-664.
[24] Zare-Reisabadi, M., Shadizadeh, S., Shahisooq, H. (2011) The Influence of In-situ Stress Anisotropy on the Optimized Wellbore Trajectory, Mogi-Coulomb Failure Criterion Application. Iranian Rock Mechanics Conference in Tehran.
[25] Al-Shaaibi, S., Al-Ajmi, A., Al-Wahaibi, Y. (2013) Three dimensional modeling for predicting sand production. Journal of Petroleum Science and Engineering. 109(5), 348-363.
[26] Xu, Y., Zhang, H., Guan, Z. (2021) Dynamic Characteristics of Downhole Bit Load and Analysis of Conversion Efficiency of Drill String Vibration Energy. Energies. 14, 229.
[27] Fan, X., Zhang, M., Zhang, Q., Zhao, P., Yao, B., Lv, D. (2020) Wellbore stability and failure regions analysis of shale formation accounting for weak bedding planes in ordos basin. Journal of Natural Gas Science and Engineering. 77, 103258.

Received: **30.11.2020**
Accepted: **06.02.2021**

CORRESPONDING AUTHOR

Liang Zhu
School of Petroleum Engineering,
Yangtze University,
Wuhan Hubei 431000 – China

e-mail: alloyer007@126.com

© by PSP Volume 30– No. 05/2021 pages 5149-5160 Fresenius Environmental Bulletin

AGROINJECTION TECHNIQUE FOR TRANSIENT GENE EXPRESSION AS RAPID AND HIGHLY EFFICIENT METHOD FOR POTATO AGROBACTERIUM-BASED TRANSFORMATION BY CRY1CA GENE

Mohei EL-Din Solliman[1,2,*], Heba Allah A Mohasseb[1,2], Abdullatif A Al-Khateeb[1], Suliman A Al-Khateeb[3], Wael F Shehata[1,4], Mohammed I Aldaej[1]

[1]Plant Biotechnology Department, College of Agricultural and Food Sciences, King Faisal University, P.O. Box 400, Al-Ahsa 31982, Kingdom of Saudi Arabia
[2]Plant Biotechnology Department, National Research Centre, Dokki -Egypt, Cairo, P.O. Box 12622, Egypt
[3]Environment and Natural Resources Department, College of Agriculture and Food Sciences, King Faisal University, P.O. Box 400, Al-Ahsa, 31982, Kingdom of Saudi Arabia
[4]Plant Production Department, College of Environmental Agricultural Science, El–Arish University, North Sinai; P.O. Box. 45511, Egypt

ABSTRACT

Potato is one of the major food crops and considered the fourth most important food crops worldwide. The insect and fungal infections are the significant constraints for potato production in the Arab countries, causing yield losses reaching more than 20%. We have used and developed a rapid and low-cost transient transformation assay by using in-planta agroinfiltratoin in potato seeds slide, which transformation efficiency is higher than those of the conventional transient assays are. Polymerase chain reaction (PCR) was used to amplify a single copy of Bacillus thuringiensis Crystal Protein Cry1Ca (cry1Ca) gene from extracted DNA to screen for the presence or absence of this gene. Potato slices were agroinjected with plasmid pRI201-AN-GUS DNA for transient assay of β-glucuronidase gene (GUS). The transformation was performed using the disarmed A. tumefaciens strain LBA4404 harboring a binary vector pRI201-AN-GUS- Cry1Ca. Genetically modified potato plants were selected on kanamycin-containing Murashige and Skoog medium (MS-media) and subcultured later to MS-media supplemented with 1.0 mg l-1 6-Benzylaminopurine (BA) and 1.5 mg l-1 ∞-Naphthaleneacetic acid (NAA). A. tumefaciens strain LBA4404 carried out the plant binary vector pRI201-AN-GUS, and pRI201-AN-GUS-Cry1Ca were used for transient expression assay. The Synthetic Cry1Ca (cry1Ca) gene, under the control of a CaMV 35S and the caste, also contained β-glucuronidase (GUS) gene. Agroinjection is an efficient transient uidA expression assay for reporter gene and analysis of candidate genes in plants. The successful transformation of Cry1Ca gene potato plants will contribute to increasing yield and food security in the future. Finally we describe here a protocol for the genetic transformation of potato based on agroinjection using A. tumefaciens carrying a plasmid (pRI201-AN-GUS-Cry1Ca) expressing a reporter uidA gene in addition to describing transient expression evidence based on histological and molecular assays. Successful transformation of transgenic potato plants will contribute to increasing the yield and food security in Saudi Arabia in the near future.

KEYWORDS:
Agrobacterium, Agroinjection, Cry1Ca gene, Potato, Transformation

INTRODUCTION

Potato has economic importance and agricultural uses throughout man's history. The insect and fungal infections are the major constraints affecting Potato production in Arab countries, causing yield losses reaching more than 20%. The applications of new biotechnological approaches focus mainly on improving potato crop for cultivation in diverse agro-climatic conditions worldwide [1, 2]. Expression of Bacillus thuringiensis Crystal Protein Cry1Ca gene has been engineered to be used for the production of transferred transgenic plant to increase resistance against certain lepidopteran insects. The coding sequence of those genes has an active insecticidal protein that has been expressed in many transgenic plants such as potato [3]. One Bacillus thuringiensis Crystal Protein (Cry1Ca) gene is a three-domain Cry protein [4, 5, 6], similar in structure to the Cry1andCry1 δ family used in transgenic crops and endotoxin binding in determining potency during Lepidopteran larval development [4, 7, 8]. The control of a plant disease includes gene transfection, biological control, molecular breeding, conventional crop breeding, and plant transformation as well as genetically modified crops [9]. In addition, there are vast applications of different agro-chemicals and their combinations in integrated pest management approaches to control insect, pests, and diseases [10].

The use of transient gene expression in plant biological system is advantageous over stable transformation methods for the generation of transgenic plants. It seems quite convincing to use transient gene expression analysis to confirm that the gene of interest in functional and expressed stably, before its application on a larger scale to generate transgenic plants [11, 12]. The transient gene expression systems are quick, malleable and most importantly have no influence from positional effects of the genes and ultimately overcome biased gene-expression [12, 13]. At the advanced developmental stage of the plant, heterologous gene expression is encouraged to escape possibly any adverse effects on the newly developed plant. Besides bacterial plasmids, the use of viral plants vectors to get transient gene expression of the gene of interest are well popularized commercially for production of specific proteins [13]. The production of transgenic plants is a routine work on a commercial scale as well as in a molecular biology laboratory. The genetic transformation has now become an everyday science for most of the crop species. The introduction of gene expression at a high level in a plant is still a big challenge, especially, to develop transgenic crop plants expressing insecticidal, antifungal, antibacterial, and antiviral proteins [14, 9].

The expected resistance to insects and fungal disease obtained with somatic hybridization could be enhanced by inserting an essential trait to the new cell line [15]. As an example, the increase in chitinase enzyme production seemed to be an ideal choice. It has been reported that chitinase plays a critical role in the enhancement of general plant resistance against fungal diseases as it degrades chitin incorporated in the construction of fungal cell wall causing fungal mycelium to collapse [16,17]. There are many advantages for expressed genes that were transformed into plants over the generation of a stable introduction of transformed plants that appear appropriate to verify that the gene product is functional and stable before going into production of transgenic plants on large-scale [11,12].

The expected outcome of the proposed task can be translated as new resistant or tolerant lines of potato plant to insect, safe time, and environment, increase the plant yield, and ultimately increase in the national income. Some trials achieved in our lab to use *Agrobacterium tumefaciens* strain LB4404 carrying binary vector pRI201-AN-GUS and pRI201-AN-GUS-Cry1Ca were used for transformation in economically important potato cultivar such as potato spunta cultivar. Using of co-cultivation Agrobacterium culture methods can be proved indispensable for successful transformation. Leaf disk was used for transformation studies. Binary vector pRI201-AN-GUS has been confirmed as an efficient method for transformation. This study describes a protocol of agroinjection using *A. tumefaciens* carrying a plasmid (pRI201-AN-GUS-Cry1Ca) expressing a reporter *uidA* gene for the genetic transformation of potato in addition to describing transient expression evidence based on histological and molecular assays.

RESULTS AND DISCUSSION

Potato is a major food crop produced in the world and widely grown under different climatic conditions. Potato has had economic importance and agricultural uses throughout human history (International Potato Center, n.d.). The insect and fungal infections are the major constraints affecting potato production, causing a yield reduction of more than 20%. To address this problem, heavy chemical treatments as well as sprays with *Bacillus thuringiensis* insecticidal formulations have been used. These have proven to be environmentally damaging and of limited efficiency. Conventional breeding for that trait has been proven difficult. An 850 bp synthetic gene was constructed from oligonucleotides that are chemically synthesized in order to improve transgenic protein expression of the Cry1Ca gene from *Bacillus thuringiensis* var. *tenebrionis* in transgenic potato. The expression of foreign genes in transient plant tissues is a valuable tool for plant transformation technology. The transient plant transformation assays offer a valuable analysis of a candidate gene expression in the transgenic potato seeds in the shortest period. This method is called fruit agroinjection, which rendered high levels of 35S promoter β-glucuronidase protein transient expression in the potato seeds, with higher expression levels in tubers. The transformation we carried out using disarmed *A. tumefaciens* strain LBA4404 harbouring a binary vector pRI201-AN-GUS and pRI201-AN-GUS-Cry1Ca Usefulness of potato seeds agroinjection was assayed in our case study: the Cry1Ca- β-glucuronidase (Cry1Ca -GUS) genes expressions in potato seeds. We proved the efficiency of this reliable technology as a tool for assay transgene expression in potato plants.

Cry1Ca Gene Synthesis, Sequence and Construction. Primers were synthesized by (Bioneer Corporation Company, Korea). The designed DNA sequence of the Cry1Ca gene (according to GenBank AN. : gb|MK184477.1|) was synthesized as one fragment ending with NcoI from 5' end and HindIII, BamHI and BglII cleavage sites from the 3' end.

Synthetic Cry1Ca (cry1Ca) gene. Sequence containing a synthetic nucleotide sequence encoding a Cry1Ca (cry1Ca) gene protein are synthesized as shown in the following sequence Figure 1.

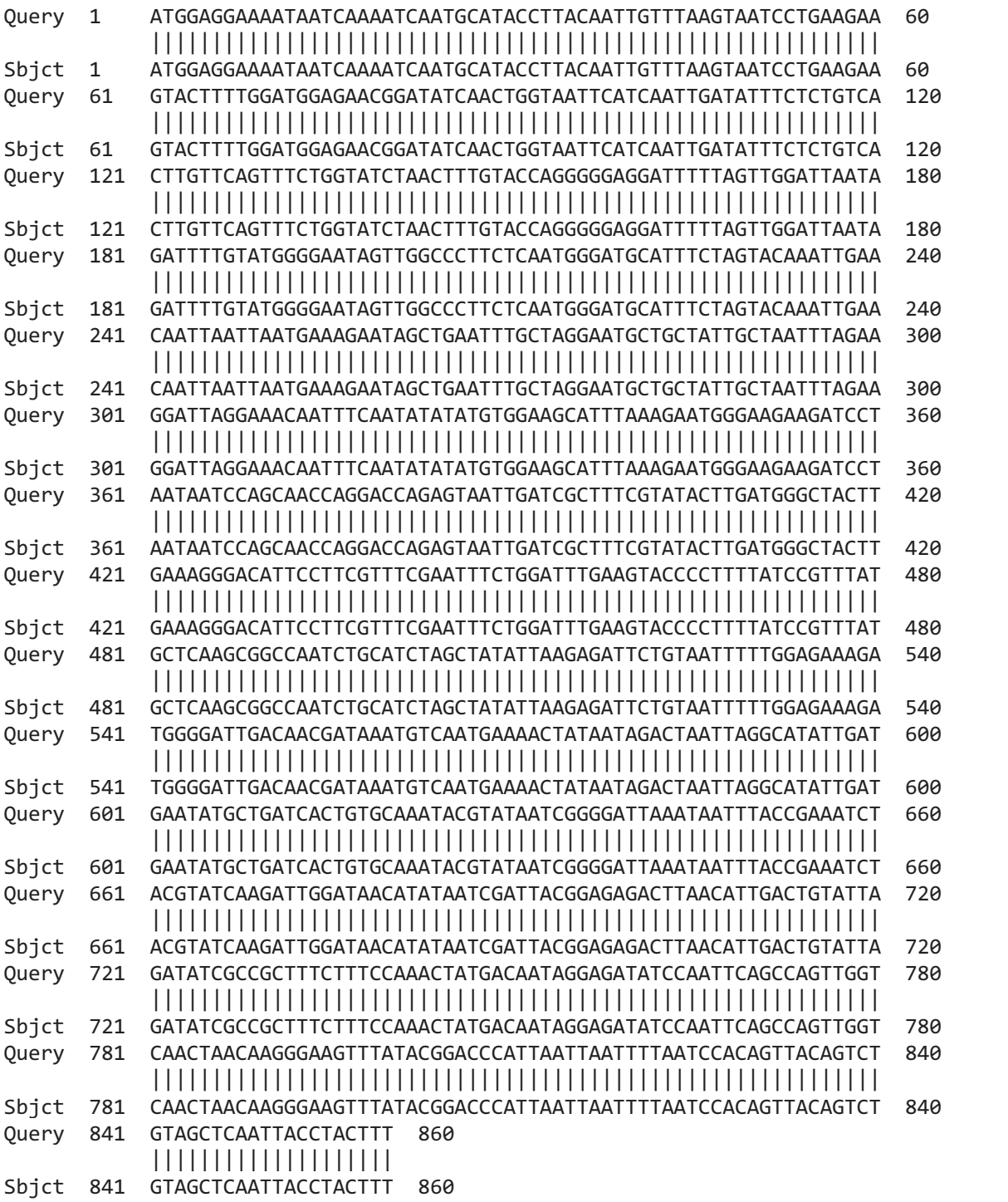

FIGURE 1

Nucleotide sequence of the Bacillus thuringiensis strain ABTS-1857 insecticidal crystal protein Cry1Ca (cry1Ca) gene. The Synthetic *Cry1Ca* gene fragments matched with the published sequences in Genbank, and the photo shows the homology of Synthetic Cry1Ca gene sequence to published matching to Cry1Ca gene sequence ID: gb|MK184477.1| in Genbank.

The coding sequences we used in pRI201-AN-GUS-Cry1Ca gene constructs as expression cassettes for the transformation and expression in potato plants.

Bacillus thuringiensis strain ABTS-1857 insecticidal crystal protein Cry1Ca gene, complete cds. Sequence ID: MK184477.**1** Length: 3570Number of Matches: 1

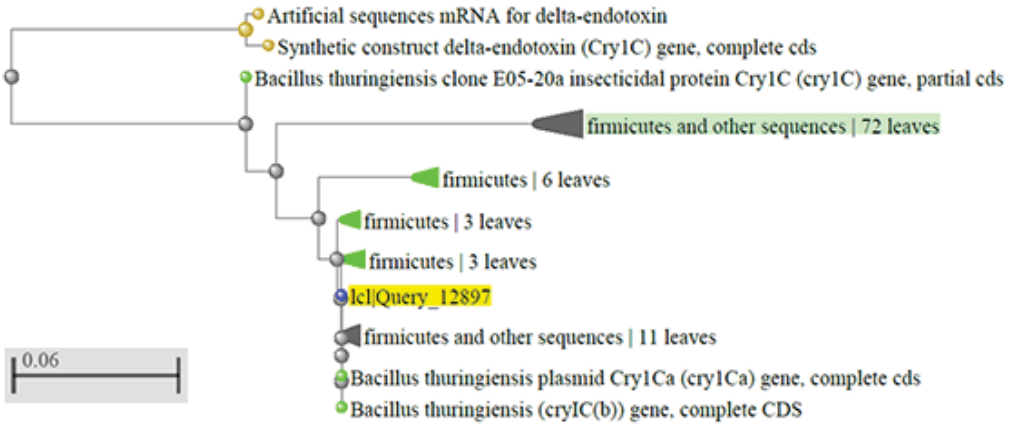

FIGURE 2

Phylogenetic relationships between the Cry1Ca gene using the (a), gene structure predictions (b) and conversed protein motifs. Phylogenetic analysis of *Bacillus thuringiensis* strain ABTS-1857 insecticidal crystal protein Cry1Ca (cry1Ca).

Gene Sequence analysis. Results show that the fragment was 850 bp for synthetic construct truncated Cry1Ca (cry1Ca) gene and 850 bp for Cry1Ca stander genes (Accession number: GenBank accession no. ID: gb|MK184477.1). GenScan and CLC analysis both predicted that the synthetic construct truncated had the same two active repeat sides, containing a full-length open reading frame (ORF) of 850 bp 270 amino acids.

BLAST result showed that the predicted ORF was 89% identical to the published nucleotide sequence of *B. thuringiensis* Cry1Ca gene Stander gene (GenBank accession no. ID: gb|MK184477.1), which is a member of the *B. thuringiensis* Cry1Ca gene Stander gene, nucleotide binding, and cry protein repeat family. The potential ORF encodes for 87 amino acid residues and contains a potential repeat motif. The synthetic truncated construct sequence showed extensive homology with each other and the conserved active repeats. Synthetic truncated construct Cry1Ca gene, matched Cry1Ca gene sequence ID: gb|MK184477.1| in Genbank as shown in Figure 2. BLAST was used to compare the sequences as shown in Figure 1, the expected bands were obtained between 830- 850bp, while, Figure 2 shows the same fragment with stop cod DH5 Bacteria**.**

Sequencing for isolated Cry1Ca gene. PCR primers contained unique restriction enzyme cleavage sites used for cloning the amplified double-stranded DNA fragments into pBHA Figures 3 and 4. The Cry1Ca gene was PCR-amplified by a forward primer Cry1Ca _Fr carrying a NcoI site, and reverse primer Cry1Ca_Rr Figures 3 and 4.

The purified Cry1Ca gene bands we used for subsequent PCR reaction to restriction sites Figure 5, while Figure 6 show the use of restriction enzymes such as XbaI and BamHI for digestion of clone of Cry1Ca gene after cloned the Cry1C gene in pRI2O1-CaMV35S-gus vector.

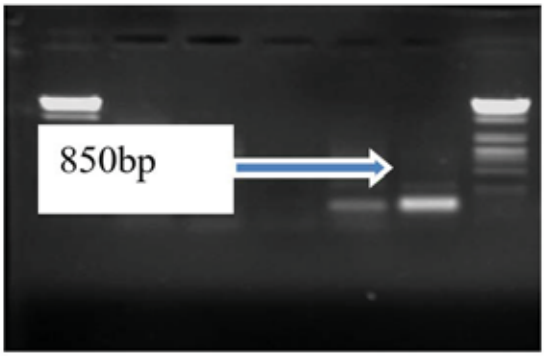

FIGURE 3

PCR amplification showing the expected size (850bp) of the amplified PCR product using specific primers, Lanes 2-6 show PCR Amplification products of Synthetic Cry1Ca (cry1Ca) gene with Cry1C-F and CryIC-R primers. M contains DNA digested with lambda HindIII used as a size marker.

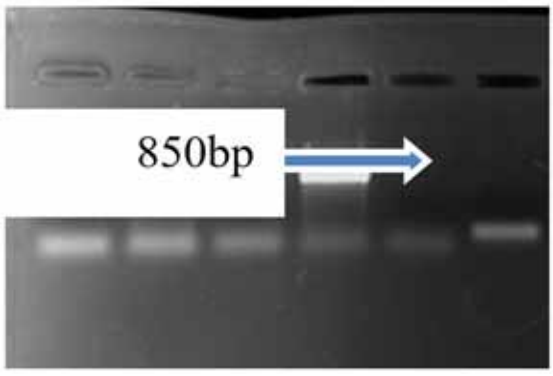

FIGURE 4

PCR screenings for the presence of Cry1Ca gene using PCR amplification using different clones. Lane from 2 to 4 using CryIC-F forward and CryIC-R reverse primers.

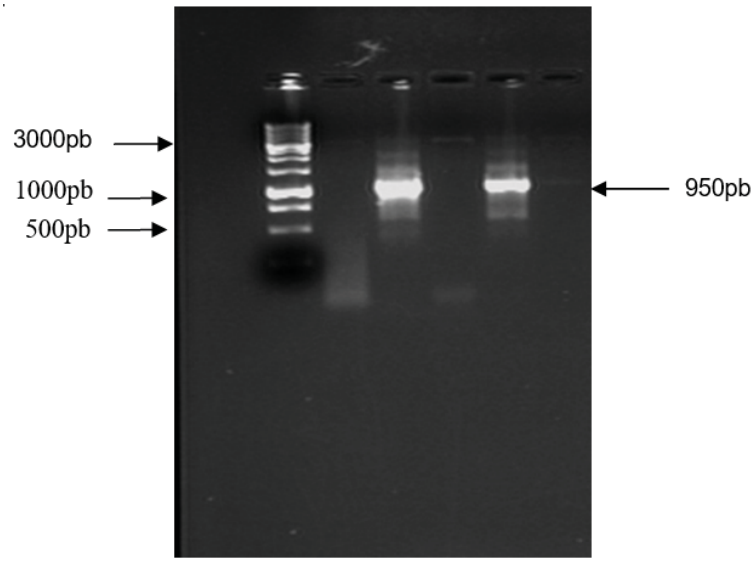

FIGURE 5
PCR amplification for Screenings of the presence of Cry gene with different clone lanes from 1to 4 using T7 and SP6 primers and DNA Marker.

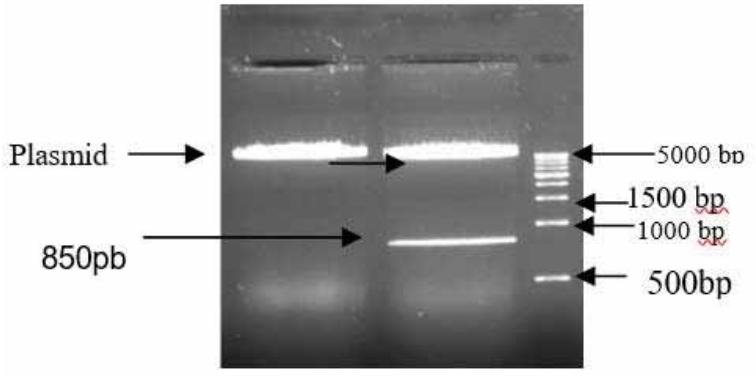

FIGURE 6
Restriction digestion products for clones of Cry1Ca gene after cloning the cry gene in pRI2O1-CaMV35S-gus vector and digested by Xba1 and *BamH*I.

Polymerase chain reaction. PCR confirmation of cloned Cry1Ca–GUS in the final plasmid DNA cassette (pRI201-AN-Cry1Ca–GUS) using the forward GUS-5 and reverse GUS-3 primers present in the pRI201-AN-GUS vector is shown in Figure 5.

Culture media and culture conditions for transformation to test the protocol of Potato before going to use the Cry1Ca gene clone. Production of transgenic potato plants. Establishment of the efficient transformation plasmids into A. tumefaciens and then get transgenic potato plants is of great practical importance. Transformation was done according to the freeze-thaw methods by [19]. However, fast results were obtained by agroinjection as a transient expression system that refers to the successful transformation in potato plants (Figure 7). Here we show the establishment of the protocol for culture conditions and Agrobacterium–mediated transformation by using pRI201-AN-GUS plasmid for potato explants transformation and growing the regenerated plant on MS regeneration medium (Figures 7- 8).

Plant growth regulators we examined to obtain adventitious shoot initiation from the calli and explants following *Agrobacterium* cocultivation. The plant growth regulator combinations examined were in mg l^{-1}: Kin and NAA. For evaluation of the effect of a second combination of plant growth regulators on transformation efficiency, the plant growth regulator combinations examined were in mg l^{-1} kin 1.0/NAA 0.1 it is the best medium.

The results refer that potato explants from the potato spunta cultivars could give callus have the ability for regeneration (Figures 7a and b, 8 and 9).

The establishment protocols of regeneration potato plants from explants-derived callus. Transformation media to be used for callus production and regeneration after selection on the same media for agrobacterium transformation Figures (7a and b, 8 and 9).

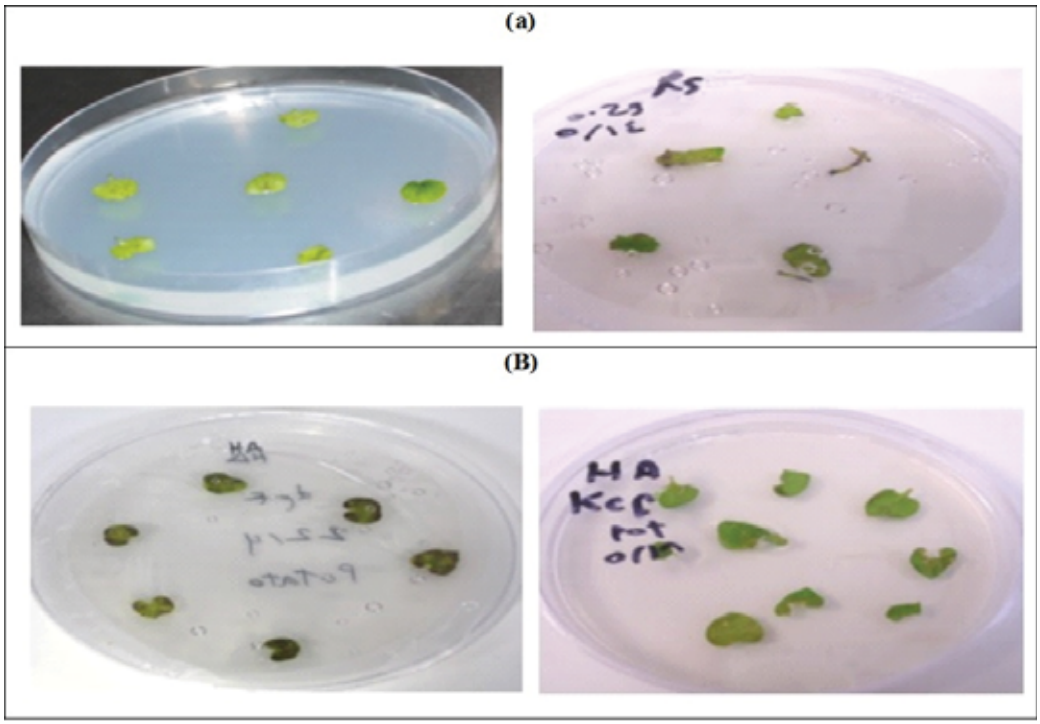

FIGURE 7

(a) Place infected tissue on MS-medium containing kanamycin. Explants after infecting the wounded plant tissue with Agrobacterium. (b) Potato Callus with embryonic like structures giving regenerated plants.

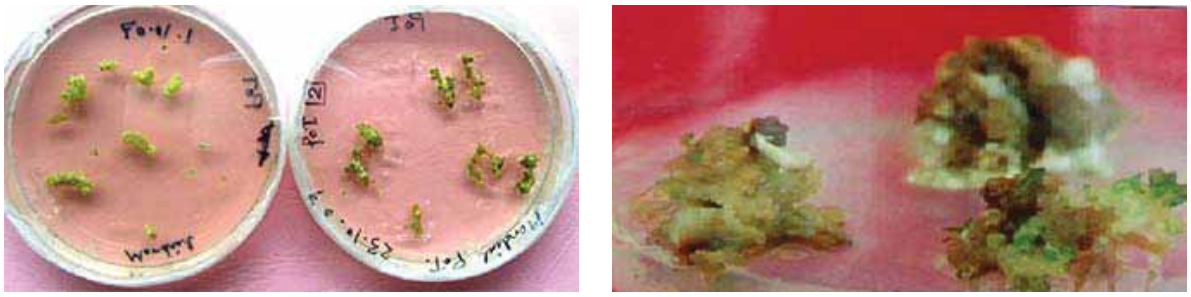

FIGURE 8

In Vitro Potato regenerated plants showing normal good growing shoots.

FIGURE 9

In Vitro Potato regenerated plants showing normal good growing roots. The adapted Potato plants trans-formed with cryI Ca gene confer to the greenhouse. The establishment protocols of regeneration potato plants from explants-derived callus. Transformation media to use for callus production and regeneration after selection on the same media for agrobacterium transformation.

However, the regenerated plants could be developed for further growth giving normal plantlets have shoots and roots Figures (7) and (8).

Agrobacterium method to transfer DNA from the bacterium into plants. Figure 9 shows the developed method for agroinjection-based system, which allows transient expression of foreign genes directly in potato tubers tissues. The traits that are used for expression must be limited to specific tissues, organs, or in response to specific stimuli [22, 23, and 14].

Agrobacterium-Based Transient Transformation. These potato seeds agroinjection methods and expression systems are designed to deliver superior protein yields compared to alternative transient systems, saving you precious time, incubator space, and plastic ware costs. Now you can express the same amount of β-glucuronidase protein in the potato seeds in a single flask with high expression levels in f potato tubers that other transient expression systems express in 20 or more flasks. *Agrobacterium tumefaciens* strain LBA4404 carried out a plant binary vector pRI201-AN-GUS and pRI201-AN-GUS-Cry1Ca we used for transient expression assay. The Synthetic Cry1Cagene, under the control of a CaMV 35S promoter and the caste, also contained the β-glucuronidase (GUS) gene.

The Beta-glucuronidase (Gus) gene under control of the 35S-promotor, with an intron, is commonly used as the reporter gene [21]. The genetically engineered *A. tumefaciens* strain LBA4404 was also used as a vector for infection in the transformation experiment, which contains plasmid pRI201-AN-GUS-Cry1Ca. The results indicated that exposing potato seeds slide to Agrobacterium inoculums for one day at 37^0C, GUS expression we observed in the potato seeds and did not turn the potato tubers out of control. PCR amplification of DNA extracted from tissues showed a generation amplicon corresponding to the expected bands of Cry1Cagenes. To the best of the researcher's knowledge, this result strongly emphasizes the successful transformation of potato varieties from Saudi Arabia for the first time. Moreover, this protocol explained the way to solve the problem of potato yield losses because of insect diseases including other economically important crops.

The results indicated that the Cry1Ca genes we introduced into the genome of the potato. The results of this study could be considered as a step towards the production of genetically modified Saudi Arabia potatoes, which is disease-free and insect resistant. Insect diseases are the most dangerous diseases for potato based on yield losses. Most of the published procedures for potato transformation are genotype dependent and still far from routine and universal methods [4].

Reliable regeneration protocol for the target plant material (Potato we optimized *in vitro*. The regeneration occurred directly or indirectly from stem and leaf segments of potato explants. Potato callus showed the embryonic-like structures giving regenerated plants, which developed to whole plantlets in vitro. The plantlets have been adapted to research laboratory conditions and successfully grown in pots packed with fertilized peat moss out-of-doors in the greenhouse.

FIGURE 10
GUS transient assay for potato seeds slices after agroinjection with pRI201-CaMV35S–GUS plasmid. Note the presence of blue spots on the agroinjected slices. Blue color reveals the tissues we reached by the infiltrated culture. No blue spots could be seen on control slices (non-agroinjected).

Agroinjection as a Transient Expression System Expression of GUS under the control of CaMV 35S. Transient assays we used to test the expression of GUS in potato seed slide tissue. The *uidA* gene under the regulation of cauliflower mosaic virus 35S (CaMV 35S) promoter in pRI201 was used as a positive control. As a negative control, no *uidA* gene we used. Potato tubers were agroinjected with various constructs using agrobacterium mediated transformation method. When assayed for GUS activity through the histochemical method, blue spots we observed in the potato tubers tissue that was infected with pRI201-CaMV-35S-GUS vector DNA (Figure 8). No activity of GUS we observed in control of plasmid DNA samples. Similar experiments using potato tubers tissue revealed the expression of GUS when infected with pRI201-CaMV35S-GUS plasmid DNA (Figure 10). No blue spots could be seen in potato seed slices with control DNA.

Efforts we made to obtain stably transformed potato plants to study the expression of GUS. This method has been used to examine the genetically modified plants [21] and allows screening and checking the expression of *uidA* (GUS) gene in most genetically modified plants. For the potato, plant regeneration from different explants, such as leaf disks and cotyledon is possible. In such studies, it has been clearly demonstrated that there is regeneration capacity among cultivars. In this respect, regeneration conditions have been studied for the hypocotyl, cotyledons and leaf sections (explants) of potato cultivars.

Volubility for expression of foreign transient genes in plant tissues is a tool for plant biotechnology as described by [24]. Histochemical detection of GUS activity was performed [21]. Negative controls, consisting of nonagroinjected potatoes, pRI201-CaMV35S–GUS agroinjected potatoes, and pRI201-CaMV35S–GUS–Cry1Ca agroinjected potatoes collected and fixed 30 min after agroinjection, did not render significant blue staining. Agrobacterium infection plays a vital role in the efficiency of the agroinjection methodology [11]. To shorten the time of gene functional analysis in potato, the researchers developed methods for transient that could be applied to potato seeds. Similar results were described earlier by [25] for the agroinjection of potato leaf in which they found that using needles was removed and Agrobacterium cultures were introduced in the intercellular spaces showed good results.

This technique is rapid and well suited for gene expression, gene function analysis in plants [26, 27], and transient expression using agroinjecation proved helpful for measuring the activity of gene constructs before stable transformation. The reasons for the differences in efficiency are not well labeled and, some of them are compression of the tissue, innervations pattern, type of plants, monocotyledon or dicotyledon plants, tissue parts, and bacteria-host compatibility with plasmids constructs [28].

MATERIALS AND METHODS

Growing Conditions. For plant transformation studies, potatoes (Solanum tuberosum L.) we grown at 25±2^{0}C with duration of 8-16 hours in dark/light inside an incubator chamber [18].

Protocol for Potato Transformation. For potato transformation, the pRI201-AN-GUS-Cry1Ca vector we transferred into Agrobacterium tumefaciens (LBA4404) and made competent by the liquid nitrogen freeze-thaw method. This protocol is designed for potato stem internodes on MS-medium, but might work for leaf pieces as well. Potato slide discs we transformed with either pRI201-AN-GUS or pRI201-AN-GUS-Cry1Ca independently [19] with few modifications according to Elkashef et al, [18].

Establishment of Potato Tissue Culture Growth and Selection of the Transgenic Potato Plants. *A*fter co-cultivating with Agrobacterium, the explants we rinsed with MS-media containing 50 mg l^{-1} Acetosyringone. The explants we then transferred to the solid MS-media in culturing plants containing 200 mg l^{-1} Kanamycin, 500µg/ml Carbenicillin, 1 mg l^{-1} BAP and 0.1 mg l^{-1} NAA. After 3-4 weeks, shoots we separated from the regenerated explants and transferred to the rooting media in separate jars. After the emergence of the root, the plantlets we removed and transferred to the vermiculite pots and covered with plastic bags for acclimatization. After 10-15 days, the plastic bags we removed and the plants were exposed. The hardened plants we transferred to potting soil and the pots we shifted to the glass house for further growth and development.

Potato In Vitro Regeneration. Potato Plant Regeneration Started by callus inductions. As described by [18], callus proliferation and plant regeneration were carried out from the leaf explants using different combinations of BAP, NAA and 2, 4-D. The primary calli we characterized and subcultured after four weeks on MS media supplemented with the BA (1.5 mg l^{-1}) and NAA (1.0 mg l^{-1}).

Potato shoot inductions and formation as methods described by Elkashef [18], were followed by using MS-media with 1.5 mg l^{-1} BAP (Fig. 6).

Potato root formation. The root proliferation was done based on the methods described by Elkashef [18], were the shoots was transferee to MS-medium supplemented with 0.3 mg l^{-1} NAA. After 21 days, the potato plants we transferred to the greenhouse for further growth and development.

Genomic Potato Plant DNA Isolation. Isolation of genomic DNA according to the methods

utilized by [14, 9] was achieved. The construction of a synthetic Cry1Ca Gene containing the β-glucuronidase (GUS) on pRI201-AN-GUS plasmid was conducted by using pRI201-AN (TaKaRa comp.). The Codon-modified Cry1Ca gene was designed according to the description of Xiang-Qian [16]. The Cry1Ca gene we synthesized by assembling the entire gene de novo from 330 to 334-mer oligonucleotides (BIONEER Company) and inserting them into the pBHA vector (BIONEER). Next genes we sub-cloned into the plant-expression binary vector, pRI201-AN-GUS, using NcoI and BamHI cloning sites.

Plasmids Structure Used for the Transgenic of Potato. In this experiment, the practical introduction of plasmids construction into A. tumefaciens is critical. The treatment using calcium chloride or the freeze-thaw methods [19]. This technique we used in dicots crops [19]. However, the result reflected the successful transformation in potato plants. The Cry1Ca products we sub-cloned in pBHA (2002bp) vector then digested with XbaI /BamHI and cloned under CAMV 35 S promoter pRI201-AN-GUS, which we already digested with XbaI and SacI downstream CAMV 35 S promoter. These constructs we then utilized for potato transformation. The amplification bands of 850 bp Cry1Ca gene we inserted into the plasmid pRI201-AN-GUS to generate the construct pRI201-AN-GUS-Cry1Ca. The positive clones having Cry1Ca gene we confirmed by restriction digestion with the restriction endonucleases XbaI and SacI.

Cry1Ca gene cloning and transformation. Cry1Ca gene we cloned into the vector pBHA (BIONEER, Korea) and the recombinant plasmid with Cry1Ca gene was transformed into Escherichia coli DH5α competent cells with the freeze-thaw method. The positive bacterial colonies we used to raise bacterial cultures and the plasmid DNA was isolated using the Wizard® Plus SV Minipreps DNA Purification Systems (Promega).

PCR amplification of Cry1Ca. PCR reaction we carried out using the Synthetic Cry1Ca gene fragment, which contains the stop codon and the restriction sites of BamHI and NcoI to be used for Cry1Ca -DNA digestion after PCR amplification. The reaction mix was, 2.5µl of Dream Taq buffer, 0.5µl diluted Dream Taq, 0.5µl dNTPs, 0.5µl of CryIC-F and 0.5µl CryIC-R primers, 2.5µl DNA template (purified original Cry1Ca fragment), and 18µl free nuclease water.

Primer name and primer sequence. CryIC_Fr as forward primer, 5'- TGTAGAAGAG-GAAGTCTATCCA-3 and for the reverse primer CryIC_Rr, 5'- TATCGGTTTCTGGGAAGTA -3.

Agrobacterium-Based Transient Transformation. Agroinjection procedure. Agroinjection carried out as described by [11]. Agrobacterium tumefaciens strain LB4404 we grown at 29°C in L-broth supplemented with 50-µg ml^{-1} kanamycin and 25-µg ml^{-1}streptomycin. All the Agrobacterium strains harboured the pRI201-AN-GUS DNA (TaKaRa comp.). The culture of Agrobacterium carrying the pRI201-AN-GUS-Cry1Ca (cry1Ca) gene construct was brought to an optical density (OD_{600}) of 1.0. Transient co-expression of the pRI201-AN-GUS and pRI201-AN-GUS- Cry1Ca constructs was at OD_{600} of 0.5 and 0.8, respectively.

Transformation of Agrobacterium. *Agro-bacterium tumefaceins* (LBA4404) competent cells we transformed with pRI201-AN-GUS and pRI201-AN-GUS-Cry1Ca constructs using the freeze-thaw method [20].

Molecular verification of transformed plants. PCR analysis of the presence of Cry1Ca (cry1Ca) gene: PCR amplification of Cry1Ca (cry1Ca) gene was carried out using Taq DNA polymerase enzyme, dNTPs mix and convergent primers Cry1c_Forward and Cry1c _Reverse. The PCR reaction conditions were as follows: initial denaturation at 94ºC for 5 minutes followed by 30 cycles for denaturation at 94^0C for 30 seconds. Next, annealing at 55ºC for 30 seconds and extension at 72ºC for either 90 seconds for cloned DNA in plasmid or 2.0 minutes for GUS gene fusion, final extension at 72ºC for 5 min. After completion of the PCR reaction, the amplicons were analyzed using 0.8 % agarose gel.

GUS Histochemical Assay. Histochemical analysis of GUS staining was performed for screening transgenic potato plants and potato potato tubers according to [21] and (2006) [11] with some modifications. To allow for the verification of the expression of *uid*A gene in potato tubers, the wild type (control) and treated potato tubers using agroinjection technique we collected, sliced and the slices were rinsed in 50 mM Na-phosphate buffer. The sliced potato tubers tissues were stained in 2 mM 5-Bromo-4-chloro-3-indolyl β-D- galactopyranoside (X-gal) (Sigma-Aldrich) and 50mM of Na-phosphate buffer (pH 7.0), followed by short-term filtering in vacuum. These potato tubers slices we then incubated overnight at 37ºC in a complete darkness. After staining, potato tubers we rinsed thoroughly in ethanol to remove all chlorophyll contents before further studies. Blue spots we recorded on the developed potato tubers-slice.

Generation of Stable Transgenic Potato Plants. The transformation was carried out using disarmed A. tumefaciens strain LBA4404 harbouring a binary vector pRI201-AN-GUS-Cry1Ca. The transgenic potato plants we selected on

hygromycin-containing medium and subsequent regeneration on Murashige and Skoog medium supplemented with 1.0 mg L^{-1} benzyl adenine (BA) and 1.5 mg L^{-1} napthalene acetic acid (NAA). PCR amplification of DNA extracts from the transformed tissues was used for testing the presence or absence of Cry1Ca gene. One of the significant challenges of modern agriculture that facing us today is controlling the plant disease which is an eco-friendly and satisfactory device [29, 30 and 31].

CONCLUSION

For the potato, plant regeneration from different explants, such as leaf disks and cotyledon is possible. In such studies, it has been clearly demonstrated that there is regeneration capacity among cultivars. In this respect, regeneration conditions have been studied for the hypocotyl, cotyledons and leaf sections (explants) of potato cultivars. Potato genetic transformation via Agrobacterium was performed successfully in the laboratory. Agroinjection is an efficient transient expression assay for reporter genes and analysis of candidate genes in plants. With the importance of the potato cultivar in the world, the successful transformation of Cry1Ca gene into potato spunta cultivar and generation of insect transgenic potato plants will contribute to increase the yield and food security in the world in the near future. This implies that agroinjection can be applied to many plants. To shorten the time of gene functional analysis in potatoes, the researchers developed methods for transients that could be applied to potato seeds. Similar results we described earlier for the agroinjection of potato leaf in which they found that using needles was removed and Agrobacterium cultures were introduced in the intercellular spaces showed good results. It demonstrated that subcellular localization of proteins evaluated by using this method was same as that by other transient transformation assays. Since it is rapid, efficient and low-cost, this method is suitable for large-scale analyses of protein subcelluar localization.

ACKNOWLEDGEMENT

This work was financed by the grant No. 150151 from the Deanship of Research at King Faisal University.

Informed Consent: Informed consent was obtained from all individual participants included in the study.

Authors' contributions: Mohei EL-Din Solliman and Heba Allah A. Mohasseb conceived and designed research. Mohei EL-Din, Abdullatif A Al-Khateeb and Suliman A Al-Khateeb conducted experiments. Wael F. Shehata analyzed data. Mohei EL-Din Solliman, Heba Allah A. Mohasseb wrote the manuscript. All authors read and approved the final manuscript.

REFERENCES

[1] Mandal, A.B. and Sheeja, T.E. (2003) *In vitro* flowering and fruiting in potato (*Solanum tuberosum* L.). Asia Pac. J. Mol. Biol. Biotechnol. 11, 37-42.

[2] Solliman, M.M., Elkazzaz, A., Taha, H., Al-Khateeb, A.A. and Mohasseb, H.A. (2013) Molecular and genetic characterization of transgenic potato expressing N gene confers resistance to ToMV. Journal of Applied Sciences Research. 9 (1), 451-459.

[3] Perlak, F.J., Stone, T.B., Muskopf, Y.M., Peterson, L.J., Parker, G.B., Mcpherson, S.A., Wyman, J., Love, S., Reed, G., Biever, D., and Fischhoff, D.A. (1993) Genetically improved potatoes: protection from damage by colorado potato beetles. Plant Mol. Biol. 22, 313-321.

[4] Durmaz, E.Y.H., Raffi A.V. and Todd R. K. (2016) Intracellular and Extracellular Expression of Bacillus thuringiensis Crystal Protein Cry5B in Lactococcus lactis for Use as an Anthelminthic. Appl. Environ. Microbiol. 82(4), 1286–1294.

[5] Hu, Y., Georghiou, S.B., Kelleher, A.J., Aroian, R.V. (2010) *Bacillus thuringiensis* Cry5B protein is highly efficacious as a single-dose therapy against an intestinal roundworm infection in mice. PLoS Neglect. Trop. Dis. 4, 614-621.

[6] Cappello, M., Bungiro, R.D., Harrison, L.M., Bischof, L.J. Griffitts, J.S., Barrows, B.D., Aroian, R.V. (2006) A purified *Bacillus thuringiensis* crystal protein with therapeutic activity against the hookworm parasite Ancylostoma ceylanicum. Proc. Natl. Acad. Sci. USA. 103, 15154–15159.

[7] Hu, Y. and Aroian, R.V. (2012) Bacterial pore-forming proteins as anthelmintics. Invertebr. Neurosci. 12, 37–41.

[8] Gilliland, A. Catherine E. Chambers, Eileen J. Bone, and David J. E. (2002) Role of Bacillus thuringiensis Cry1 δ Endotoxin Binding in Determining Potency during Lepidopteran Larval Development. Appl Environ Microbiol. 68(4), 1509–1515.

[9] Solliman, M.M., Mohasseb H.A., Al-Khateeb A.A., and Al-Khateeb S.A. (2016) *In vitro* reliable regeneration protocol of tomato plants and efficient transformation system for transient gene expression in transgenic tomato varieties resistance to fungi. J. Food Agric. Environ. 14(3/4), 29–36.

[10] Copping, L.G. and Menn, J.J. (2000) Biopesticides: a review of their action, applications and efficacy. Pest. Management Science. 56 (8), 651-676.

[11] Diego, O., Sophie, M., Willemien Wieland, H. and Granell, A. (2006) Agroinjection of potato fruits. A tool for rapid functional analysis of transgenes directly in fruit. Plant Physiology. 140(1), 3-11.

[12] Kapila, J., DeRycke, R., VanMontagu, M., and Angenon, G. (1997) An Agrobacterium-mediated transient gene expression system for intact leaves. Plant Sci. 122, 101–108.

[13] Scholthof, K.-B.G. and Peterson, P.D. (2006) The role of Helen Purdy Beale in the early development of plant serology and virology. Adv. Appl. Microbiol. 59, 221– 241.

[14] Solliman, M.M. (1998) "Isolation and Characterization of Plant Promoters for High Level and Tissue Specific Expression of Foreign Genes in Transgenic Plants" PhD from ICGEB 1998 - 2002, India. Pages 1-255.

[15] Romeis, J., Meissle, M. and Bigler, F. (2006) Transgenic crops expressing *Bacillus thuringiensis* toxins and biological control. Nature Biotechnology. 24, 63-71.

[16] Xiao, Y.H., Li, X.B., Yang, X.Y., Luo, M. and Hou, L. (2007) Cloning and characterization of a balsam pear class I chitinase gene (*Mcchil1*) and its ectopic expression enhances fungal resistance in transgenic plants. Biosci. Biotechnol. Biochem. 71, 1211–1219.

[17] Keegstra, K. (2010) Plant cell walls. Plant Physiol. 154, 483–486.

[18] Elkashef, E.M., Solliman M.M., Kkobeasy, M.I., and El-Shemy, H.A. (2012) Isolation and sequencing of the cryIC-like delta endotoxin gene from Egyptian strains of *Bacillus thuringiensis* toxic against Lepidoptera. African Journal of Biotechnology. 11(14), 3235-3243.

[19] Horsch, R.B., Fry, J.F., Hoffman, N.L., Eichholtz, D., Rogers, S.G., and Fraley, R.T. (1985) A simple and general method for transferring genes into plants. Science. 227, 226-228.

[20] Holsters, M., Dde Waele, D., Depicker, A., Messens, E., Vvan Montagu, M., and Schell, J. (1978) Transfection and transformation of *Agrobacterium tumefaciens*. Mol. Gen. Genet. 163, 181-187.

[21] Jefferson, R.A. (1987) Assaying chimeric genes in plants: the GUS gene fusion system. Plant Mol. Biol. Rep. 5, 387–405.

[22] Costa, G.M., Nogueira, F.T.S., Otoni, W.C., and Brommonschenkel, S.H. (2000) *In vitro* regeneration of processing potato (*Lycopersicon esculentum* Mill.) IPA-5 and IPA-6. Ciencia-e-Agrotecnologia. 24, 671-678.

[23] Venkatachalam, P., Geetha, N., Priya, P., Rajaseger, G. and Jayabalan N. (2000) High frequency plantlet regeneration from hypocotyl explants of potato (*Lycopersicon esculentum* Mill.) via organogenesis. Plant Cell. Biotech. Mol. Biol. 1, 95-100.

[24] Trujillo-Moya, C., Carmina, G., Vilanova, S., and Nuez F. (2011) Localization of QTLs for *in vitro* plant regeneration in tomato. BMC Plant Biol. 11, 140-149.

[25] Liu, Y.L., Schiff, M., and Dinesh-Kumar, S.P. (2002) Virus-induced gene silencing in potato. Plant J. 31, 777–786.

[26] Shah K.H., Almaghrabi B. and Bohlmann H. (2013) Comparison of expression vectors for transient expression of recombinant proteins in plants. Plant Mol. Biol. Rep. 31(6), 1529–1538.

[27] Hellens, R.P., Allan, A.C., Friel, E.N., Bolitho, K., Grafton, K., Templeton, M.D., Karunairetnam S., Gleave, A.P., and Laing, W.A. (2005) Transient expression vectors for functional genomics, quantification of promoter activity and RNA silencing in plants. Plant Methods. 1, 13- 21.

[28] Solliman, M. M. (2017) Towards production of transgenic Date palm using Agroinjection for transient expression of plant and *Agrobacterium-mediated* transformation. Date Palm Biotechnology Protocols Volume II: Germplasm Conservation and Molecular Breeding. Springer. Nature. 2 (1637), 295-305.

[29] Lorito, M., Woo, S.L., Garcia, I., Fernandez, G., Colucci Harman, G.E., Pintor-Toro, J.A., Filippone, E., Muccifora Lawrence, S.C.B., Zoina, A., Tuzun, S. and Scala, F. (1998) Genes from mycoparasitic fungi as a source for improving plant resistance to fungal pathogens. Proceedings of the National Academy of Sci. USA. 95, 7860-7865.

[30] Mohei EL-Din S., Heba Allah, A. Mohasseb, A.A., Al-Khateeb, S., Al-Khateeb, A. and Shehata, W.F. (2020) Induce of new tomato varieties resistance to fungal using Agrobacterium-mediated Transformation. Fresen. Environ. Bull. 29 (12), 11535-11544.

[31] Mohasseb, H.A.A., Solliman, M.E.-D., Al-Mssallem, I.S., Ba Abdullah, M., Shehata, W.F. and El-Shemy, H.A. (2020). Salt tolerant phenomena, sequencing and characterization of a glyoxalase I (Jojo-Gly I) gene from Jojoba in comparison with other glyoxalase I genes. Plants. 9(10), 1285-1293.

Received: **30.11.2020**
Accepted: **03.02.2021**

CORRESPONDING AUTHOR

Mohei El-Din Solliman
Plant Biotechnology Department,
National Research Centre,
Dokki Cairo P.O. Box 12622
Egypt

e-mail: msolliman@kfu.edu.sa

© by PSP Volume 30– No. 05/2021 pages 5161-5168 Fresenius Environmental Bulletin

TECTONIC EVOLUTION OF THE NORTHWESTERN MARGIN IN THE JUNGGAR BASIN AND CALCULATION OF ITS STRUCTURAL SHORTENING

Baocheng Wu[1,2,*], Zongyu Lu[1,2], Jiangang Shi[2], Chao Xiong[2], Wei Zhang[2]

[1]China University of Petroleum (Beijing), Beijing 102249, China
[2]Research Institute of Engineering Technology, PetroChina Xinjiang Oilfield Company, Karamay, Xinjiang 834000, China

ABSTRACT

The sedimentary and structural features of the marginal zone of the sedimentary basin are very complicated. In addition, strong erosion in such areas is generally considered to be detrimental to the preservation of oil and gas, so the degree of oil and gas exploration in such areas is very low. In this paper, taking the Mesozoic and Cenozoic in the northwestern margin of the Junggar Basin, China as an example, we use the abundant seismic, logging, and core data in this area to study the mesozoic and Cenozoic tectonic evolution, and calculate the tectonic shortening in this area. The results show that the Mesozoic and Cenozoic tectonic evolution in the area since the Triassic can be divided into four stages: (1) Compression-torsional deformation stage of the Indosinian period (T); (2) During the Jurassic sedimentary period, namely the early Yanshanian period, the northwestern margin of the Junggar Basin is still in a compression-torsional deformation stage; (3) During the Cretaceous sedimentary period, namely the late Yanshanian period, the basin was in a relatively stable compression and deformation stage; (4) After the Paleogene, the Junggar Basin gradually entered the Himalayan period, during which the basin was in the tensile and shear deformation stage. Based on the principle of area conservation, the structural shortening of the seismic profile was calculated. The amount of shortening before K deposition is 3.1% ~ 4.1%; the amount of shortening before E deposition is 5.9% ~ 6.7%; the amount of shortening before N deposition is 8.2% ~ 8.4%; and the current amount of shortening is 11.4% ~ 11.8%. The research in this paper has certain reference value for promoting the Meso-Cenozoic oil and gas exploration in this area.

KEYWORDS:
Junggar Basin, tectonic evolution, tectonic shortening, erosion thickness, hydrocarbon distribution

INTRODUCTION

The Junggar Basin is located in the western section of the Central Asian Orogenic Belt. It is located at the intersection of the Kazakh plate, the Siberian plate and the Tali wooden plate, and belongs to the ancient plate of Kazakhstan. The Junggar Basin is a typical intra-continental sedimentary basin developed from Late Carboniferous to Quaternary (C3-Q) surrounded by Paleozoic sutures [1-4]. The west of the basin is the western Junggar Orogenic Fold Belt, the northeast and east of the basin are the Altai Fold Orogenic Belt and the eastern Junggar Fold Orogenic Belt at the southern edge of the ancient Siberian Plate, and the southern edge of the basin is the northern Tianshan Orogenic Fold Belt. It can be seen that the tectonic setting of the Junggar Basin is closely related to the tectonic movement of the three adjacent plates and the formation and evolution of the basin-edge orogenic belt.

The basement of the Junggar Basin is a continental crust basement and has a dual structure, namely, a precambrian crystalline basement and a Paleozoic fold basement [5-9]. The lithology of the basement is relatively complicated, including acidic rocks, basites, ultrabasites, sedimentary rocks (sandstones), and deep metamorphic rocks, but it is mainly composed of granite, medium acid rocks, and sedimentary metamorphic rocks. The original gravity distribution of the basin is abnormal, and the basement morphology of the basin today is generally a monoclinic structure with a north to south dip. There are some basement uplifts (protrusions), depressions (sags) and slopes of varying scales developed on it, and the basin is asymmetrical from east to west.

The Junggar Basin is surrounded by mountain systems. The northwest boundary is Zaire Mountain and Xiemistai Mountain, the northeast boundary is Altai Mountain, Qinggridi Mountain, and Kelameili Mountain, and the south boundary is North Tianshan Mountain and Bogda Mountain. The study area is located in the northwestern margin of the Junggar Basin, and the Ke-Xia-Hongche fault zone is distributed in this area.

Mesozoic and Cenozoic structural evolution in the study area is closely related to hydrocarbon distribution [10-12]. In the study area, a set of lacustrine mudstones containing organic matter were deposited during the Late Triassic (T3). Then, a set of lacustrine-facies coal-bearing rock series was deposited in the early Jurassic and early Middle Jurassic. Among

them, the Lower Jurassic and the Lower Middle Jurassic Xishanyao Formation gradually overlaid towards the rim of the basin. From the beginning of the Late Triassic to the end of the deposition of the Xishanyao Formation, the basin received the Upper Triassic Baijiantan Formation, the Lower Jurassic Badaowan Formation, the Sangonghe Formation, and the Middle Jurassic Xishanyao Formation in approximately 60 Ma. The three layers of the Lower-Middle Jurassic are all sedimentary constructions of gray-black sandstone and mudstone interbedded with coal seams. Therefore, under the relatively stable tectonic background of this period, favorable oil and gas reservoir deposition and construction were formed. Relatively high terrain may be a favorable location for oil and gas distribution [13-15]. Therefore, a systematic study of structural evolution and calculation of structural shortening in this area has important reference value for oil and gas exploration. However, because the area is located at the edge of the basin, the sedimentary and structural features are very complex, and strong erosion is generally considered to be detrimental to the preservation of oil and gas. Therefore, the degree of oil and gas exploration in such areas is very low.

Tectonic evolution is closely related to hydrocarbon distribution. In this paper, taking the Mesozoic and Cenozoic in the northwestern margin of the Junggar Basin as an example, we use the abundant seismic, logging, and core data in this area to study the mesozoic and Cenozoic tectonic evolution, and calculate the tectonic shortening in this area. This research has certain reference value for promoting oil and gas exploration in the area.

MATERIALS AND METHODS

We use the latest seismic data in the construction area to explain the structure and faults. The strata studied are Mesozoic and Cenozoic strata, ie from Triassic to Quaternary strata. Figure 1 shows the stratigraphic division and unconformity distribution in the Junggar Basin. At the same time, the erosion thickness of the unconformity formation is calculated by the acoustic wave time difference method, which has good applicability to the strong erosion area on the edge of the basin.

Stratigraphic system		Code	Reflective layer code	Stratigraphic contact		Unconformity scale	Seismic sequence	Subsequence	Tectonic movement
Quaternary		Qx	T_{Qx}	Bottom cut	↘↘↘	Regional unconformity	Ⅷ		Himalayan Movement
Neogene		N	T_N	Top cut Bottom overlap	↗↗↗ ↘↘↘	Regional unconformity	Ⅶ		
Paleogene		E	T_E	Top cut Bottom overlap	↗↗↗ ↘↘↘	Regional unconformity	Ⅵ		
Cretaceous	Upper	K_2	T_{K2}	Top cut Bottom overlap	↗↗↗ ↘↘↘	Regional unconformity	Ⅴ	Ⅴ2	Late Yanshan Movement
	Lower	K_1	T_{K1}	Top cut Bottom overlap	↗↗↗ ↘↘↘	Regional unconformity		Ⅴ1	
Jurassic	Toutunhe Fm.	J_2t	T_{J2t}	Top cut	↗↗↗	Regional unconformity	Ⅳ	Ⅳ4	Middle Yanshan Movement
	Xishanyao Fm.	J_2x	T_{J2x}	Top cut	↗↗↗	Local unconformity		Ⅳ3	Early Yanshan Movement
	Sangonghe Fm.	J_1s	T_{J1s}	Top cut	↗↗↗			Ⅳ2	
	Badaowan Fm.	J_1b	T_{J1b}	Top integrated contact		Regional unconformity		Ⅳ1	
Triassic	Huang-Hao Fm.	T_3hs-T_3hb	T_{T3hs}-T_{T3hb}	Top cut	↗↗↗		Ⅲ	Ⅲ3	Indosinian Movement
	Kelamayi Fm.	$T_{2-3}k$	T_{T2-3k}	Top integrated contact				Ⅲ2	
	Upper Cangfang Fm.	T_2ch	T_{T2ch}	Top integrated contact		Regional unconformity		Ⅲ1	
Permian	Upper Wuerhe Fm.	P_2w	T_{P2w}	Top cut	↗↗↗	Regional unconformity	Ⅱ	Ⅱ5	Late Hercynian Movement
	Lower Wuerhe Fm.	P_2w	T_{P2w}	Top cut	↗↗↗	Regional unconformity		Ⅱ4	
	Xiazijie Fm.	P_2x	T_{P2x}	Top cut Bottom overlap	↗↗↗ ↘↘↘	Regional unconformity		Ⅱ3	
	Fengcheng Fm.	P_1f	T_{P1f}	Top cut	↗↗↗	Regional unconformity		Ⅱ2	
	Jiamuhe Fm.	P_1j	T_{P1j}	Top cut Bottom overlap	↗↗↗ ↘↘↘	Regional unconformity		Ⅱ1	
Carboniferous		C		Top cut	↗↗↗		Ⅰ		Hercynian Movement

FIGURE 1
Vertical distribution of unconformities in the Junggar Basin.

The acoustic wave time difference method can be effectively used to estimate the erosion thickness of the unconformity surface with large erosion and shallow burial. The thickness of the sediment above the unconformity surface must be less than the erosion thickness. In this paper, we have improved the conventional acoustic time difference method [16-17]. For the strata in the same sedimentary area within the basin, the amount of erosion did not change much in a certain period, and the effective information that can reflect the formation sedimentation compaction and erosion is still included in the mudstone acoustic time difference logging data.

When calculating the amount of formation erosion using conventional acoustic time difference method, the threshold value of acoustic time difference of sandstone is considered to be 620-650 μs/m. Comparison with the actual measured value of ablation shows that the prediction accuracy of this method is high and the method is feasible. Therefore, this method can be used as a feasible method for calculating the erosion of Meso-Cenozoic strata in Junggar Basin.

At the same time, the structural evolution model of the seismic profile is made using the balanced profile technique, and the amount of structural shortening is calculated according to the principle of area conservation. The principle of area conservation is that the area (profile) occupied by the strata before and after deformation remains unchanged. When the rock layer deforms along the slippage surface, the area of the profile above the slippage surface remains unchanged before and after the deformation, and the depth of the slippage surface can be calculated based on this. The length of each mark layer after recovery should be equal, otherwise there must be a discontinuity between the long layer and the short layer, such as the occurrence of branch faults, fault-related folds, and displacement transformation zones.

RESULTS

Mesozoic and Cenozoic tectonic evolution background. From the beginning of the Triassic to the Paleogene (T-E), the Junggar Basin gradually entered the squeezed depression basin stage. The formation of the prototype of the Junggar Basin occurred during the Late Hercynian Movement at the end of the Permian and the Indosinian Movement during the Early and Middle Triassic. From the Late Triassic to Early Middle Jurassic, the Junggar Basin was in the stage of basin expansion. After the Indosinian movement in the late Middle Triassic, the Junggar Basin entered a relatively stable period of structural development. The magmatic activity is weak, and the upper Triassic lacustrine and marsh facies are deposited in the basin with a large thickness. Since the Jurassic period, the Tarim block shifted from north to south, and at this time, the Junggar Basin may be in a mild inland expansion state. Strike-slip faults and normal faults mainly occurred during this period [18]. Due to the influence of faults, the thickness of the strata in the Late Triassic and Early and Middle Jurassic changes. The lake basin in the west of the Junggar Basin continued to exist, and the sedimentary center of the lake basin in the south moved to the southwest. At the same time, an asymmetrical piedmont basin appeared in front of the Altai Mountains in the north. The Baiyanghe Basin in West Junggar, the Kupu- Zhifang Basin in East Junggar, and the southern part of the Santanghu Basin were all depression areas at that time.

At the end of the late Jurassic, the Yanshan movement was very active in the Junggar Basin. The Bogda Mountain was squeezed strongly and rose again. The late Jurassic lateral compression event in the southern Junggar Basin is probably related to the northward collision of the Lhasa block. However, in the east and north of the Junggar Basin, it may be related to the significantly accelerated closure of the Mongolian-Okhotsk Basin.

During the Cretaceous period, the Mongolian-Okhotsk belt was basically closed, and the Junggar Basin showed the characteristics of pan-basin depression type sedimentation, indicating that the whole area may be in a quasi-plain environment. In particular, the Lower Cretaceous Tugulu Group is a set of rivers and alluvial plains. The thickness changes steadily and slowly, indicating a relatively stable sedimentary environment [19-20]. Its depositional range involves some mountain depressions around the lake basin. These characteristics all indicate that the sinking of the basin at this time is controlled by the equilibrium of lithospheric cooling-shrinking-gravity. Therefore, the Cretaceous was the period when the stress activity was relatively stable and the deposition rate was the lowest since the formation of the Junggar Basin.

The water body of the Upper Cretaceous began to shrink, and the eastern part of the Junggar Basin began to uplift without sedimentation. The late Yanshan movement at the end of the Cretaceous period showed an overall block uplift in the eastern Junggar Basin. Krameliet Mountain and Bogda Mountain in the south also experienced a certain degree of uplift.

Since entering the Cenozoic, the Indian subcontinent has continued to move northward, and has collided strongly with Eurasia around 50 Ma. As a result of this continuous and intense collision, the Tianshan Mountain, which had been severely eroded, once again uplifted and thrust into the north of the basin. In the front of the Tianshan Mountain, a deep-sagged piedmont basin was formed again, and huge thick Cenozoic channel-shaped sediments were accumulated in the Junggar Basin. Since the Miocene, the uplift of Tianshan has accelerated.

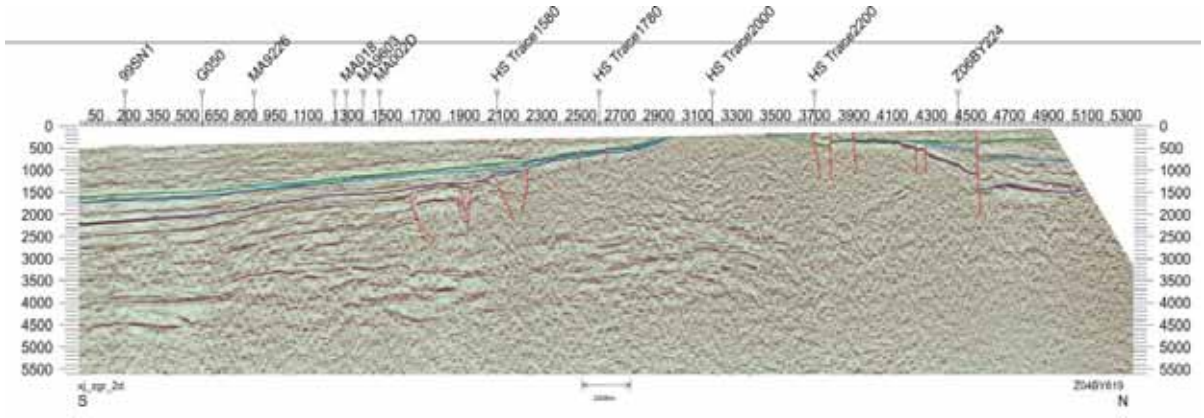

FIGURE 2
Tectonic interpretation of a seismic line in the northwestern margin of Junggar.

The activities of the northern margin of the Junggar Basin since the Cenozoic may be related to the southward movement of the Siberian Plate and the uplift of the central region of Baikal-Mongolia. According to the polar shift curve of the Siberian plate obtained from paleomagnetic research data in recent years, the southward movement of the Siberian plate is obvious from the Jurassic to the end of the Cretaceous. It caused a strong uplift in western Mongolia, and the Yanshanian tectonic movement in the northern margin of the Junggar Basin was also related to this. This effect continued until the early stage of the Himalayan movement. From the end of the Early Pleistocene to the early Middle Pleistocene, the central part of the basin gradually uplifted and stopped depositing. From the late Middle Pleistocene to Holocene, the Luliang Uplift divided the Junggar Basin into southern and northern parts. Eventually, the present tectonic pattern of the Junggar Basin was formed.

Distribution of faults in the northwestern margin of the Junggar Basin. Since the Paleozoic, the western margin of the Junggar Basin has undergone superposition and transformation of multi-stage structural deformations in Hercynian, Indosinian, Yanshanian, and Himalayan periods. Eventually a series of post-expansion thrust fault combinations were formed.

It can be seen from the seismic profile in Figure 2 that strata above the Triassic mainly develop strike-slip faults such as high-angle normal faults and Y-shaped faults. Only some faults can be broken through to the surface. The fault distance for the faults break to the surface is relatively large, and the fault distance for the faults that have not break to the surface is significantly smaller.

The Meso-Cenozoic in the northwestern margin of Junggar mainly developed four structural styles: high-angle fault, medium-low angle fault, flower-shaped fault and Y-shaped fault. Among them, low- and medium-angle faults are relatively rare, and their scale is generally small, and mostly formed late. The remaining three structural styles are widely distributed and the scale is also significantly larger. These faults are not only formed in the late period, but also formed in the early stage and continue to be active in the later period.

High-angle faults are mainly formed by strike-slip structures. There are both normal and reverse faults. Among them, the Mesozoic period mainly suffered from torsional slip and developed reverse faults, while the faults formed since the Cenozoic were mainly normal faults. The seismic profile (Figure 2) shows that during the Meso-Cenozoic period, the number of various faults was not large, and high-angle faults accounted for a relatively large proportion.

Flower-shaped faults and Y-shaped faults are important signs of strike-slip structure. Its profile shows that the main fault is steep, straight down to the base, and the upward branch fault is scattered like a flower or palm tree structure, which is a sign of aggregate type twisting action. Fault folds related to thrust faults are mainly developed in the study area.

Tectonic evolution profile. The Junggar Basin is a large-scale composite and superimposed basin that has undergone multi-phase tectonic movement transformation. Due to the composite superposition of different types of prototype basins and the characteristics of oscillatory tectonic movements, multiple regional and local unconformities have developed in the basin. These unconformities have obvious control effects on the accumulation of oil and gas in the basin. In particular, the unconformity at the bottom of the Cretaceous formed in the middle of the Yanshan Movement is of greater significance to the evolution of the basin and the control of hydrocarbon accumulation. The Hercynian is mainly manifested in the unconformity of the Carboniferous and Permian and the early and late Permian. The Indosinian period mainly showed the unconformity between the late Triassic and early and middle Jurassic. The Yanshanian period is mainly characterized by regional unconformity between the Middle and Late Jurassic and between the Jurassic and Cretaceous. The Himalayan period is mainly manifested in the

regional unconformity between the Paleogene and Neogene and between the Neogene and Quaternary.

In this study, based on the interpretation of two-dimensional seismic profiles and by comprehensively considering the structural evolution characteristics of the area, one NE-direction and one NW-direction seismic profiles were selected in the backbone seismic survey lines for analysis [21]. Based on the Move2009 software, after the time-depth conversion and considering the decompacting correction of the stratum, the principle of balanced geological profile was used to make the structural evolution profile. In the early Caledonian area, the study area was in a tensile environment and formed a series of early tensile normal faults. By the middle Caledonian period, the basin was in an extruded environment, and the faults in the study area were structurally reversed, from normal faults to reverse faults, and the terrain was high in the south and low in the north. In the early period of Hercynian, the southern part of the study area maintained a high terrain, and some NE faults and NE faults formed during this period. The middle Hercynian Movement period was a period of tectonic subsidence, and tectonic activity was relatively weakened. In the late Hercynian period, the northern part of the study area began to uplift and the degree of fault development increased. During the Himalayan period, the fault activity was further enhanced, the uplift degree in the northern part of the study area increased, and the uplift in the south gradually submerged.

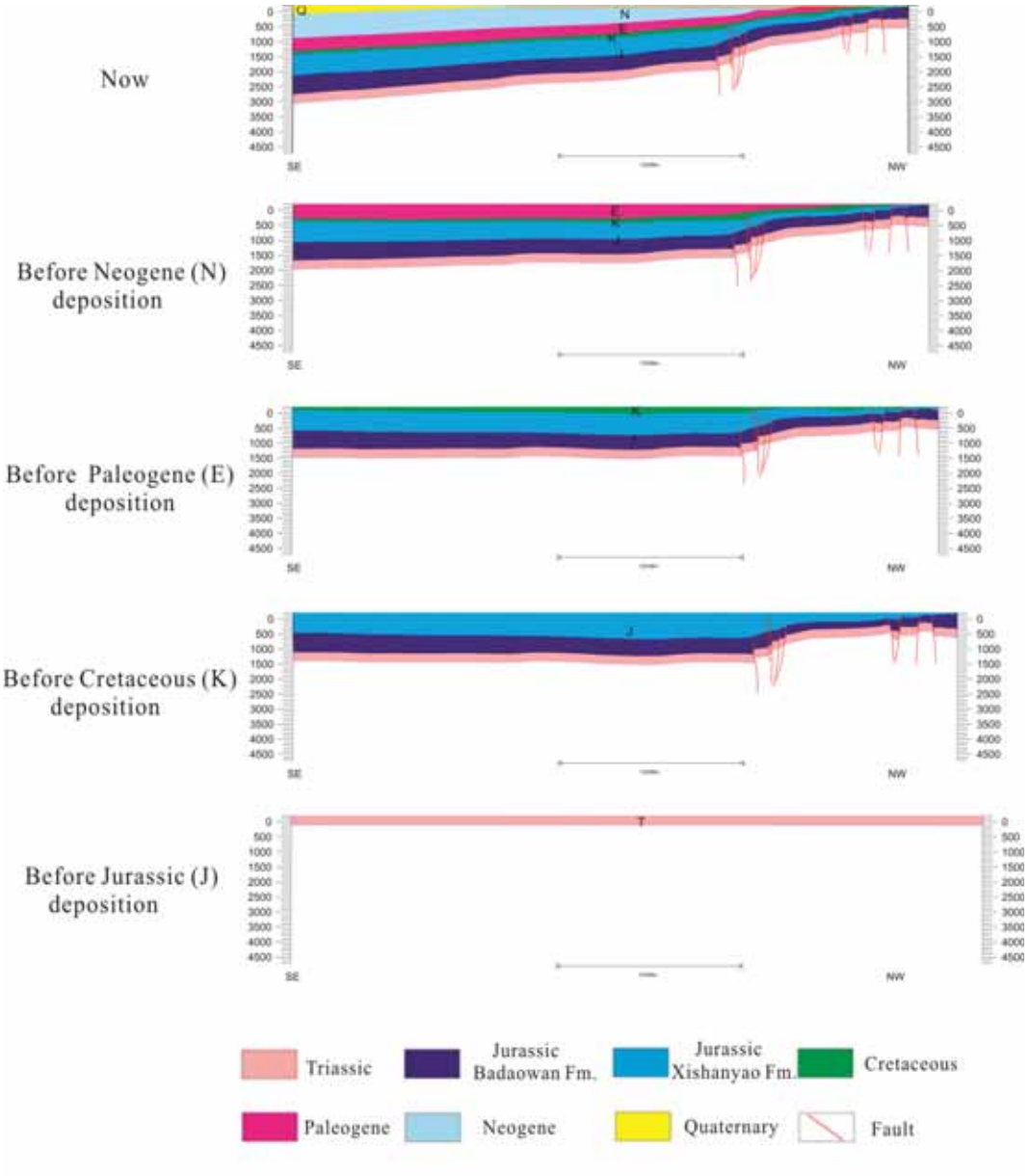

FIGURE 3
Tectonic evolution profile of seismic line in northwestern margin of Junggar Basin.

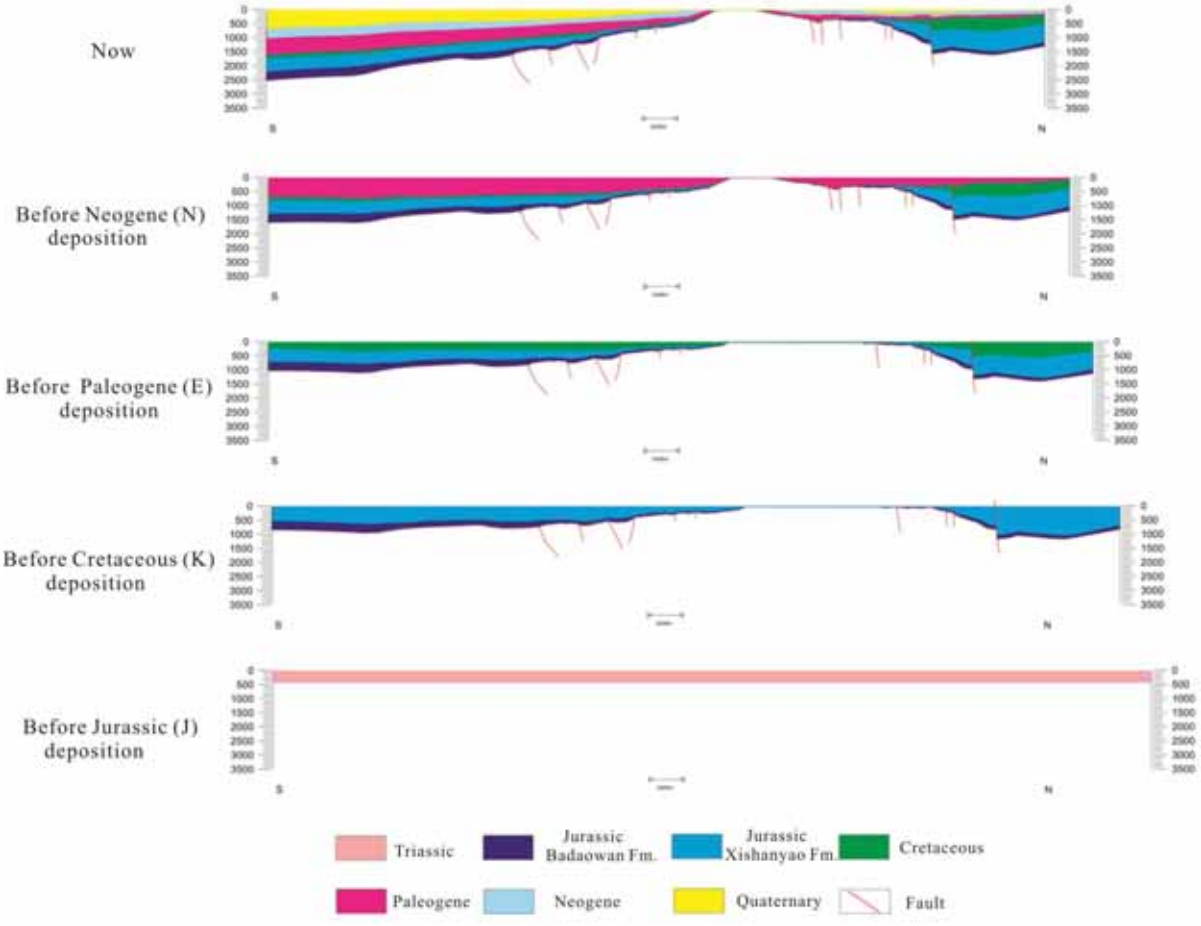

FIGURE 4
Tectonic evolution profile of seismic line in northwestern margin of Junggar Basin.

We made balanced profiles to key seismic lines in the northwestern margin of the Gar basin, as shown in Figure 3 and Figure 4. The Meso-Cenozoic tectonic evolution in this area since the Triassic can be divided into four stages:

(1) Compression-torsional deformation stage of the Indosinian period (T). At this stage, the prototype of the basin was formed, and the relief of the Triassic stratum was small. Some early-formed faults mainly developed below the Jurassic unconformity and cut the Triassic strata. At this time, under the compressive stress environment in the near-north-south direction of the region (Figure 3, profile 1), the few pre-formed faults were mainly compression-torsion thrust faults or their combinations. At this time, fault-related folds are developed. With the further development of lateral faults in the NW direction, tectonic deformation exhibits obvious segmentation characteristics. The distribution pattern of uplifts and depressions is initially formed.

(2) During the Jurassic sedimentary period, namely the early Yanshanian period, the northwestern margin of the Junggar Basin is still in a compression-torsional deformation stage. During this period, the fault developed below the Cretaceous unconformity, and the fault cut the Jurassic strata. In the northwestern marginal area, the scale of the fault is relatively small. However, there are many newly formed faults in the northernmost part of the study area.

(3) During the Cretaceous sedimentary period, namely the late Yanshanian period, the basin was in a relatively stable compression and deformation stage. During this period, the faults in the northwestern marginal area cut the bottom boundary of the Cretaceous and developed mainly on the upper wall of the main fault on the boundary. The extension direction of the fault is roughly the same as that of the main fault on the boundary. The scale of these faults is small, the distribution is discrete, and most of them are inherited faults. There are fewer newly formed faults.

(4) After the Paleogene, the Junggar Basin gradually entered the Himalayan period, during which the basin was in the tensile and shear deformation stage. During this period, the structural deformation in the northwestern margin of the Junggar Basin was mainly concentrated in the southern region. The fault is mainly manifested as a nearly vertical tensile fault developed in the Cenozoic strata. The vertical distance is usually in the range of several meters to tens of meters, and the extension length is usually several meters to hundreds of meters, which cuts the Neogene to Quaternary strata

(Figure 4, profile 2). These nearly upright normal faults indicate that some strata in this area have strike-slip characteristics. There is no obvious difference in the thickness of the strata between the two plates, indicating that they do not control the deposition. The faults in the study area are mainly in the NNE and NNN directions. This indicates that these faults represent tensile-shear deformation developed under the action of near-SN compression stress. It is consistent with the direction of the whole compressive stress of the basin during this period.

Structural shortening calculation. As for structural shortening, there is not much difference between the shortenings of the survey lines in the northwestern margin. In this paper, we use the survey lines in Figure 3 (profile 1) and Figure 4 (profile 2) as examples to calculate the amount of structural shortening.

For profile 1 of the northwestern margin of the Junggar Basin, before the J deposition, the profile length was 46.6 km; before the K deposition, the profile length was 44.7 km, the reduction was 4.1%; before the E deposition, the profile length was 43.5 km, the reduction was 6.7%; Before N deposition, the profile length was 42.7 km, with a reduction of 8.4%; today, the profile length is 41.3 km, with a reduction of 11.4%.

For profile 2, before J deposition, the profile length was 61.2 km; before K deposition, the profile length was 59.3 km, and the reduction was 3.1%; before E deposition, the profile length was 57.6 km, and the reduction was 5.9%; before N deposition, the profile length is 56.2 km, and the reduction is 8.2%; today, the length of the profile is 54 km, and the reduction is 11.8%.

In this paper, we systematically study the tectonic evolution and shortening of the Mesozoic and Cenozoic in the northwestern margin of the Junggar Basin. This study has certain reference value for promoting oil and gas exploration in this area.

CONCLUSIONS

(1) In this paper, taking the Mesozoic and Cenozoic in the northwestern margin of the Junggar Basin as an example, we use the abundant seismic, logging, and core data in this area to study the mesozoic and Cenozoic tectonic evolution, and calculate the tectonic shortening in this area.

(2) The Mesozoic and Cenozoic tectonic evolution in the area since the Triassic can be divided into four stages: 1) Compression-torsional deformation stage of the Indosinian period (T); 2) During the Jurassic sedimentary period, namely the early Yanshanian period, the northwestern margin of the Junggar Basin is still in a compression-torsional deformation stage; 3) During the Cretaceous sedimentary period, namely the late Yanshanian period, the basin was in a relatively stable compression and deformation stage; 4) After the Paleogene, the Junggar Basin gradually entered the Himalayan period, during which the basin was in the tensile and shear deformation stage.

(3) Based on the principle of area conservation, the structural shortening of the seismic profile was calculated. The amount of shortening before K deposition is 3.1% ~ 4.1%; the amount of shortening before E deposition is 5.9% ~ 6.7%; the amount of shortening before N deposition is 8.2% ~ 8.4%; and the current amount of shortening is 11.4% ~ 11.8%.

ACKNOWLEDGEMENTS

No funds support this work and the authors would like to show thank the techniques who have helped this work.

REFERENCES

[1] Henry, P. (1996) Analysis of sonic well logs applied to erosion estimates in the Bighorn basin, Wyomin. AAPG Bulletin. 80(5), 630-646.
[2] Magara, K. (1976) Thickness of removed sedimentspaleoporepressure and paleotemperature southwestern part of Western Canada Basin. AAPG Bulletin. 63(5), 812-815.
[3] Watson, M. (1987) Plate tectonic history, basin development and petroleum source rock deposition. Marine Petroleum and Geology. 4(3), 205-225.
[4] Caillet, G., Judge, N., Bramwell, N. (1997) Overpressure and hydrocarbon traping in the Chalk of the Norwegian Central Graben. Petroleum Geoscience. 1997, 3(1), 33-42.
[5] Holm, G. (1998) How abnormal pressures affect hydrocarbon exploration, exploitation. Oil & Gas Journal. 96, 79-84.
[6] Whelan, J., Kennicutt II, M. Brooks, J., Schumacher, D., Eglington, L. (1994) Organic geochemical indicators of dynamic fluid flow process in petroleum basins. Organic Geochemistry. 22(4), 587-615.
[7] Ghaith, A., Chen, W., Ortoleva, P. (1990) Oscillatory methane release from shale sourcer ock. Earth Science Reviews. 29(3), 241-248.
[8] Wang, S., Fang, G., Jiao, W., Yu, C., Cheng, L., Deng, Z., Zhang, Z., Yu, Z. (2019) Geological Conditions for Shale Gas Enrichment in the Upper Permian Dalong Formation, the Northeastern Chongqing Area, China. Fresen. Environ. Bull. 28(12), 9610-9619.

[9] Feng, J., Dai, J., Li, X., Luo, P. (2018) Soft collision and polyphasic tectonic evolution of wuxia foreland thrust belt: Evidence from geochemistry and geophysics at the northwestern margin of the junggar basin. Journal of Geodynamics. 118, 32-48.
[10] Ma, D., He, D., Li, D., Tang, J., Liu, Z. (2015) Kinematics of syn-tectonic unconformities and implications for the tectonic evolution of the Hala'alat Mountains at the northwestern margin of the Junggar Basin, Central Asian Orogenic Belt. Geoscience Frontiers. 6(2), 247-264.
[11] Roberts, S., Nunn, J. (1995) Episodic fluid expulsion from geopressured sediments. Marine and Petroleum Geology. 12(2), 195-20.
[12] Cartwright, J. (1994) Episodic basin-wide fluid expulsion from geo-pressured shale sequence in the North Seabasin. Geology. 22(3), 447-450.
[13] Hogg, A., Hamilton, P. (1998) Mycintyre R M. Mapping diagenetic fluid flow with in a reservoir: K-Ardating in the Alwyn area (UK North Sea). Marine and Petroleum Geology. 10, 279-294.
[14] Lee, M., Aronson, J., Savin, S. (1999) K-Ardating of time of gas emplacement in Rotliegendes Sandstone, Netherlands. Bulletin of the American Association Petroleum Geology. 69, 381-1385.
[15] Wang, D., Guo, J., Deng, W. (2019) Diagenesis of Tight Sandstone and its Influence on Reservoir Quality: A Case Study of the Triassic Chang 8 Member in the Xiasiwan area, Ordos Basin, China. Fresen. Environ. Bull. 28(11), 8865-8873.
[16] Xu, Q., Yuan, G., Ding, J., Zhang, W., Xin, H., Deng, C. (2019) Cenozoic tectonic and paleoenvironmental evolution of northwestern china: evidence from two deep boreholes in the jartai basin. Journal of Asian Earth Sciences. 173, 98-112.
[17] Ye, H., Li, X., Li, Z., Zhang, C. (2008) Age and origin of high Ba-Sr appinite-granites at the northwestern margin of the tibet plateau: Implications for early paleozoic Tectonic Evolution of the Western Kunlun Orogenic Belt. Gondwana Research. 13(1), 126-138.
[18] Liewig, N., Clauer, N., Sommer, F. (1987) Rb-Sr and K-Ardating of clay diagenesis in Jurassic sandstone oil-reservoir, NorthSea. Bulletin of the American Association Petroleum Geology. 71, 1461-1474.
[19] George, S., Krieger, F., Eadington, P. (1997) Geochemical comparison of oil bearing fluid inclusions trapped in quartz grains and live oil from the Toro Sandstone, Papua New Guinea. Organic Geochemistry. 26, 155-173.
[20] Nedkvitne, T., Karlsen, D., Bjorlykke, K. (1999) Relationship between reservoir diagenetic evolution and petroleum emplacement in the Ula-field, North Sea. Marine and Petroleum Geology. 10, 255-270.
[21] Elmore, R., Leach, M. (1998) Paleo-magnetism of the Rushsprings sandstone, Cement, Oklahoma: Implications for dating hydrocarbon migration, aero magnetic exploration, and understanding remagnetization mechanism. Geology. 18, 124-127.

Received: **01.12.2020**
Accepted: **03.02.2021**

CORRESPONDING AUTHOR

Baocheng Wu
China University of Petroleum (Beijing),
Beijing 102249 – China

e-mail: wubc@petrochina.com.cn

© by PSP Volume 30– No. 05/2021 pages 5169-5175 Fresenius Environmental Bulletin

RESEARCH ON SEISMIC RESISTANCE OF SIMPLE SUPPORTED BEAM BRIDGES IN MOUNTAINOUS AREAS BASED ON THE NEW SEISMIC RESISTANCE CODE

Miao Zhang[1,*], Chunxia Xie[2]

[1]Sichuan College of Architectural Technology, Department of Transport And Municipal Engineering, Chengdu Sichuan, 610399, China
[2]Sichuan College of Architectural Technology, Department of Civil Engineering, Chengdu Sichuan, 610399, China

ABSTRACT

Western China is an earthquake-prone environment with frequent earthquakes and high intensity. Affected by complex conditions such as topography, geomorphology, and hydrogeology, bridge structures in these areas generally have the typical characteristics of large pier heights and obvious differences in pier heights between adjacent piers. In this paper, taking a multi-joint simply supported beam bridge in a mountainous area in western China as an example, the bridge numerical analysis software Midas Civil is used to systematically study the structural response and anti-falling beam and anti-collision measures under earthquake action. Based on the requirements of seismic input load in the new seismic code "Code for Seismic Design of Highway Bridges", the difference in structural response of bridge structures under the new and old seismic codes, as well as measures to prevent falling beams and collisions, are analyzed. The results show that the load effect value of bridge seismic design using the new seismic code is greater, so the design result is safer. The peak displacement response of the pier top calculated on the basis of the 20 rules is about 1.4 times the calculation result of the 08 detailed rules, which reaches 21 cm. For a simply supported beam bridge in mountainous areas with a period ratio of 0.5, the relative displacement between the expansion joints under the action of an earthquake can reach up to 40 cm. Therefore, it has the possibility of collision or falling beam damage. The period difference of adjacent structures can be effectively adjusted by changing the stiffness of the plate rubber bearing, and the structural response of the simply supported beam bridge under earthquake action can be significantly improved. When the period ratio changes from 0.5 to 1.0, the relative displacement peak value decreases from 40 cm to only 2 cm. This study can provide a basis for the design and calculation of similar bridges.

KEYWORDS:
Simple beam bridge, mountainous area, seismic response, seismic code, period ratio, bridge earthquake damage environment

INTRODUCTION

Western China is an earthquake-prone area with frequent earthquakes and high intensity. Affected by complex conditions such as topography, geomorphology, and hydrogeology, bridge structures in these areas generally have the typical characteristics of large pier heights and obvious differences in pier heights between adjacent piers [1-2]. The reduction of earthquake damage to bridges under the action of an earthquake can ensure the safety of people's lives and property. At present, the research on the seismic design of bridges mainly concentrates on seismic mitigation and isolation technology [3-8], anti-collision and anti-falling beam measures [9-19], and pier ductility seismic design [20-21]. In terms of seismic isolation technology, Hameed et al. [3] analyzed the impact of lead rubber bearings (LRB) on the seismic response of bridge structures, and proposed a design scheme based on LRB seismic isolation bridges under different ground motion conditions. Xu et al. [4] analyzed the response of a multi-span continuous girder bridge with double-concave friction pendulum bearings for seismic isolation under unstable random seismic excitation with the characteristics of discontinuity, traveling wave effect and site effect. In terms of anti-collision and anti-falling beam measures, Wang et al. [10] studied the influence of period ratio and expansion joint gap on the collision response of continuous beam bridges. Won et al. [13] studied the impact of collision and period difference on the response of simply supported beam bridge piers. Bi et al. [14] studied the impact of spatial excitation on the collision of simply supported beam bridges. In terms of pier ductility seismic design, Wang et al. [20] proposed a displacement-based seismic design method for reinforced concrete piers that can achieve multi-level performance goals by improving the capacity spectrum method. Liu et al. [21] derived a simplified equation for the displacement shape of the superstructure of a continuous beam bridge under transverse seismic action.

In this paper, taking a multi-joint simply supported beam bridge in a mountainous area in western China as an example, the bridge numerical analysis software Midas Civil is used to systematically study

the structural response and anti-falling beam and anti-collision measures under earthquake action. Based on the requirements of seismic input load in the new seismic code "Code for Seismic Design of Highway Bridges", the difference in structural response of bridge structures under the new and old seismic codes, as well as measures to prevent falling beams and collisions, are analyzed. This study can provide a basis for the design and calculation of similar bridges.

MATERIALS AND METHODS

Model construction. In this paper, we take a five-joint simply supported beam bridge in the mountainous areas of western China as an example to carry out a case study. The upper structure adopts prestressed simply supported T-beams with a span of 30m, and the lower structure adopts double-column piers. The height of the bridge pier is 13m~48m, and the support is a plate rubber support.

The dynamic analysis model was established with the bridge numerical analysis software Midas Civil. The main beams, bridge piers and cap beams all adopt elastic beam elements. The support adopts an elastic connection unit, and the sliding support characteristics and fixed support characteristics of the plate rubber support are realized by adjusting the spring connection stiffness. In addition, the foundation is a rock-socketed pile on a hard rock layer, which ignores the influence of pile-soil interaction (consolidation of the pier bottom). The bridge model is shown in Figure 1.

Comparison of earthquake input load. The new version of "Code for Seismic Design of Highway Bridges" (JTG/T 2231-01-2020) was released in 2020. It replaces the "Detailed Rules for Seismic Design of Highway Engineering" (JTG/T B02-01-2008) issued and implemented in 2008. They have made major changes in the requirements for ground motion input loads. Changes in the input load will significantly affect the seismic response of the bridge structure.

The standard response spectrum curve stipulated in the 08 rules is shown in formula (1) [7, 22]:

$$S(T)=\begin{cases} S_{\max}(5.5T+0.45) & T<0.1 \\ S_{\max} & 0.1\le T\le T_g \\ S_{\max}(T_g/T) & T>T_g \end{cases}$$
$$S_{\max}=2.25C_iC_sC_dA \quad (1)$$

In the formula, T is the period, Tg is the characteristic period, Smax is the maximum design acceleration response spectrum, Ci, Cs, Cd are the site importance coefficient, site coefficient, damping adjustment coefficient, and A is the horizontal basic ground motion peak acceleration.

The response spectrum curve specified in the 20 rules is shown in formula (2):

$$S(T)=\begin{cases} S_{\max}(0.6T/T_0+0.4) & T\le T_0 \\ S_{\max} & T_0<T\le T_g \\ S_{\max}(T_g/T) & T_g<T\le 10 \end{cases}$$
$$S_{\max}=2.5C_iC_sC_dA \quad (2)$$

In the formula, T0 is the maximum period of the linear rising section of the response spectrum, which is 0.1 s, and the rest are consistent with formula (1).

It can be seen from the formulas (1) and (2) that these two rules have very different regulations on the standard response spectrum, especially the regulations on the maximum design acceleration response spectrum Smax. According to the bridge type and site type of the simply supported girder bridge studied (the bridge seismic fortification type is Type B bridge, the engineering site type is Type II site, the site characteristic period is 0.45s, and the seismic fortification intensity is 8 degrees), the comparison curve of the code response spectrum is drawn (Figure 2). It can be seen from Figure 2 that the response spectrum curves of the two types of rules are significantly different in the rising section, the platform section and the falling section. In addition, the design acceleration values corresponding to the 20 anti-seismic rules are all greater than the 08 anti-seismic rules.

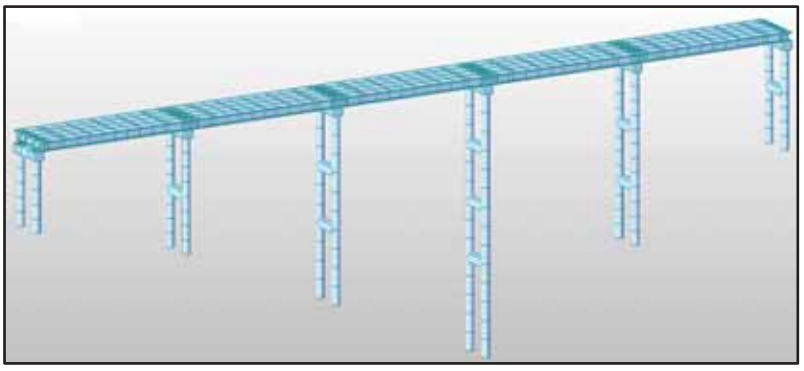

FIGURE 1
Schematic diagram of a simply supported beam bridge model.

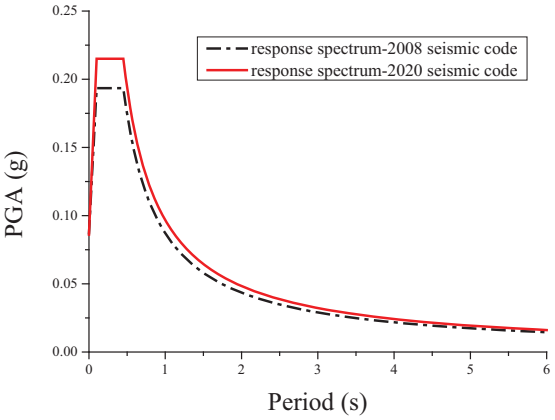

FIGURE 2
Comparison of the response spectra of the two types of specifications.

RESULTS

Differences in earthquake response of bridges under two types of standard conditions. The structural response of a simply supported girder bridge under earthquake mainly refers to the displacement level of the pier top and the force level of the pier bottom. In view of the large differences in the input load requirements between the two types of codes, the difference between the top displacement of the pier and the force on the bottom of the pier under the action of different codes was compared. The seismic response results of the bridge piers under the action of the two types of response spectrum functions are shown in Table 1. It can be seen from Table 1 that regardless of the displacement at the top of the pier or the shear and bending moments at the bottom of the pier, the structural response under the response spectrum load specified in the 20 seismic rules is greater than the calculation results of the 08 seismic rules. In addition, the displacement at the top of the pier, the shear force at the bottom of the pier and the bending moment at the bottom of the pier are magnified by 1.11 times. Therefore, the 20 anti-seismic rules are more safe.

In order to further observe the influence of the two types of codes on the structural response, we calculated the difference in the structural response under the excitation of artificial seismic waves generated according to the same rule. The response results under two artificial time history excitations are shown in Figure 3.

From the comparison result of the displacement time history curve of the pier top in Figure 3, it can be seen that similar to the analysis result of the response spectrum, the structural response corresponding to the 20 rules is greater than the corresponding analysis result of the 08 rules. But the difference is that the degree of amplification of the response is different. For example, the peak responses of the pier tops of 3# pier and 4# pier are respectively enlarged by 1.38 times and 1.4 times.

From the above response spectrum analysis and time history analysis results, it can be seen that the analysis results of simply supported beam bridges based on the 20 rules are greater than those based on the 08 rules. Therefore, the load effect value of bridge seismic design using the new seismic code is greater, so that the designed result is safer and more reasonable.

Analysis of the measures to prevent falling beams and anti-collision of simple beam bridges in mountainous areas. Through the analysis of the difference in the seismic response of the bridge under the action of the two types of codes, it can be seen that under the action of the seismic load, the peak displacement of the pier top of the bridge may exceed 20 cm. The relative displacement of adjacent bridge spans caused by this may be much larger than the gap between the bridge expansion joints or the overlap length between the main girder and the bridge pier, which may cause the main girder to collide or fall. Therefore, it is necessary to study the related content of beam drop prevention and collision prevention of simply supported beam bridges in mountainous areas.

The time-history curve of the relative displacement between the main girder of the simply supported beam bridge under the excitation of the artificial seismic wave generated by the new seismic code response spectrum and the peak relative displacement under the excitation of the time-history load are shown in Figure 4. Among them, the seam 2# represents the relative displacement between the expansion joints on the 2# pier. The other situation is similar.

It can be seen from Figure 4(a) that the relative displacement trend between the expansion joints is quite different, but they are all maintained at a higher level. According to Figure 4(b), it can be seen that the relative displacement between the expansion joints of the simply supported beam bridge under the action of the earthquake is basically greater than 25 cm. Among them, the relative displacement of 4# expansion joint is the largest, reaching 36 cm, which is much larger than the gap value of expansion joint (generally less than 20 cm). In this case, there is a possibility of collision damage between adjacent main beams. The opposite displacement of 3# expansion joint is close to 40 cm, and the main beam may be damaged by falling beam. Whether it is collision damage or falling beam damage, it may cause serious casualties and economic losses, and increase the disaster degree of earthquake rescue after the earthquake.

TABLE 1
Comparison of analysis results of seismic response of bridge piers.

Pier number	Pier top displacement (m)		Shear force at pier bottom (kN)		Bending moment at pier bottom (kN/m)	
	08 rules	20 rules	08 rules	20 rules	08 rules	20 rules
1#	0.020	0.023	120.75	134.16	1 715.08	1 905.65
2#	0.046	0.051	94.44	104.93	1 678.05	1 864.50
3#	0.076	0.084	94.05	104.49	1 381.42	1 534.91
4#	0.093	0.103	71.73	79.70	1 150.06	1 277.85
5#	0.086	0.095	101.21	112.46	1 664.62	1 849.57
6#	0.066	0.073	161.13	179.03	3 032.04	3 368.94

Notes: The order of piers 1#~6# in the table is from the left pier to the right pier.

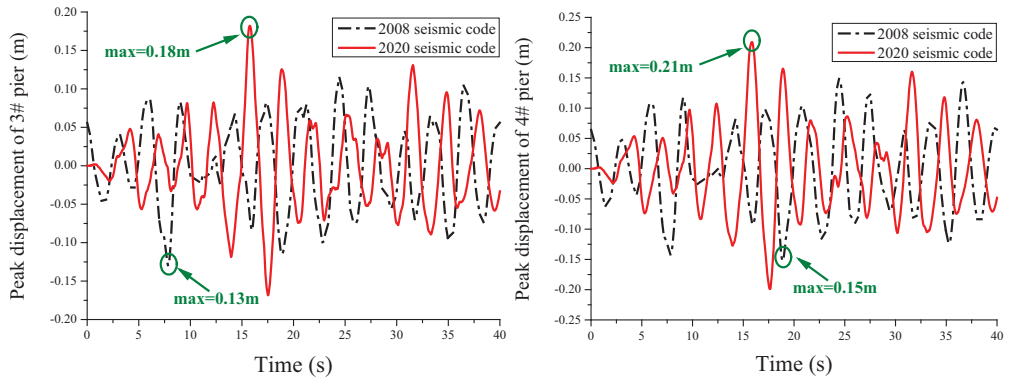

(a) 3# pier top (b) 4# pier top

FIGURE 3
Comparison of the time history curves of the displacement of the top of the pier.

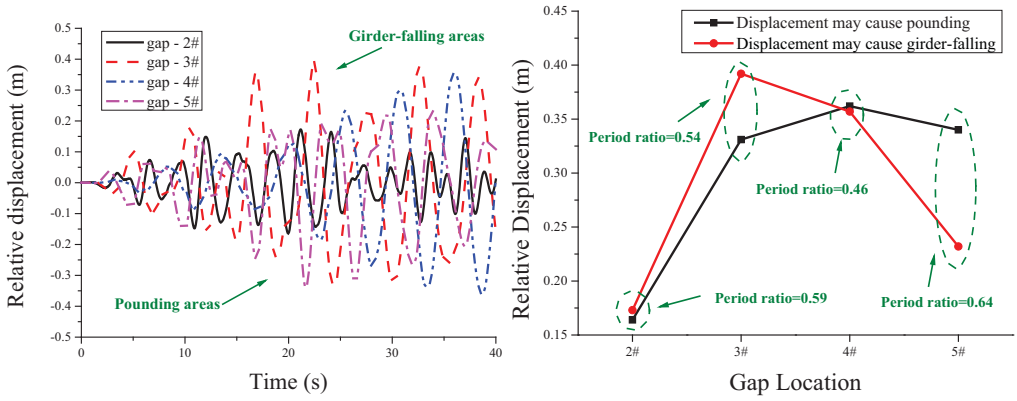

(a) Time history curve of relative displacement (b) Peak relative displacement curve

FIGURE 4
The peak relative displacement and its time history change.

Relevant studies on existing bridges have shown that the periodic difference of adjacent structures is one of the most important causes of collision and falling beam damage [10]. When the cycle ratio of adjacent connections (the ratio of a bridge with a small cycle to a bridge with a large cycle) is less than 0.7, the risk of collision and beam damage is significantly increased. Through modal calculation, the period of each connection of the simply supported beam bridge studied in this paper, and the period ratio of each adjacent connection are obtained. It can be seen from Figure 4(b) that due to the difference of pier height and other factors, the period difference of each adjacent connection of the multi-span simply supported beam bridge studied in this paper is relatively large. The maximum period ratio has reached 0.46, which is far higher than the general requirement that the adjacent period ratio is greater than 0.7. At the same time, it can be seen from Figure4(b) that the larger the period difference, the larger the relative displacement. For example, the period ratios of the adjacent joints at both ends of the expansion joints on the 3# pier and 4# pier are 0.54 and 0.46, respectively, and the corresponding relative displacements under the earthquake action are all greater than 35 cm.

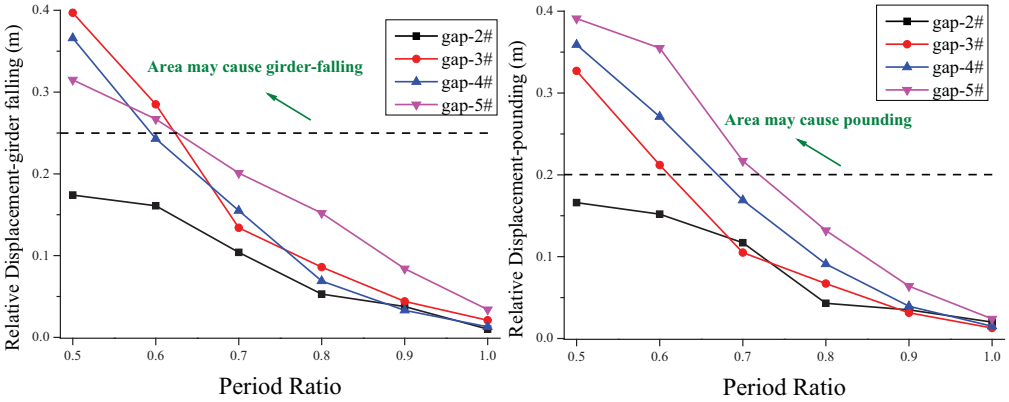

(a) Reverse peak displacement curve (b) Positive displacement peak curve

FIGURE 5

The change of relative displacement peak value under different period ratio conditions.

From the above analysis, it can be seen that for bridge structures with excessively large periods, the relative displacement between each expansion joint under the action of an earthquake is relatively large. Therefore, it has the possibility of collision or falling beam damage.

The large period difference is one of the important factors that cause the relative displacement of adjacent links to be too large, and the adjustment of the period ratio of adjacent structures can achieve the purpose of preventing falling beams and collisions. The adjustment of the period ratio can be achieved by adjusting the height of the pier, the stiffness of the pier, the stiffness of the support, etc. Due to the restrictions of the terrain and geomorphology of the mountainous areas in western China, it is difficult to adjust the height and stiffness of the bridge piers. Therefore, the period ratio of adjacent structures can be adjusted by adjusting the stiffness of the support. In the program, the period ratio of adjacent structures can be adjusted by adjusting the stiffness of the elastic connecting element. Figure 5 shows the curve of the relative displacement peak value between the main beams under different period ratios.

From the curve of relative displacement peak value under different period ratio conditions (Figure 5), it can be seen that as the period difference between adjacent structures decreases, the relative displacement between expansion joints continues to decrease. When the period ratio changes from 0.5 to 1.0, the relative displacement decreases from the maximum value of about 40 cm to only 2 cm. The greater the period difference, the more sensitive the relative displacement is affected by the period ratio. For example, when the period ratio changes from 0.5 to 0.6, the relative displacement decreases by about 30% on average. However, when the period ratio changes from 0.9 to 1.0, the relative displacement only drops below 5%.

From the above analysis, it can be seen that by adjusting the stiffness of the support, the structural response of the simply supported beam bridge under earthquake action can be significantly improved. At the same time, it can also effectively avoid the occurrence of collision or falling beam earthquake damage, and provide traffic guarantee for post-earthquake rescue and disaster relief.

CONCLUSIONS

Based on the earthquake response analysis and calculation of the simple-supported beam bridge in mountainous areas based on the new earthquake code, the following main conclusions are drawn:

(1) In this paper, taking a multi-joint simply supported beam bridge in a mountainous area in western China as an example, the bridge numerical analysis software Midas Civil is used to systematically study the structural response and anti-falling beam and anti-collision measures under earthquake action.

(2) The load effect value of bridge seismic design using the new seismic code is greater, so the design result is safer. The peak displacement response of the pier top calculated on the basis of the 20 rules is about 1.4 times the calculation result of the 08 detailed rules, which reaches 21 cm. For a simply supported beam bridge in mountainous areas with a period ratio of 0.5, the relative displacement between the expansion joints under the action of an earthquake can reach up to 40 cm. Therefore, it has the possibility of collision or falling beam damage.

(3) The period difference of adjacent structures can be effectively adjusted by changing the stiffness of the plate rubber bearing, and the structural response of the simply supported beam bridge under earthquake action can be significantly improved. When the period ratio changes from 0.5 to 1.0, the relative displacement peak value decreases from 40 cm to only 2 cm.

ACKNOWLEDGEMENTS

This work was financially supported by any funds. We want to thank all the techniques who have contributed to this work and all the authors of the references.

REFERENCES

[1] Gao, Y. (2010) Research on Nonlinear Seismic Response Characteristics of Bridges Considering Impact Effect. Chengdu: Southwest Jiaotong University. 19-22.
[2] Chen, F. (2010) Research on seismic damage investigation and seismic conceptual design principles of simply supported bridges. Chengdu: Southwest Jiaotong University. 72-75.
[3] Hameed, A., Koo, M., Do, T., Jeong, J. (2008) Effect of Lead Rubber Bearing Characteristics on the Response of Seismic-isolated Bridges. KSCE Journal of Civil Engineering. 12(3), 187-196.
[4] Xu, B., Yao, Y., Chang, J., Wang, Y., Zhang, M. (2020) Orthogonal sensitivity analysis of cascade slope stability under rainfall and earthquake applied in geology based on the principles of ecological and environmental protection. Fresen. Environ. Bull. 29(8), 6944-6950.
[5] Yuan, W., Wang, B., Cheung, P., Cao, X., Rong, Z. (2012) Seismic performance of cable-sliding friction bearing system for isolated bridges. Earthquake Engineering and Engineering Vibration. 11(2), 173-183.
[6] Hu, Z., Li, Z., Liu, J., Liu J. (1998) Research on Design Parameters of Lead Rubber Bearing for Bridge Journal of Xi'an Highway University. 18(4), 3-5.
[7] Wang, L., Yan, W., Yan, G. (2004) Influence of Lead Rubber Bearing Parameters on the Dynamic Response of Isolated Bridges. Journal of Beijing University of Technology. 30(3), 304-308.
[8] Wang, H., Fu, W., Liu, W., Yu, D., Cheng, S. (2006) Research on the equivalent simplified model of regular isolation structure. Engineering Mechanics. 23(8), 138-143.
[9] Wang, D., Feng, Q., Wang, G. (2004) The collision analysis model of adjacent beams for bridge seismic response based on straight-bar coaxial collision theory. Engineering Mechanics. 21(2), 157-166.
[10] Wang, J., Li, J., Fan, L. (2005) Research on Parameters of Longitudinal Seismic Impact Response of Continuous Beam Bridge. Journal of China Highway and Transport. 18(04), 42-47.
[11] Desroches, R., Muthukumar, S. (2002) Effect of Pounding and Restrainers on Seismic Response of Multiple-Frame Bridges. American Society of Civil Engineers. 128, 860-869.
[12] Wang, J., Li, J., Fan, L. (2007) Current Research Status of Bridge Structure Seismic Impact Effect and Anti-falling Beam Measures. Journal of Highway and Transportation Research and Development. 24(05), 71-75.
[13] Won, J., Mha, H., Kim, S. (2015) Effects of the earthquake-induced pounding upon pier motions in the multi-span simply supported steel girder bridge. Engineering Structures. 93, 1-12.
[14] Bi, K., Hao, H. (2013) Numerical simulation of pounding damage to bridge structures under spatially varying ground motions. Engineering Structures. 46, 62-76.
[15] Jankowski, R., Wilde, K., Fujino, Y. (1998) Pounding of superstructure segments in isolated elevated bridge during earthquakes. Earthquake Engineering & Structural Dynamics. 27(5), 487-502.
[16] Kun, C., Jiang, L., Chouw, N. (2017) Influence of pounding and skew angle on seismic response of bridges. Engineering Structures. 148, 890-906.
[17] Chouw, N., Hao, H. (2008) Significance of SSI and nonuniform near-fault ground motions in bridge response I: Effect on response with conventional expansion joint. Engineering Structures. 30(1), 141-153.
[18] Li, B., Bi, K., Chouw, N., W, J., Hao, H. (2012) Experimental investigation of spatially varying effect of ground motions on bridge pounding. Earthquake Engineering & Structural Dynamics. 41(14), 1959-1976.
[19] Guo, W., Shen, Y. (2002) Analysis of Nonlinear Impact Seismic Response of Elevated Simple Beam Bridge. Earthquake Engineering and Engineering Vibration. 22(04), 108-113.
[20] Wang, D., Li, H., Zhao, Y., Wang, G. (2006) Displacement-based seismic design method of reinforced concrete bridge piers. China Civil Engineering Journal. 39(10), 80-86.
[21] Liu, C., Zhao, C. (2012) Research on Target Displacement Determination Method of Continuous Beam Bridge Directly Based on Displacement. Earthquake Engineering and Engineering Vibration. 32(03), 47-56.
[22] Markiz, N., Jrade, A. (2014) Integrating a fuzzy-logic decision support system with bridge information modelling and cost estimation at conceptual design stage of concrete box-girder bridges. International Journal of Sustainable Built Environment. 3(1), 135-152.

Received: **01.12.2020**
Accepted: **03.02.2021**

CORRESPONDING AUTHOR

Miao Zhang
Sichuan College of Architectural Technology,
Department of Transport and Municipal Engineering,
Chengdu Sichuan 610399 – China

e-mail: 8376330@qq.com

© by PSP Volume 30– No. 05/2021 pages 5176-5186 Fresenius Environmental Bulletin

ANALYSIS OF ULTIMATE BEARING CAPACITY FACTOR OF BURIED STRIP FOUNDATION ADJACENT TO SLOPE BASED ON TERZAGHI THEORY OF FOUNDATION ULTIMATE BEARING CAPACITY

Yang Jiang*, Wenhu Gu, Jiarui Chen

Faculty of Architecture and Civil Engineering, Huaiyin Institute of Technology, Huai'an, 223001, China

ABSTRACT

Considering the contribution of soil strength after the slope to the ultimate bearing capacity of foundation adjacent to slope, the strength of soil after the slope was reduced, and the reduction factor m was used to characterize its strength. A bilateral asymmetric slip failure model was established. Based on Terzaghi theory of foundation, the ultimate bearing capacity of buried strip foundation adjacent to slope was divided into three parts, represented by three bearing capacity factors N_r, N_q, and N_c. Based on the condition that the triangular elastic wedge under the foundation should satisfy the static equilibrium equation, a trial algorithm was used to obtain the value of m, and the expressions for three bearing capacity factors were obtained. The effect of multiple parameters on the three bearing capacity factors of buried strip foundation adjacent to slope was analyzed through programming calculations.

KEYWORDS:
Ultimate bearing capacity factor, buried strip foundation, foundation adjacent to slope, Terzaghi theory, influencing factors

INTRODUCTION

In actual engineering, a large number of foundations are located near a slope. This type of foundation is known as the foundation adjacent to a slope. Compared with ordinary horizontal foundations, the ultimate bearing capacity of a foundation adjacent to a slope has many differences in its failure form and ultimate bearing capacity.

The classical analytical methods for the determination of ultimate bearing capacity of horizontal foundations are based on the superposition principle and are characterized by the ultimate bearing capacity factors, such as Terzaghi [1], Meyerhof [2], Hansen [3], and Vesic [4-5]. Extensive studies have been conducted on the ultimate bearing capacity factor of horizontal foundations.

Bolton et al. [6], Kumar [7], Hjiaj et al. [8], Simth [9], and many others have used the slip-line theory and finite difference method to calculate the bearing capacity factor of a foundation. Diaz-Segura [10] summarized the estimation methods of bearing capacity factor N_r on sandy soil foundations developed by 60 existing scholars, and analyzed and summarized the calculation results. Zhu et al. [11], Ukritchon [12] and Kumar et al. [13], and other scholars used slip-line method, limit analysis finite element method, and other methods to study the effect of factors such as the size of foundation and the roughness of foundation on the bearing capacity factor N_r. Zhan et al. [14] carried out a systematic finite element calculation on the bearing capacity of saturated and undrained clay ground, sandy ground, and soil with a friction angle and cohesion other than 0, and analyzed the trend of each coefficient with influencing factors such roughness of side of foundation, strength parameters of foundation soil, and level of overload. Qin et al. [15] applied the multi-block upper bound method to calculate the bearing capacity factor of foundation N_c under a wide range of cohesive strength with nonuniformity and anisotropy, and obtained the corresponding calculation curve. Wang [16] studied the calculation and engineering application of bearing capacity factor N_c of cohesive soil foundation under undrained conditions.

Based on the limit equilibrium method and superposition principle, the ultimate bearing capacity of a foundation adjacent to slope can also be expressed by three bearing capacity factors N_r, N_q, and N_c. The abovementioned related studies on the ultimate bearing capacity factor of foundation are all directed to the horizontal foundation. The research on ultimate bearing capacity factor of foundation adjacent to slope generally assumes that the foundation is in one-side slip failure mode, and the research is performed by using numerical calculation or experimental methods.

Zhou et al. [17]) used the discontinuous layout optimization (DLO) numerical simulation technology to analyze the bearing capacity of strip foundation adjacent to slope and summarize the failure

mode. Kusakabe et al. [18] established a one-side slip failure mode based on the deformation and failure of foundation soil adjacent to slope in model experiments and calculated the ultimate bearing capacity corresponding to several different sliding surfaces. Yang et al. [19] studied the one-side failure mode of foundation when the foundation was placed on the top of a slope. Castelli et al. [20] used a single-sided sliding failure mode to establish an arc-like sliding failure surface. The ultimate bearing capacity of foundation under static or dynamic loads was solved using the ultimate equilibrium method, and the bearing capacity factor was evaluated based on the failure face.

The abovementioned studies on foundations adjacent to slopes assume that the foundation is a single-sided slip failure mode, and they do not consider the contribution of soil after the slope. In fact, the strength of soil after the slope also has a certain effect on the bearing capacity of slope foundation. To improve the calculation accuracy of ultimate bearing capacity of foundation adjacent to a small slope, the contribution of soil after the slope should be considered, and the two-sided slip failure model should be used for analysis.

Based on the Terzaghi theory of ultimate bearing capacity of foundation, a two-sided asymmetric slip failure model was established. The strength of soil on the back side of slope is reduced. The ultimate bearing capacity of foundation adjacent to slope is also expressed as three bearing capacity factor expressions. The characteristics of bearing capacity factor were studied systematically.

CALCULATION MODEL

Assume that the foundation slope has sufficient height, the foundation slips along the imaginary sliding surface on the side of slope, and a virtual slip surface is present on the back side of slope. A triangular elastic wedge is present below the base, which will slide with the foundation. In a state of elastic balance, the calculation model is shown in Figure 1.

Basic assumptions. (1) The foundation is a shallow buried foundation, and the weight of covered soil above the base is regarded as equivalent overload.

(2) The base is rough, and the linear sliding surface of elastic wedge forms φ_m and φ angles with the base.

(3) The soil slides according to the imaginary failure surface.

(4) The soil is an ideal elastoplastic body and obeys the Mohr-Coulomb failure criterion.

$$\tau = c + \sigma \tan\varphi \tag{1}$$

Where

τ = the shear stress on the shear surface of soil;

σ = the normal stress on the shear surface of soil;

c = the cohesive force of soil;

φ = angle of internal friction of soil.

Foundation failure model. (1) The sliding surface of foundation divides the soil into five zones (as shown in Figure. 1).

Zone I (ADE): In the elastic compaction state, the sliding surface is a set of sliding surfaces passing through the base corner points A and D, and the triangular elastic wedge ADE moves along with the base bottom. Zone II (AEK): logarithmic spiral shear zone (plastic state), the sliding surface of which is a logarithmic spiral EK. Zone III (DEF): logarithmic spiral shear zone (plastic state), the sliding surface of which is a logarithmic spiral EF. Zone IV (DFG): Rankine passive state zone, the sliding surface along the FG line. Zone V (AKJ): Rankine passive state zone, the sliding surface along the AK line.

(2) Soil failure mode before the slope. The logarithmic spiral shear zone AEK is in a plastic state, and the center of spiral is located at point A or its extension line. The center angle can be determined by trial calculation. According to the soil flow law, the displacement vector of soil forms φ angle with the sliding surface (angle of internal friction). Therefore, the velocity direction of shear zone AEK at point E forms φ angle with the tangential direction of spiral sliding surface EK, and the velocity direction is perpendicular to the AE direction. Therefore, the direction of AE line at point A forms an angle (90°+φ) with the tangential direction of EK. According to the Terzaghi hypothesis [2], the AE plane forms an angle φ with the horizontal, and the tangent of logarithmic spiral EK at point E must be vertical.

(3) Soil failure mode after the slope. The fracture surface DEFG is an imaginary sliding surface; EF is a logarithmic spiral; and FG is a straight line. It can be considered that the soil strength after the slope is not fully exerted when the foundation reaches the ultimate bearing capacity, and the feature can be characterized by factor m (reduction factor). At this time, the strength parameters of soil after the slope can be expressed as c_m (cohesion), φ_m (angle of internal friction), and τ_m (shear strength). The soil after the slope also follows the coulomb yield criterion: $\tau_m = m(c + \sigma\tan\varphi) = c_m + \sigma\tan\varphi_m$, i.e., $c_m = mc$; $\tan\varphi_m = m\tan\varphi$. Similar to the soil before the slope, the DE surface forms an angle φ_m with the horizontal; the center of the spiral EF is at point D or its extension.

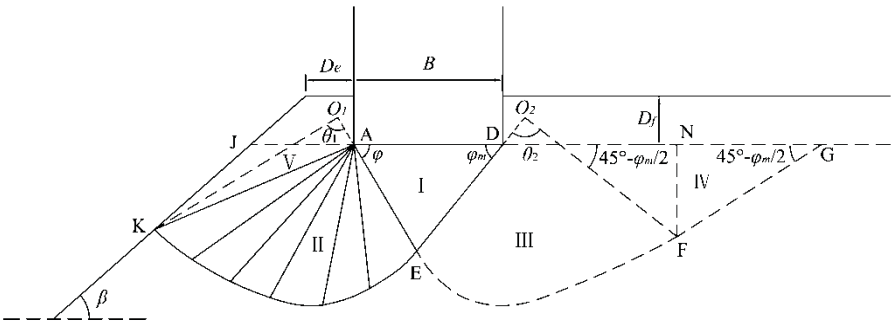

FIGURE 1
Calculation model for foundations adjacent to slopes

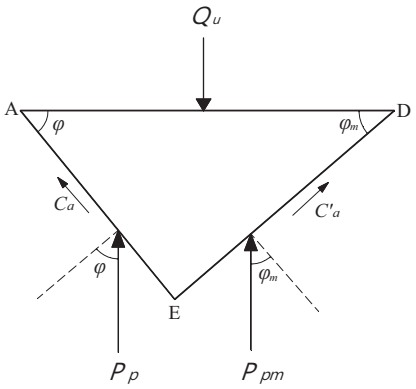

FIGURE 2
Forces on elastic wedge ADE

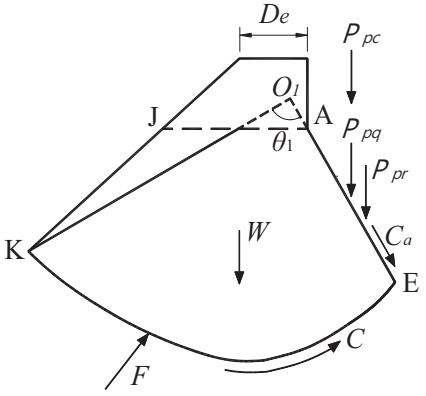

FIGURE 3
Forces on soil mass AEKJ

Principle of calculation. Based on the formula of ultimate bearing capacity of foundation derived from Terzaghi, the ultimate bearing capacity of foundation adjacent to slope is decomposed into three parts: the resistance from the gravity of foundation soil (for $c = q = 0$); the resistance from foundation depth or the overload above the base (for $c = \gamma = 0$); the resistance from the cohesion of foundation soil (for $q = \gamma = 0$). These three resistance effects can be expressed by three bearing capacity factors, namely N_r, N_q, and N_c. Then, the ultimate bearing capacity of the foundation can be expressed as follows:

$$Q_u = B(\frac{1}{2}\gamma B N_r + \gamma D_f N_q + cN_c) \quad (2)$$

For the triangular elastic wedge ADE (shown in Figure 2), which should satisfy the static balance conditions: (a) horizontal force balance: $c_m = mc$; $\tan\varphi_m = m\tan\varphi$; (b) force balance of vertical direction: $Q_u = P_p + P_{pm} + C_a\sin\varphi + C'_a\sin\varphi_m$; (c) rotational moment balance: There must be a reduction factor m which can lead to the moment balance of triangular elastic wedge ADE; also, the factor can be determined by trial calculation according to this condition.

In Figure 2,

$$C_a = c\,.\,AE = \frac{c\,.\,B\sin\varphi_m}{\sin(\varphi+\varphi_m)} \quad (3)$$

$$C'_a = c_m\,.\,DE = m\,.\,c\,.\,DE = \frac{m\,.\,c\,.\,B\sin\varphi}{\sin(\varphi+\varphi_m)} \quad (4)$$

Therefore,

$$Q_u = P_p + P_{pm} + \frac{(1+m)cB\sin\varphi_m\sin\varphi}{\sin(\varphi+\varphi_m)} \quad (5)$$

The passive earth pressure P_P of soil on the side of slope consists of three parts, namely, P_{pr}, P_{pq}, and P_{pc}. The passive earth pressure of the soil on the back side of slope is also composed of three parts, namely, P_{pmr}, P_{pmq}, and P_{pmc}.

Equation (5) can be further expressed as follows:

$$Q_u = (P_{pr} + P_{pq} + P_{pc}) + (P_{pmr} + P_{pmq} + P_{pmc}) + \frac{(1+m)cB\sin\varphi_m\sin\varphi}{\sin(\varphi+\varphi_m)} \quad (6)$$

Comparing Equations (2) and (6), three bearing capacity factors can be obtained:

$$N_r = \frac{2P_{pr} + 2P_{pmr}}{\gamma B^2} \quad (7)$$

$$N_q = \frac{P_{pq} + P_{pmq}}{\gamma D_f B} \quad (8)$$

$$N_c = \frac{P_{pc} + P_{pmc}}{cB} + \frac{(1+m)\sin\varphi_m \sin\varphi}{\sin(\varphi+\varphi_m)} \quad (9)$$

where P_{pr}, P_{pq}, and P_{pc} can be obtained according to the equilibrium condition of soil AEKJ at $c=q=0$, $c=\gamma=0$ and $q=\gamma=0$ (the balance of rotational moment of diagonal point A), as shown in Figure. 1 and 3. P_{pmr}, P_{pmq}, and P_{pmc} can be obtained according to the equilibrium condition of soil DEFN at $c=q=0$, $c=\gamma=0$, and $q=\gamma=0$ (the balance of rotational moment of diagonal point D), as shown in Figure 1 and 4.

Known conditions include: the gravity of soil γ, cohesion c, angle of internal friction φ, angle of slope β, width of foundation B, depth of foundation D_f, distance from the top of the slope D_e, and set the reduction factor m.

MATERIALS AND METHODS

Calculation of P_{pr} and P_{pmr}. As $\tan\varphi_m = m\tan\varphi$, then $\varphi_m = \arctan(m\cdot\tan\varphi)$. Figure 1 shows that $AJ = D_e + D_f\cdot\cot\beta$. According to the geometric relationship of ΔADE, $AE = \frac{B\cdot\sin\varphi_m}{\sin(\varphi+\varphi_m)}$ can be obtained. According to the foundation model, the sliding surface EK is set to a pair of spirals, then:

$$AK = AE\cdot e^{\theta_1\tan\varphi} = \frac{B\cdot\sin\varphi_m}{\sin(\varphi+\varphi_m)}\cdot e^{\theta_1\tan\varphi} \quad (10)$$

In addition, according to the geometric relationship of ΔAKJ,

$$AK = \frac{AJ\cdot\sin\beta}{\sin(\beta+\theta_1+\varphi-180^0)} \quad (11)$$

In the simultaneous Equations (10) and (11), the logarithmic spiral center angle θ_1 can be obtained by trial calculation.

Referring to Figure 3, the moment of gravity of logarithmic spiral shear zone AEK against point A can be expressed as follows:

$$M\_AKE = \int_0^{\theta_1}\gamma\cdot\frac{1}{2}AE^2e^{2\theta\tan\varphi}d\theta \cdot\frac{2}{3}AEe^{\theta\tan\varphi}\sin(\theta+\varphi-90^0) = -\frac{1}{3}\cdot\gamma\cdot AE^3 \cdot\frac{e^{3\theta_1\tan\varphi}[\sin(\theta_1+\varphi)+3\tan\varphi\cos(\theta_1+\varphi)]-4\sin\varphi}{1+9\tan^2\varphi} \quad (12)$$

By substituting the θ_1 value into Equation (10) or (11), the AK value can be obtained. $AJ = D_e + D_f\cdot\cot\beta$, so the moment of gravity of ΔAKJ against point A can also be obtained:

$$M\_AKJ = \frac{1}{2}\cdot\gamma\cdot AJ^2\cdot AK\cdot\cos(\theta_1+\varphi-90^0) + \frac{1}{2}\cdot\gamma\cdot AK\cdot\cos(\theta_1+\varphi-90^0)\cdot[AK\cdot\sin(\theta_1+\varphi-90^0)-AJ]\cdot[\frac{1}{3}AK\cdot\sin(\theta_1+\varphi-90^0)+\frac{2}{3}AJ]-\frac{1}{6}\cdot\gamma\cdot AK\cdot\cos(\theta_1+\varphi-90^0)\cdot[AK\cdot\sin(\theta_1+\varphi-90^0)]^2 \quad (13)$$

As shown in Figure 3, the passive earth pressure P_{pr} of soil before the slope acts on the third position of AE. Thus, according to the balance of rotational moment of soil AEKJ against corner point A, it can be concluded that:

$$P_{pr} = (M\_AKE + M\_AKJ)/(\frac{2}{3}AE\cdot\cos\varphi) \quad (14)$$

As shown in Figure 1, the central angle of logarithmic spiral EF is $\theta_2 = 135^0 - \varphi_m/2$.

The horizontal earth pressure P_r generated by soil △NFG acts at the third point of NF line, so the moment of P_r applied to point D can be expressed as follows:

$$M\_P_r = \frac{1}{3}\cdot\gamma\cdot[\frac{B\cdot\sin\varphi\sin(45^0-\varphi_m/2)}{\sin(\varphi+\varphi_m)}\cdot e^{\theta_2\tan\varphi_m}]^3 \quad (15)$$

The moment of gravity of △DNF against point D is:

$$M\_DNF = \frac{1}{6}\cdot\gamma\cdot[\frac{B\cdot\sin\varphi}{\sin(\varphi+\varphi_m)}\cdot e^{\theta_2\tan\varphi_m}]^3 \cdot\cos\varphi_m\cos(45^0-\varphi_m/2) \quad (16)$$

The moment of gravity of logarithmic spiral sliding soil DEF to point D is:

$$M\_DEF = -\frac{1}{3}\cdot\gamma\cdot DE^3 \cdot\frac{e^{3\theta_2\tan\varphi_m}[\sin(\theta_2+\varphi_m)+3\tan\varphi_m\cos(\theta_2+\varphi_m)]-4\sin\varphi_m}{1+9\tan^2\varphi_m} \quad (17)$$

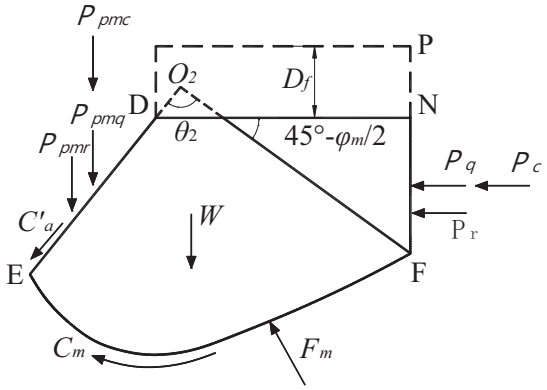

FIGURE 4
Forces on soil mass DEFN

As shown in Figure 4, the passive earth pressure $P_{pm\gamma}$ of soil after the slope acts at the third point of DE, so according to the balance condition of rotation torque of soil DEFN at the corner point D,

$$P_{pm\gamma} = (M\_P_r + M\_DNF + M\_DEF) / (\frac{2}{3} DE \cdot \cos\varphi_m) \tag{18}$$

Therefore, according to the moment balance condition of triangular elastic wedge ADE, the reduction factor m of soil after the slope for $c = q = 0$ can be calculated using the trial algorithm, i.e., Equation (19) must be satisfied as follows:

$$P_{p\gamma} \cdot \frac{1}{3} AE \cdot \cos\varphi + (P_{p\gamma} + P_{pm\gamma}) \cdot (\frac{B}{2} - AE \cdot \cos\varphi) = P_{pm\gamma} \cdot \frac{1}{3} DE \cdot \cos\varphi_m \tag{19}$$

Calculation of P_{pq} and P_{pmq}. As shown in Figure 3, the passive earth pressure P_{pq} from overload before the slope acts on the midpoint of AE, and the soil AEKJ is regarded as a rigid body. Therefore, the balance of rotational moment at the corner point A can be expressed as follows:

$$P_{pq} = \gamma \cdot [D_e^2 \cdot D_f + D_f^2 \cdot \cot\beta \cdot (D_e + \frac{1}{3} D_f \cot\beta)] / (AE \cdot \cos\varphi) \tag{20}$$

As shown in Figure 4, the passive earth pressure P_{pmq} from overload after the slope acts on the midpoint of DE, so according to the balance condition of rotational moment of soil DEFN against the corner point D,

$$P_{pmq} = \gamma D_f B^2 \cdot \frac{\sin^2\varphi}{DE \cdot \sin^2(\varphi + \varphi_m)\cos\varphi_m} \cdot e^{2\theta_2 \tan\varphi_m} \tag{21}$$

Therefore, according to the moment balance condition of triangular elastic wedge ADE, the reduction factor m of soil after the slope for $c = \gamma = 0$ can be calculated using the trial algorithm, i.e., Equation (22) must be satisfied:

$$P_{pq} \cdot \frac{1}{2} AE \cdot \cos\varphi + (P_{pq} + P_{pmq}) \cdot (\frac{B}{2} - AE \cdot \cos\varphi) = P_{pmq} \cdot \frac{1}{2} DE \cdot \cos\varphi_m \tag{22}$$

Calculation of P_{pc} and P_{pmc}. Referring to Figure. 1 and 3, the moment of cohesive force on the logarithmic spiral sliding surface EK before the slope against the corner point A is:

$$M\_C_{EK} = \int_0^{\theta_1} c \cdot r^2 d\theta = \frac{1}{2} c \cdot AE^2 \cot\varphi (e^{2\theta_1 \tan\varphi} - 1) \tag{23}$$

As shown in Figure 3, the passive earth pressure P_{pc} from the cohesive force before the slope acts on the midpoint of AE, and the soil AEKJ is regarded as a rigid body. Therefore, the balance of rotational moment at the corner point A can be expressed as follows:

$$P_{pc} = M\_C_{KE} / (\frac{1}{2} AE \cdot \cos\varphi) \tag{24}$$

The moment of P_c against point D is:

$$M\_P_c = \frac{1}{2} DE^2 \cdot c_m \cdot \tan(45^0 - \varphi_m / 2) e^{2\theta_2 \tan\varphi_m} \tag{25}$$

Referring to Figure 1 and 4, the moment of cohesive force on the logarithmic spiral sliding surface EF after the slope against the corner point D is:

$$M\_C_{EF} = \frac{1}{2} c_m \cdot DE^2 \cot\varphi_m (e^{2\theta_2 \tan\varphi_m} - 1) \tag{26}$$

As shown in Figure 4, the passive earth pressure P_{pmc} from the cohesive force after the slope acts on the midpoint of DE, so according to the balance condition of rotational moment of soil DEFN against the corner point D,

$$P_{pmc} = (M\_P_c + M\_C_{EF}) / (\frac{1}{2} DE \cdot \cos\varphi_m) \tag{27}$$

Therefore, according to the moment balance condition of triangular elastic wedge ADE, the reduction factor m of soil after the slope for $q = \gamma = 0$ can be calculated using the trial algorithm, i.e., Equation (28) must be satisfied:

$$P_{pc} \cdot \frac{1}{2} AE \cdot \cos\varphi + [P_{pc} + P_{pmc} + AE \cdot c \cdot \sin\varphi + DE \cdot m \cdot c \cdot \sin\varphi_m] \cdot (\frac{B}{2} - AE \cdot \cos\varphi) = P_{pmc} \cdot \frac{1}{2} DE \cdot \cos\varphi_m \tag{28}$$

In summary, the trial algorithm is used to determine the soil reduction factor m after the slope, and then according to Equations (14), (18), (20), (21), (24), and (27), these values, including $P_{p\gamma}$, P_{pq}, P_{pc}, $P_{pm\gamma}$, P_{pmq}, and P_{pmc} can be obtained. By substituting the above results into Equations (7), (8), and (9), the three bearing force coefficients N_r, N_q, and N_c can be obtained. The process is implemented by Fortran programming.

RESULTS

Analysis of bearing capacity factor. Through the program calculation, the values of three bearing capacity factors, namely, N_r, N_q, and N_c were determined when the relative distance from the top of the slope D_e/B = 0-2, relative depth of foundation D_f/B = 0-2, angle of slope β = 0-60°, and angle of internal friction φ = 5-45°.

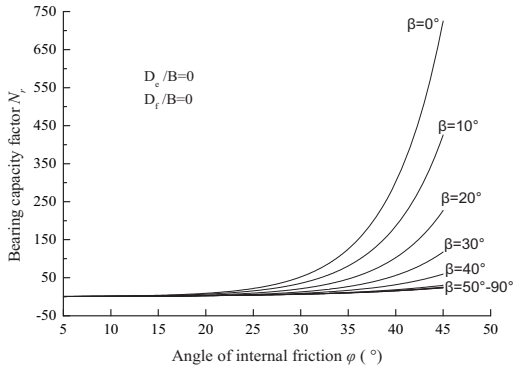

(1) $D_e/B = 0, D_f/B = 0$

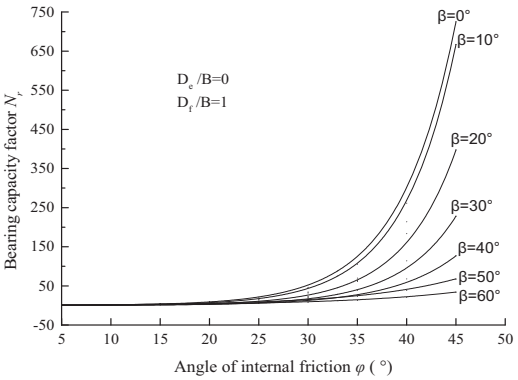

(2) $D_e/B = 0, D_f/B = 1$

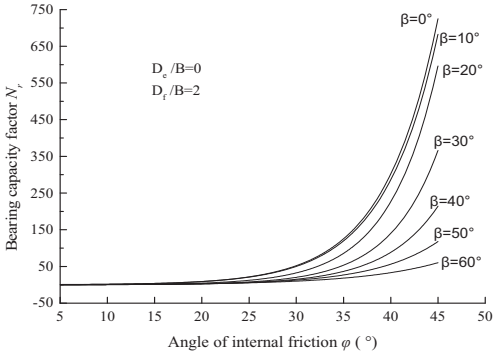

(3) $D_e/B = 0, D_f/B = 2$

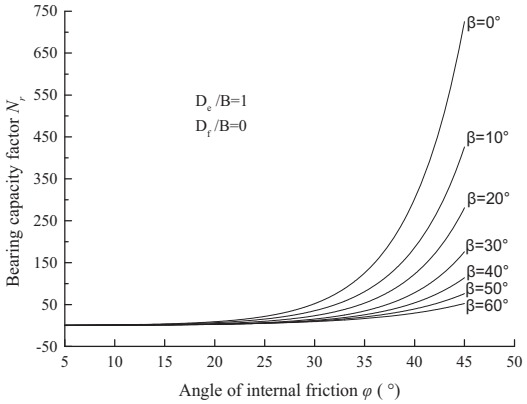

(4) $D_e/B = 1, D_f/B = 0$

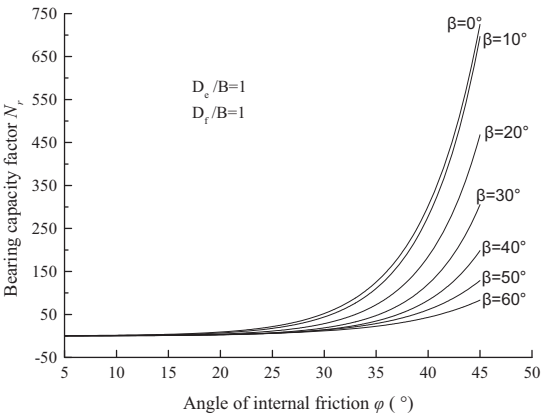

(5) $D_e/B = 1, D_f/B = 1$

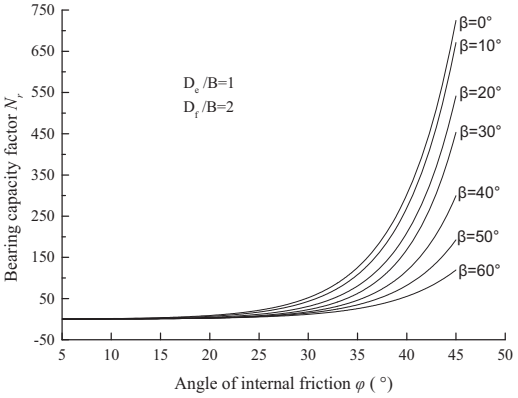

(6) $D_e/B = 1, D_f/B = 2$

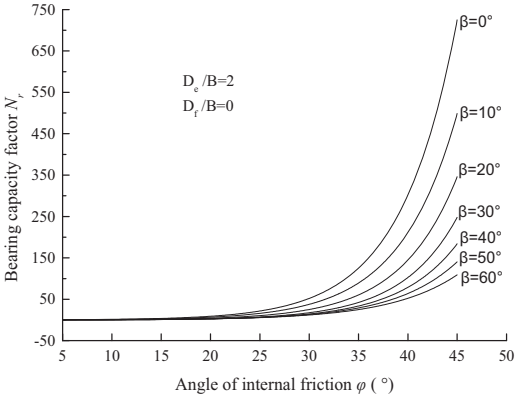

(7) $D_e/B = 2, D_f/B = 0$

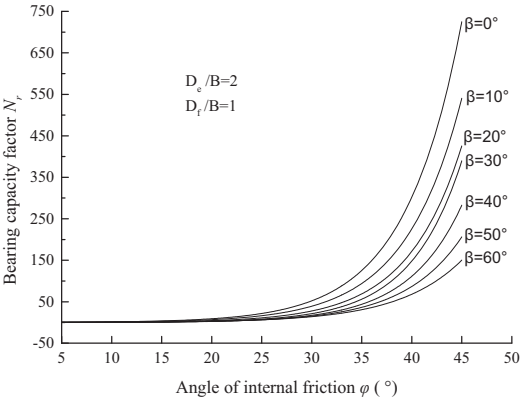

(8) $D_e/B = 2, D_f/B = 1$

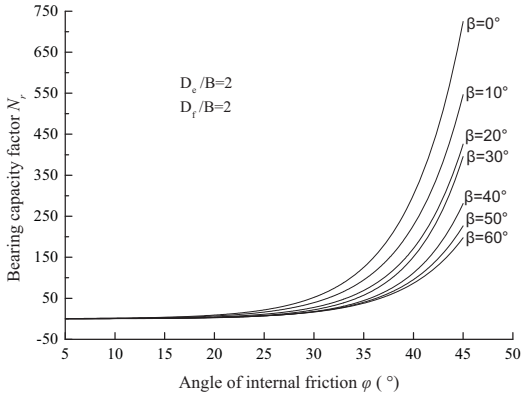

(9) D_e/B=2, D_f/B=2

FIGURE 5
Relation curves of bearing capacity factor N_r vs angle of internal friction φ

Figure 5 shows that,

(1) The value of N_r increases rapidly with the increase in φ. The regression analysis shows that the curve of N_r and φ agrees with the distribution of exponential function, and the value of φ has the most significant effect on the bearing capacity factor N_r of foundation.

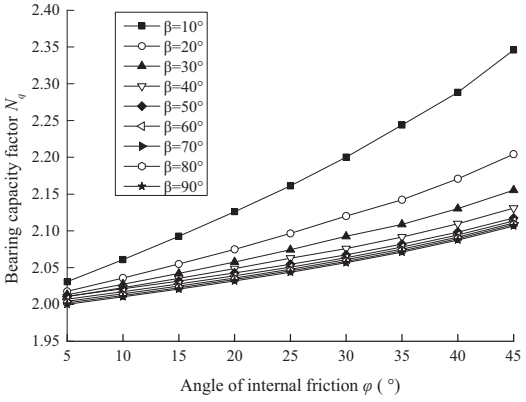

(1) D_e/B= 0, D_f/B= 0

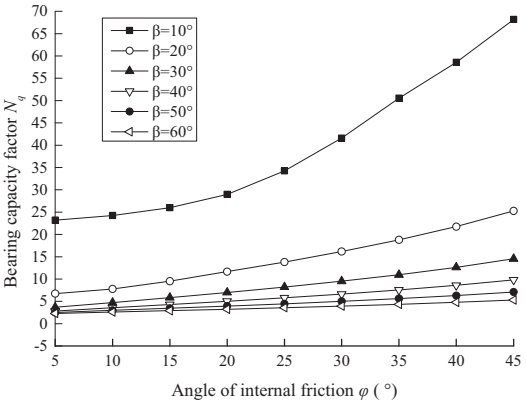

(2) D_e/B= 0, D_f/B= 1

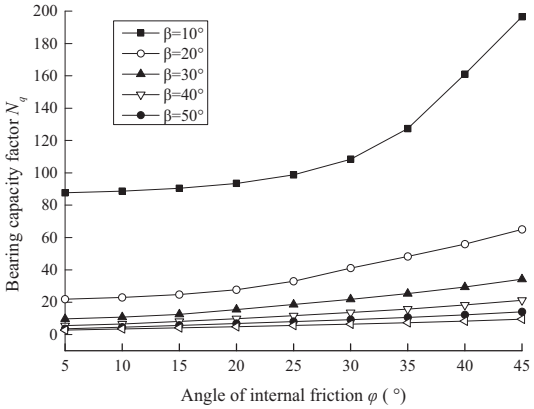

(3) D_e/B= 0, D_f/B= 2

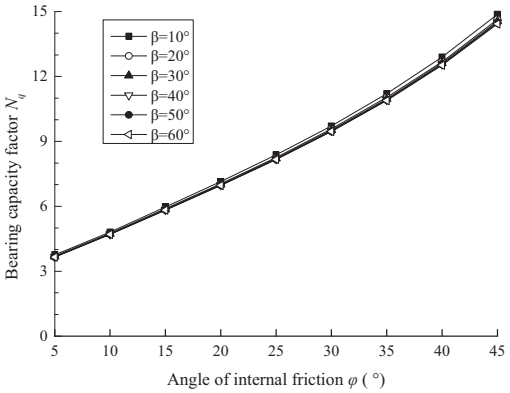

(4) D_e/B= 1, D_f/B= 0

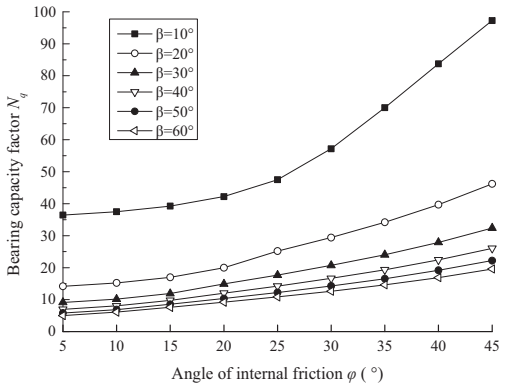

(5) D_e/B= 1, D_f/B= 1

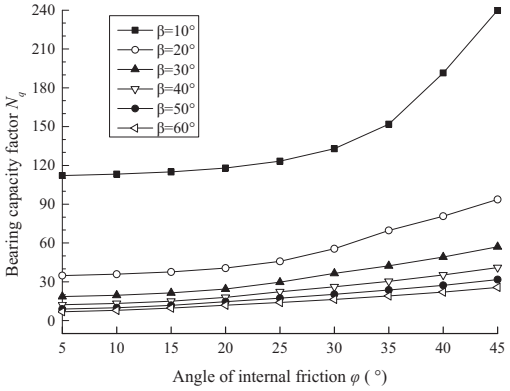

(6) D_e/B= 1, D_f/B= 2

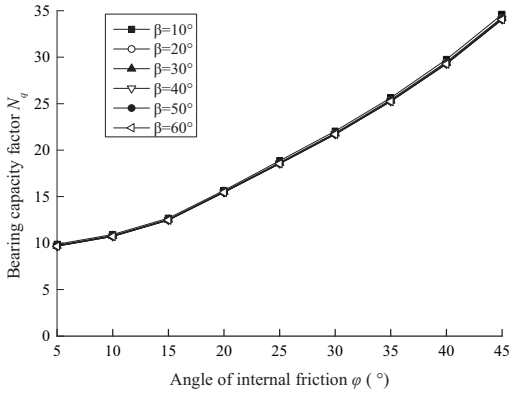

(7) $D_e/B = 2, D_f/B = 0$

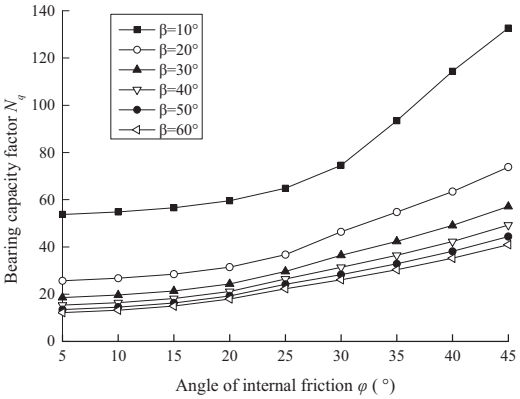

(8) $D_e/B = 2, D_f/B = 1$

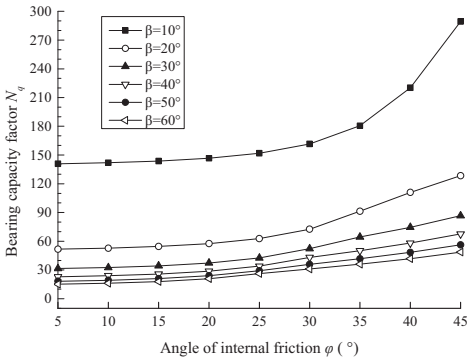

(9) $D_e/B = 2, D_f/B = 2$

FIGURE 6
Relation curves of bearing capacity factor N_q vs angle of internal friction φ

(2) When D_e/B and D_f/B are constant, the smaller the β, the greater the effect of φ on the bearing capacity factor N_r.

(3) The value of N_r increases with the increase in D_e/B and D_f/B, and decreases with the increase in β.

(4) When the angle of internal friction φ is small, D_e/B, D_f/B, and β have less effect on N_r. The larger the φ, the greater the effect of D_e/B, D_f/B, and β on N_r. Because the angle of internal friction of soil reflects the frictional characteristics of soil, it is generally considered to contain three parts: the surface friction of soil particles, the bite force generated by intercalation, and the interlocking action between the particles. When the value is large, the soil of foundation side has a more constraining effect on the foundation, causing the N_r value to increase rapidly with the increase in D_e/B, D_f/B or the decrease in β.

(5) When the angle of internal friction φ is large, i.e., D_e/B, D_f/B, and β may have a significant effect on N_r, the magnitude of β determines the degree of influence of D_e/B and D_f/B on N_r. At this time, when the value of φ is constant, the larger the β, the more obvious the effect of D_e/B and D_f/B on N_r, and vice versa. When β approaches 0, the value of N_r does not substantially change with changes in D_e/B and D_f/B.

(6) The calculation shows that the larger the φ and β, the greater the effect of D_e/B and D_f/B on N_r. When the soil $\varphi \leq 20°$ and $\beta \leq 10°$, the N_r value is slightly affected by D_e/B and D_f/B.

Figure 6 shows that,

(1) The value of bearing capacity factor N_q increases as the angle of internal friction φ increases. When the slope angle $\beta < 20°$, the value of N_q shows a significant nonlinear change with φ. In the front part of curve, i.e., when φ is small, the curve is smoother. In the latter part of curve, i.e., when φ is large, the curve is steep. When the slope angle $\beta \geq 20°$, the value of N_q gradually changes linearly with φ. The larger the β, the more obvious the linear feature.

(2) By comparing the values of N_q at different D_e/B in Figure 6, it can be observed that the value of N_q increases as D_e/B increases. It can be considered that under the condition of a certain burial depth, the greater the distance from the top of the slope, the greater the effect of overloaded soil on the stability of foundation on slope.

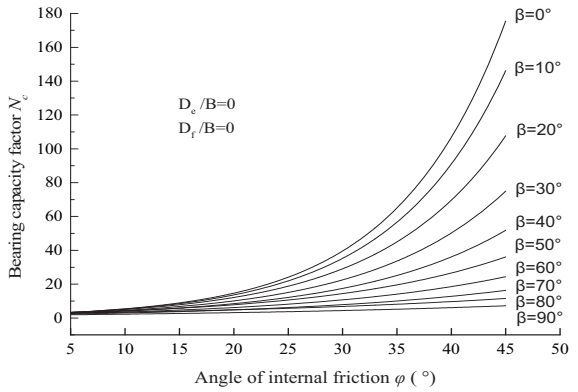

(1) $D_e/B=0, D_f/B=0$

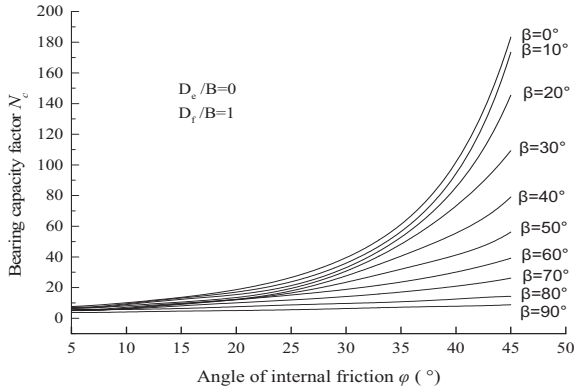

(2) $D_e/B=0, D_f/B=1$

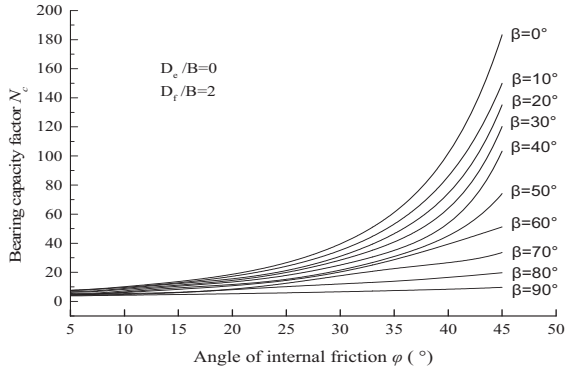

(3) $D_e/B=0, D_f/B=2$

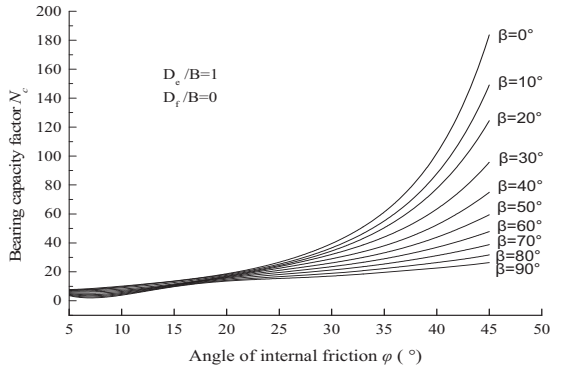

(4) $D_e/B=1, D_f/B=0$

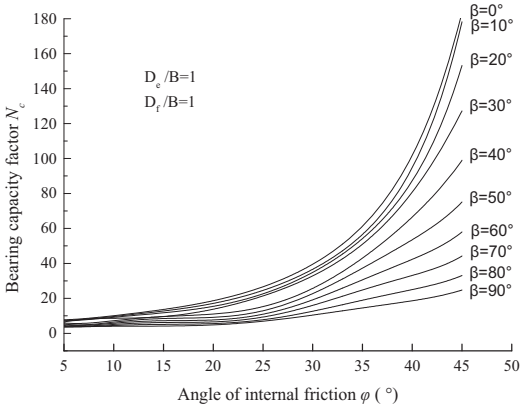

(5) $D_e/B=1, D_f/B=1$

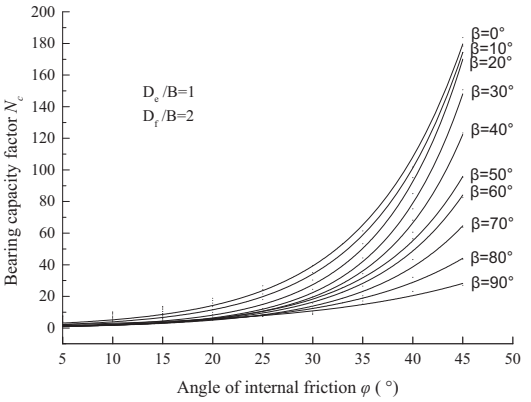

(6) $D_e/B=1, D_f/B=2$

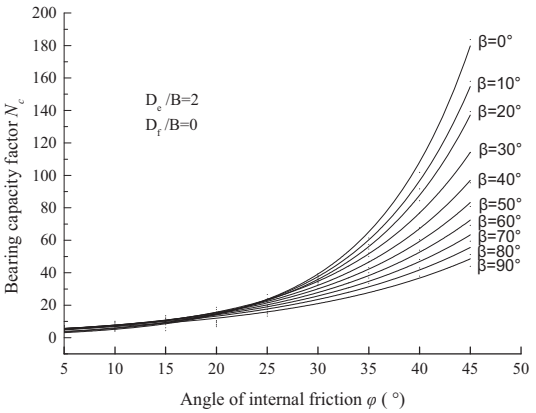

(7) $D_e/B=2, D_f/B=0$

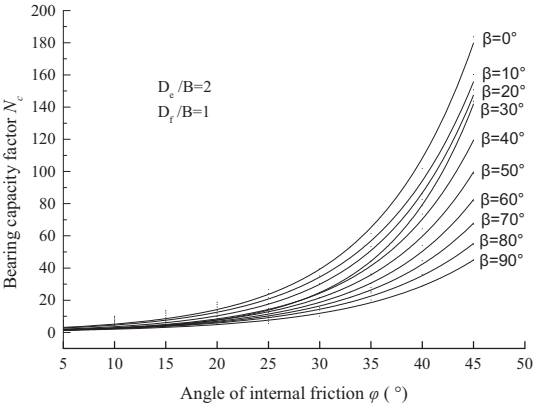

(8) $D_e/B=2, D_f/B=1$

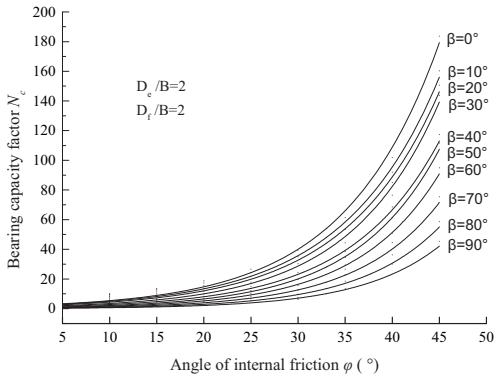

(9) $D_e/B = 2$, $D_f/B = 2$

FIGURE 7
Relation curves of bearing capacity factor N_c vs angle of internal friction φ

(3) Comparing the values of N_q at different D_f / B in Figure 6, it can be observed that N_q increases as the D_f / B increases.

(4) The larger the angle of slope β, the smaller the N_q. When the value of β is small, the change of β has a greater effect on N_q. In contrast, when the value of β is larger, the change of β has less effect on N_q.

Figure 7 shows the value of bearing capacity factor N_c when the relative distance from the top of slope D_e/B = 0-2, relative depth of foundation D_f/B = 0-2, angle of slope β = 0-90 °, and angle of internal friction φ = 5-45 °. As observed,

(1) The φ value of foundation soil has a significant effect on N_c, and the variation curve of N_c and φ is consistent with the distribution function of exponential function.

(2) The value of N_c increases as D_e/B and D_f/B increase, and decreases as β increases.

(3) When D_e/B and D_f/B are fixed, the smaller the β, the greater the effect of φ on the foundation bearing capacity factor N_c.

(4) When φ is small, the changes in D_e/B, D_f/B, and β have slight effect on N_c. The larger the φ, the more sensitive the N_c to the changes in D_e/B, D_f/B, and β. That is, the sensitivity of N_c to D_e/B, D_f/B, and β is closely related to the φ of soil.

(5) Comparing Figure. 7 (1)-(9), it can be observed that when N_c changes significantly with the changes in D_e/B, D_f/B, and β parameters, the difference in β value determines the sensitivity of N_c to the D_e/B and D_f/B parameters. That is, when φ is constant, the larger the β, the more sensitive the N_c to the D_e/B and D_f/B parameters, and vice versa.

CONCLUSIONS

A two-sided asymmetric failure model was used to fully consider the strength of soil on the back side of slope. Based on the limit equilibrium method and superposition principle, the ultimate bearing capacity of foundation adjacent to slope is decomposed into three parts, with three bearing capacity factors N_r, N_q, and N_c to characterize it.

The effects of angle of internal friction φ, angle of slope β, relative distance from the top of slope D_e/B, and relative depth of foundation D_f/B on bearing capacity factors N_r, N_q, and N_c of the foundation adjacent to slope were analyzed by performing programming calculations. The results show that:

(1) The change curve of N_r and φ agrees with the distribution of exponential function. The value of φ has the most significant effect on the bearing capacity factor N_r of foundation. When D_e/B and D_f/B are constant, the smaller the value of β, the more the value of φ affects the bearing capacity factor N_r of foundation. The value of N_r increases with the increase in D_e/B and D_f/B, and decreases with the increase in β. The larger the value of φ and β, the greater the effect of D_e/B and D_f/B on the value of N_r.

(2) The bearing capacity factor N_q increases as the angle of internal friction φ increases. When the angle of slope β is less than 20°, the value of N_q shows a significant nonlinear change with the value of φ. When the angle of slope β is greater than 20°, the value of N_q gradually changes linearly with the value of φ. The larger the value of β, the more obvious the linear characteristics. The value of N_q increases as the values of D_e / B and D_f / B increase. The larger the value of angle of slope β, the smaller the value of N_q, and when the value of β is smaller, the change of β has a greater effect on N_q.

(3) The φ value of foundation soil has a significant effect on N_c, and the variation curve of N_c and φ is more consistent with the exponential function distribution characteristics. The value of N_c increases with the increase in D_e/B and

D_f/B, and decreases with the increase in β. When D_e/B and D_f/B are constant, the smaller the β, the greater the effect of φ on the foundation bearing capacity factor N_c. The larger the φ, the more sensitive the N_c to the changes in D_e/B, D_f/B, and β. When φ is constant, the larger the β, the more sensitive the N_c to the parameters D_e/B and D_f/B.

REFERENCES

[1] Terzaghi, K. (1943) Theoretical soil mechanics. John Wiley and Sons Inc., New York, 112-118.

[2] Meyerhof, G.G. (1951) The ultimate bearing capacity of foundations. Geotechnique. 2, 301-332.

[3] Hansen, J.B. (1970) A revised and extended formula for bearing capacity. Bulletin of the Danish Geotechnical Institute. 28, 5-11.

[4] Vesic, A.S. (1973) Analysis of ultimate loads of shallow foundations. Journal of the Soil Mechanics and Foundations Division. 99(1), 45-73.

[5] Vesic, A.S. (1975) Bearing capacity of shallow foundations. In: Foundation Engineering Handbook. Van Nostrand Reinhold Company, New York. 121-145.

[6] Bolton, M.D. and Lau, C.K. (1993) Vertical bearing capacity factors for circular and strips on Mohr-Coulomb soil. Canadian Geotechnical Journal. 30, 1024-1033.

[7] Kumar, J. (2003) Nγ for rough strip footing using the method of characteristics. Canadian Geotechnical Journal. 40(3), 669-674.

[8] Hjiaj, M., Lyamin, A.V. and Sloan, S.W. (2005) Numerical limit analysis solutions for the bearing capacity factor Nγ. International Journal of Solids and Structures. 42(5-6), 1681-1704.

[9] Simth, C.C. (2005) Complete limiting stress solutions for the bearing capacity of strip footings on a Mohr-Coulomb soil. Geotechnique. 55(8), 607-612.

[10] Diaz-Segura, E.G. (2013) Assessment of the range of variation of Nγ from 60 estimation methods for footings on sand. Canadian Geotechnical Journal. 50, 793-800.

[11] Zhu, F.Y., Clark, J.I. and Phillips, R. (2001) Scale effect of strip and circular footings resting on dense sand. Journal of Geotechnical and Geoenvironmental Engineering. 127(7), 613-621.

[12] Ukritchon, B. (2003) Calculations of bearing capacity factor Nγ using numerical limit analyses. Journal of Geotechnical and Geo-environmental Engineering. 129(6), 468-474.

[13] Kumar, J. and Khatri, V.N. (2008) Effect of footing width on bearing capacity factor Nγ for smooth strip footings. Journal of Geotechnical and Geo-environmental Engineering. 134(9), 1299-1310.

[14] Zhan, Y.G., Yuan, F.F. and Luan, M.T. (2008) Numerical Study of Bearing Capacity Factors For Strip Footing Embedded in Homogeneous Subsoil. Chinese Journal of Rock Mechanics and Engineering. 27(s2), 3408-3415.

[15] Qin, H.L., Huang, M.S. and Wang, Y.J. (2010) Calculations of Nc for anisotropic and nonhomogeneous soils. Chinese Journal of Geotechnical Engineering. 32(8), 1194-1199.

[16] Wang, H.X. (2016) Estimation and engineering application of bearing capacity factors (Nc) in clay strata under undrained condition. Chinese Journal of Geotechnical Engineering. 38(3), 546-553.

[17] Zhou, H.Z., Zheng, G. and Yin, X. (2018) The bearing capacity and failure mechanism of a vertically load strip footing placed on the top of slopes. Computers and Structures. 94, 12-21.

[18] Kusakabe, O., Kimura, T. and Yamaguchi, H. (1981) Bearing capacity of slopes under strip load on the surfaces. Soils and Foundations. 21(4), 29-35.

[19] Yang, F., Yang, J.S., and Zhang, X.M.; Zhao, L. (2010) One-side slip failure mechanism and upper bound solution for bearing capacity of foundation on slope. Engineering Mechanics. 27(6), 162-168.

[20] Castelli, F., and Motta, E. (2010) Bearing capacity of strip footings near slopes. Journal of Geotechnical and Geological Engineering. 28(2), 187-198.

Received: **02.12.2020**
Accepted: **07.02.2021**

CORRESPONDING AUTHOR

Yang Jiang
Faculty of Architecture and Civil Engineering,
Huaiyin Institute of Technology,
Huai'an, 223001 – China

e-mail: jy_12345678@163.com

© by PSP Volume 30– No. 05/2021 pages 5187-5193 Fresenius Environmental Bulletin

A SURVEY RESEARCH ON ENVIRONMENTALLY FRIENDLY CONSUMPTION BEHAVIOR

Sule Turhan[1,*], SefaCakir[2], SelinTugba Varoglu[2,3]

[1]Bursa Uludag University, Faculty of Agriculture, Department of Agricultural Economics, Bursa, Turkey
[2]Republic of Turkey, Ministry of Agriculture and Forestry, Kocaeli, Turkey
[3]PhD Student, Bursa Uludag University, Faculty of Economics, Department of Econometrics, Bursa, Turkey
[4]Republic of Turkey, Ministry of Agriculture and Forestry, Igdir, Turkey

ABSTRACT

This study applies conjoint analysis in order to evaluate consumer preferences for the product attributes of apple and it aims to forecasting the importance of the product charachter and attribute levels. In addition, environmental awareness of consumers, and environmentally friendly consumption behavior researched. A previous study by Manola (1990) has shown conjoint analysis provides results that might not be obtained from a survey where respondents are asked to directly state their assessment of the importance attributes. The results give us information about the trade-offs that consumers make between price, crispness, size, flavor, color of apple. According to the conjoint analysis results and the survey findings price is an important attribute that consumers take into account during the decision process of buying apples. The results show that price is the most critical attribute; it is almost twice as important as the second critical attribute which is color.

KEYWORDS:
Apple, consumption, conjoint approach, Turkey

INTRODUCTION

While the apple production in Turkey was 109 thousand tons per year in 1950, this amount reached up to 2,5 million tons per year in 2017[1]. About 76 million tonnes of apples were grown worldwide in 2017, and China produced almost half of this total, followed by the USA Turkey, Italy, India and Poland. As a result of the relevance of the ecological conditions, apple can be produced many places in TURKEY. Bursa, which the study was done in, is a major apple manufacturer city in our country. Apples which are beneficial to human health, have become an indispensable fruit in today's healthy nutrition trends because of its usage in diets and its lack of fat. The big amount of the apples produced in Turkey is being consumed in domestic market and apple is one of the fruit which has a high consumption in domestic market. Because, almost all consumption is realized during the year, it does not allow for stock. The apple consumption per capita in Turkey has shown an upward trend in recent years, the average per capita consumption of 25 kg [2].Although there are many products that are gained by processing apples, consumers usually use apples as fresh fruits. Thus, to execute a good classification, maintaining quality and creating a price policy that can compete in domestic and international markets which will stop consumers from buying low quality products with high prices, are importants issues that must be considered important[3-4].

In this article discusses the relative importance of locally produced apple in the consumer structure of preferences. Also, consumers' perceptions about sustainable consumption and environment are examined.The study has been carried out in Bursa. The purpose of this study, consumption of apple consumption in the Bursa region of Turkey is to identify factors in their choice. Conjoint analysis is used for this.

MATERIALS AND METHODS

A questionnaire was administered to a convenient sample of 141 consumers in Bursa in 2015. The aim of the questionnaire was to establish the product attributes that affect the purchasing decisions of the consumers and the importance of these attributes along with the demographic information. Conjoint data were collected as a separate part of an extensive survey held in a central location in each of the Turkey-Bursa regions mentioned above during the period April 2015–July 2015.In the survey each product attribute was asked to be ranked as very important, important, doesn’tmatter, hot very important and not important by the respondent.They applied a special design model. They examined the ordering of 18 combinations reflecting the highest and lowest preference among the participants in the study. According to the ranveing data obtained from the respondents is analyzed by ordinary least squares regression (OLS). Wittink and Cattin found in their research that OLS is an appropriate estimation method to be used in combined analysis. [5].The commercial use of compound analysis has been documented in the United States by Cattin and Wittink(1992)[6] and

Wittink and Cattin (1989)[5]. Cattin and Wittink obtained information from 17 firms which collectively had completed about 700 projects from 1971 through 1980. Almost three out of every four applications involved new product/concept identification as one of the purposes. Pricing and market segmentation were also frequently mentioned as reasons for conjoint projects. Conjoint (trade-off) analysis is one of the most widely-used quantitative methods in Marketing Research and in a relatively short time, become a popular research tool for commercial applications. [6-7-8-9-10-11-12-13].It is used to measure preferences for product features, to learn how changes to price affect demand for products or service, and to forecast the likely acceptance of a product if brought to market [14]. Louviere 1988, was first used to assess the commercial appeal of consumer goods (for a review of such studies, see Green and Srinivasan 1990[8]) and later was adopted by environmental and agricultural economists and formally embedded in a utility-theoretic framework to assess the welfare effects of altering nonmarket goods (e.g., environmental protection) and introducing goods with novel attributes (e.g., genetically modified ingredients). In the applied study, Umberger et al. (2002) explained that 69% of the consumers had positive WTP estimates for labeled beef produced in the USA.Also, in a different study by Loureiro and Umberger in 2004 [15] use conjoint analysis. Its to estimate WTP for CoOL versus other safety labels on beef. They show that CoOL labeling does not generate a positive WTP, whereas food safety certification and traceability certification do. Mabiso et al. (2005)[16] used an auction experiment to show that the CoOL label garnered premiums for fresh produce. In the case of apples (tomatoes), 79 (72)% paid a premium with the average premium being $0.48 ($0.49).

Murphy et al. (2000)[17], showed that the ideal honey profile for 153 Irish consumers of honey was one with a thick texture, a dark golden colour, made by a small-scale producer, at a price of IR£1.95 and packaged in a 454g (1lb) plain glass jar.Gil and Sanchez (1999)[18], Examines and compares wine attribute preferences within and between two different Spanish regions, Aragón and Navarra, by means of the weighted least squares approach for conjoint analysis.Comparing the different attribute levels, consumers from Aragón preferred locally produced “and cheaper wines, while consumers from Navarra preferred Rioja and more expensive wines. Identifies and characterizes four wine consumer segments. Describes how a market simulation experiment was designed to simulate market shares of three alternative wine profiles.

RESULTS

Demographics Results. In this section, the sexes, ages, education levels and the incomes of the subjects that were surveyed as sample of the consumer market can be found (Table 1).^

The primary results obtained from the surveys are presented in Table 2.

As seen from Table 2. %53 of the respondents stated that crispness is the most important attribute flowed by flavor (%48) and price(%47), on the other

TABLE 1
Demographics results

Gender	%	Age	%
Female	59	0-18	4
Male	41	19-35	43
Education	%	35-55	44
Primary education	26	55-	9
Secondaryeducation	44	**Income**	**%**
Undergraduate education	26	-350$	61
Graduate	4	351-500$	25
		501$-	14

TABLE 2
Importance of apple attributes as stated by the respondents (%)

Attribute	Degree of importance				
	Very important	Important	Doesn’t matter	Not very important	Not important
Size	22	45	6	21	6
Color	27	30	6	29	8
Price	47	29	6	17	1
Crispness	53	35	3	8	1
Flavor	48	36	3	13	0

hand size(%45) and color(%30) are stated to be important by the respondents.

Conjoint Analysis. Today, Conjoint Analysis is widely used, especially for commercial research.In 1978, Green and Srinivasan conducted research and developments in the region using the latest technologies.They suggested conjoint analysis in their marketing work. They used it to test the adequacy of the participants' data. They applied alternative information processing rules in mathematical psychology. An update of their review, with a discussion of new developments in conjoint analysis, appeared only recently[8-19].

Depending on the ranking of the attributes by the respondents, conjoint analysis has been used to answer the question of how much more important one attribute. The answer would lead the producers to make strategic decision related to production and marketing of apple. Each of the attributes has two or three levels which are presented in Table 3.

Respondents were asked to rank 5 attributes, 3 of these attributes had 3 levels and the remaining 2 attributes had 2 levels that lead to 108 possible attribute combinations for the respondent to rank and evaluate. However, since 108 is a very large number to be evaluated in a survey, a special experimental design which is called an orthogonal array is used. In terms of an orthogonal array only a subset of the total number of combinations is chosen. Addelman(1962)[20] developed several basic plans in order to generate orthogonal arrays for various attributes and attribute levels. The 18 combination plan that applies to our case is presented in Table 4.

Respondents were asked to rank the 18 combinations using 1 and 18 to indicate their highest and lowest preferences. The results obtained from the respondents are analyzed with OLS regression. The OLS equation is (McFadden, 1999);

$Yin=\beta0+\beta1X1in+\beta2X2in+\beta3X3in+\beta4X4in+\beta5X5in+\beta6X6in+\beta7Xin+\beta8X8in+ein$

$İ=1,2\ldots\ldots\ldots,18 \quad n=1,2\ldots..,142$

Where Yin=the rank given by the rth respondent to the ith combination

X1in……X8in=level of the attribute size in the combination

(i,e,xi1 and xi2 represent the level of size, xi3

TABLE 3
Attributes and levels in the apple conjoint analysis

Size	Crispness	Price Tl/Kg
Small	Crispy	1.00 TL
Medium	Soft	1.75 TL
Large		2.50 TL
Color	Flavor	
Uniform red	Sweet	
Uniform green	Sour	
Uniform yellow		

TABLE 4
Orthogonal array of 18 combinations Attributes

Number	Size	Color	Price/kg	Crispness	Flavor	Utilities Score
1	Small	Red	1.00	Soft	Sweet	-26.5378
2	Small	Green	1.75	Soft	Sour	10.797
3	Small	Yellow	2.50	Crispy	Sweet	-6.2332
4	Medium	Red	1.75	Crispy	Sour	-4.1119
5	Medium	Green	2.50	Soft	Sweet	2.9608
6	Medium	Yellow	1.00	Soft	Sweet	-10.3229
7	Large	Red	2.50	Soft	Sour	-4.4909
8	Large	Green	1.00	Crispy	Sweet	-23.3863
9	Large	Yellow	1.75	Soft	Sweet	9.6754
10	Small	Red	2.50	Crispy	Sweet	-18.9481
11	Small	Green	1.00	Soft	Sour	-11.4439
12	Small	Yellow	1.75	Soft	Sweet	8.418
13	Medium	Red	1.00	Soft	Sweet	-23.0378
14	Medium	Green	1.75	Crispy	Sweet	1.0972
15	Medium	Yellow	2.50	Soft	Sour	10.4666
16	Large	Red	1.75	Soft	Sweet	-3.0395
17	Large	Green	2.50	Soft	Sweet	0.7182
18	Large	Yellow	1.00	Crispy	Sour	-15.8805

and xi4 represent the level of color, xi5 and xi6 represent the level of price xi7 represents the level of crispness and xi8 represents the level of flavor) The xn is a dummy variable for which the effects of coding (Cohen and Cohen) are used. For the three level attribute size: x1=1 if the level is small and 0 if not; x2=1 if the level is medium and 0 if not; and eventually the level will automatically be large if both x1 and x2 are equal to 0. For example for the 5th combination shown in table 3 (medium. Green, 1.75, soft, sweet) the independent variables will be X1=0, X2=1, X3=0, X4=1, X5=0, X6=1, X7=0, X8=1

Conjoint Analysis Results. In the consumer theory approach presented by Deacon and Lancester (1988)[21] consumers derive utility from the attributes of the product rather than the product itself. The basic principle of conjoint analysis underlies the fact that a product is composed of attributes and consumers preferences vary depending on the importance they assign to the alternative combinations pf attribute levels. The estimation technique assigns a value to each attribute level and that value is called part-worth which indicates the relative importance of that level to the consumer[22].In this study conjoint analysis is applied to estimate part-worths for each individual afterwards cluster analysis groups the consumers based on the singularity of their part-worths.

The regression results are presented in Table 5. The part-worths are estimated from the regression coefficients (Table 6). ln order to illustrate the estimation of the part-worthslets take a look at the attribute level part-worths for price. The adjusted part-worths for the 1.00 TL/kg, 1.75 TL/kg and 2.50 TL/kg were derived respectively as follows: l-13.4659-8.7750l=22.2409, l8.7750-8.7750l=0, l2.3812-8.7750l=6.3938. When we look at the adjusted part-worth we can conclude that the consumers prefer a lower price to a higher price and this conclusion is consistent with the economic theory.

TABLE 5
Estimation results of the regression model

Variable	Estimate
B_1	-1.2574 (-0.3245)
B_3	-3.5000 (-0.9114)
B_4	3.3333 (0.8680)
B_o	-0.76.99 (-0.1658)
B_5	9.5449 (3.0910)
B_6	3.1511 (0.8332)
B_7	4.1287 (1.2387)
B_8	2.6212 (0.7859)

R2=o.6269, F ratio=1.8906 (t ratios are given in parentheses)

TABLE 6
Attribute Level Part-worths

Attributes and Levels	Expressed in terms of regression Coefficients	Estimated part-worths	Adjusted part-worths
Size			
Small	B_0-B_1-B_2	-5.5273	7.5546
Medium	B_0+B_1	-2.0273	0
Large	B_0+B_2	-4.2699	6.2972
Color			
Uniform red	B_0-B_3-B_4	-7.5123	12.7149
Uniform green	B_0+B_3	2.6392	2.5634
Uniform yellow	B_0+B_4	5.2026	0
Price			
1.00TL/kg	B_0-B_3-B_6	-13.4659	22.2409
1.75TL/kg	$B_{0+}B_5$	8.7750	0
2.54TL/kg	B_0+B_4	2.3812	6.3938
Crispness			
Crisp	B_0-B_7	-4.8986	8.2494
soft	B_0+B_7	3.3588	0
Flavor			
Sweet	B_0-B_8	-3.3911	4.9424
Sour	$B_{0+}B_8$	1.5513	0

TABLE 7
Relative importance of apple attributes based on the estimated part-worths

Attribute	Importance	Percent
Size	7.5546	13.56
Color	12.7149	22.83
Price	22.2409	39.93
Crispness	8.2494	14.81
Flavor	4.9424	8.87
Total	55.7022	100

Since we have calculated the part-worths we can determine the total worth of different combinations and these combinations weight not be in the orthogonal array. The most preferred combination would be small uniform red crisp and sweet apple with a price of 1.00TL/kg. The total worth of this combination is
7.5546+12.7149+22.2409+8.2449+4.9424=55.7022.

Among the combinations presented in Table 7, combination 1(small,red,soft and sweet with a price of 1.00TL/kg) has the highest total worth.(47.4528). The difference between the part-worths of the most desired and the least desired level gives us the opportunity to measure the importance of the attribute. The importance weight for an attribute is measured by the adjusted part-worth of the most desired level. Afterwards this value is compared with the values of other attributes. The greater the importance weight is the more important the attribute is. The relative importances of apple attributes are presented in Table 6. In order to make the comparison easier the importance values are also given in percentage. As you can see from Table price is the most important attribute and flavor is the least important attribute.

On the other hand in terms of the classification of goods in economic theory; fruits and vegetables are classified as necessities and thus apple is a necessity. Necessities have inelastic demand which means that the quantity demanded does not respond strongly to the changes in price. However the conjoint analysis results do not exactly confirm the survey findings. According to the survey findings crispness is the attribute that was stated to be the most important attribute not price. 53%of the respondents think that crispness is the most important attribute followed by taste (%48) ad price (%47).

In our case, according to the conjoint analysis results and the survey findings price is an important attribute that consumers take into account during the decision process of buying apples. The conjoint analysis results show that price is the most important attribute and the respondents have stated that price is also a very important factor that affects the buying decision. These results may be reflecting the effect of the income level of the respondents along with the effect of the global economic crisis everyone is experiencing. Even though the economic theory states that the price of apple, which is a necessity, does not change the quantity demanded; In our case this statement could be ignored because the %41 of the respondents are in the low income group and the traumatic effects of the global economics crisis are still increasing in dimension.

Information on the relative importance of attributes and their levels would ait producers to manage production and marketing of apples. The results show that price is the most critical attribute; it is almost twice as important as the second critical attribute which is color. This finding suggests that producers should focus on strategic pricing. If price and the least important attribute instead was not the most important attribute, it could be interpreted as the consumers would not mind paying a higher price. However, in our case if the price increases the amount bought by the respondents are sensitive to changes in price. Thus, the producers should set the price strategically and should not risk to lose the potential buyers.

Ignoring all the attributes but the two most important ones price and color; apple with the price of 1.00 Tl/Kg and the color red would have a total worth of 22.2409+12.7149=34.9558. If the consumer is offered an apple with 1.00 Tl/Kg price but not red and green or yellow instead, the worth of that apple would only be 22.2409. The total worth would increase by 12.7149 because the consumer is getting an apple with a desired price but not the desired color If a red but expensive apple was sold to the consumer then the total worth of the apple would be 12.7149 and would decrease by 22.2409. Comparing the three choices 1) 1.00 Tl/Kg and red, 2) 1.00 Tl/Kg and green, 3) 1.75 Tl/Kg and red; the consumer would prefer the 1st choice and the 2nd would be preferred over the 3rd one.

Producers way use attributes to increase the total worth of the apple if one or more of the desired levels are not available. For instance,if the producer is selling sweet and small apples, the total worth would be 0+7.5546=7.5546. Consumers will not prefer sour and small apples to sweet and small apples but the producer can increase the amount that would be purchased by supplying sweet and large apples to the consumers, and that combination would have a total worth of 4.9424+6.2972=11.2396. Which is higher than the total worth of the sour and small combination. As one can realize, the above examples illustrate how a producer can benefit from the findings of the conjoint analysis. Conjoint analysis is

used by many marketing research firms for new product identification, market segmentation, product positioning, pricing and competitive analysis.

Environmental Perceptions of Consumers. Increasing the use of pesticides every year in our country.The use of agricultural pesticides in the last decade has increased from 60 thousand to 100 thousands.Environmentally friendly consumption; ecological, recyclable and consuming as much products as we need exhibit environmentally friendly products that do not pollute nature, support environmental projects and companies can also be shown by purchasing their products.In order to determine the awareness levels of the consumers participating in the study, the harmful effects of the agricultural pesticides on the environment were asked.In terms of nature centrism, it was understood that female respondents received a higher score than men.92% of consumers think that pesticides used in apple cultivation are harmful to the environment.When we examine the reasons of this consumption, 91% of consumers think that there are remnants of pesticides in apples due to excessive spraying.As a result, good agricultural practices are needed in apple production in our country.

Consumers are going through environmental issuesthey believe they will reach more serious dimensions.Also to consumers environmental eventsthey buy some products due to their viewpoints and some of them do notas they can afford to pay more to buy sensitive productsresults have been reached.

CONCLUSIONS

According to the conjoint analysis results and the survey findings price is an important attribute that consumers take into account during the decision process of buying apples. The conjoint analysis results show that price is the most important attribute and the respondents have stated that price is also a very important factor that affects the buying decision. The results show that price is the most critical attribute; it is almost twice as important as the second critical attribute which is color. This finding suggests that producers should focus on strategic pricing. If price and the least important attribute instead was not the most important attribute, it could be interpreted as the consumers would not mind paying a higher price.

According to the results of conjoint analysis; 39.93 percent of consumers' preferences for consumption of apple price (price); 22.83% color (color); 14.81% vitality (crispness); 13.56% size (size); 8,87% affect the taste.In the Table 4, benefit scores were calculated for each card. The card number 2 has the highest benefit with a score of 10,797.

Maksimum Utility= Medium + Uniform yellow + 1.75 TL/kg + Soft + Sour
=-2,0273+5,2026+8,7750+3,3588+1,5513=16.8604

The maximum benefit was found to be 16,8604 as calculated above. As a result, the customers' preference of medium-sized, yellow color, the price was 1.75 TL, soft and sour.

Consumers want, the products they buy are only healthy, quality and reliableto ensure that these products are produced without harming the nature and the environment. As the number of conscious consumers increases, Good Agricultural Practice production is expected to increase.Environmental, human and animal health without harming, traceability in agriculture, sustainability and food safetydissemination is very important for consumers.Therefore, raising awareness on the subject for stakeholders would be beneficial for the development of the practices.

REFERENCES

[1] TURKSTAT (2019) Turkish Statistical Institute Annual Reprots. ISBN:978-605-7613-39-4pp.163.
[2] TMOAF (2020),Republic of Turkey Ministry of Agriculture and Forestry. Business Report. pp. 416.
[3] Oglu, M., Bilgic, A., Topu, B.K., Ardali, Y. (2016). Factors Affecting the Students' Environmental Awareness, Attıtudes and Behavıors InOndokuzMayıs Unıversıty, Turkey. Fresen. Environ. Bull. 25(4), 1243-1257.
[4] Turhan Ş., Rehber, E., Erdal, B., Vural, H. (2018). Toward an Integrated Safe and Sustainable Food System, Germany.Fresen. Environ. Bull. 27(5), 2607-2611.
[5] Witting D.R., Cattin, P. (1989). Commercial Use of Conjoint Analysis: An Update, Journal of Marketing. 53, 91-96.
[6] Wittink, D.R., Vriens, M., Burhenne, W.(1992). Commercial Use of Conjoint Analysis in Europe: Results and Critical Reflections, Sawtooth Software Research Paper Series.
[7] Green, P.E., Srinivasan, V. (1978). "Conjoint Analysis in Consumer Research: Issues and Outlook," Journal of Consumer Research. 5 (September) 103-23.
[8] Green, P.E., Srinivasan, V. (1990). "Conjoint Analysis in Marketing: New Developments with Implications for Research and Practice," Journal of Marketing. 54 (October), 3-19.
[9] Mahajan, V., Wind J. (1991). "New Product Models: Practice, Shortcomings, and Desired Improvements," Marketing Science Institute, Cambridge, Massachusetts.Report. No. 91-125.

[10] Weinberg, B.D. (1990). "Roles for Research and Models in Improving New Product Development," Marketing Science Institute, Cambridge, Massachusetts.Report. No. 90-120.
[11] Bryan, S., Buxton, M., Sheldon, R., Grant, A. (1998). Magnetic resonance imaging for the investigation of knee injuries: an investigation of preference. Health Econ.7, 595–604.
[12] Ratcliffe, J., Buxton, M. (1999). Patients' preferences regarding the process and outcomes of life saving technology: an application of conjoint analysis to liver transplantation. Int. J. Technol. Assess. Health Care.15, 340–351.
[13] Greene, W. (1995). LIMDEP version 7.0. New York: Econometric Software.
[14] Louviere J.J. (1988). Analyzing Decision Making Metric Conjoint Analysis, Sage Publications, Newbury Park, London. N. 67.
[15] Umberger, W.J., Fuez, D.M., Calkins, C.R.,Killenger-Mann, K. (2002), U.S. Consumer Preference and Willingness-to-Pay for Domestic Corn-Fed Beef Versus International Grass-Fed Beef Measured Through an Experimental Auction, Agribusiness. 18, 491-504.
[16] Mabiso, A., Sterns, J., House, L., Wysocki, A. (2005). Estimating Consumers' Willingness-To-Pay for Country-Of-Origin Labels in Fresh Apples and Tomatoes: A Double-Hurdle Probit Analysis of American Data Using Factor Scores, Selected Paper prepared for presentation at the American Agricultural Economics Association Annual Meeting, Providence, Rhode Island, July 24-27
[17] Murphy, M., Cowan, C.,Henchion, M., O'Reilly, S. (2000). Irısh Consumer Preferences for Honey: A Conjoint Approach, British Food Journal, MCB University Press. 102(8), 585-597.
[18] Gil, M.J., Sanchez, M. (1997). Consumer Preferences for Wine Attributes: A Conjoint Approach, British Food Journal 99/1 MCB University Press.
[19] Burhenne, W. (1992). Commercial Use of Conjoint Analysis in Europe: Results and Critical Reflections Dick Wittink, Cornell University Marco Vriens, University of Groningen and-WimBurhenne, Interview.
[20] Addelman, S. (1962). Orthogonal Main Effect Plans for AsymmetrcalExperiments, Technometrics. 4, 21-46.
[21] Deacon, J.,Lancester, N. (1988), Late Quaternary palaeoenvironments of Southern Africa, Oxford & New York: Oxford University Press; ISBN 0-19-854449-9 hardback 225.
[22] Hatırlı, A.,Demircan, Y., Aktaş, A. (2004). Analysis of Fish Consumption of Families in Isparta Province. SüleymanDemirel University, Journal of Faculty of Economics. 9 (1). 245-256.

Received: **02.12.2020**
Accepted: **07.02.2021**

CORRESPONDING AUTHOR

Sule Turhan
Faculty of Agriculture,
Department of Agricultural Economics,
Bursa Uludag University,
Gorukle Bursa 16059 – Turkey

e-mail: sbudak@uludag.edu.tr

© by PSP Volume 30– No. 05/2021 pages 5194-5210 Fresenius Environmental Bulletin

A STUDY ABOUT RECYCLING INTO THE NATURE AND THE REHABILITATION OF OPEN MINES THROUGH "MURGUL" SAMPLE CASE

Hilal Surat[1,*], Mustafa Aybar[2]

[1]Art and Design Faculty, Artvin Coruh University, Artvin, Turkey
[2]Program of Forestry and Forest Products, Department of Artvin Vocational School, Artvin Coruh University, Artvin, Turkey

ABSTRACT

The rehabilitation for the distorted, destructed areas as a result of industrial usage through natural restoration and the increase of the biologic production capability to increase the inherent landscape quality necessitate that environmental problems like air, water, soil, noise and visual pollution, occurred again as a result of the distortion of natural landscape and the economic and social conditions of the close community be improved. In the scope of this study, the rehabilitation of the mining areas where the mining activity is completed and the restoration to its original landscape have been evaluated within researced in the case of "Murgul Bakır Madeni" project. With this study, heavy metal pollution appeared as a result of mining activities of Murgul Copper Operation, in direction of surface flow in route of waste water discharged and in order to identify heavy metal pollution soil and plant samples will be taken from 0-20 cm depth of 3 different locations in every point. In order to determine heavy metal pollution, indications of Mg, Cr, Mn, Fe, Ni, Cu, Zn, Cd and Pb elements has be done in ICP-OES tool of Artvin Coruh University Science-Technology Application and Research Center. The importance of plant species in the recovery process of a damaged area due to mining activities are great. Selection of appropriate plant species will increase the success of the repair work done.

KEYWORDS:
Heavy Metal, Mineral Fields, Landscape Restoration, Natural Plants

INTRODUCTION

Increasing global industrialization and resulting increased need for raw materials lead to mining of natural minerals. Mining activities cause serious environmental problems and affect the quality of physical environment (soil, water, air). Soil, water, noise and air pollution, alteration of the natural structure of the soil, destruction of fertile topsoil, animals and vegetation, mass migration of animal species are among the adverse effects of mining [1].

Waste generated by mining activities particularly lead to soil pollution [2]. Because mining activities produce large amounts of heavy metal-laden waste that is released without control and cause widespread pollution of the ecosystem [3, 4, 5].

Environmental stabilization of an area that was destroyed by mining activities is required to protect the natural legacy of future generations and to maintain a viable and clean environment. However, without intervention, it could take several years for a damaged area to reach an ecological balance and repair itself. Humans could restoring the efficiency, ecological, economic and aesthetic values in a destroyed area with restoration or repair studies on damaged areas without waiting for the consequences.

Biological and vegetation reclamation (phytoremediation) plays an important role in the recovery of damaged areas [6]. Based on the conditions of the study area, it is possible to plant correct plant species with adequate planting techniques to recreate and reclaim the ecological, economic and aesthetic values in the area.

After mining activities, reclamation of the natural structure as close to its original state as possible is generally analyzed in ecosystem restoration, and the work that entails the regeneration of natural vegetation is one of the most important stages of ecosystem restoration.

It is important to identify indigenous plant species in contaminated areas to determine the factors that could ensure the removal of the pollution and rehabilitation and reclamation of the previous ecosystem in mining areas. Thus, the habitat is reorganized with local plants in degraded or damaged ecosystems to reclaim the previous healthy habitat. The soil heavy metal pollution levels were investigated in the immediate vicinity of the Murgul copper mining area, the study area. Furthermore, the availability of the identified plant species in restoration and the availability of these plant species as a hyperaccumulator based on the idea that these could be indicator plants for different metals were investigated.

FIGURE 1
Sampling map of the study area

MATERIALS AND METHODS

Material. The main study material included soil and plant samples collected from Murgul copper mine site, its hinterland, and the dross dump site. The study area included the copper mine site, the stream that the wastewater was discharged, and the dross dump site within the borders of Artvin Regional Directorate of Forestry, Borcka Forestry Management Directorate, Göktaş Forestry Operation Directorate (Figure 1). It was determined that certain areas on the flow direction are privately owned and used for agricultural purposes.

In the study, 8 sampling locations were determined in the stream downstream, starting from the copper mine site. Furthermore, 2 sampling locations were determined, namely the lowest section and the beginning section of the dross dump site. Each sampling location was 100m². 20 soil samples were collected from 2 different points at each location at 0-10 and 10-20 cm depth and approximately 1-1.5 kg at each depth. All samples taken were placed in nested polyethylene bags. For both soil and plant samples, the sample number and the layer identification card were placed between the nested bags for easy identification.

Method. The soil samples were laid on newspapers at a suitable space in the laboratory and prepared for analysis. Each sample label was fixed on the newspaper with a pin. The laid samples were air-dried, grinded adequately in a mortar and passed through a 2 mm sieve, and the fine pieces were transferred into jars, and rocky sections were placed in polyethylene bags [7]. The air-dried soil samples were prepared for analysis based on the principles reported by Chapman et al. The soil sample reactions were measured with the glass electrode method. The actual acidity was determined with the measurements conducted on 1/2.5 soil-water mixture by mass after overnight storage [8].

2 ml HNO3 and 3 ml H2O2 were added to 0.3 g ground soil samples and the samples were kept in this solution for 20 minutes. The samples were then burned at 145°C for 5 minutes, and then again at 180°C for 10 minutes, and again at 100°C for 10 minutes. In the final stage, after the sample temperature was equal to the ambient temperature after 15 minutes, they were analyzed in ICP-MS, and the soil samples were dissolved with microwave acid digestion [9]. Method and the metal concentrations were determined with an ICP-OES device. Mn, Zn, Cd, Pb, Co, Cr content were analyzed at ppb level and converted to ppm level.

RESULTS

Determination of Heavy Metal Levels in Soil Samples. Accumulation levels of heavy metals such as cadmium (Cd), chromium (Cr), manganese (Mn), nickel (Ni), zinc (Zn), copper (Cu), lead (Pb), iron (Fe) and cobalt (Co) were determined in the Murgul Copper Mine and vicinity in the present study. Soil samples were collected from 2 depths on two different periods (March-May/June-August) in the mine site and vicinity. Analyzes were conducted to determine the heavy metal accumulation levels in

TABLE 1
Heavy metal concentrations in soil samples collected at 2 different depths at Murgul Copper Mine vicinity and dross dump site

						March-May					
ÖA No	Soil Depth	Cd ppm	Co ppm	Cr ppm	Cu ppm	Fe ppm	Mn ppm	Ni ppm	Pb ppm	Zn ppm	
1	0-10 cm	11,3	1,1	9,8	227,7	224,5	80,6	7,3	21,1	138,8	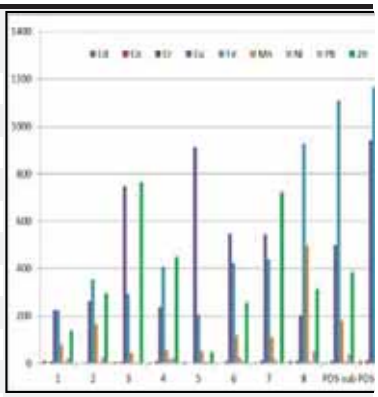
2		2,4	1,1	5,5	261,6	352,7	166,9	3,7	23,9	293,4	
3		7,3	0,9	7,7	748,5	292,2	45,5	4,6	5,3	766,3	
4		4,7	1,1	8,5	238,2	410,5	55,3	18,8	21,5	447,8	
5		7,1	0,3	3,3	915,8	207,1	52,3	7,9	7,9	48,58	
6		1,9	1,7	8,4	546,7	423,1	116,7	26,2	10,4	252,8	
7		5,5	2,1	14,2	544,3	439,1	113	18,4	5,11	723,6	
8		11,1	1,3	11,8	202,6	929,5	494,9	6,1	51,6	314,4	
PDS-sub		4,4	1,3	12,8	497,3	1109	182,9	9,4	37,3	382,8	
PDS-top		11,5	2,5	13,9	944,5	1166	955,9	73,2	28,4	451,5	
Mean		6,7	1,3	9,5	512,7	555,4	226,4	17,6	21,3	382	
1		1,8	1,499	4,22	68	100,9	394	4,8	7,1	535	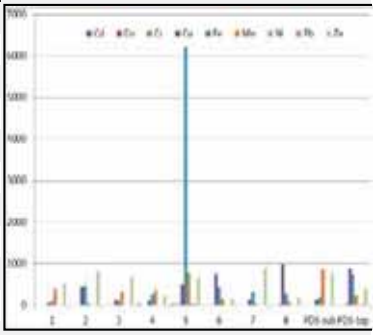
2	10-20	1,12	0,905	3,91	453,1	469,4	53,04	14,96	4,77	824,7	
3	cm	5,78	0,884	0,37	128,8	111,1	321,6	1,63	5,1	669,1	
4		22,74	1,58	7,86	101,9	262,9	380,2	1,65	10,78	222,6	
5		31,06	4,21	29,87	507,8	6229	785,8	33,52	30,88	644,9	
6		4,78	0,461	6,98	754	433,6	157,3	2,97	6,52	148,6	
7		1,32	0,923	12,96	130,5	320,6	35,68	10,22	3,14	901,4	
8		12,5	1,069	16,99	974,7	281,2	93,93	12,21	9,96	176,8	
PDS-sub		3,31	0,92	7,26	130,3	187,7	867,2	16,28	2,1	774,5	
PDS-top		13,08	2,236	37,43	880,9	742,2	231,5	7,55	25,43	396	
Mean			1,46	13,12	413	913,9	332,	10,58	10,58	529,4	
						June-August					
1	0-10 cm	4,07	6,35	65,47	195,7	2838,	279,6	5,05	6,883	87,21	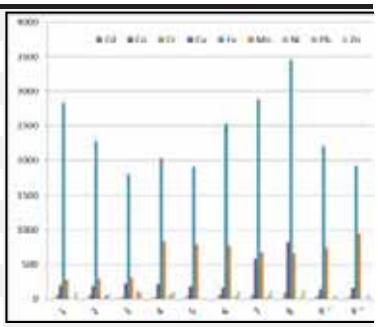
2		3,66	6,52	59,79	191,1	2280	295,7	4,91	53,53	77,48	
3		3,97	5,51	26,1	222,5	1791	313	2,302	113,3	88,67	
4		4,87	9,13	30	218,9	2029	838,2	2,89	68,74	96,16	
5		3,89	8,34	44,96	184,6	1901	795,3	3,69	3,6	8,25	
6		4,52	9,76	71,72	165,3	2530	767,2	5,93	34,12	112	
7		1,82	7,34	62,64	584,9	2890	678,7	4,05	32,45	119,3	
8		2,83	10,1	97,33	824,1	3454	661,8	5,92	24,6	133,8	
PDS-sub		1,36	10,4	38,98	141,8	2212	749,8	3,02	15,05	51,43	
PDS-top		1,54	7,99	34,53	154,7	1931	947,7	2,61	1,15	47,08	
Mean			8,144	53,15	288,4	2386	632,7	4,037	35,35	82,14	
1		1,54	7,99	34,53	154,7	1931	67,71	4,757	4,815	66,42	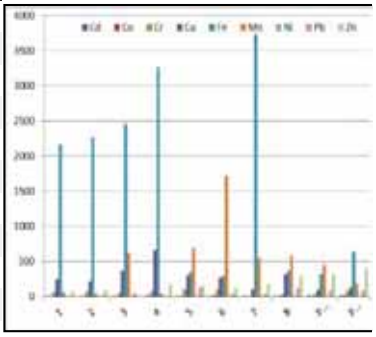
2	10-20	3,95	8,876	67,75	247,1	2173	35,47	5,419	22	86,88	
3	cm	5,16	7,665	65,69	226	2276	605,2	5,717	49,42	11,84	
4		5,71	10,99	64,53	371,2	2460	42,22	7,821	2,635	182,1	
5		14,38	18,64	76,37	658,7	3256	690,4	7,954	126,9	154,8	
6		5,36	11,35	108,2	305,5	350	1729	7,731	37,56	117,8	
7		4,07	17,00	99,89	267,3	293,6	558,8	2,871	37,77	176,4	
8		6,57	7,818	11,37	107,1	3733	578	5,684	126,9	294,8	
PDS-sub		9,99	10,09	23,51	320,8	366	451,6	3,669	82,68	314,7	
PDS-top		15,01	11,10	27,54	101,4	326,8	184,1	4,489	89,56	403,8	
Mean			12,07	63,48	273,7	1588	494,2	5,611	58,03	181	

collected samples. Soil analysis results are presented in Table 1.

Table 1 demonstrates that the average heavy metal accumulation levels in the samples collected in the March-May period could be ranked as Fe> Cu> Zn> Mn> Pb> Ni> Cr> Cd> Co, while the average heavy metal accumulation levels in the samples collected in the June-August period ranked as Fe> Mn> Cu> Zn> Cr> Pb> Co> Cd> Ni (Table 1). The review of the findings revealed that Fe

heavy metal was high during both periods. It was fund that Fe, Mn, Cu, Zn content was high in soil samples taken in both periods and at both soil depths, Cd, Cr, Pb, Ni and Co heavy metal content was at lower levels.

The average Cd content was 8.24 ppm, Co amount was 1.41 ppm, Cr content was 11.36 ppm, Fe content was 734.62 ppm, Cu content was 462.86 ppm, Mn content was 279.22 ppm, Zn content was 455.68 ppm, Ni content was 14.08 ppm, and Pb content was 15.92 ppm in soil samples collected from all locations in the study area in the March-May period The average Cd content was 5.91 ppm, Co content was 10.11 ppm, Cr content was 58.32 ppm, Fe content was 1986.57 ppm, Cu content was 281.03 ppm, Mn content was 563.46 ppm, Zn content was 131.55 ppm, Pb content was 46.69 ppm and Ni content was 4.82 ppm in soil samples collected from all locations in the study area between June and August. The analysis of the four elements with highest accumulation levels in the study area revealed that the highest Fe content was determined at a depth of 0-10 cm at upper dross deposit site (DDS-upper) as 1166 ppm and at lower dross deposit site (DDS-lower) as 1109 ppm, it was 6229 ppm at location 5 at 10-20 cm, depth, the highest Cu content was determined at a depth of 0-10 cm at upper dross deposit site (DDS-upper) as 944.5 ppm and location 5 as 915.8 ppm, while at 10-20 cm depth, it was 974.7 ppm at location 8, and 880.9 ppm at upper dross deposit site (DDS-upper), the highest Zn content was determined at 0-10 cm depth as 766.3 ppm at location, 901.4 ppm at 10-20 cm depth at location 7, and finally, the highest Mn content was determined as 955.9 ppm at 0-10 cm depth at upper dross deposit site (DDS-upper), and 867.2 ppm at 10-20 cm depth at the lower dross deposit site (DDS-lower) (Table 1).

The study findings were compared with the PEC (Probable Effects Concentration) soil heavy metal toxicity limits based on pH (Table 2). The chart that reflects over the limit heavy metal content is presented in Figure 1. It could be observed in the figure that Cd, Cu, Mn, Zn exceeded these limits in both collection periods at all stations. While Fe, Co, Cr, Ni, Pb remained below the limits in both periods, it was observed that only Ni content exceeded the limit in the dross dump site (DDS) in the March-May period, while Pb samples collected at locations 2, 3, 4 and 8, Cr collected in location 5 exceeded the limit in the June-August period. The analysis of the samples collected at location 5, which was agricultural land, revealed that Cu, Fe, Mn and Zn content was above the limit (Figure 1).

A total soil Cd content of more than 1 ppm is considered Cd pollution. Higher soil Cd content has negative effects on the plants and the toxicity increases even more after 3 ppm [10, 11]. The review of the Cd content in the areas where the samples were collected in the study demonstrated that it varied between 11.82 ppm and 16.48 ppm, which was above the limit (Table 1, Figure 1). Furthermore, Cd content figures were compared with the values reported for Belgium, the Netherlands, Germany, Ireland, Sweden, England and Spain. The reported CD content was 1.5 ppm in Belgium, Germany, Ireland and England, 1 ppm in Sweden and the Netherlands, and 2 ppm in Spain [12, 13, 14, 15].

Cu is stationary in soil and soil CU concentration is between 5 and 100 mgkg-1. Naturally, the total soil Cu content varies based on the Cu content in the soil base. Due to the intensity of mineral decomposition and the effect of growing plants, the Cu concentration is higher in the topsoil. Generally, the total Cu content is lower in highly decomposed and scoured soil. It is quite stationary as it binds strongly to copper particles in the soil. Thus, Cu content decreases towards the lower profile in most soil [16]. Cu is a metal observed in soil formed by the decomposition of alkali rocks and could easily interact with both organic and inorganic substances based on pH [17]. Due to the high solubility of Cu compounds at low pH, Cu susceptibility is high in

TABLE 2
Soil heavy metal limits (ppm) based on pH [14, 55, 56]

Limit value of Trace Elements in the Soils				
	pH < 5- 6	**pH>6**	**pH<7**	**pH≥7**
Heavy Metal (Total)	Kiln Dry Soil mg / kg	Kiln Dry Soil mg / kg	Kiln Dry Soil mg / kg	Kiln Dry Soil mg / kg
Pb	50	300	70	100
Cd	1	3	1	1,5
Cr	100	100	60	100
Cu	50	140	50	100
Ni	30	75	50	70
Zn	150	300	150	200
Mn	50	50		
Fe	50000		50000	
Co	50		80	

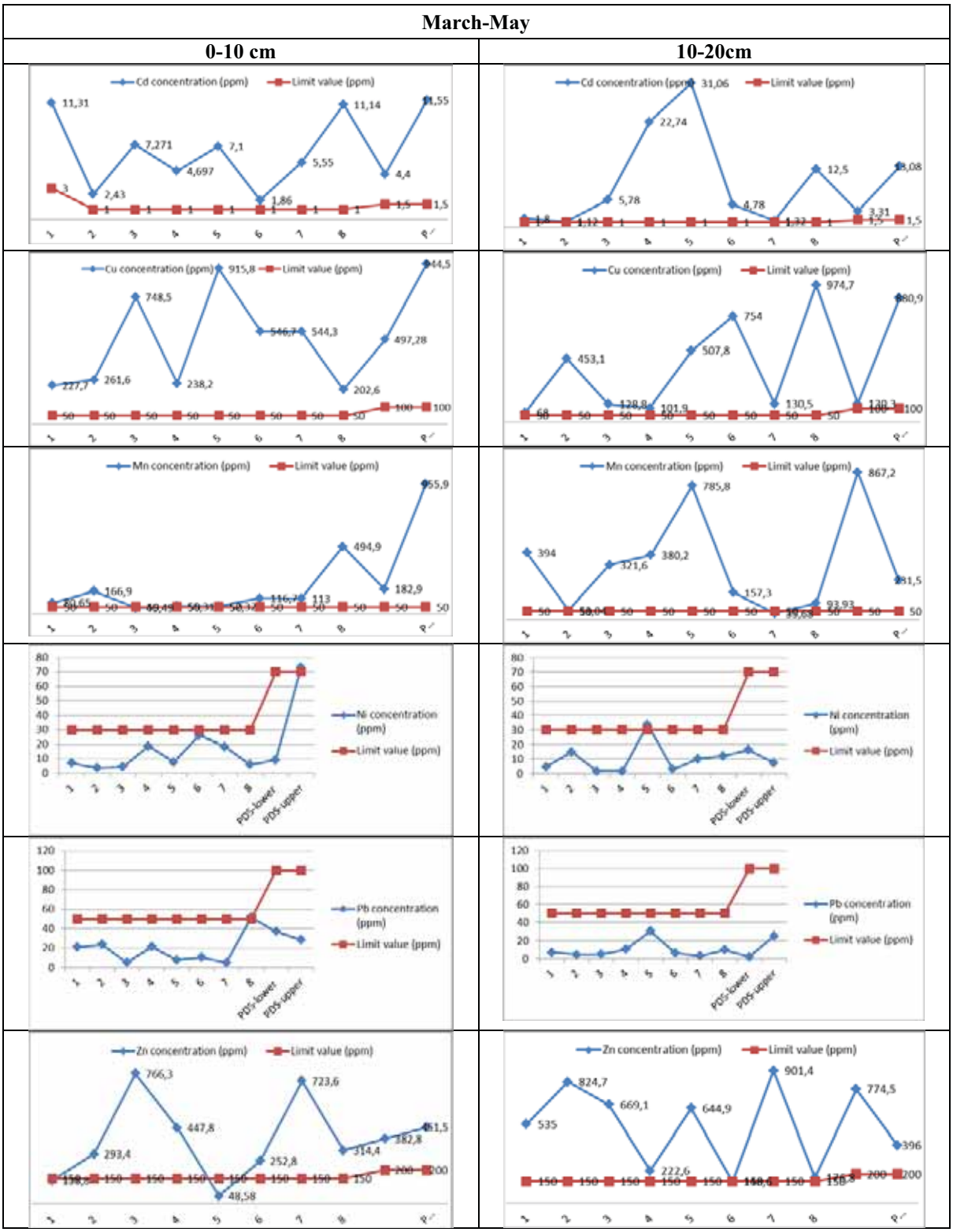

FIGURE 2
Comparison with PEC (Probable Effects Concentration) soil heavy metal toxicity limits based on pH values

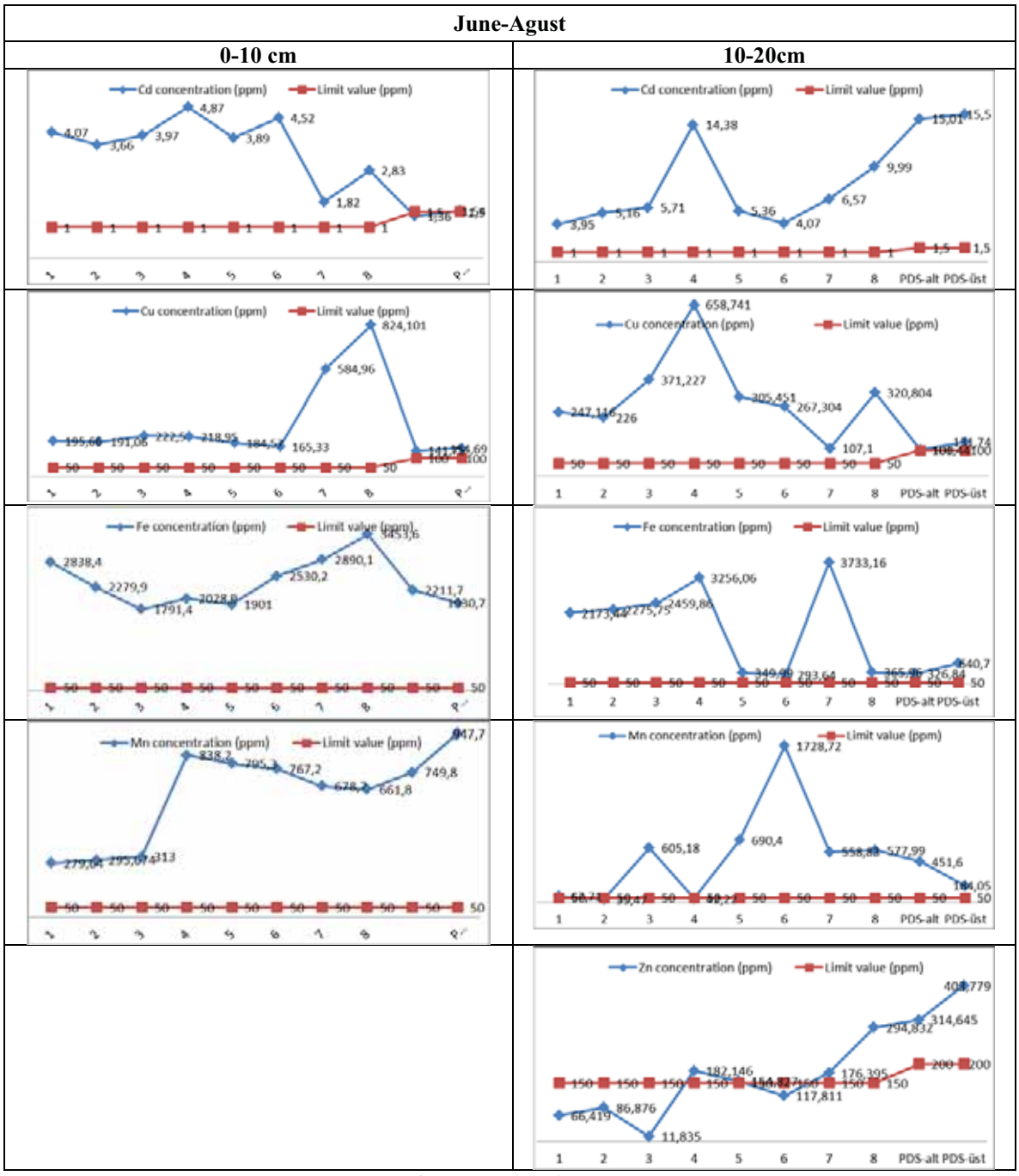

FIGURE 2 (Continue)

acidic soil and has toxic effects [18]. Cu content at 0-10 cm depth varied between 288.4 ppm (March-May) and 512.7 ppm (June-August), while this figure varied between 273.7ppm (March-May) and 413 ppm (June-August) at 10-20 cm depth (Table 1). The review of Table 1 demonstrated that the Cu content was above the limit at all locations (Figure 2). Soil Cu concentration in polluted areas was reported as 210 ppm in Australia, 240 ppm in Poland, 415-733 ppm in England, 456-2020 ppm in Japan, and 0.2-58 ppm in Zambia. The comparisons revealed that the Cd content determined in the present field study was much higher when compared to the figures reported for Belgium, Germany, Ireland, the UK, Sweden, the Netherlands and Spain. Soil Zn content is generally between 10 and 300 ppm, and on average 30 - 50 ppm. Zn levels are as low as 10 - 30 ppm in acidic soil with high scouring. Zinc is only toxic at high concentrations (Seven et al., 2018). Soil Zn content at 0-10 cm depth in the study area was 381.99 ppm (March-May) and 529.4 ppm (March-May) at 10-20 cm depth. In the March-May period, the mean Zn content in soil samples collected at 10 locations was 455.68 ppm (Table 1). In this period, the review of Zn content in samples collected in 0-10 cm depth revealed that the Zn content in 3rd, 4th, 7th, 8th locations and dross dump area exceeded the limit of 300 ppm. the

review of Zn content in samples collected in 10-20 cm depth revealed that the Zn content in 1st, 2nd, 3rd, 5th, 7th locations and dross dump area exceeded the limit of 300 ppm (Figure 2). However, in the June-August period, it was observed that Zn content was below the limit except the dross dump area.

The soil Mn content varied between 226.41 ppm (March-May) and 632.7 ppm (June-August) at all locations at 0-10 cm depth, and between 332.02 ppm (March-May) and 494.22 ppm (June-August) at 10-20 cm depth (Table 1). Mn content was below 50 ppm at the 3rd location at 0-10 cm in the March-May period, at 7th location at 10-20 cm, at the 2nd and 4th locations at 10-20 cm in the June-August period. Otherwise, Mn content was determined over the limit value at all locations (Figure 2). Table 1 reflected that Ni content was above the limit in soil samples collected in the upper dross dump site at 0-10 cm depth in the March-May period, while Pb content was above the limit in soil samples collected in 2nd, 3rd, and 4th locations at 10-20 cm depth in both periods.

There are several studies on soil heavy metal content in Turkey. The studies reported that the element levels in soil with heavy metal content for various reasons had high toxicity levels. For example, a study conducted in Edirne analyzed roadside soil Pb, Cu, Ni and Zn content. In the study, topsoil element levels were determined as follows: Pb (0.885-12.38 mg/kg), Cu (6.64-25.81 mg/kg), Ni (53.31-272.1 mg/kg) and Zn (161.5-485.6 mg/kg) [19]. In another study conducted in Elazığ, roadside soil and plant Pb, Cd and Cu content were analyzed, where the road was the source of pollution, and it was determined that the heavy metal concentrations increased with the traffic density [20]. Yalçın et al [21] analyzed roadside soil Fe, Cu, Pb, Zn, Cd, Cr, Co, Mn, Ti, Sn, Mo and As concentrations along D805-D750 and TEM highways, and reported that all heavy metal concentrations were at toxic levels. Önder et al. [22] and Malkoç et al. [23] reported that heavy metals such as Fe, Pb, Zn, Co, Cu, Ni, Cr, Mn and Cd were at high concentration levels above the limits specified in the Soil Pollution Control Regulation in soil samples collected around contaminant sources and vicinity.

The review of the studies conducted in various countries and cities around the world demonstrated that in a study conducted in Kathmandu region in Nepal, the variations in heavy metal concentrations in farm soil near the pollutant source were analyzed. Topsoil Cu content was 19.99 ± 6.91 mg/kg, Zn content was 76.3 ± 52.54 mg/kg), Cd content was 0.36 ± 0.46 mg/kg), and Pb content was 22.57 ± 23.81 mg/kg. The reported concentrations were above international standards [24]. In a study conducted in Xi'an-Baoji city in China, topsoil Pb, Zn, Cu and Cr levels were investigated (at 0-20 cm depth), and it was determined that topsoil Pb, Zn, Cu and Cr concentrations were high [25]. In a study conducted in Dinajpur-Ragpup in Bangladesh, roadside soil and vegetable heavy metal concentrations were determined as follows: Ni> Pb> Cr> Cd [26].

Determination of heavy metal levels in plant samples. Cadmium (Cd), Chromium (Cr), Manganese (Mn), Nickel (Ni), Zinc (Zn), Copper (Cu), Lead (Pb), Iron (Fe) and Cobalt (Co) heavy metal concentrations were determined in the present study conducted to reveal the heavy metal accumulations and pollution in Murgul Copper Mine site and vicinity. Leaf, shoot and branch samples were collected from plants indigenous to the mine site in two periods (March-May/June-August). Analyzes were conducted to determine the heavy metal levels in the collected samples. Plant analysis results are presented in Table 3.

Table 3 demonstrated that the mean heavy metal concentrations in plant samples could ranked as follows: Fe> Mn> Zn> Cu> Cr> Ni> Pb> Cd> Co (Table 3). The findings revealed that Fe, Mn, Zn, Cu, Cr concentrations were high in plant samples, while Cd, Pb, Ni and Co heavy metal concentrations were at lower levels.

As seen in Table 3 and Figure 3, Fe content was over 1000 ppm in *Pilosella officinarum* subsp. micradenia, Cirsium echinus, Cerastium gnaphalodes, Cota tinctoria L. J. Gay species, between 500-1000 ppm in *Scleranthus perennis* L. subsp. *perennis*, *Cerastium gnaphalodes*, *Cerastium* sp., *Quercus petraea* subsp. *iberica*, *Vicia cracca* L., *Sanguisorba* minor Scop. subsp. minor species, and between 200-500 ppm in *Rhododendron luteum*, *Ranunculus dissectus, Hypericum orientale* L., *Rhododendron smirnovii, Plantago lanceolata* L., *Trifolium alpestre* L., *Smilax excelsa* L., *Rumex acetosella* L., *Cornus sanguinea* L., *Salix caprea* L., *Silene armeria* L., *Vicia sativa* L. subsp. sativa, *Securigera varia* L., *Salix caucasica*, *Dryopteris* sp., *Betula pendula* Roth., *Leontodon hispidus* L., *Lotus corniculatus* L., *Onobrychis stenostachya*, *Melilotus officinalis* L. Pall. subsp. *officinalis* species. Kacar and İnal [27] reported that plant Fe content varied between 10 and 1000 mgkg-1, adequate Fe content was 50-250 mgkg-1, and deficiency symptoms are observed in plants with less than 50 mgkg-1 Fe content. Plant Fe toxicity is observed as dark green leaves, shortened roots and stem, and purple to dark brown leaf color.

Although the manganese toxicity depends on plant species, it could be generally observed over 100 mgkg-1 Mn concentration in dry matter. Manganese toxicity could be observed as brown spots on mature leaves in most plants. Over time, the stained areas become fungal. This phenomenon is a clear indicator of Mn toxicity. Often, symptoms of Mn toxicity are observed in the chlorotic and necrotic areas between the vessels [28]. In the study, higher than 400 ppm Mn content was determined in

Betula pendula Roth., *Rhododendron ponticum* L. subsp. *ponticum*, *Bellis perennis* L., species in the study (Table 3).

Plant dry matter Zn concentration is generally between 5 and 100 mgkg-1. Zinc toxicity usually starts after 400 mgkg-1 concentration in plants. In zinc toxicity, root and shoot growth decreases, roots become thinner, young leaves curl, and chlorosis is observed, cell growth and elongation are inhibited, cell organelles are broken down and chlorophyll synthesis is reduced in plants [29, 30]. Plant Zn concentrations varies between 5 and 100 ppm in healthy plants. It is known that high soil Zn content affects chlorophyll synthesis. This leads to a decrease in root and shoot growth, thinning of the roots, curling of young leaves and chlorosis, inhibition of cell growth and elongation and fragmentation of cell organelles in plants [31]. In the study, it was determined that Zn concentrations were between 80 and 200 ppm in *Salix caucasica*, *Salix caprea* L. *Pilosella officinarum* subsp. *micradenia*, *Lotus alpinus, Plantago lanceolata* L., *Betula pendula* Roth., *Silene armeria* L., *Vicia sativa* L. subsp. *sativa, Rumex alpinus* L., *Pilosella hoppeana*, and *Cota tinctoria* L., J.Gay species (Table3).

As seen in Table 3, Cu concentrations were over 100 ppm in *Scleranthus perennis* L. subsp. *perennis*, *Lotus corniculatus* L., *Rumex alpinus* L., *Vicia cracca* L., *Pilosella* hoppeana plant species. The extractable plant dry matter Cu content of more than 15-30 mgkg-1 could lead to cause toxic effects. Copper toxicity is generally observed in plant root systems. It leads to the inhibition of certain physiological events such as protein synthesis, photosynthesis, respiration, ion uptake, and cell membrane stability in the plant. 100 mg/kg CU content in soil and 15-30 mg/kg in plant dry matter is toxic [32, 33], investigated the effects of high soil Cu levels on soil pH and plant nutrient intake in their studies. They reported that high Cu levels led

TABLE 3
Plant species indigenous to the study area and their heavy metal content

Familya	Type	Cd (ppm)	Co (ppm)	Cr (ppm)	Cu (ppm)	Fe (ppm)	Mn (ppm)	Ni (ppm)	Pb (ppm)	Zn (ppm)
Pinaceae	*Picea orientalis* (L.)	<0.0	<0,0	0,2	19,3	107,3	324,5	1,4	<0,0	14,9
Ericaceae	*Rhododendron luteum*	<0,0	<0,0	0,5	12,2	**361,3**	213,7	16,5	<0,0	27,8
Asteraceae	*Pilosella officinarum* subsp. *micradenia*	1,3	0,2	2,0	61,5	**1024,6**	281,1	3,6	7,0	**144,6**
Fabaceae	*Lotus alpinus*	0,6	0,6	1,3	12,5	**1198,0**	75,9	3,6	2,6	**88,7**
Caryophyllaceae	*Scleranthus perennis* L. subsp. *perennis*	<0,0	<0,0	2,2	**260,1**	**560,2**	253,5	0.03	0,2	43,8
Plantaginaceae	*Plantago lanceolata* L.	0,2	<0,0	0,2	26,4	**446,6**	251,3	**48,9**	<0,0	**98,2**
Fabaceae	*Trifolium alpestre* L.	<0,0	<0,0	0,5	28,0	**320,8**	130,6	5,1	<0,0	**365,4**
Ranunculaceae	*Ranunculus dissectus*	<0,0	<0,0	<0,0	16,3	**491,3**	115,6	0,6	<0,0	44,9
Scrophulariaceae	*Scrophularia lucida* L.	<0,0	0,5	0,7	67,1	**1780,1**	150,8	4,9	3,0	46,7
Asteraceae	*Cirsium echinus*	0,8	0,5	0,8	23,8	**1268,8**	78,4	1,9	<0,0	77,5
Caryophyllaceae	*Cerastium gnaphalodes*	<0,0	0,2	2,0	24,3	**620,0**	195,8	1,4	<0,0	39,1
Plantaginaceae	*Veronica officinalis* L.	1,2	0,6	0,9	79,1	**1467,2**	188,7	1,4	11,3	**256,6**
Betulaceae	*Betula pendula* Roth.	0,7	1,0	0,6	20,8	**285,3**	**1802,2**	3,1	<0,0	**286,0**
Salicaceae	*Salix caprea* L.	1,0	0,2	0,8	13,5	**245,1**	70,0	1,3	<0,0	**592,6**
Caryophyllaceae	*Silene armeria* L.	0,8	0,3	0,8	17,7	**320,0**	**2332**	0,4	2,2	**162,6**
Fabaceae	*Vicia sativa* L. subsp. *sativa*	1,0	0,2	1,6	12,0	**239,5**	43,8	3,3	<0,0	**168,2**
Caryophyllaceae	*Cerastium sp.*	<0,0	0,2	2,0	24,3	**620,0**	195,8	1,4	<0,0	39,1
Salicaceae	*Salix caucasica*	**10,2**	0,2	0,8	13,5	**245,1**	70,0	1,3	<0,0	**592,6**
Fagaceae	*Quercus petraea* subsp. *iberica*	0,6	0,5	0,6	47,5	**952,5**	82,1	0,6	<0,0	51,0
Asteraceae	*Cota tinctoria* (L.) J.Gay.	2,9	0,8	0,7	91,6	**2360,8**	145,1	1,0	4,6	**112,1**
Asteraceae	*Pilosella hoppeana*	2,6	2,7	4,1	**321,8**	**6860,2**	184,6	3,0	22,6	**107,5**
Fabaceae	*Vicia cracca* L.	0,2	0,3	0,6	**160,1**	**546,8**	52,8	0,8	<0,0	**126,6**
Polygonaceae	*Rumex alpinus* L.	0,8	<0,0	<0,0	**139,6**	156,8	76,5	0.63	<0,0	76,9
Fabaceae	*Lotus corniculatus* L.	2,6	0,7	1,1	**468,0**	**382,0**	248,0	1,0	1,8	31,8
Rosaceae	*Sanguisorba minor* Scop. subsp. *minor*	0,7	0,3	0,6	21,5	**642,41**	77,12	0,528	<0,0	39,223
Fabaceae	*Onobrychis stenostachya*	<0,0	<0,0	<0,0	11,5	**307,43**	101,7	**109,9**	<0,0	41,412

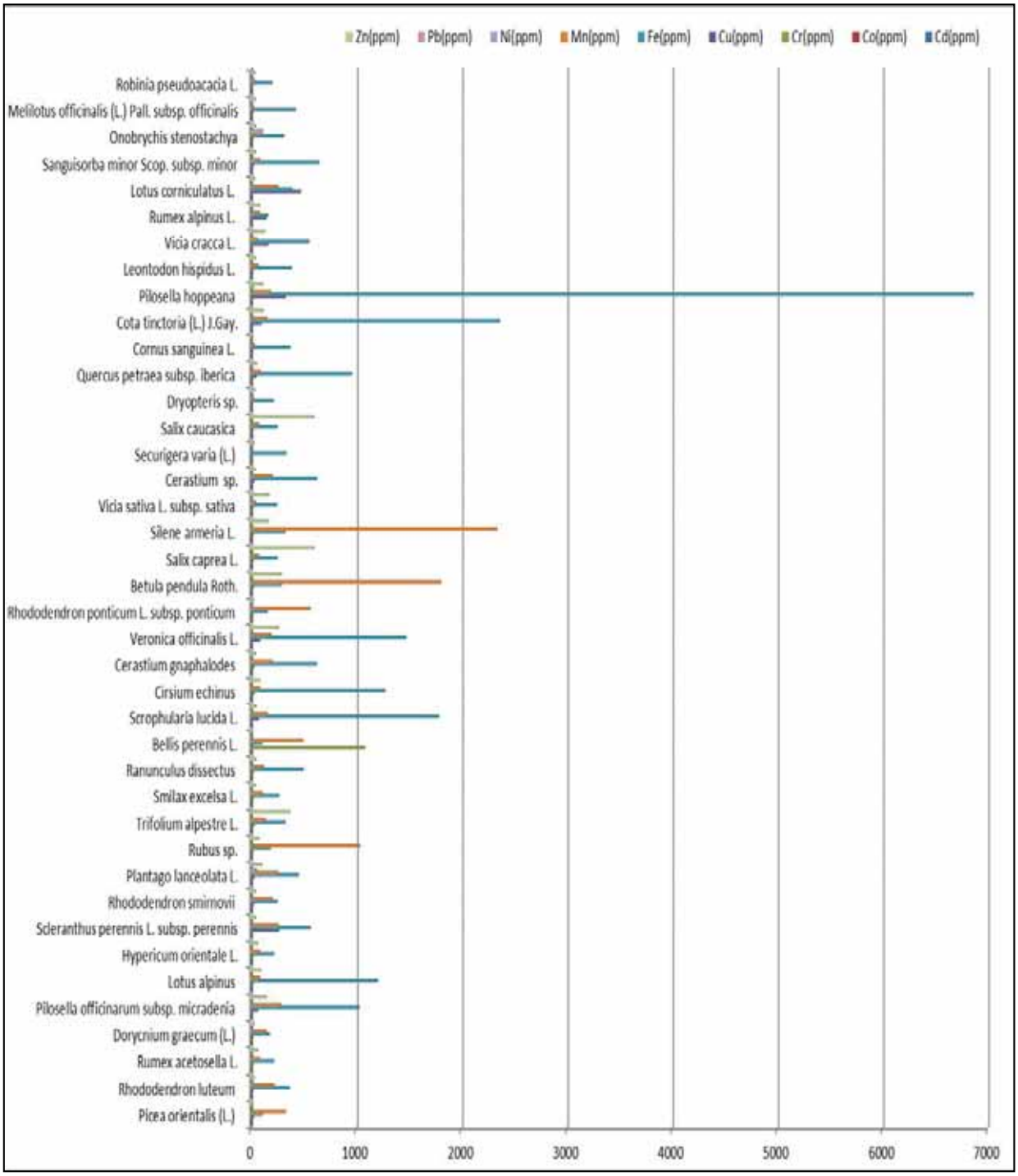

FIGURE 3
Heavy metal concentrations in plant species

to a decrease in soil pH, variable magnesium and the iron availability, and increases in total N, the available P, variable K, Zn and Cu content in the plant.

As seen Figure 4, Fe and Mn concentrations were high *in Picea orientalis* L., *Rhododendron luteum* in location 1, and Fe, Mn and Zn concentrations were high in *Rumex acetosella* L., *Dorycnium graecum* L., in location 2, Fe and Cu concentrations were high in *Pilosella officinarum* subsp. *micradenia* and *Scleranthus perennis* L. subsp. *perennis*, Fe and Zn concentrations were high in *Trifolium alpester* L., *Smilax excelsa* L., Fe concentration was high in Lotus alpinus, *Rhododendron smirnovii, Hypericum orientale* L., Cu concentration was high in *Plantago lanceolata* L., *Rubus* sp., Fe concentration was high in *Ranunculus dissectus, Scrophularia lucida* L., *Cirsium echinus* in location 4, Mn and Cr concentrations were high in *Bellis perennis* L., Fe and Zn concentrations were high in *Veronica officinalis* L. in location 5, Fe and Mn

concentrations were high in *Cerastium gnaphalodes*, Fe, Mn and Zn concentrations were high in *Betula pendula* Roth in location 6, Mn concentration was high in *Rhododendron ponticum* L. subsp. *ponticum,* Fe concentration was high in *Cota tinctoria* L., J.Gay., *Quercus petraea* subsp. *iberica*, *Pilosella hoppeana* in location 7, Mn concentration was high in Silene armeria L., Fe and Mn concentrations were high in *Leontodon hispidus* L., in location 8, Fe, Mn and Cu concentrations were high in *Lotus corniculatus* L., Fe and Cu concentrations were high in *Rumex alpinus* L., Fe and Zn concentrations were high in *Vicia cracca* L., Mn, Fe and Ni concentrations were high in *Onobrychis stenostachya*, Fe and Cu concentrations were high in *Rumex alpinus* L., Fe concentration was high in *Sanguisorba minor* Scop. subsp. *minor*, *Melilotus officinalis* L., Pall. subsp. o*fficinalis*, and the Fe concentration was high in *Robinia pseudoacacia* L., in location 10 (upper dross dump).

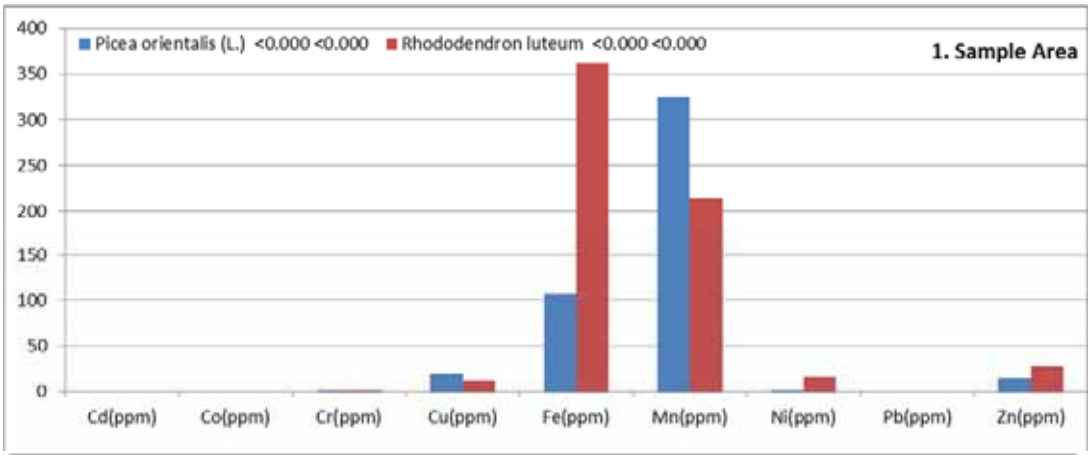

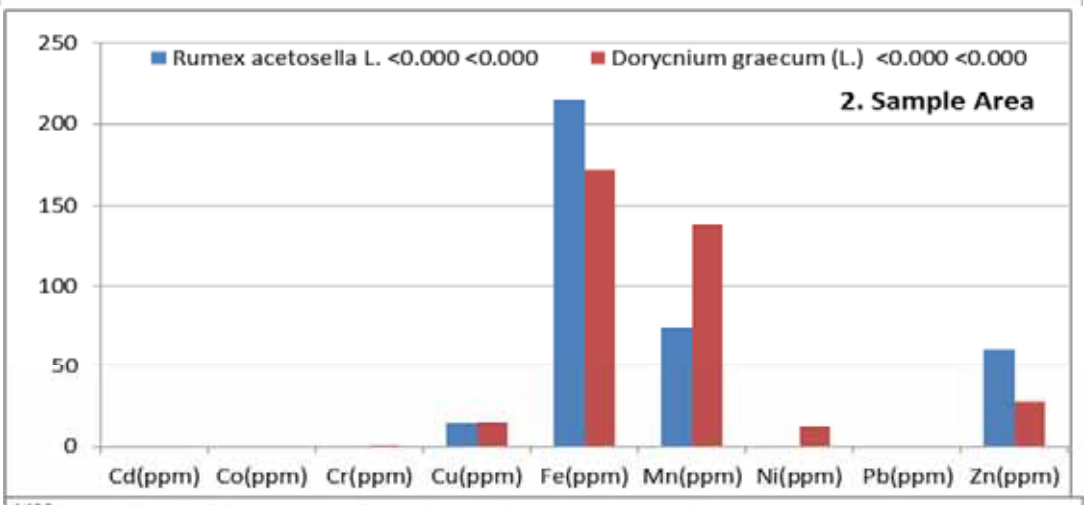

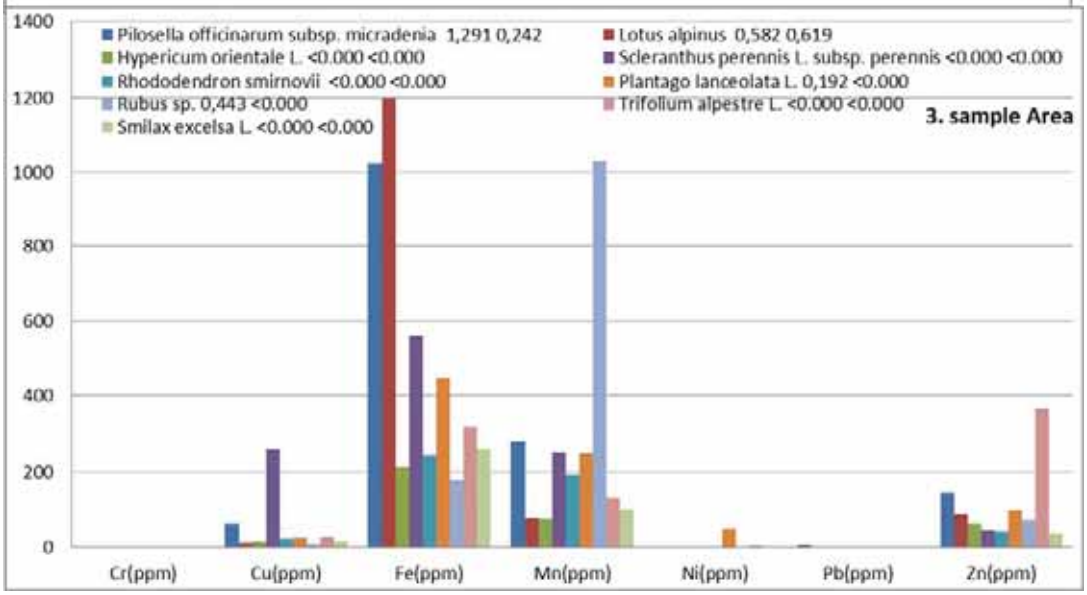

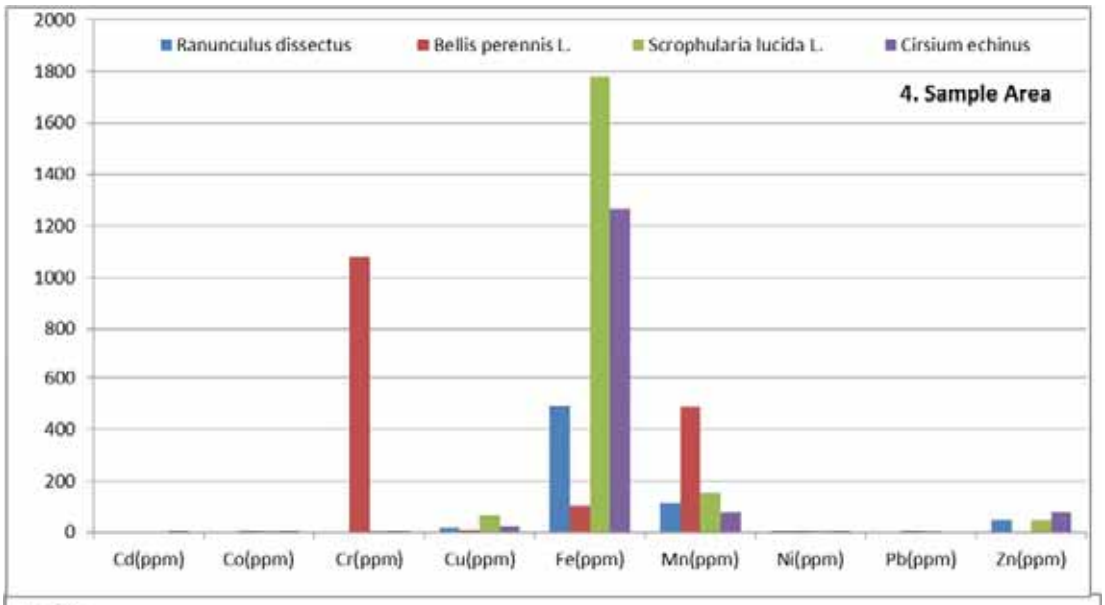
Ranunculus dissectus
Bellis perennis L.
Scrophularia lucida L.
Cirsium echinus
4. Sample Area
2000
1800
1600
1400
1200
1000
800
600
400
200
0
Cd(ppm)
Co(ppm)
Cr(ppm)
Cu(ppm)
Fe(ppm)
Mn(ppm)
Ni(ppm)
Pb(ppm)
Zn(ppm)

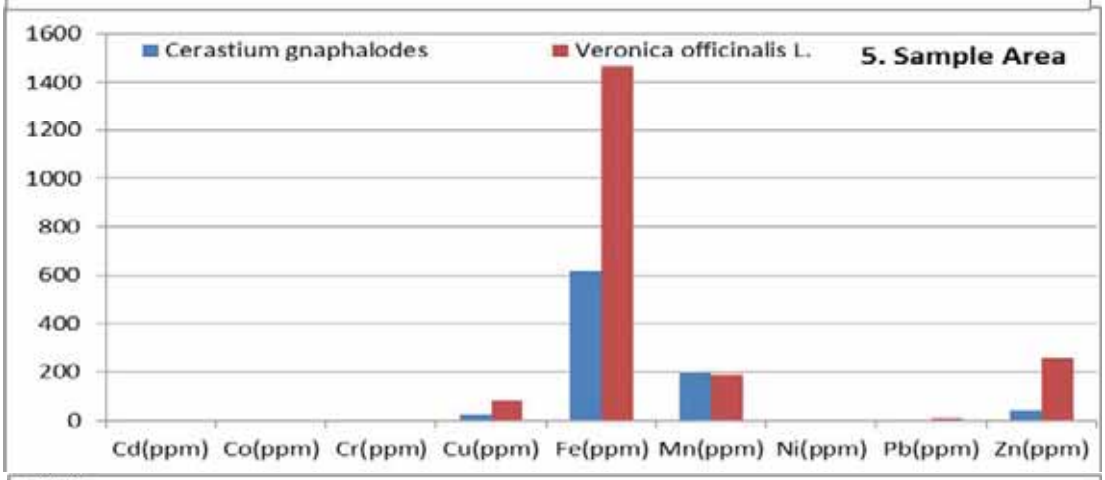
Cerastium gnaphalodes
Veronica officinalis L.
5. Sample Area
1600
1400
1200
1000
800
600
400
200
0
Cd(ppm)
Co(ppm)
Cr(ppm)
Cu(ppm)
Fe(ppm)
Mn(ppm)
Ni(ppm)
Pb(ppm)
Zn(ppm)

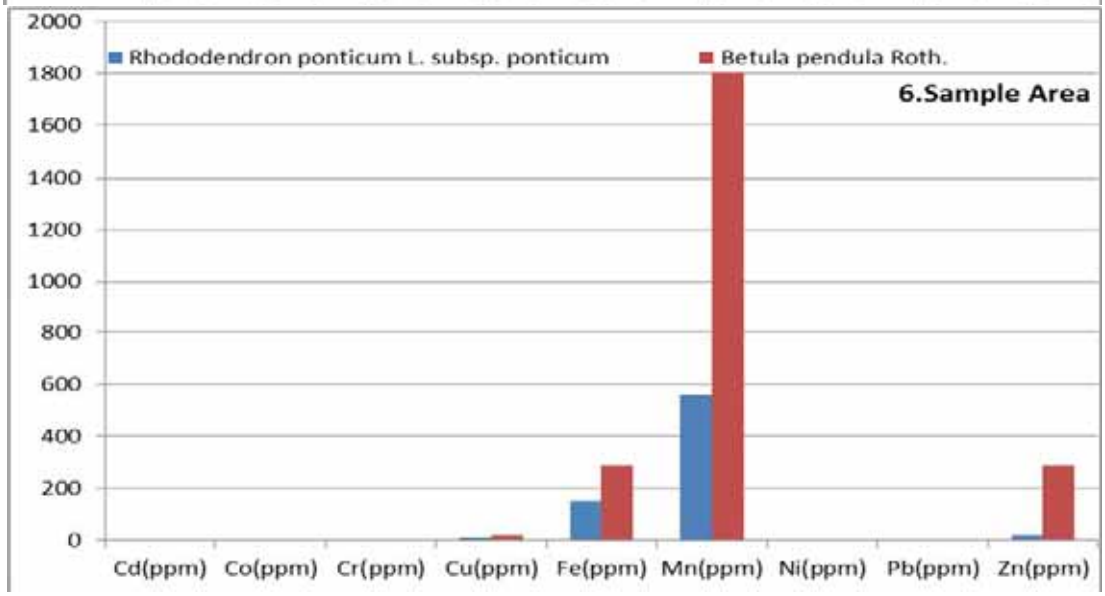
Rhododendron ponticum L. subsp. ponticum
Betula pendula Roth.
6.Sample Area
2000
1800
1600
1400
1200
1000
800
600
400
200
0
Cd(ppm)
Co(ppm)
Cr(ppm)
Cu(ppm)
Fe(ppm)
Mn(ppm)
Ni(ppm)
Pb(ppm)
Zn(ppm)

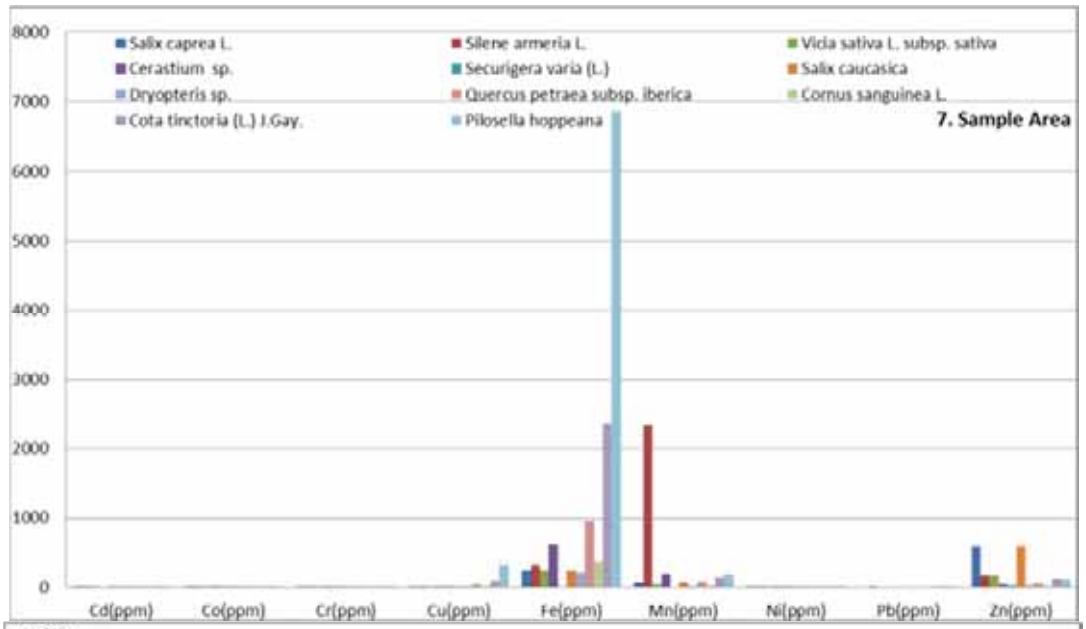
Salix caprea L.
Silene armeria L.
Vicia sativa L. subsp. sativa
Cerastium sp.
Securigera varia (L.)
Salix caucasica
Dryopteris sp.
Quercus petraea subsp. iberica
Cornus sanguinea L.
Cota tinctoria (L.) J.Gay.
Pilosella hoppeana
7. Sample Area
8000
7000
6000
5000
4000
3000
2000
1000
0
Cd(ppm)
Co(ppm)
Cr(ppm)
Cu(ppm)
Fe(ppm)
Mn(ppm)
Ni(ppm)
Pb(ppm)
Zn(ppm)

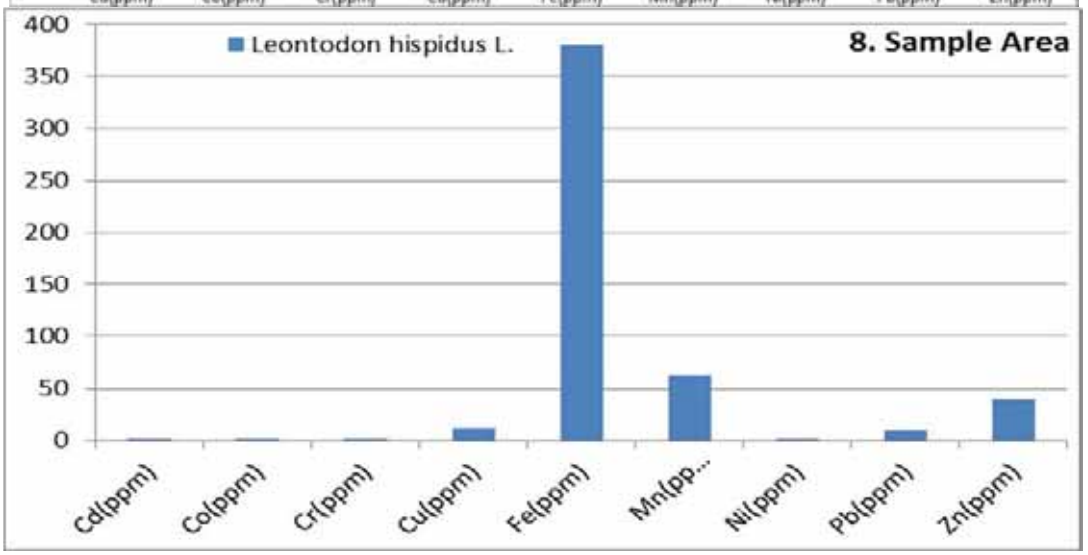
Leontodon hispidus L.
8. Sample Area
400
350
300
250
200
150
100
50
0
Cd(ppm)
Co(ppm)
Cr(ppm)
Cu(ppm)
Fe(ppm)
Mn(pp...
Ni(ppm)
Pb(ppm)
Zn(ppm)

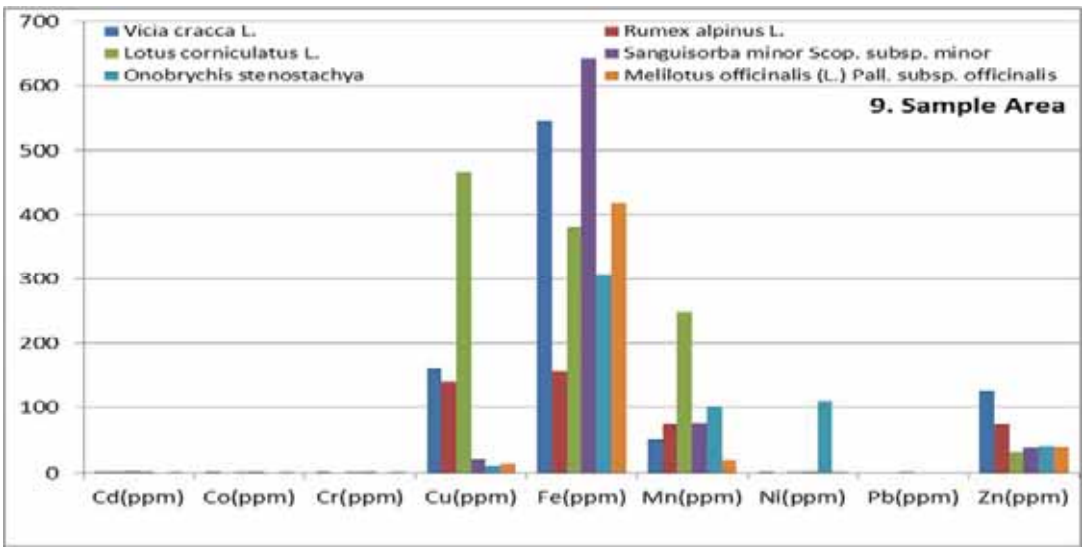
Vicia cracca L.
Rumex alpinus L.
Lotus corniculatus L.
Sanguisorba minor Scop. subsp. minor
Onobrychis stenostachya
Melilotus officinalis (L.) Pall. subsp. officinalis
9. Sample Area
700
600
500
400
300
200
100
0
Cd(ppm)
Co(ppm)
Cr(ppm)
Cu(ppm)
Fe(ppm)
Mn(ppm)
Ni(ppm)
Pb(ppm)
Zn(ppm)

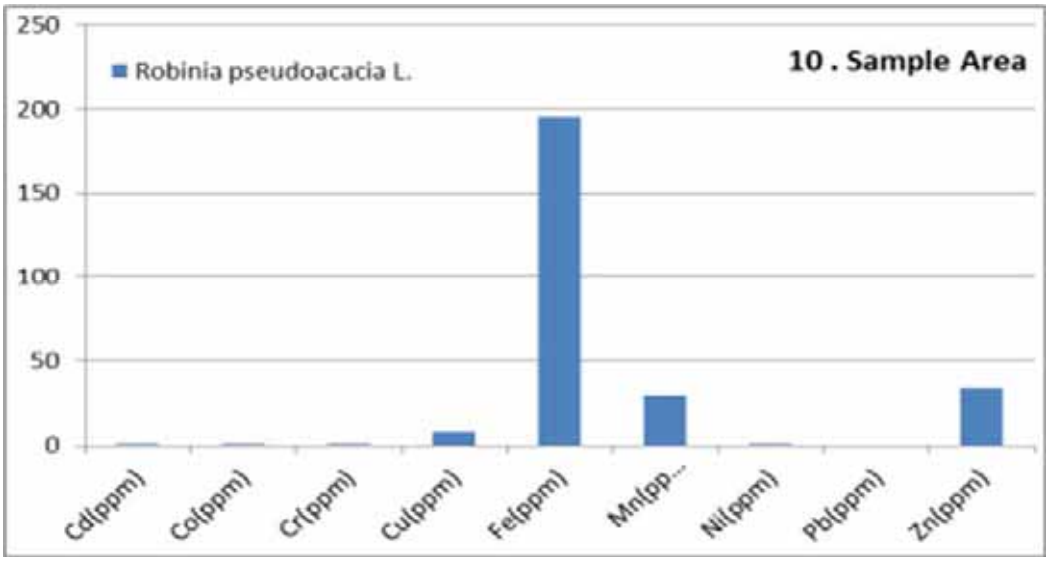

FIGURE 4
Heavy metal concentrations in plant species in sample areas

TABLE 4
Normal and toxic heavy metal concentrations in various plant species (34, 35, 36, 37, 18).

Limit value of Trace Elements in Plant		
Heavy Metal	**Sufficient-Normal (ppm)**	**Excess or Toxic (ppm)**
Pb	5-10	30-300
Cd	0,01-0,2	5-30
Cr	0,1-0,5	5-10
Cu	5-30	100
Ni	0,2-5	25-40
Zn	27-80	80-200
Mn	30-300	400-1000
Fe	10-50	50-200
Co	0,02-1	15-50

The comparison of present study findings and normal and toxic heavy metal concentrations in various plant species (Table 4) revealed that Fe concentrations in *Rhododendron luteum*, *Rumex acetosella* L., *Pilosella officinarum* subsp. *micradenia*, *Lotus alpinus*, *Hypericum orientale* L., *Scleranthus perennis* L. subsp. *perennis*, *Rhododendron smirnovii, Plantago lanceolata* L., *Trifolium alpestre* L., *Smilax excelsa* L., *Ranunculus dissectus, Scrophularia lucida* L., *Cirsium echinus, Cerastium gnaphalodes, Veronica officinalis* L., *Rhododendron ponticum* L. subsp. *ponticum*, Betula pendula Roth., *Salix caprea* L., *Silene armeria* L., *Vicia sativa* L. subsp. *sativa*, *Cerastium* sp., *Securigera varia* L., *Salix caucasica*, *Dryopteris* sp., *Quercus petraea* subsp. *iberica, Cornus sanguinea* L., *Cota tinctoria* L., J.Gay., *Pilosella hoppeana*, *Leontodon hispidus* L., *Vicia cracca* L., *Rumex alpinus* L., *Lotus corniculatus* L., *Sanguisorba* minor Scop. subsp. minor, *Onobrychis stenostachya, Melilotus officinalis* (L.) Pall. subsp. *officinalis* plant species were above 200 ppm toxic limit. Furthermore, it was observed that Cd concentration in *Salix caucasica* was between 5-30 toxic limit, Cr concentration was over 5-10 ppm toxic limit in *Bellis perennis* L., Cu concentrations were were over 100 ppm toxic limit in *Vicia cracca* L., *Rumex alpinus* L., *Lotus corniculatus* L., *Scleranthus perennis* L. subsp. p*erennis*, *Pilosella hoppeana*, Mn concentrations were between 400-1000 ppm toxic limit in *Betula pendula* Roth., *Silene armeria* L*., Rubus* sp., Ni concentrations were over the toxic limit of 25-40 ppm in Onobrychis stenostachya, *Plantago lanceolata.* L., and Zn concentrations were above the toxic limit of 80-200 ppm in *Pilosella officinarum* subsp. *micradenia*, *Plantago lanceolata* L., *Trifolium alpestre* L., *Betula pendula* Roth., *Salix caprea* L., *Silene armeria* L., *Vicia sativa* L. subsp. *sativa*, *Veronica officinalis* L., *Salix caucasica*, *Cota tinctoria* L., J.Gay., *Pilosella hoppeana*, and *Vicia cracca* L.

The plant species identified in the study area and the heavy metal concentrations over the limit and mean concentrations in soil samples collected at plant locations are presented in Tables 3 and Figure 3. As seen in Table 4, Fe, Cu, Zn and Mn concentrations were above the limit in the study area. In areas with higher than limit deposits, it was observed that 40 plant species presented in Table 3 were resistant to heavy metal soil content and they spread naturally. Wang et al [38] investigated the resistance of various plant species in heavy metal contaminated regions in China to these metals. They determined that *Rumex acetosella* L. plant near a heavy metal furnace accumulated 900 mg kg Zn in its roots and shoots. In the present study, it was determined that *Rumex acetosella* L. accumulated 214,801 ppm Fe, while *Rumex alpinus* L. accumulated 139,57 ppm Cu [39, 40]. Vural [41], in a study conducted in Gümüşhane province in Turkey in 2013, investigated heavy metal

concentration in *Robinia pseudoacacia* along a highway that goes through the urban center. The study data demonstrated that Cu, Fe, Mo, Ni, Sr and Zn concentrations *Robinia pseudoacacia* shoots were above and/or exceeded normal values. In the present study, it was determined that the Fe concentration in *Robinia pseudoacacia* was above the normal level.

Previous studies reported that families that include heavy metal pollution resistant species included *Fabaceae, Asteraceae, Caryophyllaceae, Poacea, Brassicaceae, Salicaceae* families. Also, the same studies reported that plant species in these families such as *Silene, Salix, Trifolium, Plantago, Thlaspi, Urtica, Chenopodium, Polygonum* and *Alyssum* could accumulate cadmium, copper, lead, nickel and zinc, and emphasized the importance of cultivation of these plants in contaminated soil [42, 43, 44].

CONCLUSION AND RECOMMENDATIONS

The quality and natural structure of the physical environment changes depending on the distance in and around the areas where mining activities are carried out [45]. The mining waste lead to large heavy metal deposits, especially in the soil and in the plant species that grow in the soil. It is important to investigate and determine heavy metal levels that adversely affect soil and plant quality, pose a threat to human health and cause environmental pollution.

In the present study, while Fe, Mn, Cu, Zn concentrations were high in soil samples, Cd, Cr, Pb, Ni and Co heavy metals were at lower levels. The comparison of the present study findings and pH-based PEC (Probable Effects Concentration) soil heavy metal toxicity limits revealed that Cd, Cu, Mn, Zn content exceeded these limits. It was observed that only in the dross dump site (DDS) Ni content, while Pb exceeded the limit at locations 2, 3, 4 and 8, Cr exceeded the limit at location 5. The analysis of the samples collected in location 5, which is agricultural land, demonstrated that Cu, Fe, Mn and Zn concentrations were above the limits.

The employment of certain plant species commonly found in the nature to clean ecosystems contaminated with heavy metals, and to restore damaged or destroyed ecosystems has recently been emphasized. Ecosystem restoration organizes the habitat using local plants, ensuring the restoration of destroyed or damaged ecosystems [46]

Studies demonstrated that natural species have the potential to grow in areas with heavy metal pollution, and also plantation of these species is important to reclaim these environments, restore biological productivity, and improve the soil.

The field studies conducted in the study area included the collection of indigenous plant species at locations where soil samples were collected and the collected plant species were identified. Thus, 40 plant species in 17 families were identified in the study area. Heavy metal accumulation was determined in samples collected from 40 plant species. It was observed that the mean heavy metal concentration levels in these species were ranked as follows: Fe> Mn> Zn> Cu> Cr> Ni> Pb> Cd> Co. The analysis of the findings revealed that Fe, Mn, Zn, Cu, Cr concentrations were high in plant samples, while Cd, Pb, Ni and Co heavy metal consentrations were at lower levels. The comparison of present study findings and normal and toxic heavy metal concentrations in various plant species revealed that Fe concentrations in *Rhododendron luteum, Rumex acetosella* L., *Pilosella officinarum* subsp. *micradenia*, *Lotus alpinus*, *Hypericum orientale* L., *Scleranthus perennis* L. subsp. *perennis, Rhododendron smirnovii, Plantago lanceolata* L., *Trifolium alpestre* L., *Smilax excelsa* L., *Ranunculus dissectus*, *Scrophularia lucida* L., *Cirsium echinus, Cerastium gnaphalodes, Veronica officinalis* L., *Rhododendron ponticum* L. subsp. *ponticum*, *Betula pendula* Roth., *Salix caprea* L., *Silene armeria* L., *Vicia sativa* L. subsp. *sativa*, *Cerastium* sp., *Securigera varia* L., *Salix caucasica, Dryopteris* sp., *Quercus petraea* subsp. *iberica*, *Cornus sanguinea* L., *Cota tinctoria* (L.) J.Gay., *Pilosella hoppeana*, *Leontodon hispidus* L., *Vicia cracca* L., *Rumex alpinus* L., *Lotus corniculatus* L., *Sanguisorba minor* Scop. subsp. *minor, Onobrychis stenostachya, Melilotus officinalis* (L.) Pall. subsp. officinalis plant species were above 200 ppm toxic limit. Furthermore, it was observed that Cd concentration in *Salix caucasica* was between 5-30 toxic limit, Cr concentration was over 5-10 ppm toxic limit in *Bellis perennis* L., Cu concentrations were were over 100 ppm toxic limit in *Vicia cracca* L., *Rumex alpinus* L., *Lotus corniculatus* L. ., *Scleranthus perennis* L. subsp. p*erennis*, *Pilosella hoppeana*, Mn concentrations were between 400-1000 ppm toxic limit in *Betula pendula* Roth., Silene armeria L., *Rubus* sp., Ni concentrations were over the toxic limit of 25-40 ppm in *Onobrychis stenostachya*, *Plantago lanceolata.* L., and Zn concentrations were above the toxic limit of 80-200 ppm in *Pilosella officinarum* subsp. *micradenia, Plantago lanceolata* L., *Trifolium alpestre* L., *Betula pendula* Roth., *Salix caprea* L., *Silene armeria* L., *Vicia sativa* L. subsp. *sativa*, *Veronica officinalis* L., *Salix caucasica*, Cota *tinctoria* (L.) J.Gay., *Pilosella hoppeana*, and *Vicia cracca* L.

The employment of certain common plant species commonly found in the nature to clean ecosystems contaminated with heavy metals, and to restore damaged or destroyed ecosystems has

recently been emphasized. Plants that could accumulate 50 to 500 times more metal in their above-ground organs when compared to underground ones are called hyperaccumulators. It was reported that there are approximately 400 plant species that accumulate metals. In other words, hyperaccumulator plants could accumulate heavy metals in their above-ground organs 100 to 1000 times more than other plant species without exhibiting any toxicity symptoms. Most could concentrate Ni biologically, approximately 30 could absorb Co, Cu and/or Zn, and very few could accumulate Mn and Cd. The above mentioned level is toxic for several similar species that could not adapt to living in soil with high heavy metal content. When compared to non-hyperaccumulator species, the roots of hyperaccumulator plants absorb heavy metals from the soil at a very high rate, transfer them to the stem at a higher speed, and store them in the stem and leaves in high amounts. [47; 48].

Thompson [42] reported that approximately 400 plants in 11 families clean the soil by collecting heavy metals in a literature review. [49] employed indigenous metal resistant plant species to remove metal contamination in the UK. They reported that long-term fertilization in metal-resistant plant cultivation yields excellent vegetative sections and soil stabilization. The idea of using plants to extract metals from contaminated soil was reintroduced and developed by Chaney [50], Chaney et al.[51] and Malaisse and Brooks [52] observed that the copper hyperaccumulator Haumaniastrum katangense could easily grow in copper mine waste [53]

The growth of natural vegetation in mines may take 70-80 years and even longer [54]. Thus, the surface should be in the "pre-planting" stage, which is one of the stages of mine site restoration, and it is important to plant "permanent vegetation" with major plant species. For this purpose, the employment of species such as *Trifolium alpestre* L., *Dorycnium graecum* (L.) Ser., *Lotus alpinus, Hypericum orientale* L., *Scleranthus perennis* L. subsp. *perennis, Cerastium gnaphalodes,* etc. would contribute to the growth of natural meadow grass and woody plants. In the next bushing stage, plants such as *Rhododendrom ponticum, Quercus petraea, Rubus* sp. could be used. *Robinia pseudoacacia, Quercus petraea, Picea orientalis, Betula pendula* and *Salix* sp. that are found in the study area could be used in biological soil reclamation due to the ability of their roots to bind nitrogen and suitability of the C/N ratio in fallen leaves. Thus, it will be possible to reclaim the natural ecosystem and introduce new occupancies in the after these activities.

Based on the literature review, it is possible to reclaim the natural vegetation through ecosystem restoration after mining activities with Rumex acetosella L., *Hypericum orientale* L., *Betula pendula* Roth., *Plantago lanceolata* L., *Trifolium alpestre* L., *Silene armeria* L., *Pilosella officinarum* C.H. & F.W. Schultz subsp. *micradenia* (NP.) Sell & West, *Lotus alpinus* (DC.) *Ramond., Bellis perennis* L., *Cerastium gnaphalodes* Fenzl, *Vicia cracca* L., *Robinia pseudoacacia* L., *Melilotus officinalis* (L.) Pall. subsp. *officinalis, Onobrychis stenostachya* Freyn species in *Asteraceae, Brassicaceae, Caryophyllaceae, Cyperaceae, Cunouniaceae, Fabaceae, Flacourtiaceae, Lamiaceae, Poaceae, Violaceae,* and *Euphobiaceae* families that are resistant to heavy metal pollution and indigenous to the study area.

ACKNOWLEDGEMENT

This study was supported by Artvin Çoruh University's Scientific Research Project Unit (No: 2016.F12.02.02)

REFERENCES

[1] Oladipo, O. G., Olayinka, A., Awotoye, O. O. 2014. Ecological İmpact of Mining on Soils of Southwestern Nigeria. Environmental and Experimental Biology. 12, 179-186.

[2] Weissenstein, K., Sinkala, T. (2011). Soil Pollution with Heavy Metals in Mine Environments, İmpact Areas of Mine Dumps Particularly of Gold and Copper Mining İndustries in Southern Africa. Arid Ecosystems. 1(1), 53-65.

[3] Fashola, M., Ngole-Jeme, V., Babalola, O. (2016) Heavy Metal Pollution From Gold Mines: Environmental Effects and Bacterial Strategies For Resistance. International Journal of Environmental Research and Public Health. 13(11), 1047-1067.

[4] Kahvecioğlu, Ö., Kartal, G., Güven, A., and Timur, S. (2003). Environmental Effects of Metals-I. Journal of Metallurgy. 136, 47-53.

[5] Kır, İ., Tekin-Özan, S., & Tuncay, Y. (2007). The Seasonal Variations of Some Heavy Metals in Kovada Lake's Water and Sediment. E.U. Journal of Fisheries & Aquatic Sciences 2007 Cilt/Volume 24, Sayı/Issue (1-2): 155–158

[6] Aybar, M., Bilgin, A., and Sağlam, B. (2015). Removing Heavy Metals from the Soil with Phytoremediation, Journal of Natural Hazards and Environment. 1 (2), 59-65 (in Turkish).

[7] Chapmann, N.D., Pratt, P.F. and Parker, F. (1961). Methods of Analysis for Soils, Plants And Waters. Univ. of Calif. Div. Agr. Sci. Riverside. 68-72.

[8] Gülçur, F. (1974) Physical and Chemical Analysis Methods of Soil, İ.Ü. Publications Publication No: 1970, Faculty of Forestry Publication No:201, Kurtuluş Press, Istanbul. 225-226.
[9] EPA-3052 (1996). U.S. Environmental Protection Agency, EPA-Method 3052, Microwave assisted acid digestion of siliceous and organically based matrices, U.S. Government Printing Office, 1-20, Washington, DC.
[10] Kabata Pendias, A., Pendias, H. (1992). Trace Elements in Soils and Plants, 2 Nd. Edition Crc Press, Boca Raton, Ann Arnbor London. 287-301.
[11] Tok, H.H. (1997). Environmental Pollution. Anadolu Printing, Istanbul, 154-162.
[12] Öztürk, M., Bildik, B. (2005). Compost Production in Animal Farms. Ministry of Environment and Forestry, Ankara. 6-8 (in Turkish).
[13] Öztürk, M. (2017). Compost Production from Animal Manure and Waste. 182-183.
[14] Özkan, A., Özkan, V., Sungur, Ş., Birses, H. 2017. Heavy Metal Pollution Around İnternational Hatay Airport. Natural and Engineering Sciences. 2(1), 18-24.
[15] Mentese, S., and Böbrek, O. (2020). Effect of Mining Activities on Heavy Metals in Soil (As, Cd, Co, Fe andNi): The Case of Orhaneli and Büyükorhan (Bursa). , İzmir-Turkey. Aegean Geographical Journal. 29 (1), 45-56
[16] Kabata-Pendias, A., and Pendias, H. (2001). Trace elements in soils and plants CRC Press Inc. Boca Raton, 3-9, FL, USA.
[17] Sasmaz, A., and Yaman, M. (2008). Determination Of Uranium and Thorium in Soil And Plant Parts Around Abandoned Lead–Zinc–Copper Mining Area. Communications in Soil Science and Plant Analysis. 39(17-18), 2568-2583.
[18] Deveci, T. (2012). Determınatıon of Trace Elements (Cu, Co, Mn and Zn) and Iron Concentratıons in Soıl and Vegetables Irrıgated wıth Domestic and Industrıal Wastewaters of Gazıantep City, Turkey, MSc. Thesis, Kilis 7 Aralık University Graduate School of Natural and Applied Sciences Department of Chemistry, Kilis. 10-11.
[19] Aktaş, Y.K., Kocabaş, A (2010). Heavy Metal Content of Roadside Soil İn Edirne, Turkey. Analytical Letters. 43, 1869-1878.
[20] Bakirdere, S, Yaman, M. (2008) Determination of Lead, Cadmium and Copper in Roadside Soil and Plants in Elazig, Turkey. Environmental Monitoring and Assessment.136, 401-410.
[21] Yalçın, E., Maraş, M., and Çavuşoğlu, K. (2007). The Effect of Lead and Mercury Heavy Metal İons on Body Weight and Serum Alkaline Phosphatase Level in Albino Mice. Journal of Balıkesir University Institute of Science and Technology. 9(1), 61-67 (in Turkish).
[22] Onder, S., Dursun, S., Gezgin, S., & Demirbas, A. (2007). Determination of Heavy Metal Pollution in Grass and Soil of City Centre Green Areas (Konya, Turkey). Polish Journal of Environmental Studies. 16(1),145-154.
[23] Malkoc, S., Yazıcı, B., and Savas Koparal, A. (2010). Assessment of The Levels of Heavy Metal Pollution in Roadside Soils of Eskisehir, Turkey. Environmental Toxicology and Chemistry. 29(12), 2720-2725.
[24] Zhang, J.X., Yao, N. (2008). Indicator and Multivariate Geostatistic for Spatial Prediction. Geo-Spatial Information Science. 11(4), 243-246.
[25] Fan, S. (2014). Assessment of spatial distribution and pollution with heavy metals in roadside soils along Xi'an-Baoji Highway in northwest China. Environmental Engineering & Management Journal (EEMJ). 13(12), 3161-3171.
[26] Ali, M. M., Ali, M. L., Islam, M. S., Rahman, M. Z. (2016). Preliminary assessment of heavy metals in water and sediment of Karnaphuli River, Bangladesh. Environmental Nanotechnology, Monitoring & Management. 5, 27-35
[27] Kaçar, B, İnal, A (2008) Plant Analysis. Nobel Publications No: 1241, 891, Ankara.
[28] Kacar, B., and Katkat, A. V. (2007). Plant nutrition. Nobel Publication. 849, 3.
[29] Rout, G.R. And Das, P. (2003).Effect of Metal Toxicity on Plant Growth and Metabolism: I.Zinc. Agronomie. 23, 3-11
[30] Asri, F. Ö., Sönmez, S. (2006). The Effect of Heavy Metal Toxıcıty on Plant Metabolısm. Derim. 23(2), 36-45 (in Turkish).
[31] Özbek, H., Kaya, Z., Gök, M and Kaptan, H., (1995). Soil Science. Çukurova University Faculty of Agriculture. General Publication No: 73 Textbooks Publication No: 16, 85-92 Adana
[32] Sossé, B.A., Genet, P., Dunand-Vinit, F., Toussaint, L.M., Epron, D and Badot, P.M. (2004). Effect of Copper on Growth in Cucumber Plants (Cucumis Sativus) and İts Relationships with Carbonhydrate Accumulation and Changes in İon Contents. Plant Science. (166), 1213-1218
[33] Sönmez, S., Kaplan, M., Sönmez, N.K and Kaya, H. (2006) B. Effects of High Level Copper Applications to Soil on pH and Nutrient Element Contents of Soil. Mediterranean Agricultural Sciences. 19(1), 151-158.

[34] Demirezen, D. (2002) 'Investigation of Heavy Metal Pollution at Aquatic Ecosystems in Sultan Sazlıgı and It's Environs', Ph.D. Thesis, University of Gazi, Institute of Science and Technology, 149, Ankara.
[35] Aksoy, A., Demirezen, D., Duman, F. (2005). "Bioaccumulation, Detection and Analyses of Heavy Metal Pollution in Sultan Marsh And İts Environment." Water, Air, and Soil Pollution. 164(1-4), 241-255.
[36] Kabata-Pendias, A., Mukherjee, A.B., (2007). Trace Elements from Soil to Human. Spring er Science & Business Media Book, 31-33.
[37] Khan, S., Cao, Q., Zheng, Y. M., Huang, Y. Z., and Zhu, Y. G. (2008). Health risks of heavy metals in contaminated soils and food crops irrigated with wastewater in Beijing, China. Environmental Pollution. 152(3), 686-692.
[38] Wang, W., Vinocur, B., and Altman, A. (2003). Plant responses to drought, salinity and extreme temperatures: towards genetic engineering for stress tolerance. Planta. 218(1), 1-14.
[39] Malko, A. (2002) Investigations on the active ingredient content, cadmium absorption and susceptibility to red wilts of *Hypericum Perforatum* L. Shaker, Aachen. 113-121. (in German).
[40] Schneider M, Marquard R (1996) Medicinal Herb. 1, 111–116, (in German).
[41] Vural, A. (2013). Assessment of Heavy Metal Accumulation in the Roadside Soil and Plants of Robinia Pseudoacacia, in Gumushane, Northeastern Turkey. Ekoloji. 22(89), 1-10.
[42] Thompson, L. (1997). Exciting Environmental Technologies. 159-172.
[43] Mulligan, C. N., Yong, R. N., and Gibbs, B. F. (2001). Remediation Technologies for Metal-Contaminated Soils and Groundwater: An Evaluation. Engineering Geology. 60(1-4), 193-207.
[44] Özay, C., Mammadov, R. (2013). Heavy Metals and Potential Availability of Ornamental Plants for Phytoremediation. Balıkesir University Institute of Science and Technology C. 15(1), 67-76 (in Turkish).
[45] Sağlam, B., Bilgin, A., and Aybar, M. (2020). Assessment of Heavy Metal Pollution in Soil and Sediments of Murgul Copper Mine and its Surroundings. Kastamonu University Journal of Forestry Faculty. 20(1), 25-37.
[46] Parch, L. (2004). Do You Need a Guru, Natural Health-Massachusetts Then Woodland Hılls CA. 34, 100-105.
[47] Clemens, S. (2006) Toxic Metal Accumulation, Responses to Exposure and Mechanisms of Tolerance in Plants, Biochimie, 88, 1707-1719.
[48] Rascio, N., Navari-Izzo, F. (2011). Heavy Metal Hyperaccumulating Plants: How and Why Do They Do İt? And What Makes Them so İnteresting? Plant Science 180 (2), 169–181
[49] Smith, R.A.H., Bradshaw, A.D. (1979). The Use of Metal Tolerant Plant Populations for the Reclamation of Metalliferous Wastes. J Applied Ecol 16, 595-612
[50] Chaney, R.L. (1983). Plant Uptake of İnorganic Waste Constituents. In: Parr. If, Marsh Pı3. Kia Jm, Eds. Land Treatment of Hazardous Wastes. Park Ridge, Nj: Noyes Data Corp. 50-76.
[51] Chaney, W.R., Pope, P.E., Byrnes, W.R. (1995). Tree Survival and Growth After Twelve Years on Mined Land Reclaimed in Accord with the 1977 Surface Mining Control and Reclamation Act. J. Environ. Qual. 24, 630-634.
[52] Malaisse, F., and Brooks, R.R. (1982). Colonisation of Modified Metalliferous Environments in Zaire by the Copper Flower Haumaniastrum Katangense. Plant and Soil. 64(2), 289-293.
[53] Morrey Dr, Balkwjll K, Balkwill Mj, 1989. Studies on Serpentine Flora: Preliminary Analyses of Soils and Vegetation Associated with Scrpentiniie Rock Formations in The South-Doğu Transvaal. South Afr. J. Hot. 55, 171-177
[54] Özalp, G., Dirik, H., Kuvan, Y., Güneş, Y., Orhan S. (2008). Evaluation of Mining Initiatives in Kaz Mountains in Terms of Conservation-Use Balance, İ.Ü. Report Prepared by the Faculty of Forestry. 8-10.
[55] Özkul, C. (2008). The Effect of Industrialization on Soil Heavy Metal Concentration in Izmit (Kocaeli). Journal of Applied Earth Sciences. 7 (2), 1-9.
[56] Akyıldız, M., Karataş, B. (2018). Investigation of Heavy Metal Pollution in Soils at Adana City Center. Çukurova University Faculty of Engineering and Architecture Journal. 33 (2), 199-214. (in Turkish).

Received: **03.12.2020**
Accepted: **09.02.2021**

CORRESPONDING AUTHOR

Hilal Surat
Art and Design Faculty
Artvin Coruh University,
Artvin – Turkey

e-mail: hilal1881@artvin.edu.tr

© by PSP Volume 30– No. 05/2021 pages 5211-5219 Fresenius Environmental Bulletin

A DYNAMIC MODEL FOR CALCULATING THE THERMAL PARAMETERS OF HORIZONTAL WELLS WITH STEAM HUFF AND PUFF

Qingchun Gao[1,2], Zhiming Wang[1,*], Quanshu Zeng[1]

[1]State Key Laboratory of Petroleum Resources and Prospecting, China University of Petroleum, Beijing 102249, P.R. China
[2]CNPC Greatwall Drilling Company Engineering Technology Research Institute, Panjin 124010, P.R. China

ABSTRACT

In the process of thermal recovery of heavy oil, the energy exchanges with its surrounding environment during steam migration in a tube, so as to heat will be lost and the steam enthalpy will decrease gradually. It will seriously affect the steam-simulation effect of heavy oil wells if string structure, horizontal section length, steam injection volume, and steam dryness are not reasonably designed. Therefore, the accurate calculation and forecast of thermodynamic parameters of steam along the wellbore, such as pressure, temperature, and dryness, is the key to evaluate the gas injection effect. It also has great significance for the optimization of steam-simulated parameters. In this paper, a dynamic model for calculating thermal parameters in horizontal wells with steam huff and puff is established based on one-dimensional unsteady heat-transfer theory, in which the characteristics of the variable mass flow in the horizontal segment is considered. The results shows that the maximum relative error between the calculation results and the measured data is less than 5%, which proves the accuracy of the model. The effect of wellhead steam parameters on the distribution of steam thermodynamic parameters in horizontal wellbore is almost consistent. The steam-injection rate is in direct proportion to the horizontal wellbore extension distance. In addition, the influence of steam-injection time on steam temperature, pressure, and dryness can be ignored.

KEYWORDS
Recovery, heavy oil, surrounding environment, thermodynamic parameters, wellbore, steam huff and puff

INTRODUCTION

During thermal recovery of heavy oil, the distribution of thermal physical parameters after steam injection is very important for evaluating the effect of steam simulation and optimizing production parameters [1-3]. The calculation and prediction of the pressure, temperature, and dryness of steam along the wellbore is the key to understanding the change in thermodynamic state in the process of steam migration from the wellhead to the formation [4]. After steam injection, the movement of hot steam in the horizontal wellbore is a complex and variable mass flow [5]. Therefore, in order to accurately describe the heat dissipation law of steam in the whole process, it is necessary to establish a fine thermal parameter calculation model that considers the influence of variable mass flow in the horizontal well section.

In the process of horizontal wellbore production, some researchers have carried out considerable research on variable mass flow and the wellbore heat-transfer model [6-8]. Regarding variable mass flow in horizontal wellbores, Landman et al. [9] studied the influence of hole-density distribution on the inflow profile for horizontal well perforation completion. Harald et al. [10] regarded the perforations of perforating completion as one microelement well section, half of the interval between perforations as the reservoir supply radius, and the length of perforations as the microelement well section length. The influence of perforating completion parameters on the wellbore flow law has been calculated and analyzed. Wang et al. [11] comprehensively considered the reservoir seepage and wellbore pipe flow under the variable flow rate of horizontal wells, based on the control principle of the inflow velocity profile of horizontal wells. They established the sectional combination optimisation model of perforating parameters of horizontal wells. The influence of perforation parameters on the inflow profile of perforated completion wells has also been studied [12]. The results show that the more optimised the parameters are, the better the optimisation effect of the inflow velocity profile of horizontal wells. In relation to the wellbore heat-transfer model, Ramey et al. [13] proposed a simplified model that was more consistent with the actual production situation. The famous Ramey formula, established a relationship between temperature in the wellbore, well depth, and production

time. Satter et al. [14] optimized the wellbore heat-transfer model proposed by Ramey and Willhite et al., so that the total heat-transfer coefficient in the wellbore became a function of well depth and temperature. Galate et al. [15] combined the pressure-drop equation with the heat-transfer equation to solve the problem, which improved the accuracy of their calculations. Xu et al. [16] established the radial heat-transfer model of fluid production and wellbore and calculated the total heat-transfer coefficient according to wellbore structure. Based on previous studies, Wang et al. [17] considered the heat loss caused by the change in wellbore pressure during the process of steam injection and established a mathematical model for comprehensive heat transfer in the wellbore. Zhou et al. [18] introduced PVT parameters of superheated steam into the model, and comprehensively considered the conservation of momentum, mass, and energy, establishing the parameter distribution model of superheated steam along the wellbore.

This paper establishes a numerical model for calculating thermal parameters of horizontal wells with steam huff and puff, based on one-dimensional unsteady heat-transfer theory. The characteristics of the variable mass flow, such as steam pressure, temperature, dryness, and heat loss along the horizontal wellbore, was analyzed according to the equations of energy conservation and momentum conservation.

MATERIALS AND METHODS

Due to the complexity of the model and the large number of calculation variables, the double-iteration method of pressure and dryness increments is adopted to solve the problem. The accuracy and reliability of this method are proved by comparing the model with the field data from a low-permeability heavy oil block of Liaohe, China.

RESULTS

Establishment of the model. Different from the heat-diffusion mode of steam in vertical wellbores, injected steam will flow into the formation along the perforation holes after entering horizontal wellbores, resulting in a continuous change in the mass flow of steam in the wellbore [19]. This means the flow of steam in the horizontal section belongs to the variable mass flow. In the case of variable mass flow, the volume flow rate and flow rate of steam will continue to decrease due to the continuous decrease in steam mass flow, which will reduce acceleration. Therefore, the loss caused by acceleration cannot be ignored when building the model. Due to the pressure loss in the direction of horizontal wellbores, the pressure distribution at each perforation hole of a horizontal wellbore is uneven from the heel end to the toe end, so the radial flow rate is not the same. Because of the above characteristics of steam flow in horizontal wellbores, the calculation model for pressure and temperature distribution of common circular pipe will not be applicable. By establishing a corresponding calculation model for pressure drop and temperature distribution according to the variable mass flow characteristics of steam in horizontal wellbores, we can more accurately describe the distribution law of steam thermal parameters in horizontal wellbores.

Basic assumptions are as follows: the reservoir is a homogeneous reservoir with a thickness of h and infinite horizontal extension. The heat transfer from the wellbore to the cement sheath is one-dimensional steady-state heat transfer, and the heat transfer from the cement sheath to the formation is one-dimensional unsteady heat transfer. The coupling heat transfer is not considered, and the heat transfer along the horizontal direction of the steam is ignored [20]. The injection pressure, dryness, and mass flow of the steam are maintained at the heel of the horizontal well and the steam flow in the horizontal wellbore is steady.

Conservation equation of mass. Take a microelement section at any position of the horizontal wellbore and the steam flow condition in the microelement section, as shown in Figure 1.

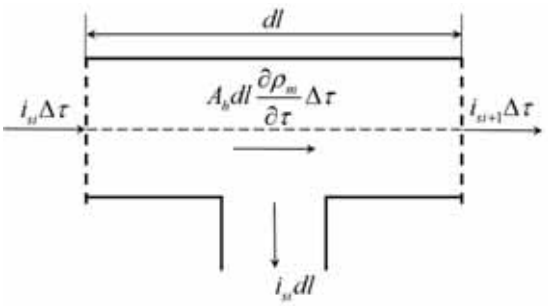

FIGURE 1
Diagram of mass conservation of steam flow in micro segment

According to the principle of conservation of mass, the difference between the mass of steam flowing in and out of the microelements in unit time is equal to the mass increment of the microelements. Based on the assumption that steam flows in a horizontal wellbore in a steady state, establish the mass conservation equation for the microelements shown in Figure 1, as follows:

$$i_{si}\Delta\tau - i_{si+1}\Delta\tau - i_{is}dl\cdot\Delta\tau = A_h dl\frac{\partial\rho_m}{\partial\tau}\Delta\tau \quad (1)$$

Where, i_s is the mass flow of steam in the wellbore, *kg/s*. $\Delta\tau$ is the time, *s*. A_h is the cross-sectional area of the micro element section, m^2. ρ_m is the steam deity in the micro element section, kg/m^3. i_{is} is the suction capacity of the formation, $kg/m\cdot s^{-1}$. $i_{si}\Delta\tau$ is the mass of steam flowing into the micro element within the time, *kg/s*. It refers to the mass increment of microelements in time, $i_{si+1}\Delta\tau$ is the mass of steam flowing out of microelements in time, *kg,* and $i_{is}dl\cdot\Delta\tau$ is the mass of steam flowing into the formation of microelements in time, *kg*. According to the hypothesis, the steam flow in horizontal wellbore is steady state.

Energy conservation equation. Since steam flows in a horizontal direction in a horizontal wellbore, the energy change caused by gravity can be ignored. A schematic diagram is shown in Figure 2.

According to the law of conservation of energy, in unit time and unit length, the reduced steam energy is the sum of heat loss friction loss and increase of formation energy. The energy conservation equation for the microelements shown in Figure 2 is established as follows:

$$\frac{dW}{dl} + i_{is}\left(h_m + \frac{v_r^2}{2}\right) + \frac{dQ}{dl} = -\frac{d}{dl}\left[i_s(h_m + \frac{v_m^2}{2})\right] \quad (2)$$

In which, *dW* is the work done by friction force in unit time, *kJ*. *dl* is the length of micro element segment, *m*. *dQ* is the heat loss of steam in micro element segment in unit time, *kJ*. h_m is the heat enthalpy of wet saturated steam mixture in micro element segment, *kJ/kg*. v_r is the speed of steam flowing into reservoir in radial direction in micro element segment, *m/s*. v_m is the flow speed of steam in horizontal direction in micro element segment, *m/s*.

Through the energy-conservation equation, the dryness change in steam in the wellbore can be deduced. The flow of steam in the horizontal wellbore is a gas liquid two-phase flow, and its enthalpy value can be expressed as follows:

$$h_m(x,t) = x\cdot h_s + (1-x)h_w \quad (3)$$

Where, h_s is the enthalpy of gas phase in the saturated wet steam in the micro element section, *kJ/kg*. h_w is the enthalpy of the liquid phase in the saturated wet steam in the micro element section, *kJ/kg*.

The enthalpy of water vapor is also a function of steam pressure, and then the equation (4) and (5) can be obtained:

$$\frac{dh_m}{dl} = (h_s - h_w)\frac{dx}{dl} + \frac{dh_w}{dP}\frac{dP}{dl} + \left(\frac{dh_s}{dP} - \frac{dh_w}{dP}\right)\frac{dP}{dl}x \quad (4)$$

When steam flows in a horizontal wellbore, its volume flow rate of gas phase is much larger than that of liquid phase, so it can be regarded as an ideal gas [21]. According to the ideal gas state equation, it can be obtained.

In order to simplify the formula, the value of N_1, N_2 and N_3 can be expressed [22]. Therefore, we can obtain equation (6):

$$\frac{dx}{dl} + \frac{N_2}{N_1}x = -\frac{N_3}{N_1} \quad (6)$$

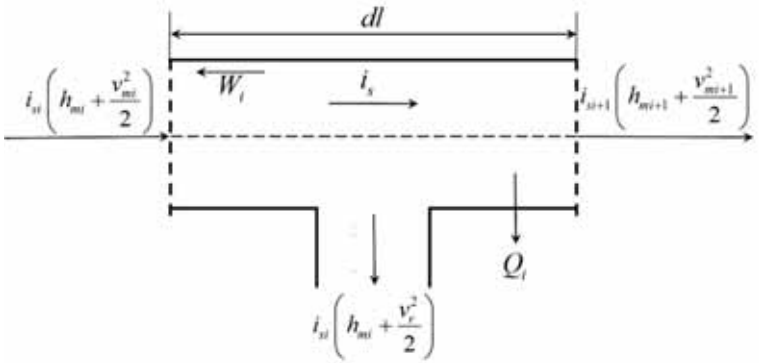

FIGURE 2
Schematic diagram of energy conservation of steam flow in micro segment

$$\frac{d}{dl}\left(\frac{v_m^2}{2}\right) = v_m\frac{dv_m}{dl} = v_m\frac{d}{dl}\left(\frac{i_s}{\rho_m A_h}\right) = \frac{v_m}{\rho_m A_h}\frac{di_s}{dl} + \frac{v_m i_s}{A_h}d\left(\frac{1}{\rho_m}\right) \quad (5)$$

When the positions of the calculated points are known, N_1, N_2 and N_3 are all constants, so equation (6) is a first order ordinary differential linear equation. After solving the differential equation, the distribution of steam dryness in the wellbore can be obtained. It can be seen from the above equations that if the heat loss, friction work, and pressure drop in the process of steam flow can be obtained, the dryness value at any position of the wellbore can be calculated.

It can be seen from the above formula that if the heat loss, friction work and pressure drop in the process of steam flow can be obtained, the dryness value at any position of the wellbore can be calculated. When the steam flows in the horizontal wellbore, it is possible to change the steam dryness to zero at a certain position of the horizontal wellbore due to the existence of heat loss. At this time, the energy equation can be obtained.

When the steam flows in the horizontal wellbore, due to the existence of heat loss, it is possible to change the steam dryness to zero at a certain position of the horizontal wellbore. At this time, the energy equation can be expressed.

Conservation equation of momentum. The momentum conservation diagram of injected steam flowing in the micro segment is shown in Figure 3. It can be seen that the forces that steam receives in the flow process mainly include the forces generated by the differential pressure at both ends of the microelement section and the friction resistance between the steam and the inner surface of the casing. The momentum conservation equation for the element segment is established, and the calculation model of steam pressure distribution in a horizontal wellbore can be obtained [23]:

$$\frac{dP}{dl} = -\frac{1}{A_h}\frac{2v_m\frac{di_s}{dl}+\frac{\tau_c}{dl}}{\left[1+\left(\frac{1}{T}\frac{dT}{dP}-\frac{1}{P}\right)\frac{v_m i_s}{A_h}\right]} \quad (7)$$

Where, τ_c is the friction between the inner wall of the casing and the steam, N. dP is the pressure drop of the selected micro segment, MPa, and dl is the steam absorption of the corresponding formation of the current micro segment, $kg/(m{\cdot}s^{-1})$.

Work done by friction. In the process of steam flow, there will be shear friction with the inner wall of the casing, the direction of which is opposite to that of steam flow, so the work of friction is negative. In unit time, the expression of the work done by the friction force on the infinitesimal segment of length can be obtained.

The friction coefficient is mainly composed of the friction coefficient between the fluid and the pipe wall, and the friction coefficient when the steam flows through the perforating hole. The calculation for the friction coefficient between fluid and pipe wall adopts the conventional pipe flow calculation method.

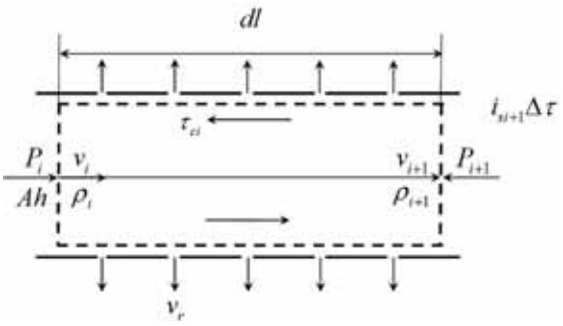

FIGURE 3
Diagram of momentum conservation of steam flow in micro segment

Calculation of physical parameters of saturated wet steam. For different flow patterns, the calculation method of liquid holdup is different [24]. The density of saturated wet steam is the weighted sum of the density of saturated water and the density of dry steam, and the velocity of saturated wet steam is the sum of the velocity of saturated water and the velocity of dry steam.

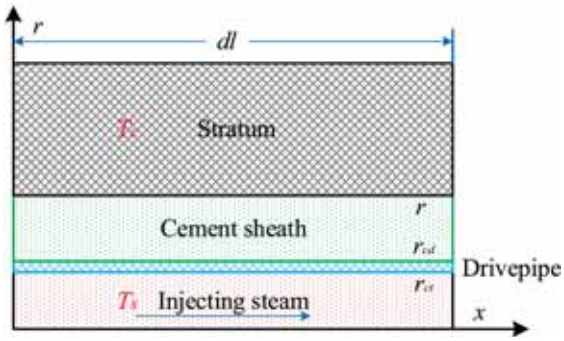

FIGURE 4
Temperature distribution diagram of steam injection process

Calculation of wellbore heat loss. According to the assumed conditions, since the horizontal well is located in the infinite formation, the reservoir has infinite heat capacity. This means that while the formation near the cement sheath can be slowly heated by steam, the formation temperature far away from the wellbore remains unchanged in the original state, which belongs to unsteady heat transfer. Therefore, the heat-transfer process from the horizontal wellbore to the formation can be simplified as: from the wellbore to the outer edge of the cement sheath is steady-state heat transfer, and from the outer edge of the cement sheath to the

formation is unsteady heat transfer, as shown in Figure 4.

Solution of the model. Because of the complexity of the model, it is difficult to directly calculate the steam pressure, temperature, dryness, and other parameters, so the double-iteration method of pressure and dryness increments is used. The solving process is shown in Figure 5, and the specific solution steps are as follows: the steam pressure, temperature, dryness and mass flow at the heel of horizontal well are known. The whole horizontal section is divided into *N* sections with the heel of horizontal well as the starting point. The variation of dryness and pressure drop in the length are estimated as the initial value of iterative calculation, and the average pressure and temperature in this section are calculated in turn. The method of beggs-Brill is used to determine the physical properties and flow parameters of the wet steam mixture at the average pressure and temperature. Calculate the steam absorption of the formation, and use equation to calculate the friction force between the steam and the screen tube. The pressure gradient of this section is calculated, and then the pressure drop of the length is obtained. The wellbore heat loss in the micro element section is calculated. On this basis, the dryness and dryness change of steam in the micro element section are calculated. Compare the calculated result with the estimated result in step, and if the calculation result is reasonable, continue, otherwise, return to recalculation. Repeat to calculate the pressure, temperature and dryness distribution of steam on each micro segment until the accumulated length of each micro segment is greater than or equal to the total length of horizontal wellbore.

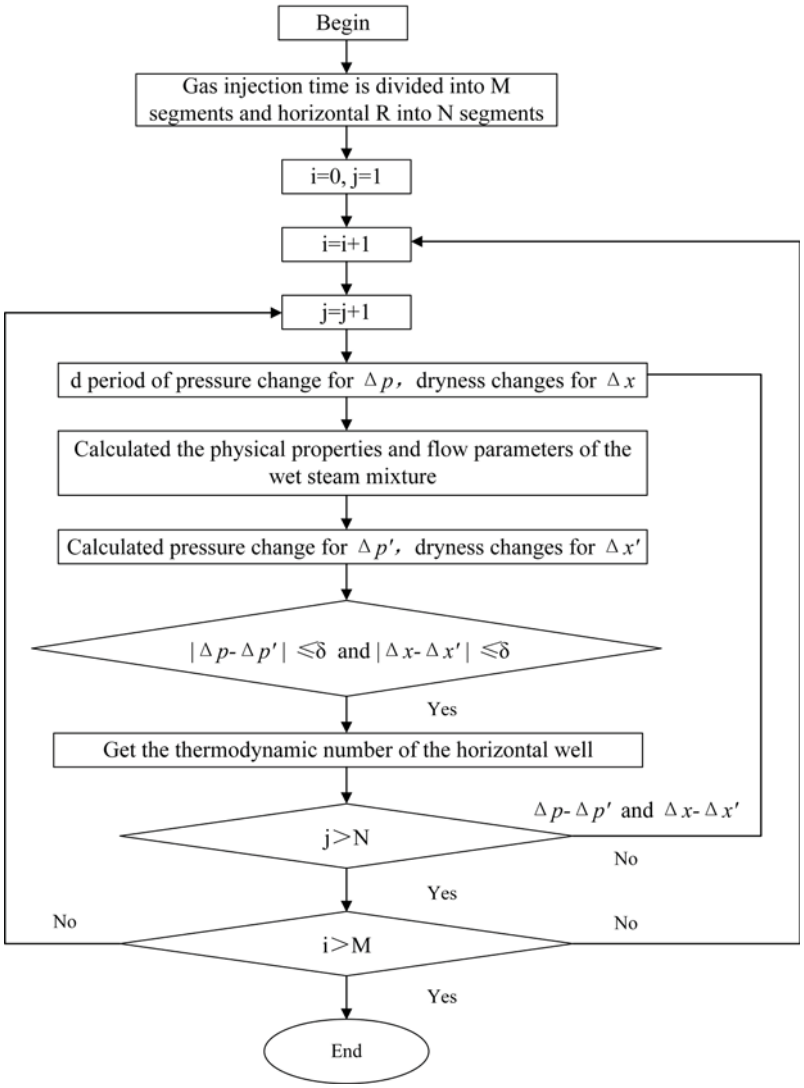

FIGURE 5
Solving process of the model

TABLE 1
Thermal parameters of horizontal wellbore

Parameters	Value	Parameters	Value
Thickness/(m)	287	Length of horizontal well/(m)	195.3
Temperature/(°C)	18.8	Inner diameter of casing/(m)	0.0807
Pressure/(MPa)	2.38	Outer diameter of casing/(m)	0.0889
Permeability/(mD)	1940	Wellbore radius/(m)	0.12
Porosity	0.32	Perforation density/(m^{-1})	12
water saturation	0.35	Perforation radius/(m)	0.0075
Viscosity of oil/(mPa·s)	1366	Formation heat conductivity/(W/m/°C)	1.730
Volume factor of oil/(m^3/m^3)	1.05	Thermal conductivity of cement/(W/m/°C)	0.933
Water volume coefficient	1.01	Wellhead steam pressure/(MPa)	5.13
Thermal diffusivity	0.108	Wellhead steam temperature/(°C)	336.5
Drainage area/(km^2)	29700	Rate of gas injection rate/(kg/s)	6.23

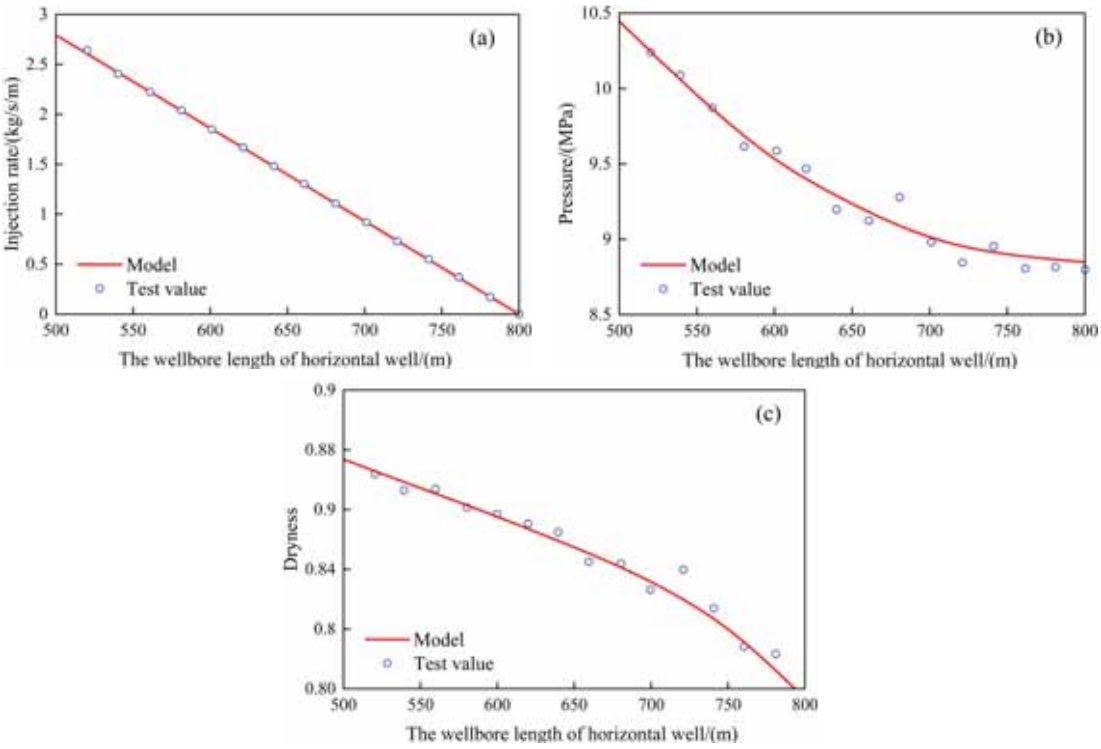

FIGURE 6
Validation of the model

Validation of the model. To verify the accuracy of the model, a huff and puff horizontal well in a low-permeability heavy oil block of Liaohe, China, is taken as an example to calculate the steam temperature, pressure, and dryness along the well [25]. Table 1 shows the reservoir physical property parameters, wellbore structure parameters, and wellhead steam-injection parameters.

The steam temperature, pressure, and dryness values calculated by the model are compared with the measured data, and the results are shown in Figure 6. It can be seen from the figures that the maximum relative error between the calculation results and the measured data is less than 5%, which proves the accuracy of the model.

Sensitivity analysis of parameters. The distribution of steam temperature, pressure, and dryness in horizontal wellbores is affected by many factors. The influence of the steam-injection rate, wellhead dryness, wellhead pressure, and injection time on the distribution of steam temperature, pressure, and dryness is obtained by using the above-mentioned model for calculating thermal physical parameters and heat loss along the horizontal wellbore, as shown in Figure 7.

The results show that the influence of wellhead steam parameters on the distribution of steam thermodynamic parameters in horizontal wellbores is basically the same. However, with the continuous injection of steam into the formation, injection effi-

ciency and dryness will be significantly reduced. The smaller the steam-injection rate, the shorter the extended distance of steam in the horizontal wellbore. The larger the steam-injection rate, the longer the extended distance of steam in the horizontal wellbore. In other words, the extended distance of steam in a horizontal wellbore decreases with the increase in wellhead steam pressure. Hence, the effect of steam-injection time on steam temperature, pressure, and dryness in horizontal wellbores can be ignored.

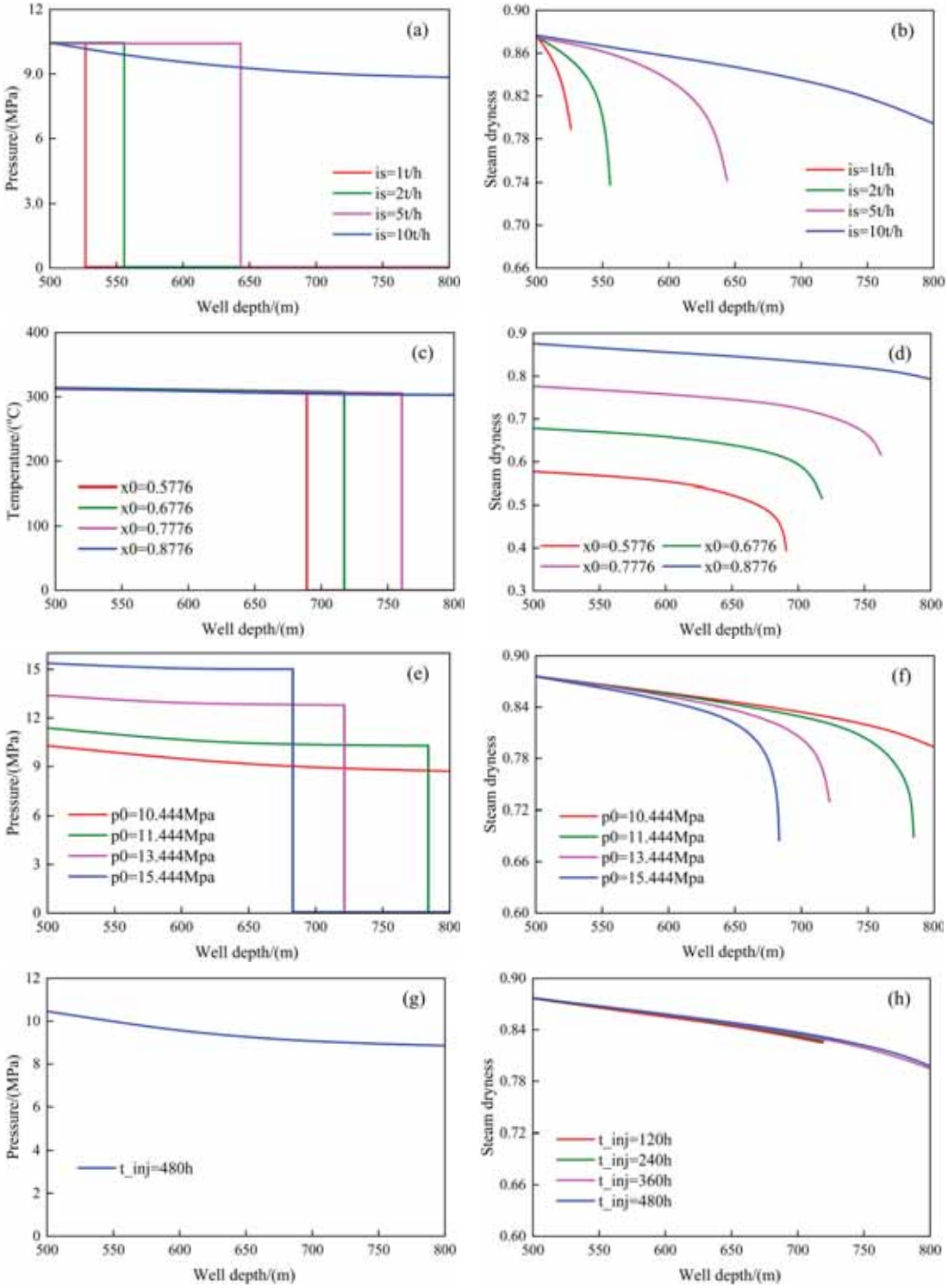

FIGURE 7
Effect of different parameters on the steam temperature, pressure, and dryness

CONCLUSIONS

In this paper, a dynamic model for calculating thermal parameters in horizontal wells with steam huff and puff is established based on one-dimensional unsteady heat-transfer theory. To reduce the number of iterations and speed up the convergence, the double-iteration method of pressure and dryness increments is used. The results shows that considering the variable mass flow of steam in the horizontal section, the maximum relative error between the calculation results from the model and the measured data is less than 5%, which is more accurate than the traditional method, and more consistent with the actual situation. The numerical results indicated that the influence of wellhead steam parameters on the distribution of steam thermodynamic parameters in horizontal wellbores is basically the same. The steam-injection rate is directly proportional to the extended distance of steam in horizontal wellbores. The influence of steam-injection time on steam temperature, pressure, and dryness can be ignored.

ACKNOWLEDGEMENTS

We thank LetPub (www.letpub.com) for its linguistic assistance during the preparation of this manuscript.

REFERENCES

[1] Sun, F., Yao, Y., Li, X., Yu, P., Zhao, L., Zhang, Y. (2017) A numerical approach for obtaining type curves of superheated multi-component thermal fluid flow in concentric dual-tubing wells. International Journal of Heat and Mass Transfer. 111(8), 41-53.

[2] Zhengbin, W., Huiqing, L., Zequan, Z., Xue, W. (2018) A novel model and sensitive analysis for productivity estimate of nitrogen assisted cyclic steam stimulation in a vertical well. International Journal of Heat and Mass Transfer. 126(4), 391-400.

[3] Dittaro, L.M., Dickson, J.L., Boone, T.J. (2013) Integrating the key learnings from laboratory simulation and field tests to assess the potential for solvent assisted-steam assisted gravity drainage. SPE Drilling & Completion. 22(10), 79-84.

[4] Li, Q.Y., Yue, M.C., Hong, Y.W., Li, T. (2007) Physical and numerical simulation of steam assisted gravity drainage with vertical and horizontal well combination in extra heavy oil reservoir. Journal of China University of Petroleum. 11(2), 32-28.

[5] Kufahl, R.H., Saha, S. (1990) A theoretical model for stress-generated fluid flow in the canaliculi-lacunae network in bone tissue. Journal of Biomechanics. 23(2), 170-180.

[6] Sun, F., Yao, Y., Li, X., Li, G., Huang, L., Liu, H. (2018) Exploitation of heavy oil by supercritical CO2: effect analysis of supercritical CO2 on H2O at superheated state in integral joint tubing and annuli. Greenhouse Gases Science & Technology. 147(5), 1461-1467.

[7] Brewster, D.B., Grosberg, P., Nissan, A.H. (1959) The stability of viscous flow between horizontal concentric cylinders. Mathematical Physical & Engineering Sciences. 251(12), 76-91.

[8] Harald, A., Piet, O. (2007) Determination of perforated schemes to control production and injection Profiles along horizontal wells. SPE Drilling & Completion. 12(1), 13-18.

[9] Wang, Z.M., Wei, J.G., Wang, X.Q., Li, H.X. (2018) Sectional combination optimization model of perforating parameters in horizontal wells. Oil exploration and development. 35(6), 725-730.

[10] Willhite G.P. (2015) Overall Heat Transfer Coefficients in Steam and Hot Water Injection Well. JPT. 607-619.

[11] Xu, X.S., Liao, R.Q., Guan, Z.H. (2013) Numerical simulation of pressure and temperature field in the production process of huff and puff wells. Journal of applied foundation and Engineering Science. 11(4), 378-383.

[12] Wang, X., Su, Y.L., Zhao, Y.J, Li, H. (2016) Calculation of heat loss considering pressure change of steam injection wellbore. Drilling and Production Technology. 29(3), 60-68.

[13] Zhou, T.Y., Cheng, L.S. (2019) Calculation model of parameters along the wellbore of superheated steam injection. Journal of Southwest Petroleum University (Natural Science Edition). 31(1), 153-155.

[14] Chen, H., Li, M., Wang, Y., Jiarela, N., Zhang, Y. (2015) Numerical simulation in steam injection wells for optimizing the distribution of thermal parameters in horizontal wells with slotted liners. Petroleum Drilling Techniques. 22(3), 109-115.

[15] Yao, Y., Yuan, X., Qiu, G. (1995) Thermal recovery of a thin-beded reservior by horizontal wells in Lean heavy oilield. Petroleum Journal. 16(3), 48-54.

[16] Li, J., Zhao, X., Chen, Z. (2011) Design and numerical study of a new hybrid css-sagd process using horizontal wells for recovering heavy oil. Petroleum Science & Technology. 29(24), 2578-2591.
[17] Xue, S., Proulx, P., Boulos, M.I. (2003) Effect of the coil angle in an inductively coupled plasma torch: a novel two-dimensional model. Plasma Chemistry & Plasma Processing. 23(2), 245-263.
[18] Chen, K.S., Ku, A.C., Chan, T.M., Yang, S.Z. (1990) Flow in the half-filled annulus between horizontal concentric cylinders in relative rotation. Journal of Fluid Mechanics. 213(1), 149-169.
[19] Nguyen, D., Rahman, S.S. (2000) A mathematical model for laminar displacement of one non-newtonian fluid by another in horizontal concentric annuli. Chemical Engineering Communications. 177(1), 215-230.
[20] Boberg, T.C., Rotter, M.B., Stark, S.D. (1992) History match of multiwell simulation models of the cyclic steam stimulation process at cold lake. Spe Reservoir Engineering. 7(3), 321-328.
[21] Jorshari, K.R., Hara, B., Jones, R.W. (2013) Sagd-pair performance optimization:a field case study of recovery enhancement. The Journal of Canadian Petroleum Technology. 52(2), 101-111.
[22] Zhang, Q. (2017) A multi-linear flow model for multistage fractured horizontal wells in shale reservoirs. Journal of Petroleum Exploration & Production Technology. 7(3), 747-758.
[23] Yang, Z., Liu, Y., Ping, Z., Li, X., Yi, L. (2018) A model for calculating formation breakdown pressure in cbm vertical wells. Acta Petrolei Sinica. 12(5), 67-72.
[24] Wang, J., Jia, A., Wei, Y., Qi, Y., Yu, D. (2018) Laplace-domain multiwell convolution for simulating pressure interference response of multiple fractured horizontal wells by use of modified stehfest algorithm. Journal of Petroleum Science & Engineering. 161, 231-247.
[25] Shiddiq, A.M.I., Christiantoro, B., Syafri, I., Abdurrokhim, A., Resesiyanto, H. (2017) A comprehensive comparison study of empirical cutting transport models in inclined and horizontal wells. Journal of Engineering & Technological Sciences. 49(2), 275-289.

Received: **03.12.2020**
Accepted: **20.01.2021**

CORRESPONDING AUTHOR

Zhiming Wang
State Key Laboratory of Petroleum Resources and Prospecting,
China University of Petroleum,
Beijing 102249 – P.R. China

e-mail: oszcbs@163.com

© by PSP Volume 30– No. 05/2021 pages 5220-5229 Fresenius Environmental Bulletin

RESEARCH ON THE CONSTRUCTION STRATEGY OF GREEN CIVILIZATION MORAL EDUCATION IN COLLEGES AND UNIVERSITIES FROM THE PERSPECTIVE OF ECOLOGICAL CIVILIZATION

Jia Liu*

College of Fine Arts, Tangshan Normal University, Tangshan Hebei, 063000, China

ABSTRACT

As the backbone of social development and progress in the future, college students are the main audience of green civilization moral education. In order to cultivate college students' consciousness of "protecting ecological environment with systems", this paper studies the construction strategies of green civilization moral education in Colleges and universities from the perspective of ecological civilization. Based on the individual characteristics of modern college students and the real life of college students, this study takes 10 universities in China as an example, mainly with the method of investigation and research, supplemented by literature research and comprehensive analysis, carries out a questionnaire survey and summary of the results of 1000 students, combs and analyzes the current situation of the construction of green civilization moral education in Colleges and universities in China, and puts forward the existing problems. The corresponding construction strategy play its due role in the University ecological moral education, in the combination of theory and practice to improve college students' awareness of the active protection of the ecological environment, accept the values and outlook on life education of ecological civilization construction. Meanwhile, it truly achieves the unity of knowledge and practice, improve the ecological environment with the construction of green civilization moral education in Colleges and universities, and improve the reality of modern ecological civilization construction Effectiveness and controllability.

KEYWORDS:
Ecological civilization perspective, green civilization moral education, construction status, construction strategy

INTRODUCTION

At present, natural resources have been unlimited development and consumption, and a large number of industrial wastes will be produced every year, which challenges the sustainable development of human society. According to the United Nations report, "the pressure on human beings caused by the unprecedented decline of nature is increasing", "one million species of animals and plants are in danger of extinction within decades." nearly three quarters of the land and 66% of the marine environment have been significantly changed by human beings, and more than 85% of the wet land area has disappeared. ". Under the severe situation of increasingly tense resource constraints, increasing environmental pollution and deteriorating ecological environment, how to ensure the sustainable development of human society in a healthy, safe, orderly and controllable environment has become a common concern of governments, international organizations and relevant circles [1]. People are the main body of social development, and education plays a fundamental and leading role in social development. In the face of the grand historical task of ecological civilization construction, education shoulders the important tasks of cultivating talents, disseminating ideas, scientific and technological innovation, and leading demonstration. Therefore, the research on the construction of green civilization moral education in Colleges and universities from the perspective of ecological civilization is conducive to coping with the realistic dilemma of ecological crisis, responding to the call of the era of ecological civilization construction, to the comprehensive and coordinated development of individuals, and to cultivating self-awareness of complying with ecological system [2].

Wang et al. [3] explored the current situation of the cultivation of ecological civilization concept in Ningxia universities as an example, and then put forward corresponding paths and Countermeasures to improve the cultivation quality and ecological protection of ecological civilization concept in Ningxia universities. Meng et al. [4] conducted a questionnaire survey on college students to understand the current situation and main problems of ecological moral education in China's colleges and universities, and on this basis, to explore the Countermeasures for organizing ecological moral education. Zou et al. [5] conducted random sampling survey on college

Questionnaire on the current situation of ecological moral education of College Students

Hello, classmate. Thank you very much for taking time out of your busy schedule to participate in my questionnaire survey. The purpose of this survey is to truly and objectively reflect the basic situation of College Students' ecological moral education, which is only used for academic research. This questionnaire adopts the method of anonymous survey, and your information and results will be completely confidential and will not cause any adverse effects on you. Please do not have any worries. Thank you for your support. Wish you success in your studies!

Basic information of respondents

1. Your gender () A. male B. female
2. Your nationality () A. Han nationality B. minority nationality
2. Your education: A. junior college B. bachelor degree C. graduate student
3. Your major category () A. literature and history B. science and engineering C. others
4. Your school is located in ()
A. Urban areas of municipalities directly under the central government and prefecture level cities
B. Urban areas of county-level cities
C. Township
D. Others
5. Your political situation () A. masses B. League members C. party members (including preparation)

The current situation of College Students' Ecological Morality

1. Do you know when the world environment day is ()
A familiar
B about it
C doesn't know
2. Do you know that a waste battery can pollute ten cubic meters of water ()
A familiar
B about it
C doesn't know
Do you know that for every 4000 cards you make, you have to cut down a big tree ()
A familiar
B about it
C doesn't know
4. Do you pay attention to energy saving signs when purchasing household appliances
A concerns
B doesn't matter
C doesn't care
5. The Yangtze River may become the second yellow river. Do you care about it
A concerns

B doesn't matter

C doesn't care

6. When dining in the school canteen, do you insist on using public chopsticks ()

A yes

B look at the mood

C will not

7. If you see other students littering everywhere, will you resolutely stop it ()

A yes

B look at the mood

C will not

8. If you see a faucet with continuous water flow, will you report to the logistics department for maintenance ()

A often

B occasionally

C never will

Questionnaire on the current situation of ecological moral education of College Students

9. Will you use less detergent or phosphate free detergent as much as possible

A often

B occasionally

C never will

10. Will you try to choose the goods with simple packing ()

A often

B occasionally

C never will

Current situation of ecological moral education in Colleges and Universities

1. Do you think it is necessary to carry out ecological moral education in Colleges and universities

A very necessary

B has little effect

C no need

2. Do you think the key to environmental protection in China is ()

A school education

B legal constraints

C. supervision by public opinion

3. Has your school offered courses related to ecological moral education ()

A has opened

B no opening

4. Do you think schools attach importance to ecological moral education

A takes it seriously

B General

C doesn't pay attention to it

5. Does your school implement ecological moral education in Ideological and moral cultivation courses

A yes

B just mentioned

C didn't mention it

6. Is ecological moral education involved in your major courses

A yes

B involves very little

C is not involved

7. Does your school have a special team of teachers to implement ecological moral education

A yes

B No

8. Are you willing to participate in the practical activities of ecological moral education organized by the school ()

A is willing to participate

B seldom takes part

C is not willing to participate

9. Which of the following are the effective ways to implement ecological moral education in Colleges and universities (multiple choices are allowed) ()

A. set up relevant compulsory courses and optional courses

B organize lectures on relevant aspects

C. carry out practical activities of environmental protection

D building ecological campus culture

10. What is the most important way for you to get information about Ecological Moral Education ()

A mass communication (TV, newspapers, magazines)

B government publicity

C school education

FIGURE 1
Questionnaire on the construction of green civilization moral education in Colleges and universities from the perspective of ecological civilization.

TABLE 1
Gender distribution of the respondents.

Sex	Number	Proportion/%
Male	537	54.08
Female	456	45.92
Total	993	100

students from ten colleges and universities in Heilongjiang Province, and conducted in-depth interviews with the cultivation workers of ecological civilization concept of college students in Heilongjiang Province, and then sorted out and analyzed them to provide data support for the proposal of Cultivation Strategies of ecological civilization concept of College Students in Heilongjiang Province.

On the basis of previous research experience, this research takes ten universities in China as an example to conduct a questionnaire survey, obtains the current situation of the construction of green civilization moral education from the perspective of ecological civilization in Colleges and universities in China, and puts forward construction strategies, so as to provide reference and suggestions for the in-depth study of the cultivation of College Students' ecological civilization concept.

MATERIALS AND METHODS

As the backbone of national development and progress, colleges and universities are the base and cradle of personnel training. Starting from the convenience of colleges and universities and from the perspective of ecological civilization, it is one of the fundamental ways out for the construction of ecological civilization.

Materials. In order to objectively and truly reflect the current situation of the construction of green

civilization moral education of contemporary college students, using the method of literature survey, consulting a large number of relevant materials, and on this basis, designed a questionnaire survey on the current situation of green civilization moral education construction in Colleges and universities from the Perspective of ecological civilization [8]. The content of the questionnaire involves two aspects: the current situation of College Students' ecological morality and the current situation of College Students' ecological moral education. The details are shown in Figure 1.

The questionnaire survey lasted one month, and a total of 1000 questionnaires were distributed to 10 universities in China, 100 for each university. Among them, 997 questionnaires were returned and 993 were valid [9]. The recovery rate was 99.7%, and the effective rate was 99.6%. The specific situation of the respondents is shown in table 1-3.

Methods. There are three main methods used in this study, namely, literature research, investigation and comprehensive analysis. Among them, the investigation method is the main method, and the other two methods are auxiliary. The following three methods are analyzed in detail.

(1) Literature research method. Literature research method is the most basic method used by many scholars and experts in writing papers. This method serves the purpose of research by searching and consulting the materials related to the research subject. For example, through the library, Internet and other channels to collect and ecological civilization from the perspective of green civilization moral construction strategy books, books, journals, papers, newspapers, conference videos, forum speeches and

TABLE 2
Educational background distribution of respondents.

Education	Number	Proportion/%
Junior college students	111	11.18
Undergraduate	558	56.19
Graduate student	324	32.63
Total	993	100

TABLE 3
Distribution of major categories of respondents.

Major	Number	Proportion/%
Literature and history	267	26.89%
Science and Engineering	576	58.01%
Other	150	15.10%
Total	993	100%

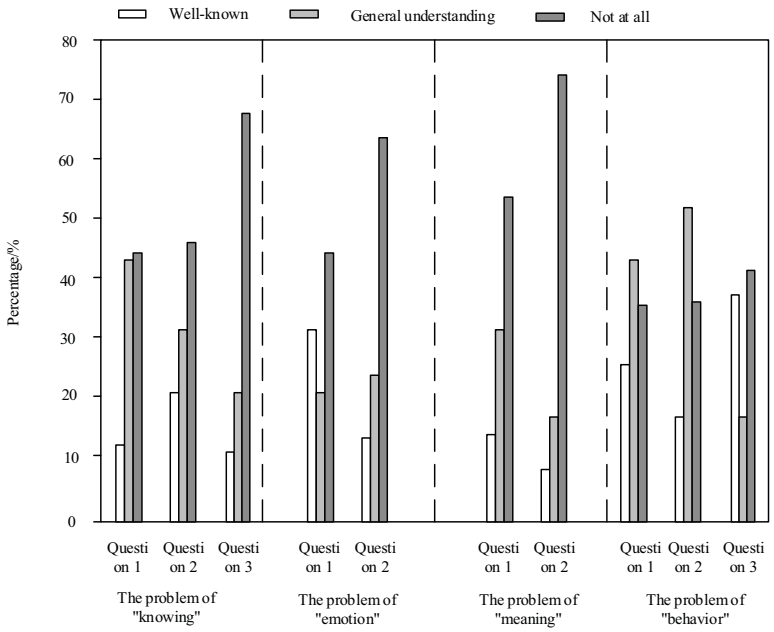

FIGURE 2
Investigation results of college students' green civilization and morality.

other materials, and then summarize and sort out these materials, in order to provide a theoretical basis for the next step of research, and to construct the overall research ideas.

(2) Investigation and research method. Investigation and research method was the research content and core method of this paper. It refers to the research method to understand the objective situation through investigation, obtain relevant data directly, and analyze these data [6]. Through the comparison, induction and analysis of the survey results, we can understand the current situation of College Students' green civilization moral education construction from the perspective of ecological civilization, and provide guidance and basis for the excavation of the follow-up key construction goals and training ways.

(3) Comprehensive analysis method. The comprehensive analysis method is based on the data obtained by literature research method and investigation research method in the later stage of this paper to sort out the comprehensive conclusion [7]. This method involves many subjects, and the research power of this paper should be based on the actual situation of college students in our country, starting from the cultivation of ecological civilization concept, comprehensive consideration, to complete the writing of this paper.

After a month of questionnaire collection, sorting, statistics and analysis, this chapter analyzes the current situation of the construction of green civilization moral education in colleges and universities from the perspective of ecological civilization, including the analysis of the current situation of college students' green civilization morality and the analysis of the current situation of college green civilization moral education [[10].

RESULTS

The results of the survey. (1) The results of the investigation on the current situation of college students' green civilization morality. This paper analyzes the current situation of college students' green civilization morality from the four aspects of knowledge, emotion, intention and behavior of the investigated objects. The results are shown in Figure 2.

Figure 2 shows that most students have a serious lack of awareness of energy conservation and environmental protection, and nearly half or more of the students choose "don't know" [11]. People's behavior is dominated by people's subjective consciousness, that is to say, when students have insufficient understanding of ecological morality, they cannot produce corresponding strong supervision consciousness and emotion, and restrain their own behavior. Among them, the results of the first, second and third questions support this point. When students see the phenomenon of violating the concept of ecological civilization, most students will choose "occasionally" or "never", and when the four aspects of knowledge, emotion, intention and action are missing, it is difficult for students to achieve self-discipline in daily life, and even lead to behavior anomie [12]. Thus, we can draw the following conclusions: from the survey results of students' knowledge, emotion, will and behavior, the green civilization moral quality of college students in China is generally not high, which is quite different from the demand and training goal of college students' green civilization moral quality, which does not meet the requirements of the development of contemporary college students' personality integrity.

(2) Investigation on the current situation of green civilization moral education in colleges and universities. In Figure 3, the answers to the questions are shown in Table 4 below.

Form the results in the Figure 3, some conclusions were got:

1) The concept of green civilization moral education in colleges and universities is weak. Colleges and universities are places for students to learn knowledge, cultivate and establish their world outlook, outlook on life and values. Therefore, higher education is very important. However, from the survey results in Figure 3, the concept of ecological moral education in colleges and universities in China is relatively weak, which is directly related to the characteristics of China's education. China's education attaches great importance to students' academic performance, relatively neglects the education of moral quality, let alone the cultivation of ecological civilization concept. Most of them only appear in the curriculum and teaching of environmental majors, and the requirements for non environmental majors are not high [13]. From the specific problems of the questionnaire survey, although most students think it is necessary to implement ecological moral education in colleges and universities, from the results of the third, fourth and fifth questions, the concept of green civilization moral education of college students is relatively weak. The software and hardware of all aspects of ecological moral education construction in colleges and universities investigated are not mature, the development of ecological moral education is seriously lagging behind, and college students' autonomy in practicing the concept of green civilization ecological moral education in colleges and universities is poor [14-16].

2) The content system of green civilization moral education in colleges and universities is not complete. The content system of green civilization moral education in colleges and universities is not complete, which is mainly reflected in the following aspects:First, the green civilization moral education carried out in colleges and universities is at the stage

of primary school teaching theory knowledge, which is relatively vague. Second, there is no scientific curriculum, no special courses to teach the moral knowledge of green ecological civilization, most of which involve ideological and moral education courses, but rarely in the professional courses I studied. Finally, there is no construction specialty in colleges and universities, and many ecological moral education teachers are part-time teachers [17], which cannot meet the needs of students for green and civilized moral education.

3) The way of green civilization moral education in colleges and universities is single. The way of ecological moral education in colleges and universities in China is explained, described or illustrated by examples. Such a single education method lacks vitality and flexibility, which makes students lose interest in the understanding of green civilization

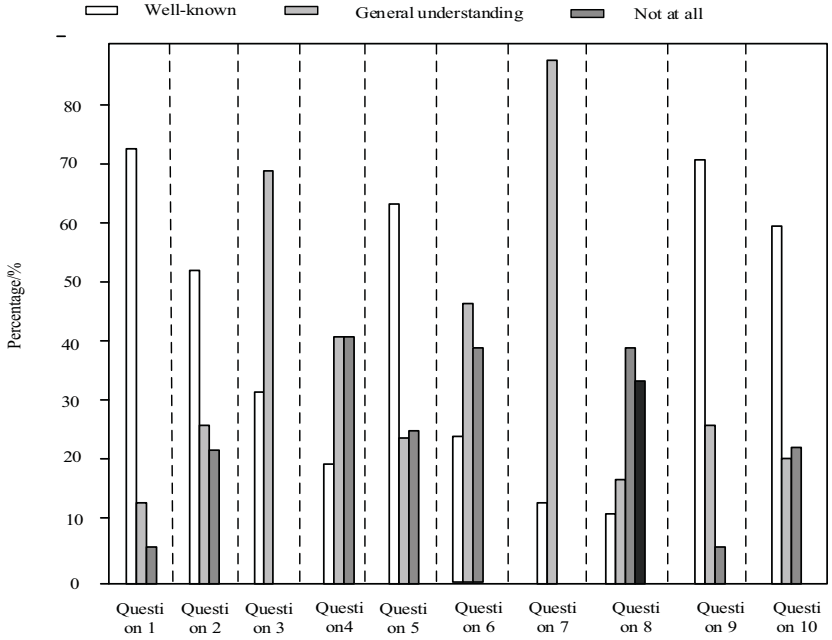

FIGURE 3
The investigation results of green civilization moral education in colleges and universities.

TABLE 4
Answer to question.

Question	Answer	Question	Answer
Question 1	Be necessary Not much Unnecessary	Question 6	Yes It involves very little Not involved
Question 2	Higher education Legal constraints Public opinion	Question 7	Yes No
Question 3	Opened No opening	Question 8	Set up relevant compulsory courses and elective courses Lectures on related aspects Carrying out the practice of environmental protection Creating ecological campus culture
Question 4	Very important	Question 9	Willing to participate
Question 5	Yes Just mention it Not mentioned	Question 10	Mass communication (TV, newspapers, magazines) Government propaganda Higher education

moral knowledge, cannot arouse students' psychological and emotional resonance, and even reject green civilization moral education, which affects the education effect [18]. The proportion of answers to. question 8 proves this. Most students think that the education mode of colleges and universities is the degradation of the classroom, and they seldom choose other education methods, such as offering relevant compulsory courses and elective courses, conducting lectures on relevant aspects, carrying out environmental protection practice activities, and creating ecological campus culture

Construction strategy analysis. According to the above analysis about the current situation of college students' green civilization moral concept and the current situation of college green civilization moral education, the corresponding strategies of college green civilization moral education construction from the perspective of ecological civilization are put forward.

(1) Promote the unity of moral education concept and behavior. In view of the current situation of the weak concept of green civilization moral education in colleges and universities, firstly, colleges and universities should realize the importance of green civilization moral education and reform from many aspects. In specific moral education, moral content can be integrated into moral virtual events [19]. Moral education is the interaction of moral cognition, moral emotion and moral behavior, and a process of the unity of cognition and practice. Moral education is the premise of moral education. The emotion of moral education comes into being with the cognition and behavior of moral education. The two cannot be separated and exist alone. After all, teaching is the main form of school moral education. How to realize the unity of knowledge and practice in class? In the process of moral education, schools can provide virtual moral education for students to experience moral situation, feel moral conflict and make value judgment. This is a kind of moral education content based on virtual life. Learning this content is of great significance to change people's moral cognition and attitude, because the time of learning moral cognition and changing moral attitude is very short. It can also solve the problem of learning boring political theory knowledge, because it can make political theory knowledge concrete moral conflict events, and can also choose moral events according to the content. When the goal is clear, we should choose the moral situation which is closer to students' life and experience according to the needs of moral development of different age groups, and encourage students to participate independently [19]. In essence, this is a change in the content and way of moral education, which is mainly manifested in the unity of moral cognition, moral emotion and moral behavior in the process of moral education, which can effectively solve the contradiction between students' moral level and behavior. The necessary conditions for the unity of moral education concept and behavior are as follows:

1) In the form of broadcasting, school newspapers and learning materials, colleges and universities should publicize the connotation and importance of ecological civilization construction; 2) The leaders and teachers in colleges and universities need to receive the education and edification of ecological knowledge regularly and change their teaching ideas; 3) Colleges and universities should build professional teachers of green civilization education course; 4) Colleges and universities should create a good atmosphere of green ecological education; 5) Construct the condition support system of ecological moral education in colleges and universities, and re arrange the curriculum [17], so as to ensure the smooth progress of efficient ecological moral education;

(2) Improve the content system of green civilization moral education in Colleges and universities. Constructing and improving the content of green civilization moral education is the primary goal and task of colleges and universities at this stage. This paper will improve the content system from two aspects of ecological moral consciousness education and ecological values education. The former includes the following contents:

1) Ecological crisis awareness education. The survival and development resources obtained by human beings have been robbed, causing serious damage to the natural ecology, and human beings have always been facing the survival crisis [20]. As the successors of socialism, college students should be fully aware of the ecological crisis in the process of education, establish correct values of green civilization, internalize into a kind of self-consciousness, and ultimately affect their study, work and life; 2) Ecological responsibility education. After being aware of the ecological crisis, we should strengthen the students' awareness of ecological crisis and guide them to consciously abide by and fulfill the ecological moral norms.

The latter includes the following contents:

1) The education of new view of nature. The new concept of nature emphasizes the value of nature and holds that natural resources are limited, owned and valuable. In the implementation of green civilization moral education in colleges and universities, this concept should be passed on to students as an important education content, so that students can deeply understand the ecological value, redefine the relationship between man and nature, and make correct value judgment when they encounter ecological problems in their study, work and life in the future; 2) Green consumption concept education. People's desire produces consumption behavior, and exces-

sive consumption behavior leads to serious ecological damage. Therefore, in the process of ecological education, we should first carry out reasonable and healthy consumption education for students, establish the concept of green consumption, reduce the acquisition of nature, and promote ecological sustainable development [19].

(3) We should innovate the ways of green civilization moral education in Colleges and universities. The single way of green civilization moral education in colleges and universities is the main reason for the poor effect of education. Therefore, we can start from the following aspects [6, 21]:

1) Set up the public compulsory course of ecological moral education. Although the effect of classroom education is not good, it is unrealistic to give up this kind of education completely, but it can reduce the proportion and improve the professionalism. One of the important ways to solve this problem is to set up the public compulsory course of ecological moral education. Through the public compulsory course of ecological moral education, students can more intuitively understand the environment and ecological crisis, further grasp the ecological moral knowledge, and then actively externalize into positive environmental protection behavior; 2) Carry out the infiltration teaching of various subjects. Ecological moral education involves geography, biology, economics, medicine and other disciplines. In the teaching of these subjects, it is an effective way to infiltrate the moral knowledge of green civilization, influence students' ecological consciousness imperceptibly, and establish correct ecological values; 3) In addition, we can also carry out lectures on relevant aspects, carry out ecological environmental protection practice activities, create ecological campus culture, and carry out ecological moral education in university network courses.

CONCLUSIONS

Ecological environment is the basis of human survival and development. Facing the destroyed ecological environment, people have realized the importance of ecological environment protection. Ecological environment construction is a long-term project. As the successor and builder of socialism in the future, the construction of green civilization moral education for college students is imminent. Therefore, this paper takes 10 universities in China as an example, analyzes the current situation of green civilization and moral education of college students through questionnaire survey, and puts forward the corresponding construction strategies.

(1) To improve the awareness of green and civilized moral education in colleges and universities includes increasing publicity, regular training, building professional teaching staff, creating atmosphere, establishing condition support system, timely updating or arranging courses, etc.

(2) We should improve the content system of green civilization moral education in colleges and universities, including ecological moral awareness education (ecological crisis awareness education and ecological responsibility awareness education) and ecological values education (new natural concept education and green consumption concept education).

(3) The ways to innovate green civilization moral education in colleges and universities include offering public compulsory courses, implementing multi-disciplinary infiltration teaching, lectures, practical activities, creating ecological campus culture, and developing network courses.

ACKNOWLEDGEMENTS

This work was the phased objectives of the scientific research project Study on the Path of Normal University Students Serving Elementary Education in Poverty-Stricken Areas of Hebei Province under the Value of "Establishing Moral Integrity in Cultivation" (2021B01), which was supported by Tangshan Normal University.

REFERENCES

[1] Kristján, K. (2020) An introduction to the special issue on wisdom and moral education. Journal of Moral Education. 49(1), 1-8.
[2] Ruyter, D. (2019) Does a Theory of Moral Education Need the Input of Empirical Research? Journal of Philosophy of Education. 53(4), 642-648.
[3] Tillson, J. (2019) Sympathy, Social Stability and Those Left Out: Querying A Theory of Moral Education. Journal of Philosophy of Education. 53(4), 649-655.
[4] Lin, Z., Zhao, L. (2019) Evaluation and analysis of coordinated development of ecological environment and economy. Fresen. Environ. Bull. 28(5), 4049-4053.
[5] Jing, M. (2018) The Practical Path of Education under the Background of New Era. Journal of HeiLongJiang Vocational Institute of Ecological Engineering. 31(04), 105-108.
[6] Hu, J. (2020) Comparison of building resilience in the international typical green building evaluation system based on the concept of ecological and environmental protection. Fresen. Environ. Bull. 29(8), 7147-7155.
[7] Darnell, C., Gulliford, L., Kristjansson, K., Paris, P. (2019) Phronesis and the Knowledge-Action Gap in Moral Psychology and Moral Education: A New Synthesis?. Human Development. 62(3), 1-29.

[8] Li, J., Qu, M. (2018) Preliminary exploration of ecological moral education resources in traditional customs of ethnic minorities in Guizhou. Environmental Science and Management. 30(12), 1-2.
[9] Zandvliet, D. (2019) Ecological education via "islands of discourse": teacher education at the intersection of culture and environment. Journal of Outdoor and Environmental Education. 22(2), 145-157.
[10] Luo, X., Pan, S. (2019) A Study on the New Paths of Moral Education in Colleges and Universities from the Perspective of Spiritual Civilization. Yinshan Academic Journal. 32(01), 103-108.
[11] Zhang, C., Zhang, Y. (2019) Research on Construction Strategy of Public Innovation Space in Universities Based on Niche Theory. Science and Technology Management Research. 39 (08), 82-87.
[12] Zhang, M., Dong, Y. (2020) The Ecological Construction of Normal Education Reform and Development in Universities. Contemporary Education and Culture. 12(03), 69-74.
[13] Xiao, N. (2018) Rationality analysis of non anthropocentrism as ecological moral education values. Educational Theory and Practice. 38 (04), 44-47.
[14] Zhou, T. (2019) The Strategic Thinking on the Construction of First-class Disciplines and the Development of Inferior Disciplines in Colleges and Universities from the Perspective of Value Ecology. Jiangsu Higher Education. 217(03), 50-55.
[15] Huang, Y., Xiong, X., Zheng, Y. (2020) Green Economy Development Strategy of Hunan Province under the Background of Ecological Civilization Construction. Journal of Hunan University (Social Sciences). 34(1), 75-82.
[16] Wang, J., Zhai, T., Lin, Y., Kong, X., He, T. (2018) Spatial imbalance and changes in supply and demand of ecosystem services in China. Science of the Total Environment. 657, 781-791.
[17] Wang, R., Sun, X., Cheng, J., Qi, R. (2020) Impact of ecological civilization education on College Students' garbage classification behavior: An Empirical Study Based on 152 universities in China. Journal of Arid Land Resources and Environment. 34(5), 21-27.
[18] Kong, Z., Ma, Y., Wu, L. (2020) Implementing ecological civilization education in classroom teaching of Microbial Ecology Microbiology. 47(4), 1248-1253.
[19] Li, Z., Zhao, Z. (2018) Low Carbon Innovation Ideas of the County Town in View of Ecological Civilization. Scientific Management Research. 36(2), 54-57.
[20] Liu, Z., Li, A., Li, C., Zhao, Y. (2018) A Research of Assessment on Civil Ecological Environment Awareness and Its Influencing Factors. Ecological Economy. 34(6), 217-222.
[21] Wang, W., Gong, C., Zhang, Z., Chen, L. (2018) Research Status and Prospect of the Subsurface Hydrology and Ecological Effect in Arid Regions. Advances in Earth Science. 33(7), 702-718.

Received: **04.12.2020**
Accepted: **03.02.2021**

CORRESPONDING AUTHOR

Jia Liu
College of Fine Arts,
Tangshan Normal University,
Tangshan Hebei 063000 – China

e-mail: 15140983@qq.com

© by PSP Volume 30– No. 05/2021 pages 5230-5237 Fresenius Environmental Bulletin

OPTIMIZATION OF ENERGY-SAVING AND ENVIRONMENTALLY FRIENDLY B & B BUILDING UNDER THE CONCEPT OF GREEN COUNTRYSIDE-TAKING SOUTHWEST ZHEJIANG AREA FOR EXAMPLE

Yuchun Zheng*

Department of Architectural Engineering, Jinhua Polytecnich, Jinhua, Zhejiang, 321007, China

ABSTRACT

The current optimization methods of energy-saving and environmentally friendly B & B buildings pay more attention to rural culture and cultural landscape, ignoring the energy-saving transformation of building structure, resulting in poor indoor insulation effect and high energy consumption of building refrigeration and heating. Taking the residential project in Southwest Zhejiang Province as an example, this paper puts forward the optimization method of energy-saving and environment-friendly B & B buildings under the concept of green countryside. Making corn straw insulation board, transforming the wall structure of B & B building to form composite wall enclosure, replacing ordinary doors and windows with single frame double glass windows, adopting energy-saving door and window materials, standardizing the ratio of window to wall, filling the gap between doors and windows, installing thermal insulation ceiling and ultra-thin vacuum insulation floor, using integrated network to control energy consumption equipment, arranging water heater and air heat pump. Through the establishment of typical building model of B & B in Southwest Zhejiang Province, comparative experiments were carried out. The experimental results show that the minimum thermal resistance of the wall enclosure is increased by 0.06 $m^2 \cdot K/W$ and 0.09 $m^2 \cdot K/W$ respectively; the heat transfer coefficient of the wall is reduced by 0.08 $m^2 \cdot K/W$ and 0.05 $m^2 \cdot K/W$; the energy saving rate of the building structure is increased by 4.6% and 6.0% respectively. The indoor thermal insulation effect is good, which can effectively improve the energy saving rate of B & B buildings and reduce the energy consumption of building refrigeration and heating.

KEYWORDS:
B & B building, energy saving transformation, wall enclosure, insulation ceiling, equipment energy consumption

INTRODUCTION

At present, B & B buildings are growing rapidly, but rural B & B renovation pays more attention to rural culture and natural landscape, ignoring building energy consumption. Most of the B & B only use air conditioning to satisfy the comfort of the interior space of the building. However, in the energy consumption of rural tourism, building energy consumption occupies an important part, which not only causes environmental pollution, but also brings economic burden to rural tourism. Therefore, through the study of energy conservation and environmental protection of B & B buildings, it is of great significance to transform the structure of B & B buildings, reduce energy waste and promote the sustainable development of B & B buildings [1].

Foreign energy-saving transformation technology research is relatively mature. In reference [2], the building energy consumption was analyzed by temperature measurement. It includes indoor thermal environment, environmental conditions, thermal performance and so on. Through the parameters of building lighting, room acoustics, thermal energy saving and building sunshine, and using Ecotect software to simulate the parameters. All the parameters are imported into the plane for point tracing modeling, which can quickly simulate the physical performance of buildings, and calculate the energy consumption of indoor air conditioning and the heat gain and loss of heat of peripheral structures. Ecotect software provides different glass properties, sky light, window layout and building orientation, compares the physical data of different models, displays the illumination data of different positions in the building, compares the natural lighting of buildings under different conditions, analyzes the optimization degree of simulation results, and selects the optimal energy-saving transformation scheme. Domestic energy-saving transformation technology research has also made great progress. Literature [3] according to the main building materials, usage, lighting energy sources, conditions and floor number, combined with the rural local climate environment, using the idea of passive priority, the relationship between environmental elements and climate construction was

analyzed, so as to improve the sunshine ventilation, heating mode, enclosure structure and energy utilization form of buildings. At the same time, according to the building type of B & B, the energy consumption is classified, the influencing factors of energy consumption are sorted out, and the targeted protective measures are proposed to reduce the building energy consumption.

On the basis of the above theory, taking the residential project in Southwest Zhejiang as an example, this paper puts forward the optimization method of energy-saving and environmental protection type B & B building under the concept of green countryside. the general continuous energy consumption mode is adopted to optimize the thermal performance of building walls, windows, roofs and floors, so as to ensure the thermal insulation and energy saving effect of the residential buildings.

MATERIALS AND METHODS

Optimize the wall enclosure structure of B & B building. Based on the analysis of the original wall of B & B in Southwest Zhejiang Province, the flatness and damage degree of the external surface of the wall are evaluated, and the indoor heat loss is reduced by means of enclosure and insulation. The exterior wall adopts the composite wall form, uses corn straw insulation board to replace the common thermal insulation materials of residential buildings in Southwest Zhejiang Province, and obtains a new composite exterior wall. The corn straw insulation board was prepared by using agricultural waste in rural areas. Firstly, the corn stalk which is divided into small segments is put into the dryer for drying, and the pulp of the stalk is removed. Use the electronic balance with high precision to weigh the straw skin to be used. Repeat the drying process until the weight remains unchanged, and crush the straw skin into small pieces of about 2 cm [4]. Then use air compressor to mix corn straw, adhesive, flame retardant and waterproof agent in proportion. Use a hot press to evenly put the mixed straw into the auxiliary cylinder and smooth it out. Press the crushed straw into a board and cool it at room temperature to obtain the corn straw insulation board [5]. A new composite wall structure was prepared by selecting Portland cement, coal gangue block, sand for cement mixing, red brick, reinforced mesh and corn straw insulation board. From the inside to the outside, the structure is followed by fire retardant coating layer, thermal insulation layer, brick wall and cement mixing. V-shaped connector made of steel wire is used to connect the bearing layer wall and corn straw insulation board [6]. The specific wall structure and V-hook arrangement are shown in Figure 1.

The ratio of cement to sand is 1:2. The cement shall be plastered and compacted inside the brick wall to make the thickness of cement before setting be 2 ~ 3mm. The bound reinforcement grid shall be fixed on the side of the brick wall and pasted on the cement mortar of the bottom layer. Then, V-shaped connector shall be used to hang on the gap of the reinforcement grid according to the layout distance, and finally the fire-retardant coating layer shall be evenly applied [7].

The indoor walls of B & B buildings are also made of composite thermal insulation materials. According to the different positions of thermal insulation materials, the interior wall structure is divided into internal insulation, sandwich insulation and external insulation [8]. Use bonding mortar to repair the cracked part of the wall, and then repair the damaged part of the wall facing layer by combining the bonding mortar, internal and external insulation [9]. The EPS board is used for external insulation, combined with polystyrene particles to form rigid foam composite thermal insulation board, so as to update the facade of the indoor wall and avoid condensation phenomenon of the wall structure. Polyurethane thermal insulation material is used for internal insulation, so that the indoor temperature of B & B building is fast [10]. In the repair process, the thermal insulation material is used as the insulation core material, which is pasted on the outside of the wall, and the insulation layer is anchored with anchors as the covering layer of the wall. The bonding area of the wall base is controlled to make it greater than 40% of the area of the insulation board, so as to play the role of anti-seepage and anti cracking [11]. Finally, the optimization of the wall enclosure structure of B & B building is completed.

Energy saving transformation of residential building doors and windows. Improve the connection between doors and windows and walls, improve the window to wall ratio of building facade, and replace doors and windows with stronger energy-saving performance. First of all, according to the orientation of B & B buildings, the ratio of window to wall should be standardized to make it less than 0.34 in the south direction, less than 0.26 in the north direction, and less than 0.30 in the East and west directions [12]. Then on the basis of meeting the lighting requirements, the thermal insulation performance of doors and windows is improved. Stick straw insulation board around the window gap, adjust the lower insulation board to protrude by 2cm, and keep the two sides and the upper part horizontal with the window, so that the window forms a closed insulation surface [13]. During the installation process, the bottom of the window is placed on the straw insulation board to fit the thermal insulation materials around the window, and the joints are filled with Styrofoam. At the same time, return air groove and high-low joint are set at the gap, and rubber sealing strip is used to improve the sealing performance of the window [14]. For the door gap of B & B building, first fill with elastic and soft material, add polystyrene

board into the cavity of door leaf; then apply rubber sealant with good sealing performance to the outside of the door, and add glass wool wrapped with leather on one side of the room [15]. After the treatment of the gap between doors and windows, the common doors and windows that do not meet the requirements in the southwest of Zhejiang Province will be replaced. Adopt energy-saving door and window materials, take the thermal conductivity < 2.4 as the selection standard of window type and material. The calculation formula of thermal conductivity is [7, 16]:

$$Q = -sb\left(\frac{kf}{c}\right)a \qquad (1)$$

In formula (1), a is the area of the glass plate of the door and window, B is the projected area of the door and window frame, f is the visible perimeter of the door and window glass panel, s is the thermal conductivity of the glass plate, c is the thermal conductivity coefficient of the door and window frame, and k is the linear heat transfer coefficient of the frame and the glass plate, and the liner material passing through the gap [17]. Based on the investigation and analysis of door and window materials, the window types and materials with thermal conductivity Q meeting the standard are selected. They are single frame double glass window with air layer thickness more than 25, broken bridge thermal insulation aluminum alloy double glass window and plastic steel Low-E double glass window. Considering the influence of windows on indoor lighting and the cost of windows, the ordinary doors and windows are replaced by plastic steel single frame double glass windows, and multi lock point hardware and stainless steel materials are selected for installation. After the replacement, add a sunshade component outside the window. From the static and dynamic point of view of solar shading, the active external shading method is adopted to control the amount of solar radiation and adjust the component angle according to the radiation intensity [18-19]. In winter, adjust the sunshade components, add a single layer of tempered glass with the thickness of 4-5mm, and add rubber sealing strip in the edge of the component glass and the metal slot to change the sunshade component into a single-layer wooden glass [20]. So far, the energy-saving transformation of the doors and windows of B & B buildings has been completed.

Optimize the roof and floor of B & B buildings. Energy saving transformation of residential building roof and floor, reduce heat transfer in the roof and ground, ensure the integrity of the building insulation layer. Increasing the thermal resistance of roof materials and reducing the direct sunlight exposure are two aspects of roof optimization. On the basis of maintaining the roof facade style, thermal insulation ceiling is installed to reduce the net height of B & B buildings, so as to reduce the actual heating area. At the same time, the insulation ceiling, intermediate air layer and roof form a new thermal insulation individual [21]. Expanded perlite and EPS insulation board are selected as the main materials of the insulation roof. The hay, plant ash, sawdust, rice husk and common vegetation materials are dried and compacted as the filling materials of the insulation roof. The thickness of the insulation roof is controlled to be more than 23mm to play the role of thermal insulation. During the installation process, combined with the original roof structure of homestay in Southwest Zhejiang, the original tarpaulin was installed, and the insulation ceiling was fixed by purlin. When the load allowed, water heater, air conditioning and other equipment were set above the insulation ceiling to save energy consumption of the equipment. In order to improve the building ground, the method of slab tile insulation is adopted to reconstruct the building ground. Considering the foundation soil and bottom base of the residential buildings in Southwest Zhejiang Province, the ultra-thin vacuum insulation material is selected as the thermal insulation material of the building ground. The thickness of the insulation layer is controlled to be 90 ~ 100 mm and then plastered with cement mortar. So far, the optimization of the roof and floor of B & B building has been completed.

Optimize the energy consumption equipment of B & B buildings. Use integrated network, increase energy efficiency of equipment, use new energy, reduce carbon emission of B & B buildings. According to the actual layout of the B & B building, the generic cabling technology, including vertical wiring, multimode optical fiber, twisted pair and horizontal wiring, is adopted to closely connect the equipment with the building structure. Then, using information network technology and taking computer network as the center, multiple switches are installed in the B & B buildings to form the basic network of personal LAN, so as to form wireless connection between electrical equipment and network, and enter into TCP / IP Internet, including heating equipment, lighting equipment, etc [4, 21]. According to the unified technical agreement standard, information sharing, resource sharing and automatic control linkage can be carried out among various equipment to avoid waste of equipment energy consumption. Above the roof, solar water heaters and air heat pumps are arranged to adjust the energy consumption structure of buildings. When the number of guest rooms in B & B building is hotel type, 3 ~ 4 vacuum tube integrated water heaters are arranged; when B & B building is single-layer courtyard type, 1 vacuum tube or flat plate water heater is directly used. The calculation formula of collector area s of water heater is [22]:

$$S = \frac{eF\lambda\rho}{J(1-\eta)} \qquad (2)$$

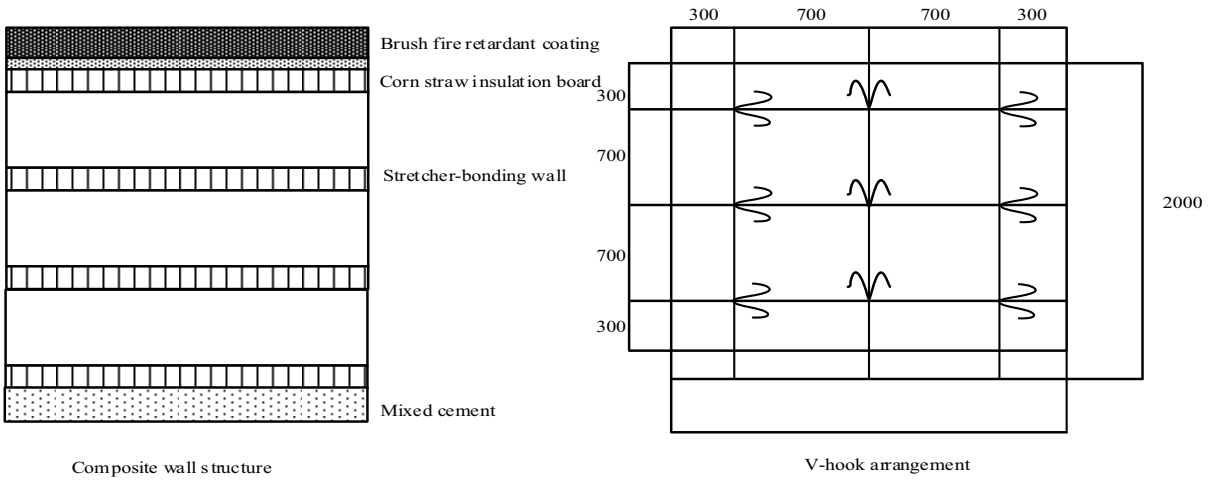

FIGURE 1
V-shaped wall and external wall layout.

FIGURE 2
Typical building model of B & B in Southwest Zhejiang.

In formula (2), J is the daily hot water consumption of B & B, η is the solar energy guarantee rate of water, e is the solar radiation amount on the daylighting surface of the collector, F is the annual average heat collection efficiency of the integrated device, λ is the heat loss rate of water storage tank and pipeline, and ρ is the water density. Formula (2) is used to determine the collector area of the water heater. Finally, the optimal inclination angle of the collector is selected on the roof, and the pipeline in the insulation ceiling space is used to transmit heat to the building interior, so as to realize the optimization of energy consumption equipment of B & B buildings. So far, the optimization method design of energy-saving and environment-friendly B & B buildings under the concept of green countryside has been completed.

RESULTS

In order to verify the effectiveness of the optimization method of energy-saving and environment-friendly B & B buildings under the concept of green countryside, a comparative experiment was conducted. The design method was recorded as group A, the method in reference [2] was recorded as group B, and method [3] was used as group C. three methods were used for energy-saving transformation of B & B buildings, and the energy-saving effects after optimization were compared.

Preparation for the experiment. The typical B & B buildings in Southwest Zhejiang were selected as the experimental objects. The plane layout, enclosure structure and heating area were simulated by using design builder software. The model of B & B building was established as shown in Figure 2.

According to the current situation of B & B buildings, the model parameters are set, as shown in Table 1.

The three methods respectively aim at the weak link of B & B building to optimize energy saving.

Experimental results. (1) Experimental results of heating and cooling and building energy consumption. After optimization by three methods, the thermal insulation performance of the wall is compared. Before the reconstruction, the building wall was built with stone without thermal insulation layer. The thickness of the wall was 350mm. The facade was plastered with cement. Only the original texture of the brick wall could be seen in the courtyard. The indoor wall adopts the form of internal thermal insulation, the thickness is 220mm, the thermal insulation material is 40mm thick granular mortar, and its structural parameters are shown in Table 2.

By using design builder software, the building envelope optimized by three methods is simulated. Firstly, the minimum heat transfer resistance of three groups of experiments is compared. The greater the heat transfer resistance is, the better the indoor insulation effect is, and the lower the building cooling

TABLE 1
Parameter setting of B & B Building.

Setting item	Parameter	Setting item	Parameter
Population density	0.04 人/m²	Heating mode	Air conditioning heating, electric heating
Refrigeration set temperature	25℃	Refrigeration mode	Air conditioning refrigeration
Heating set temperature	20℃	built-up area	123m²
Equipment energy consumption	1398 KW·h	Lighting energy consumption	1086 KW·h
Heating energy consumption	11839 KW·h	Refrigeration energy consumption	5368 KW·h
Unit energy consumption	167 KW·h	Total energy consumption	20622 KW·h

TABLE 2
The structural parameters of the front wall are not optimized.

Structural level	Thickness (m)	Heat transfer resistance (m²·K/W)	Thermal conductivity (W/m·K)
Fair faced wall	0.03	0.12	1.12
Limestone	0.05	0.23	1.02
Cement stone, mortar and plaster shall be leveled in different times	0.12	0.14	1.02
Water resistant putty of surface course shall be troweled in different times	0.06	0.15	1.82
Thermal insulation granular mortar	0.08	0.11	1.12
Latex paint	0.2	0.01	1.02

and heating energy consumption is. The calculation formula of minimum heat transfer resistance is:

$$R=\frac{n(A-B)C}{\Delta t} \quad (3)$$

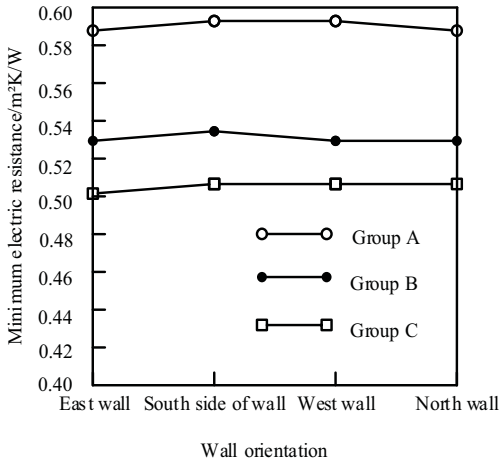

FIGURE 3
Comparison results of minimum heat transfer resistance of walls.

In formula (3), n is the temperature correction coefficient, A is the indoor calculation temperature, B is the outdoor calculation temperature of the enclosure structure, C is the internal surface heat transfer resistance, and Δt is the allowable temperature difference between the enclosure surface and the indoor air. The comparison results of minimum heat transfer resistance of wall enclosure are shown in Figure 3.

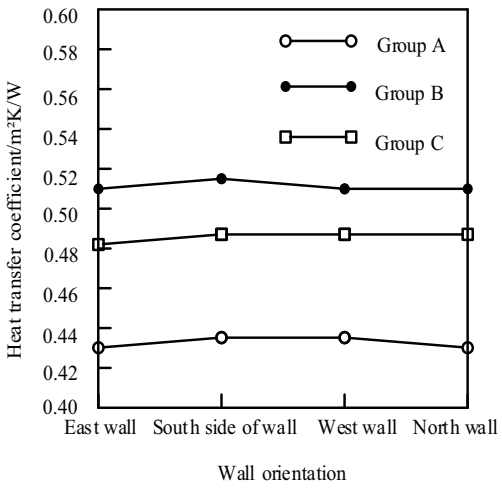

FIGURE 4
Comparison results of wall heat transfer coefficient.

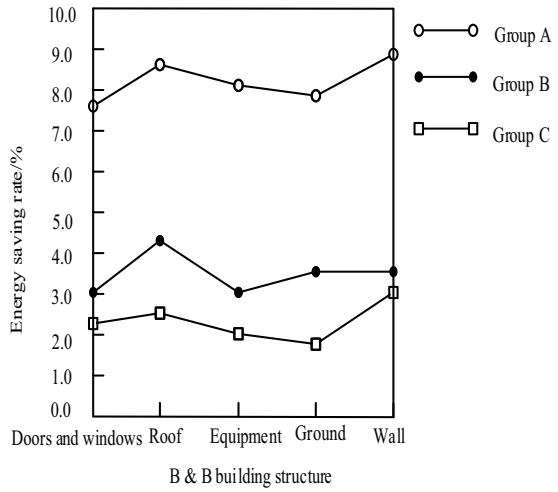

FIGURE 5
Comparison results of energy saving rate after optimization.

Figure 3 shows that the average minimum electric resistance of the wall in group A is 0.59 $m^2 \cdot K/W$, and that of group B and group C is 0.53 $m^2 \cdot K/W$ and 0.50 $m^2 \cdot K/W$, respectively. Compared with group B and group C, the minimum electric resistance of group a is increased by 0.06 $m^2 \cdot K/W$ and 0.09 $m^2 \cdot K/W$ respectively. Therefore, the minimum heat transfer resistance of the wall in group A is larger, the indoor insulation effect is better, and the building cooling and heating energy consumption is lower.

The lower the heat transfer coefficient is, the better the indoor thermal insulation effect is, and the lower the building cooling and heating energy consumption is. The calculation formula of wall heat transfer coefficient D is:

$$D=\frac{1}{E+G_r+H} \quad (4)$$

In formula (4), E is the heat transfer resistance of the inner surface of the enclosure, G_r is the heat transfer resistance of the outer surface, and H is the thermal resistance of the wall. The comparison results of heat transfer coefficient of wall enclosure are shown in Figure 4.

Figure 4 shows that the average heat transfer coefficient of the wall in group A is 0.43 $m^2 \cdot K$, and that of group B and group C is 0.51 $m^2 \cdot K$ and 0.48 $m^2 \cdot K$, respectively. Compared with group B and group C, the heat transfer coefficient of group a wall enclosure is reduced by 0.08 $m^2 \cdot K$ and 0.05 $m^2 \cdot K$, respectively. It can be seen that the heat transfer coefficient of wall enclosure of group A is lower, the indoor insulation effect is better, and the energy consumption of building refrigeration and heating is lower.

(2) Experimental results of building energy saving rate. After the optimization of wall enclosure structure, the doors and windows, roof, equipment and ground are optimized to compare the overall energy saving effect of B & B buildings. The traditional aluminum alloy windows are used in the residential buildings before the transformation. The window shading is horizontal external shading, only two wooden strips are used to support the wood board, and the external protruding eaves are used for shading directly. The roof structure from top to bottom is respectively thick and thin, with grass clay, thick tiles and tarpaulin. The roof height is 1.8m and the roof span is 1.6m. The floor is plastered with cement mortar. The cement: Sand: Gravel ratio is 1:2:2, and the thickness is 90 ~ 100 mm. The energy equipment is mainly electric energy, mainly including air conditioning, television, water heater and kitchen and bathroom appliances. According to the total energy consumption before and after optimization, the energy saving rate comparison results of the three groups of experiments are shown in Figure 5.

The average energy-saving rate of group A and group B is 8.4% and 8.4% respectively compared with group A and group C, which shows that the energy-saving rate of group A and group B is 8.4%, respectively. It can be seen that the energy saving rate of B & B buildings in experimental group A is higher. To sum up, the design method compared with the reference [2] and reference [3] energy-saving and environmental protection type residential building optimization method, improve the minimum heat transfer resistance of wall enclosure, reduce the wall heat transfer coefficient, and ensure the indoor thermal insulation performance of the building. At the same time, the energy-saving rate of doors and windows, roof, equipment, ground and wall is improved, and the energy consumption of B & B buildings is significantly reduced after optimization.

CONCLUSIONS

With the vigorous development of rural tourism, as an ecological product, rural B & B meets the needs of seeking knowledge and returning to nature. Therefore, it is imperative to introduce new energy-saving concepts into the optimal design of B & B buildings. Therefore, aiming at the problem of high energy consumption of B & B buildings in Southwest Zhejiang Province, the optimization method of energy-saving and environment-friendly B & B buildings under the concept of green countryside is proposed:

(1) Starting from the wall enclosure structure, the form of doors and windows, roof and ground structure, energy equipment, we choose composite wall, insulation ceiling and other transformation methods, change the window wall and door and window installation form, and take solar energy and air source heat pump as new energy utilization forms.

(2) Compared with the experimental group B and group C, the minimum thermal resistance of wall enclosure increased by 0.06 $m^2 \cdot K/W$ and 0.09

$m^2 \cdot K/W$ respectively, and the wall heat transfer coefficient decreased by 0.08 $m^2 \cdot K$ and 0.05 $m^2 \cdot K$, respectively. The energy-saving rate of the building structure is increased by 4.6% and 6.0% respectively, which improves the indoor thermal insulation performance of the building, reduces the energy consumption of the B & B building, and improves the indoor comfort greatly.

However, there are still some deficiencies in this study. Only for the residential environment in Southwest Zhejiang, in the future research, the technology maturity will be improved, and the optimization method will be applied to large-scale building reconstruction.

ACKNOWLEDGEMENTS

This work was supported by the Philosophy and Social Science Research Project in Zhejiang Province Named "Research on the new business form of homestay in ancient villages in Southwest Zhejiang Province from the perspective of traditional cultural change"(Number: 21NDJC305YBM). Meanwhile, we want to thank all the techniques who have helped this research and the authors of the references.

REFERENCES

[1] Liu, B., Tang, C., Xu, X. (2020) Analysis on Key Green Energy-saving Technologies of Large Exhibition Buildings. Refrigeration & Air Conditioning. 34(04), 493-499.

[2] Manigandan, S., Gunasekar, P., Devipriya, J., Anderson, A., Nithya, S. (2018) Energy-saving potential by changing window position and size in an isolated building. International Journal of Ambient Energy. 39(5-8), 462-466.

[3] Qiao, W., Guo, H., Li, W., Qin, G. (2020) Implementation Mechanism of Multi-agent Multi-objective Integrated Hierarchical Optimization for Existing Residential Buildings Energy-saving Renovation. Resource Development & Market. 36(08), 801-806.

[4] Zheng, B. (2020) Low Energy Consumption Passive House Design. Green Building. 12(03), 69-73.

[5] Chen, P. (2020) Optimization method of building energy saving for early design stage. City & House. 27(03), 131-132.

[6] Teng, J., Li, M., Wang, W., Mu, X. (2020) A Study on Energy-saving Rate of Ventilation and Shading Technical Plans of Residential Buildings in Severely Cold Areas. Journal of Engineering Management. 34(04), 69-73.

[7] Chen, Y. (2020) Effective Measures of Energy-Saving Retrofitting for Campus Building in a University. Building Energy Efficiency. 48(02), 118-120+155.

[8] Ding, Y., Guo, X., Huo, H. (2020) Optimization research on the green building based on BIM technology. Sichuan Building Materials. 46(02), 62-64.

[9] Montazeri, H., Blocken, B. (2018) Extension of generalized forced convective heat transfer coefficient expressions for isolated buildings taking into account oblique wind directions. Building and Environment. 140, 194-208.

[10] Li, H., Zhao, Y., Feng, G., Yu, S., Sun, H. (2020) Optimization analysis of building energy-saving renovation of a public institution in Jinan. Building Technology. 50(01), 51-54.

[11] Yan, L., Shu, R. (2020) Energy consumption analysis and optimum design of energy saving scheme for commercial complex based on BIM model. Journal of Guizhou Normal University (Natural Sciences). 38(01), 112-118.

[12] Shao, T., Jin, H. (2019) Optimization Design of Energy Saving for Rural Houses in Severe Cold Regions Based on an Optimization Algorithm. Building Science. 35(12), 99-107.

[13] Wu, W., Li, X., He, Q. (2019) Study on Optimal Design of Zero Energy-Consumption Residential Buildings Under the Perspective of Ecological Optimization. Urbanism and Architecture. 16(15), 7-9+20.

[14] Yu, Z., Lu, Fei., Zou, Yu., Xu, W., Sun, D., Liu, C. (2019) A Simulation-based Multi-objective Optimization Approach for Design of Nearly Zero Energy Buildings. Building Science. 35(10), 8-15.

[15] Han, F., Lin, S. (2019) Collaborative design of energy-saving building structures based on BIM technology. Journal of Shenyang University of Technology. 41(06), 710-714.

[16] Wang, Y., Deng, Q., Li, D. (2019) Energy-saving optimization research on the envelope structure renovation of existing residential buildings in cold areas. New Building Materials. 46(12), 145-148+152.

[17] Hu, J. (2020) Comparison of building resilience in the international typical green building evaluation system based on the concept of ecological and environmental protection. Fresen. Environ. Bull. 29(8), 7147-7155.

[18] Rijal, H., Yoshida, K., Humphreys, M., Nicol, J. (2020) Development of an adaptive thermal comfort model for energy-saving building design in japan. Architectural Science Review. 1, 1-14.

[19] Han, K., Zhang, J. (2020) Energy-saving building system integration with a smart and low-cost sensing/control network for sustainable and healthy living environments: demonstration case study. Energy and Buildings. 214, 109861.

[20] Zhang, D., Yu, L., Wang, L. (2019) Research on large-scale building energy efficiency retrofit based on energy consumption investigation and energy-saving potential analysis. Journal of Energy Engineering. 145(6), 04019024.1-04019024.14.
[21] Kwon, H., Yeon, S., Lee, K., Lee, K. (2018) Evaluation of building energy saving through the development of venetian blinds' optimal control algorithm according to the orientation and window-to-wall ratio. International Journal of Thermophysics. 39(2), 30.
[22] Castaldo, V., Pisello, A., Piselli, C., Fabiani, C., Cotana, F., Santamouris, M. (2018) How outdoor microclimate mitigation affects building thermal-energy performance: A new design-stage method for energy saving in residential near-zero energy settlements in Italy. Renewable Energy. 127, 920-935.

Received: **05.12.2020**
Accepted: **03.02.2021**

CORRESPONDING AUTHOR

Yuchun Zheng
Department of Architectural Engineering,
Jinhua Polytecnich,
Jinhua Zhejiang 321007 – China

e-mail: zyc330821@163.com

© by PSP Volume 30– No. 05/2021 pages 5238-5243 Fresenius Environmental Bulletin

COMPARATION AMONG SORPTIVE CHARACTERISTICS OF CADMIUM BY SOLID WASTES-DERIVED BIOCHAR FROM AQUEOUS SOLUTION

Hao Yang[1], Chengchun Sun[2], Can Zhang[3], Wei Jiao[4], Dan Zheng[5,*]

[1]Beijing Academy of Social Sciences, Beijing 100101, P.R. China
[2]Beijing Doris Consulting co., ltd, Beijing 100086, P.R. China
[3]Jiang He Hui Yuan Technology Co., Ltd, Beijing 100190, P.R. China
[4]Shandong Provincial Key Laboratory of Water and Soil Conservation and Environmental Protection, College of Resources and Environment, Linyi University, Linyi 276000, P.R. China
[5]Biogas Institute of Ministry of Agriculture and Rural Affairs, Chengdu 610041, P.R. China

ABSTRACT

Biochar has proven to effectively remove cadmium in the environment. In this study, three common solid wastes, such as corn stalks (CS), Chinese herbal residues (HR) and sludge (SL), were used as raw materials to produce biochar, which further was modified by adding thiourea. The cadmium sorption characteristics on the six kinds of biochar derived from different biomass sources were studied. The results showed that the isothermal sorption isotherms of cadmium on biochar were better fit by the Langmuir model. The sorption capacity and sorption rate of the modified-biochar were increased by 10%-15% compared with the non-modified-biochar. The sorption rates of the six biochar were in the range of 50%-90%, following the order of modified-HR > modified-CS > HR > modified-SL > CS > SL. The results provide economical and environmentally friendly materials for the biochar production and for the effective cadmium remediation in the environment.

KEYWORDS:
Biochar, Thiourea-modified, Cadmium, Sorption, Environmental remediation

INTRODUCTION

Heavy metals in the aqueous environment pose health risks to organism and eco-environments [1-2]. Cadmium (Cd) is a notorious non-essential heavy metal with the high accumulative toxicity, mobility and activity in the environment [3]. The ascending industrial and agricultural Cd uses have induced Cd-related pollution problems multiplied [4]. Cd removal from the aqueous environment has been a hotspot in the field of environmental science for decades. Traditional adsorptive removal for Cd from contaminated water is an effective approach but with high costs, operational difficulties, and disposal problems [5-7]. The development of ecologically and environment-friendly efficient methods for Cd removal from aqueous environment is necessary.

Biochar is an effective adsorbent for the removal of various contaminants from contaminated environment such as heavy metals, pesticides and nutrients [8-11]. Biochar obtains the durable fixed carbon via thermal decomposition of carbon-rich biomass under oxygen-limited conditions [12]. The biochar has complicated surface construction and the negative surface charge and thereby performs better ability to sorb pollutants than soil organic matter [13]. Growing attention was given to researches on sorption capability dynamics with the pyrolysis process optimization and best addition to diverse types of soils [14-15]. The distinct characteristics of biochar, such as intra-pores, specific surface area and surface functional group, highly depend on the type of feedstock or biochar [16-17]. Thus, studies are necessary to consider the effect of biochar type and pyrolysis process optimization on the Cd removal efficiency.

Solid wastes with abundant biomass resources are easy to be produced as biochar [18-19]. However, biochar application in the field of environmental protection has certain limitations. The modified biochar with a higher application values can be obtained by adding active groups to the surface of the biochar and improving the surface properties of the biochar [20-21]. Thiourea is a representative organic surface modifier, which can improve the adsorption capacity of adsorbent to heavy metals by increasing the binding ability of amine and sulfhydryl functional groups [22]. Solid waste re-using is an important component of any modern, efficient and green economy [18, 23]. There are abundant solid waste resources worldwide. Therefore, the objective of the present study was to compare the effects of biochar type-derived from three common solid wastes on Cd sorption characteristics before and after modification by thiourea.

MATERIALS AND METHODS

Solid wastes such as corn straw, Chinese herbal residues and sludge, were collected in the local region as raw materials to produce biochar. The collected materials were air dried, grounded, sieved and anaerobically heated. The pyrolysis products were deashed and sieved as corn straw, Chinese herbal residues and sludge biochar (CS, HR and SL). The biochars were modified by thiourea and ultrasonic, which were accordingly recorded as TCS, THR and TSL, respectively. More details were introduced in the previous research [8].

Biochar physicochemical properties analysis The pH was measured using a pH meter at a biochar/water ratio of 1: 2.5 (mass: mass). The productivity rate and ash content were measured using the weighing method.

Biochar load experiment The six kinds of biochar were weighed into the 50 ml centrifuge tubes with 20 ml 10 mg·L-1 CdCl2 solution. Sorption rate of Cd was calculated based on the detected Cd concentration after vibrating 12 h when the equilibrium arrived.

Isothermal sorption experiment Batch isothermal sorption experiments were conducted by adding biochar into the centrifuge tubes with 20 mL 0-40 mg·L-1 CdCl2 solution and detecting the residual concentration with FAAS (Flame Atomic Absorption Spectroscopy) after vibrating 12 h. The isothermal sorption experiments results were simulated by the Freundlich and Langmuir models.

RESULTS

Selective physicochemical properties of biochar Productivity rate and ash content. Data listed in Table 1 showed that the percentage productivity rates and ash contents of unmodified biochar were in the ranges of 55.6%-193% and 9.42%-46.3%, respectively, while those of modified biochar were in the ranges of 42.7%-178% and 7.57%-41.7%, respectively. Generally, the percentage productivity rates and ash contents followed the descending series of SL > TSL > HR > THR > CS >TCS. The productivity rates and ash contents decreased by 10%-20% and by circa 5% after modification.

Comparations in pH values. As shown in Figure 1, The pH values of biochar ranged from 7.53 to 8.91. There was a descending series of SL > HR > CS for the unmodified biochars, which were increased by 0.5-2.5 after modification. However, the descending trend did not change.

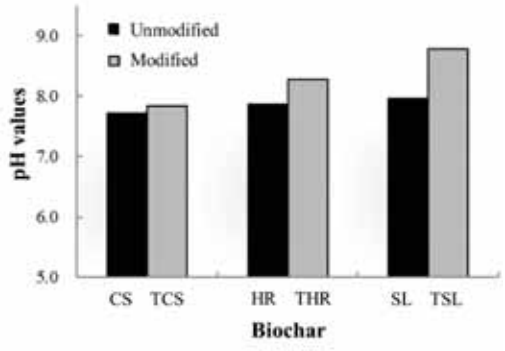

FIGURE 1
Comparations in pH values of different biochars.

Sorption capacity and rate of Cd from aqueous solution by different loads of biochar Generally, the sorption capacity of Cd gradually decreased with the unmodified biochar loads increasing from 0.02 to 0.50 g, while the sorption rate of Cd increased (Figure 2). In detail, when the biochar load was 0.20 g, the sorption rates of reached the maximum values of 91.6%, 91.9% and 79.7% for CS, HR and SL, respectively. Once the biochar loads exceeded 0.20 g, the sorption rates changed little for CS or HR, while decreasing for SL. Therefore, a ratio of 0.2g: 20 mL of biochar/solution was selected in the next batch isothermal sorption experiments after considering the comprehensive factors such as productivity, collection cost and sorption stability.

TABLE 1
Percentage productivity rate and ash content of biochar.

Index	Biochar					
	Unmodified			Modified		
	CS	HR	SL	TCS	THR	TSL
Ash content	9.42	32.9	46.3	7.57	28.9	41.7
Productivity rate	55.6	147	193	42.7	125.8	178

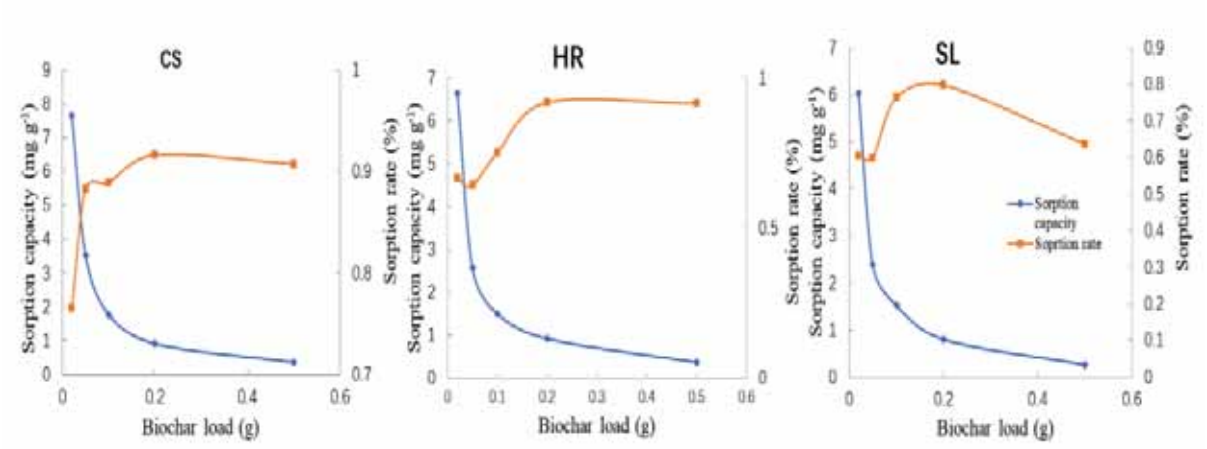

FIGURE 2
Sorption capacity and rate of Cd from aqueous solution by different loads of biochar.

Comparation in isothermal sorption characteristics of Cd on biochar. The Freundlich model fitting results showed that the sorption capacity of Cd on biochar increased with the initial Cd concentrations increasing (Figure 3). The sorption capacities of Cd on CS and SL increased after modification, whereas those on HR decreased. The sorption capacities of Cd increased sharply in the range of the relatively lower initial Cd levels (1-5.0 mg L-1), while the increments narrowed once the initial Cd levels exceeded 5.0 mg L-1. As shown in Table 2, the values of fitting parameters KF and n in the Freundlich model for the unmodified biochar were in the ranges of 0.62-1.10 (mg g-1)×(mg L-1) -n and 1.09-1.60, respectively, with the correlation coefficients ranging from 0.9185 to 0.9466. The values of fitting parameters KF in the Freundlich model for the TCS and TSL increased 2.19 and 1.47 times, respectively, with the n values over 1. However, the KF decreased by 13.6% although the value over 1.

Similar ascending trends were observed in the Langmuir model fitting results of the sorption capacities of Cd (Figure 4). The maximal apparent sorption capacity Qm in the Langmuir model for the unmodified biochar were in the ranges of 6.54-12.1 mg g-1 following the ascending series of CS > SL > HR (Table 2). A similar series was also observed in those of modified biochar with the values of 7.31-19.2 mg g-1, which were higher than those for the unmodified biochar.

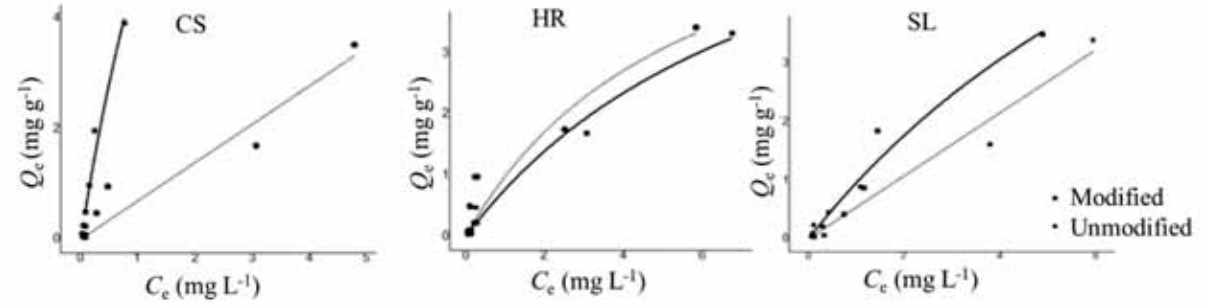

FIGURE 3
Isothermal sorption characteristics of Cd on different biochar fitting by the Freundlich and model.

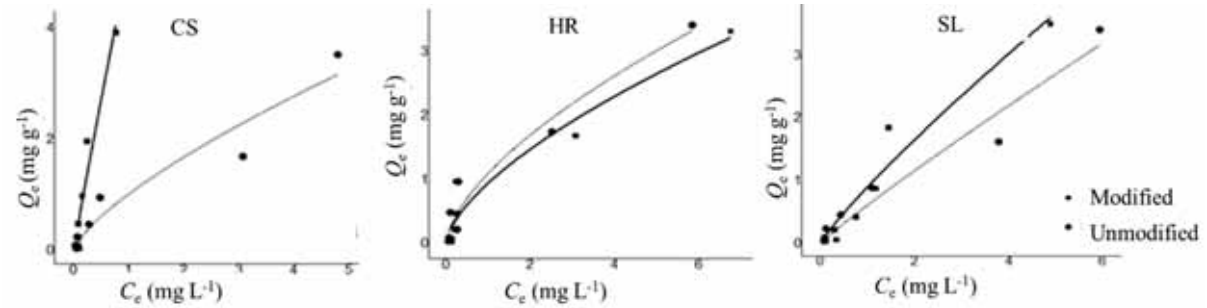

FIGURE 4
Isothermal sorption characteristics of Cd on different biochar fitting by the Langmuir model.

TABLE 2
The fitting parameters of Freundlich and Langmuir model on the Cd adsorption by biochar-amended soil response to different raw materials.

Biochar	Freundlich			Langmuir		
	K_F (mg g^{-1})×(mg L^{-1})$^{-n}$	n	R^2	K_L(L mg^{-1})	Q_m(mg g^{-1})	R^2
TCS	5.23	1.06	0.9143	0.35	19.2	0.9213
THR	0.95	1.56	0.9235	0.12	7.31	0.8905
TSL	0.91	1.15	0.9301	0.09	11.7	0.9301
CS	1.02	1.38	0.9185	1.95	12.1	0.9049
HR	1.10	1.60	0.9436	0.18	6.54	0.9126
SL	0.62	1.09	0.9466	1.18	11.7	0.9454

DISCUSSION

Biochars have different physicochemical properties after the anaerobic pyrolysis process of different raw materials even at the same temperature [24]. The ash contents and productivity rate of modified biochar were lower than those of unmodified biochar in the present study. There are many factors affecting the physicochemical properties of biochar. The raw materials used to prepare biochar usually have different physicochemical properties due to differences in their internal structure and characterization morphology. Previous study reported that the O/C and H/C ratios of pig manure-derived biochar were both lower than those of carrot-derived biochar before or after thiourea-modification [22]. Accordantly, there are differences in the pH values in the present study among different materials-derived biochars with different preparation produce even at the same temperature.

The nonlinearity sorption under low initial concentrations is mainly attributed to the surface adsorption and the specific sorption of the carbonized parts [7]. Under high initial concentrations, the surface adsorption reaches saturation and the sorption process is mainly controlled by the partitioning mechanism. Therefore, the sorption processes of different biochars for Cd mainly involve two phases. Both the Freundlich and Langmuir models well fitted the isothermal sorption data. The fact that all the non-linear parameters n values over 1 in the present study implies more sorption sites with stronger heterogeneity and higher energy [25]. The sorption processes of Cd by all the six biochars in the present study are homogeneous and linear. This is because the adsorption sites are occupied gradually with the action time increasing, while the unoccupied adsorption sites become less and less [26]. Accordingly, the adsorption rate becomes slower and slower until all the adsorption sites on the sorbent surface are occupied [27-28].

The adsorption mechanism of biochar for Cd is a very complex process, which is dependent on many factors, such as the polarity, aromaticity, specific surface area and pore structure of the adsorbent surface groups. For example, the smaller the O/C atomic ratio, the less the aliphatic related surface polar groups and the lower the hydrophilicity are. The smaller the H/C atomic ratio, the higher the degree of aromaticity is [6, 29]. Previous studies found that the surface of thiourea-modified biochar have more carboxyl, lactone, phenolic hydroxyl, carbonyl and thereby increase the hydrophilicity and polarity, increasing sorption capacity of Cd via promoting the process of exchange, precipitation, specific adsorption and complexation [6, 8]. Especially, the increased sulfydryl groups will increase the pair trend with Cd attributed to the increased sulfur lone pair electrons in thiourea-modified biochar, resulting in increases in the Cd sorption capacity via the formation of dicoordination complex or cadmium-sulfur compound precipitation [30-32]. The sulfhydryl group has a lower Lewis acidity than the oxygen-containing group, which is more conducive to the adsorption of pollutants, and the sulfhydryl-modified biochar has a more stable adsorption performance to pollutants [33-34]. Therefore, the maximal apparent sorption capacity in the Langmuir model for the unmodified biochar increased after modification by thiourea in the present study. Thiourea-modified biochar has certain effect on the removal of some pollutants in agriculture and has potential application value in the prevention and control of agricultural non-point source pollution.

CONCLUSIONS

The percentage productivity rates and ash contents followed the descending series of SL > TSL > HR > THR > CS >TCS. The productivity rates and ash contents decreased by 10%-20% and by circa 5% after modification. The pH values of biochar ranged from 7.53 to 8.91 with the descending series of SL > HR > CS for the both unmodified- and modified biochars. The pH values of thiourea-modified biochar were increased by 0.5-2.5 after modification. A ratio of 0.2g: 20 mL of biochar/solution was suggested for the Cd removal from aqueous solution after considering the comprehensive factors such as productivity, collection cost and sorption stability. The Freundlich model fitting results showed that the sorption capacity of Cd on biochar increased with the initial Cd

concentrations increasing. The sorption capacities of Cd on CS and SL increased after modification, whereas those on HR decreased. The sorption capacities of Cd increased sharply in the range of the relatively lower initial Cd levels (1-5.0 mg L-1), while the increments narrowed once the initial Cd levels exceeded 5.0 mg L-1. The maximal apparent sorption capacities of Cd in the Langmuir model were in the ranges of 6.54-12.1 mg g-1 and 7.31-19.2 mg g-1, for the unmodified- and modified biochar, respectively, following the ascending series of CS > SL > HR, which were higher for modified biochar than those for the unmodified biochar. Thiourea-modified biochar has potential application value in the Cd removal in the comminated aqueous environments.

ACKNOWLEDGEMENTS

This research benefited from financial support from the Beijing Social Science Fund of China (No.2019CN016), Youth project of Beijing Academy of Social Sciences (No.2020B2019135790), the National Natural Science Foundation of China (Grant Nos. 41701562 and 41701356) and the Central Public-interest Scientific Institution Basal Research Fund (No. 1610032019002).

REFERENCES

[1] Wang, F., Wang, X., Chen, Q., Song, N. (2021) Extension of a biotic ligand model for predicting the toxicity of metalloid selenate to wheat: the effects of pH, phosphate and sulphate. Chemosphere. 264, 128424.

[2] Wang, F., Song, N.N. (2020) Modeling of selenite toxicity to wheat root elongation using biotic ligand model: Considering the effects of pH and phosphate anion. Environ. Pollut. Article ID: 115935.

[3] Li, G., Chen, F., Jia, S., Wang, Z., He, H. (2020) Effect of biochar on cd and pyrene removal and bacteria communities variations in soils with culturing ryegrass (*Lolium perenne* L.). Environ. Pollut. 265. Article ID:114887.

[4] Wang, F., Yan, T., Zong, H., Li, S., Liu, J., Liu, Y., Hou, X. (2020) Long-term fertilization influencing agricultural diffuse heavy metal pollution and its environmental threat to a coastal city of Yellow Sea, Qingdao, East China. Fresen. Environ. Bull. 29, 5390-5398.

[5] Wang, F., Song, N. (2019). Salinity-induced alterations in plant growth, antioxidant enzyme activities, and lead transportation and accumulation in Suaeda salsa: implications for phytoremediation. Ecotoxicology. 28, 520-527.

[6] Li, Y., Wang, F., Wang, K., Song, N. (2020) Characterization and Cd removal efficiency of graphene/biochar composite derived from corn cob. Fresen. Environ. Bull. 29, 5294-5302.

[7] Liu, J., Wang, F. (2020) Simultaneous sorptive removal of typical farmland diffuse pollution on ammonium dihydrogen phosphate modified pig manure biochar in binary-solute aqueous solution. Fresen. Environ. Bull. 29, 6219-6227.

[8] Gao, W., Yang, Y., Zong, H., Liu, J., Song, N., Wang, F. (2020) Simultaneously sorptive reduction in cadmium and glyphosate diffuse loss by biochar-amended soil. Fresen. Environ. Bull. 29, 4545-4555.

[9] Shafiq, M., Alazba, A.A., Amin, M.T. (2020) Adsorption of divalent copper ions from synthetic wastewater using layered double hydroxides (NiZnFe) and its composites with banana biochar and carbon nanotubes. Water Air Soil Pollut. 231(7), 346.

[10] Wang, Y., Kang, J., Jiang, S., Li, H., Ren, Z., Xu, Q., Jiang, Q., Liu, W., Li, R., Zhang, Y. (2020) A composite of Ni–Fe–Zn layered double hydroxides/biochar for atrazine removal from aqueous solution. Biochar. 2, 455-464.

[11] Wan, S., Wang, S., Li, Y., Gao, B. (2017) Functionalizing biochar with Mg–Al and Mg–Fe layered double hydroxides for removal of phosphate from aqueous solutions. J. Ind. Eng. Chem. 47, 246-253.

[12] Lyu, H., Zhang, Q., Shen, B. (2020) Application of biochar and its composites in catalysis. Chemosphere. 240, 124842.

[13] Ahmad, M., Rajapaksha, A.U., Lim, J.E., Ming, Z., Bolan, N., Mohan, D., Vithanage, M., Sang, S.L. and Yong, S.O. (2014) Biochar as a sorbent for contaminant management in soil and water: A review. Chemosphere. 99(3), 19-33.

[14] Veksha, A., Zaman, W., Layzell, D.B. and Hill, J.M. (2014) Enhancing biochar yield by co-pyrolysis of bio-oil with biomass: impacts of potassium hydroxide addition and air pretreatment prior to co-pyrolysis. Bioresource Technol. 171, 88-94.

[15] Bashir, S., Shaaban, M., Mehmood, S., Zhu, J., Fu, Q. and Hu, H. (2018) Efficiency of C3 and C4 Plant Derived-Biochar for Cd Mobility, Nutrient Cycling and Microbial Biomass in Contaminated Soil. Bull. Environ. Contam. Toxicol. 100, 834-838.

[16] Hussain, R., Bordoloi, S., Gupta, P., Garg, A., Ravi, K., Sreedeep S., Sahoo L. (2020) Effect of biochar type on infiltration, water retention and desiccation crack potential of a silty sand. Biochar. 2, 465-478.

[17] Zhang, A., Li, X., Xing, J., Xu, G. (2020) Adsorption of potentially toxic elements in water by modified biochar: A review. J. Environ. Chem. Eng. 104196.

[18] Fang, Z., Gao, Y., Bolan, N., Shaheen, S.M., Xu, S., Wu, X., Xu, X., Hu, H., Lin, J., Zhang, F., Li, J., Rinklebe, J., Wang, H. (2020) Conversion of biological solid waste to graphene-containing biochar for water remediation: A critical review. Chem. Eng. J. 124611.
[19] Karimi, M., Diaz de Tuesta, J.L., d.P. Gonçalves, C.N., Gomes, H.T., Rodrigues, A.E., Silva, J.A. (2020) Compost from municipal solid wastes as a source of biochar for CO2 capture. Chem. Eng. Technol. 43, 1336-1349.
[20] Thomazini, A., Spokas, K., Hall, K., Ippolito, J., Lentz, R., Novak, J. (2015) GHG impacts of biochar: Predictability for the same biochar. Agr. Ecosyst. Environ. 207, 183-191.
[21] Mohan, D., Sarswat, A., Ok, Y.S., Pittman Jr, C.U. (2014) Organic and inorganic contaminants removal from water with biochar, a renewable, low cost and sustainable adsorbent–a critical review. Bioresource Technol. 160, 191-202.
[22] Gholami, L., Rahimi, G., Nezhad, A.K.J. (2020) Effect of thiourea-modified biochar on adsorption and fractionation of cadmium and lead in contaminated acidic soil. Int. J. Phytoremediat. 22(5), 468-481.
[23] Abondio, R.B., Komakech, A.J., Kambugu, R.K., Kiggundu, N., Kyamanywa, S. (2020) Assessment of municipal organic solid waste, as a potential feedstock for briquette production in Kampala, Uganda. Journal of Sustainable Bioenergy Systems. 10(2), 62-75.
[24] Cao, X.D., Harris, W. (2010) Properties of dairy-manure-derived biochar pertinent to its potential use in remediation. Bioresource Technol. 101, 5222-5228.
[25] Sarmah, A.K., Srinivasan, P., Smernik, R.J., Manley-Harris, M., Antal, M.J., Downie, A., van Zwieten, L. (2010) Retention capacity of biochar-amended new zealand dairy farm soil for an estrogenic steroid hormone and its primary metabolite. Aust. J. Soil Res. 48, 648-658.
[26] Li, S., Zong, H., Wang, F., Wang, B., Wang, C., Song, N. (2020) Effect of chitosan modified biochar on accumulations of Cu and Cd in lettuce. Fresen. Environ. Bull. 29, 2214-2221.
[27] Zong, W., Li, Y., He, S., Wang, W., Song, X., Chen, J., Liu, S., Luo, M., Song, N. (2020) Alkali modification enhanced the adsorption ability of biochars platane wood in aqueous solutions. Fresen. Environ. Bull. 29, 4479-4487.
[28] Bashir, S., Zhu, J., Fu, Q.L., Hu, H.Q. (2018) Comparing the adsorption mechanism of Cd by rice straw pristine and KOH-modified biochar. Environ. Sci. Pollut. Res. 25(12), 11875-11883.
[29] Ipeaiyeda, A.R., Choudhary, M.I., Ahmed, S. (2020) Ammonia and ammonium ccetate modifications and characterisation of activated carbons from palm kernel shell and coconut shell. Waste Biomass Valori. 11(3), 983-993.
[30] Chai, L., Li, Q., Zhu, Y., Zhang, Z., Wang, Q., Wang, Y., Yang, Z. (2010) Synthesis of thiol-functionalized spent grain as a novel adsorbent for divalent metal ions. Bioresource Technol. 101 (15), 6269-6272.
[31] Li, J., Xing, X., Li, J., Shi, M., Lin, A., Xu, C., Zheng, J., Li, R. (2018) Preparation of thiol-functionalized activated carbon from sewage sludge with coal blending for heavy metal removal from contaminated water. Environ. Pollut. 234, 677-683.
[32] Zhou, D.M., Wang, Y.J., Cang, L., Hao, X.Z., Luo, X.S. (2004) Adsorption and cosorption of cadmium and glyphosate on two soils with different characteristics. Chemosphere. 57(10), 1237-1244.
[33] Ali, J., Wang, H., Ifthikar, J., Khan, A., Wang, T., Zhan, K., Shahzad, A., Chen, Z., Chen, Z. (2018) Efficient, stable and selective adsorption of heavy metals by thio-functionalized layered double hydroxide in diverse types of water. Chem. Eng. J. 332, 387-397.
[34] Tang, N., Niu, C.G., Li, X.T., Liang, C., Guo, H., Lin, L.S., Zheng, C.W., Zeng G.M. (2018) Efficient removal of Cd2+ and Pb2+ from aqueous solution with amino- and thiol-functionalized activated carbon: isotherm and kinetics modeling. Sci. Total Environ. 635, 1331-1344.

Received: **05.12.2020**
Accepted: **22.01.2021**

CORRESPONDING AUTHOR

Dan Zheng
Biogas Institute of Ministry of
Agriculture and Rural Affairs,
Chengdu 610041 – PR China

e-mail: zhengdan@caas.cn

© by PSP Volume 30– No. 05/2021 pages 5244-5253 Fresenius Environmental Bulletin

EXPERIMENTAL STUDY ON THE THERMAL MANAGEMENT AND ACTIVE CONTROL OF DIESEL ENGINE EXHAUST PRODUCTS BASED ON ENERGY SAVING AND ENVIRONMENTAL PROTECTION REQUIREMENTS

Ke Sun, Da Li, Hao Liu, Haiyang Zhao, Guodong Zhang, Shuzhan Bai*

School of Energy and Power Engineering, Shandong University, Jinan 250061, China

ABSTRACT

With the increasingly stringent environmental standards, higher requirements are put forward for the emission of mechanical engines. Several active control methods of diesel engine optimization and their effects on exhaust emission were studied via engine bench test under medium and low loads (engine speed at 1200RPM, 20% load rate and engine speed at 1400RPM, 30% load rate). Experimental results indicate that injection advance angle and pressure are closely related to exhaust temperature. An optimized late post injection angle can increase the exhaust products temperature by 90°C. Moreover, intake throttle adjustment can also significantly increase the exhaust products temperature by 120 °C (at 20% intake throttle valve opening), accompanied by a reduction in hydrocarbon and CO emissions. Besides, the intake throttle valve opening was found to have a significant effect on the exhaust products temperature. Under medium and low loads conditions, an appropriate late post injection strategy coupled with matched intake throttle valve opening can be considered as a valid approach to increase the exhaust temperature. This study can provide a reliable reference for improving the working efficiency and exhaust emission quality of diesel engine.

KEYWORDS:
Energy saving, environmental protection requirements, engine exhaust products, exhaust temperature, emission, intake throttle, late post injection

INTRODUCTION

Diesel engine, with its good thermal efficiency, high power and torque output, has been widely applied in automotive industry for more than a century. However, with increasingly severe internal combustion engine emission laws and regulations, numerous advanced technologies have been adopted to reduce engine emissions, such as alternative fuel, optimized combustion, exhaust gas recirculation (EGR) technology and exhaust aftertreatment [1]. In Abu-Jrai's research [2], waste cooking oil was treated by a promising means and applied as renewable biodiesel to supply power for a diesel engine in various operation conditions, and the emission of CO_2 and NO_x was decreased considerably. Jebamani et al. [3]found that spray, combustion and emission are closely related to the geometrical shape of a port and valve or valves, and high swirl in the part-load condition can improve the emission performance. Serio et al. explored the influence of exhaust gas recycle system on the emission characteristics of a diesel engine, and found that emissions, including CO, CO_2 and NO_x, can be reduced by a reasonable EGR rate without significant reduction in engine power output [4].

Emission control methods without aftertreatment devices cannot meet current emission requirements. On one hand, diesel particulate filter (DPF) system, one of the most widely used aftertreatment technologies in diesel engine exhaust clarification, is increasingly indispensable. On the other hand, the regeneration of DPF which is of great significance for the efficiency and security of aftertreatment devices, requires proper engine thermal management and inner engine emission control to provide appropriate exhaust temperature and emission. Among techniques of regeneration of DPF, active regeneration is widely applied. However, thermal diffusion and fuel combustion are complex phenomena which make it difficult to evaluate soot generation process and soot load with enough accuracy. [5-6] Facing the demand of precise regeneration temperature control, efficient thermal management methods in active regeneration process are becoming increasingly critical [7-9].

DPF active regeneration requires higher temperature to activate, however, at lower loads, engine particulate emission increases, while exhaust temperature decreases. Diesel oxidation catalyst (DOC), another common aftertreatment device before DPF, oxidizes unburned hydrocarbon in the exhaust, thus exhaust temperature before DPF can increase

through proper injection and intake coupling, activate regeneration process. Besides, the precondition of oxidizing unburned hydrocarbon in exhaust under effect of catalyst inside DOC is that internal temperature reaches the ignition temperature of catalyst. It is not necessary to apply additional heating methods to increase the exhaust temperature, since proper thermal management can achieve required temperature increase, without further effect on the total thermal efficiency of the engine. Optimized exhaust thermal management strategy in diesel engine can effectively increase exhaust temperature, which is beneficial to the reduction of engine emission. While at high engine loads, the exhaust temperature is high enough to meet the requirement of ignition of catalyst in DOC, which reaches 250 °C before entering DOC. Therefore, it is of great significance to study the influence of thermal management methods on exhaust temperature behavior of diesel engine under medium and low loads [10-16].

In published literatures, researches mainly focused on either the fuel injection or the control strategy of intake and exhaust throttling, and seldom paid attention to the relative feasibility of coupling fuel injection strategy and intake throttling [17-20]. Therefore, for the same engine, it is particularly important to explore the feasibility of different methods such as fuel injection strategy and intake throttling on the improvement of engine exhaust temperature [21, 22].

In this paper, the experiment was carried out on an off-road diesel engine. Typical operating points at medium and low loads were selected to explore the influence of exhaust thermal management methods, such as injection adjustment (advance angle, pressure, late post injection) and intake adjustment (intake throttle), on diesel engine emission performance and exhaust thermal management through temperature controlling. Then exhaust thermal management methods meeting temperature requirements before DOC under different conditions were evaluated by comparing and analyzing the influence of these methods on diesel engine performance, especially exhaust temperature and emission.

EXPERIMENTS AND METHODS

Experimental device. The principal parameters of the diesel engine are showed in Table. 1.

The HORIBA Dynas3 electrodynamometer was used to measure engine speed and torque. Fuel consumption rate and emissions, such as NO_x and hydrocarbon in the exhaust, were measured by AVL 735 fuel consumption meter and HORIBA 1600 gas analyzer, respectively. The specification of these devices is shown in Table 2. And the structure of engine test bench is given in Figure 1.

TABLE 1
Principle engine parameters

Item	Parameter
Engine Type	diesel engine
Cylinder	4
Valve	4
Injection	high-pressure common-rail
Standard Power/kW	81
Standard Speed/(r·min^{-1})	2400

TABLE 2
Specification of devices

Equipment	Model	Manufacturer	Accuracy of measurement
Electric dynamometer	INDYS66JD	AVL	Speed: ±1 RPM Torque: ±0.1%FS
Exhaust gas analyzer	MEXA-7100D	HORIBA	0.01 vol%
Fuel Mass Flow Meter + Temp Control	735S+753C	AVL	0.12%

TABLE 3
Operating condition

Conditions	Speed/RPM	Torque/(N·m)	Load rate	Main injection angle	Intake air mass flow rate/(kg/h)	Exhaust Temperature/°C
A	1200	83	20%	-1.0~-2.5	201	227
B	1400	103	30%	-1.1~-2.5	229	256

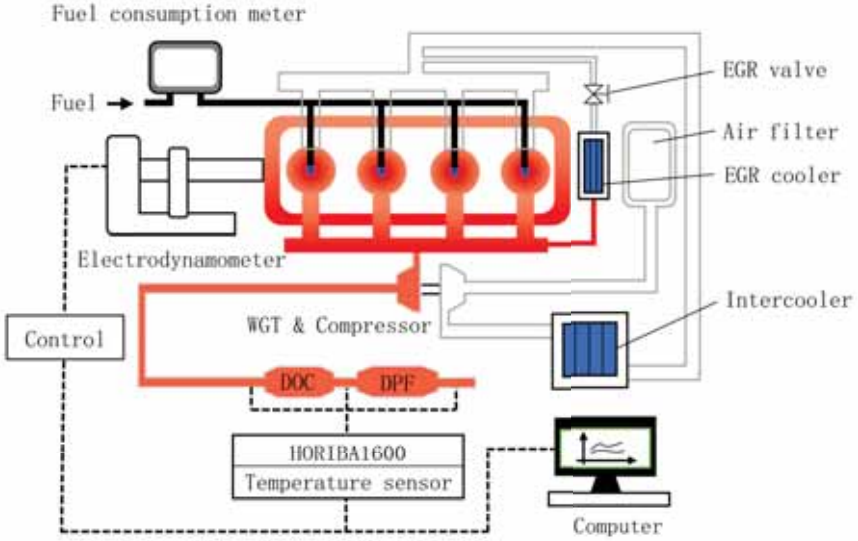

FIGURE 1
Schematic diagram of engine test bench.

Experimental methodology. The effect of aforementioned engine parameters on exhaust, especially emission and temperature, were investigated through a series of comparisons. Parameters of the high-pressure common rail diesel engine were adjusted through ECU program alteration. Injection advance angle and rail pressure were adjusted to investigate effect of injection parameters on engine exhaust emission and temperature; engine injection strategy with late post injection was adjusted to investigate effect of late post injection on engine exhaust; intake throttle valve opening was adjusted to investigate effect of intake airflow on engine exhaust. The efficient and appropriate method of exhaust thermal management at certain engine operating conditions can be evaluated through the analyzation of engine exhaust temperature and engine emission. The engine operating conditions selected in this study are shown in Table 3.

RESULTS

Injection advance angle adjustment. Exhaust temperature at different injection advance angle under the two experimental conditions is showed in Figure 2. It is shown that, exhaust temperature increases with the postponing of injection time. Under the condition A, exhaust temperature is increased from 227 °C at -2 °CA to 239 °C at 7 °CA, with an increased of 12 °C. As for the condition B, exhaust temperature is increased from 256 °C°at -1 °CA to 281 °C at 7 °CA, increased by 25 °C. The reason why exhaust temperature is increased in certain degrees under these two conditions is: with the delay of injection advance angle, cylinder pressure and instantaneous heat release rate are reduced, and energy released by fuel combustion is not fully used to push pistons to do work, but more remains in exhaust. Theoretically, with the delay of injection advance angle, the mixing time of fuel and fresh air in cylinder and the quantity of homogeneous charge are fewer, the mixing degree is lower, too. Then the ignition delay period and the rapid combustion period are decreased, and the combustion is chiefly concentrated in the slow combustion period and the post combustion period. Obviously, the result of this kind of backward movement of combustion center is: combustion duration is protracted, and specific fuel consumption is increased. In general terms, postponing the main injection advance angle results in decrease of the maximum combustion temperature and the maximum combustion pressure. Fuel injected into the cylinder cannot combust rapidly at the top dead center, the afterburning and specific fuel consumption is increased, while exhaust temperature is just increased in a low range. It can be seen that postponing injection advance angle can be adopted as an active control measures to increase exhaust temperature under the condition of low exhaust temperature increase requirement. [23-24]

Injection pressure adjustment. Exhaust temperature at different injection pressure under two conditions is showed in Figure 3. As is shown in Figure 3, with the decrease of injection pressure, exhaust temperature and BSFC (Brake specific fuel consumption) climbs gradually under both conditions. Under the condition A, the exhaust temperature is 227 °C when the injection pressure is maintained at 56 MPa, and when the injection pressure is reduced to 16MPa, the exhaust temperature rises to 241 °C, increased by 14 °C. Under the condition B, when the injection pressure is kept at 67MPa, the exhaust temperature is 256 °C, and when the injection pressure is reduced to 37MPa, the exhaust temperature rises to 281 °C, increases by 25 °C. The reason why exhaust temperature characteristics change with

injection pressure is that combustion process in diesel engine is affected by the injection pressure through influencing the spray characteristics of fuel. Different fuel injection pressure can lead to different spray penetration distance, spray particle size and uniformity of particle size. With the increase of injection pressure, the spray characteristics, the mixing effect of oil and gas and the incomplete combustion are optimized, while exhaust temperature is reduced. On the contrary, when injection pressure is decreased, the atomization effect of fuel injected into cylinder, mixing level between fuel and fresh air and combustion condition become worse, resulting in an increase in exhaust temperature. In addition, due to the uneven mixing of fuel and air, PM emission caused by inadequate oxidation is increased, and exhaust temperature is just slightly increased. [25-27].

The decrease of injection pressure can rise exhaust temperature of diesel engine. However, the subsequent deterioration of combustion effect will bring about adverse influence of higher specific fuel consumption. Under the condition A, the brake specific fuel consumption is 170.00 g/(kW*h) when injection pressure is 56 MPa. When injection pressure is reduced to 16 MPa, the brake specific fuel consumption is increased to 185.14 g/(kW*h), increased by 8.9%, which obviously has a negative impact on improvement of fuel economy of diesel engine.

In conclusion, the effect of increasing exhaust temperature by reducing injection pressure is not significant, and it needs to be at the cost of increasing PM emissions. Therefore, at present, disadvantages of reducing injection pressure are greater than its benefits, and whether it can be regarded as an effective exhaust heat management method to rise exhaust temperature characteristics of diesel engine remains to be further explored in the future.

Late post injection adjustment. Under the condition B, exhaust temperature and fuel consumption at different late post injection quantity and angle are showed in Figure 4 and Figure 5, respectively. It can be seen from the two graphs that, with the increase of the proportion of post injection quantity and angle, exhaust temperature and fuel consumption generally show an upward trend. With angle at 10 °CA, exhaust temperature increase is not significant. At 30 °CA, exhaust temperature increased from 256 °C to 342 °C, increased significantly by 33.6%. The reason is: under the circumstance that post injection angle is fixed, increase of post injection quantity will lead to decrease of main injection quantity and duration of main combustion phase. Then the post combustion period is prolonged, and exhaust temperature of diesel engine is increased. When post injection angle increases to about 40 °CA, the fuel atomization effect and combustion conditions of post-injection fuel deteriorated, large proportion of which cannot be oxidized in cylinder, resulting in a less significant increase of exhaust temperature. At even larger post injection angle, fuel combustion further deteriorates, causing less significant exhaust temperature increase. [28,29] When late post injection angle is set at about 30 °CA, the exhaust temperature increases obviously, and the fuel consumption penalty is in the medium level. Therefore, considering the exhaust temperature rise and the influence of fuel consumption comprehensively, it can be considered that the reasonable matching of late post injection angle and late post injection quantity can be used as a method to improve exhaust temperature under medium and low loads.

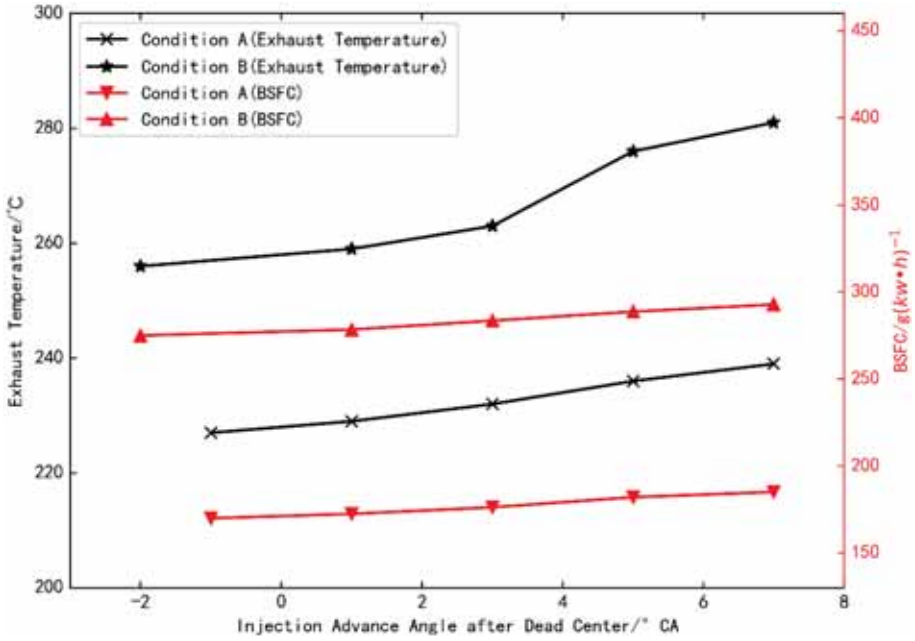

FIGURE 2
Exhaust temperature at different injection advance angle.

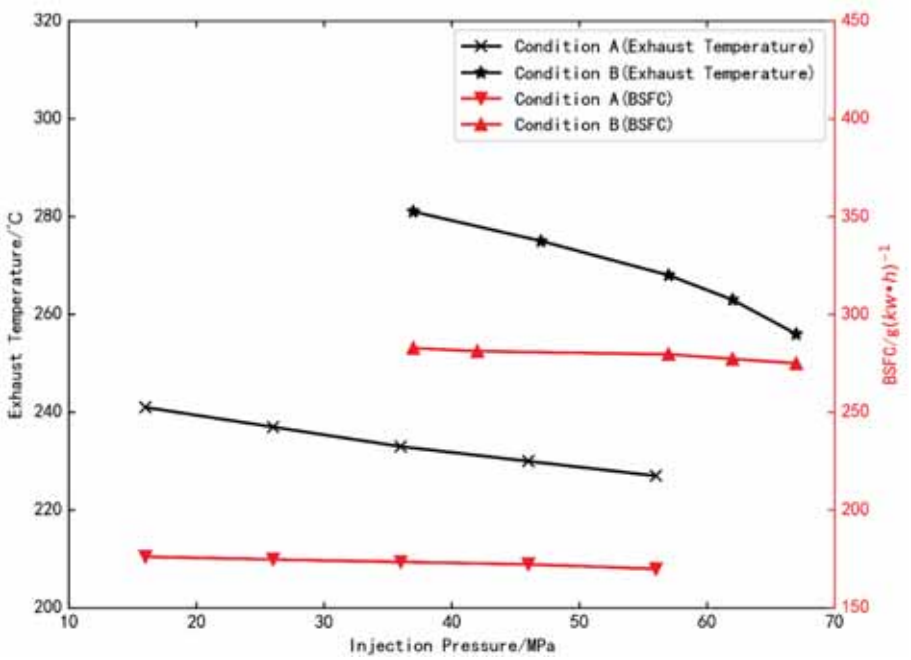

FIGURE 3
Exhaust temperature at different injection pressure.

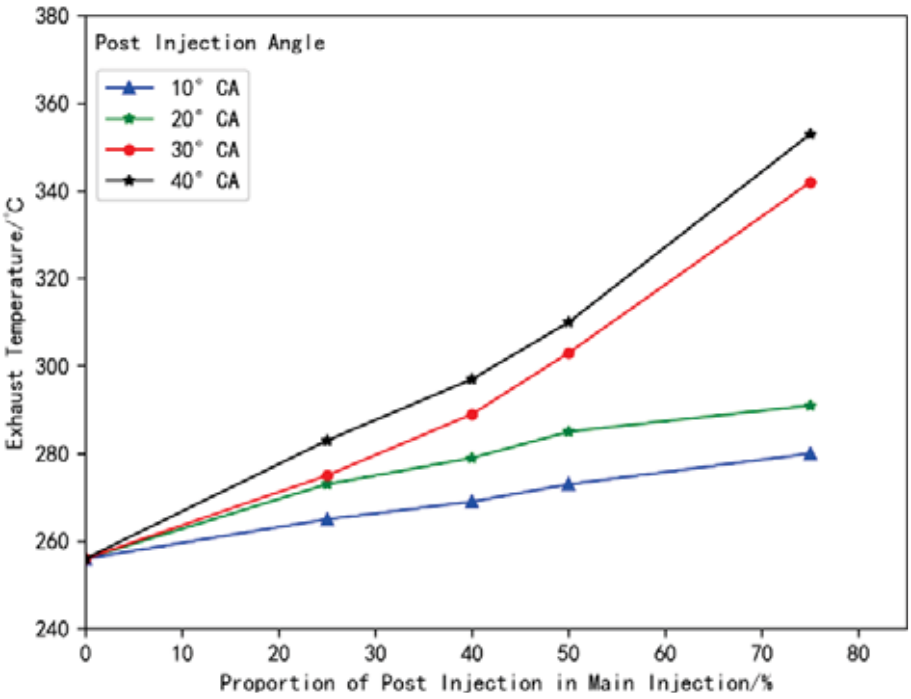

FIGURE 4
Exhaust temperature at different late post injection quantity.

Intake throttle opening adjustment. Effect of opening of intake throttle valve on exhaust temperature and emission performance of diesel engine was studied under the condition B. Intake air inflow at different intake throttle valve opening is showed in Figure 6. It can be seen from Figure 6 that the decrease of the opening of the intake throttle valve reduces the quantity of fresh air inflow through reducing effective area of intake cross-section. When the opening is reduced to less than 40%, the intake resistance is increased sharply and air inflow is decreased significantly.

According to the law of conservation of energy, if the heat generated through fuel combustion is constant, decreasing the amount of low-temperature air intake of diesel engine will increase the exhaust temperature accordingly. The main reason of exhaust temperature increase is air inflow decrease. Exhaust temperature at different intake throttle valve opening is showed in Figure 7. It can be seen from Figure 7

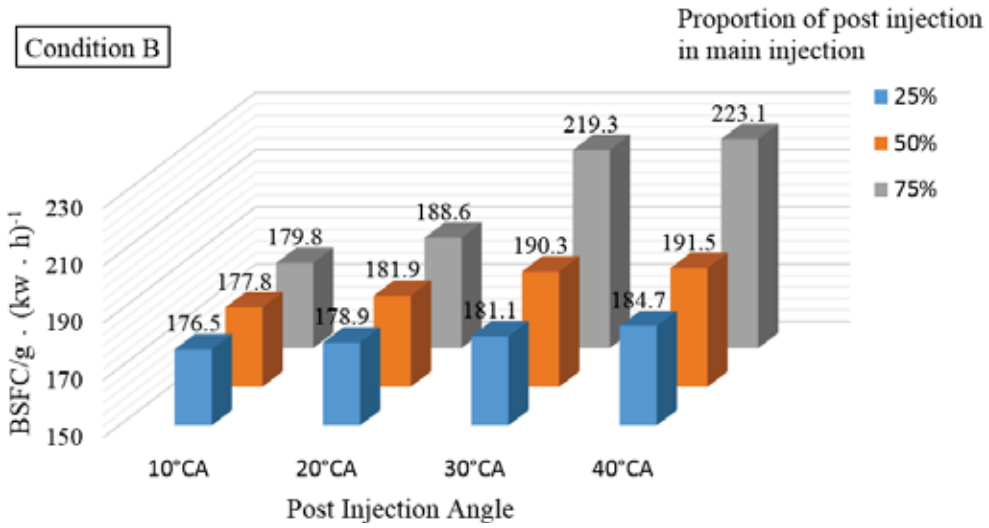

FIGURE 5
BSFC at different late post injection quantity and late post injection angle.

that as the valve opening decreases from 100% to 20%, exhaust temperature increased from 256 °C to 385 °C, increased by 51%. Therefore, reducing opening of intake throttle valve can greatly improve exhaust temperature. Generally, the excess air coefficient of diesel engine is high, especially in condition of medium and low loads and low injection quantity per cycle. The influence of intake throttle opening on fuel consumption is shown in Figure 8. The reduction of air intake changes the combustion conditions and results in the increase of fuel consumption rate, which will further increase the exhaust temperature [30-31]. In theory, the quantity of intake airflow can be reduced properly to meet the needs of improving exhaust temperature with the minimum impact on engine performance [32-33].

HC Emission at different intake throttle valve opening is showed in Figure 9. With decrease of intake throttle valve opening, a downward trend is showed in HC emission under the condition B. The HC emission mainly comes from the lean mixing area on the outer edge of fuel injection. The decrease of the opening of the intake throttle valve reduces the intake volume, prolongs the ignition delay period, and protracts the mixing time of the fuel and gas, which helps to reduce the amount of lean mixture in cylinder. In addition, the increase of average temperature in cylinder reduces the probability of misfire, resulting that the amount of HC production is decreased with the decrease of air intake.

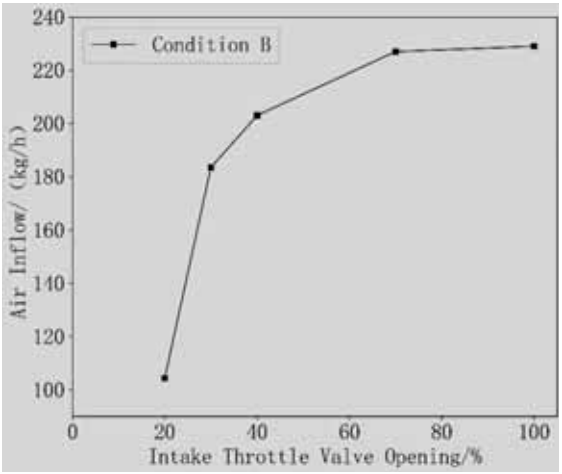

FIGURE 6
Intake air inflow at different intake throttle valve opening.

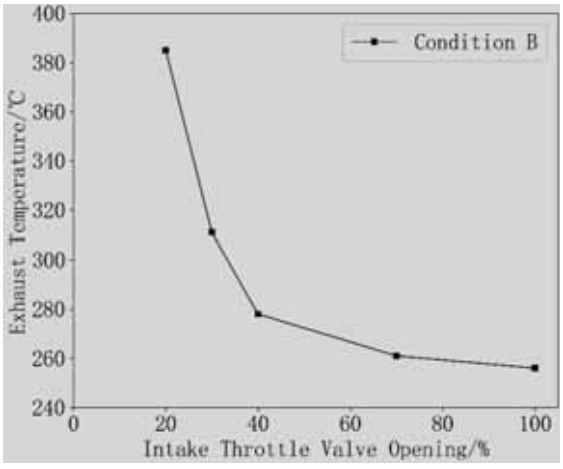

FIGURE 7
Exhaust temperature at different intake throttle valve opening.

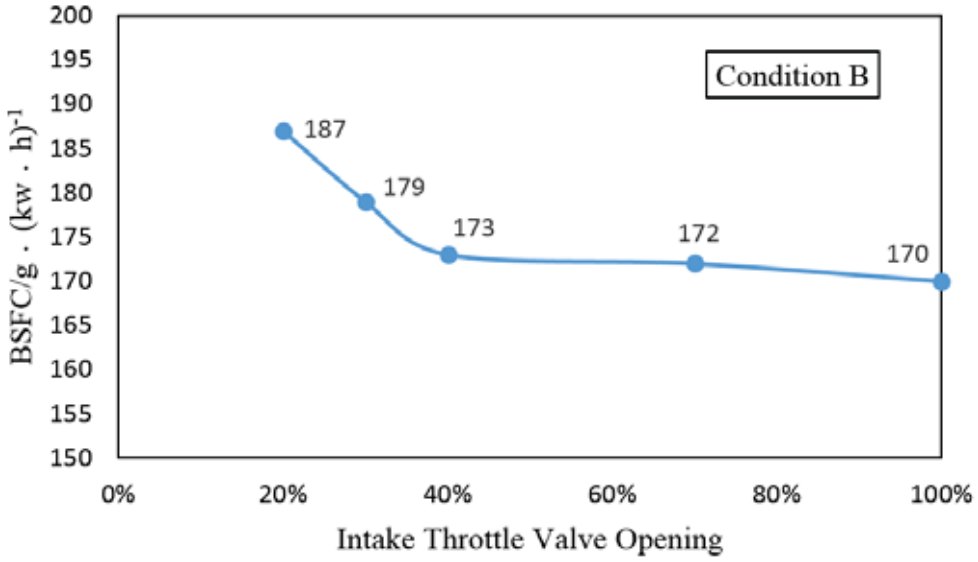

FIGURE 8
BSFC at different intake throttle valve opening.

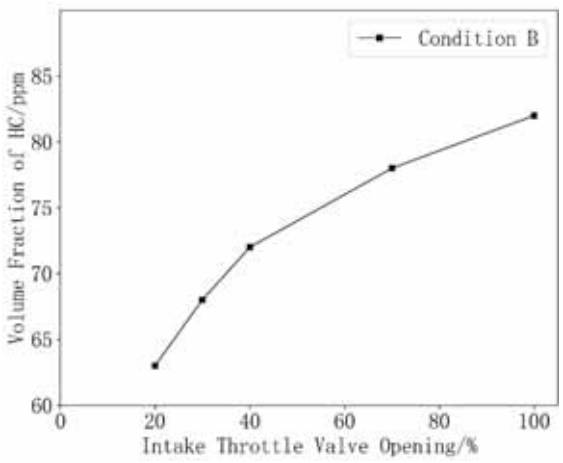

FIGURE 9
HC Emission at different intake throttle valve opening.

CO Emission at different intake throttle valve opening are showed in Figure 10. It can be seen from Figure 10 that CO emission is increased with the decrease of intake throttle valve opening. The specific performance is: when the throttle valve opening is reduced from 100% to 20%, the CO emission is increased by 78 ppm, with an increase of 48%. When the opening of the throttle valve is reduced to 20%, the coefficient of excess air in the cylinder is lower, so the region of concentrated mixture in cylinder is increased, and the probability of incomplete combustion caused by partial oxygen insufficiency is increased.

CONCLUSIONS

Based on the demand of energy conservation and environmental protection, effect of thermal management methods on exhaust temperature characteristics and emission performance of diesel engine were studied via engine bench test. Different control methods, including injection advance angle, injection pressure, late post injection and intake throttle, were taken into account. The results of steady experiment under medium and low loads conditions show that:

(1) Injection parameter adjustment can affect exhaust temperature with only limited amount. Reduced injection pressure will lead to inhomogeneous mixing effect, which has a negative effect on the normal operation of diesel engine.

(2) Exhaust temperature of diesel engine under medium and low loads can be greatly increased by proper matching of the late post injection angle and quantity, and the late post injection angle affects exhaust temperature more significantly at about 30 °CA.

(3) Reducing throttle valve opening can significantly reduce air inflow and improve exhaust temperature. However, decrease throttle valve opening will affect the stability diesel engine operation, and even result in engine's misfire.

(4) Injection parameter adjustment is not recommended as a major method for the increase and management of exhaust temperature. It is rational to adjust the late post injection angle and quantity and regard this thermal management method as a method to improve exhaust temperature under conditions of medium and low loads. Selecting the appropriate opening of throttle valve can be an effective thermal management method to rise exhaust temperature of diesel engine.

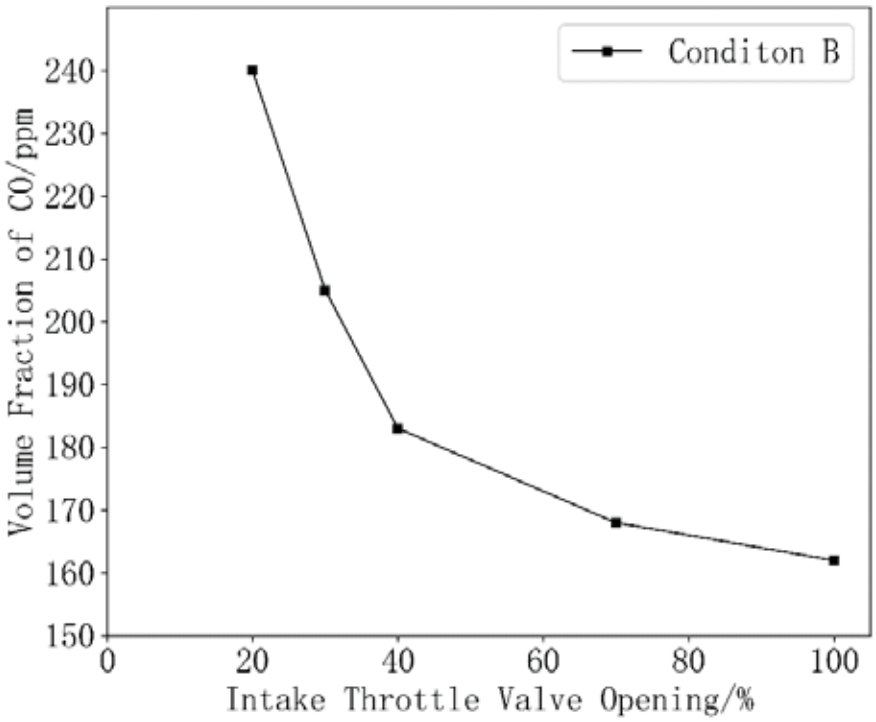

FIGURE 10
CO Emission at different intake throttle valve opening.

ACKNOWLEDGEMENT

This work was supported by the Ministry of Education of the People's Republic of China [grant numbers NELMS2017A09]. Moreover, thanks for reviewers' constructive and detailed critique contributed to the quality of this paper. Besides, I would like to appreciate the contribution of my team members, and the love and caring from my family.

REFERENCES

[1] Joshi, A. (2020) Review of vehicle engine efficiency and emissions. SAE International Journal of Advances and Current Practices in Mobility. 2(5), 2479-2507.

[2] Abu-Jrai, A., Yamin, J., Al-Muhtaseb, A., and Hararah, M. (2011) Combustion characteristics and engine emissions of a diesel engine fueled with diesel and treated waste cooking oil blends. Chemical Engineering Journal. 172(1), 129-136.

[3] Rathnaraj, J., Raja Bose, B., and Kumar, M. (2006) Simulation and experimental investigation of variable swirl intake port in DI diesel engine using CFD. Proceedings of the ASME 2006 2nd Joint U.S.-European Fluids Engineering Summer Meeting Collocated With the 14th International Conference on Nuclear Engineering. Volume 1: Symposia, Parts A and B. 17-20 July, 2006, Miami, Florida, USA.

[4] De Serio, D., de Oliveira, A., and Sodré, J. (2017) Effects of EGR rate on performance and emissions of a diesel power generator fueled by B7. Journal of the Brazilian Society of Mechanical Sciences and Engineering. 39(6), 1919-1927.

[5] Liang, J., Song, Z., and Zhang, P. (2019) An experimental study on fuel combustion under external irradiance. Fluid Dynamics & Materials Processing. 15(4), 445-458.

[6] Mousavi, S., Yousefi, T., and Saghir, Z. (2017) Experimental investigation on thermal diffusion in ternary hydrocarbon mixtures. Fluid Dynamics & Materials Processing. 13(4), 213-220.

[7] Honardar, S., Busch, H., Schnorbus, T., Severin, C., Kolbeck, A., and Korfer, T. (2011) Exhaust temperature management for diesel engines assessment of engine concepts and calibration strategies with regard to fuel penalty. 10th International Conference on Engines & Vehicles. 11-15 September, 2011, Capri, Napoli, Italy.

[8] Yamamoto, K., and Sakai, T. (2015) Simulation of continuously regenerating trap with catalyzed DPF. Catalysis Today. 242, 357-362.

[9] Basaran, H., and Ozsoysal, O. (2017) Effects of application of variable valve timing on the exhaust gas temperature improvement in a low-loaded diesel engine. Applied Thermal Engineering. 122, 758-767.

[10] Sun, K., Li, D., Liu, H. and Bai, S. (2020) Influence of diesel engine intake throttle and late post injection process on the rise of temperature in the diesel oxidation catalyst. Fluid Dynamics & Materials Processing. 16(3), 573-584.
[11] Liu, Y., Ge, Y., Tan, J., and Li, N. (2019) Experimental study on temperature characteristics of DPF active regeneration. Internal Combustion Engine & Powerplant. 36(2), 1-6. (in Chinese)
[12] Ramesh, A., Gosala, D., Allen, C., Joshi, M., McCarthy Jr, J., Farrell, L., Koeberlein, E., and Shaver, G. (2018) Cylinder deactivation for increased engine efficiency and aftertreatment thermal management in diesel engines. SAE Technical Paper. 2018-01-0384.
[13] Ding, C., Roberts, L., Fain, D., Ramesh, A., Shaver, G., McCarthy Jr, J., Ruth, M., Koeberlein, E., Holloway, E., and Nielsen, D. (2016) Fuel efficient exhaust thermal management for compression ignition engines during idle via cylinder deactivation and flexible valve actuation. International Journal of Engine Research. 17(6), 619-630.
[14] Gosala, D., Ramesh, A., Allen, C., Joshi, M., Taylor, A., Van Voorhis, M., Shaver, G., Farrell, L., Koeberlein, E., McCarthy Jr, J., and Stretch, D. (2018) Diesel engine aftertreatment warm-up through early exhaust valve opening and internal exhaust gas recirculation during idle operation. International Journal of Engine Research. 19(7), 758-773.
[15] Roberts, L., Magee, M., Shaver, G., Garg, A., McCarthy, J., Koeberlein, E., Holloway, E., Shute, R., Koeberlein, D., and Nielsen, D. (2015) Modeling the impact of early exhaust valve opening on exhaust aftertreatment thermal management and efficiency for compression ignition engines. International Journal of Engine Research. 16(6), 773-794.
[16] Li, Y., Gao, F., Wang, Q., Liu, H., and Huang, S. (2019) Research on control strategy of DOC-aided DPF system for china VI heavy-duty diesel emission regulation based on model. Auto Electric Parts. (10), 41-44. (in Chinese)
[17] Basaran, H. (2020) Utilizing exhaust valve opening modulation for fast warm-up of exhaust after-treatment systems on highway diesel vehicles. International Journal of Automotive Science and Technology. 4(1), 10-22.
[18] Basaran, H., and Ozsoysal, O. (2017) Effects of application of variable valve timing on the exhaust gas temperature improvement in a low-loaded diesel engine. Applied Thermal Engineering. 122, 758-767.
[19] Deppenkemper, K., Schoenen, M. and Koetter, M. (2019) Super ultra-low NOx emissions under extended RDE conditions - evaluation of light-off strategies of advanced diesel exhaust aftertreatment systems. SAE Technical Paper. 2019-01-0742.
[20] Ramesh, A., Shaver, G., Allen, C., Nayyar, S., Gosala, D., Caicedo Parra, D., Koeberlein, E., McCarthy Jr, J., and Nielsen, D. (2017) Utilizing low airflow strategies, including cylinder deactivation, to improve fuel efficiency and aftertreatment thermal management. International Journal of Engine Research. 18(10), 1005-1016.
[21] Zhang, P. (2017) The effect of late-post-injection strategy on the exhaust temperature and emission of diesel engine. Tianjin: Tianjin University. (Dissertation) (in Chinese)
[22] Bermúdez, V., Serrano, J., Piqueras, P., and García-Afonso, O. (2013) Analysis of heavy-duty turbocharged diesel engine response under cold transient operation with a pre-turbo after-treatment exhaust manifold configuration. International Journal of Engine Research. 14(4), 341-353.
[23] Jiang, W., Zhang, Y., Li, H., Wang, J., Li, M., and Ding, C. (2020) Experimental research on the pilot injection timing effect of combustion and emission of diesel engine. Internal Combustion Engine & Powerplant. 37(2), 7-11. (in Chinese)
[24] Zhou, L., Yang, K., Liu, Z., Wang, Y., and Chi, M. (2019) Simulation of the effect of fuel injection rate that matches fuel injection advanced angle on the performance of ultra high pressure common rail diesel engine. Journal of Northwestern Polytechnical University. 37(2), 417-423. (in Chinese)
[25] Peng, H. (2015) Study on the formation and combustion of high pressure common rail diesel engine. Mechanical & Electrical Engineering Technology. 44(12), 69-71. (in Chinese)
[26] Benajes, J., Molina, S., De Rudder, K., and Rente, T. (2006) Influence of injection rate shaping on combustion and emissions for a medium duty diesel engine. Journal of Mechanical Science and Technology. 20(9), 1436-1448.
[27] Chen, H., Ouyang, G., and Huang, K. (2012) Research on characteristics of combustion and emissions of augment HP common-rail diesel engine. Chinese Internal Combustion Engine Engineering. 33(6), 39-44. (in Chinese)
[28] Xu, R. (2018) Research on the regeneration technology of post injection of catalytic diesel particle filter. Hefei: Hefei University of Technology. (Dissertation) (in Chinese)
[29] Zhang, Z., and Zhong, K. (2019) Analysis of method to increase diesel engine exhaust temperature. Internal Combustion Engine & Powerplant. 36(4), 15-19. (in Chinese)

[30] Guan, W., Zhao, H., Ban, Z., and Lin, T. (2019) Exploring alternative combustion control strategies for low-load exhaust gas temperature management of a heavy-duty diesel engine. International Journal of Engine Research. 20(4), 381-392.
[31] Xu, X. (2019) Study of heating control strategy for DPF active regeneration based on exhaust thermal management. Zhengjiang: Jiangsu University. (Dissertation) (in Chinese)
[32] Yao, G., Zhao, G., Deng, C., and Liu, H. (2016) An experimental study on the effects of intake throttling on diesel engine performance. Automotive Engineering. 38(5), 521-525. (in Chinese)
[33] Garg, A., Magee, M., Ding, C., Roberts, L., Shaver, G., Koeberlein, E., Shute, R., Koeberlein, D., McCarthy Jr, J., and Nielsen, D. (2016) Fuel-efficient exhaust thermal management using cylinder throttling via intake valve closing timing modulation. Proceedings of the Institution of Mechanical Engineers, Part D: Journal of Automobile Engineering. 230(4), 470-478.

Received: **05.12.2020**
Accepted: **03.02.2021**

CORRESPONDING AUTHOR

Shuzhan Bai
School of Energy and Power Engineering,
Shandong University,
Jinan 250061 – China

e-mail: baishuzhan@sdu.edu.cn

© by PSP Volume 30– No. 05/2021 pages 5254-5261 Fresenius Environmental Bulletin

EVALUATION OF CARBONIFEROUS-PERMIAN HYDROCARBON SOURCE ROCKS IN HUANGHUA SAG, BOHAI BAY BASIN, CHINA

Yun Zhao, Tao Li*

School of Geosciences, Yangtze University, Wuhan, Hubei, 430100, China

ABSTRACT

The Huanghua Sag is located in the northern part of the Bohai Bay Basin and is a Mesozoic rift basin developed on the North China platform. Carboniferous source rocks are developed in the Huanghua Sag. The basin has experienced multiple stages of complex tectonics, and uneven uplifts and deformations have appeared in the basin. In addition, magma ejection is also developed in this area. The hydrocarbon generation evolution of the source rocks in the Huanghua Sag has the characteristics of discontinuity and grade differences. In this paper, based on the detailed study of structural history, we have conducted a systematic study on the burial history, heating history and hydrocarbon generation history of source rocks in the Huanghua Sag. At the same time, the EASY%R_o numerical simulation method was used for the apatite fission track (AFT) test and fluid inclusion analysis. The results show that the maturity of source rocks gradually develops with the generation of hydrocarbons. Combined with tectonic events, we discussed the intensity and time distribution of hydrocarbon generation of the source rocks. The hydrocarbon generation analysis of the source rock shows that the Huanghua Sag occurred continuous subsidence in the late Cenozoic. In the end, we proposed the co-production of Permian-Carboniferous unconventional natural gas in the central-northern area of the Huanghua Sag in the Bohai Bay Basin.

KEYWORDS:
Permian-Carboniferous, source rock, burial history, thermal history, hydrocarbon generation, EASY% RO numerical simulation

INTRODUCTION

The Bohai Bay Basin is the largest petroliferous basin in China [1]. The study area is located in the Huanghua Sag, which is developed on the Paleozoic Craton Basin of North China and located in the central area of the Bohai Bay Basin. It is a faulted basin in a Cenozoic rift basin with an area of 17 000 km^2. The area extends from the Cangxian Uplift in the west, the Yanshan Structural Belt in the north, and the Chengning Uplift in the southeast (Figure 1). Therefore, it has a wedge-shaped distribution in the SSE-NNW direction. This area is considered to be an asymmetric rift basin controlled by faults [2-3].

The Huanghua Sag is an oil-rich basin in northeast China. Since the 1950s, the Dagang Oilfield has achieved great success in the shallow petroleum exploration of the Cenozoic in the Huanghua Sag, but there have been few breakthroughs in the deep fields. The Permian-Carboniferous is an important area of oil and gas distribution in the world. Some studies focus on the thermal simulation of hydrocarbon generation in the Carboniferous-Permian. These studies use fluid-rock interaction to predict oil and gas distribution [4-6].

In recent years, with the continuous development and reduction of shallow oil and gas reservoirs, the exploration prospects and potential problems of Permian-Carboniferous oil and gas have attracted more and more attention. Paleozoic crude oil was discovered in the Kg_3 and Kg_4 wells in the deep zone of the Huanghua Sag, which led to the study of the Paleozoic geological conditions in the deep zone of the Bohai Bay Basin [7-8].

There are mainly three types of source rocks in the Huanghua Sag, that is, the thicker Mesozoic-Cenozoic covers the Benxi Formation of the Upper Carboniferous, the Taiyuan Formation of the Upper Carboniferous and the Shanxi Formation of the Lower Permian [9-10]. The source rock in the basin has experienced a complicated structural evolution history, which can be divided into four structural stages: (1) Hercynian-Indosinian stable subsidence stage; (2) Yanshan rift stage, with a series of northwest-trending faulted basins (3) The Himalayan movement stage at the end of the Eocene, that is, an exposed rift basin; (4) The rift stage of the Himalayan movement stage. Therefore, the current tectonic style is an integrated phenomenon composed of tectonic activities in different periods, types, and directions.

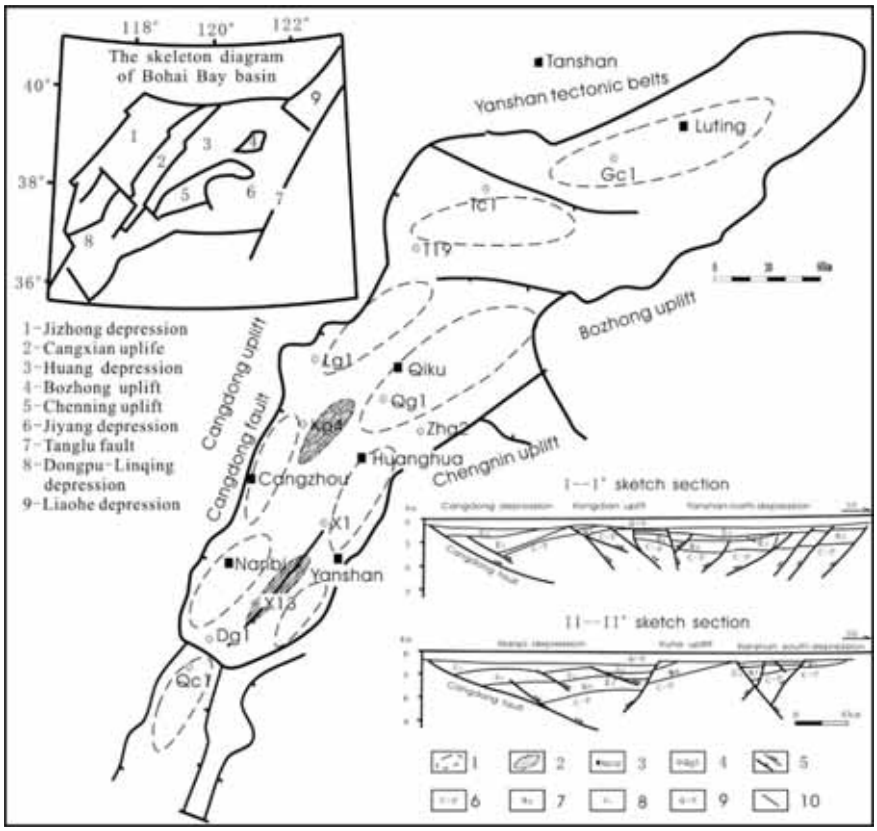

FIGURE 1
Structural distribution of the study area.

EXPERIMENTS AND METHODS

Characteristics of source rocks. The main deposits in the Permian Carboniferous are about 1 000 m thick and are divided into six groups from top to bottom, namely the Upper Carboniferous Benxi and Taiyuan Formations, Shanxi Formation, Lower Shihezi Formation, Upper Shihezi Formation and Shiqianfeng Formation. The coal-measure strata are mainly composed of Benxi Formation, Taiyuan Formation and Shanxi Formation, with a thickness of about 200 m to 300 m, which is considered to be the main source rock in Huanghua Sag. Through organic petrography analysis, organic micro-components are mainly exposed in the form of vitreous iron (Figure 2). It mainly contains type III (prone to gas) humus kerogen deposited as terrestrial marine interlayer coal-bearing clastic rocks.

The total organic carbon (TOC) values of 16 samples in the Shanxi group ranged from 0.14% to 4.7%, with an average of 2.16%, and an average of S_2 of 1.15 mg/g. The TOC values of 23 samples in the Taiyuan group ranged from 0.18% to 4.98%, with an average value of 2.5%, and an average value of S_2 of 2.21 mg/g. The 14 samples from the Benxi group had TOC values ranging from 0.06% to 4.46%, with an average of 1.64%, and an average of S_2 of 1.09 mg/g. The coal measures include coal seams with a thickness of 50 m to 60 m and dark mudstones with a thickness of 100 m to 170 m.

Burial history of source rocks. Because the source rocks were formed in the Paleozoic, and the

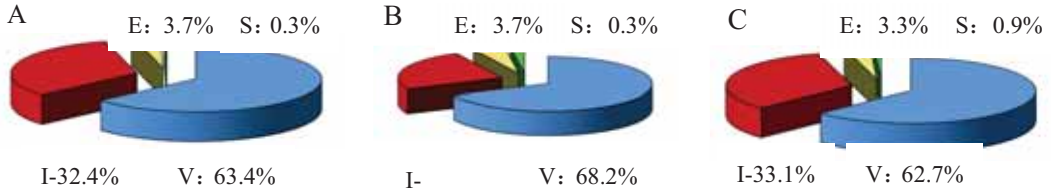

FIGURE 2
Organic composition of Permian-Carboniferous source rocks.
Notes: A-Benxi Formation; B-Taiyuan Formation; C-Shanxi Formation; V-vitrine group; I-inert group; E-chitin group; S-saprolite group.

Huanghua Sag experienced several tectonic activities from the Triassic to the Tertiary (primitive state), this led to multiple hydrocarbon generation and evolution of organic matter from the Permian to Carboniferous [11-12]. The analysis of tectonic sedimentary history shows that the burial history of the source rocks in the Huanghua Sag mainly experienced three alternate evolutionary deposition-uplift cycles: Indosinian, Himalayan and Yanshanian.

AFT thermal evolution analysis. AFT analysis has been widely used to study the thermal evolution of sedimentary basins [13-16]. Fission track annealing of apatite is mainly controlled by temperature, chemical composition of apatite and heating time. In the study, three sandstone cores (Permian Gg1-1 samples; Jurassic Kg3 and Dg1 samples) from three wells were analyzed for fission tracks. Apatite is extracted from the core using standard heavy liquid and magnetic separation techniques. In addition, the samples are tested using an external detector method to obtain track life and track length. Table 1 summarizes the fission tracks, track lengths and related errors of the three samples in Huanghua Sag.

Inversion of EASY% vitrinite reflectance. Vitrinite reflectance is the most widely used parameter to quantitatively evaluate the thermal maturity of sedimentary rocks [17-21]. Studies have shown that the reflectivity of the vitrinite of deposited organic matter is functionally related to its heating time and heating temperature [22-23]. Using the vitrinite reflection of the source rock to determine the heating time is one of the keys to determining the inverse heating temperature [24]. Many geologists have conducted extensive studies on the use of vitrinite reflectivity to restore ancient geothermal fields [25-26]. In this paper, by carrying out experiments on organic fluid inclusions in calcite needle-like zeolite in Huanghua Sag, the temperature parameters of the reflectance inversion in Huanghua Sag are obtained (Table 2).

RESULTS

The mature evolution history of source rocks. The heating process of the source rock affects its hydrocarbon generation history. Based on this, the heating history and mature evolution of the Permian-Carboniferous can be reconstructed. This is the key to accurately assessing the hydrocarbon resources of the Huanghua Sag [27-28]. However, in many cases, factors such as crustal subsidence, folds or uplifts, and erosion will cause the

TABLE 1
Experimental results of fission track of apatite in Huanghua Sag.

Well	Depth (m)	Quantity	ρ_s	ρ_I	Age(Ma)	Track length (μm)	Length correction (μm)
Kg3	3297	13	0.42 (36)	18.34 (1588)	11.7±4.9	6.8±1.4(26)	6.6±1.3(26)
Dg1	1605	9	11.24 (830)	25.17 (1855)	123.9±12.9	11.9±2(103)	11.5±2.1(103)
Gg1-1	1778	14	10.90 (801)	30.20 (2220)	87.9±2.2	11±2.1(108)	10±2.2(108)

TABLE 2
Characteristics of organic fluid inclusions in calcite needle-like zeolite in Huanghua Sag.

Well	Depth (m)	Size(μm)	Shape	Gas-liquid ratio	Phase number	Failure temperature
Qg1(O)	4 012	4~7	Ellipse	5-10%	two	126 (10)
	4 101	5~15	Ellipse	10-15%	two	118 (4)
	4 195	5~15	Square	10-15%	two	213 (6)
Kg3(O)	3 408	10±	Oblong	5-15%	two	167 (4)
	3 415	2~5	Ellipse	-	single	-
Kg4(C)	3 811	5~10	Ellipse	5-15%	two	186 (4)
GG1-1(O)	2 220	10~15	Ellipse	10-30%	two	141 (2)
Bg1(O)	2 004	10±	Ellipse	5-10%	two	128 (11)

TABLE 3
Hydrocarbon generation evolution of EASY%R_o Kg4 source rock (bottom of Taiyuan Formation, Ro=0.92).

Evolution stage	Thermal history (Ma)	Temperature (°C)	R_o (%)	Hydrocarbon generation stage
Indosinian	0.00	15.00	0.22	-
	21.30	20.80	0.28	
	51.30	26.80	0.30	
	66.30	47.85	0.34	
	81.30	86.10	0.51	Primary hydrocarbon generation
Yanshanian	103.30	32.30	0.52	-
	154.30	52.20	0.52	
	214.30	112.60	0.74	Secondary hydrocarbon generation
Early Himalayas	246.30	42.90	0.76	-
	265.80	71.50	0.76	
	275.30	87.00	0.76	
	288.00	81.70	0.76	
Late Himalayas	308.46	132.30	0.86	Last hydrocarbon generation
	311.30	136.50	0.92	

source rock's burial conditions to alternate and its heating temperature to increase [29-31]. The heating temperature difference between ancient and modern organic matter leads to unconformity of their maturation and evolution, leading to changes in the evolution of organic hydrocarbons, and it affects the evaluation of oil and gas resources.

In order to study the maturity evolution process of the entire Huanghua Sag, we dissected the test data of dozens of wells. On the basis of detailed study of structural burial history, combined with fission track test and fluid inclusion analysis, the organic maturity of source rocks in Huanghua Sag is derived using EASY%Ro numerical simulation. Table 3 shows the results of numerical simulation using EASY%R_o in well Kg4.

The results show that the maximum heating temperature of Indo-Himalayan source rocks has been increasing, which has led to a gradual increase in organic maturity (Figure 3). In this process, there are three large phase increments in the maturity of organic matter.

The first stage occurred during the Indian Ocean era, when source rocks were buried for the first time. At that time, the tectonic activity of the North China platform in North China was weak, and the crust mainly showed up and down movement. The analysis of fluid inclusions shows that the paleogeothermal flow is normal (about 3.0~3.3℃/100 m) [32-33]. The maturity period increases continuously, which is mainly controlled by the Early-Middle Triassic sediments. Studies have shown that the thickness of the Triassic in the Huanghua Sag is between 900 m and 1 400 m [34], so the deepest buried depth of the source rock does not reach 2 500 m. At the end stage, the vitrinite reflectance of the source rock does not exceed 0.7% R_o, and the organic matter belongs to the early stage of maturity in the Huanghua Sag (Figure 4A).

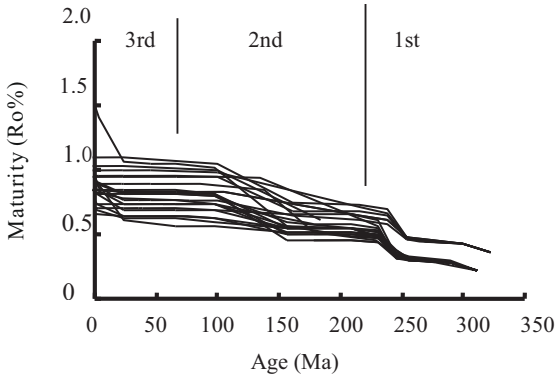

FIGURE 3
Maturity evolution curves of Taiyuan Formation in Huanghua Sag.

The second stage occurred in the Yanshan period, which corresponds to the second mature evolution of organic matter in coal measures. The structural control of the extension zone may be the subduction of the Pacific plate relative to the eastern edge of Asia. The style of the late Mesozoic structure along the edge of East Asia is related to the speed of the Pacific plate relative to the Asian plate [35]. The results show that the magmatic activity in the study area is extensive, and the paleothermal fluid is obviously abnormal. The geothermal gradient is as high as 6-7℃/100 m [21, 33-37], and the maturity of source rocks has been improved. Although the temperature conditions are relatively high, the burial depth of the source rocks is relatively shallow. The maturity of source rocks has been improved to a certain extent, but the maxi

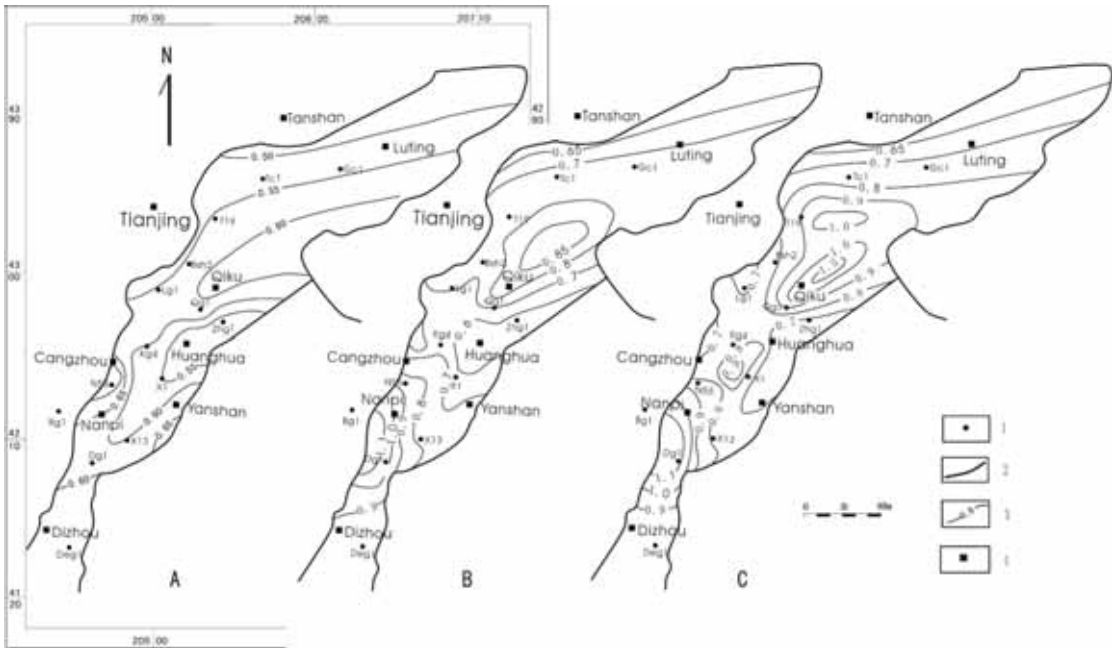

FIGURE 4
Sedimentary evolution of source rocks in Huanghua Sag.

Notes: A-Indosinian period; B-Yanshan period; C-Himalayan period. 1- well; 2- boundary; 3- source rock maturity contour (%); 4- city.

mum value does not exceed 1.1% R_o. Because the burial depth is very uneven, the maturity is exposed at different stages. The overall trend shows that the maturity of the southern part of Huanghua Sag is higher than that of the northern part. The maximum maturity in Huanghua Sag is greater than 1.1% R_o (Figure 4B).

The third stage occurred in the Himalayas. The Huanghua Sag experienced rifts in the early Tertiary and late thermal sedimentary periods from Tertiary to Quaternary. During the rifting period, the source rocks in the basalt eruptive sediments of the Huanghua Sag were buried again by the Upper Tertiary lake deposits. The ancient geothermal gradient is slightly higher, about 3.5℃/100 m. From the Tertiary to the Quaternary, the source rocks were greatly increased, especially in the northern part of the Huanghua Depression, the organic matter maturity increased significantly. The maturity is higher in the northern part of Huanghua Sag and lower in the southern part (Figure 4C).

Joint exploration of unconventional natural gas in coal measures. With sufficient gas sources and proper spatial superimposition, the coal measures in the basin are considered to be reservoirs with good exploration prospects (Figure 5).

Typical wells show that unconventional gas reservoirs can be divided into three types of secondary gas reservoirs and five types of gas reservoir combinations. According to the drainage and production theory, each type of gas reservoir combination is guided by a hydraulic fracturing matching plan suitable for its geological structure combination, thereby avoiding fracturing interference.

CONCLUSIONS

(1) In this paper, based on the detailed study of structural history, we have conducted a systematic study on the burial history, heating history and hydrocarbon generation history of source rocks in the Huanghua Sag. At the same time, the EASY%R_o numerical simulation method was used for the apatite fission track (AFT) test and fluid inclusion analysis.

(2) The Permian-Carboniferous coal measures in the Huanghua Depression have experienced a complicated structural burial history, which can be divided into three burial processes, namely, the Hercynian, Indosinian, Yanshanian and Late Himalayas. In the late Himalayas, the source rock reached the maximum burial depth, which is of great significance to the hydrocarbon generation of the source rocks.

(3) Combining fluid inclusions and Easy%R_o numerical simulation, the heating temperature of the source rock has been maintained at a high disconnection state, which leads to a gradual increase in maturity. The matu

FIGURE 5
Coexistence of various layers of source rocks in Huanghua Sag.

ration and evolution of source rocks are divided into three stages, which belong to the Indosinian, Yanshanian and Himalayan stages, and the Himalayas are subdivided into early and late stages. In most areas, especially in the north-central part of the Huanghua Sag, the late Himalayan period determined the maximum heating temperature of source rocks.

ACKNOWLEDGEMENTS

This work was not supported by any funds. We want to thank all the techniques who have contributed to this research.

REFERENCES

[1] Marra, F., Destro, E., Nikolopoulos, E., Zoccatelli, D., Borga, M. (2017) Impact of rainfall spatial aggregation on the identification of debris flow occurrence thresholds. Hydrology and Earth System Sciences. 21(9), 4525-4532.

[2] Ou, C., He, S., Xu, Q. (2015) Maccormack-tvd finite difference solution for dam break hydraulics over erodible sediment beds (vol 141, 2015). Journal Of Hydraulic Engineering. 141(5), 126-140.

[3] Ou, C., Zhou, K., Xu, Q., Yin, J., Peng, D., Wang, D. (2017) Dynamic analysis and numerical modeling of the 2015 catastrophic landslide of the construction waste landfill at Guangming, Shenzhen, China. Landslides. 14(2), 705-718.

[4] Zhang, S., Zhang, L. (2017) Impact of the 2008 wenchuan earthquake in china on subsequent long-term debris flow activities in the epicentral area. Geomorphology. 276, 86-103.

[5] Lanzoni, S., Gregoretti, C., Stancanelli, L. (2017) Coarse-grained debris flow dynamics on erodible beds. Journal of Geophysical Research: Earth Surface. 122(3), 592-614.

[6] Cama, M., Lombardo, L., Conoscenti, C., Rotigliano, E. (2017) Improving transferability strategies for debris flow susceptibility assessment: application to the saponara and itala catchments (messina, Italy). Geomorphology. 288, 52-65.

[7] Song, D., Ng, C., Choi, C., Zhou, G., Kwan, J., Koo, R. (2017) Influence of debris flow solid fraction on rigid barrier impact. Canadian Geotechnical Journal. 2016(0502), 985-1020.
[8] Albrecht, V., Turowski, J., Mcardell, B., Dieter, R., Hürlimann, S. (2017) Debrisintermixing-2.3: a finite volume solver for three-dimensional debris-flow simulations with two calibration parameters – part 2: model validation with experiments. Geoscientific Model Development. 10(11), 3963-3978.
[9] Marco C., Stefano C., Sebastiano T., Lorenzo M. (2017) Gis tools for preliminary debris-flow assessment at regional scale. Journal of Mountain Science. (12), 129-141.
[10] Morozov, V., Jin, Z., Liang, X., Korolev, E., Liu, Q., Kolchugin, A., Eskin, A., Nizamova, A., Assumption, B., Liu, G. (2021) Comparison of source rocks from the Lower Silurian Longmaxi Formation in the Yangzi Platform and the Upper Devonian Semiluksk Formation in East European Platform. Energy Geoscience. 2(1), 63-72.
[11] Iverson, R., Ou, C. (2015) Entrainment of bed material by earth‐surface mass flows: review and reformulation of depth‐integrated theory. Reviews of Geophysics. 53(1), 756-773.
[12] Pan, H, Niu, Y, Wang, W. (2004) Logging data extraction of Chinese mainland scientific drilling ppi pore rock properties. Journal of Engineering Geophysics. 1(1), 10-16.
[13] Tao, H, Cheng, R, Zhao, X, Sun, F, Yu, Z. (2011) Logging response and application of volcanic clastic rocks in Hailaer Basin. Chinese Journal of Geophysics. 54(2), 534-544.
[14] Li, L. (2018) Well Logging Response Mechanism and Lithology Identification of XingmaArchean Buried Hill in Liaohe Basin. China Petroleum and Chemical Industry Standards and Quality. 38(3), 103-104.
[15] Wang, J, Shun L, Liu, H, Song, Y. (2008) Identification of the igneous rock reservoir fracture by well logging. Journal of Southwest Petroleum University.
[16] Wu, T., Li, L., Li, W., Gai, Y., Qiu, Y., Pan, G., Chen, L. (2021) A quantitative study on source rocks in the western Leidong Depression, northern South China Sea. Energy Geoscience. 2(1), 73-82.
[17] Ou, C., He, S., Xu, Q., Luo, Y., Zhang, W. (2013) A maccormack-TVD finite difference method to simulate the mass flow in mountainous terrain with variable computational domain. Computers & Geosciences. 52, 1-10.
[18] Huang, B, Pan, B. (2001) Logging response characteristics and lithology division of deep igneous rocks in the northern Songliao Basin. Petroleum Geophysical Exploration. 40(3), 42-47.
[19] Shi, Q. (1996) Research on igneous rock logging interpretation method. China Offshore Oil and Gas. (6), 402-406.
[20] Liu, Z, Wang, Z, Liu, J, Feng, Y, Qu D. (2015) Characteristics of logging curves of intermediate-based igneous rocks in the eastern sag of Liaohe Basin. Petroleum Geophysical Prospecting. 54(6), 787-795.
[21] Jing, J, Pan, H, Dong, Z. (2009) Logging response characteristics of Permian igneous rocks in Tahe area. Journal of Engineering Geophysics. 6(4), 490-493.
[22] Jiang, D, Gao, J,Guo, Q. (2009) Logging response characteristics and lithology identification of igneous rocks in Santanghu Basin. Inner Mongolia Petrochemical. 35(7), 128-130.
[23] Provenzale, A. (1999) Transport by coherent barotropic vortices. Annual Review of Fluid Mechanics. 31(1), 55-93.
[24] Coussot, P., Laigle, D., Arattano, M., Deganutti, A., Marchi, L. (1998) Direct determination of rheological characteristics of debris flow. Journal of Hydraulic Engineering. 126(2), 865-868.
[25] García, D., Machuca, S., Medina, E. (2019) Dynamic and geomorphic characterizations of the mocoa debris flow. Landslides (Springer). 16(3), 597-609.
[26] Hashimoto, H., Hirano, M. (2010) Model of deposition of grains from debris flow. Open Criminology Journal. 110(3), 9-47.
[27] Zhou, G., Hu, H., Song, D., Zhao, T., Chen, X. (2018) Experimental study on the regulation function of slit dam against debris flows. Landslides (Springer). 16(4), 75-90.
[28] Li, Y., Chao, M., Wang, Y. (2019) Landslides and debris flows caused by an extreme rainstorm on 21 july 2012 in mountains near beijing, china. Bulletin of Engineering Geology & the Environment. 78(2), 1265-1280.
[29] Ding, F., Xie, C., Zhou, X., Jiang, C., Li, K., Wan, L., Zhang, P., Niu, H. (2021) Defining stratigraphic oil and gas plays by modifying structural plays: A case study from the Xihu Sag, east China Sea Shelf Basin. Energy Geoscience. 2(1), 41-51.
[30] Zheng, L., Yu, Y., Xi, L., Cheng, L. (2017) Preliminary study on the damping effect of a lateral damping buffer under a debris flow load. Applied Sciences. 7(2), 201-210.
[31] Li, S. (2016) Logging evaluation technology of Carboniferous igneous rock in the northwestern margin of Junggar Basin. (Doctoral dissertation, China University of Petroleum (East China).

[32] Xu, F, Deng, S, Fan, Y, Cheng, X, Liu, P. (2006) Summary of progress in logging evaluation of igneous reservoirs. Progress in Exploration Geophysics. 29(4), 239-243.
[33] Yan, W. (2009) Response characteristics of dual laterolog for net-fractured igneous reservoir. Journal of Jilin University. 39(1), 158-162.
[34] Han, Y. (2017) Study on the relationship between rock type and logging response of Niuxinyi buried hill. Chemical management.24(1), 144-149.
[35] Sundberg, J, Back, P, Ericsson, L, Wrafter, J. (2009) Estimation of thermal conductivity and its spatial variability in igneous rocks from in situ density logging. International Journal of Rock Mechanics & Mining Sciences. 46(6), 1023-1028.
[36] Xu, Y., Zhang, H., Guan, Z. (2021) Dynamic Characteristics of Downhole Bit Load and Analysis of Conversion Efficiency of Drill String Vibration Energy. Energies. 14, 229.
[37] Huang, B, Pan, B. (2004) Characteristics of log responses and lithology determination of igneous rock reservoirs. Journal of Geophysics & Engineering. 1(1), 51-55.

Received: **06.12.2020**
Accepted: **31.01.2021**

CORRESPONDING AUTHOR

Tao Li
School of Geosciences,
Yangtze University,
Wuhan, Hubei 430100 – China

e-mail: ltm817@163.com

© by PSP Volume 30– No. 05/2021 pages 5262-5269 Fresenius Environmental Bulletin

ANALYSIS OF CHINA'S ENVIRONMENTAL KUZNETS CURVE FROM THE PERSPECTIVE OF PM2.5 INDEX

Yan Yue*, Yirong Ying

Shanghai University, Shanghai 200444, China

ABSTRACT

Over 30 years of extensive development has caused inevitable damage to China's environment. Finding the optimal path between environmental pollution and economic growth is of outstanding importance and urgency. This paper uses cross-sectional data and spatial econometric models of more than 100 major cities in China in 2014. Based on the extended traditional environmental Kuznets curve hypothesis, this study uses PM2.5 concentration as a proxy indicator of environmental pollution to analyze the environmental pollution spatial correlation, the shape of the environmental Kuznets curve and its influencing factors. The results show that the urban environmental pollution in China has an obvious positive spatial correlation. The environmental Kuznets curve simulated by the cross-sectional data shows an "inverted U shape", and the environmental Kuznets curve hypothesis has been confirmed at the urban scale in China. The proportion of the secondary industry, population density, car ownership, etc. are positively related to environmental pollution. The coordinated regional development, control of urban car ownership, and multi-city joint governance are conducive to the improvement of urban environmental quality.

KEYWORDS:
Environmental Kuznets curve, PM2.5, Moran index, Spatial measurement model

INTRODUCTION

Economic development will inevitably consume environmental resources. The sustainable economic development must find a win-win path between economic development and environmental quality. In the early 1990s, through the study of the environmental effects related to the North American Free Trade Agreement (NAFTA), Grossman and Krueger first examined the relationship between environmental pollution and per capita income and found that there is an "inverted U-shaped" curve relationship between them. The Environmental Kuznets Curve Hypothesis (EKC) is proposed, that is, the environmental quality level will gradually deteriorate with the economic development, and then gradually improve with the economic development [1] (Figure 1). After that, many scholars have analyzed and studied the curve [2-5]. Selden et al. [6] selected data from most developed countries in the early 1990s and proved that there is indeed an "inverted U-shaped" trend between air pollutant emissions and per capita income. Holtz-Eakin et al. [7] studied the EKC curve with CO2 emissions as a proxy indicator of environmental pollution. Kaufmann [8] collected data on SO2 emissions from thirteen developed countries and ten developing countries to study the relationship between environmental pollution and per capita income. Suri et al. [9] explain the EKC curve from the difference between developed countries and developing countries. They found that manufacturing industries with higher environmental pollutant emissions are mainly concentrated in developing countries, while high-tech industries with lower environmental pollution emissions are mainly concentrated in developed countries. Careon [10] collected the time series data of seven common air pollutants in the 50 states of the United States from the late 1980s to the early 1990s. The research results show that the amount of pollutants discharged, and the per capita income level are negatively correlated. Lindmark [11] studied the relationship between Swiss CO2 emissions and Swiss economic growth and gave the three most important factors affecting CO2 emissions. Egli [12] found that there is an "inverted U-shaped" and "N-shaped" relationship between the emissions of nitric oxide (NO) and ammonia (NH3) and German economic growth, respectively. Mazzanti et al. [13] introduced new variables into the model studied and concluded that the "inverted U-shaped" EKC curve exists in Italy.

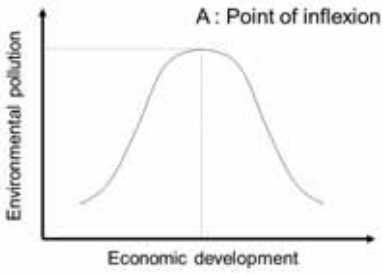

FIGURE 1
Environmental Kuznets Curve.

However, the current research still has shortcomings: First, the lack of independent variables. In the regression model, there are usually only per capita income or per capita GDP and related items without considering other variables; Second, in the selection of environmental indicators, a single environmental pollution indicator is often selected instead of a comprehensive environmental pollution indicator. At the same time, the choice of these indicators is not too close to people's daily life. Therefore, this article selects the PM2.5 concentration that people can feel every day as a proxy indicator of environmental pollution, uses spatial econometrics models to control the impact of spatial autocorrelation effects, and adds some other independent variables that affect environmental pollution to study the EKC curve at the city level in China.

MATERIALS AND METHODS

(1) Spatial measurement model theory. Spatial autocorrelation. Spatial autocorrelation refers to that if areas are close to each other, there is little difference between the values of the same variable. If the value of a variable in some neighboring areas is high or low, it is positive spatial autocorrelation, otherwise it shows the negative spatial autocorrelation [14-16]. If the distribution of high and low values is relatively uniform, there is no spatial autocorrelation. Among the methods for measuring spatial autocorrelation, the most common one should be the "Moran Index". The calculation formula is as follows [17-18]:

$$I = \frac{\sum_{i=1}^{n}\sum_{j=1}^{n}(w_{ij}(x_i-\bar{x})(x_j-\bar{x}))}{S^2\sum_{i=1}^{n}\sum_{j=1}^{n}(w_{ij})} \quad (1)$$

Where S is the sample variance. The value range of Moran index l is between 0 and 1. More than 0 indicates a positive relationship, less than 0 indicates a negative relationship, and equal to 0 indicates no spatial relationship. The larger the absolute value, the stronger the relationship. Before using the spatial measurement model, it is necessary to judge whether this set of data has the spatial dependence. If the set of data has the spatial dependence, the spatial econometric model must be used.

Spatial econometric model. Spatial econometric models can be divided into Spatial Lag Model (SLM) and Spatial Error Model (SEM).

The calculation formula of the spatial lag model is as follows [19-20]:

$$y_i = \rho\sum_{i\neq j} w_{ij}\, y_j + x_i\beta + \varepsilon_i \quad (2)$$

Among them, y_i is the dependent variable; w is the spatial weight matrix of order nxn; $\sum_{i\neq j} w_{ij}\, y_j$ is the weighted sum of dependent variables in all neighboring regions, as the spatial lag of the dependent variable, ρ is a parameter to measure the spillover effect of the dependent variable, which is also called the spatial autoregressive coefficient; x_i is the independent variable matrix of nxk, β is the parameter, reflecting the degree of influence of the independent variable on the dependent variable; ε_i is the random error term.

When the spatial dependence of the dependent variable exists in the random disturbance term, the spatial error model can be considered [21-22]:

$$y_i = x_i\beta + \mu_i \quad (3)$$

$$\mu_i = \lambda\sum_{i\neq j} w_{ij}\, y_j + \varepsilon_i \quad (4)$$

Among them, μ_i is the random error term; λ is the autoregressive coefficient of μ_i, which is used to measure the influence of the weighted sum of the error terms of the dependent variable y_i in the neighboring area $\sum_{i\neq j} w_{ij}\, y_j$ on the error term of the dependent variable y_i; ε_i is the random error term of the normal distribution.

(2) model establishment. Model research object and variable selection. This paper collected data from some major cities in China in 2014. Most of the selected cities are located on the east side of the first line of Heihe-Tengchong. These cities have big differences in terms of per capita GDP, population density, and the spatial and geographic location, which can better reflect the development status of cities in our country.

The model variables selected in this paper mainly include: (1) PM2.5 concentration (PM25), (2) per capita gross domestic product (AAGGDP), (3) car ownership (CARNUM), (4) total rainfall (RAINFALL), (5) The proportion of the secondary industry (INDUSTRY), (6) POPDENSITY, (7) Whether it is north of the Qinling Mountains and Huaihe River (ISNORTH): This indicator is treated as a dummy variable, and the city north of Qinling Mountains and Huai River is taken as 1, otherwise it is taken as 0. The Qinling-Huaihe line divides China geographically into the north and the south, and it is also a humanistic dividing line. China implements collective heating in autumn and winter, and most of the heating cities are located north of the Qinling-Huaihe line. Heating will consume a lot of energy and cause a lot of environmental pollution. This article assumes that this variable has a positive correlation with the PM2.5 concentration, that is, under the same conditions, the PM2.5 concentration in the north of the Qinling Mountains and Huai River will be higher than in the south part.

Model construction. In this paper, PM25, AVGGDP, CARNUM, RAINFALL and POPDENSITY these variables are logarithmically processed, and the following two spatial measurement models are established according to formulas (2)-(4), namely, the spatial lag model (SLM) and the spatial error Model (SEM):

Spatial Lag Model (SLM):

$$lnPM25_i = \rho \sum_{i \neq j} w_{ij}\, lnPM25_i + \beta_0 + \beta_1 \ln AVGGDP_i + \beta_2 \ln^2 AVGGDP_i + \beta_3 \ln CARNUM_i + \beta_4 \ln RAINFALL_i + \beta_5 lnPOPDENSITY_i + \beta_6 IDUSTRY_i + \beta_7 ISNORTH_i + \varepsilon_i \quad (5)$$

Spatial Error Model (SEM):

$$lnPM25_i = \rho \sum_{i \neq j} w_{ij}\, lnPM25_i + \beta_0 + \beta_1 \ln AVGGDP_i + \beta_2 \ln^2 AVGGDP_i + \beta_3 \ln CARNUM_i + \beta_4 \ln RAINFALL_i + \beta_5 lnPOPDENSITY_i + \beta_6 IDUSTRY_i + \beta_7 ISNORTH_i + \mu_i \quad (6)$$

Where

$$\mu_i = \lambda \sum_{i \neq j} w_{ij}\, lnPM25_i + \varepsilon_i \quad (7)$$

RESULTS

(1) The relationship between air pollution indicators and economic development. While collecting PM2.5 concentration data, this article also collects data on other atmospheric pollutants, including PM10 concentration, sulfur dioxide concentration, carbon monoxide concentration, nitrogen dioxide concentration, ozone concentration, and Air Quality Index (AQI). In this paper, firstly, after logarithmization of these seven air pollution indicators and per capita GDP, a quadratic function is fitted. The PM2.5 concentration, PM10 concentration, carbon monoxide concentration, sulfur dioxide concentration, nitrogen dioxide concentration, air quality index and per capita GDP shows a downward quadratic curve relationship, which can be initially considered as the existence of an "inverted U-shaped" EKC curve relationship between PM2.5 concentration, PM10 concentration, CO concentration, and SO2 nitrogen dioxide as the environmental pollution indicator and the per capita GDP. There are some differences in the bending amplitude of the curve and the size of each inflection point between various environmental indicators (Figure 2).

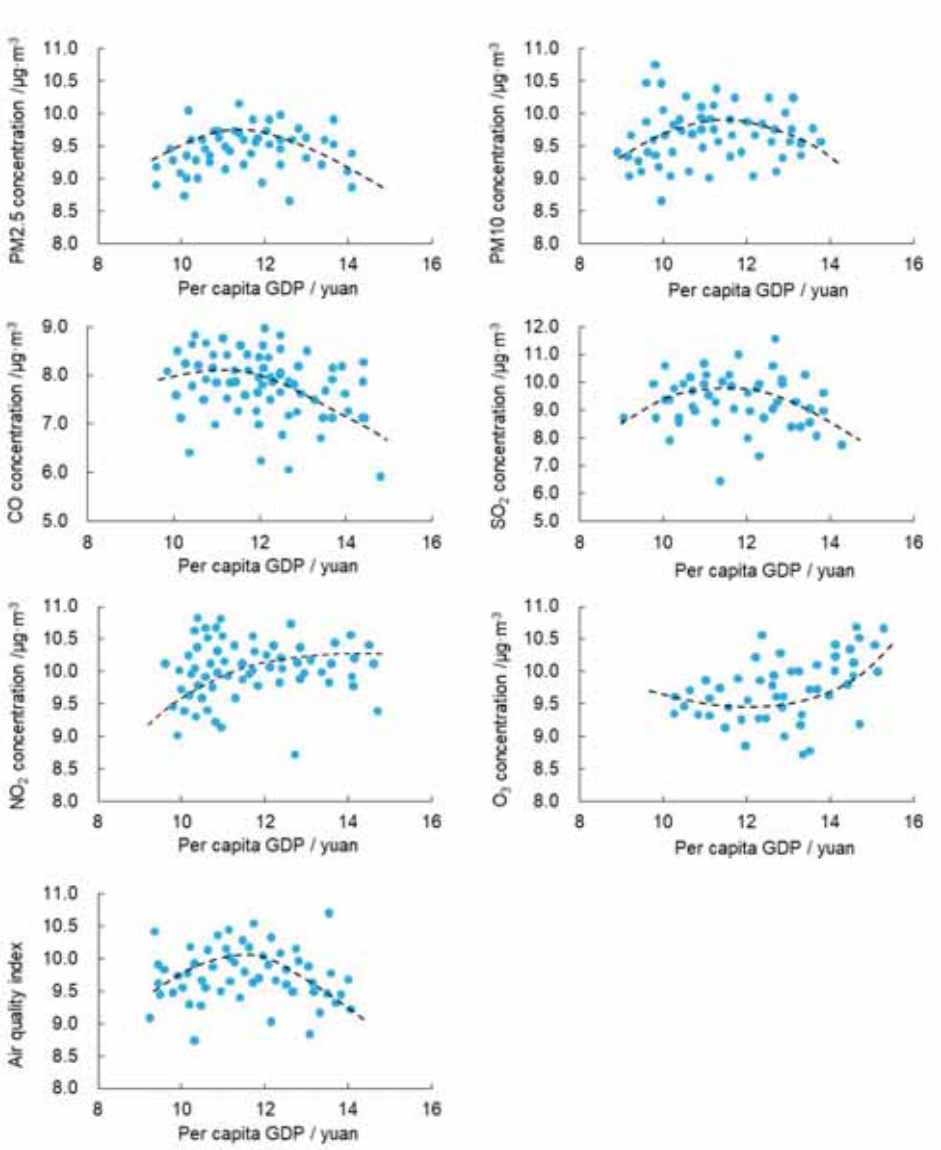

FIGURE 2
Quadratic fitting of urban pollution and per capita GDP in China.

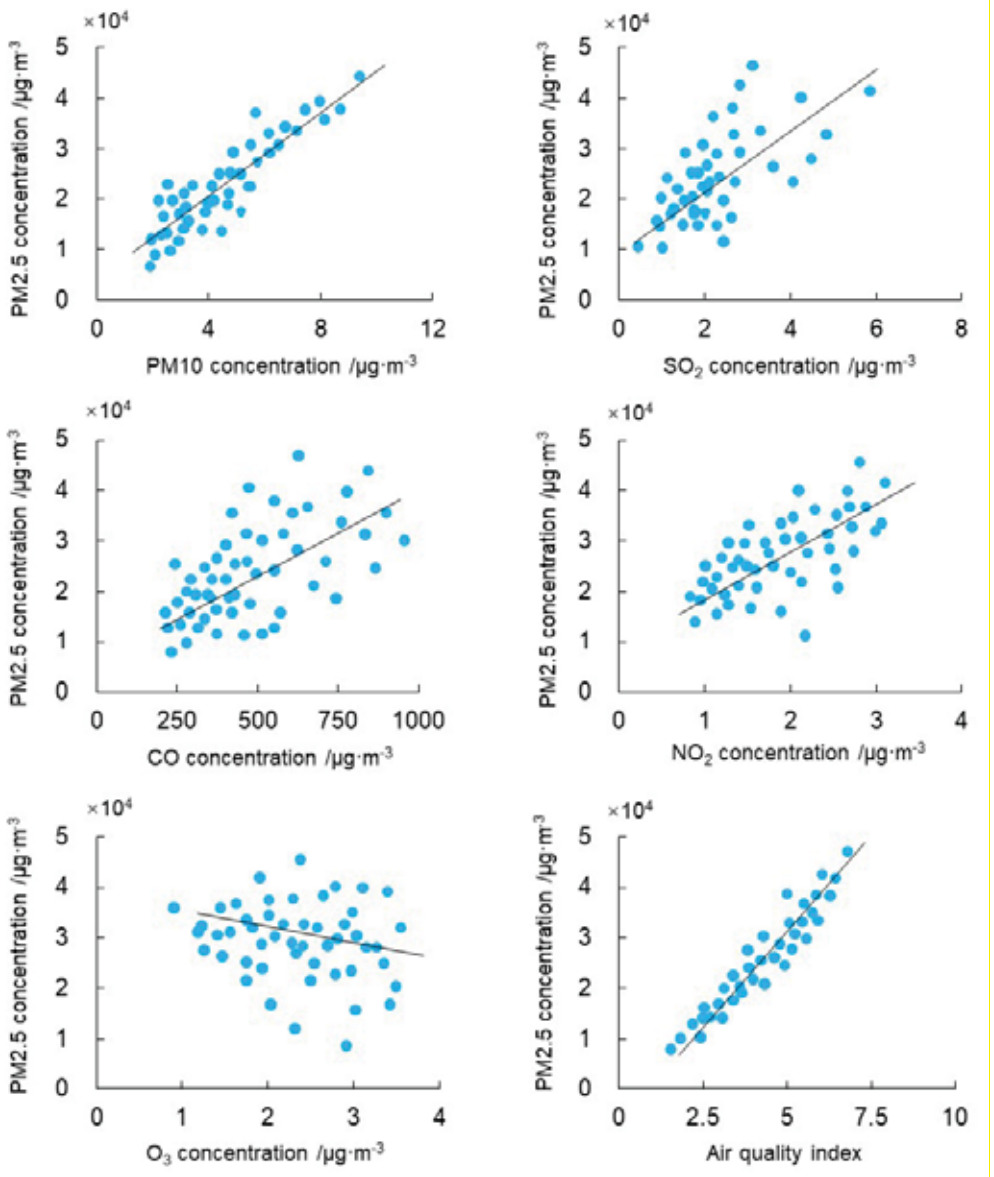

FIGURE 3
Linear fitting of PM2.5 and other environmental pollution indicators.

Figure 3 illustrates that there is a high correlation between PM2.5 concentration and PM10 concentration, and there is a positive correlation between PM2.5 concentration and sulfur dioxide concentration, nitrogen dioxide concentration and carbon monoxide concentration. A strong linear positive correlation exists between the air quality index and the PM2.5 concentration. From this part, we can get the following conclusions: first, when calculating the spatial quality index, the PM2.5 concentration index is a very important parameter standard. Second, the air quality index is a comprehensive index of air pollution, and at the same time it has a strong positive correlation with the concentration of PM2.5, which further shows that the concentration of PM2.5 is also a good comprehensive index of air pollution.

(3) Data description and spatial autocorrelation test. A preliminary statistical description of the data is used by the model to perform global spatial autocorrelation test on the corresponding variable data of more than 100 selected cities. The test results show that: the Moran index of PM2.5 concentration, rainfall, population density, per capita GDP, and whether it is north of the Qinling and Huaihe River are 0.498, 0.472, 0.234, 0.365, 0.842, respectively, which all passed the significance test, showing that these variables have obvious positive autocorrelation in the spatial distribution. There is no obvious spatial autocorrelation between the proportion of the secondary industry and car ownership. Based on the above data analysis, we can draw the following conclusions: First, the fine particles in the atmosphere will indeed continue to diffuse in the air, and then affect the air quality in the surrounding areas. Second, the rainfall between regions is also correlated, indicating that the rainfall in the neighboring cities is

generally evenly distributed. Third, there is a positive spatial autocorrelation between population density and per capita income between neighboring cities, that is, the development of neighboring cities has a certain driving effect, and the development of this city will promote the development of surrounding cities. Based on the above results, the spatial effect between cities cannot be ignored when studying the Kuznets curve of the urban environment.

(4) Regression results of spatial lag model and spatial error model. 1) Regression results of spatial lag model. In order to compare and analyze the spatial measurement results of the environmental Kuznets curve of the urban cross section, this paper uses Stata software to carry out the spatial lag model and obtain the results, as shown in Table 1.

TABLE 1
Results of Models from SLM analysis

Variable	Value	P
InAVGGDP	3.132	0.072
ln^2AVGGDP	-0.164	0.043
InCARNUM	0.052	0.032
InRAINIALL	-0.067	0.425
InPOPDENSm	0.917	0.018
INDUSTRY	0.958	0
ISNORTH	0.189	0.032
Intercept	-7.013	0.48
P/λ	0.034	0
R^2	0.493	/

TABLE 2
Results of Models from SEM analysis

Variable	Value	P
InAVGGDP	3.921	0.008
ln^2AVGGDP	-0.192	0.005
InCARNUM	0.084	0.04
InRAINIALL	-0.078	0.424
InPOPDENSm	1.131	0.015
INDUSTRY	0.9124	0
ISNORTH	0.178	0.029
Intercept	-10.83	0.157
P/λ	-0.032	0.157
R^2	0.314	/

Considering the spatial correlation between air pollution, and taking the spatial autocorrelation into the model as the residual lag term, the regression results with the spatial error model show that the coefficient of InAVGGDP is 3.132, and its P value is 0.072 which is in the 90% confidence interval. The coefficient of the quadratic term of InAVGGDP is -0.164, and its P value is 0.043, which is within the 95% confidence interval. The above two values indicate that there is an "inverted U-shaped" environmental Kuznets curve, from which the inflection point is 9.549 and the per capita GDP is 31720 yuan. The regression coefficient of car ownership on environmental pollution is 0.052. passing the 5% significance level test, showing that, without considering other factors, every 1% increase in car ownership will increase environmental damage by 0.052%. Large-scale car ownership puts greater pressure on environmental protection. The regression coefficient of population density to environmental pollution is 0.917, which has passed the 5% significance level test, indicating that for every 1% increase in population density, the environmental loss will increase by 0.917%.

The amount of rainfall reflects the climatic differences between cities. In the south, where there is more rainfall. Some impurities in the environment will be washed away, which is conducive to the self-purification and restoration of the environment. That is, under other factors unchanged, the more rainfall, the better the environment. Whether the city is in the north of Qinling Mountains and Huaihe River (ISNORTH) has a regression coefficient of 0.189 for environmental pollution, which has passed the 5% significance test. Based on the Qinling Mountains and Huaihe River, China is divided into the south and the north from a geographical perspective. Northern cities will use central heating in winter, while southern cities do not. In northern cities, heating in winter will inevitably cause environmental losses, which is consistent with the regression results of the model. The regression coefficient of the proportion of the secondary industry to the environment is 0.958, which has passed the 1% significance level test, indicating that every 1% increase in the proportion of the secondary industry will increase the environmental loss by 0.958%. The secondary industry is dominated by manufacturing, which consumes a lot of natural resources and causes unavoidable damage to the environment. Among the coefficients of the model, the regression coefficient of the proportion of the secondary industry is the largest, indicating that among the factors listed in the model, the proportion of the secondary industry has the greatest impact on the environment, further showing the importance of industrial structure adjustment to environmental protection.

2) Regression results of spatial error model. Similarly, this article uses Stata software to estimate the spatial error model, and the experimental results are shown in Table 2.

The regression results of the spatial error model show that the coefficient of lnAVGGDP is 3.921, and its P value is 0.008, which is within the 99% confidence interval. The coefficient of the quadratic term of lnAVGGDP is -0.192, and its P value is 0.005, which is within the 99% confidence. The above

two parameters showed that there is an "inverted U-shaped" environmental Kuznets curve. The value of the inflection point is 10.21 and the per capita GDP is 34,259 yuan. The coefficient of InCARNUM is 0.084, which means that for every 1% increase in car ownership, the PM2.5 concentration increases by 0.084%, and its P value is 0.031, which is significant (95% confidence interval). The coefficient of InRAINFULL is -0.078, which indicates that the more rainfall, the better the air quality when other conditions remain unchanged. The coefficient of POPDENSITY is 1.131, which is the largest coefficient except for InAVGGDP, indicating that population density has a huge impact on air pollution. The higher the population density, the more air pollution is produced. The coefficient of INDUSTRY is 0.9124, indicating that the proportion of the secondary industry has a very large impact on air pollution. Its P value is 0.000, which is very significant. The coefficient of ISNORTH is 0.178, which shows that the difference between north and south in China is still very obvious.

In general, even if there are some differences between the spatial lag model and the spatial error model, the regression results show that the urban-level data in China supports the environmental Kuznets curve hypothesis, and the inflection point of the "inverted U" curve derived from these two models is not exceed RMB 40,000 per capita GDP.

Figure 4 shows the spatial distribution of cities with a per capita GDP of less than RMB 40,000 among the cities surveyed. From this figure, we can get the following conclusions: First, there are a large number of cities with per capita GDP less than 40,000 yuan distributed around the Beijing-Tianjin-Hebei region. This phenomenon raises a problem, that is, the excessive absorption of talents and resources in large or super large cities such as Beijing and Tianjin did not play a role in economic radiation, but formed a blood draw effect on its surrounding cities, which was not conducive to the development of surrounding cities. Therefore, the "Round Capital Poverty Zone" appeared. Second, many cities are located in the eastern, central and western regions, and they lack economic resources, human resources, etc., so their economy is still in a less developed stage. Third, in the southeast coast, especially Guangdong, there are few cities with a per capita GDP of less than 40,000 yuan, which shows that there is a certain imbalance in the development of Guangdong area.

(5) Recommendations. Based on the above research conclusions, we put forward the following policy recommendations for improving the relationship between environmental pollution and economic growth in my country:

FIGURE 4
Urban spatial distribution with per capita less than 40,000 yuan.

(1) Establish a sound environmental protection legal system. In terms of legislation, China must first continue to intensify its efforts to establish and improve the judicial system related to environmental protection laws. At the same time, it must consider the procedures and implementation to ensure that there are laws to follow. In the treatment of environmental pollution, it is necessary to adopt a simultaneous policy of prevention and treatment, implement strict audits on economic development projects, and conduct environmental impact assessments. In addition, China needs to strengthen environmental management, gradually establish and improve relevant laws and regulations, and corresponding standard systems.

(2) Strictly control automobile exhaust emissions. The government should formulate macro-control policies to control the number of urban motor vehicles within a range that can maintain the urban ecological balance. The government should also implement a motor vehicle exhaust management mechanism and establish an independent exhaust gas regulatory agency. In addition, they need strictly check and control vehicles with excessive exhaust gas and increase law enforcement and penalties, compulsorily eliminate old vehicles with excessive pollution emissions. What's more, they need promote clean technology, install filters on motor vehicle exhaust pipes to eliminate exhaust pollution from the source, and at the same time encourage the use of clean energy motor vehicles in policy.

(3) Coordinate regional development and joint environmental governance. As the environmental pollution at the urban level in China is spatially autocorrelated. Neighboring cities can adopt the joint legislation-through consultations between cities and jointly formulate regional environmental pollution prevention and control laws and regulations.

CONCLUSIONS

(1) According to the results of the Moran index and the spatial econometric model, the environmental pollution between cities in China has obvious positive spatial autocorrelation, that is, the urban environmental pollution has a diffusion effect, which affects the environment of surrounding cities situation. Therefore, the spatial autocorrelation effect needs to be considered when establishing the measurement model.

(2) According to the results of the spatial lag model and the spatial error model, when using PM2.5 concentration as an indicator of environmental pollution, there is an "inverted U-shaped" environmental Kuznets curve at the urban level in China. The environmental Kuznets curve hypothesis has been confirmed at the urban scale in China. At the same time, the inflection points of the environmental Kuznets curve given by the spatial lag model and the spatial error model are slightly different, but both are between RMB 30,000 and RMB 40,000 per capita GDP.

(3) According to the results of the models in this study, the proportion of the secondary industry has a positive effect on environmental pollution, that is, the higher the proportion of the secondary industry, the heavier the environmental pollution. Population density also plays a positive role in environmental pollution, that is, the higher the population density of the city, the more serious the environmental pollution. The number of motor vehicles and environmental pollution are also positively correlated, that is, the greater the number of motor vehicles, the more serious the urban pollution. The rainfall is negatively related to environmental pollution, that is, rainfall can play a role in cleaning the atmosphere, thereby improving environmental quality. In addition, the environmental pollution of cities in China is also affected by the north-south distribution of cities. The urban environmental pollution of the cities distributed in the north of Qinling Mountains and Huaihe River is relatively heavy, and the urban environmental pollution of the cities in the south part is relatively light.

ACKNOWLEDGEMENTS

This work was supported by the national natural science foundation of China of funder grant number 71171128.

REFERENCES

[1] Grossman, G.M., Krueger, A.B. (1995) Economic growth and the environment. The Quarterly Journal of Economics. 110(2), 353-377.
[2] Cole, M.A., Rayner, A.J., Bates, J.M. (1997) The environmental Kuznets curve: an empirical analysis. Environment and Development Economics. 2(4), 401-416.
[3] Dasgupta, S., Laplante, B., Wang, H., Wheeler, D. (2002) Confronting the environmental Kuznets curve. Journal of Economic Perspectives. 16(1), 147-168.
[4] Harbaugh, W.T., Levinson, A., Wilson, D.M. (2002) Reexamining the empirical evidence for an environmental Kuznets curve. Review of Economics and Statistics. 84(3), 541-551.
[5] Stern, D.I., Common, M.S. (2001) Is there an environmental Kuznets curve for sulfur? Journal of Environmental Economics and Management. 41(2), 162-178.

[6] Selden, T.M., Song, D. (1995) Neoclassical growth, the J curve for abatement, and the inverted U curve for pollution. Journal of Environmental Economics and Management. 29(2), 162-168.
[7] Holtz-Eakin, D., Selden, T.M. (1995) Stoking the fires? CO2 emissions and economic growth. Journal of Public Economics. 57(1), 85-101.
[8] Kaufmann, R.K., Davidsdottir, B., Garnham, S., Pauly, P. (1998) The determinants of atmospheric SO2 concentrations: reconsidering the environmental Kuznets curve. Ecological Economics. 25(2), 209-220.
[9] Suri, V., Chapman, D. (1998) Economic growth, trade and energy: implications for the environmental Kuznets curve. Ecological Economics. 25(2), 195-208.
[10] Miglietta, P. P., De Leo, F., Toma, P. (2017) Environmental Kuznets curve and the water footprint: an empirical analysis. Water and Environment Journal. 31(1), 20-30.
[11] Lindmark, M. (2002) An EKC-pattern in historical perspective: carbon dioxide emissions, technology, fuel prices and growth in Sweden (1870–1997). Ecological Economics. 42(1-2), 333-347.
[12] Ali, G., Ashraf, A., Bashir, M.K., Cui, S. (2017) Exploring environmental Kuznets curve (EKC) in relation to green revolution: a case study of Pakistan. Environmental Science & Policy. 77, 166-171.
[13] Polemis, M.L. (2017) Revisiting the environmental Kuznets curve: a semi-parametric analysis on the role of market structure on environmental pollution. Letters in Spatial and Resource Sciences. 11(1), 1-9.
[14] Legendre, P. (1993) Spatial autocorrelation: trouble or new paradigm? Ecology. 74(6), 1659-1673.
[15] Smouse, P.E., Peakall, R. (1999) Spatial autocorrelation analysis of individual multiallele and multilocus genetic structure. Heredity. 82(5), 561-573.
[16] Basu, S., Thibodeau, T.G. (1998) Analysis of spatial autocorrelation in house prices. The Journal of Real Estate Finance and Economics. 17(1), 61-85.
[17] Chen, L., Chen, S. (2015) The estimation of environmental Kuznets curve in China: nonparametric panel approach. Computational Economics. 46(3), 405-420.
[18] Shen, C., Li, C., Si, Y. (2016) Spatio-temporal autocorrelation measures for nonstationary series: A new temporally detrended spatio-temporal Moran's index. Physics Letters A. 380(1-2), 106-116.
[19] Bidanset, P.E., Lombard, J.R. (2014) Evaluating spatial model accuracy in mass real estate appraisal: A comparison of geographically weighted regression and the spatial lag model. Cityscape. 16(3), 169-182.
[20] Wang, L. (2011) A nonparametric analysis on the environmental Kuznets curve. Environmetrics. 22(3), 420-430.
[21] Wilhelmsson, M. (2002) Spatial models in real estate economics. Housing, Theory and Society. 19(2), 92-101.
[22] Elhorst, J.P. (2003) Specification and estimation of spatial panel data models. International Regional Science Review. 26(3), 244-268.

Received: **06.12.2020**
Accepted: **20.01.2021**

CORRESPONDING AUTHOR

Yan Yue
Shanghai University,
Shanghai 200444 – China

e-mail: yueyan815@163.com

© by PSP Volume 30– No. 05/2021 pages 5270-5291 Fresenius Environmental Bulletin

THE STRUCTURE OF SPERMATHECA IN THE SUBGENUS C*ASSIDA* (*CASSIDA*) LINNAEUS, 1758 (COLEOPTERA: CHRYSOMELIDAE: CASSIDINAE) AND ITS TAXONOMIC SIGNIFICANCE

Huseyin Ozdikmen, Neslihan Bal*

Gazi University, Science Faculty, Department of Biology, 06500 Ankara, Turkey

ABSTRACT

Spermathecae of 9 species including the type species *Cassida nebulosa* Linnaeus, 1758 belonging to the subgenus *Cassida* (*Cassida*) Linnaeus, 1758 from Turkey have been studied and figured. Spermathecal structures of these species were evaluated under both a stereo microscope and Scanning Electron Microscope (SEM).Vasculum, ampulla, ductus glandula auxiliaris and ductus spermatheca are generally constant in shape within species, but distinct and useful in comparison with other species.Based on the structure of these four parts of spermatheca, six morphological groups have been distinguishedand defined in the subgenus *Cassida* (s.str.).According to the structures of spermathecae, it was revealed that the subgenus *Cassida* (*Cassida*) Linnaeus, 1758 is a polymorphic and polyphyletic group, not a monophyletic.In accordance with the results obtained in this study, the problematic taxonomic position of the subgenus *Cassida* (*Cassida*) is discussed. Accordingly, three new subgenera are described. The following three names are proposed for the new subgenera of *Cassida* Linnaeus, 1758; *Cassida* (*Longiampulla*) subgen. nov. with the type species *Cassida vibex* Linnaeus, 1767; *Cassida* (*Diversivascula*) subgen. nov. with the type species *Cassida sanguinolenta* Müller, 1776 and *Cassida* (*Reliquacassida*) subgen. nov. with the type species *Cassida rubiginosa* Müller, 1776.

KEYWORDS:
Coleoptera, Chrysomelidae, Cassidinae, *Cassida*, morphology, spermatheca

INTRODUCTION

The genus *Cassida* Linnaeus, 1758, a member of the tribe Cassidini Gyllenhal, 1813, has a large number of species spread almostall over the world (Palaearctic, Nearctic, Oriental, Afro-tropical, Madagascar and Australian). In the Palaearctic region where Turkey is located, this genus comprises at present 167 species [1, 2].To date, *Cassida* Linnaeus, 1758 has a total of 15 subgenera proposed for the species spreading in the Palaearctic and Oriental regions. There are no subgenera proposed for species in other regions. Therefore, it can be said that the subgeneric arrangement of this genus is not sufficient and complete [1, 3]. In Turkey, there are 41 species of 11 subgenera belonging to this genus [4-6]. However, 5 species of 5 subgenera as *Cassida* (*Cassida*) *seladonia* Gyllenhal, 1827, *C.* (*Lordiconia*) *canaliculata* Laicharting, 1781, *C.* (*Mionycha*) *azurea* Fabricius, 1801, *C.* (*Mionychella*) *hemisphaerica* Herbst, 1799 and *C.* (*Tylocentra*) *persica* Spaeth, 1926 have been recorded only as "Anatolia" without the actual locality record by Kısmalı & Sassi (1994), Warchalowski (2003, 2010) and Borowiec & Sekerka (2010) [2, 7-9]. Therefore, the presence of these species in Turkey is questionable and must be confirmed. According to the factual records, *Cassida* fauna of Turkey consists of 36 species belonging to 9 subgenera. The nominative subgenus*Cassida* (*Cassida*) Linnaeus, 1758 is represented in the world with 47 species with *Cassida inopinata* Sassi & Borowiec, 2006 (46 in the Palaearctic region and 1 in the Nearctic region) (Borowiec, 2007). Turkey's fauna consists of 21 species [4- 6].

According to Bordy & Doguet (1987), Borowiec & Świętojańska (2001) and Borowiec (2007), aedeagal morphology in the genus *Cassida* Linnaeus, 1758 is not diagnostic. Spermathecal morphology is partially diagnostic. With this study, the mentioned opinions were supported for the species group.However, so far, genital morphology has been overlooked in the arrangement of the upper categories from species group level, though with the effect of the mentioned opinions. As stated by Borowiec (2007), currently proposed subgenera are based on questionable characters (some only 3-5 adult characters, some partially larval characters and some only pupal characters). Whereas, according to our study, it can be said that the similarities and differences in spermathecal morphology can be easily used in the arrangement of the subgenera [1, 10, 11].

Male genitalia in the genus *Cassida*, like in most genera of the tribe Cassidini, are uniform and do not offer good diagnostic characters. Contrary to the homogenity of male genitalia, studies on spermathecae of a few species of Cassidini suggested quite large diversity of spermathecal structure [12-14]. These positive results stimulated us to study spermathecae of the large and polymorphic genus *Cassida* Linnaeus.

MATERIALS AND METHODS

We studied 179specimens of 9 species of *Cassida* (*Cassida*)collected from various provinces in Turkey in 1991, 1993, 1996, 1997, 2001, 2003, 2004, 2014, 2015, 2018. Most of the specimens were obtained from the private collection of Prof. Dr. Hüseyin Özdikmen at the Department of Biology, Science Faculty of Gazi University (Turkey, Ankara). Some specimens were obtained from Nazife Tuatay Plant Protection Museum (NTM) (Turkey, Ankara). They were identified by Prof. Dr. Hüseyin Özdikmen.

The spermathecae were dissected from the abdomen, and the remaining tissue was removed with fine tweezers. For light microscopic examination after cleaning, the samples were placed 70% ethanol and examined with an Olympus SZX7 stereomicroscope. For scanning electron microscopy (SEM), cleaned samples were dehydrated using an ascending series of ethanol (70%, 80%, 90%, and 100%) and then air dried. After that, the specimens were mounted onto SEM stubs using a double-sided adhesive tape, coated with gold using a Polaron SC 502 Sputter Coater, and examined with a JEOL JSM 6060 Scanning Electron Microscope (SEM) at 10 kV.In this study, figure 1 was used for the terminology of spermathecal structures.

RESULTS

In this work, structures observed by stereo microscope and SEM of spermathecae of 9 species belonging to the subgenus *Cassida* (*Cassida*) (Coleoptera: Chrysomelidae: Cassidinae) from Turkey are presented. The studied species are given in alphabetical order. Obtaining data are presented as follows:

Genus ***Cassida*** Linnaeus, 1758
Subgenus ***Cassida*** Linnaeus, 1758

Cassida atrata Fabricius, 1787 (Figure 2)

Structure of spermatheca. Vasculum is in the form of eggplant or boxing gloves. It is distinctively curved, relatively wide-angle, asymmetrical C-shaped (the apical part of cornu is more proturuded forward). In vasculum, cornu is much thicker than nodulus especially in the apical part. The apical part of cornu is noticeably swollen and dark colored. Cornu's apex is rounded. The nodulus is quite short, almost parallel, and not swollen. In stereo microscope, nodulus is dark colored on the inner surface of the basal part. In SEM, this part carries an integument, the back edge of which is extended backwards in the form of a wavy fringe. Ampulla is in the form of a

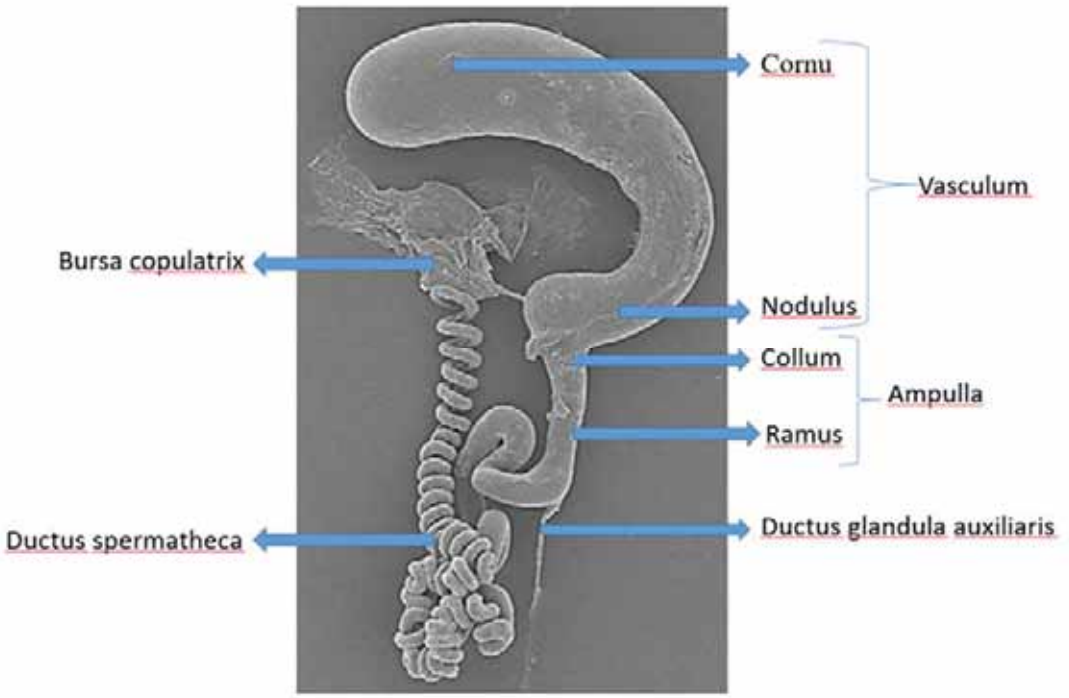

FIGURE1
Terminology of spermathecal structures.

duct or tube,which is very distinct, elongated and is laterally connected to nodulus on the outer surface of its basal part. It is slightly thinner than the thickness of nodulus. Collum is quite short, but distinct. Ramus is very distinct. It is in the form of a long, straight and thick duct or tube, which is slightly enlarged in the middle part. The widest part of ramus is slightly thinner than nodulus. Ductus glandula auxiliaris (ductus spermathecal gland) is attached to ramus on the outer surface at the end of ramus. Ductus spermatheca is connected straightly to ramus, which is thick and long. It is in the form of a flat tube, forming wide folds in the proximal part. It is thinner in the next big part and is spirally curved regularly. Ductus spermatheca is slightly thinner than ramus or approximately equal width with ramus in the proximal part and is much thinner than ramus in the spiral part.Ductus spermatheca is about 4-5 times longer than vasculum.In SEM, spermatheca carries scattered, irregular and sparsely ultrastructural pits on various parts.

Material examined.Turkey,Kayseri prov.: Develi, Kocahacılı, 38°11'15"N 35°23'50"E, 07.V.2018, 1092 m,1 ex.; **Niğde prov.:** Melendiz, between Hançerli-Küçükköy, 03.VII.1996, 1 ex; Çamardı, 29.VI.1996, 1 ex.

Cassida fausti Spaeth & Reitter, 1926 (Figure3)

Structure of spermatheca. Vasculum is in the form of an eggplant or boxing gloves. It is distinctively curved, relatively wide-angle, asymmetrical C-shaped (the apical part of cornu is more proturuded forward). In vasculum, cornu is much thicker than nodulus especially in the apical part. The apical part of cornu is noticeably swollen. Cornu's apex is rounded. Nodulus is quite short, almost parallel, and not swollen. In stereo microscope, nodulus is dark colored on the innersurface of the basal part. In SEM, this part carries an integument, the back edge of which is extended backwards in the form of a wavy fringe. Ampulla is in the form of a duct or tube that is very distinct, elongated and is laterally connected to nodulus on the outer surface of its basal part. It is much thinner than nodulus. Collum is quite short, but distinct. Ramus is very distinct. It is in the form of a long, straight and thick duct or tube. Ramus is much thinner than nodulus. Ductus glandula auxiliaris (ductus spermathecal gland) is attached to ramus on the outer surface at the end of ramus. Ductus spermatheca is connected straightly to ramus, which is thick and long. It is in the form of a flat tube, which forms wide folds in the proximal part. It is thinner in the next big part and is spirally curved regularly. Ductus spermatheca is only approximately equal width with ramus in the proximal part and is much thinner than ramus in the spiral part.Ductus spermatheca is about 2-3 times longer than vasculum.In SEM, spermatheca carries scattered, irregular and sparsely ultrastructural pits on various parts.

Material examined.Turkey,Ankara prov.: Çubuk, 1 ex.; **Bolu prov.:** Bolu-Gerede road, return of Susuz-Kınık villages, exit of Bolu, 17.V.2003, 720 m, 1 ex.; **Kastamonu prov.:** Kastamonu- Araç road, Kastamonu police forest, exit of Kastamonu 1st km, 16.V.2003, 975 m, 1 ex.; **Kayseri prov.:** İncesu, Bahçelievler, 38˚37’58’’N 35˚11’48’’E, 08.V.2018, 1072 m, 2 exs.; **Konya prov.:** Kulu, Tavşanlı, 17.V.1997, 1000 m, 1 ex.

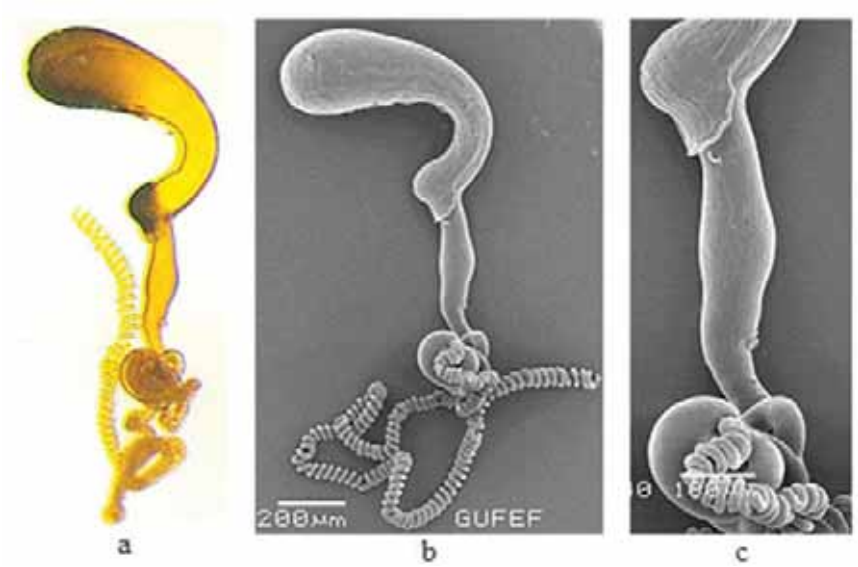

FIGURE 2
Spermathecae of *Cassida atrata*, a. view in stereo microscope, b-c. view in SEM.

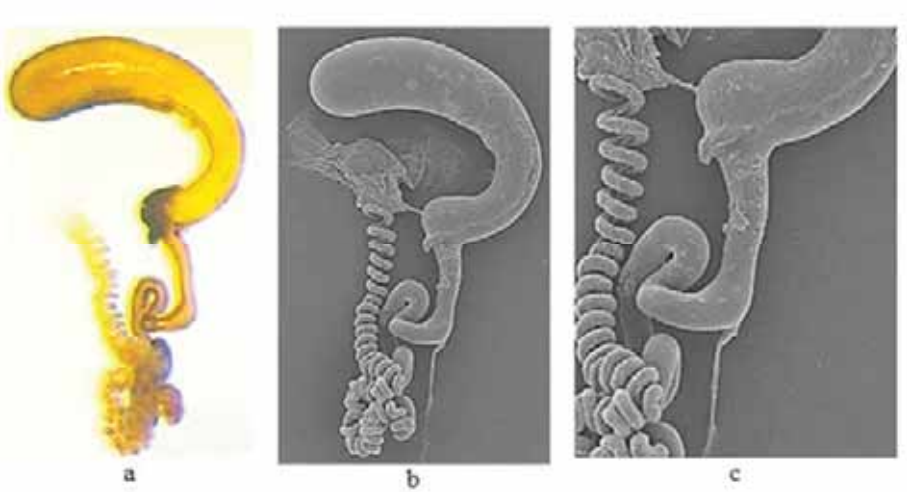

FIGURE 3
Spermathecae of *Cassida fausti*, a. view in stereo microscope, b-c. view in SEM.

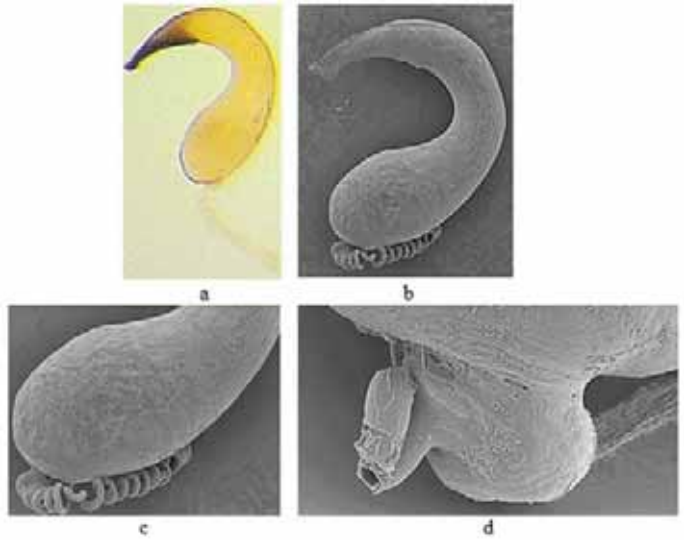

FIGURE 4
Spermathecae of *Cassida nebulosa*, a. view in stereo microscope, b-d. view in SEM.

Cassida nebulosa Linnaeus, 1758(Figure 4)

Structure of spermatheca. Vasculum is in the form of an opened hook or bird beak-shaped. It is distinctively curved, relatively wide-angle, symmetrical C-shaped. In vasculum, nodulus is much thicker than cornu especially in the basal part.Apical part of cornu is clearly sharpened and dark colored. Cornu's apex is pointed. Apical part of cornu extended to the front of its apex with an integument. The nodulus is quite long, not parallel, distinctly swollen and bulbous. In SEM, nodulus carriesa wide integument on the inner surface of the basal part. The back edge of the integument isnot extended backwards.Ampulla is very small. It is in the form of a tubercle and is connected to nodulus on the outer surface of its basal part.It is incomparably smaller than nodulus. Collum is invisible, vague or very reduced. Ramus is clearly visible and in the form of a tubercle. Ductus glandula auxiliaris (ductus spermathecal gland) is attached to the end of ramus. Ductus spermatheca is connected to ramus on the outer surface of its middle part. Ductus spermatheca is very long, quite thin, and is spirally curved regularly along almost over its entire length.It is much thinner than ampulla.Ductus spermatheca is about 10 times longer than vasculum.In SEM, spermatheca carries scattered, irregular and sparsely ultrastructural pits on various parts.

Material examined: Turkey,Konya prov.: Akşehir, Dereçine, 05.VIII.1993, leg. A. Kalkandelen, 4 exs.

Cassida palaestinaReiche, 1858(Figure 5)

Structure of spermatheca. Vasculum is in the form of a boomerang or payphone. It is distinctively curved, relatively wide-angle, asymmetrical C-shaped (the apical part of cornu is slightly protruded forward). In vasculum, cornu is much thicker than nodulus especially in the apical part. The

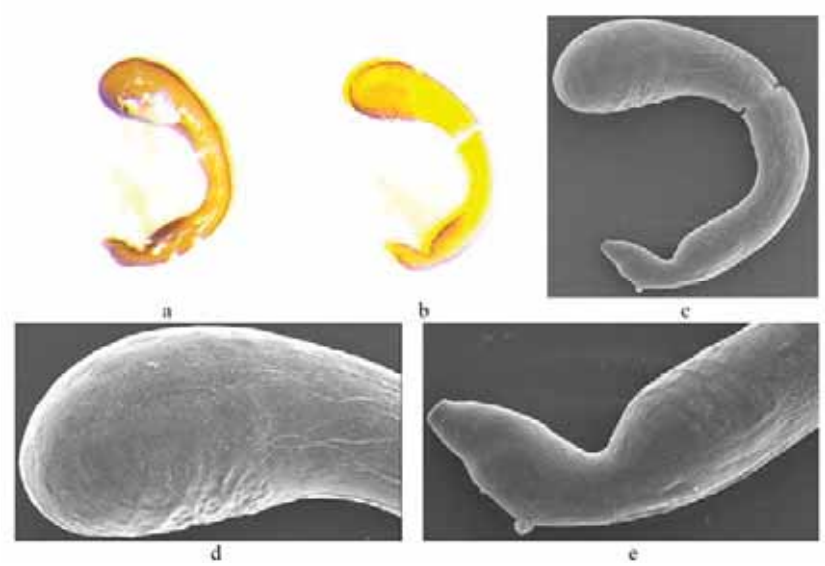

FIGURE 5
Spermathecae of *Cassida palaestina*, a-b. view in stereo microscope, c-e. view in SEM.

apical part of cornu is noticeably swollen. Cornu's apex is rounded. In SEM, the underside of the apical part of cornu has almost an integument-like thickening.Therefore, this part appears somewhat dark in stereo microscope.The nodulus is quite short, almost parallel, and not swollen. In stereo microscope, nodulus is somewhat dark colored on the inner surface of the basal part. In SEM, this part carries an integument-like thickening.Ampullais distinct. It is tubercular, quite short and is attached flat (parallel) at the bottom to the basal end of nodulus. It is slightly thinner than nodulus. Collum is quite distinct and is in the form of a short stem.Collum is much thinner than nodulus.Ramus is distinct and isin the form of a tuber or cone-like, quite small, swollen and more or less protruding outwardin the middle part.Ramus is slightly thinner than nodulus in its widest part.Ductus glandula auxiliaris (ductus spermathecal gland) is attached to ramus on the outer surface of its middle part.Ductus spermatheca is connected straightly to ramusin the middle at the end of ramus, but is broken in the examined sample.However, it is understood from the broken pieces that it is probably quite thin and spirally curved over its entire length. Ductus spermateka is much thinner than ramus.Ductus spermatheca is probably about 2-3 times longer than vasculum. In SEM, spermatheca carries scattered, irregular and sparsely ultrastructural pits on various parts.

Material examined: Turkey, Aksaray prov.: 5. km after crossing the Aksaray-Ulukışla junction, 29.V.2001, 1275 m, 4 specimens.

Cassida pannonica Suffrian, 1844(Figure6)

Structure of spermatheca. Vasculum is in the form of an eggplant or boxing gloves. It is distinctively curved, relatively wide-angle, asymmetrical C-shaped (the apical part of cornu is more proturuded forward). In vasculum, cornu is much thicker than nodulus especially in the apical part. The apical part of cornu is noticeably swollen. Cornu's apex is rounded. In SEM, apex has a very small bud-shaped process. The nodulus is quite short, almost parallel, and not swollen. In stereo microscope, nodulus is dark colored on the inner surface of the basal part. In SEM, this part carries an integument, the back edge of which is extended backwards in the form of a wavy fringe. Ampulla is in the form of a duct or tube that is very distinct, elongated and is laterally connected to nodulus on the outer surface of its basal part. It is much thinner than nodulus. Collum is quite short, but distinct. Ramus is very distinct and is in the form of a long, straight and thickish duct or tube. Ramus is much thinner than nodulus. Ductus glandula auxiliaris (ductus spermathecal gland) is attached to ramus on the outer surface at the end of ramus. Ductus spermatheca is connected straightly to ramus, which is thick and long. It is in the form of a flat tube, which forms wide folds in the proximal part. It is thinner in the next big part and is spirally curved regularly. Ductus spermatheca is approximately equal width with ramus in the proximal part and is much thinner than ramus in the spiral part. Ductus spermatheca is about 7-8 times longer than vasculum. In SEM, spermatheca carries scattered, irregular and sparsely ultrastructural pits on various parts.

Material examined:Turkey,Adana prov.: ReturnPozantı-Mersin-Çamlıyayla, 20th km, 30.V.2001, 285 m, 2 exs.; **Ankara prov.:** Kızılcahamam, Aköz village, 28.V.1997, 1150 m, 1 ex.; **Bolu prov.:** Düzce, Gavurpınarı (Between İğneler-Dibektaş), Yığılca, 1 ex.; **Çankırı prov.:** Kızılırmak, exit of Karamürsel village, Halimintepe, 40˚24'N 34˚02'E, 24.IV.2014, 550 m, 1 ex.;

Kızılırmak, entry of Kemalli village, 40˚18'N 34˚02'E, 24.IV.2014, 686 m, 1 ex.; Kızılırmak, Between Bostancı-Hacılar villages, 40˚19'N 33˚51'E, 25.IV.2014, 565 m, 1 ex.; Centre, Salt cavern district, 40˚31'N 33˚45'E, 25.IV.2014, 699 m, 1 ex.; Centre, Between Pehlivanlı-Alaçatı villages, 40˚34'N 33˚52'E, 26.IV.2014, 925 m, 1 ex.; Centre, Aşağıçavuş-Yukarıçavuş return, 40˚40'N 33˚35'E, 09.V.2015, 837 m, 1 ex.; Centre, Balıbağı village, 40˚34'N 33˚46'E, 15.V.2015, 1037 m, 1 ex.; Centre, between Ovacık-Kuzuköy village, 40˚32'N 33˚53'E, 15.V.2015, 919 m, 1 ex.; Centre entry of Karadayı, 40˚24'N 33˚45'E, 16.V.2015, 856 m, 2 exs.; Kızılırmak, Yukarıalagöz village, 40˚22'N 33˚53'E, 16.V.2015, 642 m, 1 ex.; Kızılırmak, Kavaklı, 40˚22'N 34˚1'E, 16.V.2015, 542 m, 1 ex.; Yapraklı, Bugay village, 40˚42'N 33˚46'E, 25.V.2015, 897 m, 1 ex.; Yapraklı, entry of Çevrecik, 40˚39'N 33˚49'E, 25.V.2015, 953 m, 1 ex.; Yapraklı, Kirliakça village, 40˚37'N 33˚54'E, 26.V.2015, 914 m, 3 exs.; Ilgaz, entry of Yaylaören village, 40˚52'N 33˚30'E, 17.VI.2015, 914 m, 1 ex.; Ilgaz, entry of Şeyhyunus village, 40˚50'N 33˚31'E, 18.VI.2015, 1421 m, 1 ex.; Bayramören, Harmancık village road, 41˚2'N 33˚13'E, 21.VI.2015, 861 m, 1 ex.; Atkaracalar, Budakpınarı village, 40˚51'N 33˚8'E, 22.VI.2015, 1096 m, 1 ex.; Yapraklı, Entry of Kaymaz village, 40˚43'N 33˚54'E, 29.VI.2015, 1011 m, 1 ex.; Yapraklı, Yüklü-Çevrecik return, 40˚40'N 33˚45'E, 29.VI.2015, 926 m, 1 ex.; **Çorum prov.:** Göletdere, 5 miles to Karagöl village, 16.VI.2003, 1120 m, 1 ex.; **Karabük prov.:** Eflani, Yağlıca village, 15.V.2003, 975 m, 1 ex.; **Kayseri prov.:** Sarız, Çörekdere, 38˚28'50''N 36˚27'29''E, 6.V.2018, 1637 m, 1 ex.

Cassida rubiginosa Müller, 1776(Figure7)

Structure of spermatheca. Vasculum is in the form of a boomerang or payphone. It is distinctively curved, relatively wide-angle, asymmetrical C-shaped (the apical part of cornu is slightly protruded forward). In vasculum, cornu is much thicker than nodulus especially in the apical part. The apical part of cornu is noticeably swollen. Cornu's apex is rounded. The apical part of cornu is dark colored. In SEM, the underside of the apical part of cornu has almost an integument-like thickening. Therefore, this part appears somewhat darker in stereo microscope.The nodulus is quite short, almost parallel, and not swollen. Nodulus is more or less dark colored on the inner surface of the basal part. In SEM, this part carries an integument-like thickening. Ampulla is tubercular, quite short but distinct and is attached flat (parallel) at the bottom to the basal end of nodulus. It is slightly thinner than nodulus. Collum is distinct and it is in the form of a short stem.Collum is much thinner than nodulus. Ramus is distinct and is in the form of a tuber or cone-like, quite small, swollen and more or less protruding outwardin the middle part. Ramus is slightly thinner than nodulus in its widest part. Ductus glandula auxiliaris (ductus spermathecal gland) is attached to ramus on the outer surface in the middle part of ramus.Ductus spermatheca is connected straightly to ramusin the middle at the end of ramus, very thin and spirallycurved regularly over its entire length.It is much thinner than ramus.Ductus spermatheca is aproximately equal length with vasculum or about 2 times longer than vasculum.In SEM, spermatheca carries scattered, irregular and sparsely ultrastructural pits on various parts.

Material examined: Turkey, Adana prov.: Pozantı, Tekir plateau, 23.VI.1997, 1300 m, 1 ex.; **Ankara prov.:** Kızılcahamam, Aköz village, 28.V.1997, 1150 m, 1 ex.; **Bolu prov.:** Yedigöller, Between Özbağı-Çıplaklar, Devrek (45 km to Yedigöller), 13.V.2003, 160 m, 1 ex.; **İçel prov.:** Sertavul pass, 26.VI.2001, 1410 m, 1 ex.; **Karabük prov.:** Üçevler, 14.VI.2003, 1000 m, 1 ex.; Safranbolu, Bulak village, Hazar district, 14.V.2003, 740 m, 1 ex.; **Kayseri prov.:** Sarız, Yedioluk, 38˚33'27''N 36˚27'01''E, 29.V.2018, 1770 m, 20 exs.; Melikgazi, Yeşilyurt, 04.VII.2018, 1090 m, 1 ex.; Sarız, Darıdere, 05.VII.2018, 1555 m, 1 ex.; Sarız,

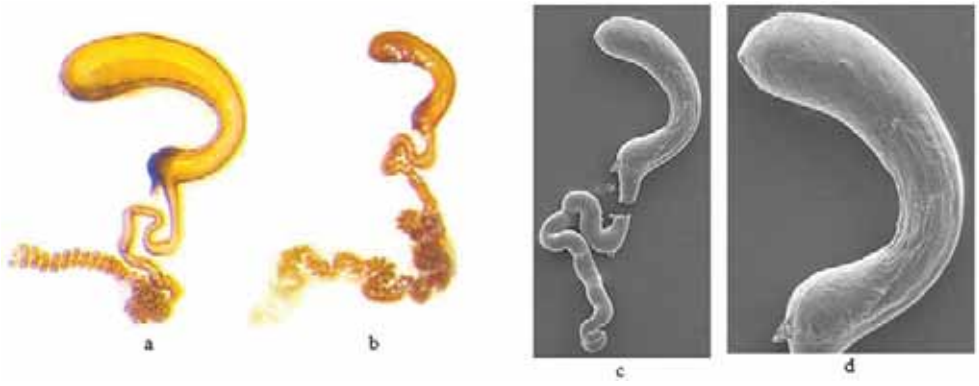

FIGURE 6
Spermathecae of *Cassida pannonica*, a-b. view in stereo microscope, c-d. view in SEM.

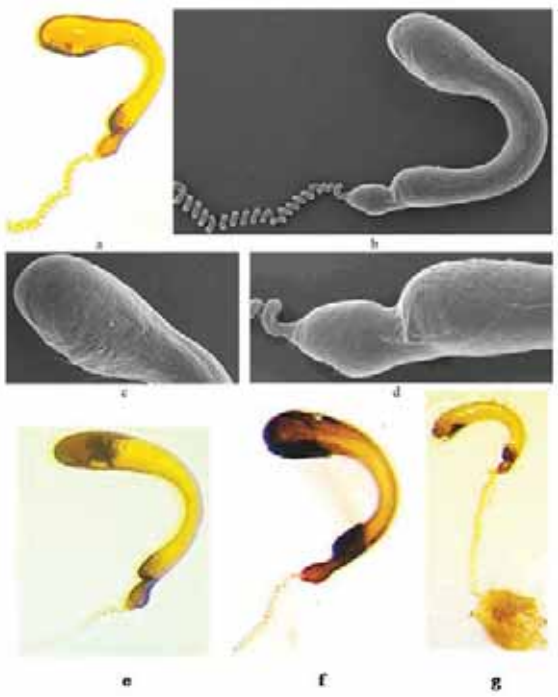

FIGURE 7
Spermathecae of *Cassida rubiginosa*, a, e-g. view in stereo microscope, b-d. view in SEM.

Yedioluk, 38°33’33’’N 36°27’16’’E, 05.V.2018, 1812 m, 6 exs.; Pırnarbaşı, Kılıçkışla, 38°39’48’’N 36°12’37’’E, 05.VII.2018, 1433 m, 24 exs.; **Konya prov.:** Kulu, Tavşanlı, 31.V.1997, 1000 m, 2 exs.; **Nevşehir prov.:** Avanos, 20.VII.1992, 1000 m, 1 ex.; Göreme, 19.V.1997, 1260 m, 1 ex.; **Niğde prov.:** Azatlı Tepeköy road, 21.VIII.1996, 1 ex.; Kayaardı, Niğde vineyard, 17.VI.1997, 6 exs.; Bor, Derbent district, 06.VII.1997, 6 exs.; Tepeköy plateau, Altınhisar-Çiftlik road, 29.IV.1997, 4 exs.

Cassida sanguinolenta Müller, 1776(Figure8)

Structure of spermatheca. Vasculum is in the form of an eggplant or boxing gloves. It is distinctively curved, relatively wide-angle, asymmetrical C-shaped (the apical part of cornu is much more protruded forward). In vasculum, cornu is much thicker than nodulus especially in the apical part.The apical part of cornu is very swollen. Cornu's apex is probably rounded.The nodulus is quite short, almost parallel, and not swollen. In SEM, nodulus has almost an integument-like thickening. Therefore, this part appears somewhat dark in stereo microscope.Ampulla is in the form of a wavy duct or tubethat is distinct, thickish, slightly elongated, and is attached flat (parallel) at the bottom to the basal end of the nodulus. The ramus of ampulla is recessed on the outer surface where it connects to the collum. Therefore, ampulla has taken a comma-like wavy shape in general view. Ampulla is slightly thinner than nodulus. Collum is quite short, distinct, and in the form of a wide stem. Ramus is in the form of a wavy duct or tubethat is short but distinct and thickish. Ductus glandula auxiliaris (ductus spermathecal gland) is laterally attached to ramus on the outer surface at the end of ramus. Ductus spermatheca islaterally connected straightly to ramuson the inner surface at the end of ramus.Ductus spermateka is broken. However, it is understood from the remaining fragments that it is probably very thin and spirally curved regularly over its entire length. Ductus spermateka is much thinner than ramus. Ductus spermatheca is about 2 times longer than vasculum.In SEM, spermatheca carries scattered, irregular and sparsely ultrastructural pits on various parts.

Material examined: Turkey, Çankırı prov.: Yapraklı, Kirliakça village, 40°37'N 33°54'E, 26.V.2015, 1 ex.; **Mersin prov.:** Entry of Fındıkpınarı**,** Municipal board, 31.V.2001, 1 ex.

Cassida stigmatica Suffrian, 1844 (Figure 9)

Structure of spermatheca. Vasculum is in the form of an eggplant or boxing gloves. It is distinctively curved, relatively wide-angle, asymmetrical C-shaped (the apical part of cornu is much more protruded forward). In vasculum, cornu is thicker than nodulus especially in the apical part. The apical part of cornu is swollen and dark colored. Cornu's apex is rounded. The nodulus is quite short, almost parallel, and not swollen. In stereo microscope, nodulus is dark colored on the inner surface of the basal part. In SEM, this part carries an integument. Ampulla is in the form of a wavy duct or tubethat is distinct, thickish, slightly elongated, and is attached flat (parallel) at the bottom to the basal

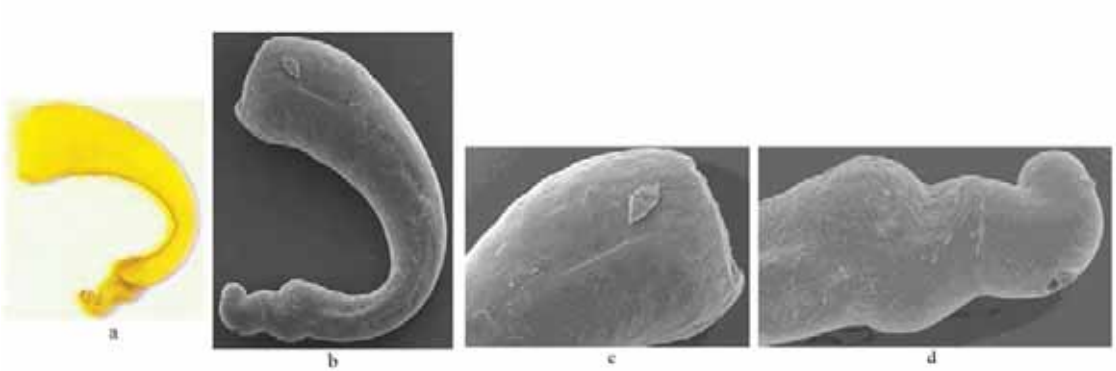

FIGURE 8
Spermathecae of *Cassida sanguinolenta*, a. view in stereo microscope, b-d. view in SEM.

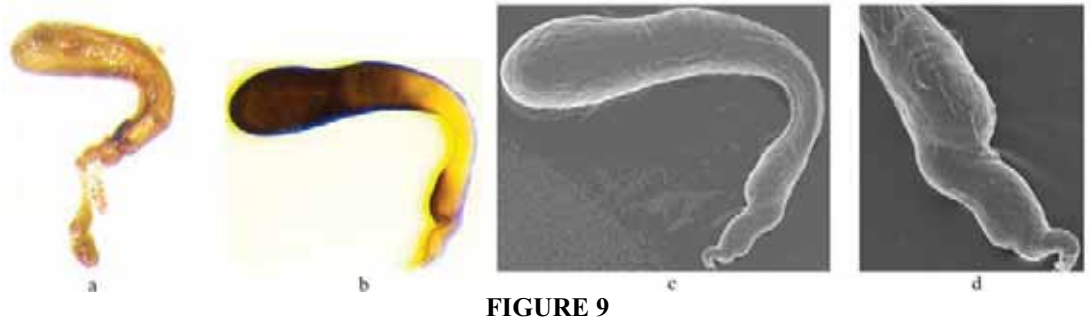

FIGURE 9
Spermathecae of *Cassida stigmatica*, a-b. view in stereo microscope, c-d. view in SEM.

end of the nodulus. The ramus of ampulla is recessed on the outer surfacewhere it connects to the collum. Therefore, ampulla has taken a comma-like wavy shape in general view. Ampulla is slightly thinner than nodulus. Collum is quite short, distinct, in the form of a wide stem. Ramus is in the form of a wavy duct or tubethat is short but distinctand thickish. Ductus glandula auxiliaris (ductus spermathecal gland) is laterally attached to ramus on the outer surface at the end of ramus. Ductus spermatheca islaterally connected straightly to ramuson the inner surface at the end of ramus, short, very thin and spirally curved regularly over its entire length.Ductus spermatheca ismuch thinner than ramus.Ductus spermatheca is approxymately equal length with vasculum. In SEM, spermatheca carries scattered, irregular and sparsely ultrastructural pits on various parts.

Material examined: Turkey, Ankara prov.: Kızılcahamam, Soğuksu National Park, 03.VII.1991, 1400 m, 2 exs.; Kızılcahamam, Güvem village, 28.V.1997, 1100 m, 4 exs.; Kızılcahamam, Aköz village, 30.VIII.1997, 1150 m, 1 ex.; **Bolu prov.:** Gerede-Bolu road, 8 km to Bolu, 17.V.2003, 710 m, 1 ex.; Pazarköy-Eskipazar road, enter of Kayılar village, 20.V.2004, 1 ex.; **Çankırı prov.:** Ilgaz, Between Beyköy-Saraycık villages, 40˚59'N 33˚44'E, 19.VI.2015, 1195 m, 1 ex.; Yapraklı, Yukarıöz, wooded area, 40˚51'N 33˚44'E, 25.VI.2015, 1380 m, 2 exs.

Cassida vibex Linnaeus, 1767 (Figure 10)

Structure of spermatheca. Vasculum is in the form of an eggplant or boxing gloves. It is distinctively curved, relatively wide-angle, asymmetrical C-shaped (the apical part of cornu is more proturuded forward). In vasculum, cornu is thicker than nodulus especially in the apical part. The apical part of cornu is swollen and dark colored. Cornu's apex is rounded. The nodulus is quite short, almost parallel, and not swollen. In stereo microscope, nodulus is dark colored on the inner surface of the basal part. In SEM, this part carries an integument, the back edge of which is extended backwards in the form of a wavy fringe. Ampulla is in the form of a duct or tube that is very distinct, slightly elongated and is laterally connected to nodulus on the outer surface of its basal part. It is slightly thinner than nodulus. Collum is quite short but distinct. Ramus is very distinct and is in the form of a longish, straight and thick duct or tube. Ramus is slightly thinner than nodulus. Ductus glandula auxiliaris (ductus spermathecal gland) is attached to ramus on the outer surface at the end of ramus. Ductus spermatheca is connected straightly to ramus, thick and longish. It is in the form of a flat tube, which makes wide folds in the proximal part. The next big part is spirally curved regularly. The spirally curved part of ductus spermatheca approximately equal width withits proximal part.Ductus spermatheca is approximately equal width with ramus over its entire length. Ductus spermatheca is about 2 times longer than vasculum. In SEM, spermatheca carries scattered, irregular and sparsely ultrastructural pits on various parts.

Material examined:Turkey, Bolu prov.: Entry of Mengen (Devrek-Mengen road), 18.VI.2003, 650 m, 1 ex.; **Çankırı prov.:** Atkaracalar, entry of Hüyük village, 40˚51'N 33˚3'E, 25.IV.2015, 1331 m, 1 ex.; Kızılırmak, between Küçükbahçeli-Büyükbahçeli villages, 40˚23'N 33˚58'E, 01.V.2015, 583 m,1 ex.; Centre, Aşağıçavuş village, 40˚41'N 33˚36'E, 09.V.2015, 847 m, 2 exs.; Centre, Alanpınar- Başeğmez villages return, 40˚41'N 33˚35'E, 09.V.2015, 822 m, 2 exs.; Kurşunlu, Dağören-Sünürlü villages return, 40˚48'N 33˚16'E, 10.V.2015, 996 m, 1 ex.; Eldivan, Oğlaklı village, 40˚32'N 33˚33'E, 13.V.2015, 1027 m, 2 exs.; Eldivan, entry of Elmacı village, 40˚28'N 33˚33'E, 13.V.2015, 937 m, 1 ex.; Eldivan, entry of Çiftlik village, 40˚34'N 33˚30'E, 14.V.2015, 844 m, 1 ex.; Centre, Tuzlu village-Yapraklı return, 40˚35'N 33˚40'E, 15.V.2015, 885 m, 1 ex.; Centre, Balıbağı village, 40˚34'N 33˚46'E, 15.V.2015, 1037 m, 1 ex.; Kızılırmak, Yukarıalagöz village, 40˚22'N 33˚53'E, 16.V.2015, 642 m, 2 exs.; Ilgaz, exit of Belören village, 40˚51'N 33˚30'E, 27.V.2015, 903 m, 6 exs.; Ilgaz, Belören village, 40˚51'N 33˚30'E, 18.VI.2015, 914 m, 4 exs.; Ilgaz, Sazak village, 40˚56'N 33˚43'E, 18.VI.2015, 1144 m, 1 ex.; Ilgaz, Kırkpınar Highland, 41˚00'N 33˚41'E, 19.VI.2015, 1230 m, 1 ex.; Yapraklı, Yukarıöz village, 40˚51'N 33˚44'E, 25.VI.2015, 1380 m, 1 ex.; **Çorum prov.:** Tosya-Kargı road, 2 miles to Akçayazı (Zincirlikuyu env.), 16.VI.2003, 655 m, 1 ex.; Göletdere, 5 miles to Karagöl village, 16.VI.2003, 1120 m, 1 ex.; **İçel prov.:** Fındıkpınarı, exit of Çağlayan, 25.VI.2001, 1070 m, 1 ex.; **Kastamonu prov.:** Exit of Kastamonu 6th km (between Kastamonu-Araç), 16.V.2003, 1000 m, 1 ex.; **Kayseri prov.:** Tomarza, Toklar, 10.VI.2015, 1425 m, 1 ex.; **Niğde prov.:** Between Niğde-Bor, Derbent district, 17.VI.1997, 2 exs.; Niğde Mountains, Karyağdı, 17.VI.1997, 1 ex.; Çamardı, Yelatan village, 23.VI.1997, 1280 m, 1 ex.; exit of Ulukışla, Bahçelik, 29.V.2001, 1445 m, 1 ex.

Structure of spermatheca in the subgenus Cassida (Cassida) Linnaeus, 1758. *Cassida nebulosa* Linnaeus, 1758 is the type species of both the genus *Cassida* Linnaeus, 1758, and therefore the nominative subgenus *Cassida* (*Cassida*) Linnaeus, 1758. Therefore, as a rule, being able to question whether there are other species belonging to this subgenus makes it necessary to firstly define the spermathecal morphology of *Cassida nebulosa* Linnaeus, 1758. The spermathecal structure of the type species should characterize this subgenus. The structure of spermatheca in *Cassida nebulosa* Linnaeus, 1758 is given in the text.

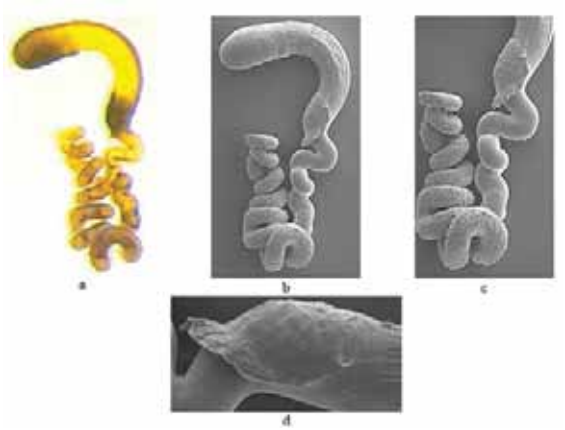

FIGURE 10
Spermathecae of *Cassida vibex*, a. view in stereo microscope, b-d. view in SEM.

Vasculum, ampulla, ductus glandula auxiliaris and ductus spermatheca are generally constant in shape within species, but distinct and useful in comparison with other species. Based on the structure of these four parts of spermatheca we divided the species of the subgenus *Cassida* (s.str.) into six groups :

Group I (*Cassida nebulosa* group**): Vasculum** is in the form of an opened hook or bird beak-shaped. It is symmetrical C-shaped. Nodulus is much thicker than cornu especially in the basal part. Apical part of cornu clearly sharpened and dark colored. Cornu's apex is pointed. Apical part of cornu extended to the front of its apex with an integument. The nodulus is quite long, not parallel, distinctly swollen and bulbous. In SEM, nodulus carries a wide integument on the inner surface of the basal part. **Ampulla** is very small. It is in the form of a tubercle and is connected to nodulus on the outer surface of its basal part. It is incomparably smaller than nodulus. Collum is invisible, vague or very reduced. Ramus is clearly visible and in the form of a tubercle. **Ductus glandula auxiliaris** (ductus spermathecal gland) is attached to ramus at the end of ramus. **Ductus spermatheca** is connected to ramus on the outer surface in the middle part of ramus. Ductus spermatheca is very long, quite thin, and is spirally curved regularly almost over its entire length. It is much thinner than ampulla. Ductus spermatheca is at least 6 times longer than vasculum. Here: *Cassida nebulosa* Linnaeus, 1758 (Figures 4, 12). In addition, *Cassida flaveola* Thunberg, 1794 (under Bordy, 2009) [15].

Group II (*Cassida vibex* group**): Vasculum** is in the form of an eggplant or boxing gloves. It is asymmetrical C-shaped (the apical part of cornu is more protruded forward). Cornu is usually much thicker than nodulus especially in the apical part. The apical part of cornu is usually noticeably swollen. Cornu's apex is rounded. The nodulus is quite short, almost parallel, and not swollen. In stereo

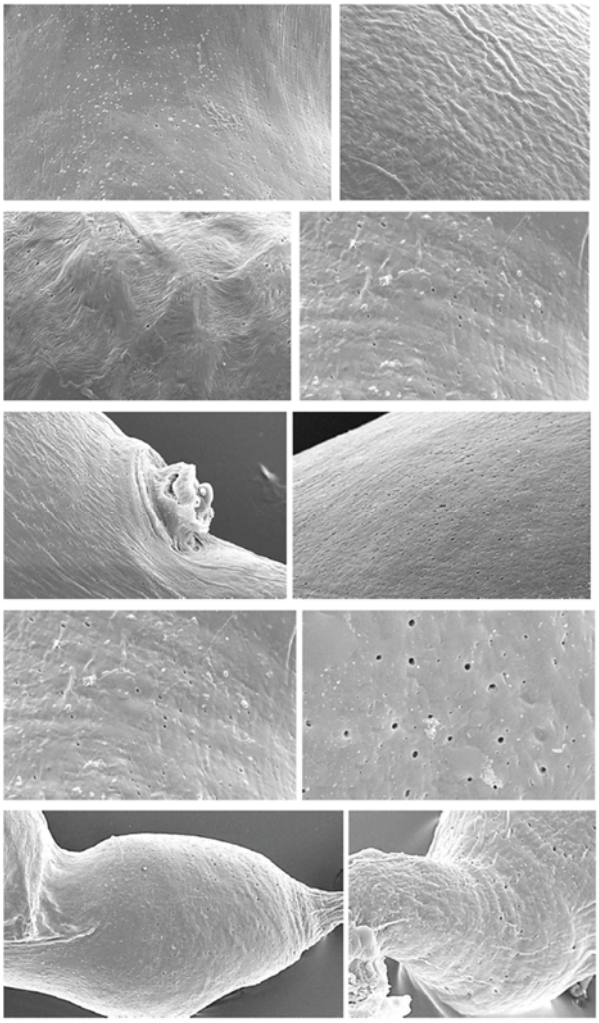

FIGURE 11
The ultrastructural pits on various parts of spermatheca in the subgenus *Cassida* (*Cassida*) Linnaeus, 1758 (SEM).

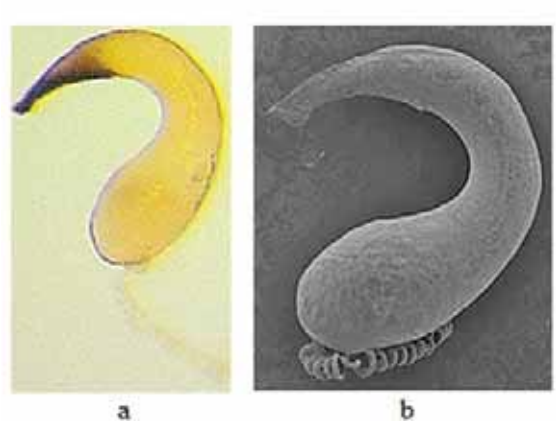

FIGURE 12
Spermathecae of *Cassida nebulosa*, a. view in stereo microscope, b-d. view in SEM.

microscope, nodulus is dark colored on the inner surface of the basal part. In SEM, this part carries an integument, the back edge of which is extended backwards in the form of a wavy fringe. **Ampulla** is in the form of a duct or tube that is very distinct, elongated and is laterally connected to nodulus on the outer surface of its basal part. It is much or slightly thinner than nodulus. Collum is quite short, but distinct. Ramus is very distinct. It is in the form of a long, straight and thick duct or tube. Ramus is much or slightly thinner than nodulus. **Ductus glandula auxiliaris** (ductus spermathecal gland) is attached to ramus on the outer surface at the end of ramus. **Ductus spermatheca** is connected straightlyto ramus, thick or thickish and long or longish. It is in the form of a flat tube, which forms wide folds in the proximal part. It is thinner in the next big part and is spirally curved regularly. Ductus spermatheca is slightly thinner than ramus or approximately equal width with ramus in the proximal part and is usually much thinner than ramus in the spiral part. Ductus spermatheca is at least more than 2 times longer than vasculum. Here: *Cassida atrata* Fabricius, 1787 (Figures 2, 13), *Cassida fausti* Spaeth & Reitter, 1926 (Figures 3, 13), *Cassida pannonica* Suffrian, 1844 (Figures 6, 13), *Cassida vibex* Linnaeus, 1767 (Figures 10, 13). In addition, *Cassida bergeali*

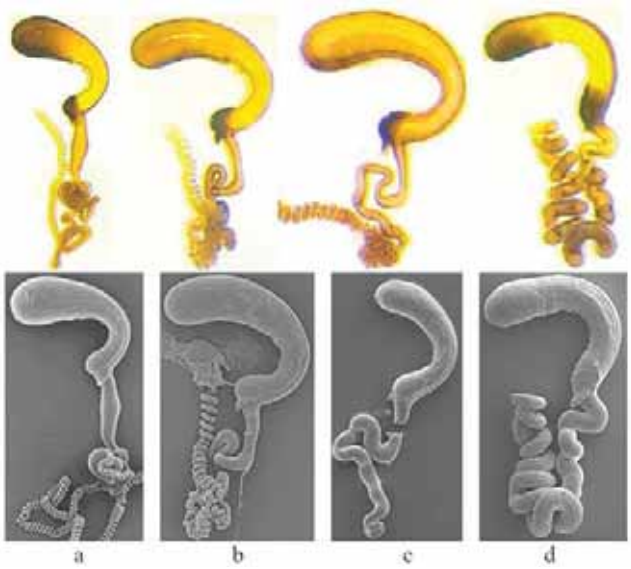

FIGURE 13
Spermathecae in stereo microscope and SEM. a. *Cassida atrata*, b. *Cassida fausti*, c. *Cassida pannonica*, d. *Cassida vibex*.

Bordy, 1995, *Cassida elongata* Weise, 1893, *Cassida inopinata* Sassi & Borowiec, 2006, *Cassida major* Kraatz, 1874 (under Sassi & Borowiec, 2006), *Cassida bergeali* Bordy,1995,*Cassida ferruginea* Goeze, 1777, *Cassida humeralis* Kraatz, 1874, *Cassida panzeri* Weise, 1907 (under Bordy, 2009) and *Cassida ferruginea* Goeze, 1777, *Cassida mongolica* Boheman 1854 (under Suenaga, 2013) [15, 16].

Group III (*Cassida rubiginosa* group**): Vasculum** is in the form of a boomerang or payphone. It is asymmetrical C-shaped (the apical part of cornu is slightly protruded forward). Cornu is much thicker than nodulus especially in the apical part.The apical part of cornu is noticeably swollen. Cornu's apex is rounded. In SEM, the underside of the apical part of cornu has almost an integument-like thickening. Therefore, this part appears somewhat dark in stereo microscope. The nodulus is quite short, almost parallel, and not swollen. In stereo microscope, nodulus is somewhat dark colored on the inner surface of the basal part. In SEM, this part carries an integument or integument-like thickening. **Ampulla** is tubercular, quite short but distinct and is attached flat (parallel) at the bottom to the basal end of nodulus. It is slightly thinner than nodulus. Collum is distinct and is in the form of a short stem.Collum is much thinner than nodulus. Ramus is in the form of a tuber or cone-like, quite small but distinct, swollen and more or less protruding outwardin the middle part. Ramus is slightly thinner than nodulus in its widest part. **Ductus glandula auxiliaris** (ductus spermathecal gland) is attached to ramus on the outer surface in the middle part of ramus. **Ductus spermatheca** is connected straightly to ramusin the middle at the end of ramus, very thin and spirally curved regularly over its entire length. It is much thinner than ramus. Ductus spermatheca is approximately equal length with vasculum or more than 2 times longer than vasculum.Here: *Cassida palaestina* Reiche, 1858 (Figures 5, 14), *Cassida rubiginosa* Müller, 1776 (Figures 7, 14),In addition, *Cassida deflorata* Suffrian, 1844, *Cassida prasina* Illiger, 1798 and *Cassida rufovirens* Suffrian, 1844 (under Bordy, 2009) [15].

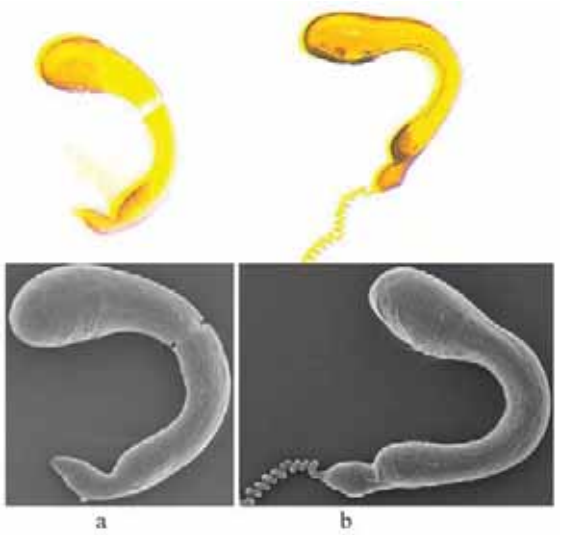

FIGURE 14
Spermathecaein stereo microscope and SEM. a. *Cassida palaestina*, b. *Cassida rubiginosa.*

Group IV (*Cassida sanguinolenta* group**): Vasculum**is in the form of an eggplant or boxing gloves. It is asymmetrical C-shaped (the apical part of cornu is much more protruded forward). Cornu is thicker than nodulus especially in the apical part.The apical part of cornu is swollen. Cornu's apex is rounded.The nodulus is quite short, almost parallel, and not swollen. In SEM, nodulus has almost an integument-like thickening on the inner surface of the basal part. Therefore, this part appears somewhat

dark in stereo microscope. **Ampulla** is in the form of a wavy duct or tubethat is distinct, thickish, slightly elongated, and is attached flat (parallel) at the bottom to the basal end of the nodulus. The ramus of ampulla is recessed on the outer surface where it connects to the collum. Therefore, ampulla has taken a comma-like wavy shape in general view. Ampulla is slightly thinner than nodulus. Collum is quite short, distinct, and in the form of a wide stem. Ramus is in the form of a wavy duct or tubethat is short but distinct and thickish. **Ductus glandula auxiliaris** (ductus spermathecal gland) is laterally attached to ramus on the outer surface at the end of ramus. **Ductus spermatheca** islaterally connected straightly to ramuson the inner surface at the end of ramus, short, very thin and spirally curved regularly over its entire length.Ductus spermatheca ismuch thinner than ramus.Ductus spermatheca is approximately equal length with vasculum or about 2-3 times longer than vasculum.Here: *Cassida sanguinolenta* Müller, 1776 (Figures 8, 15), *Cassida stigmatica* Suffrian, 1844 (Figures 9, 15). In addition, *Cassida coralline* Boheman, 1862(under Bordy, 2009) [15].

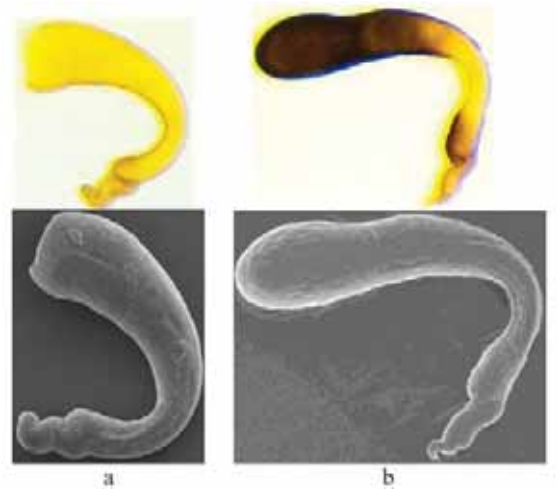

FIGURE 15
Spermathecae in stereo microscope and SEM. a. *Cassida sanguinolenta*, b. *Cassida stigmatica*.

Group V(*Cassida seladonia* group**): Vasculum**is in the form of an eggplant or boxing gloves. It is asymmetrical C-shaped (the apical part of cornu is more protruded forward). Cornu is thicker than nodulus especially in the apical part.The apical part of cornu is swollen. Cornu's apex is rounded.The nodulus is quite short, almost parallel, and not swollen. Nodulus is usually darkened on the inner surface of the basal part. **Ampulla** is in the form of a more or less wavy duct or tubethat is distinct, thick, elongated, and is attached flat (parallel) at the bottom to the basal end of nodulus.Ampulla is slightly recessed on the outer surface in its middle part where it connects to the ductus glandula auxiliaris. Ampulla is slightly thinner than nodulus. Collum is quite short, distinct, and in the form of a wide stem. Ramus is in the form of a more or less wavy duct or tubethat is longish, distinct and thick. **Ductus glandula auxiliaris** (ductus spermathecal gland) is laterally attached to ramus on the outer surface in the middle part of ramus. **Ductus spermatheca** is connected straightly to the end of ramus. It is usually in the form of a quite short, thin, flat tube, which forms small folds almost over its entire length. Sometimes it is spirally curved regularlyover its entire length. Ductus spermatheca is much thinner than ramus. Ductus spermatheca is less than vasculum or approximately equal length with vasculum.Here: *Cassida algirica* Lucas, 1849, *Cassida denticollis* Suffrian, 1844 (Figure 16), *Cassida hexastigma* Suffrian, 1844, *Cassida inquinata* Brullé, 1832 and *Cassida seladonia* Gyllenhal, 1827 (under Bordy, 2009) [15].

FIGURE 16
Spermatheca of *Cassida seladonia*in stereo microscope(taken from B. Bordy, 2009) [15].

Group VI (*Cassida sanguinosa* group**): Vasculum** is in the form of an eggplant or boxing gloves. It is asymmetrical C-shaped (the apical part of cornu is slightly protruded forward). Cornu is thicker than nodulus especially in the apical part. The apical part of cornu is swollen and the underside is darkened. Cornu's apex is rounded. However, apex has a very small bud-shaped process. The nodulus is quite short, slightly swollen, and not parallel. Nodulus is usually darkened on the inner surface of the basal part. **Ampulla** is in the form of a more or less wavy duct or tube that is distinct, thick, elongated, and is attached flat (parallel) at the bottom to the basal end of nodulus. Ampulla is slightly recessed on the outer surface in its middle part where it connects to the ductus glandula auxiliaris. Ampulla is thinner or slightly thinner than nodulus. Collum is quite short, distinct, and in the form of a wide stem. Ramus is in the form of a more or less wavy duct or tube that is longish, distinct and thick or thickish. **Ductus glandula auxiliaris** (ductus spermathecal gland) is laterally attached to ramus on the outer surface in the middle part or basal part near the middle of ramus. **Ductus spermatheca** is connected straightly to the end of ramus. It is usually in the form of a longish, more or less thin, flat tube, which forms small folds almost over its entire length. Sometimes it is spirally curved regularly over its entire length. Ductus spermatheca is much thinner than ramus. Ductus spermatheca is about 1.5-2 times longer than vasculum. Here: *Cassida alpine* Bremi-Wolf, 1855, *Cassida*

leucanthemi Bordy, 1995 and *Cassida sanguinosa* Suffrian, 1844 (Figure 17) (under Bordy, 2009) [15].

FIGURE 17
Spermatheca of *Cassida sanguinosa* in stereo microscope (taken from B. Bordy, 2009) [15].

DISCUSSION

Sassi & Borowiec (2006) stated that most taxonomic studies on Cassidinae are based only on external morphology and feeding preferences, and ignored morphology of genitalia. The structure of both male and female genitalia in many groups of cassids is very uniform and various authors suggested that they are not useful in determining species and in systematic studies. This is a rather old fashioned systematic approach.The taxonomic importance of Cassidinae internal anatomy has been considered by a growing amount of scientific studies[10-14, 16-18]. Therefore, it is expected that the use of these new traits reserves interesting novelties even within species groups.Under these circumstances, the morphology of the spermatheca seems to be more effective in delimiting a natural group.

Studies on the structure of spermatheca so far are based only on stereo microscopic studies.Bordy (2009) is a remarkable work in terms of the structure of spermathecaeof the species belonging to the subgenus *Cassida*(s.str.) in Turkey [15]. As known, *Cassida* (s.str.) includes 46 species in the world. Bordy (2009) studied spermathecae of twenty-four species belonging to *Cassida* (s.str.) as well as other *Cassida* speciesin France only in stereo microscope. Among them, fifteen species occur also in Turkey. A total of 21 speciesin this subgenus is already known from Turkey.

Among them, eight species as *C. atrata*, *C. nebulosa*, *C. pannonica*, *C. prasina*, *C. rubiginosa*, *C. sanguinolenta*, *C. stigmatica* and *C. vibex* were examined in both stereo microscope and scanning electron microscope (SEM) in this study. These species were also studied by Bordy (2009). The other two species were also examined in this study, however, E-European *C. fausti* and Turano-E-Mediterranean *C. palaestina* have not been studied because it is off his topic by Bordy (2009). Moreover, eight species known to be in Turkey but not examined in this study were studied by Bordy (2009). These are *C. algirica*, *C. denticollis*, *C. ferruginea*, *C. flaveola*, *C. inquinata*, *C. rufovirens*, *C. sanguinosa*and *C. seladonia*. Thus, structuresof spermathecae of totally eighteen species known from Turkey were evaluated by Bordy (2009) and this study [15]. After all, only the remaining 3 species reported from a single locality from Turkeyhave not been studied. These are *Cassida elongate* Weise, 1893 (just known from Konya province), *Cassida lineola* Creutzer, 1799 (just known from Kars province) and *Cassida reitteri* Weise, 1892 (just known from Ankara province). On the other side, most of the species examined in this study were evaluated by SEM for the first time.

Based on the spermathecal definition of the type species given in the text and the research results given in the literatures (Sassi & Borowiec, 2006; Bordy, 2009; Suenaga, 2013), the similarities and differences in spermathecal morphologies of the studied 10 species belonging to the subgenus *Cassida* (s.str.) were evaluated. Accordingly, no species like the type species were found among the species examined in this study currently accepted in the subgenus *Cassida* (s.str.) [15, 16, 18]. Besides, according to Bordy (2009), only the spermathecal morphologyof *Cassida flaveola* Thunberg, 1794is similar to that of the type species [15].

As mentioned, based on the structure of vasculum, ampulla, ductus glandula auxiliaris and ductus spermatheca we divided the species of the subgenus *Cassida* (s.str.) into sixdistinct groups.Based on theresults of this study, relationships among the groups can be evaluated as follows.

According to the structure of vasculum, Group III (*Cassida rubiginosa* group), Group IV (*Cassida sanguinolenta* group), Group V (*Cassida seladonia* group) and Group VI (*Cassida sanguinosa* group) seem to be more or less similar to each other. Group I (*Cassida nebulosa* group) and Group II (*Cassida vibex* group) are different from each other and the other groups.According to the structure of ampulla, Group IV (*Cassida sanguinolenta* group), Group V (*Cassida seladonia* group) and Group VI (*Cassida sanguinosa* group) seem to be more or less similar to each other. Group I (*Cassida nebulosa* group), Group II (*Cassida vibex* group) and Group III (*Cassida rubiginosa* group) are different from each other and the other groups.According to the connection to the ramus of ductus glandula auxiliaris, Group III (*Cassida rubiginosa* group), Group V (*Cassida seladonia* group) and Group VI (*Cassida sanguinosa*

group) seem to be more or less similar to each other. Besides, Group II (*Cassida vibex* group) and Group IV (*Cassida sanguinolenta* group) seem to be also more or less similar to each other. Group I (*Cassida nebulosa* group) is different from the other groups.According to the structure of ductus spermatheca, each group is different from the other.

Based on all these results, it can be said that-**Group I** (*Cassida nebulosa* group) is different from other groups in terms of all structures.**Group II** (*Cassida vibex* group) also has a very different structure than other groups. It can be said that the closest relative to this group is Group IV (*Cassida sanguinolenta* group) compared to other more distant groups. **Group III** (*Cassida rubiginosa* group) also has a quite different structure than other groups. Compared to other more distant groups, this group is close to Group V (*Cassida seladonia* group) and Group VI (*Cassida sanguinosa* group). **Group IV** (*Cassida sanguinolenta* group) has a quite different structure than other groups, and seems to be more or less close to Group V (*Cassida seladonia* group) and Group VI (*Cassida sanguinosa* group) compared to other more distant groups. **Group V** (*Cassida seladonia* group) and **Group VI** (*Cassida sanguinosa* group) seem to be closely relatedto other groups.

This is a proof that the subgenus is not a monophyletic, but a polyphyletic group. Already, Borowiec (2007) stated that this subgenus is not monophyletic, and a few subgroups can be separated in this group according to similar adult morphology and nutritional preferences [1]. Accordingly, similar species of the species examined according to the adult external morphology in the subgenus *Cassida* (s.str) and species for the mentioned six groups accepted in this study according to the structure of spermathecae based on the results of this study and the literature is given in Table 1. Also, at the end of the study, the habitus of adults of the species examined are given in plate I, and a diagnostic key based

TABLE 1

Similar species of the species examinedaccording to the adult external morphology in the subgenus *Cassida* (s.str) and species for the groups accepted according to the sturucture of spermathecaein this study.

Species	Similar species	Species for the groups in this study
Group I (**-***nebulosa* group**)** *C.nebulosa*		*C.nebulosa - C. flaveola*
Group II (**-***vibex* group**)**		*C.atrata - C. bergeali -C. elongata - C.fausti - C. ferruginea - C. humeralis - C. inopinata - C. major -C.mongolica- C.pannonica - C. panzeri - C.vibex*
C.atrata	*C.mongolica*	
C.fausti	*C. bergeali - C. elongata - C. inopinata C. pannonica - C. vibex*	
C.pannonica	*C. bergeali - C. elongata - C. fausti – C. inopinata - C. vibex*	
C.vibex	*C. bergeali - C. elongata- C. fausti – C. inopinata - C. pannonica*	
Group III (**-***rubiginosa* group**)**		*C. deflorata -C. palaestina-C. prasina -C. rubiginosa-C. rufovirens*
C.palaestina	*C. algirica - C. alpina - C. deflorata - C. rubiginosa*	
C.rubiginosa	*C. algirica- C. alpina - C. deflorata - C. palaestina*	
Group IV (**-***sanguinolenta* group**)**		*C. corallina -C. sanguinolenta-C. stigmatica*
C.sanguinolenta	*C. aurora - C. denticollis - C. prasina - C. rufovirens*	
C.stigmatica		
Group V (**-***seladonia* group**)**		*C. algirica - C. denticollis - C. hexastigma - C. inquinata C. seladonia*
Group VI (**-***sanguinosa* group**)**		*C. alpina - C. leucanthemi - C. sanguinosa*

on external and spermathecal morphological characters of adults is also provided.

As clearly seen from the table, the six groups are partly correlated with similar species of the species examinedaccording to the adult external morphological characters.It is understood from this table that the grouping we have made according to the spermathecal structure will be a more accurate approach for grouping this subgenusthan the grouping that can be done according to the external morphological characters.This approach is explicitly supported in Table 2, where the host plants of the species studied in this study are given.

In accordance with our grouping, the host plants of the type species *Cassida nebulosa* are members of Amaranthaceae and Chenopodiaceae, unlike other studied species.The host plants of the other species are members of the Asteraceae family, with the exception of *Cassida atrata*whose host plants are Lamiaceae species.This situation reveals an important and valuable explanation in terms of the fact that type species *Cassida nebulosa* differs from the other species examined in our study due to the sturucture of spermatheca and that it remains alone in group I. Also host plants of *Cassida flaveola* which regarded a member of group I is members of Caryophyllaceae family according to Bordy (2009). The grouping of other species seems to be partly correlated with the genera of their host plant family given in Table 2.

As another output revealed by the study, is that male and female genital structures in the genus *Cassida* have distinctive importance in different categories and levels in terms of the taxa examined.In general, aedeagal characters are distinctive at the family group level, and spermatecal characters are distinctive at the genus group level. Although spermatecal characters are found to be particularly useful at the species group level, most of the aedeagal characters

TABLE 2
The host plants of the species examinedin the subgenus *Cassida* (s.str) [7, 15, 19-35].

Species	Host family	Host genera	Literatures
Group I (**-***nebulosa* group**)**			
C.nebulosa	Amaranthaceae	*Amaranthus*	Chujô & Kimoto, 1961; Bordy, 2009
	Chenopodiaceae	*Atriplex*, *Beta, Chenopodium*	Kleine, 1916; Chujô & Kimoto, 1961; Kosior, 1975; Brovdij, 1983; Lee & Choo, 2006
Group II (**-***vibex* group**)**			
C.atrata	Lamiaceae	*Salvia*	Spaeth & Reitter, 1926; Bechyne, 1944; Sekerka, 2008
C.fausti	Asteraceae	*Arctium*, *Cynara*	Brovdij, 1983; Kismali & Sassi, 1994
C.pannonica	Asteraceae	*Centaurea*, *Cynara*,*Erodium*,*Jurinea*	Bechyne, 1944; Brovdij, 1983; Bordy, 1986; Bordy & Doguet, 1987; Kismali & Sassi, 1994; Bordy, 2009
C.vibex	Asteraceae	*Arctium*, *Carduus*, *Centaurea*,*Cirsium*, *Tanacetum*	Bechyne, 1944; Chujô & Kimoto, 1961; Kosior, 1975; Brovdij, 1983
Group III (**-***rubiginosa* group**)**			
C.palaestina	Asteraceae	*Carthamus*, *Cirsium*, *Cousinia*, *Cynara, Sylibium*	Berti & Rapilly, 1973; Lopatin, 1977; Al-Ali & Abbas, 1981; Borowiec et al., 1997
C.rubiginosa	Asteraceae	*Arctium*, *Artemisia*,*Centaurea*,*Cirsium*, *Carduus*, *Cynara*, *Inula*, *Onopordum*, *Pulicaria*,*Saussurea*,*Serratula, Silybum*, *Tanacetum*	Kleine, 1917a,b; Bechyne, 1944; Chujô & Kimoto, 1961; Jolivet, 1967; Kosior, 1975; Brovdij, 1983; Bourdonne & Bordy, 1993; Majka & Lesage, 2008; Bordy, 2009
Group IV (**-***sanguinolenta* group**)**			
C.sanguinolenta	Asteraceae	*Achillea*,*Tanacetum*	Bechyne, 1944; Brovdij, 1983; Bordy, 2009
C.stigmatica	Asteraceae	*Achillea*, *Artemisia, Tanacetum*	Bechyne, 1944; Brovdij, 1983

are similar among species and therefore unusable. However, it cannot be concluded that genital morphology should not be used at the species group level.It is quite clear that evaluations with SEM, in particular, will be more efficient in this respect and that it can provide diagnostic characters that cannot be evaluated under a stereo microscope.

TAXONOMY

The taxonomic position of the subgenus is under discussion. In accordance with the results obtained in this study, Borowiec (2007) stated that the group is not monophyletic becauseat least the type species *Cassida nebulosa* and *Cassida reitteri* Weise, 1892 are probably not congenericwith most of other species. Also the position of *Cassida lineola* Creutzer, 1799 and *Cassida flaveola* Thunberg, 1794 is doubtful. The four problematic species have some details about adult morphology or immaturestages unlike other taxa. On the other hand, within *Cassida* s. str.we can create several subgroups with similar morphology and feeding preferences.

Steinhausen (2002) proposed the name *Betacassida* for the wide-spread Palaearctic *Cassida nebulosa* Linnaeus, 1758 based on the structure of the pupa [36]. *Betacassida* is an objective synonym in terms of *Cassida nebulosa* is the type species of *Cassida* Linnaeus. Steinhausen (2002) also proposed the name *Pseudocassis* for the wide-spread Palaearctic *Cassida flaveola* Thunberg, 1794 based on the structure of the pupa. According to Borowiec (2007), its position within *Cassida* is still unclear. This situation, proposalof *Betacassida* and *Pseudocassis*, supported the mentioned opinions of Borowiec (2007) [1, 36].

Despite these opinions, Borowiec (2007) also stated other Palaearctic species belonging to the nominotypical subgenus except for the four problematic species form a coherent group. Consequently, he did not propose any subgeneric name for the remaining species in the nominotypical subgenus [1].

Based on all these, it is necessary that severalgroups found to be distinctly different in terms of spermathecal structures are described as new subgenera. We do not refrain from this responsibility, and we propose the new subgenera based on the groups given in the text. In accordance with the results obtained in this study, the proposed names of the new subgenera and the recommended species of them are presented.

Genus ***Cassida***Linnaeus, 1758

Subgenus ***Cassida***Linnaeus, 1758

Cassida Linnaeus, 1758: 362 (type species: *Cassida nebulosa* Linnaeus, 1758, designated by Spaeth, 1914: 92) [37].

Description of the spermathecal structure is given as group I (*Cassida nebulosa* group).

Here: *Cassida nebulosa* Linnaeus, 1758 and*Cassida flaveola*Thunberg, 1794 [38] (Tables 3, 4).

Host plants: The members of the Amaranthaceae, Chenopodiaceae, Caryophyllaceae families.

Note: Although there is the name *Pseudocassis* proposed by Steinhausen (2002) based on the structure of the pupa for *Cassida flaveola* Thunberg, 1794 whosehost plants are members of the Caryophyllaceae family, its spermathecal sturucture is more or less similar to *Cassida nebulosa* Linnaeus, 1758.On the other side, I agree with Steinhausen (2002) that this is not close to other members of Palaearctic *Cassida* (s.str.). Its position within *Cassida* is stillunclear [36].

Subgenus ***Longiampulla*** **subgen. nov.**

Longiampulla subgen. nov. (type species: *Cassida vibex* Linnaeus, 1767).

Description of the spermathecal sturucture is given as group II (*Cassida vibex*group).

Here:*Cassida atrata* Fabricius, 1787; *Cassida bergeali* Bordy, 1995; *Cassida elongate* Weise, 1893; *Cassida fausti* Spaeth & Reitter, 1926; *Cassida ferruginea* Goeze, 1777; *Cassida humeralis*-Kraatz, 1874; *Cassida inopinata* Sassi & Borowiec, 2006; *Cassida major* Kraatz, 1874; *Cassida mongolica* Boheman 1854; *Cassida pannonica*Suffrian, 1844; *Cassida panzeri* Weise, 1907; *Cassida vibex* Linnaeus, 1767 (Tables 3,4).

Host plants: The members of the Asteraceae family.

Etymology: The new subgenus is named after combining “longus” in Latin (meaning long in English) and the spermathecal sturucture “ampulla” words.

Subgenus ***Diversivascula*** **subgen. nov.**

Diversivascula subgen. nov.(type species:*Cassida sanguinolenta* Müller, 1776).

Description of the spermathecal sturucture is given as group IV (*Cassida sanguinolenta* group).

Here: *Cassida corallina* Boheman, 1862; *Cassida sanguinolenta* Müller, 1776; *Cassida stigmatica* Suffrian, 1844 (Tables 3,4).

Host plants: The members of the Asteraceae family.

Etymology: The new subgenus is named after combining “diversus” in Latin (meaning different in English) and the spermathecal sturucture “vasculum” words.

Subgenus ***Reliquacassida*** **subgen. nov.**

Reliquacassida subgen. nov.(type species: *Cassida rubiginosa* Müller, 1776).

Description of the spermathecal sturucture is given as group III (*Cassida rubiginosa* group), group

V (*Cassida seladonia* group) and group VI (*Cassida sanguinosa* group).

Here: *Cassida algirica* Lucas, 1849; *Cassida alpine* Bremi-Wolf, 1855; *Cassida deflorata* Suffrian, 1844; *Cassida denticollis* Suffrian, 1844; *Cassida hexastigma* Suffrian, 1844; *Cassida inquinata* Brullé, 1832; *Cassida leucanthemi* Bordy, 1995; *Cassida palaestina* Reiche, 1858; *Cassida prasina* Illiger, 1798; *Cassida rubiginosa* Müller, 1776; *Cassida rufovirens* Suffrian, 1844; *Cassida sanguinosa* Suffrian, 1844; *Cassida seladonia* Gyllenhal, 1827(Tables 3,4).

Host plants: The members of the Asteraceae family.

Etymology: The new subgenus is named after "reliqua" in Latin (meaning remainder in English).

As known, the nominative subgenus *Cassida* (s.str.) includes forty-seven species with *Cassida inopinata* Sassi & Borowiec, 2006 (forty-six in the Palaearctic region and one in the Nearctic region) in the world [18]. After all, thirty species currently regarded in *Cassida* (s.str.) are recommended to four subgenera of the genus *Cassida* with this work.

Cassida reitteri Weise, 1892 and *Cassida lineola* Creutzer, 1799, two of the remaining seventeen species, are problematic species as stated. As Borowiec (2007) mentioned, *Cassida reitteri* Weise, 1892is not congeneric at least with *Cassida nebulosa* Linnaeus, 1758.Also the position of *Cassida lineola* Creutzer, 1799 is doubtful. According to external morphological characters, *Cassida reitteri* Weise, 1892 is unique, and is more or less similar to *Chiridula semenovi*Weise, 1889 which is the type species of the monotypic genus *Chiridula* Weise, 1889. Also *Cassida lineola* Creutzer, 1799 is unique morphologically, and its position is still doubtful and unclear [1]. These species need to be confirmed and are therefore not recommended for any subgeneramentioned here. The remaining fifteen species that have not been recommended in any subgenerain this study,need further confirmation.

Fifteen species uncertain position, however, are discussed as follows:

The W Mediterranean species *Cassida angustifrons* Weise, 1891is unique morphologically. Its position is still uncertain.

The C and E European *Cassida aurora*Weise, 1907 is more or less similar to *Cassida rufovirens*-Suffrian, 1844 morphologically. Its host plants are the members of Asteraceae family. Therefore, it may belong to *Cassida* (*Reliquacassida*) subgen. nov.

The Caucasian species *Cassida circassica*Medvedev, 1962is unique morphologically. However, Borowiec & Świętojańska (2018) noted that its paratype is conspecific with *Cassida palaestina* ab. *nigrofemorata*. Therefore,it may belong to *Cassida* (*Reliquacassida*) subgen. nov. [39].

The position of S African species *Cassida distinguenda*Spaeth, 1928 is uncertain as most of the other African species.

The E Asiatic species *Cassida fuscorufa* Motschulsky, 1866and *Cassida jacobsoni*Spaeth, 1914is more or less similar to each other morphologically.The host plants of *Cassida fuscorufa*are the members of the Asteraceae family. Under this circumstance, it may belong to *Cassida* (*Longiampulla*) subgen. nov. or to a new subgenus that can be proposed with *Cassida jacobsoni* Spaeth, 1914, *Cassida japana* Baly, 1874, *Cassida piperata* Hope, 1842 and*Cassida pallidicollis* Boheman, 1856 according to external morphologically.

The Spanish endemic species *Cassida hyalina* Weise, 1891is more or less similar to*Cassida coralina* Boheman, 1862 morphologically. Therefore, it may belong to *Cassida* (*Diversivascula*) subgen. nov.

The Tanzanian endemic *Cassida impompalis* Spaeth, 1924is uncertain as most of the other African species.

The E Asiatic species *Cassida mandli* Spaeth, 1921is more or less similar to the recommended species in *Cassida* (*Reliquacassida*) subgen. nov. morphologically. Its host plants are the members of the Asteraceae family. Therefore, it may belong to *Cassida* (*Reliquacassida*) subgen. nov.

The Far Eastern species *Cassida japana* Baly, 1874 and *Cassida piperata*Hope, 1842is more or less similar to each other morphologically.The host plants of *Cassida piperata* Hope, 1842 are the members of the Amaranthaceae and Chenopodiaceae families.Under this circumstance, it may belong to *Cassida* (*Longiampulla*) subgen. nov. or to a new subgenus that can be proposed with *Cassida fuscorufa* Motschulsky, 1866, *Cassida jacobsoni* Spaeth, 1914 and*Cassida pallidicollis* Boheman, 1856 according to external morphologically.

The E Palaearctic species *Cassida pallidicollis* Boheman, 1856 is more or less similar to *Cassida mongolica* Boheman 1854. Its host plants are the members of Chenopodiaceae family. Under this circumstance, it may belong to *Cassida* (*Longiampulla*) subgen. nov. or to a new subgenus that can be proposed with *Cassida fuscorufa* Motschulsky, 1866, *Cassida jacobsoni* Spaeth, 1914, *Cassida japana* Baly, 1874 and *Cassida piperata* Hope, 1842 according to external morphologically.

The American species *Cassida relicta* Spaeth, 1927 is more or less similar to *Cassida ferruginea* Goeze, 1777 and *Cassida panzeri* Weise, 1907 morphologically. Therefore, it may belong to *Cassida* (*Longiampulla*) subgen. nov.

The E European-C Asiatic *Cassida sareptana* Kraatz, 1873 is more or less similar to the recommended species in *Cassida* (*Reliquacassida*) subgen. nov. morphologically. Its host plants are the members of the Asteraceae family. Therefore, it may belong to *Cassida* (*Reliquacassida*) subgen. nov.

TABLE 3
Proposed subgenera and their species according to this study

Subgenus *Cassida* (*Cassida*)	
Cassida nebulosa Linnaeus, 1758	*Cassida flaveola* Thunberg, 1794
Uncertain position to *Cassida* (*Cassida*)	
*Cassida angustifrons*Weise, 1891	*Cassida distinguenda* Spaeth, 1928
*Cassida impompalis*Spaeth, 1924	*Cassida lineola* Creutzer, 1799
*Cassida reitteri*Weise, 1892	
Subgenus *Cassida* (*Longiampulla*) subgen. nov.	
Cassida vibex Linnaeus, 1767	*Cassida atrata* Fabricius, 1787
Cassida bergeali Bordy, 1995	*Cassida elongata* Weise, 1893
Cassida fausti Spaeth & Reitter, 1926	*Cassida ferruginea* Goeze, 1777
Cassida humeralis Kraatz, 1874	*Cassida inopinata* Sassi & Borowiec, 2006
Cassida major Kraatz, 1874	*Cassida mongolica* Boheman 1854
Cassida pannonica Suffrian, 1844	*Cassida panzeri* Weise, 1907
Uncertain position to *Cassida* (*Longiampulla*)	
?*Cassida fuscorufa*Motschulsky, 1866	?*Cassida jacobsoni*Spaeth, 1914
?*Cassida japana*Baly, 1874	?*Cassida pallidicollis*Boheman, 1856
?*Cassida piperata*Hope, 1842	*Cassida relicta*Spaeth, 1927
Subgenus *Cassida* (*Diversivascula*) subgen. nov.	
Cassida sanguinolenta Müller, 1776	*Cassida corallina* Boheman, 1862
Cassida stigmatica Suffrian, 1844	
Uncertain position to *Cassida* (*Diversivascula*)	
*Cassida hyalina*Weise, 1891	?*Cassida spaethi*Weise, 1900
Subgenus *Cassida* (*Reliquacassida*) subgen. nov.	
Cassida rubiginosa Müller, 1776	*Cassida algirica* Lucas, 1849
Cassida alpina Bremi-Wolf, 1855	*Cassida deflorata* Suffrian, 1844
*Cassida denticollis*Suffrian, 1844	*Cassida hexastigma*Suffrian, 1844
Cassida inquinata Brullé, 1832	*Cassida leucanthemi* Bordy, 1995
Cassida palaestina Reiche, 1858	*Cassida prasina* Illiger, 1798
Cassida rufovirens Suffrian, 1844	*Cassida sanguinosa* Suffrian, 1844
Cassida seladonia Gyllenhal, 1827	
Uncertain positionto *Cassida* (*Reliquacassida*)	
*Cassida aurora*Weise, 1907	*Cassida circassica*Medvedev, 1962
*Cassida mandli*Spaeth, 1921	*Cassida sareptana*Kraatz, 1873

TABLE 4
Turkısh species according to the subgenera proposed in this study

Subgenus *Cassida* (*Cassida*)	
Cassida nebulosa Linnaeus, 1758	*Cassida flaveola* Thunberg, 1794
Uncertain position to *Cassida* (*Cassida*)	
Cassida lineola Creutzer, 1799	*Cassida reitteri*Weise, 1892
Subgenus *Cassida* (*Longiampulla*) subgen. nov.	
Cassida vibex Linnaeus, 1767	*Cassida atrata* Fabricius, 1787
Cassida elongata Weise, 1893	*Cassida fausti* Spaeth & Reitter, 1926
Cassida ferruginea Goeze, 1777	*Cassida pannonica* Suffrian, 1844
Subgenus *Cassida* (*Diversivascula*) subgen. nov.	
Cassida sanguinolenta Müller, 1776	*Cassida stigmatica* Suffrian, 1844
Subgenus *Cassida* (*Reliquacassida*) subgen. nov.	
Cassida rubiginosa Müller, 1776	*Cassida algirica* Lucas, 1849
*Cassida denticollis*Suffrian, 1844	*Cassida inquinata* Brullé, 1832
Cassida palaestina Reiche, 1858	*Cassida prasina* Illiger, 1798
Cassida rufovirens Suffrian, 1844	*Cassida sanguinosa* Suffrian, 1844
Cassida seladonia Gyllenhal, 1827	

The E Palaearctic species *Cassida spaethi* Weise, 1900 is more or less similar to the recommended species in *Cassida* (*Diversivascula*) subgen. nov. morphologically. Its host plants are the members of the Asteraceae family. Therefore, it may belong to *Cassida* (*Diversivascula*) subgen. nov.

The species recommended for the subgenera proposed in this study with the species uncertain position are given in Table 3.

Consequently, the taxonomic position of the subgenus is still under discussion. It is hoped that the result of this study will contribute to the solution of this problem. It is hoped that this work will create a reference for future discussions, comments and new arrangements that can be made about the taxonomic position of the subgenus.

A key to the species examined.

1. Pronotum on both sides laterally more or less rounded…..……..……..... **2**

-. Pronotum on both sides laterally more or less narrowed……..…….....**3**

2. Primary puncturation of elytra arranged in regular rows, without any punctures between rows 3 and 4. On elytra with numerous small black spots. Underside completely black. Legs entirely yellow. In spermatheca, vasculum is symmetrical C-shaped, nodulus is much thicker than cornu, apex of cornu pointed.Ductus spermatheca about 10 times longer than vasculum.Length 6.0-7.0 mm. Asiatic-European species. Habitus in Figure 18a.....
.....***Cassida* (*Cassida*) *nebulosa* Linnaeus, 1758**

-. Elytra not regularly seriate-punctate, at least with some extra punctures between rows 3 and 4. Pronotum on both sides laterally more or less narrowed. Upper side black, on anterior margin of pronotum two pale fused spots. Underside mostly black, but borders of abdomen pale. Legs completely black. In spermatheca, vasculum asymmetrical C-shaped, cornu much thicker than nodulus, apex of cornu rounded.Ductus spermatheca about 4-5 times longer than vasculum.Length 5.1-7.0 mm. C- and E-European species. Habitus in Figure 18b……
…***Cassida* (*Longiampulla*) *atrata* Fabricius, 1787**

3. On elytra intervals covered by very short, white hairs. Ampulla laterally connected to nodulus on the outer surface of its basal part. In spermatheca, ductus spermatheca in the form of a flat tube which makes wide folds in the proximal part, spirally curved regularly in its next big part distally……...……...……..
. **4**

-. On elytra intervals bare. Ampulla attached flat (parallel) at the bottom to the basal end of nodulus.In spermatheca, ductus spermatheca uniformly shaped over its entire length.....**6**

4. Elytra with a triangular darkened area (not sharply limited) on sides and behind the scutellum basally. Femora at least in basal half black. In spermatheca, ductus spermatheca is about 2-3 times longer than vasculum, its spiral part thin.Length 5.7-6.4 mm. E-European species. Habitus in Figure 18 c……
***Cassida* (*Longiampulla*) *fausti* Spaeth & Reitter, 1926**

-. Elytra with a great darkened area prolonged along the suture to apical area.In spermatheca, ductus spermatheca is about 2 or 7-8 times longer than vasculum. If it about 2 times longer than vasculum, so its spiral part much thicker…….…….....…..……..
…..**5**

5. Femora not or feebly darkened. In spermatheca, ductus spermatheca about 7-8 times longer than vasculum. It approximately equal width with ramus in its proximal part and much thinner than ramus in its spiral part.Length 6.5-8.2 mm. Sibero-European species. Habitus in Figure 18d.. …....***Cassida* (*Longiampulla*) *pannonica* Suffrian, 1844**

-. Femora at least in basal half black. In spermatheca, ductus spermatheca is about 2 times longer than vasculum. It approximately equal width with ramus over its entire length.Length 5.6-7.0 mm. Asiatic-European species. Habitus in Figure 18e……
…...***Cassida* (*Longiampulla*) *vibex* Linnaeus, 1767**

6. Clypeus narrow, at least 1.25 timeslonger than broad.In spermatheca, vasculum asymmetrical C-shaped, the apical part of cornu slightly protruded forward.....……..….. **7**

-. Clypeus broad, approximately square.In spermatheca, vasculum asymmetrical C-shaped, the apical part of cornu much more protruded forward……..…….....…... **8**

7. Clypeus shining, smooth, rather scarcely punctate. Femora usually entirely pale or only basal third black. In spermatheca, nodulus of vasculum relatively thinner basally. Length 6.5 mm. Turano-E-Mediterranean species. Habitus in Figure 18 f……
***Cassida* (*Reliquacassida*) *palaestina* Reiche, 1858**

-. Clypeus matt, reticulate, more densely punctate. Femora mostly black, at most only apical third yellowish. Elytra with a dark dot behind the scutellum and a few darkened spots on both sides of scutellum. In spermatheca, nodulus of vasculum relatively thicker basally. Length 6.5-7.5 mm. Holarctic species. Habitus in Figure 18g
.....
***Cassida* (*Reliquacassida*) *rubiginosa* Müller, 1776**

8. Pronotum as broad as elytra.In spermatheca, cornu of vasculum relatively thicker apically. Ductus spermatheca is about 2 times longer than vasculum. Length 5.0-5.9 mm. Sibero-European species. Habitus in Figure 18i
…….....
***Cassida* (*Diversivascula*) *sanguinolenta* Müller, 1776**

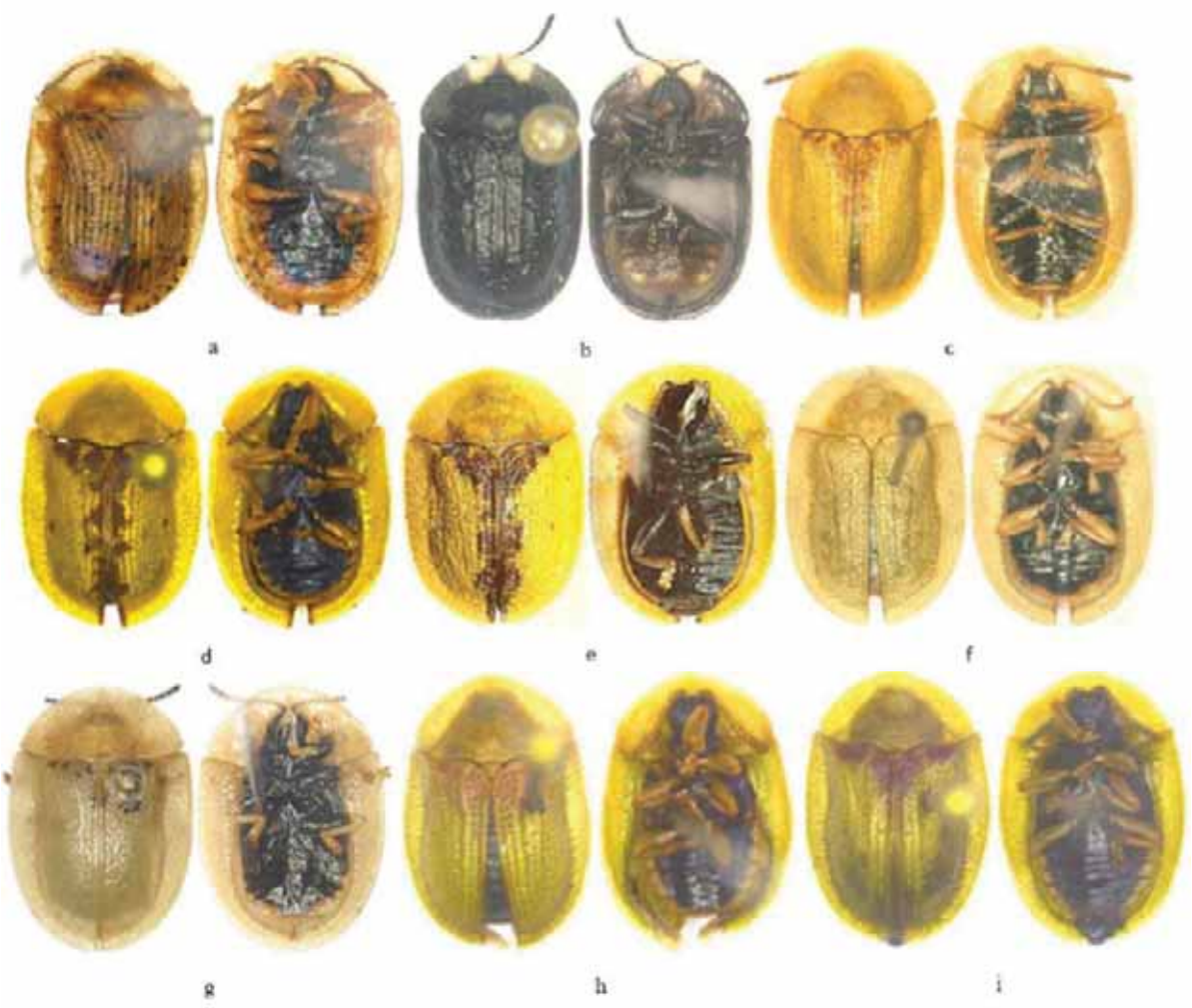

FIGURE 18

Habitus of, a. *Cassida nebulosa*Linnaeus, b. *Casida atrata* Fabricius, c. *Cassida fausti* Spaeth & Reitter, d. *Cassida pannonica* Suffrian, e. *Cassida vibex* Linnaeus, f. *Cassida palaestina* Reihe, g. *Cassida rubiginosa* Müller, h. *Cassida sanguinolenta* Müller, i. *Cassida stigmatica* Suffrian.

-. Pronotum distinctly narrower than elytra. In spermatheca, cornu of vasculum relatively thinner apically. Ductus spermatheca is approxymately equal length with vasculum.Length 5.4-5.9 mm. Palaearctic species. Habitus in Figure 18k……..... .***Cassida* (*Diversivascula*) *stigmatica* Suffrian, 1844**

ACKNOWLEDGEMENTS

We would like to thank Prof. Dr. Zekiye Suludere (Turkey) for her tremendous support in the process of picturing my study material with Scanning Electrone Microscope, Didem Coral Şahin for providing some specimens studied in this work and Damla Amutkan Mutlu (Turkey) for valuable assistance in preparing specimens for SEM examination.

REFERENCES

[1] Borowiec, L.(2007) Two new species of *Cassida* Linnaeus, 1758 (Coleoptera: Chrysomelidae: Cassidinae) from Madagascar and notes on subgenera of the genus *Cassida*. Zootaxa. 1586, 47-58.

[2] Borowiec, L. and Sekerka, L. (2010) Cassidinae: pp. 64-65, 368-390. In: I. Löbl, A. Smetana (eds.), Catalogue of Palaearctic Coleoptera, Volume 6, Chrysomeloidea. Apollo Books.1-924.

[3] Özdikmen, H. and Bal, N. (2019) On the subgenus *Alledoya* Hincks, 1950 (Coleoptera: Chrysomelidae: Cassidinae). Munis Entomology & Zoology. 14 (2), 350-357.

[4] Ekiz, A. N., Şen, İ., Aslan, E. G. and Gök, A. (2013) Checklist of leaf beetles (Coleoptera: Chrysomelidae) of Turkey, excluding Bruchinae. Journal of Natural History. 47 (33-34), 2213-2287.

[5] Özdikmen, H., Mercan, N., Cihan, N., Kaya, G., Topcu, N. N. and Kavak, M. (2014) The importance of superfamily Chrysomeloidea for Turkish biodiversity (Coleoptera). Munis Entomology & Zoology. 9 (1), 17-45.

[6] Özdikmen, H. and Kaya, G. (2014) Chorotype identification for Turkish Chrysomeloidea (Coleoptera) Part I – Chrysomelidae: Hispinae and Cassidinae. Munis Entomology & Zoology. 9 (1), 58-70.

[7] Kısmalı, Ş. and Sassi, D. (1994) Preliminary list of Chrysomelidae with notes on distribution and importance of species in Turkey. II. Subfamily Cassidinae Spaeth. Türkiye Entomoloji Dergisi. 18, 141-156.

[8] Warchałowski, A. (2003) Chrysomelidae: the leaf beetles of Europe and the mediterranean Area. Warszawa: Natura Optima Dux Foundation. 1-600.

[9] Warchalowski, A. (2010) The Palaearctic Chrysomelidae. Identification keys. Vol. 1 & 2. Warszawa*:* Natura optima dux Foundation. 1-1212.

[10] Bordy, B. and Doguet, S. (1987) Contribution to the knowledge of Cassidinae of France. Study of their spermatheca (Coleoptera, Chrysomelidae). Nouvelle Revue d'Entomologie (N.S.). 4, 161-176 (in French).

[11] Borowiec, L. and Świętojańska, J.(2001) Revision of *Cassida litigiosa* group from southern Africa (Coleoptera: Chrysomelidae: Cassidinae). Annales Zoologici Warszawa. 51, 153-184.

[12] Ataş, F., Özdikmen, H., Bal, N., Amutkan Mutlu, D. and Suludere, Z. (2019a) A SEM study on aedeagus and spermatheca of *Cassida seraphina* Ménétries, 1836 (Coleoptera: Chrysomelidae: Cassidinae) from Turkey. Munis Entomology & Zoology. 14 (2), 395-411.

[13] Ataş, F., Özdikmen, H., Bal, N., Amutkan Mutlu, D. and Suludere, Z. (2019b) A SEM study on aedeagus and spermatheca of *Cassida hablitziae* Motschulsky, 1838 (Coleoptera: Chrysomelidae: Cassidinae) from Turkey. Munis Entomology & Zoology. 14 (2), 519-529.

[14] Özdikmen, H., Bal, N., Amutkan Mutlu, D. and Suludere, Z. (2020) A SEM study on aedeagus and spermatheca of *Cassida nebulosa* Linnaeus, 1758 (Coleoptera: Chrysomelidae: Cassidinae) from Turkey. Munis Entomology & Zoology. 15 (1), 252-261.

[15] Bordy, B. (2009) Coleopteres Chrysomelidae (Second edition). Hispinae and Cassidinae. Wildlife of France. 85, FFSSN, Paris. 1-260 (in French).

[16] Suenaga, H. (2013) Notes on *Cassida ferruginea* and *Cassida mongolica* in Japan, with descriptions of their reproductive systems (Coleoptera: Chrysomelidae: Cassidinae). Genus. 24, 325-333.

[17] Borowiec, L. and Skuza, M.(2004) The structure of spermatheca in the genus *Chelymorpha* Chevrolat, 1837 (Coleoptera: Chrysomelidae: Cassidinae) and its taxonomic significance. Annales Zoologici Warszawa. 54, 439-451.

[18] Sassi, D. and Borowiec, L.(2006) *Cassida inopinata,* a new species from Italy and Balkan Region (Coleoptera: Chrysomelidae: Cassidinae). Genus. 17 (4), 545-560.

[19] Chujô, M. and Kimoto, S.(1961). Systematic catalog of Japanese Chrysomelidae. Pacific Insects. 3, 117-202.

[20] Kleine, R. (1916) Cassida nebulosa L. and her feeding image. A biological observation. Entomologische Zeitang. 77, 187-216 (in French).

[21] Kosior, A. (1975) Biology, ecology and economic importance of Cassids (Coleoptera, Chrysomelidae, Cassidinae) of the Ojcow National Park. Acta Zoologica Cracoviensia. 20, 251-392.

[22] Brovdij, V. M. (1983) Leaf beetles, Cassidinae and Hispinae. In: Fauna of Ukraine, Tom 19, vyp. 20, Kiev. 1-188 pp (in Russian).

[23] Lee, J. E. and Cho, H. W. (2006) Leaf Beetles in the crops (Coleoptera: Chrysomelidae). Economic Insects of Korea 27. Insecta Koreana, Suppl. 34, Suwon, Korea. 1-127 pp.

[24] Spaeth, F. and Reitter, E. (1926) Destination tables of the European coleopters. 95 Issue. Cassidinae of the Palaearctic region, Emmerich Reitter, Troppau. 1-68 pp (in German).

[25] Bechyne, J. (1944). Cassididae and Hispidae in Bohemia and. Moravia. Entomologické Listy (Brno), 7, 74-86 (in Czech).

[26] Sekerka, L. (2008) *Cassida aurata* Fabricius, 1792 (Coleoptera: Chrysomelidae). Faunistic records from the Czech Republic - 267. Klapalekiana. 44, 297-298.

[27] Bordy, B. (1986) Cassida pannonica Suffrian in France (Col. Chrysomelidae). Nouvelle Revue d'Entomologie (N.S.). 3, 1-160 (in French).

[28] Lopatin, I. K. (1977) Further contributions to the knowledge of the Chrysomelid Faunader Mongolia (Coleoptera). Annales Historico-Natureles Musei Nationalis Hungarici. 69, 153-155 in German).

[29] Al-Ali, A. S. and Abbas, S. A. (1981) Biology of *Cassida palaestina* Reiche (Coleoptera, Cassidinae) on safflower in Iraq. Pakistan Journal of Zoology. 13, 179-184.

[30] Borowiec, L., Chikatunov, V. and Halperin, J. (1997) Cassidinae (Coleoptera: Chrysomelidae) of Israel. Israel Journal of Entomology. 31, 147-152.

[31] Bourdonné, J.-C. and Bordy, B. (1993) Materials for a catalog of the Coleoptera of the Pyrenees. Third note. L 'Entomologiste. 49 (2), 79-89 (in French).

[32] Kleine, R. (1917a) Cassiden studies IV. About Cassida chloris Suffr. Entomologische Blätter. 13, 78-82 (in French).
[33] Kleine, R.(1917b) Cassiden Studies III. Via Cassida rubiginosa Müll., Entomologische Blätter. 13, 63-73 (in French).
[34] Jolivet, P. (1967) Systematic and ecological notes on Moroccan Chrysomelids (Coleoptera) (2nd note). Bulletin de la Société des Sciences naturelles et physiques du Maroc. 1966, 305-394 (in French).
[35] Majka, C. G. and Lesage, L. (2008) Introduced leaf beetles of the Maritime Provinces, 7: *Cassida rubiginosa* Müller and *Cassida flaveola* Thunberg (Coleoptera: Chrysomelidae). Zootaxa. 1811, 37-56.
[36] Steinhausen, W. (2002) The pupae Central European leaf beetles-A preliminary determination table Part 2 (Col. Chrysomelidae). Mitteilungen der Münchner Entomologischen Gesellschaft. 92, 5-36 (in German).
[37] Spaeth, F. (1914) Chrysomelidae*:* 16. Cassidinae. In: W. Junk, S. Schenkling, Coleopterorum Catalogus, Pars 62, Berlin, 1-182 pp.
[38] Linnaeus, C. (1758) The system of Nature, through of three kingdoms of nature, according to classes, orders, genera, species, with characters, differences, synonymis, places. Edition of Compass, reformata. I. Stockholm, IV. 824 pp (in Latin).
[39] Borowiec & Świętojańska (2018) A monograph of the Afrotropical Cassidinae (Coleoptera: Chrysomelidae). Part 5. Revision of the genus Aethiopocassis Spaeth. Zootaxa (Monograph). 4488 (1), 1-99 pp.

Received: **22.04.2020**
Accepted: **02.02.2021**

CORRESPONDING AUTHOR

Neslihan Bal
Gazi University,
Science Faculty, Department of Biology,
06500 Ankara – Turkey

e-mail: neslihansilkin@gmail.com

© by PSP Volume 30– No. 05/2021 pages 5292-5301 Fresenius Environmental Bulletin

STUDY ON LIGHT REFLECTION MATERIAL CHARACTERISTICS OF DELINTED COTTONSEED AND ITS RELATIONSHIP WITH GERMINATION

Hongzhou Zhang[1,2], Qiaohua Wang[1,3,*]

[1]College of Engineering, Huazhong Agricultural University, Wuhan Hubei 430070, China
[2]College of Mechanic and Electrical Engineering, Tarim University, Alaer Xinjiang 843300, China
[3]Key Laboratory of Agricultural Equipment in Mid-Lower Yangtze River; Ministry of Agriculture, Wuhan Hubei 430070, China

ABSTRACT

The purpose of this study was to find the light reflection material characteristics of the delinted cottonseed and its relationship with the germination. To this end, selecting cottonseeds of different species and varieties as objects of study, the spectrometer approach was adopted to collect the spectral reflection material characteristic curve of the cottonseeds, and the germination test was also carried out on the cottonseeds strictly in accordance with national standards. Thus, the results obtained in this study include that the spectral material characteristics of different cottonseed varieties were analysed to obtain the sensitive spectrum and material characteristic wavelengths of cottonseeds; the polynomial fitting and stepwise regression analysis were used to establish the light reflection material characteristics estimation model of the cottonseeds, which was also validated. The results showed that the spectral reflectance of the four delinted cottonseed varieties such as Xinluzao 57, Xinluzhong 66, Zhongmian 86 and Zhongmian 641 were related to the seed species, and within a certain wavelength range, the reflectance of different species differs obviously; the reflectance of the four cottonseed species and their relationship with the germination time were also obtained, and by fitting and stepwise regression models, the coefficients R2 of the four species are 0.8892, 0.9476, 0.9173 and 0.9287 respectively; finally, the four cotton species were tested about the germination time, to conclude that the accuracy rate for the 3, 6, 9, and 12 days is up to 94%. The impacts of the obtained results are that this study provides a theoretical basis for the rapid and efficient sorting of delinted cottonseeds based on the spectral characteristics model.

KEYWORDS:
Light reflection, Material characteristics, Delinted cottonseeds, Germination

INTRODUCTION

Crop seed is the most basic production means for agricultural production [1-2]. Affected by various factors such as soil conditions, climatic conditions, cultivation and management conditions and natural disasters etc., the quality of seeds varies widely. Xinjiang cotton area is the largest one among China's five major cotton areas, and its cotton planting area has been increasing year by year. The quality of cottonseeds directly affects the cotton production. Therefore, the detection and sorting of cottonseed quality is particularly important. But the traditional cottonseed sorting is mainly based on mechanical vibration and blast screening etc. [3-6], and the traditional seed screening method cannot eliminate the sterile saturated seeds, thereby reducing the germination rate of cottonseeds, and affecting the development of precision seeding technology.

In recent years, crop seed screening technology has developed rapidly. Xiao Daren [7] quantitatively measured the photometric and colorimetric indicators of the seed coat colour of Brassica napus L by spectral analysis, and divided the variation of its seed colour into eight grades. The results showed that the higher the grade, the darker the colour. Besides, the correlation and regression analysis showed that there was a significant negative correlation between seed coat colour and seed oil content of Brassica napus L. in the same genetic background. Chen Yuping and Liu Houli studied the changes of seed coat colour during the development of Brassica napus L, finding that the chlorophyll, lutein and anthocyanin content of seed coat increased with the development of seeds. Zhang Xuekun, Li Jiana et. of Southwest University [7-10] have long been engaged in research on rapeseed genetics and breeding. By taking the Brassica napus L as the objects of study, they conducted studies on the Brassica napus with different seed coats from the perspectives such as developmental characteristics, inherited characteristics and oil content etc., which confirmed the close relationship between these factors.

Spectrum is the pattern of the monochromatic light that is dispersive and arranged in order accord-

ing to the wavelength (or frequency) after the polychromatic light is divided through the dispersion system (such as prism and grating). It is called optical spectrum [11]. The largest part of the visible spectrum is the visible part of the electromagnetic spectrum. The electromagnetic radiation in this wavelength range is called visible light. The spectrum does not contain all the colors that the human brain can see differently, such as brown and pink. Light waves are electromagnetic radiation produced by electrons in the process of atomic motion. The motion of electrons inside the atoms of various substances is different, so the light waves they emit are also different [12]. It is of great theoretical and practical significance to study the light emission and absorption of different substances, which has become a special subject spectroscopy. The infrared absorption spectrum of molecules is generally used to study the vibration spectrum and rotation spectrum of molecules, in which the vibration spectrum of molecules has always been the main research topic [13-14].

According to the production mode, the spectrum can be divided into emission spectrum, absorption spectrum and scattering spectrum. Some objects can emit light by themselves. The spectrum formed by the light directly generated by them is called the emission spectrum. Emission spectrum can be divided into three different categories: linear spectrum, band spectrum and continuous spectrum [15-16]. The linear spectrum is mainly produced by atoms, which are composed of some discontinuous bright lines; the band spectrum is mainly produced by molecules, which are composed of some dense light within a certain wavelength range; the continuous spectrum is mainly produced by incandescent solid, liquid or high-pressure gas excited to emit electromagnetic radiation, which is composed of light of all wavelengths of continuous distribution [17]. When the white light passes through the gas, the gas will absorb the light with the same wavelength as its characteristic spectrum from the white light passing through it, so that the dark line appears in the continuous spectrum formed by the white light. In this case, the spectrum generated by absorption of certain wavelengths of light in the continuous spectrum is called the absorption spectrum [18]. Generally, the characteristic spectral lines seen in the absorption spectrum are less than the linear spectrum. According to the nature of production, the spectrum can be divided into molecular spectrum and atomic spectrum. In molecules, the energy of electronic state is 50-100 times larger than that of vibrational state, and the energy of vibrational state is 50-100 times larger than that of rotational state. Therefore, in the transition between the electronic states of molecules, there are always vibration transition and rotation transition, so many spectral lines are concentrated together to form the molecular spectrum. Therefore, the molecular spectrum is also called band spectrum. In an atom, when the atom is promoted from ground state to higher energy state in some way, the energy inside the atom increases, and some electrons in the atom are promoted to excited state. However, the excited state cannot be maintained [19]. After a short period of random time, the excited atom will return to the original state with lower energy. In the atom, the excited electrons release a photon when they return to the orbit with lower energy, these energies will be emitted in the form of light, thus generating the emission spectrum of the atom, that is, the atomic spectrum. Because the change of atomic energy state is discontinuous quantum, the spectrum produced is also composed of some discontinuous bright lines, so the atomic spectrum is also called line spectrum. When the light hits the material, inelastic scattering will occur. In addition to the elastic component (Rayleigh scattering) which is the same as the excited light wave length, there are longer and shorter components than the excited light wave [20]. The latter phenomenon is called Raman effect. This phenomenon was discovered by Indian scientist Raman in 1928. Therefore, the scattering of light with new wavelength is called Raman scattering, and the generated spectrum is called Raman spectrum or Raman scattering spectrum [21].

In this paper, the germination test was conducted in the outdoor environment by the spectrum technology in strict accordance with national standards. It explored the correlation ship between the light-reflecting characteristics of cottonseeds and the two important indexes (germination potential and the germination rate) of cottonseed quality, in order to confirm that the light reflection characteristics of cottonseeds has a significant correlation with its germination. Besides, the regression analysis was carried out for the cottonseed quality and light reflection characteristics, to find the characteristic wavelength best reflecting the quality of the delinted cottonseeds. Thus, the optimal screening model suitable for the quality of delinted cottonseed was established. This shall provide a theoretical basis for the sorting of cottonseeds according to optical characteristics, and a scientific basis for exploring an effective sorting method for delinted cotton according to optical characteristics.

MATERIALS AND METHODS

(1) Test materials. The test cottonseeds were selected from Tahe Seed Industry Company of Alar City. Before the test, 400 seeds of Xinluzao 57 and Xinluzhong 66 in Xinlu seed species, and Zhongmian 86 and Zhongmian 641 of the Zhongmian seed species were prepared respectively. All samples were divided into the training set and the prediction set at the ratio of 3:1 for each cotton variety, and all the test samples were also numbered.

(2) Main instruments The main instruments include USB2000+VIS-NIR spectrometer (350-1000nm), and GXZ-300A intelligent illumination incubator of germination test. The main parameters of this illumination incubator are: temperature control range 0-50°C, temperature fluctuation ±1.0°C, temperature deviation ±0.5°C, temperature unevenness ≤1.5°C, and the illuminance range between 0-3,000 Lx.

(3) Operation steps The test was taken in the laboratory from 13:00 to 15:00 every day. First, the cottonseeds of each species were placed on the sample stage of the spectrometer in turn, to determine the spectral reflectance of each group separately. Then, these measured seeds were boiled with boiling water. After that, we carried out the germination test, while recording the germination time and germination status, and collecting the spectral reflectance characteristics of each species.

(4) Test principle The light reflectance of the cottonseeds is R = Lt/L w, where Lt is the reflected radiance; Lw is the incident radiance, that is, the ratio of the radiance of the target to the radiance of the control whiteboard.

The germination trend, germination rate and germination time of seeds are three important indicators reflecting the seed quality. They are defined as:

Seed germination trend refers to the percentage of the normally germinated seeds in the tested seeds under the specified conditions and time at the early stage of seed germination test.

Seed germination rate refers to the percentage of all normal germinated seeds in the tested seeds under the specified conditions and time at the final stage of seed germination test.

Seed germination time refers to the time required from the start of the germination test to the germination of the seed under the specified conditions during the germination of the seed.

The high seed germination trend and short germination time indicate that the seed has strong viability with uniform germinating. The high germination rate means that the utilization value of the seeds is high. They are all important indicators for evaluating seed quality. In general, if the crop seeds have high germination rate, strong germination trend and short germination time, it indicates that the emergence of seedlings shall fast and tidy, and the seedlings be strong; if the seed has high germination rate, weak germination trend, and long germination time, the seedling emergence shall be uneven and weak. In order to better reflect the quality of cottonseeds species, the germination time was selected as an important indicator for evaluating cottonseed quality in this test.

(5) Cottonseeds germination test design Germination test was conducted on October 22 to November 10, 2018. Germination test site: The First Laboratory of Agricultural Products Processing and Testing, Key Laboratory of Modern Agricultural Engineering, Tarim University, Xinjiang Uygur Autonomous Region.

According to the germination test method, under the specific environment, the germination limit time of cottonseed is 12 days. Firstly, the delinted cottonseeds tested and selected in section 1.4 were boiled with hot water for 15 minutes respectively to break the hard seed in accordance with the requirements of GB/T3543.4-1995. After that, they were arranged at equal intervals on the sand bed of a 100 mm × 100 mm × 100 mm germination box, and then covered with loose sand of 15 to 20 mm thickness, and finally placed in GXZ- 300A intelligent light incubator. Furthermore, the sand bed should have uniform sand size, with the diameter of 0.05-0.80 mm, under the thorough washing and high temperature disinfection for 10h at 130°C, and the water content of the sand bed is 80% of its saturated water content. The light incubator is set to 24h a day, 12h daytime and night; the daytime temperature is set to 27°C, and the illuminance is 1250 Lx, while the night temperature is set to 20°C and illuminance 0 Lx.

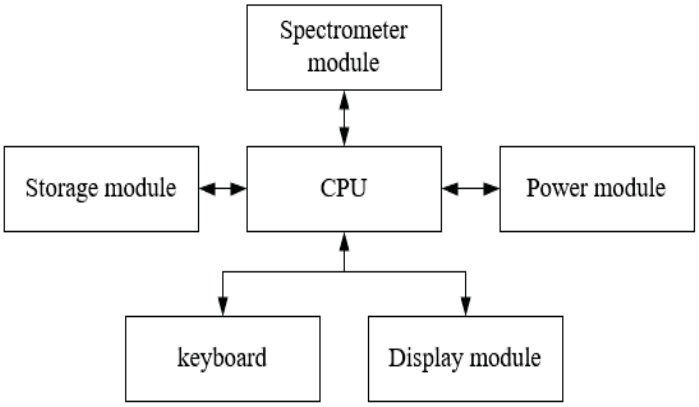

FIGURE 1
The configuration diagram of test system for cottonseed light reflection characteristics.

(6) Germination time measurement and data processing. When the germination test was carried out for 3d, 6d, 9d, and 12d, the number of cottonseeds that had been germinated in each species at each time node was quickly counted, and the mark of the germinated cottonseed was recorded. Then, polynomial regression analysis was used to analyse the correlation between the light reflection characteristic parameters of delinted cotton and its corresponding test data of germination time.

Figure 1 shows the general hardware framework of the test system for cottonseed light reflection characteristics: after inputting the pre-set value from the keyboard, the spectrometer module extracts the light reflection characteristic data of the cottonseed. Then, the computer processes the characteristic data and saves it to the storage module for data processing, while simultaneously displaying the signal processing result on the display module.

RESULTS

(1) Cottonseeds species and their light reflection characteristics. Figure 2 shows the average spectral characteristic curve of the test cottonseeds. It can be seen from the Figure that the spectral reflectance characteristics of different cottonseeds species are significantly different in any band. The test results show that within a certain wavelength range, the cottonseed species can be discriminated by its light reflectance. In the visible light range of 450-990nm, the light reflectance of the Xinlu seed species is $0.2 \leq R \leq 0.6$, and that of the Zhongmian seed species is $0.5 \leq R \leq 0.9$. When the wavelength is over 600nm, the reflectance of the Zhongmian is greater than that of Xinlu species.

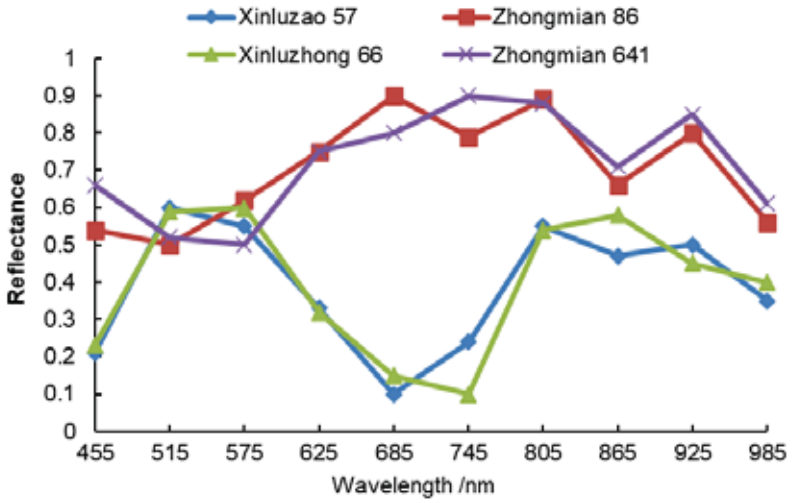

FIGURE 2
Light reflection characteristics of Xinlu cottonseeds and Zhongmian cottonseeds.

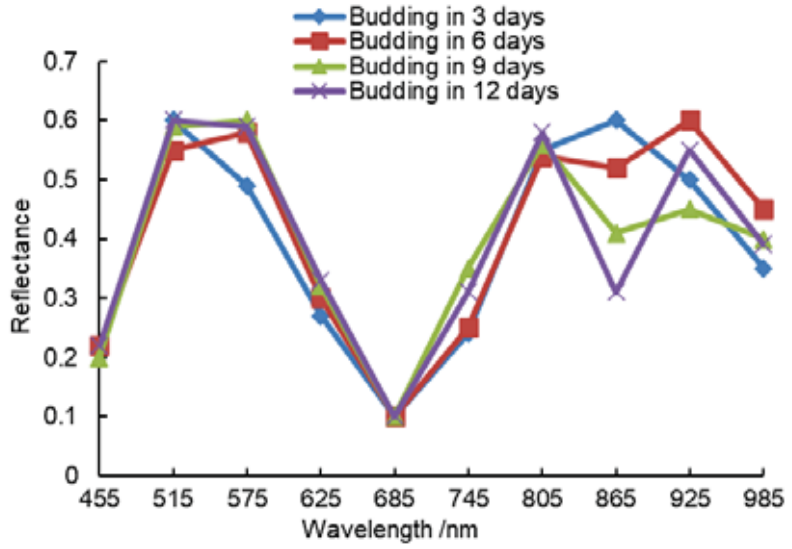

FIGURE 3
Light reflection characteristic curve of Xinluzao 57 cottonseed at different germination time.

(2) Correlation between light reflection characteristics and germination time of different cottonseeds. Figure 3, 4, 5 and 6 show the light reflection characteristic curve of the four delinted cottonseed varieties (Xinluzao 57, Xinluzhong 66, Zhongmian 86 and Zhongmian 641) at four germination time points respectively. According to the spectral characteristic curve, it can be found that the cottonseed of Xinluzao variety have the strongest absorption near the 685nm waveband, strong reflection near the 550nm band, and great difference in reflectance near the 860nm band; the cottonseeds of Zhongmian variety have stronger absorption near the 575nm waveband, a strong reflection near the 805nm band, and great difference in reflectance near the 510nm band. In addition, the light reflection sensitive wavelength of the Xinluzhong species is 860nm in the visible light range; that of the Zhonglu species is 510nm in the visible light range.

At these two sensitive wavelengths, we obtained the reflectance of cottonseeds at different germination time, andthe relationship between the reflectance and the germination time, as shown in Figure 7, 8, 9, and 10.

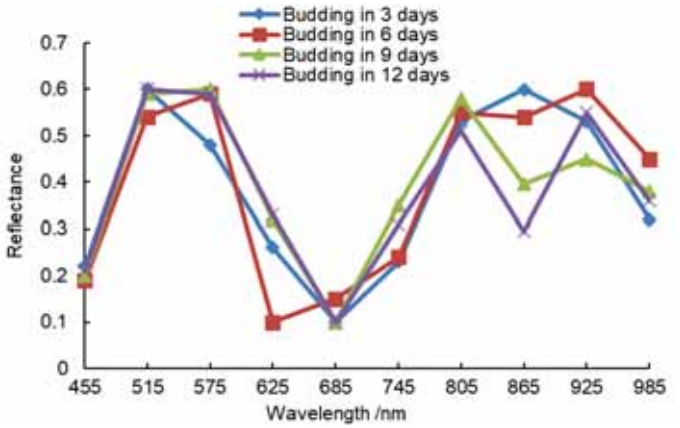

FIGURE 4

Light reflection characteristic curve of Xinluzhong 66 cottonseed at different germination time.

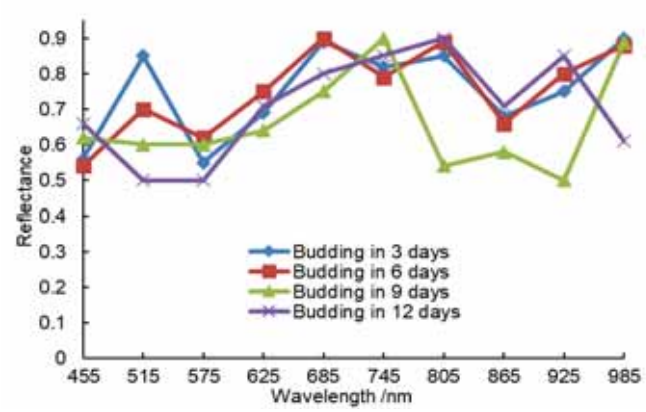

FIGURE 5

Light reflection characteristic curve of Zhongmian 86 cottonseed at different germination time.

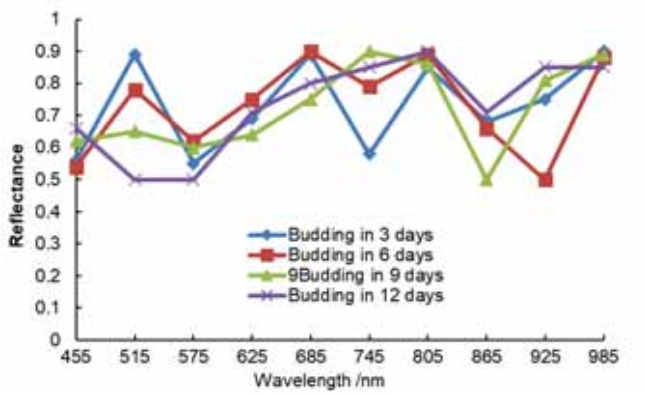

FIGURE 6

Light reflection characteristic curve of Zhongmian 641 cottonseed at different germination time.

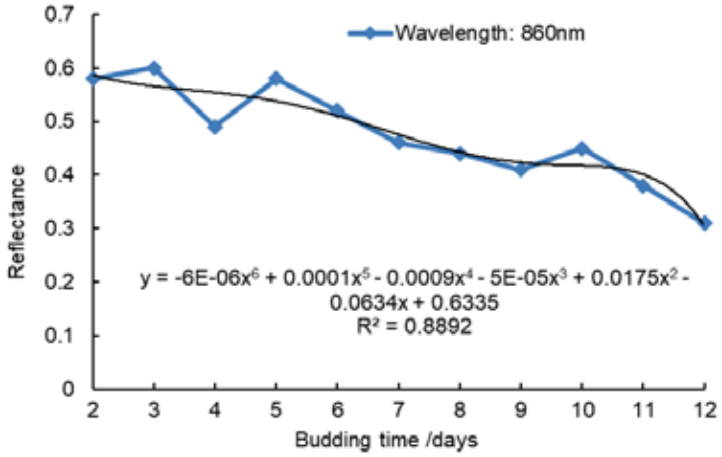

FIGURE 7
Germination time and reflectance curve of Xinluzao 57 cottonseed.

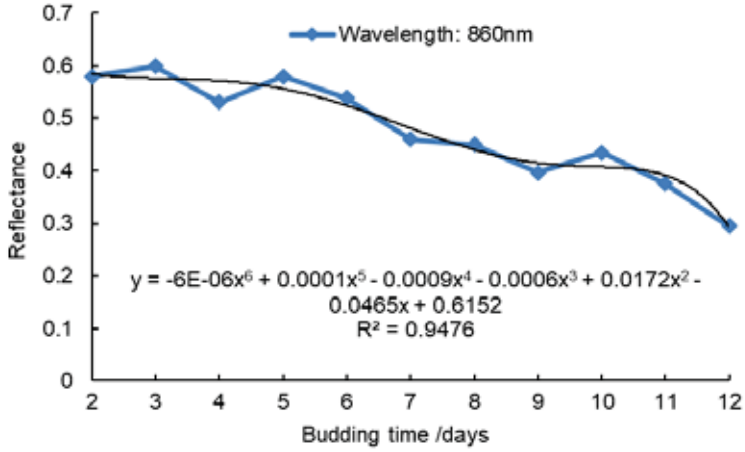

FIGURE 8
Germination time and reflectance curve of Xinluzhong 66 cottonseed.

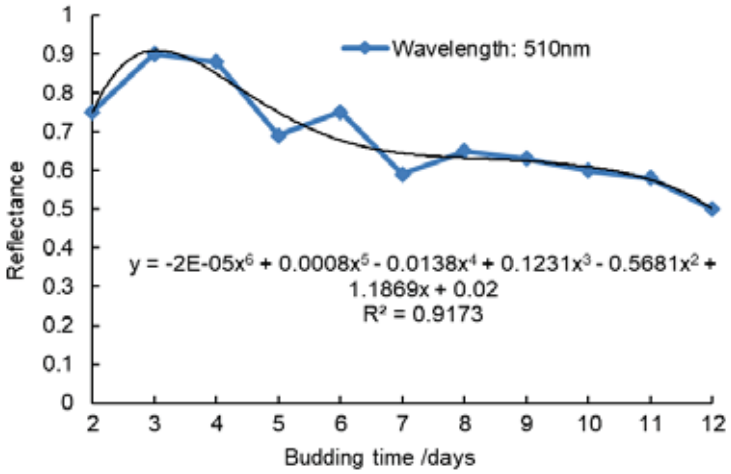

FIGURE 9
Germination time and reflectance curve of Zhongmian 86 cottonseed.

For the germination time and reflectance curve of Xinluzao 57 cottonseed, the polynomial fitting was used to obtain the regression equation: y = -6E-6x6 + 0.0001x5 - 0.0009x4 - 5E-05x3 + 0.0175x2 - 0.0634x + 0.6335. For the germination time and reflectance curve of Xinluzhong 66 cottonseed, the polynomial fitting was used to obtain the regression equation: y = -6E-6x6 + 0.0001x5 - 0.0009x4 - 5E-5x3 + 0.0175x2 - 0.0634x + 0.6335. For the germination time and reflectance curve of Zhongmian 86 cottonseed, the polynomial fitting was used to obtain the regression equation: y = -2E-5x6 + 0.0008x5 -

$0.0138x4 + 0.1231x3 - 0.5681x2 + 1.1869x + 0.02$. For the germination time and reflectance curve of Zhongmian 641 cottonseed, the polynomial fitting was used to obtain the regression equation: $y = 5E\text{-}5x6 - 0.0016x5 + 0.0218x4 - 0.1306x3 + 0.3357x2 - 0.2904x + 0.8675$. In the analysis of polynomial regression equations, the decision coefficient R2 is used to measure the proportion of the variance in the dependent variable that is predictable from the independent variable, so as to judge the explanatory power of the statistical model. The determination coefficient R2 of the fitted regression equation is 0.8892, 0.9476, 0.9173, 0.9287, respectively, indicating that the reflectance is linearly related to the linear equation containing the germination time of the independent variable. Emission spectrum analysis is to calculate the content of the measured atom or molecule according to the intensity of the characteristic spectrum emitted in the excited state. The absorption spectrum is based on the characteristic spectrum of the element to be measured, and the content is calculated by the weakened intensity after the ground state atomic absorption of the measured element in the sample steam. The atom of any element is composed of the nucleus and the electrons moving around the nucleus. The electrons outside the nucleus form different energy levels according to their energy levels. Therefore, an atomic nucleus can have multiple energy levels. The lowest energy level state is called the ground state level (E0 = 0), the other energy levels are called the excited state level, and the lowest energy level is called the first excited state. Under normal conditions, the atom is in the ground state, and the extranuclear electrons move in the orbits with the lowest energy. If a certain amount of external energy such as light energy is provided to the ground state atom, when the external light energy E is exactly equal to the energy level difference e between the ground state and a higher energy level in the ground state atom, the atom will absorb the light of this characteristic wavelength, and the outer electron will transition from the ground state to the corresponding excited state. The spectral lines of the original energy providing light are missing some characteristic spectral lines, so the atomic absorption spectrum is produced. After 10-8 seconds, the excited state electron will return to the ground state or other lower energy level, and the energy absorbed by the electron transition will be released in the form of light. This process is called atomic emission spectrum. The process of atomic absorption spectrum absorbs radiation energy, while the process of atomic emission spectrum releases radiation energy. According to the law of conservation of energy, Er = Ef+ Ex + Et, where Er is the energy of incident light; Ef is the energy of reflected light; Ex is the energy of absorbed light; Et is the energy of transmitted light. When the incident light is constant, light reflection is negatively correlated with light absorption and light transmission energy. Through the analysis of spectral reflectance characteristics of different varieties of cottonseed, the following conclusions are obtained: the reflectance of cottonseed is related to its color depth, which is consistent with the law of conservation of energy. The absorption of light energy by dark cottonseed is far greater than that of light colored cottonseed, and on the contrary, the reflected energy is small.

Spectral data is high-dimensional data. It takes a long time to analyze directly with high-dimensional data, and some spectra are invalid information for the results. In order to further optimize the data, it is necessary to reduce the dimension of spectral data and extract the feature information. There are two main methods to extract the feature information of the whole band, one is to map the high and low space of the information, the other is to select the feature wavelength. The idea of competitive adaptive reweighting algorithm is that each input variable is regarded as an independent individual, the wavelength with larger absolute value of regression coefficient in the model is selected by adaptive weighted sampling technology, the wavelength with smaller weight is removed, and the wavelength combination corresponding to the minimum RMS error of model interactive verification is optimized by interactive verification. Therefore, for spectral data, the feature wavelength can be selected by continuous projection method to achieve dimensionality reduction. The idea of PCA is to transform the data into a new coordinate system, so that the first variance of data projection is on the first principal component, the second variance is on the second principal component, and so on. The dimension of data set is reduced by keeping low-order principal components and ignoring high-order principal components. Low order components tend to retain the most important aspects of the data. Enhanced regression tree is a kind of self-learning method based on classification regression tree algorithm. This method can improve the stability and prediction accuracy of the model by self-learning and random selection. In the operation process, a certain amount of data is randomly selected for many times to analyze the influence of independent variables on dependent variables. The remaining data is used to experiment the fitting results. Finally, the mean value of the generated multiple regression is taken and output. This method can improve the stability and accuracy of the results, and get the correlation between independent variables and dependent variables.

In view of light reflection characteristics for cottonseeds, the paper proposes a new set of sorting methods suitable for the characterization of cottonseed activity, and then conducts validation analysis by sorting test. The sorting results are shown in Table 1.

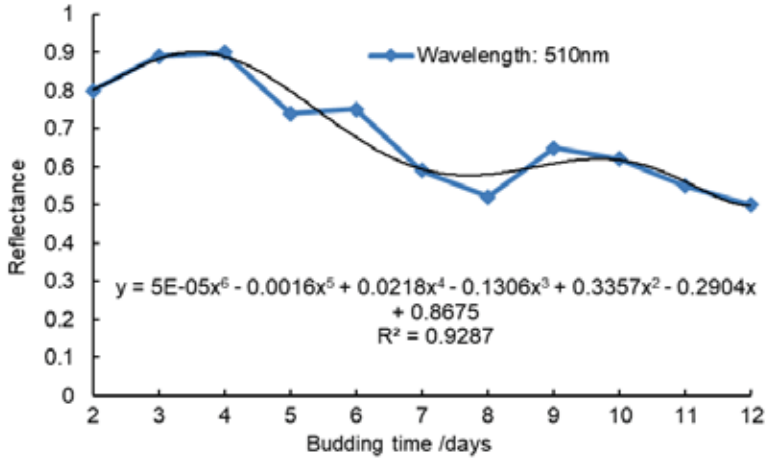

FIGURE 10
Germination time and reflectance curve of Zhongmian 641 cottonseed.

TABLE 1
Sorting results

Sorting type		Actual number	Correct number	Accuracy/%
Xinluzao 57	3d	45	44	
	6d	30	27	
	9d	14	12	
	12d	11	9	
	Total	100	92	92
Xinluzhong 66	3d	43	43	
	6d	37	36	
	9d	13	10	
	12d	7	5	
	Total	100	94	94
Zhongmian 86	3d	30	27	
	6d	32	28	
	9d	25	23	
	12d	13	10	
	Total	100	88	88
Zhongmian 641	3d	28	27	
	6d	31	26	
	9d	23	21	
	12d	18	15	
	Total	100	89	89

CONCLUSIONS

(1) In a certain wavelength range, the light reflection characteristics of the delinted cottonseeds are related to its species.There are some color differences on the outside of cotton seeds of different lines, and the thickness of seed coat is different. The color of cotton seed coat of Xinlu is darker, and that of Zhongmian is lighter. In the visible light range of 450-990nm, the light reflectance of the Xinlu seed species is $0.2 \leq R \leq 0.6$, and that of the Zhongmian is $0.5 \leq R \leq 0.9$. When the wavelength is greater than 600nm, the reflectance of Zhongmian is over that of the XinLu.

(2) Through theoretical derivation and correlation analysis, the correlation model between light reflection characteristics and budding time was established. The results showed that the budding time of cotton seeds of the two lines increased with the decrease of their reflectance, and the high-order fitting effect was better, and the Xinlu strain was more obvious, and the determination coefficient of regression equation was significantly higher than that of Chinese cotton line.The correlation model between light reflection characteristics and germination time of delinted cottonseed was obtained. Through the sorting test, the model was validated, with the accuracy rate of sorting up to 94%.

(3) This paper studies the qualitative relationship between budding time and its light reflection characteristics, which is an important index of the

quality of cashmere cotton. The quantitative relationship between reflectance and budding time is determined to a certain extent by fitting the correlation between reflectance and budding time. this paper studies the quantitative relationship between the germination time and the light reflection characteristics which reflect the quality of the delinted cottonseeds as the important indicators. This shall provide a scientific basis for the rapid non-destructive identification of the activity information of the delinted cottonseeds based on the spectral technology, and also theoretical support for the development of delinted cottonseeds sorting equipment.

ACKNOWLEDGEMENTS

The work was supported by the National Natural Science Foundation of China under Grant No.61701334, the Science and Technology Support Program for Key Industries of the Southern of Xinjiang production and Construction Corps No.2018DB001, the union Foundation of Tarim University and Huazhong Agricultural University No.HNLH202002, and the union Foundation of Tarim University and China Agricultural University No.TDZNLH201703.

REFERENCES

[1] Garea, A.S., Heras, D.B., Arguello, F. (2019) Caffe CNN-based classification of hyperspectral images on GPU. Journal of Supercomputing. 75(3), 1065-1077.

[2] Zhang, R., Kan, Z., Ma, R., Cao, W., Li, J. (2010) Relationship between color features and germination of delinted cottonseed based on RGB color model. Transactions of the Chinese Society of Agricultural Engineering. 26(10), 172-177.

[3] Su, D., Zhou, Z., Xie, J., Lang, L., Wu, C. (2011) Biomass oxygen enriched-steam gasification in an atmospheric fluidized bed for syngas production. Transactions of the Chinese Society of Agricultural Machinery. 42(3), 100-104.

[4] Yao, C., Teng, Y., Huang, L. (2015) Evaluation index system construction and empirical analysis on food security in China. Transactions of the Chinese Society of Agricultural Engineering. 31(4), 1-10.

[5] Tantaswadi, P., Vilainatre, J., Tamaree, N., Viraivan, P. (1999) Machine vision for automated visual inspection of cotton quality in textile industries using color is discrimination contour. Computers & Industrial Engineering. 37(1-2), 347-350.

[6] Li, D., Yang, W., Wang, S. (2010) Classification of foreign fibers in cotton lint using machine vision and multi-class support vector machine. Computers & Electronics in Agriculture. 74(2), 274-279.

[7] Mathew, P. (2008) Parallel algorithm for GPU processing; for use in high speed machine vision sensing of cotton lint trash. Sensors. 8(2), 817-829.

[8] Moreira, V. R., Satter, L. D., Harding, B. (2004) Comparison of conventional linted cottonseed and mechanically delinted cottonseed in diets for dairy cows. Journal of Dairy Science. 87(1), 131-138.

[9] Green, J. A., Minton, E. B. (1980) Influence of mechanical damage and fungicide seed treatments on germination and stand with cottonseed. Crop Science. 20(2), 235-239.

[10] Pratt, C., Wender, S. H. (1959) Identification of rutin and isoquercitrin in cottonseed. Journal of the American Oil Chemists' Society. 36(9), 392-394.

[11] Minton, E. B., Quisenberry, J. E. (1980) Comparison of cottonseed delinting methods in evaluating seed-treatment fungicides1. Agronomy Journal. 72(3), 573-575.

[12] Filho, F.S.O.R., Lago, A.A.D., Cia, E., Ferraz, C.A.M. (1978) Preservation of cottonseeds delinted by different methods. Bragantia. 38(1), 107-113.

[13] Hopper, N.W., Hinton, H. R. (1979) An anhydrous hydrochloric acid method for delinting small samples of cottonseed. Journal of Seed Technology. 4(1), 7-11.

[14] Santhoshkannada, A.N., Umesha, S., Hariprasad, P., Niranjana, S.R. (2008) Bacterial blight pathogen concentration in cotton seeds; its role in seed quality parameters of fuzzy and acid delinted seeds. Archiv Fr. Pflanzenschutz. 41(8), 597-607.

[15] Lopes, K.P., Bruno, R.D.L.A., Costa, R.F.D., Bruno, G.B., Rocha, M.D.S. (2006) Effects of seed processing on physiological and sanitary qualities of seeds of herbaceous cotton. Revista Brasilra de Engenharia Agrícola e Ambiental. 10(2), 426-435.

[16] Shende, S.T., Singh, M., Singh, V.P. (1987) Effect of seed bacterization with azotobacter chroococcum on germination and seedling height of upland cotton. Indian Journal of Agricultural Ences (India). 57(3), 183-185.

[17] Chen, P., Ji, P., Cao, Z.J., Li, S.L. (2007) Effect of processing whole cottonseed on yield and composition of milk in dairy cows. Journal of Animal & Feed Sciences. 16(5), 531-536.

[18] Costa, M.L.N., Dhingra, O.D., Silva, J.L.D. (2005) Influence of internal seedborne fusarium semitectum on cotton seedlings. Tropical Plant Pathology. 30(2), 183-186.

[19] Raikar, S.D., Shashidhar, S.D., Vyakarnahal, B.S., Meharwade, M.N., Basarkar, P.W. (2010) Effect of delinting, seed treatment and packaging material on seed storability of cotton genotypes. Bericht Über Die Zusammenkunft Deutsche Ophthalmologische Gesellschaft. 70(4), 128-133.
[20] Ylinen, A.M., Pellinen, T., Valtonen, J., Puolakka, M., Halonen, L. (2011) Investigation of pavement light reflection characteristics. Road Materials & Pavement Design. 12(3), 587-614.
[21] Brodskii, A.M., Urbakh, M.I. (2010) On the dependence of light reflection from metals on adatom characteristics. Physica Status Solidi. 83(2), 633-644.

Received: **06.12.2020**
Accepted: **10.01.2021**

CORRESPONDING AUTHOR

Qiaohua Wang
College of Engineering,
Huazhong Agricultural University,
Wuhan Hubei 430070 – China

e-mail: 309011160@qq.com

© by PSP Volume 30– No. 05/2021 pages 5302-5311 Fresenius Environmental Bulletin

COMPARISONS OF AGRICULTURAL USING BETWEEN SEWAGE SLUDGE AND LIVESTOCK MANURE FOR NUTRIENT LOADING, ECOLOGICAL RISK AND POTENTIAL IN TAIYUAN METROPOLITAN AREA

Baoling Duan[1,2], Qiang Feng[1], Yushan Bu[2,*]

[1]College of Resources and Environment, Shanxi University of Finance and Economics, Taiyuan, Shanxi 030006, China
[2]College of Resources and Environment, Shanxi Agricultural University, Taigu, Shanxi 030801, China

ABSTRACT

The increase in nutrients (nitrogen, phosphorus and potassium) loadings from agriculture nonpoint source pollution has been one of the major sources of water pollution or eutrophication. Comparisons between sewage sludge and livestock manure for nutrients loading, ecological risk and agricultural using potential were investigated in Taiyuan metropolitan area of Shanxi to determine which one was more suitable for agricultural using in the studying area. The mean organic matter and nitrogen, phosphorus and potassium in sewage sludge were 350.12 g/kg, 36.14 g/kg, 21.50 g/kg and 12.00 g/kg, and the contents of organic matter and nutrients (N+P+K) all exceeded the specified values formulated by Disposal of Sludge from Municipal Wastewater Treatment Plant-Control Standards for Agricultural Use (CJ/T 309-2009). In contrast to livestock manure, sewage sludge had a comparable advantage for agricultural using due to the contents of organic matter and nutrients as well as the proportion of N:P:K. The mean loadings of nitrogen, phosphorus and potassium can be ranked in the following decreasing orders as N>P>K for sewage sludge, and N>K>P for livestock manure, and all mean loadings of nitrogen, phosphorus and potassium did not exceed the ecological safety threshold values of 125 kg/ha•a, 62.5 kg/ha•a and 62.5 kg/ha•a, which were published by the Ecological County, Ecological City and Ecological Province Construction Index (revised draft), besides the mean loading of phosphorus for sewage sludge. In particular, loadings of nitrogen and potassium were higher for livestock than sewage sludge, and loadings of phosphorus were higher for sewage sludge than livestock in different districts. According to the mean values of the monomial ecological risk index, nutrients can be ranked in the decreasing order of P>N>K for sewage sludge and K>N>P for livestock manure, and they were all below the safety threshold value of 0.5. In general, the ecological risks of nitrogen and potassium were higher for livestock manure than sewage sludge, and those of phosphorus were higher for sewage sludge than livestock manure. The mean potentials of agricultural using of sewage sludge and livestock manure were 1.07 t/ha•a and 4.59 t/ha•a respectively; livestock manure had higher potential than sewage sludge; and the restrictive factor were nitrogen and phosphorus for sewage sludge, nitrogen and potassium for livestock manure. In detail, the districts having negative potential were more for livestock manure using than sewage sludge using, furthermore, the negative potential for sewage sludge using was determined by phosphorus, and for livestock manure were all determined by potassium. Combining all the analysis with the local soil condition of low nitrogen, low phosphorus and high potassium, sewage sludge was more suitable for agricultural using than livestock manure in the ecological safety manner in the studying area.

KEYWORDS:
Sewage sludge, livestock manure, nutrients loadings, ecological risk, agricultural using potential, Taiyuan metropolitan area

INTRODUCTION

Sewage sludge can be regarded as the by-product of wastewater handling [1-4]; likewise, livestock manure is the by-product of livestock feedings [5,6]. The rapid increase in economic development will likely cause a sharp rise in the output of sewage and livestock manure [3,6,7,8]. Up to now, the annual production of dewatered sewage sludge will soon exceed 30 million tons, and the annual production of feces has reached 243 million tons, urine has reached 163 million tons in China [9,10]. Disposal of a large amount of sewage sludge and livestock manure has become a critical environmental problem [11-14].

Owing to the abundant nutriment contained in sewage sludge and livestock manure, such as organic matter and nutrients (nitrogen, phosphorus and potassium), which are necessary for intensive farming and can improve crop yields [1,14-19], sewage sludge and livestock manure are widely used as soil fertilizers across the world and as the recommended organic fertilizers by the government of China

[1,15,18,20-22]. Moreover, agriculture use of sewage sludge and livestock manure is regarded as a way of waste recycling, and the most economical disposal method compared with other methods of handing [1,2,14,23,24]. But this widespread land use of sewage sludge and livestock manure in agriculture can not only take advantage of the nutrients contained in it but also cause serious environmental problems which cannot be ignored. [1,13,16,17,21,25-28]. Literatures show that, contrary to continuously increasing crop yields, long-term and unreasonable use of organic fertilizers results in water eutrophication by both leaching processes and run-off of surface water, which is closely related to nitrogen, phosphorus and potassium contamination originating from agriculture [16,29-34]. The leaching and runoff intensity of nitrogen, phosphorus and potassium will be improved when a greater quantity of sewage sludge or livestock manure enter into soils, and nutrient loadings for soils will also be intensified [1,31,33-36], this will pose a potential threat to soil and water [37]. If the amount of consumption of sewage sludge and livestock manure exceeds the capacity of farmland, serious consequences of this environmental pollution that threatens the environment's safety and human health will occur [30,38]. To protect the environment and human health from the adverse effects of nutrients which were applied on the farmland, the European Union formulated directives 86/278/EEC and 91/271/EEC to regulate the land application of fertilizer [23]. And the Nitrates Directive (91/676/EEC) were also developed to improve water quality by protecting water against pollution caused by nitrates from agricultural sources, in particular, it is about promoting better management of animal manures, chemical nitrogen fertilizer and other nitrogen-containing materials spread onto land [39]. Therefore, nutrients in sewage sludge and livestock manure have become the critical controlling parameters for safe and long-term use of them as soil conditioners [16,30]. To prevent harm to soil, human and other ecological systems by agricultural using of sewage sludge and livestock manure, sewage sludge and livestock manure intended for farmland must be prior evaluated to use in the terms of the contents of nutrients and assessed for the risk which may be caused by it. In this condition, studies often focus on nutrients loadings, ecological risk for agricultural using of sewage sludge or livestock manure [1,17,20,23,32,40,41], but fewer surveys evaluate the differences between sewage sludge and livestock manure.

To use sewage sludge and livestock manure in an environmentally safe manner and compare the differences between these two kinds of organic fertilizers, nutrients loadings, ecological risk and agricultural using potential should be evaluated. The Ecological county, Ecological City and Ecological Province Construction Index (revised draft), which was published to standardize the quality of fertilizers and guarantee the ecological safety of agricultural soil, is the foundation of this study. The aims of this study are to: (a) compare the contents of organic matter, nutrients in sewage sludge and livestock manure; (b) evaluate the nutrients loadings for sewage sludge and livestock manure and compare the difference between it; (3) assess and compare the ecological risk of agricultural using of sewage sludge and livestock manure; and (4) calculate the potential of agricultural using of sewage sludge and livestock manure, compare it; (5) determine sewage sludge or livestock manure which one was more suitable for agricultural using in the ecological safety manner.

MATERIALS AND METHODS

Study area Taiyuan metropolitan area, the growth pole of Shanxi, contains three parts: the main city zone, the co-construction zone and the modern industrial park. And Taiyuan city is the center of this metropolitan area, Yuci is the co-construction zone, and Qingxu and Taigu are the modern industrial parks. As the organizational core of the whole province's urban system and the growth pole of economic transformation and development, the developing of Taiyuan metropolitan area is crucial for Shanxi, not only for economics but also for society and ecological safety [42].

Data collection and processing Sewage sludge samples were collected from 8 municipal wastewater treatment plants located in Taiyuan metropolitan area as indicated in Figure 1. Four subsamples were collected from different sites in the same municipal wastewater treatment plants to ensure adequate representation. Samples were dried in a clean environment at room temperature, then sieved through mesh pores of sizes 0.25 mm, 0.25 mm, 0.149 mm and 0.149 mm for organic matter, total nitrogen, total phosphorus and total potassium respectively, and stored in jars at room temperature. The contents of organic matter, total nitrogen, total phosphorus and total potassium were analyzed in accordance with national standards of China as GB 9834-88, GB7173-87, GB8937-88 and GB 9836-88. When the content of organic matter was more than 150 g/kg, the analyzed results were not exact due to incomplete oxidation. In this condition, samples of 0.1 g were mixed with samples of 0.9 g which had been burned by high temperature to remove the total organic matter, and then a sample of one-tenth extracted to calculate the result.

To compare the differences between sewage sludge and livestock manure of nutrient loadings, ecological risk and potential of agricultural using, the annual productions of sewage sludge and livestock manure, contents of organic matter and nutrient for livestock manure were collected from the Environmental Bulletin of Wastewater Treatment Plant

of Shanxi, Shanxi Statistical Yearbook and related literatures.

Nutrient loadings The indices of nutrient loadings are used to express the environmental pollution of chemical fertilizer and organic fertilizer. Currently, sewage sludge and livestock manure are mainly disposed as organic fertilizers, the nutrients loadings on arable land are the load capacity of sewage sludge and livestock manure [20,43,44].

To calculate the nutrients loadings of sewage sludge and livestock manure, there are three steps to be followed: first, calculate the nutrients from sewage sludge or livestock manure; second, calculate the arable land area; third, calculate nutrients loadings as following equations [45]:

$$L_{Sewage\ sludge\ i} = \frac{C_i \times Q_i \times 10^3}{S_{arable\ land}}$$

Where $L_{sewage\ sludge\ i}$ is the ith nutrients loading of sewage sludge, and i presents nitrogen, phosphorus and potassium, kg/hm2•a; C_i is the concentration of the ith nutrients in sewage sludge, g/kg; Q_i is the annual quantity of sewage sludge, t/a; and $S_{arable\ land}$ is the area of effective arable land, hm2.

$$L_{Livestock\ manure\ i} = \frac{N_m \times t_m \times R_m \times C_{m\ i}}{S_{arable\ land}}$$

Where $L_{Livestock\ manure\ i}$ is the ith nutrients loading of livestock manure, kg/hm2•a; N_m is the annual amount of the mth livestock on hand, and m presents pigs, cattle, sheep and chicken, head; t_m is the feeding cycle of the mth livestock, days, and it was 180days, 365days, 180days and 80 days for hogs, cattle, sheep and chicken respectively [46, 47]; R_m is the daily excretion coefficient for the mth livestock, kg/head•day, presented in Table 1; and $C_{m\ i}$ is the concentration of the the mth livestock of the ith nutrients in livestock manure, g/kg.

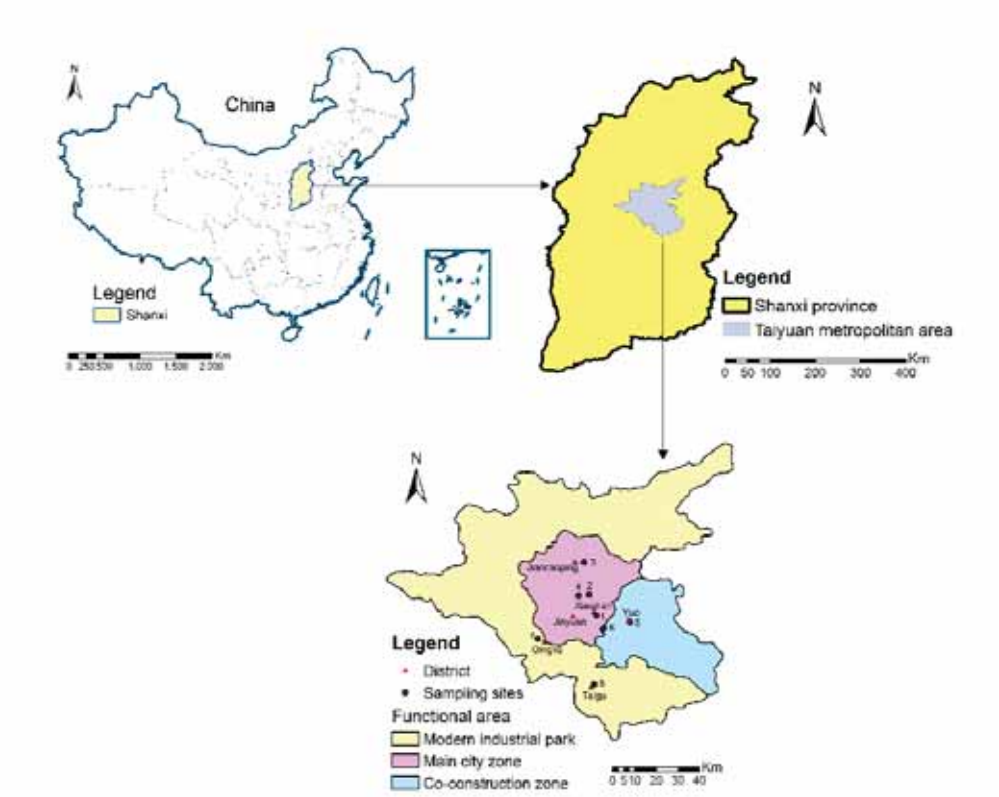

FIGURE 1
Sampling sites of wastewater treatment plants (WWPTs) and the functional area and districts located in Taiyuan metropolitan area

TABLE 1
The daily excretion coefficient for different livestock (kg/head•day) [48]

Livestock	Feces	Urine
Pigs	3.5	4.8
Cattle	15.0	10.0
Sheep	1.5	0.5
Chicken	0.11	-

TABLE 2
Classification of monomial ecological risk index [49]

Classes	R_i	Type of environmental risk	Criteria： times of fertilizers than the safety threshold
0	Ri≤0.35	Safety	Less than or equal to 0.5 times
1	0.35< Ri≤0.5	Relative safety	Less than or equal to 1 times
2	0.5 <Ri≤0.65	Low risk	Less than or equal to 2 times
3	0.65 <Ri≤0.75	Moderate risk	Less than or equal to 3 times
4	0.75<Ri≤0.8	High risk	Less than or equal to 4 times
5	Ri >0.8	Very high risk	More than 4 times

Ecological risk assessment The risk assessment of nutrients in sewage sludge and livestock manure for arable land using was formulated according to the Hakanson potential ecological risk assessment; the equation is as follows [49]:

$$R_i = \frac{F_i}{F_i + T_i}$$

Where R_i is the monomial ecological risk index for the ith nutrients in sewage sludge or livestock; F_i is the intensity agricultural using of nutrients for sewage sludge or livestock manure, kg/hm2•a; and T_i is the ecological safety threshold of nutrients for agricultural land, kg/hm2•a.

The Ecological County, Ecological City and Ecological Province Construction Index (revised draft) was issued by State Environmental Protection Administration of China in 2007. In this document, the ecological standard of fertilizer using was restricted as 250 kg/hm2, and the ecological safety loading threshold of nitrogen, phosphorus and potassium were 125 kg/hm2, 62.5 kg/hm2 and 62.5 kg/hm2 based on the proportion of 1: 0.5: 0.5 which was the nutrients proportion of nitrogen, phosphorus and potassium in developed country [50].

According to this method, the degree of ecological risk was divided into six different grades. The monomial ecological risk coefficient of 0.5 was taken as the safety threshold value. When the coefficient was lower than 0.5, there was no ecological risk for using sewage sludge or livestock manure as fertilizers on farmland, on the contrary, it was not safe. The classification of monomial ecological risk index is shown in Table 2.

Potential of sewage sludge and livestock manure for agricultural using The potential of sewage sludge and livestock manure for agricultural using was evaluated based on the threshold value of ecological safety loading as following equations:

$$P_i = \frac{L_{si} - L_i}{C_i}$$

$$P = P_{i\ Min}$$

Where P_i is the potential index of sewage sludge or livestock manure used as fertilizers according to the ith nutrient, t/ha•a; L_{si} is the threshold value of ecological safety loading of the ith nutrients, kg/hm2•a; C_i is the content of the ith nutrients in sewage sludge or pigs manure, the potential of the livestock manure used for farmland has converted by pigs manure to facilitate express the potential, g/kg; and $P_{i\ Min}$ is the minimum potential of sewage sludge or livestock manure used for agriculture based on the ith nutrients, t/ha•a.

RESULTS AND DISCUSSION

The contents of organic matter and nutrients The contents of organic matter and nutrients in sewage sludge were determined and presented in Table 3. The contents of organic matter varied from 217.90 to 432.22 g/kg, with the mean value of 337.45 g/kg. The minimum content of organic matter was higher than 200 g/kg, which was the specified standard value limited by Disposal of Sludge from Municipal Wastewater Treatment Plant-Control Standards for Agricultural Use (CJ/T 309-2009). Comparing the mean content of organic matter in sewage sludge in the studying area with that of China in sewage sludge and pigs, cattle, sheep and chicken manure presented in Table 4, it was much higher. This result indicated that the content of organic matter in sewage sludge in studying area had come up to the requirement of agricultural use, and in contrast to the pigs, cattle, sheep and chicken manure, sewage sludge had advantage.

The mean contents of nutrients in sewage sludge were in the following decreasing order: N>P>K. The mean contents of nitrogen, phosphorus and potassium were 36.11 g/kg, 22.46 g/kg and 12.71 g/kg, respectively; and they were varied from 22.68 to 47.44 g/kg, 16.32 to 45.58 g/kg and 8.36 to 15.51 g/kg. Nutrients (N+P+K) in different samples were all higher than the specified value of 30 g/kg, which was formulated by Disposal of Sludge from Municipal Wastewater Treatment Plant-Control Standards for Agricultural Use (CJ/T 309-2009). Comparing the mean contents of nitrogen, phosphorus and potassium in the studying area with the mean values of sewage sludge in China in Table 4, they were all higher, except for the content of phosphorus which was lower [42,43]. When sewage sludge was

contrasted with pigs, cattle, sheep and chicken manure, the contents of nutrients in sewage sludge were all significantly higher than that in livestock manure.

The mean values of N:P:K were 1:0.62:0.35 for sewage sludge, and the proportion for pigs, cattle, sheep and chicken manure were 1:0.16:0.33, 1:0.17:0.19, 1:0.17:0.16 and 1:0.21:0.22 respectively. Based on proportion of the N:P:K was 1:0.49:0.42 in China and 1:0.5:0.5 in the developed countries for its fertilizer, and in combination with the soil condition of low nitrogen, low phosphorus and high potassium in Shanxi, sewage sludge was more suitable for agricultural using than livestock manure [40,44,45].

Nutrients loadings of sewage sludge and livestock manure The nutrients loadings in sewage sludge were calculated and presented in Table 5. The mean loadings of nitrogen, phosphorus and potassium can be ranked in the following decreasing order as: N>P>K for sewage sludge, and N>K>P for livestock manure. The mean loadings of nitrogen, phosphorus and potassium were 91.27 kg/ha•a, 77.55 kg/ha•a and 29.80 kg/ha•a for sewage sludge and 92.35 kg/ha•a, 12.85 kg/ha•a and 54.11 kg/ha•a for livestock manure. The mean loading of nitrogen was higher than phosphorus and potassium, no matter sewage sludge or livestock manure.

TABLE 3
Statistical analysis of organic matter (OM) and nutrients contents in sewage sludge from municipal wastewater treatment plants in Taiyuan metropolitan area (g/kg)

Functional area	Sampling sites	N	P	K	OM	N:P:K
Main city zone	1	28.81	16.47	12.65	320.00	1: 0.57: 0.44
	2	47.44	24.29	12.49	385.90	1: 0.51: 0.26
	3	38.52	16.32	11.72	333.81	1: 0.42: 0.30
Co-construction zone	4	22.68	45.58	8.36	217.90	1: 2.01: 0.37
	5	36.23	20.02	13.84	352.93	1: 0.55: 0.38
	6	33.56	17.79	15.51	341.66	1: 0.53: 0.46
Modern industrial park	7	36.47	16.62	11.67	315.15	1: 0.46: 0.32
	8	45.16	22.58	15.43	432.22	1: 0.50: 0.34
Min		22.68	16.32	8.36	217.90	-
Max		47.44	45.58	15.51	432.22	-
Mean		36.11	22.46	12.71	337.45	1:0.62:0.35
Std.dev		8.07	9.81	2.32	61.75	-

TABLE 4
Organic matter (OM) and nutrients contents in different solid wastes in China (g/kg) [48,51,52]

Solid wastes	N	P	K	OM	N:P:K
Mean values of Sewage sludge in China	29.6	22.2	5.83	280	1:0.75:0.20
Pigs manure	5.6	0.87	1.83	150	1:0.16:0.33
Cattle manure	3.2	0.55	0.62	145	1:0.17:0.19
Sheep manure	6.5	1.09	1.04	280	1:0.17:0.16
Chicken manure	16.3	3.36	3.53	255	1:0.21:0.22

TABLE 5
Nutrients loadings of sewage sludge from municipal wastewater treatment plants and livestock manure in Taiyuan metropolitan area (kg/ha•a)

Functional area	District	Sewage sludge			Livestock manure		
		N	P	K	N	P	K
Main city zone	Jinyuan	89.35	51.08	39.23	129.69	19.17	73.10
	Xiaodian	379.13	377.78	112.73	65.04	8.10	29.10
	Jiancaoping	52.18	22.11	15.88	121.23	14.16	62.95
Co-construction zone	Yuci	22.70	12.30	9.55	49.77	6.66	28.09
Modern industrial park	Qingxu	1.93	0.88	0.62	61.53	8.46	37.69
	Taigu	2.34	1.17	0.80	126.81	20.54	93.70
Min		1.93	0.88	0.62	49.77	6.66	28.09
Max		379.13	377.78	112.73	129.69	20.54	93.70
Mean		91.27	77.55	29.80	92.35	12.85	54.11
Std.dev		144.90	148.24	43.04	37.21	6.02	26.75

Comparing the threshold loadings values of nitrogen, phosphorus and potassium of 125 kg/ha•a, 62.5 kg/ha•a and 62.5 kg/ha•a, which were limited by Ecological County, Ecological City and Ecological Province Construction Index (revised draft), the mean nutrients loadings for sewage sludge and livestock manure were all lower than that, except the loading of phosphorus for sewage sludge.

Further detailed, the loadings of nitrogen, phosphorus and potassium for sewage sludge in Xiaodian, and loadings of nitrogen and potassium for livestock manure in Jinyuan, Jiancaoping and Taigu were all higher than the threshold values. This indicated that a potential ecological pressure would exist when the total annual output of sewage sludge was used as fertilizer in Xiaodian and livestock manure in Jinyuan, Jiancaoping and Taigu. For sewage sludge, the high nutrients loadings in Xiaodian were caused by the huge production of sewage sludge. For livestock manure, the high nutrient loadings in Taigu were caused by the big numbers of animal breeding, and the high nutrient loadings in Jinyuan and Jiancaoping were resulted by the smaller area of farmland.

In the main, loadings of nitrogen and potassium were higher for livestock manure than sewage sludge, and loadings of phosphorus were higher for sewage sludge than livestock manure in the studying area. No matter sewage sludge or livestock manure, nitrogen loading was the main for nutrients loadings [26]. The nitrogen loading in studying area was less than the mean value of the east of China, but higher than the west of China, and it was also higher than the mean value of Shanxi [38], consistent with the trends of developed regions has high nutrients loadings and underdeveloped regions has low nutrients loadings [29,53]. This might be induced by that developed regions have great production of sewage sludge and livestock manure but small area, however underdeveloped regions have small production of sewage sludge and livestock manure but large area [29,53,54].

Ecological risk assessment of sewage sludge and livestock manure The ecological risk assessments of sewage sludge and livestock manure for agricultural using are shown in Table 6. Based on the mean values of the monomial ecological risk index, nutrients can be ranked in the decreasing order P>N>K for sewage sludge, and K>N>P for livestock manure. The ecological risks of nitrogen, phosphorus and potassium were 0.28, 0.29 and 0.23 for sewage sludge, and 0.41, 0.17 and 0.44 for livestock manure. Phosphorus was the main risky elements for sewage sludge agricultural using, and potassium was for livestock manure. The ecological risks for sewage sludge and livestock manure based on the mean were all lower than the safety threshold value of 0.5, and the ecological risks of nitrogen and potassium for livestock manure were higher than that for sewage sludge.

For sewage, the ecological risks of nitrogen, phosphorus and potassium were all lower than the safety threshold value of 0.5 in different districts, except Xiaodian. The ecological risk of nitrogen, phosphorus and potassium in Xiaodian were 0.75, 0.86 and 0.64 which all higher than the relatively safety threshold value of the 0.5, in Jinyuan were 0.42, 0.45 and 0.39 which all higher than the safety threshold value of 0.35, and in other districts were all below 0.35, this indicated that agricultural use of annual output of all sewage sludge in local farmland has high ecological risk in Xiaodian, relatively safe in Jinyuan and completely safe in Jiancaoping, Yuci, Qingxu and Taigu. The results depicted that agricultural using of sewage sludge had no ecological risks in all districts except Xiaodian, which was caused by the large amount of annual production of sewage sludge.

For livestock, the ecological risks of phosphorus were lower than 0.35 in all districts, which suggested that agricultural using livestock manure would not induce ecological risk by phosphorus. However, the ecological risks of nitrogen and potassium in Jinyuan were 0.51 and 0.54, and potassium in Taigu was 0.60, all higher than 0.5. This indicated that agricultural use of livestock manure would result in low ecological risk in Jinyuan due to nitrogen and potassium and in Taigu due to potassium; the ecological risks of nitrogen and potassium in Jiancaoping were 0.49 and 0.50 and nitrogen in Taigu was 0.50, values which were all between 0.35 and 0.5, showing that livestock manure used as fertilizers in Jiancaoping and Taigu were relatively safe; and the ecological risks of all nutrient elements in Xiaodian, Yuci and Qingxu were all fewer than 0.35, depicting that it was completely safe to use livestock manure as fertilizer in these districts. Jinyuan and Taigu should be taken more attention when livestock manure was used on farmland, which would cause low ecological risks.

According to the ecological risk assessment, not all districts are suitable for establishing sewage sludge or livestock manure farm [55], like Xiaodian was not suitable for sewage sludge farm, Jinyuan and Taigu were not suitable for livestock farm. To protect the ecological safety, Xiaodian should restrict the dosage of sewage sludge for agricultural using, and Jinyuan and Taigu should restrict the dosage of livestock manure using. And in contract to chemical fertilizer, the ecological risks of agricultural using of sewage sludge and livestock manure were lower [49]. Combining the higher potassium loadings for livestock manure than sewage sludge with the soil condition of low nitrogen, low phosphorus and high potassium in Shanxi, sewage sludge was more suitable for agricultural using than livestock manure in the studying area to protect the environmental safety.

The potential of sewage sludge and livestock manure for agricultural using The potential of

sewage sludge and livestock manure used as fertilizers were shown in Table 7. According to the mean potential index, nutrient can be sorted in the following decreasing orders: K>N>P for sewage sludge, with phosphorus as the restrictive factor, and P>N>K for pigs manure, with potassium as the restrictive factor. The potential of sewage sludge used as farmland fertilizers according to the nitrogen, phosphorus and potassium were 1.18 t/ha•a, 1.07 t/ha•a and 2.42 t/ha•a, and for livestock manure, which had been replaced by pigs manure, they were 5.83 t/ha•a, 56.50 t/ha•a and 4.59 t/ha•a. Comparing them, the mean potential of livestock manure was higher than that of sewage sludge.

For sewage sludge, the potential indices by nitrogen, phosphorus and potassium were -3.62 t/ha•a, -4.51 t/ha•a and -2.41 t/ha•a in Xiaodian, which were all less than zero, this indicated that the annual production of sewage sludge had surpassed the environmental capacity of farmland in Xiaodian. The potential of agricultural using of sewage sludge in Qinxu, Taigu, Jiancaoping, Yuci and Jinyuan were 3.37 t/ha•a, 2.72 t/ha•a, 1.89 t/ha•a, 1.33 t/ha•a and 0.69 t/ha•a; the restrictive factors of these districts were nitrogen, nitrogen and phosphorus, nitrogen, phosphorus and phosphorus, respectively. The higher potential of Qinxu and Taigu could be attributed to the low output of sewage sludge and large area of farmland; and the lower potential of Xiaodian and Jinyuan can be attributed to the high yield of sewage sludge and small farmland area of this district.

For livestock manure, the potential indices by nitrogen, phosphorus and potassium were -0.32 t/ha•a, 47.66 t/ha•a and -17.05 t/ha•a in Taigu, -0.84 t/ha•a, 49.22 t/ha•a and -5.79 t/ha•a in Jinyuan, 0.67 t/ha•a, 54.99 t/ha•a and -0.25 t/ha•a in Jiancaoping, the potential for using livestock manure as fertilizers were negative in these districts, and potassium was the restrictive factor in all. The potentials for agricultural using of livestock manure were 13.43 t/ha•a, 11.33 t/ha•a and 10.71 t/ha•a in Yuci, Qingxu and Xiaodian, respectively, and nitrogen was the restrictive factor in these three districts. The negative potential in Taigu was due to the great yield of livestock manure, in Jinyuan was because of the small area of farmland; and Jiancaoping was induced by a combination of the two factors. The high potential of agricultural using of livestock manure in Yuci, Qinxu and Xiaodian could be put down to the large area of farmland and the lower production of livestock manure.

TABLE 6
Ecological risk assessment of sewage sludge from municipal wastewater treatment plants and livestock manure for agricultural using in Taiyuan metropolitan area

Functional area	District	Sewage sludge			Livestock manure		
		N	P	K	N	P	K
Main city zone	Jinyuan	0.42	0.45	0.39	0.51	0.23	0.54
	Xiaodian	0.75	0.86	0.64	0.34	0.11	0.32
	Jiancaoping	0.29	0.26	0.20	0.49	0.18	0.50
Co-construction zone	Yuci	0.15	0.16	0.13	0.28	0.10	0.31
Modern industrial park	Qingxu	0.02	0.01	0.01	0.33	0.12	0.38
	Taigu	0.02	0.02	0.01	0.50	0.25	0.60
Min		0.02	0.01	0.01	0.28	0.10	0.31
Max		0.75	0.86	0.64	0.51	0.25	0.60
Mean		0.28	0.29	0.23	0.41	0.17	0.44
Std.dev		0.28	0.32	0.25	0.10	0.06	0.12

TABLE 7
The potential of sewage sludge from municipal wastewater treatment plants and livestock manure for agricultural using in Taiyuan metropolitan area (t/ha•a)

Functional area	District	Sewage sludge				Livestock manure			
		N	P	K	P_{min}	N	P	K	P_{min}
Main city zone	Jinyuan	1.24	0.69	1.84	0.69	-0.84	49.22	-5.79	-5.79
	Xiaodian	-3.62	-4.51	-2.41	-4.51	10.71	61.95	18.25	10.71
	Jiancaoping	1.89	2.48	3.98	1.89	0.67	54.99	-0.25	-0.25
Co-construction zone	Yuci	1.47	1.33	1.80	1.33	13.43	63.60	18.81	13.43
Modern industrial park	Qingxu	3.37	3.71	5.30	3.37	11.33	61.55	13.56	11.33
	Taigu	2.72	2.72	4.00	2.72	-0.32	47.66	-17.05	-17.05
Min		-3.62	-4.51	-2.41	-4.51	-0.84	47.66	-17.05	-17.05
Max		3.37	3.71	5.30	3.37	13.43	63.60	18.81	13.43
Mean		1.18	1.07	2.42	1.07	5.83	56.50	4.59	4.59
Std.dev		2.48	2.93	2.73	2.82	6.64	6.91	14.62	12.02

CONCLUSIONS

Nutrients and organic matter contents, ecological risk, nutrients loadings and the potential of agricultural using were compared between sewage sludge and livestock manure in the Taiyuan metropolitan area. The minimum values of organic matter and nutrients (N+P+K) in sewage sludge were all higher than the mean values of pigs, cattle, sheep and chicken manure, except the organic matter for sheep manure, and the proportion of N:P:K for sewage sludge was more suitable for agricultural using than livestock manure. The mean nutrients loadings of N>P>K for sewage sludge, N>K>P for livestock manure, and all mean nutrients loadings were below the ecological safety threshold values, except the loading of phosphorus for sewage sludge. Furthermore, the mean loadings of nitrogen and potassium for livestock manure were higher than sewage sludge, and the loading of phosphorus for sewage sludge was higher than livestock manure. Based on the mean monomial ecological risk index, the ecological risk was P>N>K for sewage sludge, and K>N>P for livestock manure. The ecological risks of nitrogen and potassium for livestock manure were higher than that for sewage sludge, and the mean values were all within the safety threshold value of 0.5. Comparing the potential of sewage sludge agricultural using with livestock manure, livestock manure was higher than sewage sludge in all districts, but the districts having negative potential were more for livestock using than sewage sludge. The restrictive factors were nitrogen and phosphorus for sewage sludge using, nitrogen and potassium for livestock manure using, and the negative potential for sewage sludge using was determined by phosphorus, for livestock manure using were all determined by potassium.

Comprehensively, according to the contents of organic matter and nutrients and combining with the proportion of N:P:K, sewage sludge was more suitable for agricultural using than livestock manure. To consider the ecological safety, and combining the local soil condition, livestock manure had advantage than sewage sludge in agricultural using.

ACKNOWLEDGEMENTS

This work was supported by the comprehensive laboratory of environmental chemical analysis of College of resources and environment in Shanxi agricultural university. We are also grateful to the Department of environmental protection of Shanxi province for their support in the data collecting. And in samples colleting, municipal wastewater treatment plants in the studying area also give greatly help to this work.

REFERENCES

[1] Mohamed, B., Mounia, K., Aziz, A., Ahmed, H., Rachid, B., Lotfi, A. (2018) Sewage sludge used as organic manure in Moroccan sunflower culture: Effects on certain soil properties, growth and yield components. Sci. Total Environ. 627, 681-688.

[2] Liu, J.Y., Zhuo, Z.X., Sun, S.Y., Ning, X.A., Zhao, S.Y., Xie, W.M., Wang, Y.J., Zheng, L., Huang, R., Li, B. (2015) Concentrations of heavy metals in six municipal sludges from Guangzhou and their potential ecological risk assessment for agricultural land use. Pol. J. of Environ. Stud. 24, 165-174.

[3] Dong, B., Liu, X., Dai, L., Dai, X. (2013) Changes of heavy metal speciation during high-solid anaerobic digestion of sewage sludge. Bioresource Technol. 131, 152-158.

[4] Guo, G.H., Chen, T.B., Yang, J., Zheng, G.D., Gao, D. (2014) Regional distribution characteristics and variation of heavy metals in sewage sludge of China. Acta Scientiae Circumstantiae. 34, 2455–2461.

[5] Gao, D., Chen, T.B., Liu, B., Zheng, Y.M., Zheng, G.D., Li, Y.X. (2006) Releases of pollutants from poultry manure in China and recommended strategies for the pollution prevention. Georg. Res. 25, 311-319.

[6] Gao, M.F., Qiu, J.J., Li, C.S., Wang, L.G., Li, H., Gao, C.Y. (2014) Modeling nitrogen loading from a watershed consisting of cropland and livestock farms in China using Manure DNDC. Agr. Ecosyst. Environ. 185, 88-98.

[7] Liu, J.Y., Zhuo, Z.X., Sun, S.Y., Ning, X.N., Zhao, S.Y., Xie, W.M., Wang, Y.J., Zheng, L., Huang, R., Li, B. (2015) Concentrations of heavy metals in six municipal sludges from Guangzhou and their potential ecological risk assessment for agricultural land use. Pol. J. Environ. Stud. 24, 165-174.

[8] Qiu, L.F, Zhu, J.X, Pan, Y., Hu, W., Amable, G.S. (2017) Multi-criteria land use suitability analysis for livestock development planning in Hangzhou metropolitan area, China. J. Clean. Prod. 161, 1011-1019.

[9] Zhou, Q.H. (2018) Analysis on municipal sludge disposal technology. Tech. Wind. 353, 113-113.

[10] Yang, S.Q., Han, R.Y., Liu, C. (2016) Study on the given amount per unit field and load capacity of livestock and poultry manure at province scale. J. China Agr. Univ. 21, 142-151.

[11] Fytili, D., Zabaniotou, A. (2008) Utilization of sewage sludge in EU application of old and new methods-A review. Renew. Sust. Energ. Rev. 12, 116-140.

[12] Kulikowska, D., Gusiatin, Z.M. (2015) Sewage sludge composting in a two-stage system: Carbon and nitrogen transformations and potential ecological risk assessment. Waste Manage. 38, 312-320.
[13] Schou, J.S., Skop, E., Jensen, J.D. (2000) Integrated agri-environmental modelling: A cost-effectiveness analysis of two nitrogen tax instruments in the Vejle Fjord watershed, Denmark. J. Environ. Manage. 58, 199-212.
[14] Nascimento, A. L., José de Souza, A., Oliveira, F. C. (2020) Chemical attributes of sewage sludges: Relationships to sources and treatments, and implications for sludge usage in agriculture[J]. J. Cleaner Prod. 258, 120746.
[15] Schlegel, A.J., Assefa, Y., Bond, H.D., Haag, L.A., Stone, L.R. (2017) Changes in soil nutrients after 10 years of cattle manure and swine effluent application. Soil Till. Res. 172, 48-58.
[16] Pedizzi, C., Noya, I., Sarli, J., González-García, S., Lema, J.M., Moreira, M. T., Carballa, M. (2018) Environmental assessment of alternative treatment schemes for energy and nutrient recovery from livestock manure. Waste Manage. 77, 276-286.
[17] Quan, Z., Lu, C.Y., Shi, Y., Chen, X., Huang, B., Wang, Y.Z., Zhao, Y., Ma, J. (2015) Manure increase the leaching risk of soil extractable organic nitrogen in intensively irrigated greenhouse vegetable cropping systems. Acta Agr. Scand. B-S. P. 65, 199-207.
[18] Liu, W., Zeng, D., She, L. (2020) Comparisons of pollution characteristics, emission situations, and mass loads for heavy metals in the manures of different livestock and poultry in China. Sci. Total Environ. 734, 139023.
[19] Rui, Y., Sanford, G.R., Hedtcke, J.L. (2020) Legacy effects of liquid dairy manure in grain production systems[J]. Agr. Syst. 181, 102825.
[20] Yan, B.J., Shi, W.J., Yan, J.J., Chun, K.P. (2017) Spatial distribution of livestock and poultry farm based on livestock manure nitrogen load on farmland and suitability evaluation. Comput. Electron. Agr. 139,180-186.
[21] Hou, Y., Bai, Z., Lesschen, J.P., Staritsky, I.G., Sikirica, N., Ma, L., Velthof, G., Oenema, O. (2016) Feed use and nitrogen excretion of livestock in EU-27. Agr. Ecosyst. Environ. 218, 232-244.
[22] Li, Y., Wang, Y., Tumbalam, P. (2019) Spatio-temporal distribution of chemical fertilizer application and manure application potential in China. Environ. Eng. Sci. 36, 1337-1347.
[23] Fumagalli, M., Perego, A., Acutis, M. (2013) Modelling nitrogen leaching from sewage sludge application to arable land in the Lombardy region (northern Italy). Sci. Total Environ. 461-462, 509-518.
[24] Kendir, E., Kentel, E., Sanin, F.D. (2015) Evaluation of heavy metals and associated health risks in a metropolitan wastewater treatment plant's sludge for its land application. Hum. Ecol. Risk Assess. 21, 1631–1643.
[25] Yoshida, H., Hoeve, M.T., Christensen, T.H., Bruun, S., Jensen, L.S., Scheutz, C. (2017) Life cycle assessment of sewage sludge management options including long-term impacts after land application. J. Clean. Prod. 174.
[26] Vizzari, M., Antognelli, S., Pauselli, M., Benincasa, P., Farneselli, M., Morbidini, L. (2016) Potential Nitrogen Load from Crop-Livestock Systems: A Spatial Database for a Multi-Scale Assessment and Mapping. Int. J. Agr. Environ. Inf. Syst. 7, 21-40.
[27] Cucina, M., Ricci, A., Zadra, C. (2019) Benefits and risks of long-term recycling of pharmaceutical sewage sludge on agricultural soil [J]. Sci. Total Environ. 695, 133762
[28] Zheng, L., Zhang, Q., Zhang, A. (2019) Spatio-temporal characteristics of the bearing capacity of cropland based on manure nitrogen and phosphorus load in mainland China[J]. J. Cleaner Prod. 233, 601-610.
[29] Zhang, X.M., Dong, Y.H., Wang, H., Shen, D. (2007) Structure of livestock and variation of fecal nitrogen pollution load in China. Environ. Sci. 28, 1311-1318.
[30] Corrêa, R.S., White, R.E., Weatherley, A.J. (2006) Effect of compost treatment of sewage sludge on nitrogen behavior in two soils. Waste Manage. 26, 614-619.
[31] Yang, R., Li, Y.Y., Wei, H.A., Gao, R., Shi, H., Wu, J.S. (2011) Study on the nitrogen and phosphorus mineralization of livestock manure in red soil. Plant Nutr. Fertilizer Sci. 17, 600-607.
[32] Ojeda, G., Tarrason, D., Ortiz, O., Alcaniz, J.M. (2006) Nitrogen losses in runoff waters from a loamy soil treated with sewage sludge. Agr. Ecosyst. Environ. 117, 49-56.
[33] Kumaragamage, D., Flaten, D., Akinremi, O.O., Sawka, C., Zvomuya, F. (2011) Soil test phosphorus changes and phosphorus runoff losses in incubated soils treated with livestock manures and synthetic fertilizer. Can. J. Soil Sci. 91, 375-384.
[34] Xia, F., Mei, K., Xu, Y. (2020) Response of N2O emission to manure application in field trials of agricultural soils across the globe [J]. Sci. Total Environ. 733, 139390.
[35] Gao, M.F., Qiu, J.J., Li, C.S., Wang, L.G., Li, H., Gao, C.Y. (2012) Modelling nitrogen pollution from livestock breeding using Manure-DNDC model. T. Chinese Soc. Agr. Eng. 28, 183-189.
[36] Luo, W., O'Brien, P. L., Hatfield, J. L. (2019) Crop yield and nitrous oxide emissions following swine manure application: a meta-analysis. Agric. Environ. Lett. 4 (1).

[37] Font-Palma, C. (2019) Methods for the Treatment of Cattle Manure-A Review. J. Carbon Res. 5, 27.
[38] Yan, B.J., Pan, Y.C. (2015) Estimation of nitrogen pollution load of farmland from livestock manure in China based on grid. Bull. Soil Water Conserv. 35, 133-137.
[39] The Council of the European Communities. (1991) Council Directive of 12 December 1991 concerning the protection of waters against pollution caused by nitrates from agricultural sources (91/676/EEC), Brussels, Belgium..
[40] Yan, B.J., Zhao, C.J., Pan, Y.C., Yan, J.J., Guo, X. (2010) Estimation of livestock manure nitrogen load and pollution risk evaluation of farmland in Daxing district. Environ. Scie. 31, 437-443.
[41] Lin, L.U., Liao, X.D., Luo, X.G. (2017) Nutritional strategies for reducing nitrogen, phosphorus and trace mineral excretions of livestock and poultry. J. Integr. Agr. 16, 2815-2833.
[42] Mi, J. (2017) An empirical study of Taiyuan metropolitan governance based on "Bow-String-Arrow" model. J. Taiyuan Univ. (Soc. Sci. Edit.). 18, 16-22.
[43] Foissy, D., Vian, J.F., David, C. (2013) Managing nutrient in organic farming system: reliance on livestock production for nutrient management of arable farmland. Org. Agr. 3,183-199.
[44] Yang, Q.C., Tian, H.Q., Li, X., Ren, W., Zhang, B.W., Zhang, X.S., Wolf. J. (2016) Spatiotemporal patterns of livestock manure nutrient production in the conterminous United States from 1930 to 2012. Sci. Total Environ. 544, 1141.
[45] DARD. (2014) Nitrates action programme 2011-2014 and phosphorus regulations workbook. Department of Agriculture and Rural Development, Cookstown, UK.
[46] Wang, L.G., Li, H., Wang, Y., Qiu, J. (2011) Changes in livestock operation systems and their contributions to manure nitrogen pollution loading in Xiaoqinghe watershed, China. J. Agro-Environ. Sci. 30, 986-992.
[47] Wu, S.S., Tan, M.Y., Long, Y.L., Huang, H., Gan, D.X., Zhu. H. (2009) Nitrogen pollution and environmental cost of livestock manure in Dongting lake area. T. Chinese Soc. Agr. Eng. 25, 229-234.
[48] Hu, A.T., Zhou, L.X. (2003) Nutrition of plants, 2nd ed.; China agricultural university press: Beijing, China. 210-216.
[49] Liu, Q.P. (2015) Regional difference of NPK fertilizers application and environmental risk assessment in Jiangsu Province, China. Chinese J. Appl. Ecology. 26, 1477-1483.
[50] Song, X.J., Chen, D.J., Zhang, X. (2010) The structural adjustment of planting and controlling of non-point source pollution by fertilizers. China Acad J. Electron. Publishing. 1, 784-787.
[51] Guo, G.H., Yang, J., Chen, T.B., Zheng, G.D., Gao, D., Song, B., Du, W. (2009) Concentrations and variation of organic matter and nutrients in municipal sludge of China. China Water Wastewater. 25, 120-121.
[52] National Agro-Technical Popularization Service Center. (1999) Records of Nutrients in Organic Fertilizer in China, 1st ed.; China Agricultural press: Beijing, China. 5-21.
[53] Yang, F., Yang, S.Q., Zhu, Y.Q., Wang, J.L. (2013) Analysis on livestock and poultry production and nitrogen pollution load of cultivated land during last 30 years in China. T. Chinese Soc. Agr. Eng. 29, 1-11.
[54] Song, K.Y., Li, Y., Ouyang, W., Hao, F.H., Wei, X.F. (2012) Manure Nutrients of Pig Excreta Relative to the Capacity of Cropland to Assimilate Nutrients in China. Procedia Environ. Sci. 13, 1846-1855.
[55] Yan, B.J., Shi, W.J., Yan, J.J., Chun, K.P. (2017) Spatial distribution of livestock and poultry farm based on livestock manure nitrogen load on farmland and suitability evaluation. Comput. Electron. Agr. 139, 180-186.
[56] Li, T., Li, W., Li, X.M., Dong, Z.X., Liu, F.W., Zhang, W.P., Bu, Y.S. (2015). Agricultural potential and security application of sewage sludge in Shanxi province. Chinese J. Environ. Eng. 9, 3455-3461.
[57] Ding, Y.C., Jiao, X.Y., Nie, D., Cheng, B., Zhao, R., Liu, P. (2012) Contents and distribution of exchangeable magnesium and their relationship with the chemical properties of main farm soils in Shanxi province, China. J. Nat. Resources. 27, 311-321.

Received: **07.12.2020**
Accepted: **10.01.2021**

CORRESPONDING AUTHOR

Yushan Bu
College of Resources and Environment,
Shanxi Agricultural University,
Taigu Shanxi 030801 – China

e-mail: yushan_bu@126.com

© by PSP Volume 30– No. 05/2021 pages 5312-5319 Fresenius Environmental Bulletin

SORPTIVE REMOVAL OF CADMIUM BY SULFURIC ACID/ULTRASONIC-MODIFIED STRAW BIOCHAR FROM SIMULATED EUTROPHIC WATER

Chunxue Yu[1], Weikang Gao[2], Bai Yu[3], Wei Jiao[4,*]

[1]Research Center for Eco-environmental Engineering, Dongguan University of Technology, Dongguan 523808, PR China
[2]Qingdao Engineering Research Center for Rural Environment, School of Resources and Environment, Qingdao Agricultural University, Qingdao 266109, PR China
[3]Agricultural Technology Promotion Station of Zhaowangzhuang Town, Laiyang 265200, PR China
[4]Shandong Provincial Key Laboratory of Water and Soil Conservation and Environmental Protection, College of Resources and Environment, Linyi University, Linyi 276000, PR China

ABSTRACT

Aiming at a dual purposes of resource conservation and environmental remediation, this study prepared corn straw- and wheat straw-derived biochar and modified them by sulfuric acid and ultrasonic wave for the cadmium removal from artificially different eutrophic water. Results showed that the removal rates of cadmium on biochar were in the ranges of 73.5%-100% and 64.6%-100% from 0.3 and 10 mg/L of cadmium solution, respectively, which were both increased with the pH increasing. Under different conditions of TN and TP concentrations, the removal rates of the two concentrations of cadmium were 57.4%-100% and 40.1%-100%, respectively. With the increasing TN and TP concentrations, the variations of Cd on biochar altered differently in the low and high cadmium solutions. With the increasing eutrophication level, the removal rates of two concentrations of cadmium solution has a downward trend. The Cd removal rate highly depended on biochar types, environmental pH, TN and TP concentrations. Generally, the modified biochar had higher Cd removal rates than unmodified biochar. The modified wheat straw biochar performed the best in the cadmium removal from different eutrophic water with a maximal removal rate of 100%. The study provides an effective and environmental tool for heavy metals-contaminated eutrophic water body.

KEYWORDS:
Cadmium (Cd), Eutrophication, modified biochar, Simultaneous environmental remediation

INTRODUCTION

With the quick development of industry in China, heavy metal pollution in water has become one of the most severe environmental problems. As a severely hazardous one, the cadmium (Cd) wastewater can discharge from mining, electroplating and chemical industry. It can not only cause direct or indirect heavy metal pollution to water bodies but also bring a considerable threat to human health [1-3]. It is urgent to study how to treat Cd-containing wastewater efficiently. The main treatment measures for Cd-containing wastewater include ion exchange, membrane separation, reverse osmosis, adsorption and chemical precipitation [4]. Due to the feature of no additional chemical reagent, simple operation and low energy consumption, adsorption treatment is regarded as an environmentally friendly and effective treatment compared with other methods. Commonly, adsorption mainly includes graphene, carbon nanotubes, activated carbon, etc. Although they all have strong adsorption capacity to heavy metals, they cannot be applied to heavy metals-containing wastewater treatment on a large scale due to their high costs [5]. The vital issue for adsorption is to find adsorbents with low price, comprehensive sources of raw materials and little interference with the environment in the treatment of heavy metal pollution.

Recently, as an environmentally friendly, low-cost and widely sourced adsorbent, biochar has attracted extensive attention in wastewater treatment. Biochar refers to a stable, carbon-rich and highly aromatized solid material produced by pyrolysis-carbonization of biomass materials at a low temperature (<700°C) under the entirely or partially anoxic condition [6-8]. Biomass itself has a good pore structure, and it will get higher porosity and specific surface after carbonization. What's more, the surface of biochar is also rich in lots of functional groups such as carbonyl, phenolic hydroxyl and carbonyl group, so it has particular surface activity and is more efficient in adsorbing heavy metals.

However, the access to active sites and the adsorption capacity could be inhibited for removing heavy metals from the environment because of the un-homogeneities and non-uniformity of biochar surface [9-10]. Due to the different methods of preparing biochar, some substances like ash and minerals could be attached to the surface and pores. Hence,

it is normal that the biochar is activated physically and chemically by cleaning the redundant materials. Among all the physical methods, ultrasound is one of an ideal way for modification [11-13]. Sajjadi et al. [14] found that the biochar modified with phosphorus and ultrasound could remove >99% of 100 mg Ni(II)/ml in only six hours.

Besides heavy metal pollution, eutrophication also has become a global problem. It mainly refers to the fact that the self-purification ability of water bodies cannot meet the requirements of accepting a large number of elements (mainly nitrogen and phosphorus) from the enclosed body of water, leading to the deterioration of water quality and ecological destruction [15]. Deng et al. [16] found that the adsorption capacity of heavy metals by biochar modified with choro-phosphate can be improved. Also, it can be suggested from the result that the combination of biochar with phosphate materials can both enhance the adsorption performance and weaken the risk of eutrophication due to the abuse of phosphate materials. What's more, different forms of heavy metals show different behaviours and strength of toxicity under different environmental conditions [17]. Therefore, it is of considerable significance to explore the influence of eutrophication water body on biochar adsorption of substantial cadmium restoration.

As a vast agricultural country since ancient times, China produced about 1.04 billion tons of crop straws in 2015, accounting for nearly a third of global output [18]. Since the 1980s, crop straw is no longer used as a heating material in rural areas, and open burning has become a common way for the disposal of the waste crop. However, it leads to the emission of a large number of gases and particulate pollutants, causing severe environmental problems [19-22]. Therefore, using corn and wheat straw as raw materials to prepare biochar can recycle not only agricultural wastes but also provide new content for remediation of polluted water [23].

In this study, agricultural solid wastes corn and wheat straw were used to prepare biochar, which was also modified with sulfuric acid/ultrasonic wave. The removal efficiency of Cd from water with different levels of eutrophication. The research results are of considerable significance to the recycling of agricultural waste and the remediation of polluted water bodies.

MATERIALS AND METHODS

Biochar preparation. The biochar preparation flow was shown in Figure1. Before biochar production, clean and air-dried straw was cut into small segments (around 2 cm in length), separately put into the muffle furnace at 400 °C for 4 h. The pyrolysis product was then screened using 0.15-mm sieve and soaked with 0.1 mol/L hydrochloric acid for 24 h to remove the ash. Washed them with distilled deionized water to neutral, dried them in the oven at 105°C. Named the corn and wheat straw biochar as CS and WS, respectively. Modified them at the ratio of 1g biochar to 20 mL sulfuric acid under 200W ultrasonic wave (30°C) for 90 min. Named the modified corn and wheat straw biochar as MCS and MWS, respectively.

Effect of pH on the sorptive removal of cadmium. According to the preliminary experiment results, the biochar addition ratio was 2 mg. 20 mL of 0.3 and 10 mg/L Cd solution was added to the 50 mL centrifuge tubes containing 2 mg MCS, CS, MWS and WS, respectively. The pH values of the solutions were adjusted to 3.25, 4.35, 5.00, 6.00, 7.00, 8.00 and 9.00 with 1 mol/L NaOH and HCl, respectively. After 24 hours of vibration on a shaker at 150 rpm, the filtrate was taken, and the residual cadmium content in the solution was determined.

Effect of nitrogen and phosphorus on the sorptive removal of cadmium. The experiment composed of two groups with 20 mL 0-25 mg/L nitrates and 0-10 mg/L phosphates, respectively. Different levels of nitrogen and phosphorus in solutions were added to 50 mL centrifuge containing 2 mg C1, C2, C3 and C4, respectively. Then followed the steps in "The effects of pH experiment".

FIGURE 1
Flow of biochar preparation.

TABLE 1
Simulated eutrophic water.

Sewage levels	TN (mg/L)	TP (mg/L)
I	2.0	0.4
II	15	0.5
III	20	1.0
IV	20	3.0

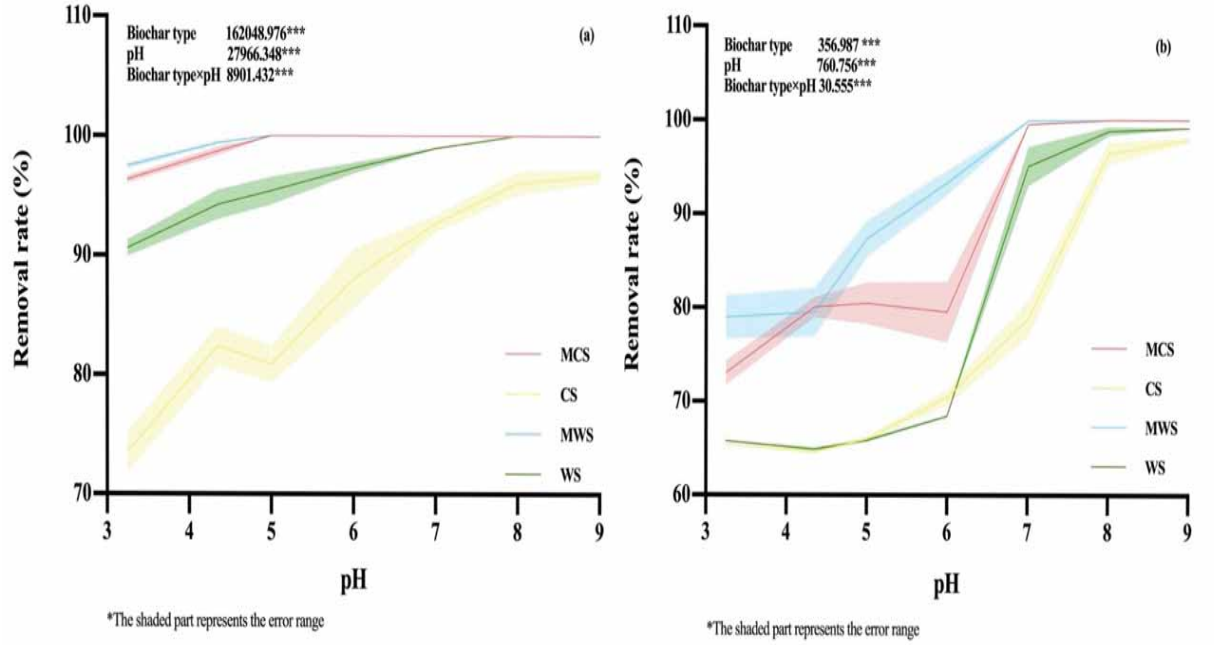

FIGURE 2
Removal rate of cadmium in aqueous solution by for biochar under different pH.

Sorptive removal of cadmium in simulated eutrophic water. Four nitrogen (TN) and phosphorus (TP) levels of simulated eutrophic water were used to remove Cd by biochar. The eutrophic water was prepared with both 10 mL of TN and TP solution listed in Table 1. Then followed the steps in "The effects of pH experiment".

Duplicates and method blanks were used to assess the quality assurance and quality control. All chemicals were of analytical grade or better, and all glassware and centrifuge tubes were previously soaked in acid (10% HNO3) and rinsed with distilled deionized water. Cd in the solution were detected by atomic absorption spectrometry (AAS), with an average recovery of 97.8 ± 5.03%. Triplicate samples were analyzed. The detected data were expressed as the means, and the standard error was within 5%.

RESULTS

Effect of pH on the adsorption of Cd. As a primary factor for a metal ion adsorption experiment, the pH of solution could influence not only the change of the metal ion morphology but also the adsorption mechanism, the surface charge polarity of the isoelectric point and adsorption capacity [24-26]. When the solution was under alkaline condition, Cd(II) could be easily formed insoluble and stable compounds, like CdCO3 and Cd(OH)2. In this experiment, the effect of solution pH in the range of 3.25-9 on Cd(II) adsorption of four biochar was studied.

The removal rate of cadmium in aqueous solution by for biochar under different pH is shown in Figure 2, and it indicated that the removal rate of biochar increased substantially with the growth of pH under both the low- and high initial Cd concentrations. According to Figure 2a, when the initial Cd concentration was 0.3 mg/L, the removal rate reached an equilibrium and maximum (100%) after the pH was 5, it was significantly different from the pH of 3.25 and 5. The removal rate reached the maximum (96.7%) when the pH was 9, it was significantly different from that of other pH conditions except when the pH was 8. The removal rate reached an equilibrium and maximum (100%) after the pH was 5, it was significantly different from the pH of 3.25 and 5. The removal rate reached the maximum (100%) when the pH was 9. It was significantly different from that of other pH conditions except when the pH was 8. At all pH values, the modified biochar's removal rate (97.1%-100%) was higher than the unmodified biochar's (73.53%-100%).

According to Figure 2b, when the initial Cd concentration was 10 mg/L, the removal rate reached an equilibrium and maximum (100%) after the pH was 8, it was significantly different from that under the previous pH conditions. The removal rate reached the maximum (97.9%) when the pH was 9. It was significantly different from that of other pH conditions except when the pH was 8. The removal rate reached an equilibrium and maximum (100%) after the pH was 8, it was significantly different from that of other pH conditions except when the pH was 7 and 9. The removal rate reached the maximum (99.2%) when the pH was 9. It was significantly different from that of other pH conditions except when the pH was 8. At all pH values, the modified biochar's removal rate (75.4%-100%) was higher than the unmodified biochar's (64.6%-99.2%).

According to Figure 3b, when the initial Cd concentration was 10 mg/L, on the whole, the removal rate showed a cyclical trend of decreasing and then increasing volatility. The removal rate reached an equilibrium and maximum (100%) when the TN was 6-10 mg/L, it was significantly different from that under other TN conditions except the TN was 0 and 20 mg/L. The removal rate reached the maximum (99.9%) when the TN was 8 mg/L, it was significantly different from that under other TN conditions except for the TN 6 mg/L. The removal rate reached an equilibrium and maximum (100%) when the TN was 6-10 mg/L, it was significantly different from that under other TN conditions except when the TN was 0 and 20 mg/L. The removal rate reached the maximum (100%) when the TN was 10 mg/L, it was significantly different from that under other TN conditions. At all TN conditions, the modified biochar's removal rate (96.1%-100%) was higher than the unmodified biochar's (90.2%-100%)..

Influence of phosphorus on the adsorption of Cd. The removal rate of cadmium in aqueous solution by biochar under different concentration of TP was shown in Figure 4, and the removal rate of all biochar reached a minimum at the relatively intermediate level. The removal rate of 0.3 mg/L cadmium solution was shown in Figure 4a, when the initial Cd concentration was 0.3 mg/L, the removal rate reached maximum (100%) when the TP was 3 and 5 mg/L, it was significantly different from that under other TP conditions. The removal rate reached the maximum (100%) when the TP was 5 mg/L, it was significantly different from that under other TP conditions. The removal rate reached maximum (100%) when the TP was 3 and 5 mg/L, it was significantly different from that under other TP conditions. The removal rate reached the maximum (100%) when the TP was 3 and 5 mg/L, it was significantly different from that under other TP conditions. At all TP conditions, the modified biochar's removal rate (48.2%-100%) was higher than the unmodified biochar's (40.1%-100%)

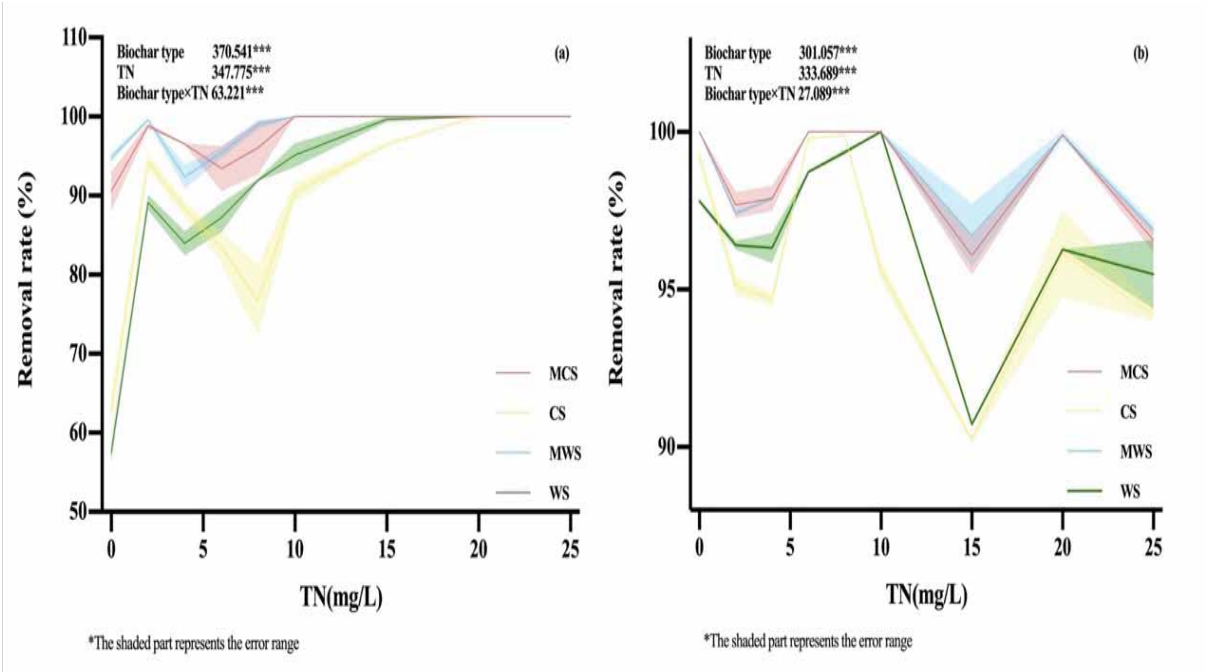

FIGURE 3
Removal rate of cadmium in aqueous solution by for biochar under different concentrations of TN.

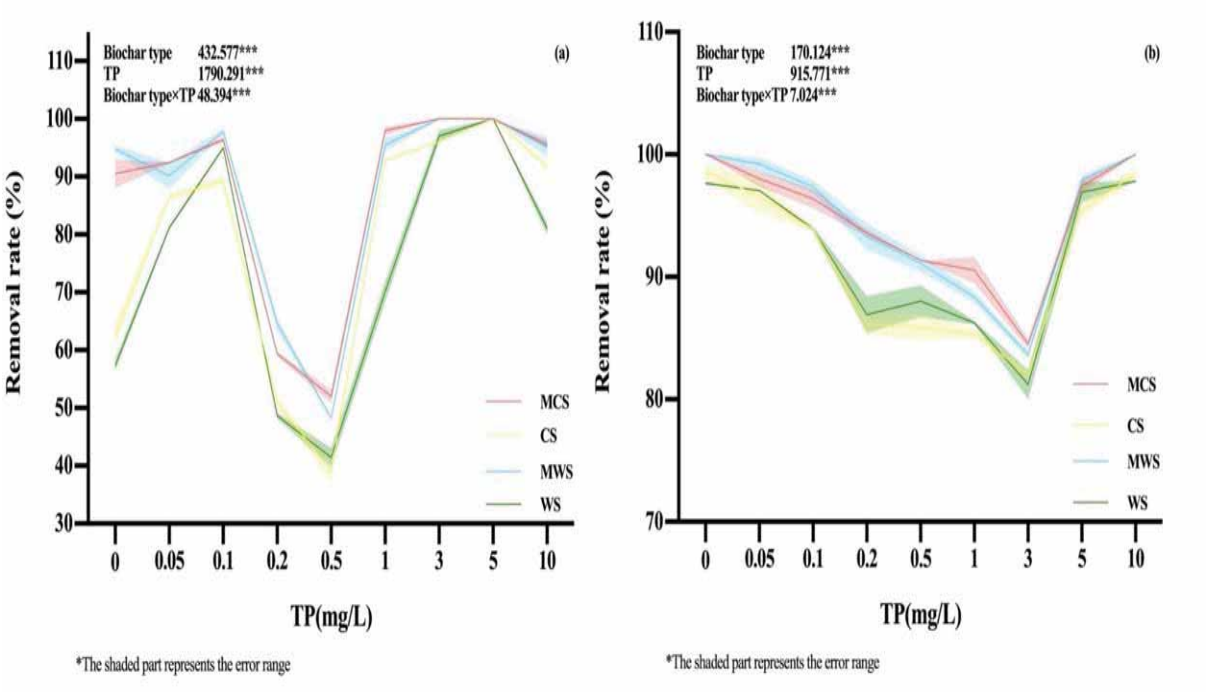

FIGURE 4
Rremoval rate of cadmium in aqueous solution by for biochar under different concentrations of TP.

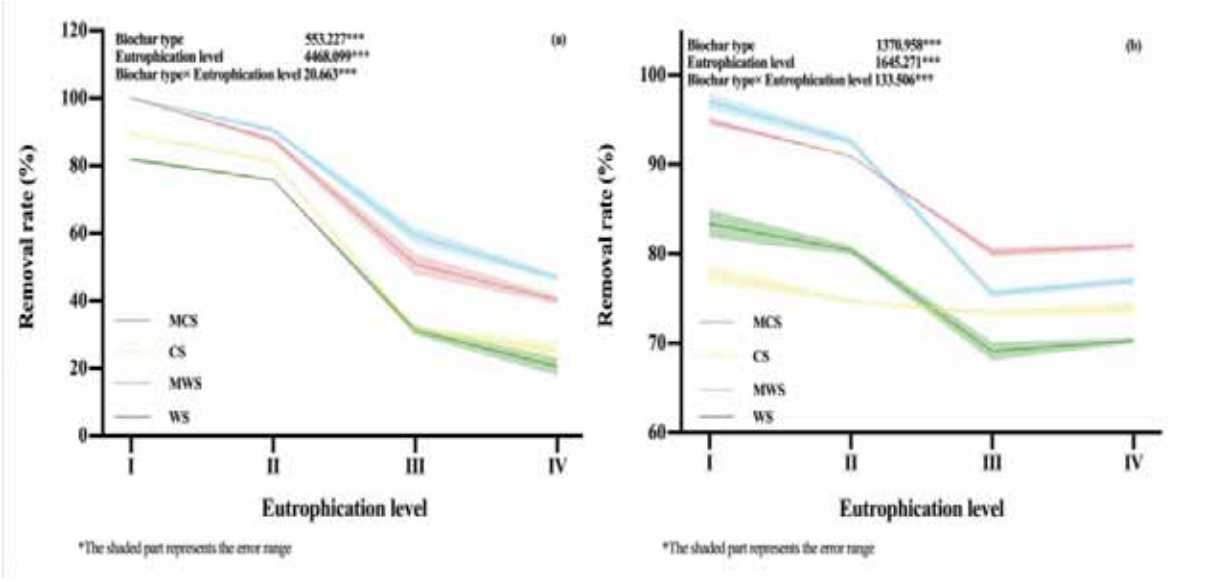

FIGURE 5
Removal rate of Cd in aqueous solution by biochar under different eutrophication levels.

The removal rate of 10 mg/L cadmium solution was shown in Figure 4b, the removal rate reached the maximum (100%) when the TP was 10 mg/L, it was significantly different from that under other TP conditions except when the TP was 0 mg/L. The removal rate reached the maximum (99.3%) when the TP was 0 mg/L, it was significantly different from that under other TP conditions except when the TP was 10 mg/L. The removal rate reached the maximum (100%) when the TP was 10 mg/L, it was significantly different from that under other TP conditions except when the TP was 0 mg/L. The removal rate reached maximum (97.8%) when the TP was 0 mg/L, it was significantly different from that under other TP conditions except when the TP was 10 mg/L. At all TP conditions, the modified biochar's removal rate (83.6%-100%) was higher than the unmodified biochar's (81.2%-99.3%).

Influence of eutrophication level on the adsorption of Cd. The removal rate of cadmium in aqueous solution by biochar under different eutrophication level was shown in Figure 5 and it indicates that the removal rate of biochar decreased with the increase of eutrophication levels. The removal rate of 0.3 mg/L Cd solution was shown in Figure 5a, the

removal rate reached maximum (100%) at the level 1, it was significantly different from that under other conditions. The removal rate reached maximum (89.3%) at the level I, it was significantly different from that under other conditions. The removal rate reached maximum (100%) at the level I, it was significantly different from that under other conditions. The removal rate reached maximum (81.8%) at the level I, it was significantly different from that under other conditions. At all situations, the modified biochar's removal rate (40.2%-100%) was higher than the unmodified biochar's (20.4%-89.3%).

The removal rate of 10 mg/L cadmium solution was shown in Figure 5b, the removal rate reached the maximum (94.9%) at the level I, it was significantly different from that under other conditions. The removal rate reached maximum (77.8%) at the level I, it was significantly different from that under other conditions. The removal rate reached maximum (96.6%) at the level I, it was significantly different from that under other conditions. The removal rate reached maximum (93.4%) at the level I, it was significantly different from that under other conditions. At all situations, the modified biochar's removal rate (76.4%-96.6%) was higher than the unmodified biochar's (70.3%-83.4%).

Due to the characteristics that biochar has developed pore structure, abundant oxygen-containing functional groups and large surface area, except for the adsorption of Cd(II) on biochar, biochar can also have ion-exchange with NH4+ and PO43- through Van dear Waals' force and even can produce irreversible adsorption through stable bonds [30-31]. In the presence of all NH4+ concentrations, the adsorption of NH4+ on biochar consists of mono-layer adsorption and multilayer adsorption, and it is influenced by the process of liquid membrane diffusion, surface adsorption and particle diffusion. Furthermore, NH4+ and Cd(II) are coexisting cations that compete for the adsorption sites on biochar and the adsorption process of NH4+ by biochar is relatively easy, causing adverse effect to the adsorption of Cd(II) on biochar and making the removal rate of Cd(II) on biochar show a volatile trend. In the presence of all PO43- concentrations, there's not only the adsorption of Cd(II) and PO43- by biochar, but also the reaction between Cd(II) and PO43- which CdHPO+4, CdH2PO+4 or other compounds will be produced, Cd(II) in the form of these compound increased its mobility. It was not suitable for the adsorption of biochar. So, under the condition that the amount of biochar added and Cd(II) remained the same, the removal rate of Cd(II) by biochar decreased before a relative TP concentration. After that, the TP concentration was too big to have the reaction that combines PO43- with Cd(II) and the biochar mainly absorbed Cd(II) and its compound, so the removal rate increased a lot.

When NH4+ and PO43- coexist in the solution and cause eutrophication, it will inhibit the adsorption of Cd on biochar, which contributes to the decrease in adsorption of Cd(II) with the increase of eutrophication level [32]. The ecological significance of applying biochar to restore cadmium-polluted water. As an environmentally friendly, inexpensive and high-efficiency adsorbent, biochar derived from straw resources is a promising means to remove Cd(II) from water and has attracted enormous attention. Some studies have shown that there are about 0.8-billion-ton per year op straws in China [33]. Applying biochar to water can absorb not only Cd(II), but also nitrogen and phosphorus to reduce eutrophication and adjust pH. Furthermore, using crop straw as the raw material can be seen as reuse of agricultural wastes to ease environment burden.

CONCLUSIONS

The sorptive removal rates of Cd significantly depended on the biochar types, pH values, the contents of TN and TP in both the low- and high-Cd-level initial Cd aqueous solutions. The impact of biochar types was enhanced by the environmental factors such as pH values, the contents of TN and TP. The removal rate of Cd increased with the pH values increasing, whereas it showed an irregular trend with the TN or TP content increasing. The modified biochar generally performed better than the unmodified biochar except wheat straw biochar. The removal rates of Cd were in the ranges of 20.4%-100% and 69.1%-96.6% from the low- and high-level initial Cd aqueous solutions, respectively, which were also depended on biochar types and decreased with the eutrophic levels increasing. Both the two sulfuric acid/ultrasonic wave-modified straw biochars were proposed to apply for the heavy metal remediation in contaminated soil and water environment.

ACKNOWLEDGEMENTS

This research benefited from financial support from the National Natural Science Foundation of China (Grant Nos. 41701562, 41701356 and 51709045) and the Central Public-interest Scientific Institution Basal Research Fund (No. 1610032019002).

REFERENCES

[1] Wang, F., Song, N. (2020) Modeling of selenite toxicity to wheat root elongation using biotic ligand model: considering the effects of pH and phosphate anion. Environ. Pollut. Article ID: 115935.

[2] Abbas, T., Rizwan, M., Ali, S., Adrees, M., Mahmood, A., Zia-ur-Rehman, M., Ibrahim, M., Arshad, M., Qayyum, M.F. (2018) Biochar application increased the growth and yield and reduced cadmium in drought stressed wheat grown in an aged contaminated soil. Ecotoxicol. Environ. Saf. 148, 825-833.

[3] Wang, F., Wang, X., Chen, Q., Song, N. (2021) Extension of a biotic ligand model for predicting the toxicity of metalloid selenate to wheat: The effects of pH, phosphate and sulphate. Chemosphere. 264, 128424.

[4] Regmi, P., Moscoso, J.L.G., Kumar, S., Cao, X.Y., Mao, J.D., Schafran, G. (2012) Removal of copper and cadmium from aqueous solution using switchgrass biochar produced via hydrothermal carbonization process. J. Environ. Manage. 109, 61-69.

[5] Chen, T., Zhou, Z.Y., Han, R., Meng, R.H., Wang, H.T., Lu, W.J. (2015) Adsorption of cadmium by biochar derived from municipal sewage sludge: Impact factors and adsorption mechanism. Chemosphere. 134, 286-293.

[6] Wang, Z.Y., Zhao, J., Song, L., Mashayekhi, H., Chefetz, B., Xing, B.S. (2011) Adsorption and desorption of phenanthrene on carbon nanotubes in simulated gastrointestinal fluids. Environ. Sci. Technol. 45(14), 6018-6024.

[7] Yu, J.S., Zhao, Y.C., Li, Y.D. (2014) Utilization of corn cob biochar in a direct carbon fuel cell. J. Power Sources. 270, 312-317.

[8] Xia, C., Li, Y., Tian, Y., Liu, Q.H., Wang, Z.M., Jia, L.J., Zhao, Y.C., Li, Y.D. (2010) Intermediate temperature fuel cell with a doped ceria–carbonate composite electrolyte. J. Power Sources. 195(10), 3149-3154.

[9] Abdul, G., Zhu, X.Y., Chen, B.L. (2017) Structural characteristics of biochar graphene nanosheet composites and their adsorption performance for phthalic acid esters. Chem. Eng. J. 319, 9-20.

[10] Beesley, L., Moreno-Jimenez, E., Gomez-Eyles, J.L., Harris, E., Robinson, B., Sizmur, T. (2011) A review of biochars' potential role in the remediation, revegetation and restoration of contaminated soils. Environ. Pollut. 159(12), 3269-3282.

[11] Chemat, F., Rombaut, N., Sicaire, A.G., Meullemiestre, A., Fabiano-Tixier, A.S., Abert-Vian, M. (2017) Ultrasound assisted extraction of food and natural products. Mechanisms, techniques, combinations, protocols and applications. A Review. Ultrason. Sonochem. 34, 540-560.

[12] Chen, J.Y., Chen, Y.Z., Li, H.L., Lai, S.Y., Jow, J. (2010) Physical and chemical effects of ultrasound vibration on polymer melt in extrusion. Ultrason. Sonochem. 17(1), 66-71.

[13] Chukwumah, Y.C., Walker, L.T., Verghese, M., Ogutu, S. (2009) Effect of frequency and duration of ultrasonication on the extraction efficiency of selected isoflavones and trans-resveratrol from peanuts (Arachis hypogaea). Ultrason. Onochem. 16(2), 293-299.

[14] Sajjadi, B., Broome, J.W., Chen, W.Y., Mattern, D.L., Egiebor, N.O., Hammer, N., Smith, C.L. (2019) Urea functionalization of ultrasound-treated biochar: A feasible strategy for enhancing heavy metal adsorption capacity. Ultrason. Sonochem. 51, 20-30.

[15] Zhang, M., Gao, B., Yao, Y., Xue, Y.W., Inyang, M. (2012) Synthesis of porous MgO-biochar nanocomposites for removal of phosphate and nitrate from aqueous solutions. Chem. Eng. J. 210, 26-32.

[16] Deng, R., Huang, D.L., Wan, J., Xue, W.J., Lei, L., Wen, X.F., Liu, X.G., Chen, S., Yang, Y., Li, Z.H., Li, B. (2019) Chloro-phosphate impregnated biochar prepared by co-precipitation for the lead, cadmium and copper synergic scavenging from aqueous solution. Bioresource Technol. 293, 122102.

[17] Du, L.G., De Vos, R., Vandecasteele, B., Lesage, E., Tack, F.M.G., Verloo, M.G. (2008) Effect of salinity on heavy metal mobility and availability in intertidal sediments of the Scheldt estuary. Estuarine, Coastal Shelf Sci. 77(4), 589-602.

[18] Li, H., Dai, M.W., Dai, S.L., Dong, X.J. (2018) Current status and environment impact of direct straw return in China's cropland-A Review. Ecotoxicol. Environ. Saf. 159, 293-300.

[19] Satyendra, T., Singh, R.N., Shaishav, S. (2013) Emissions from crop/biomass residue burning risk to atmospheric quality. Int. Res. J. Earth Sci. 1(1), 24-30.

[20] Lai, C.H., Li, H.C., Chen, K.S. (2009) Source characterization and environment impact of open burning of rice straw residues on polycyclic aromatic hydrocarbons in agricultural county. Taiwan Env. Eng. Manag. J. 19(2), 79-88.

[21] Zhang, X.Y., Qin, W.L., Xie, J.N. (2016) Improving water use efficiency in grain production of winter wheat and summer maize in the North China Plain: a review. Front Agr. Sci. Eng. 3(1), 25-33.

[22] Zhou, Y., Xing, X., Lang, J., Chen, D., Cheng, S., Wei, L., Wei, X., Liu, C. (2017) A comprehensive biomass burning emission inventory with high spatial and temporal resolution in China. Atmos. Chem. Phys. 17(4), 2839-2864.

[23] Lu, K.P., Yang, X., Shen, J.J., Robinson, B., Huang, H.G., Liu, D., Bolan, N., Pei, J.C., Wang, H.L. (2014) Effect of bamboo and rice straw biochars on the bioavailability of Cd, Cu, Pb and Zn to Sedum plumbizincicola. Agric. Ecosyst. Environ. 191, 124-132.

[24] Li, N.A., Zhang, L.D., Chen, Y.Z., Tian, Y., Wang, H.M. (2011) Adsorption behavior of Cu(II) onto titanate nanofibers prepared by alkali treatment. J. Hazard. Mater. 189, 265-272.
[25] Iftikhar, A.R., Bhatti, H.N., Hanif, M.A., Nadeem, R. (2009) Kinetic and thermodynamic aspects of Cu(II) and Cr(III) removal from aqueous solutions using rose waste biomass. J. Hazard. Mater. 161, 941-947.
[26] Lin, J.W., Zhan, Y.H., Zhu, Z.L. (2011) Adsorption characteristics of copper (II) ions from aqueous solution onto humic acid-immobilized surfactant-modified zeolite. Colloids Surf. A. 384, 9-16.
[27] Wang, F., Yan, T., Zong, H., Li, S., Liu, J., Liu, Y., Hou, X. (2020) Long-term fertilization influencing agricultural diffuse heavy metal pollution and its environmental threat to a coastal city of Yellow Sea, Qingdao, East China. Fresen. Environ. Bull. 29, 5390-5398.
[28] Wang, F., Song, N. (2019). Salinity-induced alterations in plant growth, antioxidant enzyme activities, and lead transportation and accumulation in Suaeda salsa: implications for phytoremediation. Ecotoxicology. 28, 520-527.
[29] Liu, J., Wang, F. (2020) Simultaneous sorptive removal of typical farmland diffuse pollution on ammonium dihydrogen phosphate modified pig manure biochar in binary-solute aqueous solution. Fresen. Environ. Bull. 29, 6219-6227.
[30] Tao, Y.Q., Xue, B., Zhong, J.C., Yao, S.C., Wu, Q.L. (2012) Influences of pH, heavy metals and phosphate and their co-influences on the sorption of pentachlorophenol on cyanobacterial biomass. Water Res. 46(11), 3585-3594.
[31] Hale, S.E., Alling, V., Martinsen, V., Mulder, J., Breedveld, G.D., Cornelissen, G. (2013) The sorption and desorption of phosphate-P, ammonium-N and nitrate-N in cacao shell and corn cob biochars. Chemosphere. 91(11), 1612-1619.
[32] Sumaraj Padhye, L.P. (2017) Influence of surface chemistry of carbon materials on their interactions with inorganic nitrogen contaminants in soil and water. Chemosphere. 184, 532-547.
[33] Wei, S.Y., Zhu, M.B., Song, J.Z., Peng, P.A. (2017) Comprehensive characterization of biochars produced from three major crop straws of China. Bioresource. 12, 3316-3330.

Received: **07.12.2020**
Accepted: **22.01.2021**

CORRESPONDING AUTHOR

Wei Jiao
Shandong Provincial Key Laboratory of Water and Soil Conservation and Environmental Protection,
College of Resources and Environment,
Linyi University,
Linyi 276000 – PR China

e-mail: jiaowei19856261@163.com

© by PSP Volume 30– No. 05/2021 pages 5320-5331 Fresenius Environmental Bulletin

MONITORING THE VEGETATION PHENOLOGICAL CHARACTERISTICS IN MEADOW STEPPE USING SOLAR-INDUCED CHLOROPHYLL FLUORESCENCE

Tong Dong, Hongqi Wu, Pingan Jiang*, Junhui Cheng, Nurmemet Erkin, Haibin Gu, Yongkang Li

Xinjiang Key Laboratory of Soil and Plant Ecological Processes, College of Grassland and Environmental Sciences, Xinjiang Agricultural University, Urumqi 830052, China

ABSTRACT

The accurate monitoring of vegetation phenological information in meadow steppe has great significance for understanding regional and global climate change and the grassland ecosystem carbon cycle. We used the MODIS normalized different vegetation index (NDVI), enhanced vegetation index (EVI), GOSIF solar-induced chlorophyll fluorescence (SIF) and carbon flux gross primary productivity (GPP) data to estimate the phenology of Changling meadow steppe in China from 2007 to 2010 and compared the differences in the NDVI, EVI and SIF in estimating the phenology of meadow steppe. The results showed that the R^2 of SIF and GPP was 0.82, which indicated that SIF could be used to monitor the growth of meadow steppe. Further analysis of the phenological information showed that the phenological information monitored by the NDVI, EVI and SIF lagged behind that of the carbon flux GPP. In addition, SIF was better than the NDVI and EVI in monitoring meadow steppe end date of the growing season (EOS) ($R^2 = 0.72$). Meanwhile, the NDVI, EVI, SIF and GPP of meadow steppe had the same sensitivities to environmental factors. Therefore, SIF has the potential to monitor the phenological information of meadow steppe and can better reflect the date of the EOS in meadow steppe, providing an important basis for the in-depth study of the terrestrial ecosystem carbon cycle and its response to climate change.

KEYWORDS:
Vegetation phenology, solar-induced chlorophyll fluorescence, carbon flux, vegetation index, meadow steppe

INTRODUCTION

Vegetation phenology is the study of recurring biological events that occur during the development stage of plants caused by biotic and abiotic factors and their interaction with environmental conditions [1-4]. Vegetation phenology plays a crucial role in regulating the exchanges and fluxes of water, CO_2 and energy between the biosphere and atmosphere [5,6]. In the phenological period, the start date of the growing season (SOS) and end date of the growing season (EOS) are two important transition points used to control plant growth, and the length of the growing season (LOS) reflects the duration of carbon absorption [7,8]. Several studies have shown that in most terrestrial ecosystems in the mid-high latitudes of the Northern Hemisphere, the advance of the SOS in spring or the delay of the EOS in autumn will increase ecosystem gross primary productivity (GPP), thereby increasing ecosystem net carbon absorption [9,10].

In recent decades, optical remote sensing has been widely used in vegetation phenology monitoring due to its capacity to monitor a large area with long-term continuous observation [11-14]. From the perspective of canopy structure, the normalized different vegetation index (NDVI), enhanced vegetation index (EVI), land surface water index (LSWI) and leaf area index (LAI) were extracted to estimate vegetation phenological parameters such as the SOS, EOS, and LOS. However, optical remote sensing still has uncertainties in vegetation phenology monitoring due to the influences of snow cover [15-18], land use/cover changes [19] and land surface temperature [20,21] on vegetation index signals.

The flux tower can continuously and effectively detect the exchanges of CO_2, water and energy between near-surface vegetation and the atmosphere by the eddy covariance technique and record real-time vegetation photosynthesis and vegetation growth dynamics through carbon flux observation data at a step size of 30 minutes. This method has outstanding technical advantages in phenology observations and is considered an effective way to monitor vegetation phenology [22]. The monitoring range of the flux tower is generally a few hundred to thousands of meters depending on the height of the tower body and the height of the underlying surface vegetation, and this range is comparable to that of remote sensing data of similar spatial scales [8,23]. Previously, scholars have verified vegetation phenology with vegetation ecological parameters, such as net ecosystem carbon exchange and GPP by flux towers, and they have indicated that flux towers are an effective calibration tool for satellite remote sensing inversion of vegetation phenology, which has

been widely studied by many vegetation phenology researchers [24-27]. However, the establishment of the flux tower is restricted by many conditions, such as topography, underlying surface vegetation type, and atmospheric structure, and this method is limited to a few kilometers around the flux tower; thus, it cannot be used to realize large-scale vegetation phenological monitoring [28,29].

As a research hotspot and frontier in the field of remote sensing of vegetation, solar-induced chlorophyll fluorescence (SIF) is the spectral signal (650-800 nm) emitted by plants from photosynthetic centers under solar conditions. It has two peaks: red light (690 nm) and near-infrared (740 nm) [30,31]. Compared with the "greenness"-based vegetation index used to detect "potential photosynthesis", SIF is considered to be an effective probe for vegetation photosynthesis because it has obvious technical advantages in the detection of vegetation photosynthetic physiology, which can directly reflect the dynamic changes in plant photosynthesis [32-34]. It has been proven that SIF and GPP can be expressed by the product of absorbed photosynthetic active radiation and light-use efficiency or fluorescence yield [35,36]. The establishment of the correlation theory of SIF-GPP has promoted the study of vegetation phenology monitoring based on SIF. Joiner et al. [37] first used GOME-2 SIF data to extract vegetation phenological information. Since then, SIF has been widely used in the phenological monitoring of evergreen coniferous forests [38], deciduous broadleaved forests [39], mid-high latitude forests [40], mixed forests, and farmlands [41].

However, there are few reports about SIF monitoring in relation to grassland phenology. Grassland ecosystems, as important and widely distributed vegetation cover layers in terrestrial ecosystems, store one-third of the global terrestrial carbon pool and contribute 30% of the global land vegetation purification capacity. Grassland ecosystems play a key role in the biosphere and ecosystem [42-44]. Moreover, grassland phenology is sensitive to changes in climate and the natural environment, and it is regarded as an indicator that can be used to measure the impact of terrestrial ecosystems on regional and global climate change [45-49]. Therefore, the accurate monitoring of grassland phenological information is of great significance to predict the carbon balance of grassland ecosystems [50]. In this paper, a typical meadow steppe was selected in Northeast China. There were three aims of this work: (i) to investigate whether SIF could effectively monitor the change in GPP in meadow steppe compared with the carbon flux detected by the eddy covariance technique, (ii) to examine whether SIF had the potential to extract meadow steppe phenology compared with carbon flux and a traditional optical remote sensing vegetation index and (iii) to confirm whether SIF had a consistent sensitivity to environmental changes compared with GPP and a vegetation index. Through this study, we hope that a better understanding of meadow steppe seasonal dynamics and transitions can be achieved using SIF.

MATERIALS AND METHODS

Research site. The selected site for this study is the Changling meadow steppe ecological observation station (44° 35′ N, 123° 30′ E), which is located in Changling County, Jilin Province, south of Songnen Plain in Northeast China, and along the eastern edge of Eurasian grassland. The climate type in this area is a temperate semiarid continental monsoon climate, which is cold and dry in winter and warm and humid in summer. The annual average temperature is 5°C; the annual precipitation is 350 mm, mainly concentrated in June to August; and the annual evaporation is 1200 – 1600 mm, which is 3 to 4 times the average precipitation. The soil types are mainly chernozem, alkaline soil and saline soil. *Leymus chinensis* is the dominant species in the plant community in this area, with a total coverage of more than 80%. Associated species include *Phragmites australis*, *Carex duriuscula*, *Kalimeris integrifolia*, *Puccinellia distances* and *Chloris virgata*. The relatively singular grassland vegetation type at the Changling ecological station can prevent the influence of differences in phenology among different species, which can better confirm the remote sensing phenology [51].

Vegetation indices. Compared with the LSWI, which is sensitive to water content [52], the NDVI and EVI are more sensitive to increases in the red band and decreases in the green band [53,54]. The LAI is indirectly derived from satellite remote sensing indicators such as the NDVI with additional uncertainty [55]. Therefore, two typical vegetation indices (NDVI and EVI) were selected to extract the phenological information of meadow steppe. According to the longitude and latitude coordinates of the Changling station, the MODIS surface reflectivity product MOD13A2 V006 version time series NDVI and EVI vegetation index dataset and quality control dataset were extracted (https://lpdaacsvc.cr.usgs.gov/appeears/). The MOD13A2 product has a spatial resolution of 1 km, a temporal resolution of 16 days, and 23 data issues per year. The time range of extraction is consistent with the time range of the flux station, covering a total of 92 issues from 2007 to 2010. The MOD13A2 data contain noise due to environmental conditions, sensor accuracy and other factors. Therefore, before calculating the phenological index, the following three steps are used to process the time series vegetation indices. 1) The quality control dataset is used to eliminate the data with poor reliability caused by noise such as ice and snow cover, cloud cover and aerosol, and the data marked as 0 (with credibility)

and 1 (with more credibility) are retained. 2) The NDVI and EVI time series datasets are generated by the linear interpolation method. 3) The Savizky Golay (S-G) filtering method is used to remove outliers in the time series data to make the time series curve smoother [56,57].

Solar-induced chlorophyll fluorescence. Frankenberg et al. [58] showed that NASA's OCO-2 sensor could identify SIFs worldwide. Compared with the GOME-2 and GOSAT SIF datasets, OCO-2 has the greatest advantages in terms of the increase in measurement frequency and higher spatial resolution (1.3×2.25 km^2). However, the cost of the high spatial resolution is that OCO-2 cannot provide continuous observations in space and has a low temporal resolution (16 days). Therefore, Li et al. [59] developed a GOSIF dataset with a high spatial and high temporal resolution (0.05° and 8 days, respectively) based on the discrete OCO-2 SIF combined with MODIS and meteorological data. The dataset not only solves the spatial distribution of OCO-2, which leads to the phenomenon that the SIF data of these research sites are empty in some periods, but also solves the problem of low accuracy of phenology estimation caused by the low time resolution and can make up for the deficiency of OCO-2 SIF. Therefore, the GOSIF dataset was selected to estimate the phenological information of meadow steppe, and the SIF data of Changling station from 2007 to 2010 were extracted by Python 2.7 and ArcGIS 10.7 according to the longitude and latitude coordinates of the flux stations, ultimately generating 184 time series SIF datasets.

Carbon flux. FLUXNET is an international flux observation and research network that publishes valuable global flux datasets through cooperation with several regional flux networks (https://fluxnet.fluxdata.org/). The FLUXNET dataset provides half-hourly, daily, monthly, and yearly scales of ecosystem CO_2, heat flux and meteorological variable data at 212 sites across the globe, based on the standard flux-partitioning method for gap-filling and quality control [60-63]. It provides strong data support for the regional or global scale simulation of the carbon flux cycle of ecosystems. In this study, the Changling meadow steppe ecosystem observation station (CN-cng) in a typical grassland area of China was selected. The GPP product (GPP_DT_VUT_REF) used in this study was calculated with the variable USTAR filtering approach and daytime partitioning method [64]. The daily GPP dataset from 2007 to 2014 (1461 issues in total) was used to determine the SOS, EOS and LOS. The daily average daytime air temperature dataset (TA_F), precipitation dataset (P_F), downward solar shortwave radiation dataset (SW_IN_F), soil temperature dataset (TS_F_MDS), soil water content dataset (SWC_F_MDS) and vapour pressure deficiency dataset (VPD_F) from FLUXNET-2015 were also used to explore the relationship between environment and phenology. To match the MODIS vegetation index and GOSIF step size, the precipitation data were taken as 16-day and 8-day cumulative values, and the other environmental factors were taken as 16-day and 8-day average values.

Estimation method for vegetation phenology. An asymmetric Gaussian function fitting method was proposed by Jonsson et al. [65] It can effectively monitor the start and end dates of the vegetation phenological season, and this information is more consistent with the overall characteristics of the original vegetation index curve and is closest to the upper envelope of the original data; additionally, it can effectively suppress the impact of noise. Therefore, in this study, the asymmetric Gaussian function fitting method was used to estimate the phenological information of the meadow steppe by using TIMESAT 3.2 of the MATLAB platform, and the dynamic threshold method was used to extract the SOS (threshold set at 0.2), the EOS (threshold set at 0.6), and the LOS [66].

Sensitivity analysis. The coefficient of determination (R^2) and root mean square error (RMSE) were used to validate the NDVI, EVI, SIF and their extracted phenological information for meadow steppe using GPP data of the carbon flux as measured values. The response of vegetation phenology to environmental change was analyzed by using the Pearson correlation coefficient.

RESULTS

Temporal variations in the vegetation index and their correlations with the carbon flux GPP. The temporal vegetation index reflects the seasonal change in vegetation growth and indirectly shows the intensity of plant photosynthesis and its inter-annual and intra-annual seasonal differences. From 2007 to 2010, the NDVI, EVI, SIF and carbon flux GPP in the meadow grassland of Changling station showed similar seasonal periodic changes, and the change amplitudes were similar (Figure 1). In 2008, the NDVI, EVI, SIF and GPP were higher than those in other years, indicating that the overall grassland growth in 2008 was greater than that in other years. The daily carbon flux GPP data are very sensitive to the monitoring of grassland growth and change, especially in summer when the grassland is flourishing, and the GPP value monitored by the flux tower is always higher than the NDVI, EVI and SIF. Nevertheless, due to the high sensitivity of the flux tower to monitoring grassland GPP, the GPP value in early 2010 was relatively discrete; thus, it could not accurately express the growth time series curve of

meadow steppe in this period. The NDVI and EVI growth season morphology curves were roughly consistent with the carbon flux GPP, and the NDVI value was higher than the EVI value; however, the NDVI and EVI failed to capture the change characteristics of the peak growth season of meadow steppe. The growth season curve of SIF showed a "peak" shape; after reaching the peak, it rapidly decayed and entered the ageing stage. Compared with the peak values of GPP and SIF from 2007 to 2010, the SIF time series curve was closer to GPP, indicating that SIF was more sensitive than the NDVI and EVI in terms of monitoring vegetation growth status. The multiyear mean values of the NDVI, EVI, SIF and GPP from 2007 to 2010 were calculated to represent the seasonal dynamics of their respective curves (Figure 2). The NDVI, EVI, SIF and GPP entered a rapid growth stage in April (90th day), formed the peak shape of the growth season in July (210th day), decreased rapidly after August (240th day), and tended to be flat

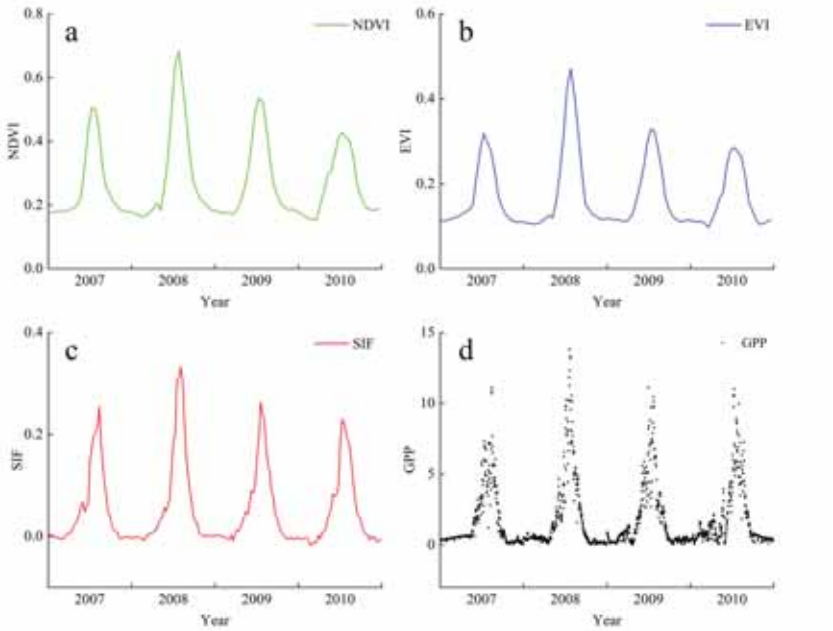

FIGURE 1
Interannual variation characteristics of the NDVI (a), EVI (b), SIF (c) and GPP (d) from 2007 to 2010

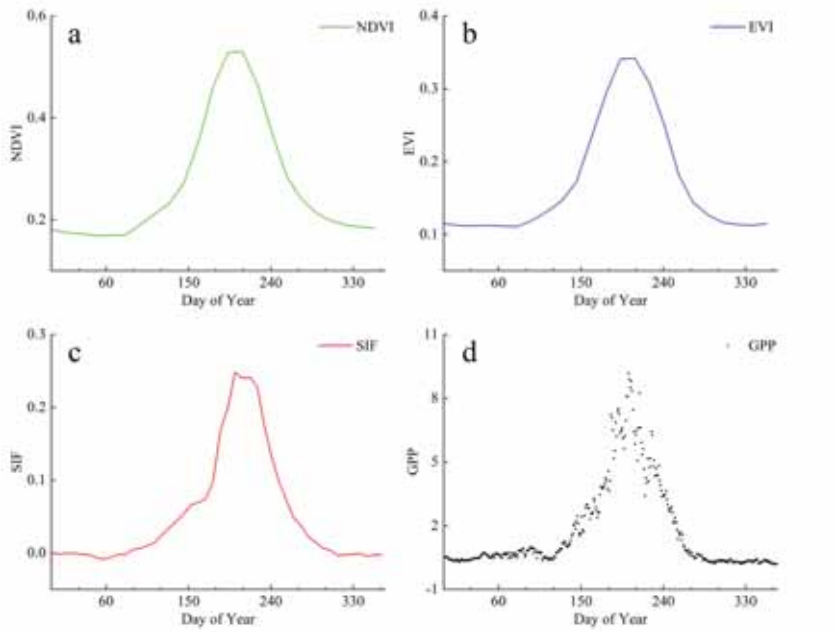

FIGURE 2
Variation characteristics of the NDVI (a), EVI (b), SIF (c) and GPP (d) within a year

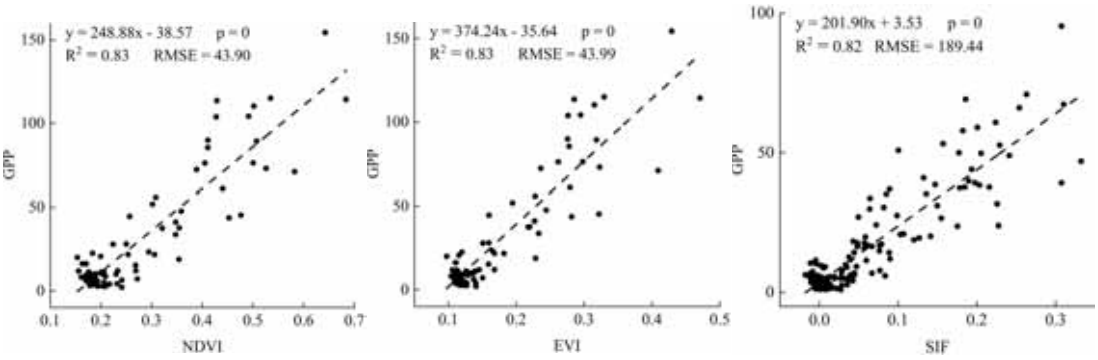

FIGURE 3
Correlation between the NDVI, EVI, SIF and GPP

until October (300th day). Compared with SIF and GPP, the NDVI and EVI started earlier in the spring phenological growth season, and SIF was closer to GPP in the curve time change; at the end of the autumn phenological growth season, GPP was earlier than the NDVI, EVI and SIF, and SIF was earlier than the NDVI and EVI. Therefore, there is a lag between the "greenness" of vegetation and the intensity of photosynthesis. The NDVI and EVI monitor the SOS in spring and the EOS in autumn to be later than the actual photosynthesis detected by GPP and SIF.

The linear regression of the NDVI, EVI, SIF and carbon flux GPP was established. There was a good linear relationship between the three remote sensing indices and carbon flux GPP ($P < 0.0001$), which showed that the seasonal variation was relatively consistent (Figure 3). Moreover, the correlation between the NDVI, EVI, SIF and GPP was high, with R^2 values of 0.83 (GPP-NDVI), 0.83 (GPP-EVI), and 0.82 (GPP-SIF), which indicated that the NDVI, EVI and SIF could accurately reflect the dynamic change in vegetation growth time at the Changling station.

Comparison of remote sensing phenology and carbon flux GPP phenology. Analysis of the interannual variation in phenological information estimated by GPP from 2007 to 2010 (Figure 4 and Table 1) showed that the year with the earliest SOS was in 2009, on the 142nd day, and the year with the latest SOS was 2008, on the 156th day, with a difference of 24 days between the two years. The year with the earliest EOS was 2009, on the 226th day; the year with the latest EOS was 2007, on the 248 day, with 22 days between the two years. The longest and shortest growing seasons (LOSs) were 92 and 78 days in 2009 and 2008, respectively, with a difference of 14 days between the two years. The results show that the vegetation phenology of the Changling station meadow grassland has obvious fluctuating changes.

The average value of phenological information over the years was calculated and compared with the phenological information extracted by the NDVI, EVI, SIF and GPP. The average SOS of the NDVI, EVI, SIF and GPP were 147, 149, 159 and 149 days, respectively. The SOS_{NDVI} was the earliest, 2 days earlier than the SOS_{GPP}; the SOS_{EVI} was the same as the SOS_{GPP}; and the SOS_{SIF} was 10 days later than the SOS_{GPP}. The average EOSs of the NDVI, EVI, SIF and GPP were 252, 253, 244 and 235 days, respectively; the EOS_{GPP} was the earliest; the EOS_{NDVI}, EOS_{EVI} and EOS_{SIF} values were 17, 18 and 9 days later than GPP, respectively. The average LOSs of the NDVI, EVI, SIF and GPP were 106, 104, 85 and 86 days, respectively. The difference between the LOS_{GPP} and LOS_{SIF} was the smallest, which was 1 day. The LOS_{NDVI} and LOS_{EVI} were 20 and 18 days longer than the LOS_{GPP}, respectively. SIF was the closest to GPP in the EOS and LOS estimations. Considering that the temporal resolution of the NDVI and EVI is 16 days and the temporal resolution of SIF is 8 days, the errors of the NDVI, EVI and SIF in estimating grassland phenological information meet the accuracy requirements.

TABLE 1
Phenological parameters of the NDVI/EVI/SIF and carbon flux GPP

Year	NDVI			EVI			SIF			GPP		
	SOS	EOS	LOS	SOS	EOS	LOS	SOS	EOS	LOS	SOS	EOS	LOS
2007	162	246	84	155	251	96	162	249	87	156	248	92
2008	163	255	92	164	253	89	168	244	76	153	231	78
2009	144	248	104	144	251	107	158	243	85	142	226	84
2010	118	260	142	130	256	126	148	242	94	146	235	89
Average	147	252	106	149	253	104	159	244	85	149	235	86

*Note: Unit / day

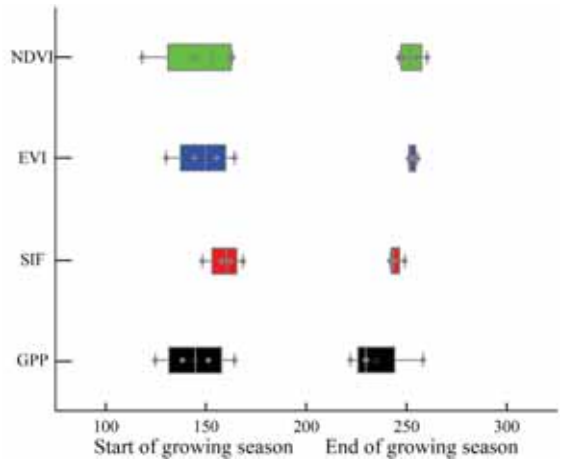

FIGURE 4
Phenological comparison of the NDVI, EVI, SIF and carbon flux GPP

The phenological information estimated by the NDVI, EVI and SIF from 2007 to 2010 was regressed with that estimated by carbon flux GPP (Figure 5). The results showed that the SOS_{NDVI} (R^2 = 0.46, P = 0.32), SOS_{EVI} (R^2 = 0.45, P = 0.33), SOS_{SIF} (R^2 = 0.35, P = 0.41), NDVI and EVI are better than SIF in estimating the SOS of meadow steppe. The EOS_{SIF} (EOS_{GPP} = 0.29 EOS_{SIF} + 176.23, R^2 = 0.72, P = 0.15) was significantly better than the EOS_{NDVI} (R^2 = 0.10, P = 0.69) and EOS_{EVI} (R^2 = 0.01, P = 0.91), which was similar to the EOS_{GPP} and showed a trend of correlation. The LOS_{EVI} (R^2 = 0.59, P = 0.23) was superior to the LOS_{NDVI} (R^2 = 0.15, P = 0.62) and LOS_{SIF} (R^2 = 0.02, P = 0.87) in monitoring the LOS.

Relationship between meadow steppe and environmental factors. The effects of different environmental factors (air temperature, precipitation, downward solar shortwave radiation, soil temperature, soil water content and vapour pressure deficiency) on the growth status (NDVI, EVI, SIF, and GPP) of meadow steppe in different seasons (winter, spring, summer and autumn) were analyzed. The results showed that the change in winter air temperature (Figure 6a) and soil temperature (Figure 6d) had little effect on the growth of meadow steppe, and the increase in air temperature and soil temperature in spring and autumn significantly improved the growth of meadow steppe. Precipitation (Figure 6b) and soil water content (Figure 6e) showed that the effects of seasonal changes on the meadow steppe deepened throughout the year. After entering the hot and dry summer, sufficient heat would no longer restrict the growth of meadow steppe, and the increase in precipitation and soil water content would significantly promote the growth of meadow steppe. The downward solar shortwave radiation (Figure 6c) and vapour pressure deficiency (Figure 6f) showed that the growth of meadow steppe was inhibited in winter and summer, while it was enhanced in summer and autumn. In general, the correlation trend of the NDVI, EVI, SIF and GPP with environmental factors was consistent, while the correlation between the SIF and environmental factors was closer than that of the vegetation indices, i.e., NDVI and EVI.

DISCUSSION

Monitoring the phenological potential of meadow steppe using SIF. In this study, we found that although the carbon accumulation capacity of meadow steppe ecosystems was weaker than that of forest and farmland ecosystems, SIF could still accurately capture the changes in meadow grassland photosynthesis, and it had a high correlation with meadow grassland GPP, indicating that SIF could effectively be used to monitor the carbon cycle of meadow grassland ecosystems. Furthermore, the potential of SIF in phenological monitoring of meadow steppe was analyzed. Compared with the phenological information monitored by GPP, the results of SIF, NDVI and EVI lagged behind, but SIF was closer to the change in GPP. This result was because the vegetation index mainly

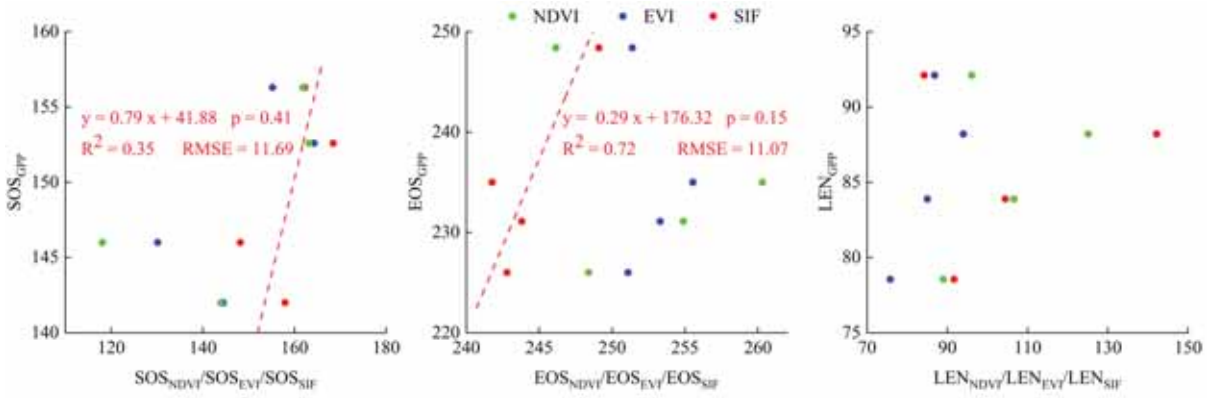

FIGURE 5
Phenological comparison of the NDVI/EVI/SIF and carbon flux GPP

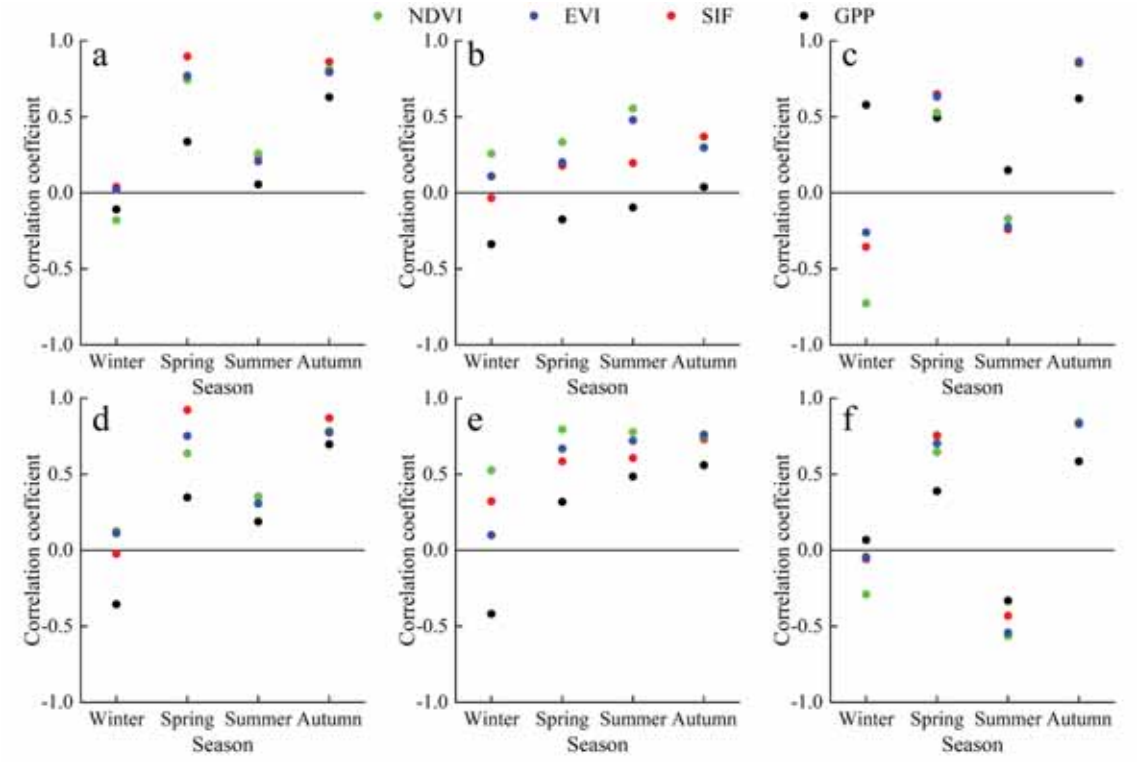

FIGURE 6

Response of meadow steppe to temperature (a), precipitation (b), downward solar shortwave radiation (c), soil temperature (d), soil moisture content (e), and saturated water vapor pressure difference (f)

represented the composite information about the vegetation canopy coverage, leaf area and canopy structure. The change in vegetation canopy often lags behind vegetation photosynthesis [67]. Previous studies have also shown that the change in the vegetation index lags behind the GPP [68-70]; thus, the phenological information of a vegetation index estimation is usually later than the actual state of the vegetation. Because of its direct detection of vegetation photosynthesis, SIF can effectively eliminate the interference of background information such as soil, water, snow and clouds [71]. Although there is still a certain lag, the results of SIF and GPP monitoring phenological information are closer to reality, which is consistent with the conclusion of Wang et al.,[41] who studied forest phenology monitoring. In addition, SIF is superior to the vegetation index in determining the EOS, which is consistent with the research results of Lu et al.,[40] who conducted mid- and high-latitude forest phenology studies in Europe and North America. This result is because the leaves of forest and grassland wither rapidly after autumn, and the values of the NDVI and EVI based on the green degree decrease, but the plant leaves are still photosynthetic, and SIF can still monitor the vegetation growth status of meadow steppe at this stage; therefore, SIF is better than the vegetation index in terms of monitoring the EOS. Although SIF has potential and advantages in phenological monitoring of meadow steppe in this study, the application of SIF in other grassland types, such as alpine meadow affected by snow cover and desert meadow with sparse vegetation in arid areas, needs to be further verified. The results of Chang et al. [39] showed that SIF could be used to effectively monitor the phenological information of snow forests. In future research, it is necessary to further analyse whether SIF can effectively monitor the alpine meadow, which is more affected by snow cover and desert grassland in arid areas with short growth cycles and sparse vegetation.

Uncertainty analysis and improvement of the model. In this study, the MODIS vegetation index and SIF of the GOSIF dataset were used to estimate the vegetation phenology of meadow steppe effectively. However, there are still some uncertain factors. This uncertainty is due to the scale effect of remote sensing data; on the spatial scale, the effective observation range of fluxes is from hundreds of meters to kilometres [72], the spatial resolution of the MODIS vegetation index is 1 km, and the spatial resolution of SIF is 0.05°× 0.05°. Although this study chose a meadow grassland with a relatively single underlying vegetation type, the SIF, vegetation index and GPP were not completely matched on a spatial scale, and the inconsistency of the observation range would inevitably produce errors in the observation results. On the time scale, GPP carbon flux is the cumulative value with a sampling frequency of 10 Hz and a sampling interval of 30 minutes [60,61], SIF is an instantaneous value with an interval of 8 days, and the NDVI and EVI have instantaneous value intervals of 16 days. Data with different temporal resolutions may cause deviations from the

analysis results of phenological information. Especially for meadow steppe, the growth and decline rate of vegetation is higher than that of forest, and the length of the growing season is relatively short [73]. Therefore, higher temporal resolution sampling can better reflect the dynamic changes in vegetation growth in meadow steppe.

In addition, there is no satellite sensor specifically used to detect vegetation fluorescence. Most of the existing satellites that acquire SIF data were originally designed to detect atmospheric chemistry. However, the chlorophyll fluorescence signal is very weak compared with surface reflection, and it is affected by atmospheric absorption and scattering caused by upward radiation transmission, resulting in noisier SIF data [32]. It is necessary to further enhance the signal-to-noise ratio and spectral, spatial and temporal resolutions of the solar-induced chlorophyll fluorescence data to further understand the land surface vegetation phenology in a more detailed and comprehensive way.

CONCLUSIONS

This study confirmed the application of SIF in the study of meadow steppe phenology. At the meadow grassland ecological observation station in Changling County, Jilin Province, China, the SIF dataset of GOSIF was significantly correlated with the GPP detected by the vorticity covariance technique, and the R^2 was 0.82. Meanwhile, the phenological information of meadow steppe estimated by GOSIF was closely matched with the estimated results of carbon flux GPP. Especially at the end of the autumn growing season, SIF performed better than the MODIS NDVI and EVI, with an R^2 of 0.72. In addition, the correlation analysis of SIF, carbon flux GPP and environmental factors showed that the correlation trends of SIF, GPP and environmental factors were consistent. In conclusion, SIF is closely related to the GPP of meadow steppe; thus, the phenological information estimated by SIF is consistent with that estimated by carbon flux GPP. Therefore, SIF is a new and effective way to monitor the phenological information of meadow steppe, which is of great significance for ecological research and agricultural production.

Although the phenological information was extracted and verified by SIF in this paper, good results were achieved. However, grassland ecosystems are very complex and dynamic, and grasslands are very sensitive to global climate change. In the future, it is necessary to verify the phenological information extraction of SIF in different grassland ecosystems to improve the accuracy and universality of SIF in grassland phenology extraction.

REFERENCES

[1] Morisette, J.T., Richardson, A.D., Knapp, A.K., Fisher, J.I., Graham, E.A., Abatzoglou, J., Wilson, B.E., Breshears, D.D., Henebry, G.M., Hanes, J.M. and Liang, L. (2009) Tracking the rhythm of the seasons in the face of global change: phenological research in the 21st century. Frontiers in Ecology and The Environment. 7, 253–260.

[2] Chen, X. (2017) Plant Phenology of Natural Landscape Dynamics, Spatiotemporal Processes of Plant Phenology, 1st ed., Springer: Berlin, Germany. 1–5.

[3] Zhu, W., Zheng, Z., Jiang, N. and Zhang, D. (2018) A comparative analysis of the spatiotemporal variation in the phenologies of two herbaceous species and associated climatic driving factors on the Tibetan Plateau. Agricultural and Forest Meteorology. 248, 177–184.

[4] Liu, X., Zhang, A., Xie, Y., Hua, J. and Liu, H. (2019). Detecting long-term trends of vegetation change at local scale through time-series image analysis: a case study in inner Mongolia, China. Fresen. Environ. Bull. 28, 1881-1895.

[5] Keenan, T., Baker, I., Barr, A., Ciais, P., Davis, K., Dietze, M., Dragoni, D., Gough, C.M., Grant, R., Hollinger, D., Hufkens, K., Poulter, B., McCaughey, H., Raczka, B., Ryu, Y., Schaefer, K., Tian, H., Verbeeck, H., Zhao, M. and Richardson, A.D. (2012) Terrestrial biosphere model performance for inter-annual variability of land-atmosphere CO_2 exchange. Global Change Biology. 18, 1971–1987.

[6] Richardson, A.D., Anderson, R.S., Arain, M.A., Barr, A.G., Bohrer, G., Chen, G., Chen, J.M., Ciais, P., Davis, K.J., Desai, A.R., Dietze, M.C., Dragoni, D., Garrity, S.R., Gough, C.M., Grant, R., Hollinger, D.Y., Margolis, H.A., McCaughey, H., Migliavacca, M., Monson, R.K., Munger, J.W., Poulter, B., Raczka, B.M., Ricciuto, D.M., Sahoo, A.K., Schaefer, K., Tian, H., Vargas, R., Verbeeck, H., Xiao, J. and Xue, Y. (2012) Terrestrial biosphere models need better representation of vegetation phenology: results fromthe North American Carbon Program Site Synthesis. Global Change Biol. 18, 566–584.

[7] Xiao, J., Chevallier, F., Gomez, C., Guanter, L., Hicke, J.A., Huete, A.R., Ichii, K., Ni, W., Pang, Y., Rahman, A.F., Sun, G., Yuan, W., Zhang, L. and Zhang X. (2019) Remote sensing of the terrestrial carbon cycle: A review of advances over 50 years. Remote Sensing of Environment. 233, 111383.

[8] Richardson, A.D., Black, T.A., Ciais, P., Delbart, N., Friedl, M.A., Gobron, F.N., Hollinger, D.Y., Kutsch, W.L., Longdoz, B., Luyssaert, S., Migliavacca, M., Montagnani, L., Munger, J.W., Moors, E., Piao, S., Rebmann, C., Reichstein, M., Saigusa, N., Tomelleri, E., Vargas, R. and Varlagin, A. (2010) Influence of spring and autumn phenological transitions on forest ecosystem productivity. Philosophical transactions - Royal Society. Biological Sciences. 365, 3227–3246.

[9] Bao, G., Chen, J., Chopping, M., Bao, Y., Bayarsaikhan, S., Dorjsuren, A., Tuya, A., Jirigala, B. and Qin, Z. (2019) Dynamics of net primary productivity on the Mongolian Plateau: Joint regulations of phenology and drought. Int. J. International Journal of Applied Earth Observation and Geoinformation. 81, 85–97.

[10] Nuarsa, I.W., As-syakur, A.R., Gunadi, I.G.A. and Sukewijaya, I.M. (2018) Changes in Gross Primary Production (GPP) over the Past Two Decades Due to Land Use Conversion in a Tourism City. ISPRS International Journal of Geo-Information. 7, 57.

[11] Matsumoto, K., Ohta, T., Irasawa, M. and Nakamura, T. (2003) Climate change and extension of the Ginkgo biloba L. growing season in Japan. Global Change Biology. 9, 1634–1642.

[12] Zhang, X., Friedl, M.A. and Schaaf, C.B. (2006) Global vegetation phenology from Moderate Resolution Imaging Spectroradiometer (MODIS): Evaluation of global patterns and comparison with in situ measurements. Journal of Geophysical Research-Biogeosciences. 111, G04017.

[13] Xin, Q., Broich, M., Zhu, P. and Gong, P. (2015) Modeling grassland spring onset across the Western United States using climate variables and MODIS-derived phenology metrics. Remote Sensing of Environment. 161, 63–77.

[14] Bolton, D.K., Gray, J.M., Melaas, E.K., Moon, M., Eklundh, L. and Friedl, M.A. (2020) Continental-scale land surface phenology from harmonized Landsat 8 and Sentinel-2 imagery. Remote Sensing of Environment. 240. Article ID: 111685.

[15] Jin, H., Jönsson, A.M., Bolmgren, K., Langvall, O. and Eklundh, L. (2017) Disentangling remotely-sensed plant phenology and snow seasonality at northern Europe using MODIS and the plant phenology index. Remote Sensing of Environment. 198, 203–212.

[16] Yang, W., Kobayashi, H., Wang, C., Shen, M., Chen, J., Matsushita, B., Tang, Y., Kim, Y., Bret-Harte, M.S., Zona, D., Oechel, W. and Kondoh, A. (2019) A semi-analytical snow-free vegetation index for improving estimation of plant phenology in tundra and grassland ecosystems. Remote Sensing of Environment. 228, 31–44.

[17] Xie, J., Jonas, T., Rixen, C., Jong, R.D., Garonna, I., Notarnicola, C., Asam, S., Schaepman, ME. and Kneubuhler, M. (2020) Land surface phenology and greenness in alpine grasslands driven by seasonal snow and meteorological factors. Science of the Total Environment. 725. Article ID: 138380.

[18] Qiao, D. and Wang, N. (2019) Relationship between Winter Snow Cover Dynamics, Climate and Spring Grassland Vegetation Phenology in Inner Mongolia, China. ISPRS International Journal of Geo-Information. 8, 42.

[19] Moon, M., Zhang, X., Henebry, G.M., Liu, L., Gray, J.M., Melaas, E.K., and Friedl, M.A. (2019) Long-term continuity in land surface phenology measurements: a comparative assessment of the MODIS land cover dynamics and VIIRS land surface phenology products. Remote Sensing of Environment. 226, 74–92.

[20] Xu, X., Zhou, G., Du, H., Mao, F., Xu, L., Li, X. and Liu, L. (2020) Combined MODIS land surface temperature and greenness data for modeling vegetation phenology, physiology, and gross primary production in terrestrial ecosystems. Science of the Total Environment. 726. Article ID:137948.

[21] Ci, P. and Xu, M. (2018). Patterns and dynamics of degradation induced grassland productivity change in Tibet. Fresen. Environ. Bull. 27, 5619-5628.

[22] Xu, X., Du, H., Fan, W., Hu, J., Mao, F. and Dong, H. (2019) Long-term trend in vegetation gross primary production, phenology and their relationships inferred from the FLUXNET data. Journal of Environmental Management. 246, 605–616.

[23] Piao, S., Liu, Q., Chen, A., Janssens, I.A., Fu, Y., Dai, J., Liu, L., Lian, X., Shen, M. and Zhu, X. (2019) Plant phenology and global climate change: Current progresses and challenges. Global Change Biology. 25,1922–1940.

[24] Balzarolo, M., Vicca, S., Nguy-Robertson, A.L., Bonal, D., Elbers, J.A., Fu, Y.H., Grünwald, T., Horemans, J.T., Papale, D., Peñuelas, J., Suyker, A. and Veroustraete, F. (2016) Matching the phenology of Net Ecosystem Exchange and vegetation indices estimated with MODIS and FLUXNET in-situ observations. Remote Sensing of Environment. 174, 290–300.

[25] Peng, D., Zhang, X., Wu, C., Huang, W., Gonsamo, A., Huete, A.R., Didanf, K., Tang, B., Liu, X. and Zhang, B. (2017) Intercomparison and evaluation of spring phenology products using National Phenology Network and AmeriFlux observations in the contiguous United States. Agricultural and Forest Meteorology. 242, 33–46.

[26] Wu, C., Peng, D., Soudani, K., Siebicke, L., Gough, C.M., Arain, M.A., Bohrer, G., Lafleur, P.M., Peichl, M., Gonsamo, A., Xu, S., Fang, B. and Ge, Q. (2017) Land surface phenology derived from normalized difference vegetation index (NDVI) at global FLUXNET sites. Agricultural and Forest Meteorology. 233, 171–182.

[27] Goulden, M.L., Daube, B.C., Fan, S.M., Sutton, D.J., Bazzaz, A., Munger, J.W. and Wofsy, S.C. (1997) Physiological responses of a black spruce forest to weather. Journal of Geophysical Research - Atmospheres. 102, 28987–28996.

[28] Baldocchi, D., Falge, E., Gu, L., Olson, R., Hollinger, D., Running, S., Anthoni, P., Bernhofer, C., Davis, K., Evans, R. and Fuentes, J. (2001) FLUXNET: A new tool to study the temporal and spatial variability of ecosystem-scale carbon dioxide, water vapor, and energy flux densities. Bulletin of the American Meteorological Society. 82, 2415–2434.

[29] Massman, W.J. and Lee, X. (2002) Eddy covariance flux corrections and uncertainties in long-term studies of carbon and energy exchanges. Agricultural and Forest Meteorology. 113, 121–144.

[30] Zhang, Z., Wang, S., Qiu, B., Song, L. and Zhang, Y. (2019) Retrieval of sun-induced chlorophyll fluorescence and advancements in carbon cycle application. Journal of Remote Sensing. 23, 37–52.

[31] Sener, M. and Arslanoglu, M. C. (2019). Selection of the most suitable Sentinel-2 bands and vegetation index for crop classification by using artificial neural network (ANN) and google earth engine (GEE). Fresen. Environ. Bull. 28, 9348-9358.

[32] Mohammed, G.H., Colombo, R., Middleton, E.M., Rascher, U., van der Tol, C., Nedbal, L., Goulas, Y., Pérez-Priego, O., Damm, A., Meroni, M., Joiner, J., Cogliati, S., Verhoef, W., Malenovský, Z., Gastellu-Etchegorry, J., Miller, J.R., Guanter, L., Moreno, J., Moya, I., Berry, J.A., Frankenberg, C. and Zarco-Tejada, P.J. (2019) Remote sensing of solar-induced chlorophyll fluorescence (SIF) in vegetation: 50 years of progress. Remote Sensing of Environment. 231. Article ID: 111177.

[33] Guanter, L., Frankenberg, C., Dudhia, A., Lewis, P.E., Gómez-Dans, J., Kuze, A., Suto, H. and Grainger, R.G. (2012) Retrieval and global assessment of terrestrial chlorophyll fluorescence from GOSAT space measurements. Remote Sensing of Environment. 121, 236–251.

[34] Li, X., Xiao, J., He, B., Altaf Arain, M., Beringer, J., Desai, A.R., Emmel, C., Hollinger, D.Y., Krasnova, A., Mammarella, I., Noe, S.M., Ortiz, P.S., Rey-Sanchez, A.C., Rocha, A.V. and Varlagin, A. (2018) Solar-induced chlorophyll fluorescence is strongly correlated with terrestrial photosynthesis for a wide variety of biomes: First global analysis based on OCO-2 and flux tower observations. Global Change Biology. 24, 3990–4008.

[35] Guanter, L., Zhang, Y., Jung, M., Joiner, J., Voigt, M., Berry, J.A., Frankenberg, C., Huete, A.R., Zarco-Tejada, P., Lee, J., Moran, M.S., Ponce-Campos, G., Beer, C., Camps-Valls, V., Buchmann, N., Gianelle, D., Klumpp, K., Cescatti, A., Baker, J.M. and Griffis, T.J. (2014) Global and time-resolved monitoring of crop photosynthesis with chlorophyll fluorescence. Proceedings of the National Academy of Sciences of the United States of America. 111, E1327–E1333.

[36] Sun, Y., Frankenberg, C., Jung, M., Joiner, J., Guanter, L., Köhler, P. and Magney, T. (2018) Overview of Solar-Induced chlorophyll Fluorescence (SIF) from the Orbiting Carbon Observatory-2: Retrieval, cross-mission comparison, and global monitoring for GPP. Remote Sensing of Environment. 209, 808–823.

[37] Joiner, J., Yoshida, Y., Vasilkov, A.P., Schaefer, K., Jung, M., Guanter, L., Zhang, Y., Garrity, S., Middleton, T.S., Huemmrich, K.F., Gu, L. and Marchesini, L.B. (2014) The seasonal cycle of satellite chlorophyll fluorescence observations and its relationship to vegetation phenology and ecosystem atmosphere carbon exchange. Remote Sensing of Environment. 152, 375–391.

[38] Magney, T.S., Bowling, D.R., Logan, B.A., Grossmann, K., Stutz, J., Blanken, P.D., Burns, S.P., Cheng, R., Garcia, M.A., Köhler, P., Lopez, S., Parazoo, N.C., Raczka, B., Schimel, D. and Frankenberg, C. (2019) Mechanistic evidence for tracking the seasonality of photosynthesis with solar-induced fluorescence. Proceedings of the National Academy of Sciences of the United States of America. 116, 11640–11645.

[39] Chang, Q., Xiao, X., Jiao, W., Wu, X., Doughty, R., Wang, J., Du, L., Zou, Z. and Qin, Y. (2019) Assessing consistency of spring phenology of snow-covered forests as estimated by vegetation indices, gross primary production, and solar-induced chlorophyll fluorescence. Agricultural and Forest Meteorology. 275, 305–316.

[40] Lu, X., Cheng, X., Li, X., Chen, J., Sun, M., Ji, M., He, H., Wang, S., Li, S. and Tang, J. (2018) Seasonal patterns of canopy photosynthesis captured by remotely sensed sun-induced fluorescence and vegetation indexes in mid-to-high latitude forests: A cross-platform comparison. Science of the Total Environment. 644, 439-451.

[41] Wang, F., Chen, B., Lin, X. and Zhang, H. (2020) Solar-induced chlorophyll fluorescence as an indicator for determining the end date of the vegetation growing season. Ecological Indicators. 109, 105755.
[42] Scurlock, J.M.O. and Hall, D.O. (1998) The global carbon sink: a grassland perspective. Global Change Biology. 4, 229–233.
[43] Zhou, W., Gang, C., Zhou, L., Chen, Y., Li, J., Ju, W. and Odeh, I. (2014) Dynamic of grassland vegetation degradation and its quantitative assessment in the northwest China. Acta Oecologica. 55, 86–96.
[44] Chen, Y., Mu, S., Sun, Z., Gang, C., Li, J., Padarian, J., Groisman, P., Chen, J. and Li, S. (2016) Grassland carbon sequestration ability in China: a new perspective from terrestrial aridity zones. Rangeland Ecology & Management. 69, 84–94.
[45] Cleland, E.E., Chiariello, N.R., Loarie, S.R., Mooney, H.A. and Field, C.B. (2006) Diverse responses of phenology to global changes in a grassland ecosystem. Proceedings of the National Academy of Sciences of the United States of America. 103, 13740–13744.
[46] Cong, N., Piao, S., Chen, A., Wang, X., Lin, X., Chen, S., Han, S., Zhou, G. and Zhang, X. (2012) Spring vegetation green-up date in China inferred from SPOT NDVI data: A multiple model analysis. Agricultural and Forest Meteorology. 165, 104–113.
[47] Richardson, A.D., Keenan, T.F., Migliavacca, M., Ryu, Y., Sonnentag, O. and Toomey, M. (2013) Climate change, phenology, and phenological control of vegetation feedbacks to the climate system. Agricultural and Forest Meteorology. 169, 156–173.
[48] Peng, D., Zhang, X., Wu, C., Huang, W., Gonsamo, A., Huete, A.R., Didan, K., Tan, B., Liu, X. and Zhang, B. (2017) Intercomparison and evaluation of spring phenology products using National Phenology Network and AmeriFlux observations in the contiguous United States. Agricultural and Forest Meteorology. 242, 33–46.
[49] Alganci, U. (2019). The use of broadband vegetation indices in cultivated land detection with Landsat 8 OLI multi-temporal images. Fresen. Environ. Bull. 28,739-744.
[50] Chai, X., Shi, P., Song, M., Zong, N., He, Y., Zhao, G. and Zhang, X. (2019) Carbon flux phenology and net ecosystem productivity simulated by a bioclimatic index in an alpine steppe-meadow on the Tibetan Plateau. Ecological Modelling. 394, 66–75.
[51] Jiang, L., Zhu, T., Ma, L., Shi, L., Hou, W. and Guo, J. (2011) Responses of ecosystem's carbon and water fluxes to global change on the Songnen steppe. Science & Technology Review. 29, 35–42.
[52] Delbart, N., Kergoat, L., Le Toan, T., Lhermitte, J. and Picard, G. (2005) Determination of phenological dates in boreal regions using normalized difference water index. Remote Sensing of Environment. 97, 26–38.
[53] Dragoni, D. and Rahman, A.F. (2012) Trends in fall phenology across the deciduous forests of the Eastern USA. Agricultural and Forest Meteorology. 157, 96–105.
[54] Zhang, X., Tan, B. and Yu, Y. (2014) Interannual variations and trends in global land surface phenology derived from enhanced vegetation index during 1982–2010. International Journal of Biometeorology. 58, 547–564.
[55] Kang, S., Running, S.W., Lim, J.H., Zhao, M., Park, C.R. and Loehman, R. (2003) A regional phenology model for detecting onset of greenness in temperate mixed forests, Korea: an application of MODIS leaf area index. Remote Sensing of Environment. 86, 232–242.
[56] Savitzky, A. and Golay, M.J. (1964) Smoothing and differentiation of data by simplified least squares procedures. Analytical Chemistry. 36, 1627–1639.
[57] Chen, J., Jönsson, P., Tamura, M., Gu, Z., Matsushita, B. and Eklundh, L. (2004) A simple method for reconstructing a high-quality NDVI time-series data set based on the Savitzky–Golay filter. Remote Sensing of Environment. 91, 332–344.
[58] Frankenberg, C., O'Dell, C., Berry, J., Guanter, L., Joiner, J., Köhler, P., Pollock, R. and Taylor, T.E. (2014) Prospects for chlorophyll fluorescence remote sensing from the Orbiting Carbon Observatory-2. Remote Sensing of Environment. 147, 1–12.
[59] Li, X. and Xiao, J. (2019) A global, 0.05-degree product of solar-induced chlorophyll fluorescence derived from OCO-2, MODIS, and reanalysis data. Remote Sensing. 11, 517.
[60] Reichstein, M., Falge, E., Baldocchi, D., Papale, D., Aubinet, M., Berbigier, P., Bernhofer, C., Buchmann, N., Gilmanov, T., Granier, A., Grünwald, T., Havránková, K., Ilvesniemi, H., Janous, D., Knohl, A., Laurila, T., Lohila, A., Loustau, D., Matteucci, G., Meyers, T., Miglietta, F., Ourcival, J.M., Pumpanen, J., Rambal, S., Rotenberg, E., Sanz, M., Tenhunen, J., Seufert, G., Vaccari, F., Vesala, T., Yakir, D. and Valentini, R. (2005) On the separation of net ecosystem exchange into assimilation and ecosystem respiration: review and improved algorithm. Global Change Biology. 11, 1424–1439.

[61] Papale, D., Reichstein, M., Aubinet, M., Canfora, E., Bernhofer, C., Kutsch, W., Longdoz, B., Rambal, S., Valentini, R., Vesala, T. and Yakir, D. (2006) Towards a standardized processing of Net Ecosystem Exchange measured with eddy covariance technique: algorithms and uncertainty estimation. Biogeosciences. 3, 571–583.

[62] Lasslop, G., Reichstein, M., Papale, D., Richardson, A.D., Arneth, A., Barr, A., Stoy, P. and Wohlfahrt, G. (2010) Separation of net ecosystem exchange into assimilation and respiration using a light response curve approach: critical issues and global evaluation. Global Change Biology. 16, 187–208.

[63] Barr, A.G., Richardson, A.D., Hollinger, D.Y., Papale, D., Arain, M.A., Black, T.A., Bohrer, G., Dragoni, D., Fischer, M.L., Gu, L., Law, B.E., Margolis, H.A., McCaughey, J.H., Munger, J.W., Oechel, W. and Schaeffer, K. (2013) Use of change-point detection for friction–velocity threshold evaluation in eddy-covariance studies. Agricultural and Forest Meteorology. 171–172, 31–45.

[64] Kumar, J., Hoffman, F.M., Hargrove, W.W. and Collier, N. (2016) Understanding the representativeness of FLUXNET for upscaling carbon flux from eddy covariance measurements. Earth Syst. Sci. Data Discuss.

[65] Jonsson, P. and Eklundh, L. (2002) Seasonality extraction by function fitting to time-series of satellite sensor data. IEEE Trans. Geosci. Remote Sensing. 40, 1824–1832.

[66] Yu, H., Luedeling, E. and Xu, J. (2010) Winter and spring warming result in delayed spring phenology on the Tibetan Plateau. Proceedings of the National Academy of Sciences of the United States of America. 107, 22151–22156.

[67] Wu, C., Gonsamo, A., Gough, C.M., Chen, J.M. and Xu, S. (2014) Modeling growing season phenology in North American forests using seasonal mean vegetation indices from MODIS. Remote Sensing of Environment. 147, 79–88.

[68] Zhang, X., Friedl, M.A., Schaaf, C.B., Strahler, A.H., Hodges, J.C., Gao, F., Reed, B.C., Huete, A. (2003) Monitoring vegetation phenology using MODIS. Remote Sensing of Environment. 84, 471–475.

[69] Hmimina, G., Dufrêne, E., Pontailler, J.Y., Delpierre, N., Aubinet, M., Caquet, B., De Grandcourt, A., Burban, B., Flechard, C., Granier, A. and Gross, P. (2013) Evaluation of the potential of MODIS satellite data to predict vegetation phenology in different biomes: An investigation using ground-based NDVI measurements. Remote Sensing of Environment. 132, 145–158.

[70] Baumann, M., Ozdogan, M., Richardson, A.D. and Radeloff, V.C. (2017) Phenology from Landsat when data is scarce: Using MODIS and Dynamic Time-Warping to combine multi-year Landsat imagery to derive annual phenology curves. Int. J. International Journal of Applied Earth Observation and Geoinformation. 54, 72–83.

[71] Joiner, J., Yoshida, Y., Vasilkov, A.P. and Middleton, E.M. (2011) First observations of global and seasonal terrestrial chlorophyll fluorescence from space. Biogeosciences. 8, 637.

[72] Schmid, H.P. (2002) Footprint modeling for vegetation atmosphere exchange studies: a review and perspective. Agricultural and Forest Meteorology. 113, 159–183.

[73] Wu, C., Peng, D., Soudani, K., Siebicke, L., Gough, C.M., Arain, M.A., Bohrer, G., Lafleur, P.M., Peichl, M., Gonsamo, A., Xu, S., Fang, B. and Ge, Q. (2017) Land surface phenology derived from normalized difference vegetation index (NDVI) at global FLUXNET sites. Agricultural and Forest Meteorology. 233, 171–182.

Received: 09.12.2020
Accepted: 19.01.2021

CORRESPONDING AUTHOR

Pingan Jiang
Xinjiang Key Laboratory of Soil and Plant Ecological Processes,
College of Grassland and Environmental Sciences,
Xinjiang Agricultural University,
Urumqi 830052 – China

e-mail: jiang863863@sina.com

© by PSP Volume 30– No. 05/2021 pages 5332-5339 Fresenius Environmental Bulletin

A NOVEL MASS METEOROLOGICAL DATA STORAGE SYSTEM BASED ON HADOOP ECOSYSTEM

Quanpeng Ji*

College of Artificial Intelligence, Chongqing University of Arts and Sciences, Yongchuan 402160, China

ABSTRACT

When using the original system to store massive meteorological data, when the data volume is in the range of 100.25 TB-130.25 TB, it usually has the problem of slow data transmission rate. Therefore, in this paper, we propose a massive meteorological data storage system based on the Hadoop ecosystem. The hardware of the system includes a server module and a weather data storage module. Among them, the server module is composed of a database remote server, an application server, etc.; the meteorological data storage module is composed of a Vault Power TM module, a main server, etc. The software of the system includes data visualization module, data processing module and database module. The data visualization module can realize the data visualization processing of meteorological point elements and meteorological linear elements. The data processing module can realize scalable, efficient and reliable distributed data processing of massive meteorological data. While the database module is composed of system management tables, file library management and meteorological data tables. The combination of hardware and software effectively realizes the storage of massive meteorological data. Finally, through comparative experiments and verification, from the perspective of ecological environment protection, the data transmission rate of the system is higher than the original system in the range of 100.25TB-130.25TB, and the data transmission performance is improved.

KEYWORDS:
Hadoop ecosystem, Weather data, Data storage system, SCSI hard disk, Ecological environment

INTRODUCTION

As an important part of the computer application field, the data storage system involves data collection, preprocessing, processing, transmission, and conversion. Moreover, its processing is very complicated. Therefore, in the process of storing and processing massive meteorological data, data cross operations are prone to occur. In recent years, the meteorological field has developed at an amazing speed, which can provide a solid meteorological guarantee for government decision-making and the production and life of the masses [1]. With the rapid development of the national economy, how to protect massive meteorological data under the sustainable development of the ecological environment has become one of the most important tasks facing people. Under the guidance of old concepts and methods, it is difficult for people to pay attention to the protection of meteorological data. It is necessary to implement the protection of meteorological data in the ecological environment, and the protection of meteorological data throughout the entire work process. At present, the actual development of China's meteorological services is characterized by a sharp increase in the data and types of upstream meteorological data. With the continuous expansion and deepening of meteorological services, more and more meteorological observation projects have increased the number and types of data uploaded by observatories to the Meteorological Information Center and Meteorological Bureau, including meteorological processing data, meteorological observation data, and other information, etc. [2]. Among them, weather processing data refers to data formed by processing weather observation data. Meteorological observation data refer to the primary meteorological products and direct observation data obtained through meteorological observation instruments. Other data include disaster assessment meteorological information, weather forecast conference system and TV conference data, and meteorological department documents and office data. Under the above background, there is an urgent need to build a unified massive meteorological data storage system to break the chaotic storage state of the current meteorological information database [3].

Countries all over the world attach great importance to the study of massive meteorological data storage systems. People began to study massive meteorological data storage systems in the 1970s. Some scholars have proposed a massive meteorological data storage system based on a relational database, which mainly implements the construction of a massive meteorological data storage system by building a relational database. However, China's research on massive meteorological data storage systems started late. Some scholars have proposed a massive meteorological data storage system based on information

sharing technology, which mainly builds a massive meteorological data storage system through information sharing technology. Reference [4] proposed the design and implementation of a cloud-native mass data storage system based on Kubernetes. This storage system uses an object storage model to meet high-frequency and large-capacity file storage. At the same time, the use of Kubernetes' rich automated tool chain improves resource utilization, making it easier to deploy and expand than other storage systems. This kind of storage system has a certain improvement in performance and stability compared with the current mainstream object storage and file systems when reading more than writing. Reference [5] proposed a mobile weather radar storage system design based on Java and cluster analysis, using mobile terminals to optimize data storage, and solved the shortcomings of existing radar systems. The software system adopts MVC mode, based on database and Android technology, realizes the remote control of the mobile terminal, and has functions such as display products and fault warning. It uses the strong echo positioning algorithm and Baidu Weather API to realize the identification and positioning of multiple strong centers of radar data. Facts have proved that the system can effectively carry out radar control and fault warning, and it has high flexibility and reliability. However, when using the above system to store massive meteorological data, when the data volume is in the range of 100.25 TB-130.25 TB, there is a problem of slow data transmission rate. Therefore, in this paper, we propose a massive meteorological data storage system based on the Hadoop ecosystem. The hardware part of the system consists of a server module and a weather data storage module. The software part is composed of data visualization module, data processing module and database module. It can combine the software and hardware of the massive meteorological data storage system, facing the Hadoop ecosystem, and realize the storage of massive meteorological data.

MATERIALS AND METHODS

Hardware design of mass meteorological data storage system. In the concept of sustainable development of the ecological environment, the massive meteorological data storage system is a new type of storage system. It has strong scalability, high parallelism and compatibility with a variety of standard equipment. The host is the root node of the system, in order to give play to the structural advantages of relational data organization. It maximizes the use of the parallelism of the underlying equipment in data transmission to achieve block storage of data. The hardware composition of the massive meteorological data storage system based on the Hadoop ecosystem includes: a server module and a meteorological data storage module [6].

Design server module. Among them, the server module is composed of a database remote server, an application server, and a client application interface. Among them, the database remote server is responsible for the maintenance and read-write management of massive meteorological data [7]. As the main body of the application, the application server contains enterprise logic such as management model, operation method, and planning. The function is to receive the input and return the result after processing. The main function of the client application interface is to provide the user interface of the system, and can guide the operator to use the interface [8].

The specific technical indicators of database remote server and application server are shown in Table 1.

TABLE 1
The specific technical indicators of the database remote server.

Server type	Serial number	Project	Data
Database remote server	1	Management interface	Graphical interface
	2	Quantity	3 sets
	3	Development tools	Java
	4	Accessible client	PHP, C^{++}, Python
	5	Management interface	Graphical interface
	6	Development language	erlang
	7	Implementation agreement	AMQP
	8	Download method	Progressive
	9	Support function	Anti-hotlinking, progress dragging
Application server	1	Quantity	1 set
	2	Development tools	Java
	3	Development language	erlang
	4	Server framework	High concurrency framework
	5	Transfer Protocol	RTMP
	6	Management interface	Graphical interface
	7	Support message interaction model	Distributed transaction, distributed transaction, remote procedure call

Design weather data storage module. The meteorological data storage system is developed under sustainable conditions and needs to conform to

the concept of sustainable development. The weather data storage module is composed of Vault Power TM modules (2), RAID 4 PERC controller card and main server [9]. Each of the main servers can be connected to a maximum of eight Vault Power TM modules, and each Vault Power TM module can be connected to 14 SCSI hard disks, with a storage capacity of 500 GB [10].

The configuration of the main server is: 14 pieces of 10 000-RPM high-performance hard drives; the dense capacity type is 3U rack space; Dell clusters, hot-swappable power supplies, hot-swappable cooling units, and hot-swappable hard drives support kits; 50, RAID support for levels 10, 5, 1, and 0; bandwidth is U230; throughput is 460 MB/s; modular design; PowerVault, Power App, and PowerEdge compatible servers; Windows server 2008 operating system; dual-channel RAID , Dual-core CPU, Intel 4.2 GHz processor, 4 GB memory, 2 100 M network cards, 800 GB storage capacity and rack-mount architecture.

The configuration of Vault Power TM module is: MSCS cluster support, keyboard, rack, LCD configuration hardware, Ultra SCSI 320 hard disk technology, dense rack support environment, redundancy function using hot swap redundancy, load balancing equipment using 750 W cooling redundancy Heat-swappable fan, load balancing redundant hot-swappable power supply, Intel TM Xeon processor, dual-core CPU and EM68T support technology.

Software design of mass meteorological data storage system. In the concept of sustainable development of the ecological environment, the establishment of system software follows four principles: the principle of green concept, the principle of sustainable development, the principle of economic development and the principle of recycling. The software composition of the massive meteorological data storage system based on the Hadoop ecosystem includes: data visualization module, data processing module, and database module [11].

TABLE 2
Visualize the content of the meteorological point elements after processing.

Serial number	Meteorological point elements	Visualization pictures	Serial number	Meteorological point elements	Visualization pictures
1	Smoke		17	Light rain	
2	Haze		18	No wind	
3	Sand dust		19	Thunderstorm	
4	Rotating wind		20	Fog	
5	Cloudy day		21	Mist	
6	Cloudy		22	Frost	
7	Sunny day		23	Typhoon	
8	Strong sandstorm		24	Shower	
9	Sandstorm		25	Freezing rain	
10	Floating dust		26	Extraordinary rainstorm	
11	Snow showers		27	Torrential rain	
12	Blizzard		28	Intense fall	
13	Heavy snow		29	Heavy rain	
14	Moderate snow		30	Moderate rain	
15	Light snow		31	Light rain	
16	Hail			-	-

Design data visualization module. Among them, the data visualization module can realize the data visualization processing of meteorological point elements and meteorological linear elements [12]. The data visualization processing flow of meteorological point elements is as follows: draw the system meteorological element symbols and generate their corresponding pictures [13]. The meteorological point-like elements are rendered based on each meteorological element category. Then, the actual longitude and latitude coordinates of the meteorological point elements are transformed and converted into the current screen coordinates, so as to realize the visual processing of the meteorological point elements in the front-end interface of the system [14]. The content of the meteorological point elements after visualization processing is shown in Table 2.

The remote sensing and monitoring process of meteorological information after visual processing is as follows:

In the first step, a network can be established using sensor nodes to monitor the nodes and monitored variables in real time or regularly;

The second step is to monitor the node temperature, acceleration, air pressure and other parameters in real time, and transmit them to the monitoring center for display through the remote network. Furthermore, the gateway system can be used to transmit information data to the mobile network through the network, and the operator's instructions are transmitted to the network through the gateway;

The third step is to establish a server and a database, control the storage of monitoring data, and provide customers with a series of information query services;

The fourth step is to configure the sensor network for the client at all times, and at the same time it can query and retrieve the monitoring data and historical data; The client terminal displays the overall topology and geographic positioning network of the monitored location at any time; It monitors the status of a certain parameter in real time, and transmits alarm information to the center when it is assumed to exceed the set value; The weather information remote sensing and monitoring module can be configured in two modes, user and self-use, that is, when an emergency occurs, it will automatically send alarm information;

The fifth step is to obtain GPS coordinates in real time. For the wind element, a special meteorological point element, its symbol attributes will change, and it needs to be drawn independently based on its drawing rules, as shown in Figure 1.

The wind symbol has two components: wind plume and wind pole. The direction of the wind can be identified by these two elements [15]. Among them, the wind plume can be used to identify the strength of the wind force, half of the wind plume represents the first wind, one wind plume represents the second wind, and a triangle represents the level 8 wind [16]. From the perspective of ecological and environmental protection, in the data visualization module, the coordinates of the wind elements are first converted through the coordinate conversion function, and converted into the current screen coordinates. Then, the screen coordinates are regarded as the coordinates of the end of the wind pole, and the wind elements are drawn based on the wind force. Furthermore, according to the direction of the wind, the drawn wind elements are rotated to realize the visualization of the wind elements [17].

The data visualization processing flow of meteorological linear elements is as follows: the point coordinate sequence in the linear meteorological data is smoothed by line smoothing to make it into a curve. Then, on both sides of the line, different types of geometric figures, such as semicircles, triangles, etc., are drawn at a certain interval based on the type of meteorological data [18-19].

Design data processing module. The data processing module is designed based on the Hadoop ecosystem, and the designed data processing module can perform scalable, efficient, and reliable distributed data processing of massive meteorological data through the Hadoop ecosystem [20-21]. The specific structure of the data processing module is shown in Figure 2.

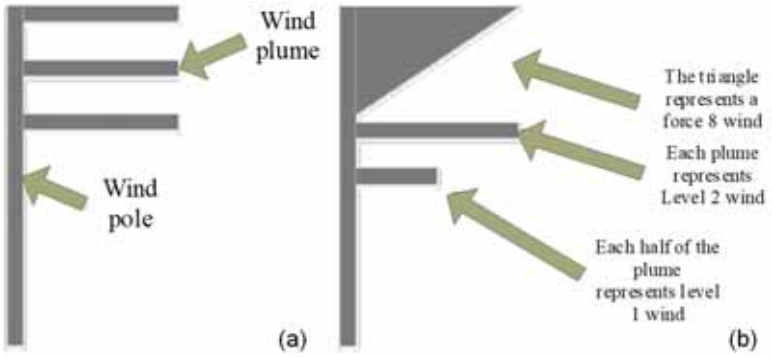

FIGURE 1
The shape of the basic wind symbol.
(a) Basic shape 1, (b) Basic shape 2.

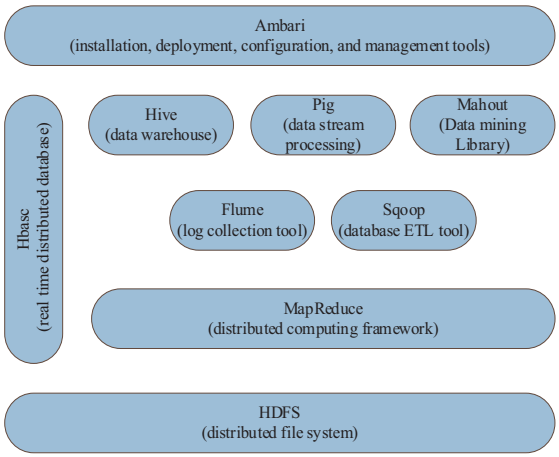

FIGURE 2
The specific composition of the data processing module.

Design database module. The database module is composed of three database tables, including system management tables, file library management, and meteorological data tables [22-23]. Its specific structure is as follows: system management table type, file library management type, weather data table type.

System management tables need to set data storage schedule. The file library management class needs to define the meta file category and define the file address. The meteorological data table needs to define the circulation index table, the station table, the watershed table and the related data of the automatic weather station.

RESULTS

Experimental design. In order to verify the performance of the designed massive meteorological data storage system based on the Hadoop ecosystem, experimental tests were carried out. The experimental topology of the system test in the experiment is shown in Figure 3.

From the perspective of the experimental topology environment and ecological environment protection, we use the designed massive meteorological data storage system based on the Hadoop ecosystem to carry out massive meteorological data storage experiments [7, 22]. The massive amount of experimental meteorological data comes from the database of the Meteorological Department of a certain place, which includes various types of meteorological data. Among them, the weather forecast platform interface is shown in Figure 4.

In this paper, we use the data transfer rate in the range of 100.25 TB-130.25 TB as the experimental data. In addition, the original two systems are used as the comparison system in the experiment for comparison experiments, which are the massive meteorological data storage systems based on a relational database and based on an information sharing technology.

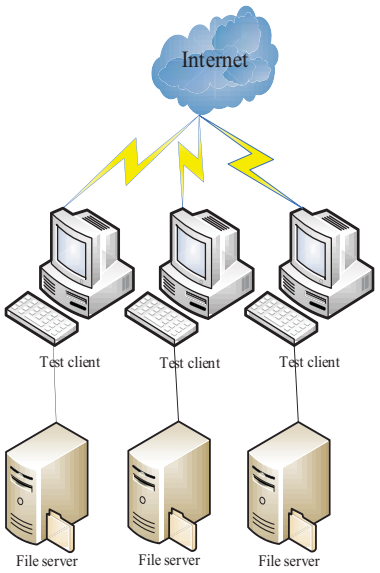

FIGURE 3
The experimental topology of the system test in the experiment.

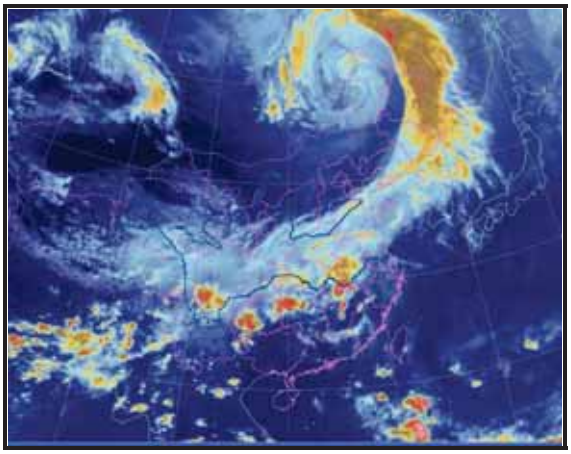

FIGURE 4
The platform interface for weather forecasting.

Results and analysis. From the perspective of ecological environment protection, when the amount of data is in the range of 100.25 TB-115.25 TB, the data transmission rate of the massive meteorological data storage system based on the Hadoop ecosystem is compared with other systems. The specific results of the experimental data are shown in Table 3.

According to the data transmission rate comparison experimental data in Table 3, when the data volume is in the range of 100.25 TB-115.25 TB, the data transmission rate of the massive meteorological data storage system based on the Hadoop ecosystem is higher than that of the massive meteorological data storage system based on relational database and information sharing technology [23-24].

TABLE 3
Experimental data for data transfer rate comparison.

Data volume (TB)	Data transfer rate (Gbps)		
	System based on Hadoop ecosystem	System based on relational database	System based on information sharing technology
100.25	2.547	1.236	1.589
101.25	2.646	1.256	1.645
102.25	2.656	1.363	1.669
103.25	2.744	1.414	1.698
104.25	2.761	1.525	1.748
105.25	2.813	1.563	1.863
106.25	2.892	1.614	1.945
107.25	2.947	1.796	2.012
108.25	3.041	1.878	2.132
109.25	3.151	1.915	2.241
110.25	3.214	2.036	2.314
111.25	3.223	2.147	2.458
112.25	3.314	2.225	2.512
113.25	3.465	2.314	2.636
114.25	3.648	2.436	2.747
115.25	3.765	2.514	2.815

TABLE 4
Experimental data for data transfer rate comparison.

Data volume (TB)	Data transfer rate (Gbps)		
	System based on Hadoop ecosystem	System based on relational database	System based on information sharing technology
116.25	3.615	2.615	2.945
117.25	3.747	2.736	3.052
118.25	3.818	2.811	3.126
119.25	3.967	2.876	3.278
120.25	4.025	2.944	3.321
121.25	4.115	3.054	3.414
122.25	4.289	3.196	3.578
123.25	4.387	3.231	3.636
124.25	4.451	3.324	3.724
125.25	4.585	3.426	3.814
126.25	4.641	3.496	3.896
127.25	4.741	3.554	3.946
128.25	4.815	3.696	4.096
129.25	4.963	3.712	4.187
130.25	5.015	3.820	4.245

When the data volume is in the range of 116.25 TB-130.25 TB, the data transmission rate comparison between the massive meteorological data storage system based on Hadoop ecosystem and the massive meteorological data storage system based on relational database and information sharing technology is shown in Table 4.

According to the data transmission rate comparison experimental data in Table 4, it can be seen that within the range of 116.25 TB-130.25 TB, the data transmission rate of the massive meteorological data storage system based on the Hadoop ecosystem is higher than that based on relational databases and the massive meteorological data storage system based on information sharing technology.

In summary, when the data volume is in the range of 100.25 TB-130.25 TB, the data transmission rate of the designed system is higher than other systems. The reason is that the system designed in this article transforms the actual longitude and latitude coordinates of the meteorological point elements and converts them into the current screen coordinates [25-26]. In this way, the visual processing of meteorological point-like elements in the front-end interface of the system is realized, which is conducive to the increase of data transmission rate.

CONCLUSIONS

From the perspective of ecological environment protection, for data in the range of 100.25TB-115.25TB, the data transmission rate of the massive meteorological data storage system based on the Hadoop ecosystem is higher than the Weather Data Storage System that based on relational databases and information sharing technology.

When the data volume is in the range of 116.25 TB-130.25 TB, the data transmission rate of the massive meteorological data storage system based on the Hadoop ecosystem is higher than that of the massive meteorological data storage system based on relational database and information sharing technology.

The massive meteorological data storage system based on the Hadoop ecosystem has realized an increase in data transmission rate, which is of great significance for realizing the unified storage of massive meteorological data.

ACKNOWLEDGEMENTS

The authors would like to show thanks to those techniques who have helped this research and all the authors of the references.

REFERENCES

[1] Li, W., Wang, X., Guo, B., Chen, D., Gao, Y. (2019) Design of Wireless Data Acquisition System for Prediction of Airport Runway Icing. Machine Tool and Hydraulics. 47(6), 38-45.

[2] Brownlie, T., Bishop, T., Parry, M. (2020) Predicting the Periodic Risk of Anthrax in Livestock in Victoria, Australia, Using Meteorological Data. International Journal of Biometeorology. 64(6), 1-10.

[3] Song, Z. (2019) Improvement of Data Service Capability of Provincial CIMISS - Based on Distributed Storage Technology. Meteorological Science and Technology. 47(3), 433-438.

[4] Liu, F., Li, J., Wang, Y., Li, L. (2020) Design and Implementation of Cloud Native Massive Data Storage System Based on Kubernetes. Journal of Computer Applications. 40(2), 547-552.

[5] Chen, Z., Hong, T. (2019) Design of Mobile Terminal Weather Radar Management System Based on Java and Clustering Analysis. Modern Electronics Technique. 42(2), 62-66.

[6] Qiu, C., Wang, W. (2018) Construction of Hydrology Big Data Cloud Platform based on Cloud Computing Architecture. Yangtze River. 49(5), 31-35.

[7] Battista, G., Roberto, D. (2017) Correlation between Air Pollution and Weather Data in Urban Areas: Assessment of the City of Rome (Italy) as Spatially and Temporally Independent Regarding Pollutants. Atmospheric Environment. 165, 240-247.

[8] Vin, R., Han, W., Gao, Z., Wang, G. (2019) A Study on Longwave Infrared Channel Selection Based on Estimates of Background Errors and Observation Errors in the Detection Area of FY-4A. Acta Meteorologica Sinica. 77(5), 898-910.

[9] Han, Q., Zheng, J., Zhao, R. (2019) Data Compression Algorithm of Early Warning Affected Area Issued by Beidou Satellite. Science Technology and Engineering. 19(23), 156-162.

[10] Wu, H., Xing, H., Wu, H., Liu, G., Yan, Y., Yu, P., Dai, X. (2019) Farmland Information Collection System Based on Internet of Things Model. Chinese Journal of Electron Devices. 42(4), 1056-1062.

[11] Chen, H., Wang, S., Liang, D., Su, Y. (2019) Big Data Analysis Research of Power Saving in Consumer Side. Power System Technology, 43(4), 1345-1353.

[12] Ferreira, L., Cunha, F., De Oliveira R.A., Fernandes. F. (2019) Estimation of Reference Evapotranspiration in Brazil with Limited Meteorological Data Using ANN And SVM - A New Approach. Journal of Hydrology. 572(9), 556-570.

[13] Liu, B., Chang, J., Xu, F., Li, H., Zhu, L., Dou, X. (2018) Design of Lidar Data Acquisition System Based on FPGA Chip. Electronics Optics and Control. 25(12), 72-76.

[14] Chen, Y., Bu, Z., Wang, Z. (2018) A Doppler Wind Lidar Based on Image-Reject Homodyne Technology. Transactions of Beijing Institute of Technology. 38(2), 205-210.

[15] Zhao, Y., Cheng, F., Wei, Y. (2019) High Quality Spatial Data Storage and Query Algorithm towards Massive Datasets Based on Cloud Computing Platform. Journal of Geomatics Science and Technology. 36(2), 185-189.

[16] Yang, D., Chen, Y., Liu S. (2018) Storage System Design for Fast Reading and Writing of Health Big Data. Computer Engineering and Design. 39(10), 3063-3067.

[17] Rebetez, M., Von, Arx, G., Gessler, A., Pannatier, E., Innes, J., Jakob, P. (2018) Meteorological Data Series from Swiss Long-Term Forest Ecosystem Research Plots since 1997. Annals of Forest Science. 75(2), 41-47.

[18] Gao, S., Li, L., Li, W., Janowicz, K., Zhang, Y. (2013) Constructing Gazetteers from Volunteered Big Geo-Data Based on Hadoop. Computers Environment and Urban Systems. 61, 172-186.

[19] Xu, X., Lei, H., Zhang, H., Ma, X. (2019) Design and Implementation of Cloud Storage System for Farmland Internet of Things Based on Nosql Database. Transactions of the Chinese Society of Agricultural Engineering. 35(1), 172-179.
[20] Qu, Z., Yuan, S., Fan, M. (2019) Double Column Family Storage Design for Massive Data of Power Quality Online Monitoring System. Power System Protection and Control. 47(2), 154-160.
[21] Lin, F., Huang, K., Lin, T., Hwang, R. (2018) Generating Hourly Local Weather Data with High Spatially Resolution and the Applications in Bioclimatic Performance. Science of the Total Environment. 653, 1262-1271.
[22] Wang, S., Lü, J., Wang, R., Wu, J., Ma, S. (2018) A Multimedia File Cloud Storage System to Support Data Deduplication and Logical Expansion. Journal of Computer Research and Development. 55(5), 1034-1048.
[23] Jose, A., Miguel, V., Goberna, M. (2018) Trait-based Selection of Nurse Plants to Restore Ecosystem Functions in Mine Tailings. Journal of Applied Ecology. 55(3), 125-131.
[24] Colston, J., Tahmeed, A., Cloupas, M., Kang, G., Kosek, M., Sousa, J. (2018) Evaluating Meteorological Data from Weather Stations, and from Satellites and Global Models for a Multi-Site Epidemiological Study. Environmental Research. 165, 91-109.
[25] Santos, J., Cunha, F., Filgueiras, R., Gustavo, H., DaSilva, G. (2020) Performance of SAFER Evapotranspiration Using Missing Meteorological Data. Agricultural Water Management. 233(12), 106-112.
[26] Bernardo, P., Charles-Dominique, T., Barakat, M., Ortet, P., Fernandez, E., Filloux, D. (2018) Geometagenomics Illuminates the Impact of Agriculture on the Distribution and Prevalence of Plant Viruses at the Ecosystem Scale. The ISME Journal. 12(1), 173-184.

Received: **10.12.2020**
Accepted: **20.01.2021**

CORRESPONDING AUTHOR

Quanpeng Ji
College of Artificial Intelligence
Chongqing University of Arts and Sciences
Yongchuan 402160 – China

e-mail: 125191408@qq.com

© by PSP Volume 30– No. 05/2021 pages 5340-5349 Fresenius Environmental Bulletin

COMPARATIVE EFFICIENCY OF NEW HERBICIDES FOR WEED CONTROL ON QUALITY YIELD AND ITS COMPONENT IN MAIZE (*ZEA MAYS*)

Abd El-Wahed A El-Sayed[1], Azza E Khaffagy[2], Fatma E M Shaheen[1],Yaser Hafez[3], Khaled Abdelaal[3,*], Fahmy A S Hassan[4], Dalia A Elhag[1]

[1]Agron. Dept, Fac. Agric., Kafrelsheik University, Kafrelsheikh, Egypt
[2]Weed Research Central Laboratory Agric. Res. Center, Giza, Egypt
[3]EPCRS Excellence Center, Plant Pathology and Biotechnology Lab., Agric. Botany Dept., Fac. Agric., Kafrelsheikh Univ., 33516 Egypt
[4]Department of Biology, College of Science, Taif University, P.O.Box 11099, Taif 21944, Saudi Arabia

ABSTRACT

A field experiment was carried out at the Experimental Farm of Sakha Agricultural Research Station at Kafr El-Sheikh Governorate, Egypt during 2018 and 2019 summer seasons to evaluate the effect of weed control treatments on the productivity and quality of maize plants. The treatments were arranged in a Randomized Complete Block Design with four replications. Weeds were controlled by all treatments compared with untreated check; however, hand weeding twice was not superior to herbicide treatments. Among the herbicidal treatments, Sonic + Maister power (504+600) cm3/ha was proved to be better in controlling weeds, increasing ear length, number of rows/ear, number of grains/row,100-grain weight in the two seasons but ear diameter and ear grains weight in the first season. As protein percentage was increased with used Stomp extra and Maister power (1800+600) cm3/ha. Application of weed control treatments resulted in less weed biomass and greater maize yield. It was concluded that the use of herbicides, especially Sonic + Maister power (504+600) cm3 /ha in weed control, was suitable and enhanced maize yield as well as controlled the associated weeds.

KEYWORDS:
Maize (*Zea mays* L.), Yield, Herbicide, Weeds control, Pendimethalin, Acetochlor, S-metolachlor and Foramsulfuron

INTRODUCTION

Maize (Zea mays, L.) is one of the most important among the cereal crops in the world's agricultural economy. Maize grains are used for human consumption, feed for poultry and livestock, for extraction of edible oil and also for starch and glucose industry [1-5]. There are many stresses affect agricultural production such as abiotic stress [6-9] and biotic stress [10-16]. Weeds infestation is one of biotic stresses and it is a serious pest that interferes with maize crop through competition resulting in direct loss to quantity and quality of the product. The idea of weeds as undesirable plants developed, when man began to produce plants for food and other different purposes [17]. Pannacci and Onofri [18] found that crop yield losses in the untreated check compared to the highest obtained yield with herbicides treatments, ranging from 33 to 91 %. Weed control in maize fields is very essential for obtaining good yield. Therefore it is important to increase, ear length, ear diameter, number of rows/ear, number of grains/row, ear grains weight; 100-grain weight, protein% and grain yield /ha. [19-22]. It has been shown that maize yield components can be reduced if weeds are not controlled [23]. Different weed control methods have been used to manage the weeds, but mechanical and chemical methods are more frequently used for the weeds control than any other control methods. Mechanical methods including hand hoeing twice are still useful but are getting expensive; laborious and time–consuming [24]. Chemical weed control is a better supplement to conventional methods and forms an integral part of the modern crop because it is cheaper, faster and it gives better control [24]. Keeping all these in view, the present study was carried out to evaluate the effect of weed control treatments on productivity of maize and growth of associated weeds

MATERIALS AND METHODS

Two field experiments were carried out at the Experimental Farm of Sakha Agricultural Research Station at Kafr El-Sheikh Governorate, Egypt during 2018 and 2019 summer seasons to evaluate the effect of weed control treatments on productivity of maize and growth of associated weeds. A randomized complete block design (RCBD) with four replicates, was used in the two seasons. The experimental field was well prepared and calcium super phosphate (15.5%

P2O5) and potassium sulphate (48% K2O) were applied during soil preparation at the rate of 200 and 50kg/ha.., respectively. Each plot contained five ridges with 5 meters in long and 70 cm in width.

Maize grains were planted by the rate of 36 kg/ha.. of hybrid three-way cross "321" in hills at 25cm distance with two grains in hill on one side of ridge during the 28th May and 3rdJune in both seasons, respectively.

Plants were thinned to one plant per hill before the 1st irrigation to give plant stand of 24000 plants per ha.dan. Nitrogen fertilizer was applied in the form of urea (46%N) at the rate of 120 kg N/ha.., in two equal doses before the first and second irrigations. Herbicides were applied post sowing and before sowing irrigation as pre-emergence and at 25 days post maize crop emergence (4-6) leaves stage of maize. As post-emergence using "Knapsack hand sprayer CP3 20 liter "equipped with one nozzle even flat fan calibrated to deliver spray volume of 200 L/ha.

Harvested was done on 27th and 29th September in both seasons respectively. The preceding crops were wheat (Triticum aestivum) in the first season and sunflower (Helianthus annus, L) in the second season. The treatments of the experiment were as follows:

1-Stomp extra (pendimethalin 45.5% EC) N-(1-ethylpropyl)-3,4-dimethyl-2,6-dinitrobenzenamine at the rate of 3.6 L/ha. as Soil surface application directly, (T1).

2- Harness (Acetochlor EC 84%) 2-chloro-N-(ethoxymethyl)-N-(2-ethyl-6 methylphenyl)acetamide at the rate of 2.4 L/ha. as soil surface application directly, (T2).

3- Sonic (S-metolachlor EC 96%) Amixture of (s)-2-chloro-N-(2-ethyle-6-methylphenyl) N-(2-methoxy-1- methyletyl) acetamide and-2-chloro-N-(2- ethyle-5-methylphenyl) acetamide in the proportion 80-100% to 20-0% at the rate of 1008 cm3/ha.as soil surface application directly,(T3).

4- Stomp extra 1800cm3 / ha. + Maister power at the rate of 600 cm3/ha. (T4).

5- Harness 1200cm3/ha.+ Maister power at the rate of 600 cm3/ha. (T5).

6- Sonic at the rate of 504 cm3/ha. + Maister power at the rate of 600 cm3/ha. (T6).

7- Maister power OD 4.53% (Foramsulfuron sodium 3.35% + Iodosulfuron – methyl sodium 0.11% + Thiencarbazone – methyl 1.07%) 2-[[[[(4, 6-dimethoxy-2-pyrimidinyl) amino] carbonyl] amino] sulfonyl]-4-(formylamino)-N, N-dimethylbenzamide. + methyl 4-iodo-2-[[[[(4-methoxy-6-methyl-1,3,5-triazin-2yl) amino] carbonyl] amino] sulfonyl] benzoate, sodium salt + methyl 4-[[[(4,5-dihydro-3-methoxy-4-methyl-5-oxo-1H-1,2,4-triazol-1-yl) carbonyl] amino] sulfonyl]-5-methyl-3-thiophenecarboxylate at the rate of 1200 cm3/ha. at 25 days after sowing, (T7).

8- Hand hoeing twice, (T8).

9- Untreated check, (T9).

Weed control efficiency (WCE): it was calculated from weed control treatments in controlling weeds as follow:

$$WCE\% = \frac{WDC - WDT}{WDC}$$

WCE = weed control efficiency:
WDC = weed dry matter in control;
WDT = weed dry matter in a treatment

TABLE 1
Chemical group and mode of action of the herbicides used according to Ashton and Crafts [25].

Common name	Chemical group	Mode Of action
Pendimethalin	Dinitroaniline	Root growth inhibitors by interrupt cell division (mitosis) in germinating seedlings and stop lateral root formation. Roots on susceptible plants will be stubby and thick, especially lateral roots
Acetochlor	Chloroacetamide	Inhibit very long chain fatty acid (VLCFA)synthesis results in stunted growth and eventually death due to lack of membranes for cellular integrity
S-metolachlor	Chloroacetamide	Inhibit very long chain fatty acid (VLCFA)synthesis Results in stunted growth and eventually death due to lack membranes for cellular integrity
Foramsulfuron sodium 3.35%+ Iodosulfuron – methyl sodium 0.11% + Thiencarbazone–methyl .07%	Sulfunylurea	Inhibit acetoacetate synthase (ALS) a key enzyme in the biosynthesis of the branched-chain amino acids isoleucine, leucine, and valine, which is necessary for formation of plant protein.

1. Weeds growth and development:
2. Samples of weeds from one square meter were chosen at random at 50 and 75 days after sowing from each plot and were hand pulled out and identified into the species according to Tackholm [26], then separated into two group's i.e. broad leaved and grassy weed. Thereafter, weeds were air dried for three days and then were oven dried at 70 C for 24 hr., until constant weight of each weed species within each group and the dry weight of each group as (g/m2) was recorded.

Maize growth and yield. 2 lines were harvested in the middle of the plots, and 10 plants were selected from them to estimate the yield and its components.

A. Maize yield and its components. 1- Ear length (cm). 2- Ear diameter (cm). 3- Number of rows/ear. 4- Number of grains/row. 5- Ear grains weight (g). 6- 100- grain weight (g). 7- Grain yield in ton/ha. was estimated based on grain yield/plot.

B. Maize grains quality. Determination of protein in maize grains: the total nitrogen was determined by micro-Kjeldahl method according to A.O.A.C. [27].

Determination of carbohydrates in maize grains: the total carbohydrate percentage was determined according to A.O.A.C. [27].

C. Correlation study. Simple correlation matrix was carried out for the two seasons to investigate the relationship between dry weight of different weed categories and maize yield and its components according to Steel and Torrie [28].

TABLE 2
Scientific, common and family names for weed species recorded in corn crop during 2018 and 2019 seasons.

No.	Scientific name	Common name	Family
	Broad-leaved weeds		
1	*Xanthium strumarium* L.	Cocklebur.	Compositae.
2	*Corchorus olitorius* L.	Nalta jute.	Tiliaceae.
3	*Hibiscus trionum,*L.	Bladder hibiscus.	Malvaceae
4	*Amaranthus retroflexus,*L.	Redroot pig weed	Amaranthaceae
5	*Portulaca oleracea,* L.	Common purslane	Portulacaceae
6	*Ammania aegyptiaca*	Tooth cup	Compositae
7	*Sida alba,* L.	Prickly sida	Malvaceae
	Grassy weeds		
1	*Echinochloa colonum* L.	Jungle rice.	Gramineae.
2	*Brachiaria reptans* L	Signal grass.	Gramineae.
3	*Dinebra retroflexa*	(Vahl.)panz	Gramineae.

TABLE 3
Effect of weed control treatments on dry weight of total weeds at 50 and 75 from days after sowing DAS in 2018 and 2019 seasons.

Weed control treatments	**2018 season**				**2019 season**			
	Dry weight of total weeds (g/m^3) days after sowing DAS							
	50 DAS	WCE%	75 DAS	WCE%	50 DAS	WCE%	75 DAS	WCE%
T1	38.62	66.2	129.91	85.2	105.74	78.1	132.6	84.4
T2	46.51	59.3	140.37	84.0	137.26	71.5	146.4	82.7
T3	21.73	80.9	119.25	86.4	90.85	81.2	112.02	86.8
T4	14.61	87.2	114.32	86.9	82.99	82.7	88.97	89.5
T5	17.86	84.4	77.97	91.1	86.91	81.9	90.31	89.3
T6	9.57	91.6	54.38	93.7	62.30	87.1	68.82	91.9
T7	11.99	89.5	103.83	88.2	90.74	81.1	104.4	87.7
T8	8.93	92.1	202.25	76.9	100.99	79.1	112.1	86.8
F- test	**		**		**		**	
LSD 5%	**11.43**		**52.96**		**21.59**		**45.82**	

"**" = high Significance at 5% level of probability

Statistical analysis. All data were statistically analyzed according to technique of analysis of variance (ANOVA) for the randomized complete block design as mentioned by Gomez and Gomez [29]. The differences among means of treatment were compared by least of significant difference (LSD) at 5% level of significance. Data are presented as untransformed means.

RESULTS

Data in Table (3) indicated that all weed control treatments significantly decreased the dry weight of total weeds (g/m2) at 50, 75 DAS in the both seasons, as compared with untreated check. Treatment 6 Provided the most effective control of total weeds and recorded the lowest dry weed (9.57 and 62.3 g/m2) after 50 DAS and (54.38 and 68.82 g/m2) after 75 DAS in the both seasons, respectively. On the other hand (T9) untreated check recorded the highest values of dry weight after 50 and 75 DAS (114.3, 878.73, 482.15 and 850.7 g/m2) in both seasons, respectively. These treatments gave excellent weed control effect by 91.6, 93.7, 81.1 and 87.7% *R%: Weed control efficiency. These results are in line with those reported by Roy et al. [30], Skoko and Zivanovic [31], Vanbiljon et al. [32] and Haseeb et al. [33]. They reported that there has been significant difference in weed and was different among the various herbicidal treatment due to difference in their mode of action might be the main reason for significantly different control. On the other hand Soren, et al. [34] they found highest weed control efficiency was recorded in hand weeding twice at 20 and 40 days after sowing.

Effect of weed control treatments on maize yield and its components. Data in Tables 4 and 5 indicated that the differences among ear length were highly significant in both seasons, ear diameter were highly significant in the first season and significant in the second season, number of rows/ear were highly significant in the first season and significant in the second season and number of grains/row were significant in both seasons which affected by different herbicidal treatments as compared with untreated check in the both seasons.

Ear length (cm). Comparison of ear length among various treatments is given in Tables (4 and 5) which show that highly significant differences in ear length between the various weed control treatments in both seasons. Chemical weed control treatments significantly affected ear length in both seasons compared with untreated check. (T6) recorded the highest ear length (22.00cm) and (23.01cm) were observed in without any significant with T4 and T8 in the first season, meanwhile there were significant differences among weed control in the second season. Untreated check (T9) had recorded the short ear length (17.66 and 16.0 cm) in both seasons, respectively. The Variation in ear length of maize in all weed control treatments could be attributed to varying effect of weed competition duration for available resources offered by different weed densities in different weed control practices. Weed control play a good roll for decreases the competition between maiz plant and different weeds. This result is in agreement with Tahir et al. [19] who found that weed competition caused a significant reduction in the value of ear length. Also less weed competition period in these treatments which allowed the maize plant to produce more photosynthetic material by using available nutrients. These results are confirmatory with those of Stefanovic et al. [35]. They founded that greater ear length in weed control treatments and smallest cob length in weedy check plots

TABLE 4
Effect of weed control treatments on maize yield components in 2018 season.

Weed control treatments	Ear length(cm)	Ear diameter(mm)	Number of rows/ear	Number of grains/row
T1	19.58	32.13	14.00	40.33
T2	19.77	33.20	13.73	40.73
T3	19.67	33.33	14.02	41.76
T4	20.60	34.36	14.20	42.00
T5	19.70	32.36	13.93	42.13
T6	22	33.96	14.36	43.03
T7	19.80	32.20	14.16	38.76
T8	20.40	32.90	14.33	42.95
T9	17.66	24.23	9.66	31.03
F- test	**	**	**	*
LSD 5 %	1.78	1.87	0.46	2.16

* and** indicate P >0.05 and P>0.01, respectively .

TABLE 5
Effect of weed control treatments on maize yield components in 2019 season.

Weed control treatments	Ear length(cm)	Ear diameter(mm)	Number of rows/ear	Number of grains/row
T1	18.93	32.26	14.00	40.13
T2	21.16	32.80	13.96	42.53
T3	20.80	33.12	14.13	43.56
T4	20.20	34.26	14.33	44.96
T5	20.33	32.66	13.60	45.20
T6	23.01	35.94	14.53	46.96
T7	21.16	32.66	14.13	45.33
T8	21.56	33.12	14.00	42.97
T9	16.00	28.32	11.96	37.53
F- test	**	*	*	*
LSD 5 %	1.42	1.82	0.74	2.55

* and** indicate P >0.05 and P>0.01, respectively .

Ear diameter (mm). Data in Tables (4 and 5) indicated that all weed control treatments significantly increased ear diameter (mm) in the both seasons compared with untreated check (T9). Treatment (T6 and T4) were recorded the highest values of ear diameter (34.36, 34.26, 33.96 and 35.94 cm) in the first and second seasons, respectively. The increases in ear diameter indicated that maize plant unaffected by any competition with uses weed control and all nutrient and water needed were available for growth and development of plant. These results are confirmatory with those of El-Metwally et al. [20] who found that weed competition caused significant reduction in the value of ear diameter.

Number of rows/ear. Number of rows/ear is one of the important yield components. It is apparent from the data recorded in Tables (4 and 5) that higher increase in number of rows/ear was registered through the most of weed control and the superior treatments were (T6) which recorded the highest values of number of row (14.36 and 14.53 row/ear) compared with (T9) which recorded the less values (9.66 and 11.96 row/ear) in the both seasons, respectively. In general, decreases of competition between weeds and maize plants increases number of row/ear. These results are in line with those of El-Metwallyet al. [20] who found that weed competition caused a significant reduction in the value of number of rows/ear.

Number of grains/row. Significant differences in number of grains/row between the various weed controls treatments were registered Tables (4 and 5) in the both seasons. The highest number of grains/row was obtained by (T6) which recorded the highest values of number of grain/row (43.03 and 46.96) without insignificant with T3, 4, 5 and 8 in the first season and with (T4, 5 and 7) in the second season. The highest number of grains per row in manual hoeing was because of very less number of weeds and consequently more photosynthates are available for plant growth and development. These results are confirmatory to Tanveer *et al*. [35]. They concluded that all weeds control treatments significantly increase the number of grain rows and number of grains per ear. These results are in harmony with those of El-Metwally et al. [20] who found that weed competition in treatment of untreated check caused significant reduction in the value of number of grains/row.

Ear grains weight (g) . Data in Tables (6 and 7) indicated that all weed control treatments significantly increased ear grains weight (g) in the both seasons The superior treatment in increasing ear grains weight (g) in the first season was (T6 and T4) which recorded the highest ear grain weight (244.26 and 273.09) in the first and second seasons, respectively. There were insignificant differences among weed control (T4, 7 and 8) in the first season. T4 and T6 and in the first season and T6 in the second season were the superior weed control in general. This treatment significantly increased ear grains weight as compared to the untreated check. These results are in confirmatory with those reported by El-Metwally et al. [20] who found that weed competition caused significant reduction in the value of ear grains weight.

100- Grain weight. Data in Table 6 and 7 showed the effect of weed control treatments on 100-grain weight in 2018 and 2019 seasons. The weight of 100-grain was increased with all weed control treatments compared with untreated check, In regard to 100-grain weight, the highest 100-grain weight was obtained by treatments (T6 and 4) which recorded (41.98 and 40.13 g) in the first season and (T6) recorded (39.25 g) in the second season, comparing with the lowest 100 grain weight 32.57 and 31.98 g which treated by (T9) in both seasons, respectively. These results are confirmatory with those of Tahir et al. [19] who found that weed competition caused significant reduction in the value of 100-grain weight. The significant variation for 100-grain weight in weed control treatments than weedy check was due to vigorous growth and development of maize plants,

which resulted in more photosynthates assimilation in grains thus more 100-grains weight. These results are in line with those of Tanveer et al. [36]. Extreme weeds growth in corn field leads to 66-80% reduction in crop yield [37,38]. Weeds compete for space, water, light and nutrients with main crop and thereby decreasing crop yield and increasing production cost. Baye and Bouchache [39], who concluded that 100-grain weight was greater in various controlled treatments than in weedy check in maize

Protein content on maize grains. Data presented in Tables 6 and 7 indicated that the effect of weed control treatments on protein percentage of maize in 2018 and 2019 seasons was significantly in the first season and highly significant in the second season. Treatments T1, 4, 5 and 6 were recorded the highest protein percentage (7.45, 7.59, 7.01 and 7.35) in the first season. T3, 4 and 6 recorded the highest protein percentage in the second season compared with T9 which recorded 5.74 and 6.31% in both seasons, respectively. This treatment significantly increased protein percentage of maize grains similar results were observed by El-Metwally et al. [20], Sharara et al. [22] and Raga'a et al. [40], had noted increase in protein content of maize grain as untreated check.

TABLE 6
Effect of weed control treatments on maize yield components, protein and carbohydrate content in 2018 season.

Weed control treatments	Ear grains weight(g)	100-grain weight(g)	Protein %	carbohydrate %	Grain yield t/ha.
T1	226.10	39.52	7.45	82.64	3.662
T2	235.92	39.23	6.93	83.07	3.606
T3	238.98	38.05	6.88	83.12	3.682
T4	273.09	40.13	7.59	82.98	3.746
T5	245.83	38.74	7.01	82.65	3.598
T6	248.25	41.98	7.35	84.26	3.822
T7	214.86	37.43	6.60	83.39	3.522
T8	245.41	36.87	6.56	83.52	3.318
T9	197.56	32.57	5.74	82.41	1.596
F- test	*	*	*	*	**
LSD 5 %	21.71	2.34	0.60	0.60	0.246

* and** indicate P >0.05 and P>0.01, respectively .

TABLE 7
Effect of weed control treatments on maize yield components, protein and carbohydrate content in 2019 season.

Weed control treatments	Ear grains weight(g)	100-grain weight(g	Protein %	carbohydrate %	Grain yield t/ha.
T1	202.62	35.53	7.40	87.59	3.4594
T2	226.09	35.54	6.95	88.04	3.6568
T3	215.64	36.57	7.90	87.09	3.7142
T4	226.75	35.72	8.35	87.28	3.7674
T5	222.75	37.19	7.71	87.73	3.6708
T6	244.26	39.25	8.08	88.69	3.8556
T7	231.33	36.57	7.26	86.91	3.7674
T8	228.81	36.22	7.12	87.88	3.7716
T9	179.43	31.98	6.31	86.65	2.1112
F- test	*	*	**	**	**
LSD 5 %	17.67	1.97	0.47	0.47	0.382

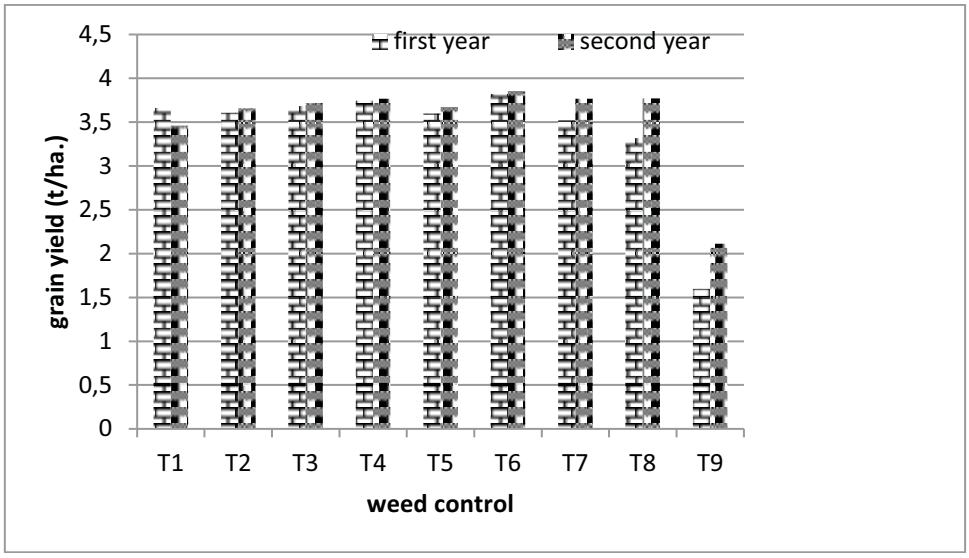

FIGURE 1
Mean of maize grain yield as affected by different weed control treatments in 2018 and 2019 growing seasons

TABLE 8
Correlation coefficient between all studied characters and maize yield analysis 2018 and 2019 seasons

Correlation analysis 2018 season

Characters	Grassy weeds	Total weeds.	Ear length	LAI	Ear di-ameter	N0.of row./ ear	No. grain/ row	100- grain weight	Ear grains weight	Grain yield
Broadleaf weeds	.857**	.997**	-.568**	-.757**	-.863**	-.944**	-.793**	-.657**	-.460*	-.947**
Grassy weeds	1	.895**	-.634**	-.650**	-.763**	-.808**	-.672**	-.707**	-.381*	-.800**
Total weeds.		1	-.589**	-.755**	-.864**	-.941**	-.789**	-.677**	-.456*	-.942**
Ear length			1	.528**	.618**	.657**	.731**	.625**	.633**	.589**
LAI				1	.655**	.698**	.660**	.598**	.458*	.668**
Ear diameter					1	.904**	.743**	.683**	.497**	.810**
N0.of row./ ear						1	.789**	.628**	.505**	.910**
No. grain/ row							1	.615**	.649**	.739**
100- grain weight								1	.583**	.577**
Ear grains weight									1	.438*
Grain yield										1

Correlation analysis 2019 season

Broadleaf weeds	.813**	.999**	-.716**	-.657**	-.632**	-.693**	-.694**	-.687**	-.570**	-.560**
Grassy weeds	1	.841**	-.592**	-.558**	-.592**	-.662**	-.542**	-.536**	-.687**	-.480*
Total weeds.		1	-.716**	-.658**	-.638**	-.700**	-.691**	-.684**	-.589**	-.562**
Ear length			1	.623**	.547**	.567**	.721**	.377	.681**	.504**
LAI				1	.470*	.729**	.572**	.448*	.598**	.873**
Ear diameter					1	.547**	.532**	.524**	.643**	.492**
N0.of row./ ear						1	.636**	.510**	.388*	.735**
No. grain/ row							1	.444*	.501**	.644**
100- grain weight								1	.498**	.544**
Ear grains weight									1	.550**
Grain yield										1

*Significant at 5% level of probability **Significant at 1% level of probability

Carbohydrate percentage. Data in Tables 6,7 showed the effect of weed control treatments on carbohydrate percentage of maize grains in 2018 and 2019 seasons. Data indicated that all weed control treatments significantly increased carbohydrate percentage of maize grains as compared with untreated check in the both seasons, the superior treatment in increasing carbohydrate percentage of maize grains in the both seasons, was (T6) which recorded (84.26 and 88.69%) in both seasons, respectively. Untreated check (T9) recorded the lowest percentage (82.41 and 86.65%) in both seasons, respectively. Similar results were observed by Soliman and Amany Hamz [41] who found that uncontrolling weed caused a significant reduction in total soluble carbohydrates percentage

Grain yield. Data regarding the effect of weed control treatments on grain yield (t/ha) are shown in Tables 6 and 7 and fig. 1, which clearly indicates grain yield (t/ha) to be highly significant affected by weed control treatments. The significantly higher grain yield (3.822 and 3.855 t./ha.) was observed under treatment T6 However, the minimum grain yield of 1.596 and 2.112 ton ha^{-1} was noted in treatments 9 (Untreated check). The variation in grain yield as compare to weedy check plots was different in all weed controlled treatments. This was mainly due to more number of grain rows, ear diameter, 100-grain weight and ear grains weight over weedy check. The lowest grain yield was recorded in weedy check could be attributed to maximum weed density which suppressed the growth and development of maize plants by competing for moisture, light and nutrients. The efficiency of various chemicals and other weed control practices in enhancing grain yield had also been observed by Stefanovic et al. [35]. Haseeb et al. [33] revealed that hand weeding gives significantly higher grain yield which was followed by weed control, also Din et al. [42], Tesfay et al. [43] and Ahmad et al. [44] reported that various weed control methods specifically with hoeing significantly enhanced grain yield of maize crop and the lowest was observed in weedy check.

Correlation between all studied characteristics and maize yield and its components. Data presented in Tables (8) indicated that the correlation coefficient between the dry weight of grassy, broad leaf weeds and their total as well as maize yield was statistically significant and inversely in both seasons**.** With all the correlation coefficient between yield components i.e. ear length, LAI, ear diameter, number of row/ear, number of grain/row, 100.grain weight, ear weight and grain yield in two seasons. Hence, weed control play a major role in increasing maize productivity, if applied at the suitable time, rate and stage of weed growth. Also, correlation analysis revealed that the yield increases due to type of weed group competition were positively contributed to the increases in growth characters and yield components. The correlation between total weeds and maize yield was highly statistically significant. Hence, weed control play a major role in increasing maize productivity, if applied at the suitable time, rate and stage of weed growth.

CONCLUSIONS

It was concluded that the use of herbicides in weed control was suitable and enhanced of maize yield as well as controlled the associated weeds. Among the herbicidal treatments, Sonic + Maister power (504+600) cm3/ha was the best treatment in weed control, increasing ear length, number of grains/row and 100-grain weight in the two seasons. Protein percentage was increased with application of Stomp extra and Maister power (1800+600) cm3/ha. Application of weed control treatments resulted in less weed biomass and improved maize yield.

ACKNOWLEDGEMENTS

The authors acknowledge Taif University Researchers Supporting Project number (TURSP-2020/143), Taif University, Taif, Saudi Arabia. The authors would like to thank all members of Plant Pathology and Biotechnology Lab., (ISO/17025 Accredited) and EPCRS Excellence Centre (Certified according to ISO/9001, ISO/14001 and OHSAS/18001), Dept. of Agric. Botany, Fac. of Agric., Kafrelsheikh University, Kafr-Elsheikh, Egypt.

REFERENCES

[1] Kumar, R., Bohra, J.S., Kumawat, N., Kumar, A., Kumariand, A., Singh, A.K. (2016) Root growth, Productivity and profitability of baby corn (*Zea mays* L.) as influenced by nutri levels under irrigated ecosystem. Research on Crops. 17, 41-46.

[2] Majid, M.A., Saiful Islam, M., EL Sabagh, A., Hasan, M.K., Saddam, M.O., Barutcular, C., Ratnasekera, D., Abdelaal, Kh.A.A., Islam, M.S. (2017) Influence of varying nitrogen levels on growth, yield and nitrogen efficiency of hybrid maize (*Zea mays*) Journal of Experimental Biology and Agricultural Sciences. 5(2), 134-142.

[3] Abdelaal, Kh.A.A., Hafez, Y.M., El Sabagh, A., Saneok, H. (2017) Ameliorative effects of Abscisic acid and yeast on morpho-physiological and yield characteristics of maize plant (Zea mays L.) under water deficit conditions, Fresen. Environ. Bull. 26(12), 7372-7383.

[4] Hafez, E.M., Abdelaal, Kh.A.A (2015) Impact of Nitrogen fertilization levels on morphophysiological characters and yield quality of some Maize hybrids (*Zea mays* L.), Egyption J. Agron. 37 (1), 35- 48.

[5] EL Sabagh, A., Hossain, A., Barutçular, C., Abdelaal, Kh.A.A., Fahad, S., Anjorin, F.B., Islam, M.S., Ratnasekera, D., Kizilgeçi, F., Yadav, S., Yıldırım, M., Konuskan, O., Saneoka, H. (2018) Sustainable maize (*Zea mays* L.) production under drought stress by understanding its adverse effect, Survival mechanism and drought tolerance indices, Journal of Experimental Biology and Agricultural Sciences. 6 (2), 282-295.

[6] Abdelaal, Kh.A.A., Hafez, Y.M., El-Afry, M.M., Tantawy, D.S., Alshaal, T. (2018) Effect of some osmoregulators on photosynthesis, lipid peroxidation, antioxidative capacity and productivity of barley (*Hordeum vulgare* L.) under water deficit stress Environmental Science and Pollution Research. 25, 30199–30211

[7] Abdelaal, Kh.A.A., Attia, K.A., Alamery, S.F., El-Afry, M.M., Ghazy, A.I., Tantawy, D.S., Al-Doss, A.A., El-Shawy, E.E., Abu-Elsaoud, A., Hafez, Y.M. (2020) Exogenous Application of Proline and Salicylic Acid can mitigate the Injurious Impacts of Drought Stress on Barley Plants Associated with Physiological and Histological Characters. Sustainability. 12, 1736.

[8] Abdelaal, Kh.A.A. (2015) Effect of Salicylic acid and Abscisic acid on morpho-physiological and anatomical characters of faba bean plants (*Vicia faba* L.) under drought stress. Journal of Plant Production Mansoura University. 6, 1771-1788.

[9] Abdelaal, Kh.A.A., Hafez, Y.M., EL Sabagh, A., Saneoka, H. (2017) Ameliorative effects of Abscisic acid and yeast on morpho-physiological and yield characteristics of maize plant (*Zea mays* L.) under drought conditions. Fresen. Environ. Bull. 26, 7372-7383.

[10] Abdelaal, Kh.A.A., Hafez, Y.M., Badr, M.M., Youseef, W.A., Esmaeil, S.M. (2014) Biochemical, histological and molecular changes in susceptible and resistant wheat cultivars inoculated with stripe rust fungus Puccinia striiformis f.sp. tritici, Egyptian Journal of Biological Pest Control. 24, 421-429.

[11] Hafez, Y.M., Abdelaal, Kh.A.A. (2015) Investigation of susceptibility and resistance mechanisms of some Egyptian wheat cultivars (*Triticum aestivum* L.) Inoculated with *Blumeria graminis* f. sp. *tritici* Using certain biochemical, Molecular characterization and SEM, Journal of Plant Protection and Pathology Mansoura Univ. 6, 431- 454.

[12] Abdelaal, Kh.A.A., Omara, R.I., Hafez, Y.M., Esmail, S.M., EL Sabagh, A. (2018) Anatomical, biochemical and physiological changes in some Egyptian wheat cultivars inoculated with *Puccinia graminis* f.sp. *tritici*, Fresen. Environ. Bull. 27, 296-305.

[13] Esmail, S.M., Omara, R.I. Abdelaal, Kh.A.A., Hafez, Y.M. (2019) Histological and biochemical aspects of compatible and incompatible wheat-Puccinia striiformis interaction. Physiological and Molecular Plant Pathology. 106, 120-128.

[14] Hafez, Y., Emeran, A., Esmail S., Mazrou, Y., Abdrabbo, D., Abdelaal, Kh.A.A. (2020) Alternative treatments improve physiological characters, yield and tolerance of wheat plants under leaf rust disease stress. Fresen. Environ. Bull. 29(6), 4738-4748.

[15] Omara, R.I., El-Kot, G., Fadel, F.M. Abdelaal, Kh.A.A., Saleh, E.M. (2019) Efficacy of certain bioagents on patho-physiological characters of wheat plants under wheat leaf rust stress Physiological and Molecular Plant Pathol.. 106, 102-108.

[16] Omara, R.I., Abdelaal, Kh.A.A. (2018) Biochemical, histopathological and genetic analysis associated with leaf rust infection in wheat plants (*Triticum aestivum* L.) Physiological and Molecular Plant Pathology. 104, 48-57.

[17] Dangwal, L.R., Singh, A., Singh, T., Sharma, A., Sharma, C. (2010) Common weeds of Rabi (winter) crops of tehsil Nowshera, District Rajouri (Jammu & Kashm ir), India. Pak. J. Weed Sci. Res. 16(1), 39-45.

[18] Pannacci, E., Onofri, A. (2016) Alternatives to terbuthylazine for chemical weed control maize. Communications in Biometry and Crop Sci. 11(1), 51-63.

[19] Tahir, M., Javed, M.R., Tanveer, A., Nadeem, M.A., Bukhari, S.A.H., Rehman, J. U. (2009) Effect of different herbicides on weeds, growth and yield of spring planted maize *(Zea mays* L.). Pak. J. of Life Soc. Sci. 7 (2), 168-174.

[20] El-Metwally, I.M., El-Salam, M.S.A., Tagour, R.M.H., Abouziena, H.F. (2012) Efficiency of Plant population and reduced herbicides rate on maize productivity and associated weeds. J. of Appl. Sci. Res. (April). 2342-2349.

[21] Kandil, E.E.E., Kordy, A.M. (2013) Effect of hand hoeing and herbicides on weeds, growth, yield and yield components of maize (*Zea mays* L.). J. Appl. Sci. Res. 9(4), 3075-3082.

[22] Sharara, F.A., El-Shahawy, T.A., El-Rokiek, K.G. (2005) Effect of some novel herbicides on the controlling weeds associated with maize plants. J. Agron. 4(2), 88-95.

[23] Patel, V.J.P.N., Upadhyay, J.B., Patel, B.D. (2006) Evaluation of herbicide mixtures for weed control in maize (*Zea mays* L.) under middle Gujarat conditions. The J. Sci. 2 (1), 81-86.

[24] Chikoye, D., Udensi, U.E., Lum, F.A. (2005) Evaluation of a new formulation of atrazine and metolachlor mixture for weed control in maize in Nigeria. Crop Protection. 24, 1016-1020.
[25] Ashton, F.M., Crafts, A.S. (1981) Mode of action of Herbicides, Wily- Inter Science. Publication John Wiley &Sons. Second Edition.
[26] Tackholm, V. (1974) Student,s Flora of Egypt. 2nd ed. Cairo University Cairo. 888
[27] A.O.A.C. (2000). Methods of analysis association of official agriculture chemistry. 17th Ed. Washington D.C.
[28] Steel, R.G.D., Torrie, J.H. (1980) Principles and Procedures of Statistics. Mc. Graw Hill Book company Inc. NewYork. 481.
[29] Gomez, K.A., Gomez, A.A. (1984) Statistical Procedures for Agricultural Research (2nd Ed.). John Wiley and Sons New York. 680
[30] Roy, C., Guggiari, F., Compagnon, J.M. (2002) Smetolachlor; herbicide for maize, sorghum and sunflower. Syngenta Agro. SAS Phytoma France. 548, 51-53.
[31] Skoko, H., Zivanovic, D. (2002) Weed control byherbicide in maize under agro-ecologicalconditions of Semberia. Weed Sci. Society of Bosnia and Herzegovina. 3, 99-105.
[32] Vanbiljon, J.J., Hugo, K.J., Vandermerve, C.J., vanmark, L.J. (2007) Pre-emergence weed control with metolachlor/ flumetsulum / mixtures. South African J. Plant and Soil. 16, 42-95.
[33] Haseeb, A., Shafi, M., Liaqat, W., Jan, M.F., Anjum, M.M., Ali, N., Rehan, W. (2018) Maize performance in response to tillage and weed control methods Pure Appl. Biol. 7(2), 518-526.
[34] Soren, C., Chowdary, K.A.G. Sathish, B., Patra, C. (2018) Weed Dynamics And Yield Of Rabi Maize (Zea Maysl.) As Influenced By Weed anagement Practices. J. Exp. Biology and Agricultural Scie. 6(1), 150–158
[35] Stefanovic, L., Milivojevic, M., Husic, I., Samic, M., Hojka, Z. (2004) Selectivity of the sulfonylurea herbicide group in the crop of commercial KL maize inbred lines. Institute-ze-Kukuruz, Herboglia, Serbis and Montenegro. 5(1), 53-63.
[36] Tanveer, A., Ayub, M., Ali, M., Ahmed, R., Ayub, M. (1999) Weed crop competition in maize in relation to row spacing and duration. Pak. J. of Biol. Sci. 2, 363-364
[37] Adigun, J.A. (2001) Control of weeds with preemergence herbicides in maize-pepper mixture in the Nigerian northern Guinea Savanna. J. Sustainable Agric. Environ. 3, 378-383.
[38] Shah, W.A., Khan, M.A., Khan, N., Zarkoon, M.A., Bakht, J. (2003) Effect of weed management at various growth stages on the yield and yield components of wheat (Triticum aestivum L). Pak. J. Weed Sci. Res. 9(2), 41-48.
[39] Baye, Y., Bouhache, M. (2007) Competition between silver leaf night shade (Solanum elaeagnifolium Cav.). Bulletin-DEPP EPPO Bulletin. 37, 129-131.
[40] Raga'a, O., Osman, F.A., Ahmed, F., Kalil, A.M., Ali S. (1988) Effect of some herbicides as plant growth regulators on the chemical composition of Zea maize grains. Food Chemistry. 28(3), 167-1760.
[41] Soliman, I.E., Hamza, A.M. (2014) Effect of some weed control treatments on yield associated weeds and chemical composition for maize grains. J. Plant Production Mansoura Univ. 5 (10), 1729-1743.
[42] Din, W.U., Naveed, K., Iqbal, S., Ali, A., Khan, S.M., Ali, N., Hussain, I. (2016) Effect of different weeding intervals and methods on the yield and yield components of maize hybrid. J. Agric. Bio. Sci. 11(3), 100-106.
[43] Tesfay, A., Amin, M., Mulugeta, N. (2014) Management of weeds in maize (Zea mays) through various pre and post emergency herbicides. Adv. Crop Sci. Tech. 2(5), 151-155
[44] Ahmad H., Shafi, M., Liaqat, W., Jan, M.F., Anjum, M.M., Ali, N., Rehan, W. (2018) Maize performance in response to tillage and weed control methods. Pure Appl. Biol. 7(2), 518-526.

Received: **13.12.2020**
Accepted: **02.02.2021**

CORRESPONDING AUTHOR

Khaled A Abdelaal
Plant Pathology and Biotechnology Lab.,
Agric. Botany Dept.,
Kafrelsheikh University,
33516 – Egypt.

e-mail: khaled_elhaies@yahoo.com

© by PSP Volume 30– No. 05/2021 pages 5350-5355 Fresenius Environmental Bulletin

A NOVEL MEASUREMENT METHOD OF KEY NODES IN ECOSYSTEM PUBLIC OPINION COMMUNICATION NETWORK

Huaibin Qin*

College of Information Science and Technology, Shihezi University, Shihezi 832003, China

ABSTRACT

In the ecosystem public opinion communication network composed of individual nodes and their propagation paths, each network node is not equally important in the process of ecological public opinion dissemination. It is of great significance for the control and management of ecological public opinion communication network to study and analyze the key network nodes and their mutual ecological public opinion communication relations in the ecological public opinion communication network. Based on the investigation of the complex network environment theory, this paper constructs the ecological public opinion communication network map. This paper measures the nodes of ecological public opinion communication network from the aspects of degree centrality, betweenness centrality, kernel centrality, eccentricity centrality, compactness centrality and eigenvector centrality. Finally, a simplified diagram of part of the structure of the ecological public opinion communication network is analyzed. The verification results show that different measurement methods and indicators can better measure and identify the key nodes in the ecological public opinion communication network from different angles. The results provide a reference for researchers and managers to analyze the ecological public opinion communication network and identify key nodes from the local and overall perspectives.

KEYWORDS:
Ecosystem, Complex network environment, Ecological public opinion communication network, Key nodes, Measurement method

INTRODUCTION

With the rapid development of China's society, people pay more and more attention to the ecological environment, and all kinds of ecological public opinion information is also growing at a certain speed. Some ecological public opinion information can affect the formulation of national policies, and some ecological public opinion information may be used by hostile forces [1-3].

Ecological public opinion communication network is composed of many individual nodes. In addition to its own characteristics and functions (such as making ecological public opinion information, judging ecological public opinion information, etc.), the individual node also transmits information with other individual nodes of ecological network, as shown in Figure 1. In the process of studying the ecological public opinion communication network, each individual of ecological public opinion communication is abstracted as a node, and the ecological public opinion communication between each two individuals is abstracted into a huge network. Research shows that the ecological public opinion communication network is a complex network environment with the characteristics of self-organization, scale-free and small world [4-7].

In the complex network environment structure composed of ecological network nodes. Due to the different function of each network node, the impact on the whole network is different. Some key network nodes have a greater impact on the ecological public opinion communication network, and even become the key nodes affecting the overall communication performance of the ecological public opinion communication network [8-9]. It is of great significance for the control and management of ecological public opinion communication network to study and analyze the key network nodes and their mutual ecological public opinion communication relations in the ecological public opinion communication network.

The research route of this thesis is shown in Figure 2. Firstly, centrality, an index to judge the key network nodes in the ecological public opinion communication network, is given. Secondly, on this basis, this paper gives the methods to judge the key network nodes in the ecological public opinion communication network, such as degree centrality, betweenness centrality, kernel centrality, eccentricity centrality, compactness centrality and eigenvector centrality. Finally, taking an ecological public opinion communication network as an example, the specific verification is carried out.

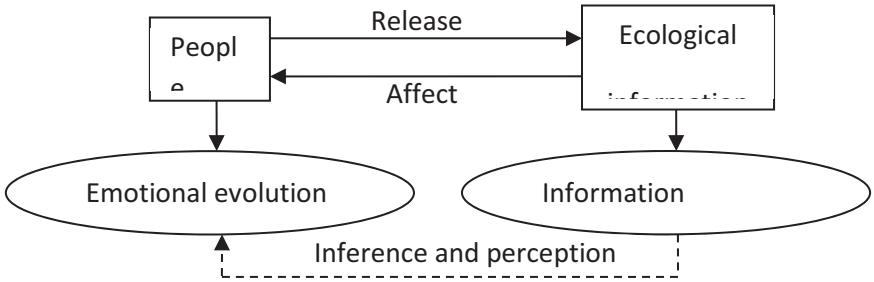

FIGURE 1
Information interaction of ecological public opinion communication network.

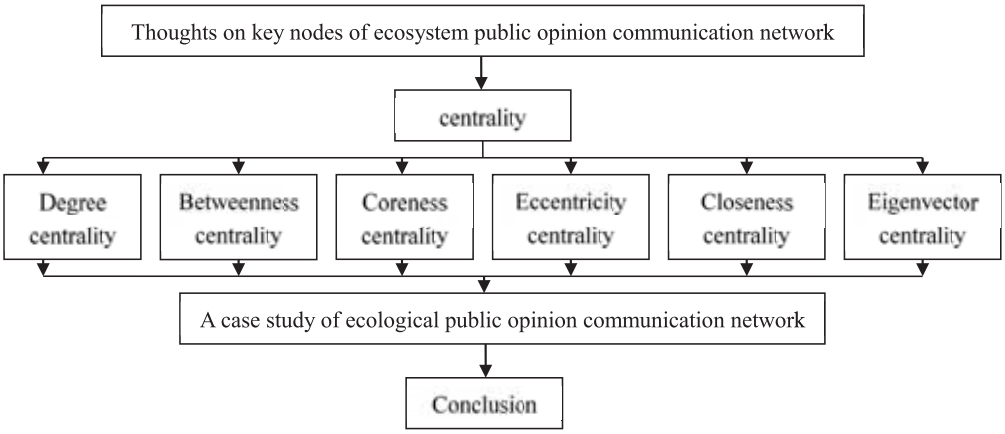

FIGURE 2
Research route of thesis.

MATERIALS AND METHODS

Ecological public opinion communication network. Centrality. Centrality is an indicator to judge the importance of nodes in the ecological network [10]. In the study of ecological public opinion communication network, each node of ecological public opinion communication network is assigned an important function value H(x). The larger the value of H(x), the more central node x is, the larger the influence range is. In the public opinion communication network of an ecosystem as shown in Figure 3, node a is the central node for the network because node a is in the center of the network.

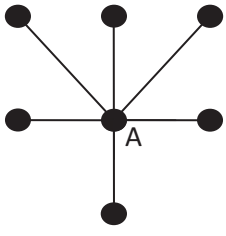

FIGURE 3
Public opinion communication network of an ecosystem.

Centrality is defined in definition 1:

Equation (1) ecological public opinion communication network is abstracted as a graph G = (V, E, f, H), among them:

1. $V=\{V_1, V_2, \ldots, V_n\}$ is the node set of ecological public opinion communication network;

2. $E=\{E_1, E_2, \ldots, E_n\}$ is the set of propagation edges among nodes of ecological public opinion communication network;

3. $F = \{< V_i, V_j >\}$ is a relational set, where $V_i \in V$, $V_j \in V$, and $i \neq j$;

4. For any node u and v, if H(u) > H(v), then the network node u is considered to be more important than the network node v;

5. N = | V | is the total number of ecological public opinion communication network nodes, and L = | E | is the total number of communication sides;

6. The propagation edge E_i in E corresponds to the network node pair < u, v > in V;

7. If the network node pairs < u, v > and < v, u > in E are the same propagation side, then it is undirected ecological public opinion communication network, otherwise, it is directed ecological public opinion communication network; if the length of all communication sides in E is 1, it is no right ecological public opinion transmission network, otherwise

it is weighted ecological public opinion transmission network [10-11].

In order to simplify the research, the following networks of this paper are all non directional and unauthorized ecological public opinion communication networks.

The centrality measurement method of ecological public opinion communication network nodes. This paper mainly measures the ecological public opinion communication network nodes from the degree centrality, the intermediate centrality, the core centrality, the eccentricity centrality, the compactness centrality and the eigenvector centrality.

Key node measurement method. The degree centrality of network nodes. The degree of nodes in ecological public opinion communication network: the degree k_v of node v refers to the number of nodes directly transmitting ecological public opinion information with the node. The greater the degree of node v, the greater the impact of the node in the whole ecological public opinion communication network [12].

The degree of network node is defined as :

$$k_v=\sum_{l\in E}\delta_l^v \qquad (1)$$

Among them, δ_l^v is 1, when f (L) = < X, Y >, there is v = X or v = Y; otherwise, it is 0. That is,

$$\delta_l^v=\begin{cases}1, if\ v=f(l)\\0, if\quad not\end{cases} \qquad (2)$$

The betweenness centrality of network nodes. Betweenness of nodes in the ecological public opinion communication network: the betweenness of node v refers to the proportion of the number of paths passing through the node v in the total number of shortest paths in the ecological public opinion communication network [11-13].
The betweenness of network nodes is defined as:

$$C_B(v)=\sum_{s\neq v\neq t\in V}\frac{\delta_{st}(v)}{\delta_{st}} \qquad (3)$$

Among them, δ_{st} is the number of shortest propagation paths from network node s to network node t, and $\delta_{st}(v)$ is the number of shortest propagation paths passing through network node v in the shortest propagation path from network node s to network node t.

The coreness centrality of network nodes. The coreness of nodes in the ecological public opinion communication network: The coreness of node v is used to express the depth of node v in the ecological public opinion communication network. The larger the value is, the greater the network depth is. In the ecological public opinion communication network, such nodes have high centrality and importance, and also have indirect dependence and communication relationship with a large number of other network nodes.

The k-core of an ecological public opinion communication network refers to the remaining sub network structure after repeatedly removing the nodes whose degree is less than or equal to k. If a network node v exists in the k-core and is removed from the (k + 1) - core, then the number of cores of the network node v is k. It is found that the coreness of network nodes with ownership degree of 1 must be 0, and the maximum of all network nodes is called the core number of ecological public opinion communication network [14-16].

The centrality of eccentricity of network nodes. The eccentricity of nodes in ecological public opinion communication network: the eccentricity of node v refers to the maximum value in the shortest propagation path from node v to all other nodes. The eccentricity of network node v is defined as the function ec (v). The larger the eccentricity, the more the network node v deviates from the center of the ecological public opinion communication network, the less important it is and the smaller the influence range. The reciprocal of eccentricity of network node v is taken as its centrality value.

The centrality of eccentricity of network nodes is defined as [9, 17]:

$$L_{ec}(v)=\frac{1}{ec(v)} \qquad (4)$$

Among them, $ec(v)=\max\{d(v,u): u\in V\}$, $V=\{V_1, V_2, \ldots, V_n\}$ is the set of network nodes, and d (v, u) is the shortest propagation path length from network node v to network node u.

The centrality of closeness of network nodes. Closeness of nodes in ecological public opinion communication network: the compactness of node V is the reciprocal of the sum of the shortest propagation path length from node V to other network nodes. In the ecological public opinion communication network, the greater the sum of the shortest propagation path length between network node V and other network nodes, the influence of the network node on other network nodes is lower [18-19].

The centrality of closeness of network nodes is defined as:

$$L_{cl}(v)=\frac{1}{\sum_{u\in V}d(v,u)} \qquad (5)$$

Among them, V = {V_1, V_2, ... , V_n} is the set of network nodes, and d (v, u) is the shortest propagation path length from network node v to network node u.

The centrality of eigenvectors of network nodes. Eigenvector of network node of ecological public opinion dissemination: centrality of feature vector of network node v refers to the importance of network node v in the whole ecological public opinion communication network, which is related to the importance of other network nodes connected by network node v. The eigenvectors of network nodes are characterized by a set of linear equations. The eigenvectors corresponding to the maximum eigenvalue λ (λ is a constant) of the equations are the central values of each network node [20].

The central value of the eigenvector of the network node is defined as:

$$L_{ei}(v)= \frac{1}{\lambda}\sum_{u\in V}^{n} A_{v,u}L_{ei}(u) \qquad (6)$$

Among them, V={V_1, V_2, ... , V_n} is the set of network nodes, $A_{v,u}$ is the adjacency matrix of ecological public opinion communication network. If the network node v and the network node u have ecological public opinion propagation connection edge, then $A_{v,u}$ is 1, otherwise $A_{v,u}$ is 0.

RESULTS

Among the above measurement methods, each method measures the centrality of network nodes from different angles. For the same ecological public opinion communication network structure, the measurement results of different measurement methods may be quite different. As an example, Figure 4 shows the simplified structure of an ecological public opinion communication network, in which seven network nodes A, B, C, D, E, F, G are included. According to the above different measurement methods, the measurement results are shown in Table 1.

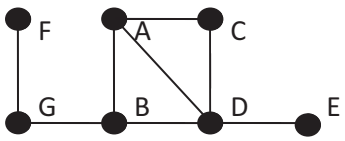

FIGURE 4
Simplified diagram of part structure of an ecological public opinion communication network.

The advantage of the degree centrality value of network node is simple and intuitive, but the disadvantage is that the measurement value only reflects the local nature of the network node in the ecological public opinion communication network. As shown in Figure 4, the degree values of network node A and network node B are 3. From the perspective of degree centrality, A and B are equally important. However, if network node A is deleted, the ecological public opinion dissemination network is still connected. If the network node B is deleted, the ecological public opinion communication network will become disconnected. From this point of view, the control and management of network node B is more important than the management of network node A.

TABLE 1
Measurement results.

Network node	K	C_B	Coreness	L_{ec}	L_{cl}	L_{ei}
A	3	1.50	2	0.33	0.10	0.51
B	3	8.00	2	0.50	0.11	0.45
C	2	0.00	2	0.25	0.08	0.38
D	4	6.50	2	0.33	0.11	0.56
E	1	0.00	1	0.25	0.07	0.20
F	1	0.00	1	0.25	0.06	0.07
G	2	5.00	1	0.33	0.08	0.19

The value of the betweenness centrality of the network node reflects the role and influence of the network node in the whole ecological public opinion communication network. The disadvantage is that the time complexity is high [21-22]. In Figure 4, the degree values of network nodes A, B, and D are 3, 3, and 4 respectively, but the dielectric values are 1.50, 8.00, and 6.50, respectively. From the perspective of betweenness centrality, the impact of network node B on the whole ecological public opinion communication network is greater than that of network nodes A and D.

The centrality value of the coreness of the network node directly reflects the depth of the network node in the whole ecological public opinion communication network structure. The disadvantage of this method is that if the network structure of ecological public opinion communication presents tree network structure, it can not adapt to it. In Figure 4, from the perspective of network organization and centrality, network nodes A, B, C, D are at the core level of ecological public opinion communication network structure, and network nodes E, F, G are at the non core level of ecological public opinion communication network structure.

The centrality of the eccentricity of network nodes can reflect the relationship between the current network nodes and the network center of ecological public opinion communication. The disadvantage is that the centrality of eccentricity only considers a single propagation path. In Figure 4, the eccentricity of network nodes A, D and G are all 0.33, indicating that network nodes A, D and G are also close to the network center of ecological public opinion dissemination. Although network node C is at the core level of ecological public opinion communication network structure, and the degree value and network node G are both 2, network node G is closer to the center of ecological public opinion communication network than network node C.

The advantage of the centrality of closeness of network nodes is that it can reflect the propagation path length relationship between the current network nodes and the center of the node dense area of the ecological public opinion communication network [23-24]. The disadvantage is that the time complexity is high, and it is not suitable for dynamic or random networks. In Figure 4, the closeness values of network nodes C and G are both 0.08, which indicates that from the centrality of closeness, the propagation paths of network nodes C and G from the center of ecological public opinion propagation network are the same. In this case, network node C and network node G are equally important and have the same influence.

The advantage of centrality of feature vectors of network nodes is that it fully considers the importance of neighbor network nodes connected with current ecological network nodes. The disadvantage is that the time complexity of calculation is relatively high. In Fig. 4, although the degree value and compactness value of network node C and network node G are the same, the neighbor network node of network node C is more important than that of network node G (the center value is higher). From the centrality of eigenvector, network node C is more important than network node G.

CONCLUSIONS

Based on the theory of complex network environment, according to the centrality idea, this paper studies the measurement method of key nodes in the ecological public opinion communication network, and studies the degree centrality, betweenness centrality, coreness centrality, eccentricity centrality, closeness centrality and eigenvector centrality are studied and verified by examples. The verification results show that each measurement method has a strict mathematical theoretical basis, and different measurement methods and indicators can measure and identify the key nodes in the ecological public opinion communication network from different angles. The results provide a reference for researchers and managers to analyze the rationality of ecological public opinion communication network and identify key nodes from the local and overall perspectives. However, the above case analysis and comparison results of different methods also show that for the same ecological public opinion communication network, the results of different centrality measurement methods may be different, and there may be greater differences. Therefore, in the follow-up study, the research group intends to continue to study from the following two aspects: first, for different ecological public opinion communication networks, according to the specific situation, give the measurement method of key network nodes suitable for the characteristics of ecological public opinion communication network; second, according to the advantages and disadvantages of each measurement method and index, a measurement model combining multiple measurement methods is proposed.

ACKNOWLEDGEMENTS

This work was not supported by any funds. We want to thank all the techniques who have helped this research and the authors of the references.

REFERENCES

[1] Ma, Y., Du, Y. (2018) Research on the Evolution of Public Opinion Based on the Deffuant Model of Complex Networks. Journal of Intelligence. 37(6), 91-95, 159.
[2] Erbas, C., Erbas, B. (2015) Modules and Transactions: Building Blocks for a Theory of Software Engineering. Science of Computer Programming. 101, 6-20.
[3] Breivold, H., Cmkovic, I., Larsson, M. (2012) A Systematic Review of Software Architecture Evolution Research. Information and Software Technology. 54(1), 16-40.
[4] Iliopoulou, C., Kepaptsoglou, K. (2019) Integrated Transit Route Network Design and Infrastructure Planning for On-Line Electric Vehicles. Transportation Research Part D: Transport and Environment. 77, 178-197.
[5] Gao, B., Wang, L. (2019) Propagation Model and Analysis Method of Network-derived Public Opinion. Information Studies: Theory and Application. 42(3), 166-170, 165.
[6] Xie, J., Qin, Q., Wu, W. (2019) Case Reasoning Model of Network Public Opinion Based on Ontology. Journal of Intelligence. 38(1), 79-86.
[7] Newman, M., Girvan, M. (2004) Finding and Evaluating Community Structures in Networks. Physical Review. 69(2), 26113.
[8] Seol, K., Kim, J., Baik, D. (2016) Common Neighbour Similarity-Based Approach to Support Intimacy Measurement in Social Network. Journal of Information Science. 42(2), 128-137.
[9] Dong, S., Deng, Y., Huang, Y. (2017) SEIR Model of Rumor Spreading in Online Social Network with Varying Total Population Size. Communication in Theoretical Physics. 68(4), 545.
[10] Peng, X. (2017) Methods for the Identification of Key Nodes in Bionetworks. Journal of Biology. 34(8), 104-109.
[11] Diao, C. (2019) Complex Network-Based Time Series Remote Sensing Model in Monitoring the Fall Foliage Transition Date for Peak Coloration. Remote Sensing of Environment. 229, 179-192.

[12] Fauzi, M. (2019) Word2Vec Model for Sentiment Analysis of Product Reviews in Indonesian Language. International Journal of Electrical and Computer Engineering. 9(1), 525.
[13] Dubey, T., Jain, A. (2019) Sentiment Analysis of Keenly Intellective Smart Phone Product Review Utilizing SVM Classification Technique. 2019 10th International Conference on Computing, Communication and Networking Technologies (ICCNT). IEEE. Kanpur, India, 1-8.
[14] Wang, J., Wang, Y. (2015) SIR Rumor Spreading Model with Network Medium in Complex Social Networks. Chinese Journal of Physics. 53(1), 020702-02710.
[15] Sun, J., Gao, J., Hu, X. (2018) Research of the Prediction of Network Public Opinion Based on Improved Attention Model. Journal of Intelligence. 37(11), 116-121.
[16] Chen, B., Wang, X., Li, Y., Yang, Q., Li, J. (2019) Energy-induced Mercury Emissions in Global Supply Chain Networks: Structural Characteristics and Policy Implications. Science of The Total Environment. 670, 87-97.
[17] Lan, Y., Wang, F., Dong, X. (2016) Study on the Heat Model of Public Crisis of Network Public Opinion. Information Science. 35(2), 32-36.
[18] Qiu, X., Zhao, L., Wang, J. (2016) Effects of Time-Dependent Diffusion Behaviors on the Rumor Spreading in Social Networks. Physics Letters A. 380(24), 2054-2063.
[19] Zhang, H. (2018) Node Importance Ranking of Complex Networks identified by Cohesion and Closeness Centrality. Computer and Digital Engineering. 46(10), 2053-2056.
[20] Wang, X., Wang, B., Xia, Y. (2017) Evaluation Method of Node Centrality for Brain Network Based on Betweenness Centrality and K-Shell. Computer Engineering and Application. 53(11), 44-49.
[21] Duan, X., Jin, G. (2018) Emergy Evaluation of Complex Network Center Nodes under Cloud Computing. Computer Simulation. 35(11), 352-355.
[22] Qin, H., Zheng, Y., Guo, L. (2019) Description and Quality Assessment of Software Architecture Based on Complex Network Theory. Journal of Shihezi University (Natural Science). 37(4), 259-264.
[23] Fellini, S., Salizzoni, P., Soulhac, L., Ridolfi, L. (2019) Propagation of Toxic Substances in the Urban Atmosphere: A Complex Network Perspective. Atmospheric Environment. 198, 291-301.
[24] Chatfield, A., Scholl, H., Brajawidagda, U. (2013) Tsunami Early Warnings via Twitter in Government: Net-Savvy Citizen's Co-Production of Time-Critical Public Information Services. Government Information Quarterly. 30(4), 377-386.

Received: **13.12.2020**
Accepted: **20.01.2021**

CORRESPONDING AUTHOR

Huaibin Qin
College of Information Science and Technology
Shihezi University
Shihezi 832003 – China

e-mail: hbqin1023@163.com

© by PSP Volume 30– No. 05/2021 pages 5356-5361 Fresenius Environmental Bulletin

THE EVALUATION OF INDIGENOUS GRAPEVINE PRODUCTION KNOWLEDGE BY SOIL CARBON IN A SEMI-ARID REGION SOUTHEASTERN TURKEY

Gokhan Buyuk[1,*], Ceren A Bayram[1], Erhan Akca[2]

[1]Adiyaman University, Faculty of Agriculture, 02040, Kahta, Adiyaman, Turkey
[2]Adiyaman University, School of Technical Programs, 02040, Adiyaman, Turkey

ABSTRACT

Not only nature but human activities also provide ecosystem services alike agriculture and agroforestry which both host a wide range of ecosystem services besides providing food and fiber for humans and animals. The efficiency of ecosystem services of a cultivated land depends on agricultural management choices. Current conventional land management approaches, that are generally unsustainable by causing various environmental problems such as pollution, loss of biodiversity and organic carbon, need to be well-defined for designing land use for agricultural production. This manuscript focuses on tillage and crop-pattern effect on soil organic carbon, which is a vital component not only for enhancing soil quality but for mitigation of climate change and desertification. The monitored plants for 10-year were peach (Prunus persica), apricot (Prunus armeniaca), cherry (Prunus avium L.), quince, pear, plum, grapevine, wheat, barley and pine that are under various land management methods namely tillage, minimum and no-tillage, cover crops, mineral/organic fertilization. The soil organic carbon trends revealed that in the studied semiarid climate zone for rainfed cultivation grapevine, and for irrigated cropping apricot had the highest organic carbon accumulation potential along with optimal C:N ratio.

KEYWORDS:
Soil organic carbon, C:N ratio, land management, semi-arid region

INTRODUCTION

Agriculture in general reduce natures ecosystem services by causing pollution, soil compaction, loss of soil biodiversity and organic matter due to unproper land management [1]. Among these soil threats summarized by FAO and ITPS [2], soil organic carbon loss is the crosscutting parameter of climate, land degradation and biodiversity. Thus, mitigating against agriculture's negative impact on organic carbon is crucial both for food security and global environmental threats. The soil organic carbon (SOC) and nitrogen (N) determine agricultural production by effecting several soil properties such as water holding capacity, nutrient balance, microorganism activity and soil aggregation [3]. Moreover, its role on plant growth, fertility and several chemical and physical processes are unique [4]. The high SOC dynamics reduces greenhouse gas emissions that is accepted as the main climate change mitigation tool [5]. Climate is one of the driving forces that determine soil organic carbon accumulation. Humid areas provide more favorable conditions for SOC increase whereas in semi-arid and arid lands enhancing SOC is quite challenging [6]. Studies show that even in 50 years of protection in an arid land soil carbon only increased less than 1% [7] which is far lower in agricultural lands [8]. Soil organic carbon increase in agricultural lands necessitates appropriate soil management particularly tillage type and crop pattern. In 20th century, intensive continuous tillage applications and the density of greenhouse gases in the world causes a decrease in SOC stock varied from 42 to 78 gigatons of carbon [9]. One of the main prerequisites for the sustainable management of the agricultural system is the maintaining the land cover. Several crop types are tested for achieving optimal protection and yield balance in agricultural lands for increasing SOC [10]. Legumes determined as the main crop providing high soil organic carbon input. However, in some agro-ecological zones legumes cultivation are not profitable due to volatile market prices and farmers choose other crops [11]. So, determining appropriate crop or crops which both secure organic carbon enhancement for the soil and income for the farmers would be an utmost goal for sustainable land management [10]. The success of this management strategy depends on the selection of adequate crop pattern/type that meet the criteria for adaptation to the climate change and natural conditions of the cultivation area [12,13]. Although, agricultural practices in general decrease soil organic carbon as manifested by Novara et al. [14], the conversion of natural vegetation to vineyard and olive increased SOC to levels by 27% to 50%.

Therefore, crop pattern should be well-planned for C sequestration in cultivated lands. In semi-arid parts of the world, which are forecasted as the most

prone areas to climate change and desertification, increasing soil carbon is challenging due to lack of moisture and biomass input [15]. Several studies reported that without farm manure or chemical fertilizer input increasing soil carbon is almost unachievable [16]. For example, in semi-arid loess region of China, manure, nitrogen and phosphorous application increased soil carbon sequestration by 30.6% [17]. Determined up to 80% increase in soil total organic carbon under conservation agriculture coupled with rice-wheat-mung bean system following 6 years of treatment [18]. In this study, for providing a useful information for farmers and decision makers for sustainable land management a long-term field management effect on SOC, N and related soil properties on different plantations were analyzed and evaluated in a semi-arid area which presents the app. 15% of the Earth's land surface.

In this study, organic carbon and C/N ratios, which are produced with different patterns of organic farming practices and accumulated after 10-years, were determined on conventional agricultural lands in Adıyaman (semi-arid climate zone) located in the upper basin of the South East Anatolia of Turkey with an ultimate aim of determining the suitable crop that can be employed for mitigating climate change in this fragile region.

MATERIALS AND METHODS

The site is situated in 37S 449812.29 E, 4181196,65N at an altitude of 700m from sea level with mean annual temperature of about 17.3°C, and precipitation of 674 mm. The evaporation varies from 1000mm to 1250mm in the region from May to October, which makes the region a semi-arid area [19]. The study evaluated the monitoring soil analyses results of 2019 with the ones in 2009 at Adıyaman University Research Feld (Adıyaman, SE Turkey) on 13 ha land with various crop covers (apricot, plum, cherry, quince, pear, peach, apple, vineyard, wheat, barley, vegetables and pine). Before agricultural production, soil organic carbon in the field was determined as 19.2 t C ha-1 at a depth of 0-20 cm and 15.8 t C ha-1 at a depth of 20-40 cm. The C/N ratio is calculated as 23.6 at 0-20 cm and 21.8 at 20-40 cm depth.

Barley, wheat and vegetables are under conventional tillage whereas orchards are cultivated with minimum tillage. Orchards are grown without fertilizer application while 80 kg P_2O_5 ha-1 and 150 kg N ha-1 are provided to wheat and barley, and 20 t ha-1 farm manure is applied to vegetables. The laboratory analyzes were made in 3 replications and the averages of the results were given.

Disturbed and undisturbed soil samples from various crop covers were collected from 0-20 cm, and 20-40 cm depths in 2019 following harvest of vegetables and grains and compared with the analysis undertaken in 2009.

The soil of the experimental field is classified as Calcaric Leptosol Colluvic [20]. Soils were air-dried, ground, and sieved to 2 mm. Soil analyses of EC (dS.m-1), pH (1:1 saturated paste), carbonate (%), texture (% sand-silt-clay), organic carbon (t C ha-1) were undertaken according to analyses described in Soil Survey Field and Laboratory Methods Manual [21].

RESULTS

The studied soils do not have serious limitations for plant growth such as steep slopes, shallow depth, low organic matter, alkaline reaction, and salinity for plant growth. The texture of the soil samples varies from clay loam and loam with a pH of 7.64-7.92, organic matter: 2.7-4.6%, total N:0.13-0.89%, Olsen-P=1.8-5.9 kg da^{-1}, CaCO3: 8.6-38.9%, EC:0.45-0.90 dsm^{-1}. For assessing soil organic carbon status in various crop covers and tillage methods soil properties, vegetation cover and tillage vs soil organic carbon were determined.

Soil Organic Carbon and Soil Properties. As, soil properties of texture, pH, carbonate content, nitrogen, phosphorous and EC are effective soil carbon dynamics, they were compared for determining each parameter input on SOC.

TABLE 1
Relationships between soil and soil properties (r)

	Organic Matter	$CaCO_3$	Phosphorus	Texture	pH	EC
$CaCO_3$	0.562*					
Phosphorus	-0.293	0.096				
Texture	0.549*	0.048	-0.628*			
pH	-0.318	0.649*	-0.527	0.351		
EC	0.055	-0.273	-0.421	0.796**	0.511	
Nitrogen	-0.429	-0.136	0.285	-0.431	-0.13	-0.522

*Correlation is significant at the 0.05 level; * Correlation is significant at the 0.01 level

Relationships Between Some Soil Properties. It has been determined that there are positive and negative relationships between some physical and chemical properties of the soils (Table 1). Significant positive relationship at the level of 5% between calcium carbonate and organic matter (0.562); significant positive relationship at the level of 5% between texture and organic matter (0.549); significant positive relationship between pH and CaCO3 at the level of 5% (0.649) were determined. There was a significant negative correlation (-0.628) between texture and phosphorus at the 5% level and a significant positive correlation (0.796) at 1% level between EC and texture. Similar results were obtained by various studies [22, 23, 24 and 25]

Soil Organic Carbon Content vs Vegetation Cover. SOC is one of the soil parameters that can provide sound information for evaluating land use effect on soil quality even it is used as a sole parameter for assessing sustainable management [7, 26]. SOC affects soil viability, humus, microorganism activity, basic fertilizer needs with soil CO_2 emissions and plants' ability to provide resources. SOC stock is mainly dependent to the vegetation cover [27, 28, 29]. The high biomass producing natural plants resistant to abiotic conditions such as drought, salinity and pH increased soil carbon content in wild life, however cropping with high fertilizer input and tillage negatively affect soil carbon. Determination of optimal income generating crop with high carbon production for soil is crucial for mitigating climate change and land degradation as well as sustaining soil fertility [8, 30].

In this study, SOC's under various vegetation covers were measured at 0-20 and 20-40 cm soil depths. We evaluated SOC at three compartments of the soil profile namely surface (0-20), subsurface (20-40) and both depths as SOC reservoir of the root zone.

The SOC ranged from 34 and 60.2 t C ha^{-1} in surface horizons. The highest SOC with 60.2 t C ha^{-1}, was measured in the cherry orchard while lowest SOC was determined at vegetable plot with 34 t C ha^{-1} (Figure 1). The high SOC of surface at cherry is most probably the irrigation during summer moths which prevents decomposition of organic matter. Moreover, the litter accumulated under the canopy is not disturbed with tillage and lack of nitrogen fertilizer application is also beneficial for the persistence of organic matter. The low SOC at vegetable covers is probably harvesting whole plant from soil and leaving no biomass even this plot has been fertilized with animal manure. Pear, quince and apple followed cherry plot with more than 50 t C ha^{-1} (Figure 1) which are all irrigated without tillage and fertilizer application. However, apricot's surface SOC level is relatively low than cherry, quince, pear and apple, which may be attributed to low level of litter accumulation due its relatively larger canopy compared to other trees.

The SOC at 20-40 cm depth ranged from 36.6 to 62.8 t C ha-1. The highest SOC at 20-40 cm was measured in vineyard. The lowest SOC was determined at cherry orchard with 35.3 t C ha^{-1} contrary to its high SOC at surface. The low subsurface SOC of cherry manifested irrigations negative impact on root propagation as plant readily reaches water due to irrigation, it does not develop wide root network for reaching water alike rainfed crops. This low subsurface SOC value is also seen in almost all irrigated orchards except apricot with 58.9 t C ha^{-1} (Figure 1). In the study site, apricot is relatively less irrigated compared to other trees as irrigation decreases apricot's resistance to gummosis [31].

Vineyards revealed the highest SOC accumulation in subsurface horizons. This is most probably grapevines widely distributed root network which is a traditional rainfed cultivation practices. Pine and apricot followed grapevine for high subsurface SOC content. Apricot is cultivated in vast areas of the region particularly high plains of Malatya bordering on the north of Adıyaman which set a sustainable crop management for organic matter enrichment of soils.

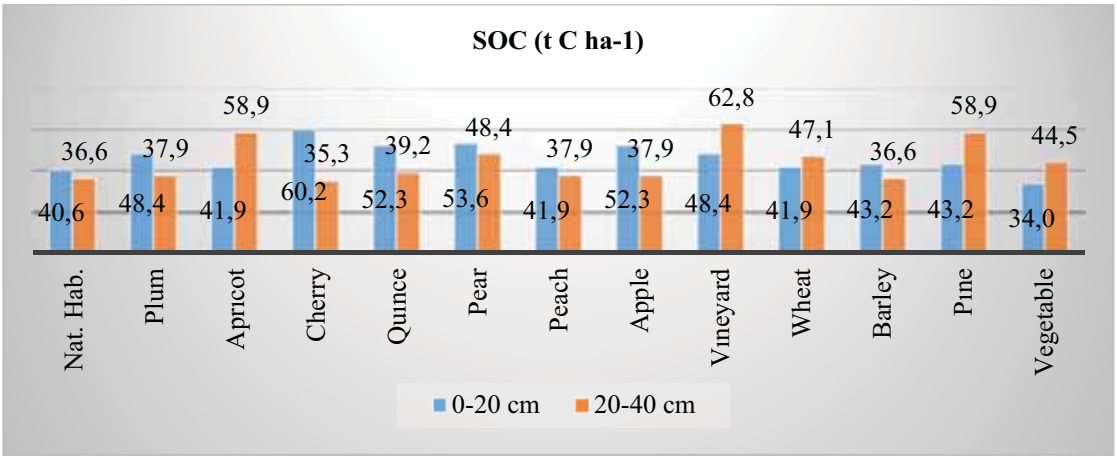

FIGURE 1
The amount of SOC in the different plantations.

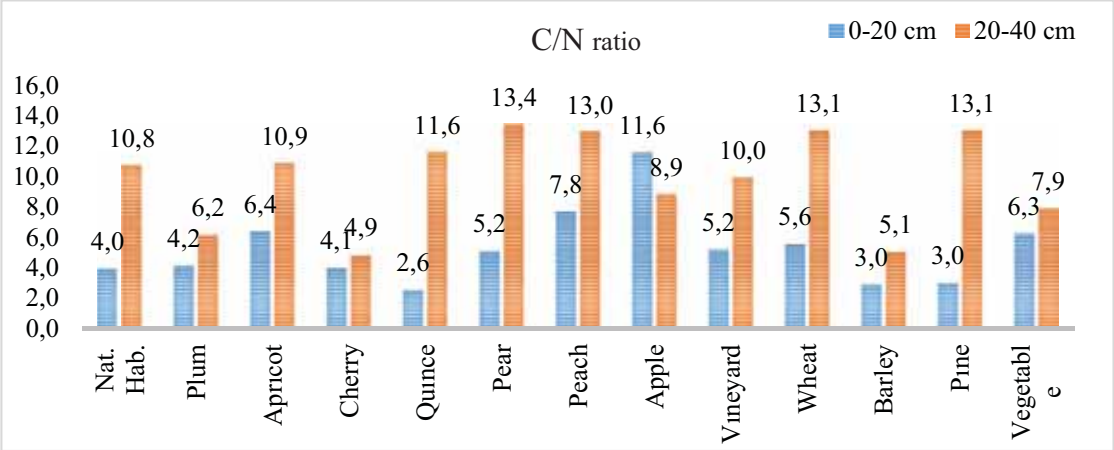

FIGURE 2
The C:N ratio in the studied site at different land uses

For both depths, the total SOC value is highest in rainfed vineyard soils with 111.2 t C ha^{-1} (Figure 1) followed by pine (102.1 t C ha^{-1}) and apricot (100.8 t C ha^{-1}). The lowest SOCs were determined at degraded natural vegetation with 77,2 t C ha^{-1}, and at vegetable plot with 78.5 t C ha^{-1} followed with 79,8 t C ha^{-1} at peach and barley plots. The relatively low organic carbon of natural vegetation is most probably due to excess grazing and sparse root network of annual C3 type grasses. [32] reviewed the excess grazing effect and suggest that SOC decreased by an average 18% in C3-dominated grasslands as is the case for Adıyaman. At vegetable cultivated plots, most of the plant tissue is harvested and removed from field that may also cause inadequate biomass input to soil for high SOC value. The low SOC at peach is most probably due to its small canopy with low litter input to soil along with sparse root network due to irrigation. Similar results were reported in some studies which they state that traditional viticulture has increased soil organic carbon even as high as 144% compared to natural areas [33, 34, 35].

C:N Ratio. The mineralization and fertilization management of cultivated soils can be planned by determining C:N ratio. At C:N ratios from 1 to 15, rapid mineralization and N release for plant uptake occurs. However, at low C:N ratio, nitrogen will be released more rapidly and crops use N immediately. However, at C:N ratio higher than 35 microbial immobilization develops which makes N not available for plants [36]. In this study, C:N ratio in surface horizons varied from 2.6 to 7.8, and in sub-surface it ranged from 4.9 to 13.4. Total C:N ratio on surface and subsurface soils were between 8.1 to 20.5 (Figure 2). Thus, for all types of vegetation cover in the studied site, it can be said that N is readily available for plants uptake so microbial immobilization is not an issue. The lowest C:N in surface soils was determined at quince with 2.8, followed by pine and barley with a C:N of 3. The high C:N which was 11.8 is determined at apricot plots. For 0-40cm average C:N is lowest at barley with 8,1. Cherry plot has the second lowest C:N ratio with 9. The C:N ratio was higher in the subsurface than surface of all plantations. This is most probably litter accumulation and mixing plant residues to the soil in experimental areas.

CONCLUSIONS

Soil organic carbon is often the only parameter used especially as an indicator of sustainable use of agricultural soils. Moreover, increasing soil organic carbon particularly in semi-arid agricultural areas where soil organic matter is quite low compared to natural lands is a way to mitigate climate change and land degradation and desertification. In this study, the orchards namely cherry, apple, pear and quince had the high SOC contents at surface compared to cereals, natural vegetation, and rainfed vineyard and apricot. However, this high figure is achieved by irrigating which is well know that preserves soil organic matter decomposition. But in semi-arid areas where water availability is becoming a serious issue, thus it is advised to cultivate rainfed or drought tolerant crops for food security. C:N ratio at all plots were below 20 which shows that at minimum tillage and controlled fertilization any plant type can provide a good N availability in Adıyaman region. We suggest that rainfed grapevine along with apricot cultivation is an optimal solution both for soil organic carbon and C:N ratio while not decreasing farmers income. Thus, suggested agricultural ecosystem for a semi-arid area will provide better ecosystem services compared to excess fertilizer and water applied conventional tillage.

REFERENCES

[1] Swinton, M.S., Lupi, F., Robertson, G.P., Hamilton, S.K. (2007) Ecosystem services and agriculture: Cultivating agricultural ecosystems for diverse benefits. Ecological Economics. 64(2), 245-252.

[2] FAO and ITPS (2015) Status of the World's Soil Resources (SWSR) – Main Report Food and Agriculture Organization of the United Nations an Intergovernmental Technical Panel on Soils, Rome, Italy.

[3] Zhang, T., Wang, Y., Wang, X., Wang, Q., Han, J. (2009) Organic carbon and nitrogen stocks in reed meadow soils converted to alfalfa fields. Soil Tillage Research. 105, 143–148.

[4] Lal, R. (2005) Soil erosion and carbon Dynamics. Soil and Tillage Research. 81(2), 137-142.

[5] Ogle, S.M., Alsaker, C., Baldock, J., Bernoux, M., Breidt, F.J., McConkey, B., Regina, K., Vazquez-Amabile, G. (2019) Climate and soil characteristics determine where no-till management can store carbon in soils and mitigate greenhouse gas emissions. Scientific Reports. 9(1), 1-8.

[6] Kutsch, W.L., Bahn, M., Heinemeyer, A. (Eds.). (2010) Soil carbon dynamics: an integrated methodology. Cambridge University Press.

[7] Büyük, G., Akça, E., Kume, T., Nagano, T. (2020) Biomass Effect on Soil Organic Carbon in Semi-Arid Continental Conditions in Central Turkey. Polish Journal of Environmental Studies. 29(5), 3525-3533.

[8] Büyük, G., Zucca, C., Akça, E. (2017) Effect of animal manure on decreasing chemical fertilizer use in degraded farm fields in semiarid region of Central Turkey. Biharean Biologist. 11(1), 48.

[9] Lo´pez, M.V., Blanco-Moure, N., Limo´n, M.A., Gracia, R. (2012) No tillage on rainfed Aragon (NE Spain): Effect on organic carbon in the soil surface horizon. Soil Tillage Res. 118, 61–65.

[10] Lal, R. (2008) Soils and sustainable agriculture. A review. Agronomy for Sustainable Development. 28(1), 57-64.

[11] Virto, I., Barré, P., Burlot, A., Chenu, C. (2012) Carbon input differences as the main factor explaining the variability in soil organic C storage in no-tilled compared to inversion tilled agrosystems. Biogeochemistry. 108(1-3), 17-26.

[12] Caetano, J.O., Benites, V.M., Silva, G.P., Silva, I.R., Assis, R.L., Cargnelutti Filho, A. (2013) Organic matter dynamics of a Cerrado Ne-ossol from cerrado converted to ulti in succession of soybeans and millet.. Rev. Bras. Cienc. Solo. 37, 1245-55. (in Portugese)

[13] Souza, L.D., Santos, C.V., Souza, L.S., Pereira, B.L.S. (2013) Resistance to penetration in Yellow Latosol of Coastal Tabuleiros, under vegetation cover with legumes. Embrapa Cassava and Fruits - Research and Development Bulletin, Report No. 58 (in Portuguese).

[14] Novara, A., La Mantia, T., Barbera, V., Gristina, L. (2012) Paired-site approach for studying soil organic carbon dynamics in a Mediterranean Semiarid Environment Catena. 89(1), 1-7.

[15] Manna, M.C., Swarup, A., Wanjari, R.H., Ravankar, H.N., Mishra, B., Saha, M.N., Sarap, P.A. (2005) Long-term effect of fertilizer and manure application on soil organic carbon storage, soil quality and yield sustainability under sub-humid and semi-arid tropical India. Field Crops Research. 93(2-3), 264-280.

[16] Liu, Y., Dang, Z.Q., Tian, F.P., Wang, D., Wu, G L. (2017) Soil organic carbon and inorganic carbon accumulation along a 30-year grassland restoration chronosequence in semi-arid regions (China). Land Degradation and Development. 28(1), 189-198.

[17] Zibilske, L.M., Bradford, J.M., Smart, J.R. (2002) Conservation tillage induced changes in organic carbon, total nitrogen and available phosphorus in a semi-arid alkaline subtropical soil. Soil and Tillage Research 66(2), 153-163.

[18] Jat, H. S., Datta, A., Choudhary, M., Yadav, A.K., Choudhary, V., Sharma, P.C., McDonald, A. (2019) Effects of tillage, crop establishment and diversification on soil organic carbon, aggregation, aggregate associated carbon and productivity in cereal systems of semi-arid Northwest India. Soil and Tillage Research. 190, 128-138.

[19] MGM. (2020) Evaluation of 2019 free surface evaporation. General Directorate of Meteorology. https://www.mgm.gov.tr/arastirma/buharlasma.aspx?s=2019.

[20] IUSS Working Group WRB. (2015) World Reference Base for Soil Resources (2014), update (2015) International soil classification system for naming soils and creating legends for soil maps. World Soil Resources Reports. No. 106. FAO, Rome.

[21] Soil Survey Staff. (2014) Soil Survey Field and Laboratory Methods Manual. Soil Survey Investigations Report No. 51, Version 2.0. R. Burt and Soil Survey Staff (ed.). U.S. Department of Agriculture, Natural Resources Conservation Service.

[22] Taşkın, M.B., Balcı, M., Soba, M.R., Kaya, E.C., Özer, P., Tanyel, G., Kabaoğlu, A., Turan, M.A., Taban, S. (2015) Nitrogen, phosphorus, potassium, calcium, magnesium and sulfur status of tea cultivation soils and tea plants in the Eastern Black Sea Region. Journal of Soil and Water 4(2), 30-40 (in Turkish).

[23] Balcı, M., Taşkın, M.B., Kaya, E.C., Soba, M.R., Özer, P., Kabaoğlu, A., Turan, M.A., Taban, S. (2016) Iron, copper, zinc and manganese conditions of tea cultivation soils and tea plants in the Eastern Black Sea Region. Journal of Soil and Water 5(2), 65- 74 (in Turkish).
[24] Bayram, S.E. (2019) The Relationships Between Some Physical-Chemical Properties and the Nutrient Content of Soils Where Tobacco is Cultivated in the Gediz Basin. Turkish Journal of Agriculture-Food Science and Technology. 7(11), 1917-1923.
[25] Akça, H., Taban, N., Turan, M.A., Taban, S., Ouedraogo, A.R. (2017) The fertility status of the garlic cultivated soils of Turkey. Journal of Soil Science and Plant Nutrition 5(2), 93-100 (in Turkish).
[26] Raiesi, F. (2017) A minimum data set and soil quality index to quantify the effect of land use conversion on soil quality and degradation in native rangelands of upland arid and semiarid regions. Ecological Indicators. 75, 307-320.
[27] Peregrina, F., Larrieta, C., Ibáñez, S., García-Escudero, E. (2010) Labile organic matter, aggregates, and stratification ratios in a semiarid vineyard with cover crops. Soil Sci. Soc. Am. J. 74, 2120–2130.
[28] Steenwerth, K., Belina, K.M. (2008) Cover crops enhance soil organic matter, carbon dynamics and microbiological function in a vineyard agroecosystem. Appl. Soil Ecology. 40, 359–369.
[29] Ruiz-Colmenero, M., Bienes, R., Eldridge, D.J., Marques, M.J. (2013) Vegetation cover reduces erosion and enhances soil organic carbon in a vineyard in the central Spain. Catena 104, 153-160.
[30] Lal, R. (2016) Beyond COP 21: potential and challenges of the "4 per Thousand" initiative. Journal of Soil and Water Conservation. 71(1), 20A-25A.
[31] Rumbos, I.C. (1997) Apricot decline and integrated plant protection. In XI International Symposium on Apricot Culture. 488, 635-642.
[32] McSherry, M.E., Ritchie, M.E. (2013) Effects of grazing on grassland soil carbon: a global review. Global Change Biology. 19(5), 1347-1357.
[33] Keesstra, S., Nunes, J., Novara, A., Finger, D., Avelar, D., Kalantari, Z., Cerdà, A. (2018) The superior effect of nature-based solutions in land management for enhancing ecosystem services. Science Total Environment. 610–611, 997–1009.
[34] Vicente-Vicente, J.L., García-Ruiz, R., Francaviglia, R., Aguilera, E., Smith, P. (2016) Soil carbon sequestration rates under Mediterranean woody crops using recommended management practices: a meta-analysis. Agric. Ecosyst. Environment. 235, 204–214.
[35] Galati, A., Gristina, L., Crescimanno, M., Barone, E., Novara, A. (2015) Towards more efficient incentives for agri-environment measures in degraded and eroded vineyards. Land Degradation and Development. 26(6), 557-564.
[36] Brust, G.E. (2019) Management Strategies for Organic Vegetable Fertility. In: D Biswas and S A Micallef (eds), Safety and Practice for Organic Food Academic Press. 193-212.

Received: **14.12.2020**
Accepted: **09.02.2021**

CORRESPONDING AUTHOR

Gokhan Buyuk
Faculty of Agriculture,
Adiyaman University,
Kahta Adiyaman 02040 – Turkey

e-mail: gbuyuk@adiyaman.edu.tr

© by PSP Volume 30– No. 05/2021 pages 5362-5369 Fresenius Environmental Bulletin

RESEARCH ON CALCULATION METHOD OF STEAM ABSORPTION IN STEAM INJECTION THERMAL RECOVERY TECHNOLOGY

Rui Deng[1,*], Ming Li[2], Song Linghu[3], Ruixiang Yang[3], Jingping Xie[4]

[1]Key Laboratory of Exploration Technologies for Oil and Gas Resources, Ministry of Education (Yangtze University), Wuhan, Hubei, 430100, China
[2]Well Testing Company, PetroChina Qinghai Oilfield Company, Mangya, Qinghai, 817500, China
[3]CNPC Logging Company Limited, Xian, Shaanxi, 710077, China
[4]Exploration Division of Huabei Oilfield Company, CNPC, Renqiu, Hebei 062552, China

ABSTRACT

The world's heavy oil resources are very rich, and its geological reserves far exceed conventional crude oil reserves. Steam injection thermal recovery technology is widely used in heavy oil fields around the world, and steam absorption calculation is an important part of steam injection thermal recovery technology. In this paper, the test principle of the high-temperature five-parameter steam absorption profile tester is introduced in detail, and a calculation model for reservoir steam absorption is constructed. Finally, the wells in Kazakhstan have been used for calculation of steam absorption, and the interpretation results have been compared with actual production. The research results show that as the pipeline grows, the heat loss gradually increases, and the dryness decreases to a large extent. When it reaches the wellhead, the dryness is only 57%. This is mainly due to the serious heat loss caused by the excessively long pipeline, which has a great influence on the steam injection effect. The calculation error of the vapor absorption percentage of the oil layer is within 5%, and the calculation result of the vapor absorption percentage is consistent with the on-site interpretation result. The interpretation conclusion verifies the reliability of the method in this paper.

KEYWORDS:
Heavy oil, steam injection thermal recovery technology, steam absorption profile, steam absorption, error

INTRODUCTION

The world's heavy oil resources are very rich, and its geological reserves far exceed conventional crude oil reserves [1-5]. So far, the proven reserves have reached 300 billion tons, while only 170 billion tons of thin oil resources can be exploited. Heavy oil is an important resource in the 21st century [6-9]. At this stage, the main method of heavy oil exploitation is thermal exploitation. This can greatly reduce the viscosity of crude oil [10-12]. This kind of technology is complicated and the investment is relatively high, and its economic risk is greater than that of ordinary oil reservoir development [13-15]. Therefore, it is necessary to calculate the amount of steam absorption reasonably during the steam injection process. Through the quantitative analysis of the steam absorption of each layer, it provides a reference for the oilfield to adjust the development plan in time. That is to say, the logging interpretation of steam injection profile can adjust steam injection parameters in real time, improve the heat utilization rate of steam, reduce energy waste, and improve the recovery effect of heavy oil [16-19].

The steam stimulation method is the so-called Cyclic Steam Injection or Steam Stimulation. It periodically injects high-temperature and high-pressure steam into the heavy oil well, so that a large amount of heat carried by the steam enters the oil layer [20-22]. The crude oil within a certain range is heated to reduce its viscosity and be recovered. The injected steam greatly reduces the viscosity of crude oil and improves the flow capacity of crude oil in the oil well, thereby increasing production [23-25]. The steam huff and puff oil recovery method is a technology with low investment and simple process. For ordinary heavy oil or extra-heavy oil reservoirs, steam huff and puff has almost no technical and economic risks. Therefore, this method has become the main method of heavy oil production.

The steam stimulation technology is shown in Figure 1. As can be seen from Figure 1, the steam stimulation process includes the following three aspects: (1) Steam injection stage. Firstly, the process parameters such as the pressure, speed, dryness and steam injection amount of the injected steam are determined based on experience. Under normal circumstances, 70-120 tons of steam are injected into the reservoir per meter, and the steam injection time is usually a few days to a few weeks. (2) Simmering stage. The well will be shut in immediately after the steam injection is completed, so that the heat carried by the steam can be fully and effectively exchanged in the oil layer to achieve the purpose of heating the

oil layer. The shut-in time cannot be too long or too short, and it is generally about 2-5 days [26-27]. (3) Oil production stage. This stage generally includes a self-injection stage and a pumping stage. The spouting phase generally lasts for several days and mainly produces condensed water around the oil well and a large amount of heated crude oil. Due to the high temperature and high pressure steam injection, the bottom hole pressure is higher, which provides energy for the spouting. When the bottom hole flow pressure is close to the formation pressure and less than the self-jet flow pressure, it is transferred to the oil pumping stage, which lasts from several months to more than one year. This is the main period of crude oil production.

For most heavy oil reservoirs, no matter shallow (200-500 m) or deep (1 000-2 000 m), when the first steam huff and puff is carried out, the oil layer pressure remains at the original pressure level, and the oil can be spun out for a period of time during oil production. When the crude oil can't self-spray, it should be pumped down immediately. When the output in the pumping stage reaches the economic limit, the next throughput cycle begins.

Steam injection thermal recovery technology is widely used in heavy oil fields around the world. When the high temperature and high pressure steam generated by the boiler enters the oil reservoir through surface pipelines and wellbore, it is bound to be accompanied by heat loss, which directly affects the effect of thermal recovery. The calculation of steam absorption for steam injection thermal recovery technology is an important part of steam injection thermal recovery technology.

In this paper, the test principle of the high-temperature five-parameter steam absorption profile tester is introduced in detail, and a calculation model for reservoir steam absorption is constructed. Finally, the wells in Kazakhstan have been used for calculation of steam absorption, and the interpretation results have been compared with actual production.

MATERIALS AND METHODS

Test instrument. In the development of steam injection in heavy oil wells, it is usually necessary to conduct a steam absorption profile test in the wellbore to analyze the effect of steam injection. The high temperature multi-parameter steam absorption profile tester can measure the temperature, pressure and flow rate of the fluid in the wellbore. Furthermore, the oil layer steam absorption is calculated based on these data to determine the oil layer's steam absorption effect. At present, there are two-parameter, three-parameter, four-parameter and five-parameter testers commonly used in downhole high temperature multi-parameter testers in steam injection wells in heavy oil fields. This article mainly uses a high-temperature five-parameter steam absorption profile tester.

The high-temperature five-parameter steam absorption profile tester is mainly for direct quantitative testing of several parameters such as downhole steam temperature, pressure, flow rate and magnetic positioning in heavy oil wells. According to the test data, the steam absorption percentage and steam absorption of each reservoir can be calculated, and the complete steam absorption profile of the steam injection well can be obtained.

During steam injection thermal recovery, the downhole temperature is usually as high as 400 °C. In order to adapt to the high temperature and high pressure environment in the well, a high temperature resistant metal thermal insulation bottle is added to the thermal recovery five-parameter steam absorption profile tester. It puts electronic components, pressure sensors, batteries and other parts that are not resistant to high temperatures in a metal insulated bottle, which solves the temperature resistance problem of the instrument. The structure diagram of the instrument is shown in Figure 2.

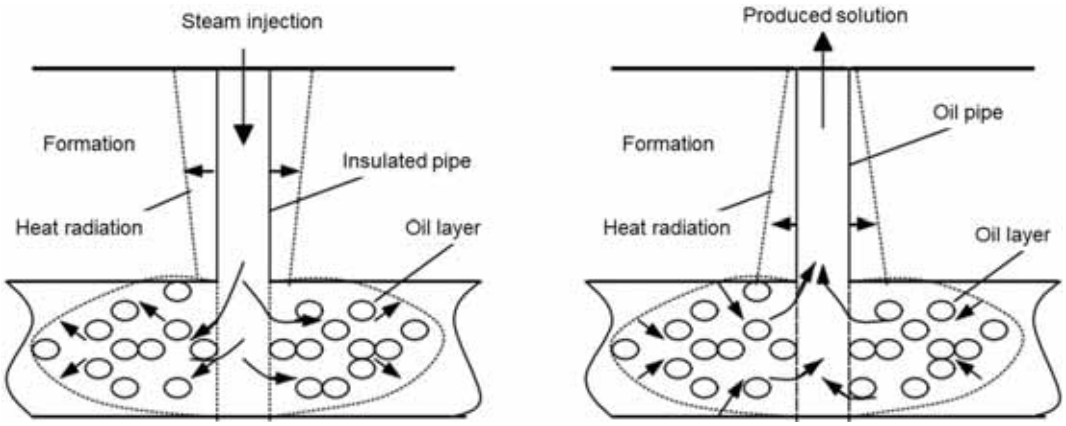

FIGURE 1
Schematic diagram of steam stimulation process.

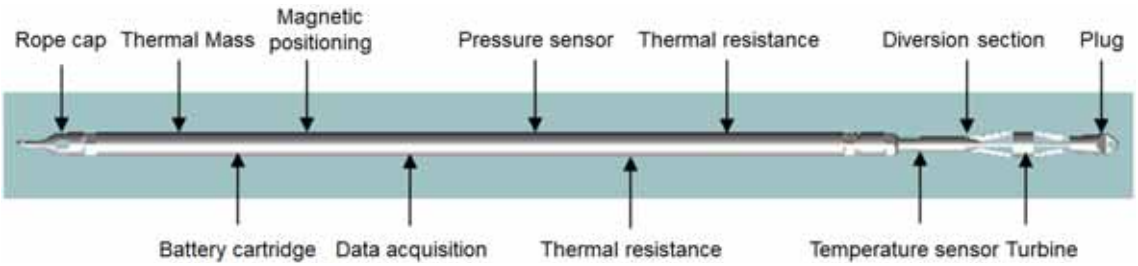

FIGURE 2
The structure of the thermal recovery five-parameter steam absorption profile tester.

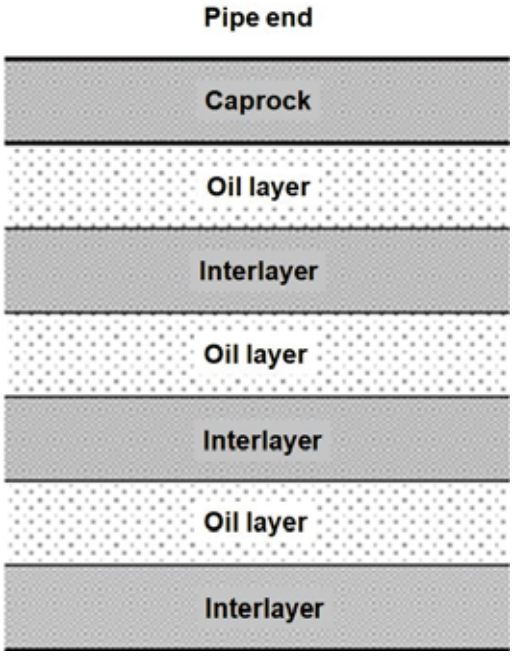

FIGURE 3
Schematic diagram of geological stratification.

The technical indicators of the instrument are as follows: instrument outer diameter: 38mm; instrument length: 1 800 mm; temperature measurement range: 0-400 °C; measurement accuracy: ±1%; pressure measurement range: 0-40 MPa; measurement accuracy: 0.2% FS; turbine Rotation range: 0-50 000 rpm; measurement accuracy: 0.08%; magnetic positioning measurement range: 0-2 V; continuous working time in underground: 4 hours.

Test principle. The thermal recovery five-parameter steam absorption profile tester is a storage electronic tester, which is powered by a high-energy battery after it goes down the well. The temperature measurement uses a thermocouple as the sensor; the pressure measurement uses a static pressure sensor; the flow measurement uses a turbine flowmeter to measure the flow rate of the fluid center.

(1) Pressure and temperature measurement method. The temperature sensor of the five-parameter tester uses an external armored platinum thermistor (Pt1000). The biggest feature of the platinum thermistor is its fast response speed and large output signal. Therefore, the temperature sensor has the characteristics of high measurement accuracy, stable linearity and good reliability. The pressure measurement uses a bridge piezoelectric sensor. The signal is output from the pressure and temperature sensor, through amplification, shaping and analog-to-digital conversion, and finally transmitted to the single-chip data acquisition system.

(2) Flow measurement method. There is a two-phase flow of soda and water in the wellbore. It requires the test point to be 1 000 meters deep down the well and in a high temperature and high pressure environment. It is difficult for general flow measurement devices to work in this environment. The turbine flow test structure of this instrument uses titanium alloy wheel blades and cemented carbide bearings, with small starting displacement and high sensitivity. The turbine sensor can measure the flow velocity of vapor phase and water phase medium. The combination of the diversion effect of the instrument itself in the well can measure the flow of water vapor. This turbine flow test structure uses titanium alloy wheel blades and hard alloy bearings.

(3) High temperature and high pressure metal insulation technology. The high-temperature five-parameter tester usually needs to be measured in a 1 000-meter-deep well, with a wellbore temperature of up to 400 °C and a pressure of 30 MPa. Therefore, the instrument uses high temperature and high pressure metal insulation technology. Based on the development status of high-temperature heat insulation technology, the existing metal insulated bottles are improved. We use multi-layer vacuum insulation, thicken the vacuum layer, and use high-efficiency heat-absorbing agents to develop high-temperature and high-pressure metal insulation bottles suitable for thermal recovery testing. The temperature rise of the heat-insulating bottle is less than 90 °C when working for 4 hours at a high temperature of 400 °C.

Calculation model of steam absorption. Assuming there are n oil layers (Figure 3), the sum of the vapor absorption percentages of each oil layer is 100%; the depth of the bell mouth is D0, the top and bottom depths of the oil layers are Ti and Di, i=1, 2, ..., n.

From the measured data, select m test data corresponding to the depth of the caprock well section (the bell mouth to the top of the first oil layer): Lj and Vj, j=1, 2, ..., m. Lj is the well depth at the test

point, and Vj is the turbine speed at the test point. It is required that the well depth of the test point is sequentially increasing: D0≤L1＜L2＜…＜Lm≤T1.

Equation (1) is used to calculate the average turbine speed of the cap fluid:

$$\overline{V_1} = \frac{1}{m}\sum_{j=1}^{m} V_j \tag{1}$$

We use the same method to calculate the average turbine speed of the fluid from the first interlayer (from the bottom of the first oil layer to the top of the second oil layer) to the n-1th interlayer fluid, and we can get $\overline{V_2}$, $\overline{V_3}$, …, $\overline{V_n}$.

Let $\overline{V}_{n+1}=0$, that is, we set the average turbine speed of the formation under the last oil layer to 0. Then the relative flow of steam in each oil layer can be calculated:

$$Q_i = \frac{\overline{V}_i - \overline{V}_{i+1}}{\overline{V}_1} \times 100, i = 1, 2, \cdots, n \tag{2}$$

In the formula, Qi is the relative flow rate of the i-th layer of steam, that is, the percentage of steam absorbed by the i-th layer, %.

In order to reduce the influence of artificial factors and instrument operation on the reliability of test data, it is generally necessary to perform multiple tests at different instrument loading (uplifting) speeds. For example, the lowering (upward) speed of the instrument is 300 m/h, 600 m/h, 900 m/h, etc. When calculating the vapor absorption of the oil layer, the relative flow calculated from the multiple test results should be arithmetic averaged.

Assuming that a total of k tests have been performed, and the speed of the instrument loading (uplifting) is different each time, a total of 2k sets of test data are obtained. The relative flow rate of the p-th set of data is calculated (1≤p≤2k), and the relative flow rate data of the oil layer is as follows:

$$Q_{i,p}, i = 1, 2, \cdots, n \tag{3}$$

Then the steam absorption of each oil layer is:

$$\overline{Q_i} = \frac{1}{2k}\sum_{p=1}^{2k} Q_{i,p} \tag{4}$$

The steam absorption strength is:

$$\eta_i = \frac{\overline{Q_i}}{100\left(D_i - T_i\right)} \times \eta \tag{5}$$

In the formula, η is the steam output of the boiler outlet, t/h; ηi is the steam absorption strength of the oil layer, t/(h·m).

RESULTS

In order to verify the correctness of the steam injection profile log interpretation method and interpretation model, the SIP module was used to process and interpret the overseas high temperature steam injection log data of Great Wall Drilling. At the same time, we analyze and compare the calculated results of the module with the measured results. There are a total of 5 test wells, these wells are from the Karazhanbas Oil Field and TBM Oil Field in Kazakhstan.

Basic Information. In the Kazakh region, the oilfields that have tested steam injection wells include the Karazhanbas Oil Field in the Aktau area and the TBM Oil Field in the Zaisan area, both of which are heavy oil reservoirs.

Karazhanbas Oil Field is located in the Ujin uplift belt in western Kazakhstan. It is a fault-back structural oil reservoir, and there are also some small-scale lens lithologic oil reservoirs. The oil reservoirs are mainly located in the Middle Jurassic and Lower Cretaceous, with an average buried depth of 300 meters. The Middle Jurassic is composed of fluvial-delta facies sand and mudstone, and the lower chalk is shallow marine facies sand and mudstone. The reservoir has good petrophysical properties, and the average porosity is between 30%-35%. The source rocks are mainly Middle and Upper Carboniferous shale and Jurassic mudstone. Crude oil has a specific gravity of about 0.94 and a high viscosity (high content of heavy components and asphaltenes). The formation pressure of the reservoir is low, and its caprock is mainly mudstone of Tertiary and Cretaceous.

The TBM Oil Field is located in the Jaisan Basin between Southern Altai and the Saul-Talbagate Mountains, which is the easternmost point of Kazakhstan. The Jaisang Basin is part of the Permian-Mesozoic depression system in the northern Junggar Basin. The reservoir is located in the Upper Permian and is a heavy oil reservoir. At present, the burial depth of the heavy oil reservoirs in the Upper Permian system developed by steam injection is about 1 500-1 700 meters, and their formation pressures are higher than 20 MPa.

Steam injection profile interpretation result. After the basic information and related parameters of the zq1 well are input, the SIP steam injection interpretation module is used to calculate the heat loss and steam absorption profile parameters of the zq1 well.

According to the basic parameters of the surface pipeline of well zq1, the pipeline is longer (2 605 m). Therefore, we calculated the pressure drop, heat loss and dryness of the surface pipeline along the step length of 78 m. At the same time, we drew the wellbore heat loss and dryness curves, as shown in Figure 4.

It can be seen from the calculation results that as the pipeline grows, the heat loss gradually increases, and the dryness decreases greatly. When it reaches the wellhead, the dryness is only 57%. This is mainly due to the serious heat loss caused by the excessively long pipeline, which has a great influence on the steam injection effect.

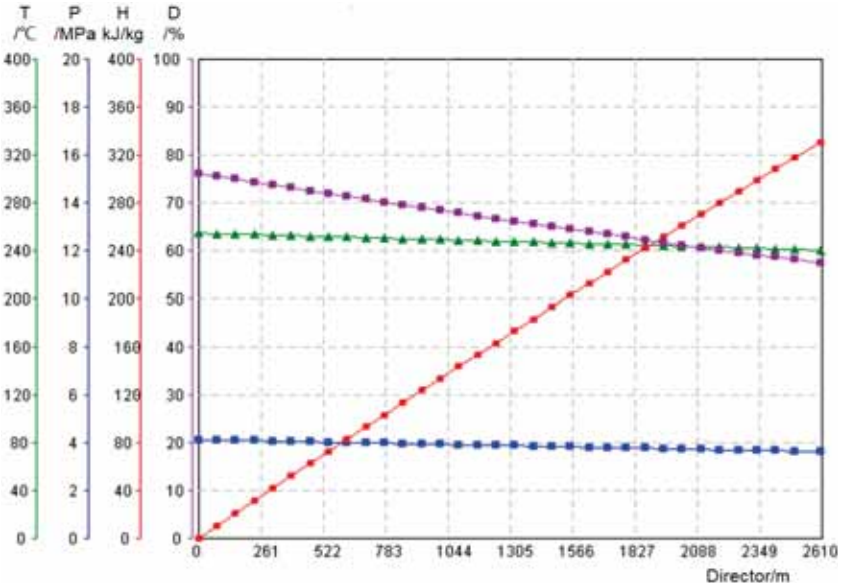

FIGURE 4
Heat loss curves of surface pipelines in well zq1.

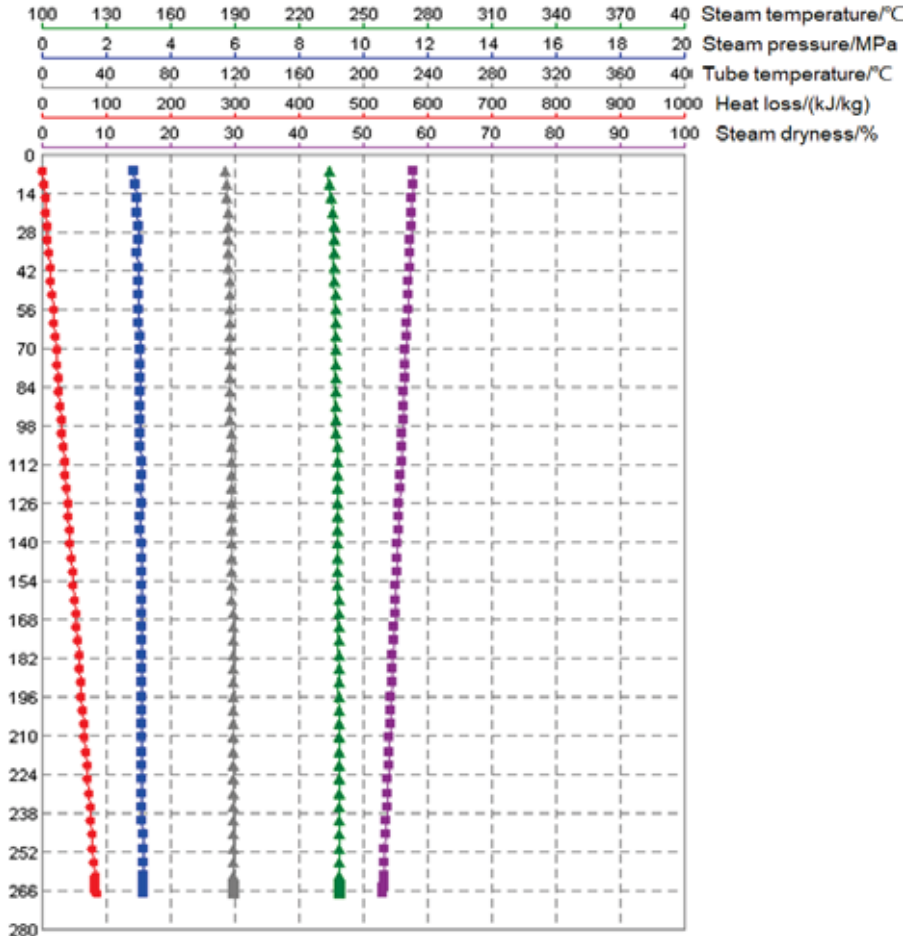

FIGURE 5
Heat loss curves in the wellbore of well zq1.

TABLE 1
Calculation results of the steam suction profile parameters of well zq1.

Layer number	Starting depth (m)	End depth (m)	Percentage of steam absorption (%)	Steam absorption (t/d)	Steam absorption strength (t/(d·m))	Interpretation
1	272.2	274.2	51.342	65.205	32.602	Good steam absorption
2	286.0	289.0	48.658	61.795	20.598	Good steam absorption
3	290.2	292.0	0.000	0.000	0.000	Poor steam absorption

TABLE 2
Comparison of calculation results of steam absorption percentage.

Well name	Layer number	Starting depth (m)	End depth (m)	Percentage of steam absorption (%)		Relative error （%）
				SIP explanation	On-site explanation	
zq1	1	272.2	274.2	51.342	51.342 3	0.00
	2	286.0	289.0	48.658	48.657 7	0.00
	3	290.2	292.0	0.000	0.000 0	0.00
zq2	1	308.8	309.8	8.333	8.300 0	0.00
	2	317.0	318.0	14.080	14.100 0	0.00
	3	321.5	326.0	77.586	77.600 0	0.00
	4	330.2	331.2	0.000	0.000 0	0.00
	5	339.5	340.5	0.000	0.000 0	0.00
	6	341.5	351.0	0.000	0.000 0	0.00
zq3	1	352.6	354.6	58.333	58.330 0	0.00
	2	356.9	358.2	8.333	8.330 0	0.00
	3	365.6	367.6	33.333	33.330 0	0.00
	4	368.5	369.7	0.000	0.000 0	0.00
zq4	1	352.6	354.6	7.227	7.317 1	1.23
	2	356.9	358.2	92.773	92.682 9	0.10
zq5	1	932.0	940.0	52.475	52.475 2	0.00
	2	945.0	954.4	20.792	20.792 1	0.00
	3	960.0	972.0	26.733	26.732 7	0.00

According to the test data of the thermal injection parameters of well zq1 and the five parameters of wellbore high temperature, the Hasan formula is selected to calculate the time function. The wellbore heat loss and dryness curves are obtained, as shown in Figure 5. From the calculation results, it can be seen that due to the position of the horn is not deep, the heat loss of steam in the wellbore is not large, and the steam reaching the oil layer has a higher dryness.

Four steam absorption profile tests were conducted in Well zq1. We calculated the steam absorption and steam absorption intensity of each perforation using the measured data of the on-site turbine flowmeter. The results are shown in Table 1.

Comparison of calculation results of steam absorption percentage. The five wells tested have been tested for multiple steam absorption profiles. According to the flow data and the average rotation speed of the turbine flowmeter in the interval above each perforation layer at different rotation speeds, the percentage of steam absorption for each perforation layer is calculated. The relative error of the calculation result is shown in Table 2.

From the above comparison results, it can be seen that the calculation error of the oil layer vapor absorption percentage is within 5%, and the calculation result of the vapor absorption percentage is consistent with the on-site interpretation result. The interpretation conclusion verifies the reliability of the method in this paper.

CONCLUSIONS

(1) In this paper, the test principle of the high-temperature five-parameter steam absorption profile tester is introduced in detail, and a calculation model for reservoir steam absorption is constructed. Finally, the wells in the Karazhanbas Oil Field in Kazakhstan have been used for calculation of steam absorption.

(2) The research results show that as the pipeline grows, the heat loss gradually increases, and the

dryness decreases to a large extent. When it reaches the wellhead, the dryness is only 57%. This is mainly due to the serious heat loss caused by the excessively long pipeline, which has a great influence on the steam injection effect.

(3) The calculation error of the vapor absorption percentage of the oil layer is within 5%, and the calculation result of the vapor absorption percentage is consistent with the on-site interpretation result. The interpretation conclusion verifies the reliability of the method in this paper.

ACKNOWLEDGEMENTS

This word was supported by the Key Project of Science and Technology Research Program of Hubei Provincial Department of Education (grant number D20191302), and the Open Fund of State Key Laboratory of Oil and Gas Reservoir Geology and Exploitation (Chengdu University of Technology, PLC20190501).

REFERENCES

[1] Sobhaniaragh, B., Mansur, W., Peters, F. (2016) Three-dimensional investigation of multiple stage hydraulic fracturing in unconventional reservoirs. Journal of Petroleum Science and Engineering. 146, 1063-1078.

[2] Wang, H. (2016) Numerical investigation of fracture spacing and sequencing effects on multiple hydraulic fracture interference and coalescence in brittle and ductile reservoir rocks. Engineering Fracture Mechanics. 157, 107-124.

[3] Mahdi, H., Kamy, S. (2015) XFEM-Based CZM for the Simulation of 3D Multiple-Cluster Hydraulic Fracturing in Quasi-Brittle Shale Formations. Rock Mechanics and Rock Engineering. 49, 1-18.

[4] Nicolas, L., Valdiviezo, M. (2016) Rock physics templates for integrated analysis of shales considering their mineralogy, organic matter and pore fluids. Journal of Petroleum Science and Engineering. 137, 33-41.

[5] Goodway, B., Perez, M., Varsek, J. (2010) Seismic petrophysics and isotropic- anisotropic AVO methods for unconventional gas exploration. The Leading Edge. 29(12), 1500-1508.

[6] Sayers, C. (2005) Seismic anisotropy of shales. Geophysical Prospecting. 53, 667-676.

[7] Ortega, J., Ulm, F., Abousleiman, Y. (2007) The effect of the nano- granular nature of shale on their poroelastic behavior. Acta Geotechnica. 2, 155-182.

[8] Kan, W., Jon, E. (2016) Mechanisms of Simultaneous Hydraulic-Fracture Propagation From Multiple Perforation Clusters in Horizontal Wells SPE Journal. 21(3), 1000-1008.

[9] Varahanaresh, S., Ahmad, G. (2015) A numerical study of sequential and simultaneous hydraulic fracturing in single and multi-lateral horizontal wells. Journal of Petroleum Science and Engineering. 132, 65-76.

[10] Wang, X., Liu, C., Wang, H. (2016) Comparison of consecutive and alternate hydraulic fracturing in horizontal wells using XFEM-based cohesive zone method. Journal of Petroleum Science and Engineering. 143, 14-25.

[11] Berryman, J., Pride, S., Wang, H. (2002) A differential scheme for elastic properties of rocks with dry or saturated cracks. Geophysical Journal International. 151, 597- 611.

[12] Armstrong, R., Wildenschild, D., Bay, B. (2015) The effect of pore morphology on microbial enhanced oil recovery. Journal of Petroleum Science and Engineering. 130, 16- 25.

[13] Farrell, N., Healy, D., Taylor, C. (2014) Anisotropy of permeability in faulted porous sandstones. Journal of Structural Geology. 63, 50- 67.

[14] Robert, G., Xu, S. (2002) An approximation for the Xu- White velocity. Geophysics. 67(5), 1406-1414.

[15] Gholami, R., Rasouli, V., Sarmadivaleh, M., Minaeian, V., Fakhari, N. (2016) Brittleness of gas shale reservoirs: A case study from the north Perth basin, Australia. Journal of Natural Gas Science and Engineering. 33, 1244-1259.

[16] Yu, W., Luo, Z., Javadpour, F., Varavei, A., Sepehrnoori, K. (2014) Sensitivity analysis of hydraulic fracture geometry in shale gas reservoirs. Journal of Petroleum Science and Engineering. 113, 1-7.

[17] Zhang, D., Ranjith, P., Perera, M. (2016) The brittleness indices used in rock mechanics and their application in shale hydraulic fracturing: A review. Journal of Petroleum Science and Engineering. 143, 158-170.

[18] Suman, P., Rima, C. (2011) Determination of in-situ stress direction from cleat orientation mapping for coal bed methane exploration in southeastern part of Jharia coalfield ,India: International Journal of Coal Geology. 87, 87- 96.

[19] Wang, S., Sloan, S., Fityus, S. (2013) Numerical Modeling of Pore Pressure Influence on Fracture Evolution in Brittle Heterogeneous Rocks. Rock Mechanics and Rock Engineering. 46(5), 1165-1182.

[20] Ma, S., Guo, J., Li, L. (2015) Influence of pore pressure on tensile fracture growth in rocks：a new explanation based on numerical testing. Frontiers of Earth Science. 9(3), 412-426.

[21] Gong, D., Qu, Z., Li, J. (2016) Extended finite element simulation of hydraulic fracture based on ABAQUS platform. Rock and Soil Mechanics. 37(5), 1513-1520.

[22] Boone, T., Ingraffea, A. (1990) Numerical procedure for simulation of hydraulically driven fracture propagation in poroelastic media. International Journal of Numerical Analysis and Modeling. 14(1), 27-47.
[23] Altamar, R., Marfurt, K. (2014) Mineralogy-based brittleness prediction from surface seismic data: Application to the Barnett shale. Interpretation. 2(4), T255- T271.
[24] Yasin, Q., Du, Q., Sohail, G., Ismail, A. (2017) Impact of organic contents and brittleness indices to differentiate the brittle-ductile transitional zone in shale gas reservoir: Geosciences Journal. 21(5), 779-789.
[25] Larry, K., Jerry, S. (2009) The geomechanics of a shale play: What makes a shale prospective. SPE 125525, Charleston, West Virginia USA. 23-25.
[26] Huang, J., Dong, D., Li, J. (2016) Reservoir characteristics and its influence on continental shale: An example from Triassic Xujiahe Formation shale, Sichuan Basin Earth Science Frontiers. 23(2), 158-166.
[27] Xue, B., Zhang, G., Wu, H. (2008) Three-dimensional numerical simulation of hydraulic fracture in oil wells. Journal of University of Science and Technology of China. 38(15), 1323-1325.

Received: **23.12.2020**
Accepted: **31.01.2021**

CORRESPONDING AUTHOR

Rui Deng
Key Laboratory of Exploration Technologies for Oil and Gas Resources,
Ministry of Education,
Yangtze University,
Wuhan Hubei 430100 – China

e-mail: dengrui@yangtzeu.edu.cn

© by PSP Volume 30– No. 05/2021 pages 5370-5376 Fresenius Environmental Bulletin

DETERMINATION OF DESIGN PARAMETERS OF DAIRY CATTLE FOOT BATH WITH OZONATED WATER SYSTEM

Erkan Gonulol[1], Goksel Tirpanci Sivri[2,*], Mehmet Recai Durgut[1], Ahmet Refik Onal[3]

[1]Department of Biosystem Engineering, Faculty of Agriculture, Tekirdag Namik Kemal University Tekirdag, Turkey
[2]Department of Food Engineering, Faculty of Agriculture, Tekirdag Namik Kemal University Tekirdag, Turkey
[3]Department of Animal Science, Faculty of Agriculture, Tekirdag Namik Kemal University Tekirdag, Turkey

ABSTRACT

Ozon is one of the most widely used antibacterial agent playing a vital role in disinfection processes. Since the maintenance of a healthy environment which requires cleaning and disinfection is obligated, the livestock production industry has to own an effective disinfection method. Ozone is proved as an effective and environment-friendly reagent compared to alternatives disinfectants for several years. The aim of this paper is to consider the biosecurity of the livestock industry while mainly focusing on foot bathing as a routine control to protect animals against several diseases. This investigation was performed in order to determine the design parameters of the footbath with ozonated water in cattle farms an ozonated water application system was developed. The concentration of ozone in water, foot exposure time, time for preparation of ozonated water, and the effect of ozone on microorganisms were founded as the design parameters. The experimental work presented here delivers one of the first investigations into how ozonated water systems might be beneficial in the foot bathing process.

KEYWORDS:
Ozone disinfection, biosecurity, footbath, environment friendly, ozonated water

INTRODUCTION

Ozone (O_3) is the highly unstable triatomic oxygen molecule that is formed by the addition of an oxygen atom to molecular diatomic oxygen (O_2) [1]. Ozone is generated commercially by-passing oxygen molecules (O_2) through an electrical charge [2]. Thus, molecular oxygen is split into two atoms of oxygen which are highly reactive moieties. When a free oxygen atom (O.) encounters molecular oxygen (O_2), it combines to form the highly unstable ozone molecule (O_3). Because ozone is unstable, it rapidly degrades back to molecular oxygen (O_2) with the released free oxygen atom (O.) combining with another free oxygen atom (O.) to form molecular oxygen (O_2) or combining with other chemical moieties to cause oxidation. Upon the release of the third oxygen atom, ozone acts as a strong oxidizing agent [3]. Ozone is a powerful germicidal. Its potent germicidal activity is doubtless due to its oxidizing power, and it has been extensively employed for the sterilization of public water supplies, for the treatment of wounds in hospitals, and for various purposes of sterilization [4,5].

As in all economic activities, the aim in livestock production is to obtain the highest efficiency and maximum profit in the current conditions. Therefore, animal breeding is commonly done with an intensive production model. This production model needs an intensive work, routine work, a long-term schedule, and planning. In addition, this method of production requires animal welfare, professional feeding, and breeding management as well as production in high-yielding animals.

Animal comfort means that an animal well adapts to his environment has fewer stress and has less health problems. Issues such as animal behavior in the barn, work efficiency, and hygiene should be taken into account. Another issue related to animal comfort is biosecurity. Biosecurity in livestock production has been used to describe measures taken to reduce the risk of the spread of animal disease on farms and defense against biological weapons, such as the deliberate introduction of smallpox or anthrax into human populations [6].

The most important element of biosecurity is disinfection. Disinfection of some sensitive areas such as; maternity area, milking parlor, milk room, and calves' area should be done regularly and properly. Some of the disinfection applications are directly on the animal for example; udder cleaning before and after milking and foot baths. Footbath is used to protect cattle against digital dermatitis. Footbathing is of paramount importance and must be used regularly, on a permanent basis, as a routine control measure [7]. It is placed on walk-through of cattle such as the exit of milking parlor or exit of the barn (on the way paddock). Since disinfectants and antibiotics concentrations are used in footbaths these rules must be followed strictly; -To protect the animal chemicals respiration, the area of the footbath should be well ventilated. -Animals should be prevented from drinking the footbath water. -The water

in the footbaath should not be drained towards manure storage. Since the effectivness of disease control depends on the transmission method, disinfection may have a pivotal role in controlling the diseases which are transmitted through contact with polluted surfaces such as housing, feed and, water.

There are some studies about the use of ozone, especially in veterinary applications, but equipment that can be used on a daily bases, such as foot bathing on farms has not yet been developed. The main purpose of the project is to find design parameters of the footbath used ozone instead of other disinfectants. The concentration of ozone in water, foot exposure time, time for preparation of ozonated water and, effect of ozone on microorganisms were defined as the design parameters. Moreover, the efficiency of ozonated water in the footbath as a disinfectant was determined by evaluation of microbial count.

MATERIALS AND METHODS

In order to determine the design parameters of the footbath with ozonated water in cattle farms, an ozonated water application system was developed. This applicator has basically consisted of ozone generation, an ozonated water tank, pump, hose and, electronic parts.

The main parts of the ozone application system are shown in Figure 1. The ozone generated in the cabin (1) was delivered to the ozonated water tank by a feeding pump. A stainless steel (A304) bucked (2) is used for the tank of ozonized water. The ozonized water was pumped by a pump (3) made of stainless steel (A304) as well. The task of the air tank on the pump is to provide continuous pumping of ozonated water (4). A silicone hose (5) is connected to the pump and a shower attachment is to the end of the hose. All parts of the applicator that are contacted with ozone or ozonated water are made of ozone-resistant material.

The cabin containing the ozone generation system and electronic parts are given in Figure 2. The ozone generator (1) is connected to a high voltage adaptor (2). The air required for the ozone generator is provided by an air pump (3). Pump switch, ozone generator switch, timer and, signal lamp is placed on the door.

Ozone was produced with the coronal-dischage method. Production capacity was 6 g/h (3-5 L/m^3 O_2 feeding) or 1,2 g/h (3-5 L/m^3 air feeding). The power of the generator was 100 W and the voltage was 220 V.

The experiments were held on the Research Dairy Farm of Tekirdag Namik Kemal University.

In order to better dissolve ozone in the water (coming from the tab) was passed through filtration and purified from minerals. A basic water filter system was displaced between the tab and the applicator. After filling the bucket with purified water, the ozone generator was started and generated ozone was delivered into the bucked.

Dissolved ozone concentration was determined by oxidation reduction potential (ORP). It was converted to ppm by using the table that mentioned Catal and Ibanoğlu, [8]. ORP value has reached a maximum of 950 mV (approximately 2 ppm) and then remained stable after 10 minutes. During the trials, tab water temperature was 18 °C.

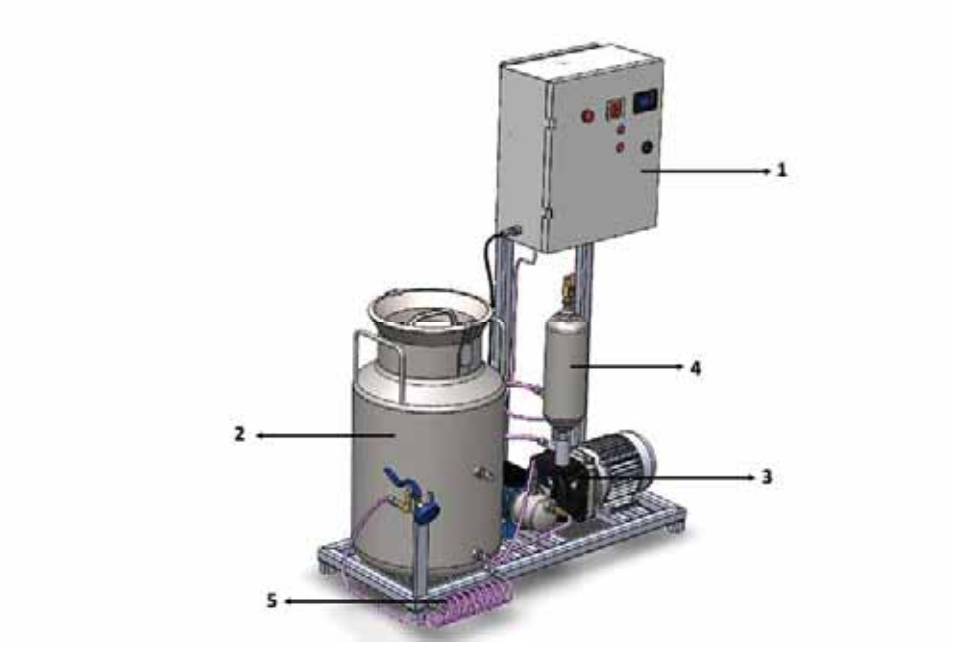

FIGURE 1
The main parts of the ozone application system
(1- Cabin for ozone generation and electronic parts, 2- Bucked of ozonated water, 3- Ozonated water pump, 4- Air tank, 5- Hose and shower attachment for ozonated water).

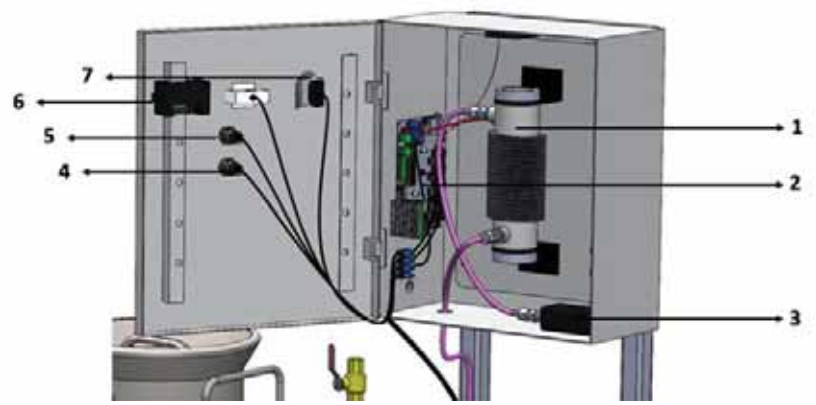

FIGURE 2
The cabin containing the ozone generation system and electronic parts
(1. Ozone generator, 2- High voltage adaptor, 3- Air pump, 4- Pump ON/OFF switch, 5- Ozone generator ON/OFF switch, 6- Timer, 7- Energy lamp

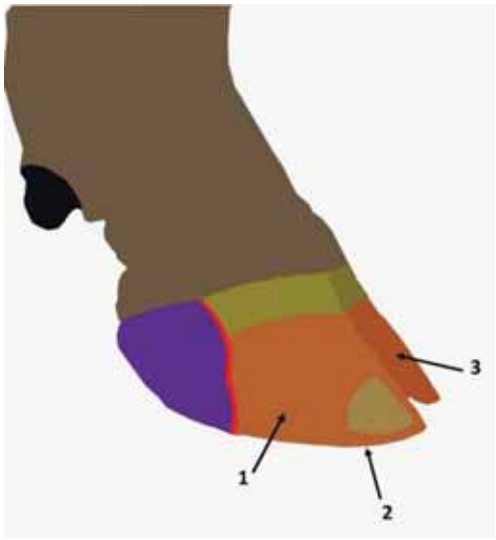

FIGURE 3
Sample points on bovine foot; Right wall (1), sole (2) and left wall (3)

Two lactating cows (Holstein) were carried out for the trials. One of them had healthy feet and the other had a lesioned foot. The feet of the cows were washed with ozonated water for 10 seconds. Before and after the washing, swap samples from healthy and lesioned foot were taken. Each foot sample was taken from three different points; the right wall (1), sole (2) and, the left wall (3) as indicated in Figure 3.

The three Rs principles used in animal experiments. The concept of Three Rs aims to ensure that animals are only used when no Replacements are available; that the number of animals used is Reduced to the minimum needed to achieve the scientific objective; and that the experiments are Refined so that only the minimum degree of animal suffering is caused [9]. The trials in the study were conducted according to animal welfare principles therefore, there were no cases of animal suffering or suffering.

To evaluate the antimicrobial effects of washing healthy and lesioned feet with ozonated water, samples were taken from three different parts of the feet, basically left and right wall and sole, with a sterile wet swab both before and after the treatment. Total Mesophilic Aerobic Bacteria Count and Total Yeast-Mold Count were performed for microbiological evaluation.

Total Mesophilic Aerobic Bacteria Count (TMAB): using samples taken under aseptic conditions, necessary dilutions were prepared and inoculated on Plate Count Agar (Merck 1.05463) by spread plate method. After incubating at 32°C for 48 hours, colony count was done, and TMAB count was calculated as log kob/cm^2. All inoculations were completed in parallels [10].

Total Yeast-Mold Count (TYM): Appropriate dilutions prepared for total yeast-mold analysis using surface samples taken from cow feet were inoculated on Potato Dextrose Agar, which has been adjusted to a pH of 3,5 by adding 10% tartaric acid, by spread plate method. After incubating for 5 days at 24 °C, colony count was made, and TYM count

was calculated as log kob/cm^2 [11].

Statistical Analysis: Data collected throughout the study was evaluated using JMP 5.0.1.a software. Analysis of variance was applied to the data through ANOVA and Tukey comparison test was applied for the comparison of variances. α value is defined as 0,05 in statistical analyses.

RESULTS

To evaluate the antimicrobial effect of washing healthy (HF) and lesioned feet (LF) with ozonated water, samples were taken from three different parts of the feet, basically left and right wall and sole, with a sterile wet swab both before (1) and after (2) the washing. Results indicating Total Mesophilic Aerobic Bacteria Count (TMAB) and Total Yeast-Mold Count (TYM) are as follows.

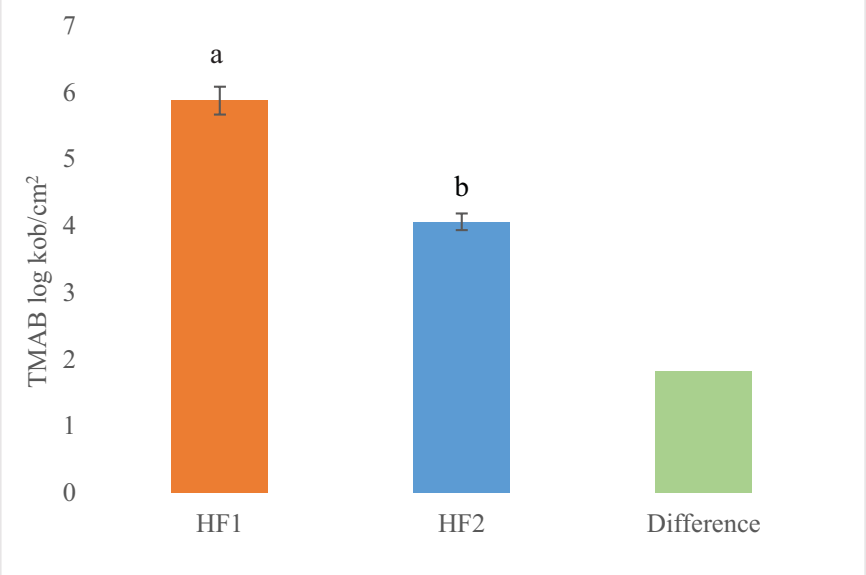

FIGURE 4

TMAB counts of samples taken from the healthy feet before (HF1) and after (HF2) ozone treatment

a, b: Results are means obtained from 3 different parts of the feet analyzed in duplicate and averaged (n=6); values with different superscript letters are significantly different ($p < 0.05$; Tukey's test).
Difference= HF1-HF2

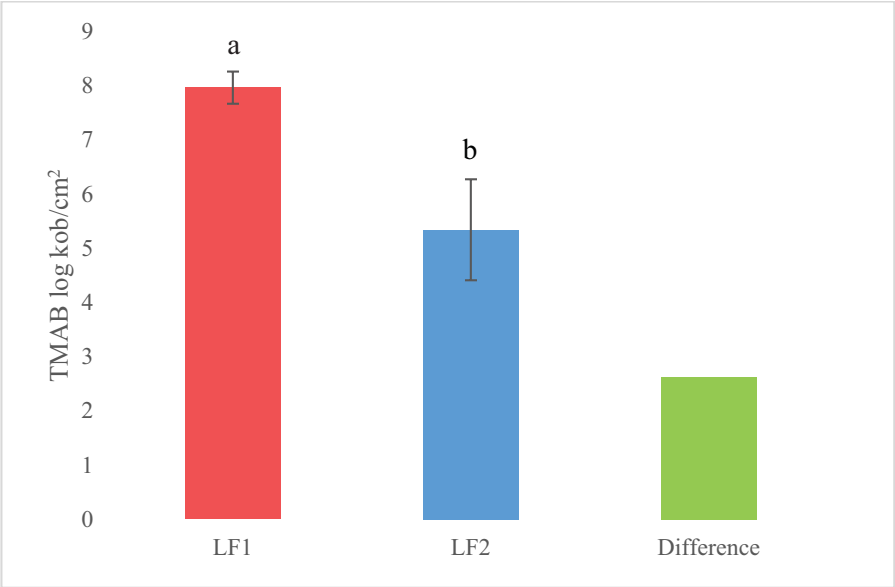

FIGURE 5

TMAB counts of samples taken from the lesioned feet before (LF1) and after (LF2) ozone treatment

a, b: Results are means obtained from 3 different parts of the feet analyzed in duplicate and averaged; values with different superscript letters are significantly different ($p < 0.05$; Tukey's test).
Difference= LF1-LF2

The TMAB count of samples taken from the healthy feet (HF) before and after ozone treatment was shown in Figure 4.

TMAB count of healthy feet before washing with ozonated water was found as 5,9 log kob/cm^2. There was a statistically significant decrease after ozone treatment and it was found as 4,1 log kob/cm^2 ($p<0,05$). The applied treatment with ozonated water has led to a decrease of 1,8 log in the number of total plate count in the healthy feet.

The TMAB count of samples taken from the lesioned feet (LF) before and after ozone treatment was shown in Figure 5.

When samples taken from the feet with lesions were analyzed, the TMAB count before the treatment was found as 7,9 log kob/cm^2 (Figure 3.2). As compared with healthy feet, feet with lesions contain 2 logs more microorganisms. There was a decrease of 2,6 log after washing with ozonated water and the plate count in the feet with lesions was found to be 5,3 log kob/cm^2 after washing with ozonated water. Total bacteria count before and after washing are statistically significantly different from each other ($p<0,05$). In a study where ozone application was tested for the treatment of feet with lesions, a decrease in the bacteria count which was quite parallel to this study, was reported. In addition, it was reported that, after 14 days of ozone application, the lesions in the hoofs and the swelling of the legs both have decreased significantly [12].

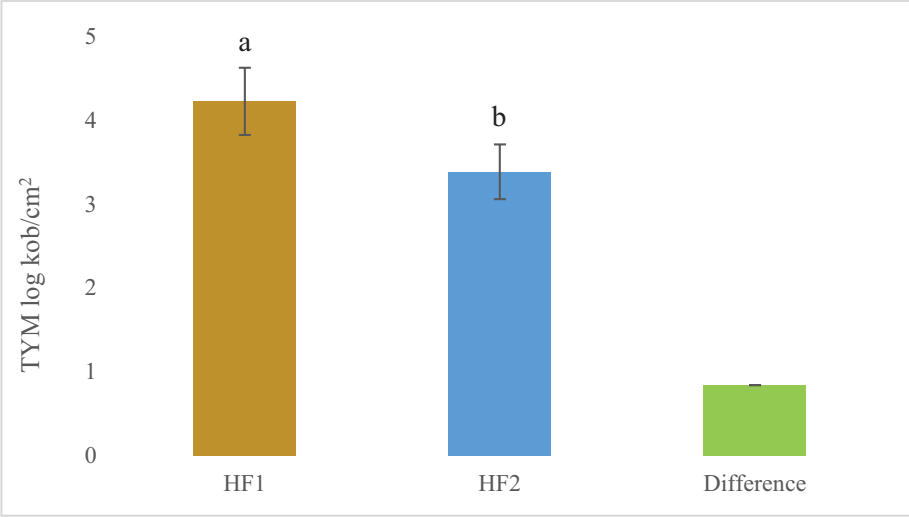

FIGURE 6

TYM counts of samples taken from the healthy feet before (HF1) and after (HF2) ozone treatment

a, b: Results are means obtained from 3 different parts of the feet analyzed in duplicate and averaged; values with different superscript letters are significantly different ($p < 0.05$; Tukey's test).
Difference= HF1-HF2

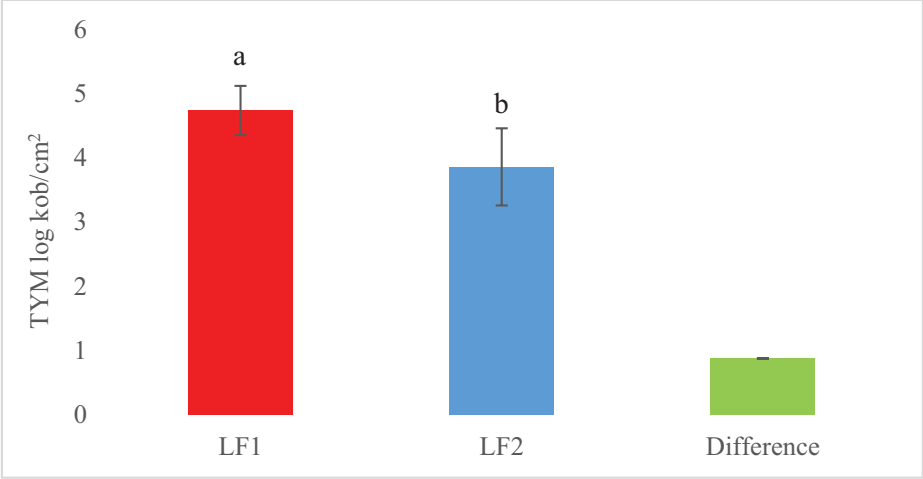

FIGURE 7

TMAB counts of samples taken from the healthy feet before (LF1) and after (LF2) ozone treatment

a, b: Results are means obtained from 3 different parts of the feet analyzed in duplicate and averaged; values with different superscript letters are significantly different ($p < 0,05$; Tukey's test).
Difference= LF1-LF2

The TYM count of samples taken from the healthy feet (HF) before and after ozone treatment was shown in Figure 6.

TYM count in the samples taken from the healthy feet before washing was 4,2 log kob/cm^2 whereas this count was defined as 3,4 log kob/cm^2 after washing with ozone water. Ozone application has caused a decrease of 0,8 log. This decrease is statically significant ($p<0,05$).

The TMAB count of samples taken from the lesioned feet (LF) before and after ozone treatment was shown in Figure 7.

When samples taken from feet with lesions were evaluated, the TYM count found before treatment was 4,7 log kob/cm^2. This value was found 3,8 log kob/cm^2 after ozone application. Ozone application has caused a decrease of 0,9 log. This decrease is statically significant ($p<0,05$).

The concentration of ozone in the bucked was reached maximum of 2 ppm under atmospheric condition and temperature of tab water (18 °C). According to Scrollavezza et al. [5] the ozone concertation in water for disinfectant purposes can be 3 ppm. If the concentration would be set as 3 ppm in the project, much more effective disinfection could be done. This concentration can be achieved by supplying enriched oxygenated air to the ozone generator.

CONCLUSIONS

Determined design parameters of the footbath used ozone in this study are;

- The tank of ozonized water and the parts that are used for delivering ozonized water should be made of ozone oxidation resistant material.
- The concentration of ozone should be at least 2 ppm in bathing water. This level was reached approximately 10 min in this project.
- Cattles should remain at least 10 seconds in the footbath while proceeding.
- The footbath should be drained of polluted water after every 15-20 cattle passes and filled with regenerated ozonized water.

It is advised that washing feet with a shower system can be more effective than a footbath system. Besides, an instant dissolving system can be more useful than preparing and keep ozonized water in the tank. For this purpose, a more powerful generator and enriched oxygen supplier are needed.

ACKNOWLEDGEMENTS

This project was supported by University of Tekirdag Namik Kemal, Scientific Research Projects Unit (BAP) as project NKUBAP.03.YLGA.18.144

REFERENCES

[1] Khadre, M.A., Yousef, A.E., Kim, J.G. (2001) Microbiological Aspects of Ozone Applications in Food: A Review. Journal of Food Science. 66, 1242–1252.

[2] Horvath, M., Bilitzky, L., Huttner, J. (1985) Ozone. New York: Elsevier. 350

[3] Guzel-Seydim, Z., Bever Jr, P.I., Grene, A.K. (2004). Efficacy of Ozone to Reduce Bacterial Populations in the Presence of Food Components. Food Microbiology. 21, 475-479.

[4] Viebahn-Hansler, R. (1991) Ozone therapy: the under- lying therapeutical concept and models of efficacy. Erfahrungsheilkunde. 40, 4-9.

[5] Scrollavezza, P., Ansaloni, F. and Polidori, P. (2002) Ozonized Autohemotherapy, a New Method to Treat Dairy Cow Acute Interdigital Phlegmon. Comparison with ceftiofur and oxytetracycline. Italian Journal of Animal Science. 3, 211-216.

[6] Waage, J.K., Mumford, J.D. (2008) Agricultural biosecurity. Phil. Trans. R. Soc. B. 363, 863–876

[7] Brizzi, A. (1993) Bovine Digital Dermatitis, American Asssociation of Bovine Practitioners, open access distributions. 33-37

[8] Catal, H. and Ibanoglu, S. (2013) Effects of Ozonation on Thermal, Structure and Rheological Properties of Rice Starch in Aqueous Solution. FOOD. 38 (2), 63-70.

[9] Passantino, A. (2008). Application of the 3Rs Principles for Animals Used for Experiments at the Beginning of the 21st Century. Annual Review of Biomedical Sciences. 10, 27-32.

[10] Clark, W.S., Brazis, A.R., Fowler, J.L., Johns, C.K. Venelson, F.E. (1978) Standard Plate Count Method. E. H. Marth (Ed.), Standard methods for the examination of dairy products Washington, DC: American Public Health Association. (14. ed., 77).

[11] Beuchat, L.R. (1978) Comparison of Acidified and Antibiotic-supplemented Potato Dextrose Agar from Three Manufacturers for its Capacity to Recover Fungi from Foods. J. Food Prot. 42(5), 427–428.

[12] Lee, S.J., Cho, S.W., Jun, M.H., Kim, D.H., Park, C.S., Han, H.R. and Kim, M.C. (2006) The Efficacy of Ozonated Water Therapy on Pododermatitis of Dairy Cows. J. Vet. Clin. 23(3), 272–278.

Received: **25.12.2020**
Accepted: **03.02.2021**

CORRESPONDING AUTHOR

Goksel Tirpanci Sivri
Department of Food Engineering,
Faculty of Agriculture,
Tekirdag Namik Kemal University,
Tekirdag – Turkey

e-mail: gtirpanci@nku.edu.tr

© by PSP Volume 30– No. 05/2021 pages 5377-5384 Fresenius Environmental Bulletin

MICRO-PORE STRUCTURE CHARACTERISTICS OF THE CHANG 6 MEMBER SANDSTONE RESERVOIR IN HUANGJIANG OILFIELD ORDOS BASIN CHINA

Jianmin Yang*, Fu Leng, Haisheng Yu, Yuping Zhao

PetroChina Changqing Oilfield Company Oil Production Plant No.7, Xi'an, 710000, China

ABSTRACT

The Ordos Basin is the second largest sedimentary basin in China. The oil and gas resources in the basin are very rich, and there is great potential for oil and gas exploration and development. The Chang 6 member of the Triassic Yanchang Formation is the main oil-bearing formation of Huanjiang Oilfield. The Chang 6 reservoir of Huanjiang Oilfield currently has the problem of insufficient understanding of reservoir geological laws, especially in the southern part of the oilfield. In this paper, the microscopic pore structure of the Chang 6 member of Huanjiang Oilfield was systematically studied by means of mineral composition analysis, thin section analysis, scanning electron microscopy analysis and mercury intrusion experiments. Experimental results show that the Chang 6 reservoir in Huanjiang Oilfield is a low-porosity, ultra-low permeability reservoir, but there are still some relatively high porosity and high permeability reservoirs in some local areas. The Chang 6 reservoir has an average porosity of 7.43% and an average permeability of 0.15×10-3 μm2. The pore types of the target layer are mainly intergranular pores and feldspar dissolution pores, and a small amount of lithic dissolution pores, intergranular dissolution pores, intercrystalline pores and microcracks are also developed. The mercury intrusion experiment showed that the pores of the Chang 6 member were poorly sorted and the pore structure was complicated. Diagenesis is the main factor affecting the pore structures of the reservoir.

KEYWORDS:
Ordos Basin, Upper Triassic, Chang 6 Member, sandstone reservoir, rock characteristics, pore structure

INTRODUCTION

With the continuous deepening of oil and gas exploration and development, the research of oil and gas reservoirs has received more and more attention [1-4]. At present, the progress of oil and gas reservoir research is mainly reflected in the following three aspects [5-9]: (1) Reservoir research is increasingly developing from the macroscopic to the microscopic direction. That is, it not only studies the macroscopic geometry and spatial distribution characteristics of the reservoir, but also goes deep into the microscopic pore structure of the reservoir, the clay minerals in the pores and their influence on oil and gas recovery; (2) Reservoir description and prediction are increasingly developing from qualitative to quantitative. It uses reservoir sedimentology, geostatistics, geological model high-resolution seismic technology, and qualitatively describes the three-dimensional spatial distribution of reservoir sandstone and its various parameters, and can establish a quantitative three-dimensional reservoir model. These studies have become an important development trend in reservoir geology in the past ten years; (3) Reservoir research has developed from a single subject to a multidisciplinary comprehensive research direction.

Reservoir evaluation needs to focus on the needs of oil and gas exploration and development, and develop integrated seismic, well logging, well testing and sedimentary geology, mathematical geology, computer and other technical means to cooperate with multiple disciplines to solve practical problems in exploration and development. The diagenesis of the reservoir is an important part of the study of reservoir evaluation. Diagenesis plays a very important role in understanding the quality of the reservoir, the evolution process of pores, and the distribution of pores [10-13]. Early studies on reservoir diagenesis focused on the analysis of the mechanism of secondary pore generation, and recent studies have mainly involved the diagenesis mechanism of pore preservation. The study of diagenesis is based on petrology, which includes studies on diagenetic signs, diagenetic events, diagenetic sequences, diagenetic facies, diagenetic evolution models, and prediction of favorable development zones. In addition, the research methods and ideas that combine the diagenesis history, pore evolution history, structural development history, and hydrocarbon migration and accumulation history of reservoir rocks have injected new content into reservoir research. The content of sedimentary diagenesis research includes: compaction, pressure solution, cementation, hydration and dehydration, microbial action, recrystallization and dissolution, etc., as well as various diagenesis stages.

The above diagenesis research can help people understand more clearly the pore distribution law, pore structure and pore genetic types, the genesis and development conditions of secondary pores, and various geological factors affecting pore development. The most constructive diagenesis in the process of carbonate diagenesis is dissolution and dolomitization. Schmidt et al. [14] proposed that there are extensive secondary pores in sandstone. In the 1980s and 1990s, the theory of dissolution developed rapidly. Many researchers have enriched and developed the theory of burial dissolution from different research directions [15-18], and it has been widely used in the study of carbonate diagenesis. The development trend of reservoir research is always from macro to micro, from qualitative to quantitative, from shallow to deep, from high permeability and high porosity to low permeability and low porosity reservoirs.

The Huanjiang area is the main area where PetroChina Changqing Oilfield Branch has increased reserves and production in recent years [19-20]. Finding high-quality geological reserves in the Chang 6 Member of the Upper Triassic is still the focus of oil and gas reserves in the next stage. In addition, it is particularly important for the rapid development of Huanjiang Oilfield to further find the production potential area of Chang 6 oil reservoir. At present, the understanding of the geological law of Chang 6 reservoir in Huanjiang Oilfield is insufficient, especially the research on the pore structure of the reservoir is very few. In this paper, the microscopic pore structure of the Chang 6 member of Huanjiang Oilfield was systematically studied by means of mineral composition analysis, thin section analysis, scanning electron microscopy analysis and mercury intrusion experiments.

MATERIALS AND METHODS

The geotectonic location of the Ordos Basin belongs to the western part of the North China Platform, which is a rectangular basin extending in the north-south direction. It has Yinshan, Daqingshan and Langshan in the north, Qinling in the south, Helan and Liupan Mountains in the west, and Luliang and Zhongtiao Mountains in the east. Its total area is 37×104 km2, and it is the second largest sedimentary basin on land in China. The Ordos Basin is a craton marginal depression basin. The base of the basin is the crystalline base of Archean and Proterozoic metamorphic rocks. And its upper part is the Paleozoic, Mesozoic and Cenozoic caprock deposits. According to the tectonic evolution history and current structural morphology, the Ordos Basin can be divided into six first-level structural units: Yimeng Uplift, Weibei Uplift, Jinxi Flexural Fold Zone, Yishan Slope, Tianhuan Sag, and Western Margin Thrust Fault Structural Belt [21-23] (Figure 1).

The Ordos Basin is a residual inland craton basin formed by the superimposition of multiple tectonic movements. There are many sets of strata deposited in the basin since the Paleozoic, among which the Triassic and Jurassic strata are generally developed in the study area. According to the characteristics of sedimentary sequence and stratigraphic lithology, the Triassic Yanchang Formation is divided into five lithological sections. In addition, according to the longitudinal distribution of oil layers, it can be divided into 10 oil layer groups from top to bottom, namely, Chang 1 to Chang 10 members. Huanjiang Oilfield is a sedimentary basin with a stable ascending type. Lake facies and delta front facies have relatively stable sedimentary cycles and marker layers. In this paper, with the deposition model as the guide, the marker layer and the deposition cycle as the reference, we use the dynamic and static combination method to divide the strata. Finally, the Chang 6 oil layer group in the study area is divided into Chang 61, Chang 62, and Chang 63.

In this paper, we have performed ordinary thin sections, cast thin sections and scanning electron microscope observations on the core samples of the Chang 6 oil layer group. At the same time, combined with the experimental results of mercury injection curve analysis, X-ray diffraction analysis, porosity and permeability, the petrological characteristics, pore structure characteristics and diagenesis characteristics of the reservoir were systematically studied. This research can provide a basis for the prediction and evaluation of favorable reservoirs.

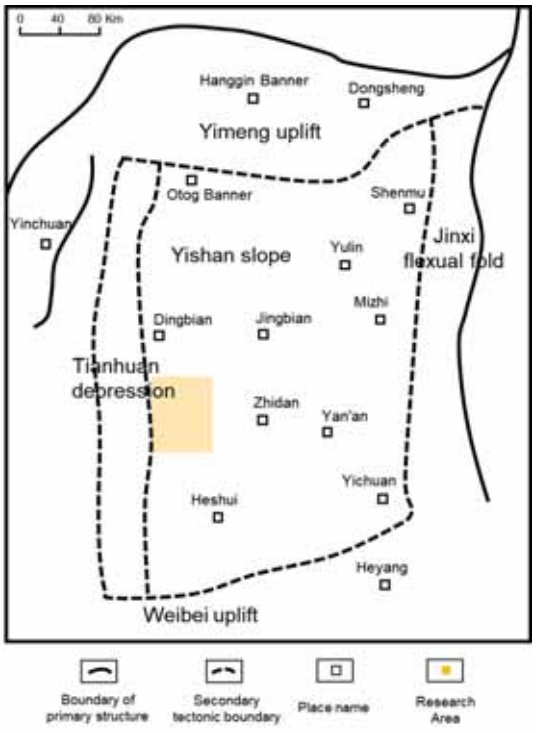

FIGURE 1
Location of the study area.

RESULTS

Reservoir petrological characteristics. The rock and mineral characteristics of the reservoir refer to the rock clastic composition, the type and content of interstitial materials, the way of cementation and arrangement of particles, and the rounding and sorting. They often determine the petrophysical properties of the reservoir and are also the internal factors that control the diagenesis of sandstone. Its effect is not only reflected in the water-rock reaction of sandstone, but also reflected in the compaction of sandstone. In a certain diagenetic background, it determines the speed and scale of sandstone diagenesis, thus affecting the pore evolution of sandstone. Therefore, the petrological characteristics of the reservoir determine the diagenesis, porosity, permeability, pore structure, and throat type of the reservoir, which are the basis for the study of reservoir petrophysical properties.

Rock type and clastic composition of the reservoir. In sandstone, component maturity refers to the degree to which the clastic components in sandstone approach the final product under the alteration of weathering, transportation and sedimentation. Therefore, the research on maturity must start from the relative stability of the detrital components. Generally speaking, immature sandstone is accumulated close to the provenance area and contains many unstable debris, such as rock debris, feldspar and iron-magnesium minerals. High maturity sandstone is the product of long-distance transportation and transformation, and it is almost entirely composed of quartz. Therefore, the types and relative abundance of cuttings and detrital minerals present in sandstone, that is, the maturity of the composition, are a reflection of the geological conditions, degree of weathering and transportation distance in the provenance area. At present, the classification of sandstone generally uses triangle diagrams. The three-component system mainly classifies sandstone according to the three sand-grade clastic components of sandstone, such as quartz, feldspar, lithic debris and mica. Based on the thin section identification results, a triangular classification map of sandstone clastic components was drawn (Figure 2). It can be seen that the Chang 6 reservoir is composed of feldspar sandstone, lithic feldspar sandstone, and feldspathic lithic sandstone. The clastic composition is mainly feldspar, followed by quartz and lithic sandstone.

Features of interstitial materials. Miscellaneous bases and cements in clastic rocks are collectively referred to as interstitials, which are the common products of sedimentation and diagenesis. There are many types of interstitials, mainly clays, carbonates, feldspars and zeolites, which are formed in different diagenetic stages. The main components of the interstitials of Chang 6 reservoir in this area are kaolinite, hydromica, chlorite, calcite, dolomite, siliceous and a small amount of iron minerals. Due to the difference in diagenesis, the content of interstitial material in each strata series is different, which results in the difference in the petrophysical properties of the reservoirs, and thus the oil enrichment degree of each strata reservoir. The sandstone interstitial content of Chang 6 reservoir in the study area is generally 16.19%. The main components of the interstitial material are hydromica, iron calcite, siliceous and dolomite, among which hydromica content is 4.90%, iron calcite content is 4.35%, siliceous content is 2.43%, and dolomite is 2.06% (Table 1)

Petrophysical characteristics. Through core analysis of 1 264 rock samples from 29 wells in Chang 6 reservoir, the porosity of Chang 6 is concentrated between 6.0-12.0%, which accounts for 79.67% of the total analyzed rock samples; the permeability is concentrated between 0.05-0.50×10-3 μm2, which accounts for 93.5% of the total rock samples analyzed (Figure 3 and Figure 4).

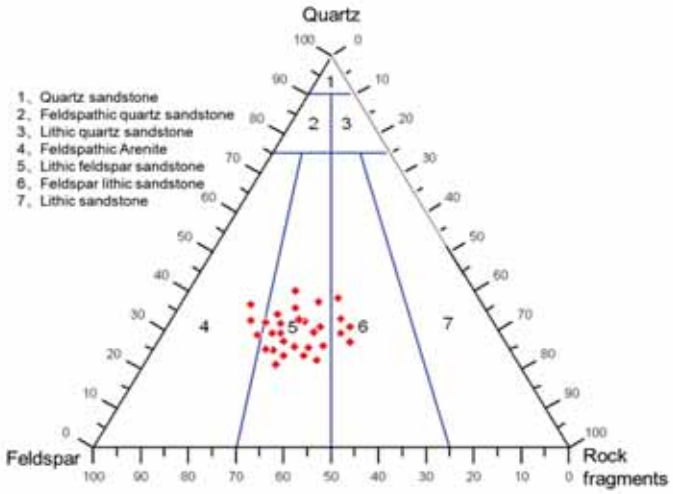

FIGURE 2
Types of sandstone in Chang 6 reservoir.

TABLE 1
The content of interstitial components in Chang 6 reservoir in Huanjiang area.

Horizon	Interstitial material (%)							
	Kaolinite	Hydromica	Chlorite film	Iron calcite	Dolomite	Siliceous	Iron minerals	Number of samples
Chang6	1.03	4.90	1.20	4.35	2.06	2.43	0.22	79

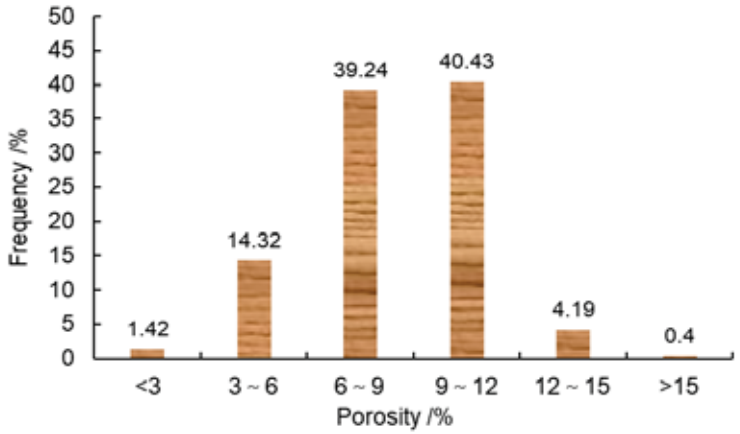

FIGURE 3
Porosity distribution of Chang 6 reservoir.

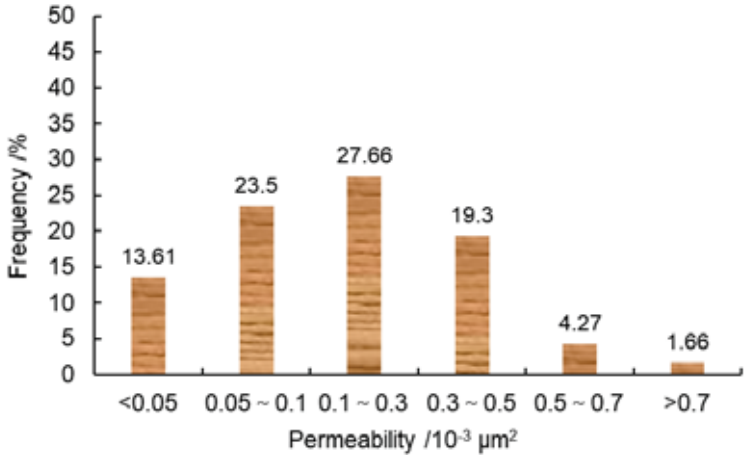

FIGURE 4
Permeability distribution of Chang 6 reservoir.

TABLE 2
Statistical results of core petrophysical properties.

Horizon	Storage space (%)			Permeability ($\times 10^{-3}$ μm^2)		
	Minimum	Maximum	Average	Minimum	Maximum	Average
Chang 6	0.37	15.95	7.43	0.001	7.991	0.15

The statistical results of core petrophysical properties are shown in Table 2:

The petrophysical property statistics show that the Chang 6 member of the Huanjiang area belongs to a low-porosity-ultra-low permeability reservoir with relatively high porosity and high permeability locally. The average porosity of the reservoir is 7.43%, and the average permeability is 0.15×10-3 μm2.

Pore type and structure. The pore types of the reservoirs in this area are mainly intergranular pores and feldspar dissolved pores. In addition, a small amount of lithic dissolved pores, intergranular dissolved pores, intercrystalline pores and micro-cracks are also developed (Table 3).

TABLE 3
Proportion of different types of pores in Chang 6 reservoir in Huanjiang area.

Horizon	Storage space (%)						
	Intergranular pore	Intergranular dissolution pore	Feldspar dissolution pore	Rock debris dissolution pore	Intercrystalline pore	Microcrack	Number of samples
Chang6	1.51	0.09	0.71	0.14	0.31	0.02	79

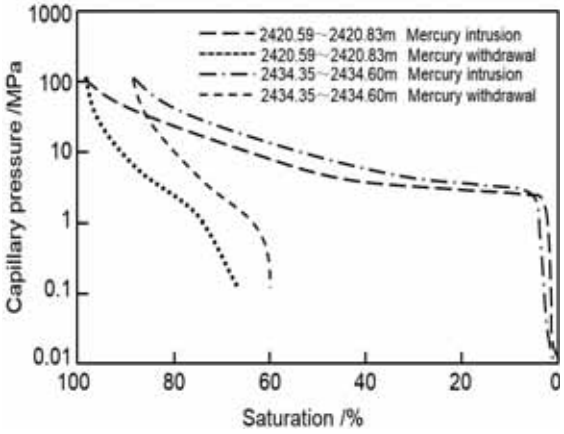

FIGURE 5
Characteristics of mercury injection curves of Chang 6 reservoir.

It can be seen from Table 3 that the pore types in the study area include intergranular pores, intergranular dissolved pores, feldspar dissolved pores, lithic dissolved pores, intercrystalline pores and micro-cracks. Among them, intergranular pores and feldspar dissolved pores are the main ones, and the distribution of pore types in each formation is completely different. The pores of the Chang 6 member are dominated by intergranular pores, with an average content of 1.51%. The pores in this area are dominated by primary intergranular pores and secondary dissolution pores. The dissolved pores are mainly feldspar dissolved pores, and these dissolved pores are greatly affected by the later diagenesis, especially the strong carbonate cementation (iron calcite cementation). Most of the remaining intergranular pores are surrounded by chlorite membrane rings, so where the chlorite membrane is developed, the remaining intergranular pores are also relatively developed, and the diagenesis is relatively weak. The dissolution intergranular pores have suffered strong diagenesis, such as those formed by the dissolution of feldspar. It will also be formed by some rock cuttings and clay fill materials after later transformation and dissolution.

The mercury injection curve of Chang 6 reservoir in this area is shown in Figure 5. Some sandstones have obvious curve platforms, and the displacement pressure is relatively high, with an average of 1.78 MPa. The median pressure is 6.12 MPa, and the median throat radius is 0.12 μm. The maximum degree of mercury intrusion is 98.44%, and the mercury removal efficiency is 30.26%. Therefore, the reservoir has developed micro-pores and the pore structure is general. From the above analysis, we can see that the small pores in the Chang 6 reservoir in the study area are developed, the pore sorting is poor, and the pore structure is complicated.

Types and characteristics of diagenesis. Diagenesis is an important factor affecting the pore structure of the reservoir. After thin section and scanning electron microscopy analysis, X-ray diffraction test and cathodoluminescence test of a large number of samples, it can be concluded that the diagenesis in this area mainly includes compaction, pressure solution, cementation, metasomatism and dissolution [38-39].

(1) Compaction, pressure solution. Compaction and pressure solution mainly occur in the early stage of diagenesis. It is the process of reducing the total volume of the rock except for the dissolution of the skeleton particles under the gravity of the overlying rock. Simply put, it is caused by mechanical compaction of rock pressure and the weight of the overlying sediment.

Compaction is common in this area, and its strength is mainly related to rock burial depth, ground temperature and clastic mineral composition. This is mainly achieved through the sinking of particles, the reduction of the distance between particles, and the shrinkage of sediment volume (Figure 6). Pressure dissolution occurs to varying degrees in the strata in the study area, which is manifested by the secondary increase of quartz and feldspar.

(2) Cementation. Cementation is the process by which minerals precipitate between particles and consolidate into rock, which reduces the pore space. The basic condition is that the pore fluid system is not closed, and saturated fluid is constantly supplied. It is an important factor that attenuates the storage space. Cementation can occur in various stages of diagenesis. The sandstone of the Yanchang Formation in the study area has strong cementation, which mainly includes clay mineral cementation, siliceous cementation, and carbonate cementation.

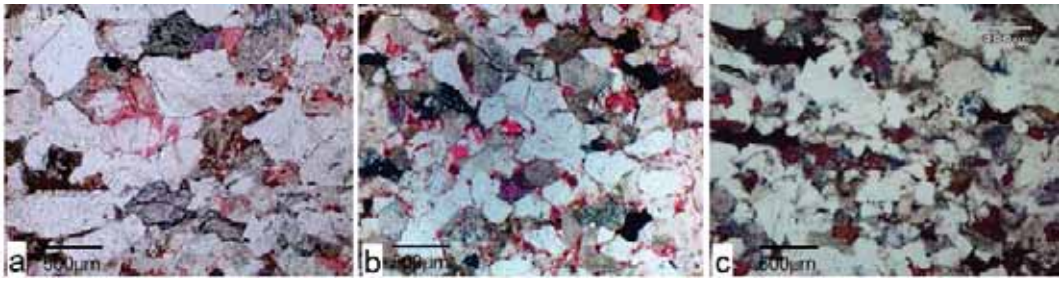

FIGURE 6
Compaction (close-fitting of particles).

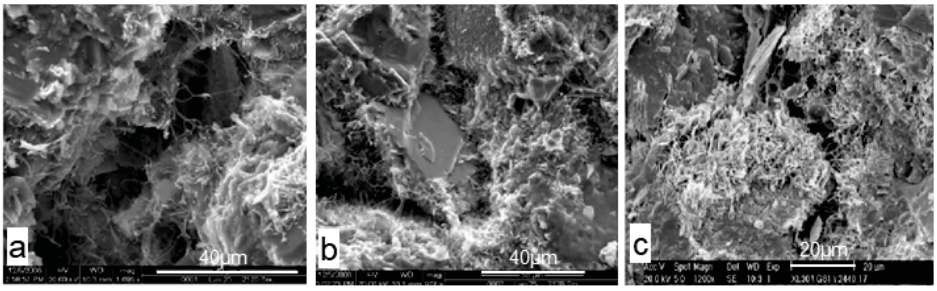

FIGURE 7
Different types of clay mineral cementation (a, illite clay cementation; b, illite clay cementation; c, chlorite cementation).

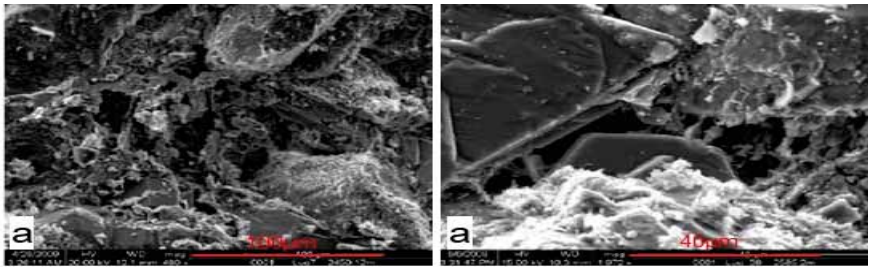

FIGURE 8
Microscopic characteristics of carbonate cementation and siliceous cementation (a-quartz cementation; b-quartz cementation).

①Cementation of authigenic clay minerals. The main cements developed in the Chang 6 member of the study area are chlorite and kaolinite. Chlorite cementation is generally developed in all layers. The chlorite film hinders the contact between the clastic particles and the pore water, which hinders the secondary growth of quartz and is beneficial to the preservation of primary pores. Kaolinite cementation is widely developed in the reservoir, and authigenic kaolinite is mostly packed between clastic particles, which reduces the porosity of the reservoir. Electron microscope observation showed that kaolinite was a flake, book page or worm-like aggregate (Figure 7).

②Carbonate cementation. Cathodoluminescence can reflect brilliant crystal calcite and iron calcite. Under cathodoluminescence, calcite is orange-yellow-brown, and iron-containing calcite is generally orange-brown, which is mainly related to the amount of ferrous ions in calcite. Ferrous ion is one of the quenchers of cathodoluminescence. The higher its content, the darker the color under cathodoluminescence. Therefore, iron-containing calcite appears darker than ordinary calcite under cathodoluminescence. Flake staining and cathodoluminescence show that the carbonate is dominated by calcite. The calcite formed in the early diagenesis is mostly distributed in granular form among the clastic particles, and sometimes it can be partially cemented in continuous crystal form. However, iron-containing or non-iron-containing calcite formed in late diagenesis is re-precipitated after dissolution, and it often appears in the form of metasomatic quartz or feldspar. The phenomenon of iron calcite surrounding calcite can be seen under the mirror, which can explain that the formation of iron calcite is later than that of calcite. The cementation of carbonate has a certain destructive effect on the reservoir. Although some dissolved pores of calcite appear, the amount of such dissolved pores is very limited. There are four types of carbonate cements: iron calcite, iron dolomite, calcite and dolomite cement, among which iron calcite cement is the main type. Carbonate ce-

mentation is mainly dolomite and iron calcite cementation in the study area. The authigenic carbonate minerals are locally inlaid and densely cemented (Figure 8).

③ **Siliceous cement.** The source of silica in the study area may mainly come from four aspects: one is from groundwater and surface water. These fluids contain a certain amount of silica. When the external conditions reduce the solubility, some silica will precipitate in certain parts of the edge of the debris particles; the second is derived from the aforementioned pressure solution. The dissolution of quartz will generate a certain amount of silica; the third is from the transformation of clay minerals. With the strengthening of diagenesis, silica will be precipitated during the conversion process of the Imonite mixed layer to illite; the fourth is from the inconsistent dissolution of silicate minerals. The feldspar in the study area generally has weak and medium clayiness, and silica will be precipitated during the kaolinization of potash feldspar.

CONCLUSIONS

(1) The Chang 6 reservoir is composed of feldspar sandstone, lithic feldspar sandstone and feldspar lithic sandstone. The clastic composition is mainly feldspar, followed by quartz and lithic feldspar. The average interstitial content of sandstone in Chang 6 reservoir in the study area is 16.19%.

(2) Experimental results show that the Chang 6 reservoir in Huanjiang Oilfield is a low-porosity, ultra-low permeability reservoir, but there are still some relatively high porosity and high permeability reservoirs in some local areas. The Chang 6 reservoir has an average porosity of 7.43% and an average permeability of 0.15×10-3 μm2. The pore types of the target layer are mainly intergranular pores and feldspar dissolution pores, and a small amount of lithic dissolution pores, intergranular dissolution pores, intercrystalline pores and micro-cracks are also developed.

(3) The mercury intrusion experiment showed that the pores of the Chang 6 member were poorly sorted and the pore structure was complicated. Diagenesis is a major factor affecting the pore structure of the reservoir. The diagenesis experienced by this reservoir mainly includes compaction, pressure solution, cementation, metasomatism and dissolution.

ACKNOWLEDGEMENTS

This work was not supported by any funds. And we wish to show sincere thanks who have helped this research and all the authors of the references.

REFERENCES

[1] King, E., Valley, J., Stockli, D., Wright, J. (2004) Oxygen isotope trends of granitic magmatism in the Great Basin: Location of the Precambrian craton boundary as reflected in zircons. Geological Society of America Bulletin. 116(3-4), 451-462.

[2] Rong, Y., Pu, W., Zhao, J., Li, K., Li, X., Li, X. (2016) Experimental research of the tracer characteristic curves for fracture-cave structures in a carbonate oil and gas reservoir. Journal of Natural Gas Science and Engineering. 31, 417-427.

[3] Yang, J., Kang, Y., Sang, Y., Li, Q. (2009) Research on diffusibility of the gas in tight sand gas reservoir. Journal of southwest Petroleum University (Science and Technology Edition). 31(6), 76.

[4] Hickman, A. (2012) Review of the Pilbara Craton and Fortescue Basin, Western Australia: Crustal evolution providing environments for early life. Island Arc. 21(1), 1-31.

[5] Djuraev, U., Jufar, S., Vasant, P. (2017) A review on conceptual and practical oil and gas reservoir monitoring methods. Journal of Petroleum Science and Engineering. 152, 586-601.

[6] Tan, Y., Pan, Z., Feng, X.T., Zhang, D., Connell, L.D., Li, S. (2019) Laboratory characterization of fracture compressibility for coal and shale gas reservoir rocks: A review. International Journal of Coal Geology. 204, 1-17.

[7] Chen, J., Kang, Y., You, L., Fang, J. (2011) Review and prospect about study on stress-sensitivity of low-permeability reservoir. Natural Gas Geoscience. 22(1), 182-189.

[8] Rui, Z., Lu, J., Zhang, Z., Guo, R., Ling, K., Zhang, R., Patil, S. (2017) A quantitative oil and gas reservoir evaluation system for development. Journal of Natural Gas Science and Engineering. 42, 31-39.

[9] Hong, D., Cao, J., Wu, T., Dang, S., Hu, W., Yao, S. (2020) Authigenic clay minerals and calcite dissolution influence reservoir quality in tight sandstones: Insights from the central Junggar Basin, NW China. Energy Geoscience. 1(1-2), 8-19.

[10] Xu, C., Kang, Y., You, Z., Chen, M. (2016) Review on formation damage mechanisms and processes in shale gas reservoir: known and to be known. Journal of Natural Gas Science and Engineering. 36, 1208-1219.

[11] Giles, M., Stevenson, S., Martin, S., Cannon, S., Hamilton, P., Marshall, J., Samways, G. (1992) The reservoir properties and diagenesis of the Brent Group: A regional perspective. Geo-logical Society, London, Special Publications. 61(1), 289-327.

[12] Taylor, T., Giles, M., Hathon, L., Diggs, T., Braunsdorf, N., Birbiglia, G., Espejo, I. (2010) Sandstone diagenesis and reservoir quality prediction: Models, myths, and reality. AAPG Bulletin. 94(8), 1093-1132.
[13] Swarbrick, R. (1994) Reservoir diagenesis and hydrocarbon migration under hydrostatic palaeopressure conditions. Clay Minerals. 29(4), 463-473.
[14] Schmidt, V., McDonald, D. (1979) The role of secondary porosity in the course of sandstone diagenesis. SEPM. 26, 175-207.
[15] Ali, S., Clark, W., Moore, W., Dribus, J. (2010) Diagenesis and reservoir quality. Oilfield Review. 22(2), 14-27.
[16] Yuan, G., Cao, Y., Jia, Z., Gluyas, J., Yang, T., Wang, Y., Xi, K. (2015) Selective dissolution of feldspars in the presence of carbonates: The way to generate secondary pores in buried sandstones by organic CO2. Marine and Petroleum Geology. 60, 105-119.
[17] Valencia, F., Laya, J. (2020) Deep-burial dissolution in an Oligocene-Miocene giant carbonate reservoir (Perla Limestone), Gulf of Venezuela Basin: Implications on microporosity development. Marine and Petroleum Geology. 113, 104144.
[18] Dong, S., Zeng, L., Lyu, W., Xia, D., Liu, G., Wu, Y., Du, X. (2020) Fracture identification and evaluation using conventional logs in tight sandstones: A case study in the Ordos Basin, China. Energy Geoscience. 1(3-4), 115-123.
[19] Bevan, J., Savage, D. (1989) The effect of organic acids on the dissolution of K-feldspar under conditions relevant to burial diagenesis. Mineralogical Magazine. 53(372), 415-425.
[20] Ehrenberg, S., Walderhaug, O., Bjørlykke, K. (2012) Carbonate porosity creation by mesogenetic dissolution: Reality or illusion? AAPG Bulletin. 96(2), 217-233.
[21] Zhang, Y., Long, H. (2012) Reservoir characteristics and influencing factors of Chang 6 reservoir in Huanjiang Oilfield. Petrochemical Industry Application. 31, 66-71.
[22] Longlong, L., Jinliang, Z., Zhongqiang, S., Ruoshan, W., Tao, Y. (2017) Diagenesis of Chang 6 formation of Hu 2 block, Huanjiang Oilfield, Ordos Basin. Petroleum Science and Technology. 35(24), 2296-2302.
[23] Yang, Y., Li, W., Ma, L. (2005) Tectonic and stratigraphic controls of hydrocarbon systems in the Ordos basin: A multicycle Cratonic Basin in central China. AAPG Bulletin. 89(2), 255-269.

Received: **25.12.2020**
Accepted: **03.02.2021**

CORRESPONDING AUTHOR

Jianming Yang
PetroChina Changqing Oilfield Company Oil Production Plant No.7,
Xi'an, 710000 – China

e-mail: 2948979328@qq.com

© by PSP Volume 30– No. 05/2021 pages 5385-5394 Fresenius Environmental Bulletin

SENSITIVITY ANALYSIS OF STEAM INJECTION PARAMETERS OF STEAM INJECTION THERMAL RECOVERY TECHNOLOGY

Rui Deng[1,*], Ming Li[2], Song Linghu[3], Ruixiang Yang[3]

[1]Key Laboratory of Exploration Technologies for Oil and Gas Resources, Ministry of Education (Yangtze University), Wuhan, Hubei, 430100, China
[2]Well Testing Company, PetroChina Qinghai Oilfield Company, Mangya, Qinghai, 817500, China
[3]CNPC Logging Company Limited, Xian, Shaanxi, 710077, China

ABSTRACT

Heavy oil resources are an important part of the future energy structure worldwide. The main method of heavy oil extraction is thermal extraction. Reasonable selection of steam injection parameters is of great significance to reduce the heat loss of pipelines and wellbore, increase the service life of pipes and wellbore, and improve the economic benefits of heavy oil production. In this paper, the actual field data is used to analyze the sensitivity of various steam injection parameters including boiler outlet parameters and wellhead injection parameters. The research results show that under the same steam injection rate, the heat loss rate increases with the increase of pipeline length; as the steam injection rate increases, the heat loss rate gradually decreases. The steam quality of the bottom hole increases slightly with the increase of steam injection time, but the increase is not very large. The bottom hole steam pressure gradually decreases with the increase of steam injection rate. For the same steam injection rate, when the steam injection rate is small (steam rate $\leqslant$ 150 t/d), the bottom steam pressure is greater than the wellhead steam pressure; on the contrary, when the steam rate is large When, the bottom steam pressure is less than the wellhead steam pressure. As the dryness of the injected steam at the wellhead increases, the heat loss rate at the bottom of the well gradually decreases. With the increase of wellhead injection steam pressure, the bottom hole heat loss rate continues to increase, and the steam dryness continues to decrease. This research is of great significance for improving the economic benefits of heavy oil production.

KEYWORDS:
Heavy oil resources, steam injection thermal recovery technology, sensitivity of steam injection parameters, heat loss rate, economic benefits.

INTRODUCTION

The distribution of heavy oil reservoirs is very wide. Almost every oil producing country in the world has heavy oil, but heavy oil reservoirs are mainly distributed in the United States, Canada, Venezuela and Russia [1-4]. China's heavy oil resources are also very rich and widely distributed [5-8]. At present, a large number of heavy oil reservoirs have been discovered in 12 large and medium oil-bearing basins and regions including Songliao Basin, Bohai Bay Basin, Junggar Basin, Nanxiang Basin and Erlian Basin [9-14]. In the past, the development of heavy oil was mainly concentrated in the American continent, and some countries have a history of mining for more than a hundred years. In the past 30 years, the Asian heavy oil development industry has also begun to rise [15-18]. By the early 1980s, China's heavy oil resources had also begun to be developed. At present, China's annual production of heavy oil has reached 13 million tons, accounting for 10% of China's total crude oil production [19-21]. It has become an important part of the petroleum industry. China has become one of the four major heavy oil mining countries [22-24]. Heavy oil resources are a huge potential resource in China and play a vital role in the future energy structure [25-27].

The main method of heavy oil extraction is thermal extraction. It mainly uses steam stimulation technology, that is, heating water to 300-400 °C to become saturated steam, and then injecting the steam into the oil layer, thereby reducing the viscosity of heavy oil. The sensitivity analysis of steam injection parameters is an important evaluation content in steam injection thermal recovery technology [28-30].

Since the 1950s, some scholars have studied the heat loss and pressure loss during steam injection [31-34]. The initial research focused on the calculation of heat loss in the wellbore [35-36]. For example, Moss and White et al. studied the heat loss in the wellbore when hot or cold fluid was injected through the casing. Hans studied the heat loss from the tubing and from the casing, and proposed that the heat loss from the tubing is actually less.

With the extensive exploitation of heavy oil

fields in China, a group of scholars have also made significant contributions to the study of heat transfer during steam injection [37-38]. Hu expounded the concept and simple calculation method of the total heat transfer coefficient of the wellbore on the basis of the predecessors. Later, Wang proposed that the total heat transfer coefficient of the wellbore is a function of time and depth, and the calculation of the heat loss in the wellbore should be done in sections. Based on the comprehensive model of two-phase flow and heat transfer, Shen analyzed the flow state of wet steam in surface pipelines and wellbore and the unstable heat transfer process in the wellbore, and calculated the heat loss, pressure loss and steam loss in surface pipelines and wellbore. Ma et al. made a detailed analysis of the steam flow along the wellbore, and proposed that heat transfer includes three methods: heat transfer, convection and radiation.

Reasonable selection of steam injection parameters is of great significance to reduce the heat loss of pipelines and wellbore, increase the service life of pipes and wellbore, and improve the economic benefits of heavy oil production. In this paper, the actual field data is used to analyze the sensitivity of various steam injection parameters including boiler outlet parameters and wellhead injection parameters. This research is of great significance for improving the economic benefits of heavy oil production.

DATABASES AND METHODS

Steam flooding is also known as Steam Drive. It is a process of continuously injecting steam into the well through an appropriate injection-production well pattern, forming a saturated steam zone around the steam injection well, heating the crude oil, and driving the crude oil to the surrounding production wells (Figure 1). Generally, heavy oil reservoirs are first swallowed and puffed by steam, and then transferred to steam flooding. Steam huff and puff can only produce crude oil in the reservoirs near each oil well, leaving a large number of dead oil areas between the wells. Therefore, the general crude oil recovery rate is only 10%-20%. When steam flooding is used, a large amount of high-temperature and high-pressure steam is continuously injected into the injection well to drive the crude oil to the surrounding production wells for production, which increases the crude oil recovery rate by 20-30% or even more. Steam flooding is more complicated, more difficult, and more risky than steam stimulation technology. However, steam flooding is an effective method to significantly improve the recovery of heavy oil, so it is the main thermal recovery technology.

In the process of steam flowing through surface pipelines, the boiler outlet steam injection parameters have a great influence on the steam reaching the wellhead. Unreasonable boiler outlet steam parameters will increase the heat loss of the ground pipeline and affect the steam dryness. In this paper, field data is used to conduct sensitivity analysis on various

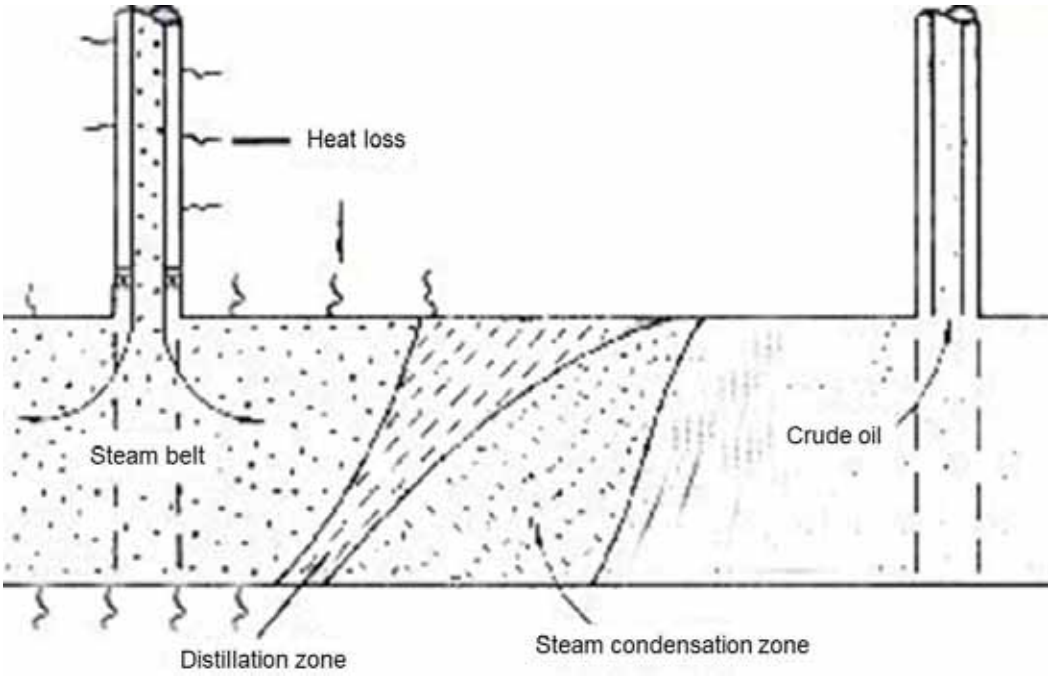

FIGURE 1
Schematic diagram of steam flooding process.

TABLE 1
Basic data of ground pipelines.

Name and unit	Value
Pipeline length (m)	1 000.00
Inner diameter of pipeline (m)	0.20
Outside diameter of pipe (m)	0.22
Insulation layer thickness (m)	0.05
Thermal conductivity of insulation (W/m°C)	0.05
Ambient temperature (°C)	10.00
Local wind speed (m/s)	2.00
Blackness of outer surface of insulation layer	0.25

TABLE 2
Basic wellbore data.

Insulation material thickness (m)	0.01		Formation thermal diffusivity (m^2/s)		9.972E-7	
Thermal conductivity (W/m°C)	Annulus liquid	0.26	Strata	2.65	Cement ring	0.52
	Annulus gas	0.07			Insulation materials	0.91
Formation temperature (°C)	Temperature gradient (°C /m)	0.02			Surface temperature (°C)	10.00
Wall blackness	Outer wall of tubing	0.65			Inner wall of casing	1.00
Bell mouth depth (m)	268				Wellbore radius (m)	0.13
Casing	Outer radius (m)	0.085 0			Inner radius (m)	0.080
Tubing	Outer radius (m)	0.036 5			Inner radius (m)	0.031

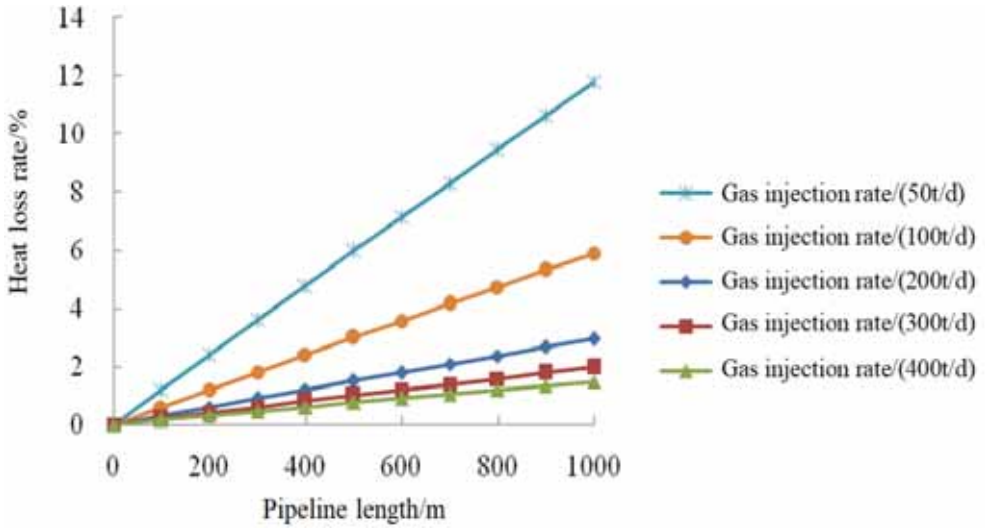

FIGURE 2
The heat loss rate along the pipeline at different steam injection rates.

steam injection parameters of surface pipelines. We mainly analyzed the influence of boiler outlet steam rate, steam quality, and steam pressure on the heat loss rate of surface pipelines. The basic data used is shown in Table 1.

In steam injection wells, the wellhead steam injection parameters not only have a great impact on the bottom-hole steam injection conditions, but also affect the casing temperature and the area where the steam acts on the formation. In this paper, actual data from on-site steam injection wells are used to calculate the wellbore steam injection parameters and analyze the influence of each parameter on bottom hole steam injection conditions and casing temperature. It mainly includes the influence of wellhead steam injection time, steam injection dryness, steam injection rate and steam injection pressure on the bottom hole (bell mouth) heat loss rate, dryness, casing temperature and bottom hole pressure respectively. The basic data used is shown in Table 2.

RESULTS

Influence of steam injection rate on heat loss in pipeline. The steam injection rate is a very important parameter in the steam injection process. The steam injection rate will directly affect the oil displacement efficiency and the development effect of heavy oil. Moreover, the higher the steam injection rate, the higher the cost. Therefore, choosing a reasonable steam injection rate can take into account the thermal recovery effect and the mining cost.

When the boiler outlet pressure is 4.1 MPa, the temperature is 252℃, and the steam quality is 0.76, different boiler outlet steam injection rates are selected for calculation. The change of steam heat loss rate along the pipeline is analyzed as shown in Figure 2.

It can be seen from Figure 2 that when other injection conditions are constant and the same steam injection rate, the heat loss rate increases with the increase of the pipeline length. As the steam injection rate increases, the heat loss rate gradually decreases. The reason is that the larger steam flow rate reduces the contact time of the hot steam with the pipeline, thereby reducing the heat transferred to the environment. But when the steam injection rate is very large, reaching 300 t/d and 400 t/d, the degree of heat loss reduction is not very obvious.

Influence of steam quality on heat loss in pipeline. When the boiler outlet pressure is 4.1 MPa, the outlet temperature is 260℃, and the steam rate is 127 t/d, different steam injection dryness is selected to analyze its influence on the surface pipeline heat loss rate. The analysis result is shown in Figure 3.

It can be seen from Figure 3 that when other injection conditions are constant, the heat loss rate increases with the increase of the pipeline length under the same steam injection dryness. When the steam dryness increases, the heat loss rate gradually decreases. The reason is that in the saturated state, the temperature and pressure of the steam remain the same, so the heat loss remains the same. However, the increase in steam quality will increase the enthalpy value of the steam and increase the total heat content of the injected steam, so the heat loss rate is reduced.

Influence of steam pressure on heat loss in pipeline. When the steam is saturated, the temperature of the steam is determined by the pressure of the

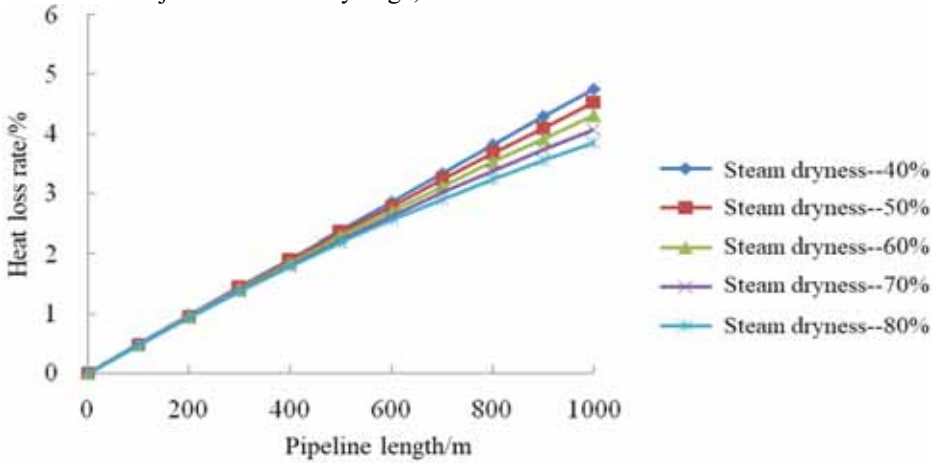

FIGURE 3
The change of heat loss rate along the pipeline under different steam injection dryness.

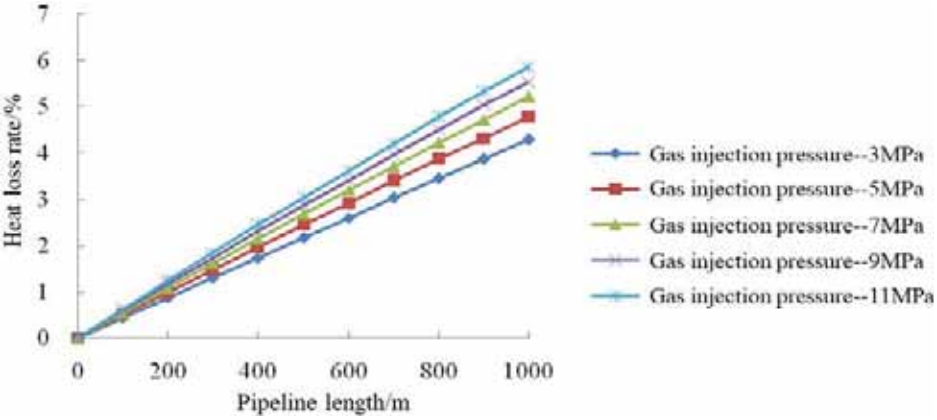

FIGURE 4
The heat loss rate along the pipeline under different steam injection pressures.

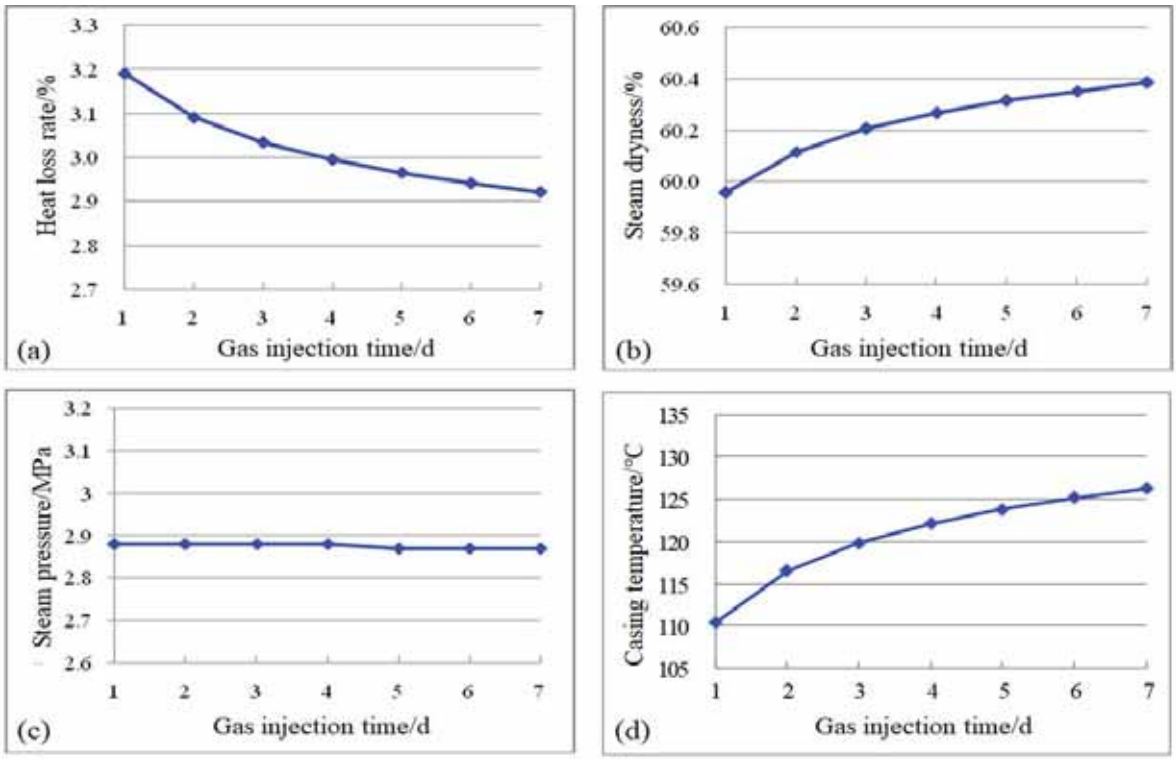

FIGURE 5
Sensitivity analysis of steam injection time.
Notes: (a) Bottom hole heat loss rate; (b) Bottom hole steam quality; (c) Bottom hole steam pressure; (d) Bottom hole heat loss rate.

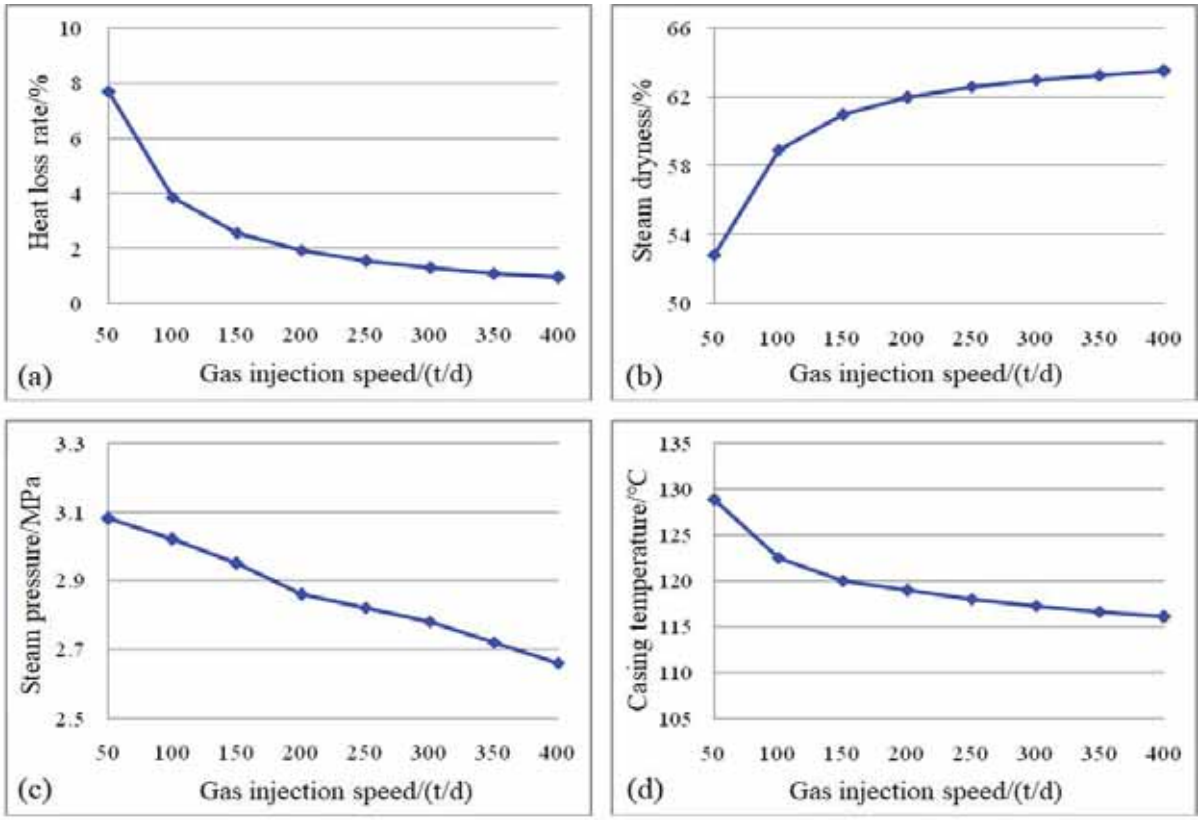

FIGURE 6
Sensitivity analysis of steam injection rate.
Notes: (a) Bottom-hole heat loss rate; (b) Bottom-hole steam dryness; (c) Bottom-hole steam pressure; (d) Bottom-hole casing temperature.

steam. The higher the pressure, the higher the steam temperature, so we only analyze the effect of steam pressure on the heat loss of the pipeline. When the boiler outlet steam temperature is 260℃, the rate is 127 t/d, and the steam quality is 0.76, different boiler outlet pressures are selected to analyze the influence of the change of steam injection pressure on the heat loss rate of surface pipelines. The analysis result is shown in Figure 4. It can be seen from Figure 4 that under the same steam pressure, the heat loss rate increases as the length of the pipeline increases; when the steam pressure increases, the heat loss rate also increases. The reason is that when the steam pressure increases, the steam temperature increases, and the greater the heat transfer from the steam to the outside. Therefore, the heat loss rate is greater.

Sensitivity of steam injection time. In the case of wellhead steam injection pressure of 3.2 MPa, steam temperature of 237.5℃, steam rate of 180 t/d, and wellhead steam dryness of 65%, Figure 5 shows the calculation results of bottom hole steam parameters and wellbore heat loss rate.

It can be seen from Figure 5a that when the steam injection time increases, the heat loss rate at the bottom of the well continues to increase. In addition, it can be seen from Figure 5b that the steam quality at the bottom of the well increases slightly with the increase of steam injection time, but the increase is not very large. This is mainly because the temperature of the formation around the wellbore will continue to rise with the increase of steam injection time, which causes the temperature difference between the formation and the steam to gradually decrease, and the heat transfer decreases. The heat loss rate of the wellbore is gradually reduced, and the steam dryness will also be reduced.

It can be seen from Figure 5c that the pressure of steam in the wellbore basically does not change with the steam injection time. The bottom hole casing temperature gradually increases with the injection time (Figure 5d). This is because as the injection time increases, steam continuously transfers heat to the formation through the casing, so the casing temperature gradually increases.

Sensitivity of steam injection rate. For the wellhead steam injection pressure of 2.9 MPa, steam temperature of 232.5℃, steam dryness of 65%, steam injection time of 3 days, Figure 6 shows the bottom hole steam parameters and the calculation results when the wellhead steam rate is 50 t/d to 400 t/d.

It can be seen from Figure 6a that the bottom hole heat loss rate gradually decreases with the increase of the steam injection rate. After the steam injection rate increases to 150 t/d, the heat loss rate is not significantly reduced. This is because at a certain steam injection pressure, the steam injection rate increases, which reduces the time the steam stays in the wellbore. Correspondingly, the steam dryness of the wellbore will increase (Figure 6b). Therefore, in order to increase the dryness of steam injected into the bottom of the well, the steam injection rate should be appropriately increased. However, the steam injection rate is related to the formation conditions, and the actual steam injection rate should not be higher than this value.

It can be seen from Figure 6c that the bottom-hole steam pressure gradually decreases with the increase of steam injection rate. For the same steam injection rate, when the steam injection rate is small (steam rate ≤150 t/d), the bottom-hole steam pressure is greater than the wellhead steam pressure. On the contrary, when the steam rate is high, the bottom steam pressure is lower than the wellhead steam pressure. This is because when steam flows downwards in the wellbore, gravity causes the pressure of the steam to increase. When the steam rate is small, the frictional resistance in the wellbore is small, and the gravity of the steam offsets part of the frictional resistance, which increases the pressure of the steam along the wellbore. As the steam rate increases, the frictional resistance gradually increases. If the steam gravity exceeds the steam gravity, the steam pressure in the wellbore will decrease along the wellbore.

As the steam injection rate increases, the bottom hole casing temperature gradually decreases, as shown in Figure 6d. This is because as the steam rate increases, the heat transfer from the wellbore to the formation decreases, and the bottom hole heat loss decreases, so the casing temperature decreases.

Sensitivity of steam dryness. For the wellhead injection steam pressure of 3.2 MPa, steam temperature of 237.5℃, steam rate of 180 t/d, and steam injection time of 3 days, Figure 7 shows the calculation results of wellhead steam quality of 30% to 80%, bottom hole steam parameters and wellbore heat loss rate.

It can be seen from Figures 7a and 7b that as the dryness of the injected steam at the wellhead increases, the heat loss rate at the bottom of the hole gradually decreases, and the steam dryness at the bottom of the hole gradually increases. Therefore, if we want to improve steam injection efficiency and reduce heat loss, we should try our best to increase steam injection dryness when economic benefits allow.

It can be seen from Figure 7c that the bottom-hole steam pressure gradually decreases with the increase of steam injection quality. This is because as the dryness increases, the volume flow rate of wet steam increases, which in turn increases the frictional resistance. The final pressure loss will also increase. With the increase of steam injection dryness, the bottom hole casing temperature gradually decreases (Figure 7d). This is because the increase in steam quality leads to a decrease in the heat loss rate

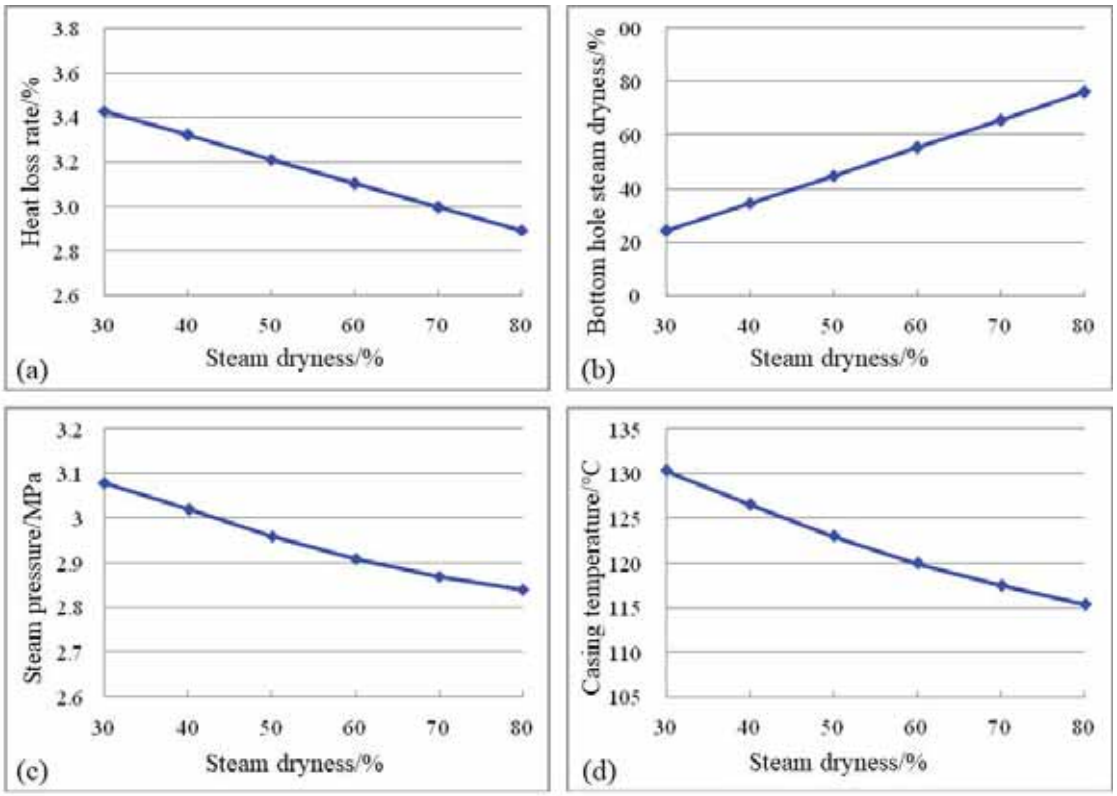

FIGURE 7
Sensitivity analysis of steam dryness.
Notes: (a) Bottom-hole heat loss rate; (b) Bottom-hole steam dryness; (c) Bottom-hole steam pressure; (d) Bottom-hole casing temperature.

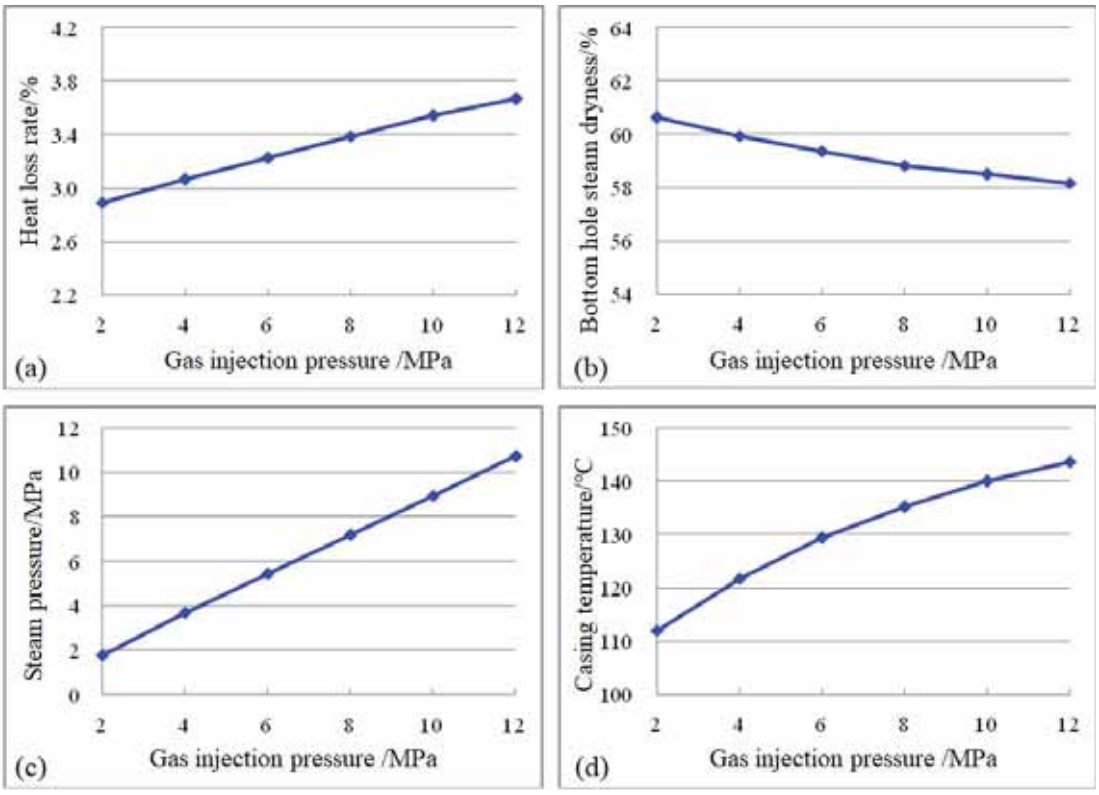

FIGURE 8
Sensitivity analysis of steam injection pressure.
Notes: (a) Bottom-hole heat loss rate; (b) Bottom-hole steam dryness; (c) Bottom-hole steam pressure; (d) Bottom-hole casing temperature.

of the wellbore, so the heat transferred to the formation by the steam decreases, which in turn reduces the casing temperature.

Sensitivity of steam injection pressure. For the wellhead steam dryness is 65%, the steam injection time is 3 days, and the steam rate is 180 t/d, Figure 8 shows the calculation results of bottom hole steam parameters and wellbore heat loss rate when the wellhead steam pressure is 2 MPa to 12 MPa.

It can be seen from Figure 8a and Figure 8b that with the increase of steam injection pressure at the wellhead, the bottom hole heat loss rate continues to increase, and the steam dryness continues to decrease. The reason is that if the steam flows down from the wellhead, the higher the temperature of the steam, the more heat it transfers to the formation, and the faster the dryness decreases. The casing temperature is determined by the heat transferred and the heat transfer coefficient. In the case of a constant heat transfer coefficient, the higher the steam pressure, the more heat transferred, and the higher the temperature of the casing (Figure 8c-d).

CONCLUSIONS

(1) In this paper, the actual field data is used to analyze the sensitivity of various steam injection parameters including boiler outlet parameters and wellhead injection parameters.

(2) The research results show that under the same steam injection rate, the heat loss rate increases with the increase of pipeline length; as the steam injection rate increases, the heat loss rate gradually decreases. The steam quality of the bottom hole increases slightly with the increase of steam injection time, but the increase is not very large.

(3) The bottom hole steam pressure gradually decreases with the increase of steam injection rate. For the same steam injection rate, when the steam injection rate is small (steam rate $\leqslant$150 t/d), the bottom steam pressure is greater than the wellhead steam pressure; on the contrary, when the steam rate is large When, the bottom steam pressure is less than the wellhead steam pressure.

(4) As the dryness of the injected steam at the wellhead increases, the heat loss rate at the bottom of the well gradually decreases. With the increase of wellhead injection steam pressure, the bottom hole heat loss rate continues to increase, and the steam dryness continues to decrease.

ACKNOWLEDGEMENTS

This word was supported by the Key Project of Science and Technology Research Program of Hubei Provincial Department of Education (grant number D20191302) and the Open Fund of State Key Laboratory of Oil and Gas Reservoir Geology and Exploitation (Chengdu University of Technology, PLC20190501).

REFERENCES

[1] Mahdi, H., Kamy, S. (2015) XFEM-Based CZM for the Simulation of 3D Multiple-Cluster Hydraulic Fracturing in Quasi-Brittle Shale Formations. Rock Mechanics and Rock Engineering. 49, 1-18.

[2] Mandal, D., Tewari, D., Rautela, M. (2004) Analysis of Micro-fractures in coal for coal bed methane exploitation in Jharia coal field. 5th conference and exposition on petroleum geophysics. Hyderabad India Jan. 15-17. 904-909.

[3] Che, C. (2006) A new round of national oil and gas resource evaluation results report of coalbed methane resource, Beijing: Ministry of Land and Resources of PRC.

[4] Kan, W., Jon, E. (2014) Simultaneous multifracture treatment: fully coupled fluid flow and fracture mechanics for Horizontal Wells. SPE. 167626, 1-9.

[5] Clarkson, C., Bustin, R., Seidle, J. (2007) Production-data analysis of single-phase (gas) coalbed-methane Wells. SPE. 100313-PA, 312-330.

[6] Bumb, A., McKee, C. (1988) Gas-well testing in the presence of desorption for coal bed methane and Devonian Shale. SPE. 15227-PA, 179- 184.

[7] Nicolas, L., Valdiviezo, M. (2016) Rock physics templates for integrated analysis of shales considering their mineralogy, organic matter and pore fluids. Journal of Petroleum Science and Engineering. 137, 33-41.

[8] Goodway, B., Perez, M., Varsek, J. (2010) Seismic petrophysics and isotropic- anisotropic AVO methods for unconventional gas exploration. The Leading Edge. 29(12), 1500-1508.

[9] Sayers, C. (2005) Seismic anisotropy of shales. Geophysical Prospecting. 53, 667-676.

[10] Ortega, J., Ulm, F., Abousleiman, Y. (2007) The effect of the nano- granular nature of shale on their poroelastic behavior. Acta Geotechnica. 2, 155-182.

[11] Sobhaniaragh, B., Mansur, W., Peters, F. (2016) Three-dimensional investigation of multiple stage hydraulic fracturing in unconventional reservoirs. Journal of Petroleum Science and Engineering. 146, 1063-1078.

[12] Wang, H. (2016) Numerical investigation of fracture spacing and sequencing effects on multiple hydraulic fracture interference and coalescence in brittle and ductile reservoir rocks. Engineering Fracture Mechanics. 157, 107-124.

[13] Wu, K., Jon, E. (2016) Mechanisms of Simultaneous Hydraulic-Fracture Propagation From Multiple Perforation Clusters in Horizontal Wells SPE Journal. 21(3), 1000-1008.
[14] Varahanaresh, S., Ahmad, G. (2015) A numerical study of sequential and simultaneous hydraulic fracturing in single and multi-lateral horizontal wells Journal of Petroleum Science and Engineering. 132, 65-76.
[15] Ramagost, B., Farshad, F. (1981) P/Z Abnormally Pressured Gas Reservoirs. SPE. 10125, 4-7.
[16] Seidle, J. (1993) Long-term gas deliverability of a dewatered coalbed. Journal of Petroleum Technology. 45(6), 564-568.
[17] Maghadam, S., Jeje, O., Mattar, L. (2011) Advanced gas material balance in simplified format. Journal of Canadian Petroleum Technology. 90-98.
[18] Pletcher, J. (2000) Improvements to reservoir material balance methods. SPE. 62882, 1-4.
[19] El-Banbi, A., Wattenbarger, R. (1998) Analysis of linear flow in gas flow production. SPE. 39972, 15-18.
[20] Huang, J., Dong, D., Li, J. (2016) Reservoir characteristics and its influence on continental shale: An example from Triassic Xujiahe Formation shale, Sichuan Basin. Earth Science Frontiers. 23(2), 158-166.
[21] Xue, B., Zhang, G., Wu, H. (2008) Three-dimensional numerical simulation of hydraulic fracture in oil wells. Journal of University of Science and Technology of China. 38(15), 1323-1325.
[22] Wang, X., Liu, C., Wang, H. (2016) Comparison of consecutive and alternate hydraulic fracturing in horizontal wells using XFEM-based cohesive zone method. Journal of Petroleum Science and Engineering. 143, 14-25.
[23] Armstrong, R., Wildenschild, D., Bay, B. (2015) The effect of pore morphology on microbial enhanced oil recovery. Journal of Petroleum Science and Engineering. 130, 16-25.
[24] Farrell, N., Healy, D., Taylor, C. (2014) Anisotropy of permeability in faulted porous sandstones. Journal of Structural Geology. 63, 50-67.
[25] Zhang, D., Ranjith, P., Perera, M. (2016) The brittleness indices used in rock mechanics and their application in shale hydraulic fracturing: A review. Journal of Petroleum Science and Engineering. 143, 158-170.
[26] Wang, S., Sloan, S., Fityus, S. (2013) Numerical Modeling of Pore Pressure Influence on Fracture Evolution in Brittle Heterogeneous Rocks. Rock Mechanics and Rock Engineering. 46(5), 1165-1182.
[27] Nobakht, M., Clarkson, C., Kaviani, D. (2012) New and improved methods for performing rate-Transient Analysis of Shale Gas Reservoirs. SPE147869, 335-349.
[28] Rahman, N., Anderson, D., Mattar, L. (2006) New rigorous material balance equation for gas flow in a compressible formation. SPE 100563, 15-17.
[29] Klinkenberg, L. (1941) The permeability of porous media to liquids and gases. API Drilling & Production Practice. 200-212.
[30] Ma, S., Guo, J., Li, L. (2015) Influence of pore pressure on tensile fracture growth in rocks：a new explanation based on numerical testing. Frontiers of Earth Science. 9(3), 412-426.
[31] Gong, D., Qu, Z., Li, J. (2016) Extended finite element simulation of hydraulic fracture based on ABAQUS platform. Rock and Soil Mechanics. 37(5), 1513-1520.
[32] Boone, T., Ingraffea, A. (1990) Numerical procedure for simulation of hydraulically driven fracture propagation in poroelastic media. International Journal of Numerical Analysis and Modeling. 14(1), 27-47.
[33] Robert, G., Xu, S. (2002) An approximation for the Xu- White velocity. Geophysics. 67(5), 1406-1414.
[34] Gholami, R., Rasouli, V., Sarmadivaleh, M., Minaeian, V., Fakhari, N. (2016) Brittleness of gas shale reservoirs: A case study from the north Perth basin, Australia. Journal of Natural Gas Science and Engineering. 33, 1244-1259.
[35] Yu, W., Luo, Z., Javadpour, F., Varavei, A., Sepehrnoori, K. (2014) Sensitivity analysis of hydraulic fracture geometry in shale gas reservoirs. Journal of Petroleum Science and Engineering. 113, 1-7.
[36] Altamar, R., Marfurt, K. (2014) Mineralogy-based brittleness prediction from surface seismic data: Application to the Barnett Shale. Interpretation. 2(4), 255-271.
[37] Yasin, Q., Du, Q., Sohail, G., Ismail, A. (2017) Impact of organic contents and brittleness indices to differentiate the brittle-ductile transitional zone in shale gas reservoir. Geosciences Journal. 21(5), 779-789.
[38] Larry, K., Jerry, S. (2009) The geomechanics of a shale play: What makes a shale prospective. SPE 125525, Charleston, West Virginia USA. 23-25.

Received: **25.12.2020**
Accepted: **03.02.2021**

CORRESPONDING AUTHOR

Rui Deng
Key Laboratory of Exploration Technologies for Oil and Gas Resources,
Ministry of Education
Yangtze University,
Wuhan Hubei 430100 – China

e-mail: dengrui@yangtzeu.edu.cn

© by PSP Volume 30– No. 05/2021 pages 5395-5399 Fresenius Environmental Bulletin

INVESTIGATION OF THE ANTIMICROBIAL AGENT POTENTIAL OF 1,5-DIKETONE DERIVATIVES

Gursel Korkmaz[1,*], Ugur Tutar[2], Hayreddin Gezegen[3]

[1]Sivas Cumhuriyet University, Sivas Vocational School of Technical Sciences, Department of Textile Technology, Sivas, Turkey
[2]Sivas Cumhuriyet University, Faculty of Pharmacy, Department of Basic Pharmaceutical Sciences, Sivas, Turkey
[3]Sivas Cumhuriyet University, Faculty of Health Science, Department of Nutrition and Dietetics, Sivas, Turkey

ABSTRACT

In this study, 1,5-diketones were synthesized by adding of cyclohexanone to five different chalcone derivatives (1a-e) via the 1,4-Michael addition reaction. Antimicrobial activities of synthesized compounds were investigated by microdilution method against two gram negative (*Klebsiella pneumoniae, Pseudomonas aeruginosa*) two gram positive (*Staphylococcus aureus, Enterococcus faecalis*) bacteria and one fungal strain (*Candida albicans*). Minimum inhibitory concentration (MIC) values of 3a-e compounds were determined in the range of 62.5-250 μg/mL.

As a result, the compounds with the best activity were 3a, 3b and 3d against *E. faecalis* gram positive bacteria strain with the same MIC value (62.5 μg / mL) as the standard drug TPZ.

KEYWORDS:
1,5-diketone, chalcone, antimicrobial, antibacterial, microdilution

INTRODUCTION

Many bacterial infectious diseases such as tuberculosis, plague and gonorrhea have led to devastating epidemics that have resulted in the deaths of many people. Today, millions of people are still infected by pathogenic bacteria and, as a result, high mortality is observed [1]. Antibiotics have been used for over 60 years to control bacterial infections [2]. Biological or synthetic origin antibiotics have two different effects that kill pathogens (bactericidal) or control their reproduction (bacteriostatic) [3].

Antimicrobial resistance caused by the misuse of antimicrobials has limited the treatment possibilities [4] and the search for new antibiotics has become a great requirement [5]. Antibiotic resistance increases day by day and it causes more than 40% of infectious diseases in some countries [6]. Economic output of 100 trillion dollars is under risk due to the increase in drug-resistant infections [6]. The Global Antibiotic Research and Development Partnership aims to develop up to four new treatments by 2023, by improving available antibiotics and accelerating new antibiotic studies [7].

Chalcones were reported in the many study to have antimicrobial effects [5,8,9]. These compounds were attract attention as synthetic and plant-based therapeutic alternatives despite the undesirable effects of currently used drugs [9]. Chalcones are α, β-unsaturated ketones that play role in the biosynthesis of flavonoids commonly found in plants [10]. In their structure, two aromatic rings are connected by three carbons and α, β-unsaturated carbonyl or a saturated carbonyl group are observed in its straight chain (Figure 1). Studies on chalcones have shown that these compounds have many biological activities such as anticancer [11], antimalarial [12], antioxidant [13], antifungal [14] and antibacterial [15].

Chalcones are very active compounds synthetically as well as their biological activities. 1,5-Diketone derivatives, that very important intermediates in the synthesis of heterocyclic compounds [16], can be synthesized from chalcones by the 1,4-Michael addition reaction easily [16]. Although studies on the synthesis of 1,5-diketones are reported in the literature, studies on their biological activities are rare. Kharchenko et al. (1988) synthesized chlorine-substituted 1,5 diketones and some of their cyclization products (thiopyrlium salts, 3-chloropyridines and 2-benzoylpyrroles) to investigate their biological activity [17]. They found that 2,4-dichloro-substituted 1,5-diketones exhibited antimicrobial activity against *Staphylococcus aureus*, *Escherichia coli*, *Pseudomonas aeruginosa*, *Candida albicans* microorganisms with an MIC of 50-100 μg / mL. These compounds also exhibited antiviral effects by inactivating MS-2 phage in the range of 25-43%. In the light of this information, we aimed to investigation of antimicrobial agents potential of the 1,5-diketone derivatives (3a-e) that obtained by 1,4-addition of cyclohexanone to 5 different chalcone derivatives (1a-e).

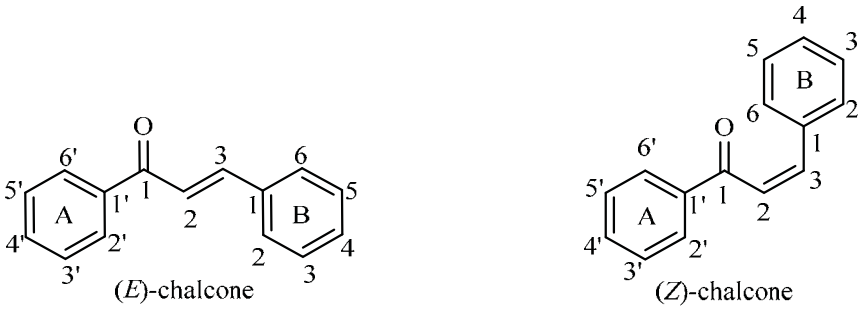

FIGURE 1
General structure of chalcones

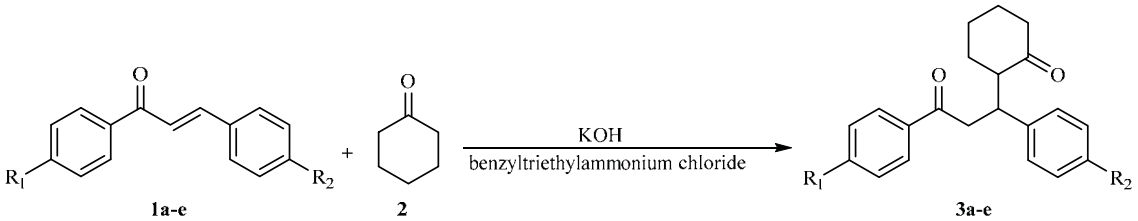

	3a	3b	3c	3d	3e
R_1	$-OCH_3$	$-OCH_3$	$-CH_3$	$-CH_3$	$-OCH_3$
R_2	-Br	-Cl	$-CH_3$	$-OCH_3$	$-CH_3$

FIGURE 2
Synthesis of 1,5-diketones compounds

MATERIALS AND METHODS

Material. Two gram negative (*Klebsiella pneumoniae* ATCC 10031, *Pseudomonas aeruginosa* ATCC 27853), two gram positive (*Staphylococcus aureus* ATCC 25923, *Enterococcus faecalis* ATCC 29212) bacterial strain and one fungal strain (*Candida albicans* ATCC 29212) was used to evaluate the biological activities of 1,5-diketone compounds. Microorganisms were supplied from Sivas Cumhuriyet University Health Services Application and Research Hospital Microbiology Laboratory. Piperacillin / tazobactam (TPZ) at a ratio of 8/1 was used as the standard drug.

Method. Synthesis of 1,5-Diketones (3a-e). 1,5-Diketones (3a-e) were synthesized by treatment of the cyclohexanone (2) (6 mmol) to chalcones (1a-e) (3 mmol) presence of benzyltriethylammonium chloride (10% mol) and KOH (5M, 0.2 mL) in CH_2Cl_2 (5 mL) at room temperature for 3h (Fig. 2). After the reaction is complete obtained product was extracted with CH_2Cl_2 (3x10 mL). Extract was dried (Na_2SO_4), and the solvent was evaporated in vacuum. The crude product was crystallized from EtOH/Et_2O 3:1 [18,19]. Spectral analysis of the synthesized 1,5-diketones (3a-e) was made in comparison with previous studies [19].

Preparation of microorganisms. Microorganism solutions were prepared in 5 mL of broth to revitalization ATCC strains kept at -20 °C. The solutions were incubated at 37 °C for 24 hours. At the end of this period, it was determined that the microorganisms were alive.

Antimicrobial activity. Dilutions of 1,5-diketone compounds were prepared in accordance with the literature [20]. Stock solutions at a concentration of 1000 µg/mL were prepared in the presence of DMSO. The prepared solutions were mixed in vortex mixers until a homogeneous mixture was obtained. Second dilutions (500 µg/mL) were obtained by mixing the stock solutions and pure Muller Hinton Broth at a ratio of 1/1. This dilution process was repeated 4 more times for each compound. Thus, six dilutions in the range 1000-31.25 µg / mL were obtained for each compound (3a-e).

Microorganism strains prepared according to 0.5 Mc Farland standard ($1x10^8$ cfu/mL) were added to the microplate wells in a volume of 100 µL [21] . Dilutions of the 1,5-diketone compounds were added to the wells in decreasing concentrations from top to bottom at a ratio of 1/1. Negative control with pure Mueller Hinton Broth and positive control groups with TPZ were prepared. The prepared microplates were incubated at 37 °C for 24 hours. At the end of this period, the turbidity in the wells was compared with the negative control group. Among the wells without turbidity in a same column, the lowest concentration was recorded as the MIC value [20].

Statistical analysis. The data were analyzed in SPSS 22.0 program with "One-way randomized block design" and Tukey test. Minimum and maximum values, arithmetic mean and standard deviation

values were calculated. Tukey test was performed for pairwise comparisons. Statistical analysis was performed with the significance level set at $p < 0.05$.

RESULTS

This study was carried out considering that 1,5-diketone derivatives obtained from chalcone compounds may also have antimicrobial effects like chalcones. 1,5-diketone compounds were obtained by adding cyclohexanone to chalcone derivatives [22]

Exothermic reaction was observed in the preparation of stock solutions. Clear and homogeneous stock solutions were obtained in the presence of DMSO. The MIC values of 1,5-diketone compounds (3a-e) and standard drug (TPZ) are given in Table 1.

One way randomized block design was performed to examine whether MIC values of the compounds differed significantly. Minimum and maximum values, arithmetic mean and standard deviation values were shown in Table 2 and Table 3. In the ANOVA table (Table 4), there was no significant difference between microorganisms ($p > 0,05$). However, a significant difference was found between 1,5-diketone compounds ($p < 0,05$). By Tukey test, 3a-e compounds were examined as paired groups. According to the results, a significant difference was found between 3a and 3e, 3b and 3e, 3c and 3e, and 3d and 3e ($p < 0.05$).

TABLE 1
MIC values of the 1,5-diketone compounds

Microorganisms	MIC (µg/mL) values					
	3a	**3b**	**3c**	**3d**	**3e**	**TPZ**
K. pneumoniae	125	125	125	125	250	31,25
P. aeruginosa	125	250	250	125	250	62,5
S. aureus	125	125	125	250	250	62,5
E. faecalis	62,5	62,5	250	62,5	250	62,5
C. albicans	125	62,5	125	125	250	15,6

MIC: Minimum inhibitory concentration
TPZ: Piperacillin/tazobactam (standart drug)

TABLE 2
Descriptive statistics on microorganisms

Microorganism	N	Minimum	Maximum	Mean	Standard Deviation
K. pneumoniae	5	125,00	250,00	150,00	55,90
P. aeruginosa	5	125,00	250,00	200,00	68,46
S. aureus	5	125,00	250,00	175,00	68,46
E. faecalis	5	62,50	250,00	125,00	76,54
C. albicans	5	62,50	250,00	137,50	68,46

TABLE 3
Descriptive statistics on 1,5-diketon compounds

Compound	N	Minimum	Maximum	Mean	Standard Deviation
3a	5	125,00	250,00	150,00	55,90
3b	5	125,00	250,00	200,00	68,46
3c	5	125,00	250,00	175,00	68,46
3d	5	62,50	250,00	125,00	76,54
3e	5	62,50	250,00	137,50	68,46

TABLE 4
ANOVA for randomized block design of 1,5-Diketone test

Sources of Variation	SS	DF	MS	F_s	p
Model	707324,219[a]	9	78591,580	54,331	,001*
Microorganisms	8886,719	4	2221,680	1,536	,239
Compounds	69042,969	4	17260,742	11,932	,001*
Error	23144,531	16	1446,533		
Total	730468,750	25			

dF: Degree of freedom, **SS:** Sum of square, **MS:** Mean square, **F_s:** F statistic

As seen from the Table 1. compounds 3a-e showed moderate-weak and weak activity (125-250 µg/mL) on *P. aeuruginosa*, *S. aureus* and *K. pneumoniae* bacterial strains relative to the standard drug (31,25-62,5 µg/mL). Compound 3b had moderate-weak activity (62.5 µg/mL) on *C. albicans* fungus strain compared to the standard drug (15.6 µg/mL), while all other compounds had weak activity. On the *E. faecalis* gram positive bacterial strain, it was determined that compound 3a with -OCH_3 and -Br substituents, compound 3b with -OCH_3 and -Cl substituents, and compound 3d with -CH_3 and OCH_3 substituents had as potent activity as the standard drug (62,5 µg/mL). Compound 3e −another compound with -CH_3 and -OCH_3 substituents like the 3d− exhibited a weak activity (250 µg/mL) against all microorganism strains. It appears that the activity results are affected by the binding of the –CH_3 and –OCH_3 substituents to the compounds at different points. These results show how the activity changes depending on the structure.

CONCLUSIONS

In this study, we investigated the antimicrobial activities of five 1,5-Diketone compounds derived from chalcone derivatives by microdilution method against *Klebsiella pneumoniae*, *Pseudomonas aeruginosa*, *Staphylococcus aureus*, *Enterococcus faecalis* bacteria strains and *Candida albicans* fungal strain. 1,5-diketone compounds were obtained from cyclohexanone addition to chalcone derivatives by 1,4 Michael Reaction. The MIC values of the compounds were found to range from 62.5 - 250 µg / mL. Compounds 3a, 3b, 3d with the same MIC value (62.5 µg / mL) as the standard drug TPZ against *E. faecalis* gram positive bacteria strain exhibited a good antimicrobial agent potential. In further studies, these biologically active compounds may play role in investigation of novel therapeutic agents.

ACKNOWLEDGEMENT

This study is a part of Gürsel Korkmaz' s Master Thesis titled "Investigation of the antimicrobial activity of 1,5-diketones obtained from chalcones" (Adviser: Uğur Tutar).

REFERENCES

[1] Khan, S.A., Asiri, A.M. (2017) Green synthesis, characterization and biological evaluation of novel chalcones as anti bacterial agents. Arabian Journal of Chemistry. 10, S2890–S2895.

[2] Osório, T.M., Monache, F.D., Chiaradia, L.D., Mascarello, A., Stumpf, T.R., Zanetti, C.R., Silveira, D.B., Barardi, C.R.M., Smania, E.F.A., Viancelli, A., Garcia, L.A.T., Yunes, R.A., Nunes, R.J., Smania, A. (2012) Antibacterial activity of chalcones, hydrazones and oxadiazoles against methicillin-resistant Staphylococcus aureus. Bioorganic & Medicinal Chemistry Letters. 22(1), 225–230.

[3] Topal, M., Uslu Şenel, G., Arslan Topal, E.I., Öbek, E. (2015) Antibiotics and usage areas. Erciyes University Journal of the Institute of Science and Technology. 31(3), 121–127.

[4] Drew, R.H. (2007) Emerging Options for Treatment of Invasive, Multidrug-Resistant Staphylococcus aureus Infections. Pharmacotherapy. 27(2), 227–249.

[5] Suwito, H., Ni'matuzahroh, B., Kristanti, A.N., Hayati, S., Dewi, S.R., Amalina, I., Puspaningsih, N.N.T., (2016) Antimicrobial Activities and In silico Analysis of Methoxy Amino Chalcone Derivatives. Procedia Chemistry. 18(Mcls 2015), 103–111.

[6] World Antibiotic Awareness Week (2019). https://www.who.int/campaigns/world-antibiotic-awareness-week/world-antibiotic-awareness-week-2019/landing. [Accessed November 18, 2020].

[7] Antimicrobial resistance. https://www.who.?nt/en/news-room/fact-sheets/deta?l/ant?m?crob?al-res?stance. [Accessed November 18, 2020].

[8] Mazimba, O. (2015) Antimicrobial activities of heterocycles derived from thienylchalcones. Journal of King Saud University Science. 27(1), 42–48.

[9] Costa, G.M., Endo, E.H., Cortez, D.A.G., Nakamura, T.U., Nakamura, C.V., Dias Filho, B.P. (2016) Antimicrobial effects of Piper hispidum extract, fractions and chalcones against Candida albicans and Staphylococcus aureus. Journal de Mycologie Médicale Journal of Medical Mycology. 26(3), 217–226.

[10] Burmaoğlu, S. (2017)[Fluoro-Substituted chalcones as the compounds having anticancer activity. Karaelmas Science and Engineering Journal. 7(2), 658–664.

[11] Park, S., Kim, E.H., Kim, J., Kim, S.H., Kim, I. (2018) Biological evaluation of indolizine-chalcone hybrids as new anticancer agents. European Journal of Medicinal Chemistry. 144, 435–443.

[12] Domínguez, J.N., León, C., Rodrigues, J., Gamboa de Domínguez, N., Gut, J., Rosenthal, P.J. (2005) Synthesis and antimalarial activity of sulfonamide chalcone derivatives. Il Farmaco. 60(4), 307–311.

[13] Shenvi, S., Kumar, K., Hatti, K.S., Rijesh, K., Diwakar, L., Reddy, G.C. (2013) Synthesis, anticancer and antioxidant activities of 2,4,5-trimethoxy chalcones and analogues from asaronaldehyde: Structure–activity relationship. European Journal of Medicinal Chemistry. 62, 435–442.
[14] Ming, L.S., Jamalis, J., Al-Maqtari, H.M., Rosli, M.M., Sankaranarayanan, M., Chander, S., Fun, H-K. (2017) Synthesis, characterization, antifungal activities and crystal structure of thiophene-based heterocyclic chalcones. Chemical Data Collections. 9–10, 104–113.
[15] Gopi, C., Sastry, V.G., Dhanaraju, M.D. (2016) Synthesis and spectroscopic characterisation of novel bioactive molecule of 3-(2-substituted)-1H-indol-3-yl)-1-(thiophen-2yl)prop-2-en-1-one chalcone derivatives as effective anti-oxidant and anti-microbial agents. Beni-Suef University Journal of Basic and Applied Sciences. 5(3), 236–243.
[16] Liu, W., Xu, Q., Liang, Y., Chen, B., Liu, W., Ma, Y. (2001) Preparation of 1,5-diketone derivatives containing ferrocenyl by Michael reaction under solvent-free condition. Journal of Organometallic Chemistry. 637–639, 719–722.
[17] Kharchenko, V.G., Chalaya, S.N., Kulikova, L.K., Litvinov, O.V. (1988) ChemInform Synthesis and Biological Activity of Chloro-Substituted 1,5-Diketones and Their Cyclization Products. ChemInform. 19(9), 500–503.
[18] Ceylan, M., Gezegen, H. (2008) Preparation of 1,5-diketones by addition of cyclohexanone to chalcones under solvent-free phase transfer catalyst condition. Turkish Journal of Chemistry. 32(1), 55–61.
[19] Gezegen, H., Tutar, U., Ceylan, M. (2016) Synthesis and antimicrobial activity of racemic 1,5-Diols: 2-(1,3-Diaryl-3-hydroxypropyl)cyclohexan-1-ol derivatives. Helvetica Chimica Acta. 99(8), 608–616.
[20] Tutar, U., Çelik, C., Gezegen, H., Hepokur, C. (2017) Determining antifungal, anti-biofilm and anti- cancer activities of "1,3-di(thiophen-2-yl) prop-2- en-1-one" chalcone derivative. Cumhuriyet Medical Journal. 39(2), 466–472.
[21] Tutar, U. (2018) Anti-Biofilm, antimicrobial and cytotoxic activity of Achillea millefolium L. essential oil. Fresen. Environ. Bull. 27(5A), 3713–3720.
[22] Gezegen, H. (2006) Synthesis of some chalcone derivatives and investigation of their reaction. Unpublished master thesis. Gaziosmanpaşa University, Institute of Science, Tokat.

Received: **25.12.2020**
Accepted: **03.02.2021**

CORRESPONDING AUTHOR

Korkmaz Gursel
Department of Textile Technology,
Sivas Vocational School of Technical Sciences
Sivas Cumhuriyet University,
Sivas 58140 – Turkey

e-mail: gurselkorkmaz7@gmail.com

© by PSP Volume 30– No. 05/2021 pages 5400-5404 Fresenius Environmental Bulletin

ANTIOXIDANT ANTIMICROBIAL OXIDANT AND ELEMENTS CONTENTS OF *XYLARIA POLYMORPHA* AND *X. HYPOXYLON* (XYLARIACEAE)

Beste Gizem Ozbey Saridogan[1], Cemil Islek[2], Hayri Baba[3], Ilgaz Akata[1,*], Mustafa Sevindik[4]

[1]Department of Biology, Faculty of Science, Ankara University, Ankara, Turkey
[2]Department of Biotechnology, Faculty of Art and Sciences, Nigde Omer Halisdemir University, Nigde, Turkey
[3]Department of Biology, Faculty of Art and Sciences, Hatay Mustafa Kemal University, Hatay, Turkey
[4]Department of Food Processing, Bahçe Vocational High School, Osmaniye Korkut Ata University, Osmaniye, Turkey

ABSTRACT

In the current study, antioxidant, oxidant, and antimicrobial potentials of *Xylaria polymorpha* (Pers.) Grev. and *X. hypoxylon* (L.) Grev. were determined. Also, the levels of elements accumulated by these fungi were measured. The samples were extracted with ethanol in soxhlet apparatus. Antioxidant and oxidant potentials were determined using Rel Assay kits. Antimicrobial activities were tested using the agar dilution method. Element contents were determined using atomic absorption spectrophotometer. As a result of the studies, TAS, TOS, and OSI values of *X. hypoxylon* were determined as 3.794±0.188, 8.609±0.171, and 0.228±0.015, respectively. TAS, TOS, and OSI values of *X. polymorpha* were determined as 5.390±0.176, 14.738±0.126, and 0.274±0.008, respectively. Besides, it was observed that the antimicrobial activities of the extracts of mushrooms were effective at 50-400 µg/mL concentrations. Element contents were determined to be at normal levels compared to literature data. As a result, it was determined that *X. polymorpha* and *X. hypoxylon* have antioxidant and antimicrobial potentials.

KEYWORDS:
Antimicrobial, Antioxidant, medicinal mushrooms, Oxidant, Xylaria

INTRODUCTION

Fungi comprise diverse groups of organisms from various lineages and lifestyles and they have crucial roles in ecosystems as well as biodegradation, pharmacology, and food industry. Globally, well over 120.000 fungal species have been described and reported to date and the earth's total fungal diversity is estimated to include 2.2 to 3.8 million species [1]. Macrofungi constitute a sub-section of the kingdom fungi, whose sporophores are recognizable with unaided eye and they comprise two divisions: Ascomycota and Basidiomycota with large, easily distinguishable spores bearing fruit bodies [2]. Humans have utilized macrofungi as nutrient sources and medicinal purposes since long ago. Fruit bodies of mushrooms are rich in vitamins, amino acids, beneficial elements such as iron, zinc, potassium, phosphorus, etc., and polysaccharides, especially including β-glucans. It is ideal for low-fat diets. Other than their nutritional traits, mushrooms exhibit various biological activities such as antimicrobial, antiviral, antioxidant, antitumor, DNA preservative, antiaging, antidiabetic, and anti-inflammatory activities [3-8].

Xylaria is an ascomycetous genus of the family Xylariaceae and its members often grow on dead wood stumps. The genus name was originated from the Greek word "xylon", which means wood. The most well-known and common species of the genus are *X. hypoxylon* and *X. polymorpha*. *X. hypoxylon* (common names: stag's horn and candle-snuff fungus) whose ascocarps have characteristic horn-like appearance. *X. polymorpha* (common name: dead man's fingers) grows in clusters from the tree base or in the woody part just beneath the soil surface [9,10]. The aim of this study is to determine antioxidant, oxidant, antimicrobial potentials and element contents of *X. hypoxylon* and *X. polymorpha*.

MATERIALS AND METHODS

X. polymorpha and *X. hypoxylon* samples were collected from Bolu and Antalya provinces respectively, in 2020. The samples were dried in the dryer at 40 °C. 10 g of the dry samples were taken and pulverized. Powder samples were extracted at 50 °C for 6 hours with ethanol in the soxhlet apparatus. A rotary evaporator was then used to remove the solvents.

Total Antioxidant and Oxidant Status. Antioxidant and oxidant values of mushroom samples were determined using Rel Assay kits. Trolox was used as a standard in antioxidant kits and hydrogen peroxide as a standard in oxidant kits [11,12]. Oxidative stress index (Arbitrary unit: AU) was calculated by proportioning oxidant values to antioxidant

values using the following formula:

$$OSI\ (AU) = \frac{TOS,\ \mu mol\ H2O2\ equiv./L}{TAS,\ mmol\ Trolox\ equiv./L\ X\ 10}$$

Element Level Test. 0.5g of mushroom samples were taken and mineralized in a mixture of 9 mL HNO3 + 1 mL H_2O_2 in a microwave solubilizer (Milestone Ethos Easy). Tests were performed in 5 replicates for each mushroom sample. Fe, Cu, Zn, Pb, Cr, Mn, Ni, Co, and Cd contents were determined using an atomic absorption spectrophotometer device (Agilent 240FS AA) [13].

Antimicrobial activity tests. The antimicrobial activities of EtOH extract obtained from mushroom samples were determined by using the agar dilution method against standard bacteria and fungus strains [14-16]. *Staphylococcus aureus* ATCC 29213, *S. aureus* MRSA ATCC 43300, *Enterococcus faecalis* ATCC 29212, *Escherichia coli* ATCC 25922, *Pseudomonas aeruginosa* ATCC 27853, *Acinetobacter baumannii* ATCC 19606 were used as bacterial strains. *Candida albicans* ATCC 10231, *C. krusei* ATCC 34135, *C. glabrata* ATCC 90030 were used as fungus strains. The concentrations of the extracts that inhibit microbial growth were determined as minimal inhibitory concentrations (MIC). Bacteria were pre-cultured in Muller Hinton Broth medium and fungus strains in RPMI 1640 Broth medium. Fluconazole, Amphotericin B was used as a reference (positive control) drug for fungi. Amikacin, Ampicillin, and Ciprofloxacin were used as reference (positive control) drugs for bacteria [17-19].

RESULTS

Antioxidant and Oxidant Status. Living organisms produce different levels of reactive oxygen species in their bodies with environmental effects. When these oxidant compounds reach high levels, oxidative stress occurs [20]. Depending on the severity of oxidative stress, different diseases such as Parkinson's, Alzheimer's, cancer, and cardiological disorders may occur in humans [21]. Organisms use antioxidant compounds that they produce in their bodies to reduce the effect of oxidative stress. These endogenous antioxidants prevent the negative effects of oxidative stress by suppressing the effect of oxidant compounds. However, when endogenous antioxidants are insufficient, supplemental antioxidants play an important role in combating oxidative stress [22]. In recent years, many studies have reported that mushrooms are important sources of antioxidants [23-25]. In our study, the antioxidant and oxidant status of EtOH extracts of *X. hypoxylon* and *X. polymorpha* mushrooms were determined. The findings obtained are shown in Table 1.

TAS, TOS, and OSI values of *Xylaria* species were not previously determined in the literature. In this study, TAS, TOS, and OSI values of *X. hypoxylon* and *X. polymorpha* were determined for the first time. As a result of the study, TAS, TOS, and OSI values of *X. polymorpha* were determined to be higher than *X. hypoxylon*. TAS value is an indicator of the whole antioxidant compounds produced by the living organisms [26]. In studies using Rel Assay kits, TAS, TOS, and OSI values of *Lepista nuda* were reported as 3.102, 36.920, and 1.190, respectively [27]. TAS, TOS, and OSI values of *Infundibulicybe geotropa* were reported as 1.854, 30.385, and 1.639, respectively [28]. TAS, TOS, and OSI values of *Lactifluus rugatus* were reported as 3.237, 8.187, and 0.254, respectively [29]. TAS, TOS, and OSI values of *Helvella leucopus* were reported as 2.181, 14.389, and 0.661, respectively [30]. Compared to these studies, TAS values of *X. hypoxylon* and *X. polymorpha* were determined to be higher than *L. nuda, I. geotropa, L. rugatus,* and *H. leucopus.* The differences in antioxidant levels among mushrooms are thought to be due to the differences in mushrooms' antioxidant compound production potentials. Also, these results show that *X. hypoxylon* and *X. polymorpha* have high antioxidant potential.

TOS values are an indicator of the total oxidant compounds in living organisms [26]. As a result of our study, the TOS value of *X. hypoxylon* was determined lower than *L. nuda, I. geotropa, H. leucopus,* and higher than *L. rugatus*. The TOS value of *X. polymorpha* was lower than *L. nuda* and *I. geotropa* and higher than *H. leucopus* and *L. rugatus*. It is thought that the differences found in TOS values among mushrooms would be due to the environmental differences in the regions where the fungal samples are collected and their potential to produce oxidant compounds. As a result, it is seen that *X. hypoxylon* and *X. polymorpha* produce oxidant compounds at normal levels.

TABLE 1
TAS, TOS, and OSI Values of *Xylaria* species

	TAS	TOS	OSI
X. hypoxylon	3.794±0.188	8.609±0.171	0.228±0.015
X. polymorpha	5.390±0.176	14.738±0.126	0.274±0.008

Values are presented as mean±S.D.; n=5

The OSI value shows the degree of the suppressive effects of antioxidant compounds on oxidant compounds produced by living organisms. It shows that as the OSI value increases, antioxidant compounds are insufficient to suppress oxidant compounds [26]. As a result of our study, although the antioxidant potential of *X. hypoxylon* is lower than that of *X. polymorpha*, its OSI value has been determined lower due to its lower oxidant compound levels. Also, *X. hypoxylon* suppressed oxidant compounds more than L. nuda, I. geotropa, L. rugatus, and *H. leucopus. X. polymorpha* suppressed oxidant compounds more than *L. nuda, I. geotropa,* and *H. leucopus* and less than *L. rugatus*.

Element Contents. Mushrooms play a role in the decay of organic cover in the ecosystem. In this decomposition process, depending on the content of the substrate they use, they accumulate different levels and types of elements in their bodies [31]. Due to these features, they can be used as pollution indicators in nature. In our study, Fe, Cu, Zn, Pb, Cr, Mn, Ni, Co, and Cd contents of *X. hypoxylon* and *X. polymorpha* were determined. The findings obtained are shown in Table 2.

Mushrooms are spread in different habitats. Element levels vary according to the content of the substrate from which they emerge. In previous studies, the maximum and minimum intervals of the elements found in wild mushrooms were reported. These intervals have been reported as 14.60-1714.00 for Fe, 1.90-180.00 for Cu, 7.63-240.00 for Zn, 0.18-16.54 for Pb, 9.63-42.70 for Cr, 18.10-103.00 for Mn, 0.67-5.14 for Ni, and 2.71-7.50 for Cd [32-37]. Compared to these data, it was determined that the element levels of *X. hypoxylon* and *X. polymorpha* used in our study are within the literature ranges.

Antimicrobial activity. Many diseases from the past to the present have been caused by microorganisms. Antimicrobial drugs are very important in the prevention of microorganism-based diseases. However, microorganisms have gained resistance to various antimicrobial compounds such as antibiotics in recent years, especially due to their unconscious use [38,39]. This resistance has prompted researchers to explore natural products and their potentials for the discovery of new drugs against microorganisms [40]. In this study, the antibacterial and antifungal potentials of wild mushrooms *X. hypoxylon* and *X. polymorpha* were investigated. The findings obtained are shown in Table 3.

In our study, it was observed that EtOH extracts of *X. hypoxylon* and *X. polymorpha* were effective against the test bacteria at 100-400 µg/mL concentrations. They have also been determined to be effective against fungus strains at 50-200 µg/mL concentrations. In previous studies, it has been reported that the EtOH extract of *X. hypoxylon* is effective against *Bacillus subtilis, B. subtilis, Candida albicans, C. albicans, Enterobacter aerogenes, Enterococcus durans, E. faecalis, E. faecium, Escherichia coli, E. coli CFAI, Klebsiella pneumoniae, Listeria innocula, L. monocytogenes, Pseudomonas aeruginosa, P. fluorescence P1, Salmonella enteritidis, S. infantis, S. kentucky, S. typhimurium, Staphylococcus aureus, S. carnosus, S. epidermidis* and *Streptococcus agalactiae* at different concentrations in disk diffusion method [41]. It has been reported that the EtOH extract of *X. polymorpha* is effective against *Escherichia coli, Staphylococcus aureus, Pseudomonas aeruginosa, Proteus vulgaris, Bacillus cereus, Micrococcus luteus, Candida albicans, Rhodotorula rubra, Geotrichum capitatum, Debaryomyces hansenii, Kluyveromyces fragilis* and *Cryptococcus neoformans* at different concentrations in disk diffusion method [42]. In our study, the antibacterial and antifungal potentials of EtOH extracts of *X. hypoxylon* and *X. polymorpha* were determined using the agar dilution method. As a result of the study, it was found that the extracts are more effective especially against fungus strains (*C. albicans, C. glabrata* and *C. krusei*). As a result, it has been determined that *X. hypoxylon* and *X. polymorpha* have antimicrobial potentials.

TABLE 2
Heavy metals contents of *Xylaria* species

	Fe	Cu	Zn	Pb	Cr	Mn	Ni	Cd
X. hypoxylon	542.09±22.55	88.39±1.37	36.70±2.78	6.88±0.93	15.26±0.88	55.19±2.59	1.10±0.16	5.58±0.30
X. polymorpha	776.82±11.30	62.29±1.59	47.86±1.93	5.94±0.44	21.54±1.31	35.92±1.50	2.85±0.51	3.59±0.24

Values are presented as mean±S.D.; n=3 (Experiments were made as 3 parallel)

TABLE 3
MIC values of *Xylaria* species

	A	B	C	D	E	F	G	H	I
X. hypoxylon	200	100	200	200	200	400	50	50	50
X. polymorpha	100	100	100	200	400	200	100	200	100

The MIC values are presented in units of µg/mL
A: *S. aureus,* B: *S. aureus MRSA,* C: *E. faecalis,* D: *E. coli,* E: *P. aeruginosa,* F: *A. baumannii,* G: *C. albicans,* H: *C. glabrata,* I: *C. krusei*

CONCLUSIONS

Being one of the constant elements of natural ecosystems, mushrooms have many biological activities. In this study, the antioxidant and antimicrobial potentials of wild mushrooms *X. hypoxylon* and *X. polymorpha* were determined. Besides, the levels of the elements that these species accumulate were determined. As a result of the studies, it was seen that *X. hypoxylon* and *X. polymorpha* have important antioxidant potential. It was also determined that their antifungal activity is higher than antibacterial activity. Furthermore, it was found that the element contents are within the literature ranges. As a result, it is thought that X. *hypoxylon* and *X. polymorpha* can be used as natural materials in pharmacological designs.

REFERENCES

[1] Altuntaş, A., Bozok, F., Taşkın, H., Kabaktepe, Ş., Allı, H., Akata, I. (2021) New additions to Turkish Mycota from Ankara, Balıkesir and Kütahya provinces. Turkish Journal of Botany. 45, 83-94

[2] Sahin, E., Akata, I. (2018) Viruses infecting macrofungi. Virus Dis. 29(1), 1–18.

[3] Ivanova, T.S., Krupodorova, T.A., Barshteyn, V.Y., Artamonova, A.B., Shlyakhovenko, V.A. (2014) Anticancer substances of mushroom origin. Experimental Oncology. 36(2), 58.

[4] Krupodorova, T.A., Barshteyn, V.Y., Zabeida, E.F., Pokas, E.V. (2016) Antibacterial activity of macromycetes mycelia and culture liquid. Microbiol. Biotechnol. Lett. 44(3), 246-253.

[5] Lemieszek, M.K., Nunes, F.M., Rzeski, W. (2019) Branched mannans from the mushroom Cantharellus cibarius enhance the anticancer activity of natural killer cells against human cancers of lung and colon. Food & Function. 10(9), 5816-5826.

[6] Sevindik, M. (2019) The novel biological tests on various extracts of *Cerioporus varius*. Fresen. Environ. Bull. 28(5), 3713-3717.

[7] Zeng, D., Zhao, J., Luk, K.H., Cheung, S.T., Wong, K.H., Chen, T. (2019) Potentiation of in vivo anticancer efficacy of selenium nanoparticles by mushroom polysaccharides surface decoration. Journal of Agricultural and Food Chemistry. 67(10), 2865-2876.

[8] Mushtaq, W., Baba, H., Akata, İ., Sevindik, M. (2020) Antioxidant Potential and Element Contents of Wild Edible Mushroom *Suillus granulatus*. Kahramanmaraş Sütçü İmam University Tarım ve Doğa Dergisi. 23(3), 592-595.

[9] Krug, J.C., Benny, G.L., Keller, H.W. (2004) Coprophilous fungi. Biodiversity of Fungi: Inventory and Monitoring Methods. 467-499.

[10] Robinson, S.C., Laks, P.E. (2010) Culture age and wood species affect zone line production of *Xylaria polymorpha*. The Open Mycology Journal. 4, 18-21.

[11] Erel, O. (2004) A novel automated direct measurement method for total antioxidant capacity using a new generation, more stable ABTS radical cation. Clinical Biochemistry. 37(4), 277-285.

[12] Erel, O. (2005) A new automated colorimetric method for measuring total oxidant status. Clinical Biochemistry. 38(12), 1103-1111.

[13] Sevindik, M., Akgul, H., Akata, I., Alli, H., Selamoglu, Z. (2017) *Fomitopsis pinicola* in healthful dietary approach and their therapeutic potentials. Acta Alimentaria. 46(4), 464-469.

[14] CLSI (The Clinical and Laboratory Standards Institute). (2012). Antimicrobial Susceptibility Testing of Anaerobic Bacteria; Approved Standard—Eighth Edition. (M11-A8).

[15] EUCAST (European Committee on Antimicrobial Susceptibility Testing). (2014). Breakpoint tables Fungal isolate for interpretation of MICs. Version 7.0.

[16] EUCAST (European Committee on Antimicrobial Susceptibility Testing). (2015). Breakpoint tables for Bacteria interpretation of MICs and zone diameters. Version 5.0

[17] Bauer, A.W., Kirby, W.M., Sherris, J.C., Turck, M. (1966) Antibiotic susceptibility testing by a standardized single disk method. Am. J. Clin. Pathol. 45, 493-96.

[18] Hindler, J., Hochstein, L., Howell, A. (1992). Preparation of routine media and reagents used in antimicrobial susceptibility testing. Part 1. McFarland standards, In H. D. Isenberg (ed) Clinical microbiology procedures handbook, vol. 1. American Society for Microbiology, Washington, D.C. 5.19.1-5.19.6.

[19] Matuschek, E., Brown, D.F., Kahlmeter, G. (2014). Development of the EUCAST disk diffusion antimicrobial susceptibility testing method and its implementation in routine microbiology laboratories. Clin. Microbiol. Infect. 20, 255-266.

[20] Foyer, C.H., Shigeoka, S. (2011) Understanding oxidative stress and antioxidant functions to enhance photosynthesis. Plant Physiology. 155(1), 93-100.

[21] Ebadi, M., Srinivasan, S.K., Baxi, M.D. (1996) Oxidative stress and antioxidant therapy in Parkinson's disease. Progress in Neurobiology. 48(1), 1-19.

[22] Prochazkova, D., Sairam, R.K., Srivastava, G.C., Singh, D.V. (2001) Oxidative stress and antioxidant activity as the basis of senescence in maize leaves. Plant Science. 161(4), 765-771.

[23] Cheung, L.M., Cheung, P.C., Ooi, V.E. (2003) Antioxidant activity and total phenolics of edible mushroom extracts. Food Chemistry. 81(2), 249-255.
[24] Jayakumar, T., Thomas, P.A., Geraldine, P. (2009) In-vitro antioxidant activities of an ethanolic extract of the oyster mushroom, Pleurotus ostreatus. Innovative Food Science & Emerging Technologies. 10(2), 228-234.
[25] Selamoglu, Z., Sevindik, M., Bal, C., Ozaltun, B., Sen, İ., Pasdaran, A. (2020) Antioxidant, antimicrobial and DNA protection activities of phenolic content of *Tricholoma virgatum* (Fr.) P. Kumm. Biointerface Research in Applied Chemistry. 10(3), 5500-5506.
[26] Korkmaz, A.I., Akgul, H., Sevindik, M., Selamoglu, Z. (2018) Study on determination of bioactive potentials of certain lichens. Acta Alimentaria. 47(1), 80-87.
[27] Bal, C., Sevindik, M., Akgul, H., Selamoglu, Z. (2019) Oxidative Stress index and Antioxidant Capacity of *Lepista nuda* Collected from Gaziantep/Turkey. Sigma. 37(1), 1-5.
[28] Sevindik, M., Akgul, H., Selamoglu, Z., Braidy, N. (2020) Antioxidant and Antigenotoxic Potential of *Infundibulicybe geotropa* Mushroom Collected from Northwestern Turkey. Oxidative Medicine and Cellular Longevity. Article ID: 5620484
[29] Sevindik, M. (2020) Antioxidant and antimicrobial capacity of *Lactifluus rugatus* and its antiproliferative activity on A549 cells. Indian Journal of Traditional Knowledge. 19(2), 423-427.
[30] Sevindik, M., Akata, I. (2020) Antioxidant, oxidant potentials and element content of edible wild mushroom *Helvella leucopus*. Indian Journal of Natural Products and Resources. 10(4), 266-271.
[31] Brzezicha-Cirocka, J., Grembecka, M., Grochowska, I., Falandysz, J., Szefer, P. (2019) Elemental composition of selected species of mushrooms based on a chemometric evaluation. Ecotoxicology and Environmental Safety. 173, 353-365.
[32] Kalač, P., Svoboda, L. (2000). A review of trace element concentrations in edible mushrooms. Food Chemistry. 69(3), 273-281.
[33] Sarikurkcu, C., Copur, M., Yildiz, D., Akata, I. (2011). Metal concentration of wild edible mushrooms in Soguksu National Park in Turkey. Food Chemistry. 128(3), 731-734.
[34] Mallikarjuna, S.E., Ranjini, A., Haware, D.J., Vijayalakshmi, M.R., Shashirekha, M.N., Rajarathnam, S. (2013) Mineral composition of four edible mushrooms. Journal of Chemistry. Article ID: 805284
[35] Gebrelibanos, M., Megersa, N., Taddesse, A.M. (2016) Levels of essential and non-essential metals in edible mushrooms cultivated in Haramaya, Ethiopia. International Journal of Food Contamination. 3(1), 2.
[36] Sevindik, M., Akgul, H., Bal, C., Selamoglu, Z. (2018) Phenolic contents, oxidant/antioxidant potential and heavy metal levels in *Cyclocybe cylindracea*. Indian Journal of Pharmaceutical Education and Research. 52(3), 437-441.
[37] Krupodorova, T., Sevindik, M. (2020) Antioxidant potential and some mineral contents of wild edible mushroom *Ramaria stricta*. AgroLife Sci. J. 9, 186-191.
[38] Davidson, P.M., Juneja, V.K. (1990) Antimicrobial agents. Food Additives. 83-137.
[39] Khaneghah, A.M., Hashemi, S.M.B., Limbo, S. (2018) Antimicrobial agents and packaging systems in antimicrobial active food packaging: An overview of approaches and interactions. Food and Bioproducts Processing. 111, 1-19.
[40] Baba, H., Sevindik, M., Dogan, M., Akgul, H. (2020) Antioxidant, antimicrobial activities and heavy metal contents of some myxomycetes. Fresen. Environ. Bull. 29(09), 7840-7846.
[41] Canli, K., Akata, I., Altuner, E.M. (2016) In vitro antimicrobial activity screening of *Xylaria hypoxylon*. African Journal of Traditional, Complementary and Alternative Medicines. 13(4), 42-46.
[42] Hacioglu, N., Akata, I., Dulger, B. (2011) Antimicrobial potential of *Xylaria polymorpha* (Pers.) Grev. African Journal of Microbiology Research. 5(6), 728-730.

Received: **28.12.2020**
Accepted: **07.02.2021**

CORRESPONDING AUTHOR

Ilgaz Akata
Department of Biology,
Faculty of Science,
Ankara University,
Ankara – Turkey

e-mail: akata@science.ankara.edu.tr

© by PSP Volume 30– No. 05/2021 pages 5405-5414 Fresenius Environmental Bulletin

COAL SEAM PERMEABILITY ENHANCEMENT TECHNOLOGY AND HIGH-VOLTAGE ELECTRICAL PULSE NEW TECHNOLOGY RESEARCH PROGRESS AND TREND

Bin Li[1,*], Sheng Xue[1,2,3]

[1]School of Safety Science and Engineering, Anhui University of Science and Technology, Huainan, Anhui Province 232001, China
[2]State Key Laboratory of Mining Response and Disaster Prevention and Control in Deep Coal Mine, Anhui University of Science and Technology, Huainan, Anhui Province 232001, China
[3]Key Laboratory of Industrial Dust Control and Occupational Health, Ministry of Education, Anhui University of Science and Technology, Huainan, Anhui Province 232001, China

ABSTRACT

Coal mine gas is an important clean and green energy. Safe and efficient exploitation of gas resources is not only of great significance to national energy security but also can greatly reduce greenhouse gas emissions and protect the global environment. It is an important means to enhance the permeability of coal seam to maximize gas resource drainage. This study summarizes the development history and research status of current permeability enhancement technologies in my country, and then analyzes the advantages and disadvantages of various permeability enhancement technologies and their scope of application. Besides, this paper introduces a new method of high-voltage electrical pulse(HVEP) to increase permeability, which can be repeated and has less damage to coal seam. Through analysis, the cracking coal mechanism of HVEP and its technical advantages are obtained. It also points out the development trend of HVEP and coal seam permeability enhancement technology in the future, which provides the basis for coal mine gas resource utilization and environmental safety. In this paper, the following main conclusions are obtained: (1) in the future, two or more permeability enhancement methods should be collaborative operation to deal with the gas resource problem; (2) the future coal mine gas control and utilization will develop towards the Internet of things and intellectualization.

KEYWORDS:
Coal mine gas, green energy, permeability enhancement technology, high-voltage electrical pulse (HVEP), development trend, intellectualization

INTRODUCTION

Coal is the energy base of human activities and an important type of energy. In 2018, coal accounted for 59% of China's primary energy consumption structure [1], which played an important role in China's economic construction and industrial development. 90% of China's coal mines are underground mining [2], which belongs to confined space, and its working environment is harsh. With the coal mining will produce a variety of toxic and harmful gases, causing the work will face some disasters that threaten the lives of miners, leading to the safety production of underground coal mine face serious challenges. The major hazard sources that hinder the safe production of coal mines are rockburst, coal dust, gas, water disaster, fire, and so on [3], especially the accidents caused by gas are the most serious. Gas accidents are easy to cause mass casualties [4].

China's shallow coal resources are exhausted, most of the coal mines have been mined to the deep. Because of the complexity of China's geological structure and the characteristics of coal seam gas occurrence [5], coal mines have the typical characteristics of high stress, high temperature, high gas pressure, and low permeability. As a result, the coal seams in our country are generally low permeability coal seams, which is challenging for the control of gas disasters and the exploitation of coalbed methane(CBM) resources. The theory of coal and gas co-mining put forward by Academician Yuan [6] is the fundamental measure to solve the gas disaster. Its core idea is to exploit CBM resources while exploiting coal resources, to achieve the purpose of gas control and resource exploitation maximization. Taking measures to enhance coal seam permeability and increase gas drainage [7] is an effective way to implement the theory of coal and gas co-mining. This can not only eliminate gas disasters but also provide clean energy and reduce greenhouse gas emissions [8] and protect the environment.

This paper summarizes the existing methods of improving the permeability of single low permeability coal seam and gas control. And It introduces a new method of improving gas permeability and gas control by high-voltage electrical pulse(HVEP). The current situation of its theoretical research and engineering application is discussed. It also points out the development trend of gas control and coal industry

in the future. This study will provide strong support for energy security and environmental security.

MATERIALS AND METHODS

For a long time, all countries attach great importance to the healthy development of the coal industry and have invested a lot of safety funds for coal mining enterprises, which makes the world coal mine safety production situation has improved significantly. According to the relevant data of China's National Bureau of Statistics [3], the statistical chart of China's raw coal production and million-ton mortality from 2000 to 2019 is shown in Figure 1, and the statistics of coal mine safety production accidents and deaths after accidents from 2000 to 2019 are shown in Figure 2. It can be seen from Figure 1 that China's coal production increased year by year before 2013. After 2013, due to the adjustment of China's energy structure and policy control, the raw coal production decreased, but increased year by year after 2016 again. It can be seen from Figure 1 and Figure 2 that since 2002, the death rate per million tons, the number of accidents, and the number of deaths in China's coal mines have decreased year by year. In 2018, the death rate per million tons of coal mines in China was 0.093, which dropped to below 0.1 for the first time. In 2019, it will continue to maintain a good state of development, and this number will drop to 0.083, reaching the best result in China's history. However, compared with the developed countries in the world, there is still a gap in China. The average mortality rate per million tons in the United States in recent 10 years is 0.028, the coal industry in Australia is one of the safest industries, and the mortality rate per million tons in coal mines is below 0.02 [9]. Therefore, China must increase high-tech investment in the field of coal mine safety, strengthen the system construction and intensify the research and development of modern and intelligent equipment, so as to ensure the continuous improvement of China's coal mine safety situation.

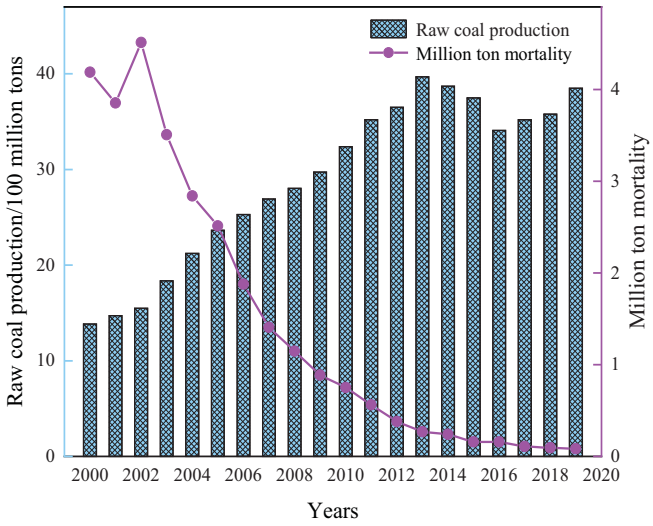

FIGURE 1
Statistics of China's raw coal production and million-ton mortality from 2000 to 2019

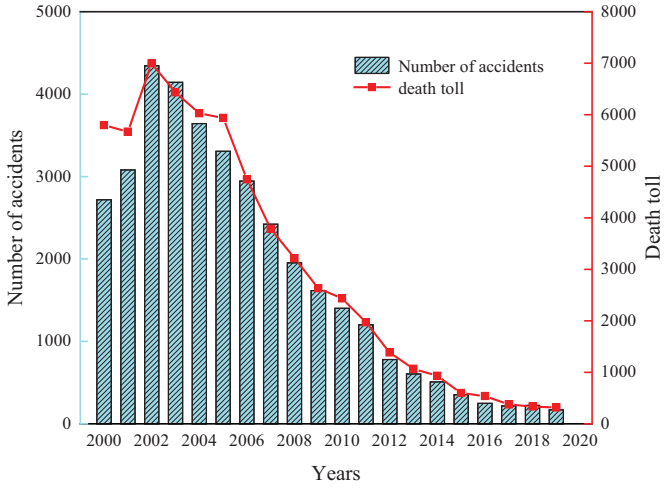

FIGURE 2
Statistics of coal mine accidents and deaths in China from 2000 to 2019

Coal mine gas is a major hazard source threatening coal mine safety, which can lead to serious coal mine safety accidents, such as gas explosion, coal and gas outburst, gas combustion and so on. But coal mine gas is also known as coalbed methane (CBM). If effective measures are taken to drainage valuable CBM resources, it can be used as excellent energy. China is rich in CBM resources. According to the statistics of the Ministry of Land and Resources [3], the geological resources of CBM buried depth is less than 2000m in China are 30 trillion cubic meters, and the recoverable resources are 12.5 trillion cubic meters. In 2016, in the process of coal mining in China, the gas released was 13.5 billion cubic meters, only 35% of the resources were extracted and utilized, and the rest 65% were discharged into the atmosphere, which not only caused the waste of resources, but also caused environmental pollution. Because the main component of CBM is methane, methane (CH_4) is a very destructive greenhouse gas [10], it can destroy the ozone layer of the atmosphere, causing global climate change, so we should increase the drainage and utilization of CBM.

Technical methods of enhancing coal seam permeability. The ways of gas control include regional control technology and local control technology. According to different coal seam situations, corresponding measures should be taken to turn hazard gas into treasure, and provide us with clean, efficient and green unconventional energy, and then protect the atmospheric environment. For the coal seam group with high gas and low permeability, the regional control technology should be adopted, that is, the method of protective seam mining. This method is the first to mine the safety coal seam with low gas content and low pressure. In the process of mining the safety coal seam, the adjacent layer will move, expand and relieve pressure. At this time, 80% of the gas in the adjacent layer can be transformed into free state, the gas content and pressure in the adjacent layer will be reduced, and then the adjacent layer will become a safety coal seam. In this process, the corresponding roadways and boreholes will be arranged to drainage the coal seam gas. Mining protective layer has been proved to be the most mature and effective way in theory and practice [11].

China's coal seam geological conditions are complex, so many coal mines do not have the conditions of protective seam mining. For a single coal seam with high gas and low permeability, gas drainage is the most difficult, so local pressure relief and permeability enhancement technology must be adopted. The commonly used local control methods in China's coal mines are densely drilling, hydraulic technology, explosive blasting permeability enhancement technology, etc., which have achieved certain effects in improving the gas drainage rate, but there are still some shortcomings. The following is an overview of the existing main enhancement permeability technology, aiming to find the best enhancement permeability technology and method suitable for the field coal, so as to maximize the extraction of coal mine gas resources.

Densely drilling technology for enhancing permeability. Coal seam drilling construction is a traditional method of pressure relief and permeability enhancement, which uses grid format, cross type and other special drilling layouts in coal seam to improve gas drainage efficiency [12]. Yi [13] studied the mechanical properties of coal mass near Dense Boreholes, analyzed the permeability of coal mass and the effect of gas pre-drainage. Gao [14] aimed at the problem of easy collapse of drilling holes in soft coal seams and difficulty in forming holes. He proposed the technology of adding screens to the drilling, optimized the structure of PVC screens, and developed supporting equipment.

Explosive blasting technology for enhancing permeability. Since the 1950s, loose blasting method has been used at home and abroad to improve the effect of coal seam gas drainage [15]. In 1956, the Kalgan coalfield of the former Soviet Union carried out the experiment of coal seam blasting to increase permeability. After blasting to increase permeability, the gas drilling flow per meter increased by 70%, and the influence radius reached 6m. In the mid-1960s, Lianshao and Beipiao Mining Bureau [16] carried out coal seam blasting enhancement permeability test. The results show that after the blasting, the gas drainage capacity of borehole is significantly increased. It indicated that the blasting method can effectively improve the permeability of coal seam, which also has a positive effect on the control of coal mine gas.

Blasting enhancing permeability technology to control coal mine gas mainly uses the comprehensive effects of explosion shockwave, high-temperature and high-pressure gas, and high-speed blasting stress wave after the explosive explosion. This action has a huge impact and destruction on the coal mass, resulting in cracks in the coal mass and the formation of crack loose circle. In this way, the stress and seepage state of coal and rock mass are changed, and the permeability of coal seam is improved. After that, coal seam gas was successfully extracted to achieve the purpose of gas control and utilization. Cai et al. [17] established the dynamic damage constitutive model of coal under blasting load and verified the model by LS-DYNA software. Finally, the influence range of the explosion stress wave is 4.8m. Zhang et al. [18] experimented with increasing permeability by blasting in the laboratory, and adopted a variety of experimental monitoring means to monitor experimental data. It is concluded that the coal cracking is the result of the combined action of shockwave,

stress wave, and explosive gas. Shaped charge blasting is to change the charge structure of the explosive [19] so that the energy after explosion can be concentrated from a certain direction [20], to achieve the enhancement permeability effect in a specific direction. Liu [21] experimented with permeability enhancement by shaped charge blasting in the laboratory, and obtained the law of stress evolution and crack expansion of shaped charge blasting. The field experiment shows that the gas drainage volume of coal seam gas is greatly improved after shaped charge blasting. Pan [22] carried out a test on coal seams containing gangue shaped charge blasting in the laboratory. He studied the damage range and stress state around the blasting hole, and concluded that shaped charge blasting has a broad application prospect in weakening of gangue.

Hydraulic technology. Hydraulic technology also uses high-pressure water as power to inject water with certain energy into the coal seam. The energy of water is the expansion and extension of the original fissures in the reservoir or the artificial formation of new cavities, slots and fissures, to make the coal and rock displace and achieve the purpose of transforming the energy storage and increasing the pressure relief and permeability. The commonly used hydraulic technology includes water jet slotting, hydraulic fracturing, hydraulic punching, etc. [23] Since the first use of hydraulic fracturing technology in the United States in 1947, great progress has been made in the theory and engineering application of hydraulic technology, which has become an effective way to increase the production of oil and gas and coal seam gas [24].

Hydraulic slotting technology. Hydraulic slotting technology is to use high-pressure water to cut a certain length of seam slot in coal seam, change the stress state of coal, and provide a seepage channel for gas. With the increase of seam slot number in coal, the effect of pressure relief and permeability increase of coal seam is achieved. In the 1970s, the field test of hydraulic slotting enhanced extraction was carried out in coal mines in China. In the aspect of theoretical research, Singh [25] first researched the mechanism of rock fracture under dynamic load in 1961 and put forward the stress wave fracture theory of rock failure and failure under the action of jet. Crow [26] believes that the main reason for rock failure in the process of water jet impacting rock is the cavitation effect caused by pressure difference. Heymann [27] thinks that the velocity of shock wave has a great influence on the jet impact pressure, and puts forward the calculation method of water hammer pressure. Li [28] made a comprehensive study from theory, numerical simulation to field application, and concluded that hydraulic cutting can improve coal seam permeability and gas drainage rate. After the technology is applied in the field, the gas extraction volume has increased by 7.8 times. Liu [29] studied the spatial distribution of slot in coal after hydraulic slotting, and determined the optimal spatial distribution mode of slotting. Zhou et al. [30] used the stress wave theory to explain the transverse crack phenomenon of rock under the impact of water jet. Lin [31] proposed the use of high-pressure abrasive jet technology, developed the corresponding equipment, and successfully applied it in Pingdingshan coal mine. It significantly improves the seam slotting ability and gas drainage concentration, which is of great significance to gas drainage work.

Hydraulic fracturing technology. Hydraulic fracturing is a method to press the high-pressure liquid mixed with proppant into the coal mass in the borehole, to make the coal mass break and form a fracture with high gas flow capacity. It enhances the coal seam permeability through a large number of fractures formed in the coal [32]. In the 1960s, the former Soviet Union introduced this technology into coal mines for the first time, and conducted hydraulic fracturing permeability enhancement tests in Karaganda and dunbas mining areas for the first time, and achieved good results [24]. In terms of theoretical research, Meng et al. [33] studied the relationship between effective stress and permeability in coal seam during hydraulic fracturing. It is concluded that the effective stress of reservoir is closely related to permeability, and slowing down the change of effective stress in the production process has a positive effect on the reduction of permeability. LV et al. [34] combined with the temporal and spatial evolution characteristics of CBM production, studied the influence relationship of seven factors such as coal seam thickness, permeability, pressure effect, and geological structure on gas production. Hubbert et al. [35] studied in detail the pressure problem in rock drilling during hydraulic fracturing through field tests. He believed that the cracking surface is always perpendicular to the direction of the minimum principal stress regardless of whether the liquid penetrates into the rock mass. Hossain et al. [36] used the theory of elasticity to study fracture pressure, fracture initiation direction, and propagation law.

Hydraulic punching technology. Hydraulic punching is to protect the rock pillar or coal pillar as a safety barrier to impact in the cavity of the target coal. The impact force of a high-pressure water jet is used to scour the hole wall to expand the diameter of the hole and flush out the pulverized coal in the hole, to achieve the purpose of increasing the permeability in the hole [37]. Hydraulic punching can also eliminate the danger of outburst because the gas potential in coal, coal elastic properties, and surrounding rock stress will be greatly reduced after hydraulic punching.

Since the 1980s, the technology of hydraulic

punching has first been widely used in the development of CBM in the San Juan Basin of the United States [38]. Currently, nearly 1500 wells in the basin have been completed by hydraulic punching technology, and the output of CBM is 20 times that of hydraulic fracturing. In terms of theoretical research, Wang et al. [39] investigated the application effect of hydraulic punching technology in soft and low permeability outburst coal seam. The results show that the outburst elimination effect of regional drainage is remarkable, the single hole washes out 7t coal, and the effective influence radius of borehole drainage is increased by 2 ~ 3 times. Wang et al. [40] used the method of combining numerical simulation and field experiments to study the change law of coal seam permeability around the borehole after the implementation of hydraulic punching. The results show that the closer to the punching position, the greater the decrease of surrounding rock stress and coal seam gas content, and the greater the improvement of coal seam permeability coefficient.

The common method of controlling coal seam gas disasters is to inject high energy material into coal, so that the injected high energy material and coal have physical changes. In this way, the coal structure and its physical and mechanical properties are changed, and cracks are produced in the coal, to achieve the purpose of pressure relief and increase the permeability of the coal seam. When the permeability of coal seam changes, the adsorption state of gas in coal will change, and a large number of adsorbed gas will be transformed into free gas, so that the gas can be extracted smoothly and the gas content in coal seam can be reduced. Through the implementation of enhancement permeability measures, we can achieve the best in the three aspects of safety, energy, and environmental protection, that is, safe mining of coal resources, maximizing the extraction of clean and green gas resources, and reducing greenhouse gas emissions.

RESULTS

Although the above methods have played a good role in the transformation of gas reservoir in a certain period, they still have limitations in some coal mine applications. For example, densely drilling will damage the mechanical properties of coal seam. During drilling construction, problems such as connection and penetration of two boreholes and sticking of boreholes may occur [16]. In soft coal seam, boreholes are not easy to form and collapse, which may cause borehole scrapping and seriously affect the extraction efficiency of boreholes. Densely drilling also has the problem of high drilling cost, and the specific drilling technology and drilling layout need to be determined according to the actual situation of the underground, which cannot be generalized.

There are three main problems in the technology of increasing permeability by blasting: (1) in coal with high gas pressure, the blasting technology is easy to induce outburst and has poor safety. (2) This method has strict management and complicated processes. (3) The probability of "explosion failure" is relatively high. In case of explosion failure, the subsequent treatment work is more dangerous, the measures are more cumbersome and time-consuming.

For hydraulic fracturing technology, the hardware problems are that the existing technology cannot manufacture high-pressure pump equipment that can fully meet the application of coal mine underground. The existing equipment either has low pump pressure and small flow, which cannot meet the fracturing requirements, or the pump pressure is too large and the volume is too large, which is not suitable for underground operation. Therefore, the technical process and corresponding equipment of hydraulic fracturing system need to be further improved. In the aspect of application effect, it is found that the fracture will close again soon after fracturing, which is not conducive to the gas drainage of coal seam. There are also some problems, such as difficult hole sealing and difficult control of fracturing effects. It is suitable for use in tight and hard reservoirs, but not in soft coal seams.

The biggest problem of hydraulic slotting technology is that water consumption is small, and the mixture of coal powder and coal block cannot be treated in time. When the mixture is too much to block the drilling hole, the permeability increasing operation will be forced to stop, especially in the soft coal seam. Therefore, this technology is not suitable for permeability increasing operation in soft coal seam.

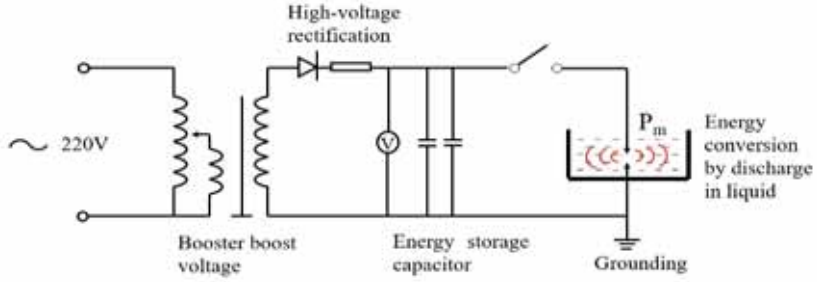

FIGURE 3
Schematic diagram of circuit principle of HVEP energy conversion

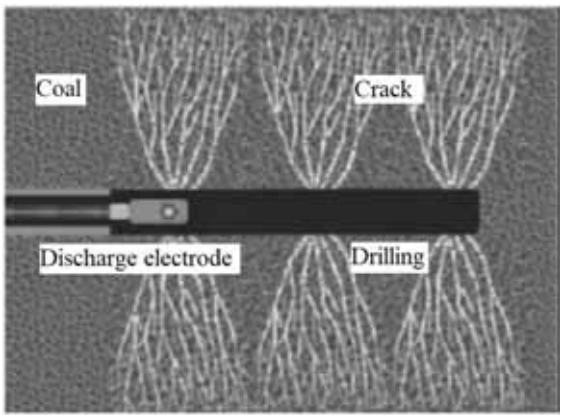

FIGURE 4
Schematic diagram of HVEP on-sites enhancing permeability operation

The new technology of HVEP enhancing permeability is put forward under this background [41]. Its enhancing permeability principle is based on the electro-hydraulic effect of Yutkin [42]. By using a special circuit, the 220V AC is transformed into high-voltage DC through boosting and rectifying, and then the electric energy is stored in the pulse capacitor. The special electrode connected with high-voltage and low-voltage electrode discharges in water to convert the electric energy into mechanical energy. In this process, the weak compressibility of water is used to transfer energy, and the transformed energy is used to crack coal and rock mass, which is a new technology of enhancement permeability. The circuit principle of HVEP energy conversion is shown in Figure 3. The main fracture mechanism of HVEP is shear cracking. When the HVEP discharges, the channel between the positive and negative electrodes expands rapidly, and the discharge channel does external work to form the pulse stress wave. When the pulse wave pressure is greater than the strength of coal, new cracks will be formed in coal. Under the action of repeated electric pulse, the coal will appear fatigue damage, its strength will decrease, and it is easier to produce new cracks and form the fracture network. The shear effect of pulse stress wave can expand the pores of coal, reduce the adsorption force between gas and solid or liquid. In this way, the gas adsorption state is improved and the gas seepage property is improved. The comprehensive effect of all the processes makes the coal produce a complex fracture network, which greatly improves the permeability of coal seam and greatly increases the gas drainage.

After the exploration and research of some scholars, the preliminary application has been carried out in the field [43], and relatively good results have been achieved. An et al. [44] applied HVEP to enhance permeability in Baode coal mine and investigated the effect of different impact densities on coal seam permeability. It is concluded that for high gas and low permeability coal seam with f value of 0.72, 0.5 times/m impact density is the best. Zhang et al. [45] carried out HVEP field permeability enhancing operation in Zhongjing coal mine, Shuicheng mining area, Guizhou Province. After the operation, the single hole gas drainage volume and gas concentration increased by more than 2.3 times, and the effective radius of permeability enhancement easing reached 40-60m, which greatly improved the coal seam permeability.

The schematic diagram of HVEP field enhancing permeability operation [43] is shown in Figure 4. Drill in the place where it needs to work in the coal and rock strata, fill the hole with water, and put the equipment deep into the operation site. The equipment can act repeatedly at each action point, and implement the impact fracturing at intervals, and then form a fracture network in the coal seam, to increase the permeability of the coal seam. HVEP causes little damage to coal, and only produces crack channels that can promote gas flow, which not only protects coal resources but also is conducive to the extraction of coal seam gas resources. It will not cause larger deformation cracks, destroy coal structure, and waste coal resources like other means of enhancing permeability. Therefore, HVEP has three major technical advantages: first, it is widely used, easy to operate, and can adapt to different properties of coal and rock by arbitrarily adjusting the energy of impact cracking. Second, it can be repeated at the same point, which can ensure the best enhancing permeability effect. The third is low damage to coal, no pollution, and no damage to coal resources.

In theoretical research, Li et al. [46] conducted an experimental study on the microstructure change of fat coal under the action of repetitive pulse. It is concluded that repetitive pulse can change the pore structure of coal and effectively improve its permeability. Bao et al. [47] used CT scanning and fractal dimension to quantitatively describe the fracture propagation law of coal mass after HVEP fracturing. It is concluded that HVEP has a good effect on coal cracking. Lin et al. [48] applied high and low voltage electrodes to coal mass directly and studied the fracture law of coal containing fractures and minerals caused by high voltage pulsed plasma. It is concluded that both fractures and minerals are important factors affecting the fracture changes of coal. Shi et al. [49] studied the coal mass with different pore structures under repeated HVEP impact and concluded that the fracture mode of coal mass is different due to different pore structures. The sensitivity of bituminous coal to impact is greater than anthracite, and the pore structure of bituminous coal has a significant contribution to the initiation and expansion of fractures.

The development trend of HVEP. The technology of HVEP fracturing coal is still in the primary stage. Although it has been applied in engineering practice, the effect cannot be guaranteed in the field

application. Sometimes it can improve the gas drainage amount well, sometimes the effect of gas drainage is not obvious after the action of HVEP. The pace of theoretical research has not kept up with the pace of field application, and the basic theoretical research of HVEP cracking needs to be further strengthened. For example, under different in-situ stress environment, the effect of HVEP on coal and rock mass, and the study of HVEP on gas-containing coal masses are rarely reported. The conditions at the coal mine site are harsh and the geological conditions are more complicated. The basic research of HVEP should be consistent with the site conditions. The next step is to study the adaptability of HVEP under different environmental conditions and study its quantitative effect to ensure that the technology can guide the field applications. Only in this way can the HVEP enhancing permeability technology be fully applicable to coal mines and better serve the development of the coal industry, the exploitation and utilization of gas resources, and the protection of the earth's environment.

Development trend of permeability enhancement technology for single low permeability coal seam. Due to the complexity of coal resources and coal seam gas occurrence conditions, there are two important development directions of coal seam permeability enhancement technology in the future. One is to vigorously develop new and more adaptable permeability enhancement technologies, such as the HVEP permeability enhancement technology mentioned above. The other is the development of synergistic permeability enhancement technology, which is a method that two or more kinds of enhancing permeability technology work together on coal mass. Every single enhancing permeability technology often has inevitable technical shortcomings. By using the technology of synergetic permeability enhancement, the disadvantages of one technology can be avoided, and the advantages of each technology can be brought into full play. The two technologies are coupled together to increase the permeability of coal seam, which has the effect of $1 + 1 > 2$. This puts forward new requirements for scientific and technological workers. It is a challenging research topic to study how to strengthen the collaborative operation of two or more technologies to maximize gas drainage.

Now, the era of 5G network and intellectualization has come [2]. In the future, how to connect the 5G network, intellectualization, and other digital information technology with the coal industry is an important direction of industrial development. Intellectualization requires the application of intelligent equipment in the whole process of coal and gas resources mining, and may even develop into Robotic Mining in the future. This will bring us many new problems and challenges, which require scientific and technological workers to solve one by one.

CONCLUSIONS

To adapt to the development of coal mines under the new situation, it is an important way to adjust the energy structure and environmental safety to extract clean, efficient, and green coal seam gas resources as much as possible while mining coal. HVEP technology is a new method that is suitable for the development of coal mines and can increase the permeability of coal seam. After the development in recent years, it has been successfully applied to the coal mine and achieved good results. However, we need to strengthen basic research work to provide a strong theoretical basis for on-site construction. Through the review of the existing technology and the discussion of HVEP technology, the following conclusions are drawn:

(1) Densely drilling enhancing permeability technology is not suitable for soft coal seam, drilling in the soft coal seam is not easy to form, prone to sticking, hole collapse phenomenon, not only affect the drilling drainage rate but also cause the possibility of outburst accident. The technology of enhancing permeability by blasting is complex, and there are some potential safety hazards. When the gas pressure is too high, the blasting technology will also induce outburst accidents. Hydraulic fracturing technology has a large scale and high cost, and it is not easy to control the fracturing effect of coal. Hydraulic fracturing is suitable for hard coal and rock, but not good for soft coal. Hydraulic slotting is not easy to be applied in soft coal, and coal powder is easy to block the drilling hole, thus interrupting the permeability enhancement operation. Hydraulic punching technology is only used for medium hard coal and soft coal.

(2) High-voltage electrical pulse (HVEP) technology is a low-cost, easy to manage, safe and feasible new technology to enhance coal seams permeability, which has broad application prospects. Its three remarkable advantages are: ① it has a wide range of applications and is easy to operate. It can adapt to different properties of coal and rock by arbitrarily adjusting the energy of impact cracking. ② It can work repeatedly at the same point of action, which can ensure the best enhancing permeability effect. ③ The operation of enhancing permeability has less damage to coal mass, no pollution, and no damage to coal resources.

(3) The development trend of coal seam permeability enhancement technology is to develop new technology with stronger adaptability, and the other is to develop synergistic permeability enhancement technology. Try to avoid the disadvantages of a certain technology, give full play to the advantages of each technology, and adapt to the new trend of coal mine development.

(4) The era of the 5G network, Internet of things and artificial intelligence has come, and the

connection with high-tech digital information technology is an important direction for the future development of the coal industry. The application of intellectualization in the coal industry requires scientific and technological workers to continuously tackle key technical problems, to better achieve energy security and environmental security.

ACKNOWLEDGEMENTS

The authors would like to thank all the persons who have helped this research and all the authors of all the references. This work was supported by the National Key R&D Program of China (2018YFC0808000).

REFERENCES

[1] Xie, H., Wu, L., Zheng, D. (2019) Prediction on the energy consumption and coal demand of China in 2025 Journal of China Coal Society. 44(7), 1949-1960.

[2] Ge, S., Hu, E., Pei, W. (2020) Classification system and key technology of coal mine robot Journal of China Coal Society. 45(1), 455-463.

[3] Wu, Q., Tu, K., Zeng, Y., Liu, S. (2019) Discussion on the main problems and countermeasures for building an upgrade version of main energy (coal) industry in China Journal of China Coal Society. 44(6), 1625-1636

[4] Li, T., Cai, M., Wang, J., Li, D., Liu, J. (2005) Discussion on relativity between rockburst and gas in deep exploitation. Journal of China Coal Society. 30(5), 562-567.

[5] Pan, Y. (2020) Gas geological occurrence regularity and coal and gas outburst research progress. Fresen. Environ. Bull. 29(3), 1763-1770.

[6] Yuan, L. (2016) Strategic thinking of simultaneous exploitation of coal and gas in deep mining Journal of China Coal Society. 41(1), 1-6.

[7] Zhang, L., Zhang, H.Z., Guo, H. (2017) A case study of gas drainage to low permeability coal seam. International Journal of Mining Science and Technology. 27(4), 687-692.

[8] Karacan, C.O., Ruiz, F.A., Cote, M. (2011) Coal mine methane: A review of capture and utilization practices with benefits to mining safety and to greenhouse gas reduction. International Journal of Coal Geology. 86(2-3), 121-156.

[9] Qi, H. (2015) Analysis on production status and safety situation for developed country of coal industry. China Coal. 41(8), 140-143.

[10] Zhang, Q., Wu, Q., Zhang, H., Zhang, B., Xia, T. (2018) Effect of montmorillonite on hydrate-based methane separation from mine gas. Journal of Central South University. 25(1), 38-50.

[11] Zhao, B., Wang, H. (2014) Different Technologies of Permeability Enhancement of Single Coal Seam in China and New Technique of High Pressure Gas Shock. Blasting. 31(3), 32-41.

[12] Liu, Q., Tong, B., Fang, Y., Tu, Q., Guo, S. (2014) High Efficient Gas Drainage Technology with Fast Full Length Screen Pipe for Borehole Protection in Soft Seam. Coal Science and Technology. 42(12), 58-61.

[13] Yi, L., Yu, Q. (2010) Numerical Test of Gas Predrainage with Dense Boreholes in Outburst Coal Seam. Safety in Coal Mines. 41(2), 1-4.

[14] Gao, Y. (2014) Gas Drainage Based on Screen Pipe Placing in Borehole Technology Without Drilling Rod Lifting in Soft Seam. Coal Science and Technology. 42(9), 115-118.

[15] Yuan, L., Liu, Z., Huang, W., Zhu, F., Zhang, W., Liu, J., Cai, F., Fu, J. (2018) Deep hole presplitting blasting in coal seam. In: Gas control technology and application of deep hole presplitting blasting in coal mine. (1st ed) Science Press, Beijing. 3-9.

[16] Yu, B. (2005) Methods of improving gas drainage capacity of mining seam. In: Technical manual for prevention and utilization of coal mine gas disaster. (Revised edition) Coal Industry Press, Beijing. 263-266.

[17] Cai, F., Liu, Z., Luo, Y. (2014) Propagation and attenuation characteristics of stress waves generated by explosion in high-gas coal-beds. Journal of China Coal Society. 39(1), 110-114.

[18] Zhang, S., Liu, Z., Liu, J., Li, Z., Gao, K. (2017) Tests for control hole's enhanced permeability mechanism under blasting load. Journal of Vibration and Shock. 36(24), 213-219.

[19] Birkhoff, G., Macdougall, D., Pugh, E., Taylor, G. (1948) Explosives with Lined Cavities. Journal of Applied Physics. 19(6), 563-582.

[20] Guo, D., Pei, H., Song, J., Qin, F., Liu, X. (2008) Study on spliting mechanism of coal bed deephole cumulative blasting to improve permeability. Journal of China Coal Society. 33(12), 1381-1385.

[21] Liu, J., Liu, Z., Gao, K., Ma, Y., Li, Z., Guo, L. (2014) Experimental Study and Application of Directional Focused Energy Blasting in Deep Boreholes. Chinese Journal of Rock Mechanics and Engineering. 33(12), 2490-2496.

[22] Pan, Y. (2020) Experimental Study on Damage Characteristics of Dirt Band by Shaped Charge Blasting in Coal Seam. Fresen. Environ. Bull. 29(4A), 2982-2992.

[23] Yuan, L., Lin, B., Yang, W. (2015) Research progress and development direction of gas control with mine hydraulic technology in China coal mine. Coal Science and Technology. 43(1), 45-49.

[24] Lu, Y., Xia, B., Ge, Z., Tang, J. (2016) Introduction. In: Theory and technology of hydraulic coal seam permeability enhancement. (1st ed) Science Press, Beijing, 1-15.
[25] Singh, M.M., Hartman, H.L. (1961) Hypothesis for the Mechanism of Rock Failure under Impact. The 4th U.S. Symposium on Rock Mechanics (USRMS). University Park, Pennsylvania.
[26] Crow, S.C. (1973) A theory of hydraulic rock cutting. International Journal of Rock Mechanics and Mining Sciences. 10(6), 567–584.
[27] Heymann, F.J. (1969) High-Speed Impact between a Liquid Drop and a Solid Surface. Journal of Applied Physics. 40(13), 5113-5122.
[28] Li, X., Lu, Y., Zhao, Y., Kang, Y., Zhou, D. (2008) Study on improving the permeability of soft coal seam with high pressure pulsed water jet. Journal of China Coal Society. 33(12), 1386-1390.
[29] Liu, S., Zhu, C., Lin, B., Liu, T. (2020) The effect of spatial distribution mode of hydraulic slotting on pressure relief and permeability enhancement of the coal seam. Journal of Mining & Safety Engineering. 37(5), 983-990.
[30] Zhou, Q., Li, N., Chen, X., Xu, T., Hui, S., Zhang, D. (2009) Analysis of water drop erosion on turbine blades based on a nonlinear liquid-solid impact model. International Journal of Impact Engineering. 36(9), 1156-1171.
[31] Lin, B., Lu, Y., Li, B., Zhai, C. (2007) High-pressure abrasive hydraulic cutting seam technology and its application in outbursts prevention. Journal of China Coal Society. 32(9), 959-963.
[32] Huang, B. (2010) Research on theory and application of hydraulic fracture weakening for coal-rock mass. Journal of China Coal Society. 335(10), 1765-1766.
[33] Meng, Z., Zhang, J., Wang, R. (2011) In-situ stress, pore pressure and stress-dependent permeability in the Southern Qinshui Basin. International Journal of Rock Mechanics and Mining Sciences. 48(1), 122-131.
[34] Lv, Y., Tang, D., Xu, H., Luo, H. (2012) Production characteristics and the key factors in high-rank coalbed methane fields: A case study on the Fanzhuang Block, Southern Qinshui Basin, China. International Journal of Coal Geology. 96(1), 93-108.
[35] Hubbert, M.K., Willis, D.G. (1957) Mechanics of Hydraulic Fracturing. Transactions of the American Institute of Mining and Metallurgical Engineers. 210(6), 153-163.
[36] Hossain, M.M., Rahman, M.K., Rahman, S.S. (2000) Hydraulic fracture initiation and propagation: roles of wellbore trajectory, perforation and stress regimes. Journal of Petroleum Science and Engineering. 27(3), 129-149.
[37] Morita, N., Fuh, G.F., Black, A.D. (1996) Borehole breakdown pressure with drilling Fluids .2. Semi-analytical solution to predict borehole breakdown pressure. International Journal of Rock Mechanics and Mining Sciences. 33(1), 53-69.
[38] Duan, M., Gao, D., Zhang, H., Wang, D. (2008) Mechanical mechanism of aerodynamic cave completion in coalbed methane wells. (2008) Coalbed Methane Symposium. Jinggangshan, Jiangxi.
[39] Wang, Z., Fan, Y., Li, S. (2012) Application of Borehole Hydraulic Flushing Technology to Soft and Outburst Seam with Low Permeability. Coal Science and Technology. 40(2), 52-55.
[40] Wang, K., Li, B., Wei, J., Li, P. (2013) Change regulation of coal seam permeability around hydraulic flushing borehole. Journal of Mining and Safety Engineering. 30(5), 778-784.
[41] Qin, Y., Qiu, A., Zhang, Y. (2014) Experiment and Discovery on Permeability Improved Technology of Coal Reservoir Based on Repeated Strong Pulse Waves of High Energy Accumulation. Coal Science and Technology. 42(6), 1-7.
[42] Yutkin, L.A. (1962) Phenomena near discharge region in liquid. In: Electrohydraulic effect. (1st ed.) Science Press, Beijing. 3-5.
[43] Zhang, Y., Qiu, A., Qin, Y. (2017) Principle and engineering practices on coal reservoir permeability improved with electric pulse controllable shock waves. Coal Science and Technology. 45(9), 79-85.
[44] An, S., Chen, D., Zhang, Y., Kong, D., Li, Y., Zhang, D., Wang, Y. (2020) Application of controllable electric pulse wave permeability-enhancing technology in the low-permeability coal seams. Coal Geology and Exploration. 48(4), 138-145.
[45] Zhang, Y., Meng, Z., Qin, Y., Zhang, Z., Zhao, Y., Qiu, A. (2019) Innovative engineering practice of soft coal seam permeability enhancement by controllable shock wave for mine gas extraction: A case of Zhongjing Mine Shuicheng, Guizhou Province, China. Journal of China Coal Society. 44(8), 2388-2400.
[46] Li, H., Qin, Y., Zhang, Y., Shi, Q., Zhou, X. (2015) Experimental study on the effect of strong repetitive pulse shockwave on the pore structure of fat coal. Journal of China Coal Society. 40(4), 915-921.
[47] Bao, X., Liu, Y., Guo, J., Cao, J., Zhao, J., Wu, J. (2020) Quantitative evaluation of fracturing effect of coal-rock masses under high-voltage discharge actions in water. Chinese Journal of Rock Mechanics and Engineering. 39(4), 715-725.
[48] Lin, B., Zhang, X., Li, Y., Zhu, C. (2019) Experiment and simulation of selective cracking of coal samples by plasma. Journal of China Coal Society. 44(11), 3472-3479.

[49] Shi, Q., Qin, Y., Li, H., Qiu, A., Zhang, Y., Zhou, X., Zheng, S. (2016) Response of pores in coal to repeated strong impulse waves. Journal of Natural Gas Science and Engineering. 34, 298-304.

Received: **29.12.2020**
Accepted: **06.02.2021**

CORRESPONDING AUTHOR

Bin Li
School of Safety Science and Engineering,
Anhui University of Science and Technology,
Huainan, Anhui Province 232001 – China

e-mail: 545284034@qq.com

© by PSP Volume 30– No. 05/2021 pages 5415-5420 Fresenius Environmental Bulletin

EVALUATION OF YIELD AND QUALITY CHARACTERISTICS OF BREAD WHEAT GENOTYPES GROWN IN THE TYPIC HAPLOXERERT SUBGROUP SOILS

Duygu Boyraz Erdem[1,*], Ferruh Feza Yilmaz[2]

[1]Namık Kemal University, Agricultural Faculty Department of Soil Science and Plant Nutrition Tekirdag, Turkey
[2]Thrace Union of Soil Laboratory Tekirdag, Turkey

ABSTRACT

This study was carried out in order to determine the grain yield and some quality characteristics of three different wheat varieties (Golya, Secretariat, Syrena Odeska) during two years in the soils of Typic Haploxerert subgroup in the dry conditions of Trakya Region, Turkey. The quality characteristics as grain yield and protein amount, text weight, 1000 grain weight, moisture content, gluten content, gluten index, normal sedimentation value, retired sedimentation value was examined in the study. The difference between wheat varieties grown in the soil of Typic Haploxerert subgroup was found to be statistically significant in terms of grain yield, moisture content, gluten content, protein amount, normal sedimentation and retired sedimentation values in the first year and the Secretaria and Syrena Odeska varities gave the high results. There was no difference between wheat varieties in text weight and 1000 grain weight in the first year. The protein content was found to be statistically significant in Golya and Secretariat varieties and the grain yield was found to be important in Golya and Syrena Odeska varieties in the second year. There was no difference between wheat varieties in text weight and 1000 grain weight, moisture content and gluten index in the second year. As a result, it has been revealed that there may be differences between wheat varieties grown in the same soil in terms of soil requirements and environmental factors, with differences in yield and quality parameters.

KEYWORDS:
Vertisol Order, bread wheat, quality characteristics

INTRODUCTION

Since wheat is the main food source of the world, it makes it a strategic product. Many parameters have an important effect on the yield and quality characteristics of wheat. In addition to the physical, chemical and technological features that make up the quality of wheat, climate and soil structure have an important impact on environmental conditions [1]. Bhatt and Derera (1975) [2] stated that the importance of genotype-environment interactions for quality characteristics in the summer wheat should be evaluated in several different environments in order to fully estimate the quality potential of the breeding lines.

The first goal is to develop high-quality varieties in breeding studies. Relationships between some agricultural characteristics and quality parameters of wheat were evaluated in different studies. This is due to the fact that the cultivars used and cultivated environments have different soil and climate characteristics. The number of studies evaluating these variable relationships detected in the literature and questioning their reasons is limited. Cangir and Boyraz (2000) [3] classified the territory of the Vertisol ordos in 3 subgroups in the detailed soil survey mapping study in Sultanköy town, Turkey, and determined that four series were first degree suitable for wheat cultivation with the need for bottom blasting.

There are many studies on wheat yield and quality parameters. Boyacı (2013) [4] determined the yield and some quality characteristics of some bread wheat varieties under Çukurova conditions. According to the variance analysis results, it was determined that the varieties are different in terms of yield and quality characteristics, and an inverse relationship between quality characteristics and yield values was reported. Aktar (2011) [5] determined the ones suitable for Çanakkale region by examining the yield and quality characteristics of some bread wheat varieties. In the study; relationships between yield and other characteristics were investigated and significant and positive relationships between plant height, hectolitre weight and grain weight in spike were determined. The wheat quality parameters were obtained as 600-674 kg da-1 in grain yield, 40- 43 g in 1000 grain weight, 10.4-12.1% in protein amount, 80.5-80,8 kg/100lt in hectolitre weight, 11- 11.4% in moisture content by, 25.6- 29.9% in gluten content, 81- 93% in gluten index, 34- 40 ml in normal sedimentation value, 41-55 ml in retired sedimentation by Boyraz Erdem and Yılmaz (2016) [6]. However, in these studies, its relation with soil properties draws attention as an issue that is not emphasized. For this reason, it is aimed to determine the relation-

ship between the soil characteristics of the wheat varieties grown in the territory of the Vertisol orders, which is one of the dominant soils of the Thrace region, and the product relationship. The aim of this study is to evaluate the relationships between quality characteristics and grain yield of wheat depending on the soil factor for Thrace Region, Turkey.

MATERIALS AND METHODS

This study was carried out in three different replications according to the randomized block design in the agricultural land belonging to the Vertisol Orders in Tekirdag with 41o01'54" latitude 27o54'41" longitude during two years growing season. In the research, 3 different wheat varieties (Golya, Secretaria, Syrena Odeska) were grown under farmer conditions in two years growing periods. Between the two growing seasons, sunflower cultivation was carried out. The research was carried out on a total area of 3600 m2, each with 180x20 m2 treatment plot. With the cultivation on the land, 10 kg da-1 20.20.0 composite fertilizer and 5 kg da-1 urea in both years; ammonium nitrate (33%) at 24 kg da-1 at the beginning of tillering; 12 kg da-1 ammonium nitrate fertilizers (33%) at the stem elongation were applied.

Climate characteristics. Some climatic parameters measured in the wheat growing periods and their average values for long years are summarized in Table 1 [7]. The 312.3 mm and 304.8 mm rainfall were measured in the two-year growing periods, respectively. Although the precipitation values were not different in the two growing periods, the temperature values were higher especially in April and May, when the plant's spiking and grain filling periods took place.

Soil Analysis. Soil samples were taken from experimental area and sieved using 4 mm sieve. Particle size distribution (texture) was determined by the hydrometer method [8]. To label texture classes, a texture triangle was used [9]. Lime was determined by the volumetric calcimeter method [10]. A pH meter was used to measure pH in saturation mud and organic matter content (%) was determined via Modified Walkley Black Wet Combustion Method [11]. Salt concentration was measured in 1/2.5 soil-water suspension with electrical conductivity tool [12]. The beneficial phosphorus contents of the soils were determined according to the sodium bicarbonate blue colour method [13]. The amount of potassium that passes to neutral 1N ammonium acetate extract in soil samples was determined in the photogram meter [14], Ca-Mg amounts were determined in the atomic absorption spectrophotometer (AAS) [15]. Also, Fe+3, Mn+2, Zn + 2 and Cu + 2 were determined in the atomic absorption spectrophotometer (AAS) [16].

TABLE 1
Some climatic parameters for two years and long-term periods

Month	First year growing period			Second year growing period			Long -term		
	Avg. rainfall (mm)	Avg. temp. (°C)	Avg. humidity (%)	Avg. rainfall (mm)	Avg. temp. (°C)	Avg. humidity (%)	Avg. rainfall (mm)	Avg. temp. (°C)	Avg. humidity (%)
November	35.2	12.9	79.2	48.5	13.8	80.7	75.6	11.0	82.0
December	3.2	6.2	74.2	0.6	7.3	79.9	84.9	7.1	82.8
January	37.0	8.2	89.6	70.7	5.6	80.0	67.0	4.8	82.6
February	5.4	7.8	84.8	68.4	9.7	85.5	55.5	5.2	80.5
March	65.6	10.3	80.5	30.6	10.4	80.3	54.7	7.5	80.0
April	40.5	13.9	82.7	22.9	15.6	72.2	42.1	11.9	77.1
May	65.2	18.1	80.8	28.1	17.9	74.4	37.2	16.9	76.0
June	60.0	22.0	75.5	35.0	23.6	72.2	36.8	21.4	72.0

Plant Analysis. In the research, grain yield, 1000 seed weight, text weight, moisture content, gluten content, gluten index, protein content was determined according to [17]. The normal sedimentation value and retired sedimentation value were determined by Atlı et.al. [18-19].

Statistical analysis. Data obtained from treatments were analysed using of variance (ANOVA). The least significant test (LSD) was used to compare and rank treatments [20]. Differences were declared significant at $p < 0.05$ or 0.01.

RESULTS

Some physical, chemical and nutrient analysis results of the soils of the experimental area are given in Table 2 and 3. The experimental area soils are classified in the Typic Haploxerert subgroup according to their pedological characteristics and analysis results [21]. Vertisol order soils are clay type class with high adhesiveness, high crackiness, cracks that can go up to 1 m in dry time in summer, with high adhesiveness and plasticity. The soil reaction to the depth of 39 cm of the profile is neutral, while the deeper are slightly alkaline. Potassium contents are sufficient until the AC horizon. While the calcium and magnesium levels of the whole profile are high, zinc values are low and manganese values are very low. It is sufficient in terms of copper contents and iron values are low.

The grain yield, 1000 seed weight, text weight, moisture content, gluten content, gluten index, protein content, normal sedimentation and retired sedimentation of treatments are presented in Table 4 and 5 for two years. According to the data of first year, there were statistically 5% significance differences in the grain yield among wheat varieties (Table 4). According to LSD test, Secretariat (641 kg da-1) and Syrena Odeska (674 kg da-1) among the cultivars grown in the soil of the Typic Haploxerert subgroup statistically took place in the same group. According to the data of second year, statistical differences were found in 1% in the grain yield among wheat varieties and according to LSD test, Golya (660 kg da-1) and Syrena Odeska (650 kg da-1) statistically the best yield was obtained from the seed varieties grown in the soil of the Typic Haploxerert subgroup (Table 5). In evaluating the two-year results, the highest grain yield value was obtained from Syrena Odeska wheat varieties. It is reported that the differences between the cultivars in terms of grain yield vary depending on the variety characteristics and environmental factors [22-25].

There were no statistically significant differences in text weight and 1000 seed weight parameters between 3 different wheat seed varieties grown in the soil of the Typic Haploxerert subgroup. While there was a statistically significant 5% significance in the moisture content value among wheat varieties in first year, it was found insignificant for second years. According to moisture content values from first years, Secretariat and Syrena Odeska (11.4%) were statistically highlighted in the LSD test grouping.

TABLE 2
Some physical and chemical analysis results of the experimental area

Profile/ depth (cm)	pH (1/2.5 soil-water)	EC (1/2.5 soil-water) (ms/cm)	Organic matter %	Lime %	Sand %	Silt %	Clay %	Texture Class
Ap/ 0-15	7.33	0.186	1.18	1.22	32.20	20.36	47.44	Clay (C)
Ad/15-39	7.30	0.141	1.07	1.04	32.20	20.36	47.44	Clay (C)
Ass/1 39-76	7.55	0.144	0.48	2.96	34.20	16.36	49.44	Clay (C)
Ass2/ 76-97	7.72	0.173	0.54	5.39	33.28	18.00	48.72	Clay (C)
AC/ 97-116	8.20	0.213	0.32	6.10	34.92	14.36	50.72	Clay (C)
C/ 116+	8.48	0.280	0.30	10.97	31.28	20.00	48.72	Clay (C)

TABLE 3
Some nutrient analysis results of horizons in Typic Haploxerert subgroup

Profile/ depth (cm)	Ca (ppm)	K (ppm)	Mg (ppm)	Cu (ppm)	Fe (ppm)	Mn (ppm)	Zn (ppm)	P_2O_5 ($kgda^{-1}$)
Ap/ 0-15	6573	233.8	687.3	0.918	1.248	3.779	0.318	11.04
Ad/15-39	6418	169.2	699.4	0.850	1.066	1.876	0.112	5.66
Ass/1 39-76	7428	149.3	1091	0.876	1.139	1.095	0.038	1.19
Ass2/ 76-97	6871	168.7	1323	0.973	1.315	1.274	0.037	0.91
AC/ 97-116	6368	125.8	1471	0.945	1.054	1.163	0.038	0.84
C/ 116+	6255	132.7	1520	1.016	1.224	1.709	0.035	0.77

TABLE 4
Yield and quality parameters of wheat genotypes for first years growing period

Parameters	Wheat genotypes			Statistical analyses
	Golya	Secretaria	Syrena Odeska	
Grain yield (kg da^{-1})	600 b*	641 a	674 a	$LSD_{0.05:}$ 34.375
1000 seed weight (g)	42	43	40	ns
Text weight (kg/ 100 L)	80.8	80.8	80.5	ns
Moisture content (%)	11.1 b *	11.4 a	11.4 a	$LSD_{0.05:}$ 0.227
Gluten content (g)	25.6 b**	29.9 a	29.1 a	$LSD_{0.01:}$ 0,882
Protein content (%)	10.4 b**	12.1 a	11.8 a	$LSD_{0.01:}$ 1.189
Gluten index (%)	93a**	81 b	93 a	$LSD_{0.01:}$ 5.316
Normal sedimentation (ml)	34 b**	39 a	40 a	$LSD_{0.01:}$ 2.170
Retired sedimentation (ml)	41 b**	54 a	55.33 a	$LSD_{0.01:}$ 3.962

**: P < 0.01, *: P < 0.05, ns: not significant

TABLE 5
Yield and quality parameters of wheat genotypes for second years growing period

Parameters	Wheat genotypes			Statistical analyses
	Golya	Secretaria	Syrena Odeska	
Grain yield (kg da^{-1})	660 a **	560 b	650 a	$LSD_{0.01:}$ 83.495
1000 seed weight (g)	40	45	45	ns
Text weight (kg/ 100 L)	75.76	76.61	75.47	ns
Moisture content (%)	11.2	11.1	11.1	ns
Gluten content (g)	25.7 b**	30.1 a	23.0 b	$LSD_{0.01:}$ 3.441
Protein content (%)	13.1 a*	13.1 a	12.1 b	$LSD_{0.05:}$ 0.632
Gluten index (%)	91	92	93	ns
Normal sedimentation (ml)	35 b**	45 a	39 b	$LSD_{0.01:}$ 4.771
Retired sedimentation (ml)	41 b*	56 a	46 b	$LSD_{0.05:}$ 7.108

**: P <0.01, *: P <0.05, ns: not significant

The amount of gluten was statistically different at 1% level in both years. According to the LSD test results, the Secretariat (29.9 g) and Syrena Odeska (29.1 g) among the seed varieties in first year and the Secretariat (30.1 g) in second year was found statistically significant.

Protein ratio is one of the criteria used in determining wheat quality [26]. Ünal (2002) [27] reports that the amount of protein in wheat varies between 6-22% depending on the species, variety, environmental conditions and production technique, and the amount of protein in Tukey varies between 10-15% in bread wheat and 11-17% in durum wheat. The amount of protein content is significantly affected by genotype and environmental conditions [28]. The amount of protein content among wheat varieties was found to be statistically 1% significant in first year and according to LSD test, the Secretariat (12.1%) and Syrena Odeska (11.8%) were found statistically significant. There were statistically significant differences at 5% significance level in second year, and in the grouping made according to the LSD test, the seed varieties Golya and Secretariat were statistically significant with 13.1% values. Secretariat seed variety has been important in both years in terms of protein amount. It has been reported by many researchers that there are significant differences between genotypes in terms of protein ratio [29-30-1]. In addition to the seed variety, the amount of precipitation, the distribution of precipitation by months, temperature, soil characteristics and cultural practices and also affect the protein ratio and quality [31-32].

In terms of gluten index values among wheat varieties, statistically, differences were found at 1% significance level in the first year of the study. According to the LSD test performed between these values, the Golya and Syrena Odeska varieties were found to be statistically significant with 93% value. In the second year, gluten index values among seed varieties were found to be statistically insignificant.

In both years, a statistically significant difference of 1% was found in the normal sedimentation value between wheat varieties. According to the LSD test performed between the normal sedimentation values of the seed varieties in the first year, secretariat was found to be statistically significant with 39 ml and Syrena Odeska 40 ml, while the second year Secretariat was found to be significant with 45 ml.

In the retired sedimentation value between wheat varieties, a statistically significant difference

of 1% in first year and a difference of 5% in second year was obtained. According to LSD results among the retired sedimentation values, the Secretariat and Syrena Odeska varieties in first year and the Secretariat in the second year were found to be statistically significant.

CONCLUSIONS

A statistical evaluation of the quality parameters of Golya, Secretariat and Syrena Odeska wheat varieties grown in two years on the soil of Vertisol Orders which spreads to approximately 16% of the Thrace region, Turkey has been made. According to the data of first year, the Secretariat and Syrena Odeska varieties were statistically significant in terms of grain yield, moisture content, gluten content, protein content, normal sedimentation and retired sedimentation values.

It has been reported that the protein ratio varies between 6-25% and the protein ratio of the grain is affected more by soil, climate and fertilizer applications rather than the variety [33]. However, as a result of this study, it was statistically determined that there was a difference in protein ratio between varieties. There was no difference between wheat varieties in terms of text weight and 1000 grain weight. Golya and Syrena Odeska varieties were statistically significant in gluten index.

According to second year data, the gluten content, normal sedimentation, retired sedimentation was found to be statistically significant in seed varieties. The protein content was found to be statistically significant in Golya and Secretariat varieties and the grain yield was found to be important in Golya and Syrena Odeska varieties. There was no difference between wheat varieties in text weight and 1000 grain weight, moisture content and gluten index.

As a result, as the cultivated plants differ in soil types, it has been revealed that there may be differences between wheat varieties grown in the same soil in terms of soil requirements and environmental factors, with differences in yield and quality parameters.

REFERENCES

[1] Atlı, A. (1999) Quality of wheat and its products Symposium on Problems and Solutions of Grain Farming in Central Anatolia 8-11 June Konya. 498-506.

[2] Bhatt, G.M., Derera, N.F. (1975) Genotype X Environment Interactions For, Heritabilities of and comelations among qality trits in wheat. Euphytica. 24, 597-604.

[3] Cangir, C., Boyraz, D. (2000) Detailed Soil Survey and Mapping of Sultanköy Town (İpsala-Edirne) Lands, Land Use Planning. TU. Tekirdağ Faculty of Agriculture Soil Department-Ministry of Agriculture and Rural Affairs General Directorate of Agricultural Reform. Tekirdağ. 186.

[4] Boyacı, A. (2013) Determination of yield and some quality characteristics of some types of bread wheat (Triticum aestivum L.) under Çukurova conditions. Master Thesis, Mustafa Kemal University, Institute of Science, Department of Field Crops. p:83.

[5] Aktar, M. (2011) Examining the yield and quality characteristics of some bread wheat varieties and determining the ones suitable for Çanakkale region. Master Thesis, Çanakkale Onsekiz Mart University, Institute of Science, Department of Field Crops. pp:78.

[6] Boyraz Erdem, D., Yılmaz, F.F. (2016) The Comparison Of Yield And Quality Parameters For Bread Wheat Varieties Grown In Vertisol Order Soils. Eurosoil 2016 Istanbul. 253-253. (Summary statement).

[7] Turkish State Meteorological. (2014) Meteorological Statistic. Turkish State Meteorological Service Turkey, 2014. (In Turkish).

[8] Bouyoucos, G.Y. (1951) A Recalibration of the Hydrometer for Making Mechanical Analysis of Soils. Agronomy Journal. 43 (5), 434.

[9] Soil Survey Division Staff. (1993) Soil survey manual Soil Survey Division Staff Soil Conservation Service, United States Department of Agriculture Handbook No: 18, Washington, D C, USA. 437.

[10] Saglam, M.T. (2008) Chemical Analysis Methods of Soil and Water. Namık Kemal University, Lesson Book :2, Tekirdag (In Turkish).

[11] Kacar, B. (1995) Plant and Soil Chemical Analysis. III. Soil Analysis. Ankara University Agricultural Faculty, Number:3, Ankara, (In Turkish).

[12] U.S. Salinity Lab. Staff (1969) Diagnosis and Improvement of Saline and Alkali Soils. USDA N: 60. USA.

[13] Olsen, S.R., Cole, C.V., Watanabe, F.S., Dean, L.A. (1954) Estimation of available phosphorus in soils by extraction with sodium bicarbonate. US. Dept. of Agric. Cric. 939.

[14] Carson, P.L. (1980) Recommended potassium test. In: Recommended chemical soil test procedures for the North Central Region. Rev.ed. North Central Regional Publication no.221. North Dakota Agric. Exp. Stn. North Dakota State University. Fargo. USA. 20-21.

[15] Thomas, G.W. (1982) Exchangeable cations Chemical and Microbiological Properties. Agronomy Monograph No. 9 (2nd Ed). ASA-SSSA, Madison, Wisconsin, USA. 159-165.

[16] Lindsay, W.L., Norvell, W.A. (1978) Development of a DTPA soil test for zinc, iron, manganese and copper. Soil Sci. Soc. Am. J. 42, 421-428.
[17] Elgün, A., Türker, S., Bilgiçli, N. (2001) Analytical Quality Control of Grains and Products. Selcuk University Faculty of Agriculture, Department of Food Engineering Lecture Notes. Konya Commodity Exchange Publication Number:2 Konya.
[18] Atlı, A., Köksel, H., Dağ, A. (1988) Methods developed for the determination of flour and sunflower damage and research on the applicability of these methods. Field Crops Central Research Institute Publications. General Publication Number: 1988/3, Res. Broadcasting: 1988/2, Agricultural Printing.
[19] ICC Standard. (1972) ICC Standard No: 116. Determination of the Sedimentation Value (According to Zeleny) as an Approximate Measure of Baking Quality. Standard Methods of the International Association for Cereal Chemistry (ICC). Verlag Moritz Schafer. Detmold.
[20] Yurtsever, N. (1984) Experimental Statistical Methods. General Directorate of Rural Services. Publications No: 56. Ankara.
[21] Soil Survey Staff. (2010) Keys to Soil Taxonomy by Soil Survey Staff. United States Department of Agriculture Natural Resources Conservation Service, USA.
[22] Feil, B. (1992) Breeding Progress in Small Grain Cereals. A Comparison of Old and Modern Cultivars. Plant Breeding. 108, 1-11.
[23] Genç, İ. Y., Yağbasanlar, T., Özkan, H., Kılınç, M. (1993) Research on the adaptation of selected durum wheat lines to irrigated conditions in Southeast Anatolia. Durum Wheat and Products Symposium. Ankara 261-272.
[24] Aydın, N., Tugay, E., Sakin, M.A., Gökmen, S. (1999) A research on determination of yield and quality characteristics of durum wheat varieties in Tokat Kazova conditions. Symposium on Problems and Solutions of Grain Farming in Central Anatolia 8-11 June Konya. 621-625.
[25] Özberk, İ., Özberk, F. (1993) Relationships between yield components and yield in durum wheat. Durum Wheat and Products Symposium. 275-285.
[26] Atlı, A., Koçak, N., Aktan, M. (1999) Evaluation of environmental conditions of our country in terms of suitability for growing high quality durum wheat. Symposium on Problems and Solutions of Grain Farming in Central Anatolia 8-11 June Konya. 345-351.
[27] Ünal, S. (2002) Methods used in determining and the importance the quality in wheat. Cereal Products Technology Congress and Exhibition. 3-4 October Gaziantep. 25-37.
[28] Bonfil, D.J., Karnieli, A., Raz, M., Mufradi, I., Asido, S., Egozi, H., Hoffman, A. Schmilovitch, Z. (2004) Decision support system for improving wheat grain quality in the Mediterranean area of Israel. Field Crops Res. 89, 153-163.
[29] Gökmen, S., Sencar, Ö. (1989) Research on yield and yield components in 28 wheat varieties and planted in the fall line in Tokat. Juornal of Cumhuriyet University Tokat Faculty of Agriculture. 1, 357-368.
[30] Budak, H., Karaltın, S., Budak, F. (1997) Determination of quality characteristics of some bread wheat varieties (Triticum aestivum L. Em Thell) by physical and chemical methods. 2. Field Crops Congress of Turkey. 22-25 September. Samsun. 534-536.
[31] Bushuk, W. (1982) Grains and Oilseeds. 3. Edition. Canadian International Grains Institute, Winnipeg Manitoba.
[32] Çağlayan, M., Elgün, A. (1999) Research on some technological features of bread wheat lines and varieties grown under different environmental conditions. Symposium on Problems and Solutions of Grain Farming in Central Anatolia (8-11 June 1999), Konya. 513-518.
[33] PBI Cambridge. (1990) Cereals. PBI Cambridge, Plant Breeding International. Cambridge.

Received: **29.12.2020**
Accepted: **06.02.2021**

CORRESPONDING AUTHOR

Duygu Boyraz Erdem
Faculty of Agriculture,
Department of Soil Science Plant Nutrition,
Namık Kemal University,
59030 Tekirdag – Turkey

e-mail: dboyraz@nku.edu.tr

© by PSP Volume 30– No. 05/2021 pages 5421-5428 Fresenius Environmental Bulletin

THE EFFECT OF DIFFERENT SALINITY LEVELS ON BIOMASS PRODUCTIVITY OF DIATOM SPECIES AND ACCUMULATION OF FUCOXANTHIN

Leyla Uslu[1,*], Oya Isik[1], Mahamad Ahmat Hamid[2], Burcu Ak Cimen[1]

[1]Cukurova University, Fisheries Faculty, Basic Science Department, Adana, Turkey
[2]Cukurova University, Department of Biotechnology, Adana, Turkey

ABSTRACT

Fucoxanthin is an orange pigment found in brown sea algae, diatoms, and dinoflagellates. Fucoxanthin, known to have anticancer, antihypertensive, antipyretic, high antioxidant activity and antiobesity effects. Considering that brown algae rich in fucoxanthin are of great importance, the search for alternative sources of this carotenoid has been ongoing for a long time. The study was conducted to determine the effect of different salinity concentrations on the biomass productivity and fucoxanthin contents of *Phaeodactylum tricornutum*, *Thalassiosira weissflogii* and *Nitzschia closterium* forma minutissima biomass. While the highest biomass amounts of the three diatom species *P. tricornutum* and *N. closterium* f. minutissima were determined at 40‰ salinity, *T. weissflogii* was determined at 30‰ salinity. In terms of species, the highest amount of biomass was determined in *N. closterium* f. minutissima with 0.523gL^{-1}. The lowest biomass content was detected in *T. weissflogii*. The highest fucoxanthin contents were determined in *T. weissflogii* and *N. closterium* f. minutissima in 30‰ salinity, while the lowest value was determined in *P. tricornutum* with 30‰ salinity. From the perspective of both biomass and fucoxanthin, *N. closterium* f. minutissima showed the best improvement in 30‰ salinity.

KEYWORDS:
Phaeodactylum tricornutum, Thalassiosira weissflogii, Nitzschia closterium forma minutissima, fucoxanthin, salinity

INTRODUCTION

Algae are photosynthetic organisms living in marine and freshwater environments with high nutritional value. Algae constitute 90% of the plants in the marine environment. Although there are about 200000 algal species, only 200 algae species are used commercially. It is known that algae are rich in protein, amino acids, vitamins and various mineral substances, and their usage area is wide due to their valuable metabolites such as polysaccharide, sterol and fatty acids [1]. Because of these properties, algae are used in many areas such as medicine, cosmetics, food support, water treatment, live feed source. High value compounds derived from algae; multiple unsaturated fatty acids (PUFA), polysaccharide, protein, pigments, sterols, vitamins and other compounds. Obtained these compounds are known to prevent diabetes, oxidation, inflammation and high cholesterol since they contain anti-oxidant, anti-tumor, anticoagulant, anti-inflammatory, anti-viral and immunomodulating components [2]. Pigments that give color to algae are chemical compounds and play an important role in photosynthesis. Natural pigments are classified as chlorophyll, carotenoids and phycobilins. While chlorophylls are found in higher plants and photosynthetic algae, carotenoids are found in most algae species, phycobilins are found only in cyanobacteria and some red algae [3-4].

Chlorophyll is one of the valuable pigments produced by microalgae. It is generally preferred as a natural colorant. In addition, it is widely used in pharmacological products because it accelerates the cell renewal and wound healing process. Chlorophyll is also used in ulcer treatment and oral sepsis [5]. In addition, chlorophylls are used in the food and cosmetic industry. Chlorophyll a is found in all algae groups, chlorophyll b in green algae, chlorophyll c in brown algae, chlorophyll d in red algae [6].

Carotenoids in algae are pigments that play an important role in photosynthesis. These are structures that collect light, provide the structure and continuity of the photosynthesis complex, prevent the formation of free radicals, remove reactive oxygen species and distribute excess energy [7]. Carotenoids are generally grouped into four main groups as carotenes, xanthophyll, carotenoid ketones and carotenoid acids. If it contains carbon in the carotene structure, it is called carotenoid, if it contains oxygen, it is called xanthophyll. Beta carotene, lutein, astaxanthin, fucoxanthin are the most important commercial carotenoids. Fucoxanthin belongs to the group of carotenoid ketones [8].

Fucoxanthin is an orange pigment found in brown sea algae, diatoms, and dinoflagellates, a pigment that takes brown or olive green color together with chlorophyll [9]. Fucoxanthin, known to have

anticancer, antihypertensive, antipyretic, high antioxidant activity and antiobesity effects [10-11] also protects the blood vessels of the liver, brain, bone, skin and eyes [12]. Fucoxanthin was first isolated from *Fucus*, *Dictyota* and *Laminaria* species in 1914 [13], later in studies it was obtained from macroalgae Laminaria japonica, *Eisenia bicyclis* and *Undaria pinnatifida* [14]. Considering that brown algae rich in fucoxanthin are of great importance, the search for alternative sources of this carotenoid has been ongoing for a long time.

The study was conducted to determine the effect of different salinity concentrations on the biomass productivity and fucoxanthin contents of *Phaeodactylum tricornutum*, *Thalassiosira weissflogii* and *Nitzschia closterium* forma minutissima biomass.

MATERIALS AND METHODS

Algae and culture conditions. In the study, *Phaeodactylum tricornutum*, *Thalassiosira weissflogii* and *Nitzschia closterium* f. minutissima were cultured at 20 °C, 40 µmol photon $m^{-2}s^{-1}$ with 16:8h light and dark cycles, in the Algal Biotechnology Laboratory. Illumination was measured with a radiation sensor LI-COR (LI-250). Walne broth with silica was used as the nutrient medium and the salinity was adjusted to 20‰, 30‰ and 40‰. The inoculation ratio was adjusted to 10%. One liter bottles were used and 900 mL sterile nutrient medium were added to the each bottles in aseptic conditions. All the treatments were made in three replicates. Experiments of the different treatments were completed on different times.

Analytical methods. Dry weight (biomass) and optical density (OD) analysis were performed daily. Dry weight was determined according to Qiang and Richmond [15]. Cell concentration, for *P. tricornutum* at 680 nm [16], for *T. weissflogii* at 680 nm [17] and for *N. closterium* f. minutissima at 750 nm [18], was determined by measuring with a UV-visible spectrophotometer (Shimadzu, UV mini, model 1240, Japan). Chlorophyll a and fucoxanthin analysis were performed every other day. Chlorophyll a analysis was performed according to Sartory and Grobbelaar [19] with 95% ethanol method. The spectrophotometer readings were made at 470, 649 and 665 nm wavelengths, and chlorophyll a was calculated according to the formula below. All measurements were made in five replicates.

Chlorophyll a (µgmL^{-1}) (Chla)= 13.7xA665-5.76xA649

Fucoxanthin analysis was performed according to Wang et al. [20]. 20 mL of cells were collected and 20 mL of ethanol was added, then the sample was incubated at 45°C for 2 hours and mixed with a vortex shaker every half hour. Finally, the pigment solution was separated by centrifugation at 4000xg. The supernatant solution was read in the spectrophotometer at 445 nm, 663 nm and 750 nm. The formula for calculating the concentration of fucoxanthin was as follows

Cfuc (µgmL^{-1})= 6.39×A445-5.18×A663+0.312×A750-5.27

A445 and A663 represent the measurement of the absorbance of microalgae suspended in ethanol and A750 nm indicates the measurement of the absorbance of the microalgae culture.

Statistical analysis. Data were analyzed by using IBM SPSS-12 statistically and the graphs were drawn by Microsoft Excel (2010 Microsoft Corporation, USA) program. The Statistical Package for the Social Sciences (SPSS) (Version 12.0, SPSS, Chicago, IL) [21] was adapted to a personal computer. The differences were considered at a significance level of α= 0.05.

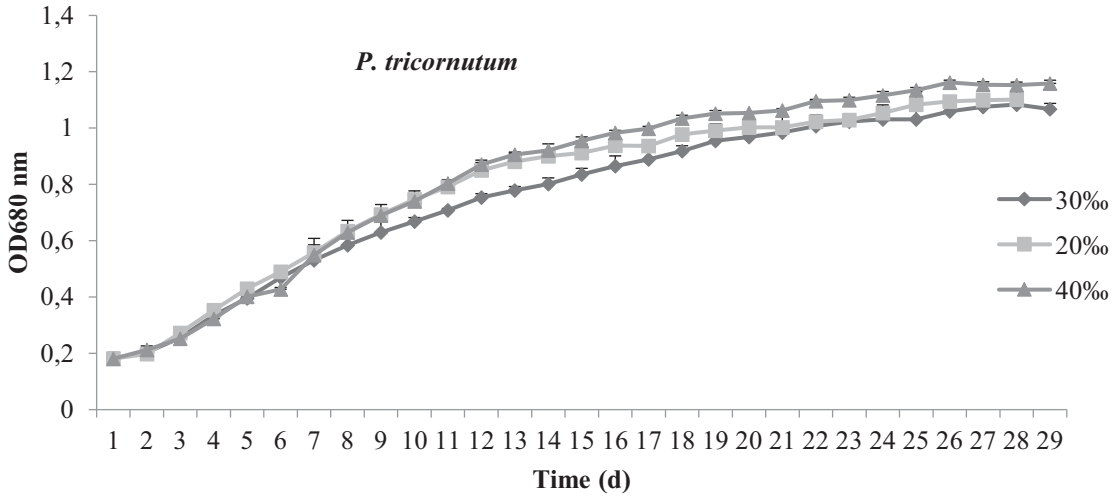

FIGURE 1
Optical density values of *P.tricornutum* cultures of different salinity.

RESULTS

In this study, the effects of different salinity rates of 20‰, 30‰ and 40‰ on the chlorophyll a and fucoxanthin of *P. tricornutum*, *T. weissflogii* and *N. closterium* f. minutissima were determined. At the same time the growth curve created and biomass productivity of the algae species were observed in the different salinities.

The growth of *P. tricornutum* was completed in 28 days in culture at 20‰ salinity and completed in 29 days in cultures at 30‰ and 40‰ salinities. The highest OD values of 1.158 was determined at 40‰ on the last day in *P. tricornutum* culture and differed from the other two groups ($p<0.05$) (Figure 1).

Growth of *T. weissflogii* was completed on 28th day in all groups. The highest optical density was determined as 0.729 in the culture at 30‰ salinity, while the lower OD value was reported as 0.667 for the culture at 40‰ salinity and the lowest OD value was determined as 0.628 in the group containing 20‰ salinity ($p<0.05$) (Figure 2).

Growth in *N. closterium* f. minutissima was completed on 28th day in of 20‰, 30‰ and 40‰ salinity groups. While the optical density values were similar in the cultures at 30 and 40‰ salinities with the values of 0.780, the optical density was lower in the culture at 20‰ salinity with 0.739 ($p<0.05$) (Figure 3).

When optical density values are compared at 20‰, 30‰ and 40‰ salinity levels, on the basis of diatom species, in *P. tricornutum* and *N. closterium* f. minutissima cultures, OD values were higher at 40 ‰ salinity, followed by *T. weissflogii* having the highest OD value at 30‰ salinity. All three species showed a low OD value in the cultures at 20‰ salinity.

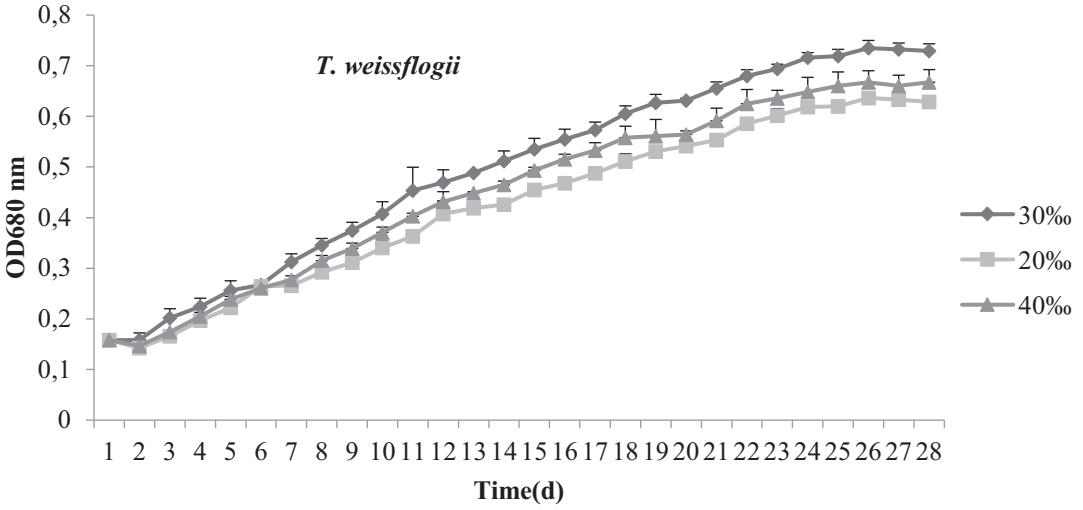

FIGURE 2
Optical density values of *T. weissflogii* cultures of different salinity.

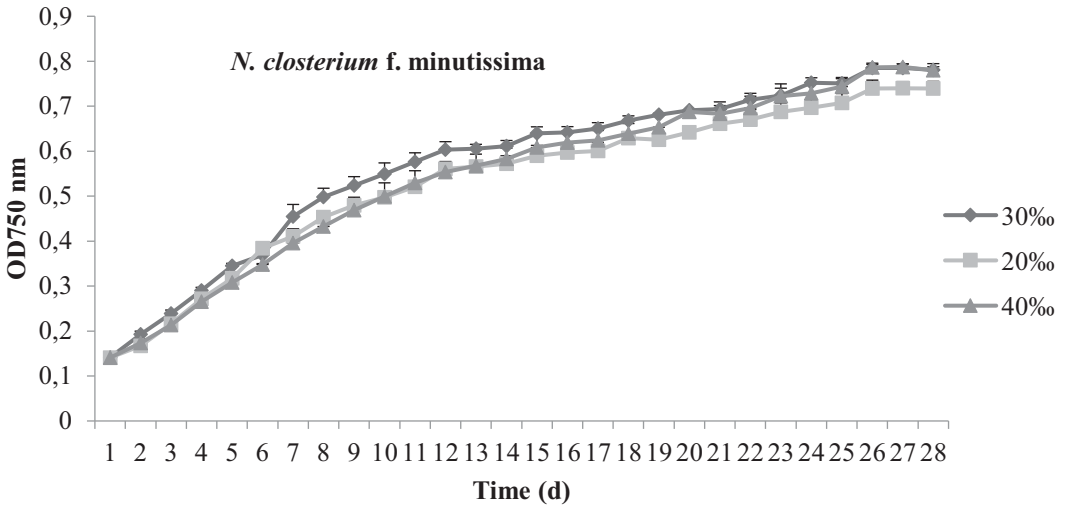

FIGURE 3
Optical density values of *N. closterium* f. minuttisima cultures of different salinity.

Growth of microalgae varies according to many physical, chemical and environmental conditions. In particular, the change in the nutrient content of the culture may cause a decrease or increase of the amount of valuable metabolites in microalgae. The most important indicator that slows growth is NaCl [22]. Ji et al., [23] reported that, high salinity concentrations inhibited growth of algae cell, and that excessive salinity can cause cell death. Qiao et al., [24] cultured *P. tricornutum* in 15, 20, 28 and 35 ppt salinity and they obtained the best biomass to the 28 ppt. Ishika et al. [25] in their study, they reported that they obtained the highest biomass at 45‰ salinity in *P. tricornutum*. In our study, the highest biomass was obtained at the culture of which salinity was 40‰ with *P. tricornutum*. It can be thought that the differences in the studies are due to the fact that the microalgae are different strains. García et al., [26] reported that *T. weissflogii* cultivated at different salinity, the best growth was observed at 25-30 ppt salinity. Vrieling et al., [27] reported that two marine diatoms (*T. punctigera* and *T. weissflogii*) developed better at low salinity (25 and 33 psu). These results were similar to ours that the highest OD and dry weight was observed at 30‰ salinity. Yu et al., [28] reported that *N. closterium* f. minuttisima can maintain growth to a certain level in high salinity (60-70 ppt), with the best growth in normal salinity seawater. At the same time the amount of chlorophyll a decreased by half at 70ppt salinity compared to normal seawater salinity. Jackson et al., [29] determined that, while the best growth of *Nitzschia pungens* f. multiseries was in 30-45‰ salinity and *N. pungens* f. pungens growth well between 15-30‰ salinity. We had also determined that the best OD, dry weight and chlorophyll a values *for N. closterium* f. minuttisima at 30-40‰ salinity, similarly.

The culture conditions have a very important effect on the growth and biochemical composition of diatoms. Especially abiotic factors such as light intensity, presence/absence of nutrients and the utilization of carbon are factors affecting growth and biochemical structure. Other factors are temperature, salinity, culture system models etc. There are many abiotic factors that also affect the amount of fucoxanthin in diatoms. However, light intensity, nitrogen and carbon utilization are among the most influential factors in fucoxanthin [30]. There are not many studies on fucoxanthin contents of diatoms at different salt concentrations.

The biomass production of *P. tricornutum* was the best with 0.457 gL^{-1} at 40‰ salinity compared to other groups. Biomass of the other two groups of salinity was found similar with 0.439 and 0.426 gL^{-1} at 20‰ and 30‰ salinities, respectively. In *P. tricornutum* cultured at 30‰ and 40‰ salinities, the highest chlorophyll a values was 3.355, 3.354 μgmL^{-1}, respectively. The highest fucoxanthin content of 4.720μgmL^{-1} was determined at 40‰ salinity (Table 1).

TABLE 1
Comparison of the growth values of *P. tricornutum*

	20‰	30‰	40‰
Parameter			
$DW_{initial}$	0.08	0.08	0.08
DW_{last}	0.439±0.02^{b}	0.426±0.01^{b}	0.457±0.01^{a}
$OD_{initial}$	0.181	0.181	0.180
OD_{last}	1.101±0.1^{b}	1.067±0.1^{b}	1.158±0.2^{a}
Chl $a_{initial}$	0.280	0.282	0.288
Chl a_{last}	3.202±0.2^{b}	3.355±0.1^{a}	3.354±0.2^{a}
$Cfuc_{initial}$	0.486	0.484	0.483
$Cfuc_{last}$	4.590±0.2^{a}	4.00±0.1^{b}	4.720±0.1^{a}

There is a statistically significant difference between the averages of the lines symbolized by the letters a, b $p < 0.05$), (n = 5).

TABLE 2
Comparison of the growth values of *T. weissflogii*

	20‰	30‰	40‰
Parameter			
$DW_{initial}$	0.07	0.07	0.07
DW_{last}	0.336±0.02^{b}	0.391±0.02^{a}	0.346±0.01^{b}
$OD_{initial}$	0.158	0.158	0.158
OD_{last}	0.628±0.01^{c}	0.729±0.01^{a}	0.667±0.02^{b}
Chl $a_{initial}$	0.305	0.303	0.301
Chl a_{last}	2.829±0.2^{a}	2.895±0.1^{a}	2.554±0.2^{b}
$Cfuc_{initial}$	0.269	0.273	0.270
$Cfuc_{last}$	4.79±0.1^{a}	4.990±0.2^{a}	4.216±0.2^{b}

There is a statistically significant difference between the averages of the lines symbolized by the letters a, b $p < 0.05$), (n = 5).

TABLE 3
Comparison of the growth values of *N. closterium* f. minutissima

	20‰	30‰	40‰
Parameter			
$DW_{initial}$	0.06	0.06	0.06
DW_{last}	0.494±0.02[b]	0.523±0.02[a]	0.523±0.02[a]
$OD_{initial}$	0.141	0.140	0.141
OD_{last}	0.739±0.02[b]	0.780±0.01[a]	0.780±0.01[a]
Chl $a_{initial}$	0.374	0.373	0.376
Chl a_{last}	3.078±0.2[b]	3.249±0.1[a]	3.209±0.1[a]
$Cfuc_{initial}$	0.582	0.588	0.582
$Cfuc_{last}$	4.725±0.2[b]	4.904±0.3[a]	4.816±0.3[a]

There is a statistically significant difference between the averages of the lines symbolized by the letters a, b p <0.05), (n = 5).

TABLE 4
Comparison of biomass amounts (gL^{-1}) of the species

	20‰	30‰	40‰
P. tricornutum	0.439±0.02[b]	0.426±0.01[b]	0.457±0.01[a]
T. weissflogii	0.336±0.02[b]	0.391±0.02[a]	0.346±0.01[b]
***N. closterium* f. minutissima**	0.494±0.02[b]	0.523±0.02[a]	0.523±0.02[a]

There is a statistically significant difference between the averages of the lines symbolized by the letters a, b p <0.05), (n = 5).

TABLE 5
Comparison of fucoxhantin contents (μgmL^{-1}) of the species

	20‰	30‰	40‰
P. tricornutum	4.590±0.2[a]	4.00±0.1[b]	4.720±0.1[a]
T. weissflogii	4.79±0.1[a]	4.990±0.2[a]	4.216±0.2[b]
***N. closterium* f. minutissima**	4.725±0.2[b]	4.904±0.3[a]	4.816±0.3[a]

There is a statistically significant difference between the averages of the lines symbolized by the letters a, b (p <0.05), (n =5).

The highest biomass, optical density and pigment amounts were obtained in *Thallasiosira* cultures of 30‰ salinity. Fucoxanthin and chlorophyll a production were higher in 20‰ salinity (Table 2).

In *N. closterium* f. minutissima cultures, fucoxanthin and chlorophyll a production were higher in 30% and 40% salinity than 20% (Table 3).

Papry et al. [31] reported that low and high (<5 and> 35) salinity slows growth in marine diatoms. Rai et al. [32] reported in their study that the protein and chlorophyll content did not change in *Chlorella*, which they cultivated at different salinity, but the lipid content increased. Danesi et al. [33] stated that microalgae biomass and chlorophyll content were related, and the amount of chlorophyll increases with the increase in cell density. In our results, it was determined that the salinity and the amount of chlorophyll did not change much, and changed depending on the biomass amount. Liang et al. [34] reported that the chlorophyll content of *P. tricornutum* also increased at different salinity, but the best value was 30‰ salinity. Akyıl et al. [35] using different methods, tried to determine the maximum amount of fucoxanthin in *P. tricornutum*. They found that the highest fucoxanthin was 5.60 mg/g by homogenized extraction method. Derwenskus et al. [36] determined the amount of fucoxanthin in *P. tricornutum* using different solvents and found that the best solvent was ethanol with 18.8 mg/g fucoxanthin. Kim et al., [14] reported that ethanol was the best solvent for extracting fucoxanthin from *P. tricornutum* in their study. We also used ethanol as a solvent in our study. Ishika et al. [25] noted that algae had 12% to 90% higher fucoxanthin content at their optimal salinity than when grown at non-optimal salinity. They stated that fucoxanthin productivity was directly related to biomass productivity and that marine microalgae performed best at <55 ppt and halotolerant microalgae at> 55 ppt salinity. They found that the best growth and fucoxanthin amount for *P. tricornutum* was obtained at 45‰ salinity. In our study, the best

growth and fucoxanthin was obtained at 40‰ salinity for *P.tricornutum*. Wang et al. [37], in their study, took two types of diatoms into culture at different salinity (5, 20 and 30 ppt). They reported that the highest fucoxanthin content of *P. tricornutum* (0.74%) was obtained at 20 ‰ salinity. Both Kim et al. [38] and Carreto and Catogglo [39], reported that factors such as small changes in culture conditions and the difference of microalgae strains may cause changes in the biochemical structure of microalgae and make it difficult to compare between studies. For example, Kim et al. [38], they reported differences of up to 300% in fucoxanthin content in different strains of *P. tricornutum* and *I. galbana*.

While the highest biomass amounts of the three diatom species *P. tricornutum* and *N. closterium* f. minutissima were determined at 40‰ salinity, *T. weissflogii* was determined at 30‰ salinity. In terms of species, the highest amount of biomass was determined in *N. closterium* f. minutissima. The lowest biomass content was detected in *T. weissflogii* (Table 4). The highest fucoxanthin contents were determined in *T. weissflogii* and *N. closterium* f. minutissima in 30‰ salinity, while the lowest value was determined in *P. tricornutum* with 30‰ salinity (Table 5). From the perspective of both biomass and fucoxanthin, *N. closterium* f. minutissima showed the best improvement in 30% salinity.

CONCLUSIONS

Fucoxanthin, the most important carotenoid obtained from diatoms, has been used in many areas, especially in the health field. Our aim in this study was to determine the amount of biomass and fucoxanthin of three diatom species cultivated at different salinity concentrations. It was *N. closterium* f. minutissima with the highest biomass and also the highest fucoxanthin content. Considering the findings, diatom *N. closterium* f. minutissima has a potential about fucoxanthin production on an industrial scale.

REFERENCES

[1] El-Sheekh, M.M., Osman, M.E., Dyab, M.A. and Amer, M.S. (2006) Production and characterization of antimicrobial active substance from the cyanobacterium *Nostoc muscorum*. Environmental Toxicology and Pharmacology. 21(1), 42-50.

[2] Akyıl, S., İlter, I., Koç, M. and Kaymak, Ertekin, F. (2016) High Value Compounds Obtained from Algae and Their Bioactive/Biological Applications. Academic Food Journal. 14(4), 418-423.(In Turkish)

[3] Spolaore, P., Joannis-Cassan, C., Duran, E. and Isambert, A. (2006) Commercial applications of microalgae. Journal of Bioscience and Bioengineering. 101(2), 87-96.

[4] Koller, M., Muhr, A. and Braunegg, G. (2014) Microalgae as versatile cellular factories for valued products. Algal Research. 6, 52-63.

[5] Scotter, M. J., Castle, L. and Roberts, D. (2005) Method development and HPLC analysis of retail foods and beverages for copper chlorophyll (E141 [i]) and chlorophyllin (E141 [ii]) food colouring materials. Food Additives and Contaminants. 22(12), 1163-1175.

[6] Dural, B. (1989) Taxonomic investigation of the order Ulvales in Çandarlı Bay II. Ulvaceae A) *Ulva* L. species. Doğa Turkish Journal of Botany. 13, 474-486.

[7] Del Campo, J.A., García-González, M. and Guerrero, M.G. (2007) Outdoor cultivation of microalgae for carotenoid production: current state and perspectives. Applied Microbiology and Biotechnology. 74(6), 1163-1174.

[8] Bağdatlıoğlu, N. and B. Demirbuker. (1999) Advances in Carotenoids in Food Processing. Food. 9, 48-51.(In Turkish)

[9] Chandini, S.K., Ganesan, P. and Bhaskar, N. (2008) In vitro antioxidant activities of three selected brown seaweeds of India. Food Chemistry. 107(2), 707-713.

[10] Heo, S.J., Yoon, W.J., Kim, K.N., Ahn, G.N., Kang, S.M., Kang, D.H. and Jeon, Y. J. (2010) Evaluation of anti-inflammatory effect of fucoxanthin isolated from brown algae in lipopolysaccharide-stimulated RAW 264.7 macrophages. Food and Chemical Toxicology. 48(8-9), 2045-2051.

[11] Maeda, H., Hosokawa, M., Sashima, T., Funayama, K. and Miyashita, K. (2005) Fucoxanthin from edible seaweed, Undaria pinnatifida, shows antiobesity effect through UCP1 expression in white adipose tissues. Biochemical and Biophysical Research Communications. 332(2), 392-397.

[12] Kelman, D., Posner, E.K., McDermid, K.J., Tabandera, N.K., Wright, P.R. and Wright, A.D. (2012) Antioxidant activity of Hawaiian marine algae. Marine Drugs. 10(2), 403-416.

[13] Peng, J., Yuan, J.P., Wu, C.F. and Wang, J.H. (2011) Fucoxanthin, a marine carotenoid present in brown seaweeds and diatoms: metabolism and bioactivities relevant to human health. Marine Drugs. 9(10), 1806-1828.

[14] Kim, S.M., Jung, Y.J., Kwon, O.N., Cha, K.H., Um, B.H., Chung, D. and Pan, C.H. (2012) A potential commercial source of fucoxanthin extracted from the microalga *Phaeodactylum tricornutum*. Applied Biochemistry and Biotechnology. 166(7), 1843-1855.

[15] Qiang, H. and Richmond, A. (1994) Optimizing the population density in *Isochrysis galbana* grown outdoors in a glass column photobioreactor. Journal of Applied Phycology. 6(4), 391-396.
[16] Griffiths, M.J., Van Hille, R.P. and Harrison, S.T.L. (2010) Selection of direct transesterification as the preferred method for assay of fatty acid content of microalgae. Lipids. 45(11), 1053-1060.
[17] Huo, S., Zhou, W., Wang, Z., Zhu, S., Dong, L., Huang, W. and Dong, R. (2015) Biomass measurement of microalgae cultivated under photoautotrophic conditions for biofuels. Energy Sources, Part A: Recovery, Utilization, and Environmental Effects. 37(13), 1447-1454.
[18] Sriharan, S., Bagga, D. and Sriharan, T.P. (1989) Environmental control of lipids and fatty acid production in the diatom *Navicula saprophila*. Applied Biochemistry and Biotechnology. 20(1), 281-291.
[19] Sartory, D.P. and Grobbelaar, J.U. (1984) Extraction of chlorophyll a from freshwater phytoplankton for spectrophotometric analysis. Hydrobiologia. 114(3), 177-187.
[20] Wang, L.J., Fan, Y., Parsons, R.L., Hu, G.R., Zhang, P.Y. and Li, F.L. (2018) A rapid method for the determination of fucoxanthin in diatom. Marine Drugs. 16(1), 33-45.
[21] Zar, J.H. (1999) Biostatistical Analysis. Upper Saddle River. 4th edn. Prentice Hall, New Jersey, Cap. 12, 231-272.
[22] Forieri, I., Hildebrandt, U. and Rostás, M. (2016) Salinity stress effects on direct and indirect defence metabolites in maize. Environmental and Experimental Botany. 122, 68-77.
[23] Ji, X., Cheng, J., Gong, D., Zhao, X., Qi, Y., Su, Y. and Ma, W. (2018) The effect of NaCl stress on photosynthetic efficiency and lipid production in freshwater microalga-*Scenedesmus obliquus* XJ002. Science of the Total Environment. 633, 593-599.
[24] Qiao, H., Cong, C., Sun, C., Li, B., Wang, J. and Zhang, L. (2016) Effect of culture conditions on growth, fatty acid composition and DHA/EPA ratio of *Phaeodactylum tricornutum*. Aquaculture. 452, 311-317.
[25] Ishika, T., Moheimani, N.R., Bahri, P.A., Laird, D.W., Blair, S. and Parlevliet, D. (2017) Haloadapted microalgae for fucoxanthin production: Effect of incremental increase in salinity. Algal Research. 28, 66-73.
[26] García, N., López-Elías, J.A., Miranda, A., Martínez-Porchas, M., Huerta, N. and García, A. (2012) Effect of salinity on growth and chemical composition of the diatom T*halassiosira weissflogii* at three culture phases. Latin American Journal of Aquatic Research. 40(2), 435-440.
[27] Vrieling, E.G., Sun, Q., Tian, M., Kooyman, P.J., Gieskes, W.W., van Santen, R.A. and Sommerdijk, N.A. (2007) Salinity-dependent diatom biosilicification implies an important role of external ionic strength. Proceedings of the National Academy of Sciences. 104(25), 10441-10446.
[28] Yu, J.L., Xia, J.R. and Zou, Y.D. (2011) Response of carbon anhydrase activity and photosynthesis to high salinity stress in *Nitzschia closterium* f. minutissima. Journal of Fisheries of China. 35(4), 515-523.
[29] Jackson, A.E., Ayer, S.W. and Laycock, M.V. (1992) The effect of salinity on growth and amino acid composition in the marine diatom *Nitzschia pungens*. Canadian Journal of Botany. 70(11), 2198-2201.
[30] Arora, N. and Philippidis, G.P. (2021) Fucoxanthin Production from Diatoms: Current Advances and Challenges. In: Mandotra S.K., Upadhyay A.K., Ahluwalia A.S. (eds) Algae. Springer, Singapore.
[31] Papry, R.I., Ishii, K., Al Mamun, M.A., Miah, S., Naito, K., Mashio, A.S. and Hasegawa, H. (2019) Arsenic biotransformation potential of six marine diatom species: effect of temperature and salinity. Scientific Reports. 9(1), 1-16.
[32] Rai, M.P., Gautom, T. and Sharma, N. (2015) Effect of salinity, pH, light intensity on growth and lipid production of microalgae for bioenergy application. OnLine Journal of Biological Sciences. 15(4), 260-267.
[33] Danesi, E.D.G., Rangel-Yagui, C.O., Sato, S. and Carvalho, J.C.M.D. (2011) Growth and content of *Spirulina platensis* biomass chlorophyll cultivated at different values of light intensity and temperature using different nitrogen sources. Brazilian Journal of Microbiology. 42(1), 362-373.
[34] Liang, Y., Sun, M., Tian, C., Cao, C. and Li, Z. (2014) Effects of salinity stress on the growth and chlorophyll fluorescence of *Phaeodactylum tricornutum* and *Chaetoceros gracilis* (Bacillariophyceae). Botanica Marina. 57(6), 469-476.
[35] Akyıl, S., İlter, I., Koç, M., Demirel, Z., Erdoğan, A., Conk-Dalay, M. and Kaymak-Ertekin, F. (2020) Effects of Extraction Methods and Conditions on Bioactive Compounds Extracted from *Phaeodactylum tricornutum.* Acta Chimica Slovenica. 67(4), 1250-1261.
[36] Derwenskus, F., Metz, F., Gille, A., Schmid-Staiger, U., Briviba, K., Schließmann, U. and Hirth, T. (2019) Pressurized extraction of unsaturated fatty acids and carotenoids from wet *Chlorella vulgaris* and *Phaeodactylum tricornutum* biomass using subcritical liquids. Gcb Bioenergy. 11(1), 335-344.

[37] Wang, H., Zhang, Y., Chen, L., Cheng, W. and Liu, T. (2018) Combined production of fucoxanthin and EPA from two diatom strains *Phaeodactylum tricornutum* and *Cylindrotheca fusiformis* cultures. Bioprocess and Biosystems Engineering. 41(7), 1061-1071.
[38] Kim, S.M., Kang, S.W., Kwon, O.N., Chung, D. and Pan, C.H. (2012) Fucoxanthin as a major carotenoid in *Isochrysis aff. galbana*: Characterization of extraction for commercial application. Journal of the Korean Society for Applied Biological Chemistry. 55(4), 477-483.
[39] Carreto, J.I. and Catoggio, J.A. (1976) Variations in pigment contents of the diatom *Phaeodactylum tricornutum* during growth. Marine Biology. 36(2), 105-112.

Received: **29.12.2020**
Accepted: **06.02.2021**

CORRESPONDING AUTHOR

Leyla Uslu
Fisheries Faculty,
Basic Science Department,
Cukurova University,
Adana – Turkey

e-mail: hizarcil@cu.edu.tr

© by PSP Volume 30– No. 05/2021 pages 5429-5436 Fresenius Environmental Bulletin

LOW-ALTITUDE UAV REMOTE SENSING TECHNOLOGY AND ITS APPLICATION IN SURVEYING AND MAPPING OF A BAUXITE MINE

Jiuling Tian*

Department of Urban Construction, Henan Polytechnic Institite, Nanyang Henan 473000, China

ABSTRACT

With the liberalization of low-altitude domain restrictions, low-altitude flight and aircraft low-altitude technology control applications have become a new direction. Low-altitude UAV remote sensing technology is often used by people in many fields, such as surveying and mapping, terrain surveying, data collection, tourism development, geological disaster prevention, agricultural irrigation, pest control, etc. In this study, the research site is the Heitutian bauxite mine in Qingzhen City, and the DJI Z-1 UAV is selected to operate remote sensing technology in the 0-500M airspace of the low-altitude field. The cycle is 3 days, and the total lift is 6 times (2 times each day). The complete topographic surveying and mapping results of the corresponding bauxite mines are collected, and the surveying and mapping data are sorted and counted. According to the relevant results of the bauxite mines surveyed and drawn, a report plan is formed. The results show that the distance between the low-altitude drone surveying and mapping area and point 1 is 1,677.55m, which is 1.45m away from the field surveying and mapping distance. The point distance between the low-altitude drone surveying and mapping area and point 2 is 2340.23m, which is 1.0 m away from the field surveying and mapping distance. The point distance between the low-altitude drone surveying and mapping area and point 3 is 1190.23m, which is 0 m away from the field surveying and mapping distance. The measurement result meets the requirements, and the accuracy is high. The operation of UAV remote sensing technology in the low-altitude field can help users to survey and map the precise location and various information of bauxite mines in detail which is of great help to the collection of data in the early stage of development and the collection of specific development information.

KEYWORDS:
Low-altitude UAV, Remote sensing technology, Bauxite, Mine surveying and mapping

INTRODUCTION

Low-altitude drones have been gradually released, and there are continuous innovations in the field of remote sensing technology. UAV surveying and mapping has become the main technical means for land exploration and geological exploration. In carrying out surveying and mapping of bauxite, UAV has many advantages, which can reduce costs and risks of surveying and mapping. If the staff do not use effective methods to solve the problem, they will miss the best time to deal with it, which will inevitably bring great economic losses to the enterprise. However, UAV remote sensing technology has its own characteristics of high monitoring efficiency, which can well assist surveying and mapping personnel to deal with various emergency matters more efficiently and accurately [1].

The UAV remote sensing technology system has good compatibility. When the UAV remote sensing technology is used to implement the measurement, it will not be affected by the complicated terrain and harsh environmental factors. The gradual improvement under the situation of multi-technology joint application fundamentally improves the compatibility of remote sensing technology systems. The information processing speed of UAV remote sensing technology is fast [2]. With UAV remote sensing technology, surveyors can quickly process all data information within the target range and can take advantage of information collection and discrimination within the scope of surveying and mapping [3]. After using the dazzling technology of drones, the work can quickly obtain relevant information, the work cost is relatively low, the data obtained is more accurate, and the geological environment information and database are updated and upgraded in time [4]. In the process of land and geological environment management, relevant departments should apply corresponding technical methods.

Using drone technology to remotely sense and control the range that the drone passes through can allow data information to be transmitted to the platform database in real time, which is very efficient. In the process of data information processing, the use of UAV remote sensing technology can supplement

the technical defects. When monitoring the designated area, it can quickly process the area information, and fundamentally further ensure the accuracy of the measurement work [5].

Nowadays, the UAV remote sensing technology used in China is basically the UAV flying in the low-altitude field. It is necessary to add and load professional equipment and facilities in the surveying and mapping to improve the accuracy of the surveying and mapping technology. The UAV is small and fast, which are very helpful to the surveying and mapping [6-7]. The drone must be photographed when it is flying. Under disorderly conditions, the image must have an inclination angle, resulting in severe ghosting. The operating system is difficult to correct and target related parameters are not easy to be repaired [8].

MATERIALS AND METHODS

Experimental equipment and materials. The research site selected the Heitutian bauxite mine in Qingzhen City. Qingzhen City is under the jurisdiction of Guiyang City, Guizhou Province which has abundant mine reserves. The DJI Z-1 model drone is selected for this investigation in the low-altitude field. The remote sensing technology operation is carried out in the 500M airspace, with a period of 3 days and 6 lifts, to collect the complete topographic surveying and mapping results of the corresponding bauxite mines and organize the surveying and mapping data.

The auxiliary data used for bauxite mine modeling includes 7 satellite-derived raster datasets. LULC data shows a strong relationship with the distribution of bauxite mines, especially those that indicate the types of bauxite mine settlements. The land cover dataset contains 14 types of land cover, which are used as auxiliary data. Net primary productivity (NPP) is the key driving force for the distribution of bauxite mines. We take MODIS 17 A3 annual NPP as our NPP data. The precipitation, temperature, slope, and altitude in a region also affect the model of mountain measurement of the bauxite mines to a certain extent which may be directly related to the distribution of bauxite mines [9]. In this case, we use digital elevation data and its derived slope data from the advanced spaceborne thermal emission and reflection radiometer (ASTER) Global Digital Elevation Model (GDEM). NTL is a more direct indicator of distribution of bauxite mines. We use Suomi National Polar Orbiting Partnership Visible Infrared Imaging Radiometer Suite (NPP-VIIRS) 500 m resolution NTL data as auxiliary data, which has a spatial resolution higher than 1 km of DMSP-OLS [10]. The UAV surveying and mapping program uses vector data (that is, composed of geometric figures such as points, lines, and polygons) as auxiliary data, including POI, road, and surveyed object data. POI are various places with location information, some of which are related to bauxite mining activities. The road network is obtained from AutoNavi map service, which is one of the largest online map service providers in China [11]. The area and height of the surveyed objects are very useful for accurate estimation of bauxite mines, especially in urban areas with dense bauxite mines.

In surveying and mapping, the embedded board used is the NVIDIA-Jetson-TX2 board, which is the fastest and most energy-efficient embedded artificial intelligence computing device. It is built around an NVIDIA Pascal™ GPU, loaded with 8GB of memory and 59.7GB/s memory bandwidth, with multiple standard hardware interfaces. We also use the OneNET platform to realize the remote, wireless, and real-time transmission. The OneNET platform is an open and free cloud platform that simplifies the access of IoT devices to the cloud. The OneNET platform has been used in various surveying, mapping, and surveying applications [12].

Research method. Data collection and organization. After receiving the mission, the UAV remote sensing system investigates the mission, determines the mission and the target, and then uses the flying platform and remote sensing equipment to investigate the geological and climatic conditions of the region and select the best time for UAV remote sensing work. We collect ground data and integrate all data in combination with field exploration [13].

Take-off site selection. After the investigation area is determined, we select the appropriate drone flight platform to take off the drone on open flat ground or on the highway to ensure that the equipment and personnel are safe to carry out the flight work. In view of the unpredictability and potential safety hazards of flight, in the development of UAV test flight operations, take-off and landing sites should be surveyed and selected reasonably [14]. The requirements for the take-off and landing sites of UAVs are not high, but safety issues must be focused on to effectively prevent various accidents [15].

Flight plan design. A reasonable take-off plan can effectively reduce the number and time of UAV take-offs. On the basis of understanding the location and information of the area, the flight efficiency needs to be combined to effectively reducing the route, thus comprehensive obtaining the image data in a timely manner.

The airborne flight control system check. During the flight of the UAV, the remote sensing equipment is installed in it. During each take-off and landing stage, the various components of the UAV should be closely inspected and checked to ensure

that the aircraft is in the normal operation of the equipment [16].

Flight quality and impact quality inspection. After the flight of the UAV is completed, the flight quality of the UAV and the quality of the remote sensing image acquisition should be checked to obtain high-quality raw data and then facilitate the processing of the later data [17]. In the link of UAV remote sensing data acquisition, due to the high-altitude air currents, the UAV flight will be unstable, and the UAV will have the problem of deviation. In the link of quality inspection of UAVs, the overlap and inclination of UAVs should be effectively calculated to achieve the most scientific and reasonable aerial data collection [18].

Flight data collection. We collect the recorded and surveyed data to complete bauxite mine surveying and mapping.

RESULTS

The advantages of UAV remote sensing measurement technology are very significant, and the characteristics are also well displayed. According to the specific environmental surveying and mapping work, targeted detailed surveys should be carried out. The flying height of the drone is controlled within 500m. The remote sensing and mapping technology of the drone is strengthened. The remote wireless signal transmitter One-Tek technology is used to enhance the radio frequency signal [19]. The collected information results are as follows:

Results of UAV monitoring improvement map. As shown in Figure 1, the original vector of the UAV is intended to be used for aerial photography. For some large-scale surveying and mapping, it is necessary to implement basic terrain and orthographic impact drawings for measurement. In the actual measurement, it is necessary to analyze the actual situation of specific surveying and mapping. This surveying and mapping is regarded as the fundamental basis of agricultural production. The task of surveying and mapping is relatively heavy, time is relatively tight, the distribution of surveying and mapping is relatively decentralized, and the measurement is becoming more and more difficult [20]. UAV surveying technology is used in this surveying and mapping. During the implementation of aerial photography, it is implemented in strict accordance with design standards to ensure that the safety and stability of the flight is maintained throughout the entire stage of aerial photography and the turning radius is controlled. The requirements are also more extensive in order to obtain accurate information data from GPS measurements [21].

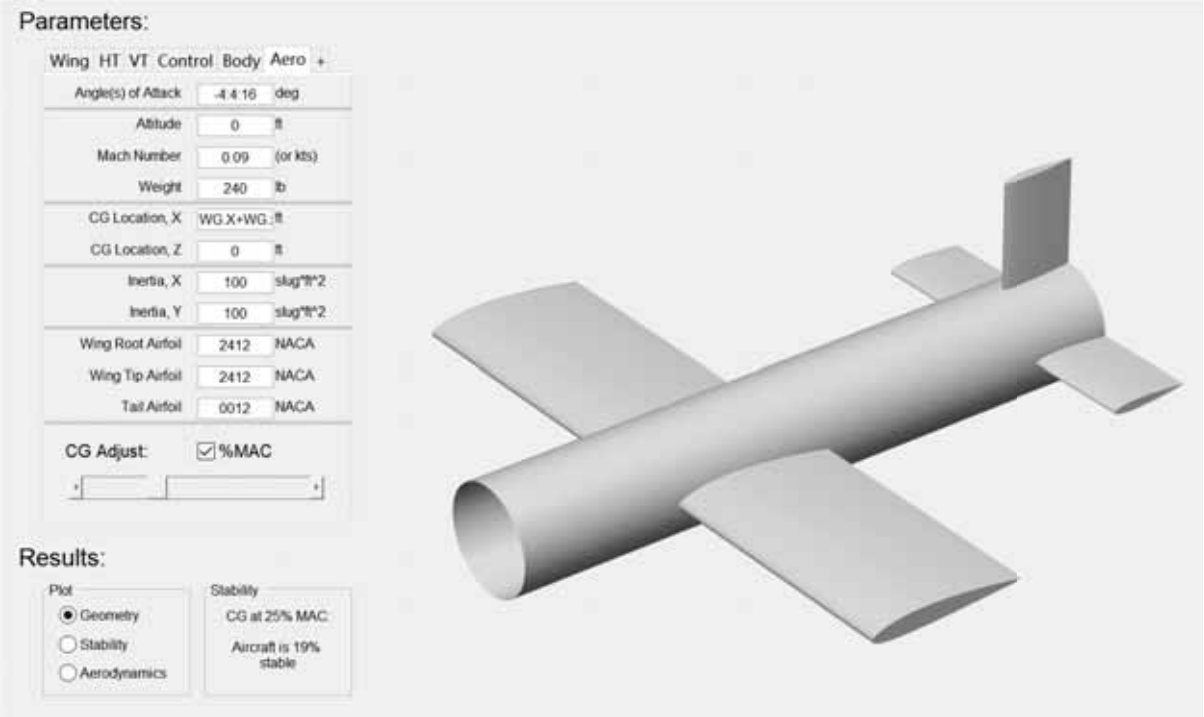

FIGURE 1
Schematic diagram of the original vector model of UAV.

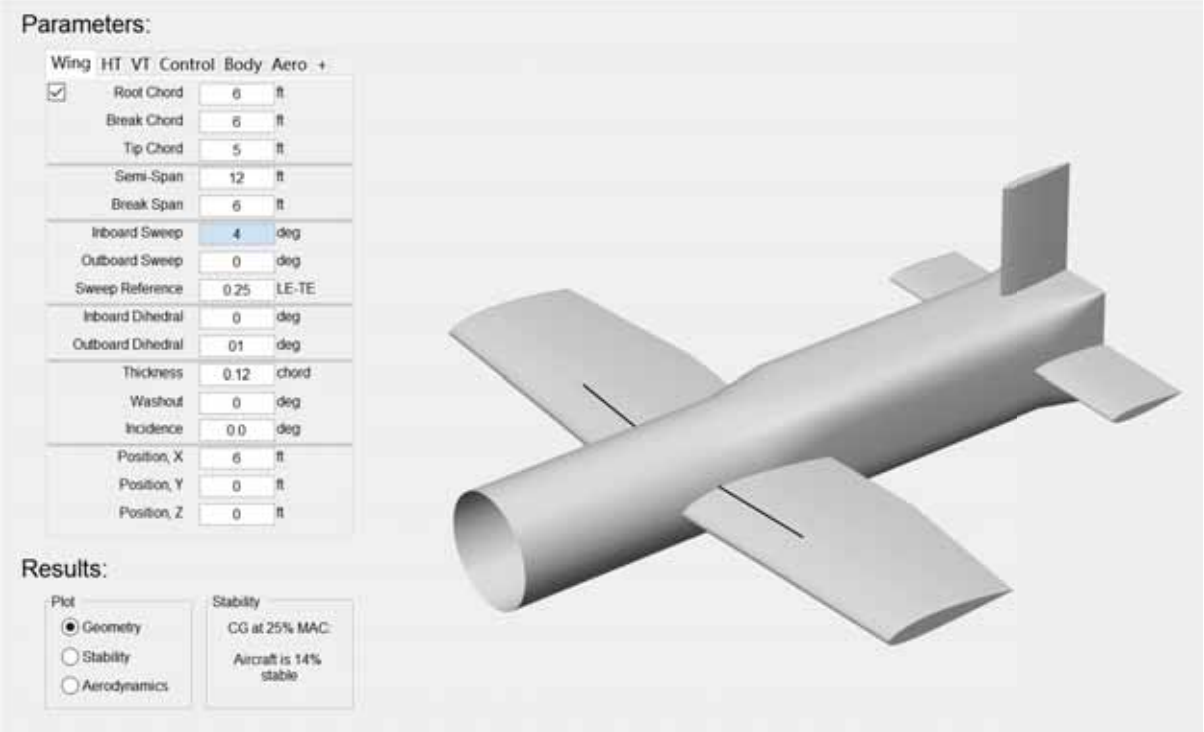

FIGURE 2
Schematic diagram of the vector model of UAV improved surveying and mapping technology equipment.

As shown in Figure 2, the UAV's improved surveying and mapping technology equipment vector model adds a red area marked surveying and mapping professional technical equipment. This type of equipment presents technical advantages mainly in improving the drone's performance under the control of remote sensing technology in the low altitude field with a surveying and mapping capability within a 500m range. This surveying and mapping technology can well survey and map professional terrain and mineral deposits [22].

Image surveying and mapping results in the upstream area of the mine. Compared with traditional information processing methods, UAV remote sensing measurement technology can prevent problems caused by manual measurement. In the current stage of the development of new measurement technologies, drone remote sensing measurement technology is more prominent in detecting natural resources, such as mines, land, and waters [23]. When processing remote sensing image information, the combination of drones and navigation and positioning implementation technologies will implement necessary conversion and transmission of the acquired data, which will inevitably increase the application level of surveying and mapping data information. The image collection results in the upstream area of the mine are shown in Figure 3.

FIGURE 3
The results of images collected from the upper and upper reaches of the bauxite mine.

The research site selects the Heitutian bauxite mine in Qingzhen City to collect the complete topographic surveying and mapping results of the corresponding bauxite mine. Through the information collection surveying and mapping statistic results, the specific range planning and the effective value of the upstream collection range are marked, and the marking result is shown in Figure 4.

As shown in Figure 4, the area marked by the black triangle is 4.5km^2. The crystals of the bauxite sample gibbsite involved in the range are extremely small, and the crystals gather into nodules, beans or soil, showing white with glassy luster, and reddish if it contains impurities. They are mainly secondary minerals produced after weathering of aluminum-containing minerals such as feldspar (Table 1).

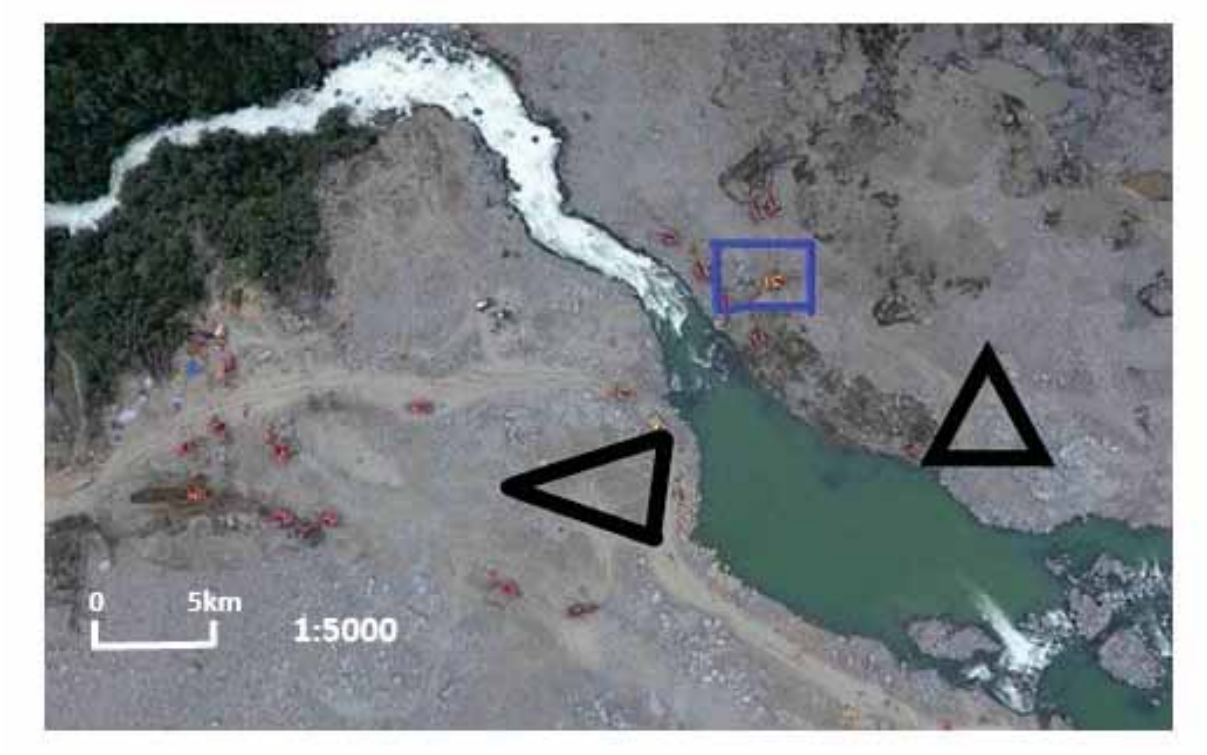

FIGURE 4
The results of mapping and marking of images collected from the upper and upper reaches of the bauxite mine.

TABLE 1
Statistical results of bauxite content

Type	Structure	Content
Bauxite (AlO(OH) and $Al_2O_3 \cdot H_2O$)	The orthorhombic crystal system, the crystals intact are columnar, plate, scale, needle, and prismatic.	TiO_2、SiO_2、Fe_2O_3、Ga_2O_3、Nb_2O_5、Ta_2O_5、TR_2O_3

As shown in Table 1, the main chemical elements of bauxite are AlO(OH) and $Al_2O_3 \cdot H_2O$.. The diaspore in the ore in the upstream area generally contains TiO_2、SiO_2、Fe_2O_3、Ga_2O_3、Nb_2O_5、Ta_2O_5、TR_2O_3 and other mixed substances of different quantity and quality.

The sample collection area is visible upstream of the bauxite mine, and the blue box represents the best setting location for the sample measurement and collection safety area in the upper and upstream area of the bauxite mine. When surveying mines, the application of drone remote sensing surveying and mapping technology can accurately detect mine resources, which can significantly improve the level of survey information and data.

Image mapping results in the downstream area of the mine. In the process of image mapping in the downstream area of the mine, a relatively residential area is found as shown in Figure 5. However, the Juzhuyuan is 10km away from the location, which has a good transportation and production environment for bauxite production.

As shown in Figure 5, it can be seen that there is a good production area in the downstream area of the bauxite mine, and the conditions for the production of the bauxite mine are already in place.

Measurement results of bauxite mining. The mine development of bauxite is carried out within the mining area of bauxite mines. The development of bauxite itself should specifically find the key direction and scope of bauxite development, minimize the development scope, and develop bauxite with higher purity. For mineral sources, certain surveying and mapping should be conducted for bauxite mines.

As shown in Figure 6, it can be seen that bauxite mining in the red area is more suitable, with a range of $9km^2$. The basic conditions of bauxite are constructed within the mining area. The distance measurement statistics of the surveying and mapping points are shown in Table 2.

FIGURE 5
Schematic diagram of the results of image mapping in the downstream area of the mine.

FIGURE 6
The results of the measurement image of bauxite mining.

TABLE 2
Statistics results of distance measurement of UAV low-altitude surveying points

Point distance number	1	2	3
Site surveying and mapping distance of the whole station (m)	1678.89	2341.23	1190.23
Low-altitude drone surveying and mapping (m)	1677.44	2340.23	1190.23
Difference (m)	1.45	1.0	0

As shown in Figure 6 and Table 2, the results show that the error between the UAV monitoring results and the field measurement is within 2m. Low-altitude drone remote sensing mapping technology is more stringent than the previous traditional aerial survey photography technology for regional terrain environmental standards. For surveying, UAV surveying is subject to relatively small factors in the terrain and environment, which to a large extent can guarantee the accuracy of surveying and mapping. For those situations where the topography is relatively complicated or the climatic environment, we can choose to use a new type of drone remote sensing measurement technology, which can not only ensure the measurement level, but also increase the accuracy of the surveying and mapping technology. In addition, during the measurement, the UAV remote sensing measurement technology is used to promote the observation value in the field measurement work to match the tolerance value within the range specified by the measurement adjustment.

CONCLUSION

Based on the above results, the low-altitude UAV remote sensing surveying and mapping technology has innovative and detectable high-value returns compared to the previous traditional methods of traditional aircraft surveying or unmanned aerial vehicle remote sensing surveying and mapping technology. With future technological breakthroughs and more high-tech cooperation, we can build a big data database and use post-processing software to obtain aerial image photos.

The application effect of bauxite mine surveying and mapping under UAV remote sensing technology is good, and the surveying and mapping methods are scientific and effective in monitoring, surveying, and mapping. The UAV remote sensing WebGIS supervision platform is used to supervise a series of functions such as target image recognition, on-site verification, investigation, and process monitoring. Therefore, the adopted digital information management system needs to accurately analyze the location and spatial information of illegal entities, which is the main function of GIS. The WebGIS system mainly adopts the browser/server (B/S) model. The B/S model simplifies the client software, develops system functions, maintains and updates the identification method on the application server. Compared with the B/S mode and the traditional independent client mode, the management and maintenance are more convenient, the demand for the client is the least, and the use and promotion are more convenient.

Compared with the traditional GIS software platform, the system platform constructed by WebGIS can access data from any platform. The spatial database can be used for data management, effectively improving efficiency and accuracy. The comprehensive demonstration module uses UAV remote sensing data to process each surveying and mapping construction project into orthophotos, digital surface models, three-dimensional models, and panoramic images. These images can comprehensively display the inspection surveying and surveying conditions, vividly show the status of surveying, mapping, and measurement. The main task of the image database and management module is to manage and dispatch the preprocessed UAV remote sensing images, and provide basic services for the entire management system, including the establishment of an image database, the import of multi-format image data, and the image management such as data browsing and display, image data location and scope. The vector database and management module is mainly used to manage and schedule the original data of surveying and mapping planning provided by relevant departments and related vector data generated by vector data processing. By superimposing the vector data on the image and comparing it with the original measurement, it can accurately survey the deviation of the measurement.

ACKNOWLEDGEMENTS

This work was not supported by any funds. The authors would like to show sincere thanks to those techniques who have contributed to this research.

REFERENCES

[1] Musaoglu, N., Seker, D.Z., Kabdasli, S., Kaya, S., Duran, Z. (2004) Using Remote Sensing And GIS for the Assessment Of Visual Attributes: A Case Study of the South Coastal Zone of Turkey. Fresen. Environ. Bull. 13(9), 854-859.

[2] Coskun, H.G. (2009) Remote Sensing and GIS Techniques for Temporal Evaluation of Environmental Impacts on Major Drinking Water Dam and Basin of Metropolis Istanbul. Fresen. Environ. Bull. 18(3), 261-269.

[3] Xu, S., Wang, T., Sun, S. (2011) The Application of Remote Sensing Technology to Coal Resources Prospecting and Evaluation in Zhaotong, Yunnan. Energy Exploration and Exploitation. 29(1), 77-86.

[4] Dos Reis, A.A., Franklin, S.E., De Mello, J.M., Acerbi Junior, F.W. (2019) Volume Estimation in a Eucalyptus Plantation Using Multi-Source Remote Sensing and Digital Terrain Data: A Case Study in Minas Gerais State, Brazil. International Journal of Remote Sensing. 40(7-8), 2683-2702.

[5] Perakis, K., Kyrimis, K., Kungolos, A. (2000) Monitoring Land Cover Change Detection with Remote Sensing Methods in Magnesia Prefecture in Greece. Fresen. Environ. Bull. 9(9), 659-666.
[6] Tao, D., Jia, G., Zhao, H. (2014) End-to-end Simulation Model of Rover-Based Hyperspectral Remote-Sensing Systems: Application to VNIS. International Journal of Remote Sensing. 35(20), 7279-7302.
[7] Duran, Z., Musaoglu, N., Seker, D. Z. (2006) Evaluating Urban Land Use Change in Historical Peninsula, Istanbul, by Using GIS and Remote Sensing. Fresen. Environ. Bull. 15(8A), 806-810.
[8] Tanik, A. (2006) Determination of Land-Use Change in an Urbanized District of Istanbul via Remote Sensing Analysis. Fresen. Environ. Bull. 15(8A), 798-805.
[9] Goksel, C., Mercan, D.E., Kabdasli, S., Bektas, F., Seker, D.Z. (2004) Definition of Sensitive Areas in a Lakeshore by Using Remote Sensing and GIS. Fresen. Environ. Bull. 13(9), 860-864.
[10] Husak, G., Grace, K. (2016) In Search of a Global Model of Cultivation: Using Remote Sensing to Examine the Characteristics and Constraints of Agricultural Production in the Developing World. Food Security. 8(1), 1-11.
[11] Kavzoglu, T., Colkesen, I. (2011) Entropic Distance Based K-Star Algorithm for Remote Sensing Image Classification. Fresen. Environ. Bull. 20(5), 1200-1207.
[12] Kavzoglu, T., Colkesen, I. (2011) Assessment of Environmental Change and Land Degradation Using Time Series of Remote Sensing Images. Fresen. Environ. Bull. 20(1A), 274-281.
[13] Estep, L., Terrie, G., Davis, B. (2004) Technical note: Crop Stress Detection Using AVIRIS Hyperspectral Imagery and Artificial Neural Networks. International Journal of Remote Sensing. 25(22), 4999-5004.
[14] Iatrou, G., Mourelatos, S., Zartaloudis, Z., Iatrou, M., Kalaitzopoulou, S. (2016) Remote Sensing for the Management of Verticillium Wilt of Olive. Fresen. Environ. Bull. 25(4), 3622-3628.
[15] Sengupta, D. K., Som, S. K., Misra, U. (1991) Lineaments and Tectonic Analysis through Landsat Imagery and Its Implications on the Evaluation of Bauxite and Laterite Deposits in and around Panchpatmali Area, Koraput District, Orissa. Journal of the Indian Society of Remote Sensing. 19(3), 187-194.
[16] Kox, S., Bugliaro, L., Ostler, A. (2014) Retrieval of Cirrus Cloud Optical Thickness and Top Altitude from Geostationary Remote Sensing. Atmospheric Measurement Techniques. 7(10), 3233-3246.
[17] Kulkarni, A.V. (2010) Monitoring Himalayan Cryosphere Using Remote Sensing Techniques. Journal of the Indian Institute of Science. 90(4), 457-469.
[18] Wright, V.F., Brown, B.A., Harris, M.A. (2011) Quenching of Phosphorus Fixation with Organic Wastes in a Bauxite Mine Overburden. Environmental Earth Sciences. 63(3), 469-476.
[19] Knobelspiesse, K., Diedenhoven, B. V., Marshak, A., Dunagan, S., Slutsker, I. (2015) Cloud Thermodynamic Phase Detection with Polarimetrically Sensitive Passive Sky Radiometers. Atmospheric Measurement Techniques. 8(3), 1537-1554.
[20] Chabot, D., Francis, C. M. (2016) Computer-Automated Bird Detection and Counts in High‐Resolution Aerial Images: A Review. Journal of Field Ornithology. 87(4), 343–359.
[21] Zhang, J., Zhang, T., Yang, Z., Li, B., Wu, Y. (2020) Altitude and Number Optimisation for UAV-Enabled Wireless Communications. IET Communications. 14(8), 1228-1233.
[22] Hong, Y., Adler, R., Verdin, J. (2007) Use of 21st Century Satellite Remote Sensing Technology in Natural Hazard Analysis. Natural Hazards. 43(2), 165-166.
[23] Pandey, K. (2015) Information Extraction Using Remote Sensing Technology to Study the Impact on Climate. Diabetes Care. 26(4), 1321-1322.

Received: **30.12.2020**
Accepted: **06.02.2021**

CORRESPONDING AUTHOR

Jiuling Tian
Department of Urban Construction
Henan Polytechnic Institute
Nanyang Henan 473000 – China

e-mail: tian810630@126.com

© by PSP Volume 30– No. 05/2021 pages 5437-5444 Fresenius Environmental Bulletin

RESEARCH ON THE INTERNATIONAL DEVELOPMENT OF CHINESE THIRD-PARTY PAYMENT PLATFORMS BASED ON THE TWO-SIDE MARKET THEORY-A PERSPECETIVE OF GREEN DEVELOPMENT

Cheng Cheng[1], Xiaobin Li[2], Jiapeng Wang[3,*]

[1]School of Business Administration, Northeastern University, Liaoning, China
[2]School of Business, East China University of Science and Technology, Shanghai, China
[3]Business School, The University of New South Wales, Sydney 2052, Australia

ABSTRACT

Currently, the pressure on global ecological environmental protection remains high, due to the influence of economic structure, energy structure, and the new COVID-19 pandemic, etc., which causing great uncertainty to economic and social development. For this reason, it is necessary to strengthen the development of green technology innovation. As China's international trade volume has gradually increased, the development of China's third-party payment platform has become crucial in the context of economic globalization. Based on the two-side market theory, this article discusses whether the profit model is beneficial to China's third-party payment platform with the case study of Paypal. The findings indicated that the pricing model is better than the revenue model for a complex third-party payment platform and the precipitation-fund profit serves as a stable profit source. The researchers further analyzed the risks that platforms may encounter in the process of internationalization to help promote the international development of China's third-party payment platform and create new momentum for green development.

KEYWORDS:
Environmental pollution, Two-side market, Resources, Payment environment

INTRODUCTION

Due to the tightening of resource constraints, serious environmental pollution and degradation of ecosystems, the task of finding a green development approach is extremely urgent. To protect the ecological environment is to protect the productivity [1]. On the one hand, we must recognize the importance of ecology for wealth production, and improving environmental pollution and reducing resource consumption can effectively develop productivity [2]. On the other hand, changing the input pattern of productivity factors through scientific and technological innovation can lead to sustainable high-quality economic development [3] (Figure 1). With the rapid development of the internet and society, the term "platform" has become very familiar to people. Platforms are links between different users. Platform operators specify different price strategies for services or products provided by different users on both sides of the platform, mainly to attract users on both sides of the platform to trade on the platform so that users on both sides of the platform are willing to participate in the platform. This special market structure is known as the "two-side market." In the real world, two-side markets have completely penetrated the daily lives of residents. For example, according to Rapier, the international Uber and Chinese Didi taxi platforms connect private car owners and ordinary passengers to facilitate people's travel [4].

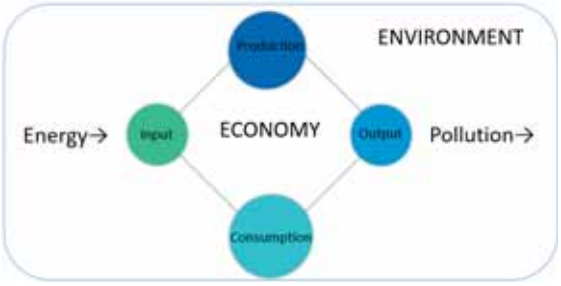

FIGURE 1
Economic System and Environment.

In 2020, because of the outbreak of COVID-19, international trade conditions have fallen sharply, and unemployment rates in various countries have risen sharply. Therefore, many unemployed people have begun to join some international bilateral market platforms such as Alibaba International Station and Fiverr to gain a source of income through online work. According to data on the Fiverr platform, as of June 30, 2020, there were 2.8 million active buyers, up from 2.2 million on June 30, 2019, yielding a year-on-year increase of 28% [5]. In these cross-border two-side markets, certain instrumental platforms

play a vital role in the cross-border third-party payment platform. The emergence of third-party payment platforms has reduced costs, reduced pollution, and realized a green development approach in which economic development and ecological environmental protection are in harmony and symbiosis (Figure 2).

In fact, the development of China's third-party payment is at the forefront of the global economy. In 2018, the penetration rate of third-party payment in China peaked at 71%, while the proportion of mobile payment in the United States was 50%, the United Kingdom was at 48%, Germany was at 49%, and France was at 40%. Despite being the country that originated mobile payments, as Qianzhan stated, Japan's proportion of mobile payments was only 30% [6]. Although the utilization rate of domestic third-party payment platforms in China is the highest of any country in the world, the world's largest multinational third-party payment platform is the company PayPal. PayPal mainly relies on the business development of the eBay e-commerce platform and has gradually begun to develop its international business.

PayPal's market share in the U.S. far exceeds that of rivals such as Amazon Pay, Visa Checkout, and Google Pay. According to the results of analysis by Morgan Stanley [7]. PayPal is far ahead of its peers in the U.S. mobile payment market. In fact, excluding Amazon, 77% of the top-500 online retail companies in the U.S. use PayPal to make payments. Amazon's Amazon Pay payment platform ranks second, with a market penetration rate of about 13%. However, excluding the use of Amazon's own website, Amazon Pay's penetration rate is only 4%, which is far lower than PayPal's 80% penetration rate. The third- and fourth-ranked U.S. electronic payments are Visa Checkout and Google's Google Pay. However, Visa Checkout and Google Pay have a market share of only 6% and 3% of the top-500 online retail stores, respectively, which is far behind that of PayPal.

Compared with other companies that have been affected by the new COVID-19 pandemic, the average company's profitability has declined, and it is now on the verge of bankruptcy. In contrast, PayPal's profitability has increased, potentially as a result of an increase in the number of participants on bilateral outsourcing platforms, such as Fiverr. A large number of unemployed people have chosen to become freelancers to make ends meet during the pandemic by selling their skills. PayPal CEO Dan Schulman mentioned in a conference call on May 7, 2020 that PayPal's net new active accounts reached the highest level in history on April 2020, higher than levels in January and February. On average, about 250,000 net new active accounts were opened per day that month, representing a 140% increase in new account openings compared with the data in March 2020. Additionally, in April 2020, PayPal added 7.4 million new customers, setting a historical record. According to PayPal's fiscal year 2020 second-quarter financial report, PayPal's second-quarter net revenue was $5.261 billion USD, an increase of 22% compared to $4.305 billion USD in the same period last year; net profit was $1.530 billion USD compared to the figure in the same period last year, representing an increase of 86% compared to $823 million USD. Similarly, earnings per share were $1.29 USD, an increase of 86% compared to $0.69 USD in the same period last year [8].

China has the fastest growing consumer market in the world with the largest volume and huge potential, and is an important mainstay in promoting stable growth of the world economy. According to data from the "China Third-Party Payment Mobile Payment Market Quarterly Monitoring Report for the Second Quarter of 2019," in the second quarter of 2019, the transaction volume of China's third-party payment mobile payment market reached 49,098.46 billion CNY, an increase of 2.93% from the previous quarter. YiGuan Search found that the expansion of social application scenarios and the increase in the scale of commercial transactions driven by e-commerce festivals have enabled China's third-party mobile transaction market to maintain steady growth [9]. According to a survey by Wang, in the third-party payment market in China in 2017, the top market shares included Alipay, Tencent Finance, One Wallet, Lianlian Pay, UMF, Yibao, Kuaiqian, and Baidu Wallet [10]. Among them, Alipay accounted for 53.73% of the market share, and Tencent Finance accounted for 39.33%. This means that Alipay under the Alibaba Group has also entered the same development situation as PayPal, but it is still in its infancy. Moreover, some small and medium Chinese enterprises have also joined this market. As PayPal has fully developed in the domestic market, it has begun to promote the internationalization of its business, and has gradually become a fully international third-party payment platform. At present, Alipay has also fully developed in the domestic market. The purpose of this article is also to analyze some of the influencing factors in the development of the international market through an analysis of the fully international third-party payment platform-PayPal so as to provide some references for Chinese third-party payment platforms, such as Alipay.

Problem Statement. Although limited by the impact of the Sino–U.S. trade war, China's share of exports to the United States has decreased to a certain extent in recent years, but its overall export quota has increased. According to data from the Ministry of Commerce of China, from January to August 2020, China's total import and export volume was 20.05 trillion yuan, a year-on-year decrease of 0.6% [11]. Of this volume, exports represented 11.05

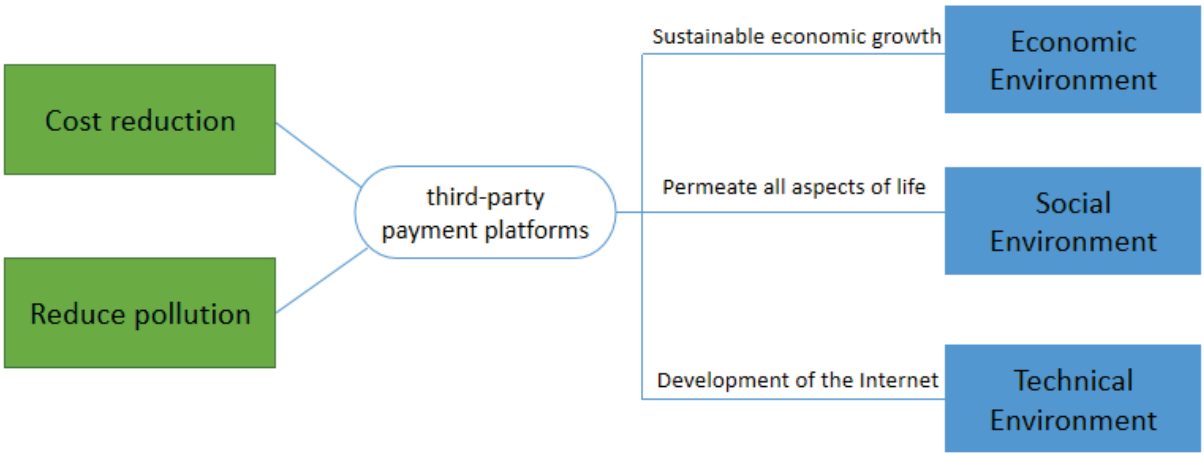

FIGURE 2
The relationship between environment and payment.

trillion yuan, an increase of 0.8%; imports represented 9 trillion yuan, a decrease of 2.3%. Moreover, the Chinese export share is increasing each year. In addition, with the development of the internet bilateral market, more small and medium enterprises participate in international trade through platforms such as Alibaba International Station, Amazon, and Fiverr. The multinational third-party payment platform is the main settlement method for the development of the international two-side market. However, in the current international two-side market, Chinese platforms occupy very little market share. Therefore, it is necessary to explore the profitability and development model of successful multinational third-party payment platforms such as PayPal. Through a case analysis of PayPal and a risk analysis of the current overseas development of China's third-party payment platform, the researchers provide suggestions in this paper that can benefit the long-term development of China's third-party payment platform overseas.

Research Aims and Objectives. The purpose of this study was to take PayPal as a case study, analyze the factors that influence its success, and provide some suggestions for Chinese third-party payment platform enterprises. The main focuses of the study were the factors affecting PayPal's revenue, how it has developed a reasonable revenue model, and whether China's third-party payment platforms can replicate PayPal's revenue model and develop rapidly in the international market. In addition, according to PayPal's income model and real cases, this paper discusses the possible risks of such a model in the internationalization of China's third-party payment platforms, and provides suggestions to help China's third-party payment platforms develop more effectively. In order to successfully achieve the above analysis objectives, the following study objectives were established: (1) Develop a reasonable replica of the PayPal revenue model. (2) Assess the current risks of Chinese third-party payment platforms in overseas markets and provide recommendations to improve their development.

MATERIALS AND METHODS

Related Two-side Market Theory. Regarding the characteristics of the two-sided market, Katz and Shapiro were the first to correlate the two-sided market with the characteristics of network externalities [12]. Moreover, Rochet & Tirole indicated that the middle layer or platform must price the two products or services it provides at the same time [13-14]. Earlier, Rochet and Tirole indicated that the two-sided market has the following characteristics: (1) price non-neutrality; (2) one type of end user does not have an internalized welfare impact on other types of users when it uses the platform. Similarly, Holland posited that the bilateral market has the following two characteristics: (1) The bilateral market platform increases the value of the platform by allowing two groups of consumers to interact or reduce transaction volume costs; (2) The interdependence of demand: That is, the sales volume on one side of the platform impacts that on the other side [15]. There is a close relationship between the sales volume on both sides. Further, Hagiu summarized the literature on the characteristics of all bilateral markets and obtained three important characteristics of bilateral markets, including the non-neutrality of the price structure, the mutual dependence and complementarity of users on both sides, and the externality of the cross network [16]. At present, most scholars agree with these three characteristics of bilateral markets.

In terms of recent research on third-party payment, Irene S Y. Kwan *et al.* posited that whether users can attract enough attention from e-commerce companies is the key to the success of e-commerce, as users can be accepted by e-commerce platforms [17]. In other words, users have to attract and participate in the platform. Similarly, Ziqi, Liao, and Tow

Cheung analyzed consumer psychology and behavior in e-commerce, and their findings indicated that improvement in e-banking service quality influences the customer attitudes to e-banking. The EU's policies and supervision of third-party payments for e-commerce was analyzed [18]. The results indicated that the transparency of e-commerce can build the confidence of the consumer and business [19-20]. Similarly, the relationship between the industrial market and B2B third-party payment e-commerce were predicted [21]. Kim pointed out that many third-party payment platform services exist in various fields of e-commerce online transactions, such as consumer confidence organizations, credit card transaction authorization agencies, banks, and consumer online privacy protection agencies [22]. The analysis pointed out that one case, the seller did send the goods until the third-party payment company confirmed that it had received the buyer's payment. In addition, the company did not send the payment to the seller before the buyer received the goods, thus protecting the interests of both parties. The transaction fee was typically paid by the buyer.

Research methods. According to the above findings, is the researchers noticed that PayPal has already achieved profitability in the international market, so whether the design of its profit model can be used as a universal model for China's internationalization of the third-party payment platform is of significance. To determine this, the researchers conducted a case study of PayPal. It started with the explanation of the revenue model used by PayPal. Then, MATLAB software was used to model the existing models and data of PayPal. This section also discusses the profitability of third-party payment platforms.

PayPal Revenue Model. As a two-sided market, a third-party payment platform typically charges users registration fees that are irrelevant to their platform interactions, and handling fees for each transaction apply place to the platform. However, considering that the PayPal third-party payment platform belongs to a highly oligopolistic market structure, the pricing strategy of "charging user fees and adopting a two-part fee system for merchants" is suitable for the PayPal market.

Based on the research and analysis of the Annstrong pricing model, an important scholar in two-side markets, the network externalities and the classic Hotelling model were introduced to obtain the general expression of the consumer utility function [17]:

$$u = \alpha N - P,\ \alpha > 0 \quad (1)$$

In Equation (1), the general expression α represents the coefficient of strength outside the network, N represents the size of the user's network, αN represents the network value of the product, and P refers to the value of the product itself.

The revenue model may be too simple for a complex third-party payment platform, and the problems and results illustrated were not representative or profound. Therefore, this utility function should be further deepened to replicate the actual situation of users and merchants. For example, when the fixed cost and variable cost of the second-party platform rises, the pricing of the third-party platform increases the user fee and merchant registration fee to ensure the profit of the second-party platform fee. But if so, it lowers the registration of merchants, which leads to a decrease in revenue. Thus, there is an imbalance between the third-party platform cost and revenue. This pricing strategy doesn't work, so the third-party payment platform immediately reduces the fees charged by the merchant. The third-party payment platform can charge merchants for the registration fee, which is negatively correlated with the fees charged by the merchants.

Second, when the number of transactions increases, the user fee and the merchant registration fee are reduced. Therefore, PayPal, to reduce fees and the number of businesses who must register users, increases the merchants' handling fee. This pricing strategy not only allows PayPal to broaden the coverage of the user and attract more merchants, but also further increases the number of PayPal transactions the platform's visibility and credibility, and eventually, the company's profits. When either the number of transactions or the merchants' handling fee increases, PayPal reduces the user fees and merchant registration fees and increases the merchant fees. This indicates that the scale and quantity of users on third-party payment platform are more attractive to merchants.

In addition, precipitation funds are also one of the main benefits of PayPal. These are deposit funds temporarily stored in the PayPal platform account. They derive mainly from the interest income generated when deposit funds are deposited in the commercial bank during the temporary deposit period:

$$\sum_{1}^{n} Mj = \sum_{1}^{n} \frac{(F_j T_j)}{360},\ j = 1,2,3\ldots,n \quad (2)$$

By solving the above model and algorithm, the researchers concluded that in the short-term future, PayPal's service-fee profit will show an upward trend, and then the growth rate will slow over time. As for the precipitation-fund profit, it will start to rise and finally become a stable value that fluctuates. For total profit, if P (for user preference) and P2 (for merchant preference) are both negative, total profit will also be negatively positive; that is, the firm will be profitable.

RESULTS

According to the revenue model of PayPal mentioned in the previous article, combined with the income model, this section discusses which specific factors may affect the overseas development of China's third-party payment platform. The researchers evaluated the possible risks of that development in combination with actual cases, using Alipay (the largest third-party platform in the current Chinese market) as the research object, and PEST as the research method.

Political Risk. Because of differences in the economic environment and legal systems around the world, in some countries, especially in developing countries, third-party payments are still in infancy, and there is no complete legal system to clearly set forth the division of responsibilities and labor for all parties involved in the payment process. As such, there is no corresponding law as a guarantee. It can be said that in the current legal system, most countries have not established a special legal system for mobile payments. When disputes arise in the actual payment process, it is difficult to divide responsibilities according to the current legal framework. Moreover, in the expansion of overseas markets, Alipay is subject to strict market access and compliance supervision. As the payment service system serves as the financial foundation of a country and the focus of national financial security, strict supervision of payment security has always been an important responsibility of central banks. In overseas expansion, the main problem Alipay faces is compliance, that is, how to obtain a paid license. In addition, various allegations on the grounds of safety supervision have been made by various countries and have the potential to become lawsuits, which may affect the expansion. In April 2017, Ant Financial announced that it would buy MoneyGram for $1.2 billion USD. However, due to the interference and investigation by the U.S. Foreign Investment Commission, Alipay was unable to obtain an acquisition license, which led it to announce in January 2018 that it would abandon the acquisition.

Economic Risk. The economic system of various countries can also significantly impact third-party payment platforms, China is a country with very strict foreign exchange control; individual Chinese residents can only exchange $5 W each year. This has a great impact on the international development of third-party payment platforms. China's economic system has determined that the business of banks must be guaranteed, but this restricts the liquidity of foreign exchange to a certain extent. It is difficult for non-state-operated companies and groups to obtain financial photos, whereas state-owned companies are relatively too large to flexibly take on some effective regulatory measures. Although Alipay has obtained a financial license at present, it is still subject to great restrictions. For example, People's Bank of China stated in 2015, under the designated policy of the People's Bank of China, individual users can pay up to 200,000 CNY per year through third-party payments through non-domestic banks, which has greatly limited the platform's development. In international business, the policy also means that its international development has been restricted by China's economic policies.

Social Risk. Alipay currently has more users than PayPal largely because of China's huge population base of 1.4 billion. However, in the expansion of overseas markets, China's huge population has served little benefit. The difference in culture is also an important factor. Alipay has been recognized by the Chinese in China, and its operation and operating model conform to Chinese culture. However, that model is different from the coexistence of business models in the expansion of Alipay in overseas markets. Although operators and financial institutions have established cooperative relations with Alipay, there are still major operating models in the dominant and cooperative parties.

There is also the factor of uncertainty. For example, banks and offline merchants in overseas markets choose to work with Alipay, to a large extent because they are driven by self-interest, and they make choices based on the pros and cons. With the changing times, if benefits do not meet expectations or new payment giants emerge in the future, Alipay's payment interface may be negatively affected until the partnership is closed and terminated. As such, resistance to third-party payment interfaces may exist for a long time. For example, Niu and Cao pointed out that Walmart China does not support Alipay [20]. Moreover, at the beginning of the expansion of overseas markets, Alipay was built around the tourism scene of Chinese tourists, but from a practical viewpoint, the consumption and demand of tourists are limited to an extent. Both overseas businesses and Alipay must come together to figure out how to promote business growth and consumption.

Technology Risk. Compared with traditional payment methods, third-party payment, as an emerging product, has bottlenecks. A key bottleneck hindering the rapid development of mobile payment has been how to ensure payment security and establish a reassuring payment environment. In the mobile payment process, not only are buyers and sellers involved in payment scenarios, but also hidden telecom operators, financial institutions, payment companies, system platforms, software operators, and other corporate entities. Ensuring that data transmission is safe from viruses and hackers and avoids payment risks (such as information leakage and theft of funds) is one of the primary considerations in third-

party payments. When buying abroad, because of the influence of the consumption environment and consumption characteristics, customers are often concerned about the security of the payment environment and worried about privacy protection and improper disclosure of personal information. In fact, data leakage has always been the focus of major internet companies and the focus of reinforcement. In March 2018, BBC indicated that Facebook's data breach plunged the company into a huge crisis of trust, and various doubts followed [22]. In the era of big data, Chinese third-party payment companies also need to consider how to keep private information from being stolen and ensure the security of the payment environment itself, so as to gain the trust and recognition of customers.

RECOMMENDATIONS AND CONCLUSIONS

Use Policy Opportunities to Expand Overseas Markets. With the implementation of China's "One Belt One Road" strategy, the economic and trade relations between the countries along the route and China can expected to become closer, and contacts in various fields to become deeper. Whether it is tourism or investment, countries along the route will enjoy huge preferential policies. However, many of the countries along the “Belt and Road” are developing countries. Limited by the development of internet technology and mobile terminals, third-party payment is still in its infancy. China's third-party payment companies have rich experience in product operation. With the help of many years of domestic experience, they can play a leading role in the development of third-party payment in these countries and help these countries complete the construction of mobile payments as soon as possible. In recent years, in southeast Asia, the internet has developed rapidly, and the penetration rate of mobile terminals has increased. Traditional credit or debit card payment methods require costly financial infrastructure. However, if these countries adopt third-party payments, huge facility construction costs can be saved.

Localization Strategies to Open Overseas Markets. China's third-party payment companies are facing regulatory confinement and competition from many other domestic companies as they attempt to expand into overseas markets. If these companies enter the market as sole proprietorship, a lot of financial resources and energy may be expended. Therefore, it is recommended that Chinese companies use capital injection, mergers and acquisitions, equity participation, and other methods to realize the market expansion of third-party payment in the expansion of overseas markets. They should attempt to realize localized operation and obtain maximum market benefits at the minimum cost. In the development of platform-level company businesses, third-party payments play an important function in both traffic and scenarios and represent an important breakthrough.

Speed Up Technology Research and Development to Effectively Improve the Security of Third-party Payments. Data security is an important topic that cannot be neglected in the internet era. In third-party payment, security issues are also attracting attention. First, payment security is not only concerned with identity verification, information exchange, and data transmission of both parties to the transaction, but also the non-repudiation of the transaction. Therefore, ensuring data security and a secure payment environment requires Chinese companies to continuously conduct R&D and technological innovation in the field of security control technology. At the same time, the state must continue to improve the legal system for third-party payments and provide clear instructions for security-related control technologies. Only if legislation continues to improve and platforms continue to innovate can third-party payments become more secure and users' privacy and property rights be protected. The first step to accomplish that is to actively adopt public key design infrastructure, improve certificate management strategies, and continually conduct vulnerability tests to establish a secure wireless network communication environment. Second, China's third-party payment companies must focus on two levels of hardware and software: They must carry out security reinforcement and cut off the possibility of intrusion from the top-level design. Third, they must continue to strengthen the safety awareness of consumers and improve the self-protection of users.

Strengthen International Cooperation and Establish International Uniform Legal Rules. In recent years, with the development of international economy and trade and the progress of the internet, the third-party payment is showing strong vitality and vitality. In the future, it can be expected to become one of the main payment methods. Therefore, in the development of cross-border third-party payments, China should work with major countries to jointly explore universally recognized mobile payment laws and regulations, actively coordinate mobile payments between countries, and strive to build a unified mobile payment platform and clearing agency to realize trade facilitation and the convenience of development. At present, although the market space for third-party payment in China is continuing to shrink, there is still a huge room for development in the international market. Therefore, relevant Chinese state departments should issue policy plans as soon as possible to help China's third-party payment companies achieve internationalization, thereby helping China's economic development.

This article discusses the international development of China's third-party payment platform based on the bilateral market theory in a perspective of green development. This article is mainly divided into five parts. In the first part, a certain introduction is given to the current development status of the internationalization of third-party payment platforms in China and the world. Although China currently has the highest penetration rate of third-party payments, in the international market, PayPal occupies the highest market share. Therefore, its profit model is an issue that needs to be discussed. In addition, the international development risks of China's third-party payment platforms also need to be considered. In the second part, the researcher describes a revenue model that was developed based on PayPal's data and development model, the main purpose of which was to provide a reference for the international development of China's third-party payment platform. In the third part, the risk research of China's third-party payment platform was carried out based on the actual case of Alipay. Researchers mainly used PEST research methods to conduct risk research from four aspects: politics, economy, society, and technology. Finally, based on PayPal revenue model and the risk research, some suggestions are given to China's third-party payment platforms, including the use of current policy opportunities, cooperation with local countries, the use of localization strategies to open the market, and the improvement of third-party payment platform technology to ensure the safety of users. In addition, the establishment of unified payment standards in laws and regulations can also better help the development of third-party payment platforms.

In general, the international development of China's third-party payment is still in its infancy. Chinese enterprises and governments need to actively face risks in the international market and continuously improve their strengths.

ACKNOWLEDGEMENTS

We thank LetPub (www.letpub.com) for its linguistic assistance during the preparation of this manuscript.

REFERENCES

[1] Xi, J. (2010) Hand in Hand to Promote Green and Sustainable Development in Asia - Speech at the Opening Ceremony of the Boao Forum for Asia 2010 Annual Meeting, Journal of People's Daily. 11 April 2010.

[2] Hua, Z. (2015) On Xi Jinping's "Eco-environmental Productivity" - A Marxist View of Productivity in Contemporary China. Academic Forum. No. 9.

[3] Lin, Z., Zhao, L. (2019) Evaluation and Analysis of Coordinated Development of Ecological Environment and Economy. Fresen. Environ. Bull. 28(5), 4049-4053.

[4] Lee, J., Ryu, M., Lee, D. (2019) A study on the reciprocal relationship between user perception and retailer perception on platform-based mobile payment service. Journal of Retailing and Consumer Services. 48, 7-15.

[5] Yao, M., Di, H., Zheng, X., Xu, X. (2018) Impact of payment technology innovations on the traditional financial industry: A focus on china. Technological Forecasting and Social Change. 135, 199-207.

[6] Yu, J., Wen, Y., Jin, J., Zhang, Y. (2019) Towards a service-dominant platform for public value co-creation in a smart city: evidence from two metropolitan cities in china. Technological Forecasting and Social Change. 142, 168-182.

[7] Guan, Y. (2019) China Third-Party Payment Mobile Payment Market Quarterly Monitoring Report for the Second Quarter of 2019.Beijing University of Posts and Telecommunications, Beijing, China.

[8] Pollini, J. (2009) Agroforestry and the Search for Alternatives to Slash-and-Burn Cultivation: From Technological Optimism to a Political Economy of Deforestation. Agriculture Ecosystems and Environment. 133(1-2), 48-60.

[9] Katz, M., Shapiro, C. (1994) Systems Competition and Network Effects. Journal of Economic Perspectives. 8(2), 93-115.

[10] Wu, Y., Mo, Z., Peng, Y., Skitmore, M. (2018) Market-driven land nationalization in China: A new system for the capitalization of rural homesteads. Land Use Policy. 70, 559-569.

[11] Rochet, J., Tirole, J. (2008) Tying in Two-Sided Markets and the Honor All Cards Rule. International Journal of Industrial Organization. 26(6), 1333-1347.

[12] Holland, M. (2007) Two-Sided Markets: A Challenge to Competition Policy, First Annual Competition Commission. University of the Witwatersrand, Johannesburg.

[13] Hagiu, A. (2009) Two-sided Platforms: Product Variety and Pricing Structures. Journal of Economics and Management Strategy. 18(4), 1011-1043.

[14] Kwan, I., Fong, J., Wong, H. (2005) An E-customer Behavior Model with Online Analytical Mining for Internet Marketing Planning. Decision Support Systems. 41(1), 189-204.

[15] Liao, Z., Cheung, M. (2005) Service Quality in Internet E-banking: A User-based Core Framework, 2005 IEEE International Conference on E-Technology, E-Commerce and E-Service, IEEE, Hong Kong, China.

[16] Kye, C. (2001) EU E-Commerce Policy Development: E-Commerce in the EU: Bringing Businesses and Consumers Aboard. Computer Law and Security Review. 17(1), 25-27.
[17] Claycomb, C., Iyer, K., Germain, R. (2005) Predicting the Level of B2B E-commerce in Industrial Organizations. Industrial Marketing Management. 34(3), 221-234.
[18] Kim, H. (2005) Consumer Profiles of Apparel Product Involvement and Values. Journal of Fashion Marketing and Management: An International Journal. 9(2), 207-220.
[19] Ya, R., Kong, F., Zhang, T. (2019) Evaluation and Analysis of Coordinated Development of Eco-Environment and Ethnic Region Economy. Fresen. Environ. Bull. 29(3), 1672-1676.
[20] Armstrong, M. (2006) Competition in Two-sided Markets. The RAND Journal of Economics. 37(3), 668-691.
[21] Li, J., Hou, L. (2019) A reflection on the taxi reform in china: Innovation vs. tradition. Computer Law & Security Report. 35(3), 251-262.
[22] Xu, J., Xiao, Y., Xie, G., Wang, Y., Jiang, Y. (2019) Computing payments for wind erosion prevention service incorporating ecosystem services flow and regional disparity in yanchi county. Science of the Total Environment. 674, 563-579.

Received: **30.12.2020**
Accepted: **20.01.2021**

CORRESPONDING AUTHOR

Jiapeng Wang
Business School,
The University of New South Wales,
Sydney 2052 – Australia

e-mail: wangjiapenguni@163.com

© by PSP Volume 30– No. 05/2021 pages 5445-5465 Fresenius Environmental Bulletin

FOLIAR-APPLIED HYDROGEN PEROXIDE AND PROLINE MODULATES GROWTH, YIELD AND BIOCHEMICAL ATTRIBUTES OF WHEAT (*TRITICUM AESTIVUM L.*) UNDER VARIED N AND P LEVELS

Naila Asghar[1], Nudrat Aisha Akram[2], Amina Ameer[1], Huma Shahid[1], Shameem Kausar[1], Ansa Asghar[1], Tayyaba Idrees[1], Sahar Mumtaz[3], Hafiz M Asfahan[4], Muhammad Sultan[4,*], Istakhar Jahangir[5]

[1]Department of Botany, University of Agriculture, Faisalabad 38040, Pakistan
[2]Department of Botany, Government College University, Faisalabad 38000, Pakistan
[3]Department of Botany, Division of Science and Technology, University of Education, Lahore 54770, Pakistan
[4]Department of Agricultural Engineering, Bahauddin Zakariya University, Bosan Road, Multan 60800, Pakistan
[5]Department of Environmental Remote Sensing and Geoinformatics, University of Trier, 54296, Germany

ABSTRACT

Better crop yield and precise future farming system is a dire need to meet the chronic food insecurity predominant these days. Positive interaction between Nitrogen, Phosphorus fertilizers and better plant growth are well known; in contrast no information is available about their role when applied in combination with (Proline+ H_2O_2). The present experiment was conducted to assess the modulation in grain yield related attributes and biochemical parameters through foliar application of bio-chemicals (Proline+ H_2O_2) and fertilizer (N+P) application as rooting medium for two wheat cultivars Millat -06 and Shafaq-11. The results exhibited that most of the yield related and biochemical attributes responded positively and significantly to NP fertilizer application. NP treatments, 80-60 kg/ha and 120-90 kg/ha both levels almost equally contributed to increase all studied attributes. It was deducted that application of Proline and H_2O_2 as foliar spray also caused improvement in term of yield related attributes, but effect was more prominent in biochemical attributes. Application of H_2O_2 increased the activities of Ascorbate per oxidase (APX), Ascorbic acid (AsA), while foliar spray of proline enhanced accumulation of Phenolic contents. Catalase activity (CAT) significantly increased with bio-chemicals (Proline+ H_2O_2) but showed differential response in both cultivars. Foliar spray of biochemical especially H_2O_2 decreased lipid peroxidation. Concerning the accumulation of endogenous H_2O_2 contents reached its maximum value with foliar spray of exogenous H_2O_2. However, foliar spray of bio-chemicals mitigated the deleterious effects of any stressful condition and activate plant antioxidative defense system that ultimately resulted in better growth and productivity. Wheat Millat-11 was better in Plant height, fertile and non-fertile spikelets and Ascorbic acid (Vitamin c) attributes, while Shaafaq-06 was better in 100-grains weight. Overall, our results suggest that improvement in yield and biochemical parameters was associated with NP fertilizers as well as foliar spray of Proline and H_2O_2.

KEYWORDS:
Fertilizers, foliar application, hydrogen peroxide, wheat, biochemical constituents, lipid peroxidation, antioxidative defense

INTRODUCTION

Wheat (Triticum aestivum L.) belongs to the family Poaceae, is one of the major and widely grown cereal food crop in the world. It is primary source of carbohydrate and its dietary contribution for human being as well as for livestock cannot be ignored. In Pakistan, it is effectively covering an extensive area of about 9062 thousand hectares which accounts for annual production of about 23.4 million tons. In Pakistan average yield of wheat (2585 kg/ha) is generally low in comparison with world average yield (3010 kg/ha) or even far away from average yield of regional countries like India and China [1]–[3]. The wheat essential prerequisite is gradually and progressively increasing due to its massive use on daily basis, there is no aggravation in claiming that Pakistan's human population is increasing continuously but its average yield is low to fulfill food's need. The yield gap in country can only be covered by increasing productivity per unit area. There are several causes comprising physiological and agronomic practices but poor soil management especially inadequate application of fertilizer is the major prime factor attributed for decline in wheat yield [4]. The judicious use of suitable fertilizers can markedly enhance the fertilizer use efficiency as well as yield by 50% [5] - [6].

Nitrogen and phosphorous are major among essential nutrients for plants, but it is matter of regret that most of Pakistani soils are severely deficient in

these essential nutrients because of nutrients mining and soil infertility [7]. The optimum amount of fertilizer application at appropriate time holds substantial influence on wheat yield potential [8]. Nitrogen acts as a leading driver for plant metabolism because of its involvement in the chlorophyll formation, protein and nucleic acid [9]. Adequate fertilization with nitrogen could be attribute to strengthened the photosynthetic efficiency which resulting in healthy vegetative growth [10]. Nitrogen is mobilized within plant organs and used maximum during the grain filling stage of crop plant and hence, improve grains protein contents. Phosphorous deficiency is common in agricultural soil of Pakistan. In plants, Phosphorus also involved in physiological as well as in structural and metabolic processes. Application of phosphorous fertilizer play vital role for crop production as it is necessary to initiate the seed germination [11]. Application of sufficient Phosphorous ensuring to attain 20% more plant height, promotes the tiller emergence and consequently, the more wheat grain yield, it has been suggested that exogenous application of P fertilizer sharply regulate the uptake and utilization of Nitrogen and phosphorous [12]–[14].

Wheat production is severely threatened by various abiotic stresses including nutrients stress. Most of these stresses triggers the osmotic stress by lowering water potential of the plant cell, affecting membrane turgidity and ultimately plant growth. Plants show wide range of different responses to fluctuating adverse environmental conditions to maintain their cell volume as well as their survival. Rapid response associated with changes in plant metabolism through production of array of different osmolytes particularly proline. Proline serve as compatible osmolyte, considering most beneficial and widely distributed compatible solute among plants under unfavorable condition. Many studies reported its diverse role in balancing the osmotic potential, stabilizing the membrane and protein, regulation of osmolarity that helps to retain turgidity required for proper growth of plant under osmotic stress. Apart from the influential role of proline as osmoregulatory, it contributes in regulating cellular redox homeostasis, as well as eliminates the toxicity of free radicles [15]. Exogenous application of proline at low concentration has also shown tremendous effects in producing tolerance against range of stresses. As proline act as a multifunctional osmolyte, it facilitates the nutrient uptake, besides this it is great source of nitrogen and improve CO_2 assimilation [16]. However, much research work is still required to understand the precise mechanism of proline in response to changing environmental conditions. Many previous studies have also discussed the harmful effects of proline for plants when applied in high concentration [17].

Exogenous application of different chemical pave a way to confer plant tolerance to deleterious environmental conditions. Hydrogen peroxide (H_2O_2) is a principal chemical ensuing better plant growth through regulation of different enzymatic and non-enzymatic antioxdative system. Although, (H_2O_2) is well recognized due to its disintegrating effect on cellular membrane [18] - [19]. Relationship between plant and (H_2O_2) always challenging. At high concentration H_2O_2 can result in extensive oxidative damage in plant which eventually induce the death of plant cell [20]. At low concentration, its pivotal role associated with induction of resistance in plants against stresses especially oxidative stress [21]. H_2O_2 is produced as a result of plant metabolism under normal conditions and very stable ROS. H_2O_2 now widely acknowledged as signaling molecule because of its potential performance as regulatory substance in plant metabolism instead of the potent dangerous product of metabolism as well as because of its constancy and diffusibility. H_2O_2 also well known for the activation of antioxidative defense system [22]. Bright et al. [23] suggested that exogenous applied H_2O_2 is effective in improving different process including stomatal movement, Senescence, developmental process [24] - [25] as well as modulate the photosynthesis and respiration [26]. H_2O_2 involved in regulation of water relations through controlling the biosynthesis of different osmolytes as well as soluble protein during osmotic adjustment [27]. Therefore, present investigation was planned with the aim of finding out the effect of varying levels of NP fertilizer on yield related attributes and grains biochemical constituents of two wheat (*Triticum aestivum* L.) cultivars and also study the extent to which exogenous application of proline are helpful in improving growth, yield and wheat grains biochemical constituents as well as stress tolerance. And whether exogenous application of hydrogen peroxide show positive contribution to improve yield and biochemical constituents through upregulation of different enzymatic and non -enzymatic antioxidants.

MATERIALS AND METHODS

The field experiment was conducted at Ayub Agricultural Research Institute (AARI) Faisalabad, Pakistan, from November 2011 to April 2012 to analyze the effects of varied levels (Nitrogen + Phosphorus) fertilizers and exogenously applied biochemicals (proline and H_2O_2) on growth, grain yield related attributes and biochemical constituents of wheat. Seeds of two wheat (*Triticum aestivum* L.) cultivars namely Millat-11 and Shafaq-06 were supplied by the "wheat section" at AARI, were sown in the plots of net size (1.62 m × 5 m). The seeds were sown with the help of 6 rows Power Planter (seed rate was 100 kg/ha) keeping row to row spacing of 27 cm on 10th November 2011. Experiment was conducted under factorial completely randomized block design (RCBD) comprising of three NP level

and three foliar spray with three replicates for each treatment. Three different levels of N & P fertilizers with one control plot (no fertilizer) i.e., 0-0, 80-60 and 120-90 kg/ha, was supplied as rooting medium. After about 110 days of seed germination, three foliar treatments (with one control) of two bio-chemicals control, Proline (20 mM) and hydrogen peroxide (10 mM) were foliarly applied at heading stage. After 1 month and 12 days of foliar treatment, three plant per treatment were harvested. Plants were used for yield related attributes, while grains were collected and preserved for biochemical analysis. The data were recorded for the following attributes during study:

Growth and yield attributes. Plant height, Number of spikes and spikelets per plant, fertile and non-fertile spikelets per plant, main stem spike length using meter rod, number of grains per plant, total number of grains per plant.100- grains weight was recorded with electric balance.

Biochemical analysis (Enzymatic and non-enzymatic antioxidants). Extraction of enzymes and protein. For the purpose of extraction already preserved wheat grains was used. Briefly, the dry wheat seeds (1g) was grounded in 10ml of pre-chilled phosphate buffer (pH 7.0). During the extraction process, pre-cooled pestle and mortar were used. Obtained grains extract was centrifuged for 20 minutes at 12000rpm. Then supernatant was stored at -800C and later used for estimation of enzymatic antioxidants such as CAT and APX.

Catalase (CAT) activity. The method described by Chandlee and Scandalios [28] was used for estimation of CAT. Already extracted sample was used for estimation. 0. 2 mL of sample extract was added to 2.7 mL of potassium phosphate buffer (pH 7) and 0.1 mL of 45 mM H_2O_2 in cooled state. The decomposition of H_2O_2 was followed by decline in absorbance at 240 nm. The enzyme activity was represented in unit mg-1 protein.

Ascorbate peroxidase (APX) activity. The method ascribed by Asada and Takahashi [29] was followed for Ascorbate peroxidase activity in wheat grains with some changes. The reaction mixture (3ml) contained 2.4 mL of 50 mM potassium phosphate buffer, 0.2 mL of 0.5 mM ascorbic acid solution,0.2 mL of sample extract and 2 mL of 45 mM H_2O_2. Then, decrease in absorbance was noted at 290 nm with the help of spectrophotometer against the blank.

Ascorbic acid (AsA) content. Determination of ascorbic acid contents following the method described by method Mukherjee and Choudhuri [30] with minor changes. 0.1g grains were grounded using 5ml of 7% trichloroacetic acid (TCA) solution. After centrifugation, 0.5ml of supernantant was mixed with DTC reagent (0.5 mL of 9 N sulfuric acid solution containing 2,4 dinitrophenyl hydrazine, thiourea and copper sulfate at the rate of 2 g, 4 g & 0.08 g respectively). Reaction mixture was kept in oven at 37ºC for 3hours. Then added 1.5 mL of ice cold 65% sulfuric acid solution after cooling. During that process, sample mixture was kept cooled at 00C. optical density were then noted at 530nm with spectrophotometer. The concentration of ascorbic acid was measured using standard curve prepared from serial grades of AsA standards.

Total phenolic content. Total phenolic contents were computed according the method ascribed by Folin Ciocalteu [31]. Briefly, (0.1 g) wheat grains were grounded in 5 mL 80% methanol solution. Obtained supernatant after centrifuged at 12000 rpm for 15 mins was used for estimation.1mL of enzyme extract was mixed with 2.5 mL Folin-Ciocalteu reagent. which is previously diluted with water 1:10 (v/v) and 2 mL of (75g/l) sodium carbonate. vortex and permit the tubes to stand at 40ºC until development of colour. Absorbance was read at 765 nm with the help of spectrophotometer (Hitachi U-2100).

Estimation of Protein content. Quantification of total protein in Previously buffer extracted sample was done according to the method developed by Bradford method [32] 100 µL of sample extract was mixed with 2ml of Bradford reagents. Absorbance value for reaction mixture was noted at 595nm and protein contents in mixture was calculated by using standard curve prepared from standard series of bovine serum albumin (200–1400 mg/kg).

Oxidative damage measurements (MDA concentration). Lipid peroxidation was estimated by determining MDA contents according to the method ascribed by Cakmak and Horst [33]. Wheat grains (0.1 g) were extracted in 0.1% trichloroacetic acid (TCA) solution (5 ml). After centrifugation 2 ml of supernatant was mixed with 2 mL of 0.6% thiobarbituaric acid (TBA) solution which was prepared in 20% TCA solution. The mixture was incubated in an oven at 100 0C for 20 min. After centrifugation and cooling the optical density of supernatant was recorded at 532 and 600 nm using spectrophotometer. MDA concentration in the wheat grains was calculated with absorbance coefficient 156 mmol−1 cm−1.

Hydrogen peroxide (H_2O_2) determination. Determination of (H_2O_2) was achieved following method described by Velikova et al. [34]. In short, 0.1 g wheat grains were homogenized in TCA (7%) in an ice bath. Material was centrifuged at 12,000 rpm. After centrifugation 1ml of supernatant was

mixed with 1ml of potassium iodide (KI). The absorbance of the resulting solution was recorded at 390 nm.

Statistical Analysis. The design of experiment was three factor (Cultivars, Fertilizer NP and Foliar application) factorial completely randomized block with three replications for each treatment. Data recorded for different attributes were subjected to analysis of variance (ANOVA) to study the effect of fertilizer (NP), foliar application (Control, proline and H_2O_2) and their interaction on yield related component and biochemical attributes of wheat grains. Various statistical approaches including Principal component analysis (PCA) and correlation studies of studied yield and biochemical attribute were employed using R Software version 3.6.2.

RESULTS

Different Yield Related Attributes of Wheat Treated with Proline and H_2O_2 under different Levels of NP. A significant increase was recorded ($p \leq 0.001$) in plant height of both studied wheat cultivars under T3(120-90 kg/ha) closely followed by T2(80-60 kg/ha) when compared to plants grown under control conditions. However, foliarly applied proline and Hydrogen peroxide (H_2O_2) also significantly affect ($p \leq 0.05$) the plant height of both wheat cultivars. Among biochemical, effect of H_2O_2 was noted slightly better than proline in increasing the plant height. In case of cultivars, slight more improvement was recorded in Millat-11 with combined application of fertilizer and biochemical. The interaction between cultivars and NP was also significant($p \leq 0.001$) (Figure.1A; Table 1).

Analysis of result revealed that NP fertilizer showed significant progress ($p \leq 0.01$) in attaining maximum number of tillers specially at T2 (80-60 kg/ha) where proline was sprayed at heading stage followed by T3 respectively. Both chemicals did not contribute significantly to number of tillers. Despite that proline improved in ability to show slightly better response as compared to control and H_2O_2. Both cultivars showed same pattern of response to all treatment and did not differ significantly (Figure1B and Table 1).

The data pertaining to number of spikes showed that there was no significant variation between both cultivars and show almost similar trend for NP fertilizer. Number of spikes followed exactly same trend as number of tillers with T2 followed by T3 with minor differences. Both cultivars gave maximum number of spikes with T2 (80-60 kg/ha). As far as foliar application is concerned, Proline combined with NP (80-60 kg/ha) gave maximum number of spike prior to H_2O_2. The interaction between cultivars, fertilizers and foliar biochemical was also significant ($p \leq 0.05$). However, minimum results were recorded from plants in control (Figure1C and Table 1).

Data showed that both cultivars had no statistically significant difference for number of spikelets. Increasing level of NP imparted significant ($p \leq 0.01$) improvement in spikelets. Of all treatment NP level (80-60 kg/ha) showed significant beneficial effect for cv. Millat-11 while shafaq responded slightly better at T3(120-90 kg/ha) in term of spikelets. Foliar application did not cause any significant impact on number of spikelets (Figure 1D and Table 1).

The effects of various level of NP fertilizer and foliar treatment was significant on number of fertile spikelets per plant in both cultivars ($p \leq 0.001$and $p \leq 0.01$). Different NP treatments and foliar application was helpful in improving the number of fertile spikelets. Both cultivars significantly($p \leq 0.05$) differ from each other. Among both cultivars, highest number of fertile spikelets was recorded in cv. Millat-11 under T2 along with foliar spray of proline (Table 1; Figure.1E). However, regarding the non-fertile spikelets per plant, both cultivars showed significant variation ($p \leq 0.05$). Each increment in NP level along with foliar spray resulted in decline this attribute. Maximum number of non-fertile spikelets were recorded by cv. Millat-11 under control treatment. Among foliar application, both chemicals contributed equally in improving spikelet fertility. However, interaction between all factors were non-significant (Figure 1F and Table 1).

The significant ($p \leq 0.001$) effect of NP fertilizer on main stem spike length was observed. Both verities showed same positive response to increased level of fertilizer. Moreover, the maximum spike length was recorded from T3 closely followed by T2 treatments over T1(Control). Addition of proline and H_2O_2 as a foliar spray at heading stage showed similar trend in increasing the spike length. The combined use of NP fertilizer and foliar spray not only increase the spike length but also improve the grain nutritional quality and yield (Figure 1G and Table 1).

Yield in term of number of grains per plant was significantly ($p \leq 0.01$) increased under different levels of fertilizer. The results showed that NP levels (T3,120-90 kg/ha) and (T2,80-60 kg/ha) alone and along with foliar application of proline and H_2O_2 gave maximum grains per plant as compared to plants from control treatment. In case of cultivar, data showed no significant changes. But this attribute was achieved maximum under T3 for cv. Millat-11, while for cv. shafaq-06 maximum received from plot supplied with T2 followed by T3. Overall, the response of proline was little more but not significant than H_2O_2 and both showed effect. The interaction of NP fertilizer with cultivars had significant effect on grain number (Figure 1H; Table 1).

TABLE 1
Mean squares from analysis of variance (ANOVA) for different yield related attributes and biochemical constituents of wheat plants treated with different NP and foliar application of proline and H_2O_2

SOV	df	Plant height(cm)	No. of tillers	No. of spikes	No. of spikelet's	No. of fertile spikelet's
Cultivars (CV)	1	1054.3***	0.463 ns	0.6667 ns	64.5 ns	600.1*
Fertilizers (NP)	2	1996.4 ***	6.889**	0.9074 ns	961.6**	998.7***
Foliar application (FA)	2	58.6*	1.722 ns	2.9074*	296.4 ns	653.9**
CV×NP	2	255.4 ***	0.963 ns	0.0556 ns	46.8 ns	13.6 ns
CV×FA	2	36.7ns	0.241 ns	0.3889 ns	0.4 ns	88.7 ns
NP×FA	4	35.0	1.028 ns	1.2963 ns	23.3 ns	89.7 ns
CV×NP×FA	4	41.1	1.991ns	2.7778*	74.4 ns	126.1 ns
Error	34	15.8	1.183	0.744	134.8	0.01752

SOV	df	No. of non-fertile spikelet's	Main stem spike length	No. of grains	100-grains wt	CAT
Cultivars (CV)	1	124.52*	0.019 ns	793 ns	10.226***	0.0783 ns
Fertilizers (NP)	2	12.80 ns	24.609***	13558**	24.759***	0.0434ns
Foliar application (FA)	2	16.46 ns	0.946.	490	0.759.	0.5410**
CV×NP	2	10.91 ns	1.117.	1413*	0.152 ns	0.2207 ns
CV×FA	2	42.91 ns	0.274 ns	273 ns	0.210 ns	0.2613 *
NP×FA	4	9.80 ns	0.538 ns	23 ns	0.093 ns	0.1182ns
CV×NP×FA	4	17.30 ns	0.077 ns	51 ns	0.136 ns	0.1881 ns
Error	34	18.33	0.376	350	0.291	0.0725

SOV	df	APX	AsA	Total phenolic	Protein	MDA
Cultivars (CV)	1	2.63.	264.4***	0.00140 ns	0.004370 ns	0.059 ns
Fertilizers (NP)	2	54.31***	892.6***	0.12966***	0.016455***	22.0608***
Foliar application (FA)	2	21.19***	417.3***	0.09097**	0.004552 ns	13.509***
CV×NP	2	6.66**	550.9***	0.03425 ns.	0.008725*	1.508**
CV×FA	2	1.63 ns	33.9***	0.00097 ns	0.005597 ns	0.100 ns
NP×FA	4	1.69 ns	72.3***	0.04122*	0.002160 ns	1.201**
CV×NP×FA	4	2.34*	109.5***	0.01808 ns	0.001861 ns	0.787*
Error	34	0.81	2.8	0.01303	0.001748	0.239

SOV	df	H_2O_2
Cultivars (CV)	1	10.60**
Fertilizers (NP)	2	34.53***
Foliar application (FA)	2	5.73**
CV×NP	2	12.89***
CV×FA	2	0.42
NP×FA	4	8.73***
CV×NP×FA	4	4.23**
Error	34	0.84

Note: ns = non-significant; *, ** and *** = significant at 0.05, 0.01 and0.001 levels, respectively; CAT: Catalase; APX: Ascorbate per oxidase; AsA: Ascorbic acid; H2O2: Hydrogen peroxide; MDA: Malondialdehyde.

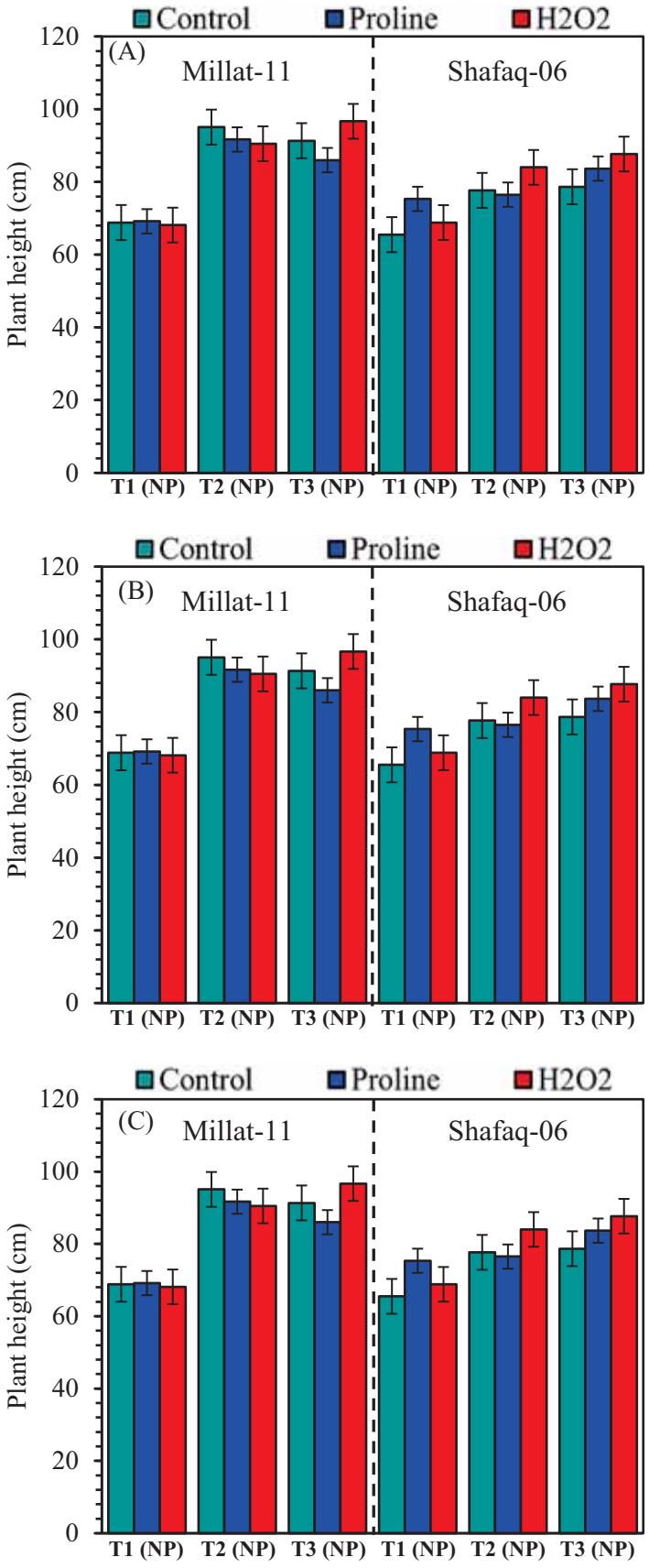
Control
Proline
H2O2
(A)
Millat-11
Shafaq-06
Plant height (cm)
0
20
40
60
80
100
120
T1 (NP)
T2 (NP)
T3 (NP)
T1 (NP)
T2 (NP)
T3 (NP)
(B)
(C)

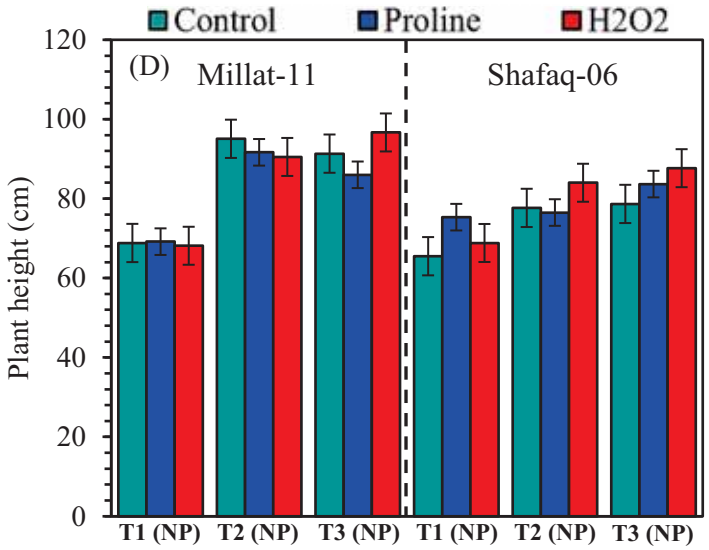
Control
Proline
H2O2
(D)
Millat-11
Shafaq-06
Plant height (cm)
0
20
40
60
80
100
120
T1 (NP)
T2 (NP)
T3 (NP)
T1 (NP)
T2 (NP)
T3 (NP)

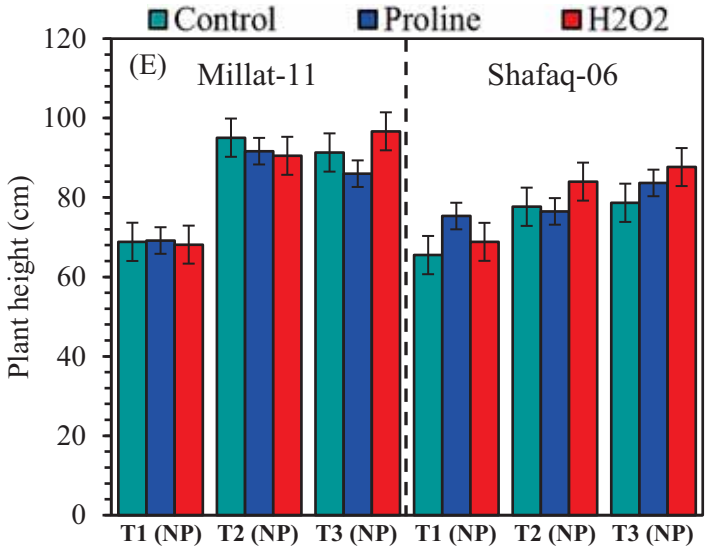
Control
Proline
H2O2
(E)
Millat-11
Shafaq-06
Plant height (cm)
0
20
40
60
80
100
120
T1 (NP)
T2 (NP)
T3 (NP)
T1 (NP)
T2 (NP)
T3 (NP)

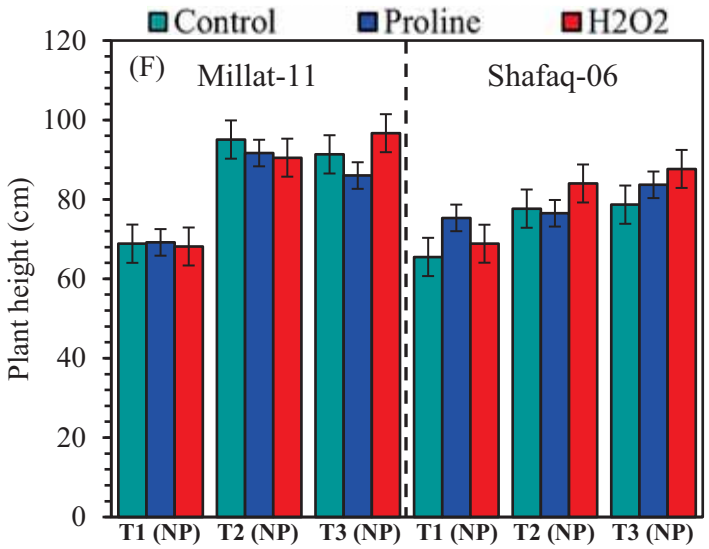
Control
Proline
H2O2
(F)
Millat-11
Shafaq-06
Plant height (cm)
0
20
40
60
80
100
120
T1 (NP)
T2 (NP)
T3 (NP)
T1 (NP)
T2 (NP)
T3 (NP)

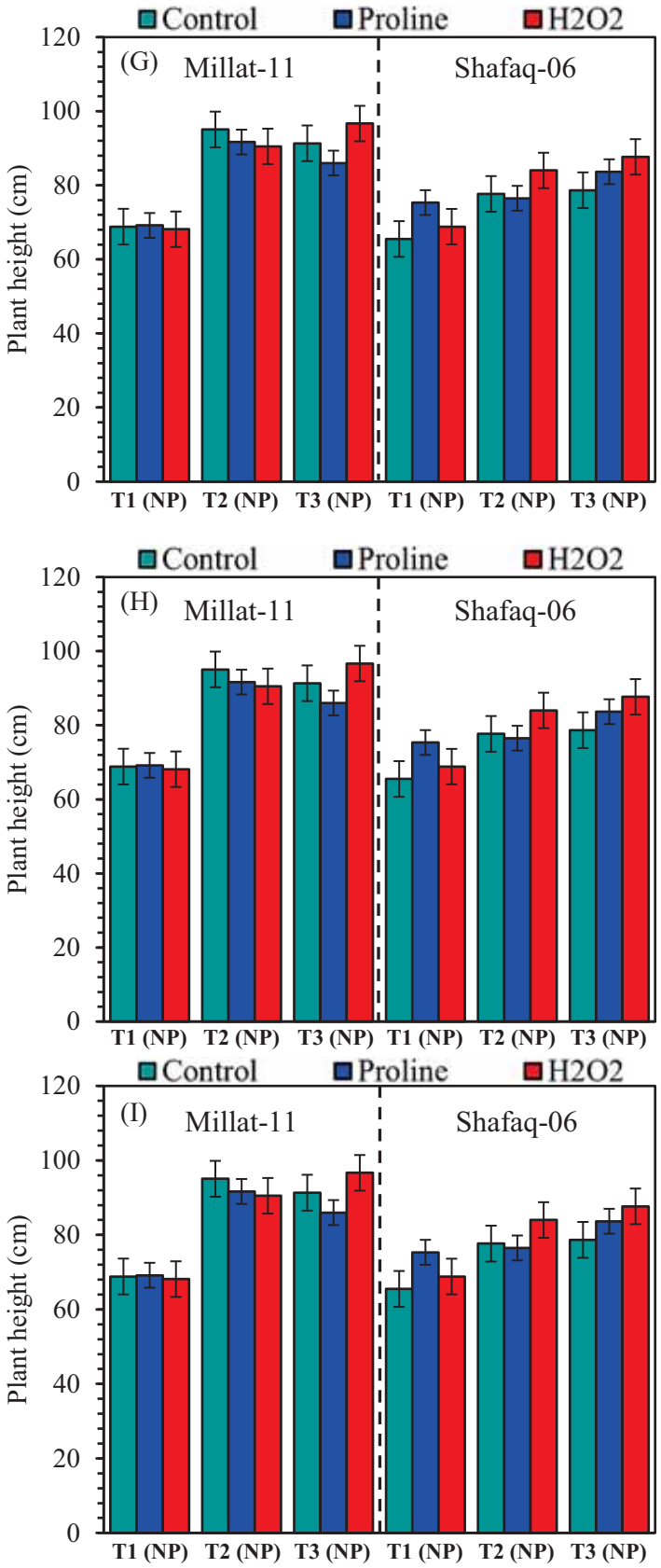

FIGURE 1

(A) Plant height, (B) Number of tillers per plant, (C) Number of spikes per plant, (D) Number of spikelet's per plant, (E) Number of fertile spikelet's per plant, (F) Number of non-fertile spikelet's per plant, (G) Main stem spike length, (H) Number of grains per plant and 100-grains weight per plant (I) of wheat plants treated with different NP and foliar application of proline and H_2O_2

Results in relation to 100-grain weight exposed significant ($p \leq 0.001$) variation in both cultivars as responded positively to different levels of NP and highest value for 100-grian weight recorded in (T3,120-90 kg/ha) which was followed closely by (T2,80-60 kg/ha). NP and foliar application together result in maximum yield. Foliar application alone did not show any significant difference. As far as selection of better cultivar is concerned, Shafaq-06 gave maximum weight of grains in combination with foliar application of H_2O_2. Increment in weight of grains was noticed as fertilizer level increasing progressively (Figure 1I and Table 1).

Activity of Enzymatic, Non-enzymatic Antioxidants and Protein Content of Wheat Treated with Proline and H_2O_2 under Different Levels of NP. For CAT activity in wheat grain no significant variation was noticed in both the wheat cultivars under all NP treatments. However, both foliar applications significantly($p \leq 0.05$) regulate CAT activity in both cultivars. Of different foliar treatment, Proline spray was observed more effective for cv. Millat-11, while H_2O_2 was helpful for improving catalase activity in cv. shafaq-06. Overall, application with NP fertilizer individually did not significantly increase CAT activity but along with foliar application showed pronounced improvement. Significant interaction ($p \leq 0.05$) was found between cultivars and foliar application (Figure.2A; Table 1). For APX activity in wheat grains significant ($p \leq 0.001$) improvement was found under different NP treatments and foliar applied biochemical. NP treatment individually or combined with foliar application, further ameliorated the APX activity in both studied cultivars. For APX activity, NP (T2, T3) and foliar application of (H_2O_2) was more effective as compared to control and proline. However, regarding cultivars, both millat and shafaq were equally effective and did not exhibited any significant difference except some minor variation in their response to NP level as cv. Millat-11 showed maximum APX activity under T3 while Shafaq showed under T2 for this studied trait. Significant ($p \leq 0.01$, $p \leq 0.05$) interaction effect of cultivars with NP (CV×NP) and their combined interaction CV×NP×FA was recorded (Figure. 2B; Table 1).

For ascorbic acid (AsA) content in wheat grains a notable increase ($p \leq 0.001$) contents were recorded in both cultivars under various NP fertilizer and foliar treatments. The effect of foliar application with H_2O_2 was more known as compared with other treatment i.e., proline and control. cv. Millat-11 was superior to cv. Shafaq-06 in this regard. Among different treatments combination of NP (T2, T3) and application of foliar H_2O_2 exhibited positive results. Significant interaction between all factors ($p \leq 0.001$) contributed positively to increase this variable (Figure 2C; Table 1).

Different levels of NP fertilizer considerably ($p \leq 0.001$) increase phenolic contents in wheat grains. In addition to fertilizer, the significant increase ($p \leq 0.01$) in phenolic contents was also recorded with foliar application of different treatments such as proline and H_2O_2. Phenolic contents showed little variation from (80-60 kg/ha) to (120-90 kg/ha) as maximum were obtained by (T2, 80-60 kg/ha) as compared to control and T3. And these results were similar for both cultivars. However, among foliar treatments, proline performed little better than H_2O_2 and control in improving phenolic contents. Furthermore, NP level and foliar application showed significant ($p \leq 0.05$) interaction for phenolic contents between them. Overall, cv. Millat-11 did not show significant difference from cv. Shafaq-06 (Figure 2D; Table 1).NP fertilization caused considerable ($p \leq 0.01$) improvement in grain protein contents. On the other hand, exogenously applied proline and H_2O_2 did not displayed any difference for both cultivars. In comparison, highest protein contents were found under (T2, l80-60 kg/ha) along with foliar treatment in both cultivars over (T1 and T3). About interaction, data analysis showed that combination of NP with cultivars gave significant ($p \leq 0.05$) protein contents (Figure 2E; Table 1).

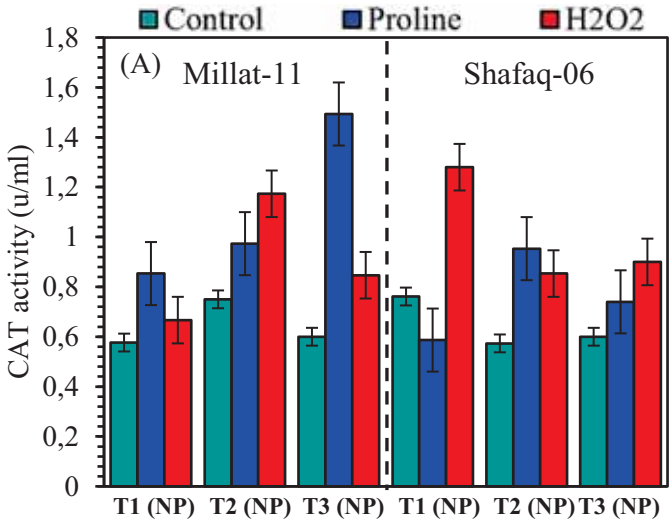

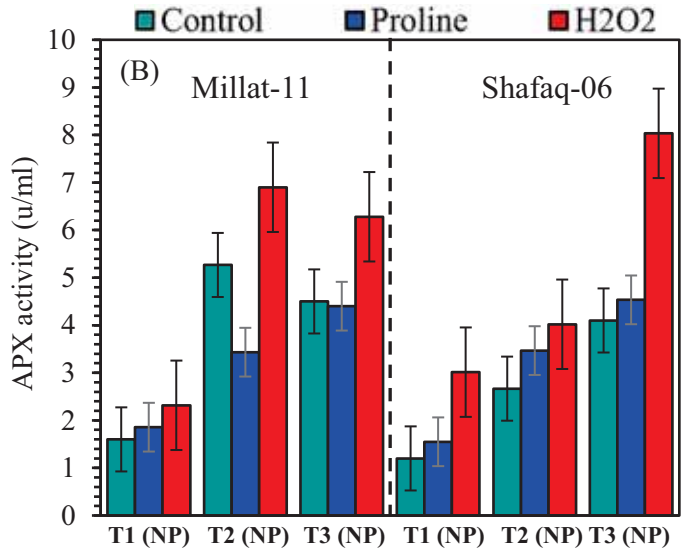
Control
Proline
H2O2
(B)
Millat-11
Shafaq-06
APX activity (u/ml)
0
1
2
3
4
5
6
7
8
9
10
T1 (NP)
T2 (NP)
T3 (NP)
T1 (NP)
T2 (NP)
T3 (NP)

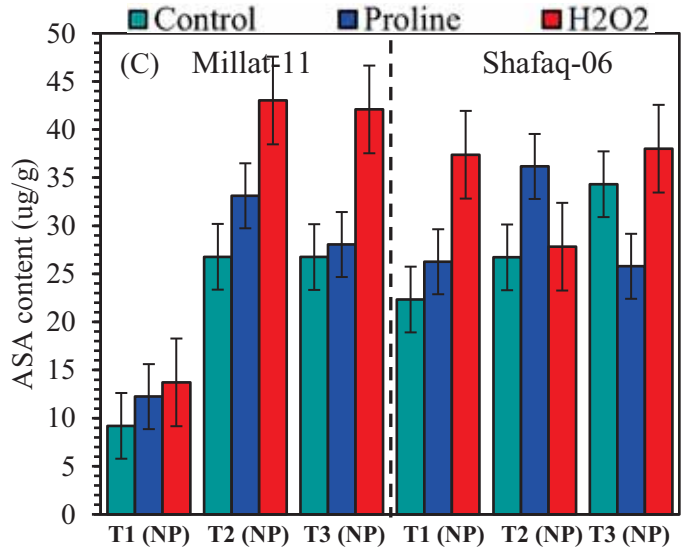
Control
Proline
H2O2
(C)
Millat-11
Shafaq-06
ASA content (ug/g)
0
5
10
15
20
25
30
35
40
45
50
T1 (NP)
T2 (NP)
T3 (NP)
T1 (NP)
T2 (NP)
T3 (NP)

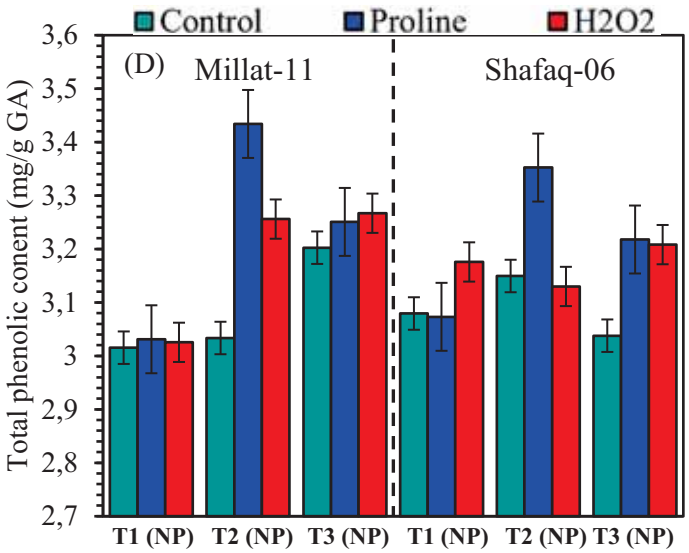
Control
Proline
H2O2
(D)
Millat-11
Shafaq-06
Total phenolic conent (mg/g GA)
2,7
2,8
2,9
3
3,1
3,2
3,3
3,4
3,5
3,6
T1 (NP)
T2 (NP)
T3 (NP)
T1 (NP)
T2 (NP)
T3 (NP)

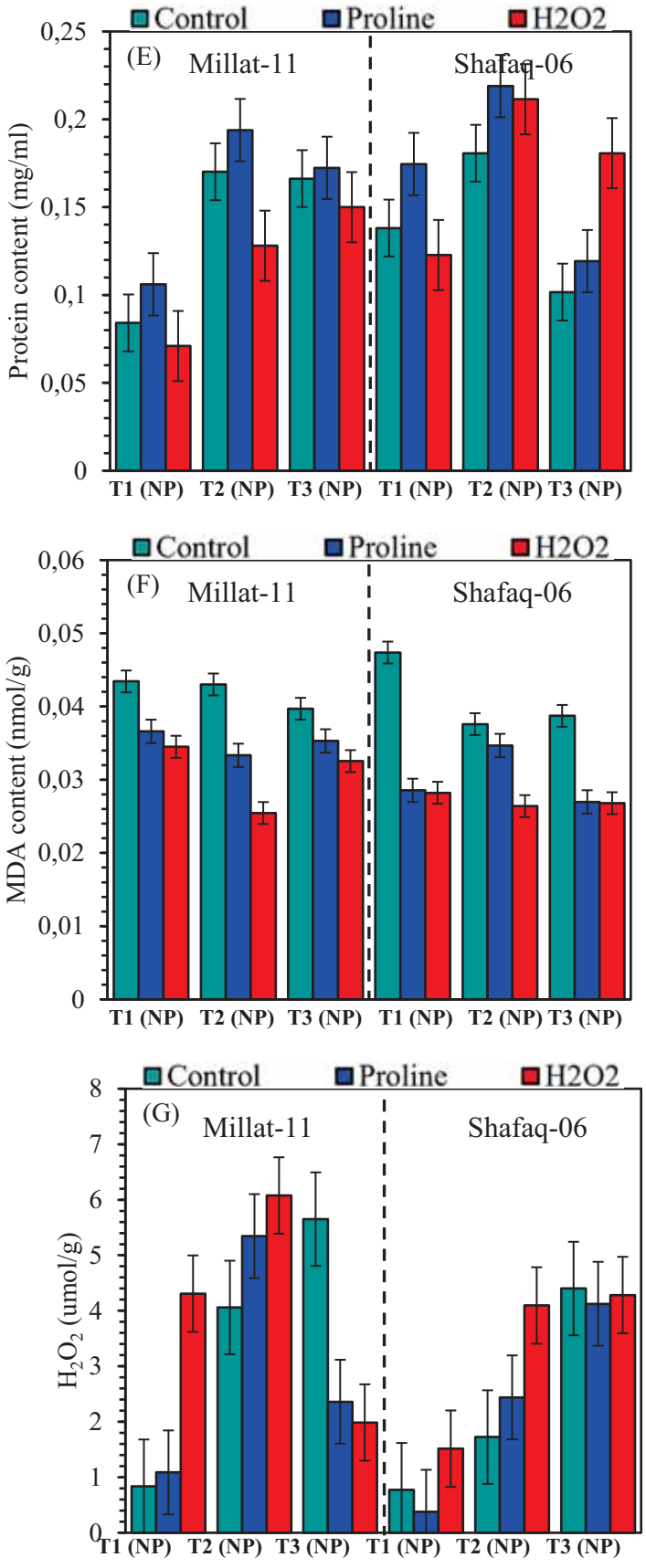

FIGURE 2

(A) Catalase activity (CAT), (B) Ascorbate per oxidase, (C) Ascorbic acid, (D) Total phenolic content, (E) protein content, (F) Malondialdehyde, (G) Hydrogen peroxide of wheat plants traeated with different NP and foliar application of proline and H_2O_2

Oxidative Damage Measurements: MDA and H_2O_2 Contents of Wheat Treated with Proline and H_2O_2 under different Levels of NP. No significant change was observed in grains MDA content under all NP application in both studied cultivars. Regardless of NP levels, exogenously applied proline and H_2O_2 significantly ($p \leq 0.001$) reduced the MDA content in both cultivars. But improvement was observed with H_2O_2 rather than proline in both cultivars (Figure. 2 F; Table 1). Results exposed highly significant ($p \leq 0.001$) improvement in grains H_2O_2 accumulation under different NP application. Foliar application of biochemical had pronounced ($p \leq 0.01$) effect on this trait. Exogenous- applied H_2O_2 alone and in combination (proline and NP (80-60 kg/ha) was effective in improving internal H_2O_2 contents for Millat-11 while this combination of proline and H_2O_2 works better under NP (120-90 kg/ha) for Shafaq-06 respectively. Overall, H_2O_2 treatment alone was proved more effective in reduction of lipid peroxidation in comparison with other treatments for both cultivars. Moreover, this enhancement showed similar trend to Synergistic effect of NP and foliar biochemical. Analysis of result revealed Fertilizer level, foliar application interaction and their combined interaction with cultivars had significant ($p \leq 0.01$) effect on H_2O_2 (Figure 2G; Table 1).

Correlation Analysis. Correlation analysis between yield related attribute and grains biochemical parameters obtained from different NP and foliar biochemical treatments are presented in Table. 2. Correlational studies showed significant positive correlation among different yield trait, NSLP, PH, NFSP, NGP, MSSL, NSP HGWP. While among biochemical attributes, positive significant correlation was found among APX, AsA, phenolic, protein and H_2O_2 contents. Results showed strong positive correlation between yield and biochemical attributes, PH, MSSL and HGWP showed strong positive correlation with APX, AsA, and H_2O_2 contents. MSSL showed highest positive correlation with Phenolic contents respectively. In vice versa, MDA contents negatively correlated with almost all studied traits but, HGWP, APX, AsA shows strong negative correlation with MDA contents. No correlation was found between CAT activity and all yield attributes

Principal Component Analysis. Principal component analysis (PCA) is a multivariate analysis or novel approach of data reduction often used to reduce the dimensionality of interrelated variables using new reduced set of uncorrelated variables (Principal components). The results of PCA presented in Figure 3 and in Table 2 revealed that first dimension (Dim-1) accounted for 46% of variation, while Dim-2 explained 13.1% of variation for studied traits in PCA. The first two dimensions of PCA explained about 59.3% of total variance which showing a good contribution. The contribution of variables to Dim-1 was largely determined by MSSL, NSLP, HGWP, PH, NGP, Phenolic, AsA and APX. Whereas contribution of variables to Dim 2 was related to MDA, NFSP and CAT.

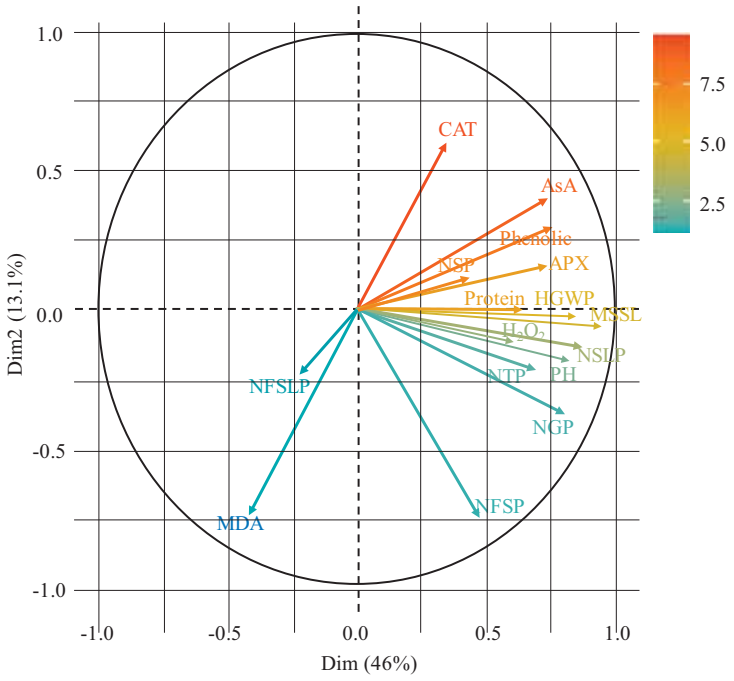

FIGURE 3
Principal component analysis of yield related attributes and biochemical constituents of wheat plants treated with different NP and foliar application of proline and H_2O_2..

TABLE 2
Pearson correlation coefficient (r) between all yield related attributes and biochemical constituents of wheat plants treated with different NP and foliar application of proline and H_2O_2

	PH	NTP	NSP	NSLP	NFSP	NFSLP	MSSL	NGP	HGWP	CAT	APX	AsA	Phenolic	Protein	MDA	H_2O_2
PH	1	0.337*	0.096ns	0.453***	0.463***	0.058ns	0.68***	0.452***	0.467***	0.196ns	0.6**	0.499***	0.409**	0.317*	-0.153ns	-0.493**
NTP		1	0.458***	0.389**	0.084ns	0.007ns	0.346*	0.292*	0.416**	0.155ns	0.1ns	0.179ns	0.321*	0.312*	-0.193ns	-0.005ns
NSP			1	0.537***	0.157ns	0.222ns	0.2ns	0.201ns	0.196ns	0.206ns	0.148ns	0.216ns	0.308*	0.136ns	-0.148ns	-0.008ns
NSLP				1	0.558***	0.277*	0.533***	0.614***	0.396**	0.153ns	0.385**	0.315*	0.412**	0.172ns	-0.288*	0.274*
NFSP					1	0.185ns	0.447***	0.568***	0.259ns	0.000ns	0.285*	0.117ns	0.014ns	0.094ns	0.128ns	0.396**
NFSLP						1	0.093ns	0.043ns	0.167ns	0.059ns	0.007ns	0.318ns	0.087ns	0.057ns	0.107ns	0.006ns
MSSL							1	0.621***	0.681***	0.232ns	0.578***	0.591***	0.492***	0.351**	-0.179ns	0.509***
NGP								1	0.637***	0.003ns	0.399**	0.333*	0.312*	0.259ns	-0.196ns	0.342*
HGWP									1	0.044ns	0.633***	0.584***	0.301*	0.374**	-0.392**	0.474***
CAT										1	0.273*	0.319*	0.285*	0.262ns	-0.285*	0.073ns
APX											1	0.663***	0.298*	0.253ns	-0.399**	0.525***
AsA												1	0.518***	0.356**	-0.381**	0.326*
Phenolic													1	0.274*	-0.198ns	0.172ns
Protein														1	-0.077ns	0.112ns
MDA															1	-0.212ns
H_2O_2																1

DISCUSSION

A variety of strategies are being applied to alleviate the destructive effects of adverse conditions and improved tolerance in many plant species, including application of some chemical such as H_2O_2, exogenous use of many growth regulator phytohormones, mineral nutrient as well as osmoprtactant amino acid particularly proline [35]–[37] Number of studies have been reported the beneficial effect of mineral nutrient fertilization, most notably nitrogen (N) and phosphorus (P) to meet optimum productivity [38] but detailed information about effects of NP fertilizer in combination with (Proline and H_2O_2) on yield and biochemical constituent of wheat was missing so far. For this purpose, two wheat varieties were selected for testing the effects of varied level of NP fertilizer and foliar application of biochemical (Proline + H_2O_2) on yield related attribute and grains biochemical constituents. In the present study root-growing medium application of different NP levels (0-0, 80-60 and 120-90) improved all yield related traits. The present investigation showed that, plant height increases in linear manner with NP at (120-90 kg/ha). Similar to the present findings, Rashid et al. [39] and Wakene et al.[40] also noted linear increase in height of barely plants with corresponding increasing NP level. Fana et al. [41] and Gerba et al. [42] while, working with wheat plants claimed that

plant height increased with each increment in nitrogen fertilizer and the probable reason might be that higher level of nitrogen played role in accelerating vegetative growth. Tillering considered as an important determinant for grain production in wheat. Balanced nutrition level considerably influenced yield and its component [43]. In the present results, (80-60 kg/ha) had significant correlation with number of tillers per plant. Our outcomes are fully supported by Jogi et al. [44] and Rakshit et al. [45] who observed beneficial effects in wheat as well as in rice yield and its components with optimum application of NP and reported that excess NP fertilizers is not productive for plants. These present results confirmed the findings that optimum NP could also attributed to increased number of productive tillers. Previous studies reported similar outcome [46].

Nitrogen and phosphorous has relatively larger effect on vegetative growth than reproductive stage, as optimum availability of nitrogen ensures the production of growth regulating cytokinin hormone which subsequently play vital role in cell division. Whereas phosphorous help in acquiring, and storage and use of energy, so they did not considerably affect the number of spikes. Present results are consistent with this statement as different application of NP did not significantly affect the number of spikes. our investigation contradicts the results of Rahman et al. [47]. Many researchers claimed the increase in number of spikes with possible increase in nutrient absorption by plants [48]. Grain yield has direct association with yield attributes such as plant height, tillers number, total spikes, fertile spikelet's, main stem spike length, grains number and 100-grains weight per plant. In the present investigation, number of spikelet's per plant, fertile spikelet's and main stem spike length were positively affected due to synergistic effect of Nitrogen and phosphorus on these studied traits. Highest number of spikelet's per plant and fertile spikelets were attained by cv. Millat -11 with NP rate of (80-60 kg/ha) while cv. Shafaq-06 obtained maximum values for these studied traits with highest dose of NP (120-90 kg/ha). This minor difference in their response to NP at different rate mainly associated with genetic variability of these studied cultivars. This obtained result was similar with research finding of [49]. Main stem spike considered as an important yield contributing trait for wheat. The present findings showed that fertilizer NP (120-90 kg/ha) gave maximum spike length which revealed that spike length gradually improved toward each accretion in NP dose up to (120-90 kg/ha). In line with results of [50] who reported that increased NP dose significantly increased spike length. The present obtained results for yield components show conformity with outcomes of Akram and Ashraf [51] who appraise the positive role of mineral fertilizers and noted that fertilizer treated wheat plant gave 224% more increment in yield elements than control plants.

Addition of balanced nutrition resulted in more grain number along with higher grain weight. Higher grains per plant represents high yield. Our study regarding grains number revealed that this studied attribute significantly increased in response to NP fertilizer at (80-60 kg/ha) and (120-90 kg/ha). As both cultivars did not differ significantly from each other, but they show response at different NP level to attain their maximum. Wheat variety cv. Millat-11 gave maximum number of grains atT3 (120-90 kg/ha), while cv. shafaq-06 gave from the plot where NP at (80-60 kg/ha) was applied as this result statistically like tillers and spikes number where higher values for these attributes was found at (80-60 kg/ha). This is in agreement with Imtiaz et al. [52] who reported simulative effect of fertilizer on spikelets count and number of grains if applied in balance proportion. Fertilizer applied in appropriate ratio stimulating the development of better root system ensure nutrient uptake by plant in effective manner as well as decrease the chance of seed deterioration and ultimately resulted in magnificent production [53]–[55].

100-grain weight is considered one of the most paramount attributes that had greatest influence on wheat yield as well as showed positive association with grain yield and other yield factors like tillers and fertile spikelets. Increased 100 grain weight attributed to the synergistic effect of NP fertilizer on biomass production. In the present study, maximum 100-grain weight was found in T3 (120-90 kg/ha) which indicate the profound role of fertilizers in both cultivars. Subsequent fertilization increased chlorophyll contents as well as improved photosynthetic efficiency which in turn ensuring translocation of photosynthates during final period of grain filling. Our results are according to the observation of Ali et al. [56] who found the key role of NP fertilizers in increasing 100 grain weight as well as wheat grain yield. Apart from our findings, such NP-induced yield improvement has previously been reviewed in many crop plant such as maize, rice and sunflower [57]–[59]. Chaudhry et al. [60] find out the correspondence of high grain yield and number of spikes with optimum (120-90-60 kg/ha) NPK level. Moreover, foliar application of proline and hydrogen peroxide (H_2O_2) has been known for their diverse role predominately in of agricultural applications [35][61]. Different adverse environmental conditions reduced cell division and negatively affect various aspect of plant life like reduce plant height, leaf area, photosynthetic pigment and apparatus which at the same time caused considerable growth and biomass reduction. The results of the present study regarding proline and H_2O_2 induced improvement in all yield related component has previously been noticed by [62]. They reported that Foliar application of proline ameliorated the plant height, dry biomass and number of grains. Ameliorating effect of foliar spray of proline on growth, physiological and biochemical process might be due to their regulatory

role in leaf photosynthetic pigment production [63], active participation in osmotic adjustment through synthesis of compatible solutes [64], stabilization of membrane and protein, enhancing enzyme and antioxidants activities and their metabolic role [65], preventing oxidative damage [66] - [67] and act as a nitrogen reserve which aid in achieving optimum yield. Exogenous low dose application of proline and H_2O_2 encourage vigorous root system which is major factor influencing nutrient uptake by root and ensuring better growth and yield attributes in wheat plant [68] - [69]. Application of H_2O_2 helps in up-regulation of various metabolic and enzyme activity linked to plant growth and developmental process [70].

Lipid peroxidation is common phenomenon under stresses and used as indices to access the extent of ROS induce oxidative damage. Magnitude of lipid peroxidation is measured in term of MDA accumulation. In present investigation, NP applied through rooting- zone medium did not play significant role in lowering MDA concentration, but they reduced to some extent in wheat grains of both cultivars. Sabrina et al. [71], claimed recovery of NPK treated strawberry plant through reduction in lipid peroxidation. According to presented findings, lipid peroxidation prevented with foliar proline and exogenous low dose of H_2O_2. Apart from proline, exogenous low dose of H_2O_2 had significant impact in reducing the accumulation of MDA contents in grains of both wheat cultivars. Many authors reported that proline foliar application lowers the accumulation of MDA and decelerates the lipid peroxidation [61] - [72]. In response to this concern, many previous author Li et al. [73] and Terzi et al. [74] claimed that exogenous H_2O_2 treatment avoided the progressive increase in MDA contents.

In addition to MDA, high concentration of endogenous H_2O_2 is one of the toxic effects and major contributor to oxidative stress. According to Neill et al. [75] and Queval et al. [76] H_2O_2 effects are dose specific and at very low concentration it serves as fundamental signaling molecules Results of present study indicated that NP fertilizer application helps to induced the pronounced accumulation of wheat grains H_2O_2 contents. Addition of mineral nutrient application further promote the higher accumulation H_2O_2 contents in the wheat plants. But Gallego et al. [77] found completely opposite trend in durum wheat, where NP application lowers the H_2O_2 contents in roots because it improved the ascorbate peroxidase (APX) and APX activities which in turn suppressed the endogenous accumulation of H_2O_2 concentration. However, In the present investigation results showed that exogenously- applied H_2O_2 leading to excessive increase in grain H_2O_2 accumulation expressively. Exogenous low dose H_2O_2 induced enhanced endogenous accumulation of this biochemical correlates well with the findings of Orabi et al. [78] who mentioned that endogenous H_2O_2 concentration completely depended on the delicate balance between its production rate versus the rate at which it is utilized by enzymatic and non-enzymatic antioxidants to alleviate the effects of lipid peroxidation. Lapshina et al. [79] while working with tobacco plants, found that tobacco leaves treated with exogenous H_2O_2 elevated both the accumulation of endogenous H_2O_2 Contents as well as CAT activity. Considering previous reports, it is suggested that amelioration in Catalase activity in parallel with increased accumulation of endogenous H_2O_2 may confirm its central role as signaling molecule leading to induction of catalase [80]–[82].

Activation of enzymatic antioxidants (CAT, APX, AsA, Phenolic content) is a potential adaptive biochemical strategy which plant usually experience under stressfull condition to mitigate the injurious effects of oxidative stress injury [19]. Catalase (CAT) considered as a biomarker to evaluate the harmful effects of different stress status [82]. In our study, NP did not contribute significantly to change in fertilizer (NP) level. On the contrary, Sabrina et al. [71] found that presence of nitrates and nitrites in durum wheat caused significant enhancement in CAT enzyme activity. Results of our study show up regulation of grains CAT enzyme activity with H_2O_2 application in cv. Millat-11. These results agree with the finding of Wang et al. [83] who reported that over expression of CAT assisted by low dose H_2O_2 when it was applied at different developmental stages especially at heading stage. Besides hydrogen peroxide, elevated the expression of grains CAT enzyme under exogenous proline was recorded for Cv. Shafaq-06. These result gets additional support from the findings of Hayat et al. who observed enhancement of CAT activity in response to foliar spray of proline? The probable reason behind this may be the potential of exogenous proline as an oxidative scavenger. However, our findings from present study demonstrate that both proline and H_2O_2 trigger grains CAT activity. Accumulation of principal antioxidant enzyme APX considered as an indicator of oxidative stress tolerance as it detoxify the oxidative stress -induced free radicals in crop plants [82] - [84]. In this relation, the activity of APX was also estimated. Our findings show considerable enhancement in grains APX enzyme activity in NP and H_2O_2 treated plants. According to Sabrina et al. [71] NPK treatments aided in getting high activity of this antioxidant enzymes. The comparative analysis of results obtained for wheat grains with previous research findings showed the activities of enzymatic antioxidants obtained its maximum values when plants sprayed with H_2O_2. There were other reports indicating significant increase in enzymes activities such as CAT, PPO, APX, POX when grains of wheat plant treated with 50 and 100 μM of H_2O_2 [85].

Furthermore, non-enzymatic secondary metabolites ascorbic acid (AsA) is vitamin C act as a key

substrate antioxidant to enzymatically minimize the consequences of lipid peroxidation. AsA contents modulate plant growth through hormonal signaling [86] - [87]. Present studies clearly show that Application of NP was significantly effective for improving AsA contents in grains of both wheat cultivars treated with T2and T3. Similarly, a considerable H_2O_2 - induced escalation has been viewed in AsA contents in grains of both wheat cultivars. Overall, response of cv. Millat -06 in term of Ascorbic acid contents to NP and H_2O_2 application was better. According to Azzedine et al. [88] exogenous H_2O_2 in low doses attributed to increase in endogenous ascorbic acid. Exogenous H_2O_2 triggered ascorbic acid contents might be due to its antioxidative defense mechanism [89] - [90].

Common cellular metabolite phenolic also have potential antioxidative defense mechanism [91] - [92]. Main function of phenolics in plant is to stabilize the free radical produced under stress and strengthen the membrane integrity from burst [82] - [93] - [94]. In the present study, chemical fertilizers as well as foliar application positively and significantly contributed for higher grains phenolics contents. Higher phenolics accumulation was noted when supplied fertilizer level i.e., 80-60 kg/ha with proline spray. It was even also revealed in shoots of Orengano (Origanum vulgare L.), that exogenous-applied proline responsible for greater accumulation of phenolic contents which might be due to role of proline in pentose phosphate cycle [95]. In view of nutritious requirement, nitrogen is most essential nutrient influenced wheat production, protein yield and contents followed by phosphors and potassium. Apart from the direct effect of nitrogen, many previous studies indicated better positive interaction between nitrogen and phosphorous [96] - [97]. Nitrogen found to be a building block for protein synthesis Giambalvo et al. [98] while phosphorous uphold the effects of nitrogen, stimulate the synthesis, partitioning and translocation of carbohydrate from source to seed hence better assimilation [99]. Present findings suggested the improvement in grain protein contents due to NP fertilizers. Exogenous application of proline and H_2O_2 did not showed any difference in improvement for both cultivars. However, scientific literature is still unavailable regarding combined effect of NP fertilizer and exogenous proline and H_2O_2 application in increasing grain protein contents.

CONCLUSIONS

From the findings, it can be concluded that application of NP fertilizers significantly improved the almost all of yield and bio-chemical parameters. NP levels,80-60 kg/ha and 120-90 kg/ha was proved effective in improving all the above studied characters. At the same time improvement in yield related attribute after foliar spray of proline and H_2O_2 may also be associated with decreased lipid peroxidation and antioxidative enzyme activities. Enzymatic and non-enzymatic antioxidative enzymes i.e., CAT, APX, AsA, Phenolics increased significantly after foliar spray of proline and H_2O_2. Although among both chemicals (proline + H_2O_2) H_2O_2 has high affinity to reduce the grains MDA contents. H_2O_2 is itself a reactive oxygen species (ROS) but its endogenous concentration was improved by exogenous application of H_2O_2, the reason behind may be to increase the antioxidative activity to prevent membrane deterioration and improve growth and productivity. This investigation provides an open way for all readers to observe how NP fertilizers and foliar-applied biochemicals induced modulation in wheat grain yield factors and biochemical constituent. In addition, low dose of H_2O_2 can be helpful in better functioning of plant. Proline also contribute to lessen the adverse effects of H_2O_2. Wheat cultivars showed better performance which was due to NP fertilizers and biochemical application as NP alones can improve the grain yield, but foliar biochemical application further ameliorates the effect of NP fertilizer by increasing functioning of antioxidative system.

ACKNOWLEDGEMENTS

The authors would like to express their heartfelt gratitude to Ayub Agricultural Research Institute, Faisalabad for allowing to conduct this field experiment.

REFERENCES

[1] Nasim, W., Ahmad, A., Wajid, S. A., Hussain, A., Khaliq, T., Usman, M., Hammad, H. M., Sultana, S. R., Mubeen, M., and Ahmad, S. (2010), Simulation of different wheat cultivars under agro-ecological condition of Faisalabad-Pakistan. Crop Environment. 1, 44–48.

[2] Shakeel, M. and Azam, S. (2012), Cytological and morphological characterization of selected synthetic hexaploid wheats derived from tetraploid durums and diploid Aegilops tauschii. Journal of Medicinal Plants Research. 6(16), 3228–3232.

[3] Atesoglu, A., Akturk, E., Rasouli, A., Erpay, S., And Ozel, H. B. (2020), Monitoring of Land-Cover/Land- Use Changes In Syria By Involving the Collect Earth Methodology Approch. Fresen. Environ. Bull. 29, 11032–11041.

[4] Andrews, M., Lea, P. J., Raven, J. A., and Lindsey, K. (2004), Can genetic manipulation of plant nitrogen assimilation enzymes result in increased crop yield and greater N-use efficiency? An assessment, Annals of Applied Biology. 145(1), 25–40.

[5] Hassan, I., Chattha, M. B., Chattha, T. H., and Ali, M. A. (2010), Factors affecting wheat yield: A case study of mixed cropping zone of Punjab. J. Agric. Res. 48(3), 403.
[6] Laghari, G. M., Oad, F. C., Shamasuddin, T., Gandahi, A. W., Siddiqui, M. H., Jagirani, A. W., and Oad, S. M. (2010), Growth, yield and nutrient uptake of various wheat cultivars under different fertilizer regimes. Sarhad Journal of Agriculture. 26(4), 489–497.
[7] Ahmed, S., Jan, N. E., Khan, R., and Din, N. (2010) Wheat response to phosphorus under climatic conditions of Juglote, Pakistan. Journal Name. 26(2), 229–233.
[8] Jan, T., Jan, M. T., Arif, M., Akbar, H., and Ali, S. (2007), Response of wheat to source, type and time of nitrogen application. Sarhad Journal of Agriculture. 23(4), 871.
[9] Jilani, M., Afzal, M., and Waseem, K. (2008), Effect Of Different Nitrogen Levels On Growth and Yield of Brinjal (Solanum Melongena L.).
[10] Ahmed, S., Ahmed, F., and Hussain, M. (2003), Effect of different NPK levels on the growth and yield of kohlrabi (Brassica caulorapa L.) at northern areas of Pakistan. Asian Journal of Plant Sciences. 2(3), 336–338.
[11] Ziadi, N., Bélanger, G., Cambouris, A. N., Tremblay, N., Nolin, M. C., and Claessens, A. (2008), Relationship between phosphorus and nitrogen concentrations in spring wheat. Agronomy Journal. 100(1), 80–86.
[12] Murad, A., Khalil, S. K., and Khalid, N. (2000), Response of sunflower hybrids to various levels of nitrogen and phosphorus. Sarhad Journal of Agriculture. 16(5), 477–483.
[13] Jiang, Z., Feng, C., Huang, L., Guo, W., Zhu, X., And Peng, Y. (2006), Effects of phosphorus application on dry matter production and phosphorus uptake in wheat (Triticum aestivum L.) Plant Nutrition and Fertilizer Science. 5(004).
[14] Telesinski, A., Platkowski, M., Cybulska, K., Telesinska, N., Wr-obel, J., and Pawlowska, B. (2018), Response of Soil Enzymes to Two Antibiotics: Polymyxin B and Penicillin G. Fresen. Environ. Bull. 27, 3873–3845.
[15] Banu, M.N.A., Hoque, M.A., Watanabe-Sugimoto, M., Matsuoka, K., Nakamura, Y., Shimoishi, Y., and Murata, Y. (2009), Proline and glycinebetaine induce antioxidant defense gene expression and suppress cell death in cultured tobacco cells under salt stress. Journal of Plant Physiology. 166(2), 146–156.
[16] Ali, Q., Ashraf, M., and Athar, H.-U.-R. (2007), Exogenously applied proline at different growth stages enhances growth of two maize cultivars grown under water deficit conditions, Pakistan. Journal of Botany. 39(4), 1133–1144.
[17] Nanjo, T., Fujita, M., Seki, M., Kato, T., Tabata, S., and Shinozaki, K. (2003), Toxicity of free proline revealed in an Arabidopsis T-DNA-tagged mutant deficient in proline dehydrogenase. Plant and Cell Physiology. 44(5), 541–548.
[18] PB, K. K., Sangam, S., Amrutha, R. N., Naidu, K. R., Rao, K., Rao, S., Reddy, K. J., Theriappan, P., and Sreenivasulu, N. (2005), Regulation of proline biosynthesis, degradation, uptake and transport in higher plants: its implications in plant growth and abiotic stress tolerance. Current Science. 88(3), 424–438.
[19] Hossain, M.A., Bhattacharjee, S., Armin, S.-M., Qian, P., Xin, W., Li, H.-Y., Burritt, D. J., Fujita, M., and Tran, L.-S. P. (2015), Hydrogen peroxide priming modulates abiotic oxidative stress tolerance: insights from ROS detoxification and scavenging. Frontiers in Plant Science. 6, 420.
[20] Arora, A., Sairam, R. K., and Srivastava, G. C. (2002), Oxidative stress and antioxidative system in plants, Current Science. 1227–1238.
[21] He, L. and Gao, Z. (2009), Pretreatment of seed with H2O2 enhances drought tolerance of wheat (Triticum aestivum L.) seedlings. African Journal of Biotechnology. 51–6157.
[22] Apel, K. and Hirt, H. (2004), Reactive oxygen species: metabolism, oxidative stress, and signal transduction, Annu. Rev. Plant Biol. 55, 373–399.
[23] Bright, J., Desikan, R., Hancock, J. T., Weir, I. S., and Neill, S. J. (2006), ABA-induced NO generation and stomatal closure in Arabidopsis are dependent on H2O2 synthesis. The Plant Journal. 45(1), 113–122.
[24] Ishibashi, Y., Yamaguchi, H., Yuasa, T., Iwaya-Inoue, M., Arima, S., and Zheng, S.-H. (2011), Hydrogen peroxide spraying alleviates drought stress in soybean plants. Journal of Plant Physiology. 168(13), 1562–1567.
[25] Liao, W.-B., Zhang, M.-L., Huang, G.-B., and Yu, J.-H. (2012), Ca 2+ and CaM are involved in NO-and H 2 O 2-induced adventitious root development in marigold. Journal of Plant Growth Regulation. 31(2), 253–264.
[26] Peng, L.-T., Jiang, Y.-M., Yang, S.-Z., and Pan, S.-Y. (2005), Accelerated senescence of fresh-cut Chinese water chestnut tissues in relation to hydrogen peroxide accumulation. Zhi wu sheng li yu fen zi sheng wu xue xue bao= Journal of Plant Physiology and Molecular Biology. 31(5), 527.
[27] Hossain, M. A., Hoque, M. A., Burritt, D. J., and Fujita, M. (2014) Proline protects plants against abiotic oxidative stress: biochemical and molecular mechanisms, in Oxidative damage to plants, Elsevier. 2014, 477–522.

[28] Chandlee, J. M. and Scandalios, J. G. (1984) Analysis of variants affecting the catalase developmental program in maize scutellum. Theoretical and Applied Genetics. 69(1), 71–77.
[29] Asada, K. (1987), Production and scavenging of active oxygen in photosynthesis. Photoinhibition. 227–287.
[30] [30] Mukherjee, S. P. and Choudhuri, M. A. (1983), Implications of water stress-induced changes in the levels of endogenous ascorbic acid and hydrogen peroxide in Vigna seedlings. Physiologia Plantarum. 58(2), 166–170.
[31] Wolfe, K., Wu, X., and Liu, R. H. (2003), Antioxidant activity of apple peels. Journal of Agricultural and Food Chemistry. 51(3), 609–614.
[32] Bradford, M. M. (1976), A rapid and sensitive method for the quantitation of microgram quantities of protein utilizing the principle of protein-dye binding. Analytical Biochemistry. 72(1–2), 248–254.
[33] Cakmak, I. and Horst, W. J. (1991), Effect of aluminium on lipid peroxidation, superoxide dismutase, catalase, and peroxidase activities in root tips of soybean (Glycine max). Physiologia Plantarum. 83(3), 463–468.
[34] Velikova, V., Yordanov, I., and Edreva, A. (2000), Oxidative stress and some antioxidant systems in acid rain-treated bean plants: protective role of exogenous polyamines. Plant Science. 151(1), 59–66.
[35] Ashraf, M. and Foolad, M. R. (2007), Roles of glycine betaine and proline in improving plant abiotic stress resistance. Environmental and Experimental Botany. 59(2), 206–216.
[36] Babu, M. A., Singh, D., and Gothandam, K. M. (2012), The effect of salinity on growth, hormones and mineral elements in leaf and fruit of tomato cultivar PKM1. J. Anim. Plant Sci. 22(1), 159–164.
[37] Beyaz, R., Gurosy, M., Aycan, M., and Yildiz, M. (2018), The Effect Of Boron On The Morphological And Physiological Reponses Of Sunflower Seedlings (Helianthus Annuus L.). Fresen. Environ. Bull. 27, 3224–3560.
[38] Rehman, O., Zaka, M. A., Rafa, H. U., and Hassan, N. M. (2006), Effect of balanced fertilization on yield and phosphorus uptake in wheat-rice rotation. J. Agric. Res. 44(2), 105–115.
[39] Rashid, A., Khan, R. U., and Khan, D. J. (2008), Comparative effect of varieties and fertilizer levels on Barley (Hordeum vulgare). International Journal of Agriculture and Biology. 10(1), 124–126.
[40] Tigre, W., Worku, W., and Haile, W. (2014), Effects of nitrogen and phosphorus fertilizer levels on growth and development of barley (Hordeum vulgare L.) at Bore District, Southern Oromia, Ethiopia. American Journal of Life Sciences. 2(5), 260–266.
[41] Fana, G., Deressa, H., Dargie, R., Bogale, M., Mehadi, S., and Getachew, F. (2012), Grain Hardness, Hectolitre Weight, Nitrogen and Phosphorus Concentrations of Durum Wheat (Triticum turgidum L. var. Durum) as Influenced by Nitrogen and Phosphorus Fertilisation. World Applied Sciences Journal. 20(10), 1322–1327.
[42] Gerba, L., Getachew, B., and Walelign, W. (2013), Nitrogen fertilization effects on grain quality of durum wheat (Triticum turgidum L. var. durum) varieties in central Ethiopia. Agricultural Sciences. 4(3), 123–130.
[43] Hasanuzzaman, M., Ahamed, K. U., Rahmatullah, M., Akhter, N., Nahar, K., and Rahman, M. L. (2010), Plant growth characters and productivity of wetland rice (Oryza sativa L.) as affected by application of different manures. Emirates Journal of Food and Agriculture. 46–58.
[44] Jogi, Q., Kandhro, M. N., and Qureshi, A. A. (2017), Effect of Balanced Fertilizer for Enhanceing Wheat Growth And Yield July-Augus, Science International. 29(4), 981–984.
[45] Rakshit, A., Sarkar, N. C., and Sen, D. (2008), Influence of organic manures on productivity of two varieties of rice. Journal of Central European Agriculture. 9(4), 629–633.
[46] Prystupa, P., Slafer, G. A., and Savin, R. (2003), Leaf appearance, tillering and their coordination in response to NxP fertilization in barley. Plant and Soil. 255(2), 587–594.
[47] Rahman, M. Z., Islam, M. R., Islam, M. T., and Karim, M. A. (2014), Dry matter accumulation, leaf area index and yield responses of wheat under different levels of nitrogen. Bangladesh Journal of Agriculturist. 7(1), 27–32.
[48] Mosanaei, H., Ajamnorozi, H., Dadashi, M. R., Faraji, A., and Pessarakli, M. (2017), Improvement effect of nitrogen fertilizer and plant density on wheat (Triticum aestivum L.) seed deterioration and yield. Emirates Journal of Food and Agriculture. 899–910.
[49] Nehe, A. S., Misra, S., Murchie, E. H., Chinnathambi, K., and Foulkes, M. J. (2018), Genetic variation in N-use efficiency and associated traits in Indian wheat cultivars. Field Crops Research. 225, 152–162.
[50] Ashraf, M., Afzal, M., Ahmad, R., Ali, S., Shahzad, S. M., Aziz, A., and Ali, L. (2011), Growth and yield components of wheat genotypes as influenced by potassium and farm yard manure on a saline sodic soil. Soil & Environment. 30(2), 115–121.

[51] Akram, M. S. and Ashraf, M. (2011), Exogenous application of potassium dihydrogen phosphate can alleviate the adverse effects of salt stress on sunflower, Journal of Plant Nutrition. 34(7), 1041–1057.
[52] Imtiaz, M., Shah, S. K. H., Khan, P., Siddiqui, S., Memon, M. Y., and Aslam, M. (2003), Response of wheat genotype" SI-91195" to increasing N and P levelsand their ratios under agro-climatic conditions of Sindh [Pakistan]. Pakistan Journal of Soil Science (Pakistan). 22(4), 58–63.
[53] Brink, G. E., Pederson, G. A., Sistani, K. R., and Fairbrother, T. E. (2001), Uptake of selected nutrients by temperate grasses and legumes. Agronomy Journal. 93(4), 887–890.
[54] Sieling, K., Stahl, C., Winkelmann, C., and Christen, O. (2005), Growth and yield of winter wheat in the first 3 years of a monoculture under varying N fertilization in NW Germany. European Journal of Agronomy. 22(1), 71–84.
[55] Khan, P., Imtiaz, M., Aslam, M., Shah, S. K. H., Depar, N., Memon, M. Y., and Siddiqui, S. H. (2008), Effect of different nitrogen and phosphorus ratios on the performance of wheat cultivar “Khirman,” Sarhad J. Agric. 24, 233–240.
[56] Ali, J., Bakht, J., Shafi, M., Khan, S., and Shah, W. A. (2002), Uptake nitrogen as affected by various combinations of nitrogen and phosphorus. Asian Journal of Plant Sciences. 1(4), 367–369.
[57] Vranová, E., Inzé, D., and Van Breusegem, F. (2002), Signal transduction during oxidative stress. Journal of Experimental Botany. 53(372), 1227–1236.
[58] Akram, M. S., Ashraf, M., and Akram, N. A. (2009), Effectiveness of potassium sulfate in mitigating salt-induced adverse effects on different physio-biochemical attributes in sunflower (Helianthus annuus L.). Flora-Morphology, Distribution, Functional Ecology of Plants. 204(6), 471–483.
[59] Sun, H.-J., Zhang, Y., Ndayambaje, E., Dong, W.-Q., Lin, H.-J., Chen, J.-R., and Hong, H.-C. (2018), The Effect Of Short-Term Exposure To Low Ph/Aluminum on The Ion Regulation, Related Atpase Activites And Haematological Parameters Of Juvenile Common Carp. Fresen. Environ. Bull. 27, 3318–3325.
[60] Chaudhry, G. A., Nawaz, S., Hussain, R., Asghar, A., and Kashif, S. R. (2000), Fertilizer requirements of new wheat genotypes under rainfed conditions. Pakistan Journal of Soil Science (Pakistan). 18(1–4), 105–109.
[61] Kamran, M., Shahbaz, M., Ashraf, M., and Akram, N. A. (2009), Alleviation of drought-induced adverse effects in spring wheat (Triticum aestivum L.) using proline as a pre-sowing seed treatment. Pak. J. Bot. 41(2), 621–632.
[62] Merwad, A.-R. M. A., Desoky, E.-S. M., and Rady, M. M. (2018), Response of water deficit-stressed Vigna unguiculata performances to silicon, proline or methionine foliar application. Scientia Horticulturae. 228, 132–144.
[63] Shahid, M. A., Balal, R. M., Pervez, M. A., Abbas, T., Aqeel, M. A., Javaid, M. M., and Garcia-Sanchez, F. (2014), Exogenous proline and proline-enriched Lolium perenne leaf extract protects against phytotoxic effects of nickel and salinity in Pisum sativum by altering polyamine metabolism in leaves. Turkish Journal of Botany. 38(5), 914–926.
[64] Dawood, M. G., Taie, H. A. A., Nassar, R. M. A., Abdelhamid, M. T., and Schmidhalter, U. (2014), The changes induced in the physio-logical, biochemical and anatomical charac-teristics of Vicia faba by the exogenous application of proline under seawater stress, South African Journal of Botany, 93, 54–63.
[65] Hayat, S., Hayat, Q., Alyemeni, M. N., Wani, A. S., Pichtel, J., and Ahmad, A. (2012), Role of proline under changing environments: a review, Plant Signaling & Behavior. 7(11), 1456–1466.
[66] Öztürk, L. and Demir, Y. (2002), In vivo and in vitro protective role of proline. Plant Growth Regulation. 38(3), 259–264.
[67] Anshula, S. and Gurpreet, S. (2013), Studies on the effect of Cu (II) ions on the antioxidant enzymes in chickpea (Cicer arietinum L.) cultivars. Journal of Stress Physiology & Biochemistry. 9(1).
[68] Liao, M., Fillery, I. R. P., and Palta, J. A. (2004), Early vigorous growth is a major factor influencing nitrogen uptake in wheat. Functional Plant Biology. 31(2), 121–129.
[69] Niu, L. and Liao, W. (2016), Hydrogen peroxide signaling in plant development and abiotic responses: crosstalk with nitric oxide and calcium. Frontiers in Plant Science. 7, 230.
[70] Barba-Espín, G., Diaz-Vivancos, P., Job, D., Belghazi, M., Job, C., And Hernández, J. A. (2011), Understanding the role of H2O2 during pea seed germination: a combined proteomic and hormone profiling approach. Plant, Cell & Environment. 34(11), 1907–1919.
[71] Sabrina, B., Reda, D. M., and Houria, E. B. (2012), Induction of antioxidant enzyme system by a nitrogen fertilizer Npk in wheat Triticum durum. Advances in Environmental Biology, 85–89.

[72] Siddiqui, M. H., Al-Whaibi, M. H., Sakran, A. M., Ali, H. M., Basalah, M. O., Faisal, M., Alatar, A., and Al-Amri, A. A. (2013), Calcium-induced amelioration of boron toxicity in radish. Journal of Plant Growth Regulation. 32(1), 61–71.

[73] Li, J.-T., Qiu, Z.-B., Zhang, X.-W., and Wang, L.-S. (2011), Exogenous hydrogen peroxide can enhance tolerance of wheat seedlings to salt stress. Acta Physiologiae Plantarum. 33(3), 835–842.

[74] Terzi, R., Kadioglu, A., Kalaycioglu, E., and Saglam, A. (2014), Hydrogen peroxide pretreatment induces osmotic stress tolerance by influencing osmolyte and abscisic acid levels in maize leaves. Journal of Plant Interactions. 9(1), 559–565.

[75] Neill, S., Desikan, R., and Hancock, J. (2002), Hydrogen peroxide signalling. Current Opinion in Plant Biology. 5(5), 388–395.

[76] Queval, G., Hager, J., Gakière, B., and Noctor, G. (2008), Why are literature data for H2O2 contents so variable? A discussion of potential difficulties in the quantitative assay of leaf extracts. Journal of Experimental Botany. 59(2), 135–146.

[77] Chen, L.-M., Lin, C. C., and Kao, C. H. (2000), Copper toxicity in rice seedlings: changes in antioxidative enzyme activities, H2O2 level, and cell wall peroxidase activity in roots. Botanical Bulletin of Academia Sinica, 41.

[78] Orabi, S. A., Abou-Hussein, S. D., and Sharara, F. A. (2017), Role of Htdrogen peroxide and α-tocopherol in alleviating the harmful effect of low temperature on cucumber (Cucumis sativas L.) plants. Middle East J. Appi. Sci. 7(04), 914–926.

[79] Lapshina, L. A., Reunov, A. V, and Nagorskaya, V. P. (2016), Effects of exogenous H 2 O 2 on the content of endogenous H 2 O 2, activities of catalase and hydrolases, and cell ultrastructure in tobacco leaves. Biology Bulletin. 43(5), 419–425.

[80] Gechev, T. S. and Hille, J. (2005), Hydrogen peroxide as a signal controlling plant programmed cell death. The Journal of Cell Biology. 168(1), 17–20.

[81] Yang, Y. L., Zhang, Y. Y., Lu, J., Zhang, H., Liu, Y., Jiang, Y., and Shi, R. X. (2012), Exogenous H 2 O 2 increased catalase and peroxidase activities and proline content in Nitraria tangutorum callus. Biologia plantarum. 56(2), 330–336.

[82] Ashraf, M. (2009), Biotechnological approach of improving plant salt tolerance using anti-oxidants as markers. Biotechnology Advances. 27(1), 84–93.

[83] Wang, Y., Li, J., Wang, J., and Li, Z. (2010), Exogenous H_2 O_2 improves the chilling tolerance of manilagrass and mascarenegrass by activating the antioxidative system. Plant Growth Regulation. 61(2), 195–204.

[84] Mittler, R. (2002), Oxidative stress, anti-oxidants and stress tolerance. Trends in Plant Science. 7(9), 405–410.

[85] Orabi, S. A. And Sadak, M. S. H. (2015), Alleviation of adverse effects of salinity stress on wheat (Triticum aestivum L.) by exogenous application of hydrogen peroxide. Journal of Basic and Applied Research International. 287–303.

[86] Shaheen, S., Naseer, S., Ashraf, M., and Akram, N. A. (2013), Salt stress affects water relations, photosynthesis, and oxidative defense mechanisms in Solanum melongena L. Journal of Plant Interactions. 8(1), 85–96.

[87] Habib, N., Ali, Q., Ali, S., Javed, M. T., Zulqurnain Haider, M., Perveen, R., Shahid, M. R., Rizwan, M., Abdel-Daim, M. M., and Elkelish, A. (2020), Use of Nitric Oxide and Hydrogen Peroxide for Better Yield of Wheat (Triticum aestivum L.) under Water Deficit Conditions: Growth, Osmoregulation, and Antioxidative Defense Mechanism. Plants. 9(2), 285.

[88] Azzedine, F., Gherroucha, H., and Baka, M. (2011), Improvement of salt tolerance in durum wheat by ascorbic acid application. J. Stress Physiol. Biochem. 7(1), 27–37.

[89] Liu, Z.-J., Guo, Y.-K., and Bai, J.-G. (2010), Exogenous hydrogen peroxide changes antioxidant enzyme activity and protects ultrastructure in leaves of two cucumber ecotypes under osmotic stress. Journal of Plant Growth Regulation. 29(2), 171–183.

[90] Saglam, A., Kalaycioglu, E., Guven, F. G., Saruhan, N., Kadioglu, A., and Demiralay, M. (2014), Hydrogen peroxide extends postharvest life of Ctenanthe setosa leaf cuts under osmotic stress by reducing leaf. Rolling, Horticulture, Environment, and Biotechnology. 55(4), 308–314.

[91] Noreen, Z. and Ashraf, M. (2009), Assessment of variation in antioxidative defense system in salt-treated pea (Pisum sativum) cultivars and its putative use as salinity tolerance markers. Journal of Plant Physiology. 166(16), 1764–1774.

[92] Li, Z.-H., Wang, Q., Ruan, X., Pan, C.-D., and Jiang, D.-A. (2010), Phenolics and plant allelopathy, Molecules, 15(12), 8933–8952.

[93] Shetty, K. and McCue, P. (2003), Phenolic antioxidant biosynthesis in plants for functional food application: integration of systems biology and biotechnological approaches. Food Biotechnology. 17(2), 67–97.

[94] Burguieres, E., McCue, P., Kwon, Y.-I., and Shetty, K. (2007), Effect of vitamin C and folic acid on seed vigour response and phenolic-linked antioxidant activity. Bioresource Technology. 98(7), 1393–1404.
[95] Lattanzio, V., Cardinali, A., Ruta, C., Fortunato, I. M., Lattanzio, V. M. T., Linsalata, V., and Cicco, N. (2009), Relationship of secondary metabolism to growth in oregano (Origanum vulgare L.) shoot cultures under nutritional stress. Environmental and Experimental Botany. 65(1), 54–62.
[96] Hussain, I., Khan, M. A., and Khan, E. A. (2006), Bread wheat varieties as influenced by different nitrogen levels. Journal of Zhejiang University Science B. 7(1), 70–78.
[97] Molla-Ali-Akbari, M. and Lotfollahi, M.-A. (2015), Influence of different levels of nitrogen and phosphorus on some traits of wheat (Triticum aestivum L.). International Journal of Biosciences. 6(5), 147–151.
[98] Giambalvo, D., Ruisi, P., Di Miceli, G., Frenda, A. S., and Amato, G. (2010), Nitrogen use efficiency and nitrogen fertilizer recovery of durum wheat genotypes as affected by interspecific competition. Agronomy Journal. 102(2), 707–715.
[99] Crista, F., Radulov, I., Sala, F., Crista, L., And Berbecea, A. (2012), Influence of NPK fertilizers upon winter wheat grain quality. Research Journal of Agricultural Science. 44(3), 30–35.

Received: **01.01.2021**
Accepted: **03.02.2021**

CORRESPONDING AUTHOR

Muhammad Sultan
Department of Agricultural Engineering,
Bahauddin Zakariya University,
Bosan Road, Multan 60800 – Pakistan

e-mail: muhammadsultan@bzu.edu.pk

© by PSP Volume 30– No. 05/2021 pages 5466-5475 Fresenius Environmental Bulletin

THE EFFECT OF HEAT STRESS ON THE COMPOSITION AND MICROBIOLOGICAL QUALITY OF BULK TANK MILK IN DAIRY CATTLE

Ayse Deniz Cardak*

Aydin Adnan Menderes University, Faculty of Agriculture, Department of Dairy Science and Technology, Aydin, Turkey

ABSTRACT

In this study, the effects of heat stress on titratable acidity (°SH), fat, protein, dry matter, ash content and total aerobic mesophilic bacteria (TAMB), yeast and mold, micrococcus/staphylococcus, and coliform bacteria count of bulk tank milk in the milk collection center were investigated, and 156 cow's milk belonging to the Holstein breed was analyzed for three years (2011-2103), once a week. Temperature-humidity index (THI) was used to determine heat stress, and THI≥70 was evaluated as heat stress. THI≥70 is seen in June-September in 2011 and 2012, and in June-August in 2013. THI values of the day one day before sampling were taken into account when conducting the analysis. It was concluded that the effect of THI on the protein and ash content, the quantity of TAMB, yeast and mold, micrococcus/staphylococcus and coliform counts of milk was significant at the level of P≤0.001; also its effect on the dry matter was significant at the level of P≤0.05. It was found that when THI<50, the °SH, ash content of milk, TAMB, yeast and mold, micrococcus/staphylococcus and coliform counts were minimal, it reached maximum values when THI≥70. The correlation between THI and °SH, milk ash content, TAMB, yeast and mold, micrococcus/staphylococcus and coliform counts was positive and the correlation between THI and milk fat, protein, and dry content was negative. The importance of the correlation was found to be P≤0.001 for °SH, protein and ash content of milk, and the quantity of TAMB, yeast and mold, micrococcus/staphylococcus and coliform found to be P>0.05 for the content of fat and dry matter. The number of positive samples for Listeria spp. and Salmonella spp. was determined as 31 (19.87%) and 28 (17.95%), respectively.

KEYWORDS:
Temperature-Humidity Index, Yeast and Mold, Micrococcus/Staphylococcus, Coliform, Listeria spp., Salmonella spp., Season

INTRODUCTION

At the top of today's biggest environmental problem is climate change. Climate change, which has emerged with the industrial revolution and increased its speed by the 20th century, shows itself with global warming. Global warming is seen as a threat to the sustainability of many species, ecosystems, and livestock production systems [1]. Climate change increases the sensitivity of animals to diseases and can lead to mutations in disease and parasite factors, an increase in zoonotic diseases, and the emergence of some new diseases [2-4].

The combined factors that cause normal body temperature to rise in dairy cattle are called "Heat Stress". It is reported that hot and humid environments will cause changes in many physiological functions in dairy cattle, which will cause stress associated with a decrease in feed consumption, an increase in water consumption and respiratory rate, deterioration in health, a decrease in reproductive and yield performance in the process of adapting to climate change [5-12].

There are different indexes to determine the level of heat stress in dairy cattle. These indexes are generally called the "temperature-humidity index (THI)", which was first described for dairy cattle by Berry et al [13]. In some studies, it has been found that heat stress begins when the THI value increases to 72 and above [14,15]. It is also suggested that the threshold at which heat stress begins in Holstein cattle may be 65-69, or even lower [16-20].

In this study, it is aimed to determine the effect of heat stress on the titratable acidity (°SH) of cow's milk, fat, protein, dry matter and ash content, TAMB, yeast and mold, micrococcus/staphylococcus, and coliform count, and the presence of Listeria spp. and Salmonella spp. in the milk collection centers of small-medium-sized dairy farming enterprises located in Koçarlı district, which is 22 km away from the central district of Aydın and 253 m in altitude. Although there have been many studies in the literature on the effect of heat stress on milk yield, studies on the effect of milk on microbiological quality have not been found. This study is important because of the contribution of the results to the literature.

MATERIALS AND METHODS

Material. Between 2011 and 2013, 156 bulk tank milk samples belonging to the Holstein breed, which constituted the research material, were collected once a week for three years from the Agricultural Development Cooperative Milk Collection Center in Koçarlı district of Aydın. After the samples were taken from refrigerant tankers to 500 ml sterile containers under aseptic conditions, they were preserved with the cold chain at ≤6°C, and analysis was started on the same day.

Meteorological data for 2011-2013 belong to station 17234 at 37°8402' north latitude and 27°8379' south longitude.

Method. Chemical Analyses: Acidity determination in raw milk was determined by the alkali titration method and the results were expressed in Soxhlet Henkel (°SH) [21]. Dry matter and ash ratios in raw milk were determined using the gravimetric method and the results were expressed as a percentage [22,23]. The fat ratio was determined as a percentage according to Gerber method using a special milk butyrometer with 0-8 grades [24]. After the samples were exposed to wet decomposition, the protein ratio was calculated by detecting nitrogen amounts of samples by the Micro Kjeldahl method and multiplying the amount of nitrogen by the factor of 6.38 [25].

The chemicals used in the analysis were obtained from Merck and Sigma Aldrich.

Microbiological Analysis: For the purpose of counting total aerobic mesophilic bacteria (TAMB), yeast and mold, micrococcus/staphylococcus, and total coliform, parallel cultures were made on Plate Count Agar (PCA, Merck), Yeast Extract Glucose Chloramphenicol Agar (YGC, Merck), Baird Parker Agar (BPA, Merck) and Violet Red Bile Dextrose Agar (VRBA, Merck), respectively, and then incubated for 48 hours at 35°C, 5 days at 25°C, 24-48 hours at 37°C and 24 hours at 37°C, respectively [26]. After incubation, the weighted average results of the cultures made with two consecutive dilutes was taken and the quantities in the samples were calculated, then the result was given as log cfu/ml after being subjected to logarithmic transformation. The formula N=C/[Vx(n1+0.1xn2)xd] was used in the calculation. In the formula, N= the number of microorganisms in 1 ml of samples, C= the sum of the number of colonies in the Petri boxes, V= the volume transferred to the Petri boxes, n1= the number of Petri boxes in the counts made from the first dilution, n2= the number of Petri boxes in the counts from the second dilution, d= the dilution rate of the concentrate dilution from the two consecutive dilutions in which the count was performed [27].

The determination of the existence of Listeria spp. and Salmonella spp. was carried out as explained by Çardak [28].

Statistical Analysis: The formula THI=(0.8xT)+[(RH÷100)x(T-14.4)]+46.4 was used to calculate the Temperature-Humidity Index (THI) [29]. In the formula, T shows the average temperature value and RH shows the relative humidity. THI values of the day one day before sampling were taken into account when conducting the analysis.

Variance analysis was applied to the chemical and microbiologic properties of milk to investigate the effects of THI, sampling period, and year, and the Tukey test was used to compare the sub-group averages. For this purpose, THI (1=<50, 2= ≥50 <60, 3= ≥60 <70, 4= ≥70) and sampling period (Q1= January, February, March, Q2= April, May, June, Q3=July, August, September, Q4= October, November, December) were divided into four groups. Statistical analysis was done with SPSS 21.0 package software.

RESULTS

The means and standard deviations of meteorological data of the study years by month are given in Table 1; The minimum, maximum, average, and standard deviation values for the parameters and meteorological data of the sampling days are given in Table 2; The means of the titratable acidity (°SH), fat, protein, dry matter and ash content of milk and the total counts of aerobic mesophilic bacteria, yeast-mold, micrococcus/staphylococcus, and coliforms are given in Table 3 together with their standard errors; Positive sample numbers and rates for Listeria spp. and Salmonella spp., are given in Table 4 by THI values, sampling periods and years; and the correlation coefficients for variables are given in Table 5 with significance levels.

It was seen that April, June-August, and October-December of 2012 had the highest value of average temperatures. In terms of average humidity, January, March-August, and October of 2011 reached the highest value. THI≥70 is observed in June-September of 2011 and 2012, and in June-August of 2013 (Table 1). It is noteworthy that the highest rainfall was in January-March and October-November of 2013, and in April-June and December of 2012. In 2011-2013, the number of rainy days was recorded as 81, 85, and 82 days, respectively.

Taking into account meteorological data from the day before the milk samples were collected, the average temperature was the minimum of 3.20°C, maximum of 31.90°C; the relative humidity was the minimum of 31.80%, maximum of 96.30%; THI was the minimum of 42.22, maximum of 79.26 (Table 2). It was noteworthy that the number of days with THI≥70 during the three years (N=156 days) of the study was 49.

TABLE 1
Meteorological data by year and month (mean±standard deviation)[1]

	2011	2012	2013	2011	2012	2013	2011	2012	2013
	Maximum Temperature (°C)			**Minimum Temperature (°C)**			**Average Temperature (°C)**		
January	12.83±2.61^{b}	9.95±2.77^{c}	13.36±3.42^{a}	4.31±2.82^{b}	2.39±2.93^{c}	5.35±4.00^{a}	7.67±2.19^{b}	5.61±2.41^{c}	8.66±3.59^{a}
February	15.46±2.71^{a}	12.36±4.27^{c}	15.43±3.34^{b}	5.35±2.69^{b}	3.33±3.31^{c}	6.95±2.72^{a}	9.51±2.21^{b}	7.15±3.26^{c}	10.59±2.63^{a}
March	17.46±4.12^{c}	18.05±4.17^{b}	19.31±3.33^{a}	6.54±3.33^{b}	6.19±3.46^{c}	8.92±3.39^{a}	11.33±3.40^{c}	11.44±3.52^{b}	13.37±2.98^{a}
April	20.98±2.25^{c}	24.19±3.34^{b}	24.28±4.73^{a}	9.61±2.61^{c}	11.81±1.92^{a}	11.24±2.65^{b}	14.51±1.72^{c}	17.30±2.36^{a}	17.04±3.12^{b}
May	26.82±3.41^{c}	27.32±2.91^{b}	30.17±4.10^{a}	14.21±2.65^{c}	15.23±1.44^{b}	16.82±2.27^{a}	19.54±2.68^{c}	20.57±1.85^{b}	22.69±2.69^{a}
June	32.42±2.75^{c}	35.81±3.38^{a}	33.36±3.52^{b}	18.70±1.95^{c}	20.22±2.97^{a}	19.48±2.47^{b}	24.94±2.24^{c}	27.45±2.96^{a}	25.96±2.86^{b}
July	36.31±1.91^{b}	38.42±1.86^{a}	36.17±1.96^{c}	21.58±1.82^{b}	23.63±1.12^{a}	21.58±1.31^{c}	28.41±1.69^{b}	30.42±1.21^{a}	28.29±1.36^{c}
Aug.	35.76±2.01^{c}	37.48±2.03^{a}	37.07±1.51^{b}	21.32±1.29^{c}	22.09±2.16^{a}	22.09±0.98^{b}	27.84±1.38^{c}	29.18±2.01^{a}	28.70±1.14^{b}
Sept.	33.43±2.88^{b}	33.59±2.42^{a}	32.06±2.21^{c}	18.46±1.56^{a}	18.18±1.59^{b}	17.03±1.86^{c}	24.94±2.19^{a}	24.61±1.73^{b}	23.75±1.81^{c}
Oct.	23.42±3.95^{c}	28.48±3.53^{a}	25.64±3.32^{b}	11.40±3.62^{b}	15.86±1.94^{a}	11.17±2.73^{c}	16.33±3.39^{c}	20.99±2.32^{a}	17.05±2.64^{b}
Nov.	17.80±2.68^{c}	21.34±2.77^{a}	20.30±3.30^{b}	5.38±2.34^{c}	11.56±3.61^{a}	10.09±2.65^{b}	10.31±2.15^{c}	15.43±3.10^{a}	14.12±2.37^{b}
Dec.	14.46±2.95^{a}	14.28±3.86^{b}	13.26±3.20^{c}	5.61±4.01^{b}	6.94±4.12^{a}	3.55±3.42^{c}	9.14±3.14^{b}	10.08±3.80^{a}	7.36±3.04^{c}
	Average Humidity (%)			**Total Precipitation (mm)**			**Temperature-Humidity Index**		
January	80.06±9.30^{a}	76.24±11.73^{c}	76.39±9.79^{b}	4.37±8.52^{b}	3.84±8.31^{c}	5.05±7.71^{a}	47.23±3.33^{b}	44.41±2.87^{c}	49.14±4.98^{a}
February	72.95±11.50^{b}	70.24±14.38^{c}	75.33±8.90^{a}	2.26±4.04^{c}	4.97±8.51^{b}	5.25±8.91^{a}	50.57±2.95^{b}	47.13±4.62^{c}	51.86±4.21^{a}
March	69.17±9.70^{a}	60.47±12.05^{c}	63.89±11.04^{b}	0.77±2.12^{c}	1.18±3.89^{b}	2.95±6.78^{a}	53.39±4.91^{c}	53.73±4.81^{b}	56.47±4.27^{a}
April	69.25±10.47^{a}	62.20±9.50^{b}	59.04±11.24^{c}	1.61±2.68^{c}	2.05±5.55^{a}	1.71±4.95^{b}	58.13±2.54^{c}	61.89±3.32^{a}	61.33±3.96^{b}
May	63.39±11.51^{a}	62.94±7.93^{b}	53.98±14.14^{c}	1.43±3.12^{c}	1.75±4.27^{a}	1.48±4.76^{b}	65.14±3.59^{c}	66.63±2.38^{b}	68.71±2.89^{a}
June	52.79±10.15^{a}	49.10±8.83^{b}	47.82±9.67^{c}	0.49±2.66^{b}	1.32±6.93^{a}	0.15±0.80^{c}	71.80±2.53^{c}	74.57±3.21^{a}	72.52±3.02^{b}
July	47.45±5.52^{a}	43.38±10.05^{b}	43.12±9.27^{c}	0.00±0.00^{b}	0.01±0.04^{a}	0.00±0.00^{c}	75.74±1.93^{b}	77.65±1.68^{a}	74.97±1.58^{c}
Aug.	47.09±7.30^{a}	37.72±8.28c	43.55±5.61^{b}	0.02±0.08^{a}	0.01±0.04^{b}	0.00±0.00^{c}	74.94±1.41^{c}	75.28±2.33^{b}	75.54±0.96^{a}
Sept.	49.44±12.54^{b}	52.88±10.07^{a}	46.56±10.64^{c}	0.73±3.94^{a}	0.00±0.00^{c}	0.21±1.13^{b}	71.34±2.03^{b}	71.42±2.00^{a}	69.68±2.10^{c}
Oct.	65.19±14.41^{a}	60.66±8.46^{b}	55.89±8.67^{c}	1.68±5.93^{b}	1.14±4.67^{c}	2.25±10.05^{a}	60.67±4.83^{c}	67.07±2.99^{a}	61.57±3.67^{b}
Nov.	56.87±8.23^{c}	71.18±7.43^{b}	73.77±11.08^{a}	0.01±0.04^{c}	0.77±2.27^{b}	3.31±7.54^{a}	52.34±2.98^{c}	59.48±4.63^{a}	57.40±3.58^{b}
Dec.	72.33±12.02^{b}	80.37±11.11^{a}	62.50±9.83^{c}	0.53±1.34^{b}	5.95±10.26^{a}	0.30±0.72^{c}	49.95±4.71^{b}	50.84±5.74^{a}	48.03±3.99^{c}
	Number of Rainy Days			81	85	82			
	Days without Rain			284	280	283			

The difference among the means indicated by different letters on the same line is significant (P≤0.05)

TABLE 2

Minimum, maximum, mean and standard deviation values for the meteorological data of the days of sampling and for the analyzed parameters (N=156)

	Minimum	Maximum	Mean	Stand. Dev.
Minimum Temperature (°C)	8.00	41.10	25.03	9.15
Maximum Temperature (°C)	-1.40	25.00	12.71	6.89
Average Temperature (°C)	3.20	31.90	18.05	7.97
Humidity (%)	31.80	96.30	59.84	15.19
Precipitation (mm)	0	22.00	1.37	4.47
Temperature-Humidity Index (THI)	42.22	79.26	62.19	10.62
Titratable acidity (°SH)	7.00	12.30	8.96	1.27
Fat content (%)	2.50	4.80	3.84	0.44
Protein content (%)	2.47	4.10	3.18	0.26
Dry matter (%)	11.29	13.42	12.43	0.42
Ash content (%)	0.50	1.12	0.85	0.13
TAMB (log cfu/ml)	4.72	8.15	6.68	1.19
Yeast and Mold (log cfu/ml)	2.81	6.14	4.64	1.11
Micrococcus/Staphylococcus (log cfu/ml)	3.05	6.24	4.79	0.78
Coliform (log cfu/ml)	3.21	6.09	4.73	0.96

TABLE 3

Means (±std error) of titratable acidity (°SH), fat, protein, dry matter, and ash content (%) of milk, and the total counts of aerobic mesophilic bacteria, yeast-mold, micrococcus/staphylococcus, and total coliforms (log cfu/ml) 1

	N	°SH	Fat	Protein	Dry Matter	Ash	TAMB	YM	MS	Coliform
Temperature-Humidity Index										
1	26	7.59±0.11^{d}	3.83±0.09	3.26±0.05^{a}	12.32±0.08	0.80±0.02^{b}	4.81±0.01^{d}	2.89±0.01^{d}	3.11±0.02^{d}	3.45±0.02^{d}
2	45	8.12±0.09^{c}	3.96±0.07	3.28±0.04^{a}	12.58±0.06	0.83±0.02^{b}	5.93±0.01^{c}	3.95±0.01^{c}	4.05±0.02^{c}	3.97±0.01^{c}
3	36	8.86±0.10^{b}	3.79±0.07	3.15±0.04^{ab}	12.38±0.07	0.84±0.02^{b}	7.03±0.01^{b}	4.93±0.01^{b}	5.01±0.02^{b}	4.95±0.01^{b}
4	49	10.53±0.08^{a}	3.78±0.06	3.08±0.04^{b}	12.37±0.06	0.92±0.02^{a}	8.10±0.01^{a}	5.98±0.01^{a}	6.20±0.02^{a}	5.95±0.01^{a}
P		***	n.s.	***	*	***	***	***	***	***
Sampling Period										
Q1	38	7.85±0.10^{c}	3.93±0.07	3.23±0.04^{ab}	12.44±0.07	0.79±0.02^{b}	5.42±0.11^{d}	3.47±0.10^{d}	3.62±0.10^{d}	3.73±0.08^{d}
Q2	39	9.20±0.10^{b}	3.89±0.07	3.11±0.04^{b}	12.45±0.07	0.86±0.02^{ab}	7.22±0.10^{b}	5.11±0.10^{b}	5.29±0.10^{b}	5.11±0.08^{b}
Q3	40	10.62±0.10^{a}	3.78±0.07	3.11±0.04^{b}	12.41±0.07	0.92±0.02^{a}	7.98±0.10^{a}	5.87±0.10^{a}	6.07±0.10^{a}	5.84±0.08^{a}
Q4	39	8.09±0.10^{c}	3.77±0.07	3.29±0.04^{a}	12.39±0.07	0.84±0.02b	6.04±0.10^{c}	4.04±0.10^{c}	4.12±0.10^{c}	4.18±0.08^{c}
P		***	n.s.	**	n.s.	***	***	***	***	***
Year										
2011	52	9.12±0.18	3.84±0.06	3.17±0.04	12.47±0.06	0.89±0.02^{a}	6.61±0.17	4.56±0.16	4.74±0.16	4.65±0.13
2012	52	8.98±0.18	3.94±0.06	3.14±0.04	12.45±0.06	0.81±0.02^{b}	6.74±0.17	4.72±0.16	4.87±0.16	4.81±0.13
2013	52	8.78±0.18	3.75±0.06	3.24±0.04	12.35±0.06	0.86±0.02^{ab}	6.68±0.17	4.64±0.16	4.76±0.16	4.73±0.13
P		n.s.	n.s.	n.s.	n.s.	*	n.s.	n.s.	n.s.	n.s.

1.TAMB: Total aerobic mesophilic bacteria; YM: Yeast&Mold; MS: Micrococcus/Staphylococcus; THI: Temperature-Humidity Index,

1: THI<50, 2: 50≥THI<60, 3: 60≥THI<70, 4: THI≥70; Q1: January-March, Q2: April-June, Q3: July-September, Q4: October-December,N: Number of sample, n.s.: P>0.05, *: P≤0.05, **: P≤0.01, ***: P≤0.001; a,b,c,d: The difference among the means indicated by different letters on the same column is significant (P≤0.05

It was concluded that the effect of THI on milk titratable acidity (°SH), protein, ash content; TAMB, yeast-mold, micrococcus/staphylococcus, and coliform counts was significant at the level of P≤0.001, the effect of THI on the dry matter content of milk was significant at the level of P≤0.05. Titratable acidity, ash content, TAMB, yeast and mold, micrococcus/staphylococcus, and coliform counts were found to be minimal when THI<50, while they reached maximum values when THI≥70 (Table 3). As shown in Table 3, when THI≥70, the fat and protein content of milk decreases by 1.3% and 5.5%, respectively, compared to THI<50.

The effect of sampling period on milk titratable acidity (°SH), ash content, TAMB, yeast and mold, micrococcus/staphylococcus, and coliform counts was found to be significant at the level of P≤0.001; the effect of sampling period on milk protein content was found to be significant at P≤0.01 (Table 3). It is noting that the titratable acidity of milk, ash content, TAMB, yeast and mold, micrococcus/ staphylococcus, and coliform counts are the maximum in July-September and the minimum in January-March. The protein content of milk reached the maximum value in the October-December period (Table 3).

It was found that the effect of the year on the ash content of milk was significant at the level of P≤0.05 (Table 3). It is observed that the ash content of milk was at a maximum level in 2011 and a minimum level in 2012 (Table 3). It was determined that the effect of the year on titratable acidity, fat, protein, and dry content of milk, TAMB, yeast and mold, micrococcus/staphylococcus, and coliform counts was not significant (P>0.05) (Table 3).

TABLE 4
Number and rate of positive samples for Listeria spp. and Salmonella spp. according to the temperature-humidity index, sampling period, and year 1

		THI				Sampling Period				Year			Total
		1	2	3	4	Q1	Q2	Q3	Q4	2011	2012	2013	N=156
		N=26	N=45	N=36	N=49	N=38	N=39	N=40	N=39	N=52	N=52	N=52	
Listeria spp.	n	8	15	3	5	7	4	4	16	9	12	10	31
	%	30.77	33.33	8.33	10.20	18.42	10.26	10.00	41.03	17.31	23.08	19.23	19.87
Salmonella spp.	n	4	7	8	9	4	6	12	6	11	9	8	28
	%	15.38	15.56	22.22	18.37	10.53	15.38	30.00	15.38	21.15	17.31	15.38	17.95

1 THI: Temperature-Humidity Index, 1: THI<50, 2: 50≥THI<60, 3: 60≥THI<70, 4: THI≥70; Q1: January-March, Q2: April-June, Q3: July-September, Q4: October-December, N: Number of sample, n: Number of positive sample, %: Positive sample rate

TABLE 5
Correlation coefficients, and levels of significance 1

	°SH	F	Pr	DM	Ash	TAMB	YM	MS	C
THI	0.867***	-0.095n.s.	-0.301***	-0,066n.s.	0,316***	0,999***	0,999***	0,993***	0,988***
Sampling Period	0.187*	-0.152n.s.	0.080n.s.	-0,051n.s.	0,161*	0,242**	0,242**	0,221**	0,238**
Year	-0.109n.s.	-0.076n.s.	0.114n.s.	-0,112n.s.	-0,088n.s.	0,026n.s.	0,028n.s.	0,008n.s.	0,030n.s.
°SH		-0.121n.s.	-0.231**	-0,052n.s.	0,322***	0,867***	0,871***	0,883***	0,885***
F			-0.036n.s.	0.781***	-0.251**	-0.095n.s.	-0.091n.s.	-0.089n.s.	-0.108n.s.
Pr				0.384***	-0.150n.s.	-0.302***	-0.302***	-0.317***	-0.313***
DM					-0.042n.s.	-0.064n.s.	-0.060n.s.	-0.075n.s.	-0.092n.s.
Ash						0.312***	0.311***	0.310***	0.313***
TAMB							0.992***	0.993***	0.988***
YM								0.993***	0.988***
MS									0.988***

1 THI: Temperature-Humidity Index, °SH: Titratable acidity (Soxhelet Henkel), F: Fat content, Pr: Protein content, DM: Dry matter, TAMB: Total aerobic mesophilic bacteria, YM: Yeast&Mould, MS: Micrococcus/Staphylococcus, C: Total coliform; n.s.: P>0,05, *: P≤0.05, **: P≤0.01,***: P≤0.001

Among all examined samples, the number of positive samples for Listeria spp. and Salmonella spp. was determined as 31 (19.87%) and 28 (17.95%), respectively. When examined by years, it is seen that the number of positive samples for Listeria spp. and Salmonella spp. was maximum in 2012 (23.1%) and 2011 (21.2%), respectively (Table 4). 50≥THI <60 ranks first with 15 (33.3%) Listeria spp. positive samples, 60≥THI <70 ranks last with 5 (10.2%) positive samples. The number of positive samples for Salmonella spp. was 4 (15.38%) when THI <50, 7 (15.56%) when 50≥THI <60, 8 (22.22%) when 60≥THI <70 9 when THI≥70 9 (18.37%). It is seen that the number of positive samples for Listeria spp. was 16 (41%) between October-December, 7 (18.42%) in January-March, 4 (10%) in April-June and July-September (Table 4). It is stated in Table 4 that the number of positive samples for Salmonella spp. was 12 (30%) in the July-September period, 6 (15.38%) in March-May and October-December periods, and 4 (10.53%) in the January-March period.

Table 5 shows that the correlation between THI and milk's titratable acidity (°SH), ash content, TAMB, yeast and mold, micrococcus/staphylococcus, and coliform counts was positive (P≤0.001) and the correlation between THI and milk's fat, protein, and dry matter content was negative. It was found that the correlation between THI and fat, dry matter content was insignificant (P> 0.05), and the correlation between protein content and THI was significant at P≤0.001 (Table 5). A positive correlation was found between the sampling periods and the titratable acidity (°SH), protein content, ash content, TAMB, yeast and mold, micrococcus/staphylococcus, and coliform counts of milk; and a negative but insignificant (P>0.05) correlation was found between the sampling period and the fat and dry matter content of milk (Table 5). A negative correlation (P≤0.001) was observed between the titratable acidity of milk and the fat, protein, and dry matter content of milk; and a positive correlation was observed between the titratable acidity and the ash content, TAMB, yeast and mold, micrococcus/staphylococcus and coliform counts (Table 5). A positive (P≤0.001) correlation was found between the fat content of milk and the dry matter content and a negative (P≤0.01) correlation was found between the fat content and ash content (Table 5). In Table 5, there was a positive (P≤0.001) correlation between the protein content of milk and the dry matter content, and a negative (P≤0.001) correlation between the TAMB, yeast and mold, micrococcus/staphylococcus, and coliform counts. The correlation between the ash content of milk and the TAMB, yeast and mold, micrococci/staphylococcus, and coliform counts was found to be positive (P≤0.001) (Table 5).

DISCUSSION AND CONCLUSIONS

In this study, which investigated the effect of heat stress on the chemical and microbiological quality of bulk tank milk, THI was divided into four groups and the fourth group is THI≥70. In previous studies, it was stated that the threshold value is THI≥72 to determine the heat stress that causes a negative effect on dairy cattle. When the THI data for this study were examined, it was observed that the minimum-maximum THI values and the number of days with THI≥70 and THI≥72 were 70.91-77.43, 16 and 15 days in 2011, and 71.41-79.26, 17 and 16 days in 2012, and 70.13-76.50, 16 and 11 days in 2013, respectively. According to these data, it was considered appropriate to determine the threshold value for heat stress as THI≥70. Bryant et al. [17] reported that Holstein-Friesian (HF) cattle are more susceptible to increasing environmental temperature than New Zealand Jersey (NZJ) cattle and that the temperature-humidity index thresholds for the change of milk composition in Holstein-Freisian, HFxNZJ hybrid, and NZJ breeds are 68, 69 and 75, respectively. In studies on milk yield and the number of somatic cells of individual animals, which are planned to be carried out later, the threshold value for heat stress is recommended to be considered THI≥65, as stated by Zimbelman and Collier [18], Brügeman et al. [19] and Herbut et al. [20].

Brügeman et al. [30] indicated that the decrease in daily protein yield is associated with an increase in THI. Bertocchi et al. [31] investigated the relationship between the seasonal variation of milk composition and THI in Holstein cows between 2003 and 2009 and concluded that the fat content of milk was the maximum in winter and minimum in summer, the protein content was the maximum in autumn and the minimum in summer. Lambertz et al. [32] reported that the relationship between the increase in the temperature-humidity index and the decrease in milk fat content was significant. Hagiya et al. (2017) [33] found that heat stress was associated with milk composition, the number of somatic cells in milk, and the incidence of mastitis. In a study conducted in Holstein-Friesian cattle, it was shown that there was a negative relationship between the temperature-humidity index and the fat content of milk, and milk fat decreased by 0.17% as a result of increasing the temperature-humidity index. In a study in which milk of Holstein and Simmental breeds were compared in terms of fat and protein content, it was reported that fat and protein content in both breeds decreased when the temperature-humidity index value was in the range of 66-80 [35]. A study conducted by Maggiolino et al. (2020) [36] found that the fat content of milk in dairy cows belonging to the Italian Brown Swiss breed was not affected by heat stress, the amount of fat was affected by heat stress in the first, second and third lactations but not affected by heat

stress in the fourth lactation and that the protein content was negatively affected by heat stress. It seems that the results of this study on the content of milk are consistent with the literature data. It is thought that the reduction in milk's fat and protein content due to heat stress may be due to reduced animal feed consumption, the consumption of extra energy to balance body temperature. It is also thought that changes in the animal's endocrine system due to heat stress can cause changes in the composition of milk.

Due to its complex biochemical structure and high water capacity, milk forms a suitable nutrient environment for various saprophytes and pathogenic microorganisms. In this study, TAMB, yeast and mold, micrococcus/staphylococcus, and coliform counts are seen to be maximum in the period of July-September and minimum in the January-March period. Any study that determined the effect of heat stress on the microorganism quantities in milk was not found. For this reason, the results of the studies on the effect of season on the microbiological quality of milk were compared with the results of this study.

Souto et al. [37] investigated the relationship between the presence of pathogens that cause mastitis in dairy cows and the hygienic quality of raw milk and reported a positive correlation between the TAMB, yeast and mold content of raw milk of dairy cows and the presence of Staphylococcus. Bertocci et al. [31] concluded that the total count of bacteria in milk is the maximum in summer and the minimum in winter. Bogdanovicova et al. [38] found that the total count of bacteria in raw milk in the Czech Republic was the maximum in autumn; the minimum in winter, the presence of S. aureus was the maximum in winter and the minimum in spring. Ferdous et al. [39] studied the microbiological characteristics of raw milk in Morocco, reporting that the count of TAMB is maximum in spring, minimum in summer; the count of molds was maximum in spring, minimum in winter; the count of coliforms was maximum in autumn, minimum in summer; the count of S. aureus was maximum in summer, minimum in spring. Smith et al. [12] concluded that heat stress causes an increase in the count of somatic cells in the Holstein and Jersey cows. Vitali et al. [40] reported that the risk of clinical mastitis was high in summer, especially in July, while the incidence of mastitis was maximum when THI>79, and minimum when THI<70.

Titratable acidity above 8.89 in SH is considered to indicate an excess of microbial development in milk [41]. In this study, it was found that the correlation between TAMB, yeast and mold, micrococcus/staphylococcus, and coliform count of milk was positive. In addition, a positive correlation between the ash content of milk and the count of micrococcus/staphylococcus reveals the possibility of a mastitis infection. A high number of yeast and mold can be associated with non-hygienic milking and delivery to the collection center without following the necessary preservation and hygiene rules.

Kalorey et al. [42] reported that the presence of Listeria spp. and L. monocytogenes in raw milk in India was 6.75% and 5.10%, respectively, and the presence of L. monocytogenes in spring, summer, autumn, and winter was 3.76%, 5.28%, 7.96%, and 4.17%, respectively.

Bouymajane et al. [43] found that the presence of L. monocytogenes was 19.44 (7/36) in loose milk in Morocco and that there was more L. monocytogenes in winter and spring than in summer and autumn. In this study, the presence of Listeria spp. was found to be 18.42%, 10.26%, 10%, and 41.03% in January-March, April-June, July-September, October-December, respectively. The reason for the high presence of Listeria spp. is thought to be the year-round feeding of dairy cows with silage. Sharifzade et al. [44] investigated the presence of L. monocytogenes in silages in Iran, reported that rainy and humid weather conditions affected the presence of L. monocytogenes of silage and that L. monocytogenes was not observed in the milk of animals that did not feed on silage. The study investigating the presence of L. monocytogenes in corn silage, feces, and tank milk in dairy cow enterprises found that the presence of Listeria spp. was 18%, 14%, and 11%, respectively, and that Listeria spp. can easily pass from the cow's gastrointestinal tract to milk [45].

Almashhadany and Osman [46] investigated the presence of Salmonella spp. in raw milk sold in Iraq, isolating Salmonella spp. with the rate of 4.76% and 16.13% respectively in January-March and April-June, and they reported that Salmonella spp. presence was the most in June (23.81%). In this study, the presence of Salmonella spp. was 15.38 (6/39) in the period of April-June and 30% (12/40) in the period of July-September. Pangloli et al [47] investigated the seasonal change of Salmonella spp. presence in dairy cows, calves, and farms, reporting that the presence of Salmonella spp. in tank milk was 6%, 17%, 29%, and 7% in January-March, April-June, July-September, and October-December, respectively. The high presence of Salmonella spp. in summer was associated with cross-contamination from the environment; it was also determined that the presence of Salmonella spp. in the milking unit, bird droppings, and insects were at the maximum level in summer [47].

There are some handicaps in comparing the results of this study, which investigated the effect of heat stress on the chemical and microbiological quality of bulk tank milk, with the results of previous studies. The effect of heat stress on milk yield was investigated in many studies, and the effect of heat stress on milk composition was the subject of a small number of studies. No studies have been found on the effect of heat stress on the microbiological quality of milk. As a result, the correlation between heat stress and protein content of milk was negative, and the correlation between heat stress and ash content,

TAMB, yeast and mold, micrococcus/staphylococcus, and coliform count of milk was positive. From the point of view of dairy technology, the protein content of milk and the microbiological quality of milk are very important, therefore, various measures should be taken to prevent milk cows from being affected by heat stress. In places with hot and humid climates, so that the non-sanitary climates do not affect the climate conditions inside the shelter, it is recommended to provide shading areas in shelters, no walls in the shelters, and a fan and ventilation system to ensure that the animals are cooled in the shelter. Since the feeding habits of the animals will change due to heat stress, it is advised to prepare rations containing high-quality roughage that meet the energy and protein needs of the animals, to feed frequently and during cool hours of the day, to provide cool and clean water that the animals can easily access, and to add water to the feed if necessary.

ACKNOWLEDGEMENTS

The author thanks the General Directorate of Meteorology of the Ministry of Agriculture and Forestry of the Republic of Turkey for meteorological data.

REFERENCES

[1] Moss, A.R., Jounany, J.P. and Neevbold, J. (2000). Methane production by ruminants: Its contribution to global warming. Ann. Zootech. 49, 231-253.

[2] Harvell, C.D., Mitchell, C.E., Ward, J.R., Altizer, S., Dobson, A.P. and Ostfeld, R.S. (2002). Climate warming and disease risks for terrestrial and marine biota. Science. 296 (5576), 2158-2162.

[3] Thorne, P.S. (2007). Environmental health impacts of concentrated animal feeding operations: anticipating hazards-searching for solutions. Environ. Health Perspect. 115, 296-297.

[4] Tirado, M.C., Clarke, R., Jaykus, L.A., McQuatters-Gollop, A. and Frank, J.M. (2010). Climate change and food safety: A review. Food Research International. 43(7), 1745-1765.

[5] West, J.W. (2003). Effects of heat-stress on production in dairy cattle. J. Dairy Sci. 86, 2131–2144.

[6] Dikmen, S. and Hansen, P.J. (2009). Is the temperature-humidity index the best indicator of heat stress in lactating dairy cows in a subtropical environment? J. Dairy Sci. 92, 109–116.

[7] Rhodas, M.L., Rhodas, R.P., Van Baale, M.J., Collier, R.J., Sanders, S.R., Weber, W.J. and Crooker, B.A. (2009). Effects of heat stress and plane of nutrition on lactating Holstein cows: I. Production, metabolism, and aspects of circulating somatotropin. J. Dairy Sci. 92, 1986-1997.

[8] Akyuz, A., Boyacı, S. and Cayli, A. (2010). Determination of critical period for dairy cows using temperature humidity index. J. Anim. & Veterinary Advances. 9(13), 1824-1827.

[9] Vermunt, J.J. and Tranter, B.P. (2011). Heat stress in dairy cattle–a review, and some of the potential risks associated with the nutritional management of this condition. In review of AVA QLD Division Conference 25-27/3/10 Australian Veterinary Association. (212-221).

[10] Wheelock, J.B., Rhoads, R.P., Van Baale, M.J., Sanders, S.R. and Baumgard, L.H. (2010). Effects of heat stress on energetic metabolism in lactating Holstein cows. J. Dairy Sci. 93, 644–655.

[11] Tao, S., Bubolz, J.W., Amaral, B.C., Thompson, M., Hayen, M.J., Johnson, S.E. and Dahl, G.E. (2011). Effect of heat stress during the dry period on mammary gland development. J. Dairy Sci. 94, 5976–5986.

[12] Smith, D.L., Smith, T., Rude, B.J. and Ward, S.H. (2013). Short communication: Comparison of the effects of heat stress on milk and component yields and somatic cell score in Holstein and Jersey cows. J. Dairy Sci. 96(5), 3028-3033.

[13] Berry, I.L., Shanklin, M.D. and Johnson, H.D. (1964). Dairy shelter design based on milk production decline as affected by temperature and humidity. Trans. Am. Soc. Ag. Eng. 7, 329–331.

[14] Bohmanova, J., Misztal, I. and Cole, J.B. (2007). Temperature-humidity indices as indicators of milk production losses due to heat stres. J. Dairy Sci. 90, 1947–1956.

[15] Gaughan, J.B., Mader, T.L., Holt, S.M. and Lisle, A. (2008). A new heat load index for feedlot cattle. J. Anim. Sci. 86, 226–234.

[16] Bouraoui, R., Lahmar, M., Majdoub, A., Djemali, M. and Belyea, R. (2002). The relationship of temperature-humidity index with milk production of dairy cows in a Mediterranean climate. Anim. Res. 51, 479–491.

[17] Bryant, J.R., López-Villalobos, N., Pryce, J.E., Holmes, C.W. and Johnson, D.L. (2007). Quantifying the effect of thermal environment on production traits in three breeds of dairy cattle in New Zealand. New Zealand Journal of Agricultural Research. 50, 327–338.

[18] Zimbelman, R.B. and Collier, R.J. (2011). Feeding strategies for high producing dairy cows during periods of elevated heat and humidity. Tri-State Dairy Nutrition Conference, Fort Wayne. ID. 111-125.

[19] Brügemann, K., Gernand, E., von Borstel, U.K. and Konig, S. (2012). Defining and evaluating heat stress thresholds in different dairy cow production systems. Arch. Anim. Breed. 55, 13–24.
[20] Herbut, P., Bieda, W. and Angrecka, S. (2015). Influence of hygrothermal conditions on milk production in a free stall barn during hot weather. Anim. Sci. Pap. Rep. 33, 49–58.
[21] Association of Official Analytical Chemists (AOAC) (1980). Acidity in cheese. Official Methods of Analysis. AOAC, Washington, 266 p.
[22] IDF (1964). Determination of the ash content of processed cheese products. International Dairy Federation, Brussels, Belgium (IDF Standard 27).
[23] IDF (1987). Milk, cream and evaporated milk. Determination of total solids content. International Dairy Federation, Brussels, Belgium (IDF Standard 21B).
[24] IDF (1996). Milk. Determination of fat content. International Dairy Federation, Brussels, Belgium (IDF Standard 1D).
[25] IDF (1993). Milk. Total nitrogen content (Kjeldahl method). International Dairy Federation, Brussels, Belgium (IDF Standard 20B).
[26] Çardak, A.D. and Yılmaz, M. (2011). Survey of the bacteriological quality of dairy products in the province of Aydin, Turkey. Milchwissenschaft-Milk Science International. 66(3), 304.
[27] Halkman, K. (2005). Analysis methods of microorganism. In: Food microbiology applications, Ankara, 89-124. (in Turkish)
[28] Çardak, A.D. (2013). Gross composition and the presence of *Listeria monocytogenes* and *Salmonella* spp. in raw milk and dairy products in Aydin, Turkey. Journal of Food Agriculture & Environment. 11(3&4), 55-62.
[29] Mader, T.L., Davis, M.S. and Brown-Brandl, T. (2006). Environmental factors influencing heat stress in feedlot cattle. J. Anim. Sci. 84, 712-719.
[30] Brügemann, K., Gernand, E., von Borstel, U.U. and König, S. (2011). Genetic analyses of protein yield in dairy cows applying random regression models with time-dependent and temperature x humidity-dependent covariates. J. Dairy Sci. 94, 4129–4139.
[31] Bertocchi, L., Vitali, A., Lacetera, N., Nardone, A., Varisco, G. and Bernabucci, U. (2014). Seasonal variations in the composition of Holstein cow's milk and temperature–humidity index relationship. Animal. 8(4), 667–674.
[32] Lambertz, C., Sanker, C. and Gauly, M. (2014). Climatic effects on milk production traits and somatic cell score in lactating Holstein-Friesian cows in different housing systems. J. Dairy Sci. 97(1), 319-329.
[33] Hagiya, K., Hayasaka, K., Yamazaki, T., Shirai, T., Osawa, T., Terawaki, Y. and Suzuki, M. (2017). Effects of heat stress on production, somatic cell score and conception rate in Holsteins. Animal Science Journal. 88(1), 3-10.
[34] Nasr, M.A. and El-Tarabany, M.S. (2017). Impact of three THI levels on somatic cell count, milk yield and composition of multiparous Holstein cows in a subtropical region. Journal of Thermal Biology. 64, 73-77.
[35] Gantner, V., Bobić, T., Gregić, M., Gantner, R., Kuterovac, K., and Potočnik, K. (2017). The differences in heat stress resistance due to dairy cattle breed. Mljekarstvo. 67(2), 112-122.
[36] Maggiolino, A., Dahl, G.E., Bartolomeo, N., Bernabucci, U., Vitali, A., Serio, G., Cassandro, M., Centoducati, G., Santus, E. and De Palo, P. (2020). Estimation of maximum thermo-hygrometric index thresholds affecting milk production in Italian Brown Swiss cattle. J. Dairy Sci. 103 (in press)
[37] Souto, L.I., Minagawa, C.Y., Telles, E.O., Garbuglio, M.A., Amaku, M., Dias, R.A. and Benites, N.R. (2008). Relationship between occurrence of mastitis pathogens in dairy cattle herds and raw-milk indicators of hygienic-sanitary quality. The Journal of Dairy Research. 75(1), 121-127.
[38] Bogdanovičová, K., Vyletělová-Klimešová, M., Babák, V., Kalhotka, L., Koláčková, I. and Karpíšková, R. (2016). Microbiological quality of raw milk in the Czech Republic. Czech J. Food Sci. 34(3), 189–196.
[39] Ferdous, N., Hnini, R., Merzouki, M., Bahi, L., Chigr, F. and Najimi, M. (2017). Microbiological characteristics of raw cow milk in Beni Mellal Area (Morocco). International Journal of Science and Engineering Applications. 6(10), 344-349.
[40] Vitali, A., Bernabucci, U., Nardone A. and Lacetera, N. (2106). Effect of season, month and temperature humidity index on the occurrence of clinical mastitis in dairy heifers. Advances in Animal Biosciences. 7(3), 250–252.
[41] Kesenkaş, H. and Akbulut, N. (2010). Determination of characteristics of street milk sold in İzmir province and milk produced in medium and large scale farms. Journal of Agricultural Faculty Aegean University. 47(2), 161-169. (in Turkish)
[42] Kalorey, D.R., Warke, S.R., Kurkure, N.V., Rawool, D.B. and Barbuddhe S.B. (2008). Listeria species in bovine raw milk: A large survey of Central India. Food Control. 19, 109–112

[43] Bouymajane, A., Filali, F.R., Benhallam, F., Eddra, A., El Allaoui, A., Chaiba, A., Aboulkacem, A. and Hou, M.A. (2019) Quantitative and qualitative microbial diversity of the raw cow's milk sold by street trading in Meknes, Morocco. Malaysian Journal of Microbiology. 15(6), 425-431.
[44] Sharifzadeh, A., Momeni, H., Ghasemi-Dehkordi, P. and Doosti, A. (2015). Presence of Listeria monocytogenes in silage products of Shahrekord city. Asian Pacific Journal of Tropical Disease. 5(Suppl. 1), S133-S136.
[45] Aydın, R., Gökmen, M., Kara, R., Önen, A. and Ektik, N. (2019). The prevalence and molecular characterization of Listeria monocytogenes in corn silage, feces and bulk tank milk samples in dairy cattle farms in Balıkesir, Turkey. Israel Journal of Veterinary Medicine. 74 (4), 184-189.
[46] Almashhadany, D.A. and Osman, A.A. (2019). Isolation, serotyping, and antibiogram of Salmonella isolates from raw milk sold at retail vending in Erbil City, Iraq. Bulletin of University of Agricultural Sciences and Veterinary Medicine Cluj-Napoca Animal Science and Biotechnologies. 76(2), 116-122.
[47] Pangloli, P., Dje, Y., Ahmed, O., Doane, C.A., Oliver, S.P. and Draughon, F.A. (2008). Seasonal incidence and molecular characterization of Salmonella from dairy cows, calves, and farm environment. Foodborne Pathogens and Disease. 5(1), 87-96.

Received: **04.01.2021**
Accepted: **10.02.2021**

CORRESPONDING AUTHOR

Ayse Deniz Cardak
Faculty of Agriculture,
Department of Dairy Science and Technology
Aydin Adnan Menderes University,
09100 Aydin – Turkey

e-mail: adenizcardak@yahoo.de

© by PSP Volume 30– No. 05/2021 pages 5476-5485 Fresenius Environmental Bulletin

POPULATION FLUCTUATIONS OF THE PISTACHIO TWIG BORER, *KERMANIA PISTACIELLA* AMSEL AND ITS PARASITOIDS

Cevdet Kaplan*, Mustafa Cemal Ciftci

Siirt University, Faculty of Agriculture, Department of Plant Protection, 56220, City Center, Siirt, Turkey

ABSTRACT

This study was conducted in Siirt, Turkey in 2016-2017 to determine the distribution, population fluctuations, and parasitoids of the pistachio twig borer, *Kermania pistaciella* Amsel, 1964 (Lepidoptera: Oinophilidae). The population fluctuations of *K. pistaciella* were monitored by pheromone traps in four orchards. The distribution and the identification of its parasitoids were performed by visual examination in a total of 66 orchards and by rearing in the laboratory. Parasitoids were obtained from *K. pistaciella* pupae kept in boxes at room conditions. *Kermania pistaciella* males were started to be caught by pheromone traps on April 8 and April 12 in the first and second years, respectively. The adult flight continued until May 16 in the first year and June 4 in the second year. The peak of the adults caught by traps occurred on April 25-29 in the first year, and on April 26-May 4 in the second year, respectively. Three parasitoid species were identified from the pupae of *K. pistaciella*, including *Centistidea* (*Paracentistidae*) *pistaciella* van Achterber & Mehrnejad, 2002 (Hymenoptera: Braconidae), *Chelonus chetini* Beyarslan & Şahan, 2019 (Hymenoptera: Braconidae), and *Gelis areator* (Panzer, 1804) (Hymenoptera: Ichneumonidae). *Centistidea pistaciella* parasitoid species is the first records of *K. pistaciella* parasitoid in Turkey.

KEYWORDS:
Kermania pistaciella, parasitoid, pheromone trap, pistachio, population fluctuations

INTRODUCTION

Pistachio (*Pistacia vera*, L) is one of the agricultural products that provide significant added value to the Turkish economy. Pistachio is in great demand as a snack and in the baklava industry and has a significant economic return in domestic and foreign markets. While almost all of the pistachios produced in Turkey are consumed in the domestic market, a very little part of them is exported. Pistachio provides important nutrients for human life, including linoleic fatty acids [1]. Since pistachio is a valuable fruit, it is also known as the "Golden Tree," "Fruit of Kings," and "Green Gold" among the people.

The main countries producing pistachio in the world are Iran, the USA, Turkey, and Syria. Of the pistachio production in the world, 90% is carried out in these countries. The pistachio production in Turkey was approximately 240,000 tons in 2018. Approximately 17% of the world's production of pistachios is realized in Turkey [2]. Due to its special climatic requirements, pistachios are mostly grown in the provinces of the Southeastern Anatolia region in Turkey. The pistachio production of Siirt province varies by years, is around 15-20 thousand tons and meets approximately 12-15% of the production in Turkey. The Siirt pistachio variety is grown in Siirt province. Since the Siirt pistachio variety is large, its shell split clearance is large, and its shell is white, it has a good buyer audience as a snack in both domestic and foreign markets.

There are many pest species that cause yield and quality loss in pistachio orchards. One of the common and intense species among these pest species is the pistachio twig borer, *Kermania pistaciella* Amsel, 1964 (Lepidoptera: Oinophilidae). It is one of the common pests with a high infestation rate in the Southeastern Anatolia Region in Turkey, where pistachio is cultivated [3; 4; 5; 6; 7]. Mehrnejad [8] stated that *K. pistaciella* is among the main pests of pistachio in Iran.

Kermania pistaciella adult moths emerge at the beginning of April. They usually lay their eggs on the ends of new shoots or fruit branches. The hatched larvae enter the one- and two-year-old shoot and fruit clusters. The larvae feed on the xylem and pith by making tunnels in shoots and fruit branches. *Kermania pistaciella* has one generation a year and spends the winter in shoots as mature larvae [3; 9; 10]. Since the larvae feed on shoots and fruit branches, it causes the weakening and drying of shoots and branches, fruit and fruit eye drop [3; 11]. The first study on the biology of *K. pistaciella* in Turkey was carried out by Küçükarslan [3] in the pistachio areas in Gaziantep. However, there are many studies on the chemical control and parasitoids of *K. pistaciella* [4; 5; 12; 13; 14].

Insecticides are applied in Iran and Turkey to control the populations of *K. pistaciella*. However, the untimely and unconscious use of insecticides and natural enemies pose a serious threat to it. Therefore, insecticide applications against *K. pistaciella* should be used in the period when pests are intense and active in nature and when parasitoids are less and not active [15;13].

Environmentally friendly practices were needed to reduce the adverse effects caused by the use of chemical insecticides. To this end, the sex pheromone of the pistachio twig borer has been identified and is currently used to monitor the activities of males and to determine the most appropriate insecticide application time [16].

Kermania pistaciella is distributed over a wide area in the Southeastern Anatolia Region in Turkey. The reasons for this are the facts that the biology of the pest is not known sufficiently, cultural precautions against the pest are not taken enough, and the time of chemical control against the pest is not determined correctly [6]. There are some studies conducted up to the present day in Turkey on the biology of *K. pistaciella*, its prevalence, parasitoids and parasitism rate, chemical control and mass trapping [3; 4; 5; 13; 17]. Likewise, studies were conducted in Iran, an important pistachio producer country, on the chemical control of *K. pistaciella*, parasitism rate, parasitoids, population changes, and the best pheromone trap type [15; 18; 19; 20; 10).

In the pest control, knowing the issues, such as the geographical distribution of the species, the habitats of the species, and the determination of the species distribution, in advance helps to manage the species control better [21; 22].

The determination of population changes and the biology of pest species is one of the important parameters in the control of pest species. This non-chemical control time, the release time of natural enemies, the appropriate time for the use of mineral compounds, the time to set up pheromone traps, etc. play an essential role in determining the most appropriate time for the use of chemical pesticides [23]. Recently, pheromones and other insect-attracting devices have been used for the detection of pest species populations, their biology, and the development of a mass trapping method for pest control. These methods are especially required in the control programs of pest species all over the world [24; 25; 26].

The population densities of pests, the periods of their occurrence in nature, their flight periods, and their peak periods vary from region to region. The temperature of the air and relative humidity influence these listed issues. Due to the dams built in Siirt province in recent years, humidity has increased, and changes are also expected in temperature values. It is necessary to investigate the population fluctuations of the pest within the year and the factors affecting this to develop the best method of the control of *K. pistaciella*, which causes significant damage in pistachio orchards in Siirt province of Turkey. There is no sufficient study on the condition of K. pistacella, which is common and intense in pistachio plantations in the Southeastern Anatolia Region, in Siirt province. In this study, the distribution of K. pistaciella, population fluctuations, and larval-pupal parasitoids were determined in the scope of the detection of pests in pistachio areas in Siirt province in 2016-2017 and the determination of the critical periods in the control of important species, and it was attempted to create data in future control programs

MATERIALS AND METHODS

The main material of the study was composed of Siirt pistachio trees and different biological periods (adult, larva, pupa) of the pistachio twig borer, *Kermania pistaciella*. Pheromone traps and laboratory equipment formed other auxiliary materials.

Determination of the distribution area of the pistachio twig borer, *Kermania pistaciella* Observations and investigations were made between 2016-2017 to determine the distribution area of *K. pistaciella*. To this end, surveys and observations were made in a total of 66 orchards in district centers and 24 villages in Siirt Center, Aydınlar, Kurtalan, Eruh, Şirvan, and Pervari districts where pistachio is cultivated. Surveys were carried out at intervals of 2-4 weeks during the whole vegetation period in four regions of each district, in different directions, and in two orchards in each region, selected to characterize that region. Orchards, where disinfection was mostly not performed, were selected as control orchards.

In the sampled orchards, 1-2-year-old shoots and fruit branches of trees were checked by visual inspection based on the study carried out by Grigorov [27] and Karadag et al. [9].

Determination of the population fluctuations of the pistachio twig borer, *Kermania pistaciella* by pheromone traps. The monitoring of the adult population of *K. pistaciella* in delta and Pherocon traps and the determination of the critical periods of control were carried out in 2016-2017 in 4 orchards located in different regions of Siirt (Central district) and of which characteristics are specified in Table 1.

One-two traps were hung in each orchard, and adult emergence was monitored by weekly controls. The traps were hung on a tree in the middle of the orchard, at a height of 1.5-2 m on the southern branch of the tree. Pheromones were changed every 4-6 weeks. The trap plates were changed as they became dirty. The counts in the traps were performed once a week [9]. Pheromone [(0,25 mg. (2-S, 12-Z)-2-acetoxy-12-heptadecene/dispenser] and traps were supplied by Scentomos Research and Development Inc. CANADA

TABLE 1
Orchards, where the population monitoring of *Kermania pistaciella* by pheromone traps was performed in Siirt province (Central district) in 2016-2017 and their characteristics

Place		Variety	Tree		Geographical characteristic
			Age	Number	
Siirt Center	Center plantation1	Siirt	30-35	440	N (37°56'25'') E (41°58'07'') 1000 m
	Center plantation2	Siirt	25-30	320	N (37°56'24'') E (41°58'05'') 1004 m
	Center plantation3	Siirt	25-30	360	N (37°56'16'') E (41°57'58'') 1020 m
	Kezer plantation	Siirt	18-20	200	N(37°57'32'') E (41°50'39'') 615 m

Determination of parasitoids of the pistachio twig borer, *Kermania pistaciella*. In the orchards sampled in February-April, ten trees in each orchard and five 1-2-year-old shoots on each tree were inspected visually. Shoots with pest pupae and larvae damage on them were brought to the laboratory and cultured. In 2016-2017, a total of 120 pest pupae were reared. Shoots with pupae on them were cultured according to the study of Ozgen et al.[13]. The shoots infested with the pest pupae were kept under room conditions in the laboratory. The emerging parasitoids and adult *K. pistaciella* individuals were counted. The parasitoids were identified by the subject experts Dr. Janko KOLAROV (Faculty of Pedagogy, University of Plovdiv, Plovdiv, Bulgaria) and Prof. Dr. Ahmet Beyarsaln (Bitlis Eren University, Faculty of Arts and Science, Department of Biology).

RESULTS

Determination of the distribution area of the pistachio twig borer, *Kermania pistaciella*. In the survey studies conducted between 2016-2017 in the pistachio production areas of Siirt province, K. pistaciella was determined in 66 orchards of Siirt Center, Aydınlar, Kurtalan, Eruh, Şirvan, and Pervari districts and their villages where observations and investigations were performed. K. pistaciella was found to be widespread in all orchards where the Siirt pistachio variety was grown in Siirt province and to be among the most important pests.

Adult population fluctuations of the pistachio twig borer, *Kermania pistaciella*. Adult insects caught in pheromone traps in 2016-2017 in the orchards where the studies were carried out are given in Figure 1-4.

In the orchards observed, the first pupa of the pest was detected on March 9 in the first year and on March 12 in the second year. When the adult population fluctuations of *K. pistaciella* were examined, the adult emergence period of *K. pistaciella* in the first year lasted for approximately 37 days from April 9 to May 16. The highest adult emergence was determined on April 29 in the traps detected in orchards no. 1, 2, and 3 in Siirt Center, respectively (Figure 1). In Siirt Kezer orchard, the adult emergence period started on April 8 in the first year and continued until May 2. The adult flight period lasted for 24 days. The highest adult emergence occurred on April 25 (Figure 2).

In the second year of the study, the adult flight period, first emergence, and peak point were similar in orchards no. 1-3 in Siirt Center. In these orchards, the first adult emergence in pheromone traps occurred on April 21, and the adult flight continued until June 2. The highest adult emergence in 3 orchards was determined on May 4. The adult flight period lasted for 41 days (Figure 3). The first adult emergence in Kezer orchard was determined on April 12, and the last adult flight was determined on May 10. The highest adult emergence occurred on April 26. The adult flight period continued for 28 days in this orchard (Figure 4).

In the orchards where the population fluctuations of *K. pistaciella* were observed, the number of *K. pistaciella* adults caught in traps throughout the year was 1353, 732, 705, and 375 adults, respectively, in the first year in orchards no. 1, 2, 3 in Siirt Center and Kezer orchard, while it was 1033, 422, 237, and 129, respectively, in the second year. The highest number of *K. pistaciella* adults was caught in orchard no. 1 in Siirt Center, and the lowest number was determined in the orchard in Kezer. The number of adults caught in the first year in all orchards was higher compared to the second year (Table 2).

As a result of the study, it was observed that climatic parameters such as temperature and relative humidity (Figure 5) affected the emergence of *K. pistaciella* adults and the flight period. The highest adult emergence occurred at the end of April when the air temperature was 20-25ºC. Since the relative humidity in April in the second year of the study was higher than the relative humidity in the first year and the number of rainy days was higher, the adult emergence occurred later, and the adult flight period was longer. It was observed that the location and altitude where the orchards were located affected adult emergence and duration. Since the orchard in the Kezer location is situated at a lower altitude than the other orchards, the pest's emergence occurred earlier, and the flight period was shorter.

TABLE 2
The total number of adults (adult number/trap/year) of *Kermania pistaciella* caught in sex pheromone traps in 3 orchards in the Central district of Siirt and in the orchard in Kezer during 2016-2017

	Siirt Center Orchard-1	Siirt Center Orchard-2	Siirt Center Orchard-3	Kezer	
Years	Adult number/Trap (Pherocon)	Adult number/Trap (Delta)	Adult number/Trap (Delta)	Adult number/Trap (Delta)	Adult number/Trap (Pherocon)
2016	1353	732	705	375	
2017	1033	422	237	57	201
TOTAL	2386	1154	942	432	201

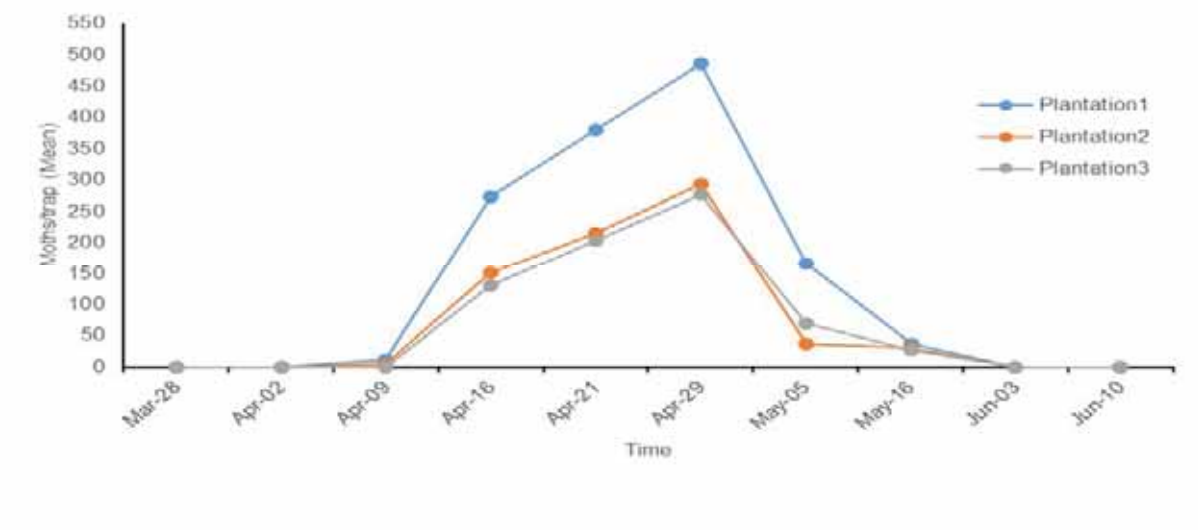

FIGURE 1
Population fluctuations of *Kermania pistaciella* in the pheromone traps in the studied orchards (Siirt Center) in 2016.

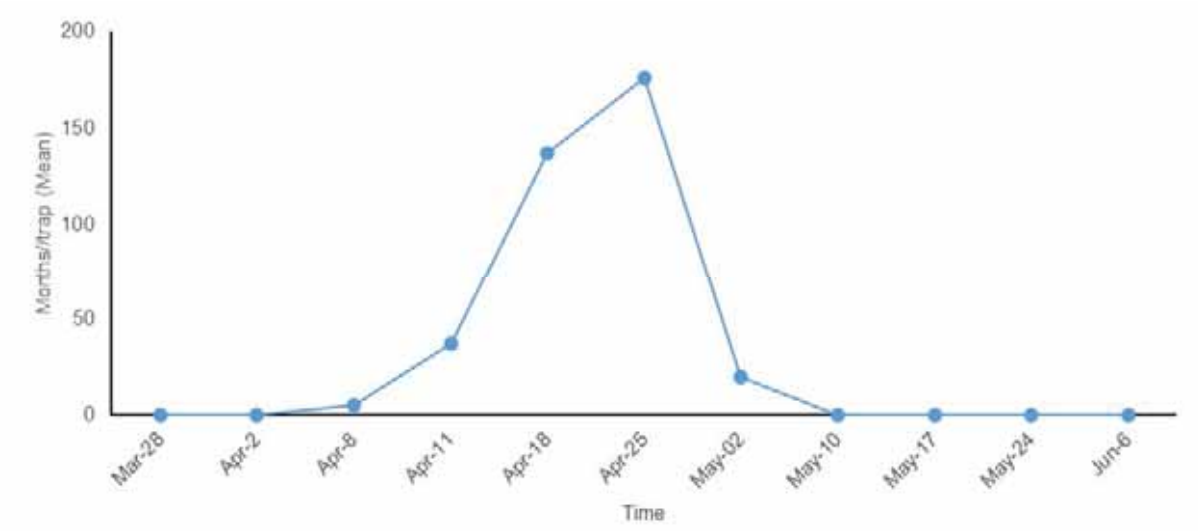

FIGURE 2
Population fluctuations of *Kermania pistaciella* in the pheromone traps in the studied orchard (Siirt Kezer) in 2016.

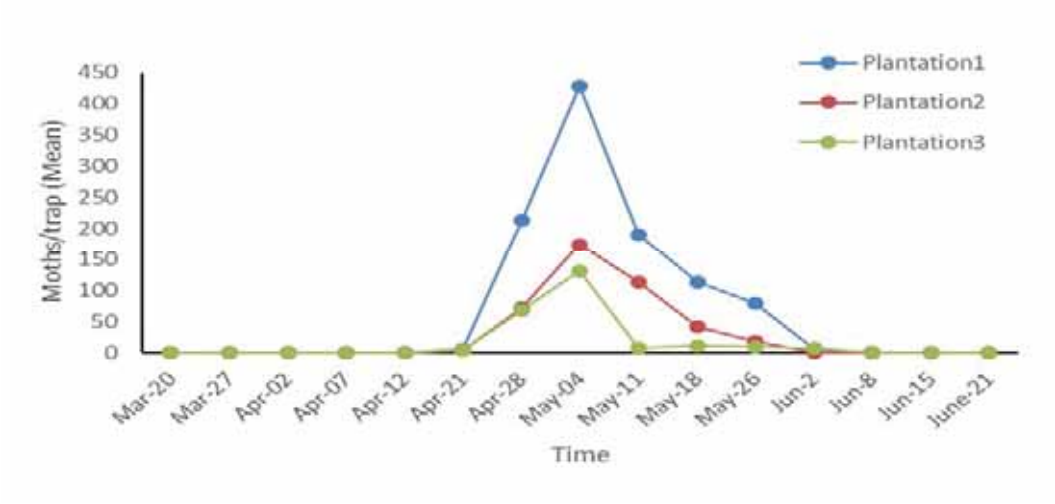

FIGURE 3
Population fluctuations of *Kermania pistaciella* in the pheromone traps in the studied orchards (Siirt Center) in 2017.

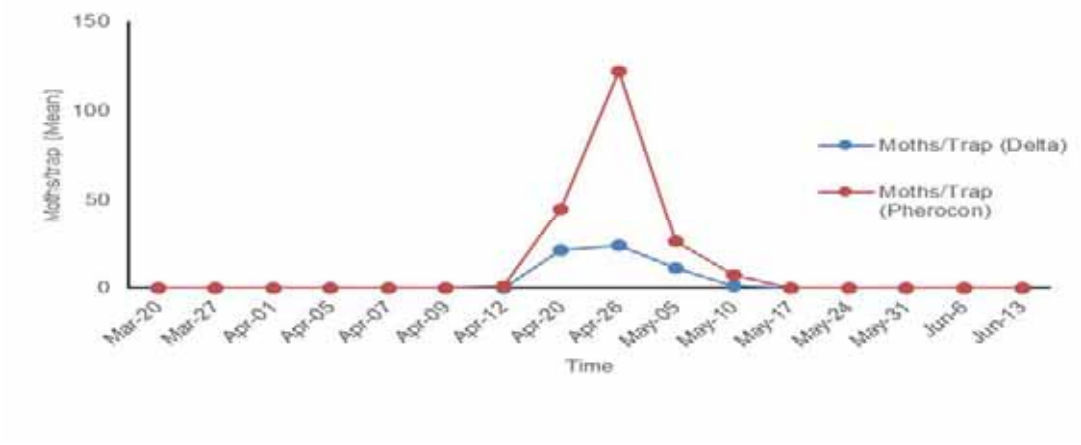

FIGURE 4
Population fluctuations of *Kermania pistaciella* in the pheromone traps in the studied orchard (Siirt Kezer) in 2017.

TABLE 3
Parasitoid species reared from cocoons of *Kermania pistaciella* in pistachio plantation areas of Siirt province, Turkey

Family	species	host	locality
Braconidae	*Centistidea* (*Paracentistidae*) *pistaciella*	*K. pistaciella*	Merkez, Kezer, Eruh- Bayramlı
Braconidae	*Chelonus chetini*	*K. pistaciella*	Merkez, Eruh- Bayramlı
Ichneumonidae	*Gelis areator*	*K. pistaciella*	Eruh, Bayramlı, Siirt Merkez

Identification of parasitoids. As a result of the study, three parasitoid species were identified from the pistachio twig borer pupae cultured (Table 3). The identified parasitoid species are as follows: *Centistidea* (*Paracentistidae*) *pistaciella* van Achterber& Mehrnejad, 2002 (Hymenoptera: Braconidae, Miracinae), *Chelonus chetini* Beyars & Şahan, 2019 (Hymenoptera: Braconidae, Cheloninae), and *Gelis areator* (Panzer, 1804) (Hymenoptera: Ichneumonidae)

***Centistidea* (*Paracentistidae*) *pistaciella* van Achterber& mehrnejad, 2002.** Material examined. Siirt Merkez: 37°56'25"N/ 41°58'07"E, 2.V.2016, 1000 m, 2 ♀♀, 2 ♂♂, Eruh Bayramlı: 37°50'32"N/ 42°07'44"E, 950 m, 30.III.2017, 2 ♀♀, ♂, (Figure 6).

Distribution in Turkey. New record for Turkish fauna

Distribution in World. Iran [12; 19; 28].

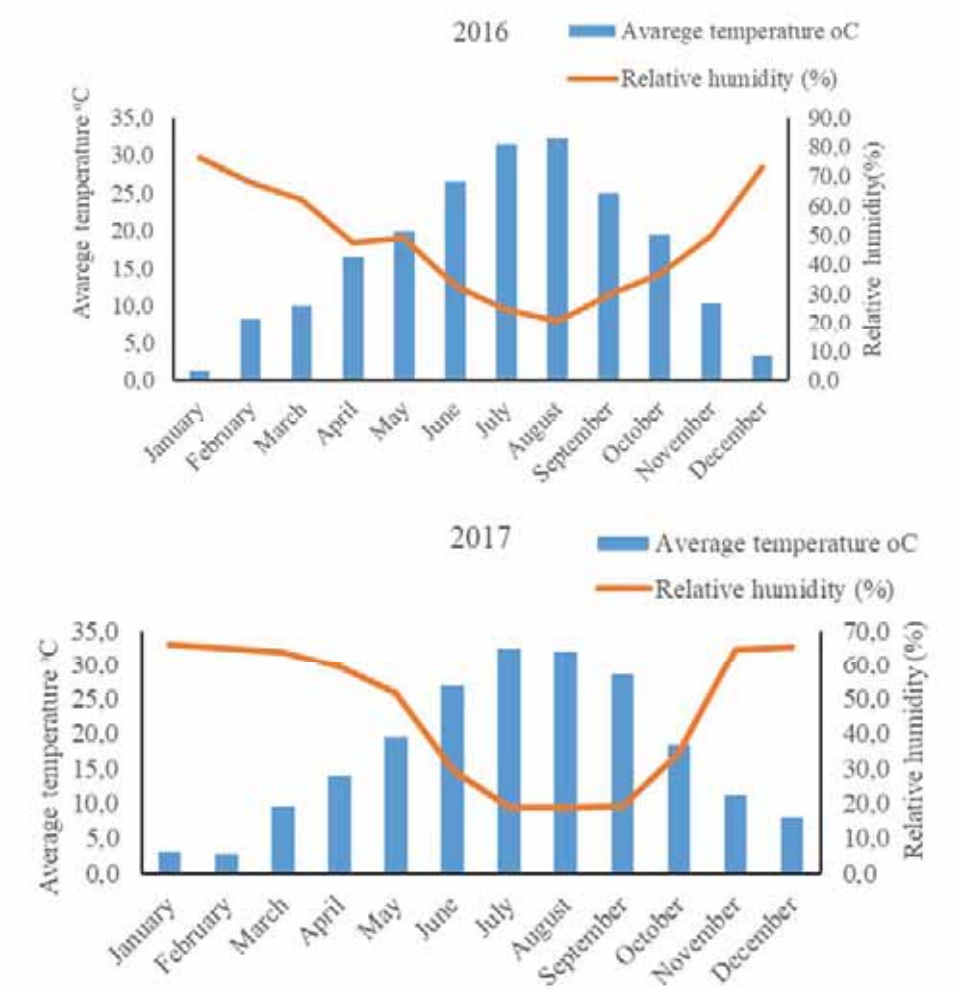

FIGURE 5
Climatic data of Siirt province for the years 2016-2017.

FIGURE 6
Centistidea* (*Paracentistidae*) *pistaciella

FIGURE 7
Chelonus chetini

FIGURE 8
Gelis areator

***Chelonus chetini* Beyarslan & Şahan, 2019.** Material examined. Eruh Bayramlı: 37°50'32"N/ 42°07'44"E, 950 m, 28.IV.2016, 2 ♀♀, ♂, Siirt Merkez: 37°56'25"N/ 41°58'07"E, 2.V.2016, 1000 m, 2 ♀♀, 2 ♂♂ (Figure7).

Distribution in Turkey. Gaziantep (Şahinbey, Nizip-Alahacı) [14], new record for Siirt Province.

Distribution in World. Turkey

***Gelis areator* (Panzer, 1804).** Material examined. Eruh Bayramlı: 37°50'32"N/ 42°07'44"E, 950 m, 28.IV.2016, 2 ♀♀, ♂ 10.V.2016, ♀, Siirt Merkez: 37°56'24"N/ 41°58'05"E, 1004 m, 28 .IV.2016, ♀, (Figure 8).

Distribution in Turkey. Edirne [29], new record for Siirt Province.

Distribution in world. In Afrotropical Region; South Africa. In Palearctic Region; Austria, Azerbai-

jan, Belguim, Bulgaria, Czech Republic, Czechoslovakia, Denmark, Faroe Is., Finland, France, Germany, Greece, Hungary, Iran, Ireland, Italy, Latvia, Lithuania, Moldova, Netherlands, Norway, Poland, Romania, Russia, Slovakia, Spain, Sweden, Turkey, Ukraine, United Kingdom, Yugoslavia. In Oriental Region; Japan, Korea [30; 29].

DISCUSSION

In this study, it was revealed that the pistachio twig borer is one of the most important and common pest species observed in the pistachio areas of Siirt province. The pest was detected in all orchards observed. *Kermania pistaciella* was identified for the first time by Küçükarslan [3] in the pistachio orchards of Gaziantep in Turkey. In the previous studies, *K. pistaciella* was among the widespread pests with a high infestation rate in the Southeastern Anatolia Region, where pistachio cultivation is performed in Turkey [3; 4; 5; 6]. Mehrnejad [8] and Fakhri & Abbasipour [10] stated that K. pistaciella was among the main pests of pistachio in Iran with the highest pistachio production in the world.

The pistachio twig borer, *K. pistaciella* males started to be caught in pheromone traps on April 8 in the first year and on April 12 in the second year. The adult flight continued until May 16 in the first year and until June 4 in the second year. The adult flight period varied by orchards. The flight period ended in 24 and 37 days in the first year and in 28 days and 41 days in the second year. In the orchards, the highest adult emergence occurred in the last week of April in Kezer orchard in both years, while it occurred at the end of April in the first year and at the beginning of May in the second year in the orchards in Siirt Center. This period is the most important time in pest control. Although not detailed, it was determined in the study that Pherocon traps attracted more adults than delta traps. The efficacy trials of different trap types to attract *K. pistaciella* adults to be made in the future will provide clearer results.

In previous studies, Yanık & Yücel [5] have stated that *K. pistaciella* is found in a wide area in Şanlıurfa and the Southeastern Anatolia Region and causes significant damage. In the collected pupae, the adult and parasitoid emergence was observed in the laboratory. They indicated that the adult emergence occurred mostly in the last week of April and in the first week of May and it peaked in this period, and this period was important for pesticide application against adults.

Zamani et al. [20] determined the first emergence, peak point, and last capture in the trap of *K. pistaciella* in 2012 to be on April 20, May 9, and May 30, respectively. They compared funnel and delta traps. The traps caught a large number of *K. pistaciella*, but there was no significant difference in terms of the attractiveness of traps between the trap types and geographic locations. In the study conducted in Bozova district of Şanlıurfa, Yanık & Yıldırım [17] stated that the first adult emergence of *K. pistacella* occurred in the beginning and middle of April, and the adult flight continued for 4-5 weeks.

In the Rafsanjan pistachio orchards in Iran, the emergence of *K. pistaciella* adults continued from the beginning of April to early May, and the peak in flight was between April 25 and April 30 [31]. In another study, Zamani et al. [20] investigated the shape of pheromone traps, the direction of hanging the traps, the place of hanging the traps on the tree, and attracting adult pests by geographic locations in order to control the population of *K. pistaciella*. According to the study results, the first adult capture, the flight peaks, and the end of the flight period in 2012 occurred on April 20, May 9, and May 30, respectively. The funnel trap caught more moths compare to the delta trap. No significant difference was determined between the direction of hanging the traps on the tree and the geographical location in terms of attracting insects.

As a result of the study, it was observed that the air temperature and relative humidity affected the emergence time of *K. pistaciella* adults, the number of emerging adults, and the flight period. Therefore, since the weather was rainy in the second year of the study, especially at the beginning of April, the adult emergence in the orchards at high altitudes occurred later in comparison with the first year, and the adult flight period continued for a longer time compared to the first year. The adult emergence was mostly concentrated at temperatures in the range of 20-25ºC, and the peak point occurred at this temperature. It is thought that the moths caught in pheromone traps in two consecutive years were different due to the different weather conditions, and especially the amount of rainfall in these orchards in both years. The reason for the low number of adults caught in the same orchards in the second year of the study compared to the first year may originate from the fact that some of the adults were caught in traps in the first year.

The data obtained in the study were similar to those obtained in the previous studies. Among the previous studies, Fakhri & Abbasipour [10] determined that air parameters, such as temperature and relative humidity, had a significant effect on the number of pistachio twig borer adults. The peak point of adult moths occurred at 20-25ºC. The highest number of *K. pistaciella* moths caught in the traps occurred between April 17-23 when the air temperature was around 25ºC.

As a result of the study, three parasitoid species were identified from the pistachio twig borer pupae cultured. The identified parasitoid species were as follows: *Centistidea* (*Paracentistidae*) *pistaciella* van Achterber& mehrnejad, 2002, *Chelonus chetini* Beyars & Şahan, 2019, and *Gelis areator* (Panzer, 1804) *Centistidea* (*Paracentistidae*) *pistaciella* and

Gelis aerator species are the first records of the larval-pupal parasitoids of *Kermania pistaciella* in Turkey.

In the study previously conducted in Siirt province in Turkey, *Chelonus flavipalpis* and *Mirax rufilabris* species were identified as the parasitoid species in *K. pistaciella* pupae [13]. Beyarslan & Şahan [14] obtained *Chelonus chetini* Beyarslan and Şahan sp. nov in the larval pupae of *K. pistaciella* in Gaziantep province and defined it as a new species and introduced it to the scientific world. Achterberg & Mehrnejad [12] detected two species (*Chelonus kermakiae* (Tobias, 2001) (Cheloninae) and *Centistidea pistaciella* spec. nov. (Miracinae)) from the Braconidae family among the *K. pistaciella* pupae in Iran. Two ichenumonid species, namely *Gelis exareolatus* (*nigritus*) and *G. liparae* were reared from pupae of pistachio twig borer moth in Kerman province of Iran. *Gelis exareolatus* was reared from pupae of both *K. pistaciella* and braconid *Chelonus kermakiae*. *Gelis liparae* was the most common hyperparasitoid of *K. pistaciella* in Kerman province [19]. Aydoğdu & Beyarslan [32] defined 13 Chelonus species and stated that five of them were the first record for the fauna of Turkey. It is observed that the parasitoid species identified in the study are similar to the species determined in the previous studies conducted in Turkey and Iran.

CONCLUSIONS

As a result of the study, *K. pistaciella* was found to be widespread and the most important pests of pistachio. The Delta and Wing pheromone traps were efficient in capturing a large number of *K. pistaciella* male adults. Males were started to be caught in pheromone traps on April 8 and April 12 in the first and second years, respectively. The adult flight continued until May 16 in the first year and until June 4 in the second year. The peak of the adults caught in traps occurred on April 25-29 in the first year, and on April 26-May 4 in the second year, respectively. *Centistidea* (*Paracentistidae*) *pistaciella* van Achterber & Mehrnejad, 2002, *Chelonus chetini* Beyarslan & Şahan, 2019, and *Gelis areator* (Panzer, 1804) were identified parasitoid species from the pupae of *K. pistaciella*. *Centistidea pistaciella* parasitoid species is the first records of parasitoid in Turkey. If all pistachio growers use pheromone traps against this pest it would be an effective management. In addition, for effective pest management mass traping and diffrent types of traps of efficiency studies are recomended

ACKNOWLEDGEMENTS

This study was carried out within the scope of the project entitled " Identification of Pistachio (Pistacia vera L.) Diseases and Pests in Siirt Province and Determination of the Critical Period for the Control of Important Species " supported by the Scientific Research Projects Department of Siirt University. The authors thank to Siirt University Scientific Research Projects Department for their financial support.

Moreover, We would like to express our gratitude to Prof. Dr. Ahmet Beyarslan (Bitlis Eren University, Faculty of Arts and Science, Department of Biology) and Dr. Janko KOLAROV (Faculty of Pedagogy, University of Plovdiv, Plovdiv, Bulgaria) who identified parasitoid species.

REFERENCES

[1] Garcia, J.M., Agar, I.T., Streif, J. (1992) Fat content and fatty acid composition in individual seeds of pistachio varieties grown in Turkey. Gartenbauwissenschaft. 57(3), 130-133.

[2] TÜİK (2018) Turkish Statistical Institute, Ankara. (Web page: www.tuik.gov.tr) (Date accessed: September: 2019).

[3] Küçükarslan, N. (1966) Pistachio of Harmful branch Moth (Kermania pistaciella Amsel) (lepidoptera: Oinophilidae) of Biology an Chemical Control. Sabri A.Ş. Basımevi, İstanbul, Türkiye. 64 s. (in Turkish)

[4] Mart, C., Celik, M.Y., Yigit, A. (1995) Biological observations and chemical control of pistachio twig borer, Kermania pistaciella Ams. (Lepidoptera: Oinophilidae), injurious in pistachio orchards in Turkey. Acta Horticulturae. 419, 373-378.

[5] Yanık, E., Yücel, A. (2001) The pistachio (*P. vera* L.) pests, their population development and damage stage in Sanliurfa province. In: XI. GREMPA Seminar on Pistachios and Almonds. Volume 56 . CIHEAM Cahiers Options Méditerranéennes , Zaragoza, 301-309.

[6] Bolu, H. (2002) Investigations on the fauna of insects and mites in pistachio areas in South Eastern Anatolia Region of Turkey. Turkish Journal of Entomology. 26 (3), 197-208.

[7] Kaplan, C., Ciftci, M.C., Cakmak, S. (2018) “Insect pests in pistachio producing areas of Turkey, 10-16”. The Book of full text of Ejons 4. International Congress on Mathematic, Engineering and Natural Sciences-IV (August 11-13, 2018 Kiev, Ukraine). 339.

[8] Mehrnejad, M.R. (2001) "The current status of pistachio pests in Iran, 315-322". In: XI GREMPA Seminar on Pistachios and Almonds. Zaragoza: CIHEAM (Cahiers Options Méditerranéennes; n. 56). 11. GREMPA Seminar on Pistachios and Almonds, 1999/09/01-04, Sanliurfa (Turkey). (Ed. B. E. Ak). 416.

[9] Karadag, S., Sarpkaya, K., Kalkancı, N., Baran, B, Canıhos, E., Oztop, A., Tekşem, I., Elekcioglu, N. Z., Karaca, M., Kaplan, C., Velioglu, A.S, Başaran, M.S., Arpacı, S., Acar, İ., Bilim, H.İ., Erdogan, C., Caner, O.K., Aydar, A., Duran, H., Kodan, M., Elibuyuk, A., Ozaslan, C. (2011). Technical instruction of integrated management of pistachio. T.C. Ministry of Food, Agriculture and Livestock, General Directorate of Agricultural Research and Policies, Department of Plant Health Research, Ankara, Turkey. 73. (in Turkish)

[10] Fakhri, N., Abbasipour, H. (2019) Population fluctuations of the pistachio twig borer, *Kermania pistaciella* Amsel, (1964) (Lepidoptera: Oinophylidae) using delta pheromone trap. Acta Agriculturae Slovenica. 114 (1), 13-20.

[11] Tezerji, Z.S. (2011) Determination of damages of pistachio twig borer moth *Kermania pistaciella* Amsel, to fruit cluster of pistachio trees. Acta Horticulturae. 912, 701-707.

[12] van Achterberg, C., Mehrnejad, M.R. (2002) The braconid parasitoids (Hymenoptera: Braconidae) of *Kermania pistaciella* (Lepidoptera: Tineidae: Hieroxestinae) in Iran. Zoologische Mededelingen. 76 (17-24), 27-40.

[13] Özgen, İ., Bolu, H., Beyarslan, A. (2012) *Chelonus flavipalpis* Szépligeti, (1896) and *Mirax rufilabris* Haliday, (1833) (Hymenoptera, Braconidae): two new larva-pupa parasitoids of Pistachio twig borer *Kermania pistaciella* Amsel, (1964) (Lepidoptera: Oinophilidae) with the parasitization ratios from Turkey. Munis Entomology & Zoology. 7 (1), 238-242.

[14] Beyarslan, A., Şahan, Y.B. (2019) A new species of Chelonini (Hymenoptera: Braconidae) from pistachio twig borer moth (*Kermania pistaciella* Amsel (Lepidoptera: Tineidae)) in Gaziantep. Turkish Journal of Zoology. 43, 388-392.

[15] Mehrnejad, M.R. (2002) The natural parasitism ratio of the pistachio twig borer moth, *Kermania pistaciella*, in Iran. Acta Horticulturae. 591, 541-544.

[16] Gries, R., Khaskin, G., Daroogheh, H., Mart, C., Karadag, S., Kubilay, E., Britton, R., Gries, G. (2006) (2S,12Z)-2acetoxy-12-heptadecene: major sex pheromone component of pistachio twig borer, *Kermania pistaciella*. Journal of Chemical Ecology. 32, 2667-2677.

[17] Yanık, E., Yıldırım, Y. (2016). Effectiveness of mass trapping for control of the pistachio twig borer, *Kermania pistaciella*. Bulletin of Insectology. 69 (1), 35-40.

[18] Abbaszadeh, G., Seyedoleslami, H., Samih, M.A., Hatami, B. (2006) Bioecology of pistachio twig borer moth *Kermania pistaciella* Amsel, in Rafsanjan and Isfahan-Iran. Communications in Agricultural and Applied Biological Sciences. 71(2 Pt B), 563-569.

[19] Mehrnejad, M.R., Basirat, M. (2009). Parasitoid complex of the pistachio twig borer moth, *Kermania pistaciella*, in Iran. Biocontrol Science and Technology. 19 (5), 499-510.

[20] Zamani, Z., Khajehali, J., Sabrazalian, M.R. (2012) Influence of trap type, trapping location and cardinal direction on the capture of the pistachio twig borer moth, *Kermania pistaciella* Amsel. (Lepidoptera: Tineidae) in Isfahan. Plant Pest Research. 2 (2), 59-61.

[21] Pearson, R.G., Raxworthy, C.J., Nakamura, M., Peterson, A.T. (2007) Predicting species distribution, from small numbers of occurrence records: a test case using cryptic geckos in Madagascar. Journal of Biogeography. 34 (1), 102-117.

[22] Tognelli, M.L., Roig-Junet, S.A., Marvaldi, A.E., Flores, G.E., Lobo, J.M. (2009) An evaluation of methods for modelling distribution of Patagonian insects. Revista Chilena de Historia Natural. 82 (3), 347-360.

[23] Bassirat, M. (2008). Estimating the heat requirements for Pistachio twig moth, *Kermania pistaciella* Amsel in field condition. Journal of Science and Technology of Agriculture and Natural Resources. 12 (45), 339-349.

[24] Carde, R.T. (1990) "Principles of Mating Disruption, 47-71". In: Behavior-Modifying Chemicals for Insect Management, Applications of Pheromones and Other Attractants (Eds. R. L. Ridgway, R. M. Silverstein & M. N. Inscoe). Marcel Dekker, INC, New York. 733.

[25] Cronin, J.T., Hayes, J.L., Turchin, P. (2000). Evaluation of traps used to monitor southern pine beetle aerial populations and sex ratios. Agricultural and Forest Entomology. 2 (1), 69-76.

[26] Devetak, M., Bohinc, T., Kač, M., Trdan, S. (2014) Seasonal dynamics of the cabbage armyworm (*Mamestra brassicae* [L.]) and the bright-line brown-eyes moth (*Mamestra oleracea* [L.]) in Slovenia. Horticultural Science. 41 (2), 80-88.

[27] Grigorov, S.P. (1974) Plant Quarantine, Zemizdat, Sofya. 346. (in Bulgarian)

[28] Yu, D.S., van Achterberg, C., Horstmann, K. (2012) World Ichneumonoidea (2005). Taxonomy, biology, morphology and distribution [Braconidae]. Taxapad (2006) (Scientific names for information management) Interactive electronical catalogue on DVD/CDROM. Vancouver.

[29] Okyar, Z., Yurtcan, M., Beyarslan, A., Aktaş, N. (2012) The Parasitoid complex of White-spotted Pinion *Cosmia diffinis* (Linnaeus, 1767) (Lepidoptera: Noctuidae) on Ulmus minor Miller (Ulmaceae) in Edirne Province (European Turkey). Journal of the Kansas Entomological Society. 85 (2), 91-96.
[30] van Noort, S. (2020). WaspWeb: Hymenoptera of the Afrotropical region. (Web page: www.waspweb.org) (Date accessed: 28/09/2020).
[31] Bassirat, M. (2006) Determination of heat requirements for pistachio twig borer moth, *Kermania pistaciella*. Acta Horticulturae. 726, 519-524.
[32] Aydoğdu, M., Beyarslan, A. (2009) A review of the tribe Phanerotomini (Hymenoptera, Braconidae, Cheloninae) in Turkey, with a new host record for *Phanerotoma* (*Bracotritoma*) *permixtellae*. Biologia. 64 (4), 748-756.

Received: **09.01.2021**
Accepted: **07.02.2021**

CORRESPONDING AUTHOR

Cevdet Kaplan
Faculty of Agriculture,
Department of Plant Protection,
Siirt University,
56220 Siirt – Turkey

e-mail: cevdetkaplan@siirt.edu.tr

© by PSP Volume 30– No. 05/2021 pages 5486-5497 Fresenius Environmental Bulletin

WATER STRESS EFFECT ON CONFECTIONERY HYBRID SUNFLOWER (*HELIANTHUS ANNUUS* L.) CULTIVARS IN DIFFERENT GROWTH PERIODS

Ismail Naneli*, Ferzat Turan

Department of Field Crops, Faculty of Agriculture, Sakarya Applied Sciences University, Sakarya, Turkey

ABSTRACT

Drought is one of the factors that cause serious yield losses in agricultural production. Severe drought events from global warming seriously affect plants and cause yield losses. Confectionary sunflower is involved in the production as a very important plant for in Turkey. However, the drought stress that may occur periodically causes this product to lose efficiency. In this study, water stress was applied in different development periods (head formation, flowering, seed-filling periods) of two hybrid confectionery sunflowers. The trial was conducted as split-plot design based on 3 replications between 2018-2019 years. According to the results obtained, many characteristics were affected by water stress during the flowering period. Particularly, seed yield, head diameter, 1000 seed weight, seed length, and hull ratio characteristics show significant differences. To seed filling period, water stress adversely affected the oil content. However, the water stress in the head formation period weren't affect the plant properties compared to the control parcel. As a result; seed yield, seed length, and oil ratio characteristics, flowering, and seed-filling period were determined as an important step for confectionery hybrid sunflower.

KEYWORDS:
Confectionery hybrid sunflower, Cultivar, Development periods, Drought stress, Yield

INTRODUCTION

Sunflower (Helianthus annuus L.) is grown in mild and subtropical climates in 72 countries and is one of the most produced seed plants in the world after soybean, rapeseed, and peanut [1]. Climate change and rainfall shortages limit agricultural production. The effects of climate change on drought's production of agriculture under rain have a significant impact on the production of rain-fed crops. Small and medium-sized rain-fed farms are highly vulnerable to climate change, and to a greater extent, small and medium-sized rain-fed farms have adopted greater coping mechanisms for climate change compared to large farms [2]. In addition, it has a significant number of uses as confectionery, ornamental, silage, animal, and bird feed. Although it is the most important oil plant in Turkey, it is consumed extensively as a confectionery [3]. Sunflower is affected by many abiotic and biotic stress factors such as yield and product quality during growth and development periods [4]. Today, drought is caused by the decrease in the amount of precipitation, increasing temperatures, evaporation, loss of water, and the amount of water available in the soil. Drought is among the common abiotic stresses in plants [5, 6]. The negative effects of drought on plants along with global climate change have made it necessary to produce resistant and drought tolerant plant varieties that can complete their life cycle in the presence of limited water in the soil [7-9]. In order to ensure sustainable water management in agriculture, on-site development work such as leveling, consolidation, and drainage must be undertaken in conjunction with irrigation systems. It should be noted that the success of irrigation projects depends on the regulation of soil water-human relations in the field of a physical infrastructure project. The agricultural water user sector is ranked first as the most water usage sector in Turkey. Therefore, the use of tools and techniques that provide effective water use in agriculture should be among the primary targets of Turkey. Completion of work to ensure that surface storage facility and groundwater reservoirs are kept at the highest level with maximum feeding, proper water collection application methods, and effective water use methods must be developed according to land use types [10]. On the other hand, determining the non-critical stages, especially during plant growth periods, prevents unnecessary irrigation. In this context, water resources and soil fertility increase. The response of plants to drought stress varies significantly depending on the intensity and duration of the stress, the plant variety, and the growth stage [11, 12]. In studies on water stress during the development period of plants, Human et al. [13] applied water stress, taking into account the water potential in the leaf during the sunflower heading, pollination, and seed setting periods. Patil and Gangavane [14] performed the water stress with water evaporation test in three different

periods 0-30, 30-60, 60-90 after planting. Subramanian and Maheswari [15] applied water stress based solely on the flowering period. The study aim is to determine the effect of water stress on yield and yield components in some stages of the vegetation period in some hybrid sunflower varieties.

MATERIALS AND METHODS

This research was conducted in Eskişehir Çifteler district (altitude 875 m) during to periods of 2018 and 2019. The study was conducted on Palancı and Ahmetbey hybrid confectıonery sunflower varieties. The trial was conducted as a split-plot design based on 3 replications. The trial establishment dates for 2018 and 2019 were in the first week of May, and the harvest was carried out in the first week of September. In the experiment, water stress (control, head formation, flowering, and seed formation period) was applied in four different plant growth stages. In the study, development periods were located in main plots and varieties in subplots. According to the soil analysis results of the experimental area, it is seen that the soil has a slightly alkaline reaction and a clayey-loam structure. Phosphorus content is high, organic matter is medium and potassium is sufficient (Table 1). Each parcel is 5 m long and consists of 4 rows. The row spacing is 70 cm and the row top is 26 cm. After planting, maintenance (hoe, etc.) operations were carried out at the four-leaf level and in different periods. Half of the nitrogenous fertilizer applications were applied at planting and the other half at four-leaf levels. In all parcels, the first irrigation was carried out with planting. In 10 plants randomly selected by applying edge effect on plots; plant height, head diameter in the plant, hull ratio, seed width, seed length, 1000 seed weight, seed yield, and oil rate were investigated. The research consists of four main plots. Water stress applications were applied to the varieties in three main plots during heading formation, flowering, and seed formation periods. The fourth main plot is the control group and is not exposed to water stress. In the examination of the meteorological data of the experimental area, no precipitation was observed during the water stress periods (Table 1). The data obtained as a result of the research were subjected to the MSTAT-C statistical analysis method according to the Two Factor Randomized Complete Block Design with Split Plot Combined over years and variance analysis was performed. Differences between applications were determined with the Duncan test [16].

RESULTS AND DISCUSSION

Drought is the most serious environmental factor affecting almost all living organisms as a result of global warming. The average Duncan test results obtained in the study are significant at 1% and 5% level and are given in tables 3, 4, 5, 6, 7, 8, 9, 10. Many features examined by Radic et al. [17]; head diameter, hull ratio, seed width, seed length, 1000 seed weight, and seed yield characteristics in the plant are affected by water stress during the flowering period.

Plant Height (cm). Plant height is an important parameter in determining the vegetative growth level. In the study, a significant difference at $p < 0.01$ level was determined as a result of the combined analysis of variance for confectionery sunflower hybrid varieties for two years. In terms of plant height, the Palancı1 variety (191.85 cm) has a longer height than the Ahmetbey variety (183.90 cm) (Table 3). The interaction of water stress in different periods applied to the cultivars and water stress, which is the main factor, was not found to be significant. Water stress applied during the specified periods did not cause any interaction with the plant height (Table 3). Water stress haven't affect the growth of the stem in the last stage of plant height, head formation in sunflower, and the final stage of growth until the flowering stage [18]. Goksoy et al. [19] limited irrigation reduces plant height in sunflower. Vilalobos et al. [20] and Osborne et al. [21] observed during their research that the plant height of sunflower increased with increasing irrigation water and decreased when stress was applied. In our research, water stress; there was no significant difference in plant height as it was applied in the last stage of plant growth during the table formation, flowering, and seed filling periods (Table 3). It can be concluded that sunflower maintains that feature of growing vegetatively until the beginning of the blooming period.

TABLE 1
Trial area climate characteristics*

Climate Factors	Years	Months					Total/Mean
		May	June	July	August	September	
Precipitation (mm)	2018	67.4	49.4	8.2	6.4	8.6	140.0
	2019	27.4	102.6	16.4	18.2	3.4	168.0
	Long Years	50.1	42.8	19.5	14.1	11.4	137.9
Temperature (° C)	2018	16.5	19.9	22.5	22.6	17.8	19.9
	2019	16.0	20.4	20.6	21.4	17.6	19.2
	Long Years	15.2	19.4	22.3	22.5	17.7	19.4

*: General Directorate of Meteorology

TABLE 2
Soil analysis results of the trial site for 2018 and 2019**

Years	N (%)	P (kg/da)	K (kg/da)	pH	Organic Matter (%)	Lime (%)	EC (dS/m)	Structure
2018	0.12	9.68	203.19	7.78	2.52	38.32	0.52	Clay-loam
2019	0.11	8.32	198.20	7.68	2.36	38.50	0.55	Clay-loam

**: Professional Environmental Analysis Laboratory Food Agriculture and Quality.

TABLE 3
Data on plant height (cm) of hybrid sunflower varieties affected by water stress in different growth periods

	Plant Height (cm)								
	Control		Head Formation		Flowering		Seed-Filling Periods		Mean
	Palancı1	Ahmetbey	Palancı1	Ahmetbey	Palancı1	Ahmetbey	Palancı1	Ahmetbey	
2018	192.67	183.33	189.67	182.67	191.67	184.00	192.00	184.02	187.42
2019	193.48	184.91	190.31	184.52	191.59	185.29	193.41	182.39	188.24
Variety×DDP	193.08	184.12	189.99	183.60	191.63	184.65	192.71	183.21	
Mean DDP	188.60		186.79		188.14		187.96		
Mean Variety	191.85 **A**	183.90 **B**							

DDP; Different development period

TABLE 4
Data on the head diameter (mm) of the cookie hybrid sunflower varieties affected by water stress in different growth periods

	Head Diameter (cm)								
	Control		Head Formation		Flowering		Seed-Filling Periods		Mean
	Palancı1	Ahmetbey	Palancı1	Ahmetbey	Palancı1	Ahmetbey	Palancı1	Ahmetbey	
2018	20.67	21.00	19.83	18.83	16.50	16.83	18.67	19.17	18.93
2019	20.42	21.43	19.98	19.28	16.42	17.98	18.49	18.92	19.12
Variety×DDP	20.55	21.22	19.91	19.06	16.46	17.41	18.58	19.05	
Mean DDP	20.88 **A**		19.48 **B**		16.93 **C**		18.81 **B**		
Mean Variety	18.87	19.18							

DDP; Different development period

Head Diameter (cm). In water stress applications during the development period, the average of varieties is 16.93 cm minimum head flowering period, and it is 20.88 cm less than the control group. The difference between the averages was found to be statistically significant (Table 4). There was no statistical difference between the cultivars and the interaction of water stress. The water stress applied according to the results obtained haven't create significant differences between the varieties in the diameter of head. The water stress applied during the flowering period in terms of the variety averages of different growth periods negatively affected the head diameter (Figure 1), and the interaction between different growth periods and the cultivar averages was found to be statistically insignificant (Table 4). Consequently, the main reason for the sensitivity of the head diameter to stress during the flowering and pollination period can be attributed to the gradual growth of flowers on the head during this period. Thus, at the beginning of the flowering stage, the flower head is relatively small.

The flower head and the increase in the number of flowers occur together. The water stress applied during the flowering period negatively affected the flowering amount and the diameter of the head. In this context, generative period water stress can cause negative situations in sunflower head development [19, 22, 23].

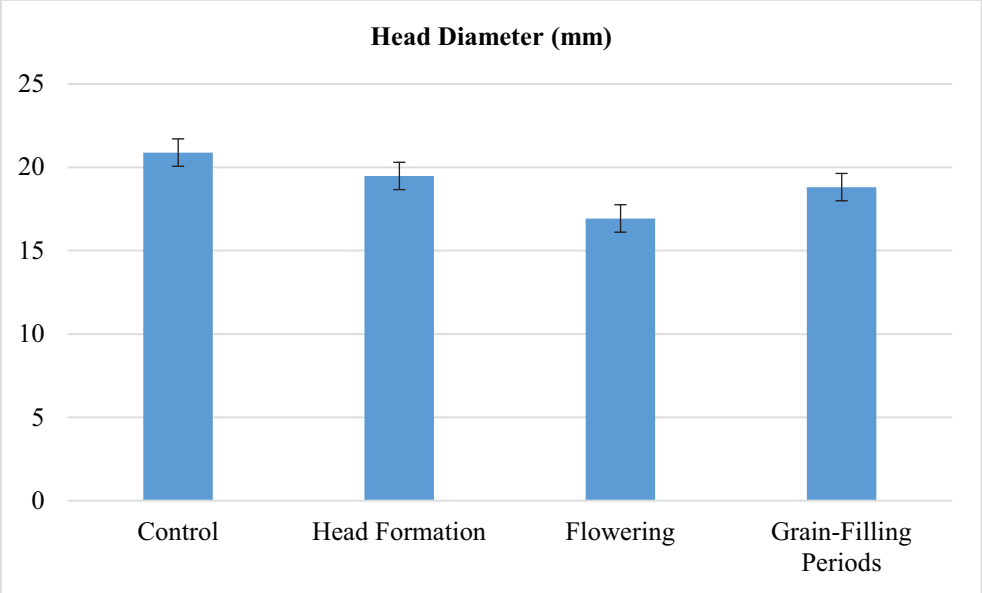

FIGURE 1
Average of different growth periods of confectionery hybrid sunflower varieties in terms of head diameter (mm)

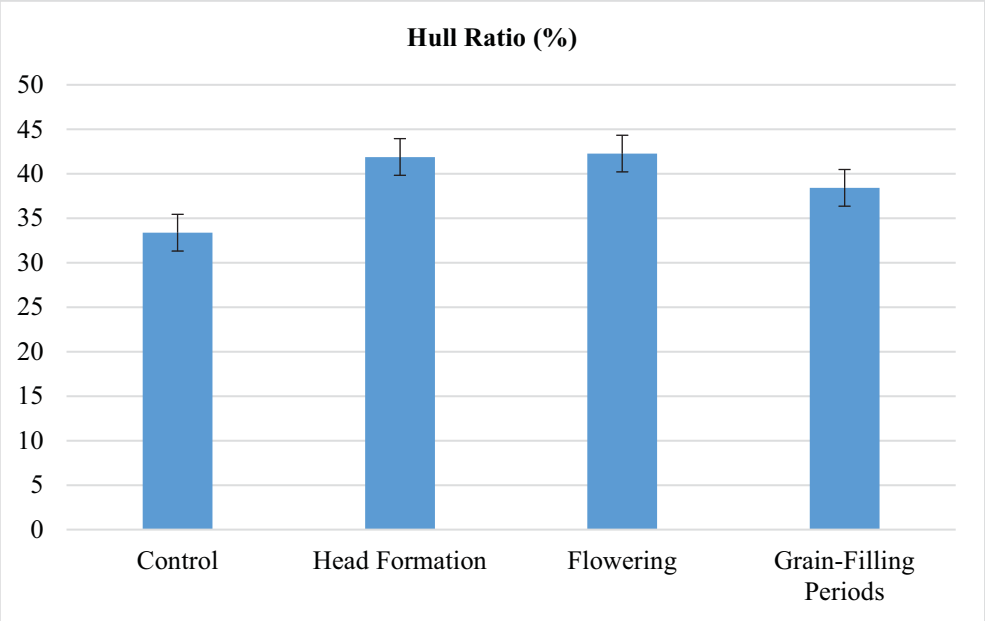

FIGURE 2
Average of different growth periods of confectionery hybrid sunflower varieties in terms of hull ratio (%)

Hull Rate (%). According to the results obtained in the study, the highest hull rate was found in the Ahmetbey variety with 43.72% during the flowering period and at least in the Palancı1 variety with 32.99% in the control application (Table 5). Considering that there is an inverse proportion between the hull ratio and the seed length, the most sensitive development process according to the average Duncan table (Table 5) in terms of hull ratio was determined as the flowering period (Figure 2). In terms of the interaction between the variety averages and the different growth period, the highest value was obtained with 43.72% in the water stress application of the Ahmetbey variety during the flowering period, while the lowest hull rate was found in the control application to the Palancı1 variety with 33.38% (Figure 3, Table 5). The hull ratio is the stage where the seed length is determined, and the water stress applied in the specified periods causes an increase in the hull ratio and small seed. Besides the hull ratio of large seeds is low, the particle ratio of small seeds is high. Kaya [24] found that different irrigation practices differ in the hull ratio of hybrid sunflower varieties.

TABLE 5
Data on the hull ratio (%) of confectionery hybrid sunflower varieties affected by water stress in different growth periods

	Hull Rate (%)								
	Control		Head Formation		Flowering		Seed-Filling Periods		Mean
	Palancı1	Ahmetbey	Palancı1	Ahmetbey	Palancı1	Ahmetbey	Palancı1	Ahmetbey	
2018	32.67	34.33	39.50	43.67	41.00	44.00	36.33	41.00	39.06
2019	33.32	33.18	40.25	44.12	40.65	43.44	35.98	40.35	38.91
Variety×DDP	32.99 f	33.75 e	39.87 c	43.89 a	40.82 b	43.72 a	36.15 d	40.67 b	
Mean DDP	33.38 C		41.89 A		42.27 A		38.42 B		
Mean Variety	37.46 B	40.51 A							

DDP; Different development period

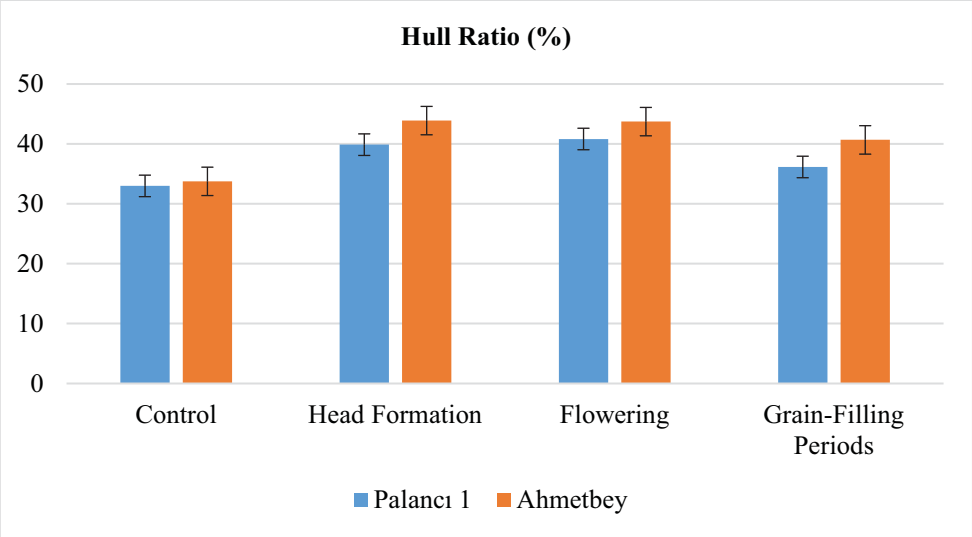

FIGURE 3
Variety × DDP (different development periods) interaction data in terms of hull ratio (%)

TABLE 6
Data on the seed width (mm) of confectionery hybrid sunflower varieties affected by water stress in different growth periods

	Seed Width (mm)								
	Control		Head Formation		Flowering		Seed-Filling Periods		Mean
	Palancı1	Ahmetbey	Palancı1	Ahmetbey	Palancı1	Ahmetbey	Palancı1	Ahmetbey	
2018	7.83	7.20	7.77	6.93	5.67	5.73	6.57	6.63	6.79
2019	7.87	7.35	7.74	6.89	5.75	5.60	6.66	6.81	6.83
Variety×DDP	7.85 a	7.27 b	7.76 a	6.91 b	5.71 d	5.66 d	6.62 c	6.72 c	
Mean DDP	7.56 A		7.34 A		5.69 C		6.67 B		
Mean Variety	6.86	6.67							

DDP; Different development period

Seed Width (mm). The average water stress applications in different growth periods was the lowest with 5.69 mm during the flowering period, while the highest value was obtained with 7.56 mm in the control group (Figure 4, Table 6). In the control application of the cultivar averages and the interaction of different growth periods, the Palancı1 variety was the highest with 7.85 mm, and the Ahmetbey variety

was found to be the lowest with 5.66 mm in the flowering period water stress application (Figure 5, Table 6). Kaya et al. [25] extreme temperatures in sunflower, especially during the seed filling period, cause rapid moisture loss in the seeds in the sunflower heads, stated situation decreases the seed length and leads to the formation of thin seeds.

Seed Length (mm). Although the seed length is a feature of the variety, it is closely related to the head diameter and the number of seeds in the head. Also, it is one of the most important features in confectionery sunflower. As the length of the confectionery sunflower increases, there is an increase in the product prices. In the research, in the water stress applied during the flowering period of the Palancı1 variety in 2018-2019. While the shortest seed length was obtained with 15.40 mm and 15.44 mm, the longest seed length was obtained in the control application of 19.23 mm Ahmetbey variety (Table 7). Different growth period averages are the lowest in the flowering period 15.59 mm and the highest in the control group with 18.74 mm (Figure 6, Table 7). Interaction of cultivar average and different growth periods Palancı1 and Ahmetbey varieties had the lowest values with 15.44 mm and 15.75 mm in the flowering period, while Palancı1 and Ahmetbey varieties were in the higher groups with 18.25 mm and 19.22 mm in the control group (Figure 7, Table 7). Pekcan [26] reported that the seed length increased 4.3% approximately with irrigation during flowering and 5.8% with two irrigation applications at the end of flowering and flowering period.

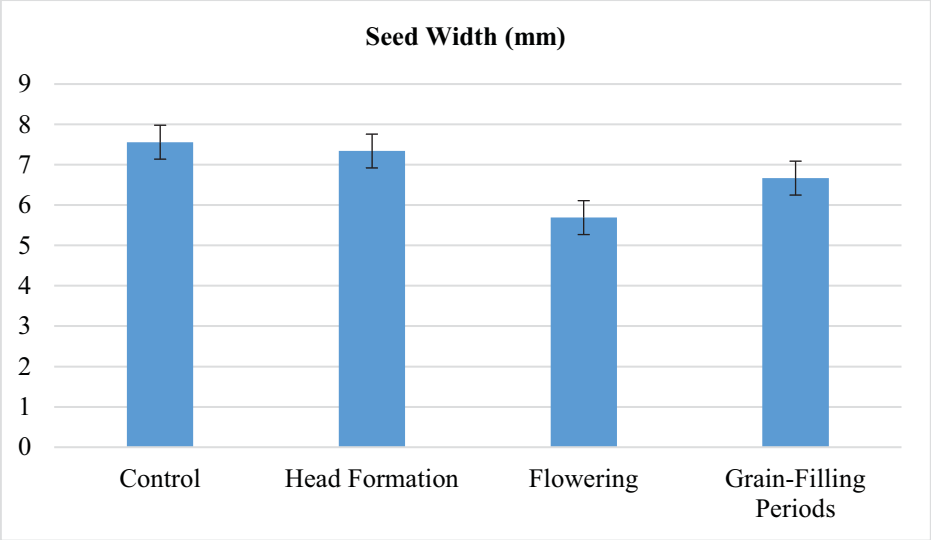

FIGURE 4
Average of different growth periods of confectionery hybrid sunflower varieties in terms of seed width (mm)

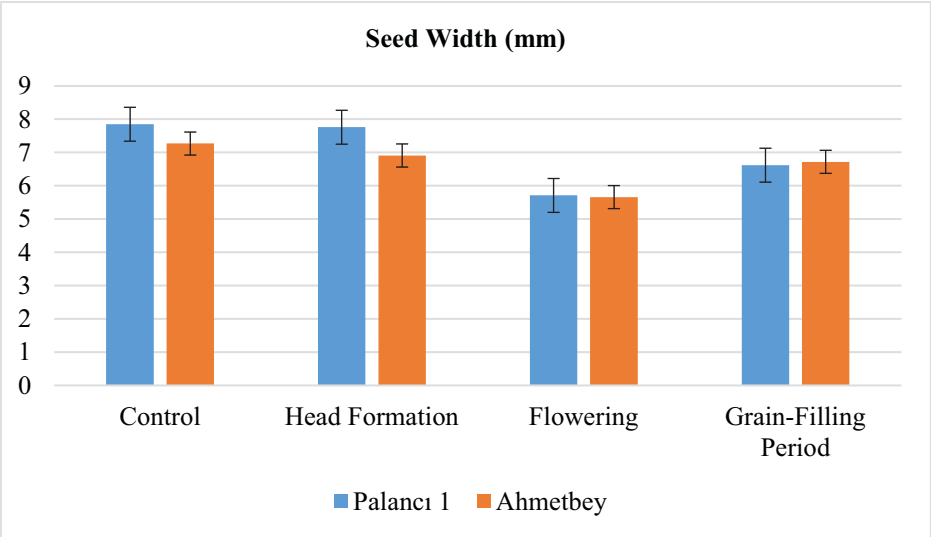

FIGURE 5
Variety × DDP (different development periods) interaction data in terms of seed width (mm)

TABLE 7
Data on the seed length (mm) of confectionery hybrid sunflower varieties affected by water stress in different growth periods

	Seed Length (mm)								
	Control		Head Formation		Flowering		Seed-Filling Periods		Mean
	Palancı1	Ahmetbey	Palancı1	Ahmetbey	Palancı1	Ahmetbey	Palancı1	Ahmetbey	
2018	18.23	19.23	17.90	18.30	15.40	15.77	16.63	16.67	17.26
2019	18.27	19.21	17.82	18.22	15.44	15.75	16.55	16.72	17.24
Variety×DDP	18.25 **b**	19.22 **a**	17.86 **b**	18.26 **b**	15.42 **d**	15.76 **d**	16.59 **c**	16.69 **c**	
Mean DDP	18.74 **A**		18.06 **B**		15.59 **D**		16.64 **C**		
Mean Variety	17.03 **B**	17.48 **A**							

DDP; Different development period

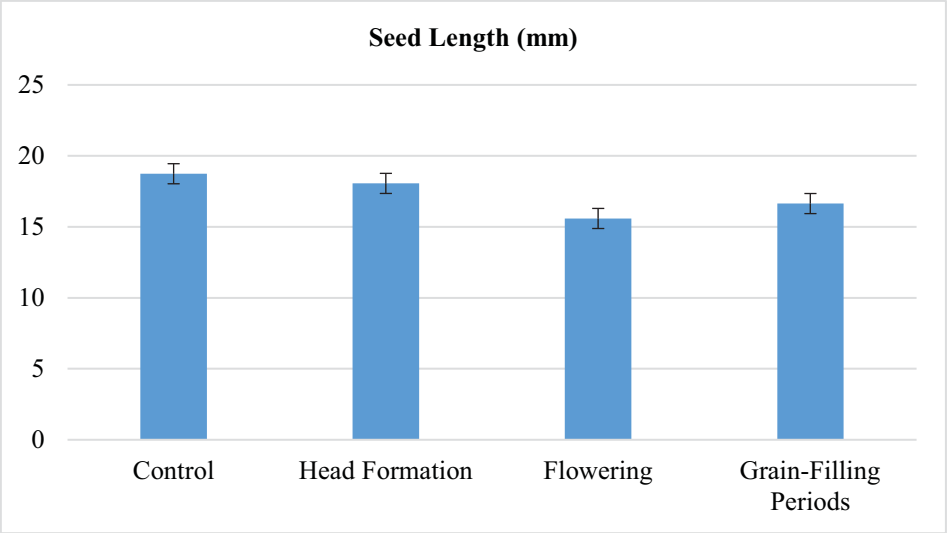

FIGURE 6
Average of different growth periods of confectionery hybrid sunflower varieties in terms of seed length (mm)

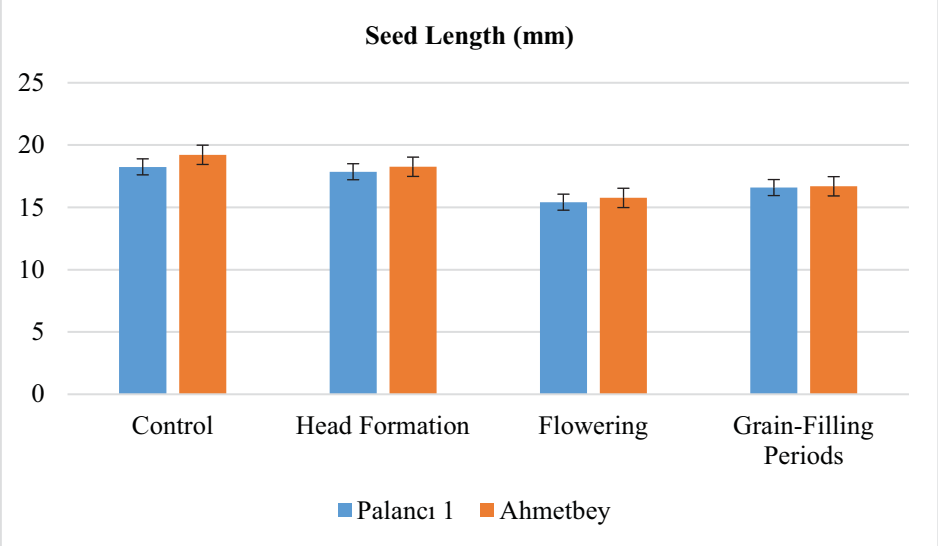

FIGURE 7
Variety × DDP (different development periods) interaction data in terms of seed length (mm)

TABLE 8
Data on the 1000 seed weight (g) of confectionery hybrid sunflower varieties affected by water stress in different growth periods

	1000 Seed Weight (g)								
	Control		Head Formation		Flowering		Seed-Filling Periods		Mean
	Palancı1	Ahmetbey	Palancı1	Ahmetbey	Palancı1	Ahmetbey	Palancı1	Ahmetbey	
2018	126.00	111.00	124.67	110.33	106.00	101.00	112.67	106.17	112.22
2019	126.41	112.22	123.97	110.83	105.88	100.97	112.91	106.97	112.52
Variety×DDP	126.20 **a**	111.61 **d**	124.32 **b**	110.58 **d**	105.94 **e**	100.98 **f**	112.79 **c**	106.57 **e**	
Mean DDP	118.91 **A**		117.45 **A**		103.46 **C**		109.68 **B**		
Mean Variety	117.31 **A**	107.44 **B**							

DDP; Different development period

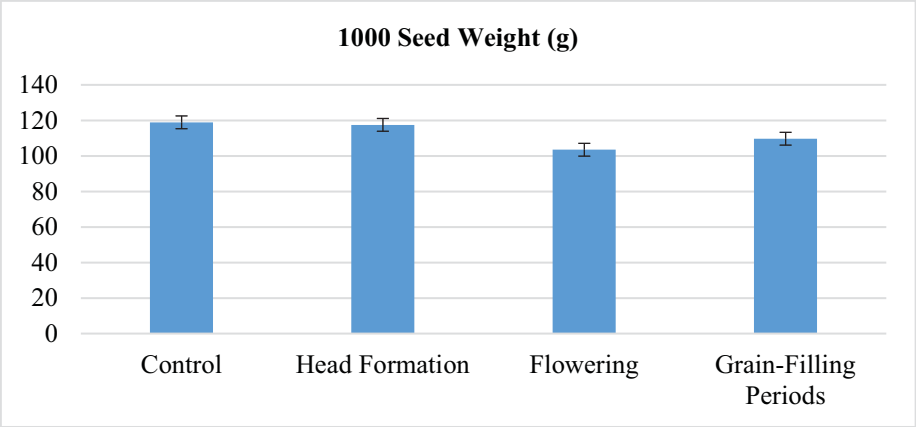

FIGURE 8
Average of different growth periods of confectionery hybrid sunflower varieties in terms of 1000 seed weight (g)

1000 Seed Weight (g). Varieties and water stress applications in different periods were found statistically significant to p <0.01 level in terms of thousand-seed weight. While the highest thousand-seed weight was observed in the control application of 126.20 g Palancı1 variety, the lowest thousand-seed weight was observed in the Ahmetbey cultivar with 100.98 g in the flowering period water stress application (Table 8). According to the different growth period averages, the control group (118.91 g) and the head formation (117.45 g) were among the high groups, while the flowering period (103.46 g) was in the low groups (Figure 8, Table 8).

In terms of the interaction between the cultivar average and the different growth periods, the maximum value was obtained from the Palancı1 variety with 126.20 g in the control group and the minimum value from the Ahmetbey variety with 100.98 g in the flowering period (Figure 9, Table 8). Thousand-seed weight is a feature that directly affects the yield. The plant exposed to water stress during the flowering period physiologically shows a decrease in the number of seeds as a result of the decrease in the number of flowers in the head. Subramanian et al. [15] water stress decreased in the number of flowers in the head before and during the flowering period. In some studies, the findings we obtained regarding a thousand-seed weight are that the shortening of the irrigation interval increases the weight of a thousand seeds [27, 28].

Seed Yield (kg/da). In the study, as a result of the analysis of variance regarding confectionery hybrid sunflower varieties to water stress in different periods, a significant difference was found at the level of p <0.01 in the water stress application periods. Variety averages of different growth periods were obtained in the control group and seed formation period, and the minimum value was obtained with 323.16 kg/da in the flowering period (Figure 10, Table 9). The water stress applied on the yield components causes the final performance of the product to decrease. According to the results, water stress seen before the generative period haven't affect the seed yield negatively [29, 30].

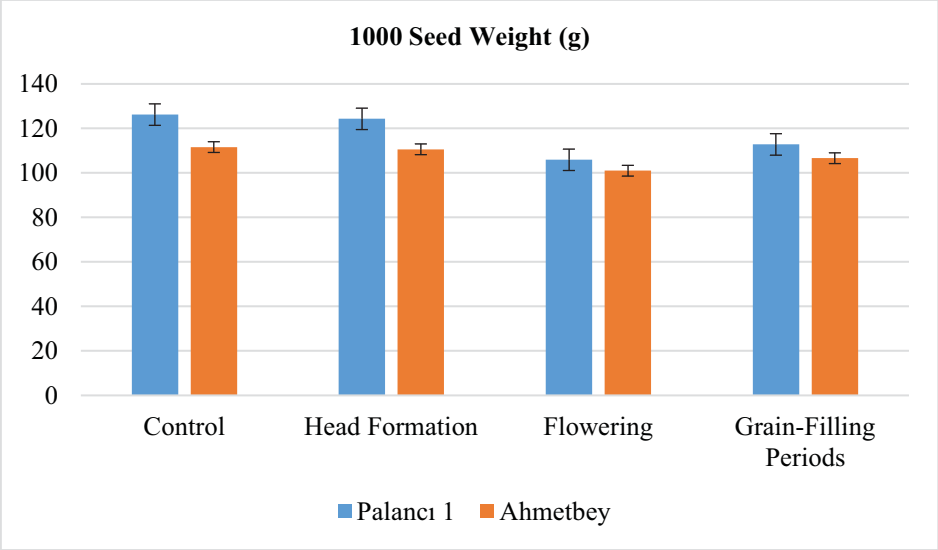

FIGURE 9
Variety × DDP (different development periods) interaction data in terms of 1000 seed weight (g)

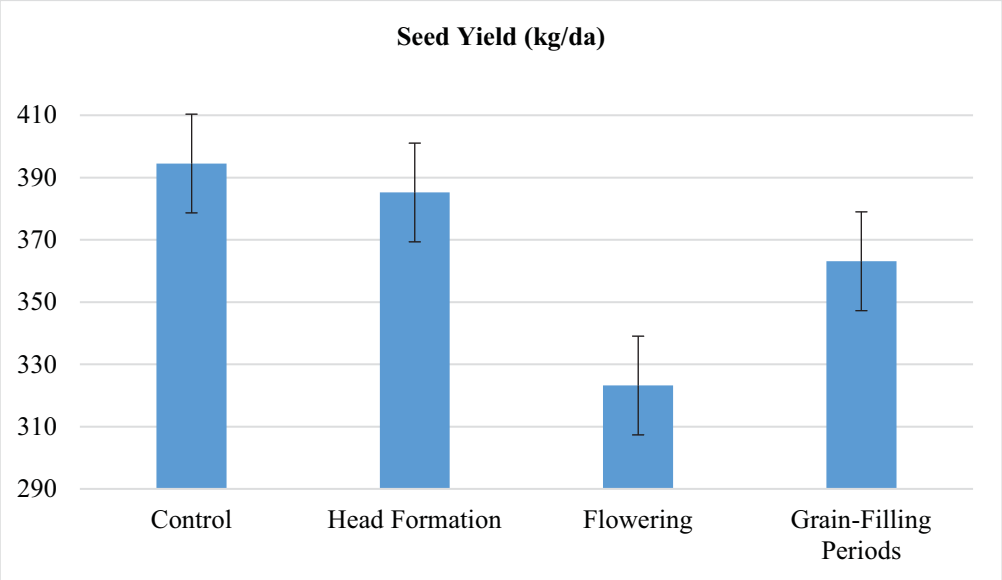

FIGURE 10
Average of different growth periods of confectionery hybrid sunflower varieties in terms of seed yield (kg/da)

TABLE 9
Data on the seed yield (kg/da) of confectionery hybrid sunflower varieties affected by water stress in different growth periods

	Seed Yield (kg/da)								
	Control		Head Formation		Flowering		Seed-Filling Periods		Mean
	Palancı1	Ahmetbey	Palancı1	Ahmetbey	Palancı1	Ahmetbey	Palancı1	Ahmetbey	
2018	379.00	390.00	377.33	388.00	321.00	330.67	354.00	362.00	362.75
2019	395.75	413.35	380.15	395.23	315.75	325.22	361.84	374.55	370.23
Variety×DDP	387.38	401.68	378.74	391.62	318.38	327.95	357.92	368.28	
Mean DDP	394.53 **A**		385.18 **A**		323.16 **C**		363.10 **B**		
Mean Variety	360.60 **B**	372.38 **A**							

DDP; Different development period

TABLE 10
Data on the oil ratio (%) of confectionery hybrid sunflower varieties affected by water stress in different growth periods

	Oil Ratio (%)								
	Control		Head Formation		Flowering		Seed-Filling Periods		Mean
	Palancı1	Ahmetbey	Palancı1	Ahmetbey	Palancı1	Ahmetbey	Palancı1	Ahmetbey	
2018	24.33	20.57	23.67	19.33	22.00	18.17	19.33	15.50	20.36
2019	25.34	19.58	23.88	19.89	22.45	17.98	19.26	15.59	20.50
Variety×DDP	24.84 **a**	20.08 **bc**	23.78 **ab**	19.61 **c**	22.23 **ab**	18.08 **cd**	19.30 **c**	15.55 **d**	
Mean DDP	22.46 **A**		21.69 **B**		20.15 **C**		17.42 **D**		
Mean Variety	22.53 **A**	18.33 **B**							

DDP; Different development period

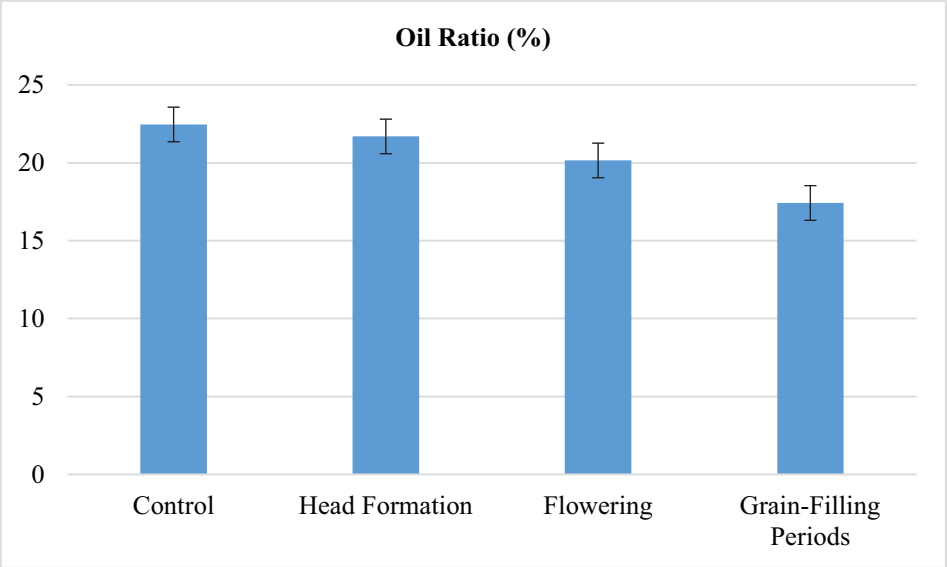

FIGURE 11
Average of different growth periods of confectionery hybrid sunflower varieties in terms of oil ratio (%)

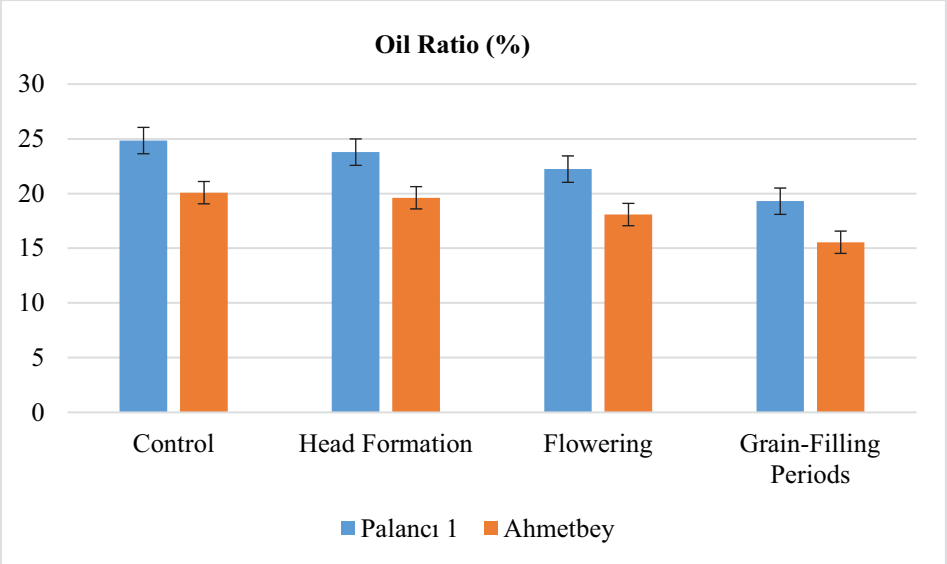

FIGURE 12
Variety × DDP (different development periods) interaction data in terms of oil ratio (%)

Oil ratio (%). There was a statistically significant difference at $p < 0.01$ between the cultivars and the application periods in the water stress application applied in different growth periods with the confectionary hybrid sunflower varieties. In water stress applications to different periods, the highest oil ratio was found in the control application with 22.46%, and the lowest oil ratio was found in the seed-filling period with 17.42% (Figure 11, Table 10). Palancı1 variety had the highest oil rate with 24.84% in the control group, and the Ahmetbey variety had the lowest oil rate with 15.55% in the seed-filling period to the interaction of the variety average and different growth periods (Figure 12, Table 10). The decrease in the seed oil ratio in the plant subjected to water stress application in the generative period emphasizes the importance of the specified period in terms of oil ratio compared to the vegetative period. Tabatabaei et al. [31] reported that the oil rate they obtained under water stress conditions was 17.61% lower than the irrigation conditions.

CONCLUSIONS

This study was carried out with applying water stress in hybrid sunflower for two confectionery varieties in different vegetative and generative periods of the plant to irrigate the plant in certain periods when the plant is affected to water stress, to make an economic contribution to the companies that sell as confectionery and to offer a high quality standard product to the consumer. Significant differences were observed in the statistical analysis and average values of the examined properties. With the water stress applied during the flowering period significant reductions were determined on head diameter, hull ratio, seed width, seed length, 1000 seed weight, and seed yield characteristics. For the oil ratio feature, the seed filling period has been determined as the most sensitive period in water stress application. According to the two-year results obtained from the research, one of the most important factors that producers should pay attention to during the cultivation of sunflowers for confectionery is not to expose the plant to water stress during the flowering period.

REFERENCES

[1] Seiler, G.J., Qi, L.L., Marek, L.F. (2017) Utilization of sunflower crop wild relatives for cultivated sunflower improvement. Crop Science. 57(3), 1-19.

[2] Kuzucu, M., Dökmen, F., Güneş, A. (2016) Effects of climate change on agriculture production under rain-fed condition. International Journal of Electronics, Mechanical and Mechatronics Engineering. 6(1), 1057-1065.

[3] Gaytancıoğlu, O. (1999) Production and foreign trade problems of confectionery sunflower. In: Confectionary sunflower foreign trade seminar. 9 June, Istanbul, 21-28 (In Turkey).

[4] Škorić, D. (2009) Sunflower breeding for resistance to abiotic stresses. Helia. 32(50), 1-16.

[5] Joshi, R., Wani, S.H., Singh, B., Bohra, A., Dar, Z.A., Lone, A.A., Pareek, A., Singla-Pareek, S.L. (2016) Transcription factors and plants response to drought stress: current understanding and future directions. Frontiers in Plant Science. 7, 1-15.

[6] Yadav, S., Sharma, K.D. (2016) Molecular and morphophysiological analysis of drought stress in plants. In: Plant Growth. Rijeka, IntechOpen: London, UK. 149-173.

[7] Shanker, A.K., Maheswari, M., Yadav, S., Desai, S., Bhanu, D., Attal, N.B., Venkateswarlu, B. (2014) Drought stress responses in crops. Functional & Integrative Genomics. 14(1), 11-22.

[8] Samancıoğlu, A., Yıldırım, E. (2015) The effects of bacterial applications that promote plant growth on increasing drought tolerance in plants. Mustafa Kemal University Journal of Agricultural Faculty. 20(1), 72-79 (In Turkey).

[9] Mahmood, H.N., Towfiq, S.I., Rashid, K.A. (2019) The sensitivity of different growth stages of sunflower (Helianthus annuus L.) under deficit irrigation. Applied Ecology and Environmental Research. 17(4), 7605-7623.

[10] Güneş, A. (2018) The importance of water use under climate change effects in semi-arid agricultural areas. International Journal of Advanced Engineering Research and Science. 5(3), 226-229 (In Turkey).

[11] Jaleel, C.A., Gopi, R., Panneerselvam, R. (2008) Growth and photosynthetic pigments responses of two varieties of catharanthus roseus to triadimefon treatment. Comptes Rendus Biologies. 331(4), 272-277.

[12] Hasanuzzaman, M., Hossain, M.A., da Silva, J.A.T., Fujita, M. (2012) Plant response and tolerance to abiotic oxidative stress: antioxidant defense is a key factor, crop stress and its management. In: Crop Stress and Its Management: Perspectives and Strategies, Springer, Dordrecht. 261-315.

[13] Human, J.J., Du Toit, D., Bezuidenhout, H.D., De Bruyn, L.P. (1990) The influence of plant water stress on net photosynthesis and yield of sunflower (Helianthus annuus L.). Journal of Agronomy and Crop Science. 164(4), 231-241.

[14] Patil, B.P., Gangavane, S.B. (1990) Effect of water stress imposed of various growth stages on yield of ground nut and sunflower. Journal of Maharashtra Agricultural University. 15(3), 322-324.

[15] Subramanian, V.B., Maheswari, M. (1991) Physiological and yield responses of sunflower to water stress at flowering. Indian Journal Plant Physiology. 34(2), 153-159.
[16] Düzgüneş, O., Kesici, T., Kavuncu, O., Gürbüz, F. (1987) Research and experimental design. In: Statistical Methods II. Ankara University Agricultural Faculty Press, Ankara. 1-295 (In Turkey).
[17] Radic, V., Balalic, I., Miladinov, Z., Ciric, M., Vasiljevic, M., Jocic, S., Marjanovic-Jeromela, A. (2020) Genotype x environment interaction of some traits in sunflower (Helianthus annuus L.) lines. Applied Ecology and Environmental Research. 18(1), 1707-1719.
[18] Anwar, M., Schneiter, M., Jones, M. (1995) Response of sunflower varieties to different irrigation regimes during kharif season in Peshawar valley. Journal of Maharashtra Agricultural University. 11(3), 273-278.
[19] Goksoy, A.T., Demir, A.O., Turan, Z.M., Dagustu, N. (2004) Responses of sunflower to full and limited irrigation at different growth stages. Field Crops Research. 87(2-3), 167-178.
[20] Vilalobos, F.J., Hall, A.J., Ritchie, J.R., Orgaz, F. (1996) Oilcrop-sun: a development, growth, and yield model of the sunflower crop. Agronomy Journal. 88(3), 403-415.
[21] Osborne, S.L., Schepers, S., Francis, D.D., Schlemer, M.R. (2002) Use of spectral radiance to in-season biomass and grain yield in nitrogen and and water stressed corn. Crop Sciences. 42(1), 165-171.
[22] Wise, R.R., Frederick, J.R., Alm, D.M., Kramer, D.M., Hesketh, J.D., Crofts, A.R., Ort, D.R. (1990) Investigation of the limitations to photosynthesis induced by leaf water deficit in field-grown sunflower (Helianthus annuus L.). Plant Cell and Environment. 13(9), 923-931.
[23] Taiz, L., Zeiger, E. (2002) Photosynthesis: physiological and ecological considerations. In: Plant physiology. Sinauer Associates Inc., Sunderland, 171-192.
[24] Kaya, M.D. (2006) The effects of irrigation applied in different growth periods on yield and yield components in sunflower (Helianthus annus L.), Ankara University Faculty of Agricultura, Ankara, 1-95 (In Turkey).
[25] Kaya, Y., Evci, G., Durak, S., Pekcan, V., Gücer, T. (2005) The effect of the grain filling period yield on sunflower grain yield and other important yield components. In: Field Crops Congress, 5-9 September, Antalya. 1-6 (In Turkey).
[26] Pekcan, V. (2014) Determination of the effects of irrigation, nitrogen (n) doses and plant density on yield and quality traits in confectionery sunflower (Helianthus annuus L.), Namık Kemal University Field Crops Department, 1-140 (In Turkey).
[27] El-Hafez, S.A.A., El-Sabbagh, A.A., El-Bably, A.Z., Abou-El, A. (2002) Evaluation of sprinkler irrigated sunflower in North Delta, Egypt. Alexandria Journal of Agricultural Research. 47(1), 147-152.
[28] Flagella, Z., Rotunno, T., Tarantino, E., Caterina, R., Caro, A., Di Caterina, R., Di Caterina, A., De-Caro, A. (2002) Changes in seed yield and oil fatty acid composition of high oleic sunflower (Helianthus annuus L.) hybrids in relation to the sowing date and the water regime. European Journal of Agronomy. 17(3), 221-230.
[29] Oride, J.R. (1984) Yield & Water use efficiency sunflower concontration and quality of dryland sunflower grow thin high plains. Agronomy Journal. 76(2), 229-235.
[30] Unger, P.W. (1992) Time and frequency if irrigation effects on sunflower production and water use. Soil Science Society of American Journal. 46(5), 1072-1076.
[31] Tabatabaei, S.A., Rafiee, V., Shakeri, E., Salmani, M. (2012) Responses of sunflower (Helianthus annuus L.) to deficit Irrigation at different growth stages. International Journal of Agriculture Research and Review. 2(5), 624-629.

Received: **11.01.2021**
Accepted: **10.02.2021**

CORRESPONDING AUTHOR

Ismail Naneli
Department of Field Crops,
Faculty of Agriculture,
Sakarya Applied Sciences University,
Sakarya – Turkey

e-mail: ismailnaneli@subu.edu.tr

© by PSP Volume 30– No. 05/2021 pages 5498-5509 Fresenius Environmental Bulletin

COMPARABLE ANALYSIS ATMOSPHERIC DEFICITS AND WATER REGIME DURING DIFFERENT SEASON ON ALLUVIAL FLOOD FOREST HABITAT AT EAST SREM

Milena A Andelic*

Forestry Faculty, University of Belgrade, 11000, Republic Serbia

ABSTRACT

Anthropogenic activities at East Srem during 20th century has led to drastic water regime changes and affected hygrophilous alluvial forest with penduculate oak as edificatory specie. After rising embankments and cessation floods only two water-resources are available for oak, precipitation (AW – atmospheric water) and groundwater (GW). In this area GW and river Sava (SW – surface water) are hydraulically connected; GW charges with SW and precipitation and discharges via evapotranspiration. RHMSS (Republic hydro-meteorological Service of Serbia) is the referential organization for weather forecasts and monitoring SW and GW level on territory Serbia. RHMSS stations located at East Srem are selected and collected data are analyzed for the period 1992-2018. Objective of this paper is to indicate degree of changes in available water quantity to oak during different seasons with methods synthesis and comparable analysis. In this area lithological environment could be permeable, semi - permeable or not permeable and during dry season these parameters dictates available water through-out capillary rising GW from which oak depends. During dry seasons one of the adaptation mechanism is prolonging root in direction accessible soil moisture. Lighting up water availability conditions will contribute in better planning water recourses at East Srem for protection penduculate oak.

KEYWORDS:
Alluvial plane, groundwater, vapor pressure deficit, Quercus robur L., East Srem

INTRODUCTION

According to Anex I Habitats Directive (2006/105/EC) the cod 91F0 represents alluvial flood mixed forest with species Quercus robur, Ulmus laveisi, Ulmus minor, Fraxinus excelsior or Fraxinus angustifolia along large rivers in Serbia [21]. Penduculate oak and narrow-leafed ash association at Srem is most hygrophilous variant of forest and represents syndynamic connection with monodominantly narrow-leafed ash forest [24].

Alluvial flood forest ecosystems were under biggest changes in biological and ecological balance relative to other forest ecosystems [22]. Autochthonous flora, fauna, watery and humid meadow and forest ecosistems last 100 yr suffered drastic changes under anthropogenic influences (construction embarkments, exploatation wells, drainage network) [14]. Most of the old penduculate oak forest were replaced with new associations and drying is explaninig with decrease groundwater level [24].

Many trees in water-limited areas survive because of groundwater. Extending root hair in direction available moisture, such species survive dry season by taking-up water directly from groundwater zone or through capillary rising [12]. During dry period precipitation supplies only minor part of evapotranspiration and trees need to rely on groundwater [3].

Precise understanding vegetation role in hydrological cycle is very important [13]. Arid areas occupies nearly 1/3 Earth surface which inhabits 38% world population. Withdraws groundwater for domestic use and spreading agriculture will lead to decrease groundwater level and put in danger terrestrial ecosystem. These factors affect biodiversity, degradation, desertification and balance with consequences on social and economic development [9].

In this paper water regime change (atmospheric-water (AW), groundwater (GW), surface-water (SW)) and atmospheric deficits are analyzed during period 1992-2018 on example unit “Progarska ada – Crni lug – Zidine – Drenska” located at East Srem. Results give insight interaction GW and vegetation during different season and improves understanding of possible oak response to water regime change. Interpretation general response vegetation by defined pattern represents practical approach in water-management.

Study area and data. Forest unit “Progarska ada – Crni lug – Zidine – Drenska” is situated between 20°08’00” - 20°19’00” East geographical longitude 44°39’00” - 44°44’00” North geographical latitude. Total unit surphace amounts 1318.23 ha and 84% territory occupies forest [4].

Main purpose of this unit was defined after formation hunting area, exploitation wells and embankments. Part of forest at Progarska ada have water supplies purpose, Crni lug hunt-tourist, Drenska protection from water, and Zidine currently only production [4].

Climatic conditions at experimental site. Climatic conditions observed on meteorological stations (m.st.) Surčin (44º49'; 20º17' and 96 m a.s.l.) and Sremska Mitrovica (45º01'; 19º33' and 82 m a.s.l.) during period 1992-2018 [20] are analyzed using the following parameters (Figure 1): air temperature; precipitation and relative air humidity. Long-term month average is determined as ratio between month sum value and total number of data. Seasonal value is shown as tree month average: winter – December, January and February; spring – March, April and May; summer – Jun, July and August; autumn – September, October and November.

Spatial distribution of average relative air humidity shows highest value during January and December, and lowest during April, May, July and August. Seasonal lowest relative air humidity value is registered during spring and summer, and highest during winter (Figure 1). On Pannonian plain relative annual precipitation oscillation (ratio between difference highest and lowest month and annual precipitation) riches minimum of 5-6% [25]. According to Figure 1 at this area precipitation are evenly distributed (6.7%). Average long-term annual precipitation amounts 616.6 mm, with highest value during summer (30% from total) and lowest during winter (20% from total). Highest month precipitation is during June (76.2 mm or 12.4%) and lowest during February (34.7 mm or 5.6%). Average long-term annual air temperature is 12.1ºC (Figure 1) with highest value during summer (22.1ºC), and lowest during winter (1.8 ºC). Monthly air temperature riches higest values during July (22.7ºC) and August (22.5ºC), and lowest during January (0.80ºC).

Vegetation and type of soil at investigation area. Best penduculate oak forests, located in Slavonia and Srem, are worldwide known for quality wood. They are located on aluviall plane of river Sava and its tributaries, on alluvial, sandy-loam or clay soil, on terrain whit relative high GW level and occasional floods [10]. At Srem most present forest associations, syndynamically connected, are penduculate oak and narrow-leafed ash (Fraxino angustifolie – Quercetum roboris) and penduculate oak, narrow-leafed ash and hornbeam (Carpino – Fraxino – Quercetum roboris). These associations are represented on surface of 22181 ha or 58% [2].

Within forest unit "Progarska ada – Crni lug – Zidine – Drenska" two soil type are [4]: alluvium and chernozem. According to vertical distribution forest belongs complex [4]:

I Complex (zone): alluvial – hygrophilous type forest, covers large number forest and smaller number shrubs associations developed during conditions intensive moisturizing at alluvial plane. Within Complex present hygrophilous species are: alder, willows, penduculate oak and narrow-leafed ash. Gradual humidity decrease has influenced on species shift and Complex dissect further on ceno-ecological groups:

a)Ceno–ecological forest type white willows and poplar (Salicion albae) at different semi-gley soil;

b)Ceno–ecological forest type penduculate oak and alder (Alno-Quercion roboris) at semi–gley and some automorph soils.

Ceno–ecological forest type further dissect on groups of ecological units:

- Forest white and black poplar (Populetum albo-nigrae) at different alluvial soils.
- Forest penduculate oak and narrow-leafed ash (Fraxino-Quercetum roboris) at moist semi-gley and drier gley soil.

Relief and lithological environment at investigation field. Forest unit "Progarska ada – Crni lug – Zidine – Drenska" lay along left side of river Sava, partly on its inundation and also at Progarska ada. Biggest forest unit surface (Crni lug and Zidine) lay at part which is protected from flood with embankments [4]. Relief of this forest unit was developed with constantly alluvial river enforcement, flooding and suspending material such as sand, gravel and mud. Relief consist of micro-elevations and depressions which represent former parts of river flow direction. Altitude of terrain is between 72-74 m a.s.l. [15].

Geological environment is composed from diluvium and alluvial deposits. During geological history river sediments were deposited on Tertiary clay and loam, and soil-gravel material forms the base [16]. According to [7] soil-gravel deposits have good filtration characteristic (10^{-1} cm·s^{-1}); beside soil-gravel complex in the base also appears clay, sandy clay of Neogene period; and upper layer complex have considerably lower value coefficients filtration (10^{-3}-10^{-4}-10^{-5} cm·s^{-1}).

Penduculate oak habitat are located on alluvial formations (two-layered porous environment) with established direct hydraulic connection between river and GW [16]. Oscillation GW depends on SW level and evapotranspiration. In this area largest reserves GW are accumulated in inter-granular porous deposits Neogene and Quartery age [18]. At widely alluvial plane and river bed Sava, thanks to spatial and hypsometric ratio presented lithological environment, sub-artesian aquifer is formed [15].

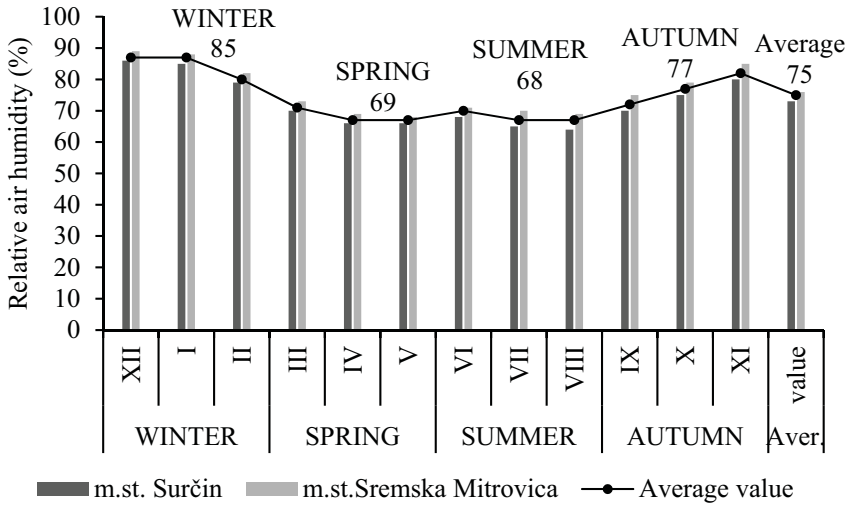

(a)

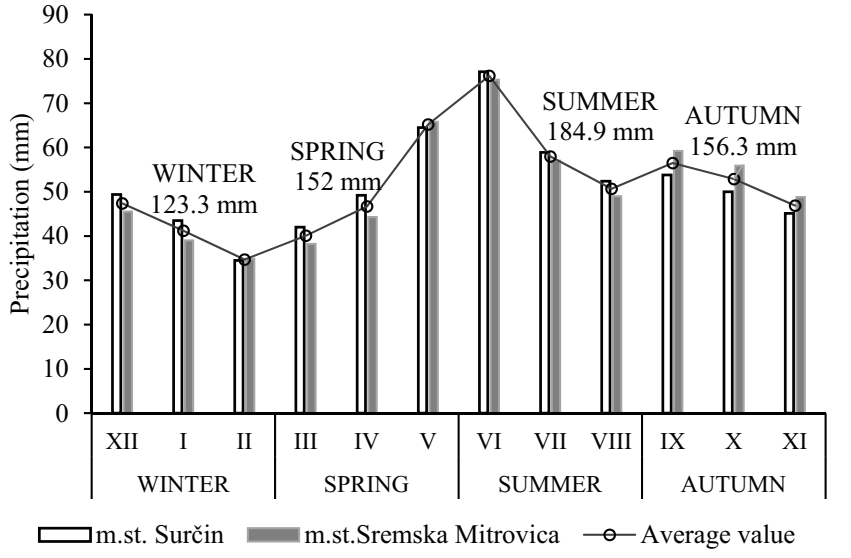

(b)

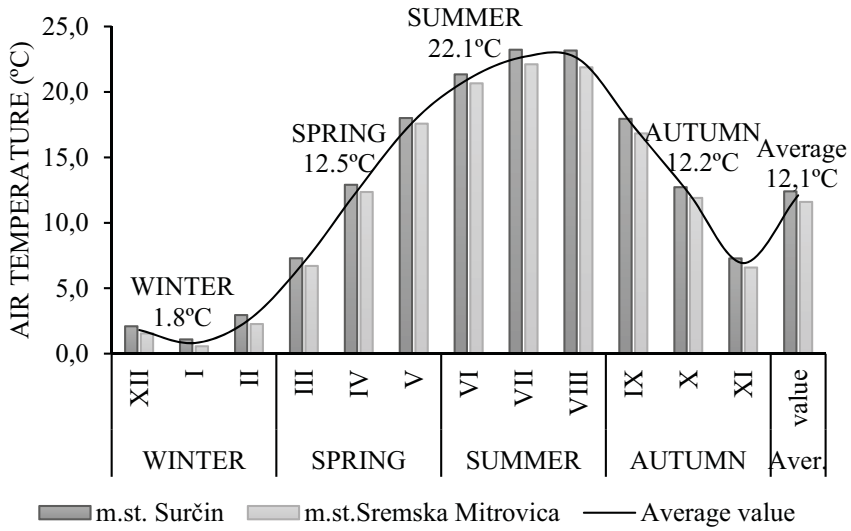

(c)

FIGURE 1
Climatological conditions at East Srem for period 1992-2018 (a, relative air humidity; b, precipitation; c, air temperature)

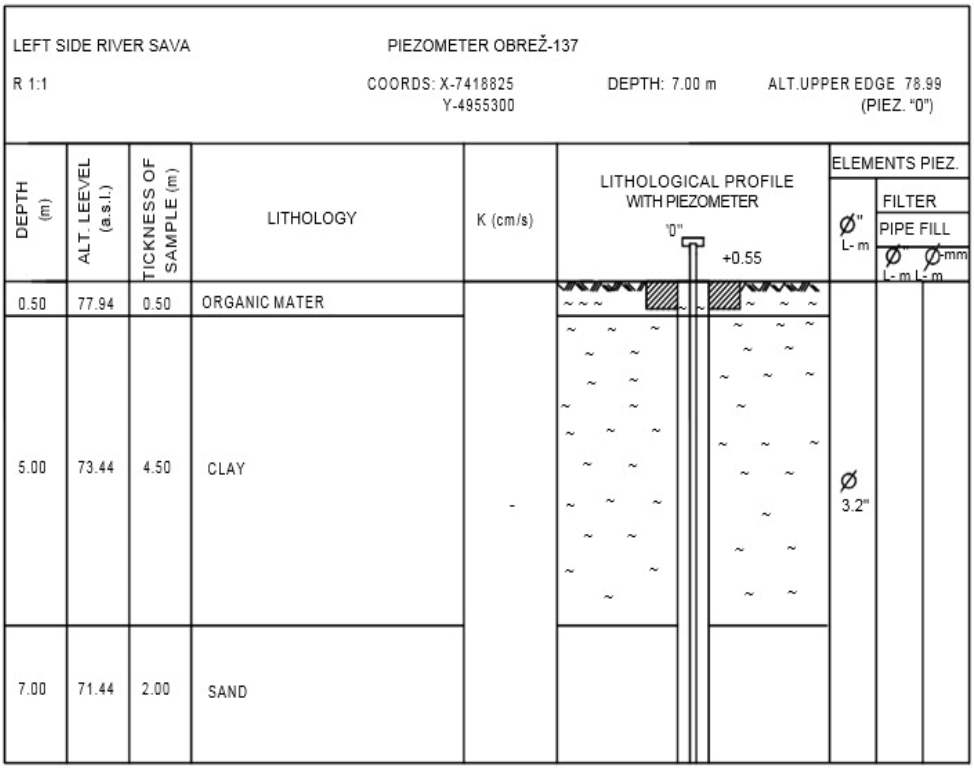

FIGURE 2
Piezometer construction Obrež (137) RHMSS (Location piezometer is 44°44'15"N and 19°58'30"E; altitude most upper spot of piezometer is 78.99 m a.s.l; level of terrain is 78.44 m a.s.l; altitude of part of piezometer above terrain is 0.55 m; diameter of piezometer is 80/73 mm; piezometer longitude is 7.55 m; piezometer depth is 7 m)

Lithological environment at East Srem on example forest unit "Progarska ada – Crni lug – Zidine – Drenska" is interpreted with piezometer Obrež (137) [20]. At this area lithological samples show the presence of clay till 5 m depth, and sands are deeper (Figure 2). Most important physical characteristics connected with capillary rising are [11]: maximal capillary rising - function of porosity, moisture accumulation capacity, capillary rising - function of nonsaturated hydraulic conductivity. Clay has highest capillary rising and longest capacity for keeping moisture.

MATERIALS AND METHODS

Material in paper. For purpose of this paper registrated data (atmosferic water (AW), graoundwater (GW), surface-water (SW) and climatological parameters used for calculation different atmosperic deficits) are colected from annual books for following RHMSS stations [20]: meteorological station (m.st.) Surčin and Sremska Mitrovica; hydrological station (h.st.) Šabac; and piezometer Obrež (137).

Hydrological and meteorological annual books are composed from data observed with stations distributed on territory Serbia [20]:

Climatological data include measuring and observation different parameters in time interval 07, 14 and 21 hour. Beside basic measured values, annual books show different meteorological measurement such as relative air humidity.

Hydrological annual books contain two parts: surface water (SW) and groundwater (GW). At hydrological stations, limnigraph, digital and batten are used for SW level monitoring. Annual books show minimal, maximal and average month and annual SW level.

Network GW stations (piezometers) are formed within lithological environment of inter-granular porosity or phreatic and sub-artesian aquifers. Annual books show for every piezometer absolute high ("0"), depth and altitude (part above surface terrain). Annual books contain piezometer data and minimal, maximal and average month and annual GW level.

Methods. Collected parameters value from annual books [20] are separately analyzed for period 1992-2018, with focus on last four years, and divided in two groups: climatological and hydrological data group. In this paper used scientific methods are: method synthesis and comparable method.

Climatological observation and atmospheric demands at investigation area. Precipitation, relative air humidity and temperature observed on m.st. Surčin and m.st. Sremska Mitrovica are used for cal-

culation following variables: (1) potential evapotranspiration (ETp), (2) vapor pressure deficit (VPD), (3) atmospheric humidity (NS), (4) precipitation deficit, (5) water-limited conditions.

(1) Potential evapotranspiration (ETp). According to Tornthwaite method following formulas are used for calculation ETp [5]:

$$ET_p = 1.6 \cdot \left(10 \cdot \frac{T}{I}\right)^a \quad (1)$$

$$a = 0.000000675 \cdot I^3 - 0.000077 \cdot I^2 + 0.01792 \cdot I + 0.492 \quad (2)$$

$$I = \left(\frac{T}{5}\right)^{1.514} \quad (3)$$

ETp – potential evapotranspiration (mm); T – mean month air temperature (°C); I – annual thermal index, a - index.

ETp value has to be corrected with duration day coefficient [5]. Longitude of duration day is shown according to location m.st. Surčin and m.st. Sremska Mitrovica. In calculations average value is used.

(2) Vapor pressure deficit (VPD) is calculated as maximal vapor pressure (e_S) and represent function of air temperature [23]:

$$e_s = 0.6108 \exp\left(\frac{17.27+T_a}{T_a+237.3}\right) \quad (4)$$

e_S – maximal vapor pressure (kPa); Ta – air temperature (°C).

Coefficient in formula depends of sigh air temperature [23]: T (°C) > 0 parameters amount C1 = 6.1078, C2 = 17.08085, C3 = 234.175; T (°C) < 0 parameters amount C1 = 6.1078, C2 = 17.84362, C3 = 245.425.

Actual vapor pressure (e_a) is determined as function maximal vapor pressure (e_S) and relative air humidity [23].

$$e_a = e_s \cdot \left(\frac{RH}{100}\right) \quad (5)$$

e_a – actual vapor deficit (kPa), RH – relative air humidity (%).

(3) Meyer quotient (NS) or atmosphere humidity is calculated with value vapor pressure deficit. Cernesc value for classification climate are following [25]: NS=200 climate conditions are between arid and humid, NS<200 climate is arid, NS>200 climate is humid. Following formula is used for calculation Meyer quotient [25]:

$$NS = \frac{H}{E-e} \quad (6)$$

H – average annual precipitation (mm), E – maximal vapoure pressure which is equal to average annual air temperature (kPa), e – average actual vapor pressure during year (kPa).

(4) Precipitation deficit. represents difference between potential evapotranspiration and precipitation [3].

(5) Water limited conditions. represents ratio between precipitation and potential evapotranspiration - $P \cdot ETp^{-1}$. According to [12] value $P \cdot ETp^{-1}$ less or equal to 0.75 represent water limited conditions for vegetation.

Hydrological observation [20] (1) Water level of river Sava. SW (surface-water) level observed at hydrological station (h.st.) Šabac (72.61 m a.s.l.) is represented according to absolute value.

(2) Groundwater level. GW (groundwater) level observed in piezometer Obrež (137) (78.44 m a.s.l.) is represented according to absolute value.

RESULTS

On example forest unit "Progarska ada – Crni lug – Zidine – Drenska" at East Srem water regime changes and atmospheric deficits are analyzed during different seasons (winter, spring, summer and autumn) for period 1992-2018. This chapter shows calculations and analysis: atmospheric deficits with boundary values; oscillation GW and SW level; synthesis and comparable analyzes GW, SW and AW.

Atmospheric deficits at investigation field. Atmospheric deficits are defined with four parameters: precipitation deficit (Δ=P-ETp^{-1}), vapor pressure deficit (VPD), atmospheric humidity (NS) and water-limited conditions ($P \cdot ETp^{-1}$).

Wet and dry seasons for vegetation are defined with following precipitation deficits [3]: 170 (150 to 200) mm and 380 (350 to 400) mm respectively. Daily vapor pressure deficit values higher than 3 kPa affect transpiration (becomes excessive) and plant abruptly loses water [19]. Water-limited conditions are characterized with significant temporal and spatial precipitation variability, short infiltration events often only partially rewetting root zone, limited soil moisture availability exerting water stress on plants, adaptation vegetation to water stress [12].

At investigation field long-term annual precipitation deficit, calculated as difference ETp (735.4 mm) and precipitation (616.6 mm) amounts -118.8 mm (Table 1). Long-term values shows precipitation deficit from April to September, but July (-85.2 mm) and August (-80.3 mm) have highest values. Compared to the long-term average, last four years (2015-2018) have larger precipitation deficit values (Table 1): -149.4 mm (2015 yr.); -267.3 mm (2017 yr.) -186.3 mm (2018 yr.). During 2016 yr. precipitation deficit is below long-term average (Table 1). Precipitation deficit last four vegetation periods is present in almost all months. Highest month deficit during last four years are (Table 1): Jun (-100.9 mm) and July (-151.7 mm) 2015 yr.; July (-94 mm) and August (-79.7 mm) 2016 yr.; Jun (-120.1 mm) and August (-118.2 mm) 2017 yr.; August (-114.7 mm) 2018 yr. In most cases these values are above long-term

average.

Critical months with highest vapor pressure deficit are May, July and August (Table 2). March, April and August have most arid atmospheric conditions (Table 3). During some months in 2015 and 2017 yr vapor pressure deficit has excessive rising. Average month vapor pressure deficit value during 2015 and 2017 yr. is larger than 3 kPa and also indicate on extremely high daily values (Table 2). During last four vegetation periods, according to boundary classification (NS≤200), months with extreme aridity are (Table 3): April (105), Jun (107) and July (34) 2015 yr.; April (202) and August (207) 2016 yr.; March (130), April (204), Jun (93), July (192) and August (85) 2017 yr; April (151), May (204), August (113), September (57) and October (58) 2018 yr. These values show extremly atmospheric aridity during July 2015 yr., August 2017 yr., September 2018 yr.

TABLE 1
Comparative representation value of precipitation and ETp

Yr.	Month	I	II	III	IV	V	VI	VII	VIII	IX	X	XI	XII	Average value
1992-2018	ETp	1.1	5	23.2	56.7	101.1	127.7	143.2	131	80	45.8	17.9	2.8	735.4
	P	41.2	34.7	40.1	46.7	65.2	76.2	58	50.7	56.5	52.9	46.9	47.4	616.6
	Δ	40.2	29.7	16.9	-9.9	-35.9	-51.5	-85.2	-80.3	-23.5	7.1	29.1	44.6	-118.8
2015	ETp	4.6	5.2	22.5	51.7	102.5	125.4	162.3	144	87.5	40.3	18.4	5.3	769.6
	P	55.9	54.3	73.7	28.6	91.9	24.6	10.7	80.3	76.4	64.5	57.6	2.1	620.2
	Δ	51.3	49	51.1	-23.1	-10.6	-100.9	-151.7	-63.7	-11.1	24.2	39.2	-3.2	-149.4
2016	ETp	1.6	21.5	26.6	65.4	93.2	133.5	145.7	120	85.7	36.3	16.4	0	746
	P	42.9	36.2	80.9	48.25	57.8	121.0	51.8	40.3	63.8	64.0	61.8	1.9	670.5
	Δ	41.3	14.7	54.3	-17.2	-35.4	-12.6	-94	-79.7	-21.9	27.7	45.4	1.9	-75.6
2017	ETp	0	8.4	34.8	49	97.2	145.4	153.4	144.2	76.5	44.2	16.8	6.4	776.4
	P	15.8	21.6	28.5	50.4	86.2	25.3	53.5	26.0	71.0	46.6	34.6	49.7	509.1
	Δ	15.8	13.2	-6.4	1.4	-11.1	-120.1	-99.9	-118.2	-5.5	2.4	17.8	43.3	-267.3
2018	ETp	7.2	1.7	15	80.7	118.8	127.5	136.9	140.6	83.9	56.9	19.2	2	790.5
	P	39.6	67.3	58.9	39.1	52.6	109.5	94.7	25.9	14.3	14.3	33.0	55.3	604.2
	Δ	32.4	65.6	43.9	-41.7	-66.3	-18	-42.2	-114.7	-69.6	-42.7	13.7	53.2	-186.3

TABLE 2
Comparative review value vapor pressure deficit (VPD)

Month	I	II	III	IV	V	VI	VII	VIII	IX	X	XI	XII
1992-2018	0.9	1.3	1.9	2.2	2.3	2.2	2.3	2.4	1.9	1.6	1.2	0.8
2015	1.0	1.1	1.9	2.7	2.4	2.3	3.1	2.7	1.9	1.1	1.4	0.5
2016	1.0	1.5	1.6	2.4	2.1	1.9	2.2	1.9	2.0	1.3	1.4	1.2
2017	1.0	1.5	2.2	2.5	2.0	2.7	2.8	3.0	2.1	1.8	1.1	1.1
2018	1.2	1.0	1.4	2.6	2.6	1.9	1.8	2.3	2.5	2.5	1.5	0.9

TABLE 3
Comparative review value atmospheric humidity (NS)

Month	I	II	III	IV	V	VI	VII	VIII	IX	X	XI	XII
1992-2018	463	267	208	209	284	353	250	214	292	336	396	563
2015	543	495	389	105	391	107	34	299	402	569	406	44
2016	448	238	509	202	271	631	234	207	319	480	447	16
2017	164	141	130	204	424	93	192	85	332	255	301	452

2018	321	679	408	151	204	572	532	113	57	58	216	597

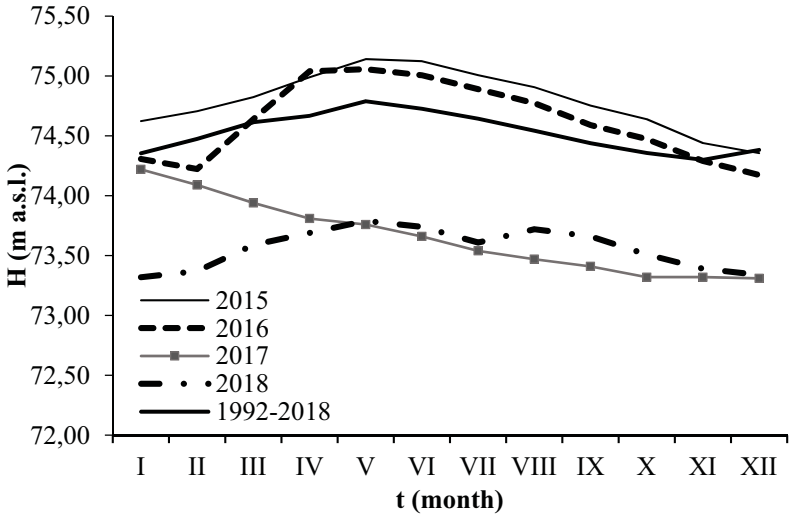

FIGURE 3
Comparative review GW level in piezometer Obrež (137)

Long-term average values show the prevalence of water-limited conditions ($P \cdot ETp^{-1}$) from May (0.64) till August (0.39) (Table 1). Interval values constantly decline during this months. Although these values in September (0.71) rising still indicate on aridity presence (Table 1). Months with arid conditions ($P \cdot ETp^{-1}$) are: May (0.62), July (0.36) and August (0.34) 2016 yr; Jun-August (0.17-0.35) 2017 yr; April (0.48), May (0.44) and July-October (0.17-0.69) 2018 yr. Lowest $P \cdot ETp^{-1}$ value is presented in July 2015 yr (0.07). These value indicate extreme aridity for plants.

Ground and surface water regime at investigation field. GW contributes to process moisturizing soil. This contribution depends directly from hydrogeological conditions and anthropogenic activities [16]. In order to prevent flooding, along river Sava was constructed embankment and hydraulic connection between wetlands and river was interrupted during period high water levels [15]. According to [15] drainage network on agriculture surfaces and exploitation wells probably influenced on decrease GW level. Long-term GW level observed in piezometer Obrež-137 (Figure 2) rises from January till May, decreases from Jun till November, and rises during December (Figure 3). During 2017 and 2018 yr. GW level is below long-term average and lower than 2015 and 2016 yr. (Figure 3). During 2015 and 2016 yr. GW level is highest in April and May, and lowest in December. Compared to long-term average, GW level in January and February 2016 yr is lower. During 2017 yr. GW level constantly declines. GW level in July 2018 yr decline.

Long-term average SW level observed at h.st. Šabac riches maximum in April, declines from May till August, and rises from September till December (Figure 4). Compared to long-term average SW level has different oscillations during last four years:

2015 yr.: From January till March and October is above, during April till December (except Jun and October) below long-term average.

2016 yr.: In January and April is below long-term average, from Jun till August in average, from September till October (and December) below average. In February, March, May and November is above long-term average.

2017 yr.: In January and from April till August is below long-term average, during February and September in average, from October till November below average, in December above average. In March is slightly above long-term average.

2018 yr.: From January till April is above average, from May till Jun below average, in July above average, in August in average, from September till December below average.

Synthesis and comparable analyses atmospheric, ground and surface water. Comparative review values AW (m.st. Surcin and m.st. Sremska Mitrovica), SW (h.st. Šabac) and GW (piezometer Obrež 137) level during period 1992-2018 yr. and 2015-2018 is shown on Figure 5. From synthesis reviewed data following conclusions are (Figure 5):

During period 1992-2018 precipitation highest amount is registered in Jun. GW level declines from May till November. SW level decreases from April till August.

During 2015 yr. precipitation lowest amount is registered in April, Jun, July and December and larger amount during March, May, August and September. GW level from January till May rises and from Jun till December declines. SW level decreases from March till September, and rises during October.

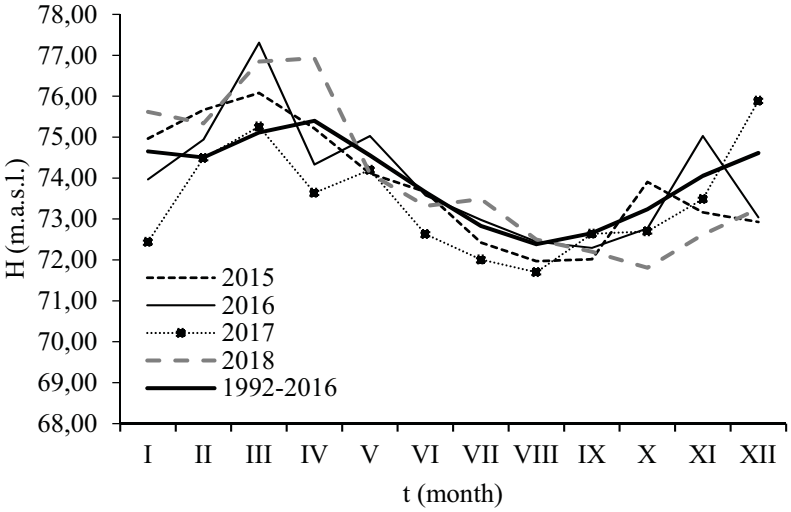

FIGURE 4
Comparable review SW level at h.st. Šabac

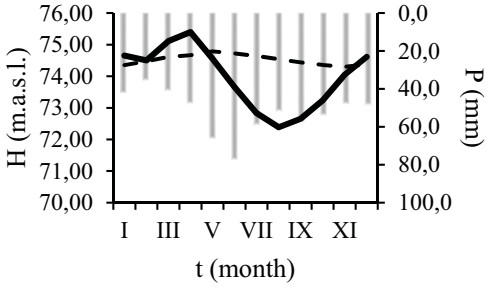

(a)

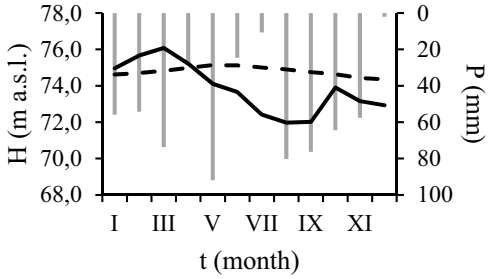

(b)

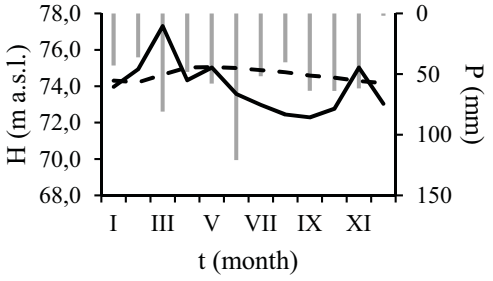

(c)

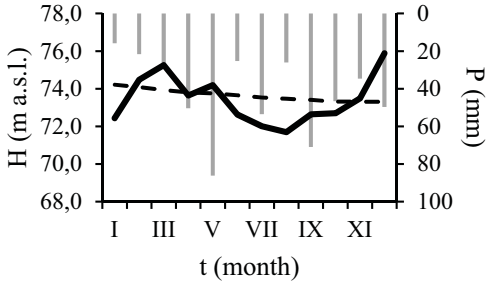

(d)

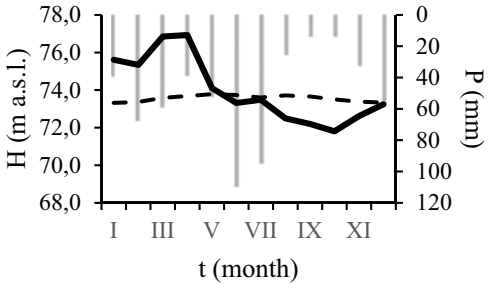

(e)

FIGURE 5
Comparative review precipitation, GW and SW level values
(a, 1992-2018; b, 2015; c, 2016; d, 2017; e, 2018).

During 2016 yr. precipitation larger amount is registered in March and Jun. During other months precipitation are below or in long-term average. GW level rises from February till April, and after that decreases gradually. SW level decreases from April till September.

During 2017 yr. precipitation are above long-term average. In Jun precipitation are significantly below long-term average. GW level declines evenly during whole year. SW rising is registered in May and September.

During 2018 yr. larger amount of precipitation is registered in Jun and July. Precipitation amount, from August till October, is significantly below long-term average. GW level rises from February till August (minor decreases is registered in July), after that decreases. SW level rises during April and July then decreases till October and after that rises again.

DISCUSSION

High ETp values indicate loosing water in soil subsurface and surface via evaporation and transpiration. This exspecially refers to dry seasons. In water-limited conditions high ETp value signify that actuall ET is main component of watery balance [12]. Soil moisture moves according to following directions [5]: capillary movement - from zone with higher capillary potential to lower, deeper moisture to the surface by water vapor (temperature and pressure gradient influence on movement). Capillary water is most important water for plants because of longest retention. Amount of water which passes through plant depends on physiology and enviromental factors. Plant spends large water amount for optimal functioning. For example to synthesize 1 gram dry matter plant need to spend 500 grams of water [6]. For production 1 kg dry matter oak transpires 340 $l \cdot kg^{-1}$ [17].

On experimental field "Progarska ada – Crni lug - Zidine – Drenska" at East Srem precipitation amount during 2017 yr. (509.1 mm) and 2018 yr. (604.2 mm) is significantly below long-term average (616.6 mm) and 2015 yr. (620.2 mm), 2016 yr. (670.5 mm). Precipitation from May till October (except September) 2017 yr. are below long-term average, uppermost in Jun (25.3 mm) and August (26 mm). Also during 2018 yr. precipitation are below long-term average from August (25.9 mm) till November (33 mm).

Largest precipitation deficit is present 2017 (-267.3 mm) and 2018 yr. (-186.3 mm) compared to long-term average and 2015, 2016 yr. According to standard values [3] precipitation deficit during 2017 yr. belongs upper limit and indicates to extremely arid conditions for vegetation (NS<200 mm).

Compared to long-term average, vapor pressure deficit is increased during last four years. This increasing indicate high atmospheric aridity with negative impact on transpiration (become excessive) during summer months mostly in July. Water-limited conditions during 2017-2018 yr. are below limit (≤0.75) and twice as much below long-term average and indicate to intensification aridity. Extremely low values of atmospheric humidity last four years are represented during spring and summer season. In the future vapor pressure and precipitation deficit, atmospheric humidity and water limited conditions are likely to change from season to season with different impact on transpiration.

GW balance depends from charging and discharging and special detailed review balance components with their connections to other components of watery cycle gives important information for assessment sustainability GW resources and efficiently management [8]. GW charges during high water level river Sava and precipitation (on places where aquifer is opened to the surface) [16]. Observation GW level in piezometer Obrež (137) and SW level at h.st. Šabac during analyzed period showed following:

During spring and summer 2015 and 2016 yr. GW level is above long-term average. During 2015 yr. SW level is below long-term average, and during 2016 yr. in long-term average.

During 2017 and 2018 yr. GW level is below long-term average and 2015, 2016 yr. During 2017 yr. SW level is below long-term average and 2015 yr. During first half of 2018 yr. SW level is above long-term average but from August till December below long-term average and 2015-2017 yr.

Results indicate that in situation higher vapor pressure and precipitation deficits penduculate oak depends on hydrogeological conditions in terms available moisture. Penduculate oak in younger age develops roots which goes 2.00 m in depth, later that roots lags behind in rising and lateral roots replacing it [10]. GW capillary rise is very important for surviving oak during larger precipitation deficits. However united effects of watery deficits in wide range might have different impact on vegetation. After construction embankments, flood water is absent, and penduculate oak depends only on AW and GW. At investigation field during dry season different configuration terrain with presence micro-elevations and depressions and permeable, semi-permeable and non-permeable lithology becomes additional aggravating factor for availability capillary water to root system.

According to [1] increasing demand for water could lead to excessive draw aquifers. This draw could lead to price increase and have negative influence on water quality. Due to strong competitions between industrial, urban and agriculture systems, future demands for fresh water will increase and more endanger vegetation. Groundwater management should directed in way that draw do not excess natural charging. Natural charging can amount less

than 1% average precipitation in arid and semi-arid regions, 20% average precipitation in Mediterranean climate type, till 50% in cold humid climate regions.

On one side overall assessment fresh water use covers benefits and on other cost of management including investments for environment protection. Greater competition between different sectors indicate that within water management has to be included conservation strategy and applying appropriate use of fresh water. Main goal would be evenly water distribution for all sectors [1]. Among the others, range of water distribution will depend from correct assessment of used amount water by vegetation.

CONCLUSIONS

During 19th and 20th century hygrophilous alluvial forest with penduculate oak as edificatory specie located at East Srem were brought in condition of natural sparseness and drying under influence different anthropogenic activities. In this context two important periods are: period of primitive cuts of trees and hydro-technical works (channels, exploitation wells, embankments). Last decades special attention is directed to climate change, primarily on precipitation regime and air temperature.

On example forest unit "Progarska ada – Crni lug – Zidine – Drenska" at East Srem water regime change (AW, GW and SW) and atmospheric deficits are analyzed during period 1992-2018 with special focus on last four years. Values of selected parameters observed with RHMSS stations located at East Srem are collected from annual books. In this paper climatic and hydrological conditions are analyzed separately, boundary values for atmospheric deficit are shown, GW and SW level oscillation, with methods synthesis and comparable analysis is roughly shown water availability for penduculate oak.

Results indicates on larger and smaller water deficits during different seasons and years with different effects on plants. In situation larger precipitation deficit, penduculate oak need to rely on GW capillary rising. In this paper special attention is dedicated to vapor pressure deficit. Daily values vapor pressure deficit above 3 kPa have negative impact on transpiration. During 2015-2018 yr. monthly vapor pressure deficit is increased and beyond boundary value. Atmospheric humidity and water-limited conditions during 2015-2018 yr. also indicate on extremely arid climatic conditions at experimental field.

At East Srem on example forest unit "Progarska ada – Crni lug – Zidine – Drenska" results and relevant literature showed following conclusions:

In this area sub-artesian aquifer is formed. Aquifer reserves are accumulated in lithological environment with inter-granular porosity. Two-layered porous environment is composed from permeable sands and semi- and non-permeable clays (upper layers). Coefficients filtration ranges from 10^{-1} to 10^{-2} $cm \cdot s^{-1}$ (sands) and 10^{-4} to 10^{-5} $cm \cdot s^{-1}$ (clay).

Between GW and river Sava direct hydraulic connection is developed; GW charges during high SW level and with precipitation, and discharges via evapotranspiration.

Lithological samples in piezometer Obrež (137) indicate presence semi-permeable and non-permeable clay till 5.0 m depth. Clays have highest capillary rising and longest water retention. Deeper layers are composed from sands with good permeability properties but low retention. During dry season capillary rising is crucial for maintaining functional stability penduculate oak.

Relief this forest unit contains micro-elevations and depressions. These could be additional limited factor for capillary rising and water availability to penduculate oak (root system goes into 2.0 m depth).

Atmospheric deficits analysis has shown larger vapor pressure and precipitation deficit and also presence of higher aridity during 2017 and 2018 yr. compared to long-term average.

Water-limited conditions during 2017 and 2018 yr. are below boundary value ($\leq$0.75) and twice as lower then long-term average. This value indicates on extremely arid climate conditions.

Compared to the long-term average, GW level is lowest during 2017. and 2018 yr. More or less, during 2017 and 2018 yr., SW level is below long-term average. Observation of these values is important in analysis extremely arid atmospheric conditions impact on penduculate oak.

Comparative analysis GW, SW and AW during 1992-2018 yr and 2015-2018 yr. indicate presence of non-equally distribution precipitation last four years and during both periods GW regime follows regime of river Sava. Besides atmospheric deficits during vegetation period 2015 and 2016 yr., GW level is on favorable depth for oak root system comparative to 2017 and 2018 yr. During 2015 and 2016 yr atmospheric aridity is not so large (except July 2015 yr.).

Arid climatic conditions, characterized with variable precipitation distribution and air temperature increasing, may have significant effect on hygrophilous species such as penduculate oak. Strategy of precise technology gives good assessment tool for used water in wide range during sulfurous and deficit and represent one of the measure for achieving this goal. Results of this paper represent contribution in lighting up watery and atmospheric conditions on habitat penduculate oak at East Srem.

REFERENCES

[1] Bouwer, H. (1994) Role of groundwater and artificial recharge in future water resources management. Future Groundwater Resources at Risk. Book of Proceedings of the Helsinki Conference. 222, 491-497.

[2] Bobinac, M. (2009) Effects of common oak regeneration on a permanent sample plot in Srem – after two decades. Works of the Faculty of Forestry. University of Sarajevo. 1, 9-19.

[3] Čermak, J., Prax, A. (2001) Water balance of a Southern Moravian floodplain forest under natural and modified soil water regimes and its ecological consequences. Annals of Forest Science. 58(1), 15-29.

[4] Dražić, G., Dražić, S. (2010) Special forest management basis for unit Progarska ada – Crni lug – Zidine – Drenska". Ministry of Agriculture, Forestry and Water Economy Serbia. Forest Service.

[5] Đorović, M. (1995) Horizontal pipe drainage. Naučna knjiga (Scientific book). Belgrade. 1-181.

[6] Đukić, M. (2006) Plant physiology. Forestry faculty. University of Belgrade. Belgrade. 1-227.

[7] Filipović, B., Krunić, O., Lazić, M. (2005) Regyonal hydrology of Republic Serbia. Faculty of Mining and Geology. University of Belgrade. 1-403.

[8] Foster, S., Perry, C. (2009) Improving groundwater resource accounting in irrigated areas: a prerequisite for promoting sustainable use. Hydrogeology Journal. 18, 291–294.

[9] Huang, F., Zhang, D., Chen, X. (2019) Vegetation response to groundwater variation in arid environments: visualization of research evolution, synthesis of response types, and estimation of groundwater threshold. Int. J. Environ. Res. Public Health. 16 (10), 1849.

[10] Jovanović, B. (2000) Dendrology. Forestry faculty. University of Belgrade. Belgrade. 1-536.

[11] Liu, Q., Yasufuku, N., Miao, J., Ren, J. (2014) An approach for quick estimation of maximum height of capillary rise. Soils and Foundations 54, 1241-1245.

[12] Lubczynski, M. (2009) The hydrogeological role of trees in water-limited enviroments. Hydrogeology Journal. 17, 247-259.

[13] Lundblad, M., Lagergren, F., Lindroth, A. (2001) Evaluation of heat balance and heat dissipation methods for sap flow measurments in pine and spruce. Ann. For. Sci. 58, 625-638.

[14] Mataruga, Z., Jarić, S., Karadžić, B., Mitrović, M., Kostić, O., Marković, M., Pavlović, P. (2016) Contribution to the knowledge of the allochthonous flora in the lower course of the Sava River. Acta Herbologica. 25, 57-70.

[15] Nikić, Z. (2003) Good water supply for the "Crni lug" hunting area [Serbia, Serbia & Montenegro], present state and future. Conference "Voda 2003" Zlatibor. 373-376.

[16] Nikić, Z., Letić, L., Nikolić, V., Filipović, B. (2010): Procedure for underground water calculation regime of Pedunculata oak habitat in Plain Srem. Bulletin of the Faculty Forestry. 101, 125-138.

[17] Nikić, Z., Pavlović, R. (2012) Hydrogeology with geomorphology. Forestry Faculty. University of Belgrade. 1-404.

[18] Polomčić, D., Stevanović, Z., Bajić, D., Hajdin, B., Vakanjac-Ristić, V., Dokmanović, P., Milanović, S. (2012) Water supply and sustainable management of groundwater resources in Serbia. Vodoprivreda. 44, 225-231.

[19] Reyes-Acosta, J.L., Lubczynski, M.W. (2012) Optimization of dry-season sap flow measurments in an oak semi-arid open woodland in Spain. Ecohydrology. 7 (2), 258-277.

[20] RHMSS. Rebublic Hydro-meteorological Service Serbia (2020) Annual books. Official web: hidmet.gov.rs.

[21] Sekulić, N., Šinžar-Sekulić, J. (2010): Emerald ecological network in Serbia. Serbian Government Ministry of Environment and Spatial Planning Institute for Nature Conservation of Serbia. Belgrade. 1-95.

[22] Tikvić, I., Zečić, Ž., Ugarković, D., Posarić, D. (2009) Damage of Forest Trees and Quality of Timber Assortmets of Pedunculate Oak on Spačva Area. Forestry. (5–6), 237-248.

[23] Tendayi, R. (2010) Evapotranspiration in water limited enviroments: up – scaling from the crown canopy to the eddy flux footprint. Thesis. International institute for geo – information science and earth observation Enschede, the Netherlands. 1-81.

[24] Tomić, Z. (2004) Forestry phytocenology. Forestry faculty. University of Belgrade. Belgrade. Book. 1-250.

[25] Unkašević, M. (2005): Forestry ecoclimatology. Forestry faculty. University in Belgrade. Belgrade. Book. 1-231.

Received: **04.09.2020**
Accepted: **15.02.2021**

CORRESPONDING AUTHOR

Milena A Andelic
Forestry faculty,
University in Belgrade.
Belgrade 11000 – Republic Serbia

e-mail: milenaandjelic911@hotmail.rs

© by PSP Volume 30– No. 05/2021 pages 5510-5515 Fresenius Environmental Bulletin

RESEARCH ON THE DEVELOPMENT OF CULTURAL CREATION PRODUCTS OF ENVIRONMENTAL CERAMICS UNDER THE BACKGROUND OF DIGITAL CREATIVE INDUSTRY

Xiaobo Lian[1], Sangyoung Lee[2,*]

[1]Sanming University, No. 25, Jingdong Road, Sanyuan District, Sanming City, Fujian Province, China
[2]TongMyong University, No.428 Shenxian Road, South District, Busan Metropolitan City, South Korea

ABSTRACT

Under the background of the rapid development of the digital creative industry, as the urbanization process continues to advance, environmental ceramics as part of it also shines in public art. The development of environmental ceramics is an inevitable trend in the construction of public space. For traditional ceramic art, China has a long history of ceramic art and exquisite craftsmanship. However, with the continuous development of the traditional ceramic art technology, it has presented various unsuitable drawbacks in the specific application. Environmental ceramics has successfully solved these problems, and naturally it is integrated into public facilities, making the overall environmental building uniquely appealing. Only by combining the traditional Chinese cultural elements with the modern people's way of thinking, so that the environmental ceramic art reflects the modern people's living habits, can the environmental ceramic works be accepted by more people, and people's living standards can be continuously improved.

KEYWORDS:
Digital creative, Cultural creation products, Creative industry

INTRODUCTION

In recent years, with the continuous development of network technology, industries closely integrated with Internet technology are also booming. Network literature, creative design, VR and many other fields have successfully achieved the perfect combination of Internet technology. The combination of creative design and computer technology has become an important part of the digital creative industry. Under the premise of innovation and development as the background of the whole society, the digital creative industry was included in the country's five strategic emerging industries for the first time in December 2016, marking the development of the digital creative industry into a new golden age. The digital creative industry refers to a new type of industry that relies on innovative ideas based on high technology. The development of the digital creative industry is very rapid, showing a trend of linear growth and its association with information technology, high-end manufacturing and other industries is called the five new pillars supporting economic development.

With the strong development of the digital creative industry, the structure of the corresponding cultural industry and the ecological environment for the development of cultural and creative products are constantly being adjusted and improved. Culturally creative products, in particular, are sold as a cultural idea and the artistic value behind the product. The same production process, with the addition of the cultural and artistic value that the public appreciates, has a different visual experience. The value of the goods it has is also incalculable. Traditional folk art works have great artistic value, but they have not been well developed due to their low work efficiency and limited communication channels. The marketed products produced by the machine are often not distinctive, so they are not highly competitive, and the economic benefits brought by nature are not good. Therefore, the emergence and development of cultural and creative products.

With its unique expressive power, environmental ceramics gradually enters the human eye. Environmental ceramic art is an art developed on the basis of traditional ceramic art. It is more practical for the construction of public environment. The traces of environmental ceramics can be seen in various public areas such as the square park. The environmental ceramic art of each area is combined with the historical background of its geographical environment to make it unique. And representative. And the spiritual ideas revealed in environmental ceramics are more and more easily understood and accepted by the public.

DIGITAL CREATIVE INDUSTRY

The development of digital creative industries. The digital creative industry is an industry that combines advanced digital technology with the excellent creative ideas of human beings. The digital creative industry is the driving force for the continuous development of the technology field and the inexhaustible source of cultural creativity. At the core of the digital creative field is the creative concept. Only with a good creative concept can it be realized through high-tech science and technology.

The digital creative industry has been widely recognized by the public for its simplicity, generosity and rapid dissemination. At the same time, in the modern digital creative industry, one must also add to the research and development of energy-saving and environmental protection functions. Joining the concept of environmental protection enables the digital creative industry to have greater competitiveness and ultimately achieve sustainable development of the industry. The comprehensive promotion of economic development, convenient communication methods and energy saving and environmental protection have made the digital creative industry an important part of emerging industries in various countries.

Figure 1 shows the spatial distribution of the global creative industry.

It can be seen from the results in Figure 1. The development of the global cultural and creative industries is extremely uneven. The global cultural and creative industry development centers are mainly concentrated in the North America with the United States as the core, the European region with the UK as the core, and China and Japan. South Korea is the core Asian region. And the proportion of the Asian region is small, but the historical and cultural background of the Asian region is relatively strong. China accounts for 4% of the total, which is the smaller proportion of the countries. This is inconsistent with China's 5,000-year history. Therefore, China still has a long way to go for the development of cultural and creative industries.

The connotation of digital creative industry. The specific contents of the cultural and creative industries mainly include creative groups in radio, film and television, animation, audiovisual, media, visual arts, performing arts, crafts and design, sculpture, environmental art, advertising and decoration, fashion design, software and computer services.

According to the contents of the "China Cultural and Financial Development Report 2018" recently released by the National Finance and Development Laboratory, the contents of the digital creative industry mainly include the following five ways in which data visualization is commonly used include:

Figure 2 shows the overall framework of the digital creative industry, which systematically demonstrates the digital creative industry in two ways. First of all, in terms of the content used in the digital creative industry, the breadth of its content is designed in various fields, from film and television photography to literary works, to creative design, and even to online education. Secondly, in the technical means used in the digital creative industry, technology introduces digital technology from reality and virtual, visual and tactile aspects to complete the final effect.

DEVELOPMENT OF CULTURAL CREATIVE PRODUCTS AND ENVIRONMENTAL CERAMICS

Cultural and creative products. The creation of contemporary cultural and creative products is inseparable from the application of modern technology, and cultural and creative products must have rich historical and cultural characteristics. If a product wants to have a high added value, it must attach a certain cultural connotation to it. The products constructed with modern science and technology established by relying on the wisdom of mankind and the cultural resources of the nation are Cultural and creative products. On the whole, real cultural and creative products can be defined by the following formula:

Cultural and creative products = culture + innovation + products

The design process of Cultural and creative products not only needs to pursue the shape and beauty of the products, but also needs to incorporate the historical background elements contained in the products. And further introduction of the story behind the elements of historical and cultural background, through the introduction of related stories, can also arouse public interest. Only by adding emotions to the designer, the designer first touches the work and can further influence the work.

Traditional products, or more than enough culture, lack of innovation. Or follow the trend, only pursue fashion, ignoring the cultural connotation of the product. In summary, modern craft products mainly include the following three shortcomings:

The lack of traditional culture and craftsmanship. In ancient China, there were 5,000 years of historical origins. The artifacts found in ancient tombs can also be seen in the wisdom of the working people of ancient China. For the crystallization of the wisdom summed up from the labor life process, we have not achieved good inheritance and innovation. As a highly creative clan, it should be based on the inheritance of excellent ancient culture and ancient techniques, and combine it with modern high-tech to develop outstanding cultural and creative products

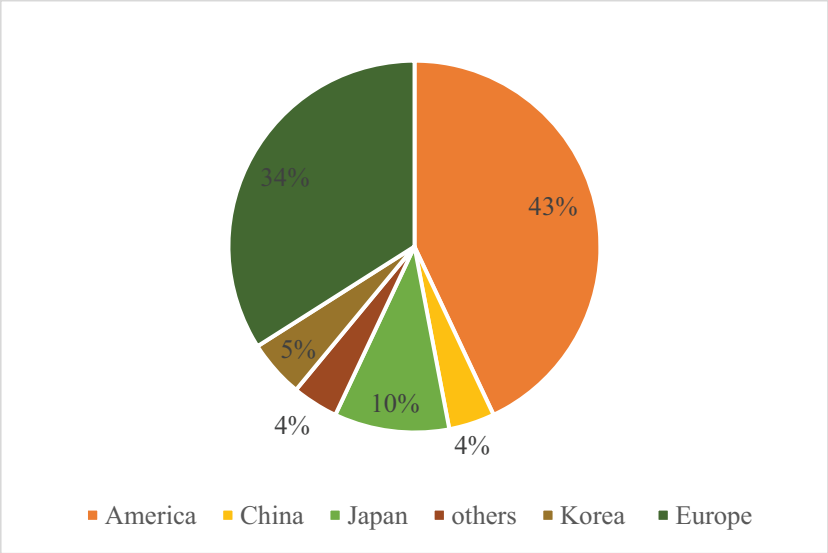

FIGURE 1
The spatial distribution pattern of global creative industries

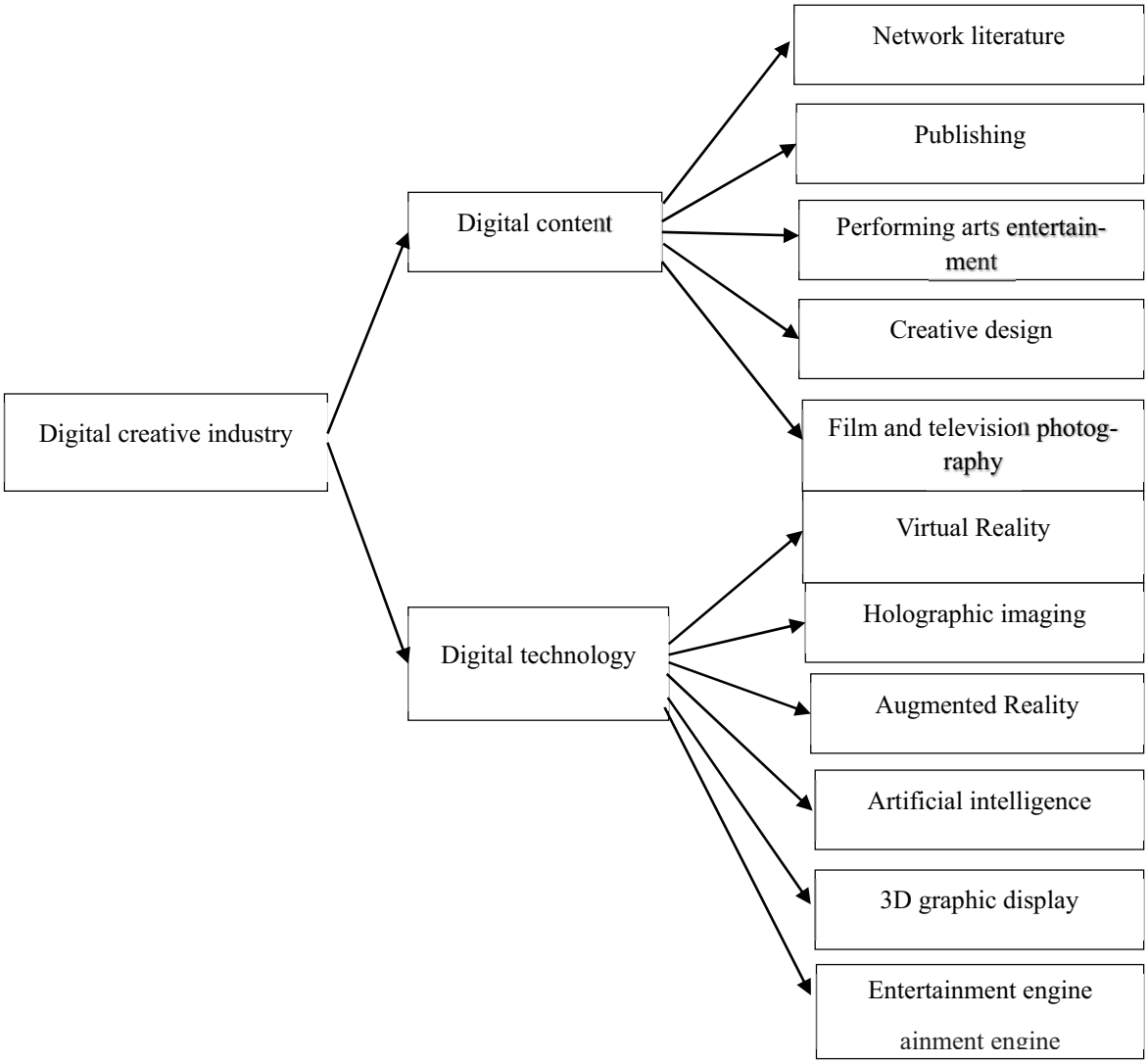

FIGURE 2
Digital creative industry framework

with more innovation and competitiveness. It is not something that only pursues the trend, and ignores the historical and cultural products that are enough to become the basis of the trend.

At the same time as modern technology continues to develop, it is inevitable that some traditional processes are missing. Although traditional artisan craftsmanship is less efficient than high-tech, its craftsmanship and refinement in the creative process are irreplaceable for the mechanized production of machinery. At the same time, the lack of craft spirit in the product is also a major problem that cannot be ignored. For the separation of traditional culture, the faults and lack of classical civilization are one of the root causes of the current vitality of innovation.

Excellent products lack communication channels. Of course, there is no shortage of cultural and creative products in today's society, and there are not many excellent cultural and creative products. However, the channels for disseminating cultural and creative products are scarce, and it is difficult for excellent cultural and creative products and cultural ideas to have opportunities for wide-ranging communication. How to make good design concepts and design works can enter the society, and can lead the trend of the society and resonate with the times. It is an urgent problem to be considered.

Aesthetics and design concepts have not yet gained popularity. Due to insufficient understanding of the design background of Cultural and creative products , many literary products cannot be accepted by the public. Therefore, there are many aesthetic inconsistencies. Many elements of historical culture cannot be accepted by the public and become a major problem in the sales channel. For example, the Peking Opera element, the public knows a lot about it, so the sales of literary products including elements such as Beijing Opera costumes and Peking Opera masks are quite impressive.

Environmental Ceramics. Environmental ceramics refers to the extension of traditional ceramic products. As the name suggests, environmental ceramics mainly consists of two parts, one refers to traditional ceramic technology, and the other refers to the effective use of environmental elements. Through the effective combination and utilization of environmental space and environmental architecture, the combination of the two is more in line with the viewer's aesthetic vision to achieve the best visual effect. At the same time, environmental ceramics as a part of cultural and creative products will also have the characteristics of Cultural and creative products. Environmental ceramics will also incorporate new materials and new technologies, as well as new concepts of design innovation. Therefore, environmental ceramics must be a combination of tradition and modernity, art and craftsmanship. The technical means used in environmental ceramics are also diverse, and their forms of expression are more varied. Environmental ceramic art has penetrated into all aspects of people's lives, and plays an irreplaceable role in improving human living standards and improving public aesthetic fatigue. The performance of environmental ceramics has great tension, great flexibility and creativity, and the effectiveness of its central expression is unmatched by other art forms.

Through the division of the use space, the environmental ceramic art can be divided into two types: indoor environmental ceramics and outdoor environmental ceramics. Different types of expressions are different, and the performance effects presented are different, but in essence, the effects of the two are the same for purifying the physical and mental and the liberation of the spirit.

Indoor environment. The indoor environment pottery art combines the pottery art with the interior decoration, and through the design of the interior decoration, it is the sentiment of the human mind. A good indoor environment pottery is enough to show the designer's inner world and spiritual level, as well as its longing for nature. Simple and elegant interior

(a) (b)

FIGURE 3
Comparison of indoor and outdoor environmental ceramics

design is very helpful for people's spiritual relaxation. The quaint and elegant indoor environment ceramic design will be enjoyable. As shown in (a) of Figure 3, it is a typical indoor pottery work.

Outdoor environment. The outdoor environment ceramics is mostly used in public places and some more important environments. The ceramic art technology is perfectly integrated into large buildings, which can improve the recognition, enjoyability and harmony of the surrounding environment. In today's era, the development of outdoor environment ceramic art has become an indispensable part of the public environment, environmental ceramic art has become an important part of the outdoor environmental planning structure. Through the planning of the outdoor environment ceramic art, the emotions to be expressed can be perfectly integrated into the environmental ceramic art design, and the ceramic art design is fully integrated with the design idea and the public aesthetic. At the same time, the outdoor environment ceramics is more like a vast project than the small and delicate ceramics in the indoor environment. The large outdoor space provides plenty of space for the creation of environmental ceramics, but at the same time it brings a lot of creative challenges to the creators. How to reasonably plan the outdoor environment space, so that the overall design will not split the outdoor space without making the space display too dense. As shown by (b) in Figure 3, it is a representative of a typical outdoor pottery.

Measures to change the environment of ceramic art creation. In the design process of environmental ceramics, in order to solve the problems, it is necessary to increase the following three aspects:

Constantly join the traditional cultural elements of China. As a craft product set up in China, ceramic art needs to pay more attention to the consideration of traditional cultural elements in its creative process, but at the same time it needs to add new elements in the development of modern society. Only by truly returning to China's cultural traditions, combining modern and classical, combining craftsmanship with technology, can environmental ceramics continue to innovate.

Add modern people's thinking and thinking habits to environmental ceramics. If the environmental ceramic art is to be recognized by the public as soon as possible, only the public's way of thinking should be properly incorporated into the creative process of environmental ceramics, so that the public can slowly receive the cultural information transmitted from the environmental ceramics. In this way, the environmental ceramics and the public are constantly adapting to each other and eventually moving forward.

Use traditional cultural symbols to convey cultural information. Today, with the increasing popularity of online language and multi-language, the public's awareness of traditional Chinese characters and traditional cultural information has gradually declined. Therefore, in the process of creating environmental ceramics, we also need to pay attention to the use of traditional cultural symbols. Only by understanding traditional culture and then analysing traditional culture can we make more appropriate use of traditional cultural symbols.

CONCLUSIONS

While the digital creative industry is increasingly deepening into people's lives, the emphasis on indoor and outdoor environmental ceramics should also be quickly put on the agenda. In the context of such an era, environmental ceramics has been limited by the original means of transmission, and the unacceptable plight of the public has been increasingly accepted and appreciated by people. With the continuous improvement of living standards, environmental ceramics plays an irreplaceable role in improving the living standards of the public and releasing the spiritual level. Combining the traditional history and culture of the nation with high-tech is the direction for the digital creative industry to move forward.

ACKNOWLEDGEMENTS

1. Research on the development strategy of tourism and cultural creative industry in Western Fujian under the guidance of "digital creative industry"

Youth Social Science Project of Education Department of Fujian Province, Project No.: JAS19350 / A201919

2. Research on "mass entrepreneurship and innovation" teaching mode and reform practice of product design specialty under the guidance of results -- Taking Sanming University as an example, Sanming University Institute of higher education, Project No.:SHE1905

REFERENCES

[1] Mingyan, W., Qinghua, C. (2012) Research on Regional Expression of Environmental Ceramics. Popular Art. 12

[2] Xingzhou, Z. (2012) A Comparative Study of Environmental Ceramic Art and Public Art. Popular Art. 21.

[3] Na, W., Wen, H., Yi, Y. (2015) Application of Ceramic Art in Environmental Art Design. Literary Life. (11), 165-165.

[4] Yanyun, C., Hua, Z., Liang, T. (2014) On the Importance of Ecological Design Concept of Environmental Ceramic Art. Literary Life·Art Theory. 12, 77-77.
[5] Cockburn, B., Fu, Z.X., Hungria, A., Ji, L.Y., Sanchez, M.A., Sayas, F.J. (2017) Stormer-Numerov HDG Methods for Acoustic Waves. Journal of Scientific Computing. 75(2), 597-624.
[6] Fu, Z.X., Heuer, N., Sayas, F.J. (2017). A nonsymmetric coupling of Boundary Elements with the Hybridizable Discontinuous Galerkin method. Computers & Mathematics with Applications. 74 (11), 2752-2768.
[7] Yang, X.H. (2018) On the Inner Logic of Direct Thinking in Modern Ceramic Art Creation. Art Review. 3, 172-175.
[8] Liu, Y.J. (2008) Application of Chinese original painted pottery modeling and decorative language in modern ceramic art. Dalian University of Technology. 1-5.
[9] Wenjuan, L. (2011) Research on Folk Art Elements in Modern Chinese Ceramic Art. Literary Life Journal. 11, 179-179.
[10] Wei, X., Zhimin, C. (2005) Semiotics in Ceramic Art Design. Chinese Ceramics. 41(5).
[11] Fu, Z.X., Heuer, N., Sayas, F.J. (2018). Coupling of HDG with a double-layer potential BEM. Mathematics. 2018, 1-25.
[12] Yang, F.Y. (2012). Analysis of Mathematical Models in Ceramic Art Design. China Ceramic Industry. 19(4), 1-8.
[13] Gao, L. (1992) Progress in Computer Applications and Mathematical Methods in the Field of Ancient Ceramics Research in China. Chinese Ceramics. 2, 57-61
[14] Lee, K.N., Eldridge, J.I., Robinson, R.C. (2005). Residual Stresses and Their Effects on the Durability of Environmental Barrier Coatings for SiC Ceramics . Journal of the American Ceramic Society. 88(12), 3483-3488.
[15] Lee, K.N., Fox, D.S., Bansal, N.P. (2005) Rare earth silicate environmental barrier coatings for SiC/SiC composites and Si3N4 ceramics. Journal of the European Ceramic Society. 25(10), 1705-1715.
[16] Lian, J.J., Wang, X.Q., Zhang, W.J., Ma, B., Liu, D.M. (2017) Multi-Source Generation Mechanisms for Low Frequency Noise Induced by Flood Discharge and Energy Dissipation from a High Dam with a Ski-Jump Type Spillway. International Journal of Environmental Research and Public Health. 14(12), 1482.
[17] Zou, P., Wang, J., Yin, H. (2007) Research on dynamic characteristics of original rock in the scour pit of energy dissipation of ski-jump. Journal of Hydroelectric Engineering. 26(4), 71-75.
[18] Feng, J., Wang, L., Li, R., Li, K., Pu, X., Li, Y. (2018) Operational regulation of a hydropower cascade based on the mitigation of the total dissolved gas supersaturation. Ecological Indicators. 92, 124-132.
[19] Hojjati, S.H., Hojjati, S.H., Neyshabouri, S.A.A.S. (2017) The objective design of triangular bucket for dam's spillway using Non-dominated Sorting Genetic Algorithm II: NSGA-II. Scientia Iranica. 24(1), 19-27.
[20] Kong, D.X., Miao, C.Y., Wu, J.W., Borthwick, A.G.L., Duan, Q.Y., Zhang, X.M. (2017) Environmental impact assessments of the Xiaolangdi Reservoir on the most hyperconcentrated laden river, Yellow River, China. Environmental Science and Pollution Research. 24(5), 4337-4351.
[21] Xing, Z., Wang, J., Zhang, J. (2018) Expansion of environmental impact assessment for eco-efficiency evaluation of China's economic sectors: An economic input-output based frontier approach. Science of the Total Environment. 635, 284.
[22] Guo, Z.L. (2000) Methods for Environmental Impact Assessment of Agricultural Water Conservancy Projects. Transactions of the Chinese Society of Agricultural Engineering. 16(5), 16-19.
[23] Koyano, M. (2008) The significance of the Convention on Environmental Impact Assessment in a Transboundary Context (Espoo Convention) in international environmental law: examining the implications of the Danube Delta case. Impact Assessment and Project Appraisal. 26(4), 299-314.
[24] Wei, W., Deng, J., Liu, B. (2013) Influence of aeration and initial water thickness on axial velocity attenuation of jet flows. Journal of Zhejiang University-SCIENCE A. 14(5), 362-370.

Received: **08.06.2020**
Accepted: **16.12.2020**

CORRESPONDING AUTHOR

Sangyoung Lee
TongMyong University,
Busan Metropolitan City,
No.428 Shenxian Road – South Korea

e-mail: leesangyoung@tom.com

© by PSP Volume 30– No. 05/2021 pages 5516-5520 Fresenius Environmental Bulletin

STUDY ON PROPERTIES OF CHEMICALLY MODIFIED DIAMOND LIKE CARBON FILMS

Jin-mei Wu*

North China University of Water Resources and Electric Power, Zhengzhou, China

ABSTRACT

Diamond like carbon (DLC) films were deposited on silicon substrates by plasma enhanced chemical vapor deposition (PECVD) technique and chemically modified by H2 plasma treatment. Properties of chemically modified diamond carbon films are investigated. The results of orthogonal test showed that the best wear resistance could be gained with the addition of particle diameter 150 nm, and the wear rate decreases by 50% under 1 m/s and 50 N. COD removal of oily wastewater was achieved more than 80% when chemically modified diamond carbon films is used. BOD5/COD ratio is now 0.55. This ratio is sufficient in many cases for biological treatment.

KEYWORDS:
DLC, PECVD, properties, orthogonal test, COD removal, oily wastewater

INTRODUCTION

Diamond-like carbon films (DLC) have attracted much attention due to an excellent combination of favourable properties such as high hardness, chemical inertness, high thermal conductivity, optical transparencies in a broad range, etc. [1]. A considerable amount of research has been done on preparation of DLC films by various vapour phase deposition techniques [2-4]. Since Namba first pioneered the concept of electrodeposition from organic solutions (as opposed to gas phase) for production of diamond phase carbon films in 1992 [5], the liquid-phase deposition method is attracting more and more interests and attention due to its attractive advantages such as a low deposition temperature, a low cost, and a simple experimental installation over the gas-phase techniques. The practicability of the DLC film growth has been demonstrated by a cathodic deposition mode under the action of electric current on various organic solvents (ethanol, methanol, dimethylformamide, acetronitrile, etc.) or their mixtures with deionized water [6-9] and diamond phases have been identified in the deposited DLC films [10, 11]. Furthermore, DLC films exhibit super lubricity when the tribo-test is carried out in hydrogen atmosphere. Such a characteristic is related to the saturation of covalent dangling carbon bonds by forming C–H bonds at the sliding interface [12]. Moreover the surface hydrogen in amorphous hydrogenated (a-C:H) films play a significant role in super lubricity [13]. In this respect, mainly the hydrogen content and nature of carbon hybridization determine the friction and wear behavior of DLC films [14].

Oily wastewater is wastewater mixed with oil under a wide range of concentrations. The oil mixed in water can be fats, hydrocarbons, and petroleum fractions such as diesel oil, gasoline, and kerosene. Nowadays, many industries generate a large amount of oily wastewaters, which have various adverse impacts on the surrounding environment, such as air pollution caused by the evaporation of oil and hydrocarbon contents to the atmosphere. In addition, they can affect groundwater, seawater, or drinking water as a result of the percolation of contaminants in produced water into the water resources beneath the soil [15]. A variety of treatment methods geared toward the removal of the oil impurities can be used to minimize or avoid the adverse effects of oily wastewater. Examples are electrochemical treatment, membrane filtration, use of biological media, adsorption, flotation and chemical coagulation, treatment using ultrasound-dispersed nanoscale zero-valent iron particles, titanium dioxide, vacuum ultraviolet and natural minerals, and hybrid technologies, among others [16].

In the present paper, Properties of these films were studied in respect of physical and chemical changes after the H_2 plasma treatment. Also considered in the present work is the determination of the change of the ratio of biological oxygen demand to chemical oxygen demand. Such a ratio is generally regarded as an important index of biodegradability of the treated high-strength industrial wastewater.

MATERIALS AND METHODS

DLC films were grown on silicon (100) substrates using PECVD technique. Prior to deposition, single crystal Si (100) wafer substrates were ultrasonically cleaned in ethanol for 10 min. Subsequently, Si wafers were loaded into the vacuum chamber and the chamber was evacuated to 5×10^{-6} mbar. The process chamber was purged with high pure Ar gas at least twice to reduce the oxygen partial pressure.The chemical bonding nature of DLC films were characterized by Raman spectroscopy using Renishaw in-Via model spectrometer equipped with 514 nm wavelength laser source of 50 mW power. Before commencement of these measurements, low power sputtering of the samples for 1 min duration was carried out to remove surface contamination and other adsorbed impurity layers. The spectrometer was attached with a monochromatic X-ray source having an energy resolution of 0.6 eV. Contact angle (CA) at the surface of these films was measured by sessile drop method with a Kruss Easy Drop contact angle instrument (EasyDrop DSA 100-1). The volume of the water droplets was ~1 μL. These measurements were carried out at room temperature and an atmospheric pressure with a relative humidity of ~70%. Standard deviations of the CA measurements were typically ±2°. Friction and wear behavior of these films were measured by a ball-on-disk tribometer (CSM, Switzerland) operating in a linear reciprocating mode. The Al_2O_3 ball of 6 mm diameter was used as a sliding counter body against all the test specimens. The normal load and sliding speeds were kept constant at 1 N and 3 cm/s, respectively. A stroke length of 3 mm was used during the course of each experiment. The tests were carried out in ambient (dry and unlubricated) conditions with relative humidity of 72±1%. All measurements were repeated 3 times on each sample and data was found to be reproducible.

The COD of the collected liquid are measured by potassium dichromate method of Chinese Standard 11914-89 and BOD_5 is measured by Chinese Standard 7488-87.

RESULTS AND DISCUSSION

Effect of loading on tribological properties. Figure 1 shows variation of the friction coefficient of with loading at a sliding speed of 0.1 m/s. It is seen that friction coefficient increases with the increase in loading firstly, and then decreases with the load when the applied loading is higher than 50 N.

Effect of sliding speed on tribological properties. Figure 2 shows variation of the friction coefficient of with different sliding speed at a loading of 50 N. It is seen that the friction coefficient increases with the increase of sliding speed.

Analysis of orthogonal test results. From Table 1 and 2, loading is the primary factors on copper yield, followed by particle diameter and sliding speed. The wear is selected for objective

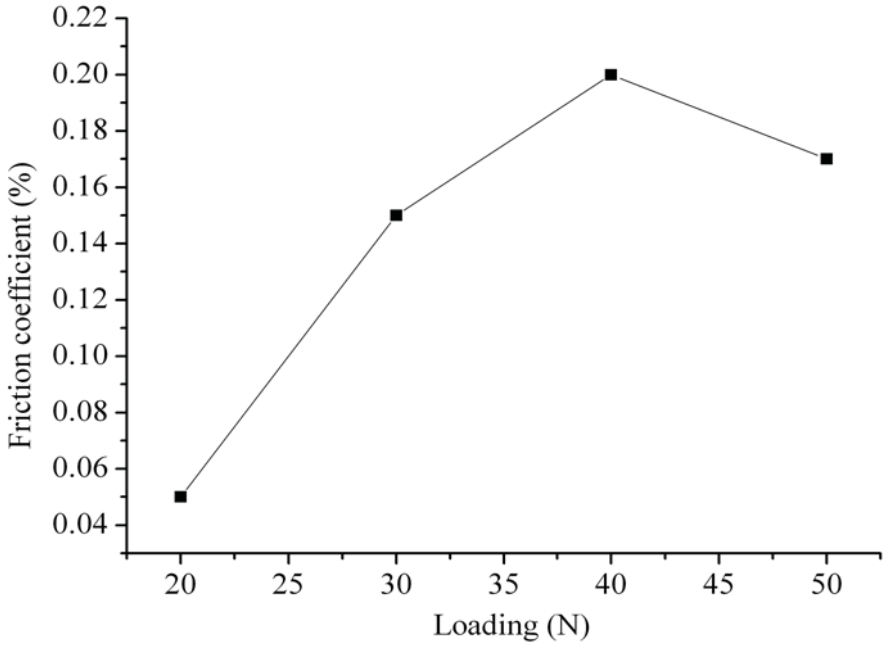

FIGURE 1
Effect of loading on Tribological properties

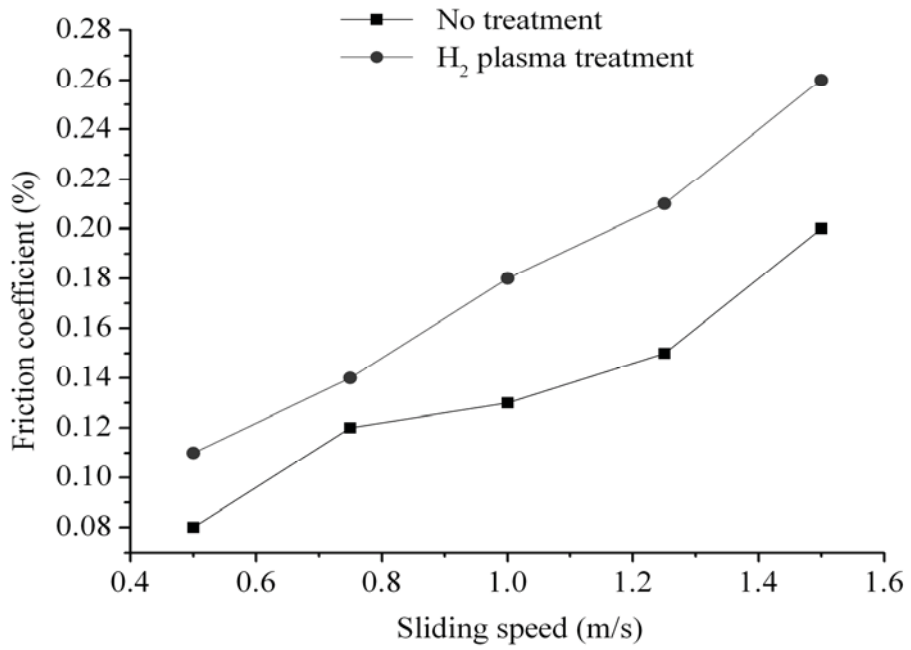

FIGURE 2
Effect of sliding speed on Tribological properties

TABLE 1
Orthogonal factor level table $L_9(3^4)$

Level	Loading (N)	Particle diameter (nm)	Sliding speed (m/s)
1	30	50	0.5
2	40	75	0.75
3	50	150	1

TABLE 2
Orthogonal experimental data and results

No.	Loading (N)	Particle diameter (nm)	Sliding speed (m/s)	Wear (g)
1	1	1	1	0.0008
2	1	2	2	0.0008
3	1	3	3	0.00086
4	2	2	3	0.00098
5	2	3	1	0.00098
6	2	1	2	0.00092
7	3	3	2	0.00099
8	3	1	3	0.00097
9	3	2	1	0.00098
R_1	0.00084	0.000914	0.00093	
R_2	0.00096	0.00093	0.000916	
R_3	0.00098	0.0000948	0.000941	
Range	0.00014	0.000033	0.000025	

R means sum of the test results for factors.

function, which is a combination of optimal conditions: loading 50 N, particle diameter 150 nm and sliding speed 1 m/s. The wear rate decreases by 50 % under under optimal conditions.

Chemically modified diamond carbon films catalysed wet oxidation of oily wastewater. It is shown that significant COD removal from oily wastewater occurred (Figure 3). COD removal increased with increasing chemically modified diamond carbon films. The maximum amount of COD that could be removed was approximately 86.6% in 10 min in the presence of chemically modified diamond carbon films as opposed to approximately 58.4% without chemically modified diamond carbon films addition.

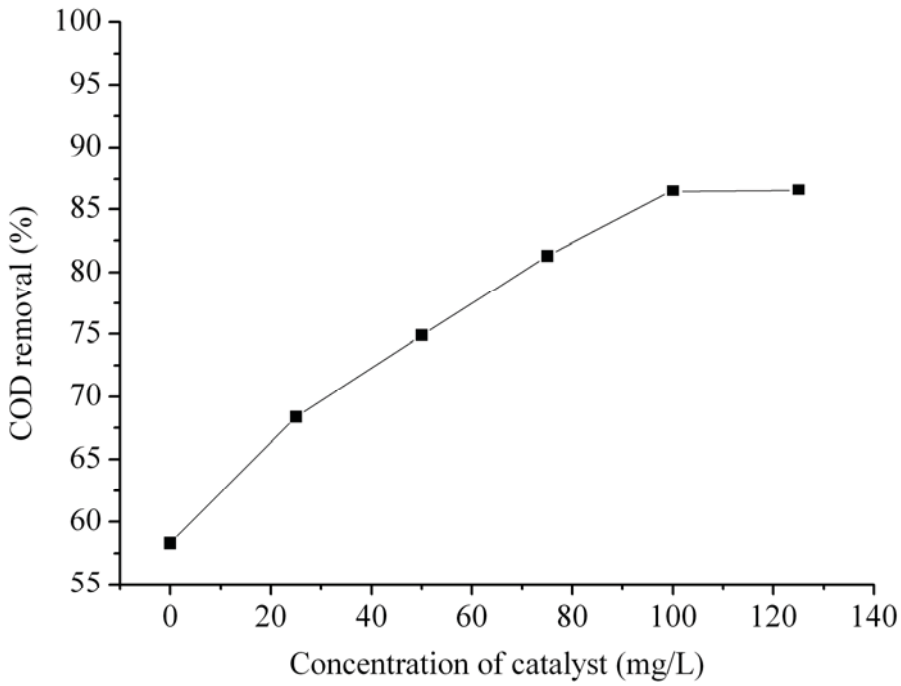

FIGURE 3
Effect of increasing chemically modified diamond carbon films on COD removal

BOD_5/COD. BOD_5/COD ratio is a very important indexfor any waste to be biodegradable. Normally, an industrial wastewater with a BOD_5/COD ratio of about 0.5 or above is considered as a biodegradable waste. Therefore, in this study, BOD_5/COD ratio of some reactor effluents was determined. Initial BOD_5 and COD of our oily wastewater are 400 and 2000 mg/L; respectively. So, the initial BOD_5/COD ratio is about 0.2. This result indicates that our wastewater is not suitable for biological treatment. After the WPO process, at a temperature of 330°C for 20 min, the BOD_5 and COD of the effluent were found as 110 and 200 mg/L; respectively. So, BOD_5/COD ratio is now 0.55. This ratio is sufficient in many cases for biological treatment.

CONCLUSIONS

DLC films have been successfully prepared using electrochemical method. DLC films can be obtained at a relative low potential with a higher growth rate. The DLC films deposited in the present study have nearly the same outstanding friction wear behaviours as those by magnetron sputtering technique. It is seen that the friction coefficient increases with the increase of sliding speed and loading. The results of orthogonal test showed that the best wear resistance could be gained with the addition of particle diameter 150 nm, and the wear rate decreases by 50% under 1 m / s and 50 N. COD removal of oily wastewater was achieved more than 80% when chemically modified diamond carbon films is used. BOD_5/COD ratio is now 0.55. This ratio is sufficient in many cases for biological treatment.

REFERENCES

[1] Bouzakis, K. D., Michailidis, N., Gerardis, S., Katirtzoglou, G., Lili, E., Papa, M., Brizuela, M., Garcia-Luis, A., Cremer, R. (2008) Impact Resistance of Doped CrAlN PVD Coatings Correlated with Their Cutting Performance in Milling Aerospace Alloys. J. Balkan Tibological Association. Conference Proceedings. (IKEE) 14 (3), 292.

[2] Karamis, M.B., Cerit, A.A., Nair, F. (2009) Failure and Damage Analyses of Al-7075 Matrix Composite Reinforced with SiCp after Ballistic Impact. Oxid. Commun. 32 (1), 130.

[3] Kandeva, M., Karastoianov, D., Ivanova, B., Pozhidaeva, V. (2013) Influence of Nano-diamond Particles on the Tribological Characteristics of Nickel Chemical Coatings. J. Balkan Tibological Association. 19 (4), 596.

[4] Thagard, S.M., Takashima, K., Mizuno, A. (2009) Electrical discharges in polar organic liquids. Plasma Processes and Polymers. 6, 741.

[5] Ramesham, R., Welch, W., Neely, W.C., Rose, M. F., Askew, R. F. (1997) Plasma etching and patterning of CVD diamond at <100 ◦C for microelectronics applications. Thin Solid Films. 304, 245.
[6] Urruchi, W. I., Massi, M., Maciel, H.S., Otani, C., Nishioka, L.N. (2000) Etching of DLC films using a low intensity oxygen plasma jet. Diamond and Related Materials. 9, 685.
[7] Feldshtein, E.E., Dyachkova, L. N. (2016) The Use of Nanodiamonds to Improve Tribological Properties of Sintered Antifriction Materials. J. Balkan Tibological Association. 22 (1), 227.
[8] Yan, X. B., Xu, T., Chen, G., Liu, H. W., Yang, S.R. (2004) Effect of deposition voltage on the microstructure of electrochemically deposited hydrogenated amorphous carbon films. Carbon. 42, 3103.
[9] Ronning, C. (2003) Ion beam synthesis and growth mechanism of diamond-like materials. Applied Physics A. 77, 39.
[10] Neuville, S., Mattews, A. (2007) A perspective on the optimization of hard carbon and related coatings for engineering applications. Thin Solid Films. 515, 6619.
[11] Bahadur, S., Gong, D., Anderegg, J.W. (1992) The role of copper compounds as fillers in transfer film formation and wear of nylon. Wear. 154, 207.
[12] Cadman, P., Gossedge, G.M. (1979) The chemical nature of metalpolytetrafluoroethlene tribological interactions as studied by X-ray photoelectron spectroscopy. Wear. 54, 211.
[13] Wang, Y., Alsmeyer, D.C., Mccreery, R.L. (1990) Raman spectroscopy of carbon materials: structural basis of observed spectra. Chemistry of Materials. 2, 557.
[14] Ferrari, A.C., Robertson, J. (2000) Interpretation of Raman spectra of disordered and amorphous carbon. Physical Review B. 61, 14095.
[15] Li, J., Li, Z.D., Yan, S., Zhang, H.X. (2018) Treatment of oily wastewater via supercritical water oxidation (SCWO) and electrochemical process. Fresen. Environ. Bull. 27, 6960-6965.
[16] Zhang, H.X., Li, Y., Li, Z.D., Dong, G.T., Wang, P., Li, W. (2017) Experimental study of petrochemical oily wastewater treatment for reuse. Fresen. Environ. Bull. 26, 516-519.

Received: **10.12.2019**
Accepted: **10.08.2020**

CORRESPONDING AUTHOR

Jin-mei Wu
North China University of Water Resources and Electric Power, Zhengzhou – China

e-mail: wujinmei8889@163.com

© by PSP Volume 30– No. 05/2021 pages 5521-5528 Fresenius Environmental Bulletin

EVALUATION ON CONSUMER ATTITUDES TOWARDS TO THE PURCHASE OF ECO-LABELED PRODUCTS

Mirela Panainte-Lehadus[1], Valentin Nedeff[1,2], Narcis Barsan[1,*], Emilian Mosnegutu[1], Antonina Temea[1], Claudia Tomozei[1], Oana Irimia[1], Dana Chitimus[1]

[1]Department of Environment Engineering and Mechanical Engineering, Faculty of Engineering, Vasile Alecsandri University of Bacau, 156 Calea Marasesti, 600115, Bacau, Romania
[2]Gheorghe Ionescu Sisesti, Academy of Agricultural and Forestry Sciences Bucharest, 61 Marasti, 011464, Bucharest, Romania

ABSTRACT

The use of eco-labeled products are specific tools used for promoting sustainable consumption, so it is important to guide and educate consumers on choosing these products. The paper presents the results of a market study conducted during the period 2010-2013, within the LIFE + project - "Green Products Promotion", a study that aimed to identify the buyers' decision regarding the environment when pur-chasing some products. The results show that over 46 % from respondents know the most significant ef-fects, 62.46% consider its environmental impact and 45.8% believe that the Ecolabel plays an important role in their purchasing decision.

KEYWORDS:
Environment, Eco – labels, Consumers, Product

INTRODUCTION

Today's society is increasingly confronted with numerous issues related to environmental protection and their implications: climate change, fire, drought, etc.

A Eurobarometer survey shows that 52 % of Europeans believe that the most pressing environmental concern is climate change, 35 % atmospheric pollution, 31 % maritime pollution, 28 % deforestation and waste. In this context, the adoption of viable consumption patterns, the application of measures to reduce the impact on the environment, to reduce the impact of climate change, to protect the atmosphere are urgently needed [1-3].

Environmental health and protection have become an increasingly important issue, so it is necessary to adopt sustainable practices and focus on green procurement. The demographic increase (it is expected that by 2050 the overall population will reach 9.4 billion), implies the need for a huge quantity of products to meet the needs of the people. Many of these have an impact on the environment at differ-ent stages of the life cycle. Thus, it is essential to guide consumers in choosing organic products and to promote sustainable consumption [3-7].

Ecological labels play an important role in the policies of implementation of sustainable consumption. Product eco-labeling is the measure by which consumers are helped to make decisions that reduce the impact on the environment and allow them to influence the way products are made.

Ecological labels are tools to inform consumers about the green characteristics of products in a visual way. Eco-labeling can be considered as a product innovation process, because it favors the emergence of new environmentally friendly products, new cleaner production methods [5-10].

Studies in the field have shown that large-scale changes in consumption methods and the adoption of green products are considered ways to address environmental issues and limit the effects of climate change [8-14].

Scientific research points to increasing energy efficiency and reducing energy consumption as ways to reduce greenhouse gas emissions. Energy consuming products are mainly involved in the production of greenhouse gas emissions, studies show that 75 % of greenhouse gas emissions are due to the use phase of the products. From this category, household appliances make up 25 % of the total European energy consumption. In this context, the UE has developed two directives to increase the energy efficiency of this type of product, the directives aim is to save energy by transforming the market, stimulating the supply, and adapting the products, supporting consumers in purchasing energy efficient products. Some research highlights the fact that an increasing number of consumers are changing their consumption patterns and using increasingly sustainable products. There is a wide range of green products on the market: electrical devices, furniture and wood products, clothing, paper products. In Europe in 2015 the market for eco-labeled paper products represented 72 % of total sales [10-18].

In the Nordic countries there are eco-labels for 55 product groups and 2800 products. In Japan, 64 product groups have established criteria for the eco-label and more than 5000 products have been accepted. In Romania there are 10 categories of eco-labeled products and 31 products, 21 producers have

eco-labeled products. Although there is a wide range of eco-labeled products, actual sales of eco-labeled products have remained at moderate levels. The low share of sales of green products is justified by the small percentage of the market for green products. Consciousness of the importance of environmental protection is considered a prerequisite for the purchase of green products, the consumer segment of green products is 10-15 %, if there are categories of products that do not have eco-labeled products, this segment is expected to remain limited [15-25].

In recent years, many modern consumers tend to be concerned about organic products and how they are identified. This tendency is supported by the personal beliefs of the consumers as well as their expectations regarding the high quality of the products However, the share of sales is low. Studies in the field indicate that the market for green products is almost non-existent due mainly to poor promotion, non-consumer information, modest size of the green market segment [12-25].

The paper presents the results obtained after conducting market research conducted in several Roma-nian cities to identify the level of consumer knowledge regarding green products.

MATERIALS AND METHODS

The study presented in the paper was carried out in the period 2010 - 2013, being targeted 5 cities: Bacau, Bucharest, Timisoara, Sibiu, and Cluj. In choosing the cities in which the study was implemented, it was considered to cover a considerable percentage of the population of the country. The study was carried out in three stages: at the beginning of the project (2010), after the first year of project implementation (2011) and at the end of the project (2013).

According to the established methodology, a questionnaire was structured in five parts: perception on environmental issues; criteria for the selection of purchased products; the degree of knowledge of green products and their interest in them; issues related to the identification and promotion of green products; buyer profile.

In the present work will be analyzed the aspects regarding: criteria for the selection of products bought the level of know about the green products and the interest about them.

RESULTS

At the question "How much do you know about the impact that the products you buy and use have on the environment" over 46 % of buyers indicated that "I know the most significant effects", but what is most relevant is the gradual increase of buyers who are "fully informed" from 9.8 % in 2010 to 16.2 % in 2013. The share of buyers who "know little things" is on average 30 %, but their tendency is decreasing according to of the last study (Figure 1). A significant decrease is also represented by the percentage of people who "know nothing" 4.3 % in 2010 to 3.5 % in 2013.

Regarding the importance of the "Impact of the product on the environment" on the purchase decision, it is found that an increasing number of buyers take this into account, respectively 75 % of buyers in 2010, 77.3 % of buyers in 2011 and 79.3 % of buyers in 2013 (Figure 2).

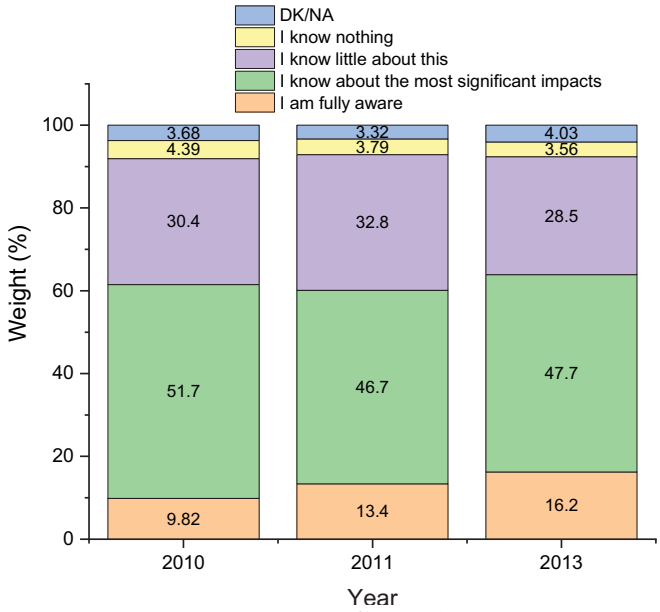

FIGURE 1

Distribution of the answers to the item "How much do you know about the environmental impact of the products you buy and use?"

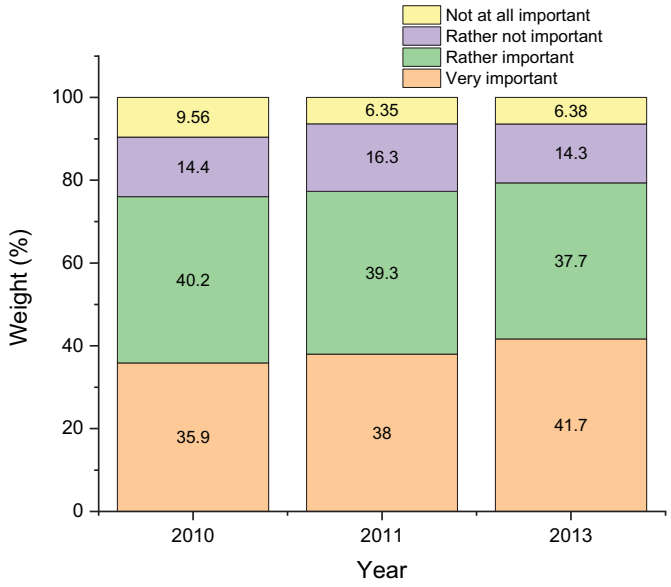

FIGURE 2
Distribution of the answers to the item "Impact of the product on the environment".

This change of mindset, of the buyers, is mainly due to their information on the impact generated by different industries on the environment (information obtained both through the media and through the different projects carried out for this purpose) but also on the awareness on climate change.

As for the price of the product, a very large share of buyers, when buying a product, consider the price of the product, so over 85 % of buyers consider the price of the product important. The 2013 study shows a slight decrease in the percentage of those who consider the price of the product very important (Figure 3).

Regarding the quality of the product, if in the first study 75 % of the buyers think that the quality of the product plays an important role in the decision to purchase a product, this weight increases in the 2011 study to 77 %, followed by a decrease of 6 % within of the last study (Figure 4).

The brand of purchased products plays a very important role in the decision to buy the products, the importance of this is given by the percentage of positive answers, an increase can be observed from 27.89 % in the 2010 study to 33.58 % in the 2013 study (Figure 5).

In many cases, by the brand of the product, the buyer perceives better quality, which entails a higher cost price, this fact being corroborated with the results obtained regarding the price of the product and its quality.

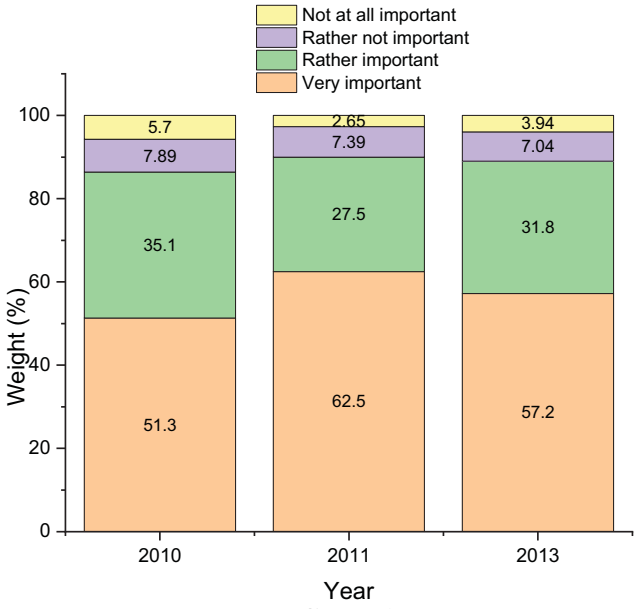

FIGURE 3
Distribution of the answers to the item "how importance is the price of the product?"

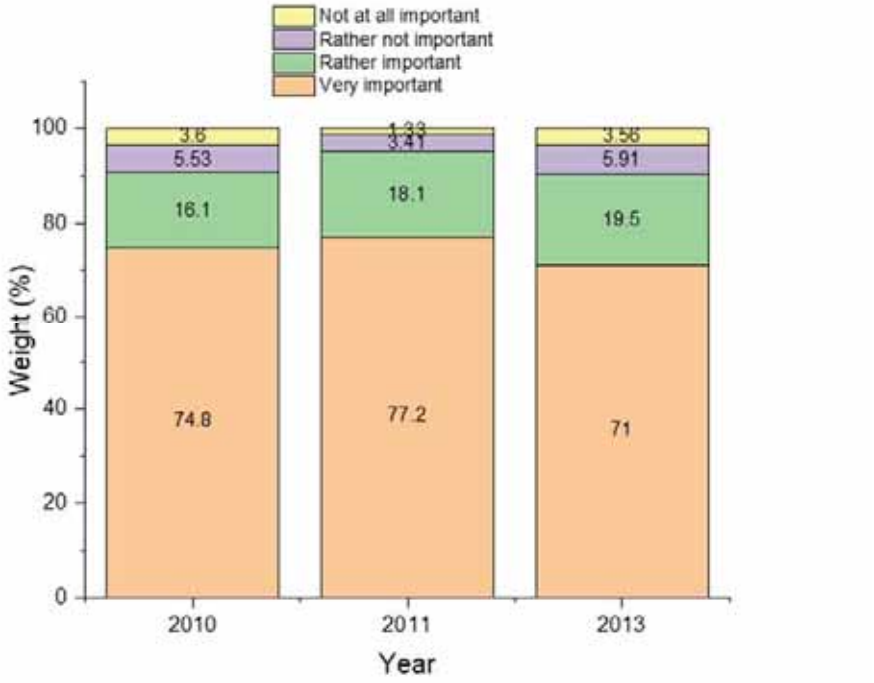

FIGURE 4
Distribution of the answers to the item "how importance are the quality of the product?"

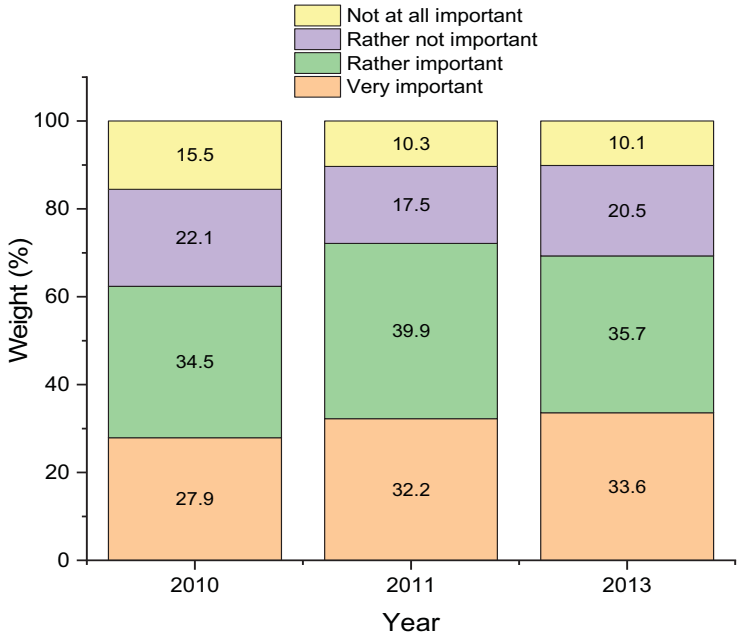

FIGURE 5
Distribution of the answers to the item "how importance are the brand name of the product?"

Regarding the role played by the ecological label in the purchase decision, the percentage of those who consider that this plays an important role has increased from 43.1 % in 2010 to 45.8 % in 2013. The same variation is found and in the case of those who consider that the eco-label does not play an important role in the purchasing decisions (Figure 6). It is worth noting that the percentage of those who never read the product label has decreased.

At the item "Do you know any labels?" the share of those who answered NO to this question decreased significantly from 46.1 % in the 2010 to 39 % in the 2013 (Figure 7).

At the item "Have you identified green products in Romanian markets" states that (Figure 8).

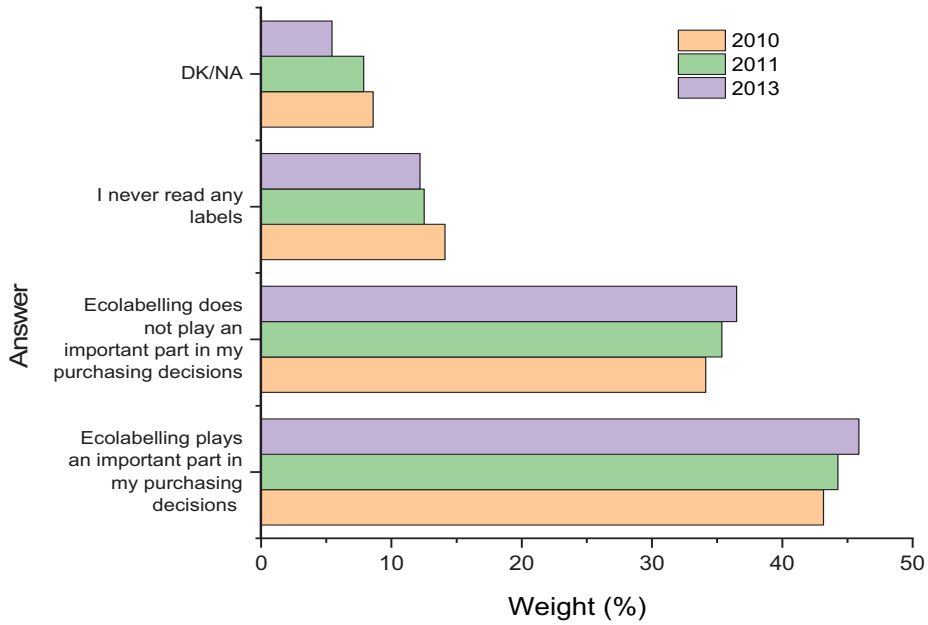

FIGURE 6
Distribution of the answers to the item "How important is the eco-label in the decision to buy a product?"

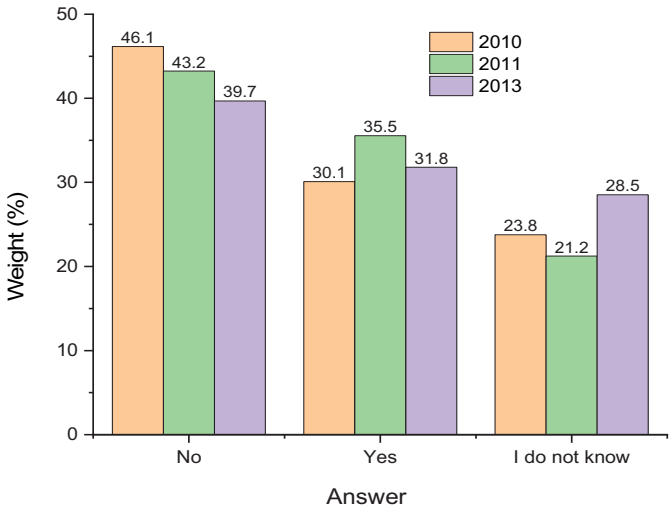

FIGURE 7
Distribution of the answers to the item "Do you know any labels?"

If the first study on green products shows that only 46.5 % of the respondents knew about green products, in the next campaign, in 2011, the highest share of positive answers was obtained (54 %), but this decreased by 7 % in the next analysis. One of the factors that led to the decline of this indicator is that it is the crisis that has affected the economy of the whole of Europe. However, we can say that campaigns made to popularize green products have had an impact on the way buyers make decisions about choosing a product. The share of those who did not identify green products on the Romanian market remained constant (about 16 %) for all three studies. However, a significant number of buyers are not sure or do not know (27 % with a tolerance of + 2 % and -3 %) of the existence of green prod-ucts. From the category of green products indicated by the buyers participating in these surveys, we notice light bulbs, washing machines and televisions (Figure 8).

When asked "Why do you think green products are better?" the vast majority of those who answered this question opted for the answer "are recyclable" in proportion of over 40 % and over 32 % of the respondents opted for the answer "consume little energy" (Figure 9).

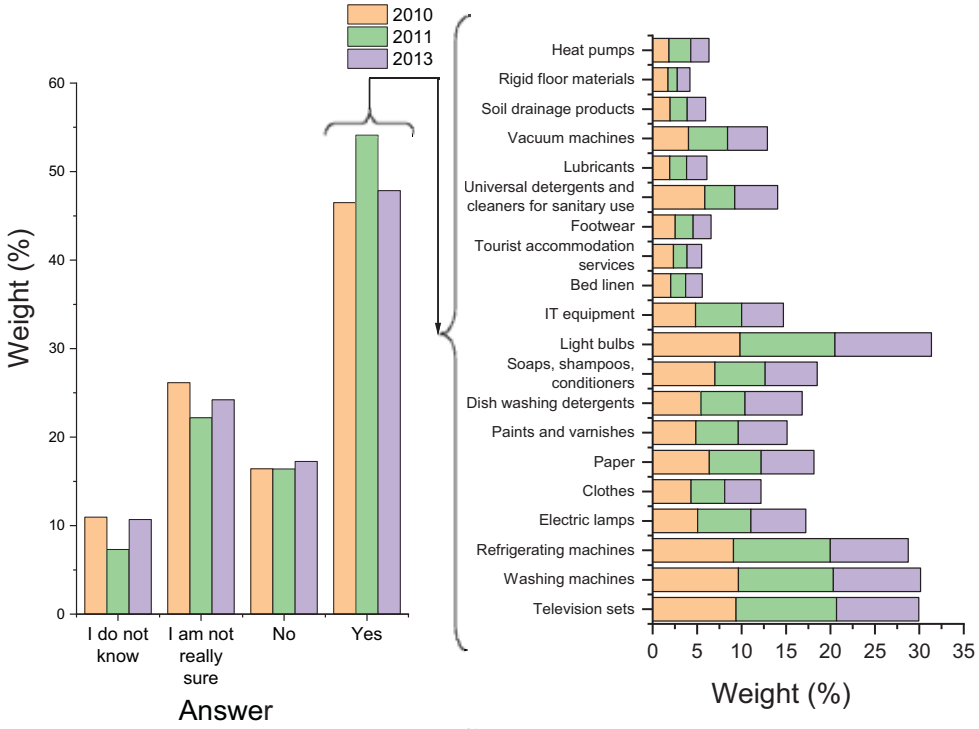

FIGURE 8
Distribution of the green products indicated by the buyers.

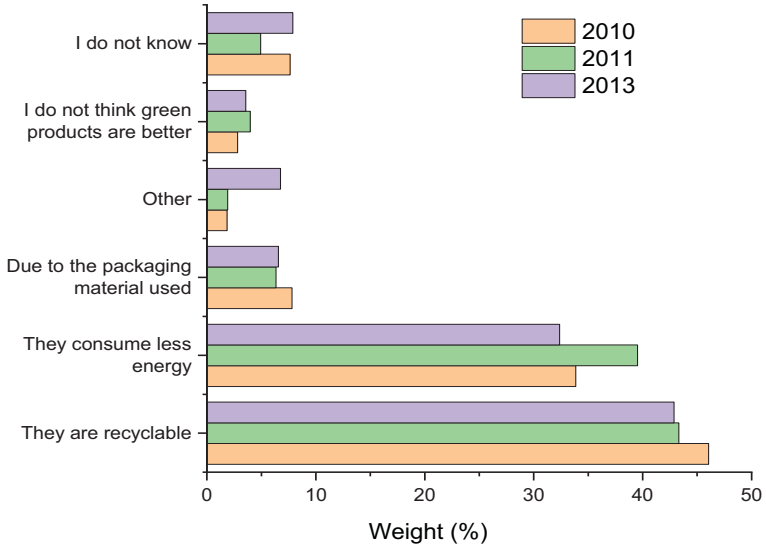

FIGURE 9
Distribution of o the answers to the item " Why do you consider that green products are better?"

CONCLUSIONS

From the analysis of the data presented, it can be noticed that consumers give importance to the impact that the products they market may be over the environment and that the eco-label plays an important role in their purchasing decision, although the percentage of those who know ecolabels is relative low. The results of the studies have highlighted that the reasons why consumers believe that green products are better are: recyclability, low energy consumption, packaging.

Also important is the level of knowledge of consumers regarding green products, durability as the de-cision to choose a product rests with the buyer's conviction.

ACKNOWLEDGEMENTS

The “Promoting Green Products” project (LIFE+08/INF/RO/000507) was financed by the European Commission through the LIFE+ program.

REFERENCES

[1] Song, L., Lim, Y., Chang, P., Guo, Y., Zhang, M., Wang, X., Yu X., Lehto, M.R. (2019) Ecolabel's Role in Informing Sustainable Consumption: A Naturalistic Decision Making Study Using Eye Tracking Glasses. Journal of Cleaner Production. 218, 685-695.

[2] Rex E., Baumann, H. (2007) Beyond Ecolabels: What Green Marketing Can Learn from Conventional Marketing. Journal of Cleaner Production. 15(6), 567-576.

[3] Banyte, J., Brazioniene, L., Gadeikiene, A. (2010) Investigation of Green Consumer Profile: A Case of Lithuanian Market of Eco-Friendly Food Products. Economics and Management. 15, 374-383.

[4] Panainte-Lehadus, M., Nedeff, V., Mosnegutu, E., Lazar, G., Caraman, I., Tomozei, C., Chitimus, D., Barsan, N. (2014) Study Regarding Public Perception on Environmental Issues Relating to Romania. International Conference on Production Research - Regional Conference Africa, Europe and the Middle East and 3rd International Conference on Quality and Innovation in Engineering and Management, ICPR-AEM. Technical University Cluj-Napoca, Cluj-Napoca, Romania. 393-396.

[5] Bratt, C., Hallstedt, S., Robert, K.H., Broman, G., Oldmark, J. (2011) Assessment of Eco-Labelling Criteria Development from a Strategic Sustainability Perspective. Journal of Cleaner Production. 19, 1631-1638.

[6] Rubik, F., Frankl, P. (2005) The Future of Eco-Labelling. Making Environmental Product Information Systems Effective Sheffield. Routledge, London, 5-74.

[7] Amstel, M., Driessen, P., Glasbergen, P. (2008) Eco-labeling and Information Asymmetry: A Comparison of Five Eco-Labels in the Netherlands. Journal of Cleaner Production. 16, 263-276.

[8] Lavallee, S., Plouffe, S. (2004) The Eco Label and Sustainable Development. International Journal of Life Cycle Assessment. 9, 349-354.

[9] Panainte, M., Caraman, I., Nedeff, V., Inglezakis, V., Venetis, C., Coutsikos, P., Gabriel Lazar, G., Barsan, N. (2014) Green Market: A Comparative Study in Romania. Fresen. Environ. Bull. 23(11), 2870-2875.

[10] Atanasoaie, G., (2013) Eco-Label and Its Role in the Development of Organic Products Market. Economy Transdisciplinarity Cognition. 16(1), 122-129.

[11] Prieto-Sandoval V., Alfaro, J.A., Mejía-Villa, A., Ormazabal, M. (2016) ECO-Labels as a Multidimensional Research Topic: Trends and Opportunities. Journal of Cleaner Production. 135, 806-818.

[12] Panainte, M., Inglezakis, V., Caraman, I., Nicolescu, M., Mosnegutu E.F., Nedeff, F.M. (2014) The Evolution of Eco-Labeled Products in Romania. Environmental Engineering and Management Journal. 13(7), 1665-1671.

[13] Thogersen, J., Haugaard, P., Olesen, A., (2010) Consumer Responses to Ecolabels. European Journal of Marketing. 44(11/12), 1787-1810.

[14] Schumacher, I. (2010) Ecolabeling, Consumers' Preferences and Taxation. Ecological Economics. 69(11), 2202-2212.

[15] Cerri, J., Testa, F., Rizzi, F. (2018) The More I Care, the Less I Will Listen to You: How Information, Environmental Concern and Ethical Production Influence Consumers' Attitudes and the Purchasing of Sustainable Products. Journal of Cleaner Production. 175, 343-353.

[16] Panainte-Lehadus, M., Nedeff, V., Mosnegutu, E., Caraman, I., Barsan, N. (2015) Production and Distribution of Green Products in Romania. International Multidisciplinary Scientific GeoConference Surveying Geology and Mining Ecology Management, SGEM. 2(5), 397-404.

[17] Chakravarthy, Y., Potdar, A., Singh, A., Unnikrishnan, S., Naik, N. (2016) Role of Ecolabeling in Reducing Ecotoxicology, Ecotoxicology and Environmental Safety. 134(2), 383-389.

[18] Sogn-Grundvåg, G., Asche, F., Zhang, D., Young, J.A. (2019) Eco-labels and Product Longevity: The Case of Whitefish in UK Grocery Retailing. Food Policy. 88, 101750.

[19] Russo, A.C., Rossi, M., Germani, M., Favi, C. (2018) Energy Label Directive: Current Limitations and Guidelines for the Improvement. Procedia CIRP. 69, 674-679.

[20] MMEDIU (2020) List of Economic Operators in Romania that Have Obtained the European Eco-Label. Available online at: http://www.mmediu.ro/articol/lista-operatorilor-economici-din-romania-care-au-obtinut-eticheta-ecologica-europeana/3154 (accessed: 5.02.2020) (in Romanian).

[21] Tiwari, S., Mani Tripathi, D., Srivastava, U., Yadav, P.K. (2011) Green Marketing – Emerging Dimensions. Journal of Business Excellence. 2(1), 18-23.

[22] Ucenic, C., Bacali, L. (2007) Attitude of Romanian Consumers and Producers toward Ecological Products, Proceedings of the 2nd IASME/WSEAS International Conference on Energy and Environment held in Portoroz, Slovenia. 15-17 May 2007.

[23] Grimmer, M., Bingham, T. (2013) Company Environmental Performance and Consumer Purchase Intentions. Journal of Business Research. 66, 1945-1953.

[24] Grundey, D., Zaharia, R. (2008) Sustainable Incentives in Marketing and Strategic Greening: The Cases of Lithuania and Romania, Technological and Economic Development. Baltic Journal on Sustainability. 14(2), 130-143.
[25] Temea, A., Comoglio, C., Botta, S., Nedeff, V., Panainte-Lehadus, M., Danu, M., Barsan, N. (2016) Developing a Green Register of Eco-labeled Products in Romania. Environmental Engineering and Management Journal. 15(8), 1873-1878.

Received: **09.12.2020**
Accepted: **19.01.2021**

CORRESPONDING AUTHOR

Narcis Barsan
Faculty of Engineering
University of Bacau
Bacau 600115 – Romania

e-mail: narcis.barsan@ub.ro

© by PSP Volume 30– No. 05/2021 pages 5529-5536 Fresenius Environmental Bulletin

NOTICE

RESEARCH ON COORDINATED DEVELOPMENT OF REGIONAL ECOLOGICAL ENVIRONMENT AND ECONOMY

Qiyue Chen[1], Shijun Chen[2], Tao Fan[3,*]

[1]School of East China Normal University, Shanghai 312000, China
[2]Institute of New Rural Development, Tongji University, Shanghai 200241, China
[3]School of Economic and Management, Tongji University, Shanghai 200092, China

ABSTRACT

In the present society, modernization grew rapidly and the situation of ecological development has been gained great concern domestically or even globally. With the constant development of economy, the ecological environment is facing unprecedented pressure to some extent. In accordance with sustainable development policy requirements, coordinated development between the ecological environment and the economy should be given priority by nation and government. Taking Guangzhou as an example and based on evaluation indicator of ecological environment and economic development, this study established a scheduling model of them and analyzed the relationships of coordination degree between ecological environment and economic development in Guangzhou. On the basis of successful economic development, environmental protection must be attached great importance. This study will not only serve as a reference for coordination degree between ecological environment and economic development in Guangzhou, but also it will provide case reference for other cities and nations.

KEYWORDS:
Ecological environment, Economy, Coordinated development, Guangzhou

INTRODUCTION

Since reform and opening up in China, the productive forces have been liberated, various industries have been greatly developed, national economy has been soared and people's living have gradually transferred from hunger and cold to food and clothing, then well-off, which have realized a significant leap in economic conditions and material life. However, it should be paid attention that, when economic development soared, ecological environment paid a enormous cost and in turn affected economic development. Ecological environment is the material environment human beings depends on, and its destruction exerted a great impact on human life. Therefore, at present, the important task is to protect ecological environment. The ecological environment and economic development are mutually influenced and promoted. Only by truly achieving sustainable development between ecological environment and economic development can people truly obtain the healthy and happy social life. Guangzhou, the capital of Guangdong, is one of the cities with the fastest and most stable economic development in South China. It has won many honors and awards about economic indicators. However, the ecological environment in Guangzhou is stuck in difficulties behind steady economic growth[1]. Based on the idea of sustainable development and choosing Guangzhou as an example, this study analyzed the dynamic track of ecological environment and economic development in over a decade and obtained the relevant data of the coordinated development between ecology and economy, which was of guiding significance in coordinated development of ecology and economy in Guangzhou and other cities.

MATERIALS AND METHODS

Research Area. Guangzhou, the capital of Guangdong, covered by hilly land with marine subtropical monsoon climate. Located in water rich area of Southern China, it riches in river system with numerous rivers and large water coverage. Guangzhou is an important central city, international trade center and comprehensive transportation hub of China approved by the State Council. Located in the southern China, Guangzhou is on the northern edge of the South China Sea and the Pearl River Delta, and it is the first coastal open city, the central city of Greater Bay Area, the Pearl River Delta Economic Zone and the hub city of One Belt

One Road Initiative[2]. At the end of 2018, permanent population of Guangzhou reached 14.9044 million, urban population reached 12.8744 million and urbanization rate was up to 86.38%. As the political, military, economic, cultural, scientific and educational center of South China, Guangzhou has become one of the cities with the fastest economic development and high per capita income[3].

Guangdong was the pioneer to implement reform and opening up, so that its economy was greatly promoted. And Guangzhou, as its capital, has become one of the most developed and active cities in Guangdong Province. According to relevant analysis, in 2017, Gross Regional Product (GDP) reached 2150.315 billion yuan, a year-on-year growth of 7.0%. In addition, per capita GDP reached 150678 yuan, converted into 22317 US dollars at the average exchange rate. What's more, the regional fiscal revenue was 594.7 billion yuan, an increase of 14.0%. Among them, the added value of urban agriculture in the primary industry was 23.349 billion yuan, a decrease of 1.0%; the added value of industries in the secondary industry was 601.529 billion yuan, a growth of 4.7%; and the added value of commerce in the tertiary industry was 1525.437 billion yuan, an increase of 8.2%. The proportion of added value of the primary, secondary and tertiary industries was 1.09: 27.97: 70.94. The contribution rate of the secondary industry to economic growth was 20.9% and the contribution rate of the tertiary industry to economic growth was 79.3% , increasing by 2.3% over the previous year.

While admiring steady and rapid development of Guangzhou, ecological environment was under intense pressure and suffered from severe destruction because of industrial transformation, increasing proportion of industrial and commercial development, and a large number of resource use and energy consumption[4]. When it came to atmospheric environment, rapid development of industry and automobile industry resulted in an increasing number of smoke and waste emissions, which was more serious than third and fourth tier cities in Guangdong. When it came to water resources, the overdue treatment or neglect of sewage and waste water discharge led to a certain contamination of water quality[5]. The quality of water and air must be ensured because they were the most basic material conditions for human beings. Therefore, it has been urgent and significant to coordinate ecological environment and economic development.

Selection of Evaluation Indicator. The basis and key to evaluate coordinated development of ecological environment and economy was to establish evaluation indicators of both of them. This study synthesized the development history and the important economic situation status of Guangzhou and based on sustainable development between ecological environment and economy. Aiming at ensuring the evaluation indicator system was scientific, rational and concise, eight indicators were selected from ecological environment and economic development respectively for parallel comparison and connection. Furthermore, the coordinated development of ecological environment and economy can be analyzed.

Selection of Ecological Environment Evaluation Indicator. Ecological environment refers to the sum of all kinds of natural (including the second nature formed under artificial intervention) forces (material and energy) or functions that affect human life and production activities. It mainly includes water resources, land resources, biological resources and climate resources and closely relates to the composite ecosystem of social and economic sustainable development[6]. The problem of ecological environment refers to negative feedback effect which does harm to human survival caused by the environmental destruction and pollution when human beings make use of nature with the aim of survival and development[7]. After consulting relevant data, ecological environmental indicators are analyzed and evaluated from two dimensions, including first-level indicators and secondary indicators. The first level indicators are divided from a macro perspective, including water environment, air quality, climate change and vegetation cover; the secondary indicators makes the first-level indicators more detailed, including water resources per capita, effective irrigation area ratio, exhaust emission intensity, the annual average temperature, the annual average rainfall, forest cover rate. See Table 1[8].

Selection of Economic Development Evaluation Indicator. The level of economic development refers to the scale, speed and level of a country's economic development. It is the transformation process that a nation or society strives for getting rid of poverty and backwardness and obtaining affluence and happiness. It is also the basis for realizing well-off society[9]. The level of economic development reflects the quality of life and culture of a country or a city to a large extent [10]. The industry structure is so extremely complicated that there are numerous factors that affect a city's economic development level. Analyzing relevant researches, the definition of a city's economic development level can be divided into economic environment, social harmony, quality of life and cultural education[11]. Moreover, they can be divided into GDP per capita, R & D expenditures as a percent

TABLE 1
Evaluation indicators of Ecological Environment

First-level indicators	Secondary indicators	
	Indicators	Explanation
Water Environment	Water resources per capita	Ratio of available freshwater resources to corresponding total population
	Effective irrigation area ratio	Sum of normal irrigated paddy fields and irrigated land as a percentage of total area
Air quality	Exhaust emission intensity	Amount of exhaust gas emitted per unit area
	Waste solid emission intensity	Amount of solid waste discharged per unit area
Climate change	The annual average temperature	Average of multi-day average temperature (or multi-month average temperature)
	Annual mean precipitation	Average of total rainfall divided by years
Vegetation cover	Woodland area per capita	Ratio of forest land area to corresponding total population
	Forest cover rate	Forest area as a percentage of land area

TABLE 2
Economic Development Evaluation Indicators

First-level indicators	Secondary indicators	
	Indicators	Explanation
Economic development	GDP per capita	GDP to total population
	R & D expenditures as a percentage of GDP	Ratio of R & D expenditure to GDP indicators
	Proportion of value added of tertiary industry to GDP	Tertiary industry value added as a percentage of GDP
Social Harmony	Income ratio of urban and rural residents	Ratio of urban per capita disposable income to rural per capita net income
Quality of Life	Urban disposable income	The portion of income that households can use for their daily lives
	Rural per capita net income	Rural households can use the non-investment and productive income
Cultural education	Average years of education	Number of years of academic education per capita
	Culture and entertainment	Proportion of cultural, educational and Entertainment expenditures as a proportion of expenditures

age of GDP, income ratio of urban and rural residents, urban disposable income, rural per capita net income, proportion of cultural, educational and entertainment expenditures, and average years of education. See Table 2[12].

Establishment of Coordinated Model. Coordination refers to the phenomenon that two or more modules can be connected, and they are interacted and mutual effected [13]. The coordination between ecological environment and economic development refers to the process to establish interaction between ecology and economy by adopting financial and technological methods within the affordability of ecological environment[14]. For the reason that coordination refers to the relevance between modules, so the greater the coordinated degree is, the more collaborative the cooperation between the two modules is, therefore, the stronger the mutual influence between them will be. Therefore, the coordinated degree between ecological environment and economic development can be defined as the degree of interaction between them. The greater the coordinated degree is, the more collaborative between ecological environment and economic development is [15].

Standardization of Indicator Data. Due to different units and variation degrees among indicators, aiming at eliminating the impact of Dimensionalization on the analysis results, magnitude difference between the indicators are supposed to be reduced to make them comparable. Therefore, this study adopted the range transformation method

to standardize the indicator data, which can be divided into positive indicator and negative indicator.

$$A_i^{'} = \frac{A_i - A_{min}}{A_{max} - A_{min}} \quad \text{positive indicator (1)}$$

$$A_i^{'} = \frac{A_{max} - A_i}{A_{max} - A_{min}} \quad \text{negative indicator (2)}$$

In formula (1) (2), $A_i^{'}$ is the standardized indicator value, A_i is the original standardized indicator value, A_{min} is the minimum standard index value and A_{max} is the maximum standard index value with the same series before processing.

Adoption of Weight. Except for the influence of the magnitude difference of the indicator value, the evaluation indicator may also be interfered by some human factors. Therefore, this study adopted the entropy method in the objective weighting method, that was, the objective weight was determined according to the variation of each indicator. This method can be compared with the subjective weighting method, and it was based on the amount of information provided by each indicator, so that it could reduce interference on evaluation indicator caused by human factors to a certain extent.

Construction of Coordinated Degree Model. In order to better evaluate the coordinated development degree of ecological environment and economic development in Guangzhou, this study adopted coordinated degree and coordinated degree model, which was essential to judge the interaction intensity and the corresponding time interval between ecological environment and economic development. The calculation formulas are as follows:

$$f(x) = \sum_{m=1}^{9} e_m \times X_m^{'} \quad (3)$$

$$g(y) = \sum_{n=1}^{7} h_n \times Y_n^{'} \quad (4)$$

In the formula above, e_m is the M-th ecological environment, e_m is the n-th economic development indicator weight, and $X_m^{'}$ is the standardized value of ecological environment indicator data and $Y_n^{'}$ is standardized value of economic development indicator data . According to the calculation of ecological environment comprehensive evaluation function $f(x)$ and economic development comprehensive evaluation function $g(y)$, G, the deviation coefficient of ecological environment and economic development, can be obtained. Deviation coefficient can reflect relationships between both of them. The calculation formula is as follows:

$$G = \sqrt{f(x) \times g(y) \div [(f(x) + g(y) \div 2)]^2} \quad (5)$$

The coordinated degree is represented by K, reflecting the comprehensive evaluation value between ecological environment and economic development. The coordinated degree is indispensable, represented by Q, which can more truly and comprehensively reflect the coordination level between ecological environment and economic development in the study field. The smaller the coordinated development degree is, the more harmonious the ecological environment and economic development is, and vice versa [16]. The calculation formulas are as follows:

$$K = \alpha f(x) + \beta g(y) \quad (6)$$

$$Q = \sqrt{G \times K} \quad (7)$$

In the formula mentioned above, α, β are undetermined coefficients. This study begins with the idea that ecological environment and economic development ware of equal importance. So α and β are both 0.5.

RESULTS AND DISCUSSION

Measurement of Coordinated Degree of Ecological Environment and Economic Development. Through collection of relevant indicator data of Guangzhou from 2009 to 2019, standardiza-

tion of data of each indicator value and adoption of entropy method to determine the weight value of each evaluation indicator, the comprehensive evaluation index of ecological environment $f(x)$ and comprehensive evaluation index of economic development $g(y)$ were obtained through analysis. The results are shown in Table 3.

On the basis of the results of the above formula, coordinated degree, coordinated development degree model and discrimination standard, this study respectively calculated the dispersion coefficient G, coordinated degree K and coordinated development degree Q of Guangzhou from 2009 to 2019. In addition, based on coordinated development division and coordinated development type in Table 4, the coordination of ecological environment and economic development of Guangzhou can be better reflected. The results are shown in Table 5[17].

Analysis on the Coordinated Development of Ecological Environment and Economy. Comparing and analyzing the coordination of ecological environment and economic development in Table 4 and Table 5 from 2009 to 2019, it can be found that the coordinated degree of ecological environment and economic development in Guangzhou was on the steady rise. From 2009 to 2014, the coordinated development of ecology and economy

TABLE 3
Comprehensive Evaluation Index of Ecological Environment and Economy

years	2009	2010	2011	2012	2013	2014	2015	2016	2017	2018	2019
Ecological development status	0.365	0.412	0.527	0.592	0.668	0.763	0.843	0.936	0.991	1.085	1.126
The level of economic development	0.341	0.468	0.612	0.695	0.755	0.902	1.238	1.308	1.421	1.488	1.509

TABLE 4
Division of Coordinated Development Degree

Coordinated Development Division	Coordinated Development Type
0.00~0.10	Severe disorders
0.11~0.3	Moderate disorder
0.31~0.4	Mild disorders
0.41~0.5	Barely Coordinating
0.51~0.6	Primary coordinated development
0.61~0.7	Intermediate Coordinated Development
0.71~0.9	Well coordinated development
>0.9	High-quality coordinated development

TABLE 5
Coordinated Evaluation Results of Ecological Environment and Economic Development in Guangzhou

years	Coefficient of dispersion	Coordination	Coordinated development	Coordination type
2009	0.16	0.586	0.4	Mild disorders
2010	0.156	0.598	0.478	Barely Coordinating
2011	0.172	0.654	0.556	Primary coordinated development
2012	0.193	0.646	0.589	Primary coordinated development
2013	0.245	0.682	0.661	Intermediate Coordinated Development
2014	0.283	0.731	0.699	Intermediate Coordinated Development
2015	0.326	0.741	0.798	Well coordinated development
2016	0.398	0.785	0.869	Well coordinated development
2017	0.485	0.837	0.899	Well coordinated development
2018	0.61	0.869	1.091	High-quality coordinated development
2019	0.683	0.968	1.215	High-quality coordinated development

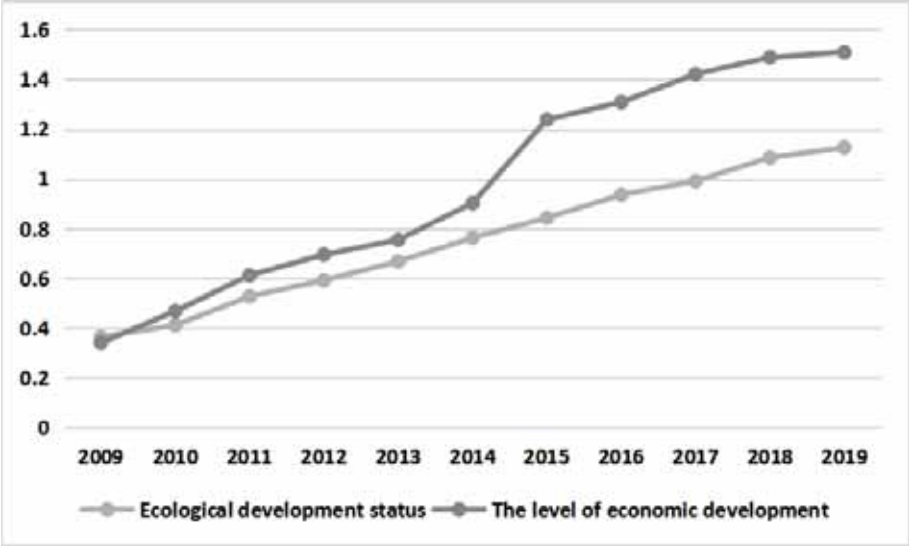

FIGURE 1
Coordinate Degree Evolution of Ecological Environment and Economic Development in Guangzhou from 2009 to 2019

still remained negative, reflecting that the ecological environment in Guangzhou was damaged. However, from 2015 to 2017, the coordinated development of ecology and economy was improved obviously. From 2018 to 2019, it even reached high-quality coordinated development, showing that the measures carried out by Guangzhou in the ecological environment were effective. It was worth learning that protection and concern of the ecological environment should be given more attention while developing a city's economy and industry.

According to the data of coordinated development degree of ecological environment and economy, the coordinate degree evolution of ecological environment and economic development in Guangzhou from 2009 to 2019 was drawn. It is shown in Figure 1. It can be seen from the figure that the broken line of square node is the comprehensive evaluation index of ecological environment, and the broken line of circular node is the comprehensive evaluation index of economic development. It can be discovered from the figure that from 2009 to 2019, the comprehensive evaluation indexes of Guangzhou's economic development were always apt to increase; while the comprehensive evaluation indexes of ecological environment were on the rise except for the first two years. Therefore, the ecological environment in Guangzhou was also highly valued with constant economic development, indicating that the coordination between the ecological environment and economic development of Guangzhou was positive[18].

Ecological Environment and Economy Coordinated Development Initiative. Guangzhou, one of the most developed cities in South China, excels at model and demonstration. However, it should be alarming that consumption of ecological resources is the price of economic development. Therefore,one of the most important issues for cities is to learn that how to coordinate the ecology and economy and how to protect the living environment [19]. It is worth learning that ecological environment has been patiently protected and economy has been steadily promoted in Guangzhou in a recent decade. In order to improve the construction of coordinated development of ecology and economy, there are a few aspects that can make contributions: ① Strengthening laws and regulations of ecological environment protection and formalizing measures of ecological protection; ② Increasing vegetation coverage, afforestation and accelerating the construction of urban landscape; ③ Effectively coping with industrial pollution and reducing the emission of waste gas and solid waste;④ Effectively classifying the urban garbage and advocating people to reduce the use of plastic bags and other non degradable products; ⑤ Supporting the development and use of renewable energy [20]. Only in the bearable range for ecological environment to develop economy can human society develop in a eternal and sustainable way. In addition, Other cities can learn from Guangzhou's experience in balancing coordinated development of ecology and economy to further create cities with flourished economy and splendid ecology.

CONCLUSION

In this study, a scheduling model of them and analyzed the relationships of coordination degree between ecological environment and economic development in Guangzhou is established. On the basis of successful economic development, environmental protection must be attached great importance. This study will not only serve as a reference for coordination degree between ecological environment and economic development in Guangzhou, but also it will provide case reference for other cities and nations.

REFERENCES

[1] Liang, Q., Sun, H.Y., Wu, X.Y., Ou, X.L., Gao, G.Q., Jin, Y., Tong, D.Y. (2018) Development of New mRNA Markers for the Identification of Menstrual Blood. Annals of Clinical & Laboratory Science. 48(1), 55-62.

[2] Lv, J., Song, W.J., Lin, S.L., Chen, M.B., Feng, Z.P., Li, Y.L., Ding, Y.L. (2017). Influence of equalization on $LiFePO_4$ battery inconsistency. International Journal of Energy Research. 41(8), 1171-1181.

[3] Chen, K.L., Gong, J.Z., Chen, X.Y. (2017). Spatial pattern and differentiation characteristics of Urban heat Island intensity in Guangzhou city. Chinese Journal of Ecology. 36(3), 792-799.

[4] Wohlfarth, M., Schnurr, D., Krämer, J. (2019) Winners, Losers, and Facebook: The Role of Social Logins in the Online Advertising Ecosystem. Management Science. 65(4), 1678-1699.

[5] Javid, A. (2015) Recent Record of Scotophilus heathii From Wheat-Rice Based Agroecosystem of Punjab. Pakistan Journal of Zoology. 46(4), 1175-1179.

[6] Dong, X.H., Xu, M., Lin, M.Z., Li, Y., Yang, X.D. (2019). Lake sediment evidences historical patterns of lake ecosystem services and their tradeoff/synergy mechanism: Progress, case studies and prospective. Journal of Ecology and Rural Environment. 35(1), 28-37.

[7] Pavlova, A.S., Kashulin, N., Denisov, D., Terentev, P.M., Kashulina, T.G., Dauval'ter, V.A. (2019) Distribution of Chemical Elements between the Components of the Ecosystem of Arctic Lake Bolshoy Vudyavr (Khibiny, Murmansk Oblast). Contemporary Problems of Ecology. 12(3), 280-297.

[8] Cuesta, F., Llambí, L.D., Huggel, C., Drenkhan, F., Gosling, W.D., Muriel, P., Jaramillo, R., Tovar, C. (2019). New land in the Neotropics: a review of biotic community, ecosystem and landscape transformations in the face of climate and glacier change. Regional Environmental Change. 19 (6), 1623-1642.

[9] Miletić, G.M., Žmuk, B., Mišetić, R. (2018). Second homes and local socio-economic development: the case of Croatia. Journal of Housing & the Built Environment. 33(2), 301-318.

[10] Dai, E., Wu, Z., Du, X. (2018) A gradient analysis on urban sprawl and urban landscape pattern between 1985 and 2000 in the Pearl River Delta, China. Frontiers of Earth Science. 12(4), 791-807.

[11] Fuzhan, X. (2019). China's Economic Development and Development Economics Innovation. Social Sciences in China. 40(2), 100-110.

[12] Zhu, F.B., Fang, Y.P., Yang, X.T., Qiu, X.P., Yu, H. (2018) Effects of altitude on county economic development in China. Journal of Mountain Science. 15(2), 406-418.

[13] Gomes, D.A., Nurbekyan, L., Prazeres, M. (2017) One-Dimensional Stationary Mean-Field Games with Local Coupling. Dynamic Games and Applications. 8(2), 315-351.

[14] Zhao, F.L., Liu, Q.F., Yan, X., Bo, H.L., Zeng, C., Tan, S.C. (2019). Droplet Motion and Phase Change Model with Two-Way Coupling. Journal of Thermal Science. 28(4), 826-833.

[15] Bao, T.Q., Fellner, K., Latos, E. (2018) Well-posedness and exponential equilibration of a volume-surface reaction-diffusion system with nonlinear boundary coupling. Annales De L Institut Henri Poincare Non Linear Analysis. 35(3), 643-673.

[16] Dossey, B.M., Rosa, W.E., Beck, D.M. (2019) Nursing and the Sustainable Development Goals: From Nightingale to Now. The American Journal of Nursing. 119(5), 44-49.

[17] Zinabu, E., Kelderman, P., Van Der, Kwast, J., Irvine, K. (2019). Monitoring river water and sediments within a changing Ethiopian catchment to support sustainable development. Environmental Monitoring and Assessment. 191(455), 1-20.

[18] Liu, D.Q., Zhang, J.X., Gong, J., Cao, E.J. (2019) Ecological function zoning in Bailongjiang Watershed of Gansu based on production-living-ecological function clusters. Chinese Journal of Ecology. 38(4), 1258-1266.

[19] Asghari, M., Noaparast, M., Shafaie, S.Z., Ghassa, S. (2018) Recovery of coal particles from a tailing dam for environmental protection and economical beneficiations. International Journal of Coal Science & Technology. 5(2), 253-263.
[20] Wang, Z.W., Li, X., Chen, H. (2018). Preparation of Environmental Protection and High Efficiency Lead-Free Solder Paste. Key Engineering Materials. 789, 216-220.

Received: **28.05.2020**
Accepted: **20.10.2020**

CORRESPONDING AUTHOR

Tao Fan
School of Economic and Management,
Tongji University
Shanghai 200092 – China

e-mail: yuyu889a@163.com

© by PSP Volume 30– No. 05/2021 pages 5537-5549 Fresenius Environmental Bulletin

NOTICE

COVID-19 MANAGEMENT: TRADITIONAL CHINESE MEDICINE VS. WESTERN MEDICINAL ANTIVIRAL DRUGS, A REVIEW AND META-ANALYSIS

Muhammad Adnan Shereen[1], Nadia Bashir[1], Mubarak Ali Khan[2], Abeer Kazmi[2], Suliman Khan[3], Luo Zhen[4], Jianguo Wu[1,4,*]

[1]State Key Laboratory of Virology, College of Life Sciences, Wuhan University, Wuhan, PR China
[2]Department of Biotechnology, Faculty of Chemical and Life Sciences, Abdul Wali Khan University Mardan (AWKUM), Mardan 23390, Pakistan
[3]The Department of Cerebrovascular Diseases, The Second Affiliated Hospital of Zhengzhou University, Zhengzhou, PR China
[4]Guangdong Provincial Key Laboratory of Virology, Institute of Medical Microbiology, Jinan University, Guangzhou, Guangdong 510632, China

ABSTRACT

SARS-CoV-2 causing COVID-19 spread to more than 200 countries with 109 M infected patients and 2.41 M deaths (6.98% mortality rate). Currently, there is no approved drug or vaccine available to treat COVID-19 patients, though some combinations of already used broad-spectrum Western medicines, such as antibiotics, antivirals, and interferons are exploited against SARS-CoV-2. Among the Western medicines used, Chloroquine, Hydroxychloroquine, Chloroquine Phosphate, Remdesivir, and Umifenovir (Arbidol) were the most effective antivirals against SARS-CoV-2 at high or frequent dose. These drugs limited the viral infection by inhibiting attachment of virus to ACE2 receptor of human cell or by interfering and terminating the viral genome replication, but also induced severe adverse effects on the patients. Due to high and frequent dose of antivirals, patients reported with Hepatic, renal, and cardiac complications along with vomiting, diarrhea, muscle cramps, skin complications, anemia, abdominal pain, bleeding from nose, nausea, swelling of legs and ankles, hearing, and mental complications. Different vaccines are in trail phases might take long time to be available for COVID-19 patients, so an alternate therapy is required with no or minimal adverse effects. Chinese health workers significantly recovered the COVID-19 patients (92.4% recovery rate) by using their Traditional Chinese Medicine (TCM). The current review article contains details about the adverse effects of certain Western medicines, like antivirals on the COVID-19 patients and the efficacy of therapeutic herbal Traditional Chinese Medicine (TCM) for clinical recovery of COVID-19 patients in China.

KEYWORDS:
SARS-CoV-2, COVID-19, Western Medicine, Antiviral drugs, Traditional Chinese Medicine

INTRODUCTION

SARS-CoV-2 found in Wuhan, China caused the deadliest COVID-19 pandemic worldwide [1,2]. COVID-19 can be diagnosed by CT-scan, RT-PCR, dd-PCR, and ICT kits, however, until now, RT-PCR is the only confirmatory test, which has been widely recommended. Currently, there is no approved drug or vaccine available to treat or prevent COVID-19, but few Western medicines like antiviral, antibiotics, and interferon have shown promising results [3]. Although combinational therapies with conventional antiviral and antibiotic drugs are effective, however, they cause several adverse effects, such as mental illness, nausea, muscle cramps, and hepatic and kidney complications [4]. On the other hand, treatment with Traditional Chinese Medicines (TCM) alone or in combination with Western Medicine (antiviral drugs) resulted in the recovery of over 75000 patients (with approximately more than 90% recovery rate) from COVID-19 in China [5], suggesting that TCM play a critical role in clinical recovery. According to the published literature, using TCM against COVID-19 is effective and safe [5,6]. In this review, we discuss the adverse consequences associated with some of the Western Medicines, including chloroquine and other antiviral drugs. Furthermore, we highlight the effective role of herbal Traditional Chinese Medicine (TCM) alone and in combination against COVID-19. Like other human coronaviruses, SARS-CoV-2 also uses angiotensin-converting enzyme 2 (ACE2) human cell receptor for attachment and entry. After entry, virus is transported to the endosomes for un-coating, followed by transcription and translation of viral genome in cytoplasm. Replication of positive-strand viral genomic RNA is transcribed into a negative RNA strand that is used as a template for the synthesis of viral mRNA. Before assembly and release of virions, viral proteins undergo post translational modifications. Chloroquine increases the acidification of endosomes and inhibits the formation of the autophagosome or

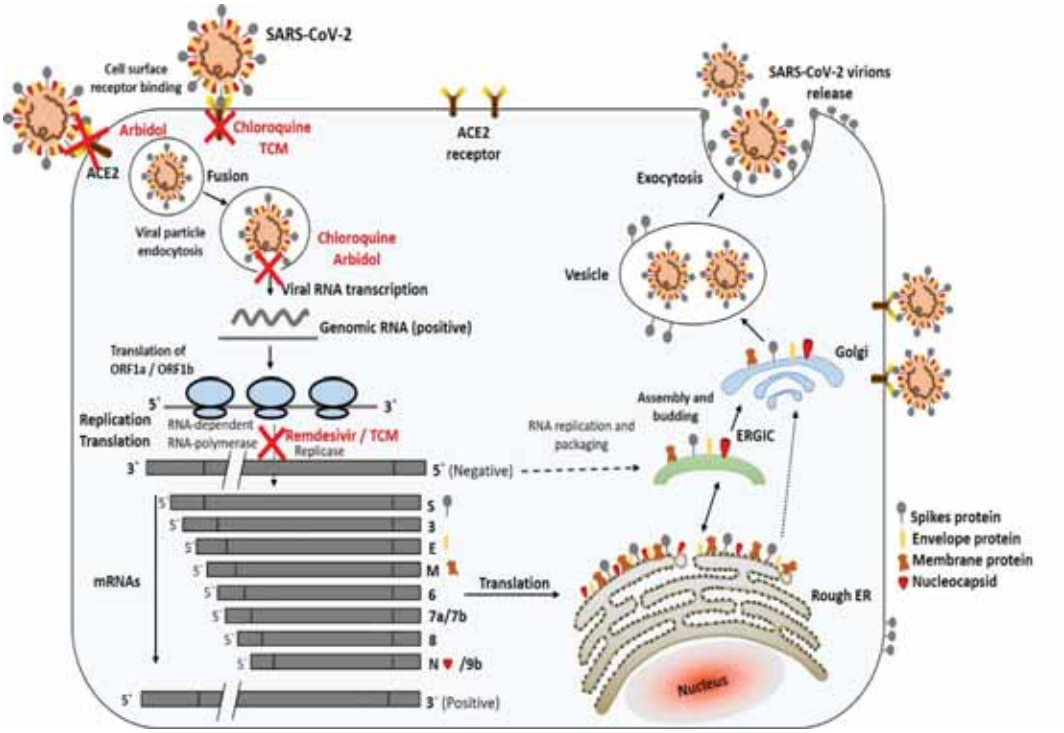

FIGURE 1
Schematic representation of the possible effects of chloroquine, Remdesivir and Arbidol on the severe acute respiratory syndrome coronavirus 2 (SARS-CoV-2) replication cycle.:

inhibits virus replication by reduction of cellular mitogen-activated protein kinase activity. Moreover, chloroquine could alter M protein maturation and interfere with virion assembly and budding. Arbidol interacts with glycoprotein of SARS-CoV-2 and causes mutation in it therefore virus become unable to recognize and attach to ACE2 receptor of human cells. The active triphosphate and nucleotide analog of Remdesivir attach to the i+3 position of RNA polymerase and inhibit RNA polymerase activity and cause termination of viral genome replication.

Western Medicine. Western medicines are widely using around the world to treat various diseases, the novel approaches and techniques in the 21st century have enhanced the efficacy of modern Western medicines. Western medicines are commercialized after a series of experiments in order to minimize the adverse effects of the chemical compounds [7]. To treat COVID-19 patients variable Western medicines were applied, including broad spectrum antivirals. The patients have recovered after treatment, though the frequent use of higher concentration of drugs have caused severe complications. Few of these drugs, their antiviral efficacy against COVID-19 and adverse side effects are briefly discussed as follow.

Chloroquine. Chloroquine belongs to 4-aminoquinoline class of drugs and was discovered in 1934 by Hans Adersag and introduced for Malaria treatment and prevention, in 1947. Later on, it was used against Human Coronaviruses, Dengue virus, flavi-viruses, retro-viruses, Influenza, Ebola, HCV, HBV, HIV, and autoimmune disorders, such as rheumatoid arthritis, amebiasis, and lupus erythematosus [8-10]. Chloroquine was introduced in the form of tablets in combination with sulfate, phosphate, or hydrochloride salts, under the trade name Resochin, Lariago, Chloroquine FNA, and Dawaquin [11]. Malaria parasite digests the protein unit of hemoglobin and release heme in nontoxic form by crystallizing it to form hemozoin. The main mechanism of Chloroquine is to inhibit the formation of hemozoin, thus toxic heme is release that lyse the membranes and kill the malaria parasite [12,13]. The chloroquine also has potential to increases the lysosomal and endosomal pH that inhibits the viral nucleic material release and replication initiation. Chloroquine allows zinc transportation to cells which restricts viral RNA-polymerase activity [14,15]. Chloroquine is effective against autoimmune diseases especially rheumatoid arthritis by enhancing Interleukin-1 (IL-1) and enzymes production and Reactive Oxygen Species (ROS), by lysosomes and macrophages [16]. Due to the presence of hydroxyl group (N-ethyl), Hydroxychloroquine is diverse from chloroquine, similarly the addition of phosphate group, Chloroquine phosphate is diverse from both. Hydroxychloroquine and Chloroquine Phosphate has the same mechanism of action like chloroquine, with rapid gastrointestinal absorption and renal elimination [10].

The death rate due to overdose of Chloroquine is 20% reported in a study [17]. Chloroquine fluctuates the pH of a renal and hepatic cells and tissues, and causes enzymatic variations in kidney and liver

which may lead to cause organ failure and death. Chloroquine and hydroxychloroquine have remarkable bioavailability and oral absorption with extended plasma elimination half-life, takes 6 to 7 months to fully eliminate from the body and about half of the drug metabolites undergo unmodified renal clearance. Therefore, the patient may face major and minor negative effects even after discontinuation of the medicine [18]. Chloroquine can easily pass through placenta and even excreted from breast milk, may cause complications in child and mother [19-21].

Chloroquine and its salts cause corneal deposits, posterior subcapsular lens opacity, ciliary body dysfunction, and irregularity in the macular pigmentation in early phase. Other deleterious effects of chloroquine and its derivatives include vomiting, diarrhea, muscle cramps, skin complications, abdominal pain, bleeding from nose, nausea, swelling of legs and ankles, hearing and mental complications, and anemia [22,23].

Role of Chloroquine against COVID-19. Chloroquine inhibits viral replication [24], hence reduce the viral load, therefore, it was found effective against COVID-19 as reported by Chinese medical researchers. Chloroquine phosphate limit the viral attachment and entry to the cell by interfering glycosylation of receptor (Figure 1) [25,26]. 500mg of chloroquine was given to COVID-19 patients BD in mild and severe conditions [26]. The health authorities of Korea, China, and Italy approved chloroquine for clinical trials and experimental studies for COVID-19, later on, the authorities observed negative impacts of chloroquine and limited its use. Chloroquine cause severe adverse effects, especially in COVID-19 patients, including cardiac and diabetic complications, as it increase arrhythmia risk [27]. 11 out of 40 COVID-19 patients died in Brazil, treated with higher concentration of chloroquine for 6 days [28,29]. On March 27th, food and drug administration (FDA) from US issued a guideline mentioned that chloroquine or chloroquine phosphate should not be recommended for COVID-19 treatment [30]. Similar guidelines were also issued by European Medicines Agency (EMA) on April 1 2020 [31].

Remdesivir. Remdesivir is a single stereoisomer monophosphoramidate antiviral drug, introduced in October 2015 by Gilead Sciences (American Bio-pharmaceutical Company) to treat Ebola and Marburg virus. Initially, it was experimented by US Army Medical Research Institute of Infectious Diseases (US-AMRIID) on Ebola infected Rhesus Monkey. Remdesivir is nucleotide analog that inhibit viral replication by interfering with viral RNA transcription [32,33]. Remdesivir metabolize into its active form GS-441524 which interferes and limit the replicating and proof-reading activity of viral RNA polymerase and exoribonuclease enzymes, respectively. In some viruses, it pause the RNA polymerase activity and induces irreversible nucleotide chain termination [33,34]

At higher or repeated dose, remdesivir also possess typical antiviral negative effects, such as cramps, nausea, headache, and vomiting. Pregnant women and those who have plans to conceive are restricted to use remdesivir as it affects fetus with severe pregnancy outcomes [35]. In animal model study, remdesivir effected kidneys development in fetus. In animal model study the higher levels of radioactivity of remdesivir were detected in kidney, kidney medulla, liver, and arterial wall, while minimal radioactivity was detected in brain tissues of rats. Remdesivir caused injury to the cortical and basophilic tubules and karyomegaly in the renal cells of the male rats. It also increased the weight of kidney in both male and female rats, and exhibited OAT3- dependent cytotoxicity by 15 folds. Remdesivir reduced the amount of viable embryos and reduced the size and weight of ovary, oviduct and uterus of female rat [36]. It is also reported that major systemic metabolites, GS-704277 and nucleoside analog GS-441524 of Remdesivir fluctuates the level of hepatic enzymes and cause serious liver damage [35].

Role of Remdesivir against COVID-19. The Remdesivir blocks the SARS-CoV-2 replication in human cell by the similar mechanism as it uses against SARS-CoV, Ebola virus and MERS-CoV. The active triphosphate and nucleotide analog of Remdesivir attach to the i+3 position of RNA polymerase and inhibit RNA polymerase activity and cause termination of viral genome replication as shown in Figure 1 [37]. Initially, due to less efficacy and severe negative effects of Remdesivir, Gilead Sciences stopped clinical trials against Ebola virus, but now in January 2020, Gilead Sciences re-began laboratory testing of Remdesivir against SARS-CoV-2 [38]. On January 21st, Chinese health authorities and Wuhan institute of Virology tested Remdesivir in clinical trial against COVID-19 in infected patients, resulted in clinical recovery [39]. 94% oxygen saturation value of COVID-19 patient was improved in USA when treated with Remdesivir [40]. Studies concluded that remdesivir is more effective when used during early or mild conditions of COVID-19 infection [41]. The Johns Hopkins University declared Remdesivir as the most efficient drug against COVID-19, on the other hand, US scientists reported that Remdesivir cause kidneys and liver complications in COVID-19 patients, by fluctuating the enzymatic level and result in death [35].

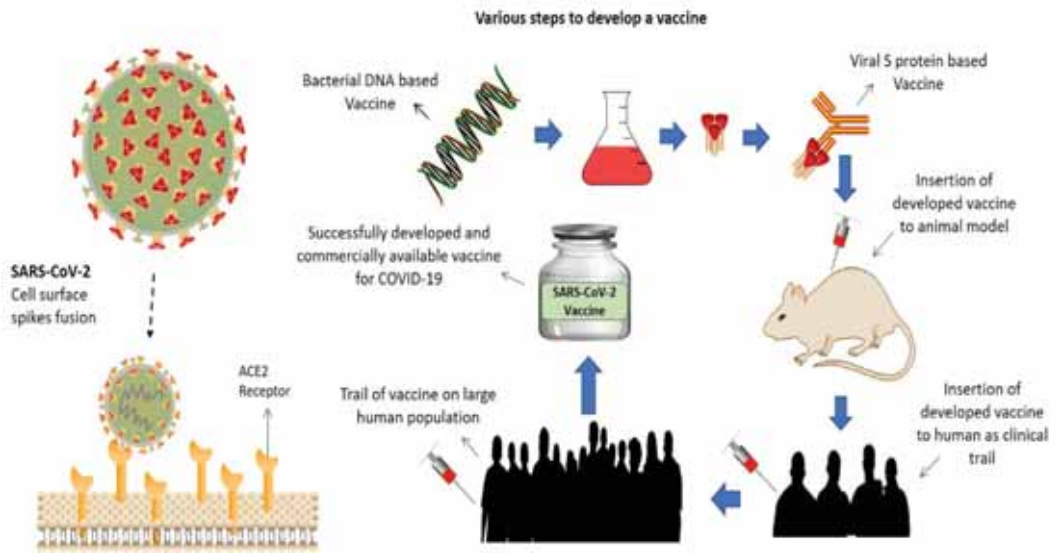

FIGURE 2
The various strategies and trail phases involved in the development and commercialization of an effective COVID-19 vaccine.

Umifenovir (Arbidol). Umifenovir is an indole base, hydrophobic antiviral drug manufactured by a Russian company, Pharmstandard in 1974. The drug was commercialized under a trade name 'Arbidol' in China and Russia, though the drug is not approved by US-FDA for prevention and treatment of influenza and limited to few countries [42]. Umifenovir effects virus by both ways such as viricidal activity (directly acting) or by blocking viral replication at a several stage of viral life cycle. Due to hydrophobic nature of Umifenovir, molecules are capable of interaction with amino acids (tyrosine, tryptophan), which enhances its ability to directly kill viruses. Umifenovir may also interact with aromatic compounds of the viral glycoproteins which are responsible for targeted human cell recognition and fusion [43]. Umifenovir also act as an antioxidant and stimulates immune response by enhancing interferon production and macrophages activity [44]. Different studies proved that Umifenovir is more efficient against RNA viruses as compare to DNA viruses. The drug effectiveness is reported against Ebola virus, HCV, HBV, Herpes virus, and polio virus [45-47].

The higher dose of Umifenovir causes allergic reactions, hypertension, and hypersensitivity while in children it causes sensitization. Other side effects include nausea, diarrhea, muscle cramps, headache, laziness, and elevated serum transaminase [48]. The commercialization of Arbidol to treat Influenza was criticized by the Russian academy of medical sciences and reported that the drug efficacy is not proven and the claims to treat influenza and rapid recovery is false [49].

Role of Umifenovir (Arbidol) against COVID-19. Arbidol significantly reduced the SARS-CoV-2 induced COVID-19 infection in a similar mechanism as it applied against influenza viruses. The active compound of Umifenovir interact with the glycoproteins of SARS-CoV-2 and prevents recognition and attachment of SARS-CoV-2 with ACE2 receptor of human cells, as shown in Figure 1 [50]. In February 2020, National health commission of China declared Arbidol in combination with Darunavir as a potential drug to treat COVID-19 pandemic [51]. In recent reports, it is concluded that Arbidol can be effective only at early (asymptomatic) stages, while showed no effect on patients with mild and moderate COVID-19 conditions [52].

Vaccines for COVID-19. Up to date, no approved vaccine is available against SARS-CoV-2, though some research centers and pharmaceuticals industries struggling to develop an effective vaccine, as listed in Table 1 (Figure 2). Chinese Centre for Disease Control and Prevention, Johnson & Johnson, Stermina therapeutics, US National Institute of Allergy and Infectious Diseases, GeoVax-BravoVax industry, Vir Biotechnology, Novavax, and Clover Biopharmaceuticals are approaching various techniques to design a vaccine for COVID-19. They target as, mRNA-based vaccine, inactivated virus vaccine, protein subunit-trimer based vaccine, and DNA based vaccine. Some of these vaccines are in 2nd or 3rd phase of trail progress [3,53,54]. Recently, Sinovac Biotech designed a vaccine named 'PiCoVacc' through inactivation method and tested effective against 11 various strains of SARS. Rats, mice, and non-human primates were used as animal model for testing vaccine [55]. Another vaccine prepared using dendritic cells modified with artificial antigens, by Shenzhen GenoImmune Medical Institute, that can produce antibodies against COVID-19, named LV-SMENP-DC, and is in animal trail phase [56].

TABLE 1
Different approaches applied by various pharmaceutical industries and research centers to develop efficient vaccine for COVID-19

Type/ name of Vaccine	Manufacturer	Preparation strategy
SARS-CoV-2 vaccine	US National Institute of Allergy and Infectious Diseases	m-RNA based vaccine
	Stermirna Therapeutics	
Nucleic Acid Based vaccine	CureVac	
	Moderna	
BNT162	Pfizer and BioNTech	
INO-4800	Inovio Pharmaceuticals	
Nasal Vaccine for COVID-19	University of waterloo	Bacterial DNA encoding SARS-CoV-2 spike protein
Opencorona	Cobra Biologics and Karolinska Institute	
bacTRL-Spike	Symvivo Corporation	
Inactivated viral vaccine	Chinese Centre for Disease Control and Prevention	Viral strain
Corona vaccine	GeoVax and BravoVax	MVA-VLP vaccine platform and SARS-CoV-2 genetic sequences
SARS-CoV-2 vaccine	Clover Biopharmaceuticals	recombinant 2019-nCoV S protein subunit-trimer based vaccine
Whole virus vaccine	Johnson & Johnson	Adenovirus-vectored vaccine using AdVac® and PER.C6® technology
Whole virus vaccine	Codagenix and serum institute of India	Live attenuated vaccine
Subunits based vaccine	University of Queensland	Protein-based vaccine using Molecular Camp platform
	Vaxart	Vaccine using Oral recombinant protein
Nanoparticle	Novavax	Recombinant protein nanotechnology
Antibody based vaccine	Vir Biotechnology	Monoclonal antibodies
Subunit based Vaccine	New York blood center, Fudan University New York	RBD protein of coronavirus-based vaccine
Whole virus	University of Oxford	Protein modified whole virus
PiCoVacc	Sinovac Biotech	Inactivated SARS-CoV-2 virus
Whole Inactivated Virus	Wuhan Institute of Biological Products	
Ad5-nCoV	CanSino Biologics	recombinant adenovirus type 5 vector (using spike protein)
LV-SMENP-DC	Shenzhen Geno-Immune Medical Institute	Dendritic cells modified with artificial antigens

TRADITIONAL CHINESE MEDICINE (TCM)

TCM is a branch of traditional herbal medicines from Chinese medical practices to treat various infectious diseases from last 3500 years [57]. It has made indelible contributions to the well- being of the Chinese people. TCM are alluring and alternative medicines based on nontoxic herbal remedies that can be used against viruses, such as Jinhua Qinggan granule and Xuebijing injection are effective against various strains of Influenza, SARS and MERS coronaviruses, and Avian flu [58,59]. TCM played a vital role in recovery of patients from COVID-19 in China, 92.4% of people recovered from COVID-19 in China [6]. There are few most effective TCM against COVID-19, discussed in this article.

Jinhua Qinggan granule. Jinhua Qinggan granule is a mixture of 12 different medicinal plants including mint and licorice. The drug was developed against Influenza virus. The major role of Jinhua Qinggan granule is to protect and detoxify lungs and enhance the proliferation of lymphocytes and white blood cells. The drug was also used in current COVID-19 pandemic in China and resulted in recovery of patients within a week [60,61].

Xuebijing injection. Xuebijing injection is composed of 5 various Herbs, it was introduced during 2003 SARS-CoV epidemic in China. The major function of the drug is to detoxify lungs and recover infected organ, it can also remove blood stasis and suppress inflammatory response. Later on, the in vitro studies proved the antiviral efficiency of Xuebijing injection as it blocks the viral replication and inhibits the inflammation induced by virus. Xuebijing injection was examined on 712 COVID-19 patients in 32 hospitals of China, resulted in reduction of mortality rate by 8.9% in severe COVID-19 patients and recovered patients 5 days prior to the other patients (regular treatment) [62].

Lung Cleansing and Detoxifying Decoction. The old TCM book written in 220 A.D (Shang Han Za Bing Lun) was used to prepare decoction from 21 different herbal components, currently known as Lung Cleansing and Detoxifying Decoction. The major function of decoction is to protect lungs and sinus from deleterious effects of pathogens and contaminated air (smog). It is also effective to treat cough, fatigue, fever, and lungs complications. It was proved from the reports that lung cleansing and detoxifying decoction can up-regulates the cell signaling pathways and inhibits the cell components to replicate viral genome. During COVID-19 pandemic, 1258 patients in 11 different provinces of China were treated with lung cleansing and detoxifying decoction, resulted in 96.3 % of clinical recovery [5,6].

Huashi Baidu. Huashi Baidu is another TCM prepared by the Academy of Chinese Medical Sciences from 14 various herbs after the clinical practices at Wuhan Jinyintan Hospital. It is mainly used to detoxify lungs, remove dampness and relief cough. Huashi Baidu was also used to treat COVID-19 patients in China, resulted in significant reduction of viral load and improved lung conditions of severely infected patients. Huashi Baidu reduced 30% of viral load in COVID-19 infected guinea pigs [6,61].

Mechanism of TCM against SARS-CoV-2 . Lianhuaqingwen (LQ) is a traditional Chinese medicine with immunoregulatory effect and antiviral potential against various strains of influenza [63]. Recently, Lianhuaqingwen was used against SARS-CoV-2 containing Vero E6 cells. A remarkable reduction in production of pro-inflammatory cytokines was observed at the level of mRNA, resulted in inhibition of viral replication. Lianhuaqingwen also affected the virion assembly, cells contained virions with irregular morphology [64]. Lianhuaqingwen is also an effective TCM used against SARS-CoV-2, available in the form of Capsule/Granule. During in vitro study, Lianhua Qingwen remarkably reduced the viral load by inhibiting the viral replication and affected viral morphology. Lianhua Qingwen significantly reduced mRNA expression levels of TNF-α, IL-6, CCL-2/MCP-1, and CXCL-10/IP-10 and enhanced the expression of connexins in alveolar epithelial cells and pulmonary vascular endothelial cells [65]. The compounds in Kangbingdu Granules (a TCM) reduced the viral attachment and infection to host cell by binding to the ACE2 receptor of human cell and viral glycoproteins [66].

Key ingredients of TCM. On the basis of sign and symptoms, Chinese health worker prescribed different Traditional Chinese medicine to the COVID-19 patients which include, Huoxiang Zhengqi Shui, Lianhua Qingwen, Shufeng Jiedu Capsules, Jinhua Qinggan Granules, Qingfei Paidu Tang, Xiyanping, Xuebijing, Re-Du-Ning, Tan-Re-Qing, and Xingnaojing Injection [67]. Patients with critical conditions were treated with, Shenfu and Shengmai San injections, Suhe Xiang Wan and Angong Niuhuang Wan Pills [68]. Most of the traditional Chinese medicine are composed of more than 10 medicinal herbs, though *Astragalus membranaceus, Glycyrrhizae uralensis*, *Saposhnikoviae divaricata, Atractylodis macrocephalae*, *Lonicerae Japonicae Flos, Fructus Forsythiae, Atractylodis Rhizoma, Radix platycodonis, Agastache rugosa, Cyrtomium fortune J. Sm, Eupatorii Herba*, *Agastache rugosa, Ophiopogon japonicas, Scrophularia ningpoensis, Rhizoma phragmitis*, *Adeinophora stricta Miq,* and *Dendrobium nobile Lindl* are the most common medicinal plants found effective TCMs used against COVID-19 [69,70]. Roots, leaves, stems, or Rhizomes of these plants are used for effective TCM production, as these plants contain especial secondary metabolites which are responsible for treatment of various diseases and infections. The major secondary metabolites and their chief bioactivities are enlisted in Table 2.

TCM IN COMBINATION WITH WESTERN MEDICINES

To minimize the adverse effects and enhance the efficacy of Western Medicines to cope COVID-19, combination of Western and Traditional Chinese Medicine is an effective approach. In a recent study, a 51-year-old woman, 27-year-old nurse, and 53-year-old man infected with COVID-19 were treated at Tongji Hospital China, with combination of Jinyebaidu granules (TCM) and oseltamivir (75mg per day), Shuanghuanglian oral liquid (SHL) and intervenes injection of immunoglobulin (IVIG) (5g per day), Jinyebaidu granules (TCM) and Arbidol, SHL (20 mL) and Arbidol, respectively. After few days of treatment, significant recovery was observed in COVID-19 patients, including normal breathing, body temperature dropped from 39 ^{o}C to 36.5^{o}C and negative SARS-CoV-2 diagnostic test [71].

TABLE 2
Key plants of Traditional Chinese medicines (TCMs) used for treatment of COVID-19 patients

Plant specie	Family	Chinese name	Plant part used	Active metabolites	Effectiveness	References
Astragalus membranaceus	Fabaceae	Huangqi	Roots	Astragaloside IV, cycloastragenol, calycosin-7-O-β-D-glucoside, calycosin, ononin and formononetin	Treat fatigue, allergies, common cold, upper respiratory infections, fibromyalgia, diabetes, and cardiac complications	[73]
Glycyrrhizae uralensis	Fabaceae	Ganca o	Legumes, Roots	Triterpene saponins and various types of flavonoids, including glycyrrhetinic acid, glycyrrhizic acid, liquiritigenin, isoliquiritigenin, liquiritin and licochalcone A.	Antiulcer, anti-inflammatory, anti-allergic, antichrombotic, antidiabetic, hepatoprogenic, and neuroprotective	[74]
Saposhnikoviae divaricate	Apiaceae	Fangfeng	Roots, Leaves	Chromones and coumarins, flavonoids, flavones, prim-O-glucosylcimifugin, 4′-O-β-D-glucosyl-5- O-methylvisamminol, cimifugin, Sec-O-glucosylhamaudol, and 5-O-methylvisamminol	Rheumatism and allergic rhinitis, anti-inflammatory, analgesic, immunoregulatory, antioxidative, and anti-proliferative, antimicrobial	[75]
Atractylodes macrocephala	Asteraceae	Baizhu	Rhizomes	Sesquiterpenoids, triterpenoids, polyacetylenes, coumarins, phenylpropanoids, flavonoids and flavonoid glycosides, steroids, benzoquinones, and polysaccharides	Antimicrobial, antitumor, anti-inflammatory, anti-aging, antioxidative, anti-osteoporotic, neuroprotective, immunomodulatory, improve gastrointestinal function, and gonadal hormone regulation.	[76]
Lonicera japonica	Caprifoliaceae	Jinyinhua	Flowers, Leaves, Buds	Caffeoylquinic acids, 3,5-dicaffeoylquinic acid butyl ester, organic acids, flavonoids, iridoids, triterpenoids, and volatile oils	Anti-inflammatory, antiviral, antidiabetic, antiallergic, and antioxidant	[77]
Forsythia suspensa	Oleaceae	Lianqiao	Fruits	Lignans and phenylethanol glycosides, phenols, furofurans	Anti-inflammatory, analgesic, antiallergic antimicrobial, antiviral, antidiabetic, treat bronchiolitis, fever, vomiting, and heart diseases	[78]
Atractylodes lancea	Asteraceae	Cangzhu	Rhizomes	Atractylodin, *β*-eudesmol, atractylon, hinesol, atractyloside A, atractyloside F, atractyloquinone, and atractylochromene	Antimicrobial, treat rheumatic diseases, anti-cancer, anti-obesity, and anti-inflammatory	[79]
Agastache rugosa	Lamiaceae	Huoxiang	Leaves, Stems	Phenylpropanoids, terpenoids, rosmarinic acid, methyleugenol, pulegone, menthone,	Antimicrobial, antiviral, anti-mutagenic, cytotoxic activity to can-	[80]

				isomenthone, spathulenol, acacetin, tilianin, agastachoside, and agastachin	cer cell lines, anti-nociceptive, anti-inflammatory, anti-atherogenic, antioxidant	
Cyrtomium fortunei J. Sm	Dryopteridaceae	Guanzhong	Rhizomes	6'-methylglucuronide-5-hydroxy-chromone, ethyl α-d-glactopyranoside, neoechinulin A, 9,12,13-trihydroxyoctadeca-10(E),15(Z)-dienoic acid and phellopterin	Analgesic, anthelmintic, antibacterial, anticoagulant, antiviral, depurative, febrifuge and haemostatic	[81]
Eupatorium perfoliatum	Asteraceae	Peilan	Leaves, Stems, Roots	Flavonoids, sesquiterpene, lactones, triterpenes, steroids, volatile oil, polysaccharide, Caffeic acid, pyrrolizidine alkaloids	Immunostimulant, anti-inflammatory, antibacterial, antiprotozoal, antiviral, treat rheumatism, fever, vomiting, pneumonia, and constipation	[82]
Ophiopogon japonicas	Asparagaceae	Maidong	Roots	Steroidal saponins, Homoisoflavonoids, Polysaccharides, alicylic acid, p-hydroxybenzoic, vanillic acid, p-hydroxybenzaldenhyde, trans-p-coumaric acid, oleanolic acid, azelaic acid, n-tricosanoic acid, tianshic acid	Antioxidant, anticancer, antimicrobial, antidiabetic, immunomodulator, antimyocardial ischemia, anti-inflammatory, antitussive,	[83]
Scrophularia ningpoensis	Scrophulariaceae	Xuanshen	Leaves, Roots	Iridoid Glycosides, Glycoside esters, triterpenoids	Anti-inflammatory, analgesic, antimicrobial, hepatoprotective, and wound healing activity	[84]
Adenophora stricta	Campanulaceae	Shashen	Root	Beta-sitosterol, beta-sitosterol-O-beta-D-glucopyranoside, taraxerone and octacasanoic acid	Antitussive, expectorant, treatment of dry coughs, chronic bronchitis and tuberculosis	[85]
Dendrobium nobile	Orchidaceae	Shihu	Stem	Polysaccharides, alkaloids, phenanthrenes, bibenzyls, dendrobine	Treat fever, antidiabetic, antiinfection, anticancer, protect eyesight, improve appetite, digestion, astringent, analgesic, antipyretic, and anti-inflammatory	[86]
Nigella sativa	Ranunculaceae	Hakjungchou	Seeds	Thymoquinone, Thymohydroquinone, Dithymoquinone, Thymol, Nigellicine, carvacrol, terpineol, tanethol, nigellidine, nigellone,	Diuretic, antihypertensive, bronchodilator, gastroprotective, hepatoprotective, antidiabetic, anticancer, immunomodulatory, analgesic, antimicrobial, analgesics, anti-inflammatory, spasmolytic, renal protective, and antioxidant	[87]

TCM (Shuang Huang Lian Kou Fu Ye, Bu Huan Jin Zheng Qi San, Da Yuan Yin, Xue Bi Jing Injection, and Qing Fei Pai Du Tang) in combination with some WM, including ritonavir, lopinavir, oseltamivir remdesivir, and favipiravir or Chloroquine phosphate also played a vital role in recovery of COVID-19 patients in China. These combinations remarkably inhibited the viral proliferation and triggered inflammation pathway in COVID-19 patients [72].

CONCLUSION AND FUTURE PERSPECTIVES

As there is no approved drug or vaccine available to treat COVID-19, though some previously used broad spectrum Western Medicines are effective against the virus. Remdesivir, Chloroquine, Chloroquine Phosphate, and Arbidol (Umifenovir) are the efficient antivirals to encounter SARS-CoV-2, but due to frequent and high dose, patients face several adverse effects. Arbidol and remdesivir are effective during early or mild stages, but no significant results were obtained during severe or critical conditions of COVID-19. Patients with severe conditions were treated bd-daily of Chloroquine at higher concentration, were recovered but high dose of chloroquine and its salts resulted 20% of mortality rate in elder patients. The antivirals at higher dose cause kidney and hepatic complications by fluctuating organ enzymatic level. Other common side effects include vomiting, nausea, muscle cramps, headache, mental complications, and hearing problems. The fatality rate is increasing day by day around the world, as vaccine production takes long time, so yet no positive progress has been observed. The world must look for an alternative option to cure infected patients as the Chinese health authorities did.

Traditional Chinese Medicine (TCM) are used in China and various parts of world from more than 3500 years. The Traditional Chinese Medicines are the complex combination of various herbal extracts with bioactive compounds which can be an alternative drug to encounter SARS-CoV-2 and other resistant microbes due to its high efficacy and minimal or no side effects. Different combinations and concentrations of TCM were given to COVID-19 patients at early, mild, moderate, and severe conditions. At highly critical conditions, patients were treated with Shenfu and Shengmai San injections, Suhe Xiang Wan and Angong Niuhuang Wan Pills. More than 90% of COVID-19 patients recovered in China by treating with Traditional Chinese Medicines (TCM). The USA, UK, and other European countries with higher COVD-19 mortality rate must also use TCM either alone or in combination with lower dose of antiviral and antibiotics. It is the time for developed countries to invest in herbal medicines industry as well and take benefit from old Chinese books and herbalists.

Due to minute size and broad-spectrum antimicrobial activity of nanoparticles, such as metallic nanoparticles are widely used against various microorganisms including Human Coronaviruses. Until now 40 different strains of SARS-CoV-2 are identified which are rapidly evaluating and adapting to the environment, they might be resistant to several antiviral and antibacterial drugs, but they are not prone to nanomedicines. Thus, the metallic nanoparticles (Gold, Silver, Zinc, Iron or Copper) synthesize by using TCM or plants with antiviral potential (green synthesis of nanoparticles) can be an effective approach towards encountering SARS-CoV-2 pandemic.

ACKNOWLEDGEMENT

Authors Contributions. All the authors contributed equally to this work and authors read and approved the final manuscript.

Ethics approval. Ethics approval was not required for this study.

REFERENCES

[1] Worldometer. (2020) COVID-19 coronavirus pandemic. Availabe online: https://www.worldometers.info/coronavirus/ (Accessed on 22 march).

[2] Shereen, M.A., Kazmi, A. (2020) SARS-CoV-2 pandemic: causes and current situation, historical lessons, and strategical therapeutic interventions. Biomedical Research and Therapy. 7, 3807-3812.

[3] Shereen, M.A., Khan, S., Kazmi, A., Bashir, N., Siddique, R. (2020) COVID-19 infection: origin, transmission, and characteristics of human coronaviruses. Journal of Advanced Research. 24, 91-98 es.

[4] Singh, R., Sripada, L., Singh, R. (2014) Side effects of antibiotics during bacterial infection: mitochondria, the main target in host cell. Mitochondrion. 16, 50-54.

[5] Zhang, Z.-j., Wu, W.-y., Hou, J.-j., Zhang, L.-l., Li, F.-f., Gao, L., Wu, X.-d., Shi, J.-y., Zhang, R., Long, H.-l. Active constituents and mechanisms of Respiratory Detox Shot, a traditional Chinese medicine prescription, for COVID-19 control and prevention: network-molecular docking-LC-MSE analysis. Journal of Integrative Medicine . 18(3), 229-241.

[6] Daily, C. (2020) 6 effective TCM recipes for COVID-19. Availabe online: http://covid-19.chinadaily.com.cn/a/202003/24/WS5e795bb6a3101282172816c2.html (Accessed on April).

[7] Wallace, B.A. (2018) Look at East vs West Medicine. Availabe online: https://healthcare inamerica.us/a-look-at-east-vs-west-medicine-92edfcaeca18 (Accessed on June).
[8] Savarino, A., Di Trani, L., Donatelli, I., Cauda, R., Cassone, A. (2006) New insights into the antiviral effects of chloroquine. The Lancet Infectious Diseases. 6, 67-69.
[9] Keyaerts, E., Li, S., Vijgen, L., Rysman, E., Verbeeck, J., Van Ranst, M., Maes, P. (2009) Antiviral activity of chloroquine against human coronavirus OC43 infection in newborn mice. Antimicrobial agents and chemotherapy. 53, 3416-3421.
[10] Devaux, C.A., Rolain, J.-M., Colson, P., Raoult, D. (2020) New insights on the antiviral effects of chloroquine against coronavirus: what to expect for COVID-19? International Journal of Antimicrobial Agents. Article ID: 105938.
[11] Krafts, K., Hempelmann, E., Skórska-Stania, A. (2012) From methylene blue to chloroquine: a brief review of the development of an antimalarial therapy. Parasitology Research. 111, 1-6.
[12] Homewood, C., Warhurst, D., Peters, W., Baggaley, V. (1972) Lysosomes, pH and the anti-malarial action of chloroquine. Nature. 235, 50-52.
[13] Ginsburg, H., Famin, O., Zhang, J., Krugliak, M. (1998) Inhibition of glutathione-dependent degradation of heme by chloroquine and amodiaquine as a possible basis for their antimalarial mode of action. Biochemical Pharmacology. 56, 1305-1313.
[14] Al-Bari, M.A.A. (2015) Chloroquine analogues in drug discovery: new directions of uses, mechanisms of actions and toxic manifestations from malaria to multifarious diseases. Journal of Antimicrobial Chemotherapy. 70, 1608-1621.
[15] Savarino, A., Gennero, L., Chen, H.C., Serrano, D., Malavasi, F., Boelaert, J.R., Sperber, K. (2001) Anti-HIV effects of chloroquine: mechanisms of inhibition and spectrum of activity. Aids. 15, 2221-2229.
[16] Thomé, R., Lopes, S.C.P., Costa, F.T.M., Verinaud, L. (2013) Chloroquine: modes of action of an undervalued drug. Immunology Letters . 153, 50-57.
[17] Wong, A.L.N., Cheung, I.T.F., Graham, C.A. (2008) Hydroxychloroquine overdose: case report and recommendations for management. European Journal of Emergency Medicine.15, 16-18.
[18] Stokkermans, T.J., Trichonas, G. (2019) Chloroquine And Hydroxychloroquine Toxicity.
[19] Kalia, S., Dutz, J.P. (2007) New concepts in antimalarial use and mode of action in dermatology. Dermatologic Therapy. 20, 160-174.
[20] Rainsford, K., Parke, A.L., Clifford-Rashotte, M., Kean, W. (2015) Therapy and pharmacological properties of hydroxychloroquine and chloroquine in treatment of systemic lupus erythematosus, rheumatoid arthritis and related diseases. Inflammopharmacology. 23, 231-269.
[21] Ullberg, S., Lindquist, N., Sjöstrand, S.(1970) Accumulation of chorio-retinotoxic drugs in the foetal eye. Nature. 227, 1257-1258.
[22] Martins, A.C., Cayotopa, A.D.E., Klein, W.W., Schlosser, A.R., Silva, A.F.d., Souza, M.N.d., Andrade, B.W.B., Filgueira-Júnior, J.A., Pinto, W.d.J., da Silva-Nunes, M. (2015) Side effects of chloroquine and primaquine and symptom reduction in malaria endemic area (Mâncio Lima, Acre, Brazil). Interdisciplinary Perspectives on Infectious Diseases.
[23] Bogaczewicz, A., Sobów, T. (2017) Psychiatric adverse effects of chloroquine. Psychiatria i Psychologia Kliniczna. 17, 111-114.
[24] Wang, M., Cao, R., Zhang, L., Yang, X., Liu, J., Xu, M., Shi, Z., Hu, Z., Zhong, W., Xiao, G. (2020) Remdesivir and chloroquine effectively inhibit the recently emerged novel coronavirus (2019-nCoV) in vitro. Cell Research. 1-3.
[25] Gao, J., Tian, Z., Yang, X. (2020) Breakthrough: Chloroquine phosphate has shown apparent efficacy in treatment of COVID-19 associated pneumonia in clinical studies. BioScience Trends. 11-23..
[26] Singh, A.K., Singh, A., Shaikh, A., Singh, R., Misra, A. (2020) Chloroquine and hydroxychloroquine in the treatment of COVID-19 with or without diabetes: a systematic search and a narrative review with a special reference to India and other developing countries. Diabetes & Metabolic Syndrome: Clinical Research & Reviews.
[27] Servick, K. (2020) Antimalarials widely used against COVID-19 heighten risk of cardiac arrest. How can doctors minimize the danger? Availabe online: https://www.sciencemag.org/news/2020/04/antimalarials-widely-used-against-covid-19-heighten-risk-cardiac-arrest-how-can-doctors (Accessed on April).
[28] Thomas, K. (2020) Small Chloroquine Study Halted Over Risk of Fatal Heart Complications. Availabe online: https://www.nytimes.com/2020/ 04/ 12/health/chloroquine-coronavirus-trump.html (Accessed on April).
[29] Sykes, T. (2020)Chloroquine Study Ended in Brazil After Patients Developed Irregular Heart Rates. Availabe online: https://www.thedailybeast.com/chloroquine-study-ended-in-brazil-after-patients-developed-irregular-heart-rates (Accessed on April).

[30] FDA. (2020) FDA Letter to Stakeholders: Do Not Use Chloroquine Phosphate Intended for Fish as Treatment for COVID-19 in Humans. Availabe online: https://www.fda.gov/animal-veterinary/product-safety-information/fda-letter-stakeholders-do-not-use-chloroquine-phosphate-intended-fish-treatment-covid-19-humans (Accessed on April).

[31] EMA. (2020) COVID-19: chloroquine and hydroxychloroquine only to be used in clinical trials or emergency use programmes Availabe online: https://www.ema.europa.eu/en/news/covid-19-chloroquine-hydroxychloroquine-only-be-used-clinical-trials-emergency-use-programmes (Accessed on April).

[32] Warren, T.K., Jordan, R., Lo, M.K., Ray, A.S., Mackman, R.L., Soloveva, V., Siegel, D., Perron, M., Bannister, R., Hui, H.C. (2016) Therapeutic efficacy of the small molecule GS-5734 against Ebola virus in rhesus monkeys. Nature. 531, 381-385.

[33] Agostini, M.L., Andres, E.L., Sims, A.C., Graham, R.L., Sheahan, T.P., Lu, X., Smith, E.C., Case, J.B., Feng, J.Y., Jordan, R. (2018) Coronavirus susceptibility to the antiviral remdesivir (GS-5734) is mediated by the viral polymerase and the proofreading exoribo-nuclease. MBio. 9, e00221-00218.

[34] Tchesnokov, E.P., Feng, J.Y., Porter, D.P., Götte, M. (2019) Mechanism of inhibition of Ebola virus RNA-dependent RNA polymerase by remdesivir. Viruses . 11, 326.

[35] Cunha, J. (2020) Remdesivir (RDV). Availabe online: https://www.rxlist.com/consumer_remdesivir_rdv/drugs-condition.htm (Accessed on April).

[36] EMA. (2020) Summary on compassionate use of Remdesivir Gilead. Availabe online: https://www.ema.europa.eu/en/documents/other/summary-compassionate-use-remdesivir-gilead_en.pdf (Accessed on April).

[37] Gordon, C.J., Tchesnokov, E.P., Woolner, E., Perry, J.K., Feng, J.Y., Porter, D.P., Gotte, M. (2020) Remdesivir is a direct-acting antiviral that inhibits RNA-dependent RNA polymerase from severe acute respiratory syndrome coronavirus 2 with high potency. Journal of Biological Chemistry. RA120. 013679.

[38] de Wit, E., Feldmann, F., Cronin, J., Jordan, R., Okumura, A., Thomas, T., Scott, D., Cihlar, T., Feldmann, H. (2020) Prophylactic and therapeutic remdesivir (GS-5734) treatment in the rhesus macaque model of MERS-CoV infection. Proceedings of the National Academy of Sciences. 117, 6771-6776.

[39] Barmann, J. (2020r) Bay Area-Based Gilead Sees Potential Legal Conflict With China Over Its Coronavirus Drug. Availabe online: https://web.archive.org/web/20200326060714/https://sfist.com/2020/02/06/bay-area-based-gilead-donates-experimental-anti-viral-drug-to-china/ (Accessed on April).

[40] Holshue, M.L., DeBolt, C., Lindquist, S., Lofy, K.H., Wiesman, J., Bruce, H., Spitters, C., Ericson, K., Wilkerson, S., Tural, A. (2020) First case of 2019 novel coronavirus in the United States. New England Journal of Medicine.

[41] Dong, L., Hu, S., Gao, J. (2020) Discovering drugs to treat coronavirus disease 2019 (COVID-19). Drug Discoveries & Therapeutics. 14, 58-60.

[42] Poveda, E., Wyles, D.L., Mena, Á., Pedreira, J.D., Castro-Iglesias, Á., Cachay, E. (2014) Update on hepatitis C virus resistance to direct-acting antiviral agents. Antiviral Research. 108, 181-191.

[43] Haviernik, J., Štefánik, M., Fojtíková, M., Kali, S., Tordo, N., Rudolf, I., Hubálek, Z., Eyer, L., Ruzek, D. (2018) Arbidol (Umifenovir): a broad-spectrum antiviral drug that inhibits medically important arthropod-borne flaviviruses. Viruses. 10, 184.

[44] Proskurnina, E.V., Izmailov, D.Y., Sozarukova, M.M., Zhuravleva, T.A., Leneva, I.A., Poromov, A.A. (2020) Antioxidant Potential of Antiviral Drug Umifenovir. Molecules. 25, 1577.

[45] Boriskin, Y.S., Pécheur, E.-I., Polyak, S.J. (2006) Arbidol: a broad-spectrum antiviral that inhibits acute and chronic HCV infection. Virology Journal. 3, 56.

[46] Pécheur, E.-I., Borisevich, V., Halfmann, P., Morrey, J.D., Smee, D.F., Prichard, M., Mire, C.E., Kawaoka, Y., Geisbert, T.W., Polyak, S.J. (2016) The synthetic antiviral drug arbidol inhibits globally prevalent pathogenic viruses. Journal of Virology. 90, 3086-3092.

[47] Hulseberg, C., Fénéant, L., Szymańska-de Wijs, K., Kessler, N., Nelson, E., Shoemaker, C., Schmaljohn, C., Polyak, S., White, J. (2019) Arbidol and other low-molecular-weight drugs that inhibit Lassa and Ebola viruses. Journal of Virology. 93, e02185-02118.

[48] Huang, L., Zhang, L., Liu, Y., Luo, R., Zeng, L., Telegina, I., Vlassov, V.V. (2015) Arbidol for preventing and treating influenza in adults and children. Cochrane Database of Systematic Reviews .

[49] Golunov, I. (2020) 13 most popular flu cures: do they work? Availabe online: https://republic.ru/posts/l/1037105#1.%20%D0%90%D0%A0%D0%91%D0%98%D0%94%D0%9E%D0%9B.%20%D0%9E%D0%B1%D1%8A%D0%B5%D0%BC%20%D0%BF%D1%80%D0%BE%D0%B4%D0%B0%D0%B6%20-%205%20%D0%BC%D0%BB%D1%80%D0%B4%20%D1%80%D1%83%D0%B1 (Accessed on April).

[50] Chen, C., Huang, J., Cheng, Z., Wu, J., Chen, S., Zhang, Y., Chen, B., Lu, M., Luo, Y., Zhang, J. (2020) Favipiravir versus Arbidol for COVID-19: a randomized clinical trial. medRxiv.

[51] Ng, E. (2020) Coronavirus: are cocktail therapies for flu and HIV the magic cure? Bangkok and Hangzhou hospitals put combination remedies to the test. Availabe online: https://www.scmp.com/business/companies/article/3048888/could-cocktail-therapies-hiv-and-flu-be-magic-cure-new (Accessed on April).

[52] Press, C. (2020) Lopinavir/ritonavir and Arbidol not effective for mild-to-moderate COVID-19 in adults. Availabe online: https://medical xpress.com/ news/2020-04-lopinavirritonavir-arbidol-effective-mild-to-moderate-covid-.html (Accessed on May).

[53] Johnson, J. (2020) Our COVID-19 Response Efforts. Availabe online: https://www.jnj.com/coronavirus (Accessed on 17 April).

[54] Gao, Q., Bao, L., Mao, H., Wang, L., Xu, K., Li, Y., Zhu, L., Wang, N., Lv, Z., Gao, H. (2020) Rapid development of an inactivated vaccine for SARS-CoV-2. bioRxiv 2020.

[55] Mestrovic, T. (2020) PiCoVacc vaccine candidate for COVID-19 effective in animal trials. Availabe online: https://www.news-medical.net/news/20200421/PiCoVacc-vaccine-candidate-for-COVID-19-effective-in-animal-trials.aspx (Accessed on May).

[56] Le, T.T., Andreadakis, Z., Kumar, A., Román, R.G., Tollefsen, S., Saville, M., Mayhew, S. (2020) The COVID-19 vaccine development landscape. Nat. Rev. Drug Discov.

[57] Tang, J.-L., Liu, B.-Y., Ma, K.-W. (2008) Traditional chinese medicine. The Lancet. 372, 1938-1940.

[58] Tao, Z., Yang, Y., Shi, W., Xue, M., Yang, W., Song, Z., Yao, C., Yin, J., Shi, D., Zhang, Y. (2013) Complementary and alternative medicine is expected to make greater contribution in controlling the prevalence of influenza. BioScience Trends. 7, 253-256.

[59] Ma, Y., Chen, M., Guo, Y., Liu, J., Chen, W., Guan, M., Wang, Y., Zhao, X., Wang, X., Li, H. (2019) Prevention and treatment of infectious diseases by traditional Chinese medicine: a commentary. Apmis. 127, 372-384.

[60] Li, G., Zhao, J., Tu, Z., Li, J., Liu, Q., Shi, L., Miao, Q., Yuan, H., Liu, X., Long, Y. (2013) Treating influenza patients of wind-heat affecting Fei syndrome by jinhua qinggan granule: a double-blinded randomized control trial. Zhongguo Zhong xi yi jie he za zhi Zhongguo Zhongxiyi jiehe zazhi= Chinese Journal of Integrated Traditional and Western Medicine. 33, 1631-1635.

[61] Ho, L.T., Chan, K.K., Chung, V.C., Leung, T.H. (2020) Highlights of traditional Chinese medicine frontline expert advice in the China national guideline for COVID-19. European Journal of Integrative Medicine. 101116.

[62] Li, C., Zhang, X., Liu, S., Shang, H. (2020) Current evidence and research prospects of Xuebijing injection in treating novel corona-virus-infected pneumonia (COVID-19). World Sci Technol Modern Tradit. Chin. Med. Mater. Med. 02-19.

[63] Ding, Y., Zeng, L., Li, R., Chen, Q., Zhou, B., Chen, Q., leng Cheng, P., Yutao, W., Zheng, J., Yang, Z. (2020) The Chinese prescription lianhuaqingwen capsule exerts anti-influenza activity through the inhibition of viral propagation and impacts immune function. BMC Complementary and Alternative Medicine. 17, 130.

[64] Runfeng, L., Yunlong, H., Jicheng, H., Weiqi, P., Qinhai, M., Yongxia, S., Chufang, L., Jin, Z., Zhenhua, J., Haiming, J. (2020) Lianhua-qingwen exerts anti-viral and anti-inflammatory activity against novel coronavirus (SARS-CoV-2). Pharmacological Research. 104761.

[65] Yangxin, S. (2020) Summary Report on Lianhua Qingwen Capsule/Granule for the Treatment of Influenza, Cold and Coronavirus Disease 2019 (COVID-19). Frontiers in Pharmacology. 11, 1066..

[66] Yan, Y.-M., Shen, X., Cao, Y.-K., Zhang, J.-J., Wang, Y., Cheng, Y.-X. (2020) Discovery of anti-2019-nCoV agents from Chinese patent drugs via docking screening. Journal of Diabetes & Metabolic Disorders. 1-9.

[67] Han, Y., Zhao, M., Shi, B., Song, Z., Zhou, S., He, Y. (2020) Application of integrative medicine protocols on treatment of coronavirus disease 2019. Chin Tradit Herb Drugs. 02-18.

[68] Yang, Y., Islam, M.S., Wang, J., Li, Y., Chen, X. (2020) Traditional Chinese medicine in the treatment of patients infected with 2019-new coronavirus (SARS-CoV-2): a review and perspective. International Journal of Biological Sciences. 16, 1708.

[69] Xu, X., Zhang, Y., Li, X., Li, X. (2020) Analysis on prevention plan of corona virus disease-19 (COVID-19) by traditional Chinese medicine in various regions. Chin. Tradit. Herb. Drugs. 51, 1-8.

[70] Luo, H., Tang, Q.-l., Shang, Y.-x., Liang, S.-b., Yang, M., Robinson, N., Liu, J.-p. (2020) Can Chinese medicine be used for prevention of corona virus disease 2019 (COVID-19)? A review of historical classics, research evidence and current prevention programs. Chinese Journal of Integrative Medicine. 1-8.
[71] Ni, L., Zhou, L., Zhou, M., Zhao, J., Wang, D.W. (2020) Combination of western medicine and Chinese traditional patent medicine in treating a family case of COVID-19 in Wuhan. Frontiers of Medicine. 1-5.
[72] Lem, F.F., Opook, F., Herng, D.L.J., Na, C.S., Lawson, F.P., Tyng, C.F. (2020) Molecular mechanism of action of repurposed drugs and traditional Chinese medicine used for the treatment of patients infected with COVID-19: A systematic review. MedRxiv.
[73] Liu, Y., Liu, J., Wang, Y., Abozeid, A., Tang, Z.-H. (2016) Simultaneous determination of six active metabolites in Astragalus mongholicus (Fisch.) Bge. under salt stress by ultra-pressure liquid chromatography with tandem mass spectrometry. SpringerPlus. 5, 927.
[74] Yin, L., Guan, E., Zhang, Y., Shu, Z., Wang, B., Wu, X., Chen, J., Liu, J., Fu, X., Sun, W. (2018) Chemical profile and anti-inflammatory activity of total flavonoids from glycyrrhiza uralensis fisch. Iranian Journal of Pharmaceutical Research: IJPR. 17, 726.
[75] Jenny, K., Edwin, P., George, B.-L. (2017) Saposhnikoviae divaricata: a phytochemical, pharmacological, and pharmacokinetic review. Chinese Journal of Natural Medicines. 15, 255-264.
[76] Zhu, B., Zhang, Q.-l., Hua, J.-w., Cheng, W.-l., Qin, L.-p. (2018) The traditional uses, phytochemistry, and pharmacology of Atractylodes macrocephala Koidz.: A review. Journal of Ethnopharmacology. 226, 143-167.
[77] Senfeng, S., Xue, J. (2017) Research Progress on Chemical Constituents from Lonicera Japonica. Chemical Industry Times. 8.
[78] Wang, Z., Xia, Q., Liu, X., Liu, W., Huang, W., Mei, X., Luo, J., Shan, M., Lin, R., Zou, D. (2018) Phytochemistry, pharmacology, quality control and future research of Forsythia suspensa (Thunb.) Vahl: a review. Journal of Ethnopharmacology. 210, 318-339.
[79] Jun, X., Fu, P., Lei, Y., Cheng, P. (2018) Pharmacological effects of medicinal components of Atractylodes lancea (Thunb.) DC. Chinese Medicine. 13, 59.
[80] Anand, S., Pang, E., Livanos, G., Mantri, N. (2018) Characterization of physico-chemical properties and antioxidant capacities of bioactive honey produced from Australian grown Agastache rugosa and its correlation with colour and poly-phenol content. Molecules. 23, 108.
[81] Yang, S.-J., Liu, M.-C., Liang, N., Xiang, H.-M., Yang, S. (2013) Chemical constituents of Cyrtomium fortumei (J.) Smith. Natural Product Research. 27, 2066-2068.
[82] Colegate, S.M., Upton, R., Gardner, D.R., Panter, K.E., Betz, J.M. (2018) Potentially toxic pyrrolizidine alkaloids in Eupatorium perfoliatum and three related species. Implications for herbal use as boneset. Phytochemical Analysis. 29, 613-626.
[83] Wang, Y., Liu, F., Liang, Z., Peng, L., Wang, B., Yu, J., Su, Y., Ma, C. (2017) Homoisoflavonoids and the antioxidant activity of Ophiopogon japonicus root. Iranian Journal of Pharmaceutical Research: IJPR .16, 357.
[84] Xie, G., Jiang, Y., Huang, M., Zhu, Y., Wu, G., Qin, M. (2020) Dynamic analysis of secondary metabolites in various parts of Scrophularia ningpoensis by liquid chromatography tandem mass spectrometry. Journal of Pharmaceutical and Biomedical Analysis.113307.
[85] Wang, C., Zhang, N., Wang, Z., Qi, Z., Zheng, B., Li, P., Liu, J. (2017) Rapid characterization of chemical constituents of Platycodon grandiflorum and its adulterant Adenophora stricta by UPLC-QTOF-MS/MS. Journal of Mass Spectrometry. 52, 643-656.
[86] Li, R., Liu, T., Liu, M., Chen, F., Liu, S., Yang, J. (2017) Anti-influenza A virus activity of dendrobine and its mechanism of action. Journal of Agricultural and Food Chemistry. 65, 3665-3674.
[87] Kazmi, A., Khan, M.A., Ali, H. (2019) Biotechnological approaches for production of bioactive secondary metabolites in Nigella sativa: an up-to-date review. International Journal of Secondary Metabolite. 6, 172-195.

Received: **21.10.2020**
Accepted: **28.10.2020**

CORRESPONDING AUTHOR

Jianguo Wu
State Key Laboratory of Virology,
College of Life Sciences,
Wuhan University,
Wuhan – PR China

e-mail: jwu@whu.edu.cn

© by PSP Volume 30– No. 05/2021 pages 5550-5556 Fresenius Environmental Bulletin

NOTICE

STUDY ON LOW-CARBON ECONOMY BASED ON ECOLOGICAL PERSPECTIVE

Shuling Wang*

ZheJiang Industry & Trade Vocational College, Wenzhou 325000, Zhe Jiang, China

ABSTRACT

The traditional high-carbon economic development mode has caused great damage to the ecological environment while accelerating economic development. On the contrary, the green low-carbon economic mode pays more attention to energy conservation, emission reduction and ecological environment protection while developing the economy. This study introduces the relevant theories of low-carbon economy and corporate financial management, and extends the differences between high-carbon and low-carbon economic development modes. By analyzing the impact of low-carbon economy on the corporate financial goals, such as profit maximization, enterprise value maximization, shareholder wealth maximization, earnings per share maximization and shareholders' equity maximization, as well as the impact on the corporate financial management principles, such as net benefit principle, signaling principle, self-interest principle and risk-reward trade-off principle, this paper emphasizes that the low-carbon economic development mode is the general trend and plays a key role in the sustainable energy-saving society. Therefore, the idea of low-carbon economy should be applied to the corporate financial goals and financial management principles in practice.

KEYWORDS:
Ecological perspective, Low-carbon economy, Principles, Sustainable development

INTRODUCTION

With the development of social economy, the concepts of green environmental protection, energy conservation and emission reduction have become increasingly popular. The traditional high-carbon economic development mode blindly pursues economic benefits while ignoring the ecological environment protection, resulting in incalculable ecological losses. This economic development mode is obviously not suitable for the development of modern economy [1]. The low-carbon economic mode is emerging quietly and gradually forming a new trend to guide corporate innovation. The low-carbon economic mode requires paying attention to the ecological environment protection and realizing sustainable development while developing economy. The traditional corporate financial management focuses on maximizing the enterprise economic benefits while lacking the sense of social responsibility to protect the ecology. Therefore, it is particularly necessary to study the corporate financial goals and financial management principles under the low-carbon economy, reform and innovate them, and apply them to enterprise development so as to achieve sustainable development.

MATERIALS AND METHODS

Relevant Theories. Low-carbon Economy. Since ancient times, the development of human society and economy has always been "highly carbonized", using a large amount of natural resources in exchange for social and economic development. Although this high-carbon economic development mode has accelerated the development of social economy, it has used a large amount of natural energy, and the ecological environment has been destroyed unscrupulously, sacrificing the homeland on which human beings depend. Nowadays, human beings are already facing severe ecological environment problems, which seriously restrict sustainable development [2,3]. With the depletion of natural resources and the destruction of ecological environment, the concept of sustainable development is deeply rooted in people's hearts. Obviously, the high-carbon economic development mode is not suitable for the development of modern economy and is replaced by the low-carbon economic development mode. Low-carbon economy ensures the continuous reduction of natural resource usage while ensuring the stable and rapid development of economy. Its comparison with the past high-carbon economic development mode is shown in Figure 1. According to the guidance of the concept of sustainable development, low-carbon economy realizes low-carbon city through low-carbon industry policy, technology policy and market policy, coupled with innovative reform of production system, innovative and iterative development of technology, development of

green energy and international cooperation, thus constructing a low-carbon society, as shown in Figure 2. Low-carbon society, while ensuring stable economic development, minimizes the use of high-carbon resources, improves the utilization rate of natural energy, greatly reduces the emission of greenhouse gases such as carbon dioxide, reduces the generation of pollutants, and achieves coordinated development of economy and ecological protection [4]. Therefore, low-carbon economy is a green development mode, which is based on the theories of resource economics, environmental economics, recycling economics and sustainable development, with the characteristics of integrity, gradualness, goal and systematicness, achieving the reform and transformation of the traditional high-carbon economic mode and setting off another revolutionary wave of economic development.

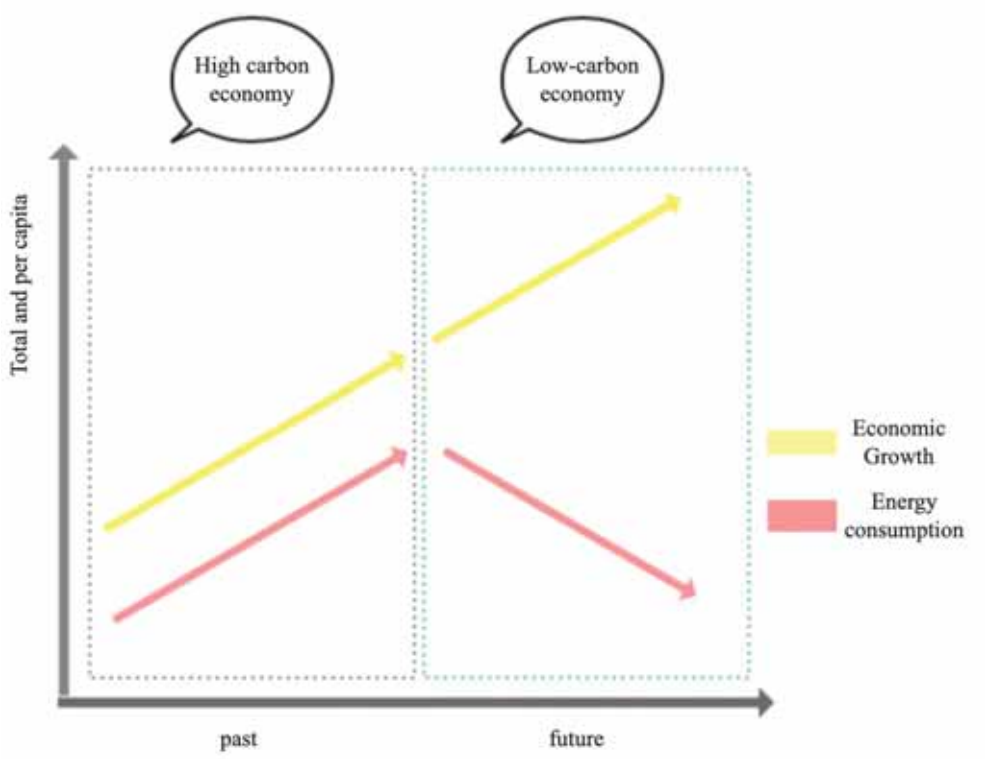

FIGURE 1
Comparison between High-carbon Economy and Low-carbon Economy

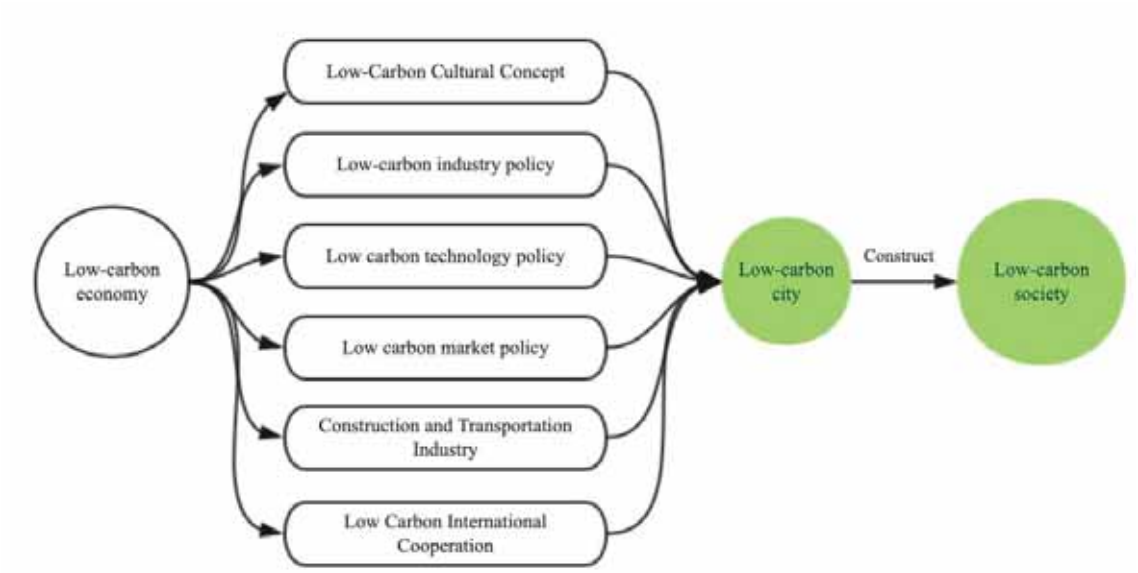

FIGURE 2
Formation of Low-carbon Society

RESULTS AND DISCUSSION

Corporate Financial Goals. Corporate financial goals, in general, are the ultimate goals to be achieved by the corporate financial-related activities under specific conditions. As the basic standard to determine the financial management, corporate financial goals are generally used to evaluate the rationality of the financial-related work of an enterprise. Corporate financial goals play an important role in enterprise development, drive the enterprise to continuously strengthen its own management and improve its income and profits, which is of great significance to the long-term development of the enterprise.

Corporate financial goals can be divided into five types, including profit maximization, enterprise value maximization, shareholder wealth maximization, earnings per share maximization and shareholders' equity maximization [5,6]. Among them, profit maximization believes that profits represent the enterprise's wealth, and only by increasing corporate profits can the enterprise survive; enterprise value maximization believes that through reasonable financial management and financial strategies, enterprises can increase the benefit and maximize its value, including the enterprise's intangible assets and its future potential; shareholder wealth maximization holds that the total value of the stock market represents the enterprise's wealth, and when the stock price of the enterprise reaches the highest, its financial goals are also maximized; earnings per share maximization believes that the enterprise's income and profits should be linked to the invested capital of the enterprise's shareholders and examine the relationship between the enterprise's profit and the invested capital; while shareholders' equity maximization holds that the shareholders' equity is fully linked to the stock market price of the enterprise; the higher the stock market price, the greater the shareholders' equity. These five kinds of corporate financial goals are determined based on the enterprise, shareholders and the stock market, and they all have certain internal connections, as shown in Figure 3.

Corporate Financial Management Principles. Corporate financial management principles include net benefit principle, signaling principle, self-interest principle and risk-reward trade-off principle [7-9]. Among them, net benefit principle belongs to the principle of value creation, signaling principle and self-interest principle belongs to the principle of environment competition-related, risk-reward trade-off principle belongs to the principle of financial transaction, and its relationship is shown in Figure 4. Net benefit principle is the most important principle in the corporate economic development, which is related to the corporate income, expenditure and output of net profit. Different enterprise decisions play different roles, and net benefit principle is the guarantee

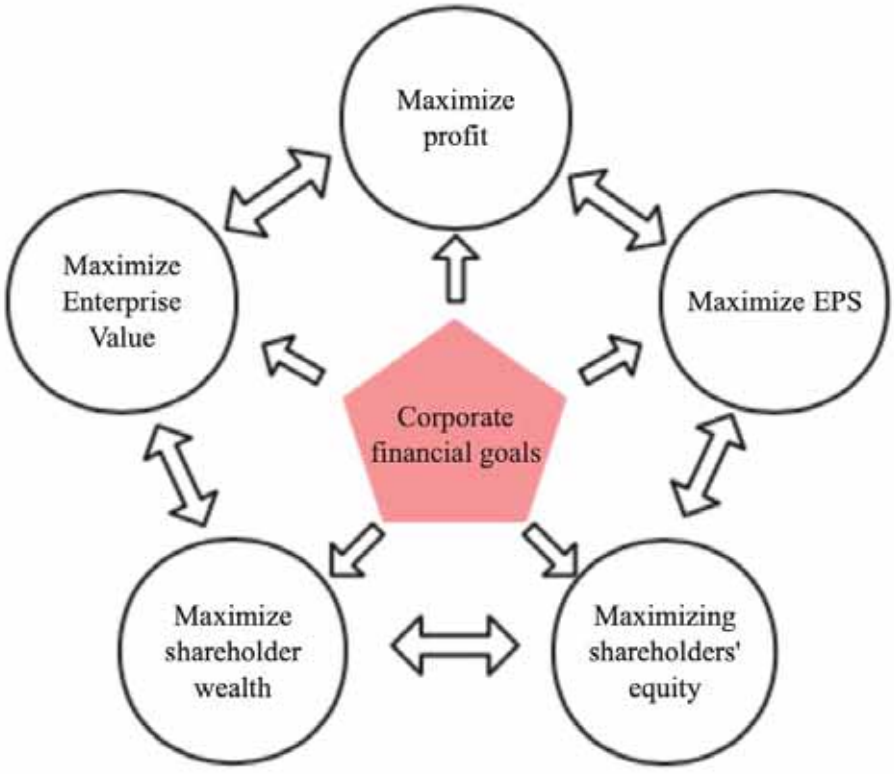

FIGURE 3
Five Types of Corporate Financial Goals

principle for the stable development of an enterprise. Signaling principle refers to that in the process of information transmission, enterprises are more persuasive through specific forms than oral statements. Self-interest principle refers to the most basic principle that enterprises follow in the economic development, under the supervision of laws and regulations, to carry out various projects in line with their own development, in order to maximize the interests. Risk-reward trade-off principle is the embodiment of the relationship between risk and reward in enterprise economic development. In order to balance the subtle relationship between risk and reward, it is necessary for every enterprise to achieve the financial goal of low risk and high reward to the greatest extent in enterprise economic development.

Impact of Low-carbon Economy on Corporate Financial Goals and Financial Management Principles. Impact of Low-carbon Economy on Corporate Financial Goals. With the development of social economy, five different types of corporate financial goals have been derived, including profit maximization, enterprise value maximization, shareholder wealth maximization, earnings per share maximization and shareholders' equity maximization [10]. These five types of financial goals are all for the purpose of increasing the enterprise's wealth, focusing on the generation of economic benefits, but ignoring the ecological benefits of sustainable development. It can be said that under the traditional high-carbon economic mode, enterprises often assume more their own economic responsibilities and lack of social responsibility for ecological environment protection and sustainable development [11]. Since ancient times, the development of enterprise economy has brought great

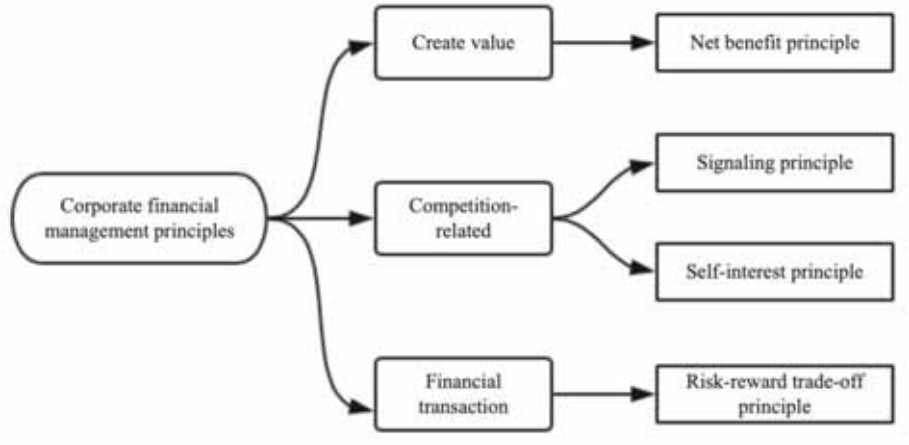

FIGURE 4
Framework of Corporate Financial Management Principles

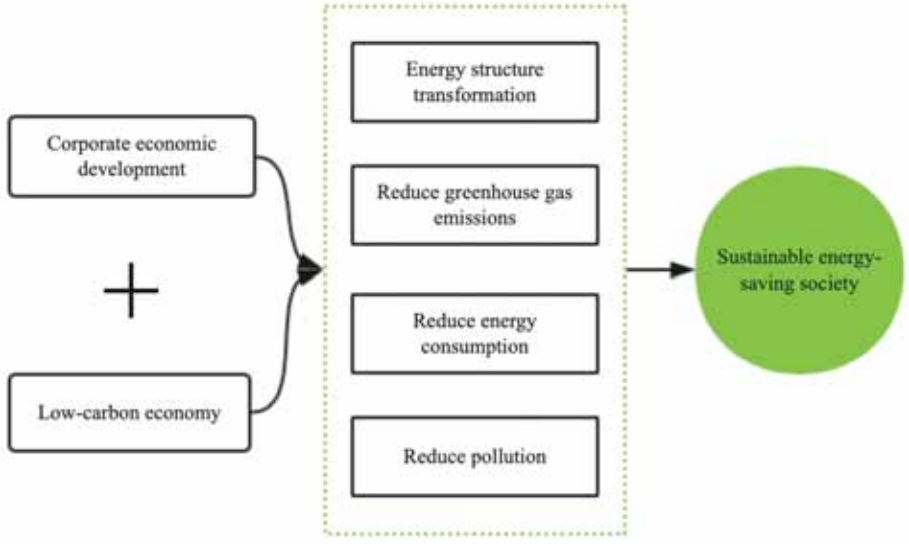

FIGURE 5
Sustainable Energy-saving Society

pressure to the ecological environment, and the deteriorating ecological environment has sounded a warning to human beings. In order to realize sustainable development and protect our common ecological homeland, while realizing financial goals and seeking profits, enterprises should assume more social responsibilities for ecological environment protection. With the combination of low-carbon economic development mode, enterprises should rationally develop ecological resources, increase the recycling of ecological resources, carry out energy structure transformation, reduce resource and energy consumption, reduce pollution, reduce the emission of greenhouse gases such as carbon dioxide, etc., and realize a sustainable energy-saving society, as shown in Figure 5.

Under the influence of low-carbon economic development mode, the formulation of corporate financial goals should not only emphasize the corporate income and profits, but also reflect on the green ecological environment protection and sustainable development. Even though the wealth and internal value of the enterprise have been maximized, if the ecological environment protection value has not been generated, it still belongs to the high-carbon economic development mode. Obviously, the financial goals of this mode are not conform to the trend of the times development, and will be eliminated eventually [12]. Therefore, under the low-carbon economy, the financial goals of an enterprise should be the sum of its own value goal and ecological and environment protection goal. In the low-carbon economy, in order to achieve financial goals, enterprises reduce the use of high-carbon energy, reduce greenhouse gas emissions, and change the energy structure of economic development as much as possible, their ecological and environment protection value will be improved, and their financial goals will be achieved faster; similarly, if the high-carbon economic development mode continues to be used, the ecological and environment protection value will be greatly reduced, the achievement of modern financial goals will be slower. With the concept of sustainable development becoming more and more popular today, enterprises that destroy the ecological environment for their own economic development will not only suffer from legal sanctions, but will also be despised by more people and their partners will be reduced, which will undoubtedly become a stumbling block for the economic development of enterprises [13].

Impact of Low-carbon Economy on Financial Management Principles. Net Benefit Principle. As the most important principle in the economic development of an enterprise, net benefit principle is related to the corporate income, expenditure and output of net profit, emphasizes the net economic benefits of enterprise development. Under the influence of low-carbon economy, enterprises regard ecological environment protection benefits as part of their net benefits and increase the protection of ecological resources while seeking economic benefits [14,15]. Meanwhile, the idea of low-carbon and environmental protection will be applied to the corporate financial management decision-making. The operating costs of adopting traditional high-carbon economic mode and modern low-carbon economic mode will be evaluated and compared in many aspects, including low-carbon investment costs, project budgets and future economic benefits of sustainable development. The difference value of benefits between traditional high-carbon economy and modern low-carbon economy will be roughly evaluated, and the cost of enterprises will be minimized on the premise of protecting the ecological environment.

Signaling Principle. Compared with the traditional high-carbon economic development mode, in the low-carbon economic mode, enterprises will have more clear goals and more initiative for their own financial goals, and there will be more effective methods to implement in risk assessment and strategy formulation [16]. Under the influence of low-carbon economy, enterprises should not only set financial goals, but also consider the impact of financial management on the external ecological environment. If it is a positive impact, it should be maximized by practical actions, while the negative impact is the opposite. Not only that, for the enterprise's stakeholders, such as shareholders, more information should be transmitted to reflect the measures taken in the corporate financial management activities and the impact on the ecological and environment protection.

Self-interest Principle. Self-interest principle is the most basic principle of enterprise development. Under the traditional high-carbon economic development mode, enterprises follow the self-interest principle to develop economy, self-interest is everything, emphasizing interest but neglecting society, blindly pursuing their own economic development while completely ignoring the ecological environment protection. Such self-interest enterprise behavior is difficult to survive in the modern low-carbon economic mode with sustainable development. Under the influence of low-carbon economic mode, enterprises can better follow the self-interest principle, because the development of enterprises cannot be separated from the impact of the external environment. Enterprises can reduce energy consumption, increase green environmental protection efforts, and reduce the pollution to the ecological environment as much as possible. Not only can they publicize their own reputation for environmental protection, but also the external ecological environment will be improved, which also provides more possibilities for enterprises to develop economy [17,18]. Therefore,

the self-interest principle and the low-carbon economic development mode are not opposite to each other, but complementary.

Risk-reward Trade-off Principle. Under the influence of sustainable development and low-carbon economic mode, the operation of corporate financial management requires enterprises to have more analysis and grasp of relevant policies issued by the government, timely access to policy information, and rapid grasp of market information, which are of vital importance to enterprises and play a key role in controlling risks and rewards in enterprise economic development [19,20]. Nowadays, the low-carbon economic mode is the inevitable choice for the economic development of enterprises. Only by accurately grasping the policy regulation and control, implementing the precise arrangement of corporate financial management, and then carrying out scientific planning, can enterprises carry out the green innovation and ecological environment protection reform from the inside out, and at the same time, control the risks and profits of enterprise development to the greatest extent, so as to realize the rapid development of enterprises under the low-carbon economic mode [21].

CONCLUSION

The traditional high-carbon economic development mode is no longer applicable to the development of modern economy, while the low-carbon economic mode is the general trend. At present, the low-carbon reform of corporate financial management is not mature and lacks some successful experience and perfect theoretical practice. However, with the increasing popularity of the concept of energy conservation, environmental protection and sustainable development, and the continuous development of science and technology, the low-carbon and environment-friendly corporate financial management mode will be promoted, and the relevant theoretical concepts and practical systems will be improved, thus contributing to the ecological environment protection and the realization of a sustainable energy-saving society.

REFERENCES

[1] Xie, H. (2014) Legal Regulation of Low-Carbon Economy. Ieri Procedia. 8, 170-175.

[2] Lou, S.H., Zhang, L.J., Wu, Y.W., Wang, Y.C. (2017) Coordination Operation of Electric Vehicles and Power System under Low-Carbon Economy. Transactions of China Electrotechnical Society. 32(5), 176-183.

[3] Huan, X., Wei, L., Shi, L. (2017) Berth allocation model under low-carbon economy and its algorithms implementation . Computer Engineering & Applications. 50(6), 219-225.

[4] Lohani, B.N., Kawai, M., Anbumozhi, V. (2016) Managing the Transition to a Low-Carbon Economy. Washington: Brookings Institution Press.

[5] Long-Fei, C. (2019) Green certification, e-commerce, and low-carbon economy for international tourist hotels. Environmental Science & Pollution Research International. 26(18), 17965-17973.

[6] Dai, Q.Z., Li, Y.J., Xie, Q.W., Liang, L. (2014) Allocating Tradable Emissions Permits Based on the Proportional Allocation Concept to Achieve a Low-Carbon Economy. Mathematical Problems in Engineering. 3, 1-8.

[7] Heffron, R.J. (2018).The Just Transition To a Low-Carbon Economy. Renewable Energy Law & Policy Review. 3, 39-41.

[8] Niamir, L., Filatova, T., Voinov, A., Bressers, H. (2018) Transition to low-carbon economy : Assessing cumulative impacts of individual behavioral changes. 118, 325-345.

[9] Jing, X., Na, X., Lin, Z. (2017) Industrial Low-Carbon Economy in Hebei Province and Countermeasures Based on Driving Force State Response Algorithm. Journal of Computational and Theoretical Nanoscience. 14(5), 157-161.

[10] Zhong, X.Z. (2016) Making China the Transition to a Low-Carbon Economy: Key Challenges and Responses. Ccep Working Papers. 3, 187-202.

[11] Bernardo, G., D'Alessandro, S. (2014). Transition to sustainability? Feasible scenarios towards a low-carbon economy, 7991, 190-197.

[12] Pozzoli, M., Paolone, F. (2017). Corporate Financial Distress. Springer International Publishing. 29-43.

[13] Regina, M.L., Bautista, C.C. (2016). Firm Heterogeneity and Corporate Financial Distress. Social Science Electronic Publishing. 6, 537-539.

[14] Street, T., Jackson, J. (2016) Aligning corporate strategy with financial targets. New Zealand Management. 62(1), 24-25.

[15] Holynskyy, Y. (2017). The Importance Of Financial Management Principles In The State Budget Execution. Social Science Electronic Publishing. 17(4), 19.

[16] Korotina, N. (2017). Theoretical bases of state and municipal financial management. Social Science Electronic Publishing. 22(6), 28.

[17] Coe, C.K. (2016). Financial stewardship and management. John Wiley & Sons, Inc. 140-167.

[18] Wilkinson, S., Hajibandeh, M., Remoy, H. (2014) Sustainable Development. Science. 304(5671), 12-21.

[19] Butnaru, G.I., Mirela, S. (2014) Tourism And Sustainable Development. Ces Working Papers. 6(2), 32-45.
[20] Ekinci, M.B. (2014). The Cittaslow philosophy in the context of sustainable tourism development; the case of Turkey. Tourism Management. 41, 178-189.
[21] Idowu, S.O. (2013) World Business Council for Sustainable Development. Encyclopedia of Corporate Social Responsibility. Springer, Berlin, Heidelberg.

Received: **31.10.2020**
Accepted: **10.01.2021**

CORRESPONDING AUTHOR

Shuling Wang
Zhe Jiang Industry & Trade Vocational College,
Wenzhou 325000 ZheJiang – China

e-mail: 15548816852@189.cn

© by PSP Volume 30– No. 05/2021 pages 5557-5563 Fresenius Environmental Bulletin

NOTICE

ANALYSIS OF LOGISTICS EFFICIENCY BASED ON GREEN SUPPLY CHAIN

Li Zhang*

School of Business, Shandong University of Political Science and Law, Jinan 250014, Shandong, China

ABSTRACT

As an industry with high energy consumption and low efficiency, cold chain logistics has been criticized by people for its lack of environmental protection. In order to realize the sustainable development of cold chain logistics in resource utilization, the integration of green supply chain management concept provides a huge possibility for cold chain logistics to reach the standard of green environmental protection. This study analyzes the current situation of cold chain logistics in China by elaborating the related theoretical concepts of green supply chain and cold chain logistics, points out the defects of domestic cold chain logistics in its own system, technical management and backward facilities, and further analyzes the main factors affecting cold chain logistics based on green supply chain from two aspects of green environmental protection and cold chain logistics. Finally, the paper puts forward suggestions for the development of cold chain logistics, and analyzes the improvement strategies from the perspectives of government and cold chain logistics enterprises. This research is of great significance to the development of domestic cold chain logistics and to reduce the gap between China and foreign countries.

KEYWORDS:
Green supply chain, cold chain logistics, efficiency analysis, sustainable development

INTRODUCTION

With the improvement of people's living standards, the demand for various seafood, fresh fruits and vegetables and other products is also increasing year by year, while these products are perishable and difficult to preserve, which puts forward extremely strict requirements for long-distance transportation of cold chain logistics [1, 2]. Nowadays, cold chain logistics has become one of the key indicators to measure a country's scientific and technological development, so it is of great benefit to speed up the development of cold chain logistics technology and realize the convenience of domestic cold chain logistics product supply and the advancement of technology. However, at present, the development of domestic cold chain logistics is slow and its efficiency is far lower than that of developed countries abroad. There are still many defects, such as extremely lax market supervision, backward cold chain technology, lack of standardized management system, low energy utilization rate and packaging recycling rate, and great pressure on the ecological environment. Therefore, the traditional cold chain logistics will be eliminated by the modern energy-saving and environment-friendly society and replaced by the cold chain logistics based on the green supply chain [3]. As a new mode of cold chain logistics for sustainable development, cold chain logistics based on green supply chain can conform to the trend of the times and is of great significance for ecological environment protection and sustainable development.

MATERIALS AND METHODS

Relevant Theory and Current Situation Analysis. Green Supply Chain. Economic development is accompanied by the consumption of natural resources. In recent years, with the rapid development of the world, the consumption of natural resources has become faster and faster, and resource waste and shortage have occurred from time to time. In order to realize the ecological strategy of sustainable development and achieve the economic development while maintaining the sustainable development of energy, the ecological concept of green supply chain management has been introduced. The concept of green supply chain management closely combines "protecting ecology" and "developing economy". As an effective way to achieve sustainable development strategy, it is particularly important for today's industrial structure globalization [4].

Green supply chain is the derivative of traditional manufacturing supply chain that has the characteristics of high consumption and low efficiency. On the basis of traditional supply chain, green supply chain calculates the optimization rate and utilization rate of resources, and then combines the calculation of pressure on the ecological environment to formulate corresponding measures according to the calculation results, so as to improve the utilization rate of

resources, save ecological energy and reduce the pressure on the ecological environment. The traditional supply chain (as shown in Figure 1) controls the temperature of the whole process from product-cold storage-distribution center-seller-consumer, through the long-distance transportation and delivery, and then carries out the sales packaging and processing before reaching sellers.

Based on the traditional supply chain, the green supply chain adds the green recycling link, which can make the waste generated in the supply chain be reused, improve the energy utilization rate, reduce the waste emission, and realize the coordination of ecological protection and economic development [5, 6]. As a modern management mode of supply chain, green supply chain takes natural resources and ecological environment as the starting point, supply chain management technology and green production theory as the basis, controls capital flow, supply flow and information flow in the whole supply chain process from the beginning to obtaining product materials, to designing products, manufacturing products, transporting products, selling products, using products and recycling products. In addition, the green supply chain technology integrates the green theory into the supply chain management technology, realizing the green supply chain network structure (as shown in Figure 2) with the manufacturer as the starting point, the intermediate link as suppliers, distributors and retailers, the end point as customers, embedded with the energy-saving and environmental protection link and the connection of relevant enterprise departments, thus realizing the maximization of supply chain benefits, which not only improves the recycling and utilization rate of products but also protects the ecological environment and reduces environmental pollution [7].

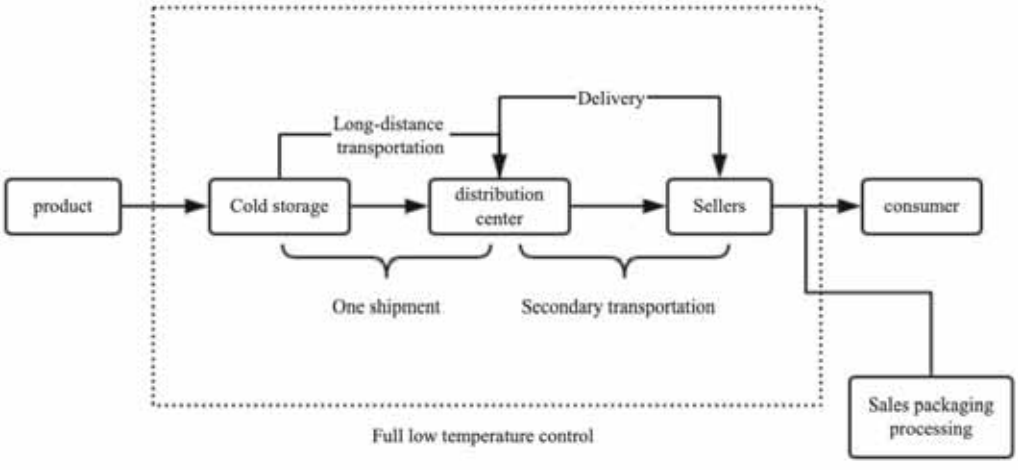

FIGURE 1
Traditional Agricultural Product Supply Chain

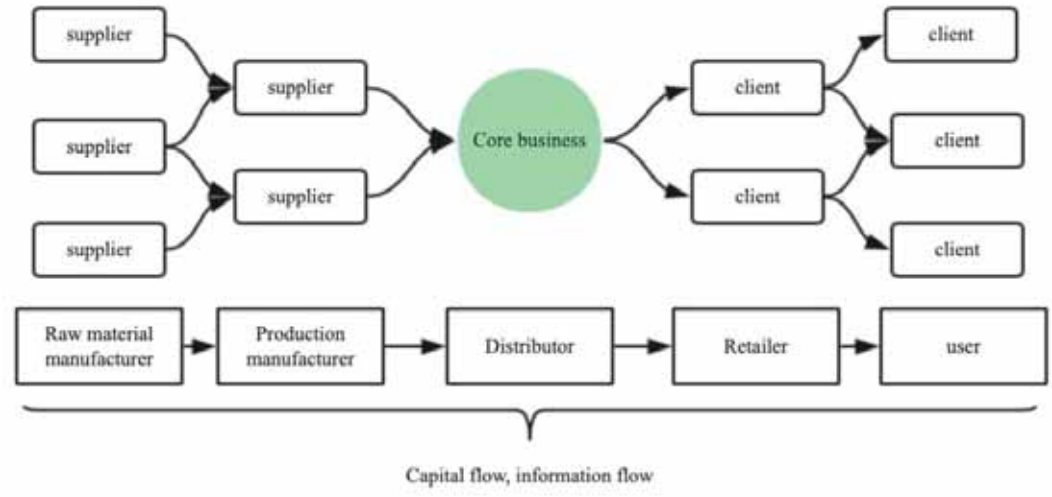

FIGURE 2
Model of Green Supply Chain Network Structure

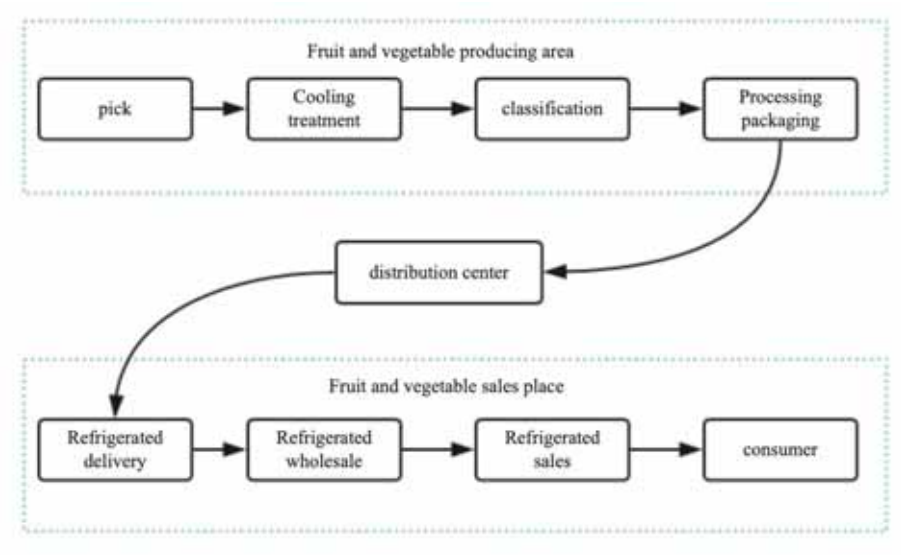

FIGURE 3
Cold Chain Logistics Operation Mode of Fruit and Vegetable Products

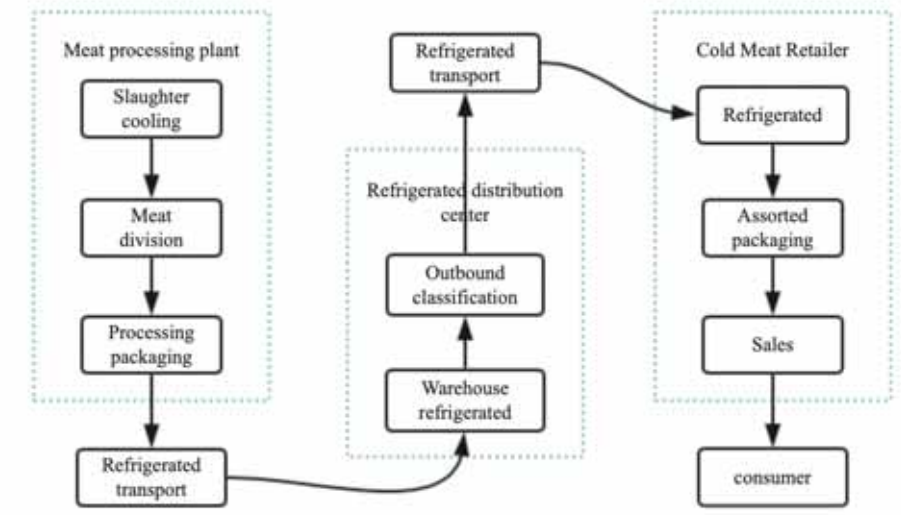

FIGURE 4
Cold Chain Logistics Operation Mode of Meat Products

Cold Chain Logistics Technology. Cold chain logistics technology is mainly used in fresh products, fruits and vegetables, meat products and other industries. These products are perishable and difficult to preserve, which causes difficulties in long-distance transportation. Therefore, cold chain logistics technology emerges as the times require. Cold chain logistics technology has the advantages of large transportation capacity, stable temperature control, extremely high freshness-preservation degree, and a large number of connected distributors, which adds a lot of convenience to the long-distance transportation of such products, so it is of great significance to study the efficiency of cold chain logistics technology [8].

With the development of social economy, cold chain logistics technology has been continuously improved and perfected. Until now, the technology has become mature. Common types of cold chain logistics include cold chain logistics of fruit and vegetable products and cold chain logistics of meat products. Among them, the cold chain logistics of fruit and vegetable products includes picking, cooling, sorting, processing and packaging of fruits and vegetables at the picking place, and distribution to the selling place for wholesale sales. The specific process is shown in Figure 3. Cold chain logistics of meat products includes processing plants, transportation centers, distribution centers and retail merchants. Each link has different functional divisions, and the specific process is shown in Figure 4. Cold chain logistics technology strictly requires products to maintain a long-term fresh and low-temperature state in the chain process, so as to prevent the product quality from declining, even corruption and deterioration, resulting in incalculable losses. The basis of cold chain logistics technology is "cold chain",

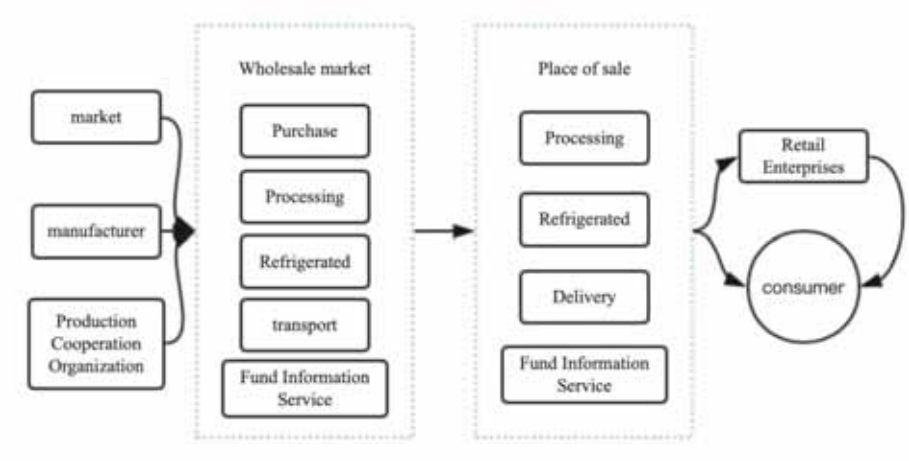

FIGURE 5
Cold Chain Logistics Mode in Wholesale Market

that is to store and process some products that are perishable or can only be stored at low temperature by controlling the appropriate low temperature in the whole process, so as to isolate external pollution to the greatest extent, fully maintain the product quality and minimize the losses caused by long-distance transportation [9, 10]. As the core system of cold chain logistics technology, low temperature control system plays a key role, for the efficiency of cold chain logistics largely depends on the function of the system. Through the temperature control of the whole process by the low temperature control system, the production, storage, transportation and sales of cold chain products are strictly controlled to ensure the product quality.

Status Analysis. As the largest product manufacturing country in the world, China has countless cold chain products for long-distance transportation every year, and the use of cold chain technology has become increasingly mature. However, compared with advanced and perfect cold chain logistics systems in developed countries, there is still a large gap [11].

Incomplete Cold Chain Logistics System. Cold chain products have the problem of difficult storage, coupled with numerous logistics links, through producers, transporters, distributors and wholesalers, etc., which is a test for the long-term quality maintenance of cold chain products. In order to ensure the quality of cold chain products to the greatest extent, the cost is considerable. Therefore, there are only a few of large enterprises of cold chain logistics in China, which is closely related to the lack of a perfect cold chain logistics system. At present, the domestic common cold chain logistics system is often directly formulated by suppliers, collectively referred to as cold chain logistics in the wholesale market, which is directly transported to the wholesale market by manufacturers through cooperative organizations, distributed to the sale place after cold chain treatment in the wholesale market, and then sold through retail enterprises, as shown in Figure 5. The scale of cold chain logistics in the wholesale market is extremely small, and the management is nonstandard, even good and poor products are mixed up. There are still high limitations on the logistics distribution in remote areas and the distribution during peak periods. Therefore, the whole country lacks systematic planning and management [12]. Besides, for the logistics system is directly formulated by enterprises or suppliers, in order to reduce costs and improve profits, in the absence of market supervision, tax evasion of enterprises is serious. There are also shortcomings such as low and unprofessional management level, unreasonable distribution of supply chain, too simple transportation package, too single transportation mode, mostly truck transportation, lack of cohesion and insufficient communication in all aspects of logistics, making it difficult to ensure the quality of cold chain products after long-distance transportation, causing incalculable losses.

Backward Cold Chain Logistics Technology

The advancement of cold chain logistics technology is directly related to the quality of cold chain products. The level of cold chain logistics is determined by supply chain systems such as warehouse systems, temperature control systems, transportation and distribution systems, and quality assurance systems [13]. However, the current level of domestic cold chain logistics technology is still in a relatively backward stage. Due to the low popularity of the concept of green supply chain at this stage, coupled with the long technical cycle, high investment that less than the return, and the great risk, as a result, the investment cost of cold chain logistics for most enterprises is not high, and the management also lacks financial, human and material support, so the current management development level of cold chain technology and the transformation of management concepts are at an extremely slow stage. In addition, in-

formation technology is also essential for the development of cold chain logistics technology. The network coverage in some areas is not high or the network speed is slow, especially in mountainous areas, which causes some difficulties in the communication of some aspects in cold chain logistics. Furthermore, there are efficiency issues and a large uncertainty in the product collection and distribution.

Lax Market Supervision. Domestic cold chain logistics system is generally in a chaotic situation, and the most critical reason is the lax market supervision. The stable and healthy operation of the industry is inseparable from strict market supervision. As products that need to be guaranteed quality under specific conditions, cold chain products have extremely strict time and quality requirements for all links of the whole logistics system. If there are more links, market supervision will have loopholes, which will often be exploited. At present, cold chain logistics is such a phenomenon. Some links lack of necessary processing, coupled with tax evasion, all of which highlight the problems caused by the lack of market supervision in cold chain logistics. Therefore, the government should strengthen market supervision on the development of cold chain logistics, manage and supervise all links, and ensure the healthy and stable operation of the whole cold chain logistics system [14, 15].

Lack of Guidance and Support from Large-scale Enterprises. Cold chain logistics technology requires the guidance and support of large-scale enterprises. By formulating standardized schemes, unified planning and management of cold chain logistics can be carried out [16]. At present, most domestic cold chain logistics lack a fixed system standard, and the classification rules of cold chain products are relatively vague, resulting in the lack of sufficient competitiveness of cold chain logistics in the logistics market. Moreover, there are various kinds of cold chain products in China, but the number of cold chain enterprises, intermediate distributors and other links are small, which leads to the limited and fixed transportation demand that the domestic cold chain logistics system can only provide today. This can neither promote the development of domestic cold chain logistics, but also has been in a conflicting stage. Nowadays, the domestic cold chain logistics technology is backward, and the problems in each link are increasingly prominent. A large part of the reason is the lack of guidance and support of large-scale enterprises' technology, the lack of optimized allocation of cold chain logistics resources, and the lack of green management concept.

RESULTS AND DISCUSSION

Analysis of Cold Chain Logistics Efficiency Based on Green Supply Chain. Green Environmental Protection. As a technology with high energy consumption, cold chain logistics has great pressure on the ecological environment. The integration of green supply chain makes cold chain logistics reduce the consumption of natural resources and play an important role in the ecological environment protection. The cold chain logistics of green supply chain is based on the concept of sustainable development, which can minimize the energy consumption from the aspects of loss rate and packaging recycling rate [17].

In the cold chain logistics system based on green supply chain, resource consumption rate and product packaging recycling rate are the key points in the analysis of cold chain logistics efficiency in terms of green environmental protection. Resource consumption rate is a key factor in efficiency evaluation. The process of product packaging, transportation and storage makes extensive use of energy equipment such as refrigerators and refrigerated trucks, which can reflect the rationality of resource utilization. The packaging recycling rate is reflected in the high efficiency of cold chain product packaging in the process of production, recycling and reuse [18]. The resource consumption rate is lower and the packaging recycling rate is higher, which indicates that cold chain logistics is better in green environmental protection and conforms to the concept of green supply chain. However, the resource consumption rate remains high and the product packaging recycling rate has been always low, indicating that cold chain logistics is extremely unfriendly to ecological environment protection. The proportion of green environmental protection investment, as another efficiency consideration, refers to the proportion of the enterprise's investment in environmental protection to the total investment of the enterprise, which directly reflects the green environmental protection degree of the enterprise for cold chain logistics. The larger the proportion, the higher the degree, and vice versa.

Nowadays, people pay more and more attention to the concept of green environmental protection. On the basis of the continuous maturity of cold chain logistics technology, cold chain logistics enterprises invest more funds in developing green supply chain to improve the proportion of green environmental protection investment. By reducing energy use and product packaging, improving the product packaging recycling rate, and adopting more advanced green environmental protection technology, these measures have achieved certain results in the ecological environment protection [19].

Cold Chain Logistics. In the whole process of

cold chain logistics from product acquisition to cooling storage, processing and transportation to sales, the efficiency of cold chain logistics is reflected in storage and transportation. Based on the principle of green supply chain, considering that cold chain products have the characteristics of large quantity and difficult storage, cold chain logistics has extremely strict requirements for storage technology [20]. At the same time of reducing energy consumption and promoting environmental protection, in order to reduce the shock of cold chain products during transportation and ensure the product quality, stricter technical requirements are put forward for long-distance cold chain transportation. In this case, for the sake of improving the efficiency of storage and transportation, reducing the use of natural resources and achieving the successful operation of the whole cold chain logistics at a lower cost, the cold chain logistics enterprises have greatly reduced the pressure on the ecological environment while reducing the enterprise costs and increasing profits.

The utilization rate of cold chain warehouse is the main indicator of storage efficiency in the cold chain logistics system. Cold chain warehouse is the most basic facility of cold chain logistics. The higher the utilization rate of cold chain warehouse, the better the equipment runs, and the higher the utilization rate of resources, the more energy-saving and environmental protection concept can be embodied, also the greater the cost saved by the enterprise. However, due to the backwardness of domestic cold chain warehouse equipment, the lack of systematic and professional guidance and management, and the far insufficient investment in human and material resources and funds, the utilization rate of cold chain warehouse has been at a relatively low level in recent years. The loss rate of cold chain products is another key indicator to reflect the logistics efficiency of cold chain products. It usually refers to the proportion of the value lost after the products are transported in the cold chain to the total value. The smaller loss rate, the higher the cold chain logistics efficiency, and vice versa.

CONCLUSION

In order to realize the sustainable development of natural resources and social economy, cold chain logistics based on green supply chain has become the trend of the times. However, compared with the advanced level of cold chain logistics in developed countries abroad, the domestic development has been relatively backward and the efficiency of cold chain logistics has been at a relatively low level for a long time. Therefore, it can be rectified from the following aspects: first, the government supports and guides the establishment of cold chain market scale, the building of core enterprises, unified and standardized management, and the improvement of market competitiveness. Second, perfect the cold chain logistics system, formulate appropriate laws and regulations, integrate the concepts of green environmental protection and sustainable development, manage and supervise all links. Third, invest more human and material resources and funds, introduce foreign advanced technology, equipment and management methods to maximize the efficiency of cold chain logistics, thus realizing the rapid development of cold chain logistics enterprises in China.

REFERENCES

[1] Voith, M. (2017) A green supply chain. Chemical and Engineering News. 88(31), 16-22.
[2] Rola, R. (2016) ISO 14001 Certification- a step ahead towards implementation of green supply chain management practices in chemical industries. International Journal of Scientific Research. 17(19), 399-401.
[3] Qie, H. (2014) The Research Progress of the Cold Chain Logistics of Agricultural Products. Asian Agricultural Research. 06(9).
[4] Brunetti, G., Simunek, J., Bautista, E. (2018). A hybrid finite volume-finite element model for the numerical analysis of furrow irrigation and fertigation. Computers & Electronics in Agriculture. 150, 312-327.
[5] Chen, C.C., Chen, T.E., Zhang, C., Xie, G.Z. (2015) Research on Agricultural Products Cold-Chain Logistics of Mobile Services Application. IFIP Advances in Information and Communication Technology. 420, 247-254.
[6] Chen, B., Zhou, A. (2016) An Analysis of the Cold Chain Logistics concerning Agricultural Products in Chongqing City. Asian Agricultural Research. 8(1), 19-21.
[7] Li, Y.Y., Liu, G.Q., Xu, S. (2014) Programming of Guangxi agricultural product logistics common information platform based on cloud computing. Journal of Southern Agriculture. 45(6), 1117-1120.
[8] Liu, S.C., Zhao, C.J., Yang, X.Y., Qian, J.P., Wang, G.L., Zhong, S.Y. (2014) Design and application of control charts in pork sensory quality during cold chain logistics. Transactions of the Chinese Society for Agricultural Machinery. 45(7), 177-182.
[9] Shu, C.Y. (2014) The application of fuzzy multiple criteria to assess the selection of suppliers from dealers in the supply chain of plastics industry. European Journal of Haematology. 43(4), 352-354.
[10] Nie, Y.S., Sun, G.R., Zhang, X.L. (2014) Design of Green Processing Chain for Processing of Ginseng Fruit Vinegar. Advanced Materials Research. 933, 988-993.

[11] Tang, Y.R., Xie, J., Li, N.W., Xu, H.W., Su, H., Li, L., Pan, W.L. (2014) Effects of different cold chain logistics situations on quality and microstructure of tuna (Thunnus obesus) fillets. Transactions of the Chinese Society of Agricultural Engineering. 30(5), 285-292.
[12] Ya, B. (2016) Study of Food Cold Chain Logistics Demand Forecast Based on Multiple Regression and AW-BP Forecasting Method on System Order Parameters. Journal of Computational and Theoretical Nanoscience. 13(7), 4019-4024.
[13] Zhao, G.W. (2014) Food-Related Cold-Chain Logistics Management in China. Advanced Materials Research. 962-965, 2373-2376.
[14] Sun, T., Shen, Q.Q. (2020) Coupling and coordination analysis between tourism development and ecological environment in Jiangsu province. Fresen. Environ. Bull. 29(5), 3671-3678.
[15] Qian, J.P., Fan, B.L., Zhang, X., Du, X.W., Sun, L.T., Wang, Y.Z. (2017) Temperature monitoring in cold chain chamber based on temperature sensing RFID labels. Transactions of the Chinese Society of Agricultural Engineering. 33(21), 282-288.
[16] Tang, Y.R., Xie, J., Xu, H.W., Zhang, N., Gao, L. (2015) Application of cold storage phase-change technology in cold chain logistics of tuna (thunnus obesus). Modern Food Science and Technology. 31(1), 173-178.
[17] Lailossa, G.W. (2015) The new paradigm of cold chain management systems and it's logistics on Tuna fishery sector in Indonesia. AACL Bioflux. 8(3), 381-389.
[18] Zhao, C.J., Han, J.W., Yang, X.T., Qian, J.P., Liu, S.C. (2015) Digital simulation technology of computational fluid dynamics in agricultural cold-chain logistics applications. Transactions of the Chinese Society of Agricultural Machinery. 46(3), 214-222.
[19] Yu, H.Y., Zhang, R., Li, S.Y. (2014) Simulation Modeling of Post-Earthquake Vaccine Cold-Chain Emergency Transportation Based on ExtendSim. Applied Mechanics and Materials. 599-601, 2220-2224.
[20] Tao, W., Wei, Z., Li, B. (2017) Pricing of urban food cold chain joint distribution based on non-cooperative game. Journal of Beijing Jiaotong University. 41(3), 28-33.

Received: **01.11.2020**
Accepted: **13.12.2020**

CORRESPONDING AUTHOR

Li Zhang
School of Business
Shandong University of Political Science and Law
Jinan 250014, Shandong – China

e-mail: zhangli889@tom.com

AUTHOR INDEX

A

Abdelaal, K. 5340
Abdelaal, K. A. 4935
Abdelhafez, E. 4893
Ahmad, K. 4975
Ahmed, A. 4901
Ahmed, I. 4975
Ahmed, T. 4901
Aisha, G. 5015
Akata, I. 5400
Akbar, R. 5098
Akca, E. 5356
Akpulat, H. A. 4868
Akram, N. A. 5445
Alam, S. 5093
Al-Antary, T. M. 4771
Aldaej, M. I. 5149
Alhudaib, K. A. A. 5131
Ali, S. 5093
Alkhateb, B. A. A. H. 4771
Al-Khateeb, A. A. 5149
Al-Khateeb, S. A. 5149
Al-Shamary, W. F. A. 4771
Alyami, M. Z. 5131
Ameer, A. 5445
Andelic, M. A. 5498
Asfahan, H. M. 5445
Asghar, A. 5445
Asghar, N. 5445
Assra, A. A. 4935
Atas, M. 4868
Aybar, M. 5194
Aykol, G. 4749
Azhar, M. F. A. 4742

B

Baba, H. 5400
Bai, S. 5244
Bal, N. 5270
Barsan, N. 5521
Bashir, H. 4975
Bashir, N. 5537
Bayraktar, C. 4719
Bayram, C. A. 5356
Boylu, O. A. 4928
Bu, Y. 5302
Buyuk, G. 5356

C

Caglar, O. 4921
Cao, Q. 4953
Cardak, A. D. 5466
Cavusoglu, K. 4842
Celik, H. 4787
Cetin, M. D. 4868
Ceylan, R. F. 4719
Channa, Q. A. 5015
Chen, J. 4730, 5176
Chen, Q. 5529
Chen, S. 4836, 5529
Chen, X. 5002
Cheng, C. 5437
Cheng, J. 5320
Chitimus, D. 5521
Ciftci, M. C. 5476
Cimen, B. A. 5421
Cokkizgin, A. 4928

D

Dai, H. 4888
Dartay, M. 5054
Deng, R. 5362, 5385
Deng, Y. 4850
Dong, T. 5320
Dongfeng, Y. 4756
Du, Y. 4994
Duan, B. 5302
Durgut, M. R. 4779, 5370

E

Eid, A. 4804
Ejaz, M. 5093
El-Bably, A. 4804
El-Ganainy, S. M. 5131
Elhag, D. A. 5340
Elhity, M. A. 4935
El-Sayed, A. E. A. 5340
Erdem, D. B. 5415
Ergul, M. 4868
Erkin, N. 5320
Eruygur, N. 4868
Eski, A. 4749

F

Fadila, A. S. K. 4984
Fan, T. 5529
Farooq, M. 4742
Fatima, A. 4984
Feng, Q. 5302
Feng, Y. 5002

G

Gandahi, N. 5015
Gao, L. 5108
Gao, Q. 5211
Gao, W. 5312
Gezegen, H. 5395
Ghani, E. T. A. 4771
Girgel, U. 4928
Gonulol, E. 5370
Gu, H. 5320
Gu, W. 5176
Guclu, G. 4868
Guo, Y. 4855
Guven, M. 4719

H

Hafez, F. E. M. S. Y. 5340
Hafez, Y. M. 4935
Hamdan, M. 4893
Hamid, M. A. 5421
Han, C. 5140
Han, J. 4875
Hanci, F. 4763
Haq, I. H. 5093
Hassan, F. A. S. 5340
Hassan, M. M. 4935
He, G. 4994
He, Q. 5140
He, Z. 4730

I

Idrees, T. 5445
Irimia, O. 5521
Isik, O. 5421
Islek, C. 5400

J

Jahangir, I. 5445
Jahanzaib, J. 4742
Jatoi, T. A. 5015
Jatoi, W. A. 5015
Ji, Q. 5332
Jiang, J. 4830
Jiang, P. 5320
Jiang, Y. 4875, 5176
Jiao, W. 5002, 5238, 5312
Jihao, C. 4756

K

Kahlel, A.-M. S. 4771
Kang, J. 4888
Kang, S. 4830
Kang, X. 5075
Kaplan, C. 5476
Kausar, S. 5445
Kazmi, A. 5537
Khaffagy, A. E. 5340
Khan, I. A. K. 5098
Khan, M. A. 5537
Khan, M. M. 5093
Khan, S. 5537
Khan, Z. I. 4975
Khurshid, A. 5093
Korkmaz, G. 5395
Kunene, S. S. 4787
Kutlar, I. 4719

L

Lee, S. 5510
Lehadus, M. 5521
Lei, Z. 4756
Leng, F. 5377
Li, B. 5405
Li, D. 5244
Li, J. 4850, 5108
Li, M. 4888, 5362, 5385
Li, Q. 5059
Li, T. 5254
Li, X. 5437
Li, Y. 5320
Lian, X. 5510
Lin, J. 5040, 5047
Lin, S. 4836
Linghu, S. 5362, 5385
Liu, C. 5040, 5047
Liu, H. 4953, 5244
Liu, J. 5220
Liu, S. 4798
Liu, Y. 5026, 5033
Liu, Z. 5140
Lou, Y. 5140
Lu, X. 5108
Lu, Z. 5161
Luo, L. 4943
Luo, Q. 4850
Luo, Y. 4730
Lu, H. 4861

M
Macar, O. 4842
Macar, T. K. 4842
Maitlo, W. A. 5015
Mao, L. 4823
Mao, T. 5059
Mao, X. 5108
Memon, S. 5015
Mercan, S. 4749
Mohasseb, H. A. A. 5149
Mosnegutu, E. 5521
Muhammad, A. 5093
Mumtaz, S. 5445

N
Naneli, I. 5486
Nawaz, R. 4901
Nazar, S. 4975
Nedeff, V. 5521

O
Okasha, A. 4804
Omer, A. H. M. 4935
Onal, A. R. 5370
Ozdikmen, H. 5270

P
Pervez, M. A. P. 4742
Pinar, H. 4763

Q
Qadir, I. 4742
Qi, L. 5108
Qin, H. 5350
Qin, L. 5108

R
Rajput, L. 5015
Rezk, A. A. 5131
Rizwan, M. 4975

S
Saridogan, B. G. O. 5400
Sarra, S. 4984
Sattar, M. N. 5131
Sayin, S. 5119
SefaCakir, S. 5187
Sevindik, M. 5400
Shah, W. H. 5093
Shahid, H. 5445
Shehata, W. F. 5149
Shen, Y. 5067
Shereen, M. A. 5537
Shi, J. 5161
Shu, Y. 4830
Simsek, D. 4763
Sivri, G. T. 5370
Solangi, A. H. 5015
Solliman, M. E. S. 5149
Solmaz, F. G. S. 4749
Sultan, M. 5445
Sun, C. 5238
Sun, K. 5244
Sun, Y. 5067
Surat, H. 5194

T
Temea, A. 5521
Tian, J. 5429
Tomozei, C. 5521
Topkara, E. F. T. 4749
Toprak, S. 4763
Turan, F. 5486
Turhan, S. 5187
Tutar, U. 5395

U
Ucar, E. 4868
Uslu, L. 5421

V
Varoglu, S. 5187
Veesar, N. F. 5015

W
Wang, B. 4943
Wang, J. 5437
Wang, Q. 5292
Wang, R. 4888, 5108
Wang, S. 5550
Wang, T. 4994
Wang, Y. 5108
Wang, Z. 5211
Wu, B. 5161
Wu, H. 5067, 5320
Wu, J. 5516, 5537

X

Xian, F. 5047
Xie, C. 5108, 5169
Xie, J. 5362
Xinjuan, C. 4756
Xiong, C. 5161
Xu, S. 4911
Xue, S. 5405
Xue, W. 4875

Y

Yalcin, E. 4842
Yan, T. 5002
Yan, Z. 4953, 5108
Yanar, O. 4749
Yang, B. 5084
Yang, H. 5002, 5238
Yang, J. 5377
Yang, R. 5362, 5385
Yang, T. 4836
Yarar, B. 4779
Yasin, G. 4742
Ye, H. 4823
Yildirim, U. 4962
Yilmaz, F. F. 5415
Ying, Y. 5262
You, Q. 4888
Yu, B. 5312
Yu, C. 5312
Yu, H. 4730, 5377
Yuan, H. 5108
Yue, L. 4756
Yue, Y. 5262

Z

Zayed, B. A. 4935
Zeng, H. 4943
Zeng, Q. 5211
Zeng, X. 4943
Zhang, C. 5238
Zhang, G. 5244
Zhang, H. 5292
Zhang, J. 4888
Zhang, L. 5557
Zhang, M. 5169
Zhang, R. 4730, 4730
Zhang, W. 5161
Zhang, Y. 4730, 5075
Zhao, H. 5244
Zhao, Q. 5084
Zhao, S. 4994
Zhao, X. 4730
Zhao, Y. 5254, 5377
Zhen, L. 5537
Zheng, D. 5238
Zheng, Y. 5230
Zhou, J. 5067
Zhou, W. 4861
Zhu, L. 5140
Zhu, W. 4798
Zou, J. 4875
Zubair, M. 4742
Zuo, F. 5026, 5033

SUBJECT INDEX

A

Accumulation 4787
ACE2 inhibitors 5119
Acetochlor 5340
Agricultural development 4836
Agricultural informatization 4836
Agricultural land 4901
agricultural products 4719
agricultural using potential 5302
Agrobacterium 5149
Agroforestry 4742
Agroinjection 5149
Air conditioning 4850
Albizia lebbeck 4742
Algae 5119
Alluvial plane 5498
amino acids 4975
analytic hierarchy process 4994
antibacterial 5395
Antibacterial growth 5040
Anticancer 4868
antimicrobial 4868, 5395, 5400
Antioxidant 4842, 4868, 5400
antioxidative defense 5445
Antiviral drugs 5537
Apple 5187
Artificial Neural Network 4893

B

B & B building 5230
Bacillus thuringiensis 4749
Bauxite 5429
Beautiful countryside 5059
Big data 4836
Big data environment 4953
BIM technology 4911
Biochar 5238
biochemical constituents 5445
Biodiversity 4975
biosecurity 5370
borehole stability 5140
bread wheat 5415
Bread wheat genotypes 4921
bridge earthquake damage environment 5169
burial history 5254
buried strip foundation 5176

C

C. maculatus 5098
C:N ratio 5356
Cadmium 4787, 5238
Cadmium (Cd) 5312
calorific value 4756
Carbohydrate 4749
Carbon emission reduction 4994
carbon flux 5320
Carbon risk 5084
Cassida 5270
Cassidinae 5270
Cellular characteristics 4943
chalcone 5395
Chang 6 Member 5377
chemical energy 4779
chlorophyll concentration 4875
chlorophyll content 4935
chlorophyll fluorescence characteristics 4875
Chrysomelidae 5270
Climate change 4901
CMIP5 models 5002
Coal mine gas 5405
COD removal 5516
Coherence 4943
cold chain logistics 5557
Coleoptera 5270
Coliform 5466
collapse pressure 5140
Complex network environment 5350
Confectionery hybrid sunflower 5486
conjoint approach 5187
construction status 5220
construction strategy 5220
consumer preference 4719
Consumers 5521
consumption 5187
Cooperative coupling 4823
Coordinated development 4798, 4855, 5529
Coordination model 4855
Corn 4842
Coronavirus 4893
Correlation 4861
correlations 5015
Cotton 5015
Countermeasure 5059
coupling and coordination 5075
COVID-19 4719, 4893, 5537
Creative industry 5510
Cry1Ca gene 5149
Cucumber breeding 4763
Cultivar 5486
Cultural creation products 5510
Cyclic redesign 4830

D

Data storage system 5332
Delinted cottonseeds 5292
Desertification 4901
desulfurization 4756
Development periods 5486
development trend 5405
diagnosis 5067
Digital creative 5510
DLC 5516
Drought stress 4730, 5486
Dry Bean 4928
dry yield 4787
duration 5067

E

East Srem 5498
EASY% RO numerical simulation 5254
Eco – labels 5521
ecological 4953
Ecological civilization 4823
Ecological civilization perspective 5220
ecological compensation 4994
Ecological environment 4798, 4855, 5075, 5332, 5529
Ecological environment protection 4830
ecological function zone 4994
Ecological perspective 5550
Ecological planning 4888
Ecological public opinion communication network 5350
Ecological resource 4830
ecological risk 5302
economic benefits 5385
Economic development 4798
Economic Efficiency 4804
Economy 5529
Ecosystem 5350
Ecotourism 4861
efficiency analysis 5557
electrical energy 4779
ELISA 5093
embryogenesis 4763
emission 5244
Energy 5033
Energy saving 5244
energy saving transformation 5230
energy savings 4911
engine exhaust products 5244
Environment 4911, 5521
environment friendly 5370
Environmental Kuznets curve 5262
Environmental pollution 4830, 4861, 5437
environmental protection requirements 5244
Environmental remediation 5238
Enzyme 4749
Enzyme inhibitory 4868
equipment energy consumption 5230
erosion thickness 5161
error 5362
Eutrophication 5312
evaluation index 5075
exhaust temperature 5244
Exponential strength criterion 5140

F

feasibility 4911
Fertilizers 5445
financial support 5075
flooding risk 4962
flume experiment 5108
foliar application 5445
footbath 5370
foundation adjacent to slope 5176
fucoxanthin 5421
Fuelwood 4742

G

Gas exchange attributes 4875
Genotype 4928
geographic information system 4962
Germination 4730, 5292
Ghost fishing 5054
gillnets 5054
GMO 4842
Green building 4911
green civilization moral education 5220
green energy 5405
Green supply chain 5557
groundwater 5498
Growth 4771
Guangzhou 5529

H

Hadoop ecosystem 5332
Haihe River Basin 5002
haploidy 4763
health 4787
heat loss rate 5385
Heat pump energy efficiency 4850
Heavy Metal 5194
heavy metals 4787
Heavy oil 5211, 5362
Heavy oil resources 5385
heavy rain 5067
Hepatitis B virus 5093
Hepatitis D virus 5093
Herbicide 5340
high-voltage electrical pulse (HVEP) 5405
Horqin Sandy Land 4730
Huaihe River Basin 4994
hydrocarbon distribution 5161
hydrocarbon generation 5254
hydrogen peroxide 5445

I

indland waters 5054
Infection 4749
influencing factors 5176
Information technology 4836
Informatization 5084
Insect Mortalities 5098
insulation ceiling 5230
intake throttle 5244
Integration 5059
intellectualization 5405
interflow 5108
Internet of Things 5084
Irrigation 4921
Irrigation intervals 4771

J

Junggar Basin 5161

K

Kalman filter 5026, 5033
Kermania pistaciella 5476
Key nodes 5350
Konjak 5040, 5047

L

Land cover change 4901
land management 5356
Landscape Restoration 5194
large-scale atmospheric variable 5002
late post injection 5244
Light reflection 5292
lipid peroxidation 5445
Listeria spp. 5466
livestock manure 5302
logit 4719
lost gear 5054
Low intensity ultrasound 4943
Low latitudes environment 5067
Low power consumption 5033
Low-altitude UAV 5429
Low-carbon economy 5550

M

machine vision 4953
Maize (*Zea mays* L.) 5340
manual energy 4779
Material characteristics 5292
meadow steppe 5320
Measurement method 5350
mechanical energy 4779
medicinal mushrooms 5400
Medicinal tree 4742
Micrococcus/Staphylococcus 5466
Microcystis 4943
microdilution 5395
Mine surveying and mapping. 5429
Mineral Fields 5194
Model 4888
modified biochar 5312
Molecular Characterization 5131
molecular docking 5119
molecular dynamics simulation 5119
Molecular markers 4928
Moran index 5262
morphology 5270
Morphometric analysis 4962
mountainous area 5169
Multi parameter 5026

N

NaCl 4875
Namal valley 4975
Natural Plants 5194
Nitzschia closterium forma minutissima 5421
nutrients loadings 5302

O
oily wastewater 5516
On-Farm Irrigation Management 4804
Ordos Basin 5377
Organic fertilizer 5040
orthogonal test 5516
Oxidant 5400
ozonated water 5370
Ozone disinfection 5370

P
paper and cardboard 4779
parasitoid 5476
Payment environment 5437
PECVD 5516
Pendimethalin 5340
performance 4911
performance evaluation 5002
period ratio 5169
Perlite 4771
permeability enhancement technology 5405
Permian-Carboniferous 5254
Ph. vulgaris 4928
Phaeodactylum 5421
pheromone trap 5476
phosphorus spray 4935
physiological response 4730
Phyto-chemicals 5098
pistachio 5476
Plant extracts 5098
plateau areas 5067
PM2.5 5262
population fluctuations 5476
pore structure 5377
Ports 5084
Potassium iodide 4921
Potato 5149
Potato plant 4771
Potato virus Y 5131
Pregnancy 4984
Prevention 5047
Principles 5550
Product 5521
Proline 4921
properties 5516
Protein 4749
Protein expression 4943
pyrolysis 4756

Q
quality characteristics 5415
Quercus robur L. 5498

R
R410A 4850
Rats 4984
Recombination 5131
Recovery 5211
Refrigerant 4850
Remote sensing technology 5429
Reproduction 4984
Resources 5437
Rice 4935
Risk assessment 4888
RNG k-ε turbulence model 5108
rock characteristics 5377
RT- PCR 5093
Rural tourism 4823

S
sales point 4719
saline sodic soil 4935
salinity 5421
Salmonella spp. 5466
Salt range 4975
sandstone reservoir 5377
SARS-CoV-2 5119,
Saudi Arabia 5131
scenario analysis 4719
SCFAs 5119
screening 5015
SCSI hard disk 5332
Season 5466
Seedling 4842
seedling stage 5015
seismic code 5169
seismic response 5169
semi-arid region 5356
Semi-coke 4756
sensitivity of steam injection parameters 5385
Service quality 4861
S-metolachlor and Foramsulfuron 5340
soil erosion 4962
Soil organic carbon 5356
Soil-borne disease 5047
Solanum tuberosum 5131
solar-induced chlorophyll fluorescence 5320
Sorption 5238
sorting robot 4953
source rock 5254
Southern blight 5040
Spatial measurement model 5262
Spatio-temporal change 4901
spermatheca 5270
SSR 4928
steam absorption 5362
steam absorption profile 5362
steam huff and puff 5211
steam injection thermal recovery technology 5362, 5385
stratified reservoir 5108
surrounding environment 5211
Sustainable 4798

Settleability 4943
Sewage sludge 5302
Simple beam bridge 5169
Simultaneous environmental remediation 5312
sustainable development 5059, 5550, 5557
SYRIII 5131
system realization path 4953

T
Taiyuan metropolitan area 5302
Tangible 4742
tectonic evolution 5161
tectonic shortening 5161
temperature and precipitation 5002
Temperature-Humidity Index 5466
Terminalia arjuna 4742
Terzaghi theory 5176
Thalassiosira weissflogii 5421
thermal history 5254
thermodynamic parameters 5211
Thiourea-modified 5238
Thymus pectinatus 4868
Tillage Practices 4804
Tourism industry 4855
Toxicity 4787, 5098
Traditional Chinese Medicine 5537
trammel nets 5054
Transformation 5149
Transgenic 4842
traps 5054
true triaxial rock strength 5140
Turbidity currents 5108
Turkey 5054, 5187
Two-side market 5437

U
Ultimate bearing capacity 5176
Ultrasonic water meter 5026, 5033
Upper Triassic 5377
Urban gas pipeline 4888
Urbanization construction 4823
Urbanization process 5075

V
vapor pressure deficit 5498
vegetation index 5320
Vegetation phenology 5320
Vertisol Order 5415
Vitamin E 4984

W
wall enclosure 5230
Walnut shell wood vinegar 5047
Wastewater treatment 4779
water management 4962
water potential 4730
Water Productivity 4804
Water stress 4921
Water Table 4804
watershed hydrology 4962
weather 5067
Weather data 4893, 5332
Weeds control 5340
weight 5075
well stress distribution 5140
wellbore 5211
Western Medicine 5537
wheat 5445
Wheat (Triticum aestivum L.) 4804

X
Xylaria 5400

Y
Yeast and Mold 5466
Yield 4771, 4928, 5340, 5486
Yield components 4921

Z
Zea mays L 4842
Zinc Deficiency 4984

1, 2, 3…., 9, 0
1,5-diketone 5395

FEB – GUIDE FOR AUTHORS

General

FEB accepts original papers, review articles, short communications, research abstracts from the entire sphere of environmental-chemistry,-biology,-microbiology,- technology, -biotechnology and-management, furthermore, about residue analysis/ and ecotoxicology of contaminants.

Acceptance or no acceptance of a contribution will be decided, as in the case of other scientific journals, by a board of reviewers. Papers are processed with the understanding that they have not been published before (except in form of an abstract or as a part of a published lecture, review or thesis);that they are not under consideration for publication elsewhere; that their publication has been approved by all co-authors, if any, as well as- tacitly or explicitly- by the responsible authorities at the institute where the work has been carried out and that, if accepted, it will not be published elsewhere in the same form, in either the same or another language, without the consent of the copyright holders.

Language

Papers must be written in English. Spelling may either follow American (Webster) or British (Oxford) usage but must be consistent. Authors who are less familiar with the English language should seek assistance from proficient colleagues in order to produce manuscripts that are grammatically and linguistically correct.

Size of manuscript

Review articles should not exceed 30 typewritten pages. In addition up to 5 figures may be included.

Original papers must not exceed 14 typewritten pages. In addition up to 5 figures may be included.

Short-Communications should be limited to 4 typewritten pages plus not more than 1 illustration.

Short descriptions of the authors, presentation of their groups and their research activities (with photo) should together not exceed I typewritten page. Short research abstracts should report in a few brief sentences (one-fourth to one page) particularly significant findings. Short articles by relative newcomers to the chemical innovation arena highlight the key elements of their Master and PhD-works in about I page.

Book Reviews are normally written in-house, but suggestions for books to review are welcome.

Preparation of manuscript

Dear authors,

FEB is available both as printed journal and as online journal on the web. You can now e-mail your manuscripts with an attached file. Save both time and money. To avoid any problems handling your text please follow the instructions given below:

When preparing your manuscripts have the formula K/SS (Keep It Simple and Stupid) in mind. Most word processing programs such as MS-Word offer a lot of features. Some of them can do serious harm to our layout. So please do not insert hyperlinks and/or automatic cross-references, tables of contents, references, footnotes, etc.

1. Please use the standard format features of your word processor (such as standard.dot for MS Word).
2. Please do not insert automatisms or secret link-ups between your text and your figures or tables. These features will drive our graphic department sometimes mad.
3. Please only use two fonts for text or tables "Times New Roman" and for graphical presentations "Arial".
4. Stylesheets, text, tables and graphics in shade of grey
5. Turn on the automatic language detection in English (American or British)
6. Please - check your files for viruses before you send them to us!!

Manuscripts should be uploaded on our website prt-parlar.de

Thank you very much!

STRUCTURE OF THE MANUSCRIPT

Title page: The first page of the manuscript should contain the following items in the sequence given: A concise title of the paper (no abbreviations). The names of all authors with at least one first name spelled out for every author. The names of Universities with Faculty, City and Country of all authors.

Abstracts: The second page of the manuscript should start with an abstract that summarizes briefly the contents of the paper (except short communications). Its length should not exceed 150-200 words. The abstract should be as informative as possible. An extended repetition of the paper's title is not considered to be an abstract.

Keywords: Below the Summary up to 6 key words have to be provided which will assist indexers in cross-indexing your article.

Introduction: This should define the problem and, if possible, the frame of existing knowledge. Please ensure that people not working in that particular field will be able to understand the intention. The word length of the introduction should be 150 to 300 words.

Materials and methods:
Please be as precise as possible to enable other scientists to repeat the work.

Results: Only material pertinent to the subject must be included. Data must not be repeated in figures and tables.

Acknowledgements: Acknowledgements of financial support, advice or other kind of assistance should be given at the end of the text under the heading "Acknowledgements". The names of funding organisations should be written in full.

References: Responsibility for the accuracy of references rests with the authors. References are to be limited in number to those absolutely necessary. References should appear in numerical order in brackets and in order of their citation in the text. They should be grouped at the end of the paper in numerical order of appearance. Abbreviated titles of periodicals are to be used according to Chemical or Biological Abstracts, but names of lesser known journals should be typed in full. References should be styled and punctuated according to the following examples:

ORIGINAL PAPERS:
l. Author, N.N. and Author, N.N. (Year) Full title of the article. Journal and Volume, first and last page.

BOOK OR PROCEEDING:
2. Surname, N., Surname, N.N., Surname, N.N., Surname, N. (Year) Title of the contribution. In: Title of the book or proceeding. Volume, Publisher, City, first and last page

DOCTORAL THESIS:
3. Author, N.N. (Year) Title of the thesis, University and Faculty, City

UNPUBLISHED WORK:
Papers that are unpublished but have been submitted to a journal may be cited with the journal's name followed by "in press". However, this practice is acceptable only if the author has at least received galley proofs of his paper. In all other cases reference must be made to “unpublished work" or "personal communication".

Discussion and Conclusion: This part should interpret the results in reference to the problem outlined in the introduction and of related observations by the author/s or others. Implications for further studies or application may be discussed. A conclusion should be added if results and discussion are combined.

Corresponding author: The name of the corresponding author with complete postal address